Cover Picture



Hong Lin and Samuel J. Danishefsky*

The Art of Synthesis and the beauty of Nature lure so many chemists into total synthesis. The cover picture shows yellow jasmine in full bloom, from which the poisonous alkaloid gelsemine was isolated. The formula of gelsemine and important intermediates from six total syntheses are overlaid on the photograph. From these syntheses, we can learn which strategies represent the fastest and/or most efficient routes to the target. More about this fascinating compound and organic synthesis at its best can be found in the Review by S. J. Danishefsky and H. Lin on pg. 36 ff.

You're only as good as your last success

Thank you John, thank you Steve!

The October issue of *Chemical Reviews*, one of the journals published by the American Chemical Society, is dedicated to the topic "Recoverable Catalysts and Reagents". The Editor of that issue (and Associate Editor of the journal) is *John* A. Gladysz, Professor at the Universität Erlangen-Nürnberg, who writes in the last paragraph of his Editorial "It presages an era in which syntheses of all types may be conducted in toto with recoverable catalysts and reagents. Indeed, the dawn of this epoch was recently evinced by a multistep total synthesis of an amaryllidaceae alkaloid that used only supported reagents and scavengers (Baxendale, I. R.; Ley, S. V.; Piutti, C., *Angew. Chem.* 2002, *114*, 2298; *Angew. Chem. Int. Ed.* 2002, *41*, 2194)—no less than 13 immobilized systems!" The cited publication from *Steve* Ley, Professor at the University of Cambridge and the most recent president of the Royal Society of Chemistry, is a perfect example of the type of Communication that *Angewandte Chemie* publishes. Even if not every Communication published in this journal marks the beginning of a new epoch, then it is certainly to be expected that as many of this type of article as possible, from the full spectrum of chemistry, are to be found in the pages of "*Angewandte*."

Excellent work must also be excellently presented. In this respect *Angewandte Chemie* has certainly led the way in the past and it has been the model for the development of many scientific journals. However, keeping in mind that the old sayings "you don't keep ahead by standing still" and "you're only as good as your last success" bear more than a grain of truth, then the change to weekly publication is the ideal time to make some changes from which readers and authors will profit. In discussions with the German Chemical Society's (GDCh's) Editorial and International Advisory Board, as well as in the publishing house, and in particular with the Editorial team the structure and the layout of the journal have been revised, as you can see from the issue or computer screen in front of you. What has changed and what has stayed the same?

1. On the cover, the trademark round picture naturally remains. However, the typeface of the title has been altered. Instead of very bold block capitals the title is now a lighter, but still striking, standard text in the Scala Sans font and the word *Chemie* is in blue: *Angewandte Chemie* is full of life, colorful, and multifaceted as shown by the title text itself. The frequently and affectionately used short form of the title "*Angewandte*" can of course continue to be used (Germans like to use derived versions of this too).

2. The sequence of the sections has been rearranged so that the shorter sections come together in a block after the Table of Contents. Up to now the Essays and Highlights, which take up only a few pages, were sandwiched between the longer Review articles and the substantial Communications section, and the Book and Website reviews were somewhat tacked on the end. Now you will find these smaller important sections, which add to the liveliness of the journal, grouped together at the front of the issue. In the future this will also be the place for reports on selected conferences, in which the current state of a field, and not a list of the lectures, should be given. In addition, obituaries of scientists who have made outstanding contributions to their subject areas will be published here. These short sections will often be followed by a Minireview, then usually a Review, and finally the Communications. The indexes remain at the end of the issue, as does the preview of the next issue, which has also undergone a facelift.

3. The layout changes that really stand out are: The distinctive round cover-picture motif, which has become a trademark of the quality of contributions in *Angewandte Chemie*, is now featured in several variations, not just on the cover. The full-page graphics at the start of Reviews and the beginning of the Communications section (the frontispieces) are also in this circular form. In addition small circular icons serve as a guiding element in the headers throughout an issue. For the benefit of speed readers, short eye-catching headlines have been added in prominent banners above the actual titles of the articles; these banners are color coded in the Table of Contents for the different sections of the journal. These headlines have the function, not only of helping readers to find their way rapidly through the issue, but also to act as a lure to the article.

Angewandte International Edition Chemie

Setting up lures to entice the reader is, after the selection of articles to publish, one of the most important roles of the Editorial team. Readers want to have their curiosity aroused, and authors want their article to receive as much attention as possible. To ensure both these aims are realized there are many other small changes to the journal that I have not mentioned.

"When the new issue hits the reader's desk, he says, "Okay, startle me!" That's the editor's challenge."
Dennis Flanagan, former Editor of *Scientific American*

All the above naturally applies to the printed as well as the elec-

© 2003 Wiley-VCH Verlag GmbH & Co. KGaA, Weinheim
1433-7851/03/4201-0004 $ 20.00+.50/0

Table 1: Editors, chairmen of the Editorial Boards, and Impact Factors of *Angewandte Chemie*, *Chemistry—A European Journal*, *ChemBioChem* and *ChemPhysChem*, as well as the *European Journal of Inorganic Chemistry* and the *European Journal of Organic Chemistry*.

Journal	Editor	Chairman of the Editorial Board	Impact Factor
Angew. Chem.	Peter Gölitz	Horst Kessler	8.255
Chem. Eur. J.	Neville Compton	Jan-Erling Bäckvall	4.614
ChemBioChem	Peter Gölitz[a]	Alan R. Fersht/Jean-Marie Lehn	2.920
ChemPhysChem	Peter Gölitz[b]	James T. Hynes/Frans C. De Schryver	4.217
Eur. J. Inorg. Chem.	Karen J. Hindson	Ivano Bertini	2.475
Eur. J. Org. Chem.	Haymo Ross	Henning Hopf	2.193

[a] Deputy Editor: Kathryn Wright. [b] Associate Editor: Carol Stanier.

tronic version of *Angewandte Chemie*. Worldwide more and more people read the journal online; within 18 months the number of full-article downloads has doubled and it is not unknown for an individual article to be downloaded over ten thousand times (and we hope that it is actually read). Everyone, not only subscribers, can receive the Table of Contents of the issue by e-mail when it is published ("Content Alerts"), and now you can also receive automatically thematic information about titles and authors of the current articles ("Profiled Alerts"). More information about this service can be found under www.interscience.wiley.com/alerts. Further improvements to the online presentation of *Angewandte Chemie* are in progress. Since March last year it has been possible to submit manuscripts online; this saves postage costs and time, and our authors have been very fast in taking advantage of this service: around 80% of manuscripts reach us this way. Naturally, whenever possible, we send manuscripts to the referees electronically, and more than 90% of the referee reports are now returned by this means. A complete online platform for the submission and refereeing of manuscripts as well as for the production process has been developed by the publishing house, and a prototype is currently being tested with the *European Journal of Inorganic Chemistry*.

Table 2: Country of origin of Communications submitted between January and November 2001 and 2002. Manuscripts with authors from several countries are assigned to the country of the submitting author.

Country	2001	%	2002	%
USA	373	(19)	417	(19)
Japan	272	(14)	323	(14)
Germany	337	(17)	322	(14)
China (P.R.)	210	(11)	321	(14)
Great Britain	105	(5)	119	(5)
Spain	67	(3)	87	(4)
France	93	(5)	84	(4)
South Korea	71	(3)	82	(4)
India	67	(3)	70	(3)
Italy	56	(3)	58	(3)
Switzerland	52	(3)	47	(2)
Canada	48	(2)	47	(2)
Netherlands	30	(2)	29	(1)
Taiwan (R.C.)	25	(1)	30	(1)
Israel	26	(1)	23	(1)
Poland	11	(1)	15	(1)
Sweden	11	(1)	14	(1)
Greece	8	(0.5)	13	(1)
Singapore	13	(1)	13	(1)
Russia	9	(0.5)	11	(1)
Others	74	(4)	82	(4)
Total	1958	100	2207	100

On the theme of the European Journals: Since the start of this year, all the journals in the "family" have adopted the same structure, modeled on *Angewandte Chemie*. The aims and scope of a journal, as well as advising and supervising the Editors, is the responsibility of the Editorial and Advisory Boards of the societies co-owning the journals; the daily running is the responsibility of well-trained Editors, whose offices are close to each other (for more information see Table 1). This arrangement facilitates the rapid transfer of manuscripts from one journal to another, as the format or degree of specialty of the manuscript requires. To date, manuscripts that were too long or too specialized for *Angewandte Chemie* could be transferred to *Chemistry—A European Journal*, *ChemBioChem*, or *ChemPhysChem*. In spite of the increased frequency of publication, the rejection rate for *Angewandte Chemie* of over 60% in 2002 will in all probability increase further, given the continuous increase in submissions over the last decade. Last year alone 15% more Communications were received than in 2001! Table 2 gives a breakdown of their origins and a comparison with the submissions for 2001.

We hope that this year you will again find many epoch-making publications in the pages of this journal, whether they are from John or Steve, from other famous and established authors, or from those who are just at the start of their careers. Daniel Bellus, a member of the International Advisory Board of *Angewandte Chemie*, once said to me: "The best never rest". With that in mind I am confident that we can offer you a highly exciting *Angewandte* in 2003.



Peter Gölitz

PS: The short Notice to Authors describing the different sections of the journal can be found in this issue after the Table of Contents; full details for the preparation of manuscripts, as well as templates for the design of cover pictures and frontispieces are published on our homepage (www.angewandte.org).

 © 2003 Wiley-VCH Verlag GmbH & Co. KGaA, Weinheim 1433-7851/03/4201-0005 $ 20.00+.50/0

Contents

Obituary

George Porter (1920–2002) —— **18–19** — Kinetics Research and the Public Understanding of Science — *J. M. Thomas, R. Mason*

Web Sites

http://www.exploratorium.edu/cooking —— **20** — Whats's Cooking on the Web? — *H. This*

Books

Computational Molecular Spectroscopy —— **21** — Per Jensen, Philip R. Bunker — *C. Mück-Lichtenfeld*

Glycoscience —— **22** — Bertram Fraser-Reid, Kuniaki Tatsuta, Joachim Thiem — *T. Opatz, H. Kunz*

The One Culture? —— **22** — Jay A. Labinger, Harry Collins — *P. Laszlo*

Highlights

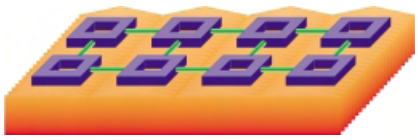
Surface Nanotechnology

Stefan Hecht* —— **24–26**

Welding, Organizing, and Planting Organic Molecules on Substrate Surfaces—Promising Approaches towards Nanoarchitectonics from the Bottom up

Keywords:
nanomaterials · scanning probe microscopy · self-assembly · single molecules

Single molecule reactivity, self-assembly, and self-directed growth can be used to generate patterns on the nanometer scale. For example, molecular building blocks can be organized on substrate surfaces (see picture). New approaches that take advantage of single-molecule reactivity and self-organization, as well as stabilization of structures on substrate surfaces, are introduced.

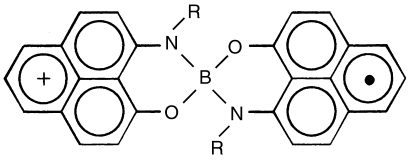


Structural Control of Properties

Joel S. Miller* —— **27–29**

Bistable Electrical, Optical, and Magnetic Behavior in a Molecule-Based Material

Keywords:
bistability · conducting materials · dimerization · hysteresis · spiro compounds



Neutral alkyl-substituted spirobiphenalenyl radicals (see formula) were recently reported that exhibit bistability as a consequence of temperature-dependent hysteretic switching. The high- and low-temperature forms display significant differences in their electrical, optical, and magnetic properties.

© 2003 Wiley-VCH Verlag GmbH & Co. KGaA, Weinheim

1433-7851/03/4201-0006 $ 20.00+.50/0



Success squared! The French mathematician Jacques Hadamard (1865–1963; pictured) significantly improved the analysis of complex signals by introducing a decomposition based on square waves. A review is presented of the application of the Hadamard transform to time-of-flight mass spectrometry. The primary benefit of this technique is the gain in signal-to-noise ratio associated with signal multiplexing.

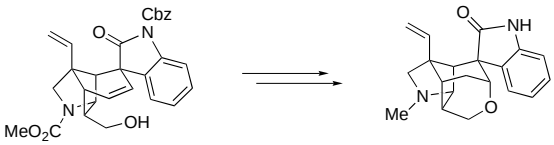
Minireviews

High-Speed Mass Spectrometry

Richard N. Zare,* Facundo M. Fernández, Joel R. Kimmel ——— **30–35**

Hadamard Transform Time-of-Flight Mass Spectrometry: More Signal, More of the Time

Keywords:
analytical methods · Hadamard transform · mass spectrometry · signal multiplexing



1

Reviews

Total Syntheses of Gelsemine

Hong Lin, Samuel J. Danishefsky* ——— **36–51**

Gelsemine: A Thought-Provoking Target for Total Synthesis

Keywords:
natural products · polycycles · stereoselective synthesis · total synthesis

Seven total syntheses of the title compound **1** have already been reported. In this Review, the authors discuss the fascinating strategies (e.g. see scheme) employed in the various assemblies of the key fragments, including the quaternary center C20, the oxindole moiety, and the bicyclooctane residue.

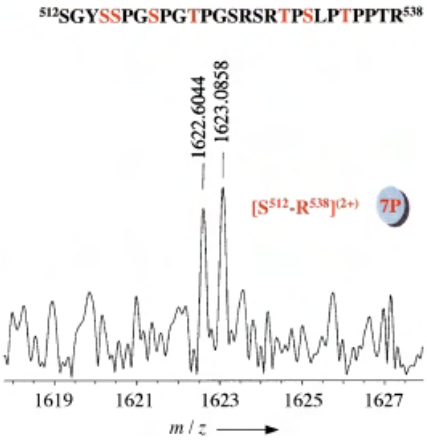
Communications

Mass Spectrometry of Biopolymers

Joël S. Rossier, Nikolay Youhnovski, Niels Lion, Eugen Damoc, Susanne Becker, Frédéric Reymond, Hubert H. Girault, Michael Przybylski* ——— **54–58**

Thin-Chip Microspray System for High-Performance Fourier-Transform Ion-Cyclotron Resonance Mass Spectrometry of Biopolymers

Keywords:
analytical methods · biopolymers · combinatorial chemistry · mass spectrometry · proteomics



Microchip innovation: A thin-film microchip system has been developed for microelectrospray Fourier-transform ion-cyclotron resonance mass spectrometry. Application perspectives include the analysis of combinatorial libraries and high-performance proteomics (as shown for the peptide fragment of the phosphorylation domain (512–538) of human neurofibrillary tau protein; the seven phosphorylation sites are indicated in red).

For the USA and Canada:
ANGEWANDTE CHEMIE International Edition (ISSN 1433-7851) is published weekly by Wiley-VCH PO Box 191161, D 69451 Weinheim, Germany. Air freight and mailing in the USA by Publications Expediting Inc. 200 Meacham Ave., Elmont, NY 11003. Periodicals postage paid at Jamaica NY 11431. US POSTMASTER: send address changes to *Angewandte Chemie*, Wiley-VCH, 111 River Street, Hoboken, NJ 07030. Annual institutional subscription price for institutions: Europe € 2998.00/3148.00. Outside Europe US$ 3718.00/3904.00 (valid for print or electronic/print and electronic delivery); for individuals who are personal members of a national chemical society, or whose institution already subscribes, or who are retired or self-employed consultants, print only (including postage and handling charges): Europe € 248.00/Outside Europe US$ 348.00.

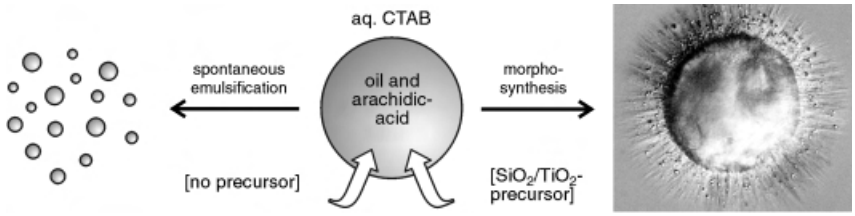
 © 2003 Wiley-VCH Verlag GmbH & Co. KGaA, Weinheim 1433-7851/03/4201-0007 $ 20.00+.50/0

Contents

Biomineralization

Dirk Volkmer,* Stefano Tugulu, Matthias Fricke, Tim Nielsen — **58–61**

Morphosynthesis of Star-Shaped Titania–Silica Shells



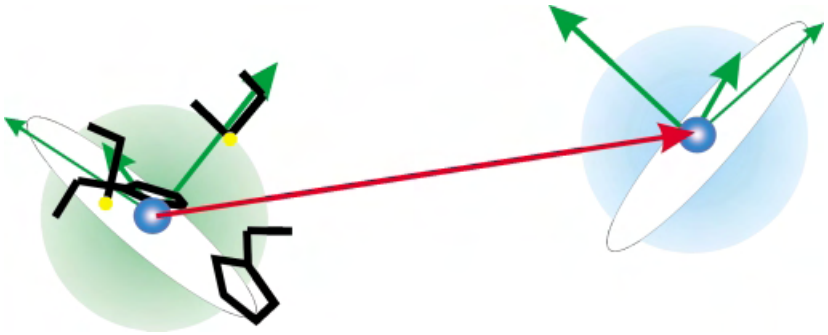
Keywords:
bioinorganic chemistry · biomimetic synthesis · biomineralization · emulsions · surfactants

A self-organized dynamic growth process ("morphosynthesis") involving mineral formation at a membrane-type surface leads to discrete inorganic shells of star-shape morphology (see picture). CTAB = cetyltrimethylammonium bromide.

Distances Given by Pulsed EPR

Irene M. C. van Amsterdam, Marcellus Ubbink, Gerard W. Canters, Martina Huber* — **62–64**

Measurement of a Cu—Cu Distance of 26 Å by a Pulsed EPR Method



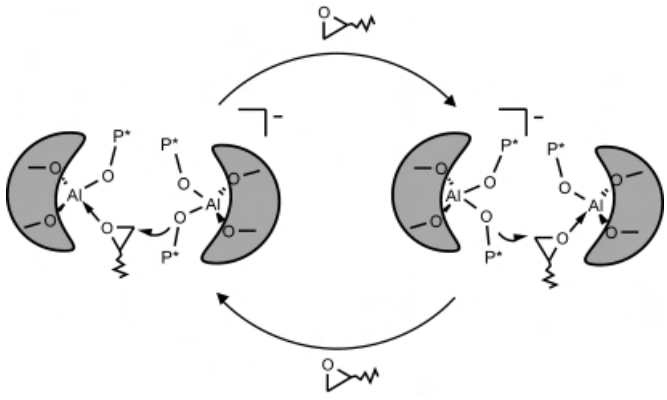
Keywords:
copper · EPR spectroscopy · metalloproteins · structure elucidation

Distances between paramagnetic transition-metal ions in compounds can be studied by using the pulsed electron–electron double-resonance method. Hereby, the relative orientation (red arrow) of the metal centers (Cu^{II}, blue sphere), as well as the principal axes of the *g* tensor (green arrows) relative to the ligands play an important role (schematic representation: dimer of the copper protein azurin).

Propylene Oxide Polymerization

Wigand Braune, Jun Okuda* — **64–68**

An Efficient Method for Controlled Propylene Oxide Polymerization: The Significance of Bimetallic Activation in Aluminum Lewis Acids

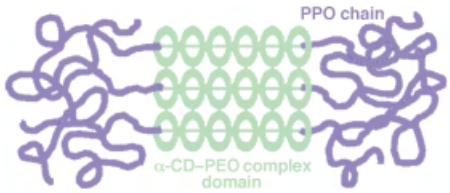


Keywords:
aluminum · epoxides · O ligands · regioselectivity · ring-opening polymerization

Combined strength: Only the combination of aluminate complexes with their neutral Lewis acids allows the controlled regioregular ring-opening polymerization of industrially important propylene oxide. The chain propagation proceeds at both aluminium centers according to a novel mechanism (see scheme).

© 2003 Wiley-VCH Verlag GmbH & Co. KGaA, Weinheim

1433-7851/03/4201-0008 $ 20.00+.50/0



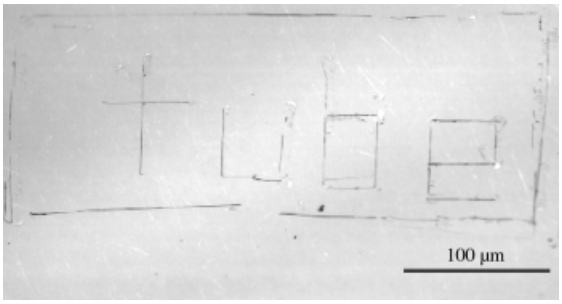
Polypseudorotaxanes

Jun Li,* Xiping Ni, Kam Leong — 69 – 72

Block-Selected Molecular Recognition and Formation of Polypseudorotaxanes between Poly(propylene oxide)-Poly(ethylene oxide)-Poly(propylene oxide) Triblock Copolymers and α-Cyclodextrin

Keywords:
block copolymers · cyclodextrins · inclusion compounds · molecular recognition · pseudorotaxanes

Although a poly(propylene oxide) (PPO) chain was previously thought to be impenetrable to α-cyclodextrin, the middle poly(ethylene oxide) (PEO) block of PPO-PEO-PPO triblock copolymers can be selectively recognized and included by α-cyclodextrin to form polypseudorotaxanes (see schematic representation), even though it is flanked by two PPO blocks.



Lipid Nanotubes

Hiroshi Frusawa, Akihiro Fukagawa, Yuki Ikeda, Jun Araki, Kohzo Ito,* George John, Toshimi Shimizu* — 72 – 74

Aligning a Single-Lipid Nanotube with Moderate Stiffness

Keywords:
lipids · nanotubes · self-assembly · supramolecular chemistry

Bendy tubes: Lipid nanotubes can be aligned by a novel and simple method, whereby a fine line of a single nanotube is drawn freely by microinjecting the aqueous dispersion onto a glass plate. This technique is simple and highly adaptable; even words can be written (see picture)! The tubes can be bent and their Young's modulus measured by manipulation with optical tweezers.

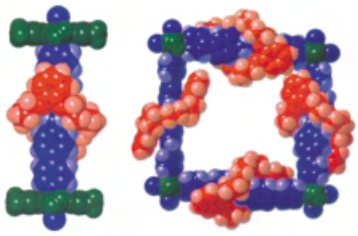
Metal-Based Polyrotaxanes

Gregory J. E. Davidson, Stephen J. Loeb* — 74 – 77

Channels and Cavities Lined with Interlocked Components: Metal-Based Polyrotaxanes That Utilize Pyridinium Axles and Crown Ether Wheels as Ligands

Keywords:
coordination polymers · crystal engineering · rotaxanes · self-assembly · supramolecular chemistry

One- and two-dimensional coordination polymers (see picture) in which the bridging ligands are coated with crown ethers (red) can be prepared by metal–ligand self-assembly. These metal-based polyrotaxanes contain channels and cavities that are lined with mechanically linked molecular components. This structural design has significant potential for tuning the physical properties of internal cavities and the production of materials that contain functional molecular entities that may be addressable or controllable.



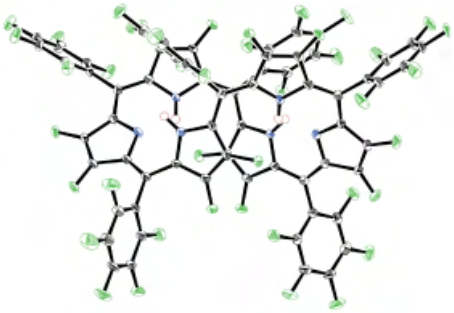
 © 2003 Wiley-VCH Verlag GmbH & Co. KGaA, Weinheim 1433-7851/03/4201-0009 $ 20.00+.50/0

Contents

Expanded Porphyrins

Soji Shimizu, Ji-Young Shin, Hiroyuki Furuta,* Rami Ismael, Atsuhiro Osuka* ——— **78 – 82**

Perfluorinated *meso*-Aryl-Substituted Expanded Porphyrins



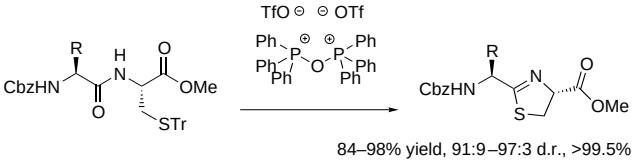
Twisted figure-of-eight structures are found for the perfluorinated *meso*-aryl-substituted expanded porphyrins synthesized from 3,4-difluoropyrrole and pentafluorobenzaldehyde under modified Rothemund–Lindsey conditions. The crystal structure of the [26]hexaphyrin (see picture) consists of two almost planar tripyrrolic subunits which are tilted by approximately 60° in which a distinct alternation in the bond lengths of the π-electronic system is evident.

Keywords:
aromaticity · fluorinated ligands · macrocyclic ligands · porphyrinoids

Biomimetic Heterocycle Synthesis

Shu-Li You, Hossein Razavi, Jeffery W. Kelly* ——— **83 – 85**

A Biomimetic Synthesis of Thiazolines Using Hexaphenyloxodiphosphonium Trifluoromethanesulfonate



Most chemical syntheses of thiazolines use serine residues, whereas nature employs cysteine residues. In a biomimetic approach, $[(Ph_3P^+)_2O](OTf^-)_2$ was used to promote triphenylmethyl (Tr) deprotection and dehydrocyclization of simple cysteine *N*-amides to give thiazolines in excellent chemical and optical yields (see scheme). This mild method was extended to the synthesis of, for example, thiazolines from cysteine-containing dipeptides in high yield and without significant loss of chirality at the C2-exomethine carbon atom. TF = trifluoromethanesulfonyl, Cbz = benzyloxycarbonyl

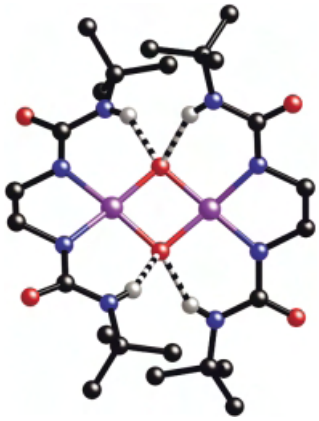
Keywords:
asymmetric synthesis · biomimetic synthesis · cyclization · dehydrogenation · heterocycles

H-Bond-Supported Oxo Bridges

Peter L. Larsen, Terry J. Parolin, Douglas R. Powell, Michael P. Hendrich, A. S. Borovik* ——— **85 – 89**

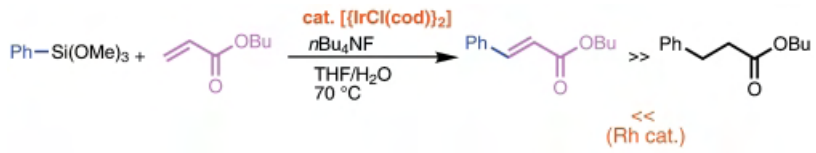
Hydrogen Bonds around $M(\mu\text{-}O)_2M$ Rhombs: Stabilizing a $\{Co^{III}(\mu\text{-}O)_2Co^{III}\}$ Complex at Room Temperature

Hydrogen bonds to metal complexes located within the active sites of proteins have been implicated in the regulation of function. Incorporation of these noncovalent interactions into a synthetic system with bridging oxo ligands is reported. Unprecedented thermal stability of a complex with a $\{Co^{III}(\mu\text{-}O)_2Co^{III}\}$ core is observed (see picture), in which intramolecular hydrogen bonds to the oxo ligands are present.



Keywords:
cobalt · hydrogen bonds · IR spectroscopy · isotope effects · oxo ligands

© 2003 Wiley-VCH Verlag GmbH & Co. KGaA, Weinheim
1433-7851/03/4201-0010 $ 20.00+.50/0



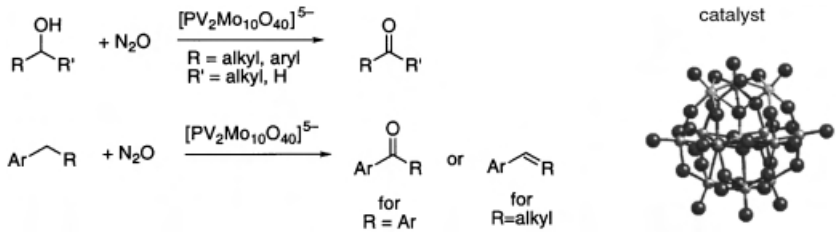
Ir-Catalyzed C-C Bond Formation

Tooru Koike, Xiaoli Du, Tomoyuki Sanada, Yasuaki Danda, Atsunori Mori* ——— 89 – 92

Iridium-Catalyzed Mizoroki–Heck-Type Reaction of Organosilicon Reagents

Keywords:
alkoxysilanes · C–C coupling · homogeneous catalysis · iridium · silicon

Independent of substrate and solvent, the C–C bond-forming reaction of organosilicon reagents with α,β-unsaturated carbonyl compounds can be catalyzed by an iridium complex to give exclusively the Mizoroki–Heck-type addition/elimination product (see scheme). This result sharply contrasts the analogous reaction with a rhodium catalyst under similar conditions in which the 1,4-addition product is obtained preferentially. cod = cycloocta-1,5-diene.



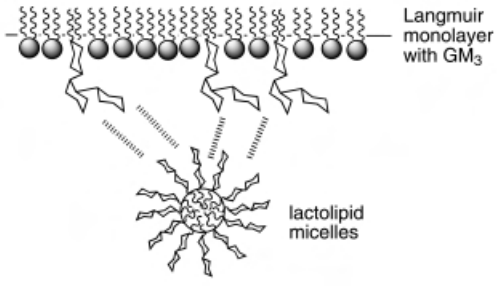
Polyoxometalate Catalysts

Revital Ben-Daniel, Ronny Neumann* ——— 92 – 95

Activation of Nitrous Oxide and Selective Oxidation of Alcohols and Alkylarenes Catalyzed by the $[PV_2Mo_{10}O_{40}]^{5-}$ Polyoxometalate Ion

Keywords:
alcohols · homogeneous catalysis · nitrogen oxides · oxidation · polyoxometalates

A vanadium-substituted polyoxomolybdate ion ($[PV_2Mo_{10}O_{40}]^{5-}$, top right) can activate nitrous oxide to promote the highly selective catalytic oxidation of primary and secondary alcohols to aldehydes and ketones, and the oxidation of various alkylaromatic substrates (see scheme).



Carbohydrate–Carbohydrate Interactions

Paul V. Santacroce, Amit Basu* ——— 95 – 98

Probing Specificity in Carbohydrate–Carbohydrate Interactions with Micelles and Langmuir Monolayers

Keywords:
carbohydrates · glycolipids · membranes · molecular recognition · noncovalent interactions

The epimerization of a single axial hydroxy group in a carbohydrate can affect carbohydrate–carbohydrate interactions significantly. Glycolipid micelles and glycolipid-containing Langmuir monolayers (see picture) were used to model these key interactions on the molecular level. (GM_3 is the ganglioside sialosyl-lactosylceramide found on the surface of melanoma cells.)

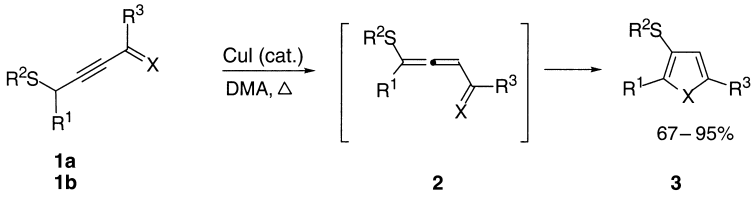
 © 2003 Wiley-VCH Verlag GmbH & Co. KGaA, Weinheim 1433-7851/03/4201-0011 $ 20.00+.50/0

Contents

Synthesis of Pyrroles and Furans

Joseph T. Kim, Alexander V. Kel'in, Vladimir Gevorgyan* ——— **98 – 101**

1,2-Migration of the Thio Group in Allenyl Sulfides: Efficient Synthesis of 3-Thio-Substituted Furans and Pyrroles



1a
1b
2
3

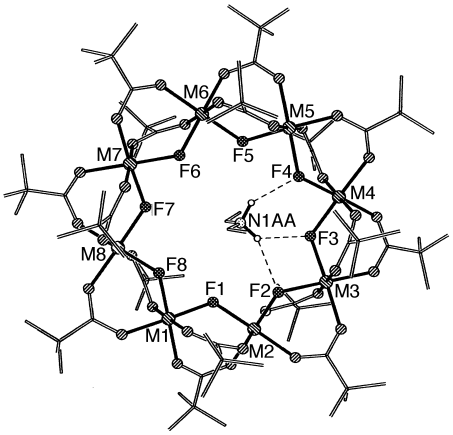
The copper-catalyzed cycloisomerization of thioalkynyl ketones **1a** and thioalkynyl imines **1b** allows the efficient synthesis of 3-thio-substituted furans **3a** and pyrroles **3b**, an important class of heterocyclic unit previously inaccessible by standard cycloisomerization techniques. A plausible mechanism for this unusual cascade involves a 1,2-migration of the thio group in the intermediate keto- and iminoallenyl sulfides **2**. DMA = *N*,*N*-dimethylacetamide.

Keywords:
cyclization · heterocycles · homogeneous catalysis · nitrogen heterocycles · sulfur

Heterometallic Wheel Complexes

Finn K. Larsen, Eric J. L. McInnes, Hassane El Mkami, Jacob Overgaard, Stergios Piligkos, Gopalan Rajaraman, Eva Rentschler, Andrew A. Smith, Graham M. Smith, Val Boote, Martin Jennings, Grigore A. Timco,* Richard E. P. Winpenny* ——— **101 – 105**

Synthesis and Characterization of Heterometallic $\{Cr_7M\}$ Wheels



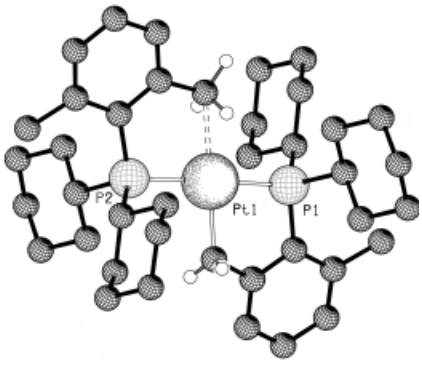
A new set of wheels: Substituting a chromium ion in $[Cr_8F_8(O_2CCMe_3)_{16}]$ with one of a number of alternative transition metals has yielded an unprecedented family of heterometallic wheel complexes (see picture), supported at their centers by secondary ammonium ions. Both 3d (Mn, Fe, Co, Ni) and 4d (Cd) metals have been employed to produce such structures, the magnetic and spectroscopic properties of which are discussed.

Keywords:
cage compounds · chromium · EPR spectroscopy · heterometallic complexes · magnetic properties

14-Electron Platinum(II) Complexes

Walter Baratta,* Sergio Stoccoro,* Angelino Doppiu, Eberhardt Herdtweck, Antonio Zucca, Pierluigi Rigo ——— **105 – 109**

Novel T-Shaped 14-Electron Platinum(II) Complexes Stabilized by One Agostic Interaction



The stereoelectronic properties of the $PR_2(2,6\text{-}Me_2C_6H_3)$ (R = Ph, Cy) ligand can be used to stabilize an unprecedented class of 14-electron platinum(II) complexes. The X-ray analysis of the cyclometalated cyclohexyl derivative reveals an agostic interaction between the Pt center and an *o*-methyl moiety (see picture). The fast and reversible formation of three-coordinate platinum–hydrido complexes occurs by reaction with H_2, and is achieved through the cleavage of a platinum–carbon bond.

Keywords:
agostic interactions · phosphane ligands · platinum · X-ray diffraction

© 2003 Wiley-VCH Verlag GmbH & Co. KGaA, Weinheim

1433-7851/03/4201-0012 $ 20.00+.50/0

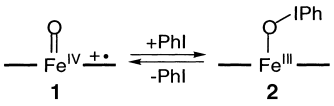
Iron Porphyrin Complexes

Wonwoo Nam,* Sun Kyung Choi, Mi Hee Lim, Jan-Uwe Rohde, Inwoo Kim, Jinheung Kim, Cheal Kim, Lawrence Que, Jr.* 109 – 111

Reversible Formation of Iodosylbenzene–Iron Porphyrin Intermediates in the Reaction of Oxoiron(IV) Porphyrin π-Cation Radicals and Iodobenzene

Keywords:
enzyme models · epoxidation · iron · porphyrinoids · radical ions

The electronic nature of iron porphyrin complexes and iodobenzene derivatives markedly influences the formation of iodosylbenzene–iron(III) porphyrin intermediates **2**, which are generated in the reaction of oxoiron(IV) porphyrin cation radicals **1** and iodobenzene. Epoxidation



1 **2**

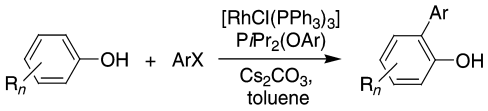
of olefins by **2** affords high yields of epoxide products.

Direct Aryl Halide Phenol Coupling

Robin B. Bedford,* Simon J. Coles, Michael B. Hursthouse, Michael E. Limmert 112 – 114

The Catalytic Intermolecular Orthoarylation of Phenols

Keywords:
arylation · homogeneous catalysis · P ligands · phenols · rhodium



(1)

The use of Wilkinson's catalyst with diisopropylphosphinite ligands acting as cocatalysts allows the catalytic ortho-arylation of phenols [Eq. (1)], a process that relies on a C–H activation of a phenol that has been incorporated into the cocatalyst by transesterification.

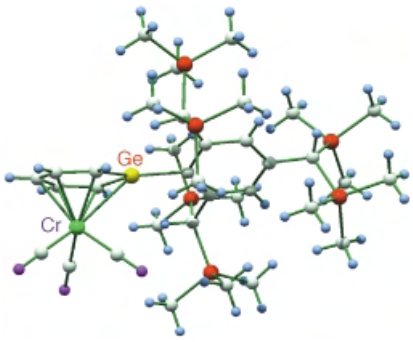
Aromaticity of Germabenzenes

Norio Nakata, Nobuhiro Takeda, Norihiro Tokitoh* 115 – 117

η^6-Germabenzene Complexes of Chromium and Molybdenum

Keywords:
arene ligands · coordination modes · germanium · metallacycles · transition metals

η^6-Bonding characteristics are exhibited by stable germabenzene complexes that are stabilized with the extremely bulky 2,4,6-tris[bis(trimethylsilyl)methyl]phenyl ligand. The ring system coordinates to transition-metal centers (M = Cr, Mo; see picture) to give the first evidence of the aromatic character in germabenzene complexes, from the standpoint of their chemical reactivity.



 © 2003 Wiley-VCH Verlag GmbH & Co. KGaA, Weinheim 1433-7851/03/4201-0013 $ 20.00+.50/0

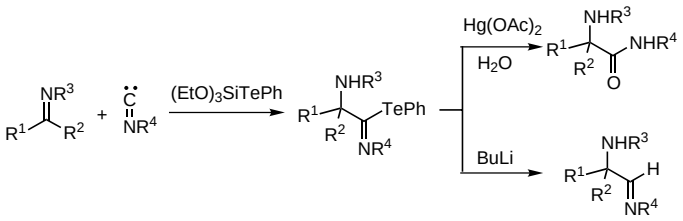
Contents

Synthesis of Amino Acid Derivatives

Shigeru Yamago,* Hiroshi Miyazoe, Takeyoshi Nakayama, Masaki Miyoshi, Junichi Yoshida* _____ **117 – 120**

A Diversity-Oriented Synthesis of α-Amino Acid Derivatives by a Silyltelluride-Mediated Radical Coupling Reaction of Imines and Isonitriles

Keywords:
C–C coupling · multicomponent reactions · radical reactions · synthetic methods · tellurium



A radical idea: A diversity-oriented synthesis of α-amino acid derivatives is realized by the silyltelluride-mediated radical coupling of imines and isonitriles followed by various transformations of the carbon–tellurium bond of the coupling products (see scheme). The α-amino radical generated from the imine and the silyltelluride is the key intermediate in the coupling reaction.

VIP Communications labeled with this symbol have been judged by two referees as being "very important papers".

The publication of Communications labeled with this symbol has been accelerated because of their topical or highly competitive nature.

Supporting information for articles labeled with this symbol can be found at www.angewandte.org or www.interscience.wiley.com.

Sources

Product and Company Directory

You can start the entry for your company in "Sources" in any issue of *Angewandte Chemie*.

If you would like more information, please do not hesitate to contact us.

Wiley-VCH Verlag – Advertising Department
Tel.: 0 62 01 - 60 65 65
Fax: 0 62 01 - 60 65 50
E-Mail: MSchulz@wiley-vch.de

Service

Keywords _____ *122*

Authors _____ *123*

Angewandte's Sister Journals _____ *124 – 125*

Preview _____ *127*

 © 2003 Wiley-VCH Verlag GmbH & Co. KGaA, Weinheim 1433-7851/03/4201-0014 $ 20.00+.50/0

Surface nanotechnology

Welding, Organizing, and Planting Organic Molecules on Substrate Surfaces—Promising Approaches towards Nanoarchitectonics from the Bottom up**

*Stefan Hecht**

Keywords:
nanomaterials · scanning probe microscopy · self-assembly · single molecules

The rapidly evolving field of nanotechnology[1] has so far primarily benefited from the development of instrumentation by the physical community, which enables visualization and manipulation of matter down to the atomic level.[2] These major advances have propelled us chemists into the unique position of gaining fundamental insights into the dynamics and reactivity of single molecules[3] and furthermore to exploit this knowledge for the bottom-up approach to nanofabrication, which promises to revolutionize future device miniaturization and electronics.[1,4]

Our ability to custom-design and synthesize programmed molecular objects will be crucial to construct functional nanoscale architectures. These molecules will serve as the functional building blocks of molecular construction sets[5] and inherit the desired electronic or magnetic properties, adopt a well-defined shape, and incorporate specific handles such as reactive groups and recognition motifs. In order to assemble these individual building blocks into larger integrated systems, several issues will have to be addressed: 1) The surface should be locally activated, either by inducing a chemical process in individual molecules or by changing the substrate directly; 2) the molecules should preferably be organized on the substrate by self-assembly; 3) the generated features should be stabilized and permanently fixed to the substrate. Recent advances in these areas utilizing organic molecules will be highlighted here from a synthetic chemist's point of view.[6]

The concept of inducing a chemical reaction by using tunneling electrons of a scanning tunneling microscope (STM) tip was suggested by Ho in the late 1990s.[7] However, there are still few experiments which demonstrate single-molecule reactivity in the sense of a classical bond-forming event.[8] In a key experiment, Rieder and co-workers recently carried out an "Ullmann reaction", which involved the homocoupling of two iodobenzene molecules to afford biphenyl, step by step at the step edge of a Cu(111) surface using a low-temperature, ultrahigh-vacuum STM (Figure 1).[9] First, selective breaking of the weakest bond (the C-I bond) was induced by applying the appropriate sample bias. Single tunneling electrons presumably cause C–I bond dissociation and the resulting phenyl radical intermediate is stabilized by π interaction with the surface as well as σ interaction

[*] Dr. S. Hecht
Institut für Chemie/Organische Chemie
Freie Universität Berlin
Takustrasse 3, 14195 Berlin (Germany)
Fax: (+49) 30-838-52551
E-mail: shecht@chemie.fu-berlin.de

[**] S.H. is indebted to Karl-Heinz Rieder (Freie Universität Berlin), Shiyoshi Yokoyama (Communications Research Laboratory, Iwaoka), Kerry W. Hipps (Washington State University, Pullman), Yuji Okawa (Surface and Interface Laboratory, RIKEN, Waco), and Robert Wolkow (Steacie Institute for Molecular Sciences, Ottawa) for providing the STM images. Generous support by the Sofja Kovalevskaja Award of the Alexander von Humboldt Foundation, endowed by the Federal Ministry of Education and Research (BMBF) within the Program for Investment in the Future (ZIP) of the German Government, is gratefully acknowledged.

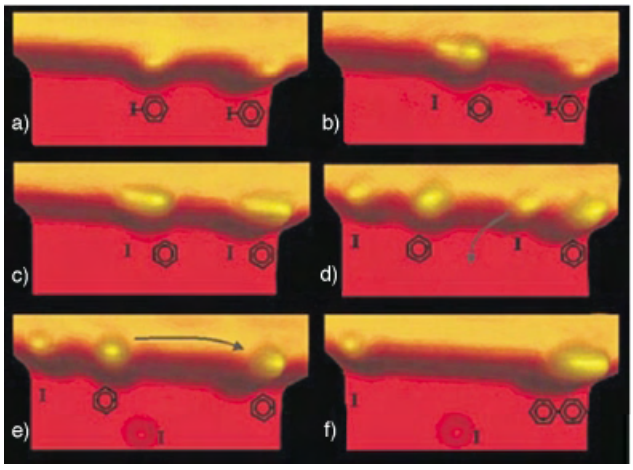


Figure 1. STM images of the surface "Ullmann reaction":[9] a) adsorption of two iodobenzene molecules at a Cu(111) step edge; b), c) successive iodine abstraction using a voltage pulse (1.5 V); d) removal of iodide by-product; e) moving both phenyl fragments into close proximity; f) bond formation by excitation (second voltage pulse: 0.5 V) to yield biphenyl.

 © 2003 Wiley-VCH Verlag GmbH & Co. KGaA, Weinheim 1433-7851/03/4201-0024 $ 17.50+.50/0

of the radical center with a Cu atom of the step edge. After moving two such "surface cuprates" into close proximity, an additional excitation of the system by inelastic tunneling is required to stimulate the rotation of the phenyl radical necessary for bond formation. Although sophisticated nanostructures could in principle be built up molecule-by-molecule by utilizing such a welding process, this approach intrinsically lacks the potential of through-put.[10]

Though it is not yet clear how the bottom-up approach to nanofabrication could be developed into an industrial process, the aspect of self-assembly as a tool to pattern large substrate areas will certainly play a central role. Supramolecular chemistry[11] has been indispensable for the organization of organic molecules on substrate surfaces. Significant advances in this area have recently been made by arranging large functional macrocycles into nanosized regular patterns using the specificity and directionality of noncovalent interactions. In elegant work,[12] Yokoyama et al. took advantage of the dipole–dipole interaction between cyano groups to force benzonitrile-type moieties into either antiparallel-dimer or trigonal-trimer configurations. By using a porphyrin skeleton to organize the cyanophenyl substituents in space, discrete ensembles such as trimers, tetramers, and long chains were formed. For example, when deposited on an Au(111) surface, *trans*-5,15-bis(4-cyanophenyl)-10,20-bis(3,5-di-*tert*-butylphenyl)porphyrin (**1**) assembled into straight supramolecular wires (Figure 2a) of lengths above 100 nm, with some branching arising from the incorporation of the trimer motif. In another approach, Hipps et al. could generate highly organized mixed assemblies of nickel(II) tetraphenylporphyrin (**2**) and cobalt(II) hexadecafluorophthalocyanine (**3**) macrocycles on an analogous substrate (Figure 2b).[13] Multiple H–F interactions are primarily responsible for a long-range order that extends to approximately 100 nm.

While the functionality of the self-organized molecular species promises interesting properties of the resulting material that could potentially be useful in electronic and sensing applications, it should be advantageous to lock the assembly covalently in a consecutive step to secure the stability of the structure. Okawa and Aono recently accomplished just that by locally inducing a diacetylene chain polymerization in self-assembled monolayers of 10,12-nonacosadiynoic acid on graphite (Figure 3a).[14] After the creation of an artificial defect using the STM tip by application of a positively pulsed sample bias, the polymerization of one diacetylene monolayer chain was initiated at another location with an opposing voltage pulse. After progression, the polymer chain was terminated at the defect site. This experiment combines the advantage of topochemical reactions for nanoscale patterning of substrate surfaces[15] with the ability to induce reactivity locally (see above), however, covalent fixation of the aggregate to the substrate has not been achieved by this method. An alternative, and conceptually very different, approach relies on the substrate acting as a directing template for an anisotropic growth process. While no preorientation of the reactants in the form of a well-defined self-assembly is necessary, a permanent and covalent surface modification is achieved. This concept of self-directed growth has been demonstrated by Wolkow and co-workers, who generated molecular lines on H-terminated Si(100) surfaces (Figure 3b).[16] By creating "dangling bonds" at the surface and exposing them to styrene vapor, a surface benzyl radical is formed that is stabilized by H abstraction from the neighboring Si–H site, which thereby regenerates the propagating species, that is, a dangling bond. This process leads to the formation of lines by planting individual phenyl moieties on the surface that line up in a typical π–π-stacking fashion and therefore indicate a potential use as a molecular wire.

While the examples presented here are certainly encouraging, only a vigorous multidisciplinary effort including both the chemical and physical communities will be able to transform these approaches into real life techology.

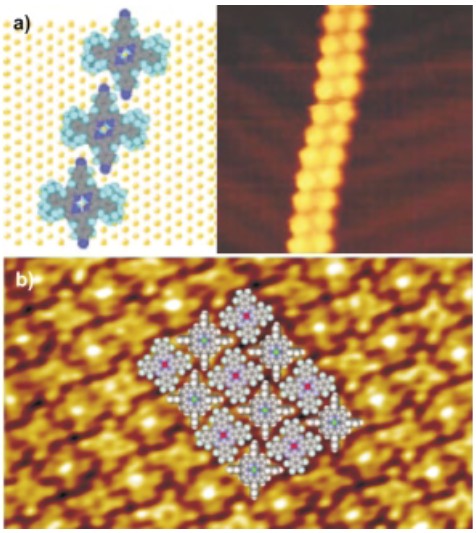


Figure 2. STM images of self-assembled macrocycles on Au(111): a) antiparallel arrangement of cyanophenyl groups in **1** leads to formation of straight wires;[12] b) alternating assembly of a mixture of **2** and **3**.[13]

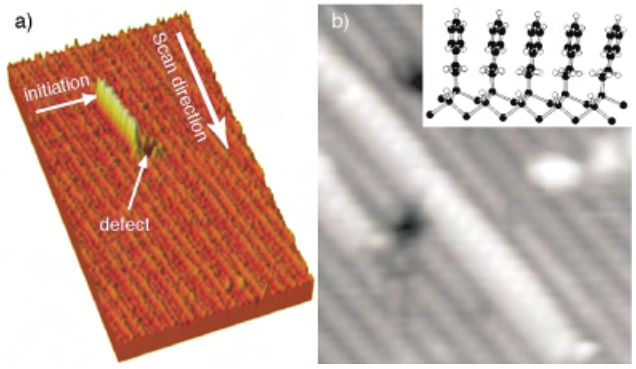


Figure 3. STM images of grown nanostructures: a) diacetylene polymerization in a self-assembled monolayer on graphite, initiated using an STM tip (−4 V) and terminated at an intentionally placed artificial defect (+ 5 V);[14] b) self-directed growth of styrene lines on H-terminated Si(100) initiated by surface dangling bonds.[16]

 © 2003 Wiley-VCH Verlag GmbH & Co. KGaA, Weinheim 1433-7851/03/4201-0025 $ 17.50+.50/0

[1] a) *Sci. Am.* **2001**, *285*, 32 – 91 (special issue: "Nanotechnology"); b) *Chem. Eng. News* **2000**, *78*(42), 24 – 42.

[2] a) A. Yazdani, C. M. Lieber, *Nature* **1999**, *401*, 227 – 230; b) G. S. McCarthy, P. S. Weiss, *Chem. Rev.* **1999**, *99*, 1983 – 1990; c) S. Bunk, *Nature* **2001**, *410*, 127 – 129.

[3] a) J. K. Gimzewski, C. Joachim, *Science* **1999**, *283*, 1683 – 1688 (special issue: "Single Molecules"); b) H. L. Anderson, *Angew. Chem.* **2000**, *112*, 2552 – 2554; *Angew. Chem. Int. Ed.* **2000**, *39*, 2451 – 2453.

[4] a) C. Joachim, J. K. Gimzewski, A. Aviram, *Nature* **2000**, *408*, 541 – 548; b) J. M. Tour, *Acc. Chem. Res.* **2000**, *33*, 791 – 804.

[5] *Modular Chemistry* (Ed.: J. Michl), Kluwer, Dordrecht, **1997**.

[6] Many inorganic building blocks, such as various types of nanowires, have been described, see for example: a) M. S. Gudiksen, L. J. Lauhon, J. Wang, D. C. Smith, C. M. Lieber, *Nature* **2002**, *415*, 617 – 620; b) M. R. Diehl, S. N. Yaliraki, R. A. Beckman, M. Barahona, J. R. Heath, *Angew. Chem.* **2002**, *114*, 363 – 366; *Angew. Chem. Int. Ed.* **2002**, *41*, 353 – 356; c) Y. Huang, X. Duan, Y. Cui, L. J. Lauhon, K.-H. Kim, C. M. Lieber, *Science* **2001**, *294*, 1313 – 1317; d) A. Bachtold, P. Hadley, T. Nakanishi, C. Dekker, *Science* **2001**, 294, 1317 – 1320; e) Y. Cui, C. M. Lieber, *Science* **2001**, *291*, 851 – 853; f) Y. Huang, X. F. Duan, Q. Q. Wei, C. M. Lieber, *Science* **2001**, *291*, 630 – 633; g) V. Derycke, R. Martel, J. Appenzeller, P. Avouris, *Nano Lett.* **2001**, *1*, 453 – 456.

[7] W. Ho, *Acc. Chem. Res.* **1998**, *31*, 567 – 573.

[8] a) H. J. Lee, W. Ho, *Science* **1999**, *286*, 1719 – 1722; b) in a related approach, large cylindrical nanoobjects based on dendronized polymers have very recently been covalently connected using atomic force microscopy (AFM) manipulation followed by photochemical fixation: J. Barner, F. Mallwitz, L. Shu, A. D. Schlüter, J. P. Rabe, Angew. Chem. **2003**, *115*, in press; Angew. Chem. Int. Ed. **2003**, *42*, in press.

[9] a) S. W. Hla, L. Bartels, G. Meyer, K.-H. Rieder, *Phys. Rev. Lett.* **2000**, *85*, 2777 – 2780; b) S. W. Hla, G. Meyer, K.-H. Rieder, *ChemPhysChem* **2001**, *2*, 361 – 366.

[10] This problem could partially be alleviated in nanolithography by using AFM in combination with tip arrays. See for example: M. Lutwyche, C. Andreoli, G. Binnig, J. Brugger, U. Drechsler, W. Häberle, H. Rohrer, H. Rothuizen, P. Vettiger, G. Yaralioglu, C. Quate, *Sens. Actuators A* **1999**, *73*, 89 – 94.

[11] *Science* **2002**, *295*, 2400 – 2421 (special issue: "Supramolecular Chemistry and Self-Assembly").

[12] T. Yokoyama, S. Yokoyama, T. Kamikado, Y. Okuno, S. Mashiko, *Nature* **2001**, *413*, 619 – 621.

[13] K. W. Hipps, L. Scudiero, D. E. Barlow, M. P. Cooke, *J. Am. Chem. Soc.* **2002**, *124*, 2126 – 2127.

[14] Y. Okawa, M. Aono, *Nature* **2001**, *409*, 683 – 684.

[15] For related work on topochemical large-area patterning consult: a) S. De Feyter, A. Gesquière, M. M. Abdel-Mottaleb, P. C. M. Grim, De Schryver, C. Meiners, M. Sieffert, S. Valiyaveettil, K. Müllen, *Acc. Chem. Res.* **2000**, *33*, 520 – 531; b) S. De Feyter, J. Hofkens, M. Van der Auweraer, R. J. M. Nolte, K. Müllen, F. C. De Schryver, *Chem. Commun.* **2001**, 585 – 592; c) M. M. S. Abdel-Mottaleb, S. De Feyter, A. Gesquière, M. Sieffert, M. Klapper, K. Müllen, F. C. De Schryver, *Nano Lett.* **2001**, *1*, 353 – 359. Similar approaches have been applied to materials chemistry in the past for example, to generate polymerized functional vesicles: S. Okada, S. Peng, W. Spevak, D. Charych, *Acc. Chem. Res.* **1998**, *31*, 229 – 239.

[16] G. P. Lopinski, D. D. M. Wayner, R. A. Wolkow, *Nature* **2000**, *406*, 48 – 51.

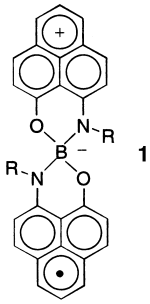
Structural Control of Properties

Bistable Electrical, Optical, and Magnetic Behavior in a Molecule-Based Material**

*Joel S. Miller**

Keywords:
bistability · conducting materials · dimerization · hysteresis · spiro compounds

The control of physical properties by controlling the structure of materials has reached new dimensions with the recent report by Haddon and co-workers[1] which shows that significant electrical, optical, and magnetic properties can be switched between two states through thermal control of the structure of two neutral alkyl-substituted spirobiphenalenyl radicals (**1**, R = Et, *n*Bu). While virtually every structural transformation leads to changes in numerous physical properties, typical changes are inconsequential for memory or sensor applications. Additionally, such applications require changes that are rapid and reversible, and the altered property provides the means to store or sense as well as read information. Color or optical changes as well as changes in electrical conductivity or magnetization are frequently used for memory or sensing applications. A useful system possesses a modulation in one of these properties. It is rare to identify a system with two useful properties being simultaneously modulated, such as spin-crossover materials,[2,3] however, Haddon and co-workers have extended the number of useful properties being simultaneously modulated to three.



1

The unpaired electrons associated with the spirobiphenalenyl radicals **1** provide the basis for the observed structural transformation to dimers at low temperature and the consequent change in the electronic structure from independent radicals to a π dimer. Compound **1** has an unpaired electron delocalized over both phenalenyl units, as expected from Pauling's description of resonance. However, in the solid state **1** (R = Et, *n*Bu) has reduced symmetry, with each of the phenalenyl units in different environments (Figure 1) within the crystal, and can be considered as valence-ambiguous or valence-tautomeric, akin to several cobalt semiquinone complexes.[4]

Analysis of the bond lengths as a function of temperature led Haddon and co-workers to conclude that in the low-temperature phase (for R = Et or *n*-Bu) the unpaired electrons reside in the phenalenyl units that are in proximity to each other (Figure 2), an arrangement which is characterized by an intradimer separation of 3.2 Å. In the high-temperature form, however, the unpaired electrons are located on the alternative phenalenyl units. The intradimer separation for this form is increased to 3.3 Å, which is indicative of the reduction of

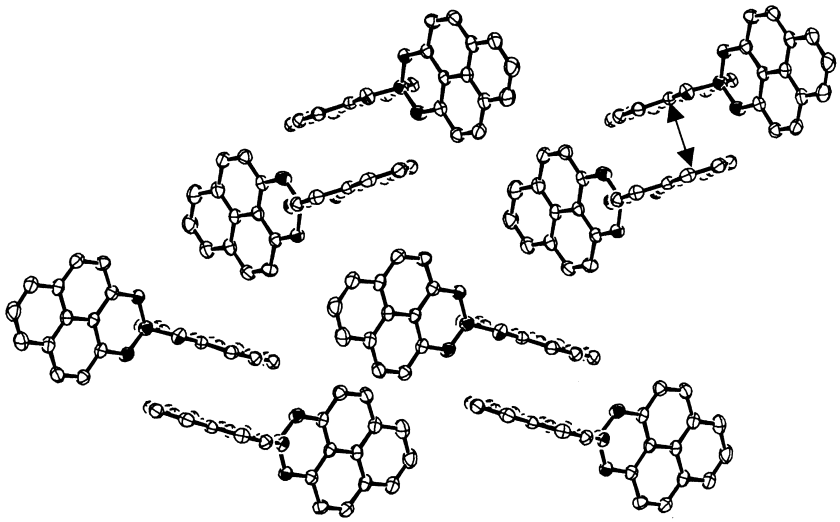


Figure 1. Packing diagram of the spirobiphenalenyl radical **1** (R = Et). The intradimer separation decreases from approximately 3.3 Å in the high-temperature phase to approximately 3.2 Å in the low-temperature phase. The structure of radical **1** with R = *n*Bu is similar. Reprinted with permission from ref. [1].

[*] Prof. J. S. Miller
Department of Chemistry
University of Utah
315 S. 1400 E. RM 2124
Salt Lake City, UT 84112-0850 (USA)
Fax: (+1) 801-581-8433
E-mail: jsmiller@chem.utah.edu

[**] The author gratefully acknowledges partial support from the ACS-PRF (PRF No. 36165-AC5), the U.S. Department of Energy (Grant No. DE-FG03-93ER45504), the National Science Foundation (Grant No. CHE 0110685), and the Air Force Office of Scientific Research (Grant No. F49620-00-1-0055). Figures 1, 2, and 3 are reprinted with permission from M. E. Itkis, X. Chi, A. W. Cordes, R. C. Haddon, *Science* **2002**, *296*, 1443. Copyright 2002 American Association for the Advancement of Science.

 © 2003 Wiley-VCH Verlag GmbH & Co. KGaA, Weinheim 1433-7851/03/4201-0027 $ 20.00+.50/0

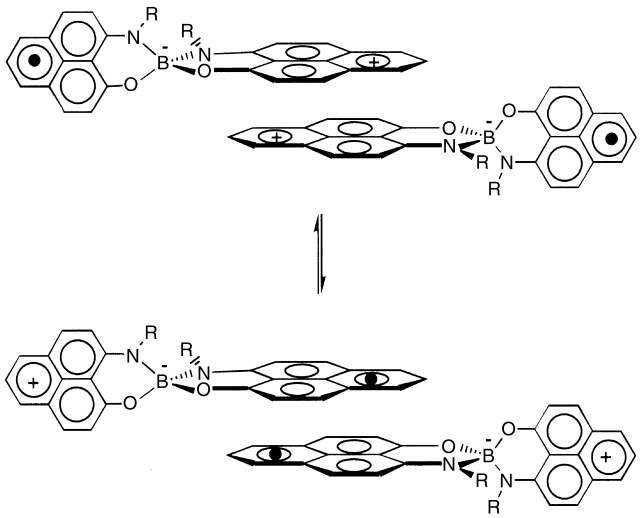


Figure 2. Interconversion between the high- (top) and low-temperature (bottom) structures for spirobiphenalenyl radicals (**1**, R = *n*Bu). Reprinted with permission from ref. [1].

the electronic interaction, as a consequence of the increased separation of the unpaired electrons. At low temperatures the unpaired electrons couple in a singlet ground state, and give rise to a diamagnetic response. In contrast, at higher temperatures the reduced interaction leads to paramagnetic behavior (Figure 3). Most surprisingly, the conductivity increases by two orders of magnitude in the low-temperature diamagnetic state (Figure 3B). Hence, the temperature-dependent movement of the unpaired electrons leads to a structural alteration and significant changes in the conductivity, magnetic, and IR absorption properties of the material.

Information storage media require hysteretic behavior, as both states need to have a finite lifetime; in other words, they must exhibit bistability.[5] Haddon and co-workers show that the changes in the conductivity, magnetic, and IR absorption properties persist for both the high-temperature and low-temperature states. This enables information to be "locked in" until erasure occurs, by cooling for R = *n*Bu, but not for R = Et.

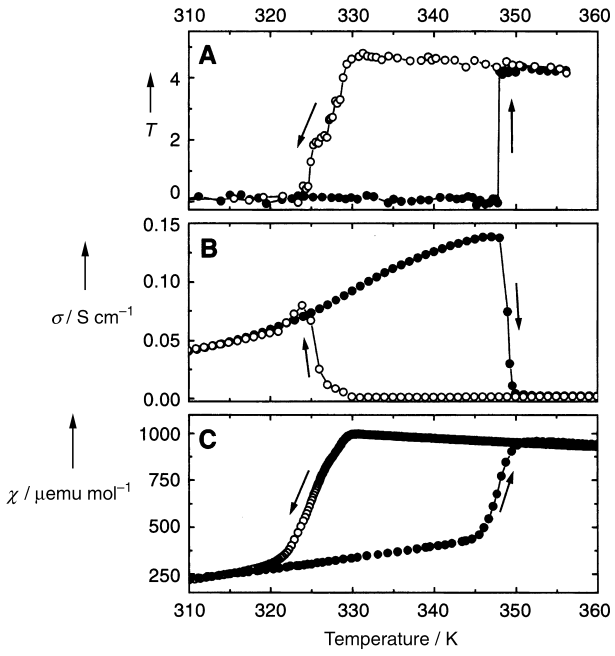


Figure 3. Hysteretic behavior of the IR transmittance at 2600 cm^{-1} (A), dc electrical conductivity (B), and magnetic susceptibility (C) for the *n*-butyl spirobiphenalenyl radical **1** as a function of temperature. Reprinted with permission from ref. [1].

Although **1** (R = *n*Bu) exhibits significant changes in three important physical properties, as well as hysteresis in these properties, which are all useful attributes for memory/sensor devices, it is unlikely that it is a candidate as a next-generation memory/sensor element, as a result of its slow reversible response which occurs at too high a temperature, and perhaps also the changes in the observed effects are too small. Speed is very important in our modern "gigahertz" world. Hence, transformations brought about by heating/cooling are limited by heat transfer rates and their associated times to reach equilibrium, which are slow compared to electronic-driven transformations. The observed effects occur between 320 and 350 K, which being significantly above room temperature would be at a temperature too high to be considered for most practical applications, as heating would be required. The hysteretic region of approximately 30 K is beneficial, but it would be more useful if it hovered above and below room temperature (for example, 295 ± 15 K). It should be noted that it is rare to fault a material because of the required transformation occurring at too high a temperature, as typically an effect is only evident at lower temperatures. Also, this suggests that it is most important to study materials above 300 K as, for example, our standard 2–300 K magnetization studies would have never led to the identification of materials with transitions above 300 K.

Additionally, spin-crossover materials exhibit a change in their paramagnetic response, but the absolute change in magnitude of the magnetic susceptibility is too low to be practical, and the useful property for device applications is the concomitant abrupt change in color.[3,6] While **1** (R = Et, *n*Bu) undergoes changes in its IR absorption spectra, a color change was not reported, and the change in susceptibility is less than that observed for spin-crossover materials. Perhaps the change in conductivity could be utilized in an application, but then this system, with three useful properties being simultaneously modulated, reduces to a system with only one. Nevertheless, Haddon and co-workers have made a major leap forward with their demonstration that materials, and in this case a molecule-based material, can be made that have three useful properties that can, in principle, be used in future devices. A goal for the future is the development of materials in which three physical properties can be independently altered, for example, by changing only the magnetic behavior,

 © 2003 Wiley-VCH Verlag GmbH & Co. KGaA, Weinheim 1433-7851/03/4201-0028 $ 20.00+.50/0

or changing both the magnetic and electrical properties, or both the magnetic and optical properties, so that a three- property system with an eightfold enhancement of data storage density might be achieved.

[1] M. E. Itkis, X. Chi, A. W. Cordes, R. C. Haddon, *Science* **2002**, *296*, 1443.

[2] For example: P. Gütlich, A. Hauser, H. Spiering, *Angew. Chem.* **1994**, *106*, 2109; *Angew. Chem. Int. Ed. Engl.* **1994**, *33*, 2024.

[3] O. Kahn, C. J. Martinez, *Science* **1998**, *279*, 44; O. Kahn, J. Kröber, C. Jay, *Adv. Mater.* **1992**, *4*, 718.

[4] P. Gütlich, A. Dei, *Angew. Chem.* **1997**, *109*, 2852; *Angew. Chem. Int. Ed. Engl.* **1997**, *36*, 2734.

[5] O. Kahn, J. P. Launay, *Chemtronics* **1988**, *3*, 140.

[6] Room-temperature spin-crossover materials have been "crystal engineered": J. Kröber, E. Codjovi, O. Kahn, O. Groliere, C. Jay, *J. Am. Chem. Soc.* **1993**, *115*, 9810.

 © 2003 Wiley-VCH Verlag GmbH & Co. KGaA, Weinheim 1433-7851/03/4201-0029 $ 20.00+.50/0

High-Speed Mass Spectrometry

Hadamard Transform Time-of-Flight Mass Spectrometry: More Signal, More of the Time

Richard N. Zare, Facundo M. Fernández, and Joel R. Kimmel*

Keywords:
analytical methods · Hadamard transform · mass spectrometry · signal multiplexing

Hadamard transform time-of-flight mass spectrometry (HT-TOF MS) is a type of mass analysis that was developed to couple continuous ion sources to the inherently pulsed nature of time-of-flight measurements. Unlike conventional TOF MS, the Hadamard transform method offers a duty cycle of 50 %, with the possibility of extending it to 100 %. Because it is a multiplexing technique, the attainable signal-to-noise ratio (SNR) is also significantly higher than that of conventional TOF MS. This review covers the basic principles behind HT-TOF MS. We illustrate, through examples, the source of the high-duty cycle and the increase in SNR. These features translate to a mass spectral storage rate that is the fastest among similar instruments, which enables its use as a detector for high-speed separations.

1. Introduction

A mass spectrometer is a device for weighing molecules. It converts a neutral molecule into a positively or negatively charged ion, and it subjects the ion to known electric or magnetic fields. The subsequent motion of the ion depends on its mass and charge. An analysis of the ion's motion allows its mass-to-charge ratio (m/z) to be determined, and hence its molecular weight. Many types of mass spectrometry exist. By far the simplest and least expensive method is time-of-flight (TOF) mass spectrometry (MS), in which ions of different masses are given the same kinetic energy but different velocities, each ion experiencing the same potential drop. After acceleration, the flight time of the ion is measured over a fixed distance between a starting point and the ion detector. It is easily shown that the square of the flight time t is directly proportional to the mass-to-charge ratio of the ion m/z. Our review concerns a new method for carrying out TOF MS that has the advantages of high efficiency and rapid acquisition of mass spectra.

[*] Prof. R. N. Zare, Dr. F. M. Fernández, J. R. Kimmel
Department of Chemistry
Stanford University
Stanford, CA 94305-5080 (USA)
Fax: (+1) 650-723-9262
E-mail: zare@stanford.edu

In TOF MS, the ion source is pulsed to create packets of ions. In the conventional procedure, the system waits for all the ions in a packet to reach the detector before injecting the next packet of ions. This pulsing creates inherent complications when TOF MS is coupled to a continuous ion source. Such coupling is often accomplished by an orthogonal extraction scheme in which a packet from a continuous stream of ions is pushed at a right angle to the ion stream and directed toward the ion detector. Because of the system delay between packet extractions, the duty cycle of an orthogonal extraction instrument is usually between 5–15 %. This degree of merit means that up to 95 % of the information contained in the ion stream is lost. In contrast, we describe here an on-line modulation–demodulation scheme that allows, on average, half of the ions in the ion stream to strike the ion detector to give a duty cycle of 50 %. Moreover, because we modulate this beam at a frequency of 10 to 20 MHz, mass spectra can be collected, one after the other, at a rate of more than 250 second^{-1}. The advantage of such a high sampling rate and good ion-collection efficiency is that TOF MS done in this manner can be combined with some fast chromatographic or electrophoretic separation technique prior to ionization, to give a large dynamic range and a large capacity factor for what can be separated, detected, and quantified in a complex mixture.

To make our discussion more concrete, let us consider a very simple example of mass determination, namely, weighing three bananas of slightly different mass. This example might seem silly at first, but it provides deep insights into the weighing process. Suppose our weighing device is a single-pan scale (Figure 1) that takes one second to make a weight measurement and whose response has an uncertainty given by

 © 2003 Wiley-VCH Verlag GmbH & Co. KGaA, Weinheim 1433-7851/03/4201-0030 $ 17.50+.50/0

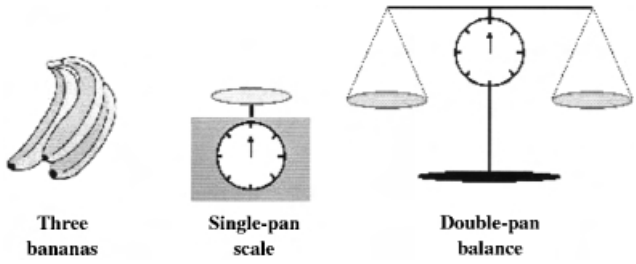


Figure 1. Weighing three bananas with two types of scales.

the square root of the signal, that is, the square root of the mass. What is the optimum strategy for weighing the bananas?

Initially, the answer appears to be straightforward. Each banana is placed on the pan and weighed separately for one second. Yet, with a bit of reflection we realize that a better strategy is to weigh the bananas together as three different pairs and then subtract the weight of one pair from another to get the individual weights of the three bananas. The second procedure gives the same answer but with less uncertainty. Why? The single-pan scale spends the same time weighing more bananas. Similarly, we seek a means to multiplex signals so that the time-of-flight mass spectrometer spends more time detecting the ions contained in the ion stream.

Let us explore further the challenge of devising an optimum weighing strategy for the three bananas by replacing the single-pan scale with a double-pan balance (Figure 1). With two pans, the best weighing procedure is to put one banana on one side of the balance and the other two on the opposite side. This weighing is repeated twice more, and each time a different banana is chosen as the lone counterbalancing weight. The double-pan balance is superior to the single-pan scale, because with two pans all three bananas are being weighed all the time, which thus increases the quality of the information. We will discuss how a similar procedure can be implemented in time-of-flight mass spectrometry to increase the duty cycle from 50 to 100%. But first we will describe how to achieve a 50% duty cycle.

Conventional TOF MS can be compared to the weighing method in which each banana is weighed separately on a single-pan scale. The ion source is pulsed at a constant rate that allows ions of only one m/z value to strike the detector in a given time bin. As with the bananas, it is also possible to modulate and detect ions in such a way that the measurement in each time bin yields information about all m/z values. We accomplish this task by gating a continuous beam on and off at a rate so rapid that multiple ion packets exist in the flight chamber of the instrument at the same time. Differences in ion velocities cause the packets to overlap as they drift; thus, the detector registers multiple m/z values. Interpretation of the signal requires knowledge of the gating sequence. We provide the ion gate with a sequence of on and off pulses that may be represented by "1"s and "0"s. If the sequence contains a 1, a packet of ions is launched at the detector; if the sequence contains a 0, the ions are deflected to miss the detector. The best sequence consists of about as many "1"s as "0"s. In this manner, the detector has a 50% duty cycle.



Richard N. Zare graduated from Harvard (B.A. in Chemistry and Physics, 1961; Ph.D. in Chemical Physics, 1964) and was at the Massachusetts Institute of Technology (1965), University of Colorado (1966–1969), and Columbia University (1970–1977) before moving to Stanford in 1977. He has received numerous honors and honorary doctorates and has authored and co-authored over 650 publications.



Dr. Facundo M. Fernández was born in Buenos Aires, Argentina in 1970. He received his MSc in Chemistry from the College of Exact and Natural Sciences (1995) and his Ph.D. in Analytical Chemistry from Buenos Aires University in (1999). In August 2000, he joined the research group of Prof. Richard N. Zare in the Department of Chemistry at Stanford University. In 2002, he joined the group of Prof. Vicki Wysocki in the Department of Chemistry at the University of Arizona.



Joel R. Kimmel received his BS in Chemistry from Colorado State University in Fort Collins, Colorado in 1999. He is currently a Ph.D. candidate in the Department of Chemistry at Stanford University, where he works with Prof. Zare on the development of Hadamard transform time-of-flight mass spectrometry.

One way to make these on and off pulses sharply defined in space and time is to use a "Bradbury–Nielsen gate" (BNG) (Figure 2).[1,2] The BNG consists of two electrically isolated sets of equally spaced wires that lie in the same plane but alternate in potential, between positive and negative. When no potential is applied to the wires, the trajectory of the charged ion beam is undeflected by the BNG. To deflect the beam, potentials of equal magnitude and opposite polarity are applied to the two wire sets, which causes the ion beam to miss the detector. To feel the force of the charged wires, ions must

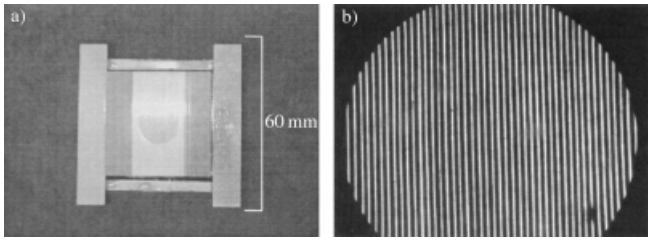


Figure 2. a) Finely spaced Bradbury–Nielsen gate (front view, 100 μm spacing) and b) closer view of the optical aperture showing the two interleaved wire sets.

 © 2003 Wiley-VCH Verlag GmbH & Co. KGaA, Weinheim 1433-7851/03/4201-0031 $ 17.50+.50/0

be within a distance of the gate approximately equal to the wire spacing. Consequently, it is possible to modulate the ion beam on and off in a controlled manner at a sharply localized starting point.

Brock et al.[3,4] first reported the use of the BNG to achieve on-axis modulation of an ion stream by means of a well-defined pseudorandom sequence of pulses that transmits or deflects the ions. This BNG may be regarded as chopping the ion stream into packets of different lengths. The ions in these packets travel through the flight tube between the BNG and the ion detector at different velocities, with typical flight times of hundreds of microseconds. At the BNG, the temporal width of an ion packet and the time between adjacent ion packets is three orders of magnitude shorter than these flight times (ns versus μs). Consequently, as the ion packets travel the length of the flight tube, faster ions in one packet overtake slower ions in earlier packets, which causes the packets to interpenetrate and overlap. The response of the detector appears to be noise (Figure 3a), but this assessment is incorrect. Actually, the signal output of the detector is the convolution of many conventional TOF mass spectra, each shifted in time according to the pseudo-random binary modulation sequence. Hence, the TOF mass spectrum can be extracted from this data by demodulating the output signal using knowledge of the applied sequence (Figure 3b). The demodulation corresponds mathematically to an "inverse Hadamard" transform. Thus, the procedure is called Hadamard transform time-of-flight mass spectrometry (HT-TOF MS). Under ideal circumstances, in which the sequence applied to the ions is known exactly, the transform returns the mass spectrum with no distortion.

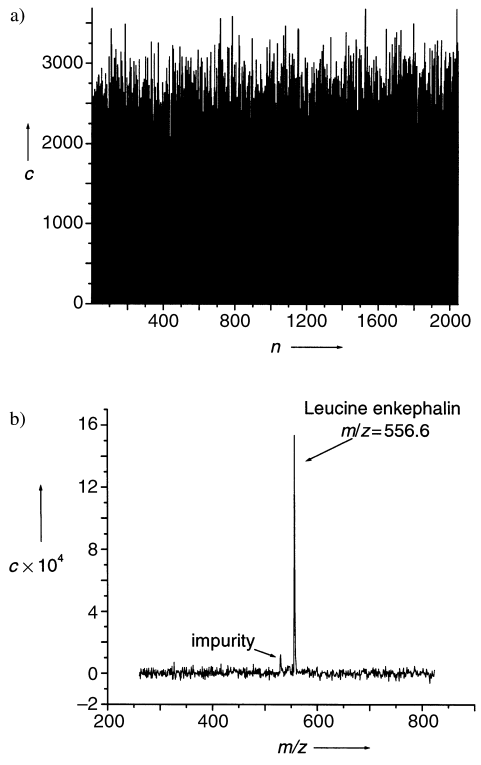


Figure 3. Electrospray ionization–HT-TOF mass spectrum of 1.4 pmol of the peptide leucine enkephalin (1+) dissolved in methanol:water:-acetic acid 50:50:1. The acquisition time was 2 s. Diagram a) shows the raw (convoluted) data and b) shows the deconvoluted mass spectrum obtained in low resolution mode.[19] The pseudorandom binary sequence consisted of $(2^{11}-1) = 2047$ elements, each of 100 ns duration. c = counts, n = bin number.

The Hadamard transform belongs to the same family of transforms as that of the more familiar Fourier transform.[5] In the Fourier transform, the basis functions used to express the signal function in the time domain are an infinite series of sine and cosine functions. In contrast, for the Hadamard transform we use as a basis set a finite series of binary elements. As a consequence, the Hadamard transform is significantly faster to compute, and it does not suffer from aliasing effects (the process by which smooth curves and other lines become jagged because the resolution of the device or file is not high enough to represent a smooth curve (the process in which the signal becomes distorted because the sampling rate is not sufficiently high to capture the signal features). Hadamard transforms have already been used in many different chemical applications such as Raman imaging[6] capillary electrophoresis,[7,8] and Fourier-transform mass spectrometry.[9] They are applicable to any phenomenon in which a series of on and off signals are recorded. Because Hadamard transforms are rather unfamiliar, the bulk of this review is devoted to working through a simple example. We close with one recent application of HT-TOF MS to the analysis of a mixture of peptides—an application that hints at the power of combining separations with HT-TOF MS analysis.

2. The Basics of HT-TOF MS

We will explain the basics of HT-TOF MS with the aid of a simple example. The first step is to build a virtual TOF spectrum. Our virtual sample is an aqueous solution that contains the peptide P ($M_w = 1620$ Da) and a protein such as a protease ($M_w = 56\,000$ Da). One way to produce gas-phase ions from this sample is to use electrospray ionization (ESI). In ESI, the sample is nebulized through a needle that has a high potential relative to the mass spectrometer.[10] This electrical field causes a spray of finely divided, charged droplets. As solvent evaporates, the surface charge density of the droplets increases, which leads to a Coulombic explosion that causes the droplets to fission into yet smaller droplets. Evaporation and fission continue, which result in a beam of "naked", positively charged gas-phase ions. Basic compounds such as peptides and proteins often carry more than one charge per molecule and consequently appear in the TOF spectrum with a mass-to-charge ratio lower than their molecular weight.

To record the TOF spectrum of our virtual sample in a conventional TOF instrument, the BNG would be opened for a fixed period of time (a few hundreds of ns) and then closed. Ions in the packet that passed the open gate would drift through the instrument and be recorded as they arrived at the detector. Ions reaching the gate when it is energized would be deflected and miss the detector. Counts are usually collected in time bins that are a few ns wide, by using a time-to-digital converter. However, to simplify the calculations and reduce the size of the Hadamard matrices needed, we chose to use

much larger time bins in our example. If a 10 kV field were used to accelerate ions and the flight path were 50 cm long, the flight times of the components in our sample mixture would be 1.56 μs for H_3O (1+), 10.24 μs for substance P (2+), and 26.94 μs for the protease (10+). To record the full mass spectrum, we chose to set up the acquisition system to acquire ion counts in seven time bins, each 5 μs wide. This arrangement is sufficient to record a maximum flight time of 35 μs, which corresponds to an upper mass cutoff of 9560 Da.

The recorded spectrum looks something like Figure 4. The intensity of each solute peak reflects the abundance of the component in solution multiplied by the ionization efficiency. We arbitrarily chose the three peaks to have the ratio 3:2:1. The peaks originating from the solvent reflect only the amount of charge carried by ionized solvent molecules[11] and do not usually carry analytical information. Notice that each peak in the TOF spectrum shown in Figure 4 has some background noise associated with it. This noise is proportional to the square root of the ion intensity.[12] In this particular case of the protease, we chose a background noise level of ten counts per bin ($\sqrt{100}=10$). In this scenario, the signal-to-noise ratio (SNR) for the protease peak is $100/10=10$. Time bins showing no peaks will have only the detector dark noise.

Let us perform the same TOF experiment using Hadamard multiplexing. A Hadamard matrix H_n of order n is a matrix of $+1$ and -1 with the property that the scalar product of any two different rows or columns is 0.[13] As we mentioned before, a mass spectrometer is used to weigh molecules. To record the $+1$ and -1 states in a Hadamard matrix, we would need a spectrometer furnished with two detectors, which is analogous to the double-pan balance in our example of weighing bananas. Hadamard multiplexing can also be done with only one detector if we use a type of Hadamard matrix that contains only $+1$ and 0. Such matrices, called Simplex matrices, are easily derived from Hadamard matrices.[13] Using a Simplex matrix is like weighing bananas in bunches with a single-pan scale. As in the conventional TOF example, we need to accommodate a maximum flight time of 35 μs in seven bins. Hence, we require a 7×7 Simplex matrix (Figure 5).

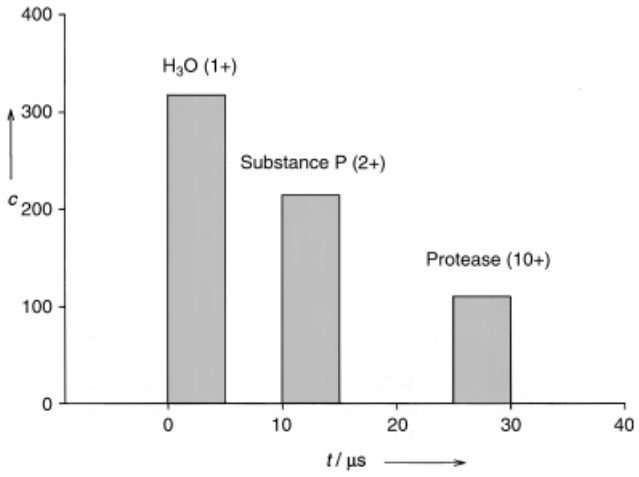


Figure 4. TOF mass spectrum used in the example of the peptide model.

What is the meaning of this matrix? Its first row contains the sequence of voltage pulses that are sent to the ion gate at 5 μs intervals. A sequence of "1 1 1 0 1 0 0" means that the beam state is "on, on, on, off, on, off, off." Notice that the second ion packet is injected into the flight chamber immediately after the first. Consequently, we will record a signal much more complex than with conventional TOF. Mathematically, the spectrum acquired in HT-TOF MS is found by multiplying the TOF distribution, regarded as a seven-element column vector, by a 7×7 Simplex matrix and adding a seven-element column noise vector. The resulting vector shows hits from different compounds in the same time bin. For example, the last element of the convoluted spectrum is obtained by multiplying the fifth row of the Simplex matrix by the TOF spectrum. The obtained value of 449 counts accounts for hits of protease and H_3O^+ injected during the first and fifth time bins, respectively, and it includes the background noise. Also notice that the noise level is higher than in the conventional TOF spectrum (49 counts versus 10 counts). Because we have analyzed four ion packets, the total signal is larger, and the noise increases with increasing signal ($\sqrt{2400}\approx49$). For reasons explained later, there is still a gain in overall signal-to-noise ratio as a result of multiplexing. Figure 7 shows the result of the convolution presented in Figure 6. Figure 3a is the equivalent of Figure 7, but with an 8191×8191 matrix.

$$S=\begin{bmatrix}1&1&1&0&1&0&0\\1&1&0&1&0&0&1\\1&0&1&0&0&1&1\\0&1&0&0&1&1&1\\1&0&0&1&1&1&0\\0&0&1&1&1&0&1\\0&1&1&1&0&1&0\end{bmatrix}$$

Figure 5. Simplex matrix 7×7 used in the example.

The TOF spectrum is deconvoluted from this signal by multiplying the experimental vector by the inverse of the Simplex matrix (Figure 8). This multiplication can be done in real time because the matrix inverse needs to be calculated only once and is then stored in the computer. Moreover, the inversion process requires only additions and subtractions.

Is there an advantage in using Hadamard multiplexing? Figure 9 compares the outcomes of a conventional and an HT-TOF MS experiment. As we can see, the noise (12.25 counts bin^{-1}) in the HT-TOF MS experiment is larger than the noise (10 counts bin^{-1}) of the protease peak in the conventional TOF experiment but smaller than the noise (17 counts bin^{-1}) in the H_3O^+ peak. The SNR from HT-TOF MS is 8.2 compared to 10 from conventional TOF MS for the protease peak and 24.5 compared to 17.3 in the H_3O^+ peak, respectively. It might seem at first that Hadamard multiplexing offers no clear gain, but this conclusion fails to take into account how the SNR scales with sequence length for the same mass resolution. It has been shown that the SNR is a function of the square root of the matrix size.[12] If a much

$$\begin{bmatrix}1&1&1&0&1&0&0\\1&1&0&1&0&0&1\\1&0&1&0&0&1&1\\0&1&0&0&1&1&1\\1&0&0&1&1&1&0\\0&0&1&1&1&0&1\\0&1&1&1&0&1&0\end{bmatrix}\times\begin{bmatrix}300\\0\\200\\0\\0\\100\\0\end{bmatrix}+\begin{bmatrix}49\\49\\49\\49\\49\\49\\49\end{bmatrix}=\begin{bmatrix}549\\349\\649\\149\\449\\249\\349\end{bmatrix}$$

Figure 6. Matrix form of the Hadamard convolution.

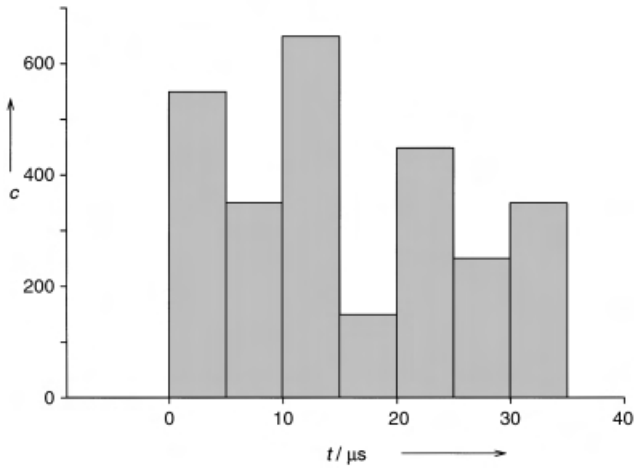


Figure 7. TOF spectrum used in the example after convolution with a Simplex matrix derived from a Hadamard matrix.

$$\frac{1}{4}\times\begin{bmatrix} 1 & 1 & 1 & -1 & 1 & -1 & -1\\ 1 & 1 & -1 & 1 & -1 & -1 & 1\\ 1 & -1 & 1 & -1 & -1 & 1 & 1\\ -1 & 1 & -1 & -1 & 1 & 1 & 1\\ 1 & -1 & -1 & 1 & 1 & 1 & -1\\ -1 & -1 & 1 & 1 & 1 & -1 & 1\\ -1 & 1 & 1 & 1 & -1 & 1 & -1 \end{bmatrix}\times\left(\begin{bmatrix}500\\300\\600\\100\\400\\200\\300\end{bmatrix}+\begin{bmatrix}49\\49\\49\\49\\49\\49\\49\end{bmatrix}\right)=\begin{bmatrix}312.25\\12.25\\212.25\\12.25\\12.25\\112.25\\12.25\end{bmatrix}$$

Figure 8. Hadamard deconvolution. The noise vector is shown separately for clarity.

larger matrix is used in place of the 7×7 matrix in the example, we can expect a significant gain in SNR.

In many experiments we use a sequence length of $N=(2^{13}-1)=8191$. According to the work by Wilhelmi and Gompf,[14] the expected maximum SNR gain for a 8191×8191 matrix varied between $\sqrt{(8191/2)}=64$ and $\sqrt{8191}/2=45$, depending on the background level. The SNR gain is also a function of spectrum sparsity, and the best results are obtained for spectra with very few, strong mass peaks. Experiments in our laboratory have shown that the experimental SNR gain is in accordance with these theoretical values.[12]

3. Applications and Outlook

The principal advantage of multiplexing in TOF MS is increased sensitivity, which leads to lower detection limits. This increased SNR enables a larger spectral storage rate. If instead of a continuous ion beam of constant composition, the output of a capillary separation technique is directly coupled to the ESI source in the HT-TOF MS, we face the challenge of analyzing an ion beam with fast, transient signals corresponding to the eluting compounds. The sensitivity of modern TOF spectrometers requires that several spectra must be averaged in order to display a single spectrum with a good SNR. This fact limits the spectral storage rate of the mass spectrometer. If the peak widths of the eluting compounds become smaller, such as in microchip separations,[15] high-speed gas chromatography,[16] or ultrafast capillary electrophoresis,[17] the MS detector may not be able to keep up with the speed of separation. As a result, peak shapes become drastically distorted.[18] Owing to its improved SNR, HT-TOF MS provides a faster storage speed than conventional TOF spectrometers, which makes it an ideal tool for capillary and other high-speed separations.

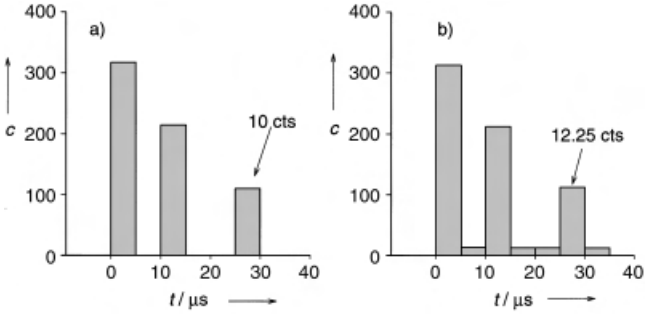


Figure 9. Comparison of SNR obtained in a) the conventional TOF spectrum and b) the deconvoluted HT-TOF spectrum used in the example ($N=7$). cts = noise counts.

Recently, we demonstrated the feasibility of detecting the capillary electrophoretic separation of a mixture of nine peptides with HT-TOF MS.[19] The results are shown in Figure 10. In this same study, we acquired spectra across peaks with widths of the order of hundreds of milliseconds and obtained a maximum spectral storage rate of 277 mass spectra s^{-1}, nearly 3.5 times faster than the best conventional instrument operating over the same mass range.

It might be wondered whether saturation is a problem when so many ion packets are incident on the ion detector at essentially the same time. We have observed response linearity in the 10–200 micromolar range for peptides, which suggests that no saturation is occurring. Ion counts from solvent and buffer components have been suppressed by efficient desolvation in the ESI source to reduce unwanted signals and to avoid detector saturation.

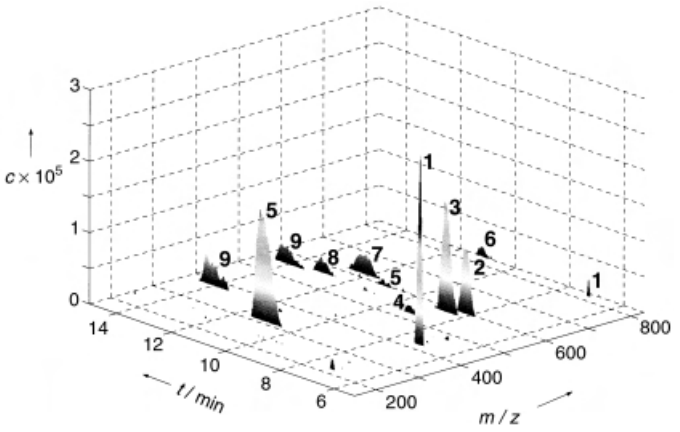


Figure 10. Separation of a nine-peptide mixture by pressure-assisted capillary electrophoresis and ESI–HT-TOF MS. Peak assignments: **1**: bombesin, **2**: bradykinin (fragment 1–5), **3**: leucine enkephalin, **4**: oxytocin, **5**: methionine enkephalin, **6**: substance P, **7**: human luteinizing release hormone, **8**: Arg 8-vasopressin, and **9**: bradykinin.

Although obtaining a 50% duty cycle is a big step toward high-efficiency TOF mass spectrometry, the advantages of the Hadamard transform can be pursued even further. Installation of a position-sensitive ion detector that is able to sense both the deflected and undeflected beams in different zones of its active area would allow the use of Hadamard matrices instead of Simplex matrices in the deconvolution process.

Drawing an analogy between a two-detector experiment and weighing bananas with a double-pan balance is not exact, but, for both bananas and ions, the principal advantage of two detectors is clear: no species goes unmeasured. Moving to this mode of operation would increase the SNR by 40%,[13] raise the duty cycle to 100%, and, ultimately, increase the spectral storage rate of the MS. Although fully position-sensitive ion detectors based on resistive anode encoders are already available,[20,21] high-resolution (x,y) information is not necessary for implementing a full Hadamard encoding. Instead, a conventional microchannel plate (MCP) detector assembly with a two-zone patterned anode can be used. A schematic of such a device is shown in Figure 11. A modified HT-TOF MS spectrometer that uses full Hadamard encoding is under development in our laboratory at the present time.

To appreciate what promise HT-TOF MS may hold, let us make a conservative estimate of how many different mass peaks might be determined in a chemical analysis that combines a fast capillary-format separation (GC, for example) with this type of mass spectrometric detection. Let us imagine that a peak has a full width at half maximum of 200 ms and that the separation of the mixture is completed in 400 s. During that time, between 2000 peaks (the maximum possible) and 740 (37%, based on statistical considerations[22]) might be recorded. But the HT-TOF MS can easily have a mass resolution of 1000 and record a mass range m/z up to 5000,[23] which means that more than 1000 different species that co-elute with the same retention time can be distinguished. This amount also depends on the number of isotopomers and charged species produced per analyte by the electrospray ionization source, but a conservative estimate is that about one million different compounds could be detected in this two-dimensional format. Certain other forms of mass spectrometry offer higher resolution, but this gain in resolution comes at the expense of acquisition time. Notice that in order to monitor a chromatographic peak that is 100 ms wide, a spectral storage speed of 100 mass spectra s^{-1} or more is needed, if it is assumed that ten points are required to define the peak.

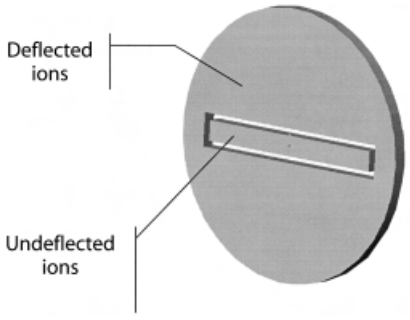


Figure 11. Patterned anode of the position-sensitive MCP detector. The central square detects the undeflected portion of the ion beam and the peripheral segment detects the deflected portion.

As we move toward faster and more complex separations, the need for MS with moderate resolution and high acquisition rate becomes increasingly urgent. The HT-TOF MS technique, coupled to a fast separation technique, begins to approach two-dimensional gel electrophoresis in its resolution of different components in a mixture, but with the marked advantages of an enormous gain in sample throughput and identification power.

We thank the U.S. Air Force Office of Scientific Research for support of this work.

Received: May 6, 2002 [M01572]

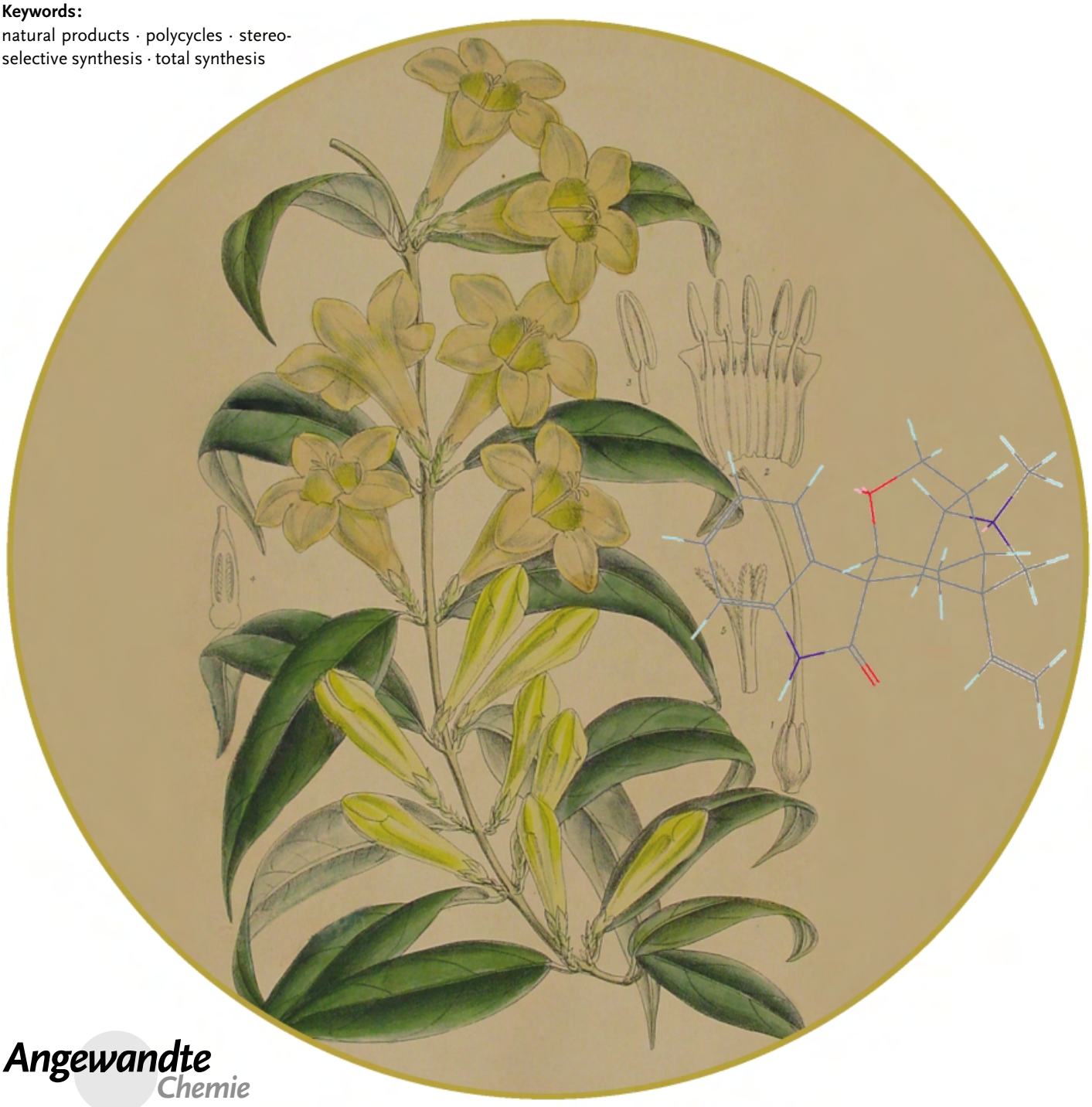
[1] N. E. Bradbury, R. A. Nielsen, *Phys. Rev.* **1936**, *49*, 388–393.
[2] R. Weinkauf, K. Walter, C. Weickhart, U. Boesl, E. W. Schlag, *Z. Naturforsch. A* **1989**, *44*, 1219–1225.
[3] A. Brock, N. Rodriguez, R. N. Zare, *Rev. Sci. Instrum.* **2000**, *71*, 1306–1318.
[4] A. Brock, N. Rodriguez, R. N. Zare, *Anal. Chem.* **1998**, *70*, 3735–3741.
[5] A. G. Marshall, *Fourier, Hadamard, and Hilbert Transforms in Chemistry*, Plenum, New York, **1982**.
[6] D. C. Tilotta, R. D. Freeman, W. G. Fateley, *Appl. Spectrosc.* **1987**, *41*, 1280–1287.
[7] T. Kaneta, Y. Yamaguchi, T. Imasaka, *Anal. Chem.* **1999**, *71*, 5444–5446.
[8] T. Kaneta, *Anal. Chem.* **2001**, *73*, 540A–547A.
[9] E. R. Williams, S. Y. Loh, F. W. McLafferty, *Anal. Chem.* **1990**, *62*, 698–703.
[10] P. Kebarle, L. Tang, *Anal. Chem.* **1993**, *65*, 972A–986A.
[11] A. D. Smith, M. Moini, *Anal. Chem.* **2001**, *73*, 240–246.
[12] F. M. Fernandez, J. M. Vadillo, F. Engelke, J. R. Kimmel, R. N. Zare, N. Rodriguez, M. Wetterhall, K. Markides, *J. Am. Soc. Mass Spectrom.* **2001**, *12*, 1302–1311.
[13] M. D. Harwit, N. J. Sloane, *Hadamard Transform Optics*, Academic Press, London, **1979**.
[14] G. Wilhelmi, F. Gompf, *Nucl. Instrum. Methods* **1970**, *81*, 36–44.
[15] F. von Heeren, E. Verpoorte, A. Manz, W. Thormann, *Anal. Chem.* **1996**, *68*, 2044–2053.
[16] C. Leonard, A. Grall, R. Sacks, *Anal. Chem.* **1999**, *71*, 2123–2129.
[17] C. A. Monnig, J. W. Jorgenson, *Anal. Chem.* **1991**, *63*, 802–807.
[18] J. F. Banks, T. Dresch, *Anal. Chem.* **1996**, *68*, 1480–1485.
[19] F. M. Fernandez, J. M. Vadillo, J. R. Kimmel, M. Wetterhall, K. E. Markides, N. Rodriguez, R. N. Zare, *Anal. Chem.* **2002**, *74*, 1611–1617.
[20] T. Mizogawa, H. Shiromaru, M. Sato, Y. Ito, *Int. J. Mass. Spectrom.* **2002**, *215*, 141–149.
[21] F. A. Rajgara, D. Mathur, T. Nishide, T. Kitamura, H. Shiromaru, Y. Achiba, N. Kobayashi, *Int. J. Mass. Spectrom.* **2002**, *215*, 151–162.
[22] J. M. Davis, J. Calvin Giddings, *Anal. Chem.* **1983**, *55*, 418–424.
[23] Resolution in HT-TOF MS is primarily governed by the frequency at which the BNG is switched. In contrast to conventional TOF MS, the detector response time and digitizing rate play a secondary role. For example, a resolution $\Delta m/m$ of 2000 at $m/z = 1000$ could be achieved at 25 MHz if the fidelity of the modulation is maintained at this frequency. The mass range of a HT-TOF mass spectrometer is a function of the sequence length and the mass cutoff of the BNG. For an in-depth discussion of these topics see ref. [12].

Total Syntheses of Gelsemine

Gelsemine: A Thought-Provoking Target for Total Synthesis**

*Hong Lin and Samuel J. Danishefsky**

Keywords:
natural products · polycycles · stereoselective synthesis · total synthesis



© 2003 Wiley-VCH Verlag GmbH & Co. KGaA, Weinheim

1433-7851/03/4201-0036 $ 20.00+.50/0

Gelsemine and 21-oxogelsemine have been synthesized through several routes. This Review focuses on the comparison of the different strategies to assemble the bicyclo[3.2.1]octane core, to introduce the bridgehead quaternary C20 to form the pyrrolidine moiety, to construct the oxindole residue, and to close the tetrahydropyran ring en route to gelsemine.

From the Contents

1. Introduction 37

2. Strategies for the Assembly of the Bicyclo[3.2.1]octane Skeleton 37

3. Strategies to Introduce the Quaternary Center (C20) and to Construct the Pyrrolidine Ring 43

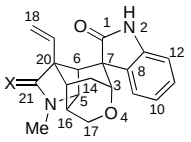
4. Strategies for Introduction of the Spirooxindole Moiety 46

5. Strategies to Construct the Tetrahydropyran Ring 49

6. Conclusion 50

1. Introduction

Gelsemine, isolated from *gelsemium sempervirens*, was first noted in the literature in 1870.[1] Its structure was determined in 1959 by Conroy and Chakrabarti.[2a] The novel construction, which Conroy proposed for the alkaloid, constituted an accommodation of the degradative and spectroscopic data then available. Fortunately, his deduction was proven to be correct in a simultaneous but independent crystallographic determination reported by Lovell et al.,[2b] who showed unambiguously that gelsemine is correctly represented as structure **1**. Accordingly, structure **2** corresponds to 21-oxogelsemine, also a natural product.



1: X = H, H
2: X = O

The degree of attention which has been lavished by many laboratories on total syntheses of gelsemine surely did not arise from any documented information suggesting that this alkaloid might have valuable properties. Actually, reports concerning any biological activity associated with gelsemine are at best sketchy and often anecdotal in style.[3] Rather, the attraction to gelsemine as a target in total synthesis has been driven by its fascinating three-dimensional architecture. It is in the solution of such problems that much new chemistry is often learnt.

This review will, in the first instance, deal with issues inherent in the successful total syntheses of **1**. However, the primary agenda of this paper deals with insight gained from various efforts directed at the synthesis of gelsemine. Ultimately, synthesis is the expression of our collective understanding of the underlying science of chemistry. It is not unlikely that these forays will be of greater consequence than the total syntheses themselves. For instance, a striking example will be seen in the use of a rather hindered, tetrasubstituted olefin in an intramolecular Heck reaction, described by Overman and co-workers in their total synthesis of gelsemine.[4] The advance has subsequently been applied as an essential key step in syntheses of many complex natural products.[5]

To date, seven total syntheses of **1** have been reported.[4,6–11] These attest to the multitude of perceptions and strategies that this highly compact hexacyclic indole alkaloid has stimulated. Our goal in writing this Review was not to provide a comprehensive collection of the literature published related to the synthesis of gelsemine. Rather, we emphasize the diversity of analyses that have been directed to reach **1**. We place particular emphasis on comparative solutions for assembling various subsections of the molecule, such as the bicyclo[3.2.1]octane skeleton, the C20 stereogenic center, the C7 stereogenic center anchoring the spirooxindole, the pyrrolidine moiety, and the very hindered tetrahydropyranyl ring on the concave face of the molecule. Accordingly, we have organized the Review around these structural elements rather than on recapitulations of each of the total syntheses in a serial format. In this way, we hoped to foster appreciation and comparative analyses of the various works.

2. Strategies for the Assembly of the Bicyclo[3.2.1]-octane Skeleton

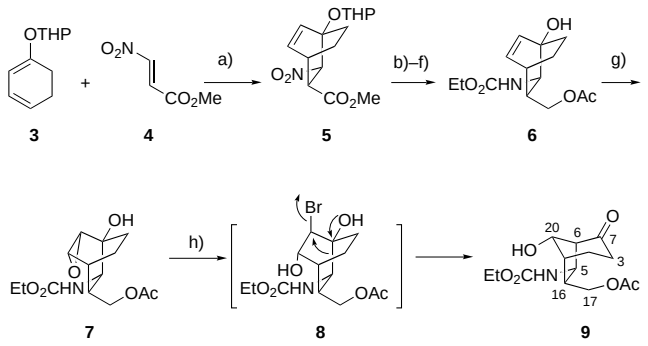
2.1. The Formation of the C5–C6 Bond—The Fleming, Overman, and Johnson Approaches

The approach of Fleming and co-workers to fashion the bicyclo[3.2.1]octane skeleton exploited Lewis acid promoted epoxide opening and ring fragmentation of a functionalized [2.2.2]octane **8** to form the C5–C6 bond (Scheme 1).[12] Diels–Alder condensation of diene **3** and β-nitroacrylate (**4**) afforded **5** and an isomer in which the nitro group had the *exo* configuration. The nitro group of **5** was reduced to the amine with Al/Hg in MeOH, and the amine was protected as its

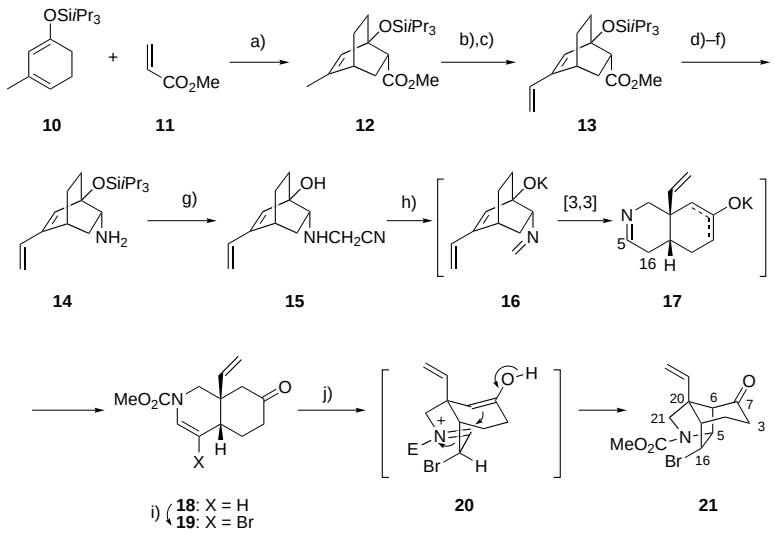
[*] S. J. Danishefsky, H. Lin
Bioorganic Laboratory
Sloan-Kettering Institute for Cancer Research
New York, NY 10021 (USA)
Fax: (+1) 212-772-8691
E-mail: s-danishefsky@ski.mskcc.org
S. J. Danishefsky
Department of Chemistry, Columbia University
New York, NY 10021 (USA)

[**] Frontispiece courtesy of the Luesther T. Mertz Library, The New York Botanical Gardens.

 © 2003 Wiley-VCH Verlag GmbH & Co. KGaA, Weinheim 1433-7851/03/4201-0037 $ 20.00+.50/0



Scheme 1. Synthesis of a bicyclo[3.2.1]octane by Fleming and co-workers. Conditions and reagents: a) pyrogallol (cat.), benzene, 0 °C→RT, 43 % + 39 % of *exo* product; b) Al/Hg, MeOH; c) EtO_2CCl, Et_3N; d) $LiAlH_4$; e) AcCl, Et_3N; f) PPTS, EtOH, 81 % over five steps; g) *p*-nitroperbenzoic acid, CH_2Cl_2, 85 %; h) $MgBr_2{\cdot}Et_2O$, benzene/THF, 65 °C, 78 %. PPTS = pyridinium *p*-toluenesulfonate.



Scheme 2. Approach used by Overman and co-workers in the synthesis of the tricyclic core. Conditions and reagents: a) $AlCl_3$, CH_2Cl_2, −78 °C, 76–83 %; b) SeO_2, dioxane, 100 °C; c) $Ph_3P{=}CH_2$, THF, −78→0 °C, 62–90 % over two steps; d) KOH, EtOH/H_2O, 90 °C; e) 1) $(ClCO)_2$, CH_2Cl_2, 0 °C; 2) NaN_3, acetone/H_2O; 3) toluene, reflux; f) KOH, dioxane/H_2O, 23 °C, 64 % over three steps; g) 1) $ClCH_2CN$, Bu_4NI (2 mol %), iPr_2NEt, THF, 67 °C; 2) Bu_4NF, THF, 0 °C, 90 %; h) 1) KH, [18]crown-6, THF, room temperature; 2) $ClCO_2Me$, DTBMP, −78 °C→RT; 3) KOH, MeOH, H_2O, room temperature, 81 %; i) Br_2, 1,2,2,6,6-pentamethylpiperidine, CH_2Cl_2, −78 °C; j) TFA, reflux, 67 % over 2 steps. DTBMP = 2,6-di-*tert*-butyl-4-methylpyridine, TFA = trifluoroacetic acid.

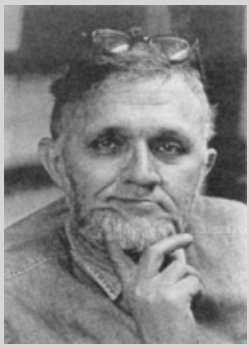
ethyl carbamate derivative. The ester function was reduced to an alcohol, which was protected as its acetate. Acidic hydrolysis of the THP protecting group afforded **6**. Remarkably, peracid-induced epoxidation of **6** preferentially occurred from its more hindered α face to give epoxide **7**. The latter was treated with $MgBr_2$ to provide rearrangement product **9**, presumably through the bromide intermediate **8**. Although the selectivity of the Diels–Alder reaction was low, it did allow a quick access to **9**, in which was embedded the functionality and stereochemistry required for the further elaboration.

The synthesis of the bicyclo[3.2.1] skeleton by Overman and co-workers also commenced with a Diels–Alder reaction. His scheme took advantage of an *N*-acyliminium Mannich cyclization as the key step to produce the C5−C6 bond (Scheme 2).[13] A straight forward Diels–Alder reaction of diene **10** and methyl acrylate (**11**) afforded bicyclo[2.2.2]octene **12** with apparently high *endo* selectivity. Allylic oxidation with selenium dioxide, followed by Wittig reaction of the aldehyde provided **13**. A Curtius rearrangement sequence converted ester **13** into amine **14**. The latter was subjected to alkylation with $ClCH_2CN$, followed by desilylation to afford **15**. Base-catalyzed aza-Cope rearrangement was accomplished by treatment of **15** with excess KH. The imine enolate **17** was bisacylated by deprotonation followed by quenching with excess methyl chloroformate. Finally selective cleavage of the carbonate afforded *cis*-hexahydroisoquinolinone **18**. The enecarbamate functional group in this molecule was selectively brominated and the product **19** was heated at reflux to provide azatricyclodecanone **21** as a single diastereomer. Apparently, the acyliminium intermediate **20**, bearing the *exo* bromine substituent, has the ideal geometry to deliver tricyclic product **21** in which the quaternary C20 carbon atom and the pyrrolidine moiety were already embedded. By using this extensively optimized sequence, compound **21** was prepared from commercially available 3-methylanisole in 12 steps and 16 % yield.

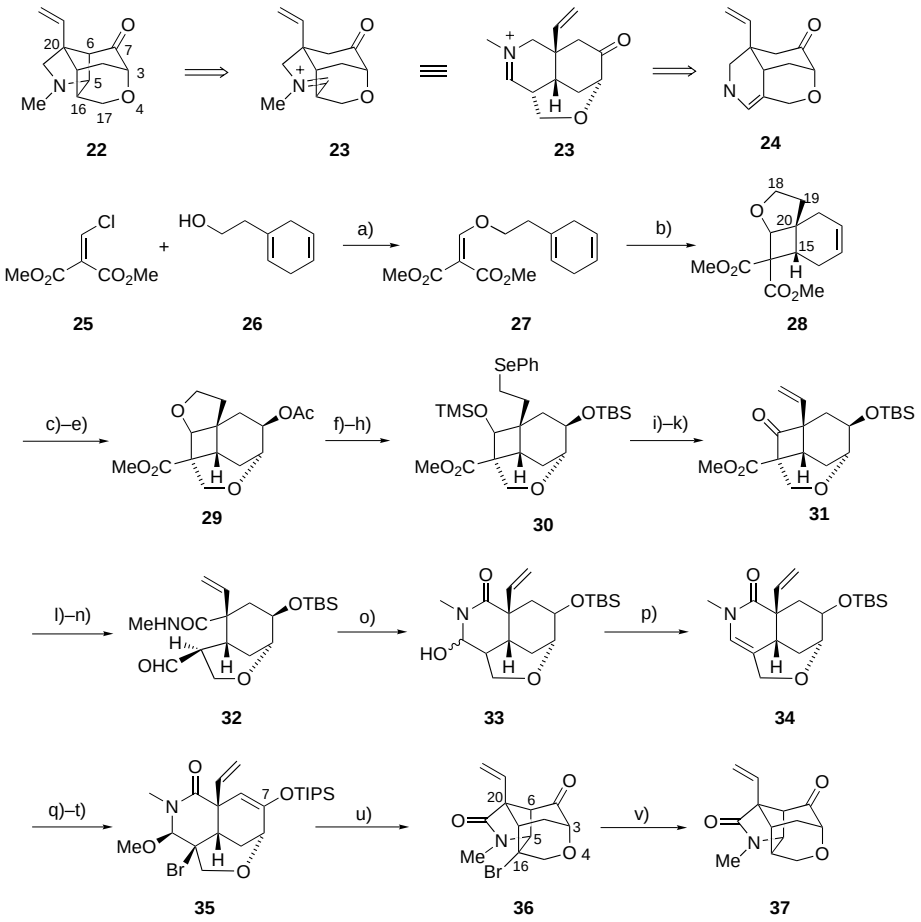
The strategy employed by Johnson and co-workers to form the C5−C6 bond also involved



Hong Lin was born in Nanjing, People's Republic of China, in 1970. She received a B.S. degree from Nanjing University in 1991 and a M.S. degree from the Shanghai Institute of Organic Chemistry in 1994. She received a Ph.D. degree in 2000 from Brandeis University, where she focused on the total synthesis of biologically intriguing and structurally novel natural alkaloids under the guidance of Professor Barry B. Snider. As an NIH postdoctoral fellow under the mentorship of Professor Samuel J. Danishefsky at the Memorial Sloan-Kettering Cancer Center, she completed the total synthesis of gelsemine. She is currently a medicinal chemist at GlaxoSmithKline.



Samuel J. Danishefsky was born in 1936. He received a B.S. degree at Yeshiva University, NY (1956). He obtained a Ph.D. in 1962 at Harvard University under the direction of Professor Peter Yates. From 1961 to 1963 he was a Postdoctoral Fellow at Columbia University under the mentorship of Gilbert Stork. From 1963 to 1979 he was on the faculty at the University of Pittsburgh, before moving to Yale University where he was Professor from 1980 to 1993. In 1993 he returned to New York as Professor of Chemistry at Columbia University. He is currently Head of Bioorganic Chemistry at the Memorial Sloan-Kettering Cancer Center. He is the recipient of numerous awards and prizes.



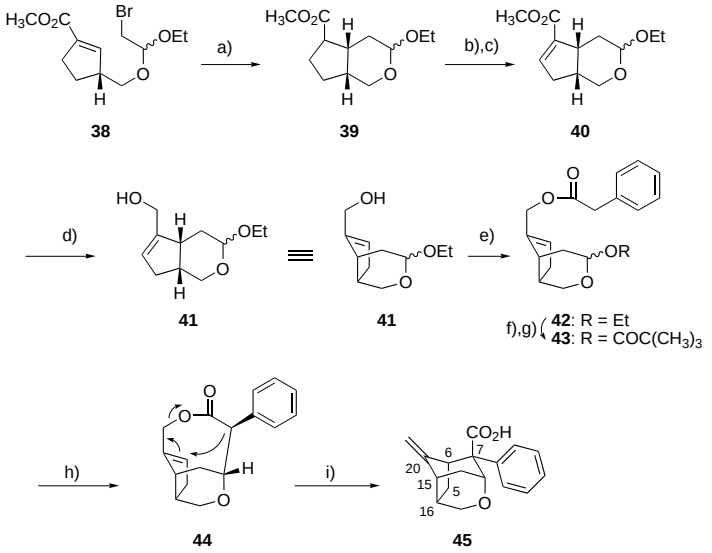
Scheme 3. Synthesis of the tetracyclic skeleton by Johnson and co-workers. Conditions and reagents: a) pyridine, 73%; b) *hν*, MeOH, trace HOAc, 53%; c) $LiAlH_4$, THF; d) AgOAc, I_2, HOAc, 44% over two steps; e) $RuCl_3$, $NaIO_4$, MeCN, CCl_4, H_2O; then CH_2N_2, Et_2O; f) K_2CO_3, MeOH, THF; g) TBSOTf, 2,6-lutidine, CH_2Cl_2, −5 °C, 85% over three steps; h) $PhSeSiMe_3$, ZnI_2, PhMe, reflux, 94%; i) *m*CPBA, THF, −25 °C; then Pr_2NH, CCl_4, reflux, 92%; j) K_2CO_3, MeOH, THF; k) DMSO, TFAA, −70 °C, Et_3N, 92% over two steps; l) $MeNH_2$, MeOH, THF, 86%; m) $LiBH_4$, MeOH, Et_2O; n) CrO_3, pyridine, CH_2Cl_2, 95%; o) K_2CO_3, MeOH, 88%; p) TsOH, CH_2Cl_2; q) Br_2, MeOH, 97% over two steps; r) Bu_4NF, THF; s) DMSO, $(COCl)_2$, Et_3N, 96% over two steps; t) TIPSOTf, Et_3N, 97%; u) TFA, reflux, 15 min, 74%; v) Bu_3SnH, AIBN, benzene, reflux. TBS = *tert*-butyldimethylsilyl, Tf = trifluoromethanesulfonyl, *m*CPBA = *m*-chloroperbenzoic acid, TFAA = trifluoroacetic anhydride, Ts = *p*-toluenesulfonyl, DMSO = dimethyl sulfoxide, TIPS = triisopropylsilyl, AIBN = 2,2′-azobisisobutyronitrile.

an intramolecular Mannich reaction, but on the more advanced intermediate iminium **23**, with the tetrahydropyran ring already incorporated (Scheme 3).[7] The synthesis of **24** commenced with *O*-alkylation of **26** with **25**, followed by the photoinduced cycloaddition of triene **27**. This sequence gave the key tricyclic diester intermediate **28**. At this stage, the functionality for the future C20 vinyl group is in the required *cis* relationship to the 15-H at the ring fusion. Reduction of **28** with $LiAlH_4$ afforded the diol, which was treated with AgOAc and I_2 to establish the tetrahydropyran ring. The remaining hydroxy group was oxidized to the corresponding acid and esterified to provide **29**. The base-labile acetate of **29** was replaced with a TBS protecting group, and the tetrahydrofuran ring was cleaved by the action of $PhSeSiMe_3$ in the presence of catalytic ZnI_2. Oxidative deselenylation of **30** provided the vinyl group and careful desilylation (to avoid the retroaldol reaction, which occurs under more basic conditions) followed by immediate oxidation afforded cyclobutane-β-ketoester **31**. Treatment of **31** with methylamine resulted in cleavage of the strained β-ketoester linkage, thus affording an amido ester. Following reduction of the ester and subsequent oxidation, aldehyde **32** was in hand. The aldehyde was epimerized with methanolic K_2CO_3, thereby triggering cyclization to hydroxylactam **33**, which was readily dehydrated to afford enamide **34**. Treatment of the latter with methanolic bromine followed by functional-group modification at C7 provided compound **35**. In a key step, this compound was converted into bromoketone **36** through an intramolecular Mannich reaction. Following reductive debromination, the well-advanced tetracyclic intermediate **37** was in hand. Of course, in both this compound and its less oxidized counterpart **22**, there remained the daunting task of spirooxindole insertion at C7 to reach gelsemine.

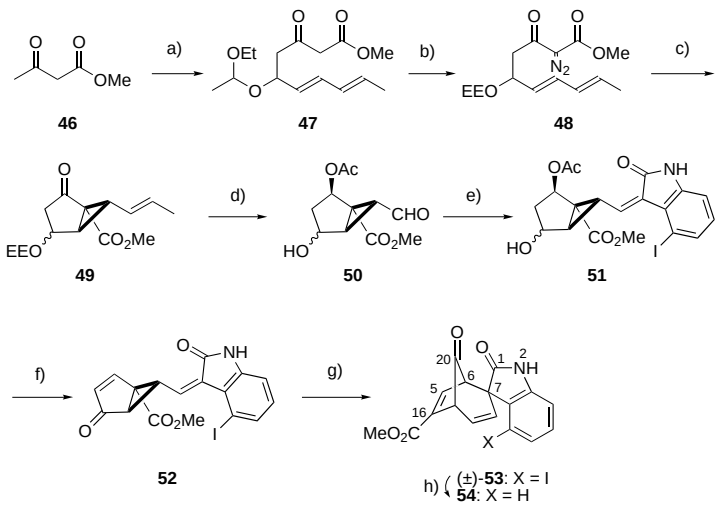
2.2. C6–C7-Bond Formation—Four Approaches

Another strategy to synthesize a highly functionalized bicyclo[3.2.1] skeleton involved the formation of the critical C6–C7 bond as in the model study by Stork and co-workers through a Claisen rearrangement. The total synthesis by Fukuyama and co-workers (and our own) exploited divinylcyclopropane bond reorganization to the same end.

The approach used by Stork and co-workers to prepare the gelsemine skeleton exploited an elegant radical-initiated cyclization of **38** to provide bicyclic ester **39**.[14] This product was easily converted into unsaturated ester **40** by selenation and oxidative elimination (Scheme 4). This sequence led to a 6:1 mixture of **40** and its tetrasubstituted isomer. Reduction of **40** afforded allylic alcohol **41**, which was acylated with phenylacetic acid to give ester **42**. The ethoxy group of **42** was replaced with a more active leaving group (pivaloate) to afford **43**. The crucial bond formation between the anomeric center and the α-methylene group of the phenylacetic ester occurred via the TMS ketene acetal derived from **43**. Cyclization was accomplished through the use of TMSOTf



Scheme 4. Synthesis of the tricyclic core by Stork and co-workers through C6–C7-bond formation. Conditions and reagents: a) Bu_3SnH, AIBN (cat., 0.02 M in benzene), reflux, 3 h, 95%; b) 1) LDA, THF, −78→−30 °C; 2) −78 °C, PhSeSePh, 93%; c) 1) *m*CPBA, CH_2Cl_2, −40 °C, 1 h; 2) Et_3N, room temperature, 98% of a 6:1 mixture of **40** and tetrasubstituted unsaturated ester; d) DIBALH, Et_2O, 0 °C, 1 h, 95%; e) phenylacetic acid, DCC, DMAP, CH_2Cl_2, room temperature, 30 min, 79%; f) Amberlite-H^+, THF/H_2O (20:1), 1–2 h, 65 °C, 90%; g) PivCl, DMAP, Et_3N, CH_2Cl_2, room temperature, 1 h, 85%; h) 1) LDA, TMSCl, THF, −78 °C; 2) diluted with CH_2Cl_2/THF (1:1) to 0.002 M, TMSOTf, −78→−20 °C, 67%; i) LDA, TMSCl, THF, −78 °C; then room temperature, 24 h, 96%. DIBALH = diisobutylaluminum hydride, DCC = dicyclohexylcarbodiimide, DMAP = 4-dimethylaminopyridine, LDA = lithium diisopropylamide, Piv = 2,2,2-trimethylacetyl.

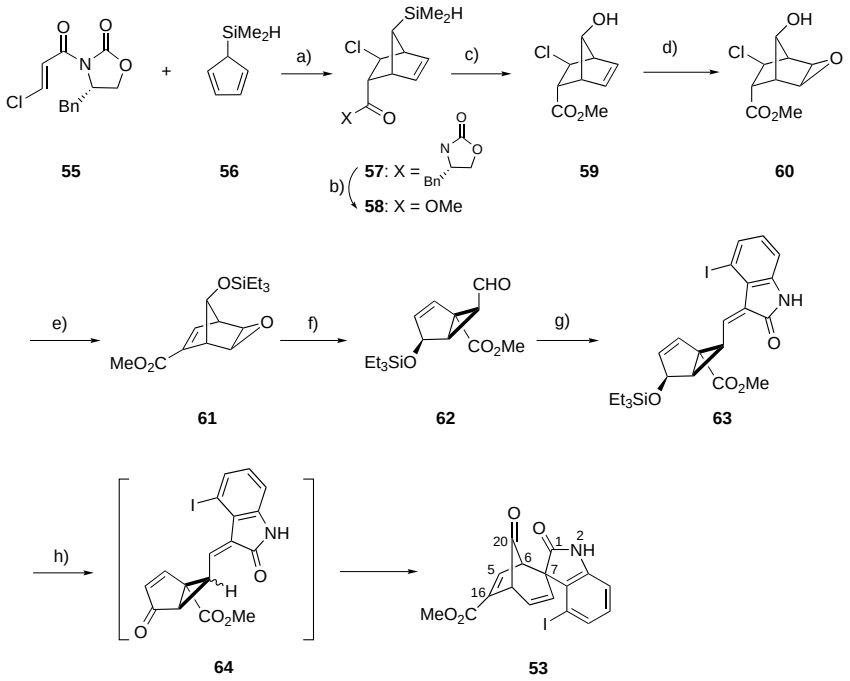


Scheme 5. Synthesis of the bicyclo[3.2.1] Core by Fukuyama and co-workers by divinylcyclopropane rearrangement. Conditions and reagents: a) 1) NaH, THF, 0 °C; then BuLi; 2) sorbic aldehyde, 0→23 °C; ethyl vinyl ether, $POCl_3$, CH_2Cl_2, 0→23 °C, 53%; b) TsN_3, Et_3N, CH_2Cl_2, 0 °C, 83%; c) [Cu(acac)$_2$] (cat.), $CuSO_4$, benzene, 85 °C, 3 h, 68%; d) 1) $NaBH_4$, MeOH, 0 °C; 2) Ac_2O, pyridine, 23 °C; 3) TsOH, *i*PrOH/H_2O, 23 °C, 74%; 4) O_3, MeOH/CH_2Cl_2 (10%), −78 °C, then Me_2S, −78 to 23 °C, 89%; e) 4-iodooxindole, piperidine (cat.), MeOH, 23 °C, 89%; f) 1) DCC, DMSO, pyridinium trifluoroacetate, 23 °C; 2) Et_3N, CH_2Cl_2, 23 °C, 91%; g) toluene/CH_3CN (1:1), 90 °C, 45 min, 98%; h) Bu_3SnH, AIBN (cat.), toluene, 95 °C, 1 h, 85%. EE = ethoxyethyl.

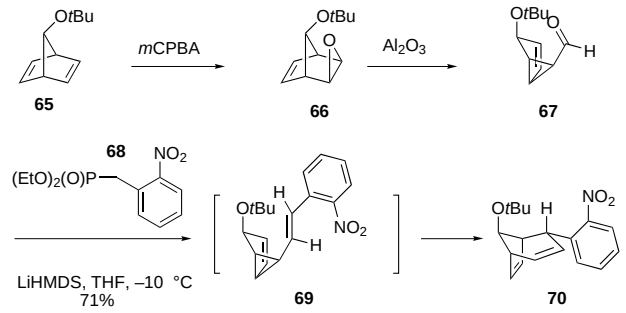
to afford the strained lactone **44** as a single diastereomer. The key Claisen rearrangement step was then realized *via* the enol silyl ether of **44** thereby providing acid **45**. This highly imaginative assembly leads to a significant portion of the carbon skeleton of gelsemine in a stereospecific way. Moreover, compound **45** includes functionalities for the construction of the oxindole moiety at C7.

In the first-generation approach by Fukuyama and co-workers to gelsemine,[9] the spirooxindole functionality was installed stereoselectively through a sequence involving intermediates **50**, **53**, and **54**. His approach took advantage of earlier findings of Kondo et al.[15a] and of Taber[15b] in establishing a vinylcyclopropane intermediate (Scheme 5). Addition of the dianion derived from methyl acetoacetate (**46**) to sorbic aldehyde followed by protection of the resulting alcohol gave ethoxyethyl ether **47**. A Regitz diazo-transfer reaction conducted on **47** furnished **48**. The latter underwent copper-mediated cyclopropanation to provide bicyclic ketone **49**. Sequential reduction of ketone **49**, acetylation of the resulting alcohol, hydrolysis of the ethoxyethyl ether, and finally, ozonolysis of the olefin led to aldehyde **50**. Knoevenagel-like condensation of this compound with 4-iodooxindole gave exclusively the alkylidene indoline (*Z*)-**51**, which is thermodynamically much more stable than its *E* isomer. Pfitzner–Moffatt oxidation of alcohol **51** followed by elimination of acetic acid furnished enone **52**, which underwent divinylcyclopropane–cycloheptadiene rearrangement at 90 °C to provide the racemic spirooxindole (±)-**53**. Subsequent deiodonation afforded the key bicyclo[3.2.1] intermediate **54**.

The second-generation approach by Fukuyama and co-workers resulted in a stereospecific total synthesis of (+)-gelsemine.[10] The bicyclo[3.2.1] core structure was again assembled through a divinylcyclopropane rearrangement, but from an optically active intermediate **64** prepared from a chiral-auxiliary-controlled asymmetric Diels–Alder reaction (Scheme 6). Dienophile **55** and 5-dimethylsilylcyclopentadiene (**56**) underwent a Diels–Alder reaction in the presence of Et_2AlCl to give adduct **57** as a single isomer. Its stereochemistry was confirmed by X-ray crystallographic analysis. The chiral auxiliary was removed and the dimethylsilyl group was oxidized to give alcohol **59**. Epoxidation of the olefinic linkage led to **60**. Protection of the alcohol followed by dehydrochlorination furnished α,β-unsaturated ester **61**. The rearrangement of the *exo* epoxide was best carried out by treatment with bis(2,6-di-*tert*-butyl-4-methylphenoxide)methylaluminum (MAD) in toluene at −20 °C to afford exclusively the α-methyl ester epimer **62**. Condensation of aldehyde **62** and 4-iodooxindole afforded only the alkylidene indolinone (*Z*)-**63**. Subjection of the latter to desilylation and Jones oxidation gave a mixture of isomeric **64** and rearrangement product



Scheme 6. Asymmetric synthesis of the bicyclo[3.2.1] core by Fukuyama and co-workers. Conditions and reagents: a) Et_2AlCl, CH_2Cl_2, −78 °C, 88%; b) $Sm(OTf)_3$ (cat.), MeOH, 99%; c) H_2O_2 (30%), KF, $KHCO_3$, THF/MeOH, 53%; d) $[VO(acac)_2]$, *t*BuOOH, benzene, 100%; e) 1) TESOTf, 2,6-lutidine, CH_2Cl_2, 97%; 2) *t*BuOK, benzene, 98%; f) MAD, toluene, −20 °C; g) 4-iodooxindole, piperidine (cat.), MeOH, 60% over two steps; h) 1) TBAF, THF, 87%; 2) CrO_3, H_2SO_4, acetone; 3) toluene/MeCN, 90 °C, 83%. TES = triethylsilyl, MAD = bis(2,6-di-*tert*-butyl-4-methylphenoxide)methylaluminum, TBAF = tetra-*n*-butylammonium fluoride.



Scheme 7. Divinylcyclopropane rearrangement to bicyclo[3.2.1] core by Danishefsky and co-workers.

53. The mixture was heated at 90 °C to furnish **53** as an enantiomerically pure intermediate.

Our synthesis of the bicyclo[3.2.1] core commenced with the known aldehyde **67** (Scheme 7),[11] prepared by regioselective epoxidation of norbornadiene **65** followed by the rearrangement of unstable *exo* epoxide **66** to **67**. *o*-Nitrobenzylidenation of aldehyde **67** with phosphonate **68** led to **70** presumably *via* divinylcyclopropane **69**. Our route was unique in that it projected the late-stage introduction of a critical one-carbon fragment at C7.

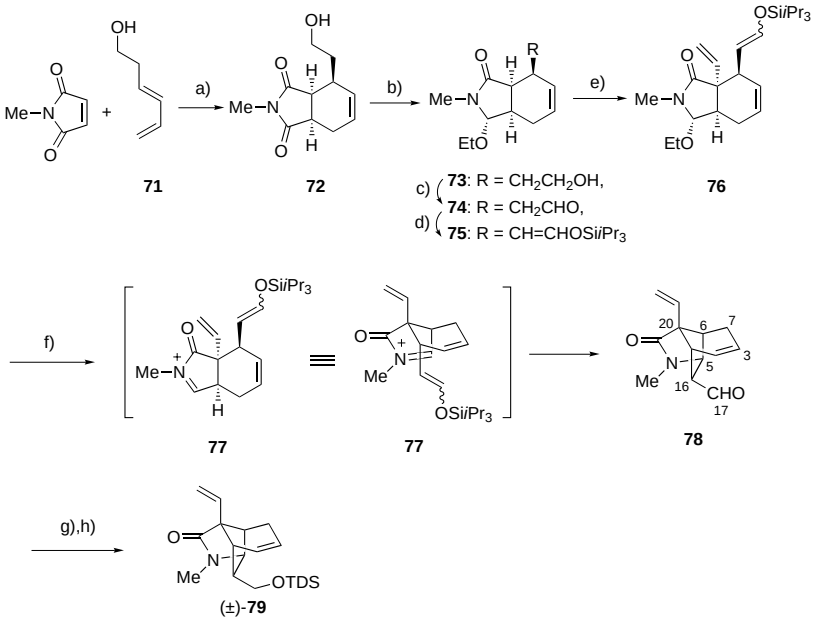
2.3. C5–C16-Bond Formation—The Hart, Speckamp, and Cha Approaches

A third strategy to assemble the appropriate skeleton for reaching gelsemine was the formation of the C5–C16 bond in the total syntheses by Speckamp and co-workers and by Hart and co-workers, as well as in the model study by Cha and co-workers.

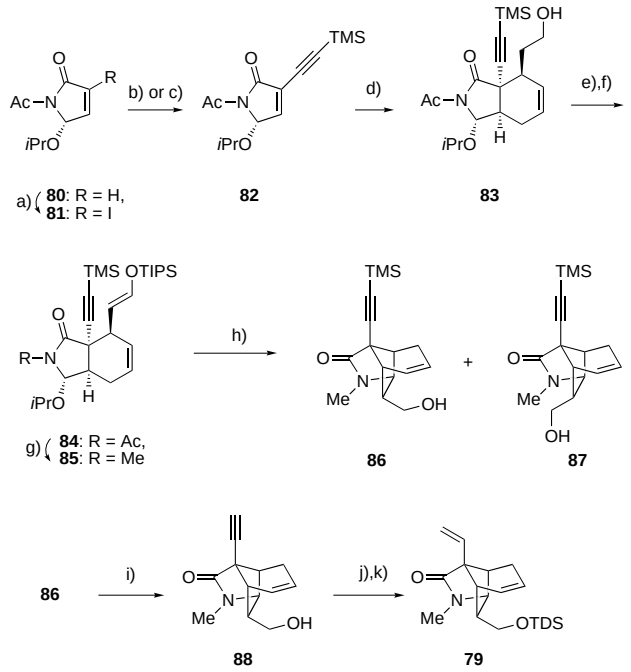
The key step in the approach of Speckamp and co-workers was an intramolecular *N*-acyliminium cyclization (see Scheme 8) similar to that in the Overman and Johnson demonstrations discussed above. However, in the case of Speckamp, the C5–C16 bond, rather than the C5–C6 bond, was established.[16,17] Diels–Alder reaction of diene **71** and *N*-methylmaleimide only gave *endo*-adduct **72**. Regioselective partial reduction of imide **72** followed by ethanolysis afforded **73** as the major product in a complex mixture. Aldehyde **74** was easily purified and then transformed into an inseparable mixture of *E*/*Z* (70:30) silyl enol ether **75**. The vinyl group at the quaternary C20 was introduced by the aldol condensation of the enolate of lactam **75** with 2-(phenylseleno)ethanal. Subsequent elimination of the mesylate of the aldol adduct afforded **76**. The Mannich-like cyclization of **76**, via presumed acyliminium intermediate **77**, gave a 70:30 mixture of **78** and its C16 epimer. Reduction of the mixture followed by recrystallization afforded the pure desired alcohol, which was protected as the silyl ether (±)-**79**.

In the later asymmetric synthesis by Speckamp and co-workers en route to (+)-gelsemine,[17] optically active **79** was prepared from chiral pyrrolinone **80** by using a modified sequence (Scheme 9). Iodination of **80** afforded **81**, which was subjected to either Stille or Sonogashira[18] coupling to provide acetylene **82**. Diels–Alder reaction of **82** and diene **71** proceeded with excellent selectivity to give **83** as a single isomer. The hydroxy group of **83** was converted into the crude silyl enol ether **84** in which the *E* isomer was the predominant product. Cleavage of the *N*-acetyl group followed by *N*-methylation afforded **85** as a pure *E* isomer. The *N*-acyliminium cyclization reaction of **85** was best achieved by treatment with TMSOTf to afford a 4:1 mixture of aldehydes. Reduction of this mixture gave rise to a 4:1 mixture of **86** and **87**. Base-induced desilylation of **86** provided **88**, which was protected as its silyl ether. Following partial reduction of the alkyne, the enantiomerically pure **79** was in hand.

The approach of Hart and co-workers to the synthesis of gelsemine contemplated the formation of the C5–C16 bond through radical cyclization.[8,19] Their route also commenced with the Diels–Alder reaction of *N*-methylmaleimide with diene **89** to give **90** (Scheme 10). Acidic hydrolysis of the silyl enol ether and the THP protecting group in the presence of



Scheme 8. Synthesis of the tricyclic core through C6–C15-bond formation by Speckamp and co-workers. Conditions and reagents: a) toluene, reflux, 95%; b) 1) $NaBH_4$ (excess), EtOH, H_2SO_4 (cat.), 0°C, 2 h; 2) H_2SO_4 (6 N) in EtOH; c) CrO_3, pyridine, CH_2Cl_2, 4.5 h, 20°C, 44% over two steps; d) TIPSOTf, Et_3N, CH_2Cl_2, *E*/*Z* (70:30), 100%; e) 1) LDA, THF, −78°C, $PhSeCH_2CHO$; 2) MsCl, Et_3N, CH_2Cl_2, 70%; f) $BF_3{\cdot}OEt_2$, CH_2Cl_2, 10°C, 10 min, 70% + 30% of C16-epimer of **78**; g) $NaBH_4$, EtOH, 90%; h) TDSCl, imidazole, DMF. Ms = mesyl = methanesulfonyl, TDS = thexyldimethylsilyl, DMF = *N*,*N*-dimethylformamide.



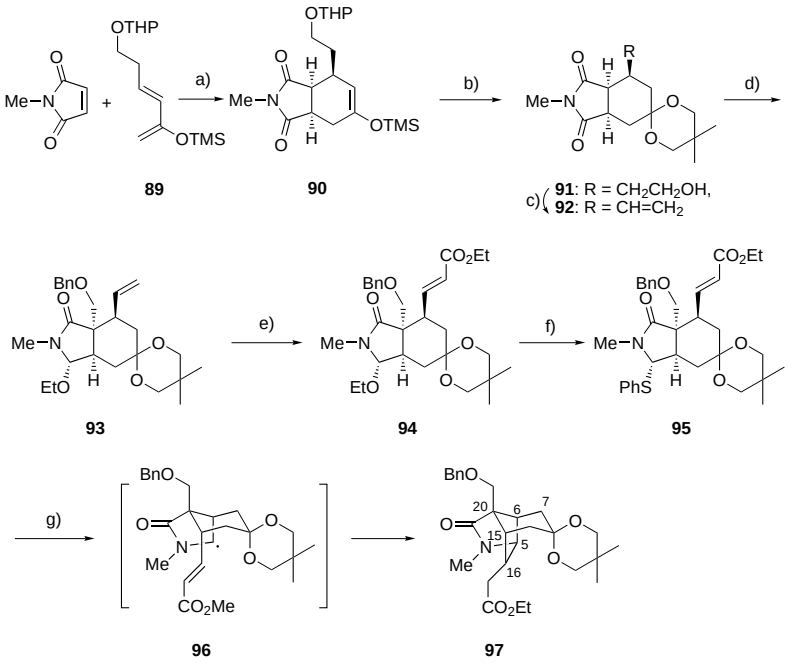
Scheme 9. Asymmetric approach to the tricyclic core by Speckamp and co-workers. Conditions and reagents: a) I_2, pyridine, CCl_4, 0°C→RT, 68 h, 88%; b) $TMSCCSnBu_3$, $[PdCl_2(MeCN)_2]$ (5%), DMF, room temperature, 15 min, 89%; c) TMSCCH, CuI (10%), $[PdCl_2(MeCN)_2]$ (5%), diisopropylamine (3 equiv), THF, room temperature, 1 h, 91%; d) ammonia-rinsed flask, **71**, hydroquinone (trace), toluene, 100°C, 40 h, 93%; e) Dess–Martin periodonane, CH_2Cl_2, 0°C→RT, 2 h; f) TIPSOTf, Et_3N, CH_2Cl_2, 0°C→RT, 2 h; g) 1) Me_2NH (excess), CH_2Cl_2, 0°C→RT, 2 h, 65% over three steps; 2) MeI, THF, LiHMDS, −78°C→RT, 98%; h) TMSOTf, CH_2Cl_2, −13°C, 25 min, **86**/**87** 4:1; then $NaBH_4$, EtOH, 0°C, 66%; i) K_2CO_3, MeOH, room temperature, 98%; j) TDSCl, imidazole, DMF, room temperature; k) Lindlar catalyst, H_2 (1 atm), quinoline, EtOAc, 20 min, 99%. HMDS = hexamethyldisilazanide.

2,2-dimethyl-1,3-propanediol afforded ketal **91**. The latter, when subjected to the dehydration conditions reported by Grieco et al. (*o*-$NO_2C_6H_4SeCN$, nBu_3P, then H_2O_2),[20] gave **92**. Partial reduction of imide **92**, *O*-alkylation of the resulting alcohol, and alkylation of the lithium enolate of the amide furnished **93**. Ozonolysis of the vinyl group of **93** followed by Wittig olefination provided α,β-unsaturated ester **94**. After ethoxy–thiophenoxy exchange, **95** was in hand. Finally, a free radical cyclization of **96**, which adopted a boatlike conformation possibly to avoid the interaction between the ketal and α,β-unsaturated ester functions, furnished the tricyclic **97** with the undesired stereochemistry at C16. Fortunately, this problem was eventually solved.

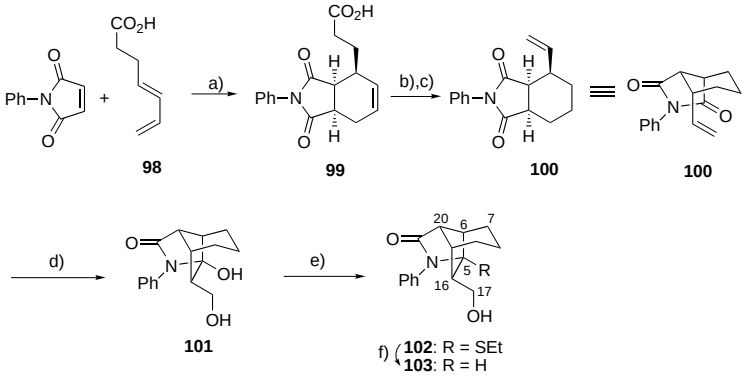
A strategy that was complimentary to Speckamp's nucleophilic addition to an *N*-acyliminium species and Hart's amidomethinyl α-acylamine radical cyclization, was the Ti^{II}-mediated cyclization of a ω-vinylimide by Cha and co-workers (Scheme 11).[21] Thus, Diels–Alder reaction of *N*-phenylmaleimide and diene **98** afforded acid **99**, which was subjected to hydrogenation and subsequent oxidative decarboxylation to afford ω-vinylimide **100**. Treatment of **100** with excess cyclopentylmagnesium chloride in the presence of 1.5 equivalents of $ClTi(OiPr)_3$ followed by autooxidation prior to aqueous workup, afforded the desired cyclization product **101**. Finally, the *N*-acylaminal functionality was reduced in a two-step sequence to provide **103** via **102**.

2.4. A Photochemical Approach

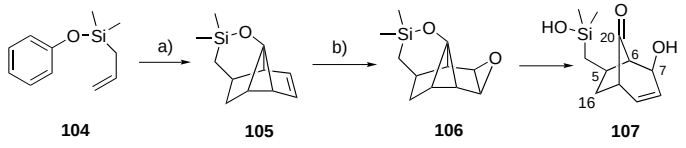
An interesting photochemical approach to the bicyclo[3.2.1] skeleton of gelsemine was reported by Penkett and co-workers (Scheme 12).[22] Photolysis of 3-(phenoxydimethylsilyl)prop-1-ene (**104**) afforded the desired photoadduct **105**[23] as the major product. Treatment of **105** with *m*CPBA gave **107**, presumably from fragmentation of epoxide **106**.



Scheme 10. Synthesis of the tricyclic skeleton by Hart and co-workers through C5–C16-bond formation/free-radical cyclization. Conditions and reagents: a) toluene, reflux; b) TsOH, 2,2-dimethylpropan-1,3-diol, 39% over two steps; c) 1) *o*-$NO_2C_6H_4SeCN$, *n*Bu_3P, THF; 2) H_2O_2, 79%; d) 1) $NaBH_4$, MeOH, −23 °C; 2) NaH, EtI, THF, 71%; 3) LDA, THF, $PhCH_2OCH_2Cl$, 96%; e) 1) O_3, CH_2Cl_2, MeOH, then Me_2S, 76%; 2) $Ph_3P{=}CHCO_2Et$, 82%; f) PhSH, TsOH (cat.), CH_2Cl_2, 76%; g) AIBN (cat.), Bu_3SnH, benzene, 64%.



Scheme 11. Ti^{II}-mediated cyclization of ω-vinylimides in the approach by Cha and co-workers to the tricylic core. Conditions and reagents: a) $NaHCO_3$, H_2O, 90%; b) H_2, Pd/C; c) $Pb(OAc)_4$, $Cu(OAc)_2$, pyridine, chlorobenzene, 50%; d) *c*-C_5H_9MgCl, $ClTi(OiPr)_3$, Et_2O, 0 °C, then O_2, 42%; e) EtSH, $BF_3{\cdot}Et_2O$, CH_2Cl_2, 85%; f) Raney nickel, H_2, EtOH, 80%.



Scheme 12. Photochemical approach to the bicyclo[3.2.1] skeleton by Penkett and co-workers. Conditions and reagents: a) *hν*, 254 nm, hexane, 38%; b) *m*CPBA, 56%.

3. Strategies to Introduce the Quaternary Center (C20) and to Construct the Pyrrolidine Ring

3.1. C5–C6-Bond Formation—Overman Approach through Aza-Cope Rearrangement

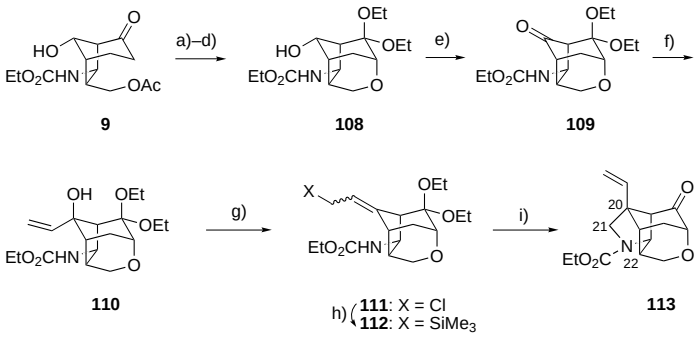
One of the challenges in any total synthesis of gelsemine is that of stereoselectively constructing the bridgehead (C20) quaternary center of the pyrrolidine moiety. In the above-mentioned synthesis by Overman and co-workers (Scheme 2), the C20 quaternary center was introduced by an aza-Cope rearrangement (**15**→**18**). In essence, the stereochemical outcome—*cis* relationship between 15-H and C20 vinyl group—was determined from the initial *endo* Diels–Alder cycloaddition. Upon formation of the C5–C6 bond through a Mannich reaction (**19**→**21**), the pyrrolidine moiety also became accessible.

3.2. C19–C20-Bond Formation—Aldol Condensation and Alkylation

The strategies of Speckamp and co-workers[6,16] and of Hart and co-workers[8,18] to construct the C20 quaternary center and the pyrrolidine ring of **1** are very similar. In both of these syntheses, *N*-methylmaleimide served as the source of the pyrrolidine moiety. The C20 quaternary center was formed by either an aldol condensation (Scheme 8, **75**→**76**) or by alkylation of the amide enolate (Scheme 10, **92**→**93**) with further elaboration to the vinyl group. In both cases, the stereochemistry at C20 was totally controlled by the initial relative stereochemistry (C5, C6, and C15) set up in the *endo* Diels–Alder reactions.

3.3. C20–C21-Bond Formation—Intramolecular [2+2] Photocycloaddition

In the synthesis of **1** by Johnson and co-workers,[7a] the *cis* relationship between 15-H and the vinyl group at C20 was assured by the [2+2] photocycloaddition and the vinyl group was masked as a tetrahydrofuran ring (Scheme 3, **27**→**28**). A lactam equivalent of the pyrrolidine moiety was formed via an acyliminium Mannich reaction through C5–C6 formation (**35**→**36**), similar to approach of Overman and co-workers.



Scheme 13. Synthesis of the C20 quaternary center and the pyrrolidine ring by Fleming and co-workers. Conditions and reagents: a) $PhNMe_3Br_3$; b) DHP, H^+; c) K_2CO_3, H_2O; d) PPTS, EtOH, 62% over four steps; e) PCC, Al_2O_3, 91%; f) $CH_2{=}CHMgBr$, 90%; g) $SOCl_2$, 97%; h) $(Me_3Si)_2CuLi$, 84%; i) $(CH_2O)_3$, HCO_2H, 85%. DHP = dihydropyran, PCC = pyridinium chlorochromate.

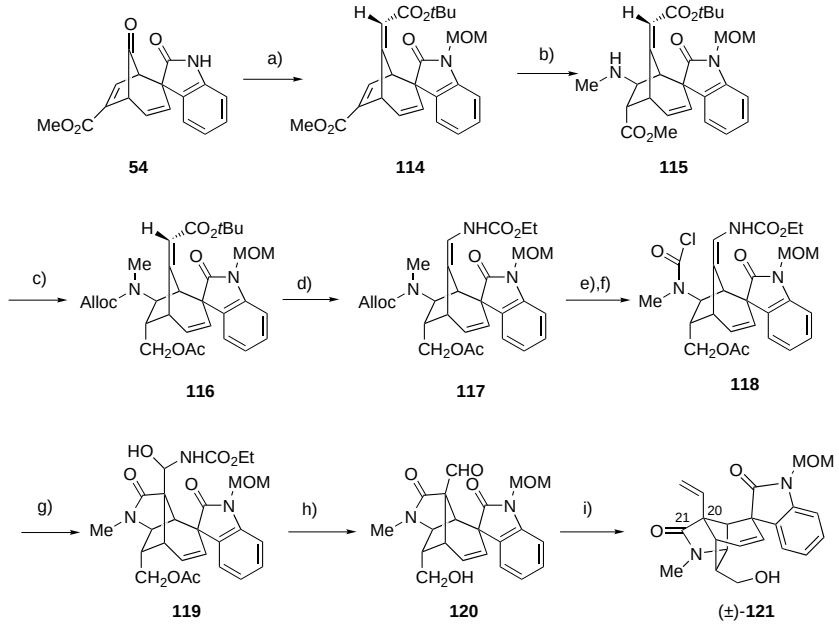
3.4. Fleming's Approach

In a model study by Fleming and co-workers (Scheme 13),[12] the fully functionalized bicyclo[3.2.1]octanone **9** was brominated and the bridgehead hydroxy group was protected. Basic hydrolysis of the acetate released the oxy anion, which displaced a bromide group to give rise to the desired tetrahydropyran ring. Subsequent acidic ethanolysis removed the THP protecting group and afforded ketal **108**. Oxidation of alcohol **108** afforded ketone **109**, which upon treatment with vinylmagnesium bromide, furnished tertiary alcohol **110**. Allylsilane **112** was prepared from allyl chloride **111**, derived from chlorination of tertiary alcohol **110**. Treatment of **112** with formaldehyde under acidic condition furnished **113**, presumably through nucleophilic addition of allylsilane to the *N*-acyliminium intermediate. In this way, the quaternary C20 center and the pyrrolidine ring moiety were assembled through the C20–C21-bond formation.

3.5. C20–C21-Bond Formation: Fukuyama's Approach

Fukuyama and co-workers assembled the quaternary center at C20 and the pyrrolidine ring through C20–C21-bond formation (Scheme 14).[9] Selective elongation of the bridgehead ketone group was quite difficult, but was eventually achieved. In a one-pot sequence, treatment of **54** with $(EtO)_2P(O)CH(Li)CO_2tBu$ followed by protection of the indolinone nitrogen atom afforded a single isomer of **114**. Interestingly, the Michael addition of methylamine occurred exclusively at the α,β-unsaturated methyl ester, in preference to the α,β-unsaturated *tert*-butyl ester **115**. Protection of the amine, selective reduction of the methyl ester, and acetylation of the resulting alcohol yielded **116**. The *tert*-butyl ester of **116** was converted into ethyl urethane **117** by a classical Curtius rearrangement. Deprotection of the Alloc group of **117** followed by treatment of the resulting amine with phosgene provided carbamoyl chloride **118**, which cyclized to lactam **119** in the presence of AgOTf and Ag_2CO_3. Acidic hydrolysis of aminal urethane **119** caused concomitant hydrolysis of the acetate to yield aldehyde **120**. Methylenation of the sterically hindered aldehyde was best effected by treatment with Tebbe reagent to give **121**.

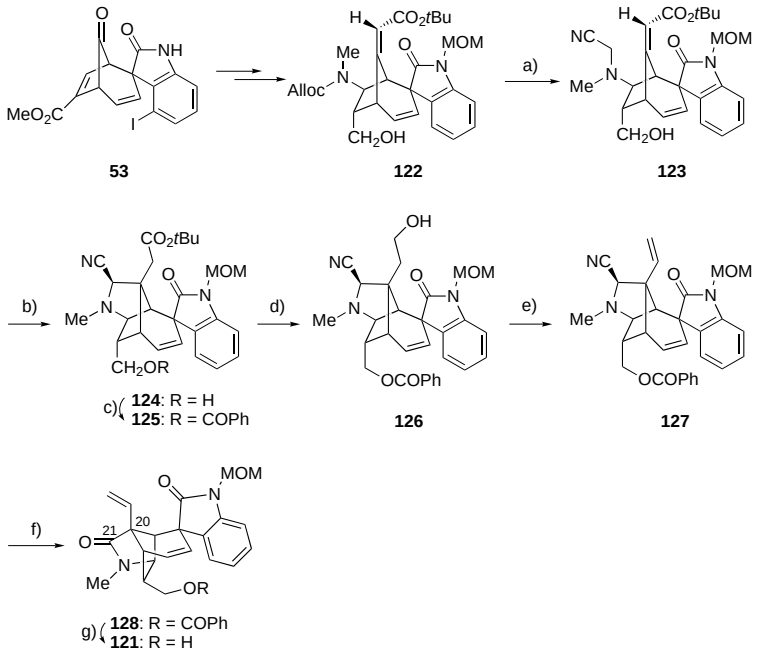
In the second-generation asymmetric synthesis of **1** by Fukuyama and co-workers, an intramolecular Michael addition was applied to establish the C20–C21 bond (Scheme 15).[10] Optically pure **53** was converted into **122** by following similar transformations to those used in the racemic series. Removal of the Alloc group, followed by *N*-cyanomethylation afforded aminonitrile **123**. The latter underwent Michael addition upon treatment with KHMDS to yield pyrrolidine **124**. Protection of the hydroxy group of **124** afforded benzoate ester **125**. Progression of the *tert*-butoxycarbonylmethyl group to the required vinyl group was accomplished via alcohol **126**, in turn obtained by chemoselective reduction of a mixed anhydride. Alcohol **126** was then converted into vinyl compound **127**, as described by Grieco et al.[20] Oxidation of cyanopyrrolidine **127** with *m*CPBA in a Polonovsky-like reaction, afforded lactam **128**. Basic hydrolysis of benzoate **128** gave rise to alcohol **121**.



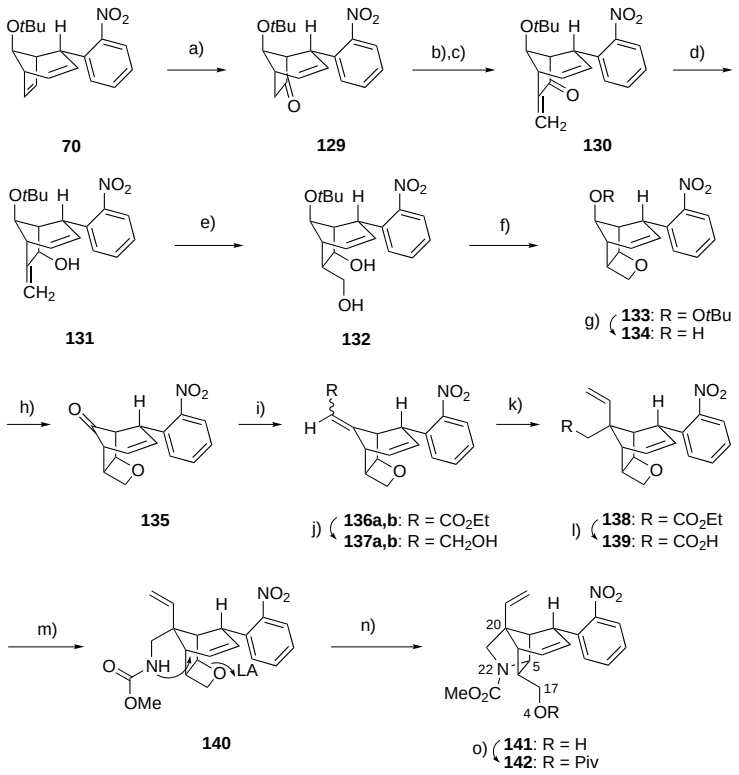
Scheme 14. Formation of the C20 quaternary center and of the pyrrolidine ring by Fukuyama and co-workers. Conditions and reagents: a) $(EtO)_2P(O)CH_2CO_2tBu$, BuLi, THF, 65 °C, then MOMCl, *t*BuOK, 23 °C, 70%; b) $MeNH_2$, MeOH, 23 °C, 100%; c) 1) $ClCO_2CH_2CH{=}CH_2$, pyridine, DMAP, CH_2Cl_2, 0 °C; 2) $LiBH_4$, $LiBEt_3H$ (cat.), THF, 23 °C; 3) Ac_2O, pyridine, 73%; d) 1) HCO_2H, 23 °C, 79%; 2) $ClCO_2Et$, Et_3N, THF, 0 °C; 3) nBu_4NN_3; 4) toluene, Et_3N (cat.), reflux, then EtOH, 23 °C, 76%; e) $[Pd(PPh_3)_4]$, PPh_3, pyrrolidine, CH_2Cl_2, 23 °C; f) $COCl_2$, 2,6-lutidine, CH_2Cl_2, 0 °C, 95%; g) AgOTf, Ag_2CO_3, CH_2Cl_2, 45 °C, 15 min, 52%; h) HCl (3 N), THF, 23 °C, 18 h; i) $[Cp_2TiMe_2]$, THF, −40→0 °C, 3 h, 65%. MOM = methoxymethyl, Alloc = allyloxycarbonyl.

3.6. C5–N22-Bond Formation—Claisen Rearrangement and Oxetane Ring Opening

A Lewis acid catalyzed intramolecular displacement of the C5–O4 bond of a strategic oxetane ring



Scheme 15. Second-generation approach to the formation of the C20 quaternary center and the pyrrolidine ring by Fukuyama and co-workers. Conditions and reagents: a) 1) $[Pd(PPh_3)_4]$, pyrrolidine, THF; 2) ICH_2CN, iPr_2NEt, MeCN, 60 °C, 78 %; b) KHMDS, THF, −78→0 °C, 62 %; c) PhCOCl, pyridine, DMAP (cat.), CH_2Cl_2, 92 %; d) 1) HCO_2H, 96 %; 2) $ClCO_2Et$, NEt_3, THF, then $NaBH_4$, H_2O, 80 %; e) 1) *o*-$NO_2C_6H_4SeCN$, PBu_3, THF; 2) *m*CPBA, then NEt_3, 97 %; f) *m*CPBA, THF/H_2O, then NEt_3, 83 %; g) K_2CO_3, MeOH, 96 %.



Scheme 16. Our strategy to construct the C20 quaternary center and to form the pyrrolidine ring. Conditions and reagents: a) 1) BH_2Cl·DMS, Et_2O, 0 °C, then $NaOH/H_2O_2$, 77 % + 7 % of C16 regioisomer; 2) $(COCl)_2$, DMSO, Et_3N, CH_2Cl_2, 99 %; b) 1) LiHMDS, TESCl, Et_3N, THF, −78→0 °C; 2) Eschenmoser salt, CH_2Cl_2, 91 %; c) 1) MeI, CH_2Cl_2/Et_2O; 2) Al_2O_3, CH_2Cl_2, 95 %; d) $NaBH_4$, $CeCl_3·7H_2O$, MeOH, 99 %; e) 1) 9-BBN dimer, THF; 2) $NaOH/H_2O_2$, 88 %; f) 1) MsCl, Et_3N, CH_2Cl_2, −78 °C; 2) NaHMDS, THF, −78→0 °C, 91 %; g) TFA/CH_2Cl_2, 0 °C, 81 %; h) $(COCl)_2$, DMSO, Et_3N, CH_2Cl_2, −78 °C, 81 %; i) triethylphosphonoacetate, NaH, THF, 0 °C, 3:2, 92 %; j) DIBALH, CH_2Cl_2, −78 °C, 88 %; k) $CH_3C(OEt)_3$, propionic acid (cat.), toluene, reflux, 64 %; l) NaOH/THF/EtOH, 86 %; m) 1) diphenylphosphoryl azide, Et_3N, benzene, 25 °C→reflux; 2) MeOH, reflux; 89 %; n) $BF_3·Et_2O$, CH_2Cl_2, −78→12 °C, 64 %; o) PivCl, Et_3N, DMAP, CH_2Cl_2, 0→25 °C, 92 %. DMS = dimethyl sulfide, Eschenmoser salt = $(CH_3)_2N{=}CH_2I$, Piv = pivalyl = 2,2,2-trimethylacetyl, BBN = 9-borabicyclo[3.3.1]nonane.

was central to the approach of our group for constructing the pyrrolidine ring en route to gelsemine. The quaternary C20 carbon was formed by a surprisingly stereospecific Claisen rearrangement (Scheme 16).[11a] Treatment of **70** with BH_2Cl·DMS followed by oxidative workup afforded the C5-OH and C16-OH products in an 11:1 ratio. The remote olefin had controlled the sense of the hydroboration step. This control was critical for the synthesis of the oxetane with desired regiochemistry.[24] The stereochemistry of the oxetane arose from sequential β-face additions to C5 and C16. Oxidation of the C5-OH group afforded ketone **129**. Mannich reaction of the silyl enol ether derived from **129** followed by quaternization of the nitrogen atom and base-induced elimination afforded α-methyleneketone **130**. Taking advantage of β-face addition to both sp^2 centers (C5 and C16), hydride delivery at C5 in a Luche reaction afforded **131**, and hydroboration of **131** also occurred from the β face, generating diol **132**. From this diol intermediate, the α-face oxetane **133** was fashioned in a straightforward way as shown. Following the cleavage of *tert*-butyl ether **133**, the resulting alcohol function in **134** was oxidized to afford ketone **135**. Emmons-type condensation was successful in terms of overall yield, but led to a 3:2 mixture of β,β-disubstituted stereoisomers **136a** and **136b**. Each compound was reduced to its allylic alcohol counterpart (**137a** and **137b**, respectively). These isomers were treated individually with triethylorthoacetate. Remarkably, each allylic alcohol gave rise to a single and identical γ,δ-unsaturated ester **138** with the

desired configuration of the β-vinyl and α-carboxymethyl functions at C20.

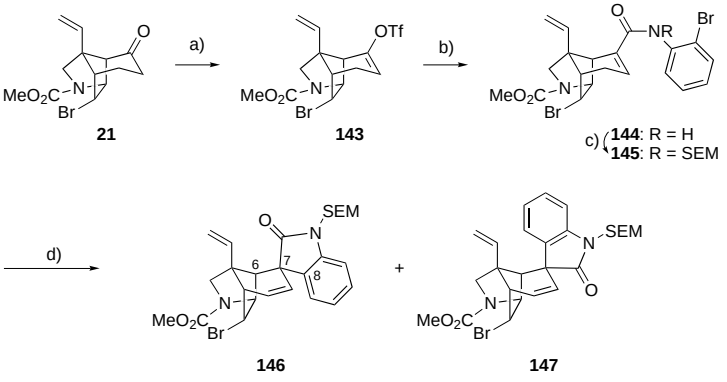
Regardless of the reasons for this convergence, it provided smooth access to the key intermediate **138**. Alkaline hydrolysis of the ethyl ester function served to release the free acid **139**. Subjection of the latter to Curtius degradation as reported by Shiori and co-workers[25] afforded urethane **140**. As anticipated, the hitherto robust oxetane linkage, which had survived in the sequence that started with **133**, was opened by the urethane nitrogen atom under Lewis acid activation ($BF_3{\cdot}OEt_2$) and compound **141** was in hand. Protection of alcohol **141** afforded pivaloate **142**.

4. Strategies for Introduction of the Spirooxindole Moiety

4.1. Formation of C7–C8 Bond

One idea to construct the spirooxindole moiety, relying on C7–C8 formation through an intramolecular Heck reaction, was reported by Overman and co-workers and by Speckamp and co-workers. In a related approach, radical cyclization in the synthesis by Hart and co-workers and Johnson and co-workers had accomplished the same goal.

As a pioneering group in the exploration of the intramolecular Heck reaction in the syntheses of complex natural products, Overman and co-workers successfully prepared the advanced pentacyclic intermediate **146** with good diastereoselectivity (Scheme 17).[13b,26] Conversion of **21** into the enol triflate **143** followed by palladium-mediated carbonylation in the presence of 2-bromoaniline provided **144**. Following alkylation with SEMCl, **145** was in hand. It was found that the palladium catalysts, the additives, and the solvents affected the diastereoselectivity of the Heck reaction of **145**.[26] A 9:1 ratio of **146** and **147** was observed when **145** was subjected to "ligandless" Heck conditions ($[Pd_2(dba)_3]$, Et_3N, toluene). Unfortunately, attempts to install the hydroxy group at C17 for further elaboration of the tetrahydropyran ring proved to be unsuccessful.



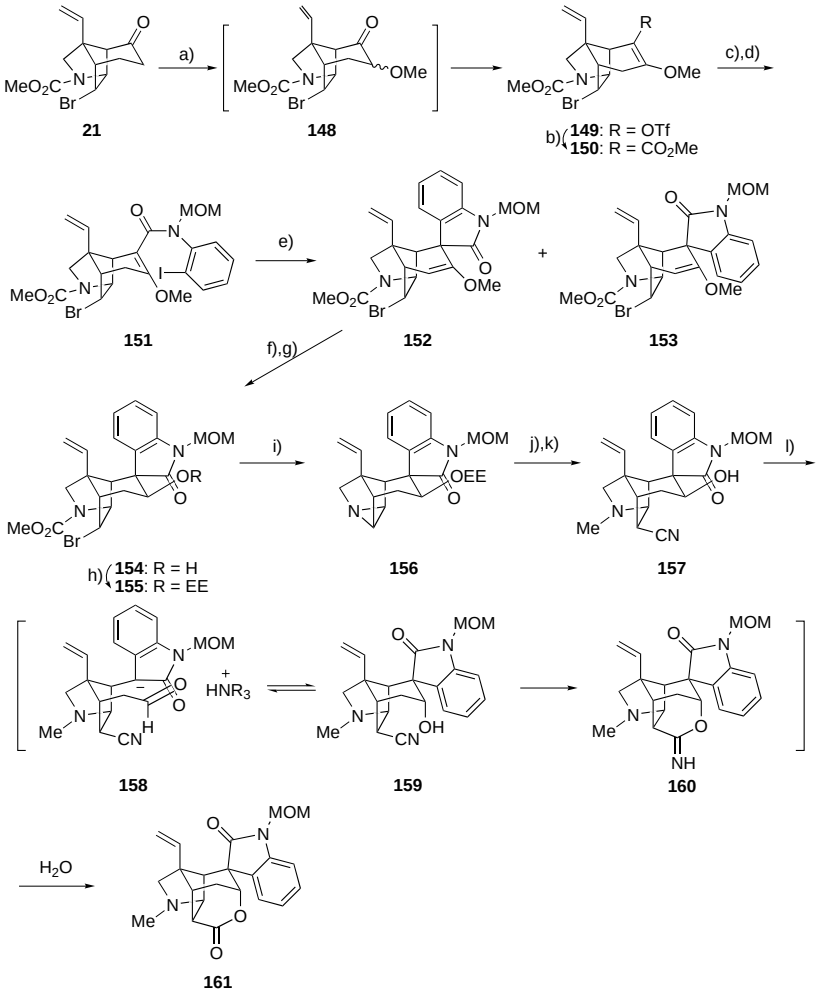
Scheme 17. Intramolecular Heck reaction to construct the oxindole moiety (Overman and co-workers). Conditions and reagents: a) LDA, $PhNTf_2$, THF, −78→0 °C, 100%; b) $[Pd(PPh_3)_4]$ (1 mol%), 2-bromoaniline, CO, 1 atm, DMF, 80 °C, 79%; c) NaH, SEMCl, THF, 23 °C; d) $[Pd_2(dba)_3]$ (10–20 mol%), Et_3N, toluene, 110 °C, 89–95% of **146** and **147** (89:11). SEM = 2-(trimethylsilyl)ethoxymethyl, dba = dibenzylideneacetone.

Accordingly, Overman and co-workers directed their attention to the introduction of a oxygen-containing functional group at C3. Such a group could be employed to form the pyran ring of **1** (Scheme 18).[11] This objective was accomplished by initial oxidation of the silyl enol ether derived from **21** to generate enol triflate **149** via methoxy ketone **148**. Palladium-catalyzed carbonylation of **149** in the presence of methanol afforded methyl ester **150**. Treatment of this compound with the dimethylaluminum amide derivative of iodoaniline resulted in the coupled product. The resulting secondary amide was protected as its MOM tertiary amide **151**. An intramolecular Heck reaction of **151** was difficult, as this substrate corresponds to a tetrasubstituted vinylogous carbamate. However, cyclization did occur efficiently under cationic conditions ($[Pd_2(dba)_3]{\cdot}CHCl_3$, Ag_3PO_4, Et_3N, THF), providing a mixture of **152** and **153** (13:1). The major product was the "wrong" stereoisomer with respect to gelsemine. Hydrolysis of methyl ether **152** followed by reduction of the resulting ketone afforded equatorial alcohol **154** as the major product. Protection of this alcohol to form **155** followed by treatment with NaCN in DMSO yielded aziridine **156**. Methylation of **156** with MeOTf, with subsequent regioselective opening of the resulting aziridinium salt at C16 with NaCN and removal of the 1-ethoxyethyl group provided **157**.

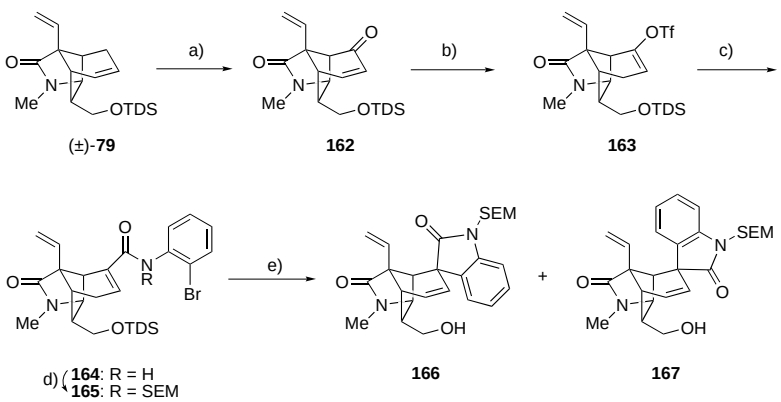
At this stage, the oxindole of **157** with the undesired configuration at the spiro center C20 was epimerized by the action of DBU. Presumably, the mechanism of the epimerization reaction involves a retro-aldol cleavage of the C3–C7 bond to generate an intermediate such as **158**. After rotation about the C6–C7 and C3–C14 bonds, aldol closure afforded **159** in which both the oxindole and C3 hydroxy group were epimerized. Addition of the axial OH group to the proximal nitrile afforded the cyclic imidate **160**, which was hydrolyzed to lactone **161**. This route, although lengthy, constituted a clever reconfiguration at C20.

An intramolecular Heck reaction was also applied by Speckamp and co-workers in their total synthesis of **1** (Scheme 19).[6] Allylic oxidation of (±)-**79** afforded enone **162**, which was reduced in a 1,4-selective manner with L-selectride. Trapping of the resulting enolate furnished enol triflate **163**. Palladium-catalyzed carbonylation of **163** in the presence of 2-bromoaniline provided **164**, which was treated with SEMCl to give **165**. Under the "ligandless" Heck conditions used by Overman and co-workers,[26] **165** did undergo cyclization and subsequent desilylation to yield a mixture of **166** and **167** (2:1). Fortunately, the diastereomer with the "correct" stereochemistry at C7 relative to gelsemine was the major product.

In the total synthesis of gelsemine by Hart and co-workers, the oxindole was assembled by free-radical cyclization, thereby establishing the C7–C8 bond (Scheme 20).[8a,b] Ester **97** was converted into **168** by twofold addition of the Grignard reagent phenyl magnesium bromide, and subsequent *O*-methylation, afforded **169**. Hydrolysis of the ketal provided ketone **170**. The empirical result showed that enolization of **170** occurred preferentially at C7: Treatment of **170** with *o*-bromophenylisocyanate in the presence of KH yielded **171**. Following acetylation of **171** at both the oxygen and the nitrogen atoms, compound **172** was in hand.



Scheme 18. Revised intramolecular Heck reaction route (Overman and co-workers). Conditions and reagents: a) 1) KHMDS, Et_3SiCl, THF, −78 °C; 2) $(PhIO)_n$, $BF_3{\cdot}OEt_2$, MeOH, CH_2Cl_2, −78→0 °C; 3) KHMDS, Comins' reagent, THF, −78 °C, 61%; b) CO (3.5 bar), $[PdCl_2(dppf)_2]{\cdot}CH_2Cl_2$, MeOH, $(n\text{Bu})_3N$, DMF, 80 °C, 94%; c) 2-iodoaniline, Me_3Al, CH_2Cl_2, 0 °C→RT, 91%; d) NaH, MOMCl, THF, 86%; e) $[Pd_2(dba)_3]{\cdot}CHCl_3$, Ag_3PO_4, Et_3N, THF, reflux, 61–78% of **152** + **153** (13:1); f) HCl (conc.), MeOH, room temperature, 98%; g) $(i\text{Bu})_3Al$, PhMe, −78 °C→RT, 71%; h) ethyl vinyl ether, PPTS, CH_2Cl_2, room temperature, 85%; i) NaCN, Me_2SO, 150 °C, 99%; j) MeOTf, DTBMP, CH_2Cl_2, 0 °C; NaCN, Me_2SO, 90 °C, 85%; k) $TsOH{\cdot}H_2O$, CH_2Cl_2, MeOH, room temperature, 99%; l) DBU, PhMe, reflux, 80%. Comins reagent = Tf_2NPh, dppf = 1,1′-bis(diphenylphosphanyl)ferrocene, DTBMP = 2,6-di-*tert*-butyl-4-methylpyridine, DBU = 1,8-diazabicyclo[5.4.0]undec-7-ene.



Scheme 19. Intramolecular Heck reaction to construct the oxindole moiety (Speckamp and co-workers). Conditions and reagents: a) CrO_3, 3,5-dimethylpyrazole, CH_2Cl_2, −30 °C; b) L-selectride, THF, −78 °C, then Tf_2NPh, room temperature, 18 h, 65%; c) $Pd(OAc)_2$, PPh_3, Et_3N, CO, 2-bromoaniline, DMF, room temperature, 24 h, 70%; d) NaH, SEMCl, THF; e) 1) $[Pd_2(dba)_3]$, Et_3N, toluene, reflux, 4 h; 2) Bu_4NF, THF, room temperature, 60% + 30% of **167**. L-selectride = lithium tri-*sec*-butylborohydride.

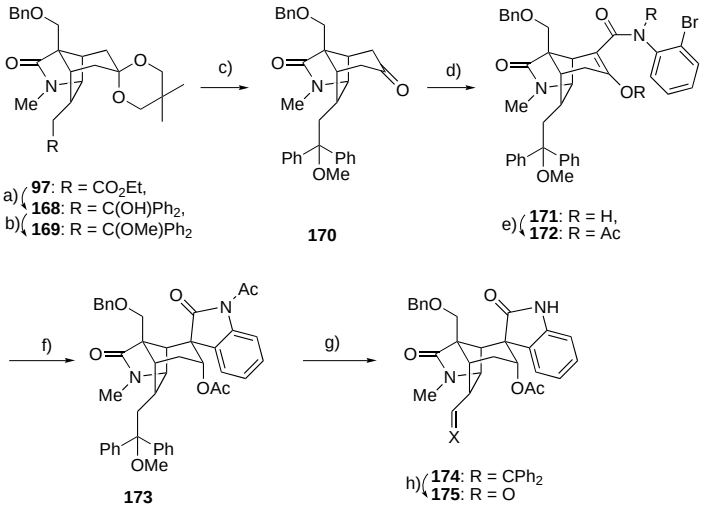
Remarkably, it was found that free-radical cyclization of **172** provided **173** with good selectivity. Subsequent elimination and deacetylation gave **174**, which was subjected to ozonolysis to afford aldehyde **175**. The progression of this compound is discussed in Section 5.2.

Radical cyclization toward the synthesis of the oxindole moiety by Johnson and coworkers was initiated by the irradiation of a mixture of *N*-alkenylbenzotriazoles **177** and **178** derived from the condensation of ketone **37** with lithiated benzotriazole **176** (Scheme 21).[7b] Cyclization products **179** and **180** were obtained in a 1:2 ratio. The minor isomer, **179** could be converted into 21-oxogelsemine (**2**) by hydrolysis. Further reduction of **2** with DIBALH afforded gelsemine (**1**).

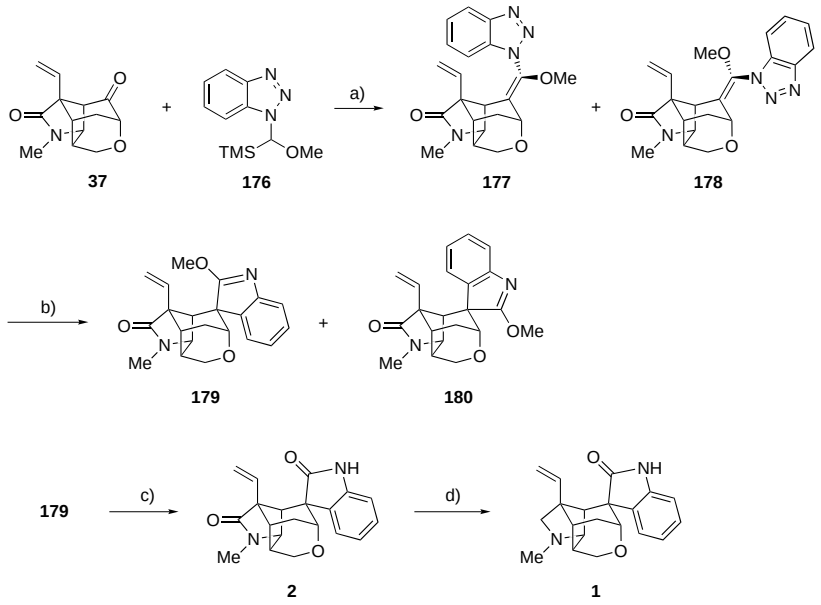
4.2. Formation of the C6–C7 Bond

We have seen that installation of the spirooxindole moiety with good stereoselectivity has been one of the major challenges in the synthesis of gelsemine. This problem was solved in an elegant synthesis by Fukuyama and co-workers (Schemes 5 and 6). By introducing a bulky iodide in the oxindole framework, the geometry of the double bond was totally controlled in the Knoevenagel condensations leading to the formation of alkylidene indolinones **51** and **63**. The subsequent divinylcyclopropane rearrangement afforded only one isomer with the desired stereochemistry. In this rearrangement, the quaternary C7 center was assembled by means of C6–C7-bond formation.

In the model study by Stork and coworkers, the quaternary C7 center was also introduced by C6–C7-bond formation through a stereospecific Claisen rearrangement (Scheme 4, **44**→**45**). It will be recalled



Scheme 20. Radical cyclization to form the oxindole (Hart and co-workers). Conditions and reagents: a) PhMgBr, 87%; b) NaH, DMSO, CH_3I, 100%; c) TsOH, acetone, 94%; d) NaH, KH, $oBrC_6H_4N{=}C{=}O$, THF, 80%; e) Ac_2O, DMAP, Et_3N, DMF, 98%; f) Bn_3SnH, AIBN (cat.), PhH, $h\nu$, 42% + 16% of C7 isomers (9% α + 7% β acetates); g) TsOH, CH_2Cl_2, then MeOH, 93%; h) O_3, CH_2Cl_2, MeOH, then Me_2S, 65%.



Scheme 21. Synthesis of the oxindole moiety by Johnson and co-workers. Conditions and reagents: a) LDA, 65%; b) $h\nu$, MeCN, pyrex, purification by silica-gel chromatography, 12% of **179** + 24% of **180**; c) HCl, H_2O, THF; d) DIBALH, 63%.

that the configuration of C7 was governed at the stage of the radical *cis* cyclization of **38** to **39**. Acid **45** could be potentially converted into the oxindole moiety by known methods.

4.3. Formation of the C1–C7 Bond

Another strategy towards the spirooxindole unit was through C1–C7-bond formation through an Eschenmoser–Claisen rearrangement. This was a key feature of our synthesis of gelsemine (Scheme 22).[11b] Bromination of **136** afforded **181**. Acetolysis of **181** with AgOAc provided **182**; the otherwise unusual retention of configuration attests to the highly hindered nature of the α-face of C14. Reduction of the nitro group afforded the amine, which was protected with CbzCl to provide **183**. Deprotection of the acetate afforded **184**.

Major efforts were directed at the use of the C14 β-OH group to introduce a β-orientated one-carbon fragment at C7 by suprafacial allylic transposition. Such attempts were uniformly unsuccessful. Apparently, formidable steric forces prevent C–C-bond formation even by intramolecular means. Fortunately, it was found that the Eschenmoser amide acetal version of the Claisen rearrangement took place in the desired [3,3] sense.[27] Subjection of **184** to the conditions shown led to **185**, which cyclized on silica gel during chromatography to yield lactam **186**.

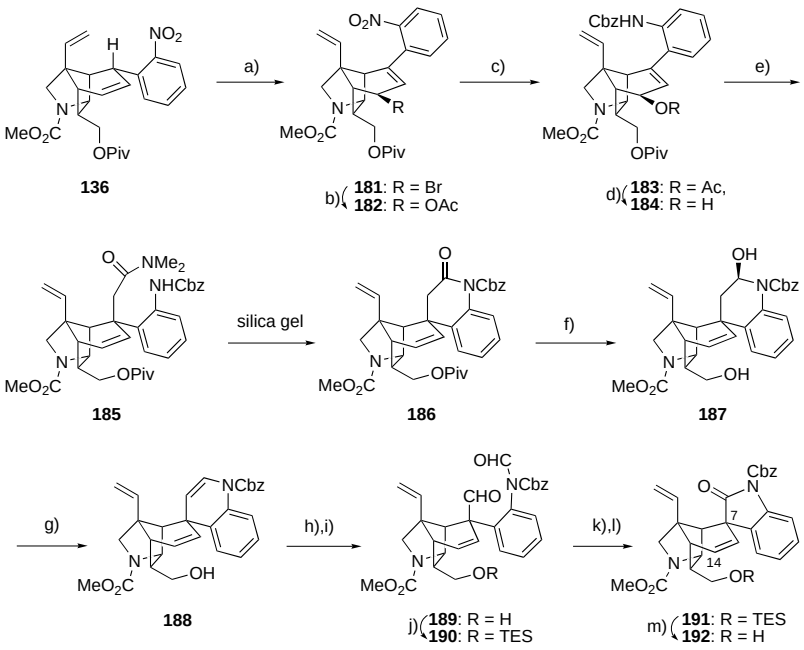
The sequence to shrink the six-membered lactam to a five-membered spiroanilide for the purposes of reaching gelsemine began with reduction of **186** to afford aminal **187**, which was dehydrated to furnish enamide **188**. Dihydroxylation of **188** across the more electron-rich enamide double bond provided a trihydroxy intermediate, which was subjected to oxidative cleavage. This degradation provided **189** in 45% yield, containing an all-important β-face aldehyde at C7. Protection of the hydroxy group of **189** led to silyl ether **190**. Methanolysis of this compound resulted in concurrent *N*-deformylation and ring closure to a cyclic hemiaminal. The latter, following oxidation, gave rise to oxindole **191**. Desilylation of **191** led to **192** in which the extremely hindered free hydroxymethyl group on the α-face (initially derived by intramolecular oxetane opening) could now effect cyclization to the tetrahydropyran ring upon activation of the proximal double bond.

In an early approach by Hart and co-workers to fashion the oxindole, an alkoxymethylation of indole was proposed through C1–C7-bond formation (Scheme 23).[28] It was planned that Fischer indolization of **193** would provide **194**, which might undergo alkoxymethylation to afford **195**. Indeed, alkoxymethylation did work well on the model compound **196** to form **197**. However, it failed on the more complicated substrate **194**.

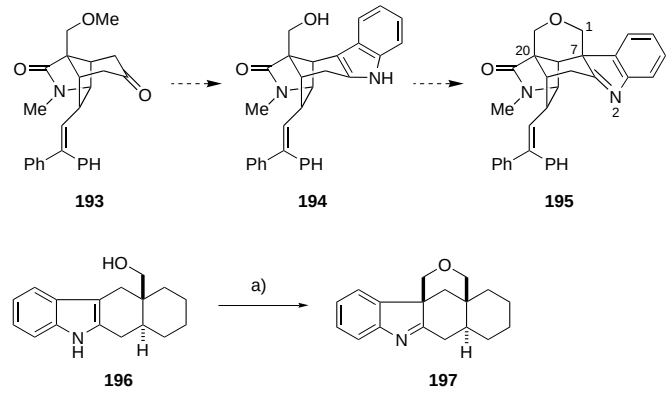
C1–C7-bond formation towards the synthesis of the oxindole unit was also accomplished by Fukuyama and co-workers through a radical-initiated aryl isonitrile cyclization (Scheme 24).[29,30] In the model study, a facile cyclization occurred upon treatment of isonitrile **198** with thiophenol and AIBN. Indeed, the thioimidate **199** was hydrolyzed to oxindole **200**. Unfortunately, attempted applications of this chemistry to more advanced intermediates that would have provided an opportunity to reach gelsemine were unsuccessful.

4.4. Fleming's Model Study

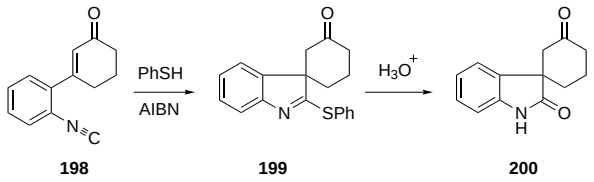
During the course of their study toward the synthesis of gelsemine, Fleming and co-workers discovered several new



Scheme 22. Our approach to the oxindole moiety. Conditions and reagents: a) NBS, AIBN, *hν*, CCl_4/CH_2Cl_2, 55–60 °C, 60% based on recovered starting material; b) AgOAc, HOAc, 52%; c) 1) zinc dust, THF/HOAc; 2) CbzCl, $NaHCO_3$, CH_2Cl_2, 94% over two steps; d) K_2CO_3, MeOH, 90%; e) $CH_3C(OMe)_2NMe_2$, *m*-xylene, 45%; f) DIBALH, CH_2Cl_2, −78 °C; g) TsOH·H_2O, CH_2Cl_2, reflux, 50% over two steps; h) 1) OsO_4, THF, −25 °C; 2) aqueous Na_2SO_3; i) $NaIO_4$, THF/H_2O, 45%; j) TESOTf, Et_3N, CH_2Cl_2, 0 °C, 80%; k) NaOMe, MeOH; l) TPAP, NMO, CH_2Cl_2, 4 Å molecular sieves, 50% over two steps; m) TBAF/HOAc 1:1, THF, 80%. NBS = *N*-bromosuccinimide, Cbz = benzyloxycarbonyl, TPAP = tetrapropylammonium perruthenate, NMO = 4-methylmorpholine *N*-oxide.



Scheme 23. Model study of the alkoxymethylation of indoles (Hart and co-workers). Conditions and reagents: a) $(MeO)_2CH_2$, CH_2Cl_2, $EtAlCl_2$, −78→RT, 59%.



Scheme 24. Radical-initiated aryl isonitrile cyclization towards the spirooxindole—model study by Fukuyama and co-workers.

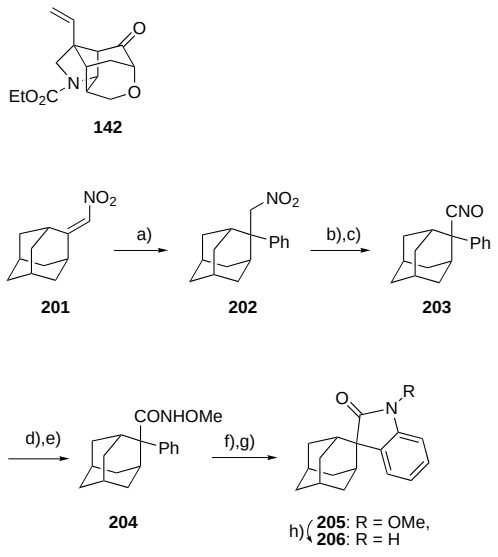
oxindole syntheses in anticipation of building the C7 quaternary center.[31] The approach shown in Scheme 25 appeared to be synthetically useful. The addition of Ph_3Al to α,β-unsaturated nitro compound **201** derived from adamantanone gave **202**. Dehydration of this compound afforded the hindered nitrile oxide **203**. Hydration of **203** followed by methylation provided methyl hydroxamate **204**. Chlorination of **204** followed by cyclization of the resulting *N*-chlorohydroxamate with Ag^I as Lewis acid afforded *N*-methoxy oxindole **205**. Reduction of **205** led to oxindole **206**. Unfortunately, this methodology did not lend itself to reaching gelsemine *via* **142**.

5. Strategies to Construct the Tetrahydropyran Ring

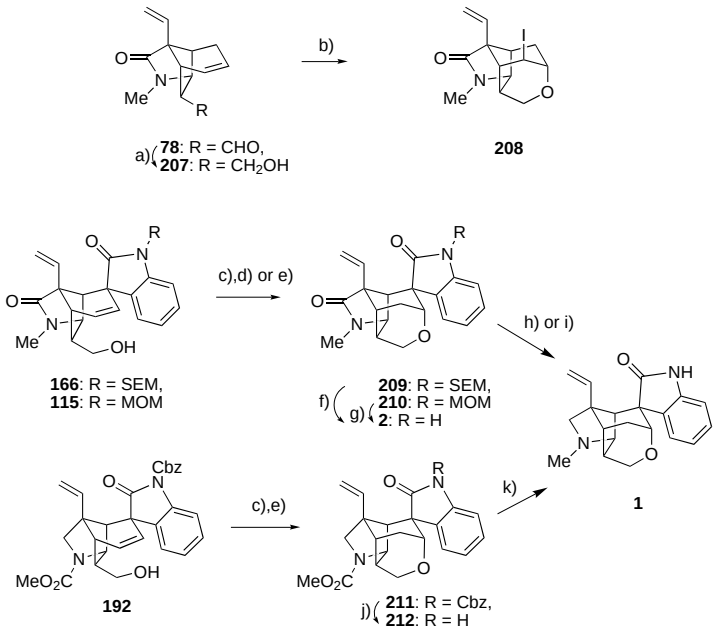
5.1. Formation of the C3–O4 Bond

As we have seen, most planned routes to gelsemine anticipated building the tetrahydropyran ring by means of C3–O4-bond formation (Scheme 3, **28**→**29**; Scheme 26, **207**→**208**; or Scheme 13, **9**→**108**).

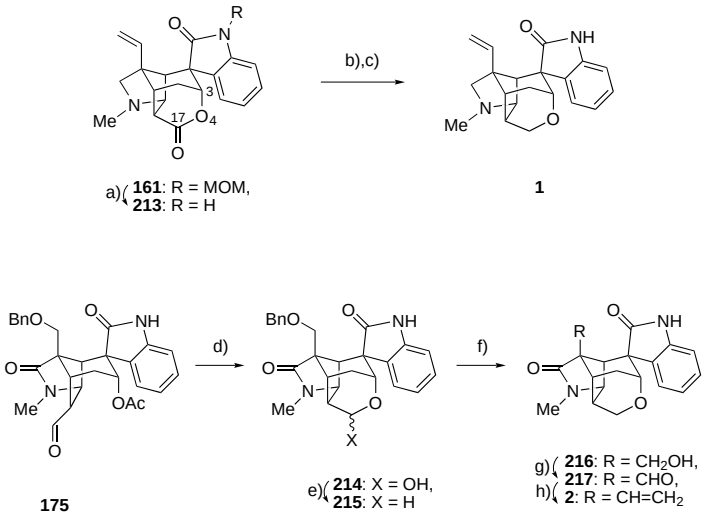
Oxymercuration was applied in the total syntheses by Speckamp and co-workers and by Fukuyama and co-workers, as well as in our own (Scheme 26). In the sequence adopted by Speckamp and co-workers, alcohol **166** was treated with $Hg(OTf)_2$·*N*,*N*-dimethylaniline followed by reductive de-



Scheme 25. Model study towards the synthesis of the oxindole unit by Fleming and co-workers. Conditions and reagents: a) Ph_3Al, 0 °C, 91%; b) NaOMe; c) AcCl; d) H_2SO_4, acetone, 75 °C; e) Na_2CO_3, MeI, 69% over four steps; f) *t*BuOCl, CH_2Cl_2, room temperature, exclusion of light; g) $Zn(OAc)_2$, CH_3NO_2, reflux, 85% over two steps; h) Na/Hg, MeOH/Et_2O 1:1, 0 °C, 100%.



Scheme 26. Oxymercuration to furnish the tetrahydropyran ring—Strategies of Speckamp, Fukuyama, and Danishefsky. Conditions and reagents: a) $NaBH_4$, EtOH, 70%; b) I_2, Na_2CO_3, CH_3CN, 20°C, 5 days, 49%; c) $Hg(OTf)_2$·*N*,*N*-dimethylaniline, CH_3NO_2, 60–90%; d) $NaBH_4$, NaOH, CH_2Cl_2, EtOH, 80%; e) $NaBH_4$, NaOH, $BnEt_3NCl$, CH_2Cl_2/H_2O, 60%; f) Bu_4NF, THF, molecular sieves (4 Å), reflux, 4 h, 90%; g) TMSCl, NaI, CH_3CN; NEt_3, MeOH, 63%; h) AlH_3, THF, −65–0°C, 4 h, 50%; i) DIBALH, toluene, 82%–90%; j) NaOH (10%), THF, 91%; k) $LiAlH_4$, THF, 0–25°C, 81%. Bn = benzyl.



Scheme 27. Synthesis of the tetrahydropyran unit by Overman and co-workers and Hart and co-workers . Conditions and reagents: a) 1) HCl (conc.), $(MeOCH_2)_2$, 55°C; 2) $(iPr)_2NEt$, MeOH, 55°C, 90%; b) 1) $(iBu)_2AlH$, toluene, 0°C→RT; 2) Et_3SiH, TFA, CH_2Cl_2, reflux, 65% over two steps; d) HCl, H_2O, DME, 48°C, 16 h, 65%; e) Et_3SiH, TFA, CH_2Cl_2, 83%; f) BBr_3, CH_2Cl_2, 95%; g) Dess–Martin periodinane, 71%; h) $[Cp_2TiMe_2]$, 87%. DME = 1,2-dimethoxyethane.

mercuration to afford the tetrahydropyran **209**. Desilylation of **209** provided 21-oxogelsemine (**2**) and subsequent reduction afforded gelsemine itself. The sequence used by Fukuyama and co-workers was similar, except for the use of different protecting groups (**115**→**210**→**2**→**1**). Our synthesis did not proceed through the 21-oxo congener of gelsemine. Instead, the terminal phase of this effort involved reduction of the methyl carbamate of **212** to afford **1**.

5.2. Formation of the O4–C17 Bond

Another strategy to construct the tetrahydropyran ring was through lactone or hemiacetal formation, exploiting O4–C17-bond formation. This concept was nicely demonstrated in the concluding phases of the total syntheses by Overman and co-workers and by Hart and co-workers (Scheme 27). The Overman route proceeded through a two-stage reduction of the lactone to the tetrahydropyran moiety of gelsemine. In the synthesis by Hart, **175** (derived from *N*-acyl amine radical cyclization and with the undesired configuration at C16) was epimerized in a hemiacetal-forming step under acidic conditions (**175**→**214**). Reduction of hemiacetal **214** afforded tetrahydropyran **215**. The late-phase transformation of the C20 benzyloxymethyl group of **215** following classical types of reactions afforded 21-oxogelsemine (**2**).

6. Conclusion

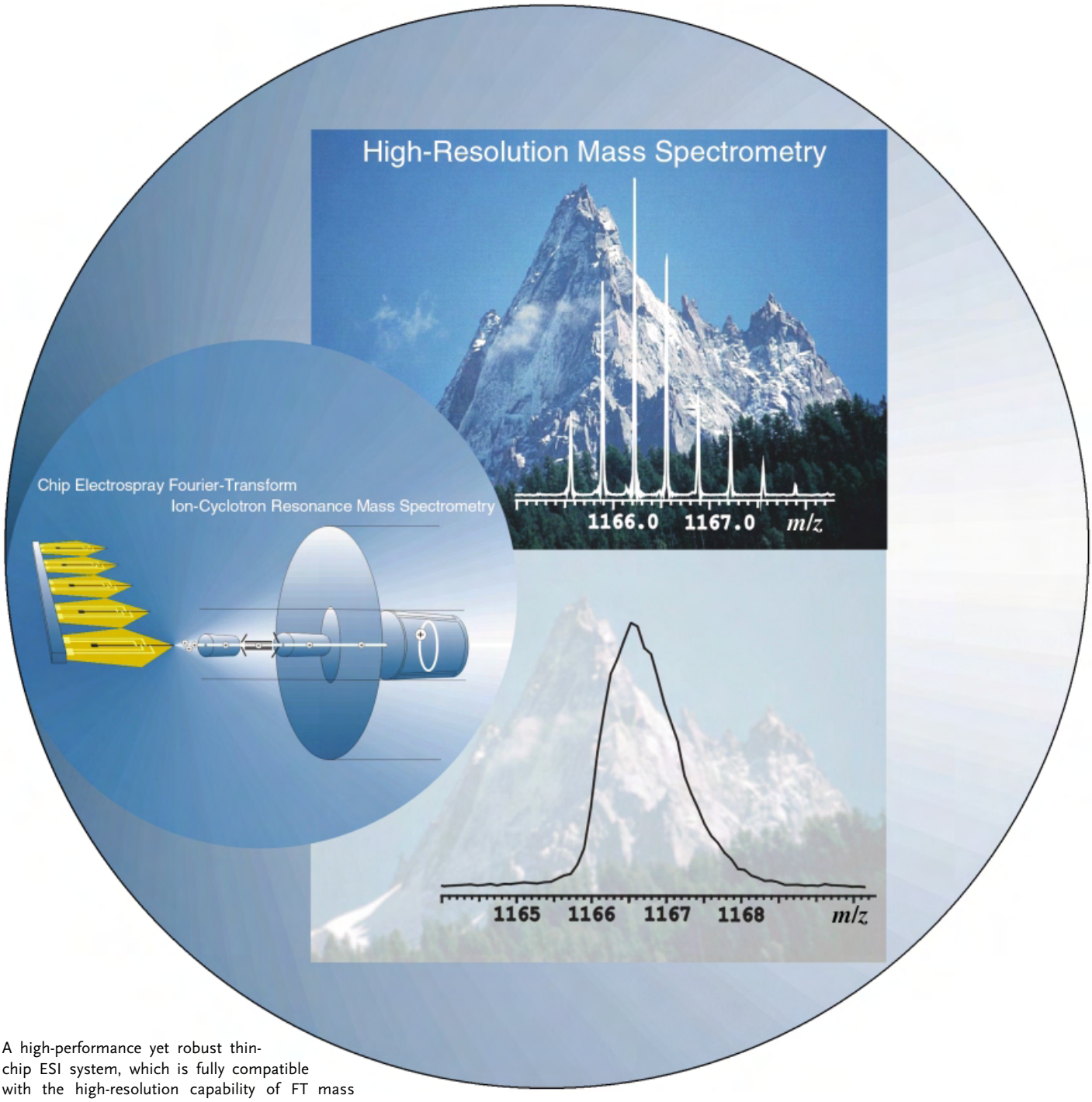
In summary, partially developed and fully completed programs to build gelsemine in the laboratory have been rich in intellectual excitement and have been valuable learning experiences. The synthetic studies towards gelsemine summarized here have not only shown the power of classical synthetic methods, but also demonstrated how a well-selected target (e.g. **1**) can evoke the discovery of new reactions and provide new insight into molecular architecture. Total synthesis remains a valuable medium for increasing our fascination with chemistry, as we pry loose its secrets.

This work was supported by grants from the National Institutes of Health (grant HL25848). H.L. thanks NIH Cancer Pharmacology Training Grant (T32-CA62948) for a postdoctoral fellowship and the Texaco Foundation for providing chemicals. The receipt of a Pfizer Award to S.J.D. for Creative Work in Organic Synthesis is gratefully acknowledged.

Received: June 5, 2002 [A00538]

[1] J. E. Saxton in *The Alkaloids, Vol. 8* (Ed.: R. H. F. Manske), Academic Press, New York, **1965**, pp. 93 – 117.
[2] a) H. Conroy, J. K. Chakrabarti, *Tetrahedron Lett.* **1959**, *4*, 6 – 13; b) F. M. Lovell, R. Pepinsky, A. J. C. Wilson, *Tetrahedron Lett.* **1959**, *4*, 1 – 5.
[3] Z.-J. Liu, R.-R. Lu in *The Alkaloids, Vol. 33* (Ed.: R. H. F. Manske), Academic Press, New York, **1988**, pp. 83 – 140.
[4] A. Madin, C. J. O'Donnell, T. Oh, D. W. Old, L. E. Overman, M. J. Sharp, *Angew. Chem.* **1999**, *111*, 3110 – 3112; *Angew. Chem. Int. Ed.* **1999**, *38*, 2934 – 2936.
[5] a) J. T. Link, L. E. Overman, *CHEMTECH* **1998**, *28*, 19; b) L. E. Overman, J. T. Link in *Metal-Catalyzed Cross-Coupling Reactions* (Eds.: F. Diederich, P. J. Stang), Wiley-VCH, Weinheim, **1998**, pp. 231 – 270.
[6] N. J. Newcombe, F. Ya, R. J. Vijn, H. Hiemstra, W. N. Speckamp, *J. Chem. Soc. Chem. Commun.* **1994**, 767 – 768.
[7] a) Z. Sheikh, R. W. Steel, A. S. Tasker, A. P. Johnson, *J. Chem. Soc. Chem. Commun.* **1994**, 763 – 764; b) J. K. Dutton, R. W. Steel, A. S. Tasker, V. Popsavin, A. P. Johnson, *J. Chem. Soc. Chem. Commun.* **1994**, 765 – 766.
[8] a) S. Atarashi, J.-K. Choi, D.-C. Ha, D. J. Hart, D. Kuzmich, C.-S. Lee, S. Ramesh, S. C. Wu, *J. Am. Chem. Soc.* **1997**, *119*, 6226 – 6241; b) D. Kuzmich, S. C. Wu, D.-C. Ha, C.-S. Lee, S. Ramesh, S. Atarashi, J.-K. Choi, D. J. Hart, *J. Am. Chem. Soc.* **1994**, *116*, 6943 – 6944.
[9] T. Fukuyama, G. Liu, *J. Am. Chem. Soc.* **1996**, *118*, 7426 – 7427.
[10] S. Yokoshima, H. Tokuyama, T. Fukuyama, *Angew. Chem.* **2000**, *112*, 4239 – 4241; *Angew. Chem. Int. Ed.* **2000**, *39*, 4073 – 4075.
[11] a) F. W. Ng, H. Lin, Q. Tan, S. J. Danishefsky, *Tetrahedron Lett.* **2002**, *43*, 545 – 548; b) H. Lin, F. W. Ng, S. J. Danishefsky, *Tetrahedron Lett.* **2002**, *43*, 549 – 551.
[12] C. Clarke, I. Fleming, J. M. D. Fortunak, P. T. Gallagher, M. C. Honan, A. Mann, C. O. Nübling, P. R. Raithby, J. J. Wolff, *Tetrahedron* **1988**, *44*, 3931 – 3944.
[13] a) W. G. Earley, E. J. Jacobsen, G. P. Meier, T. Oh, L. E. Overman, *Tetrahedron Lett.* **1988**, *29*, 3781 – 3784; b) W. G. Earley, T. Oh, L. E. Overman, *Tetrahedron Lett.* **1988**, *29*, 3785 – 3788.
[14] G. Stork, M. E. Krafft, S. A. Biller, *Tetrahedron Lett.* **1987**, *28*, 1035 – 1038.
[15] a) K. Kondo, T. Umemoto, K. Yato, D. Tunemoto, *Tetrahedron Lett.* **1978**, *19*, 3927 – 3930; b) D. F. Taber, *J. Am. Chem. Soc.* **1977**, *99*, 3513 – 3514.
[16] a) R. J. Vijn, H. Hiemstra, J. J. Kok, M. Knotter, W. N. Speckamp, *Tetrahedron* **1987**, *43*, 5019 – 5030; b) H. Hiemstra, R. J. Vijn, W. N. Speckamp, *J. Org. Chem.* **1988**, *53*, 3882 – 3884.
[17] J. Dijkink, J.-C. Cintrat, W. N. Speckamp, H. Hiemstra, *Tetrahedron Lett.* **1999**, *40*, 5919 – 5922.
[18] See reference [20] cited in reference [17].
[19] J.-K. Choi, D.-C. Ha, D. J. Hart, C.-S. Lee, S. Ramesh, S. Wu, *J. Org. Chem.* **1989**, *54*, 279 – 290.
[20] P. A. Grieco, S. Gilman, M. Nishizawa, *J. Org. Chem.* **1976**, *41*, 1485 – 1486.
[21] M. J. Sung, C.-W. Lee, J. K. Cha, *Synlett* **1999**, 561 – 562.
[22] A. G. Avent, P. W. Byrne, C. S. Penkett, *Org. Lett.* **1999**, *1*, 2073 – 2075.
[23] P. A. Wender, L. Siggel, J. M. Nuss, *Comprehensive Organic Synthesis, Vol. 5* (Eds.: B. M. Trost, I. Fleming, L. A. Paquette), Pergamon, Oxford, **1991**, p. 645.
[24] F. W. Ng, P. Chiu, S. J. Danishefsky, *Tetrahedron Lett.* **1998**, *39*, 767 – 770.
[25] See reference [19] cited in reference [11a].
[26] A. Madin, L. E. Overman, *Tetrahedron Lett.* **1992**, *33*, 4859 – 4862.
[27] See reference [11] cited in reference [11b].
[28] D. J. Hart, S. C. Wu, *Heterocycles* **1993**, *35*, 135 – 138.
[29] T. Fukuyama, G. Liu, *Pure Appl. Chem.* **1997**, *69*, 501 – 505.
[30] H. Tokuyama, T. Yamashita, M. T. Reding, Y. Kaburagi, T. Fukuyama, *J. Am. Chem. Soc.* **1999**, *121*, 3791 – 3792.
[31] a) I. Fleming, M. A. Loreto, I. H. M. Wallace, *J. Chem. Soc. Perkin Trans. 1* **1986**, 349 – 359; b) I. Fleming, R. C. Moses, M. Tercel, J. Ziv, *J. Chem. Soc. Perkin Trans. 1* **1991**, 617 – 626.

Communications



A high-performance yet robust thin-chip ESI system, which is fully compatible with the high-resolution capability of FT mass spectrometry, is described. Major advantages of the thin-chip are flexible volumes, long spraying times at high sensitivity, and substantially lower background and contamination problems. With this system for biopolymer analysis, applications to high-performance proteomics and combinatorial libraries are possible. For more information see the article by Przybylski et al. on the following pages.

 © 2003 Wiley-VCH Verlag GmbH & Co. KGaA, Weinheim 1433-7851/03/4201-0053 $ 17.50+.50/0

Mass Spectrometry of Biopolymers

Thin-Chip Microspray System for High-Performance Fourier-Transform Ion-Cyclotron Resonance Mass Spectrometry of Biopolymers**

*Joël S. Rossier, Nikolay Youhnovski, Niels Lion, Eugen Damoc, Susanne Becker, Frédéric Reymond, Hubert H. Girault, and Michael Przybylski**

The recent dramatic development of biopolymer analysis would be unthinkable without new high-performance analytical tools.[1] For example, the completion of the human genome sequence has substantially profited from advances in highly sensitive automated tools for sample preparation and analysis.[2] Proteome analysis (proteomics)[3] is a particular challenge for which new analytical methods of high sensitivity are required, for example, for the characterization of post-translational structure modifications.[4,5] Electrospray-ionization mass spectrometry (ESI-MS) has become a powerful molecular tool for protein primary-structure determination, the study of conformational states and folding pathways, the characterization of noncovalent supramolecular complexes, and the analysis of complex mixtures by combination with microseparation methods (HPLC, capillary electrophoresis (CE)).[6–8] Most recently Fourier-transform ion-cyclotron-resonance mass spectrometry (FT-ICR-MS) has enabled a breakthrough for the ultra-high-resolution mass spectrometric analysis of biopolymers by using both ESI and MALDI ionization.[9] A unique attribute of FT-ICR-MS in comparison to other MS methods is its ability to simultaneously provide high mass resolution ($>10^6$), mass-determination accuracy (<1 ppm), and sensitivity.[10] Of particular interest is the versatility of FT-ICR-MS^n-techniques for structure determination using fragmentation by collision-induced dissociation (CID) or IR laser multiphoton dissociation (IRMPD),[11] and the coupling with micro/nano-ESI.[12]

The coupling of microscale devices with mass spectrometry has gained broad interest in the analysis of peptides and proteins, for example, as an alternative to chip-fluorescence methods.[13] The coupling with ESI-MS benefits from the general compatibility of flow rates in microchips with those generated in micro/nano-electrospray, which renders the combination of microchip technology with the analytical potential of ESI-MS highly attractive.[14] However, the coupling is not straightforward, and chip material, microstructure design, and surface properties are of critical importance for the analytical performance of the combination. Furthermore, the chip-fabrication process must yield disposable, low-cost devices to enable large-scale bioanalytical applications. Most work to date has employed glass or silicon substrates which, however, are generally hydrophilic and lead to spilling of the Taylor cone around the chip outlet and to instability in spray generation.[14] Some studies use low-cost polymer substrates such as polydimethylsiloxane (PDMS), however, its mechanical strength as a thin foil is limited.[15]

Herein we describe the development of a thin-polymer microspray-chip FT-ICR-MS system that enables high-performance ESI-MS analyses of biopolymers.[16] The microchip employed is produced from plasma-ablated polyimide foils by using techniques analogous to those in microelectronics.[17] First analytical applications demonstrate chip-ESI-FT-ICR spectra with high resolution and mass accuracy, with several advantages compared to nano-ESI-MS; furthermore, we show its suitability for the analysis of complex mixtures such as combinatorial peptide libraries and for high-performance proteome analysis.

A main goal for the chip system was to provide low-cost, disposable devices, yet suitable for high-performance ESI-MS. To this end, the choice of the material becomes critical. In contrast to the adjunction of glass or fused silica tips, which is inadequate for mass production, the present chips were made of plasma-ablated polyimide foils by using techniques developed in the microelectronics industry (e.g. Dyconex, Zurich). A resist is patterned on a copper-coated polyimide foil which is then copper-etched and plasma-etched. This technique enables etching of inlet and outlet during the fabrication of microchannels, as well as the integration of gold-coated microelectrodes within the microstructure. The structure and build-up of the chip is shown in Figure 1. As a result of the high mechanical strength of polyimide, no bending was observed even with a thickness of only 10 μm around the nozzle. Furthermore, the surface properties of the microstructure can be adjusted by the oxidative or reductive nature of the plasma used. The present technology provides disposable, hydrophobic devices well suited for the coupling with ESI-MS.[18] Particularly attractive are the high reproducibility (exact channel and outlet dimensions), flexibility of chip design, and low-cost production.

Examples of chip-ESI-FT-ICR spectra are shown in Figure 2 for bovine insulin B-chain and ubiquitin. The chip-FT-ICR-MS measurements provided mass determination accuracies of 1.4 ppm for insulin and 2.0 ppm for ubiquitin by using routine broad band (BB) mode and side-kick (SK) trapping method, at mass resolutions in the BB mode of 57000 (ubiquitin) and 91000 (insulin B-chain). However, mass resolution is readily increased up to $>10^6$ by using the

[*] Prof. Dr. M. Przybylski, Dr. N. Youhnovski, Dipl.-Chem. E. Damoc, Dipl.-Chem. S. Becker
University of Konstanz, Department of Chemistry
Laboratory of Analytical Chemistry
78457 Konstanz (Germany)
Fax: (+49) 7531-88-3097
E-mail: Michael.Przybylski@uni-konstanz.de
Dipl.-Chem. N. Lion, Prof. Dr. H. H. Girault
Laboratoire d'Éléctrochimie
École Polytechnique Fédérale de Lausanne
1015 Lausanne (Switzerland)
Dr. J. S. Rossier, Dr. F. Reymond
DiagnoSwiss S.A., Rte de L'Ile au bois 2
1870 Monthey (Switzerland)

[**] This work was supported by the European Union, 5th Framework Research Programme QoL-2000, QLRT-2000-01903; Deutsche Forschungsgemeinschaft (Biopolymer Mass Spectrometry), Bonn (Germany), and the Office Fédéral de L'Éducation et de la Science (OFES grant No 01.0182).

 © 2003 Wiley-VCH Verlag GmbH & Co. KGaA, Weinheim 1433-7851/03/4201-0054 $ 20.00+.50/0

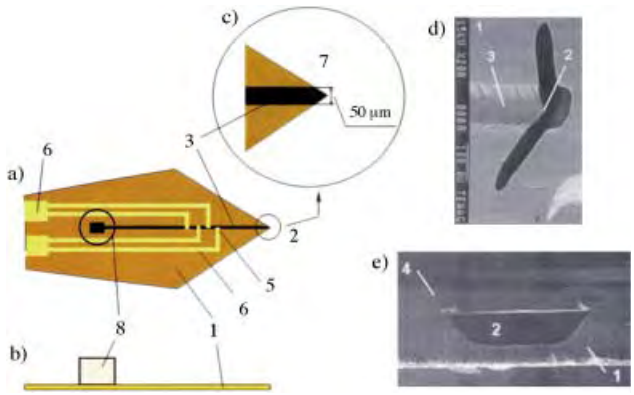


Figure 1. Schematic representation and electron micrographs of thin-layer ESI-microchip. a) Top view of the chip structure prepared for the FTICR-interface, b) side view of the chip with the microfluid reservoir, c) expanded view of the chip showing the microchannel spray exit, d) SEM image showing the top view of a portion of the micro-electrospray system before sealing, e) SEM image of the chip, showing the cross-section of the central channel **3** prepared by plasma etching, where the substrate **1** is polyimide and the sealing layer **4** a 30-µm-thick polyethylene/polyethelene terephthalate laminate. **1** polyimide thin layer substrate, **2** ESI-spray exit, **3** microchannel fabricated by plasma ablation of the polyimide substrate, **4** a 30-µm-thick sealing layer of polyethylene/polyethylene terephthalate laminate, **5** electrode for high-voltage application, **6** electrode contacts, **7** sharp tip angle prepared by plasma etching of the substrate, **8** microfluidic sample reservoir.

high-resolution mode. At standard resolution (BB mode) the charge states of ions were readily defined from the mass difference of two adjacent isotopes, without the necessity of deconvolution techniques (Figure 2). This situation is of importance, for example, for the analysis of noncovalent complexes where a low charge distribution may yield only few peaks that are difficult to deconvolute. The high resolution of the chip-FT-ICR spectra routinely provides monoisotopic peaks with mass-determination accuracies around 1 ppm.

The characterization of complex mixtures, such as from natural products and combinatorial libraries, often requires preliminary fractionation or separation (e.g. by HPLC or CE). In such applications the high resolution and accuracy of FT-ICR-MS proves to be extremely useful, for example, to detect mixture components with closely adjacent masses.[19] The feasibility of the chip-ESI-FT-ICR system is illustrated in Figure 3 for a combinatorial peptide library derived from the core epitope of mucin-2 gastrointestinal glycoprotein, a marker protein for colon cancer.[20] In a combinatorial peptide sublibrary of the epitope motif, TQTXT,[21] the chip-ESI-FT-ICR-MS analysis was capable of distinguishing, and provided identification of all components of the library at monoisotopic resolution. Protonated molecular ions were observed with a relative-abundance distribution reflecting the composition of components, except for the peptide TQTHT, whereas the ion signal of the two isobaric peptides, TQTIT and TQTLT, were twice as abundant as the other components. The chip-ESI spectrum provided unequivocal resolution of the "isobaric" peptides, TQTKT and TQTQT with molecular masses, 578.3071 and 578.2708 ($\Delta m = 0.0364$ amu). The accuracies

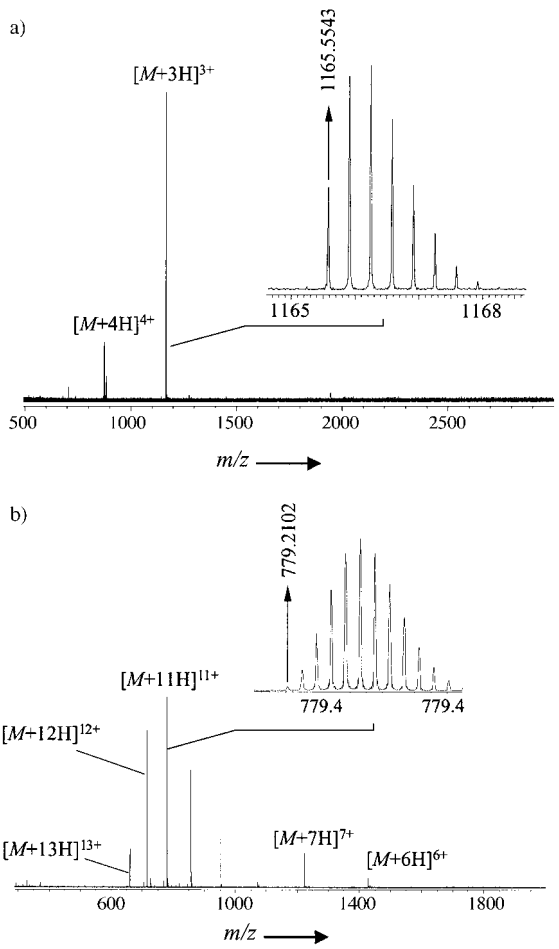


Figure 2. Chip-ESI-FT-ICR mass spectra of a) oxidized bovine insulin B-chain, (0.0071 mg mL^{-1} in 2% aqueous acetic acid/methanol, 1/1), b) bovine ubiquitin (0.02 mg mL^{-1} in 3% aqueous acetic acid/methanol, 1/1).

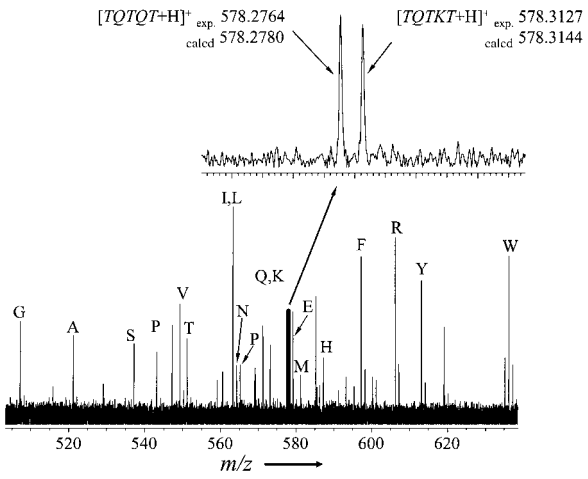


Figure 3. Chip-ESI-FT-ICR mass spectrum of the combinatorial peptide sub-library TQTXT (where X = all proteinogenic amino acids except Cys). The peaks corresponding to the isobaric peptides TQTIT and TQTLT overlap. The insert shows the base-line separated peaks corresponding to the protonated molecular ions of peptides TQTQT and TQTKT (see Table 1).

 © 2003 Wiley-VCH Verlag GmbH & Co. KGaA, Weinheim 1433-7851/03/4201-0055 $ 20.00+.50/0

Table 1: Elemental compositions of components of the TQTXT peptide library determined by chip-ESI-FT-ICR-MS.

Amino acid X	$[TQTXT+H]^+$ calcd	$[TQTXT+H]^+$ exp.	Δm	ppm	Elemental composition
A	521.2566	521.25547	0.00113	2.2	$C_{20}H_{36}N_6O_{10}$
D	565.2464	565.24558	0.00082	1.5	$C_{21}H_{36}N_6O_{12}$
E	579.2621	579.26044	0.00166	2.9	$C_{22}H_{38}N_6O_{12}$
F	597.2879	597.28656	0.00134	2.2	$C_{26}H_{40}N_6O_{10}$
G	507.2409	507.23953	0.00137	2.7	$C_{19}H_{34}N_6O_{10}$
H	587.2784	587.27640	0.00200	3.4	$C_{23}H_{38}N_9O_{10}$
I	563.3035	563.30182	0.00168	3.0	$C_{23}H_{42}N_6O_{10}$
K	578.3144	578.31271	0.00169	2.9	$C_{23}H_{43}N_7O_{10}$
L	563.3035	563.30182	0.00168	3.0	$C_{23}H_{42}N_6O_{10}$
M	581.2599	581.25877	0.00113	1.9	$C_{22}H_{40}N_6O_{10}S$
N	564.2624	564.26118	0.00122	2.2	$C_{21}H_{37}N_7O_{11}$
P	547.2722	547.27080	0.00140	2.6	$C_{22}H_{38}N_6O_{10}$
Q	578.2780	578.27636	0.00164	2.8	$C_{22}H_{39}N_7O_{11}$
R	606.3206	606.31884	0.00176	2.9	$C_{23}H_{43}N_9O_{10}$
S	537.2515	537.24984	0.00166	3.1	$C_{20}H_{36}N_6O_{11}$
T	551.2671	551.26583	0.00127	2.3	$C_{21}H_{38}N_6O_{11}$
V	549.2879	549.28638	0.00152	2.8	$C_{22}H_{40}H_6O_{10}$
W	636.2988	636.29657	0.00223	3.5	$C_{28}H_{41}N_7O_{10}$
Y	613.2828	613.28049	0.00231	3.8	$C_{26}H_{40}N_6O_{11}$
		Average:	0.00155	2.7	
		Standard deviation:	0.00038	0.6	

of mass determinations yielded the elemental compositions of all the library components (Table 1).

Similar results were obtained for a number of polypeptides and proteins within an approximate molecular-weight range of between 1 and 35 kDa (data not shown). The chip-ESI-FT-ICR-MS interface provides a stable spray of 0.1–3 μL sample solutions for at least 15 min, which enables analysis of low sample concentrations, that is, attomol sensitivity for oligopeptides as shown previously for nano-ESI-FT-ICR-MS[4b] (see Figure 2). However, for peptides in the lower mass range a significant advantage of the chip-ESI-system was found in the absence of the background and/or contamination that is frequently found with nano-ESI capillaries.[12] Furthermore, spraying times with the chip are sufficient to carry out the complete range of fragmentation experiments, one of the key features of FT-ICR-MS.[9] Fragmentation experiments of the model peptide angiotensin were carried out in the ESI source low vacuum region (source CID), as well as in the ICR-cell, after isolation of ions using 1) Ar as collision gas (SORI-CID), or 2) IRMPD.[10] The MS/MS feasibility of the chip-ESI-FT-ICR system was demonstrated by IRMPD fragmentation of angiotensin yielding results comparable to those obtained using the nano-ESI source (Table 2). First multistage (MS^n) experiments were performed up to the MS^3 level by using both SORI-CID and IRMPD.

A first application of the chip-FTICR system to a complex multicomponent mixture in proteome analysis is shown in Figure 4 with an in-gel digested tryptic peptide mixture of the human microtubule-associated tau protein which has recently aroused interest as a target protein in neurofibrillary tangles characteristic of Alzheimer's disease. The pathophysiological aggregation of tau in fibrillary tangles has been shown to be associated with structural changes by multi-(hyper)-phosphorylation which has therefore become the subject of recent studies.[22] In the chip-ESI spectrum the complete primary structure including 18 serine- and threonine-phosphorylations could be directly identified from the tryp-

Table 2: FT-ICR-fragmentation experiments of angiotensin I by IRMPD and source-CID.

MS/MS fragmentation	Isolated ions	Sequence determined	Resolution	Accuracy [ppm]
IRMPD	$[M+2H]^{2+}$ $[M+3H]^{3+}$	DYIHP	50000	6
source-CID	–	IHPFHL	60000	3

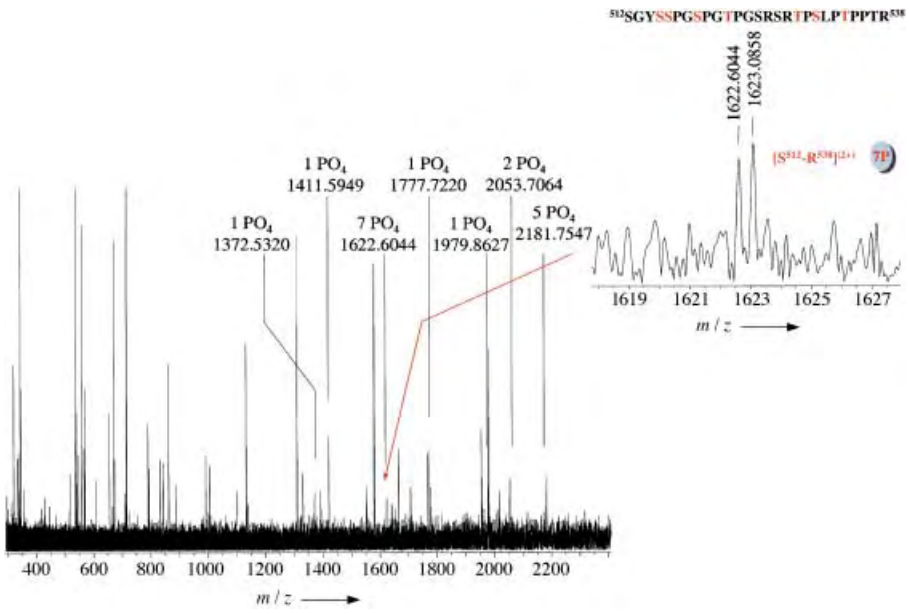


Figure 4. Chip-ESI-FTICR mass spectrum of tryptic digest mixture of multiphosphorylated human neurofibrillary tau protein. Mass assignments with m/z detection range, 200–2500, and partial sequences are shown for phosphorylated peptides. The insert shows the peptide fragment of the phosphorylation domain (512–538); the seven phosphorylation sites, identified using information from the NiceProt View of Swiss-Prot database (primary accession number P10636), are indicated in red ($C_{113}H_{191}N_{36}O_{61}P_7$, doubly protonated; calcd: 1622.55513; found: 1622.60435, $\Delta = 30$ ppm).

 © 2003 Wiley-VCH Verlag GmbH & Co. KGaA, Weinheim 1433-7851/03/4201-0056 $ 20.00+.50/0

tic peptides, partially with very low abundances, which clearly demonstrates the high analytical performance of the chip-FTICR-MS. Mass determinations yielded accuracies of 5–20 ppm within the phosphorylated peptide sequences; this provided the direct identification of 7 and 5 phosphorylation sites in the multi-phosphorylation domains, (512—538; see insert in Figure 4, and (382—398; T386, S388, T395, T396, S397).

In summary, we have developed a high performance yet robust thin-chip ESI system which is fully compatible with the high-resolution capability of FT-ICR-MS. With the present plasma-etched microchip, alignment to the ESI-FT-ICR ion source is straightforward. Low voltages for biopolymer ionization can be applied, such as for the study of noncovalent complexes, low flow rates can be used and multiplexing is easy. Furthermore, the design of the microchannel tip is suitable for micro-CE applications without the necessity of a sheath liquid. In comparison to the standard nano-ESI-FTICR capillary system in our laboratory,[10b,12] major advantages of the microchip are flexible volumes, long spraying times at high sensitivity, substantially lower background and contamination problems and, particularly, the suitability for micro-immobilization chemistry, for example, with gold surfaces. In addition, first studies in our laboratories show that the chip-microfluidic-MS coupling is especially attractive for high performance proteomics applications.

Experimental Section

Production of microchips: The fabrication of microchips (Figure 1) has been described in refs. [16,17] Briefly, 30 × 40 cm polyimide foils of 50 μm thickness were coated on both sides with a 5 μm copper layer and fixed in a frame. The surface was coated with a liquid photoresist which was exposed and developed by standard printed-circuit manufacturing processes. The copper was etched with an aqueous solution of CuCl and H_2O_2, and the substrate then exposed to a low-pressure plasma formed in an O_2/CF_4 gas mixture with an O_2 content of about 80%. The exposed polymer areas were etched isotropically at an ablation rate of about 1–2 μm min^{-1}. The channels were then etched in arrays, and the copper is further patterned to serve as electrode or conductive tracks. Electroplating of gold was performed to form an inert metal layer covering the copper tracks, and the channels were finally sealed by lamination with a 30 μm-thick polyethylene/polyethylene terephthalate sheet.

Preparation and alignment of chips for ESI-FT-ICR-MS coupling: The chip-ESI-FT-ICR-MS coupling interface was constructed in a self-built chip holder, prepared for fixation of up to five chips. The holder is equipped with *x*,*y*,*z*-fine adjustment screws for movement and positioning of the chips in front of the capillary entrance. The ESI voltage was applied onto the chip contacts or by using an electrode in the chip reservoir. The standard multiport entrance of the ESI ion source was removed, and placed 1–2 mm in front of the capillary entrance (Figure 1).

Mass spectra were obtained with a 7T Bruker Daltonik Apex II FTICR mass spectrometer equipped with an APOLLO electrospray/nano-ESI source. Sample solutions of 0.5–5 μL (0.0005–0.01 μg μL^{-1}) were applied to the chip reservoir, and the chip fixed into the sample holder. The spray voltage was slowly increased from 0 V to the working voltage of 1000–2300 V, and the onset of the spray inspected with a microscope. Mass spectra were obtained by acquisition of, typically, 4–32 single scans at 45–70 V capillary exit voltage, 9.14 V of skimmer 1, 8.82 V of skimmer 2, 2500 μs ionization pulse time, 0.001 s ionization delay time, 1.2 μs excitation sweep pulse. Oxidized bovine insulin B-chain, was dissolved in water/methanol/acetic acid (49.5/49.5/1) to a final concentration of 0.0071 mg mL^{-1}. Bovine ubiquitin was dissolved in a solution of 3% aqueous acetic acid/methanol (1/1) to yield a final concentration of 0.002 mg mL^{-1}. In-gel digestion with trypsin (2 h) and sample preparation of human tau protein was performed as previously described.[5,9d]

IRMPD experiments were performed with Ar as the cooling gas at the following experimental steps: 5000 μs empty ESI source, empty ICR cell: 5000 μs hexapole accumulation; 1800 μs ion injection, 40000 μs IR laser in cell; 30 μs detection delay. The CID experiments were performed at a capillary exit voltage of 70–120 V.

Single peptides and peptide libraries comprising the mucin-2 epitope motif, TQTXT, were synthesized by solid-phase peptide synthesis (SPPS) on a chloromethylated polystyrene resin with the portioning-mixing method, using Boc/benzyl (Boc = *tert*-butoxycarbonyl) protection chemistry.[20] Coupling steps were monitored by ninhydrin and the Boc group removed with 33% TFA (TFA = trifluoroacetic acid). Final cleavage from the resin was performed by treatment with anhydrous HF for 1 h, and crude libraries and single peptides were purified by HPLC before analysis by MALDI-TOF-MS and ESI-FT-ICR-MS.

Received: May 29, 2002
Revised: August 15, 2002 [Z19388]

[1] J. H. Chan, A. T. Timpermann, D. Quin, R. Aebersold, *Anal. Chem.* **1999**, *71*, 4437 – 4444.
[2] B. Zhang, H. Liu, L. Karger, F. Foret, *Anal. Chem.* **1999**, *71*, 3258 – 3264.
[3] The term proteome was recently proposed to describe the large scale study of the proteins expressed from a genome.
[4] a) T. Rabilloud, *Proteomics* **2002**, *2*, 3 – 10; b) M. Przybylski, N. Youhnovski, K. Bruns, E. Damoc, C. Damoc, R. Knippers, M. Kohlmann, R. Cecal, X. Tian, F. Reymond, J. Rossier, *Proteomics* **2002**, in press.
[5] a) S. Meri, M. Baumann, *Biomol. Eng.* **2001**, *18*, 213 – 220; b) M. R. Larson, G. L. Soerensen, S. J. Fey, P. M. Larsen, P. Roepstorff, *Proteomics* **2001**, *1*, 223 – 238.
[6] a) M. S. Wilm, M. Mann, *Int. J. Mass Spectrom. Ion Processes* **1994**, *136*, 167 – 180; b) M. Przybylski, *Adv. Mass Spectrom.* **1995**, *13*, 257 – 283; c) G. Valaskovic, N. L. Kelleher, F. W. McLafferty, *Science* **1996**, *273*, 1199 – 1202.
[7] a) J. A. Loo, *Mass Spectrom. Rev.* **1997**, *16*, 1 – 23; b) M. Przybylski, M. O. Glocker, *Angew. Chem.* **1996**, *108*, 878 – 899; *Angew. Chem. Int. Ed. Engl.* **1996**, *35*, 806 – 823; c) R. D. Smith, J. E. Bruce, Q. Wu, Q. P. Lei, *Chem. Soc. Rev.* **1997**, *26*, 191 – 202.
[8] a) M. T. Davis, T. D. Lee, *J. Am. Soc. Mass Spectrom.* **1998**, *9*, 194 – 201; b) D. Figeys, R. Aebersold, *Anal. Chem.* **1998**, *70*, 3721 – 3727
[9] a) A. G. Marshall, C. L. Hendrickson, G. S. Jackson, *Mass Spectrom. Rev.* **1998**, *17*, 1 – 35; b) M. E. Belov, M. V. Gorshkov, H. R. Udseth, G. A. Anderson, A. V. Tolmachev, D. C. Prior, R. Harkewicz, R. D. Smith, *J. Am. Soc. Mass Spectrom.* **2000**, *11*, 19 – 23; c) M. R. Emmett, F. M. White, C. L. Hendrickson, S. D. Shi, A. G. Marshall, *J. Am. Soc. Mass Spectrom.* **1998**, *9*, 333 – 340; d) S. H. Bauer, M. F. Wiechers, K. Bruns, M. Przybylski, C. A. O. Stuermer, *Anal. Biochem.* **2001**, *298*, 25 – 31.
[10] a) T. B. Walk, A. W. Trautwein, H. Richter, G. Jung, *Angew. Chem.* **1999**, *111*, 1877 – 1880; *Angew. Chem. Int. Ed.* **1999**, *38*, 1763 – 1765; b) T. A. Fligge, C. Reinhard, C. Harter, F. T. Wieland, M. Przybylski, *Biochemistry* **2000**, *39*, 8491 – 8496.
[11] G. Baykut, R. Jertz, M. Witt, *Rapid Commun. Mass Spectrom.* **2000**, *14*, 1238 – 1247.
[12] a) T. A. Fligge, M. Przybylski, J. P. Quinn, A. G. Marshall, *Eur. Mass Spectrom.* **1998**, *4*, 401 – 404; b) T. A. Fligge, J. Kast, K.

Bruns, M. Przybylski, *J. Am. Soc. Mass Spectrom.* **1999**, *10*, 112–116.
[13] R. D. Oleschuk, D. J. Harrison, *TrAC Trends Anal. Chem.* **2000**, *19*, 379–388.
[14] T. C. Rohner, J. S. Rossier, H. H. Girault, *Anal. Chem.* **2001**, *73*, 5353–5357.
[15] a) J.-S. Kim, D. R. Knapp, *J. Am. Soc. Mass Spectrom.* **2001**, *12*, 463–469; b) J. S. Kim, D. R. Knapp, *Electrophoresis* **2001**, *22*, 3993–3999.
[16] M. Przybylski, N. Youhnovski, F. Reymond, J. Rossier, UK Patent GB0121590.4 **2001**.
[17] J. Rossier, F. Reymond, P. E. Michel, *Electrophoresis* **2002**, *23*, 858–867.
[18] V. Gobry, J. Van Oostrum, M. Martinelli, T. Rohner, J. Rossier, H. H. Girault, *Proteomics* **2002**, in press.
[19] E. Windberg, F. Hudecz, A. Marquardt, F. Sebestyen, A. Kiss, S. Bosze, H. Medzihradszky-Schweiger, M. Przybylski, *Rapid Commun. Mass Spectrom.* **2002**, *16*, 834–839.
[20] K. Uray, M. R. Price, F. Hudecz, *J. Pept. Sci.* **1998**, *4*, 319–326.
[21] A. Marquardt, E. Windberg, X. Tian, M. Kohlmann, F. Hudecz, M. Przybylski in *Proceedings of the 18th Symposium on Combinatorial Chemistry*, Mayflower, Kingswinford, **2002**, in press.
[22] a) M. L. Billingsley, R. L. Kincaid, *Biochem. J.* **1997**, *323*, 577–591; b) K. C. Wilhelmsen, *Proc. Natl. Acad. Sci. USA* **1999**, *96*, 7120–7121.

Biomineralization

Morphosynthesis of Star-Shaped Titania–Silica Shells**

Dirk Volkmer, Stefano Tugulu, Matthias Fricke, and Tim Nielsen*

Biomineralizing organisms such as diatoms or radiolaria develop intricately shaped inorganic casings mainly consisting of amorphous silica.[1] In spite of the ubiquity of these organisms the morphogenetic foundations of cell development yielding a species-specific shell design are poorly understood. However, a few details of silica metabolic pathways in diatoms and other silicifying organisms have been discovered recently, including hitherto unknown classes of enzymes (silicateins[2]) and peptides (silaffins,[3] frustulins,[4] pleuralins (formerly HEPs),[5] SP41[6]) being either associated with silicic acid polycondensation, precipitation, or shell development.

The unicellular diatoms are particularly interesting model organisms that may give rise to novel biomimetic strategies for producing complex, hierarchically structured materials.[7] Shell development in diatoms occurs within a highly specialized membrane compartment, the so-called silica deposition vesicle (SDV).[8] There is still much debate about the processes that serve to mould the SDV into its final shape.[9] SDVs occur among a broad range of protists (testate amoebae, heliozoa, and radiolaria), which hints to a common secretory mechanism for the production of siliceous structures.[10] Clearly, the formation of hierarchically structured silicified cell walls involves distinct differentiation/growth steps at the characteristic length scales, ranging from nano- to micron-sized structures, and thus a distinction between micro- and macromorphogenesis has been proposed recently.[11]

Herein we present our first endeavors to set up a biomimetic model system of shell formation in unicellular organisms such as diatoms or radiolaria. The model system consists of a surfactant-stabilized oil droplet which is microinjected into an aqueous solution. The oil droplet contains small amounts of a monomeric metal oxide precursor, which starts to hydrolyze when brought in contact to the aqueous phase, finally leading to formation of a mineralized shell at the oil–water interface. The progress of mineralization is monitored in situ by means of video microscopy. This relatively simple system was chosen because it shows decisive features characteristic of biological systems. It has a primitive silicon "metabolism" that liberates monomeric silicic acid from a masked storage deposit. The release of hydrolytically unstable metal oxide precursors occurs at a membrane-type surface. The oil droplet dimensions are comparable to the sizes of typical silicifying unicellular organisms (10–100 μm). Owing to the limited amount of metal oxide precursor contained within the oil droplet, the shell formation process is intrinsically self-terminating. Finally, but most importantly, appropriately chosen organic additives dissolved in the oil phase (or the aqueous solution, respectively) may induce dynamic self-organization processes that ultimately lead to formation of discrete hollow shells of complex shapes.

Among the many experiments conducted so far, our attention was attracted by a particular system which leads to the morphosynthesis of discrete star-shaped shells bearing a striking resemblance to the silicified skeletons of radiolaria. The basic reaction system consists of a small droplet of chlorocyclohexane that contains arachidic acid ($c =$ 42.4 mM).[12] The aqueous phase consists of a highly diluted solution of cetyltrimethylammonium bromide (CTAB, $c =$ 55.6 μM). Upon microinjection, the surface of the oil droplet starts to become corrugated within a few minutes (Figure 1). We observe the growth of small liquid-filled spines extruding from the surface of the oil droplet. The spines sometimes reach a length of approximately 90 μm, while typical diameters range from 3 to 15 μm.

[*] Dr. D. Volkmer, S. Tugulu
University of Bielefeld
Faculty of Chemistry, AC1
33501 Bielefeld (Germany)
Fax: (+49) 521-106-6003
E-mail: dirk.volkmer@uni-bielefeld.de
M. Fricke, Dr. T. Nielsen
University of Bielefeld
Faculty of Physics, D3 (Germany)

[**] This work was supported by the Deutsche Forschungsgemeinschaft (DFG Schwerpunktprogramm 1117 "Prinzipien der Biomineralisation"; DFG grant Vo 829/2-1). D.V. thanks the DFG for a habilitation scholarship (DFG grant Vo 829/1-1).

Supporting information (instrumentation and preparation procedures) for this article is available on the WWW under http://www.angewandte.org or from the author.

 © 2003 Wiley-VCH Verlag GmbH & Co. KGaA, Weinheim 1433-7851/03/4201-0058 $ 20.00+.50/0

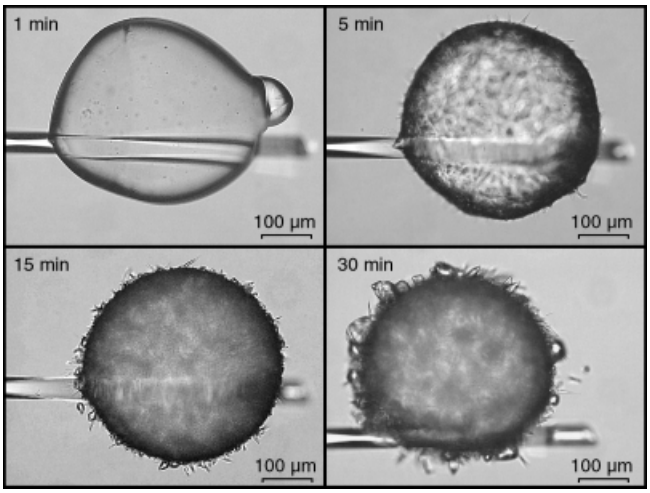


Figure 1. Timelapse recording of the spontaneous emulsification of a chlorocyclohexane droplet containing arachidic acid ($c = 42.4$ mM) after microinjection into an aqueous solution of CTAB ($c = 55.6$ µM) (bright-field optical micrographs).

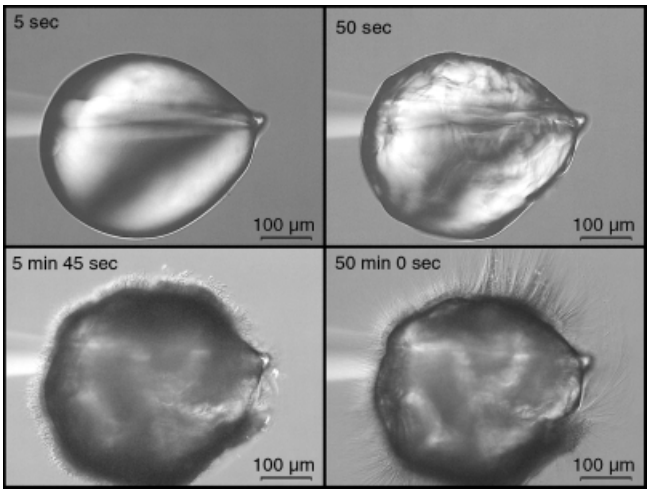


Figure 2. Timelapse recording of spine formation of a chlorocyclohexane droplet containing arachidic acid ($c = 42.4$ mM) and tetra-*tert*-butyl orthotitanate (TBOT, 4 wt%) after microinjection into an aqueous solution of CTAB ($c = 0.556$ mM) (differential interference contrast optical micrographs).

Upon reaching a critical size, the spines start to tie up and form a corona of submicroscopic droplets around the original oil droplet. The dissipation process continues until most of the original droplet is divided into smaller size microemulsion droplets which subsequently start to spread out into the aqueous solution. Similar dynamic self-organization processes have been reported and are commonly referred to as *spontaneous emulsification*.[13] It is noteworthy that under the chosen experimental conditions the emulsification process only occurs when oppositely charged surfactants are used within the two different liquid phases. Substituting arachidic acid with arachidyl alcohol, for instance, or omitting one surfactant, does not lead to spontaneous emulsification at all. Thus it is anticipated that electrostatic interactions between the oppositely charged surfactants contribute a great deal to the driving force of the process.[14]

The challenge here was to couple the mineralization process to the spontaneous dissipation of the oil droplet while preserving the metastable star-shape morphology. This is achieved by proper choice of the metal oxide precursor being added to the oil phase and careful adjustment of surfactant concentrations. We were first unable to establish a simple silica-based model system that would have led to robust silica shells at ambient conditions (i.e. room temperature, aqueous solution at pH ≈ 7) in a suitable time frame.[15] A major improvement was achieved by employing titania or mixtures of titania/silica precursors that are hydrolytically less stable than typical silica precursors (tetramethoxysilane (TMOS), tetraethoxysilane (TEOS)) used within initial experiments (see Supporting Information).[16] Using admixtures of tetra-*tert*-butyl orthotitanate (TBOT) we are able to produce smooth and robust, mineralized shells at the oil–water interface within a few minutes to hours, depending on the experimental conditions.

Figure 2 shows a timelapse recording of optical micrographs similar to those in Figure 1. The oil droplet now contains a small amount of titania precursor (TBOT). Again, formation of a star-shape morphology is observed, but in contrast to the system without metal oxide precursor, the dissipation process becomes frozen at an intermediate stage after a few minutes. A closer inspection of the particles thus obtained shows that the mineralized surface consists of thin hollow spines (av. diameter: 1 µm) that may grow up to a length of some 100 µm. The star-shaped titania particles are completely stable if kept in aqueous solution but they rapidly decompose upon drying in air. Attempts to preserve the morphology by freeze-drying procedures have failed so far. Scanning electron micrographs of freeze-dried samples reveal hollow mineralized shells (av. wall thickness ≈ 1 µm), while the characteristic spines have completely disappeared. According to scanning electron micrographs the remaining mineral shell consists of a mesoporous network of partially coalesced titania colloid particles with typical diameters ranging from 40–70 nm. The fact that the spines are completely lost during sample drying points to a low mineral content of these structural elements.

A systematic variation of surfactant and precursor concentrations, respectively, shows that the genesis of star-shaped titania particles is a highly concentration-dependent process: The most uniform particles are obtained at a TBOT starting concentration of about 4 wt%. At TBOT contents below 3 wt%, the dissipation process is slowed down compared to the precursor-free system, but eventually leads to formation of microemulsion droplets; TBOT contents exceeding 5 wt%, in contrast, yield massive mineral shells encompassing the oil droplet, which lack radial undulations.

The putative composition of spines that develop during emulsification led us to employ fluorescence microscopy to answer the principle question, as to whether or not the growing spines are filled with organic solvent. By adding a hydrophobic fluorescent probe (coumarin 153) to the chlorocyclohexane solution, we were able to image the time-dependent spatial distribution of the immiscible liquid phases by real-time laser-scanning microscopy. We employed a novel multibeam two-photon microscope with diffraction limited

 © 2003 Wiley-VCH Verlag GmbH & Co. KGaA, Weinheim 1433-7851/03/4201-0059 $ 20.00+.50/0

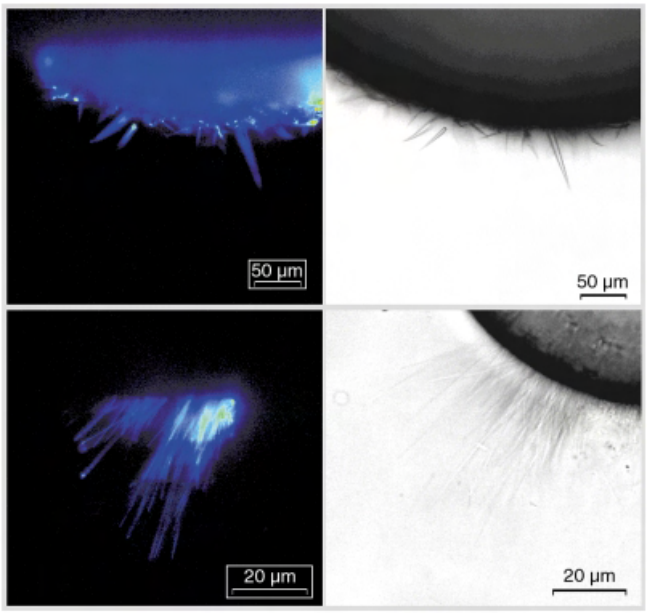


Figure 3. Fluorescence images (left side) and bright-field optical micrographs (right side) taken from the oil droplet periphery during spine development. Pictures correspond to the system lacking precursor (top row) and containing a titania precursor (bottom row). The spines and the laser-dissected fraction of the oil droplet appear in blue or green colors against the dark (nonfluorescent) background.

three-dimensional spatial resolution and fast scanning capability (frame rates up to 60 Hz) to record optical sections of the droplets and the spines.[17] The fluorescence signal is taken as a measure of the coumarin concentration and can be used to visualize the distribution of the organic solvent.

Figure 3 shows representative fluorescence images (left side) as opposed to bright field optical micrographs (right side) taken from the droplet periphery during spine development. The pictures in the top row correspond to the system without precursor. The spines and the laser-dissected fraction of the oil droplet appear in blue or green colors against the dark (nonfluorescent) background. Colors represent different fluorescence intensity levels. It is clearly seen that the fluorescence intensity is uniform throughout the main body of the oil droplet *and* the spines, which is indicative of a homogeneous distribution of the fluorescent probe and the organic solvent, suggesting a continuous transition between oil droplet and spines. A similar picture is gained from the fluorescence images of the precursor-containing system (Figure 3, bottom), which shows a comparably uniform fluorescence throughout the thin spines radiating from the surface of the oil droplet. We conclude that spine formation in both systems is governed by a similar self-organization process that involves surfactant-mediated development of interface curvature between two immiscible liquid phases.

Based on these experiments we currently rule out that complex surfactant aggregates, for example, surfactant multilayer tubules,[18] are involved in spine formation as found, for instance, in fluid-rod structures of hydrated solid lecithin surfaces ("myelin figures"). By employing single droplet microinjection experiments, we were able to narrow the optimum concentration range of chemical components. As a

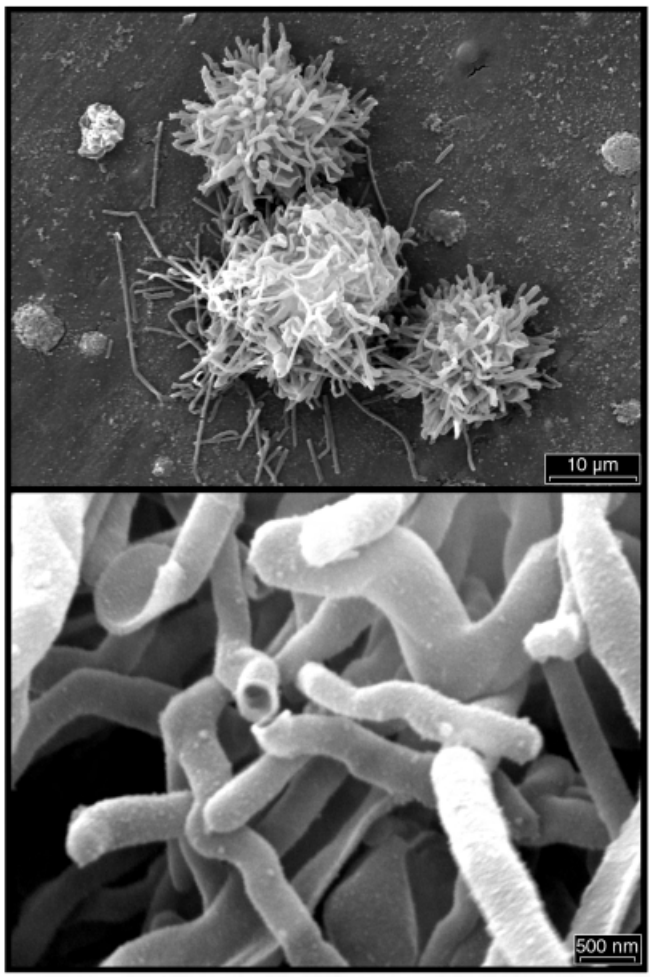


Figure 4. Scanning electron micrographs of star-shaped titania–silica shells from bulk sample preparation procedures. Top: Typical morphology of an air-dried sample demonstrating the robust nature of the mineralized shells. Bottom: Fractured sample indicating the hollow tubular nature of mineralized spines.

remaining challenge we finally transferred our insights gained from video microscopy investigations to a technically simple bulk sample preparation procedure. This was achieved by adding a silica precursor (TMOS) to the oil phase or the aqueous solution. Mechanically robust mineralized star-shaped particles are then obtained by adding a small volume of chlorocyclohexane, which contains a TBOT/TMOS precursor, to a pre-hydrolyzed aqueous solution of TMOS. The suspension is gently shaken a few times in a closed vial and the suspension is left to stand quiescent for a few days, while sedimentation of the emulsion droplets occurs. Light microscopic examination of the particles that have settled at the bottom of the vial reveal high yields of star-shaped particles that possess a narrow size distribution with average diameters ranging from 10–100 µm. The fraction of particles with small diameters (10–20 µm) are found to be quite robust which simplifies preparation of samples suitable for electron microscopic investigations. In fact, sample morphology is completely preserved after air drying and subjecting the particles to an argon plasma at reduced pressure.

 © 2003 Wiley-VCH Verlag GmbH & Co. KGaA, Weinheim 1433-7851/03/4201-0060 $ 20.00+.50/0

Figure 4 (top) displays the typical particle morphology obtained from bulk sample preparations. It is seen that the spines emerging from the outer shell surface are completely stable. These hollow mineralized spines have an average diameter of some 400–600 nm, while the average wall thickness amounts to approximately 60 nm, as can be seen from scanning electron micrographs of fractured samples at high magnification (Figure 4, bottom). The elemental composition was determined at selected sample areas by using energy-dispersive X-ray (EDX) fluorescence. EDX spectra spotted at the inner droplet surface and at the surface of discrete spines confirm the presence of both Si and Ti.

While there are many reports that make use of organic templates (e.g. liquid crystalline mesophases,[19] vesicles,[20] polymer latex spheres,[21] macromolecules,[22] or oil/water microemulsions[23]) to produce inorganic (silica) materials with well-defined porosity, our approach differs in that a dynamic dissipation process (i.e. the spontaneous emulsification of oil droplets) is used to shape the inorganic matrix.[24] In this regard our approach is certainly related to natural biomineralization processes, although there might be only a faint relation to the various, highly specialized (macro-)molecular constituents of biosilicifying organisms. We anticipate that a closer relation may be achieved once more insight into the functional properties of these macromolecules in biological systems becomes available. Future investigations will focus on the mechanisms that govern the formation of star-shaped particle morphologies.

Received: May 17, 2002
Revised: September 23, 2002 [Z19325]

[1] a) C. C. Perry, T. Keeling-Tucker, *J. Biol. Inorg. Chem.* **2000**, *5*, 537–550; b) *Silicon and Siliceous Structures in Biological Systems* (Eds.: T. L. Simpson, B. E. Volcani), Springer, New York, **1981**.

[2] a) J. N. Cha, K. Shimizu, Y. Zhou, S. C. Christiansen, B. F. Chmelka, G. D. Stucky, D. E. Morse, *Proc. Natl. Acad. Sci. USA* **1999**, *96*, 361–365; b) K. Shimizu, J. Cha, G. D. Stucky, D. E. Morse, *Proc. Natl. Acad. Sci. USA* **1998**, *95*, 6234–6238.

[3] a) N. Kröger, R. Deutzmann, M. Sumper, *J. Biol. Chem.* **2001**, *276*, 26066–26070; b) N. Kröger, R. Deutzmann, C. Bergsdorf, M. Sumper, *Proc. Natl. Acad. Sci. USA* **2000**, *97*, 14133–14138; c) N. Kröger, R. Deutzmann, M. Sumper, *Science* **1999**, *286*, 1129–1132.

[4] N. Kröger, C. Bergsdorf, M. Sumper, *Eur. J. Biochem.* **1996**, *239*, 259–264.

[5] a) N. Kröger, R. Wetherbee, *Protist* **2000**, *151*, 263–273; b) N. Kröger, G. Lehmann, R. Rachel, M. Sumper, *Eur. J. Biochem.* **1997**, *250*, 99–105.

[6] T. F. Schultz, L. Egerton-Warburton, S. A. Crawford, R. Wetherbee, *Protist* **2001**, *152*, 315–327.

[7] E. G. Vrieling, T. P. M. Beelen, R. A. van Santen, W. W. C. Gieskes, *J. Biotechnol.* **1999**, *70*, 39–51.

[8] a) D. Volkmer, *Chem. Unserer Zeit* **1999**, *33*, 6–19; b) E. G. Vrieling, W. W. C. Gieskes, T. P. M. Beelen, *J. Phycol.* **1999**, *35*, 548–559.

[9] For different working hypotheses on the mechanisms of pattern formation in diatom biosilica see: a) R. Gordon, R. W. Drum, *Int. Rev. Cytol.* **1994**, *150*, 243–372; b) A. M. M. Schmid, R. K. Eberwein, M. Hesse, *Protoplasma* **1996**, *193*, 144–173; c) E. G. Vrieling, T. P. M. Beelen, R. A. van Santen, W. W. C. Gieskes, *Angew. Chem.* **2002**, *114*, 1613–1616; *Angew. Chem. Int. Ed.* **2002**, *41*, 1543–1546; d) M. Sumper, *Science* **2002**, *295*, 2430–2433.

[10] O. R. Anderson, *Protoplasma* **1994**, *181*, 61–77.

[11] R. Wetherbee, S. Crawford, P. Mulvaney, *The Nanostructure and Development of Diatom Biosilica* in: *Biomineralization* (Ed.: E. Baeuerlein), Wiley-VCH, Weinheim, **2000**, pp. 189–205.

[12] Chlorocyclohexane was chosen because of its specific density of 1.0 $g\,cm^{-3}$, which avoids droplet buoyancy in aqueous solution.

[13] Selected references: a) N. Shahidzadeh, D. Bonn, J. Meunier, M. Nabavi, M. Airiau, M. Morvan, *Langmuir* **2000**, *16*, 9703–9708; b) T. Nishimi, C. A. Miller, *Langmuir* **2000**, *16*, 9233–9241; c) C. A. Miller, *Colloids Surf.* **1988**, *29*, 89–102; d) O. Theissen, G. Gompper, *Eur. Phys. J. B* **1999**, *11*, 91–100; e) M. J. Rang, C. A. Miller, *J. Colloid Interface Sci.* **1999**, *209*, 179–192; f) R. Granek, R. C. Ball, M. E. Cates, *J. Phys. II* **1993**, *3*, 829–849; g) W. J. Benton, C. A. Miller, T. Fort, *J. Dispersion Sci. Technol.* **1982**, *3*, 1–44.

[14] Mixtures of cationic and anionic surfactants often lead to spontaneous formation of (thermodynamically stable) vesicles: a) E. W. Kaler, A. K. Murthy, B. E. Rodriguez, J. A. N. Zasadzinski, *Science* **1989**, *245*, 1371–1374; b) S. A. Safran, P. Pincus, D. Andelman, *Science* **1990**, *248*, 354–355; c) C. Tondre, C. Caillet, *Adv. Colloid Interface Sci.* **2001**, *93*, 115–134.

[15] The formation of hollow silica shells using an oil/water microemulsion template has been reported by different research groups. However, silicic acid condensation occurs under either strongly acidic or basic conditions: a) S. Schacht, Q. Huo, I. G. Voigt-Martin, G. D. Stucky, F. Schüth, *Science* **1996**, *273*, 768–771; b) C. E. Fowler, D. Khushalani, S. Mann, *Chem. Commun.* **2001**, 2028–2029.

[16] R. J. Davis, Z. Liu, *Chem. Mater.* **1997**, *9*, 2311–2324.

[17] T. Nielsen, M. Fricke, D. Hellweg, P. Andresen, *J. Microsc.* **2001**, *201*, 368–376.

[18] J. H. Fuhrhop, W. Helfrich, *Chem. Rev.* **1993**, *93*, 1565–1582.

[19] a) C. T. Kresge, M. E. Leonowicz, W. J. Roth, J. C. Vartuli, J. S. Beck, *Nature* **1992**, *359*, 710–712; b) G. S. Attard, J. C. Glyde, C. G. Göltner, *Nature* **1995**, *378*, 366–368.

[20] a) S.S Kim, W. Z. Zhang, T. J. Pinnavaia, *Science* **1998**, *282*, 1302–1305; b) P. T. Tanev, T. J. Pinnavaia, *Science* **1996**, *271*, 1267–1269.

[21] a) F. Caruso, R. A. Caruso, H. Möhwald, *Science* **1998**, *282*, 1111–1114; b) B. T. Holland, C. F. Blanford, T. Do, A. Stein, *Chem. Mater.* **1999**, *11*, 795–805.

[22] a) C. Göltner, S. Henke, M. C. Weißenberger, M. Antonietti, *Angew. Chem.* **1998**, *110*, 633–636; *Angew. Chem. Int. Ed.* **1998**, *37*, 613–616; b) J. N. Cha, G. D. Stucky, D. E. Morse, T. J. Deming, *Nature* **2000**, *403*, 289–292; c) D. Y. Zhao, J. L. Feng, Q. S. Huo, N. Melosh, G. H. Fredrickson, B. F. Chmelka, G. D. Stucky, *Science* **1998**, *279*, 548–552; d) M. Templin, A. Franck, A. DuChesne, H. Leist, Y. M. Zhang, R. Ulrich, V. Schadler, U. Wiesner, *Science* **1997**, *278*, 1795–1798.

[23] a) S. Schacht, Q. Huo, I. G. Voigt-Martin, G. D. Stucky, F. Schüth, *Science* **1996**, *273*, 768–771; b) P. Schmidt-Winkel, W. W. Lukens Jr. , P. Yang, D. I. Margolese, J. S. Lettow, J. Y. Ying, G. D. Stucky, *Chem. Mater.* **2000**, *12*, 686–696.

[24] Dynamic transformation processes leading to complex morphologies have been reported. The precise function of the organic template, however, is in most cases not well established. Selected reviews on this subject: a) S. Mann, G. A. Ozin, *Nature* **1996**, *382*, 313–318; b) G. A. Ozin, *Acc. Chem. Res.* **1997**, *30*, 17–27; c) S. Mann, S. L. Burkett, S. A. Davis, C. E. Fowler, N. H. Mendelson, S. D. Sims, D. Walsh, N. T. Whilton, *Chem. Mater.* **1997**, *9*, 2300–2310; d) S. Mann, *Angew. Chem.* **2000**, *112*, 3532–3548; *Angew. Chem. Int. Ed.* **2000**, *39*, 3392–3406; e) L. A. Estroff, A. D. Hamilton, *Chem. Mater.* **2001**, *13*, 3227–3235.

 © 2003 Wiley-VCH Verlag GmbH & Co. KGaA, Weinheim 1433-7851/03/4201-0061 $ 20.00+.50/0

Distances Given by Pulsed EPR

Measurement of a Cu–Cu Distance of 26 Å by a Pulsed EPR Method**

*Irene M. C. van Amsterdam, Marcellus Ubbink, Gerard W. Canters, and Martina Huber**

Methods for determining accurate distances in biological and chemical systems are becoming increasingly important. They provide structural information for systems that cannot be crystallized or are otherwise not accessible to the traditional tools of structure determination. In particular, methods are needed to measure long distances to complement existing techniques. In this context, the advantage of electron paramagnetic resonance (EPR) is becoming increasingly apparent since it combines specificity and the potential to measure long distances.[1,2] Herein we demonstrate that long distances between copper ions in biological systems can be measured by using a pulsed electron electron double resonance (DEER) method.[3] We have investigated covalently linked dimers of an electron transfer protein, the copper protein azurin—these dimers are model compounds for electron transfer (ET).[4,5] The models consist of two azurin protein molecules linked through a surface cysteine group introduced by site-directed mutagenesis (N42C mutant); in az-**1** directly by a cystine bond (Figure 1) and in az-**2** by a flexible linker (1,1′-[oxydi(methylene)]bis(maleimide); BMME).[4,5]

In the DEER technique, three pulses at the observing frequency ν_{obs} and one pulse at the pump frequency ν_{pump} are combined in the four-pulse sequence shown in Figure 2. With the exception of one unsuccessful attempt to determine the distance between two metal centers in a protein,[6] previous applications of DEER have been limited to nitroxide spin labels, for which distances of about 30 Å have been determined.[3]

The importance of reactive metal centers in biological reactions underlines the need to extend the use of the DEER method to paramagnetic transition-metal ions. For the dimers investigated here, ET occurs between the two copper ions, which makes the Cu–Cu distance an important parameter in interpreting the ET rates determined by NMR spectroscopy.[4,5] It is not self-evident that Cu^{II} ions can be investigated by the DEER method, since the g- and hyperfine anisotropies of Cu^{II} ions are significantly larger than for nitroxide spin labels. This results in a pronounced dependence of the EPR spectra on the orientation of the magnetic field: only molecules with a particular orientation to the external magnetic field are excited (orientation selection).

Here we show that copper–copper interactions can be measured by the DEER method, and we present a model that

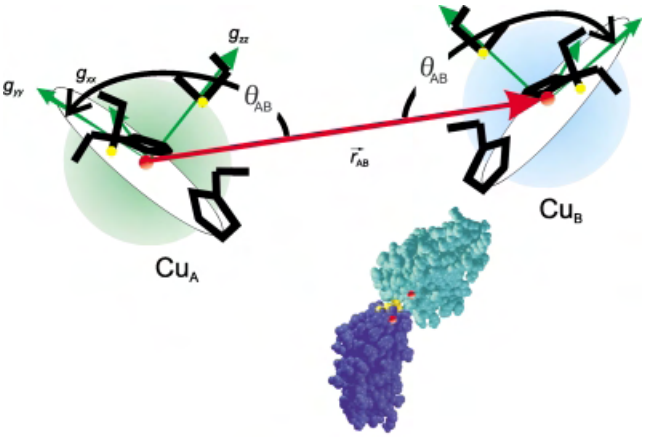


Figure 1. Structure of az-**1** dimer. Schematic representation: Relative orientation of the two copper sites Cu_A and Cu_B in the dimer as well as the principal axes of the *g* tensor with respect to the ligands. $\vec{r}_{AB}$: vector between Cu_A and Cu_B; θ_{AB}: dipolar angle for B_0 in the g_{xx}, g_{yy} plane. Insert: space-filling model of the dimer structure from X-ray crystallography.[4]

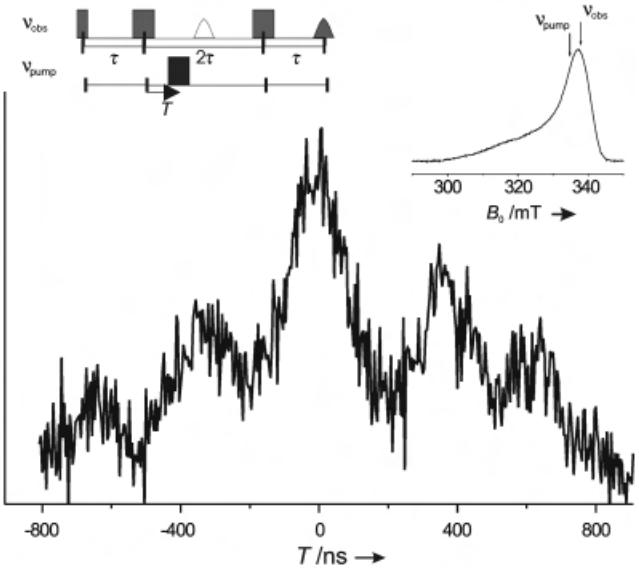


Figure 2. Result of the DEER experiment on az-**1**, showing the electron spin echo intensity as a function of the time *T*. The modulation amplitude accounts for about 3% of the total echo intensity. Temperature: 10 K, total measurement time: 75 min. Time increments in *T*: 4 ns. Insert: DEER pulse sequence (left); echo-detected (absorption type) EPR spectrum (right), with turning points at the principal values of the *g* tensor $g_{xx}=2.04$, $g_{yy}=2.06$, and $g_{zz}=2.27$.[8] ν_{obs}: B_0 field at which experiment is performed, ν_{pump}: field corresponding to the frequency offset $\nu_{obs}-\nu_{pump}$ of 75 MHz.

[*] Dr. M. Huber
Department of Molecular Physics
Leiden University
P.O. Box 9504, 2300 RA Leiden (The Netherlands)
Fax: (+31) 71-527-5819
E-mail: mhuber@molphys.leidenuniv.nl
I. M. C. van Amsterdam, Dr. M. Ubbink, Prof. Dr. G. W. Canters
Leiden Institute of Chemistry
Gorlaeus Laboratories
Leiden University
P.O. Box 9504, 2300 RA Leiden (The Netherlands)

[**] We thank E. J. J. Groenen and J. Schmidt for enlightening discussions and support of this work. Contributions by S. S. Eaton, G. R. Eaton, and G. Jeschke are gratefully acknowledged. The work was performed under the auspices of the BIOMAC Research School of the Leiden and Delft Universities.

 © 2003 Wiley-VCH Verlag GmbH & Co. KGaA, Weinheim 1433-7851/03/4201-0062 $ 20.00+.50/0

takes into account orientation selection. X-ray crystal structure analysis data for the dimers investigated were available; however, since potential differences between the conformation of the dimers in the crystal and in the (frozen) solution could have an impact on the interpretation of ET rates measured in solution, additional information was sought regarding distances and conformations in solution.

DEER experiments were performed on both dimers. The electron spin echo intensity plotted as a function of the time T for az-**1** (Figure 2) shows distinct modulations, which qualitatively agree with those of the nitroxide spin probes.[3] The Fourier transformation of the signal provides a frequency spectrum (Figure 3a) in which the maximum intensity is observed at the dipolar frequency $\nu_{dip} = 2.7$ MHz. In the second dimer, az-**2**, no modulations were observed under the same experimental conditions. The modulations in Figure 2 show that the DEER method can be applied to Cu^{II} centers. In the following we will discuss the frequency spectrum and the differences between the two dimers.

The frequencies reflect the dipolar interaction, which, in the point dipole approximation, is given by Equation (1).

$$\nu_{dip} = \frac{\mu_0 g_A g_B \beta_e^2}{4\pi h} \frac{1}{r_{AB}^3} (3\cos^2\theta_{AB} - 1) \quad (1)$$

It contains r_{AB}, the distance between the paramagnetic centers A and B, g_A and g_B the g values of the two radical fragments, and θ_{AB} the dipolar angle of the magnetic field B_0 and the inter-radical vector $\vec{r}_{AB}$ (Figure 1).

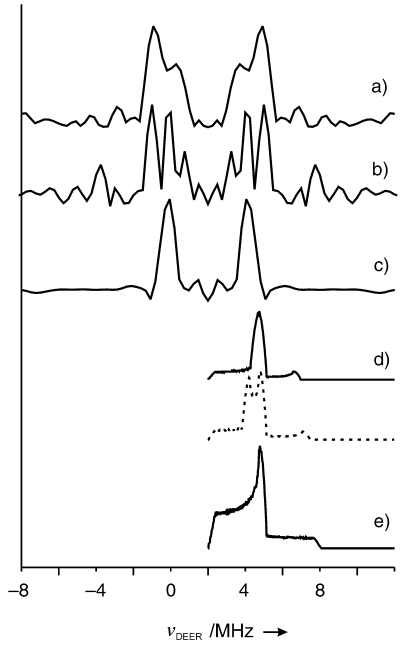


Figure 3. a) Fourier transform of the experimental data (curve from Figure 2). b) Simulation of the powder pattern (e) after inverse Fourier transformation to reconstruct the time trace. These data were reduced to the length of the experimental time trace (1.6 μs), followed by a Fourier transformation as in a. c) Fourier transform of the sum of simulated dipolar frequencies of Cu_A and Cu_B (d), data manipulation as for b. d) Simulation of dipolar frequencies with orientation selection: Cu_A (solid), Cu_B (dashed); ν_{dip} values calculated for 1° intervals; resonance positions superimposed with Gaussian lines (linewidth 10.0 kHz). e) Simulation of the dipolar spectrum for random orientation.

The Fourier transform of the DEER response curve for az-**1** contains frequencies between 0.7 and 3.6 MHz (Figure 3a), which reflect the distance between the two Cu^{II} centers, r_{AB}, and the dipolar angle θ_{AB}. For random frozen solutions the frquency spectrum of ν_{dip} can be calculated (θ_{AB} between 0° and 90°), which, for example, has been described by Larsen et al.[7] for nitroxide systems. The simulation of the frequency spectrum for az-**1** without orientation selection is shown in Figure 3e. For Cu^{II}, excitation of the EPR spectrum at the positions indicated in Figure 2 selects only those dimers which have a defined orientation relative to the magnetic field. For these orientations B_0 is close to the g_{xx}, g_{yy} plane (Figure 1), effectively reducing the accessible values of θ_{AB}. The range of θ_{AB} is determined by the orientation of the two g tensors relative to $\vec{r}_{AB}$. The orientation of the g tensor with respect to the copper ligand environment is known from high-field EPR spectroscopy on single-crystals of azurin,[8] and the relative orientation of the two copper centers in the dimer is taken from the X-ray structure analysis of az-**1**.[4,5] To calculate the effect of the orientation selection on ν_{dip} we assume that the g tensor is axially symmetric, that is, B_0 is taken to lie in a cone around the unique g_{zz} direction. The orientation of the two copper centers (Cu_A and Cu_B, Figure 1) in the dimer relative to $\vec{r}_{AB}$ is not equivalent, therefore, the frequency distribution of ν_{dip} differs for Cu_A and Cu_B (Figure 3d). Coincidentally, the orientation of the two copper centers in az-**1** is such that the most abundant orientations cause frequencies close to the maximum in the powder pattern for the same distance (Figure 3e). The simplified model neglects an additional orientation selection, which is imposed by the fact that only those molecules show modulation in which Cu_A is excited at ν_{obs} and Cu_B at ν_{pump} and vice versa.[7] Therefore, the actual frequency distribution is expected to be narrower than the one calculated by using the model. However, the observed spectrum (Figure 3a) is broader than the calculated one(Figure 3d). This could be a result of the limited time window T over which the modulation was measured. To test this, the frequency distribution of the simulation was treated in the same way as the experimental data (see caption for Figure 3). This causes distinct changes in the lineshape (Figure 3c). After this treatment the experimental spectrum (Figure 3a) is broader than the simulated spectrum (Figure 3a). It is less broad, however, than the simulated spectrum obtained by the same method from the simulation of a random sample (Figure 3b). Thus we conclude that the dimer can assume more configurations in frozen solution than in the crystal, without, however, resulting in a random orientation.

The absence of a modulation for the dimer az-**2** is attributed to the shorter copper–copper distance (r_{AB} = 25.9 Å (az-**1**) and 14.6 Å (az-**2**))[4,5] resulting in a larger dipolar interaction between the centers (az-**1**: $\nu_{dip} = 3.0$ MHz, az-**2**: $\nu_{dip} = 17.2$ MHz for $\theta_{AB} = 90°$, see [Eq. (1)]). The ν_{dip} value for az-**2** is larger than the experimental excitation bandwidth (see Experimental Section), which explains the absence of modulations for az-**2**.

 © 2003 Wiley-VCH Verlag GmbH & Co. KGaA, Weinheim 1433-7851/03/4201-0063 $ 20.00+.50/0

In summary, the results of the measurements and the simulations demonstrate that orientation selection affects the DEER response. For az-**1** it suggests that in solution more conformations are accessible than in the crystal, an aspect which is currently undergoing detailed analysis. With respect to the determination of distances in other systems, usually enough information about the relative *g* tensor orientation is known to allow the distances to be determined with sufficient accuracy. If the relative orientation is not known, the dipolar frequency ν_{dip} will differ by a factor of 2 between the two extreme angles $\theta_{AB} = 0°$ and 90°. The resulting difference in r_{AB} of 25% is therefore the maximum uncertainty expected from orientation effects. Finally, the study demonstrates that DEER can be applied to the determination of structures of compounds which contain paramagnetic transition-metal ions, and thus provides an additional method for structural investigations on biological systems. This is particularly important given the physiological significance of metal ions.

Experimental Section

Spectra were measured on a Bruker Elexsys E680 spectrometer with modifications to the microwave bridge to introduce the second microwave frequency analogous to those described by Pannier et al.[3] using a HP synthesizer HP 83752B and a microwave amplifier (Microwave Amplifiers AL 16-9–10-15). The four-pulse DEER sequence[3] with pulse lengths of 16 ns for $\pi/2$, 32 ns for π pulses, and $\tau = 896$ ns was employed. Pulse powers were adjusted to equal intensity at ν_{obs} and ν_{pump}. The maximum frequency separation of ν_{obs} and ν_{pump} was estimated by detuning the measurement frequency from the resonator frequency. At offsets of ± 37.5 MHz attenuation of the signal was observed, leading to the choice of $\nu_{obs} - \nu_{pump}$ of 75 MHz. At that separation, the echo is reduced by less than a factor of 2. The excitation bandwidth of the pulses is smaller than in the experiments described by Pannier et al., where a maximum of 25 MHz is given.[3] In the Fourier transformation (by using the Origin program (Microcal(TM) Northhampton, USA) of the modulation, a Gaussian background was subtracted from the experimental data, the resulting curve was filtered with a Hamming window, and filled with zeros to 1024 points to a total time of 3.2 μs.

Received: June 20, 2002 [Z19574]

[1] *Distance Measurements in Biological Systems by EPR*, (Eds.: L. J. Berliner, S. S. Eaton, G. R. Eaton), Kluver Academic, New York, **2000**.

[2] P. P. Borbat, A. J. Costa-Filho, K. A. Earle, J. K. Moscicki, J. H. Freed, *Science* **2001**, *291*, 266–269.

[3] M. Pannier, S. Veit, A. Godt, G. Jeschke, H. W. Spiess, *J. Magn. Res.* **2000**, *142*, 331–340.

[4] I. M. C. van Amsterdam, M. Ubbink, O. Einsle, A. Messerschmidt, A. Merli, D. Cavazzini, G. L. Rossi, G. W. Canters, *Nat. Struct. Biol.* **2002**, *9*, 48–52.

[5] I. M. C. van Amsterdam, M. Ubbink, L. J. C. Jeuken, M. P. Verbeet, O. Einsle, A. Messerschmidt, G. W. Canters, *Chem. Eur. J.* **2001**, *7*, 2398–2406.

[6] R. Codd, A. V. Astashkin, A. Pacheco, A. M. Raitsimring, J. H. Enemark, *J. Biol. Inorg. Chem.* **2002**, *7*, 338–350.

[7] R. G. Larsen, D. J. Singel, *J. Chem. Phys.* **1993**, *98* 5134–5146.

[8] J. A. Coremans, O. G. Poluektov, E. J. Groenen, G. W. Canters, H. Nar, A. Messerschmidt, *J. Am. Chem. Soc.* **1994**, *116*, 3097–3101.

Propylene Oxide Polymerization

An Efficient Method for Controlled Propylene Oxide Polymerization: The Significance of Bimetallic Activation in Aluminum Lewis Acids**

*Wigand Braune and Jun Okuda**

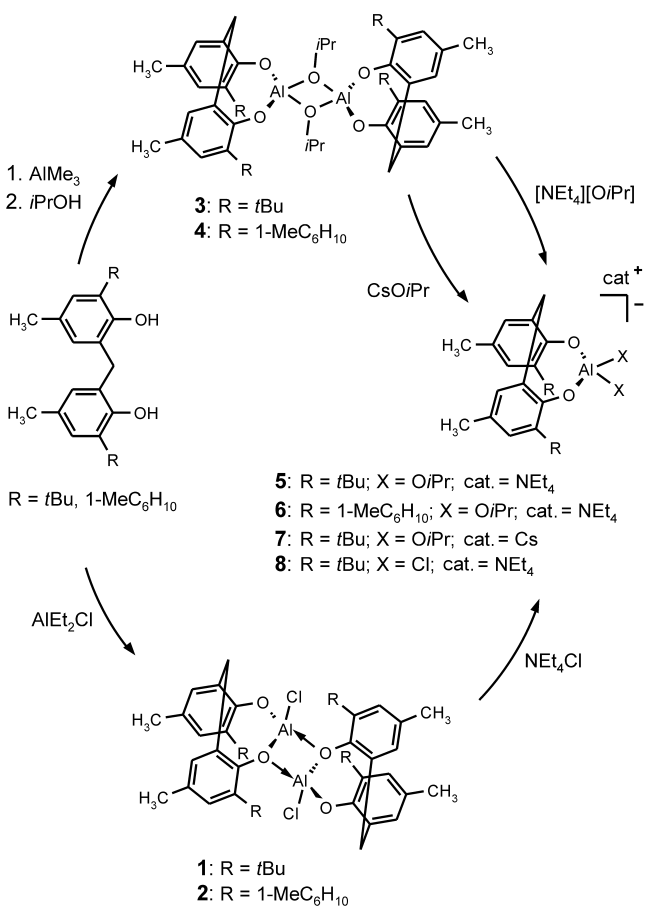
Propylene oxide (PO) is with a worldwide production of 4.5 million tons a significant intermediate of the petrochemical industry. Two-thirds of the propylene oxide is converted by ring-opening polymerization into polypropylene glycols and propoxylated products of polyurethane.[1] The classical initiator for this reaction is KOH, whose high basicity leads to deprotonation of the methyl group, resulting in side reactions.[2] Rapid and controlled PO polymerization has recently become possible through so-called double-metal cyanide compounds (DMC), whose structure and mechanism is, however, still unclear.[3] Only a small number of structurally characterized initiators for living coordination PO polymerization has been published so far: aluminum complexes with tri- or tetradentate ligands (porphyrins, phthalocyanine, tetraazaannulene, salen-type ligands, diethylenetriamine) polymerize PO by a mechanism based on chain growth at a single metal center by reaction of the monomer with the coordinated alkoxo ligand (in addition, *cis* migration, rear attack, and participation of two metal centers are also assumed).[4] The sterically demanding Lewis acidic organoaluminum complexes accelerate the coordination ring-opening polymerization.[5] We report here the targeted synthesis of new aluminate complexes and their polymerization properties in combination with their neutral Lewis acid precursors. Our results prove for the first time that PO polymerization does not occur at a single Lewis acidic metal center and confirm the earlier proposal of bimetallic activation by Price and Vandenberg.[6,7]

$[\{Al(L)Cl\}_2]$ (**1**: L = mbmp, **2**: mmcp), easily obtained by reaction of $AlEt_2Cl$ with 2,2′-methylenebis(6-*tert*-butyl-4-methylphenol) ($mbmpH_2$) or 2,2′-methylenebis(4-methyl-6-(1-methylcyclohexyl)phenol) ($mmcpH_2$), as well as the isopropanolato complexes $[\{Al(L)(\mu\text{-}OiPr)\}_2]$ (**3**: L = mbmp, **4**: mmcp), obtainable from trimethylaluminum in a two-step procedure, did at first appear to be suitable for ring-opening polymerization of PO (Scheme 1).[8,9] With these initiators we could, however, only observe slow (> 24 h) and regioirregular oligomerization of PO.[10,11] We suspect that the ring opening

[*] Prof. Dr. J. Okuda, Dipl.-Chem. W. Braune
Institut für Anorganische Chemie und Analytische Chemie
Johannes Gutenberg-Universität Mainz
Duesbergweg 10–14, 55099 Mainz (Germany)
Fax: (+49) 6131–39–25605
E-mail: okuda@mail.uni-mainz.de

[**] This work has been supported by Bayer AG and the Fonds der Chemischen Industrie. We are grateful to Dr. J. Hofmann for helpful discussions, Dr. T. P. Spaniol for the crystallographic studies, and Prof. Dr. M. Schmidt for the MALDI-TOF mass spectra.

 © 2003 Wiley-VCH Verlag GmbH & Co. KGaA, Weinheim 1433-7851/03/4201-0064 $ 20.00+.50/0



Scheme 1. Compounds **1**–**8**.

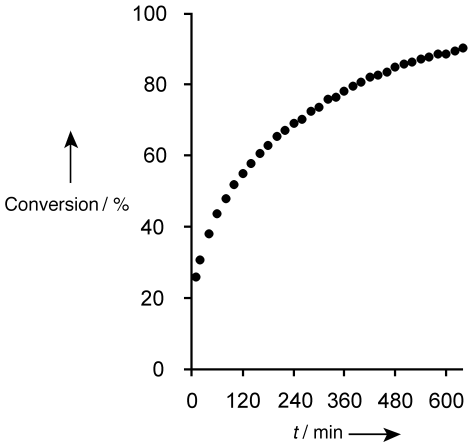


Figure 1. Polymerization of PO (0.21 mL) initiated by **3** and **5** ($[\mathbf{3}]_0/[\mathbf{5}]_0/[PO]_0 = 1:1:200$) in $CDCl_3$ (0.45 mL) at room temperature.

is, at least partly, induced by the chelating bisphenolato ligands.

By reaction of $[NEt_4][OiPr]$ with **3** or **4** at −20 °C, the aluminate $[NEt_4][Al(L)(OiPr)_2]$ (**5**: L = mbmp; **6**: mmcp) could be isolated in yields from 63 to 74 % (Scheme 1). The ^1H NMR spectra of these complexes in $CDCl_3$ at room temperature showed the presence of C_s symmetry, with two sharp doublets for the methyl protons for each of the *syn*- and *anti*-isopropoxy ligands (**5**: $\delta = 1.07$, 1.15 ppm with $^3J_{H,H} = 5.9$ Hz; **6**: $\delta = 1.15$, 1.12 ppm with $^3J_{H,H} = 5.9$ Hz). A crystal structure determination of the aluminate (ate) complexes confirmed the expected tetrahedral coordination of the aluminum centers within the anion, which has merely an electrostatic interaction with the cation.[12] To exclude the possibility of participation of the cation in the polymerization, the cesium aluminate $Cs[Al(mbmp)(OiPr)_2]$ (**7**) was prepared by reaction of **3** with CsO*i*Pr. We obtained the related dichloroaluminate $[NEt_4][Al(L)Cl_2]$ (**8**) quantitatively by direct reaction between **1** and NEt_4Cl. Like the neutral compounds **1**–**4**, aluminates **5**–**8** were not reactive towards ring-opening polymerization of PO.

When neutral complexes **1**, **3**, and **4** were combined with ate complexes **5**–**8** to form initiator systems $[Al(L)(X)]_2/[Al(L)(X)_2]^-$ (L = mbmp, mmcp; X = Cl, O*i*Pr), ring-opening polymerization of PO occurred with pronounced speed and control at room temperature. Figure 1 shows the ^1H NMR spectroscopically observed conversion of PO (0.21 mL) in $CDCl_3$ (0.45 mL) at room temperature with the initiator system formed from equimolar quantities of **3** and **5**, and with a monomer/initiator ratio of 50:1 in accordance to the mechanism discussed below. In Table 1, the polymerization conversions at room temperature obtained with Lewis acid precursor (LA) to aluminate (AT) ratios of 1.0 and 1.5 are compared.

Polymerization initiated by the isopropanolato systems is clearly faster than that initiated by the corresponding chloro systems. The most active initiator system was the combination of **4** and **6** (Experiment 3, Table 1) with a conversion of 77 % after 180 min. The 1-methylcyclohexyl substituent of the bisphenolato ligand mmcp in **4** may cause a significant shift of the monomer–dimer equilibrium in favor of the Lewis acidic monomeric species.[8a] The cesium aluminate **7** in combination with **3** did not initiate polymerization, addition of crown ether ([18]crown-6), however, allowed an activity comparable to

Table 1: Polymerization of PO (2 mL) in CH_2Cl_2 (2 mL) with various systems composed of neutral Lewis acid precursors (LA) and ate complexes (AT).

Exp.	LA	AT	[LA]/[AT]	*t* [min]	Ratio PO/active centers[a]	Conversion [%]	M_n [g mol^{-1}]	$M_{theor.}$ [g mol^{-1}]	M_w/M_n
1	**1**	**8**	1.0	180	100	22	1190	1280	1.09
2	**3**	**5**	1.0	180	100	49	2500	2850	1.18
3	**4**	**6**	1.0	180	100	77	3580	4470	1.22
4	**3**	**7**	1.0	180	100	0	–	–	–
5	**3**	**7**[b]	1.0	180	100	42	2270	2440	1.19
6	**3**	**7**[c]	1.0	180	100	33	1680	1920	1.12
7	**3**	**5**	1.5	180	100	49	2320	2850	1.20
8	**4**	**6**	1.5	180	100	65	3090	3780	1.22

[a] The active centers are the alkoxo and chloro ligands of the initiator system. [b] With addition of two molar equivalents of [18]crown-6. [c] With addition of one molar equivalent of [18]crown-6.

 © 2003 Wiley-VCH Verlag GmbH & Co. KGaA, Weinheim 1433-7851/03/4201-0065 $ 20.00+.50/0

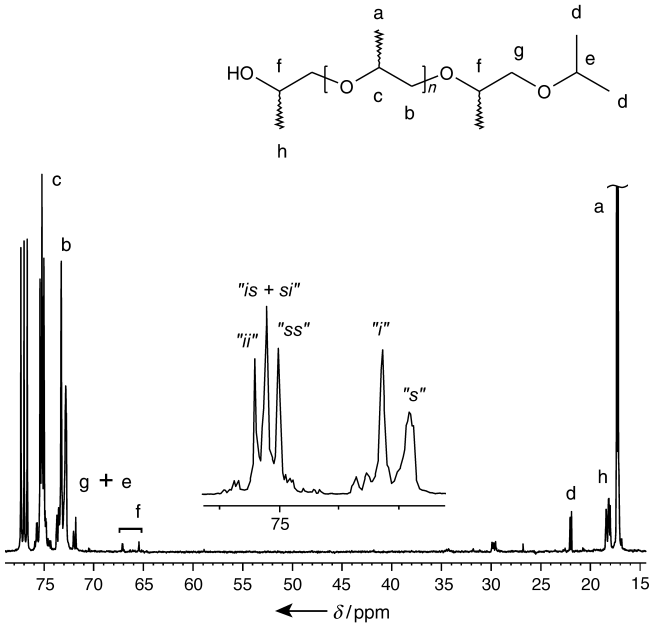
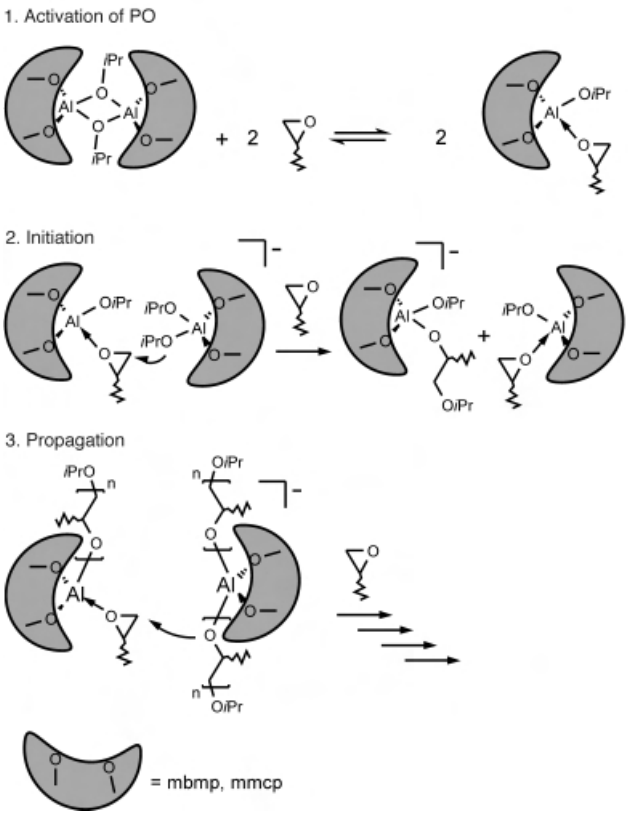


Figure 2. ^{13}C NMR spectrum ($CDCl_3$) of the polyether obtained with initiators **3** and **5** ($[\mathbf{3}]_0/[\mathbf{5}]_0/[PO]_0 = 1:1:400$, 49% conversion).

that of Experiment 2 to be achieved. GPC measurements of the polyether showed polydispersities between 1.09 and 1.22. To examine the polymer end groups more closely, we separated the initiators obtained from equimolar combinations of either **1** with **8** or **3** with **5** from their polymers with molecular weights of $2.4 \times 10^3\ g\,mol^{-1}$ and $2.5 \times 10^3\ g\,mol^{-1}$, respectively, by column chromatography. Figure 2 shows the ^{13}C NMR spectrum of the polyether obtained with isopropanolato complexes **3** and **5** in $CDCl_3$.

The signals of the CH_3- (a), CH_2- (b), and CH groups (c) appeared at $\delta = 17.2, 17.4$ (a), 72.8, 73.2 (b), and 75.0, 75.2, 75.4 (c) ppm, and showed a chiral polymer with exclusive head-to-tail bonding, with the four possible head-to-tail triads appearing with the same frequencies in a purely statistical distribution.[13,7a] The weak signals arose from the end groups: the isopropoxy group appeared at $\delta = 21.9$, 22.0 ($CH(\mathit{C}H_3)_2$ (d)), and 71.8 ppm ($\mathit{C}H(CH_3)_2$ (e)), and the terminal methine carbon atom CHOH (f) appeared at $\delta = 65.4$ and 67.1 ppm.[5b,14] The resonance signal of the terminal methylene carbon atom $\mathit{C}H_2O\mathit{i}Pr$ (g) was found at $\delta = 72.0$ ppm.[15] The relatively strong resonance signals at $\delta = 18$ ppm therefore stem not only from the methyl groups CH_3 (h) at the ends of the regularly obtained polymer, but also from those at the ends of the very low-molecular-weight oligomers ($M_n < 600\ g\,mol^{-1}$) resulting from the bisphenolato ligands.[16] The ^{13}C NMR spectrum of the polyether obtained with chloro complexes **1** and **8** gave the same statistical distribution of triads and the same resonance signals corresponding to the end groups (CH_2Cl: $\delta = 47.4$ ppm; CHOH: $\delta = 65.4$, 67.1 ppm). The MALDI-TOF mass spectra (dithranol, K, THF) of the polymers examined showed a monomodal weight distribution. The mass difference was 58 in each case, and the detected masses confirmed the end groups determined from the ^{13}C NMR spectra.[17]

We propose that the ring-opening polymerization proceeds as shown in Scheme 2 under the synergic interaction of a phenolatoaluminum complex with the corresponding ate complex. The first step consists of the reaction of the dimeric neutral complex with PO to form a labile adduct (step 1 in Scheme 2).[8a,c,18] Ring opening of the epoxide activated by the monomeric complex proceeds by transfer of an alkoxy group from the corresponding ate complex; this is accompanied by simultaneous regeneration of the aluminate (steps 2 and 3 in Scheme 2). The activity of the initiator system based on the cesium alkoxide with added crown ether shows that separation of the ion pairs is a requirement for efficient transfer of the alkoxy group. When the initiator consisted of a combination of **1** and **8**, the chloro complexes underwent a prior reaction with PO to form the corresponding 1-chloro-2-propanolato complexes. During polymerization, the neutral phenolato aluminum complexes bear one growing polymer chain, and the aluminate two (step 3 in Scheme 2). The average initiator efficiency (number of polymer chains initiated per aluminum atom) should therefore depend on the ratio of neutral to anionic complexes. To check the proposed mechanism, we carried out the polymerization of PO with four different initiator efficiencies until complete conversion had taken place (Figure 3).



Scheme 2. The concept of coordination anionic polymerization with chain transfer.

The ratio of monomer to the total number of centers active for polymerization was deliberately kept constant (a: 50; b: 100). In good agreement with the hypothesis, the molecular weights obtained in the experimental series hardly

 © 2003 Wiley-VCH Verlag GmbH & Co. KGaA, Weinheim 1433-7851/03/4201-0066 $ 20.00+.50/0

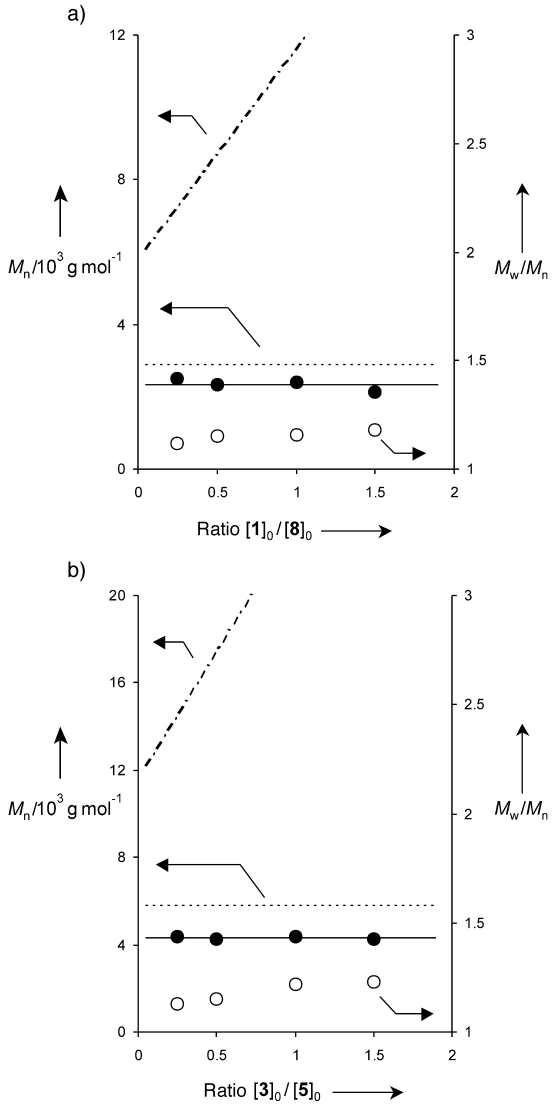


Figure 3. Polymerization of with PO (2 mL) a) variable ratios $[1]_0/[8]_0$ and constant ratio $[PO]_0/[\text{active centers}]_0 = 50{:}1$ (calculated according to a coordination anionic mechanism with chain transfer) in CH_2Cl_2 (1 mL) at room temperature and b) variable ratios $[3]_0/[5]_0$ and constant ratio $[PO]_0/[\text{active centers}]_0 = 100{:}1$ in CH_2Cl_2 (2 mL) at room temperature. Plotted are M_n (●), M_w/M_n (○), the theoretical course when a coordination anionic mechanism with chain transfer is assumed (- - - -), and the theoretical course when a simple anionic mechanism is assumed (•–•–).

differed from each other. With a simple anionic mechanism without simultaneous chain growth at all metal centers, the molecular weight would have been linearly dependent on the number of ate complexes or neutral phenolatoaluminum complexes used.

In summary, we have confirmed here that ring-opening polymerization of PO cannot occur at simple Lewis acidic centers, but that nucleophilic ate complexes must be present at the same time. The fundamentally new mechanism reported herein should have far-reaching consequences for understanding PO polymerization, and should allow the design of new, structurally characterized initiators, also for the stereoselective polymerization of PO.[19]

Experimental Section

5: At 70 °C, sodium (46 mg, 2.0 mmol) was dissolved with generation of hydrogen gas in isopropyl alcohol (10 mL). This solution was added dropwise at −20 °C to a solution of NEt_4Cl (331 mg, 2.0 mmol) in isopropyl alcohol (3 mL); this resulted in precipitation of NaCl. To reduce the solubility of the NaCl, diethyl ether (20 mL) was added at −20 °C. In another reaction flask, **3** (849 mg, 1.0 mmol) was suspended in diethyl ether (5 mL) cooled to −20 °C, and isopropyl alcohol (5 mL) was added. The precooled solution of the tetraethylammonium isopropoxide was added dropwise to this suspension; the reaction mixture dissolved as a result. The solution was stirred at below 0 °C for 45 min, and then the solvent was removed in vacuo. The residue was dissolved in dichloromethane (3 mL) and filtered. After the addition of diethyl ether (15 mL), the aluminate was recrystallized at −30 °C. Yield: 910 mg (74 %) of **5** as colorless crystals. Complex **6** was prepared similarly.

^{1}H NMR (400 MHz, $CDCl_3$, 25 °C): $\delta = 0.85$ (t, $^3J_{H,H} = 7.4$ Hz, 12 H; NCH_2CH_3), 1.07 (d, $^3J_{H,H} = 5.9$ Hz, 6 H; $CH(CH_3)_2$), 1.15 (d, $^3J_{H,H} = 5.9$ Hz, 6 H; $CH(CH_3)_2$), 1.37 (s, 18 H; 6-$C(CH_3)_3$), 2.13 (s, 6 H; 4-CH_3), 2.46 (q, $^3J_{H,H} = 7.4$ Hz; NCH_2CH_3), 3.00 (d, $^2J_{H,H} = 13.7$ Hz, 1 H; 2-CH_2), 4.19 (septet, $^3J_{H,H} = 5.9$ Hz; $CH(CH_3)_2$), 4.36 (septet, $^3J_{H,H} = 5.9$ Hz; $CH(CH_3)_2$), 3.75 (d, $^2J_{H,H} = 13.7$ Hz, 1 H; 2-CH_2), 6.72 (d, $^4J_{H,H} = 2.0$ Hz, 2 H; 5-H), 6.83 ppm (d, $^4J_{H,H} = 2.0$ Hz, 2 H; 3-H); ^{13}C NMR (100.6 MHz, $CDCl_3$, 25 °C): $\delta = 7.3$ (NCH_2CH_3), 20.9 (4-CH_3), 28.0 ($CH(CH_3)_2$), 28.2 ($CH(CH_3)_2$), 30.1 (6-$C(CH_3)_3$), 33.8 (6-$C(CH_3)_3$), 34.9 (2-CH_2), 52.0 (NCH_2CH_3), 62.4 ($CH(CH_3)_2$), 62.6 ($CH(CH_3)_2$), 122.7, 125.1, 128.6, 131.4, 138.0 (phenyl 2-C to 6-C), 156.2 ppm (*ipso*-phenyl-C); elemental analysis (%) calcd for $C_{37}H_{64}AlNO_4$ (613.91): C 72.39, H 10.51, N 2.28; found: C 72.30 H 10.64 N 2.71.

Received: July 9, 2002
Revised: September 19, 2002 [Z19702]

[1] a) X. Zuwei, Z. Ning, S. Yu, *Science* **2001**, *292*, 1139 – 1141; b) K. Weissermel, H.-J. Arpe, *Industrielle Organische Chemie*, 4th ed., Wiley-VCH, Weinheim, **1994**, chap. 11.

[2] S. D. Gagnon, *Encyclopedia of Polymer Science and Engineering, Vol. 6*, 2nd ed., Wiley-VCH, Weinheim, **1994**, pp. 275 – 307.

[3] The polymerization of alkylene oxides by double and multimetal cyanide compounds has been comprehensively patented. Examples: a) P. Ooms, J. Hofmann, C. Steinlein, S. Ehlers, PCT Int. Appl. WO 0134297 **2001**; b) T. Ostrowski, K. Harre, P. Zehner, J. Müller, D. Stützer, G. H. Grosch, J. Winkler, PCT Int. Appl. WO 0162826 **2001**.

[4] For living coordination polymerization of PO, see: a) T. Aida, R. Mizuta, Y. Yoshida, S. Inoue, *Makromol. Chem.* **1981**, *182*, 1073 – 1079; b) T. Aida, S. Inoue, *Macromolecules* **1981**, *14*, 1162 – 1166; c) T. Aida, S. Inoue, *Macromolecules* **1981**, *14*, 1166 – 1169; d) T. Aida, Y. Maekawa, S. Asano, S. Inoue, *Macromolecules* **1988**, *21*, 1195 – 1202; e) T. Aida, K. Wada, S. Inoue, *Macromolecules* **1987**, *20*, 237 – 241; f) V. Vincens, A. Le Borgne, N. Spassky, *Makromol. Chem. Macromol. Symp.* **1991**, *47*, 285 – 291; g) A. Le Borgne, V. Vincens, M. Jouglard, N. Spassky, *Makromol. Chem. Macromol. Symp.* **1993**, *73*, 37 – 46; h) D. A. Atwood, J. A. Jegier, D. Rutherford, *Inorg. Chem.* **1996**, *35*, 63 – 70; i) N. Emig, H. Nguyen, H. Krautscheid, R. Réau, J.-B. Cazaux, G. Bertrand, *Organometallics* **1998**, *17*, 3599 – 3608. For the proposed mechanisms, see h), i) and: K. Shimasaki, T. Aida, S. Inoue, *Macromolecules* **1987**, *20*, 3076 – 3080.

[5] a) H. Sugimoto, C. Kawamura, M. Kuroki, T. Aida, S. Inoue, *Macromolecules* **1994**, *27*, 2013 – 2018; b) M. Akatsuka, T. Aida, S. Inoue, *Macromolecules* **1994**, *27*, 2820 – 2825; c) T. Aida, S. Inoue, *Acc. Chem. Res.* **1996**, *29*, 39 – 48; d) H. Sugimoto, S. Inoue, *Adv. Polym. Sci.* **1999**, *146*, 39 – 119.

 © 2003 Wiley-VCH Verlag GmbH & Co. KGaA, Weinheim 1433-7851/03/4201-0067 $ 20.00+.50/0

[6] a) C. C. Price, R. Spector, *J. Am. Chem. Soc.* **1965**, *87*, 2069 – 2070; b) E. J. Vandenberg, *J. Polym. Sci.* **1960**, *47*, 486 – 489; c) E. J. Vandenberg, *J. Polym. Sci. Polym. Chem. Ed.* **1969**, *7*, 525 – 567.

[7] Chisholm's microstructure analysis of the oligomers obtained by phenolato complexes is indicative of the necessity of two metal centers during the polymerization process. The inversion of the chiral carbon atoms in the head-to-head linkages partially found can only be explained by this, see: a) B. Antelmann, M. H. Chisholm, S. S. Iyer, J. C. Huffman, D. Navarro-Llobet, M. Pagel, W. J. Simonsick, W. Zhong, *Macromolecules* **2001**, *34*, 3159 – 3175; b) M. H. Chisholm, D. Navarro-Llobet, W. J. Simonsick, *Macromolecules* **2001**, *34*, 8851 – 8857.

[8] a) I. Taden, H.-C. Kang, W. Massa, T. P. Spaniol, J. Okuda, *Eur. J. Inorg. Chem.* **2000**, 441 – 445; b) Y.-C. Liu, B.-T. Ko, C.-C. Lin, *Macromolecules* **2001**, *34*, 6196 – 6201; c) H.-L. Chen, B.-T. Ko, B.-H. Huang, C.-C. Lin, *Organometallics* **2001**, *20*, 5076 – 5083.

[9] $mmcpH_2$ was kindly donated by Baerlocher GmbH.

[10] Polymerization example with **1**: A molar ratio $[PO]_0/[Al]_0$ of 200/1 for a reaction time of five days at room temperature in bulk gave a regioirregular oligomer in 15 % yield ($M_n = 940$, $M_w/M_n = 1.33$).

[11] A system obtained by reacting $AlEt_2Cl$ with 25,27-dimethoxy-26,28-dihydroxy-*p*-*tert*-butyl-calix[4]arene shows similarity with the bisphenolato compound described herein. These authors report a regioregular PO polymerization that proceeds only at elevated temperatures and a reaction time of several days and resulted in only low conversion: W. Kuran, T. Listos, M. Abramczyk, A. Dawidek, *J. Macromol. Sci. Pure Appl. Chem.* **1998**, *A35*, 427 – 437.

[12] Crystallographic data of **6**: Colorless needles were obtained at −30 °C from a mixture of dichloromethane and diethyl ether, Bruker-AXS diffractometer, $\lambda = 0.71073$ Å, $a = 19.466(2)$, $b = 20.181(1)$, $c = 22.539(2)$ Å, $V = 8854(1)$ Å^3; orthorhombic, *Pbca*, $Z = 8$, $T = 193$ K, $2\theta_{max.} = 46°$; 32347 reflections collected, of which 6400 independent ($R_{int} = 0.1843$), Structure solution with direct methods, refinement against F^2, 482 refined parameters, $R_1 = 0.0666$, $wR_2 = 0.1529$ (observed data). CCDC-193556 contains the supplementary crystallographic data for this paper. These data can be obtained free of charge via www.ccdc.cam.ac.uk/conts/retrieving.html (or from the Cambridge Crystallographic Data Centre, 12, Union Road, Cambridge CB21EZ, UK; fax: (+44) 1223-336-033; or deposit@ccdc.cam.ac.uk).

[13] For a detailed study of the microstructure of atactic polypropylene oxides by ^{13}C NMR spectroscopy, see: F. C. Schilling, A. E. Tonelli, *Macromolecules* **1986**, *19*, 1337 – 1343.

[14] The assignments of the signals according to the literature was checked by comparison of both polymer spectra and by DEPT-135 experiments.

[15] The weak signals at $\delta = 30$ ppm are assigned to the *tert*-butyl carbon atoms $C(CH_3)_3$ of the bisphenolato ligands, which despite its chelate structure evidently polymerized PO under ring-opening to a minor extent. Assignment according to the ^{13}C NMR spectrum of $mbmpH_2$: $\delta = 29.8$ ($C(CH_3)_3$).

[16] The MALDI-TOF mass spectrum of the polymer showed above m/z 600 exclusively masses separated by m/z 58 without any intermediate masses.

[17] Number of monomer units $N = (M_{det} - M_+ - M_{end})/M_{PO}$, with M_{det}: detected mass; M_+: mass of cations; M_{end}: mass of the end group; M_{PO}: 58.08 (mass of PO).

[18] a) C.-H. Lin, L.-F. Yan, F.-C. Wang, Y.-L. Sun, C.-C. Lin, *J. Organomet. Chem.* **1999**, *587*, 151 – 159; b) B.-T. Ko, C.-C. Wu, C.-C. Lin, *Organometallics* **2000**, *19*, 1864 – 1869.

[19] T. Tsuruta, *J. Polym. Sci. Part D* **1972**, *6*, 179 – 250, and references therein.

 © 2003 Wiley-VCH Verlag GmbH & Co. KGaA, Weinheim 1433-7851/03/4201-0068 $ 20.00+.50/0

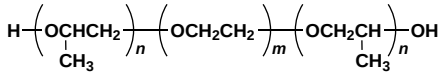
Polypseudorotaxanes

Block-Selected Molecular Recognition and Formation of Polypseudorotaxanes between Poly(propylene oxide)-Poly(ethylene oxide)-Poly(propylene oxide) Triblock Copolymers and α-Cyclodextrin**

Jun Li, Xiping Ni, and Kam Leong*

Inclusion complexes (ICs), particularly the ones leading to supramolecular assemblies, continue to be a fascinating topic in modern organic chemistry as they serve as models for understanding molecular recognition and as materials for biological applications. Polyrotaxanes, which are formed by multiple macrocycles threading over a polymer chain, are such an example.[1,2] Cyclodextrins (CDs) constitute a series of cyclic oligosaccharides composed of six, seven, or eight D(+)-glucose units linked by α-1,4-linkages, and named α-, β-, or γ-CD, respectively. The geometry of CDs gives a hydrophobic cavity having a depth of approximately 7.0 Å, and an internal diameter of about 4.5, 7.0, and 8.5 Å for α-, β-, and γ-CD, respectively.[3] Various molecules can fit into the cavity of CDs to form ICs, which have been extensively studied as models for understanding the mechanism of molecular recognition.[3,4] Recently, polypseudorotaxanes,[5] namely, ICs with necklacelike supramolecular structures formed by cyclodextrins and polymers, have attracted special interest.[6–12]

The correlation between the cross-sectional area of the polymer chains and the internal diameter of the CD cavities has been a key factor in the formation of ICs. Poly(ethylene oxide) (PEO) and oligoethylene of various molecular weights form ICs with α-CD, but not with β-CD and γ-CD, to give crystalline polypseudorotaxanes in high yields.[7] Conversely, poly(propylene oxide) (PPO) can form ICs with β-CD and γ-CD in high yields, but not with α-CD.[8] The assumption is that the PPO chain is too large to penetrate the inner cavity of α-CD. There were also studies performed on the formation of ICs between CDs and pluronic PEO-PPO-PEO triblock copolymers, in which thinner PEO blocks flank a middle PPO block; β-CD could selectively thread the middle PPO block to form a polypseudorotaxane,[9] while α-CD selectively includes the flanking PEO blocks.[10] Recently, we reported the formation of an IC between poly[(ethylene oxide)-*ran*-(propylene oxide)] and α-CD, and demonstrated that α-CD can pass over a PO unit randomly placed in the PEO chain to form ICs with EO units.[11] Herein, we report the unexpected observation that PPO-PEO-PPO triblock copolymers, in which two thicker PPO blocks flank a middle PEO block, can form ICs with α-CD to give polypseudorotaxanes in high yields. We demonstrate that α-CD can slide over the flanking bulky PPO blocks to selectively form stable complexes with the middle PEO block of the triblock copolymers.



The molecular characteristics of the PPO-PEO-PPO triblock copolymers used in this study are presented in Table 1. The PPO-PEO-PPO triblock copolymers are known as "reverse" pluronic (pluronic-R) copolymers.[13] The terminal secondary hydroxy groups of pluronic-R have lower reactivity and acidity than the terminal primary hydroxy groups of pluronic PEO-PPO-PEO triblock copolymers. We found the PPO-PEO-PPO triblock copolymers formed ICs with α-CD as well as with β-CD and γ-CD to give polypseudorotaxanes. The α-CD/PPO-PEO-PPO ICs were formed in very high yields, thus indicating that the IC formation is not the result of any contamination of the copolymers. The polypseudorotaxanes dissolved slowly when they were resuspended in a large amount of water, which indicates that the formation of the IC is reversible, and the polypseudorotaxanes are in equilibrium with their components in solution.

Figure 1 shows the X-ray powder diffraction patterns of α-CD/PPO-PEO-PPO and other ICs formed with α-CD. The pattern obtained for the α-CD/propionic acid IC (Figure 1a) is consistent with the α-CD ICs having a cage-type structure.[14] The pattern of the α-CD/PEO IC, with a number of sharp reflections and the main one at $2\theta = 19.4°$ ($d = 4.57$ Å) in Figure 1b, represents the channel-type structure of crystalline necklacelike polypseudorotaxanes of α-CD and PEO,[11,14] which is totally different from that of α-CD/propionic acid IC. The patterns of α-CD/PPO-PEO-PPO ICs (Figure 1c–e) are similar to that of α-CD/PEO IC, but different from that of the α-CD/propionic acid IC, which suggests that the α-CD/PPO-PEO-PPO polypseudorotaxanes are isomorphous with the channel-type structure formed by the α-CD/PEO IC.

The α-CD/PPO-PEO-PPO ICs were quantitatively studied by using ^{1}H NMR spectroscopy. A comparison between the integral intensities of peaks for α-CD and those for PPO-PEO-PPO gives the compositions and molecular weights of the α-CD/PPO-PEO-PPO ICs (Table 1). There are three possible structures for the α-CD/PPO-PEO-PPO ICs: a) the α-CD molecules are selectively threaded on the middle PEO

[*] Dr. J. Li, X. Ni, Prof. K. Leong
Molecular and Bio-Materials Cluster
Institute of Materials Research and Engineering (IMRE)
3 Research Link, Singapore 117602 (Republic of Singapore)
Fax: (+65) 6872-0785
E-mail: jun-li@imre.a-star.edu.sg
Dr. J. Li
Division of Bioengineering
Faculty of Engineering, National University of Singapore
Singapore 117576 (Republic of Singapore)
Prof. K. Leong
Department of Biomedical Engineering
Johns Hopkins University
Baltimore, MD 21205 (USA)

[**] This work was financially support by A*STAR (Agency of Science, Technology, and Research, Singapore). The authors thank Mr. Z. Zhou and Mr. B. Chen for NMR and X-ray diffraction measurements, respectively.

Supporting information for this article is available on the WWW under http://www.angewandte.org or from the author.

 © 2003 Wiley-VCH Verlag GmbH & Co. KGaA, Weinheim 1433-7851/03/4201-0069 $ 20.00+.50/0

Table 1: Characteristics of the PPO-PEO-PPO triblock copolymers and the α-CD/PPO-PEO-PPO ICs.

PPO-PEO-PPO triblock copolymer[a]			α-CD/PPO-PEO-PPO IC[d]				
composition[b]	M_n [g mol^{-1}][c]	M_w/M_n[c]	M_n [g mol^{-1}][e]	x[e]	m/x[f]	$2n/x$[g]	$(2n+m)/x$[h]
$PO_8EO_{23}PO_8$	1.99×10^3	1.03	1.31×10^4	11.4	2.0/1	1.4/1	3.4/1
$PO_{15}EO_{24}PO_{15}$	2.74×10^3	1.03	1.38×10^4	11.4	2.1/1	2.6/1	4.7/1
$PO_{25}EO_{12}PO_{25}$	3.45×10^3	1.03	8.90×10^3	5.6	2.1/1	8.9/1	11.1/1

[a] The copolymers are denoted $PO_nEO_mPO_n$ where n and m are average block lengths in repeat units. [b] Determined by combination of ^{1}H NMR spectroscopic and GPC results. [c] Determined by GPC. [d] The ICs are denoted $(\alpha\text{-CD})_x{\cdot}PO_nEO_mPO_n$ where x is the number of α-CD molecules per single copolymer chain. [e] Determined by ^{1}H NMR spectroscopy. [f] Molar ratio of EO unit to α-CD. [g] Molar ratio of PO unit to α-CD. [h] Molar ratio of total number of EO and PO units to α-CD.

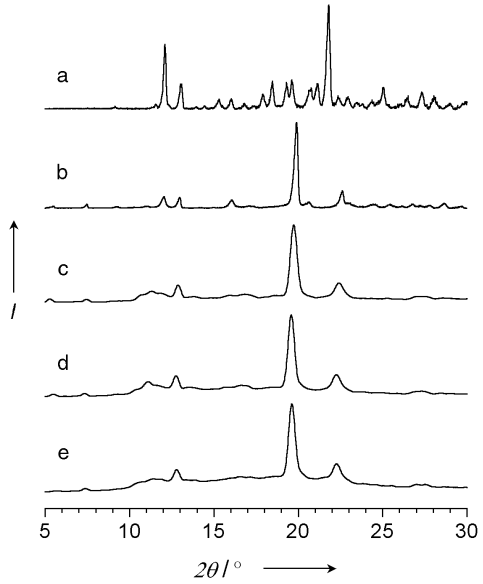


Figure 1. X-ray powder diffraction patterns for the α-CD/propionic acid IC (a), α-CD/PEO ($M_n = 1000$) IC (b), α-CD/$PO_8EO_{23}PO_8$ IC (c), α-CD/$PO_{15}EO_{24}PO_{15}$ IC (d), and α-CD/$PO_{25}EO_{12}PO_{25}$ IC (e). X-ray measurements: nickel-filtered $Cu_{K\alpha}$ radiation ($\lambda = 1.542$ Å), voltage: 40 kV, current: 40 mA, scanning speed: 0.6° per min.

block, while the PPO blocks remain uncovered; b) the α-CD molecules are selectively threaded on the flanking PPO blocks, while the middle PEO block remains uncomplexed; c) the α-CD molecules are threaded on both PEO and PPO blocks. As shown in Table 1, the molar ratio of EO unit to α-CD (m/x), which corresponds to the assumption (a), is 2/1 for all three polypseudorotaxanes, which matches perfectly the stoichiometry of the α-CD/PEO ICs reported previously.[7b] This result strongly suggests that only the middle PEO block in the α-CD/PPO-PEO-PPO polypseudorotaxanes is closely included by α-CD molecules, while the flanking PPO blocks are uncovered. In contrast, the molar ratios of PO unit to α-CD ($2n/x$) or total number of PO and EO units to α-CD ($(2n+m)$/x), which corresponds to the assumptions (b) or (c), show no consistency with any reasonable stoichiometry.

On the basis of these findings we can reasonably hypothesize that the IC formation is driven by the strong interaction between α-CD and the PEO segments,[15] and aided by the flexible molecular motion of α-CD and the copolymer chain. The proposed structure is also in accordance with the broadening X-ray powder patterns for the α-CD/PPO-PEO-PPO ICs (Figure 1c–e), which show that the α-CD/PPO-PEO-PPO ICs have a lower crystallinity than the stoichiometric α-CD/PEO ICs. This effect is most likely caused by the existence of the uncovered amorphous PPO blocks. Mayer et al.[16] have performed computational studies on the IC formation between α- or β-CD and oligomers of PEO, PPO, or the PEO-PPO diblock copolymer up to EO_4PO_4. Their simulation estimated a total complexation energy of -52.4 kJ mol^{-1} for α-CD/PEO compared to -43.3 kJ mol^{-1} for α-CD/PPO, which supports our hypothesis that there is an incentive for α-CD to overcome an energy barrier to reach the middle PEO block.

The kinetics of the threading process and formation of the ICs were studied with turbidity measurements. Figure 2 shows the change in absorption during formation and precipitation of the polypseudorotaxanes formed between α-CD and PPO-PEO-PPO triblock copolymers in aqueous solution. The curves show a region where the absorption remains zero, followed by a region where the absorption sharply increases. The first region corresponds to the threading and sliding of α-CD onto the polymer chains, and so this region is defined as "threading time" (t_{th}).[8d] The stable polypseudorotaxanes are formed after time t_{th} and start to aggregate into crystalline particles. Therefore, the absorption starts to increase sharply in the second region. Figure 2 shows that the value of t_{th}

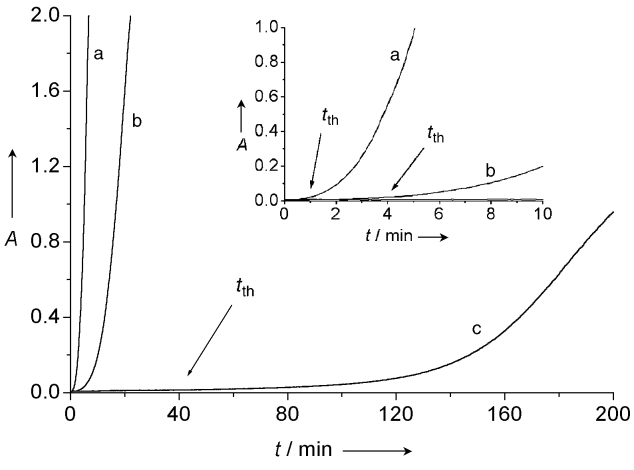


Figure 2. Plot of the absorption at 600 nm against time for aqueous solutions containing 126 mg mL^{-1} of α-CD and 6.5 mg mL^{-1} of triblock copolymer $PO_8EO_{23}PO_8$ (a), $PO_{15}EO_{24}PO_{15}$ (b), and $PO_{25}EO_{12}PO_{25}$ (c) at 20 °C. The arrows indicate the region where absorption remains zero. The inset shows an expanded plot for 0 to 10 min.

 © 2003 Wiley-VCH Verlag GmbH & Co. KGaA, Weinheim 1433-7851/03/4201-0070 $ 20.00+.50/0

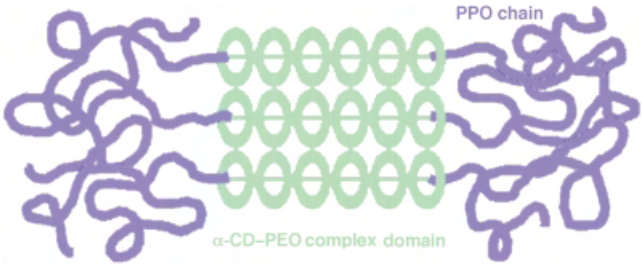


Figure 3. Schematic representation of the proposed structures of α-CD/PPO-PEO-PPO polypseudorotaxanes.

increases from about 1.0 min for $PO_8EO_{23}PO_8$ ($n=8$), to about 4.0 min for $PO_{15}EO_{24}PO_{15}$ ($n=15$) and about 40 min for $PO_{25}EO_{12}PO_{25}$ ($n=25$). The value of t_{th} strongly depends on the length of the PPO blocks since the α-CD molecules have to first overcome the energy barrier of threading and sliding over the flanking PPO blocks to form a stable IC with the middle PEO block.

In summary, PPO-PEO-PPO triblock copolymers can form ICs with α-CD to give polypseudorotaxanes in high yields. It is proposed that only the middle PEO block in the polypseudorotaxanes is closely included by α-CD molecules to form crystalline IC domains with a channel structure, while flanking PPO blocks are uncovered and remain amorphous (Figure 3). The finding contradicts the conventional wisdom that α-CD would not be large enough to slip over a PPO chain. This observation may have intriguing implications in designing new cyclodextrin ICs and polypseudorotaxanes using novel functional block copolymers for molecular machines, sensors, or other interesting applications.

Experimental Section

Three PPO-PEO-PPO pluronic-R triblock copolymers ("reverse" pluronics) were purchased from Aldrich. The pluronic-R copolymers are well studied in the literature.[13] We determined the molecular characteristics of the samples by using ^{1}H NMR and GPC[17] (data shown in Table 1), which were found to be within the specifications of the supplier.

The α-CD/PPO-PEO-PPO ICs were prepared as follows. Bulk PPO-PEO-PPO triblock copolymers (75.0 mg) were added to an excess of an aqueous solution of α-CD (4.57 mL, 0.145 g mL^{-1}) in a test tube at room temperature. The dissolving of the copolymer could be facilitated by immersing the tubes in an ultrasonic waterbath or vortexing.[18] The solutions gradually became turbid, eventually producing ICs in the form of crystalline precipitates. The ICs were isolated by filtration or centrifugation, washed with a limited amount of water, and dried under vacuum. The percentage yields were calculated on the basis of the compositions of the ICs given in Table 1. α-CD/$PO_8EO_{23}PO_8$ IC: Yield, 390 mg (73 %); m.p. 293–300 °C (decomp); ^{1}H NMR (400 MHz, [D$_6$]DMSO, 22 °C): $\delta=5.51$ (s, ca. 68 H, O(2)H of CD), 5.43 (s, ca. 68 H, O(3)H of CD), 4.80 (d, ca. 68 H, H(1) of CD), 4.48 (t, ca. 68 H, O(6)H of CD), 3.77 (t, ca. 68 H, H(3) of CD), 3.64 (m, ca. 136 H, H(6) of CD), 3.58 (m, ca. 68 H, H(5) of CD), 3.51 (s, ca. 92 H, H of PEO block), 3.25–3.47 (br m, ca. 185 H, H of PPO backbone, H(2) and H(4) of CD), 1.04 ppm (m, ca. 48 H, CH_3 of PPO block); elemental analysis (%) calcd for $C_{94}H_{190}O_{40}\cdot12\,C_{36}H_{60}O_{30}\cdot24\,H_2O$: C 44.91, H 6.52; found: C 44.45, H 6.89. α-CD/$PO_{15}EO_{24}PO_{15}$ IC: Yield, 331 mg (83 %); m.p. 293–300 °C (decomp); ^{1}H NMR (400 MHz, [D$_6$]DMSO, 22 °C): $\delta=5.51$ (s, ca. 68 H, O(2)H of CD), 5.43 (s, ca. 68 H, O(3)H of CD), 4.80 (d, ca. 68 H, H(1) of CD), 4.47 (t, ca. 68 H, O(6)H of CD), 3.77 (t, ca. 68 H, H(3) of CD), 3.64 (m, ca. 136 H, H(6) of CD), 3.58 (m, ca. 68 H, H(5) of CD), 3.51 (s, ca. 96 H, H of PEO block), 3.25–3.47 (br m, ca. 227 H, H of PPO backbone, H(2) and H(4) of CD), 1.04 ppm (m, ca. 90 H, CH_3 of PPO block); elemental analysis (%) calcd for $C_{138}H_{278}O_{55}\cdot12\,C_{36}H_{60}O_{30}\cdot24\,H_2O$: C 45.87, H 6.74; found: C 45.43, H 7.21. α-CD/$PO_{25}EO_{12}PO_{25}$ IC: Yield, 146 mg (71 %); m.p. 293–300 °C (decomp); ^{1}H NMR (400 MHz, [D$_6$]DMSO, 22 °C): $\delta=5.51$ (s, ca. 34 H, O(2)H of CD), 5.43 (s, ca. 34 H, O(3)H of CD), 4.80 (d, ca. 34 H, H(1) of CD), 4.47 (t, ca. 34 H, O(6)H of CD), 3.77 (t, ca. 34 H, H(3) of CD), 3.64 (m, ca. 67 H, H(6) of CD), 3.58 (m, ca. 34 H, H(5) of CD), 3.50 (s, ca. 48 H, H of PEO block), 3.25–3.48 (br m, ca. 217 H, H of PPO backbone, H(2) and H(4) of CD), 1.04 ppm (m, ca. 150 H, CH_3 of PPO block); elemental analysis (%) calcd for $C_{174}H_{350}O_{63}\cdot6\,C_{36}H_{60}O_{30}\cdot12\,H_2O$: C 49.29, H 7.53; found: C 48.86, H 8.09.

Received: June 21, 2002
Revised: September 30, 2002 [Z19580]

[1] H. W. Gibson, H. Marand, *Adv. Mater.* **1993**, *5*, 11–21; F. M. Raymo, J. F. Stoddart, *Chem. Rev.* **1999**, *99*, 1643–1663; J.-P. Sauvage, C. Dietrich-Buchecker, *Molecular Catenanes, Rotaxanes and Knots*, VCH, Weinheim, **1999**; J. A. Semlyen, *Cyclic Polymers*, Kluwer, Boston, **2000**.

[2] P. E. Mason, W. S. Bryant, H. W. Gibson, *Macromolecules* **1999**, *32*, 1559–1569; F. M. Raymo, M. D. Bartberger, K. N. Houk, J. F. Stoddart, *J. Am. Chem. Soc.* **2001**, *123*, 9264–9267; C. Reuter, W. Wienand, C. Schmuck, F. Vogtle, *Chem. Eur. J.* **2001**, *7*, 1728–1733.

[3] M. L. Bender, M. Komiyama, *Cyclodextrin Chemistry*, Springer, Berlin, **1978**.

[4] J. Szejtli, *Chem. Rev.* **1998**, *98*, 1743–1754; K. B. Lipkowitz, *Chem. Rev.* **1998**, *98*, 1829–1874.

[5] There is also an opinion that such supramolecular species should be called pseudopolyrotaxanes, since pseudopolyrotaxanes bear the same relationship to polyrotaxanes as pseudorotaxanes do to rotaxanes.

[6] G. Wenz, B. Keller, *Angew. Chem.* **1992**, *104*, 201–204; *Angew. Chem. Int. Ed. Engl.* **1992**, *31*, 197–199; G. Wenz, *Angew. Chem.* **1994**, *106*, 851–870; *Angew. Chem. Int. Ed. Engl.* **1994**, *33*, 803–822; S. A. Nepogodiev, J. F. Stoddart, *Chem. Rev.* **1998**, *98*, 1959–1976.

[7] a) A. Harada, J. Li, M. Kamachi, *Nature* **1992**, *356*, 325–327; b) A. Harada, J. Li, M. Kamachi, *Macromolecules* **1993**, *26*, 5698–5703; c) J. Li, A. Harada, M. Kamachi, *Bull. Chem. Soc. Jpn.* **1994**, *67*, 2808–2818.

[8] a) A. Harada, M. Kamachi, *J. Chem. Soc. Chem. Commun.* **1990**, 1322–1223; b) A. Harada, M. Okada, J. Li, M. Kamachi, *Macromolecules* **1995**, *28*, 8406–8411; c) J. Pozuelo, F. Mendicuti, W. L. Mattice, *Polym. J.* **1998**, *30*, 479–484; d) P. L. Nostro, J. R. Lopes, C. Cardelli, *Langmuir* **2001**, *17*, 4610–4615.

[9] H. Fujita, T. Ooya, N. Yui, *Macromolecules* **1999**, *32*, 2534–2541.

[10] J. Li, X. Li, Z. Zhou, X. Ni, K. W. Leong, *Macromolecules* **2001**, *34*, 7236–7237.

[11] J. Li, X. Li, K. C. Toh, X. Ni, Z. Zhou, K. W. Leong, *Macromolecules* **2001**, *34*, 8829–8831.

[12] M. Born, H. Ritter, *Macromol. Rapid Commun.* **1996**, *17*, 197–202; O. Noll, H. Ritter, *Macromol. Chem. Phys.* **1998**, *199*, 791–794; C. C. Rusa, A. E. Tonelli, *Macromolecules* **2001**, *34*, 5321–5324; H. Jiao, S. H. Goh, S. Valiyaveettil, *Macromolecules* **2002**, *35*, 1980–1983; J. Li, K. C. Toh, *J. Chem. Soc. Perkin Trans. 2* **2002**, 35–40.

[13] Z. Zhou, B. Chu, *Macromolecules* **1994**, *27*, 2025–2033; K. Mortensen, W. Brown, E. Jorgensen, *Macromolecules* **1994**, *27*, 5654–5666; K. Mortensen, *Macromolecules* **1997**, *30*, 503–507.

 © 2003 Wiley-VCH Verlag GmbH & Co. KGaA, Weinheim 1433-7851/03/4201-0071 $ 20.00+.50/0

[14] K. Takeo, T. Kuge, *Agric. Biol. Chem.* **1970**, *34*, 1787–1794; K. McMullan, W. Saenger, J. Fayos, D. Mootz, *Carbohydr. Res.* **1973**, *31*, 37–46.
[15] The strong interaction comes from the size/steric fittings, the hydrophobic interaction between α-CD and PEO, and the intermolecular hydrogen bonding of α-CDs (also see ref. [6]), thus giving a large favorable enthalpy that becomes the driving force for α-CD to slide over the PPO segments and then form a stable complex with the PEO block.
[16] B. Mayer, C. T. Klein, I. N. Topchieva, G. J. Kohler, *Comput.-Aided Mol. Des.* **1999**, *13*, 373–383.
[17] Two phenogel 5 μ 50 and 1000 Å columns (size: 300 × 4.6 mm) in series and a refractive detector were used with THF as the eluent at a flow rate of 0.30 mL min^{-1} at 40 °C. The calibration curve was obtained from monodispersed poly(ethylene glycol) standards.
[18] The sonication was proved not to degrade either the copolymers or α-CD, as evident by means of ^{1}H NMR spectroscopy, GPC, and TLC. Also see ref. [6].

Lipid Nanotubes

Aligning a Single-Lipid Nanotube with Moderate Stiffness**

Hiroshi Frusawa, Akihiro Fukagawa, Yuki Ikeda, Jun Araki, Kohzo Ito, George John, and Toshimi Shimizu**

Many types of amphiphilic molecules have been found to self-assemble into cylindrical tubules in aqueous solutions.[1–12] The synthetic lipid tubules can provide intriguing hydrophilic internal and external surfaces, unlike carbon nanotubes,[13] and therefore they have unique potential not only as cytomimetic tubules but also as hollow nanospaces for chemical reactions, the transferral of biomolecules, etc. The mechanical properties of lipid nanotubes, however, have not been investigated to date, in contrast to extensive studies on microtubules[14,15] or carbon nanotubes.[16] We have measured the Young's modulus of a single-lipid nanotube that consists of renewable-resource-based synthetic glycolipids (cardanyl-β-D-glucopyranoside)[17] by using optical tweezers. Herein we report that the Young's moduli of the present lipid nanotubes are similar to those of microtubules[15] with outer and inner diameters of the same order. Furthermore, because of the moderate stiffness, we have succeeded in aligning the single-lipid nanotube on a glass plate by microextrusion of the aqueous dispersion.

To measure accurately the flexural rigidity of the single nanotube, we should pay careful attention to the aggregation in an aqueous dispersion. Figure 1 is a transmission electronic microscopy (TEM) image which shows that the lipid nanotubes are completely isolated and form no bundles. TEM images of higher resolution have further shown that the outer and inner diameters are 50 and 10 nm, respectively,[17] which is similar to the values (25 and 10 nm) of microtubules.[18]

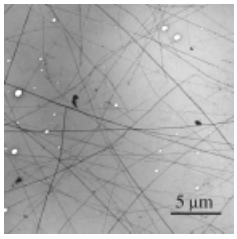


Figure 1. TEM image of lipid nanotubes in an aqueous dispersion, which were used for flexural rigidity measurements.

A drop of the aqueous dispersion was placed on a glass slide for optical traps, and pressed between coverslip and slide. Because some nanotubes were thereby forced to adhere firmly to the substrate, we had no difficulty in finding a target fixed well at only one end. Using optical tweezers (Sigma Koki LMS-46755), the monoattached nanotube was bent as follows: A laser beam was focused onto the target, the lipid nanotube was trapped in the focal point in a similar way to microtubules.[14,15] This trapping occurs because of the difference in refractive index between the nanotube and the surrounding medium, water. Therefore, while it is possible to manipulate the tubule in a direction perpendicular to its long axis, we cannot do this along the long axis, except by manipulation at either end. We can thus bend the nanotubes by moving the stage and capturing the tube near the free end.

The laser beam was switched off after some bending had occurred, and the resulting bow-shaped nanotube started to relax to its initial straight form. From the relaxation time τ, we can evaluate the flexural rigidity K, because the balance condition between elastic and hydrodynamic force[15] yields the time-dependence of relaxation of the free end, as shown in Equations (1) and (2). Here, y is the ordinate perpendicular to the initial straight line, L is the contour length, η is the viscosity, and d is the outer diameter.

$$y(L,t) = y(L,0)\exp(-t/\tau) \quad (1)$$

$$\tau = \frac{11\pi\eta L^4}{60\,\mathrm{K}\ln(L/2\,\mathrm{d})} \quad (2)$$

[*] Prof. Dr. K. Ito, A. Fukagawa, Dr. J. Araki
Graduate School of Frontier Sciences
University of Tokyo
Hongo 7-3-1, Bunkyo-ku, Tokyo 113-8656 (Japan)
Fax: (+81) 3-5841-8738
E-mail: kohzo@exp.t.u-tokyo.ac.jp
Prof. Dr. T. Shimizu
Nanoarchitectonics Research Center (NARC)
National Institute of Advanced Industrial Science and Technology (AIST)
Tsukuba Central 5, 1-1-1 Higashi, Tsukuba, Ibaraki 305-8565 (Japan)
Fax: (+81) 298-614-545
E-mail: tshmz-shimizu@aist.go.jp
Dr. H. Frusawa, Y. Ikeda
Department of Applied Physics, University of Tokyo
Hongo 7-3-1, Bunkyo-ku, Tokyo 113–8656 (Japan)
Dr. G. John
CREST, Japan Science and Technology Corporation (JST)
Tsukuba Central 4, 1-1-1 Higashi, Tsukuba, Ibaraki 305-8562 (Japan)
[**] This work was supported by the JST-CREST.

 © 2003 Wiley-VCH Verlag GmbH & Co. KGaA, Weinheim 1433-7851/03/4201-0072 $ 20.00+.50/0

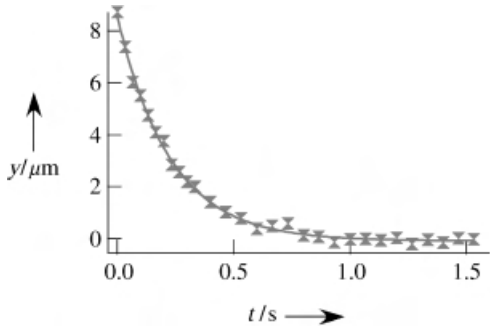


Figure 2. Time course of the free end relaxing from its bent position to the initial point. Closed circles represent a result obtained by image processing, and the solid line shows a fit to the exponential decay, that is, Eq. (2).

Figure 2 is a plot of $y(L, t)$ versus time for the free end of the tube, measured at 23 °C. Fitting of Eq. (2) to the curve gives the relaxation time $\tau \approx 0.22$ s, from which we obtain the bending rigidity $K \approx 2.2 \times 10^{-22}\,\mathrm{N\,m^2}$. In the evaluation, we assume that the viscosity η mainly comes from the solvent, water, and ignore the friction between nanotube and slide. We also evaluated the stiffness of other nanotubes using the water viscosity, and obtained almost identical values to the first value, which supports the above assumption.

To compare the present lipid nanotube with microtubules, we first converted the bending stiffness K into the Young's modulus $E = K/I$. Here I is the geometrical moment in inertia and is given for the tubes as $I = (d_o^4 - d_i^4)\pi/64$ with outer diameter d_o and inner diameter d_i. The evaluation gives $E \approx$ 720 MPa for the present nanotube, and $E \approx 1000$ MPa for microtubules.[14] We therefore conclude that the glycolipid nanotube is a cytomimetic tubule, in that both the elasticity and the diameter size are similar to those of microtubules. Our lipid nanotube and microtubules differ, however, in their persistence lengths L_p, which measures the crossover from a rodlike to a flexible form. Estimating from the relation $L_p = K/k_BT$, we have $L_p \approx 5$ cm for the lipid nanotube, which is longer than those of microtubules, $L_p \approx 0.1$ cm.[14] The difference is ascribable to a thicker (10–15 nm) cylinder wall for the present nanotubes than the microtubules: because the wall thickness is twice as large as that of microtubules, the persistence length is not identical, but the Young's modulus is similar.

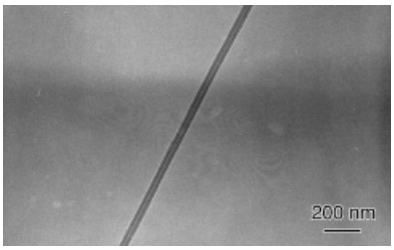


Figure 4. TEM image of a single lipid nanotube which is aligned by our manipulation method onto Formvar (poly(vinyl formal)) film spread on a copper grid.

Considering that our nanotubes have modest Young's moduli as well as long persistence lengths, one may envisage the possibility of aligning them. Indeed we demonstrate below that a microextrusion of aqueous nanotube dispersion is a simple method for directing single nanotubes.

Figure 3 illustrates the microextrusion process. We have exploited a microinjection system (eppendorf FemtoJet + InjectMan), and have used a dispersion with the same concentration as that of the above bending measurement; nanotubes are fully dispersed before microextrusion. The first step (Figure 3 a) involves touching the microneedle (500 nm inner diameter) lightly onto the slide, which allows a small amount of lipid nanotube dispersion to drop onto it. The water component evaporates away quickly because of the irradiation from the halogen lamp needed for microscopy, during which time an edge of the single nanotube adheres to the glass plate. We can hence freely draw a fine line with a single lipid nanotube, by moving the microneedle in an arbitrary direction. In practice the manipulation does not work well every time, because nanotubes are not always contained in the first drop; we sometimes inject only water which soon evaporates.

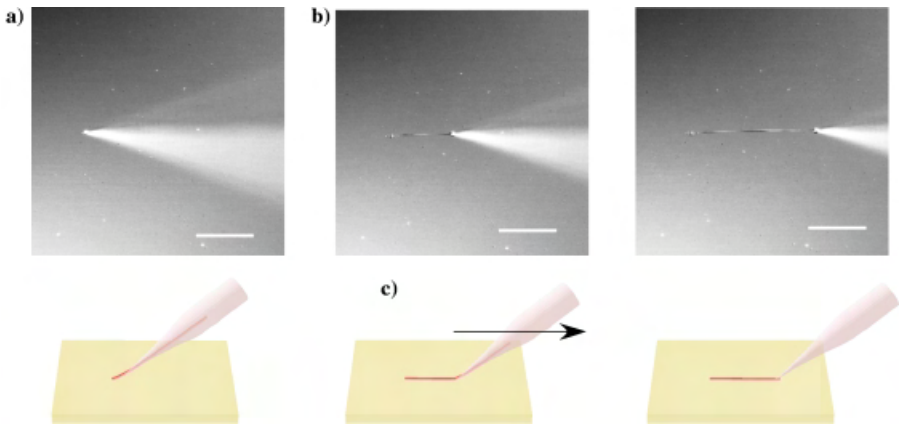


Figure 3. Confocal laser scanning micrographs (Carl Zeiss LSM510) of a fine line drawn with single nanotubes by microextrusion, and its explanatory schematics. The white triangles in the images correspond to the tip of the needle: a) the needle end touches a glass slide. because a positive pressure is applied against backward flow, even before injection, a very small amount of solution drops onto the glass. As a consequence, while water quickly evaporates, the nanotubes become attached; b) by slowly moving the needle linearly, nanotubes are extruded one after another; c) when the injection is stopped, the line ends.

Of course, it must be checked whether the microextruded line observed by optical microscopy is truly a single nanotube or not. To this end we drew a line using the above microextrusion technique onto Formvar (poly(vinyl formal)) film spread onto a copper grid. Figure 4 is the TEM image of this line, and shows that the line is indeed a single lipid nanotube. Remarkably, this

 © 2003 Wiley-VCH Verlag GmbH & Co. KGaA, Weinheim 1433-7851/03/4201-0073 $ 20.00+.50/0

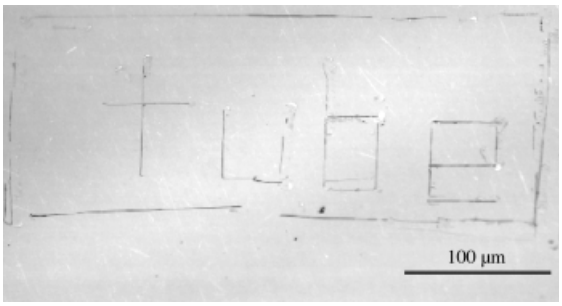


Figure 5. Confocal laser scanning micrograph of the word "tube" drawn with single nanotubes using our microinjection system. The frame, also drawn using single nanotubes, is 0.37 mm long and 0.15 mm wide. A higher magnification of this is shown in Figure 4.

manipulation easily aligns a single tube in an arbitrary direction. For demonstration we have further written the word "tube", as shown in Figure 5.

In summary, we found that the glycolipid nanotube could be a good candidate for a cytomimetic tubule in terms of its mechanical properties. Moreover, exploiting the moderate rigidity, we have developed a novel but simple aligning method: a fine line of the single nanotube is drawn freely simply by microextruding the aqueous dispersion on glass plate. Our manipulation methodology promises to open up fascinating possibilities for lipid nanotubes beyond only a substitute for microtubules; for example, a nanoneedle could be realized by extruding half of the single nanotube and fixing it at the tip of a microextrusion needle; also bridging or branching of the nanotubes on glass or metal substrates might be used as a mold for the formation of a wire and hub inside them, in molecular electronic devices; lastly, a single nanotube channel and its assembled array should provide 1D nanospace for the separation of advanced macromolecules beyond the submicro total analysis system (subμTAS).

Experimental Section

Preparation of single lipid nanotubes: These were prepared in water through self-assembly of renewable-resource-based, synthetic glycolipid cardanyl-β-D-glucopyranoside, which is a mixture of 1-*O*-3′-*n*-(8′(*Z*),11′(*Z*), 14′-pentadecatrienyl)-phenyl- β -D-glucopyranoside (ca. 29 wt%), 1-*O*-3′-*n*-(8′(*Z*),11′(*Z*)-pentadecadienyl) phenyl-β-D-glucopyranoside (ca. 16 wt%), 1-*O*-3′-*n*-(8′(*Z*)-pentadecenyl) phenyl-β-D-glucopyranoside (ca. 50 wt%), and 1-*O*-3′-*n*-(pentadecyl) phenyl-β-D-glucopyranoside (ca. 5 wt%), as reported elsewhere.[17] Nanotube structures with 10–15 nm inner diameter and high axial ratios were confirmed by TEM, field-emission scanning electron microscopy (FE-SEM), confocal laser scanning microscopy, and atomic force microscopy (AFM). On the basis of X-ray diffraction studies, the tubular membrane wall consists of three to four interdigitated lipid bilayers. Combination of a hydrogen-bond network between the glucose headgroups, π–π stacking interactions between phenyl rings, and hydrophobic interactions between long alkyl chains are responsible for the stabilization of noncovalently formed nanotube architectures.

Received: July 31, 2002 [Z19858]

[1] P. Yager, P. E. Schoen, *Mol. Cryst. Liq. Cryst. Sci. Technol., Sect. A,* **1984**, *106*, 371 – 381.
[2] J. M. Schnur, B. R. Ranta, J. V. Selinger, G. Jyothi, K. R. K. Easwaran, *Science* **1994**, *264*, 945 – 947.
[3] B. N. Thomas, C. R. Safinya, R. J. Plano, N. A. Clark, *Science* **1995**, *267*, 1635 – 1638.
[4] N. Nakashima, S. Asakuma, T. Kunitake, *J. Am. Chem. Soc.* **1985**, *107*, 509 – 510.
[5] J. H. Fuhrhop, D. Spiroski, C. Boettcher, *J. Am. Chem. Soc.* **1993**, *115*, 1600 – 1601.
[6] F. Giulieri, F. Guillod, J. Greiner, M. P. Krafft, J. G. Riess, *Chem. Eur. J.* **1996**, *2*, 1335 – 1339.
[7] S. Stewart, G. Liu, *Angew. Chem.* **2000**, *112*, 348 – 352; *Angew. Chem. Int. Ed.* **2000**, *39*, 340 – 344.
[8] P. Ringler, W. Muller, H. Ringsdorf, A. Brisson, *Chem. Eur. J.* **1997**, *3*, 622 – 625.
[9] J. H. Fuhrhop, U. Bindig, U. Siggel, *J. Am. Chem. Soc.* **1993**, *115*, 11 036 – 11 037.
[10] T. Shimizu, M. Kogiso, M. Masuda, *Nature* **1996**, *383*, 487 – 488.
[11] M. Kogiso, S. Ohnishi, K. Yase, M. Masuda, T. Shimizu, *Langmuir* **1998**, *14*, 4978 – 4986.
[12] J. M. Schnur, *Science* **1993**, *262*, 1669 – 1676.
[13] S. Iijima, *Nature* **1991**, *354*, 56 – 58.
[14] F. Gittes, B. Mickey, J. Nettleton, J. Howard, *J. Cell Biol.* **1993**, *120*, 923 – 934.
[15] H. Felgner, R. Frank, M. Schliwa, *J. Cell Sci.* **1996**, *109*, 509 – 516.
[16] M. M. J. Treacy, T. W. Ebbesen, J. M. Gibson, *Nature* **1996**, *381*, 678 – 680.
[17] G. John, M. Masuda, Y. Okada, K. Yase, T. Shimizu, *Adv. Mater.* **2001**, *13*, 715 – 718.
[18] L. A. Amos, T. S. Baker, *Nature* **1979**, *279*, 607 – 612.

Metal-Based Polyrotaxanes

Channels and Cavities Lined with Interlocked Components: Metal-Based Polyrotaxanes That Utilize Pyridinium Axles and Crown Ether Wheels as Ligands**

*Gregory J. E. Davidson and Stephen J. Loeb**

The formation of polyrotaxanes by metal–ligand self-assembly is a viable method for the programmed organization of mechanically linked molecular components into a repeating framework. This has significant potential for producing materials that contain functional molecular entities that may be addressable or controllable.[1] The challenges of designing, synthesizing, and crystallizing such materials are many and

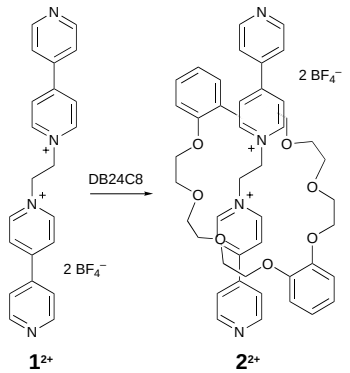
[*] Prof. S. J. Loeb, G. J. E. Davidson
Department of Chemistry and Biochemistry
University of Windsor
Windsor, ON N9B 3P4 (Canada)
Fax: (+1) 519-973-7098
E-mail: loeb@uwindsor.ca

[**] We thank NSERC of Canada and PRF-ACS for financial support of this research. G.K.H. Shimizu and A. P. Côté of the Department of Chemistry, University of Calgary are thanked for providing the thermogravimetric analysis data.

 © 2003 Wiley-VCH Verlag GmbH & Co. KGaA, Weinheim 1433-7851/03/4201-0074 $ 20.00+.50/0

very few well-characterized examples exist.[2–6] To date, the only set of compounds to realize this combination are those prepared by Kim et al. in which a diaminoalkane "string" and cucurbituril (CB) "bead" are linked by a transition metal or lanthanide ion. This method was successfully employed to produce 1D, 2D, and 3D metal-containing polyrotaxanes,[2,3] and in one case large cavities and channels were shown to be possible.[4] In an effort to expand the number of known examples of this concept and to introduce some structural flexibility into the components, we present herein examples of metal-based polyrotaxanes constructed by using pyridinium "axles", crown ether "wheels", and transition metal ion "nodes". In particular, this design will allow investigations of some interesting concepts: 1) the effective volume of a dynamic mechanical component (crown ether) may be useful in eliminating interpenetration in metal–ligand (ML) nets[7,8] allowing the formation of large cavities, 2) the ability to change crown ethers without effecting the basic structure of a ML net could result in tremendous structural flexibility and allow the control of cavity properties and function, and 3) the dynamic motion of an interlocked component that is threaded on to an ML net may be useful in the design of addressable solid-state materials. None of these features are presently possible with known polyrotaxanes.

Scheme 1 shows how the dipyridinium axle $\mathbf{1}^{2+}$ can be threaded through dibenzo-[24]crown-8 ether, DB24C8, to produce the [2]pseudorotaxane $\mathbf{2}^{2+}$. We have previously demonstrated that this [2]pseudorotaxane can act as a ligand and that employing metal complexes as stoppers is a versatile method for producing [2]rotaxanes in good yield.[9–12] Herein, we report that this same supramolecular motif can be involved in metal–ligand self-assembly (crystal engineering) reactions and thereby be extended to polymeric systems; linear 1D and square-grid 2D metal-based polyrotaxanes.



Scheme 1. The [2]pseudorotaxane $\mathbf{2}^{2+}$ is easily prepared from the dipyridinium salt $\mathbf{1}^{2+}$ and DB24C8 in a solvent such as CH_2Cl_2, acetone, MeCN, or $MeNO_2$.

One equivalent of $\mathbf{1}[BF_4]_2$ was mixed with two equivalents of DB24C8 and one equivalent of $[M(H_2O)_6][BF_4]_2$ (M = Co, Zn) in MeCN. The bulk of the solid material was isolated in good yield by reducing the volume of the mixture to about 20% of the original amount; 71% (Co), 92% (Zn). X-ray quality crystals[13] of $\{[Co(H_2O)_2(MeCN)_2(\mathbf{2})][BF_4]_4\cdot(MeCN)_2(H_2O)_2\}_x$ (**3**) were produced by slow evaporation of the

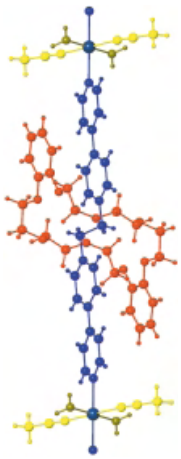


Figure 1. Ball-and-stick representation of the repeating metal–ligand unit in **3**. Key: blue: $\mathbf{1}^{2+}$ axle; red: DB24C8 wheel; dark blue: metal ion; green: H_2O; yellow: MeCN.

reaction mixture. Figure 1 shows that the use of Co^{II} ions in MeCN results in an octahedral coordination geometry comprising two [2]pseudorotaxane ligands, two MeCN molecules, and two water molecules all with *trans* orientations. The result is a 1D coordination polymer in which every bridging ligand is a [2]rotaxane. The Zn^{II} version $\{[Zn(H_2O)_2(MeCN)_2(\mathbf{2})][BF_4]_4\cdot(MeCN)_2(H_2O)_2\}_x$ (**4**) is isomorphous with **3**. Although the linker $\mathbf{1}^{2+}$ could adopt either an *anti* or *gauche* conformation at the central ethylene unit, only the *anti* conformation is possible when $\mathbf{1}^{2+}$ is threaded through a 24-membered crown ether as part of a [2]pseudorotaxane or rotaxane.[9–12,14] This combination of a *trans* geometry at the metal ion and a linear [2]pseudorotaxane ligand produces a linear 1D polymer with a repeat distance between Co atoms of 22.1 Å.

Figure 2 shows how these linear cationic 1D polyrotaxanes pack side-by-side in parallel chains in the solid state. Infinite 1D channels are formed between the polymer strands and are filled with the counterions and solvents of crystallization; in this case four BF_4^- ions, two molecules of MeCN and two molecules of water per monomer unit. Calculations

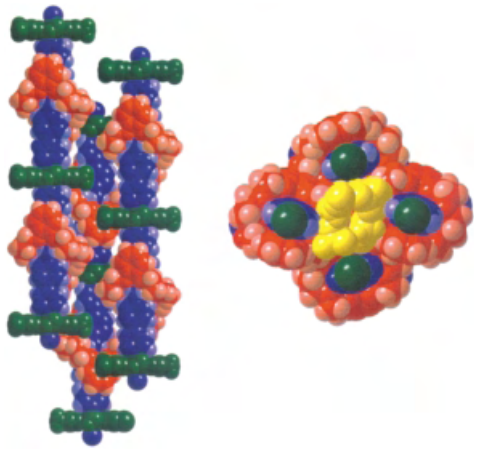


Figure 2. Space-filling representations of parallel chains of polyrotaxane **3** with solvent and anion removed for clarity (left) and a view down the chains showing the channels filled with anions and solvent (right). Key: blue: $\mathbf{1}^{2+}$ axle; red: DB24C8 wheel; green: metal with bound H_2O and MeCN ligands; yellow: anions and solvent molecules.

 © 2003 Wiley-VCH Verlag GmbH & Co. KGaA, Weinheim 1433-7851/03/4201-0075 $ 20.00+.50/0

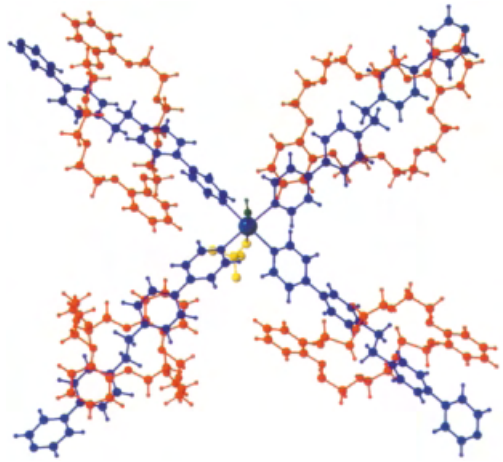


Figure 3. Ball-and-stick representation of the coordination sphere of the metal center in **5**. Key: blue: $\mathbf{1}^{2+}$ axle; red: DB24C8 wheel; green: H_2O; yellow: BF_4.

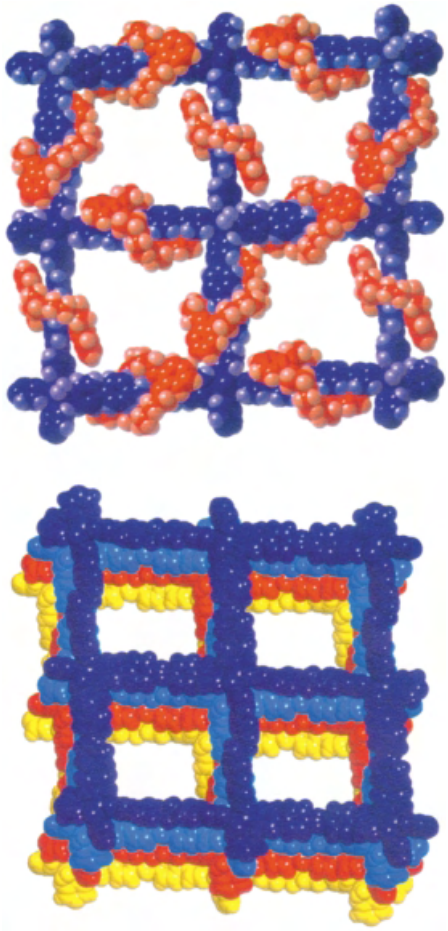


Figure 4. Top: A space-filling model showing four square-grids of **5**. ($MeNO_2$ solvent molecules and noncoordinated BF_4 anions are omitted for clarity). Key: blue: metal–ligand lattice; red = DB24C8. Bottom: Four layers of the grid are shown to emphasize the infinite channels and the open framework of the solid (DB24C8 molecules, $MeNO_2$ solvent molecules, and noncoordinated BF_4 anions are omitted for clarity).

from the X-ray structural parameters show that the accessible void space in the channels occupied by anions and solvent is 33.9 %; 13.2 % for solvent only.[15]

Since, the linear 1D polyrotaxanes **3** and **4** contain an octahedral metal ion in which the ancillary ligands are solvent molecules (H_2O and MeCN), we reasoned it should be possible to induce higher orders of dimensionality by employing one or a combination of noncoordinating solvents, anhydrous metal salts, and a greater amount of [2]pseudorotaxane ligand. Ultimately, we were successful in increasing the dimensionality by reacting two equivalents of $\mathbf{1}[BF_4]_2$ with four equivalents of DB24C8 and one equivalent of $[Cd(H_2O)_6][BF_4]_2$ in $MeNO_2$.[16,17] X-ray quality crystalline material was produced in good yield (> 80 %) by vapor diffusion of isopropyl ether into the reaction mixture. Figure 3 shows that the use of Cd^{II} ions in the noncoordinating solvent $MeNO_2$ results in an octahedral coordination geometry comprising *four* [2]pseudorotaxane ligands in a square-planar arrangement, one water molecule, and one coordinated BF_4^- anion. Figure 4 (top) shows how propagation of these units results in a 2D square net coordination polymer $\{[Cd(H_2O)(BF_4)(\mathbf{2})_2][BF_4]_5(MeNO_2)_{15}\}_x$ (**5**) in which every bridging ligand is a [2]rotaxane. The sides of the square net are defined by Cd···Cd distances of 22.2 Å, while the interlayer spacings are 12.0 and 10.0 Å, respectively, in an AB alternating pattern down the *c* axis (22.0 Å). Figure 4 (bottom) shows how this pattern gives rise to openings that are large infinite channels lined with crown ethers. These channels are not completely perpendicular to the 2D net but offset slightly as the 2D layers are knitted together by a series of H···F and H···O hydrogen bonds, which utilize the Cd–OH_2 unit of one layer, the neighboring Cd–BF_4 group in an adjacent layer, and intervening solvent molecules (there are 15 noncoordinated molecules of $MeNO_2$ per Cd^{II} ion). Calculations estimate that the accessible void space occupied by anions and solvent is 49.7 %; 38.0 % for solvent only.[15]

The stability of the polyrotaxane frameworks in **3**–**5** were probed by thermogravimetric analysis.[18] This showed that although the solid materials easily lost molecules of crystallization (MeCN at > 70 °C, H_2O at > 100 °C, $MeNO_2$ from 30 to 100 °C) and coordinated solvent molecules (H_2O and MeCN at > 150 °C), the rotaxane framework did not breakdown and lose crown ether until > 250 °C. Presumably at this temperature, there is complete decomposition of the metal–ligand coordination polymer. This demonstrates that although the crown is initially held in position by weak noncovalent bonds in the template formation of the [2]pseudorotaxane and only interacts with the polymer by way of these residual noncovalent interactions, a covalent or strong metal–ligand bond must be broken to release this component. Therefore, incorporation of molecular machine-like units into solid-state structures by self-assembly of metal–ligand coordination polymers offers a viable route for creating functional materials and there is nothing inherently unstable about the individual rotaxane components.

From these preliminary results, we can conclude that 1) the design of open framework materials with interlocked components can be expanded to include pyridinium axles and crown ether wheels, and 2) interpenetration does not appear

 © 2003 Wiley-VCH Verlag GmbH & Co. KGaA, Weinheim 1433-7851/03/4201-0076 $ 20.00+.50/0

to be a problem as large square openings and infinite channels are possible. Further detailed experiments are needed to determine if the lack of interpenetration can be attributed to the dynamic nature of the crown units in solution and during crystallization. Future investigations will focus on the effect of changing crown ethers on the physical properties of the cavities and channels in these open framework materials.

Received: August 2, 2002 [Z19875]

[1] a) V. Balzani, A. Credi, F. M. Raymo, J. F. Stoddart, *Angew. Chem.* **2000**, *112*, 3484; *Angew. Chem. Int. Ed.* **2000**, *39*, 3348; b) A. N. Shipway, I. Willner, *Acc. Chem. Res.* **2001**, *34*, 421.

[2] K-M. Park, D. Whang, E. Lee, J. Heo, K. Kim, *Chem. Eur. J.* **2002**, *8*, 498.

[3] A dinuclear Tb^{III} center acts as the metal ion node for the 3D polyrotaxane; E. Lee, J. Heo, K. Kim, *Angew. Chem.* **2000**, *112*, 2811; *Angew. Chem. Int. Ed.* **2000**, *39*, 2699.

[4] E. Lee, J. Kim, J. Heo, D. Whang, K. Kim, *Angew. Chem.* **2001**, *113*, 413; *Angew. Chem. Int. Ed.* **2001**, *40*, 399.

[5] B. F. Hoskins, R. Robson, D. A. Slizys, *Angew. Chem.* **1997**, *109*, 2430; *Angew. Chem. Int. Ed. Engl.* **1997**, *36*, 2336.

[6] C. S. A. Fraser, M. C. Jennings, R. J. Puddephatt, *Chem. Commun.* **2001**, 1310.

[7] M. Zaworotko, *Chem. Commun.* **2001**, 1.

[8] N. G. Pschirer, D. M. Ciurtin, M. D. Smith, U. H. F. Bunz, H.-C. zur Loye, *Angew. Chem.* **2002**, *114*, 663; *Angew. Chem. Int. Ed.* **2002**, *41*, 583.

[9] S. J. Loeb, J. A. Wisner, *Chem. Commun.* **1998**, 2757.

[10] G. J. E. Davidson, S. J. Loeb, N. A. Parekh, J. A. Wisner, *J. Chem. Soc. Dalton Trans.* **2001**, 3135.

[11] a) K. Chichak, M. C. Walsh, N. R. Branda, *Chem. Commun.* **2000**, 847; b) M. J. Gunter, N. Bampos, K. D. Johnstone, J. K. M. Sanders, *New J. Chem.* **2001**, *25*, 166.

[12] Y. Diskin-Posner, G. K. Patra, I. Goldberg, *Eur. J. Inorg. Chem.* **2001**, 2515.

[13] Crystal data[19] for **3**: $C_{54}H_{72}B_4CoF_{16}N_8O_{12}$, $M_r = 1431.4$, yellow-orange blocks, ($0.28 \times 0.24 \times 0.20$ mm) monoclinic, $P2_1/c$, $a = 14.2776(1)$, $b = 11.8122(2)$, $c = 20.6360(2)$ Å, $\beta = 104.084(1)°$, $V = 3375.64(7)$ Å^3, $Z = 2$, $\rho_{calcd} = 1.408$ g cm^{-3}, $\mu = 0.360$ mm^{-1}, min/max trans. = 0.1083/0.1525, $2\theta_{max} = 50.0°$, $Mo_{K\alpha}$ $\lambda = 0.71073$ Å, $T = 293(2)$ K, 5861 total reflections (R(int) = 0.0157), $R1 = 0.0744$, wR2 = 0.2193 ($I > 2\sigma I$), $R1 = 0.0806$, $wR2 = 0.2270$ (all data), GoF (F^2) = 1.072, $N_o/N_v = 5861/440$. Crystals of **4** were of poorer quality than those obtained for **3** but the data was good enough to determine that the two structures are isomorphous with Zn replacing Co at the metal linking node. **4**: $C_{54}H_{72}B_4F_{16}N_8O_{12}Zn$, $M_r = 1437.8$, yellow blocks, ($0.24 \times 0.20 \times 0.18$ mm) monoclinic, $P2_1/c$, $a = 14.2776(1)$, $b = 11.8122(2)$, $c = 20.6360(2)$ Å, $\beta = 104.084(1)°$, $V = 3375.64(7)$ Å^3, $Z = 2$, $\rho_{calcd} = 1.415$ g cm^{-3}, $\mu = 0.469$ mm^{-1}, min/max trans. = 0.0964/0.1423, $2\theta_{max} = 42.0°$, $Mo_{K\alpha}$ $\lambda = 0.71073$ Å, $T = 293(2)$ K, 3269 total reflections (R(int) = 0.1136), $R1 = 0.1676$, $wR2 = 0.3766$ ($I > 2\sigma I$), $R1 = 0.2161$, $wR2 = 0.4140$ (all data), GoF (F^2) = 1.199, $N_o/N_v = 3269/421$. **5**: $C_{107}H_{151}B_6CdF_{24}N_{23}O_{47}$, $M_r = 3144.8$, yellow blocks, ($0.34 \times 0.26 \times 0.24$ mm) triclinic, $P\bar{1}$, $a = 17.331(2)$, $b = 20.345(2)$, $c = 22.006(2)$ Å, $\alpha = 83.692(2)$, $\beta = 80.080(2)$, $\gamma = 72.306(2)°$, $V = 7267.9(13)$ Å^3, $Z = 2$, $\rho_{calcd} = 1.437$ g cm^{-3}, $\mu = 0.269$ mm^{-1}, min/max trans. = 0.7885, $2\theta_{max} = 50.0°$, $Mo_{K\alpha}$ $\lambda = 0.71073$ Å, $T = 173.5(2)$ K, 25248 total reflections (R(int) = 0.0511), $R1 = 0.1075$, $wR2 = 0.3067$ ($I > 2\sigma I$), $R1 = 0.1431$, $wR2 = 0.3469$ (all data), GoF (F^2) = 1.345, N_o/N_v/restraints = 25248/1878/1294. Crystals of **3** and **4** were mounted on a glass fiber at room temperature, those for **5** were frozen in paratone oil inside a cryoloop. Reflection data were integrated from frame data obtained from hemisphere scans on a Bruker APEX diffractometer with CCD detector. Decay (< 1%) was monitored by 50 standard data frames measured at the beginning and end of data collection. Diffraction data and unit cell parameters were consistent with assigned space groups. Lorentzian polarization corrections and empirical absorption corrections, based on redundant data at varying effective azimuthal angles, were applied to the data sets. The structures were solved by direct methods, completed by subsequent Fourier syntheses, and refined with full-matrix least-squares methods against $|F^2|$ data. All non-hydrogen atoms were refined anisotropically. Hydrogen atoms were treated as idealized contributions. Scattering factors and anomalous dispersion coefficients are contained in the SHELXTL 5.03 program library (G. M. Sheldrick, Madison, WI). CCDC-182287 (**3**), CCDC-182288 (**4**), and CCDC-190997 (**5**) contain the supplementary crystallographic data for this paper. These data can be obtained free of charge via www.ccdc.cam.ac.uk/conts/retrieving.html (or from the Cambridge Crystallographic Data Centre, 12, Union Road, Cambridge CB21EZ, UK; fax: (+44) 1223-336-033; or deposit @ccdc.cam.ac.uk).

[14] S. J. Loeb, J. A. Wisner, *Angew. Chem.* **1998**, *110*, 3010; *Angew. Chem. Int. Ed.* **1998**, *37*, 2838.

[15] The accessible void volumes were calculated with the program PLATON by using a probe with a radius of 1.2 Å. A. M. C. T. PLATON, Utrecht University, Utrecht, The Netherlands, A. L. Spek, **1998**.

[16] Preliminary X-ray results for crystals of the Co^{II}, Ni^{II}, and Cu^{II} complexes, generated in exactly the same manner, indicate that the materials are isomorphous with **5**.

[17] **Note added in proof** (October 8, 2002): After submission of this manuscript, we determined the structure of the Cd^{II} complex in which crystals were formed under exactly the same conditions as those used to create the 2D net, but omitting the DB24C8 component. The resulting material is a 1D polymer, $\{[Cd(H_2O)_2(BF_4)_2(\mathbf{1})][BF_4]_2\}_x$, which forms a tightly packed herringbone pattern and contains no channels or cavities; details will be reported in due course.

[18] Thermogravimetric analysis were performed on a Netzsch STA449C Instrument under $N_2(g)$ atmosphere at a scan rate of 5 °C min^{-1}.

[19] Ball-and-stick and space-filling diagrams were prepared using DIAMOND-Visual Crystal Structure Information System CRYSTAL IMPACT, Postfach 1251, 53002 Bonn.

Expanded Porphyrins

Perfluorinated *meso*-Aryl-Substituted Expanded Porphyrins**

Soji Shimizu, Ji-Young Shin, Hiroyuki Furuta, Rami Ismael, and Atsuhiro Osuka**

In recent years there has been a considerable upsurge in the development of expanded porphyrins with five or more conjugated pyrrolic rings, because of their ability to exhibit a variety of interesting optical, electrochemical, stereochemical, and coordination properties.[1,2] Among such macrocyclic systems, there are only scattered reports on *meso*-aryl-substituted expanded porphyrins that are structurally homologous to tetrakis-*meso*-aryl porphyrin in respect of the alternate conjugative arrangement of pyrrole and methine carbon atoms. Recently, we reported that simple modified Rothemund–Lindsey reaction of pentafluorobenzaldehyde and pyrrole unexpectedly allowed the formation of a series of *meso*-aryl-substituted expanded porphyrins ranging from pentaphyrin to dodecaphyrin.[3] *meso*-Aryl-substituted expanded porphyrins thus formed have received particular attention as a result of their ability to chelate multimetal ions as well as the multitude of oxidation states. In addition, *meso*-aryl-substituted expanded porphyrins can be structurally diverse, depending on the ring size, the metalation, and the degree of protonation.[3,4] For example, in the solid states, [26]hexaphyrin takes a flat rectangular conformation with two inverted pyrrole rings,[4] [36]octaphyrin exhibits a figure-of-eight conformation,[3] and the [42]nonaphyrin-trifluoroacetic acid (TFA) complex shows a butterfly conformation with a central cleft in which TFA is bound by two inverted pyrrole rings.[3] Finally, these *meso*-aryl-substituted expanded porphyrins and other related large macrocycles offer a good opportunity to study the interplay between the aromaticity/non-aromaticity that may be brought about by the two-electron oxidation/reduction of the macrocycle.

Provided that the successful formation of *meso*-aryl-substituted expanded porphyrins is mainly a consequence of the steric congestion around the formyl group and the electron-deficient property of the aryl aldehyde, the similar reaction of pentafluorobenzaldehyde and 3,4-difluoropyrrole[5,6] may be facilitated by the additional steric crowding as well as by the electron-deficient nature of the fluorine substituents in the pyrrole ring. Furthermore, perfluorinated *meso*-aryl-substituted expanded porphyrins may be interesting as robust oxidation catalysts and functional dyes.[7]

Here we report the synthesis of a series of perfluorinated expanded porphyrins that possess fluorine substituents at both the *meso*-aryl and β-pyrrole positions. In a typical synthesis, a solution of 3,4-difluoropyrrole and pentafluorobenzaldehyde (66.7 mM each) in CH_2Cl_2 was stirred for 8 h with $BF_3{\cdot}OEt_2$. After oxidation with DDQ for 10 h, chromatographic separation on silica gel gave porphyrin **1** (6–9%),[7] pentaphyrin **2** (about 1%),[8] hexaphyrin **3** (2–5%), heptaphyrin **4** (4–6%), octaphyrin **5** (4–7%), nonaphyrin **6** (~2%), and decaphyrin **7** (about 2%; Scheme 1). The X-ray crystal structures of the hexaphyrin and octaphyrin were found to be particularly interesting, in that both these structures are quite different from those of the corresponding β-hydrogen (β-H) expanded porphyrins.

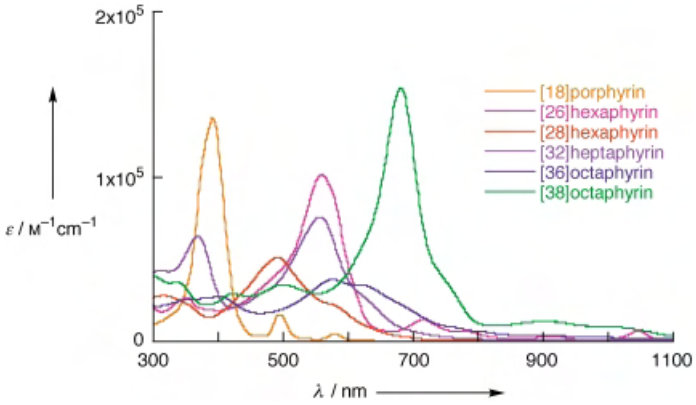


Figure 1. UV/Vis spectra of *meso*-aryl-substituted expanded porphyrins.

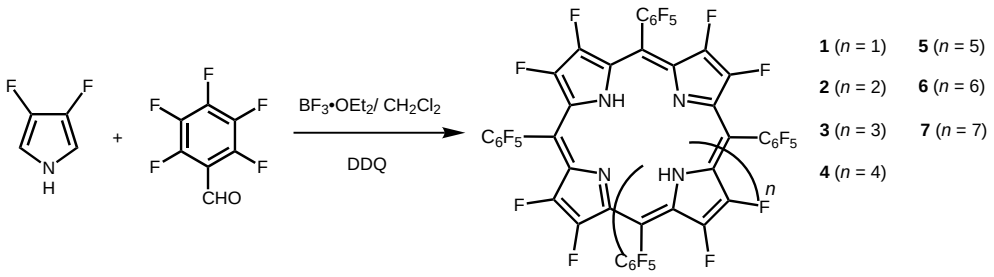
The yield of the initial hexaphyrin product **3** was variable for each batch, probably because of its very poor solubility in common organic solvents. The isolated hexaphyrin **3** exhibited a sharp Soret-like band at 560 nm ($\varepsilon = 1.0 \times 10^5\,M^{-1}\,cm^{-1}$) and Q-type bands at 717, 779, 907, and 1048 nm in the UV/Vis spectrum (Figure 1). These band positions are quite similar to those of β-H [26]hexaphyrin and suggest that **3** has aromatic character. This hexaphyrin was converted into a reduced form upon treatment with $NaBH_4$ which was found to be more soluble in many solvents. Thus, a better yield (about 5–7%) of hexaphyrin has been constantly achieved by the treatment of the product mixture with $NaBH_4$ before the chromatographic separation. The reduced hexaphyrin was quantitatively oxidized back to its poorly soluble oxidized form upon treatment with DDQ. The reduced hexaphyrin exhibits two singlets at $\delta = 15.39$ and 11.93 ppm in the ^1H NMR spectrum (Table 1) and a broad band at 492 nm ($\varepsilon = 5.1 \times 10^4\,M^{-1}\,cm^{-1}$) without a Q-band-like absorption band, which suggests it has non-aromatic character (Figure 1). The structure of the reduced hexaphyrin has been revealed by X-ray crystallography to be [28]hexaphyrin (Scheme 2), with a twisted figure-of-eight-like

[*] Prof. H. Furuta, Prof. A. Osuka, S. Shimizu, Dr. J.-Y. Shin, Dr. R. Ismael
Department of Chemistry
Graduate School of Science
Kyoto University
Sakyo-ku, Kyoto 606–8502 (Japan)
Fax: (+81) 75-753-3970
E-mail: hfuruta@cstf.kyushu-u.ac.jp
osuka@kuchem.kyoto-u.ac.jp

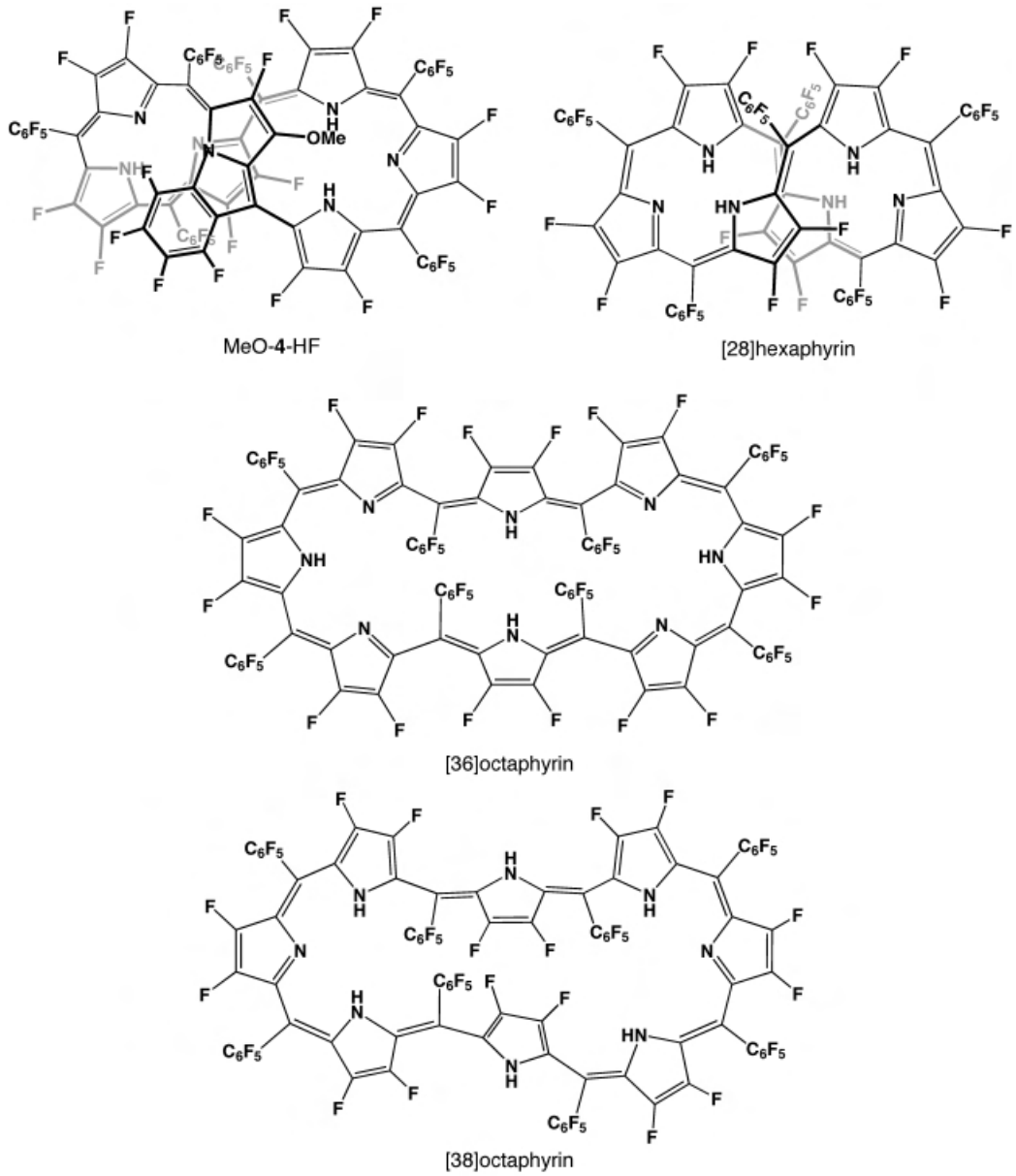
[**] This work was supported by Grant-in-Aids for Scientific Research from the Ministry of Education, Culture, Sports, Science, and Technology of Japan, CREST (Core Research for Evolutional Science and Technology) of the Japan Science and Technology Corporation (JST).

Supporting information for this article is available on the WWW under http://www.angewandte.org or from the author.

 © 2003 Wiley-VCH Verlag GmbH & Co. KGaA, Weinheim 1433-7851/03/4201-0078 $ 20.00+.50/0



Scheme 1. DDQ = 2,3-dichloro-5,6-dicyano-1,4-benzoquinone.



Scheme 2. Structures of selected *meso*-aryl-substituted perfluorinated porphyrins.

conformation consisting of two tripyrrolic "hemimacrocycles", in which the two tripyrrolic subunits are almost planar and the two planes are canted by approximately 60° (Figure 2).[9] It is interesting to note that a distinct alternation in the bond lengths of the π-electronic system is evident from the detailed analysis of its X-ray structure, and this is, to the best of our knowledge, the smallest expanded porphyrin that takes a twisted figure-of-eight conformation.

The heptaphyrin **4** exhibited a parent ion at *m*/*z* 1959 (calcd: *m*/*z* 1957) in the FABMS spectrum and quite simple

 © 2003 Wiley-VCH Verlag GmbH & Co. KGaA, Weinheim 1433-7851/03/4201-0079 $ 20.00+.50/0

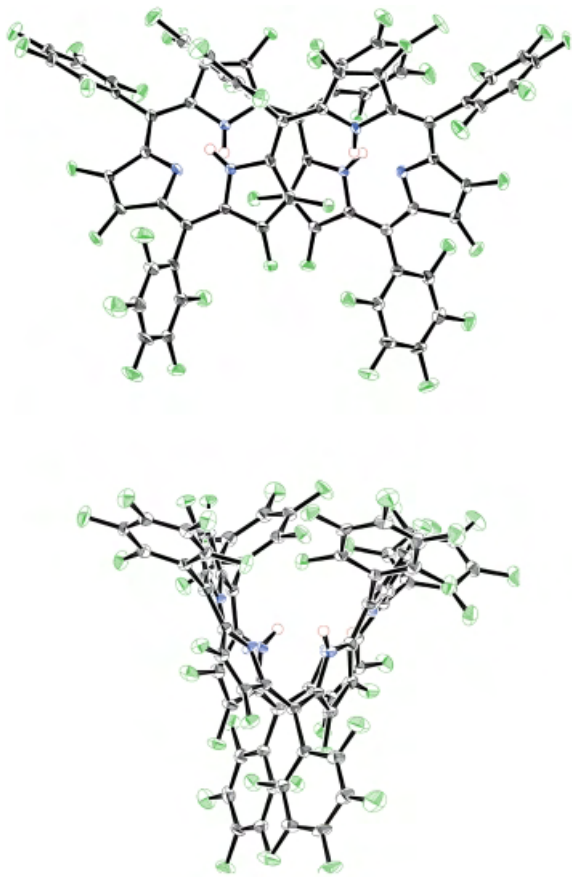


Figure 2. X-ray crystal structure of [28]hexaphyrin **3**. Top view (top) and side view (bottom).

^{1}H NMR and ^{19}F NMR spectra (see below), which suggests it has a symmetric conformation in $CDCl_3$ solution, although its detailed X-ray structure has not been determined. The signals of the inner NH protons appear at $\delta = 14.25$ and 11.34 ppm in the ^{1}H NMR spectrum of the compound, which suggests there is no specific ring current effect. The UV/Vis spectrum of heptaphyrin **4** exhibits an absorption band at 557 nm without any low-energy band. During many attempts to make single crystals, we found that **4** was converted slowly into its fused form (**4**–HF) in solutions containing methanol, as evident from the parent ion in the FAB mass spectrum. The fused form exhibited a parent molecular ion peak at *m*/*z* 1938, which was smaller than the original heptaphyrin by an equivalent of HF (*m*/*z* 20). Unlike the case with **4**, it was possible to obtain crystals of the fused heptaphyirn **4**–HF suitable for X-ray analysis (Figure 3).[10,11] The structure is a methanol adduct of N-fused [32]heptaphyrin, MeO-**4**–HF, in which the macrocycle adopts a twisted figure-of-eight-like conformation with a fused tripyrrolic ring formed by a nucleophilic substitution of the *ortho* fluorine atom by the inverted pyrrole nitrogen atom and with the β-fluorine atom of the fused pyrrole ring substituted by methanol. MeO-**4**–HF exhibits the bond alternation and shows signals for the inner NH protons at $\delta = 13.59$, 12.97, and 12.21 ppm, and its absorption spectrum is similar to that of nonfused heptaphyrin **4** with some bathochromic shifts. Collectively, N-fused

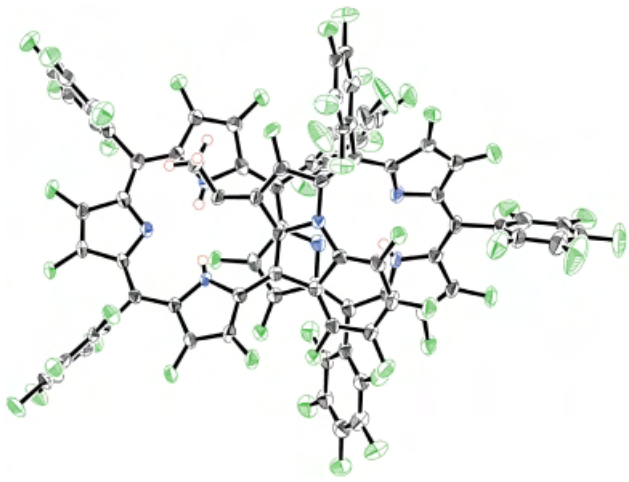


Figure 3. X-ray crystal structure of methanol-adduct of N-fused [32]heptaphyrin MeO-**4**–HF.

[32]heptaphyrins, **4**–HF and MeO-**4**–HF, can be considered to be non-aromatic.

The FAB mass spectrum of octaphyrin **5** (obtained from the reaction mixture) exhibits a molecular ion at *m*/*z* 2236 (calcd: *m*/*z* 2236) and the ^{1}H NMR spectrum shows four NH signals at $\delta = 13.80$, 12.42, 11.30, and 7.95 ppm. The UV/Vis spectrum shows broad bands at 401, 576, and 616 nm without noticeable Q-band-like transitions in the longer wavelength region. All these data suggest that it has a non-aromatic character that may be delineated as a 36π-electronic system. The firm structural evidence for this supposition came from its X-ray crystal structure, which shows a cyclic ellipsoidal conformation, in which two sets of three pyrrole rings (1), (2), and (4)′, and (1)′, (2)′, and (4), constitute a relatively planar arrangement but the pyrrole rings (3) and (3)′ are largely canted from such planes (Figure 4).[12] As seen in the side view, the (3) and (3)′ pyrrole rings are almost parallel with their nitrogen atoms pointing inward toward the center of the macrocycle. Of the eight pyrrole rings, the (1), (3), (1)′, and (3)′ rings bear hydrogen atoms while (2), (4), (2)′, and (4)′ do not. In line with the assignment as a 36π-electron non-aromatic system, the bond alternation of the conjugated double bonds is evident from the X-ray structure. It is interesting to note that the solid-state structure of the present [36]octaphyrin is a rare example, since most of the octaphyrin derivatives reported so far take figure-of-eight conformations.[2d,3b,13] This [36]octaphyrin was reduced to [38]octaphyrin upon stirring with $NaBH_4$. This reduced octaphyrin exhibited a molecular ion peak at *m*/*z* 2238 (calcd: *m*/*z* 2238) in the mass spectrum and showed a sharp Soret-like band at 681 nm ($\varepsilon = 1.5 \times 10^5\,\text{M}^{-1}\text{cm}^{-1}$) and Q-band-like absorptions at 907 and 1020 nm in the UV/Vis spectrum. The ^{1}H NMR spectrum revealed the presence of six NH signals at $\delta = 7.95$, 7.46, 7.19, 5.38, 5.31, and 5.23 ppm, while the ^{19}F NMR spectrum revealed 16 signals for the *ortho* F atoms, which suggests that the [38]octaphyrin has a nonsymmetric structure. In comparison to [28]hexaphyrin, the reoxidation of [38]octaphyrin with DDQ was found to be rather slow. The X-ray structure of [38]octaphyrin shows a twisted macrocyclic

 © 2003 Wiley-VCH Verlag GmbH & Co. KGaA, Weinheim 1433-7851/03/4201-0080 $ 20.00+.50/0

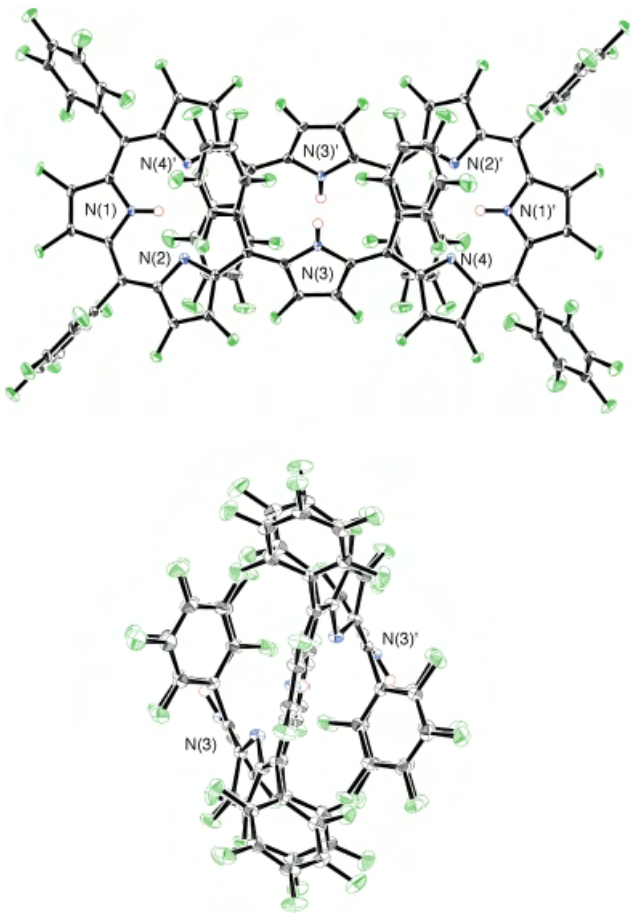


Figure 4. X-ray crystal structure of [36]octaphyrin **5**. Top view (top) and side view (bottom).

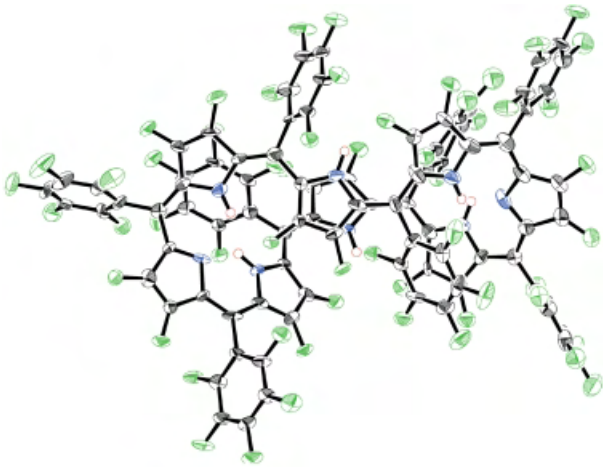


Figure 5. X-ray crystal structure of [38]octaphyrin (**5** + 2 H).

conformation consisting of the two-edge iminopyrroles and the rest six aminopyrroles (Figure 5).[14]

An interesting correlation exists between the absorption spectral properties and the number of π electrons in the conjugated rings. The spectral characteristic for $[4n]$-π electronic systems is the presence of only a single broad Soret-like band without Q-band-like low energy bands in the

Table 1: Selected physical data for [28]hexaphyrin, [32]heptaphyrin, N-fused [32]heptaphyrin, [36]octaphyrin, and [38]octaphyrin.

[28]hexaphyrin: ^{1}H NMR (500 MHz, $CDCl_3$, 303 K): $\delta = 15.39$ (s, 2H; NH), 11.93 ppm (s, 2H; NH); ^{19}F NMR (470.40 MHz, $CDCl_3$, 222 K, C_6F_6): $\delta = -136.64$ (d, $^3J = 18.3$ Hz, 2F; *o*-F), −137.54 (d, $^3J = 21.2$ Hz, 2F; *o*-F), −140.87 (d, $^3J = 21.2$ Hz, 2F; *o*-F), −141.12 (d, $^3J = 21.2$ Hz, 2F; *o*-F), −141.85 (brs, 2F; *o*-F), −142.56 (brs, 2F; *o*-F), −147.79 (t, $^3J = 18.3$ Hz, 2F; *p*-F), −148.08 (s, 2F; β-F), −149.15 (t, $^3J = 21.6$ Hz, 2F; *p*-F), −149.38 (s, 2F; β-F), −151.65 (t, $^3J = 21.2$ Hz, 2F; *p*-F), −153.57 (s, 2F; β-F), −153.82 (s, 2F; β-F), −154.37 (s, 2F; β-F), −157.98 (t, $^3J = 24.5$ Hz, 2F; *m*-F), −160.16 (t, $^3J = 21.2$ Hz, 2F; *m*-F), −160.31 (s, 2F; β-F), −160.50 (t, $^3J = 15.5$ Hz, 2F; *m*-F), −161.57 ppm (m, 6F; *m*-F); UV/Vis (CH_2Cl_2): λ_{max} (ε[M^{-1} cm^{-1}]) = 492 nm (51000); FABMS: *m*/*z* (% intensity): 1678 (100) [M^+]

[32]heptaphyrin: ^{1}H NMR (500 MHz, $CDCl_3$, 296 K): $\delta = 14.25$ (2H; NH), 11.34 ppm (s, 2H; NH); ^{19}F NMR (470.40 MHz, $CDCl_3$, 297 K, C_6F_6): $\delta = -137.06$ (d, $^3J = 21.2$ Hz, 2F; *o*-F), −138.97 (d, $^3J = 21.6$ Hz, 2F; *o*-F), −139.44 (m, 2F; *o*-F), −140.44 (m, 6F; *o*-F), −141.69 (d, $^3J = 27.8$ Hz, 2F; *o*-F), −146.00 (s, 2F; β-F), −148.52 (s, 2F; β-F), −149.26 (t, $^3J = 18.35$ Hz, 2F; *p*-F), −150.20 (t, $^3J = 21.6$ Hz, 2F; *p*-F), −150.33 (s, 2F; β-F), −151.16 (t, $^3J = 18.35$ Hz, 2F; *p*-F), −151.63 (s, 2F; β-F), −151.85 (t, $^3J = 21.2$ Hz, F; *p*-F), −151.95 (s, 2F; β-F), −153.71 (s, 2F; β-F), −156.82 (s, 2F; β-F), −159.77 (t, $^3J = 24.0$ Hz, 2F; *m*-F), −161.58 ~162.29 ppm (12F; *m*-F); UV/Vis (CH_2Cl_2): λ_{max} (ε[M^{-1} cm^{-1}]) = 557 (76000), 368 nm (64000); FABMS: *m*/*z* (% intensity): 1958 (100) [M^++H]

N-fused [32]heptaphyrin: ^{1}H NMR (500 MHz, $CDCl_3$, 296 K): $\delta = 12.91$ (1H; NH), 12.68 (s, 1H; NH), 11.82 ppm (s, 1H; NH); ^{19}F NMR (470.40 MHz, $CDCl_3$, 297 K, C_6F_6): $\delta = -136.70$ (m, 3F; *o*-F), −137.91 (d, $^3J = 18.3$ Hz, 2F; *o*-F), −140.05 (d, $^3J = 18.3$ Hz, 1F; *o*-F), −140.17 (d, $^3J = 21.2$ Hz, 1F; *o*-F), −140.54 (d, $^3J = 18.3$ Hz, 2F; *o*-F), −140.78 (2F; *o*-F), −141.46 (d, $^3J = 18.3$ Hz, 1F; *o*-F), −141.66 (s, 1F; β-F), −141.86 (s, 1F; β-F), −142.50 (s, 2F; β-F), −142.80 (d, $^3J = 9.41$ Hz, 1F; *o*-F), −145.63 (s, 1F; β-F), −145.78 (s, 1F; β-F), −146.65 (t, $^3J = 16.0$ Hz, 1F; *p*-F), −147.65 (t, $^3J = 18.3$ Hz, 1F; *p*-F), −148.34 (s, 1F; β-F), −149.03 (s, 1F; β-F), −149.50 (t, $^3J = 21.6$ Hz, 1F; *p*-F), −150.62 (t, $^3J = 21.6$ Hz, 1F; *p*-F), −150.95 (m, 2F; *p*-F), −151.44 (t, $^3J = 21.6$ Hz, 1F; *p*-F), −152.80 (t, $^3J = 17.4$ Hz, 1F; *p*-F), −153.17 (s, 1F; β-F), −154.76 (s, 1F; β-F), −155.45 (s, 1F; β-F), −158.57 (s, 2F; β-F), −158.72 (s, 1F; β-F), −160.44–−162.55 ppm (14F; *m*-F); UV/Vis (CH_2Cl_2): $\lambda_{max} = 385$, 607 nm; FABMS: *m*/*z* (% intensity): 1938 (100) [M^+]

[36]octaphyrin: ^{1}H NMR (500 MHz, $CDCl_3$, 223 K): $\delta = 13.79$ (s, 1H; NH), 12.42 (s, 1H; NH), 11.30 (1H; NH), 7.97 ppm (1H; NH); UV/Vis (CH_2Cl_2): λ_{max} (ε[M^{-1} cm^{-1}]) = 616 (68000), 576 (74000), 401 nm (53000); FABMS: *m*/*z* (% intensity): 2236 (100) [M^+]

[38]octaphyrin: ^{1}H NMR (500 MHz, $CDCl_3$, 296 K): $\delta = 7.96$ (1H; NH), 7.46 (s, 1H; NH), 7.19 (s, 1H; NH), 5.39 (1H; NH), 5.31 (s, 1H; NH), 5.23 ppm (s, 1H; NH); ^{19}F NMR (470.40 MHz, $CDCl_3$, 297 K, C_6F_6): $\delta = -135.72$ (d, $^3J = 24.5$ Hz, 1F; *o*-F), −136.56 (d, $^3J = 21.2$ Hz, 1F; *o*-F), −136.68 (d, $^3J = 18.3$ Hz, 1F; *o*-F), −137.12 (d, $^3J = 21.2$ Hz, 1F; *o*-F), −139.62 (d, $^3J = 21.2$ Hz, 1F; *o*-F), −139.80 (d, $^3J = 21.6$ Hz, 1F; *o*-F), −140.43 (d, $^3J = 21.6$ Hz, 1F; *o*-F), −140.92 (d, $^3J = 27.8$, 1F; *o*-F), −141.88 (m, 2F; *o*-F), −142.34 (brs, 1F; *o*-F), −142.70 (d, $^3J = 24.5$ Hz, 1F; *o*-F), −143.65 (brs, 1F; *o*-F), −145.13 (brs, 1F; *o*-F), −147.10 (brs, 1F; *o*-F), −147.60 (m, 1F; *o*-F), −148.95 (s, 1F; β-F), −149.42 (t, $^3J = 33.9$ Hz, 5F; *p*-F), −149.72 (s, 1F; β-F), −150.48 (s, 5F; β-F), −151.09 (t, $^3J = 18.3$ Hz, 1F; *p*-F), −151.46 (t, $^3J = 18.3$ Hz, 1F; *p*-F), −151.56 (s, 1F; β-F), −151.94 (t, $^3J = 21.6$ Hz, 1F; *p*-F), −152.53 (s, 1F; β-F), −153.71 (s, 1F; β-F), −154.69 (s, 1F; β-F), −155.18 (s, 1F; β-F), −157.20 (s, 1F; β-F), −157.42 (s, 1F; β-F), −158.21 (s, 1F; β-F), −164.18 (s, 1F; β-F), −158.41–−163.84 ppm (16F; *m*-F); UV/Vis (CH_2Cl_2): λ_{max} (ε[M^{-1} cm^{-1}]) = 681 nm (154000); FABMS: *m*/*z* (% intensity): 2238 (100) [M^+]

 © 2003 Wiley-VCH Verlag GmbH & Co. KGaA, Weinheim 1433-7851/03/4201-0081 $ 20.00+.50/0

UV/Vis spectrum ([28]hexaphyrin, [32]heptaphyirn, and [36]octaphyrin), whereas the [4*n*+2]-π electronic systems have a remarkably sharp Soret-like band with several Q-band-like low energy absorption bands ([26]hexaphyrin and [38]octaphyrin). This trend seems to suggest that the Hückel rule may still be valid for the prediction of absorption properties of the *meso*-aryl-substituted expanded porphyrins. However, the upfield shifts for the inner NH protons of [38]octaphyrin are only modest, thus not indicating a strong ring current. The detailed analysis of the X-ray structure has revealed an alternation in the bond length of this octaphyrin, thus posing a question on the aromaticity of this large expanded porphyrin macrocycle.

In summary, a range of perfluorinated *meso*-aryl-substituted expanded porphyrins are readily formed from the reaction of 3,4-difluropyrrole and pentafluorobenzaldehyde followed by the oxidation with DDQ. Of these, the solid-state structures of the perfluorinated [28]hexaphyrin and [36]octaphyrin are markedly different from those of their β-H counterparts. The [36]octaphyrin has been reduced with $NaBH_4$ to [38]octaphyrin and generated large structural changes. Furthermore, the perfluorinated heptaphyrin has been shown to be readily converted into its fused form upon treatment with alcohol. The absorption spectral characteristics have been found to be a function of the number of π electrons. The porphyrin-like sharp Soret band and low-energy Q-band-like bands are observed for macrocycles with [4*n*+2]-π electrons, which do not exhibit a strong ring current effect. The applications of these perfluorinated expanded porphyrins as robust oxidation catalysts and as long-wavelength absorbing dyes are interesting future targets and such studies are actively in progress.

Received: August 9, 2002 [Z19941]

[1] a) J. L. Sessler, A. Gebauer, S. J. Weghorn, *The Porphyrin Handbook, Vol. 2* (Eds.: K. M. Kadish, K. M. Smith, R. Guilard), Academic Press, San Diego, **1999**, chap. 9; b) E. Vogel, *J. Heterocycl. Chem.* **1996**, *33*, 1461; c) T. D. Lash, *Angew. Chem.* **2000**, *112*, 1833; *Angew. Chem. Int. Ed.* **2000**, *39*, 1763; d) B. Franck, A. Nonn, *Angew. Chem.* **1995**, *107*, 1941; *Angew. Chem. Int. Ed. Engl.* **1995**, *34*, 1795.

[2] a) J. L. Sessler, M. J. Cyr, V. Lynch, E. MaGhee, J. A. Ibers, *J. Am. Chem. Soc.* **1990**, *112*, 2810; b) J. L. Sessler, T. Morishima, V. Lynch, *Angew. Chem.* **1991**, *103*, 1018; *Angew. Chem. Int. Ed. Engl.* **1991**, *30*, 977; c) J. L. Sessler, S. J. Weghorn, V. Lynch, M. R. Johnson, *Angew. Chem.* **1994**, *106*, 1572; *Angew. Chem. Int. Ed. Engl.* **1994**, *33*, 1509; d) E. Vogel, M. Bröring, J. Fink, D. Rosen, H. Schmickler, J. Lex, K. W. K. Chan, Y.-D. Wu, D. A. Plattner, M. Nendel, K. N. Houk, *Angew. Chem.* **1995**, *107*, 2705; *Angew. Chem. Int. Ed. Engl.* **1995**, *34*, 2511; e) J. Setsune, S. Maeda, *J. Am. Chem. Soc.* **2000**, *122*, 12405; f) V. G. Anand, S. K. Pushpan, S. Venkatraman, A. Dey, T. K. Chandrashekar, B. S. Joshi, R. Roy, W. Teng, K. R. Senge, *J. Am. Chem. Soc.* **2001**, *123*, 8620; g) N. Sprutta, L. Latos-Grazynski, *Chem. Eur. J.* **2001**, *7*, 5099; h) D. Siedel, V. Lynch, J. L. Sessler, *Angew. Chem.* **2002**, *114*, 1480; *Angew. Chem. Int. Ed.* **2002**, *41*, 1422.

[3] a) J.-Y. Shin, H. Furuta, A. Osuka, *Angew. Chem.* **2001**, *113*, 639; *Angew. Chem. Int. Ed.* **2001**, *40*, 619; b) J.-Y. Shin, H. Furuta, K. Yoza, S. Igarashi, A. Osuka, *J. Am. Chem. Soc.* **2001**, *123*, 7190.

[4] *meso*-Pentafluorophenylhexaphyin has been prepared in a low yield under different conditions, see M. G. P. M. S. Neves, R. M. Martins, A. C. Tomé, A. J. D. Silvestre, A. M. S. Silva, V. Félix, M. G. B. Drew, J. A. S. Cavaleiro, *Chem. Commun.* **1999**, 385.

[5] E. K. Woller, V. V. Smirnov, S. G. DiMagno, *J. Org. Chem.* **1998**, *63*, 5706.

[6] Ring-expanded calixpyrroles were prepared by the reaction of acetone and 3,4-difluoropyrrole, see J. L. Sessler, P. Anzenbacher, Jr., J. A. Shrinver, K. Jursikova, V. M. Lynch, M. Marquez, *J. Am. Chem. Soc.* **2000**, *122*, 12061.

[7] a) S. Tsuchiya, M. Seno, *Chem. Lett.* **1989**, 263; b) E. K. Woller, S. G. DiMagno, *J. Org. Chem.* **1997**, *62*, 1588.

[8] This pentaphyrin product was considered to be a fused pentaphyrin as judged from its parent ion signal (*m*/*z* 1379) on the basis of FABMS, see ref. [3a]. We, however, noted the formation of nonfused pentaphyrin, the complete characterization of which could not be carried out because of its instability.

[9] Crystal data of [28]hexaphyrin **3**: $C_{66}H_4F_{42}N_6$, $M_r = 1678.7(1)$, triclinic, space group $P\bar{1}$, $a = 11.5000(5)$, $b = 14.7625(9)$, $c = 19.673(1)$ Å, $\alpha = 71.876(1)$, $\beta = 83.702(2)$, $\gamma = 86.999(2)°$, $V = 3154.4(3)$ Å^3, $Z = 2$, $\rho_{calcd} = 1.822$ g cm^{-3}, $T = 123$ K, crystal size $0.50 \times 0.20 \times 0.10$ mm^3, $R = 0.071$, $R_w = 0.081$, GOF = 2.177 for 10238 reflections with $I > 2.0\sigma(I)$. CCDC-185842 (**3**), CCDC-185846 (MeO-**4**–HF), CCDC-185847 (**5**), and CCDC-190412 (**5**+2H) contains the supplementary crystallographic data for this paper. These data can be obtained free of charge via www.ccdc.cam.ac.uk/conts/retrieving.html (or from the Cambridge Crystallographic Data Centre, 12, Union Road, Cambridge CB21EZ, UK; fax: (+44) 1223-336-033; or deposit @ccdc.cam.ac.uk).

[10] Crystal data of methanol-adduct of N-fused [32]heptaphyrin MeO-**4**–HF: $C_{78}H_6F_{47}N_7O$, $M_r = 1949.8(5)$, triclinic, space group $P\bar{1}$, $a = 14.4773(7)$, $b = 16.305(2)$, $c = 17.212(2)$ Å, $\alpha = 96.39(1)$, $\beta = 110.150(4)$, $\gamma = 92.28(1)°$, $V = 3777.4(7)$ Å^3, $Z = 2$, $\rho_{calcd} = 1.807$ g cm^{-3}, $T = 123$ K, crystal size $0.10 \times 0.10 \times 0.05$ mm^3, $R = 0.092$, $R_w = 0.094$, GOF = 0.120 for 8688 reflections with $I > 2.0\sigma(I)$.

[11] In a similar manner, the single crystals of a fused heptaphyrin obtained from a solution of CH_2Cl_2 and *i*PrOH showed the almost same crystal structure (see Supporting Information).

[12] Crystal data of [36]octaphyrin **5**: $C_{88}H_4F_{56}N_8$, $M_r = 2235.9(7)$, triclinic, space group $P\bar{1}$, $a = 11.0672(2)$, $b = 13.8090(9)$, $c = 19.033(1)$ Å, $\alpha = 93.641(2)$, $\beta = 96.243(4)$, $\gamma = 108.931(3)°$, $V = 2719.9(2)$ Å^3, $Z = 1$, $\rho_{calcd} = 1.720$ g cm^{-3}, $T = 123$ K, crystal size $0.50 \times 0.25 \times 0.25$ mm^3, $R = 0.081$, $R_w = 0.087$, GOF = 2.366 for 9209 reflections with $I > 2.0\sigma(I)$.

[13] Quite recently, a completely flat ring-shape [30]octaphyrin(0.0.0.0.0.0.0.0) was reported, see: ref. [2h].

[14] Crystal data of [38]octaphyrin (**5** + 2H): $C_{88}H_6F_{56}N_8$, $M_r = 2237.9(8)$, triclinic, space group $P\bar{1}$, $a = 13.839(2)$, $b = 18.629(2)$, $c = 19.712(2)$ Å, $\alpha = 61.763(3)$, $\beta = 74.599(5)$, $\gamma = 71.470(8)°$, $V = 4204.4(9)$ Å^3, $Z = 2$, $\rho_{calcd} = 1.802$ g cm^{-3}, $T = 123$ K, crystal size $0.20 \times 0.20 \times 0.05$ mm^3, $R = 0.084$, $R_w = 0.104$, GOF = 1.216 for 5530 reflections with $I > 2.0\sigma(I)$.

 © 2003 Wiley-VCH Verlag GmbH & Co. KGaA, Weinheim 1433-7851/03/4201-0082 $ 20.00+.50/0

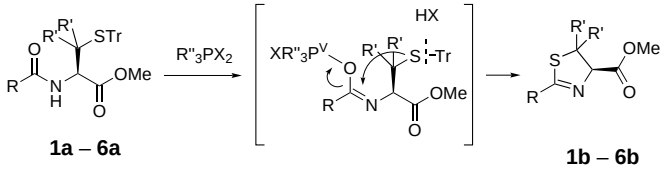
Biomimetic Heterocycle Synthesis

A Biomimetic Synthesis of Thiazolines Using Hexaphenyloxodiphosphonium Trifluoromethanesulfonate**

*Shu-Li You, Hossein Razavi, and Jeffery W. Kelly**

Thiazoline heterocycles are found in many bioactive natural products of peptide origin.[1] This substructure confers conformational rigidity and serves as a recognition site for DNA, RNA, and protein binding. Thiazolines are biosynthesized from peptides by nucleophilic attack of the cysteine thiol group on the amide carbonyl group of the preceding residue, followed by dehydration.[2] Although the biosynthesis of thiazolines employs cysteine residues, most chemical syntheses use serine residues, whereby the side chain is transformed into an electrophile that is attacked by the thioamide group of the preceding residue.[3] Here we report a facile and efficient biomimetic synthesis of thiazolines by treating N-acylated cysteine substrates with hexaphenyloxodiphosphonium trifluoromethanesulfonate to activate the amide group. The reaction proceeds in high yield with retention of configuration at the C4- and C2-exomethine carbon atoms of the thiazoline. Previous reports describe the scope and limitations of a mechanistically similar transformation with a Ti^{IV} reagent.[4]

Dehydrocyclization of a fully protected *N*-acyl cysteine residue requires activation of the amide bond, as well as deprotection of the side chain. We envisioned that the oxophilicity and Lewis acidity of phosphonium salts or phosphoranes should enable them to perform both transformations simultaneously (Scheme 1). To test this hypothesis, a number of commercially available or easily prepared



Scheme 1. Proposed mechanism for the synthesis of thiazolines with a P^V reagent.

phosphonium salts and phosphoranes were evaluated, a few of which are outlined in Table 1. We discovered that phosphorus reagent **C**, derived from triphenylphosphane oxide and triflic anhydride, converted fully protected cysteine **1a** (Scheme 1; R = Ph, R′ = H) to the corresponding thiazoline **1b** (Table 1, entry 3). Interestingly, phosphorus reagents **A** and **B** did not react with **1a** (Table 1, entries 1 and 2).

Although reagent **C** is known to activate and dehydrate amide carbonyl groups to afford nitriles, likely through a oxo-bridged diphosphonium salt,[5–6] its structure has never been conclusively determined.[7] Hence, this water-sensitive phosphorus reagent was crystallized, and X-ray diffraction revealed an O-bridged bis-phosphonium salt (Figure 1).

To ensure that the solid-state structure is relevant to the reactive species in solution, the ^{31}P NMR spectrum of the crystallized reagent was compared to those of reagents

Table 1: Synthesis of thiazoline **1b** from **1a** under a variety of reaction conditions.[a]

Entry	Reagent[b]	Solvent	*t*	Yield [%][c]	*ee* [%][d]
1	**A**	CH_2Cl_2	48 h	–	–
2	**B**	CH_2Cl_2	48 h	–	–
3	**C**	CH_2Cl_2	10 min	98	> 99.5
4[e]	**C**	Et_2O	48 h	98	> 99.5
5	**C**	THF	48 h	75	> 99.5
6	**C**	CH_3CN	10 min	96	> 99.5

[a] Reactions were carried out at 0 °C unless otherwise indicated. [b] **A**: hexamethylphosphoramide (3.0 equiv)/Tf_2O (1.5 equiv); **B**: Ph_3PBr_2 (1.5 equiv); **C**: Ph_3PO (3.0 equiv)/Tf_2O (1.5 equiv). [c] Yield of isolated product based on **1a**. Treating **1a** with triflic anhydride alone affords 55% yield of **1b**. [d] Determined by HPLC on a Chiralcel OD column. [e] Reaction at 25 °C.

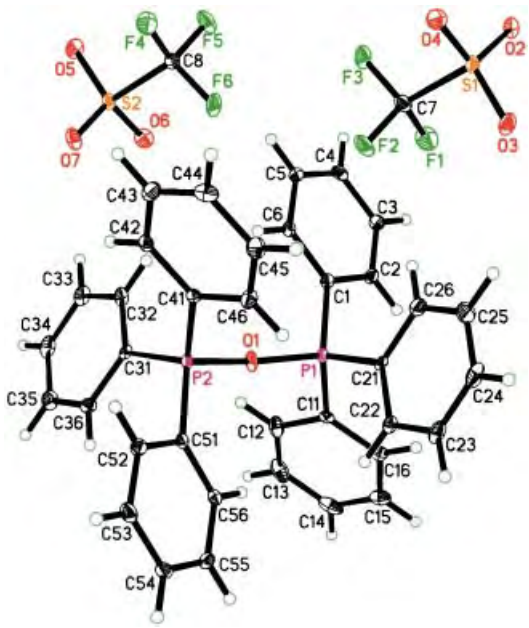


Figure 1. X-ray crystal structure of phosphorus reagent **C**. CCDC-192890 contains the supplementary crystallographic data for this paper. These data can be obtained free of charge via www.ccdc.cam.ac.uk/conts/retrieving.html (or from the Cambridge Crystallographic Data Centre, 12, Union Road, Cambridge CB21EZ, UK; fax: (+ 44) 1223-336-033; or deposit@ccdc.cam.ac.uk).

[*] Prof. J. W. Kelly, S.-L. You, H. Razavi
Department of Chemistry and
The Skaggs Institute of Chemical Biology
The Scripps Research Institute
La Jolla, CA 92037 (USA)
Fax: (+1) 858-784-9899
E-mail: jkelly@scripps.edu

[**] We gratefully acknowledge NIH grant GM63212 and the Skaggs Institute of Chemical Biology for generous financial support and a postdoctoral fellowship (H.R.). We thank Professor Dale Boger for use of his analytical chiral HPLC, Dr. Raj K. Chadha for the X-ray structure determination, and Professor Evan T. Powers for helpful discussions.

Supporting information for this article is available on the WWW under http://www.angewandte.org or from the author.

 © 2003 Wiley-VCH Verlag GmbH & Co. KGaA, Weinheim 1433-7851/03/4201-0083 $ 20.00+.50/0

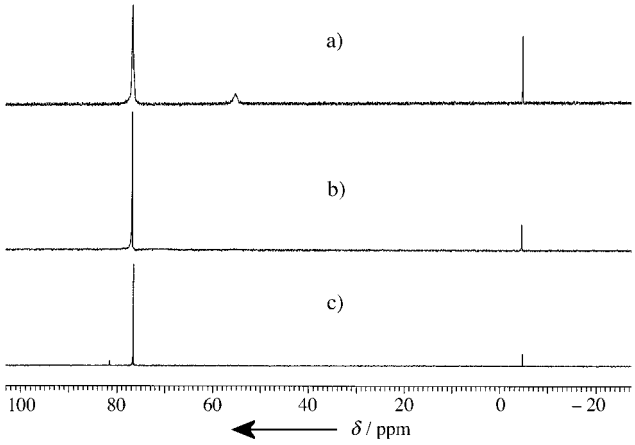


Figure 2. ^{31}P NMR spectra of crystallized **C**, and of **C** prepared in solution. All spectra were recorded in CD_3CN at 400 MHz (Ph_3P as the internal standard in a microtube, $\delta = -4.7$ ppm). a) Crystallized reagent **C**; b) Ph_3PO (2 equiv) and Tf_2O (1 equiv); c) Ph_3PO (1 equiv) and Tf_2O (1 equiv).

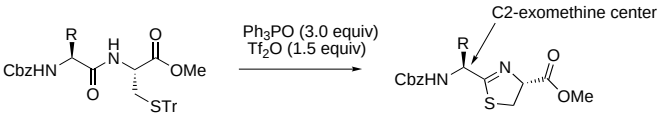
generated with different reaction stoichiometries of triphenylphosphane oxide and triflic anhydride (Figure 2). This study showed that reagent **C**, characterized crystallographically (Figure 1), is the sole species in solution, irrespective of whether one or two equivalents of triflic anhydride are used with two equivalents of triphenylphosphane oxide.

To examine the scope and limitations of this reaction, a few fully protected cysteine *N*-amide derivatives were synthesized and subjected to the optimized reaction conditions (Table 2). In general, these reactions afforded optically pure products in moderate to high yields, without any appreciable substituent effects on stereoselectivity. Lower optical purity was observed only with the *p*-NO_2-substituted substrate with extended reaction time (over 15 min). It is feasible to utilize a catalytic amount of triphenylphosphane oxide in the preparation of thiazoline **1b** without a significant decrease in yield or stereoselectivity (Table 2, entry 6).

To apply this mild method to the synthesis of thiazolines from peptides, four Cbz-protected dipeptides were synthesized (**7a**–**10a**, see Table 3). Thiazolines derived from these dipeptides are of particular interest, since these motifs are routinely found in bioactive marine metabolites.[2,8] In all cases, thiazolines were synthesized in high yields and with minimal loss of stereochemical integrity at the C2-exomethine centers.

To demonstrate the utility of this method in one-pot tandem cyclodehydrations, the fully protected Cys–Cys dipeptide **11a** was synthesized.[9] The reaction of this substrate was sluggish at 0 °C. However, it proceeded smoothly at ambient temperature to give the corresponding thiazole–thiazoline product **11b** in very high chemical yield and optical purity (Scheme 2). Rapid selective oxidation of bis-thiazolines to thiazole–thiazoline products was previously established.[1a,b,10]

Table 3: Synthesis of thiazolines from cysteine-containing dipeptides.[a]



7a–10a **7b–10b**

R	*T* [°C]	*t* [min]	Starting material (d.r.)	Yield [%][b]	Product (d.r.)[d]	*ee* [%][d]
Bn	0	10	**7a** (>99:1)	84	**7b** (93:7)[c]	>99.5
Bn	−20	120	**7a** (>99:1)	98	**7b** (97:3)[c]	>99.5
Me	−20	120	**8a** (99:1)	84	**8b** (91:9)	>99.5
*i*Pr	−20	120	**9a** (98:2)	86	**9b** (97:3)	>99.5
*s*Bu	−20	120	**10a** (96:4)	95	**10b** (96:4)	>99.5

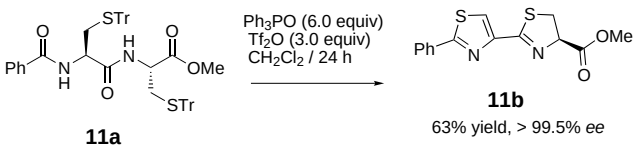
[a] Reactions with 3 equiv Ph_3PO and 1.5 equiv Tf_2O in dichloromethane. [b] Yields of isolated products. Treatment of the protected dipeptide **7a** with triflic anhydride alone yields a very complex reaction mixture. [c] Diastereomeric ratio of the crude reaction mixture was determined by NMR spectroscopy at 500 MHz. [d] Diastereomeric ratio was determined by HPLC on a Chiralcel OD or OD-H column; *ee* is that of the major product.

Table 2: Synthesis of thiazolines from simple cysteine derivatives under optimized conditions.[a]

Entry	Substrate (config.)	R	R′	Product (Yield [%])[b]	*ee* [%][c]
1	**2a** (D)	Ph	H	**2b** (98)	>99.5
2	**3a** (L)	Ph	Me	**3b** (98)	99
3	**4a** (L)	4-$MeOC_6H_4$	H	**4b** (92)	>99.5
4[d]	**5a** (L)	4-$NO_2C_6H_4$	H	**5b** (86)	>99.5
5	**6a** (L)	$PhCH_2CH_2$	H	**6b** (84)	>99.5
6[e]	**1a** (L)	Ph	H	**1b** (96)	>99.5

[a] Reactions were carried out with 3 equiv Ph_3PO and 1.5 equiv Tf_2O in dichloromethane at 0 °C for 10 min. [b] Yield of isolated product based on the cysteine substrate. [c] Determined by HPLC on a Chiralcel OD column. [d] The reaction was quenched after 5 min. [e] Reaction with 0.1 equiv Ph_3PO and 1.5 equiv Tf_2O in dichloromethane at 0 °C for 60 min.

In conclusion, the O-bridged bistriphenylphosphonium salt **C** promotes deprotection and dehydrocyclization of simple cysteine *N*-amides to give the corresponding thiazolines in excellent chemical and optical yields. This mild method was extended to the synthesis of thiazolines from



11a **11b**
63% yield, > 99.5% *ee*

Scheme 2. Synthesis of a thiazole–thiazoline bisheterocycle from a fully protected Cys–Cys dipeptide.

 © 2003 Wiley-VCH Verlag GmbH & Co. KGaA, Weinheim 1433-7851/03/4201-0084 $ 20.00+.50/0

cysteine-containing dipeptides in high yield and without significant loss of chirality at the C2-exomethine carbon atom. Finally, the application of this method to one-pot tandem dehydrocyclizations afforded a thiazole–thiazoline product in good overall yield and with excellent stereocontrol.

Experimental Section

General procedure for synthesis of thiazolines: Trifluoromethanesulfonic anhydride (50 μL, 0.3 mmol) was added slowly to a solution of triphenylphosphane oxide (167 mg, 0.6 mmol) in dry CH_2Cl_2 (2 mL) at 0 °C. The reaction mixture was stirred for 10 min at 0 °C and then adjusted to the desired reaction temperature, followed by addition of the fully protected cysteine *N*-amide (0.2 mmol). The reaction progress was monitored by TLC. The reaction mixture was quenched with 10% aqueous $NaHCO_3$ solution. The aqueous layer was extracted with CH_2Cl_2, and the combined organic layers were dried over Na_2SO_4, filtered, and concentrated. The resultant crude product was purified by flash chromatography with EtOAc/hexanes. More details and characterization data of the products can be found in the Supporting Information.

Received: July 26, 2002 [Z19833]

[1] a) S. Carmeli, R. E. Moore, G. M. L. Patterson, T. H. Corbett, F. A. Valeriote, *J. Am. Chem. Soc.* **1990**, *112*, 8195; b) S. Carmeli, R. E. Moore, G. M. L. Patterson, *Tetrahedron Lett.* **1991**, *32*, 2593; c) R. J. Boyce, G. C. Mulqueen, G. Pattenden, *Tetrahedron* **1995**, *51*, 7321; d) for reviews, see P. Wipf, *Chem. Rev.* **1995**, *95*, 2115.

[2] a) H. M. Patel, C. T. Wash, *Biochemistry* **2001**, *40*, 9023; b) for reviews, see R. S. Roy, A. M. Gehring, J. C. Milne, P. J. Belshaw, C. T. Wash, *Nat. Prod. Rep.* **1999**, *16*, 249.

[3] a) C. D. J. Boden, G. Pattenden, *J. Chem. Soc. Perkin Trans. 1* **2001**, 875; b) P. Wipf, P. C. Fritch, *Tetrahedron Lett.* **1994**, *35*, 5397; c) P. Wipf, P. C. Fritchm, *J. Am. Chem. Soc.* **1996**, *118*, 12358; d) B. Mckeever, G. Pattenden, *Tetrahedron Lett.* **2001**, *42*, 2573; e) P. Wipf, Y. Uto, *J. Org. Chem.* **2000**, *65*, 1037.

[4] a) M. A. Walker, C. H. Heathcock, *J. Org. Chem.* **1992**, *57*, 5566; b) R. L. J. Parsons, C. H. Heathcock, *Synlett* **1996**, 1168; c) P. Raman, H. Razavi, J. W. Kelly, *Org. Lett.* **2000**, *2*, 3289.

[5] J. B. Hendrickson, S. M. Schwartzman, *Tetrahedron Lett.* **1975**, 277.

[6] Other applications of this reagent: a) J. B. Hendrickson, M. S. Hussoin, *J. Org. Chem.* **1987**, *52*, 4137; b) J. B. Hendrickson, M. S. Hussoin, *Synthesis* **1989**, 217; c) J. B. Hendrickson, M. S. Hussoin, *Synlett* **1990**, 423; d) J. B. Hendrickson, M. A. Walker, A. Varvak, M. S. Hussoin, *Synlett* **1996**, 661; e) F. Yokokawa, Y. Hamada, T. Shioiri, *Synlett* **1992**, 153.

[7] A. Aaberg, T. Gramstqd, S. Husebye, *Tetrahedron Lett.* **1979**, 2263.

[8] L. A. Morris, J. J. Kettenes van den Bosch, K. Versluis, G. S. Thompson, M. Jaspars, *Tetrahedron* **2000**, *56*, 8345.

[9] Compounds were synthesized in solution by standard protocols using 1-hydroxybenzotriazole (HOBT, 1.1 equiv), 2-(1*H*-benzotriazol-1-yl)-1,1,3,3-tetramethyluronium hexafluorophosphate (HBTU, 1.1 equiv), and diisopropylethylamine (DIEA, 2.1 equiv) in DMF to mediate amide bond formation.

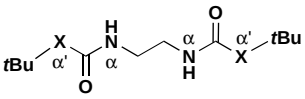
[10] A. B. Charette, P. Chua, *J. Org. Chem.* **1998**, *63*, 908.

H-Bond-Supported Oxo Bridges

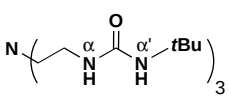
Hydrogen Bonds around $M(\mu\text{-}O)_2M$ Rhombs: Stabilizing a $\{Co^{III}(\mu\text{-}O)_2Co^{III}\}$ Complex at Room Temperature**

*Peter L. Larsen, Terry J. Parolin, Douglas R. Powell, Michael P. Hendrich, and A. S. Borovik**

Species with $\{M(\mu\text{-}O)_2M\}$ rhombs containing late 3d transition metal ions are proposed as key intermediates in biological and chemical processes.[1–4] Studies on metalloenzymes suggest that noncovalent interactions between the protein-derived active-site structures and the $\{M(\mu\text{-}O)_2M\}$ cores are often necessary for function.[1b,5] These types of interactions, such as hydrogen bonds (H-bonds), are often difficult to replicate in synthetic systems,[6] which may partially explain the thermal instability of many complexes containing $\{M(\mu\text{-}O)_2M\}$ cores: reported examples that contain Co^{III}, Ni^{III}, and Cu^{III} ions are only stable at temperatures below −20 °C. Herein we describe the preparation and characterization of $[Co^{III}H_2\mathbf{1}(\mu\text{-}O)]_2^{2-}$, which is stable at room temperature, in part, because of intramolecular H-bonds that form with the bridging oxo ligands of the $\{Co^{III}(\mu\text{-}O)_2Co^{III}\}$ core. These results add to the growing body of evidence that demonstrates the importance of noncovalent interactions in regulating the properties of metal–oxo complexes.



$H_4\mathbf{1}$ X = NH
$H_2\mathbf{2}$ X = O



$H_6\mathbf{3}$

We have recently shown that monomeric Fe^{III} and Mn^{III} complexes with a terminal oxo or hydroxo ligand can be isolated by confining the $\{M^{III}\text{–}O(H)\}$ units within rigid H-bond cavities.[7] These complexes were prepared with the

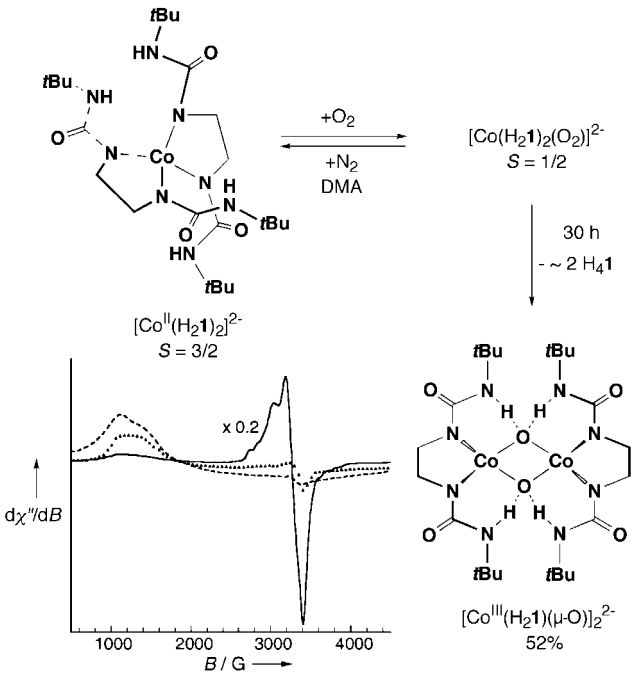
[*] Prof. Dr. A. S. Borovik, P. L. Larsen, Dr. D. R. Powell
Department of Chemistry
University of Kansas
2010 Malott Hall, 1251 Wescoe Dr., Lawrence, KS 66045-7582 (USA)
Fax: (+1) 785-864-5396
E-mail: aborovik@ku.edu
T. J. Parolin, Prof. Dr. M. P. Hendrich
Department of Chemistry
Carnegie Mellon University
Pittsburgh, PA 15213 (USA)

[**] Acknowledgement is made to the NIH (GM50781 to A.S.B. and GM49970 to M.P.H.) for financial support of this research. The X-ray diffraction instrumentation was purchased with funds from the National Science Foundation (CHE-0079282) and the University of Kansas. We thank Drs. C. E. MacBeth and R. Gupta, and Professor T. N. Sorrell for helpful discussions.

Supporting information for this article is available on the WWW under http://www.angewandte.org or from the author.

tripodal ligand $[H_3\mathbf{3}]^{3-}$, which uses monodeprotonated *N*-ethylene-*N*′-*tert*-butyl-urea groups as a scaffold for the H-bond cavity. While useful to generate these unique monomeric complexes, $[H_3\mathbf{3}]^{3-}$ has yet to yield polynuclear species with single-atom bridges. In contrast, $[H_2\mathbf{1}]^{2-}$ has a less constrained H-bond framework that could support complexes with bridging groups, such as oxo ligands. Deprotonation of the urea α-NH groups in $H_4\mathbf{1}$ generate N^- sites, which bind to metal ions. The α′-NH groups remain protonated and serve as H-bond donors to other coordinated ligands. Intramolecular H-bonds are expected because thermodynamically favored six-membered rings are formed. Because urea groups have been successfully used to promote the formation of H-bonds to terminal M–O units, we anticipated that a similar type of intramolecular interaction would aid in the isolation of complexes with $\{M(\mu\text{-}O)_2M\}$ rhombs.

The preparation of $[Co^{III}H_2\mathbf{1}(\mu\text{-}O)]_2^{2-}$ is outlined in Scheme 1. Bubbling dry O_2 through a solution of the four-coordinate $[Co^{II}(H_2\mathbf{1})_2]^{2-}$ [8] complex ($E_{1/2} = -0.33$ V versus a saturated calomel electrode (SCE)) in *N*,*N*-dimethylacetamide (DMA) at room temperature produces observable changes in the optical and EPR spectra. In the presence of excess O_2, $[Co^{II}(H_2\mathbf{1})_2]^{2-}$ (λ_{max} (ε_M) = 292 (2100), 498 (90), 575 nm (160)) converts to a species with $\lambda_{max} = 444$ nm. Concomitant changes are found in the EPR spectra; the broad X-band (9.3 GHz) EPR spectrum of the high-spin $[Co^{II}(H_2\mathbf{1})_2]^{2-}$ complex ($S = 3/2$) changes to a spectrum with *g* values centered around 2. These changes in spectral properties are consistent with the formation of a $Co–O_2$ adduct,[9] which is proposed to have the formula $[Co(H_2\mathbf{1})_2(O_2)]^{2-}$. This process is partially reversible; bubbling N_2 through a solution of $[Co(H_2\mathbf{1})_2(O_2)]^{2-}$ converts approximately 50% of the sample back to $[Co^{II}(H_2\mathbf{1})_2]^{2-}$ (inset, Scheme 1). The incomplete reversion of $[Co(H_2\mathbf{1})_2(O_2)]^{2-}$ to $[Co^{II}(H_2\mathbf{1})_2]^{2-}$ at room temperature implies that the $Co–O_2$ adduct reacts further to yield new cobalt species with ligands that may be derived from O_2. In fact, after 30 h at room temperature, a reddish-purple complex was isolated with absorbance features at $\lambda_{max}(\varepsilon_M) = 308$ (8500), 435 (4500), 518 (5500), and 1014 nm (370).



Scheme 1. Preparative route for $[Co^{III}H_2\mathbf{1}(\mu\text{-}O)]_2^{2-}$. Inset: X-band (9.3 GHz) EPR spectra measured at 4 K for $[Co^{II}(H_2\mathbf{1})]_2^{2-}$ (– – –), $[Co(H_2\mathbf{1})_2O_2]^{2-}$ (——), and $[Co(H_2\mathbf{1})_2O_2]^{2-}$ + N_2 (▲).

The identity of this reddish-purple complex was confirmed as $[Co^{III}H_2\mathbf{1}(\mu\text{-}O)]_2^{2-}$ by an X-ray diffraction study. $K_2[Co^{III}H_2\mathbf{1}(\mu\text{-}O)]_2\cdot 4\,DMA\cdot 0.5\,C_4H_{10}O\cdot 0.25\,H_2O$ crystallized in the orthorhombic space group $P2_12_12_1$, with four independent, but virtually identical, anions in the asymmetric unit (denoted $[Co^{III}H_2\mathbf{1}\mathbf{a}\text{–}\mathbf{d}(\mu\text{-}O)]_2^{2-}$). Figure 1 illustrates the molecular structure of $[Co^{III}H_2\mathbf{1}\mathbf{a}(\mu\text{-}O)]_2^{2-}$, with selected metrical parameters listed in the legend. Each Co^{III} ion in the $[Co^{III}H_2\mathbf{1}(\mu\text{-}O)]_2^{2-}$ unit is ligated by two urea nitrogen and two oxo-bridging oxygen atoms in a distorted square planar arrangement. The planes formed by N8a-Co1a-N11a and N23a-Co2a-N28a are twisted 26.6 and 27.0°, respectively, from the planar $Co^{III}(\mu\text{-}O)_2Co^{III}$ core. Four-coordinate Co^{III} complexes are rare[10] and typically have square-planar coordination geometry. The distortions from planarity in the $[Co^{III}H_2\mathbf{1}(\mu\text{-}O)]_2^{2-}$ ion are only exceeded by a Co^{III} complex with a tetraazamacrocyclic tropocoronand ligand, which has a 41° twist angle.[10g]

In $[Co^{III}H_2\mathbf{1}\mathbf{a}(O)]_2^{2-}$ the average Co^{III}–N and Co^{III}–O distances are 1.885(3) and 1.817(3) Å. Additional structural values include an average O_{oxo}-Co-O_{oxo} angle of 99.49(8)°, a

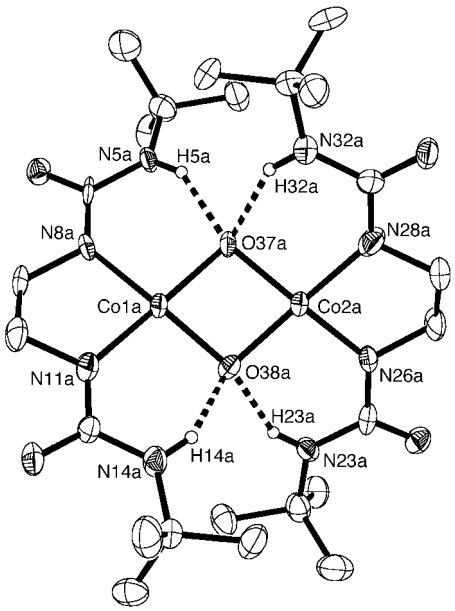


Figure 1. Molecular structure of $[Co^{III}H_2\mathbf{1}\mathbf{a}(\mu\text{-}O)]_2^{2-}$. Thermal ellipsoids are drawn at the 50% probability level and only urea hydrogen atoms are shown. Selected bond lengths [Å] and angles [°]: Co1a-O37a 1.799(5), Co1a-O38a 1.821(5), Co1a-N8a 1.890(6), Co1a-N11a 1.899(7), Co2a-O37a 1.814(5), Co2a-O38a 1.832(5), Co2a-N26a 1.849(6), Co2a-N30a 1.903(7), Co1a···Co2a 2.7368(13); O37a-Co1a-O38a 82.5(2), O37a-Co1a-N8a 98.2(2), O38a-Co1a-N8a 161.5(3), O37a-Co1a-N11a 162.9(3), O38a-Co1a-N11a 98.9(3), N8a-Co1a-N11a 85.9(3), O37a-Co2a-O38a 81.8(2), O37a-Co2a-N26a 162.6(3), O38a-Co2a-N26a 99.5(2), O37a-Co2a-N30a 98.2(2), O38a-Co2a-N30a 161.4(3), N26a-Co2a-N30a 86.1(3).

 © 2003 Wiley-VCH Verlag GmbH & Co. KGaA, Weinheim 1433-7851/03/4201-0086 $ 20.00+.50/0

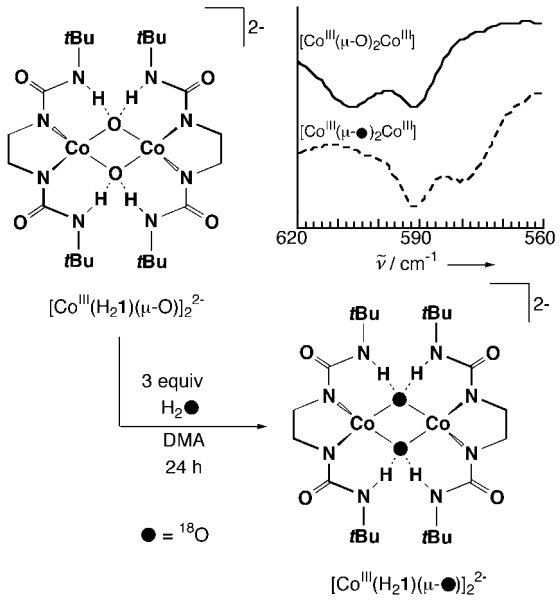
$Co^{III}\cdots Co^{III}$ separation of 2.736(1) Å, and an O···O separation of 2.375(4) Å. These metrical values are comparable to those found in the structures of other late 3d metal complexes containing $\{M(\mu\text{-}O)_2M\}$ rhombs. In particular, the structural parameters of the $\{Co^{III}(\mu\text{-}O)_2Co^{III}\}$ core within the $[Co^{III}H_2\mathbf{1}(\mu\text{-}O)]_2^{2-}$ ion nearly match those found in $[Co^{III}Tp^{Me_n}(\mu\text{-}O)]_2$ ($n=2,3$), the only other structurally characterized cobalt complexes with bis-μ-oxo cores.[3,11] For instance, $[Co^{III}Tp^{Me_3}(\mu\text{-}O)]_2$ (Tp^{Me_3} = hydrotris(3,4,5-trimethyl-1-pyrazolyl)borate), with five-coordinate Co^{III} centers, has a $Co^{III}\cdots Co^{III}$ separation of 2.728(2) Å and an O_{oxo}-Co-O_{oxo} angle of 99.3(2)°.

A unique structural feature of $[Co^{III}H_2\mathbf{1}(\mu\text{-}O)]_2^{2-}$ is the network of intramolecular H-bonds that surround the $\{Co^{III}(\mu\text{-}O)_2Co^{III}\}$ rhomb. Each bridging oxo ligand forms two intramolecular H-bonds with the urea α′-NH groups of the $[H_2\mathbf{1}]^{2-}$ ligands. All the $N_{urea}\cdots O_{oxo}$ separations are less than 2.75 Å, which is indicative of the presence of H bonds.[12] Support for this assignment comes from solid-state FTIR results on $[Co^{III}H_2\mathbf{1}(\mu\text{-}O)]_2^{2-}$ that show one broad peak for the $\tilde{\nu}$(NH) vibrations at 3184 cm^{-1}. This peak occurs at lower energy and is broader than the comparable signal found in $[Co^{II}(H_2\mathbf{1})_2]^{2-}$ ($\tilde{\nu}(NH)=3340\ cm^{-1}$), which does not contain intramolecular H-bonds.[8,13]

The presence of $NH\cdots O_{oxo}$ bonds in $[Co^{III}H_2\mathbf{1}(\mu\text{-}O)]_2^{2-}$ may explain its unusual stability at room temperature. $[Co^{III}H_2\mathbf{1}(\mu\text{-}O)]_2^{2-}$ can be prepared, purified, and stored for weeks at room temperature under anhydrous conditions without measurable decomposition. The urea α′-NH groups in $[Co^{III}H_2\mathbf{1}(\mu\text{-}O)]_2^{2-}$, which are strong H-bond donors, help control the secondary coordination sphere around the $\{Co^{III}(\mu\text{-}O)_2Co^{III}\}$ core. The combination of H-bond interactions and a highly anionic ligand field around the Co^{III} ions apparently provides enough stabilization to allow isolation of $[Co^{III}H_2\mathbf{1}(\mu\text{-}O)]_2^{2-}$ at room temperature. In contrast, other Co^{III}, Ni^{III}, and Cu^{III} complexes with an $\{M(\mu\text{-}O)_2M\}$ rhomb lack these features, and have limited lifetimes at room temperature. For instance, $[Co^{III}Tp^{Me_3}(\mu\text{-}O)]$ is only stable at or below −50 °C; at higher temperatures it decomposes through pathways that oxidize a methyl group on the Tp^{Me_3} ligands.[3a,e]

Frozen solutions of $[Co^{III}H_2\mathbf{1}(\mu\text{-}O)]_2^{2-}$ do not have observable X-band EPR spectra at either 4.2 or 77 K. This finding is consistent with magnetization studies carried out on solid samples of $K_2[Co^{III}H_2\mathbf{1}(\mu\text{-}O)]_2$ using a SQUID magnetometer in the temperature range of 5 to 250 K and an applied magnetic field of 0.5 T. A computer simulation of the data (Figure S1, Supporting Information) shows a large antiferromagnetic exchange interaction between the Co^{III} ions, with $J=-190(10)\ cm^{-1}$ for $S_1=S_2=1$ and $g_1=g_2=2.6$.[14] This strong coupling reflects the presence of two efficient exchange pathways furnished by the bis(μ-oxo) ligands.[15]

The oxo ligands in $[Co^{III}H_2\mathbf{1}(\mu\text{-}O)]_2^{2-}$ are exchangeable with water. Treating $[Co^{III}H_2\mathbf{1}(\mu\text{-}^{16}O)]_2^{2-}$ with 3 equivalents of $H_2{}^{18}O$ in DMA for 24 h affords the ^{18}O-labeled complex, $[Co^{III}H_2\mathbf{1}(\mu\text{-}^{18}O)]_2^{2-}$ (Scheme 2).[16] FTIR spectroscopy was used to evaluate the incorporation of the $[^{18}O]^{2-}$ ligands into the complex. The FTIR spectrum of $[Co^{III}H_2\mathbf{1}(\mu\text{-}^{16}O)]_2^{2-}$ has a peak at 607 cm^{-1} (inset, Scheme 2), which is tentatively



Scheme 2. Reaction of $[Co^{III}H_2\mathbf{1}(\mu\text{-}O)]_2^{2-}$ with ^{18}O-labeled water. Inset: FTIR spectra (Nujol) of $[Co^{III}(H_2\mathbf{1})(\mu\text{-}^{16}O)]_2^{2-}$ (——) and $[Co^{III}(H_2\mathbf{1})(\mu\text{-}^{18}O)]_2^{2-}$ (– – –). The peak at approximately 590 cm^{-1} is from DMA.

assigned as the $\tilde{\nu}_{asym}(Co^{III}(\mu\text{-}O)_2Co^{III})$ vibration.[17] In $[Co^{III}H_2\mathbf{1}(\mu\text{-}^{18}O)]_2^{2-}$ this peak is shifted to 580 cm^{-1}, which is the expected shift based on a harmonic Co–O oscillator model. $[Co^{III}H_2\mathbf{1}(\mu\text{-}^{18}O)]_2^{2-}$ can also be prepared from $[Co^{II}(H_2\mathbf{1})_2]^{2-}$ and 3 equivalents of $^{18}O_2$ by the procedure outlined in Scheme 1. This result suggests that the source of the oxo ligands in $[Co^{III}H_2\mathbf{1}(\mu\text{-}O)]_2^{2-}$ is derived from dioxygen. However, FTIR spectra of the product contain a small peak (less than 20%) at 607 cm^{-1}, indicating that $[Co^{III}H_2\mathbf{1}(\mu\text{-}^{16}O)]_2^{2-}$ is also present. Because water exchange with the $\{Co^{III}(\mu\text{-}O)_2Co^{III}\}$ core occurs in the same timeframe as dimer formation, we attribute the presence of the ^{16}O complex to oxo exchange of $[Co^{III}H_2\mathbf{1}(\mu\text{-}^{18}O)]_2^{2-}$ with adventitious $H_2{}^{16}O$ in the solvent.

To our knowledge, $[Co^{III}H_2\mathbf{1}(\mu\text{-}O)]_2^{2-}$ is the first complex where definitive evidence exists for the formation of H bonds to a $\{M(\mu\text{-}O)_2M\}$ rhomb. These noncovalent interactions are proposed to aid in extending the thermal stability of $[Co^{III}H_2\mathbf{1}(\mu\text{-}O)]_2^{2-}$ to a temperature more than 70 °C higher than reported for comparable cobalt complexes. Furthermore, $[H_2\mathbf{1}]^{2-}$ species can be readily modified to probe the influences of H bonds on metal ion reactivity; for example, the four-coordinate complex anion $[Co^{II}(\mathbf{2})_2]^{2-}$ has carbamate groups instead of urea groups, and therefore lacks the H-bond donors that are present in $[Co^{II}(H_2\mathbf{1})_2]^{2-}$. Preliminary studies show that the reaction between $[Co^{II}(\mathbf{2})_2]^{2-}$ and O_2 produces species that do not have spectroscopic properties consistent with complexes containing $\{Co^{III}(\mu\text{-}O)_2Co^{III}\}$ cores. Additional studies are planned to probe the formation and stabilization of the $\{M(\mu\text{-}O)_2M\}$ core at room temperature.

Experimental Section

$K_2[CoH_2\mathbf{1}(O)]_2$: A solution of $K_2[Co(H_2\mathbf{1})_2]\cdot 4DMA$[8] (0.705 g, 0.706 mmol) in DMA (10 mL) was purged with a stream of O_2 at

room temperature. After 25 min, the bubbling was discontinued and the reaction mixture was allowed to stir for 30 h. Volatiles were removed under reduced pressure and the resulting red-brown solid was dissolved in DMA (5 mL) and crystallized by layering with diethyl ether saturated with O_2. During crystallization a white solid was also obtained, the spectral properties of which matched those of H_4**1**. Analytically pure $K_2[CoH_2$**1**$(O)]_2$ was obtained after three recrystallizations to afford 0.174 g (0.183 mmol, 52%) of reddish-purple crystals. Elemental analysis (%) calcd for $K_2[CoH_2$**1**$(O)]_2 \cdot 2$DMA$\cdot 0.5 C_4H_{10}O \cdot 0.25 H_2O$ ($C_{34}H_{71.5}Co_2K_2N_{10}O_{8.75}$): C 42.69, H 7.53, N 14.63; found: C 42.89, H 7.51, N 14.65. FTIR (Nujol): $\tilde{\nu} = 3184$ (NH, b), 1640 (CO, s), 607 cm^{-1} (Co–O, m). ^{1}H NMR (500 MHz, [D$_6$]DMSO, 24 °C): $\delta = 84.1$ (s, 4H; -CH_2-), 74.1 (s, 4H; -CH_2-), 16.4 (s, 4H; NH), 0.5 ppm (s, 36H; $C(CH_3)_3$).

X-ray structural analysis for $K_2[Co^{III}H_2$**1**$(\mu\text{-}O)]_2 \cdot 4DMA\cdot 0.50 C_4H_{10}O \cdot 0.25 H_2O$: $0.37 \times 0.23 \times 0.12$ mm, orthorhombic, space group $P2_12_12_1$, $a = 18.8952(10)$, $b = 26.5923(14)$, $c = 46.360(2)$ Å; $V = 23\,294(2)$ Å^3, $\rho_{calcd} = 1.290$ Mg m^{-3}, $Z = 16$, $2\theta_{max} = 3.30$ to 50.00°; $Mo_{K\alpha}$ radiation ($\lambda = 0.71073$ Å), $F(000) = 9656$, $T = 100(2)$ K, total reflections = 131 198 collected on a Bruker SMART diffractometer equipped with an APEX CCD area detector, independent reflections = 45 748 ($R_{int} = 0.0539$), observed data = 32 000 ($I > 2\sigma(I)$), restraints(para)$^{-1}$ ratio = 1397(2752)$^{-1}$, absorption correction: SADABS, max(min) transmission, 0.9130(0.7632)$^{-1}$; direct methods, SHELXTL-V5.0; hydrogen atom positions were initially determined by geometry and refined by a riding model and nonhydrogen atoms were refined with anisotropic displacement parameters; full-matrix least-square refinement on F^2; $R1(wR2) = 0.0887$ (0.2413), GOF = 1.088, 3.957, -0.712 e Å^{-3}, residual based on $I > 2\sigma(I)$. The absolute structure was determined by refinement of the Flack parameter.[18] 16 DMA molecules, two diethyl ether molecules, and one water molecule were also present in the asymmetric unit. Five of the DMA molecules were disordered and modeled in two orientations. Restraints on the positional and displacement parameters of the disordered atoms were required for the refinement to converge.

Received: June 17, 2002
Revised: October 2, 2002 [Z19547]

[1] Recent review: a) J. Du Bois, T. J. Mizoguchi, S. J. Lippard, *Coord. Chem. Rev.* **2000**, *200–202*, 443 – 485; b) M. Merkx, D. A. Kopp, M. H. Sazinsky, J. L. Blazyk, J. Müller, S. J. Lippard, *Angew. Chem.* **2001**, *113*, 2860 – 2888; *Angew. Chem. Int. Ed.* **2001**, *40*, 2782 – 2807; c) L. Que, Jr., W. B. Tolman, *Angew. Chem.* **2002**, *114*, 1160 – 1185; *Angew. Chem. Int. Ed.* **2002**, *41*, 1114 – 1137.

[2] {$Cu^{III}(\mu\text{-}O)_2Cu^{III}$}, selected examples: a) J. A. Halfen, S. Mahapatra, E. C. Wilkinson, S. Kaderli, V. G. Young, Jr., L. Que, Jr., A. D. Zuberbühler, W. B. Tolman, *Science* **1996**, *271*, 1397 – 1400; b) W. B. Tolman, *Acc. Chem. Res.* **1997**, *30*, 227 – 237, and references therein; c) V. Mahadevan, Z. Hou, A. P. Cole, D. E. Root, T. K. Lal, E. I. Solomon, T. D. P. Stack, *J. Am. Chem. Soc.* **1997**, *119*, 11 996 – 11 997; d) S. Itoh, H. Nakao, L. M. Berreau, T. Kondo, M. Komatsu, S. Fukusumi, *J. Am. Chem. Soc.* **1998**, *120*, 2890 – 2899; e) M. J. Henson, P. Mukherjee, D. E. Root, T. D. P. Stack, E. I. Solomon, *J. Am. Chem. Soc.* **1999**, *121*, 10 332 – 10 345.

[3] {$Ni^{III}(\mu\text{-}O)_2Ni^{III}$} and {$Co^{III}(\mu\text{-}O)_2Co^{III}$}: a) S. Hikichi, M. Yoshizawa, Y. Sasakura, M. Akita, Y. Moro-oka, *J. Am. Chem. Soc.* **1998**, *120*, 10 567 – 10 568; b) K. Shiren, S. Ogo, S. Fujinami, H. Hayashi, M. Suzuki, A. Uehara, Y. Wantanabe, Y. Moro-oko, *J. Am. Chem. Soc.* **2000**, *122*, 254 – 262; c) S. Itoh, H. Bandoh, M. Nakagawa, S. Nagatomo, T. Kitagawa, K. D. Karlin, S. Fukusumi, *J. Am. Chem. Soc.* **2001**, *123*, 11 168 – 11 178; d) B. S. Mandimutsira, J. L. Yamarik, T. C. Brunold, W. Gu, S. P. Cramer, C. G. Riordan, *J. Am. Chem. Soc.* **2001**, *123*, 9194 – 9195; e) K. H. Theopold, O. M. Reinaud, D. Doren, R. Konecny in *3rd World Congress on Oxidation Catalysis*, (Eds.: R. K. Grasselli, S. T. Oyama, A. M. Gaffney, J. E. Lyons), Elsevier Science, New York, **1997**, pp. 1081 – 1088; f) S. Hikichi, M. Yoshizawa, Y. Sasakura, H. Komatsuzaki, Y. Moro-oka, M. Akita, *Chem. Eur. J.* **2001**, *7*, 5012 – 5028; f) D. E. Benson, A. E. Haddy, H. W. Hellinga, *Biochemistry* **2002**, *41*, 3262 – 3269.

[4] {$Fe(\mu\text{-}O)_2Fe$}: a) Y. Dong, H. Fujii, M. P. Hendrich, R. A. Leising, G. Pan, C. R. Randall, E. C. Wilkinson, Y. Zang, L. Que, Jr., B. G. Fox, K. Kaffmann, E. Münck, *J. Am. Chem. Soc.* **1995**, *117*, 2778 – 2792; b) H. Zheng, Y. Zang, Y. Dong, V. G. Young, Jr., L. Que, Jr., *J. Am. Chem. Soc.* **1999**, *121*, 2226 – 2235, and references therein; c) H.-F. Hsu, Y. Dong, L. Shu, V. G. Young, Jr., L. Que, Jr., *J. Am. Chem. Soc.* **1999**, *121*, 5230 – 5237; d) M. Costa, J.-U. Rohde, A. Stubna, R. Y. N. Ho, L. Quaroni, E. Münck, L. Que, Jr., *J. Am. Chem. Soc.* **2001**, *123*, 12 931 – 12 932.

[5] B. D. Dunietz, M. D. Beachy, Y. Cao, D. A. Whittington, S. J. Lippard, R. A. Friesner, *J. Am. Chem. Soc.* **2000**, *122*, 2828 – 2839.

[6] Selected examples: a) G. E. Wuenshell, C. Tetreau, D. Lavalette, C. A. Reed, *J. Am. Chem. Soc.* **1992**, *114*, 3346 – 3355; b) J. P. Collman, X. Zhang, K. Wong, J. I. Brauman, *J. Am. Chem. Soc.* **1994**, *116*, 6245 – 6251; c) M. Momenteau, C. A. Reed, *Chem. Rev.* **1994**, *94*, 659 – 698; d) J. E. Kickham, S. J. Loeb, S. L. Murphy, *J. Am. Chem. Soc.* **1993**, *115*, 7031 – 7032; e) D. M. Rudkevich, W. Verboom, Z. Brzozka, M. J. Palys, W. P. R. V. Stauthamer, G. J. Van Hummel, S. M. Franken, S. Harkema, J. F. J. Engbersen, D. N. Reinhoudt, *J. Am. Chem. Soc.* **1994**, *116*, 4341 – 4351; f) N. Kitajima, H. Komatsuzaki, S. Hikichi, M. Osawa, Y. Moro-oka, *J. Am. Chem. Soc.* **1994**, *116*, 11 596 – 11 597; g) P. H. Walton, K. N. Raymond, *Inorg. Chim. Acta* **1995**, *240*, 593 – 601; i) W. Yao, R. H. Crabtree, *Inorg. Chem.* **1996**, *35*, 3007 – 3011; h) A. Wada, M. Harata, K. Hasegawa, K. Jitsukawa, H. Masuda, M. Mukai, T. Kitagawa, H. Einaga, *Angew. Chem.* **1998**, *110*, 874 – 875; *Angew. Chem. Int. Ed.* **1998**, *37*, 798 – 799; i) C.-Y. Yeh, C. J. Chang, D. G. Nocera, *J. Am. Chem. Soc.* **2001**, *123*, 1513 – 1514.

[7] a) B. S. Hammes, V. G. Young, Jr., A. S. Borovik, *Angew. Chem.* **1999**, *111*, 744 – 746; *Angew. Chem. Int. Ed.* **1999**, *38*, 666 – 669; b) Z. Shirin, B. S. Hammes, V. G. Young, Jr., A. S. Borovik, *J. Am. Chem. Soc.* **2000**, *122*, 1836 – 1837; c) C. E. MacBeth, A. P. Golombek, V. G. Young, Jr., C. Yang, K. Kuczera, M. P. Hendrich, A. S. Borovik, *Science* **2000**, *289*, 938 – 941; d) C. E. MacBeth, B. S. Hammes, V. G. Young, Jr., A. S. Borovik, *Inorg. Chem.* **2001**, *40*, 4733 – 4741; e) R. Gupta, C. E. MacBeth, V. G. Young, Jr., A. S. Borovik, *J. Am. Chem. Soc.* **2002**, *124*, 1136 – 1137.

[8] C. E. MacBeth, P. L. Larsen, T. N. Sorrell, D. R. Powell, A. S. Borovik, *Inorg. Chim. Acta*, in press.

[9] a) F. A. Walker, *J. Am. Chem. Soc.* **1970**, *92*, 4235 – 4244; b) B. M. Hoffman, D. L. Diemente, F. Basolo, *J. Am. Chem. Soc.* **1970**, *92*, 61 – 65; c) F. A. Walker, J. Bowen, *J. Am. Chem. Soc.* **1985**, *107*, 7632 – 7635; d) J. H. Bowen, N. V. Shokhirev, A. M. Raitsimring, D. H. Buttlaire, F. A. Walker, *J. Am. Chem. Soc.* **1997**, *119*, 683 – 8691.

[10] Selected examples: a) R. Williams, E. Billig, J. H. Waters, H. B. Gray, *J. Am. Chem. Soc.* **1966**, *88*, 43 – 50; b) R. Fibar, S. A. Koch, M. M. Millar, *Inorg. Chem.* **1985**, *24*, 3311 – 3312; c) T. J. Collins, T. G. Richmond, B. D. Santarsiero, T. G. R. T. Treco, *J. Am. Chem. Soc.* **1986**, *108*, 2088 – 2090; d) C. P. Rao, J. R. Dorfman, R. H. Holm, *Inorg. Chem.* **1986**, *25*, 428 – 439; e) T. J. Collins, R. D. Powell, C. Slebodnick, E. S. Uffelman, *J. Am. Chem. Soc.* **1991**, *113*, 8419 – 8425; f) A. L. Balch, M. Mazzanti, B. C. Noll, M. M. Olmstead, *J. Am. Chem. Soc.* **1994**, *116*, 9114 – 9122; g) L. H. Doerrer, M. T. Bautista, S. J. Lippard, *Inorg. Chem.* **1997**, *36*, 3578 – 3579; h) T. Yagi, H. Hanai, T. Komorita,

 © 2003 Wiley-VCH Verlag GmbH & Co. KGaA, Weinheim 1433-7851/03/4201-0088 $ 20.00+.50/0

T. Suzuki, S. Kaizaki, *J. Chem. Soc. Dalton Trans.* **2002**, 1126–1131.
[11] A $[Co_8O_4]^{4+}$ cubane molecular aggregate has been characterized which contains $\{Co(\mu\text{-}O)_2Co\}$ units. The oxo ligands in this system interact with four cobalt centers. K. Dimitrou, J.-S. Sun, K. Folting, G. Christou, *Inorg. Chem.* **1995**, *34*, 4160–4166.
[12] a) J. Elmsley, *Chem. Soc. Rev.* **1980**, *9*, 91–124; b) M. C. Etter, *Acc. Chem. Res.* **1990**, *23*, 120–126.
[13] Shifts to lower energy and broadening of $\tilde{\nu}$(NH) signals are indicative of intramolecular H-bonds in organic compounds: see G. B. Liang, G. P. Dado, S. H. Gellman, *J. Am. Chem. Soc.* **1991**, *113*, 3994–3995.
[14] The Hamiltonian, $\mathscr{H} = -2JS_1S_2 + g_1\mu_B BS_1 + g_2\mu_B BS_2$ was used to fit the data. The data were corrected for ligand diamagnetism ($\chi_{dia} = 0.0067\,J(T)^{-2}mol^{-1}$), temperature-independent paramagnetism ($\chi_{TIP} = 0.022\,J(T)^{-2}mol^{-1}$), and a mononuclear cobalt impurity of less than 2%. The assignment of $S_1 = S_2 = 1$ is based on the magnetic properties determined for a previously reported four-coordinate monomeric Co^{III} complex.[10g] The magnetization data for $[Co^{III}H_2\mathbf{1}(\mu\text{-}O)]_2^{2-}$ can not distinguish between $S_1 = S_2 = 1$ or $S_1 = S_2 = 2$; the derived value of J from our data is the same for both calculations. The system spin manifolds for the former are $S = 0, 1, 2$ and the latter, $S = 0, 1, 2, 3, 4$. The ability to distinguish between these two systems requires the possibility of populating the $S = 3$ manifold. However, the large J value and temperature limitations of the instrument do not allow detection above a system spin value of $S = 2$.
[15] Strong antiferromagnetic coupling has also been observed in a complex containing an $\{Fe^{III}(\mu\text{-}O)_2Fe^{III}\}$ rhomb.[4b]
[16] $K_2[Co(H_2\mathbf{1})_2]$ (0.021 mmol, 0.020 g) was treated with 1.1 μL (0.063 mmol) of $H_2{}^{18}O$ in DMA (5 mL)for 24 h. A small amount (less than 10%) of free ligand was also found in the FTIR spectrum, which did not hinder detection of the changes in $\tilde{\nu}_{asym}(\{Co^{III}(\mu\text{-}O)_2Co^{III}\})$.
[17] Similar asymmetric vibrations have been observed in other $\{M(\mu\text{-}O)_2M\}$ complexes,[1c,2e] also see: P. L. Holland, C. J. Cramer, E. C. Wilkinson, S. Mahapatra, K. R. Rodgers, S. Itoh, M. Taki, S. Fukuzumi, L. Que, Jr., W. B. Tolman, *J. Am. Chem. Soc.* **2000**, *122*, 792–802.
[18] H. D. Flack, *Acta Crystallogr. Sect. A* **1983**, *39*, 876–881.

Ir-Catalyzed C-C Bond Formation

Iridium-Catalyzed Mizoroki–Heck-Type Reaction of Organosilicon Reagents

*Tooru Koike, Xiaoli Du, Tomoyuki Sanada, Yasuaki Danda, and Atsunori Mori**

Iridium-catalyzed C–C bond-forming reactions have recently attracted much attention.[1] However, the reaction with main group organometallic reagents containing elements such as boron, tin, and silicon has not been demonstrated so far. Although carbon–carbon bond formation with such main group reagents with an α,β-unsaturated carbonyl compound has been reported recently to undergo a Mizoroki–Heck-type or conjugate addition reaction with palladium,[2] rhodium,[3] and ruthenium[4] catalysts, the specific nature of the metal catalysts largely influences the reaction mechanism as well as the reaction course. Herein, we report that an iridium catalyst effects the Mizoroki–Heck-type addition/elimination reaction of α,β-unsaturated carbonyl compounds with several organosilicon reagents, and constitutes the first C–C bond formation with a main group reagent.[5]

The reaction of $PhSi(OMe)_3$ (**1**) with butyl acrylate (**2a**) in the presence of 5 mol% of $[\{IrCl(cod)\}_2]$ (cod = 1,5-cyclooctadiene) and tetrabutylammonium fluoride (TBAF) in toluene/H_2O (6/1) at 120°C for 24 h afforded the addition/elimination product **3a** in 71% yield while the conjugate addition product **4a** was not obtained at all. This result sharply contrasts that of the related reaction with the rhodium catalyst $[\{RhCl(cod)\}_2]$ at 60°C in THF/H_2O (6/1), which affords the conjugate adduct **4a** as the major product with high selectivity, **3a**/**4a** = 3/97 (Scheme 1).[6] In contrast to the combination of silicon reagent **1** and TBAF under anhydrous conditions, which is highly effective for the palladium-catalyzed cross-coupling reaction with organic halides,[7] the rhodium- or iridium-catalyzed reaction of this combination with **2a** proceeded only very slightly without the addition of water.

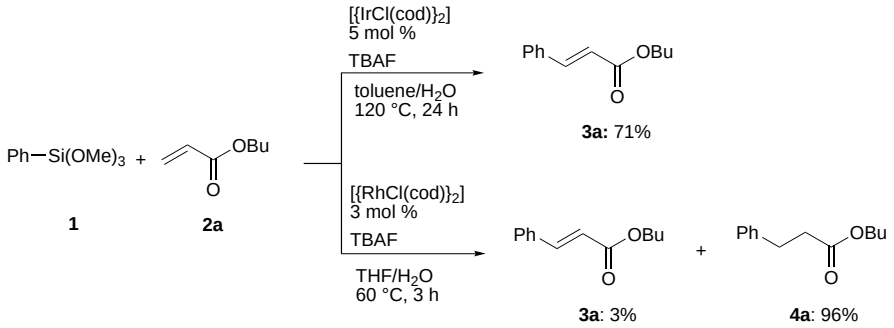
Table 1 summarizes the iridium-catalyzed Mizoroki–Heck-type addition/elimination reactions of several organosilicon reagents with α,β-unsaturated carbonyl compounds. Both iridium chloride and methoxide exhibited similar reactivities in the reactions with TBAF. The reaction also proceeded in THF/H_2O at lower temperature (70°C), although a small amount of conjugate addition product was formed (70/5). Several aryl silanes bearing a substituent on the aromatic ring also effected the reaction. Although the reaction of an *ortho*-substituted aryl silane was found to be slightly slower, the Mizoroki–Heck-type product was selectively obtained over the 1,4-addition product. Alkenylsilanes, which were prepared by hydrosilylation of alkynes, could also effect the reaction to afford a diene in 67% yield.

Aryl silanediols (**7**–**9**) were also found to participate in the addition/elimination reaction. By contrast to alkoxysilanes, silanediols effected the reactions without addition of TBAF and water. However, no reaction occurred when $[\{IrCl(cod)\}_2]$ was used as the catalyst. Only $[\{Ir(OMe)(cod)\}_2]$ was found to be an effective catalyst. Worthy of note is that the reaction with silanediols can be a halogen-free process, which is in contrast to the palladium-catalyzed Mizoroki–Heck reaction with aryl halides. Reactions of other main group reagents such as those derived from boron and tin were found to proceed in a similar manner. Methyl vinyl ketone (**2b**) also underwent reaction to give **3b** in good yields.

In contrast to our recent report on rhodium catalysts in which addition/elimination versus conjugate addition of esters was controlled by the addition of water, while ketones underwent conjugate addition with or without water,[3e] the iridium-catalyzed reaction predominantly proceeded through

[*] Prof. Dr. A. Mori, T. Koike, X. Du, T. Sanada, Y. Danda
Chemical Resources Laboratory
Tokyo Institute of Technology
4259 Nagatsuta, Yokohama 226–8503 (Japan)
Fax: (+81) 45–924–5224
E-mail: amori@res.titech.ac.jp

 © 2003 Wiley-VCH Verlag GmbH & Co. KGaA, Weinheim 1433-7851/03/4201-0089 $ 20.00+.50/0



Scheme 1.

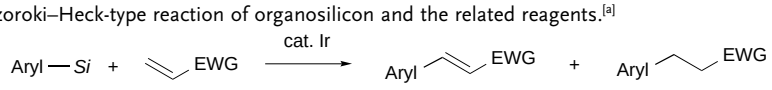
the addition/elimination reaction to form **3**, irrespective of the substrate species and the solvent system used.[8]

The iridium-catalyzed Mizoroki–Heck-type reaction proceeds as shown in Scheme 2. Similar to the rhodium case reported recently,[3e] migration of the organic group of the silicon reagent to the iridium center and insertion of **2** to the thus formed organoiridium species would afford intermediate **A**. In contrast to the rhodium-catalyzed reaction, which proceeds through a competition of β-hydride elimination and protonolysis to afford the Mizoroki–Heck-type or conjugate-addition product, the iridium-catalyzed reaction proceeds preferentially through β-hydride elimination to exclusively give **3** and the hydridoiridium **B** as a result of the lower reactivity of the carbon–iridium bond of **A** toward protonolysis.

Further transformation of **B** is also markedly different from that obtained with palladium and ruthenium catalysts, which are reported to involve redox process of metallic species to reduce the corresponding H–Pd^{II} or H–Ru^{II} species to their lower oxidation states.[2,4] Hence, an additional oxidant such as $Cu(OAc)_2$ is required in the palladium- or ruthenium-catalyzed reaction. On the other hand, the iridium-catalyzed reaction proceeds without an oxidant, and the metal species would be Ir^{I} throughout the catalytic cycle. The iridium hydride **B** might be hydrolyzed to *Ir*–OH to effect further catalytic reaction. Alternatively, **B** could react with **2** to give **A′**, which is then hydrolyzed by water or subjected to further insertion of **2**. Indeed, formation of butyl propanoate and the dimerized product **11** (EWG = COOBu) was confirmed in the reaction of butyl acrylate (**2a**).[9]

As shown in the last entry of Table 1, only the conjugate-addition product was obtained from the iridium-catalyzed reaction of methyl vinyl ketone (**2b**) with $PhSi(OMe)_3$ (**1**) and TBAF. Nevertheless, the reaction is also considered to proceed by a pathway different from the rhodium-catalyzed reaction, which proceeds through the protonolysis of intermediate **A**. The iridium-catalyzed formation of the conjugate adduct could take place by the reduction of the Mizoroki–Heck-type product **3b** with the formed hydridoiridium **B**.

Table 1: Iridium-catalyzed Mizoroki–Heck-type reaction of organosilicon and the related reagents.[a]

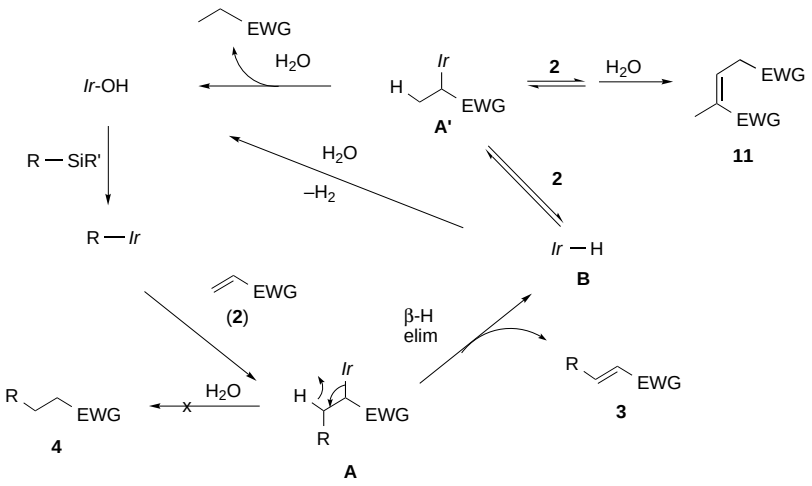


2

Silicon reagent	**2**, EWG	Catalyst (mol%)[b]	Solvent(s)[c]	*T* [°C]	Yield [%] MH	1,4-
$PhSi(OMe)_3$ (**1**)/TBAF	COOBu (**2a**)	$[\{IrCl(cod)\}_2]$ (5)	toluene/H_2O (6/1)	120	71	0
		$[\{Ir(OMe)(cod)\}_2]$ (5)		120	70	5
		$[\{IrCl(cod)\}_2]$ (5)	THF/H_2O (6/1)	70	62	3
$(4\text{-}MeOC_6H_4)Si(OEt)_3$(**5**)/TBAF				70	70	0
$(2\text{-}MeC_6H_4)Si(OEt)_3$/TBAF (**6**)		$[\{IrCl(cod)\}_2]$ (7.5)		70	61	0
$PhEtSi(OH)_2$ (**7**)		$[\{Ir(OMe)(cod)\}_2]$ (3)	toluene	120	64	0
		$[\{IrCl(cod)\}_2]$ (3)		120	0	0
$(4\text{-}MeC_6H_4)EtSi(OH)_2$ (**8**)		$[\{Ir(OMe)(cod)\}_2]$ (5)	toluene/H_2O (6/1)	120	63	0
$(4\text{-}MeOC_6H_4)EtSi(OH)_2$ (**9**)				120	62	0
$(4\text{-}MeC_6H_4)SnBu_3$/TBAF				70	79	2
$PhB(OH)_2$		$[\{Ir(OMe)(cod)\}_2]$ (3)	DME/H_2O (2/1)	80	72	0
(*E*)-PhCH=CHSiMe$(OEt)_2$/TBAF (**10a**)	COOEt(**2a′**)	$[\{IrCl(cod\}_2]$ (5)	THF/H_2O (6/1)	70	41	0
(*E*)-PhCH=CHSi$(OEt)_3$/TBAF (**10b**)				70[d]	67	0
7	COMe (**2b**)	$[\{Ir(OMe)(cod)\}_2]$ (3)	toluene	120	50	4
			toluene/H_2O (6/1)	120	41	8
8				120	52	0
1/TBAF		$[\{IrCl(cod)\}_2]$ (5)		120	0	52

[a] Unless noted, the reaction was carried out with 0.3 mmol of silicon reagent, 0.9 mmol of **2** (and 0.3 mmol of TBAF), with stirring for 24 h. The product was obtained as an unseparable mixture of Mizoroki–Heck-type (MH-type) and 1,4-addition products, whose ratio was determined by ^1H NMR analysis. [b] The catalyst loading is shown based on the amount of silicon reagent used. [c] The solvent ratio is shown in parenthesis. [d] The reaction was carried out for 8 h. DME = 1,2-dimethoxyethane.

 © 2003 Wiley-VCH Verlag GmbH & Co. KGaA, Weinheim 1433-7851/03/4201-0090 $ 20.00+.50/0



Scheme 2. EWG = electron-withdrawing group. *Ir* = iridium catalyst.

When the iridium-catalyzed reaction of butyl acrylate (**2a**) with **1**/TBAF was carried out in the presence of **3b**, which was the Mizoroki–Heck product of **2b**, reduction of **3b** took place to afford **4b** together with **3a** [Eq. (1)]. This observation suggests that the resulting formation of the conjugate-addition product would be the sequential Mizoroki–Heck-type addition/elimination followed by conjugate reduction. The similar reaction with $[\{Rh(OH)(cod)\}_2]$ instead of the analogous iridium catalyst resulted in a trace amount of **4b** and the recovery of **3b**.[10] Hence, **3b** can serve as a hydride acceptor to avoid the use of excess amounts of acrylate **2a**.

In summary, an iridium-catalyzed Mizoroki–Heck-type reaction, which is a new class of iridium-catalyzed C–C bond-forming reaction, with organosilicon reagents was described. In contrast to related rhodium-catalyzed reactions, the preference for a Mizoroki–Heck-type reaction pathway is independent of the substrate and solvent system. This difference could be caused by the formation of a stable iridium–carbon bond at the position α to the carbonyl group in the intermediate.

Experimental Section

3a: A 1M solution of TBAF (0.2 mL) in THF was added to a mixture of phenyltrimethoxysilane (0.037 mL, 0.2 mmol), butyl acrylate (0.086 mL, 0.6 mmol), and $[\{IrCl(cod)\}_2]$ (6.7 mg, 0.01 mmol) in THF (2 mL) and H_2O (0.33 mL) under an argon atmosphere. The resulting solution was allowed to warm to 70 °C and the reaction was continued for 24 h. After cooling the solution to room temperature it was passed through a short celite pad and the filtrate was concentrated under reduced pressure to leave a crude oil, which was purified by column chromatography on silica gel to afford 31 mg of the product as a mixture of **3a** and **4a**, whose ratio was estimated to be 70/5 by ^{1}H NMR analysis. ^{1}H NMR (300 MHz, $CDCl_3$): $\delta = 6.48$ (d, $J = 16$ Hz, 1H; PhC*H*=CHCOO-), 7.77 (d, $J = 16$ Hz, 1H; PhCH=C*H*COO-) for **3a** (major product), 2.64 (t, $J = 7.8$ Hz, 2H; PhCH_2CH$_2$COO-), 2.96 ppm (t, $J = 7.8$ Hz, 2H; PhCH$_2$CH_2COO-) for **4a** (minor product).

Received: June 27, 2002
Revised: October 11, 2002 [Z19625]

[1] a) N. Chatani, S. Ikeda, K. Ohe, S. Murai, *J. Am. Chem. Soc.* **1992**, *114*, 9710–9711; b) C.-H. Jun, Z. Lu, R. H. Crabtree, *Tetrahedron Lett.* **1992**, *33*, 7119–7120; c) P. M. Maitlis, A. Haynes, G. I. Sunley, M. J. Howard, *Dalton Trans.*, **1996**, 2187–2196; d) S.-I. Murahashi, H. Takaya, *Acc. Chem. Res.* **2002**, *33*, 225–233; e) M. Murakami, K. Itami, M. Ubukata, I. Tsuji, Y. Ito, *J. Org. Chem.* **1998**, *63*, 4–5; f) R. Takeuchi, M. Kashio, *Angew. Chem.* **1997**, *109*, 268–270; *Angew. Chem. Int. Ed. Engl.* **1997**, *36*, 263–265; g) S. Sakaguchi, T. Kubo, Y. Ishii, *Angew. Chem.* **2001**, *113*, 2602–2604; *Angew. Chem. Int. Ed.* **2001**, *40*, 2534–2536; h) T. Ohmura, Y. Yamamoto, N. Miyaura, *Organometallics* **2000**, *19*, 365–367; i) T. Shibata, K. Takagi, *J. Am. Chem. Soc.* **2000**, *122*, 9852–9853.

[2] B: a) C. S. Cho, S. Uemura, *J. Organomet. Chem.* **1994**, *465*, 85–92; b) X. Du, M. Suguro, K. Hirabayashi, A. Mori, T. Nishikata, N. Hagiwara, K. Kawata, T. Okeda, H.-F. Wang, K. Fugami, M. Kosugi, *Org. Lett.* **2001**, *3*, 3313–3316; Sn: c) K. Fugami, S. Hagiwara, H. Oda, M. Kosugi, *Synlett* **1998**, 477–478; d) K. Hirabayashi, J. Ando, Y. Nishihara, A. Mori, T. Hiyama, *Synlett* **1999**, 99–101; Si: e) K. Hirabayashi, Y. Nishihara, A. Mori, T. Hiyama, *Tetrahedron Lett.* **1998**, *39*, 7893–7896; f) K. Hirabayashi, J. Ando, J. Kawashima, Y. Nishihara, A. Mori, T. Hiyama, *Bull. Chem. Soc. Jpn.* **2000**, *73*, 1409–1417.

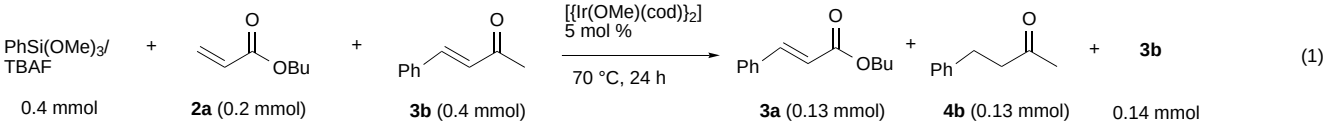
[3] B: a) Y. Takaya, M. Ogasawara, T. Hayashi, M. Sakai, N. Miyaura, *J. Am. Chem. Soc.* **1998**, *120*, 5579–5580; b) M. Lautens, A. Roy, K. Fukuoka, K. Fagnou, B. Martin-Matúte, *J. Am. Chem. Soc.* **2001**, *123*, 5358–5359; Sn: c) S. Oi, M. Moro, Y. Inoue *Chem. Lett.* **1998**, 83–84; d) Y. Meng, C. J. Li, *J. Am. Chem. Soc.* **2000**, *122*, 9538–9539; Si: e) A. Mori, Y. Danda, T. Fujii, K. Hirabayashi, K. Osakada, *J. Am. Chem. Soc.* **2001**, *123*, 10774–10775; f) T. Koike, X. Du, A. Mori, K. Osakada *Synlett* **2002**, 301–303; g) S. Oi, Y. Honma, Y. Inoue *Org. Lett.* **2002**, *4*, 667–669; h) M. Murata, R. Shimazaki, M. Ishikura, S. Watanabe, Y. Masuda, *Synthesis*, **2002**, 717–719; i) T. S. Huang, C. J. Li, *Chem. Commun.* **2001**, 2348–2349.

[4] B: E. J. Farrington, J. M. Brown, C. F. J. Barnard, E. Rowsell, *Angew. Chem.* **2002**, *114*, 169–171; *Angew. Chem. Int. Ed.* **2002**, *41*, 161–163.

[5] Although the Mizoroki–Heck reaction of organic halides instead of an organometallic reagent with a rhodium or iridium catalyst is reported, a high temperature (150 °C) must be applied: S. Iyer, *J. Organomet. Chem.* **1995**, *490*, C27–C28.

[6] X. Du, T. Koike, Y. Danda, A. Mori, unpublished results; a part of this work was presented at the 81st Annual Meeting of the Chemical Society of Japan, 4G644 (**2002**).

[7] a) M. E. Mowery, P. DeShong, *J. Org. Chem.* **1999**, *64*, 1684–1688; b) K. Tamao, K. Kobayashi, Y. Ito, *Tetrahedron Lett.* **1989**,



(1)

30, 6051 – 6054; c) K. Shibata, K. Miyazawa, Y. Goto, *Chem. Commun.* **1997**, 1309 – 1310.
[8] Although we have examined other α,β-unsaturated carbonyl compounds bearing substituents at the α and/or β positions, no desired addition/elimination reaction product was obtained.
[9] H. Nakagawa, S. Sakaguchi, Y. Ishii, 81st Annual Meeting of the Chemical Society of Japan, 1G549 (**2002**). In our present study, the reaction of (4-MeC_6H_4)EtSi$(OH)_2$ (0.3 mmol) with butyl acrylate **2a** (0.9 mmol) in toluene/H_2O at 120 °C in the presence of [{Ir(OMe)(cod)}$_2$] (3 mol %) afforded the Mizoroki–Heck-type product(46 %), in which 36 % of **2a** was converted into **9**.
[10] The rhodium-catalyzed reaction under similar conditions (3 mol % of [{Rh(OH)(cod)}$_2$], 4-$MeC_6H_4SiEt(OH)_2$ (0.6 mmol), **2a** (0.3 mmol), and **3b** (0.6 mmol) in THF (3 mL) at 70 °C for 24 h) afforded 27 % of the Mizoroki–Heck-type product **3a** and 3 % of **4b** with 75 % recovery of **3b**.

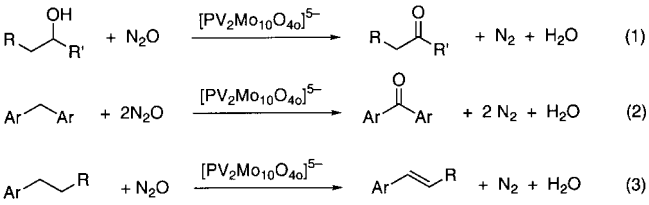
Polyoxometalate Catalysts

Activation of Nitrous Oxide and Selective Oxidation of Alcohols and Alkylarenes Catalyzed by the $[PV_2Mo_{10}O_{40}]^{5-}$ Polyoxometalate Ion**

*Revital Ben-Daniel and Ronny Neumann**

Nitrous oxide is a potentially interesting oxidant for selective oxidation of organic substrates since it contains 36 wt % oxygen, and the by-product of an oxidation reaction would be environmentally benign molecular nitrogen. These advantages are difficult to realize since N_2O is generally considered to be both inert[1] and a poor ligand.[2] Thus, very few catalysts have been reported for the activation of N_2O and its use as a selective oxidant in hydrocarbon oxidation. In the area of heterogeneous catalysis, various metal oxides have been investigated.[3] The most effective catalysts appear to be iron-containing acidic zeolites[4] which at elevated temperatures are thought to yield surface-activated iron–oxo species (α-oxygen).[5] These species are capable of oxygen transfer to rather inert hydrocarbons, such as benzene and methane, to yield phenol and methanol, respectively.[6] In homogeneous media, noncatalytic oxygen transfer from nitrous oxide to alkyl, alkyne, and imido ligands of transition-metal complexes has been observed.[7] Molybdenum(III) complexes have cleaved nitrogen–nitrogen bonds[8] and N_2O has been decomposed at subambient temperatures to N_2 and O_2 using a ruthenium complex.[9] More relevant to the work reported herein is the reported oxygen transfer from nitrous oxide to form metal–oxo species.[10] In one particular case,[11] a ruthenium porphyrin has been used to prepare a high-valent ruthenium–dioxo species capable of oxygen-transfer to nucleophiles such as alkenes and sulfides. Under more extreme conditions (140 °C, 10 atm N_2O), the ruthenium porphyrin has recently been shown to catalyze oxygen transfer to trisubstituted alkenes,[12] and the oxidation of alcohols to ketones.[13]

With regard to the ongoing interest in the catalytic activity of polyoxometalates in oxidation reactions,[14] especially with benign oxidants such as O_2 and H_2O_2, we have very recently found that a manganese-substituted "sandwich"-type polyoxometalate can also activate N_2O and lead to the highly selective epoxidation of alkenes.[15] In this paper we will describe a different set of N_2O-activation reactions involving the vanadium-containing Keggin-type polyoxomolybdate, [{nBu$_4$N}$_5${$PV_2Mo_{10}O_{40}$}]. In this case, selective oxidation by C–H bond activation was possible leading to the oxidation of a) primary and secondary alcohols to aldehydes and ketones, respectively (Equation (1)) and b) alkyl aromatics to ketones (Equation (2)), or alternatively leading to their oxydehydrogenation (Equation (3)).



For the oxidation of alcohols (Table 1) it was shown that secondary and primary alcohols were oxidized selectively (greater than 99.9 %) to ketones and aldehydes, respectively,

Table 1: Oxydehydrogenation of alcohols with N_2O catalyzed by [{nBu$_4$N}$_5${$PV_2Mo_{10}O_{40}$}].[a]

Substrate	Product	Conversion [mol %]
1-octanol	1-octanal	42.5
2-octanol	2-octanone	48.1
cyclohexanol	cyclohexanone	68.2
cyclooctanol	cyclooctanone	89
cis-2-hexen-1-ol	2-hexenal[b]	50.5
trans-2-hexen-1-ol	2-hexenal[b]	50.3
1-octene-3-ol	1-octen-3-one	56.8
benzyl alcohol	benzaldehyde	> 99

[a] Reaction conditions: alcohol (1 mmol), [{nBu$_4$N}$_5${$PV_2Mo_{10}O_{40}$}] (0.02 mmol), N_2O (1 atm), benzonitrile (1 mL), 150 °C, 15 h. Selectivity to the aldehyde or ketone was > 99.9 %. [b] The configuration of the unsaturated aldehyde was not definitively determined. However, since the catalytic system is inert to alkenes it is likely, but not certain, that the configuration was retained.

[*] R. Neumann, R. Ben-Daniel
Department of Organic Chemistry
Weizmann Institute of Science
76100 Rehovot (Israel)
Fax: (+972) 8-934-4142
E-mail: ronny.neumann@weizmann.ac.il

[**] This research was supported by the Basic Research Foundation administered by the Israeli Academy of Science and Humanities and the Israeli Ministry of Science. Dr. Lev Weiner is thanked for the ESR measurements. R.N. is the Rebecca and Israel Sieff Professor of Organic Chemistry.

Supporting information for this article is available on the WWW under http://www.angewandte.org or from the author.

 © 2003 Wiley-VCH Verlag GmbH & Co. KGaA, Weinheim 1433-7851/03/4201-0092 $ 20.00+.50/0

with no further oxidation of aldehydes to carboxylic acids.[16] Acyclic primary, secondary, and allylic alcohols showed similar reactivity; yields between approximately 40–60% were possible. Higher yields were obtained for cyclic secondary alcohols (approximately 60–80%), while benzylic alcohols gave quantitative yields of products. Attempts at increasing the conversion in the cases of 1-octanol and 2-octanol by lengthening the reaction time, coupled with addition of more N_2O or increasing the reaction temperature were not successful. Similar reaction conversions and selectivity were obtained. An increase in the amount of catalyst to 5 mol% unfortunately led to a decrease in reaction selectivity. Importantly, when using O_2 in place of N_2O there was no reaction. One should note that in the past we have reported on the use of the $[PV_2Mo_{10}O_{40}]^{5-}$ polyoxometalate ion in the aerobic oxidation of alcohols; however in those cases the catalyst is only active when supported on active carbon;[17] $[\{n\mathrm{Bu}_4\mathrm{N}\}_5\{PV_2Mo_{10}O_{40}\}]$ is inactive.

The results of the oxidation of alkyl aromatic compounds are summarized in Table 2. For substrates without a hydrogen atom at the α-position, with respect to the position of the benzylic carbon atom, there was oxygenation at the benzylic position and selective formation (greater than 99.9%) of the diaryl ketone or triaryl alcohol as sole products. Lengthening the reaction time coupled with repressurization of the reaction vessel could increase the yields. For other substrates, such as ethylbenzene and *i*-propylbenzene, the presence of an α-hydrogen atom led to oxydehydrogenation and the formation of vinyl benzene products. Control reactions with molecular oxygen gave much lower yields and reaction mixtures typical for autooxidation pathways. $[\{n\mathrm{Bu}_4\mathrm{N}\}_5\{PV_2Mo_{10}O_{40}\}]$ did not catalyze the alkene epoxidation of 1-octene, cyclooctene, or cyclohexene. In the latter case, some oxydehydrogenation, 3 mol% conversion to 1,3-cyclohexadiene and then to benzene was observed. It should also be noted that although the examples given in Table 1 and Table 2 describe the use of quite polar benzonitrile as solvent, similar reactions with alcohol and alkylaromatic substrates such 1-octanol, 2-octanol, and diphenylmethane with apolar decalin (decahydronaphthalene) as solvent gave almost identical results. In contrast fluorobenzene, which was previously used in epoxidation reactions with nitrous oxide,[15] did not lead to selective oxidation, especially in the case of the oxidation of alkylaromatic substrates.

Table 2: Oxidation of alkylaromatics with N_2O catalyzed by $[\{n\mathrm{Bu}_4\mathrm{N}\}_5\{PV_2Mo_{10}O_{40}\}]$.[a]

Substrate	Product	Conversion [mol%][a]
triphenylmethane	triphenylmethanol	52.4 (89)
diphenylmethane	benzophenone	6.2 (32)
toluene	no product	0
fluorene	fluoren-9-one	11.1 (50)
xanthene	xanthen-9-one	14.0 (54)
ethylbenzene	styrene	6.8
i-propylbenzene	α-methylstyrene	27.6

[a] Reaction conditions: substrate (1 mmol), $[\{n\mathrm{Bu}_4\mathrm{N}\}_5\{PV_2Mo_{10}O_{40}\}]$ (0.01 mmol), N_2O (1 atm), benzonitrile (1 mL), 150°C, 8 h. Selectivity to the product was > 99.9%. [b] Yields in parentheses are those after 48 h, with reintroduction of N_2O after 24 h.

Another notable observation is that the quantification of N_2O, N_2, and O_2 by gas chromatography showed no nonproductive decomposition of N_2O to N_2 and O_2 at 150–180°C in the absence or presence of a reaction substrate such as benzyl alcohol or xanthene. In the presence of the aforementioned substrates, N_2 formation was consistent with the degree of reaction of the organic substrate within a 10% margin of error.

Some preliminary insight into the mode of N_2O activation and the reaction pathway is most warranted. First, heating $[\{n\mathrm{Bu}_4\mathrm{N}\}_5\{PV_2Mo_{10}O_{40}\}]$ (0.01 M) in benzonitrile or decalin at 150°C in a N_2O atmosphere (1 atm) yielded a green solution (UV/Vis shows an absorption at 750 nm) indicative of the oxidation of N_2O by the polyoxometalate, which is reduced accordingly (Figure 1).

The degree of reduction, calculated by calibration with the reduction of pure $[n\mathrm{Bu}_4\mathrm{N}]_5[PV_2Mo_{10}O_{40}]$ by Zn, is approximately 55% after 6 h. In the absence of N_2O, that is, by heating $[\{n\mathrm{Bu}_4\mathrm{N}\}_5\{PV_2Mo_{10}O_{40}\}]$ in benzonitrile or decalin only, slight polyoxometalate reduction (approximately 5%) was observed within 6 h. Importantly, the apparent reduction of the $[\{n\mathrm{Bu}_4\mathrm{N}\}_5\{PV_2Mo_{10}O_{40}\}]$ polyoxometalate is reversible, that is, upon removal of N_2O, the $[\{n\mathrm{Bu}_4\mathrm{N}\}_5\{PV_2Mo_{10}O_{40}\}]$ is reoxidized. Additionally, an ESR spectrum of this solution yielded an anisotropic spectrum which can be assigned to a reduced $[PV_2Mo_{10}O_{40}]$ species (see Supporting Information). Under the same reaction conditions the ^{15}N NMR peaks of $^{15}N_2O$ at $\delta = 150$ and 210 ppm disappeared, apparently because of a paramagnetic peak-broadening effect caused by the reduction of the polyoxometalate by N_2O. These lines of evidence seem to suggest an unusual and unexpected redox or donor–acceptor (D–A) interaction between N_2O and $[\{n\mathrm{Bu}_4\mathrm{N}\}_5\{PV_2Mo_{10}O_{40}\}]$ (Equation (4)).

$$\mathrm{POM}^0 + \overset{+}{\mathrm{N}}\equiv\overset{-}{\mathrm{N}}\text{–}\mathrm{O} \rightleftharpoons \mathrm{POM}^{1-} \left|\overset{+}{\mathrm{N}}\equiv\overset{\bullet}{\mathrm{N}}\text{–}\mathrm{O}\right. \quad (4)$$

Such a reaction is rather surprising considering the high ionization potential of N_2O (approximately 12.8 eV),[18] but may conceivably be explained by an outer-sphere electron transfer, in which the polyanionic nature of polyoxometalates energetically increases the favorability of such D–A inter-

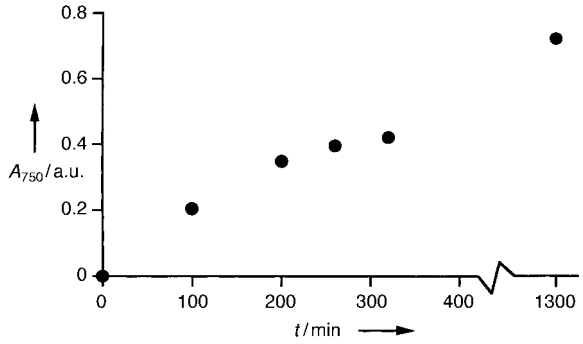


Figure 1. The reduction of $[\{n\mathrm{Bu}_4\mathrm{N}\}_5\{PV_2Mo_{10}O_{40}\}]$ by N_2O. Reaction conditions: $[\{n\mathrm{Bu}_4\mathrm{N}\}_5\{PV_2Mo_{10}O_{40}\}]$ (0.01 M) in benzonitrile, 150°C, N_2O (1 atm).

 © 2003 Wiley-VCH Verlag GmbH & Co. KGaA, Weinheim 1433-7851/03/4201-0093 $ 20.00+.50/0

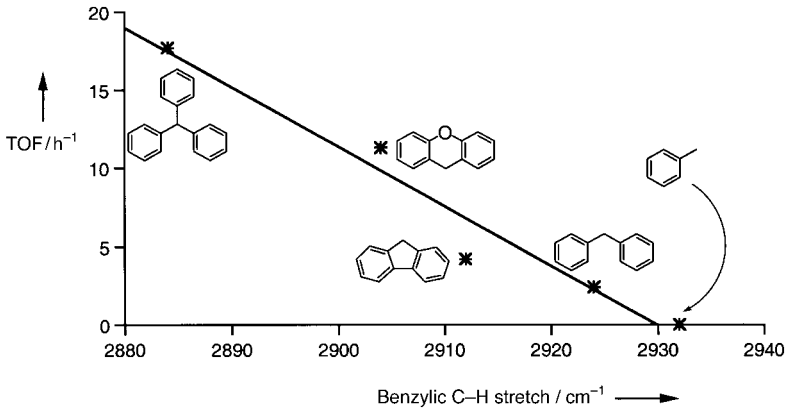


Figure 2. Reactivity for oxygenation of alkyl aromatics as a function of benzylic C–H bond energy (from gas phase IR C–H stretch vibration). Reaction conditions: alkylarene (1 mmol), $[\{n\mathrm{Bu_4N}\}_5\{\mathrm{PV_2Mo_{10}O_{40}}\}]$ (0.01 mmol), N_2O (1 atm), benzonitrile (1 mL), 150 °C.

actions and the formation of D–A complexes.[19] A similar redox interaction has been recently observed between a manganese(III)-substituted polyoxometalate and N_2O.[15]

For further insight into the mode of activation of the alkyl arene and alcohol substrate, a correlation between reactivity and a relevant property of the substrates was sought. In the oxidation of alkyl arenes, the conversion initially increased linearly as a function of time indicating a zero-order reaction in the organic substrate. Using these data, one may observe that the relative reactivity towards the oxidation of alkyl arenes was in the order: triphenylmethane > xanthene > fluorene > diphenylmethane > toluene, and was well correlated ($r^2 = 0.96$) to C–H homolytic bond strength at the benzylic position (Figure 2).[20] Notably, the use of approximately 70% ^{18}O-labeled $[\{n\mathrm{Bu_4N}\}_5\{\mathrm{PV_2Mo_{10}O_{40}}\}]$ (xanthene (1 mmol), $[\{n\mathrm{Bu_4N}\}_5\{\mathrm{PV_2Mo_{10}O_{40}}\}]$ (1 mmol), N_2O (1 atm), benzonitrile (1 mL), 150 °C) yielded only the unlabeled product indicating that the source of oxygen in the product was N_2O.[21]

Similarly, a Hammett plot of the oxidation of a series of benzylic alcohols yielded $\rho = 0.59$ ($r^2 = 0.97$, Figure 3). The low ρ value is consistent with the formation of a radicaloid species at the benzylic carbon in the transition state of the rate-determining step. Thus, for both alkyl arenes and alcohols, there is initial evidence indicating homolytic C–H bond cleavage in the rate-determining oxidation step. This is supported by kinetic isotope effects (KIE) which gave $k_H/k_D = 11.0$ and 15.9 for benzyl alcohol/[D_2]benzyl alcohol and xanthene/[9-D_2]xanthene, respectively.

Although it is premature to present a full picture of the reaction scheme, the initial results on the novel selective oxidation reactions presented above indicate that initially there is activation by the electron transfer of N_2O by the polyoxometalate species, as suggested by UV/Vis, ESR, and ^{15}N NMR spectroscopy. The activated N_2O then reacts with (or activates) the organic substrate leading to H abstraction from the latter, as supported by the correlation between the rate of alkyl arene oxidation, the C–H homolytic bond strength, and the low ρ value obtained for benzylic alcohol oxidation; the measured KIEs support such a scheme. In the case of alcohol oxidation, initial H abstraction is presumably followed by additional dehydrogenation to yield the aldehyde or ketone. In the case of alkyl arene oxidation, the intermediate radical species is probably oxidized through oxygen transfer from nitrous oxide.

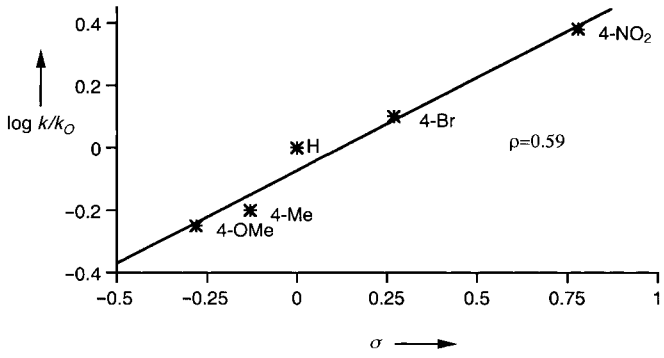


Figure 3. Hammett plot for the oxidation of benzylic alcohols. Reaction conditions: benzylic alcohol (1 mmol), $[\{n\mathrm{Bu_4N}\}_5\{\mathrm{PV_2Mo_{10}O_{40}}\}]$ (0.01 mmol), N_2O (1 atm), benzonitrile (1 mL), 150 °C.

Experimental Section

Reactions were carried out in 15-mL glass pressure tubes. Typically, appropriate amounts (see Table and Figure captions) of the substrate (all highest purity commercial products) and the $[\{n\mathrm{Bu_4N}\}_5\{\mathrm{PV_2Mo_{10}O_{40}}\}]$ catalyst were dissolved in the reaction solvent. N_2O (greater than 99.95% purity) was introduced to the pressure tube by four consecutive pump–thaw cycles using a Schlenk line. Conversions of the organic substrate were measured by GLC (HP 6890) using a 5% phenylmethylsilicone (30 m, 0.32 mm internal diameter, 0.25 μm coating) column. The identity of the products was verified by GC-MS.

Received: July 10, 2002
Revised: October 8, 2002 [Z19706]

[1] R. G. S. Banks, R. J. Henderson, J. M. Pratt, *J. Chem. Soc. A* **1968**, 2886–2889.
[2] F. Bottomley, I. J. B. Lin, M. Mukaida, *J. Am. Chem. Soc.* **1980**, *102*, 5238–5342.
[3] K. J. Zhen, M. M. Khan, C. H. Mak, K. B. Lewis, G. A. Somorjai, *J. Catal.* **1985**, *94*, 501–507; H. F. Liu, R. S. Liu, K. Y. Liew, R. E. Johnson, J. H. Lunsford, *J. Am. Chem. Soc.* **1984**, *106*, 4117–4121.
[4] G. I. Panov, *CATTECH* **2000**, *4*, 18–32; G. I. Panov, A. Uriate, M. A. Rodkin, V. I. Sobolev, *Catal. Today* **1998**, *41*, 365–385.
[5] N. P. Notte, *Top. Catal.* **2000**, *13*, 387–394.
[6] M. A. Rhodkin, V. I. Sobolev, K. A. Dubkov, N. H. Watkins, G. I. Panov, *Stud. Surf. Sci. Catal.* **2000**, *130A*, 881–886.
[7] P. Mansunaga, G. L. Hillhouse, A. L. Rheingold, *J. Am. Chem. Soc.* **1993**, *115*, 2075–2077; G. A. Vaughan, D. Chadwick, G. L. Hillhouse, A. L. Rheingold, *J. Am. Chem. Soc.* **1989**, *111*, 5491–5493; A. M. Baranger, T. A. Hanna, R. G. Bergman, *J. Am. Chem. Soc.* **1995**, *117*, 10041–10046.

 © 2003 Wiley-VCH Verlag GmbH & Co. KGaA, Weinheim 1433-7851/03/4201-0094 $ 20.00+.50/0

[8] A. R. Johnson, W. M. Davis, C. C. Cummins, S. Serron, S. P. Nolan, D. J. Masaev, K. Morokuma, *J. Am. Chem. Soc.* **1998**, *120*, 2071 – 2085; C. E. Laplaza, A. L. Odom, W. M. Davis, C. C. Cummins, J. D. Protasiewicz, *J. Am. Chem. Soc.* **1995**, *117*, 4999 – 5000.
[9] C. B. Pamplin, E. S. F. Ma, N. Safari, S. J. Rettig, B. R. James, *J. Am. Chem. Soc.* **2001**, *123*, 8596 – 8597.
[10] R. R. Conry, J. M. Mayer, *Inorg. Chem.* **1990**, *29*, 4862 – 4867; W. A. Howard, G. Parkin, *J. Am. Chem. Soc.* **1994**, *116*, 606 – 615.
[11] J. T. Groves, J. S. Roman, *J. Am. Chem. Soc.* **1995**, *117*, 5594 – 5595.
[12] T. Yamada, K. Hashimoto, Y. Kitaichi, K. Suzuki, T. Ikeno, *Chem. Lett.* **2001**, 268 – 269.
[13] K. Hashimoto, Y. Kitaichi, H. Tanaka, T. Ikeno, T. Yamada, *Chem. Lett.* **2001**, 922 – 923.
[14] N. Mizuno, M. Misono, *Chem. Rev.* **1998**, *98*, 171 – 199; C. L. Hill, C. M. Prosser-McCartha, *Coord. Chem. Rev.* **1995**, *143*, 407 – 455; I. V. Kozhevnikov, *Chem. Rev.* **1998**, *98*, 171 – 198; R. Neumann, *Prog. Inorg. Chem.* **1998**, *47*, 317 – 370.
[15] R. Ben-Daniel, L. Weiner, R. Neumann, *J. Am. Chem. Soc.* **2002**, *124*, 8788 – 8789.
[16] It should be noted that alcohols can also be oxidized with benign oxidants such as O_2 and H_2O_2, but the reaction is rarely selective for aliphatic primary alcohols, see: R. A. Sheldon, *Catal. Today* **2000**, *57*, 157 – 166.
[17] A. M. Khenkin, I. Vigdergauz, R. Neumann, *Chem. Eur. J.* **2000**, *6*, 875 – 882; R. Neumann, M. Levin, *J. Org. Chem.* **1991**, *56*, 5707 – 5710.
[18] There is no exact correlation between the gas-phase ionization potential and the solution oxidation potential which is the more relevant, but unknown, parameter.
[19] I. A. Weinstock, *Chem. Rev.* **1998**, *98*, 113 – 170; A. M. Khenkin, L. Weiner, Y. Wang, R. Neumann, *J. Am. Chem. Soc.* **2001**, *123*, 8531 – 8542.
[20] Benzylic C–H bond strengths are proportional to the benzylic C–H stretch vibration, as taken from the gas-phase IR spectra. IR data from NIST at http://webbook.nist.gov/chemistry.
[21] The inverse experiment using $N_2{}^{18}O$ is also desirable; $N_2{}^{18}O$ was not commercially available and is prohibitively expensive to synthesize.

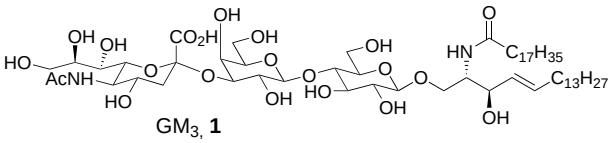
Carbohydrate–Carbohydrate Interactions

Probing Specificity in Carbohydrate–Carbohydrate Interactions with Micelles and Langmuir Monolayers**

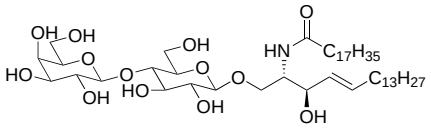
*Paul V. Santacroce and Amit Basu**

Carbohydrate–carbohydrate interactions (CCIs) between cell surface glycolipids are important mediators of cell adhesion during development, metastasis, and signal transduction.[1] CCIs are also important for the higher-order structure of polysaccharides, compaction of the myelin sheath, sperm–egg cell adhesion, and proteoglycan-mediated sponge cell aggregation.[2] The interaction has been studied by a variety of techniques including vesicle adhesion,[3a,b] surface plasmon resonance (SPR) spectroscopy,[3c,d] atomic force microscopy (AFM),[3e] nuclear magnetic resonance (NMR) spectroscopy,[3f,g] mass spectrometry (MS),[3h,i] infrared (IR) spectroscopy,[3j] surface force measurements,[,3k] quartz crystal microbalance (QCM) measurements,[3l] and Langmuir monolayer compression isotherms.[3m] These interactions, which are generally calcium ion dependent, require multivalent carbohydrate-–carbohydrate contacts, and the oligomeric nature of the association has hampered efforts to structurally characterize the carbohydrate aggregates at high resolution. In this communication we report a new method for detecting CCIs by monitoring the interactions of glycolipid micelles with a glycolipid monolayer. We show that small changes in carbohydrate structure significantly affect glycolipid association.

The adhesion of a melanoma cell to an endothelial cell is mediated by carbohydrate–carbohydrate recognition between the melanoma cell surface ganglioside sialosyllactosylceramide (GM_3, **1**) and the glycosphingolipid lactosylcera-



GM_3, **1**



LacCer, **2**

[*] Prof. A. Basu, P. V. Santacroce
Department of Chemistry
Box H, Brown University
Providence, RI 02912 (USA)
Fax: (+1) 253-540-0698
E-mail: amit_basu@brown.edu

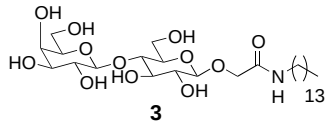
[**] We gratefully acknowledge financial support from Brown University (startup funds; Salomon Faculty Research Award), Rhode Island Foundation, Research Corporation (Research Innovation Award), and the Petroleum Research Fund administered by the American Chemical Society. A.B. is an NSF Faculty Early CAREER awardee. P.V.S. is a Department of Education GAANN Fellow. We thank Professor Zimmt for the use of his spectrofluorometer.

 © 2003 Wiley-VCH Verlag GmbH & Co. KGaA, Weinheim 1433-7851/03/4201-0095 $ 20.00+.50/0

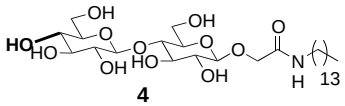
mide (LacCer, **2**) found on endothelial cells.[4] The GM_3–LacCer interaction activates signal transduction in B16 melanoma cells. The metastatic potential of the melanoma is correlated with levels of GM_3 expression in cells.[5] Multivalent lactose glycoconjugates inhibit melanoma metastasis, and a better understanding of the carbohydrate recognition event on a molecular level may aid in the design of better anti-melanoma agents.[5,6]

We sought a method for detecting this interaction which would be amenable for screening a variety of mutant glycolipids and would also allow us to modulate the membrane environment. We probed the specificity of CCIs with single-tailed glycolipids, since they readily self-assemble into polyvalent clusters in the form of micelles. Membrane morphology can be readily adjusted in Langmuir monolayers, which have been used extensively to study binding interactions at membrane interfaces.[3l,m,7] Glycolipid monolayers prepared over solutions of glycosylated polystyrenes show expanded pressure versus area isotherms and have been used to probe CCIs.[3l,m] The structure of the monolayer can be monitored readily by fluorescence or Brewster angle microscopy; the monolayers can also be transferred to solid supports for AFM, SPR, and other spectroscopic measurements.[8]

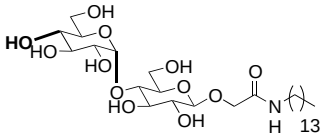
Although native glycolipid–glycolipid interactions occur in the context of a membrane environment, a ceramide tail is not required for the association, and CCI-mediated aggregation has been observed with oligosaccharides presented on a variety of multivalent platforms.[3c,d,f,l,m,9] We therefore prepared the simplified synthetic glycolipid **3** as a LacCer



3



4



5

analogue.[10] The critical micelle concentration (cmc) value for **3** was determined by monitoring the encapsulation of the fluorescent probe 1,6-diphenylhexatriene (DPH) and was found to be approximately 8 μM in 1 mM $CaCl_2$.[11]

We studied the CCI between **3** and GM_3 by preparing a Langmuir monolayer containing 10% GM_3, then injecting a micellar solution of **3** into the aqueous subphase under the monolayer.[12] After injection the change in the surface pressure ($\Delta\pi$) over time was monitored. A representative set of data showing the interaction of **3** with the GM_3 monolayer is given in Figure 1. When the concentration of **3** is well below the cmc, the values of $\Delta\pi$ decrease over time (Figure 1b). The magnitude of this decrease is similar to that observed in a "holding" experiment, in which no micelles have been injected into the subphase (Figure 1a).[13] However, at concentrations close to or above the cmc, the $\Delta\pi$ values increase over time, usually plateauing within an hour (Figure 1c–f). This increase is consistent with glycolipid insertion into the monolayer. Glycolipid **3** exhibits a concentration-dependent increase in "final" $\Delta\pi$ values ($\Delta\pi$ at 167 min), as shown in the uppermost plot in Figure 2. Additionally, injection of a methyl lactoside solution (100 μM) under the GM_3 monolayer also failed to result in any change in $\Delta\pi$ different from the "holding" experiment. The concentration dependence of $\Delta\pi$ also demonstrates that polyvalent presentation of carbohydrates is required. These

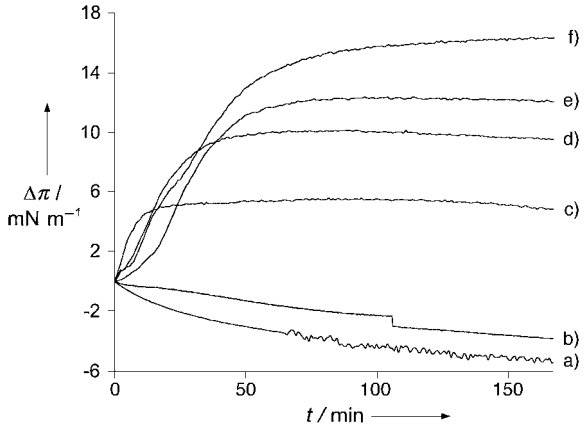


Figure 1. Plots of the change in surface pressure ($\Delta\pi$) over time for the binding of **3** to a DPPC/GM_3 (9:1) monolayer (initial pressure = 30 mN m^{-1}) at the following concentrations of **3**: a) 0 μM; b) 1 μM; c) 5 μM; d) 10 μM; e) 15 μM; f) 25 μM. DPPC = dipalmitoylphosphatidylcholine.

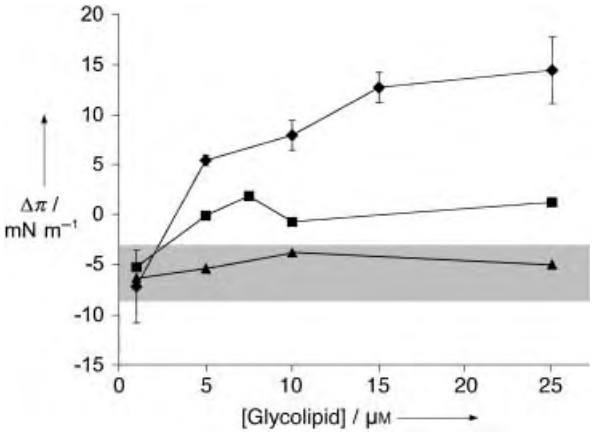


Figure 2. Final $\Delta\pi$ values ($t = 167$ min) as a function of the identity and concentration of the subphase glycolipid. The monolayer is DPPC/GM_3 (9:1); initial $\pi = 30$ mN m^{-1}). ◆ = **3**, ▲ = **4**, ■ = **5**. Each point represents the average of two or more measurements. The shaded region corresponds to the $\Delta\pi$ values observed in the absence of any micelles in the subphase (i.e. a "holding" experiment). Errors generally range from 5 to 20%, and a single representative set for measurements with glycolipid **3** is shown for clarity.

 © 2003 Wiley-VCH Verlag GmbH & Co. KGaA, Weinheim 1433-7851/03/4201-0096 $ 20.00+.50/0

results establish that CCIs can be detected with Langmuir monolayers and micelles as models for biomembranes.

To probe the fine specificity of the GM_3–Lac interaction we modified the structure of the lactose disaccharide slightly. We prepared the cellobiosyl lipid **4** (cmc ≈ 4 μM) and studied the interaction of micelles of **4** with a monolayer containing GM_3. Remarkably, the concentration-dependent response seen with **3** is not observed when minor modifications are introduced into the carbohydrate portion of the glycolipid. The conversion of a single stereocenter in the disaccharide by epimerizing the axial OH group in **3** to the equatorial OH found in **4** completely abrogates the binding at all concentrations examined (Figure 2).[14] This loss in binding might arise from a weakened interaction with the metal ion, as calcium ions preferentially bind *cis* diols on sugars.[15,16]

An alternative explanation for the smaller $\Delta\pi$ value of **4** may lie in the low intrinsic surface activity of **4**.[17] However, subsequent studies with **5** (cmc ≈ 5 μM), which has very similar surface activity to **3**, indicated that **5** did not exhibit a concentration-dependent change in $\Delta\pi$, even at glycolipid concentrations well above the cmc (Figure 2).[18] Thus, the increase in $\Delta\pi$ for **3** cannot simply be a result of its intrinsic surface activity.[19] In summary, very subtle modifications, that is, epimerization, of the carbohydrate headgroup of a lactosyl lipid result in significant changes in the interaction of the synthetic glycolipids with a GM_3-containing monolayer. This indicates that the concentration-dependent increase in $\Delta\pi$ seen with **3** is a function of carbohydrate–carbohydrate recognition.

Since the observed positive values of $\Delta\pi$ most likely arise from insertion of **3** into the monolayer, we postulated that decreasing the initial pressure of the monolayer should facilitate insertion and result in larger $\Delta\pi$ values. This is exactly what was observed in binding studies with **3** and **5** when the initial pressure of the monolayer was varied from 5 to 55 mN m^{-1} (Figure 3).[20] At each pressure at which binding was examined the $\Delta\pi$ value for **3** is consistently higher than that observed for **5**, again indicating that surface activity alone cannot explain the observations. Furthermore, **3** continues to have positive $\Delta\pi$ values at starting pressures as high as 50 mN m^{-1}, while **5** does not show any appreciable binding above 30 mN m^{-1}, consistent with GM_3–Lac interactions at the interface.

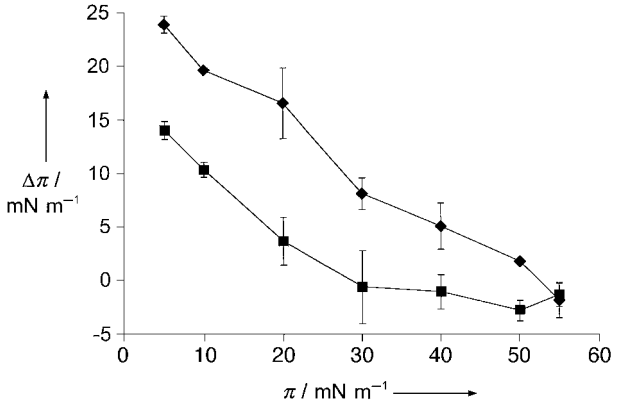


Figure 3. Plot of the final $\Delta\pi$ values as a function of initial monolayer pressure. Glycolipid concentrations of **3** and **5** are 10 μM. ◆ = **3**, ■ = **5**.

In conclusion, we have shown that CCIs can be studied by examining the interaction of glycolipid micelles with glycolipids embedded in a monolayer at the air–water interface. Furthermore, the GM_3–Lac interaction is highly specific for lactose, and very minor modifications to the structure of the carbohydrate headgroup have significant effects on binding. Our results indicate that CCIs involve very specific molecular recognition events between carbohydrates and does not arise simply from nonspecific interactions between two polyhydroxylated surfaces formed by membrane-bound glycolipids. In future studies directed towards elucidating the details of this molecular recognition phenomenon we will synthesize glycolipids that probe the role of calcium binding and examine the role of the formation of microdomains in the membrane in mediating CCIs.[4c]

Received: July 29, 2002
Revised: September 23, 2002 [Z19838]

[1] a) J. Rojo, J. C. Morales, S. Penadés, *Top. Curr. Chem.* **2002**, *218*, 45; b) N. V. Bovin, *Biochemistry (Moscow)* **1996**, *61*, 694; c) S. Hakomori, *Pure Appl. Chem.* **1991**, *63*, 473; d) D. Spillman, M. M. Burger, *J. Cell. Biochem.* **1996**, *61*, 562.

[2] a) J. E. Scott, F. Heatley, *Proc. Natl. Acad. Sci. USA* **1999**, *96*, 4850; b) R. J. Stewart, J. M. Boggs, *Biochemistry* **1993**, *32*, 10666; c) S. R. Haseley, H. J. Vermeer, J. P. Kamerling, J. F. G. Vliegenthart, *Proc. Natl. Acad. Sci. USA* **2001**, *98*, 9419; d) S. Yu, N. Kojima, S. Hakomori, S. Kudo, S. Inoue, Y. Inoue, *Proc. Natl. Acad. Sci. USA* **2002**, *99*, 2854.

[3] Vesicle adhesion: a) R. J. Stewart, J. M. Boggs, *Biochemistry* **1993**, *32*, 10666; b) F. Pincet, T. Le Bouar, Y. Zhang, J. Esnault, J.-M. Mallet, E. Perez, P. Sinaÿ, *Biophys. J.* **2001**, *80*, 1354; SPR: c) K. Matsuura, H. Kitakouji, N. Sawada, H. Ishida, M. Kiso, K. Kitajima, K. Kobayashi, *J. Am. Chem. Soc.* **2000**, *122*, 7406; d) M. Hernáiz, J. M. de la Fuente, A. G. Barrientos, S. Penadés, *Angew. Chem.* **2002**, *114*, 1624; *Angew. Chem. Int. Ed.* **2002**, *41*, 1554; AFM: e) C. Tromas, J. Rojo, J. M. de la Fuente, A. G. Barrientos, R. García, S. Penadés, *Angew. Chem.* **2001**, *113*, 3142; *Angew. Chem. Int. Ed.* **2001**, *40*, 3052; NMR: f) C. Gege, A. Geyer, R. R. Schmidt, *Eur. J. Org. Chem.* **2002**, 2475; g) B. Henry, H. Desvaux, M. Pristchepa, P. Berthault, Y. M. Zhang, J. M. Mallet, J. Esnault, P. Sinay, *Carbohydr. Res.* **1999**, *315*, 48; MS: h) K. M. Koshy, J. Wang, J. M. Boggs, *Biophys. J.* **1999**, *77*, 306; i) G. Siuzdak, Z. L. Zheng, J. Y. Rhamphal, Y. Ichikawa, K. C. Nicolaou, F. C. Gaeta, K. S. Chatman, C. H. Wong, *Bioorg. Med. Chem. Lett.* **1994**, *4*, 2863; IR: j) J. M. Boggs, A. Menikh, G. Rangaraj, *Biophys. J.* **2000**, *78*, 874; Surface force measurements: k) Z. W. Yu, T. L. Calvert, D. Leckband, *Biochemistry* **1998**, *37*, 1540; QCM: l) K. Matsuura, H. Kitakouji, A. Tsuchida, N. Sawada, H. Ishida, M. Kiso, K. Kobayashi, *Chem. Lett.* **1998**, 1293; Langmuir compressions: m) K. Matsuura, H. Kitakouji, R. Oda, Y. Morimoto, H. Asano, H. Ishida, M. Kiso, K. Kitajima, K. Kobayashi, *Langmuir* **2002**, *18*, 6940.

[4] a) N. Kojima, M. Shiota, Y. Sadahira, K. Handa, S. Hakomori, *J. Biol. Chem.* **1992**, *267*, 17264; b) N. Kojima, S. Hakomori, *J. Biol. Chem.* **1991**, *266*, 17552; c) K. Iwabuchi, S. Yamamura, A. Prinetti, K. Handa, S. Hakomori, *J. Biol. Chem.* **1998**, *273*, 9130.

[5] E. Otsuji, Y. S. Park, K. Tashiro, N. Kojima, T. Toyokuni, S. Hakomori, *Int. J. Oncol.* **1995**, *6*, 319.

[6] B. Dean, H. Ogushi, S. Cai, E. Otsuji, K. Tashiro, S. Hakomori, T. Toyokuni, *Carbohydr. Res.* **1993**, *245*, 175.

 © 2003 Wiley-VCH Verlag GmbH & Co. KGaA, Weinheim 1433-7851/03/4201-0097 $ 20.00+.50/0

[7] a) S. Wang, R. M. Leblanc, *Biochim. Biophys. Acta* **1999**, *1419*, 317; b) A. Giehl, T. Lemm, O. Bartelsen, K. Sandhoff, A. Blume, *Eur. J. Biochem.* **1999**, *261*, 650; c) R. Villard, D. Hammache, G. Delapierre, F. Fotiadu, G. Buono, J. Fantini, *ChemBioChem* **2002**, *3*, 517; d) J. Hernandez, R. Pouplana, J. Estelrich, *J. Dispersion Sci. Technol.* **1988**, *9*, 223; e) H. Zhao, A. C. Rinaldi, A. D. Giulio, M. Simmaco, P. K. J. Kinnunen, *Biochemistry* **2002**, *41*, 4425; f) I. J. Vereyken, V. Chupin, R. A. Demel, S. C. M. Smeekens, B. D. Kurijff, *Biochim. Biophys. Acta* **2001**, *1510*, 307; for an overview of the applications of lipid monolayers, see g) H. Brockman, *Curr. Opin. Struct. Biol.* **1999**, *9*, 438.

[8] a) C. M. Knobler, *Adv. Chem. Phys.* **1990**, *77*, 397; b) S. Heyse, T. Stora, E. Schmid, J. H. Lakey, H. Vogel, *Biochim. Biophys. Acta* **1998**, *85507*, 319; c) C. Yuan, L. J. Johnston, *Biophys. J.* **2000**, *79*, 2768; d) J. C. Conboy, K. D. McReynolds, J. Gervay-Hague, S. S. Saavedra, *J. Am. Chem. Soc.* **2002**, *124*, 968.

[9] N. Kojima, B. Fenderson, M. Stroud, R. Goldberg, R. Habermann, T. Toyokuni, S. Hakomori, *Glycoconjugate J.* **1994**, *11*, 238.

[10] The glycolipids were prepared from the corresponding peracetylated disaccharides by conversion into the glycosyl bromides with HBr followed by silver triflate mediated glycosylation with allyl alcohol. Subsequent ozonolysis, oxidation, and coupling to tetradecylamine followed by Zemplen deacylation provided the desired compounds. The synthetic glycolipids were characterized by ^{1}H and ^{13}C NMR spectroscopy and high-resolution mass spectrometry.

[11] A. Chattopadhyay, E. London, *Anal. Biochem.* **1984**, *139*, 408.

[12] The Langmuir monolayer experiments were carried out on a KSV minitrough equipped with a Wilhelmy plate and balance. A chloroform/methanol solution of a 10% GM_3/90% DPPC mixture was deposited with a microsyringe on a subphase of 1 mM $CaCl_2$. The solvent was allowed to evaporate over 10 min, and the monolayer was compressed at a rate of 3 mm min^{-1} until the desired initial monolayer pressure for the binding experiment was reached. Once the monolayer was at the target pressure the barriers were stopped, and the subphase was stirred gently outside the barriers. The binding experiment was initiated by injection of 1.5 mL of a concentrated glycolipid solution into the subphase outside the Teflon barriers.

[13] Negative $\Delta\pi$ values are indicative of either lipid loss from the monolayers owing to the high solubility of the glycolipids and/or rearrangements within the monolayer after compression has ceased. See a) J. Esnault, J.-M. Mallet, Y. Zhang, P. Sinäy, T. LeBouar, F. Pincet, E. Perez, *Eur. J. Org. Chem.* **2001**, 253; b) G. L. Gaines, *Insoluble Monolayers at Liquid–Gas Interfaces*, Interscience Publishers, New York, **1966**, p. 143.

[14] Single-site modifications can have measurable effects on CCIs. For examples in the context of glycopolymer recognition, see references [3c,l,m].

[15] a) W. Cook, C. Bugg, *Biochim. Biophys. Acta* **1975**, *389*, 428; b) W. Cook, C. Bugg, *J. Am. Chem. Soc.* **1973**, *95*, 6442.

[16] Another observation consistent with this hypothesis is that the cmc value of **3** is higher in 1 mM $CaCl_2$ than in deionized water. This is in contrast to **4**, **5**, and Tween-80,[18] all of which show decreases in cmc values on going from water to 1 mM $CaCl_2$, as might be expected in a solution of greater ionic strength.

[17] The surface activities or equilibrium surface pressures for **3**, **4**, and **5** are: 26, 6, and 22 mN m^{-1}, respectively.

[18] Binding studies of the GM_3 monolayer at 30 mN m^{-1} with Tween-80, a nonionic hydroxy-terminated detergent, which has an equilibrium surface pressure of 28 mN m^{-1} and a cmc of 3 μM, also failed to show a concentration-dependent increase in $\Delta\pi$.

[19] When GM_3 was omitted from the monolayer, injection of 25 μM **3** or **5** afforded a $\Delta\pi$ of 8 mN m^{-1} (30 mN m^{-1} starting pressure). The rate of increase in π was slower in the absence of GM_3 which suggests that CCIs facilitate insertion by targeting the glycolipids to the interface. These observations indicate that in the absence of CCIs intrinsic surface activity becomes the primary contributor to $\Delta\pi$.

[20] Glycolipid **4** had a $\Delta\pi$ of 2.7 mN m^{-1} at an initial pressure of 10 mN m^{-1}. At all other pressures examined the $\Delta\pi$ value was indistinguishable from the values observed in a "holding" experiment.

Synthesis of Pyrroles and Furans

1,2-Migration of the Thio Group in Allenyl Sulfides: Efficient Synthesis of 3-Thio-Substituted Furans and Pyrroles**

*Joseph T. Kim, Alexander V. Kel'in, and Vladimir Gevorgyan**

The 1,2-migration of the thio group is an important chemical transformation that is extensively used in carbohydrate chemistry for stereoselective Mitsunobu-type substitution at the anomeric center [Eq. (1)].[1] There are also reports on employment of a 1,2-shift of the thio group in the synthesis of heterocycles [Eq. (2)][1a,b] Known 1,2-migrations of the thio group can be classified as one of two types: 1) An S_N2-type attack of the lone pair of electrons of the sulfur atom at the adjacent sp^3 center in **A** produces the thiiranium intermediate **B**, which after subsequent nucleophile-assisted ring opening affords **C**, a product of 1,2-migration of the thio group [Eq. (1)].[1] 2) The migration is triggered by attack of the sulfur atom at the sp^2 carbon atom of the iminium[2a,b] or imine[2c] moiety of **D** to form the thiiranium species **E**. The latter either produces sulfide **F** through nucleophilic attack[2c] or gives the thioenamine **G** as a result of a deprotonation/ring-opening process [$R^1 = H$, Eq. (2)].[2a,b] In all cases the migrations of the thio group proceeded from an sp^3 center to either another sp^3 [Eq. (1)][1] or to an sp^2 [Eq. (2)][2] carbon center. To the best of our knowledge, there are no reports of 1,2-migration of the thio group from an olefinic carbon atom.

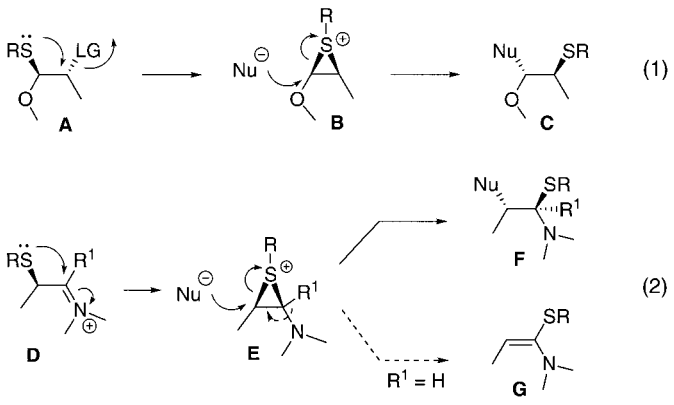
Herein we wish to report a novel 1,2-migration of the thio group from an sp^2 carbon atom in allenyl sulfides. This unprecedented migration allowed the development of an

[*] Prof. Dr. V. Gevorgyan, J. T. Kim, A. V. Kel'in
Department of Chemistry, University of Illinois at Chicago
845 West Taylor Street, Chicago, IL 60607-7061 (USA)
Fax: (+1) 312-355-0836
E-mail: vlad@uic.edu

[**] The support of the National Science Foundation (CHE-0096889) and the National Institutes of Health (GM-64444) is gratefully acknowledged.

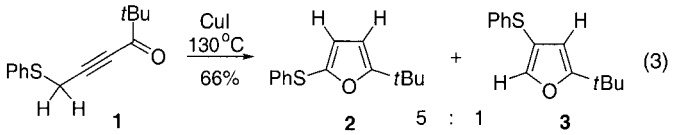
Supporting information for this article is available on the WWW under http://www.angewandte.org or from the author.

 © 2003 Wiley-VCH Verlag GmbH & Co. KGaA, Weinheim 1433-7851/03/4201-0098 $ 20.00+.50/0

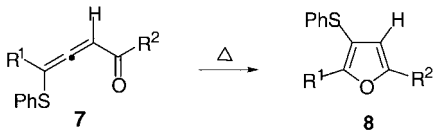


efficient method for the synthesis of 3-thio-substituted furans and pyrroles.

During the investigation of the scope of the recently found Cu-catalyzed transformation of alkynyl ketones and alkynyl imines into 2,5-disubstituted furans[3] and pyrroles,[4] we discovered that heating ketopropargyl sulfide **1** in *N*,*N*-dimethylacetamide (DMA) in the presence of CuI (10 mol%) not only gave the targeted 2,5-disubstituted furan **2**, but also a small amount of the unexpected 2,4-disubstituted furan **3** [Eq. (3)]. It was hypothesized that first, propargyl–allenyl isomerization[5] produces an allenic intermediate **4** (Scheme 1).



Next, the allenyl sulfide **4**, according to the "standard" cycloisomerization scenario (Scheme 1, path a)[3] produces the major reaction product, furan **2**.[3] It was proposed that alternatively, an intramolecular nucleophilic attack of the lone pair of electrons of the sulfur atom at the central carbon atom of the allene can transform it into the aromatic thiirenium zwitterion **5**.[6] The latter, either via Ad_N-E (**5**→**6**) or through a direct S_N2-Vin-type[7] process, affords the minor isomeric furan **3** (Scheme 1, path b). Although the role of the copper catalyst in this reaction is not completely understood, there are some indications that it facilitates propargyl–allenyl isomerization,[3,4,8] and in some cases it is also required for further transformations [Eq. (4)], probably as a result of the stabilization of carbanionic intermediates.[8] It occurred to us that if the above mechanistic proposal is correct, then replacement of H^b in allene **4** with any other nonmigrating group should enforce selective migration of the thio group to produce 2,4-disubstituted furan **3** exclusively (path b). To examine this proposal, thioallenes **7a**,**b** were prepared by independent methods and subjected to the cycloisomerization conditions described above [Eq. (4)]. Remarkably, it was found that thioallenyl phenyl ketone **7a**, even in the absence of CuI, underwent *quantitative* thermal transformation to **8a**. In contrast, attempts to perform analogous thermal cycloisomerization of thioallenyl alkyl ketone **7b** resulted in total decomposition of the starting material, whereas 82% of **8b** was isolated when the reaction was performed at room temperature in the presence of CuI (5 mol%) [Eq. (4)].

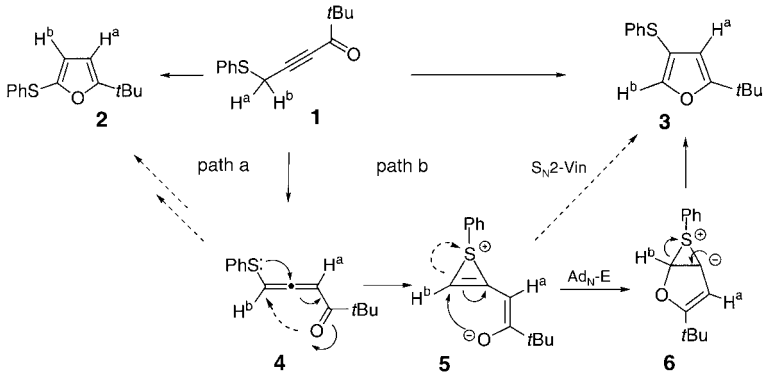


8a: $R^1 = n$Bu, R^2 = Ph (130°C, 2h, 100%)
8b: $R^1 = n$Bu, $R^2 = (CH_2)_3OMOM$ (CuI, (5 mol%), RT, 36h, 82%)

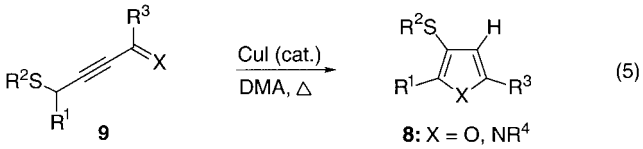
Naturally, we next attempted a selective migrative cycloisomerization of substituted propargyl sulfides, undoubtedly superior precursors when compared with allenyl sulfides from a synthetic point of view. Accordingly, a series of alkyl-substituted propargyl sulfides **9** were synthesized and subjected to the cycloisomerization reaction [Eq. (5)].

We were very pleased to find that thiopropargyl aldehyde **9c** underwent smooth and selective cycloisomerization, producing 2-butyl-3-phenylsulfanyl-furan (**8c**) in 71% yield as a *single* reaction product (Table 1, entry 1). Cycloisomerization of thiopropargyl ketones **9a**,**d**,**e** proceeded provided the trisubstituted furans **8a**,**d**,**e** in very good yields (Table 1, entries 2–4).[9] Cycloisomerization of phenylsulfanyl propargyl ketones possessing alkenyl (**9f**), ester (**9g**), and protected alcohol (**9h**) functionalities in the side chain proceeded readily to afford the corresponding trisubstituted furans **8f–h** in good to very high yields (Table 1, entries 5–7). The alkyl sulfanyl group migrated with an efficiency comparable to that of its phenylsulfanyl analogue to give the corresponding furan **8i** in 72% yield (Table 1, entry 8).

Inspired by the successful synthesis of trisubstituted furans, the cycloisomerization of thiopropargyl imines was then investigated. It was found that thiopropargyl imines **9j–o** in the presence of



Scheme 1. Different routes for the cyclization of the ketopropargyl sulfide **1** to give either furan **2** or **3**. Based on this mechanistic proposal, the reaction of ketopropargyl sulfides in which H^b of **4** is replaced with any other nonmigrating group should exclusively follow path b.

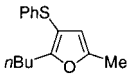
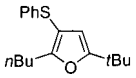
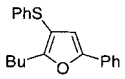
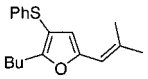
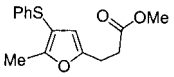
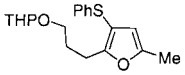
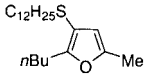
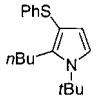
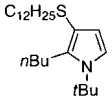
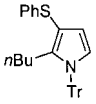
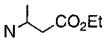
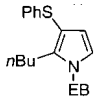
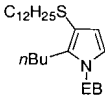
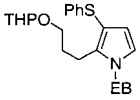


(5)

CuI underwent a similar transformation to give the corresponding 3-thio-substituted pyrroles **8j–o** in very good yields (Table 1, entries 9–14).[10] Again, the dodecyl sulfanyl group (Table 1, entry 10) migrated comparably to the phenyl sulfanyl analogue (Table 1, entry 9) and the THP-protected alcohol functionality was tolerated (Table 1, entry 14). It is worth mentioning that all synthesized pyrroles have removable groups at the nitrogen atom, for example, the *tert*-butyl (**8j**, **k**, Table 1, entries 9, 10),[11] trityl (**8l**, Table 1, entry 11),[12] and 3-ethylbutyryl[4,13] (**8m–o**, Table 1, entries 12–14) groups, and thus can be easily functionalized further at the nitrogen site.[14]

In conclusion, a novel 1,2-migration of the thio group in thioallenyl ketones and thioallenyl imines was discovered. An efficient method for the synthesis of di- and trisubstituted

Table 1: Cu-catalyzed synthesis of 3-substituted furans and pyrroles.

Entry	Substrate					Product	Yield [%][a]
	9	R^1	R^2	R^3	X	**8**	
1	**c**	*n*Bu	Ph	H	O		71
2	**d**	*n*Bu	Ph	Me	O		76
3	**e**	*n*Bu	Ph	*t*Bu	O		89
4	**a**	*n*Bu	Ph	Ph	O		91
5	**f**	*n*Bu	Ph		O		95
6	**g**	Me	Ph	$(CH_2)_2CO_2Me$	O		71
7	**h**	$(CH_2)_3OTHP$	Ph	Me	O		93
8	**i**	*n*Bu	$(CH_2)_{11}CH_3$	Me	O		72
9	**j**	*n*Bu	Ph	H	N-*t*Bu		78
10	**k**	*n*Bu	$(CH_2)_{11}CH_3$	H	N-*t*Bu		86
11	**l**	*n*Bu	Ph	H	N-Tr		85
12	**m**	*n*Bu	Ph	H			74
13	**n**	*n*Bu	$(CH_2)_{11}CH_3$	H	N-EB		67
14	**o**	$(CH_2)_3OTHP$	Ph	H	N-EB		78

[a] Yield of isolated product. THP = tetrahydropyran, Tr = trityl = triphenylmethyl, EB = ethyl butyryl.

 © 2003 Wiley-VCH Verlag GmbH & Co. KGaA, Weinheim 1433-7851/03/4201-0100 $ 20.00+.50/0

furans and trisubstituted pyrroles that possess an aryl sulfanyl or alkyl sulfanyl substituent at C3 has been developed.

Received: August 7, 2002 [Z19912]

[1] a) B. D. Johnston, B. M. Pinto, *J. Org. Chem.* **2000**, *65*, 4607; b) B. Yu, Z. Yang, *Org. Lett.* **2001**, *3*, 377; c) A. Viso, N. Poopeiko, S. Castillon, *Tetrahedron Lett.* **2000**, *41*, 407.

[2] a) R. Plate, R. J. F. Nivard, H. C. J. Ottenheijm, *Tetrahedron* **1986**, *42*, 4503; b) P. Hamel, *J. Org. Chem.* **2002**, *67*, 2854; c) A. Volontereo, M. Zanda, P. Bravo, G. Fronza, G. Cavicchio, M. Crucianelli, *J. Org. Chem.* **1997**, *62*, 8031.

[3] A. V. Kel'in, V. Gevorgyan, *J. Org. Chem.* **2002**, *67*, 95.

[4] A. V. Kel'in, A. W. Sromek, V. Gevorgyan, *J. Am. Chem. Soc.* **2001**, *123*, 2074.

[5] For an example of propargyl–allenyl isomerization, see: P. J. Garratt, S. B. Neoh, *J. Am. Chem. Soc.* **1975**, *97*, 3255.

[6] For an example of stable thiirenium ions, see: V. Lucchini, G. Modena, G. Valle, G. Capozzi, *J. Org. Chem.* **1981**, *46*, 4720; see also reference [7].

[7] a) V. Lucchini, G. Modena, L. Pasquato, *J. Am. Chem. Soc.* **1993**, *115*, 4527; b) R. Destro, V. Lucchini, G. Modena, L. Pasquato, *J. Org. Chem.* **2000**, *65*, 3367.

[8] For the cuprate-assisted transformation of propargylic thioacetals into allenyl copper species, see: a) H.-R. Tseng, C.-F. Lee, L.-M. Yang, T.-Y. Luh, *J. Am. Chem. Soc.* **2000**, *122*, 4992; b) H.-R. Tseng, C.-F. Lee, L.-M. Yang, T.-Y. Luh, *J. Org. Chem.* **1999**, *64*, 8582.

[9] Typical procedure (**9d**): A mixture of propargyl ketone **9d** (246 mg, 1.0 mmol), CuI (12 mg, 0.05 mmol), and anhydrous DMA (2.0 mL) was stirred in a Wheaton microreactor (3 mL) under an Ar atmosphere at 130 °C. The reaction was monitored by TLC and GC/MS until completion. After 12 h, the mixture was cooled to room temperature and poured into saturated aqueous NH_4Cl (20 mL). The phases were separated, and the aqueous phase was extracted (hexanes, 2×10 mL). The combined organic extracts were washed (brine, 10 mL), dried (Na_2SO_4, 2 g), and concentrated under reduced pressure. The residue was purified by means of silica-gel chromatography with hexanes to give furan **8d** (187 mg, 76 %).

[10] Cycloisomerization of **9j–o** to form pyrroles **8j–o** proceeded under slightly different reaction conditions to those in the synthesis of furans **8a–i**. See Supporting Information for details.

[11] For deprotection of *N*-*t*Bu group in pyrroles, see: a) J. Leroy, C. Wakselman, *Tetrahedron Lett.* **1994**, *35*, 8605; b) P. La Porta, L. Capuzzi, F. Bettarini, *Synthesis* **1994**, *3*, 287.

[12] For deprotection of *N*-Tr group in pyrroles, see: D. J. Chadwick, S. T. Hodgson, *J. Chem. Soc. Perkin Trans. 1* **1983**, 93.

[13] For deprotection of analogous group in pyrroles, see: E. Roder, H. Wiedenfeld, T. Bourauel, *Liebigs Ann. Chem.* **1985**, 1708.

[14] It was found that EB protecting group can very easily be removed from the pyrroles. Thus, thio-substituted pyrrole **8m** underwent a facile retro-Michael reaction in the presence of KO*t*Bu to give the corresponding pyrrole **8p** quantitatively.

Heterometallic Wheel Complexes

Synthesis and Characterization of Heterometallic {Cr_7M} Wheels**

Finn K. Larsen, Eric J. L. McInnes, Hassane El Mkami, Jacob Overgaard, Stergios Piligkos, Gopalan Rajaraman, Eva Rentschler, Andrew A. Smith, Graham M. Smith, Val Boote, Martin Jennings, Grigore A. Timco, and Richard E. P. Winpenny**

Many beautiful cyclic metal structures have been reported recently, for example, the giant wheels from Müller and co-workers,[1] the wheels using carboxylate ligands made by, among others, the Lippard group,[2] and the metallocoronands reported by Saalfrank and co-workers.[3] One question that intrigued us based on this chemistry was whether heterometallic rings could be made? A recent theoretical paper by Meier and Loss[4] suggests that such wheels may show interesting quantum coherence phenomena. We have found that an extensive family of such wheels can be made straightforwardly, and in good yield, based on the fundamental chemical principle that a cation–anion pair will have different crystallization properties than a neutral molecule.

The neutral homometallic wheel, $[Cr_8F_8(O_2CCMe_3)_{16}]$ (**1**)[5] has been widely studied, both because of its magnetic properties[6] and because it can act as a host for small organic molecules.[7] As we understand the chemistry of **1** thoroughly, it seemed a good candidate for preparing heterometallic analogues. The approach adopted was straightforward; if we replace a single chromium(III) center by a dication (M) the monoanionic species $[Cr_7MF_8(O_2CCMe_3)_{16}]^-$ will be formed. In the presence of a suitable cation, we should then be able to separate the salt from **1**, which may also be present. Using this

[*] Dr. G. A. Timco
Institute of Chemistry
Moldovan Academy of Sciences, Kishinev (Moldova)
Fax: (+3732) 737-133
E-mail: timg@nor.md

Prof. R. E. P. Winpenny, Dr. E. J. L. McInnes, S. Piligkos, G. Rajaraman, A. A. Smith, V. Boote, M. Jennings
Department of Chemistry, The University of Manchester
Oxford Road, Manchester, M13 9PL (UK)
Fax: (+44) 161-275-4616
E-mail: richard.winpenny@man.ac.uk

Prof. F. K. Larsen, J. Overgaard
Department of Chemistry, University of Aarhus
8000 Århus C (Denmark)

Dr. E. Rentschler
Max Planck Institut für Strahlenchemie
Mülheim (Germany)

Dr. H. E. Mkami, Dr. G. M. Smith
Department of Physics and Astronomy
The University of St. Andrews, St. Andrews (UK)

[**] This work was supported by the EPSRC(UK), INTAS (Contract 00–0172) and The Royal Society.

 © 2003 Wiley-VCH Verlag GmbH & Co. KGaA, Weinheim 1433-7851/03/4201-0101 $ 20.00+.50/0

methodology, we have pursued a series of reactions in which metal dications are added to the reaction matrix from which **1** is crystallized.

Two routes have been explored. The first route involves the reaction of hydrated chromium(III) fluoride and $[Ni_2(O_2CCMe_3)_4(HO_2CCMe_3)_4(H_2O)]$ (**2**)[8] or $[Co_2(O_2CCMe_3)_4(HO_2CCMe_3)_4(H_2O)]$ (**3**)[8] in a mixture of DMF and pivalic (trimethylacetic) acid. The reaction gives $[\{Me_2NH_2\}\{Cr_7NiF_8(O_2CCMe_3)_{16}\}]$ (**4**) or $[\{Me_2NH_2\}\{Cr_7CoF_8(O_2CCMe_3)_{16}\}]$ (**5**), respectively, with a trace of **1** that can be removed chromatographically; crystals of **4** or **5** can then be obtained from the eluted solutions. The formation of the $[Me_2NH_2]^+$ ion is presumably as a result of the acid hydrolysis of DMF.

A second, and superior, route is to carry out the reaction of $CrF_3 \cdot 4H_2O$ and **2** or **3** in a mixture of a secondary amine and pivalic acid. The reaction was performed in a teflon flask at 140 °C, and the products $[\{R_2NH_2\}\{Cr_7NiF_8(O_2CCMe_3)_{16}\}]$ (where R = Me (**4**), Et (**6**), *n*Pr (**7**), *n*Bu (**8**), *n*-octyl (**9**)) and $[\{R_2NH_2\}\{Cr_7CoF_8(O_2CCMe_3)_{16}\}]$ (where R = Me (**5**), Et (**10**)) crystallize with no trace of **1** or any other impurity. Other secondary amines give similar products.

The chemistry can be extended to other M^{II} ions by dissolving chromium fluoride in the pivalic acid/diethylamine mixture at 140 °C before adding an excess of the second metal salt. $[\{Et_2NH_2\}\{Cr_7MF_8(O_2CCMe_3)_{16}\}]$ (M = Mn (**11**), Fe (**12**), Cd (**13**)) can then be made with good purity in yields of around 70 %. For **11** and **12** the hydrated metal chloride salt was used, while for **13** cadmium carbonate was added. We have also made $[\{nBu_2NH_2\}\{Cr_7FeF_8(O_2CCMe_3)_{16}\}]$ (**14**) by this route.

The compounds crystallize in one of four crystal systems: primitive tetragonal, body-centered tetragonal, monoclinic, or orthorhombic.[9] Modeling some of these crystal structures is difficult, mainly because of the nature of the pivalate ligands. The methyl groups are invariably disordered and also create intermolecular voids between the large complexes, presumably containing cocrystallized volatile solvent molecules with no possibility of significant hydrogen bonding. Thus, the solvent atomic positions are ill-defined and impossible to model. Similar problems were encountered for **1**.[7] In the tetragonal crystals the fourfold symmetry of the wheel is higher than that available to the ammonium cation, thus requiring positional disorder in the side arms of the cation. The result is that while refinement proceeded well for **5**, **6**, and **7** (**10**–**13** are isostructural with **6**), for the other structures the *R* factors are high. However, the connectivity among nonhydrogen atoms in the annular structure is unequivocally established in all cases. A view of **6** is shown in Figure 1.

The structure of the anions is similar to that of the neutral wheel **1**, with each M···M vector bridged by a μ-fluoride and two 1,3-bridging pivalates. The M site is disordered over all possible metal sites. In all the structures the average Cr–F and Cr–O bond lengths are longer than in **1**, but not by statistically significant amounts, for example, the average Cr–F bond lengths range from 1.927(5) Å for **8** to 1.939(8) Å for **4** (compared with a range of 1.914(6) and 1.924(5) Å for different solvates of **1**[7]).

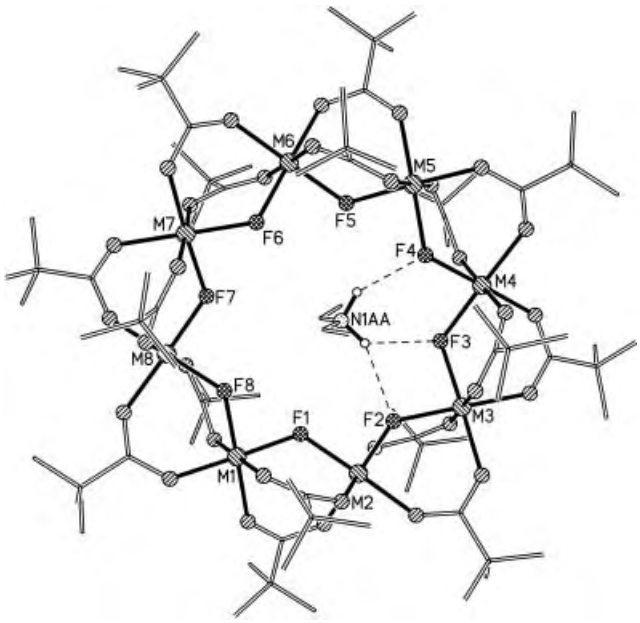


Figure 1. The molecular structure of **6**, with the hydrogen atoms omitted for clarity. Bond length ranges [Å]: M–O(OCH_3) 1.940–2.023, M–O(O_2CCH_3) 2.021–2.071, (average esd 0.0042). M is 7/8 Cr and 1/8 the second metal at each site.

For all the structures a secondary ammonium cation is found in the cavity of the macrocycle, forming three N–H···F bonds (Figure 1). The N···F distances vary from 2.47 to 3.12 Å, and appear to lengthen as the alkyl side-chains lengthen. The disorder in the structures makes the variation in distances statistically insignificant, however it is clear that in **9** there is barely space to contain the *n*-octyl chains of the cation. The presence of these cations is strong evidence that one of the Cr^{III} centers has been displaced by a dication in each case.

Support for these findings comes from elemental analysis; for all compounds we have analysis of both metals present, C, H, and N, and also F for **4** and **9**–**14**. In all cases, this fits for $[\{R_2NH_2\}\{Cr_7MF_8(O_2CCMe_3)_{16}\}]$. The excellent fluorine analysis rules out the presence of hydroxide in the bridges. Further evidence is provided by mass spectroscopy. For **4**–**14** (**7** not studied) we see the most intense peak for the anion $[Cr_7MF_8(O_2CCMe_3)_{16}]^-$ in the negative-ion spectra, with a correct isotopic distribution. In the positive-ion spectra we see the molecular ion and sometimes peaks at higher mass, indicating the incorporation of Na^+ cations.

Mössbauer spectroscopy of **14** indicates that only Fe^{II} species are present. Both the isotope shift and quadrupole splitting of 1.362 and 2.404 $mm\,s^{-1}$, respectively, are clear indications that this oxidation state is present, and there is no evidence of resonance from Fe^{III} ions.

The magnetic behavior of each wheel is broadly similar. For **1**, antiferromagnetic exchange leads to a diamagnetic ground state in zero-field.[6] In the $\{Cr_7Ni\}$ cages the imbalance in spins gives an $S = 1/2$ ground state, leading to an inflection in $\chi_m T$ versus T at low temperature for those cages studied (**4**, **6**, and **7**; Figure 2, data for **6** shown). The behavior can be modeled with one exchange interaction of around 12 cm^{-1},

 © 2003 Wiley-VCH Verlag GmbH & Co. KGaA, Weinheim 1433-7851/03/4201-0102 $ 20.00+.50/0

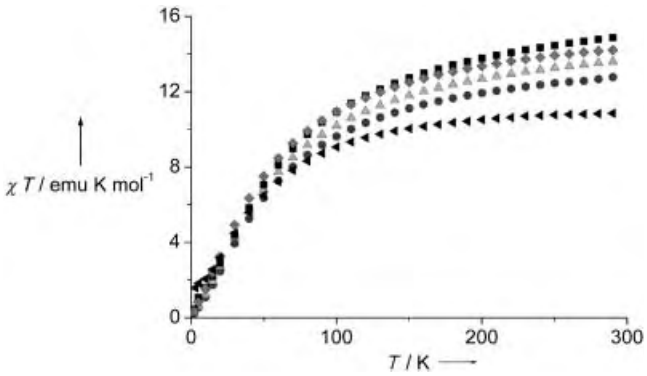


Figure 2. Plot of $\chi_m T$ versus T for **6** (●), **10** (▲), **13** (◀), **11** (■), and **14** (◆).

very similar to that reported for **1**.[6] There is no need to invoke a less symmetric magnetic model.

For **10** the high-temperature value of $\chi_m T$ is higher than for the $\{Cr_7Ni\}$ wheels, which reflects the presence of high-spin Co^{II} species, but a similar fall is seen at lower temperatures. The ground state of **10** appears to be diamagnetic. For **11** and **14** the value of $\chi_m T$ at room temperature is higher still, as high-spin Mn^{II} or Fe^{II} species are present; the low-temperature value again suggests $S = 1$ or 1/2, respectively. For **13** the value of $\chi_m T$ at room temperature is lower, as Cd^{II} ions have no spin, while at low temperature the value is equivalent to an $S = 3/2$ ground state.

Complex **1** gives well-defined EPR spectra at low temperatures[6] because of transitions within $S = 1$ and $S = 2$ excited states; the resonances have a relatively low intensity. The EPR spectra of the $\{Cr_7M\}$ wheels are entirely different. For example, **6** gives a pair of transitions at $g_{xy} = 1.781$ and $g_z = 1.740$ (Figure 3a). Therefore the spectrum resembles a transition for an $S = 1/2$ species with axial symmetry. The low g value can be justified based on the vector coupling approach,[10] assuming $g_{Cr} = 1.99$ and $g_{Ni} = 2.10$. A sample of **10** gives a much less intense but identical spectrum resulting from a small percentage (0.04%) of a Ni^{II} impurity. Complexes **11**–**13** give complex spectra consistent with ground states with S greater than 1/2 (Figure 3b, c, and d). For **12** the EPR spectrum contains a broad transition at approximately $g = 4.0$, which indicates the presence of an Fe^{III} impurity (Figure 3b), in addition to features close to $g = 2.00$. The impurity is not found by Mössbauer spectroscopy, however, this may simply reflect the greater sensitivity of EPR analysis. We have not yet fully interpreted the spectra for **11**–**13**.

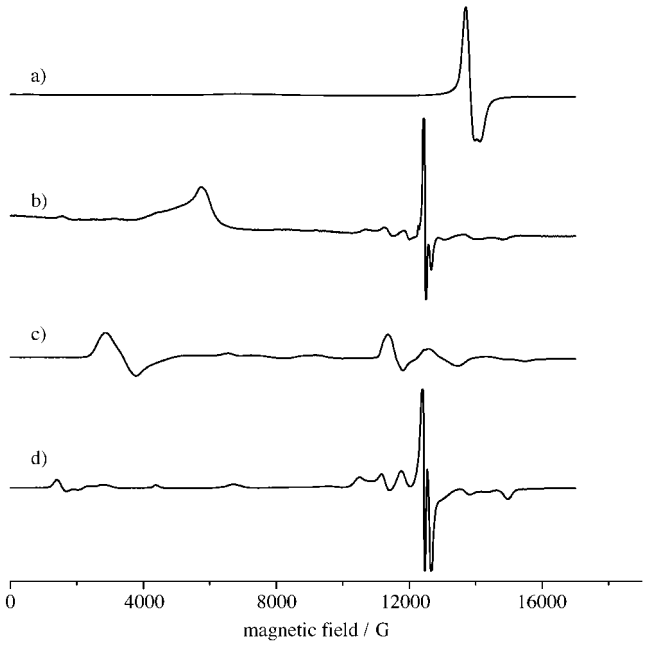


Figure 3. Q-band EPR spectra at 5 K for a) **6**, b) **12**, c) **11**, and d) **13**.

The compounds reported are the first heterometallic wheels. The method used is applicable to many other systems, if a convenient cation can be added to the system. The existence of many such wheels will allow a detailed analysis of the magnetic behavior of antiferromagnetically coupled wheels with a nondiamagnetic ground state. Previously, this has not been possible.

Experimental Section

First route: **4**: $CrF_3 \cdot 4H_2O$ (5.0 g, 27.6 mmol), $[Ni_2(O_2CCMe_3)_4(HO_2CCMe_3)_4(H_2O)]$ (2.0 g, 2.7 mmol), DMF (8.5 mL, 110.0 mmol), and pivalic acid (11.5 g, 112.6 mmol) were heated to 140 °C for 2 h while stirring in a teflon flask. During this time, chromium fluoride dissolved and a green crystalline product formed. The solution was cooled to room temperature and the following day the crystalline product was filtered, washed with DMF, then with water, and dried in air. The product was purified by column chromatography on silica gel using toluene as eluent. First the less polar impurity **1** eluted, then **4** (or **5**). The toluene was then evaporated under reduced pressure. Yield 4.0 g (45.3%). The product was recrystallized from from THF/CH_3CN.

Elemental analysis calcd (%) for $C_{82}H_{152}Cr_7F_8NNiO_{32}$: Cr 16.26, Ni 2.62, C 43.99, H 6.84, N 0.63; found: Cr 15.68, Ni 2.32, C 43.74, H 6.96, N 0.55. ES-MS (THF, m/z): −2191 $[Cr_7NiF_8(O_2CCMe_3)_{16}]^-$; +2238 $[M^+]$; +2260 $[M+Na]^+$.

5: This product was obtained by an analogous procedure to **4**, but starting from $[Co_2(O_2CCMe_3)_4(HO_2CCMe_3)_4(H_2O)]$. The product was recrystallized from acetone. Yield 3.1 g (35.1%). Elemental analysis calcd (%) for $C_{82}H_{152}CoCr_7F_8NO_{32}$: Cr 16.26, Co 2.62, C 43.99, H 6.84, N 0.63; found: Cr 16.18, Co 2.16, C 44.79, H 7.18, N 0.54. ES-MS (THF, m/z): −2191 $[Cr_7CoF_8(O_2CCMe_3)_{16}]^-$; +2238 $[M^+]$; +2261 $[M+Na]^+$.

Second route: **4·C_6H_5Me**: $CrF_3 \cdot 4H_2O$ (5.0 g, 27.6 mmol), $[Ni_2(O_2CCMe_3)_4(HO_2CCMe_3)_4(H_2O)]$ (2.0 g, 2.7 mmol), dimethylamine (2.0 M solution in THF, 5.5 mL, 11.0 mmol), and pivalic acid (14.0 g, 137.1 mmol) were stirred at 140 °C for 5 h. During this time, chromium fluoride dissolved and a green crystalline product formed. The flask was cooled to room temperature and acetone (50 mL) was added while stirring. The crystalline product was filtered, washed with a large quantity of acetone, dried in air, and recrystallized from toluene to give **4**·$C_6H_5CH_3$. Yield 6.45 g (70.1%). Elemental analysis calcd (%) for $C_{89}H_{160}Cr_7F_8N_1Ni_1O_{32}$: Cr 15.62, Ni 2.52, C 45.86, H 6.92, N 0.60, F 6.52; found: Cr 15.17, Ni 2.47, C 46.38, H 7.07, N 0.50, F 6.57. ES-MS (THF, m/z): −2191 $[Cr_7NiF_8(O_2CCMe_3)_{16}]^-$; +2239 $[M^+]$.

5·C_6H_5Me was obtained by an analogous procedure starting from $[Co_2(O_2CCMe_3)_4(HO_2CCMe_3)_4(H_2O)]$. Yield 6.15 g (66.9%). Elemental analysis calcd (%) for $C_{89}H_{160}Cr_7F_8NCoO_{32}$: Cr 15.61, Co 2.53, C 45.86, H 6.92, N 0.60; found: Cr 15.22, Co 2.45, C 46.66, H 7.24, N 0.58. ES-MS (THF): same as **5**.

 © 2003 Wiley-VCH Verlag GmbH & Co. KGaA, Weinheim 1433-7851/03/4201-0103 $ 20.00+.50/0

Compounds **6**–**11** were obtained by analogous reactions to that for **4**·C_6H_5Me replacing dimethylamine with the secondary amines listed below.

6: Et_2NH (0.85 g, 11.6 mmol); recrystallized from ethyl acetate. Yield 6.1 g (68.2 %). Elemental analysis calcd (%) for $C_{84}H_{156}Cr_7F_8N_1Ni_1O_{32}$: Cr 15.61, Ni 2.53, C 45.51, H 6.94, N 0.62, F 6.70; found: Cr 14.59, Ni 2.50, C 44.46, H 7.12, N 0.62, F 6.74. ES-MS (THF, *m*/*z*): −2191 $[Cr_7NiF_8(O_2CCMe_3)_{16}]^-$; +2266 $[M^+]$; +2289 $[M+Na]^+$.

7: nPr_2NH (1.12 g, 11.1 mmol); recrystallized from toluene. Yield 5.7 g (63.0 %). Elemental analysis calcd (%) for $C_{86}H_{160}Cr_7F_8N_1Ni_1O_{32}$: Cr 15.86, Ni 2.56, C 45.01, H 7.03, N 0.61; found: Cr 15.08, Ni 2.39, C 45.71, H 7.31, N 0.57.

8: nBu_2NH (1.43 g, 11.1 mmol); recrystallized from toluene. Yield 5.65 g (61.7 %). Elemental analysis calcd (%) for $C_{88}H_{164}Cr_7F_8N_1Ni_1O_{32}$: Cr 15.67, Ni 2.53, C 45.50, H 7.12, N 0.60; found: Cr 15.52, Ni 2.46, C 46.92, H 7.31, N 0.59. ES-MS (THF, *m*/*z*): −2192 $[Cr_7NiF_8(O_2CCMe_3)_{16}]^-$; +2345 $[M+Na]^+$.

9: $(n\text{-octyl})_2NH$ (2.65 g, 11.0 mmol); recrystallized from toluene. Yield 5.45 g (56.7 %). Elemental analysis calcd (%) for $C_{96}H_{180}Cr_7F_8N_1Ni_1O_{32}$: Cr 14.95, Ni 2.41, C 47.35, H 7.45, N 0.58, F 6.24; found: Cr 15.27, Ni 2.34, C 47.93, H 7.52, N 0.56, F 6.36. ES-MS (THF, *m*/*z*): −2191 $[Cr_7NiF_8(O_2CCMe_3)_{16}]^-$; +2225 (not assigned).

10 was obtained by an analogous procedure to **5**, replacing Me_2NH with Et_2NH (0.85 g, 11.6 mmol); recrystallized from ethyl acetate. Yield 5.8 g (64.9 %). Elemental analysis calcd (%) for $C_{84}H_{156}Co_1Cr_7F_8N_1O_{32}$: Cr 16.06, Co 2.60, C 44.50, H 6.94, N 0.62, F 6.70; found: Cr 15.31, Co 2.57, C 44.51, H 7.05, N 0.62, F 6.67, Ni 0.04 (impurity). ES-MS (THF, *m*/*z*): −2193 $[Cr_7CoF_8(O_2CCMe_3)_{16}]^-$; +2267 $[M^+]$.

11: $CrF_3{\cdot}4H_2O$ (5.0 g, 27.6 mmol), Et_2NH (0.85 g, 11.6 mmol), and pivalic acid (14.0 g, 137.1 mmol) were heated to 140 °C while stirring for 1.5 h in a teflon flask. $MnCl_2{\cdot}4H_2O$ (1.5 g, 7.6 mmol) was added to the mixture and the temperature was increased to 160 °C for 5 h, at which point a green crystalline product had formed. The flask was cooled to room temperature and acetone (50 mL) was added while stirring. The product was collected by filtration, washed with a large quantity of acetone, then dried in air and recrystallized from ethyl acetate. Yield 6.7 g (75.1 %). Elemental analysis calcd (%) for $C_{84}H_{156}Cr_7MnF_8N_1O_{32}$: Cr 16.08, Mn 2.43, C 44.58, H 6.95, N 0.62, F 6.72; found: Cr 16.18, Mn 2.56, C 44.56, H 6.90, N 0.62, F 6.75. ES-MS (THF, *m*/*z*): −2188 $[Cr_7MnF_8(O_2CCMe_3)_{16}]^-$; +2262 $[M^+]$; +2284 $[M+Na]^+$.

12 was obtained by an analogous procedure to **11** by replacing $MnCl_2{\cdot}4H_2O$ with $FeCl_2{\cdot}4H_2O$ (1.5 g, 7.5 mmol); recrystallized from ethyl acetate**.** Yield 6.7 g (75.0 %). Elemental analysis calcd (%) for $C_{84}H_{156}Cr_7F_8Fe_1N_1O_{32}$: Cr 16.08, Fe 2.47, C 44.56, H 6.95, N 0.62, F 6.71; found: Cr 15.76, Fe 2.62, C 44.62, H 6.95, N 0.60, F 6.62. ES-MS (THF, *m*/*z*): −2188 $[Cr_7FeF_8(O_2CCMe_3)_{16}]^-$; +2263 $[M^+]$; +2287 $[M+Na]^+$.

13 was obtained by an analogous procedure to **11** by replacing $MnCl_2{\cdot}4H_2O$ with $CdCO_3$ (1.2 g, 7.0 mmol); recrystallized from ethyl acetate**.** Yield 6.5 g (67.2 %). Elemental analysis calcd (%) for $C_{84}H_{156}Cr_7CdF_8N_1O_{32}$: Cr 15.69, Cd 4.84, C 43.48, H 6.78, N 0.60, F 6.55; found: Cr 15.22, Cd 4.99, C 43.76, H 6.94, N 0.63, F 6.41. ES-MS (THF, *m*/*z*): −2246 $[Cr_7CdF_8(O_2CCMe_3)_{16}]^-$; −2319 $[M^-]$; +2320 $[M^+]$; +2343 $[M+Na]^+$; +2393 (not assigned).

14 was obtained by an analogous procedure to **12** by replacing Et_2NH by nBu_2NH (1.43 g, 11.1 mmol); the product was purified by column chromatography (silica gel/toluene; **14** elutes as the second fraction) then crystallized by evaporation of the toluene. Yield 6.04 g (69.9 %). Elemental analysis calcd (%) for $C_{88}H_{164}Cr_7F_8FeNO_{32}$: Cr 15.69, Fe 2.41, C 45.56, H 7.12, N 0.60, F 6.55; found: Cr 15.35, Fe 2.37, C 46.88, H 7.10, N 0.52, F 6.51. ES-MS (THF, *m*/*z*): −2188 $[Cr_7FeF_8(O_2CCMe_3)_{16}]^-$; +2320 $[M^+]$; +2343 $[M+Na]^+$.

Measurements: Mössbauer spectra were measured at 80 K against a $^{57}Co(Rh)$ source moving at constant acceleration. Velocity calibration was carried out by using the resonance lines of metallic iron, and isomer shifts are given relative to iron metal at room temperature. EPR spectra were recorded at 5 K on a Bruker ESP 300E spectrometer at the X-, K-, and Q-bands (approximately 9.5, 24, and 34 GHz, respectively) and at the W-band (approximately 90 GHz) using a homemade spectrometer.[11]

Magnetic susceptibility measurements were performed on polycrystalline samples in the temperature range 2.0–298 K in an applied field of 1 T using a Quantum Design MPMS SQUID magnetometer. Corrections for diamagnetic contributions were applied by using Pascal's Constants. The sample holder diamagnetism was measured and subtracted from the raw data.

Received: August 19, 2002 [Z19997]

[1] A. Müller, E. Krickemeyer, J. Meyer, H. Bögge, F. Peters, W. Plass, E. Diemann, S. Dillinger, F. Nonnebruch, M. Randerath, C. Menke, *Angew. Chem.* **1995**, *107*, 2293–2295; *Angew. Chem. Int. Ed. Engl.* **1995**, *34*, 2122–2124.

[2] a) K. L. Taft, C. D. Delfs, G. C. Papaefthymiou, S. Foner, D. Gatteschi, S. J. Lippard, *J. Am. Chem. Soc.* **1994**, *116*, 823–832; b) S. P. Watton, P. Fuhrmann, L. E. Pence, A. Caneschi, A. Cornia, G. L. Abbati, S. J. Lippard, *Angew. Chem.* **1997**, *109*, 2917–2919; *Angew. Chem. Int. Ed. Engl.* **1997**, *36*, 2774–2776; c) A. Caneschi, A. Cornia, A. C. Fabretti, D. Gatteschi, *Angew. Chem.* **1999**, *111*, 1372–1374; *Angew. Chem. Int. Ed.* **1999**, *38*, 1295–1297; d) M. Frey, S. G. Harris, J. M. Holmes, D. A. Nation, S. Parsons, P. A. Tasker, R. E. P. Winpenny, *Chem. Eur. J.* **2000**, *6*, 1407–1415; e) E. J. L. McInnes, C. Anson, A. K. Powell, A. J. Thomson, S. Poussereau, R. Sessoli, *Chem. Commun.* **2001**, 85–86; f) J. K. Beattie, T. W. Hambley, J. A. Kleptko, A. F. Masters, P. Turner, *Chem. Commun.* **1998**, 45–46; g) C. P. Raptopoulou, V. Tangoulis, E. Devlin, *Angew. Chem.* **2002**, *114*, 2492–2495; *Angew. Chem. Int. Ed.* **2002**, *41*, 2386–2389.

[3] O. Waldmann, R. Koch, S. Schromm, J. Schülein, P. Müller, I. Bernt, R. W. Saalfrank, F. Hampel, E. Balthes, *Inorg. Chem.* **2001**, *40*, 2986–2995, and references therein.

[4] F. Meier, D. Loss, *Phys. Rev. B* **2001**, *64*, 224411/1–224411/14.

[5] N. V. Gerbeleu, Yu. T. Struchkov, G. A. Timco, A. S. Batsanov, K. M. Indrichan, G. A. Popovich, *Dokl. Akad. Nauk SSSR* **1990**, *313*, 1459–1462.

[6] J. van Slageren, R. Sessoli, D. Gatteschi, A. A. Smith, M. Helliwell, R. E. P. Winpenny, A. Cornia, A.-L. Barra, A. G. M. Jansen, G. A. Timco, E. Rentschler, *Chem. Eur. J.* **2002**, *8*, 277–285.

[7] J. Overgaard, B. B. Iversen, S. P. Palii, G. A. Timco, N. V. Gerbeleu, F. K. Larsen, *Chem. Eur. J.* **2002**, *8*, 2775–2786.

[8] G. Chaboussant, H. U. Güdel, A. Parkin, S. Parsons, A. A. Smith, G. A. Timco, R. E. P. Winpenny, unpublished results.

[9] Crystal data for **4** ($C_{82}H_{152}Cr_7F_8NNiO_{32}$; $M_r = 2232.05$): dark green plate, tetragonal, space group *P*4, $a = b = 19.8908(5)$, $c = 16.0395(8)$ Å, $V = 6345.9(4)$ Å^3, $Z = 2$ (the molecule lies on a fourfold axis), $T = 120.0(2)$ K, $\rho_{calcd} = 1.168$ g cm^{-1}, $F(000) = 2342$, $\mu(Mo_{K\alpha}) = 0.730$ mm^{-1}. Crystal data for **5** ($C_{82}H_{152}CoCr_7F_8NO_{32}$; $M_r = 2232.05$): dark-green plate, tetragonal, space group *I*4, $a = b = 19.8514(7)$, $c = 16.1783(7)$ Å, $V = 6375.5(4)$ Å^3, $Z = 2$ (the molecule lies on a fourfold axis), $T = 120.0(2)$ K, $\rho_{calcd} = 1.163$ g cm^{-1}, $F(000) = 2342$, $\mu(Mo_{K\alpha}) = 0.726$ mm^{-1}. Crystal data for **6** ($C_{87}H_{158}Cr_7F_8NNiO_{33}$; $M_r = 2314.14$): dark green plate, monoclinic, space group $P2_1/c$, $a = 24.9959(10)$, $b = 16.6134(7)$, $c = 30.8822(13)$ Å, $\beta = 109.957(1)$°, $V = 12054.2(9)$ Å^3, $Z = 4$, $T = 120.0(2)$ K, $\rho_{calcd} = 1.275$ g cm^{-1}, $F(000) = 4860$, $\mu(Mo_{K\alpha}) = 0.771$ mm^{-1}. Crystal data for **7** ($C_{92}H_{166}Cr_7F_8NNiO_{33}$; $M_r = 2382.26$): dark green plate, monoclinic, space group $P2_1/c$, $a = 25.2406(18)$, $b = 16.7224(11)$, $c = 31.593(2)$ Å, $\beta = 101.661(1)$°, $V = 13059.8(15)$ Å^3, $Z = 4$, $T = 120.0(2)$ K, $\rho_{calcd} = 1.212$ g cm^{-1},

 © 2003 Wiley-VCH Verlag GmbH & Co. KGaA, Weinheim 1433-7851/03/4201-0104 $ 20.00+.50/0

$F(000) = 5012$, $\mu(Mo_{K\alpha}) = 0.714\ mm^{-1}$. Crystal data for **8** ($C_{88}H_{164}Cr_7F_8NNiO_{32}$; $M_r = 2316.20$): dark-green plate, monoclinic, space group $P2_1/n$, $a = 26.067(2)$, $b = 20.3010(17)$, $c = 27.098(2)$ Å, $\beta = 112.258(1)°$, $V = 13271.5(19)$ Å^3, $Z = 4$, $T = 120.0(2)$ K, $\rho_{calcd} = 1.159\ g\,cm^{-1}$, $F(000) = 4876$, $\mu(Mo_{K\alpha}) = 0.700\ mm^{-1}$. Crystal data for **9** ($C_{96}H_{180}Cr_7F_8NNiO_{32}$; $M_r = 2428.41$): dark-green plate, orthorhombic, space group *Pnma*, $a = 23.2504(15)$, $b = 21.0031(13)$, $c = 31.451(2)$ Å, $V = 15358.4(17)$ Å^3, $Z = 4$, $T = 120.0(2)$ K, $\rho_{calcd} = 1.050\ g\,cm^{-1}$, $F(000) = 5132$, $\mu(Mo_{K\alpha}) = 0.608\ mm^{-1}$. Unit cell for **10**: dark-green plate, monoclinic, space group $P2_1/c$, $a = 25.031(1)$, $b = 16.639(1)$, $c = 30.910(1)$ Å, $\beta = 110.03(1)°$. Unit cell for **11**: dark-green plate, monoclinic, space group $P2_1/c$, $a = 25.061(4)$, $b = 16.622(3)$, $c = 30.960(5)$ Å, $\beta = 110.488(5)°$. Unit cell for **12**: dark-green plate, monoclinic, space group $P2_1/c$, $a = 25.049(2)$, $b = 16.630(1)$, $c = 30.927(2)$ Å, $\beta = 110.18(3)°$. Unit cell for **13**: dark-green plate, monoclinic, space group $P2_1/c$, $a = 25.173(7)$, $b = 16.629(5)$, $c = 31.135(8)$ Å, $\beta = 111.093(3)°$. Compounds **10**, **11**, **12**, and **13** are isostructural with **6**. Data were collected on a Bruker SMART CCD diffractometer ($Mo_{K\alpha}$, $\lambda = 0.71069$ Å). In all cases the selected crystals were mounted onto the tip of a glass pin using Paratone-N oil and placed in the cold flow (120 K) produced with an Oxford Cryocooling device. Complete hemispheres of data were collected using ω scans (0.3°, 30 s/frame). Integrated intensities were obtained with SAINT+[12] and corrected for absorption using SADABS.[12] Structure solution and refinement was performed with the SHELX-package.[12] The structures were solved by direct methods and completed by iterative cycles of ΔF syntheses and full-matrix least-squares refinement against F^2 to give for **4**: using 479 parameters and 55 restraints, $wR_2 = 0.5006$ (12935 unique reflections), $R_1 = 0.1806$ (11281 reflections with $I > 2\sigma(I)$); for **5**: using 299 parameters and 28 restraints, $wR_2 = 0.2937$ (7978 unique reflections), $R_1 = 0.0973$ (7306 reflections with $I > 2\sigma(I)$); for **6**: using 1204 parameters and 105 restraints, $wR_2 = 0.1716$ (20413 unique reflections), $R_1 = 0.0804$ (17353 reflections with $I > 2\sigma(I)$); for **7**: using 901 parameters and 108 restraints, $wR_2 = 0.3241$ (22002 unique reflections), $R_1 = 0.1140$ (13892 reflections with $I > 2\sigma(I)$); for **8**: using 827 parameters and 116 restraints, $wR_2 = 0.4806$ (30385 unique reflections), $R_1 = 0.1661$ (17629 reflections with $I > 2\sigma(I)$); for **9**: using 449 parameters and 76 restraints, $wR_2 = 0.5085$ (9688 unique reflections), $R_1 = 0.1780$ (7500 reflections with $I > 2\sigma(I)$). CCDC-191618–191623 contains the supplementary crystallographic data for this paper. These data can be obtained free of charge via www.ccdc.cam.ac.uk/conts/retrieving.html (or from the Cambridge Crystallographic Data Centre, 12, Union Road, Cambridge CB21EZ, UK; fax: (+44) 1223-336-033; or deposit@ccdc.cam.ac.uk).

[10] A. Bencini, D. Gatteschi, *EPR of Exchange Coupled Systems*, Springer, Berlin, **1989**.

[11] G. M. Smith, J. C. G. Lesurf, R. H. Mitchell, P. C. Riedi, *Rev. Sci. Instrum.* **1998**, *69*, 3924–3931.

[12] SHELX-PC Package, Bruker Analytical X-ray Systems, Madison, WI, **1998**.

14-Electron Platinum(II) Complexes

Novel T-Shaped 14-Electron Platinum(II) Complexes Stabilized by One Agostic Interaction**

Walter Baratta, Sergio Stoccoro,* Angelino Doppiu, Eberhardt Herdtweck, Antonio Zucca, and Pierluigi Rigo*

Three-coordinate 14-electron d^8-ML_3 complexes, which are generally transient species generated in situ by ligand dissociation, have received much attention because of their key role in many stoichiometric and catalytic reactions.[1] Platinum(II) complexes of the form $[L_2PtR(solvent)]^+$, which contain bidentate nitrogen ligands and a weakly bonded solvent molecule, have been found to be active in alkane C–H activation through the formation of the transient alkane σ-adduct $[L_2PtR(R'–H)]^+$.[2] Such species have eluded isolation because of the ease of displacement of the alkane moiety by solvent or anions in solution, and thus, several approaches have been used to examine their reactivity including the study of agostic complexes.[3] Orpen and Spencer have described a series of β-agostic platinum(II) complexes of the type $[Pt(R)(P–P)]^+$ (P–P = chelating diphosphane; R = alkyl), which are in equilibrium with the corresponding alkene–hydrido derivatives,[4] and which have been viewed as models for intermediates along the migratory insertion/β-elimination alkene-polymerization pathway.[3a,4c] The bulky phosphane P*t*Bu$_3$ has been used to stabilize 14-electron T-shaped platinum(II) species of the form *trans*-$[PtH(PtBu_3)_2]X$ (X = noncoordinating anion), which have been characterized by NMR analysis.[5] It is noteworthy that the analogous derivatives bearing PCy_3 or P*i*Pr$_3$ moieties led to the four-coordinate complexes *trans*-$[PtH(PR_3)_2(solvent)][BAr^f_4]$ (R = Cy,[6a] *i*Pr;[6b] $Ar^f = 3,5\text{-}(CF_3)_2C_6H_3$), with dichloromethane as solvent.

[*] Dr. W. Baratta, Prof. P. Rigo
Dipartimento di Scienze e Tecnologie Chimiche
Università di Udine
Via Cotonificio 108, 33100 Udine (Italy)
Fax: (+39) 0432–558–803
E-mail: inorg@dstc.uniud.it

Dr. S. Stoccoro, Dr. A. Doppiu, Dr. A. Zucca
Dipartimento di Chimica
Università di Sassari
Via Vienna 2, 07100 Sassari (Italy)
Fax: +39–079–229–559
E-mail: stoccoro@ssmain.uniss.it

Dr. E. Herdtweck
Anorganisch-chemisches Institut
Technische Universität München
Lichtenbergstrasse 4, 85747 Garching (Germany)

[**] This work was supported by Ministero della Ricerca Scientifica e Tecnologica (MURST), University of Sassari and the Bayerische Forschungsstiftung (FORKAT; X-ray equipment).

Supporting information for this article is available on the WWW under http://www.angewandte.org or from the author.

Among the phosphanes used to stabilize low-coordinated species, those containing the 2,6-dimethylphenyl group appear very effective since the *o*-methyl groups can easily interact in an agostic fashion. In fact, we have recently isolated a rare example of a 14-electron ruthenium(II) complex $[RuCl_2\{PPh_2(2,6\text{-}Me_2C_6H_3)\}_2]$,[7] which is stabilized by two agostic interactions. In contrast, employment of the $PPh_2(2,6\text{-}Me_2C_6H_3)$ ligand with osmium led to the formation of complexes containing a tridentate *trans*-stilbene-type ligand, which results from the coupling of two *o*-methyl groups and the activation of four C–H bonds.[8] We have now found that $PR_2(2,6\text{-}Me_2C_6H_3)$ ligands (R = Ph, Cy) can be used to prepare a new class of three-coordinate 14-electron platinum(II) complexes; the crystallographic characterization of the cyclohexyl derivative is reported herein.

Treatment of [PtMeCl(cod)] (cod = cyclooctadiene) with two equivalents of $PPh_2(2,6\text{-}Me_2C_6H_3)$ in dichloromethane afforded the *trans* derivative **1** (84% yield),[9] through the substitution of cyclooctadiene. Similarly to **1**, complex **2**[9] was obtained in 85% yield from the platinum precursor and the bulky phosphane $PCy_2(2,6\text{-}Me_2C_6H_3)$ (Scheme 1).

Complexes **1** and **2** are thermally stable in solution and show NMR parameters in accordance with those of the *trans*-$[PtMeX(PR_3)_2]$ derivatives.[10] No *cis* complexes were observed during the formation of **1** and **2**, which can be attributed to the high steric requirement of the phosphanes employed.[11]

The three-coordinate complexes **3** and **4**[12] are obtained in 85 and 76% yield, respectively, by reacting **1** or **2** with $Na[BAr^f_4]$ in CH_2Cl_2 at room temperature through the cleavage of an *o*-methyl C–H bond and extrusion of methane (Scheme 1). The ^{1}H NMR spectrum of **3** in CD_2Cl_2 at room temperature shows a resonance at $\delta = 2.35$ ppm, with a value for J(H,Pt) (that is, the coupling constant for the metal satellite resonances) of 30.3 Hz for two methyl groups. At −95 °C this signal splits into two resonances of equal intensity at $\delta = 2.95$ and 1.75 ppm, which indicates that the rotation of the 2,6-dimethylphenyl group is frozen out. The $^{13}C\{^1H\}$ NMR spectrum at 20 °C displays a signal at $\delta = 22.7$ ppm for the $PtCH_2$ moiety with a large ^1J(C,Pt) coupling constant of 840 Hz,[10,13] consistent with a "very weak" ligand *trans* to the CH_2 group, whereas the resonance for the two methyl groups is at $\delta = 17.6$ ppm with J(C,Pt) = 94 Hz. Upon cooling at −95 °C this signal splits into two peaks at $\delta = 22.8$ and 9.4 ppm, of which the latter is attributable to the agostic methyl group.[7,14] Although the NMR data for complex **4** is similar to that for **3**, no rotation of the 2,6-dimethylphenyl group occurs at room temperature. The ^{1}H NMR resonance of the agostic CH_3 group appears at $\delta = 2.70$ ppm with J(H,Pt) = 64.0 Hz, whereas its $^{13}C\{^1H\}$ NMR signal is shifted to high field ($\delta = 13.6$ ppm) with a remarkably high J(C,Pt) coupling constant of 191 Hz. The NMR data of **3** and **4** clearly suggests that rotation of the 2,6-dimethylphenyl group is affected by the steric requirements of the PR_2 (R = Ph, Cy) moiety, with cyclohexyl substituents leading to a more hindered rotation than with phenyl substituents.

To establish the previous formulation with one *o*-methyl group close to the metal center, an X-ray diffraction study was carried out on a single crystal of **4**.[15] The representation of the cation of **4** with some relevant bond lengths and angles is shown in Figure 1; the $[BAr^f_4]^-$ ion is not bound directly to the platinum center.

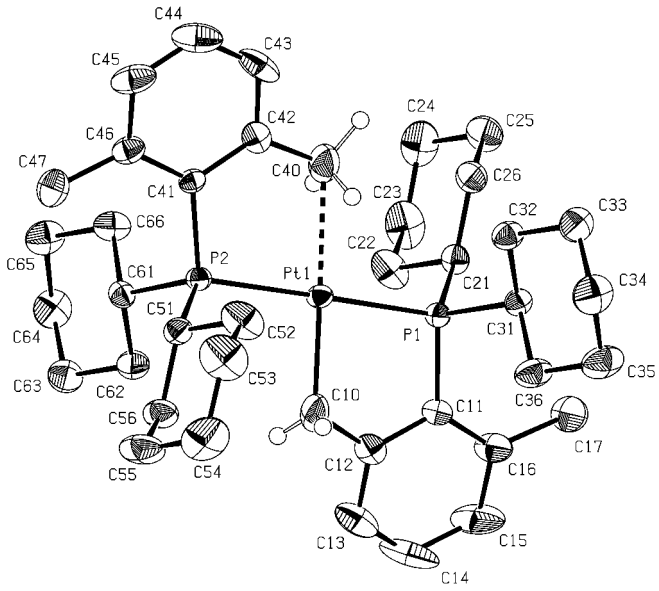
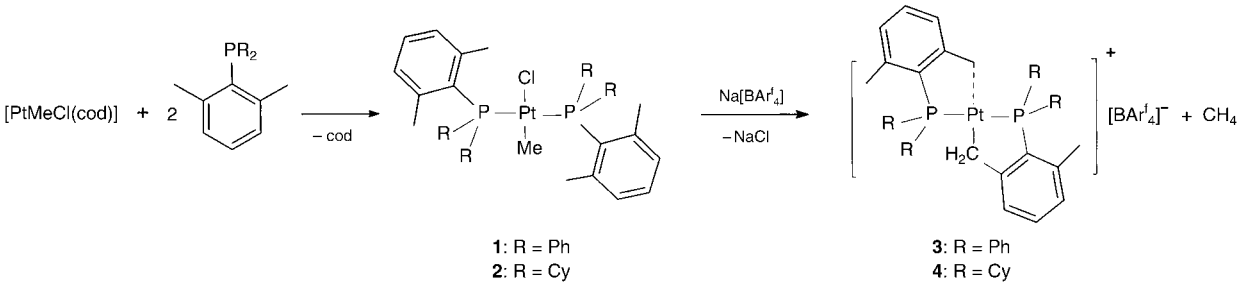


Figure 1. ORTEP-style drawing of the Pt-centered cation in the solid-state structure of **4**·0.25 CH_2Cl_2. Thermal ellipsoids are drawn at the 50% probability level. Selected bond lengths [Å] and angles [°]: Pt1–P1 2.3088(9), Pt1–P2 2.3279(9), Pt1–C10 2.088(7), Pt1···C40 2.432(6); P1-Pt1-P2 177.71(3), P1-Pt1-C10 81.91(14), P1-Pt1···C40 101.41(12), P2-Pt1-C10 97.28(14), P2-Pt1···C40 79.63(12), C10-Pt1···C40 172.94(18), Pt1-P2-C41 107.21(11).



1: R = Ph
2: R = Cy

3: R = Ph
4: R = Cy

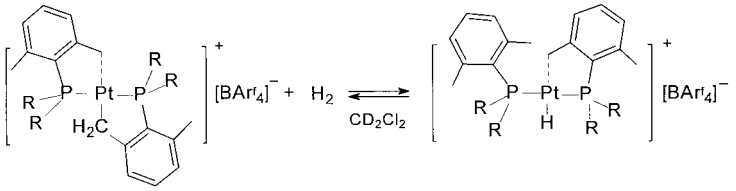
Scheme 1. Synthesis of **1**–**4**.

 © 2003 Wiley-VCH Verlag GmbH & Co. KGaA, Weinheim 1433-7851/03/4201-0106 $ 20.00+.50/0

The crystal structure consists of discrete monomeric units with the platinum center in a nearly square environment, coordinated to two *trans* phosphane groups and an alkyl group. The coordination sphere is completed by one methyl group of the 2,6-dimethylphenyl moiety. The Pt1-P2-C41 angle for the 2,6-dimethylphenyl group of **4** is 107.21(11)° and is smaller than the equivalent angles for the cyclohexyl substituents Pt1-P2-C51 (114.57(13)°) and Pt1-P2-C61 (115.11(12)°).[7] The five atoms Pt1, P1, P2, C10, and C40 are almost coplanar, and lie less than ± 0.10 Å from the mean plane, whereas the 2,6-dimethylphenyl group is bent back from this plane and is hinged about the P2–C40 axis at an angle of 8.4(2)° (as defined by the P2-Pt1-C40 and P2-C41-C42-C40 planes). The Pt1···C40 separation (2.432(6) Å) is a relatively short nonbonding distance, and is longer than the length reported for β-agostic complexes.[4a–b] It is noteworthy that the hydrogen atoms bonded to C40, which have been located and refined, are "tilted" away from the metal, a phenomenon that has been observed in $[RuCl_2\{PPh_2(2,6\text{-}Me_2C_6H_3)\}_2]$[7] and in some lanthanoid derivatives that contain the $CH(SiMe_3)_2$ ligand.[16] This may indicate an agostic interaction with the carbon atom providing a strong contribution.

As a result of the high coordinative unsaturation of **3** and **4**, these complexes react with dihydrogen in an equilibrium reaction in which the hydrido derivatives **5** and **6** are readily formed by heterolytic dihydrogen splitting and Pt–C bond cleavage [Eq. (1)].[17]

When a solution of **3** (CD_2Cl_2, 20 °C) is treated with dihydrogen (1 atm), the $^{31}P\{^1H\}$ NMR spectrum exhibits one sharp resonance at $\delta = 29.0$ ppm with $^1J(P,Pt) = 2717$ Hz for **5**, in addition to signals for **3** (**5**:**3** molar ratio = 1:4). The



3: R = Ph
4: R = Cy

5: R = Ph
6: R = Cy

(1)

^1H NMR spectrum reveals one signal at $\delta = 2.22$ ppm with $J(H,Pt) = 11.3$ Hz for the four *o*-methyl groups and one broad signal at $\delta = -20.83$ for the hydrido ligand with a remarkably high $^1J(H,Pt)$ coupling constant of 2052 Hz.[18] Similarly to **3**, the reaction of **4** with H_2 leads to the formation of complex **6** ($\delta(^{31}P) = 54.5$; $^1J(P,Pt) = 2631$ Hz), where **6** and **4** are recovered in a molar ratio of 2:1, which indicates that for the Cy derivative the equilibrium is more shifted to the right. The ^1H NMR spectrum of **6** exhibits one signal at $\delta = 2.74$ ppm with $J(H,Pt) = 15.0$ Hz for the *o*-methyl groups and one triplet at $\delta = -19.74$ ppm ($^2J(H,P) = 10.0$ Hz) with a $^1J(H,Pt)$ coupling constant of 2074 Hz. The data is similar to that of the three-coordinate derivatives $[PtH(P^tBu_3)_2]X$ (X = BF_4, PF_6, ClO_4, CF_3SO_3)[5] but differs from that of the related cyclohexyl species $[PtH(PCy_3)_2(L)][BAr^f_4]$ (L = CD_2Cl_2 and H_2)[6a] indicating that **5** and **6** are not solvato or dihydrogen[19] complexes of platinum(II), but are actually three-coordinate complexes with time-averaged agostic interactions of the four *o*-methyl groups. When the solutions containing either **5** or **6** are gently heated (40 °C) under Ar for a few minutes, the equilibrium completely shifts to the left as a result of the deprotonation of an agostic *o*-methyl group and associated H_2 extrusion. In the reversible Pt–C hydrogenolysis, H_2 probably replaces the agostic *o*-methyl group, which leads to a transient cationic dihydrogen-cyclometalated platinum(II) complex that may be in equilibrium with the 16-electron platinum(IV) dihydrido species.[1j,19] Interestingly, Milstein and co-workers have recently reported the opening of a platinum(II) metallacycle complex by reaction with dihydrogen, but under harsher conditions.[20]

In conclusion, the accessibility of 14-electron platinum(II) complexes relies on the use of the bulky ligands $PR_2(2,6\text{-}Me_2C_6H_3)$ (R = Ph, Cy) which allow protection against solvent coordination. Complexes **3** and **4** represent rare examples of three-coordinate platinum(II) complexes, characterized both in solution and in the solid state, that undergo a reversible and facile platinum–carbon hydrogenolysis through loss of the weakly bound *o*-methyl group. These complexes may be suitable precursors for new investigations of the relatively unexplored chemistry of 14-electron platinum(II) complexes.

Experimental Section

3: Na[BAr$^f_4$] (298 mg, 0.36 mmol) was added to **1** (300 mg, 0.36 mmol) dissolved in dichloromethane (20 mL), which afforded the evolution of methane and a precipitate of NaCl. After filtration of the NaCl, the solution was evaporated to dryness. The white solid was washed with cold pentane, filtered, and dried under reduced pressure. Yield 501 mg (85 %). The derivative **4** was prepared by an analogous method (76 % yield).

Received: August 26, 2002 [Z50047]

[1] a) J. P. Collman, L. S. Hegedus, J. R. Norton, R. G. Finke, *Principles and Applications of Organotransition Metal Chemistry*, University Science Books, Mill Valley, CA, **1987**; b) J. A. Maguire, W. T. Boese, M. E. Goldman, A. S. Goldman, *Coord. Chem. Rev.* **1990**, *97*, 179; c) A. Vigalok, Y. Ben-David, D. Milstein, *Organometallics* **1996**, *15*, 1839; d) R. Romeo, *Comments Inorg. Chem.* **1990**, *11*, 21; e) R. Romeo, M. R. Plutino, L. I. Elding, *Inorg. Chem.* **1997**, *36*, 5909; f) C. D. Tagge, R. D. Simpson, R. G. Bergman, M. J. Hostetler, G. S. Girolami, R. G. Nuzzo, *J. Am. Chem. Soc.* **1996**, *118*, 2634; g) E. L. Dias, M. Brookhart, P. S. White, *Chem. Commun.* **2001**, 423; h) D. J. Mindiola, G. L. Hillhouse, *J. Am. Chem. Soc.* **2001**, *123*, 4623; i) J. Cámpora, E. Gutiérrez-Puebla, J. A. López, A. Monge, P. Palma, D. del Río, E. Carmona, *Angew. Chem.* **2001**, *113*, 3753; *Angew. Chem. Int. Ed.* **2001**, *40*, 3641; j) R. J. Puddephatt, *Angew. Chem.* **2002**, *114*, 271; *Angew. Chem. Int. Ed.* **2002**, *41*, 261.

[2] a) M. W. Holtcamp, J. A. Labinger, J. E. Bercaw, *J. Am. Chem. Soc.* **1997**, *119*, 848; b) L. Johansson, O. B. Ryan, M. Tilset, *J. Am. Chem. Soc.* **1999**, *121*, 1974; c) L. Johansson, M. Tilset, *J. Am. Chem. Soc.* **2001**, *123*, 739.

[3] a) M. Brookhart, M. L. H. Green, L.-L. Wong, *Prog. Inorg. Chem.* **1988**, *36*, 1; b) R. H. Crabtree, D. G. Hamilton, *Adv.*

Organomet. Chem. **1988**, *28*, 299; c) R. H. Crabtree, *Angew. Chem.* **1993**, *105*, 828; *Angew. Chem. Int. Ed. Engl.* **1993**, *32*, 789.

[4] a) N. Carr, B. J. Dunne, A. G. Orpen, J. L. Spencer, *J. Chem. Soc. Chem. Commun.* **1988**, 926; b) N. Carr, L. Mole, A. G. Orpen, J. L. Spencer, *J. Chem. Soc. Dalton Trans.* **1992**, 2653; c) L. Mole, J. L. Spencer, N. Carr, A. G. Orpen, *Organometallics* **1991**, *10*, 49.

[5] R. M. Goel, R. C. Srivastava, *Can. J. Chem.* **1983**, *61*, 1352.

[6] a) S. S. Stahl, J. A. Labinger, J. E. Bercaw, *Inorg. Chem.* **1998**, *37*, 2422; b) M. D. Butts, B. L. Scott, G. J. Kubas, *J. Am. Chem. Soc.* **1996**, *118*, 11831.

[7] W. Baratta, E. Herdtweck, P. Rigo, *Angew. Chem.* **1999**, *111*, 1733; *Angew. Chem. Int. Ed.* **1999**, *38*, 1629.

[8] W. Baratta, E. Herdtweck, P. Martinuzzi, P. Rigo, *Organometallics* **2001**, *20*, 305.

[9] NMR data for complexes **1** and **2** are provided as Supporting Information.

[10] F. R. Hartley in *Comprehensive Organometallic Chemistry, Vol. 6* (Eds.: G. Wilkinson, F. G. A. Stone, E. W. Abel), Pergamon Press, Oxford, **1982**, p. 471.

[11] a) G. Alibrandi, M. Cusumano, D. Minniti, L. Monsù Scolaro, R. Romeo, *Inorg. Chem.* **1989**, *28*, 342; b) R. Romeo, G. Alibrandi, *Inorg. Chem.* **1997**, *36*, 4822.

[12] **3**: ^{1}H NMR (299.9 MHz, CD_2Cl_2, 20 C, TMS): $\delta = 7.78$–7.00 (m, 38 H; aromatic protons), 3.91 (d, J(P,H) = 4.6 Hz, ^2J(Pt,H) = 109 Hz, 2 H; $PtCH_2$), 2.35 (s, J(Pt,H) = 30.3 Hz, 6 H; agostic CH_3), 1.96 ppm (s, 3 H; CH_3); ^{13}C NMR (75.4 MHz, CD_2Cl_2, 20 C, TMS): $\delta = 162.2$ (q, ^1J(C,B) = 50 Hz; *ipso* aromatic carbons), 144.5–143.7 (*ipso* aromatic carbons), 135.2–125.8 (aromatic carbons), 125.0 (q, ^1J(C,F) = 272 Hz; CF_3), 117.9 (aromatic carbons), 22.7 (s, ^1J(C,Pt) = 840 Hz; $PtCH_2$), 21.6 (d, ^3J(C,P) = 3.0 Hz; CH_3), 17.6 ppm (s, J(C,Pt) = 94 Hz; agostic CH_3); ^{31}P{^{1}H} NMR (122.4 MHz, CD_2Cl_2, 20 C, H_3PO_4): $\delta = 51.3$ (d, ^2J(P,P) = 351 Hz, ^1J(Pt,P) = 2866 Hz), 39.5 ppm (d, ^2J(P,P) = 351 Hz, ^1J(Pt,P) = 2751 Hz); elemental analysis (%) calcd for $C_{72}H_{49}BF_{24}P_2Pt$: C 52.80, H 3.02; found: C 52.84, H 3.08. **4**: ^{1}H NMR (299.9 MHz, CD_2Cl_2, 20 C, TMS): $\delta = 7.68$–7.09 (m, 18 H; aromatic protons), 4.22 (d, J(P,H) = 4.6 Hz, ^2J(Pt,H) = 107 Hz, 2 H; $PtCH_2$), 2.70 (s, J(Pt,H) = 64.0 Hz, 3 H; agostic CH_3), 2.54 (s, 3 H; CH_3), 2.50 (s, 3 H; CH_3), 2.38–1.12 ppm (m, 44 H; Cy); ^{13}C NMR (75.4 MHz, CD_2Cl_2, 20 C, TMS): $\delta = 162.1$ (q, ^1J(C,B) = 50 Hz; *ipso* aromatic carbons), 143.7–141.5 (*ipso* aromatic carbons), 135.1–125.3 (aromatic carbons), 124.9 (q, ^1J(C,F) = 272 Hz; CF_3), 124.1 and 117.8 (aromatic carbons), 38.7 (d, ^1J(C,P) = 26.5 Hz; PCH of Cy), 38.0 (d, ^1J(C,P) = 27.5 Hz; PCH of Cy), 31.9 (d, ^2J(C,P) = 104.0 Hz; CH_2 of Cy), 30.9 (d, ^2J(C,P) = 63.5 Hz, ^3J(C,Pt) = 12.0 Hz; CH_2 of Cy), 27.4–26.8 (s, CH_2 of Cy), 26.1 (s; CH of Cy), 23.4 and 22.1 (s; CH_3), 17.8 (d, ^2J(C,P) = 3.0 Hz, ^1J(C,Pt) = 806 Hz; $PtCH_2$), 13.6 ppm (d, J(C,P) = 7.7 Hz, J(C,Pt) = 191 Hz; agostic CH_3); ^{31}P{^{1}H} NMR (122.4 MHz, CD_2Cl_2, 20 C, H_3PO_4): $\delta = 73.3$ (d, ^2J(P,P) = 316 Hz, ^1J(Pt,P) = 2776 Hz), 54.9 ppm (d, ^2J(P,P) = 316 Hz, ^1J(Pt,P) = 2677 Hz); elemental analysis (%) calcd for $C_{72}H_{73}BF_{24}P_2Pt$: C 52.03, H 4.43; found: C 52.65, H 4.47.

[13] B. C. Ankianiec, V. Christou, D. T. Hardy, S. K. Thomson, G. B. Young, *J. Am. Chem. Soc.* **1994**, *116*, 9963.

[14] R. H. Crabtree, E. M. Holt, M. Lavin, S. M. Morehouse, *Inorg. Chem.* **1985**, *24*, 1986.

[15] a) Crystal structure analysis of **4**·0.25 CH_2Cl_2: $4(C_{72}H_{73}BF_{24}P_2Pt)\cdot CH_2Cl_2$, $M_r = 6733.46$, triclinic, space group $P\bar{1}$, $a = 13.8101(1)$, $b = 19.2354(2)$, $c = 29.6683(3)$ Å, $\alpha = 101.466(1)$, $\beta = 93.333(1)$, $\gamma = 109.049(1)$°, $V = 7236.26(13)$ Å^3, $Z = 1$, $\rho_{calcd} = 1.545$ g cm^{-3}, $F_{000} = 3378$, $\mu = 2.105$ mm^{-1}. A suitable single crystal for the X-ray diffraction study was obtained from a CH_2Cl_2/toluene solution at 4 °C. The selected crystal was coated with perfluorinated ether, fixed in a capillary, and transferred to the diffractometer and the cold nitrogen flow (Oxford Cryosystems). Preliminary examinations and data collection were carried out on a kappa-CCD device (NONIUS MACH3) at the window of a rotating anode (NONIUS FR591) with graphite-monochromated $Mo_{K\alpha}$ radiation ($\lambda = 0.71073$ Å). Data collection was performed at 123 K within the Θ range of $1.20 < \Theta < 25.35$°. A total of 81323 reflections were integrated and corrected for Lorentz and polarization effects. A correction for absorption effects was applied with the DIFABS algorithm ($C_{min/max}$ 0.632/0.892). After merging ($R_{int} = 0.0338$), 26468 (21745: $I_o > 2\sigma(I_o)$) independent reflections remained and all were used to refine 2187 parameters. The structure was solved by a combination of direct methods and difference-Fourier syntheses. All nonhydrogen atoms were refined anisotropically. All 61 hydrogen atom positions for the Pt1 cation were found in the difference Fourier map calculated from the model containing all nonhydrogen atoms. The hydrogen positions were refined with individual isotropic displacement parameters. All of the other 104 hydrogen atoms were placed in calculated positions ($d_{C-H} = 0.95$, 0.98, 0.99, 1.00 Å). Isotropic displacement parameters were calculated from the parent carbon atom ($U_H = 1.2/1.5 \cdot U_C$). The hydrogen atoms were included in the structure factor calculations but not refined. Full-matrix least-squares refinements in 4 blocks were carried out by minimizing $w(F_o^2 - F_c^2)^2$ and converged with $R1 = 0.0348$ ($I_o > 2\sigma(I_o)$), $wR2 = 0.0825$ (all data), GOF = 1.012 and shift/error < 0.001. The asymmetric unit cell contains three crystallographically independent Pt cations. Two of them ($Pt2^+$ and $Pt3^+$) are located around a center of inversion and therefore show a disorder (in each of two positions, 50:50) which could be clearly resolved. The two anions and the CH_2Cl_2 solvent molecule are well-ordered. Neutral-atom scattering factors for all atoms and anomalous dispersion corrections for the nonhydrogen atoms were taken from *International Tables for Crystallography*. Crystallographic data (excluding structure factors) for the structure reported in this paper have been deposited with the Cambridge Crystallographic Data Centre. CCDC-191944 (**4**·0.25 CH_2Cl_2) contains the supplementary crystallographic data for this paper. These data can be obtained free of charge via www.ccdc.cam.ac.uk/conts/retrieving.html (or from the Cambridge Crystallographic Data Centre, 12, Union Road, Cambridge CB21EZ, UK; fax: (+44) 1223-336-033; or deposit @ccdc.cam.ac.uk); b) Data Collection Software for Nonius kappa-CCD devices, Delft (The Netherlands), **1997**; c) Z. Otwinowski, W. Minor, *Methods Enzymol.* **1997**, *276*, 307 ff; d) A. Altomare, G. Cascarano, C. Giacovazzo, A. Guagliardi, M. C. Burla, G. Polidori, M. Camalli, SIR92, *J. Appl. Crystallogr.* **1994**, *27*, 435; e) *International Tables for Crystallography*, Vol. C, Tables 6.1.1.4, 4.2.6.8, and 4.2.4.2 (Ed.: A. J. C. Wilson), Kluwer Academic Publishers, Dordrecht (The Netherlands), **1992**; f) A. L. Spek, PLATON, *A Multipurpose Crystallographic Tool*, Utrecht University, Utrecht, **2000**; g) G. M. Sheldrick, SHELXL-97, Universität Göttingen, Göttingen (Germany), **1998**.

[16] W. T. Klooster, L. Brammer, C. J. Schaverien, P. H. M. Budzelaar, *J. Am. Chem. Soc.* **1999**, *121*, 1381.

[17] a) A. C. Albéniz, G. Schulte, R. H. Crabtree, *Organometallics* **1992**, *11*, 242; b) A. J. Toner, S. Gründemann, E. Clot, H.-H. Limbach, B. Donnadieu, S. Sabo-Etienne, B. Chaudret, *J. Am. Chem. Soc.* **2000**, *122*, 6777; c) R. H. Morris in *Recent Advances in Hydride Chemistry* (Eds.: M. Peruzzini, R. Poli), Elsevier, Amsterdam **2001**, p. 1.

[18] Notable high ^1J(H,Pt) values have been also reported with nitrogen ligands: G. Minghetti, M. A. Cinellu, S. Stoccoro, G. Chelucci, A. Zucca, *Inorg. Chem.* **1990**, *29*, 5138.

[19] D. G. Gusev, J. U. Notheis, J. R. Rambo, B. E. Hauger, O. Eisenstein, K. G. Caulton, *J. Am. Chem. Soc.* **1994**, *116*, 7409.

[20] M. E. van der Boom, J. Ott, D. Milstein, *Organometallics* **1998**, *17*, 4263.

 © 2003 Wiley-VCH Verlag GmbH & Co. KGaA, Weinheim 1433-7851/03/4201-0108 $ 20.00+.50/0

Iron Porphyrin Complexes

Reversible Formation of Iodosylbenzene–Iron Porphyrin Intermediates in the Reaction of Oxoiron(IV) Porphyrin π-Cation Radicals and Iodobenzene**

Wonwoo Nam, Sun Kyung Choi, Mi Hee Lim, Jan-Uwe Rohde, Inwoo Kim, Jinheung Kim, Cheal Kim, and Lawrence Que, Jr.**

High-valent oxoiron(IV) porphyrin π-cation radicals **2** are generally accepted to be the key reactive intermediates in a variety of oxidation reactions by heme-containing enzymes such as cytochromes P450, peroxidases, and catalases.[1,2] Extensive studies with synthetic iron(III) porphyrin complexes and various terminal oxidants have shown that **2** is generated by heterolytic O–X bond cleavage of $[(Porp)Fe^{III}\text{-}O\text{-}X]^+$ (**1**) [path A in Eq. (1)].[3] In contrast, there are only two reported instances of the reverse reaction, O–X bond formation between **2** and X [path B in Eq. (1)], as biomimetic examples of haloperoxidases.[4] One is the oxo transfer from an oxomanganese(V) porphyrin complex to bromide (Br^-),[4a] and the other is the generation of a $[(Porp)Fe^{III}\text{-}OCl]$ complex in the reaction of **2** and Cl^-.[4b]

$$[(Porp)Fe^{III}]^+ + OX \rightleftharpoons [(Porp)Fe^{III}\text{-}O\text{-}X]^+ \ (\mathbf{1}) \underset{B}{\overset{A}{\rightleftharpoons}} [(Porp)^{+\cdot}Fe^{IV}{=}O]^+ \ (\mathbf{2}) + X \quad (1)$$

Iodosylbenzene (PhIO) has been widely used as a terminal oxidant in metal-complex-catalyzed oxidation reactions.[1d] We have shown recently that the reaction of $[Fe(TMP)(CF_3SO_3)]$[5] with PhIO generates a $[(TMP)^{+\cdot}Fe^{IV}{=}O]^+$ complex.[6] Although the presence of the iodosylbenzene–iron porphyrin intermediates, [(Porp)Fe-OIPh], has been suggested in PhIO reactions,[7] such intermediates have not been isolated or characterized previously. Herein, we report evidence for the formation of the new $[(Porp)Fe^{III}\text{-}OIPh]^+$ intermediates **3** in the reaction of $[(Porp)^{+\cdot}Fe^{IV}{=}O]^+$ complexes and iodobenzene [Eq. (2)]. We also show that the formation of **3** depends on the electronic nature of iron porphyrin complexes and iodobenzene derivatives, and that an equilibrium between **2** and **3** exists. Reactions of oxygen atom transfer from **3** to olefins are briefly discussed as well.

$$[(Porp)^{+\cdot}Fe^{IV}{=}O]^+ \ (\mathbf{2}) + PhI \rightleftharpoons [(Porp)Fe^{III}{-}O{-}IPh]^+ \ (\mathbf{3}) \quad (2)$$

Treatment of triflate iron(III) porphyrin complexes, $Fe(TDCPP)(CF_3SO_3)$ and $Fe(TDFPP)(CF_3SO_3)$,[5] with 1.2 equiv *m*-chloroperbenzoic acid (*m*-CPBA) in a solvent mixture of CH_3CN and CH_2Cl_2 at −40 °C resulted in the formation of oxoiron(IV) porphyrin π-cation radicals, $[(TDCPP)^{+\cdot}Fe^{IV}{=}O]^+$ (**2a**) and $[(TDFPP)^{+\cdot}Fe^{IV}{=}O]^+$ (**2b**), (Figure 1).[8] Upon the addition of 30 equiv PhI to the reaction solutions containing **2a** and **2b**, the color of the reaction solutions immediately changed from green to reddish brown. The formation of new intermediates, **3a** and **3b**, was confirmed by the disappearance of features characteristic of $[(Porp)^{+\cdot}Fe^{IV}{=}O]^+$ complexes (a weak Soret band and broad Q bands around 500–750 nm) and the appearance of a strong Soret band at ≈420 nm and a Q band at ≈535 nm in the UV/Vis spectra (Figure 1).

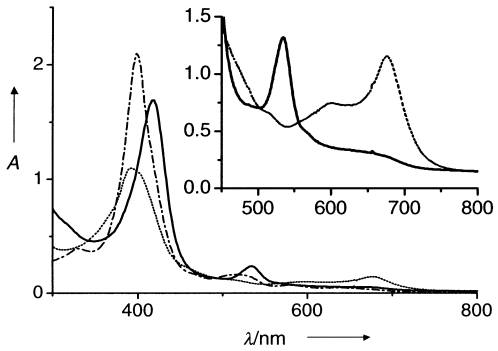


Figure 1. UV/Vis spectra of $[Fe(TDCPP)(CF_3SO_3)]$ (–·–), **2a** (····), and **3a** (——). Reaction conditions: the addition of *m*-CPBA (1×10^{-3} mmol, diluted in 50 μL of CH_3CN) into a 0.1 cm UV cuvette containing a solution of $[Fe(TDCPP)(CF_3SO_3)]$ (2×10^{-4} mmol) in a solvent mixture (1 mL) of CH_3CN and CH_2Cl_2 (3:1) at −40 °C resulted in the formation of **2a**. Subsequent addition of PhI (30 equiv, diluted in 50 μL of CH_3CN) to the cuvette containing **2a** led to the immediate formation of **3a**. Inset: Q-band region of **2a** (1 mM) and **3a** (1 mM). UV/Vis spectra were recorded on a Hewlett Packard 8453 spectrophotometer equipped with an Optostat^{DN} variable-temperature liquid-nitrogen cryostat (Oxford Instruments).

[*] Prof. Dr. W. Nam, S. K. Choi, M. H. Lim, I. Kim
Department of Chemistry and Division of Molecular Life Sciences
Ewha Womans University
Seoul 120-750 (Korea)
Fax: (+82) 2-3277-2384
E-mail: wwnam@ewha.ac.kr
Prof. Dr. L. Que, Jr., Dr. J.-U. Rohde
Department of Chemistry and Center for Metals in Biocatalysis
University of Minnesota
Minneapolis, Minnesota 55455 (USA)
Fax: (+1) 612-624-7029
E-mail: que@chem.umn.edu
Prof. Dr. J. Kim
Department of Chemical Technology
Changwon National University
Kyungnam 641-773 (Korea)
Prof. Dr. C. Kim
Department of Fine Chemistry
Seoul National University of Technology
Seoul 139-743 (Korea)

[**] This research was supported by KOSEF (R03-2001-00028, R02-2002-000-00048-0 to W.N.), the LG Yonam Foundation (W.N.), and the NIH (GM-38767 to L.Q.). We also thank KOSEF and NSF for stimulating this international cooperative research effort. J.-U.R. thanks the Deutsche Forschungsgemeinschaft (DFG) for a postdoctoral fellowship. XAS data were collected on beamline X9B at the National Synchrotron Light Source and on beamline 7-3 at the Stanford Synchrotron Radiation Laboratory, both supported by the US Department of Energy and the NIH.

Supporting information for this article is available on the WWW under http://www.angewandte.org or from the author. Table S1 contains results of ^{18}O-labeled water experiments performed with $[(Porp)Fe^{III}{-}OIPh]^+$ and $[(Porp)^{+\cdot}Fe^{IV}{=}O]^+$ intermediates (1 page). Details of the Fe K-edge XAS characterization of **2b** and **3b**, experimental data and fits (Figure S1 and S2).

Insight into the nature of **3b** has been gained from further spectroscopic studies. Upon the addition of 30 equiv PhI to **2b**, the characteristic $S = 3/2$ EPR signals of **2b** were replaced by new features at $g = 5.7$ and 2.0, which indicates the formation of an axially symmetric $S = 5/2$ species (data not shown).[8,9] This observation suggests the reduction of the oxoiron(IV) porphyrin π-cation radical to a high-spin iron(III) state. The disappearance of the high-valent iron-oxo species upon the addition of PhI was confirmed by X-ray absorption spectroscopy (Figure 2). Complex **2b** exhibits an intense 1s→3d pre-edge transition with an area of 38(2) units; this value is

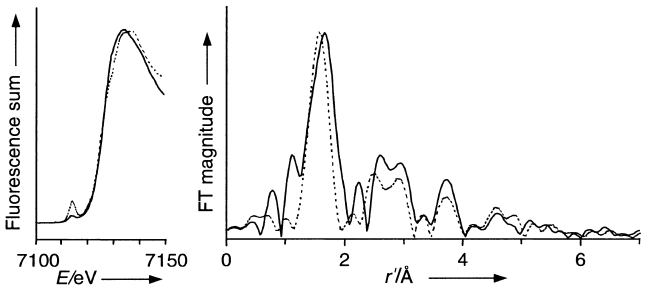


Figure 2. X-ray absorption near-edge structures (Fe K-edge XANES, fluorescence excitation, left panel) and Fourier transforms of the Fe K-edge EXAFS data (right panel) of **2b** (– – –) and **3b** (——) in frozen CH_3CN solution at $T = 10$–15 K.

much higher than is commonly observed for five-coordinate iron complexes (12–20 units)[10] and can be attributed to the significant distortion imposed by the oxo ligand on the iron coordination environment.[10,11] EXAFS analysis of **2b** shows that its first coordination sphere consists of 1 N/O at 1.67 Å,[11] assigned to the oxo ligand, and 4 N at 2.00 Å, assigned to the porphyrin nitrogen atoms (Figure S1, Supporting Information). Upon conversion into **3b**, its 1s→3d pre-edge transition is halved in intensity to 17(2) units, the 1.67 Å Fe–O distance is no longer observed, and the average Fe–N distance lengthens to 2.07 Å (Figure S2, Supporting Information). Taken together, the spectroscopic data show that PhI reduces the oxoiron(IV) porphyrin π-cation radical to a high-spin Fe^{III} complex; in turn the oxo group must then be transferred to PhI, presumably forming PhIO coordinated to the iron(III) center (see below).

The formation of the intermediates **3** in the reactions of **2** and PhI depends significantly on the electronic nature of the iron porphyrin complexes and iodobenzene derivatives. For example, **3** was not observed in the reaction of PhI and $[(TMP)^{+\bullet}Fe^{IV}{=}O]^+$, which contains an electron-rich porphyrin ligand, under identical reaction conditions. Similarly, **3a** and **3b** do not form in the reactions of **2a** and **2b** with the electron-poor F_5C_6I. Interestingly, in the intermediate case of 1,2-difluoro-4-iodobenzene ($F_2C_6H_3I$), both **2** and the new intermediate **3** were present in the reaction solutions, and the amount of **3** observed was proportional to the amount of $F_2C_6H_3I$ added to the reaction solutions (Figure 3). These results demonstrate clearly that there is an equilibrium between **2** and **3** [Eq. (2)], which favors the new intermediate **3** when the porphyrin ligand of $[(Porp)^{+\bullet}Fe^{IV}{=}O]^+$ com-

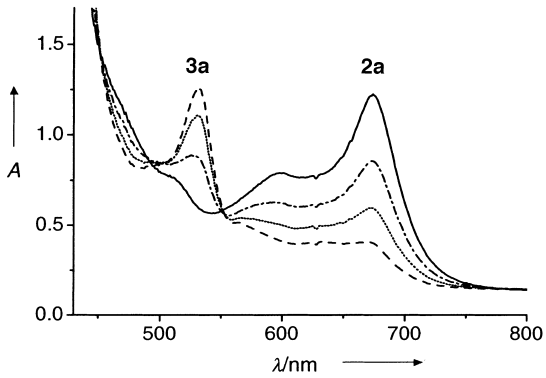


Figure 3. UV/Vis spectra showing the formation of **3a** as a function of the amount of 1,2-difluoro-4-iodobenzene ($F_2C_6H_3I$) added to the solution of **2a**. Reaction conditions: **2a** (1 mM) was prepared as described in Figure 1. $F_2C_6H_3I$ (diluted in 50 μL of CH_3CN) was added to the solution of **2a** (**2a**, ——; **2a** + 5 equiv $F_2C_6H_3I$, –•–; **2a** + 20 equiv $F_2C_6H_3I$, ····; **2a** + 60 equiv $F_2C_6H_3I$, – – –).

plexes is electron-deficient and/or the iodobenzene derivative is electron-rich.

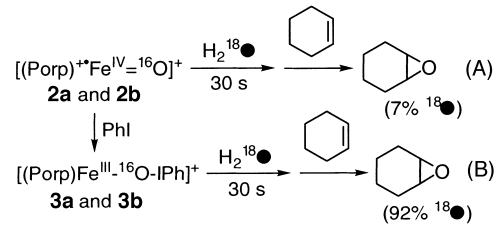
The reactivity of **3** towards olefins was then examined. Addition of olefins to **3a** and **3b** converted these intermediates immediately back into the starting iron(III) porphyrins, and analysis of the resulting solutions revealed epoxides as major products with retention of stereochemistry (Table 1). Interestingly, the epoxidation of cyclohexene by **3a** and **3b**, when performed in the presence of $H_2{}^{18}O$,[12] resulted in ≈92% ^{18}O incorporation from $H_2{}^{18}O$ into the cyclohexene oxide product, while **2a** and **2b** under the same conditions afforded 7% ^{18}O incorporation (Scheme 1; also see Table S1, Supporting Information). These results demonstrate that the intermediates **3a** and **3b** readily exchange their oxygen atoms with labeled water. Because it has been suggested previously that the exchange of the iodosylbenzene oxygen with labeled water is greatly facilitated by the coordination of iodosylbenzene to a Lewis acidic metal center [Eq. (3)],[13] the observation of such a high ^{18}O incorporation in the reactions of **3a**

Table 1: Epoxidation of olefins by in situ generated **3a** and **3b**.[a]

Substrate	Products	Yields [%][b] **3a**	**3b**
cyclohexene	cyclohexene oxide	72	65
	cyclohexenol	<2	<2
	cyclohexenone	<1	<1
cis-stilbene	*cis*-stilbene oxide	63	56
	trans-stilbene oxide	<1	<1
	benzaldehyde	<2	<2

[a] All reactions were monitored by UV/Vis spectral changes of reaction solutions. Reaction conditions: **2a** and **2b** were prepared by reacting triflate iron(III) porphyrin complexes (1×10^{-3} mmol) with 1.2 equiv *m*-CPBA (1.2×10^{-3} mmol, diluted in 50 μL of CH_3CN) in a solvent mixture (0.5 mL) of CH_3CN and CH_2Cl_2 (3:1) at −40 °C. **3a** and **3b** were prepared by adding 30 equiv PhI (3×10^{-2} mmol, diluted in 50 μL of CH_3CN) to the reaction solutions containing **2a** and **2b**. Oxygenation reactions were performed by the addition of olefins (0.1 mmol, diluted in 50 μL of CH_2Cl_2) to the reaction solutions of **3a** and **3b** at −40 °C. PPh_3 (1×10^{-2} mmol, diluted in 50 μL of CH_3CN) was added to the reaction mixture prior to product analyses. [b] Based on the amounts of **3a** and **3b** prepared. Errors are within ± 15% of the stated values.

 © 2003 Wiley-VCH Verlag GmbH & Co. KGaA, Weinheim 1433-7851/03/4201-0110 $ 20.00+.50/0



Scheme 1. Results of ^{18}O-labeled water experiments.

and **3b** strongly supports the coordination of PhIO to the iron center in **3**.[7,14,15]

$$LM^{n+}-{}^{16}O-I-Ph + H_2^{18}\bullet \rightleftharpoons LM^{n+}-{}^{18}\bullet-I-Ph + H_2^{16}O \qquad (3)$$

In summary, we have demonstrated that new [(Porp)Fe^{III}–OIPh]$^+$ intermediates are generated in the reaction of [(Porp)$^{+\bullet}$Fe^{IV}=O]$^+$ and PhI and that the electronic nature of iron porphyrin complexes and iodobenzene derivatives markedly influences the equilibrium between these two forms. The observation that olefins are epoxidized upon their addition to solutions of **3** raises the possibility that **3** itself may be the epoxidizing agent. This is an intriguing prospect, but we cannot at present exclude the possibility that the small amount of **2** present in the equilibrium between **2** and **3** is responsible for the observed reactivity.[16] Future studies will be directed towards addressing the question of whether such a "second oxidant" is involved in the olefin epoxidations.[17,18]

Received: August 30, 2002 [Z50077]

[1] a) P. R. Ortiz de Montellano, *Cytochrome P450: Structure, Mechanism, and Biochemistry*, 2nd ed., Plenum, New York, **1995**; b) M. Sono, M. P. Roach, E. D. Coulter, J. H. Dawson, *Chem. Rev.* **1996**, *96*, 2841–2887; c) J. L. McLain, J. Lee, J. T. Groves in *Biomimetic Oxidations Catalyzed by Transition Metal Complexes* (Ed.: B. Meunier), Imperial College Press, London, **2000**, pp. 91–169; d) B. Meunier, A. Robert, G. Pratviel, J. Bernadou in *The Porphyrin Handbook, Vol. 4* (Eds.: K. M. Kadish, K. M. Smith, R. Guilard), Academic Press, New York, **2000**, chap. 31, pp. 119–187.

[2] a) R. Davydov, T. M. Makris, V. Kofman, D. E. Werst, S. G. Sligar, B. M. Hoffman, *J. Am. Chem. Soc.* **2001**, *123*, 1403–1415; b) I. Schlichting, J. Berendzen, K. Chu, A. M. Stock, S. A. Maves, D. A. Benson, R. M. Sweet, D. Ringe, G. A. Petsko, S. G. Sligar, *Science* **2000**, *287*, 1615–1622; c) F. Ogliaro, S. Cohen, M. Filatov, N. Harris, S. Shaik, *Angew. Chem.* **2000**, *112*, 4009–4013; *Angew. Chem. Int. Ed.* **2000**, *39*, 3851–3855.

[3] a) Y. Watanabe in *The Porphyrin Handbook, Vol. 4* (Eds.: K. M. Kadish, K. M. Smith, R. Guilard), Academic Press, New York, **2000**, chap. 30, pp. 97–117; b) W. Nam, H. J. Han, S.-Y. Oh, Y. J. Lee, M.-H. Choi, S.-Y. Han, C. Kim, S. K. Woo, W. Shin, *J. Am. Chem. Soc.* **2000**, *122*, 8677–8684, and references therein.

[4] a) N. Jin, J. L. Bourassa, S. C. Tizio, J. T. Groves, *Angew. Chem.* **2000**, *112*, 4007–4009; *Angew. Chem. Int. Ed.* **2000**, *39*, 3849–3851; b) H.-A. Wagenknecht, W.-D. Woggon, *Angew. Chem.* **1997**, *109*, 404–407; *Angew. Chem. Int. Ed. Engl.* **1997**, *36*, 390–392.

[5] Abbreviations of porphyrin ligands: TMP = *meso*-tetramesitylporphinato dianion; TDCPP = *meso*-tetrakis(2,6-dichlorophenyl)porphinato dianion; TDFPP = *meso*-tetrakis(2,6-difluorophenyl)porphinato dianion.

[6] W. Nam, M. H. Lim, S.-Y. Oh, *Inorg. Chem.* **2000**, *39*, 5572–5575.

[7] a) J. P. Collman, A. S. Chien, T. A. Eberspacher, J. I. Brauman, *J. Am. Chem. Soc.* **2000**, *122*, 11098–11100; b) K. Machii, Y. Watanabe, I. Morishima, *J. Am. Chem. Soc.* **1995**, *117*, 6691–6697.

[8] K. Jayaraj, J. Terner, A. Gold, D. A. Roberts, R. N. Austin, D. Mandon, R. Weiss, E. Bill, M. Muther, A. X. Trautwein, *Inorg. Chem.* **1996**, *35*, 1632–1640.

[9] H. Fujii, *Coord. Chem. Rev.* **2002**, *226*, 51–60.

[10] a) A. L. Roe, D. J. Schneider, R. J. Mayer, J. W. Pyrz, J. Widom, L. Que, Jr., *J. Am. Chem. Soc.* **1984**, *106*, 1676–1681; b) C. R. Randall, L. Shu, Y.-M. Chiou, K. S. Hagen, M. Ito, N. Kitajima, R. J. Lachicotte, Y. Zang, L. Que, Jr., *Inorg. Chem.* **1995**, *34*, 1036–1039; c) T. E. Westre, P. Kennepohl, J. G. DeWitt, B. Hedman, K. O. Hodgson, E. I. Solomon, *J. Am. Chem. Soc.* **1997**, *119*, 6297–6314.

[11] a) J. E. Penner-Hahn, T. J. McMurry, M. Renner, L. Latos-Grazynsky, K. S. Eble, I. M. Davis, A. L. Balch, J. T. Groves, J. H. Dawson, K. O. Hodgson, *J. Biol. Chem.* **1983**, *258*, 12761–12764; b) T. Wolter, W. Meyer-Klaucke, M. Müther, D. Mandon, H. Winkler, A. X. Trautwein, R. Weiss, *J. Inorg. Biochem.* **2000**, *78*, 117–122.

[12] B. Meunier, J. Bernadou, in *Struct. Bonding* (Ed. B. Meunier) Springer, Berlin **2000**, *97*, 1–35, and references therein.

[13] W. Nam, J. S. Valentine, *J. Am. Chem. Soc.* **1993**, *115*, 1772–1778.

[14] Hill and co-workers isolated the [PhIO-Mn^{IV}(TPP)] adducts, [{PhI(OAc)O}$_2$Mn^{IV}(TPP)] and [{XMn^{IV}TPP(OIPh)$_2$}$_2$O], in the reactions of [Mn(TPP)(OAc)] and PhIO. The PhIO–Mn^{IV}–porphyrins oxygenated hydrocarbons and exchanged oxygen atoms with labeled water. a) J. A. Smegal, C. L. Hill, *J. Am. Chem. Soc.* **1983**, *105*, 2920–2922; b) J. A. Smegal, B. C. Schardt, C. L. Hill, *J. Am. Chem. Soc.* **1983**, *105*, 3510–3515; c) J. A. Smegal, C. L. Hill, *J. Am. Chem. Soc.* **1983**, *105*, 3515–3521.

[15] J. S. Valentine, W. Nam, R. Y. N. Ho in *The Activation of Dioxygen and Homogeneous Catalytic Oxidation* (Eds.: D. H. R. Barton, A. E. Martell, D. T. Sawyer), Plenum, New York, **1993**, pp. 183–198, and references therein.

[16] We have shown very recently that when the anionic ligand of iron(III) porphyrin catalysts is the triflate anion ($CF_3SO_3^-$), oxoiron(IV) porphyrin π-cation radicals are the reactive epoxidizing intermediate in the catalytic epoxidation of olefins by PhIO: W. Nam, S. W. Jin, M. H. Lim, J. Y. Ryu, C. Kim, *Inorg. Chem.* **2002**, *41*, 3647–3652.

[17] The existence of a "second oxidant" in catalytic oxygenation reactions has been a topic of much debate. See the following recent review articles. a) P. R. Ortiz de Montellano, J. J. De Voss, *Nat. Prod. Rep.* **2002**, *19*, 477–493; b) Y. Watanabe, *J. Biol. Inorg. Chem.* **2001**, *6*, 846–856; c) T. D. H. Bugg, *Curr. Opin. Chem. Biol.* **2001**, *5*, 550–555; d) A. D. N. Vaz, *Curr. Drug Metab.* **2001**, *2*, 1–16; e) M. Newcomb, P. H. Toy, *Acc. Chem. Res.* **2000**, *33*, 449–455.

[18] F. Ogliaro, S. P. de Visser, S. Cohen, P. K. Sharma, S. Shaik, *J. Am. Chem. Soc.* **2002**, *124*, 2806–2817.

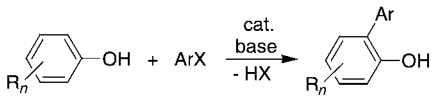
 © 2003 Wiley-VCH Verlag GmbH & Co. KGaA, Weinheim 1433-7851/03/4201-0111 $ 20.00+.50/0

Direct Aryl Halide Phenol Coupling

The Catalytic Intermolecular Orthoarylation of Phenols**

Robin B. Bedford, Simon J. Coles, Michael B. Hursthouse, and Michael E. Limmert*

The biaryl subunit is an important structural motif that is found in a wide range of compounds such as natural products, polymers, liquid crystals, and ligands for homogeneous transition-metal catalysts.[1] One class of reaction that provides particular challenges for the catalytic chemist is the synthesis of orthoarylated phenols. Currently the most commonly used catalytic routes to these compounds employ Suzuki or Stille coupling reactions.[2] These require the introduction and subsequent loss of stoichiometric amounts of either boronic acid/ester or organotin functions. Therefore the ability to couple an aryl halide *directly* with a phenol (Scheme 1) without the need for a sacrificial electrophilic boron or tin fragment would be highly desirable from both synthetic and atom-economic points of view.



Scheme 1. The catalytic orthoarylation of phenols.

The transition-metal-catalyzed *ortho*-selective arylation of phenols has been limited to a few examples of *intramolecular* couplings of aryl halides that are tethered to the phenolic substrates,[3] and the reactions of aryl halides with 1-naphthol or 2-aryl-substituted phenols.[4] In all cases the reactions proceed via the formation of stable five- or six-membered metallacycles. Simple phenols avoid orthometalation reactions with late transition metals as this would give unfavorably strained, four-membered metallacycles.[5] However when aryloxide groups are incorporated into phosphorus donors such as phosphites, $P(OAr)_3$, or phosphinites, $PR_2(OAr)$, then facile orthometalation can occur to give low-strain, five-membered metallacyles. Lewis exploited this phenomenon when he demonstrated that ruthenium triarylphophite complexes catalyze the *ortho*-specific deuteration and ethylation of phenol.[6,7] These catalytic processes rely on the reversible in situ transesterification of catalytic amounts of triaylphosphite ligands with the substrate phenols. We were interested to see whether catalytic transesterification of phenols and their subsequent C–H activation by orthometalation could be used to realize the *intermolecular* orthoarylation of these substrates (Scheme 1), a process that, to the best of our knowledge, has not been previously reported. Such a process could allow the synthesis of a wide range of selectively 2-arylated phenols.[8]

The substrates used in optimization studies were 4-bromoacetophenone and the bulky phenol 2,4-di-*tert*-butylphenol, since phosphorus donors that incorporate this aryl oxide residue have been found to undergo particularly facile orthometalation reactions.[9] Initial experiments focused on the use of either 1) palladium catalysts formed in situ from dipalladium tris(dibenzylideneacetone) with the ligands tris(2,4-di-*tert*-butylphenyl)phosphite (**1**), (2,4-di-*tert*-butylphenyl) diphenyl phosphinite (**2**), or (2,4-di-*tert*-butylphenyl) diisopropyl phosphinite (**3a**) acting as cocatalysts, or 2) preformed palladacyclic catalysts containing these ligands.[9b,c] In all cases we observed either no reaction or the oxidative coupling of the phenol to give 2,2′,4,4′-tetra-*tert*-butylbiphenol (**4**).

By contrast when Wilkinson's catalyst is employed with an appropriate cocatalyst, then the reaction proceeds as shown in Scheme 1 to give the orthoarylated phenol, 2,4-di-*tert*-butyl-6-4′-acetylphenyl phenol (**5a**). The molecular structure of this new phenol was determined and is shown in Figure 1.[10] The choice of cocatalyst is important; the reaction works with the bulky triarylphosphite ligand **1**, but a large excess (3.5 equivalents) of aryl bromide is required otherwise the major product formed is again the homocoupled biphenol **4**. The triarylphosphinite ligand **2** also functions as a cocatalyst and does not require such a large excess of aryl bromide, but when it is replaced by the aryl dialkylphosphinite **3a** then the reaction is far more efficient and higher yields of the product are obtained. In principle any OAr functional group can be incorporated into the phosphinite cocatalyst, but for ease of product identification and purification we usually employed phosphinites that contain the substrate phenol. The data from the catalytic studies with Wilkinson's catalyst and the aryl dialkylphosphinite ligands acting as cocatalysts are summarized in Table 1.

As can be seen from Table 1, entries 1–6, good to excellent conversions to the 2-arylated phenols are obtained regardless of whether the aryl bromide used is activated, nonactivated, or deactivated with respect to oxidative addition. The

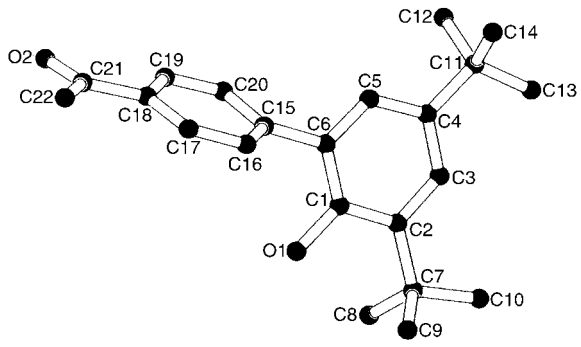


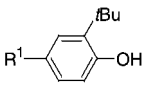
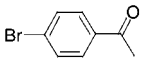
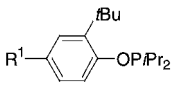
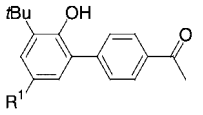
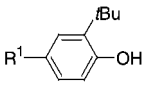
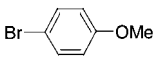
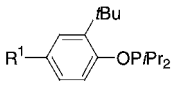
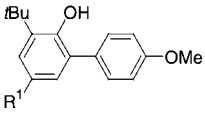
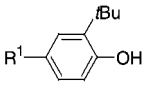
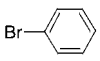
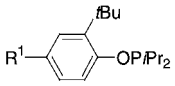
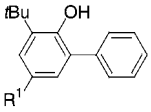
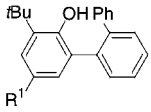
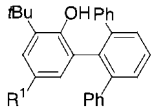
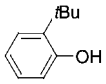
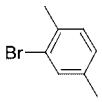
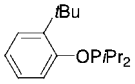
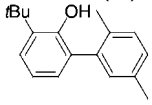
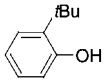
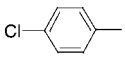
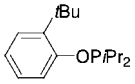
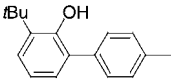
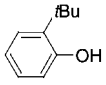
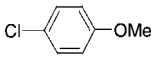
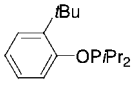
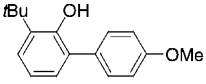
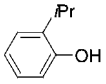
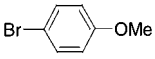
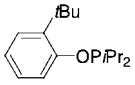
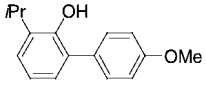
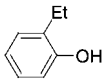
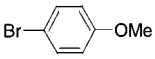
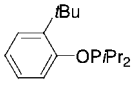
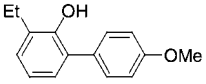
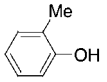
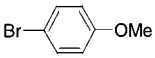
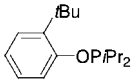
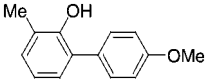
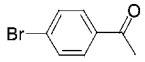
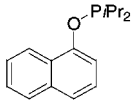
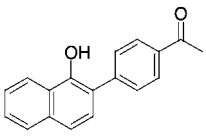
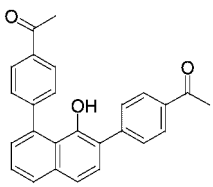
Figure 1. Molecular structure of compound **5a**.

[*] Dr. R. B. Bedford, Dr. M. E. Limmert
School of Chemistry
University of Exeter
Exeter, EX4 4QD (UK)
Fax: (+44) 1392-263-434
E-mail: r.bedford@ex.ac.uk
Dr. S. J. Coles, Prof. M. B. Hursthouse
EPSRC National Crystallography Service
University of Southampton (UK)

[**] We gratefully acknowledge the EPSRC for funding.

 © 2003 Wiley-VCH Verlag GmbH & Co. KGaA, Weinheim 1433-7851/03/4201-0112 $ 20.00+.50/0

Table 1: Catalytic orthoarylation of phenols.[a]

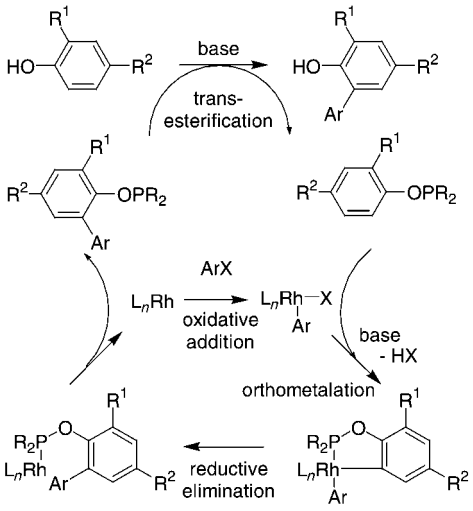
Entry	Phenol	Aryl halide	Phosphinite cocatalyst	Product (yield [%])[b]		
1 ($R^1 = t$Bu) 2 (R^1 = H)					**5a**: $R^1 = t$Bu (96) **5b**: R^1 = H (96)	
3 ($R^1 = t$Bu) 4 (R^1 = H)					**5c**: $R^1 = t$Bu (86) **5d**: R^1 = H (79)	
5 ($R^1 = t$Bu) 6 (R^1 = H)						
				5e: $R^1 = t$Bu (81) **5f**: R^1 = H (84)	**6e**: $R^1 = t$Bu (6) **6f**: R^1 = H (8)	**7e**: $R^1 = t$Bu (5)
7					**5f** (100)	
8					**5g** (25)[c]	
9					**5h** (15)	
10					**5i** (68)	
11					**5j** (53)	
12					**5k** (21)[c]	
13						
				5m (71)	**8** (23)	

[a] Reaction conditions: Phenol (1.0 mmol), aryl halide (1.5 mmol), Cs_2CO_3 (1.7 mmol), $[RhCl(PPh_3)_3]$ (0.05 mmol), $PR_2(OAr)$ (0.15 mmol), toluene (10 mL), reflux, N_2, 18 h. [b] Yield of isolated product. [c] Estimated by ^{1}H NMR spectroscopy.

reaction also proceeds smoothly when the sterically hindered aryl bromide 2-bromo-*para*-xylene is employed (Table 1, entry 7). Even aryl chlorides can be used as substrates (Table 1, entries 8 and 9), although much lower yields of coupled products result. In all cases where the phenol substrate is unsubstituted at the 4-position only orthoarylation occurs; a simple electrophilic reaction of these substrates should also lead to the formation of paraarylated products. This demonstrates that the reaction is indeed *ortho*-selective, which in turn implies that the C–H activation of the phenol occurs after it has been incorporated into the phosphinite cocatalyst. In certain cases the reaction does not stop at the simple 2-arylated products and arylation of the previously introduced 2-aryl group occurs. Such multiple arylation reactions have been observed before.[4]

It is not necessary to have a bulky *tert*-butyl group in the 2-positon of the phenol for the reaction to proceed; the incorporation of progressively smaller groups such as isopropyl and ethyl still gives good yields of the products (Table 1, entries 10 and 11). Activity was even seen with 2-methylphenol (Table 1, entry 12), however in this case the yield was somewhat lower. No activity is observed with unsubstituted phenol. The reduction in catalytic activity with decreasing steric bulk implies that the rate-determining step is probably the orthometalation of the phosphinite ligand. To accelerate this process and thus facilitate the use of phenol as a substrate

 © 2003 Wiley-VCH Verlag GmbH & Co. KGaA, Weinheim 1433-7851/03/4201-0113 $ 20.00+.50/0



Scheme 2. Plausible reaction mechanism.

we investigated the application of the bulkier phosphinite cocatalyst P*t*Bu$_2$(OPh) (**3b**), formed by reaction of P*t*Bu$_2$Cl with sodium phenoxide. In this case a number of products resulted that proved very difficult to separate. However it was possible to determine by ^{1}H NMR spectroscopy that roughly one third of the 4-bromoanisole used was incorporated into coupled products.

It is not necessary to have an alkyl group in the 2-position to facilitate the coupling reaction; 1-naphthol can also be used as a substrate (Table 1, entry 13). In this case a small amount of a second, 2,8-diarylated product (**8**), is observed. Presumably the 8-arylation occurs after the 2-arylation as there is no evidence for the formation of 8-arylated naphthol. It is possible that the 8-arylation does not proceed through the orthometalation of a phosphinite intermediate since 1-naphthol itself has been shown to undergo 8-arylation in the presence of a palladium catalyst.[4]

A plausible mechanism for the new reaction is given in Scheme 2, in which the phosphinite cocatalyst coordinates to and orthometalates at a rhodium(III) center formed previously by oxidative addition of the aryl halide. However, it is possible that the orthometalation step precedes the oxidative addition and occurs at a Rh$^{\mathrm{I}}$ center. Either way, subsequent reductive elimination of the orthometalated ligand and the aryl group leads to the reformation of the active catalyst and the liberation of a new 2-arylated aryl dialkylphosphinite ligand. This ligand then undergoes catalytic transesterification with the starting phenol to regenerate the cocatalyst and liberate the 2-arylated phenol product.

In summary, we have demonstrated for the first time the catalytic intermolecular *ortho*-selective arylation of phenols. We are currently examining the scope of this reaction with a range of phenols and related substrates and a variety of coupling partners.

Experimental Section

Typical catalytic procedure: Synthesis of **5a**: [RhCl(PPh$_3$)$_3$] (0.046 g, 0.05 mmol), **3a** (0.048 g, 0.15 mmol), 4-bromoacetophenone (0.300 g, 1.50 mmol), 2,4-di-*tert*-butylphenol (0.206 g, 1.00 mmol), and Cs_2CO_3 (0.550 g, 1.70 mmol) in toluene (10 mL) were heated at reflux under N_2 for 18 h, cooled and quenched with HCl (aq) (2 M, 5 mL). The mixture was extracted with CH_2Cl_2 (3 × 25 mL), dried ($MgSO_4$), filtered, and the solvent was removed under reduced pressure. The residue was purified by flash chromatography (silica, $CHCl_3$/hexane 1:1) to give **5a** as a colorless solid (0.313 g, 96 %).

Received: September 2, 2002 [Z50087]

[1] a) S. P. Stanforth, *Tetrahedron* **1998**, *54*, 263 – 303; b) G. Bringmann, R. Walter, R. Weirich, *Angew. Chem.* **1990**, *102*, 1006; *Angew. Chem. Int. Ed. Engl.* **1990**, *29*, 977 – 991.

[2] For recent examples see: a) M. A. Zhuravel, S. T. Nguyen, *Tetrahedron Lett.* **2001**, *42*, 7925 – 7928; b) R. Kranich, K. Eis, O. Geis, S. Mühle, J. W. Bats, H.-G. Schmalz, *Chem. Eur. J.* **2000**, *6*, 2874 – 2894; c) K. B. Simonsen, K. V. Gothelf, K. A. Jørgensen, *J. Org. Chem.* **1998**, *63*, 7536 – 7538; d) D. E. Zembower, H. Zhang, *J. Org. Chem.* **1998**, *63*, 9300 – 9305; e) S. Yonezawa, T. Komurasaki, K. Kawada, T. Tsuri, M. Fuji, A. Kugimiya, N. Haga, S. Mitsumori, M. Inagaki, T. Nakatani, Y. Tamura, S. Takechi, T. Taishi, M. Ohtani, *J. Org. Chem.* **1998**, *63*, 5831 – 5837.

[3] a) D. D. Hennings, S. Iwasa, V. H. Rawal, *J. Org. Chem.* **1997**, *62*, 2 – 3; b) D. D. Hennings, S. Iwasa, V. H. Rawal, *Tetrahedron Lett.* **1997**, *38*, 6379 – 6382.

[4] a) T. Satoh, Y. Kawamura, M. Miura, M. Nomura, *Angew. Chem.* **1997**, *109*, 1820 – 1822; *Angew. Chem. Int. Ed. Engl.* **1997**, *36*, 1740 – 1742; b) T. Satoh, J. Inoh, Y. Kawamura, Y. Kawamura, M. Miura, M. Nomura, *Bull. Chem. Soc. Jpn.* **1998**, *71*, 2239 – 2246.

[5] Miura and co-workers have demonstrated the 1-arylation of 2-naphthols. This pattern of reactivity presumably results from the high susceptibility of the 1-position to electrophilic attack rather than the formation of a highly strained four-membered palladacycle. See references [4].

[6] L. N. Lewis, *Inorg. Chem.* **1985**, *24*, 4433 – 4435.

[7] L. N. Lewis, J. F. Smith, *J. Am. Chem. Soc.* **1986**, *108*, 2728 – 2735.

[8] Very recently Yamaguchi and co-workers reported the gallium-catalyzed orthoalkynylation of phenols with haloalkynes: K. Kobayashi, M. Arisawa, M. Yamaguchi, *J. Am. Chem. Soc.* **2002**, *124*, 8528 – 8529.

[9] a) R. B. Bedford, S. Castillon, P. A. Chaloner, C. Claver, E. Fernandez, P. B. Hitchcock, A. Ruiz, *Organometallics* **1996**, *15*, 3990 – 3997; b) D. A. Albisson, R. B. Bedford, S. E. Lawrence, P. N. Scully, *Chem. Commun.* **1998**, 2095 – 2096; c) R. B. Bedford, S. L. Welch, *Chem. Commun.* **2001**, 129 – 130; d) R. B. Bedford, S. L. Hazelwood, *Organometallics* **2002**, *21*, 2599 – 2600.

[10] CCDC-192419 contains the supplementary crystallographic data for this paper. These data can be obtained free of charge via www.ccdc.cam.ac.uk/conts/retrieving.html (or from the Cambridge Crystallographic Data Centre, 12, Union Road, Cambridge CB21EZ, UK; fax: (+44) 1223-336-033; or deposit @ccdc.cam.ac.uk).

 © 2003 Wiley-VCH Verlag GmbH & Co. KGaA, Weinheim 1433-7851/03/4201-0114 $ 20.00+.50/0

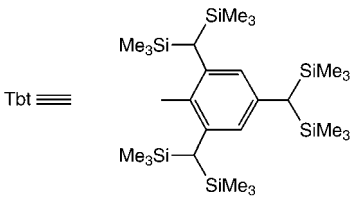
Aromaticity of Germabenzenes

η^6-Germabenzene Complexes of Chromium and Molybdenum**

*Norio Nakata, Nobuhiro Takeda, and Norihiro Tokitoh**

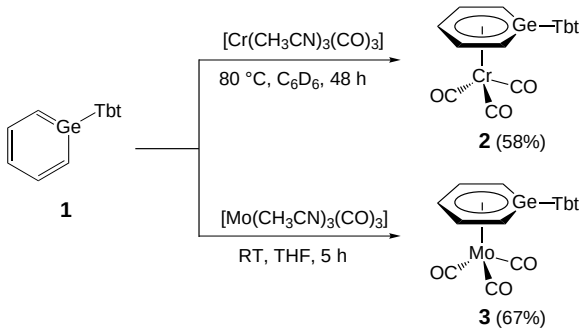
Although germabenzenes are the most fundamental germaaromatic compounds having a simple 6π-electron ring system, very little is known about their synthesis and characterization because of their extremely high reactivity. In the 1980s, Märkl et al. reported the pioneering synthesis of 1,4-di-*tert*-butylgermabenzene,[1] however, its generation was only supported by the formation of its [2+2] dimer and the trapping reaction with 2,3-dimethyl-1,3-butadiene. In addition, they described the spectroscopic detection of 1,4-dialkylgermabenzenes in the gas phase by variable temperature photoelectron spectroscopy (VTPES) experiments.[2] Kiprof and Brown have recently reported the theoretical studies of germabenzene and its valence isomers.[3] More recently, we have revealed the details of the synthesis, structure, reactivity, and aromaticity of the first stable germabenzene **1** bearing a 2,4,6-tris[bis(trimethylsilyl)methyl]phenyl (Tbt) group, the size of which provides efficient steric protection.[4]

The coordination of cyclic π-hydrocarbon ligands to transition metals has been an attractive research field since the 1960s.[5] Recently, there has been a considerable interest in transition-metal complexes that contain sila- and germaaromatic compounds as ligands, from the viewpoint of their method of coordination and their unique structures.[6] Sila- and germabenzenes are expected to be suitable ligands for transition-metal complexes because of their delocalized ring structure and aromatic character. Recently, Tilley et al. reported the characterization of the first Ru complex containing an η^6-silabenzene ligand ($[C_5Me_5Ru\{\eta^6\text{-}C_5H_5Si(t\text{-}Bu)\}][BH(C_6F_5)_3]$) by NMR and IR spectroscopy.[7] However, the molecular structures and reactivities of η^6-sila- and germabenzene complexes have not been fully reported to date. Here, we report the synthesis and characterization of the first stable η^6-germabenzene complexes, $[\{\eta^6\text{-}C_5H_5Ge(Tbt)\}M(CO)_3]$ (M = Cr (**2**), Mo (**3**)).



[*] Prof. Dr. N. Tokitoh, N. Nakata, Dr. N. Takeda
Institute for Chemical Research
Kyoto University
Gokasho, Uji, Kyoto 611-0011 (Japan)
Fax: (+81) 774-38-3209
E-mail: tokitoh@boc.kuicr.kyoto-u.ac.jp

[**] This work was partially supported by a Grant-in-Aid for COE Research on Elements Science (No. 12CE2005) and Grants-in-Aid for Scientific Research (Nos. 14204064, 11304045, and 11166250) from the Ministry of Education, Culture, Sports, Science, and Technology, Japan.



Scheme 1. Syntheses of η^6-germabenzene complexes **2** and **3**.

The ligand exchange reaction of $[Cr(CH_3CN)_3(CO)_3]$[8] with **1** at 80 °C in C_6D_6 resulted in the formation of the η^6-germabenzene–chromium complex, $[\{\eta^6\text{-}C_5H_5Ge(Tbt)\}Cr(CO)_3]$ (**2**), as yellow crystals in 58% yield (Scheme 1). The novel Mo complex, $[\{\eta^6\text{-}C_5H_5Ge(Tbt)\}Mo(CO)_3]$ (**3**), was also obtained as yellow crystals in 67% yield when $[Mo(CH_3CN)_3(CO)_3]$[9] was used as the metal source at room temperature in THF. Germabenzene complexes **2** and **3** possess reasonable thermal stability in both the solid state and in solution under argon atmosphere, and no detectable change was observed after the thermolysis of **2** and **3** in C_6D_6 at 120 °C in a sealed tube for a few days. In addition, **2** and **3** are more stable towards air and moisture than the free germabenzene **1**. These results reflect that coordination to the transition metal (Cr, Mo) leads to the thermodynamic stabilization of the reactive species **1**.

Complexes **2** and **3** were fully characterized by ^1H and ^{13}C NMR, IR, and UV/Vis spectroscopy. As expected, the ^1H NMR chemical shifts of the germabenzene ring protons for **2** ($\delta = 3.95$, 4.73, and 4.98 ppm) and **3** ($\delta = 4.05$, 4.73, and 5.17 ppm) are shifted upfield relative to those for the free germabenzene **1** ($\delta = 6.72$, 7.85 and 8.06 ppm).[4] The ^{13}C NMR signals for the germabenzene ring carbons of **2** ($\delta = 83.00$, 85.87, and 100.91 ppm) and **3** ($\delta = 81.64$, 83.77, and 103.11 ppm) also appear at much higher field than the equivalent signals for **1** ($\delta = 114.23$, 132.23, and 140.96 ppm),[4] and were observed at slightly higher field than the resonances for the corresponding η^6-arene complexes, $[(\eta^6\text{-arene})M(CO)_3]$ (M = Cr, Mo)($\delta = 92.4$–118.8 ppm).[10] Additionally, the $^{13}C{=}O$ chemical shifts for **2** and **3** ($\delta =$ 235.05 and 222.19 ppm, respectively) are quite similar to those for $[(\eta^6\text{-mesitylene})M(CO)_3]$ (M = Cr ($\delta = 235.1$ ppm), Mo ($\delta = 223.7$ ppm)).[10a] In the IR spectra, the stretching frequencies ($\tilde{\nu}_{CO}$) of **2** (1867, 1887, and 1954 cm^{-1}) and **3** (1865, 1883, and 1952 cm^{-1}) were observed at lower energy than those of the corresponding benzene complexes, $[(\eta^6\text{-}C_6H_6)M(CO)_3]$ (M = Cr ($\tilde{\nu}_{CO} = 1915$ and 1982 cm^{-1}),[11] M = Mo ($\tilde{\nu}_{CO} = 1913$ and 1983 cm^{-1})[12]). These results suggest that the benzene ligands in $[(\eta^6\text{-}C_6H_6)M(CO)_3]$ (M = Cr, Mo) are stronger electron donors than the germabenzene ligands of **2** and **3**. Furthermore, three carbonyl stretching frequencies that were calculated by vibrational analysis for the model

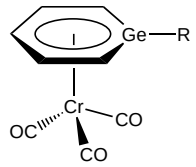
Table 1: Observed and calculated carbonyl stretching frequencies of [{η^6-$C_5H_5Ge(Tbt)$}$Cr(CO)_3$] (**2**) and [{η^6-C_5H_5GeH}$Cr(CO)_3$] (**4**).

2 (observed)[a]	**4** (calculated)[b]	Relative value (obsd/calcd)
1867	1994	0.94
1887	2011	0.94
1954	2059	0.95

[a] KBr. [b] Calculated at the B3LYP/6-311G(d,p)(LANL2DZ for Cr) level.

compound [{η^6-C_5H_5GeH}$Cr(CO)_3$] (**4**) were in good agreement with those of **2** considering the overestimation of the vibrational frequencies in the theoretical calculation (Table 1).[13]

The UV/Vis spectra of **2** and **3** in hexane showed three absorption maxima (**2**: 225 ($\varepsilon = 49000$), 279 ($\varepsilon = 17000$), and 340 ($\varepsilon = 8000$); **3**: 228 ($\varepsilon = 41000$), 287 ($\varepsilon = 10000$), and 344 nm ($\varepsilon = 13000$)). These values are slightly red-shifted compared to those for the corresponding benzene complexes (217 ($\varepsilon = 23700$), 263 ($\varepsilon = 6720$), and 315 nm ($\varepsilon = 9450$) for [(η^6-C_6H_6)$Cr(CO)_3$]; 220 (sh), 282–287 ($\varepsilon = 3980$), and 323 nm ($\varepsilon = 18400$) for [(η^6-C_6H_6)$Mo(CO)_3$], respectively).[14]



4 (R = H)
5 ($R = CH_3$)

The molecular geometry of **2** was determined by X-ray crystallographic analysis; the ORTEP diagram is given in Figure 1.[15] Complex **2** features a nearly planar germabenzene ligand (the sum of the bond angles around the central Ge atom and the sum of the interior bond angles of the germabenzene ring are 359.9 and 719.4°, respectively), which is η^6-coordinated to the {$Cr(CO)_3$} unit. The dihedral angle between the germabenzene ring and the benzene ring of the Tbt group is about 35°. In addition, the Ge atom does not reside directly above the C6 carbon atom, which is a constituent of one of the legs of the "piano stool" formed by the three CO ligands; when viewed from above the germabenzene ring, the angle formed by the Ge, Cr, and C6 atoms is 28°. These results may be attributed to the steric and electronic repulsion between the Tbt group and the CO ligand. The lengths of the two Ge–C bonds (1.859(5) and 1.878(5) Å) and the four C–C bonds (1.393(7)–1.404(7) Å) in the germabenzene ligand are slightly longer than those of the free germabenzene **1** (Ge–C: 1.827(2) and 1.829(2), C–C: 1.385(3)–1.396(3) Å).[4] While the five C–Cr bond lengths (2.186(5)–2.314(4) Å) are similar to those of [(η^6-C_6H_6)$Cr(CO)_3$] (2.217(2)–2.240(2) Å),[16] the Ge–Cr bond length of 2.5849(12) Å is somewhat longer than that which was reported for the Ge–Cr bond of the related complex, $[\{(OC)_5Cr\}I_2Ge{-}GeI_2\{Cr(CO)_5\}]^{2-}$ (2.468(1) Å).[17] In addition, theoretical calculations for the model compounds [{η^6-C_5H_5GeR}$Cr(CO)_3$] (R = H (**4**), CH_3 (**5**)) were performed for a comparison (Table 2).[18] The agreement between the experimental and theoretical values is excellent, which suggests that the Ge–C and C–C bond lengths of the germabenzene rings, in addition to the length of the Ge–Cr bonds, are little affected by substituents on the germanium atom.

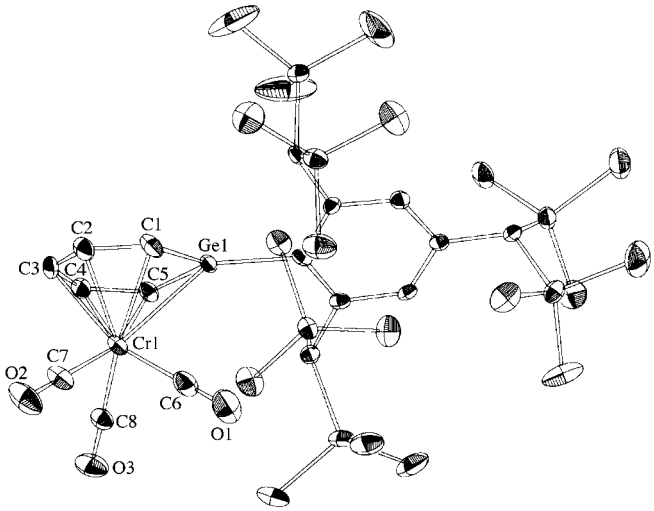


Figure 1. ORTEP diagram of [{(η^6-$C_5H_5Ge(Tbt)$}$Cr(CO)_3$] (**2,** 50% thermal ellipsoids; the fragment of solvated benzene is omitted for clarity). Selected bond lengths (Å) and angles (°): Ge1-C1 1.878(5), Ge1-C5 1.859(5), C1-C2 1.396(7), C2-C3 1.404(7), C3-C4 1.393(7), C4-C5 1.404(6), Ge1-Cr1 2.5849(12), C1-Cr1 2.300(5), C2-Cr1 2.199(5), C3-Cr1 2.186(5), C4-Cr1 2.220(5), C5-Cr1 2.314(4); C1-Ge1-C5 100.7(2), C1-Ge1-C9 128.1(2), C5-Ge1-C9 131.14(19), Ge1-C1-C2 121.0(4), C1-C2-C3 125.9(5), C2-C3-C4 124.6(4), C3-C4-C5 125.8(5), Ge1-C5-C4 121.4(4).

In conclusion, we successfully synthesized the novel η^6-germabenzene complexes **2** and **3** by the reactions of germabenzene **1** with $[M(CH_3CN)_3(CO)_3]$ (M = Cr, Mo), and their molecular structures were determined from their spectroscopic data and from X-ray structural analysis. Thus, these results convey the first description of the aromatic character of germabenzenes, from the standpoint of their chemical reactivity. Further investigations on the reactivity of **2** and **3** and the synthesis of new germabenzene complexes are currently in progress.

Experimental Section

2: In a glove-box filled with argon, **1** (50.2 mg, 0.073 mmol) and $[Cr(CH_3CN)_3(CO)_3]$ (22.6 mg, 0.087 mmol) were dissolved in C_6D_6 (0.5 mL) and the solution was placed into an NMR tube, which was then placed under vacuum and sealed. Heating the mixture at 80 °C for 48 h resulted in the disappearance of the NMR signals for **1**. The tube was then opened and the solvent was removed in vacuo. The

Table 2: Observed and calculated bond lengths [Å] of the Cr complexes **2**, **4**, and **5**.

	2 (observed)	**4** (calculated)[a]	**5** (calculated)[a]
Ge1-C1, Ge1-C5	1.878(5), 1.859(5)	1.862	1.864, 1.867
C1-C2, C4-C5	1.396(7), 1.404(6)	1.406	1.407, 1.405
C2-C3, C3-C4	1.404(6), 1.393(7)	1.417	1.415, 1.418
Ge1-Cr1	2.5849(12)	2.556	2.572

[a] Calculated at the B3LYP/6-311G(d,p) (LANL2DZ for Cr) level.

 © 2003 Wiley-VCH Verlag GmbH & Co. KGaA, Weinheim 1433-7851/03/4201-0116 $ 20.00+.50/0

residue was recrystallized from pentane at −40 °C to give **2** (34.7 mg, 58 %) as yellow crystals. m.p. 274–276 °C (decomp); ^{1}H NMR (300 MHz, C_6D_6): $\delta = 0.12$ (s, 18 H), 0.19 (s, 36 H), 1.49 (s, 1 H), 2.45 (br s, 1 H), 2.52 (br s, 1 H), 3.95 (d, ^3J(H,H) = 10.5 Hz, 2 H), 4.73 (t, ^3J(H,H) = 6.3 Hz, 1 H), 4.98 (dd, ^3J(H,H) = 6.3, 10.5 Hz, 2 H), 6.63 (br s, 1 H), 6.73 ppm (br s, 1 H); ^{13}C NMR (75 MHz, C_6D_6): $\delta = 0.61$ (q), 0.78 (q), 0.91 (q), 31.50 (d), 34.37 (d), 34.79 (d), 83.00 (d), 85.87 (d), 100.91 (d), 122.44 (d), 123.55 (s), 127.26 (d), 148.32 (s), 151.92 (s × 2), 235.05 ppm (s); IR (KBr): $\tilde{\nu} = 1867$, 1887, 1954 cm^{-1} (C≡O); UV/Vis (*n*-hexane): λ_{max} (ε) = 225 (49 000), 279 (17 000), 340 nm (8000); LRMS (FAB): *m*/*z* (%) = 826 (8) [M^+], 691 (75) [{C_5H_5Ge(Tbt)}$^+$], 521 (100) [{(Tbt)−2 CH_3}$^+$]. Although we have tried to obtain the elemental analysis of **2** on several occasions, the results have not been commensurate with the calculated values for **2** because of its highly moisture-sensitive properties (elemental analysis calcd for $C_{35}H_{64}CrGeO_3Si_6$: C 50.89, H 7.81; found: C 49.16, H 7.87).

3: In a glove-box filled with argon, [Mo(CH_3CN)$_3$(CO)$_3$] (16.3 mg, 0.054 mmol) was added to a solution of **1** (40.1 mg, 0.058 mmol) in THF (1 mL) at room temperature, and the mixture was stirred for 5 h. After the solvent was removed in vacuo, the residue was recrystallized from hexane at −40 °C to give **3** (31.4 mg, 67 %) as yellow crystals. M.p. 248–250 °C (decomp); ^{1}H NMR (300 MHz, C_6D_6): $\delta = 0.11$ (s, 18 H), 0.18 (s, 36 H), 1.47 (s, 1 H), 2.39 (br s, 1 H), 2.49 (br s, 1 H), 4.05 (d, ^3J(H,H) = 9.9 Hz, 2 H), 4.73 (t, ^3J(H,H) = 6.6 Hz, 1 H), 5.17 (dd, ^3J(H,H) = 6.6, 9.9 Hz, 2 H), 6.61 (br s, 1 H), 6.70 ppm (br s, 1 H); ^{13}C NMR (75 MHz, C_6D_6): $\delta = 0.57$ (q), 0.77 (q), 0.88 (q), 31.43 (d), 34.66 (d), 34.99 (d), 81.64 (d), 83.77 (d), 103.11 (d), 122.40 (d), 123.72 (s), 127.23 (d), 148.28 (s), 151.66 (s × 2), 222.19 ppm (s); IR (KBr): $\tilde{\nu} = 1865$, 1883, 1952 cm^{-1} (C≡O); UV/Vis (*n*-hexane): λ_{max} (ε) = 228 (41 000), 287 (10 000), 344 nm (13 000); elemental analysis calcd for $C_{35}H_{64}GeMoO_3Si_6$: C 48.32, H 7.42; found: C 47.91, H 7.48.

Received: September 4, 2002 [Z50103]

[1] G. Märkl, D. Rudnick, *Tetrahedron Lett.* **1980**, *21*, 1405.
[2] G. Märkl, D. Rudnick, R. Schulz, A. Schweig, *Angew. Chem.* **1982**, *94*, 211; *Angew. Chem. Int. Ed. Engl.* **1982**, *21*, 221.
[3] P. Kiprof, A. B. Brown, *Internet J. Chem.* **1999**, *2*, 1.
[4] N. Nakata, N. Takeda, N. Tokitoh, *J. Am. Chem. Soc.* **2002**, *124*, 6914.
[5] For a review of π-arene complexes of group 6 metals, see: M. J. Morris in *Comprehensive Organometallic Chemistry II, Vol. 5* (Eds.: E. W. Abel, F. G. A. Stone, G. Wilkinson), Pergamon, Oxford, **1995**, chap. 8.
[6] Reports on η^5-silolyl and germolyl complexes, see: a) W. P. Freeman, T. D. Tilley, A. L. Rheingold, *J. Am. Chem. Soc.* **1994**, *116*, 8428; b) J. M. Dysard, T. D. Tilley, *J. Am. Chem. Soc.* **1998**, *120*, 8245; c) J. M. Dysard, T. D. Tilley, *J. Am. Chem. Soc.* **2000**, *122*, 3097; d) W. P. Freeman, J. M. Dysard, T. D. Tilley, A. L. Rheingold, *Organometallics* **2002**, *21*, 1734.
[7] J. M. Dysard, T. D. Tilley, T. K. Woo, *Organometallics* **2001**, *20*, 1195.
[8] D. P. Tate, W. R. Knipple, J. M. Augl, *Inorg. Chem.* **1962**, *1*, 433.
[9] R. B. King, *J. Organomet. Chem.* **1967**, *8*, 139.
[10] a) B. E. Mann, *J. Chem. Soc. D* **1971**, 976; b) B. E. Mann, *J. Chem. Soc. Dalton Trans.* **1973**, 2012.
[11] C. A. L. Mahaffy, P. L. Pauson, *Inorg. Synth.* **1979**, *19*, 154.
[12] A. N. Nesmeyanov, V. V. Krivykh, V. S. Kaganovich, M. I. Rybinskaya, *J. Organomet. Chem.* **1975**, *102*, 185.
[13] Since the scaling factor at the B3LYP/LANL2DZ level was unknown, we compared the ratio of the observed carbonyl stretching frequencies to the calculated ones.
[14] M. G. Evdokimova, B. M. Yavorskii, V. N. Trembouler, N. K. Baranetskaya, V. U. Krivyk, G. B. Zaslavskaya, *Dokl. Phys. Chem.* **1978**, *239*, 394.
[15] Single crystals of **2** suitable for X-ray crystallographic analysis were grown by recrystallization from benzene. Crystal data for **2**·0.5 C_6H_6 ($C_{38}H_{67}CrGeO_3Si_6$): $M = 865.05$, $T = 103(2)$ K, monoclinic, space group $P2_1/n$ (no. 14), $a = 12.613(6)$, $b = 32.756(13)$, $c = 12.661(5)$ Å, $\beta = 115.767(6)°$, $V = 4711(3)$ Å^3, $Z = 4$, $\rho_{calcd} = 1.220$ g cm^{-3}, $\mu = 1.053$ mm^{-1}, $\lambda = 0.71070$ Å, $2\theta_{max} = 50.0°$, 28 628 measured reflections, 8231 independent reflections, 460 refined parameters, GOF = 1.246, $R_1 = 0.0700$ and w$R_2 = 0.1808$ ($I > 2\sigma(I)$), $R_1 = 0.0820$ and w$R_2 = 0.1871$ (for all data), largest difference peak and hole 0.497 and −0.491 e Å^3. The intensity data were collected on a Rigaku/MSC Mercury CCD diffractometer. The structure was solved by direct methods (SHELXS-97) and refined by full-matrix least-squares procedures on F^2 for all reflections (SHELXL-97). All hydrogen atoms were placed using AFIX instructions. CCDC-192689 contains the supplementary crystallographic data for this paper. These data can be obtained free of charge via www.ccdc.cam.ac.uk/conts/retrieving.html (or from the Cambridge Crystallographic Data Centre, 12, Union Road, Cambridge CB2 1EZ, UK; fax: (+44) 1223-336-033; or deposit@ccdc.cam.ac.uk).
[16] B. Rees, P. Coppens, *J. Organomet. Chem.* **1972**, *42*, C102.
[17] G. Renner, P. Kircher, G. Huttner, P. Rutsch, K. Heinze, *Eur. J. Inorg. Chem.* **2000**, 879.
[18] Geometry optimization for **4** and **5** was carried out using the Gaussian 98 program with density functional theory at the B3LYP level with 6-311G(d,p) basis set for Ge, C, O, and H atoms and the LANL2DZ for Cr atom.

Synthesis of Amino Acid Derivatives

A Diversity-Oriented Synthesis of α-Amino Acid Derivatives by a Silyltelluride-Mediated Radical Coupling Reaction of Imines and Isonitriles**

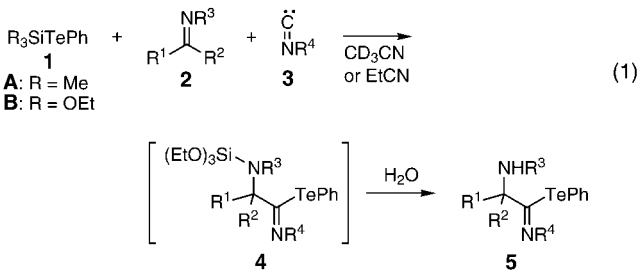
Shigeru Yamago, Hiroshi Miyazoe, Takeyoshi Nakayama, Masaki Miyoshi, and Junichi Yoshida**

Development of new and practical methods for the synthesis of α-amino acids and their derivatives is of considerable interest to researchers, because the importance of these compounds in biological systems and their exceptional utility as building blocks in organic synthesis is well known.[1,2]

[*] Prof. S. Yamago, Prof. J. Yoshida, Dr. H. Miyazoe, T. Nakayama, M. Miyoshi
Department of Synthetic Chemistry and Biological Chemistry
Graduate School of Engineering, Kyoto University
Kyoto 606-8501 (Japan)
Fax: (+81) 75-753-5911
E-mail: yamago@sbchem.kyoto-u.ac.jp
yoshida@chem.kyoto-u.ac.jp

[**] This work was partly supported by a Grant-in-Aid for the Scientific Research from Japan Society for the Promotion of Science.
Supporting information for this article is available on the WWW under http://www.angewandte.org or from the author.

Because imines are excellent acceptors for various carbon nucleophiles, numerous synthetic routes from imines to amino acids have been developed under ionic conditions as exemplified by the Ugi reaction[3] and the Strecker reaction.[4,5] However, because of the unfavorable thermodynamics in the addition of carbon-centered radicals to imines, only a few examples of radical-mediated synthesis have been reported.[6–8] We report here a new synthesis of α-amino acid derivatives that relies on a silyltelluride-mediated radical coupling[9] strategy of imines and isonitriles followed by transformation of the resulting imidoyl tellurides [Eq. (1)].[10]



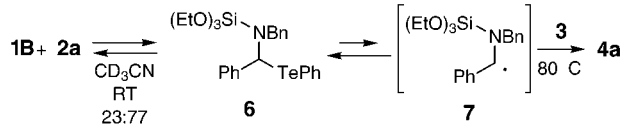
We initially examined the trimethylsilyl phenyl telluride (**1A**) mediated coupling reaction of imines and isonitriles. However, in sharp contrast to the reaction of **1A** and carbonyl compounds,[9] **1A** was totally unreactive toward imines. After screening several silyltellurides and group 14 metal tellurides, we were pleased to find that triethoxysilyl phenyl telluride (**1B**) was sufficiently reactive, providing the desired coupling product **4** with high efficiency. Thus, the reaction of **1B** (1.3 equiv), the imine **2a** (R^1 = Ph, R^2 = H, R^3 = Bn; Bn = benzyl; 1.0 equiv), and 2,6-xylylisonitrile (**3**, R^4 = 2,6-$Me_2C_6H_3$; 2.0 equiv) in CD_3CN was complete within 4 h at 80 °C and afforded the coupling product **5a** in 92 % yield after flash column chromatography (Table 1, entry 1). ^{1}H NMR spectroscopy indicated that the reaction initially afforded the silylated amine **4a**, which was hydrolyzed to **5a** during column chromatography. The NMR spectroscopic experiment also revealed the profile of the reaction (Scheme 1). The reaction of **1** and **2a** gave a 23:77 equilibrium mixture of the starting materials and the α-silylaminotelluride **6** after 0.5 h at room temperature in the absence of isonitrile, and the ratio did not change upon prolonged heating at 80 °C. However, addition of **3** (2 equiv) to the reaction mixture smoothly and completely converted **1**, **2a**, and **6** into **4a**. Because the imidoylation proceeds virtually irreversibly,[11] trapping of the α-amino radical **7**, which is reversibly generated from **6**,[12] by **3** shifted the equilibrium from the starting materials to the product.

As shown in Table 1, the current reaction is extremely versatile, and a variety of diversely substituted R^1 and R^2 groups of imines can participate in the coupling reaction. Thus, aromatic and aliphatic imines with acyclic and cyclic structures were coupled with **1B** and **3** within 4–24 h at 20–80 °C to give **4** in good to excellent yields. It is worth mentioning that the quaternary carbon center was effectively constructed by employing trisubstituted imines (entries 13 and 14). It is also interesting to observe that C–C multiple bonds were unaffected by the radical intermediates (entries 9 and 10). Because α-amino radicals undergo intermolecular addition to C–C multiple bonds only when electron-withdrawing groups are attached to the nitrogen atom,[13] the current results clearly indicate that the triethoxysilyl group is not a strong electron-withdrawing group. Moderate *anti* selectivity was observed in the reaction of the α-alkoxy imine **2c** (entry 11). Although we also examined several α-alkoxy imines with different α-alkyl substituents, such as the *iso*-propyl group, and/or a protecting group (results not shown), such as *tert*-butyldimethylsilyl (TBDMS), we could not increase the selectivity.

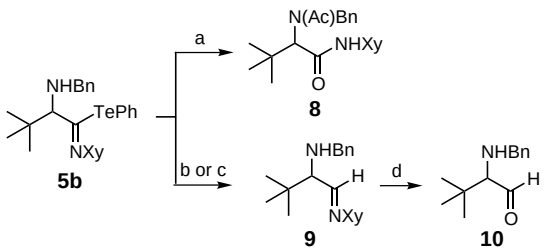
Not only do the R^1 and R^2 substituents of the imines allow for diversity, but the R^3 moiety also serves as a diversification site. Thus, the reaction of a variety of *N*-alkyl benzylidene imine derivatives (R^1 = Ph, R^2 = H), afforded the desired coupling reaction (R^3 = *n*Bu; 94 %, R^3 = $(CH_2)_2$OMe; 78 %, R^3 = allyl; 95 %), while the imines possessing electron-withdrawing groups, for example, SO_2Tol (Tol = toluyl), did not react under identical conditions.

As the reaction proceeds in a group-transfer manner, the carbon-tellurium bond in the products can also be used for the diversity-oriented transformation to a variety of amino acid derivatives (Scheme 2). Thus, mercury-mediated oxidative hydrolysis of **5b** gave the *tert*-leucine amide **8** in good yield.[14] Treatment of **5b** with *n*BuLi followed by hydrolysis of the resulting imidoyl lithium afforded the α-amino imine **9**,[15] which was further hydrolyzed to the α-amino aldehyde **10**. The tributyltin hydride-mediated radical reduction of **5b** also afforded **9** in good yield.

In summary, the combination of the silyl telluride-mediated coupling reaction of imines and isonitriles and C–Te bond manipulations allows the diversity-oriented synthesis of α-amino acid derivatives. Further synthetic studies on mechanistic and synthetic aspects as well as combinatorial applications of the reaction are currently underway.



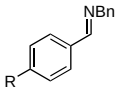
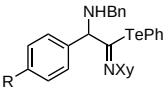
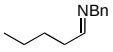
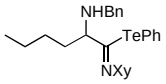
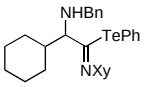
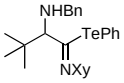
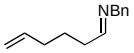
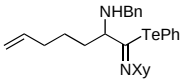
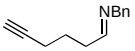
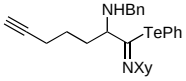
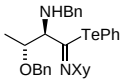
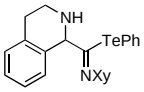
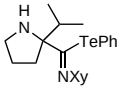
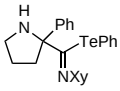
Scheme 1. The course of the coupling reaction.



Scheme 2. Transformation of the coupling product into α-amino acids and their derivatives. Conditions: a) $Hg(OAc)_2$ (1.0 equiv), BSA (1.5 equiv), H_2O/THF, RT, 0.25 h, 94 %; b) BuLi (2.2 equiv), THF, −72 °C, 0.2 h then H_3O^+, 76 %; c) Bu_3SnH (1.2 equiv), AIBN (0.1 equiv), benzene, 80 °C, 2 h, 70 % d) AcOH (1.2 equiv), THF, −72 °C, 78 %. AIBN = azobisisobutyronitrile. Xy = 2,6-dimethylphenyl

 © 2003 Wiley-VCH Verlag GmbH & Co. KGaA, Weinheim 1433-7851/03/4201-0118 $ 20.00+.50/0

Table 1: Three component coupling reactions with silyltelluride **1A**, imine **2** and isonitrile **3a**[a]

Entry	Imine	*T* [°C]	*t* [h]	Product	Yield [%]
					
1	R = H (**2a**)	80	4	(**5a**)	92
2	R = Me	80	4		93
3	R = OMe	80	4		88
4	R = NMe_2	80	4		91
5	R = CO_2Me	80	2		50
6		25	24		63
7		25	24		92
8		25	24		74 (72)[c]
9		25	24		67
10		25	24		68
11		25	24		77[b]
12		25	24		61
13		25	24		50
14		25	24		43

[a] The reaction was carried out by heating a solution of **1a** (1.3 equiv), **2** (1.0 equiv) and **3a** (2.0 equiv) in CD_3CN or MeCN. [b] A 76:24 mixture of the diastereomers was obtained. The major isomer is shown. [c] Yield using one equivalent of each reagent.

Experimental Section

Typical experimental procedure: Synthesis of **5b**. A solution of **1B** (3.69 g, 10.0 mmol), *N*-(*tert*-butylmethylidene)benzylamine (**2b**) (1.76 g, 10.0 mmol), and **3** (1.31 g, 10.0 mmol) in acetonitrile (10.0 mL) was stirred at room temperature for 24 h. After removal of the solvent, purification of the crude mixture by flash column chromatography (silica gel: 270 g, elution with 3% ethyl acetate in hexane) gave **5b** in 72% yield as a pale yellow solid (3.68 g, 7.20 mmol); m.p. 53.9–54.3 °C; IR (KBr): $\tilde{\nu}$ = 2950, 1609, 1588, 1464, 847, 804, 764, 731, 695 cm^{-1}; ^1H NMR (300 MHz, $CDCl_3$): δ = 1.04 (s, 9H), 2.27 (s, 6H), 2.39 (br s, 1H), 3.26 (s, 1H), 3.77 (d, J = 12.9 Hz, 1H), 4.26 (d, J = 12.9 Hz, 1H), 6.90–6.99 (m, 2H), 6.99–7.05 (m, 1H), 7.13 (t, J = 7.5 Hz, 2H), 7.23–7.42 (m, 6H), 7.70–7.77 ppm (m, 2H); ^{13}C NMR (75 MHz, $CDCl_3$): δ = 18.94, 19.11, 27.28, 35.99, 53.18, 71.43, 114.17, 124.55, 125.75, 126.09, 126.91, 128.00, 128.27, 128.65, 129.17, 140.80, 141.92, 150.59, 170.06 ppm; HRMS (FAB) *m*/*z*: calcd for $C_{27}H_{33}N_2Te$ $[M+H]^+$, 515.1706, found 515.1699; elemental analysis calcd for $C_{27}H_{32}N_2Te$: C 63.32, H 6.30, N 5.47, found: C 63.08, H 6.33, N 5.33.

Received: September 17, 2002 [Z50184]

[1] R. M. Williams, *Synthesis of Optically Active α-Amino Acids*, Pergamon, Oxford, **1989**; R. O. Duthaler, *Tetrahedron* **1994**, *50*, 1539; R. M. Williams, J. A. Hendrix, *Chem. Rev.* **1992**, *92*, 889.
[2] G. M. Coppola, H. F. Schuster, *Asymmetric Synthesis. Construction of Chiral Molecules Using Amino Acids*, Wiley, New York,

1987; F. J. Sardina, H. Rapoport, *Chem. Rev.* **1996**, *96*, 1825; D. J. Ager, I. Prakash, D. R. Schaad, *Chem. Rev.* **1996**, *96*, 835.

[3] A. Dömling, I. Ugi, *Angew. Chem.* **2000**, *112*, 3300; *Angew. Chem. Int. Ed.* **2000**, *39*, 3168; T. A. Keating, R. W. Armstrong, *J. Am. Chem. Soc.* **1996**, *118*, 2574.

[4] For recent representative examples, see; H. Ishitani, S. Komiyama, Y. Hasegawa, S. Kobayashi, *J. Am. Chem. Soc.* **2000**, *122*, 767; M. S. Sigman, E. N. Jacobsen, *J. Am. Chem. Soc.* **1998**, *120*, 5315; M. S. Iyer, K. M. Gigstad, N. D. Namdev, M. Lipton, *J. Am. Chem. Soc.* **1996**, *118*, 4910; F. A. Davis, P. S. Portonovo, R. E. Reddy, Y. Chiu, *J. Org. Chem.* **1996**, *61*, 440.

[5] S. Wenglowsky, L. S. Hegedus, *J. Am. Chem. Soc.* **1998**, *120*, 12468; N. A. Petasis, I. A. Zavialov, *J. Am. Chem. Soc.* **1997**, *119*, 445.

[6] For reviews on intermolecular addition of carbon-centered radicals to C–N double bonds, see; G. K. Friestad, *Tetrahedron* **2001**, *57*, 5461; A. G. Fallis, I. M. Brinza, *Tetrahedron* **1997**, *53*, 17543.

[7] a) H. Miyabe, C. Ushiro, M. Ueda, K. Yamakawa, T. Naito, *J. Org. Chem.* **2000**, *65*, 176; H. Miyabe, C. Konishi, T. Naito, *Org. Lett.* **2000**, *2*, 1443; b) M. P. Bertrand, L. Feray, R. Nouguier, P. Perfetti, *Synlett* **1999**, 1148; M. P. Bertrand, L. Feray, R. Nouguier, L. Stella, *Synlett* **1998**, 780.

[8] S. Yamago, M. Nakamura, X.-O. Wang, M. Yanagawa, S. Tokumitsu, E. Nakamura, *J. Org. Chem.* **1998**, *63*, 1694.

[9] S. Yamago, M. Miyoshi, H. Miyazoe, J. Yoshida, *Angew. Chem.* **2002**, *114*, 1465; *Angew. Chem. Int. Ed.* **2002**, *41*, 1407; H. Miyazoe, S. Yamago, J. Yoshida, *Angew. Chem.* **2000**, *112*, 3815; *Angew. Chem. Int. Ed.* **2000**, *39*, 3669; S. Yamago, H. Miyoshi, K. Iida, J. Yoshida, *Org. Lett.* **2000**, *2*, 3671.

[10] An alternative route using glycine radicals has been reported. See: C. J. Easton, *Chem. Rev.* **1997**, *97*, 53; C. J. Easton, C. A. Hutton, *Synlett* **1998**, 457; M. Sibi, Y. Asano, J. B. Sausker, *Angew. Chem.* **2001**, *113*, 1333; *Angew. Chem. Int. Ed.* **2001**, *40*, 1293, and references therein. See also, P. Renaud, L. Giraud, *Synthesis* **1996**, 913.

[11] S. Yamago, H. Miyazoe, R. Goto, M. Hashidume, T. Sawazaki, J. Yoshida, *J. Am. Chem. Soc.* **2001**, *123*, 3697; S. Yamago, H. Miyazoe, T. Sawazaki, J. Yoshida, *Tetrahedron Lett.* **2000**, *41*, 7517; S. Yamago, H. Miyazoe, R. Goto, J. Yoshida, *Tetrahedron Lett.* **1999**, *40*, 2347.

[12] S. Yamago, K. Iida, J. Yoshida, *J. Am. Chem. Soc.*, in press; S. Yamago, K. Iida, J. Yoshida, *J. Am. Chem. Soc.* **2002**, *124*, 2874; S. Yamago, M. Hashidume, J. Yoshida, *Tetrahedron* **2002**, *58*, 6805; S. Yamago, H. Miyazoe, J. Yoshida, *Tetrahedron Lett.* **1999**, *40*, 2339.

[13] A. Padwa, H. Nimmesgern, G. S. K. Wong, *Tetrahedron Lett.* **1985**, *26*, 957.

[14] For the oxidative transformation of C–Te bonds, see: S. Yamago, K. Kokubo, J. Yoshida, *Chem. Lett.* **1997**, 111; S. Yamago, K. Kokubo, H. Murakami, Y. Mino, O. Hara, J. Yoshida, *Tetrahedron Lett.* **1998**, *39*, 7905. See also ref. [11].

[15] T. Hirao, N. Kambe, A. Ogawa, M. Miyoshi, S. Murai, N. Sonoda, *Angew. Chem.* **1987**, *99*, 1221; *Angew. Chem. Int. Ed. Engl.* **1987**, *26*, 1187. While the tellurium–lithium exchange from acyl tellurides to acyl lithiums is known, there has been no report on the generation of imidoyl lithium species from imidoyl telluride compounds. See T. Hiiro, Y. Morita, T. Inoue, N. Kambe, A. Ogawa, I. Ryu, N. Sonoda, *J. Am. Chem. Soc.* **1990**, *112*, 455.

 © 2003 Wiley-VCH Verlag GmbH & Co. KGaA, Weinheim 1433-7851/03/4201-0120 $ 20.00+.50/0

Cover Picture

Christophe Copéret,* Mathieu Chabanas, Romain Petroff Saint-Arroman, and Jean-Marie Basset*



Catalysis research builds bridges between disciplines. The cover picture shows the linking position of surface organometallic chemistry between the two traditional areas of catalysis. The transfer of the concepts and tools of molecular organometallic chemistry to surfaces leads to the generation of well-defined surface species. The success of this approach results from understanding the reactions of organometallic complexes with the support. More about this field can be found in the review by Copéret, Basset, et al. on page 156ff.

Contents

News

Awards and Appointments ——— **139**

Meeting Reviews

Protein Design at the Crossroads of Biotechnology, Chemistry, Theory, and Evolution ——— **140 – 142** | 86. International Titisee Conference | *R. Jaenicke, R. Sterner*

Books

Chemical Bonding and Molecular Geometry ——— **143 – 147** | Ronald J. Gillespie, Paul L. A. Popelier | *G. Frenking*

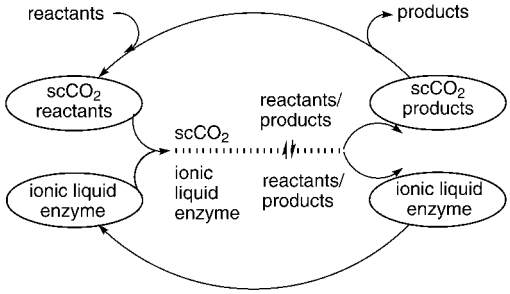
Highlights

Green Solvents

Sergei V. Dzyuba, Richard A. Bartsch* ——— **148 – 150**

Recent Advances in Applications of Room-Temperature Ionic Liquid/Supercritical CO_2 Systems

Keywords:
carbon dioxide · enzyme catalysis · green chemistry · ionic liquids · supercritical fluids



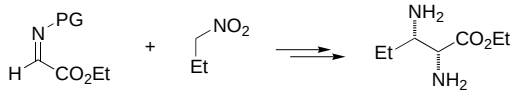
Duet of Extremes: Efficient and environmentally benign, biphasic systems consisting of ionic liquids and supercritical CO_2 ($scCO_2$) have been employed in lipase-catalyzed esterifications (see scheme). The reaction takes place in the ionic liquid with or without a solid support, and the products are removed by means of either batchwise or continuous-flow extraction with supercritical CO_2.

Aza-Henry Reactions

Bernhard Westermann* ——— **151 – 153**

Asymmetric Catalytic Aza-Henry Reactions Leading to 1,2-Diamines and 1,2-Diaminocarboxylic Acids

Keywords:
asymmetric synthesis · aza-Henry reactions · diamines · Lewis acids · Mannich reactions



In the wake of the aldol and Mannich reactions, textbook examples of asymmetric reactions, comes the aza-Henry reaction (aka nitro-Mannich reaction), which leads to 1,2-diamines or α,β-diaminocarboxylic acids (see scheme, PG = protecting group). Recent developments point to a bright future for this transformation.

 © 2003 Wiley-VCH Verlag GmbH & Co. KGaA, Weinheim 1433-7851/03/4202-0132 $ 20.00+.50/0

Reviews



All sorts of improvements to heterogeneous catalysts are possible through surface organometallic chemistry. This method allows the structures of complexes grafted onto silica surfaces to be studied (see scheme). From this data, the elementary steps of the catalytic process can be deduced and structure–activity relationships developed, which results in a better understanding of the catalytic process.

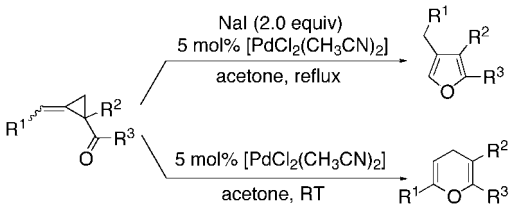
Surface Organometallic Chemistry

Christophe Copéret,* Mathieu Chabanas, Romain Petroff Saint-Arroman, Jean-Marie Basset* ——— **156 – 181**

Homogeneous and Heterogeneous Catalysis: Bridging the Gap through Surface Organometallic Chemistry

Keywords:
heterogeneous catalysis · organometallic chemistry · silica · surface chemistry · transition metals

Communications



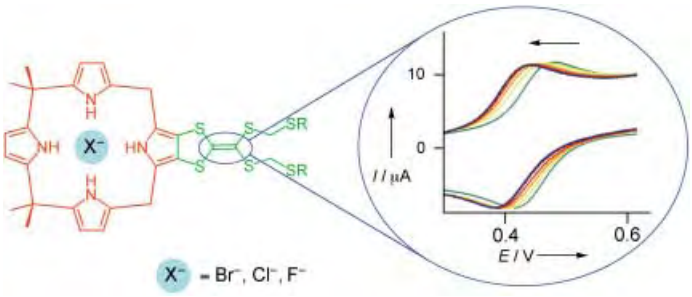
Useful building blocks are formed in this $[PdCl_2(CH_3CN)_2]$-catalyzed regioselective isomerization reaction of alkylidene cyclopropyl ketones, in which a dramatic salt effect was observed. In the presence of NaI, the reaction in refluxing acetone afforded furans, while 4*H*-pyrans were formed at RT in the absence of NaI (see scheme).

Regioselective Cyclization

Shengming Ma,*
Junliang Zhang ——— **184 – 187**

Tuning the Regioselectivity in the Palladium(II)-Catalyzed Isomerization of Alkylidene Cyclopropyl Ketones: A Dramatic Salt Effect

Keywords:
cyclization · isomerization · palladium · salt effect · small ring systems



A redox-responsive receptor based on the annulation of the calix[4]pyrrole-receptor unit and the redox-active tetrathiafulvalene transducer unit is able to bind anions (see scheme) and act as an efficient chemosensor for the detection of anions by electrochemical means.

Electrochemical Sensors

Kent A. Nielsen, Jan O. Jeppesen,*
Eric Levillain, Jan Becher* ——— **187 – 191**

Mono-Tetrathiafulvalene Calix[4]pyrrole in the Electrochemical Sensing of Anions

Keywords:
anions · cyclic voltammetry · porphyrinoids · receptors · sensors

For the USA and Canada:
ANGEWANDTE CHEMIE International Edition (ISSN 1433-7851) is published weekly by Wiley-VCH PO Box 191161, D 69451 Weinheim, Germany. Air freight and mailing in the USA by Publications Expediting Inc. 200 Meacham Ave., Elmont, NY 11003. Periodicals postage paid at Jamaica NY 11431. US POSTMASTER: send address changes to *Angewandte Chemie*, Wiley-VCH, 605 Third Ave, New York, NY 10158-0012. Annual institutional subscription price for institutions: Europe € 2998.00/3148.00. Outside Europe US$ 3718.00/3904.00 (valid for print or electronic/print and electronic delivery); for individuals who are personal members of a national chemical society, or whose institution already subscribes, or who are retired or self-employed consultants, print only (including postage and handling charges): Europe € 248.00/Outside Europe US$ 348.00.

 © 2003 Wiley-VCH Verlag GmbH & Co. KGaA, Weinheim 1433-7851/03/4202-0133 $ 20.00+.50/0

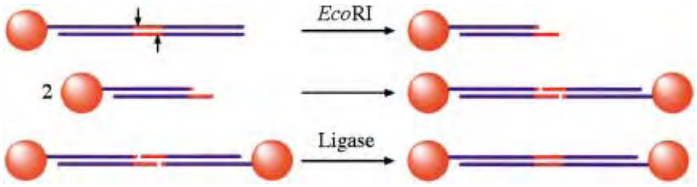
Contents

Gold/DNA Nanostructures

Antonios G. Kanaras, Zhenxin Wang, Andrew D. Bates, Richard Cosstick, Mathias Brust* ——— **191 – 194**

Towards Multistep Nanostructure Synthesis: Programmed Enzymatic Self-Assembly of DNA/Gold Systems

Keywords:
DNA · enzymes · gold · nanostructures · self-assembly



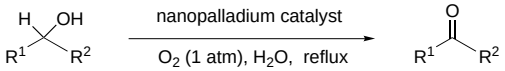
Enzyme-dependent assembly of DNA/gold nanostructures is achieved using DNA-capped gold colloids and DNA processing enzymes. Particle-bound DNA double strands are cleaved at designated sites by a restriction endonuclease (see picture). In a subsequent step the particles are linked to each other through these activated sites by a DNA ligase. This new strategy enables the multistep synthesis of nanostructures.

Oxidation of Alcohols in Water

Yasuhiro Uozumi,* Ryu Nakao ——— **194 – 197**

Catalytic Oxidation of Alcohols in Water under Atmospheric Oxygen by Use of an Amphiphilic Resin-Dispersion of a Nanopalladium Catalyst

Keywords:
catalysts · nanoparticles · oxidation · palladium



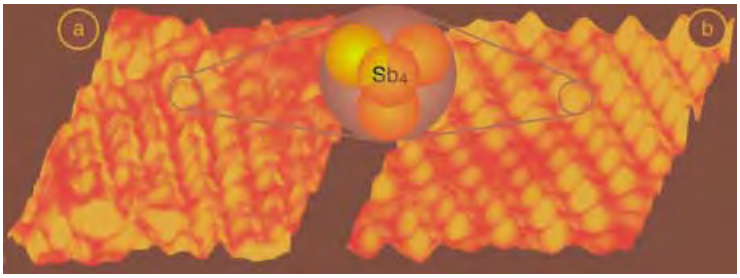
A step closer to the ideal oxidation of alcohols: Catalytic oxidation of alcohols in water under atmospheric oxygen was achieved by use of an amphiphilic resin-dispersion of a nanopalladium catalyst (see scheme). This system combines high catalytic activity owing to the large surface area of the nanoparticles and water-based reactivity provided by the amphiphilicity of the polystyrene—poly(ethylene glycol) matrix.

Antimony Tetramers

Thorsten M. Bernhardt, Bert Stegemann, Bernhard Kaiser,* Klaus Rademann ——— **199 – 202**

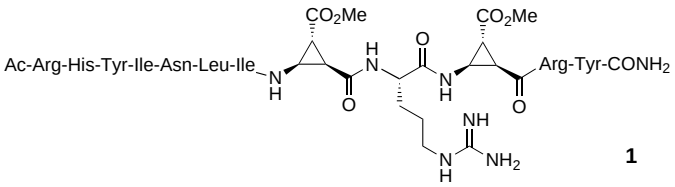
Crystalline Structures of Sb_4 Molecules in Antimony Thin Films

Keywords:
antimony · scanning probe microscopy · structure elucidation · surface analysis · thin films



Sb_4: The building block of a new solid-state modification of antimony. This is a somewhat provocative description of the fact that nanocrystalline structures of Sb_4 tetrahedrons exist on the substrates $AuSb_2(100)$ and $MoS_2(0001)$. Scanning tunneling microscopy images (see picture, ⓐ and ⓑ, respectively, each 39×39 Å^2) of thin amorphous antimony films show such local well-ordered areas with nearly cubic symmetry.

© 2003 Wiley-VCH Verlag GmbH & Co. KGaA, Weinheim
1433-7851/03/4202-0134 $ 20.00+.50/0



1

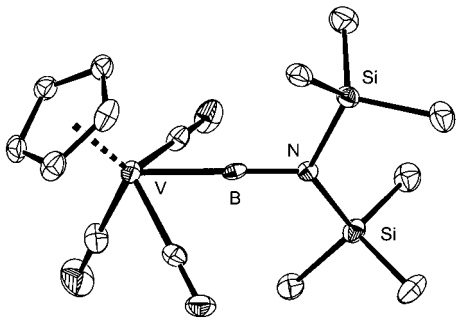
Conformationally Restricted Peptides

Norman Koglin, Chiara Zorn, Raphael Beumer, Chiara Cabrele, Christian Bubert, Norbert Sewald, Oliver Reiser,* Annette G. Beck-Sickinger* ——— 202 – 205

Analogues of Neuropeptide Y Containing β-Aminocyclopropane Carboxylic Acids are the Shortest Linear Peptides That Are Selective for the Y_1 Receptor

Unique, conformationally restricted β-amino acids are a constituent of truncated linear peptides such as **1**, which have been obtained for the first time; these species show high and selective affinity toward the Y_1 receptor. The high affinity of these ligands is dependent on the position and the configuration of this β-aminocyclopropane carboxylic acid.

Keywords:
amino acids · peptides · peptidomimetics · small ring systems · structure-activity relationships



1

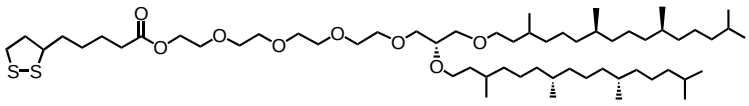
Borylene Half-Sandwich Complexes

Holger Braunschweig,* Miriam Colling, Chunhua Hu, Krzysztof Radacki ——— 205 – 208

$[(\eta^5\text{-}C_5H_5)(OC)_3V{=}B{=}N(SiMe_3)_2]$: A Half-Sandwich Complex with a Terminal Borylene Ligand

A vanadium–boron distance of 1.971 Å characterizes the first classical bond between these two elements. The novel half-sandwich complex **1** was obtained from $[(OC)_5Cr{=}B{=}N(SiMe_3)_2]$ by photochemically induced intermetallic borylene transfer.

Keywords:
boron · borylene complexes · sandwich complexes · vanadium



1

Model Systems for Membranes

Stefan M. Schiller,* Renate Naumann, Katherine Lovejoy, Horst Kunz, Wolfgang Knoll ——— 208 – 211

Archaea Analogue Thiolipids for Tethered Bilayer Lipid Membranes on Ultrasmooth Gold Surfaces

Simple vesicle fusion allowed the formation of a bilayer lipid membrane from the self-assembled monolayer of lipoic acid ester **1** (see formula). Film thicknesses determined by surface plasmon resonance (SPR) spectroscopic measurements agree with the theoretical thicknesses of the stretched conformation. Electrochemical impedance spectroscopy (EIS) of the model system shows that the latter exhibits similar electrical properties to biological membranes.

Keywords:
gold · lipids · membranes · monolayers · self-assembly

 © 2003 Wiley-VCH Verlag GmbH & Co. KGaA, Weinheim 1433-7851/03/4202-0135 $ 20.00+.50/0

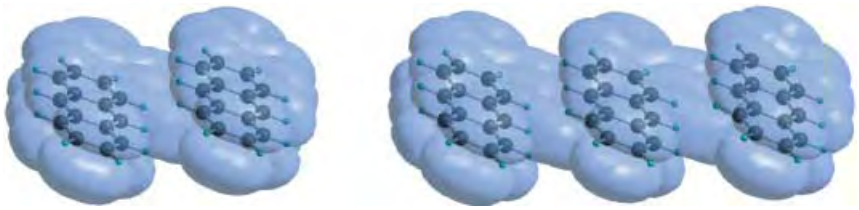
Contents

Delocalization in Arene Clusters

Jae Kyu Song, Nam Ki Lee, Seong Keun Kim* ——— **213 – 216**

Multiple Ion Cores in Anthracene Anion Clusters

Keywords:
anions · anthracene · density functional calculations · photoelectron spectroscopy



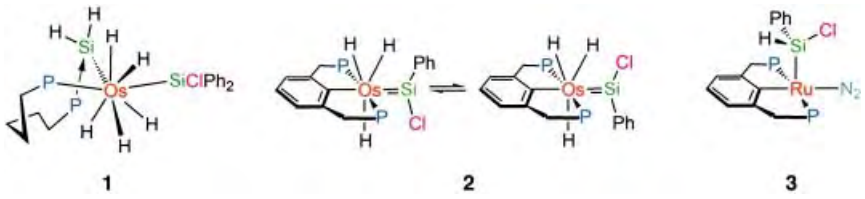
Spreading the charge: Anion clusters of anthracene, $(An)_n^-$, with n values of up to 6 were studied and found to contain a distinctly monomeric, dimeric, or trimeric ion core with a delocalized electronic charge (see figure). Coexistence of dimeric and trimeric ion cores was observed in $(An)_4^-$, but the ion core reverts to a monomeric one in $(An)_5^-$, with the completion of a solvation shell around the monomer anion.

Migration/Redistribution

Dmitry G. Gusev,* Frédéric-Georges Fontaine, Alan J. Lough, Davit Zargarian* ——— **216 – 219**

Polyhydrido(silylene)osmium and Silyl(dinitrogen)ruthenium Products Through Redistribution of Phenylsilane with Osmium and Ruthenium Pincer Complexes

Keywords:
hydrides · osmium · pincer ligands · silanes · silylene ligands



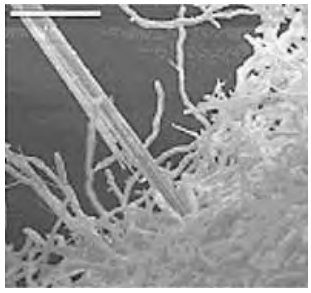
Migration/Redistribution Galore! The reaction of phenylsilane with a series of Os and Ru pincer complexes has led to the isolation of complexes **1**–**3**, thus allowing the direct observation of 1,2-addition and redistribution reactions that are so fundamental in the transformations of organosilanes in catalysis. Complex **1** represents a rare example of a complex containing a donor-stabilized SiH_2 ligand.

Asbestos Decontamination

Elena Martino, Laura Prandi, Ivana Fenoglio, Paola Bonfante, Silvia Perotto,* Bice Fubini* ——— **219 – 222**

Soil Fungal Hyphae Bind and Attack Asbestos Fibers

Keywords:
asbestos · biodecontamination · chelates · iron · siderophores



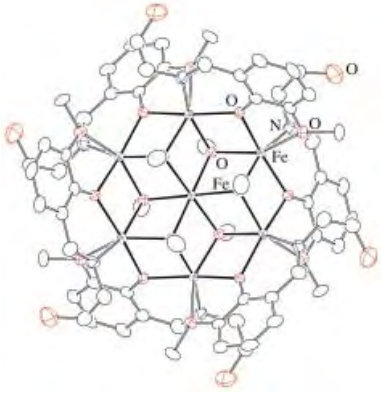
Possible agents for the decontamination and bioremediation of asbestos-polluted soils: selected soil fungi modify and bind asbestos fibers. The picture shows a single asbestos fiber in intimate contact with the hyphae of *Fusarium oxysporum* (the bar in the upper left corresponds to 20 μm). The fungi produce metal chelators which extract iron ions from the fibers.

High-Spin Iron Wheels

Hiroki Oshio,* Norihisa Hoshino, Tasuku Ito, Motohiro Nakano, Franz Renz, Philipp Gütlich ——— **223 – 225**

High-Spin Wheel of a Heptanuclear Mixed-Valent $Fe^{II,III}$ Complex

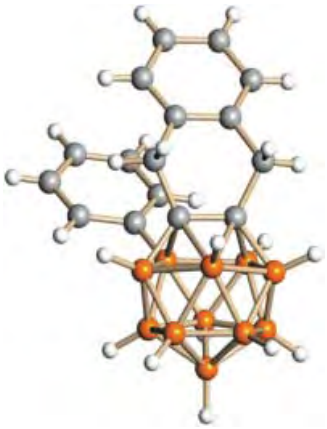
Keywords:
cluster compounds · high-spin molecules · iron · magnetic properties · mixed-valent compounds



Wheels with high spins: The reaction of a tridentate Schiff base ligand with iron(II) chloride, and subsequent oxidation with $[(tBu_4N)MnO_4]$ yielded a heptanuclear mixed-valent iron wheel (see picture) with a spin ground state of $S = 29/2$.

© 2003 Wiley-VCH Verlag GmbH & Co. KGaA, Weinheim
1433-7851/03/4202-0136 $ 20.00+.50/0

Cornering the 13th vertex: The first 13-vertex carborane (see picture, B: brown, C: gray, H: white) has been prepared by a methodology that can in principle be applied repeatedly, leading to 14-, 15-, 16-, ... vertex carboranes in the future. The 13-vertex species has a henicosahedral geometry, not the docosahedral one expected, but the two forms are found to be very close in energy by DFT calculations.

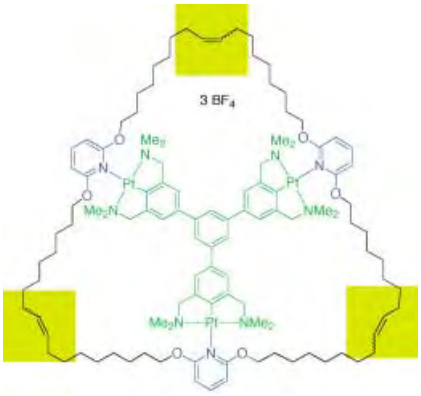


Carborane Cages

Anthony Burke, David Ellis, Barry T. Giles, Bruce E. Hodson, Stuart A. Macgregor, Georgina M. Rosair, Alan J. Welch* _____ 225 – 228

Beyond the Icosahedron: The First 13-Vertex Carborane

Keywords:
boron · carboranes · density functional calculations · structure elucidation · synthetic methods



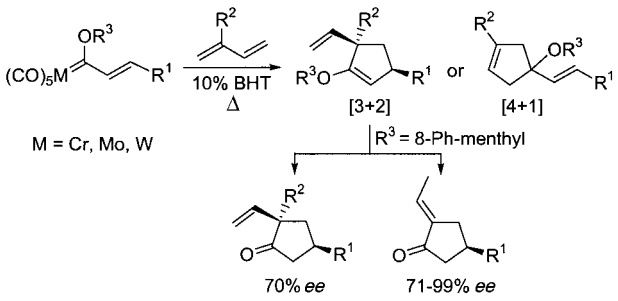
A 69-membered ring (see picture) results from a metathesis reaction that uses a metalated tris(pincer)-substituted benzene as scaffold. The macrocyclic product can be detached by the addition of Cl^- after which the template is recovered quantitatively.

Giant Rings

Aleksey V. Chuchuryukin, Harm P. Dijkstra, Bart M. J. M. Suijkerbuijk, Robertus J. M. Klein Gebbink, Gerard P. M. van Klink, Allison M. Mills, Anthony L. Spek, Gerard van Koten* _____ 228 – 230

Macrocycle Synthesis by Olefin Metathesis on a Nanosized, Shape-Persistent Tricationic Platinum Template

Keywords:
macrocyclic ligands · metathesis · N ligands · platinum · template synthesis



Regio- and stereochemically controlled formation of cyclopentenes has been achieved through the reaction of transition-metal–alkoxy(alkenyl)carbene complexes and neutral 1,3-dienes (see scheme; BHT = 2,6-di-*tert*-butyl-4-methylphenol). Reaction conditions dictate whether [3+2] or [4+1] cycloaddition products are obtained; alkenyl-substituted cyclopentanones of high enantiomeric purity are synthesized by using 8-phenylmenthyloxycarbene complexes.

Controlled Cycloadditions

José Barluenga,* Salomé López, Josefa Flórez _____ 231 – 233

[3+2] and [4+1] Cycloaddition Reactions of Fischer Alkoxy(alkenyl)carbene Complexes with Electronically Neutral 1,3-Dienes

Keywords:
asymmetric synthesis · carbene ligands · cycloaddition · cyclopentenes · diene ligands

 © 2003 Wiley-VCH Verlag GmbH & Co. KGaA, Weinheim 1433-7851/03/4202-0137 $ 20.00+.50/0

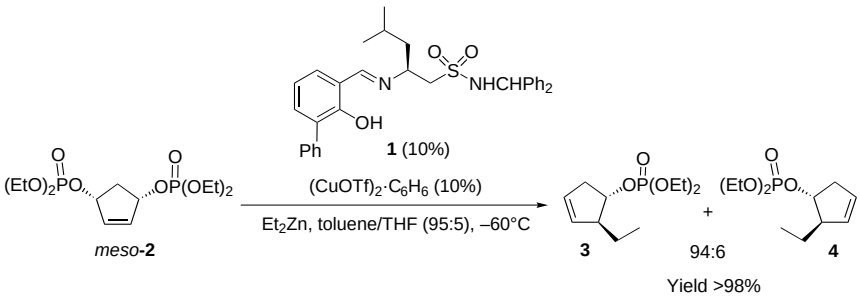
Contents

Desymmetrization of meso Compounds

Umberto Piarulli,* Philippe Daubos, Christelle Claverie, Maryline Roux, Cesare Gennari* ——— **234 – 236**

A Catalytic and Enantioselective Desymmetrization of *meso* Cyclic Allylic Bisdiethylphosphates with Organozinc Reagents

Keywords:
alkylation · asymmetric synthesis · copper · organophosphates · zinc



The chosen one: The desymmetrization of *meso*-**2** is possible with the use of diethylzinc in the presence of the Cu^{I} complex of **1** (10 mol%; Tf = CF_3SO_2). Ligand **1** was optimized from a screen of a library of 125 compounds. Other ligands from the same library favor the formation of the opposite enantiomer **4**.

VIP Communications labeled with this symbol have been judged by two referees as being "very important papers".

The publication of Communications labeled with this symbol has been accelerated because of their topical or highly competitive nature.

Supporting information for articles labeled with this symbol can be found at www.angewandte.org or www.interscience.wiley.com.



News in *Angewandte Chemie*?

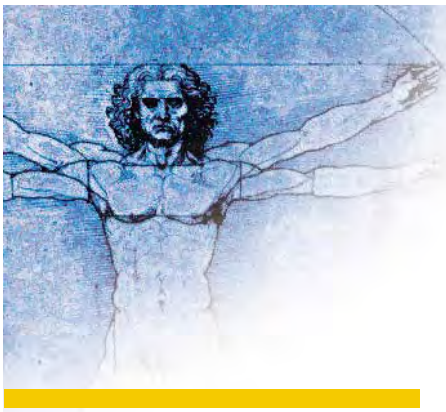
The aim of this section is to bring the scientific community closer together. The focus will be on international and interdisciplinary events, moves and awards. News items will include references to current articles in our family of journals.

Service

Classified ——— *155*
Keywords ——— *238*
Authors ——— *239*
Angewandte's Sister Journals ——— *240*
Sources ——— *A1*
Preview ——— *241*

© 2003 Wiley-VCH Verlag GmbH & Co. KGaA, Weinheim

1433-7851/03/4202-0138 $ 20.00+.50/0



Dieter Seebach and Shū Kobayashi Receive Nagoya Medals

The Nagoya Medals are awarded every year to an organic chemist who has made significant original contributions to the field in its broadest sense (gold, since 1995), and to a relatively young Japanese scientist whose research has a major impact on the field of synthetic organic chemistry (silver, since 1999). This year, the medals were presented to

- Prof. **Dieter Seebach**, ETH Zurich (Gold Medal). Seebach earned his doctorate under the guidance of Rudolf Criegee in 1964 and spent two years as a postdoc in the group of E. J. Corey. His contributions to organic synthesis include textbook classics (umpolung, natural product syntheses, Ti and Zr catalysts for chemoselective asymmetric carbonyl alkylations, TADDOLs,[1] β-peptides,[2]…), especially on the understanding of chirality. He is one of the world's most frequently cited chemistry authors.



D. Seebach

- Prof. **Shū Kobayashi**, University of Tokyo (Silver Medal), was recognized for his research on Lewis acid and other catalysts,[3] some of which may be used in micellar aqueous media or microcapsules.



S. Kobayashi

Amatore, Basset, and Raveau Elected Members of the Académie des Sciences

The prestigious French Academy of Sciences, which dates back as far as 1666, has three new members in its chemistry and materials chemistry sections:

- **Bernard Raveau**, Professor of Chemistry at the Université de Caen (Normandy, France), Member of the International Advisory Board of *Angewandte Chemie*. His main topics of research are the synthesis and study of high-T_c superconductive oxides and magnetic and ferroelectric compounds.
- **Christian Amatore**, Director of the Chemistry Department of the Ecole Normale Supérieure (Paris), Member of the Editorial Board of *ChemPhysChem*. His research is focused on microelectrodes and the theory of molecular electrochemistry.[4] Amatore is the Guest Editor of *ChemPhysChem*'s upcoming special issue on electrochemistry.
- **Jean-Marie Basset**, CNRS Research Director at CPE Lyon. His group's research is devoted to surface organometallic chemistry, especially the creation of structurally uniform active sites with catalytic properties. See his review in this issue.

German President's "Future Award" for Two Chemists

The Prize for Technology and Innovation ("Future Award") was awarded to Prof. **Maria-Regina Kula**[5] (FZ Jülich) and PD **Martina Pohl**[6] for their research on "Gentle Chemistry with Biological Catalysts" by the President of the Federal Republic of Germany.



M.-R. Kula

As a result of the efforts of the prize winners, enzymes can today be extracted from cells in a pure form to be used in industrial processes. Moreover, they developed a method for the continuous recycling of coenzyms, such as for the enzymatic production of leucine through the use of formiate dehydrogenase. NADH is additionally fixed on a membrane. Further optimization including rational protein design led to the large-scale economic use of enzymes and coenzymes today.



M. Pohl

Seeberger Moves from the MIT to Zurich

Peter Seeberger, currently a Firmenich associate professor of Chemistry at the MIT, will succeed Dieter Seebach as a professor of Organic Chemistry at ETH Zurich (Switzerland) on April 1, 2003.

Seeberger earned his Ph. D. in biochemistry under the guidance of Marvin H. Caruthers (Boulder, CO, 1995). After a postdoctoral fellowship with Samuel J. Danishefsky at the Sloan–Kettering Institute for Cancer Research in New York, he moved to the MIT in January 1998. His research is focused on the interface of biology and chemistry, in particular on the role of carbohydrates and glycoconjugates in information transfer. Research projects include the automated synthesis of glycoconjugates, the preparation of carbohydrate arrays, and drug development (such as a malaria vaccine).[7]

[1] D. Seebach, A. K. Beck, A. Heckel, *Angew. Chem.* **2001**, *113*, 96; *Angew. Chem. Int. Ed.* **2001**, *40*, 92.
[2] J. V. Schreiber, J. Frackenpohl, F. Moser, T. Fleischmann, H.-P. E. Kohler, D. Seebach, *ChemBioChem* **2002**, *3*, 424.
[3] R. Akiyama, S. Kobayashi, *Angew. Chem.* **2002**, *114*, 2714; *Angew. Chem. Int. Ed.* **2002**, *41*, 2602.
[4] C. Amatore, Y. Bouret, E. Maisonhaute, J. I. Goldsmith, H. D. Abruña, *ChemPhysChem* **2001**, *2*, 130.
[5] L. Krieg, M. B. Ansorge-Schumacher, M.-R. Kula, *Adv. Syth. Catal.* **2002**, *344*, 965.
[6] M. Pohl, B. Lingen, M. Müller, *Chem. Eur. J.* **2002**, *8*, 5288.
[7] H. A. Orgueira, A. Bartolozzi, P. Schell, P. H. Seeberger, *Angew. Chem.* **2002**, *114*, 2232; *Angew. Chem. Int. Ed.* **2002**, *41*, 2128.

 © 2003 Wiley-VCH Verlag GmbH & Co. KGaA, Weinheim 1433-7851/03/4202-0139 $ 20.00+.50/0

Protein Design at the Crossroads of Biotechnology, Chemistry, Theory, and Evolution**

Rainer Jaenicke* and Reinhard Sterner*

In the biosciences, the statement that progress in science is driven by progress in methodology has hardly ever been more evident than in the case of W. Arber's site-directed mutagenesis of proteins. It has revolutionized the "specific chemical modification" of early days, securing DNA-based specificity and allowing engineering and large-scale production of recombinant proteins. With the advent of complete genome sequences and structural bioinformatics,[1] physical biochemists are presently facing the task of finding the relationship between information at the DNA level, on the one hand, and the 3D structure, function and stability at the protein level, on the other. Routes to predict protein structure and to tailor "new and better proteins" with desired functional and physical properties have been explored during the last decade. However, the results were often disappointing, as present knowledge about the molecular principles of the self-organization, function and stability of proteins is still rudimentary, in spite of the >10000 3D structures solved and of the millions of mutants studied with respect to their biochemical and biophysical properties. Novel methods of directed in vitro protein evolution hold great promise to open new horizons.[2,3] To exploit this potential, a Titisee Conference of the Boehringer Ingelheim Fonds (with F. X. Schmid, Bayreuth and R. Sterner, Köln as organizers) brought together researchers from a variety of experimental and theoretical fields, to encourage closer interactions between groups involved in new strategies for the design of proteins, in the context of both basic and applied protein science. Topics included a) knowledge-based structure prediction, classification and design, b) protein stability and stabilization, and c) protein–protein or protein–ligand interactions and enzyme catalysis. Space only allows us to highlight a selection of the presentations; inevitably they reflect the reviewers preferences. To summarize the whole program, the excellent choice of speakers and the generosity of the sponsoring organization made the conference unique both in its scientific standards and its personal atmosphere.

At first sight, to start with regulated intramembrane proteolysis might appear surprising, given the topic of the meeting. However, the lecture given by R. T. Sauer (Cambridge, MA, USA) amply illustrated the level of complexity accessible to present-day cellular biochemistry, covering the whole spectrum of strategies available for the elucidation of the structural, energetic and functional details of stress-induced protein degradation as a basic phenomenon in proteomics.[4] S. Benkovic (Pennsylvania State University, PA, USA) in his "Perspective on Biological Catalysis" presented the complete kinetic scheme and the complementary structural details of the mechanism of dihydrofolate reductase, the central enzyme in folate biosynthesis and, for this reason, an important target in the treatment of cancer and infectious diseases. Stopped-flow kinetics together with the 3D structure of mutants not only allowed the differentiation between a closed and an open state of the active site and between rate constants of transconformation and hydrogen transfer, but also the localization of positions in- and outside the active site which are involved in the catalytic mechanism. Restriction–modification systems are the working horses of recombinant gene technology. In vivo they serve to protect the cell against foreign DNA by recognizing short palindromic DNA sequences in a concerted manner. As cleavage at noncognate sites would be lethal to the cell, restriction enzymes (REs) are among the most specific enzymes known. A. Pingoud (Gießen, Germany) reported attempts to change RE specificity by using non-natural target DNA sequences or by rational protein design and directed evolution. The aim of his ongoing studies is to create programmable REs exhibiting sequence specificities which can be altered by a variable interchangeable determinant. Such enzymes would be extremely useful for the analysis of large genomes.

Since the middle of the 1990s, confidence in the perspective that natural proteins might carry a potential for functional improvements of technically relevant proteins came mainly from hyperthermophilic enzymes. The lessons they taught us have been applied to enhance protein stability, either by rational or evolutionary protein design.[2,5] Focusing on the correlation of structure, stability and function, M. J. Danson (Bath, UK), presented a systematic study on the dimeric enzyme citrate synthase from different organisms with optimal growth temperatures between 10 and 100 °C, supporting the view that the 3D structures are highly conserved regardless a wide range of sequence variations. In accordance with studies reported by R. Ladenstein (Stockholm, Sweden), intra- and intermolecular ionic interactions, particularly in the form of ionic networks, seem to be essential for protein ultrastability. However, there is no doubt that contributions of other types of weak interactions also play a significant role.[5] At this point it is important to note that thermostability does not guarantee thermoactivity; rather, thermal inactivation may significantly precede thermal denaturation. On the other hand, the protein inventory of a specific organism does not necessarily reflect the optimum conditions of its environment; rather, individual proteins in one and the same species may differ widely in their intrinsic stabilities. The general view that

> *"Protein engineering and directed evolution methods are suitable methods to optimize [the] stability and efficiency [of enzymes], or even to alter their specificity."*

[*] R. Jaenicke
Birkbeck College, University of London, London (UK)
R. Sterner
Institut für Biochemie, Universität Köln, Köln (Germany)

[**] 86th International Titisee Conference, held in Titisee, Black Forest, October 23–27, 2002

 © 2003 Wiley-VCH Verlag GmbH & Co. KGaA, Weinheim 1433-7851/03/4202-0140 $ 20.00+.50/0

enzymes, because of the reduced consumption of water, energy and harmful chemicals, are the natural solution to industrial problems was put forward by T. V. Borchert (Bagsvaerd, Denmark), who gave a perspective over a wide range of applications and unexpectedly profitable developments during the last couple of years. Evidently, the naturally occurring enzymes do not always display the characteristics required in an industrial application, so that protein engineering and directed evolution methods are necessary to optimize their stability and efficiency, or even to alter their specificity. Industrially relevant examples in this context are the production of cyclodextrin from starch by converting α-amylase into cyclodextrin glycosyltransferase and the production of thermally stable subtilisins with high catalytic activity in the presence of organic solvents. Along the same lines, nature does not provide enantiopure compounds required for pharmaceutical purposes, because the natural enantioselectivity of enzymes is not sufficiently high. K.-E. Jaeger (Düsseldorf, Germany) demonstrated how the combination of various mutagenesis techniques (error-prone PCR, DNA shuffling, combinatorial cassette mutagenesis) with high-throughput screening is able to significantly improve the natural specificity. In the case of bacterial lipases, X-ray data, combined with molecular modelling and molecular dynamics calculations, allowed the rationalization of the effect of specific amino acid exchanges as a first step toward a detailed understanding of the structural basis of enantioselectivity.

A novel in vivo screening system allowing the rapid detection of protein folding and stability variants in the cytoplasm of *Escherichia coli* was reported by R. Glockshuber (Zürich, Switzerland). It makes use of fluorescence resonance energy transfer (FRET), and is based on the simultaneous fusion of the green (GFP) and blue (BFP) fluorescent proteins to the C- and N-terminal ends of a protein X, to be studied in its folding properties. Efficient FRET from BFP to GFP in the ternary fusion protein is only observed in vivo if X is folded, this way bringing BFP and GFP into close proximity, while FRET is lost when the two signal proteins are far apart due to unfolding or intracellular degradation. Applying the system to antibody V_L intradomains differing in their thermodynamic stabilities revealed a strong correlation between V_L stability and resistance against intracellular proteolysis.

An important goal of protein design has been the generation of polypeptide chains that specifically bind to ligands such as metal ions, organic molecules and peptides. Antibodies have been optimised by evolution to serve this purpose. Attempts to experimentally improve their specificity and affinity down to nM binding constants for various ligands were successful. However, their application still presents practical problems caused mainly by their large size and their laborious production in *E. coli* as a host. Therefore, various alternative protein scaffolds have been tailored as "binding templates". In this context, H. Kolmar (Göttingen, Germany) demonstrated how the small and extremely stable cystine-knot miniprotease inhibitors, which are held together by three intramolecular disulfide bonds, can be used as scaffolds. As a proof of concept, from a library of a cystine-knot miniprotease inhibitors (produced by randomization of the protease inhibitor loop and presented at the surface of *E. coli* cells), variants with a high-affinity binding to an antibody were isolated by fluorescence activated cell sorting. A. Skerra (München-Freising, Germany) summarized approaches towards the redesign of lipocalins for ligand binding, using rational design and directed evolution. Natural lipocalins contain a circularly closed eight-stranded anti-parallel β-sheet that supports four loops at one of its ends, thus forming the entrance to the ligand binding pocket. In a rational design approach, the Zn^{2+} binding site of carbonic anhydrase was grafted onto the retinol-binding protein. The engineered protein displayed high Zn^{2+} affinity and specificity. In the directed evolution approach, 16 amino acids from a bilin-binding protein were randomized, and variants capable of binding to fluorescein as a model hapten were isolated via phage display. X-ray data of various lipocalins revealed a high plasticity in their loop regions, suggesting that they provide a versatile framework capable of binding chemically diverse ligands.

The optimisation by design of peptide–protein and protein–protein interactions can be of significant pharmacological relevance, as was highlighted in the contributions by A. Beck-Sickinger (Leipzig, Germany) and H. Lilie (Halle, Germany). A. Beck-Sickinger described the use of fluorescence techniques to study the interaction of neuropeptide Y, a crucial player in the control of feeding, with its various G-protein coupled receptors. By systematically replacing all amino acids of the protein with L-alanine, several residues crucial for receptor binding were identified, using an elegant approach based on the induced expression of the green fluorescent protein and fluorescence-activated cell sorting. H. Lilie gave a progress report on systems for gene therapy in which viruslike capsid particles loaded with therapeutics are guided to specific tumor cells. The idea is to mediate the interaction between capsids and tumor cells by fusing the eye lens protein γ-crystallin to the capsid coat protein. The four β-sheets of γ-crystallin will then be redesigned in order to allow for its binding to tumor-specific marker proteins. In a proof of principle experiment, from a library of γ-crystallins, produced by the randomization of eight amino acids, a variant with an extremely high binding affinity to an IgG antibody was isolated.

Our knowledge on the sequence–structure–function relationship of proteins is still sparse, which makes the rational design of proteins often frustrating. However, some important progress has been made and is now being integrated into computer programs, supporting the planning and analysis of protein design experiments. In particular, algorithms modeling the conformation of amino acids by searching rotamer libraries recently yielded promising results presented by H. W. Hellinga (Durham, NC, USA), S. L. Mayo (Pasadena, CA, USA) and W. Haehnel (Freiburg, Germany). H. W. Hellinga summarized the computer-guided reconstruction of periplasmic binding protein to bind various neurotransmitters, metabolites, drugs, chemical threats and even the explosive TNT with extremely high affinity and selectivity. S. L. Mayo de-

 © 2003 Wiley-VCH Verlag GmbH & Co. KGaA, Weinheim 1433-7851/03/4202-0141 $ 20.00+.50/0

scribed how the thioredoxin scaffold, which is catalytically inert, was used to yield an enzyme that promotes the nucleophilic hydrolysis of a *p*-nitrophenyl ester. A virtual combinatorial active-site scan was performed to identify favorable positions for the catalytic histidine as well as mutations necessary for substrate recognition and binding. The top two variants identified in this theoretical scan contained two and three amino acid exchanges. They were produced and showed significant esterase activity. In this context, W. Haehnel reported on successful examples of the generation of functional 4-helix-bundle proteins by combinatorial peptide synthesis. The peptide libraries were attached to specific sites of templates bound to cellulose membranes. Screening of the immobilized peptides by UV/Vis spectroscopy allowed the identification of proteins with His-ligated heme groups displaying increased redox potentials and enzymatic heme-oxygenase activity, on the one hand, and novel proteins with Cys-ligated copper centers, on the other. In a de novo design approach, rotamer selection was applied in order to allow for a computer-guided assembly of the hydrophobic core of a protein with a β-sandwich backbone structure. The formation of the structure was verified by FTIR spectroscopy.

Many contemporary enzymes display significant similarities with respect to sequence, structure and catalytic mechanism, suggesting that they are evolutionarily related.[6] A good example are enzymes with a $(\beta\alpha)_8$-barrel structure, which is a frequently encountered and catalytically versatile fold. Moreover, $(\beta\alpha)_8$-barrels provide an ideal scaffold for enzyme design, because the parts of the structure that are important for catalytic activity and for conformational stability are spatially separated. J. Gerlt (Urbana, IL, USA) and R. Sterner (Köln, Germany) showed how laboratory evolution can provide insights into the natural evolution of $(\beta\alpha)_8$-barrels. Using similar directed evolution approaches, namely the combination of random mutagenesis in vitro with genetic selection in vivo, the catalytic activities of $(\beta\alpha)_8$-barrel enzymes were replaced by the activities of evolutionarily related ones.

D. Hilvert (Zürich, Switzerland) demonstrated how genetic selection can be elegantly used to determine the minimal requirements for a functional fold.[7] Large degenerate libraries were prepared by replacing all secondary structure in the dimeric helical bundle chorismate synthase with simple binary-patterned modules based on a limited set of four polar and four nonpolar amino acids. Two-stage in vivo selection yielded catalytically active variants possessing biophysical and kinetic properties typical of the natural enzyme even though about 80% of the protein originated from the simplified modules and >90% of the protein consisted of only eight different amino acids. Thus, a quantitative assessment of the number of sequences compatible with a given functional fold was obtained. This strategy of combining chemical information with genetic selection may be generally useful in designing protein scaffolds with tailored activities.

"These are the questions that challenge those interested in the molecular principles of protein structure and stability."

In the closing lecture, A. Plückthun (Zürich, Switzerland) highlighted three approaches to new proteins developed in his laboratory during the last couple of years. To select and further evolve proteins to high affinity and stability, "ribosome display" has been developed to mimic Darwinian evolution in a cell-free system: Depending on the selection conditions employed, the molecular properties can be altered in a predictable direction. First experiments with synthetic antibodies, for which the structures of the evolved molecules were determined, made it possible to pinpoint molecular causes for the improved binding affinities and biophysical properties. After such an analysis, they can then be introduced by rational means. A second approach allows the development of new cysteine-free antibody-like molecules which greatly surpass antibodies in stability and expression yield in *E. coli*. These look highly promising for intracellular applications, e.g. as stable and selective inhibitors in proteomics applications. They are based on fully synthetic libraries of either ankyrin- or leucine-rich repeats that are naturally involved in tight protein–protein interactions. In work with synthetic ankyrin libraries, very rapid enrichment with ribosome display was observed in a variety of protein targets, presumably as a result of their efficient folding. Specific high-affinity binders could be obtained against a variety of targets. Functional inhibitors of the kanamycin resistance protein, a structural homolog of eukaryotic kinases, could be obtained. X-ray data demonstrated the success of the synthetic library design and suggests how the synthetic molecules also surpass the natural repeat proteins in biophysical properties. Finally, attempts were made to embark on the creation of new functional proteins without any structural precedent, based on the ligation of cassettes encoding secondary structures to produce proteins of about 100 amino acids. Eventually this may help to address some fundamental questions as to why there are so few different protein folds encoded in the known genomes. Evidently, these are the problems that challenge those interested in the molecular principles of protein structure and stability. However, the ultimate goal of protein design is to construct "better proteins" with specifically tailored properties. To accomplish this, a lot more basic research and development needs to be done. The 86th Titisee Conference not only provided a state-of-the-art overview of the present tools and trends, but also gave the participants sufficient time to exchange ideas on how to make use of them. It was indeed worth the effort.

[1] A. N. Lupas, R. B. Russel, A. Engel (Eds.), Structural Bioinformatics, *J. Struct. Biol.* **2001**, *134*, 93–282.

[2] F. H. Arnold (Ed.), *Adv. Prot. Chem.* **2001**, *55*, 1–450.

[3] S. Brakmann, K. Johnsson (Eds.), *Directed Molecular Evolution of Proteins*, Wiley-VCH, Weinheim, **2002**.

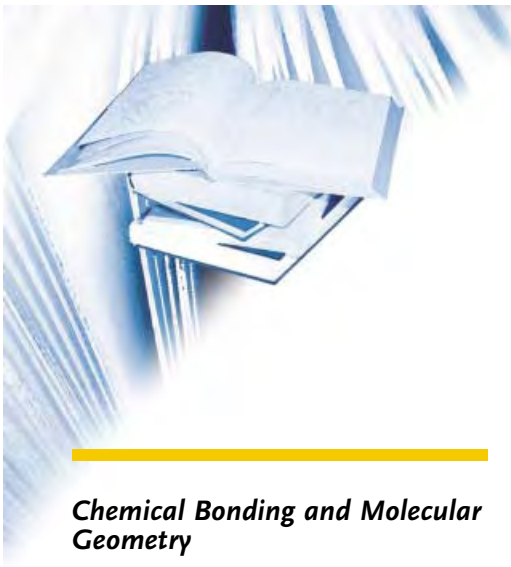
[4] F. Lottspeich, *Angew. Chem.* **1999**, *111*, 2630–2647; *Angew. Chem. Int. Ed.* **1999**, *38*, 2476–2492.

[5] M. W. W. Adams, R. M. Kelly (Eds.), *Methods Enzymol.* **2002**, *334*, 283–478.

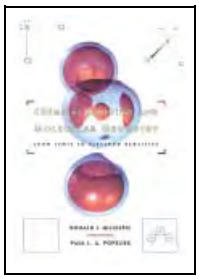
[6] J. A. Gerlt, P. C. Babbitt, *Annu. Rev. Biochem.* **2001**, *70*, 209–246.

[7] S. V. Taylor, P. Kast, D. Hilvert, *Angew. Chem.* **2001**, *113*, 3408–3436; *Angew. Chem. Int. Ed.* **2001**, *40*, 3310–3335.

 © 2003 Wiley-VCH Verlag GmbH & Co. KGaA, Weinheim 1433-7851/03/4202-0142 $ 20.00+.50/0



Chemical Bonding and Molecular Geometry



From Lewis to Electron Densities. By Ronald J. Gillespie and Paul L. A. Popelier. Oxford University Press, New York 2001. 268 pp., softcover $ 39.50.—ISBN 0-19-510496-X

The explanation of molecular geometries in terms of theoretical models is one of the most fundamental concepts in chemistry. Nearly every chemistry textbook devotes an introductory chapter to the question of how the geometrical arrangement of the atoms in a molecule can be rationalized by means of an ordering scheme, the rules of which should be as simple and comprehensive as possible. The search for an explanation of the shape of molecules has a long history, which has involved a large number of ad hoc models and other rules and models based on quantum chemistry. The well-known dilemma for students, particularly in the first semester, comes from the fact that, depending on the preference of the professor, several models for explaining molecular geometries may be discussed without explaining the connections and the frequent contradictions. It often happens that the MO and VB models, frontier orbitals and the HSAB concept, the octet rule and hybridization, the VSEPR model, and the Hückel rule are introduced without giving a deeper insight into their basic principles, which can easily lead to a state of resigned confusion. The situation becomes aggravated by the strong tendency of chemists to judge the value of a model more by its simplicity and ease of visualization than by how well it agrees with physical laws and quantum-theoretical insights. Although MO models have become important for understanding aromaticity and for the interpretation and prediction of pericyclic reactions, it cannot be said that the wavefunction has received much affection from chemists, despite its fundamental importance for chemical phenomena. The mathematical concept ψ is too abstract and too elusive for the human imagination to grasp to allow it to become the focus of orthodox chemistry, which instead strives for pictures that are accessible for the human senses.

The aim of this prologue is to try to characterize the intention of the book *Chemical Bonding and Molecular Geometry* by Ron Gillespie and Paul Popelier. The authors describe their attempt to explain in a consistent way the geometry of molecules using three complementary models or theories. The authors restrict their endeavor to molecules of the Main Group elements, because (p. 257) "the study of the shape of transition metal molecules in terms of the electron density distribution is still the subject of research and it has not reached a sufficient stage of development to enable us to discuss it in this book." The first of the three models is the VSEPR (valence shell electron pair repulsion) model, which in its original version was introduced in 1957 by Gillespie and Nyholm. The heuristic VSEPR model has become an important standard model for understanding the structure of inorganic molecular compounds. In this book it receives a quantum-chemical justification and interpretation that is based on the AIM (atoms in molecules) theory of Richard Bader, which is the second pillar of the models in this volume. Like Bader, the authors reject the wavefunction as a basis for the explanation of molecular geometries because it is not a physical observable and it cannot be measured by an experiment. They rather side with the electron density as the elementary basis for their models, because the analysis of the density is based on a physically observable property of the molecule. At this point the authors must be reminded of the ground-breaking publication by Heitler and London in 1927, which showed that the fundamental basis of the chemical bond is the resonance of the wavefunction, and it cannot be explained simply by the electron density. The latter is the *product* but not the *driving force* of the chemical bonding. That this finding can be ignored, while still obtaining a widely valid ordering scheme based on the electron density, is on the one hand a pleasing result when one seeks models based on considering simple analogies. On the other hand, however, it supports the deceptive idea that the origin of the chemical bond lies in the change of the electron density distribution. The third pillar of the models is the more recent LCP (ligand close packing) model which was introduced in 1997 and 1998 by Gillespie and Robinson.

"...the strong tendency of chemists to judge the value of a model more by its simplicitiy and ease of visualization than by how well it agrees with physical laws and quantum-theoretical insights."

The book is divided into nine chapters. Chapter 1, "The Chemical Bond: Classical Concepts and Theories", gives a short overview of the historical development of models of the chemical bond. It begins with the evolution of the Periodic System of the elements and the introduction of drawing a line as a symbol for a bond, and it ends with a critical discussion of the limitations of the Lewis model and the octet rule. It is noticeable that models which refer to the wavefunction are not mentioned at all. The $4n+2$ rule, which is based on the work of Hückel, is not even even mentioned, although the geometry and stability of aromatic compounds cannot be understood without considering the special role of π orbitals. Although one may concede that Gillespie as an inorganic chemist might have a biased viewpoint, there are several places in the book where the geometries of organic com-

 © 2003 Wiley-VCH Verlag GmbH & Co. KGaA, Weinheim 1433-7851/03/4202-0143 $ 20.00+.50/0

pounds are discussed in great detail. However, in those cases the authors carefully avoid bonding models that are based on orbitals.

Chapter 2, "Bond Properties", contains a critical discussion of elementary terms which are often used when the chemical bond is considered. These are bond distance, bond order, bond dissociation energy, force constant, dipole moment, etc. Especially noteworthy is the discussion about the connection between dipole moment and charge distribution. The authors show nicely that it is not possible to use the dipole moment, which is a vector, as an indicator for the molecular charge distribution, although this is often wrongly claimed. The electronic charge distribution in a molecule is highly anisotropic, and therefore it is also not possible to use atomic partial charges to estimate the ionic character of a bond. This part is well done and worth reading, but then on page 39 one finds some statements about the bonding situations in BF_3 and SiF_4 which involve contradictory and selective arguments. The authors say that the explanation of the shortness of the bonds in terms of resonance structures which have boron–fluorine and silicon–fluorine double bonds due to π backdonation would be inconsistent because this would lead to positive partial charges at the fluorine atom. The positive charges of the resonance structures would not agree with the calculated large negative values. Every relevant textbook, including the present work, explicitly points out that the partial charges of Lewis structures have only a formal meaning. "Formal charges may even be of opposite sign to the real charge" (p. 17). On page 39 the authors ignore what they say on page 17! In the second part of this chapter, under the heading "Resonance Structures", the authors introduce among others benzene, without addressing the question of why cyclobutadiene, which also has two equivalent resonance structures, has a rectangular geometry with two long and two short bonds.

Chapter 3, "Some Basic Concepts of Quantum Mechanics", is devoted to elementary concepts and ideas of quantum theory and to basic foundations of quantum-chemical methods such as MO and VB theory. The authors do not devote much attention to mathematical details but instead focus on the description of the most important principles and the understanding of the physical quantities. Particularly well done is the discussion about the importance of the Pauli exclusion principle, the relevance of which for the electronic structure of molecules is often neglected. Except for the final section, "Postscript", this chapter gives a concise and successful description of the elementary concepts of quantum chemistry. But then one reads (pp. 81–82): "The wave function … does not directly give us any understanding of the bonding or geometry of a molecule. To attempt to obtain such an understanding we need to interpret the wave function." This is followed (p. 82) by: "Alternatively, we can base our analysis on the electron density, which as we have seen, is readily obtained from the wave function … Because this analysis is based on a real physically observable property of a molecule, this approach appears to be more fundamental." It remains the secret of the authors why the electron density ϱ should be more fundamental than the wavefunction ψ, even though ϱ is determined by ψ and not vice versa. Since the publication by Heitler and London in 1927 we know that it is only the wavefunction that gives an explanation for the chemical bond, whereas all attempts to explain the chemical bond in terms of the electron density have failed. It is hard for human beings to accept that the fundamental principles of elementary quantities of science are not accessible to their sensory perception. It is at this point that the preference for "solid" observable quantities which is often found in chemistry becomes connected with the false statement that the latter has a higher status than a mathematical quantity. This part should be read with great caution! It is also appropriate at this point to mention that the electron density distribution is the *result* of chemical interactions but not their driving force.

> ***"At this point the authors must be reminded of the groundbreaking publication … which showed that the fundamental basis of the chemical bond is the resonance of the wavefunction, and it cannot be explaned simply by the electron density."***

Chapter 4 introduces the VSEPR model which is probably known to most readers. There have been some modifications since the time when the original version was published in 1957. The term "electron domain", which is the spatial region of a bonding or lone electron pair, has been introduced more recently. It becomes important in the context of the AIM theory which is discussed later. The authors make it clear that the repulsion of two electron domains comes mainly from Pauli repulsion and not from electrostatic forces. The other parts of this chapter are mainly concerned with comparing experimental bond angles with the predictions of the VSEPR model. The interpretation of the bonding situation and geometry of ethylene and substituted ethylenes is not convincing and ignores some facts. The construction of C_2H_4 from two CH_2 fragments in the triplet state, yielding two banana bonds ("bent bonds"), is comprehensible. However, the discussion of the bond angles of haloethylenes fails to mention that CX_2 (X = halogen) has a singlet ground state, and therefore $X_2C=CX_2$ should not be planar. When, finally, one even reads the statement (p. 106) that orbital models with σ and π bonds would not predict that ethylene is planar, it becomes clear that the viewpoint of the authors is very biased. This also becomes obvious from the discussion about the influence of electronegativity on the bond angle of AX_3 molecules (pp. 98–99). The decrease of the bond angle with higher electronegativity is explained by using the VSEPR model. There is only a discussion of those examples from Table 4.3 which agree with the VSEPR model, although the data show that on going from AH_3 to AF_3 the bond angle increases in the case where A is P, whereas it decreases where A is N or Sb. At the end of the chapter it is finally admitted that the VSEPR model may fail in two cases. These are molecules with ligand–ligand interac-

 © 2003 Wiley-VCH Verlag GmbH & Co. KGaA, Weinheim 1433-7851/03/4202-0144 $ 20.00+.50/0

tions and transition metal compounds. The second case is not discussed in the book. For the first case the authors recommend the LCP model, which is introduced in Chapter 5.

The LCP model (Chapter 5) is based on the observation that the ligand–ligand distances X–X in compounds AX_n, where A is an element of the first octal row and X is an electronegative element, have a remarkably constant value which is independent of the type of molecule. For example, the F–F distances in BF_3 und BF_4^- have the same value, 226 pm, and the F–F distance in CF_3^+ (216 pm) has nearly the same value as in CF_4 (215 pm). Also, the A–X bonds become longer when the coordination number is increased. From this the authors conclude that the ligands X are close-packed around the central atom A, and that the longer A–X distance in higher coordinated compounds is caused by ligand–ligand repulsion. It is suggested that the A–X distance of linear molecules AX_2 should be considered as the "natural" bond distance, which becomes longer in AX_3 because of steric repulsion. Accordingly, the longer C–F distance in CF_4 (131.9 pm) compared to CF_3^+ (124.4 pm) is not explained by the change from sp^3 to sp^2 hybridization but rather in terms of fluorine–fluorine repulsion. Considering the large number of quantum-chemical investigations which clearly show that the bond distance between two bonded atoms is determined primarily by their direct electronic interactions, the LCP model appears rather odd. The authors also have great difficulty in explaining why this model fails for heavier Main Group elements. For example, the A–X distances for A = Al, Si, P, S and X = F, Cl, O become shorter and not longer when the coordination number increases from four to six, and the P–F distance in PF_4^+ (145.7 pm) is significantly shorter than in PF_3 (157.0 pm) although the F–F distances are nearly the same. Although the LCP model is not very convincing here, the authors hail it as a step forward compared with the VSEPR model: "… the LCP model can be regarded as an extension and a refinement of the VSEPR model in which bond pair–bond pair repulsions are replaced by ligand–ligand repulsions" (p. 132).

"It remains the secret of the authors why the electron density should be more fundamental than the wavefunction, even though the electron density is determined by the wavefunction and not vice versa."

The AIM theory and the topological analysis of the electron density after Bader are introduced in Chapter 6. The second derivative of the electron density, the so-called Laplace distribution, is discussed separately in Chapter 7. The topological analysis of the electron density distribution which was developed by Richard Bader is, from the viewpoint of chemical models, perhaps the most attractive discipline of quantum theory, because many heuristic models of the prequantum time can be obtained by a mathematical treatment of the electron density in a quasi-natural way. Atoms in a molecule are derived as subdomains of the functional space of the electron density of molecules, and, more importantly, the bonding line between bonded atoms is revealed without making more or less arbitrary assumptions. The differences in the type of bonding, i.e., the difference between covalent and ionic interactions, can also be verified with this theory. The AIM theory has therefore become an important tool among other methods for analyzing the bonding situation in molecules. Proponents of the AIM theory prefer to see the results of the topologial analysis of the electron density not as complementary to chemical models and in particular to MO models, but rather as a substitute for them. However, this attempt has not been successful so far. Because the domains of electron concentration are very important for the AIM theory as well as for the VSEPR model, it is understandable that the two disciplines are connected. Chapters 6 and 7 summarize the most important definitions and results of the AIM theory.

"It is hard for human beings to accept that the fundamental principles of elementary quantities of science are not accessible to their sensory perception."

The two concluding chapters, 8 and 9, attempt to explain the geometries of compounds of Main Group elements on the basis of the above three models. It is reasonable that the molecules of the first octal row elements, whose coordination number is rarely larger than 4, are discussed separately in Chapter 8, while compounds of the heavier Main Group elements are discussed in Chapter 9. Chapter 8, after some introductory remarks, focuses on fluorides, chlorides, and hydrides of the elements lithium to carbon. The calculated atomic charges are then used as a basis for a superficial and biased presentation of the topic, with the headline "Polar Bonds and Ionic–Covalent Character" (p. 185), which also contains wrong statements. There is, for example, the assertion on page 187 that "… the attraction between the two atoms … in a pure covalent bond … is due only to the electron density accumulated between their nuclei". Although this explanation is frequently given, it is completely wrong! Here the dislike of the authors against considering the wavefunction goes so far that fundamental knowledge gained by quantum theory is simply ignored. This is followed by the attempt to prove the weakness of the concept of ionic and covalent bond using LiF and BF_3 as examples which, following the arguments of the authors, can only be solved with the AIM model. Because the atomic partial charges in BF_3 (fluorine: -0.81; boron: +2.43) suggest a stronger interatomic charge attraction than in LiF (fluorine: -0.92; lithium: +0.92), while at the same time the electron density at the bond critical point, in agreement with the electronegativities, indicates stronger covalent bonding in BF_3 than in LiF, the authors conclude that there is a contradiction within the accepted bonding model, because the ionic and covalent contributions cannot both increase at the same time. This argument is nothing but a con, because it should be clear to every

 © 2003 Wiley-VCH Verlag GmbH & Co. KGaA, Weinheim 1433-7851/03/4202-0145 $ 20.00+.50/0

chemist that the *absolute* strengths of the ionic and covalent contributions may both increase whereas the ionic/covalent character is determined by the *ratio* of the two values. And the statement of the authors that the ionic and covalent character of a bond cannot be clearly defined is also not correct. There have been many theoretical studies in recent years in which the absolute values and the ratio of electrostatic and covalent bonding, based on a clearly defined quantum-chemical partitioning of the bonding energy, have been given quantitatively.

The calculated partial charges are frequently used in the following discussions for explaining the geometries and other properties of molecules in terms of the above three models. Although the number of molecules discussed is not very large, it is not difficult for the careful reader to find several exceptions in the tables which are either not mentioned or are explained with questionable arguments, or are commented on laconically as on page 212: "The reasons for the large bond angles in $N(CF_3)_3$ and $N(SCF_3)_3$ are not clear". Particularly noteworthy is the highlighted discussion in a special section on page 191. It is devoted to the question of why BCl_3 is a stronger Lewis acid than BF_3, even though the partial charge of the boron atom in BF_3 (+2.43) is higher than in BCl_3 (+1.93). This finding can therefore not be explained by the electron density distribution. Because the generally accepted model suggests stronger p(π)-backdonation of fluorine compared with chlorine, thus involving the wavefunction, which is against the chemical viewpoint of the authors, they offer an alternative explanation. The authors say that BF_3 is intrinsically a stronger Lewis acid than BCl_3. Then, however, they claim that the energy which is necessary to deform planar BF_3 into a pyramidal geometry in complexes with strong bases such as NH_3 is greater than that for BCl_3. As a proof for the statement they cite a publication by Gillespie et al. (*Inorg. Chem.* **1999**, *38*, 4659) which reports on quantum-chemical calculations for such complexes. This paper shows that the energy difference between the planar equilibrium geometry and a pyramidal structure with a given tilt angle is higher for BF_3 than for BCl_3. However, the model calculations are totally irrelevant for the real molecules F_3B-NH_3 and Cl_3B-NH_3 and for the deformation energies of BF_3 and BCl_3 in the complexes! If one calculates the energies of the Lewis acids with the frozen geometries of the complexes and compares them with the energies of the equilibrium structures, it turns out that BF_3 actually has a *smaller* deformation energy than BCl_3. Thus, BCl_3 is also an intrinsically stronger Lewis acid than BF_3!

There are further absurdities in this and in the following chapter. On page 192, Table 8.3, the AIM partial charges which are praised as a basis for the nature of the chemical bond have a problem, because the calculated values for CH_4 give a small *negative* charge for the hydrogen atoms. Everybody who knows about the fundamental difference between the chemical behavior of protic and hydridic hydrogen will be startled by this. In Section 8.6.1 (pp. 204–205) there is a discussion of the geometry of the CF_3O^- anion using the LCP model, in which the authors fail to justify why they are using the radius of carbonyl oxygen for the O atom, even though the calculated partial charge of CF_3O^- (-1.26) is nearly the same as that of CH_3OH (-1.24). Why is the C–O distance of the former molecule typical of a double bond whereas that of the latter molecule is typical of a single bond? Here the authors use the observed fact as a starting point for a deceptive explanation which seemingly supports the LCP model. The power of the latter is grotesquely exaggerated by the statement (p. 206) that the shorter bond length of CO compared with CO_2 is in agreement with the LCP model. The use of Lewis structures, on the other hand, is criticized at several points using faulty arguments. For example, on page 203 in the discussion of the three Lewis structures of the carbonyl group, there is the statement that the bonding line of a C–O single bond would suggest a nonpolar covalent bond. No chemist would agree with this.

"This gives a fundamentally false unterstanding of the chemical bond."

The extremely biased presentation continues in the final chapter, where the geometries of selected molecules of the heavier Main Group elements are discussed. First there is the introduction of well-known bonding models for hypervalent compounds, such as hybridization with inclusion of d-orbitals and three-center four-electron bonds. Then there is the rejection of writing Lewis structures because, among other reasons, the 15 equivalent resonance structures of SF_6 which can be written in accordance with the octet rule would give a formal charge of +2 for sulfur, whereas the partial charge calculated by the AIM method is +3.55 (p. 230). Here again the authors ignore their explicit statement given on page 17 that the charges of Lewis structures are only formal. The following sections discuss geometries of molecules with increasingly higher coordination numbers. Conspiciously, the authors discuss only cases where there is good agreement with the VSEPR and LCP models, although one soon finds contradictions in the tabulated values. For example, the equatorial S–F distance in SF_4 (154.5 pm) is significantly shorter than in SF_2 (162.5 pm), although the LCP model predicts a longer bond. It becomes clear that the explanations for the observed geometries become more and more difficult for the authors. This becomes perfectly clear from the discussion of the C_{3v} geometries of SeF_6^{2-}, IF_6^-, and XeF_6 (p. 254). The reason why the lone electron pair of the central atom is suddenly without stereochemical significance, although it was suggested to play an important role for the C_{4v} geometry of IF_5, remains unclear. Enlightenment could be found in the nearly 20-year-old review by Kutzelnigg about the chemical bonding of heavier Main Group elements (*Angew. Chem.* **1984**, *96*, 262; *Angew. Chem. Int. Ed. Engl.* **1984**, *23*, 272), but that would mean that the wavefunction has to be considered.

To sum up: the book by Gillespie and Popelier is entertaining reading for every chemist who wants to review his or her ideas about models for molecular geometries by comparing them with the arguments of the authors. If one reads it with scepticism, it may even enrich one's

knowledge about the subject, because it clearly shows the limitations of the correlation between electron density distribution and molecular geometries. However, the greatest caution is advised, because the authors make the statement that the electron density is more fundamental than the wavefunction and that the electron density distribution would be an *explanation* for molecular structures. This gives a fundamentally false understanding of the chemical bond. Therefore, a strong warning must be made with regard to the explicit goal of the authors (preface, page xi) "to provide undergraduate students with an introduction to models and theories of chemical bonding and geometry".

Gernot Frenking
Fachbereich Chemie
Universität Marburg (Germany)

40 Years of Chemistry History



The basis for a **journey of discovery** through **all** the important developments in chemistry and related disciplines

The **authors** and **keywords** of all the reviews that have appeared in ***Angewandte Chemie*** in the last 40 years

Now available at a special price of € 19.80 (including postage)

Only available directly from:
Angewandte Chemie
Postfach 10 11 61
69451 Weinheim (Germany)
Telephone: (+49) 6201-606-265
Fax: (+49) 6201-606-331
E-mail: angewandte@wiley-vch.de

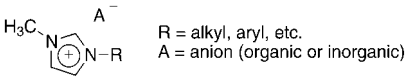
Green solvents

Recent Advances in Applications of Room-Temperature Ionic Liquid/Supercritical CO_2 Systems

*Sergei V. Dzyuba and Richard A. Bartsch**

Keywords:
carbon dioxide · enzyme catalysis · green chemistry · ionic liquids · supercritical fluids

Recent research has demonstrated that room-temperature ionic liquids such as 3-methylimidazolium (MIM) derivatives (Scheme 1) are novel media for a variety of chemical applications.[1] Because ionic liquids (ILs) are easy to prepare and modify structurally to elicit desired physical properties, they are a versatile alternative to molecular organic solvents. Based upon their negligible vapor pressure, ILs have been advocated as "green solvents".[1,2] However, the green nature of processes involving IL solvents is seriously limited by the need to use volatile and/or flammable molecular organic solvents to isolate reaction products from the ILs, as well as to recover the ILs themselves. An alternative, environmentally benign solvent that would enable efficient isolation of organic substrates is highly desirable.



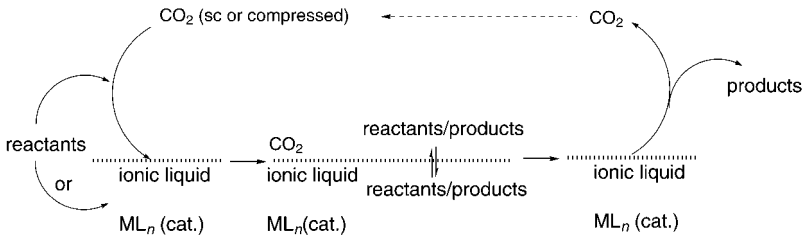
Scheme 1. Room-temperature ionic liquids.

Supercritical carbon dioxide ($scCO_2$) has received attention as a versatile, environmentally benign solvent for a variety of applications.[3] The high volatility and low polarity of $scCO_2$ make it an interesting solvent partner with nonvolatile and fairly polar ILs. The different miscibilities of $scCO_2$ and ILs lead to two-phase systems that have found application in several areas. The success of this two-phase system is based on solubility of $scCO_2$ in the IL, which is controlled by pressure, but insolubility of the IL in $scCO_2$. (The latter is quite different from the appreciable solubility of molecular organic solvents in $scCO_2$.) The solubility of $scCO_2$ in ILs also facilitates mass transfer processes by decreasing their viscosity.

The concept of combining these two completely different solvent types was first realized in the batchwise extraction of naphthalene from BMIM[PF_6] with $scCO_2$ (BMIM = 1-*n*-butyl-3-methylimidazolium).[4] Not only was the aromatic hydrocarbon extracted efficiently by $scCO_2$, but also the IL was recovered in its original purity after extraction and depressurization. This two-phase system was shown to be generally applicable: A variety of polar and nonpolar aliphatic and aromatic substrates was recovered effectively from the IL by batchwise extraction with $scCO_2$.[5] Furthermore, a theoretical basis for the phase behavior of IL/$scCO_2$ systems was established.[6]

Subsequently, biphasic IL/$scCO_2$ systems were utilized in several metal-catalyzed organic reactions (Scheme 2).[7] Both batch and continuous-flow processes were developed in which reactants were introduced into the IL directly or with a flow of CO_2 and products were recovered from the compressed or $scCO_2$. These transformations include the catalytic hydrogenation of alkenes with chiral and achiral organometallic catalysts in batch processes,[8] and hydroformylation and asymmetric hydrovinylation reactions in continuous-flow IL/$scCO_2$ systems.[9]

The use of ILs as novel media for enzyme-catalyzed transformations has attracted considerable interest as well. Lipases exhibit high stability and activity when suspended in ILs.[10] A fine balance between the IL structure and identity of the enzyme was demonstrated in the kinetic resolution of 1-phenylethanol.[11] The reactants were added to the IL/lipase mixture, and the products were extracted with hexane/propanol or distilled out. The simplicity of this approach is attractive. However, the need to utilize hazardous molecular organic solvents for product extraction is a serious drawback. Also it was noted that isolating the product by distillation led to an appreciable decrease in enzyme activity when the IL/enzyme mixture was reused.



Scheme 2. Metal-catalyzed organic reactions conducted in an ionic liquid and supercritical or compressed CO_2.

[*] Prof. R. A. Bartsch, Dr. S. V. Dzyuba[+]
Department of Chemistry and Biochemistry
Texas Tech University
Lubbock, TX 79409 (USA)
Fax: (+1) 806-742-1289
E-mail: richard.bartsch@ttu.edu
[+] Present address:
Department of Chemistry
Massachusetts Institute of Technology
Cambridge, MA 02139 (USA)

 © 2003 Wiley-VCH Verlag GmbH & Co. KGaA, Weinheim 1433-7851/03/4202-0148 $ 20.00+.50/0

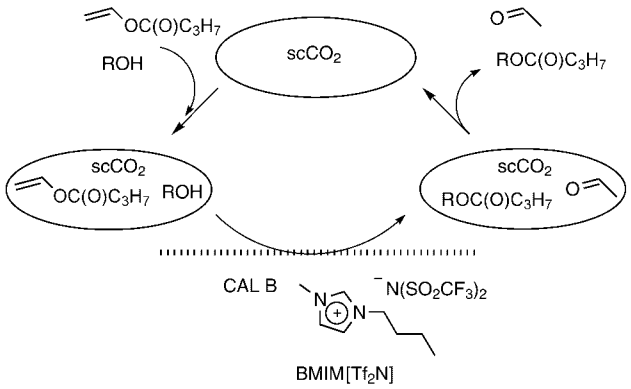
Enzyme-catalyzed reactions in $scCO_2$ have been described also.[12] Very recently, two groups almost simultaneously reported success with IL/$scCO_2$ systems for biocatalytic transesterification reactions and kinetic resolution of 1-phenylethanol.[13,14] In both investigations the ILs were 1-alkyl-3-methylimidazolium bis(trifluoromethanesulfonyl)imides.

In the first study the biocatalyst was an aqueous solution of *Candida antarctica* lipase B (CAL B) dissolved in EMIM[Tf_2N] or BMIM[Tf_2N] immobilized on glass wool (EMIM = 1-ethyl-3-methylimidazolium, Tf = trifluoromethanesulfonyl).[13] For the transesterification of vinyl butyrate and 1-butanol to form butyl butyrate (Scheme 3), a solution of the ester in hexane and a twofold excess of the alcohol was injected into $scCO_2$, which was then flowed over the immobilized IL/enzyme solution; the butyl butyrate product was recovered by depressurizatiuon through a restrictor. For reactions conducted at 40, 50, and 100 °C with 15 MPa pressure, the lowest temperature gave the least enzyme deactivation (i.e., circa 15% after the packed-bed reactor had been used eleven times). For kinetic resolution of *rac*-1-phenylethanol, the aqueous enzyme solution was dissolved in EMIM[Tf_2N] or BMIM[Tf_2N] and then immobilized on Celite. A solution of vinyl propionate and a twofold excess of 1-phenylethanol in hexane was injected into $scCO_2$, which was flowing over the immobilized IL/enzyme layer. At 50 °C (*R*)-1-phenylethyl propionate was formed in >99.9% enantiomeric excess. The efficiency was the same with both ILs, and the activity was found to be eight times greater than when the enzyme was immobilized on Celite in the absence of IL. Thus, "dissolution" of the enzyme in the IL was found to provide protection against denaturization—thermal as well as through the action of the molecular organic solvent and $scCO_2$. Since the cost of both enzymes and ILs is fairly high, their immobilization on a solid support is advantageous. Such immobilized enzyme/IL systems would also allow facile screening of various ILs to find the one most suitable for a given enzyme-catalyzed reaction.

Although this report clearly serves as a proof of principle, some important issues remain to be addressed. The true nature of the immobilized IL/enzyme layer must be explored, particularly with regard to its water content. (Although EMIM[Tf_2N] and BMIM[Tf_2N] are hydrophobic, they do dissolve a few weight percent of water.) Also, it is unclear whether the immobilized IL/enzyme layer is homogeneous or heterogeneous. Finally, what is the role of the molecular organic solvent in which the alcohol and ester are injected in the flowing $scCO_2$?

A suspension of CAL B in BMIM[Tf_2N] was used as the biocatalyst in the second study,[14] which has some distinct differences from the first one. The acylation of 1-octanol by vinyl acetate was first investigated in a batch model reaction in which the IL was used as a solvent rather than as a protective layer for the enzyme. In this case 1-octanol and a twofold excess of vinyl acetate were added directly to the IL/enzyme suspension in the reactor. After reaction for 0.5 h the reactor was connected to a CO_2 compressor and extracted for 1 h at 39 °C and 9.5 MPa. The octyl acetate, acetaldehyde, and excess vinyl acetate were collected in a cold trap and analyzed by GC. A 92% yield of octyl acetate was realized. Thus unlike the first report,[13] molecular solvents were not used in any step of the reaction, making it a truly green process. The reaction and extraction were repeated three times to give the desired ester in 97, 98, and 98% yields. Encouraged by these results, the researchers adopted a continuous-flow system in which a $scCO_2$ stream, into which the reactants were injected, was flowed through the IL-suspended enzyme. The output was almost identical to the input, and the system operated for 24 h with a yield of 0.1 kg L^{-1} of reactor volume per hour. A batch reaction system was also utilized for the kinetic resolution of *rac*-1-phenylethanol by reaction with vinyl acetate in the IL/enzyme suspension. After reaction, extraction with $scCO_2$ efficiently converted the *R* enantiomer into the corresponding acetate ester. Repeated reactions in the same IL/enzyme suspension followed by $scCO_2$ extraction of the product gave no apparent enzyme deactivation.

These results suggest a promising future for biphasic IL/$scCO_2$ systems. A primary advantage of such systems is the solubility or stability of organometallic or enzymatic catalysts in ILs and their negligible solubility in $scCO_2$. On the other hand, many organic reactants and products are reasonably soluble in $scCO_2$. The advantages of using CO_2 as an extraction medium include low cost, nontoxic nature, recoverability, and ease of separation from reaction products. Now that a number of ILs are commercially available, an earlier impediment to their broader application has been removed. The primary disadvantage of these biphasic systems is the cost of the equipment for producing and handling $scCO_2$. Another drawback is the very limited amount of information available on the toxicity and other physiological effects of ILs. For biocatalytic IL systems the enzymes are currently limited to lipases. The utility of the biocatalysis in IL solvent systems would be markedly improved if a broader assortment of enzymes, for example, peroxidases, could be applied. Furthermore, the



Scheme 3. Enzyme-catalyzed transesterification conducted in BMIM[Tf_2N] and supercritical CO_2.

 © 2003 Wiley-VCH Verlag GmbH & Co. KGaA, Weinheim 1433-7851/03/4202-0149 $ 20.00+.50/0

development of continuous-flow catalytic systems in which both the IL/catalyst and the CO_2 can be recycled would be an important advance en route to large-scale commerical applications.

[1] a) K. R. Seddon, *J. Chem. Technol. Biotechnol.* **1997**, *63*, 351 – 356; b) T. Welton, *Chem. Rev.* **1999**, *99*, 2071 – 2083; c) P. Wasserscheid, W. Keim, *Angew. Chem.* **2000**, *112*, 3926 – 3945; *Angew. Chem. Int. Ed.* **2000**, *39*, 3772 – 3789; d) "Ionic Liquids. Industrial Applications to Green Chemistry": *ACS Symp. Ser.* **2002**, *818*.

[2] M. Freemantle, *Chem. Eng. News* **1998**, *76*(13), 32 – 37.

[3] For recent selected reviews on the use of $scCO_2$ see: a) A. Baiker, *Chem. Rev.* **1999**, *99*, 453 – 474; b) P. J. Jessop, T. Ikariya, R. Noyori, *Chem. Rev.* **1999**, *99*, 475 – 493; c) J. A. Darr, M. Poliakoff, *Chem. Rev.* **1999**, *99*, 495 – 541; d) A. J. Mesiano, E. J. Beckman, A. J. Russell, *Chem. Rev.* **1999**, *99*, 623 – 633; e) J. A. Behles, J. M. DeSimone, *Pure Appl. Chem.* **2001**, *73*, 1281 – 1285.

[4] L. A. Blanchard, D. Hancu, E. J. Beckman, J. F. Brennecke, *Nature* **1999**, *399*, 28 – 29.

[5] L. A. Blanchard, J. F. Brennecke, *Ind. Eng. Chem. Res.* **2001**, *40*, 287 – 292.

[6] L. A. Blanchard, Z. Gu, J. F. Brennecke, *J. Phys. Chem. A* **2001**, *105*, 2437 – 2444.

[7] For a recent review on the use of supercritical fluids and ionic liquids see: C. M. Gordon, *Appl. Catal. A* **2001**, *222*, 101 – 117.

[8] a) R. A. Brown, P. Pollet, E. McKoon, C. A. Eckert, C. L. Liotta, P. G. Jessop, *J. Am. Chem. Soc.* **2001**, *123*, 1254 – 1255; b) F. Liu, M. B. Abrams, R. T. Baker, W. Tumas, *Chem. Commun.* **2001**, 433 – 444.

[9] a) M. F. Sellin, P. B. Webb, D. J. Cole-Hamilton, *Chem. Commun.* **2001**, 781 – 782; b) A. Bösmann, B. Franciò, E. Janssen, M. Solinas, W. Leitner, P. Wasserscheid, *Angew. Chem.* **2001**, *113*, 2769 – 2771; *Angew. Chem. Int. Ed.* **2001**, *40*, 2697 – 2699.

[10] The use of ionic liquids for enzyme-assisted transformations has been reviewed recently: R. A. Sheldon, R. M. Lau, M. J. Sorgedrager, F. van Rantwijk, K. R. Seddon, *Green Chem.* **2002**, *4*, 147 – 151.

[11] S. H. Schöfer, N. Kaftzik, P. Wasserscheid, U. Kragl *Chem. Commun.* **2001**, 425 – 426.

[12] For reviews of enzymatic reactions in $scCO_2$ see: a) A. J. Mesiano, E. J. Beckman, A. J. Russell, *Chem. Rev.* **1999**, *99*, 623 – 633; b) H. Hartmann, E. Schwabe, T. Scheper, D. Combes in *Stereoselective Biocatalysis* (Ed.: R. N. Patel), Marcel Dekker, New York, NY, **2000**, pp. 799 – 838.

[13] P. Lozano, T. de Diego, D. Carrie, M. Vaultier, J. L. Iborra, *Chem. Commun.* **2002**, 692 – 693.

[14] M. T. Reetz, W. Wiesenhöfer, G. Franciò, W. Leitner, *Chem. Commun.* **2002**, 992 – 993.

Aza-Henry Reactions

Asymmetric Catalytic Aza-Henry Reactions Leading to 1,2-Diamines and 1,2-Diaminocarboxylic Acids

*Bernhard Westermann**

Dedicated to Prof. Dr. Dieter Seebach on the occasion of his 65th birthday

Keywords:
asymmetric syntheses · aza-Henry reactions · diamines · Lewis acids · Mannich reactions

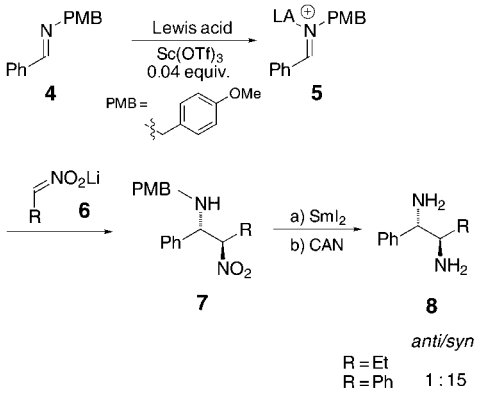
The aldol reaction, known for its remarkable diastereo- and enantioselectivity, initiated quantum leaps in the development of stereoselective synthesis. In this context the question frequently asked—"Does it work with compounds having C–N rather than C–O double bonds"—has been answered extensively in recent years.[1] A variety of synthetic procedures have been devised to carry out the Mannich and related reactions stereoselectively. Despite all these improvements one major gap remained, namely, the diastereoselective, asymmetric synthesis of vicinal diamines. This class of compounds is of particular interest owing to their broad utility, which ranges from application as antitumor reagents to employment as ligands in stereoselective organic synthesis.[2,3]

Not surprisingly, a number of methods have been developed for the synthesis of products with these functional units. Most of these procedures rely on "chiral-pool" compounds and/or chiral auxiliaries for stereocontrol. These approaches have several considerable drawbacks: the stereochemistry of the products is restricted by the limited accessibility of starting materials (often only one stereoisomer), and chiral auxiliaries, although often recyclable, may be required in equimolar amounts.

[*] Priv.-Doz. Dr. B. Westermann
Faculty of Natural Sciences, University of Paderborn
33095 Paderborn (Germany)
Fax: (+49) 5251-603-245
E-mail: bw@fb13n.uni-paderborn.de

Organometallic methodologies with potential catalytic variations are known, but often they are hampered by very narrow substrate-specificity or have limited application for the synthesis of chiral, nonracemic products. Bäckvall et al. described the aminopalladation of (*E*)-alkenes **1** and subsequent oxidation in the presence of amines which provided racemic *syn*-diamines **2** (Scheme 1).[4,5] Another attractive synthesis of 1,2-diamines is based on the derivatization of 1,2-diols and 1,2-amino alcohols, which are provided by the Sharpless asymmetric dihydroxylation and aminohydroxylation of olefins, respectively.[6]

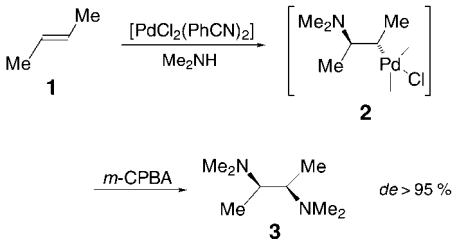
Very recently, Anderson et al. reported an interesting synthesis of 1,2-diamines.[7] First, an aza-Henry reaction (alternatively, nitro-Mannich reaction, i.e. addition of nitronates **6** to imines **5**) provided β-nitroamines **7**. To avoid retro-addition, these intermediates were then reduced with SmI_2, and the vicinal diamines **8** could be obtained in high yields and with good diastereoselectivities (Scheme 2).



Scheme 2. Diastereoselective synthesis of 1,2-diamines by means of an aza-Henry reaction (Tf = tri-triflate, CAN = ceric ammonium nitrate).

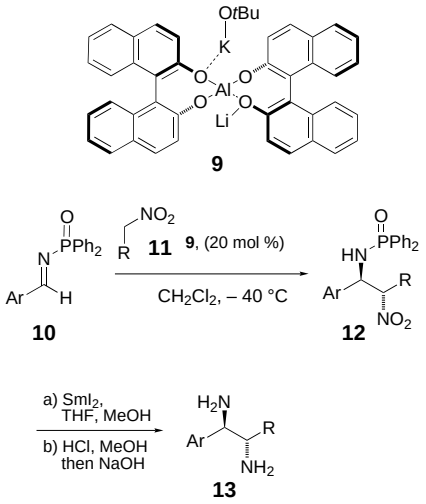
In preliminary studies imines **4** and nitroalkanes **6** were allowed to react in the presence of Brønsted acids. More recently the reaction was found to be catalyzed by Lewis acids like BF_3 and $Sc(OTf)_3$.[8] Thus, the stage was set for developing the catalytic, asymmetric variants of this sequence—goals addressed and achieved by the research groups led by Shibasaki and Jørgensen.

Shibasaki et al. investigated the aza-Henry reaction conducted with the heterodimetallic catalyst **9**, which they had developed (Scheme 3).[9,10] Since **9** shows concomitantly Brønsted-basic and Lewis-acidic behavior, both the electrophile and the nucleophile can be activated. Complexes of this



Scheme 1. Diamination of alkenes via an aminoalkyl-palladium intermediate (*m*-CPBA = *meta*-chloroperbenzoic acid).

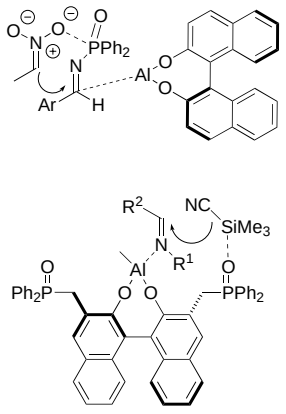
 © 2003 Wiley-VCH Verlag GmbH & Co. KGaA, Weinheim 1433-7851/03/4202-0151 $ 20.00+.50/0



Scheme 3. Asymmetric aza-Henry reaction with the heterodimetallic complex **9**.

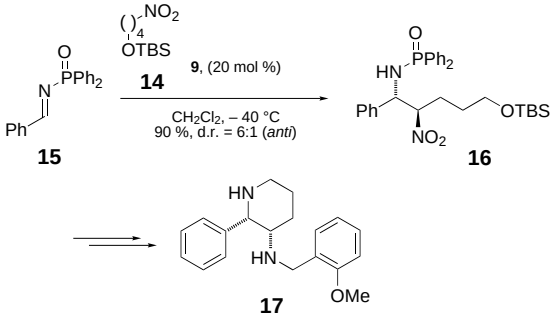
type can be considered mimics of the aldolase type II enzymes (Zn as cofactor) and have given excellent results as catalysts in aldol, Strecker, and Reissert reactions.[11]

For high selectivities it appears mandatory to include anchor groups (P=O bonds), which provide additional complexation and orientation in these heterodimetallic complexes (Scheme 4). They can be present in the catalyst itself, in the substrate, or in an additive to the reaction mixture. In the case of the aza-Henry reaction this unit is found in substrate **10** (Scheme 3). Under optimized conditions **12** could be obtained in 90% yield (*syn*:*anti* > 6:1) with an enantiomeric excess of > 80%. Among the disadvantages are the limited number of suitable nitronates **11** available



Scheme 4. The P=O bond aids in the complexation and orientation of electrophiles and nucleophiles.

(in the beginning only nitromethane), the restriction to *N*-phosphinoylimines **10**, and the large amount of catalyst (20 mol%, which corresponds to 40 mol% chiral auxiliary). One point in favor of this methodology is that vicinal diamines **13** can be obtained easily from **12** by reduction of the nitro group and cleavage of the phosphinoyl group. The effectiveness of this method has been demonstrated recently in the synthesis of the potent antagonist of substance P, CP-99994 (**17**, Scheme 5).[12] Certainly consideration



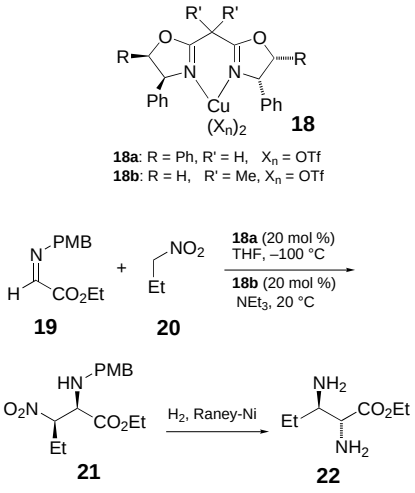
Scheme 5. Synthesis of CP-99994 (**17**) in which an aza-Henry reaction is the key step (TBS = *tert*-butyldimethylsilyl).

of this type of simultaneous Lewis-acidic/Brønsted-basic activity in the optimization of catalysts by either combinatorial or evolutional approaches may lead to very powerful catalysts for aza-Henry reactions.

The breakthrough in terms of handling, substrate variety, and practicability was achieved by Jørgensen et al. (Scheme 6).[13,14] They showed that application of C_2-symmetrical chiral Lewis acids **18a** and **18b** (20 mol%) to the addition of nitronates to imines can afford aza-Henry products **21** with high diastereo- and enantioselectivities. After reduction of the nitro moiety in **21** very valuable building blocks like α,β-diaminocarboxylic acids **22** can be obtained (Scheme 6). If silylated nitronates are employed, addition of base is not necessary. Under these reaction conditions the aza-Henry adducts **21** are stable and can be isolated. Owing to the high reactivity of the silylated nitronates, the reaction proceeds uncatalyzed even at −78°C. Reaction temperatures of −100°C were required to achieve high diastereoselectivities (*erythro*:*threo* > 25:1) and high enantioselectivities (> 95% *ee* for the *erythro* product).

This limitation can be overcome and the reaction can be conducted at room temperature when amines (NEt_3 has been the amine of choice) are added to the less reactive nitro compounds. The resulting stereoselectivities and yields are generally very high (*erythro*:*threo* > 92:8; > 93% *ee* for the *erythro* product, > 80% *ee* for the *threo* product; 60–87% yield) when Lewis acids **18a** or **18b** are used. All these features make this sequence amenable to technical applications. Decreasing the temperature to 0°C, which is easily accomplished, increased selectivities but prolonged reaction times (1 d at 20°C, 5 d at 0°C). The solvent used (CH_2Cl_2) does not need further purification and drying, and inert gas atmosphere can be avoided. The only critical point is the addition sequence of the reaction partners.

In these studies the ligands in the Lewis acids, C_2-symmetrical modified bisoxazolines, have proved to be superior to their BINOL- and TADDOL-derived congeners. The copper(II) salts employed can be copper triflate and even copper bromide despite its decreased Lewis acidity. The

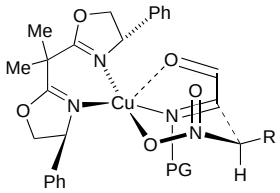


Scheme 6. Lewis acids with modified bisoxazoline ligands in aza-Henry reactions (PMB = *p*-methoxybenzyl; Tf = triflate).

 © 2003 Wiley-VCH Verlag GmbH & Co. KGaA, Weinheim 1433-7851/03/4202-0152 $ 20.00+.50/0

sole stipulation is that the protecting group on the imine should be an electron-rich aryl group.

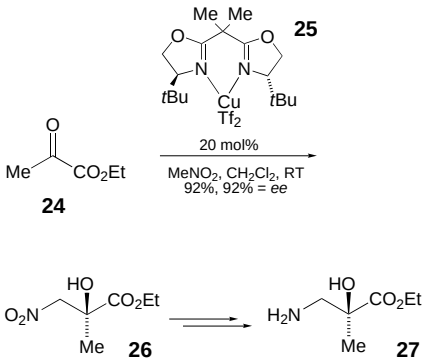
The high selectivity of the addition is attributed to a Zimmerman–Traxler transition state, in which both reaction partners are coordinated at the chiral Lewis acid. If one presumes a rapid equilibration of the *E* and the *Z* forms of the nitronate, transition state **23** (PG = protecting group) is formed exclusively, which explains the preferred formation of the *erythro* product.



23

Finally, it should be pointed out that this method can be applied to the classical Henry reaction in which ethyl pyruvate (**24**) is converted into the corresponding hydroxyaminocarboxylic acid **27** (Scheme 7). The quaternary stereogenic center is generated with high selectivity.[15]

Both approaches, that based on the bifunctional Lewis acid catalyst and that based on the copper-bisoxazolidine catalyst, have bright prospects. Even in the initial evaluation of these catalysts they have proven to be most valuable for a number of very interesting products.[16]



Scheme 7. Henry reactions giving α-hydroxy-β-aminocarboxylic acids **27**.

[1] K. Juhl, N. Gathergood, K. A. Jørgensen, *Angew. Chem.* **2001**, *113*, 3083; *Angew. Chem. Int. Ed.* **2001**, *40*, 2995, and references therein.

[2] D. Lucet, T. Le Gall, C. Mioskowski, *Angew. Chem.* **1998**, *110*, 2724; *Angew. Chem. Int. Ed.* **1998**, *37*, 2581.

[3] C. T. Lowden, J. S. Mendoza, *Tetrahedron Lett.* **2002**, *43*, 979.

[4] J. E. Bäckvall, *Tetrahedron Lett.* **1975**, 2225.

[5] J. E. Bäckvall, *Tetrahedron Lett.* **1978**, 163.

[6] Asymmetric Dihydroxylations and Aminohydroxylations, C. Bolm, J. P. Hildebrand, K. Muniz in *Catalytic Asymmetric Synthesis, 2nd ed.* (Ed.: I. Ojima), Wiley-VCH, **2000**, p. 399, and references therein.

[7] H. Adams, J. C. Anderson, S. Peace, A. M. K. Pennell, *J. Org. Chem.* **1998**, *63*, 9932.

[8] J. C. Anderson, S. Peace, S. Pih, *Synlett* **2000**, 850.

[9] K. Yamada, S. J. Harwood, H. Gröger, M. Shibasaki, *Angew. Chem.* **1999**, *111*, 3713; *Angew. Chem. Int. Ed.* **1999**, *38*, 3504.

[10] K. Yamada, G. Moll, M. Shibasaki, *Synlett* **2001**, 980.

[11] H. Gröger, *Chem. Eur. J.* **2001**, *7*, 5247, and references therein.

[12] N. Tsuritani, K. Yamada, N. Yoshikawa, M. Shibasaki, *Chem. Lett.* **2002**, 276.

[13] K. R. Knudsen, T. Risgaard, N. Nishiwaki, K. V. Gothelf, K. A. Jørgensen, *J. Am. Chem. Soc.* **2001**, *123*, 5843.

[14] N. Nishiwaki, K. R. Knudsen, K. V. Gothelf, K. A. Jørgensen, *Angew. Chem.* **2001**, *113*, 3080; *Angew. Chem. Int. Ed.* **2001**, *40*, 2992.

[15] C. Christensen, K. Juhl, R. G. Hazell, K. A. Jørgensen, *J. Org. Chem.* **2002**, *67*, 4875. A minireview on the construction of quaternary stereocenters: J. Christoffers, *Angew. Chem.* **2001**, *113*, 4725; *Angew. Chem. Int. Ed.* **2001**, *40*, 4591.

[16] Diastereoselective Henry reactions under high pressure: Y. Misumi, K. Matsumoto, *Angew. Chem.* **2002**, *114*, 1073; *Angew. Chem. Int. Ed.* **2002**, *41*, 1031.

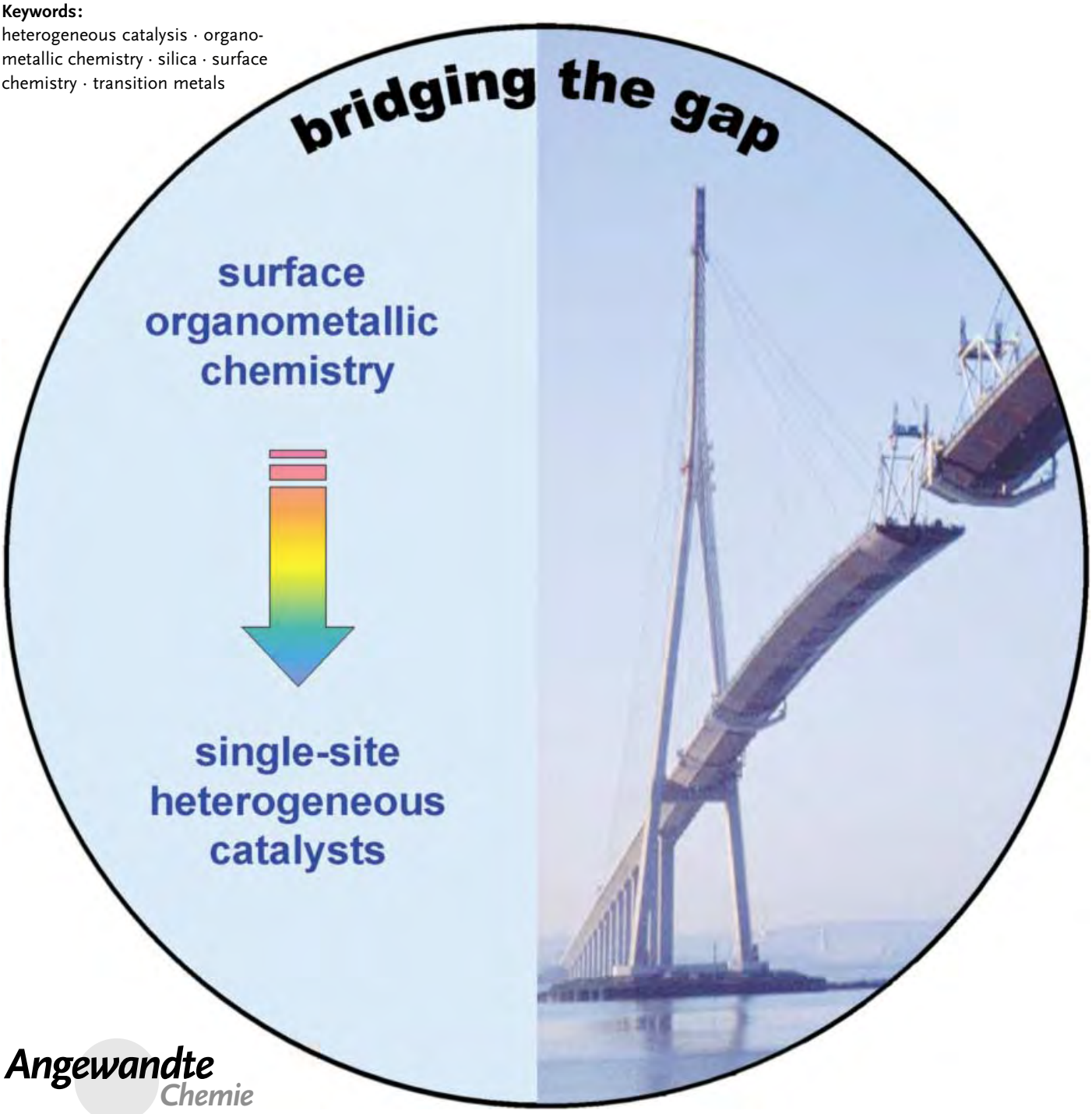
 © 2003 Wiley-VCH Verlag GmbH & Co. KGaA, Weinheim 1433-7851/03/4202-0153 $ 20.00+.50/0

Surface Organometallic Chemistry

Homogeneous and Heterogeneous Catalysis: Bridging the Gap through Surface Organometallic Chemistry

Christophe Copéret, Mathieu Chabanas, Romain Petroff Saint-Arroman, and Jean-Marie Basset**

Keywords:
heterogeneous catalysis · organometallic chemistry · silica · surface chemistry · transition metals



© 2003 Wiley-VCH Verlag GmbH & Co. KGaA, Weinheim
1433-7851/03/4202-0156 $ 20.00+.50/0

Surface organometallic chemistry is an area of heterogeneous catalysis which has recently emerged as a result of a comparative analysis of homogeneous and heterogeneous catalysis. The chemical industry has often favored heterogeneous catalysis, but the development of better catalysts has been hindered by the presence of numerous kinds of active sites and also by the low concentration of active sites. These factors have precluded a rational improvement of these systems, hence the empirical nature of heterogeneous catalysis. Catalysis is primarily a molecular phenomenon, and it must involve well-defined surface organometallic intermediates and/or transition states. Thus, one must be able to construct a well-defined active site, test its catalytic performance, and assess a structure–activity relationship, which will be used, in turn—as in homogeneous catalysis—to design better catalysts.
By the transfer of the concepts and tools of molecular organometallic chemistry to surfaces, surface organometallic chemistry can generate well-defined surface species by understanding the reaction of organometallic complexes with the support, which can be considered as a rigid ligand. This new approach to heterogeneous catalysis can bring molecular insight to the design of new catalysts and even allow the discovery of new reactions (Ziegler–Natta depolymerization and alkane metathesis). After more than a century of existence, heterogeneous catalysis can still be improved and will play a crucial role in solving current problems. It offers an answer to economical and environmental problems faced by industry in the production of molecules (agrochemicals, petrochemicals, pharmaceuticals, polymers, basic chemicals).

From the Contents

1. Introduction 157
2. Techniques in Surface Organometallic Chemistry 158
3. Surface Organometallic Chemistry on Silica 159
5. Summary and Outlook 169

1. Introduction

Catalysis remains a strategic field of chemistry because of its implication in many fields, which include industry, energy, environment, and life sciences. Whether it is homogeneous or heterogeneous (or even enzymatic), catalysis is primarily a molecular phenomenon since it involves the chemical transformation of molecules into other molecules. At the beginning of the 21st Century, even though many attempts have been made to fully erase the gap existing between these two important fields of chemistry, they still belong to different scientific communities: homogeneous catalysis is connected to molecular organometallic chemistry, and heterogeneous catalysis is closer to surface science and solid-state chemistry.

Although the physico–chemical tools of surface science have progressed tremendously in the last decades, the level of understanding of heterogeneous catalysis is still limited, especially when compared to that of molecular organometallic chemistry and homogeneous catalysis. Perhaps one of the main reasons for the difficulty in obtaining a structure–activity relationship in heterogeneous catalysis is the small number of active sites, a concept introduced in 1926 by H. S. Taylor.[1] To date, even the impressive number of physico–chemical tools available (see Section 2) do not lead to the clear detection of active sites, and it has also not been possible in most cases to get a precise description of the mechanism occurring at these active sites. By mechanism we do not mean diffusion through the pores towards the surface, or on the surface itself but the molecular transformations or elementary steps, by which the reagent molecules undergo bond making and breaking on the so-called active sites.

It is to meet this challenge—which is a century old,[2] and yet strategic (90% of the chemical industry is based on heterogeneous catalytic processes)—that surface organometallic chemistry has recently been developed. This discipline consists in bringing the concepts and the tools of molecular chemistry, especially organometallic chemistry, to surface science and heterogeneous catalysis.

One of the first aspects of this chemistry was to study the reactivity of organometallic molecules (of main-group elements, transition metals, lanthanides, and actinides) with surfaces and more particularly those of oxides, zeolites, mesoporous materials, and metals (as in metallic materials). Although pioneering work was started in the 60s by polymer scientists,[3] this field of chemistry, with a precise definition of the overall structure of the active sites is completely new in its present form.

The questions of this chemistry are numerous:

[*] Dr. C. Copéret, Dr. J.-M. Basset, M. Chabanas, R. Petroff Saint-Arroman
Laboratoire de Chimie Organométallique de Surface
UMR 9986 CNRS/CPE Lyon
43 Bd du 11 Novembre 1918, 69616 Villeurbanne Cedex (France)
Fax: (+33) 4-7243-1795
E-mail: coperet@cpe.fr
basset@cpe.fr

 © 2003 Wiley-VCH Verlag GmbH & Co. KGaA, Weinheim 1433-7851/03/4202-0157 $ 20.00+.50/0

1) Can we apply the concepts of molecular reactivity when an organometallic compound reacts with a surface? In many instances the answer to this question is yes.[4] The functional groups present at the surface of an oxide, a zeolite, or even of a metal particle have a chemical reactivity close to those of molecules and organometallic complexes in solution. Clearly, some parameters are superimposed as a result of the rigidity of the crystalline lattice which stabilizes species that could not otherwise be stable in solution.
2) Can we rationalize molecular structures of complexes on surfaces on the same basis as those of molecules in solution? The accumulated knowledge suggests that the supports behave as a rigid ligand similar to their molecular analogues. This similarity is crucial since it allows us to predict molecular surface structures on the basis of simple electron counts which is so useful in evaluating and predicting catalytic behavior.
3) Is it possible to study "elementary steps" of heterogeneous catalysis through the stoichiometric reactivity of surface organometallic fragments? This is probably the most important aspect of surface organometallic chemistry since if the answer to this question is yes, and if the elementary steps which are observed are the same as those of molecular organometallic chemistry, then the transfer of mechanistic concepts from molecular organometallic chemistry to surface chemistry will be obvious and rapid so that a real breakthrough is likely to occur in the field of heterogeneous catalysis.
4) The ultimate goal of this chemistry is to use all the above concepts to construct on the surfaces, by a true molecular engineering approach, the active sites, uniform in composition and distribution, so as to achieve single-site heterogeneous catalysts. This concept was first proposed in the field of catalytic polymerization when well-defined "homogeneous" metallocene catalysts were found to behave in a tunable way, and have been slowly replacing the "black box" of classical heterogeneous Ziegler–Natta catalysis.

Herein, we will focus on the recent advances in the surface organometallic chemistry of d-block transition-metal complexes with metal oxides, specifically silica.

2. Techniques in Surface Organometallic Chemistry

One of the main objectives of surface organometallic chemistry is to characterize surface species and thus to establish structure–activity relationships, as in homogeneous catalysis. Therefore, as in molecular chemistry, surface organometallic chemistry heavily relies on both chemical and spectroscopic methods to understand the structure of surface entities. IR spectroscopy is an essential tool for understanding the grafting step and to assess the modification



Christophe Copéret received his degree of "Ingenieur" from ESCIL (Chimie Lyon, France) in 1992. A year before, he joined the PhD program of Purdue University, Indiana (USA) where he worked on the development of synthetic methodology through organometallic chemistry and catalysis under the direction of Professor E.-i. Negishi. In 1996, after obtaining his PhD degree, he joined the Scripps Research Institute to work with Professor K. B. Sharpless on selective oxidation reactions before accepting a full-time position in the CNRS (1998), where he is currently developing the surface organometallic chemistry of transition metals on metal oxides directed towards the generation of single-site heterogeneous catalysts.



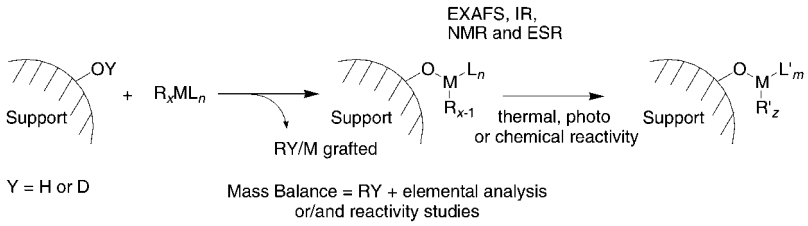
Romain Petroff Saint-Arroman received his degree of "Ingenieur" from ESCPE Lyon in 1999. During this degree, he spent one year in Dow Chemicals under the supervision of Dr. C. Piechocki and also received a Masters degree in catalysis working on the characterization of molybdenum surface complexes with Dr. C. Copéret. He then completed a PhD degree in the same laboratory, with Drs F. Lefebvre and J.-M. Basset, working on oxidation. He has recently accepted a research position at Rhodia in Lyon (France).



Mathieu Chabanas received his degree of "Ingenieur" from ESCPE Lyon in 1998. During this degree, he spent one year at BASF under the supervision of Dr. J. H. Teles. He obtained a Masters degree in catalysis in the Laboratoire de Chimie Organometallique de Surface (LCOMS) working on the hydrogenolysis of alkanes with Dr. J. Thivolle-Cazat. He then completed his PhD in the same laboratory working on the preparation and the characterization of single-site heterogeneous catalysts with Drs C. Copéret and J.-M. Basset. He is currently a research chemist at BASF AG in Ludwigshafen (Germany).



Jean-Marie Basset received his degree of Ingenieur from ESCIL in 1965 and then joined the "Institut de Recherche et de la Catalyse" (IRC) in Lyon where he obtained a PhD in 1969 under the supervision of Professor M. Prettre. After a postdoctoral period at the University of Toronto in 1969–70 in the laboratory of Prof. W. F. Gaydon he returned to the IRC where he developed a research group on olefin metathesis and the organometallic chemistry of surfaces. He founded the Laboratoire de Chimie Organometallique de Surface (LCOMS) at the ESCPE Lyon in 1993. He is a member of the French Academy of Science and of the French Academy of Technology, and is the author of more than 300 publications and 35 patents.



Scheme 1. General strategy to understand structures of surface complexes.

of the species on the surface upon various treatments (chemical, photochemical, and thermal reactivity; Scheme 1). Thus spectroscopy, in combination with quantitative measurements of product evolution during grafting and upon further chemical treatments of the surface complex, can provide a quick, yet clear, picture of the surface complex through mass-balance analysis. Typically, the latter aspect has been mainly addressed by using hydrolysis, alcoholysis, and hydrogenolysis reactions and in some specific cases pseudo-Wittig reactions (presence of an alkylidene ligand) [Eq. (1)–(5)]. Additionally grafting on deuterated silica (≡SiOD) or using deuterolysis of surface complexes (or equivalent) can give more information about the mode of grafting and the coordination sphere of the grafted organometallic complex.

$$[\equiv SiOM(CH_2R)_x] + R'OD(H) \xrightarrow{\text{solvolysis}} [\equiv SiOM(OR')_x] + x\,RCH_2D(H) \quad (1)$$

$$[\equiv SiOM(CH_2R)_x] + H_2 \xrightarrow{\text{hydrogenolysis}} [\equiv SiOMH_x] + x\,RCH_3 \quad (2)$$

$$[\equiv SiOM(=CHR)_x] + R'OD(H) \xrightarrow{\text{solvolysis}} [\equiv SiOM(OR')_{2x}] + x\,RCHD_2(H_2) \quad (3)$$

$$[\equiv SiOM(=CHR)_x] + CH_3COCH_3 \xrightarrow{\text{pseudo-Wittig}} [\equiv SiOM(=O)_x] + RCH{=}C(CH_3)_2 \quad (4)$$

$$[\equiv SiOM(\equiv CR)_x] + R'OD(H) \xrightarrow{\text{solvolysis}} [\equiv SiOM(OR')_{3x}] + x\,RCD_3(H_3) \quad (5)$$

The most powerful and commonly used tools in structural molecular organometallic chemistry are X-ray crystallography, NMR, IR (Raman), and ESR spectroscopy which give a clear and detailed picture of the coordination sphere around a metal center. In this respect, surface organometallic chemistry has used the corresponding methods for amorphous solids (Scheme 2):[5]

1) EXAFS, which provides interatomic distances as well as average coordination numbers (the number of nearest-neighbor atoms, and to some extent next-nearest-neighbor atoms).
2) IR spectroscopy (usually in situ), which is used to follow modification of both the support (especially during grafting) and the surface complex upon further treatment.
3) ESR and XANES, which can indicate the oxidation state and the geometry of the metal complex when applicable.
4) Solid-state NMR spectroscopy (1D and 2D), probably one of the most powerful methods for structure determination.

Besides these solid-state methods, molecular models, such as polyhedral oligomeric silsesquioxanes (POSS), which can mimic the surface of silica (see Section 3.2.), can also be of great help in understanding the reaction of an organometallic precursor with a surface (typically with silanol groups) and establishing the molecular structure of a surface complex (see Section 3.2.). Moreover, since surface organometallic chemistry deals with surfaces, it also uses other important methods of surface science, such as X-ray photoelectron spectroscopy (XPS), specific surface measurements (BET, porous distribution). All these stoichiometry events and spectroscopic methods help in understanding the structure of a surface complex. Several examples that illustrate this approach will be presented followed by their relevance to catalysis (Section 4.).[6]

3. Surface Organometallic Chemistry on Silica

3.1. Generalities on Silica

A key component in surface organometallic chemistry is the support. It is therefore of prime importance to understand the support in order to control its reactivity (selection of reactive functional groups) and the potential structure of the supported organometallic complexes. On a 200 $m^2 g^{-1}$ Aerosil silica from Degussa, the surface is composed of siloxane bridges (≡SiOSi≡) and silanol groups (≡SiOH). Their concentrations and their types depend on the temperature of the pretreatments.[7,8] Siloxane bridges are characterized by their size (four-, six-, eight-, …, membered ring), which decreases with an increase of the pretreatment temperature. Silanol groups are either isolated, geminal, or vicinal (Scheme 3a). Upon heating, silanols condense to produce siloxane bridges and water. This process, called partial dehydroxylation,

Molecular chemistry		**Surface organometallic Chemistry**
What are the tools to characterize a compound ?		Transfer or tools possible?
IR (Raman) Spectroscopy		Yes
NMR Spectroscopy		Yes
ESR Spectroscopy		Yes
UV Spectroscopy		Yes
Elemental Analysis	→ Transfer of Tools →	Yes
Mass Spectrometry		-
X-Ray Crystallography		EXAFS, XANES
mp, bp		-
Density		-
Color		Yes
Chemical Characterization (reactivity)		Yes
		BET
		XPS
		Porosity
		Microscopy

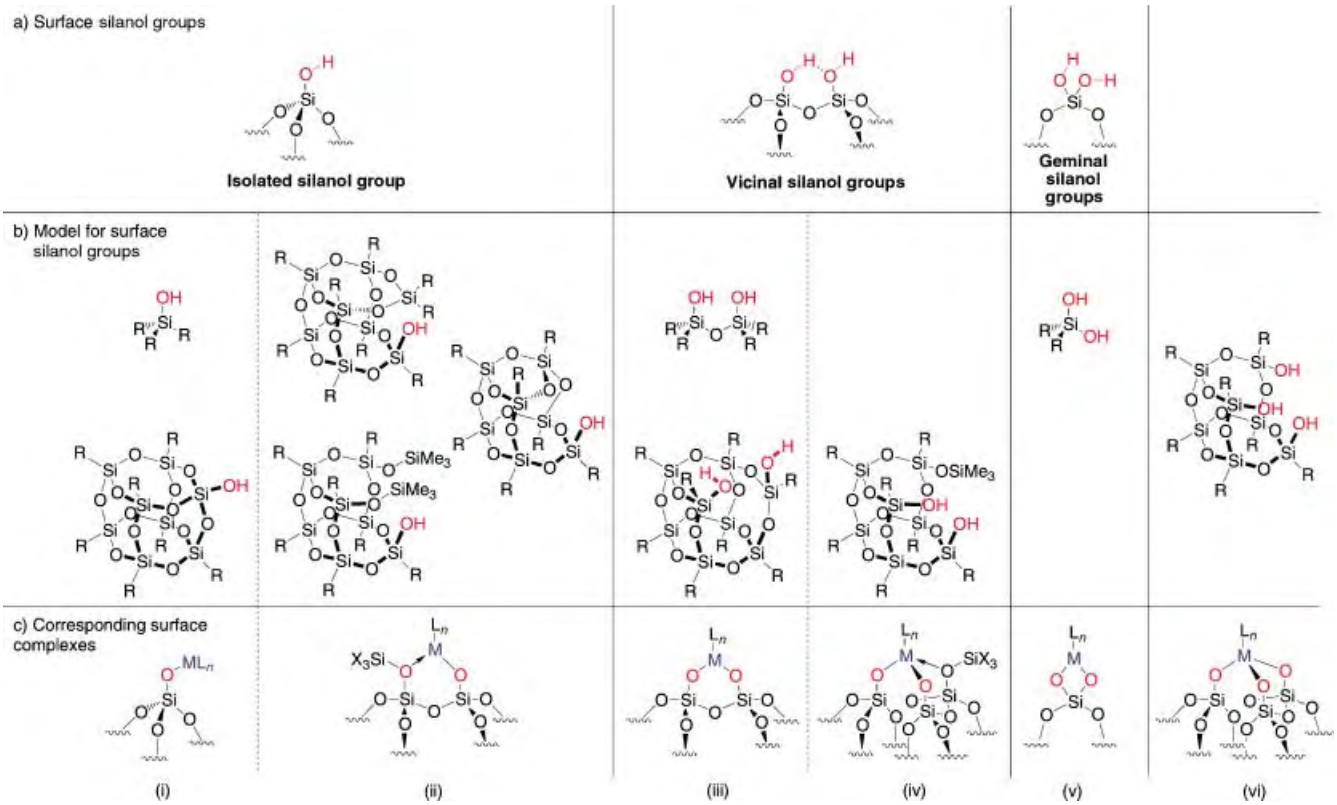
Scheme 2. Methods for characterization of heterogeneous catalysts in surface organometallic chemistry compared with those in molecular chemistry.

transforms vicinal silanol groups into isolated ones, which are the main components after a thermal treatment at 700 °C. Above 800 °C, strained four-membered-ring siloxane bridges are also produced accompanied by a significant loss of specific surface area (sintering). Typically on silica with a surface area of 200 $m^2 g^{-1}$ treated under vacuum at 200, 500, and 700 °C, there are about 2.6, 1.2, and 0.7 ± 0.2 accessible OH groups per nm^2, respectively (that is a concentration of approximately 0.86, 0.42, and 0.23 mmol OH g^{-1} of silica, respectively). These numbers probably give an estimation of accessible silanol groups for bulky organometallic precursors. In summary, functional groups on the surface of silica are either silanols or siloxane bridges, and their concentrations depend highly on the temperature of the partial dehydroxylation of the silica. Moreover silica, despite its amorphous structure, is rather homogeneous in terms of types of reactive functional groups (≡SiOH) and shows a rather low acidity (Lewis or Brønsted) compared to other supports. Therefore silica is probably the support of choice to generate well-defined surface organometallic complexes.

3.2. Molecular Analogues of Silica: Another Tool To Understand the Chemistry of Surfaces

Molecular chemistry is usually faster and easier in terms of structure characterization and reactivity understanding than solid-state chemistry. Therefore, the use of molecular models to mimic the surface of silica can help in understanding surface reactions. For example, the reaction of organometallic compounds with these models gives rise to metal complexes that are more easily characterized and that can provide important data, such as bond lengths (X-ray and/or EXAFS) and chemical shifts (solution and/or solid-state NMR spectroscopy), which can be used as reference material for data obtained for surface organometallic complexes (solid-state NMR spectroscopy and EXAFS).[9,10]

The reactive functional groups of silica are silanols and siloxane bridges. Therefore, it is necessary to have a wide range of molecular models that represent these various sites. Several different models have been used, such as trialkylsilanols and polyhedral oligomeric silsequioxanes (POSS). Surface silanol groups have been classified into three different types: isolated, vicinal, or geminal silanol. Each type of silanol can be mimicked by a corresponding molecular analogue (Scheme 3b). Note that while the molecular siloxane analogue having three silanol groups (Scheme 3b-(6)) is probably not a good model for silica, its corresponding organometallic derivatives describe trisgrafted surface complexes (Scheme 3c-(6)). Moreover, several molecular models for either mono- or bissiloxy systems exist and can be used to represent the different local environments of silica and around the grafted metal centers (Scheme 3b–c/(2)–(4)), for example, those in proximity to siloxane bridges or those close to hydrophobic groups (in the case of a silica modified with alkylsilanes). POSS and their analogues are probably the best



Scheme 3. a) Various types of surface silanol groups, b) molecular models that mimic the corresponding silanol groups of a silica surface (for POSS derivatives, R = cyclopentyl or -hexyl, for other models R = *t*Bu and Ph), and c) the corresponding surface complexes.

suited since they can mimic the environment of the different types of silanol groups and have pK_a values for ≡SiOH units close to those of silica.[9n]

The use of these analogues to understand surface reactions and to gain information about surface complexes is likely to become more systematic and should be coupled with the study of the corresponding surface reactions.

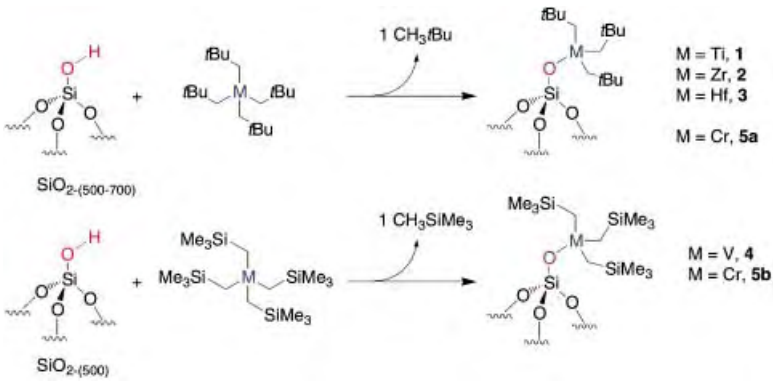
3.3. Surface Organometallic Complexes: Generalities and Examples

The interaction of organometallic complexes with silica has been investigated for some time.[3] The development of surface organometallic chemistry exactly parallels the discovery and the development of the synthesis of transition-metal organometallic complexes. In fact, the first organometallic species studied in this field were allyl derivatives of Group 4–8 transition metals.[3b,11] Yet these pioneering studies were more oriented towards the discovery of new materials and their reactivity (in catalysis and especially in polymerization) than trying to generate the appropriate coordination sphere of supported metal complexes to achieve a specific application. This approach is what probably distinguishes the earlier investigations from the current activity.

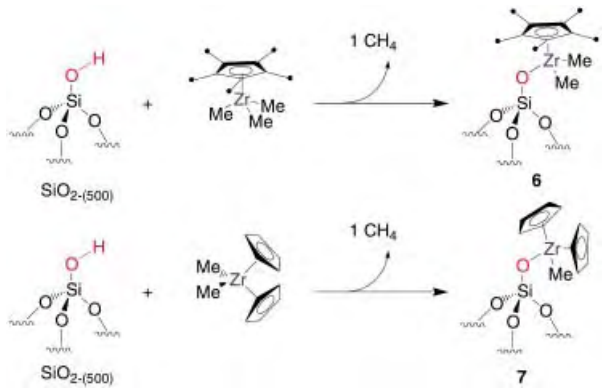
In the following section, we will discuss the formation of a wide range of well-defined surface complexes and classify them according to the number of their covalent bonds with the silica surface.

3.3.1. Monografted (Monosiloxy) Organometallic Complexes [≡SiOML$_n$]

Trisneopentylzirconium monografted to a surface of a silica pre-treated at 500 °C ($SiO_{2-(500)}$) under vacuum, [≡SiOZr(CH_2tBu)$_3$] (**2**), was the first surface complex to be fully characterized by both chemical and spectroscopic methods (Scheme 4).[12] Indeed, one equivalent of neopentane is evolved during the grafting of [Zr(CH_2tBu)$_4$] onto $SiO_{2-(500)}$ and the concomitant and total disappearance of the silanol groups of the silica surface as indicated by IR spectroscopy. Moreover, elemental analysis and the hydrolysis of **2** are consistent with the presence of three neopentyl



Scheme 4. Group 4 and first-row Group 5 and 6 surface complexes.



Scheme 5. Group 4 metallocene surface complexes.

groups around the Zr center, which is further confirmed by solid-state NMR spectroscopy (Table 1) and EXAFS (three Zr–O bonds of 1.95 Å).[13]

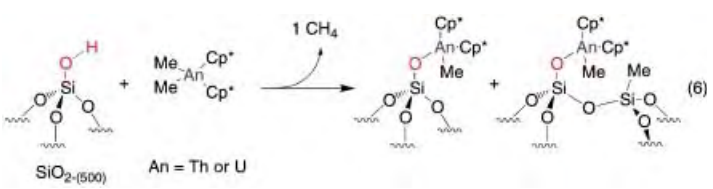
It has also been possible to generate the other corresponding Group 4 metal complexes [≡SiOM(CH_2tBu)$_3$] (Scheme 4 and Table 1), that is, those of Ti (**1**)[14,15] and Hf (**3**).[16] This can also be extended to first-row peralkyl transition-metal complexes, such as those of V^{IV} [≡SiOV(CH_2SiMe_3)$_3$] (**4**), and Cr^{IV} [≡SiOCr(CH_2EMe_3)$_3$] (**5a** E = C and **5b** E = Si).[17] Zirconium cyclopentadienyl derivatives, such as [Cp_2ZrMe_2] and [Cp*ZrMe$_3$] (Cp = C_5H_5 and Cp* = C_5Me_5) also react in a similar manner with silica, that is, with the formation of monosiloxy complexes and with the concomitant evolution of one equivalent of methane during grafting (Scheme 5). The corresponding surface complexes were also fully characterized by elemental analysis, IR and NMR spectroscopy, which included ^2H and ^{13}C labeling studies (for IR and NMR spectroscopy studies, respectively) as [≡SiOZrCp_2Me] (**6**) and [≡SiOZrCp*Me$_2$] (**7**), respectively (Table 1).[18] In contrast, the corresponding actinide complexes [Cp*$_2$AnMe$_2$] (An = Th, U) react with silica to give a more complex mixture of surface compounds by reactions with both surface silanol groups and siloxane bridges which is in accord with their stronger electrophilicity and oxophilic character [Eq. (6)].[19]

The reactivity of silica was thought to be understood until the grafting of [Ta(=CHtBu)(CH_2tBu)$_3$] was attempted on a $SiO_{2-(500)}$. In contrast to what was observed in the case of peralkyl homoleptic complexes of Group 4 and first-row transition metals, a 65:35 mixture of monosiloxy ($x = 1$, **8**) and bissiloxy ($x = 2$, **9**) surface complexes [(≡SiO)$_x$-Ta(=CHtBu)(CH_2tBu)$_{3-x}$] was obtained on a $SiO_{2-(500)}$ upon grafting, under identical conditions, according to mass-balance analysis (neopentane evolution during grafting and after hydrolysis).[20] A careful deuterium-labeling study showed that during grafting [Ta(=CHtBu)(CH_2tBu)$_3$] reacted with deuterated silica by electrophilic cleavage of a neopentyl group (≈ 20 %) and addition of the [≡SiOD] onto the alkylidene moiety to form a tetrakis(neopentyl)tantalum surface complex [(≡SiO)Ta(CH_2t-

Table 1: Solid-state NMR spectroscopic data for selected monosiloxy complexes.[a]

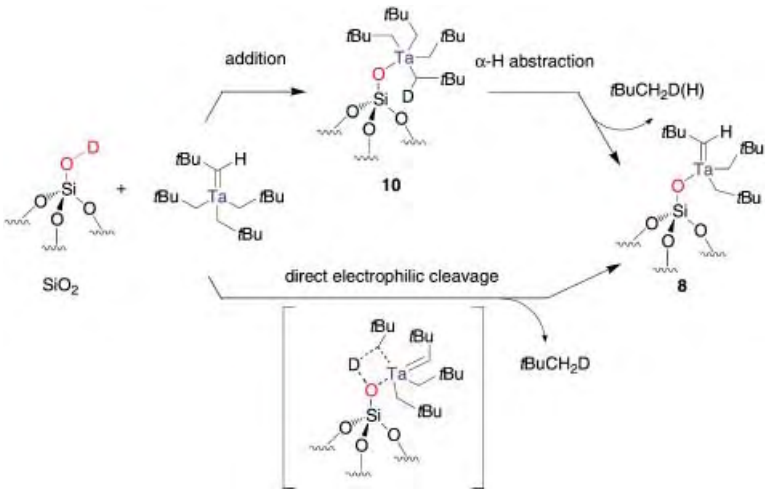
Structure	$\delta(^1H)$ [ppm]	Assignment	$\delta(^{13}C)$ [ppm]	Assignment
$[(\equiv SiO)Ti(CH_2tBu)_3]$ (**1**)	2.1	CH_2tBu	115	CH_2tBu
	0.8	$CH_2C(CH_3)_3$	34	$CH_2C(CH_3)_3$
			38	$CH_2C(CH_3)_3$
$[(\equiv SiO)Zr(CH_2tBu)_3]$ (**2**)	–	CH_2tBu	96	CH_2tBu
	1.1	$CH_2C(CH_3)_3$	–	$CH_2C(CH_3)_3$
			35	$CH_2C(CH_3)_3$
$[(\equiv SiO)Hf(CH_2tBu)_3]$ (**3**)	–	CH_2tBu	108	CH_2tBu
	0.8	$CH_2C(CH_3)_3$	36	$CH_2C(CH_3)_3$
			–	$CH_2C(CH_3)_3$
$[(\equiv SiO)Zr(CH_3)Cp_2]$ (**6**)	0.2	CH_3	22	CH_3
	5.8	C_5H_5	–	C_5H_5
$[(\equiv SiO)Zr(CH_3)_2Cp^*]$ (**7**)	−0.3	CH_3	37	CH_3
	1.7	$C_5(CH_3)_5$	120	$C_5(CH_3)_5$
			9	$C_5(CH_3)_5$
$[(\equiv SiO)Ta(=CHtBu)(CH_2tBu)_2]$ (**8**)[b]	1.0	CH_2tBu	96	CH_2tBu
	1.0	$CH_2C(CH_3)_3$	30	$CH_2C(CH_3)_3$
			–	$CH_2C(CH_3)_3$
	4.2	$=CHtBu$	246	$=CHtBu$
	1.0	$=CHC(CH_3)_3$	30	$=CHC(CH_3)_3$
			–	$=CHC(CH_3)_3$
$[(\equiv SiO)Mo(\equiv CtBu)(CH_2tBu)_2]$ (**11**)[b]	1.1	CH_2tBu	32	$CH_2C(CH_3)_3$
	2.8		–	$CH_2C(CH_3)_3$
	1.1	$CH_2C(CH_3)_3$	329	$\equiv CtBu$
	1.3	$\equiv CC(CH_3)_3$	28	$\equiv CC(CH_3)_3$
			54	$\equiv CC(CH_3)_3$
			90	CH_2tBu
$[(\equiv SiO)W(\equiv CtBu)(CH_2tBu)_2]$ (**12**)	–	CH_2tBu	32	$CH_2C(CH_3)_3$
	–		–	$CH_2C(CH_3)_3$
	1.1	$CH_2C(CH_3)_3$	318	$\equiv CtBu$
	1.3	$\equiv CC(CH_3)_3$	32	$\equiv CC(CH_3)_3$
			54	$\equiv CC(CH_3)_3$
			95	$CH_2C(CH_3)_3$
$[(\equiv SiO)Re(\equiv CtBu)(=CHtBu)(CH_2tBu)]$ (**13**)[b]	2.6	CH_2tBu	49	CH_2tBu
	3.1		32	$CH_2C(CH_3)_3$
	1.1	$CH_2C(CH_3)_3$	35	$CH_2C(CH_3)_3$
	11.1	$=CHtBu$	247	$=CHtBu$
	1.25	$=CHC(CH_3)_3$	31	$=CHC(CH_3)_3$
			45	$=CHC(CH_3)_3$
	1.4	$\equiv CC(CH_3)_3$	291	$\equiv CtBu$
			29	$\equiv CC(CH_3)_3$
			53	$\equiv CC(CH_3)_3$

[a] The structure of all compounds reported herein is consistent with mass-balance analysis, that is, the evolution of one alkane molecule per grafted metal atom during grafting and of the complementary alkane content upon hydrolysis or hydrogenolysis of the surface complex. [b] Fully characterized by 2D HETCOR solid-state NMR spectroscopy.



Bu)$_4$] (**10**) which then forms **8** by means of an α-H abstraction (≈80%; Scheme 6). A similar reactivity pattern was found for the grafting of $[W(\equiv CtBu)(CH_2tBu)_3]$ with $SiO_{2\text{-}(500)}$, which gave a mixture of mono and bisgrafted surface complexes containing various ligands (alkyl, alkylidene, and alkylidyne).[21,22] Their reactivity and in particular the pseudo-Wittig reaction suggested the presence of an alkylidene ligand, but this system is too complex to allow better characterization.

These last two examples do not follow the criterion of a homogeneous molecular structure on a surface! Increasing the temperature of partial dehydroxylation of silica leads to isolation of the silanol groups. Therefore, by using a $SiO_{2\text{-}(700)}$ it is possible to generate the monosiloxy complex **8** selectively (>95%).[23] It is important to note that unenriched solid-state NMR spectroscopy of **8** provided little information, because of the poor signal-to-noise ratio, for the detection of carbon atoms directly bonded to the metal center and more specifically for metal–alkylidene carbon atoms (the methyl groups of the *t*Bu fragment are usually the only type of carbon atom detected). Therefore, the use of partially ^{13}C-enriched organometallic precursors is usually necessary. In this case—$[\equiv SiOTa(=C^*HtBu)(C^*H_2tBu)_2]$ ^{13}C-enriched on the positions α to the metal center (noted *)—solid-state NMR spectroscopy clearly demonstrates the presence of neopentyl and neopentylidene ligands, which confirm its structure (Figure 1a).[24] Furthermore 2D HETCOR solid-state NMR spectroscopy of **8** allows its identity to be established with, for example, a clear correlation between the carbene proton ($\delta = 4.2$ ppm) and the carbon atom ($\delta = 246$ ppm; Figure 1c–d). EXAFS data are also fully consistent with the structure of **8**, and indicate the presence of four atoms around the Ta center at distances of 2.15 Å (2 Ta–C), 1.87 Å (1 Ta–O + 1 Ta=C). Moreover, a corresponding molecular complex, $[(C_5H_9)_7(Si_7O_{12})SiOTa(=CHtBu)(CH_2tBu)_2]$ (**8m**)—prepared by the reaction of a molecular analogue of an isolated silica silanol group—displays resonance signals with chemical shifts in the ^1H and ^{13}C spectra close to or identical to those of **8** (Scheme 7). This reaction, easily monitored by NMR spectroscopy has allowed the detection of a reaction intermediate $[(C_5H_9)_7(Si_7O_{12})SiOTa(CH_2tBu)_4]$ (**10m**), which is the product of the addition of the silanol group to the carbene moiety of



Scheme 6. Surface chemistry of the grafting of [Ta(=CH*t*Bu)(CH$_2$*t*Bu)$_3$] on silica.

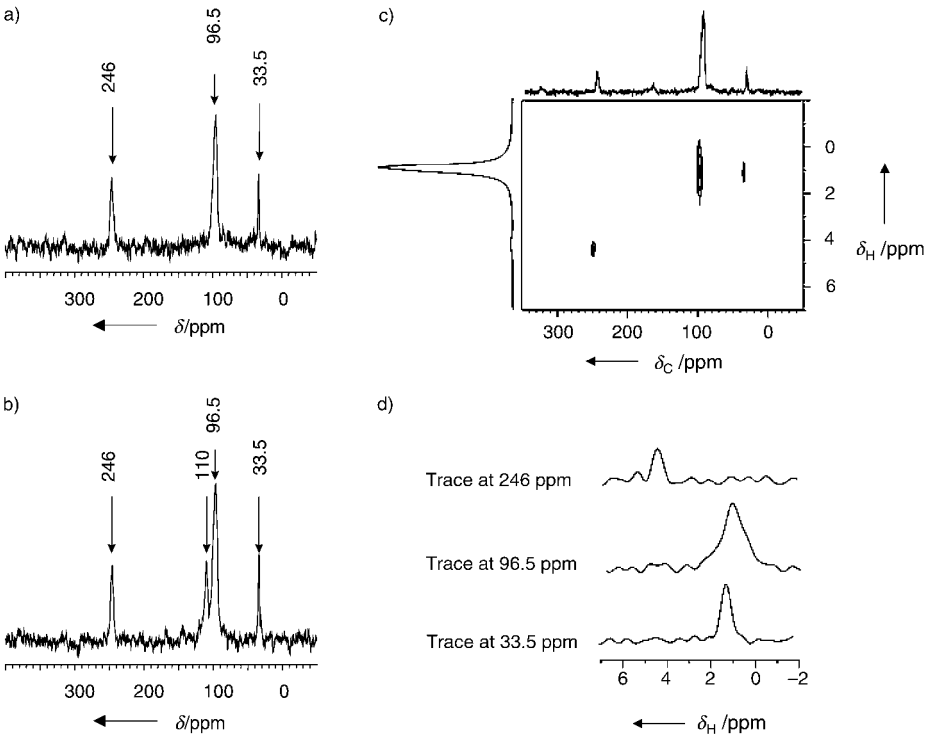
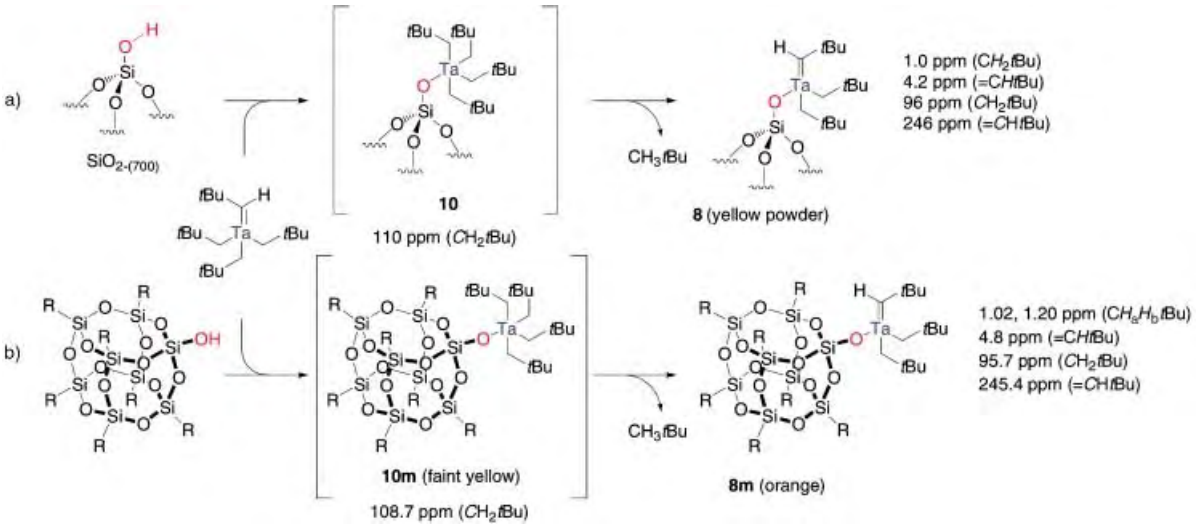


Figure 1. a) CP/MAS ^{13}C Solid-state NMR spectrum of **8**, b) CP/MAS ^{13}C solids-state NMR spectra of **8** and **10**, c) 2D ^{1}H-^{13}C HETCOR solid-state NMR spectra of **8** (2 ms of contact time), d) proton traces of the signals at $\delta = 246$, 96.5, and 33.5 ppm.

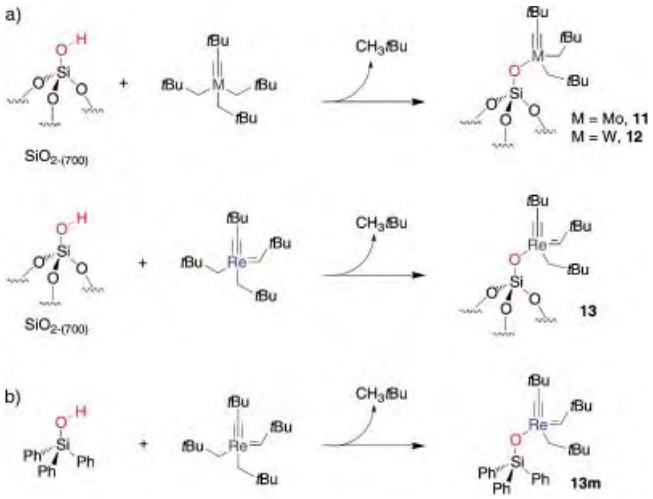
[Ta(=CH*t*Bu)(CH$_2$*t*Bu)$_3$] and which slowly decomposes by α-H abstraction into **8m**. This result led to the detection of the corresponding intermediate **10** on the silica surface by solid-state NMR spectroscopy if low temperatures and short evaporation times were used during the reaction of [Ta(=CH*t*Bu)(CH$_2$*t*Bu)$_3$] with silica (Figure 1b).

The investigation of the reactivity of transition metals with $SiO_{2\text{-}(700)}$ was extended to Groups 6 and 7, namely [M(≡C*t*Bu)(CH$_2$*t*Bu)$_3$] (M = Mo or W) and [Re(≡C*t*Bu)(=CH*t*Bu)(CH$_2$*t*Bu)$_2$]. Here again, perhydrocarbyl complexes react to give a well-defined monosiloxy surface complex, this characterization is supported by elemental analysis and gas evolution, that is, the evolution of one neopentane per grafted metal and the retention of the complementary ligands around the metal center (Scheme 8). Because of the structural complexity of the starting molecular complexes (in contrast to homoleptic complexes such as [M(CH$_2$*t*Bu)$_4$]) in these cases (M = Ta, Mo, W, and Re), NMR spectroscopy was critical in determining the structure of the surface complexes. Therefore using ^{13}C-enriched complexes, 1D solid-state NMR spectroscopy clearly indicated the presence of different type of ligands for the following structures: [≡SiOM(≡C*t*Bu)(CH$_2$*t*Bu)$_2$] (**11,** M = Mo;[25] **12,** M = W[26]) and [≡SiORe(≡C*t*Bu)(=CH*t*Bu)(CH$_2$*t*Bu)] (**13**; Table 1 and Scheme 8).[27,28] 2D HETCOR solid-state NMR spectroscopy is probably even more important for characterizing these systems. Indeed the presence of various ligands gives rise to numerous resonance signals in both the ^{1}H and ^{13}C NMR spectra. The chemical shifts of the signals arising from the different carbon atoms positioned α to the metal center are usually sufficiently different to assign the resonance signals and postulate a structure; nonetheless correlation spectroscopy can confirm these assignments and allow even more information to be extracted that is not readily available from 1D NMR spectroscopy. For example, the two signals at $\delta = 2.6$ and 3.1 ppm in the ^{1}H NMR spectrum of **13** were tentatively assigned to the two diastereotopic methylene protons of the neopentyl fragment based on the NMR spectral data obtained on the corresponding molecular complex.[28] The correlation peak in 2D HETCOR solid-state NMR spectrum between these two signals and the signal of the methylene carbon atom allows an unequivocal assignment, which is further corroborated by the similar chemical shifts in both ^{1}H and ^{13}C NMR spectra for molecular models (Scheme 8 and Table 1). Another example is the "absence" of signals for methylene protons (CH$_2$*t*Bu) of the neopentyl fragment for **8**[24] (Figure 1) and **11**[25] in the ^{1}H NMR spectra; such information can be extracted indirectly from the ^{13}C dimension in the 2D NMR spectrum.

On a $SiO_{2\text{-}(700)}$, the silanol groups are sufficiently isolated to yield monosiloxy surface complexes in all cases to date. In fact, Group 4 metals also yield monosiloxy surface complexes on a $SiO_{2\text{-}(700)}$, albeit with a lower weight content of metals than on $SiO_{2\text{-}(500)}$ because of the decrease in the surface density of silanol groups.[29]



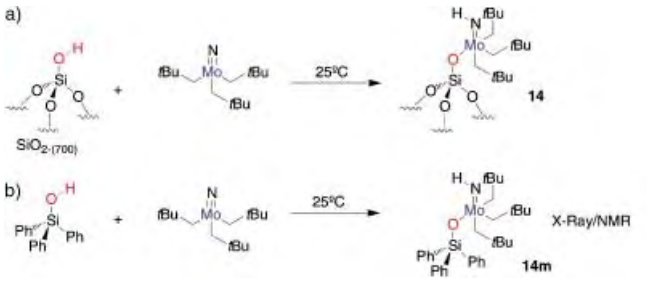
Scheme 7. Comparison of surface and molecular chemistry in the reaction of $[Ta(=CHtBu)(CH_2tBu)_3]$ with a) silica partially dehydroxylated at 700 °C and b) a POSS (R = *c*-C_5H_9), a model for the silica surface.



Scheme 8. a) Surface chemistry of Group 6 and 7 metals with silica partially dehydroxylated at 700 °C and b) a molecular analogue of **13**.

Noteworthy is also the reaction of $[Mo(\equiv N)(CH_2tBu)_3]$ with silica ($SiO_{2\text{-}(500)}$ or $SiO_{2\text{-}(700)}$), which yields $[\equiv SiOMo(=NH)(CH_2tBu)_3]$ (**14**) from the addition of the silanol to the nitrido ligand as demonstrated by IR and NMR spectroscopy as well as model studies (**14m**; Scheme 9).[30] Moreover, upon heating at 70 °C, $[\equiv SiOMo(=NH)(=CHtBu)(CH_2tBu)]$ (**15**) is formed with the release of one equivalent of neopentane by α-H abstraction. In this case the presence of the alkylidene ligand was demonstrated by the formation of one equivalent of 2,4,4-trimethyl-2-pentene by a pseudo-Wittig reaction between **15** and acetone [Eq. (7)].[30a]





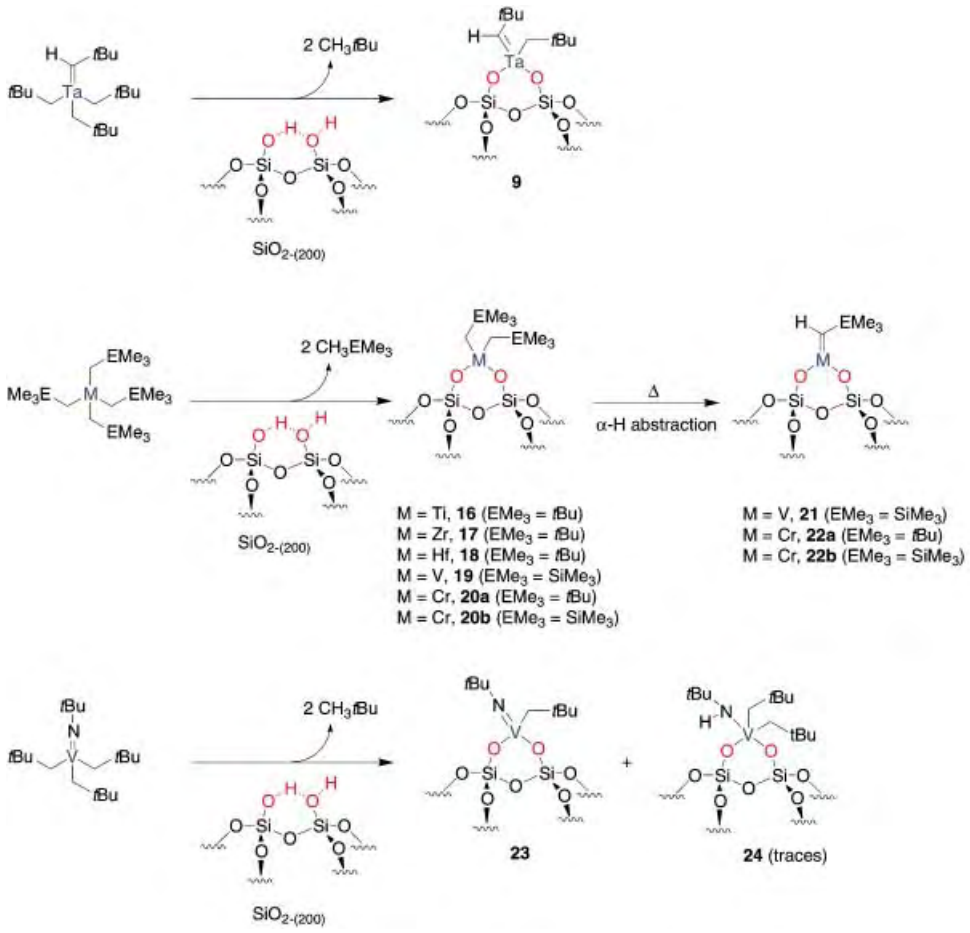
Scheme 9. a) Surface chemistry of $[Mo(\equiv N)(CH_2tBu)_3]$ with silica partially dehydroxylated at 700 °C and b) a molecular analogue of **14**.

An important feature of molecular organometallic chemistry is its ability to vary the number of bonds between the metal center and the ligands. One might ask if it is possible to control the grafting reaction to yield exclusively a bisgrafted surface complex as in the case of Ta.

3.3.2. *Bisgrafted Bissiloxy Organometallic Complexes $[(\equiv SiO)_2ML_n]$*

The use of higher temperatures (> 500 °C, e.g. 700 °C) allows the generation of isolated surface silanol groups and therefore the generation of monografted species. The use of lower temperatures of dehydroxylation should provide the reverse effect and favor the formation of bisgrafted metal complexes. Note however, that a too low temperature of dehydroxylation can induce the retention of small amounts of physisorbed water molecules, which could be significant during the grafting studies (reaction of water with the organometallic complex during or after grafting).

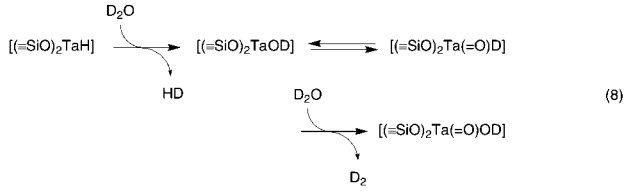
Partial dehydroxylation of silica at 200 °C ($SiO_{2\text{-}(200)}$) can be used, according to mass-balance analyses, to generate selectively well-defined bissiloxy complexes: $[(\equiv SiO)_2M(CH_2EMe_3)_2]$ (**17**, M = Zr, E = C),[31] (**19**, $M = V^{IV}$, E = Si) and ($M = Cr^{IV}$ **20a** and **20b** for E = C or Si, respectively; Scheme 10).[17,32,33] Interestingly, the latter complexes can be

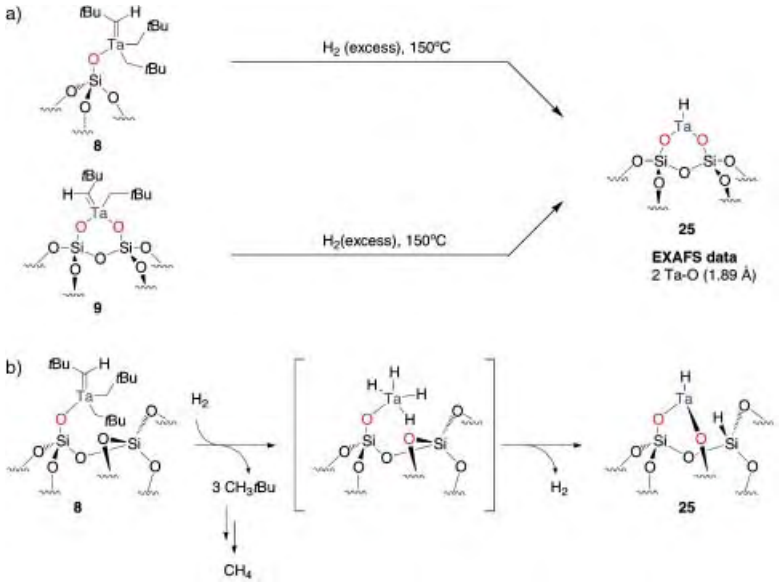


Scheme 10. Surface chemistry of Group 4 and 5 transition metals on silica partially dehydroxylated at low temperatures (< 300 °C, typically 200 °C).

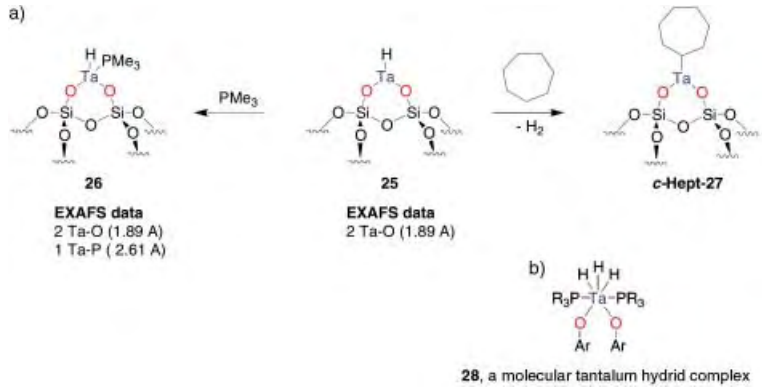
converted into the alkylidene complexes $[(\equiv SiO)_2M(=CHEMe_3)]$ (**21** M = V and E = Si; **22a** and **22b** for M = Cr with E = C and Si, respectively), upon treatment at 70 °C along with the formation of one equivalent of neopentane or tetramethylsilane. The process of elimination of neopentane was clearly established as an α-H abstraction, and kinetic studies further confirmed this pathway in the case of **20a** ($\Delta H^{\neq} = 11$ kcal mol^{-1}, $\Delta S^{\neq} = -43$ cal K^{-1} mol^{-1}).[33] Grafting of $[Ta(=CHtBu)(CH_2tBu)_3]$ on a $SiO_{2\text{-}(200)or(300)}$ also generates the bissiloxy surface complex $[(\equiv SiO)_2Ta(=CHtBu)(CH_2tBu)]$ (**9**).[23] Noteworthy is the reaction of $[V(=NtBu)(CH_2tBu)_3]$ with $SiO_{2\text{-}(200)}$ which gives $[(\equiv SiO)_2V(=NtBu)(CH_2tBu)]$ (**23**); in contrast $[V(=NtBu)(OtBu)(CH_2tBu)_2]$ does not react with SiO_2. The surface of complex **23** was characterized by ^{13}C and ^{51}V NMR spectroscopy, however, the surface chemistry is rather complex because of the presence of the imido ligand.[34] For example, a small amount of $[(\equiv SiO)_2V(NHtBu)(CH_2tBu)_2]$ is also detected, which comes from the addition of a silanol group onto the imido moiety of the molecular complex.

It is also possible to obtain bisgrafted surface complexes from monografted complexes by their thermal treatment under H_2. For example, $[(\equiv SiO)Ta(=CHtBu)(CH_2tBu)_2]$ (**8**) gives $[(\equiv SiO)_2TaH]$ (**25**) by hydrogenolysis of the perhydrocarbyl ligands and further reaction with the siloxane bridges to give **25** and surface Si–H moieties (Scheme 11).[35] The formation of the ≡SiH bonds at the surface is now a general observation: it occurs each time that a silica supported polyalkyl derivative of an early transition metal (Group 4–6) is treated under hydrogen at moderate to high temperatures (typically 50 to 300 °C). During this treatment the alkyl groups of the grafted metal are transformed into hydride units, and these hydrides are able to cleave (≡Si-O-Si≡) bridges, probably by σ-bond metathesis, which yields an additional Si-O-M bond as well as a ≡Si-H bond. This phenomenon is probably a result of the greater "oxophilicity" of the metal center than that of Si. Conversely, $[(\equiv SiO)_2Ta(=CHtBu)(CH_2tBu)]$ (**9**) is also converted into **25** under the same conditions. Therefore a mixture of **8** and **9** is in fact converted into the same surface species **25**. EXAFS data confirms the presence of two oxygen atoms 1.89 Å from the Ta center. Moreover the presence an equimolar ratio of D_2 and HD upon reaction of **25** with D_2O is clearly consistent with the presence of a Ta^{III} center [Eq. (8)].





Scheme 11. a) Generation of silica-supported tantalum hydride **25** and b) the proposed mechanism of its formation.



Scheme 12. a) Reactivity of **25** with cycloheptane and PMe_3 and b) structural comparison of **25** with a molecular analogue **28**.

The reaction of PMe_3 on $[(\equiv SiO)_2TaH]$ (**25**) gives a monophosphane adduct $[(\equiv SiO)_2TaH(PMe_3)]$ (**26**) according to IR, ^{13}C, and ^{31}P NMR spectroscopy as well as EXAFS.[36] Note that the structures of **25** and **26** are somewhat different from the molecular complex $[(ArO)_2TaH_3(PMe_3)_2]$ (**28**) which contains additional phosphane and hydride ligands (Scheme 12).[37] The presence of a single phosphane group is probably because of the surface, which is rather bulky, and can also play the role of a two-electron donor ligand (siloxane bridges). Noteworthy is that the surface complex **25** readily reacts with cycloalkanes (RH) at room temperature to give the corresponding (monocycloalkyl)tantalum(III) surface complexes, $[(\equiv SiO)_2TaR]$, with the concomitant liberation of one equivalent of H_2 (for example: ***c*-Hept-27**; Scheme 12).[35a,38]

3.3.3. *Trisgrafted Trissiloxy Organometallic Complexes, $[(\equiv SiO)_3ML_n]$*

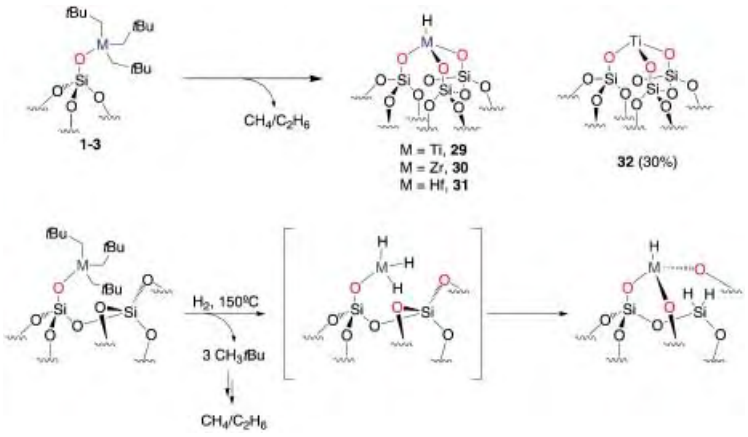
To date there is no evidence for the direct formation of a trissiloxy surface complex by the direct reaction of an organometallic complex with silica (whatever its level of dehydroxylation). On the other hand, the thermal treatment under H_2 of monosiloxyperalkyl complexes of Group 4 metals, $[(\equiv SiO)M(CH_2tBu)_3]$ (**1**–**3**), generate $[(\equiv SiO)_3MH]$ (**29**, M = Ti;[14] **30**, M = Zr;[12,13,39] **31**, M = Hf;[16] Scheme 13), by hydrogenolysis of the M–C into M–H bonds followed by further reaction with the surface siloxane to form new metal-support (M–O) bonds along with Si–H bonds.[35b] Noteworthy is the case of Ti, which also contains 30% of $[(\equiv SiO)_3M^{III}]$ (**32**) along with **29**.

These hydride complexes readily react with alkanes to give stable surface alkyl complexes and H_2. For example, the reaction of cycloheptane and **30** gives the corresponding monocycloheptyl surface complex ***c*-Hept-33** (Scheme 14).[39] Noteworthy is the high selectivity for the activation of primary carbon atoms in the activation of propane, for which a 97% selectivity towards the *n*-propyl complex ***n*Pr-33** is observed.[40] Finally it is also possible to activate methane to give **Me-33**.

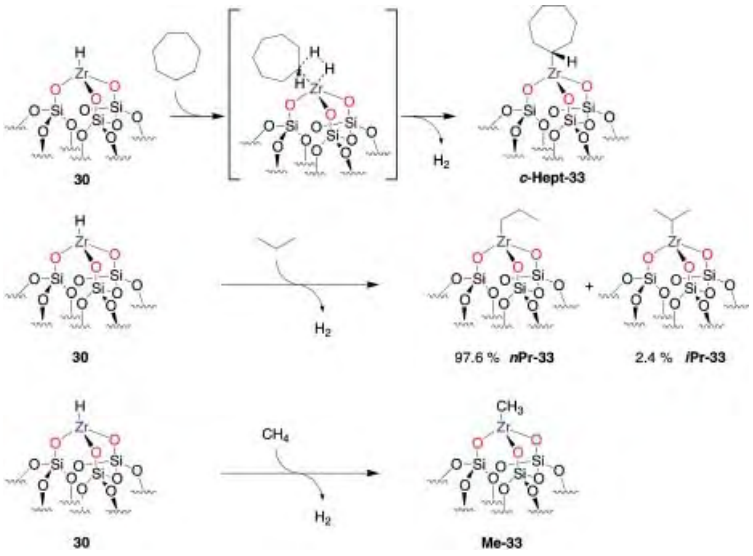
Thermal treatment under H_2 allows access to the trisgrafted or tripodal systems that are not readily obtained from the interaction of organometallic complexes directly with silica, whatever the temperature of dehydroxylation. Moreover, this treatment gives highly electron-deficient surface complexes (**29**–**32** as well as **25**), which readily activate the C–H bond of alkanes at low temperatures. Moreover, these complexes also participate in catalytic reactions that involve a C–C bond activation as a key step; this will be discussed in Section 4.4.

3.3.4. *Alkoxides and Surface Organometallic Complexes*

Understanding the surface reaction of organometallic compounds with silica allows the selective synthesis of



Scheme 13. Generation of silica-supported Group 4 transition-metal hydrides $[(\equiv SiO)_3MH]$ and the mechanism of their formation.



Scheme 14. Alkane activation with $[(\equiv SiO)_3ZrH]$ (**30**).

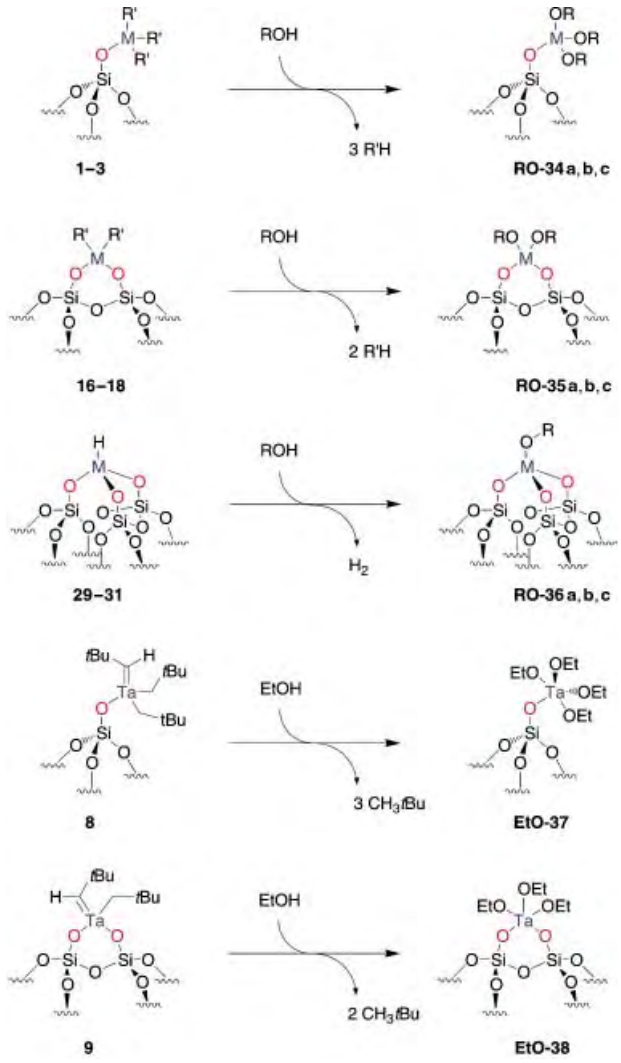
monosiloxy ($x=1$), bissiloxy ($x=2$), or trissiloxy ($x=3$) surface complexes $[(\equiv SiO)_xMY]$ (Y = H or R′), which can then be transformed into their corresponding alkoxide derivatives $[(\equiv SiO)_xMOR]$ by simple metathetical reactions with the corresponding alcohols (ROH; Scheme 15).

By using the aforementioned strategy, it is possible to generate both $[(\equiv SiO)_3TiOR]$ (**RO-36a**; R = Me or *t*Bu) and $[(\equiv SiO)Ti(OR)_3]$ (**RO-34a**; R = Me or *t*Bu) surface complexes from the reaction of the corresponding monohydrido (**29**) and trisneopentyl surface complexes (**1**) with various alcohols, for example, methanol and *tert*-butanol.[41] The same type of reaction can be used to prepare other Group 4 (**RO-34–36b** M = Zr) and Group 5 surface alkoxide complexes. For example, the ethanolysis of **8** and/or **9**, yields the corresponding alkoxides $[(\equiv SiO)Ta(OEt)_4]$ (**EtO-37**) and $[(\equiv SiO)_2Ta(OEt)_3]$ (**EtO-38**).[42]

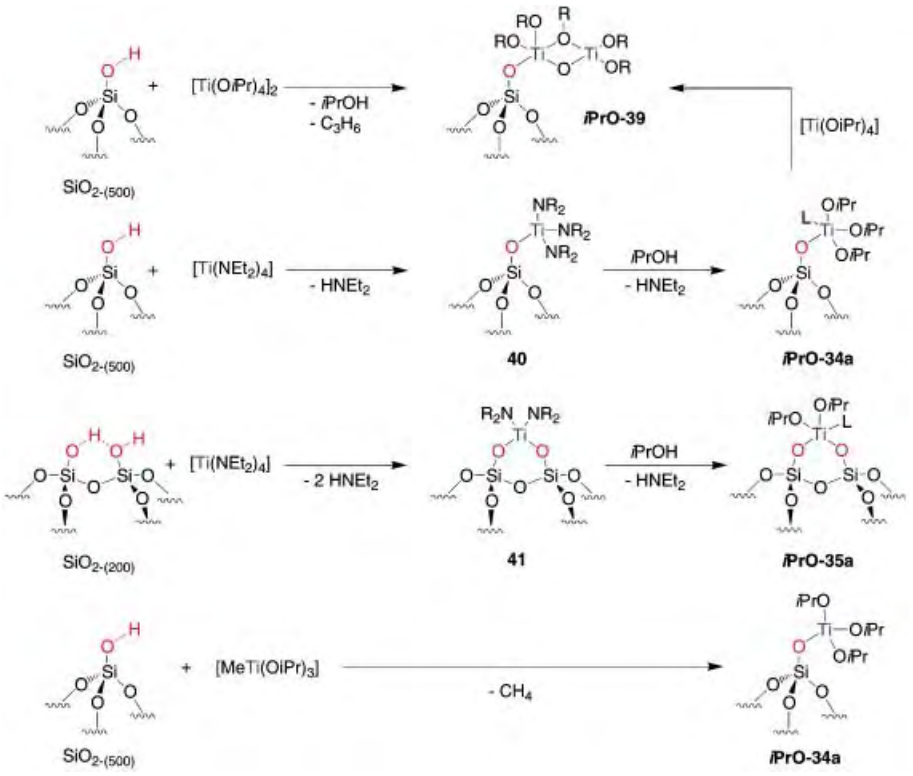
The preparation of alkoxide derivatives should not require organometallic complexes and should be possible by grafting directly metal alkoxides. This aspect of surface organometallic chemistry is still in its infancy, but several mononuclear surface alkoxides have been claimed. It is worth pointing out that molecular precursors can have a great influence on the structure of the surface complexes formed. For example, $[Ti(O\mathit{i}Pr)_4]$ yields a dimer ***i*PrO-39** (according to elemental analysis), while a monomer, $[(\equiv SiO)Ti(O\mathit{i}Pr)_3]$ (***i*PrO-34a**) can be generated by the reaction of $[Ti(NEt_2)_4]$ with silica followed by a treatment with *i*PrOH (Scheme 16).[43] In fact, the reaction of ***i*PrO-34a** with $[Ti(O\mathit{i}Pr)_4]$ also gives the dimer ***i*PrO-39**. Similarly using a $SiO_{2\text{-}(200)}$, it is possible to generate selectively $[(\equiv SiO)_2Ti(NR_2)_2]$ (**41**) which can then be transformed into $[(\equiv SiO)_2Ti(OR)_2]$ (***i*PrO-35a**). However, these alkoxide complexes are obtained with remaining alcohol ligands in their coordination sphere. Noteworthy is therefore the generation of ***i*PrO-34a** from the reaction of silica with $[CH_3Ti(O\mathit{i}Pr)_3]$ with the evolution of one equivalent of methane, the absence of alcohol formation here should provide base-free metal alkoxide surface species.[44]

The grafting of $[V(=O)(O\mathit{i}Pr)_3]$ or $[V(=O)Cl_3]$ yields the corresponding monosiloxy surface complexes $[(\equiv SiO)V(=O)(OR)_2]$ (**42**) and $[(\equiv SiO)V(=O)Cl_2]$ (**43**) independently of the temperature of pretreatment of silica (25–500 °C) according to mass-balance analysis, IR as well as ^{51}V magic-angle spinning (MAS) NMR spectroscopy. This latter technique can, in fact, easily indicate the number of Cl or OR ligands around the metal center (Scheme 17).[45] Noteworthy is the ligand exchange with alcohols in **43**. While monosubsitution is observed even with a large excess of alcohol at room temperature, to give $[(\equiv SiO)V(=O)(OR)Cl]$ (**44**), complete substitution is observed upon reaction at higher temperatures (70 °C) to give $[(\equiv SiO)V(=O)(OR)_2]$ (**42**).[46]

Acetylacetonate (acac) zirconium derivatives supported on silica can be prepared. For example, the reaction of $[Zr(acac)_4]$ with $SiO_{2\text{-}(500)}$ gives $[(\equiv SiO)Zr(acac)_3]$ (**45**) by a direct route, whereas



Scheme 15. Alcoholysis of Group 4 and 5 supported organometallic complexes, a clean preparation of surface alkoxide compounds **a**: M = Ti, **b**: M = Zr, **c**: M = Hf.



Scheme 16. Surface chemistry of molecular titanium alkoxides $[Ti(OiPr)_4]$ and amides $[Ti(NEt_2)_4]$ with silica (L = *i*PrOH or $HNEt_2$).

mal pretreatment of the support (Table 2). Generally, both the type of "molecular" ligand (such as, alkyl, hydride, carbene, carbyne, cyclopentadienyl, alkoxide, amido, imido) as well as the number of bonds between the "solid ligand" and the transition metal can be controlled. In this respect, silica can function as a tunable "ligand", which can behave either as a η^1 or η^2 ligand depending on its thermal treatment. Additionally hydrogenolysis of alkyl derivatives at temperatures typically around 150 °C can provide a clean access to bis- or trisgrafted transition-metal complexes, usually by further reaction of the surface complexes with the siloxane bridges of the silica surface under these conditions.

Finally all these systems can be converted cleanly into the corresponding alkoxide and acac derivatives. Direct routes to alkoxide derivatives have been delineated, nonetheless it seems that the structure of the precursors has a great influence on the outcome of the surface complexes.

Surface organometallic chemistry allows the synthesis of a pool of well-defined surface complexes, that can be used as catalysts. Although there are strong structural analogies with molecular structures in solution, many of them have a structure which differs from that usually obtained in solution. Their electron count (using classical formalism) shows that very electronically unsaturated species can be obtained. This is probably because of the rigidity of the surface which prevents bimolecular reactions and thereby the formation of dimers from highly coordinately unsaturated and reactive intermediates.

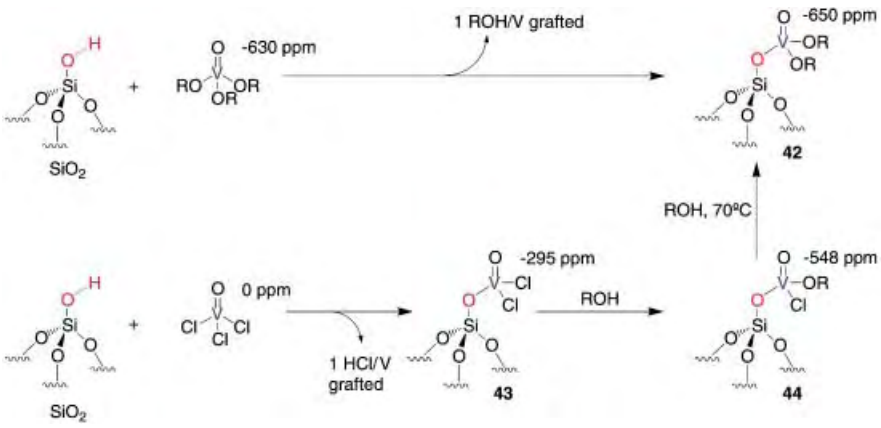
Knowledge of the structures of surface complexes should be advantageous in drawing structure–activity relationships to improve their catalyst performance. In the next Section, the use of these surface complexes as catalysts for known and unprecedented reactions will be exemplified.

$[(\equiv SiO)_3Zr(acac)]$ (**46**) was obtained by the reaction of $[(\equiv SiO)_3ZrH]$ (**30**) and acetylacetone (Scheme 18). Both surface complexes were fully characterized by elemental analysis, EXAFS, and solid-state NMR spectroscopy. The latter data were fully consistent with those obtained from molecular model studies (**45m** and **46m**).[47]

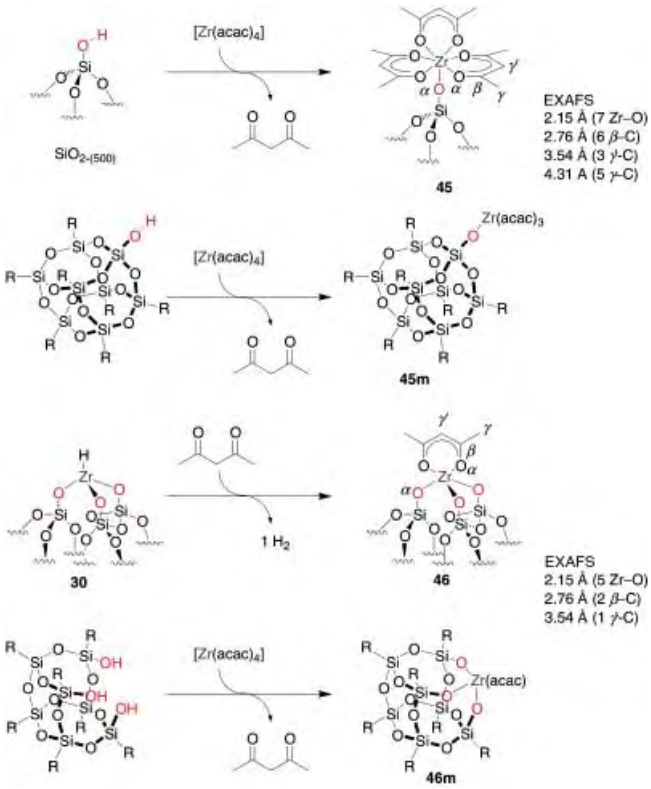
The study of the reaction of transition-metal alkoxides (and amides) with silica is in general more complex than that of alkyl derivatives. One of the reasons is that the alcohols (and amines) which are produced from alkoxides during the grafting are at least partially adsorbed on the silica (or make a base adduct with the metal center), which makes mass-balance difficult to establish. This problem does not usually occur with alkyl derivatives since alkanes are not basic! This kind of surface reaction with alkoxides will probably require very detailed spectroscopic studies as well as mass-balance analysis to further understand the surface chemistry.

3.3.5. *Grafting of Transition Metals onto Silica: Conclusions*

These investigations show that it is possible to control the mode of grafting of transition metals onto a silica through the temperature of the ther-



Scheme 17. Surface chemistry of molecular oxovanadium alkoxides and chlorides: the use of ^{51}V MAS NMR spectroscopy to discriminate surface species.



Scheme 18. Preparation and characterization of a) mono- and b) tris-grafted zirconium acetylacetonate surface complexes (R = *c*-C_5H_9).

Table 2: Influence of the temperature of partial dehydroxylation on the structure of grafted complexes.[a]

Molecular complexes	$SiO_{2-(700)}$	$SiO_{2-(500)}$	$SiO_{2-(200)}$
$[Ti(CH_2tBu)_4]$	Mono (**1**)	Mono (**1**)	–
$[Zr(CH_2tBu)_4]$	Mono (**2**)	Mono (**2**)	Bis (**17**)
$[Hf(CH_2tBu)_4]$	Mono (**3**)	Mono (**3**)	–
$[V(CH_2SiMe_3)_4]$	–	Mono (**4**)	Bis (**19**)
$[Ta(=CHtBu)(CH_2tBu)_3]$	Mono (**8**)	Mix (**8**/**9**)	Bis (**9**)
$[Cr(CH_2tBu)_4]$	–	Mono (**5a**)	Bis (**20a**)
$[Cr(CH_2SiMe_3)_4]$	–	Mono (**5b**)	Bis (**20b**)
$[Mo(\equiv CHtBu)(CH_2tBu)_3]$	Mono (**11**)	–	–
$[W(\equiv CtBu)(CH_2tBu)_3]$	Mono (**12**)	Mix[b]	–
$[Re(\equiv CtBu)(=CHtBu)(CH_2tBu)_2]$	Mono (**13**)	–	–

[a] Mono, bis, and mix refer to mono-, bisgrafted, and mixture of the two, respectively, as confirmed by mass-balance analysis in all cases.
[b] Undetermined mixtures of surface complexes.

4. Application of Surface Organometallic Chemistry to Heterogeneous Catalysis

One of the main objectives of surface organometallic chemistry is to prepare "well-defined" and ultimately "single-site" heterogeneous catalysts. The strategy is usually the following: if one wishes to realize a catalytic reaction the first step consists of drawing a mechanism deduced from elementary steps already known in molecular organometallic chemistry. From this mechanistic scheme, it is then possible to conceive a coordination sphere for the metal center with the right ligand environment, including the surface oxygen atoms.

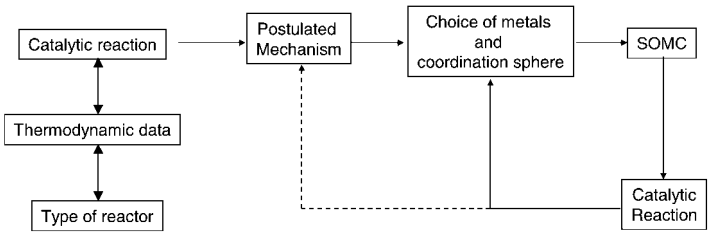


Figure 2. Targeted improvements in heterogeneous catalysis through surface organometallic chemistry (SOMC).

Then, through surface organometallic chemistry, one constructs, on the surface, this surface organometallic complex. This step is probably the most time consuming, since it requires expertise both in surface science and also in molecular organometallic techniques. When the surface organometallic complexes are prepared and sufficiently characterized, then catalysis is carried out with two sets of results: the expected reaction is observed with some degree of activity and selectivity. The strategy is then to modify the coordination sphere so as to increase activity, selectivity, and lifetime. And the loop of improvement continues (Figure 2). The other outcome is that the desired reaction does not take place, and an unexpected catalytic reaction is observed which sometimes gives even more interesting results: the discovery of the alkane metathesis reaction belongs to this second category (see Section 4.4.).

4.1. Olefin Polymerization

The presence of metal–carbon or eventually metal–hydride bond(s) in surface organometallic complexes makes them good candidates for polymerization catalysts.[3,6,48] This was in fact one of the reasons why the early work on surface organometallic chemistry started in the field of polymerization. At that time the goals were to find new heterogeneous catalysts for polymerization reactions.[3] If one excludes the Phillips catalysts, for which some Cp_2Cr^{II} precursors can be used (or at least this was claimed),[49] the first generation of supported metal-hydride, -alkyl, or -Cp complexes were not used commercially.

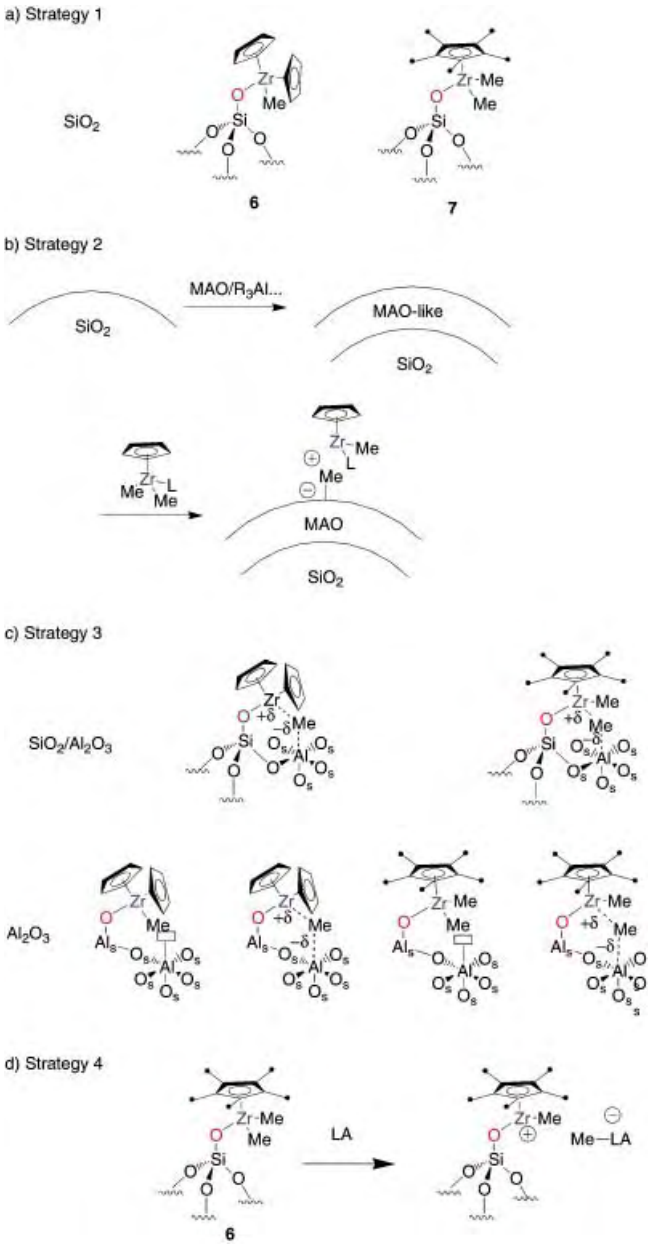
In homogeneous catalysis, one of the major developments in olefin polymerization was the discovery of the metallocene-based catalysts[50] and the possible control of the microstructure and properties of polymers by the right choice of ligands and co-catalysts, in particular methylaluminoxan (MAO).[51] Various strategies have been used to graft metallocene species onto surfaces to obtain polymerization catalysts:

1) The generation of the corresponding well-defined supported surface complexes, such as $[(\equiv SiO)ZrCp_2Me]$ (**6**) and $[(\equiv SiO)ZrCp^*Me_2]$ (**7**)[18,52,53] was investigated. However, these grafted systems showed little activity in polymerization (Table 3). This is not too surprising if one considers that they are neutral complexes, whereas active homogeneous Group 4 catalysts are usually cati-

onic.[53] Several strategies have been undertaken to avoid this problem.

2) The support can be treated first with alkylating agents, such as MAO or alkylaluminum, to eliminate OH groups and also to support the alkylating agent, and then this thus-modified silica is brought into contact with the metallocene complex. In fact, the metallocene complex is not really bound to the surface,[54] but the complex is cationic and "floats" above the surface as a kind of ion pair with the anionic surface. The complexity of this surface chemistry was investigated through model studies, which further demonstrated the diversity of the reactivity of surface aluminum alkyl derivatives with transition-metal complexes.[55]
3) Another strategy consists of directly grafting the metallocene complex onto supports other than silica with a Lewis acid center, such as silica–alumina (SiO_2/Al_2O_3) or alumina (Al_2O_3), for which the zirconium center may become partially cationic by transfer of the methyl group onto an adjacent aluminum vacant sites (Scheme 19).[18,52,53] In our laboratory we have studied ethylene polymerization in the absence of co-catalyst with the silica–alumina or alumina surface complexes, namely [$ZrCp^*Me_3/SiO_2$-Al_2O_3], [$ZrCp_2Me_2/SiO_2$-Al_2O_3], [$ZrCp^*Me_3/Al_2O_3$], and [$ZrCp_2Me_2/Al_2O_3$], which had been fully characterized by IR and NMR spectroscopy, and by EXAFS. The activities obtained in the series of alumina-supported monocyclopentadienyl zirconium complexes have always been higher, whatever the oxide used, than those found for the biscyclopentadienyl analogues (Table 3). In addition, regardless of the type of the starting zirconium complex, that is the mono- or biscyclopentadienyl series, the following order of activity has been established based on the support material: SiO_2-$Al_2O_{3(500)} < Al_2O_{3(1000)} < Al_2O_{3(500)}$. Nevertheless the activity obtained for the best catalyst, [$Cp^*ZrMe_3/Al_2O_{3(500)}$], remained low by comparison to the level of activity reported for the homogeneous systems. The same trend has been observed by Marks et al. for the activity of supported actinides.[19]
4) it is also possible to introduce an external molecular "noncoordinating Lewis acid" on the neutral grafted complexes so as to produce a "non-floating" cationic species. In this case, the zirconium center remains σ-bonded to the surface and has a cationic propagating center (e.g. a methyl group), which is generated by the Lewis acid additive abstracting a methyl group from the coordination sphere to make the cationic species. Effectively when the oxide bore acidic Lewis centers (MAO or $B(C_6F_5)_3$), the resulting surface species LA/$Cp^*ZrMe_3/SiO_{2(500)}$ and LA/$Cp^*ZrMe_3/Al_2O_{3(500)}$ (where LA = lewis acid) displayed an increase in activity (Table 3). Yet these catalysts show still moderate activity if compared to their homogeneous analogues. This could be because of p_π–d_π back donation to the zirconium center, which would decrease the electrophilicity of the zirconium center, making it less active.

The EXXON Corporation has recently disclosed in a very elegant way, a MAO-free route, which relies on the formation



Scheme 19. a) Strategy 1: direct grafting of alkyl zirconium metallocene derivatives onto partially dehydroxylated silica. b) Strategy 2: activation by passivation of the silica surface with MAO or alkylaluminum reagents. c) Strategy 3: activation by support effects. Comparison of surface species of zirconium metallocene derivatives grafted on silica (strategy 1), silica alumina, and alumina. d) Strategy 4: activation by Lewis acid (LA) additives to silica supported metallocene catalysts.

of surface cationic metal–alkyl species in which the coordination sphere is apparently well-defined and single-site. The strategy is based on the reaction of silica, sequentially with $B(C_6F_5)_3$ and dimethylaniline, to yield a modified silica with siloxyborato anilinium surface functional groups (**47,** Scheme 20), which is then treated with dialkyl transition-metal complexes to form the single-site floating cationic species **48**.[56,57] These systems indeed gave high activities in the polymerization of ethylene and propylene. The first step, the formation of the borato–anilinium complex [{≡Si-

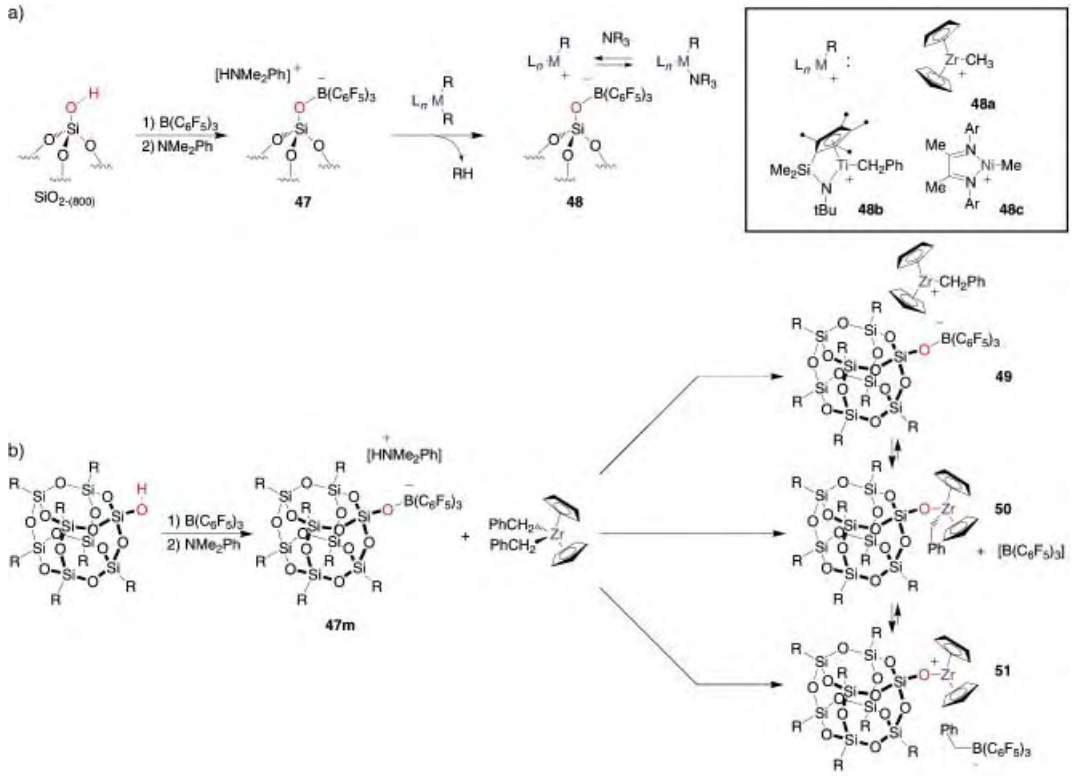
Table 3: Polymerization of ethylene with supported metallocene catalysts prepared by surface organometallic chemistry.

Catalyst	Co-catalyst	Maximum activity [kg(PE) mol (Zr)$^{-1}$ h^{-1}]	Productivity[b] [kg(PE) mol(Zr)$^{-1}$ h^{-1}]
$Cp_2ZrMe_2/SiO_{2\text{-}(500)}$ (**6**)	–	0	–
$Cp_2ZrMe_2/SiO_2\text{-}Al_2O_{3\text{-}(500)}$	–	0	–
$Cp_2ZrMe_2/Al_2O_{3\text{-}(500)}$	–	3[a]	–
$Cp_2ZrMe_2/Al_2O_{3\text{-}(500)}$	–	20[b]	13
$Cp_2ZrMe_2/Al_2O_{3\text{-}(1000)}$	–	0	–
$Cp^*ZrMe_3/SiO_{2\text{-}(500)}$ (**7**)	–	0[a,b]	–
$Cp^*ZrMe_3/SiO_{2\text{-}(500)}$ (**7**)	MAO	260[b]	230
$Cp^*ZrMe_3/SiO_{2\text{-}(500)}$ (**7**)	$B(C_6F_5)_3$	<1[b]	9
$Cp^*ZrMe_3/SiO_2\text{-}Al_2O_{3\text{-}(500)}$	–	0	–
$Cp^*ZrMe_3/Al_2O_{3\text{-}(500)}$	–	20[a]	–
$Cp^*ZrMe_3/Al_2O_{3\text{-}(500)}$	–	76–109[b]	50–90
$Cp^*ZrMe_3/Al_2O_{3\text{-}(1000)}$	–	13[a]	–

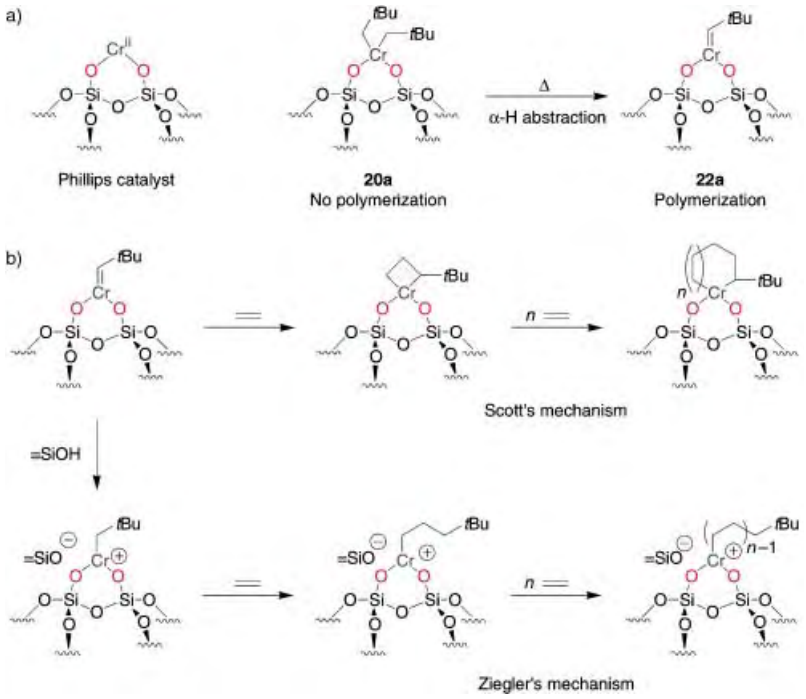
[a] Gas-phase polymerization (0.3 bar of ethylene), rate measured by IR spectroscopy and expressed in kg of PE mol $Zr^{-1}h^{-1}atm^{-1}$. [b] Liquid-phase polymerization (4 bar of ethylene); PE = polyethylene.

$OB(C_6F_5)_3\}^-(HNMe_2Ph)^+]$ (**47**), was confirmed with model (**47m**)[58] and surface studies.[59] Model studies clearly indicated the importance of the base in this system since with pyridine the borato complex is not obtained but only the pyridine–$B(C_6F_5)_3$ adduct. Moreover, these model studies have also shown that the reaction of an organometallic complex with **47m** yields a highly active polymerization catalyst, but the expected floating cationic species equivalent (**49**) would probably have a short life time (if any), since **47m** reacts with $[Cp_2Zr(CH_2Ph)_2]$ to give **50** and **51**, which are both completely inactive as polymerization catalysts. As pointed out by Duchateau et al.[58] the catalytic activity in these systems could in fact only be a result of the reaction of the excess of $B(C_6F_5)_3$ with the organometallic complex. If applicable to the surface species (which can behave very differently), this demonstrates the importance of understanding every step in surface organometallic chemistry, the use of models being a possible approach for this. In fact, it is important to stress the necessity of conducting both detailed model studies and scrupulous analysis of the surface species by using as many methods as possible to ascertain the structure of surface complexes.

Other important ethylene-polymerization processes use Cr-based catalysts (the Phillips process).[60] Scott et al. have studied $[(\equiv SiO)_2Cr(=CHtBu)_2]$ (**22**) as a model for the Phillips catalyst,[61,62] based on their kinetic and chemical reactivity data they have proposed a polymer growth by insertion of ethylene into a growing metallacycle (Scheme 21). On the other hand, based on DFT calculations, Ziegler et al. favor a



Scheme 20. Modication of a) the silica surface b) a POSS with Lewis acids to generate well-defined cationic species (R = *c*-C_5H_9).



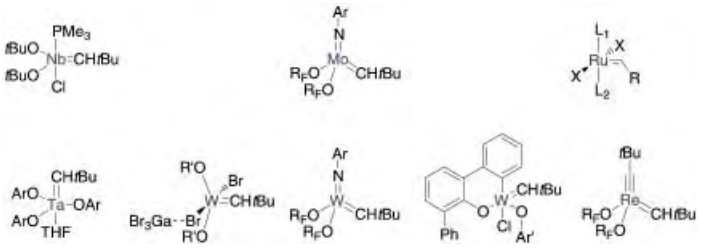
Scheme 21. a) The Phillips catalyst and the preparation of **22a** as a model for the Phillips catalyst (see Scheme 10), b) polymerization of ethylene with a well-defined Cr^{IV}-complex, **22a**.

typical insertion mechanism by a cationic chromium–alkyl intermediate, since a mechanism involving carbenes, such as Scott et al. proposed, would have a too high kinetic barrier. Ziegler et al. proposed that these cationic species would be generated by the protonation of the carbene intermediate by a source of protons, such as the remaining silanol groups of silica.[63,64]

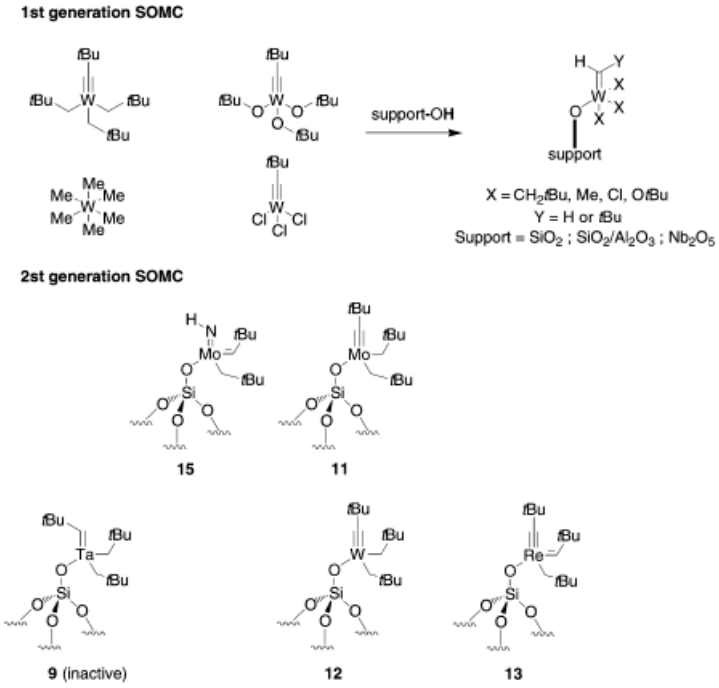
In the field of polymerization there are many examples in which all the concepts and tools of surface organometallic chemistry have been used to develop very active catalysts. The catalysts developed have catalytic behaviors which can be tuned in a very precise way as in molecular chemistry. Some of the results can even be predicted, based on the simple concepts of molecular organometallic chemistry and therefore be used to draw up structure–activity relationship.

4.2. Olefin Metathesis

Olefin metathesis was discovered by using classical heterogeneous catalysts based on transition-metal oxides, mainly MoO_3 and WO_3, supported on silica or alumina, which catalytically transformed propene into ethene and butenes.[65] A major breakthrough was the subsequent discovery in the late 1960s by British Petroleum that Re_2O_7/Al_2O_3 could catalyze this reaction at room temperature and that functionalized olefins, methyl oleate, could also be converted when alkylating agents (such as tetraalkyltin) were used, albeit in low turnovers and with the concomitant formation of inactive catalytic species that could not be regenerated. These systems have been developed into industrial processes for non-functionalized olefins, but in the following thirty years no critical advances have appeared in heterogeneous catalysis, especially for functionalized olefins. On the other hand, molecular organometallic chemistry has clearly demonstrated that metal–carbene complexes are the key intermediates[66] and has been successful in generating well-defined systems of that type.[67] Now the latest generation of homogeneous catalysts display activity, selectivity, and tolerance to functional groups often unseen for their heterogeneous competitors (Scheme 22). Very early on, the preparation of olefin-metathesis catalysts by surface organometallic chemistry was attempted.[68,69] The first rationally designed heterogeneous catalyst was prepared by the grafting of [W(≡C*t*Bu)(O*t*Bu)$_3$] on silica to generate a well-defined metal–alkylidene species from the addition of surface silanol groups to the alkylidyne ligand (Scheme 23).[21,22,70] Although the activities were good (Table 4), the presence of the alkylidene ligand was only assumed based on the chemical reactivity of the surface complex with no direct evidence for such ligands from spectroscopic methods. Further studies on the grafting of [W(≡C*t*Bu)X$_3$] (for X = Cl, O*t*Bu, and CH_2*t*Bu) also provided olefin-metathesis catalysts, but no clear identification of the surface species could be established. More recently the structures of **8, 11**–**13**, and **15** have been clearly established, and their activity in olefin metathesis investigated. While [(≡SiO)Ta(=CH*t*Bu)(CH_2*t*-Bu)$_2$] (**8**) shows little or no activity in olefin metathesis, which is not surprising for a tantalum complex,[71] good activity has been found for the well-defined alkylidyne surface complexes [(≡SiO)Mo(≡C*t*Bu)(CH_2*t*Bu)$_2$] (**11**) and [(≡SiO)W(≡C*t*Bu)(CH_2*t*Bu)$_2$] (**12**).[72] The formation of the active species (alkylidene propagating center) is as yet unclear. It is worth noting that the molecular precursors of the active species (perhydrocarbyl compounds) are completely inactive. The influence of the surface siloxy groups parallels the results from Schrock et al. on the development of efficient homogeneous catalysts for olefin metathesis based on [(RO)$_2$M(=NAr)(=CH*t*Bu)] by the tuning of the alkoxy



Scheme 22. Examples of homogenous olefin metathesis catalysts. $R_F = (CF_3)_2(CH_3)C$, R = Ph or CH=CMe$_2$, R′ = CH_2*t*Bu, Ar = Aryl; L_1/L_2 = tricyclohexylphosphane, triphenylphosphane, or carbene ligands.



Scheme 23. First and second generation of heterogeneous olefin-metathesis catalysts prepared by surface organometallic chemistry.

ligand RO ($RO = OC(CH_3)_3$, $OC(CH_3)(CF_3)_2$ activity: $OC(CH_3)_3 < OC(CH_3)(CF_3)_2$).[73] To date, one of the closest surface analogues to the Schrock catalyst is [(≡SiO)Mo(=NH)(=CH*t*Bu)(CH$_2$*t*Bu)] (**15**)[30] which has, however, shown lower activities than [$(R_{F6}O)_2$Mo(=NAr)(=CH*t*Bu)] (Table 4).

Table 4: Initial rates for the metathesis of propene with various heterogeneous catalysts.[a]

Catalyst	TOF[b]	*T* [°C]	R[c]	Ref.
8	inactive	25	1000	[72]
11	0.53	25	500	[72]
12	0.23	25	1700	[72]
13	0.25	25	500	[27]
15	0.47	25	830	[30]
$Mo(allyl)_4/SiO_2$	0.17	90	—[d]	[65b]
$W(allyl)_4/SiO_2$	0.01–0.1	100	—[d]	[65b]
$W(\equiv Ct Bu)(OtBu)_3/SiO_2$	>1.5	69	10^4[e]	[70]
WMe_6/SiO_2	—[d]	25	—[d]	[68]
MoO_3/SiO_2	0.004	400	—[d]	[65b]
WO_3/SiO_2	—[d]	400	—[d]	[65b]
Re_2O_7/SiO_2	<0.002	150	—[d]	[74]
$[Re(CO)_3OH]_4/SiO_2$	0.00074	150	—[d]	[74]
MoO_3/Al_2O_3	0.05–0.5	200	—[d]	[65b]
WO_3/Al_2O_3	0.1–1.0	300	—[d]	[65b]
Re_2O_7/Al_2O_3	0.05–0.1	25–35	—[d]	[74f]

[a] For comparison [$(R_FO)_2$M(=NAr)(=CH*t*Bu)] type catalysts display initial rates of 4–17 depending on the metal and the nature of R in the metathesis of (*Z*)-2-pentene. [b] Turnover frequency [(mol P)(mol C)$^{-1}$ s^{-1}]; P = product, C = catalyst. [c] Substrate to catalyst ratio, for which the reaction reaches at least the thermodynamic equilibrium. [d] Not readily calculated from the published data. [e] Data obtained for the metathesis of 1-octene.

In contrast the well-defined silica-supported alkylidene Re complex [(≡SiO)Re(≡C*t*Bu)(=CH*t*Bu)(CH$_2$*t*-Bu)] (**13**) has showed unprecedented activity in olefin metathesis[27,72] compared to the heterogeneous Re-based catalysts[74] and even homogeneous ones.[75] This system is even more interesting since other silica supported Re-catalysts are inactive, which suggests that the initiation step (formation of the alkylidene propagating center) is probably the critical step in classical heterogeneous silica-supported catalysts.[74] Moreover, it was possible to observe around one equivalent of the cross-metathesis products from the initiation step in contrast to classical heterogeneous catalysts for which the initiation step is often unclear (Figure 3).

It appears that a new generation of well-defined catalysts can be prepared. These catalysts are based on supported carbene or carbyne complexes of Mo, W, or Re. They exhibit activities, selectivities, and lifetimes in some cases superior to those encountered in classical heterogeneous and even homogeneous catalysis. It will probably take time before this new generation of catalysts will be of practical industrial use since a few problems still have to be solved, such as the ease of preparation and regeneration. But given the competitiveness of these systems in terms of catalytic performances, these chemical challenges should be met in the near future.

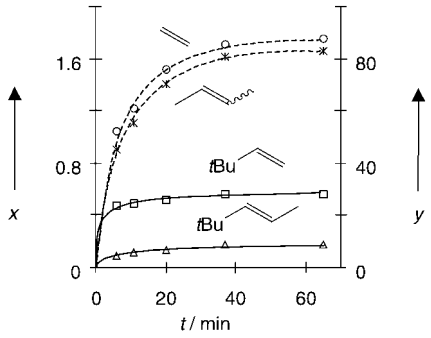
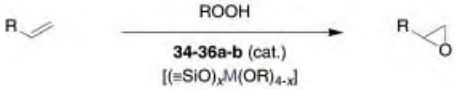


Figure 3. Quantification in the gas phase of 3,3′-dimethylbutene and (*E*)-4,4-dimethyl-2-pentene during propene metathesis (500 equivalents) catalyzed by **13** (one equivalent) at 25 °C; *x* = cross-metathesis products (3,3′-dimethylbutene and (*E*)-4,4-dimethyl-2-pentene) [mol product (mol Re)$^{-1}$], *y* = propene metathesis products (ethene and butene) [mol product (mol Re)$^{-1}$].

4.3. Well-Defined Surface Alkoxides for Oxidation and Lewis Acid Catalysts

Transition-metal alkoxides are known key precursors for epoxidation catalysts. The epoxidation of olefins by using a combined TiX_4/SiO_2 system[76] has been developed by Shell and is still being studied [Eq. (9)].[44,77,78]



(9)

One of the main problems has been to prepare a "single-site" catalyst. Using the aforementioned strategy (see, Section 3.3.4. and Scheme 15), it is in principle possible to generate [(≡SiO)$_3$TiOR] (**RO-36a**), [(≡SiO)$_2$Ti(OR)$_2$] (**RO-35a**), and [(≡SiO)Ti(OR)$_3$] (**RO-34a**) selectively by controlling all the steps from the grafting to the formation of the alkoxide. According to model studies using POSS analogues, the tripodal systems (**RO-34m**) displays better activities and selectivities than the corresponding bipodal (**RO-35m**) or tetrapodal case (**52**).[79] This result suggests that the best environment, in the case of Ti dispersed on silica, is probably that provided by the tripodal system (Scheme 24), which in fact corresponds to a compromise between the accessibility of the titanium center and an increase in the electrophilicity of the metal center, which seems to increase with the number of siloxy substituents. This trend was further confirmed by using the surface complexes **RO-34a, RO-35a,** and **RO-36a**, which have been prepared by surface organometallic chemistry and fully characterized.[41] This investigation has shown that in all cases the trisiloxy titanium (**RO-36a**) system was indeed more efficient (activity and selectivity) than the mono- (**RO-34a**) or the bissiloxy[80] (**RO-35a**; Table 5) compounds and is in agreement with model studies.[79] Choplin et al. have shown that these types of catalysts (M = Ti and Zr) are somewhat less selective when H_2O_2 is used as an oxidant.[15,81] One of the key parameters was the dispersion of the metal centers on the support, especially in the case of Zr, which readily catalyzes the ring opening of the epoxide. The use of hydrophopic silica, that is a silica partially derivatized with trimethylsilyl groups, helps to improve the activity and the selectivity in these systems.

Table 5: Influence of the structure of the alkoxy-titanium surface complexes in the epoxidation of 1-octene.[a]

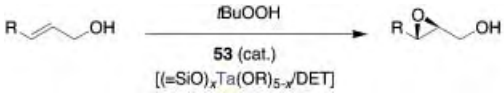
Surface complex	Initial rate[b]	Conversion [%]	Selectivity [%]	Yield [%]
HO-34a	65	99	75	74
HO-36a[c]	174	99	>99	99
X-36a[d]	450	100	96	96
MeO-34a	200	99	99	98
MeO-36a	345	100	>99	>99
***t*BuO-34a**	450	100	98	98
***t*BuO-36a**	930	100	>99	>99

[a] Experimental conditions: TBHP:1-octene:Ti = 150:3000:1. [b] Expressed in [(mol P) (mol C)$^{-1}$ h^{-1}]. [c] Prepared from **29**/**32** mixtures by hydrolysis. [d] Prepared from **29**/**32** mixtures by contact with dry O_2, for which X is probably OH from decomposition of the hydroperoxy compound. P = product, C = catalyst, TBHP = *tert*-butylhydroperoxide.

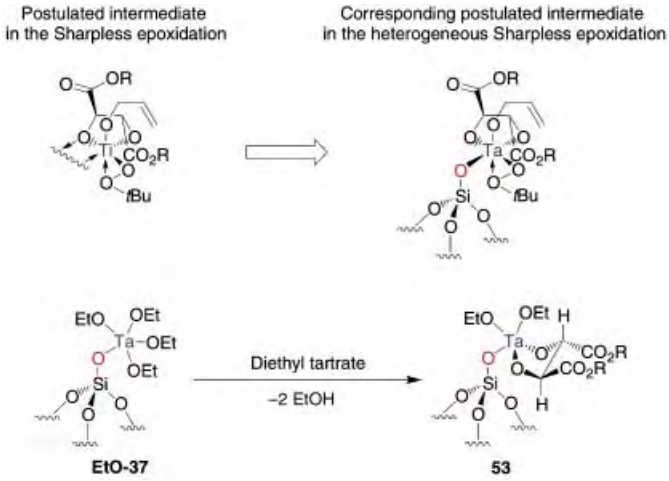


Scheme 24. Understanding the active site of heterogeneous TiX_4/SiO_2 epoxidation catalyst through the catalytic efficiency of the corresponding molecular analogues (R = *c*-C_6H_{11}).

Another example corresponds to a conceptual approach towards the synthesis of a supported Sharpless-epoxidation catalyst [Eq. (10)]. In the homogeneous system, the proposed "active" species consists of a d^0 titanium center surrounded by



the bidentate tartrate, an allyloxy (from the allylic alcohol), and a *tert*-butylperoxy (from *tert*-butylhydroperoxide, TBHP) ligands (Scheme 25).[82] Grafting a Ti complex onto a metal-oxide support could not allow the key coordination sphere described to be attained without loosing one of these three key ligands (the C_2-symmetric chiral bidentate ligand, the oxidant, and the olefin). To obtain a coordination sphere similar to that of the proposed active species for Sharpless epoxidation, one more valence electron is required, such as in



Scheme 25. Heterogeneous Sharpless-epoxidation catatysts.

tantalum, a Group 5 metal. In this case, tantalum can accommodate all the ligands necessary for asymmetric-epoxidation catalysis as well as bonding to the silica surface. Therefore, ethanolysis of **8**/**9** mixtures (prepared on $SiO_{2-(500)}$) yields a mixture of [(≡SiO)Ta(OEt)$_4$] (**EtO-37**) and [(≡SiO)$_2$-Ta(OEt)$_3$] (**EtO-38**), which, upon treatment with diethyl tartrate (det) gives the corresponding [(≡SiO)Ta(det)(OEt)$_2$] (**53**) and [(≡SiO)$_2$Ta(det)(OEt)].[42] This approach has lead to an epoxidation catalyst of activity and selectivity usually better than those obtained with the original Sharpless catalyst (Figure 4) with the advantage of being easily separable from the reaction medium with no detectable leaching. Moreover, the homogeneous tantalum–alkoxide compounds in fact have little activity and give rise to the opposite stereochemistry.

Transition-metal alkoxides are also Lewis acids, for example, [Zr(acac)$_4$] catalyzes transesterification. Its transposition into a heterogeneous catalyst has been realized.[47] Therefore, the corresponding silica-supported complexes [(≡SiO)Zr(acac)$_3$] (**45**) and [(≡SiO)$_3$Zr-

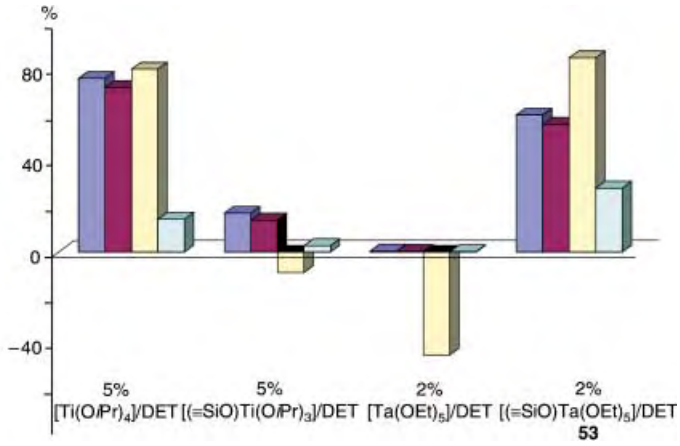
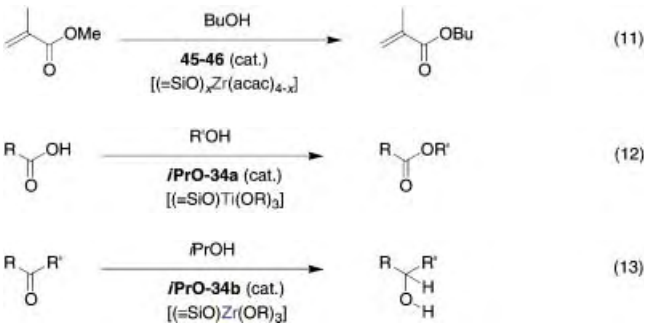


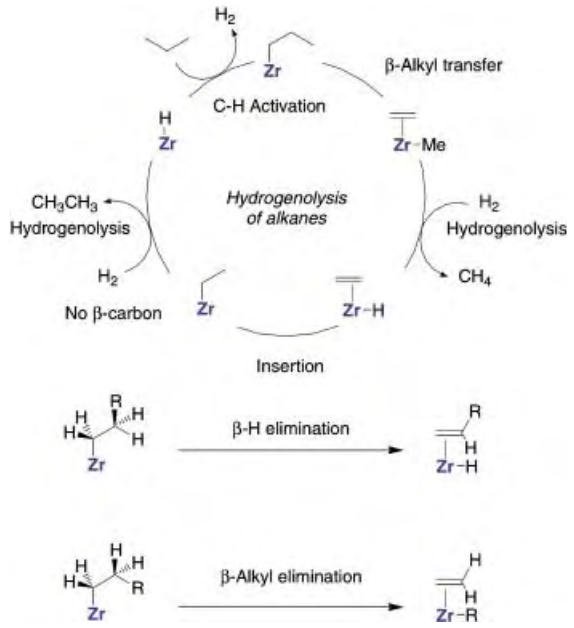
Figure 4. Comparison of asymetric-epoxidation catalysts for allylic alcohols: blue (conversion), red (yield), yellow (% ee), and green (TON).

(acac)] (**46**) show high activities in the transesterification of methyl metacrylate [Eq. (11)], albeit with lower rates than those obtained with the corresponding molecular complex [$Zr(acac)_4$]. Additionally the monosiloxy complex **45** suffered from leaching while **46** did not. Moreover, it was also shown that the loss of activity was a result of the build-up of the corresponding *n*-butoxide derivatives [$(\equiv SiO)_3Zr(OBu)$] (**BuO-36b**) on the surface, which can be circumvented by the addition of acetylacetone.[47c] It is also noteworthy that the family of surface complexes **RO-34–36** (M = Ti and Zr) are also catalysts for esterification (***i*PrO-34a;** Equation (12))[44] and the hydrogen-transfer reaction for ketone reduction (***i*PrO-34b;** Equation (13)).[83]



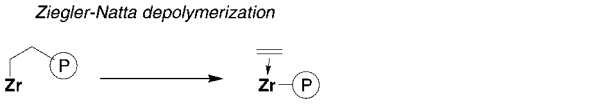
4.4. Catalytic Transformation of Alkanes

The hydrocarbyl surface organometallic species of early transition metals readily give hydrido complexes upon their treatment under a large excess of H_2 at 150 °C (see Scheme 11 and Scheme 13). In the case of Zr and Hf, the hydrido complex [$(\equiv SiO)_3MH$] (**30** and **31** for Zr and Hf, respectively) is formed, and the hydrogenolysis of the neopentyl ligands produces a 3:1 mixture of methane and ethane. This ratio is in good agreement with a β-alkyl transfer as a key step for carbon–carbon bond cleavage (Scheme 26). This mechanism has been further confirmed during the investigation of the low-temperature hydrogenolysis of alkanes, which typically shows that ethane is not cleaved under these conditions. The



Scheme 26. Low-temperature hydrogenolysis of alkanes catalyzed by **30; Zr** = {$(\equiv SiO)_3Zr$}.

ethyl surface complex, [$(\equiv SiO)_3Zr$-Et] (**Et-33**), which does not contain a carbon–carbon bond in the β-position, does not undergo carbon–carbon activation (Figure 5a,b).[39,84] The depolymerization of polyolefin catalyzed by **30** is the result of successive β-alkyl transfer and hydrogenolysis steps [Eq. (14)].[85,86] This key elementary step was further con-



firmed by theoretical investigations of Parrinello et al., which also suggested that the β-alkyl transfer and hydrogenolysis steps should occur at two different Zr centers, since the olefin produced by the β-alkyl transfer has little or no affinity for the d^0 metal center.[87] Noteworthy is the preparation of the Ti complexes [$(\equiv SiO)_3TiH$] (**29**) and [$(\equiv SiO)_3Ti$] (**32**), which gives a methane:ethane ratio of 1:1 instead of 3:1 (for Zr and Hf). Further studies on the hydrogenolysis of alkanes with **29**/**32** mixtures has suggested that hydroisomerization probably occurs in this system, thus explaining the difference in methane:ethane ratio in the hydrogenolysis of [$(\equiv SiO)$-$Ti(CH_2tBu)_3$] (**1**; Scheme 27).[14]

Secondly, [$(\equiv SiO)_3ZrH$] (**30**) catalyzes fast H/H(D) exchange in H_2/D_2 mixtures at low temperatures (liquid N_2).[88] The H/D exchange reaction for methane/D_2 mixtures was also studied in detail, which allowed activation parameters (E_a = 7 kcal mol^{-1}; $\Delta S = -27$ kcal mol^{-1}), to be obtained which are consistent with a σ-bond metathesis process (Scheme 28). σ-Bond metathesis type mechanisms are in fact typical of electrophilic d^0 metal centers.[89] Of various possible mechanisms DFT calculations on this system indicate that the H/D exchange reaction is indeed very fast for H_2/D_2 mixtures

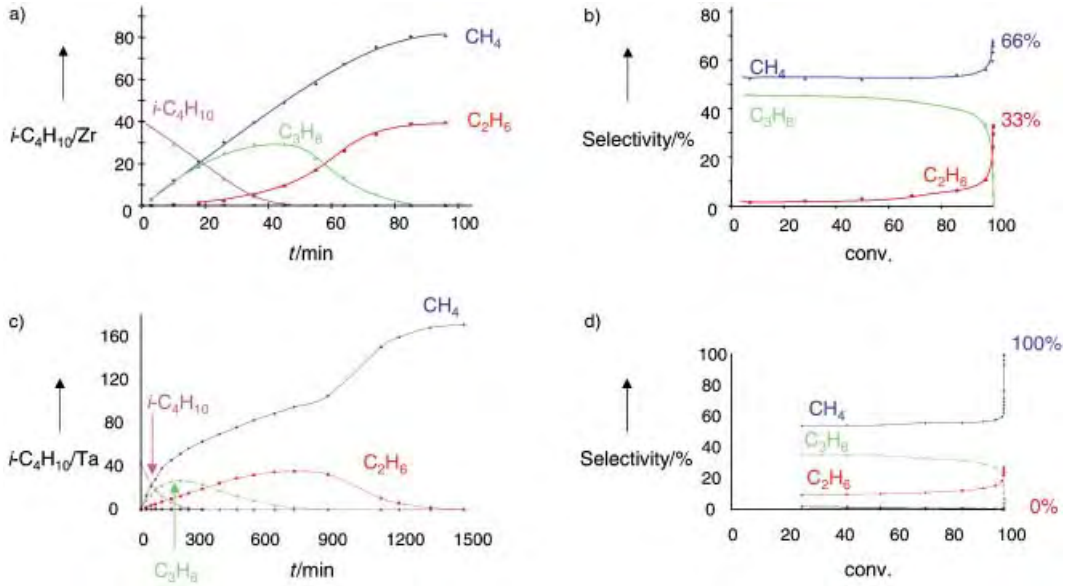
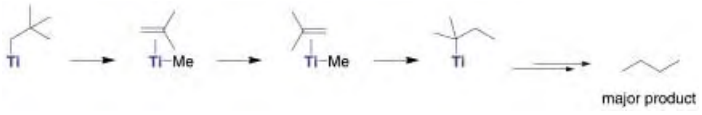
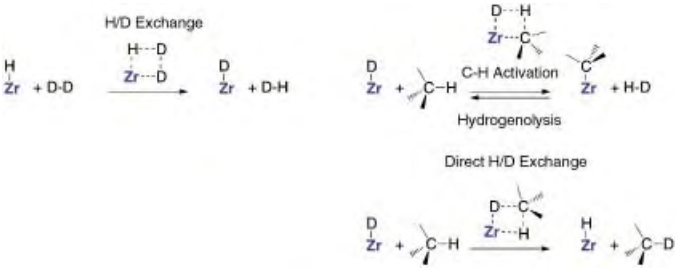


Figure 5. Low-temperature hydrogenolysis of isobutane: a) product evolution in the reaction catalyzed by **30**, b) selectivity versus conversion in the reaction catalyzed by **30**, c) product evolution in the reaction catalyzed by **25**, d) selectivity versus conversion in the reaction catalyzed by **25**.



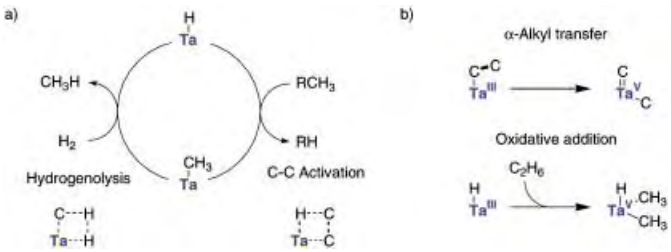
Scheme 27. Hydroisomerization of alkanes with **29; Ti** = {(≡SiO)$_3$Ti}.



Scheme 28. Pathways for H/D exchange reactions on **30; Zr** = {(≡SiO)$_3$Zr}.

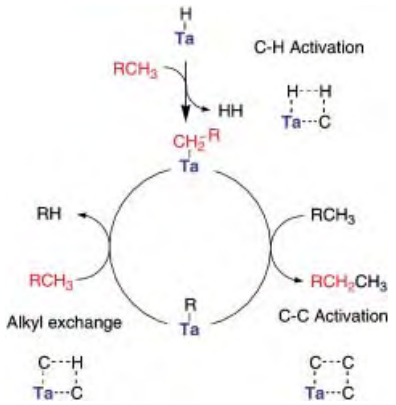
(nearly barrierless), but probably takes place by a two-step C–H activation/hydrogenolysis pathway rather than a direct exchange process in CH_4/D_2 mixtures.[90]

The extension to Group 5 metals, specifically Ta, led to the discovery of the very different hydride, [(≡SiO)$_2$TaH] (**25**) a d^2 eight-electron monohydride complex (see Scheme 11). In this case, in the presence of H_2, alkanes are transformed into methane as the sole product (Figure 5c,d),[91] which is in sharp contrast to the reaction with Group 4 metal hydrides, which do not cleave ethane under similar conditions. The proposed mechanism (a σ-bond metathesis mechanism) for the carbon–carbon bond cleavage involves a four-center transition state, in which the Ta–H and the carbon–carbon bonds interact in a concerted fashion (Scheme 29). Oxidative pathways, such as oxidative addition and α-alkyl transfer[92] cannot be excluded since **25** has a d^2 configuration.



Scheme 29. Low-temperature hydrogenolysis of alkanes catalyzed by **25**; a) through σ-bond metathesis mechanism and b) through oxidative pathways; **Ta** = {(≡SiO)$_2$Ta}.

The surface complex [(≡SiO)$_2$TaH] (**25**) also activates alkanes (RH) at low temperatures to give [(≡SiO)$_2$TaR] (**R-27**; Scheme 12),[35,38] but above 80 °C acyclic alkanes are transformed into their lower and higher homologues (Scheme 30 and Figure 6).[93] This new reaction has been named alkane σ-bond metathesis since alkyl fragments of alkanes are exchanged in contrast to the well-known alkene metathesis, for which it is the alkylidene fragments that are exchanged. A four-center σ-bond metathesis transition state has also been proposed in agreement with the product distribution and the high electrophilicity of the metal center. More recently, the surface organometallic species [(≡SiO)$_x$Ta(=CH*t*Bu)-(CH$_2$*t*Bu)$_{3-x}$] (**8** $x = 1$ and **9** $x = 2$), have also shown similar reactivities with **25** and allowed the cross-metathesis reaction to be observed (Scheme 31).[94] This reactivity has also implied that Ta^V could be an active species. Moreover, in this case, it is possible to evaluate the relative rate of the alkyl exchange reaction (C–H activation) versus cross-metathesis (C–C activation) to about 3:1. Mechanistic investigations on this reaction are still in progress. Alkane metathesis is in fact a productive event among several competitive and faster degenerate processes (Scheme 32,33). For example, ^{13}C



Scheme 30. Alkane metathesis catalyzed by **25**; **Ta** = {(≡SiO)$_2$Ta}.

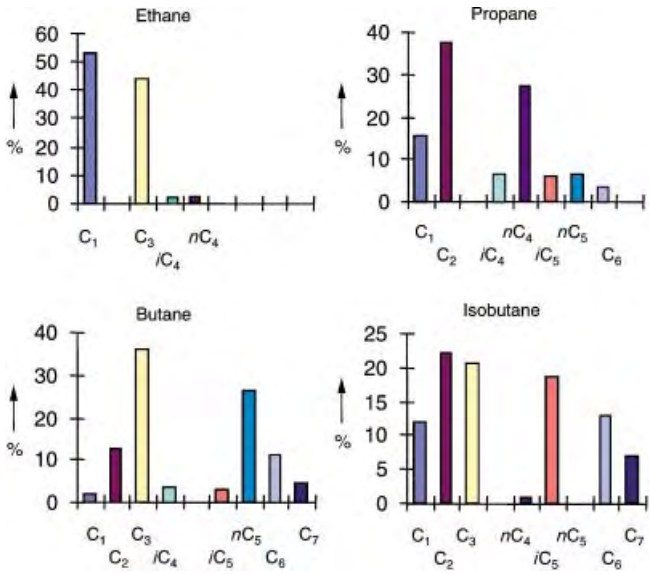
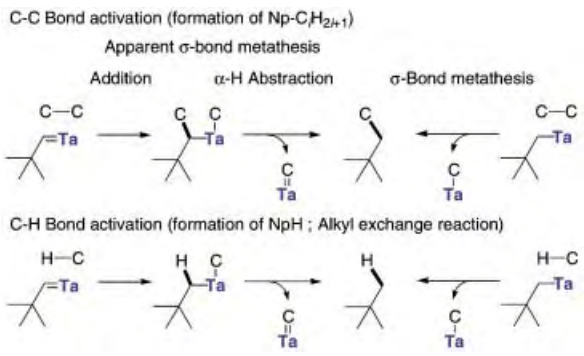
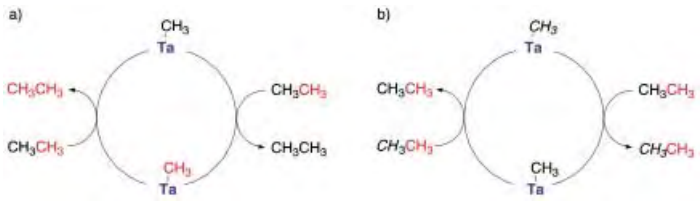


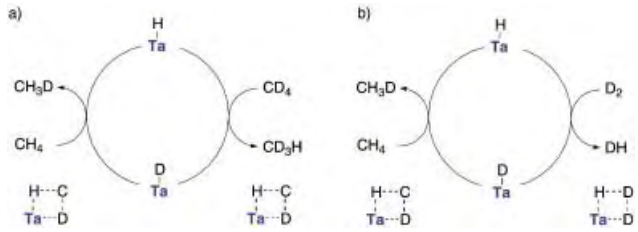
Figure 6. Alkane metathesis catalyzed by **25**. Product distribution [%] as a function of alkanes.



Scheme 31. Alkane activation and metathesis with **8**/**9** mixtures; **Ta** = {(≡SiO)$_x$Ta(CH$_2$*t*Bu)$_{3-x}$}; **8**: $x = 1$; **9**: $x = 2$; Np = neopentyl.



Scheme 32. Degenerate pathways in the alkane metathesis catalyzed by **25** a) degenerate, b) fully degenerate; **Ta** = {(≡SiO)$_2$Ta}.



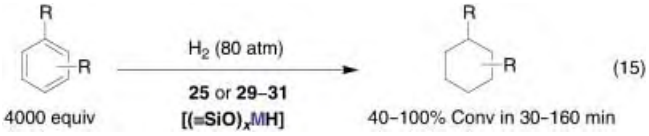
Scheme 33. Pathways for H/D exchange reactions catalyzed by **25** in a) CH_4/CD_4 or b) CH_4/D_2 mixtures; **Ta** = {(≡SiO)$_2$Ta}.

monolabeled ethane is transformed into a one-to-one mixture of non- and dilabeled ethanes; these degenerate metathesis processes are estimated to be about five-times faster than the productive metathesis, that is, the formation of propane and methane from two ethane molecules (Scheme 32).[95] H/D exchange reactions in mixtures of alkanes (CH_4/CD_4) in the presence or the absence of H_2 is even faster (about 200 times; Scheme 33).[96]

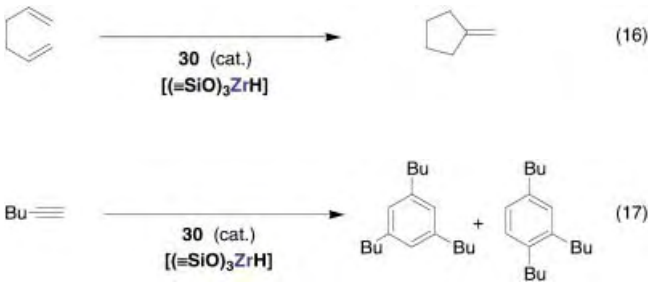
Surface organometallic chemistry can be used to generate entities that display reactivities never observed either in heterogeneous or in homogeneous catalysis. This is worth noting since molecular complexes have closely related structures but display little or no reactivity towards carbon–carbon bonds.[89,97–99] This difference is probably a result of the high electrophilicity of these surface complexes (8–10-electron complexes) in combination with a stabilization of reactive intermediates by the surface (there is no possibility of dimerization despite a high degree of unsaturation and the presence of small ligands, such as hydrides).

4.5. Other Applications of Supported Transition-Metal Hydride Species

These surface complexes (**25** and **29**–**31**), probably generated in situ from their alkyl derivatives, catalyze the hydrogenation of aromatics very efficiently [Eq. (15)].[100,101] For example, 4000 equivalents of benzene are converted into cyclohexane in 240 min in the presence of **30** and H_2 (80 atm) at 120 °C.



Finally the surface complex **30** has also been shown to catalyze carbon–carbon bond forming reactions, such as the cyclization of dienes [Eq. (16)] and cyclotrimerization of alkynes [Eq. (17)].[102]



5. Summary and Outlook

Herein, we have tried to show that a molecular approach to heterogeneous catalysis is a possible answer to the numerous questions and problems raised in this area of science, such as:

- The low number of active sites (and/or phases).
- The difficulty of understanding surface mechanisms.
- The inadequacy of the techniques of surface characterization, even in situ, with respect to the real need for comprehension in a molecular way.
- The difficulty of finding structure–activity relationships.
- A purely empirical approach to the improvement of catalysts.

Among the possible solutions to these problems, the surface-science approach on well-defined surfaces has reached a level of understanding for which it is possible to "see" the molecules dissociating and recombining on a surface to give the products,[103] which are the elementary steps of the catalytic process! This approach is extremely time consuming and limited mainly to metallic surfaces in interaction with simple molecules, such as O_2, NO, CO. Another possible solution is the combinatorial approach.

Surface organometallic chemistry is the opposite of the combinatorial approach. In the year 2002, there is a wealth of knowledge available on the various types of chemical activation of molecules and elementary steps. Therefore, by a simple transfer of concepts from molecular chemistry to surface chemistry it is now possible:

1) to prepare, at least in a limited number of cases, the so-called "active site" in a high concentration on the surface by a strategy of molecular design and engineering,
2) to study elementary steps on these species,
3) to determine the structure–activity relationships necessary for progress to be made in a rational way.

Herein we have shown that this approach allows the activity, selectivity, life time, in a variety of reactions, such as olefin metathesis, olefin epoxidation, olefin asymmetric epoxidations, olefin polymerization, and *trans*-esterification to be improved. This situation is a result of the precise design of the grafting strategy as well as the characterization of the active site at a molecular level. The use of high-resolution NMR spectroscopy techniques in combination with labeling experiments and the synthesis of molecular models, such as polyoligomeric silsesquisioxane systems, can readily help in understanding the structure of the well-defined catalysts.

We have also shown that surface organometallic chemistry allows highly electrophilic catalysts to be prepared, which can carry out catalytic reactions which have no equivalent in molecular or heterogeneous catalysis, such as alkane metathesis and Ziegler–Natta depolymerization.

The future direction of surface organometallic chemistry will probably combine several approaches:

1) understanding the interaction of more complex organometallic complexes with silica (Group 8–10 metals, lanthanides, and actinides),
2) transposition of this accumulated knowledge on the reactivity and the structure on a silica surface so as to understand other more complex (well-defined) supports,
3) understanding of reaction mechanisms through careful identification of reaction intermediates,
4) development of spectroscopic tools so as to have a finer description of the surface complex, to probe the single-site nature of active sites, as well as to understand the changes at the metal center during catalysis,[104]
5) use of theoretical calculations in combination with data obtained for elementary steps on surfaces (activation energies, structural changes) to clarify and help the design of better catalysts,
6) development of high-throughput surface organometallic chemistry to screen a wider variety of catalysts,
7) investigation of aging phenomena, to establish if they are mechanistic or a result of leaching, and to circumvent them,
8) simplification of the preparation of the catalysts,
9) rational, simplified, and economical procedure for regeneration.

In the future, the synthesis of a variety of surface structures with the proper ligands will probably generate numerous new highly active catalysts. However, we want to stress the importance of the characterization of such species, to establish structure–activity relationships from which a better understanding of the catalysts can be obtained. This is probably one of the challenges that will face this field.

The authors gratefully acknowledge the contributions of the many co-workers involved in these projects whose names are listed within the references. A special thanks to A. Lesage, S. Hediger, and L. Emsley for their collaboration on the development of solid-state NMR spectroscopy applied to our problems. This work was made possible by the support of the CNRS, ESCPE Lyon, La Région Rhône-Alpes, The French Ministry for Research and Technology (MENRT), and all our past and present industrial partners.

Received: January 24, 2002 [A500]

[1] H. S. Taylor, *Proc. R. Soc. London Ser. A* **1926**, *113*, 77.
[2] Sabatier was a pioneer of heterogeneous catalysis: P. Sabatier, J.-B. Senderens, *C. R. Hebd. Seances Acad. Sci.* **1897**, *124*, 616;

P. Sabatier, J.-B. Senderens, *C. R. Hebd. Seances Acad. Sci.* **1897**, *124,* 1358.

[3] a) D. G. H. Ballard, *Adv. Catal.* **1973**, *23*, 263; b) J. P. Candlin, H. Thomas, *Adv. Chem. Ser.* **1974**, *132*, 212; c) *Studies in Surface Science and Catalysis, Vol. 8* (Eds.: Yu. I. Yermakov, B. N. Kuznetsov, V. A. Zakharov), Elsevier, Amsterdam, **1981**; d) *Tailored Metal Catalysis* (Ed.: Y. Iwasawa), D. Reidel Publishing Company, Dordrecht, **1986**; e) J. Evans in *Surface Organometallic Chemistry : Molecular Approaches to Surface Catalysis, NATO ASI series, Vol. 231* (Eds. J.-M. Basset, B. C. Gates, J.-P. Candy, A. Choplin, M. Leconte, F. Quignard, C. Santini), Kluwer Academic Publishers, Dordrecht **1988**.

[4] a) J.-M. Basset, A. Choplin, *J. Mol. Catal.* **1983**, *21*, 95; b) S. L. Scott, J.-M. Basset, G. P. Niccolai, C. C. Santini, J.-P. Candy, C. Lécuyer, F. Quignard, A. Choplin, *New J. Chem.* **1994**, *18*, 115; c) J.-M. Basset, F. Lefebvre, C. C. Santini, *Coord. Chem. Rev.* **1998**, *178–180*, 1703.

[5] *Handbook of Heterogeneous Catalysis, Vol. 2* (Eds: G. Ertl, H. Knözinger, J. Weitkamp), Wiley-VCH, Weinheim, **1997**.

[6] C. Copéret, J. Thivolle-Cazat, J.-M. Basset *in Fine Chemicals through Heterogeneous Catalysis* (Eds.: R. A. Sheldon, H. van Bekkum), Wiley-VCH, Weinheim, **2001**, p. 553.

[7] a) B. A. Morrow, *Stud. Surf. Sci. Catal.* **1990**, *57*, A161; b) *Studies in Surface Science and Catalysis, Vol. 93* (Eds. E. F. Vansant, P. Van Der Voort, K. C. Vranchen), Elsevier, Amsterdam, **1995**; c) *The Surface Properties of Silica* (Ed.: A. P. Legrand), Wiley, New York, **1998**; d) B. A. Morrow, I. D. Gay, *Surfact. Sci. Ser.* **2000**, *90*, 9.

[8] M. E. Bartram, T. A. Michalske, J. W. Rogers, Jr., *J. Phys. Chem.* **1991**, *95*, 4453.

[9] a) J. F. Brown, Jr., L. H. Vogt, Jr., *J. Am. Chem. Soc.* **1965**, *87*, 4313; b) J. F. Brown, Jr., *J. Am. Chem. Soc.* **1965**, *87*, 4317; c) R. E. LaPointe, P. T. Wolczanski, G. D. Van Duyne, *Organometallics* **1985**, *4*, 1810; d) F. J. Feher, D. A. Newman, J. F. Walzer, *J. Am. Chem. Soc.* **1989**, *111*, 1741; e) F. J. Feher, D. A. Newman, *J. Am. Chem. Soc.* **1990**, *112*, 1931; f) F. J. Feher, T. A. Budzichowski, R. L. Blanski, K. J. Weller, J. W. Ziller, *Organometallics* **1991**, *10*, 2526; g) F. J. Feher, R. L. Blanski, *J. Am. Chem. Soc.* **1992**, *114*, 5886; h) F. J. Feher, R. L. Blanski, *Organometallics* **1993**, *12*, 958; i) F. J. Feher, T. L. Tajima, *J. Am. Chem. Soc.* **1994**, *116*, 2145; j) F. J. Feher, K. J. Weller, J. J. Schwab, *Organometallics* **1995**, *14*, 2009; k) R. Duchateau, H. C. L. Abbenhuis, R. A. Van Santen, S. K.-H. Thiele, M. F. H. Van Tol, *Organometallics* **1998**, *17*, 5222; l) F. J. Feher, D. Soulivong, G. T. Lewis, *J. Am. Chem. Soc.* **1997**, *119*, 11323; m) R. Duchateau, H. C. L. Abbenhuis, R. A. Van Santen, A. Meetsma, S. K.-H. Thiele, M. F. H. Van Tol, *Organometallics* **1998**, *17*, 5663; n) R. Duchateau, U. Cremer, R. J. Harmsen, S. I. Mohamud, H. C. L. Abbenhuis, R. A. Van Santen, A. Meetsma, S. K.-H. Thiele, M. F. H. Van Tol, M. Kranenburg, *Organometallics* **1999**, *18*, 5447; o) T. W. Dijkstra, R. Duchateau, R. A. van Santen, A. Meetsma, G. P. A. Yap, *J. Am. Chem. Soc.* **2002**, *124*, 9856.

[10] Reviews: a) F. J. Feher, T. A. Budzichowski, *Polyhedron* **1995**, *14*, 3239; b) P. T. Wolczanski, *Polyhedron* **1995**, *14*, 3335; c) P. D. Lickiss, *Adv. Inorg. Chem.* **1995**, *42*, 147; d) R. Murugavel, A. Voigt, M. G. Walawalkar, H. W. Roesky, *Chem. Rev.* **1996**, *96*, 2205; e) P. G. Harrison, *J. Organomet. Chem.* **1997**, *542*, 141; f) L. King, A. C. Sullivan, *Coord. Chem. Rev.* **1999**, *189*, 19; g) V. Lorenz, A. Fischer, S. Giessmann, J. W. Gilje, Y. Gun'ko, K. Jacob, F. T. Edelmann, *Coord. Chem. Rev.* **2000**, *206–207*, 321; h) H. C. L. Abbenhuis, *Chem. Eur. J.* **2000**, *6*, 25; i) B. Marciniec, H. Maciejewski, *Coord. Chem. Rev.* **2001**, *223*, 301; j) R. Duchateau, *Chem. Rev.* **2002**, *102*, 3525.

[11] For more recent work on allyl derivatives of Rh (a–c) and Cr (d): a) M. D. Ward, T. V. Harris, J. Schwartz, *J. Chem. Soc. Chem. Commun.* **1980**, 357; b) H. C. Foley, S. J. DeCanio, K. D. Tau, K. J. Chao, J. H. Onuferko, C. Dybowski, B. C. Gates, *J. Am. Chem. Soc.* **1983**, *105* , 3074; c) P. Dufour, C. Houtman, C. C. Santini, C. Nédez, J.-M. Basset, L. Y. Hsu, S. G. Shore, *J. Am. Chem. Soc.* **1992**, *114*, 4248; d) O. M. Bade, R. Blom, M. Ystenes, *Organometallics* **1998**, *17*, 2524.

[12] a) F. Quignard, A. Choplin, J.-M. Basset, *J. Chem. Soc. Chem. Commun.* **1991**, 1589; b) S. A. King, J. Schwartz, *Inorg. Chem.* **1991**, *30*, 3771; c) F. Quignard, C. Lécuyer, C. Bougault, F. Lefebvre, A. Choplin, D. Olivier, J.-M. Basset, *Inorg. Chem.* **1992**, *31*, 928.

[13] J. Corker, F. Lefebvre, C. Lécuyer, V. Dufaud, F. Quignard, A. Choplin, J. Evans, J.-M. Basset, *Science* **1996**, *271*, 966.

[14] C. Rozier, G. P. Niccolaï, J.-M. Basset, *J. Am. Chem. Soc.* **1997**, *119*, 12408.

[15] S. A. Holmes, F. Quignard, A. Choplin, R. Teissier, J. Kervennal, *J. Catal.* **1998**, *176*, 173.

[16] L. d'Ornelas, S. Reyes, F. Quignard, A. Choplin, J.-M. Basset, *Chem. Lett.* **1993**, 1931.

[17] J. Amor Nait Ajjou, S. L. Scott, *Organometallics* **1997**, *16*, 86.

[18] M. Jezequel, V. Dufaud, M. J. Ruiz-Garcia, F. Carrillo-Hermosilla, U. Neugebauer, G. P. Niccolai, F. Lefebvre, F. Bayard, J. Corker, S. Fiddy, J. Evans, J.-P. Broyer, J. Malinge, J.-M. Basset, *J. Am. Chem. Soc.* **2001**, *123*, 3520.

[19] a) P. J. Toscano, T. J. Marks, *J. Am. Chem. Soc.* **1985**, *107*, 653; b) P. J. Toscano, T. J. Marks, *Langmuir* **1986**, *2*, 820; c) W. C. Finch, R. D. Gillespie, D. Hedden, T. J. Marks, *J. Am. Chem. Soc.* **1990**, *112*, 6221.

[20] V. Dufaud, G. P. Niccolai, J. Thivolle-Cazat, J.-M. Basset, *J. Am. Chem. Soc.* **1995**, *117*, 4288.

[21] R. Buffon, M. Leconte, A. Choplin, J.-M. Basset, *J. Chem. Soc. Chem. Commun.* **1993**, 361.

[22] R. Buffon, M. Leconte, A. Choplin, J.-M. Basset, *J. Chem. Soc. Dalton Trans.* **1994**, 1723.

[23] L. Lefort, M. Chabanas, O. Maury, D. Meunier, C. Copéret, J. Thivolle-Cazat, J.-M. Basset, *J. Organomet. Chem.* **2000**, *593–594*, 96.

[24] M. Chabanas, A. E. Quadrelli, B. Fenet, C. Copéret, J. Thivolle-Cazat, J.-M. Basset, A. Lesage, L. Emsley, *Angew. Chem.* **2001**, *113*, 4625; *Angew. Chem. Int. Ed.* **2001**, *40*, 4493.

[25] R. Petroff Saint-Arroman, M. Chabanas, A. Baudouin, C. Copéret, J.-M. Basset, A. Lesage, L. Emsley, *J. Am. Chem. Soc.* **2001**, *123*, 3820.

[26] M. Chabanas, D. Alcor, E. Gautier, C. Copéret, J.-M. Basset, A. Lesage, S. Hediger, L. Emsley, W. Lukens, unpublished results.

[27] M. Chabanas, A. Baudouin, C. Copéret, J.-M. Basset, *J. Am. Chem. Soc.* **2001**, *123*, 2062.

[28] a) M. Chabanas, A. Baudouin, C. Copéret, J.-M. Basset, W. Lukens, S. Hediger, A. Lesage, L. Emsley, *J. Am. Chem. Soc.* **2003**, *125*, 492; b) A. Lesage, L. Emsley, M. Chabanas, C. Copéret, J.-M. Basset, *Angew. Chem.* **2002**, *114*, 4717; *Angew. Chem. Int. Ed. Engl.* **2002**, *41*, 4535.

[29] R. Petroff Saint-Arroman, F. Lefebvre, J.-M. Basset, unpublished results.

[30] a) W. A. Herrmann, A. W. Stumpf, T. Priermeier, S. Bogdanovic, V. Dufaud, J.-M. Basset, *Angew. Chem.* **1996**, *108*, 2978; *Angew. Chem. Int. Ed. Engl.* **1996**, *35*, 2803; b) Q. Yang, C. Copéret, J.-M. Basset, unpublished results.

[31] V. Riollet, Master Thesis, Université Claude Bernard, **1999**.

[32] J. Amor Nait Ajjou, S. L. Scott, V. Paquet, *J. Am. Chem. Soc.* **1998**, *120*, 415.

[33] J. Amor Nait Ajjou, G. L. Rice, S. L. Scott, *J. Am. Chem. Soc.* **1998**, *120*, 13436.

[34] S. I. Wolke, R. Buffon, U. P. Rodrigues Filho, *J. Organomet. Chem.* **2001**, *625*, 101.

[35] a) V. Vidal, A. Théolier, J. Thivolle-Cazat, J.-M. Basset, J. Corker, *J. Am. Chem. Soc.* **1996**, *118*, 4595; b) When $[(\equiv SiO)_2TaH]$ is treated under H_2 at 500 °C it is transformed

into [(≡SiO)$_3$Ta], see: G. Saggio, A. de Mallmann, B. Maunders, M. Taoufik, J. Thivolle-Cazat, J.-M. Basset, *Organometallics* **2002**, *21*, 5167.
[36] M. Taoufik, A. de Mallmann, E. Prouzet, G. Saggio, J. Thivolle-Cazat, J.-M. Basset, *Organometallics* **2001**, *20*, 5518.
[37] B. C. Ankianiec, P. E. Fanwick, I. P. Rothwell, *J. Am. Chem. Soc.* **1991**, *113*, 4710.
[38] V. Vidal, A. Théolier, J. Thivolle-Cazat, J.-M. Basset, *J. Chem. Soc. Chem. Commun.* **1995**, 991.
[39] a) F. Quignard, C. Lécuyer, A. Choplin, D. Olivier, J.-M. Basset, *J. Mol. Cat.* **1992**, *74*, 353; b) F. Quignard, C. Lécuyer, A. Choplin, J.-M. Basset, *J. Chem. Soc. Dalton Trans.* **1994**, 1153.
[40] G. P. Niccolai, J.-M. Basset, *Appl. Catal., A* **1996**, *146*, 145.
[41] C. Rozier, PhD Thesis, Université Claude Bernard Lyon I, **1999**.
[42] D. Meunier, A. Piechaczyk, A. de Mallmann, J.-M. Basset, *Angew. Chem.* **1999**, *111*, 3738; *Angew. Chem. Int. Ed.* **1999**, *38*, 3540.
[43] A. O. Bouh, G. L. Rice, S. L. Scott, *J. Am. Chem. Soc.* **1999**, *121*, 7201.
[44] C. Blandy, J.-L. Pellegatta, R. Choukroun, B. Gilot, R. Guiraud, *Can. J. Chem.* **1993**, *71*, 34.
[45] G. L. Rice, S. L. Scott, *Langmuir* **1997**, *13*, 1545.
[46] G. L. Rice, S. L. Scott, *J. Mol. Catal. A: Chem.* **1997**, *125*, 73.
[47] a) V. Capdevielle-Salinier, PhD Thesis, Université Claude Bernard Lyon I, **1996**; b) V. Dufaud, V. Salinier, J.-M. Basset, International Symposium on the relation between Homogeneous and Heterogeneous Catalysis (shhc10), July 2002; c) N. Ferret, V. Dufaud, V. Salinier, V. Dufaud, J.-M. Basset, FR 2747675 **1997**.
[48] a) C. W. Tullock, F. N. Tebbe, R. Mülhaupt, D. W. Ovenall, R. A. Setterquist, S. D. Ittel, *J. Polym. Sci., Part A: Polym. Chem.* **1989**, *27*, 3063; b) J. W. Collette, C. W. Tullock, R. N. MacDonald, W. H. Buck, A. C. L. Su, J. R. Harrel, R. Mülhaupt, B. C. Anderson, *Macromolecules* **1989**, *22*, 3851; c) C. W. Tullock, R. Mülhaupt, S. D. Ittel, *Makromol. Chem. Rapid Commun.* **1989**, *10*, 19; d) S. D. Ittel, *J. Macromol. Sci., Chem.* **1990**, *A27*, 1133; e) L. T. Nelson, S. D. Ittel, *Polym. Prep.* **1994**, 35, 665.
[49] a) F. J. Karol, C. Wu, W. T. Reichle, N. J. Maraschin, *J. Catal.* **1979**, *60*, 68; b) F. J. Karol, *Chem. Tech.* **1983**, *4*, 222.
[50] H. H. Brintzinger, D. Fischer, R. Mülhaupt, B. Rieger, R. M. Waymouth, *Angew. Chem.* **1995**, *107*, 1255; *Angew. Chem. Int. Ed. Engl.* **1995**, *34*, 1143.
[51] a) A. Andresen, H.-G. Cordes, J. Herwig, W. Kaminsky, A. Merck, R. Mottweiler, J. Pein, H. Sinn, H.-J. Vollmer, *Angew. Chem.* **1976**, *88*, 689; *Angew. Chem. Int. Ed. Engl.* **1976**, *15*, 630; b) Review: *Metalorganic Catalysts for Synthesis and Polymerisation* (Ed.: W. Kaminsky), Springer, Berlin, **1999**.
[52] K.-H. Dahmen, D. Hedden, R. L. Burwell, Jr., T. J. Marks, *Langmuir* **1988**, *4*, 1212.
[53] T. J. Marks, *Acc. Chem. Res.* **1992**, *25*, 57.
[54] a) G. G. Hlatky, *Chem. Rev.* **2000**, *100*, 1347; b) G. Fink, B. Steinmetz, J. Zechlin, C. Przybyla, B. Tesche, *Chem. Rev.* **2000**, *100*, 1377; c) E. Y.-X. Chen, T. J. Marks, *Chem. Rev.* **2000**, *100*, 1391.
[55] M. D. Skowronska-Ptasinska, R. Duchateau, R. A. van Santen, G. P. A. Yap, *Organometallics* **2001**, *20*, 3519.
[56] J. F. Walzer, Jr., US 5643847 **1997**.
[57] a) S. J. Lancaster, S. M. O'Hara, M. Bochmann in *Metalorganic Catalysts for Synthesis and Polymerisation* (Ed.: W. Kaminsky), Springer, Berlin **1999**, p. 413; b) M. Bochmann, G. Jiménez Pindado, S. J. Lancaster, *J. Mol. Catal. A: Chem.* **1999**, *146*, 179.
[58] R. Duchateau, R. A. van Santen, G. P. A. Yap, *Organometallics* **2000**, *19*, 809.
[59] N. Millot, A. Cox, C. C. Santini, Y. Molard, J.-M. Basset, *Chem. Eur. J.* **2002**, *8*, 1438.
[60] M. P. McDaniel, *Adv. Catal.* **1985**, *33*, 47.
[61] J. Amor Nait Ajjou, S. L. Scott, *J. Am. Chem. Soc.* **2000**, *122*, 8968.
[62] S. L. Scott, J. Amor Nait Ajjou, *Chem. Eng. Sci.* **2001**, *56*, 4155.
[63] R. Schmid, T. Ziegler, *Can. J. Chem.* **2000**, *78*, 265.
[64] M. P. McDaniel, M. B. Welch, *J. Catal.* **1983**, *82*, 98.
[65] a) For seminal works in this area: a) H. S. Euleterio, US 3074918 **1963**; R. L. Banks, G. C. Bailey, *Ind. Eng. Chem. Prod. Res. Dev.* **1964**, *3*, 170; b) For a comprehensive review: *Olefin Metathesis and Metathesis Polymerization* (Eds.: K. J. Ivin, J. C. Mol), Academic Press, San Diego, **1997**.
[66] J.-L. Hérisson, Y. Chauvin, *Makromol. Chem.* **1971**, *141*, 161.
[67] Review on olefin metathesis in homogeneous catalysis: a) T. M. Trnka, R. H. Grubbs, *Acc. Chem. Res.* **2001**, *34*, 18; b) R. R. Schrock, A. H. Hoveyda, *Chem. Eur. J.* **2001**, *7*, 945.
[68] a) W. Mowat, J. Smith, D. A. Whan, *J. Chem. Soc. Chem. Commun.* **1974**, 34; b) J. Smith, W. Mowat, D. A. Whan, E. A. V. Ebsworth, *J. Chem. Soc. Dalton Trans.* **1974**, 1742; c) I. A. Oreshkin, L. I. Red'kina, K. L. Makovetskii, E. I. Tinyakova, B. A. Dolgoplosk, *Izv. Akad. Nauk SSSR, Ser. Khim.* **1971**, *5*, 1123.
[69] Y. Iwasawa, Y. Nakano, S. Ogasawara, *J. Chem. Soc., Faraday Trans. 1*, **1978**, *74*, 2968.
[70] K. Weiss, G. Loessel, *Angew. Chem.* **1989**, *101*, 75; *Angew. Chem. Int. Ed. Engl.* **1989**, *28*, 62.
[71] S. M. Rocklage, J. D. Fellmann, G. A. Rupprecht, L. W. Messerle, R. R. Schrock, *J. Am. Chem. Soc.* **1981**, *103*, 1440.
[72] a) M. Chabanas, PhD Thesis, Université Claude Bernard Lyon I, **2001**; b) M. Chabanas, C. Copéret, J.-M. Basset, *Chem. Eur. J.*, in press.
[73] a) R. R. Schrock, *Acc. Chem. Res.* **1990**, *23*, 158; b) J. Feldman, R. R. Schrock, *Prog. Inorg. Chem.* **1991**, *39*, 1; c) R. R. Schrock, *Polyhedron* **1995**, *14*, 3177; d) R. R. Schrock, *Top. Organomet. Chem.* **1998**, 1; e) R. R. Schrock, *Chem. Rev.* **2002**, *102*, 145.
[74] The activity of rhenium oxides supported on silica is usually poor below 120 °C. For some examples, see: a) A. W. Aldag, C. J. Lin, A. Clark, *Recl. Trav. Chim. Pays-Bas*, **1977**, *96*, M27; b) N. Tsuda, A. Fujimori, *J. Catal.* **1981**, *69*, 410; c) L. G. Duquette, R. C. Cieslinski, C. W. Jung, P. E. Garrou, *J. Catal.* **1984**, *90*, 362; d) P. S. Kirlin, B. C. Gates, *J. Chem. Soc. Chem. Commun.* **1985**, 277; e) R. M. Edreva-Kardjieva, A. A. Andreev, *J. Catal.* **1986**, *97*, 321; f) For a comparison with Re_2O_7 supported on alumina, see: Y. Chauvin, D. Commereuc, *J. Chem. Soc. Chem. Commun.* **1992**, 462; g) For a review on this system, see: J. C. Mol, *Catal. Today* **1999**, *51*, 289; h) J. C. Mol, *Green Chemistry* **2002**, *4*, 5.
[75] a) R. Toreki, G. A. Vaughan, R. R. Schrock, W. M. Davis, *J. Am. Chem. Soc.* **1993**, *115*, 127; b) A. M. Lapointe, R. R. Schrock, *Organometallics* **1995**, *14*, 1875; c) B. T. Flatt, R. H. Grubbs, R. L. Blanski, J. C. Calabrese, J. Feldman, *Organometallics* **1994**, *13*, 2728; d) D. Commereuc, *J. Chem. Soc. Chem. Commun.* **1995**, 791.
[76] a) H. P. Wulff, GB 1,249,79 **1971**; b) M. Dusi, T. Mallat, A. Baiker, *Catal. Rev. Sci. Eng.* **2000**, *42*, 213; c) R. A. Sheldon, M. C. A. van Vliet in *Fine Chemicals through Heterogeneous Catalysis* (Eds.: R. A. Sheldon, H. van Bekkum), Wiley-VCH, Weinheim, **2001**, p. 473.
[77] a) S. Haukka, E.-L. Lakomaa, A. Root, *J. Phys. Chem.* **1993**, *97*, 5085; b) E. Jorda, A. Tuel, R. Teissier, J. Kervennal, *J. Chem. Soc. Chem. Commun.* **1995**, 1775; c) C. Cativiela, J. M. Fraile, J. I. García, J. A. Mayoral, *J. Mol. Catal. A* **1996**, *112*, 259; d) J. M. Fraile, J. I. García, J. A. Mayoral, M. G. Proietti, M. C. Sánchez, *J. Phys. Chem.* **1996**, *100*, 19484.
[78] a) For the preparation of Ti-containing catalysts by other approaches, see ref. [77c] and: J. M. Thomas, R. Raja, *Chem.*

Commun. **2001**, 675, and references therein; b) For the TS-1 system, which tolerates H_2O_2 as an oxidant, see: U. Romano, G. Perego, B. Notari, US 4410501 **1983** and ref. [76c].

[79] a) H. C. L. Abbenhuis, S. Krijnen, R. A. van Santen, *Chem. Commun.* **1997**, 331; b) T. Maschmeyer, M. C. Klunduk, C. M. Martin, D. S. Shephard, J. M. Thomas, B. F. G. Johnson, *Chem. Commun.* **1997**, 1847; c) M. Crocker, R. H. M. Herold, A. G. Orpen, *Chem. Commun.* **1997**, 2411; d) M. Crocker, R. H. M. Herold, A. G. Orpen, M. T. A. Overgaag, *J. Chem. Soc. Dalton Trans.* **1999**, 3791.

[80] a) M. Crocker, R. H. M. Herold, B. G. Roosenbrand, K. A. Emeis, A. E. Wilson, *Colloids Surf. A.* **1998**, *139*, 351.

[81] a) F. Quignard, A. Choplin, R. Teissier, *J. Mol. Catal. A: Chem.* **1997**, *120*, L27; b) S. A. Holmes, F. Quignard, A. Choplin, R. Teissier, J. Kervennal, *J. Catal.* **1998**, *176*, 182.

[82] a) T. Katsuki, K. B. Sharpless, *J. Am. Chem. Soc.* **1980**, *102*, 5974; b) Y. Gao, R. M. Hanson, J. M. Klunder, S. Y. Ko, H. Masamune, K. B. Sharpless, *J. Am. Chem. Soc.* **1987**, *109*, 5765; c) M. G. Finn, K. B. Sharpless, *J. Am. Chem. Soc.* **1991**, *113*, 113.

[83] a) P. Leyrit, C. McGill, F. Quignard, A. Choplin, *J. Mol. Cat. A: Chem.* **1996**, *112*, 395; b) F. Quignard, O. Graziani, A. Choplin, *Applied Catalysis, A: General* **1999**, *182*, 29.

[84] C. Lécuyer, F. Quignard, A. Choplin, D. Olivier, J.-M. Basset, *Angew. Chem.* **1991**, *103*, 1692; *Angew. Chem. Int. Ed. Engl.* **1991**, *30*, 1660.

[85] V. Dufaud, J.-M. Basset, *Angew. Chem.* **1998**, *110*, 848; *Angew. Chem. Int. Ed.* **1998**, *37*, 806.

[86] G. P. Niccolai, J.-M. Basset in *Catalytic Activation and Functionalisation of Light Alkanes, Nato ASI Series Vol. 3/44* (Eds.: E. R. Derouane, J. Haber, F. Lemos, F. Ramôa Ribeiro, M. Guismet), Kluwer Academic Press, Dordrecht, **1998**, p. 111.

[87] J. J. Mortensen, M. Parrinello, *J. Phys. Chem. B* **2000**, *104*, 2901.

[88] G. L. Casty, M. G. Matturo, G. R. Myers, R. P. Reynolds, R. B. Hall, *Organometallics* **2001**, *20*, 2246.

[89] a) P. L. Watson, *J. Chem. Soc. Chem. Commun.* **1983**, 276; b) P. L. Watson, *J. Am. Chem. Soc.* **1983**, *105*, 6491; c) B. J. Burger, M. E. Thompson, W. D. Cotter, J. E. Bercaw, *J. Am. Chem. Soc.* **1990**, *112*, 1566.

[90] H. Chermette, A. Grouiller, C. Copéret, J.-M. Basset, unpublished results; a) for related theoretical investigations of σ-bond metathesis processes, see: M. L. Steigerwald, W. A. Goddard III, *J. Am. Chem. Soc.* **1984**, *106*, 308; b) H. Rabaâ, J.-Y. Saillard, R. Hoffmann, *J. Am. Chem. Soc.* **1986**, *108*, 4327; c) C. A. Jolly, D. S. Marynick, *J. Am. Chem. Soc.* **1989**, *111*, 7968; d) A. K. Rappé, *Organometallics* **1990**, *9*, 466; e) E. Folga, T. Ziegler, L. Fan, *New. J. Chem.* **1991**, *15*, 741; f) E. Folga, T. Ziegler, *Can. J. Chem.* **1992**, *70*, 333; g) T. Ziegler, E. Folga, A. Bercés, *J. Am. Chem. Soc.* **1993**, *115*, 636; h) B. J. Deelman, J. H. Teuben, S. A. MacGregor, O. Eisenstein, *New. J. Chem.* **1995**, *19*, 691; i) L. Maron, O. Eiseinstein, *J. Am. Chem. Soc.* **2001**, *123*, 1036.

[91] M. Chabanas, V. Vidal, C. Copéret, J. Thivolle-Cazat, J.-M. Basset, *Angew. Chem.* **2000**, *112*, 2038; *Angew. Chem. Int. Ed.* **2000**, *39*, 1962.

[92] The reverse elementary step has been documented: a) P. R. Sharp, R. R. Schrock, *J. Organomet. Chem.*, **1979**, *171*, 43; b) J. C. Hayes, G. D. N. Pearson, N. J. Cooper, *J. Am. Chem. Soc.* **1981**, *103*, 4648.

[93] V. Vidal, A. Théolier, J. Thivolle-Cazat, J.-M. Basset, *Science* **1997**, *276*, 99.

[94] C. Copéret, O. Maury, J. Thivolle-Cazat, J.-M. Basset, *Angew. Chem.* **2001**, *113,* 2393; *Angew. Chem. Int. Ed.* **2001**, *40*, 2331.

[95] O. Maury, L. Lefort, V. Vidal, J. Thivolle-Cazat, J.-M. Basset, *Angew. Chem.* **1999**, *111*, 2121, *Angew. Chem. Int. Ed.* **1999**, *38*, 1952.

[96] L. Lefort, C. Copéret, M. Taoufik, J. Thivolle-Cazat, J.-M. Basset, *Chem. Commun.* **2000**, 663.

[97] a) H. W. Turner, S. J. Simpson, R. A. Andersen, *J. Am. Chem. Soc.* **1979**, *101*, 2782; b) S. J. Simpson, H. W. Turner, R. A. Andersen, *J. Am. Chem. Soc.* **1979**, *101*, 7728.

[98] a) T. V. Lubben, P. T. Wolczanski, G. D. van Duyne, *Organometallics* **1984**, *3*, 977; b) C. C. Cummins, S. M. Baxter, P. T. Wolczanski, *J. Am. Chem. Soc.* **1988**, *110*, 8731; c) C. C. Cummins, C. P. Schaller, G. D. van Duyne, P. T. Wolczanski, A. W. E. Chan, R. Hoffmann, *J. Am. Chem. Soc.* **1991**, *113*, 2985; d) C. C. Cummins, G. D. van Duyne, C. P. Schaller, P. T. Wolczanski, *Organometallics* **1991**, *10*, 164; e) J. L. Bennett, P. T. Wolczanski *J. Am. Chem. Soc.* **1994**, *116*, 2179; f) C. P. Schaller, C. C. Cummins, P. T. Wolczanski, *J. Am. Chem. Soc.* **1996**, *118*, 591; g) J. L. Bennett, P. T. Wolczanski, *J. Am. Chem. Soc.* **1997**, *119*, 10696.

[99] a) R. W. Chestnut, L. D. Durfee, P. E. Fanwick, I. P. Rothwell, K. Folting, J. C. Huffman, *Polyhedron* **1987**, *6*, 2026; b) C. C. Cummins, R. R. Schrock, W. M. Davis, *Organometallics* **1992**, *11*, 1452; c) M. Booij, B.-J. Deelman, R. Duchateau, D. S. Postma, A. Meetsma, J. H. Teuben, *Organometallics* **1993**, *12*, 3531; d) R. R. Schrock, K.-Y. Shih, D. A. Dobbs, W. M. Davis, *J. Am. Chem. Soc.* **1995**, *117*, 6609; e) H. Nöth, M. Schmidt, *Organometallics* **1995**, *14*, 4601; f) L. Jia, E. Ding, A. L. Rheingold, B. Rhatigan, *Organometallics* **2000**, *19*, 963.

[100] R. D. Profilet, A. P. Rothwell, I. P. Rothwell, *J. Chem. Soc. Chem. Commun.* **1993**, 42; the hydride is probably generated in situ from the starting alkyl surface complex.

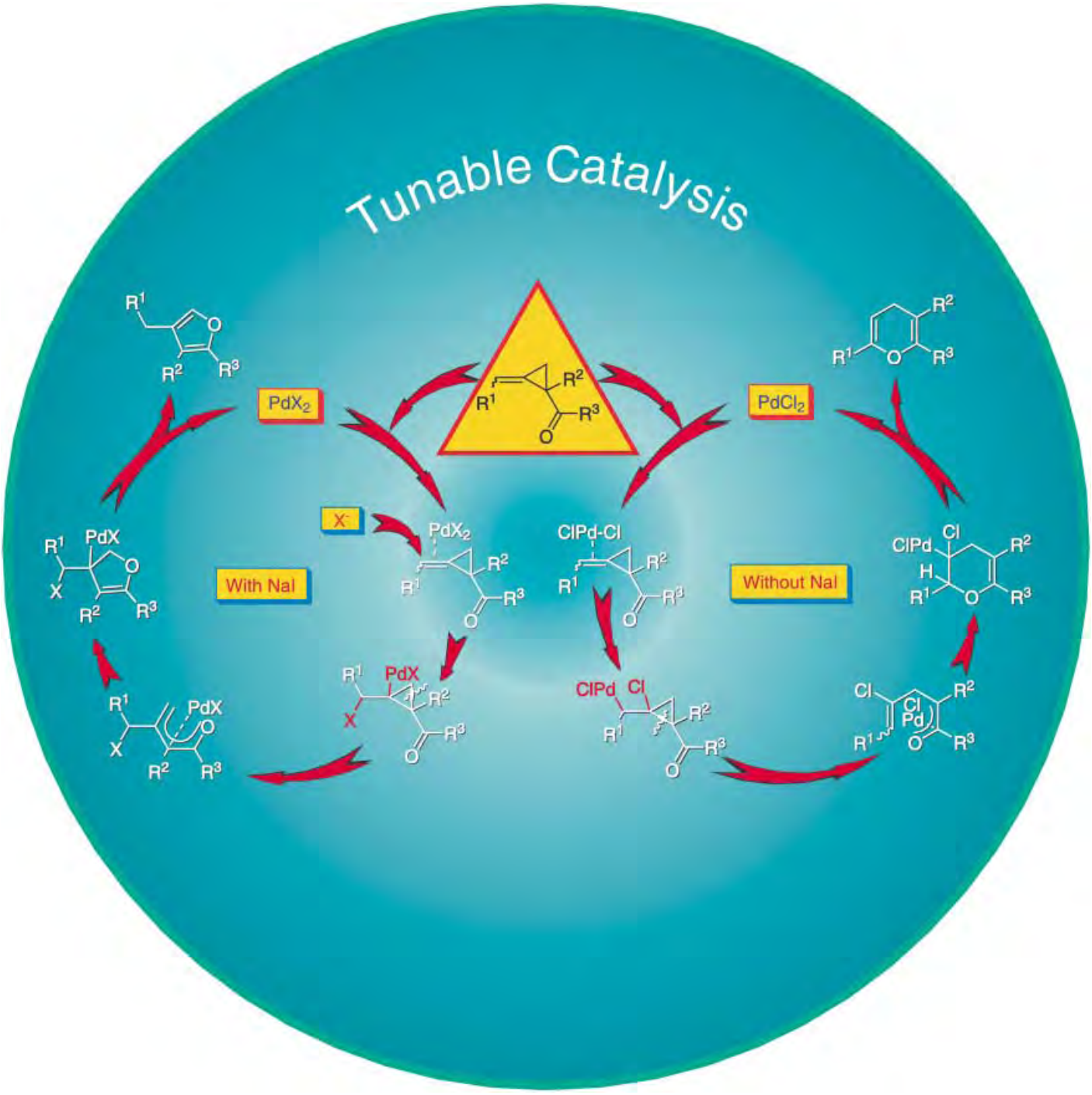
[101] For examples with supported actinide derivatives, see: a) R. D. Gillespie, R. L. Burwell, T. J. Marks, *Langmuir* **1990**, *6*, 1465; b) M. S. Eisen, T. J. Marks, *J. Am. Chem. Soc.* **1992**, *114*, 10358; c) M. S. Eisen, T. J. Marks, *J. Mol. Cat.* **1994**, *86*, 23.

[102] S. A. King, J. Schwartz, *Inorg. Chem.* **1991**, *30*, 3771. Note that the IR stretching frequencies around 2200 cm^{-1} in this publication were misassigned to $\tilde{\nu}$(Zr–H), they are in fact those of $\tilde{\nu}$(Si–H).

[103] G. Ertl, *Adv. Catal.* **2000**, *45*, 69.

[104] For in situ spectroscopy in flow reactors, see for examples: a) EXAFS: M. A. Newton, D. G. Burnaby, A. J. Dent, S. Diaz-Moreno, J. Evans, S. G. Fiddy, T. Neisus, S. Pascarelli, S. Turin *J. Phys. Chem. A* **2001**, *105*, 5965; b) 2D IR spectroscopy: F. Thibault-Starzyk, A. Vimont, C. Fernandez, J.-P. Gilson, *Chem. Commun.* **2000**, 1003; F. Thibault-Starzyk, A. Vimont, J.-P. Gilson, *Stud. Surf. Sci. Catal.* **2001**, *135*, 1828; c) Solid-state NMR spectroscopy: W. Wang, M. Seiler, I. I. Ivanova, J. Weitkamp, M. Hunger *Chem. Commun.* **2001**, 1362; J. Weitkamp, M. Hunger, *Angew. Chem.* **2001**, *113*, 3061; *Angew. Chem. Int. Ed.* **2001**, *40*, 2954; d) ESR-UV spectroscopy: A. Brückner, *Chem. Commun.* **2001**, 2122; e) G. A. Somorjai, J. M. Thomas, *Top. Catal.* **1999**, *8*, (1/8), volume devoted to spectroscopy.

Communications



From a starting material of alkylidene cyclopropyl ketones, it is possible to make both two types of useful organic building block (furans and 4*H*-pyrans) regioselectively, by a simple adjustment of the reaction conditions. For more information, see the communication by S. Ma and J. Zhang.

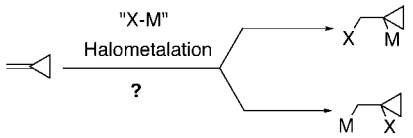
 © 2003 Wiley-VCH Verlag GmbH & Co. KGaA, Weinheim 1433-7851/03/4200-0183 $ 20.00+.50/0

Regioselective Cyclization

Tuning the Regioselectivity in the Palladium(II)-Catalyzed Isomerization of Alkylidene Cyclopropyl Ketones: A Dramatic Salt Effect**

Shengming Ma and Junliang Zhang*

In the last three decades, methylenecyclopropanes (MCPs) have been studied with numerous mechanistic,[1] biological[2] and synthetic interests.[3] Especially, mounting attention has been paid to the transition-metal-catalyzed reactions of MCPs.[4,5] Various reaction pathways, including oxidative addition of the distal or proximal C–C bond[4,6] and regioselective hydrometalation[7,8] or carbometalation[9,10] of the C=C bond, have been observed in the transition-metal-catalyzed reactions of MCPs. Although the chloropalladation reaction of MCPs with stoichiometric $[PdCl_2(PhCN)_2]$ has been studied,[11] no catalyzed reaction has been reported (Scheme 1). During our systematic study of allene chemistry,[12] we have been interested in the chemistry of its analogues, MCPs. Herein, we disclose a dramatic salt effect[13] in the palladium(II)-catalyzed regioselective cycloisomerization reaction of the alkylidene cyclopropyl ketones **1** giving the corresponding furan or 4*H*-pyran derivatives initiated with the regioselective halopalladation of the C=C bond of MCPs.



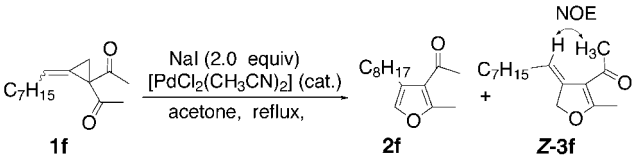
Scheme 1. Two possible modes of halometalation reactions of MCPs.

We initially examined the reaction of the methylenecyclopropyl ketone **1a**[14] in the presence of a catalytic amount of $[PdCl_2(CH_3CN)_2]$. After numerous trial and error attempts, fortunately we observed the $[PdCl_2(CH_3CN)_2]$-catalyzed regioselctive isomerization of **1a** with two equivalents of sodium iodide in THF afforded 2-phenyl-4-methylfuran **2a**[15] in 51% yield (entry 2, Table 1). The reaction can also be carried out in CH_3CN or DMF to afford the product in very low yields (entries 3 and 4, Table 1). The best results were obtained using two equivalents of sodium iodide as the additive in refluxing acetone, under the catalysis of 5 mol% $[PdCl_2(CH_3CN)_2]$ (Conditions A; entry 5, Table 1). Other salts such as tetra(*n*-butyl)ammonium iodide, tetra(*n*-butyl)ammonium bromide, and lithium bromide also showed a similar effect, albeit that **2a** was formed in lower yields (entries 6–8, Table 1).

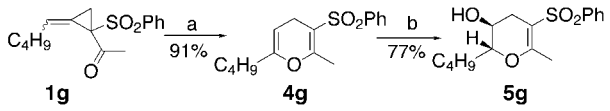
This transformation is general and some of the typical results are summarized in Table 2. The reactions of **1** under Conditions A afforded the corresponding polysubstituted furans **2** in good yields (Table 2). The reaction of **1d** with 20 mol% of sodium iodide afforded the corresponding product **2d** in a lower yield (compare entries 3 and 4, Table 2). The reaction of **1f** for 20.5 h afforded the furan **2f** in 80% yield, while 4-octylidene-4, 5-dihydrofuran *Z*-**3f** was formed in 55% yield together with **2f** (15%; Scheme 2) within 1 h, which indicates that the reaction proceeded through the intermediacy of **3f**. The stereochemistry of *Z*-**3f** was determined by an NOE study.

Furthermore, it is surprising for us to observe that the $[PdCl_2(CH_3CN)_2]$-catalyzed reaction of **1g** in acetone at RT *in the absence of NaI* (Conditions B) afforded the 4*H*-pyran **4g** in 91% yield (Scheme 3), of which the structure was determined by a X-ray diffraction study of the corresponding hydroboration–oxidation product **5g**.[16]

This transformation is also general and the results are summarized in Table 3. In the presence of 5 mol% $[PdCl_2(CH_3CN)_2]$, the reaction of the alkylidene cyclopropyl ketone **1b** at RT in acetone gave the 4*H*-pyran **4b** in 80% yield (entry 1, Table 3). In some cases, benzene is a better solvent. For example, the reaction of **1d** in benzene afforded **4d** in 80% yield, while the same reaction in acetone afforded **4d** in 69% yield (entries 3 and 4, Table 3). The reaction of **1e**, which contains the TBS-protected hydroxy group (TBS = *tert*-butyldimethylsilyl), gave **4e** in 85% yield in benzene (entry 5, Table 3). The presence of the electron-withdrawing group R^2



Scheme 2. The Pd^{II}-catalyzed cycloisomerization reaction of **1f** under Conditions A.



Scheme 3. The Pd^{II}-catalyzed isomerization reaction of **1g** under Conditions B and the subsequent hydroboration–oxidation reaction. a) 5 mol% $[PdCl_2(CH_3CN)_2]$, acetone, RT, 15 min; b) 1. $BH_3{\cdot}SMe_2$, THF, 0°C→RT, 1 h; 2. $NaOH–H_2O_2$, 0°C→RT, 6 h.

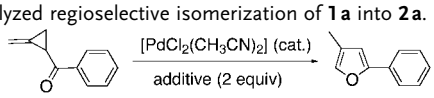
[*] Prof. S. Ma, Dr. J. Zhang
State Key Laboratory of Organometallic Chemistry
Shanghai Institute of Organic Chemistry, Chinese Academy of Sciences
354 Fenglin Lu, Shanghai 200032 (P.R. China)
Fax: (+86) 21-6416-6128
E-mail: masm@pub.sioc.ac.cn

[**] Financial support from the National Science Foundation of China, the Major State Basic Research Development Program (Grant No. G2000077500), the Chinese Academy of Sciences, and the Shanghai Municipal Committee of Science and Technology are greatly appreciated. S.M. is the recipient of the 1999 Qiu Shi Award for Young Chinese Scientific Workers issued by the Hong Kong Qiu Shi Foundation of Science and Technology (1999–2003)

Supporting information for this article is available on the WWW under http://www.angewandte.org or from the author.

 © 2003 Wiley-VCH Verlag GmbH & Co. KGaA, Weinheim 1433-7851/03/4202-0184 $ 20.00+.50/0

Table 1: Palladium(II)-catalyzed regioselective isomerization of **1a** into **2a**.

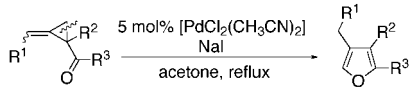


1a **2a**

Entry	Additive	Solvent	*T* [°C]	*t* [h]	Yield [%][a]
1	LiCl	CH_2Cl_2	RT	5	0
2	NaI	THF	reflux	10	51
3	NaI	CH_3CN	70	10	5
4	NaI	DMF	70	10	9
5	NaI	acetone	reflux	9	80
6	Bu_4NI	acetone	reflux	10	61[b]
7	Bu_4NBr	acetone	reflux	10	57[b]
8	LiBr	acetone	reflux	10	63

[a] 5 mol% of catalyst was used. [b] 10 mol% of catalyst was used.

Table 2: Palladium(II)-catalyzed regioselective isomerization of ketones **1**, which leads to furans **2**.[a]

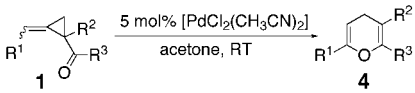


1 **2**

Entry	**1**			*t*	Yield of **2**
	R^1	R^2	R^3	[h]	[%]
1	C_7H_{15}	CO_2Et	Me (**1b**)	10	74 (**2b**)
2	C_4H_9	CO_2Et	Me (**1c**)	14	74 (**2c**)
3	Bn	CO_2Et	Me (**1d**)	13.5	78 (**2d**)
4		**1d**		24	65 (**2d**)[b]
5	$TBSO(CH_2)_3$	CO_2Et	Me (**1e**)	26	82 (**2e**)
6	C_7H_{15}	COMe	Me (**1f**)	20.5	80 (**2f**)[c]
7	H	H	$C_6H_5(CH_2)_2$ (**1h**)	12	77 (**2h**)

[a] Unless otherwise specified, the reaction was carried out using **1** (0.25–1.5 mmol) in the presence of 5 mol% $[PdCl_2(CH_3CN)_2]$ and 2 equiv of sodium iodide in 2 mL of acetone under reflux (Conditions A). [b] The reaction was carried out in the presence of 0.2 equiv of sodium iodide in 0.5 mL of acetone under reflux. [c] See the text.

Table 3: Palladium(II)-catalyzed regioselective isomerization of the ketones **1**, which leads to the 4*H*-pyrans **4**.[a]



1 **4**

Entry	**1**			*t*	Yield of **4**
	R^1	R^2	R^3	[min]	[%]
1	C_7H_{15}	CO_2Et	Me (**1b**)	15	80 (**4b**)
2	C_4H_9	CO_2Et	Me (**1c**)	15	75 (**4c**)
3	Bn	CO_2Et	Me (**1d**)	15	69 (**4d**)
4		**1d**		10	80 (**4d**)[b]
5	$TBSO(CH_2)_3$	CO_2Et	Me (**1e**)	10	85 (**4e**)[b]
6	C_7H_{15}	COMe	Me (**1f**)	40	60 (**4f**)
7	C_4H_9	SO_2Ph	Me (**1g**)	15	91 (**4g**)
8	C_8H_{17}	H	Ph (**1i**)	15	70 (**4i**)[b]

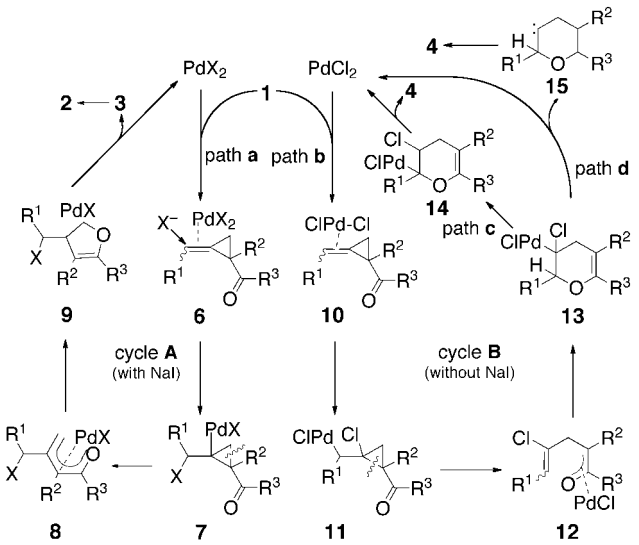
[a] Unless otherwise specified, all reactions were carried out using **1** (0.5 mmol) in the presence of 5 mol% $[PdCl_2(CH_3CN)_2]$ in 2 mL of acetone at RT (Conditions B). [b] The solvent used was benzene.

is not necessary because the reaction of **1i** was also good, affording **4i** in 70% yield (entry 8, Table 3).

A plausible rationale for the dramatic salt effect of NaI in the palladium(II)-catalyzed regioselective cycloisomerization of **1** is shown in Scheme 4**.** In the presence of NaI, the iodide anion (I^-) attacks the palladium(II)-coordinated C=C bond to afford the palladium intermediate **7** (path **a**), then β decarbopalladation involving the proximal C–C bond of the complex **7** would give the delocalized intermediate **8,** which would undergo the intramolecular *endo*-mode insertion of the C=C bond into the oxy-palladium bond followed by β halide elimination to produce the catalytically active palladium(II) species and **3**, which would furnish the furan **2** upon aromatization (cycle **A**). In the absence of NaI the reaction would go through cycle **B**. The regioselective chloropalladation[11] of the C=C bond of the alkylidene cyclopropane ketone **1** (path **b**) would afford the palladium intermediate **11**, which would undergo β decarbopalladation to afford the delocalized intermediate **12**. Subsequent intramolecular *endo*-mode insertion of the C=C bond into the oxygen–palladium bond of the intermediate **12** would afford a cyclic palladium intermediate **13**, which would undergo β-hydride elimination–hydropalladation with an opposite regioselectivity to afford the palladium intermediate **14**. Finally, β-halide elimination of **14** would produce the 4*H*-pyran **4** and regenerate the palladium(II) species (path **c**). The intermediate **13** might also undergo α-halide elimination[17] to afford a carbene intermediate **15** and regenerate palladium(II) species (path **d**). The carbene intermediate **15** would undergo intramolecular 1, 2-migration of hydrogen to afford the 4*H*-pyran **4**.

In conclusion, a dramatic salt effect was observed in the palladium(II)-catalyzed regioselective cycloisomerization of alkylidene cyclopropyl ketones **1**. In the presence of two equivalents of sodium iodide or other salts the reaction provides the furans **2** through distal-bond cleavage, while in the absence of salt, the polysubstituted 4*H*-pyrans **4** were formed by proximal-bond cleavage. Further studies into the scope, mechanism, and synthetic applications of this reaction are being carried out in our laboratory.

 © 2003 Wiley-VCH Verlag GmbH & Co. KGaA, Weinheim 1433-7851/03/4202-0185 $ 20.00+.50/0



Scheme 4. A plausible mechanism for the Pd^{II}-catalyzed isomerization reaction of **1**.

Experimental Section

Conditions A; synthesis of **2b**: $[PdCl_2(MeCN)_2]$ (17 mg, 0.65 mmol) was added to a solution of **1b** (356 mg, 1.3 mmol) and sodium iodide (400 mg, 2.7 mmol) in acetone (5 mL). The mixture was then stirred under reflux for 14 h. Evaporation of the solvent and chromatography on silica gel (petroleum ether/ether 100:1) afforded pure **2b** (256 mg, 74%) as a liquid. ^{1}H NMR (300 MHz, C_6D_6): $\delta = 6.81$ (s, 1H), 4.03 (q, $J = 7.2$ Hz, 2H), 2.61 (t, $J = 7.5$ Hz, 2H), 2.37 (s, 3H), 1.60–1.46 (m, 2H), 1.38–1.10 (m, 10H), 0.97 (t, $J = 7.2$ Hz, 3H), 0.84 ppm (t, $J = 7.2$ Hz, 3H); ^{13}C NMR (75.4 MHz, C_6D_6): $\delta = 164.10$, 160.06, 137.63, 126.76, 113.51, 59.57, 32.25, 30.08, 29.96, 29.87, 29.73, 25.17. 23.03, 14.31, 14.26, 14.24 ppm; MS (70 eV): *m/z* (%): 266 (1.14) [M^+], 168 (100) [$M^+ - C_7H_{14}$]; IR (neat): $\tilde{\nu} = 1716$, 1607, 1559 cm^{-1}; HRMS calcd for $C_{16}H_{26}O_3$: 266.18819, found: 266.18641.

Conditions B; synthesis of **4b**: $[PdCl_2(MeCN)_2]$ (6 mg, 5 mol%) was added to a solution of **1b** (133 mg, 0.50 mmol) in acetone (2 mL). The mixture was then stirred at RT for 15 min. Evaporation of the solvent and chromatography on silica gel (petroleum ether/ether 100:1) afforded pure **4b** (106 mg, 80%) as an air-sensitive liquid. ^{1}H NMR (300 MHz, $CDCl_3$): $\delta = 4.65$ (t, $J = 3.6$ Hz, 1H), 4.14 (q, $J = 6.9$ Hz, 2H), 2.90–2.80 (m, 2H), 2.20 (t, $J = 0.9$ Hz, 3H), 1.99 (t, $J = 6.9$ Hz, 2H), 1.50–1.30 (m, 2H), 1.30–1.20 (m, 8H), 1.25 (t, $J = 6.9$ Hz, 3H), 0.87 ppm (t, $J = 6.6$ Hz, 3H); ^{13}C NMR (75.4 MHz, $CDCl_3$): $\delta =$ 168.16, 160.95, 150.23, 100.27, 97.33, 59.81, 32.58, 31.76, 29.04, 28.94, 26.35, 22.62, 21.92, 19.13, 14.31, 14.05 ppm; MS (70 eV): *m/z* (%): 266 (7.89) [M^+], 43 (100) [$C_3H_7^+$]; IR (neat): $\tilde{\nu} = 1720$, 1637, 761 cm^{-1}; HRMS calcd for $C_{16}H_{26}O_3$: 266.18819, found 266.1857.

Received: July 29, 2002 [Z19842]

[1] M. G. Lazzara, J. J. Harrison, M. Rule, E. F. Hilinski, J. A. Berson, *J. Am. Chem. Soc.* **1982**, *104*, 2233.

[2] a) C. H. Hassall, K. Reyle, P. Feng, *Nature* **1954**, *173*, 356; b) C. H. Hassall, K. Reyle, *Biochem. J.* **1955**, *60*, 344; c) J. A. Carbon, W. B. Martin, L. R. Swett, *J. Am. Chem. Soc.* **1958**, *80*, 1002; d) N. D. Lenn, Y. Shih, M. T. Stankovich, H. Liu, *J. Am. Chem. Soc.* **1989**, *111*, 3065.

[3] a) R. Noyori, N. Hayashi, M. Katô, *J. Am. Chem. Soc.* **1971**, *93*, 4948; b) B. M. Trost, *Angew. Chem.* **1986**, *98*, 1; *Angew. Chem. Int. Ed. Engl.* **1986**, *25*, 1; c) S. Yamago, E. Nakamura, *J. Am. Chem. Soc.* **1989**, *111*, 7285; d) A. Brandi, A. Goti, *Chem. Rev.* **1998**, *98*, 589.

[4] For a recent review, see: I. Nakamura, Y. Yamamoto, *Adv. Synth. Catal.* **2002**, *344*, 111–129.

[5] For reviews, see: a) P. Binger, H. M. Büch, *Top. Curr. Chem.* **1987**, *135*, 77; b) T. Ohta, H. Takaya in *Comprehensive Organic Synthesis, Vol. 5* (Ed.: B. M. Trost, I. Fleming, L. A. Paquette), Pergamon, Oxford, **1991**, p. 1185; c) *"Carbocyclic Three-Membered Ring Compounds": Methoden Org. Chem. (Houben-Weyl) 4th ed., Vol. E17*, **1996**, 2217; d) M. Lautens, W. Klute, W. Tam, *Chem. Rev.* **1996**, *96*, 49.

[6] M. Suginome, T. Matsuda, Y. Ito, *J. Am. Chem. Soc.* **2000**, *122*, 11015.

[7] a) M. Lautens, C. Meyer, A. Lorenz, *J. Am. Chem. Soc.* **1996**, *118*, 10676; b) A. G. Bessmertnykh, K. A. Blinov, Y. K. Grishin, N. A. Donskaya, E. V. Tveritinova, N. M. Yur'eva, I. P. Beletskaya, *J. Org. Chem.* **1997**, *62*, 6069.

[8] a) N. Tsukada, A. Shibuya, I. Nakamura, Y. Yamamoto, *J. Am. Chem. Soc.* **1997**, *119*, 8123; b) I. Nakamura, H. Itagaki, Y. Yamamoto, *J. Org. Chem.* **1998**, *63*, 6458; c) D. H. Camacho, I. Nakamura, S. Saito, Y. Yamamoto, *Angew. Chem.* **1999**, *111*, 3576; *Angew. Chem. Int. Ed.* **1999**, *38, 3365*; d) I. Nakamura, S. Saito, Y. Yamamoto, *J. Am. Chem. Soc.* **2000**, *122*, 2661; e) D. H. Camacho, I. Nakamura, S. Saito, Y. Yamamoto, *J. Org. Chem.* **2001**, *66*, 270.

[9] a) G. Fournet, G. Balme, J. J. Barieux, J. Goré, *Tetraherdron* **1988**, *44*, 5809, 5821; b) S. Bräse, A. de Meijere, *Angew. Chem.* **1995**, *107*, 2741; *Angew. Chem. Int. Ed. Engl.* **1995**, *34*, 2545.

[10] a) R. Grigg, P. Kennewell, A. Teasdale, V. Sridharan, *Tetrahedron Lett.* **1993**, *34*, 153; b) K. H. Ang, S. Bräse, A. G. Steinig, F. E. Meyer, A. Llebaria, K. Voigt, A. de Meijere, *Tetrahedron* **1996**, *52*, 11503.

[11] a) R. Noyori, H. Takaya, *Chem. Commun.* **1969**, 525; b) P. R. Clemens, R. P. Hughes, L. D. Margerum, *J. Am. Chem. Soc.* **1981**, *103*, 2428; c) T. A. Albright, P. R. Clemens, R. P. Hughes, D. E. Hunton, L. D. Margerum, *J. Am. Chem. Soc.* **1982**, *104*, 5369; d) B. K. Dallas, R. P. Hughes, K. Schumann, *J. Am. Chem. Soc.* **1982**, *104*, 5380, and references therein.

[12] For some of the most recent results from this group, see: a) S. Ma, S. Wu, *Chem. Commun.* **2001**, 441; b) S. Ma, S. Zhao, *J. Am. Chem. Soc.* **2001**, *123*, 5578; c) S. Ma, Z. Shi, *Chem. Commun.* **2002**, 540; d) S. Ma, W. Gao, *Synlett* **2002**, 65; e) S. Ma, S. Yin, L. Li, F. Tao, *Org. Lett.* **2002**, *4*, 505; f) S. Ma, N. Jiao, S. Zhao, H. Hou, *J. Org. Chem.* **2002**, *67*, 2837; g) S. Ma, D. Duan, Y. Wang, *J. Comb. Chem.* **2002**, *4*, 239; h) S. Ma, Z. Yu, *Angew. Chem.* **2002**, *114*, 1853; *Angew. Chem. Int. Ed.* **2002**, *41*, 1775.

[13] For reviews, see: a) E. M. Vogl, H. Gröger, M. Shibasaki, *Angew. Chem.* **1999**, *111*, 1671; *Angew. Chem. Int. Ed.* **1999**, *38*, 1570; b) K. Fagnou, M. Lautens, *Angew. Chem.* **2002**, *114*, 26; *Angew. Chem. Int. Ed.* **2002**, *41*, 26.

[14] **1a, 1h**, and **1i** were prepared according to the following reference except that the corresponding *N,N*-dimethyl amide was used instead of the lithium carboxulates, see: E. W. Thomas, J. R. Szmuszkovicz, *J. Org. Chem.* **1990**, *55*, 6054; other starting MCPs were prepared by the rhodium-catalyzed cyclopropanation reaction of the diazo compounds with allenes, see: C. Cheng, T. Shimo, K. Somekawa, M. Baba, *Tetrahedron* **1998**, *54*, 2031.

[15] The structure of **2a** was determined by the comparison with the authentic sample, which was synthesized according to the following reference: Y. Wakabayashi, Y. Fukuda, H. Shiragami, K. Utimoto, H. Nozaki, *Tetrahedron* **1985**, *41*, 3655. For ^{1}H NMR spectroscopic data of **2a**, see: H. Hagiwara, H. Uda, *J. Chem. Soc. Perkin Trans. 1* **1984**, 91.

[16] X-ray data for compound **5g**: $C_{16}H_{22}O_4S$, $M_r = 310.40$, monoclinic, space group $P2(1)/c$, $Mo_{K\alpha}$, final R indices $[I > 2\sigma(I)]$, $R1 = 0.0553$, $wR2 = 0.1280$, $a = 17.931(4)$, $b = 8.4053(16)$, $c =$ 10.938(2) Å, $\alpha = 90$, $\beta = 94.494(3)$, $\gamma = 90°$, $V = 1643.5(5)$ Å^3,

 © 2003 Wiley-VCH Verlag GmbH & Co. KGaA, Weinheim 1433-7851/03/4202-0186 $ 20.00+.50/0

$T = 293$ K, $Z = 4$, reflections collected/unique: 9438/3824 ($R_{int} = 0.0457$), no observation [$I > 2\sigma(I)$] 3824, parameters 257. CCDC-190370 (**5g**) contains the supplementary crystallographic data for this paper. These data can be obtained free of charge via www.ccdc.cam.ac.uk/conts/retrieving.html (or from the Cambridge Crystallographic Data Centre, 12, Union Road, Cambridge CB2 1EZ, UK; fax: (+44) 1223-336-033; or deposit @ccdc.cam.ac.uk).

[17] S. Ma, B. Xu, B. Ni, *J. Org. Chem.* **2000**, *65*, 8532.

Electrochemical Sensors

Mono-Tetrathiafulvalene Calix[4]pyrrole in the Electrochemical Sensing of Anions**

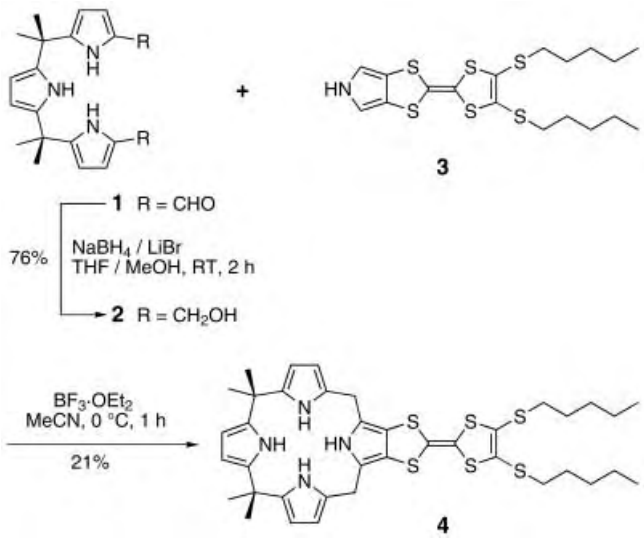
Kent A. Nielsen, Jan O. Jeppesen, Eric Levillain, and Jan Becher**

Dedicated to Professor J. Fraser Stoddart on the occasion of his 60th birthday

The advent of supramolecular chemistry[1] has stimulated the contemporary chemist's interest in the development of chemosensors capable of recognizing specific chemical species.[2] Calix[4]pyrroles[3]—first synthesized in the 19th Century by Baeyer[4]—contain four pyrrole–NH hydrogen-bond functionalities and have recently been studied for possible use as receptors for anionic and neutral substrates.[5] They have been used to prepare optical anion sensors[6] and anion-selective high-performance liquid-chromatography (HPLC) supports.[7] However, only a few electrochemically active sensors based on calix[4]pyrroles have been reported.[8] Electrochemically active sensors, designed to permit the detection of substrates by binding-induced changes in the redox properties, are generally composed of a receptor unit, which works by the covalent association of a substrate-recognition functionality, and an electrochemical-signaling capacity (redox-active unit). The redox-active tetrathiafulvalene[9] (TTF) unit can exist in three stable redox states (TTF^0, $TTF^{+\bullet}$, and TTF^{2+}) and for this reason TTF derivatives have found widespread use in materials chemistry.[9] Progress in synthetic TTF chemistry[9] has revolutionized the possibilities for the incorporation of TTF into macrocyclic, molecular, and supramolecular structures and has transformed complicated systems, such as TTF cyclophanes,[9] TTF catenanes,[9] and TTF rotaxanes/pseudorotaxanes[9,10] from chemical curiosities into a vibrant area of modern-day research. In the context of electrochemically active sensors, TTF has already been used as the redox-active unit in a number of cation responsive receptors.[11] However, to our knowledge, no anion receptor incorporating TTF as the redox-active unit has been reported. We have recently developed an efficient synthesis of the parent pyrrolo[3,4-*d*]TTF-ring system.[12] With this building block in hand, we have prepared the first example of a single molecule in which the anion-receptor abilities of the calix[4]-pyrrole system were coupled to the favorable redox properties of the TTF core through direct annulation of one TTF unit to the upper rim of the calix[4]pyrrole skeleton.

Herein, we report the synthesis of the first calix[4]pyrrole incorporating a TTF unit. Furthermore, we describe our ^{1}H NMR spectroscopic and electrochemical studies on the recognition abilities of this novel mono-TTF calix[4]pyrrole **4** system towards anions.

Our preparation of the mono-TTF calix[4]pyrrole **4** is outlined in Scheme 1. The tripyrrane dialdehyde **1** was prepared according to a literature procedure[13] by the condensation of pyrrole and acetone followed by a Clezy formylation. The reduction of the formyl groups with $NaBH_4$/LiBr in anhydrous THF/MeOH produced the bishydroxymethyltripyrrane **2** in 76% yield. The tripyrrane **2** was used immediately after purification by means of flash column chromatography on account of the low stability of the compound. Treatment of equal quantities of **2** and the newly developed pyrrolo TTF **3** with a catalytic amount of $BF_3{\cdot}Et_2O$ in anhydrous MeCN, gave the mono-TTF calix[4]pyrrole **4** as yellow crystals after purification by means of column chromatography (yield 21%).[14]



Scheme 1. Synthesis of the mono-TTF calix[4]pyrrole **4**.

[*] Dr. J. O. Jeppesen, Prof. J. Becher, K. A. Nielsen
Department of Chemistry
Odense University (University of Southern Denmark)
Campusvej 55, 5230 Odense M (Denmark)
Fax: (+45) 66-158-780
E-mail: joj@chem.sdu.dk
jbe@chem.sdu.dk
Dr. E. Levillain
Ingénierie Moléculaire et Matériaux Organiques
CNRS UMR 6501, Université d'Angers
2 Bd Lavoisier, 49045 Angers (France)

[**] We gratefully acknowledge the University of Odense for a Ph.D scholarship to K.A.N., financial support from Carlsbergfondet to J.O.J, and the French Embassy Copenhagen for a travel grant to J.B.

A high-resolution MALDI-MS of **4** showed the exact mass *m*/*z* 752.2170, corresponding to $M^{+\cdot}$ (calcd mass $M^{+\cdot}$ 752.2198). The ^{1}H NMR spectrum (250 MHz) of **4**, recorded in CD_3CN at 303 K, showed three broad singlets at $\delta = 7.81$, 7.95, and 8.22 ppm—integrating to 1H, 1H, and 2H, respectively,—which can be assigned to the three sets of chemically nonequivalent NH protons. An ^{1}H-{^{1}H}NOE-NMR experiment was carried out to assign the resonance signals associated with the pyrrole NH protons. Irradiation of the *meso*-CH_2 protons ($\delta = 3.61$ ppm) led to signal enhancements for the signals at $\delta = 7.95$ and 8.22 ppm, respectively, but no observable effect for the signal at $\delta = 7.81$ ppm. These results clearly indicate that the resonance signal at $\delta = 7.95$ ppm corresponds to the NH proton on the pyrrolo-TTF unit, whereas the resonance signal at $\delta = 7.81$ ppm corresponds to the pyrrole–NH proton opposite to the pyrrolo-TTF unit. Finally, the resonance signal at $\delta = 8.22$ ppm is assigned to the remaining two chemically equivalent pyrrole–NH protons. Solution oxidation potentials (vs Ag/AgCl) obtained from a cyclic voltammogram of compound **4** recorded in MeCN revealed two pairs of reversible redox waves at $E^1_{1/2} = 0.45$ V and $E^2_{1/2} = 0.75$ V.

By employing ^{1}H NMR spectroscopy and cyclic voltammetry (CV), **4** was shown to form complexes with Br^-, Cl^-, and F^- ions. A comparison of the ^{1}H NMR spectra (CD_3CN, 300 K) of the free receptor **4** (Figure 1a) and **4** in the presence of Br^- ions (Figure 1b) reveals significant chemical-shift differences for the resonances associated with the NH protons (downfield shifts, $\Delta\delta = 2.2$–3.2 ppm), which indicates that the Br^- ion is complexed by **4**. A continuous-variation ^{1}H NMR experiment was carried out to determine the stoichiometry of the binding between **4** and Br^- ions. The Job plot[15] obtained exhibit a maximum at 0.55, thus indicating that **4** forms a 1:1 complex with Br^- ions. To target biological analytes, the receptor **4** should function in the presence of water. Therefore, binding studies between **4** and Br^-, Cl^-, and F^- ions were performed in CD_3CN containing 0.5% v/v D_2O, as acetonitrile is water miscible, which would allow the receptor **4** to sense anions added in the form of aqueous solutions.[16] To determine the binding constant (K_a) for the 1:1 complex of Br^- ions and **4**, ^{1}H NMR titration experiments (Figure 2) were carried out. This was done by means of monitoring the changes in the chemical shift for the resonance signals associated with the three nonequivalent NH protons upon the addition of an increasing amount of nBu$_4$NBr to the receptor **4** at 300 K. The binding constant was obtained using the nonlinear curve-fitting program EQNMR[17] and gave an average K_a value of $7.6 \times 10^3\,\text{M}^{-1}$ for the **4**·Br^- complex. Similar titration experiments were carried out with solutions containing Cl^- and F^- ions. However, as a consequence of strong binding between the receptor **4** and these two anions, the titration plots tended towards linearity with increasing anion concentration, which made the nonlinear curve fitting procedure unreliable[18] for estimating K_a values. To determine the K_a values for the **4**·Cl^- and **4**·F^- complex, a competitive ^{1}H NMR spectroscopic method was used.[18] The binding constant between **4** and Cl^- ions was determined in a competitive experiment with Br^- ions under conditions of negligible free receptor concentrations. Addition of a solution containing Cl^- ions to a solution of **4** saturated with Br^- ions induced further downfield shifts (Figure 1c) of the resonance signals associated with the NH protons, which indicates that complexed Br^- has been partly replaced by Cl^- ions. Analysis[18b] of the data gave a K_a value of $1.2 \times 10^5\,\text{M}^{-1}$ for the **4**·Cl^- complex. A similar competition experiment was carried out between F^- and Cl^- (Figure 1e). These results are summarized in Table 1.

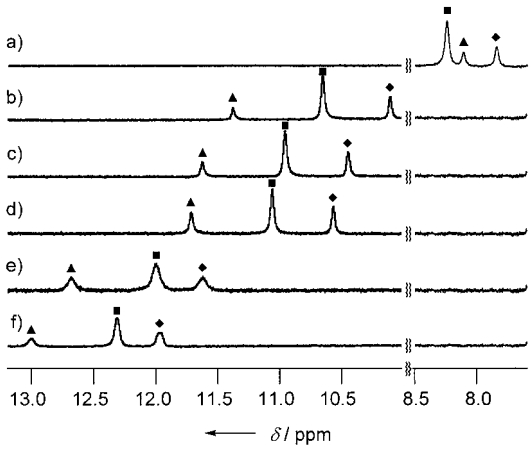


Figure 1. Partial ^{1}H NMR spectra (300 MHz) recorded in CD_3CN/0.5% v/v D_2O at 300 K of a) free receptor **4** (3.9 mM), b) **4** + Br^- (3.9 equiv), c) **4** + Br^- (3.9 equiv) + Cl^- (2.1 equiv), d) **4** + Cl^- (7.4 equiv), e) **4** + Cl^- (7.4 equiv) + F^- (2.2 equiv), f) **4** + F^- (10.5 equiv). The signals correspond to the three different pyrrole–NH protons. ▲ = NH on the pyrrolo-TTF unit, ■ = NH adjacent to the pyrrolo-TTF unit, and ◆ = NH opposite to the pyrrolo-TTF unit.

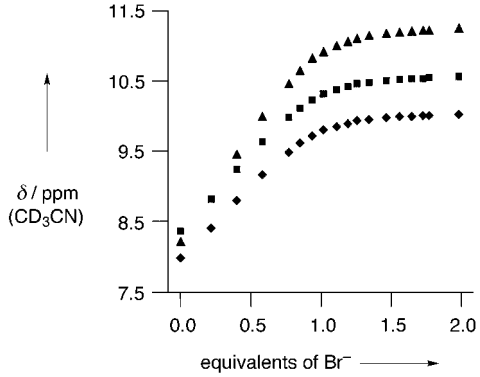


Figure 2. ^{1}H NMR titration curves of the perturbation of the three nonequivalent NH protons upon addition of increasing amounts of Br^- ions. ▲ = NH on the pyrrolo-TTF unit, ■ = NH adjacent to the pyrrolo-TTF unit, and ◆ = NH opposite to the pyrrolo-TTF unit.

The receptor **4** was designed to permit the detection of anions by binding-induced changes in the electrochemically properties of the TTF unit. CV was used to probe the changes in the redox potentials of **4** upon complexation of anions. The progressive addition of a solution containing Br^- ions to a solution of **4** in MeCN at 298 K resulted in a cathodic displacement of the first oxidation potential ($E^1_{1/2}$) of the TTF unit (Figure 3). It should be noted (Figure 3a) that the current intensity associated with second oxidation wave increases as the concentration of Br^- ions increases. This unexpected

 © 2003 Wiley-VCH Verlag GmbH & Co. KGaA, Weinheim 1433-7851/03/4202-0188 $ 20.00+.50/0

Table 1: Binding constants between **4** and the Br^-, Cl^-, and F^- ions determined by ^1H NMR spectroscopy at 300 K, and first redox potentials $E^1_{1/2}$ of the complexes **4**·X^- (where X is a halide) determined by CV at 298 K.

X^-	K_a [M^{-1}] (CD_3CN/ 0.5% v/v D_2O)	$E^1_{1/2}$ [mV] (MeCN)[a]	ΔE [mV] (MeCN)[b]
Br^-	7.6×10^3[c]	+467	−34
Cl^-	1.2×10^5[d]	+462	−43
F^-	2.1×10^6[e]	–	–

[a] Values obtained from 1:1 mixtures of **4** and nBu_4NX. [b] Maximum ΔE values (ΔE_{max}) were obtained from 1:2 mixtures of **4** and nBu_4NX. [c] A CD_3CN (0.5% v/v D_2O) solution of receptor **4** (3.9 mM) was titrated by adding a concentrated CD_3CN (0.5% v/v D_2O) solution of nBu_4NBr which also contained receptor **4** at the initial concentration to account for dilution effects. The binding constant was elucidated using the EQNMR computer program[17] and is the average of two independent experiments using the three NH protons as probes, the estimated error was <10%. [d] Determined from competitive binding experiments.[18] An average K_{rel} of 16.8 for the ions Cl^-/Br^- was obtained by analyzing a CD_3CN (0.5% v/v D_2O) solution of **4** (3.9 mM) containing Br^- (3.9 equiv) and Cl^- (either 1.6 or 2.1 equiv), estimated error was <15%. [e] Determined from competitive binding experiments.[18] An average K_{rel} of 16.9 for F^-/Cl^- was obtained by analyzing a CD_3CN (0.5% v/v D_2O) solution of **4** (3.9 mM) containing Cl^- (7.4 equiv) and F^- (either 2.0 or 2.2 equiv), estimated error was <15%.

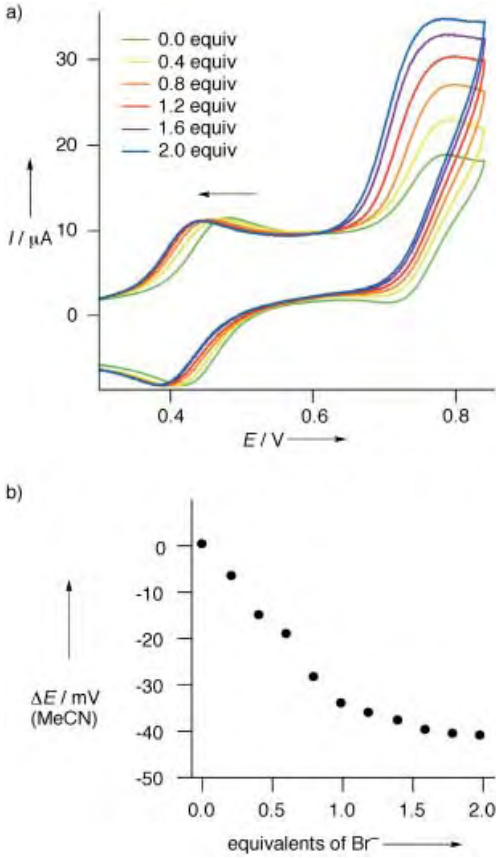


Figure 3. a) Cyclic voltammograms of the receptor **4** (0.5 mM) recorded in MeCN at 298 K with nBu_4NPF_6 (0.4 M) as the supporting electrolyte. Experiments were carried out in a glove box containing anhydrous oxygen-free (<1 vpm) argon and without light, at a scan rate of 0.5 Vs^{-1}.[25] The receptor **4** was titrated by adding concentrated MeCN solution of nBu_4NBr that also contained receptor **4** at the initial concentration, to counter the dilution effects. The potentials were referred to Ag/AgCl. b) CV titration curves showing the cathodic shift of the first oxidation potential of the receptor **4** upon addition of Br^- ions. Note that the cathodic shift of the first oxidation potential is independent of the second oxidation process.

growth of the current intensity is a consequence of the oxidation of the anion. Indeed, in the absence of the receptor **4**, the Br^- ion undergoes oxidation[19] in solution at a potential, which is close to the second oxidation potential of **4**. As a consequence of the overlapping nature of these two oxidation processes, it is not possible to obtain any information about whether complexation of the anions to **4** also affect the second oxidation potential of the TTF unit in **4**. It is evident from Figure 3b that the displacement of the first oxidation potential reach a limit ($\Delta E = -40$ mV) when approximately stoichiometric amounts of Br^- ions were added to **4**, which provides further evidence for the high stability of the **4**·Br^- complex. Similar cathodic displacements were observed when **4** was titrated with a solution containing Cl^- ions, and the results obtained are recorded in Table 1,[20] together with the results obtained from the titration of **4** with a solution containing Br^- ions. The results from the electrochemical experiments reveal that the complexation of the anions inside the cavity of **4** shift the first oxidation of the TTF unit towards more cathodic potentials,[21] which can be accounted for by delocalization of the negative charge from the binding site N–H···X^- to the TTF core.[22] The annulation of the TTF unit to the upper rim of the calix[4]pyrrole skeleton, not only transduces the binding event to an electrochemical output signal, but also substantially increases the binding abilities of the receptor towards anionic substrates as compared to other calix[4]pyrrole receptors, such as *meso*-octamethylcalix[4]pyrrole.[23] To our knowledge, **4** displays the strongest anion binding affinities yet recorded for calix[4]pyrrole receptors, and the binding constants obtained (Table 1) between **4** and Br^-, Cl^-, and F^- ions are two orders of magnitude higher than those reported for *meso*-octamethylcalix[4]pyrrole.[24] The stronger affinity of **4** towards anions is presumably a direct consequence of the pyrrolo-TTF–NH proton being more acidic than the other NH protons of **4**. This factor implies that the pyrrolo-TTF–NH proton is able to form a stronger hydrogen bond with anions upon complexation, as compared to NH protons in the parent calix[4]pyrrole. This hypothesis is supported by the fact that the pyrrolo-TTF–NH proton experience the largest difference in chemical shift ($\Delta\delta$) when solutions containing halides are added. In the case of the Br^-ion, the $\Delta\delta$ reach a value of 3.2 ppm (Figure 2), whereas the remaining pyrrole–NH protons only reach $\Delta\delta$ values in the range of 2.2–2.3 ppm.

In summary, we have prepared an efficient chemosensor—mono-TTF-calix[4]pyrrole **4**—that allows the detection of anions by electrochemical means. The incorporation of one redox-active pyrrolo-TTF unit into a calix[4]pyrrole produces a receptor with the strongest binding affinities toward Br^-, Cl^-, and F^- ions yet recorded for a calix[4]pyrrole system. To our knowledge, **4** represents the first anion sensor based on TTF and the first calix[4]pyrrole system shown to have an

 © 2003 Wiley-VCH Verlag GmbH & Co. KGaA, Weinheim 1433-7851/03/4202-0189 $ 20.00+.50/0

approximately stoichiometric CV response upon the addition of anions. These observations make the redox-responsive calix[4]pyrrole **4** and related systems very attractive for further investigations.

Experimental Section

2: $NaBH_4$ (79.0 mg, 2.09 mmol) was added in one portion to a solution of the tripyrrane dialdehyde[13] **1** (235 mg, 0.70 mmol) and anhydrous LiBr (181 mg, 2.09 mmol) in anhydrous THF-MeOH (70 mL, 2:1 v/v). The reaction mixture was stirred at room temperature for 2 h before H_2O (50 mL) was added. The mixture was extracted with CH_2Cl_2 (3 × 50 mL), and the extract was dried ($MgSO_4$). The solvent was removed under vacuum and the residue was purified by column chromatography (SiO_2; PhMe:EtOAc 1:1). The colorless band containing the product ($R_f = 0.2$) was collected and the solvent evaporated affording the bishydroxymethyl tripyrrane **2** (0.18 g, 76%) as a colorless solid. The product was used immediately after purification, on account of its low stability: ^{1}H NMR ($CDCl_3$, 300 MHz, 298 K): $\delta = 1.55$ (s, 12H), 2.41 (br, s, 2H), 4.30 (s, 4H), 5.88–5.92 (m, 4H), 5.99 (d, $J = 2.8$ Hz, 2H), 7.55 (br, s, 1H), 8.32 ppm (br, s, 2H); ^{13}C NMR ($CDCl_3$ 75 MHz, 298 K): $\delta = 29.3, 35.5, 57.7, 103.3, 103.4, 106.7, 130.1, 138.6, 140.6$ ppm.

4: Tripyrrane **2** (0.17 g, 0.50 mmol) and the pyrrolo-TTF[12] **3** (0.22 g, 0.50 mmol) was dissolved in anhydrous MeCN (50 mL) under an atmosphere of nitrogen and stirred at 0 °C for 10 min before a catalytic amount of $BF_3{\cdot}Et_2O$ (4.33 μL, ~5 mg, 5 μmol) was added to the yellow solution. Stirring was maintained for 1 h at 0 °C, the solvent was then removed under reduced pressure, and the resulting residue was dissolved in CH_2Cl_2 (80 mL), washed with an aqueous NaOH solution (0.1 M, 20 mL) and H_2O (2 × 30 mL), and dried ($MgSO_4$). The solvent was removed under reduced pressure and the resulting yellow solid was subjected to column chromatography (SiO_2; cyclohexane:CH_2Cl_2 2:1). The yellow band containing the product ($R_f = 0.3$) was collected and the solvent evaporated under vacuum affording the mono-TTF calix[4]pyrrole **4** (79.1 mg, 21%) as a yellow solid. Recrystallization from CH_2Cl_2/nC_7H_{16} gave **4** as thin yellow needles: m.p. 139.5–140.5 °C; ^{1}H NMR (CD_3CN, 250 MHz, 303 K): $\delta = 0.89$ (t, $J = 6.9$ Hz, 6H), 1.25–1.43 (m, 8H), 1.51 (s, 12H), 1.55–1.67 (m, 4H), 2.84 (t, $J = 7.3$ Hz, 4H), 3.61 (s, 4H), 5.73–5.79 (m, 2H), 5.79–5.85 (m, 4H), 7.81 (br, s, 1H), 7.95 (br, s, 1H), 8.22 ppm (br, s, 2H); HiResMALDI: m/z 752.2170 (calcd for $C_{38}H_{48}N_4S_6^{+\bullet}$ 752.2198); elemental analysis calcd (%) for $C_{38}H_{48}N_4S_6$ (753.21): C 60.59, H 6.42, N 7.44, S 25.54; found C 60.67, H 6.26, N 7.55, S 25.68.

Received: June 14, 2002
Revised: September 3, 2002 [Z19534]

[1] a) J.-M. Lehn, *Supramolecular Chemistry*, VCH, Weinheim, **1995**; b) *Comprehensive Supramolecular Chemistry, Vol. 1–11* (Eds.: J. L. Atwood, J. E. D. Davies, D. D. MacNicol, F. Vögtle, D. Reinhoudt), Pergamon, Oxford, **1996**.

[2] a) P. L. Boulas, M. Gomez-Kaifer, L. Echegoyen, *Angew. Chem.* **1998**, *110*, 226–258; *Angew. Chem. Int. Ed.* **1998**, *37*, 216–247; b) A. P. Davis, R. S. Wareham, *Angew. Chem.* **1999**, *111*, 3160–3179; *Angew. Chem. Int. Ed.* **1999**, *38*, 2978–2996; c) P. A. Gale, *Coord. Chem. Rev.* **2000**, *199*, 181–233; d) B. Valeur, I. Leray, *Coord. Chem. Rev.* **2000**, *205*, 3–40; e) P. A. Gale, *Coord. Chem. Rev.* **2001**, *213*, 79–128; f) P. D. Beer, P. A. Gale, *Angew. Chem.* **2001**, *113*, 502–532; *Angew. Chem. Int. Ed.* **2001**, *40*, 486–516.

[3] J. L. Sessler, P. A. Gale in *The Porphyrin Handbook, Vol. 6* (Eds.: K. M. Kadish, K. M. Smith, R. Guilard), Academic Press, San Diego, **2000**, pp. 257–278.

[4] A. Baeyer, *Ber. Dtsch. Chem. Ges.* **1886**, *19*, 2184–2185.

[5] a) P. Anzenbacher, Jr., A. C. Try, H. Miyaji, K. Jursýková, V. M. Lynch, M. Marquez, J. L. Sessler, *J. Am. Chem. Soc.* **2000**, *122*, 10268–10272; b) F. P. Schmidtchen, *Org. Lett.* **2002**, *4*, 431–434; c) D.-W. Yoon, H. Hwang, C.-H. Lee, *Angew. Chem.* **2002**, *114*, 1835–1837; *Angew. Chem. Int. Ed.* **2002**, *41*, 1757–1759.

[6] H. Miyaji, W. Sato, J. L. Sessler, *Angew. Chem.* **2000**, *112*, 1847–1850; *Angew. Chem. Int. Ed.* **2000**, *39*, 1777–1780.

[7] J. L. Sessler, P. A. Gale, J. W. Genge, *Chem. Eur. J.* **1998**, *4*, 1095–1099.

[8] a) J. L. Sessler, A. Gebauer, P. A. Gale, *Gazz. Chim. Ital.* **1997**, *127*, 723–726; b) P. A. Gale, M. B. Hursthouse, M. E. Light, J. L. Sessler, C. N. Warriner, R. S. Zimmerman, *Tetrahedron Lett.* **2001**, *42*, 6759–6762.

[9] For recent TTF reviews, see: a) M. R. Bryce, *J. Mater. Chem.* **2000**, *10*, 589–598; b) M. B. Nielsen, C. Lomholt, J. Becher, *Chem. Soc. Rev.* **2000**, *29*, 153–164; c) J. L. Segura, N. Martín, *Angew. Chem.* **2001**, *113*, 1416–1455; *Angew. Chem. Int. Ed.* **2001**, *40*, 1372–1409.

[10] a) J. O. Jeppesen, J. Perkins, J. Becher, J. F. Stoddart, *Org. Lett.* **2000**, *2*, 3547–3550; b) J. O. Jeppesen, J. Perkins, J. Becher, J. F. Stoddart, *Angew. Chem.* **2001**, *113*, 1256–1261; *Angew. Chem. Int. Ed.* **2001**, *40*, 1216–1221; c) C. P. Collier, J. O. Jeppesen, Y. Luo, J. Perkins, E. W. Wong, J. R. Heath, J. F. Stoddart, *J. Am. Chem. Soc.* **2001**, *123*, 12632–12641; d) J. O. Jeppesen, J. Becher, J. F. Stoddart, *Org. Lett.* **2002**, *4*, 557–560; e) Y. Luo, C. P. Collier, J. O. Jeppesen, K. A. Nielsen, E. Delonno, G. Ho, J. Perkins, H.-R. Tseng, T. Yamamoto, J. F. Stoddart, J. R. Heath, *ChemPhysChem* **2002**, *3*, 519–525.

[11] See for example: a) F. Le Derf, E. Levillain, G. Trippé, A. Gorgues, M. Sallé, R. M. Sebastian, A. M. Caminade, J. P. Majoral, *Angew. Chem.* **2001**, *113*, 224–227; *Angew. Chem. Int. Ed.* **2001**, *40*, 224–227; b) F. Le Derf, M. Mazari, N. Mercier, E. Levillain, G. Trippé, A. Riou, P. Richomme, J. Becher, J. Garin, J. Orduna, N. Gallego-Planas, A. Gorgues, M. Sallé, *Chem. Eur. J.* **2001**, *7*, 447–455; c) G. Trippé, E. Levillain, F. Le Derf, A. Gorgues, M. Sallé, J. O. Jeppesen, K. Nielsen, J. Becher, *Org. Lett.* **2002**, *4*, 2461–2464.

[12] a) J. O. Jeppesen, K. Takimiya, F. Jensen, J. Becher, *Org. Lett.* **1999**, *1*, 1291–1294; b) J. O. Jeppesen, K. Takimiya, F. Jensen, T. Brimert, K. Nielsen, N. Thorup, J. Becher, *J. Org. Chem.* **2000**, *65*, 5794–5805.

[13] C. Bucher, R. S. Zimmerman, V. Lynch, J. L. Sessler, *J. Am. Chem. Soc.* **2001**, *123*, 9716–9717.

[14] More than 20% of **3** can be recovered during chromatographic purification.

[15] H. Tsukube, H. Furuta, A. Odani, Y. Takeda, Y. Kudo, Y. Inoue, Y. Liu, H. Sakamoto, K. Kimura in *Comprehensive Supramolecular Chemistry, Vol. 8* (Eds.: J. L. Atwood, J. E. D. Davies, D. D. MacNicol, F. Vögtle, D. Reinhoudt), Pergamon, Oxford, **1996**, pp. 425–482.

[16] P. Anzenbacher, Jr., K. Jursýková, J. L. Sessler, *J. Am. Chem. Soc.* **2000**, *122*, 9350–9351.

[17] M. J. Hynes, *J. Chem. Soc. Dalton Trans.* **1993**, 311–312.

[18] a) J. A. A. de Boer, D. N. Reinhoudt, *J. Am. Chem. Soc.* **1985**, *107*, 5347–5351; b) L. Fielding, *Tetrahedron* **2000**, *56*, 6151–6170.

[19] Similar results have been observed with Cl^- ions.

[20] CV titration experiments were also carried out with solutions containing F^- ions. However, it was not possible to obtain a ΔE value for the **4**·F^- complex, because the redox events become irreversible. This may be caused by the formation of a N–F bond at the doped state, by delocalization of the positive charge from $TTF^{+\bullet}$, or by oxidation of the calix[4]pyrrole skeleton. This phenomena has previously been observed, see ref. [8].

[21] The control experiments carried out by means of the titration of **3** with solutions containing Br^- ions did not show any observable displacement of the first oxidation potential.

[22] The character of the highest-occupied molecular orbital (HOMO) of monopyrrolo TTFs has recently been calculated

 © 2003 Wiley-VCH Verlag GmbH & Co. KGaA, Weinheim 1433-7851/03/4202-0190 $ 20.00+.50/0

and shows that approximately 13% of the HOMO density is located on the outer pyrrole ring, see ref. [12b].
[23] P. A. Gale, J. L. Sessler, V. Král, V. Lynch, *J. Am. Chem. Soc.* **1996**, *118*, 5140–5141.
[24] Binding constants between *meso*-octamethylcalix[4]pyrrole and Cl^-, and F^- ions in CD_3CN/0.5% v/v D_2O at 295 K have been determined by ^1H NMR spectroscopy to be $5.0\times10^3\,M^{-1}$ and $>1.0\times10^4\,M^{-1}$, respectively, see ref. [5a]. However, calorimetric measurements carried out in anhydrous MeCN (<10 ppm) on *meso*-octamethylcalix[4]pyrrole gave binding constants of $1.9\times10^5\,M^{-1}$ and $1.5\times10^5\,M^{-1}$ for Cl^-, and F^- ions, respectively, see ref. [5b].
[25] To minimize adsorption phenomena, a high scan rate of $0.5\,V\,s^{-1}$ was used.

Gold/DNA Nanostructures

Towards Multistep Nanostructure Synthesis: Programmed Enzymatic Self-Assembly of DNA/Gold Systems**

*Antonios G. Kanaras, Zhenxin Wang, Andrew D. Bates, Richard Cosstick, and Mathias Brust**

The programmed self-assembly of nanostructures from well-defined units is an important aim in nanoscience.[1,2] The use of gold nanoparticles stabilized by thiol-modified DNA is a promising approach towards this goal.[3–8] The specificity of DNA base-pairing provides a precise means of programming interactions between particles by hybridization with specifically designed linker strands. To introduce an additional level of control, we have developed a general method by which the reactivity of initially latent DNA linking sites can be switched on deliberately. We have adapted well-developed methods of molecular biology to produce a nanoscale analogue of protecting groups. We show that linking sites can be protected by hybridization with complementary strands and deprotected by cleaving these double strands at predetermined sites with restriction enzymes. This results in cohesive ends of single-stranded DNA, which can bind by hybridization to complementary sequences present in the system. In a second enzymatic step the DNA phosphodiester backbones at the hybridization sites are covalently joined using a DNA ligase. This approach represents a generic protocol that will enable multistep nanostructure syntheses.

In addition to DNA, further biomolecular interactions have been exploited for programmed assembly. These include other specific recognition motifs such as antibody–antigen and biotin–avidin binding.[8–11] A number of nonbiomolecular systems with various degrees of complexity have also been reported.[12–16] These approaches generally have in common that the reactivity of the binding sites is determined by the initial design of the system. A reaction, once started, proceeds until all reactive sites have been consumed by binding to complementary motifs. This essentially limits programmed nanostructure assembly to single-step reactions. Conversely, modern preparative chemistry is characterized by complex multistep syntheses, which can routinely be carried out by selectively addressing certain reactive sites while others are left temporarily unreactive. This is achieved by the use of protecting groups, which are essential to practically all modern chemical syntheses. Here we introduce a comparable concept to programmed nanostructure assembly, which uses the restriction sites in double-stranded DNA as protected linking motifs and restriction endonucleases as selective deprotecting agents. The complete reaction sequence carried out to demonstrate this principle is illustrated schematically in Figure 1.

The starting point for this work was the preparation of an aqueous solution of 15 nm gold nanoparticles, which were coated and stabilized by a ligand shell of thiol-modified

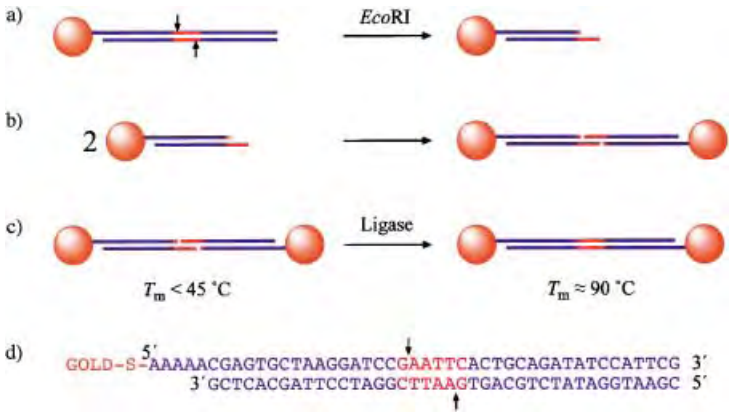


Figure 1. Schematic description of the method. a) Gold nanoparticles derivatized with double-stranded DNA are treated with restriction enzyme *Eco*RI, which cleaves the DNA to yield cohesive ends. The red color represents the recognition site of the enzyme, and the arrows indicate the sites of cleavage on each strand. In reality, each 15 nm particle has around 100 DNA ligands; b) Two cohesive ends hybridize, which leads to a weak association of particles; c) The DNA backbones are covalently joined at the hybridized site by DNA ligase to yield a stable 40-base-pair double-stranded link between particles; d) The sequences of the oligonucleotides are illustrated, together with the *Eco*RI site and positions of backbone cleavage, as in (a).

[*] Dr. M. Brust, A. G. Kanaras, Dr. Z. Wang, Dr. R. Cosstick
Centre for Nanoscale Science, Department of Chemistry
The University of Liverpool
Liverpool L69 7ZD (UK)
Fax: (+44) 151-794-3588
E-mail: m.brust@liv.ac.uk
A. G. Kanaras, Dr. A. D. Bates
School of Biological Sciences
The University of Liverpool
Liverpool L69 7ZB (UK)

[**] The authors wish to thank John Naylor for his help with TEM and Dr. Damian Parry for helpful advice. Financial support by the EPSRC, BBSRC, and the European Union (NANOMOL) is gratefully acknowledged. M.B. is the recipient of an EPSRC Advanced Research Fellowship and A.G.K. is partially supported by a University of Liverpool PhD Studentship.

 © 2003 Wiley-VCH Verlag GmbH & Co. KGaA, Weinheim 1433-7851/03/4202-0191 $ 20.00+.50/0

single-stranded DNA of 45 bases. This was achieved by essentially following the methods described by Mirkin and co-workers.[3,5,17,18] A noteworthy modification is that the derivatization of the particles with DNA was carried out while concentrating the sample in a vacuum centrifuge. This led to extraordinarily stable particles, which were unaffected by the various conditions of the subsequent enzymatic reactions. The particle-bound DNA was then converted to a double-stranded form by hybridization with a complementary single-stranded DNA. The DNA sequence was chosen so that the double strands formed on the particles would contain recognition sites for a number of restriction endonucleases. The system did not now contain any single-stranded DNA capable of hybridization with complementary linker strands. In order to create reactive sites by deprotection, the restriction enzyme *Eco*RI was used to cleave the double strands on the particles at specific recognition sites to leave a cohesive end capable of hybridization. After inactivation of the enzyme the DNA remaining on the particle surface was isolated and analyzed by gel electrophoresis. As shown in Figure 2, almost all the DNA present in the system was cleaved by the enzyme. Importantly, preliminary experiments with other restriction enzymes such as *Eco*RV, *Pst*I, *Nla*IV, *Bam*HI, and *Apo*I gave comparable results when the respective recognition sites were present.

After this first enzymatic step, hybridization between the newly created cohesive ends through the relatively labile overlap of only four complementary base pairs resulted in the formation of weakly associated aggregates of particles. This process has been investigated by transmission electron microscopy (TEM) as shown in Figure 3a and b. The formation of small aggregates is clearly seen in comparison with randomly distributed individual particles prior to enzyme treatment. In order to stabilize the system at this stage the DNA backbones at the hybridized cohesive ends were covalently joined in a second enzymatic step using T4 DNA ligase. Inspection with TEM now showed the presence of significantly larger aggregates, which are formed as a consequence of much stronger interparticle binding by the newly formed 40-base-pair double-stranded linker (Figure 3c).

The simplest and most powerful analytical tool to monitor this enzymatic two-step reaction is the "Northwestern" spot test, developed by Mirkin and co-workers.[19] This is an extremely sensitive method to discriminate between aggregated and nonaggregated gold nanoparticles in aqueous solution, based on a perceptible color change from red to blue upon aggregation. The test consists of the evaporation of a droplet of an aqueous solution of particles on a reverse-phase thin-layer chromatography plate. A blue spot indicates aggregation, while a red spot indicates the presence of freely dispersed particles. Figure 4 shows the results of the spot tests and the visible absorption spectra of the corresponding solutions at various temperatures for the free particles in solution (a), the loosely aggregated particles after the enzymatic deprotection step (b), and the strongly bound aggregates after enzymatic ligation (c). The results are consistent with the TEM study but contain important additional information regarding the stability of the aggregates, both before and after the ligation step. The free particles complexed with double-stranded DNA always give a red spot test, even at room temperature, which confirms that no aggregation of particles takes place. The absorption spectrum is typical for freely dispersed particles of this size range showing a sharp plasmon absorption band at 524 nm. After treatment with *Eco*RI, a blue spot is obtained at 25 °C indicating particle aggregation, but the aggregates dissociate (red spot) at slightly elevated temperatures (45 °C) as a result of the melting (dehybridization) of the weak four-base-pair cohesive ends. The melting temperature (T_m) of a single cohesive end will be close to room temperature, but the loose aggregates of particles will be maintained by multiple transient links that will only dissociate completely at a higher temperature. In accordance with the spot tests, the visible spectra show a slightly broadened plasmon band which is red-shifted to 534 nm at 25 °C, and the typically sharp band at

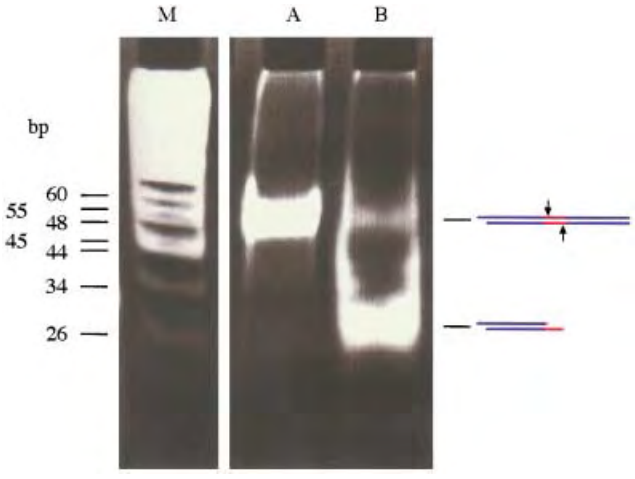


Figure 2. DNA cleavage analyzed by polyacrylamide gel electrophoresis. Particle-bound DNA was isolated before (A) and after (B) treatment with *Eco*RI and subjected to electrophoresis on a 20% polyacrylamide gel, alongside marker DNAs of known sizes (M). The numbers indicate DNA sizes in base pairs and the pictograms indicate the DNA species present, as in Figure 1.

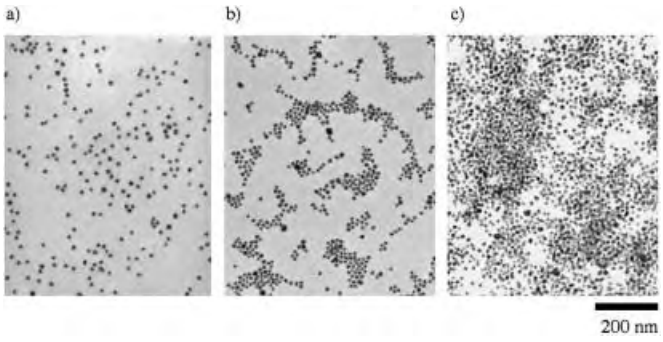


Figure 3. TEM analysis of DNA–nanoparticle complexes. Micrographs represent DNA–nanoparticle complexes analyzed before (a) and after (b) treatment with *Eco*RI, and after subsequent treatment with DNA ligase (c).

 © 2003 Wiley-VCH Verlag GmbH & Co. KGaA, Weinheim 1433-7851/03/4202-0192 $ 20.00+.50/0

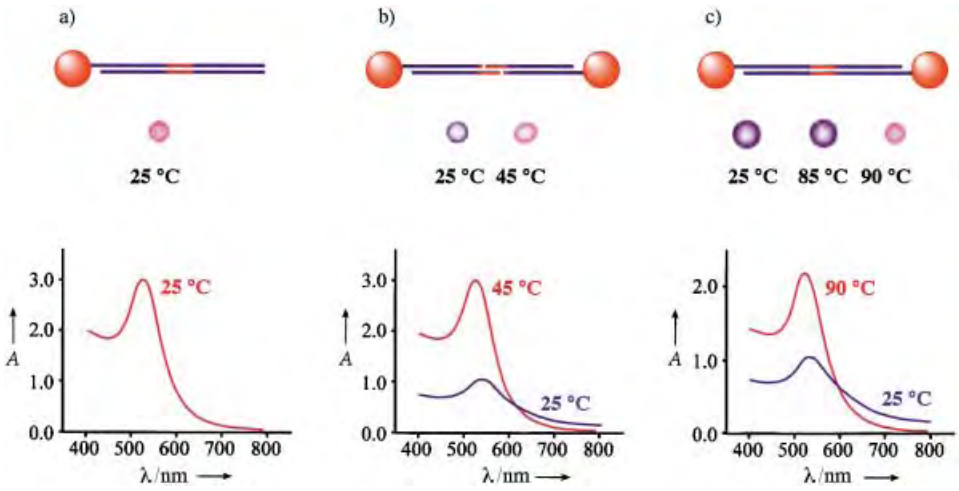


Figure 4. Spot test and absorbance spectra of DNA–nanoparticle complexes. "Northwestern" spot tests (see text) and visible absorption spectra are illustrated for DNA–nanoparticle complexes, analyzed at the temperatures shown, both before (a) and after (b) treatment with *Eco*RI, and after subsequent treatment with DNA ligase (c).

524 nm at 45 °C. A dramatic difference in the melting behavior is observed after the ligation step, which has converted the labile four-base-pair overlap into a continuous 40-base-pair double strand. The spot test remained blue up to 85 °C and changed to red sharply at 90 °C, at which temperature, the 40-base-pair double-stranded linker dehybridized. The same behavior is reflected in the absorption spectra of the solutions. This shows unequivocally that the second enzymatic step has indeed taken place and modified the properties of the system significantly. This was further confirmed by the gel electrophoresis of DNA released from the particles (not shown).

What has been demonstrated here is a new method of nanostructure manipulation. This is illustrated by a series of reactions in which randomly dispersed DNA-coated gold particles are converted first to weakly associated structures, and subsequently to an aggregated system through simple and predictable manipulation with DNA-processing enzymes. In particular, we have introduced the powerful concept of protecting and deprotecting specific reaction sites, which is new to nanoscience. The simplest possible system has deliberately been chosen for these "proof of principle" experiments. The preparation of geometrically more challenging structures by our new approach may now become possible using, for example, tailored nanoparticles with precisely one, two, or three DNA strands attached, as shown by Alivisatos and co-workers.[20] We have shown that enzymes can be employed as tools to provide crucial additional control (selective cleavage and ligation) over nanostructure assembly. This opens vast possibilities for the future use of enzymes in this area. Restriction endonucleases are very important research tools in molecular biology, and their well-established ability to cleave DNA at specific recognition sites is beginning to be applied to nanostructures.[21–25] To date, over 3000 restriction enzymes have been discovered and hundreds are commercially available.[21] This will allow for the preparation of nanostructure building blocks with a large number of protected binding sites, each of which is addressable by a different enzyme, so that the multistep syntheses of nanostructures can now be envisaged. It is to be expected that many other sophisticated biomolecular research tools will also become invaluable to nanoscience in the near future.

Experimental Section

Preparation of DNA-complexed gold nanoparticles: Near-monodisperse gold nanoparticles of 15 nm diameter were prepared in aqueous solution by the classical citrate reduction route following standard procedures.[26,27] Prior to use, the hydrosols were filtered with a 0.45 μm pore-size Millex-HA microfilter (Millipore).[5] DNA 45-mers with a 5′-thiol modification ($OPO_3(CH_2)_6$–S–S–$(CH_2)_6OH$) were either purchased (Sigma Genosys Ltd.) or prepared following standard procedures.[4,5] In a typical preparation the gold nanoparticles were derivatized with thiolated single-stranded oligonucleotides by incubating a gold sol (500 μL, 6 nM) overnight with disulfide-protected oligonucleotides (25 μL, 40 μM) in aqueous solution. Then the solution was diluted to a final volume of 1 mL containing NaCl (0.1 M) and sodium phosphate buffer (5 mM, pH 7.0) solutions. After further incubation for 2 h the volume was slowly reduced to 150 μL by vacuum centrifugation over 3–4 h at 40 °C. This is an important modification of previously published procedures and ensures a gradual and simultaneous increase in ionic strength and oligonucleotide concentration, which leads to unusually stable DNA-complexed particles. The loading of particles with DNA achieved by this method has been estimated by UV/Vis spectroscopy to be in the range of 100 ± 30 DNA molecules per particle, somewhat more than previously reported.[18] Nonspecific aggregation (precipitation) may occur due to the presence of excess oligonucleotides. This is fully reversible by diluting to 500 μL and heating briefly to 50 °C. Unbound oligonucleotides were then removed by repeated centrifugation and suspension of the pellet (Sigma 1-13 Centrifuge, 13 000 rpm, ×2). The DNA-complexed particles were stored in a solution (500 μL) containing NaCl (0.5 M) and sodium phosphate (10 mM, pH 7.0).

Hybridization of particle-bound single-stranded DNA: The single-stranded DNA oligonucleotides present on the gold particles were hybridized with non-thiolated complementary DNA (64 μL of a 15.5 μM solution) by incubating for 2 h in a hybridization buffer (500 μL, NaCl (0.5 M), sodium phosphate (10 mM, pH 7.0)). Excess free oligonucleotides were then removed by centrifugation and

 © 2003 Wiley-VCH Verlag GmbH & Co. KGaA, Weinheim 1433-7851/03/4202-0193 $ 20.00+.50/0

suspension in the hybridization buffer (13000 rpm, ×3). Particles were stored in 500 μL of the hybridization buffer.

Enzymatic digestion of particle-bound DNA: The first enzymatic reaction step was carried out by incubating the particles overnight at 37 °C in a 100 μL solution containing NaCl (50 mM), Tris-HCl (100 mM, pH 7.5), and $MgCl_2$ (10 mM) containing 200 units of *Eco*RI enzyme (New England Biolabs Ltd.).

Enzymatic ligation of particle-bound DNA: The enzymatic ligation step was carried out by incubating the particles overnight at room temperature in a buffer solution comprised of Tris-HCl (50 mM, pH 7.5), $MgCl_2$ (10 mM), and ATP (1 mM) containing 1600 units of T4 DNA ligase (New England Biolabs Ltd.).

Gel electrophoresis: After the first enzymatic reaction the enzyme was deactivated by addition of EDTA (20 mM final concentration). The particles were isolated by repeated centrifugation and redispersion into an aqueous EDTA solution (20 mM) and then incubated overnight in 20 μL of an aqueous solution of dithiothreitol (0.5 M) and EDTA (20 mM). Gel electrophoresis was carried out using a 20% polyacrylamide (19:1 acrylamide:bisacrylamide) gel in TBE (Tris-borate (90 mM, pH 8.0) and EDTA (1 mM)) and the bands were visualized by staining with ethidium bromide.

Transmission electron microscopy: Specimens for inspection by TEM were prepared by the slow evaporation of one drop of an aqueous solution of the particles onto a carbon-coated copper mesh grid. All samples were examined in a JEOL 2000 EX TEM operating at 200 kV.

Received: August 13, 2002
Revised: October 17, 2002 [Z19957]

[1] S. Mann, S. Shenton, M. Li, S. Connolly, D. Fitzmaurice, *Adv. Mater.* **2000**, *12*, 147 – 150.
[2] E. Dujardin, S. Mann, *Adv. Mater.* **2002**, *14*, 775 – 788.
[3] C. A. Mirkin, R. L. Letsinger, R. C. Mucic, J. J. Storhoff, *Nature* **1996**, *382*, 607 – 609.
[4] A. P. Alivisatos, K. P. Johnsson, X. Peng, T. E. Wilson, C. J. Loweth, M. P. Bruchez, Jr., P. G. Schultz, *Nature* **1996**, *382*, 609 – 611.
[5] J. J. Storhoff, R. Elghanian, R. C. Mucic, C. A. Mirkin, R. L. Letsinger, *J. Am. Chem. Soc.* **1998**, *120*, 1959 – 1964.
[6] C. L. Loweth, W. B. Caldwell, X. Peng, A. P. Alivisatos, P. G. Schultz, *Angew. Chem.* **1999**, *111*, 1925 – 1929; *Angew. Chem. Int. Ed.* **1999**, *38*, 1808 – 1812.
[7] J. J. Storhoff, C. A. Mirkin, *Chem. Rev.* **1999**, *99*, 1849 – 1862.
[8] C. M. Niemeyer, *Angew. Chem.* **2001**, *113*, 4254 – 4287; *Angew. Chem. Int. Ed.* **2001**, *40*, 4128 – 4158.
[9] W. Shenton, S. A. Davis, S. Mann, *Adv. Mater.* **1999**, *11*, 449 – 452.
[10] M. Li, K. K. W. Wong, S. Mann, *Chem. Mater.* **1999**, *11*, 23 – 26.
[11] S. Connolly, D. Fitzmaurice, *Adv. Mater.* **1999**, *11*, 1202 – 1205.
[12] M. Brust, D. Bethell, D. J. Schiffrin, C. J. Kiely, *Adv. Mater.* **1995**, *7*, 795 – 797.
[13] M. Brust, C. J. Kiely, D. Bethell, D. J. Schiffrin, *J. Am. Chem.* Soc. **1998**, *120*, 12367 – 12368.
[14] L. C. Brousseau, J. P. Novak, S. M. Marinakos, D. L. Feldheim, *Adv. Mater.* **1999**, *11*, 447 – 449.
[15] A. K. Boal, F. Ilhan, J. E. DeRouchey, T. Thurn-Albrecht, T. P. Russell, V. M. Rotello, *Nature* **2000**, *404*, 746 – 748.
[16] B. L. Frankamp, O. Uzun, F. Ilhan, A. K. Boal, V. M. Rotello, *J. Am. Chem. Soc.* **2002**, *124*, 892 – 893.
[17] J. J. Storhoff, A. A. Lazarides, R. C. Mucic, C. A. Mirkin, R. L. Letsinger, G. C. Schatz, *J. Am. Chem. Soc.* **2000**, *122*, 4640 – 4650.
[18] L. M. Demers, C. A. Mirkin, R. C. Mucic, R. A. Reynolds III, R. L. Letsinger, R. Elghanian, G. Viswanadham, *Anal. Chem.* **2000**, *72*, 5535 – 5541.
[19] R. Elghanian, J. J. Storhoff, R. C. Mucic, R. L. Letsinger, C. A. Mirkin, *Science* **1997**, *277*, 1078 – 1081.
[20] D. Zanchet, C. M. Micheel, W. J. Parak, D. Gerion, A. P. Alivisatos, *Nano Lett.* **2001**, *1*, 32 – 35.
[21] A. Pingoud, A. Jeltsch, *Nucleic Acids Res.* **2001**, *29*, 3705 – 3727.
[22] L. He, M. D. Musick, S. R. Nicewarner, F. G. Salinas, S. J. Benkovic, M. J. Natan, C. D. Keating, *J. Am. Chem. Soc.* **2000**, *122*, 9071 – 9077.
[23] J. C. O'Brien, J. T. Stickney, M. D. Porter, *J. Am. Chem. Soc.* **2000**, *122*, 5004 – 5005.
[24] J. M. Perez, T. O'Loughin, F. J. Simeone, R. Weissleder, L. Josephson, *J. Am. Chem. Soc.* **2002**, *124*, 2856 – 2857.
[25] C. S. Yun, G. A. Khitrov, D. E. Vergona, N. O. Reich, G. F. Strouse, *J. Am. Chem. Soc.* **2002**, *124*, 7644 – 7645.
[26] J. Turkevich, P. S. Stevenson, J. Hillier, *Discuss. Faraday Soc.* **1951**, *11*, 55 – 75.
[27] G. Frens, *Nature* **1973**, *241*, 20 – 22.

Oxidation of Alcohols in Water

Catalytic Oxidation of Alcohols in Water under Atmospheric Oxygen by Use of an Amphiphilic Resin-Dispersion of a Nanopalladium Catalyst

Yasuhiro Uozumi and Ryu Nakao*

Oxidation of alcohols to form carbonyl compounds is one of the most fundamental and important yet immature processes in organic chemistry. Thus, although a variety of methods and reagents for the oxidation have been developed, until recently the traditional oxidation reactions have been performed with stoichiometric amounts of heavy metal reagents (e.g. Cr, Mn)[1] or moisture-sensitive expensive oxidants (e.g., *N,N′*-dicyclohexylcarbodiimide (DCC), oxalyl chloride),[2] and often in environmentally undesirable media like chlorinated solvents which render them impractical. There is good reason to believe that alcohol oxidation might be feasible by aerobic oxidation in water in a reaction promoted by a heterogeneous catalyst under atmospheric pressure conditions. This would represent a much cheaper, safer, and more environmentally benign oxidation protocol. Recently, much work has appeared on the catalytic oxidation of allylic or benzylic alcohols with molecular oxygen,[3,4] and several palladium catalyst systems have been developed for the oxidation.[5,6]

We have previously reported that amphiphilic polystyrene-poly(ethylene glycol) (PS-PEG) resin-supported palladium–phosphane complexes catalyzed various palladium-mediated reactions smoothly in water.[7] With the resin-supported catalyst in aqueous media, organic substrates must

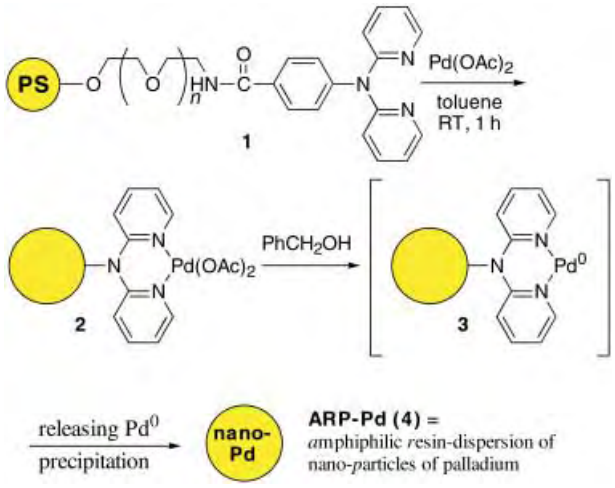
[*] Prof. Y. Uozumi, R. Nakao
Division of Complex Catalysis
Institute for Molecular Science
Myodaiji, Okazaki, 444-8585 (Japan)
Fax: (+81) 564-55-7240
E-mail: uo@ims.ac.jp

 © 2003 Wiley-VCH Verlag GmbH & Co. KGaA, Weinheim 1433-7851/03/4202-0194 $ 20.00+.50/0

diffuse into the hydrophobic PS matrix to form the highly concentrated reaction sphere in which the anchored catalyst performs efficient organic transformations in water. These observations prompted us to design and prepare PS-PEG resin-supported palladium nanoparticles,[8,9] which should combine high catalytic activity owing to the large surface area of the nanoparticles[10] and water-based reactivity provided by the amphiphilicity of the PS-PEG matrix. Catalytic oxidation of alcohol was achieved in water under an atmospheric pressure of molecular oxygen by use of amphiphilic polymer-supported palladium nanoparticles.[11]

An amphiphilic resin-dispersion of palladium nanoparticles was readily prepared by reduction of a PS-PEG resin-supported palladium(II) complex (Scheme 1). Thus, the bis-pyridine chelating ligand **1** anchored on PS-PEG amino-resin was complexed to palladium by treatment with an equimolar amount of $Pd(OAc)_2$ in toluene at 25 °C to give the stable 16-electron divalent palladium complex **2**. The complex **2** was treated with benzyl alcohol in refluxing water for 12 h to generate palladium complex **3** in situ which should readily release the neutral palladium species. The nanopalladium particles were precipitated out in a PS-PEG matrix to give the desired amphiphilic PS-PEG resin-dispersion of palladium nanoparticles (**4**, ARP-Pd) (loading value: 0.37 mmol Pd per g). Transmission electron microscopy (TEM) of the resulting palladium-resin (Figure 1a, b)shows that the palladium particles have a mean diameter of 9.1 nm with a narrow size distribution (Figure 1c).

The catalytic activity of the amphiphilic resin-dispersion of palladium nanoparticles (ARP-Pd) was examined for the catalytic aerobic oxidation of alcohols in water. Representative results are shown in Table 1. Thus, a mixture of 1 mol% palladium of ARP-Pd and benzyl alcohol was refluxed in water under an atmospheric pressure of oxygen gas for 90 min. After being cooled, the mixture was filtered and the catalyst resin was rinsed twice with a small portion of diethyl ether. The washings were concentrated in vacuo to give benzaldehyde almost quantitatively, the purity of which was analyzed by ^{1}H NMR spectroscopy and gas chromatography



Scheme 1. Preparation of amphiphilic resin-dispersion of nanoparticles of palladium (ARP-Pd; **4**).

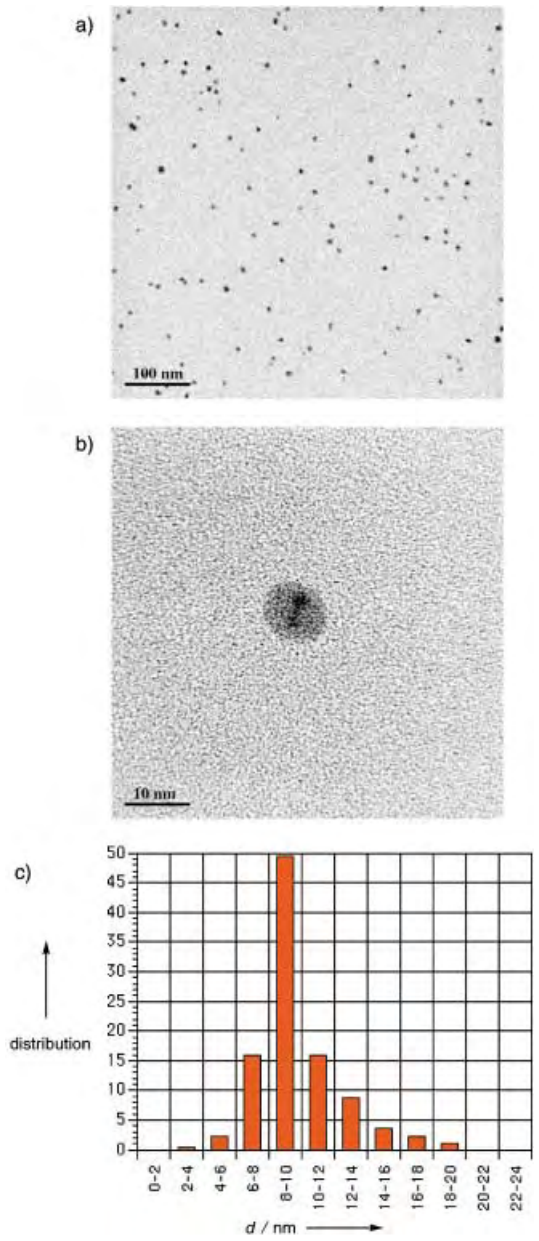


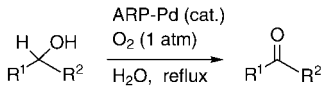
Figure 1. TEM images (a and b), and the respective histogram of particle size distribution (c) of **4**.

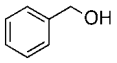
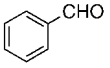
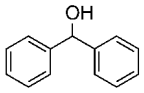
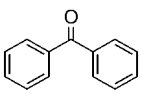
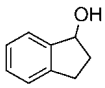
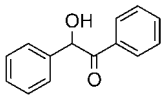
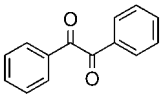
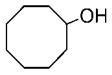
(GC) to be 97% without any chromatographic purification (Table 1, entry 1). During the reaction, no deposit of palladium black on the glass wall (a palladium mirror) was observed. The recovered ARP-Pd showed essentially the same TEM image and was reused with negligible loss of catalytic activity. After the workup, the aqueous filtrate exhibited no catalytic activity for the oxidation. These observations indicate that the palladium species does not leach into the aqueous phase under the reaction conditions.[12]

Secondary alcohols gave the corresponding ketones under essentially the same conditions. Thus, phenethyl alcohol, diphenylmethanol, and 1-hydroxyindane underwent catalytic oxidation in water to give acetophenone, benzophenone, and indanone in >99%, 85%, and 95% yield, respectively

 © 2003 Wiley-VCH Verlag GmbH & Co. KGaA, Weinheim 1433-7851/03/4202-0195 $ 20.00+.50/0

Table 1: ARP-Pd catalyzed oxidation of alcohols in water.[a]



Entry	Substrate	Product	Pd [mol%]	*t* [h]	Yield [%][b]
1			1	1.5	97
2			5	20	>99
3			5	20	85
4			5	20	95
5			1	2.5	98
6			5	20	78
7			20	20	88
8			(second run)	20	86
9			(third run)	20	83
10			(forth run)	20	87
11	*n*-$C_8H_{17}OH$[c]	*n*-$C_7H_{15}COOH$	20	40	90
12	*n*-$C_6H_{13}OH$[c]	*n*-$C_5H_{11}COOH$	20	40	98
13	*n*-C_4H_9OH[c]	*n*-C_3H_7COOH	20	40	93

[a] All reactions were carried out in refluxing water under 1 atm of oxygen gas. Pd mol%/reaction time (h): entries 1 and 5: 1/2, entries 2–5: 5/20, entry 7: 20/20, entries 11–13: 20/40; ratio of alcohol (mmol)/water (mL): 1/1.3. [b] All yields are for the pure products. [c] Oxidation of 1-alkanols were performed in 0.2 M aqueous solution of potassium carbonate.

(Table 1, entries 2, 3, and 4). The catalytic oxidation of benzoin bearing an α-ketohydroxy group and isophorol bearing an allylic hydroxy group also proceeded smoothly to give benzil and isophorone in 98% and 78% yields (Table 1, entries 5 and 6). It is noteworthy that this catalyst system was also effective for the oxidation of nonactivated alkanols. Thus, the oxidation of cyclooctanol took place in water under an atmospheric pressure of oxygen gas to give cyclooctanone in 88% yield (Table 1, entry 7). Catalytic aerobic oxidation of primary alcohols was carried out in an aqueous solution of potassium carbonate (0.2 M) under otherwise similar conditions. Thus, 1-octanol, 1-hexanol, and 1-butanol were oxidized by using 20 mol% palladium of the ARP-Pd catalyst under oxygen gas (1 atm) in refluxing water in the presence of potassium carbonate. The mixture was filtered, and the filtrate was acidified with hydrochloric acid and extracted with diethyl ether to give excellent yields of the corresponding carboxylic acids (Table 1, entries 11, 12, and 13).

Recycling experiments were examined for the oxidation of cyclooctanol. Thus, after the first run, which gave cyclooctanone in 88% yield (Table 1, entry 7), the ARP-Pd catalyst was subjected to a second oxidation from which it gave cyclooctanone in 86% yield (Table 1, entry 8); the average chemical yield for four consecutive runs was 86%, which clearly demonstrates the practical recyclability of this catalyst (Table 1, entries 7–10).

In conclusion, catalytic oxidation of alcohols was achieved in water by oxygen gas by using a novel amphiphilic resin-dispersion of palladium nanoparticles (ARP-Pd), which was designed and prepared with a view toward using it for palladium catalysis in water. Similarly, nanoparticles of various transition metals can be envisaged in a PS-PEG matrix, which would provide a wide variety of high catalytic abilities in water. We are currently investigating the scope and mechanism of this catalytic oxidation.

Experimental Section

PS-PEG resin-supported bispyridine ligand **1.** A mixture of PS-PEG amino-resin (5.0 g; average diameter = 170 μm, 1% divinylbenzene cross-linked, loading value of amino residue = 0.4 mmol g^{-1}), 1-(3-dimethylaminopropyl)-3-ethylcarbodiimide hydrochloride (EDCI) (709 mg, 3.70 mmol), 1-hydroxybenzotriazole hydrate (HOBt)

 © 2003 Wiley-VCH Verlag GmbH & Co. KGaA, Weinheim 1433-7851/03/4202-0196 $ 20.00+.50/0

(625 g, 4.63 mmol), and 4-(bis(pyrid-2-yl)amino)benzoic acid (808 mg, 2.78 mmol) in DMF (60 mL) was shaken at room temperature for 10 h. The mixture was filtered and the resulting resin beads were rinsed three times with DMF and three times with dichloromethane, then dried in vacuo to give **1**. Swollen gel-phase ^{13}C MAS NMR (100 MHz, $CDCl_3$, 25 °C, TMS; characteristic signals; signals of PS and PEG moieties are omitted for simplicity): $\delta = 117.2$, 118.5, 125.4, 128.2, 130.5, 137.4, 147.4, 148.3, 157.6, 166.4 ppm.

PS-PEG resin-supported palladium acetate bispyridine complex **2**: A mixture of **1** (5.5 g; loading value of ligand residue = 0.37 mmol g^{-1}) and palladium diacetate (457 mg, 2.04 mmol) in toluene (60 mL) was shaken at room temperature for 1 h. The mixture was filtered and the resulting resin beads were rinsed three times with dichloromethane and then dried in vacuo to give **2**. Swollen gel-phase ^{13}C MAS NMR (100 MHz, $CDCl_3$, 25 °C, TMS; characteristic signals; signals of PS and PEG moieties are omitted for simplicity): $\delta = 23.0$, 116.4, 117.2, 120.1, 129.7, 135.7, 140.0, 142.1, 150.3, 150.7, 165.5, 177.5 ppm.

PS-PEG resin-dispersion of palladium nanoparticles **4** (ARP-Pd): A mixture of **2** (5.6 g; loading value of palladium residue = 0.37 mmol g^{-1}) and benzyl alcohol (18 mL) in water (56 mL) was refluxed for 12 h (no leaching of palladium to the water phase was observed, which would have resulted in the formation of palladium black). The mixture was filtered and the resulting resin beads were rinsed three times with water and three times with acetone, then dried in vacuo to give ARP-Pd.

Catalytic oxidation of alcohols in water: Typical procedure given for the oxidation of 1-hexanol: A mixture of ARP-Pd (106 mg, 39 μmol of palladium), 1-hexanol (22 μL, 0.17 mmol), and potassium carbonate (24 mg, 0.17 mmol) in water (0.9 mL) was refluxed for 40 h under an atmospheric pressure of oxygen gas. After being cooled, the mixture was filtered, and the resin beads were rinsed three times with saturated aqueous sodium bicarbonate solution. The combined filtrate was acidified with 5% hydrochloric acid and extracted with diethyl ether. The extract was dried over magnesium sulfate and concentrated in vacuo to give hexanoic acid (20 mg; 98%) as a pure compound (> 99% purity based on GC and ^1H NMR analysis).

Received: August 26, 2002
Revised: October 10, 2002 [Z50036]

[1] For a review on metal-mediated oxidations, see: *Organic Syntheses by Oxidation with Metal Compounds* (Eds.: W. J. Mijs, C. R. H. de Jonge), Plenum, New York, **1986**.

[2] For a general review, see: M. Hudlicky, *Oxidations in Organic Chemistry*, ACS monograph 186, Washington, DC, **1990**.

[3] For aerobic oxidations with transition-metal cayalysts, see: a) I. E. Markó, P. R. Giles, M. Tsukazaki, S. M. Brown, C. J. Urch, *Science* **1996**, *274*, 2044; b) I. E. Markó, P. R. Giles, M. Tsukazaki, I. Chellé-Regnaut, C. J. Urch, S. M. Brown, *J. Am. Chem. Soc.* **1997**, *119*, 12661; c) A. Hanyu, E. Takezawa, S. Sakaguchi, Y. Ishii, *Tetrahedron Lett.* **1998**, *39*, 5557; d) R. Lenz, S. V. Ley, *J. Chem. Soc. Perkin Trans. 1* **1997**, 3291; e) A. Dijkman, I. W. C. E. Arends, R. A. Sheldon, *Chem. Commun.* **1999**, 1591; f) Y. Wang, J. L. DuBois, B. Hedman, K. O. Hodgson, T. D. P. Stack, *Science* **1998**, *279*, 537; g) P. Chaudhuri, M. Hess, U. Flörke, K. Wieghardt, *Angew. Chem.* **1998**, *110*, 2499; *Angew. Chem. Int. Ed.* **1998**, *37*, 2217; h) P. Chanudhuri, M. Hess, T. Weyhermüller, K. Wieghardt, *Angew. Chem. Int. Ed.* **1999**, *111*, 1165; *Angew. Chem. Int. Ed.* **1999**, *38*, 1095; i) P. Chaudhuri, M. Hess, J. Müller, K. Hildenbrand, E. Bill, T. Weyhermuller, K. Wieghardt, *J. Am. Chem. Soc.* **1999**, *121*, 9599; j) B. Betzemeier, M. Cavazzini, S. Quici, P. Knochel, *Tetrahedron Lett.* **2000**, *41*, 4343; k) K. Yamaguchi, K. Mori, T. Mizugaki, K. Ebitani, K. Kaneda, *J. Am. Chem. Soc.* **2000**, *122*, 7144; l) A. Dijksman, A. Marino-Gonzalez, A. Mairatai Payeras, I. W. C. E. Arends, R. A. Sheldon, *J. Am. Chem. Soc.* **2001**, *123*, 6826; m) G. Csjernyik, A. H. Ell, L. Fandini, B. Pugin, J.-E. Bäckvall, *J. Org. Chem.* **2002**, *67*, 1657; n) I. Ansari, R. Gree, *Org. Lett.* **2002**, *4*, 1507; o) R. Gianna, B. Betzemeier, S. Quici, P. Knochel, *Tetrahedron* **2002**, *58*, 3985; p) Y. Maeda, N. Kakiuchi, S. Matsumura, T. Nishimura, T. Kawamura, S. Uemura, *J. Org. Chem.* **2002**, *67*, 6718.

[4] For recent examples of mechanistic studies on palladium-catalyzed aerobic oxidaions, see: a) B. A. Steinhoff, S. R. Fix, S. S. Stahl, *J. Am. Chem. Soc.* **2002**, *124*, 766; b) S. S. Stahl, J. L. Thorma, R. C. Nelson, M. A. Kozee, *J. Am. Chem. Soc.* **2001**, *123*, 7188.

[5] For recent examples of aerobic oxidations with palladium compounds, see: a) K. P. Peterson, R. C. Larock, *J. Org. Chem.* **1998**, *63*, 3185; b) T. Nishimura, T. Onoue, K. Ohe, S. Uemura, *Tetrahedron Lett.* **1998**, *39*, 6011; c) T. Nishimura, T. Onoue, K. Ohe, S. Uemura, *J. Org. Chem.* **1998**, *63*, 6750; d) N. Kakiuchi, Y. Maeda, T. Nishimura, S. Uemura, *J. Org. Chem.* **2001**, *66*, 6620; e) T. Nishimura, Y. Maeda, N. Kakiuchi, S. Uemura, *J. Chem. Soc. Perkin Trans. 1* **2000**, 4301.

[6] As far as we know, the only previously reported successful work on catalytic aerobic oxidation of a wide range of alcohols in water is the pioneering work of Sheldon in 2000, where the oxidation of various alcohols was catalyzed by a water-soluble palladium complex under 30-bar pressure of air to give excellent yields of the corresponding carbonyl compounds, see: a) G.-J. ten Brink, I. W. C. E. Arends, R. A. Sheldon, *Science* **2000**, *287*, 1636; b) G.-J. ten Brink, I. W. C. E. Arends, R. A. Sheldon, *Adv. Synth. Catal.* **2002**, *344*, 355.

[7] For palladium-catalyzed reactions in water using amphiphilic PS-PEG resin-supported palladium complexes, see: a) Y. Uozumi, H. Danjo, T. Hayashi, *Tetrahedron Lett.* **1997**, *38*, 3557 (π-allylic substitution); b) H. Danjo, D. Tanaka, T. Hayashi, Y. Uozumi, *Tetrahedron* **1999**, *55*, 14341 (π-allylic substitution); c) Y. Uozumi, H. Danjo, T. Hayashi, *J. Org. Chem.* **1999**, *64*, 3384 (cross-coupling); d) Y. Uozumi, T. Watanabe, *J. Org. Chem.* **1999**, *64*, 6921 (carbonylation and Heck reaction); e) Y. Uozumi, H. Danjo, T. Hayashi, *Tetrahedron Lett.* **1998**, *39*, 8303 (asymmetric allylic substitution); f) Y. Uozumi, K. Shibatomi, *J. Am. Chem. Soc.* **2001**, *123*, 2919 (asymmetric allylic substitution); g) Y. Uozumi, Y. Nakai, *Org. Lett.* **2002**, *4*, 2997.

[8] For a recent review on catalytic reactions by metal nanoparticles, see: M. Králik, A. Biffis, *J. Mol. Catal. A* **2001**, *177*, 113.

[9] For examples of polymer-stabilized palladium nanoparticles, see: a) N. Toshima, Y. Shiraishi, T. Teranishi, M. Miyake, T. Tominaga, H. Watanabe, W. Brijoux, H. Bönnemann, G. Schmid, *Appl. Organomet. Chem.* **2001**, *15*, 178; b) T. Teranishi, M. Miyake, *Chem. Mater.* **1998**, *10*, 594; c) D. E. Bergbreiter, B. Chen, T. J. Lynch, *J. Org. Chem.* **1983**, *48*, 4179.

[10] J. S. Bradley in *Clusters and Colloids: From Theory to Applications* (Ed.: G. Schmid), VCH, Weinheim, **1994**, pp. 523–536.

[11] It has been reported that palladium cluster catalysts promote oxidation of allylic alcohols under an oxygen atmosphere, see: a) K. Kaneda, M. Fujii, K. Morioka, *J. Org. Chem.* **1996**, *61*, 4502; b) K. Kaneda, Y. Fujii, K. Ebitani, *Tetrahedron Lett.* **1997**, *38*, 9023.

[12] A referee has argued that the oxidation with leached homogeneous palladium species could still be plausible where the metal species may redeposit back on the heterogeneous surface. For recent examples of metal colloids as reservoirs for homogeneous metal species, see: a) S. Tasler, B. H. Lipshutz, *J. Org. Chem.* **2002**, ASAP; b) I. W. Davies, L. Matty, D. L. Hughes, P. J. Reider, *J. Am. Chem. Soc.* **2001**, *123*, 10139. See also ref. [8].

 © 2003 Wiley-VCH Verlag GmbH & Co. KGaA, Weinheim 1433-7851/03/4202-0197 $ 20.00+.50/0

Antimony Tetramers

Crystalline Structures of Sb_4 Molecules in Antimony Thin Films**

Thorsten M. Bernhardt, Bert Stegemann, Bernhard Kaiser, and Klaus Rademann*

Elemental antimony occurs in the solid bulk in a metallic as well as an amorphous modification.[1] Over a wide temperature range the gas phase of elemental antimony comprises almost exclusively of tetrameric molecules;[2] however, a solid-state modification of antimony consisting of Sb_4 molecules, comparable to white phosphorus and yellow arsenic, is not known to date. This is explained by the fact that the Sb_4 molecule is so unstable that even quenching with liquid nitrogen leads to the polymeric amorphous phase.[3]

Herein we demonstrate that scanning tunneling microscopy (STM) can be used to identify unexpected crystalline ordered areas with nearly cubic symmetry in antimony thin films that are prepared under appropriate conditions from Sb_4 molecules. The lattice constants of these structures are clearly different from the lattice constants of metallic α-antimony and are in agreement with the known structural data of tetrahedral Sb_4 molecules.[4–6] The symmetry of the well-ordered areas in the antimony films is also in accordance with the structures of the modifications of the lighter homologous elements arsenic and phosphorus which are likewise composed of tetrameric units (As_4 and P_4). The present STM data therefore indicate that a new allotropic modification of antimony composed of Sb_4 molecules exists on the nanometer scale. Substrate surfaces on which such well-ordered antimony structures can be observed, are the (0001) basal plane of MoS_2 and the (100) plane of the surface alloy $AuSb_2$. Atomically resolved STM images of both substrates are depicted in Figure 1.

Antimony thin films on various surfaces and their amorphous, nonmetallic structure have been described in the literature.[7,8] On the MoS_2(0001) surface the condensation of Sb_4 at a substrate temperature of −190 °C also results in macroscopically amorphous antimony films without apparent structural order. This can be seen from Figure 2a, which displays a two-monolayer-thick film. If such a film is investigated at the highest resolution, local, well-ordered areas

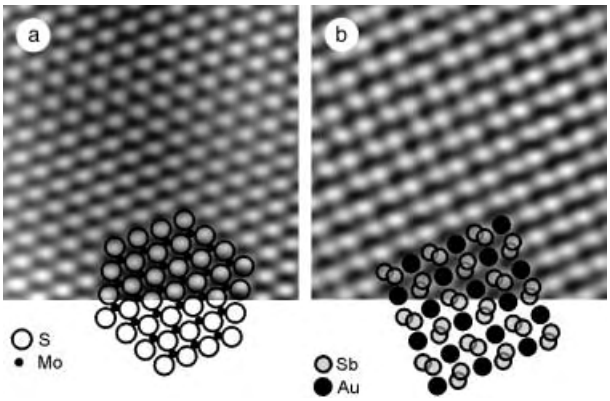


Figure 1. STM images of the substrate surfaces (39 × 39 Å²) on which the local crystalline areas can be observed after deposition of 1–2 monolayers of antimony. a) MoS_2(0001) with hexagonal structure. Tunneling parameters: −0.1 V, 2.8 nA. b) $AuSb_2$(100) with quadratic surface structure. Tunneling parameters: 0.5 V, 2.0 nA. Both images were high-frequency-filtered to minimize noise. The schematic drawings of the lattice structures enable the assignment of the bright maxima of the local density of states in the STM images: In a) the hexagonal arrangement of S atoms in the uppermost layer is shown,[13] in b) the two quadratic sublattices of Au atoms and Sb dimers, respectively, are visible. In the case of the Sb dimers the scanning tunnel microscope images show a superposition of the two atoms.[15]

(marked by arrows in Figure 2b) can be identified at coverages of 1–2 monolayers. These local structures always exhibit a simple, rectangular symmetry. In general no epitaxial

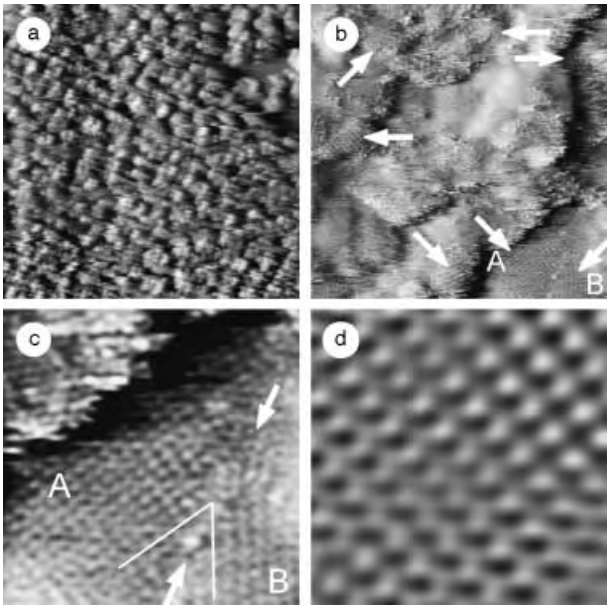


Figure 2. STM data of a two-monolayer-thick antimony film on MoS_2 at different magnifications. a) The 2480 × 2480 Å² image showing the generally amorphous structure of the film. b) The areas marked by arrows in the 310 × 310 Å² image exhibit a well-ordered structure. c) The 100 × 100 Å² magnification of the structures A and B in b). Along the line marked by arrows a grain boundary between two neighboring ordered areas is visible. The orientations of these structures are rotated by 59 ± 1° with respect to each other. d) A 39 × 39 Å² excerpt of area A. The image was high-frequency-filtered to emphasize the well-ordered structure. Tunneling parameters of all images: 0.6 V, 1.0 nA.

[*] Priv.-Doz. Dr. B. Kaiser, Dipl.-Phys. B. Stegemann, Prof. Dr. K. Rademann
Institut für Chemie
Humboldt Universität zu Berlin
Brook-Taylor-Strasse 2, 12489 Berlin (Germany)
Fax: (+49) 30-2093-5559
E-mail: bernhard.kaiser@rz.hu-berlin.de
Dr. T. M. Bernhardt
Institut für Experimentalphysik
Freie Universität Berlin
Arnimallee 14, 14195 Berlin (Germany)

[**] This work was supported by the Deutsche Forschungsgemeinschaft. We thank S. Rogaschewski and A. Laws for the preparation of gold films.

 © 2003 Wiley-VCH Verlag GmbH & Co. KGaA, Weinheim 1433-7851/03/4202-0199 $ 20.00+.50/0

orientation between film and substrate could be observed. Figure 2c displays a magnification of the areas marked with A and B. A grain boundary highlighted by the two arrows separates structure A from structure B. The lattice orientation in both areas (white lines) is rotated relative to each other by $59 \pm 1°$. This could, however, point toward an alignment of the areas along the hexagonal substrate symmetry (see Figure 1a). In Figure 2d a stronger magnification of structure A is displayed. Close analysis of this image reveals significant differences between the perpendicular lattice vectors a_1 and a_2. The statistical analysis of the lattice distances of 14 investigated, local well-ordered areas (depicted in Figure 3a) illustrates this observation. Average lattice parameters of $a_1 = 5.06 \pm 0.13$ Å and $a_2 = 4.51 \pm 0.16$ Å are obtained for the crystalline antimony structures on $MoS_2(0001)$.

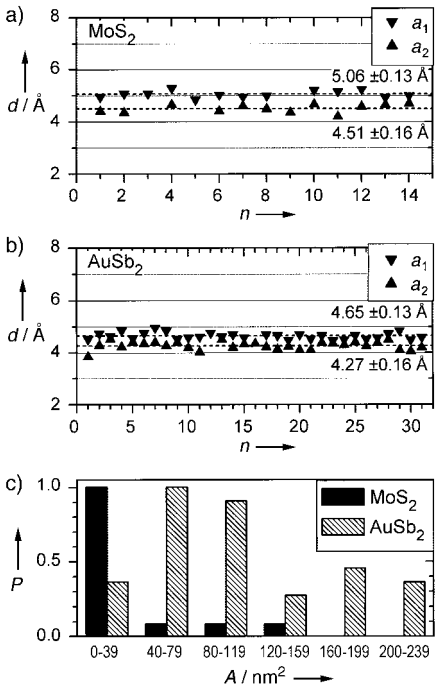


Figure 3. Statistical analysis of the lattice distances and sizes of the crystalline ordered areas. Displayed are the lattice parameters a_1 (▼) and a_2 (▼) of all analyzed structures n on a) MoS_2 and b) $AuSb_2$. The numbers given are the data averages (marked by the dashed lines) and their standard deviations. c) Size distribution of the crystalline, well-ordered areas on both substrates MoS_2 and $AuSb_2$. The relative abundance P is plotted as a function of the size A of the crystalline areas.

On a Au(111) substrate covered with the surface alloy $AuSb_2$, ordered areas can be observed even at room temperature. From Figure 4a the generally amorphous structure of a two-monolayer-thick antimony film on this substrate can be recognized. With increasing magnification, again local, well-ordered structures with rectangular symmetry appear. These are highlighted by arrows in Figure 4b. A preferred alignment of the lattice orientation in these areas with respect to the quadratic symmetry of the $AuSb_2(100)$ substrate cannot be identified. Further magnification of the structure in area A can be seen in Figure 4c. The edges and corners of the uppermost layer of the well-ordered structure are well resolved. The high-resolution image in Figure 4d shows the corrugation of the crystalline area in Figure 4c in a magnification comparable to that in Figure 2d. Close inspection reveals that also on $AuSb_2$ the antimony structures appear with clearly rectangular symmetry. In total 31 local, crystalline areas of antimony on $AuSb_2$ have been investigated, and the statistical evaluation is given in Figure 3b. In this case, the average lattice constants are $a_1 = 4.65 \pm 0.13$ and $a_2 = 4.27 \pm 0.16$ Å. These values are somewhat smaller than in the case of the MoS_2 surface. However, the lattice parameters a_1 and a_2 of the antimony structures are consistently in the ratio of 10:9 to each other on both substrates. The comparison of the size of the local well-ordered areas on both substrates in Figure 3c reveals that the average size of the nanostructures on MoS_2 is smaller (maximum at 0–39 nm) than on $AuSb_2$ (maximum at 40–79 nm). In addition the size distribution on $AuSb_2$ is clearly broader than on MoS_2.

The local crystalline areas display a three-dimensional structure. Although in both cases only the nominal amount of two-monolayer antimony was deposited, no ideal two-dimensional but a heavily structured film is formed (see Figure 2a and 4a). The observed crystalline areas appear to generally have a height of several monolayers, as can be seen from Figure 5. These images were recorded without an electronic difference filter for measuring the vertical distance. Several layers can be identified of a structure on MoS_2 (Figure 5a) as well as on $AuSb_2$ (Figure 5c), which are separated by steps.

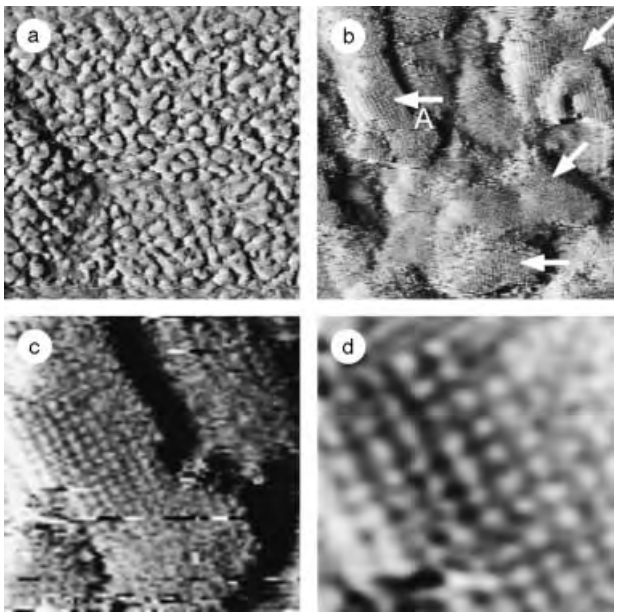


Figure 4. STM image of a two-monolayer-thick antimony film on a Au(111) surface covered by the surface alloy $AuSb_2$: a) The 2480×2480 Å^2 overview over the generally amorphous structure of the film. Tunneling parameters: 0.8 V, 1.8 nA. b) The 310×310 Å^2 STM image displays well-ordered areas in the film at the positions marked by arrows. Tunneling parameters: −0.96 V, 1.7 nA. c) Magnification of area A in b) (100×100 Å^2). d) A further enlarged view of area A (39×39 Å^2). The image was high-frequency-filtered, to enhance visibility of the well-ordered structure.

 © 2003 Wiley-VCH Verlag GmbH & Co. KGaA, Weinheim 1433-7851/03/4202-0200 $ 20.00+.50/0

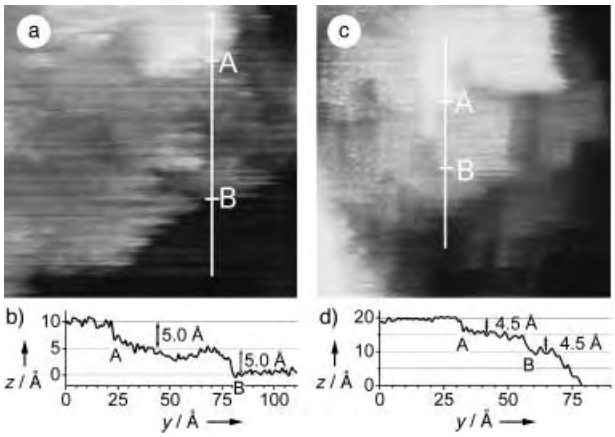


Figure 5. STM images (120×120 Å^2) of the three-dimensional structure in the well-ordered areas on a) MoS_2 (tunneling parameters: 0.6 V, 1.0 nA) and c) $AuSb_2$ (tunneling parameters: −0.25 V, 7.9 nA). The data were taken without electronic difference filter so that the gray scale represents the absolute sample height. Vertical profiles (*z* direction) along the white lines (*y* direction) are depicted below the corresponding STM images in b) and d). The given numbers are the heights of monomolecular steps at the positions marked by A and B.

The rectangular symmetry of several consecutive layers of the antimony structures in Figure 5c is particularly well resolved. Vertical profiles along the white lines are depicted below the STM images (Figure 5b and d). In both images two particular steps are marked with A and B. The measured step heights on both substrates range between 4.5 and 5.0 Å and are thus comparable to the lattice distances in the layers. Based on these results, the atomic arrangement in the local, well-ordered areas will now be discussed.

The crystal structure of metallic α-antimony is rhombohedral (space group $R\bar{3}m$). Each Sb atom in a lattice plane has three next neighbors at a distance of 2.908 Å. The smallest interatomic distance between the adjacent lattice planes is 3.355 Å.[1] The evidently larger measured distances as well as the different symmetry of the local, crystalline areas on both substrates prove that the corrugation maxima in the STM images cannot be assigned to single antimony atoms in a lattice plane of α-antimony. The presence of nanocrystallites of metallic antimony can therefore be ruled out.

However, the measured lattice distances fit well the known dimensions of the vapor-deposited Sb_4 molecules. Collision-induced fragmentation of the impinging Sb_4 molecules can be excluded at thermal deposition energies.[9] A solid-state modification of antimony based on Sb_4 molecules has not been described before, as mentioned above; however, data obtained by X-ray diffraction indicate the existence of chains and layers of tetrahedrons in antimony thin films.[8] Sb_4 was detected in liquid antimony by neutron scattering[10] and individual Sb_4 molecules were observed by STM on a Si(001) surface.[6] Sb_4 has the structure of a regular tetrahedron.[4] Ab initio calculations gave a bond length in the tetrahedron of 2.687 Å.[5]

Starting from the measured distances between the corrugation maxima in the local, well-ordered areas of the antimony thin films and based on an atomic radius of half the bond length (1.34 Å), a molecular lattice arrangement is obtained as displayed in Figure 6. Other arrangements in accord with the observed symmetry are not possible on both substrates. The observed crystalline ordered antimony structures can hence be explained, if each protrusion measured with STM, that is, the maxima of the local electronic density of states, is assigned to one undissociated Sb_4 tetrahedron molecule. This assignment of the observed corrugation is also supported by STM measurements of single Sb_4 molecules on Si(001) which gave an Sb_4 diameter of about 5 Å.[6] Taking into consideration the convolution with the STM tip, this value represents an upper limit for the lateral size of Sb_4 and thus agrees well with the measured distances.Although the detailed structures of yellow arsenic and white phosphorus, which are built of As_4 and P_4 molecules, respectively, have not been resolved yet, crystals of these modifications with cubic symmetry could be obtained.[1,11] The step heights of the observed antimony modification are comparable to the distances between the Sb_4 molecules in the lattice layers (Figure 5) and thus demonstrate the three-dimensional character of the crystalline structures. It is therefore reasonable to assume that the antimony modification presented here has a nearly cubic lattice structure.

In this respect, the well-ordered areas on $AuSb_2$ in general show besides the lateral also a stronger vertical extension. As at larger coverages (above 3 ML) no well-ordered Sb_4 areas can be identified, the smaller distances between the Sb_4 molecules on $AuSb_2$ indicate that the more extended structures in comparison to MoS_2 are closer to the critical size, at which the transition to the amorphous phase takes place.[12] A further possible explanation for the different intermolecular distances on the two substrates might lie in a different interaction of Sb_4 with MoS_2 and $AuSb_2$. Future experiments and a detailed theoretical modeling of the Sb_4 structures on the substrates will hopefully give more insight into these aspects.

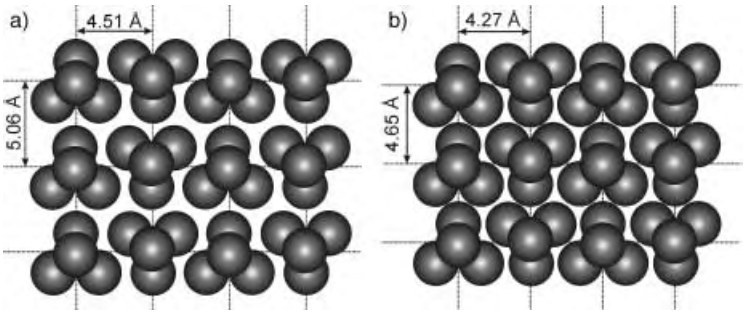


Figure 6. Structure model for the arrangement of the Sb_4 tetrahedrons in the uppermost layer of the Sb_4 antimony modification on a) the MoS_2 substrate and on b) the $AuSb_2$ substrate according to the observed symmetry and lattice distances. The scanning tunnel microscope images a superposition of the four atoms in the tetrahedron. Consequently, these arrangements are the only possible variations of rectangular lattices with the measured distances.

 © 2003 Wiley-VCH Verlag GmbH & Co. KGaA, Weinheim 1433-7851/03/4202-0201 $ 20.00+.50/0

Experimental Section

The antimony thin films were synthesized in ultra-high vacuum (base pressure: 4×10^{-11} mbar) by evaporation of Sb_4 molecules from a resistance-heated effusive oven (temperature: 330 °C; deposition rate: 0.1 nm s^{-1}; Sb: 99.9999 %, Johnson-Matthey). The layer thickness is given in monolayers of Sb atoms. The MoS_2 substrates were prepared by cleavage according to the procedure given in reference [13]. The $AuSb_2$ surface alloy was prepared starting from Au(111).[14] On this substrate the surface alloy $AuSb_2$ with the (100) orientation forms spontaneously, if less than one monolayer of antimony is deposited at room temperature.[15] The beetle-type STM[16] is located in an analysis chamber directly attached to the preparation chamber.[17] To increase image contrast, the STM data were electronically differentiated directly during acquisition. Therefore the STM images appear as if they are illuminated from the side.

Received: April 8, 2002
Revised: October 11, 2002 [Z19057]

[1] J. Donohue, *The structures of the elements*, Wiley-Interscience, New York, **1974**.
[2] J. Mühlbach, P. Pfau, E. Recknagel, K. Sattler, *Surf. Sci.* **1981**, *106*, 18.
[3] A. F. Hollemann, N. Wiberg, *Lehrbuch der Anorganischen Chemie*, 101. ed., Walter de Gruyter, Berlin, **1995**.
[4] H. Sontag, R. Weber, *Chem. Phys.* **1982**, *70*, 23.
[5] V. Kumar, *Phys. Rev. B* **1993**, *48*, 8470.
[6] Y. W. Mo, *Phys. Rev. Lett.* **1992**, *69*, 3643.
[7] J. Cohen, *J. Appl. Phys.* **1954**, *25*, 798; M. Hashimoto, K. Umezawa, R. Murayama, *Thin Solid Films* **1990**, *188*, 95; A. Hoareau, J. X. Hu, P. Jensen, P. Melinon, M. Treilleux, B. Cabaud, *Thin Solid Films* **1992**, *209*, 161; H. Murmann, *Z. Phys.* **1929**, *54*, 741; J. A. Prins, *Nature* **1933**, *131*, 760; H. Levinstein, *J. Appl. Phys.* **1949**, *20*, 306.
[8] H. Richter, H. Berckhemer, G. Breitling, *Z. Naturforsch. A* **1952**, *9*, 236.
[9] B. Kaiser, T. M. Bernhardt, B. Stegemann, J. Opitz, K. Rademann, *Nucl. Instrum. Methods Phys. Res. Sect. B* **1999**, *157*, 155; T. M. Bernhardt, B. Kaiser, K. Rademann, *Phys. Chem. Chem. Phys.* **2002**, *4*, 1192.
[10] P. Lamparter, S. Steeb, W. Knoll, *Z. Naturforsch. A* **1976**, *31*, 90.
[11] J. Eiduss, R. Kalendarev, A. Rodionov, A. Sazonov, G. Chikvaidze, *Phys. Status Solidi B* **1996**, *193*, 3.
[12] G. Fuchs, P. Melinon, F. Santos Aires, M. Treilleux, B. Cabaud, A. Hoareau, *Phys. Rev. B* **1991**, *44*, 3926.
[13] J. G. Kushmerick, S. A. Kandel, P. Han, J. A. Johnson, P. S. Weiss, *J. Phys. Chem. B* **2000**, *104*, 2980.
[14] J. A. DeRose, T. Thundat, L. A. Nagahara, S. M. Lindsay, *Surf. Sci.* **1991**, *256*, 102.
[15] B. Stegemann, T. M. Bernhardt, B. Kaiser, K. Rademann, *Surf. Sci.* **2002**, *511*, 153.
[16] K. Besocke, *Surf. Sci.* **1987**, *181*, 145.
[17] B. Kaiser, T. M. Bernhardt, K. Rademann, *Nucl. Instrum. Methods Phys. Res. Sect. B* **1997**, *125*, 223; T. M. Bernhardt, Dissertation thesis, Humboldt-University, Berlin, **1997**.

Conformationally Restricted Peptides

Analogues of Neuropeptide Y Containing β-Aminocyclopropane Carboxylic Acids are the Shortest Linear Peptides That Are Selective for the Y_1 Receptor**

Norman Koglin, Chiara Zorn, Raphael Beumer, Chiara Cabrele, Christian Bubert, Norbert Sewald, Oliver Reiser, and Annette G. Beck-Sickinger**

Dedicated to Professor Peter Welzel on the occasion of his 65th birthday.

Neuropeptide Y (NPY) is one of the most abundant neuropeptides in the mammalian central nervous system. It consists of 36 amino acids and has an amide group at the C terminus. To date NPY is the strongest known stimulator of food intake in rat and mice models. Other important biological functions are vasoconstriction in the periphery, regulation of behavior and modulation of pain and epileptic seizures.[1]

In mammals, the activities of NPY are mediated by at least three different G-protein-coupled receptors (Y_1, Y_2, and Y_5). Because NPY shows sub-nanomolar affinity towards all of them, it is still difficult to distinguish the physiological roles of each receptor in vivo. To address this problem, the knowledge of the particular bioactive conformation at each receptor is indispensable for the further development of subtype-selective ligands. Substitutions of single amino acids have revealed that especially the highly conserved C-terminal part of NPY, with its two positively charged arginine side chains in positions 33 and 35 and the tyrosine amide in position 36, plays a crucial role during the recognition process by the respective receptor. Because of its flexibility, no defined structure could be assigned to this important part of the molecule to date. It is assumed that different secondary structure motifs of the C terminus are responsible for receptor subtype selectivity.

[*] Prof. Dr. O. Reiser, Dr. C. Zorn, Dr. R. Beumer, Dr. C. Bubert
Institut für Organische Chemie
Universität Regensburg
Universitätsstrasse 31, 93040 Regensburg (Germany)
Fax: (+49) 941-9434-121
E-mail: oliver.reiser@chemie.uni-regensburg.de
Prof. Dr. A. G. Beck-Sickinger, Dipl.-Biochem. N. Koglin, Dr. C. Cabrele
Institut für Biochemie
Universität Leipzig
Talstrasse 33, 04103 Leipzig (Germany)
Fax: (+49) 341-9736-998
E-mail: beck-sickinger@uni-leipzig.de
Prof. Dr. N. Sewald
Institut für Organische und Bioorganische Chemie
Universität Bielefeld
Postfach 100131, 33501 Bielefeld (Germany)

[**] This work was supported by the Deutsche Forschungsgemeinschaft (BE1264/3-1 and RE948-4/1) and the Fonds der Chemischen Industrie and through generous chemical gifts from BASF AG, Bayer AG, and Degussa AG.

 © 2003 Wiley-VCH Verlag GmbH & Co. KGaA, Weinheim 1433-7851/03/4202-0202 $ 20.00+.50/0

It has been shown that substitutions close to these major C-terminal positions allow a distinction to be made between some receptor subtypes. For example, the introduction of a proline residue in position 34 of the NPY sequence significantly reduced the Y_2 receptor affinity and maintained the affinity toward the Y_1 and Y_5 receptors.[2] The introduction of the turn-inducing Ala–Aib sequence in positions 31 and 32, respectively, led to a Y_5-selective analogue.[3] Whereas the influence of the Ala–Aib substitution on the peptidic structure could be further elucidated by NMR spectroscopic investigations, the proline substitution at position 34 did not sufficiently restrain the C terminus to enable the structural requirements of NPY binding at other receptor subtypes to be deduced.[4] Accordingly, novel approaches are required for the identification of the bioactive conformation at the Y_1 receptor.

To rigidify the peptide backbone and to induce or to stabilize distinct secondary structure motifs, analogues of the C-terminal NPY sequence with new conformationally restricted building blocks were investigated. We expected that the incorporation of such constraints would be especially effective at positions 32 and 34, which are in direct proximity to the most important amino acids Arg33 and Arg35. By using this strategy, we identified β-aminocyclopropane carboxylic acids (β-ACC) as novel constricted building blocks that are highly effective for the stabilization of secondary structures in peptides, and moreover, complement known constrained α-amino acids such as proline or α-aminoisobutyric acid (Aib) in their properties.

The incorporation of β-ACCs into peptides, however, turned out to be challenging. Because of the 1,2-donor-acceptor substituted cyclopropane structure, β-ACCs are unstable in the N-unprotected form, which necessitates special coupling techniques to incorporate them into peptides.[5] The β-amino acid **1** (Scheme 1) can be readily synthesized in diastereo- and enantiomerically pure form starting from *N*-Boc-pyrrole.[6] We synthesized the prerequisite dipeptides **2** and **3**, which then were used as dipeptide building blocks in solid-phase peptide synthesis. The β-ACC-containing dipeptides were introduced into the growing peptide chain by a manual coupling step after TBTU activation[7] and further elongation by automated Fmoc/*tert*-butyl coupling procedures.[3] The resulting peptides were analyzed by HPLC and MALDI-MS, which confirmed the intact cyclopropyl ring system. The conformational properties of the C-terminal NPY analogues containing these β-ACC dipeptides were investigated by circular dichroism (CD) spectroscopy, and their affinity to the Y receptors was probed by competition binding assays with living cells that selectively express one receptor subtype (compounds **4**–**15**, Table 1).

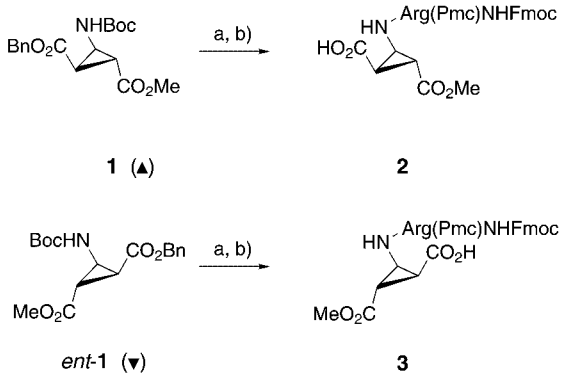
From previous studies it is known that the full-length molecule of NPY is necessary for binding to the Y_1 receptor. N-terminally truncated analogues, such as NPY(13–36) or NPY(18–36) bind only to the Y_2 receptor, whereas NPY(2–36) is recognized by Y_2 and Y_5.[2b] However, in contrast to the unsubstituted C-terminal fragment NPY(25–36)[8] we obtained β-ACC-containing NPY analogues, which bind to the Y_1 receptor (peptides **4**, **8**, and **10**, Table 1) with high affinity and selectivity.

The affinity of the β-ACC-containing NPY analogues is strongly dependent on the position of the substitution and the absolute configuration of the β-ACC derivative. The introduction of a β-ACC-moiety with the (▲)-configuration in position 34 was crucial for binding to the Y_1 receptor. Accordingly, only a single β-ACC substitution with this configuration in position 34 (peptide **4**) was sufficient to evoke nanomolar biological affinity at the Y_1 receptor and high selectivity, whereas a (▼)-configured β-ACC-residue in position 34 (peptide **5**) remained biologically inactive at all

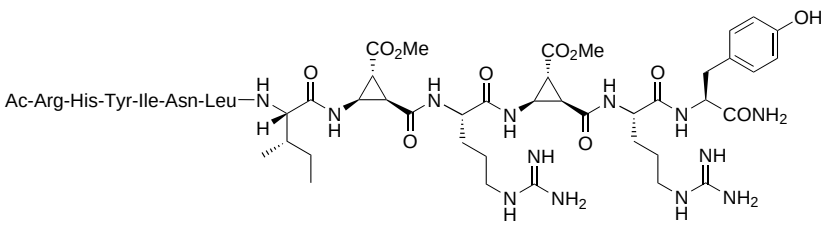
Table 1: Sequences and affinities of shortened β-ACC-containing NPY analogues at the Y receptors. The affinities are expressed as K_i values [nM].[a] For more details see text.

	Sequences[b]	Y_1	Y_2	Y_5	$\Delta[\Theta]_R$[c]
	RHYINLITRQRY-NH_2	>1000	21[d]	>1000	17.5
4	RHYINLITR▲RY-NH_2	37(±20)	>1000	724	5.6
5	RHYINLITR▼RY-NH_2	>1000	>1000	>1000	3.7
6	RHYINLI▲RQRY-NH_2	>1000	>1000	>1000	1.5
7	RHYINLI▼RQRY-NH_2	>1000	>1000	>1000	1.6
8	RHYINLI▲R▲RY-NH_2	50(±10)	>1000	617	2.9
9	RHYINLI▼R▲RY-NH_2	>150	>1000	>1000	3.5
10	RHYINL**R**▲R▲RY-NH_2	29(±13)	>1000	118	3.3
11	RHYINL**R**▼R▼RY-NH_2	1000	>1000	>1000	2.2
12	NL**R**▲R▲RY-NH_2	235	>1000	>1000	2.0
13	RHYINLITR**P**RY-NH_2	>1000	>1000	>1000	5.1
14	RHYINLI**P**R**P**RY-NH_2	>1000	>1000	>1000	1.4
15	RHYINLITR**β**RY-NH_2	>1000	>1000	>1000	9.9

For explanations of ▲ and ▼, see Scheme 1; **β** = β-homoglutamine; other substitutions are marked in bold. [a] Competitive binding assays were performed as described previously using ^{3}H-NPY (Amersham) as the radioligand.[3] The K_i values were determined by using the Cheng–Prusoff equation with K_d values for ^{3}H-NPY of 0.18 nM for the Y_1 receptor and 2.4 nM for the Y_5 receptor. [b] All peptides were N-terminally acetylated, except for peptides **6** and **7**. [c] $\Delta[\Theta]_R$ [10^{-3} deg cm^2 dmol^{-1}] is the difference of the mean-residue molar ellipticity values $[\Theta]_R$ at 222 nm, obtained from the CD spectra in buffer and in the presence of 30% TFE. Peptide concentrations were 30 μM. [d] K_i value previously published.[8]



Scheme 1. The synthesis of β-ACC-containing dipeptides for facile introduction into peptide sequences: a) 1) HCl(g)/EtOAc; 2) Fmoc-Arg(Pmc)-OH, EDC, pyridine, 88–97%; b) Pd/C, 1,4-cyclohexadiene (5 equiv), MeOH, 77–88%. Bn = benzyl, Boc = *tert*-butoxycarbonyl, EDC = 1-(3-dimethylaminopropyl)-3-ethylcarbodiimide hydrochloride, Fmoc = 9-fluorenylmethyloxycarbonyl, Pmc = 2,2,5,7,8-pentamethylchroman-6-sulfonyl.



Scheme 2. A C-terminal NPY analogue (peptide **8**) containing two (▲)-configured β-ACC residues.

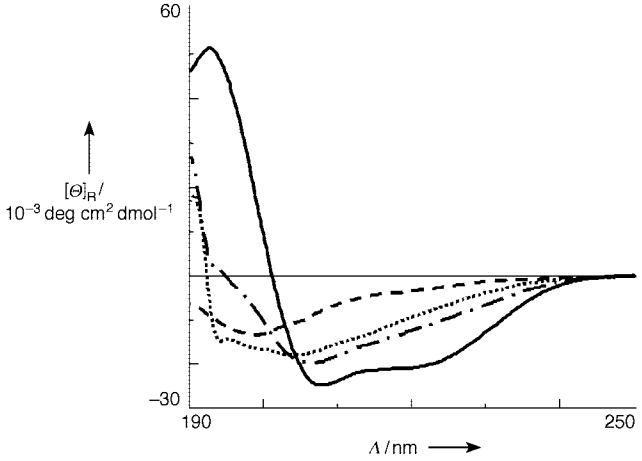


Figure 1. CD-spectra of the unsubstituted C-terminal NPY fragment NPY(25–36) in 20 mM phosphate buffer (pH 7.0; – – –) and in the presence of 30% TFE (——), in comparison with the β-ACC disubstituted analogue (peptide **8**) in buffer (••••) and in 30% TFE (•–•–), respectively. Peptide concentrations were 30 μM.

investigated receptors. Peptides **6** and **7**, which contain a β-ACC residue at position 32, were biologically inactive in both configurations. Combination of the two β-ACC-substitutions with the same (▲)-configuration of the cyclopropane ring in positions 32 and 34 did not improve affinity at the Y_1 receptor (peptides **8** and **10**, Scheme 2), but led to more rigid peptides such as can be seen in Figure 1. In peptide **10**, even the substitution of an Ile by an Arg residue in position 31 is tolerated at the Y_1 receptor, if it is combined with the bioactive (▲)-configuration of the β-ACC residues in positions 32 and 34. However, peptide **10** is slightly less selective, as its affinity at the Y_5 receptor increased by approximately five fold. This increase could arise from a new ionic interaction of the Arg31 side chain with the Y_5 receptor. If the opposite (▼)-configuration of the β-ACC residue is used in position 32 and 34, the disubstituted peptide **11** will remain biologically inactive. Peptide **9**, with the (▼)-configured β-ACC residue in position 32 but with a bioactive (▲)-β-ACC derivative in position 34, shows reduced affinity to the Y_1 receptor. Interestingly, the further shortened β-ACC-disubstituted octapeptide **12**, with two (▲)-configured β-ACCs, still shows moderate affinity. Accordingly, these four peptides (**4**, **8**, **10**, and **12**) are the first and only linear NPY segments with affinity and selectivity at the Y_1 receptor.

A recently reported disulfide-bridged, cyclic, C-terminal NPY analogue shows similar affinities at the Y_1 receptor to those of the linear β-ACC-substituted peptides **4**, **8**, and **10** reported herein.[9] Accordingly it can be assumed that β-ACC substitutions cause a similarly constrained arrangement of the critical side chains in linear peptides to that which can otherwise be obtained by simple cyclization. It is remarkable that similar NPY analogues containing the natural conformationally restricted amino acid proline are biologically inactive at all investigated receptors (peptides **13** and **14**). Similarly, the introduction of the β-amino acid β-homoglutamine[10] (**β**) into position 34 yielded also only an inactive peptide **15**. Accordingly, the observed affinities at the Y_1 receptor are exclusively evoked by a substitution with the conformationally constricted (▲)-β-ACC derivative in position 34 or in combination with a similarly configured β-ACC residue in position 32.

For the unsubstituted C-terminal fragment, conformational studies by circular dichroism (CD) showed the typical CD spectrum of a random peptide in buffer and also a high α-helical content in the presence of the α-helix-promoting additive 2,2,2-trifluoroethanol (TFE), whereas the β-ACC-containing analogues behaved completely differently (Figure 1). A higher content of structured peptide with a minimum around 206 nm was found and a significantly reduced tendency of α-helix formation was observed in the presence of TFE, as shown by the $\Delta[\Theta]_R$ values in Table 1. The $\Delta[\Theta]_R$ values are obtained by subtracting the $[\Theta]_R$ values at 222 nm in the presence of TFE from those obtained in buffer. From these studies it can be concluded that β-ACC substitutions stabilize distinct backbone conformations and thereby significantly reduce the tendency towards α-helix formation in helix-promoting environments such as TFE or membranes.

Thus the β-ACC disubstituted and truncated NPY analogues **8** and **10** are the most rigidified peptides but have still the structural requirements for biological activity at the Y_1 receptor; to date such reqirements can neither be induced with natural amino acids nor with analogous β-amino acids. These peptides are therefore most suitable for further structural investigations and for the development of new lead structures in pharmaceutical chemistry. Further studies are currently under investigation to gain more insights into the peptide structure and the influence of the configuration of the cyclopropane ring system on the secondary structure. Accordingly, we could show that β-ACC residues are extremely useful for the rigidification of peptides. The application of this concept to other systems could lead to new types of peptidomimetics.

Received: July 5, 2002 [Z19670]

[1] a) C. Cabrele, A. G. Beck-Sickinger, *J. Pept. Sci.* **2000**, *6*, 97–122; b) A. Inui, *Trends Pharmacol. Sci.* **1999**, *20*, 43–46.

[2] a) J. Fuhlendorff, U. Gether, L. Aakerlund, N. Langeland-Johansen, H. Thøgersen, S. G. Melberg, U. Bang Olsen, O. Thastrup, *Proc. Natl. Acad. Sci. USA* **1990**, *87*, 182–186; b) C. Gerald, M. W. Walker, L. Criscione, E. L. Gustafson, C. Batzl-Hartmann, K. E. Smith, P. Vaysse, M. M. Durkin, T. M. Laz, D. L. Linemeyer, A. O. Schaffhauser, S. Whitebread, K. G.

 © 2003 Wiley-VCH Verlag GmbH & Co. KGaA, Weinheim 1433-7851/03/4202-0204 $ 20.00+.50/0

Hofbauer, R. I. Taber, T. A. Branchek, R. L. Weinshank, *Nature* **1996**, *382*, 168 – 171.
[3] C. Cabrele, M. Langer, R. Bader, H. A. Wieland, H. N. Doods, O. Zerbe, A. Beck-Sickinger, *J. Biol. Chem.* **2000**, *275*, 36043 – 36048.
[4] A. Khiat, M. Labelle, Y. Boulanger, *J. Pept. Res.* **1998**, *51*, 317 – 322.
[5] a) C. Bubert, C. Cabrele, O. Reiser, *Synlett* **1997**, 827 – 829; b) C. Zorn, F. Gnad, S. Salmen, T. Herpin, O. Reiser, *Tetrahedron Lett.* **2001**, *42*, 7049 – 7053.
[6] R. Beumer, C. Bubert, C. Cabrele, O. Vielhauer, M. Pietzsch, O. Reiser, *J. Org. Chem.* **2000**, *65*, 8960 – 8969.
[7] TBTU: 1*H*-Benzotriazolium 1-[bis(dimethylamino)methylene]-tetrafluoroborate-3-oxide; β-ACC-containing dipeptide (1 equiv), TBTU (1.5 equiv), *N*,*N*′-diisopropylethylamine (3 equiv) in 0.5 M *N*-hydroxybenzotriazole in *N*,*N*-dimethylformamide; reaction time 1 h; double coupling.
[8] B. Rist, O. Zerbe, N. Ingenhoven, L. Scapozza, C. Peers, P. F. T. Vaughan, R. L. McDonald, H. A. Wieland, A. G. Beck-Sickinger, *FEBS Lett.* **1996**, *394*, 169 – 173.
[9] Y. Takebayashi, H. Koga, J. Togami, A. Inui, H. Kurihara, K. Koshiya, T. Furuya, A. Tanaka, K. Murase, *J. Pept. Res.* **2000**, *56*, 409 – 415.
[10] A. Müller, C. Vogt, N. Sewald, *Synthesis* **1998**, 837 – 841.

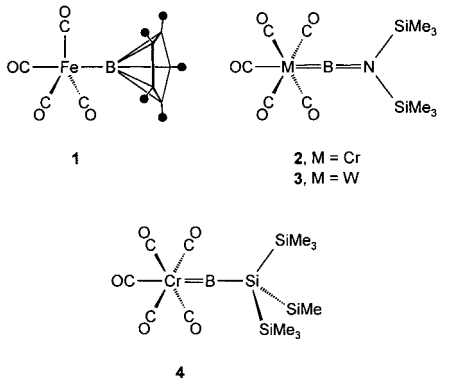
Borylene Half-Sandwich Complexes

$[(\eta^5\text{-}C_5H_5)(OC)_3V{=}B{=}N(SiMe_3)_2]$: A Half-Sandwich Complex with a Terminal Borylene Ligand**

Holger Braunschweig, Miriam Colling, Chunhua Hu, and Krzysztof Radacki*

Dedicated to Professor Thomas P. Fehlner on the occasion of his 65th birthday

In contrast to the rather well-developed chemistry of bridged borylene complexes $L_xM{-}B(R){-}ML_x$[1] their terminal counterparts $L_xM{=}B{-}R$ are still exceptionally rare and restricted to five structurally authentic examples[2]—two of which,



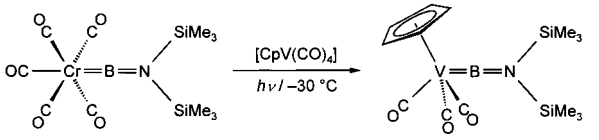
1 — 2, M = Cr; 3, M = W — 4

Figure 1. Structurally authentic terminal borylene complexes that have been obtained by salt elimination reactions.

however, comprise boron in higher coordination numbers than two.[3] Most of these borylene complexes (Figure 1) were obtained by salt elimination reactions from dianionic carbonylmetallates and suitable dihaloboranes. Although this method of preparation was initially very successful, it appears to be limited to the use of the homoleptic carbonylmetallates $Na_2[Fe(CO)_4]$ and $Na_2[M(CO)_5]$ (M = Cr, W), despite the rather broad availability of dianionic transition metal complexes and corresponding synthetic equivalents.[4] Thus, combination of terminal borylenes with any coligand other than carbonyl is precluded as yet, although such complexes with various ligands are of significant interest.[5]

Recently, we reported on the photochemically induced intermetallic borylene transfer as a novel and potentially useful way of synthesizing both bridged and terminal borylene complexes.[2b] However, as far as the latter were concerned at that time, this route provided only an alternative access to the chromium complex $[(OC)_5Cr{=}B{=}N(SiMe_3)_2]$, which we obtained somewhat earlier by conventional salt elimination.[2a] Further exploitation of this method has now led to the synthesis and full characterization of $[(\eta^5\text{-}C_5H_5)(OC)_3V{=}B{=}N(SiMe_3)_2]$ (**5**), the first half-sandwich complex with a terminal borylene ligand.

The title compound **5** was formed upon irradiation of $[(OC)_5Cr{=}B{=}N(SiMe_3)_2]$ (**2**) in the presence of $[(\eta^5\text{-}C_5H_5)V(CO)_4]$ for four days at −30 °C in toluene according to Equation (1). Compound **5** was separated by fractional crystallization and isolated in 42 % yield as a dark yellow



(1)

2 — 5

crystalline material, which is readily soluble in all common aliphatic and aromatic solvents and only modestly air- and moisture sensitive.

Single crystals of **5** suitable for X-ray structural analysis were grown from hexane solutions at −80 °C. The compound crystallizes in the space group $P2_1/c$ and the molecule adopts a

[*] Prof. Dr. H. Braunschweig,[+] Dr. K. Radacki
Department of Chemistry
Imperial College
London SW7 2AY (UK)
E-mail: h.braunschweig@mail.uni-wuerzburg.de
Dr. M. Colling, Dr. C. Hu
Institut für Anorganische Chemie
Technische Hochschule
52056 Aachen (Germany)
[+] New address:
Institut für Anorganische Chemie der Universität Würzburg
Am Hubland, 97074 Würzburg (Germany)
Fax: (+49) 0931-8884623

[**] This work was supported by the Deutsche Forschungsgemeinschaft, the Fonds der Chemischen Industrie, EPSRC, and the Royal Society. We are grateful to the Rechenzentrum of Aachen University of Technology (RWTH) for generously placing computation time at our disposal.

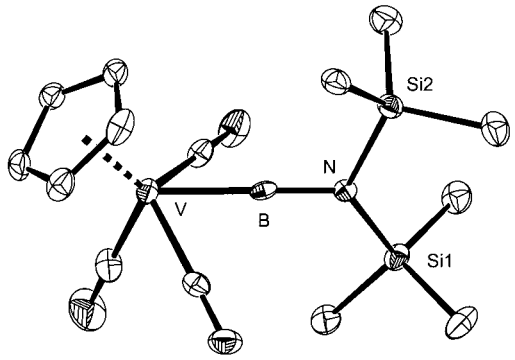


Figure 2. Structure of **5** in the crystal. Selected interatomic distances [Å] and angle [°]: V-B 1.959(6), B-N 1.378(7); V-B-N 177.9(4).

geometry close to C_s symmetry in the solid state (Figure 2).[6] The planar B-N-Si1-Si2 moiety is twisted by 12° with respect to the plane defined by Cp_m (centroid of the cyclopentadienyl ring), one carbonyl ligand, vanadium, and boron, which accounts for the distortion of the symmetry. The overall geometry of the central metal-B-N moiety and in particular its linear arrangement (V-B-N 177.9(4)°) and the small B–N distance of only 1.378(7) Å matches that of the related chromium and tungsten complexes **2** and **3**.[2a,b] The V–B distance of 1.959(6) Å is very similar to the Cr–B distance of 1.996 Å in **2** and significantly smaller than the distance for the V–C double bond in related carbene complexes of the type $[(\eta^5\text{-}C_5H_5)(OC)_3V{=}C(OR)R]$.[7] The V–$Cp_m$ and V–CO distances are unexceptional and within the range of corresponding data reported for $[(\eta^5\text{-}C_5H_5)V(CO)_4]$ and the aforementioned carbene complexes.[8] Compound **5** represents the first example for a classical, that is, electron-precise bond between vanadium and boron. Earlier reports on covalent V–B interactions were restricted to vanadacarbaboranes, and thus nonclassical, that is, electron-deficient bonds. Corresponding distances in these metallaboranes have significantly greater values (2.248–2.442 Å) due to higher coordination numbers of both atoms.[9]

Inspection of the structural data revealed unexpectedly short B–C distances of only 1.997(8) and 2.037(8) Å for the two CO ligands adjacent to the borylene group. However, the linear arrangement of all three ligands and the unexceptional V–C, C–O, and B–N distances provide no evidence for a bonding interaction. The same is true for ^{13}C and ^{11}B NMR resonance signals in solution. In addition, DFT calculations (see below) provided further evidence for the absence of two-center, two-electron (2c2e) bonds between boron and carbon atoms. Hence, the observed close proximity of the ligands may be attributed to steric reasons.

The structure of **5** in solution was derived from IR and multinuclear NMR spectra. Three CO stretching frequencies were detected at 1984, 1884, and 1842 cm^{-1}, which are slightly shifted to higher wavenumbers than those of the related carbene complex $[(\eta^5\text{-}C_5H_5)(OC)_3V{=}C(NMe_2)H]$,[10] thus indicating a similar situation with respect to vanadium-to-element π-backbonding. The significantly deshielded ^{11}B NMR resonance signal at $\delta = 98.3$ ppm matches those of the related aminoborylene complexes **2** and **3**, which were found at $\delta = 92.3$ and 86.6 ppm, respectively. The ^1H and ^{13}C NMR spectra only dsiplayed single sets of signals for the $(Me_3Si)_2N$ moiety even at −80 °C, thus indicating either a vertical arrangement of the aminoborylene ligand in solution or a very low rotational barrier. Similar studies on the related cationic carbene complex $[(\eta^5\text{-}C_5H_5)(Ph_2PCH_2CH_2PPh_2)Fe{=}CH_2][AsF_6]$ (**6**) revealed a surprisingly low rotational barrier of only 45 kJ mol^{-1} for the methylene ligand. This value, however, does not directly indicate a weak metal–carbon double bond but rather reflects the small energy difference between the horizontal and vertical arrangement of the CH_2 group.[11]

To shed further light on this topic DFT calculations were performed for both **5** and the parent aminoborylene complex $[(\eta^5\text{-}C_5H_5)(OC)_3V{=}B{=}NH_2]$ (**7**).[12] The minimum structure calculated for **5** corresponded to that found in the crystal. In particular the slight deviation from C_s symmetry caused by twisting of the B-N-Si1-Si2 moiety by 12° was exactly reproduced. The horizontal arrangement of the aminoborylene ligand resulted in a geometry that is about 19 kJ mol^{-1} higher in energy. The interatomic distances for the minimum structure were calculated to be 1–5 pm longer than those in the crystal, which corresponds well to the expected trend in comparing bond lengths in the gas and the solid phase. Chemical shifts calculated by GIAO were also found to be in very good agreement with experimental data (Table 1). For the parent complex **7** calculations revealed that the minimum structure contains the aminoborylene ligand in the horizontal orientation. Rotation of the BNH_2 moiety in nine subsequent steps of 10° is paralleled by a linear but small increase in energy. The resulting geometry with a vertically aligned borylene ligand represents a transition state on the potential energy surface, which is approximately 9 kJ mol^{-1} higher in energy than the molecule in its ground state. The preference for the slightly twisted orientation of the $(Me_3Si)_2NB$ ligand in **5** can be explained by the increased steric requirements of the Me_3Si groups. Molecular modeling studies proved that the interatomic distances especially between CO and Me groups achieve a minimal value for the horizontal arrangement.[13]

Table 1: Selected spectroscopic and structural data of **5** and **7**.

	5[a]	**5**[b]	**5**[b]	**7**[b]	**7**[b]
Si-N-V-Cp_m [°]	12.2	12.3	90	0.0	90
B-V [Å]	1.959(6)	1.967	1.990	1.939	1.925
B-N [Å]	1.378(7)	1.382	1.378	1.385	1.383
V-B-N [°]	177.9(4)	177.1	175.6	177.5	179.7
$\delta(^1H_{Me})$ [ppm]	0.21	0.43	0.49	–	–
$\delta(^1H_{Cp})$ [ppm]	4.66	4.69	4.72	5.03	5.27
$\delta(^{11}B)$ [ppm]	98.3	93.1	106.5	92.7	95.1

[a] Measured values. [b] Calculated values.

In conclusion it can be assumed that in solution the $(Me_3Si)_2NB$ ligand displays free rotation even at low temperature due to the energy difference of only 19 kJ mol^{-1} between the horizontal and the vertical orientation. This small energy difference, which is even significantly smaller than that in the aforementioned cationic carbene complexes,

 © 2003 Wiley-VCH Verlag GmbH & Co. KGaA, Weinheim 1433-7851/03/4202-0206 $ 20.00+.50/0

does not directly indicate weak V–B π-backbonding. Inspection of the molecular orbitals revealed that the [(η^5-C_5H_5)$(OC)_3$V] fragment possesses an a″-symmetrical HOMO and perpendicular to that an a′-symmetrical HOMO-1. This set of occupied metal-like orbitals can provide backbonding into an orthogonal set of empty orbitals (LUMO and LUMO + 1) of corresponding symmetry to that of the aminoborylene fragment. For both **5** and **7** the calculated V–B distances for the horizontal and vertical arrangement of the borylene ligands differ by less than 1.5 pm, which indicates a similar situation with respect to π bonding for both orientations.

Experimental Section

All manipulations were carried out by standard Schlenk techniques under N_2.

5: A solution of **2** (0.37 g, 1.02 mmol) and [(η^5-C_5H_5)V$(CO)_4$] (0.46 g, 2.04 mmol, 100% excess) in toluene (100 mL) was irradiated with a high-pressure Hg lamp (Heraeus TQ 150) at −30 °C for 10 h. After four days the yellow-green reaction mixture was allowed to come to ambient temperature and all volatile materials were removed in high vacuum. The residue was taken up in hexane (40 mL), the solution was filtered, and the solid residue was washed with hexane (10 mL). The combined yellow-green filtrates were concentrated to 20 mL in high vacuum (0 °C/0.001 Torr) and stored at −80 °C. The first solid fraction that was isolated consisted of the unreacted starting materials **2** and [(η^5-C_5H_5)V$(CO)_4$]. The remaining solution was concentrated to 10 mL and after storage at −80 °C for another four days **5** (0.16 g, 0.43 mmol, 42.2% yield) was isolated as yellow-brown needles.

All NMR spectra were recorded in [D_6]benzene at 25 °C. ^{1}H NMR (500 MHz, TMS): $\delta = 0.21$ (s, 18H; Si$(CH_3)_3$), 4.66 ppm (s, 5H; C_5H_5); ^{11}B NMR (160 MHz, $Et_2O{\cdot}BF_3$): $\delta = 98.3$ ppm (br. s); ^{13}C NMR (126 MHz, TMS): $\delta = 2.23$ (Si$(CH_3)_3$), 91.01 (C_5H_5), 211.47 ppm (CO); IR (KBr): $\tilde{\nu} = 1984$, 1884, 1842 cm^{-1} (CO); MS *m*/*z* (%): 371 (9) [M^+], 343 (1) [M^+−CO], 315 (10) [M^+−2CO], 287 (100) [M^+−3CO], 116 (62) [CpV], 98 (7) [BN$(SiMe_3)$], 73 (6) [$SiMe_3$]; elemental analysis (%) calcd for $C_{14}H_{23}BNVO_3Si_2$: C 45.29, H 6.24, N 3.77; found: C 44.89; H 6.15, N 3.89.

Received: July 22, 2002 [Z19795]

[1] a) H. Braunschweig, *Angew. Chem.* **1998**, *110*, 1882; *Angew. Chem. Int. Ed.* **1998**, *37*, 1786; b) H. Braunschweig, M. Colling, *J. Organomet. Chem.* **2000**, *614*, 18; c) H. Braunschweig, M. Colling, *Coord. Chem. Rev.* **2001**, *223*, 1; d) H. Braunschweig in *Inorganic Chemical Highlights* (Eds.: G. Meyer, D. Naumann, L. Wesemann), Wiley-VCH, Weinheim, New York, **2001**, p. 213; H. Braunschweig, M. Colling, *Eur. J. Inorg. Chem.* **2002**, in press.

[2] a) H. Braunschweig, C. Kollann, U. Englert, *Angew. Chem.* **1998**, *110*, 3355–3357; *Angew. Chem. Int. Ed.* **1998**, *37*, 3179–3180; b) H. Braunschweig, M. Colling, C. Kollann, H.-G. Stammler, *Angew. Chem.* **2001**, *113*, 2298–2300; *Angew. Chem. Int. Ed.* **2001**, *40*, 2229–2231; c) H. Braunschweig, M. Colling, C. Kollann, K. Merz, K. Radacki, *Angew. Chem.* **2001**, *113*, 4327–4329; *Angew. Chem. Int. Ed.* **2001**, *40*, 4198–4200.

[3] a) A. H. Cowley, V. Lomelí, A. Voigt, *J. Am. Chem. Soc.* **1998**, *120*, 6401–6402; b) G. J. Irvine, C. E. F. Rickard, W. R. Roper, A. Williamson, L. J. Wright, *Angew. Chem.* **2000**, *112*, 978–980; *Angew. Chem. Int. Ed.* **2000**, *39*, 948–950.

[4] a) U. Schubert, U. Kirchgässner, J. Grönen, H. Piana, *Polyhedron* **1989**, *8*, 1589–1593, and references therein; b) E. Colomer, R. P. Corriu, C. Marzin, A. Vioux, *Inorg. Chem.* **1982**, *21*, 368–373.

[5] B. Wrackmeyer, *Angew. Chem.* **1999**, *111*, 817–819; *Angew. Chem. Int. Ed.* **1999**, *38*, 771–773.

[6] Crystal structure determination of **5**: $C_{14}H_{23}BNVO_3Si_2$, $Mo_{K\alpha}$ radiation ($\lambda = 0.71073$ Å, graphite monochromator), $T = 213(2)$ K, $0.48 \times 0.16 \times 0.04$ mm, monoclinic, space group $P2_1/c$; $a = 14.7166(19)$, $b = 10.4320(14)$, $c = 12.448(2)$ Å, $\beta = 96.154(14)°$, $V = 1900.1(5)$ Å^3, $Z = 4$, $\rho_{calcd} = 1.298$ g cm^{-1}, $\mu(Mo_{K\alpha}) = 6.57$ cm^{-1}, $F(000) = 776$, measured reflections ($2.40° < \theta < 26.01°$), 3711 independent reflections with $I > \sigma(I)$, 199 variables. The intensities were measured with an Enraf–Nonius CAD4 diffractometer. Lattice parameters and orientation matrices were obtained from 25 centered reflections. Data were collected by using the $\omega/2\theta$ scan method. Data were processed by using the SDP program.[14] Empirical absorption corrections were applied by ψ scan. The structure was solved by direct methods and refined by using SHELXTL.[15] Non-hydrogen atoms were refined with anisotropic displacement parameters, and hydrogen atoms were placed in idealized positions (C–H = 0.98 Å) and included as riding with $U_{iso}(H) = 1.3\,U_{eq}$-(non-H). All refinements were made by full-matrix least-squares on F^2. *R*1 ($I > 2\sigma(I)$) = 0.0675, *wR*2 (all data) = 0.1040; GOF = 0.901. CCDC-190135 contains the supplementary crystallographic data for this paper. These data can be obtained free of charge via www.ccdc.cam.ac.uk/conts/retrieving.html (or from the Cambridge Crystallographic Data Centre, 12, Union Road, Cambridge CB2 1EZ, UK; fax: (+44) 1223-336-033; or deposit @ccdc.cam.ac.uk).

[7] It should be noted that the rather long V–C linkage was attributed to a contribution of the acylmetalate resonance structure: G. Erker, R. Pfaff, C. Krüger, S. Werner, *Organometallics* **1991**, *10*, 3559–3568.

[8] J. B. Wilford, A. Whitla, H. M. Powell, *J. Organomet. Chem.* **1967**, *8*, 495–501.

[9] a) R. G. Swisher, E. Sinn, A. Brewer, R. N. Grimes, *J. Am. Chem. Soc.* **1983**, *105*, 2079–2080; b) R. G. Swisher, E. Sinn, R. N. Grimes, *Organometallics* **1984**, *3*, 599–605; c) M. D. Wasczcak, Y. Wang, A. Garg, W. E. Geiger, S. O. Kang, P. J. Carroll, L. G. Sneddon, *J. Am. Chem. Soc.* **2001**, *123*, 2783–2790.

[10] A. J. Hartshorn, M. F. Lappert, K. Turner, *J. Chem. Soc. Dalton Trans.* **1978**, 348–356.

[11] W. B. Studebaker, M. Brookhart, *J. Organomet. Chem.* **1986**, *310*, C39–C41.

[12] a) All SCF calculations were run with the Gaussian 98 package on a cluster of workstations. The total energies E_h and the ZPVE (in Hartrees, in parentheses) were calculated at the B3LYP-level with 6-31G(d,p) basis sets for non-metal atoms and CEP-31G {A} or Wachters {B} basis sets for vanadium: **7**: vertical: −685.757456 (0.140239) {A}, −1558.431046 (0.140252) {B}, horizontal: −685.7539332 (0.139742) {A}, −1558.427663 (0.139547) {B}; **5**: vertical: −1503.172561 (0.345511) {A}, horizontal: −1503.165131 (0.34605) {A}. Gaussian 98 (Revision A.11), M. J. Frisch, G. W. Trucks, H. B. Schlegel, G. E. Scuseria, M. A. Robb, J. R. Cheeseman, V. G. Zakrzewski, J. A. Montgomery, R. E. Stratmann, J. C. Burant, S. Dapprich, J. M. Millam, A. D. Daniels, K. N. Kudin, M. C. Strain, O. Farkas, J. Tomasi, V. Barone, M. Cossi, R. Cammi, B. Mennucci, C. Pomelli, C. Adamo, S. Clifford, J. Ochterski, G. A. Petersson, P. Y. Ayala, Q. Cui, K. Morokuma, D. K. Malick, A. D. Rabuck, K. Raghavachari, J. B. Foresman, J. Cioslowski, J. V. Ortiz, B. B. Stefanov, G. Liu, A. Liashenko, P. Piskorz, I. Komaromi, R. Gomperts, R. L. Martin, D. J. Fox, T. Keith, M. A. Al-Laham, C. Y. Peng, A. Nanayakkara, C. Gonzalez, M. Challacombe, P. M. W. Gill, B. G. Johnson, W. Chen, M. W. Wong, J. L. Andres, M. Head-Gordon, E. S. Replogle, J. A. Pople, Gaussian, Inc., Pittsburgh, PA, **2001**; b) A. J. H. Wachters, *J. Chem. Phys.* **1970**, *52*, 1033–1036; c) A. J. H. Wachters, IBM Tech. Rept. RJ584, **1969**; d) W. Bauschlicher, Jr., S. R. Langhoff, L. A. Barnes, *J. Chem. Phys.* **1989**, *91*, 2399–2411; e) the basis sets were obtained from the Extensible Computational Chemistry Environment Basis Set Database, Version 5/22/02 (developed and

distributed by the Environmental and Molecular Sciences Laboratory, Richland, WA, USA, and funded by the U.S. Department of Energy.

[13] To rationalize the different steric requirements for the horizontally and vertically arranged borylene ligand a "ϕ-ψ" search was performed. In this the dihedral angles H-C-Si-N, C-Si-N-B, and C-Cp_m-V-B were changed in 5° steps over a range of 120° for the former two and 72° for the latter one, and the distances between terminal atoms of different groups, that is Cp, Me, and CO were calculated. For geometries with the smallest interatomic distances the search was repeated in 2° steps over ranges of $\pm 60°$ and $\pm 36°$. The following distances [Å] were determined; vertical: Cp–Me 1.633 (smallest distance), 2.412 (average distance), CO–Me 1.652 (smallest distance), 2.308 (average distance); horizontal: Cp–Me 1.959 (smallest distance), 2.887 (average distance), CO–Me 1.214 (smallest distance), 1.926 (average distance). While Cp–Me distances are comparable and even somewhat larger for the horizontal orientation, the very small CO–Me distances for the latter are evident. Although those results are of qualitative nature, they clearly provide evidence that the horizontal arrangement is sterically less favored.

[14] C. K. Fair, MolEN, An Interactive Intelligent System for Crystal Structure Analysis, Enraf-Nonius, Delft, The Netherlands, **1990**.

[15] G. M. Sheldrick, Program Package SHELXTL, Version 5.1. Bruker Analytical X-ray Systems, Inc., Madison, Wisconsin, USA, **1998**.

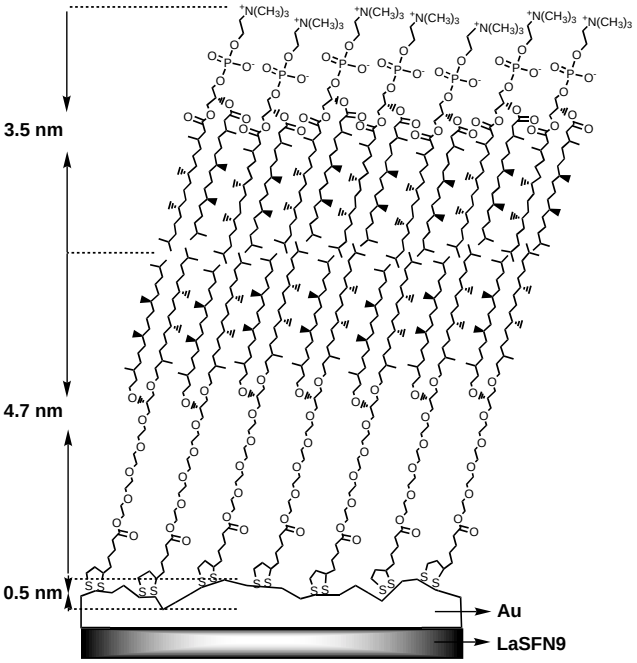


Figure 1. Schematic representation of the arrangement of the DPTL molecules to form the tBLMs. Molecular dimensions are in proportion to the ultrasmooth gold surface to guarantee the perfect alignment of the phytanyl chains in the formation of a dense mono- and bilayer. The tetraethylene glycol chains are assumed to be stretched. LaSFN9 = high-refractive-index glass.

Model Systems for Membranes

Archaea Analogue Thiolipids for Tethered Bilayer Lipid Membranes on Ultrasmooth Gold Surfaces**

Stefan M. Schiller, Renate Naumann, Katherine Lovejoy, Horst Kunz, and Wolfgang Knoll*

Tethered bilayer lipid membranes (tBLMs) mimick the biological cytoplasmic membrane and are promising tools for basic research and biosensor applications. They comprise a lipid group linked to a metal surface, preferably gold, through a thiol-modified tether as spacer unit between the lipid and the gold substrate. The tether/spacer molecules should decouple the membrane from the surface and thus provide a hydrophilic layer (between the membrane and the substrate) with the functional properties of the cytosol/cytoskeleton.[1] They should establish a water-containing submembrane space, which reduces the hydrophobic influence of the metal surface,[2] thus enabling the functional incorporation of membrane proteins.[3]

Moreover, the combination of such ultrathin tBLMs with the robustness of a gold support in a planar configuration allows the application of surface-sensitive techniques, including surface plasmon resonance spectroscopy (SPR), measurements with a quartz-crystal microbalance (QCM), surface-enhanced IR, and electrochemical techniques such as electrochemical impedance spectroscopy (EIS). The metal surface also allows the investigation of surface molecules under a defined electric field, thus extending the scope of experimental conditions significant to the study of field-sensitive processes, for example, ion transport through receptors, channels, and carriers such as valinomycin.

The tBLMs reported so far are supplemented with polar peptide,[4] oligomer,[5] or polymer[6–8] spacers. Poly- or oligomeric tether molecules based on poly- or oligo(ethylene glycol) modified with dialkyl lipids tails have been employed in many cases. However, the capacitance and impedance of these tBLMs were found in the ranges 0.5–0.7 $\mu F\,cm^{-2}$ and 0.01–0.1 $M\Omega\,cm^2$, respectively,[5,6,9,10] insufficient to match the electrical properties of biological membranes. The model

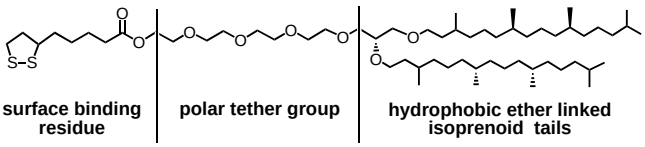
[*] Dipl.-Chem. S. M. Schiller, Dr. R. Naumann, Prof. Dr. W. Knoll
Max-Planck-Institut für Polymerforschung
Ackermannweg 10, 55128 Mainz (Germany)
Fax: (+49) 6131-379-100
E-mail: schiller@mpip-mainz.mpg.de

K. Lovejoy
Department of Chemistry, Northwestern University
Evanston, IL 60208-3113 (USA)

Dipl.-Chem. S. M. Schiller, Prof. Dr. H. Kunz
Institut für Organische Chemie, Universität Mainz
Duesbergweg 10–24, 55128 Mainz (Germany)

[**] We thank Iris Kärcher for skillful technical assistance and Krasimir Vasilev for the preparation of template-stripped gold (TSG). K.L. was a summer student at the MPIP and was supported by the Center for Polymer Interfaces and Macromolecular Assemblies (CPIMA) under NSF grant (DMR-9808677).

 © 2003 Wiley-VCH Verlag GmbH & Co. KGaA, Weinheim 1433-7851/03/4202-0208 $ 20.00+.50/0



system that best reflects the electrical properties of the biomembrane is the bilayer lipid membrane (BLM), which shows capacitance values of around 0.5 μF cm^{-2} and impedance values of $\geq$10 MΩ cm^2.[11,12] tBLMs with good electrical insulation properties were presented by Cornell et al.,[13] who used a multicomponent system consisting of a monophytanoyl spacer lipid together with a transmembrane lipid.

In contrast, the tBLM presented herein is based on a single molecule, the novel archaea analogue 2,3-di-*O*-phytanyl-*sn*-glycerol-1-tetraethylene glycol-D,L-α-lipoic acid ester lipid (DPTL). Phytanyl chains were chosen as hydrophobic tails instead of alkyl chains because of their low phase-transition temperature and their influence on the density and stability of biological membranes.[14] The phase-transition temperature of 2,3-di-*O*-phytanyl-*sn*-glycerol-1-tetraethylene glycol was determined to be <-80 °C by differential scanning calorimetry (DSC). In contrast to the system of Cornell et al.[13] which bears one phytanoyl chain, our system has two phytanyl chains bound to the spacer through a chiral glycerol unit since it is known that a single hydrophobic chain does not guarantee a stable insertion of molecules into a lipid membrane.[15] Furthermore, the 2,3-di-*O*-phytanyl-*sn*-glycerol unit contains only ether linkages to prevent hydrolytic cleaving. This moiety is known to form stable biomembranes under the extreme living conditions (e.g. high temperatures) of extremophiles or archaea.[16] The importance of the ether linkage and the absence of esters and polar phosphatidyl groups to form highly impermeable membranes was experimentally demonstrated by Mathai et al.[17]

According to FTIR spectroscopic studies, the tetraeth−ylene glycol spacer can be considered as an elongated hydrophilic chain (Figure 1), which provides the maximum decoupling distance of the lipid membrane from the substrate. Other oligoethylene glycol (OEG) moieties such as penta- to octa(ethylene glycol) moieties adopt a 7/2 helical structure; the octa(ethylene glycol) appears to have a slightly distorted helical conformation.[18] The synthesis of DPTL is illustrated in Scheme 1.

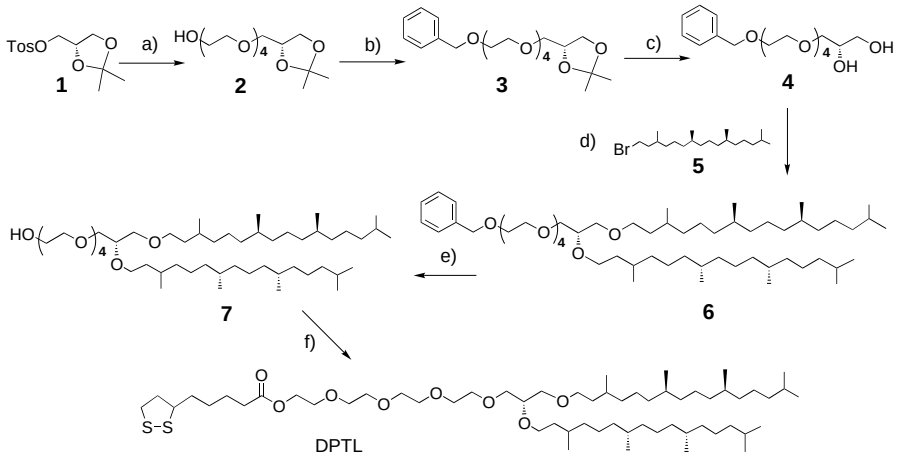
The influence of structure and morphology of the gold substrate on the preparation of self-assembled monolayers (SAMs) is often disregarded. Herein we introduce another key feature, the application of the ultrasmooth surface of template-stripped gold (TSG),[19] to form tBLMs with good insulating properties. Smooth metal surfaces such as that of mercury have been shown to be effective for the formation of tBLMs.[20]

The roughness of TSG was shown to be 0.5 nm over areas of μm^2 by AFM, one order of magnitude smaller than the molecular dimension of the DPTL molecule itself (Figure 1). This ensures the perfect supramolecular alignment of the functional units, resulting in a perfect arrangement of the monolayer. For comparison, the roughness of polycrystalline gold often used for the preparation of SAMs can be as high as 5–10 nm. Au (111), obtained by annealing the gold surfaces, has a roughness of 5 nm over an area of several μm^2 (measured by AFM, not shown). Rough surfaces seem to be a cause of the low impedance values observed in many model membranes.

High resistive tBLMs have been prepared from a SAM of DPTL on the TSG surface. The fusion of liposomes prepared from diphytanoylphosphatidylcholine (DPhyPC) gave rise to the formation of well-defined lipid bilayers as shown by SPR

Table 1: Data obtained by simulations from EIS (capacitance and resistance, Figure 2) and SPR (thickness) measurements. Molecule sizes obtained by modeling calculations with CS Chem3D Pro are added for comparison.

	C_{II} (exp.) [μF cm^{-2}]	R_{II} (exp.) [MΩ cm^2]	d (exp.) [nm]	d (calcd) [nm]
DPTL, monolayer before vesicle spreading	0.55	1.75	4.7	4.7
lipid bilayer after vesicle spreading	0.49	4.35	8.5	8.2
lipid bilayer in KCl (0.1 M) + valinomycin	0.64	0.0022		
lipid bilayer in KCl (0.1 M) + valinomycin after washing with NaCl (0.1 M)	0.61	0.31		



Scheme 1. Synthesis of DPTL: Acetal **1** was synthesized from D-mannitol according to reference [19]. a) Tetra(ethylene glycol) (20 equiv), NaH (2.5 equiv), dioxane, DMAP (cat.), Ar, 45–75 °C, 3 d; b) NaH (2 equiv), BnBr (2.5 equiv), TBAI (cat.), DMF, Ar, 0→20 °C, 2 d, 35% (over steps a) and b)); c) H_2O/THF, Dowex 50WX8, 50 °C, 18 h, 89%; d) NaH (2.1 equiv), **5** (4 equiv, synthesized from phytol according to reference [20]), DMF, Ar, room temperature,4 d, 49%; e) THF, MeOH, H_2, Pd/C (0.3 equiv), room temperature, 30 min, quant.; f) lipoic acid (5 equiv), EDC (6.6 equiv), DMAP (cat.), CH_2Cl_2, Ar, 1 d, 60%. Bn = benzyl, TBAI = tetrabutylammonium iodide, DMF = *N*,*N*-dimethylformamide, EDC = 1-ethyl-3-(3-dimethylaminopropyl)carbodiimide hydrochloride, DMAP = 4-dimethylaminopyridine.

 © 2003 Wiley-VCH Verlag GmbH & Co. KGaA, Weinheim 1433-7851/03/4202-0209 $ 20.00+.50/0

and EIS measurements. We have found only recently that SPR and EIS can be applied simultaneously not only to polycrystalline gold[21] but also to the TSG surface, provided that an optical glue is used for the preparation.[21] Hence this powerful combination of techniques was used to investigate the formation of tBLMs based on the DPTL molecule. Layer thicknesses were calculated from SPR measurements on the basis of a three-layer system of glass, gold, and the lipid layer. For the latter, a refractive index of $n = 1.5$ is assumed and the glue was assumed to have the same refractive index as glass. Results are given in Table 1. The thickness values are in agreement with the dimensions of the molecules, which were modeled with CS Chem 3D Pro (CambridgeSoft Corporation, Version 4.0). The configuration represented in Figure 1 shows a slight tilt angle of the molecular axis and the extended conformation of the OEG spacer. The increase in the thickness of the layer by fusion of the liposomes was monitored in real time by means of SPR spectroscopy and clearly showed saturation within 60 min, which indicates the unrolling of vesicles on a hydrophobic surface to form a lipid bilayer.

The impedance spectra are shown in Figure 2. From these spectra, the capacitance and the resistance of the lipid mono- and bilayer were calculated by fitting the data to the equivalent circuit.[22,24,25] The circuit consists of a RC mesh representing the lipid film, the resistance of the electrolyte solution, and the capacitance of the diffuse double layer adjacent to the gold. The results are given in Table 1. Data measured for the tBLMs varied from 0.45 to 0.8 $\mu F\,cm^{-2}$ for the capacitance and from 2 to 12 $M\Omega\,cm^2$ for the resistance. They thus compare quite well with those of the BLMs.

Also shown in Figure 2 is the effect of valinomycin on the resistance of the tBLM in the presence of potassium ions. Valinomycin is a potassium ionophore antibiotic, produced by *Streptomyces fulvissimus*,[26] which specifically includes potassium ions in its hydrophilic interior, while the hydrophobic exterior enables transmembrane transport of the potassium ions. This gives rise to the so-called inflection point in the EIS spectrum, at which point the resistance drops to the kΩ range (Table 1) and the capacitance of the diffuse double layer evolves to approximately 5 $\mu F\,cm^{-2}$, in agreement with values reported by other authors.[22,24,25]

It is concluded from these experiments that tBLMs can be prepared on SAMs of DPTL simply by vesicle fusion; the molecules are arranged almost perpendicular to the surface, particularly on ultrasmooth gold surfaces. The obtained tBLMs are stable over days and have electrical properties that resemble those of the biological membrane. The tetraethylene glycol spacer allows the formation of a diffuse double layer in the aqueous space between the lipid layer and the substrate, thus mimicking the cytoskeleton.[22,24] The tBLM presented herein can thus be seen as model system for biological membranes.

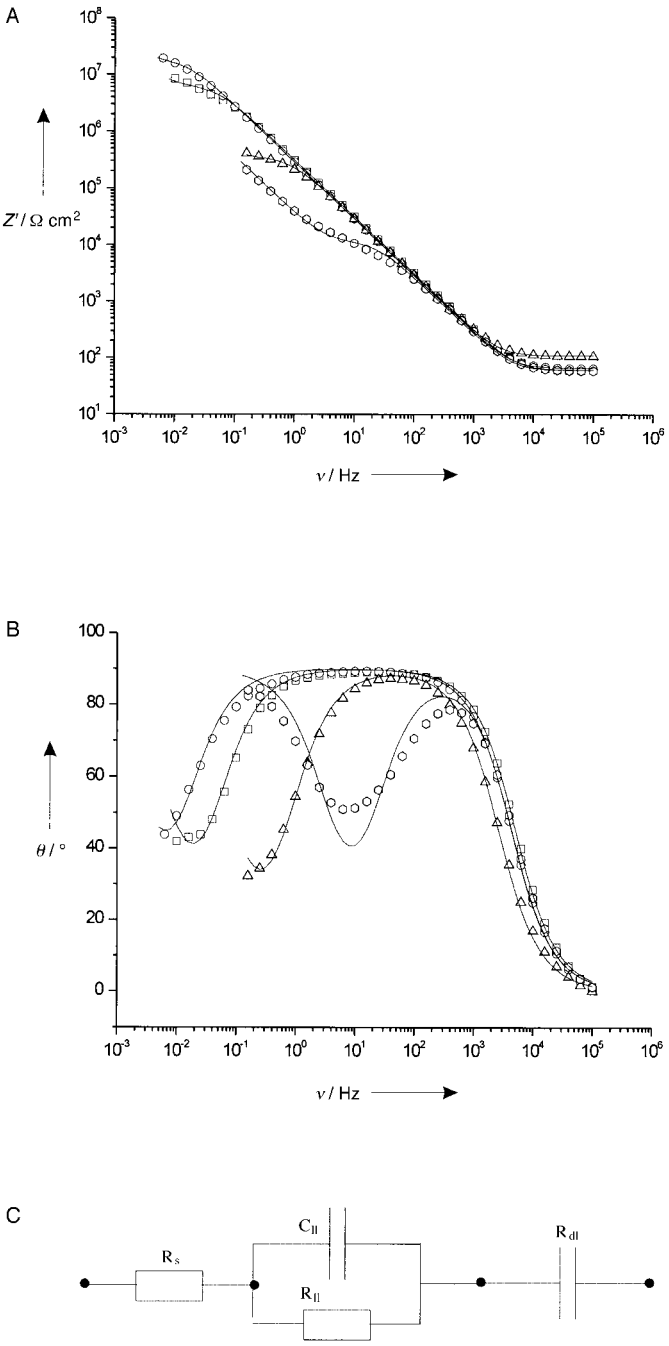


Figure 2. EIS analyses of TSG films coated with DPTL monolayers before (□) and after (○) fusion with DPhyPC liposomes in KCl solution (0.1 mol L^{-1}), the latter after adding valinomycin (0.1 μM) (hexagons), and after washing with NaCl (0.1 mol L^{-1}) (△). The solid lines represent fitted data. A) Z' (real part of the impedance) versus ν (frequency); B) θ (phase shift or phase angle) versus ν (frequency); C) equivalent circuit used for fitting purposes.

Experimental Section

Au(111) surfaces and TSG: 60-nm gold films were deposited by electrothermal evaporation (0.01–0.05 nm s^{-1}, 2×10^{-6} mbar) on freshly cleaved mica sheets. The gold surface was annealed by heating the mica sheets at 650 °C for 45 s to form Au(111). The gold surface was then glued with EPO-TEK 377 (Polytec GmbH, Waldbronn, Germany) to high-refractive-index ($n = 1.7$) glass slides and heated at 150 °C for 60 min. After cooling, these slides were immersed in THF for 30 s to allow the mica sheets to be separated from the gold film, which were then thoroughly rinsed with ethanol.

Formation of SAMs and vesicle fusion: TSG slides were placed for 24 h in an ethanolic solution of DPTL (0.2 mg mL^{-1}), rinsed in

 © 2003 Wiley-VCH Verlag GmbH & Co. KGaA, Weinheim 1433-7851/03/4202-0210 $ 20.00+.50/0

pure ethanol, and dried under a stream of nitrogen. The prepared slides were then mounted in a measuring cell described earlier[23] for simultaneous SPR and EIS experiments. The thickness of the SAMs were measured in a solution of KCl (0.1 mol L^{-1}) before and after the addition of DPhyPC vesicles (DPhyPC supplied from Avanti Polar Lipids, Inc., Alabaster, Al, USA) freshly prepared by extrusion through a 50-nm polycarbonate filter. Fusion of vesicles was carried out at 30 °C at a final concentration of 0.02 mg mL^{-1}. EIS spectra were taken before and after the addition of valinomycin (final concentration $= 4 \times 10^{-6}$ mol L^{-1}). Surface plasmons were excited by a 632.5-nm HeNe laser. EIS measurements were conducted at a bias potential of 0 V vs. Ag/AgCl, saturated NaCl reference electrode and a platinum counter electrode.

Received: August 8, 2002 [Z19921]

[1] E. Sackmann, *Science* **1996**, *271*, 43.
[2] W. J. Miller, N. L. Abbott, *Langmuir* **1997**, *13*, 7106.
[3] R. Naumann, E. K. Schmidt, A. Jonczyk, K. Fendler, B. Kadenbach, T. Liebermann, A. Offenhäusser, W. Knoll, *Biosens. Bioelectron.* **1999**, *14*, 651.
[4] E. K. Schmidt, T. Liebermann, M. Kreiter, A. Jonczyk, R. Naumann, A. Offenhäusser, E. Neumann, A. Kukol, A. Maelicke, W. Knoll, *Biosens. Bioelectron.* **1998**, *13*, 585.
[5] H. Lang, C. Duschl, H. Vogel, *Langmuir* **1994**, *10*, 197.
[6] M. L. Wagner, L. K. Tamm, *Biophys. J.* **2000**, *79*, 1400.
[7] C. Erdelen, L. Häussling, R. Naumann, H. Ringsdorf, H. Wolf, J. Yang, M. Liley, J. Spinke, W. Knoll, *Langmuir* **1994**, *10*, 1246.
[8] J. Spinke, J. Yang, H. Wolf, M. Liley, H. Ringsdorf, W. Knoll, *Biophys. J.* **1992**, *63*, 1667.
[9] S. Heyse, O. P. Ernst, Z. Dienes, K. P. Hofmann, H. Vogel, *Biochemistry* **1998**, *37*, 507.
[10] L. M. Williams, S. D. Evans, T. M. Flynn, A. Marsh, P. F. Knowles, R. J. Bushby, N. Boden, *Langmuir* **1997**, *13*, 751.
[11] G. Wiegand, N. Arribas-Layton, H. Hillebrand, E. Sackmann, P. Wagner, *J. Phys. Chem. B* **2002**, *106*, 4245.
[12] a) R. Guidelli, G. Aloisi, L. Becucci, A. Dolfi, M. R. Moncelli, F. T. Buoninsegni, *J. Electroanal. Chem.* **2001**, *504*, 1; b) W. Knoll, C. W. Frank, C. Heibel, R. Naumann, A. Offenhäuser, J. Rühe, E. K. Schmidt, W. W. Shen, A. Sinner, *Rev. Mol. Biotechnol.* **2000**, *74*, 137; c) E. K. Sinner, W. Knoll, *Curr. Opin. Chem. Biol.* **2001**, *5*, 705.
[13] B. A. Cornell, V. L. B. Braach-Maksvytis, L. G. King, P. D. J. Osman, B. Raguse, L. Wieczorek, R. J. Pace, *Nature* **1997**, *387*, 580.
[14] V. L B. Braach-Maksvytis, B. Raguse, *J. Am. Chem. Soc.* **2000**, *122*, 9544.
[15] R. M. Epand, *Biopolymers* **1997**, *43*, 15.
[16] C. R. Woese, G. E. Fox, *Proc. Natl. Acad. Sci. USA* **1977**, *74*, 5088.
[17] J. C. Mathai, G. D. Sprott, M. L. Zeidel, *J. Biol. Chem.* **2001**, *276*, 27266.
[18] D. J. Vanderah, C. P. Pham, S. K. Springer, V. Silin, C. W. Meuse, *Langmuir* **2000**, *16*, 6527.
[19] W. J. Kerr, G. G. Kirk, D. Middlemiss, *J. Organomet. Chem.* **1996**, *519*, 93.
[20] a) M. Ishiwatari, K. Yamada, R. Ishiwatari, *Chem. Lettl* **2002**, *3*, 206; b) P. G. Schouten, J. F. Van der Pol, J. W. Zwikker, W. Drenth, S. J. Picken, *Mol. Cryst. Liq. Cryst.* **1991**, *195*, 291.
[21] P. Wagner, M. Hegner, H. J. Güntherodt, G. Semenza, *Langmuir* **1995**, *11*, 3867.
[22] C. Peggion, F. Formaggio, C. Toniolo, L. Becucci, M. R. Moncelli, R. Guidelli, *Langmuir* **2001**, *17*, 6585.
[23] N. Bunjes, E. K. Schmidt, A. Jonczyk, F. Rippmann, D. Beyer, H. Ringsdorf, P. Gräber, W. Knoll, R. Naumann, *Langmuir* **1997**, *13*, 6188.
[24] B. Raguse, V. L B. Braach-Maksvytis, B. A. Cornell, L. G. King, P. D. D. Osman, R. J. Pace, L. Wieczorek, *Langmuir* **1998**, *14*, 648.
[25] G. Krishna, J. Schulte, B. A. Cornell, R. Pace, L. Wieczorek, P. D. Osman, *Langmuir* **2001**, *17*, 4858.
[26] H. Neurath, R. L. Hill, *The Proteins, Vol. 5*, Academic Press, New York, **1982**.

 © 2003 Wiley-VCH Verlag GmbH & Co. KGaA, Weinheim 1433-7851/03/4202-0211 $ 20.00+.50/0

Delocalization in Arene Clusters

Multiple Ion Cores in Anthracene Anion Clusters**

*Jae Kyu Song, Nam Ki Lee, and Seong Keun Kim**

Small aromatic hydrocarbons do not generally accommodate an excess electron to form a stable anion, and only transient anions of very short lifetime have been observed with shape resonance.[1] However, the decreasing value of the negative electron affinity with increasing ring size indicates that charge delocalization renders electron attachment to these molecules less prohibitive. For example, electron affinity changes from −1.12 eV for benzene to −0.19 eV for naphthalene.[1] Thus the large molecular framework of anthracene leads to sufficient delocalization of the excess electronic charge to give the molecule a *positive* electron affinity of 0.53 eV,[2] which makes it the smallest unsubstituted aromatic hydrocarbon with a stable valence anion state.

Anthracene has been studied as a prototypical model for a localized charge carrier system in organic molecular crystals over the last several decades.[3] A charge is known to be localized in these systems through a polarization-type interaction between the charge carrier and the local lattice environment. Since anthracene cluster anions can serve as a model for a microscopic charge-injected system, study of such anions will lead to a better understanding of the mechanism of electron localization as well as electron transfer in molecular crystals.

Another goal of this study concerns the elucidation of the ion core structure of aromatic anion clusters, of which little is known so far, in contrast to the case of aromatic cation clusters.[4–8] The cation dimer of benzene was found to form a unique ion core stabilized by what is known as charge resonance.[4–6] A similar case was also found for naphthalene and anthracene dimer cations.[4,7,8] The only sign of charge resonance observed for aromatic anions, however, was in the case of anthracene in bulk glassy solution,[9] where its anion was believed to exist as a dimeric unit.[9,10] Only very recently was the ion core of naphthalene anion clusters directly examined and found to have a monomeric charge core.[11]

In this study, we examined the ion core structure of small anthracene anion clusters, $(An)_n^-$ ($n = 1$–6), in the gas phase and found that $(An)_n^-$ can have monomeric, dimeric, and trimeric ion cores and thus undergoes multiple core switching as the cluster increases in size.

[*] Prof. Dr. S. K. Kim, J. K. Song, N. K. Lee
School of Chemistry
Seoul National University
Seoul 151-747 (Korea)
Fax: (+82) 2-889-5719
E-mail: seongkim@plaza.snu.ac.kr

[**] This work was supported by the National Creative Research Initiatives Program (99-C-CT-01-C-50) of the Ministry of Science and Technology of Korea.

Two typical mass distributions of $(An)_n^-$ clusters obtained under different conditions are shown in Figure 1. Although the overall shapes of the distributions are different, both show a mild intensity anomaly at $n = 5$, which may indicate structural stability resulting from shell closing, as in the case of benzene cluster cations, which have a magic number of $n = 14$.[12] In order to investigate this possibility in more detail, photoelectron spectroscopy and theoretical calculations were carried out for $(An)_n^-$ clusters.

The photoelectron spectra of $(An)_1^-$ obtained at four different photon energies are presented in Figure 2. The photoelectron spectrum obtained at 1064 nm displays a well-resolved structure, with a separation of 0.05 eV (about 400 cm^{-1}), which most likely reflects the totally symmetric ν_{12} vibrational mode (390 cm^{-1}).[2,13] The fourth peak, at 0.715 eV, seems to belong to a different vibrational progression because its intensity is higher than the third peak and its spacing is incommensurate with the other peaks. The energy gap between the fourth peak and the origin is 0.175 eV (1410 cm^{-1}), which probably represents another totally symmetric mode, $\nu_6 = 1408$ cm^{-1}.[13] The electron affinity of An was determined from the position of the origin band to be 0.54 eV, which agrees with the literature value of 0.53 eV.[2]

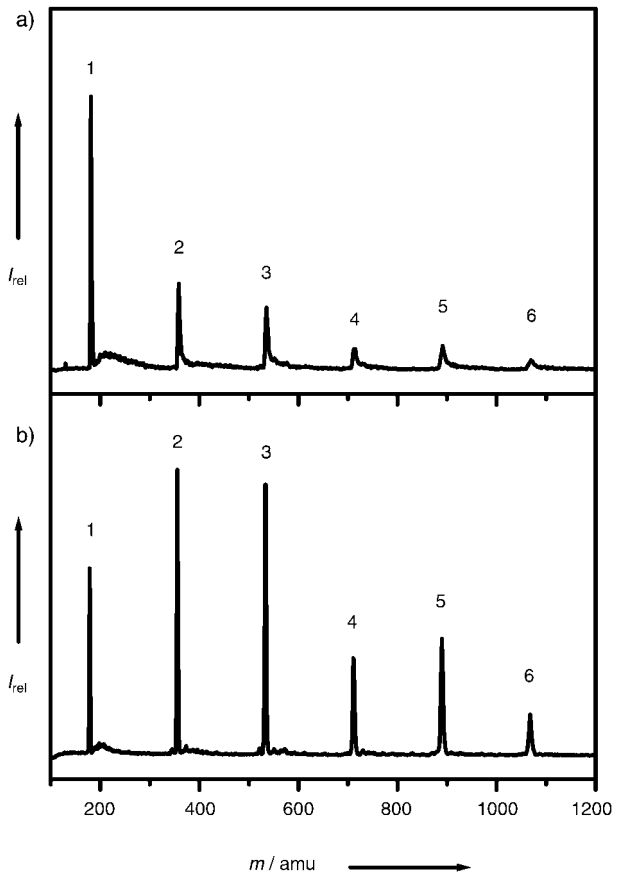


Figure 1. Mass distributions of the anthracene anion clusters, $(An)_n^-$. The spectra were obtained under different conditions chosen to enhance (a) the smaller clusters and (b) the larger ones. Both show the magic number, $n = 5$.

 © 2003 Wiley-VCH Verlag GmbH & Co. KGaA, Weinheim 1433-7851/03/4202-0213 $ 20.00+.50/0

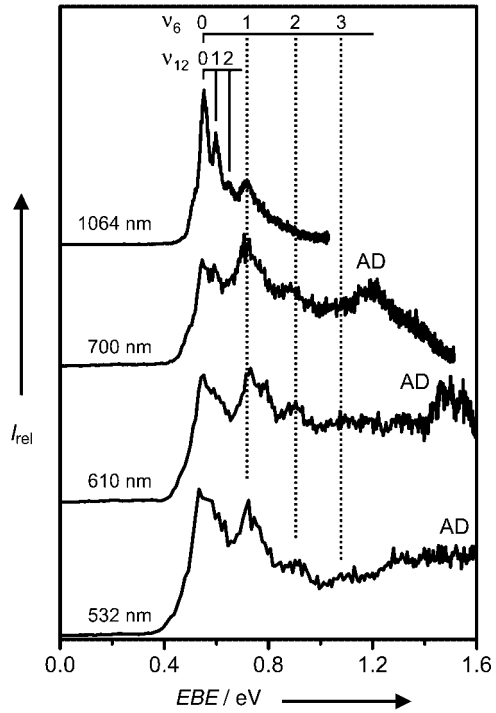


Figure 2. Photoelectron spectra of the anthracene monomer anion, $(An)_1^-$, measured by photodetachment at 1064, 700, 610, and 532 nm. The slow rise beginning near 1.0 eV of the electron binding energy (EBE) in the bottom three spectra is tentatively ascribed to autodetachment from a short-lived excited state of the anthracene anion.

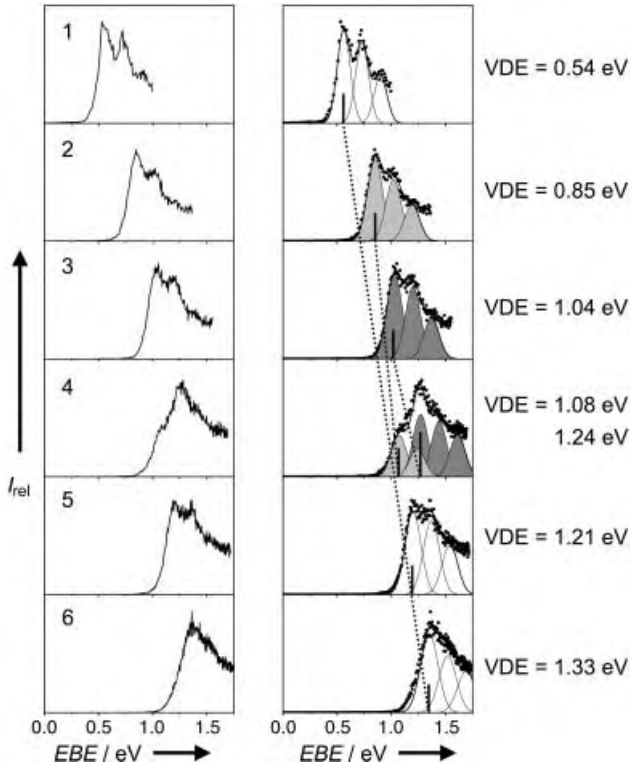


Figure 3. Left: photoelectron spectra of anthracene cluster anions, $(An)_n^-$ ($n=1$–6), measured by photodetachment at 532 nm. Right: deconvolution of the spectra with a set of Gaussian functions with a fixed spacing equal to that of the ν_6 mode. The broad band produced by autodetachment was omitted for clarity. The solid bars denote the vertical detachment energies (VDEs) and the dotted lines connect the VDEs of anions with a common ion core (discussed in the text). The monomeric ion core at $n=1$ is represented by unshaded curves, the dimeric core at $n=2$ by light gray shading, and the trimeric core at $n=3$ by dark gray shading. The spectra are plotted against electron binding energy.

The hump at the rising part of the origin band may be ascribed to a hot band transition.

The photoelectron spectra obtained at other wavelengths display totally different peak shapes. The ν_{12} mode is hardly discernable due to the limited resolution of our photoelectron spectrometer at these electron kinetic energies. Here, the only clearly identifiable vibrational progression is that observed for the ν_6 mode. The slow rise in electron binding energy beginning at 1.0 eV may be the result of autodetachment from a short-lived excited state of the An anion accessible at a photon energy above that at a wavelength of 700 nm.[1,9]

The photoelectron spectra of the entire series of $(An)_n^-$ ($n=1$–6) clusters studied are presented in the left-hand column of Figure 3. It is evident that there is an irregular change of spectral profile at $n=4$. In order to better resolve the spectra, we deconvoluted them with a set of Gaussian peaks with an energy spacing equal to that of the ν_6 mode. The results are shown in the right-hand column of Figure 3 and yield a remarkably good fit over the entire series of $(An)_n^-$ clusters.

At first glance, the seemingly gradual shift of peaks from $n=1$ to $n=3$ appears to indicate a typical solvation effect, whereby each additional solvent molecule around a common central ion stabilizes the ion in a steady, stepwise manner. But, the very anomalous shape of the spectrum at $n=4$ casts strong doubt upon this interpretation. The prospect of the failure of a simple solvation model involving a single common ion core prompted us to carry out theoretical calculations to address the character of the ions that give rise to the spectra in Figure 3. We employed density functional theory (DFT) at the B3LYP/6-31G* level by using the Gaussian 98 program suite.[14] Stable geometries were calculated by using analytical gradients with full geometry optimization. The frequencies of optimized geometries were obtained to make sure that these structures represent stable points on the potential energy surface.

The most stable geometry of the $(An)_2^-$ species was found to be a symmetric parallel-displaced (PD) structure, shown in Figure 4a. According to the charge population analysis, the excess electron is delocalized over the two moieties equally, which means that $(An)_2^-$ is a dimeric ion rather than an ion–solvent complex. It is also worth noting that the difference in VDE values between consecutive spectra in Figure 3 is by far the largest between $n=1$ and $n=2$, and this difference is comparable to the energy gain expected for charge resonance.[4]

The structure of the $(An)_3^-$ cluster was also optimized by a DFT calculation at B3LYP/6-31G*, which yielded the double parallel-displaced (DPD) geometry shown in Figure 4b as its most stable structure. In this geometry, the excess electron is quite evenly delocalized over the three molecules, with a little

 © 2003 Wiley-VCH Verlag GmbH & Co. KGaA, Weinheim 1433-7851/03/4202-0214 $ 20.00+.50/0

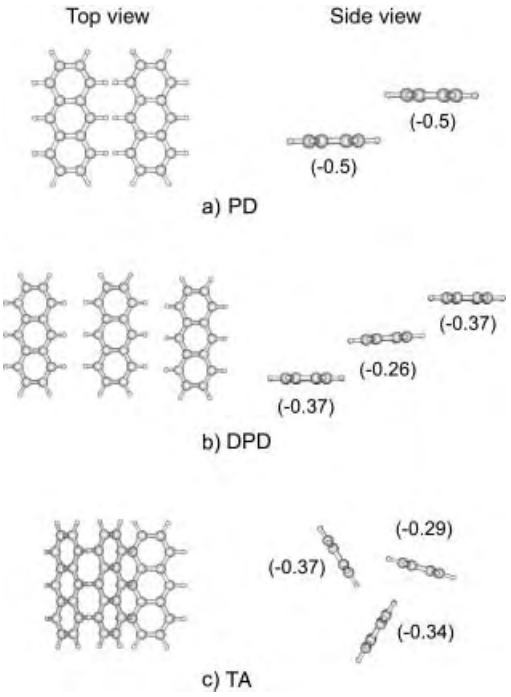


Figure 4. a) The most stable geometry of $(An)_2^-$. b) The most stable geometry of $(An)_3^-$. c) Another low-energy structure for $(An)_3^-$. The numbers in parentheses represent the charge populations on each constituent molecule obtained by Mulliken population analysis.

more charge on the two end moieties than on the middle one. A careful inspection of the geometry also shows that the three molecules are not perfectly parallel; the middle molecule is slightly tilted to face the two end moieties. Another stable geometry for the $(An)_3^-$ species is the triangular (TA) geometry shown in Figure 4c, which is similar to the known stable geometry of aromatic neutral trimers.[15,16] This structure is somewhat asymmetric, unlike neutral trimers, which have a perfect symmetry. The TA geometry is 0.05 eV higher in energy than the DPD structure. The excess electron in the TA geometry is also quite evenly delocalized over the three moieties. In either case, we conclude that $(An)_3^-$ forms a trimeric ion core rather than an ion–solvent complex with a monomeric or dimeric ion core.

The monomeric, dimeric, or trimeric nature of the ion core is indicated by shading in the right-hand column of Figure 3. The seemingly composite nature of the band profile for the $(An)_4^-$ species and the anomalous origin band suggest coexistence of different ion cores, each with their own VDE value. The deconvolution of the photoelectron spectrum with dimeric and trimeric band components gave a surprisingly good fit, which suggests that $(An)_4^-$ exists in two forms: $(An)_2^-$–$(An)_2$ and $(An)_3^-$–$(An)_1$, with a dimeric and a trimeric ion core, respectively. Recently it was reported that two stable geometries of the neutral $(An)_4$ species can also coexist with similar stability.[16] One of these geometries is built on a dimeric unit and the other on a trimeric unit.

In Figure 3, three dotted lines are drawn between anions with a common ion core in an attempt to connect the VDEs on the basis of a solvation model involving multiple ion cores. The VDE of the dimeric $(An)_4^-$ ion is connected to that of $(An)_2^-$ by a line, while the VDE of the trimeric $(An)_4^-$ is connected to that of $(An)_3^-$. The line connecting the VDEs of $(An)_5^-$ and $(An)_6^-$ leads directly to the VDE of $(An)_1^-$, which may imply that these two anions have a monomeric ion core. This result, in addition to the observed magic number of $n=5$, may indicate a shell closure around a monomeric anion core by four solvent molecules, which suggests another core switching from $n=4$ to $n=5$.

In summary, we found monomeric, dimeric, and trimeric anion core structures for the $(An)_n^-$ ($n=1$–6) clusters. Different ion cores have their own characteristic VDE values, which are different from the values anticipated from a simple stepwise solvation model involving a single common ion core. Coexistence of a dimeric and a trimeric anion core was found in $(An)_4^-$. A monomeric ion core structure is restored in $(An)_5^-$, probably because of the enhanced stability that is associated with the completion of a solvation shell with four solvent molecules around the monomeric anion.

Experimental Section

The details of our experimental apparatus have been reported elsewhere.[17,18] The molecular beam was generated by supersonic expansion of An vapor at 170 °C seeded in Ar carrier gas. The anion clusters were first mass selected and then subjected to photoelectron spectroscopy with unfocused laser light at a fluence of 2 mJ pulse^{-1} cm^{-2} to achieve photodetachment but avoid multiphoton effects.[17,19]

Received: June 24, 2002 [Z19597]

[1] P. D. Burrow, J. A. Michejda, K. D. Jordan, *J. Chem. Phys.* **1987**, *86*, 9.
[2] J. Schiedt, R. Weinkauf, *Chem. Phys. Lett.* **1997**, *266*, 201.
[3] E. A. Silinsh, V. Čápek, *Organic Molecular Crystals*, AIP, New York, **1994**.
[4] M. Meot-Ner, *J. Phys. Chem.* **1980**, *84*, 2724.
[5] H. J. Neusser, H. Krause, *Chem. Rev.* **1994**, *94*, 1829.
[6] K. Ohashi, N. Nishi, *J. Chem. Phys.* **1998**, *109*, 3971.
[7] H. Saigusa, E. C. Lim, *J. Phys. Chem.* **1994**, *98*, 13470.
[8] Y. Inokuchi, K. Ohashi, M. Matsumoto, N. Nishi, *J. Phys. Chem.* **1995**, *99*, 3416.
[9] T. Shida, S. Iwata, *J. Chem. Phys.* **1972**, *56*, 2858.
[10] J. McHale, J. Simons, *J. Chem. Phys.* **1980**, *72*, 425.
[11] J. K. Song, S. Y. Han, I. Chu, J. H. Kim, S. K. Kim, S. A. Lyapustina, S. Xu, J. M. Nilles, K. H. Bowen, *J. Chem. Phys.* **2002**, *116*, 4477.
[12] B. Ernstberger, H. Krause, H. J. Neusser, *Ber. Bunsen-Ges.* **1993**, *97*, 884.
[13] W. R. Lambert, P. M. Felker, J. A. Syage, A. H. Zewail, *J. Chem. Phys.* **1984**, *81*, 2195.
[14] Gaussian 98 (Revision A.7), M. J. Frisch, G. W. Trucks, H. B. Schlegel, G. E. Scuseria, M. A. Robb, J. R. Cheeseman, V. G. Zakrzewski, J. A. Montgomery, R. E. Stratmann, J. C. Burant, S. Dapprich, J. M. Millam, A. D. Daniels, K. N. Kudin, M. C. Strain, O. Farkas, J. Tomasi, V. Barone, M. Cossi, R. Cammi, B. Mennucci, C. Pomelli, C. Adamo, S. Clifford, J. Ochterski, G. A. Petersson, P. Y. Ayala, Q. Cui, K. Morokuma, D. K. Malick, A. D. Rabuck, K. Raghavachari, J. B. Foresman, J. Cioslowski, J. V. Ortiz, A. G. Baboul, B. B. Stefanov, G. Liu, A. Liashenko, P. Piskorz, I. Komaromi, R. Gomperts, R. L. Martin, D. J. Fox, T. Keith, M. A. Al-Laham, C. Y. Peng, A. Nanayakkara, C.

Gonzalez, M. Challacombe, P. M. W. Gill, B. G. Johnson, W. Chen, M. W. Wong, J. L. Andres, M. Head-Gordon, E. S. Replogle, J. A. Pople, Gaussian, Inc., Pittsburgh, PA, **1998**.
[15] C. Gonzalez, T. C. Allison, E. C. Lim, *J. Phys. Chem. A* **2001**, *105*, 10583; C. Gonzalez, E. C. Lim, *J. Phys. Chem. A* **1999**, *103*, 1437; C. Gonzalez, E. C. Lim, *Chem. Phys. Lett.* **2002**, *357*, 161.
[16] F. Piuzzi, I. Dimicoli, M. Mons, P. Millié, V. Brenner, Q. Zhao, B. Soep, A. Tramer, *Chem. Phys.* **2002**, *275*, 123.
[17] S. Y. Han, J. K. Song, J. H. Kim, H. B. Oh, S. K. Kim, *J. Chem. Phys.* **1999**, *111*, 4041.
[18] J. K. Song, N. K. Lee, S. K. Kim, *J. Chem. Phys.* **2002**, *117*, 1589.
[19] J. Schiedt, R. Weinkauf, D. M. Neumark, E. W. Schlag, *Chem. Phys.* **1998**, *239*, 511.

Migration/Redistribution

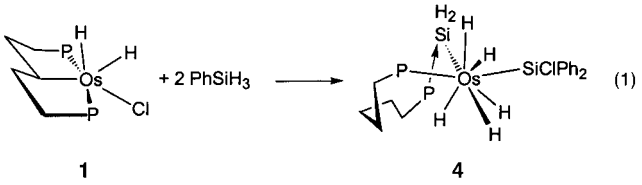
Polyhydrido(silylene)osmium and Silyl(dinitrogen)ruthenium Products Through Redistribution of Phenylsilane with Osmium and Ruthenium Pincer Complexes**

Dmitry G. Gusev, Frédéric-Georges Fontaine, Alan J. Lough, and Davit Zargarian**

Transition-metal silylene complexes, silicon analogues of metal carbenes, are reactive species believed to be important intermediates in the industrial synthesis of chloromethylsilanes,[1] the catalytic oligomerization of hydrosilanes,[2] and the redistribution chemistry of organosilanes.[3] The high reactivity of metal silylenes is related to the electron deficiency of the silicon center, which is presumably due to the very weak π bonding between the silicon atom and the transition metal.[4] Consistent with this notion, in most of the complexes reported to date[5] the silylene moiety requires stabilization from coordinating Lewis bases and/or heteroatom-based substituents (e.g., OR, SR, NR_2),[6] whereas nonstabilized silylene complexes are difficult to isolate.[7]

The tendency of Os and Ru pincer complexes to give coordinatively unsaturated alkylidene and vinylidene products in reactions with alkynes[8a] prompted us to investigate their reactivity towards hydrosilanes with the expectation that addition or 1,2 migration of the Si–H bonds might afford silylene products. Here we describe silylene and silyl complexes obtained from the reaction of $PhSiH_3$ with $[OsH_2Cl\{CH(C_2H_4PtBu_2)_2\}]$ (**1**),[8b] $[OsH_2Cl\{2,6\text{-}(CH_2PtBu_2)_2C_6H_3\}]$ (**2**),[8c] and $[RuHCl\{1,3\text{-}(CH_2PtBu_2)_2\text{-}C_6H_4\}]$ (**3**).[8d]

Addition of 2 equiv of $PhSiH_3$ to **1** in toluene afforded the pentahydrido complex **4** in 83% yield [Eq. (1), P = P*t*Bu$_2$]. A



1 **4** (1)

single-crystal X-ray analysis of **4** showed that the Os center adopts an 8-coordinate, dodecahedral geometry consisting of two orthogonal, trapezoidal planes defined by the atoms Si1,$H1_{Os}$,$H5_{Os}$,P2 and Si2,$H3_{Os}$,$H4_{Os}$,$H2_{Os}$ (Figure 1, left). The Os–Si distances for the silyl (2.374 Å) and the base-stabilized silylene (2.386 Å) ligand are in the normal range for Os–Si single bonds in hydrido(silyl)osmium complexes (3.34 to 2.49 Å).[9] The anticipated uncertainty associated with locating the hydride ligands in the solid-state structure of **4** prompted a study of its structure using ONIOM (DFT/HF) geometry optimization (Figure 1, right);[10] the closeness of the computational and experimental data indicates that the structure of this complex has been established reliably. Solution NMR data are also consistent with the proposed structure for **4** and show that the hydride ligands are highly fluxional. For example, the averaged OsH_5 resonance did not decoalesce down to −100 °C (^{1}H NMR, [D$_8$]toluene) and its

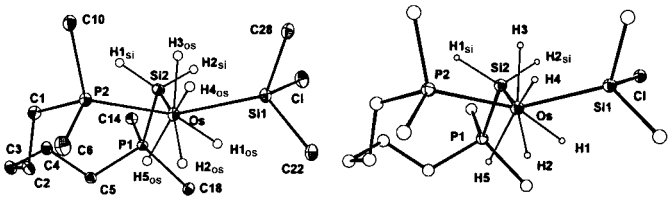


Figure 1. Partial experimental (left) and calculated (right) structures of **4** with the methyl groups and the co-crystallized toluene molecule omitted for clarity. Key experimental parameters [Å, deg]: Os-Si1 2.3739(8), Os-Si2 2.3857(8), Os-P2 2.4044(8), P1-Si2 2.361(1); P1-Si2-Os 120.29(3), P2-Os-Si1 140.63(3), P2-Os-Si2 100.96(3), Si1-Os-Si2 104.84(3), $H1_{Si}$-Si2-$H2_{Si}$ 102.9(19), H_{Si}-Si2-Os (av.) 120.2(14). Calculated parameters [Å, deg]: Os-Si1 2.417, Os-Si2 2.409, Os-P2 2.454, P1-Si2 2.363, Si1···H1 2.071, Si2···H3 2.246, Os-H1–Os-H5 1.638, 1.635, 1.670, 1.642, 1.653; P1-Si2-Os 124.3, P2-Os-Si1 142.2, P2-Os-Si2 99.8, Si1-Os-Si2 101.3, $H1_{Si}$-Si2-$H2_{Si}$ 101.0, H_{Si}-Si2-Os (av.) 120.9, H2···H5 1.883 (the shortest H···H separation).

[*] Prof. D. G. Gusev
Department of Chemistry
Wilfrid Laurier University
Waterloo, ON, N2L3C5 (Canada)
Fax: (+1) 519-746-0677
E-mail: dgoussev@wlu.ca
Dr. A. J. Lough
Department of Chemistry (X-Ray Laboratory)
University of Toronto
Toronto, ON, M5S3H6 (Canada)
Prof. D. Zargarian, F.-G. Fontaine
Département de chimie
Université de Montréal
Montréal, PQ, H3C 3J7 (Canada)
Fax: (+1) 514-343-7586
E-mail: zargarian.davit@umontreal.ca

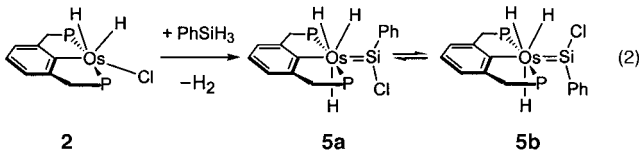
[**] We gratefully acknowledge research funding from NSERC (D.G. and D.Z.), Research Corporation (D.G.), and FCAR (D.Z.). F.-G.F. is grateful to NSERC for PGS(A&B) scholarships.
Supporting information for this article is available on the WWW under http://www.angewandte.org or from the author.

 © 2003 Wiley-VCH Verlag GmbH & Co. KGaA, Weinheim 1433-7851/03/4202-0216 $ 20.00+.50/0

average relaxation time $T1_{min}$ was long (215 ms at −20 °C and 300 MHz), which is typical of polyhydrides with no short H···H contacts.

Evidently, complex **1** and two molecules of $PhSiH_3$ have undergone a series of redistribution reactions culminating in the net hydrogenation of the Os–C bond and the generation of one silyl, one base-stabilized silylene, and five hydride ligands. Complex **4** is the first compound bearing a base-stabilized SiH_2 ligand. We have briefly probed the relative stability of the P→Si interaction in the presence of other Lewis bases. Thus, addition of 1 equiv of NEt_3 to a C_6D_6 solution of **4** reduced the intensities of the ^{31}P resonances attributed to the P nuclei coordinated to the SiH_2 moiety ($\delta =$ 14.5 ppm) and the Os center ($\delta = 56.6$ ppm), and gave rise to two new resonances at $\delta = 27.4$ and 50.3 ppm (conversion ca. 50 %). The chemical shift of one of the new resonances is very close to that of the uncoordinated bis(di-*tert*-butylphosphanyl)pentane ligand ($\delta = 27.7$ ppm in C_6D_6), indicating that this ligand is monodentate in the resulting complex. Similar observations were made when 1 equiv of PCy_3 was reacted with **4**: new ^{31}P resonances emerged at $\delta = 27.5$, 48.9, and −4.9 ppm (conversion ca. 80 %); decoupling experiments have allowed us to assign the latter resonance to the Cy_3P→ SiH_2 moiety. These preliminary observations demonstrate that good Lewis bases can displace the $PtBu_2$ group, thereby generating new donor-stabilized SiH_2 complexes.

To better understand the influence of the ligand on the reactivity of **1,** we investigated the reaction of $PhSiH_3$ with complex **2,** a direct analogue of **1** that has a pincer ligand with a more rigid backbone. In this case, the trihydrido(silylene) product **5** was obtained in 60 % yield [Eq. (2), $P = PtBu_2$].



(2)

Complex **5** undergoes a slow decomposition at room temperature, both in the solid and in solution, as evident from a gradual color change from yellow to dark brown. The thermal instability of **5** prevented crystallographic characterization, but NMR spectra collected at low temperature using samples prepared at −70 °C established the identity of the product as a trihydrido(silylene) complex that exists as two rotamers in solution, as described below. In addition, a computational study using the ONIOM (DFT/HF) methodology supported the structural assignments for both isomers (the optimized structure of **5a** is shown in Figure 2).

The $^{31}P\{^1H\}$ NMR spectrum of the isolated solid showed a single resonance ($\delta = 85.7$ ppm), whereas the $^{29}Si\{^1H\}$ NMR spectrum showed two triplets (6:1 signal intensity ratio) in a chemical shift region characteristic of silylenes ($\delta = 239.3$ (**5a**) and 246.5 ppm (**5b**), $^2J_{PSi} = 9.4$ Hz). Two sets of resonances were also observed in the hydride region of the ^1H NMR spectrum (1:2 intensity ratio within each set), implying two different trihydrido substructures. We interpret these observations to indicate that **5** is a silylene complex with a plane of symmetry that renders the two phosphorus nuclei equivalent; the rotation of the silylene moiety about the Os–Si bond gives rise to two rotamers, which were assigned the structures **5a** and **5b** on the basis of the difference NOE spectra. For example, isomer **5a** showed a strong NOE between the SiPh and the H2/H3 signals, whereas no NOE was detected between the signals for the *ortho* hydrogen atoms of SiPh and H1 (numbering according to Figure 2). In contrast, a strong NOE was detected in isomer **5b** between the *ortho* hydrogen atoms of SiPh and H1. The NOE experiments also indicated a slow exchange at −70 °C between **5a** and **5b**: irradiation of the H1 resonance of one isomer resulted in a partial saturation transfer to the corresponding hydride resonance of the other. Integration of the hydride signals allowed us to determine that the **5b**/**5a** equilibrium has a small ΔG (−0.7 kcal mol^{-1}); consistent with this, the computational study showed a very small energy difference (−0.01 kcal mol^{-1}) between the two isomers.

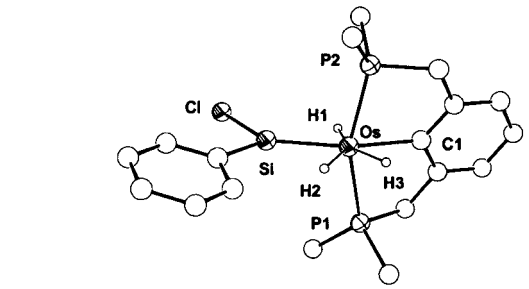
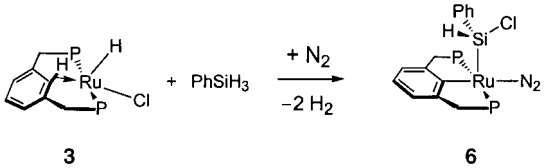


Figure 2. Partial calculated structure of **5a** with the methyl groups omitted for clarity. Key parameters [Å, deg]: Os-Si 2.281, Os-C1 2.171, Os-P1 2.387, Os-P2 2.394, Os-H1 1.670, Os-H2 1.641, Os-H3 1.651, H2···H3 1.652; P1-Os-P2 157.3, Si-Os-C1 161.9, Si-Os-H1 82.4, Si-Os-H2 63.9, C1-Os-H1 79.9, C1-Os-H3 74.3, H2-Os-H3 60.2.

The different reactivities of **1** and **2** underline the importance of the auxiliary ligand in determining the course and outcome of the reaction with $PhSiH_3$. We have also probed the importance of the metal atom by reacting $PhSiH_3$ with **3**, the Ru analogue of **2** that displays an agostic interaction between the central C–H moiety and the Ru center. This reaction gave the dinitrogen(silyl) complex **6** in 75 % yield [Eq. (3), $P = PtBu_2$]. The identity of **6** was



(3)

established by spectroscopic studies and X-ray crystallography (Figure 3), as described below.

The IR spectrum of complex **6** features strong N≡N and Si–H stretches at 2142 and 2105 cm^{-1}, respectively. The presence of the Si–H group was also evident from the NMR spectra, which showed a ^1H signal ($\delta = 5.37$ ppm, d, $^3J_{PH} =$

 © 2003 Wiley-VCH Verlag GmbH & Co. KGaA, Weinheim 1433-7851/03/4202-0217 $ 20.00+.50/0

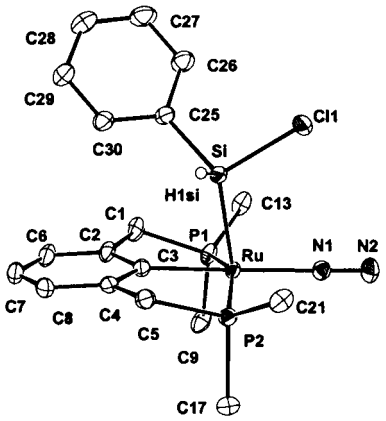


Figure 3. Partial experimental structures of **6** with the methyl groups omitted for clarity. Key parameters [Å, deg]: Ru-C3 2.068(3), Ru-Si 2.2821(7), Ru-N1 2.014(2), Ru-P1 2.3512(7), Ru-P2 2.3632(7), N1-N2 1.099(3); P1-Ru-P2 157.35(3), C3-Ru-Si 78.23(7), C3-Ru-N1 178.5(1), Si-Ru-N1 100.33(7).

17.7 Hz) featuring the anticipated Si satellites ($^1J_{SiH} = 206$ Hz) and a $^{29}Si\{^1H\}$ signal with the appropriate multiplicity ($\delta =$ 31.5 ppm, t, $^2J_{PSi} = 24$ Hz). The asymmetric nature of this silyl ligand renders the CH_2 and P*t*Bu$_2$ groups inequivalent in the NMR spectra of **6**. According to the X-ray data, the geometry around Ru in **6** is square-pyramidal with the silyl ligand occupying the apical position; the absence of a ligand *trans* to the silyl moiety is presumably responsible for the very short Ru–Si bond (2.282 Å). The Ru–N (2.014 Å) and N≡N (1.099 Å) distances are similar to the corresponding distances in related neutral dinitrogen complexes: [RuH(N$_2$)-{CH(C$_2$H$_4$P*t*Bu$_2$)$_2$}] (1.965/1.117 Å),[11a] [RuH$_2$(N$_2$){κ^3(*P,P,P*)-PhP(C$_3$H$_6$PCy$_2$)$_2$}] (2.005/1.093 Å),[11b] and [(PPh$_3$)$_2$RuH-(μ-H$_3$)Ru(N$_2$)(PPh$_3$)$_2$] (2.003/1.086 Å).[11c]

A comparison of the reactivities observed for complexes **2** and **3** provides some insight into the mechanism of their reactions with PhSiH$_3$. The following sequence of steps can be envisaged: 1) addition of PhSiH$_3$ to **2**/**3** generates the initial silyl ligand PhSiH$_2$ and releases H$_2$; 2) a redistributive SiH/MCl exchange gives the 16-electron intermediate [(PCP-ligand)MH$_2$(PhSi(H)Cl)]; 3) the Os^{IV} intermediate undergoes a 1,2 migration of SiH to give the trihydrido(silylene) complex **5**, whereas its Ru counterpart loses H$_2$ to give the dinitrogen(silyl) complex **6**. The difference in the reactivities of **2** and **3** is presumably due to the weaker Ru–H bonds (compared to Os–H bonds) and the prevalence of the +2 oxidation state in the chemistry of Ru complexes stabilized by phosphanes.

In summary, the described reactions of PhSiH$_3$ with complexes **1**–**3** have provided an opportunity to study the direct and unassisted conversion of a hydrosilane to transition-metal silylene derivatives, a transformation believed to be important in many catalytic processes involving organosilicon compounds.[12] The spontaneous silyl-to-silylene conversions observed here are rather rare, though they can be induced by photolysis[13] or assisted by Lewis acids.[14] On the other hand, silylene formation by Si–SiR$_3$ migrations has been observed with Rh^I,[15] Ir^I,[16] and Ni^{II}[17] systems. The transformations with the Os complex **1** are even more interesting, since they involve complex redistribution reactions that convert two molecules of PhSiH$_3$ to the silyl ligand Ph$_2$SiCl and the unprecedented parent silylene moiety SiH$_2$.

Experimental Section

Spectroscopic data for compounds **4**–**6** are given below; all other information pertaining to the synthetic and computational work is provided in the Supporting Information. Complete crystallographic data for the structural analyses have been deposited with the Cambridge Crystallographic Data Centre. CCDC-190307 (**4**) and CCDC-190308 (**6**) contain the supplementary crystallographic data for this paper. These data can be obtained free of charge via www.ccdc.cam.ac.uk/conts/retrieving.html (or from the Cambridge Crystallographic Data Centre, 12, Union Road, Cambridge CB21EZ, UK; fax: (+44) 1223-336-033; or deposit@ccdc.cam.ac.uk).

Complex **4**: elemental analysis calcd for $C_{33}H_{63}ClOsP_2Si_2$·toluene (895.811): C 53.63, H 7.99; found: C 53.61, H 8.40. IR (Nujol): $\tilde{\nu}$ (ν_{SiH}, ν_{OsH}) = 2079, 2066, 2001, 1913 cm^{-1}. NMR (20 °C, C_6D_6, *J* in Hz): ^1H NMR: $\delta = -9.70$ (ddt, $^2J_{HP} = 5.9$, $^3J_{HP} = 8.1$, $^3J_{HH} = 1.6$, 5H, OsH$_5$), 1.00 (d, $^3J_{HP} = 12.9$, 18H, CH$_3$), 1.16 (d, $^3J_{HP} = 12.3$, 18H, CH$_3$), 1.1–1.8 (m, 10H, CH$_2$), 4.74 (dd, $^2J_{HP} = 19.0$, $^3J_{HP} = 3.0$, $^1J_{HSi} = 179.3$, SiH$_2$), 7.12, 7.30, 8.34 ppm (m, 10H, Ph). $^{13}C\{^1H\}$ NMR: $\delta = 14.0$ (d, $J_{CP} =$ 21.7, CH$_2$), 20.3 (s, CH$_2$), 21.0 (d, $J_{CP} = 17.7$, CH$_2$), 22.9 (d, $J_{CP} = 1.6$, CH$_2$), 29.6 (dd, $J_{CP} = 8.5$, 10.2, CH$_2$), 29.4 (s, CH$_3$), 30.0 (s, CH$_3$), 34.6 (d, $J_{CP} = 17.1$, PC), 35.3 (d, $J_{CP} = 20.7$, PC), 127.0 (s, CH), 127.5 (s, CH), 135.4 (s, CH), 151.5 ppm (d, $J_{CP} = 2.7$, C). $^{31}P\{^1H\}$ NMR: $\delta = 56.6$ ($^2J_{PSi} = 27.8$), 14.5 ppm ($^1J_{PSi} = 44.6$). $^{29}Si\{^1H\}$ NMR: $\delta = 30.4$ (dd, $^3J_{SiP} = 2.8$, $^2J_{SiP} = 27.8$), −67.4 ppm (dd, $^2J_{SiP} = 5.5$, $^1J_{SiP} = 44.7$).

Complex **5**: IR (Nujol): $\tilde{\nu}$ (ν_{OsH}) = 2177, 2089, 1870 cm^{-1}. NMR (−70 °C, [D$_8$]toluene, *J* in Hz): ^1H NMR: $\delta = -7.50$ (**5a**), −7.34 (**5b**) (br, 2H, OsH$_2$), −6.98 (**5b**) (t, $^2J_{HP} = 11.4$, OsH), −6.33 ppm (**5a**) (t, $^2J_{HP} = 13.8$, OsH). $^1H\{^{31}P\}$ NMR: $\delta = 1.01$ (s, 18H, CH$_3$), 1.18 (s, 18H, CH$_3$), 3.24 (d, $^2J_{HH} = 15.9$, 2H, CH$_2$), 3.41 (d, $^2J_{HH} = 15.9$, 2H, CH$_2$), 7.0–7.3 (m, 6H, Ar), 8.66 ppm (d, $^2J_{HP} = 7.5$, 2H, Ph). $^{31}P\{^1H\}$ NMR: $\delta = 85.7$ ppm (s). $^{13}C\{^1H\}$ NMR: $\delta = 29.2$ (br, CH$_3$), 34.0 (vt, $^vJ = 10.5$, PC), 35.9 (vt, $^vJ = 12.0$, PC), 42.8 (vt, $^vJ = 14.8$, CH$_2$), 120.0 (vt, $^vJ =$ 7.8, CH, Ar), 123.3 (s, CH, Ar), 132.4 (s, CH, Ph), 128.8 (s, CH, Ph), 135.2 (s, CH, Ph), 149.3 (vt, $^vJ = 8.5$, C, Ar), 149.9 (s, C, Ph), 155.2 ppm (t, $^2J_{CP} = 3.7$, RuC). $^{29}Si\{^1H\}$ NMR: $\delta = 239.3$ (**5a**), 246.5 ppm (**5b**) (t, $^2J_{SiP} = 9.4$).

Complex **6**: elemental analysis calcd for $C_{30}H_{49}ClN_2P_2RuSi$ (664.29): C 54.24, H 7.43, N 4.22; found: C 53.90, H 7.64, N 4.02. IR (Nujol): $\tilde{\nu} = 2142$ ($\nu_{N\equiv N}$), 2105 cm^{-1} (ν_{SiH}). NMR ([D$_8$]toluene, *J* in Hz): ^1H NMR: $\delta = 5.37$ ppm (d, $^3J_{HP} = 17.7$, $^1J_{HSi} = 206$, SiH). $^1H\{^{31}P\}$ NMR: $\delta = 0.90$, 0.94, 1.20, 1.42 (s, 36H, CH$_3$), 2.56 (d, $^2J_{HH} = 16.4$, 1H, CH$_2$), 2.78 (d, $^2J_{HH} = 16.4$, 1H, CH$_2$), 3.09 (d, $^2J_{HH} = 16.7$, 1H, CH$_2$), 3.73 (d, $^2J_{HH} = 16.7$, 1H, CH$_2$), 6.9–7.1 ppm (m, 8H, Ar). $^{31}P\{^1H\}$ NMR: $\delta = 74.8$, 80.7 ppm (d, $^2J_{PP} = 217$). $^{13}C\{^1H\}$ NMR: $\delta = 30.5$, 30.6, 32.1, 32.9 (d, CH$_3$), 35.3 (d, $^1J_{CP} = 21.9$, CH$_2$), 36.3 (d, $^1J_{CP} = 19.3$, CH$_2$), 35.0, 36.6, 37.5, 38.1 (d, PC), 121.9 (d, $^3J_{CP} = 17.0$, CH, Ar), 122.5 (d, $^3J_{CP} = 16.7$, CH, Ar), 124.2 (s, CH, Ar), 126.5, 127.8, 135.6 (s, CH, Ph), 144.6 (d, $^3J_{CP} = 2.3$, SiC, Ph), 156.0 (m, C, Ar), 178.1 ppm (t, $^2J_{CP} = 2.9$, RuC). $^{29}Si\{^1H\}$ NMR: $\delta = 31.5$ ppm (t, $^2J_{SiP} = 24$).

Received: July 25, 2002 [Z19819]

[1] For details on the preparation of chloromethylsilanes from elemental silicon and chloromethane, the so-called Direct Process, see: a) M. P. Clarke, *J. Organomet. Chem.* **1989**, *376*, 165; b) M. P. Clarke, *J. Organomet. Chem.* **1991**, *408*, 149; c) for information on the reactivities of silylenes with chloroalkanes in solution see: P. W. Wanandi, P. B. Glaser, T. D. Tilley, *J. Am. Chem. Soc.* **2000**, *122*, 972.

 © 2003 Wiley-VCH Verlag GmbH & Co. KGaA, Weinheim 1433-7851/03/4202-0218 $ 20.00+.50/0

[2] a) K. A. Brown-Wensley, *Organometallics* **1987**, *6*, 1590; b) E. A. Zarate, C. Tessier-Youngs, W. J. Youngs, *J. Am. Chem. Soc.* **1988**, *110*, 4068.
[3] H. Yamashita, M. Tanaka, M. Goto, *Organometallics* **1992**, *11*, 3227.
[4] H. Jacobsen, T. Ziegler, *Organometallics* **1995**, *14*, 224, and references therein.
[5] The first transition-metal silylene complexes were reported by the groups of Tilley and Zybill: a) D. A. Straus, T. D. Tilley, A. L. Rheingold, S. J. Geib, *J. Am. Chem. Soc.* **1987**, *109*, 5872; b) C. Zybill, G. Müller, *Angew. Chem.* **1987**, *99*, 683; *Angew. Chem. Int. Ed. Engl.* **1987**, *26*, 669.
[6] For reviews on transition-metal silylene complexes see: a) C. Zybill, *Top. Curr. Chem.* **1991**, *160*, 1; b) C. Zybill, H. Handwerker, H. Friedrich, *Adv. Organomet. Chem.* **1994**, *36*, 229.
[7] a) J. D. Feldman, G. P. Mitchell, J.-O. Nolte, T. D. Tilley, *J. Am. Chem. Soc.* **1998**, *120*, 11184; b) S. K. Grumbine, T. D. Tilley, F. P. Arnold, A. L. Rheingold, *J. Am. Chem. Soc.* **1994**, *116*, 5495.
[8] a) D. G. Gusev, T. Maxwell, F. M. Dolgushin, M. Lyssenko, A. J. Lough, *Organometallics* **2002**, *21*, 1095; b) D. G. Gusev, A. J. Lough, *Organometallics* **2002**, *21*, 2601; c) D. G. Gusev, F. M. Dolgushin, M. Y. Antipin, *Organometallics* **2001**, *20*, 1001; d) D. G. Gusev, M. Madott, F. M. Dolgushin, K. A. Lyssenko, M. Y. Antipin, *Organometallics* **2000**, *19*, 1734.
[9] a) C. E. F. Rickard, W. R. Roper, S. D. Woodgate, L. J. Wright, *J. Organomet. Chem.* **2000**, *609*, 177; b) G. R. Clark, K. R. Flower, C. E. F. Rickard, W. R. Roper, D. M. Salter, L. J. Wright, *J. Organomet. Chem.* **1993**, *462*, 331; c) M. L. Buil, P. Espinet, M. A. Esteruelas, F. J. Lahoz, A. Lledos, J. M. Martinez-Ilarduya, F. Maseras, J. Modrego, E. Onate, L. A. Oro, E. Sola, C. Valero, *Inorg. Chem.* **1996**, *35*, 1250.
[10] a) The computational studies were performed on a 2.2 GHz Pentium IV PC using Gaussian 98 (Revision A.11), M. J. Frisch, G. W. Trucks, H. B. Schlegel, G. E. Scuseria, M. A. Robb, J. R. Cheeseman, V. G. Zakrzewski, J. A. Montgomery, R. E. Stratmann, J. C. Burant, S. Dapprich, J. M. Millam, A. D. Daniels, K. N. Kudin, M. C. Strain, O. Farkas, J. Tomasi, V. Barone, M. Cossi, R. Cammi, B. Mennucci, C. Pomelli, C. Adamo, S. Clifford, J. Ochterski, G. A. Petersson, P. Y. Ayala, Q. Cui, K. Morokuma, D. K. Malick, A. D. Rabuck, K. Raghavachari, J. B. Foresman, J. Cioslowski, J. V. Ortiz, B. B. Stefanov, G. Liu, A. Liashenko, P. Piskorz, I. Komaromi, R. Gomperts, R. L. Martin, D. J. Fox, T. Keith, M. A. Al-Laham, C. Y. Peng, A. Nanayakkara, C. Gonzalez, M. Challacombe, P. M. W. Gill, B. G. Johnson, W. Chen, M. W. Wong, J. L. Andres, M. Head-Gordon, E. S. Replogle, J. A. Pople, Gaussian, Inc., Pittsburgh, PA, **1998**. The geometry optimizations were carried out using the ONIOM(B3PW91:HF/LANL2MB) method[10b], and the nature of the stationary points as a minimum of energy was verified in frequency calculations. For the optimized structures of **4**, **5a**, and **5b** only real frequencies are obtained. b) M. Svensson, S. Humbel, R. D. J. Froese, T. Matsubara, S. Sieber, K. Morokuma, *J. Phys. Chem.* **1996**, *100*, 19357; F. Maseras, *Chem. Commun.* **2000**, 1821.
[11] a) D. G. Gusev, A. J. Lough, *Organometallics* **2002**, *21*, 5019; b) G. Jia, D. W. Meek, J. C. Gallicci, *Inorg. Chem.* **1991**, *30*, 403; c) B. Chaudret, J. Devillers, R. Poilblanc, *Organometallics* **1985**, *4*, 1727.
[12] a) M. D. Curtis, P. S. Epstein, *Adv. Organomet. Chem.* **1981**, *19*, 213; b) T. D. Tilley in *The Chemistry of Organic Silicon Compounds* (Eds.: S. Patai, Z. Rappaport), Wiley, New York, **1989**, Chap. 24, p. 1415; c) T. D. Tilley, *Comments Inorg. Chem.* **1990**, *10*, 37; d) T. D. Tilley in *The Silicon–Heteroatom Bond* (Eds.: S. Patai, Z. Rappaport), Wiley, New York, **1991**, Chap. 9 and 10, pp. 245 and 309; e) K. H. Pannel, H. L. Sharma, *Chem. Rev.* **1995**, *95*, 1351.
[13] R. J. P. Corriu, G. F. Lanneau, B. P. Chauhan, *Organometallics* **1993**, *12*, 2001.
[14] a) G. P. Mitchell, T. D. Tilley, *J. Am. Chem. Soc.* **1998**, *120*, 7635; b) G. P. Mitchell, T. D. Tilley, *Angew. Chem.* **1998**, *110*, 2602; *Angew. Chem. Int. Ed.* **1998**, *37*, 2524; c) J. C. Peters, J. D. Feldman, T. D. Tilley, *J. Am. Chem. Soc.* **1999**, *121*, 9871.
[15] G. P. Mitchell, T. D. Tilley, *Organometallics* **1996**, *15*, 3477.
[16] G. P. Mitchell, T. D. Tilley, G. P. A. Yap, A. L. Rheingold, *Organometallics* **1995**, *14*, 5472.
[17] S. Nlate, E. Herdtweck, R. A. Fischer, *Angew. Chem.* **1996**, *108*, 1957; *Angew. Chem. Int. Ed. Engl.* **1996**, *35*, 1861.

Asbestos Decontamination

Soil Fungal Hyphae Bind and Attack Asbestos Fibers**

Elena Martino, Laura Prandi, Ivana Fenoglio, Paola Bonfante, Silvia Perotto, and Bice Fubini**

Once a major issue in occupational health and safety, asbestos has now become a general environmental problem.[1] Several mountain areas—from the western Alps in Italy to the Sierra Nevada in the USA—are rich in asbestos and asbestiform minerals, and many defunct asbestos industries and mines have left substantial amounts of asbestos fibers on the abandoned sites. Exposure to airborne asbestos fibrils causes a severe pneumoconiosis (asbestosis) and malignancies such as bronchogenic carcinoma and pleural mesothelioma.[2–4] The decontamination of asbestos fibers dispersed over wide areas of soil and in waters obviously requires a different approach from what was proposed for asbestos localized in buildings.[5] The fibers cannot be removed but have to be inactivated in situ without damaging the environment. New, environmentally friendly techniques are thus required for

[*] Prof. Dr. S. Perotto, Dr. E. Martino,[+] Prof. Dr. P. Bonfante
Interdepartmental Center "G. Scansetti" for Studies on Asbestos and Other Toxic Particulates
University of Torino, Dipartimento Biologia Vegetale
via le Mattioli 25, 10125 Torino (Italy)
Fax: (+39) 11-670-7459
E-mail: silvia.perotto@unito.it
Prof. Dr. B. Fubini, Dr. L. Prandi,[+] Dr. I. Fenoglio
Interdepartmental Center "G. Scansetti" for Studies on Asbestos and Other Toxic Particulates
University of Torino, Dipartimento di Chimica IFM
via P. Giuria 7, 10125 Torino (Italy)
Fax: (+39) 11-670-7566
E-mail: bice.fubini@unito.it
[+] E.M. and L.P. contributed equally to the work.
[**] The research was funded in part by CNR, Finalized Project on Biotechnology (Subproject 2) and by Regione Piemonte, Italy.
Supporting information for this article is available on the WWW under http://www.angewandte.org or from the author.

application to a vast territory, whereby the physicochemical properties of the fibers are modified to shut down the pathogenic mechanism.

Iron is known to contribute to asbestos toxicity, and its removal reduces in vitro cell damage caused by asbestos fibers.[2,6] Thus, if iron could be continuously extracted by means of a "natural" process from the fibers dispersed in the environment, consequent modifications at the surface of the fibers could result in a decrease in their carcinogenic potential or even in a full inactivation of the asbestos fibers dispersed in the soil.

Several soil microorganisms are capable of scavenging iron for their own metabolism from recalcitrant substrates[7] by releasing, in the surrounding soil environment, potent chelators with different metal specificity (for example, polycarboxylic acids and other siderophores). Some ericoid mycorrhizal fungi, which are able to colonize roots symbiotically, have been reported to produce several hydroxamate siderophores known to form very stable complexes with iron(III) ions.[8] Fungi are of particular interest because they can extend through extensive volumes of soil thanks to their hyphal structures. We thus investigated the ability of some soil fungi to grow in the presence of crocidolite (fibrous riebeckite or blue asbestos) fibers, release iron chelators that modify the surface of the fibers at the atomic level, and reduce the potential of the generation of free radicals. A number of fungi with different trophic characteristics were selected because of their ability to grow on silicates, produce siderophores, and tolerate different metals.

Crocidolite, one of the most potent fibrous carcinogens and the most studied form of asbestos,[5] contains up to 29% iron in both oxidation states (Fe^{II}, Fe^{III}) in its crystal structure. When at the surface in a low oxidation state, iron ions are highly reactive centers, at which the generation of free radicals,[6,9–11] redox cycling of iron,[12] and coordination of electron-donor molecules[13] may take place. Iron is mobilized from crocidolite by various chelators[14,15] with loss of the potential to generate radicals[16,17] and damage DNA.[6a,18] None of the fungi tested was inhibited in biomass production when grown in liquid culture (9.2 mg mL^{-1} in Czapek glucose medium) when the crocidolite fibers were either in direct contact or in a chamber separated from the fibers by a dialysis membrane. Conversely, crocidolite induced a significant growth increase (>65%) in *Geomyces pannorum* and in three strains of *Oidiodendron maius* (Zn, Cd, and A). In liquid mycelial cultures, crocidolite fibers and fibrils were visibly removed from the suspension in the aqueous phase and tightly bound to the fungal hyphae, so that the supernatant was progressively cleared (Figure 1). At the ultrastructural level the fibrils appear to be in intimate contact with the fungus (Figure 2). After growth of the fungal mycelia with crocidolite (42 days) the culture supernatant contained variable amounts of iron ions. A few fungi (*G. vinaceous*, *O. maius* strains Zn, A, Cd) did not extract iron from asbestos, but the majority of species (*G. pannorum*, *Mortierella hyalina*, sterile mycelium MUT840, *O. griseum*, and *F. oxysporum*) induced the removal of substantial amounts of iron. Of these, *Fusarium oxysporum*, *M. hyalina*, and *O. maius* E were the most active in terms of moles of iron released per gram of fungal biomass (Figure 3). Note that, in the absence of fungi, crocidolite fibers did not release any detectable iron in the medium.



Figure 1. Effects of fungal mycelium on a suspension of asbestos. Fine asbestos fibers (1.5–4 μm mean diameter) form a turbid suspension when dispersed in the Czapek glucose medium (left). When the fungal mycelium, here the sterile mycelium strain MUT840, was grown in the medium containing asbestos fibers, it removed the fibers from the suspension, thus leaving a clear supernatant (right). This phenomenon was observed for all the fungi tested and indicates that the fungal hyphae can bind or entrap the asbestos material.

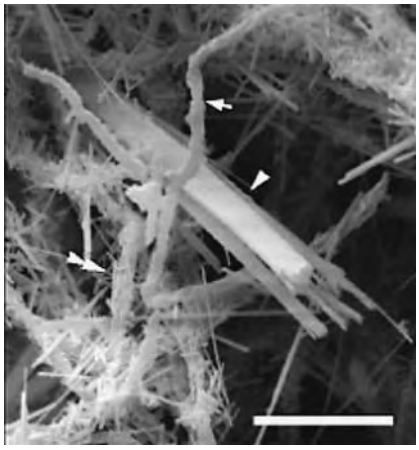


Figure 2. Scanning electron micrograph showing the fungal hyphae of *O. maius* (arrow) intertwined with asbestos fibers of different sizes. A large fiber is clearly visible in the center of the photograph (arrowhead), whereas smaller fibers (double arrowhead) can be found associated with the surface of the fungal hyphae (scale bar corresponds to 10 μm).

All fungi able to induce iron release from crocidolite fibers also secreted siderophores, detected as a clearing halo around the fungal colony on specific plate assays (Figure 4). The halo diameter, which was considered to be proportional to siderophore secretion, appears to parallel iron extraction. Thus, an enhancement of siderophore production might result in the removal of even more iron from the fibers.

In cell-free tests a 1-mM solution of the strong iron chelator desferrioxamine—a hydroxamate siderophore usually employed clinically in the treatment of hemochromatosis and other diseases related to iron-overload—extracted iron from crocidolite fibers. The amount of iron extracted greatly exceeded what was expected to be at the surface based on the crystal structure of crocidolite.[9,19] Both iron and silicon were

 © 2003 Wiley-VCH Verlag GmbH & Co. KGaA, Weinheim 1433-7851/03/4202-0220 $ 20.00+.50/0

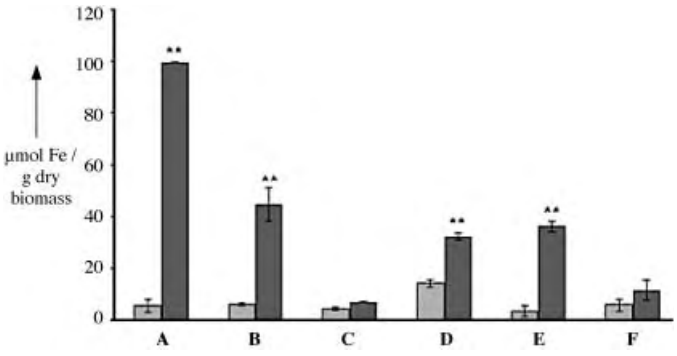


Figure 3. Iron solubilization by soil fungi. Iron was extracted from crocidolite fibers by the various mycelia tested: A = *Fusarium oxysporum*, B = *Mortierella hyalina*, C = *Geomyces pannorum*; D = sterile mycelium MUT 840, E = *Oidiodendron maius* E, F = *Oidiodendron maius* Cd). The diagram shows the amount of iron measured in the culture medium of the control (left-hand bars) and the asbestos-treated samples (right-hand bars). Data are the mean of three independent experiments ± standard deviation. Asterisks indicate significant differences between control and asbestos-containing medium ($P < 0.05$).

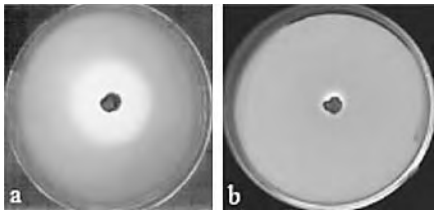


Figure 4. A specific plate assays shows the release of siderophores, detected as a clear halo. Highly solubilizing fungal strains such as sterile mycelium MUT 840 (a) produced significantly higher amounts of siderophores than less solubilizing fungi such as *Oidiodendron maius* Cd (b).

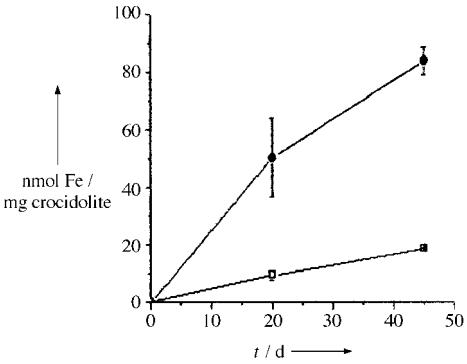


Figure 5. Amount of iron released over time from crocidolite in the presence of *Fusarium oxysporum* (open squares) and *Mortierella hyalina* (filled circles). Data are the mean of three independent experiments ± standard deviation. The amount of iron released progressively increases with the time of incubation, and no plateau values are obtained even after 45 days of culture.

found in the supernatant but with an iron:silicon ratio greater than that in the solid. This suggests that the progressive removal of iron from the bulk of the fiber by desferrioxamine is followed by diffusion of bulk iron ions in the silicate matrix, which eventually leads to collapse of the silicate structure in the outmost layers.[9,20] The newly formed surface is amorphous and is much less reactive in generating free radicals than the original surface.[6a,21] Also the amount of iron extracted by the fungal siderophores was greater than what might have found at the surface. Assuming a maximum of three to four iron atoms per nm^2, which exceeds the average value on the crystal planes of the amphibole structure, the iron mobilized by fungi corresponds to six to seven iron atoms per nm^2, which would correspond to two or more layers below the surface. The trend of iron release in the presence of *F. oxysporum* and *M. hyalina*, which is reported in Figure 5, suggests that iron extraction was far from being exhausted after 45 days of culture but would have proceeded as long as the fibers and the hyphae would have been in contact. Prolonged growth of iron-extracting fungi on the fibers is thus likely to yield transformations at the fiber surface similar to those observed after incubation in desferrioxamine.

The generation of ·OH radicals by the crocidolite fibers in the presence of H_2O_2 was evaluated by EPR spectroscopy and with 5,5-dimethyl-1-pyrroline *N*-oxide (DMPO) as a spin trap. The nitroxide radical formed upon reaction of ·OH with DMPO gives rise to a characteristic four-line EPR signal with the intensity ratio 1:2:2:1 and hyperfine coupling constants $a_N = a_H = 15$ G. The EPR spectra obtained from aqueous suspensions of the original crocidolite and of crocidolite fibers incubated for 45 days with growing *F. oxysporum* are shown in Figure 6. The original fibers, as previously reported,[17] generate substantial ·OH radicals (Figure 6a). Conversely, the fibers that had been treated with *F. oxysporum* and then washed and dried are fully inactivated in their potential to generate ·OH radicals (Figure 6b). Asbestos fibers induce single-strand breaks in DNA, and this effect is lowered by incubation with desferrioxamine.[15,16] Considering that a mild pretreatment of crocidolite fibers with desferrioxamine could prevent DNA mutations at defined loci in Chinese hamster V79 cells,[22] we may expect that, following interaction with the fungi, the biological activity of the fibers might be reduced also.

The extracellular protein profiles for fungi grown in the presence and in the absence of asbestos fibers revealed



Figure 6. EPR spectra (DMPO as spin trap) obtained from aqueous suspensions of a) crocidolite, which shows the signal of the [HO·–DMPO] adduct, and of b) crocidolite pretreated with *F. oxysporum*.

 © 2003 Wiley-VCH Verlag GmbH & Co. KGaA, Weinheim 1433-7851/03/4202-0221 $ 20.00+.50/0

substantial changes, with new proteins being induced and other ones repressed following contact with the fibers. Among the induced proteins, a manganese superoxide dismutase (Mn-SOD) was identified in *G. pannorum* by N-terminus sequencing and immuno cross-reactivity. SOD enzymes are potent antioxidant proteins that catalyze the conversion of the superoxide ion in hydrogen peroxide and oxygen. An increase in Mn-SOD enzyme was detected in type II epithelial cells of rat lungs after inhalation of crocidolite asbestos.[10] The expression of Mn-SOD in mesothelioma is also much greater than that in healthy pleural mesothelium,[23] and transfection of a Mn-SOD gene into hamster tracheal epithelial cells ameliorates asbestos-mediated cytotoxicity.[24] The cellular response to asbestos fibers may thus show some similarities in fungi and in mammalian cells.

On the basis of the results described we believe fungi may be possible agents for the decontamination of asbestos-polluted soils. Not only may adhesion of the fibrils on the fungal mycelium limit their dispersal in the specific sites where the fungi grow, but also the action of the potent siderophores could modify the fiber surface, depriving it of the free radical generating sites crucial to triggering of the carcinogenic mechanisms. Soil fungi display a huge functional and genetic biodiversity, and suitable strains with high iron-mobilizing abilities can be selected from natural sources. Alternatively, the identification of genes involved in siderophore production may be the starting point for genetically engineered organisms with increased iron mobilization from asbestos.

Received: July 25, 2002
Revised: October 7, 2002 [Z19820]

[1] EPA Asbestos Health Effects Colloquium, Oakland US 24–27 May 2001. Reference to Proceedings of EPA Asbestos Health Effects Colloquium, Oakland USA 24–27 May 2001, http://www.epa.gov/swerrims/ahec
[2] A. B. Kane in *Mechanisms of Fiber Carcinogenesis, Vol. 140* (Eds.: A. B. Kane, P. Boffetta, R. Saracci, J. D. Wilburn), International Agency for Research on Cancer Scientific Publication, Lyon, **1996**, pp. 11–35.
[3] B. T. Mossman, A. Churg, *Am. J. Respir. Crit. Care Med.* **1998**, *157*, 1666–1680.
[4] *IARC Monographs on the Evaluation of Carcinogenic Risks to Humans, Asbestos*, International Agency for Research on Cancer Scientific Publication 14, Lyon, **1977**.
[5] B. T. Mossman, J. Bignon, M. Corn, A. Seaton, J. B. L. Gee, *Science* **1990**, *247*, 294–301.
[6] a) J. A. Hardy, A. E. Aust, *Chem. Rev.* **1995**, *95*, 95–97; b) D. W. Kamp, P. Graceffa, W. A. Pryor, S. A. Weitzman, *Free. Rad. Biol. Med.* **1992**, *12*, 293–315; c) A. J. Ghio, T. P. Kennedy, A. R. Whorton, A. L. Crumbliss, G. E. Hatch, J. R. Hoidal, *Am. J. Physiol.* **1992**, *263*, 511–517; d) D. W. Kamp, S. A. Weitzman, *Thorax* **1999**, *54*, 638–652.
[7] M. L. Guerinot, *Annu. Rev. Microbiol.* **1994**, *48*, 743–772.
[8] K. Haselwandter, B. Dobernigg, W. Beek, G. Jung, A. Cansier, G. Winkelmann, *BioMetals* **1992**, *5*, 51–56.
[9] B. Fubini, C. Otero-Aréan, *Chem. Soc. Rev.* **1999**, *28*, 373–381.
[10] J. A. Holley, Y. M. Janssen, B. T. Mossman, D. J. Taatjes, *Am. J. Pathol.* **1992**, *141*, 475–485.
[11] A. J. Ghio, J. Zhang, C. A. Piantadosi, *Arch. Biochem. Biophys.* **1992**, *298*, 646–650.
[12] B. Fubini in *Use of physico-chemical and cell free assays to evaluate the potential carcinogenicity of fibers in mechanisms of fiber carcinogenesis, Vol. 140* (Eds: A. B. Kane, P. Boffetta, R. Saracci, J. D. Wilbourn), International Agency for Research on Cancer Scientific Publication, Lyon, **1996**.
[13] L. Prandi, S. Bodoardo, N. Penazzi, B. Fubini, *J. Mater. Chem.* **2001**, *11*, 1495–1501.
[14] G. Martra, G. Martra, E. Chiardola, S. Coluccia, L. Marchese, M. Tomatis, B. Fubini, *Langmuir* **1999**, *15*, 5742–5752.
[15] L. G. Lund, A. E. Aust, *Arch. Biochem. Biophys.* **1990**, *278*, 60–64.
[16] C. C. Chao, L. G. Lund, K. R. Zinn, A. E. Aust, *Arch. Biochem. Biophys.* **1994**, *314*, 1–7.
[17] B. Fubini, L. Mollo, E. Giamello, *Free. Rad. Res.* **1995**, *23*, 593–614.
[18] J. Gold, H. Amandusson, A. Krozer, B. Kasemo, T. Ericsson, G. Zaneti, B. Fubini, *Environ. Health Perspect.* **1997**, *105*, 1021–1030.
[19] B. Fubini, L. Mollo, *Toxicology Lett.* **1995**, *82–83*, 951–960.
[20] L. Prandi, M. Tomatis, N. Penazzi, B. Fubini, *Ann. Occup. Hyg.* **2002**, *46*, 140–143.
[21] "Effect of chelators on the surface properties of asbestos": L. Mollo, E. Merlo, E. Giamello, M. Volante, B. Fubini; in *Cellular and Molecular Effects of Mineral and Synthetic Dusts and Fiber*, NATO ASI Series Vol. H85 (Eds.: J. M. G. Davis, M.-C. Jaurand), Berlin/Heidelberg, Springer-Verlag, **1994**, pp. 425–432.
[22] S. H. Park, A. E. Aust, *Cancer Res.* **1998**, *58*, 1144–1148.
[23] K. Kahlos, P. Paakko, E. Kurttila, Y. Soini, V. L. Kinnula, *Br. J. Cancer* **2000**, *82*, 1022–1029.
[24] B. T. Mossman, P. Surinrut, B. T. Brinton, J. P. Marsh, N. H. Heintz, B. Lindau-Shepard, J. B. Shaffer, *Free. Rad. Biol. Med.* **1996**, *21*, 125–131.
[25] "Biochemical analysis of polygalacturonases produced by ericoid mycorrhizal fungi": S. Perotto, V. Cometti, J. D. Coisson, I. Perugini, P. Bonfante in *Mycorrhizae Manual Book* (Ed.: A. Varma), Springer, Heidelberg, **1998**, pp. 187–215.
[26] U. K. Laemmli, *Nature* **1970**, *222*, 680–685.
[27] B. Schwyn, J. B. Neilands, *Anal. Biochem.* **1987**, *160*, 47–56.

 © 2003 Wiley-VCH Verlag GmbH & Co. KGaA, Weinheim 1433-7851/03/4202-0222 $ 20.00+.50/0



High-Spin Iron Wheels

High-Spin Wheel of a Heptanuclear Mixed-Valent $Fe^{II,III}$ Complex**

Hiroki Oshio, Norihisa Hoshino, Tasuku Ito, Motohiro Nakano, Franz Renz, and Philipp Gütlich*

Iron and manganese clusters with oxygen atoms acting as bridging ligands possess a variety of structures and are of current interest in materials and bioinorganic chemistry. For example, nanosized molecules with a high-spin ground state afford single-domain magnets,[1] which may display hysteresis,[2] slow magnetic relaxation,[3] and spin-quantum tunneling characteristics of a purely molecular origin.[4] The iron-storage protein ferritin and manganese clusters have been extensively studied as a biological prototype in the inorganic systems,[5] and as models of the water-oxidizing complex in photosystem II,[6] respectively. The development of synthetic routes to metal clusters has resulted in remarkable achievements in spin chemistry and biochemistry. Among organic bridging ligands, alkoxo groups have been employed extensively for constructing metal clusters because of their versatile bridging modes (μ_2 and μ_3). Subtle changes in reaction conditions have resulted in the formation of unexpected and beautiful structures, such as cyclic polymetallic clusters.[7] Previously, we have described an alkoxo-bridged iron(II) cube, $[Fe_4(sae)_4(MeOH)_4]$ (H_2sae = 2-salicylideneamino-1-ethanol), which exhibited superparamagnetic behavior with a blocking temperature of 1.1 K.[7g] In the course of exploring the versatility of Schiff base ligands, we found that complexes with higher spin multiplicities could be synthesized from reactions involving iron(II or III) chloride and the tridentate Schiff base ligand 3-methoxy-2-salicylideneamino-1-ethanol (H_2L). Alkoxo-bridged cluster molecules with core structures of $[Fe^{II}_3Fe^{III}]$, $[Fe^{II}Fe^{III}_6]$, and $[Fe^{III}Fe^{II}_6]$ were prepared by varying the amount of oxidant used. In this communication, we report the synthesis and magnetic properties of a heptanuclear iron(II, III) wheel with the highest spin ground state in this series.

A stoichiometric amount of $[(t\mathrm{Bu}_4\mathrm{N})MnO_4]$ was added to a mixture of $FeCl_2{\cdot}4H_2O$ and H_2L in methanol. After 1–2 weeks, dark-red hexagonal blocks of $[Fe^{III}Fe^{II}_6(MeO)_6(HL)_6]Cl_3$ (**1**-Cl_3) were obtained in 50% yield. **1**-Cl_3 crystallizes in the trigonal $P\bar{3}c1$ space group,[8] in which the $\mathbf{1}^{3+}$ ion is situated on a $\bar{3}$ inversion axis. The cyclic structure is composed of seven coplanar iron ions; the core can, therefore, be regarded as a wheel with crystallographically imposed S_6 symmetry. The molecular structure of the $\mathbf{1}^{3+}$ ion, viewed perpendicular to the ring plane, is shown in Figure 1.

The Schiff base ligand (H_2L) has four possible coordination sites, namely, the methoxy, phenoxy, imino, and alcohol moieties. X-ray structural analysis showed that the alcohol groups are uncoordinated and have positional disorder. Therefore, the ligand acts as a tridentate monoanion (HL^-). In the wheel, six μ_2-phenoxo groups bridge the iron ions on the rim, which themselves are linked to the central ion through six μ_3-bridging methoxy groups that act as "spokes" to form the wheel structure. Each iron ion on the rim (Fe2) adopts an N_1O_5 configuration through coordination to the Schiff base and methoxide groups; a Jahn–Teller distortion for the Fe2 ions was observed. Coordination bond lengths about the Fe2 ions are in the range of 2.042(4)–2.362(5) Å. The coordination geometry of the central iron ion (Fe1) is octahedral with bond lengths of 2.150(4) Å (Fe1–O4 (meth-

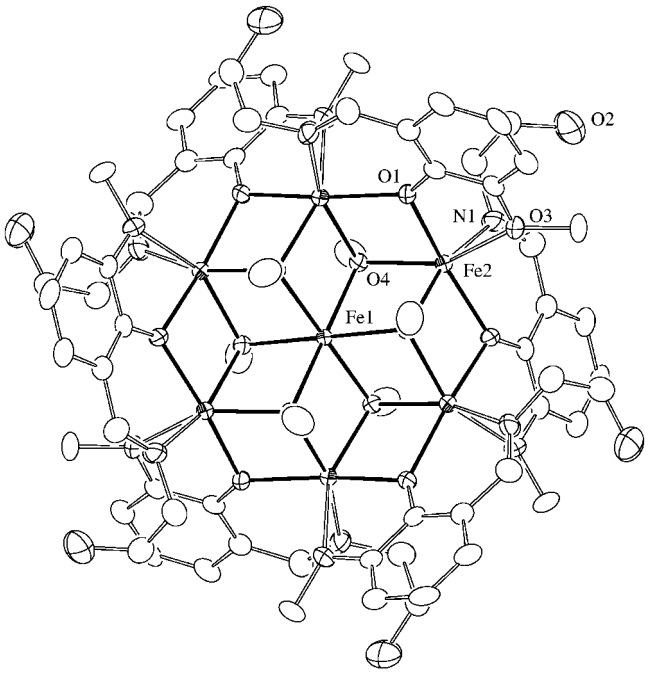


Figure 1. ORTEP diagram of the $\mathbf{1}^{3+}$ ion. Selected bond lengths [Å] and angles [°]: Fe1-O4 2.153(3), Fe2-O1A 2.041(3), Fe2-O4 2.079(3), Fe2-O1 2.092(4), Fe2-N1 2.125(5), Fe2-O4A 2.181(3), Fe2-O3 2.367(4); O4A-Fe2-O3 96.52(15), Fe2B-O1-Fe2 103.51(15), Fe2-O4-Fe1 98.43(14), Fe2-O4-Fe2B 99.28(13), Fe1-O4-Fe2B 95.37(13). Symmetry operations: A: $x-y,x-1,-z$; B: $y+1,-x+y+1,-z$.

[*] Prof. H. Oshio
Department of Chemistry
University of Tsukuba
Tennodai 1-1-1, Tsukuba 305-8571 (Japan)
Fax: (+81) 298-4238
E-mail: oshio@chem.tsukuba.ac.jp
N. Hoshino, Prof. T. Ito
Department of Chemistry
Graduate School of Science, Tohoku University
Aoba-ku, Sendai 980-8578 (Japan)
Dr. M. Nakano
Department of Molecular Chemistry
Graduate School of Engineering, Osaka University
1-16 Machikaneyama, Toyonaka, Osaka 560-0043 (Japan)
Dr. F. Renz, Prof. P. Gütlich
Institut für Anorganische Chemie und Analytische Chemie
Johannes Gutenberg Universität Mainz
Staudinger Weg 9, 55099 Mainz (Germany)

[**] This work was partially supported by a Grant-in-Aid for Scientific Research from the Ministry of Education, Science, Sports and Culture, Japan.

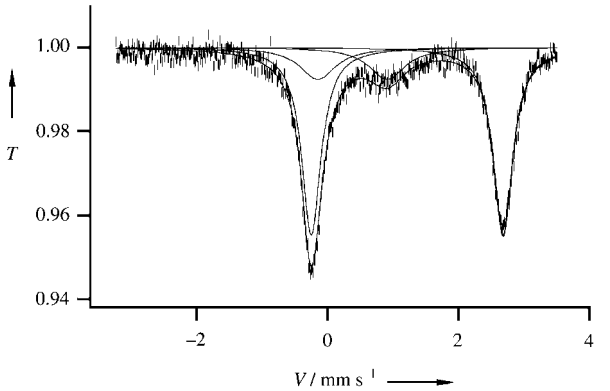


Figure 2. Mössbauer spectrum of **1**-Cl_3. The velocity scale was calibrated relative to α-iron.

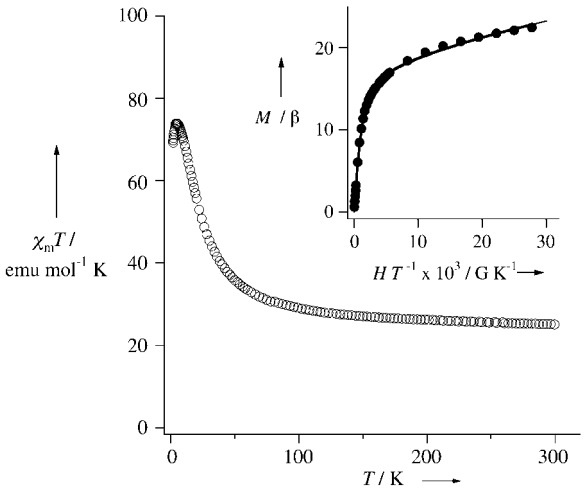


Figure 3. The $\chi_m T$ versus temperature and magnetization (M) versus field strength (H/T, inset) plots for **1**-Cl_3. The solid line results from a least-squares fit using the parameters and the equation described in the text.

oxide)). The iron ions on the rim (Fe2) and at the center (Fe1) were, therefore, assigned to be Fe^{II} and Fe^{III} ions, respectively, based on both the valence sum calculation and the presence of a Jahn–Teller distortion. This assignment was also confirmed by Mössbauer spectroscopy. The bond angles for Fe^{III}-O-Fe^{II} (95.33(15) and 98.61(16)°) are more acute than those of Fe^{II}-O-Fe^{II} (99.23(15) and 103.45(18)°).

The Mössbauer spectrum at 20 K exhibits two doublets (Figure 2). One doublet ($\delta = 0.38\ mm\,s^{-1}$ and $\Delta E_Q = 1.02\ mm\,s^{-1}$; the velocity was calibrated relative to α-iron) is characteristic of a high-spin Fe^{3+} ion, while the other ($\delta = 1.22\ mm\,s^{-1}$ and $\Delta E_Q = 2.93\ mm\,s^{-1}$) is characteristic of high-spin Fe^{2+} ion. Assuming that the Mössbauer–Lamb factors for the Fe^{3+} and Fe^{2+} ions have similar values, the Fe^{3+}/Fe^{2+} ratio calculated from the peak areas is 0.18:0.82, which is in good agreement with the ratio of 1:6 (approximately 0.14:0.86) determined from the chemical formula.

The temperature dependence of the magnetic susceptibilities was measured down to 1.8 K and is shown in Figure 3, together with a plot of magnetization versus field strength at 1.8 K (inset). The $\chi_m T$ value at 300 K is 25.2 emu mol^{-1} K, and this value increased gradually as the temperature was lowered, reaching a maximum value of 73.8 emu mol^{-1} K at 5.5 K. This magnetic behavior is characteristic of the occurrence of ferromagnetic interactions, and suggests an $S = 29/2$ spin ground state for **1**-Cl_3. The sudden decrease in the $\chi_m T$ value below 5.5 K results from magnetic anisotropy and/or through-space antiferromagnetic interactions.[9]

Magnetization data were collected as a function of the applied field up to 5 T at 1.8 K. The $M/N\mu_B$ values increased with increasing magnetic field strength, and did not show saturation up to 5 T. The $M/N\mu_B$ versus H/T data at 1.8 K were fitted assuming only that the ground state is populated. The spin-Hamiltonian was constructed using the sum of the isotropic Zeeman and axial zero-field splitting (ZFS) terms,[10] and the 30×30 matrix elements ($= (2S+1)^2$) were diagonalized to yield magnetization curves following a powder average procedure.[11] Least-squares calculations gave a best-fit parameter of $D = +0.53(2)\ cm^{-1}$, with a fixed g_{av} value of 2.046.[12] It should be noted that the calculation assuming a $S = 27/2$ ground state gave $D = +0.42(2)\ cm^{-1}$, while that for a ground state of $S = 25/2$ was divergent. Measurements of ac magnetic susceptibility were also performed in the temperature range of 1.8–4.0 K with a 3 G ac field oscillating at 250–1000 Hz, but no out-of-phase signal was observed. This is understandable, as a result of the positive D value of this compound.

In summary, we have prepared a mixed-valent high-spin wheel with a spin ground state of $S = 29/2$. The emphasis of further studies will be to prepare a high-spin wheel with a negative D value by modifying the Schiff base ligands.

Experimental Section

All synthetic procedures were carried out in Schlenk-type vessels under a nitrogen atmosphere, with solvents that were degassed prior to use. A solution of $FeCl_2 \cdot 4H_2O$ (232 mg, 1.17 mmol) in methanol (40 mL) was added to a mixture of 3-methoxysalicylaldehyde (152 mg, 1 mmol), 2-amino-1-ethanol (61 mg, 1 mmol), and Et_3N (101 mg, 1 mmol). After adding [(tBu$_4$N)MnO$_4$] (15 mg, 0.13 mmol), the resulting mixture was stored for 1–2 weeks, in which time dark-red hexagonal blocks had formed, which were collected by filtration. No manganese ions were detected by optical emission spectroscopy (Shimadzu ICPS-7000). Elemental analysis (%) calculated for $C_{66}H_{90}Cl_3Fe_7N_6O_{24}$: C 42.88, H 4.91, N 4.55, Fe 21.14; found: C 43.12, H 4.49, N 4.70, Fe 21.47.

Received: September 2, 2002 [Z50080]

[1] a) S. M. J. Aubin, M. W. Wemple, D. M. Adams, H.-L. Tsai, G. Christou, D. N. Hendrickson, *J. Am. Chem. Soc.* **1996**, *118*, 7746; b) J. Yoo, A. Yamaguchi, M. Nakano, J. Krzystek, W. E. Streib, L.-C. Brunel, H. Ishimoto, G. Christou, D. N. Hendrickson, *Inorg. Chem.* **2001**, *40*, 4604; c) A. L. Barra, D. Gatteschi, R. Sessoli, *Chem. Eur. J.* **2000**, *6*, 1608; d) A. L. Barra, A. Caneschi, A. Cornia, F. Fabrizi de Biani, D. Gatteschi, C. Sangregorio, R. Sessoli, L. Sorace, *J. Am. Chem. Soc.* **1999**, *121*, 5302; e) S. Ferlay, T. Mallah, R. Ouahes, P. Veillet, M. Verdaguer, *Inorg. Chem.* **1999**, *38*, 229; f) A. Cornia, D. Gatteschi, R. Sessoli, *Coord. Chem. Rev.* **2001**, *219*, 573; g) *Magnetism: Molecules to Materials III* (Eds.: J. S. Miller, M. Drillon), Wiley, VCH, **2002**.

 © 2003 Wiley-VCH Verlag GmbH & Co. KGaA, Weinheim 1433-7851/03/4202-0224 $ 20.00+.50/0

[2] a) R. Sessoli, D. Gatteschi, A. Caneschi, M. A. Novak, *Nature* **1993**, *365*, 141; b) A. Caneschi, D. Gatteschi, N. Lalioti, C. Sangregorio, R. Sessoli, G. Venturi, A. Vingigni, A. Rettori, M. G. Pini, M. A. Novak, *Angew. Chem.* **2001**, *113*, 1810; *Angew. Chem. Int. Ed.* **2001**, *40*, 1760; c) A. L. Barra, A. Caneschi, D. Gatteschi, D. P. Goldberg, R. Sessoli, *Solid State Chem.* **1999**, *45I*, 484.

[3] a) A. L. Barra, D. Gatteschi, R. Sessoli, *Chem. Eur. J.* **2000**, *6*, 1608; b) L. Thomas, F. Lionti, R. Ballou, D. Gatteschi, R. Sessoli, A. L. Barra, *Nature* **1996**, *383*, 145; c) J. R. Friedman, M. Sarachik, J. Tejada, R. Ziolo, *Phys. Rev. Lett.* **1996**, *76*, 3830.

[4] a) A. Yamaguchi, H. Ishimoto, K. Awaga, J. S. Yoo, M. Nakano, D. N. Hendrickson, E. K. Brechin, G. Christou, *Phys. B* **2000**, *284–*288, 1225; b) D. Gatteschi, A. Caneschi, L. Pardi, R. Sessoli, *Science* **1994**, *265*, 1054; c) A. Müller, F. Peters, M. T. Pope, D. Gatteschi, *Chem. Rev.* **1998**, *98*, 239.

[5] a) K. L. Taft, C. D. Delfs, G. C. Papaefthymiou, S. Foner, D. Gatteschi, S. J. Lippard, *J. Am. Chem. Soc.* **1994**, *116*, 823; b) R. R. Crichton, *Angew. Chem.* **1973**, *85*, 53; *Angew. Chem. Int. Ed. Engl.* **1973**, *12*, 57; c) K. L. Taft, G. C. Papaefthymiou, S. J. Lippard, *Science* **1993**, *259*, 1302.

[6] a) K. Wieghardt, *Angew. Chem.* **1994**, *106*, 765; *Angew. Chem. Int. Ed. Engl.* **1994**, *33*, 725; b) R. J. Debus, *Biochim. Biophys. Acta* **1992**, *1102*, 269; c) G. W. Bruvig, H. H. Thorp, R. H. Crabtree, *Acc. Chem. Res.* **1991**, *24*, 311; d) G. Christou, *Acc. Chem. Res.* **1989**, *22*, 328.

[7] a) A. Caneschi, A. Cornia, S. J. Lippard, *Angew. Chem.* **1995**, *107*, 511; *Angew. Chem. Int. Ed. Engl.* **1995**, *34*, 467; b) S. P. Watton, P. Fuhrmann, L. E. Pence, A. Caneschi, A. Cornia, G. L. Abbati, S. J. Lippard, *Angew. Chem.* **1997**, *109*, 2917; *Angew. Chem. Int. Ed. Engl.* **1997**, *36*, 2774; c) R. W. Saalfrank, I. Bernt, E. Uller, F. Hampel, *Angew. Chem.* **1997**, *109*, 2596; *Angew. Chem. Int. Ed. Engl.* **1997**, *36*, 2482; d) G. L. Abbati, A. Cornia, A. C. Fabretti, A. Caneschi, D. Gatteschi, *Inorg. Chem.* **1998**, *37*, 3759; e) O. Waldmann, R. Koch, S. Schromm, J. Schülein, P. Müller, I. Bernt, R. W. Saalfrank, F. Hampel, E. Balthes, *Inorg. Chem.* **2001**, *40*, 2986; f) A. L. Dearden, S. Parsons, R. E. P. Winpenny, *Angew. Chem.* **2001**, *113*, 155; *Angew. Chem. Int. Ed.* **2001**, *40*, 151; g) H. Oshio, N. Hoshino, T. Ito, *J. Am. Chem. Soc.* **2000**, *122*, 12602.

[8] Crystal data for **1**-Cl_3 ($C_{66}H_{90}Cl_3Fe_7N_6O_{24}$): dark-red block (0.2x0.2x0.3 mm^3), $M = 1848.75$, trigonal, space group $P\bar{3}c1$ (No. 165), $a = 14.5632(15)$, $c = 22.374(3)$ Å, $V = 4109.4(9)$ Å^3, $Z = 2$, $T = -70$°C; A total of 22130 (R(int) = 0.0807) unique reflections ($3° < 2\theta < 50°$) were measured. Nonhydrogen atoms were refined with anisotropic thermal parameters. Hydrogen atoms were included in calculated positions and refined with isotropic thermal parameters riding on those of the parent atoms. Full-matrix least-squares refinement on F^2 (194 variables) converged to $R1 = 0.0650$, $wR2 = 0.1785$ ($I > 2\sigma(I)$). CCDC-192326 contains the supplementary crystallographic data for this paper. These data can be obtained free of charge via www.ccdc.cam.ac.uk/conts/retrieving.html (or from the Cambridge Crystallographic Data Centre, 12, Union Road, Cambridge CB21EZ, UK; fax: (+44) 1223-336-033; or deposit @ccdc.cam.ac.uk).

[9] An iron ion has unquenched orbital momentum and the spin-Hamiltonian should include the anisotropic term. Analysis of the magnetic data has not been performed.

[10] a) G. Armoi, M. J. Knapp, J.-O. Claude, J. C. Huffman, D. N. Hendrickson, G. Christou, *J. Am. Chem. Soc.* **1999**, *121*, 5489; b) H. J. Eppley, H.-L. Tsai, N. de Vries, K. Folting, G. Christou, D. N. Hendrickson, *J. Am. Chem. Soc.* **1995**, *117*, 301.

[11] V. R. Marath, S. Mitra, *Chem. Phys. Lett.* **1974**, *27*, 103.

[12] The average g value was estimated by the Curie plot of the χ_m values in the temperature range of 200–300 K.

Carborane Cages

Beyond the Icosahedron: The First 13-Vertex Carborane**

*Anthony Burke, David Ellis, Barry T. Giles, Bruce E. Hodson, Stuart A. Macgregor, Georgina M. Rosair, and Alan J. Welch**

The chemistry of carboranes and heterocarboranes is dominated by the 12-vertex icosahedron. The first carborane reported[1] was 1-C(CH_3)CH_2-1,2-*closo*-$C_2B_{10}H_{11}$ and there are now literally thousands of heterocarboranes known based on the icosahedral geometry. The field of subicosahedral heterocarboranes is also well developed, which reflects the existence of carboranes from $C_2B_3H_5$ to $C_2B_9H_{11}$.

In contrast, the area of supraicosahedral heterocarboranes is relatively unexplored. Although the first 13-vertex metallacarborane was reported over 30 years ago,[2] there are only about a hundred such compounds currently known. The first supraicosahedral p-block metallacarborane was described only last year.[3] We are aware of only a handful of 14-vertex metallacarboranes,[4,5] and no such species of greater cluster size. Crucially, there are no reports of carboranes which extend the homologous family $C_2B_nH_{2+n}$ beyond $n = 10$ nor any reports of the parent borane ions $[B_nH_n]^{2-}$ for $n > 12$. This situation is unfortunate since several of the current applications of boron-cluster compounds, for example, in catalysis as "least-coordinating anions"[6] and in boron–neutron-capture therapy of tumors,[7] would benefit from the existence of carboranes with larger numbers of B atoms.

The most recent computational study of supraicosahedral boranes[8] concluded that a) $[B_{13}H_{13}]^{2-}$, $[B_{14}H_{14}]^{2-}$, and $[B_{15}H_{15}]^{2-}$ ions are thermodynamically unstable with respect to $[B_{12}H_{12}]^{2-}$, and b) the $[B_{12}H_{12}]^{2-} \rightarrow [B_{13}H_{13}]^{2-}$ step is particularly unfavorable and represents a synthetic bottleneck. Tantalizingly, the higher boranes $[B_{16}H_{16}]^{2-}$ and $[B_{17}H_{17}]^{2-}$ are predicted to be progressively more stable than $[B_{15}H_{15}]^{2-}$. In a separate study,[9] other workers have predicted stable, spherical, geometries for $B_{20}H_{20}$, $B_{32}H_{32}$, $B_{42}H_{42}$, and $B_{92}H_{92}$ clusters. Although similar calculations have not been performed on closo carboranes, the results of these computational studies suggest that several stable, large, carboranes could be viable synthetic targets as long as the 12-vertex→13-vertex barrier is overcome. We now report that breakthrough.

[*] Prof. A. J. Welch, A. Burke, Dr. D. Ellis, B. T. Giles, Dr. B. E. Hodson, Dr. S. A. Macgregor, Dr. G. M. Rosair
Department of Chemistry
Heriot-Watt University
Edinburgh EH14 4AS (UK)
Fax: (+44) 131-451-3180
E-mail: a.j.welch@hw.ac.uk

[**] We thank D. Ferrer, M. A. Laguna, and F. Schmidt for preliminary experiments. We acknowledge the EPSRC and the Leverhulme Trust for support of this work. We also thank A. S. F. Boyd for NMR spectra, R. Ferguson for mass spectra and G. Evans for microanalyses. A.J.W is the recipient of a Royal Society Leverhulme Trust Senior Research Fellowship.

An appealing way to prepare the 13-vertex $C_2B_{11}H_{13}$ or its derivatives from the appropriate $C_2B_{10}H_{12}$ species is by polyhedral expansion, that is, reduction of the closo precursor to the nido dianion[10] $[C_2B_{10}H_{12}]^{2-}$ followed by capitation through treatment with a BRX_2 compound,[11] analogous to the method employed to prepare the first 13-vertex metallacarborane.[2] Starting from 1,2-*closo*-$C_2B_{10}H_{12}$ we tried this many times, under a variety of conditions, and in a variety of solvents, each attempt failing to produce a supraicosahedral species. However, we did note that reduction of 1,2-*closo*-$C_2B_{10}H_{12}$, followed by treatment with BI_3, produced 3-I-1,2-*closo*-$C_2B_{10}H_{11}$, which suggests successful initial production of a 13-vertex carborane that spontaneously degraded by loss of a {BH} unit.

When 1,2-*closo*-$C_2B_{10}H_{12}$ is reduced the cage carbon atoms separate.[12] Our observation that they become adjacent again when the presumed 13-vertex carborane partially degrades suggested that a system in which such C-atom movement was prevented might represent a way forward. Tethering the cage C atoms with an α,α-*o*-xylylene bridge retains their adjacency on reduction.[13] However, the reduced species has not been structurally characterized in the absence of a coordinated metal ion,[13] so to provide a firm basis for the subsequent capitation step we have determined the structure[14] of the [7,8-μ-{$C_6H_4(CH_2)_2$}-7,8-*nido*-$C_2B_{10}H_{11}]^-$ (**1**) ion as its $[HNEt_3]^+$ salt (Figure 1). This study establishes the presence of a six-atom C_2B_4 open upper face with adjacent C atoms. The structure of the anion is broadly similar to that of the kinetic isomer of the same species coordinated to K^+[13] ions and to that established[12] for the [7,9-Me_2-7,9-*nido*-$C_2B_{10}H_{11}]^-$ ion except that the former is fully triangulated save for a flat six-membered face, and the quadrilateral CB_3 lower face of the latter is replaced by a trapezoidal C_2B_2 face here. The C_6 ring of the phenylene bridge is located over this trapezoidal face.

Removal of the bridging proton from **1** with BuLi or direct two electron (2e) reduction of 1,2-μ-{$C_6H_4(CH_2)_2$}-1,2-*closo*-$C_2B_{10}H_{10}$ with Na yields the [7,8-μ-{$C_6H_4(CH_2)_2$}-7,8-*nido*-$C_2B_{10}H_{10}]^{2-}$ ion which we assume has the same basic structure as the monoanion. Treatment of this compound with $PhBCl_2$ affords the unprecedented 13-vertex carborane 1,2-μ-{$C_6H_4(CH_2)_2$}-3-Ph-1,2-$C_2B_{11}H_{10}$ (**2**) as a moderately stable colorless crystalline solid.

Compound **2** was characterized by ^1H, ^{13}C, and ^{11}B NMR spectroscopy, mass spectrometry, and single-crystal X-ray diffraction[15] (Figure 2). Ignoring the Ph substituent, the carborane cluster has approximate C_s symmetry about the plane passing through B5, B12, and B13. All the polyhedral faces are triangulated except for C1-C2-B7-B3 which is trapezoidal. With respect to the cluster C1 and C2 are both four-connected, B5 is six-connected, and all other B atoms are five-connected. This polyhedral shape is that of a henicosahedron (**a**, Figure 3) and not the docosahedron previously predicted[8] for the 13-vertex borane $[B_{13}H_{13}]^{2-}$ (**b**, Figure 3) which has C_{2v} symmetry and is fully triangulated, but the two geometries are related by only a single diamond↔square transformation. We have used density functional calculations[16] to study both $[B_{13}H_{13}]^{2-}$ and 1,2-$C_2B_{11}H_{13}$, and find that the structure **b** is preferred over **a** by 3.8 kJ mol^{-1} for the borane dianion, whilst the reverse is the case by 7.4 kJ mol^{-1}

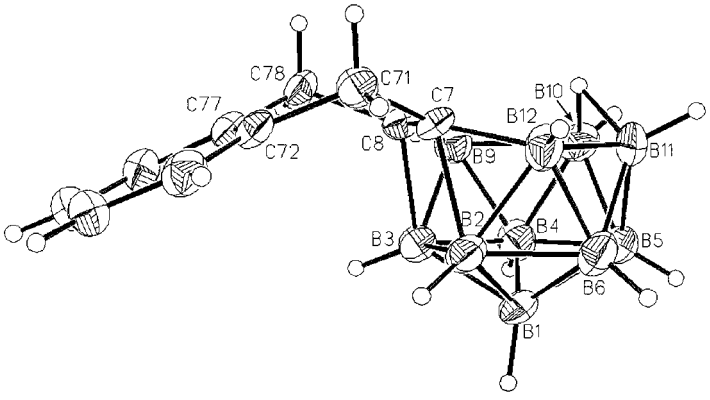


Figure 1. Perspective view of **1** (except for the H atoms, all atoms are drawn as thermal ellipsoids set at 50% probability). The anion has crystallographically imposed C_s symmetry. Selected interatomic distances [Å]: C7-C8 1.444(7), C7-B2 1.833(7), B2-B3 1.949(9), C8-B3 1.816(7), C8-B9 1.546(7), B9-B10 1.851(9), B10-B11 1.836(9), B11-B12 1.842(8), B12-C7 1.551(7).

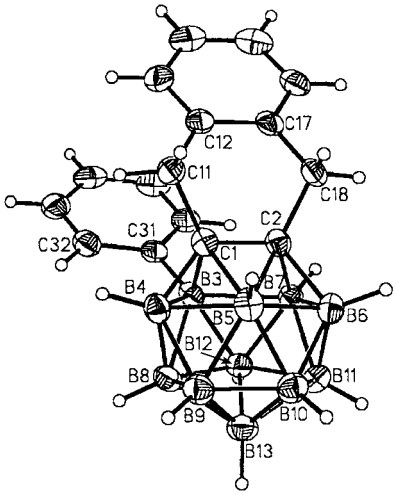


Figure 2. Perspective view of the supraicosahedral carborane **2** (except for the H atoms, all atoms are drawn as thermal ellipsoids set at 50% probability). Selected interatomic distances [Å]: C1-C2 1.427(2), C1-B3 1.898(2), C1-B4 1.569(2), C1-B5 1.841(3), C2-B5 1.917(3), C2-B6 1.632(3), C2-B7 1.766(2), B3-B7 1.987(3).

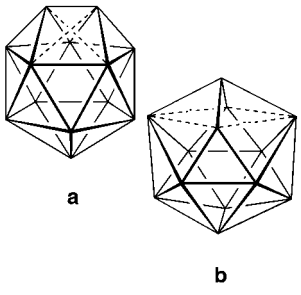


Figure 3. The cluster geometries (**a**, the henicosahedron) found in the supraicosahedral carborane **2** and (**b**, the docosahedron) predicted for the $[B_{13}H_{13}]^{2-}$ ion. Idealized point groups are C_s and C_{2v}, respectively. Theoretically, the henicosahedron is preferred for 1,2-$C_2B_{11}H_{13}$ by 7.4 kJ mol^{-1}, whereas the docosahedron is preferred for $[B_{13}H_{13}]^{2-}$ by 3.8 kJ mol^{-1}. Topologically **a** can be transformed into **b** by making either, and **b** into **a** by breaking any, of the dashed connectivities shown.

 © 2003 Wiley-VCH Verlag GmbH & Co. KGaA, Weinheim 1433-7851/03/4202-0226 $ 20.00+.50/0

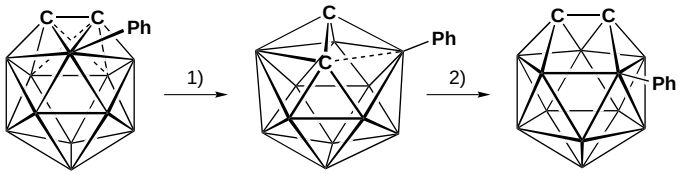


Figure 4. Suggested mechanism for the formation of **2**. The kinetic isomer (left) transforms to the observed thermodynamic isomer (right) by a square→diamond transformation (1, either dashed connectivity made) followed by a diamond→square transformation (2, dashed connectivity broken). The intermediate species has the docosahedral geometry shown as **b** in Figure 3.

for the carborane. We presume the tendency of cluster C atoms to adopt relatively low connected sites is responsible for the latter preference. In **2** the B atom bearing the Ph substituent is not the six-connected boron atom—capitation of deprotonated **1** would be expected to afford **2** in which B3(Ph) and B5(H) were interchanged. We suggest that the kinetic product does indeed have Ph group bonded to a six-connected boron atom, but that it rearranges (Figure 4) into **2** by successive square→diamond then (different) diamond→square transformations via a docosahedral intermediate. Given the marginal differences in calculated energies between the henicosahedron and the docosahedron such a rearrangement is expected to be facile.

We have demonstrated that it is possible to break through the critical 12-vertex→13-vertex bottleneck in polyhedral boron chemistry. For the borane dianions the 12-vertex→13-vertex step has been described as the most difficult to achieve, which suggests that we are now well positioned to synthesize new families of 14-, 15-, 16-, … vertex carborane clusters by successive reduction/capitation steps. Although it has been necessary to tether the cage C atoms to achieve the 12-vertex→13-vertex polyhedral expansion we clearly would not wish to be restricted to tethered supraicosahedral carboranes. We are therefore also investigating the synthesis of supraicosahedral carboranes with removable tethers. Calculations[8] suggest that the stability of 14-vertex and higher polyhedra may make tether removal feasible from this point. Amongst other things tether removal would allow study of the isomerizations of these large carboranes.

Experimental Section

$[HNEt_3]$**1**: Reduction (Na/naphthalene) of 1,2-μ-$\{C_6H_4(CH_2)_2\}$-1,2-*closo*-$C_2B_{10}H_{10}$ in THF, addition of $BF_3{\cdot}OEt_2$ (1 equiv), hydrolysis (H_2O), and treatment with $[HNEt_3]Cl$, followed by extraction into CH_2Cl_2 and crystallization from CH_2Cl_2/OEt_2 afforded $[HNEt_3]$**1** in 42% yield. IR (KBr disc): $\tilde{\nu}_{max}$ 2500 (BH) cm^{-1}; ^1H NMR ($(CD_3)_2CO$, 298 K): $\delta = 7.01$–6.99 (m, 4H, C_6H_4), 3.96 (br s, 1H, H_{endo}), 3.86 (d, $J =$ 15 Hz, 2H, $C_{bridge}H_2$), 3.69 (d, $J = 15$ Hz, 2H, $C_{bridge}H_2$), 3.43 (q, $J =$ 12 Hz, 6H, NCH_2), 1.38 ppm (t, $J = 12$ Hz, CH_3); ^{11}B-$\{^1H\}$ NMR ($(CD_3)_2CO$, 298 K): $\delta = 8.2$ (2B), 2.1 (2B), −6.5 (2B), −13.5 (2B), −16.9 (1B), −19.0 ppm (1B); ^{13}C-$\{^1H\}$ NMR ($(CD_3)_2CO$, 298 K): $\delta =$ 138.9 (2C, Ar_{quat}), 126.6 (2C, Ar), 126.4 (2C, Ar), 49.3 (2C, C_{bridge}), 48.1 (3C, NCH_2), 9.6 ppm (3C, CH_3). Satisfactory microanalytical data were obtained.

2, direct synthesis from closo carborane: Reduction (Na/naphthalene) of 1,2-μ-$\{C_6H_4(CH_2)_2\}$-1,2-*closo*-$C_2B_{10}H_{10}$ in THF followed by replacement of solvent with 40–60 petroleum ether, cooling to 0°C and addition of $PhBCl_2$ afforded **2** in 6% yield (not optimized) following workup involving extraction into CH_2Cl_2, thin layer chromatography on SiO_2 and crystallization from CH_2Cl_2/petroleum ether. IR (CH_2Cl_2): $\tilde{\nu}_{max}$ 2570 (BH) cm^{-1}; ^1H NMR ($CDCl_3$, 298 K): $\delta = 7.21$–6.76 (m, 9H, C_6H_4), 3.91 (s, 4H, CH_2); ^{11}B-$\{^1H\}$ NMR ($CDCl_3$, 298 K): $\delta = 8.4$ (2B), 5.3 (3B, including BPh as a partially obscured signal to higher frequency), 3.7 (2B), 0.6 (2B), −1.2 ppm (2B): ^{13}C-$\{^1H\}$ NMR ($CDCl_3$, 298 K): $\delta = 140.2$ (1C, Ar_{quat}), 133.2 (2C, Ar), 129.5 (2C, Ar_{quat}), 128.4 (1C, Ar), 127.1 (2C, Ar), 126.9 (2C, Ar), 125.2 (2C, Ar), 48.7 ppm (2C, C_{bridge}); MS (EI): m/z 331 [M^+], 256 [M^+−Ph], 245 [M^+−BPh]. Satisfactory microanalytical data were obtained.

Received: September 12, 2002 [Z50151]

[1] M. M. Fein, J. Bobinski, N. Mayes, N. Schwartz, M. S. Cohen, *Inorg. Chem.* **1963**, *2*, 1111.
[2] G. B. Dunks, M. M. McKown, M. F. Hawthorne, *J. Am. Chem. Soc.* **1971**, *93*, 2541.
[3] N. M. M. Wilson, D. Ellis, A. S. F. Boyd, B. T. Giles, S. A. Macgregor, G. M. Rosair, A. J. Welch, *Chem. Commun.* **2002**, 464.
[4] W. J. Evans, M. F. Hawthorne, *J. Chem. Soc. Chem. Commun.* **1974**, 38.
[5] W. M. Maxwell, R. F. Bryan, E. Sinn, R. N. Grimes, *J. Am. Chem. Soc.* **1977**, *99*, 4016; J. R. Pipal, R. N. Grimes, *Inorg. Chem.* **1978**, *17*, 6.
[6] K. Shelly, C. A. Reed, Y. L. Lee, W. R. Scheidt, *J. Am. Chem. Soc.* **1986**, *108*, 3117.
[7] for example, L. F. Tietze, U. Griesbach, U. Bothe, H. Nakamura, Y. Yamamoto, *ChemBioChem* **2002**, *3*, 219.
[8] P. von R. Schleyer, K. Najafian, A. M. Mebel, *Inorg. Chem.* **1998**, *37*, 6765.
[9] I. Boustani, A. Rubio, J. A. Alonso in *Contemporary Boron Chemistry* (Eds.: M. G. Davidson, A. K. Hughes, T. B. Marder, K. Wade), Royal Society of Chemistry, Cambridge, **2000**.
[10] D. Grafstein, J. Dvorak, *Inorg. Chem.* **1963**, *2*, 1128.
[11] M. F. Hawthorne, P. A. Wegner, *J. Am. Chem. Soc.* **1968**, *90*, 896.
[12] T. D. Getman, C. B. Knobler, M. F. Hawthorne, *Inorg. Chem.* **1990**, *29*, 158.
[13] G. Zi, H.-W. Li, Z. Xie, *Chem. Commun.* **2001**, 1110.
[14] For both structure determinations: crystals were studied at 160(2) K using a Bruker *P*4 diffractometer with $Mo_{K\alpha}$ radiation ($\lambda = 0.71073$ Å). Intensity data to θ_{max} 25° were collected by ω scans. Data were corrected for absorption by psi scans and the structures solved by direct and difference-Fourier methods. Refinement[20] was by full-matrix least-squares analysis on F^2. All non-hydrogen atoms were refined with anisotropic displacement parameters. Crystal data for $[HNEt_3]$**1**: $C_{16}H_{35}B_{10}N{\cdot}0.5 < CH_2Cl_2 < 1.0$, $M_r^* = 507.50$, monoclinic, $P2_1/c$, $a = 15.658(2)$, $b =$ 11.543(2), $c = 14.580(3)$ Å, $\beta = 110.310(10)°$, $V = 2471.4(7)$ Å^3, $Z = 4$, $\rho = 1.364$ Mg m^{-3}, $\mu^* = 0.286$ mm^{-1}, $F(000)^* = 1064$. 4545 data collected, 4294 independent reflections ($R_{int} = 0.0706$), $R_1 =$ 0.1168, $wR_2 = 0.2916$ for data with $I > 2\sigma(I)$, $S = 1.125$, largest peak 0.872 and deepest hole −0.343 e Å^{-3}. ($*M_r$, ρ, μ, and $F(000)$ values assume $0.5\,CH_2Cl_2$ of solvation). CCDC-188724 ($[HNEt_3]$**1**) and CCDC-188725 (**2**) contains the supplementary crystallographic data for this paper. These data can be obtained free of charge via www.ccdc.cam.ac.uk/conts/retrieving.html (or from the Cambridge Crystallographic Data Centre, 12 Union Road, Cambridge CB2 1EZ, UK; fax: (+44) 1223-336-033; or deposit@ccdc.cam.ac.uk).

[15] Crystal data for **2**: $C_{16}H_{23}B_{11}$, $M_r = 334.25$, monoclinic, $P2_1/n$, $a = 7.345(2)$, $b = 17.393(4)$, $c = 14.786(3)$ Å, $\beta = 99.28(2)°$, $V = 1864.2(8)$ Å^3, $Z = 4$, $\rho_{calcd} = 1.191$ Mg m^{-3}, $\mu = 0.058$ mm^{-1}, $F(000) = 696$. 4355 data collected, 3268 independent reflections ($R_{int} = 0.0336$), $R_1 = 0.0462$, $wR_2 = 0.1081$ for data with $I > 2\sigma(I)$, $S = 1.033$, largest peak 0.140 and deepest hole -0.225 e Å^{-3}.[14]
[16] R. G. Parr, W. Yang, *Density-Functional Theory of Atoms and Molecules*, OUP, New York, **1989**. Calculations used the ADF1999 program[17–19] with the BP86 functional and incorporated a treatment of relativistic effects. A double-ζ plus polarization STO basis set for all atoms and the frozen core approximation was applied (C, B: 1s).
[17] E. J. Baerends, D. E. Ellis, P. Ros, *Chem. Phys.* **1973**, *2*, 41.
[18] G. te Velde, E. J. Baerends, *J. Comput. Phys.* **1992**, *99*, 84.
[19] C. F. Guerra, J. G. Snijders, G. te Velde, E. J. Baerends, *Theor. Chem. Acc.* **1998**, *99*, 391.
[20] G. M. Sheldrick, SHELXTL Version 5.1, Bruker AXS Inc., Madison, Wisconsin, **1999**.

Giant Rings

Macrocycle Synthesis by Olefin Metathesis on a Nanosized, Shape-Persistent Tricationic Platinum Template**

*Aleksey V. Chuchuryukin, Harm P. Dijkstra, Bart M. J. M. Suijkerbuijk, Robertus J. M. Klein Gebbink, Gerard P. M. van Klink, Allison M. Mills, Anthony L. Spek, and Gerard van Koten**

Macrocyclic compounds are widely used as preorganized host molecules for the selective binding of specific guests.[1] Commonly, these guests are monometallic cations or small polar molecules, such as urea. An alternative possibility is to assemble a given set of molecules around a metal center[2] or molecular pattern[3,4] and then couple the molecules to one host–guest complex. In this reaction sequence the metal center or molecular pattern functions as template.[5] In a number of recent reports the latter strategy has been used for the synthesis of catenanes and knots,[6] and of molecular wires imbedded in an alkane double helix.[7] In these reactions, host and guest often become irreversibly integrated in an assembly with novel molecular properties.

In a recent study, we prepared a series of shape-persistent multimetallic compounds which can be easily converted into the corresponding multicationic species.[8] The cationic sites in the trication of **1** (see Scheme 1) used in the present study are fixed in a two-dimensional space and are at the corners of a triangle with edges of 1.75 nm.[8b] The NCN pincer platinum cations bind new ligands exclusively *trans* to C_{ipso} along the pseudo C_2 axis of the molecule (C_4-C_{ipso}-Pt). Accordingly, binding of pyridine ligands provides a special molecular arrangement having the planes of the tris(phenylene)benzene core and the pyridine ligands coplanar. It turns out that of the combinations ECE pincer ligand/metal/pyridine (E: N, S; metal: palladium, platinum) the NCN pincer platinum pyridine complexes are the kinetically most stable ones.[9] Moreover, the NCN-Pt complexes are the least active catalysts for the isomerization of α-olefins (see below). This makes the trication of **1** an ideal template for interconnecting the pyridine rings at the *ortho* or *meta* positions thereby forming a large tris(pyridyl) macrocyclic compound around the trication.

Here we report the selective linking of 2,6-bis(dec-9-enyloxy)pyridine substituents by alkene metathesis to form a 69-membered tris(pyridyl) macrocycle. Its detachment occurs by addition of nucleophiles, for example, Cl^-. The trisolefinic macrocycle could be hydrogenated and subsequently recoordinated to the tricationic template. This sequence (Scheme 1) provides a new approach to the selective synthesis of large-ring macrocyclic hosts which have as the only preorganization a precise atom connectivity pattern.

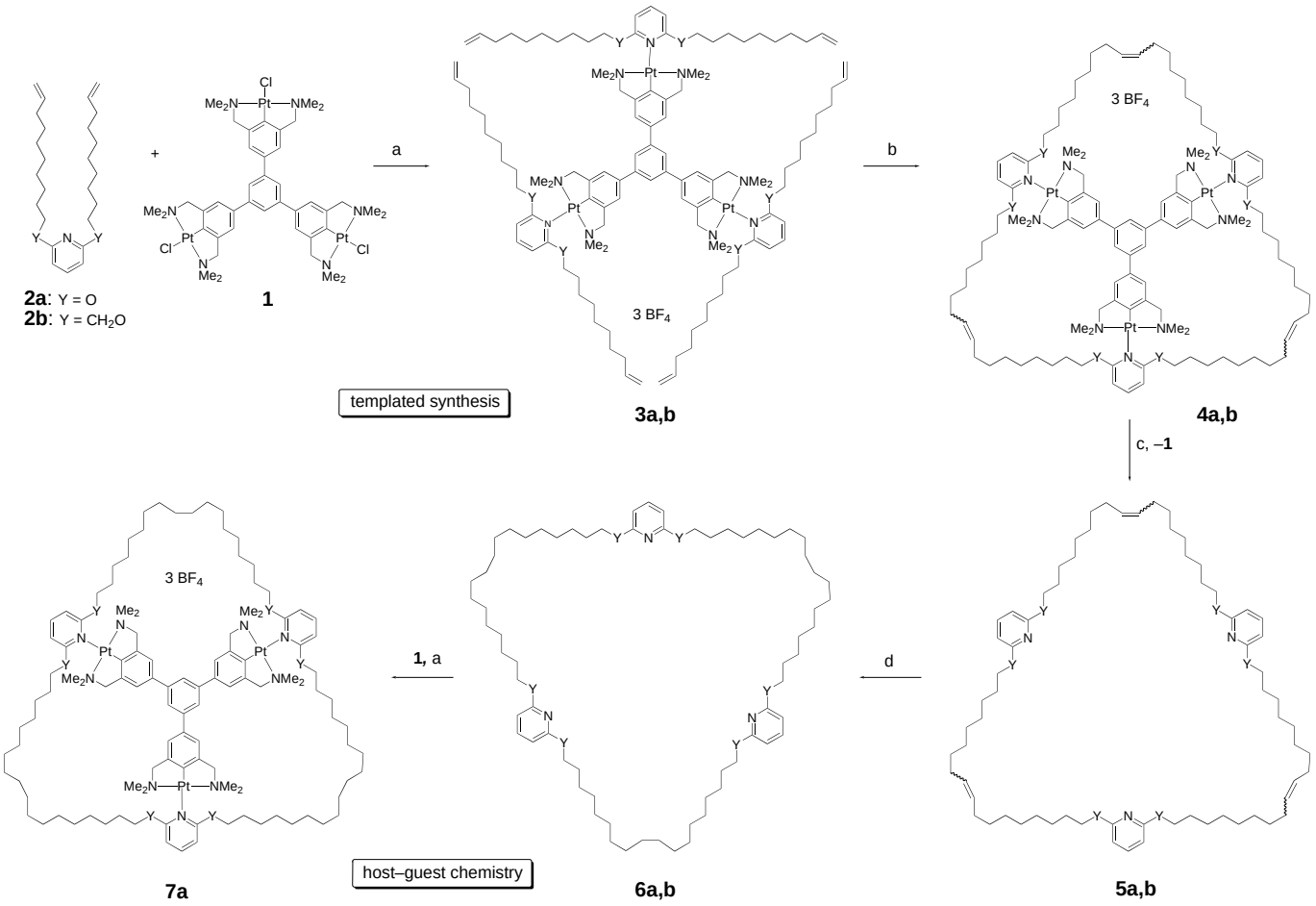
2,6-Bisolefin-substituted pyridines **2a**,**b** were prepared from 9-decen-1-ol and 2,6-dibromopyridine or 2,6-bis(chloromethyl)pyridine, respectively. The template precursor **1** (1 mmol) was reacted in CH_2Cl_2 with three equivalents of either **2a** or **2b** in the presence of suspended $AgBF_4$ to give the tricationic compounds **3a** or **3b**, respectively, in quantitative yields. A prolonged reaction time (30 min to 16 h) is necessary because of the poor solubility of $AgBF_4$ in CH_2Cl_2. The compounds **3** undergo alkene metathesis in the presence of the first-generation Grubbs catalyst, $[Cl_2(Cy_3P)_2Ru{=}CHPh]$ (5 mol% per pyridine ligand), leading to the tricationic tris-platinum heteromacrocycle complexes **4**. The alkene metathesis reactions were performed under high dilution (1×10^{-3} M) to prevent intermolecular olefin metathesis polymerization. Easy detachment of the newly formed macroheterocycle from the tricationic template was possible by reacting **4** with an aqueous NaCl solution, affording free macrocycle **5a** or **5b** and the neutral template precursor **1**. In fact, pure **1** was obtained quantitatively and could be reused in subsequent experiments.

[*] Prof. Dr. G. van Koten, Dr. A. V. Chuchuryukin, Dr. H. P. Dijkstra, B. M. J. M. Suijkerbuijk, Dr. R. J. M. Klein Gebbink, Dr. G. P. M. van Klink
Debye Institute, Department of Metal-Mediated Synthesis
Utrecht University
Padualaan 8, 3584 CH Utrecht (The Netherlands)
Fax: (+31) 30-252-3615
E-mail: g.vankoten@chem.uu.nl
Dr. A. M. Mills, Prof. Dr. A. L. Spek[+]
Bijvoet Center for Biomolecular Research
Department of Crystal and Structural Chemistry
Utrecht University
Padualaan 8, 3584 CH Utrecht (The Netherlands)
[+] Corresponding author for the crystallographic section.

[**] We thank the National Research School Combination Catalysis (NRSC-C)and the Council for Chemical Sciences of the Netherlands Foundation for Scientific Research (CW-NWO) for financial support, and C. Versluis and A. C. H. T. M. van der Kerk-van Hoof, Department of Biomolecular Mass Spectrometry, for the electrospray mass spectra.

Supporting information for this article is available on the WWW under http://www.angewandte.org or from the author.

 © 2003 Wiley-VCH Verlag GmbH & Co. KGaA, Weinheim 1433-7851/03/4202-0228 $ 20.00+.50/0



Scheme 1. a) $AgBF_4$, CH_2Cl_2; b) $[Cl_2(PCy_3)_2Ru{=}CHPh]$ 5 mol%, CH_2Cl_2; c) NaCl, H_2O/CH_2Cl_2; d) H_2, Pd/C.

The macroheterocycles **5** were isolated by preparative thin-layer chromatography (TLC) in 67 (**5a**) and 44% (**5b**) yield. Some mono-pyridine macrocycles and linear oligomers were also formed as by-products. In an attempt to increase the reaction rate and to decrease the amount of catalyst, the more active second-generation Grubbs catalyst, $[Cl_2(PCy_3)(IMes)Ru{=}CHPh]$, IMes = 1,3-bis(2,4,6-trimethylphenyl)-4,5-dihydroimidazol-2-ylidene, was used in the metathesis reaction of **3b**. However, this led to a dramatic decrease in yield of macrocycle **5b** (20%), while large amounts of oligomers were formed. These findings point to the occurrence of secondary cross- and ring-opening metathesis polymerization (ROMP) reactions.

As **5a** and **5b** were formed as mixtures of *cis*/*trans* trisolefinic heteromacrocycles, for analysis purposes they were hydrogenated over Pd/C in CH_2Cl_2 thus providing the alkane macrocycles **6a** (99%) and **6b** (80%).[10] In the case of **5b**, some hydrogenolysis of the benzylic ether bond was observed as a side reaction.[11] It should be noted that according to mass spectrometry both saturated compounds **6** contain macrocycles having one CH_2 group less as small impurities. These macrocycles are most likely formed through cross metathesis of an α-olefinic substituent with a β-olefinic one, which was formed by a prior metal-catalyzed isomerization reaction. Unfortunately, it was not possible to separate these macrocycles from the desired products by TLC.

The macrocycles **6**, which are very flexible and non-preorganized (e.g., by conformational preferences in the connecting alkanediyl chains), were further studied as hosts for highly preorganized nanosized trimetallic guests such as **1**. The reaction of **6a** with **1** gave—after work-up with acetone—complex **7a** in almost quantitative yield (96%). Characterization comprised NMR spectroscopy, elemental analysis and electrospray mass spectrometry.[10] The mass and isotopic pattern in the experimental spectrum was identical to that in the calculated spectrum for the tricationic complex **7a**.

Definite proof for the reattachment to **1** and the perfect cyclic structure of **6a** was provided by an X-ray structure determination of **7a** (with tetraphenylborate as counter anion). This salt was obtained by reaction of **7a** with $NaBPh_4$ in acetone. The molecular geometry and some selected distances and angles are given in Figure 1.[12] The central benzene ring of the template is substituted at positions 1, 3, and 5 with pincer–platinum moieties, each at a different twist angle (the dihedral angles between the planes of the central ring and the pincer aryl rings range from 25.6(3) to 85.1(5)°). The macrocyclic tris(pyridyl) ligand is ligated through its pyridine N atoms to the three peripheral metal centers *trans*

 © 2003 Wiley-VCH Verlag GmbH & Co. KGaA, Weinheim 1433-7851/03/4202-0229 $ 20.00+.50/0

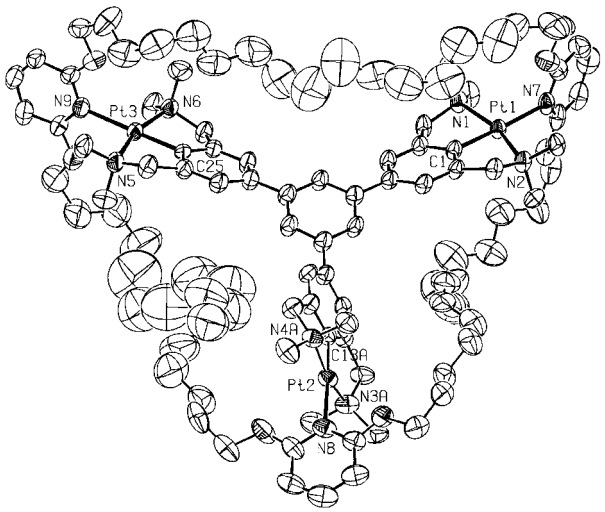


Figure 1. ORTEP representation of the cation in complex **7a**. The hydrogen atoms have been omitted for clarity. Only the major conformation of each of the disordered groups is shown. Selected bond lengths [Å] and angles [°]: Pt1-C1 1.910(5), Pt1-N1 2.104(4), Pt1-N2 2.087(4), Pt1-N7 2.191(4), Pt2-C13A 1.916(5), Pt2-N3A 2.094(6), Pt2-N4A 2.071(5), Pt2-N8 2.192(4), Pt3-C25 1.929(5), Pt3-N5 2.090(4), Pt3-N6 2.093(4), Pt3-N9 2.183(5); C1-Pt1-N1 81.72(18), C1-Pt1-N2 81.19(18), N1-Pt1-N7 94.71(15), N2-Pt1-N7 102.39(15), C1-Pt1-N7 176.32(17), N1-Pt1-N2 162.86(16), C13A-Pt2-N3A 80.4(2), C13A-Pt2-N4A 81.8(2), N3A-Pt2-N8 98.4(2), N4A-Pt2-N8 99.5(2), C13A-Pt2-N8 176.87(19), N3A-Pt2-N4A 161.8(3), C25-Pt3-N5 82.24(19), C25-Pt3-N6 81.33(19), N5-Pt3-N9 96.92(17), N6-Pt3-N9 99.55(17), C25-Pt3-N9 178.3(2), N5-Pt3-N6 163.49(18).

to C_{ipso} of the framework. The pyridine rings of the ligand are nearly perpendicular to the $PtCN_3$ ((NCN)-Pt-N(py)) coordination planes (84.3(4)–89.8(3)°), and are linked at the 2- and 6-positions by saturated $O(CH_2)_{18}O$ bridges to form a 69-membered macrocycle.

In conclusion, this report demonstrates the possibility of synthesizing large polynuclear heteromacrocycles by metathesis of olefin-substituted pyridines in the coordination sphere of symmetric, shape-persistent multimetallic templates. In addition, these multimetallic templates are quantitatively recovered. Currently, this template-directed synthesis is applied in the selective and high-yield synthesis of large heteroatomic crown ether rings.

Received: September 24, 2002 [Z50230]

[1] a) E. C. Constable, *Coordination Chemistry of Macrocyclic Compounds*, Academic, San Diego, CA, **1999**; b) L. F. Lindoy, *The Chemistry of Macrocyclic Ligand Complexes*, Cambridge University Press, Cambridge, UK, **1992**.

[2] E. B. Bauer, J. Ruwwe, J. M. Martín-Alvarez, T. B. Peters, J. C. Bohling, F. A. Hampel, S. Szafert, T. Lis, J. A. Gladysz, *Chem. Commun.* **2000**, 2261–2262, and references therein.

[3] a) J. A. Harnisch, R. J. Angelici, *Inorg. Chim. Acta* **2000**, *300–302*, 273–279; b) H. L. Anderson, J. K. M. Sanders, *J. Chem. Soc. Perkin Trans. 1* **1995**, *29*, 2223–2229, and references therein.

[4] For ring-closing reactions using dynamic combinatorial libraries see a) E. Stulz, Y.-F. Ng, S. M. Scott, J. K. M. Sanders, *Chem. Commun.* **2002**, 524–525; b) S. L. Roberts, R. L. E. Furlan, G. R. L. Cousins, J. K. M. Sanders, *Chem. Commun.* **2002**, 938–939, and references therein.

[5] For general references on templated synthesis see a) N. V. Gerbeleu, V. B. Arion, J. Burgess, *Template Synthesis of Macrocyclic Compounds*, Wiley-VCH, Weinheim, **1999**; b) F. Diederich, P. J. Stang, *Templated Organic Synthesis*, Wiley-VCH, Weinheim, **1999**.

[6] a) M. Weck, B. Mohr, J.-P. Sauvage, R. H. Grubbs, *J. Org. Chem.* **1999**, *64*, 5463–5471; b) G. Rapenne, C. Dietrich-Buchecker, J.-P. Sauvage, *J. Am. Chem. Soc.* **1999**, *121*, 994–1001.

[7] J. Stahl, J. C. Bohling, E. B. Bauer, T. B. Peters, W. Mohr, J. M. Martín-Alvarez, F. Hampel, J. A. Gladysz, *Angew. Chem.* **2002**, *114*, 1951–1957; *Angew. Chem. Int. Ed.* **2002**, *41*, 1872–1876.

[8] a) H. P. Dijkstra, M. D. Meijer, J. Patel, R. Kreiter, G. P. M. van Klink, M. Lutz, A. L. Spek, A. J. Canty, G. van Koten, *Organometallics* **2001**, *20*, 3159–3168; b) H. P. Dijkstra, C. A. Kruithof, N. Ronde, R. van de Coevering, D. J. Ramon, D. Vogt, G. P. M. van Klink, G. van Koten, *J. Org. Chem.* **2002**, ASAP; c) I. P. Beletskaya, A. V. Chuchurjukin, H. P. Dijkstra, G. P. M. van Klink, G. van Koten, *Tetrahedron Lett.* **2000**, *41*, 1081–1085.

[9] H. P. Dijkstra, A. Chuchuryukin, B. M. J. M. Suijkerbuijk, G. P. M. van Klink, A. M. Mills, A. L. Spek, G. van Koten, *Adv. Synth. Catal.* **2002**, *344*, 771–780.

[10] NMR spectroscopic, mass spectrometric and elemental analysis data are available as Supporting Information.

[11] Use of PtO_2[11a] as hydrogenation catalyst or of a nitrogen-containing base as inhibitor for the side reaction[11b] might increase the yield of **6b**. a) H. Pettersson-Fasth, S. W. Riesinger, J. E. Bäckvall, *J. Org. Chem.* **1995**, *60*, 6091–6096; b) H. Sajiki, K. Hirota, *Tetrahedron* **1998**, *54*, 13981–13996.

[12] $C_{111}H_{174}N_9O_6Pt_3 \cdot 3(C_{24}H_{20}B)$, $M_r = 3273.49$, triclinic, $P\bar{1}$ (No. 2), $a = 18.9296(1)$, $b = 20.6363(1)$, $c = 22.4100(2)$ Å, $\alpha = 80.4058(3)$, $\beta = 86.3821(3)$, $\gamma = 76.7954(3)°$, $V = 8400.66(10)$ Å^3, $Z = 2$, $\rho_{calcd} = 1.294$ g cm^{-3}; 2219 refined parameters, 3563 restraints, $R(F) = 0.0517$ $[I > 2\sigma(I)]$, $wR(F^2) = 0.1357$, $S = 1.04$, $\Delta\rho_{max}/\Delta\rho_{min} = 1.92/-1.49$ e Å^{-3}. CCDC 185367 contains the supplementary crystallographic data for this paper. These data can be obtained free of charge via www.ccdc.cam.ac.uk/conts/retrieving.html (or from the Cambridge Crystallographic Data Centre, 12, Union Road, Cambridge CB2 1EZ, UK; fax: (+44) 1223-336-033; or deposit@ccdc.cam.ac.uk).

 © 2003 Wiley-VCH Verlag GmbH & Co. KGaA, Weinheim 1433-7851/03/4202-0230 $ 20.00+.50/0

Controlled Cycloadditions

[3+2] and [4+1] Cycloaddition Reactions of Fischer Alkoxy(alkenyl)carbene Complexes with Electronically Neutral 1,3-Dienes**

José Barluenga, Salomé López, and Josefa Flórez*

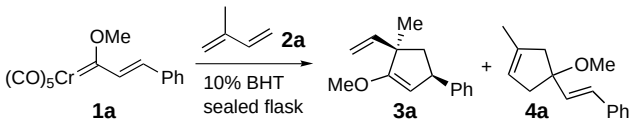
Dedicated to Professor Julio D. Martín on the occasion of his 60th birthday

Reactions of the heteroatom-stabilized carbene complexes of group 6 metals with conjugated carbodienes allow for the construction of cyclic products with different ring sizes[1] that depend upon both the nature of the reaction partners and the reaction conditions.[2] Electron-deficient 1,3-dienes are known to react when heated with alkoxy(aryl/alkyl)carbene complexes to afford $[2_D+1_C]$[3] cycloadducts with high selectivity.[4] While analogous reactions with aminocarbene complexes provide a $[4_D+1_C]$ cycloadduct with pentacarbonyl[(*N*,*N*-dimethylamino)methylene]chromium[5] or $[4_D+3_C]$ cycloadducts with molybdenum–amino(alkenyl)carbene complexes.[6] Electron-rich 1,3-dienes also react with alkoxy(alkenyl)carbene complexes, which undergo a $[4_D+3_C]$ cycloaddition reaction in the case of the chromium derivatives,[7] and a $[4_D+2_C]$ cycloaddition process when tungsten–carbene complexes are involved.[8,9] Nevertheless, the corresponding $[4_D+1_C]$ adduct was isolated when a Cr complex was mixed at room temperature with 2-methyl-1,3-dimorpholino-1,3-butadiene.[7c] In addition, the reaction of alkenylcarbene derivatives with a 1-acceptor-3-donor-substituted 1,3-diene furnished cyclopentenes, which are the $[3_C+2_D]$ adducts of the corresponding carbene ligand to the electron-rich terminal double bond of the silyloxydiene.[7d,10] Simple 1,3-dienes have been shown to undergo either a thermally selective monocyclopropanation reaction ($[2_D+1_C]$ cycloaddition) with alkoxy(alkyl/aryl)carbene complexes of Mo and Cr,[11] or a room-temperature Diels–Alder reaction ($[4_D+2_C]$ annulation) with alkoxy(alkenyl)carbene complexes of Cr and W.[8a,c,12] On the other hand, the photolytic reaction of chromium–alkoxy(alkyl/aryl)carbene complexes with simple cyclic 1,3-dienes produced bicyclic cyclobutanones ($[2_D+1_C+1_{CO}]$ annulation products) with a high degree of selectivity.[13]

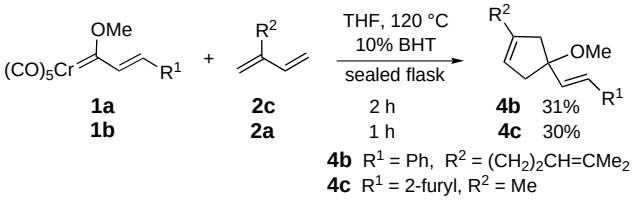
Herein, we report the first examples of $[3_C+2_D]$ or $[4_D+1_C]$ cycloaddition reactions between alkoxy(alkenyl)carbene complexes and electronically neutral 1,3-dienes. The transfer reaction of the carbene ligand as a three-carbon-atom synthon, which seems to be more general than that in which it acts as a one-carbon-atom synthon, took place with total regio- and diastereoselectivity, and high asymmetric induction can be observed when alkenylcarbene complexes derived from (−)-8-phenylmenthol are used.[14]

In the initial experiment, the standard protocol previously established for the intermolecular cyclopropanation of simple alkenes with alkenylcarbene complexes[15] was utilized to evaluate the reaction of methoxycarbene complex **1a** with isoprene (**2a**). Accordingly, this reaction was conducted in THF with five equivalents of diene **2a** in the presence of a catalytic quantity (10 mol% with respect to the diene) of 2,6-di-*tert*-butyl-4-methylphenol (BHT).[16] After heating for 9 h at 80 °C, a nearly equimolar mixture of tetrasubstituted cyclopentene enol ether **3a** and trisubstituted cyclopentene **4a** was obtained (Scheme 1). These structural isomers were easily separated by column chromatography. Compound **3a** was formed as a single diastereoisomer. We observed that performing the reaction in toluene led exclusively to the [3+2] cycloadduct **3a** in high yield, whereas heating the reaction in THF at 120 °C in a sealed flask gave only the [4+1] cycloadduct **4a**, although only in moderate yield. The reactions of other alkenylcarbene complexes with different 1,3-dienes were carried out under both of the above-mentioned reaction conditions to produce the corresponding [3+2] or [4+1] cycloadducts; the results are summarized in both Table 1 and Scheme 2.

The reaction of 3-aryl/heteroaryl- or 3-alkyl-substituted alkenylcarbene–chromium complexes **1a–d** with 1,3-dienes **2a–c** in toluene proceeded smoothly to afford the cyclopentenes **3a–f** diastereoselectively and with high efficiency (Table 1, entries 1–6). The reaction with the structurally analogous molybdenum–carbene complex **1e**, which was conducted at 45 °C, was less efficient (entry 7), while treatment with the corresponding tungsten complex **1f** gave compound **3a** with comparable yield, but required a much longer reaction time (entry 8).[17] Acid hydrolysis of enol ethers **3a–d** and **f** (where R^2 is not H) furnished cyclo-



Scheme 1. Illustration of [3+2] and [4+1] cycloaddition reactions.



Scheme 2. [4+1] Cycloaddition reactions.

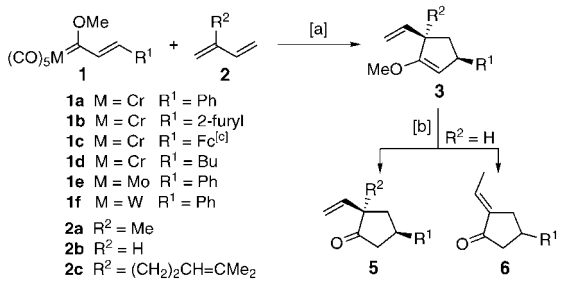
[*] Prof. Dr. J. Barluenga, S. López, Dr. J. Flórez
Instituto Universitario de Química Organometálica "Enrique Moles"
Unidad Asociada al CSIC, Universidad de Oviedo
Julián Clavería 8, 33071 Oviedo (Spain)
Fax: (+34) 98-510-3450
E-mail: barluenga@sauron.quimica.uniovi.es

[**] This research was supported by the DGICYT (PB97-1271). We thank Dr. Eduardo Rubio for assistance with the 2D NMR spectra.

Supporting information for this article is available on the WWW under http://www.angewandte.org or from the author.

 © 2003 Wiley-VCH Verlag GmbH & Co. KGaA, Weinheim 1433-7851/03/4202-0231 $ 20.00+.50/0

Table 1: [3+2] Cycloaddition reactions of alkenylcarbene complexes with simple 1,3-dienes and their subsequent hydrolysis reactions.



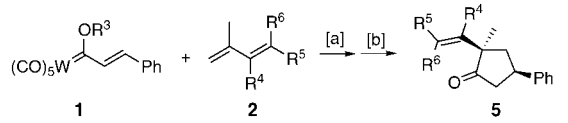
1a M = Cr R^1 = Ph
1b M = Cr R^1 = 2-furyl
1c M = Cr R^1 = Fc[c]
1d M = Cr R^1 = Bu
1e M = Mo R^1 = Ph
1f M = W R^1 = Ph

2a R^2 = Me
2b R^2 = H
2c R^2 = $(CH_2)_2CH{=}CMe_2$

Entry	1	2	*t* [h][d]	3	Yield [%][e]	5 or 6	Yield [%][f]
1	**1a**	**2a**	9	**3a**	94	**5a**	70
2	**1b**	**2a**	10.5	**3b**	91	**5b**	85
3	**1c**	**2a**	24	**3c**	94	**5c**	90
4	**1d**	**2a**	5.5	**3d**	75[g]	**5d**	90
5	**1a**	**2b**	5	**3e**	95	**6a**	86
6	**1a**	**2c**	11	**3f**	86	**5e**	78
7	**1e**	**2a**	24[h]	**3a**	50[i]		
8	**1f**	**2a**	72	**3a**	80[i]		

[a] $PhCH_3$, 5 equiv of **2**, 10% BHT (with respect to the diene), 80°C (bath temperature), sealed flask. [b] 2 N HCl, THF, room temperature, 10–15 min. [c] Fc = ferrocenyl. [d] Reaction time required for complete disappearance of starting carbene complex **1**. [e] Yield obtained from the cycloaddition reaction. [f] Yield obtained after hydrolysis. [g] Crude yield of impure product, which was submitted to hydrolysis without characterization. [h] Reaction temperature = 45 °C. [i] Crude yield.

Table 2: [3+2] Cycloadditions of tungsten–carbene complexes **1f** and **g** with 1,3-dienes **2d–f**.

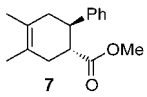


Entry	1	R^3	2	R^4	R^5	R^6	*t* [d][c]	5	Yield [%]
1	**1f**	Me	**2d**	Me	H	H	2.5	**5f**	50[d]
2	**1g**	menthyl[e]	**2d**	Me	H	H	8	**5f**	60
3	**1g**	menthyl[e]	**2e**	H	Me	H	2	**5g**	80
4	**1f**	Me	**2f**	H	Me	Me	4	**5h**	65

[a] $PhCH_3$, 5 equiv of **2**, 10% BHT (with respect to the 1,3-diene), 80°C (bath temperature), sealed flask. [b] The crude product was treated with 2 N HCl, THF, room temperature, 10–15 min (for R^3 = Me) or 1 h (for R^3 = menthyl). [c] Reaction time required for complete disappearance of starting carbene complex **1** at 80°C. [d] In this experiment compound **7** was also isolated in 25% yield. [e] (−)-Menthol was used to prepare the starting carbene complex **1g**.

pentanones **5a–e** (entries 1–4, 6), while the same hydrolysis reaction of enol ether **3e** (R^2 = H) occurred with concomitant isomerization of the terminal C=C bond to form 2-ethylidenecyclopentanone **6a** (entry 5). Both compounds **5** and **6** were isolated as unique diastereoisomers.

In addition, we have found that the more-substituted 1,3-dienes **2d** and **e** led to a complicated mixture of products when they were treated with chromium–carbene complex **1a** (5 equiv of **2**, 10% BHT, $PhCH_3$, 80°C, 8–21 h). In contrast, tungsten–carbene complexes **1f** and **g** reacted with 1,3-dienes **2d–f** to give the corresponding [3+2] cycloadducts, which after subsequent acid hydrolysis were all isolated as the 2-vinylcyclopentanones **5** as a single diastereoisomer (Table 2). The reaction of methoxycarbene complex **1f** with a disubstituted 1,3-diene, such as 2,3-dimethyl-1,3-butadiene (**2d**), provided a 2:1 mixture of cyclopentanone **5f** and cyclohexene derivative **7**, respectively (Table 2, entry 1), whereas the analogous reaction with the trisubstituted 1,3-diene **2f** afforded only the corresponding [3+2] adduct **5h** (Table 2, entry 4). Formation of the minor compound **7**, which is the formal $[4_D+2_C]$ cycloadduct/oxidation product, was completely suppressed by using the menthyloxycarbene complex **1g**, which on treatment with either of the disubstituted 1,3-dienes **2d** or **2e** afforded cyclopentanones **5f** and **g** (Table 2, entries 2 and 3).[18]



7

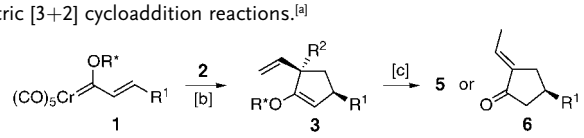
In contrast, the thermal reaction (120°C in THF) of alkenylcarbene–chromium complexes **1a** and **b** with 1,3-dienes **2a** and **c** led to cyclopentene [4+1] adducts **4b** and **c** with low efficiency. A considerable quantity of unidentified products were obtained in these experiments (Scheme 2).[19,20] The connectivity of the atoms in **3** and **4** and the stereochemistry of **3**, **5**, **6**, and **7** were ascertained by NMR experiments (including HMQC, HMBC, COSY, and NOESY).

Finally, the possibility to prepare enantiomerically enriched cyclopentanones **5** and **6** was examined using 8-phenylmenthyloxy (alkenyl)carbene–chromium complexes **1h** and **i**.[14] These chiral complexes reacted with dienes **2a** and **b** to give the [3+2] adducts **3g–i** with variable diastereomeric excesses (Table 3). The most successful result was achieved in the reaction of **1h** and **2b**, in which **3h** was obtained as a diastereomerically pure material. Acid hydrolysis of **3h** led to the isolation of the enantiomerically pure 2-ethylidene-4-phenylcyclopentanone (+)-**6a**. The geometry of (+)-**5** and (+)-**6** was assumed from X-ray analysis of a single crystal of the major enantiomer (+)-**6b**, which exhibits an absolute configuration *R* for the newly created stereogenic center, and confirmed the *E* configuration of the exocyclic C=C bond.[21]

Formation of products **3** and **4** can be rationalized, according to previous models,[5,7d,10,17d] by means of a metalla-Diels–Alder reaction, which presumably occurs after an initial thermally induced dissociation of a CO ligand, followed by reductive elimination of the metal moiety (Scheme 3). The final [3+2] adduct **3** or [4+1] adduct **4** would involve the initial formal addition of the alkenylcarbene complex as a

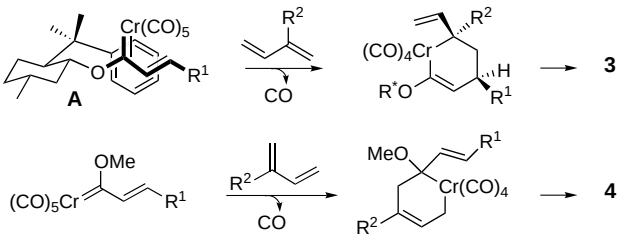
 © 2003 Wiley-VCH Verlag GmbH & Co. KGaA, Weinheim 1433-7851/03/4202-0232 $ 20.00+.50/0

Table 3: Asymmetric [3+2] cycloaddition reactions.[a]



1	R^1	2	R^2	3	Yield [%][d]	*de* [%][e]	5 or 6	Yield [%]	*ee* [%][f]
1h	Ph	**2a**	Me	**3g**	94	74	(+)-**5a**	73	70
1h	Ph	**2b**	H	**3h**	90	>99	(+)-**6a**	90	>99
1i	Fc	**2b**	H	**3i**	95	80	(+)-**6b**	85	79

[a] R* = 8-Phenylmenthyl; (−)-8-Phenylmenthol was used to prepare carbene complexes **1h** and **i**. [b] $PhCH_3$, 10 mol% BHT, 80 °C (bath temperature), sealed flask, 4–24 h. [c] 2 N HCl, THF, room temperature, 1 h. [d] Crude yield. [e] Determined by integration of ^{1}H NMR spectra of the crude product. [f] Determined by HPLC analysis on a chiral support.



Scheme 3. Proposed models for the [3+2] and [4+1] cycloaddition reactions.

1-chroma-1,3-diene and as a Cr=C dienophile, respectively. The sense of diastereochemical induction, which is in agreement with previous results,[14,17d] involves approach of the dienophile to the less-hindered face (front side in model **A**) of the metalladiene.

In conclusion, a general, selective synthesis of enantiomerically enriched alkenyl-substituted cyclopentanones is reported. The process is based on the new annulation of a three-carbon-atom unit of an alkoxy(alkenyl)carbene complex to a two-carbon-atom unit of a simple 1,3-diene. Studies of the scope of these cycloaddition reactions are currently in progress.

Received: October 2, 2002 [Z50281]

[1] H.-W. Frühauf, *Chem. Rev.* **1997**, *97*, 523.

[2] For recent reviews, see: a) K. H. Dötz, P. Tomuschat, *Chem. Soc. Rev.* **1999**, *28*, 187; b) J. W. Herndon, *Tetrahedron* **2000**, *56*, 1257; c) A. de Meijere, H. Schirmer, M. Duetsch, *Angew. Chem.* **2000**, *112*, 4124; *Angew. Chem. Int. Ed.* **2000**, *39*, 3964.

[3] The topological identification of the reaction type is used in a formal sense to describe the number of carbon atoms provided by each fragment to the final cycloadduct, regardless of the mechanism and the number of steps involved. The subscripts D and C refer to the corresponding reagent: D = 1,3-diene, C = carbene ligand (complex).

[4] a) M. Buchert, H.-U. Reissig, *Chem. Ber.* **1992**, *125*, 2723; b) M. Buchert, M. Hoffmann, H.-U. Reissig, *Chem. Ber.* **1995**, *128*, 605.

[5] M. A. Sierra, B. Söderberg, P. A. Lander, L. S. Hegedus, *Organometallics* **1993**, *12*, 3769.

[6] J. Barluenga, F. Aznar, A. Martín, *Organometallics* **1995**, *14*, 1429.

[7] a) W. D. Wulff, D. C. Yang, C. K. Murray, *J. Am. Chem. Soc.* **1988**, *110*, 2653; b) J. Barluenga, F. Aznar, A. Martín, J. T. Vázquez, *J. Am. Chem. Soc.* **1995**, *117*, 9419; c) J. Barluenga, F. Aznar, M. Fernández, *Chem. Eur. J.* **1997**, *3*, 1629; d) M. Hoffmann, M. Buchert, H.-U. Reissig, *Chem. Eur. J.* **1999**, *5*, 876.

[8] a) W. D. Wulff, W. E. Bauta, R. W. Kaesler, P. J. Lankford, R. A. Miller, C. K. Murray, D. C. Yang, *J. Am. Chem. Soc.* **1990**, *112*, 3642; b) J. Barluenga, F. Aznar, A. Martín, S. Barluenga, *Tetrahedron* **1997**, *53*, 9323. For reactions with amino(alkenyl)carbene complexes, see: c) T. S. Powers, W. Jiang, J. Su, W. D. Wulff, *J. Am. Chem. Soc.* **1997**, *119*, 6438.

[9] For reactions of acetoxy(alkenyl)carbene complexes, see: K. Takeda, Y. Okamoto, A. Nakajima, E. Yoshii, T. Koizumi, *Synlett* **1997**, 1181.

[10] M. Hoffmann, M. Buchert, H.-U. Reissig, *Angew. Chem.* **1997**, *109*, 281; *Angew. Chem. Int. Ed. Engl.* **1997**, *36*, 283.

[11] D. F. Harvey, K. P. Lund, *J. Am. Chem. Soc.* **1991**, *113*, 8916.

[12] a) W. D. Wulff, D. C. Yang, *J. Am. Chem. Soc.* **1983**, *105*, 6726; b) K. H. Dötz, W. Kuhn, G. Müller, B. Huber, H. G. Alt, *Angew. Chem.* **1986**, *98*, 826; *Angew. Chem. Int. Ed. Engl.* **1986**, *25*, 812.

[13] a) B. C. Söderberg, L. S. Hegedus, M. A. Sierra, *J. Am. Chem. Soc.* **1990**, *112*, 4364; b) S. Köbbing, J. Mattay, G. Raabe, *Chem. Ber.* **1993**, *126*, 1849.

[14] J. Barluenga, J. M. Montserrat, J. Flórez, S. García-Granda, E. Martín, *Chem. Eur. J.* **1995**, *1*, 236.

[15] J. Barluenga, S. López, A. A. Trabanco, A. Fernández-Acebes, J. Flórez, *J. Am. Chem. Soc.* **2000**, *122*, 8145.

[16] With 1,3-dienes, the presence of this additive is required to inhibit polymerization.

[17] For other [3+2] cycloadditions involving a three-carbon-atom synthon alkenylcarbene ligand, and other substrates, see for example: electron-deficient olefins: a) M. Hoffmann, H.-U. Reissig, *Synlett* **1995**, 625; Enamines: b) J. Barluenga, M. Tomás, A. Ballesteros, J. Santamaría, C. Brillet, S. García-Granda, A. Piñera-Nicolás, J. T. Vázquez, *J. Am. Chem. Soc.* **1999**, *121*, 4516; Methyl ketone enolates: c) J. Barluenga, J. Alonso, F. Rodríguez, F. J. Fañanás, *Angew. Chem.* **2000**, *112*, 2556; *Angew. Chem. Int. Ed.* **2000**, *39*, 2460; Imines: d) H. Kagoshima, T. Okamura, T. Akiyama, *J. Am. Chem. Soc.* **2001**, *123*, 7182; Alkynes: e) W. D. Wulff, B. M. Bax, T. A. Brandvold, K. S. Chan, A. M. Gilbert, R. P. Hsung, J. Mitchell, J. Clardy, *Organometallics* **1994**, *13*, 102.

[18] No asymmetric induction was observed in the cycloaddition reactions with the chiral menthyloxycarbene complex **1g**.

[19] The analogous treatment (10% BHT, THF, 120 °C, 0.5 h) of complex **1a** with **2b** exclusively provided the [3+2] adduct **3d** (75%).

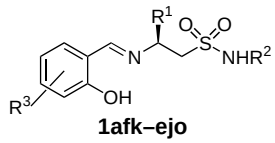
[20] For other [4+1] cycloadditions involving a one-carbon-atom synthon alkenylcarbene ligand, see: J. Barluenga, A. Ballesteros, J. Santamaría, M. Tomás, *J. Organomet. Chem.* **2002**, *643–644*, 363, and references therein.

[21] For full details of the X-ray study, see: J. F. Van der Maelen Uría, S. García-Granda, S. López, *Acta Crystallogr. Sect. E* **2002**, *58*, m613.

Desymmetrization of meso Compounds

A Catalytic and Enantioselective Desymmetrization of *meso* Cyclic Allylic Bisdiethylphosphates with Organozinc Reagents**

Umberto Piarulli, Philippe Daubos, Christelle Claverie, Maryline Roux, and Cesare Gennari**



1afk–ejo

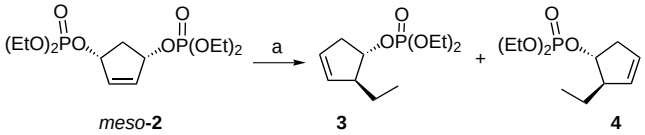
a: R^1 = Me
b: R^1 = *i*Pr
c: R^1 = *i*Bu
d: R^1 = CH_2Ph
e: R^1 = *t*Bu
f: R^2 = CH_2Ph
g: R^2 = (*R*)-CH(Me)Cy
h: R^2 = (*S*)-CH(Me)Cy
i: R^2 = *i*Pr
j: R^2 = $CHPh_2$
k: R^3 = H
l: R^3 = 3,5-*t*Bu_2
m: R^3 = 3,5-Cl_2
n: R^3 = 5,6-$(CH)_4$-
o: R^3 = 3-Ph

Catalytic enantioselective desymmetrization of *meso* compounds is a powerful tool for the construction of enantiomerically enriched functionalized products.[1] *meso* Cyclic allylic diol derivatives are challenging substrates for the asymmetric allylic substitution reaction,[2] owing to the potential competition of several reaction pathways. In particular, S_N2' and S_N2 substitutions can occur, and both with either retention or inversion of stereochemistry. In the case of S_N2 substitution, in which an allylic alcohol derivative is obtained, a second allylic substitution might occur through the S_N2' or S_N2 mechanism, with either retention or inversion of stereochemistry. Based on this complex scenario, up to 15 isomers (seven pairs of enantiomers and one *meso* compound) could, in principle, be obtained.

Herein we present a new highly regio-, diastereo-, and enantioselective desymmetrization of *meso,* cyclic allylic bisdiethylphosphates with organozinc reagents[3] catalyzed by copper(I) complexes of chiral Schiff base ligands **1**.[4] *cis*-4-Cyclopentene-1,3-diol was transformed into the corresponding bisdiethylphosphate **2** by deprotonation with *n*BuLi and reaction with diethylchlorophosphate in THF/TMEDA (4:1).[5] Reaction of *meso*-4-cyclopentene-1,3-bisdiethylphosphate (**2**) with diethylzinc in the presence of $(CuOTf)_2{\cdot}C_6H_6$ ($Tf = CF_3SO_2$) (10 mol%) and chiral ligand **1cjl** in toluene/THF (95:5 v/v) at −78°C afforded only the product arising from the S_N2' mechanism with inversion of stereochemistry, with an enantiomeric ratio **3**/**4** of 87:13 in favor of the *S,S* enantiomer (Scheme 1).[6–8] Other copper sources (CuCN, $Cu(OTf)_2$) and other solvents (pure toluene, pure THF, CH_2Cl_2, *n*-hexane) gave lower yields and poorer selectivities.

A library of 125 ligands **1**[4c] was screened: Cu^I complexes were preformed in situ by stirring a solution of ligand **1** (10 mol%) with $(CuOTf)_2{\cdot}C_6H_6$ (10 mol%) in toluene/THF (95:5) at room temperature. Diethylzinc (solution in toluene) and 4-cyclopentene-1,3-bisdiethylphosphate (**2**) were then added to the mixture at −78°C, and the reaction mixture was stirred for 15 h before quenching. The most interesting results are shown in Table 1: The best enantiomeric ratio (94:6) in favor of the *S,S* enantiomer **3** was observed in the presence of ligands **1cjo** and **1cjm**.[7,8] We found that an increase in the temperature to −60°C did not have a detrimental effect on the enantioselectivity. Instead, complete conversion and almost quantitative yield were observed (for example, ligand **1cjo**: >98% yield, 88% *ee*; ligand **1cjm**: >98% yield, 88% *ee*; ligand **1cjl**: 80% yield, 74% *ee*). Interestingly, ligands with different steric hindrance but with the same absolute configuration at the stereogenic center bearing R^1 may lead to opposite enantiomeric ratios (!) (Table 1, entries 7–9). An enantiomeric ratio of up to 76:24 in favor of (*R,R*)-**4** was obtained in the presence of ligand **1egk**. As a rule of thumb, substituted salicylaldehydes (R^3 = 3,5-Cl_2; 3-Ph; 3,5-*t*Bu; 5,6-$(CH)_4$-), bulky amines ($R^2 = CHPh_2$), and relatively small substituents at the stereogenic center (R^1 = *i*Bu, Me) favor the formation of enantiomer (*S,S*)-**3**, whereas unsubstituted salicylaldehydes (R^3 = H) and relatively small amines (e.g. $R^2 = CH_2Ph$) tend to favor the formation of enantiomer (*R,R*)-**4**.

To investigate the scope of this new reaction, different organozinc reagents were tested with bisdiethylphosphate **2** in the presence of the ligands that gave the best results in the previous screening (**1cjo, 1cjm**) (Scheme 2). In the case of dimethylzinc, the reaction gave exclusively the product



meso-**2** **3** **4**

Scheme 1. Enantioselective allylic alkylation of **2** with Et_2Zn, catalyzed by $(CuOTf)_2{\cdot}C_6H_6$/**1**. Screening of the library of ligands **1**.
a) 1) $(CuOTf)_2{\cdot}C_6H_6$ (10 mol%), **1** (10 mol%), toluene/THF (95:5), room temperature, 45 min; 2) Et_2Zn (1.1 M in toluene), −78°C, 15 h.

[*] Dr. U. Piarulli
Dipartimento di Scienze Chimiche, Fisiche e Matematiche
Università dell'Insubria
via Valleggio 11, 22100 Como (Italy)
Fax: (+39) 031-238-6449
E-mail: umberto.piarulli@uninsubria.it
Prof. Dr. C. Gennari, Dr. P. Daubos, Dr. C. Claverie, Dr. M. Roux
Dipartimento di Chimica Organica e Industriale
Centro di Eccellenza C.I.S.I., Università di Milano
Istituto di Scienze e Tecnologie Molecolari (ISTM) del CNR
via G. Venezian 21, 20133 Milano (Italy)
Fax: (+39) 02-5031-4072
E-mail: cesare.gennari@unimi.it

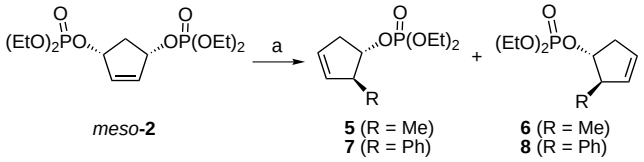
[**] We thank the European Commission (IHP Network grant "Combi-Cat" HPRN-CT-2000-00014) for financial support and postdoctoral fellowships to M. Roux (HPRN-CT-2000-00014), C. Claverie (HPRN-CT-2000-00014), and P. Daubos ("Marie Curie" HPMF-CT-2001-01318). We also thank "Merck Research Laboratories" (Merck's Academic Development Program Award to C. Gennari, 2001) for financial support. U. Piarulli thanks the Dipartimento di Chimica Organica e Industriale (Milan University) for their hospitality.

 © 2003 Wiley-VCH Verlag GmbH & Co. KGaA, Weinheim 1433-7851/03/4202-0234 $ 20.00+.50/0

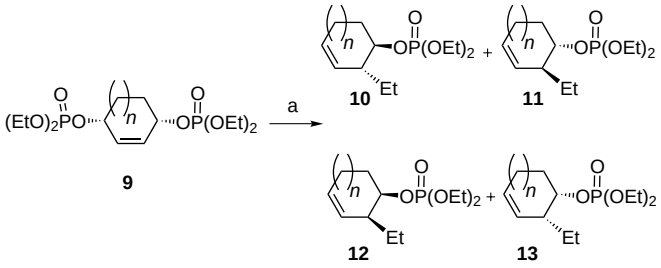
Table 1: Selected results from the high-throughput screening of the library of ligands **1**.[a]

Entry	**1**	R^1	R^2	R^3	**3**/**4**	Yield [%]
1	**cjo**	*i*Bu	$CHPh_2$	3-Ph	94:6	54
2	**cjm**	*i*Bu	$CHPh_2$	3,5-Cl_2	94:6	47
3	**cjl**	*i*Bu	$CHPh_2$	3,5-*t*Bu_2	87:13	42
4	**ajm**	Me	$CHPh_2$	3,5-Cl_2	86:14	62
5	**cjk**	*i*Bu	$CHPh_2$	H	84:16	54
6	**cjn**	*i*Bu	$CHPh_2$	5,6-$(CH)_4$-	83:17	49
7	**afk**	Me	CH_2Ph	H	31:69	13
8	**bfk**	*i*Pr	CH_2Ph	H	30:70	12
9	**egk**	*t*Bu	(*R*)-CH(Me)Cy	H	24:76	26

[a] $[CuOTf]_2{\cdot}C_6H_6$ (0.1 equiv), **1** (0.1 equiv), Et_2Zn (2.0 equiv), **2** (1.0 equiv), toluene/THF (95:5), −78 °C, 15 h.



Scheme 2. Enantioselective allylic alkylation of **2** with R_2Zn, catalyzed by $(CuOTf)_2{\cdot}C_6H_6$/**1cjo** or $(CuOTf)_2{\cdot}C_6H_6$/**1cjm**. a) 1) $(CuOTf)_2{\cdot}C_6H_6$ (10 mol%), **1cjo** or **1cjm** (10 mol%), toluene/THF (95:5), room temperature, 45 min; 2) R_2Zn, −60 °C, 15 h.



Scheme 3. Allylic alkylation of **9** with Et_2Zn, catalyzed by $(CuOTf)_2{\cdot}C_6H_6$/**1**. a) 1) $(CuOTf)_2{\cdot}C_6H_6$ (10 mol%), **1** (10 mol%), room temperature, 45 min; 2) Et_2Zn, −78 or −60 °C, 15 h.

arising from the S_N2' substitution with inversion of stereochemistry (ligand **1cjm**, −60 °C), in moderate yield (40%) and excellent enantiomeric ratio (**5**/**6** 97:3) in favor of the *S,S* enantiomer (**5**, R = Me).[7,8] Allylic phenylation was possible in the reaction of bisdiethylphosphate **2** with a mixture of diphenylzinc and dimethylzinc (2:1).[9] The phenyl group was preferably transferred (Ph transfer vs. Me transfer = 48:1), giving the product of S_N2' substitution with inversion of stereochemistry in moderate yield (60%) and fair enantiomeric ratio (**7**/**8** 84:16 with ligand **1cjo**, −60 °C) in favor of the *S,R* enantiomer (**7**, R = Ph).[7,10]

Reaction of diethylzinc with *cis*-2-cyclohexene-1,4-bisdiethylphosphate[11] (**9**, $n = 1$) (Scheme 3) gave the S_N2' products originating from either inversion (**10** and **11**) or retention of stereochemistry (**12** and **13**) with good diastereoselectivity (81:19–4:96), depending on the solvent and the ligand used. However, racemic mixtures were invariably produced.[12] Preliminary studies with *cis*-2-cycloheptene-1,4-bisdiethylphosphate[11] (**9**, $n = 2$) indicate that only the products arising from the S_N2' substitution with inversion of stereochemistry (**10** + **11**) are formed, with moderate enantiomeric excess (e.g. 56% *ee* with ligand **1cjk**, −60 °C).[10]

In conclusion, we have disclosed a new highly regio-, diastereo-, and enantioselective desymmetrization of *meso* cyclic allylic bisdiethylphosphates with organozinc reagents catalyzed by copper(I) complexes of chiral Schiff base ligands **1**. Further investigations into the scope and limitations of this reaction are currently underway.

Experimental Section

General Procedure: Ligand **1** (0.017 mmol) was dissolved in dry toluene/THF (95:5 v/v; 1.5 mL) in a flame-dried flask under argon. $(CuOTf)_2{\cdot}C_6H_6$ (4.7 mg, 0.017 mmol) was subsequently added, and the resulting greenish solution was stirred at room temperature for 45 min. The reaction mixture was cooled to −78 °C and treated with Et_2Zn (1.1 M solution in toluene; 0.310 mL, 0.340 mmol). After 10 min, *meso*-**2** (60 mg, 0.170 mmol) was added. The reaction mixture was stirred at −78 °C for 15 h, then quenched with a saturated aqueous solution of NH_4Cl (1 mL), and diluted with ethyl acetate (1 mL). The organic phase was separated and filtered through celite. *n*-Decane (0.033 mL, 0.170 mmol) was added, and a sample of the crude reaction mixture (1 μL) was then injected into a GC instrument equipped with a chiral capillary column for determination of yields and enantiomeric ratios (**3**/**4**). Column: MEGADEX DMEPEβ, OV 1701, 25 m, film 0.25 μm; carrier: H_2 (70 kPa); injector 250 °C; detector 250 °C; oven temperature 110 °C, 0.8 °C min^{-1} to 140 °C; t_R: 0.91 min (*n*-decane), 17.7 min ((1*R*,2*R*)-**4**), 18.0 min ((1*S*,2*S*)-**3**), and 39.8 min (*meso*-**2**).

Received: October 10, 2002 [Z50333]

[1] For a recent review, see: M. C. Willis, *J. Chem. Soc. Perkin Trans. 1* **1999**, 1765–1784.

[2] For leading examples of desymmetrization of *meso* cyclic allylic diol derivatives (esters, carbonates, and the closely related *meso* oxabicyclic alkenes), see: a) B. M. Trost, J. Dudash, Jr., E. J. Hembre, *Chem. Eur. J.* **2001**, *7*, 1619–1629; b) B. M. Trost, D. E. Patterson, E. J. Hembre, *Chem. Eur. J.* **2001**, *7*, 3768–3775; c) B. M. Trost, J. Dudash, Jr., O. Dirat, *Chem. Eur. J.* **2002**, *8*, 259–268; d) M. Lautens, J.-L. Renaud, S. Hiebert, *J. Am. Chem. Soc.* **2000**, *122*, 1804–1805; e) M. Lautens, S. Hiebert, J.-L. Renaud, *Org. Lett.* **2000**, *2*, 1971–1973; f) M. Lautens, S. Hiebert, J.-L. Renaud, *J. Am. Chem. Soc.* **2001**, *123*, 6834–6839; g) M. Lautens, C. Dockendorff, K. Fagnou, A. Malicki, *Org. Lett.* **2002**, *4*, 1311–1314, and references therein; h) F. Bertozzi, M. Pineschi, F. Macchia, L. A. Arnold, A. J. Minnaard, B. L. Feringa, *Org. Lett.* **2002**, *4*, 2703–2705.

[3] For copper-catalyzed allylic alkylations in the presence of dialkylzinc reagents, see: a) F. Dübner, P. Knochel, *Angew. Chem.* **1999**, *111*, 391–393; *Angew. Chem. Int. Ed.* **1999**, *38*, 379–381; b) C. A. Luchaco-Cullis, H. Mizutani, K. E. Murphy, A. H. Hoveyda, *Angew. Chem.* **2001**, *113*, 1504–1508; *Angew. Chem. Int. Ed.* **2001**, *40*, 1456–1460; c) H. Malda, A. W. van Zijl, L. A. Arnold, B. L. Feringa, *Org. Lett.* **2001**, *3*, 1169–1171; d) S.

 © 2003 Wiley-VCH Verlag GmbH & Co. KGaA, Weinheim 1433-7851/03/4202-0235 $ 20.00+.50/0

Ongeri, U. Piarulli, M. Roux, C. Monti, C. Gennari, *Helv. Chim. Acta* **2002**, 3388 – 3399.

[4] a) I. Chataigner, C. Gennari, U. Piarulli, S. Ceccarelli, *Angew. Chem.* **2000**, *112*, 953 – 956; *Angew. Chem. Int. Ed.* **2000**, *39*, 916 – 918; b) S. Ongeri, U. Piarulli, R. F. W. Jackson, C. Gennari, *Eur. J. Org. Chem.* **2001**, 803 – 807; c) I. Chataigner, C. Gennari, S. Ongeri, U. Piarulli, S. Ceccarelli, *Chem. Eur. J.* **2001**, *7*, 2628 – 2634.

[5] K. L. Yu, K. Y. Ko, B. Fraser-Reid, *Synth. Commun.* **1988**, 465 – 468.

[6] The chiral copper complex appears to be essential to obtain the reaction product. In fact, the addition of Et_2Zn in the presence of $(CuOTf)_2{\cdot}C_6H_6$ and in the absence of the chiral ligand gave only starting material and minute amounts of **3**/**4** (8 %).

[7] CuCN (3.5 equiv) mediated allylic alkylation of (1*R*,3*S*)-(+)-*cis*-4-cyclopentene-1,3-diol 1-acetate with EtMgCl (3.0 equiv) in THF at −18→0 °C gave (1*S*,2*S*)-*trans*-2-ethyl-3-cyclopenten-1-ol selectively, through S_N2' substitution of the acetate with inversion. This compound was then reacted with $(EtO)_2POCl$ (pyridine, DMAP, CH_2Cl_2) to give enantiomerically pure **3** $[\alpha]_D = +84.0°$ ($CHCl_3$, $c = 1.2$). The above synthetic sequence was also performed with MeMgCl and PhMgCl instead of EtMgCl, yielding enantiomerically pure (1*S*,2*S*)-**5** (R = Me) and (1*S*,2*R*)-**7** (R = Ph). See: a) M. Ito, M. G. Murugesh, Y. Kobayashi, *Tetrahedron Lett.* **2001**, *42*, 423 – 427; b) M. Ito, M. Matsuumi, M. G. Murugesh, Y. Kobayashi, *J. Org. Chem.* **2001**, *66*, 5881 – 5889; c) Y. Kobayashi, M. Ito, J. Igarashi, *Tetrahedron Lett.* **2002**, *43*, 4829 – 4832.

[8] The crude reaction mixture was injected into a GC instrument equipped with a chiral capillary column for the determination of *ee* values (column: MEGADEX DMEPEβ, OV 1701, 25 m, film 0.25 μm, carrier: H_2 (70 kPa)). For the determination of **3**/**4** ratio, see Experimental Section. Determination of **5**/**6** (R = Me) ratio: injector 250 °C, detector 250 °C, oven temperature 90 °C, 0.8 °C min^{-1} to 130 °C, t_R: 26.2 min ((1*R*,2*R*)-**6**) and 26.7 min ((1*S*,2*S*)-**5**).

[9] a) C. Bolm, N. Hermanns, J. P. Hildebrand, K. Muñiz, *Angew. Chem.* **2000**, *112*, 3607 – 3609; *Angew. Chem. Int. Ed.* **2000**, *39*, 3465 – 3467; b) M. Schinnerl, M. Seitz, A. Kaiser, O. Reiser, *Org. Lett.* **2001**, *3*, 4259 – 4262.

[10] The enantiomeric ratios (**7**/**8** (R = Ph), **10**:**11**, $n = 2$) was determined after reduction of the phosphate ester with $LiAlH_4$ in diethyl ether (quant. yield), and derivatization of the resulting alcohol with (*R*)-(+)-α-methoxy-α-(trifluoromethyl)phenylacetic acid, dicyclohexyl carbodiimide, 4-dimethylaminopyridine in dichloromethane (quant. yield). The ratio of the two diastereomeric Mosher esters was assessed by ^1H NMR spectroscopy; see: a) J. A. Dale, H. S. Mosher, *J. Am. Chem. Soc.* **1973**, *95*, 512 – 519; b) G. R. Sullivan, J. A. Dale, H. S. Mosher, *J. Org. Chem.* **1973**, *38*, 2143 – 2147.

[11] J. E. Bäckvall, S. E. Byström, R. E. Nordberg, *J. Org. Chem.* **1984**, *49*, 4619 – 4631.

[12] At present we do not have a convincing rationale for this unexpected result. However, a possible reason for the different behavior of the cycloalkene derivatives **2** and **9** ($n = 1$, $n = 2$) might be related to their symmetry. Indeed, whereas the cyclopentene derivative **2** and the cycloheptene derivative **9** ($n = 2$) can exist and react in a C_S conformation (plane symmetric), the cyclohexene derivative **9** ($n = 1$) is better described as a mixture of readily interconverting enantiomers.

 © 2003 Wiley-VCH Verlag GmbH & Co. KGaA, Weinheim 1433-7851/03/4202-0236 $ 20.00+.50/0

Cover Picture



Dante Gatteschi and Roberta Sessoli*

Single-Molecule Magnets have received a lot of attention over the last decade. The cover picture shows the stepped magnetic hysteresis loop, which is the fingerprint of the resonant quantum tunneling of the magnetization. This phenomenon is observed at low temperature in molecules characterized by large spin and large magnetic anisotropy, as is the case for the dodecanuclear manganese(III)–manganese(IV) oxo cluster or the octanuclear iron(III) cluster. More about the properties of such "single-molecule magnets" can be found in the Review by D. Gatteschi and R. Sessoli on page 269 ff.

Contents

Web Sites

http://www.shsu.edu/~chm_tgc/sounds/sound.html — **254**	Add a Little Flash to Your Lectures	*T. Hannon, J. Elsila, H. Bechtel*

Books

Supramolecular Organization and Materials Design — **255**	William Jones, C. N. R. Rao	*M. Epple*
In-Situ Spectroscopy in Heterogeneous Catalysis — **256**	James F. Haw	*F. Jentoft*

Highlights

Transport Mechanisms

R. Ludwig* — **258 – 260**

New Insight into the Transport Mechanism of Hydrated Hydroxide Ions in Water

Keywords:
ab initio calculations · anions · transport mechanism · water chemistry



A simple reflection of the hydrated proton does not describe how the hydrated hydroxide ion behaves in water. That both ions display a different chemistry in aqueous solution is in contradiction to traditional views in chemistry textbooks.

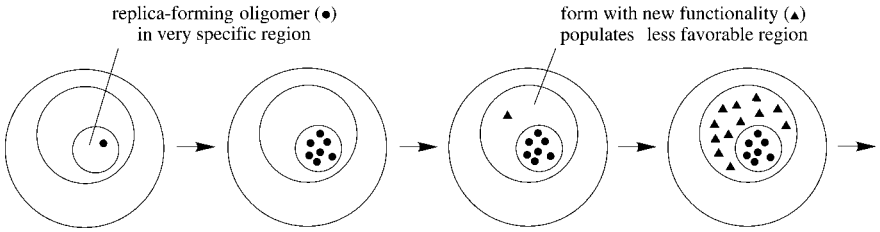
Essays

Origin of Life

H. Kuhn,* C. Kuhn — **262 – 266**

Diversified World: Drive to Life's Origin?!

Keywords:
evolution · genetic apparatus · homochirality · information emergence · origin of life · self-organization

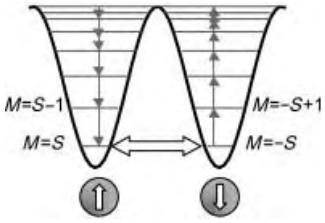


How does life originate? To uncover the fundamental mechanism of this process a series of tangible, detailed physical-chemical steps must be sought which lead to a genetic apparatus. The process in the thought experiment begins in a small singular region with a particularly special temporal-spatial structure. A continuous increase in complexity is coupled with the population of increasingly less favorable regions (see picture). A highly diversified structure is crucial to maintain this process.

© 2003 Wiley-VCH Verlag GmbH & Co. KGaA, Weinheim

1433-7851/03/4203-0246 $ 20.00+.50/0

Reviews



Single-molecule magnets (SMMs) are a new class of materials which are particularly attractive for the interplay of quantum and classical aspects in magnetism. In particular they show the tunneling effects of the magnetization which have been long looked for. To design new SMMs chemists must understand which are the structural factors determining these unusual properties. The goal of this review is to provide the necessary theoretical background and to report the state of the art of the field. The picture shows the classical energy-level diagram of a system with spin *S*.

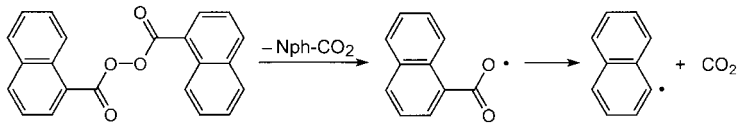
Single-Molecule Magnets

D. Gatteschi, R. Sessoli* ____ **268 – 297**

Quantum Tunneling of Magnetization and Related Phenomena in Molecular Materials

Keywords:
cluster compounds · magnetic properties · quantum tunneling · single-molecule magnets · theoretical chemistry

Communications



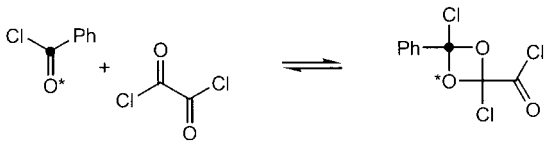
Time-resolved studies of the decomposition of organic peroxides are of fundamental interest because the time scales of formation and subsequent decay of free-radical intermediates determine the initiator efficiency in radical polymerization reactions. The photoinduced multistep decarboxylation of organic peroxides (e.g. dinaphthoyl peroxide, see scheme) in solution was monitored in real time and analyzed with quantum-chemical methods.

Femtochemistry of Peroxides

B. Abel,* J. Aßmann, M. Buback, M. Kling, S. Schmatz,* J. Schroeder ____ **300 – 303**

Ultrafast Decarboxylation of Organic Peroxides in Solution: Interplay of Different Spectroscopic Techniques, Quantum Chemistry, and Theoretical Modeling

Keywords:
density functional calculations · femtochemistry · intermediates · peroxides · transition states



Tell me where the ^{18}O atoms are, where are they to be found? This question was raised when a large amount of the ^{18}O labeling was lost in the course of the conversion of [$^{18}O_2$]benzoic acid into [^{18}O]benzoyl chloride with oxalyl chloride. That the ^{13}C marking in [carboxy-^{13}C]benzoic acid was retained fully under the same conditions made the matter even more mysterious. Equilibration with 1,3-dioxetane (see scheme) or 1,3,5-trioxane intermediates can explain the oxygen-atom exchange with retention of identity of the carbon atom of the carbonyl group.

Oxygen Labeling and Exchange

P. Haiss, K.-P. Zeller* ____ **303 – 305**

Loss of Isotope Labeling in the Conversion of [$^{18}O_2$]Benzoic Acid into [^{18}O]Benzoyl Chloride with Oxalyl Chloride

Keywords:
acid chlorides · isotope labeling · oxygen · reaction mechanisms

For the USA and Canada:
ANGEWANDTE CHEMIE International Edition (ISSN 1433-7851) is published weekly by Wiley-VCH PO Box 191161, D 69451 Weinheim, Germany. Air freight and mailing in the USA by Publications Expediting Inc. 200 Meacham Ave., Elmont, NY 11003. Periodicals postage paid at Jamaica NY 11431. US POSTMASTER: send address changes to *Angewandte Chemie*, Wiley-VCH, 605 Third Ave, New York, NY 10158-0012. Annual institutional subscription price for institutions: Europe € 2998.00/3148.00. Outside Europe US$ 3718.00/3904.00 (valid for print or electronic/print and electronic delivery); for individuals who are personal members of a national chemical society, or whose institution already subscribes, or who are retired or self-employed consultants, print only (including postage and handling charges): Europe € 248.00/Outside Europe US$ 348.00.

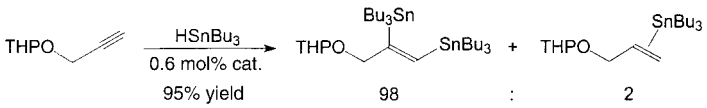
 © 2003 Wiley-VCH Verlag GmbH & Co. KGaA, Weinheim 1433-7851/03/4203-0247 $ 20.00+.50/0

Contents

Tungsten-Catalyzed Distannation

S. Braune, U. Kazmaier* ——— **306 – 308**

Development of a New Catalyst for the Distannation of Alkynes



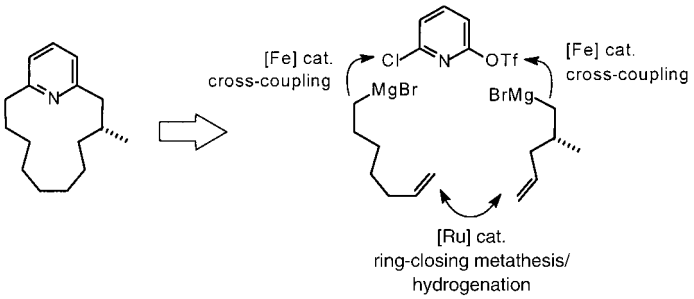
An added bonus in the optimization of a catalyst for the hydrostannation with tin hydrides was the discovery that molybdenum isonitrile complexes are also suitable for distannations. Further developments in this respect led to a new tungsten isonitrile complex, which catalyzed this reaction highly efficiently and selectively (see scheme, THP = tetrahydropyranyl).

Keywords:
isocyanide ligands · molybdenum · stannation · tungsten · vinylstannanes

Efficient Synthetic Strategy

A. Fürstner,* A. Leitner ——— **308 – 311**

A Catalytic Approach to (*R*)-(+)-Muscopyridine with Integrated "Self-Clearance"



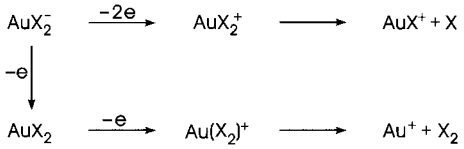
The integration of various metal-catalyzed reactions into a one-pot processes opens an unprecedentedly short and efficient route to the odoriferous alkaloid (*R*)-(+)-muscopyridine. Importantly, it is shown how metathesis can be used for a most convenient "self-clearance" of a product mixture (see scheme; OTf = CF_3SO_3).

Keywords:
cross-coupling · iron · macrocycles · metathesis · ruthenium

Gaseous Gold Dihalides

D. Schröder,* R. Brown, P. Schwerdtfeger, X. B. Wang, X. Yang, L. S. Wang, H. Schwarz ——— **311 – 314**

Gold Dichloride and Gold Dibromide with Gold Atoms in Three Different Oxidation States



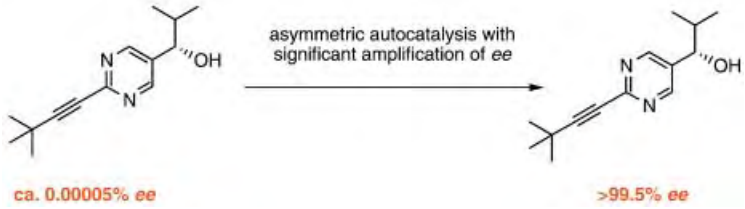
Anionic, cationic, and neutral: Gaseous gold dihalides can exist in three different oxidation states, namely: AuX_2^-, AuX_2, and AuX_2^+ (see scheme; X = Cl, Br). The dihalide structure is strongly preferred for anionic and neutral species, whereas experiment and theory suggest the presence of X–X bonds in the cations.

Keywords:
electron transfer · gold halides · mass spectrometry · photoelectron spectroscopy

Amplification of Chirality

I. Sato, H. Urabe, S. Ishiguro, T. Shibata, K. Soai* ——— **315 – 317**

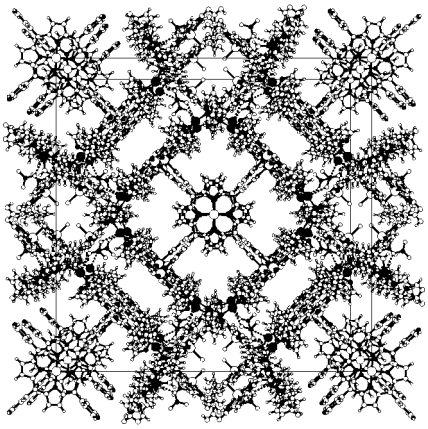
Amplification of Chirality from Extremely Low to Greater than 99.5% *ee* by Asymmetric Autocatalysis



"Single-handedly", in every sense of the word, the alkylation product shown catalyzes its own asymmetric formation from the corresponding aldehyde. In this way the miniscule initial enantiomeric excess of about 0.00005% was amplified to >99.5% *ee* after three cycles.

Keywords:
alkylations · asymmetric synthesis · autocatalysis · chirality · zinc

© 2003 Wiley-VCH Verlag GmbH & Co. KGaA, Weinheim
1433-7851/03/4203-0248 $ 20.00+.50/0



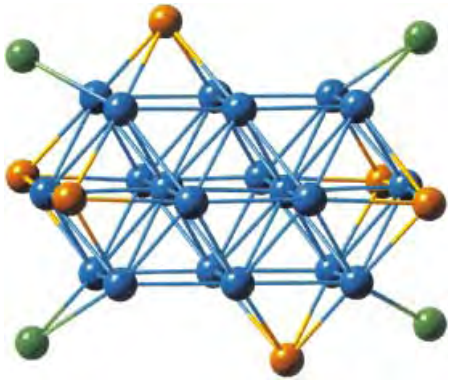
Very large free voids (more than 50% of the cell volume) and interesting stuctural motifs are found in the 2D and 3D frameworks assembled using $AgNO_3$ and 5,10,15,20-tetra(4-pyridyl)porphyrin (H_2tpyp) building blocks. The robust 3D network of $[Ag_8(Zn^{II}tpyp)_7(H_2O)_2](NO_3)_8$ is particularly fascinating in that it exhibits a unique self-penetrating topology (see figure) and can be reversibly desolvated.

Coordination Networks

L. Carlucci, G. Ciani,* D. M. Proserpio, F. Porta ——— **317 – 322**

Open Network Architectures from the Self-Assembly of $AgNO_3$ and 5,10,15,20-Tetra(4-pyridyl)porphyrin (H_2tpyp) Building Blocks: The Exceptional Self-Penetrating Topology of the 3D Network of $[Ag_8(Zn^{II}tpyp)_7(H_2O)_2](NO_3)_8$

Keywords:
coordination polymer · nanostructures · networks · porphyrinoids · silver



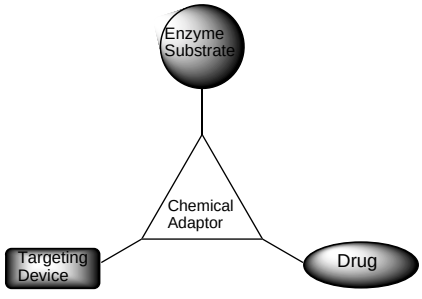
Unprecedented metal-core architectures are exhibited by the title palladium cluster compounds, the structures of which consist of twinned cuboctahedral units. The Pd_{30} core (see picture) consists of two Pd_{13} fragments that form a Pd_{20} bicuboctahedron (blue) with six common atoms, in addition to six face-capping (orange) and four wingtip (green) Pd atoms. The Pd_{54} core is a more complex, five-layered supracluster, but contains the same central Pd_{20} bicuboctahedron as observed in the Pd_{30} cluster.

Palladium Cluster Compounds

E. G. Mednikov, S. A. Ivanov, L. F. Dahl* ——— **323 – 327**

$[Pd_{30}(CO)_{26}(PEt_3)_{10}]$ and $[Pd_{54}(CO)_{40}(PEt_3)_{14}]$: Generation of Nanosized Pd_{30}- and Pd_{54}-Core Geometries Containing Interpenetrating Cuboctahedral-Based Metal Polyhedra

Keywords:
carbonyl ligands · cluster compounds · palladium · phosphane ligands · structure elucidation



Targeting tumors can be achieved by using a novel chemical adaptor system (see picture) comprising, for example, the anticancer drug epotoside, an *N*-(2-hydroxypropyl)methacrylamide (HPMA) copolymer as the tumor-targeting device, and catalytic antibody 38C2 as the triggering enzyme in a single entity. When the enzyme cleaves the substrate, it triggers a spontaneous reaction that releases the active drug from the targeting moiety.

Chemical Adaptor Systems

A. Gopin, N. Pessah, M. Shamis, C. Rader, D. Shabat* ——— **327 – 332**

A Chemical Adaptor System Designed To Link a Tumor-Targeting Device with a Prodrug and an Enzymatic Trigger

Keywords:
cancer therapy · catalytic antibodies · drug delivery systems · prodrugs · selective chemotherapy

 © 2003 Wiley-VCH Verlag GmbH & Co. KGaA, Weinheim 1433-7851/03/4203-0249 $ 20.00+.50/0

Contents

Light Harvesting with Gels

A. Ajayaghosh,* S. J. George, V. K. Praveen ——— 332 – 335

Gelation-Assisted Light Harvesting by Selective Energy Transfer from an Oligo(*p*-phenylenevinylene)-Based Self-Assembly to an Organic Dye

Keywords:
energy transfer · gels · light harvesting · phenylenevinylenes · self-assembly



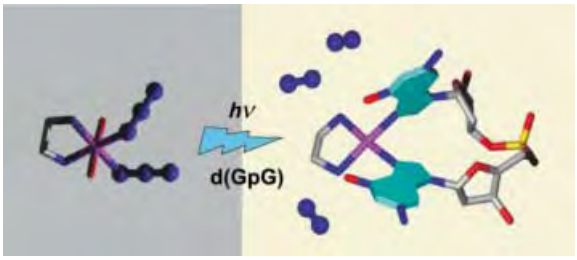
Hot gels get turned off: Gelation of the title molecules facilitate transfer of excitation energy exclusively from the self-assembled nanostructures (see scheme path a) to Rhodamine B and not from the single molecules (path b), thereby establishing the role of self-assembled gel nanostructures in light harvesting. The emission from the dye can be shut off in a thermoreversible fashion since the self-assembly breaks to form molecular, dissolved oligo(phenylenevinylene)s above the gel melting temperature (T_{gel}).

Photochemotherapeutical Drugs

P. Müller, B. Schröder, J. A. Parkinson, N. A. Kratochwil, R. A. Coxall, A. Parkin, S. Parsons, P. J. Sadler* ——— 335 – 339

Nucleotide Cross-Linking Induced by Photoreactions of Platinum(IV)–Azide Complexes

Keywords:
antitumor agents · bioinorganic chemistry · NMR spectroscopy · nucleotides · photochemistry · platinum



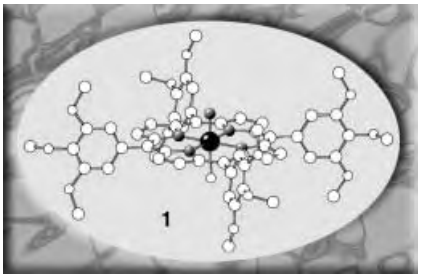
Visible light irradiation of inert [Pt^{IV}-(diam(m)ine)(diazide)] complexes leads to reductive elimination of the azide ligands, production of N_2, and formation of bifunctional adducts with guanine bases of the type which are lethal to cancer cells (see scheme).

Aminations with Ru Porphyrins

S. K.-Y. Leung, J.-S. Huang, J.-L. Liang, C.-M. Che,* Z.-Y. Zhou ——— 340 – 343

Nitrido Ruthenium Porphyrins: Synthesis, Characterization, and Amination Reactions with Hydrocarbon or Silyl Enol Ethers

Keywords:
amination · N ligands · porphyrinoids · ruthenium · structure elucidation



An unprecedented synthetic strategy was used for the preparation of nitrido ruthenium(VI) porphyrins such as **1**. The structure of **1** features a Ru–N (nitrido) distance of 1.656(5) Å. Reactions of nitrido ruthenium(VI) porphyrins with silyl enol ethers or indan, in the presence of trifluoroacetic anhydride, afforded *N*-trifluoroacetyl amines in up to 84% yield.

© 2003 Wiley-VCH Verlag GmbH & Co. KGaA, Weinheim
1433-7851/03/4203-0250 $ 20.00+.50/0

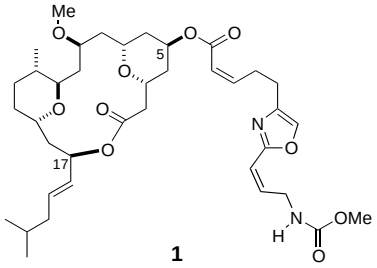
Synthesis of a Marine Macrolide

I. Paterson,* M. Tudge ——— 343 – 347

Stereocontrolled Total Synthesis of (+)-Leucascandrolide A

Keywords:
aldol reaction · antitumor agents · macrolides · natural products · total synthesis

Apparently no longer available from its natural source is the potent cytotoxic and antifungal agent leucascandrolide A (**1**), which was initially isolated from a New Caledonian calcareous sponge. A highly stereocontrolled total synthesis of this structurally unique macrolide commences with a Jacobsen asymmetric hetero Diels–Alder reaction to configure the tetrahydropyran ring. An efficient endgame relies on two Mitsunobu reactions, the first to generate the 18-membered macrolactone



1

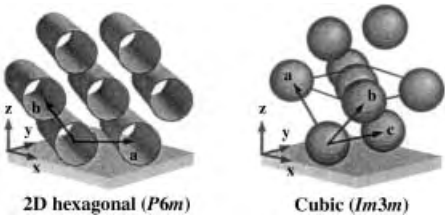
and the second to attach the oxazole-bearing side chain.

Yttria-Zirconia Thin Films

E. L. Crepaldi, G. J. de A. A. Soler-Illia, A. Bouchara, D. Grosso, D. Durand, C. Sanchez* ——— 347 – 351

Controlled Formation of Highly Ordered Cubic and Hexagonal Mesoporous Nanocrystalline Yttria–Zirconia and Ceria–Zirconia Thin Films Exhibiting High Thermal Stability

Keywords:
cerium · mesoporous materials · thin films · yttrium · zirconium



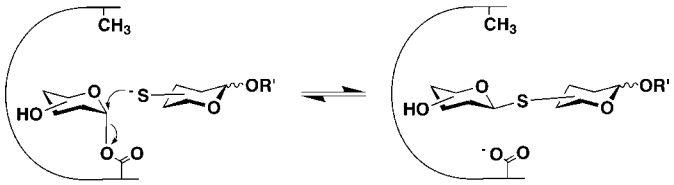
Yttria–zirconia and ceria–zirconia mesoporous thin films adopt either a cubic or 2D hexagonal mesostructure (see picture) depending on the quantity of water employed during the post-processing of the films. The hexagonal films are thermally stable above 400 °C, while the cubic forms retain their integrity up to 700 °C; both forms continue to be porous at temperatures as high as 800 °C. Such robust and easily prepared crystalline materials may have many useful applications, for example, in the design of sensors, electrode materials, and catalysts.

Glycobiology

M. Jahn, J. Marles, R. A. J. Warren, S. G. Withers* ——— 352 – 354

Thioglycoligases: Mutant Glycosidases for Thioglycoside Synthesis

Keywords:
enzyme catalysis · glycosylation · thioglycosides



Engineering of the active site of retaining glycosidases in conjunction with the appropriate modification of their substrates has led to the enzymatic synthesis of thioglycosidic linkages in thiooligosaccharides (see scheme).

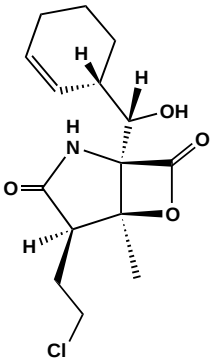
A Cytotoxic Proteasome Inhibitor

R. H. Feling, G. O. Buchanan, T. J. Mincer, C. A. Kauffman, P. R. Jensen, W. Fenical* ——— 355 – 357

Salinosporamide A: A Highly Cytotoxic Proteasome Inhibitor from a Novel Microbial Source, a Marine Bacterium of the New Genus *Salinospora*

Keywords:
cytotoxicity · inhibitors · natural products · proteases · structure elucidation

Strong and selective cytotoxicity toward a variety of cancer cell lines is shown by salinosporamide A (**1**), which was isolated from the culture extract of a unique marine actinomycete belonging to the recently discovered genus *Salinospora*.



1

 © 2003 Wiley-VCH Verlag GmbH & Co. KGaA, Weinheim 1433-7851/03/4203-0251 $ 20.00+.50/0

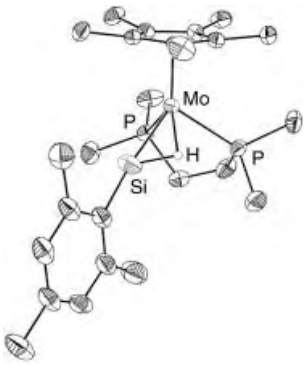
Contents

Molybdenum–Silicon Multiple Bonds

B. V. Mork, T. D. Tilley* ——— **357 – 360**

Multiple Bonding Between Silicon and Molybdenum: A Transition-Metal Complex with Considerable Silylyne Character

Keywords:
bond theory · metal–metal interactions · molybdenum · silicon · transition metals



Mo≡Si bonds a reality? The silylene complex [Cp*(dmpe)(H)Mo=Si(Cl)Mes] (Cp* = η^5-pentamethylcyclopentadienyl, dmpe = 1,2-bis(dimethylphosphanyl)-ethane, Mes = 2,4,6-trimethylphenyl) reacts cleanly with $LiB(C_6F_5)_4$ in fluorobenzene to give [{Cp*(dmpe)(H)MoSi-Mes}{$B(C_6F_5)_4$}], the first structurally determined complex with significant metal silylyne (M≡Si) character (see picture). The possibility of a silicon–hydride interaction is discussed.

VIP Communications labeled with this symbol have been judged by two referees as being "very important papers".

The publication of Communications labeled with this symbol has been accelerated because of their topical or highly competitive nature.

Supporting information for articles labeled with this symbol can be found at www.angewandte.org or www.interscience.wiley.com.

Sources

Product and Company Directory

You can start the entry for your company in "Sources" in any issue of *Angewandte Chemie*.

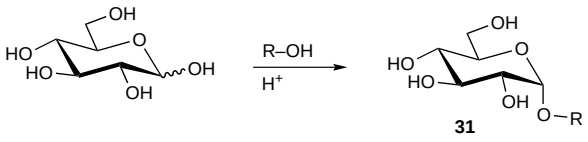
If you would like more information, please do not hesitate to contact us.

Wiley-VCH Verlag – Advertising Department
Tel.: 0 62 01 - 60 65 65
Fax: 0 62 01 - 60 65 50
E-Mail: MSchulz@wiley-vch.de

Service

Keywords ——— **362**
Authors ——— **363**
Angewandte's Sister Journals ——— **364**
Classified ——— **261**
Preview ——— **365**

Corrigendum



31

In the Essay on Emil Fischer by Horst Kunz (*Angew. Chem. Int. Ed.* **2002**, *41*, 4439 – 4451), the oxygen atoms are missing from the rings in the formulae of the glycopyranoses. For example, the correct form of Scheme 14 is shown; the formulae of other glycopyranoses in the other schemes should be corrected accordingly. According to the author, dealing with carbohydrates for many years obviously promotes a kind of occupational myopia in which one sees oxygen atoms in pyranoses even where there are none. In addition the reagent over the first arrow in Scheme 19 should be chloroacetyl chloride, on page 4443, first column, paragraph four, line three, it should be "Ludwig Knorr", on page 4449, second column, fourth from last line "Lise Meitner", and in ref [64] the correct book title is "Aus meinem Leben. Von Arbeit, Muse and Freunden". The author apologizes for these errors.

© 2003 Wiley-VCH Verlag GmbH & Co. KGaA, Weinheim

1433-7851/03/4203-0252 $ 20.00+.50/0

Transport Mechanisms

New Insight into the Transport Mechanism of Hydrated Hydroxide Ions in Water**

*Ralf Ludwig**

Keywords:
ab initio calculations · anions · transport mechanisms · water chemistry

Liquid water possesses many remarkable properties that can be explained to a large extend by its extremely high density of hydrogen bonds and the arrangement of the molecules. One of these properties is the anomalously high mobility of the proton and the hydroxide ion (OH^-) in this liquid. Both ions are much faster than ions of similar size in water. Recently, new efforts have been made to understand the nature and transport mechanism of the hydrated proton and hydroxide ion in aqueous solution. It transpired that the transport mechanism of hydroxide ions in aqueous solution differs significantly from what has been thought by generations of scientists. This was shown by Tuckerman et al.[1] using perhaps the most powerful computer simulation techniques available today. They used a combination of ab initio molecular dynamics simulations (Car-Parrinello molecular dynamics (CPMD))[2] and ab initio path integrals[3,4] to investigate the structure and dynamics of the hydrated hydroxide ion in bulk water. As a result the most widely held views on the structure and transport mechanism of the hydrated OH^- ion should be replaced by a more complex and rich picture, in which the quantum-mechanical character of the hydroxide ion plays an important role.

Since Hückel's fundamental work "Theorie der Beweglichkeiten des Wasserstoff- und Hydroxylions in wässriger Lösung"[5] (Theory of the Mobility of Hydrogen and Hydroxyl Ions in Aqueous Solution) in 1928 it was believed that the hydrated OH^- ion could be regarded as a water molecule missing a proton, and that the transport mechanism of such a "proton hole" could be inferred from an excess proton mechanism by simply reversing the polarity of the hydrogen bonds.

The main conclusion by Tuckerman et al.[1] is now that the OH^- ions behave differently from excess protons (H^+) in water.[6] The "proton hole picture" of the hydroxide ion is clearly flawed. The hydroxide ions are transported through solution in a different way. The new results on the nature and transport mechanism of the hydrated hydroxide ion have an impact in areas related to aqueous acid–base chemistry, enzymatic reactions, and organic synthesis. The reaction conditions in basic solutions are also utilized for one of the oldest chemical processes, soap manufacturing.[7]

For a better understanding of the hydrated hydroxide ion in water, we firstly consider the traditional view of the character of the hydrated proton in aqueous solution. This picture is then compared to the calculated results previously obtained by the same research group.[6] Most chemists take the hydrated proton as being the oxonium ion, H_3O^+. Within this structure the bare proton is so strongly bound to water molecules that it could not exist in isolation. This picture was refined by Eigen[8] as well as Zundel and Metzger[9] who advocated the presence of larger complexes such as $H_9O_4^+$ and $H_5O_2^+$, respectively. In the "Eigen cation" the central oxonium ion is strongly hydrogen bonded to three H_2O molecules, thus forming $(H_3O^+)(H_2O)_3$. In the "Zundel ion" the proton lies midway between two water molecules ($H_2O\cdots H^+\cdots H_2O$). Without going deeper into these viewpoints, it was already clear that the electronic structure depends strongly on the surrounding water molecules, and that nuclear quantum issues were involved. Related to the structural aspect is the mechanism of the anomalously high mobility of the proton in water; it is approximately five times higher than the mobility of ions of similar size to H_3O^+. This observation has been explained by using the famous de Grotthuss mechanism.[10] In this mechanism a proton shuttles between successive water molecules, and a proton relay takes places in the hydrogen-bonded water network. By using the ab initio molecular dynamics approach, Marx et al.[6] found that the hydrated proton has an inherently fluxional character. The Eigen and Zundel cations show up along with other intermediate structures during this process. The observed proton transport did not match with traditional views. The interconversion of the hydrated proton is not limited by the proton motion itself, but rather by rearrangements of water molecules. In this situation the "Zundel cation" $H_5O_2^+$ plays an integral role. The CPMD simulations showed that in acid the proton H^+ is often found between two water molecules and can be schematically described as $[H_2O\cdots H\cdots H_2O]^+$ (Figure 1b). It can

[*] Priv.-Doz. Dr. R. Ludwig
Physikalische Chemie
Fachbereich Chemie
Universität Dortmund
Otto-Hahn-Strasse 6, 44221 Dortmund (Germany)
Fax: (+49) 231-755-3937
E-mail: ludwig@pc2a.chemie.uni-dortmund.de

[**] I am greatful to the Deutsche Forschungsgemeinschaft and to the Fonds der Chemischen Industrie for financial support.

 © 2003 Wiley-VCH Verlag GmbH & Co. KGaA, Weinheim 1433-7851/03/4203-0258 $ 20.00+.50/0

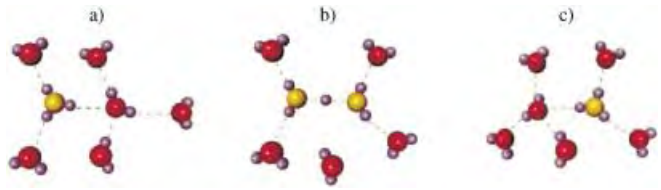


Figure 1. Transport mechanism of H_3O^+. a) The H_3O^+ ion (yellow oxygen atom) is threefold-coordinate in the complex $H_3O^+(H_2O)_3$. b) Thermal fluctuations cause an H-bond between a first and a second solvation-shell water molecule to break. As a consequence the first shell O···O distance (yellow oxygen atoms) decreases and the protons migrates to the center of the bond, thus forming an intermediate $H_5O_2^+$ ion complex. c) The complete proton transfer yields again a properly solvated H_3O^+ at a new site in the H-bond network. It should be noted that this Figure illustrates a simplified sketch of the "real" quantum processes given in ref. [6]. To aid understanding, it was necessary to omit some details. Reprinted with permission from Nature (ref. [1], copyright 2002, Macmillan Publishers Ltd).

move by diffusion and easily form H_3O^+, which itself is surrounded by three water molecules $[H_3O^+(H_2O)_3]$ (Figure 1a,c). Thus, the proton is able to diffuse throughout the entire network of hydrogen bonds in water at a rate considerably greater than that of conventional diffusion. The CPMD calculations yield this "structural diffusion" to be driven by fluctuations in the second solvation shell of H_3O^+, which reduce the number of water molecules in the first solvation shell from four to three.

Recently, new results were also presented for a better understanding of the autodissociation of water ($H_2O + H_2O \rightleftharpoons H_3O^+ + OH^-$). Geissler et al.[11] showed by CPMD simulations that the transfer of a proton in the OH···O systems represents the first step. Bakker and Nienhuys[12] used ultrafast (femtosecond) mid-infrared spectroscopy to study the excited vibrational states of the H-bonded OH groups of the water molecule. They investigated the effect of the OH···O interaction and dynamics on the spectral response of the OH stretching vibrations of liquid water. They observed that the hydrogen atom already becomes delocalized between the oxygen atoms of two neighboring water molecules in the second excited state of the OH stretching vibration. The energy required for this delocalization ($6500\ cm^{-1}$) is unexpectedly low and corresponds to less than 20% of the dissociation energy of the OH bond of the water molecule in the gas phase ($38750\ cm^{-1}$).

Until now, textbooks and articles have suggested that the hydroxide ion, and thus bases, behave in a similar way.[13–15] The analogous hydrated proton complexes would be $[OH\cdots H\cdots OH]^-$ and $OH^-(H_2O)_3$. Tuckerman et al.[1] were able to demonstrate that this "proton hole picture" of the hydroxide ion is clearly misleading, and that the reversal of the polarity of the bonds in the network of hydrogen bonds does not correctly describe the mechanism by which the hydroxide ions are transported through solution. They addressed this issue by applying a computer simulation methodology that included both the quantum-electronic and quantum-nuclear motion. Whereas classical molecular dynamics uses Newton's classical laws of motion and employ mostly empirical forces, CPMD[2] determines the forces "on the fly" by way of electronic structure calculations during the course of the dynamics. The nuclear quantum wave character is handeled by using Feynman path integral techniques.[3,4]

The main result is that the chemistry of the oxonium and hydroxide ions in water is very different. The hydroxide ion cannot diffuse its solvation structures because it is surrounded by four coordinating water molecules (Figure 2a). In this arrangement the accepted H-bonds are roughly planar and result in the formation of the $OH^-(H_2O)_4$ complex. This phenomenon was termed "hypercoordination" by the authors.[1] The stability of this structure had been previously confirmed by solution-phase[16] and quantum-chemical calculations.[17] Accepting a proton in this configuration would result in a water molecule having a 90° bond angle. Such a water molecule is energetically strongly disfavored compared to molecules with angles of 104.5° in the gas phase and about 109° in bulk water. Thus, to move a proton easily, one of the four hydrogen bonds has to break off and leave the hydroxide ion in the triply coordinated solvation structure $OH^-(H_2O)_3$ (Figure 2a,b). With one water molecule removed, the angles in the remaining structure are all much closer to the ideal bond angle and proton transfer can occur.

In classical considerations the triply coordinated complex first has to relax in its ideal geometry before it can accept another water molecule and form the complex $OH^-(H_2O)_4$ again (Figure 2c). In other words: If quantum effects are taken into account, the proton can be transferred when less ideal bond angles are present. During this structural diffusion the OH^- defect is moved about one hydrogen-bond length. This complex only exists as a "transition complex" in basic solution and turns out to be unstable relative to the corresponding structure in acids. There was also

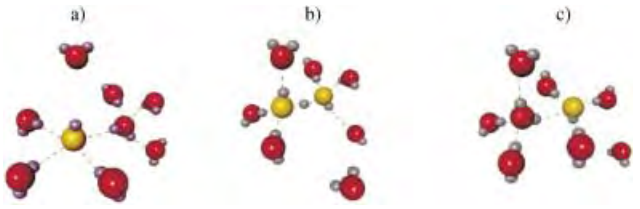


Figure 2. Transport mechanism of OH^-. a) The OH^- ion is fourfold-coordinate in the stable complex $OH^-(H_2O)_4$. b) The breaking of an H-bond by thermal fluctuations results in one of the first-solvation-shell water molecules departing and leaves the OH^- ion in a $OH^-(H_2O)_3$ complex. The O···O distance (yellow oxygen atoms) decreases and a weak hydrogen bond is formed between the OH^- hydrogen atom and the water molecule lying above. c) Complete proton transfer causes the $OH^-(H_2O)_3$ complex to migrate to a new site in the H-bond network. Finally, the new OH^- ion acquires a fourth H-bond and the $OH^-(H_2O)_4$ structure is once again complete. It should be noted that this Figure illustrates a simplified sketch of the "real" quantum processes given in ref. [1]. To aid understanding, it was necessary to omit some details. Reproduced with permission from Nature (ref. [1], copyright 2002, Macmillan Publishers Ltd).

 © 2003 Wiley-VCH Verlag GmbH & Co. KGaA, Weinheim 1433-7851/03/4203-0259 $ 20.00+.50/0

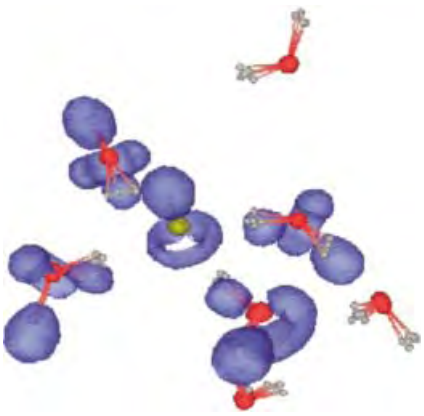


Figure 3. Stable fourfold planar $OH^-(H_2O)_4$ structure. The three lone pairs of electrons around the hydroxide oxygen atom are in a delocalized ring structure, thus supporting the hypercoordination of the OH^- ion (courtesy of D. Marx).

indication from spectroscopic measurements of microsolvated OH^- clusters[18] that there is no cationic analogue of the $OH^-(H_2O)_4$ complex and that in half of the configurations the hydroxide ion forms an additional weak H-bond, thus giving a total coordination number of 4.5. The unexpectedly high coordination number of the solvated hydroxide ion contrasts with the textbook picture that each of the three lone pairs of electrons on the oxygen atom accepts a single H-bond. The main feature of the analyzed electron localization function (ELF)[19] is a continuous ring around the OH^- bond axis (Figure 3). This pattern suggests a lack of directionality in H-bonding and, in accordance with the spectroscopic picture, supports both structural flexibility and high coordination. In particular, the scientists could show, that quantum effects accelerate the transition from $OH^-(H_2O)_3$ drastically. Tunneling protons yield the major contribution to this effect, and is completely negligible for acids.

In summary, two separate processes determine the motion of the hydroxide ion within the network of hydrogen bonds in water. Firstly, an active solvation state is formed. Here a hydrogen bond is broken in the shell of water molecules around the hydroxide complex. A small energy jump is required for this to occur. The results agree nicely with experimental spectroscopic data. Secondly, a weak hydrogen bond is formed between the hydroxide hydrogen atom and a neighboring water molecule. One water molecule is then lost, a proton accepted, and the new hydroxide ion is formed. Tuckerman et al.[1,6] showed that protons and hydroxide ions move differently in aqueous solution. Thus, current views of aqueous bases in textbooks have to be revised.

The importance of hydroxide ions for the structural and dynamical properties of water was also shown by Chen et al.[20] They carried out CPMD simulations on a series of aqueous NaOH and KOH solutions and the calculations, indeed, confirmed that significant changes in the structural and dynamical properties of water occurred on addition of hydroxide ions. The tetrahedral coordination of pure water is completely missing at high concentrations of both NaOH and KOH. The authors also found new spectroscopic features, such as a "free" OH stretch, a broadening of the normal water OH stretching band, and a large blue shift of both the vibrational band and the low-frequency translation band. Significant changes in the structural and dynamical properties of water in the presence of hydroxide ions was recently shown by neutron diffraction using isotopic substitution experiments[21] and spectroscopic measurements.[22] The structural and dynamical behavior is inextricably linked to the formation of compact hydroxide–water complexes as shown by Tuckerman et al.[1] for pure water and for aqueous KOD solutions.[23] In the latter article similarities and differences between two concentrations of aqueous KOD solutions were highlighted and a new interpretation of the measured infrared spectra was proposed.

[1] M. E. Tuckerman, D. Marx, M. Parrinello, *Nature* **2002**, *417*, 925 – 929.
[2] R. Car, M. Parrinello, *Phys. Rev. Lett.* **1985**, *55*, 2471 – 2474.
[3] D. Marx, M. Parrinello, *Z. Phys. B* **1994**, *95*, 143 – 144.
[4] D. Marx, M. Parinello, *J. Chem. Phys.* **1996**, *104*, 4077 – 4082.
[5] E. Hückel, *Z. Elektrochem. Angew. Phys. Chem.* **1928**, *34*, 546 – 562.
[6] D. Marx, M. E. Tuckerman, J. Hutter, M. Parrinello, *Nature* **1999**, *397*, 601 – 604.
[7] O. Phanstiel, E. Dueno, Q. X. Wang, *J. Chem. Educ.* **1998**, *75*, 612 – 614.
[8] M. Eigen, *Angew. Chem.* **1963**, *75*, 489 – 508; *Angew. Chem. Int. Ed. Engl.* **1964**, *3*, 1 – 19.
[9] G. Zundel, H. Metzger, *Z. Phys. Chem.* **1968**, *58*, 225 – 245.
[10] C. J. T. de Grotthuss, *Ann. Chim.* **1806**, *58*, 54 – 74.
[11] P. L. Geissler, C. Dellago, D. Chandler, J. Hutter, M. Parrinello, *Science* **2001**, *291*, 2121 – 2124.
[12] H. J. Bakker, H.-K. Nienhuys, *Science* **2002**, *297*, 587 – 590.
[13] W. J. Moore, *Basic Physical Chemistry*, Prentice-Hall, New Jersey, **1983**.
[14] G. K. Vemulapalli, *Physical Chemistry*, Prentice-Hall, New Jersey, **1993**.
[15] N. Agmon, *Chem. Phys. Lett.* **2000**, *319*, 247 – 252.
[16] M. E. Tuckerman, K. Laasonen, M. Sprik, M. Parrinello, *J. Chem. Phys.* **1995**, *103*, 150 – 161.
[17] J. J. Nova, F. Mota, C. P. delValle, M. Plans, *J. Phys. Chem. A* **1997**, *101*, 7842 – 7853.
[18] C. Chandari, Y.-S. Wang, J. C. Jiang, Y. T. Lee, H.-C. Chang, G. Niedner-Schattenburg, *Mol. Phys.* **2001**, *99*, 1161 – 1173.
[19] A. D. Becke, K. E. Edgecombe, *J. Chem. Phys.* **1990**, *92*, 5397 – 5403.
[20] B. Chen, J. M. Park, I. Ivanov, G. Tabacchi, M. L. Klein, M. Parrinello, *J. Am. Chem. Soc.* **2002**, *124*, 8534 – 8535.
[21] F. Bruni, M. Ricci, A. K. Soper, *J. Chem. Phys.* **2001**, *114*, 8056 – 8063.
[22] Y. Amo, Y. Tominga, *J. Raman Spectrosc.* **2000**, *31*, 547 – 553.
[23] Z. W. Zhu, M. E. Tuckerman, *J. Phys. Chem. B* **2002**, *106*, 8009 – 8018.

Origin of Life

Diversified World: Drive to Life's Origin?!**

Hans Kuhn and Christoph Kuhn*

Keywords:
evolution · genetic apparatus · homochirality · information emergence · origin of life · self-organization

What is decisive for the origin of life? Here we do not want to delve into the chemical details but attempt to look at the fundamental motivation which leads to the remarkable process of self-organization to simplest forms of life. That should be useful to stimulate experimentation. It is often assumed that in principle life can arise in a homogeneous medium or at a reactive interface by intrinsic necessity (see, for example, reference [1]). Processes of this type are known, but is it really possible that such a process can lead to a machine as intricate as the genetic apparatus of biosystems? The idea that life arises slowly in a chaos of lifeless matter is fascinating, but is life's emergence not a process dfferent in principle? Are not quite special highly diversified environmental conditions changing periodically in a particular way required as the driving force for the formation of increasingly more complex forms, evolving to forms of early life?

Model Pathway

To establish the plausibility of a theory of the origin of life a tangible and detailed sequence of hypothetical physical-chemical processes which leads to the basic machinery of life must be proposed. Each step would have to be as simple as possible, however, to understand the fundamentals of this type of processes. But it cannot be expected from such a way to go that a genetic apparatus as complex as that which actually exists in the biosystem will be achieved, but a less intricate apparatus with the same functional properties. Such a model pathway would have to be constantly improved on the basis of new experiments and knowledge. A description of the historical pathway is not aspired. The process should demonstrate how systems with lifelike properties are formed as well as chemically totally differently constructed supramolecular systems, or systems that could arise at suitable locations everywhere in the universe.

The extremely important questions currently of special interest in connection with the origin of life (what role do RNA, DNA, peptides, thioesters, pyrite, etc. play? And where did the process take place, in the depths of the ocean, at a volcano, on Mars, or elsewhere? How was the beginning of a replication process possible? Which enzyme-free metabolic processes were required to synthesize the building blocks of a first replica-producing system and to exploit an energy source?[2]) are not considered here. We attempt to contribute to finding answers to questions concerning further evolution of a replicating molecule toward the genetic machine by developing theoretical models. Which principle requirements, independent of the special chemistry, must be fulfilled to initiate and drive forward this process? What are the demands placed on the building blocks of the evolving systems and the environment? How can these demands be fulfilled with the resources of chemistry? Can in this way a plausible model pathway to systems with a genetic apparatus be found? In a recent publication[3] some critical steps of a simple model pathway suggested in reference [4] are simulated on a computer. The model pathway assumes that quite specific external influences are fundamentally important for the origin of life. The proposed hypothetical steps lead to a simple translation device, to a plausible explanation of the basic transformations (transition from RNA to DNA as carrier of genetic information), and to the development of the genetic code of biosystems in detail. Here we focus on general aspects of the process.

The Beginning

It is assumed that amongst the enormous diversity of regions with different properties on the prebiotic Earth there exists, by chance, somewhere a small, singular region with the following important properties:

1) the presence of certain, energy-rich monomers which were formed by fortuitously prevailing conditions and are continuously replenished. In the thought experiment two mutually complementary monomer types are assumed to be available;
2) unique, temporal-spatial environmental properties which allow the continual formation of short strands by condensation of the monomers;
3) occasionally, in a very seldom step, a short strand is formed by chance in which the monomers are connected in such a waythat the strand can act as a template for the formation of the complementary strand;

[*] Prof. Dr. H. Kuhn
Ringoldswilstrasse 50, 3656 Tschingel (Switzerland)
Fax: (+41)-33-251-3379
Dr. C. Kuhn
Gruppe Biophysik
Institut für Molekularbiologie und Biophysik
Eidgenössische Technische Hochschule
Hönggerberg, 8093 Zürich (Switzerland)

[**] C.K. is grateful to Professor Kurt Würthrich for his hospitality.

 © 2003 Wiley-VCH Verlag GmbH & Co. KGaA, Weinheim 1433-7851/03/4203-0262 $ 20.00+.50/0

4) replica formation starts and continues under the prevailing conditions, and by accidental copying errors strands are formed with different monomer sequences which display different folding structures, and selection occurs (for example, by different hydrolysis sensitivities of differently folded strands).

Despite considerable efforts it has hitherto not been possible to realize a plausible initial reproduction process experimentally,[5] although more recent approaches [6,7] are encouraging. Very diverse possibilities have been suggested as the starting point of life's origin on Earth, including processes on mineral surfaces. The question is not under discussion here, but each proposal should be substantiated by giving a plausible pathway to a system of self-replicating RNA-like chains.[8] According to the model[4] such a replicating system presumes the formation of a homochiral template strand so that the fitting together of template and the developing strand is guaranteed. Such a template is formed by chance in a racemic solution of monomers. In this accidental, initiating process is seen the origin of the homochirality of biological systems. The formation of such a symmetry break has been realized experimentally in reference [6]. The experiments in reference [7] support the idea of a complex temporal-spatial structure as fundamental already for the initial process.

The thought experiment[4] as described rests on the assumption that an appropriate self-replicating system will be realized experimentally, since fundamentally nothing speaks against it. The real puzzling feature in the origin of life emanates from the subsequent processes. How can such a system develop into an entity with a genetic apparatus?

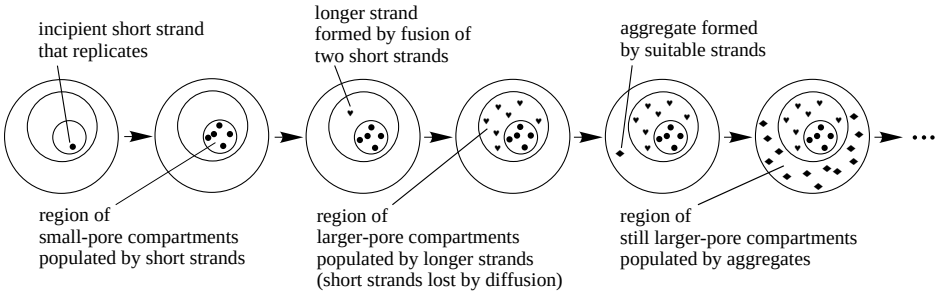


Figure 1. Highly diversified world: driving force for increase in complexity by colonizing increasingly less favorable regions. Only short strands emerge spontaneously, the occurrence of longer replica-forming strands is much too improbable. After short strands have multiplied, longer strands can easily occur by fusion. These strands may form folding structures. Aggregate-forming strands may appear.

Structural Diversity of the Environment:

Stimulus for Continuous Complexity Increase

According to the model the critical factor in the origin of life is that in the small region under consideration where multiplication of strands and selection takes place, a strand is formed fortuitously by a copying error which can survive and multiply in a neighboring region with slightly different properties, in contrast to the hitherto existing strands. The process is ongoing (Figure 1); increasingly less favorable regions are occupied with replicable forms. This requires the occurrence of increasingly more complex and more intricate systems. In this way the systems thus formed become increasingly independent upon the quite special, restrictive conditions in the region in which the process has begun. The fact that an enormous number of regions with different properties existed on the prebiotic Earth plays a central role in the model. The multiformity is the stimulus for the continuous increase in complexity. In this view of a beginning in a most particular region, sequences of very different processes (many kinds of chemical reactions, concentration and separation processes) led to building blocks for a replicating system. This view should stimulate the search for many different possibilities to obtain such building blocks.

Periodicity and Compartmentalization

Living systems are complex aggregates of mutually compatible molecules. Thus even for the first steps suitable conditions must be found which lead to the aggregates of mutually compatible molecules and to the evolution of increasingly more complex and intricate aggregates. In addition to the structural diversity, temporal periodicity and spatial compartmentalization (e.g. day–night cycle and small pores in a rock) are fundamentally important conditions.

A periodic change between totally different environmental influences, for example different temperatures, is important: aggregates must be formed through the interdiffusion and interlocking of individual molecules: these aggregates are subjected to a selection process; the aggregates must then disintegrate again into individual molecules which are replicated; and a new cycle must begin. The process continues, driven by the given periodicity.Compartmentalization is important to avoid the individual molecules diffusing apart, enabling the molecules to come together for reconstitution. The compartments must be somewhat porous so that copies of the newly produced favorable form within a compartment can gradually spread over the whole region.These general considerations are important in the search for a detailed model pathway[4] and for the determination of the parameters for computer simulation[3]. Two fundamental facts should be taken into account when considering the evolution of increasingly complex aggregates:

1) A prerequisite for aggregates of interlocking strands to be formed is that template strand and replicate are antiparallel in the double strand. Only in this case the single strands obtained after separating template and replicate can form compact folding structures required to build aggregates. Indeed, the postulated

 © 2003 Wiley-VCH Verlag GmbH & Co. KGaA, Weinheim 1433-7851/03/4203-0263 $ 20.00+.50/0

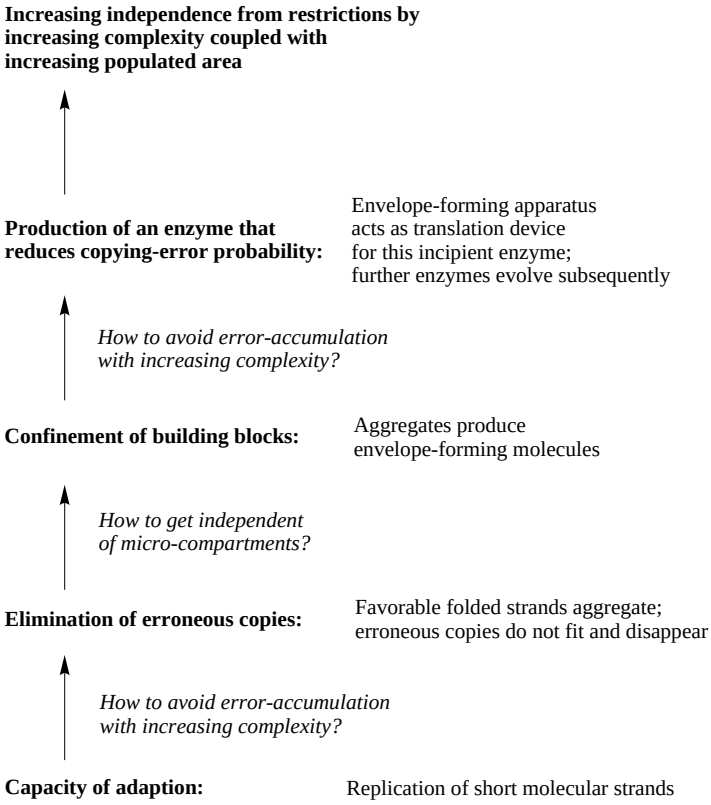


Figure 2. Early stages in the evolution of life in the thought experiment: logical steps, barriers, and their surmounting.

antiparallelity is realized in living forms.

2) A basic question is how to overcome the difficulty that evolution comes to an end at a certain level of complexity because of copying errors accumulation. This requirement is achieved automatically in the model by the formation of aggregates of mutually compatible molecules: molecules which have a changed folding through reproduction errors do not, in general, integrate and disappear. With increasing complexity of the aggregating forms the mechanism is always determinative and of fundamental importance in the evolution of increasingly intricate systems.

The first steps resulting from these considerations are given in Figure 2. They lead to a simple genetic apparatus.

Computer Simulation

Each cycle in this simulation consists of a

1) construction phase (simulation of the formation of functional aggregates by diffusion and joining together of molecular strands);
2) selection phase (aggregates—according to a feasibility parameter which determines their survival probability—are randomly selected. This parameter is held in a library for each aggregate form which is regarded as a possibility to occur in any phase in the evolution process;
3) Replication phase (aggregates break down into individual strands which serve as tempates for a replica formation after which template and replica strand separate).

The calculation results[3] underpin critical breakthroughs in the first stages of the hypothetical model (for example, the formation of an aggregate such as in Figure 3 that functions as a simple translation apparatus).

Basic Idea and Procedure

The basic principle of the model (continuous increase in complexity, associated with the colonization of increasingly less favorable regions) represents an extension of the Darwin Theory according to which during biological evolution increasingly more complex systems are formed through new ecological niches being populated. Previously empty regions are increasingly occupied. Later the creation of ecological niches by gradual expulsion of competitors becomes important.[9] The basic procedure (the search for an unbroken chain of hypothetical, physical-chemical process which leads to a genetic apparatus) represents an extension of Darwin's way to go. In the search for the mechanism of the origin of life

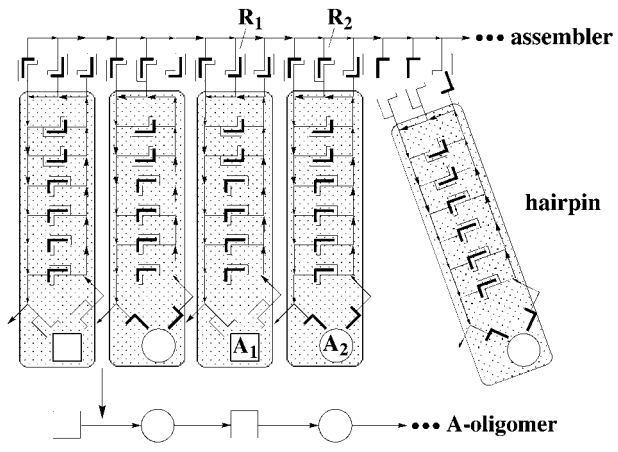


Figure 3. Translation apparatus for a binary code. Important stage in the model pathway in the computer simulation: assembler and hairpin strands of *R* monomers (R_1 and R_2). Cohesive alignment of hairpins by means of the reading frame. A-monomers (A_1 and A_2) are bound to the open end of the hairpins. A binary code relating the sequence of R_1 and R_2 in the assembler with the sequence of A_1 and A_2, which are linking to form the A-oligomer. The A-oligomer acts as an enzyme. R and A are reminiscent of a ribonucleotide and an amino acid in biosystems.

the method described should be immediately plausible by its relation to Darwin's basic ideas.

Origin of Life: Self-Organization by Intrinsic Necessity or by the Necessity to Increase Complexity with Extending Populated World?

A diversified environment, the drive to life in the present view, plays no role in the theories which are based on the assumption that the essential process in the origin of life can be considered, in principle, as a self-organization in a homogeneous phase by intrinsic necessity. It is interesting to inquire after the causes for the great fascination and the broad acceptance of this idea.Up to the beginning of the 1970s it was frequently thought that the origin of life was inconsistent with thermodynamics, but then the thermodynamic conditions for processes of self-organization in a homogeneous medium in the steady state were given.[10] Thus the described statement was considered to be disproved, the gap between physics and biology bridged, and the basic laws of a theory of the origin of life discovered. However, the fact that structures form in a homogeneous medium by self-organization does not allow one to conclude that this type of self-organization can actually lead to living systems.

Thermodynamics and the Origin of Life

The idea that the origin of life is inconsistent with thermodynamics cannot be refuted, in our view, without giving a plausible model pathway, and all the more the more detailed the pathway is. The problem of the origin of life is therefore finding such a pathway and not a question of thermodynamics since every physical-chemical process is consistent with thermodynamics.

Gradual or Sudden Manifestation of Life?

In the conception that within an in principle homogeneous phase increasingly more complex forms evolve slowly, life originates gradually. A different situation is given if in contrast we start from the concept that in a region with singular properties a clearly orientated process is set in motion: through replication, variation, and selection a development is instantaneously initiated which (jointly with an increasing expansion of the populated region) leads to increasingly complex forms. In this explosive process a property of matter emerges all of a sudden which was not previously manifest. It is useful to define physical-chemical systems with this singular behavior as living organisms even life in common sense appears much later. Thus life originates suddenly with the appearance of the first self-replicating molecule which is variable through errors in the copying process.

Genetic Information

The special feature of living organisms is that they carry information as certain sequences of building blocks, the recipe for the construction of copies (genetic information). The evolutionary process and therefore the genetic information can only be seen in connection with the given environment. The genetic information carried by the evolving forms should not be confused with the observer's information required to characterize the environment of these forms. The genetic information, quantified by the number of bits, is transferred from one generation to the next. In the described portrayal of a sudden change from the lifeless to the living, genetic information is produced with the appearance of the first self-replicating molecule. The carrier of the information (the recipe for the construction of copies) is the molecule itself. With the advance of evolution the genetically transferred information grows (measured by the number of bits), and the carrier of the information itself changes at certain stages of evolution.[8] The information grows with the extension in the information-bearing chain, and its significance increases (measured by the minimum number of bits which must be produced and rejected in order to achieve the observed evolution stage). As described above, there are very different conceptions on the nature of the initial information carrier, exemplifying the presented scenario (sudden appearance of an initial information-carrying, physical object and continuous complexity increase).[11] Genetic information is clearly defined other than in scenarios where the origin of life is considered as gradual change from the lifeless to the living.

Outlook

The driving forces inducing the emergence of life are sought by theoretical modeling. It is attempted to see motivations that lead to this process which must also be valid anywhere in the cosmos under quite different but extremely specific chemical and spatiotemporal conditions. To achieve advances in our understanding of the origin of life model pathways must be improved by an increasingly detailed determination of the environmental conditions and an ever better preparative chemical underpinning. The concept that the process begins in a particular region should stimulate a broad search for experimental possibilities.

[1] D. Segré, D. Lancet, *EMBO Rep.* **2000**, *1*, 217–222; A. D. Miller, *ChemBioChem.* **2002**, *3*, 45–46.

[2] N. Lahav, *Biogenesis: Theories of Life's Origin,* Oxford University Press, New York, **1999**; A. Brack, *The Molecular Origins of Life: Assembling the Pieces of the Puzzle,* Cambridge University Press, New York, **1998**; C. Wills, J. Bada, *The Spark of Life. Darwin and the Primeval Soup,* Oxford University Press, Oxford, **2001**; G. Wächtershäuser, *Prog. Biophys. Mol. Biol.* **1992**, *58*, 85–201; C. de Duve, *Blueprint for a Cell: The Nature and Origin of Life,* Patterson, Burlington, **1991**; I. Fry, *The Emergence of Life on Earth,* Rudgers University Press, New Brunswick, **2000**; G. F. Joyce, *Nature*, **2002**, *418*, 214—221; *Frontiers of Life, Vol. 1, The Origin of Life* (Eds.: D. Baltimore, R. Dulbecco, F. Jacob, R. Levi-Motalcini), Academic Press, San Diego, **2000**

[3] C. Kuhn, *Proc. Natl. Acad. Sci. USA* **2001**, *98*, 8620–8626.

[4] H. Kuhn, H.-D. Försterling, *Principles of Physical Chemistry. Understanding Molecules, Molecular Assemblies, Supramolecular Machines,* Wiley, New York,

2000; H. Kuhn, J. Waser in *Lock-and-key principle* (Ed.: J.-P. Behr), Wiley, New York, **1994**, p. 247 – 306; H. Kuhn, J. Waser in *Biophysics* (Eds.: W. Hoppe W. Lohmann, H. Markl, H. Ziegler), Springer, Berlin, **1983** p. 830 – 874; H. Kuhn, *Angew. Chem.* **1972**, *84*, 838 – 862; *Angew. Chem. Int. Ed. Engl.* **1972**, *11*, 798 – 820; H. Kuhn, *Naturwissenschaften* **1976**, *63*, 68 – 80; H. Kuhn, J. Waser, *Angew. Chem.* **1981**, *93*, 495 – 515; *Angew. Chem. Int. Ed. Engl.* **1981**, *20*, 500 – 520.

[5] L. E. Orgel, *Proc. Natl. Acad. Sci. USA* **2000**, *97*, 12503 – 12504.

[6] A. Eschenmoser, *Science* **1999**, *284*, 2118 – 2123; M. Bolli, R. Micura, A. Eschenmoser, *Chem. Biol.* **1997**, *4*, 309 – 320.

[7] A. Luther, R. Brandsch, G. von Kiedrowski, *Nature* **1998**, *396*, 245 – 248.

[8] For example, the first self-reproducing molecule can be a short strand similar to pyranosyl-RNA. In this case base pairing is more stable and selective than is the case with natural furanosyl-RNA.[6] This is of advantage for the start of evolution. Later, when a certain degree of complexity has been achieved that correct fitting together of the components is guaranteed, a more rapidly functioning machine built up from furanosyl-RNA would be more advantageous. But how could such a conversion come about? A genetic apparatus of a certain complexity based upon pyranosyl-RNA produces an enzyme which allows the formation of a furanosyl-RNA replica. This leads to a symbiosis until the furanosyl-RNA based system is no longer dependent upon pyranosyl-RNA system which then disappears.

[9] Darwin did not suppose, however, that his theory of the origin of the species is the way to approach the problem of the origin of life, as his famous picture of the start in a "warm little pond", which stimulated the later concept of an primeval soup, shows.

[10] M. Eigen, Naturwissenschaften **1971**, *58*, 465 – 523; I. Prigogine, D. Glansdorff, *Thermodynamic Theory of Structure, Stability and Fluctuations*, Wiley-Interscience, New York, **1971**.

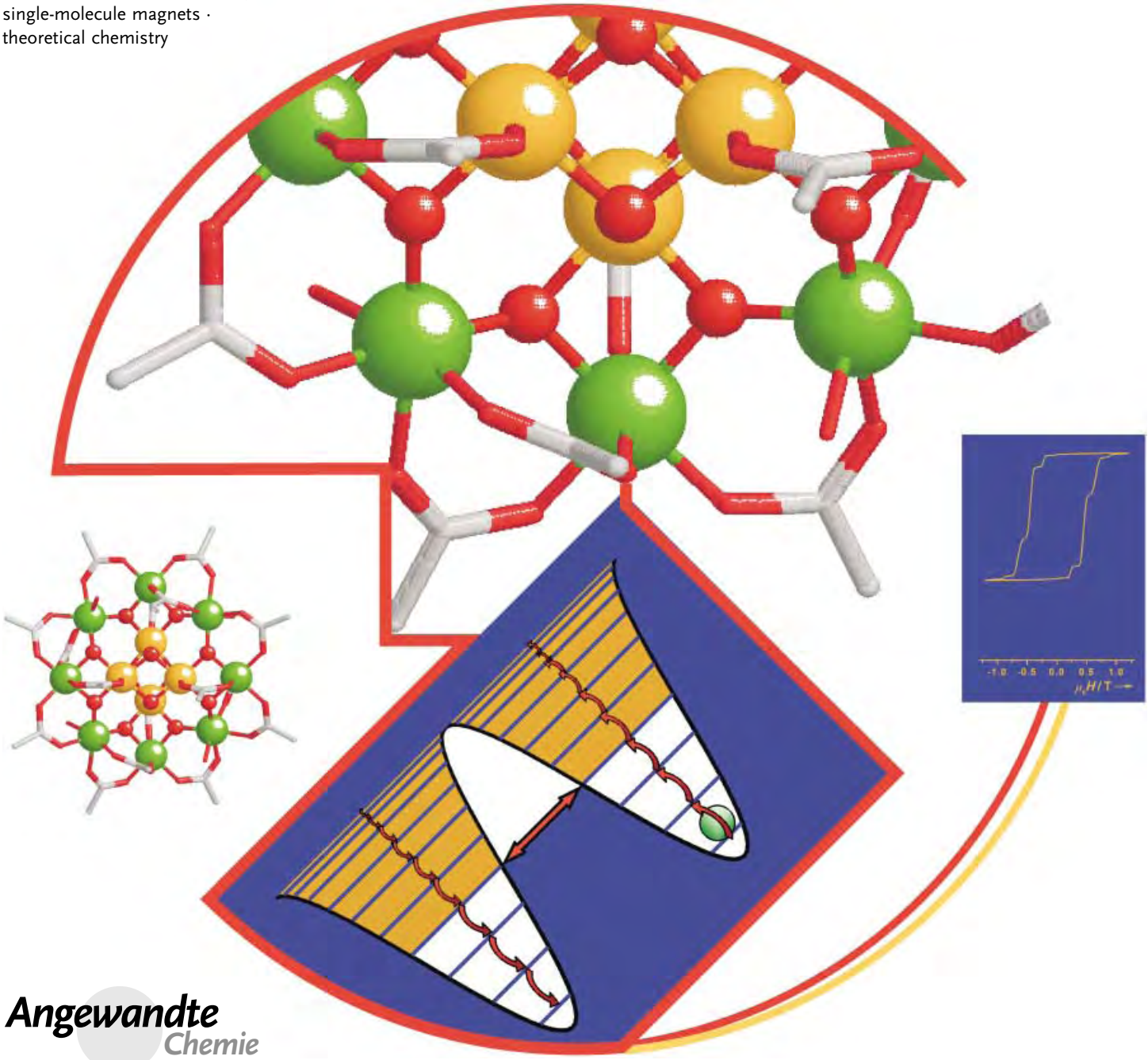
[11] The frequenly posed question "what first, metabolism or genetic apparatus?" is not relevant in this context. In the given model (life beginning in a most partcular region where chains of reactions lead to a replicating system) the former case is assumed: metabolism present in the beginning, improved and developed during the evolution of the genetic apparatus by stepwise inclusion of enzymes.

Single-Molecule Magnets

Quantum Tunneling of Magnetization and Related Phenomena in Molecular Materials

*Dante Gatteschi and Roberta Sessoli**

Keywords:
cluster compounds · magnetic properties · quantum tunneling · single-molecule magnets · theoretical chemistry



© 2003 Wiley-VCH Verlag GmbH & Co. KGaA, Weinheim

1433-7851/03/4203-0268 $ 20.00+.50/0

Molecules comprising a large number of coupled paramagnetic centers are attracting much interest because they may show properties which are intermediate between those of simple paramagnets and classical bulk magnets and provide unambiguous evidence of quantum size effects in magnets. To date, two cluster families, usually referred to as Mn12 and Fe8, have been used to test theories. However, it is reasonable to predict that other classes of molecules will be discovered which have similar or superior properties. To do this it is necessary that synthetic chemists have a good understanding of the correlation between the structure and properties of the molecules, for this it is necessary that concepts such as quantum tunneling, quantum coherence, quantum oscillations are understood. The goal of this article is to review the fundamental concepts needed to understand quantum size effects in molecular magnets and to critically report what has been done in the field to date.

From the Contents

1. Introduction	269
2. Quantum Tunneling and Quantum Coherence	270
3. Magnetic Relaxation in Systems with Large Spin	271
4. Spin Tunneling: Zero-Field Case	272
5. Tunneling in Magnetic Fields	274
6. Quantum Phenomena Starting from Classical Physics	275
7. Mn12ac and Single-Molecule Magnets	276
8. Fe8	287
9. Other Single-Molecule Magnets	291
10. Conclusions and Perspectives	292
11. Appendix	294

1. Introduction

The fields in which chemistry may have a fundamental role are increasing in number, and it is becoming more and more difficult (though stimulating) for synthetic chemists to cope with requests of new compounds with highly sophisticated properties. The movement from simplicity to complexity in molecular chemistry is one which cannot be stopped, and supramolecular chemistry is just one clear example of that.[1]

The last few years have seen the opening of many new research fields in which molecular materials have been forced, through chemical ingenuity, to acquire properties which are associated with classic inorganic materials. Perhaps the most convincing evidence for this has been the development of purely organic materials, which behave as conductors and superconductors. In addition, organic materials, because of their photorefractive and nonlinear-optical properties, are now even used to make lasers.[2,3]

Magnetism is certainly one of the fundamental properties of matter, inextricably associated with electrical properties, and molecular magnetic materials have recently become a hot topic, thanks to the efforts of many research groups. In particular the role of a pioneer of the field, the late Olivier Kahn, must be recognized.[4,5] One of the main difficulties in developing molecule-based magnets is that bulk magnetism is intrinsically a three-dimensional (3D) property in that only if a 3D lattice of interacting magnetic centers is assembled may the material show spontaneous magnetization below a critical temperature. The problem with molecular materials is that the design of genuine 3D connected lattices is not obvious, because the intrinsic low symmetry of the individual molecules tends to favor 1D or 2D arrangements. Here the difference between molecular magnets and conductors is striking, because for conductors exciting properties can be found even if 1D arrangements of individual molecules are obtained in the solid state. However, this has not scared the synthetic chemists and genuine room-temperature molecule-based magnets are now available. The field has been well reviewed in recent years and the interested reader is addressed to the cited literature.[6–9]

The difficulties in forming 3D magnets with molecular materials have been turned into advantages when it was realized that oligonuclear compounds, comprising a large, but finite, number of magnetic centers may have unique magnetic properties which have made them almost ideal systems for observing quantum size effects in magnets.[10–14] The magnetic centers can be transition-metal or rare-earth ions, or even organic radicals. The observation of quantum phenomena in mesoscopic matter[15] provides, in principle, confirmation to the so-called Copenhagen interpretation, which assumes that there is a continuous transition from the field of small objects, where quantum mechanics is required, to macroscopic objects, where classical physics operates well. Materials the properties of which are intermediate between classical and quantum nature, or where there is coexistence of the two, may be used for completely new types of devices. A particularly interesting field is that of quantum computing,[16] where information can be handled taking advantage of quantum

[*] Prof. Dr. R. Sessoli, Prof. Dr. D. Gatteschi
Department of Chemistry
University of Florence, UdR INSTM
Polo scientifico universitario, via della Lastruccia 3
50019 Sesto Fiorentino (Italy)
Fax: (+ 39)-055-4573372
E-mail: roberta.sessoli@unifi.it

 © 2003 Wiley-VCH Verlag GmbH & Co. KGaA, Weinheim 1433-7851/03/4203-0269 $ 20.00+.50/0

effects. Research is very active in this field, on systems ranging from the NMR of molecules[16] to Josephson junctions.[17] In principle it is also possible to consider magnets in this perspective,[18] as these have long been suggested to give rise to quantum effects in mesoscopic objects.

At the beginning of the 1990s it was discovered[19,20] that a molecule, comprising 12 manganese ions, and characterized by a ground state with $S = 10$, $[Mn_{12}O_{12}(CH_3COO)_{16}(H_2O)_4]$ (Mn12ac),[21] shows slow relaxation of the magnetization at low temperature (of the order of months at 2 K). Under these conditions a single molecule becomes like a tiny magnet, in the sense that if magnetized by an applied field it retains the magnetization for days. In fact it gives rise to magnetic hysteresis, which is one condition for storing information in a particle. Under this respect therefore Mn12ac behaves like a classical magnet. However, it is still small enough to also show large quantum effects. In fact Mn12ac, and other molecules which have since been investigated, provide the best examples to date of the observation of quantum effects, such as the tunneling of the magnetization, in magnets. These molecules are now often called "single-molecule magnets"[22] (SMMs). The name itself is not correct, because to have a magnet it is necessary to have an infinite number of coupled centers, but is evocative, and in our opinion it can be used provided the above *caveat* is taken into consideration.[11,23]

Herein we wish to review the current state of the art in the field of SMMs, and in particular highlight the numerous and complex quantum phenomena that can be observed in this new class of molecular materials. The field of SMMs is an interdisciplinary one, where many papers are published in physics and chemistry journals. To design new classes of molecules with enhanced SMM properties the chemical community must be aware of the development of the physical treatment of SMMs. Thus, the reader must be prepared to digest a little quantum mechanics; we will try to provide the basic introduction, in as brief and clear a form as possible.

2. Quantum Tunneling and Quantum Coherence

It all started with Schrödinger's cat: the poor animal was the first macroscopic object for which quantum phenomena were envisaged as possible, and the agonizing result was that it remained uncertain whether it was alive or dead. More seriously, macroscopic objects may be stable in two different states, but they can have only one state at a time. If we consider a ball in a container characterized by two wells (Figure 1a), it may be either in the left or in the right well, but once a choice is made it is clear that its state is described for instance by the statement: the ball is in the right well. It can change its state, by overcoming the barrier Δ_B separating the two wells, and then roll down into the left well. A quantum object on the other hand has also a wave nature, and if the wavefunction of the left-hand particle extends over to the right-hand well, and vice versa, the state of the particle must be described by a superposition of the two states. Since the wavefunction of the left well extends to the right wall with a nonzero value, the probability of observing the left ball in the right well is different from zero: therefore the ball can be both in the right- and in the left-hand well. It is as if the particle could pass from left to right without climbing the barrier, but tunneling; the effect is in fact called quantum tunneling, and is one of the most typical manifestations of quantum mechanics. Some typical examples are observed in small molecules, such as ammonia, where the inversion of the NH_3 bonds occurs exactly with this mechanism. Hydrogen tunneling has been observed in enzyme catalysis,[24] and recently also in a hydrogen-bond network containing calyx[4]arene molecules.[25] There is no theoretical limitation that in principle forbids observing quantum effects in larger particles, although it is known that the tunneling probability scales exponentially with the barrier height and the particle mass. Therefore it is expected to be most observable in small particles and at low temperatures.

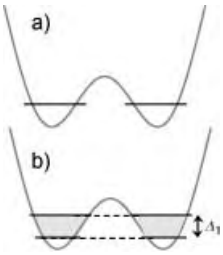


Figure 1. Tunneling in a double well system. a) Noninteracting states; b) interacting states giving rise to tunnel splitting Δ_T.

The actual possibility of observing tunneling depends on the extent of the interaction of the two wavefunctions. In fact, if the two wavefunctions overlap there must be an interaction between them which splits the two degenerate levels in the



Dante Gatteschi was born in Florence in 1945. He graduated in Chemistry at the University of Florence in 1969. He became the assistant of Professor Sacconi and in 1980 he became Professor of Chemistry in the same University. His research interests lie in the electronic structure of transition-metal complexes, in EPR spectroscopy, and in the last few years in molecular magnetism. In 1979 he was awarded by the Italian Chemical society the Nasini prize and in 1992 the Magnetic Resonance Award. In 2000 he was awarded the Bruker Prize for his contributions to EPR spectroscopy and in 2002 he shared with Roberta Sessoli and three other colleagues the Agilent Europhysics Prize.



Roberta Sessoli, born in 1963, graduated in chemistry at the University of Florence in 1987 and received her PhD in 1992 for work on molecular magnetism. She is now Associate Professor at the Faculty of Pharmacy at the University of Florence. Her current interests are the study of slow dynamics of magnetization in one-dimensional molecular compounds. For her work on the static and dynamic magnetic properties of high spin clusters she was recently awarded the 2002 Agilent Technologies Europhysics Prize that she shares with Dante Gatteschi and three other colleagues.

left and right well, giving rise to a so-called tunnel splitting, Δ_T (Figure 1b). One of the two coupled levels is of lower energy than the degenerate levels, while the other is of higher energy, exactly like a pair of bonding–antibonding levels in elementary MO theory. The possibility of tunneling is related to the relative energies of the tunnel splitting and of the barrier. The smaller the ratio between the two the smaller the possibility of observing tunneling.

So far we have considered the system of the particle in the two wells as completely separated from the environment. This is clearly an approximation, because the interaction with the environment can be minimized, but not completely eliminated. If the particle is localized in a metastable state (Figure 2), it can tunnel out of the metastable state. No energy is involved if the particle is isolated from the environment, whereas coupling to the environment means that the particle loses energy with the tunneling (as shown by the arrows in Figure 2). The interactions with the environment will tend to localize the particles, because the interactions will make one well more "attractive" than the other (that is, reduce the energy of one of the wells). In the case of strong coupling with the environment, which means that this interaction is much larger than the tunnel splitting, the particle will stay localized in one of the two wells, and will not tunnel. For intermediate coupling the particle can tunnel, but jumping incoherently from one well to the other. This means that one particle will tunnel, and localize for some time in the other well, and then tunnel again, but in an irregular way. The third case is that of weak coupling when the tunnel splitting is large compared to the interaction with the environment, and the particle oscillates coherently between the two minima. The conditions for observing coherent tunneling are severe. Evidence for coherent tunneling is the observation of energy absorption at a frequency corresponding to the tunnel splitting. In the above experiment of calyx[4]arene a peak was observed in the proton-spin lattice-relaxation rate at a field corresponding to the tunneling frequency of 35 MHz.[25]



Figure 2. Tunneling from a metastable state.

In the above discussion we did not take into account the origin of the interaction between the two wavefunctions. It is apparent that in the description we have made some implicit assumptions: 1) that an unperturbed Hamiltonian, $\mathscr{H}_0$, gives the initial description with the two equivalent wells, 2) a perturbation Hamiltonian, $\mathscr{H}_1$, is added which couples the two separate states and removes the degeneration, 3) a Hamiltonian describing the interaction with the environment, $\mathscr{H}_2$, is needed [Eq. (1)].

$$\mathscr{H} = \mathscr{H}_0 + \mathscr{H}_1 + \mathscr{H}_2 \tag{1}$$

The actual form of the three relevant Hamiltonians will depend on the nature of the system taken into consideration. In this article we will be focussing on magnetic systems, therefore we will limit the description to such systems.

3. Magnetic Relaxation in Systems with Large Spin

Let us consider a system with a well defined ground spin state, characterized by a large value of S (for example Mn12ac with $S = 10$). The unperturbed Hamiltonian includes the effect of an external magnetic field parallel to the unique axis of the cluster and of its axial splitting as a result of crystal-field effects. At this level of approximation only the second-order crystal-field effects will be included. Therefore, for the discussion we wish to develop,[26] the $\mathscr{H}_0$ Hamiltonian can be written as Equation (2) where D is a negative constant for the system of interest and H_z is the magnetic field strength in the z direction. D is one of the parameters of the so-called Zero Field Splitting (ZFS) because it removes the degeneracy of the S multiplet.

$$\mathscr{H}_0 = D\,[S_z^2 - S(S+1)/3] + g\,\mu_B\,H_z\,S_z \tag{2}$$

The energies of the spin levels corresponding to $\mathscr{H}_0$ are in fact easy to calculate as given by Equation (3), where $-S \leq M_S \leq S$.

$$E(M_S) = D\,(M_S^2 - 110/3) + g\,\mu_B\,M_S\,H_z \tag{3}$$

The energy levels can be plotted as shown in Figure 3a. When no external field is applied all the levels are degenerate pairs, except $M_S = 0$. Since D is negative the $M_S = \pm S$ levels will lie lowest. In Figure 3 the states with positive M_S are plotted in one potential well, and those with negative M_S in the other. This formalism is an extension of that commonly used for superparamagnets (see below).[27] A system like this is characterized by magnetic anisotropy along the "easy axis", which means that the magnetization is preferentially oriented parallel to the z axis.

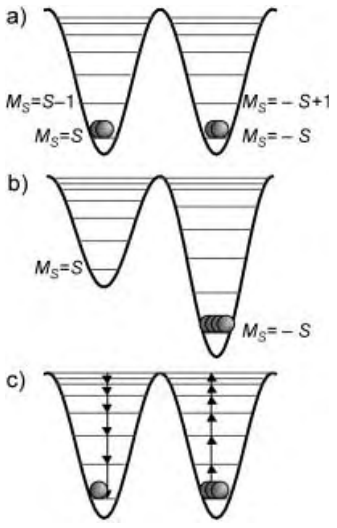


Figure 3. Energy levels for a spin state S with easy axis magnetic anisotropy. The $+M$ levels are localized in the left well and the $-M$ levels in the right well. a) In zero field the two wells are equally populated; b) the application of a magnetic field selectively populates the right well; c) after removing the field the return to equilibrium occurs through a series of steps.

When a field is applied parallel to the z axis the levels characterized by a positive M_S correspond to a projection of the magnetization antiparallel to the field, while those with negative M_S correspond to magnetization parallel to the applied external field (Figure 3b). The separation in zero field between the $|M_S|$ and $|M_S-1|$ levels is given by $(2|M_S|-1)|D|$. The system can be prepared in a magnetized state by applying a magnetic field parallel to the z axis. If T is low and H_z large the $M_S=-10$ state will be the only one populated and the magnetization reaches the saturation value. When the field is removed the system must go back to thermal equilibrium ("relaxation"; Figure 3c). This means that at the equilibrium half of the molecules must be in the $M_S=-10$ and half in the $M_S=+10$ state, with no resulting magnetization. The relaxation (the return to the equilibrium) can be monitored by measuring the magnetization as a function of time ($M(t)$). For a simple system this occurs with an exponential decay [Eq. (4); τ = relaxation time].

$$M_z(t) = M_z(t=0)\exp(-t/\tau) \tag{4}$$

The relaxation process is made possible by the coupling of the spin system to the environment. An important source of coupling is the spin-phonon interaction, which originates from the perturbation of the crystal field induced by lattice vibrations. The spin-phonon Hamiltonian contains terms quadratic in the spin operators.[28,29] Therefore, the allowed transitions are from a state $|M_S\rangle$ to $|M_S\pm1\rangle$ and $|M_S\pm2\rangle$. However, for the sake of simplicity we can consider only the terms that connect $|M_S\rangle$ to $|M_S\pm1\rangle$. In particular, by coupling to vibrations (phonon coupling) a given molecule can change its state from $M_S=-10$ to $M_S=-9$ by absorbing one quantum which corresponds to the difference in energy $E(-9)-E(-10)$. The process can be repeated to go to $M_S=-8$, then $M_S=-7$, until $M_S=0$ is reached. From this state the spin can lose its energy by emitting phonons, that is, exciting vibrational modes of the lattice, to reach the $M_S=+10$ state, or to return to the $M_S=-10$ state. The theoretical expression for the relaxation rate requires the calculation of the transition probability, γ_p^q, from one state, with $M_S=p$, to the other, with $M_S=q$, mediated by spin-phonon coupling V_{pq}. After some approximation the transition probability can be expressed as Equation (5) (for $E(q)>E(p)$) and Equation (6) (for $E(q)<E(p)$).[29]

$$\gamma_p^q \propto |V_{pq}|^2[(E(q)-E(p)]^3[1-\exp((E(q)-E(p))/kT)]^{-1} \tag{5}$$

$$\gamma_p^q \propto |V_{pq}|^2[(E(p)-E(q)]^3[\exp((E(p)-E(q))/kT)-1]^{-1} \tag{6}$$

The transition probabilities in Equation (5), which correspond to increasing the energy, become extremely small at low temperature. The probability per unit time, to go to the top of the barrier, is proportional to the product of the exponentials $\exp((E(q)-E(p))/kT)$, of the individual ladder steps to go from $M_S=-10$ to $M_S=0$, which in a weak field corresponds to $\exp((E(0)-E(-10))/kT)$. The quantity $E(0)-E(S)=\Delta E$ corresponds therefore to a barrier to be overcome in the relaxation process. By writing a set of master equations, where the variation per unit of time of the population M is related to the transition probabilities, Villain et al.[29] have obtained the Equations (7a,b) for the relaxation time τ in the limit $kT \ll \Delta E$ and a weak magnetic field, where ρ is the speed of sound in the material and c is the speed of light in a vacuum.

$$\tau = \tau_0 \exp(\Delta E/kT) \tag{7a}$$

$$\tau_0 = \frac{2\pi}{3}\frac{\hbar^2\rho c^5}{|V_{10}|}\left[\frac{S^2}{\Delta E}\right]^3 \tag{7b}$$

The spin-phonon matrix element in τ_0 is V_{10} because the last step in climbing the barrier is the slowest one, thus determining the rate of the entire process. The relaxation rate therefore follows the Arrhenius law, where the barrier ΔE is the difference in energy between the $M_S=\pm S$ states and the highest one(s), that is $-DS^2$ for integer spin and $-D(S^2-{}^1/_4)$ for half-integer spin values.

This behavior is the same as that observed for superparamagnets (classical magnetic particles). These are small particles of bulk magnets, in which the magnetic anisotropy is comparable to the thermal energy.[27] Actually they can be considered as systems with extremely high S (of the order of 10^3 or larger). The main difference to our $S=10$ system is that the energy levels within the potential wells of the superparamagnets give rise to a quasicontinuum. Another important consequence of the theoretical treatment of the preexponential factor τ_0 is that it is expected to be proportional to $[S^2/\Delta E]^3$ and therefore $\tau_0 \propto |D|^{-3}$. However, for a given ΔE barrier the higher the value of the spin S the longer the relaxation time. Therefore, rather expectedly, the strategy to observe a long relaxation time is that of synthesizing clusters with large spin S and large zero-field splitting.

4. Spin Tunneling: Zero-Field Case

At low temperature only the degenerate $M_S=\pm10$ levels will be populated, but, as long as the Hamiltonian $\mathscr{H}_0$ [Eq. (2)] is valid the two states are orthogonal to each other, and there is no possibility of tunneling. In principle, since the two states are degenerate, every linear combination will be an eigenfunction of the system. But to observe tunneling the two functions must be admixed by some suitable perturbation. Therefore, if we want to observe tunneling we must introduce the perturbation Hamiltonian $\mathscr{H}_1$ that allows the mixing of the two states. The tunneling process involving otherwise degenerate levels is named resonant tunneling.[30–32]

From the physical point of view it is possible to think of a distortion which removes the axial symmetry that we have assumed for $\mathscr{H}_0$. This situation corresponds to the introduction of an anisotropy in the xy plane, or, as it is often called, a transverse anisotropy. A convenient form for the $\mathscr{H}_1$ Hamiltonian is Equation (8) where E is a parameter, which, without loss of generality,[33] is limited to be $0 \le |E/D| \le {}^1/_3$.

$$\mathscr{H}_1 = E(S_x^2 - S_y^2) \tag{8}$$

In the case considered so far, if E is positive the spins in the xy plane will try to avoid the x axis, which is called the hard axis, while y is the intermediate axis. The Hamiltonian $\mathscr{H}_1$ does not commute with $\mathscr{H}_0$, therefore the eigenstates of the full Hamiltonian $\mathscr{H} = \mathscr{H}_0 + \mathscr{H}_1$ are an admixture of $|M_S\rangle$ states, also with different sign of M. The wavefunction is therefore partially delocalized on both wells and this may give rise to tunneling. However, Equation (8) directly couples states differing in M_S by ± 2. Therefore in first-order perturbation theory $M_S = +10$ admixes with $M_S = +8$, and $M_S = -10$ with $M_S = -8$, but no admixture of $M_S = +10$ and $M_S = -10$ is possible at this level of approximation. Of course $M_S = +8$ is coupled to $M_S = +6$, and this to $M_S = +4$, etc. Therefore an admixture is possible for the $M_S = \pm 10$ states, but only at the tenth order in perturbation theory and the tunnel splitting Δ_T of the $M_S = \pm 10$ levels will be extremely low. Matters are different for the higher energy levels where for instance the $M_S = \pm 2$ levels are split in second-order perturbation theory.

The energy levels appropriate to the Hamiltonian, which include the transverse anisotropy term [Eq. (8)], can be easily calculated by diagonalizing the 21×21 matrix of the $2S+1$ states. The results are plotted in Figure 4, which shows the energy levels in the presence of an applied magnetic field parallel to the z axis, the so-called easy axis, where the largest magnetization is observed. It is apparent that for small values of E/D the highest energy levels begin to split even in zero field, while the lowest-lying levels remain essentially degenerate, which confirms the above qualitative discussion. For the lowest-lying levels a perturbation description is still appropriate, while for the highest energy levels it loses significance. However, since we are interested at the behavior at low temperature, where only the lowest-lying levels will be populated, the perturbation approach remains valid.

The $M_S = \pm 1$ levels (remember that this notation is rigorously meaningful only for $E/D = 0$ because with $E \neq 0$ states with different M_S will be admixed) show the largest splitting (insert in Figure 4), followed by the $M_S = \pm 2$ levels, while all the others remain essentially not split. On increasing the transverse anisotropy further, matters become more complex on the high part of the graph, because of the extensive mixing of the levels. An interesting feature is that new quasidegeneracies are established, which show up clearly at the $E/D = 1/3$ limit. The levels become symmetrically spaced, with one isolated level at 0, and quasidegenerate pairs at $\pm(5.3686,\ 6.8491)\,D$, $\pm(16.95728,\ 17.12642)\,D$, $\pm(30.48692,\ 30.49622)\,D$, $\pm(46.16872,\ 46.16898)\,D$, $\pm(63.93715,\ 63.93715)\,D$. The observed degeneracies of the levels are accidental, and also for the two pairs for which it seems to be so it is only matter of the number significant digits. Any pair of quasidegenerate states on the top of the barrier is an admixture of odd and even $|M_S\rangle$ states. Therefore the states of a pair can be considered as orthogonal to each other, in contrast to the quasidegenerate states in the lower part of the barrier. What is certainly real is the symmetrical disposition around 0.

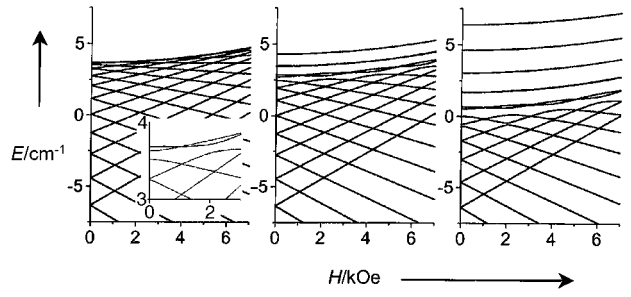


Figure 4. Energy levels for a spin state $S = 10$ as a function of an axial magnetic field. Left: $E/D = 0.01$; center: $E/D = 0.1$; right: $E/D = 1/3$, $D = 0.1\ \mathrm{cm}^{-1}$.

It is apparent that the larger $|M_S|$ the smaller the splitting. For these levels the description of the splitting as tunnel splitting is appropriate. It must be remembered here that the tunnel splitting is zero for systems with half integer S as the transverse term of the anisotropy [Eq. (8)] does not admix the ground states. These states are degenerate as predicted by the Kramers theorem,[34] according to which the minimum possible degeneracy of the states of odd-integer spin systems is two. Therefore, in principle, no tunneling is possible for a system with half-integer spin in rigorously zero field.

The split levels can, to a good approximation, be expressed as Equations (9a,b) where the $|s^*\rangle$ functions are localized states provided by perturbation theory at orders lower than S.[26]

$$|0\rangle = [|-10^*\rangle + |10^*\rangle]/\sqrt{2} \tag{9a}$$

$$|1\rangle = [|-10^*\rangle - |10^*\rangle]/\sqrt{2} \tag{9b}$$

In fact the calculation of the tenth-order perturbation may be very difficult, and an intermediate possibility is that of including perturbation say up to fourth or sixth order to have an acceptable approximation to the ground state. The amplitudes of the wavefunctions given in Equations (9) are very small through the potential barrier and large on both sides. This situation is similar to the conditions met in the tunneling of a proton in a hydrogen bond.

Tunneling may occur not only between the lowest-lying states $M_S = \pm S$, but also between pairs of degenerate excited states.[35–41] This phenomenon is called the phonon-assisted (or thermally activated) tunneling mechanism, as phonons need to be adsorbed to populate the higher M_S states involved in the tunneling process. This mechanism is very important at intermediate temperature because the tunneling frequency is expected to increase on decreasing $|M_S|$. It offers therefore a shortcut for the relaxation of the molecules. In principle a molecule may not need to go over the maximum of the barrier even at relatively high temperatures, but may find a shortcut and tunnel (Figure 5).

The process of phonon-assisted tunneling relaxation is more complex then depicted in Figure 5. It has indeed some analogies with an electric circuit[37,38] with the transition probability represented by resistances/impedances and the population of the $|M_S\rangle$ states represented by voltages. There are many paths for the current to flow through the circuit just as there are many paths for the system to relax, but some of them contribute very little to the overall process. Moreover, their contribution changes with the temperature because the

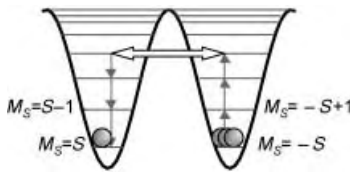


Figure 5. A possible "short cut" to magnetic relaxation through tunneling between thermally activated states.

population of the states as well as the phonon spectrum changes. A clearly visible effect of this admixed process is the fact that the height of the barrier experimentally measured for Mn12ac is smaller than that calculated as the energy difference between $E(0)$ and $E(-10)$.

In a coherent tunneling process the wavefunction, which initially is prepared to correspond to the localized $|-10^*\rangle$ state, should indefinitely oscillate as in Equation (10).

$$|\Psi(t)\rangle = |-10^*\rangle \cos(\omega_T t) + |+10^*\rangle \sin(\omega_T t) \tag{10}$$

In incoherent tunneling on the other hand the spin goes from the $|-10^*\rangle$ state to the $|10^*\rangle$ and stays there. In this process energy is exchanged with the environment. The damping of the oscillations described by Equation (10) must be associated[42] with: 1) the dipolar interaction of the spins of one molecule with those of the other molecules, 2) the interaction of the electron spins with nuclear spins present in the molecule. The dipolar interactions produce fields of a few-hundred Oersted. The hyperfine interactions depend on the nature of the nuclei present in the molecule. For instance, in Mn12ac there are twelve ^{55}Mn nuclei, each with spin $I = {}^5/_2$. These may give rise to fields of a few-hundred Oersted.

The low symmetry effects in a given multiplet will be limited to the terms of Hamiltonians in Equations (2) and (8) only if the S value is smaller than 2, otherwise other even-order terms must be added to the Hamiltonians. The first higher-order terms to be introduced are the fourth-order ones.[28] For a spin $S = 10$, in principle, all the even-order terms up to 20 should be included. It is clear that the number of parameters to be introduced in this way becomes absolutely impossible to control, and quite often a conservative approach is used, in which only the minimum number is used. In general one starts with the second-order terms, then, if some experimental data cannot be fit, the fourth-order terms are added. We are aware of only one case where terms higher than four have been explicitly taken into account.[43,44] The higher-order terms take a standard form, which can be used also for the second-order terms, using the so-called Stevens operator equivalents $\Sigma_{n,k} B_n^k O_n^k$[28] where the B_n^k are parameters to be obtained from the analysis of experimental data and O_n^k are operators of power n in the spin angular momentum. The value of k is restricted to $0 \le k \le n$. The k values to be included depend on the symmetry of the system and on the quantization axes used to define the basis set. For tetragonal symmetry $k = 0$ and 4 are allowed, for trigonal symmetry $k = 0$ and 3. For C_2 symmetry $k = 0, 2, 4$ will be needed. The k index operators couple M_S states differing by $\pm k$. The operator equivalents of the fourth order are given in the Appendix. Contrary to the second-order terms the fourth-order terms give rise to a splitting of the S multiplets even in cubic symmetry. The $k = 0$ term does not remove the degeneracy of the $\pm M_S$ levels, but simply changes the separation between neighboring levels. The $k = 4$ terms tend to remove the degeneracy of the $\pm M_S$ levels, introducing a 45° asymmetry in the xy plane. A positive value for B_4^4 places the hard axis along x and y, while a negative value places it along the bisectors of the principal axes. In trigonal symmetry the low-symmetry component has $k = 3$ and the easy axes are found every 60°.

5. Tunneling in Magnetic Fields

If a magnetic field is applied parallel to the z axis the energies of the M_S levels change rapidly, with a slope equal to $M_S g \mu_B$ (Figure 4). It is apparent that the pairs of $\pm M_S$ levels will no longer be degenerate, and the conditions for tunneling will be lost. However, since the energy of the $+M_S$ level increases and that of the $-M_S + n$ level decreases, they will have to meet somewhere, restoring the conditions for resonant tunneling. The field at which this occurs, for axial symmetry and considering only second-order anisotropy terms, is given by Equation (11) where $D' = D/g\mu_B$, and $n = 0, 1, 2\ldots$

$$H_z(n) = n D' \tag{11}$$

It is easy to show that if only the axial second-order ZFS parameter is included, all the $+M_S$ levels will cross the $-M_S + n$ levels at the same field. This is no longer true if higher-order terms are included.

Another interesting feature is provided by the behavior of the lowest-lying levels under the influence of a magnetic field applied parallel to the hard axis. Let us focus on the lowest-lying $M_S = \pm 10$ levels. If their separation from the other excited states, starting from the $M_S = \pm 9$ levels, is large compared to the Zeeman energy, their splitting in a field applied parallel to the hard axis will be very small. However, if one enlarges sufficiently the energy scale of the lowest-lying levels a characteristic oscillatory behavior is noticed (Figure 6).[45–47] At zero field the two levels are split by an amount, which depends on the E/D ratio. For the maximum value $|E/$

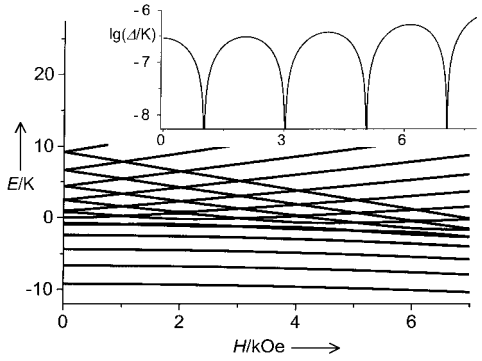


Figure 6. Energy levels of a spin state $S = 10$ in the presence of a transverse magnetic field applied parallel to the hard axis. The inset shows the tunnel splitting of the lowest $M_S = \pm 10$ pair. The curves are calculated with $D = -0.1$ cm^{-1} and $E/D = {}^1/_3$.

$D| = {}^1/_3$ the separation is $2.876 \times 10^{-6} |D|$. The splitting rapidly decreases and goes to zero for $H_x = \sqrt{E'(E'+D')}$, where $E' = E/g\mu_B$, and $D' = D/g\mu_B$. Then it increases again, goes to a maximum at $H_x = 2\sqrt{E'(E'+D')}$, then to a minimum (zero), and so on. The oscillations are repeated S times, and beyond $H_x = (2S+1)\sqrt{E'(E'+D')}$ the oscillatory behavior is quenched. If the analogous plot was reported for the M_S level the oscillations would be observed M_S times. In general the fields at which the tunnel splitting is quenched are given by Equation (12) where $n = 0, 1, 2, \ldots, S$.

$$H_x(n) = (2n+1)\sqrt{E'(E'+D')} \tag{12}$$

If the energy of the states is calculated in the presence of a field parallel to the z axis (the intensity $H_z(1)$ of which is defined by Equation (11)), the (10,−9), (9,−8), … pairs of energy levels will be quasidegenerate for $H_x = 0$. If the transverse field H_x is applied together with a $H_z(1)$ field the oscillatory behavior is also observed, but the points of the maxima and minima are shifted by half a period. In fact if n is even the fields at which the tunnel splitting is quenched are given by Equation (12), while for odd values of n they are given by Equation (13).

$$H_x(n) = 2n\sqrt{E'(E'+D')} \tag{13}$$

These parity effects have been predicted to be detectable in mesoscopic magnets,[26,45–50] but they were experimentally observed for the first time in SMMs (see Section 6).[51]

6. Quantum Phenomena Starting from Classical Physics

Up to now we have used what can be called a molecular approach, which means we have calculated the energies of the spin levels using quantum mechanics. However, we are also interested in investigating the transition from the realm of quantum mechanics to classical physics, therefore it is interesting to also use the opposite approach, seeing if it is possible to describe quantum phenomena from a classical starting point. A more classical approach and its analytic solutions have an important advantage over the quantum mechanical one and the associated numerical methods: it provides a simpler language. While an exhaustive treatment is not the scope of this review and also it overwhelms our capabilities, a description of the oscillatory behavior of the tunnel splitting using a semi-classical approach demonstrates the advantages of the semi-classical method.[31]

The basis to do that is to use Feynman's path-integral formulation of quantum mechanics. The evolution of a system from a state x' to a state x'' can be represented as a path integral [Eq. (14)][52] where the integration is done over all the allowed paths $x(t)$, $D[x(t)]$ is defined by the discrete version of the path integral, and $S[x(t)]$ is the classical action defined through the classical Lagrangian.

$$I = \int D[x(t)] e^{(i/\hbar)S[x(t)]} \tag{14}$$

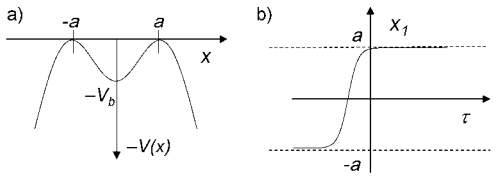


Figure 7. a) Reversed double-well potential for the imaginary time formalism; b) classical instanton solution. Modified from ref. [52].

In this formalism the tunneling of a system characterized by a two-well potential with $x'' = a$ and $x' = -a$ (Figure 7a), is made possible by introducing an imaginary time $t = i\tau$. In this way "classical" paths, $x_1(\tau)$, become possible (Figure 7b). These solutions are called instantons, because they differ from the asymptotic values $\pm a$ only for a certain "instant" of time. Evaluation of the path integral requires that all instanton solutions, $x_1, x_2, \ldots, x_n$, are taken into account.

The use of the Feynman's approach for a single spin is not straightforward, because there is no obvious coordinate or momentum representation for a spin, however, one commonly used procedure is that of using a transformation into canonical coordinates with subsequent use of configuration or phase-space path integral. In this way the tunnel behavior is described by the phase difference between two equivalent paths.

The instanton description has been used[51,53] to describe the tunnel splitting of a molecular cluster, such as Fe8 (see Section 8). It is assumed that the cluster has a large axial anisotropy with a strong transverse component, which makes x the hard axis. If the magnetization is prepared by saturating along $+z$ axis, when the field is switched off the system must return to equilibrium by switching to the $-z$ axis. The rotation will occur preferentially in the yz plane, and it can be either clockwise or anticlockwise. When a transverse field is applied, the two minima A and B are still connected by two paths, which depend on the strength of the transverse field and its orientation in the xy plane (Figure 8). If the two paths are covered in phase there will be a reinforcement and a tunnel splitting will result, while if they are dephased by $\pi/2$ then the splitting will be quenched. These topological interferences are also known as Berry phases.[54]

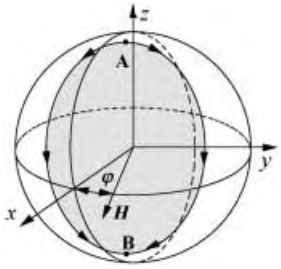


Figure 8. Unit sphere showing the classical reversal of spin. The *x*, *y*, and *z* axes are the hard, intermediate, and easy axis, respectively. The spins point toward $\pm z$ in zero field. The two degenerate minima A and B (the position of which depends on the transverse field) are connected by two paths, clockwise and anticlockwise. When the shaded area corresponds to $k\pi/S$ (k = odd integer) the two paths give destructive interference. Modified from ref. [51].

Another approach widely used for describing mesoscopic quantum tunneling is the so-called Wentzel–Kramers–Brillouin (WKB) approach.[55–59] This is an approach to find a semi-classical approximation to the solution of the quantum-mechanical Schrödinger equation and in particular how to find its eigenstates. A modified version of this approach has been used by Villain et al.[26] where the ground-state wavefunctions for a giant spin S in biaxial-type magnetic anisotropy are approximated in the limit of a high barrier, by assuming that the states can be effectively described only by admixing states belonging to the same well (see Figure 3).

7. Mn12ac and Single-Molecule Magnets

7.1. Structure and Magnetism of Mn12ac

The synthesis and the structure of the first SMM was reported by Lis[21] in 1980. The actual formula of the compound is $[Mn_{12}O_{12}(CH_3COO)_{16}(H_2O)_4]\cdot 2\,CH_3COOH\cdot 4\,H_2O$. The possibility of formation of dodecanuclear manganese acetate complexes had been suggested[60] as early as 1921 but it was only when X-ray structure determination became routine that it was possible to clearly confirm the structure (Figure 9). The crystal has tetragonal symmetry (space group $I\bar{4}$) and the dodecanuclear cluster has S_4 symmetry. It was poetically described as resembling a snowflake,[21] but the tetragonal symmetry of course is not appropriate to snowflakes. Since the molecule has tetragonal symmetry there are three independent manganese ions, namely two manganese(III) and one manganese(IV), which are octahedral coordinated (Figure 10). The manganese(III) ions can be easily recognized by the bond lengths and by the elongated structure typical of these Jahn–Teller distorted ions. The structural evidence is for a mixed-valence compound belonging to the Class I of the Robin and Day[61] classification. This assignment is further corroborated by the bond valence sums,[62] which are close to 4 and to 3, respectively, for the two types of ions. Mn1, which corresponds formally to an Mn^{IV} center, is coordinated to five oxo ligands and to one oxygen atom of an acetate group; Mn2, which corresponds to an Mn^{III} center, is bound to two oxo ligands and to four oxygen atoms of acetate molecules, while Mn3, which is also formally an Mn^{III} center, is bound to two oxo ligands, three oxygen atoms of acetate molecules, and a water molecule. All the oxo ligands form μ_3 bridges. The manganese(III) ions show the typical elongated octahedral coordination seen in most Mn^{III} complexes. The elongation axis of Mn2 makes an angle of 11° with the tetragonal axis, while that of Mn3 makes an angle of 37°. These values are important for the barrier to the reorientation of the magnetization as will be discussed below.

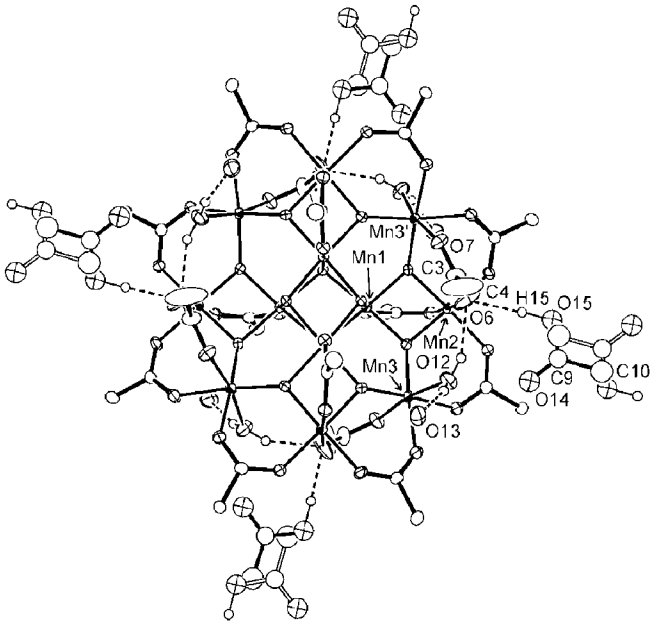


Figure 9. ORTEP view of $[Mn_{12}O_{12}(CH_3COO)_{16}(H_2O)_4]\cdot 2\,CH_3COOH\cdot 4\,H_2O$. The two symmetry related disordered acetic acid molecules are differentiated through full and empty bonds. Modified from ref. [64].

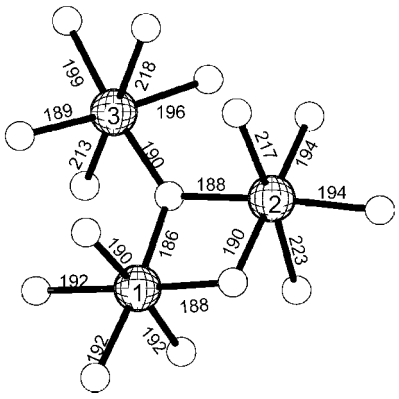


Figure 10. Coordination environment of the three independent manganese ions in Mn12ac. The labeling scheme is given in Figure 9.

Another important feature of the structure is the presence of acetic acid and water molecules of crystallization. Thermogravimetric studies[21] showed that loss of solvated molecules starts at 308 K and continues up to 463 K. Above this temperature decomposition of the compound sets in. The acetic acid molecules of solvation lie between adjacent clusters and close to a twofold axis and are therefore statistically distributed between the two symmetry-equivalent positions. They are at hydrogen-bond distances from the coordinated water molecules and the acetate ligands, as shown by low-temperature neutron diffraction studies.[63] In the original crystal structure solution of Lis[21] there was some disorder which has recently been well characterized[64] (Figure 9) thanks to a low-temperature (83 K) X-ray data collection. The main effect of the disorder is to reduce the real symmetry of most molecules present in the crystals; the relevance to the tunneling behavior is discussed in Section 7.2.

Several other carboxylate compounds were prepared, as shown in Table 1. The acetate derivative **1** is obtained by addition of permanganate to a solution of $Mn(CH_3COO)_2\cdot 4\,H_2O$ in water/acetic acid (2:3) through the reaction given in Equation (15).

$$16\,Mn^{7+} + 44\,Mn^{2+} \rightarrow 5\,(Mn^{3.33+})_{12} \qquad (15)$$

Table 1: Mn12 derivatives with reported structures.[a]

Compound	R	x	Space group	Solvent molecules	Water coordination	Ref
1	Me	4	$I\bar{4}$[b]	$2\,CH_3COOH$, $4\,H_2O$	1:1:1:1	[21]
2	Et	3	$P1m$	$4\,H_2O$		[125]
3	Et	3	$P2_1/c$			[125]
4	Me, Et	4	$I4m$	$2\,H_2O$, $4\,C_2H_5COOH$	1:1:1:1	[143]
5	$tBuCH_2$	4	$P1m$	CH_2Cl_2, CH_3NO_2	1:2:1:0	[139]
6	Ph	4	$P1m$		2:2:0:0	[65,141]
7	Ph	4	$Fdd2$	$2\,C_6H_5COOH$	2:2:0:0	[142]
8	p-Me-C_6H_4	4	$C2/c$	p-Me-C_6H_4COOH	1:2:1:0	[125]
9	p-Me-C_6H_4	4	$I2/a$	$3\,H_2O$	1:1:2:0	[125]
10	p-Cl-C_6H_4	4	$C2/c$	$8\,CH_2Cl_2$	2:2:0:0	[125]
11	m-Cl-C_6H_4	3	$P1m$	m-Cl-C_6H_4COOH	?	[144]
12	o-Cl-C_6H_4	4	$Pnn2$	CH_2Cl_2, $5\,H_2O$	1:1:2:0	[140]
13	$PhCH_2$	4	$P1m$		1:2:1:0	[139]

[a] General formula $[Mn_{12}O_{12}(RCOO)_{16}(H_2O)_x]\cdot S$. [b] Site symmetry S_4.

The reaction has an excellent yield (typically 80%). The preparation is similar to that used for preparing manganese(III) acetate, which is a polymer containing trinuclear units which are suspected to be involved in the mechanism of formation of the cluster.

The other carboxylate compounds are generally obtained by treating a slurry of the acetate derivative in a suitable solvent with the desired carboxylic acid. A typical reaction is that described for the preparation of the benzoate derivative.[65] Treatment of Mn12ac with a 100% excess of benzoic acid in CH_2Cl_2 leads to a majority, but not all, of the acetate ligands being exchanged. The black solid obtained, which contains both acetate and benzoate, is further treated with a tenfold excess of benzoic acid to give the completely substituted derivative.

The interesting feature of the class of Mn12 clusters is that they remain intact in solution, as shown by proton NMR spectroscopic measurements on the acetate, propionate, and benzoate derivatives.[66] A broad concentration-dependent peak in the spectrum of Mn12ac is assigned to the weighted average of bound and free water molecules, which indicates that the ligand exchange is fast on the NMR time scale. There are only three other resonance signals, which correspond to the three magnetically inequivalent acetate ions, of relative intensity 1:1:2, which indicates that the tetragonal symmetry of the crystal is preserved in solution. The two resonance signals which are most shifted downfield are assigned to the acetate ligands bridging the Mn^{3+} ions, while the upfield peak is assigned to the acetate groups bridging the four Mn^{3+}–Mn^{4+} pairs. The signal of double intensity is assigned to the equatorial acetate groups.

The temperature dependence of $\chi_m T$ for a polycrystalline powder sample of Mn12ac is shown in Figure 11. At room temperature its value (19.4 emu mol^{-1} K) is smaller than expected for uncoupled spins (31.5 emu mol^{-1} K). This result indicates an overall antiferromagnetic coupling. On decreasing temperature $\chi_m T$ goes through a minimum indicating ferrimagnetic behavior as a result of antiferromagnetic interactions with no compensation of the individual magnetic moments. The increase in $\chi_m T$ on further decreasing temperature gives rise to a broad maximum at approximately 55.6 emu mol^{-1} K, which is close to the value expected for a spin $S = 10$ (55 emu mol^{-1} K), but very far from the value expected for ferromagnetic coupling ($S = 22$; 253 emu mol^{-1} K), which confirms that the cluster has a ferrimagnetic spin arrangement. The decrease of $\chi_m T$ at lower temperatures may indicate a large zero-field splitting of the ground state or intercluster interactions. The former hypothesis has been independently confirmed through many different experimental techniques.

The first unambiguous evidence of the ground $S = 10$ state came from high-field (HF) magnetization studies.[19] Single-crystal magnetization data provided evidence of a very large easy-axis magnetic anisotropy (Figure 12).[67] Both the parallel (to the tetragonal axis) and perpendicular magnetization reach a saturation value of about 20 μ_B, as expected for an $S = 10$ state. However the former curve increases much more rapidly than the latter, indicating a strong Ising anisotropy.

The anisotropy has been confirmed by HF-EPR spectroscopy (Figure 13) on a polycrystalline powder at variable temperature at a frequency of 525 GHz, in applied fields up to 26 T.[19,68] Since the Zeeman energy becomes comparable to

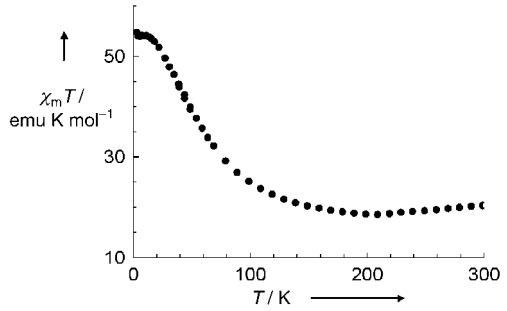


Figure 11. Temperature dependence of $\chi_m T$ for a polycrystalline powder of Mn12ac.

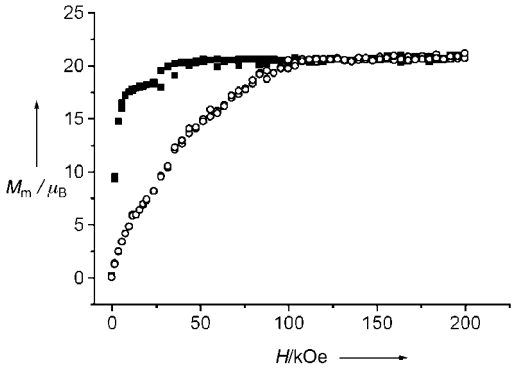


Figure 12. High-field magnetization curves for a single crystal of Mn12ac: ■ magnetic field parallel to the tetragonal axis; ○ magnetic field perpendicular to the tetragonal axis. Modified from ref. [67].

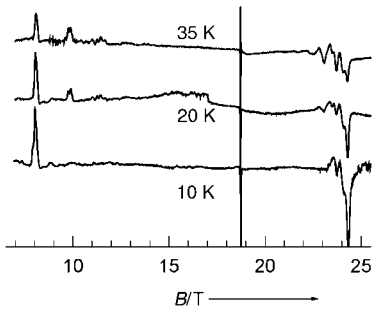


Figure 13. 525 GHz EPR spectra of a polycrystalline powder of Mn12ac at different temperatures. The narrow signal marks the $g = 2.00$ resonance.

kT at low temperature, strong depopulation effects are indicated by the HF-EPR spectra, with certain lines disappearing on decreasing temperature.[69] The features appearing at low temperature correspond to transitions between the lowest $M_S = -10$ and the first excited $M_S = -9$ levels. The experimental spectra show that the features observed at low field correspond to resonances of crystallites with the tetragonal axis parallel to the applied magnetic field, while those at high field correspond to crystallites with the magnetic field perpendicular to the tetragonal axis (i.e., in the tetragonal plane). The separation between two neighboring parallel lines should be equal to $2D/g_e\mu_B$ (where D is the parameter defined in Equation (2), Section 3). Actually the separation between pairs of neighboring lines is not a constant, which indicates that the higher-order terms of the anisotropy play some relevant role here. Single-crystal EPR measurements at different frequencies have also been reported[68] and the values of the parameters are given in Table 2. Similar values were also obtained through high-field magnetic torque measurements.[70] Two sets of values were obtained in different laboratories by using HF-EPR spectroscopy.[71] In general there is good agreement between the different sets, the major differences being on the transverse fourth-order terms, which are the most difficult to determine experimentally. A more troublesome problem, however, is the use of different Hamiltonians for interpreting the experimental data. In fact, many different forms of Hamiltonian have been used, often with the same symbols having different physical meanings. We have used the D and E parameters [Eq. (2), (3)] for the second-order terms and the Steven's operator equivalents O_n^k which are listed in the appendix, with the corresponding parameters B_n^k. It must be stressed that the value of the D parameter may be different if the fourth-order parameters are included in the fit. The O_4^0 operator also contains S_z^2 terms [Eq. (16)]. Therefore when the fourth-order term is included the S_z^2 operator is associated with the parameters $D - [30S(S+1) - 25]B_4^0$, whereas if only the second-order operators are taken into consideration it is associated with D alone.

Table 2: Zero-field splitting parameters for Mn12ac in cm^{-1}.

D	B_4^0	B_4^4	Lit.
−0.46(2)	$-2.2(2)\times10^{-5}$	$\pm4(1)\times10^{-5}$	[68]
−0.457(2)	$-2.33(4)\times10^{-5}$	$\pm3.0(5)\times10^{-5}$	[73]
−0.47	-1.5×10^{-5}	-8.7×10^{-5}	[71]
−0.46	-2.19×10^{-5}	–	[76]

$$O_4^0 = 35S_z^4 - [30S(S+1) - 25]S_z^2 - 6S(S+1) + 3S^2(S+1)^2 \qquad (16)$$

Inelastic neutron scattering is another important tool for obtaining experimental information on the spin structure and spin excitations.[72] It is a zero-field experiment; therefore the g value of the spin system is not important. Transitions between levels following the selection rules $\Delta M_S = 0, \pm1$ are allowed. High-resolution spectra of Mn12ac[73,74] (Figure 14) show that the experimental spacing of the levels is not regular; this is then an experimental indication that fourth-order terms must be introduced.

Another technique has recently become available for the measurement of the energy spacing of spin levels in zero applied magnetic field, namely a quasi-optic submillimeter backward-wave-oscillator (BWO) technique.[75] The BWO technique is operated in the frequency-scanning mode. The scanning is carried out at different points by varying the BWO supply voltage in steps. The frequency resolution of the apparatus $\Delta\nu/\nu$ is 10^{-4}–10^{-5}. Three transitions were observed[76] in the frequency range 0–35 cm^{-1}, which correspond to the transitions $\pm10 \rightarrow \pm9$, $\pm9 \rightarrow \pm8$, and $\pm8 \rightarrow \pm7$. Also in this case the irregular spacing of the levels confirmed the need of fourth-order terms.

The above spectroscopic techniques show some additional features, other than the features which can be safely assigned to transitions within the $S = 10$ ground state. These extra features have been assigned either to minority species present as unavoidable defects in the crystals or to transitions involving the lowest-lying excited states ($S = 9, 8, \ldots$). While crystal defects are now well known, the evidence for transitions involving levels other than $S = 10$ is far from conclusive.

Specific-heat measurements provided[67,77] no evidence for long-range order in the compound, thus ruling out intercluster interactions as the origin of the deviation of the χT values from those expected for $S = 10$.

The $S = 10$ ground state can be modeled at the simplest level by assuming that all the manganese(III) spins are up and the manganese(IV) spins are down. Polarized neutron-diffrac-

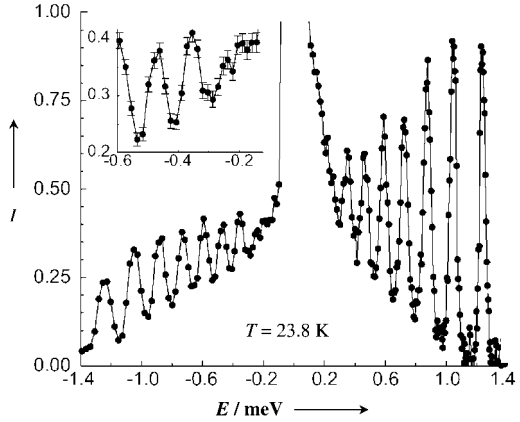


Figure 14. Inelastic neutron-scattering data obtained for Mn12ac at 23.8 K. The inset shows the low-energy range. Modified from ref. [73].

tion experiments performed on a single crystal confirmed this view.[78] Even if the calculated total magnetic moment for $S=10$ agrees with the $20\,\mu_B$ saturation value found, the spin density on each metal center is significantly reduced compared to the spin-only value. Such a trend was indeed predicted by density functional theory (DFT) calculations.[79,80] No significant spin density was found on nonmetal atoms.

Since Mn12ac is a ferrimagnetic cluster, excited spin levels with $S>10$ must be present. In principle these levels may become populated at high field, because in the limiting condition of a strong field the ferromagnetic $S=22$ state must become the ground state. Clearly high fields are needed to stabilize the high-spin states, because relatively strong exchange interactions binding the spins must be overcome. Recently extremely high pulsed fields have become technically possible. An experiment reaching 800 T showed a series of crossovers from $S=10$ to $S=11$, 12,..., up to $S=22$.[81] The crossover points are observed for fields ranging from 300 to 600 T.

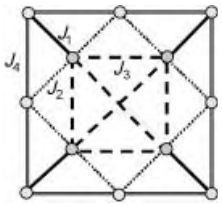


Figure 15. Scheme for calculating the spin states of Mn12ac.

Several attempts have been made to calculate the complete spectrum of the spin levels of Mn12ac.[65,82,83] The task is far from simple, because the total number of spin states is one hundred million! Initially several attempts were made by using some ad hoc assumptions. For instance it was assumed that the J_1 coupling constant, defined in Figure 15, corresponding to the interaction between manganese(III) and manganese(IV) centers mediated by a double oxo bridge, is strongly antiferromagnetic.[65] The coupling constant J_2 is between manganese(III) and manganese(IV) ions mediated by a single oxo bridge, J_3 is that between manganese(IV) ions, while J_4 corresponds to the exchange between the manganese(III) ions, and the Hamiltonian used is in the form $\mathscr{H}_{ex}=J\mathbf{S_a}\mathbf{S_b}$.

It may be assumed that the four Mn^{III}–Mn^{IV} pairs connected by J_1 are in the ground $S={}^1/_2$ state, and that the contributions from the excited $S={}^3/_2$, ${}^5/_2$, and ${}^7/_2$ states may be neglected. By using this assumption sample calculations were performed, in which the constants J_2, J_3, and J_4 were varied in a relatively small range. It was observed that the S values of the calculated ground states could vary from 8 to 10, depending on the values of the parameters used.

Later the calculations were performed again trying to fit the excited states made available by the high-field experiments described above.[81] In this case, assuming that the assignment of the experimental crossover fields is correct it is possible to perform complete calculations, because in this case the energies of the highest excited states can be calculated by diagonalizing relatively small matrices.[65] The values of the parameters changed dramatically. Unfortunately these data do not allow calculation of the ground state. Tupitsyn et al. provided further sets of parameters, which showed that the previously reported parameters did not describe the $S=10$ ground state.[82]

Recently more powerful calculation techniques have been implemented.[83] These methods use an efficient system for representing a state, in a computer, by a single number. Further, the spatial symmetry (S_4 in the case of Mn12ac) is exploited by using the valence-bond (VB) method, which employs the Rumer–Pauling rule.[84] Using the complete set of spin states it was shown that the previous approximate calculations fail to give the correct ground state. Sample calculations showed that with $J_1=149\ cm^{-1}$ and $J_2=59\ cm^{-1}$, the spin of the ground state is very sensitive to J_4 for a fixed value of J_3. Calculation of the temperature dependence of the susceptibility provides a check for the goodness of the parameters. The chosen values of the parameters were based on the assumption of a ground $S=10$ state with $S=9$ lying 35 K above. In the reported calculations, with $J_3=59\ cm^{-1}$, $J_4=-44\ cm^{-1}$, an $S=11$ excited level is present at $179\ cm^{-1}$. This should give a crossover to the ground state in a field of 192 T, not too far from the experimentally determined one, 382 T. Calculations have been also performed in the Lanczos formalism,[85,86] which for a particular S value give only the lowest-lying states. The best-fit parameters $J_1=62\ cm^{-1}$, $J_2=61\ cm^{-1}$, $J_3=0\ cm^{-1}$, $J_4=12\ cm^{-1}$ were obtained and reproduce the presence of an $S=9$ at approximately 35 K and the energies of the states with $S>10$.

The largest contribution to the origin of the magnetic anisotropy of Mn12ac comes from the single-ion anisotropy of the Jahn–Teller-distorted manganese(III) ions. With a defined ground state, and strong exchange as a limiting condition, it is possible to express the observed zero-field-splitting parameter D as a linear combination of the single-ion zero-field splitting parameters D_2 and D_3 of the two crystallographically independent manganese(III) ions, Mn2 and Mn3, respectively.[42] If the ground state is defined by a coupling scheme in which the eight manganese(III) ions are ferromagnetically coupled to give a total spin $S_A=16$, and the four manganese(IV) ions to give a total spin $S_B=6$, Equation (17) holds for the ground $S=10$ state, where $a_2=a_3=0.02845$ as calculated from spin projection techniques.[33]

$$D_{tot}=a_2D_2+a_3D_3 \tag{17}$$

Assuming, for the sake of simplicity, that $D_2=D_3$, incorporating the experimental D value in Equation (17) gives $D_2=-2.0\ cm^{-1}$, a value totally acceptable if compared to the experimental parameters observed in isolated manganese(III) complexes. Analogous relationships have been calculated for the fourth-order terms,[42] although no safe values are available for the individual ions.

To evaluate the magnetic anisotropy of Mn12ac starting from first principles treatments were attempted using DFT calculations.[79,80] These calculations start from naked $Mn_{12}O_{12}$ clusters. Rather unsurprisingly these clusters do not compare well with the structure and magnetic properties of Mn12ac. More interestingly the calculated ground state of the complete cluster is $S=10$ as experimentally observed. The unpaired spin density is essentially localized on the manganese ions, and is negative for the inner tetrahedron and positive for the outside ring. Significant spin density is also calculated on the bridging oxo groups. On introducing spin–orbit coupling into the calculations, the second-order contribution to the barrier was estimated to be in astonishingly good agreement with the experimental data.

More sophisticated phenomena have also been taken into consideration, including the contributions from spin–spin interactions to the magnetic anisotropy.[87] Among these the intracluster dipolar interactions seem to play only a minor role, while those determined by antisymmetric exchange may play a significant role. Detailed calculations have been performed assuming that J_1 is dominant.[88] To justify the experimental zero-field splitting an antisymmetric exchange contribution ranging from -1 to $+10\,cm^{-1}$ was included. Unfortunately no reliable estimate of this contribution is possible. Further, these calculations require that the molecule has a reduced symmetry.

A very powerful technique to evaluate the magnetic anisotropy of metal clusters is based on the crystal-field analysis of the magnetic anisotropy of the metal centers associated with the projection technique mentioned above.[89] It has been shown[90] that the magnetic anisotropy of manganese(III) ions can be predicted with a great accuracy by taking into account the crystal field generated by the ligands and by introducing the real geometry of the coordination sphere by using the angular-overlap (AO) model.[91] This is a ligand-field model[92] which uses molecular-orbital oriented e_σ and e_π parameters for each donor atom, and is particularly well suited to account for angular distortions in the ligand field. Its application to Mn12ac has been particularly useful in evaluating the effects of the disorder in the structure on the magnetic anisotropy.[93] If we look in more detail at the low-temperature X-ray crystal structure it is possible to model the disorder of the acetate ligand, bridging Mn2 and Mn3, which is induced by the presence of acetic acid molecules in two different positions, A and B (Figure 16). The site occupation factors are very close to 0.5, as for the acetic acid of crystallization, which, when present, form hydrogen bonds with the acetate ligands. The four different coordination environments of the manganese(III) ions, provided by the X-ray analysis, have been used in calculating the magnetic anisotropy with the AOM approach. The values of the e_σ and e_π parameters for each donor atom, taken from literature data,[89] have been corrected for the actual metal–ligand separation by assuming an exponential dependence. In Table 3 the results obtained from the calculation are reported. As can be seen, the interaction with the acetic acid molecule induces only minor changes in the D and E parameters as well as in the direction of the easy axis even if the effects on the deviation from tetragonal symmetry are sizeable. Six different isomeric forms of Mn12ac can thus be envisaged which differ in the number ($n = 0$, 1, 4) and arrangement of hydrogen-bound acetate ligands (Figure 17). Clearly, strict axial symmetry can be retained only in the case of a regular pattern of $n = 0$ and $n = 4$ isomers. However, this would lead to a supercell with doubled lattice constants ($a' = b' = 2a$) for which no experimental evidence has been found. The zero-field splitting parameters of the six different isomers can be easily calculated using Equation (18) where the D parameters are now substituted by tensors.

$$\mathbf{D}_{tot} = d_2 \sum_{i=1}^{4} \mathbf{R}_i^T \mathbf{D}_2^{\alpha(i)} \mathbf{R}_i + d_3 \sum_{i=1}^{4} \mathbf{R}_i^T \mathbf{D}_3^{\alpha(i)} \mathbf{R}_i \qquad (18)$$

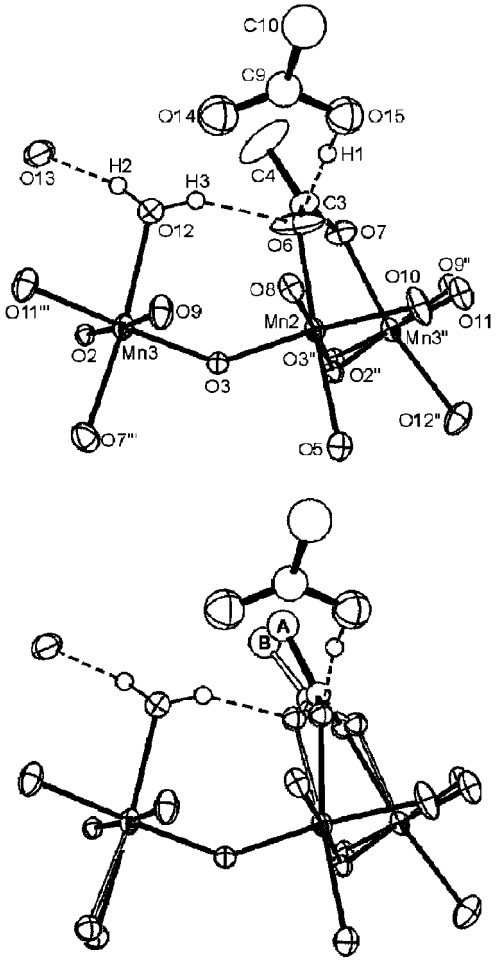


Figure 16. Coordination sphere of Mn2 and Mn3, as determined from anisotropic refinement of the displacement factors of C3, C4, O6, and O7 (top) and from an isotropic model with disorder fitting (bottom). Thermal ellipsoids are set at 50% probability. Methyl hydrogen atoms are omitted for the sake of clarity.

Table 3: Calculated Mn^{III} magnetic anisotropy parameters in Mn12ac.

Site	D [K]	E [K]	δ [°][a]
Mn2A	−4.92	0.40	11.6
Mn2B	−5.27	0.27	10.7
Mn3A	−4.57	0.10	37.2
Mn3B	−4.40	0.07	37.1
Mn3 flipped[b]	−4.64	0.06	58.4

[a] δ is the angle between the easy-axis direction of each manganese site and the crystallographic c axis. [b] The elongation axis of Mn3 has been flipped to point towards an oxo ligand (see section 7.3 and 7.5).

In Equation (18) $\alpha(i)$ describes the disorder induced by acetic acid molecules in positions A or B, $\mathbf{D}_2^{\alpha(i)}$ and $\mathbf{D}_3^{\alpha(i)}$ are the single-ion zero-field-splitting tensors for the Mn2 and Mn3 sites generated by the ith symmetry operation of the S_4 point-group. The resulting $\mathbf{D}_{tot}$ tensor turns out to be axial and diagonal in the crystal axes reference frame only for $n = 0$ and $n = 4$. In the other four cases nonzero off diagonal terms are present and diagonalization of the matrices provided the D and E parameters along with the angle θ between the easy axis and the crystallographic c axis (Table 4). The easy axis of

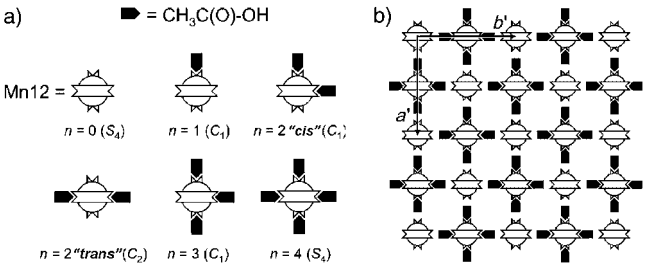


Figure 17. a) The six hydrogen-bond isomers of Mn12ac; b) a possible aggregation of isomers retaining the tetragonal symmetry.

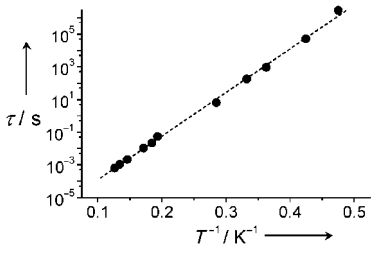


Figure 18. Temperature dependence of the relaxation time of the magnetization of Mn12ac. The dashed line corresponds to an Arrhenius law with $\tau_0 = 2.1 \times 10^{-7}$ s, $\Delta/k = 62$ K.

Table 4: Calculated magnetic anisotropy and tunnel splitting of the isomers of Mn12ac.

Isomer	c [%]	D [K]	E [K]	δ [°]	$\Delta_{-10,4}$ $(n=6)$[a]
$n=0$	6.25	0.759	0	0	0
$n=4$	6.25	0.797	0	0	0
$n=1$	25	0.769	2.34×10^{-3}	0.3	8.8×10^{-8}
$n=2$, *cis*	25	0.778	1.87×10^{-4}	0.4	7.0×10^{-9}
$n=2$, *trans*	12.5	0.778	4.70×10^{-3}	0	1.7×10^{-7}
$n=3$	25	0.788	2.35×10^{-3}	0.3	8.9×10^{-8}
"flipped"	n.a.	0.754	4.39×10^{-2}	9.0	7.3×10^{-7}

[a] The tunnel splitting is calculated at the level crossing of $M_S = -10$ and $M_S' = 4$ corresponding to $n = 6$ [see Eq. (11)] assuming for the ZFS parameters the same as in ref. [73] but including the E term here reported in the 4th column.

the different species does not deviate significantly from the crystallographic c axis. The six species have very similar D values (within $\pm 2\%$), which is in acceptable agreement with the experimental values reported in Table 2, considering the approximations involved (definition of the ground-state wavefunctions and the related projection coefficients, neglect of higher-order terms, etc.).

7.2. Slow Relaxation and Quantum Tunneling of the Magnetization of Mn12ac

The large zero-field splitting of the ground $S = 10$ provides a barrier for the reorientation of the magnetization at low temperature as explained in Section 3. If only second-order terms are included in the Hamiltonian the calculated barrier for Mn12ac is about 70 K. The relaxation time of the magnetization has been experimentally found to follow a thermally activated behavior, with $\tau_0 = 2.1 \times 10^{-7}$ s, $\Delta/k = 62$ K.[20] Figure 18 shows the temperature dependence of $\ln(\tau)$. The relaxation time becomes of the order of months at 2 K. Recent determinations suggest that below 2.0 K τ becomes slightly dependent on temperature and that at 1.5 K it is of the order of 50 years.[94]

The first evidence of slow relaxation of the magnetization came from ac susceptibility measurements (Figure 19).[19,95] In an ac experiment an out-of-phase signal, χ'', is expected to be seen if the relaxation frequency of the magnetization of the sample becomes lower than the frequency of the ac magnetic field.[27] At the temperature at which χ'' goes through a maximum the relaxation frequency of the magnetization is equal to the ac field frequency.

Since the relaxation time becomes so long magnetic hysteresis is observed.[20] Experiments performed on single crystals, with the external magnetic field applied parallel to the unique axis, showed a stepped hysteresis[96,97] as reported in Figure 20. The first reported experiment[96] was performed on a group of crystals oriented with their c axis parallel to the magnetic field. The crystals could be oriented in a high field at room temperature, taking advantage of the large shape anisotropy of the microcrystals. The origin of the steps, which is not related to the Barkhausen effect,[27] has been assigned to the thermally assisted quantum tunneling of the magnetization.[35–41] Similar conclusions had been reached on the basis of ac magnetic-susceptibility measurements.[67] The steps are observed at the fields at which pairs of levels become degenerate. They correspond to relative minima in the relaxation times, because at these fields two mechanisms are operative, namely the thermally activated and the quantum tunneling. At the fields corresponding to flat regions of the magnetic hysteresis curve the degeneracy of the levels is lost

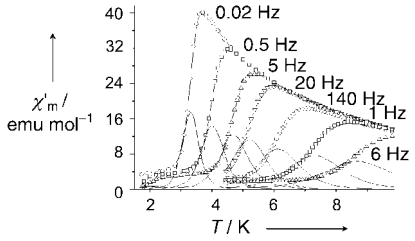


Figure 19. Temperature dependence of the in-phase ac magnetic susceptibility of Mn12ac at different frequencies.

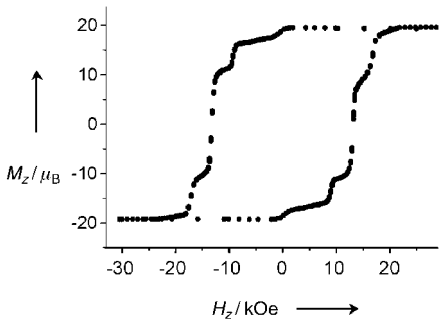


Figure 20. Magnetic hysteresis loop for a single crystal of Mn12ac with the field parallel to the tetragonal axis at 2.1 K. Modified from ref. [97].

and the tunneling mechanism is destroyed giving longer relaxation times. The field dependence of the relaxation time of the magnetization is shown in Figure 21. Many other magnetic experiments[98–103] have confirmed this picture but a similar trend has been observed using different techniques including specific-heat-capacity measurements[104–106] and NMR spectroscopy.[107,108]

Often the final proof for quantum tunneling is associated with the temperature independence of the relaxation time. This limit is never reached experimentally for Mn12ac, because below 2 K τ becomes extremely long, and reliable measurements, which require the temperature of the experiment to be fixed for very long times become practically impossible. At low temperature, however, relaxation can be still observed if a strong axial field is applied. The relaxation in fact involves the transition from the $M_S=-10$ metastable state to M_S' states. The smaller $|M_S'|$ is the larger the applied field. The relaxation is accelerated by the reduction of the barrier height as well as by the more efficient admixing in of the states with lower $|M_S'|$. In the presence of fourth-order axial anisotropy, as for Mn12ac, the resonant tunneling occurs at different field for different $M_S \rightarrow M_S'$ pairs. It has been possible[87,109–112] to determine which pairs of states are involved, and at which temperature the mechanism involves exclusively the metastable ground state $M_S=10$. It has been theoretically shown[113] and recently confirmed experimentally[111] that this crossover from thermally activated to ground tunneling can be either first or second order depending on the strength of the transverse field (Figure 22). It is important to underline that all the resonance signals are observed although the tetragonal symmetry of the transverse anisotropy would require that only every fourth step (corresponding to $M_S-M_S'=4n$) is present. The presence of second-order transverse anisotropy, which is expected in most of the Mn12ac molecules in the crystal,[93] allows $(2n)$ transitions, whereas for the odd $(2n+1)$ transitions a transverse field must be included. More recently, an accurate analysis of the dependence of the magnetization on the sweeping rate of the axial magnetic field has shown[114] that the fractions of reversed magnetization at the even transitions scale well on a single curve if plotted as a function of a scaling parameter. This parameter is proportional to the logarithm of the inverse of the field sweeping rate. Such an experimental behavior can be justified if a broad distribution of the second-order transverse anisotropy is present. It has been suggested[115] that a small concentration (0.1 %) of disordered molecules in

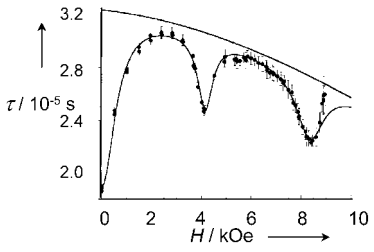


Figure 21. Field dependence of the relaxation time of the magnetization of Mn12ac ($T=8.5$ K) obtained from an ac susceptibility measurement at a frequency of 5.37 kHz. Modified from ref. [240].

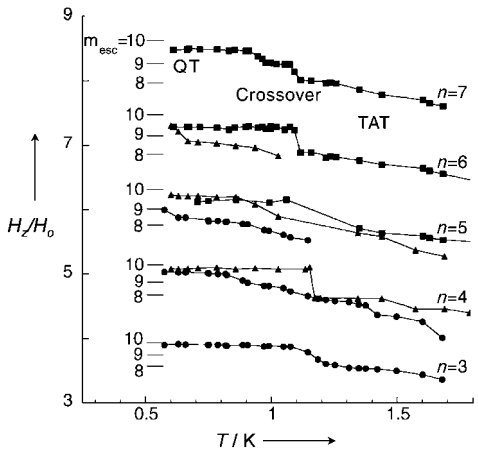


Figure 22. Temperature dependence of the peak positions in the unit $H_0=4.2$ kOe, $\theta=0°$ (■), $\theta=20°$ (▲), and $\theta=35°$ (●). QT = quantum tunneling, TAT = thermally activated tunneling. Modified from ref. [111].

the crystal structure and the associated gradient of the magnetic anisotropy, which extends over a wide distance, can give rise to the distribution in the E parameter and the consequent scaling law. Crystal-field calculations have, however, shown that the magnetic anisotropy is only slightly affected by strong perturbation of the structure (such as, the presence of a hydrogen-bonded acetic acid molecule) and therefore long-range effects of disorder are expected to be very small.[93] On the contrary the presence of several isomers with significantly different transverse anisotropy could mimic the broad distribution required to justify the experimental behavior.

An important point to be clarified is how the relaxation times are actually measured. The most direct way, which can be used when τ is sufficiently long, is to saturate the sample (better a crystal than a powder), switch off the field, and measure the decay of the magnetization as a function of time. In the simplest case, when only one decay mechanism is possible the magnetization follows the exponential law given in Equation (4). More complex behavior is usually observed, which can be fitted with stretched exponentials [Eq. (19)] where M_{eq} and $M(0)$ are the equilibrium and initial magnetization, respectively, and β is a coefficient ranging from 0 to 1.[116,117]

$$M(t) = M_{eq} + [M(0) - M_{eq}] \exp[-(t/\tau)^{\beta}] \qquad (19)$$

The stretched exponential fit has the same role as the Curie–Weiss fit of magnetic susceptibility, it takes into account all the possible deviations from simple single-exponential behavior. In Mn12ac the relaxation has been observed to deviate from single exponential at short times[94,99] (presumably because of the dipolar interactions with the neighboring molecules), and to be accurately reproduced by a single exponential at longer times. The mechanism by which the dipolar fields determine a non-exponential decay is intuitively clear. If the sample is initially saturated, when the field is removed it will be far from equilibrium, and will start to relax. The actual field felt by a

relaxing molecule will depend on the state of the neighboring molecules, each molecule feeling a different field from the others.

Sometimes the stretched exponential fit has been used for the whole set of data, alternatively the initial data are neglected and the remainder of the M/t measurement treated with the single exponential. In particular Thomas et al.[94] found that in a single crystal of Mn12ac a single exponential fit is possible above 2.8 K. Below 2.0 K the initial relaxation follows a square-root regime in Equation (20) with $M(0)$ the initial magnetization and M_{eq} the equilibrium magnetization, as anticipated for dipolar and/or hyperfine assisted tunneling, based on theoretical work by Prokof'ev and Stamp.[118,119]

$$M(t) = M(0)_{in} + ([M_{eq} - M(0)])\,(t/\tau)^{1/2} \tag{20}$$

The specific heat capacity has also been used to measure relaxation times. In a series of sophisticated experiments Fominaya et al. used a nanocalorimeter[120] to measure the specific heat of single crystals of Mn12ac as a function of frequency with a magnetic field applied parallel to the tetragonal axis. The nanocalorimeter consists of a 3-μm-thick silicon membrane suspended in a vacuum and linked to the thermal bath by twelve narrow silicon bridges. A planar NbN thermometer and a CuNi heater are placed on one side of this membrane and the samples are pasted with grease on the other side. The experimental set-up permits not only the study of extremely small crystals, but also a very accurate measurement of the sample temperature. Experimentally one can measure the absolute specific heat capacity C at frequency ω [Eq. (21)] where C_{bi} is the specific heat capacity in the bilateral regime when the levels on both sides of the barrier are accessible while in the unilateral regime, when the states on the opposite side of the barrier are not accessible, the specific heat is reduced to C_{uni}.

$$|C(\omega)| = \sqrt{C_{uni}^2 + \frac{C_{bi}^2 - C_{uni}^2}{1+\omega^2\tau^2}} \tag{21}$$

When $\omega\tau \gg 1$, that is, when $\tau \to \infty$, then Equation (21) becomes $C(\omega) = C_{uni}$, which means that the jumps over the potential barrier are impossible during the measuring time $2\pi/\omega$. At the other limit, $\omega\tau \ll 1$ (that is, when $\tau \to 0$), $C(\omega) = C_{bi}$, which is the equilibrium value. At the resonant fields, when the relaxation accelerates because of the tunnel mechanism, the bilateral regime is suddenly attained and the specific heat capacity increases significantly showing well resolved peaks (Figure 23).[106] Using Equation (21) it is possible to calculate the relaxation time [Eq. (22)]:

$$\tau = \frac{1}{\omega}\sqrt{\frac{C^2(\omega) - C_{bi}^2}{C_{uni}^2 - C^2(\omega)}} \tag{22}$$

The values of the experimentally determined relaxation times as a function of an axial magnetic field are shown in Figure 24.[105] They agree reasonably well with the values

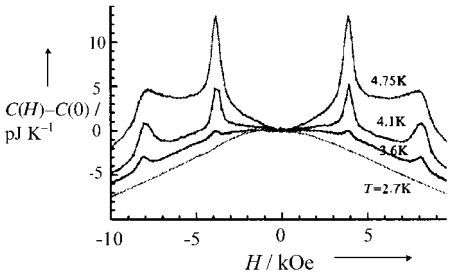


Figure 23. Field dependence of the ac specific heat (10 Hz) of a single crystal of Mn12ac. The magnetic field is applied parallel to the tetragonal axis. Modified from ref. [106].

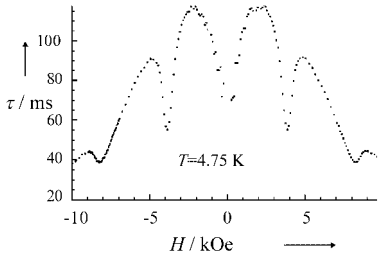


Figure 24. Field dependence of the relaxation time of the magnetization of a single crystal of Mn12ac obtained through ac specific heat capacity measurements. Modified from ref. [105].

obtained with other experimental techniques, and in particular show the wavelike behavior, with peaks and minima at $H_n = n\,H_0$ ($n = 0, 1, \ldots$; $H_0 = 0.45$ T).

7.3. Tunneling Mechanisms and Quantum Coherence in Mn12ac

All data in Section 7.2 provide a clear picture of quantum tunneling effects in Mn12ac in the thermally assisted regime. Similar theoretical results have been produced by considering the role of phonon coupling.[35,36,38–40,121] The problems for a detailed comparison with the experimental data are that acceptable values are not available for several parameters, but by and large, the theoretical picture is clear.

However, several questions are still open, such as what is the detailed relaxation mechanism at low temperature and with the limiting condition of a low transverse static field, and if it is possible to observe quantum coherence? There is no doubt that a splitting of the $\pm M$ levels is needed to observe tunneling, and there is no doubt that this splitting is small. Moreover, the selection rules imposed by the second- or fourth-order transverse anisotropy terms require that the tunneling at odd transition be quenched. Therefore other mechanisms must be available that allow the tunnel process.

Inherent sources of tunnel splitting are the hyperfine fields caused by the presence of magnetic nuclei (^{1}H, ^{2}H, ^{13}C, ^{55}Mn) and the dipolar fields caused by the presence of the other Mn12ac molecules in the lattice. Finally, it is also possible to determine a splitting of the $\pm M$ levels by using an external magnetic field applied perpendicular to the tetragonal axis. In fact the presence of disruptive external magnetic fields may be a source of error. In a single-crystal experiment it is very difficult to orient the external field

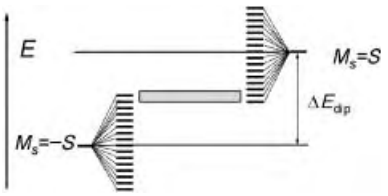


Figure 25. Internal dipolar fields change the energies of the two levels split by the tunnel interaction, and thus hinder tunneling. By effectively broadening the levels hyperfine interactions restore the matching of the left and right levels (shaded area).

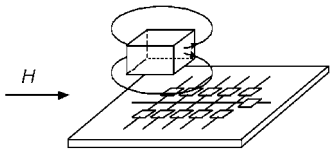


Figure 26. Schematic view of the micro-SQUID array used in the high sensitivity magnetometer. The sample is placed directly on the array. Modified from ref. [127].

exactly parallel to the tetragonal axis to provide a nonzero component in the tetragonal plane. The hyperfine field is expected to be mainly determined by the ^{55}Mn nuclei, which have $I = {}^5/_2$ and correspond to the sites where the highest spin density is concentrated. The hyperfine coupling constant is typically of the order of 10 mT for manganese ions, and in fact this value is confirmed by NMR spectra (see Section 7.4.)

The tunnel splitting of Mn12ac in the ground $M_S = \pm 10$ state is very small, of the order of 10^{-10} K and thus much smaller than the dipolar and hyperfine fields. An estimation of these contributions to the ground doublet-energy separation gives a value of Δ between 0.1 and 0.5 K. Starting from simple theoretical arguments tunneling should not be observed. However, to solve this problem Prokof'ev and Stamp[118,119] suggested a theory (PS theory), according to which the dipolar and hyperfine fields, by varying the bias at each molecular site in time, can continually bring more molecules to resonance. The point can be made clearer by considering Figure 25. The rapidly fluctuating hyperfine fields bring molecules into resonance. The dipolar fields of tunneled spins can lift the degeneracy and thus remove a large number of neighboring spins from resonance. However, a gradual adjustment of the dipolar fields across the sample (up to 0.03 T in Mn12ac) caused by tunneling relaxation, brings other molecules into resonance and allows continuous relaxation. Therefore one expects a fast relaxation at short times and slow logarithmic relaxation at long times.

Looking in detail at the PS theory, the short-time relaxation of the magnetization must follow Equation (23).

$$M(H,t) = M(0) + [M_{eq}(\mathrm{H}) - M(0)]\,[\Gamma_{sqrt}(H)t]^{1/2} \qquad (23)$$

The magnitude of $\Gamma_{sqrt}(H)$, the tunneling rate derived from the square root analysis of the decay of the magnetization, is given by Equation (24) where $P(H)$ is the normalized distribution of molecules that are in resonance at the applied field H. $P(H)$ can be determined once $\Gamma_{sqrt}(H)$ is measured as a function of the field.

$$\Gamma_{sqrt}(H) \sim (\Delta_t^2/\mathrm{h})\,P(H) \qquad (24)$$

Δ_t^2 is the tunnel splitting at the tunneling resonance. Experimental confirmation comes from micro-SQUID measurements on Mn12ac.[122] The experimental apparatus[123] is as shown in Figure 26. The sensitivity of this setup is as high as 10^{-17} emu, that is about ten orders of magnitude better than traditional SQUIDs. The magnetometer is an array of micro-SQUIDs arranged on top of a chip. The sample is placed on top of the chip so that some SQUIDs are directly under the sample, others are beside the sample.

In these experiments a fast-relaxing minor species is monitored.[124] This species is only present in small percentage (2–4 %) and is significantly different from the six isomers discussed in Section 7.1. Because of its small concentration it is undetected by X-ray analysis, however, it can be reasonably supposed that it corresponds to a dodecanuclear cluster where the elongation axis of one manganese(III) ion has flipped its direction. Such a modification has already been observed in two isomers of the *p*-methyl benzoate derivatives of Mn12ac clusters (see Section 7.5).[125] Again crystal-field calculations using the AOM approach can provide an estimation of the modification in the magnetic-anisotropy tensor of the flipped manganese centers (see Table 3). If one of these centers is present, the transverse magnetic anisotropy increases by an order of magnitude (Table 4) which provides an acceleration of the tunneling process. The experimental measurement of $\Gamma_{sqrt}(H)$ provides the normalized distribution of molecules that are in resonance at the applied field. This is done by a so-called "hole digging" procedure,[126,127] in which a fraction of molecules is allowed to relax by the tunneling process, which is only possible when the applied plus the internal field satisfy the resonance conditions. As the relaxed molecules have significantly modified their internal dipolar field, a hole appears in the field distribution of the tunnel probability. The term hole digging is used in analogy to the hole burning technique of spectroscopy, by which individual groups of molecules are addressed.[128] The experimental width of the distribution is of the order of 12 mT in the 40–300 mK range, a width comparable with the distribution of hyperfine fields. Calculations assuming reasonable values for the manganese(III) (6.9 mT) and manganese(IV) (8.5 mT) centers suggest a width of about 16 mT, in good agreement with the experimental data.[122]

The presence of quantum-mechanical tunneling therefore is well established for Mn12ac. The observation of quantum coherence on the other hand is still much more controversial.[104,129]

7.4. Characterization of Mn12ac by other Spectroscopic Methods

In addition to the spectroscopic methods used to construct the detailed map of the low-lying spin components of the ground $S = 10$ state, other spectral techniques have been used

to characterize this state. An important one is certainly NMR spectroscopy, because it gives direct access to the electron-spin–nuclear-spin interaction, which may assist the tunneling mechanism. NMR spectroscopy is sensitive to the electron spin, dominated by the so-called hyperfine interactions, and the nuclear relaxation. Worth mentioning here is the muon spin resonance and relaxation technique,[130,131] which is similar to NMR spectroscopy in that it provides a local probe which is sensitive to the electron relaxation.

^{1}H NMR spectra of Mn12ac in solution have been discussed in Section 7.1.[66] Recently it was possible to observe the ^{55}Mn NMR spectra[132,133] in a polycrystalline powder at 1.4 K (Figure 27). The spectrum was measured in zero applied field. It shows three resonance signals in the range 200–40 MHz. The low frequency sharp resonance signal is assigned to the four manganese(IV) centers and the two broad resonance signals at 280 and 370 MHz, to the crystallographically inequivalent manganese(III) centers. ^{1}H and ^{2}H NMR spectra at low temperature were also reported,[136] which show two resonance signals: one, essentially not shifted, assigned to the CH_3COO, CH_3COOH, and solvated water molecules, the other signal which is shifted, is assigned to the coordinated water molecules.

Using the time dependence of the Hahn-echo pulse sequence the relaxation of the magnetization was measured and compared to that obtained through specific-heat-capacity and dc magnetic measurements.[108] The echo is generated with a $\pi/2$-π pulse sequence at the resonance frequency. The typical $\pi/2$ pulse length was 3.5–4.5 μs and the delay τ between the two pulses approximately 50 μs. The experiments were performed on polycrystalline samples which were aligned with the anisotropy axis along the magnetic field by letting the sample sit at 4.2 K in a field of 1.8 T for several hours. The field was turned off and the system was given time to reach thermal equilibrium at the preset temperature. The field was turned on and the echo intensity was monitored as a function of time. The evolution of the magnetism with time could be reproduced with Equation (25) where h is the echo

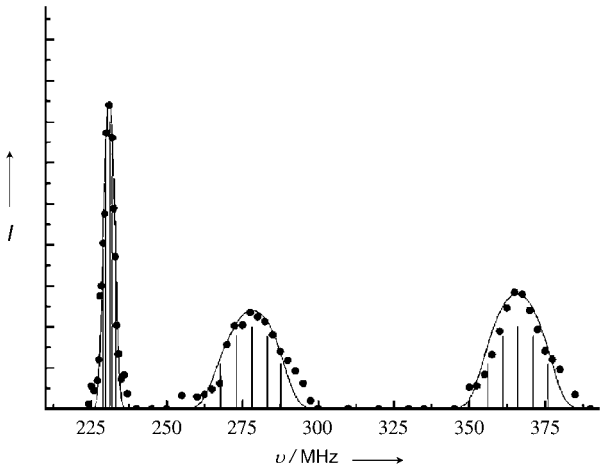


Figure 27. Spin echo intensity of the ^{55}NMR spectra of Mn12ac measured at $H = 0$ and $T = 1.4$ K. Modified from ref. [133].

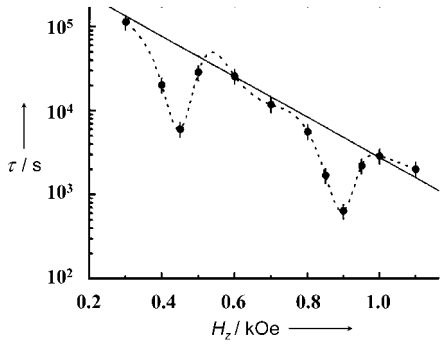


Figure 28. Field dependence of the relaxation time of the magnetization of Mn12ac at 2.4 K measured through the echo proton NMR spectroscopy. Modified from ref. [108].

magnitude and $1/W$ $(=\tau_r)$ is the relaxation time of the magnetization of Mn12ac.

$$h(t) = a[1-\exp(-Wt)] + b \tag{25}$$

The time dependence suggests that the nuclei feel an electronic relaxation process, following Equation (26) where N_p is the number of protons per molecule, N_m is the total number of molecules, and $N_p^{ch}(t)$ is the number of protons which undergo a change of average local field in the time interval separating the $\pi/2$-π pulses.

$$h(t) \propto [N_p N_m - N_p^{ch}(t)] \tag{26}$$

By suitable derivation the echo height can finally be expressed as Equation (27) where N_m^{eff} is the number of molecules with protons that are affected by the local field change as a result of a molecular spin flip.

$$h(t) = h(\infty)[1-N_m^{eff} W\tau \exp(-W\tau)] \tag{27}$$

As $\tau = 50$ μs and W are small, Equation (27) requires that $t \gg \tau$ and $W\tau \ll 1$. The temperature dependence of τ_r in a field of 0.45 T was found to follow a thermally activated mechanism with $\tau_0 = 10^{-7}$ s, and $\Delta/k = 60$ K in acceptable agreement with the values obtained through other experimental techniques. The field dependence (Figure 28) shows the anomalies at the crossing fields described in Section 7.2.

There have been numerous other reports on the use of NMR spectroscopy with Mn12ac.[107,134–138]

7.5. Mn12 Derivatives

The Mn12 derivatives for which the structure has been reported are shown in Table 1 (Section 7.1). They all have the general formula $[Mn_{12}O_{12}(RCOO)_{16}(H_2O)_x]Y$, where Y = solvent molecules.[22] The main structural difference is the presence of either four or three water molecules in the cluster. An example of the latter category is provided by $[Mn_{12}O_{12}(EtCOO)_{16}(H_2O)_3]$, which crystallizes either in a monoclinic space group, without solvent molecules, or in a triclinic space group, with four cocrystallized water molecules.[125] Also the clusters with four cocrystallized water molecules show

significant structural differences. In all the cases the manganese(III) ions are either doubly bridged to one manganese(IV) center (type I), or singly bridged to two manganese(IV) centers (type II). The water molecules are bound to type II ions. The coordination in cluster **1** (see Table 1) is such that one water molecule per type II ion is present.[21] The manganese–water direction roughly indicates the Jahn–Teller distortion axis. In other derivatives some of the type II Mn ions have either no water molecules, or two water molecules. Four different isomers have been experimentally observed, which correspond to the coordination schemes 1:1:1:1 (as in **1**),[21,125,143] 1:2:1:0,[125,139] 1:1:2:0,[125,140] and 2:2:0:0[65,125,141,142] (the notation indicates the water coordination number of the type II Mn ions).

There are some distinctive exceptions to the rule that the oxo ligands are not found on the elongation axis. In fact, the Jahn–Teller distortion axis in **8** (see Table 1) includes one of the bridging oxo ligands, so that for this Mn center the elongation axis is approximately orthogonal to the elongation axes of the other manganese(III) centers (Figure 29).[125] In **9** the elongation axes are essentially parallel to each other.[125] The two clusters therefore can be considered as distortion isomers, as frequently observed for copper(II) compounds. It is apparent that intercluster interactions, such as hydrogen bonds, may play an important role. The magnetic properties of **8** and **9** are very different from each other.

The temperature dependence of the out-of-phase susceptibility of **8** and **9**, at different frequencies, is shown in Figure 30. It is apparent that slow relaxation effects show up at higher temperatures for **9** than **8**, which suggests a higher barrier for the reorientation of the magnetization in **9**. Since the ground state in both cases is $S = 10$, the greater barrier height is associated with a larger zero-field splitting. If the zero-field-splitting parameter of the cluster depends on the projection of the individual zero-field-splitting tensors of the Jahn–Teller distorted manganese(III) center, it is apparent that the resultant must be larger in **9** (where the local distortion axes are essentially parallel to each other), than in **8** (where one of the local axes is orthogonal to the others). Distortion isomers such as these may also be responsible for the presence of two species with different relaxation properties, as frequently observed even in single crystals of Mn12 derivatives.

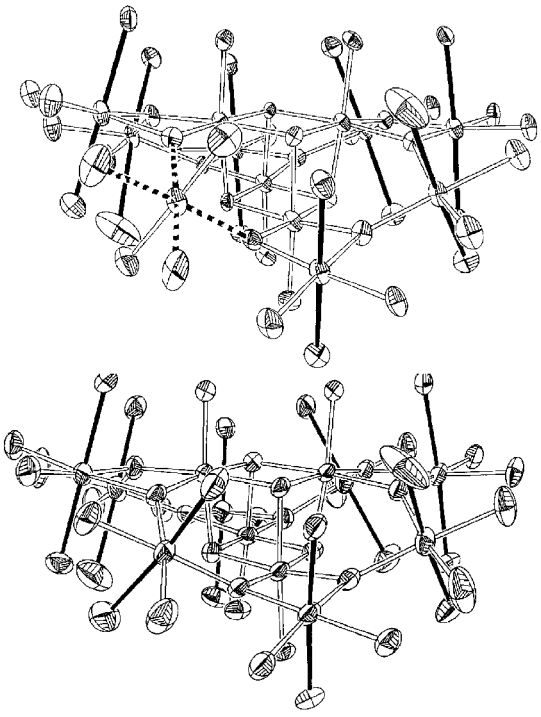


Figure 29. ORTEP views of two distortion isomers **8** (top) and **9** (bottom). The elongation axes of the manganese(III) coordination sphere are indicated by filled bonds. The dashed lines indicate an unusual orientation for the elongation axis in **8**. Modified from ref. [11].

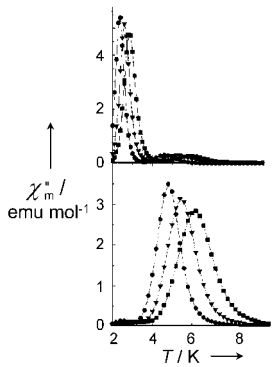


Figure 30. Plots of the out-of-phase ac magnetic susceptibility versus temperature for polycrystalline samples of **8** (upper) and **9** (lower). Modified from ref. [241].

The compounds with three cocrystallized water molecules ($x = 3$; **2**, **3**, **11** in Table 1) have one manganese(III) center which is five coordinate.[144] The overall temperature dependence of χT is not much different from that observed in Mn12ac, but an $S = 9$ ground spin state was suggested from the analysis of the magnetization. However, a good agreement to this was only observed in the derivative with R = Ph, Y = PhCOOH·CH_2Cl_2. Several derivatives show some chemical instability, such as solvent loss, which provide ambiguity in the experimental measurements.

By treating $[Mn_{12}O_{12}(RCOO)_{16}(H_2O)_4]$ derivatives with nitric acid in MeCN new compounds of formula $[Mn_{12}O_{12}(NO_3)_4(RCOO)_{12}(H_2O)_4]$ (R = CH_2tBu, Ph) were obtained.[145] The four nitrate groups are not disordered and replace bridging carboxylate groups. The ground state is still $S = 10$, and a SMM behavior is observed at low temperature. The zero-field splitting and the barrier are very similar to those observed in Mn12ac.

7.6. Reduced Mn12 Species

From the chemical point of view one of the most exciting properties of Mn12 clusters is their stability in solution, which allows a rich redox chemistry. Differential pulsed voltammetry investigations have been reported for **1** in MeCN, which shows two reversible processes, an oxidation and a reduction, and four redox processes altogether.[65] Very similar results were observed for the benzoate derivative in CH_2Cl_2. The

oxidation process occurs at 0.79 V and the reduction process at 0.11 V. The values are referred to the Cp_2Fe/Cp_2Fe^+ (Cp = C_5H_5) couple. The corresponding processes are summarized in Equation (28).

$$[Mn_{12}O_{12}]^+ \rightarrow [Mn_{12}O_{12}] \rightarrow [Mn_{12}O_{12}]^- \rightarrow [Mn_{12}O_{12}]^{2-} \rightarrow [Mn_{12}O_{12}]^{3-} \quad (28)$$

A series of benzoate derivatives, which have similar solubility in a given solvent, allowed a comparative analysis of the role of the carboxylate group in the redox potentials.[146] It was found that the potentials satisfactorily correlate with the electron-withdrawing properties of the *para* substituent in the benzene ring. An electron-withdrawing substituent causes the carboxylate group to become less basic, reducing the electron density on the metal ions thereby making the cluster easier to reduce and concomitantly harder to oxidize.

The first reduction potential is at low enough potential that mild reducing agents, such as iodide can be used to reduce the compound. The PPh_4^+ derivatives of the clusters with R = Et and R = Ph were directly obtained by adding the iodide to the appropriate unreduced Mn12 clusters. Metathesis reactions yielded the [*m*-MPYNN]$^+$ salt (*m*-MPYNN = *m*-*N*-methylpyridinium nitronyl nitroxide).[147] This cation is magnetic with a moment corresponding to one unpaired electron. $(PPh_4)[Mn_{12}O_{12}(Et\text{-}COO)_{16}(H_2O)_4]$ crystallizes in the monoclinic $P2_1/c$ space group.[66] The overall structure of the anion is very similar to that of the unreduced species. The reduction yielded a valence-localized species, one of the external manganese(III) ions being reduced to manganese(II). The identification of the reduced ion has been made on the basis of structural features and confirmed by bond valence sums.[62] It has been suggested that the reduction of manganese(III) rather than of a manganese(IV) ion is because the reduction of a manganese(IV) ion would introduce a distorted manganese(III) ion creating a strain in the apparently rigid $[Mn_4O_4]$ structure. The temperature dependence of the χT product is qualitatively similar to that of Mn12, which suggests a ferrimagnetic ground state, $S = {}^{19}/_{2}$, with a large negative zero-field splitting. The magnetic data, however, require a physically unreasonable *g* factor of 1.74. It is apparent that the ground spin state cannot be obtained simply by "exchanging" one of the $S = 2$ spins with a $S = {}^{5}/_{2}$ spin, because this would lead to either $S = {}^{21}/_{2}$, for parallel, or $S = {}^{11}/_{2}$, for an antiparallel alignment of this spin with those of the manganese(III) ions. A frustrated structure is dominant for $Mn12^-$, analogous to that which gives rise to $S = 9$ in Mn12. Similar results were obtained for the R = Ph derivative.

HF-EPR spectra have been used to obtain the zero-field-splitting parameter *D*.[146] The spectra were recorded on loose polycrystalline samples. It was assumed that a uniform orientation of the powder was achieved and the spectra were assigned on the assumption of the strong-field limit. With this simplified treatment the zero-field-splitting *D* was found to be $-0.62\ cm^{-1}$. Slow relaxation of the magnetization was observed. Accurate data for the temperature dependence of the relaxation time of the R = Ph derivative showed that it follows a thermally activated pattern with $\Delta/k = 57.5$ K. The pre-exponential factor is much larger than in Mn12ac ($\tau_0 = 3.1 \times 10^{-10}$ s). Magnetic hysteresis was also observed, with steps as observed in the unreduced compounds. A step is observed also at zero-field. If this behavior is interpreted as being a result of tunneling effects it is against the Kramers theorem, in which degeneracy cannot be removed in zero applied field. However, the dipolar fields of the other molecules may actually be responsible for this loss of degeneracy.

Recently the structure of the paramagnetic $[Fe(C_5Me_5)_2]^+$ cation and the $[Mn_{12}O_{12}(O_2CC_6F_5)_{16}(H_2O)_4]$ anion[148] have also been reported. The ground state was found to be $S = {}^{21}/_{2}$, with axial zero-field-splitting parameters of $D = -0.351\ cm^{-1}$ and $B_4^0 = -3.6 \times 10^{-7}\ cm^{-1}$, as determined by HF-EPR spectroscopy.

Experiments performed with the magnetic counterion [*m*-MPYNN]$^+$ showed much faster relaxation in agreement with the perturbation given to the cluster by the fast-relaxing radical cation.[147] No substantial change in the relaxation of the Mn_{12}^- species was observed with the $[Fe(C_5Me_5)_2]^+$ counterion.

Using carboxylate ligands with more electron-withdrawing substituents it was also possible to obtain the Mn_{12}^{2-} derivatives[149,150] $[cation]_2[Mn_{12}O_{12}(O_2CR)_{16}(H_2O)_4]$, where cation = PPh_4, $NnPr_4$, R = $CHCl_2$, C_6F_5, 2,4-$C_6H_3(NO_2)_2$. The second manganese(II) center (generated by the reduction of a Mn^{III} center) is also found on the outer ring. The ground state is reported to be $S = 10$, with an axial zero-field splitting of $D \approx -0.3\ cm^{-1}$. Slow magnetic relaxation is observed below 7 K, in agreement with the expected reduced barrier height. Measurements performed using an array of micro-SQUID measurements showed evidence of quantum phase interference effects (see Section 8).[151] A transverse variable magnetic field parallel to the hard axis can modulate the tunnel splitting. Oscillations were observed with a periodicity of about 0.4 T.

8. Fe8

The second molecule that has been intensively investigated for its SMM behavior is commonly indicated as Fe8. The formula is $[Fe_8O_2(OH)_{12}(tacn)_6]Br_8$ (tacn = 1,4,7-triazacyclononane) and comprises an octanuclear cation (Figure 31).[152] The compound is prepared by the controlled hydrolysis of $[Fe(tacn)]Cl_3$ in a water/pyridine mixture in the presence of sodium bromide. The two inner iron(III) ions are octahedrally coordinated to the two bridging oxo and four bridging hydroxy ligands. Fe3 and Fe4 coordinate to three nitrogen atoms of the tacn molecules, two hydroxy and one oxo ligand, while the outer iron(III) centers (Fe5–Fe8) coordinate three nitrogen atoms and three hydroxy groups. The presence of three different Fe sites has been also confirmed by Mössbauer spectroscopy.[153,154] The oxo ligands form μ_3 bridges, while the hydroxy ligands form μ_2 bridges. Fe1, Fe2, Fe3, Fe4 form a structure which is often encountered in polynuclear metal complexes, which has been described as a butterfly structure.[155] With some fantasy Fe1 and Fe2 define the body and Fe3 and Fe4 the wings of the

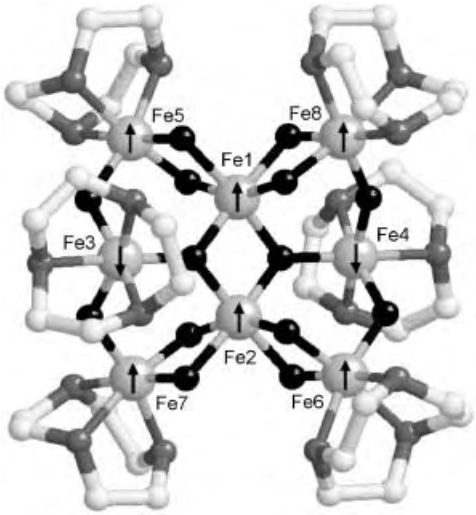


Figure 31. Schematic structure of Fe8 with the suggested preferred orientation of the individual spins.

butterfly. From the magnetic point of view this structure gives rise to spin frustration effects, which make the prediction of the ground state spin arrangement difficult.

The temperature dependence of χT clearly indicates a ferromagnetic behavior with a ground $S = 10$ state,[156] confirmed by high-field magnetization measurements. At the simplest possible approach, this ground state can be justified by putting six $S = {}^5/_2$ spins up and two down. The fit of the temperature dependence of the susceptibility suggested the spin arrangement shown by the arrows in Figure 31, which was experimentally confirmed by a polarized neutron-diffraction experiment (Figure 32).[157] The fit of the susceptibility was performed by assuming a D_2 symmetry for the cluster, which reduced the size of the matrices to be diagonalized.[158] The values of the J constants[83] compare well with the values previously reported for simple iron(III) low-nuclearity compounds with similar bridges.[159] Similar sets of values were also obtained through full-matrix calculations.[83]

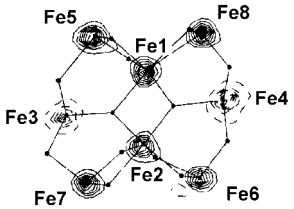


Figure 32. Spin density map of Fe8 from polarized neutron experiments. Negative contours are dashed (step 0.7 $\mu_B/Å^2$). Modified from ref. [157].

The ground $S = 10$ state is largely split in zero-field as shown by HF-EPR,[153,158] inelastic neutron scattering,[160,161] and far infrared spectroscopy.[162] The temperature dependence of the far infrared spectra is shown in Figure 33. Four clear transitions are observed with maxima at 2.45, 2.93, 3.36, and 3.8 cm^{-1} and are attributed to the transitions $\pm 7 \rightarrow \pm 6$, $\pm 7 \rightarrow \pm 8$, $\pm 8 \rightarrow \pm 9$, and $\pm 9 \rightarrow \pm 10$. Since the cluster has no symmetry the spin Hamiltonian is more complex than that used for Mn12ac. A possible form assuming D_2 symmetry is given by Equation (29), where the O_n^m operators are defined in the Appendix.

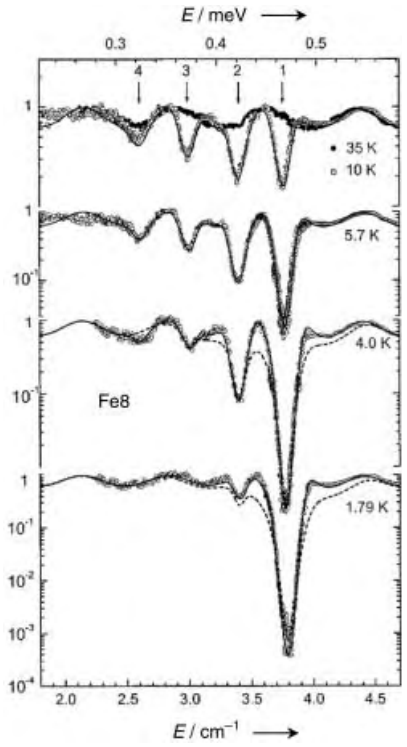


Figure 33. Far infrared spectra of Fe8 in zero field at different temperatures. Modified from ref. [162].

$$\mathscr{H} = \mathbf{D}\, S_z^2 + E\,(S_x^2 - S_y^2) + B_4^0 O_4^0 + B_4^2 O_4^2 + B_4^4 O_4^4 \qquad (29)$$

The values of the relevant parameters obtained by the fitting of several different experimental techniques are shown in Table 5. Single-crystal HF-EPR spectra have also provided the directions of the principal axes of the **D** tensor. The easy axis (that of the prevailing orientation of the individual spins) makes a small angle, about 10°, with the perpendicular to the plane of the iron ions, while the hard axis passes through the Fe1 and Fe2 ions. These results show that the splitting has a large rhombic component, mainly determined by the large value of the $|E/D|$ ratio. Consequently the energies of the M_S levels in Fe8 are much different from those of Mn12ac (Figure 34). The lowest-lying levels are almost degenerate $\pm M_S$ pairs, but approaching the top of the barrier the levels are

Table 5: Zero-field splitting parameters for Fe8.[a]

D	$\lvert E/D \rvert$	B_4^0	B_4^2	B_4^4	Lit.
−0.205	0.19	1.6×10^{-6}	-5.0×10^{-6}	-8×10^{-6}	[158]
−0.203	0.160	0.7×10^{-6}	8.06×10^{-8}	5.96×10^{-6}	[160]
−0.205	0.150	1.4×10^{-6}	8.06×10^{-8}	5.96×10^{-6}	[162]

[a] See Equation (29).

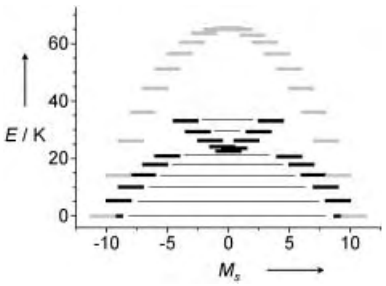


Figure 34. Calculated energy levels of the split components of the $S=$ 10 ground multiplet of Mn12ac (gray) and Fe8 (black). The levels of Fe8 in the upper part of the graph are strongly admixed and their position is arbitrary.

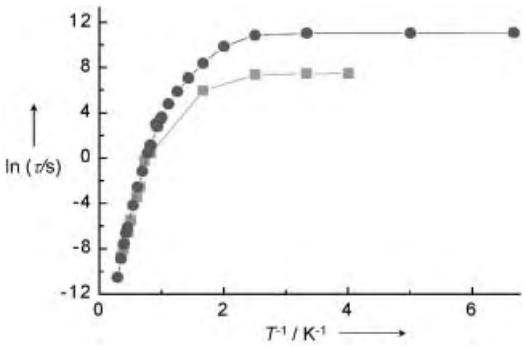


Figure 35. Temperature dependence of the relaxation time of the magnetization of Fe8 (●) and of Fe8PCl (■). Modified from ref. [178].

strongly admixed, and the M_S labeling loses any physical significance. In fact, above the levels which can be indicated as $+5$ and -5 there is a nondegenerate level, which is an admixture of states with smaller M_S. Above this again pairs of quasidegenerate levels are observed, but which cannot be labeled $\pm M_S$. It is apparent that the energy of the barrier in this case cannot be estimated as the difference in energy between the lowest and the highest energy levels. It is probably more appropriate to use the difference between the lowest lying ± 10 and the nondegenerate level. At any rate, there must be a sizeable barrier, therefore slow relaxation effects of the magnetization should be observed at low temperature.

The origin of the magnetic anisotropy responsible for the observed zero-field splitting is presumably a mixture of dipolar and single ion contributions. The dipolar contributions can be easily and rather accurately calculated assuming that the magnetic moments are localized on the iron ions and using the point dipolar approximation.[33] In this frame the calculated zero-field-splitting parameters D and E are much smaller than the experimental values. This is not an unexpected result, because similar trends were observed in other polynuclear iron(III) compounds.[163] Therefore the single ion contribution is also relevant.

Slow relaxation effects show up below 20 K in Mössbauer spectra.[153,154] This technique has a time scale of 10^{-8}–10^{-9} s therefore the blocking temperatures are comparatively higher than in ac susceptibility measurements which show slow relaxation effects only below 3 K. Below 1 K the relaxation time becomes so long that direct measurements can be performed by measuring the magnetization as a function of time. The temperature dependence of the relaxation time of the magnetization in the range 0.070–30 K is shown in Figure 35. At high temperature the Arrhenius law is approximately followed, with $\tau_0 = 2 \times 10^{-7}$ s, and $\Delta/k = 23$ K and with decreasing temperature the curve flattens out. Measurements below 400 mK show that the relaxation time becomes temperature independent ($\tau \approx 5 \times 10^5$ s), thus confirming the presence of pure quantum tunneling.[164]

Like Mn12ac, Fe8 gives rise to a stepped hysteresis.[162,165] In agreement with the smaller zero-field splitting of Fe8 the steps are separated by about 0.22 T and equally spaced. Also, in this case, the steps are attributed to thermally activated tunneling of the magnetization. The dynamic nature of the hysteresis is illustrated by the strong dependence of the curves on the sweeping rate of the field (Figure 36).[165,166] The lower the sweep rate the smaller the fraction of molecules that can relax by resonant quantum tunneling at the lower critical fields. Therefore, the steps at higher critical fields increase their height as the sweeping rate is increased. As with the relaxation time the hysteresis becomes temperature independent below 350 mK and this makes Fe8 better suited to investigate all the effects related to the tunneling process. The square-root decay of the magnetization of Equation (23) has been observed in Fe8.[165] The role of the dipolar field and its evolution as the tunneling relaxation proceeds has been monitored with the use of the hole digging micro-SQUID techniques.[127] Under experimental conditions that give the narrowest linewidth for the magnetization hole, the linewidth

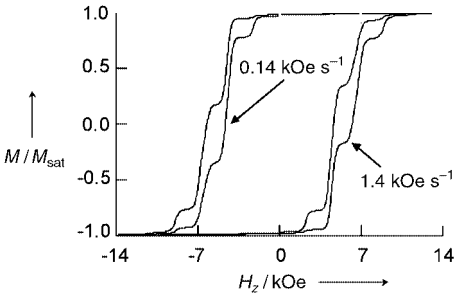


Figure 36. Dependence of the hysteresis loops of Fe8 on the field sweeping rate in the pure tunneling regime ($T=$ 0.3 K).

of the hole, about 0.8 mT, is significantly smaller than in Mn12ac, which is in agreement with the reduced hyperfine field of Fe8 in which the only magnetically active iron nucleus is ^{57}Fe, with a natural abundance of about 2%. Nevertheless hyperfine fields play an important role in the tunneling mechanism. In fact for Fe8 the tunnel splitting of the lowest $\pm$ 10 levels corresponds to a field H_t of approximately 10^{-8} T. The dipolar field H_d is of the order of 10–30 mT,[167] thus the tunneling conditions, which require $H_t > H_d$ are not fulfilled. If tunneling is suppressed, the magnetization at very low temperature is frozen and so are the dipolar fields. However the fluctuating hyperfine field H_{hyp}, generated by the magnetic nuclei ^{1}H ($I = {}^1/_2$), ^{79,81}Br ($I = {}^3/_2$), ^{14}N ($I = 1$) present in the Fe8 clusters, is of the order of 1 mT. The broadening of the ground ± 10 levels may restore the tunneling conditions for

the molecules for which $H_d < H_{hyp}$. Let us suppose that a given molecule undergoes the transition by the tunneling mechanism. Its relaxation changes the dipolar fields of the neighboring molecules in such a way that other molecules reach the tunneling conditions. Therefore the relaxation process is a continuous one.[118,168] The evolution of the magnetization with time as well as the hole digging process have been successfully simulated with Monte Carlo techniques using the tunneling scenario described above.[169,170]

The role of the nuclei in the relaxation process has been demonstrated in experiments in which Fe8 has been enriched with the magnetic ^{57}Fe ($I = {}^1/_2$) isotope and/or with ^{2}H ($I = 1$).[171,172] Enrichment with ^{57}Fe shortens the relaxation time, in agreement with the increased hyperfine field, while the enrichment with deuterium causes an enhancement of the relaxation time, in agreement with the decreased hyperfine field (Figure 37). This unusual isotope effect, which is not related to the mass (which is increased in both isotopically

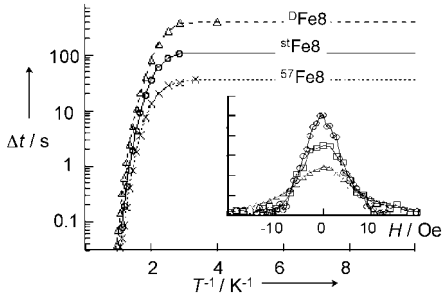


Figure 37. Temperature dependence of the elapsed time needed to relax 1% of the saturation magnetization of a deuterium enriched Fe8 crystal (^{D}Fe8), of a standard crystal (stFe8), and of a ^{57}Fe enriched one (^{57}Fe8). The inset shows the hole burnt in the distribution of tunneling rate versus applied field for the ^{D}Fe8 (○), stFe8 (□), and ^{57}Fe8 (△). Modified from ref. [171].

modified samples), seems to be related to the broadening of the tunneling resonance as confirmed by the investigation of the intrinsic linewidth by the hole-digging technique. The linewidth is larger for the ^{57}Fe enriched sample and smaller for the deuterated one (inset of Figure 37). The observed linewidth for the natural-abundance derivative is in qualitative agreement with the hyperfine fields of the protons determined by NMR spectroscopy.[173,174] The increase in linewidth observed in the enriched sample compares well with an approximation performed taking into account the contact term of the hyperfine interaction of ^{57}Fe nuclei in iron(III) systems.

It is possible to enhance the tunnel splitting by applying a field perpendicular to the easy axis. When the field is applied along the hard direction the oscillating behavior described in Section 5 should than be observed. The measurement of the tunnel splitting can be best performed by using the Landau–Zener–Stückelberg (LZS) model.[175–177] In a two-level system the crossing may occur either directly (zero tunnel splitting) or through an "avoided crossing" (nonzero tunnel splitting; Figure 38). The avoided crossing occurs if the two states are admixed. The admixture can be determined both by intrinsic

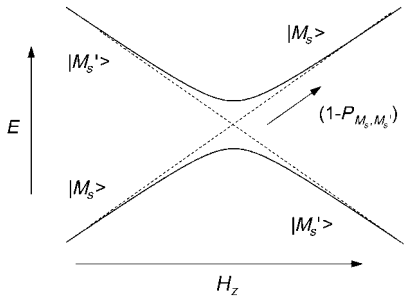


Figure 38. Crossing (– – –) and avoided crossing (——) of pairs of levels as a function of an axial magnetic field.

fields (given by terms such as $E(S_x^2 - S_y^2)$), and by external fields, applied parallel to a hard direction. By sweeping the magnetic field along the easy axis at a relatively high frequency only a small fraction of molecules can tunnel within the short period, thus the dipolar field distribution is not altered. Moreover, if the field is swept over the entire resonance, the dipolar field distribution has no effect on the overall tunnel probability. When sweeping the H_z field at a constant frequency over the avoided energy level in which crossing between the levels M_S and M_S' occurs, the tunneling probability is given by Equation (30) where dH/dt is the constant field sweeping frequency.

$$P_{M_S,M_S'} = 1 - \exp[-\pi\Delta^2_{M_S,M_S'}/(2\,h\,g\mu_B|M_S - M_S'|dH/dt)] \quad (30)$$

If the splitting is zero, P is also zero, and no tunneling occurs. If Δ is large, P tends to one, and tunneling occurs. The magnetization after N sweeps is given by Equation (31) where Γ is the overall LZS transition frequency.

$$M(N) \sim \exp[-2\,P\,N] = \exp[-\Gamma t] \quad (31)$$

Experimentally Γ, P, and Δ can be measured by saturating the magnetization, then periodically changing the field at a constant rate.

Wernsdorfer and Sessoli[51] used the micro-SQUID apparatus described in Section 7.3 and measured the tunnel splitting with the LZS model by sweeping the axial magnetic field around the values of $H_z = n\,0.22$ T, with $n = 0, 1, 2$, which correspond to the tunnel resonance conditions for the $10 \rightarrow -10$, $10 \rightarrow -9$, and $10 \rightarrow -8$ levels, respectively. The measured values of Δ as a function of the applied static transverse field H_x for the quantum transitions between $M_S = +10$ and $M_S' = -(10-n)$ are shown in Figure 39. Oscillations with a periodicity of about 0.4 T are clearly seen. These are the first observations of the destructive interference of tunneling pathways (the so-called Berry phase shown in Figure 8) in magnets. The parity effects are clearly seen: the oscillations are symmetric around $H_x = 0$, this corresponds to a maximum value of Δ for $n = 0$, 2, and a minimum for $n = 1$. If the observed values are compared with those which can be calculated using Equations (12) and (13) and the experimentally determined D and E values the agreement is far from satisfactory. An acceptable agreement is only obtained if the fourth-order transverse term is included and a B_4^4 parameter

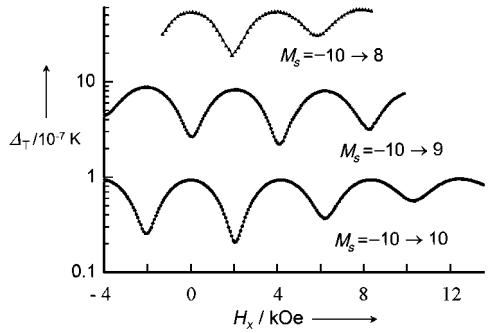


Figure 39. Transverse-field dependence of the tunnel splitting of quasi-degenerate M,M' levels measured for Fe8 at 80 mK. The three curves corresponds to different resonance fields characterized by $n=0$, $n=1$, and $n=2$. Modified from ref. [51].

about five-times larger than the value provided by HF-EPR.[158] The period of the oscillation, being related to the tunnel splitting of low-lying levels, is however very strongly affected by higher-order terms of the transverse anisotropy, for which no experimental estimates are available. This area requires further theoretical and experimental work.

A transverse field modulation can effect the shape of the hysteresis loop, promoting or suppressing tunneling as shown in Figure 40, where three hysteresis loops measured for Fe8 in

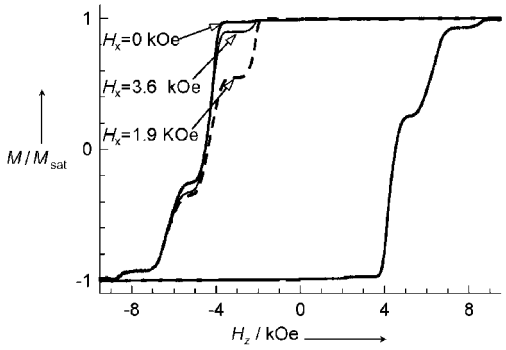


Figure 40. Transverse-field dependence of the hysteresis loop of Fe8 in the ground-state tunneling regime. Modified from ref. [235].

the quantum regime are reported. The three curves differ for the applied transverse static field. A transverse field of 0.19 T significantly enhances the quantum relaxation at the resonance field $H_z = 0.22$ T. The height of the step is larger than both in zero and in a stronger transverse field of $H_x = 0.38$ T. This anomalous behavior is only observed in SMMs, where the tunneling dominates the magnetization dynamics. In principle with the bidimensional control of the field it should be possible to influence the hard–soft magnetic character of the material, as the application of an appropriate transverse field facilitates the reversal of the longitudinal magnetization, without affecting the stability of the remnant magnetization in zero field.

Fe8 is less amenable than Mn12 clusters to ligand substitution reactions. Actually only one other derivative has been reported, $[Fe_8O_2(OH)_{12}(tacn)_6]Br_{4.3}(ClO_4)_{3.7}\cdot 6H_2O$ (Fe8PCl), in which some of the bromide ions have been replaced by perchlorate ions.[178] While Fe8 crystallizes in the triclinic space group $P1$,[152] Fe8PCl crystallizes in the monoclinic $P2_1/c$. This change of space group has consequences for the relative orientations of the molecules in the unit cell. In fact two magnetically nonequivalent sites are observed in Fe8PCl which is centrosymmetric. The magnetic properties of the two compounds are very similar to each other. The HF-EPR spectra also show a very similar splitting of the ground $S = 10$ state, with the distinct difference that the second-order transverse anisotropy is larger in Fe8PCl. ($|E/D| = 0.21$ in Fe8PCl and 0.19 for Fe8). This result has consequences for the relaxation times (see Figure 35). The relaxation times of Fe8PCl are shorter because of the larger transverse field anisotropy. The crossover from mixed thermal–quantum to quantum relaxation occurs in both cases at about 350 mK.

9. Other Single-Molecule Magnets

As expected, other clusters have been reported to have SMMs behavior, these include Fe4,[179] Mn4,[180–186] V4,[187] CrM6,[188–191] Ni12,[112] and Mn10.[193] It is apparent that for SMM behavior it is not the size of the clusters that counts but rather the value of S in the ground state and the magnetic anisotropy. However, all these molecules show slow relaxation effects at lower temperatures than Mn12ac.

$[Fe_4(OCH_3)_6(dpm)_6]$ (Fe4; Hdpm = dipivaloylmethane) has the structure shown in Figure 41.[179] The cluster Fe4 crystallizes in the monoclinic space group $C2/c$, with crystallo-

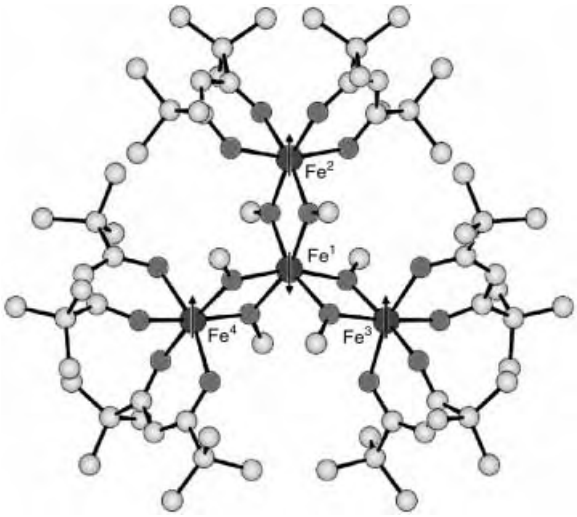


Figure 41. Structure of Fe4 with the suggested preferred orientation of the spins. Fe dark gray, C light gray, O medium gray.

graphically imposed C_2 symmetry, however, there is some disorder, resulting from the dpm units. The four iron(III) ions are antiferromagnetically coupled to give a ground $S = 5$ state, as confirmed by the temperature dependence of the magnetic

susceptibility. Polycrystalline powder HF-EPR spectra give $D = -0.20\ cm^{-1}$, which suggests a barrier for the reorientation of the magnetization of about 7 K. More accurate single-crystal investigations performed at W band frequency (95 GHz) showed the presence of three different sites, in agreement with the disordered structure, with slightly different zero-field-splitting parameters.[194] Similar results were obtained by inelastic neutron scattering experiments.[195] The spin dynamics have been studied by Mössbauer spectroscopy, which reveals slow relaxation below 30 K.[154,196] Slow magnetic relaxation was observed below 1 K ($\tau_0 = 1.1 \times 10^{-6}$ s, $\Delta/k = 3.5$ K), in reasonable agreement with the above zero-field-splitting parameters.

There are now several families of Mn_4 clusters which show SMM behavior. The first comprises a central cubane-type structure $[Mn_4(\mu_3\text{-}O)_3(\mu_3\text{-}X)]^{6+}$ (X = Cl, F, N_3, NCO, O_2CMe), for which a $[Mn^{IV}Mn^{III}_3]$ charge distribution is suggested along with a $S = {}^9/_2$ ground state, with a large zero-field splitting. The D values obtained from measurements on the temperature dependence of the magnetic susceptibility of polycrystalline powders are in the range -0.27 to $-0.32\ cm^{-1}$. Values of about $-0.54\ cm^{-1}$ were estimated from the analysis of HF-EPR spectra.[180] Below 3 K the system shows an out of phase ac susceptibility in zero field and an Arrhenius behavior of the relaxation time. Below 1 K hysteresis loops are observed with well-defined steps at $H = \pm 0.5$ T, which are in agreement with the D value estimated from HF-EPR data. More surprising is the well-defined step observed in zero field, although a half-integer spin should not show tunneling in zero field.[180] In fact, the relaxation becomes temperature independent, suggesting the presence of tunneling.

More recently, another $S = {}^9/_2$ cluster, $[Mn_4O_3(OSiMe_3)(O_2CMe)_3(dbm)_3]$ (Hdbm = dibenzoylmethane) has been extensively investigated at low temperature along with a $Mn^{II}_2Mn^{III}_2$, $S = 8$, cluster of formula $[Mn_4(O_2CMe)_2(Hpdm)_6](ClO_4)_2$ (H_2pdm = pyridine-2,6-dimethanol). Thanks to the micro-SQUID techniques and the Landau–Zener model the tunnel splitting of the ground state has been investigated as a function of the magnetic field applied perpendicularly to the easy axis.[197] The tunnel splitting increases much faster with increasing transverse field for the $S = {}^9/_2$ cluster than the $S = 8$ cluster or the Fe8 cluster which also has an integer spin state. These findings confirm that the tunneling is partially quenched in zero field for half-integer spin. The parity effect in the tunnel splitting is clearly in agreement with Kramers theorem,[34,56] and the results reported by Wernsdorfer et al. [197] are a nice experimental confirmation of it. In the compound of formula $[Mn_4O_3Cl_4(O_2CEt)_3(py)_3]$ (py = pyridine) two Mn4 clusters, each one characterized by a $S = {}^9/_2$ ground state, are connected through weak hydrogen bonds. The effects of this intercluster interaction are also visible in the tunneling of the magnetization, which is suppressed in zero field because at this field both clusters should tunnel at the same time.[198]

Another well documented type of small SMM is provided by compounds of formula $[V^{III}_4O_2(O_2CR)_7(bpy)_2]^+$ (byp = bipyridine) with a V_4O_2 core arranged in a butterfly structure.[187] Vanadium(III) is a d^2 ion which in O_h symmetry has an orbitally degenerate $^3T_{1g}$ state. However, neglecting complications associated with orbital degeneracy the temperature dependence of the magnetic susceptibility suggested a ground $S = 3$ state, with $D = -1.5\ cm^{-1}$. This result suggests an energy barrier of about 18 K, but only a very weak out-of-phase signal was observed in the ac susceptibility measurements. Similar parameters were reported for $[NEt_4][V^{III}_4O_2(O_2CR)_7(pic)_2]$ (pic = 2-picolinate) in which stronger out-of-phase signals were observed which shift on applying external magnetic fields.

The list of systems showing SMM behavior is continually increasing. Increasing the spin ground state is still the goal of the synthetic efforts of many groups. Spin states larger than ten have in fact been observed in Mn10,[199] Fe19,[200,201] and Ni12[192,200,201] clusters, as well as in heterometallic clusters containing cyanide bridges.[188–190] Despite of the larger spin of the ground state, the magnetic anisotropy is relatively small for these compounds and the blocking temperature is around or below 1 K. Evidence of the thermal-assisted tunneling of the magnetization are often limited to the observation of an Arrhenius behavior with a significantly reduced barrier height, and comparison of the magnetic anisotropy estimated from EPR and magnetic data. A larger database of well-characterized systems could help in clarifying some points, such as the role played by the excited spin states or that played by the anisotropic terms of the intracluster exchange interaction for the still relatively rare phenomenon of resonant magnetic tunneling.

10. Conclusions and Perspectives

The field of single-molecule magnets is still rapidly expanding, and there is no doubt that in the next few years there will be many more compounds available, perhaps with higher blocking temperatures and better controlled quantum effects. Further attempts will also be made to organize the SMMs into layers in which it will be possible to address individual molecules.[202–205]

Other categories of classical molecular magnetic clusters are also being studied. These include the antiferromagnetic rings, which have been suggested to give rise to tunneling effects of the Neél vector,[206,207] and individual clusters with antiferromagnetic coupling, such as V15[208–211] and Fe30.[212]

Antiferromagnetic rings of different size, but so far only even membered, have been reported. This is a pity because in odd membered rings spin frustration effects might be observed, giving rise to a rich spin dynamics. Interesting quantum effects have been observed in antiferromagnetic rings, of the type $[Fe_{10}(OMe)_2(CH_2ClCOO)_{10}]$ (Fe10), the so-called ferric wheel.[213] Below 1 K, Fe10 is in the ground $S = 0$ state, so that the low-field magnetization is zero. However, on increasing the field the excited states with $S > 0$ rapidly decrease their energies, and a crossover between the ground states $S = 0$ and $S = 1$ is observed as a step in the magnetization curve. At higher fields analogous crossovers occur, for example between $S = 2$ and $S = 1$ and, in strong pulsed fields, it was possible to observe the crossover to an $S = 9$ ground state. The position of the steps provides information on the energy separation of the excited states in zero field, assuming

that the g values are known, a reasonable assumption for iron(III) compounds. The stepped magnetization indicates the appearance of the quantum size effects in molecular clusters on a macroscopic scale. However, if the same measurements are performed on $[Mo_{72}Fe_{30}O_{252}\{Mo_2O_7(H_2O)\}_2\{Mo_2O_8H_2(H_2O)\}(CH_3COO)_{12}(H_2O)_{91}]\cdot 150\,H_2O$ (Fe30), completely different results are observed.[212] The molybdenum ions are diamagnetic, therefore the magnetic properties are associated with the 30 iron(III) ions which are located on the vertices of an icosidodecahedron. Because of the geometry of the spin sites and the antiferromagnetic exchange, spin frustration and competing ordered states are expected to occur. The temperature dependence of the magnetic susceptibility gave (using classical spins) $J \approx 1.6$ K, and the field dependence of the magnetization did not show any quantum size effect down to 0.46 K. The linear increase in magnetization for Fe30 is characteristic of an antiferromagnet. This situation suggests that for Fe30 the spin levels define a quasicontinuum and quantum effects are only expected to show up below 100 mK. In this sense Fe30 can be considered as a tiny antiferromagnet, exactly as Mn12ac can be considered as a tiny ferrimagnet.

In addition to Fe10 there are several other iron(III) antiferromagnetic rings reported (Fe6,[214–220] Fe8,[221] Fe12,[222] Fe18[223]) and also rings comprising different metal ions, such as the chromic wheels.[224–227] Several features of these antiferromagnetic rings are as yet not completely understood. There is clear indication of avoided crossing between the levels, a requisite for observing quantum tunneling in the Landau–Zener approach. Odd spin terms would be required to allow the admixture of neighboring states (with S differing by ± 1, as observed at the $S = 0 \rightarrow 1$, $S = 1 \rightarrow 2$, crossovers). The role of Dzyaloshinski–Moriya terms, that is antisymmetric exchange, has been advocated, but this demands noncentrosymmetric structures, however most of the wheels are centrosymmetric.[225,228]

A somewhat similar situation has been observed recently in $K_6[V_{15}As_6O_{42}(H_2O)]\cdot 8\,H_2O$ (V15; $S = {}^1/_2$). This is a cluster comprising fifteen vanadium(IV) ions, with a structure made up of three metal-ion layers containing six, three, and six vanadium ions, respectively.[229] The coupling between the ions in the two hexagonal V_6 layers is strongly antiferromagnetic, in such a way that these layers are in the ground $S = 0$ state at low temperature. The three spins in the triangular V_3 layer are frustrated, with a pair of degenerate spin doublets lying lowest.[208] A "butterfly" hysteresis loop was observed below 200 mK suggesting avoided crossing between the low-lying levels.[209,210] Again the role of the antisymmetric exchange terms is assumed to be important, but more experimental and theoretical work is needed to understand fully the physical properties of V15.

Of course, one of the goals is that of synthesizing larger clusters, because it would be important to obtain systems containing hundreds of magnetic atoms, systems with a size in the mesoscopic regime. The seminal results reported by Müller and co-workers[212,230–234] suggest that this route may be possible. Clearly it is not only necessary to synthesize large molecules, which contain a large number of magnetic centers; it is also necessary to promote suitable magnetic interactions between them. The role of the bridging ligands is thus of paramount importance. So far μ_2, μ_3, and even μ_6 bridging O^{2-}, OR^- groups have been found to be very versatile for promoting strong coupling between transition-metal ions. Another interesting bridging ligand is the CN^- ion, which has also the advantage of being asymmetrical thus inducing selectivity when bridging different transition-metal ions. Other ligands will certainly be investigated in the next years. Particularly promising are sulfur-based ligands, which have the advantage of forming stronger covalent bonds than oxygen, and as a consequence a stronger magnetic interaction. The use of paramagnetic bridging ligands, such as nitronyl nitroxides and semiquinones, may also be anticipated.

The physical conditions for obtaining SMM behavior are understood, an easy axis (Ising) type magnetic anisotropy is required. The physical conditions for achieving this are, for ions such as iron(III), chromium(III), manganese(III), cobalt(II) which have been intensively investigated in the last few years, increasingly clear. We remind that the sources of anisotropy are twofold, either associated with the "building blocks" (single-ion anisotropy) or to the "mortar" connecting them (spin–spin anisotropy). Since the anisotropy is a tensorial property it is determined by the tensorial sum of the local anisotropies.[235] In other words it is not sufficient (and may not even be necessary), to choose individual building blocks with the correct Ising type anisotropy, because the bulk anisotropy of the cluster will actually depend on the geometry of the whole structure. To build-up magnetic anisotropy from the anisotropy of the building blocks, it is certainly a good guideline to exploit transition-metal ions which have orbitally nondegenerate ground states. However it must be remembered that the actual anisotropy of the magnetic molecules depends on how the individual building blocks are spatially oriented one relative to the other. And frankly speaking this still seems to be beyond our control, suggesting that serendipity must play an important role in the development of SMMs.[212,230–235]

If the goal of making SMMs is that of increasing the blocking temperatures, then increasing the number of coupled spins and keeping the interactions between the individual spins as strong as possible is certainly the best way forward. In this sense the ferrimagnetic approach, that is, assembling either different antiferromagnetically coupled spins, or different numbers of antiferromagnetically coupled spins, is the easiest approach. Strong ferromagnetic coupling is rather difficult to develop.

Possible applications of magnetic clusters range from novel magnetic storage media to quantum computing. The possibility of storing information in the nanometer-size magnetic iron(III) core of Ferritin is currently being investigated[236–239] thus it is possible that other similar clusters might well be suitable. In general it may be expected that all the uses of magnetic particles might be extended to molecular clusters, for example, magnetic drug delivery, contrast agents for magnetic resonance imaging (MRI), and magnetocaloric effects. The use of smaller particles has been suggested for implementing Grover's algorithm for quantum computing.[18,239]

11. Appendix

$$M(N) \sim \exp[-2PN] = \exp[-\Gamma t] \quad (31)$$

$$O_4^2 = \{[7S_z^2 - S(S+1) - 5](S_+^2 + S_-^2) + (S_+^2 + S_-^2)[7S_z^4 - S(S+1) - 5]\}/4 \quad (A2)$$

$$O_4^4 = (S_+^4 + S_-^4)/2 \quad (A3)$$

$$O_4^3 = [S_z(S_+^3 + S_-^3) + (S_+^3 + S_-^3)S_z]/4 \quad (A4)$$

The financial support of MIUR and CNR is gratefully acknowledged. We thank P. Parri for the realization of the cover and frontispiece pictures and S. T. Hatscher for the German translation.

Received: February 12, 2002 [A516]

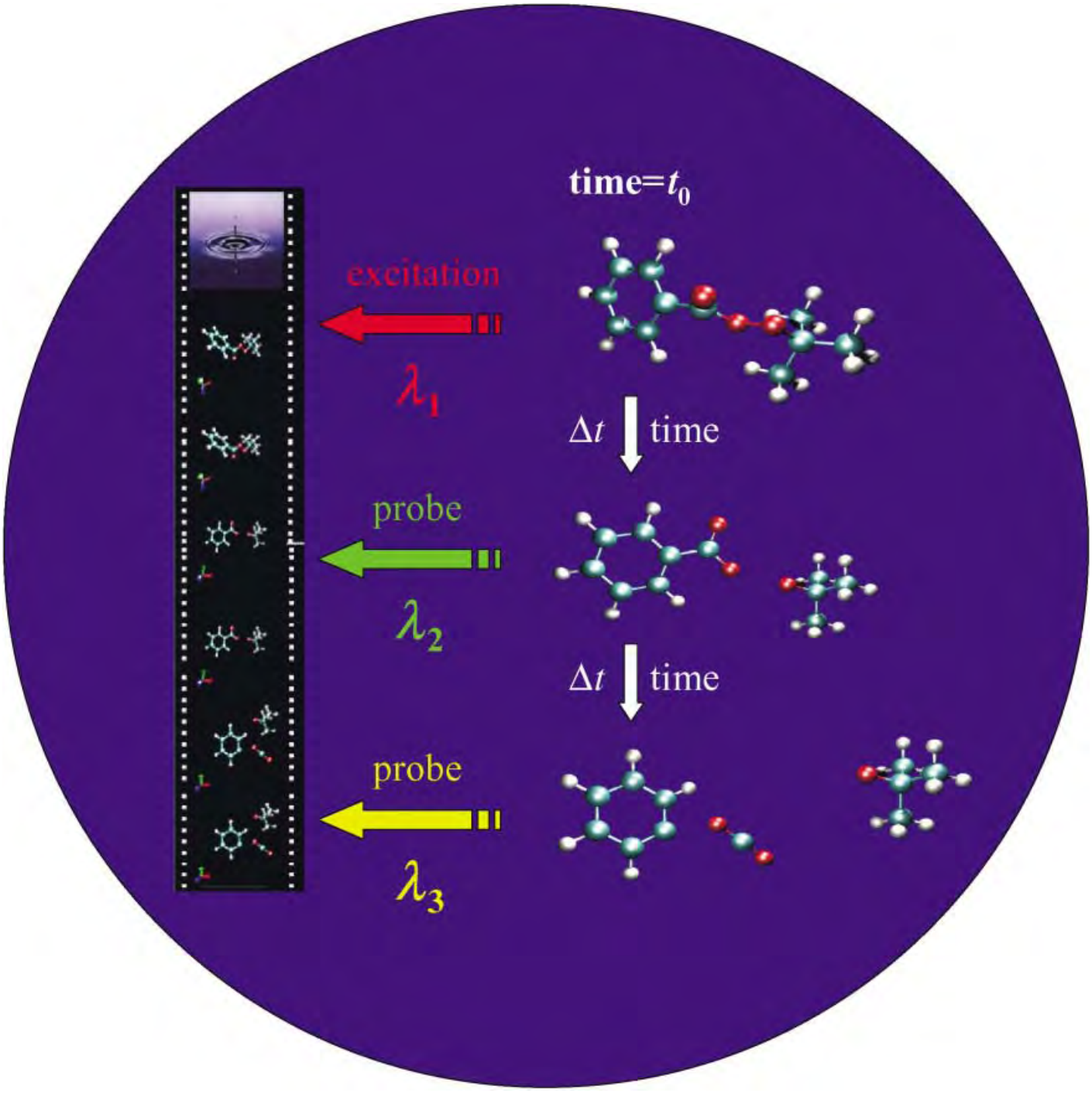
[1] J.-M. Lehn, *Supramolecular Chemistry. Concepts and Perspectives*, VCH, Weinheim, **1995**.
[2] S. Miyata, H. S. Nalwa, *Organic Electroluminescent Materials and Devices*, Gordon and Breach, Amsterdam, **1997**.
[3] C. Bosshard, R. Spreiter, U. Meier, I. Liakatas, M. Bösch, M. Jäger, S. Manetta, S. Follonier, P. Günter in *Crystal Engineering: From Molecules and Crystals to Materials, Vol. C538*, (Eds.: D. Braga, F. Grepioni, A. G. Orpen), Kluwer, Dordrecht, **1999**, p. 261.
[4] J. J. Girerd, M. Verdaguer, O. Eisenstein, *New J. Chem.* **2000**, *24*, 77.
[5] O. Kahn, *Molecular Magnetism*, VCH, Weinheim, **1993**.
[6] *Magnetism: Molecules to Materials. Molecule Based Materials, Vol. 2* (Eds.: J. S. Miller, M. Drillon), Wiley-VCH, Weinheim, **2001**.
[7] *Magnetism: Molecules to Materials. Nanosized Magnetic Materials, Vol. 3* (Eds.: J. S. Miller, M. Drillon), Wiley-VCH, Weinheim, **2002**.
[8] *Magnetism: Molecules to Materials: Models and Experiments, Vol. 1* (Eds.: J. S. Miller, M. Drillon), Wiley-VCH, Weinheim, **2001**.
[9] For a general review of the different classes of molecular magnetic materials see: *MRS Bull.* **2000**, *25*(11), special issue "molecule-based magnets".
[10] D. Gatteschi, A. Caneschi, L. Pardi, R. Sessoli, *Science* **1994**, *265*, 1054.
[11] G. Christou, D. Gatteschi, D. N. Hendrickson, R. Sessoli, *MRS Bull.* **2000**, *25*, 66.
[12] B. Barbara, L. Gunther, *Phys. World* **1999**, *12*(3) 35.
[13] P. C. E. Stamp, *Nature* **1996**, *383*, 125.
[14] E. M. Chudnovsky, *Science* **1996**, *274*, 838.
[15] A. J. Leggett in *Quantum Tunneling of Magnetization-QTM'94* (Eds.: L. Gunther, B. Barbara), Kluwer, Dordrecht, **1995**, p. 1.
[16] J. A. Jones, *Science* **1998**, *280*, 229.
[17] Y. Makhlin, G. Schon, A. Shnirman, *Nature* **1999**, *398*, 305.
[18] M. N. Leuenberger, D. Loss, *Nature* **2001**, *410*, 789.
[19] A. Caneschi, D. Gatteschi, R. Sessoli, A.-L. Barra, L. C. Brunel, M. Guillot, *J. Am. Chem. Soc.* **1991**, *113*, 5873.
[20] R. Sessoli, D. Gatteschi, A. Caneschi, M. A. Novak, *Nature* **1993**, *365*, 141.
[21] T. Lis, *Acta Crystallogr. Sect. B* **1980**, *36*, 2042.
[22] G. Aromi, S. M. J. Aubin, M. A. Bolcar, G. Christou, H. J. Eppley, K. Folting, D. N. Hendrickson, J. C. Huffman, R. C. Squire, H. L. Tsai, S. Wang, M. W. Wemple, *Polyhedron* **1998**, *17*, 3005.
[23] In a crystal the intermolecular dipolar interactions are expected to lead to magnetic order: X. Martinez-Hidalgo, E. M. Chudnovsky, A. A. Aharony, *Europhys. Lett.* **2001**, *55*, 273; J. F. Fernandez, J. J. Alonso, *Phys. Rev. B* **2000**, *62*, 53. However, if the transition temperature is very low the magnetization freezes without achieving the ordered state.
[24] D. Ringe, G. A. Petsko, *Nature* **1999**, *399*, 417.
[25] D. F. Brougham, R. Caciuffo, A. J. Horsewill, *Nature* **1999**, *397*, 241.
[26] J. Villain, A. Fort, *Eur. Phys. J.* **2000**, *17*, 69.
[27] A. H. Morrish, *The Physical Principles of Magnetism*, Wiley, New York, **1966**.
[28] A. Abragam, B. Bleaney, *Electron Paramagnetic Resonance of Transition Ions*, Dover, New York, **1986**.
[29] J. Villain, F. Hartman-Boutron, R. Sessoli, A. Rettori, *Europhys. Lett.* **1994**, *27*, 159.
[30] *Quantum Tunneling of Magnetization–QTM'94* (Eds.: L. Gunther, B. Barbara), Kluwer, Dordrecht, **1995**.
[31] E. M. Chudnovsky, J. Tejada, *Macroscopic Quantum Tunneling of the Magnetic Moments*, Cambridge University Press, Cambridge, **1998**.
[32] P. C. P. Stamp, E. M. Chudnovsky, B. Barbara, *Int. J. Mod. Phys. B* **1992**, *6*, 1355.
[33] A. Bencini, D. Gatteschi, *EPR of Exchange Coupled Systems*, Springer, Berlin, **1990**.
[34] H. A. Kramers, *Proc. R. Acad. Sci. Amsterdam* **1930**, *33*, 959.
[35] A. Fort, A. Rettori, J. Villain, D. Gatteschi, R. Sessoli, *Phys. Rev. Lett.* **1998**, *80*, 612.
[36] D. A. Garanin, E. M. Chudnovsky, *Phys. Rev. B* **1997**, *56*, 11102.
[37] M. N. Leuenberger, D. Loss, *Europhys. Lett.* **1999**, *46*, 692.
[38] M. N. Leuenberger, D. Loss, *Phys. Rev. B* **2000**, *61*, 1286.
[39] F. Luis, J. Bartolomé, J. F. Fernàndez, *Phys. Rev. B* **1998**, *57*, 505.
[40] T. Pohjola, H. Schoeller, *Phys. Rev. B* **2000**, *62*, 15026.
[41] J. R. Friedman, *Phys. Rev. B* **1998**, *57*, 10291.
[42] F. Hartmann-Boutron, P. Politi, J. Villain, *Int. J. Mod. Phys. B* **1996**, *10*, 2577.
[43] M. N. Leuenberger, D. Loss, *Phys. Rev. B* **2000**, *61*, 12200.
[44] In the treatment in ref. [43] it has been assumed that *S* is a good quantum number, but in light of experimental data this may break down.
[45] A. Garg, *Europhys. Lett.* **1993**, *22*, 205.
[46] D. Loss, D. P. Di Vincenzo, G. Grinstein, *Phys. Rev. Lett.* **1992**, *69*, 3236.
[47] J. von Delft, C. Henley, *Phys. Rev. Lett.* **1992**, *69*, 3236.
[48] A. Garg, *Phys. Rev. B* **2001**, *64*, 4413.
[49] A. Garg, *Phys. Rev. B* **2001**, *64*, 4414.
[50] M. N. Leuenberger, D. Loss, *Phys. Rev. B* **2001**, *63*, 4414.
[51] W. Wernsdorfer, R. Sessoli, *Science* **1999**, *284*, 133.
[52] R. Schilling in *Quantum Tunneling of Magnetization–QTM'94* (Eds.: L. Gunther, B. Barbara), Kluwer, Dordrecht, **1995**, p. 59.
[53] S.-Y. Lee, S.-K. Yoo, *Phys. Rev. B* **2000**, *62*, 13884.
[54] M. V. Berry, *Proc. R. Soc. London Ser. A* **1984**, *392*, 45.
[55] G. Wentzel, *Z. Phys.* **1926**, *38*, 518.
[56] H. A. Kramers, *Z. Phys.* **1926**, *39*, 826.
[57] L. Brillouin, *J. Phys. (Paris)* **1926**, *7*, 353.
[58] J. L. Van Hemmen, A. Sütö in *Quantum Tunneling of the Magnetization–QTM'94* (Eds.: L. Gunther, B. Barbara), Kluwer, Dordrecht, **1995**, p. 19.
[59] A. Garg, *Phys. Rev. Lett.* **1999**, *83*, 4385.
[60] R. F. Weinland, G. Fischer, *Z. Anorg. Allg. Chem.* **1921**, *120*, 161.
[61] M. B. Robin, P. Day, *Adv. Inorg. Chem. Radiochem.* **1967**, *10*, 247.
[62] I. D. Brown, K. K. Wu, *Acta Crystallogr. Sect. B* **1976**, *32*, 1957.
[63] P. Langan, R. Robinson, P. J. Brown, D. Argyriou, D. Hendrickson, G. Christou, *Acta Crystallogr. Sect. C* **2001**, *57*, 909.

[64] A. Cornia, A. C. Fabretti, D. Gatteschi, R. Sessoli, L. Sorace, A. L. Barra, C. Daiguebonne, T. Roisnel, *Acta Crystallogr. Sect. C* **2002**, *58,* M371.
[65] R. Sessoli, H. L. Tsai, A. R. Schake, S. Wang, J. B. Vincent, K. Folting, D. Gatteschi, G. Christou, D. N. Hendrickson, *J. Am. Chem. Soc.* **1993**, *115,* 1804.
[66] H. J. Eppley, H.-L. Tsai, N. de Vries, K. Folting, G. Christou, D. N. Hendrickson, *J. Am. Chem. Soc.* **1995**, *117*, 301.
[67] M. A. Novak, R. Sessoli in *Quantum Tunneling of Magnetization–QTM'94* (Eds.: L. Gunther, B. Barbara), Kluwer, Dordrecht, **1995**, p. 171.
[68] A. L. Barra, D. Gatteschi, R. Sessoli, *Phys. Rev. B* **1997**, *56*, 8192.
[69] A. L. Barra, L. C. Brunel, D. Gatteschi, L. Pardi, R. Sessoli, *Acc. Chem. Res.* **1998**, *31*, 460.
[70] A. Cornia, M. Affronte, A. G. M. Jansen, D. Gatteschi, A. Caneschi, R. Sessoli, *Chem. Phys. Lett.* **2000**, *322*, 477.
[71] S. Hill, J. A. A. J. Perenboom, N. S. Dalal, T. Hathaway, T. Stalcup, J. S. Brooks, *Phys. Rev. Lett.* **1998**, *80*, 2453.
[72] "Molecular Magnetism: From Molecular Assemblies to the Devices": H. U. Güdel, *NATO ASI Ser. E* **1996**, *321*, 229.
[73] I. Mirebeau, M. Hennion, H. Casalta, H. Andres, H. U. Güdel, A. V. Irodova, A. Caneschi, *Phys. Rev. Lett.* **1999**, *83*, 628.
[74] Y. C. Zhong, M. P. Sarachik, J. R. Friedman, R. A. Robinson, T. M. Kelley, H. Nakotte, A. C. Christianson, F. Trouw, S. M. J. Aubin, D. N. Hendrickson, *J. Appl. Phys.* **1999**, *85*, 5636.
[75] A. A. Volkov, Yu. G. Goncharov, G. V. Kozlov, A. A. Mukhin, A. M. Prokhorov, *Infrared Phys.* **1985**, *25*, 369.
[76] A. A. Mukhin, V. D. Travkin, A. K. Zvezdin, S. P. Lebedev, A. Caneschi, D. Gatteschi, *Europhys. Lett.* **1998**, *44*, 778.
[77] A. M. Gomes, M. A. Novak, R. Sessoli, A. Caneschi, D. Gatteschi, *Phys. Rev. B* **1998**, *57*, 5021.
[78] R. A. Robinson, P. J. Brown, D. N. Argyriou, D. N. Hendrickson, S. M. J. Aubin, *J. Phys. Condens. Matter* **2000**, *12*, 2805.
[79] M. R. Pederson, D. V. Porezag, J. Kortus, S. N. Khanna, *J. Appl. Phys.* **2000**, *87*, 5487.
[80] M. R. Pederson, S. N. Khanna, *Phys. Rev. B* **1999**, *60*, 9566.
[81] V. V. Platonov, B. Barbara, A. Caneschi, D. A. Clark, C. M. Fowler, D. G. J. D. Gatteschi, I. A. Lubashevsky, A. A. Mukhin, V. I. Plis, A. I. Popov, D. G. Rickel, R. Sessoli, O. M. Tatsenko, A. K. Zvezdin, unpublished results.
[82] I. Tupitsyn, B. Barbara in *Magnetism: Molecules to Materials. Nanosized Magnetic Materials, Vol. 3* (Eds.: J. S. Miller, M. Drillon), Wiley-VCH, Weinheim, **2002**, p. 109.
[83] C. Raghu, I. Rudra, D. Sen, S. Ramasesha, *Phys. Rev. B* **2001**, *64*, 4419.
[84] Z. G. Soos, S. Ramasesha in *Valence Bond Theory and Chemical Structure* (Eds.: D. J. Klein, N. Trinajstic), Elsevier, New York, **1990**, p. 81.
[85] N. Regnault, T. Jolicoeur, D. Gatteschi, R. Sessoli, M. Verdaguer, *Phys. Rev. B* **2002**, *66*, 054409.
[86] J. K. Cullum, R. A. Willoughby, *Lanczos Algorithm for Large Symmetric Eigenvalue Computations*, Birkhauser, Boston, **1985**.
[87] I. Chiorescu, R. Giraud, A. G. M. Jansen, A. Caneschi, B. Barbara, *Phys. Rev. Lett.* **2000**, *85*, 4807.
[88] M. I. Katsnelson, V. V. Dobrovitski, B. N. Harmon, *Phys. Rev. B* **1999**, *59*, 6919.
[89] D. Gatteschi, L. Sorace, *J. Solid State Chem.* **2001**, *159*, 253.
[90] A. L. Barra, D. Gatteschi, R. Sessoli, G. L. Abbati, A. Cornia, A. C. Fabretti, M. G. Uytterhoeven, *Angew. Chem.* **1997**, *109*, 2423; *Angew. Chem. Int. Ed. Engl.* **1997**, *36*, 2329.
[91] A. Bencini, I. Ciofini, M. G. Uytterhoeven, *Inorg. Chim. Acta* **1998**, *274*, 90.
[92] C. E. Schäffer, *Struct. Bonding (Berlin)* **1973**, *12*, 50.
[93] A. Cornia, R. Sessoli, L. Sorace, D. Gatteschi, A. L. Barra, C. Daiguebonne, *Phys. Rev. Lett.* **2002**, *89*, 257201.
[94] L. Thomas, A. Caneschi, B. Barbara, *Phys. Rev. Lett.* **1999**, *83*, 2398.
[95] M. A. Novak, R. Sessoli, A. Caneschi, D. Gatteschi, *J. Magn. Magn. Mater.* **1995**, *146*, 211.
[96] J. R. Friedman, M. P. Sarachik, J. Tejada, R. Ziolo, *Phys. Rev. Lett.* **1996**, *76*, 3830.
[97] L. Thomas, F. Lionti, R. Ballou, D. Gatteschi, R. Sessoli, B. Barbara, *Nature* **1996**, *383*, 145.
[98] J. A. A. J. Perenboom, J. S. Brooks, S. Hill, T. Hathaway, N. S. Dalal, *Phys. B* **1998**, *246*, 294.
[99] J. A. A. J. Perenboom, J. S. Brooks, S. Hill, T. Hathaway, N. S. Dalal, *Phys. Rev. B* **1998**, *58*, 330.
[100] F. Luis, J. M. Hernandez, J. Bartolome, J. Tejada, *Nanotechnology* **1999**, *10*, 86.
[101] F. Luis, J. Bartolome, J. F. Fernandez, J. Tejada, J. M. Hernandez, X. X. Zhang, R. Ziolo, *Phys. Rev. B* **1997**, *55*, 11448.
[102] J. R. Friedman, M. P. Sarachik, J. M. Hernandez, X. X. Zhang, J. Tejada, E. Molins, R. Ziolo, *J. Appl. Phys.* **1997**, *81*, 3978.
[103] J. M. Hernandez, X. X. Zhang, F. Luis, J. Tejada, J. R. Friedman, M. P. Sarachik, R. Ziolo, *Phys. Rev. B* **1997**, *55*, 5858.
[104] F. Luis, F. L. Mettes, J. Tejada, D. Gatteschi, L. J. de Jongh, *Phys. Rev. Lett.* **2000**, *85*, 4377.
[105] F. Fominaya, J. Villain, T. Fournier, P. Gandit, J. Chaussy, A. Fort, A. Caneschi, *Phys. Rev. B* **1999**, *59*, 519.
[106] F. Fominaya, J. Villain, P. Gandit, J. Chaussy, A. Caneschi, *Phys. Rev. Lett.* **1997**, *79*, 1126.
[107] A. Lascialfari, D. Gatteschi, F. Borsa, A. Shastri, Z. H. Jang, P. Carretta, *Phys. Rev. B* **1998**, *57*, 514.
[108] Z. H. Jang, A. Lascialfari, F. Borsa, D. Gatteschi, *Phys. Rev. Lett.* **2000**, *84*, 2977.
[109] B. Barbara, L. Thomas, F. Lionti, A. Sulpice, A. Caneschi, *J. Magn. Magn. Mater.* **1998**, *177*, 1324.
[110] A. D. Kent, Y. C. Zhong, L. Bokacheva, D. Ruiz, D. N. Hendrickson, M. P. Sarachik, *Europhys. Lett.* **2000**, *49*, 521.
[111] L. Bokacheva, A. D. Kent, M. A. Walters, *Phys. Rev. Lett.* **2000**, *85*, 4803.
[112] Y. C. Zhong, M. P. Sarachik, J. Yoo, D. N. Hendrickson, *Phys. Rev. B* **2000**, *62*, R9256.
[113] E. M. Chudnovsky, D. A. Garanin, *Phys. Rev. Lett.* **1997**, *79*, 4469.
[114] K. M. Mertes, Y. Suzuki, M. P. Sarachik, Y. Paltiel, H. Strickman, E. Zeldov, E. Rumberger, D. N. Hendrickson, G. Christou, *Phys. Rev. Lett.* **2001**, *87*, 227205.
[115] E. M. Chudnovsky, D. A. Garanin, *Phys. Rev. Lett.* **2001**, *8718*, 7203.
[116] R. V. Chamberlin, G. Mozurkewich, R. Orbach, *Phys. Rev. Lett.* **1984**, *52*, 867.
[117] D. K. Lottis, R. M. White, E. Dan Dahlberg, *Phys. Rev. Lett.* **1991**, *67*, 362.
[118] N. V. Prokof'ev, P. C. E. Stamp, *Phys. Rev. Lett.* **1998**, *80*, 5794.
[119] N. V. Prokof'ev, P. C. E. Stamp, *J. Low Temp. Phys.* **1996**, *104*, 143.
[120] F. Fominaya, T. Fournier, P. Gandit, J. Chaussy, *Rev. Sci. Instrum.* **1997**, *68*, 4191.
[121] J. F. Fernandez, F. Luis, J. Bartolome, *Phys. Rev. Lett.* **1998**, *80*, 5659.
[122] W. Wernsdorfer, R. Sessoli, D. Gatteschi, *Europhys. Lett.* **1999**, *47*, 254.
[123] W. Wernsdorfer, K. Hasselbach, A. Benoit, B. Barbara, D. Mailly, J. Tuaillon, J. P. Perez, V. Dupuis, J. P. Dupin, G. Giraud, A. Perex, *J. Appl. Phys.* **1995**, *78*, 7192.
[124] M. Evangelisti, J. Bartolomé, *J. Magn. Magn. Mater.* **2000**, *221*, 99.
[125] S. M. J. Aubin, Z. M. Sun, H. J. Eppley, E. M. Rumberger, I. A. Guzei, K. Folting, P. K. Gantzel, A. L. Rheingold, G. Christou, D. N. Hendrickson, *Inorg. Chem.* **2001**, *40*, 2127.

[126] W. Wernsdorfer, T. Ohm, C. Sangregorio, R. Sessoli, D. Gatteschi, C. Paulsen, *Phys. B* **2000**, *284*, 1229.
[127] W. Wernsdorfer, *Adv. Chem. Phys.* **2001**, *118*, 99.
[128] X. S. Xie, J. K. Trautman, *Annu. Rev. Phys. Chem.* **1998**, *49*, 441.
[129] F. L. Mettes, F. Luis, L. J. de Jongh, *Phys. Rev. B* **2001**, *64*, 174411.
[130] A. Schenck, *Muon Spin Rotation Spectroscopy: Principles and Applications in Solid State Physics*, Hilger, Bristol, **1986**.
[131] D. Gatteschi, P. Carretta, A. Lascialfari, *Phys. B* **2000**, *289*, 94.
[132] T. Goto, T. Kubo, T. Koshiba, Y. Fujii, A. Oyamada, J. Arai, K. Takeda, K. Awaga, *Phys. B* **2000**, *284*, 1227.
[133] Y. Furukawa, K. Watanabe, K. Kumagai, F. Borsa, D. Gatteschi, *Phys. Rev. B* **2001**, *64*, 4401.
[134] Y. Furukawa, K. Watanabe, K. Kumagai, Z. H. Jang, A. Lascialfari, F. Borsa, D. Gatteschi, *Phys. Rev. B* **2000**, *62*, 14246.
[135] D. Arcon, J. Dolinsek, T. Apih, R. Blinc, N. S. Dalal, R. M. Achey, *Phys. Rev. B* **1998**, *58*, R2941.
[136] J. Dolinsek, D. Arcon, R. Blinc, P. Vonlanthen, J. L. Gavilano, H. R. Ott, R. M. Achey, N. S. Dalal, *Europhys. Lett.* **1998**, *42*, 691.
[137] R. M. Achey, P. L. Kuhns, A. P. Reyes, W. G. Moulton, N. S. Dalal, *Phys. Rev. B* **2001**, *64*, 4420.
[138] A. Lascialfari, Z. H. Jang, F. Borsa, P. Carretta, D. Gatteschi, *Phys. Rev. B* **1998**, *81*, 3773.
[139] Z. M. Sun, D. Ruiz, E. Rumberger, C. D. Incarvito, K. Folting, A. L. Rheingold, G. Christou, D. N. Hendrickson, *Inorg. Chem.* **1998**, *37*, 4758.
[140] D. Ruiz, Z. Sun, B. Albela, K. Folting, J. Ribas, G. Christou, D. N. Hendrickson, *Angew. Chem.* **1998**, *110*, 315; *Angew. Chem. Int. Ed.* **1998**, *37*, 300.
[141] P. D. Boyd, Q. Li, V. B. Vincent, K. Folting, H.-R. Chang, W. E. Streib, J. C. Huffman, G. Christou, D. N. Hendrickson, *J. Am. Chem. Soc.* **1988**, *110*, 8537.
[142] K. Takeda, K. Awaga, T. Inabe, *Phys. Rev. B* **1998**, *57*, R11062.
[143] Y.-G. Wei, S.-W. Zhang, M.-C. Shao, Y.-Q. Tang, *Polyhedron* **1997**, *16*, 1471.
[144] J. An, Z.-D. Chen, J. Bian, J.-T. Chen, S.-X. Wang, S. Gao, G.-X. Xu, *Inorg. Chim. Acta* **2000**, *299*, 28.
[145] P. Artus, C. Boskovic, J. Yoo, W. E. Streib, L. C. Brunel, D. N. Hendrickson, G. Christou, *Inorg. Chem.* **2001**, *40*, 4199.
[146] S. M. J. Aubin, Z. Sun, L. Pardi, J. Krzystek, K. Folting, L.-C. Brunel, A. L. Rheingold, G. Christou, D. N. Hendrickson, *Inorg. Chem.* **1999**, *38*, 5329.
[147] K. Takeda, K. Awaga, *Phys. Rev. B* **1997**, *56*, 14560.
[148] T. Kuroda-Sowa, M. Lam, A. L. Rheingold, C. Frommen, W. M. Reiff, M. Nakano, J. Yoo, A. L. Maniero, L. C. Brunel, G. Christou, D. N. Hendrickson, *Inorg. Chem.* **2001**, *40*, 6469.
[149] M. Soler, S. K. Chandra, D. Ruiz, E. R. Davidson, D. N. Hendrickson, G. Christou, *Chem. Commun.* **2000**, 2417.
[150] M. Soler, S. K. Chandra, D. Ruiz, J. C. Huffman, D. N. Hendrickson, G. Christou, *Polyhedron* **2001**, *20*, 1279.
[151] W. Wernsdorfer, M. Soler, G. Christou, D. N. Hendrickson, *J. Appl. Phys.* **2002**, *91*, 7164.
[152] K. Wieghardt, K. Pohl, I. Jibril, G. Huttner, *Angew. Chem.* **1984**, *96*, 63; *Angew. Chem. Int. Ed. Engl.* **1984**, *23*, 77.
[153] A. L. Barra, P. Debrunner, D. Gatteschi, C. E. Schulz, R. Sessoli, *Europhys. Lett.* **1996**, *35*, 133.
[154] L. Cianchi, F. Del Giallo, G. Spina, W. Reiff, A. Caneschi, *Phys. Rev. B* **2002**, *65*, 064415.
[155] J. B. Vincent, C. Christmas, H.-R. Chang, Q. Li, P. D. W. Boyd, J. C. Huffman, D. N. Hendrickson, G. Christou *J. Am. Chem. Soc.* **1989**, *111*, 2086.
[156] C. Delfs, D. Gatteschi, L. Pardi, R. Sessoli, K. Wieghardt, D. Hanke, *Inorg. Chem.* **1993**, *32*, 3099.
[157] Y. Pontillon, A. Caneschi, D. Gatteschi, R. Sessoli, E. Ressouche, J. Schweizer, E. Lelievre-Berna, *J. Am. Chem. Soc.* **1999**, *121*, 5342.
[158] A. L. Barra, D. Gatteschi, R. Sessoli, *Chem. Eur. J.* **2000**, *6*, 1608.
[159] S. M. Gorun, S. J. Lippard, *Inorg. Chem.* **1991**, *30*, 1625.
[160] R. Caciuffo, G. Amoretti, A. Murani, R. Sessoli, A. Caneschi, D. Gatteschi, *Phys. Rev. Lett.* **1998**, *81*, 4744.
[161] G. Amoretti, R. Caciuffo, J. Combet, A. Murani, A. Caneschi, *Phys. Rev. B* **2000**, *62*, 3022.
[162] A. Mukhin, B. Gorshunov, M. Dressel, C. Sangregorio, D. Gatteschi, *Phys. Rev. B* **2001**, *63*, 4411.
[163] G. L. Abbati, L. C. Brunel, H. Casalta, A. Cornia, A. C. Fabretti, D. Gatteschi, A. K. Hassan, A. G. M. Jansen, A. L. Maniero, L. A. Pardi, C. Paulsen, U. Segre, *Chem. Eur. J.* **2001**, *7*, 1796.
[164] C. Sangregorio, T. Ohm, C. Paulsen, R. Sessoli, D. Gatteschi, *Phys. Rev. Lett.* **1997**, *78*, 4645.
[165] W. Wernsdorfer, T. Ohm, C. Sangregorio, R. Sessoli, D. Mailly, C. Paulsen, *Phys. Rev. Lett.* **1999**, *82*, 3903.
[166] W. Wernsdorfer, R. Sessoli, A. Caneschi, D. Gatteschi, A. Cornia, D. Mailly, *J. Appl. Phys.* **2000**, *87*, 5481.
[167] T. Ohm, C. Sangregorio, C. Paulsen, *Eur. Phys. J. B* **1998**, *6*, 195.
[168] N. V. Prokof'ev, P. C. E. Stamp, *Rep. Prog. Phys.* **2000**, *63*, 669.
[169] A. Cuccoli, A. Fort, A. Rettori, E. Adam, J. Villain, *Eur. Phys. J. B* **1999**, *12*, 39.
[170] J. J. Alonso, J. F. Fernandez, *Phys. Rev. Lett.* **2001**, *87*, 7205.
[171] W. Wernsdorfer, A. Caneschi, R. Sessoli, D. Gatteschi, A. Cornia, V. Villar, C. Paulsen, *Phys. Rev. Lett.* **2000**, *84*, 2965.
[172] R. Sessoli, A. Caneschi, D. Gatteschi, L. Sorace, A. Cornia, W. Wernsdorfer, *J. Magn. Magn. Mater.* **2001**, *226*, 1954.
[173] D. Gatteschi, A. Lascialfari, F. Borsa, *J. Magn. Magn. Mater.* **1998**, *185*, 238.
[174] Y. Furukawa, K. Kumagai, A. Lascialfari, S. Aldrovandi, F. Borsa, R. Sessoli, D. Gatteschi, *Phys. Rev. B* **2001**, *6409*, 4439.
[175] L. Landau, *Phys. Z. Sowjetunion* **1932**, *4*, 46.
[176] C. Zener, *Proc. R. Soc. London Ser. A* **1932**, *137*, 696.
[177] E. C. G. Stückelberg, *Helv. Phys. Acta* **1932**, *5*, 369.
[178] A. L. Barra, F. Bencini, A. Caneschi, D. Gatteschi, C. Paulsen, C. Sangregorio, R. Sessoli, L. Sorace, *ChemPhysChem* **2001**, *2*, 523.
[179] A. L. Barra, A. Caneschi, A. Cornia, F. F. De Biani, D. Gatteschi, C. Sangregorio, R. Sessoli, L. Sorace, *J. Am. Chem. Soc.* **1999**, *121*, 5302.
[180] S. M. J. Aubin, N. R. Dilley, L. Pardi, J. Krzystek, M. W. Wemple, L. C. Brunel, M. B. Maple, G. Christou, D. N. Hendrickson, *J. Am. Chem. Soc.* **1998**, *120*, 4991.
[181] E. K. Brechin, J. Yoo, M. Nakano, J. C. Huffman, D. N. Hendrickson, G. Christou, *Chem. Commun.* **1999**, 783.
[182] A. Yamaguchi, H. Ishimoto, K. Awaga, J. S. Yoo, M. Nakano, D. N. Hendrickson, E. K. Brechin, G. Christou, *Phys. B* **2000**, *284*, 1225.
[183] S. Y. Wang, M. S. Wemple, J. Yoo, K. Folting, J. C. Huffman, K. S. Hagen, D. N. Hendrickson, G. Christou, *Inorg. Chem.* **2000**, *39*, 1501.
[184] J. Yoo, E. K. Brechin, A. Yamaguchi, M. Nakano, J. C. Huffman, A. L. Maniero, L. C. Brunel, K. Awaga, H. Ishimoto, G. Christou, D. N. Hendrickson, *Inorg. Chem.* **2000**, *39*, 3615.
[185] N. Aliaga, K. Folting, D. N. Hendrickson, G. Christou, *Polyhedron* **2001**, *20*, 1273.
[186] A. Bhattacharjee, Y. Miyazaki, M. Nakano, J. Yoo, G. Christou, D. N. Hendrickson, M. Sorai, *Polyhedron* **2001**, *20*, 1607.
[187] S. L. Castro, Z. M. Sun, C. M. Grant, J. C. Bollinger, D. N. Hendrickson, G. Christou, *J. Am. Chem. Soc.* **1998**, *120*, 2365.
[188] T. Mallah, C. Auberger, M. Verdaguer, P. Veillet, *J. Chem. Soc. Chem. Commun.* **1995**, 61.
[189] A. Scuiller, T. Mallah, M. Verdaguer, A. Nivorozkhin, J. L. Tholence, P. Veillet, *New J. Chem.* **1996**, *20*, 1.
[190] A. Scuiller, V. Marvaud, J. Vaissermann, I. Rosenman, M. Verdaguer, *Mol. Cryst. Liq. Cryst. Sci. Technol. Sect. A* **1999**, *334*, 1165.

[191] Z. Salman, A. Keren, P. Mendels, A. Scuiller, M. Verdaguer, *Phys. B* **2000**, *289*, 106.
[192] C. Cadiou, M. Murrie, C. Paulsen, V. Villar, W. Wernsdorfer, R. E. P. Winpenny, *Chem. Commun.* **2001**, 2666.
[193] A. L. Barra, A. Caneschi, D. Gatteschi, D. P. Goldberg, R. Sessoli, *J. Solid State Chem.* **1999**, *145*, 484.
[194] A. Bouwen, A. Caneschi, D. Gatteschi, E. Goovaerts, D. Schoemaker, L. Sorace, M. Stefan, *J. Phys. Chem. B* **2001**, *105*, 2658.
[195] G. Amoretti, S. Carretta, R. Caciuffo, H. Casalta, A. Cornia, M. Affronte, D. Gatteschi, *Phys. Rev. B* **2001**, *64*, 4403.
[196] A. Caneschi, L. Cianchi, F. Del Giallo, D. Gatteschi, P. Moretti, F. Pieralli, G. Spina, *J. Phys. Condens. Matter* **1999**, *11*, 3395.
[197] W. Wernsdorfer, S. Bhaduri, C. Boskovic, G. Christou, D. N. Hendrickson, *Phys. Rev. B.* **2002**, *65*, 180403.
[198] W. Wernsdorfer, N. Allaga-Alcalde, D. N. Hendrickson, G. Christou, *Nature* **2002**, *416*, 406.
[199] D. P. Goldberg, A. Caneschi, R. Sessoli, C. D. Delfs, J. S. Lippard, *J. Am. Chem. Soc.* **1995**, *117*, 5789.
[200] A. K. Powell, S. L. Heath, D. Gatteschi, L. Pardi, R. Sessoli, G. Spina, F. Del Giallo, F. Pieralli *J. Am. Chem. Soc.* **1995**, *117*, 2491.
[201] J. C. Goodwin, R. Sessoli, D. Gatteschi, W. Wernsdorfer, A. K. Powell, S. L. Heath, A. L. Barra, *J. Chem. Soc. Dalton Trans.* **2000**, 4702.
[202] M. Clemente-Leon, H. Soyer, E. Coronado, C. Mingotaud, C. J. Gomez-Garcia, P. Delhaes, *Angew. Chem.* **1998**, *110*, 3053; *Angew. Chem. Int. Ed.* **1998**, *37*, 2842.
[203] M. Clemente-Leon, H. Soyer, C. Mingotaud, C. J. Gomez-Garcia, E. Coronado, P. Delhaes, *Synth. Met.* **1999**, *103*, 2263.
[204] M. Clemente-Leon, E. Coronado, P. Delhaes, C. J. Gomez-Garcia, C. Mingotaud, *Adv. Mater.* **2001**, *13*, 574.
[205] E. Coronado, M. Feliz, A. Forment-Aliaga, C. J. Gomez-Garcia, R. Llusar, F. M. Romero, *Inorg. Chem.* **2001**, *40*, 6084.
[206] A. Chiolero, D. Loss, *Phys. Rev. Lett.* **1998**, *80*, 169.
[207] F. Meier, D. Loss, *Phys. Rev. Lett.* **2001**, *86*, 5373.
[208] D. Gatteschi, L. Pardi, A.-L. Barra, A. Müller, J. Döring, *Nature* **1991**, *354*, 463.
[209] I. Chiorescu, W. Wernsdorfer, B. Barbara, A. Müller, H. Bögge, *J. Appl. Phys.* **2000**, *87*, 5496.
[210] I. Chiorescu, W. Wernsdorfer, A. Müller, H. Bögge, B. Barbara, *Phys. Rev. Lett.* **2000**, *84*, 3454.
[211] I. Chiorescu, W. Wernsdorfer, A. Müller, H. Bögge, B. Barbara, *J. Magn. Magn. Mater.* **2000**, *221*, 103.
[212] A. Müller, M. Luban, C. Schröder, R. Modler, P. Kögerler, M. Axenovich, J. Schnack, P. Canfield, S. Bud'ko, N. Harrison, *ChemPhysChem* **2001**, *2*, 517.
[213] K. L. Taft, C. D. Delfs, G. C. Papaefthymiou, S. Foner, D. Gatteschi, S. J. Lippard, *J. Am. Chem. Soc.* **1994**, *116*, 823.
[214] A. Caneschi, A. Cornia, A. C. Fabretti, S. Foner, D. Gatteschi, R. Grandi, L. Schenetti, *Chem. Eur. J.* **1996**, *2*, 2329.
[215] B. Pilawa, R. Desquiotz, M. T. Kelemen, M. Weickenmeier, A. Geisselmann, *J. Magn. Magn. Mater.* **1997**, *177–181*, 748.
[216] O. Waldmann, J. Schülein, P. Müller, I. Bernt, R. W. Saalfrank, H. P. Andres, H. U. Güdel, P. Allenspach, *Inorg. Chem.* **1999**, *38*, 5879.
[217] G. L. Abbati, A. Cornia, A. C. Fabretti, W. Malavasi, L. Schenetti, A. Caneschi, D. Gatteschi, *Inorg. Chem.* **1997**, *36*, 6443.
[218] A. Lascialfari, Z. H. Jang, F. Borsa, D. Gatteschi, A. Cornia, *J. Appl. Phys.* **1998**, *83*, 6946.
[219] A. Caneschi, A. Cornia, S. J. Lippard, *Angew. Chem.* **1995**, *107*, 511; *Angew. Chem. Int. Ed. Engl.* **1995**, *34*, 467.
[220] M. Affronte, J. C. Lasjaunias, A. Cornia, A. Caneschi, *Phys. Rev. B* **1999**, *60*, 1161.
[221] O. Waldmann, R. Koch, S. Scromm, J. Schülein, P. Müller, I. Bernt, R. W. Saalfrank, F. Hampel, E. Balthes, *Inorg. Chem.* **2001**, *40*, 2986.
[222] A. Caneschi, A. Cornia, A. C. Fabretti, D. Gatteschi, *Angew. Chem.* **1999**, *111*, 1372; *Angew. Chem. Int. Ed.* **1999**, *38*, 1295.
[223] S. P. Watton, P. Fuhrmann, L. E. Pence, A. Caneschi, A. Cornia, G. L. Abbati, S. J. Lippard, *Angew. Chem.* **1997**, *109,* 2917; *Angew. Chem. Int. Ed. Engl.* **1997**, *36*, 2774.
[224] M. Eshel, A. Bino, I. Felner, D. C. Johnston, M. Luban, L. L. Miller, *Inorg. Chem.* **2000**, *39*, 1376.
[225] J. Van Slageren, R. Sessoli, D. Gatteschi, A. A. Smith, M. Helliwell, R. E. P. Winpenny, A. Cornia, A. L. Barra, A. G. M. Jansen, E. Rentschler, G. A. Timco, *Chem. Eur. J.* **2002**, *8*, 277.
[226] I. M. Atkinson, C. Benelli, M. Murrie, S. Parson, R. E. P. Winpenny, *Chem. Commun.* **1999**, 285.
[227] E. J. L. McInnes, C. Anson, A. K. Powell, A. J. Thomson, S. Poussereau, R. Sessoli, *Chem. Commun.* **2001**, 89.
[228] M. Affronte, A. Cornia, A. Lascialfari, F. Borsa, D. Gatteschi, J. Hinderer, M. Horvatic, A. G. M. Jansen, M. H. Julien, *Phys. Rev. Lett.* **2002**, *88*, 167201.
[229] A. Müller, J. Döring, *Angew. Chem.* **1988**, *100,* 1790; *Angew. Chem. Int. Ed. Engl.* **1988**, *27*, 1721.
[230] A. Müller, E. Krickemeyer, S. K. Das, P. Kögerler, S. Sarkar, H. Bögge, M. Schmidtmann, S. Sarkar, *Angew. Chem.* **2000**, *112,* 1674; *Angew. Chem. Int. Ed.* **2000**, *39*, 1612.
[231] A. Müller, C. Beugholt, P. Kögerler, H. Bögge, S. Bud'ko, M. Luban, *Inorg. Chem.* **2000**, *39*, 5176.
[232] A. Müller, S. K. Das, P. Kögerler, H. Bögge, M. Schmidtmann, A. X. Trautwein, V. Schünemann, E. Krickemeyer, W. Preetz, *Angew. Chem.* **2000**, *112,* 3556; *Angew. Chem. Int. Ed.* **2000**, *39*, 3414.
[233] A. Müller, C. Beugholt, H. Bögge, M. Schmidtmann, *Inorg. Chem.* **2000**, *39*, 3112.
[234] A. Müller, P. Kögerler, *Coord. Chem. Rev.* **2000**, *199*, 335.
[235] A. Cornia, D. Gatteschi, R. Sessoli, *Coord. Chem. Rev.* **2001** , *219*, 573.
[236] K. K. W. Wong, T. Douglas, S. Gider, D. D. Awschalom, S. Mann, *Chem. Mater.* **1998**, *10*, 279.
[237] J. G. E. Harris, J. E. Grimaldi, D. D. Awschalom, A. Chiolero, D. Loss, *Phys. Rev. B* **1999**, *60*, 3453.
[238] S. Gider, D. D. Awschalom, T. Douglas, S. Mann, M. Chaparala, *Science* **1995**, *268*, 77.
[239] J. Tejada, E. M. Chudnovsky, E. Del Barco, J. M. Hernandez, T. P. Spiller, *Nanotechnology* **2001**, *12*, 181.
[240] B. Barbara, L. Thomas, F. Lionti, I. Chiorescu, A. Sulpice, *J. Magn. Magn. Mater.* **1999**, *200*, 167.
[241] S. M. J. Aubin, Z. M. Sun, I. A. Guzei, A. L. Rheingold, G. Christou, D. N. Hendrickson, *Chem. Commun.* **1997**, 2239.

Communications



Watching photoinduced chemical reactions in solution in real time by femtosecond spectroscopy. For more information, see the Communication by B. Abel and S. Schmatz et al. on the following pages.

 © 2003 Wiley-VCH Verlag GmbH & Co. KGaA, Weinheim 1433-7851/03/4203-0299 $ 20.00+.50/0

Femtochemistry of Peroxides

Ultrafast Decarboxylation of Organic Peroxides in Solution: Interplay of Different Spectroscopic Techniques, Quantum Chemistry, and Theoretical Modeling**

Bernd Abel, Jens Aßmann, Michael Buback, Matthias Kling, Stefan Schmatz,* and Jörg Schroeder*

Dedicated to Professor Dr. Lutz F. Tietze on the occasion of his 60th birthday

Studies of the decomposition of organic peroxides are of fundamental interest and importance for application-oriented polymer chemistry. The time scales of the formation of free-radical intermediates and of subsequent processes, including unimolecular decomposition of intermediates, ultimately determine the initiator efficiency in radical polymerizations.[1–4] A large body of literature on thermal peroxide decomposition has accumulated.[5,6] Photochemical decomposition has almost exclusively been investigated in the nanosecond to microsecond time domain by means of visible absorption and EPR spectroscopy.[7–10] As a result of the poor time resolution, a complete mechanistic understanding of the elementary reactions of peroxide decomposition has not been possible. Even subsequent experiments with picosecond (ps) time resolution did not provide detailed unambiguous mechanistic insight,[1–3,11,12] mostly because of insufficient time resolution and spectral overlap of transient absorption bands. More recently, the formation of CO_2 and its subsequent vibrational cooling after peroxide decomposition could be monitored with about 2–5-ps time resolution by transient IR spectroscopy.[1–3] These studies clearly indicate that femtosecond (fs) time resolution is required for a detailed understanding of the mechanisms.[1–3] While a recent paper focuses on experimental studies of peroxide decomposition on the femtosecond (fs) timescale,[13] we describe herein time-resolved monitoring of transient intermediates and products in peroxide decarboxylation with ultrafast fs spectroscopy in combination with high-level quantum chemistry and theoretical modeling. Although we have investigated a considerable number of different peroxides, we only discuss di-1-naphthoyl peroxide (DNPO) as an example of our strategy (Figure 1).

DNPO photodissociation yields 1-naphthoyloxy free-radical intermediates and, as products, naphthyl radicals and CO_2. As shown for the photodecomposition of DNPO in Figure 1, the decay of transient 1-naphthoyloxy radicals and the formation of products can be probed directly by ultrafast transient absorption spectroscopy in different spectral regions: 1-naphthoyloxy radicals can conveniently be detected in the visible region,[14] whereas CO_2 is detected through the IR absorption of ν_3 fundamental.[1] Competing processes such as vibrational cooling of hot intermediates[15–18] may also produce overlapping spectral absorptions on a similar time scale to that of photoinduced peroxide decarboxylation kinetics in solution. It was thus necessary to scan the probe wavelength over broad wavelength ranges (UV to IR) to identify suitable spectral observation windows.

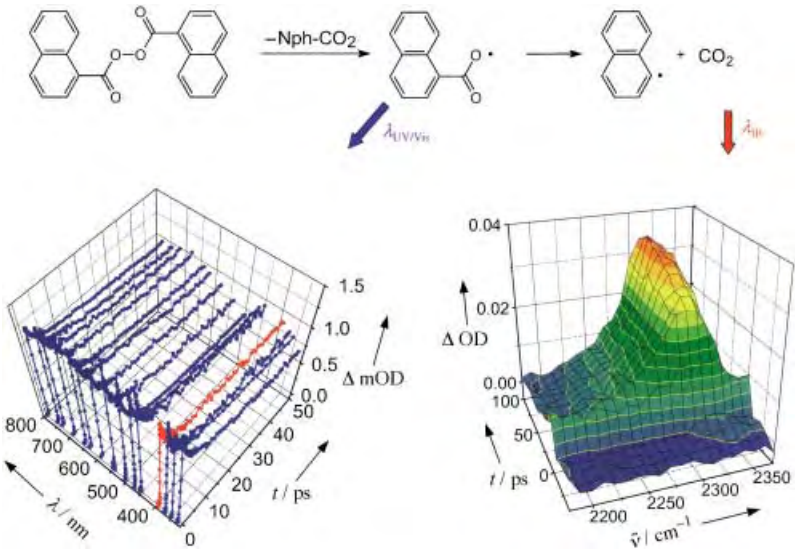


Figure 1. Decarboxylation of dinaphthoyl peroxide (DNPO). Left: transient decays at probe wavelengths in the visible spectral region; right: complementary transient spectra of nascent "hot" CO_2 with an absorption at around 2340 cm^{-1}.

Transient absorption profiles after excitation of DNPO in a solution of propylene carbonate (PC) at 266 nm and probing the subsequent transient absorption in the 300–800-nm spectral range are shown on the left-hand side of Figure 1. A characteristic feature of these traces is the rapid rise in absorbance within 1 ps, which is attributed to the extremely fast formation of "hot" 1-naphthoyloxy radicals. Whereas the hot radicals in turn dissociate on a ps time scale (as is indicated by the fast absorbance decay), the relaxed radicals decompose on a much longer timescale, which manifests itself in the "offset" of the decay traces. At long delay times, two broad absorption bands of 1-naphthoyloxy radicals can be identified, which agree with the transient spectra reported by Tateno et al.[14] From an analysis of several absorption signals,

[*] Prof. Dr. B. Abel, Priv.-Doz. Dr. S. Schmatz, Dr. J. Aßmann, Prof. Dr. M. Buback, Dr. M. Kling, Prof. Dr. J. Schroeder
Institut für Physikalische Chemie, Universität Göttingen
Tammannstrasse 6, 37077 Göttingen (Germany)
Fax: (+49) 551-39-3150
E-mail: babel@gwdg.de
sschmat@gwdg.de

[**] This work was supported by the Deutsche Forschungsgemeinschaft (SFB 357) and AKZO Nobel. The authors gratefully acknowledge interesting discussions of several aspects of this work with Prof. P. Botschwina and Prof. J. Troe.

Supporting information for this article is available on the WWW under http://www.angewandte.org or from the author.

 © 2003 Wiley-VCH Verlag GmbH & Co. KGaA, Weinheim 1433-7851/03/4203-0300 $ 20.00+.50/0

we found two nearly optimal spectral windows at 390 and 620 nm for the sensitive and unperturbed quantitative observation of the intermediate radical. The diagram on the right-hand side of Figure 1 shows a 3D plot of the time-resolved IR absorbance of the asymmetric stretch of CO_2. The nascent CO_2 product is vibrationally excited as indicated by the initially broad spectrum, which subsequently shifts and narrows as the molecule cools to ambient temperature. These spectra provide information about the rate of CO_2 formation, the initial CO_2 energy content after decarboxylation, and the vibrational cooling dynamics in the particular solvent. In Figure 2 we compare the rise of the ν_3 band integral

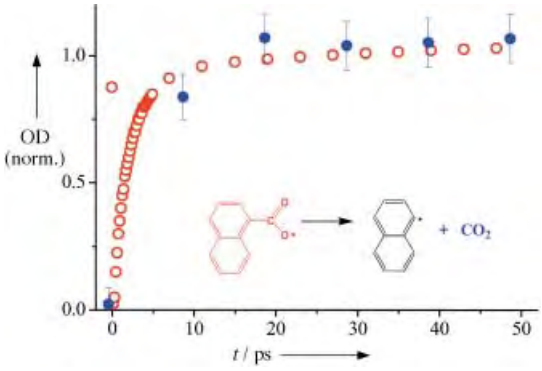


Figure 2. Comparison of the decay of the intermediate naphthoyloxy radical and formation of CO_2 from different experiments. ○: inverted (normalized) transient absorption of the 1-naphthoyloxy radical monitored at 390 nm after excitation of DNPO at 266 nm; ●: integrated absorption of the nascent CO_2 molecule at around 4.3 μm after photodissociation of DNPO at 308 nm[1] (see also Figure 1).

absorption of nascent CO_2 from Figure 1 with the inverted and normalized transient absorption decay of naphthoyloxy radicals at 390 nm. The good agreement between the two traces demonstrates that the observed transient decay of the intermediate radical in the visible spectral region correlates with the formation of CO_2.

The rigorous theoretical treatment of chemical transformations in solution is still a difficult task. Our analysis of peroxide decomposition is based upon the following approximations and assumptions: We assume that absorption at 266 nm excites the peroxide into the electronically excited (repulsive) S_1 state from which the molecule decomposes within one vibrational period and produces intermediate species in their respective electronic ground states. It is reasonable to assume that elimination of CO_2 occurs through a fast sequential mechanism (which appears to be the rule rather than the exception in the decomposition of organic peroxides).[19] The vibrationally hot intermediate radicals on the ground-state potential-energy surface (PES) rapidly dissociate in a statistical unimolecular barrier reaction to the products or cool down to ambient temperature and subsequently react in a much slower thermal reaction. Both cases can be treated quantitatively by unimolecular rate theory. The energetics for the intermediate 1-naphthoyloxy radical from DNPO dissociation is depicted in Figure 3. The rate constants of the fragmentation of the 1-naphthoyloxy

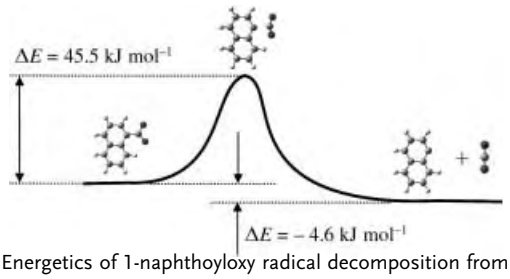


Figure 3. Energetics of 1-naphthoyloxy radical decomposition from DFT calculations. $\Delta_R H°$ (298 K) = −9.4 kJ mol^{-1} (B3LYP/6-311+G(2d,p)), zero-point energy corrected barrier height E_0 = 39.0 kJ mol^{-1} (B3LYP/6-311+G(2d,p)//6-31G(d)).

radical can be calculated by statistical unimolecular rate theory if the barrier height and the vibrational frequencies of the radical in its equilibrium and transition-state geometry are available from high-level quantum-chemical calculations. The underlying assumption of this approach is that the initial excess energy is statistically distributed among the radical fragments such that a temperature may be assigned to the intermediates and to the end products.

Our approach is actually a predictive modeling of experimental curves without parameter fitting, which—as shown below—works well for diaroyl peroxides in nonpolar and/or weakly interacting solvents. In fact, DNPO appears to be a prototype system because the corresponding intermediate naphthoyloxy radical reaction proceeds exclusively on the ground-state PES. Density-functional theory (DFT) was used to calculate the barrier height, energies of all species, and the frequencies of the normal modes on the ground-state PES.[20] The hybrid functionals B3LYP and B3PW91 were used in conjunction with basis sets of up to 393 contracted Gaussian orbitals. Kieninger et al. have reported extensive B3LYP and B3PW91 calculations for HCOO and CH_3COO radicals.[21] Furthermore, these authors report B3PW91 calculations of the energetics of the benzoyloxy radical. A comparison of their DFT calculations with results obtained on the CASPT2/ANO and MP2 level indicated that DFT calculations can provide reasonable data for free-radical species such as those used in our studies.

The microcanonical (statistical) specific rate constant for a molecule that overcomes a distinct barrier of height E_0 in a reaction to form products is given by [Eq. (1)].

$$k(E) = \frac{W(E-E_0)}{h\rho(E)} \qquad (1)$$

The terms $W(E-E_0)$ and $\rho(E)$ describe the number of energetically accessible transition-state energy levels and the density of states of the reactant molecules at energy E, respectively. The barrier was calculated to be E_0 = 39.0 kJ mol^{-1}. The calculated frequencies of the reactant and the transition state are given in the Supporting Information. The normal mode Q_{TS}, which corresponds to the reaction coordinate ($\omega_{TS} = 313i\,cm^{-1}$), is characterized by a simultaneous stretching of the nph–CO_2 bond and widening of the O-C-O angle toward linear CO_2 (Figure 3). From the excess energy $h\nu - E_0$ ($h\nu$ = photon energy at the excitation wavelength), the initial internal energy $\langle E\rangle_{ini}$ of the intermediate

 © 2003 Wiley-VCH Verlag GmbH & Co. KGaA, Weinheim 1433-7851/03/4203-0301 $ 20.00+.50/0

radical was estimated based on the assumption that the excess energy was statistically distributed among all vibrational degrees of freedom of the two fragments. For the nascent 1-naphthoyloxy radical, we found $\langle E\rangle_{ini} = 172\ kJ\,mol^{-1}$, which corresponds to an initial vibrational temperature $T_{ini} = 910\ K$. The subsequent time evolution of energy level populations $n(i,t)$ as a result of cooling and fragmentation of hot radicals was calculated with a stepladder model, which includes the rates of stepwise energy transfer to the solvent and the energy-dependent rates of the fragmentation. Energy transfer was globally taken into account by a simple model that mimics a first-order energy relaxation with an overall phenomenological vibrational energy transfer (VET) relaxation time constant of $\tau_{VET} = (7.5 \pm 1.5)$ ps. Strictly speaking, τ_{VET} is a parameter in our calculation that was taken from experimental relaxation studies in solution (propylene carbonate) for molecules of comparable complexity and with a similar number of vibrational degrees of freedom.[17,22] Normalized concentration–time profiles, $S(t)_{norm}$, of the hot 1-naphthoyloxy radical were calculated according to Eq. (2) and convolution with the cross-correlation function of the two laser pulses.

$$S(t)_{norm} = \frac{\sum_i n(i,t)}{\sum_i n(i,t=0)} \qquad (2)$$

An experimental 1-naphthoyloxy radical transient absorbance trace (○) recorded at 390 nm (compare to red curve in Figure 1) is presented in Figure 4 together with the result of a model calculation based on energies, barrier heights, and vibrational frequencies from our DFT computations (full red line). To illustrate the effective time resolution of the experiment, the cross-correlation function between pump and probe pulses is given together with the experimental signal in the insert of Figure 4. The agreement between the experiment and the theoretical model in this particular case is very satisfactory. Notably, the long-time behavior of the transients is a result of the slow thermal fragmentation of the intermediate radical at ambient temperature which is accounted for in the modeling. The excellent representation of the measured signal indicates that the rate constants as well as the calculated barriers adequately describe the ultrafast as well as the long-time kinetics (i.e., about $^1/_3$ and $^2/_3$, respectively, of the overall decarboxylation) beyond the ps timescale.

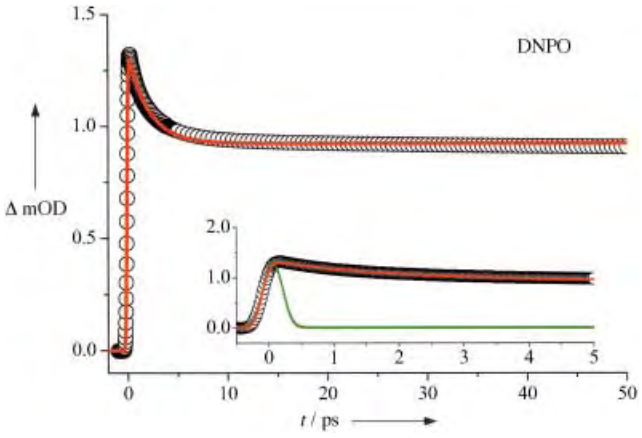


Figure 4. Experiment (○) and simulation (red solid line) of the formation and decay of the 1-naphthoyloxy radical in photoinduced DNPO decomposition in propylene carbonate. The cross-correlation of the pump and probe pulses at 266 nm and 390 nm (green line) in the insert indicates the time resolution of the experiment.

The successful modeling of the photodissociation dynamics of DNPO is probably a result of the fact that DNPO is an almost ideal system because the reaction of the intermediate proceeds exclusively on the ground-state PES. Although DFT calculations were not expected to yield barrier heights to an accuracy much better than a few $kcal\,mol^{-1}$, our calculated barrier for DNPO agrees with the experimentally determined value to within 1–2 $kcal\,mol^{-1}$.[14] However, some favorable error compensation in the calculation cannot be ruled out. Furthermore, τ_{VET} is a parameter rather than a precisely known energy-transfer coefficient, which may be significantly different for other solvents such as CCl_4.[23] Recently, the model was also used successfully for the analysis of the dissociation dynamics of other peroxides. It was found that in some cases the model needs to be extended to include direct dissociation from electronically excited states of the intermediates.[23]

In summary, we have demonstrated that ultrafast spectroscopy in the UV/Vis and in the IR spectral range in combination with quantum-chemical calculations is a powerful tool for probing and understanding photoinduced "femtochemistry" (of DNPO) in solution. A high time resolution and broad spectral tunability are indispensable to identify species unambiguously and to monitor their kinetics, whereas quantum theory and theoretical modeling provide the key to decode the experimental data.

Experimental Section

In the experiments a commercial Ti:sapphire laser system with regenerative amplification (Clark CPA-2001) and 150-fs time resolution pumped two tunable optical parametric amplifiers (NOPA, Clark and TOPAS, Light Conversion). λ_{pump} was tuned to a broad electronic absorption band of the peroxides at 266 nm, and λ_{probe} was varied between 300 and 800 nm. The two laser pulses with relative polarizations at the magic angle (54.7°) were weakly focused ($f =$ 200 mm) and overlapped in a nearly collinear pump/probe geometry (5°) in a fast-flow cell (path length: 0.1–0.2 mm). Transient absorption differences were recorded at a repetition rate of 1 kHz. The experimental setup for transient IR absorption spectroscopy with ps time resolution was described elsewhere.[24] The peroxides were synthesized and kindly provided by AKZO Nobel (Research Center Deventer, The Netherlands) and used without further purification.

Received: June 6, 2002
Revised: September 19, 2002 [Z19490]

[1] J. Aschenbrücker, M. Buback, N. P. Ernsting, J. Schroeder, U. Steegmüller, *Ber. Bunsen-Ges.* **1998**, *102*, 965.
[2] J. Aschenbrücker, M. Buback, N. P. Ernsting, J. Schroeder, U. Steegmüller, *J. Phys. Chem. B* **1998**, *102*, 5552.

 © 2003 Wiley-VCH Verlag GmbH & Co. KGaA, Weinheim 1433-7851/03/4203-0302 $ 20.00+.50/0

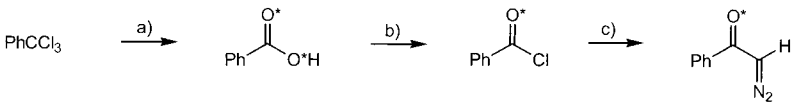
[3] M. Buback, M. Kling, M. T. Seidel, F.-D. Schott, J. Schroeder, U. Steegmüller, *Z. Phys. Chem.* **2001**, *215*, 717.
[4] C. A. Barson, J. C. Bevington, *J. Polym. Sci. Part A* **1997**, *35*, 2955.
[5] M. Buback, J. Sandmann, *Z. Phys. Chem.* **2000**, *214*, 583.
[6] Y. Sawaki in *Organic Peroxides* (Ed.: W. Ando), Wiley, New York, **1992**, p. 425.
[7] J. Hashimoto, K. Segawa, H. Sakuragi, *Chem. Phys. Lett.* **1999**, *314*, 261.
[8] J. Wang, T. Tateno, H. Sakuragi, K. Tokumaru, *J. Photochem. Photobiol. A* **1995**, *92*, 53.
[9] J. Chateauneuf, J. Lusztyk, K. U. Ingold, *J. Am. Chem. Soc.* **1988**, *110*, 2877.
[10] S. Yamauchi, N. Hirota, S. Takahara, H. Misama, K. Sawabe, H. Sakuragi, K. Tokumaru, *J. Am. Chem. Soc.* **1989**, *111*, 4402.
[11] D. E. Falvey, G. B. Schuster, *J. Am. Chem. Soc.* **1986**, *108*, 7419.
[12] E. A. Morlino, M. D. Bohorquez, D. C. Neckers, A. A. J. Rodgers, *J. Am. Chem. Soc.* **1991**, *113*, 3599.
[13] T. M. Brockman, S. M. Hubig, J. K. Kochi, *J. Org. Chem.* **1997**, *62*, 2210.
[14] T. Tateno, H. Sakuragi, K. Tokumaru, *Chem. Lett.* **1992**, *20*, 1883.
[15] A. Charvat, J. Aßmann, B. Abel, D. Schwarzer, *J. Phys. Chem. A* **2001**, *105*, 5071.
[16] A. Charvat, J. Aßmann, B. Abel, D. Schwarzer, K. Henning, K. Luther, J. Troe, *Phys. Chem. Chem. Phys.* **2001**, *3*, 2230.
[17] J. C. Owrutsky, D. Raftery, R. M. Hochstrasser, *Annu. Rev. Phys. Chem.* **1994**, *45*, 519.
[18] R. M. Stratt, M. Maroncelli, *J. Phys. Chem.* **1996**, *100*, 12981.
[19] C. Maul, K.-H. Gericke, *Int. Rev. Phys. Chem.* **1997**, *16*, 1.
[20] Gaussian 98 (Revision A.7), M. J. Frisch, G. W. Trucks, H. B. Schlegel, G. E. Scuseria, M. A. Robb, J. R. Cheeseman, V. G. Zakrzewski, J. A. Montgomery, R. E. Stratmann, J. C. Burant, S. Dapprich, J. M. Millam, A. D. Daniels, K. N. Kudin, M. C. Strain, O. Farkas, J. Tomasi, V. Barone, M. Cossi, R. Cammi, B. Mennucci, C. Pomelli, C. Adamo, S. Clifford, J. Ochterski, G. A. Petersson, P. Y. Ayala, Q. Cui, K. Morokuma, D. K. Malick, A. D. Rabuck, K. Raghavachari, J. B. Foresman, J. Cioslowski, J. V. Ortiz, A. G. Baboul, B. B. Stefanov, G. Liu, A. Liashenko, P. Piskorz, I. Komaromi, R. Gomperts, R. L. Martin, D. J. Fox, T. Keith, M. A. Al-Laham, C. Y. Peng, A. Nanayakkara, C. Gonzalez, M. Challacombe, P. M. W. Gill, B. G. Johnson, W. Chen, M. W. Wong, J. L. Andres, M. Head-Gordon, E. S. Replogle, J. A. Pople, Gaussian, Inc., Pittsburgh, PA, **1998**.
[21] M. Kieninger, O. N. Ventura, S. Suhai, *Int. J. Quantum Chem.* **1998**, *70*, 253.
[22] D. Schwarzer, J. Troe, M. Zerezke, *J. Chem. Phys.* **1997**, *107*, 8380.
[23] B. Abel, J. Aßmann, P. Botschwina, M. Buback, M. Kling, R. Oswald, S. Schmatz, J. Schroeder, T. Witte, unpublished results.
[24] J. Aschenbrücker, M. Buback, N. P. Ernsting, J. Jasny, J. Schroeder, U. Stegmüller, *Appl. Phys. B* **1997**, *65*, 441.

Oxygen Labeling and Exchange

Loss of Isotope Labeling in the Conversion of [$^{18}O_2$]Benzoic Acid into [^{18}O]Benzoyl Chloride with Oxalyl Chloride**

*Peter Haiss and Klaus-Peter Zeller**

In the course of a study on reaction mechanisms, we needed [^{18}O]2-phenyl-2-oxodiazoethane (**4***), which was prepared following the reactions given in Scheme 1. [^{18}O]Water with an enrichment of 95% ^{18}O was used as labeling source in the reactions. Based on this, benzoic acid (**2***) formed by the hydrolysis of benzotrichloride (**1**) should have a composition of 90.25% $^{18}O_2$, 9.5% $^{16}O^{18}O$, and 0.25% $^{16}O_2$. The experimental verification with the help of EI- (positive mode) and ESI-mass spectrometry (negative mode) confirms this isotope distribution (90% $^{18}O_2$, 10% $^{16}O^{18}O$, <1% $^{16}O_2$). Dissolution of the labeled benzoic acid in water/acetonitrile does not result in any decrease in the ^{18}O content.



Scheme 1. Synthesis of α-diazoketone **4***, $*=^{18}O$: a) $H_2{}^{18}O$/110°C/48 h, ampoule; b) 3 equivalents of $(COCl)_2$/77°C/1 h; c) CH_2N_2/Et_2O/0°C.

For the derivatization of the marked benzoic acid (**2***) to [^{18}O]benzoyl chloride (**3***), we chose oxalyl chloride on account of its preparative advantage, a decision which led to unexpected consequences. The reaction of benzoyl chloride (**3***) with diazomethane gives the diazoketone **4***, the carbonyl group of which unexpectedly shows two resonance signals with marginally different shifts ($\Delta\delta = 0.03$ ppm) in the ^{13}C NMR spectrum (Figure 1a).

Risley and Van Etten have also reported a similar isotope effect for the ^{13}C resonances of [^{16}O]- and [^{18}O]-carbonyl groups, in approximately the same range as ours,[2] in which the signal at a somewhat higher field strength can be assigned to the ^{18}O isotopomer. It can be seen from the intensities of the resonance signals of **4*** that the required ^{18}O-isotopomer is formed in only 40%.

At first we thought that a hydration–dehydration sequence involving the formed α diazoketone **4***, because of adventitious moisture present in ethereal diazomethane, could be responsible for the drastic loss of ^{18}O. This inference

[*] Prof. Dr. K.-P. Zeller, Dipl.-Chem. P. Haiss
Institut für Organische Chemie
Universität Tübingen
Auf der Morgenstelle 18, 72076 Tübingen (Germany)
Fax: (+49) 7071-29-5076
E-mail: kpz@uni-tuebingen.de

[**] We thank Prof. Dr. H.-J. Machulla, Sektion für Radiopharmazie, Universitätsklinikum Tübingen, for a generous gift of [^{18}O]water.

proved to be unfounded as reexamination revealed that **3*** had also been affected by loss of isotope labeling.

The ^{13}C carbonyl resonance of **3*** is split into two signals, exactly as in the subsequent product (Figure 1b). Mass spectrometry shows the hydrolysis of the intermediate **3*** (ca. 1 mg **3***, few drops of water, ultrasound bath) affords benzoic acid containing an ^{18}O content of 39.8%, and not expected 95%. Oxalyl chloride, used as a reagent in the step **2***→**3***, is thus the source for the considerable incorporation of ^{16}O observed.

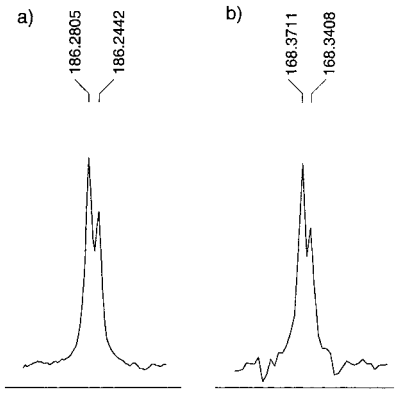
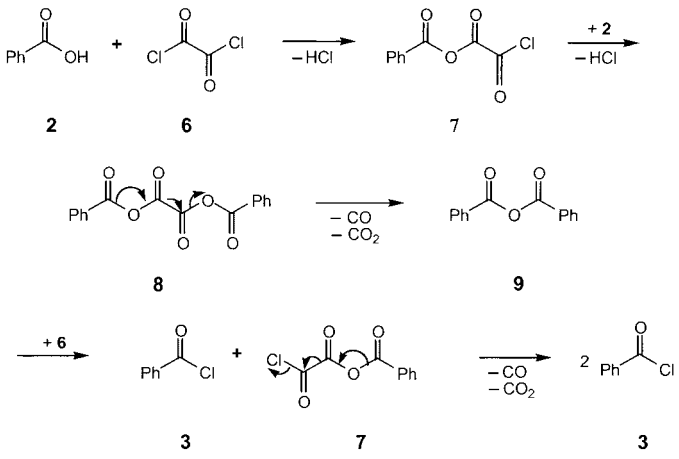


Figure 1. Carbonyl region of the ^{13}C NMR spectra of a) [^{18}O]2-phenyl-2-oxodiazoethane (**4***) and b) [^{18}O]benzoyl chloride (**3***).

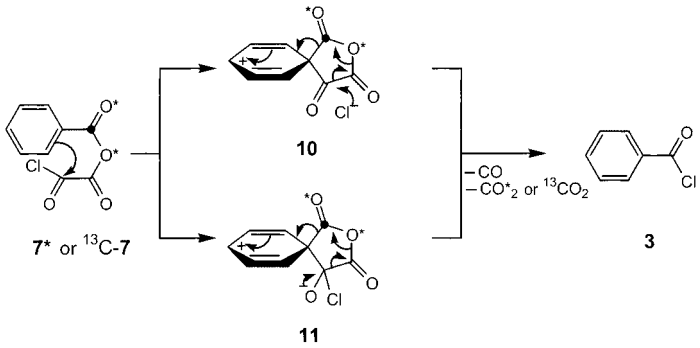
The use of oxalyl chloride (**6**) for the preparation of carboxylic acid chlorides dates back to the classical work of Adams and Ulich.[3] Depending on the amount of **6** used in the reaction with carboxylic acids, either carboxylic acid anhydrides **9** (<1 equiv) or acid chlorides (>2 equiv) are formed. Mixed anhydride **7** and in some cases isolable diacyloxalates **8** have been shown to exist as intermediates in the reaction (Scheme 2).

The carbonyl group of benzoic acid should, in principle, be found intact in benzoyl chloride irrespective of the course of the reaction. Our observation, that the oxygen atom of the carbonyl group undergoes an appreciable oxygen-atom exchange indicates that this view presents only an incomplete picture of the actual processes involved in the formation of benzoyl chloride.



Scheme 2. General reaction of carboxylic acids with oxalyl chloride, with benzoic acid given as a specific example.

An intramolecular Friedel–Crafts attack at the *ipso* position of the intermediate **7*** parallel to the collapse of **7*** to **3*** (following the mechanism postulated by Adams and Ulich[3]) is a plausible explanation for the loss of ^{18}O labeling in **3***. Thus, unlabeled **3** could be formed via a spiro-type σ-complex (either **10** or **11**) with concomitant elimination of CO and labeled CO_2 (Scheme 3). This explanation would demand that all the benzoic acid undergoing a loss of isotope labeling should in fact loose the whole carbonyl group. Thus, a corresponding loss of the ^{13}C isotope labeling should take place when using [carboxy-^{13}C]benzoic acid (^{13}C-**7**).



Scheme 3. Intramolecular *ipso* attack in the intermediate **7*** or ^{13}C-**7**; demands the loss of ^{18}O from **7*** and the loss of ^{13}C from ^{13}C-**7** (not observed), ⋆ = ^{18}O, ● = ^{13}C.

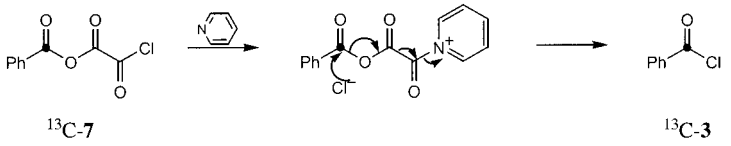
Young and Robinson[4] have converted sodium [carboxy-^{13}C]benzoate into [carbonyl-^{13}C]benzoyl chloride with complete retention of ^{13}C marking, by reaction with oxalyl chloride in the presence of pyridine. In this reaction, ^{13}C-**7** as an isotopomer of **7*** should be formed in the first partial step by elimination of NaCl. The absence of loss of ^{13}C labeling consequently excludes the intramolecular *ipso* attack. However, this could be a result of the presence of pyridine, which catalyzes the collapse to labeled [carbonyl-^{13}C]benzoyl chloride (^{13}C-**3**) and restrains the competing intramolecular Friedel–Crafts acylation (^{13}C-**7**→**3**; Scheme 4).

This consideration made it necessary to treat [carboxy-^{13}C]benzoic acid with oxalyl chloride under the same conditions as for **2*** and to conduct an isotope analysis of the benzoyl chloride thus formed. The hydrolysis of the resulting benzoyl chloride obtained to benzoic acid and the mass spectrometric analysis of the latter shows the complete retention of the ^{13}C enrichment (89.5% ^{13}C).

Our studies lead to the surprising result that in the reaction of benzoic acid with an excess of oxalyl chloride to give benzoyl chloride, the carbonyl oxygen atom is exchanged to an extent of 60%, while at the same time the carbon atom of the carbonyl group retains its identity.

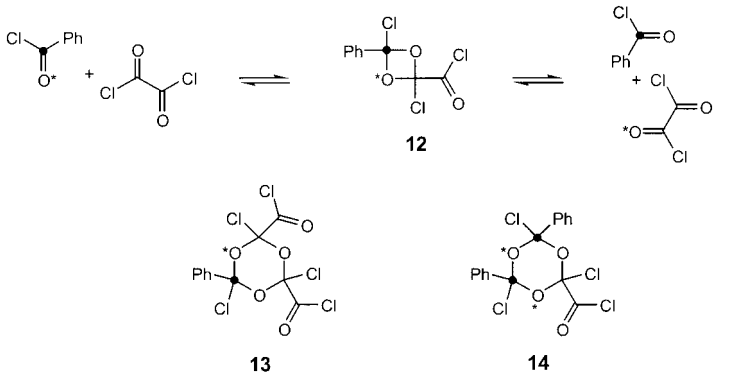
To explain these results, we propose the reversible formation of the 1,3-dioxetanes **12**[5] or alternatively the 1,3,5-trioxanes **13** or **14** from benzoyl chloride and oxalyl chloride (Scheme 5). Such processes and intermediates ex-

 © 2003 Wiley-VCH Verlag GmbH & Co. KGaA, Weinheim 1433-7851/03/4203-0304 $ 20.00+.50/0



^{13}C-**7** ^{13}C-**3**

Scheme 4. Catalytic acceleration of the breakdown of ^{13}C-**7** to ^{13}C-**3** by pyridine.



12 **13** **14**

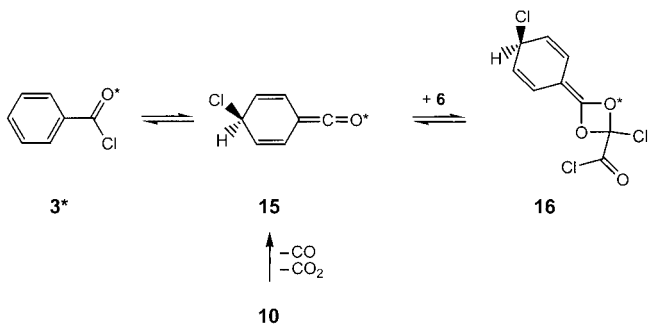
Scheme 5. Oxygen exchange between [^{18}O]benzoyl chloride (**3***) and oxalyl chloride (**6**) via 1,3-dioxetane **12** or the 1,3,5-trioxanes **13** and **14**.

plain the equilibration of the oxygen atoms of benzoyl chloride and oxalyl chloride without an intermolecular exchange of carbonyl carbon atoms in accordance with our experimental observations.

In principle, the same outcome would result from similar equilibria between the starting material benzoic acid (**2**) and the intermediates **7**, **8**, and **9** on one side, and oxalyl chloride (**6**) on the other side, these equilibria would be established simultaneously on the formation of benzoyl chloride (**3**). Because **3** possesses the highest carbonyl reactivity of all the benzoic acid derivatives present in the reaction mixture, we consider it as the most suitable candidate for this role.

Finally, as an especially reactive carbonyl compound, the formation of intermediate cyclohexadienylideneketene **15**[9] through isomerization of benzoyl chloride (**3***) or the decay of the ion pair **10** can be considered (Scheme 6). The intermediate **15** could undergo an oxygen-atom replacement with oxalyl chloride (**6**), for example, via **16** in an analogous manner.

We used exactly three equivalents of oxalyl chloride for the reaction with benzoic acid. Two equivalents from the oxalyl chloride remain after formation of benzoyl chloride (**3**) to set up the equilibrium with **12**, or **13** and **14** as intermediates. Thus, for the distribution of the oxygen atoms the ratio ^{16}O:^{18}O is 4:1. Therefore under complete equilibration, the benzoyl chloride (**3***) resulting from **2*** should contain 20% of the ^{18}O labeling. After a total reaction time of 1 hour, we find an enrichment of 39.8% ^{18}O, which shows that the oxygen-exchange process has not yet reached the equilibration stage. A further loss of ^{18}O marking is to be expected for longer reaction times.



3* **15** **16** **10**

Scheme 6. Oxygen Exchange via ketene intermediate **15**.

Received: June 28, 2002 [Z19636]

[1] R. Salmon in *Encyclopedia of Reagents for Organic Synthesis, Vol. 6* (Ed.: L. A. Paquette), Wiley, Chichester, **1995**, pp. 3814–3817.

[2] J. M. Risley, R. L. Van Etten, *J. Am. Chem. Soc.* **1980**, *102*, 4609–4614.

[3] R. Adams, L. H. Ulich, *J. Am. Chem. Soc.* **1920**, *42*, 599–611.

[4] D. J. Young, M. J. T. Robinson, *J. Labelled Compd. Radiopharm.* **2000**, *43*, 121–126.

[5] The chemistry of 1,3-dioxetanes is less known although, according to the MO calculations,[6] they should be more stable than the intensively studied 1,2-isomers.[7] A literature survey up to 1995 excludes the existence of authentic 1,3-dioxetanes.[7] Our literature search revealed that 1,3-dioxetanes are sporadically described as reactions products, for example, Ref. [8].

[6] a) P. N. V. P. Kumar, X. D. Wang, B. Lam, T. A. Albright, E. D. Jemmis, *J. Mol. Struct.* **1989**, *194*, 183–190; b) T. H. Lay, T. Yamada, P.-L. Tsai, J. W. Bozzelli, *J. Phys. Chem. A* **1997**, *101*, 2471–2477.

[7] C. R. Saha-Möller, W. Adam in *Comprehensive Heterocyclic Chemistry II, Vol. 1B* (Eds.: A. R. Katritzky, C. W. Rees, E. F. V. Scriven, A. Padwa), **1996**, pp. 1041–1082.

[8] a) L. S. Boulos, I. T. Hennawy, *Phosphorus Sulfur Silicon Relat. Elem.* **1993**, *84*, 173–179; b) D. Bankston, *J. Org. Chem.* **1989**, *54*, 2003–2006.

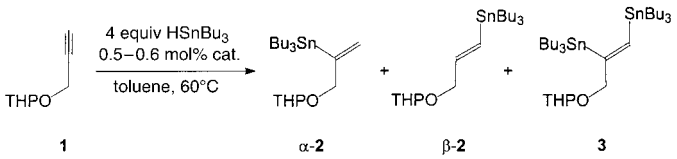
[9] We thank one of the referees for pointing out the possible participation of a ketene intermediate.

 © 2003 Wiley-VCH Verlag GmbH & Co. KGaA, Weinheim 1433-7851/03/4203-0305 $ 20.00+.50/0

Tungsten-Catalyzed Distannation

Development of a New Catalyst for the Distannation of Alkynes**

*Sascha Braune and Uli Kazmaier**



Scheme 1. Mono- and distannation of **1**. THP = tetrahydropyranyl.

Vinylstannanes have become important building blocks in natural product chemistry as a result of the diverse range of palladium-catalyzed cross-coupling reactions they undergo with halides, acid chlorides, or triflates.[1] The broad applicability and high tolerance against functional groups has stimulated a keen interest in synthesizing these organotin derivatives. The most direct route to these compounds is by hydrostannation, namely the addition of tin hydrides to C≡C bonds. Besides this route, only a small number of approaches exist to introduce two functionalities simultaneously. One is the nickel-catalyzed carbostannation of terminal alkynes, in which a tributyltin and an allylic fragment are introduced simultaneously.[3] Other possibilities are the palladium-catalyzed addition of a silyl and a stannyl group (silastannation) to an alkyne or[4] distannation, mainly developed by Mitchell et al.[5] Best results have been obtained in the palladium-catalyzed distannation of alkynes by using hexamethyldistannane, a compound that is not unproblematic to handle in terms of its toxicity. Chemoselective transformations of both tin fragments are possible, underlining the synthetic use of these distannylated (*Z*)-olefins in organic chemistry.[6] The distannation of nonterminal acetylenic esters to (*Z*)-bis(trimethyltin)alk-2-enoates was achieved by Piers et al. in high yields.[7] Herein we report that distannylated (*Z*)-olefins can not only be obtained by palladium-catalyzed reactions but also by using isonitrile transition-metal complexes of Group 6 in combination with tributyltin hydride.

Our group has been studying the regioselective hydrostannation of alkynes with $[Mo(CO)_3(CN\mathit{t}Bu)_3]$ (**A**) for several years.[8] This catalyst is very stable and reliable, and gives high selectivity for the sterically more hindered α-stannylated product. Since this catalyst does not work as well in hydrostannations of propargylic ethers as it does in the corresponding reactions with propargylic esters or alcohols, we tried to optimize the catalyst by varying the isonitrile ligands. Starting from $[Mo(CO)_6]$ and the corresponding isonitrile[9] we prepared several catalysts by ligand exchange, for example, $[Mo(CO)_3(CNPh)_3]$ (**B**).[10] This complex shows a slower conversion rate and a poor ratio of α- to β-products as well as a surprising side product: 19% (relative to the whole conversion) of the distannylated product **3** in the "hydrostannation" of the tetrahydropyranylpropargylic ether (**1**; Scheme 1). This side product was also obtained in the hydrostannation of propargylic compouds with the other catalysts, but always in less than 5%.This result was initially surprising for us, and we assumed that based on the lower reactivity of the phenyl isocyanide complex (**B**), the decomposition of the tin hydride by elimination of H_2 and the formation of the distannane competes with the hydrostannation. This would explain the formation of the distannylated product as a metal-catalyzed addition of an in situ prepared distannane to a C≡C bond. Decompositions of this type are well known for palladium-catalyzed reactions,[11] and palladium complexes also catalyze the addition of distannanes to alkynes.[5] Only recently Lautens et al. reported an analogous side product in a palladium-catalyzed hydrostannation.[4e] To verify our mechanistic hypothesis we tried to react hexabutyldistannane with **1** in the presence of our molybdenum catalysts, but in no case were we able to isolate any stannylated product. Evidently, a "free" distannane is not the reagent responsible for the addition, but the "decomposition" must take place in the coordination sphere of the metal, probably in the presence of coordinated alkyne.

It is known that tungsten and molybdenum form stable complexes with trialkyltin compounds.[12] Bel'skii et al. were able to crystallize complexes of the type Mo-$HSnBu_3$ and characterize them by X-ray crystallography in 1986.[13] Brown et al. showed that $[HMo(CO)_3Cp]$ and $HSnBu_3$ react to form a complex of the type $[Bu_3SnMo(CO)_3Cp]$ under reductive elimination of hydrogen.[14] In 1991 Schubert et al. observed that $[MesCr(CO)_3]$ forms a stable complex with triphenyltin hydride after dissociation of one carbonyl ligand. This complex contains a three-centered hydrogen bond Cr-H-Sn.[15] They were also able to detect the appearance of complexes like $[(CO)_4(Ph_3P)W(H)SnPh_3]$ by spectroscopy, but unfortunately because of the lability of the tungsten complexes they were not able to crystallize them. However, they observed that with an excess of tin hydride, hydrogen is eliminated and the corresponding distannylated complex $[(CO)_4(Ph_3P)W(SnPh_3)_2]$ is obtained.

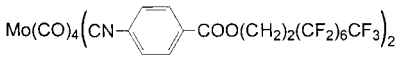
Thus, it wasn't as surprising as initially throught that we obtained the distannylated product. The next question was, how can we alter the ratio of distannation to hydrostannation. Clearly, the electron-donating *tert*-butyl group of **A** favors the hydrostannation, whereas the rather electron-withdrawing phenyl ring in the phenyl isocyanide complex **B** favors the decomposition of the tin hydride. Therefore, we explored the effects of further electron-withdrawing groups at the phenyl ring on the product ratio (see Scheme 1) and synthesized "electron-poor" isonitriles[16] and the corresponding molybdenum and tungsten isonitrile complexes **C**–**G**.[9,17]

First we examined the molybdenum complexes **C**–**E** and confirmed that electron-withdrawing groups in the isonitrile

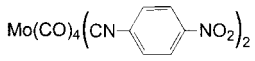
[*] Prof. Dr. U. Kazmaier, Dipl.-Chem. S. Braune
Universität des Saarlandes
Institut für Organische Chemie
Im Stadtwald, Geb. 23.2, 66123 Saarbrücken (Germany)
Fax: (+49) 681-302-2409
E-mail: u.kazmaier@mx.uni-saarland.de

[**] This work was supported by the Deutsche Forschungsgemeinschaft (SFB 247 and Ka880/5) and by the Fonds der Chemischen Industrie.

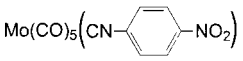
 © 2003 Wiley-VCH Verlag GmbH & Co. KGaA, Weinheim 1433-7851/03/4203-0306 $ 20.00+.50/0



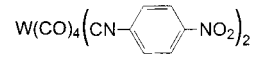
C



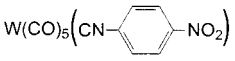
D



E



F



G

Table 1: Mono- and distannation of **1**.

Catalyst	Yield [%] α-**2**	β-**2**	**3**
A	94	1	3
B	42	18	14
C	14	2	29
D	21	2	40
E	2	1	44
F	5	4	77
G	1	1	93

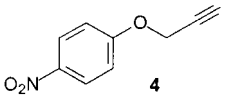
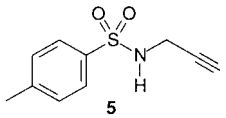
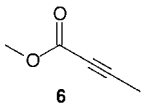
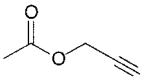
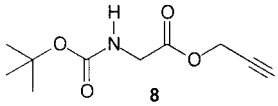
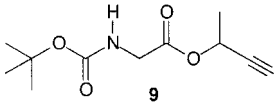
part of the complex discriminate the hydrostannation (Table 1). Surprisingly we found the best selectivity with the monoisonitrile complex **E**, which yields nearly exclusively the distannylated product. But we were not able to improve the yield above 50% even by careful optimization of the reaction parameters.

We hoped to achieve a further improvement by using the corresponding tungsten-based catalyst, since tungsten because of its larger atomic volume should be more willing to bind two sterically demanding fragments like the tributyltin groups.[15] Indeed the tungsten complexes show a higher reactivity than the corresponding molybdenum complexes, and the monoisonitrile complex **G** proved to be the best catalyst: the *cis*-distannylated products are obtained almost exclusively in near quantitative yields. Even though only 0.5–0.6 mol% of catalyst were used in all the reactions, the conversion was complete after 5 h at the most.

Furthermore we were able to show the general use of catalyst **G** in the selective distannation of functionalized terminal alkynes (Table 2). In nearly all cases the ratio of distannation/hydrostannation was better than 20/1. This was valid for ethers (**4**) as well as for amides (**5**). In the case of **6** we found only distannylated product, though the yield decreased. This example demonstrated that even substituted alkynes can be distannylated selectively. We obtained very good yields and excellent selectivities in the case of propargylic esters (**7, 8**). Steric hindrance has, however, a strong influence especially on the yields as a comparison of **8** and **9** shows. Simple alkynes are less suitable as substrates for our catalyst systems; for example, in the reaction of 1-decyne, only negligible amounts of distannylated product were obtained, and without significant selectivity.

In conclusion, we could show that the tungsten isonitrile complex **G** is a highly efficient and selective catalyst for distannations of alkynes, in which tributyltin hydride can be used as the tin source. Mechanistic studies on this exceptional reaction are in progress.

Table 2: Distannation of alkynes with the tungsten isonitrile complex **G**.

Substrate	distannation	Yield [%] α-stannation	β-stannation
 **4**	62	3	0
 **5**	76	3	1
 **6**	42	0	0
 **7**	87	1	1
 **8**	73	1	0
 **9**	32	2	1

Experimental Section

Synthesis of the catalyst **G**: *p*-Nitrophenyl isocyanide (790 mg, 5.33 mmol) dissolved in absolute toluene (10 mL) was added slowly to a suspension of $CoCl_2 \cdot 2H_2O$ (400 mg, 2.41 mmol) and $[W(CO)_6]$ (605 mg, 1.72 mmol) in absolute toluene (10 mL) at 100 °C. The mixture was refluxed for 7 h before the resulting black suspension was evaporated in vacuo. The residue obtained was purified by flash chromatography over silica using CH_2Cl_2/hexane (1/1) as eluent. Yield: 189 mg (0.40 mmol, 23%) of a yellow solid.

^{1}H NMR (300 MHz, $CDCl_3$): $\delta = 7.55$ (d, $^3J = 9.1$ Hz; (CH)C–NC), 8.32 ppm (d, $^3J = 9.1$ Hz; (CH)C–NO_2); ^{13}C NMR (75 MHz, $CDCl_3$): $\delta = 125.9$ (d; (*C*H)C–NO_2), 128.0 (d; (*C*H)C–NC), 141.8 (s; *C*–NC), 147.7 (s; C–NO_2), 194.1 (s; *cis*-CO), 195.7 ppm (s; *trans*-CO), (isonitrile-C not detected); IR (KBr): $\tilde{\nu} = 2135$ (s), 2049 (s), 1972, 1925 (vs), 1524 (m), 1344 cm^{-1} (s); FAB$^+$-HRMS [*m*/*z*, (%)]: $C_{12}H_4N_2O_7{}^{186}W$: calcd: 473.9562, found: 473.9548 (50.3); $C_{12}H_4N_2O_7{}^{184}W$: calcd: 471.9528, found: 471.9497 (56.1); $C_{12}H_4N_2O_7{}^{183}W$: calcd: 473.9521, found: 470.9500 (35.7); $C_{12}H_4N_2O_7{}^{182}W$: calcd: 469.9501, found: 469.9464 (48.0); elemental analysis (%): calcd: C 30.15, H 2.11, N 5.86; found: C 30.17, H 1.42, N 5.64.

General procedure for the distannation: The alkyne (1 mmol), catalyst **G** (3 mg, 0.6 mol%) and a point of a spatula of hydroquinone were dissolved in absolute toluene (2 mL) and heated for 15 min at 60 °C. After addition of tributyltin hydride (1 mL, 3.8 mmol), heating was continued for 12 h at 60 °C. After removal of the solvent the crude product was chromatographed over silica gel. First hexabutyldistannane and tributyltin hydride were eluted with pure hexane, then the product was isolated by using hexane/ethyl acetate/1% triethylamine (98–90% hexane).

Received: August 15, 2002 [Z19974]

[1] a) J. K. Stille, *Angew. Chem.* **1986**, *98*, 504–519; *Angew. Chem. Int. Ed. Engl.* **1986**, *25*, 508–523; b) J. E. Baldwin, R. M.

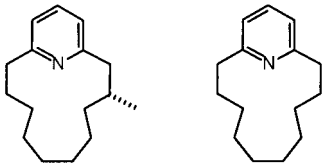
Adlington, S. H. Ramcharitar, *J. Chem. Soc. Chem. Commun.* **1991**, 940–942; c) A. G. Davies, *Organotin Chemistry*, VCH, Weinheim, **1997**.
[2] Review: N. D. Smith, J. Manusco, M. Lautens, *Chem. Rev.* **2000**, *100*, 3257–3282.
[3] E. Shirakawa, K. Yamasaki, H. Yoshida, T, Hiyama, *J. Am. Chem. Soc.* **1999**, *121*, 10221–10222.
[4] a) T. N. Mitchell, H. Killing, R. Dicke, R. Wickenkamp, *J. Chem. Soc. Chem. Commun.* **1985**, 354–355; b) B. L. Chenard, E. D. Laganis, F. Davidson, T. V. RajanBabu, *J. Org. Chem.* **1985**, *50*, 3666–3667; c) B. L. Chenard, C. M. Van Zyl, *J. Org. Chem.* **1986**, *51*, 3561–3566; d) T. N. Mitchell, A. Amamria, R. Dicke, R. Wickenkamp, U. Schneider, *J. Org. Chem.* **1987**, *52*, 4868–4874; d) J.-P. Quintard, I. Beaudet, J.-L. Parrain, *Tetrahedron Lett.* **1991**, *32*, 6333–6336; e) M. Lautens, J. Manusco, *Synlett* **2002**, 394–398.
[5] T. N. Mitchell, A. Amaria, H. Killing, D. Rutschow, *J. Organomet. Chem.* **1986**, *304*, 257–265.
[6] T. N. Mitchell, K. Kwetkat, D. Rutschow, U. Schneider, *Tetrahedron* **1989**, *45*, 969–978.
[7] E. Piers, R. T. Skerlj, *J. Chem. Soc. Chem. Commun.* **1986**, 626–627.
[8] a) U. Kazmaier, D. Schauß, M. Pohlman, *Org. Lett.* **1999**, *1*, 1017–1019; b) U. Kazmaier, D. Schauß, M. Pohlman, S. Raddatz, *Synthesis* **2000**, 914–917; c) U. Kazmaier, M. Pohlman, D. Schauß, *Eur. J. Org. Chem.* **2000**, 2761–2766; d) U. Kazmaier, D. Schauß, S. Raddatz, M. Pohlman, *Chem. Eur. J.* **2001**, *7*, 456–464.
[9] N. J. Coville, M. O. Albers, *J. Organomet. Chem.* **1980**, *199*, 55–62.
[10] U. Kazmaier, S. Braune, *J. Organomet. Chem.* **2002**, *641*, 26–29.
[11] K.-R. Pörschke, *Main Group Met. Chem.* **2002**, *25*, 45–53.
[12] a) E. E. Isaacs, W. A. G. Graham, *Can. J. Chem.* **1975**, *53*, 467–473; b) J. E. Ellis, J. T. Lin, G. P. Hagen, *Organometallics* **1983**, *2*, 1145–1150.
[13] V. K. Bel'skii, A. N. Protskii, B. M. Bulychev, G. L. Soloveichik, *Dokl. Akad. Nauk SSSR* **1986**, *287*, 857–861; *Proc. Acad. Sci. USSR Chem. Sect.* **1986**, *286/291*, 76–80.
[14] T. L. Brown, R. W. Wegman, *Organometallics* **1982**, *1*, 47–52.
[15] U. Schubert, H. Piana, U. Kirchgäßner, *Chem. Ber.* **1991**, *124*, 743–751.
[16] M. A. Mironov, V. S. Mokrushin, *Russ. J. Org. Chem.* **1999**, *35*, 719–723.
[17] In contrast to the electron-rich isonitriles which provide mainly the tris(isonitrile) complexes under the conditions described in reference [9], with electron-poor isonitriles under the same conditions the mono- and disubstituted complexes are obtained, which can be separated by flash chromatography.

Efficient Synthetic Strategy

A Catalytic Approach to (*R*)-(+)-Muscopyridine with Integrated "Self-Clearance"**

Alois Fürstner and Andreas Leitner*

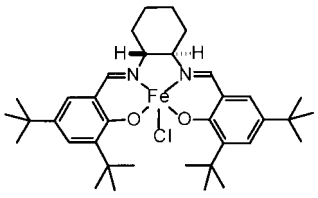
The chemist's ability to make molecules of utmost complexity[1] must not hide the fact that the practicability of many such syntheses is still low. The arithmetic demon inherent to any linear sequence constitutes one of the major hurdles in this regard. To overcome this obstacle new methodology and improved retrosynthetic logic are called for which allow more than one bond-making event to be integrated into a single synthetic operation.[2] The approaches to the odoriferous alkaloid (*R*)-(+)-muscopyridine (**1**), derived from the animal kingdom, and its naturally occurring nor-analogue **2** outlined below tackle this theme and illustrate how priority can be given to the "economy of steps"[3] by a highly orchestrated catalysis-based process. Following its isolation by Ruzicka and Prelog,[4] the unusual *meta*-pyridinophane derivative **1** has



1 **2**

been repeatedly targeted.[5–7] Despite its rather simple structure, however, none of the reported syntheses is fully satisfactory, being either unduly lengthy and/or poor yielding.[8]

Our approach to the alkaloid **1** takes advantage of the favorable application profile of an iron-catalyzed alkyl–aryl cross-coupling reaction recently developed in our laboratory as a powerful alternative to established organopalladium chemistry; in the present case the iron–salen complex **3** was applied.[9,10] The method not only allows one to replace expensive precious metal complexes by cheap iron salts, but it is also distinguished by unprecedentedly high reaction rates even at or below room temperature. While aryl chlorides as



3

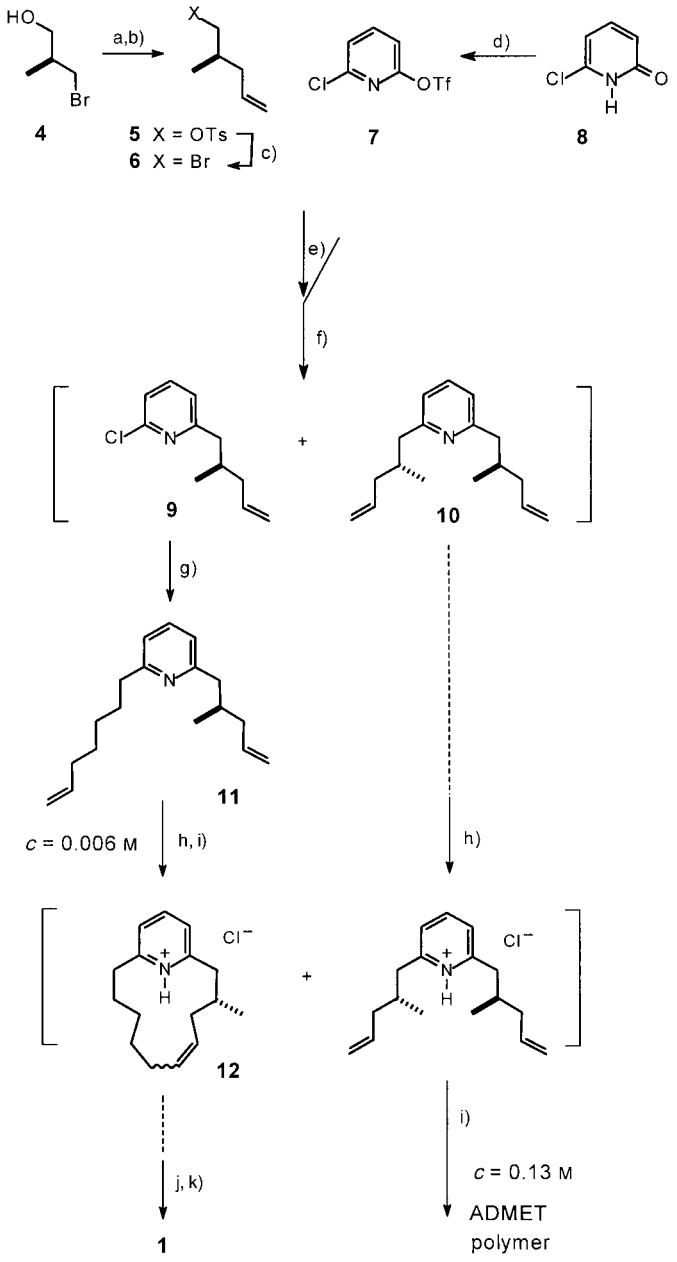
[*] Prof. A. Fürstner, Dipl.-Ing. A. Leitner
Max-Planck-Institut für Kohlenforschung
45470 Mülheim an der Ruhr (Germany)
Fax: (+49) 208-306-2994
E-mail: fuerstner@mpi-muelheim.mpg.de

[**] This work was supported by the Deutsche Forschungsgemeinschaft (Leibniz program) and the Fonds der Chemischen Industrie.

 © 2003 Wiley-VCH Verlag GmbH & Co. KGaA, Weinheim 1433-7851/03/4203-0308 $ 20.00+.50/0

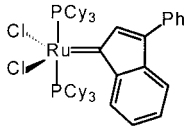
well as aryl sulfonates qualify as the substrates, the latter are usually distinctly more reactive. This chemoselectivity pattern constitutes a major design element of the synthesis depicted in Scheme 1.

Specifically, reaction of the commercially available bromo alcohol **4** with $H_2C{=}CHMgBr$ in the presence of catalytic amounts of CuI affords the rather volatile alkene (X = OH),[11] which is immediately converted without further purification into tosylate **5** to minimize losses during workup



Scheme 1. Synthesis of (*R*)-(+)-muscopyridine (**1**): a) $H_2C{=}CHMgBr$, CuI (5 mol%), THF, 0°C; b) tosyl chloride, pyridine, CH_2Cl_2, 65% (over two steps); c) LiBr, acetone, reflux, 81%; d) triflic anhydride, pyridine, 97%; e) Mg, THF, bromide **6**; f) complex **3** (5 mol%), THF/NMP, 0°C; g) 6-heptenylmagnesium bromide, complex **3** (5 mol%), 80% (combined yield, **11**:**10** ≈ 4:1); h) HCl, Et_2O; i) complex **13** (10 mol%), CH_2Cl_2, reflux, $c = 0.006$ M, 14 h; then $c = 0.13$ M, 12 h; j) H_2 (50 atm), 70°C; k) aqueous saturated $NaHCO_3$, 57% (over steps h)–k)) NMP = *N*-methylpyrrolidinone.

(65% over both steps). Subsequent treatment with LiBr in acetone affords the corresponding bromide **6**. The enantiomerically pure Grignard reagent derived therefrom is then added by syringe to a solution of the difunctional pyridine derivative **7** and the iron–salen complex **3** (5 mol%) in THF/NMP at 0°C. Monitoring of the reaction by TLC reveals that substrate **7** is completely consumed after 20 min; compound **9** forms selectively by reaction at the triflate site, together with small amounts of the dialkylation product **10**. However, rather than taking recourse to workup and purification at this point, a solution of 6-heptenylmagnesium bromide and additional **3** (5 mol%) were introduced and stirring was continued for 30 min at 0°C. The ensuing second iron-catalyzed cross-coupling reaction affords the desired diene **11**, which is contaminated with compound **10** formed in the first step (80% combined yield, **11**:**10** ≈ 4:1). Again, no attempt was made to separate these products that are indistinguishable by TLC; instead, a much more convenient chemical "self-clearance" occurs as an integral part of the subsequent metathesis cascade.



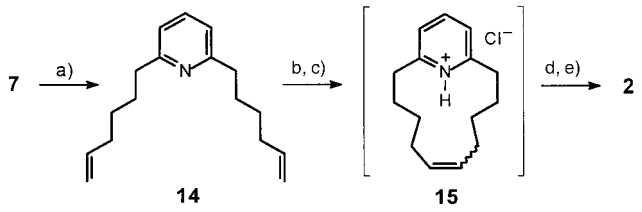
13

Conversion of the product mixture of **11** and **10** to the corresponding hydrochloride salts[12] followed by treatment with the readily available ruthenium–indenylidene complex **13** (10 mol%)[13,14] under high dilution conditions leads to the selective cyclization of diene **11** to the *meta*-pyridinophane **12** ($E,Z \approx 1.8{:}1$), while the hydrochloride of compound **10** remains unchanged. This reflects the greater ease of formation of the 13-membered ring as compared to the kinetically and thermodynamically handicapped 11-membered analogue that would derive from **10** by ring-closing metathesis (RCM).[15,16] After most of the solvent has been distilled off, however, residual **10** is forced to polymerize by acyclic diene metathesis (ADMET)[17] and thereby completely disappears from the GC trace while the macrocycle persists. Evidently, the indenylidene catalyst **13** does not lead to any noticeable reopening of the cyclic olefin **12** once it is formed, although RCM is a priori a reversible transformation.[18] Therefore this transformation constitutes a noteworthy illustration for selectivity by catalyst tuning which allows one to rigorously distinguish between terminal and disubstituted double bonds.

At this point, workup is further postponed and advantage is taken from the multifaceted behavior of the ruthenium catalyst **13**. Thus, the crude mixture containing the cyclic monomer **12**, the ADMET-polymer, and the still intact metathesis catalyst is transferred into an autoclave and is stirred under H_2 (50 atm) overnight. Thereby, the carbene complex converts into a ruthenium hydride species, which acts as an efficient hydrogenation catalyst.[19] Passing the mixture through a short pad of silica suffices to give analytically pure (*R*)-(+)-muscopyridine **1** in 57% yield, while the polymeric by-product is retained on top of the column. This streamlined approach to enantiopure **1** together with the most convenient workup outperforms all previous approaches to this natural musk by virtue of its brevity and highly integrated character.

The adaptation of this concept to the synthesis of the achiral nor-analogue **2** is straightforward (Scheme 2). Treatment of substrate **7** with an excess of 5-hexenylmagnesium

 © 2003 Wiley-VCH Verlag GmbH & Co. KGaA, Weinheim 1433-7851/03/4203-0309 $ 20.00+.50/0



Scheme 2. Synthesis of normuscopyridine **2**: a) 5-hexenylmagnesium bromide, complex **3** (10 mol%), THF/NMP, 0°C, 75%; b) HCl, Et_2O; c) complex **13** (10 mol%), CH_2Cl_2, reflux, 14 h; d) H_2 (50 atm), 70°C; e) aqueous saturated $NaHCO_3$, 68% (over steps b)–e)).

bromide[20] in the presence of catalytic amounts of complex **3** as the precatalyst provides the dialkylation product **14** in 75% yield after a reaction time of only 20 min. Exposure of the corresponding hydrochloride to the ruthenium–indenylidene complex **13** in a dilute CH_2Cl_2 solution delivers cycloalkene **15**. Subsequent hydrogenation (50 atm H_2) of the crude product affords the targeted 10-[2,6]-pyridinophane **2** in 68% overall yield.

In summary, these syntheses feature several notable aspects: They show the exceptional performance of the emerging iron-catalyzed alkyl–aryl cross-coupling method, which enables the construction of polysubstituted arenes by serial "three-component coupling" in one pot at unusually high reaction rates. Moreover, the syntheses of **1** and **2** illustrate several ways in which one can benefit from the subtleties of olefin metathesis chemistry: not only is it possible to rigorously distinguish between medium-sized rings and macrocycles as well as between terminal and internal double bonds, but it is also possible to perform "tandem catalysis" events (RCM/ADMET + hydrogenation) with a single ruthenium–carbene complex as the catalytically competent precursor.[19] Finally, the muscopyridine case study exemplifies an unprecedented "chemical" self-clearance routine that exploits the complementarity between RCM and ADMET. Further work aimed at a rational use of these and related aspects is underway.

Received: September 6, 2002
Revised: October 29, 2002 [Z50109]

[1] a) K. C. Nicolaou, D. Vourloumis, N. Winssinger, P. S. Baran, *Angew. Chem.* **2000**, *112*, 46–126; *Angew. Chem. Int. Ed.* **2000**, *39*, 44–122; b) E. J. Corey, X.-M. Cheng, *The Logic of Chemical Synthesis*, Wiley, New York, **1989**.

[2] Domino processes, for example, are an elegant way to reach this goal: a) L. F. Tietze, U. Beifuss, *Angew. Chem.* **1993**, *105*, 137–170; *Angew. Chem. Int. Ed. Engl.* **1993**, *32*, 131–163; b) L. F. Tietze, *Chem. Rev.* **1996**, *96*, 115–136.

[3] A. Fürstner, *Synlett* **1999**, 1523–1533.

[4] a) H. Schinz, L. Ruzicka, U. Geyer, V. Prelog, *Helv. Chim. Acta* **1946**, *29*, 1524–1528; b) G. Ohloff, *Riechstoffe und Geruchssinn: Die Molekulare Welt der Düfte*, Springer, Berlin, **1990**; c) see also: Y. De-Quan, B. C. Das, *Planta Med.* **1983**, *49*, 183–184.

[5] Syntheses of *rac*-**1**: a) K. Biemann, G. Büchi, B. H. Walker, *J. Am. Chem. Soc.* **1957**, *79*, 5558–5564; b) K. Tamao, S. Kodama, T. Nakatsuka, Y. Kiso, M. Kumada, *J. Am. Chem. Soc.* **1975**, *97*, 4405–4406; c) H. Saimoto, T. Hiyama, H. Nozaki, *Tetrahedron Lett.* **1980**, *21*, 3897–3898; d) F. Hadj-Abo, M. Hesse, *Helv. Chim. Acta* **1992**, *75*, 1834–1839.

[6] Syntheses of (*R*)-(+)-**1**: a) K. Utimoto, S. Kato, M. Tanaka, Y. Hoshino, S. Fujikura, H. Nozaki, *Heterocycles* **1982**, *18*, 149–152; b) H. Hagiwara, T. Katsumi, V. P. Kamat, T. Hoshi, T. Suzuki, M. Ando, *J. Org. Chem.* **2000**, *65*, 7231–7234.

[7] Syntheses of muscopyridine isomers: a) U. K. Georgi, J. Rétey, *Chem. Commun.* **1971**, 32–33; b) A. T. Balaban, M. Gavat, C. D. Nenitzescu, *Tetrahedron* **1962**, *18*, 1079–1081; c) P. Dubs, R. Stüssi, *J. Chem. Soc. Chem. Commun.* **1976**, 1021.

[8] The synthesis described by Kumada et al. that is based on a "stitching" cross-coupling reaction is seemingly one-step; this step, however, affords only 20% yield and the preparation of the aliphatic segment in racemic form requires four additional steps, the yields of which were not specified (see footnote 10 in ref. [5b]).

[9] a) A. Fürstner, A. Leitner, *Angew. Chem.* **2002**, *114*, 632–635; *Angew. Chem. Int. Ed.* **2002**, *41*, 609–612; b) A. Fürstner, A. Leitner, M. Méndez, H. Krause, *J. Am. Chem. Soc.* **2002**, *124*, 13856–13863.

[10] For related iron-catalyzed cross-coupling reactions with alkenyl halides see, for example: a) M. Tamura, J. K. Kochi, *J. Am. Chem. Soc.* **1971**, *93*, 1487–1489; b) G. Cahiez, H. Avedissian, *Synthesis* **1998**, 1199–1205, and references therein.

[11] M. El Hadrami, J.-P. Lavergne, P. Viallefont, M. Y. A. Itto, A. Hasnaoui, *Tetrahedron Lett.* **1991**, *32*, 3985–3988.

[12] Ruthenium-based metathesis catalysts are easily poisoned by amines. This problem can be circumvented by protonating the basic sites, see, for example: a) G. C. Fu, S. T. Nguyen, R. H. Grubbs, *J. Am. Chem. Soc.* **1993**, *115*, 9856–9857; b) A. Fürstner, J. Grabowski, C. W. Lehmann, *J. Org. Chem.* **1999**, *64*, 8275–8280.

[13] A. Fürstner, O. Guth, A. Düffels, G. Seidel, M. Liebl, B. Gabor, R. Mynott, *Chem. Eur. J.* **2001**, *7*, 4811–4820.

[14] For previous applications of this catalyst see: a) A. Fürstner, A. F. Hill, M. Liebl, J. D. E. T. Wilton-Ely, *Chem. Commun.* **1999**, 601–602; b) A. Fürstner, O. R. Thiel, *J. Org. Chem.* **2000**, *65*, 1738–1742; c) A. Fürstner, J. Grabowski, C. W. Lehmann, T. Kataoka, K. Nagai, *ChemBioChem* **2001**, *2*, 60–68; d) A. Fürstner, K. Radkowski, *Chem. Commun.* **2001**, 671–672; e) A. Fürstner, K. Radkowski, C. Wirtz, R. Goddard, C. W. Lehmann, R. Mynott, *J. Am. Chem. Soc.* **2002**, *124*, 7061–7069; f) A. Fürstner, F. Jeanjean, P. Razon, *Angew. Chem.* **2002**, *114*, 2203–2206; *Angew. Chem. Int. Ed.* **2002**, *41*, 2097–2101; g) A. Fürstner, M. Schlede, *Adv. Synth. Catal.* **2002**, *344*, 657–665.

[15] Reviews: a) T. M. Trnka, R. H. Grubbs, *Acc. Chem. Res.* **2001**, *34*, 18–29; b) A. Fürstner, *Angew. Chem.* **2000**, *112*, 3140–3172; *Angew. Chem. Int. Ed.* **2000**, *39*, 3012–3043; c) M. Schuster, S. Blechert, *Angew. Chem.* **1997**, *109*, 2124–2144; *Angew. Chem. Int. Ed. Engl.* **1997**, *36*, 2037–2056.

[16] For a general discussion of cyclization reactions as a function of ring size see: L. Mandolini, *Adv. Phys. Org. Chem.* **1986**, *22*, 1–111.

[17] D. Tindall, J. H. Pawlow, K. B. Wagener, *Top. Organomet. Chem.* **1998**, *1*, 183–198.

[18] In contrast, macrocyclic alkenes are *not* inert to the more active "second-generation" ruthenium catalysts. While in the present case this leads to undesirable polymerization, it is possible to use this ability to advantage: a) A. B. Smith, C. M. Adams, S. A. Kozmin, *J. Am. Chem. Soc.* **2001**, *123*, 990–991; b) A. Fürstner, O. R. Thiel, L. Ackermann, *Org. Lett.* **2001**, *3*, 449–451; c) C. W. Lee, R. H. Grubbs, *Org. Lett.* **2000**, *2*, 2145–2147; d) A. Fürstner, O. R. Thiel, N. Kindler, B. Bartkowska, *J. Org. Chem.* **2000**, *65*, 7990–7995.

[19] For previous examples of tandem RCM/hydrogenation catalysis by ruthenium–carbene complexes see: a) A. Fürstner, K. Langemann, N. Kindler Studiengesellschaft Kohle mbH, US

 © 2003 Wiley-VCH Verlag GmbH & Co. KGaA, Weinheim 1433-7851/03/4203-0310 $ 20.00+.50/0

Patent 5,936,100 **1999** (priority December 16, 1996); b) J. Louie, C. W. Bielawski, R. H. Grubbs, *J. Am. Chem. Soc.* **2001**, *123*, 11312–11313.

[20] Insertion of Mg into commercial 6-bromo-1-hexene is accompanied by partial cyclization to give (cyclopentylmethyl)magnesium bromide in addition to the desired 5-hexenylmagnesium bromide, see D. Lal, D. Griller, S. Husband, K. U. Ingold, *J. Am. Chem. Soc.* **1974**, *96*, 6355–6357. The side products resulting thereof are easily eliminated by flash chromatography and the yield of **14** refers to analytically pure product.



Gaseous Gold Dihalides

Gold Dichloride and Gold Dibromide with Gold Atoms in Three Different Oxidation States**

Detlef Schröder, Reuben Brown, Peter Schwerdtfeger, Xue-Bin Wang, Xin Yang, Lai-Sheng Wang, and Helmut Schwarz*

Dedicated to Professor Roald Hoffmann on the occasion of his 65th birthday

While the most common oxidation states of gold are 0, I, and III, gold(II) compounds are also known to exist in the condensed phase and generally contain Au–Au bonds.[1,2] However, genuine gold(II) chloride, $AuCl_2$, is not known in the condensed phase.[3] Compounds such as $CsAuCl_3$ or Au_4Cl_8 have been identified as mixed-valence species comprising Au^I and Au^{III} centers.[4,5] Further, photooxidation of $AuCl_2^-$ ions in solution gives Au^{III} directly with no indication for the presence of Au^{II} intermediates,[6] and the only report of Au^{II} in solution comes from a study by Rich and Taube in 1954 who proposed $AuCl_3^-$ as a transient in the redox reactions of Fe^{2+} and $AuCl_4^-$ ions.[7]

Herein, we report an experimental and theoretical study of gaseous gold dihalides $AuX_2^{-/0/+}$ (X = Cl, Br) bearing three different charges, that is, the AuX_2^- ions (formally containing gold(I)), neutral AuX_2 species (formally gold(II)), and the corresponding AuX_2^+ ions (formally gold(III)), provided that the latter species can still be described as ionized gold dihalides (see below).

To this end, two complementary experimental techniques are combined: photoelectron spectroscopy (PES)[8] and sector-field mass spectrometry using charge-reversal (CR) and neutralization reionization (NR) techniques in conjunction with the related neutral-and-ion decomposition difference (NIDD) method.[9,10] Both types of experiments start from the corresponding mass-selected AuX_2^- ions as precursors. In the PES study, the AuX_2^- ions (X = Cl, Br, I) are generated by electrospray ionization of diluted AuX solutions in water/methanol.[11] In the sector experiments,[12,13] fast-atom bombardment (FAB) of aqueous slurries of AuX_3 is used to generate AuX_2^- ions; this method does not work for X = I, because reduction of AuI_3 to metallic gold occurs upon contact of the metallic probe tip with the sample. Likewise, no gold-fluoride ions could be generated by FAB of an AuF_3 slurry, because of the rapid hydrolysis of gold fluorides.

The photodetachment spectra of AuX_2^- ions (X = Cl, Br, I) indicate substantial electron affinities for the corresponding neutral species (Figure 1). Thus, the vertical detachment energies amount to $VDE(AuCl_2^-) = 4.74 \pm 0.05$ eV, $VDE(AuBr_2^-) = 4.61 \pm 0.05$ eV, and $VDE(AuI_2^-) = 4.28 \pm 0.05$ eV. Adiabatic detachment energies, that is, the electron affinities (EAs) of the corresponding neutral species, can be estimated by linear extrapolation of the onsets of the first features to the baseline. This analysis leads to the values $EA(AuCl_2) = 4.60 \pm 0.07$ eV, $EA(AuBr_2) = 4.46 \pm 0.07$ eV, and $EA(AuI_2) = 4.18 \pm 0.07$ eV. The relatively small differences (≤ 0.15 eV) between the vertical and adiabatic transitions indicate similar geometries for the anionic and neutral $AuX_2^{-/0}$ species. Further, the PE spectra show several bands at higher energy which are assigned to the formation of electronically excited states in neutral AuX_2; these features will be analyzed in a forthcoming article. Here, we focus on the ground-state properties of the $AuX_2^{-/0/+}$ systems and in particular for X = Cl.

Upon collisional activation of mass-selected $AuCl_2^-$ ions in the sector-field experiments, only the $AuCl^-$ ion is detected as an anionic fragment. If the analyzer is switched to positive ions, the corresponding CR spectrum (Figure 2a) is dominated by the $AuCl^+$ fragment (100%) along with a significant recovery signal for $AuCl_2^+$ as well as the atomic Au^+ ion; a weak signal from the Cl^+ ion is detected at highest sensitivity (< 1%, not visible in Figure 2a). The NR spectrum of the $AuCl_2^-$ ion is also dominated by $AuCl_n^+$ ions ($n = 0$–2), but the relative yield of $AuCl^+$ is reduced significantly (Figure 2b).[14]

[*] Dr. D. Schröder, Prof. Dr. H. Schwarz
Institut für Chemie
Technische Universität Berlin
Strasse des 17. Juni 135, 10623 Berlin (Germany)
Fax: (+49) 30-314-21102
E-mail: df@www.chem.tu-berlin.de
Dr. R. Brown, Prof. Dr. P. Schwerdtfeger, Dr. X. B. Wang
Department of Chemistry
University of Auckland
Private Bag 92019, Auckland (New Zealand)
Dr. X. Yang, Prof. Dr. L. S. Wang
Department of Physics
Washington State University
2710 University Drive, Richland, WA 99352 (USA) and
W. R. Wiley Environmental Molecular Science Laboratory
Pacific Northwest National Laboratory
P. O. Box 999, Richland, WA 99352 (USA)

[**] This work was supported by the Deutsche Forschungsgemeinschaft, the Fonds der Chemischen Industrie, the US National Science Foundation, and the Royal Society of New Zealand (Marsden scheme). The work in Washington was performed at the W. R. Wiley Environmental Molecular Science Laboratory, a national scientific user facility sponsored by Department of Energy's Office of Biological and Environmental Research which is operated for the US Department of Energy by Batelle. The Berlin group thanks the DEGUSSA AG for a gift of gold(III) halides. R.B. thanks the Alexander von Humboldt Stiftung (Bonn) for a research fellowship.

 © 2003 Wiley-VCH Verlag GmbH & Co. KGaA, Weinheim 1433-7851/03/4203-0311 $ 20.00+.50/0

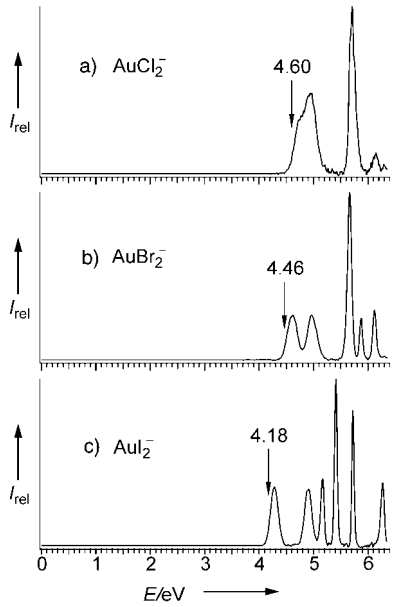


Figure 1. Photoelectron spectra of a) $AuCl_2^-$, b) $AuBr_2^-$, and c) AuI_2^- ions at 193 nm (6.424 eV). The derived adiabatic electron affinities of AuX_2 (X = Cl, Br, I) are indicated by the vertical arrows.

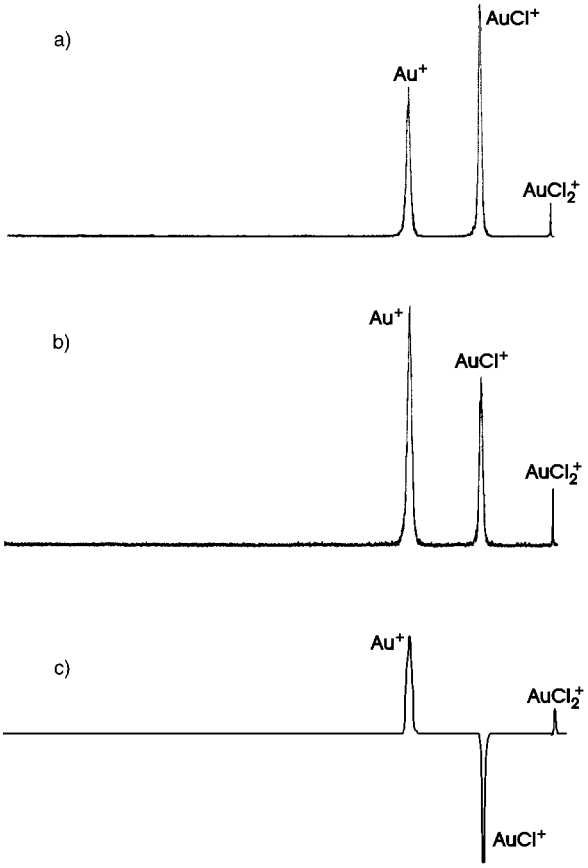


Figure 2. a) CR, b) NR, and c) NIDD mass spectra of mass-selected $AuCl_2^-$ ions generated by FAB of an aqueous slurry of gold(III) chloride.

This qualitative difference between the CR and NR spectra indicates a notable difference between the more-or-less simultaneous detachment of two electrons in CR ($AuCl_2^- \rightarrow AuCl_2^+$) and the stepwise sequence of two single-electron detachments in NR (first $AuCl_2^- \rightarrow AuCl_2$, then $AuCl_2 \rightarrow AuCl_2^+$). The NIDD scheme[10,15] allows for a quantification of the differential fragmentation behavior of $AuCl_2^-$ upon CR and NR. In the NIDD spectrum of $AuCl_2^-$ ions, the recovery signal and that of the Au^+ ions both appear on the positive scale, whereas the $AuCl^+$ fragment gives rise to a negative signal (Figure 2c).

These mass spectrometric results have the following implications. At first, the observation of an NR recovery signal demonstrates the existence of a transient neutral $AuCl_2$ species with a lifetime of at least several microseconds, that is, the time of flight between the two collision events. Next, the appearance of a recovery signal on the positive scale of the NIDD spectrum suggests that stepwise electron transfer in NR with intermediate relaxation of the neutral is associated with more favorable Franck–Condon factors than the direct CR of the anion. Likewise, the reversal of the $AuCl^+/Au^+$ ratios in CR and NR experiments suggests substantial differences of the potential-energy surfaces of anionic, neutral, and cationic $AuCl_2^{-/0/+}$ species. Furthermore, energy-resolved CR and NR measurements[16] permit the determination of the energy balances of the associated redox transitions as $\Delta E_{CR} = 16.5 \pm 1.0$ eV and $\Delta E_{NR} = 16.0 \pm 1.0$ eV, respectively.[17] To a first approximation, these energy differences correspond to those associated with the related vertical electron-transfer processes, that is, $AuCl_2^- \rightarrow AuCl_2^+$ in CR and first $AuCl_2^- \rightarrow AuCl_2$ then $AuCl_2 \rightarrow AuCl_2^+$ in NR.

For a more detailed analysis of the experimental results, the $AuCl_2^{-/0/+}$ system was studied theoretically using a scalar relativistic coupled-cluster approach (CCSD(T)).[18–21] At this level of theory, the $AuCl_2^-$ ion is predicted to have a singlet ground state ($^1\Sigma_g^+$) with a bond length of $r_{AuCl} = 2.29$ Å and an angle of $\alpha_{ClAuCl} = 180°$ in good agreement with previous results.[22] Likewise, a linear geometry is found for the neutral $AuCl_2$ species ($^2\prod_g$, $r_{AuCl} = 2.25$ Å). The minor change in bond length ($\Delta r_{AuCl} = 0.04$ Å) is consistent with the similarity of the vertical and adiabatic detachment energies of $AuCl_2^-$ ions in the PE spectra (see above). Note, however, that the Cl-Au-Cl bending potential is significantly softer for the neutral species than for the anion (Figure 3). Finally, the adiabatic and vertical detachment energies of the $AuCl_2^-$ ion are

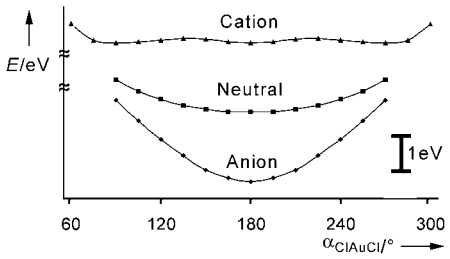


Figure 3. Schematic bending potentials of α_{ClAuCl} in $AuCl_2^-$, $AuCl_2$, and $AuCl_2^+$ according to CCSD(T) calculations. To display the variations on a reasonable scale, the linear minima of the curves are deliberately fixed for a distance of 2 eV for each charge state.

 © 2003 Wiley-VCH Verlag GmbH & Co. KGaA, Weinheim 1433-7851/03/4203-0312 $ 20.00+.50/0

calculated to be 4.77 and 4.85 eV, respectively, which is in good agreement with the experimental data.

A much more complicated situation evolves for the cationic species. For this triatomic AB_2 system, there are no less than three different low-lying minima on the singlet surface. A linear $AuCl_2^+$ ion ($^1\Pi_g$) with $r_{AuCl} = 2.21$ Å, a bent ($\alpha_{ClAuCl} = 94°$), but otherwise similar $AuCl_2^+$ structure ($^1B_1$, C_{2v}) with $r_{AuCl} = 2.24$ Å, and a bent ion having a different connectivity of the atoms and C_s symmetry, that is, $Au(Cl_2)^+$ ($^1A_1$) with $r_{AuCl} = 2.45$ Å, $r_{ClCl} = 2.06$ Å, and $\alpha_{ClAuCl} = 35°$ (this corresponds to $\alpha_{AuClCl} = 102°$). In terms of bonding schemes, the two former isomers can be viewed as gold dichlorides with a formal gold(III) center, whereas the third isomer is best described as an ion/neutral complex of atomic Au^+ and molecular chlorine.[23] At the CCSD(T) level of theory, these three isomers are 0.72, 0.72, and 1.00 eV lower in energy than the corresponding dissociation asymptote $Au^+ + Cl_2$.[24] The energetic proximity of the linear and bent $AuCl_2^+$ isomers has an analogy in the T-shaped structure of neutral $AuCl_3$ and the square-planar coordination in the corresponding dimer Au_2Cl_6.[25,26] Further, a bond strength of about 1 eV for the end-on complex of Au^+ with molecular chlorine is fully consistent with data for the ligation of gold(I) in the gas phase.[27] For the linear isomer $AuCl_2^+$ ($^1\Pi_g$), the adiabatic and vertical ionization energies are computed as 10.71 and 10.79 eV, respectively (15.55 eV in total for the vertical transition $AuCl_2^- \rightarrow AuCl_2^+$).

The computed potential-energy surfaces of $AuCl_2^{-/0/+}$ (Figure 3 and 4) nicely account for the experimental findings. Thus, vertical charge reversal of the anion leads to the gold(III) dichloride cation $AuCl_2^+$ from which atomic chlorine is lost upon consecutive fragmentation in the high-energy collision event. In contrast, neutralization of the anion provides access to the neutral species having a much flatter Cl-Au-Cl bending potential. Upon reionization of neutral $AuCl_2$, the bent $AuCl_2^+$ ion and in particular the more stable $Au(Cl_2)^+$ isomer can be formed, thereby accounting for the positive NIDD signal of the recovery ion. In addition, the structural reorganization associated with bending increases the probability of access to the low-lying $Au^+ + Cl_2$ dissociation asymptote in the NR experiment, thereby accounting for the positive NIDD signal for the Au^+ fragment. It is instructive to consider the computed Au–Cl dissociation energies (D_0) of the linear $AuCl_2^{-/0/+}$ species as a function of charge. The calculated values are, $D_0(ClAu-Cl^-) = 3.45$ eV for the anion, $D_0(ClAu-Cl) = 2.15$ eV for the neutral, and $D_0(ClAu^+-Cl) = 2.10$ eV for the cation indicate that all three species can be termed as being covalently bound metal halides. Accordingly, gaseous gold dichloride can exist in three different oxidation states.[23]

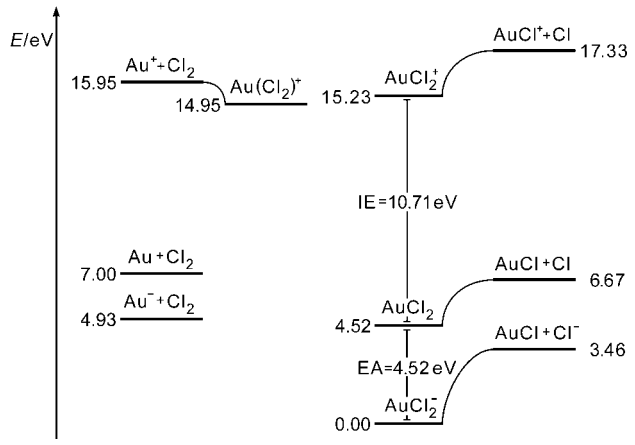


Figure 4. Redox profile of $AuCl_2^-$, $AuCl_2$, and $AuCl_2^+$ according to CCSD(T) calculations (energies [eV] relative to the anion). For the sake of clarity, the bent minimum of $AuCl_2^+$ is omitted (see text).

A comparable situation seems to occur in the $AuBr_2^{-/0/+}$ system. Thus, the PE detachment energies are similar to those of the dichloride, and the $AuBr_n^+$ fragments ($n = 0$–2) detected by CR and NR of mass-selected $AuBr_2^-$ ions (intensities in CR/NR, respectively: $AuBr_2^+$: 25/55, $AuBr^+$: 100/100, Au^+: 25/45) lead to positive NIDD signals for the $AuBr_2^+$ recovery ion as well as atomic Au^+ ion, whereas that of the $AuBr^+$ ion is negative. Preliminary theoretical calculations of the linear $AuBr_2^{-/0/+}$ isomers indicate a situation quite similar to that of $AuCl_2^{-/0/+}$.

In summary, mass spectrometric experiments demonstrate that the gold dihalides AuX_2 (X = Cl, Br) can adopt three different oxidation states, all giving rise to long-lived triatomic species in the gas phase. As far as the stability of gold(II) halides in the condensed phase is concerned, the combination of the calculated enthalpy of bonding $\Delta_f H(AuCl_2) = 30$ kcal mol^{-1}[28] as predicted by theory with $\Delta_f H(AuCl) = 50$ kcal mol^{-1}[30] and $\Delta_f H(AuCl_3) = 48$ kcal mol^{-1}[31] suggests that disproportionation of neutral gold(II) dichloride according to reaction in Equation (1) is endothermic by 38 kcal mol^{-1}.[32]

$$2\,AuCl_2 \rightarrow AuCl + AuCl_3 \qquad (1)$$

Thus, whereas $AuCl_2$ is stable against disproportionation in the idealized gas phase, it is likely to exist as $Au^+[AuCl_4]^-$ in the condensed phase. The preparation of bulk gold(II) compounds therefore requires an appropriate ligand environment to prevent disproportionation. An excellent example for such a stabilization of a gold(II) compound by ligation is the $AuXe_4^{2+}(Sb_2F_{11})_2^-$ salt recently characterized by Seidel and Seppelt.[33,34]

Received: October 21, 2002 [Z50405]

[1] R. J. Puddephatt, *The Chemistry of Gold*, Elsevier, Amsterdam, **1978**.
[2] See also: W. Grochala, R. Hoffmann, *Angew. Chem.* **2001**, *113*, 2817; *Angew. Chem. Int. Ed.* **2001**, *40*, 2742.
[3] *Gmelin Handbook of Inorganic and Organometallic Chemistry, Au, Suppl. B1*, **1992**, p. 189.
[4] N. Elliot, L. Pauling, *J. Am. Chem. Soc.* **1938**, *60*, 1846.
[5] D. Belli Dell'Amico, F. Calderazzo, F. Marchetti, S. Merlino, G. Perego, *J. Chem. Soc. Chem. Commun.* **1977**, 31, and references therein.
[6] H. Kunkely, A. Vogler, *Inorg. Chem.* **1992**, *31*, 4539.
[7] R. L. Rich, H. Taube, *J. Phys. Chem.* **1954**, *58*, 6.
[8] L. S. Wang, C. F. Ding, X. B. Wang, S. E. Barlow, *Rev. Sci. Instrum.* **1999**, *70*, 1957.
[9] N. Goldberg, H. Schwarz, *Acc. Chem. Res.* **1994**, *27*, 347.

[10] a) C. A. Schalley, G. Hornung, D. Schröder, H. Schwarz, *Chem. Soc. Rev.* **1998**, *27*, 91; b) C. A. Schalley, G. Hornung, D. Schröder, H. Schwarz, *Int. J. Mass Spectrom. Ion Processes* **1998**, *172*, 181.

[11] The PES apparatus includes a magnetic-bottle time-of-flight photoelectron analyzer and an electrospray ion source as described elsewhere.[8] In brief, 10^{-3} molar solutions of AuX in water/methanol (1/9; pH ~ 7) were sprayed through a 0.01 mm diameter syringe needle at ambient atmosphere and a potential of −2.2 kV. Negatively charged ions emerging from the source were guided by an rf-only quadrupole into an ion trap, where the ions were accumulated for 0.1 s before being pushed into the extraction zone of a time-of-flight mass spectrometer. The major anions were AuX_2^- and AuX_4^-. In the PES experiments, the anions of interest were mass-selected, decelerated, and intercepted by a 193 nm laser beam in the detachment zone of the magnetic-bottle photoelectron analyzer. The photoelectrons were collected near 100% efficiency and analyzed in a four-meter long time-of-flight tube. Photoelectron time-of-flight spectra were then converted into kinetic energy spectra and calibrated against the known spectra of O^- and I^- ions.

[12] The experiments were performed with a modified VG ZAB/HF/AMD 604 four-sector mass spectrometer of BEBE configuration (B stands for magnetic and E for electric sectors).[13] The ions of interest were generated by FAB (Xe, 8–10 kV) of aqueous slurries of AuX_3 in the negative-ion mode. The ions having a kinetic energy of 8 keV were mass-selected using B(1) and the respective mass spectra were recorded by scanning E(1). For collisional activation, helium was used as the collision gas at 80% transmission (T). In the CR and NR experiments,[9,10] oxygen was used throughout as the collision gas (80% T).

[13] C. A. Schalley, D. Schröder, H. Schwarz, *Int. J. Mass Spectrom. Ion Processes* **1996**, *153*, 173.

[14] The absolute ratio of the survivor signals in CR and NR is approximately 4:1.

[15] The NIDD intensities are derived from the NR and CR spectra using the following formula: $I_{i,NIDD} = I_{i,NR}/\Sigma I_{i,NR} - I_{i,CR}/\Sigma I_{i,CR}$; for further details, see ref. [10b].

[16] a) D. Schröder, S. Bärsch, H. Schwarz, *Int. J. Mass Spectrom.* **1999**, *192*, 125; b) D. Schröder, H. Schwarz, *Int. J. Mass Spectrom.*, in press.

[17] Note that the majority of the experimental error arises from uncertainties in the calibration of the kinetic energy scale.[16] The experimental difference of ΔE_{CR} and ΔE_{NR} is 0.5 ± 0.3 eV.

[18] The calculations were performed using the Gaussian 98 program[19] at the CCSD(T) level. For gold, an adjusted valence basis set together with a small-core scalar relativistic pseudopotential was used which consists of a $[Kr]4d^{10}4f^{14}$ core ($5s^25p^65d^{10}6s^1$ valence space).[20] For the halogen atoms, augmented, correlation-consistent, double-ζ basis sets were employed. Some initial CCSD(T) geometry optimizations were performed with single-ζ basis sets and were then repeated with the larger aug-cc-pVDZ basis set; at this level only partial re-optimization of the geometries was performed.

[19] Gaussian 98 (Revision A.7), M. J. Frisch, G. W. Trucks, H. B. Schlegel, G. E. Scuseria, M. A. Robb, J. R. Cheeseman, V. G. Zakrzewski, J. A. Montgomery, R. E. Stratmann, J. C. Burant, S. Dapprich, J. M. Millam, A. D. Daniels, K. N. Kudin, M. C. Strain, O. Farkas, J. Tomasi, V. Barone, M. Cossi, R. Cammi, B. Mennucci, C. Pomelli, C. Adamo, S. Clifford, J. Ochterski, G. A. Petersson, P. Y. Ayala, Q. Cui, K. Morokuma, D. K. Malick, A. D. Rabuck, K. Raghavachari, J. B. Foresman, J. Cioslowski, J. V. Ortiz, B. B. Stefanov, G. Liu, A. Liashenko, P. Piskorz, I. Komaromi, R. Gomperts, R. L. Martin, D. J. Fox, T. Keith, M. A. Al-Laham, C. Y. Peng, A. Nanayakkara, C. Gonzalez, M. Challacombe, P. M. W. Gill, B. G. Johnson, W. Chen, M. W. Wong, J. L. Andres, M. Head-Gordon, E. S. Replogle, J. A. Pople, Gaussian, Inc., Pittsburgh, PA, **1998**.

[20] P. Schwerdtfeger, M. Dolg, W. H. E. Schwarz, G. A. Bowmaker, P. D. W. Boyd, *J. Chem. Phys.* **1989**, *91*, 1762.

[21] For a similar approach, see: J. R. Brown, P. Schwerdtfeger, D. Schröder, H. Schwarz, *J. Am. Soc. Mass Spectrom.* **2002**, *13*, 485.

[22] P. Schwerdtfeger, P. D. W. Boyd, A. K. Burrell, W. T. Robinson, M. J. Taylor, *Inorg. Chem.* **1990**, *29*, 3593.

[23] These bonding schemes are fully consistent with Mulliken population analysis of the partial charges: $AuCl_2^-$, $q_{Au} = 0.44$, $q_{Cl} = -0.72$; $AuCl_2^0$, $q_{Au} = 0.80$, $q_{Cl} = -0.40$; $AuCl_2^+$ ($^1\Pi_g$), $q_{Au} = 1.02$, $q_{Cl} = -0.01$; $AuCl_2^+$ ($^1B_1$), $q_{Au} = 1.09$, $q_{Cl} = -0.045$; $Au(Cl_2)^+$ ($^1A_1$), $q_{Au} = 0.85$, $q_{Cl(1)} = -0.01$, $q_{Cl(2)} = 0.16$.

[24] We note that the relative energies of the three cationic isomers, differed significantly between single- and double-ζ basis sets. As also the double-ζ basis is far from being complete and spin-orbit effects are neglected, the energy order of the $[AuCl_2]^+$ isomers should accordingly be viewed as a first approximation.

[25] P. Schwerdtfeger, P. D. W. Boyd, S. Brienne, A. K. Burrell, *Inorg. Chem.* **1992**, *31*, 3411.

[26] M. Hargittai, A. Schulz, B. Reffy, M. Kolonits, *J. Am. Chem. Soc.* **2001**, *123*, 1449.

[27] D. Schröder, H. Schwarz, J. Hrušák, P. Pyykkö, *Inorg. Chem.* **1998**, *37*, 624.

[28] Calculated for 0 K using the enthalpy of the reaction $AuCl_2 \rightarrow Au + Cl_2$ computed here as 57.3 kcal mol^{-1} in conjunction with $\Delta_f H(Au) = 87.5$ kcal mol^{-1} and $\Delta_f H(Cl_2) = 0$ kcal mol^{-1} taken from ref. [29].

[29] S. G. Lias, J. E. Bartmess, J. F. Liebman, J. L. Holmes, R. D. Levin, W. G. Mallard, *J. Phys. Chem. Ref. Data Suppl. 1* **1988**, *17*.

[30] Calculated for 0 K using the values $\Delta_f H(Au) = 87.5$ kcal mol^{-1}, $\Delta_f H(Cl) = 28.6$ kcal mol^{-1}, and $D_0(Au-Cl) = 66$ kcal mol^{-1} taken from refs. [21] and [29].

[31] Calculated for 0 K using $\Delta_f H(Au_2Cl_6) = 47$ kcal mol^{-1} and the computational prediction of $D_0(Cl_3Au-AuCl_3) = 48.4$ kcal mol^{-1} taken from: a) D. D. Wagman, W. H. Evans, V. B. Parker, R. H. Schumm, I. Halow, S. M. Bailey, K. L. Churney, R. L. Nuttal, *J. Phys. Chem. Ref. Data Suppl. 1* **1982**, *11*; b) ref. [25].

[32] The directly calculated B3LYP value is 24 kcal mol^{-1}, see: R. Brown, Ph.D. Thesis, University of Auckland, New Zealand, **2001**.

[33] S. Seidel, K. Seppelt, *Science* **2000**, *290*, 117.

[34] See also: T. Drews, S. Seidel, K. Seppelt, *Angew. Chem.* **2002**, *114*, 470; *Angew. Chem. Int. Ed.* **2002**, *41*, 454.

 © 2003 Wiley-VCH Verlag GmbH & Co. KGaA, Weinheim 1433-7851/03/4203-0314 $ 20.00+.50/0

Amplification of Chirality

Amplification of Chirality from Extremely Low to Greater than 99.5% *ee* by Asymmetric Autocatalysis**

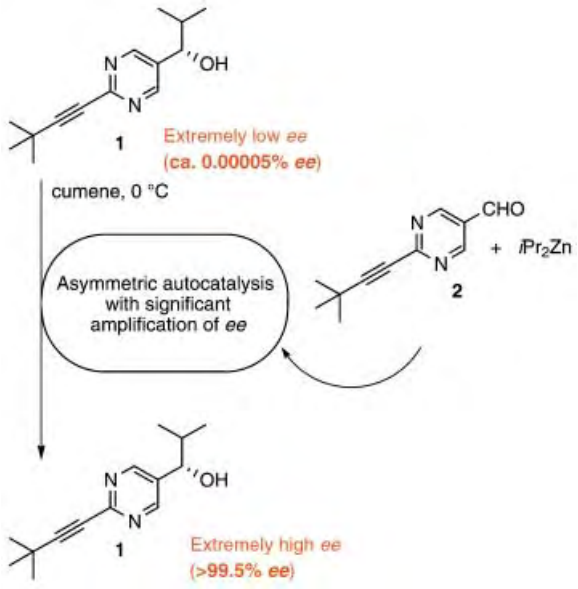
*Itaru Sato, Hiroki Urabe, Saori Ishiguro, Takanori Shibata, and Kenso Soai**

Biomolecules such as amino acids and sugars occur in Nature overwhelmingly as L and D enantiomers, respectively. The origins of chirality and the processes leading to high enantiomeric enrichment of organic compounds have been intriguing puzzles.[1] Several factors have been proposed as the origins of chirality of organic molecules.[2] However, the enantiomeric excesses (*ee*) of organic compounds induced by these factors have usually been very low (from 10^{-4} to < 2% *ee*). Circularly polarized light (CPL) induces very low selectivity (< 2% *ee*) in asymmetric photosynthesis,[2a,b] photoisomerization,[2c] photoequilibration,[2d,e] and photolysis.[2f,g] Asymmetric adsorption on and desorption from chiral surfaces induce a tiny imbalance (< 2% *ee*) in enantiomers.[2h–k] These very low levels of enantiomeric excess require an efficient method of amplification in order to explain the very high enantiomeric enrichment of organic compounds. A tiny imbalance in the enantiomeric composition of a sterically encumbered olefin induces the twist of a nematic phase into a cholesteric phase in liquid crystals.[2d] The positive nonlinear effect of asymmetric catalysis, discovered by Kagan et al.,[3a] explains how a product can have a higher *ee* than the chiral catalyst required for its production.[3] However, the selectivity of the reaction remains low to moderate when the chirality level of the asymmetric catalyst employed is low. For example, the product was produced with only 36% *ee* when a catalyst with 3% *ee* was used.[3b] On the other hand, we reported asymmetric autocatalysis in which the chiral product acts as a chiral catalyst for its own production.[4] The chirality level of the initial catalyst with 0.3–2% *ee* was enhanced to 87–88% *ee*.[5] However, considering the much lower levels of chirality induced by a physical factor,[2l] it is a challenge to develop a method for "amplifying chirality" starting from extremely small enantiomeric imbalances to give practically enantiomerically pure product.

Herein we report efficient chirality amplification by a catalyst with as low as 10^{-5}% *ee* to give practically enantiomerically pure (> 99.5% *ee*) product in only three consecutive cycles. The product formed in situ with enhanced *ee* serves as an asymmetric autocatalyst for the further formation of itself with much higher *ee*.

The initial asymmetric autocatalysts with very low levels of chirality were prepared carefully by adding calculated amounts of standardized solutions of (*S*)- and (*R*)-(2-alkynyl-5-pyrimidyl)alkanol **1** (> 99.5% *ee*)[6] to racemic **1** (Scheme 1).[7] The enantiomeric enrichment of these two solutions was roughly 0.00005% *ee* (i.e. enantiomeric ratio of ca. 50.000025:49.999975).[8] We found that the first asymmetric autocatalysis with (*S*)-**1** of approximately 0.00005% *ee* in the enantioselective addition of diisopropylzinc[9] to 2-alkynylpyrimidine-5-carbaldehyde **2** gave (*S*)-**1** in 96% yield with an enhanced selectivity of 57% *ee* (Table 1, run 1). To take advantage of asymmetric autocatalysis, the (*S*)-**1** obtained was used as an asymmetric autocatalyst for the next reaction (run 2). Indeed, by adding pyrimidine-5-carbaldehyde **2** slowly over a period of 1.5 h to the mixture of asymmetric autocatalyst **1** and iPr$_2$Zn, the *ee* of the pyrimidylalkanol **1** obtained increased to 99% and the yield was 96%. By the third cycle of asymmetric autocatalysis, the chirality level of pyrimidylalkanol reached > 99.5% *ee* (run 3). On the other hand, asymmetric autocatalysis starting with (*R*)-**1** with ca. 0.00005% *ee* instead of (*S*)-**1** produced (*R*)-**1** with 45% *ee* (run 4). The next reaction with this as the asymmetric autocatalyst and a slow addition of aldehyde **2** further enhanced the enantiomeric enrichment of (*R*)-**1** to 95% *ee* (run 5). Finally, the third reaction afforded practically enantiomerically pure (*R*)-**1** with > 99.5% *ee* (run 6).

As shown here, extremely tiny enantiomeric imbalances in the catalyst **1** on the order of 10^{-5}% *ee* with *S* and *R* configurations were effectively amplified to > 99.5% *ee* with



Scheme 1. Alkylation of **2** catalyzed by and yielding (2-alkynyl-5-pyrimidyl)alkanol **1**.

[*] Prof. Dr. K. Soai, Dr. I. Sato, H. Urabe, S. Ishiguro, Dr. T. Shibata
Department of Applied Chemistry, Faculty of Science
Tokyo University of Science
Kagurazaka, Shinjuku-ku, Tokyo 162-8601 (Japan)
Fax: (+81) 3-3235-2214
E-mail: soai@rs.kagu.tus.ac.jp

[**] This work was supported in part by Japan Space Forum, New Energy and Development Organization (NEDO), and a Grant-in-Aid for Scientific Research from the Ministry of Education, Sports, Culture, Science and Technology. This research was presented at the 81st Annual Meeting of The Chemical Society of Japan: H. Urabe, S. Ishiguro, I. Sato, K. Soai, Abstract 4GZ-16, March 2002, Tokyo.

Supporting information for this article is available on the WWW under http://www.angewandte.org or from the author.

 © 2003 Wiley-VCH Verlag GmbH & Co. KGaA, Weinheim 1433-7851/03/4203-0315 $ 20.00+.50/0

Table 1: Amplification of chirality from extremely low levels to >99.5% *ee* by asymmetric autocatalysis.

Run[a]	Set[b]	Initial autocat. **1** *ee* [%]	Config.	Initial and newly formed **1** *ee* [%][c]	Config.	Newly formed **1** Yield [%]
1[d]	A	ca. 0.00005	*S*	57	*S*	96
2[e]		57	*S*	99	*S*	96
3[e]		99	*S*	>99.5	*S*	90
4[d]	A	ca. 0.00005	*R*	45	*R*	96
5[e]		45	*R*	95	*R*	96
6[e]		95	*R*	>99.5	*R*	92
7[f]	B	ca. 0.005	*S*	86	*S*	99
8[f]	B	ca. 0.005	*R*	82	*R*	98
9[f]	C	ca. 0.0005	*S*	76	*S*	95
10[f]	C	ca. 0.0005	*R*	71	*R*	98

[a] All reactions were reproducible. Although very slight enantioselectivity was observed in the initially formed products in runs 1, 4, and 7–10, further asymmetric autocatalysis enhanced in all cases the chirality level of **1** to >99.5% *ee*. [b] The pair of *S* and *R* asymmetric autocatalysts indicated in one set were prepared by the addition of a certain amount of (*S*)- and (*R*)-**1**, respectively, to a racemic mixture. See refs. [7] and [8]. [c] Determined by HPLC analysis with a chiral stationary phase (Chiralcel OD). [d] Reactions were carried out in cumene at 0°C. Molar ratio asymmetric autocatalyst **1**:aldehyde **2**:iPr$_2$Zn = 0.008:1:2. Aldehyde and iPr$_2$Zn were added in four portions. See Experimental Section. [e] Aldehyde **2** and iPr$_2$Zn were added slowly over a period of 1.5 h with a microfeeder. Molar ratio asymmetric autocatalyst **1**:aldehyde **2**:iPr$_2$Zn = 0.02:1:1.5. [f] Molar ratio asymmetric autocatalyst **1**:aldehyde **2**:iPr$_2$Zn = 0.01:1:2. Aldehyde and iPr$_2$Zn were added in three portions.

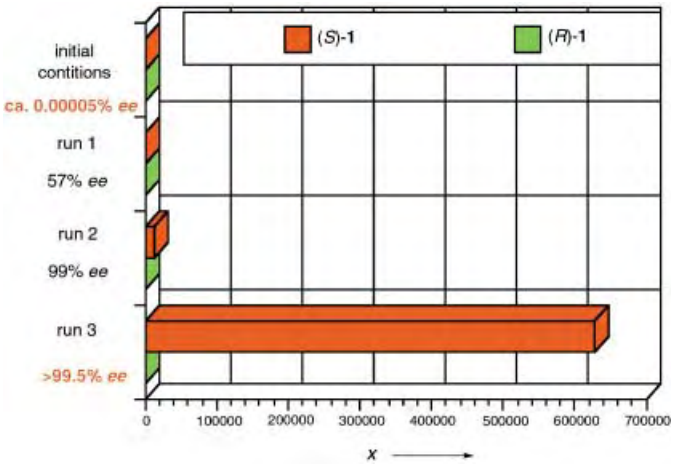


Figure 1. Plot showing the increase in the amount of *S* and *R* isomers by the factor *x* during consecutive asymmetric autocatalyses (Table 1, runs 1–3).

S and *R* configurations, respectively, in the product **1** by three consecutive cycles of asymmetric autocatalysis.[10] As shown in Figure 1, the very slightly major *S* enantiomer in the initial (*S*)-**1** with ca. 0.00005% *ee* has automultiplied by a factor of ca. 630000 after the three consecutive asymmetric autocatalyses (runs 1–3), whereas the very slightly minor enantiomer (*S*)-**1** has automultiplied by a factor of only ca. 950.

We also examined asymmetric autocatalysis using catalysts **1** with 10^{-3}–10^{-4}% *ee*. As expected, (*S*)- and (*R*)-**1** with increased *ee* were formed with (*S*)- and (*R*)-asymmetric autocatalysts **1**, respectively (runs 7–10). It should be mentioned that the subsequent asymmetric autocatalysis with the product **1** as asymmetric autocatalyst amplified the chirality level to >99.5% *ee*.[11,12]

In summary, we have demonstrated that 2-alkynylpyrimidylalkanol with a chirality level of only 10^{-5}% *ee* with *S* and *R* configurations automultiplies with significant amplification of chirality in the addition of iPr$_2$Zn to 2-alkynylpyrimidine-5-carbaldehyde, producing itself with the corresponding configurations in almost enantiomerically pure form. We believe that this reaction provides an efficient method to correlate extremely low levels of chirality induced by factors[13] related to the origin of chirality to very high levels of chirality of organic compounds.

Experimental Section

Typical experimental procedure for asymmetric autocatalysis using alkanol **1** with about 0.00005% *ee* (run 1): A solution of iPr$_2$Zn (0.1 mL of a 1.0 M solution in cumene, 0.1 mmol) was added at 0°C to a solution of (*S*)-**1** (1.3 mL of a 9.9×10^{-3} M solution in cumene, 2.9 mg, 0.013 mmol) with ca. 0.00005% *ee*, and the mixture was stirred for 15 min. A solution of aldehyde **2** (9.4 mg, 0.05 mmol) in cumene (1 mL) was then added over a period of 30 min, and the mixture was stirred for 1.5 h at 0°C. Cumene (1.3 mL), iPr$_2$Zn (0.3 mmol, 0.3 mL of a 1.0 M solution in cumene), and a solution of aldehyde **2** (28.2 mg, 0.15 mmol) in cumene (1.5 mL) were added successively, and the reaction mixture was stirred for 1 h. Then cumene (2.6 mL), iPr$_2$Zn (0.9 mmol, 0.9 mL of 1.0 M solution in cumene), and a solution of aldehyde **2** (84.6 mg, 0.45 mmol) in cumene (3.0 mL) were added successively, and the mixture was stirred at 0°C for another 1 h. After the addition of cumene (9.3 mL), iPr$_2$Zn (1.8 mmol, 1.8 mL of a 1.0 M solution in toluene) and a solution of aldehyde **2** (169 mg, 0.90 mmol) in cumene (5.0 mL), the mixture was stirred for 18 h. The reaction was quenched with hydrochloric acid (1.0 M, 4 mL), and saturated aqueous sodium hydrogencarbonate (13 mL) was then added. The mixture was filtered through Celite, and the filtrate was extracted with ethyl acetate. The combined organic layers were dried over anhydrous sodium sulfate, and concentrated under reduced pressure. Purification of the residue by silica gel chromatography (eluent, hexane:ethyl acetate = 3:1 *v*/*v*) gave (*S*)-pyrimidyl alkanol **1** with 57% *ee* (348 mg). The yield of the newly formed **1** was 96%.

Received: August 21, 2002 [Z50015]

[1] a) A. Eschenmoser, *Science* **1999**, *284*, 2118–2124; b) B. L. Feringa, R. A. van Delden, *Angew. Chem.* **1999**, *111*, 3624–3645; *Angew. Chem. Int. Ed.* **1999**, *38*, 3418–3438; c) J. Podlech, *Cell. Mol. Life Sci.* **2001**, *58*, 44–60; c) W. A. Bonner, *Origins Life Evol. Biosphere* **1991**, *21*, 59–111; d) J. S. Siegel, *Chirality* **1998**, *10*, 24–27.

[2] a) A. Moradpour, J. F. Nicoud, G. Balavoine, H. B. Kagan, G. Tsoucaris, *J. Am. Chem. Soc.* **1971**, *93*, 2353–2354; b) W. J. Bernstein, M. Calvin, O. Buchardt, *J. Am. Chem. Soc.* **1972**, *94*, 494–498; c) Y. Inoue, H. Tsuneishi, T. Hakushi, K. Yagi, H. Awazu, H. Onuki, *Chem. Commun.* **1996**, 2627–2628;

 © 2003 Wiley-VCH Verlag GmbH & Co. KGaA, Weinheim 1433-7851/03/4203-0316 $ 20.00+.50/0

d) N. P. M. Huck, W. F. Jager, B. de Lange, B. L. Feringa, *Science* **1996**, *273*, 1686 – 1688; e) Y. Zhang, G. B. Schuster, *J. Org. Chem.* **1995**, *60*, 7192 – 7197; f) J. J. Flores, W. A. Bonner, G. A. Massey, *J. Am. Chem. Soc.* **1977**, *99*, 3622 – 3625; g) H. Nishino, A. Kosaka, G. A. Hembury, H. Shitomi, H. Onuki, Y. Inoue, *Org. Lett.* **2001**, *3*, 921 – 924; h) W. A. Bonner, P. R. Kavasmaneck, F. S. Martin, J. J. Flores, *Science* **1974**, *186*, 143 – 144; i) D. S. Sholl, A. Asthagiri, T. D. Power, *J. Phys. Chem. B* **2001**, *105*, 4771 – 4782; j) G. A. Attard, *J. Phys. Chem. B* **2001**, *105*, 3158 – 3167; k) R. M. Hazen, T. R. Filley, G. A. Goodfriend, *Proc. Natl. Acad. Sci. USA* **2001**, *98*, 5487 – 5490; l) G. L. J. A. Rikken, E. Raupach, *Nature* **2000**, *405*, 932 – 935.

[3] a) C. Puchot, O. Samuel, E. Duñach, S. Zhao, C. Agami, H. B. Kagan, *J. Am. Chem. Soc.* **1986**, *108*, 2353 – 2357; b) N. Oguni, Y. Matsuda, T. Kaneko, *J. Am. Chem. Soc.* **1988**, *110*, 7877 – 7878; c) M. Kitamura, S. Okada, S. Suga, R. Noyori, *J. Am. Chem. Soc.* **1989**, *111*, 4028 – 4036; d) for the nonlinear effect in asymmetric *autoinduction*, see M. Szlosek, M. Figadère, *Angew. Chem.* **2000**, *112*, 1869 – 1871; *Angew. Chem. Int. Ed.* **2000**, *39*, 1799 – 1801; reviews: e) C. Girard, H. B. Kagan, *Angew. Chem.* **1998**, *110*, 3088 – 3127; *Angew. Chem. Int. Ed.* **1998**, *37*, 2922 – 2959; f) M. Avalos, R. Babiano, P. Cintas, J. L. Jiménez, J. C. Palacios, *Tetrahedron: Asymmetry* **1997**, *8*, 2997 – 3017; g) K. Mikami, M. Terada, T. Korenaga, Y. Matsumoto, M. Ueki, R. Angelaud, *Angew. Chem.* **2000**, *112*, 3676 – 3701; *Angew. Chem. Int. Ed.* **2000**, *39*, 3532 – 3556; h) H. B. Kagan, *Adv. Synth. Catal.* **2001**, *343*, 227—233.

[4] Reviews: a) K. Soai, T. Shibata, I. Sato, *Acc. Chem. Res.* **2000**, *33*, 382 – 390; b) K. Soai, I. Sato, T. Shibata, *Chem. Rec.* **2001**, *1*, 321 – 331; c) K. Soai, I. Sato, *Chirality* **2002**, *14*, 548 – 554; d) M. Avalos, R. Babiano, P. Cintas, J. L. Jiménez, J. C. Palacios, *Chem. Commun.* **2000**, 887 – 892; e) H. Buschmann, R. Thede, D. Heller, *Angew. Chem.* **2000**, *112*, 4197 – 4199; *Angew. Chem. Int. Ed.* **2000**, *39*, 4033 – 4036; f) G. Zubay, A. Schechter, *Chemtracts* **2001**, *14*, 291 – 296; g) M. H. Todd, *Chem. Soc. Rev.* **2002**, *31*, 211 – 222; for kinetic[4h,i] and theoretical studies[4j] on asymmetric autocatalysis, see: h) I. Sato, D. Omiya, K. Tsukiyama, Y. Ogi, K. Soai, *Tetrahedron: Asymmetry* **2001**, *12*, 1965 – 1969; i) D. G. Blackmond, C. R. McMillan, S. Ramdeehul, A. Schorm, J. M. Brown, *J. Am. Chem. Soc.* **2001**, *123*, 10103 – 10104; j) P. D. Bailey, *J. Chem. Soc. Chem. Commun.* **1995**, 1797 – 1798.

[5] a) K. Soai, T. Shibata, H. Morioka, K. Choji, *Nature* **1995**, *378*, 767 – 768; b) T. Shibata, T. Hayase, J. Yamamoto, K. Soai, *Tetrahedron: Asymmetry* **1997**, *8*, 1717 – 1719.

[6] T. Shibata, S. Yonekubo, K. Soai, *Angew. Chem.* **1999**, *111*, 749 – 751; *Angew. Chem. Int. Ed.* **1999**, *38*, 659 – 661.

[7] Racemic **1** was prepared by the lithiation of 2-alkynyl-5-bromopyrimidine followed by treatment with 2-methylpropanal.

[8] Preparation of (*S*)-**1** with ca. 0.00005 % *ee*. Pyrimidyl alkanol (*S*)-**1** (1.5 mg, > 99.5 % *ee*) was dissolved in ethyl acetate (or benzene) to make a standardized solution of (*S*)-**1** (3.2×10^{-6} mol L^{-1}). The solution (50 μL) was added to a solution of racemic **1** (75.1 mg) in ethyl acetate (or benzene). Then, a part of the solution was transferred to another flask, and the removal of solvent gave (*S*)-**1** with ca. 0.00005 % *ee* (9.9 mg). Dissolution of the whole (*S*)-**1** in 4.3 mL of cumene produced a 9.9×10^{-3} M solution of (*S*)-**1** with ca. 0.00005 % *ee*.

[9] a) K. Soai, S. Niwa, *Chem. Rev.* **1992**, *92*, 833 – 856; b) L. Pu, H.-B. Yu, *Chem. Rev.* **2001**, *101*, 757 – 824.

[10] After our experiments were completed, Singleton and Vo reported asymmetric autocatalysis using (*R*)-(2-methylpyrimidyl)alkanol[5b] with the order of 10^{-5} % *ee* [a) D. A. Singleton, L. K. Vo, *J. Am. Chem. Soc.* **2002**, *124*, 10010 – 10011]. However, they used only the catalyst with the *R* configuration. We believe that it is essentially important to examine the asymmetric autocatalysts of both configurations. The reasons are as follows: 1) The chirality level of the catalyst on the order of 10^{-5} % *ee* is below the detection level of the instruments typically used, for example, HPLC, CD, polarimeter etc. (for recent advances in the measurement of enantiomeric excesses, see: b) M. Tsukamoto, H. B. Kagan, *Adv. Synth. Catal.* **2002**, *344*, 453 – 463). 2) Only after obtaining results that the asymmetric autocatalyst with *S* configuration affords itself with *S* configuration and the asymmetric autocatalyst with *R* configuration affords itself with *R* configuration one can judge that the autocatalyst works.

[11] Autocatalyst **1** on the order of 10^{-9} % *ee* has been employed, but we have not yet received reproducible results probably because of the effect of some unexpected and unknown chiral factor.

[12] The reaction of 2-methylpyrimidine-5-carbaldehyde with $i Pr_2Zn$ without any added chiral substance had been examined in 100 experiments. After repeated asymmetric autocatalysis, (2-methylpyrimidyl)alkanol with a chirality level above the detection level formed [K. Soai, T. Shibata, Y. Kowata, Japan Kokai Tokkyo Koho JP, 9-268179 **1997**]. However, the probability of the formation of *S* and *R* enantiomers in toluene was not equal, which indicates an unexpected and unknown chiral factor affects the asymmetric induction. Similar observations have been reported by Singleton and Vo.[10a]

[13] a) K. Soai, S. Osanai, K. Kadowaki, S. Yonekubo, T. Shibata, I. Sato, *J. Am. Chem. Soc.* **1999**, *121*, 11235 – 11236; b) I. Sato, K. Kadowaki, K. Soai, *Angew. Chem.* **2000**, *112*, 1570 – 1572; *Angew. Chem. Int. Ed.* **2000**, *39*, 1510 – 1512; c) T. Shibata, J. Yamamoto, N. Matsumoto, S. Yonekubo, S. Osanai, K. Soai, *J. Am. Chem. Soc.* **1998**, *120*, 12157 – 12158.

Coordination Networks

Open Network Architectures from the Self-Assembly of $AgNO_3$ and 5,10,15,20-Tetra(4-pyridyl)porphyrin (H_2tpyp) Building Blocks: The Exceptional Self-Penetrating Topology of the 3D Network of $[Ag_8(Zn^{II}tpyp)_7(H_2O)_2](NO_3)_8$**

Lucia Carlucci, Gianfranco Ciani, Davide M. Proserpio, and Francesca Porta*

The use of suitable predetermined building blocks has assumed an increasing relevance in recent times in the crystal engineering of coordination frameworks[1] that have potential interest as zeolite-like materials.[2] In this regard, much

[*] Prof. G. Ciani, Dr. D. M. Proserpio
Dipartimento di Chimica Strutturale e Stereochimica Inorganica
Via G. Venezian 21, 20133 Milano (Italy)
Fax: (+39) 02-5031-4454
E-mail: davide@csmtbo.mi.cnr.it
Prof. F. Porta
Dipartimento di Chimica Inorganica, Metallorganica e Analitica
Via G. Venezian 21, 20133 Milano (Italy)
Dr. L. Carlucci
Dipartimento di Biologia Strutturale e Funzionale
Università dell'Insubria
Via J. H. Dunant 3, 21100 Varese (Italy)

[**] This work was supported by MURST within the project "Solid Supermolecules" 2000–2001. F.P. thanks the ISTM Centre for instrument facilities.

attention has been devoted to the networking ability of tetra-substituted porphyrins and metalloporphyrins,[3] which are potentially able to act as tetradentate planar donor groups and to produce open lattice species with large void volumes. Moreover, the nature of such building blocks can lead to synthetic supramolecular arrays with potential applications in materials chemistry as photonic devices, conductive polymers, chemical sensors, and receptors for selective catalysis. Examples of multiporphyrin architectures constructed by supramolecular interactions include species controlled by the variation of the peripheral substituent groups and/or the encapsulated metals, and those assembled through hydrogen-bonding bridges[3] or coordinative bonds to the metals of identical neighboring metalloporphyrin units[4] or to external metal centers.[5–8] The synthetic strategy based on coordinative interactions seems quite promising for the crystal engineering of robust open networks, whose structures can, in principle, be programmed by using appropriate substituents on the porphyrin groups (which are considered as large square-planar donor ligands) and external metal units with suitable coordination geometries. The pioneering work of Robson and co-workers in this area has, indeed, shown that metalloporphyrins can give coordination networks with the $CdSO_4$[5a] or the PtS topology[5b] by using Cd^{II} centers (acting as linear spacers) or tetrahedral Cu^{I} centers, respectively. Most of the reported frameworks contain external divalent metal ions, while species with trivalent[6e,8] or monovalent[6a–d] metal ions are more rare.

We are currently investigating the reactions of different silver(I) salts with the free-base 5,10,15,20-tetra(4-pyridyl)-porphyrin (H_2tpyp) and with its Zn^{II}-metalated derivative (Zntpyp). To our knowledge, only one previous example of a multiporphyrin species assembled with Ag^{I} ions, that is, $[Ag(H_2tpyp)]PF_6 \cdot 1.5\,TCE \cdot MeOH \cdot H_2O$ (TCE = tetrachloroethane), has been reported which consists of polymeric linear chains.[9] The versatility of silver cations can afford a variety of coordination geometries, but mainly gives the digonal and the tetrahedral ones. Digonal coordination affords not only 1D linear chains, but gives access to target structures comprised of 2D square grids (Ag:porphyrin 2:1) and 3D nets with the $CdSO_4$ or NbO topologies (Ag:porphyrin 2:1), while the tetrahedral geometry would only be expected to give a 3D structure of the PtS type (Ag:porphyrin 1:1), as previously found with Cu^{I} ions.[5b] We report here novel polymeric frameworks obtained from the self-assembly of $AgNO_3$ with H_2tpyp or Zntpyp, namely, the 2D species $[Ag_4(H_2tpyp)_3](NO_3)_4 \cdot x$solv (**1**) and $[Ag_2(H_2tpyp)(NO_3)](NO_3) \cdot x$solv (**2**) as well as the 3D network $[Ag_8(Zntpyp)_7(H_2O)_2](NO_3)_8 \cdot x$solv (**3**). Only compound **2** contains one of the expected structural motifs (2D square-grid layers), as also observed by us with other silver salts (such as triflate and tosylate) and which will be reported elsewhere.[10] The topologies of compounds **1** and **3** are unprecedented and the latter one is a rare case of a 3D self-penetrating net. As desired, these networks are robust and exhibit large free voids (> 50 %) full of removable guest solvent molecules.

The self-assembly processes of these species were carried out by slow diffusion of solutions containing a large stoichiometric excess (up to fivefold) of $AgNO_3$ into solutions of H_2tpyp or Zntpyp in TCE/MeOH. The solvent system plays a fundamental role in driving the processes. Compound **1** was isolated in good yield on layering a solution of $AgNO_3$ in *N,N′*-dimethylacetamide (DMA) over a solution of H_2tpyp in TCE/MeOH, after interposing a small volume of pure 3-chloroaniline between the two phases. Brown crystals formed within a few days. We have also observed the formation of variable amounts of smaller crystals of compound **2** under these conditions. However, the main product obtained on changing the solvents for the silver salt (for example, by using $EtOH/H_2O/CH_3CN$ or $DMSO/CH_3CN$ mixtures) is a different species, namely, $[Ag(H_2tpyp)](NO_3) \cdot x$solv,[11] containing simple linear chains similar to those already reported.[9] Similarly, compound **3** was obtained in good yield upon layering a solution of $AgNO_3$ in DMA over a solution of Zntpyp in TCE/MeOH, after interposition of a small volume of pure DMA between the two phases. Dark-red crystals formed within a few days, which grew bigger and of better quality on keeping the reaction vessel at low temperature. This species can also be obtained in high yields (ca. 97 %) as polycrystalline samples by adding over 1 h, under stirring, a solution of $AgNO_3$ in DMA to a solution of Zntpyp in TCE/

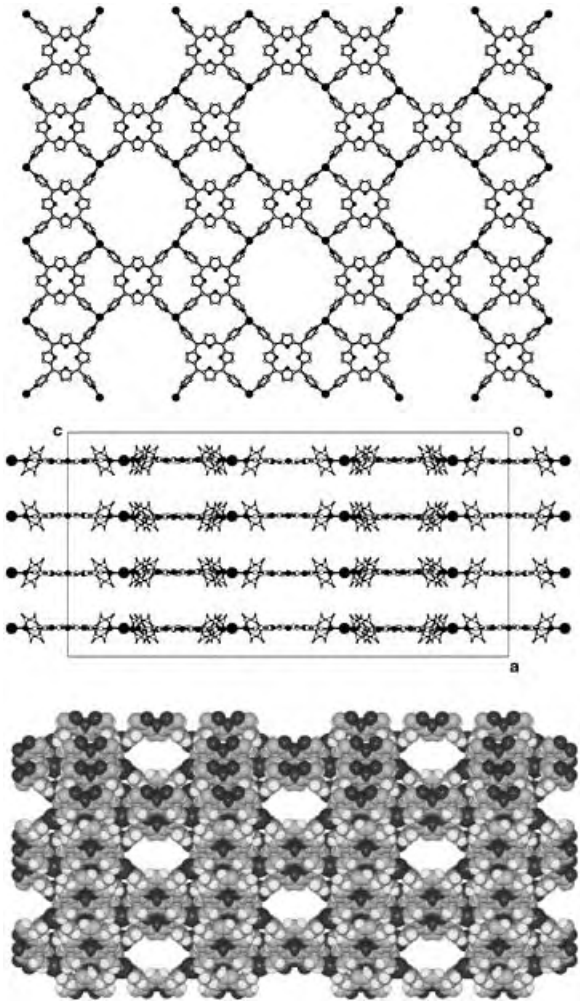


Figure 1. Structure of **1**. A single 2D layer (top), a side view of the stacked layers (middle), and a view of the packing with the channels running along [110] (bottom).

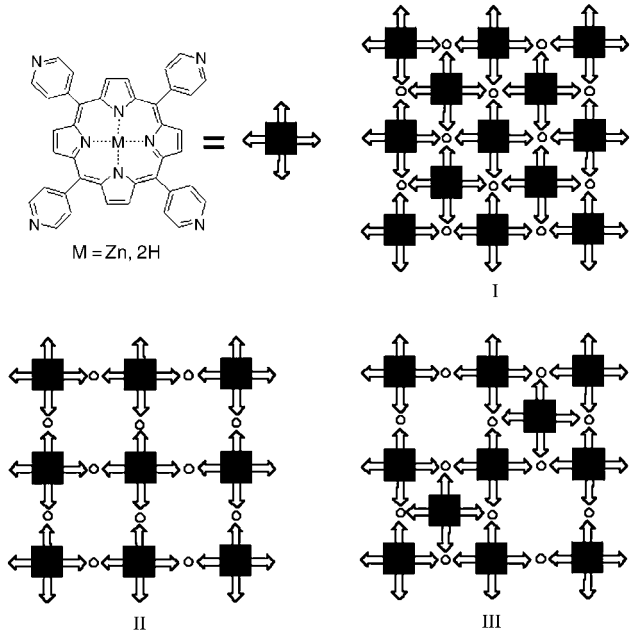
 © 2003 Wiley-VCH Verlag GmbH & Co. KGaA, Weinheim 1433-7851/03/4203-0318 $ 20.00+.50/0

MeOH in a reaction flask placed in an ice bath. All compounds were characterized by single-crystal X-ray analyses.[12]

The structure of **1** consists of two-dimensional flat layers comprised of tetracoordinate H_2tpyp centers and tricoordinate Ag^+ ions in the ratio 3:4 (Figure 1, top). This 2D net contains two types of rings: four- and eight-membered squares of alternating centers[13] with approximate edge dimensions of 10.0×10.2 and 19.9×19.9 Å, respectively. The topology is novel and can be related to the more usual square grid of (4,4) type (I in Scheme 1), as observed, for example, in the $[MCl_2(H_2tpyp)]$ (M = Pb, Cd) species.[7a] The 2D layer of larger square meshes II, which contain digonal metal centers as in compound **2**, can be obtained by eliminating one half of the H_2tpyp centers from I (see below), while the elimination of only one quarter of the H_2tpyp centers can give either the layer of type III shown in Scheme 1 or that actually observed in **1**. The coordination of the metal centers in both III and compound **1** gives a tricoordinate T-shaped geometry, which is rather common for silver cations. However, the reason is not clear why the actual structure is preferred out of the two possibilities. The arms within the T-shaped coordination of the Ag^+ ions are shorter than the third Ag–N bond (2.263(3)–2.241(4) versus 2.427(3) Å) and the corresponding bond angle is larger than the other two (156.5(1) versus 101.3(1)–102.0(1)°). The 2D layers stack along the *a* axis, with an interlayer separation of 1/4 *a* (ca. 7.19 Å) and in an ABCD sequence (Figure 1, middle). The structure does not show wide channels when viewed down the stacking direction, since the larger squares of adjacent layers are not aligned. However, channels can be observed that run with an orientation inclined with respect to the planes of the layers, that is, along [110], and show an elliptical cross-section of about 6.0×14.5 Å (when the van der Waals radii are considered; Figure 1, bottom). The framework represents only approximately 35% of the cell volume and the interlayer regions and the channels contain disordered nitrate anions and many solvent molecules, for which a reasonable refinement was not possible. It is also difficult to establish the nature and amounts of these solvents by noncrystallographic methods because of the unavoidable formation of mixtures of crystals of **1** and **2**. Solid, air-dried samples of these mixtures were suspended in deuterated dichloromethane; ^{1}H NMR analyses performed on these solutions after a few hours revealed the presence of 3-chloroaniline, TCE, and DMA in a ratio of 1:2.3:1.7, similar to the composition of the reaction mother liquor.

Compound **2** contains a more usual type of 2D layers of (4,4) topology (Figure 2, top; II in Scheme 1), with large squares of edge dimensions 19.1×19.9 Å. This structural motif was previously observed in multiporphyrin systems connected through $(-COOH)_2$ hydrogen-bond pairs,[14] instead of the pyridyl-Ag-pyridyl synthons.

In contrast to **1**, the layers of **2** are sligthly undulated (Figure 2, middle) because one of the two independent Ag^I ions exhibits a nonlinear coordination geometry as a



Scheme 1.

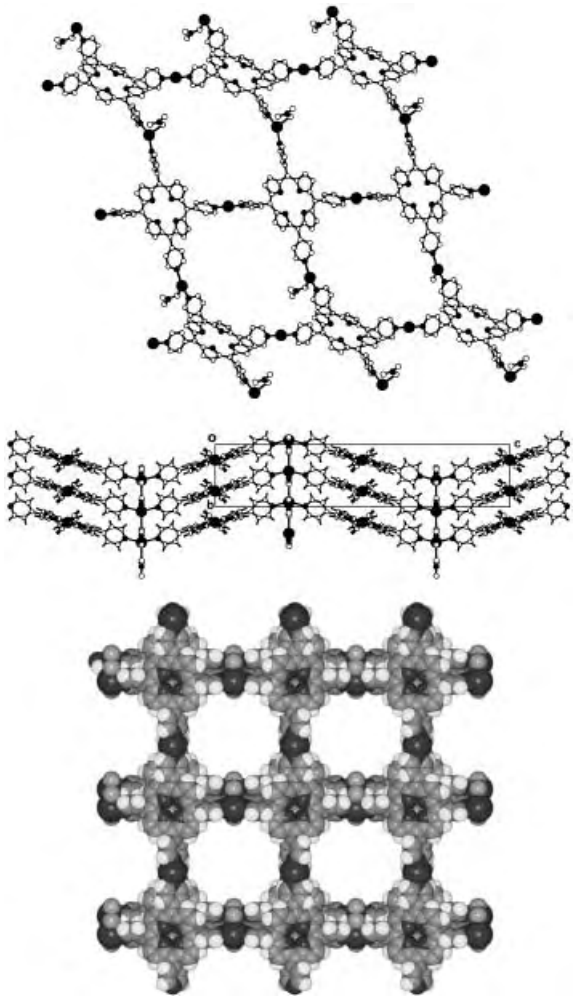


Figure 2. Structure of **2**. A single 2D layer (top), a side view of the stacked undulated layers (middle), and a view of the packing down the *b* axis showing the large square channels (bottom).

 © 2003 Wiley-VCH Verlag GmbH & Co. KGaA, Weinheim 1433-7851/03/4203-0319 $ 20.00+.50/0

result of the asymmetric interactions with two oxygen atoms of two μ-η¹ nitrate anions that bridge adjacent layers (Ag–O 2.48(2), 2.74(2) Å). These interactions generate an overall 3D network with the $CdSO_4$-type topology. The stacking of the layers occurs down the *b* axis with a separation of 1/2 *b* (ca. 4.0 Å). The sequence is ABAB because of the presence of a small offset of adjacent sheets. This arrangement creates large channels of rectangular cross-section (ca. 12.0 × 15.0 Å, when the van der Waals radii are considered) running along the *b* direction (Figure 2, bottom). Large free voids (ca. 50% of the cell volume) are thus associated with these regions, and this contrasts with **1**, in which free voids are mainly localized in the interlayer spaces.

The structure of compound **3** is influenced by the presence of the Zntpyp versus the H_2tpyp building blocks in that the Zn^{2+} ions enclosed in the porphyrin macrocycles essentially show a high tendency to increase their coordination number to five or six by axial bonding.[3] This species contains a complex 3D tetragonal open network (Figure 3), whose rationalization can be described stepwise. First of all,

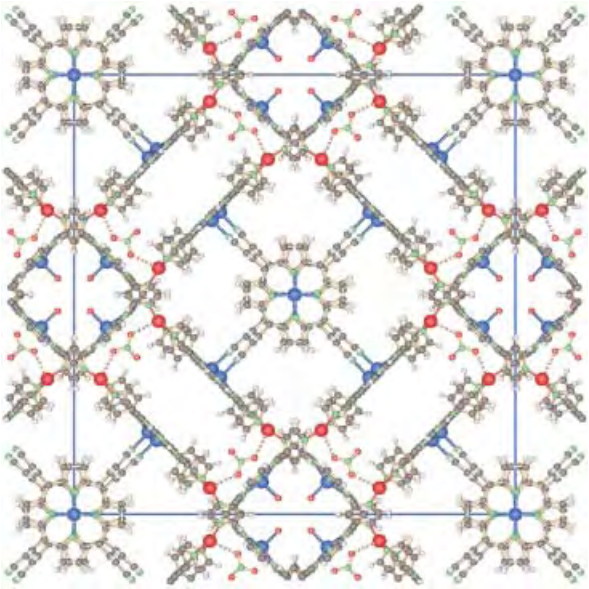


Figure 3. A view of the overall network in **3** down the tetragonal *c* axis.

it is comprised of 2D layers of composition $[Ag_4(Zntpyp)_3(H_2O)]^{4+}$ that exhibit the same topology observed in compound **1** (Figure 4, top). Second, these layers are all parallel to the tetragonal *c* axis and are disposed in two sets of pairs (average interplanar separations: within the pairs approximately 7.3 Å, and between different pairs approximately 20.5 Å) that span two mutually perpendicular directions and interpenetrate in the "so-called" inclined fashion[1c] through all the pairs of large facing windows in the paired layers (Figure 4, bottom). Third, these sets of layers are interconnected by Zntpyp units whose macrocyclic planes are perpendicular to the tetragonal *c* axis (Figure 3). The four pyridyl groups of each of these units form axial bonds towards the metalloporphyrin Zn centers in four different surrounding layers (2/3 of the Zn centers on each layer are involved). The

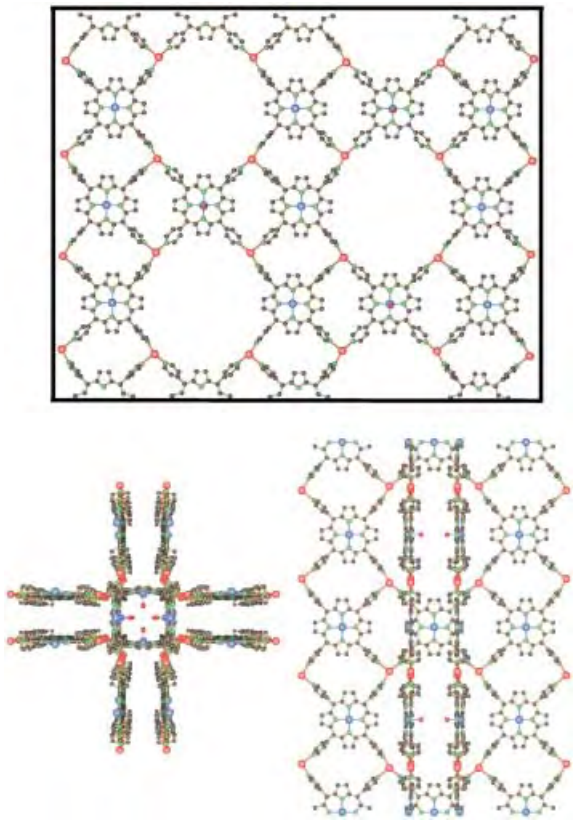


Figure 4. Portion of a 2D layer (top) and two views of the inclined interpenetration of two pairs of layers (bottom) in **3**.

overall resulting network is therefore a unique 3D self-penetrating (or polyknotted) architecture.[15] The coordination geometries of the different metal centers are as follows: within the layers the Ag centers show T-shaped tricoordinate geometry as in **1** (Ag–N 2.161(9),2.195(9), 2.389(10) Å; N-Ag-N 98.5(3), 101.7(3), 157.2(3)°), while all the Zn centers are five-coordinate square pyramidal (2/3 with axial pyridyl groups, Zn–N 2.134(8) Å, and 1/3 with axial water molecules, Zn–O 2.098(16) Å); the Zn centers in the remaining Zntpyp "bridging" groups show the less-usual square-planar coordination geometry.[16] The network contains large free volumes that are populated by many disordered solvent molecules and one half of the nitrate anions. The remaining NO_3^- ions are anchored to the framework and show weak interactions (2.751(11) Å) with pairs of silver centers (Figure 3). As illustrated in Figure 3, there are channels running along the *c* axis with square and rectangular cross-sections (with inter-wall distances of about 9.2 × 9.2 Å and 7.3 × 18.5 Å, respectively). The major voids, however, are enclosed within the large chambers delimited by the "horizontal" metalloporphyrin groups (ca. 20.5 × 20.5 × 14.5 Å; Figure 5). The overall free voids are 55% of the cell volume. These are full of a mixture of solvent molecules that have been identified (by IR and NMR methods) to be TCE, DMA, and water. The composition is rather variable, as also evidenced by elemental analyses. NMR analyses of suspensions of **3** in $CDCl_3$ after one day revealed relative molar ratios of TCE:DMA:H_2O of

 © 2003 Wiley-VCH Verlag GmbH & Co. KGaA, Weinheim 1433-7851/03/4203-0320 $ 20.00+.50/0

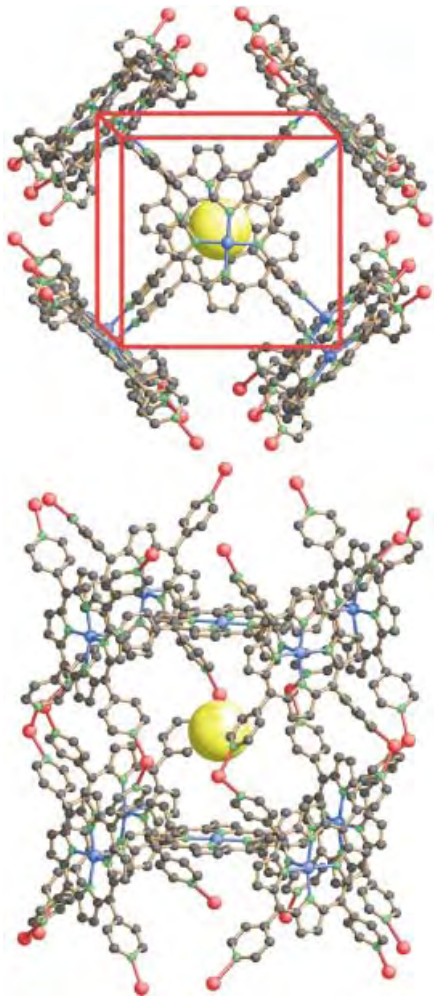


Figure 5. Two views of a large chamber between two Zn-porphyrin units perpendicular to the tetragonal axis. The central sphere (4 Å diameter) indicates the baricenter. The top view also shows an enclosed cube (having eight Zn corners) with edges of about 14 Å.

approximately 1:1.6:1.3. Compound **3** can be formulated as $[Ag_8(Zntpyp)_7(H_2O)_2](NO_3)_8{\cdot}11\,TCE{\cdot}17.5\,DMA{\cdot}12\,H_2O$, which is in agreement also with the residual volumes and electron densities obtained from the SQUEEZE-Bypass refinements.[12]

Thermal gravimetric (TG) analyses reveal an almost continuous loss of solvents in the range 40–400 °C; three overlapping steps are evident which can be attributed to the sequential loss of water, TCE, and DMA. The total solvent weight loss is about 35 % (calculated: 36.7 %). No further weight loss could be observed upon heating up to approximately 500 °C and, at this point, the compound starts to decompose, probably by dissociation of the pyridyl groups. Slow heating of samples of **3** in an oven up to 130 °C shows that the weight loss (solvent removal) is accompanied by a progressive loss of crystallinity (monitored by X-ray powder diffraction (XRPD)). Successive immersion of these depleted samples overnight in a solution having the same composition as the reaction mixture reveals that the process is reversible and that the solvent uptake is accompanied by a recovery of crystallinity. Thus, the network of **3** is maintained along the process, as confirmed by comparing the XRPD patterns with the calculated one.[17]

Experimental Section

1 and **2**: These two species were obtained as a mixture; attempts to get pure samples of **1** and/or **2** were unsuccessful. Pure 3-chloroaniline (2 mL) was layered onto a solution of H_2tpyp dissolved in a 3:1 mixture of TCE:MeOH (5 mL, 5×10^{-3} M) and then $AgNO_3$ dissolved in DMA (3 mL, 3×10^{-2} M) was layered on top. The mixture was left at room temperature for several days. The formation of a silver mirror with crystals of **1** and **2** on the walls and on the bottom of the vessel was noted. The crystals were recovered by filtration, washed with a mixture of TCE:DMA (1:1), and dried in the air (yield: 5–6 mg). ^{1}H NMR (17.4 mg, 1 mL CD_2Cl_2, at RT for 4 h): $\delta = 7.09$ (1 H, t), 6.71 (1 H, d), 6.70 (1 H, s), 6.58 ppm (1 H, d) for 3-chloroaniline; 6.07 ppm (2 H, s) for TCE; 3.01 (3 H, s), 2.91 (3 H, s), 2.05 ppm (3 H, s) for DMA; 1.3 ppm (2 H, brs) for H_2O. The relative ratio for these solvents was 1:2.17:1.61:2.42. The elemental analyses were rather variable, depending on the composition of the mixtures. Thermal gravimetric analyses (nitrogen, 10 °C min^{-1}) showed a continuous weight loss in the range 40–400 °C (overall ca. 30 %) attributed to the removal of the guest solvents. A weight loss of about 21 % was then observed in the range 450–630 °C which can be attributed to the dissociation of the pyridyl groups. IR spectroscopy on a single crystal of **1**: $\tilde{\nu} = 3332$, 3076, 2976, 1605, 1483, 1363, 1219, 1070, 976, 787, 674 cm^{-1}.

3: Pure DMA (1.5 mL) was layered onto a solution of ZnTpyP dissolved in a 3:1 mixture of TCE:MeOH (5 mL, 1.5×10^{-3} M) and a solution of $AgNO_3$ dissolved in DMA (3.2 mL, 7.26×10^{-3} M) then layered on top. The mixture was left at −20 °C, and after five days crystals of **3** that were suitable for the diffraction analyses were grown. Compound **3** was prepared in bulk by adding a solution of $AgNO_3$ (51.8 mg; 0.305 mmol) dissolved in DMA (28 mL) to a solution of ZnTpyP (42 mg, 0.0616 mmol) dissolved in a mixture of TCE:MeOH (3:1, 30 mL). After stirring the reaction mixture for 1 h at 0 °C a polycrystalline violet powder was formed, which was recovered by filtration through a teflon membrane, washed with a mixture of TCE:DMA (1:1) and dried in the air (yield: ca. 97 %). The XRPD analysis performed on this sample confirmed the pure nature of the powder as **3**. The ^{1}H NMR experiment was performed on 15.8 mg of **3** (the purity was checked by XRPD analysis) isolated from the reaction mixture, dried in the air with the use of adsorbent paper, and suspended in $CDCl_3$ (1 mL). The spectra were acquired after leaving the sample at room temperature for one day and showed signals at $\delta = 5.96$ ppm (2 H, s) attributed to TCE; 3.01 (3 H, s), 2.95 (3 H, s), 2.09 ppm (3 H, s) attributed to DMA; and at 1.73 ppm (2 H, s) attributed to H_2O. The absolute amounts of solvents have been calculated by the addition of naphthalene as an internal standard. Elemental analysis calcd (%) for $C_{372}H_{375.5}Ag_8Cl_{44}N_{81.5}O_{55.5}Zn_7$: C 45.86, H 3.86, N 11.72; found: C 46.82, H 3.64, N 10.64. thermal gravimetric analyses (nitrogen, 10 °C min^{-1}) were carried out on freshly prepared crystalline or polycrystalline samples. UV/Vis (solid): $\lambda_{max} = 392$, 561, 607 nm. IR (KBr pellets): $\tilde{\nu} = 1596$, 1383, 1205, 1071, 923, 789, 671 cm^{-1}.

Received: October 10, 2002 [Z50342]

[1] a) B. F. Hoskins, R. Robson, *J. Am. Chem. Soc.* **1990**, *112*, 1546; b) R. Robson, B. F. Abrahams, S. R. Batten, R. W. Gable, B. F. Hoskins, J. Liu, *Supramolecular Architecture*, ACS publications, **1992**, chap. 19; c) S. R. Batten, R. Robson, *Angew. Chem.* **1998**, *110*, 1558; *Angew. Chem. Int. Ed.* **1998**, *37*, 1460; d) P. J. Hagrman, D. Hagrman, J. Zubieta, *Angew. Chem.* **1999**, *111*,

2798; *Angew. Chem. Int. Ed.* **1999**, *38*, 2639; e) M. Munakata, L. P. Wu, T. Kuroda-Sowa, *Adv. Inorg. Chem.* **1999**, *46*, 173; f) A. N. Khlobystov, A. J. Blake, N. R. Champness, D. A. Lemenovskii, A. G. Majouga, N. V. Zyk, M. Schroder, *Coord. Chem. Rev.* **2001**, *222*, 155; g) M. Eddaoudi, D. B. Moler, H. L. Li, B. L. Chen, T. M. Reineke, M. O'Keeffe, O. M. Yaghi, *Acc. Chem. Res.* **2001**, *34*, 319; h) B. Moulton, M. J. Zaworotko, *Chem. Rev.* **2001**, *101*, 1629.

[2] See, for example, a) C. Janiak, *Angew. Chem.* **1997**, *109*, 1499; *Angew. Chem. Int. Ed. Engl.* **1997**, *36*, 1431; b) H. Li, M. Eddaoudi, M. O'Keeffe, O. M. Yaghi, *Nature* **1999**, *402*, 276; c) S. Noro, S. Kitagawa, M. Kondo, K. Seki, *Angew. Chem.* **2000**, *112*, 2161; *Angew. Chem. Int. Ed.* **2000**, *39*, 2082; d) L. Carlucci, G. Ciani, M. Moret, D. M. Proserpio, S. Rizzato, *Angew. Chem.* **2000**, *112*, 1566; *Angew. Chem. Int. Ed.* **2000**, *39*, 1506; e) C. J. Kepert, T. J. Prior, M. J. Rosseinsky, *J. Am. Chem. Soc.* **2001**, *123*, 10001; f) M. Eddaoudi, J. Kim, N. Rosi, D. Vodak, J. Wachter, M. O'Keeffe, O. M. Yaghi, *Science*, **2002**, *295*, 469; g) L. Carlucci, N. Cozzi, G. Ciani, M. Moret, D. M. Proserpio, S. Rizzato, *Chem. Commun.* **2002**, 1354; h) S. Noro, R. Kitaura, M. Kondo, S. Kitagawa, T. Ishii, H. Matsuzaka, M. Yamashita, *J. Am. Chem. Soc.* **2002**, *124*, 2568, and references therein.

[3] a) I. Goldberg, *Chem. Eur. J.* **2000**, *6*, 3863; b) I. Goldberg, *CrystEngComm* **2002**, *4*, 109.

[4] a) H. Krupitsky, Z. Stein, I. Goldberg, C. E. Strouse, *J. Inclusion Phenom. Mol. Recognit. Chem.* **1994**, *18*, 177; b) R. K. Kumar, S. Balasubramanian, I. Goldberg, *Inorg. Chem.* **1998**, *37*, 541; c) Y. Diskin-Posner, G. K. Patra, I. Goldberg, *J. Chem. Soc. Dalton Trans.* **2001**, 2775; d) K.-J. Lin, *Angew. Chem.* **1999**, *111*, 2894; *Angew. Chem. Int. Ed.* **1999**, *38*, 2730 Erratum: K.-J. Lin, *Angew. Chem.* **1999**, *111*, 3621; *Angew. Chem. Int. Ed.* **1999**, *38*, 3415; e) K. M. Barkigia, P. Battioni, V. Riou, D. Mansuy, J. Fajer, *Chem. Commun.* **2002**, 956; f) L. Pan, S. Kelly, X. Huang, J. Li, *Chem. Commun.* **2002**, 2334.

[5] a) B. F. Abrahams, B. F. Hoskins, R. Robson, *J. Am. Chem. Soc.* **1991**, *113*, 3606; b) B. F. Abrahams, B. F. Hoskins, D. M. Michail, R. Robson, *Nature* **1994**, *369*, 727.

[6] a) Y. Diskin-Posner, S. Dahal, I. Goldberg, *Angew. Chem.* **2000**, *112*, 1344; *Angew. Chem. Int. Ed.* **2000**, *39*, 1288; b) Y. Diskin-Posner, I. Goldberg, *New J. Chem.* **2001**, *25*, 899; c) Y. Diskin-Posner, G. K. Patra, I. Goldberg, *Eur. J. Inorg. Chem.* **2001**, 2515; d) Y. Diskin-Posner, S. Dahal, I. Goldberg, *Chem. Commun.* **2000**, 585; e) R. K. Kumar, I. Goldberg, *Angew. Chem.* **1998**, *110*, 3176; *Angew. Chem. Int. Ed.* **1998**, *37*, 3027.

[7] a) C. V. K. Sharma, G. A. Broker, J. G. Huddleston, J. W. Baldwin, R. M. Metzger, R. D. Rogers, *J. Am. Chem. Soc.* **1999**, *121*, 1137; b) C. V. K. Sharma, G. A. Broker, R. D. Rogers, *J. Solid State Chem.* **2000**, *152*, 253.

[8] D. Hagrman, P. J. Hagrman, J. Zubieta, *Angew. Chem.* **1999**, *111*, 3359; *Angew. Chem. Int. Ed.* **1999**, *38*, 3165.

[9] M. Kondo, Y. Kimura, K. Wada, T. Mizutani, Y. Ito, S. Kitagawa, *Chem. Lett.* **2000**, 818.

[10] L. Carlucci, G. Ciani, D. M. Proserpio, F. Porta, unpublished results.

[11] Crystal data for $[Ag(H_2tpyp)](NO_3)\cdot x$solv: triclinic, space group $P\bar{1}$ (no. 2), $a = 6.5177(12)$, $b = 10.445(2)$, $c = 17.908(3)$ Å, $\alpha = 83.753(7)$, $\beta = 83.487(9)$, $\gamma = 77.243(8)°$, $V = 1177.0(4)$ Å^3, $Z = 1$, final $R1$ value 0.1383 (0.0748 after SQUEEZE, see ref. [12]) for 2559 independent reflections $[I > 2\sigma(I)]$.

[12] Crystal data for **1**, $C_{120}H_{78}Ag_4N_{28}O_{12}\cdot x$solv: orthorhombic, space group *Fmmm* (no. 69), $a = 28.770(13)$, $b = 29.035(13)$, $c = 56.46(3)$ Å, $V = 47130(37)$ Å^3, $Z = 8$, final $R1$ value 0.1836 (0.0548 after SQUEEZE, see below) for 3972 independent reflections $[I > 2\sigma(I)]$. Crystal data for **2**, $C_{40}H_{26}Ag_2N_{10}O_{10}\cdot x$solv: orthorhombic, space group *Pbcm* (no. 57), $a = 19.861(7)$, $b = 8.077(3)$, $c = 38.220(13)$ Å, $V = 6131(4)$ Å^3, $Z = 8$, final $R1$ value 0.1455 (0.0870 after SQUEEZE, see below) for 1426 independent reflections $[I > 2\sigma(I)]$. Crystal data for **3**, $C_{280}H_{172}Ag_8N_{63}O_{26}Zn_7\cdot x$solv: tetragonal, space group *I*4/*mcm* (no. 140), $a = b = 39.169(2)$, $c = 28.991(2)$ Å, $V = 44478(4)$ Å^3, $Z = 4$, final *R1* value 0.1577 (0.0774 after SQUEEZE, see below) for 3021 independent reflections $[I > 2\sigma(I)]$. The data collections were performed at room temperature on a Bruker SMART CCD area-detector diffractometer, using $Mo_{K\alpha}$ radiation ($\lambda = 0.71073$ Å), by the ω-scan method, within the limits $1 < \theta < 23°$ for **1**, $1 < \theta < 22°$ for **2**, and $1 < \theta < 23°$ for **3**. Empirical absorption corrections (SADABS) were applied. The structures were solved by direct methods (SIR97) and refined by full-matrix least-squares on F^2 (SHELX-97). Anisotropic thermal factors were assigned to all the non-hydrogen atoms in **1** and **3** and to the silver atoms only in **2**. The solvent-accessible volume was assessed in these structures using the PLATON software (A. L. Spek, *Acta Crystallogr. Sect. A* **1990**, *46*, C34) and the contribution of the disordered solvent (located in the voids of the interporphyrin channel of the lattice) to the diffraction pattern is subtracted from the observed data by the "Squeeze" method as implemented in PLATON (P. Van der Sluis, A. L. Spek, *Acta Crystallogr. Sect. A* **1990**, *46*, 194: The SQUEEZE-Bypass method referred therein is widely used in crystallographic analysis of compounds containing substantial amounts of disordered solvent that cannot be located precisely from diffraction data.) All the diagrams were generated using the SCHAKAL 97 program. CCDC-194964 – 194967 contains the supplementary crystallographic data for this paper. These data can be obtained free of charge via www.ccdc.cam.ac.uk/conts/retrieving.html (or from the Cambridge Crystallographic Data Centre, 12 Union Road, Cambridge CB21EZ, UK; fax: (+44) 1223-336-033; or deposit@ccdc.cam.ac.uk).

[13] 2D nets of alternating centers are described in: A. F. Wells, *Acta Crystallogr. Sect. B* **1968**, *24*, 50; B. Zhou, J.-Y. Li, J.-H. Yu, Y.-H. Xu, W.-G. Xu, N. Shi, S.-L. Qiu, R.-R. Xu, *Comput. Chem.* **1999**, *23*, 555.

[14] Y. Diskin-Posner, I. Goldberg, *Chem. Commun.* **1999**, 1961.

[15] Some previous examples of self-penetrating nets are: a) B. F. Abrahams, S. R. Batten, M. J. Grannas, H. Hamit, B. F. Hoskins, R. Robson, *Angew. Chem.* **1999**, *111*, 1538; *Angew. Chem. Int. Ed.* **1999**, *38*, 1475; b) M. A. Withersby, A. J. Blake, N. R. Champness, P. A. Cooke, P. Hubberstey, M. Schroder, *J. Am. Chem. Soc.* **2000**, *122*, 4044; c) L. Carlucci, G. Ciani, D. M. Proserpio, S. Rizzato, *J. Chem. Soc. Dalton Trans.* **2000**, 3821.

[16] Long axial interactions with disordered solvent molecules cannot be excluded; indeed we observed small residual electron densities in the axial direction at about 2.75 Å which are difficult to rationalize and to refine.

[17] Preliminary results of an investigation on the possibility of exchanging the nitrate anions seem encouraging. A polycrystalline sample of **3** suspended overnight in an aqueous solution of $(NEt_4)PF_6$, recovered by filtration, washed several times with water, and dried in the air, showed IR signals typical of the PF_6^- ions. However, further studies are needed to establish the exact nature of the process and the fraction of exchanged anions. Indeed, the exchange may occur by a crystal-to-crystal solvent-mediated process as recently described in: A. N. Khlobystov, N. R. Champness, C. J. Roberts, S. J. B. Tendler, C. Thompson, M. Schröder, *Cryst. Eng. Comm.* **2002**, *4*, 426.

 © 2003 Wiley-VCH Verlag GmbH & Co. KGaA, Weinheim 1433-7851/03/4203-0322 $ 20.00+.50/0

Palladium Cluster Compounds

$[Pd_{30}(CO)_{26}(PEt_3)_{10}]$ and $[Pd_{54}(CO)_{40}(PEt_3)_{14}]$: Generation of Nanosized Pd_{30}- and Pd_{54}-Core Geometries Containing Interpenetrating Cuboctahedral-Based Metal Polyhedra**

*Eugeny G. Mednikov, Sergei A. Ivanov, and Lawrence F. Dahl**

Herein, we report the synthesis and structural features of the two new palladium carbonyl phosphane clusters $[Pd_{30}(\mu_2\text{-}CO)_{22}(\mu_3\text{-}CO)_4(PEt_3)_{10}]$ (**1**) and $[Pd_{54}(\mu_2\text{-}CO)_{32}(\mu_3\text{-}CO)_8(PEt_3)_{14}]$ (**2**). Their nanosized Pd_{30} and Pd_{54} cores are the first examples of so-called "twinned"-core geometries involving a previously unknown oligomeric growth pattern, comprised of interpenetrating cuboctahedra as building blocks (that is, corresponding to selective ccp/hcp layer stacking; ccp = cubic close-packed, hcp = hexagonal close-packed). These results have particular stereochemical implications concerning multi-twinned structures[1] and growth sequences of much larger ligated and nonligated palladium nanoparticles.[2–6] The previously unknown cuboctahedral-twinned palladium-core geometries in **1** and **2** provide additional stereochemical evidence that emphasizes the highly versatile nature of this unique transition metal in readily forming a remarkable array of highly condensed carbonyl–phosphane clusters with either icosahedral-, ccp-, or mixed ccp/hcp-based metal-core arrangements.[4d,7–11] Palladium clusters also have considerable general interest since palladium has special commercial importance in that it forms exceptionally efficient mono- and bimetallic catalysts for organic transformations.

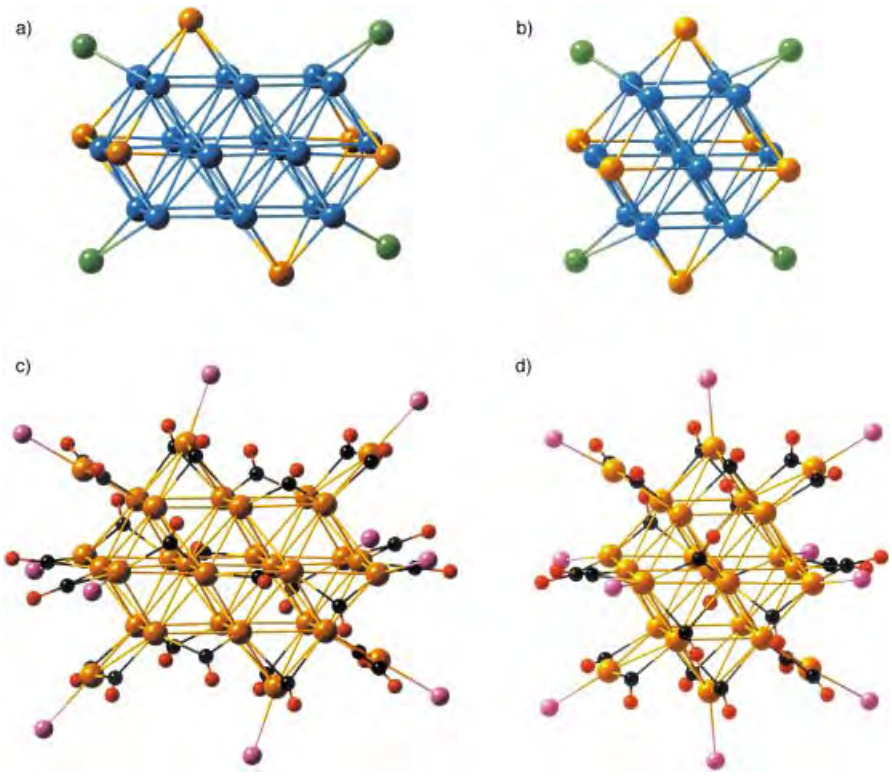


Figure 1. a) Pd_{30} pseudo-C_{2h} (2/m) core geometry in $[Pd_{30}(CO)_{26}(PEt_3)_{10}]$ (**1**). The maximum metal-core diameter (excluding the wingtip Pd atoms) between two symmetry-equivalent pairs of centrosymmetrically opposite (square-face)-capping Pd atoms (orange) is 1.01 nm; inclusion of the wingtip Pd atoms results in two symmetry-equivalent pairs of centrosymmetrically related wingtip atoms with metal-core diameters of 1.14 nm; b) Pd_{23}-core geometry in the known $[Pd_{23}(CO)_{20}(PEt_3)_{10}]$ (**3**).[10,11] The centered Pd_{13} kernel (blue) corresponds to a standard ccp arrangement about a centered atom; c) Structure of **1** which shows ten terminal PEt_3 ligands (without ethyl substituents for clarity) and 26 bridging CO groups about the Pd_{30} core. Pseudo-C_{2h} symmetry is maintained with the C_2 axis passing through two bridging CO groups and with the σ_h mirror plane (approximately coinciding with the paper) containing four bicuboctahedral Pd atoms, as well as two (square-face)-capping Pd atoms and four wingtip Pd atoms, together with their six attached phosphane P atoms. The two tetracapping $\{Pd(PEt_3)\}$ fragments lying on the mirror plane are each connected by two μ_3-CO groups to four basal Pd atoms in shell 1, while the other four tetracapping and four wingtip $\{Pd(PEt_3)\}$ fragments in shell 2 are each linked by 2 μ_2-CO groups to 14 Pd atoms in shell 1. The remaining six μ_2-CO groups are linked to three adjacent pairs of centrosymmetrically opposite bicuboctahedral Pd atoms in shell 1; d) Structure of **3** showing the analogous distribution of 10 terminal PEt_3 ligands (without ethyl substituents) and 20 bridging CO groups about the Pd_{23} core.[10,11]

Crystals of both **1** and **2** were reproducibly obtained as by-products together with $[Pd_{38}(CO)_{28}(PEt_3)_{12}]$[8h,i,12] through the deligation of $[Pd_{10}(CO)_{12}(PEt_3)_6]$ [8a,9a] with CO assistance at the initial stage of the reaction.[13,14] The molecular geometries and stoichiometries of **1** and **2** were unambiguously established from X-ray crystallographic analysis.[15]

The pseudo-C_{2h} (2/m) geometry of the Pd_{30} core of $[Pd_{30}(CO)_{26}(PEt_3)_{10}]$ (**1**; Figure 1 a) is composed of two interpenetrating centered Pd_{13} cuboctahedra (blue), which form a "twinned" centered Pd_{20} bicuboctahedron (blue, with six common atoms) that is capped on six of its eight square faces by six Pd atoms (orange) and additionally edge-bridged by four exopolyhedral wingtip Pd atoms (green). The crystallographically required centrosymmetric Pd_{30} geometry of **1** (Figure 1 a) is closely related to the Pd_{23} geometry (Figure 1 b) of the known $[Pd_{23}(CO)_{20}(PEt_3)_{10}]$ cluster (**3**), which is composed of a centered Pd_{13} cuboctahedron (blue) with six

[*] Prof. L. F. Dahl, Dr. E. G. Mednikov, Dr. S. A. Ivanov
Department of Chemistry
University of Wisconsin-Madison
1101 University Avenue, Madison, WI 53706 (USA)
Fax: (+1) 608-262-6143
E-mail: dahl@chem.wisc.edu

[**] This research was supported by the National Science Foundation (CHE-9729555). The CCD area detector system was purchased, in part, with a NSF grant (CHE-9310428). Color figures were prepared with Crystal Maker, Interactive Crystallography (version 5; David C. Palmer, P.O. Box 183, Bicester, Oxfordshire, OX26 3TA (UK)). We are indebted to Dr. Ilia Guzei (UW-Madison) for helpful crystallographic advice.

 © 2003 Wiley-VCH Verlag GmbH & Co. KGaA, Weinheim 1433-7851/03/4203-0323 $ 20.00+.50/0

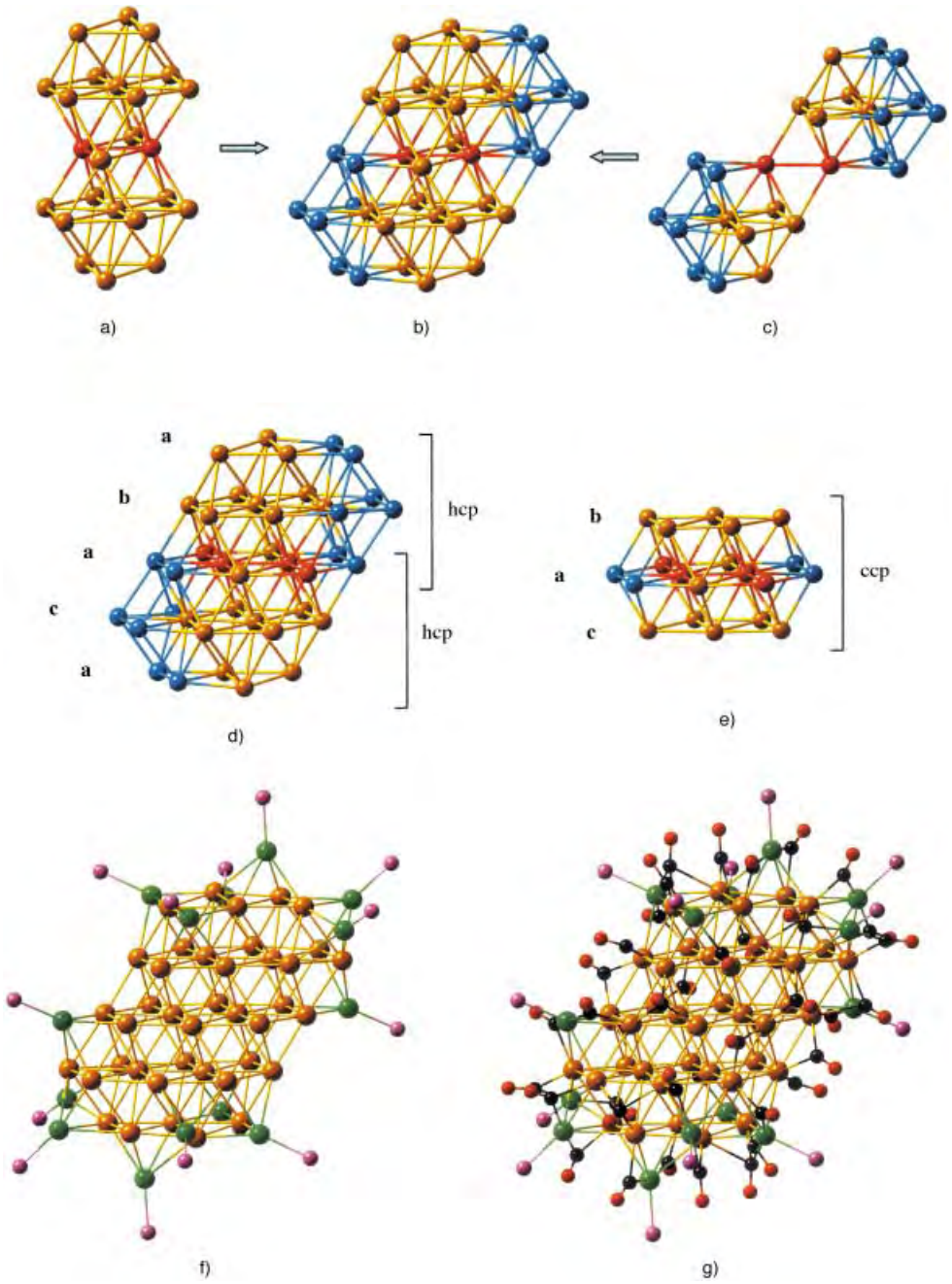


Figure 2. a) Central Pd_{38} fragment of the Pd_{54} core in C_i $[Pd_{54}(CO)_{40}(PEt_3)_{14}]$ (**2**), composed of four interpenetrating centered anti-cuboctahedra (hcp) generated by superposition of Pd_{24} fragment (left) and Pd_{26} fragment (right); b) Pd_{24} fragment consisting of two interpenetrating centered anti-cuboctahedra with a common Pd–Pd edge; c) Pd_{26} fragment consisting of two connected but non-interpenetrating centered anti-cuboctahedra. d) Pd_{40} fragment of the Pd_{54} core consists of a five-layer mixed hcp/ccp stacking arrangement formed from the central Pd_{38} fragment and two centrosymmetrically related Pd atoms (red) to the middle (equatorial) layer. The resulting 40-atom framework has a close-packed (**a**(Pd_5) **b**(Pd_{10}) **a**(Pd_{10}) **c**(Pd_{10}) **a**(Pd_5)) sequence; the top and bottom three layers may be viewed as two interpenetrating 25-atom **aba** and **aca** hcp layers with a common middle layer; e) Pd_{20} fragment of three interior 30-atom layers, which has a **bac** ccp stacking arrangement that corresponds to two interpenetrating centered cuboctahedra with six common atoms and completely coincides with Pd_{20} core of cluster **1**. f) Pd_{54}-core geometry obtained by the addition of 12 square-capping and two triangular-capping phosphane-attached Pd atoms (shell 2) to a Pd_{40} fragment composed of six interior coplanar Pd atoms forming four edge-fused equilateral triangles that are completely encapsulated by 34 Pd atoms (shell 1). Metal-core dimensions are $1.5 \times 1.2 \times 0.5$ nm; g) Structure of **2** displaying the arrangement of 14 PEt_3 ligands (without ethyl substituents) and 40 bridging CO groups about the Pd_{54} core.

 © 2003 Wiley-VCH Verlag GmbH & Co. KGaA, Weinheim 1433-7851/03/4203-0324 $ 20.00+.50/0

additional (square-face {100}) capping Pd atoms (orange) and four edge-bridging wingtip Pd atoms (green).[10,11] The 13 centered-cuboctahedral and six (square-face) capping Pd atoms in **3** may alternatively be viewed as a centered ν_2 Pd_{19} octahedron (that is, ν_n denotes $(n+1)$ equally spaced atoms along each edge) of pseudo-O_h (4/m$\bar{3}$2/m) symmetry with the other four wingtip Pd atoms lying on one of the octahedral mirror planes, such that the molecular symmetry is reduced to pseudo-D_{2h} (*mmm*). A geometrical comparison of the metal frameworks in **1** and **3** (Figure 1a, b) reveals that the pseudo-C_{2h} Pd_{30} core in **1** may be formally constructed from two of the centered Pd_{20} building-block-fragments in **3** (that is, the geometry of the Pd_{23} core, minus one face-capping and two wingtip Pd atoms) by a centrosymmetric interpenetration resulting in ten common atoms.

From a cluster shell model, both **1** and **3** may be regarded as possessing two and one interior Pd atoms, respectively, that are completely encapsulated in the first metal-coordination shell (shell 1) by 18 and 12 Pd atoms, respectively, that are not attached to PEt_3 groups; in turn, these first-shell Pd atoms are surrounded by ten bridging {$Pd(PEt_3)$} fragments in the second incomplete metal-coordination shell (shell 2) that are each connected to only the Pd atoms in shell 1. Figure 1c and d shows that a close geometrical resemblance exists between the entire ligated structures of **1** and **3**, with the CO and PEt_3 ligands in **1** occupying analogous coordination sites to those in **3**.[16,17]

The configuration of $[Pd_{54}(CO)_{40}(PEt_3)_{14}]$ (**2**) is given in Figure 2. Its close-packed "multi-twinned" Pd_{54}-core geometry of crystallographic $C_i(\bar{1})$ site-symmetry consists of a central five-layer Pd_{38} framework (Figure 2b) that may be formally considered as a fragment from a supracluster generated by the interpenetration of two anti-cuboctahedral Pd_{24} fragments (Figure 2a) and two anti-cuboctahedral Pd_{26} fragments (Figure 2c). These fragments each combine two anti-cuboctahedral (hcp) building blocks, with and without a common Pd–Pd edge, respectively. Addition of two centrosymmetrically related Pd atoms (red) to the middle (equatorial) layer of the Pd_{38} unit gives a Pd_{40} framework (Figure 2d) that is formed by the stacking of five layers in a mixed ccp/hcp (**a**(Pd_5) **b**(Pd_{10}) **a**(Pd_{10}) **c**(Pd_{10}) **a**(Pd_5)) sequence. This sequence reveals that the Pd_{40} framework can be regarded as the interpenetration of two centrosymmetrically equivalent 25-atom hcp three-layer **aba** and **aca** fragments, each containing a common middle layer (Figure 2d). 20 of the 30 Pd atoms in the inner three layers that have a **bac** ccp arrangement (Figure 2e) correspond to two interpenetrating centered Pd_{13} cuboctahedra (with six common Pd atoms). This Pd_{40} component of the Pd_{54}-core geometry of **2** may likewise be envisioned as a close-packed cluster shell-model with six interior Pd atoms conforming to a coplanar array of four edge-fused equilateral triangles that are completely surrounded by 34 Pd atoms (shell 1). Further condensation of 14 face-capping {$Pd(PEt_3)$} fragments gives rise to the incomplete second shell (Figure 2f). Figure 2g gives the configuration of **2** (without the phosphorus-attached ethyl substituents), which maintains crystallographic $C_i(\bar{1})$ symmetry. The entire Pd_{54} core is stabilized by 14 PEt_3 and 40 bridging carbonyl ligands.[16,17]

The identical geometrical conformity of the same central ccp Pd_{20} fragment in **1** (blue in Figure 1a) and **2** (Figure 2e) to a centered Pd_{20} bicuboctahedron, which formally arises through an interpenetrating "twinning" of the central cuboctahedral Pd_{13} fragment in **3** (blue in Figure 1b) suggests similar growth pathways. Prime evidence for this close architectural interrelationship of their cores is demonstrated by the fact that the mean Pd–Pd separations within the fragments are amazingly similar, in spite of the ellipsoidal Pd_{30}- and Pd_{54}-core geometries. Salient structural/bonding features and their resulting implications are: 1) Pd(i)–Pd(i) mean separations of 2.77 and 2.76 Å for the two and six interior Pd(i) atoms in the twinned cuboctahedral (ccp) and multi-twinned cuboctahedral (ccp/hcp)-based nanosized cores of **1** and **2**, respectively, which are analogous to the Pd–Pd separation of 2.75 Å found in ccp Pd metal.[18] This bond-length similarity is consistent with the interior palladium atoms being considered as having metallic character; 2) equivalent radial Pd(i)–Pd(s_1) and tangential Pd(s_1)–Pd(s_1) mean separations of 2.82–2.84 Å for the first-shell Pd(s_1) atoms that completely surround the interior Pd(i) atoms in **1**, **2**, and **3**. Their essentially identical mean separations, which are expected for ccp/hcp cores in metal nanoparticles,[19] point to analogous charge distributions for the similarly coordinated Pd(s_1) atoms, without undue strain effects being sterically imposed by the elliptical "twinned" cuboctahedral-based cores of **1** and **2**. The fact that the mean separations are approximately 0.08 Å longer than that of the interior Pd(i)–Pd(i) interactions can be attributed to ligation influences of the CO and $Pd(PEt_3)$ bridging units; 3) shorter mean Pd(s_1)–Pd(s_2) separations (by 0.024–0.062 Å), relative to the corresponding Pd(s_1)–Pd(s_1) interactions, can be readily ascribed to the bond-shortening influence of the two bridging CO groups that connect each capping {$Pd(PEt_3)$} unit (denoted as Pd(s_2)) to the Pd(s_1) atoms; and 4) their virtually identical overall mean Pd–Pd bonding connectivities of 2.81 Å which likewise signify that similar types of core geometries in palladium–carbonyl–phosphane clusters strongly influence its resulting metal–metal bonding characteristics.

A major outcome of this research is that the unprecedented metal-core architectures of **1** and **2** represent a hitherto unknown type of oligomerization as interpenetrating twinned composites of cuboctahedral (ccp/hcp) building blocks. The fact that **1** and **2** are by-products of the same reaction suggests a similar growth pattern that had not been previously encountered.

Received: October 14, 2002 [Z50363]

[1] L. D. Marks, *Rep. Prog. Phys.* **1994**, *57*, 603, and references therein.

[2] a) J. S. Bradley, E. W. Hill, S. Behal, C. Klein, B. Chaudret, A. Duteil, *Chem. Mater.* **1992**, *4*, 1234; b) C. Amiens, D. de Carlo, B. Chaudret, J. S. Bradley, R. Mazel, C. Roucau, *J. Am. Chem. Soc.* **1993**, *115*, 11638; c) M. J. Yacaman, J. A. Ascencio, H. B. Liu, J. Gardea-Torresdey, *J. Vac. Sci. Technol.* **2001**, *B19*, 1091; d) H. Bönnemann, R. M. Richards, *Eur. J. Inorg. Chem.* **2001**, 2455;

e) N. Toshima, T. Yonezawa, *New J. Chem.* **1998**, *2*, 1179, and references therein.

[3] Noncrystalline N,O-ligated (noncarbonyl) palladium nanoclusters possessing idealized formulations based upon concentric full-shell palladium cores have been reported: namely, five-shell Pd_{561} clusters[4,5] and mixtures of seven-shell Pd_{1415} and eight-shell Pd_{2057} clusters.[6]

[4] a) M. N. Vargaftik, V. P. Zagorodnikov, I. P. Stolyarov, I. I. Moiseev, V. A. Likholobov, D. I. Kochubey, A. L. Chuvilin, V. I. Zaikovsky, K. I. Zamaraev, G. I. Timofeeva, *J. Chem. Soc. Chem. Commun.* **1985**, 937; b) M. N. Vargaftik, I. I. Moiseev, D. I. Kochubey, K. I. Zamaraev, *Faraday Discuss.* **1991**, *92*, 13; c) "Catalysis with Palladium Clusters": I. I. Moiseev, M. N. Vargaftik in *Catalysis by Di- and Polynuclear Metal Cluster Compounds* (Eds.: R. D. Adams, F. A. Cotton), Wiley-VCH, New York, **1998**, p. 395; d) T. A. Stromnova, I. I. Moiseev, *Russ. Chem. Rev.* **1998**, *67*, 485.

[5] a) G. Schmid, *Polyhedron* **1988**, *7*, 2321; b) G. Schmid, *Chem. Rev.* **1992**, *92*, 1709.

[6] G. Schmid, M. Harms, J.-O. Malm, J.-O. Bovin, J. van Ruitenbeck, H. W. Zandbergen, W. T. Fu, *J. Am. Chem. Soc.* **1993**, *115*, 2046.

[7] a) N. K. Eremenko, E. G. Mednikov, S. S. Kurasov, *Russ. Chem. Rev.* **1985**, *54*, 394, and references therein; b) N. K. Eremenko, S. P. Gubin, *Pure Appl. Chem.* **1990**, *62*, 1179; c) A. D. Burrows, D. M. P. Mingos, *Transition Met. Chem.* **1993**, *18*, 129, and references therein; d) R. B. King, *Gazz. Chim. Ital.* **1992**, *122*, 383; e) K. R. Dixon, A. C. Dixon, *Comprehensive Organometallic Chemistry II, Vol. 9* (Eds.: E. W. Abel, F. G. A. Stone, G. Wilkinson, R. J. Puddephatt), Elsevier, Tarrytown, NY, **1995**, p. 194; f) T. A. Stromnova, I. I. Moiseev, *Russ. Chem. Rev.* **1998**, *67*, 485, and references therein; g) E. G. Mednikov, S. A. Ivanov, I. A. Guzei, L. F. Dahl, *Abst. of Papers*, 222nd ACS National Meeting of American Chemical Society, Chicago, IL.; American Chemical Society, Washington, DC, **2001**, INORG 331.

[8] a) $[Pd_{10}(CO)_{12}(PR_3)_6]$ (R = *n*Bu, Et): E. G. Mednikov, N. K. Eremenko, *Izv. Akad. Nauk SSSR Ser. Khim.* **1982**, 2540. [E. G. Mednikov, N. K. Eremenko, *Russ. Chem. Bull.* **1983**, *32*, 2240 (*Engl. Trans.*)]; b) $[Pd_{10}(CO)_{14}(PnBu_3)_4]$: E. G. Mednikov, N. K. Eremenko, Yu. L. Slovokhotov, Yu. T. Struchkov, S. P. Gubin, *J. Organomet. Chem.* **1983**, *258*, 247; c) $[Pd_{10}(CO)_{12}(PPh_3)_6]$: E. G. Mednikov, N. K. Eremenko, *Izv. Akad. Nauk SSSR Ser. Khim.* **1984**, 2781. [E. G. Mednikov, N. K. Eremenko, *Russ. Chem. Bull.* **1984**, *33*, 2547 (*Engl. Trans.*)]; d) $[Pd_{12}(CO)_{12}(PnBu_3)_6]$: E. G. Mednikov, Yu. T. Struchkov, Yu. L. Slovokhotov, *J. Organomet. Chem.* **1998**, *566*, 15; e) $[Pd_{16}(CO)_{13}(PEt_3)_9]$: E. G. Mednikov, Yu. L. Slovokhotov, Yu. T. Struchkov, *Metalloorg. Khim.* **1991**, *4*, 123. [E. G. Mednikov, Yu. L. Slovokhotov, Yu. T. Struchkov, *Organomet. Chem. USSR* **1991**, *4*, 65 (*Engl. Trans.*)]; f) $[Pd_{23}(CO)_{20}(PEt_3)_8]$: E. G. Mednikov, N. K. Eremenko, Yu. L. Slovokhotov, Yu. T. Struchkov, *Zh. Vsesoyuzn. Khim. O-va im. D. I. Mendeleeva*, **1987**, *32*, 101 (*in Russian*); E. G. Mednikov, *Izv. Akad. Nauk SSSR Ser. Khim.* **1993**, 1299. [E. G. Mednikov, N. K. Eremenko, Yu. L. Slovokhotov, Yu. T. Struchkov, *Russ. Chem. Bull.* **1993**, *42*, 1242 (*Engl. Trans.*)]; g) $[Pd_{23}(CO)_{22}(PEt_3)_{10}]$: E. G. Mednikov, N. K. Eremenko, Yu. L. Slovokhotov, Yu. T. Struchkov, *J. Organomet. Chem.* **1986**, *301*, C35; E. G. Mednikov, *Metalloorg. Khim.* **1991**, *4*, 885. [E. G. Mednikov, *Organomet. Chem. USSR* **1991**, *4*, 433 (*Engl. Trans.*)]; h) $[Pd_{34}(CO)_{24}(PEt_3)_{12}]$, $[Pd_{38}(CO)_{28}(PR_3)_{12}]$, (R = Et, *n*Bu): E. G. Mednikov, N. I. Kanteeva, *Izv. Akad. Nauk SSSR Ser. Khim.* **1995**, 167 [E. G. Mednikov, N. I. Kanteeva, *Russ. Chem. Bull.* **1995**, *44*, 163 (*Engl. Trans.*)]; i) $[Pd_{38}(CO)_{28}(PEt_3)_{12}]$ (**5**): E. G. Mednikov, N. K. Eremenko, Yu. L. Slovokhotov, Yu. T. Struchkov, *J. Chem. Soc. Chem. Commun.* **1987**, 218; j) E. G. Mednikov, P. V. Petrovsky, Yu. L. Slovokhotov, O. A. Belyakova, N. I. Malkina, unpublished results; k) E. G. Mednikov, unpublished results.

[9] a) $[Pd_{10}(CO)_{12}(PEt_3)_6]$ (**4**): D. M. P. Mingos, C. M. Hill, *Croat. Chem. Acta* **1995**, *68*, 745; b) $[Pd_{145}(CO)_x(PEt_3)_{30}]$: N. T. Tran, D. R. Powell, L. F. Dahl, *Angew. Chem.* **2000**, *112*, 4287; *Angew. Chem. Int. Ed.* **2000**, *39*, 4121; c) $[Pd_{16}(CO)_{13}(PMe_3)_9]$, $[Pd_{35}(CO)_{23}(PMe_3)_{15}]$, $[Pd_{39}(CO)_{23}(PMe_3)_{16}]$, $[Pd_{59}(CO)_{32}(PMe_3)_{21}]$: N. T. Tran, M. Kawano, L. F. Dahl, *J. Chem. Soc. Dalton Trans.* **2001**, 2731.

[10] Interestingly, reactions of the $[Pd_{13}Ni_{13}(CO)_{34}]^{4-}$ tetraanion[11a] with PEt_3 produced, in addition to the known Pd_{10}, Pd_{16}, and Pd_{34} clusters,[8a,e,h] a different crystal form of $[Pd_{23}(CO)_{20}(PEt_3)_{10}]$[11b] that has the same Pd_{23} framework as that previously reported by Mednikov et al.[8g] for $[Pd_{23}(CO)_{22}(PEt_3)_{10}]$ but with two fewer CO groups; a comparative molecular analysis favors the existence of both clusters.[11b,c]

[11] a) N. T. Tran, M. Kawano, D. R. Powell, L. F. Dahl, *J. Chem. Soc. Dalton Trans.* **2000**, 4138; b) J. Wittayakun, N. T. Tran, D. R. Powell, L. F. Dahl, unpublished results; c) E. G. Mednikov, L. F. Dahl, unpublished results.

[12] In contrast to the generally close-packed metal frameworks of palladium carbonyl phosphanes, such as **1** and **2**, the metal-core geometry of $[Pd_{38}(CO)_{28}(PEt_3)_{12}]$ (**5**)[8i] cannot be described in terms of close-packing without invoking considerable distortions.

[13] In a typical procedure, $[Pd_{10}(CO)_{12}(PEt_3)_6]$ (**4**, 0.150 g, 0.071 mmol) was combined with a mixture of Me_2CO (7 mL), iPr_2O (2 mL), and CF_3CO_2H (0.1 mL) in a 100-mL flask and stirred at room temperature, initially under N_2 for 1 h, then under CO for 2 h, and finally under N_2. After two weeks, easily distinguishable black end-sharpened needle-shaped crystals of **1**·2 Me_2CO and black end-flattened needle-shaped crystals of **2**·2 Me_2CO were separated under the microscope from the black block-shaped crystals of $[Pd_{38}(CO)_{28}(PEt_3)_{12}]$ (**5**). Estimated yields of crystals of **1**·2 Me_2CO (less than 5%), **2**·2 Me_2CO (less than 1%), and **5**·2 Me_2CO (55–57%). Similar yields of crystals of **1** and **2** were obtained by direct treatment under CO (70–80 min) of solutions of **4** (0.150 g) in Me_2CO (7 mL), Et_2O (2 mL), HOAc (0.17 mL), and CF_3CO_2H (0.05 mL) followed by crystallization under N_2. Compound **2** was also prepared as a minor product without the assistance of CO but in the presence of HCO_2H instead of HOAc, and either with or without CF_3CO_2H.[14] None of the reactions without CO have given **1**. IR spectra of **1** and **2** (Nujol, CaF_2 cell) exhibited bridging CO groups at 1910 (m), 1881 (s), 1864 (sh) cm^{-1} and 1920 (m), 1878 (s), 1802 (w) cm^{-1}, respectively. Crystals of **5** were identified from both single-crystal X-ray data and an IR spectrum, as previously described.[8h,i]

[14] In one of these reactions, different solvated crystals of **2** were isolated and identified from by X-ray crystallographic analysis. **2**·3 Me_2CO: triclinic; $P\bar{1}$; $a = 17.599(2)$, $b = 18.773(2)$, $c = 20.457(2)$ Å, $\alpha = 65.176(1)$, $\beta = 68.656(1)$, $\gamma = 66.086(1)°$, $V = 5452.4$ Å^3, $Z = 1$, $\rho_{calcd} = 2.648$ Mg m^{-3}. Compound **2**·3 Me_2CO has crystallographic $C_i(\bar{1})$ site symmetry. It is noteworthy that crystals of **2**·3 Me_2CO exploded in the absence of a solution environment, even in paratone(N) or epoxy components; they could only be stabilized for an X-ray diffraction study in a quickly hardening solution of polystyrene in Me_2CO/Et_2O.

[15] a) **1**·2 Me_2CO: monoclinic; $P2_1/n$; $a = 13.862(1)$, $b = 25.294(2)$, $c = 19.648(2)$ Å, $\beta = 97.882(1)°$, $V = 6824.2(9)$ Å^3; $Z = 2$, $\rho_{calcd} = 2.539$ Mg m^{-3}. $Mo_{K\alpha}$ data collected at 173(2) K with SMART CCD 1000 area detector diffractometer by 0.3ω scans over a 2θ range 3.2–56.6°; empirical absorption correction (SADABS) applied ($\mu(Mo_{K\alpha}) = 4.014$ mm^{-1}; max/min transmission, 0.856/0.379). Anisotropic refinement (695 parameters; 47 restraints) on 16927 independent reflections converged at $\omega R_2(F^2) = 0.126$ with $R_1(F) = 0.044$ for $I > 2\sigma(I)$; GOF (on F^2) = 0.92; max/min

 © 2003 Wiley-VCH Verlag GmbH & Co. KGaA, Weinheim 1433-7851/03/4203-0326 $ 20.00+.50/0

residual electron density, 2.19/−2.18 e Å^{-3}.Compound **1** has crystallographic $C_i(\bar{1})$ site symmetry such that the asymmetric part of the crystal structure consists of 1/2 of a neutral cluster and one solvated acetone molecule; b) **2**·2 Me_2CO: monoclinic; $P2_1/n$; $a = 17.517(1)$, $b = 24.471(2)$, $c = 24.216(2)$ Å, $\beta = 106.233(1)°$, $V = 9966.5(13)$ Å^3; $Z = 2$, $\rho_{calcd} = 2.878$ Mg m^{-3}. $Mo_{K\alpha}$ data collected at 173(2) K with SMART CCD 1000 area detector diffractometer by 0.3ω scans over 2θ range 2.9–56.6°; empirical absorption correction (SADABS) applied ($\mu(Mo_{K\alpha}) = 4.900$ mm^{-1}; max./min. transmission, 0.758/0.374). Anisotropic refinement (1044 parameters; 74 restraints) on 24577 independent reflections converged at $\omega R_2(F^2) = 0.158$ with $R_1(F) = 0.052$ for $I > 2\sigma(I)$; GOF (on F^2) = 0.99; max./min. residual electron density, 2.13/−2.56 e Å^{-3}. Compound **2** has crystallographic $C_i(\bar{1})$ site symmetry such that the asymmetric part of the crystal structure consists of 1/2 of a neutral molecule and one solvated acetone molecule. CCDC-195160 (**1**) and -195161 (**2**) contain the supplementary crystallographic data for this paper. These data can be obtained free of charge via www.ccdc.cam.ac.uk/conts/retrieving.html (or from the Cambridge Crystallographic Data Centre, 12, Union Road, Cambridge CB21EZ, UK; fax: (+44) 1223-336-033; or deposit@ccdc.cam.ac.uk).

[16] Observed electron counts of 372, 648, and 290 electrons were obtained for **1**, **2**, and **3**, respectively. Application of the Mingos electron-counting model[17] for a close-packed metal cluster gives rise to the following predicted electron counts: namely, 290 electrons (i.e., 12 × 18(surface) + 18(interior) + 4 × 14(wingtip)) for **3** and 378 electrons (i.e., 12 × 24(surface) + 34(two interior) + 4 × 14(wingtip)) for **1**. The highly condensed geometry of **2** prevents a reliable predicted electron count.

[17] a) D. M. P. Mingos, *J. Chem. Soc. Chem. Commun.* **1985**, 1352; b) D. M. P. Mingos, L. Zhenyang, *J. Chem. Soc. Dalton Trans.* **1988**, 1657.

[18] J. Donohue, *The Structures of the Elements*, Wiley, New York, **1974**, p. 216.

[19] In sharp contrast, corresponding mean radial Pd(i)–Pd(s_1) separations found in face-condensed icosahedral-based Pd-core geometries of high-nuclearity palladium carbonyl trimethylphosphine clusters are approximately 0.14 Å shorter than the mean tangential intrashell Pd(s_1)–Pd(s_1) separations (that is, 2.73 (av) versus 2.87 Å (av)).[9c] This large difference is ascribed to geometrically imposed radial compressions in icosahedral-based polyhedra. The close agreement of the mean Pd–Pd separations determined for the radial and tangential (intrashell) connectivities in **1**, **2**, and **3** point to the absence of geometrical distortions in the metal-core geometries of cuboctahedral-based systems.

Chemical Adaptor Systems

A Chemical Adaptor System Designed To Link a Tumor-Targeting Device with a Prodrug and an Enzymatic Trigger**

*Anna Gopin, Neta Pessah, Marina Shamis, Christoph Rader, and Doron Shabat**

Selective chemotherapy remains a key issue for successful treatment in cancer therapy. Prolonged administration of effective concentrations of chemotherapeutic agents is usually not possible because of dose-limiting systemic toxicities. Furthermore, strong side effects involving nonmalignant tissues are often observed. Therefore, much effort has been devoted to the development of new drug delivery systems that mediate drug release selectively at the tumor site. One way to achieve such selectivity is to activate a prodrug specifically by a confined enzymatic activity. In this concept, the enzyme is either expressed by the tumor cells, or brought to the tumor by a targeting moiety such as a monoclonal antibody.[1] The prodrug is converted to an active drug by the local or localized enzyme at the tumor site, thereby minimizing nonspecific toxicity to other tissues.

Here we present a new concept that combines a tumor-targeting device, a prodrug, and a prodrug activation trigger in a single entity. We designed a generic module or chemical adaptor that is based on three chemical functionalities as shown in Figure 1. The first functionality is attached to an active drug and**,** thereby, masks it to yield a prodrug. The second functionality is linked to a targeting moiety, which is responsible for guiding the prodrug to the tumor site, and the third functionality is attached to an enzyme substrate. When the corresponding enzyme cleaves the substrate, it triggers a spontaneous reaction that releases the active drug from the targeting moiety. As a result, prodrug activation will preferentially occur at the tumor site.

The central core of our chemical adaptor (Scheme 1) is based on 4-hydroxymandelic acid, which is commercially available and has three functional groups suitable for linkage. Group **I** is a carboxylic acid that is conjugated to a targeting moiety through an amide bond. The drug is linked through the benzyl alcohol group **II**, and the enzyme substrate is attached through the phenol group **III** by a carbamate bond.

[*] Dr. D. Shabat, A. Gopin, N. Pessah, M. Shamis, Dr. C. Rader
Department of Organic Chemistry
School of chemistry, Faculty of Exact Sciences
Tel Aviv University
Tel Aviv 69978 (Israel)
Fax: (+972) 3-640-9293
E-mail: chdoron@post.tau.ac.il

[**] We thank Professor Richard A. Lerner and Professor Carlos F. Barbas III of The Scripps Research Institute for providing antibody 38C2 and TEVA Pharmaceutical Industries Ltd., Israel for a gift of etoposide. We also thank Ms. Rajeswari Thayumanavan for early contributions to this work.

Supporting information for this article is available on the WWW under http://www.angewandte.org or from the author.

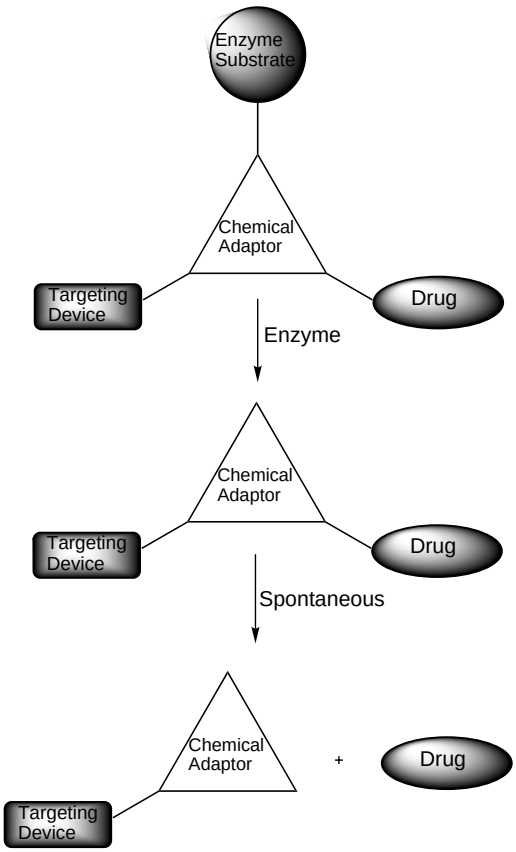
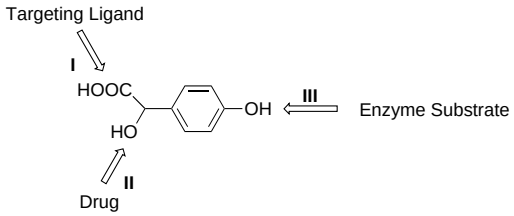


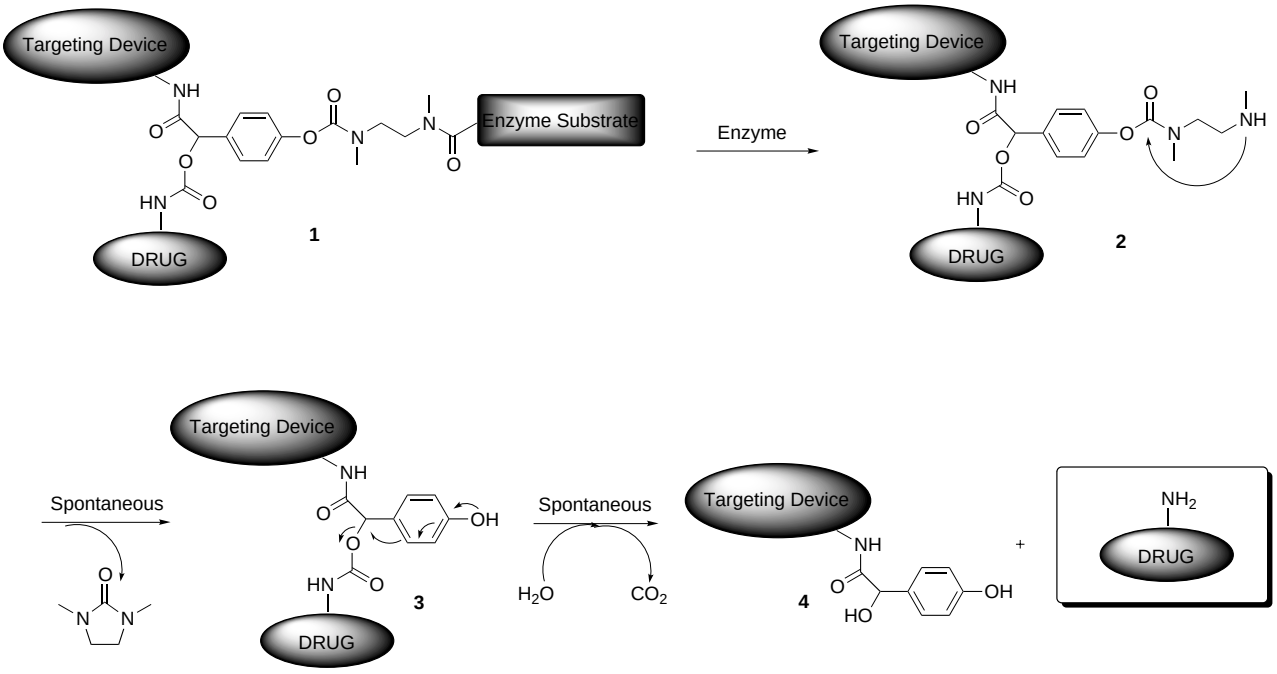
Figure 1. 4-Hydroxymandelic acid, the central core of the **c**hemical adaptor system.



Scheme 1. General design of the chemical adaptor system. Cleavage of the enzyme substrate generates an intermediate that spontaneously rearranges to release the drug from the targeting device.

Scheme 2 illustrates the release mechanism of the drug. Cleaving the enzyme substrate generates a free amine group (**2**) that spontaneously cyclizes to form a dimethyl urea derivative and phenol **3**. The latter undergoes spontaneous rearrangement to give a quinone methide intermediate (trapped by water to give benzyl alcohol **4**), which releases the drug in the form of carbamic acid, which then decarboxylates spontaneously, yielding the active drug.

The design of our generic module allows us to potentially link any targeting device to a variety of drugs and to release them with any enzyme by using the corresponding substrate as a trigger. As proof of the concept, we designed a pilot system for which we chose catalytic antibody 38C2 as the cleaving enzyme.[2] Antibody 38C2 catalyzes a sequence of retro-aldol retro-Michael reactions, using substrates that are not recognized by human enzymes, and thus, are ideal triggers for selective prodrug activation. Antibody 38C2 has proven its ability to catalyze the retro-aldol reactions with a broad range of substrates[3] and recently was conjugated to an *N*-(2-hydroxypropyl)methacrylamide (HPMA) copolymer for tumor targeting.[4] Furthermore, antibody 38C2 has demon-

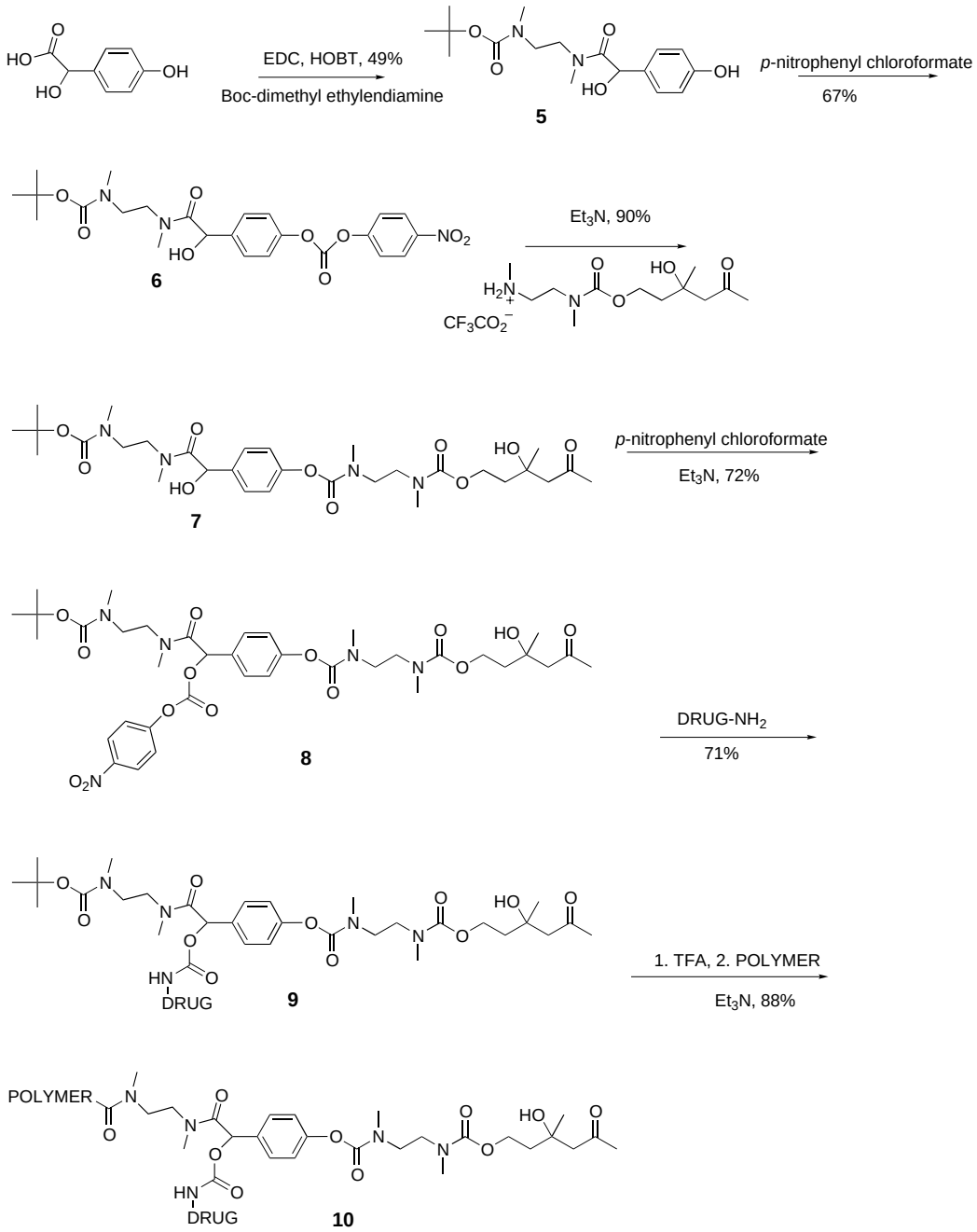


Scheme 2. General mechanism of drug release starting with specific enzymatic cleavage.

 © 2003 Wiley-VCH Verlag GmbH & Co. KGaA, Weinheim 1433-7851/03/4203-0328 $ 20.00+.50/0

strated its efficacy in activating several prodrugs in vitro and in vivo.[5] A dramatic 75% decrease in subcutaneous (s.c.) tumor size has been observed in mice that received an intratumoral injection of antibody 38C2 and systemic treatments with an etoposide prodrug.[6]

As a targeting device we chose a polymer molecule for our pilot system. Water-soluble synthetic polymers such as HPMA copolymers are biocompatible, nonimmunogenic,[7] and nontoxic. Moreover, their in vivo distribution is well characterized[8] and they are known to accumulate selectively at tumor sites due to the enhanced permeability and retention (EPR) effect.[9] This effect occurs because of the difference between the vasculature physiology of solid tumors and normal tissues. Compared with the regular ordered vasculature of normal tissues, blood vessels in tumors are often highly abnormal. The growth of the tumor creates a constant need for the continuous supply of new blood vessels. This process, termed angiogenesis, often results in the construction of vessels with leaky walls, which allows enhanced permeability of macromolecules within the tumor. In addition, poor



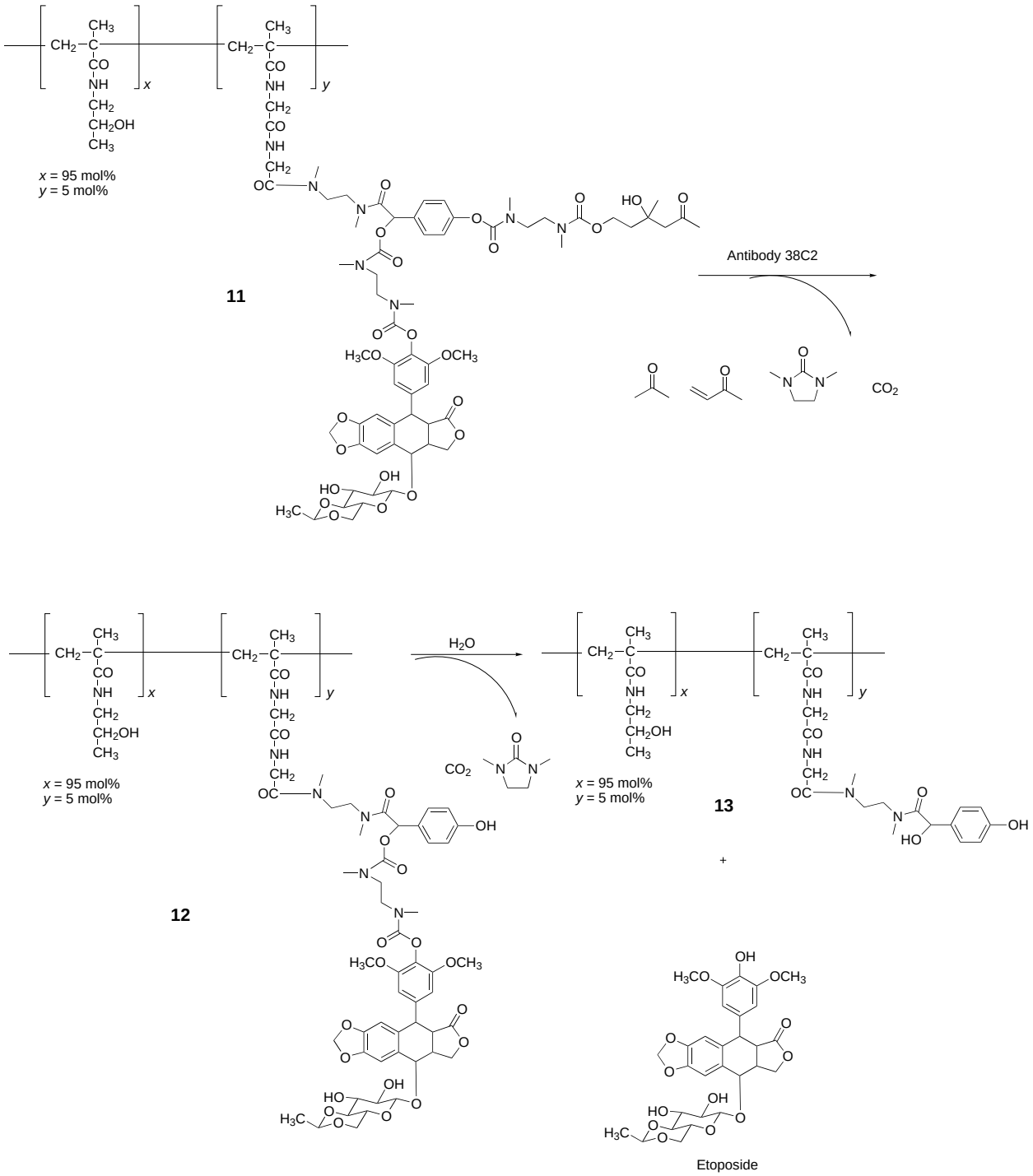
Scheme 3. Synthesis of the chemical adaptor system using catalytic antibody 38C2 as the activating enzyme, an HPMA copolymer as a targeting device, and any drug with a functional amine group. EDC = 1-[3-(dimethylamino)propyl]-3-ethylcarbodiimide, HOBT = 1-hydroxybenzotriazole, TFA = trifluoroacetic acid.

 © 2003 Wiley-VCH Verlag GmbH & Co. KGaA, Weinheim 1433-7851/03/4203-0329 $ 20.00+.50/0

lymphatic drainage at the tumor site promotes accumulation of large molecules. Based on the tumor-targeting properties of molecules derivatized with HPMA copolymers, polymer-directed enzyme prodrug therapy (PDEPT) was developed by Duncan et al. as a novel approach toward selective chemotherapy.[10]

Etoposide was selected as the drug in our pilot system. It is a well-established anticancer drug, which was approved for clinical use by the FDA in the late 1970s, after it demonstrated efficacy in chemotherapy. Etoposide exhibits its antitumor activity by inhibition of enzymes that cut and pass double-stranded DNA called topoisomerase inhibitors.[11] The phenol group of etoposide was used to link it to the complex through a carbamate bond (see Scheme 4).

Starting from 4-hydroxymandelic acid, we built the complex as described in Scheme 3. In brief, 4-hydroxyman-



Scheme 4. Mechanism of etoposide drug release from the HPMA-copolymer, using catalytic antibody 38C2 as the triggering enzyme.

 © 2003 Wiley-VCH Verlag GmbH & Co. KGaA, Weinheim 1433-7851/03/4203-0330 $ 20.00+.50/0

delic acid was coupled with monoprotected Boc-dimethylethylenediamine in the presence of EDC and HOBT to give amide **5**. Selective acylation of the phenol group with *p*-nitrophenyl chloroformate afforded carbonate **6**, which was treated with antibody 38C2- substrate to give compound **7**. Acylation of the benzylic alcohol with *p*-nitrophenyl chloroformate gave carbonate **8**, which was treated with an amine drug to give compound **9**. The Boc protecting group was removed by TFA to give the corresponding amine salt, which was immediately coupled with the *p*-nitrophenyl ester of the HPMA copolymer to give the final complex **10**. The drug–polymer conjugate was purified by dialysis against water. By measuring its UV spectrum, the number of drug molecules attached to the HPMA copolymer was determined. Based on the etoposide chromophore, which has a λ_{max} value at 280 nm, we found that on average three molecules of the drug were linked to one molecule of the HPMA copolymer.

Next we tested whether the etoposide drug can be released from complex **11** by the catalytic activity of antibody 38C2. According to our design, the drug should be spontaneously released after the generation of phenol **12** as illustrated in Scheme 4. We incubated complex **11** with catalytic antibody 38C2 in phosphate-buffered saline (PBS) (pH 7.4) at 37 °C and monitored the appearance of etoposide using an HPLC assay. As a positive control, we used a previously described etoposide prodrug[6] that is activated by antibody 38C2. As Figure 2 shows, etoposide was released by the catalytic activity of antibody 38C2 to form compound **13** and the free drug. The rate of drug release was similar to the activation rate of the known etoposide prodrug. No spontaneous etoposide release was observed in the absence of the antibody.

The general synthetic approach of introducing the drug in our chemical adaptor system as outlined in Scheme 3, involves a reaction between an amine group of the drug and a *p*-nitrophenyl carbonate of a hydroxybenzyl alcohol to form a carbamate linkage. This strategy is convenient when the drug has an available amine group such as in the case of doxorubicin. Drugs like etoposide, which have free hydroxy groups that need to be masked, are linked through an *N*,*N*-dimethylethylenediamine spacer, which spontaneously immolates to form a dimethyl urea derivative (see Scheme 4).

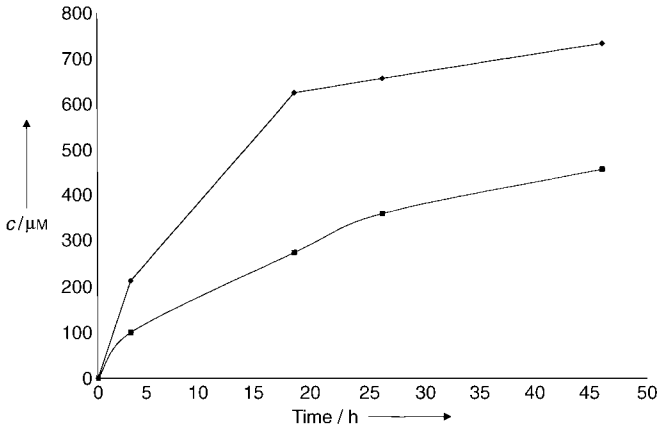


Figure 2. Determination of etoposide release from the HPMA copolymer versus drug formation from a known etoposide prodrug by catalytic antibody 38C2. ◆ Complex **11** (500 μM) with antibody 38C2 (66 μM) in PBS-7.4. ■ Etoposide prodrug (500 μM) with antibody 38C2 (66 μM) in PBS (pH 7.4). Reactions were incubated at 37 °C for the indicated time. The drug release concentration *c* was monitored by HPLC analysis.

A similar and elegant approach of enzymatic cleavage leading to a small-molecule release, was recently published by Waldmann et al.[12] An enzyme-labile linker group was attached to a solid support and a third functionality was used for solid-phase synthesis of a target molecule. The small molecule was detached from the polymeric support, starting by enzymatic cleavage, leading to generation of an intermediate that spontaneously released the product. In one example a quinone methide rearrangement was used to release the target molecule, similarly to our approach.[13] The intermediate was generated by enzymatic cleavage of an ester group, which would result in a high background if used for in vivo prodrug activation. Whereas ester functionalities are stable in organic solvents, they undergo rapid hydrolysis in aqueous solutions at physiological pH. In addition, endogenous enzymes with esterase activity further contribute to nonspecific prodrug activation. In view of these facts, we designed a chemical adaptor system that does not contain any ester linkages but utilizes rather stable amide and carbamate bonds.

In conclusion, we have developed a drug delivery system based on a chemical adaptor that provides a generic linkage of a drug with a targeting device in a manner suitable for triggering by defined enzymatic activity. The system is generic and can be applied to a variety of drugs, targeting devices, and enzymes by introducing the corresponding substrate as a trigger for drug release in the chemical adaptor. The chemical adaptor system was designed with stable chemical linkages to avoid nonspecific drug release in vivo. Proof of the concept was demonstrated by using etoposide as the drug, an HPMA copolymer as the targeting device, and catalytic antibody 38C2 as the triggering enzyme. Currently we are synthesizing a variety of chemical adaptor systems using different tumor-targeting devices, prodrugs, and enzymatic triggers. Two additional examples, comprising a penicillin amidase substrate as the enzymatic trigger and camptothecin as the anticancer drug, respectively, are described in the Supporting Information. In vivo studies aimed at testing our chemical adaptor concept for the selective targeting of tumors have been initiated.

Received: May 21, 2002
Revised: October 22, 2002 [Z19328]

[1] K. D. Bagshawe, S. K. Sharma, C. J. Springer, G. T. Rogers, *Ann. Oncol.* **1994**, *5*, 879–891.
[2] J. Wagner, R. A. Lerner, C. F. Barbas III, *Science* **1995**, *270*, 1797–1800.
[3] T. Hoffmann, G. Zhong, B. List, D. Shabat, J. Anderson, S. Gramatikova, R. A. Lerner, C. F. Barbas III, *J. Am. Chem. Soc.* **1998**, *120*, 2768–2779.
[4] R. Satchi-Fainaro, W. Wrasidlo, H. N. Lode, D. Shabat, *Bio. Org. Med. Lett.* **2002**, *10*, 3023–3029.

 © 2003 Wiley-VCH Verlag GmbH & Co. KGaA, Weinheim 1433-7851/03/4203-0331 $ 20.00+.50/0

[5] D. Shabat, C. Rader, B. List, R. A. Lerner, C. F. Barbas III, *Proc. Natl. Acad. Sci. USA* **1999**, *96*, 6925 – 6930.
[6] D. Shabat, H. Lode, U. Pertl, R. A. reisfeld, C. Rader, R. A. Lerner, C. F. Barbas III, *Proc. Natl. Acad. Sci. USA* **2001**, *98*, 7528 – 7533.
[7] B. Rihova, M. Bilej, V. Vetvicka, K. Ulbrich, J. Strohalm, J. Kopecek, R. Duncan, *Biomaterials* **1989**, *10*, 335 – 342.
[8] L. W. Seymour, K. Ulbrich, J. Strohalm, J. Kopecek, R. Duncan, *Biochem. Pharmacol.* **1990**, *39*, 1125 – 1131.
[9] H. Maeda, J. Wu, T. Sawa, Y. Matsumura, K. Hori, *J. Controlled Release* **2000**, *65*, 271 – 284.
[10] R. Satchi, T. A. Connors, R. Duncan, *Br. J. Cancer* **2001**, 1070 – 1076.
[11] K. R. Hande, *Eur. J. Cancer* **1998**, *34*, 1514 – 1521.
[12] U. Grether, H. Waldmann, *Chem. Eur. J.* **2001**, *7*, 959 – 971.
[13] B. Sauerbrei, V. Jungmann, H. Waldmann, *Angew. Chem.* **1998**, *110*, 1187 – 1190; *Angew. Chem. Int. Ed.* **1998**, *37*, 1143 – 1146.

Light Harvesting with Gels

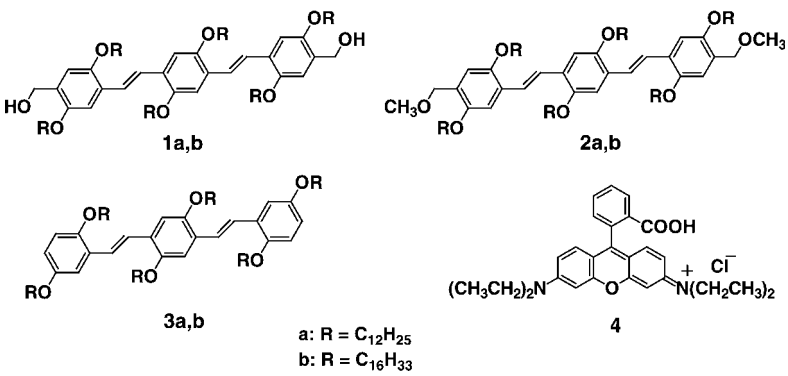
Gelation-Assisted Light Harvesting by Selective Energy Transfer from an Oligo(*p*-phenylenevinylene)-Based Self-Assembly to an Organic Dye**

Ayyappanpillai Ajayaghosh, Subi J. George, and Vakayil K. Praveen*

Dedicated to the memory of Darshan Ranganathan

Excitation energy transfer within and between molecular systems plays an important role in natural processes, such as photosynthesis. In this context, there has been widespread interest in mimicking the mechanism of solar-energy harvesting of natural photosynthesis with the aid of synthetic molecular systems. Apart from this, photoinduced energy transfer has become significant in the area of photovoltaics, organic light-emitting diodes, fluorescent labeling, and in a variety of photonic devices. In most of these cases, energy transfer is considerably influenced by the supramolecular ordering and spatial relationship of the donor and acceptor chromophores. Molecular architectures such as hydrogen-bonded systems,[1] dendrimers,[2] chromophore-linked polymers,[3] Langmuir–Blodgett films,[4] and self-assembled monolayers[5] are of extremely important in this context. Among a plethora of donor–acceptor systems investigated, energy and electron transfer from oligo(phenylenevinylene)s (OPVs) and poly(phenylenevinylene)s (PPVs) to acceptors, such as C_{60},[6] phenanthroline,[7] and doped organic dyes[8] have generated enormous interest because of their potential use in photovoltaic and light-emitting devices. From this view point, the recent reports by Meijer and coworkers on energy and electron transfer from OPV-functionalized dendrimers and supramolecular assemblies to various acceptors are of particular interest.[9] This situation has prompted us to investigate on the potential of OPV based organogels for the purpose of energy transfer and light harvesting.[10]

Small-molecule-based organogels have attracted much attention in recent years because of their interesting physical properties and architectural elegance.[11] However, organogels based on π-conjugated systems are relatively very few.[12] Recently, we have reported hydrogen-bond- and π-stack-induced supramolecular assembly of the OPV derivatives **1a**,**b**, which leads to the formation of entangled nanostructures, which induce gelation of hydrocarbon solvents.[13] The absorption and emission properties of **1a**,**b** showed dramatic changes during gelation, which is an indication of strong intermolecular π-electronic coupling of the ordered self-assembled OPV gel. Excitation of **1a**,**b** in cyclohexane at 380 and 470 nm revealed the emission corresponding to the monomeric species ($\lambda_{em} = 455$ and 483 nm, $\Phi_f = 0.40 \pm 0.01$ related to quinine sulfate, $\tau = 1.46$ ns; Figure 1, spectrum b) and self-assembled species ($\lambda_{em} = 525$ and 565 nm, $\Phi_f = 0.40 \pm 0.01$ related to Rhodamine 6G, $\tau = 1.62$ ns; Figure 1, spectrum c), which showed strong dependency on solvent polarity and temperature.



Herein we describe an interesting case of a thermoreversible fluorescence-resonance energy transfer (FRET) and light harvesting, exclusively from OPV based supramolecular gel nanostructures of **1a**,**b** to an organic dye. To study the feasibility of such an energy transfer, we chose Rhodamine B as the acceptor, the absorption ($\lambda_{max} = 555$ nm) of which

[*] Dr. A. Ajayaghosh, S. J. George, V. K. Praveen
Photochemistry Research Unit
Regional Research Laboratory, CSIR
Trivandrum-695019 (India)
Fax: (+91) 471-490-186
E-mail: aajayaghosh@rediffmail.com

[**] This work was supported by the Department of Science and Technology, Government of India under the Swarnajayanti scheme (DST/SF/C6/99-2000). We thank Mr. P. Prabhakar Rao for SEM analysis and CSIR for a research fellowship to S.J.G. This is contribution number RRLT-PRU-155.

Supporting information for this article is available on the WWW under http://www.angewandte.org or from the author.

 © 2003 Wiley-VCH Verlag GmbH & Co. KGaA, Weinheim 1433-7851/03/4203-0332 $ 20.00+.50/0

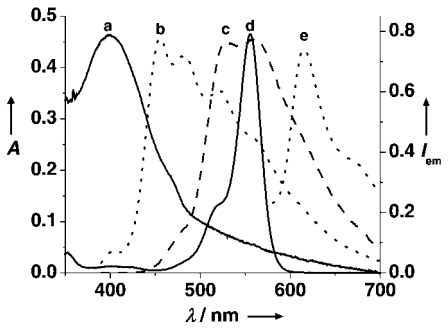


Figure 1. Individual absorption and emission spectra of **1b** and Rhodamine B in cyclohexane:chloroform (16:1). a) Absorption of **1b**, b) emission of monomeric **1b** at 380 nm excitation, c) emission of self-assembled **1b** gel at 470 nm excitation, d) absorption of Rhodamine B, e) emission of Rhodamine B ($\lambda_{ex} = 535$ nm).

matches with the emission of the self-assembled OPV ($\lambda_{em} =$ 527 and 560 nm) as indicated by their individual absorption and emission spectra (Figure 1). The absorption spectrum of a mixture of **1b** (1.01×10^{-5} M) and Rhodamine B (8×10^{-5} M) in a mixture of cyclohexane and chloroform (16:1) was recorded, which showed the characteristic absorption bands of the individual components, thereby ruling out any ground-state interaction between them.

In Figure 2a, the fluorescence emission spectra of **1b** and a mixture of **1b** and Rhodamine B in cyclohexane:chloroform (16:1) are shown. In this solvent mixture, **1b** (1.01×10^{-5} M) has a broad emission with three emission maxima at 455, 483, and 525 nm with a shoulder around 565 nm. When excited at 380 nm in the presence of Rhodamine B (8×10^{-5} M), selective quenching of the emission between 500–650 nm, corresponding to the self-assembled OPV, could be seen with the concomitant emission of Rhodamine B at 620 nm. This result is an indication of excitation energy-transfer selectively from the self-assembled OPVs to the Rhodamine B. The emission between 400–480 nm of the dissolved molecular OPV was virtually unaffected indicating no energy transfer from them. When the same solution was excited at 470 nm, the emission maxima at 527 and 560 nm corresponding to the self-assembled species were significantly quenched and the dye emission occurred at 620 nm (Figure 2b). When an optically matching solution of the dye was excited at 380 or 470 nm in the absence of **1b**, no significant emission could be seen. This situation is a clear indication that the emission from the dye occurs as a result of the energy transfer from the self-assembled gel and not by direct excitation. While, the emission profile of the optically matching solutions of the dye upon direct excitation at 535 nm and indirect excitation in the presence of **1b** at 470 nm were perfectly matching, the intensity of the latter was higher (inset of Figure 2b). This amplified emission points towards the efficient energy hopping from the donor to the acceptor by a Förster type mechanism.[14] The rate of energy transfer k_{ET} ($1.67 \times 10^{13}\,M^{-1}s^{-1}$) was estimated from the rate of fluorescence quenching k_{SV} ($2.7 \times 10^{4}\,M^{-1}$) obtained from the Stern–Volmer plot and the lifetime of the self-assembled species ($\tau =$ 1.62 ns).

Efficient energy transfer in solid film is a prerequisite for the designing of light-harvesting devices. In this context, we were keen to study the emission profile of a xerogel film of **1b** containing Rhodamine B (2:1 mol ratio). Interestingly, energy transfer occurs with high efficiency in this case (Figure 3). Emission maximum of the OPV film at 550 nm was completely quenched with the formation of a strong fluorescence from the dye ($\lambda_{max} = 620$ nm), when excited at 380 nm. However, emission of the same film upon direct excitation of the dye at 535 nm was negligible reiterating an efficient energy transfer in the former case. The apparent efficiency of energy transfer as estimated from the OPV fluorescence-

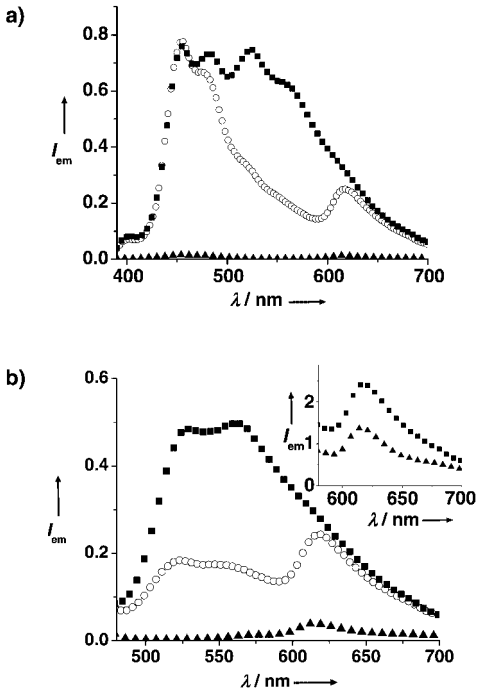


Figure 2. Energy-transfer quenching of the fluorescence of **1b** (1.01×10^{-5} M) in cyclohexane:chloroform (16:1) in the presence of Rhodamine B (8×10^{-5} M) a) at an excitation wavelength of 380 nm and b) at 470 nm. (■) fluorescence of **1b**, (○) fluorescence of **1b** + Rhodamine B, (▲) fluorescence of Rhodamine B. Inset of Figure 2b shows the emission of the dye on its indirect excitation at 470 nm (■) and direct (▲) excitation at and 535 nm illustrating the amplified emission.

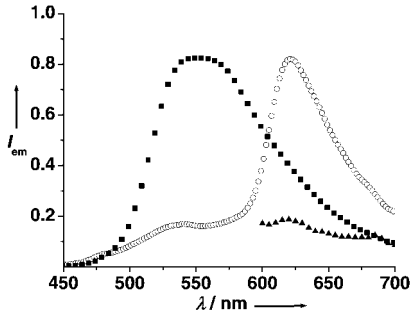


Figure 3. Normalized emission ($\lambda_{ex} = 380$ nm) from the film of **1b** (■), film of **1b** + Rhodamine B (2:1 mol ratio; ○), and from direct excitation ($\lambda_{ex} = 535$ nm) of Rhodamine B (▲), which illustrates the amplified emission from Rhodamine B by energy transfer.

 © 2003 Wiley-VCH Verlag GmbH & Co. KGaA, Weinheim 1433-7851/03/4203-0333 $ 20.00+.50/0

quenching profiles was 90% for the xerogel film and 63% for the solution. In the former case, most of the OPVs are in the form of self-assembled xerogel, where the donor and the acceptor chromophores are present well within the Förster radius, thereby facilitating efficient excitation-energy hopping when compared to that in solution. The observed emission from Rhodamine B as a result of the energy transfer from the OPV xerogel was several times more intense than that resulting from the direct excitation of the dye, which indicates efficient light harvesting in this donor–acceptor system.[15]

The role of the gel self-assembly in promoting the energy transfer is established by the temperature-dependent emission studies (Figure 4). At 5°C, more than 90% of the OPVs exist in the self-assembled form as evident from the emission spectrum. When excited at 380 nm, in the presence of the dye at 5°C, the emission of the gel was quenched and the dye emission occurred at 620 nm. Upon heating, the emission from the dye at 620 nm was decreased (>90% quenching above T_{gel}) with the concomitant increase of the molecular OPV emission at 455 and 483 nm (Figure 4, inset). Upon cooling the solution, the dye emission is regained. Since the energy transfer between the donor and acceptor is usually independent of temperature, the observed temperature effect in energy transfer is the consequence of thermoreversible breaking and forming of the self-assembled gel nanostructures. Similar results were obtained for the OPV **1a**. Interestingly, energy transfer was not predominant in the case of **2a**,**b** and **3a**,**b**, which failed to form gels (See Supporting Information).

Supramolecular organization of the donor chromophore (OPV) has a crucial role in transferring the excitation energy to the dispersed Rhodamine B (Figure 5). Detailed morphological studies of the OPV gels in the absence and presence of Rhodamine B using scanning electron microscopy (SEM) show that the dye molecules are partly trapped in the OPV-gel nanostructures and partly remain in the solvent medium.

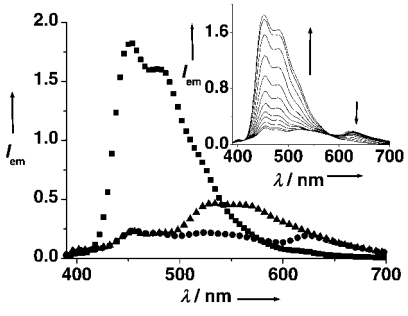


Figure 4. Temperature-dependence of energy transfer between **1b** (1.05×10^{-5} M) and Rhodamine B (5.85×10^{-5} M). (▲) emission spectrum of **1b** at 5°C, (●) emission spectrum of **1b** + Rhodamine B at 5°C, (■) emission spectrum of **1b** + Rhodamine B at 40°C. Inset shows the decrease in Rhodamine B emission with increasing temperature from 5°C to 40°C.

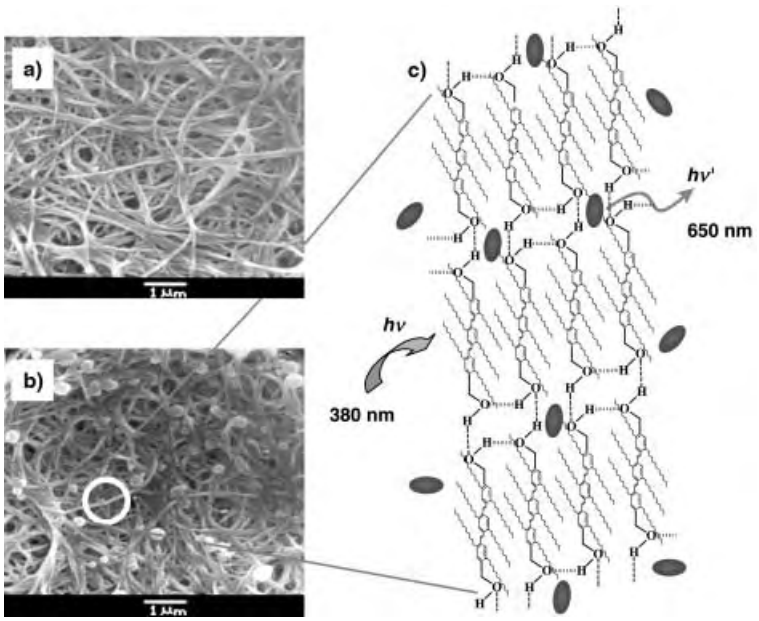


Figure 5. SEM images of the gel of **1b** from cyclohexane:chloroform (16:1) in the a) absence of Rhodamine B, and b) presence of Rhodamine B. c) Probable self-assembly of Rhodamine B dispersed OPV gel, the ellipsoids represent the trapped Rhodamine B molecules.

The energy transfer preferably occurs to the gel-trapped dye molecules, which are within the Förster radii. This may be the reason why we had to use excess concentrations of the dye relative to the OPVs for better energy transfer in the solvent medium. On the other hand, efficient fluorescence quenching and energy harvesting is possible from OPV xerogel film with lesser amount of the dye, since majority of the dye molecules are trapped in the xerogel film.

In conclusion, the role of hydrogen-bonded and π-stacked OPV self-assembly in facilitating energy transfer and light harvesting, exclusively from the gel phase is demonstrated. More importantly, the energy transfer could be thermally controlled by the reversible gelation of the OPVs. Detailed study of the role of the OPV gel morphology on energy and electron transfer to various acceptors and their use in photovoltaic devices are in progress.

Received: June 21, 2002
Revised: September 24, 2002 [Z19579]

[1] a) M. D. Ward, *Chem. Soc. Rev.* **1997**, *26*, 365–375.
[2] a) C. Devadoss, P. Bharathi, J. S. Moore, *J. Am. Chem. Soc.* **1996**, *118*, 9635–9644; b) P.-W. Wang, Y.-J. Liu, C. Devadoss, P. Bharathi, J. S. Moore, *Adv. Mater.* **1996**, *8*, 237–241; c) G. M. Stewart, M. A. Fox, *J. Am. Chem. Soc.* **1996**, *118*, 4354–4360; d) D.-L. Jiang, T. Aida, *Nature* **1997**, *388*, 454–456; e) M. Plevoets, F. Vögtle, L. DeCola, V. Balzani, *New J. Chem.* **1999**, *23*, 63–69; f) S. L. Gilat, A. Adronov, J. M. J. Fréchet, *Angew. Chem.* **1999**, *111*, 1519–1524; *Angew. Chem. Int. Ed.* **1999**, *38*, 1422–1427; g) A. Adronov, J. M. J. Fréchet, *Chem. Commun.* **2000**, 1701–1710; h) M.-S. Choi, T. Aida, T. Yamazaki, I. Yamazaki, *Angew. Chem.* **2001**, *113*, 3294–3298; *Angew. Chem. Int. Ed.* **2001**, *40*, 3194–3198.

 © 2003 Wiley-VCH Verlag GmbH & Co. KGaA, Weinheim 1433-7851/03/4203-0334 $ 20.00+.50/0

[3] a) M. Nowakowska, V. P. Foyle, J. E. Guillet, *J. Am. Chem. Soc.* **1993**, *115*, 5975 – 5981; b) D. M. Watkins, M. A. Fox, *J. Am. Chem. Soc.* **1994**, *116*, 6441 – 6442; c) X. Schultze, J. Serin, A. Adronov, J. M. J. Fréchet, *Chem. Commun.* **2001**, 1160 – 1161.
[4] P. J. Dutton, L. Conte, *Langmuir* **1999**, *15*, 613 – 617.
[5] L. A. J. Christoffels, A. Adronov, J. M. J. Fréchet, *Angew. Chem. Int. Ed.* **2000**, *112*, 2247 – 2251; *Angew. Chem. Int. Ed.* **2000**, *39*, 2163 – 2167.
[6] a) E. Peeters, P. A. van Hal, J. Knol, C. J. Brabec, N. S. Sacriciftci, J. C. Hummelen, R. A. J. Janssen, *J. Phys. Chem. B* **2000**, *122*, 10174 – 10190; b) N. Armaroli, F. Barigelletti, P. Ceroni, J.-F. Eckert, J.-F. Nicoud, J.-F. Nierengarten, *Chem. Commun.* **2000**, 599 – 600; c) J.-F. Eckert, J.-F. Nicoud, J.-F. Nierengarten, S.-G. Liu, L. Echegoyen, F. Barigelletti, N. Armaroli, L. Ouali, V. Krasnikov, G. Hadziioannou, *J. Am. Chem. Soc.* **2000**, *122*, 7467 – 7479.
[7] N. Armaroli, J.-F. Eckert, J.-F. Nierengarten, *Chem. Commun.* **2000**, 2105 – 2106.
[8] a) P. H. Bolivar, G. Wegmann, R. Kersting, M. Deussen, U. Lemmer, R. F. Mahrt, H. Bässler, E. O. Göbel, H. Kurz, *Chem. Phys. Lett.* **1995**, *245*, 534 – 538; b) J. Morgado, F. Cacialli, R. Iqbal, S. C. Moratti, A. B. Holmes, G. Yahioglu, L. R. Milgrom, R. H. Friend, *J. Mater. Chem.* **2001**, *11*, 278 – 283; c) K. Brunner, J. A. E. H. van Haare, B. M. W. Langeveld-Voss, H. F. M. Schoo, J. W. Hofstraat, A. van Dijken, *J. Phys. Chem. B* **2002**, *106*, 6834 – 6841.
[9] a) A. P. H. J. Schenning, E. Peeters, E. W. Meijer, *J. Am. Chem. Soc.* **2000**, *122*, 4489 – 4495; b) A. El-ghayoury, A. P. H. J. Schenning, P. A. van Hal, J. K. J. van Duren, R. A. J. Janssen, E. W. Meijer, *Angew. Chem.* **2001**, *113*, 3772 – 3775; *Angew. Chem. Int. Ed.* **2001**, *40*, 3660 – 3663; c) A. P. H. J. Schenning, J. v. Herrikhuyzen, P. Jonkheijm, Z. Chen, F. Würthner, E. W. Meijer, *J. Am. Chem. Soc.* **2002**, *124*, 10252 – 10253.
[10] One of the reviewers pointed out a very recent publication on light-harvesting hydrogels: T. Nakashima, N. Kimizuka, *Adv. Mater.* **2002**, *14*, 1113 – 1116.
[11] a) P. Terech, R. G. Weiss, *Chem. Rev.* **1997**, *97*, 3133 – 3159; b) J. H. van Esch, B. L. Feringa, *Angew. Chem. Int. Ed.* **2000**, *112*, 2351 – 2354; *Angew. Chem. Int. Ed.* **2000**, *39*, 2263 – 2266; c) R. Wang, C. Geiger, L. Chen, B. Swanson, D. G. Whitten, *J. Am. Chem. Soc.* **2000**, *122*, 2399 – 2400; d) F. S. Schoonbeek, J. H. van Esch, R. Hulst, R. M. Kellogg, B. L. Feringa, *Chem. Eur. J.* **2000**, *6*, 2633 – 2643; e) L. A. Estroff, A. D. Hamilton, *Angew. Chem.* **2000**, *112*, 3589 – 3592; *Angew. Chem. Int. Ed.* **2000**, *39*, 3447 – 3450; f) J. H. Jung, Y. Ono, S. Shinkai, *Angew. Chem.* **2000**, *112*, 1931 – 1933; *Angew. Chem. Int. Ed.* **2000**, *39*, 1862 – 1865; g) U. Maitra, S. Mukhopadhyay, A. Sarkar, P. Rao, S. S. Indi, *Angew. Chem.* **2001**, *113*, 2341 – 2343; *Angew. Chem. Int. Ed.* **2001**, *40*, 2281 – 2283; h) G. Mieden-Gundert, L. Klein, M. Fischer, F. Vögtle, K. Heuzé, J.-L. Pozzo, M. Vallier, F. Fages, *Angew. Chem.* **2001**, *113*, 3266 – 3267; *Angew. Chem. Int. Ed.* **2001**, *40*, 3164 – 3166; i) S. Tamaru, M. Takeuchi, M. Sano, S. Shinkai, *Angew. Chem.* **2002**, *114*, 881 – 884; *Angew. Chem. Int. Ed.* **2002**, *41*, 853 – 856.
[12] a) T. M. Swager, C. J. Gil, M. S. Wrighton, *J. Phys. Chem.* **1995**, *99*, 4886 – 4893; b) T. Brotin, R. Utermohlen, F. Fages, H. Boucas-Laurent, J.-P. Desvergne, *J. Chem. Soc. Chem. Commun.* **1991**, 416 – 417; c) F. S. Schoonbeek, J. H. van Esch, B. Wegewijs, D. B. A. Rep, M. P. de Haas, T. M. Klapwijk, R. M. Kellogg, B. L. Feringa, *Angew. Chem.* **1999**, *111*, 1486 – 1490; *Angew. Chem. Int. Ed.* **1999**, *38*, 1393 – 1397; d) M. Grell, D. D. C. Bradley, X. Long, T. Chamberlain, M. Inbasekaran, E. P. Woo, M. Soliman, *Acta Polym.* **1998**, *49*, 439 – 444; e) C. Geiger, M. Stanescu, L. Chen, D. G. Whitten, *Langmuir* **1999**, *15*, 2241 – 2245; f) W. Y. Huang, S. Matsuoka, T. K. Kwei, Y. Okamoto, *Macromolecules* **2001**, *34*, 7166 – 7171.
[13] A. Ajayaghosh, S. J. George, *J. Am. Chem. Soc.* **2001**, *123*, 5148 – 5149.
[14] Energy transfer from PPVs to organic dyes has been shown to occur by the Förster type mechanism. See ref. [8] for details.
[15] Similar observations have been made by Fréchet and co-workers in chromophore-labeled self-assembled monolayers. See ref. [5]. Also: D. T. McQuade, A. H. Hegedus, T. M. Swager, *J. Am. Chem. Soc.* **2000**, *122*, 12389 – 12390.

Photochemotherapeutical Drugs

Nucleotide Cross-Linking Induced by Photoreactions of Platinum(IV)–Azide Complexes**

*Philippe Müller, Björn Schröder, John A. Parkinson, Nicole A. Kratochwil, Robert A. Coxall, Andrew Parkin, Simon Parsons, and Peter J. Sadler**

State-of-the-art lasers and fibre optics now have the ability to reach any tissue in the body. A site-specific activation of photochemotherapeutic agents is therefore possible, which minimizes the severe side-effects of chemotherapy. Photosensitizers which catalyze the production of singlet oxygen are used in clinics for photodynamic therapy.[1] This technique relies on the presence of oxygen in the target tissue. A new approach towards the development of oxygen-independent photochemotherapeutic agents has recently been developed.[2–4] Photoactive Pt^{IV} analogues of the anticancer drug cisplatin (*cis*-$[Pt^{II}Cl_2(NH_3)_2]$) are of special interest: it has been shown that nucleotide platination by Pt^{IV}–diiododiamine compounds can be induced by visible light.[4] However, slow photoreactions and low stability against biological reducing agents such as glutathione can be a problem with this class of complexes. We have therefore sought alternative Pt^{IV} compounds that are better suited to this purpose, especially those more stable towards reducing agents.[5]

[*] Prof. Dr. P. J. Sadler, P. Müller, B. Schröder, J. A. Parkinson, N. A. Kratochwil, R. A. Coxall, A. Parkin, S. Parsons
Department of Chemistry
The University of Edinburgh, King's Buildings
West Mains Road, Edinburgh EH9 3JJ (UK)
Fax: (+44) 131-650-6452
E-mail: p.j.sadler@ed.ac.uk

[**] We thank the Swiss National Science Foundation (TMR award to P.M.), EPSRC, EC (Marie Curie Fellowship to N.A.K.), and Wellcome Trust (Edinburgh Protein Interaction Centre) for support, and Dr. Anita Jones and Dr. Trevor Ridley for their help and advice with laser technology, and colleagues in EC COST D8/D20 for stimulating discussions.

Supporting information for this article is available on the WWW under http://www.angewandte.org or from the author.

Pt^{IV}–azide coordination compounds are well known to be photoactive. Photoreactions, using UV light ($\lambda < 400$ nm), have been reported for Pt^{IV}–hexa- and –diazide compounds in water that lead to a reductive elimination of the azide ligands and the production of N_2.[6,7] We report here the first crystal structures of Pt^{IV}–diazidodiamine compounds and show that the Pt^{IV}–diazidodiam(m)ine cisplatin analogue *cis*,*trans*-[Pt^{IV}(en)$(N_3)_2(OH)_2$] (**4**; en = ethylenediamine) can be activated with visible light to give highly reactive Pt^{II} species which bind rapidly and stereospecifically to nucleotides, thereby forming known cisplatin–nucleotide cross-links. These complexes represent, therefore, a new class of potential photoactivatable platinum prodrugs.

First we determined the X-ray structures of the precursor Pt^{II} complexes *cis*-[$Pt^{II}(N_3)_2(NH_3)_2$] (**1**) and [Pt^{II}(en)$(N_3)_2$] (**3**; see Supporting Information) which were then oxidized to the corresponding Pt^{IV}–dihydroxy complexes, namely *cis*,*trans*-*cis*-[$Pt^{IV}(N_3)_2(OH)_2(NH_3)_2$] (**2**) and *cis*,*trans*-[Pt^{IV}(en)$(N_3)_2(OH)_2$] (**4**, Figure 1).[8] In the latter complexes the Pt^{IV} ion has close to octahedral geometry and the azide ligands are almost linear ($\sphericalangle N_\alpha$-N_β-N_γ: ca. 173°), with Pt-N_α-N_β angles between 115.5–119.6°. The N_β–N_γ bonds are approximately 0.07 Å shorter than N_α–N_β, which is typical for azide ligands.[12] The bond lengths and angles are in the expected range, and are in good agreement with reported Pt^{IV}–azido structures.[13–16]

The success of photochemotherapeutic agents is highly dependent on their stability under physiological conditions. NMR studies showed that complexes **2** and **4** reacted only slowly with the intracellular reducing agent glutathione (GSH) over a period of several weeks (see Supporting Information), and no reactions at all were observed in human blood plasma. 5′-GMP and d(GpG) did not react with these complexes over a period of one week at 298 K in the dark. The Pt^{IV} complexes **2** and **4** therefore possess the low chemical reactivity essential for potential photochemotherapeutic agents.

Photoreactions of the ^{15}N-labeled Pt^{IV} complexes **2** and **4** were carried out in water and in the presence of 5′-GMP and d(GpG), and followed by 1D ^{1}H, 2D [^{1}H,^{15}N] HSQC, and 2D [^{1}H,^{15}N] HSQC-TOCSY NMR spectroscopy. Photo-irradiation was carried out using an Ar-Kr ion laser equipped with a fibre optic link designed to deliver light directly into the sample within the magnet of the NMR spectrometer. The time-courses of the photoreactions of the chelated diamine-Pt^{IV}-diazide complex **4** in the presence of two molar equivalents of 5′-GMP or one molar equivalent of d(GpG) are shown in Figures 2 and 3 (for the structures and numbering of the complexes see the Supporting Information). The signals arising from **4** and 5′-GMP (en(CH_2): $\delta = 2.83$, H8: $\delta = 8.00$, Figure 2) decreased during irradiation with low-power visible light ($\lambda_{irr} = 457.9$ nm, 15 mW) and two new signals appeared in both the en(CH_2) and 5′-GMP H8 regions of the spectrum at $\delta = 2.71$ (***7b***), 2.58 (***8b***), 8.43 (***7a***), and 8.48 ppm (***8a***).

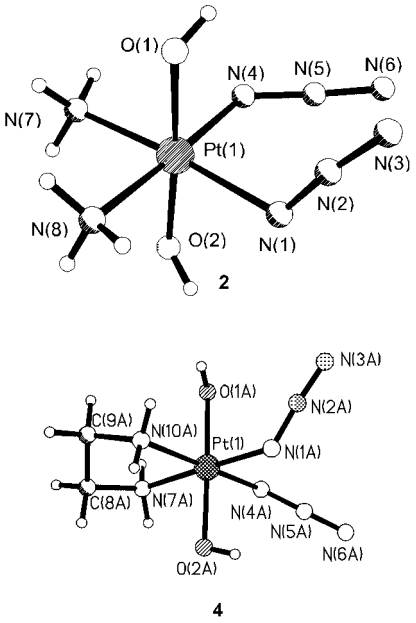


Figure 1. Molecular structures of complex **2** (top) and one of the two molecules of complex **4** which form the asymmetric unit. Selected bond lengths [Å] and angles [°]: **2**: Pt(1)-N(1) 2.036(9), Pt(1)-N(4) 2.038(9), Pt(1)-N(7) 2.043(8), Pt(1)-N(8) 2.022(9), Pt(1)-O(1) 2.005(7), Pt(1)-O(2) 2.007(7), N(1)-N(2) 1.201(13), N(2)-N(3) 1.167(13), N(4)-N(5) 1.224(13), N(5)-N(6) 1.158(13); N(1)-Pt(1)-N(4) 93.0(3); N(1)-N(2)-N(3) 172.9(10), N(2)-N(1)-Pt(1) 117.3(7), N(5)-N(4)-Pt(1) 115.2(6); **4** (molecule 1): Pt(1)-O(1A) 1.994(3), Pt(1)-O(2A) 2.001(3), Pt(1)-N(1A) 2.033(4), Pt(1)-N(4A) 2.040(5), Pt(1)-N(7A) 2.040(4), Pt(1)-N(10A) 2.045(4), N(7A)-C(8A) 1.477(7), C(8A)-C(9A) 1.506(7), N(1A)-N(2A) 1.207(6), N(2A)-N(3A) 1.147(6), N(4A)-N(5A) 1.211(6), N(5A)-N(6A) 1.139(6); N(7A)-Pt(1)-N(10A) 83.71(17), N(1A)-Pt(1)-N(4A) 93.7(2), C(8A)-N(7A)-Pt(1) 109.0(3), Pt(1)-N(1A)-N(2A) 117.4(4), Pt(1)-N(4A)-N(5A) 119.6(4), N(1A)-N(2A)-N(3A) 173.8(5).

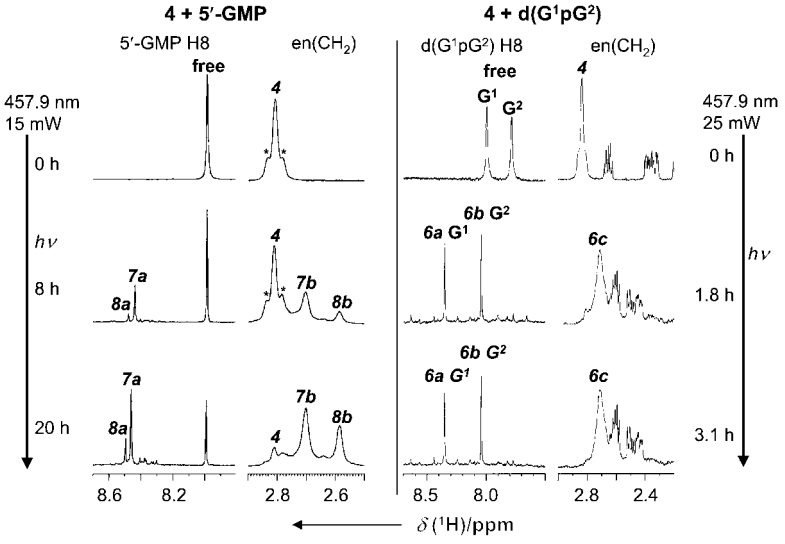


Figure 2. Selected regions of 500 MHz 1D ^{1}H NMR spectra acquired during the photoreactions of *cis*,*trans*-[Pt^{IV}(en)$(N_3)_2(OH)_2$] (**4**) in the presence of two molar equivalents of 5′-GMP, or one molar equivalent of d(G^1pG^2) ($\lambda_{irr} = 457.9$ nm, 15/25 mW, 1 mM, pH 5, at 298 K). ^{195}Pt satellites are indicated by *. Assignments in italics correspond to signals associated with a particular compound.

 © 2003 Wiley-VCH Verlag GmbH & Co. KGaA, Weinheim 1433-7851/03/4203-0336 $ 20.00+.50/0

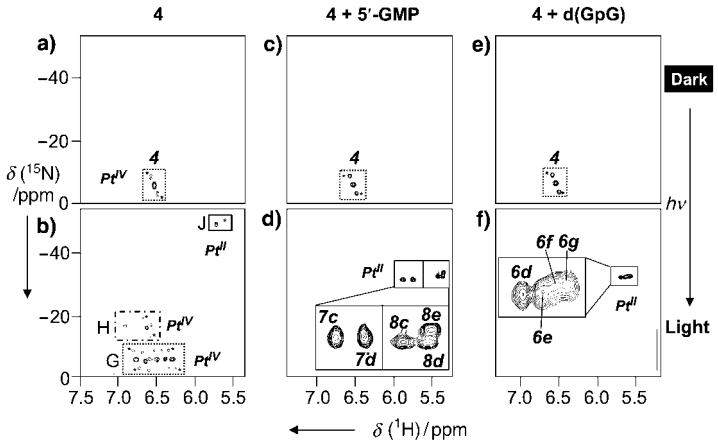


Figure 3. 2D [^{1}H,^{15}N] HSQC NMR spectra acquired during photoreactions (λ_{irr} = 457.9 nm) of *cis*,*trans*-[Pt^{IV}(en)(N$_3$)$_2$(OH)$_2$] (**4**) in water, in the presence of 5′-GMP (molar ratio 1:2, 2 mM) and d(GpG) (molar ratio 1:1, 1 mM) at irradiation times of a) 0 h, b) 4 h, c) 0 h, d) 20 h, e) 0 h, and f) 1.78 h, pH 5, 295 K. Asterisks indicate ^{195}Pt satellites.

Such a high frequency shift for the H8 resonance of 5′-GMP is typical of metal coordination to N7 of 5′-GMP.[17,18] Peaks ***7a*** (major) and ***8a*** (minor) accounted for 60% of the initial H8 signal intensity of 5′-GMP after 20 h irradiation. The 2D [^{1}H,^{15}N] HSQC NMR spectrum after 20 h irradiation (Figure 3d) exhibited two sets of ^{1}H/^{15}N cross-peaks, ***7c/d*** and ***8c/d/e*** (Table 1), which relate to the peaks ***7a/b*** and ***8a/b*** in the corresponding 1D ^{1}H NMR spectrum, as shown in the 2D HSQC-TOCSY NMR spectrum (see Supporting Information). Such ^{1}H/^{15}N chemical shifts are characteristic of {Pt^{II}N-H$_2$(en)} *trans* to an N atom rather than a Pt^{IV} complex, and the δ values of cross-peaks ***7c/d*** are the same as those reported previously for [Pt^{II}(^{15}N-en)(5′-GMP-*N7*)$_2$]$^{2+}$ (**7**; the charges on the nucleotides are ignored in the formulas).[17,18] No protonation at the 5′-GMP-*N7* site (pK_a = 2.48[19]) was observed for compounds **7** and **8** (no change in the chemical shift for H8 between pH 1–4) confirming platinum coordination to *N7* (Figure 4a).[20] No intermediate compounds were detected during the irradiation. The presence of **7** was confirmed by ESI-MS (see Supporting Information). Complex **8**, which may contain a modified 5′-GMP, was not further characterized.

In contrast to the above reaction, irradiation of **4** (λ_{irr} = 457.9 nm, 25 mW) in the presence of one molar equivalent of d(G^{1}pG^2) led to only one major product **6** (Figures 2 and 3e/f). A high frequency shift of 0.4 ppm was observed in the ^{1}H NMR spectrum for the d(G^{1}pG^2) H8 resonances (peaks ***6a/b***) after 1.8 h irradiation indicating platinum binding to d(G^{1}pG^2)-*N7^1*,*N7^2*. Four ^{1}H/^{15}N cross-peaks with equal intensity separated into two pairs associated with distinct ^{15}N shifts (δ(^{1}H/^{15}N) = 5.68 (***6d***), 5.63 (***6e***)/−30.9, 5.58 (***6f***), 5.55 (***6g***)/−31.22 ppm) appeared simultaneously. These values are in agreement with those reported for [Pt^{II}(^{15}N-en){d(G^{1}pG^2)-*N7^1*,*N7^2*}]$^{2+}$ (**6**).[17,21] The presence of complex **6** was further confirmed by a pH titration for ^{1}H peaks ***6a/b*** (Figure 4b). The pH

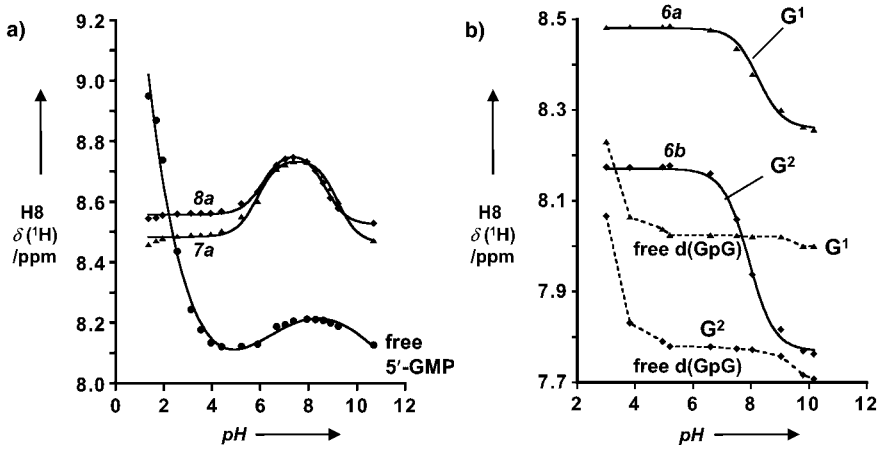


Figure 4. Variation of the chemical shift of H8 with pH value of a) 5′-GMP, and b) d(G^{1}pG^2) before and after the photoreactions with *cis*,*trans*-[Pt^{IV}(en)(N$_3$)$_2$(OH)$_2$] (**4**; λ_{irr} = 457.9 nm) at 298 K.

Table 1: ^{1}H and ^{15}N chemical shifts and coupling constants ^1J(^{195}Pt,^{15}N) [Hz].

Pt complex	NH_3/NH_2		CH_2	^2J(^{1}H,^{195}Pt)	^1J(^{15}N,^{195}Pt)
	δ(^{1}H) [ppm]	δ(^{15}N) [ppm]	δ(^{1}H) [ppm]		
cis-[Pt^{II}(N$_3$)$_2$(NH$_3$)$_2$] (**1**)	3.86	−69.5		57	305
cis,*trans*-[Pt^{IV}(N$_3$)$_2$(OH)$_2$(NH$_3$)$_2$] (**2**)	5.20	−39.8		46	258
[Pt^{II}(en)(N$_3$)$_2$] **3**	5.10	−33.8	2.61	53	337
cis,*trans*-[Pt^{IV}(en)(N$_3$)$_2$(OH)$_2$] (**4**)	6.50	−5.9	2.83	43	275
cis-[Pt^{II}(NH$_3$)$_2$\{d(GpG)-*N7^1*,*N7^2*\}]$^{2+}$ (**5**)	4.45/4.38	−68.3/−68.5			
[Pt^{II}(en)\{d(GpG)-*N7^1*,*N7^2*\}]$^{2+}$ (**6**)	5.65/5.56	−30.9/−31.2	2.84		
[Pt^{II}(en)(GMP-*N7*)$_2$]$^{2+}$ (**7**)	5.75/5.88	−30.7	2.71		
8	5.38/5.33	−31.7	2.58		
	5.35	−32.9			
G[a]	6.2 to 6.8	−6.0		43	277
H[a]	6.67/6.95	−16.21/−16.72		44	306
J[a]	5.70/5.59	−48.4/−49.9			

[a] See Figure 3.

 © 2003 Wiley-VCH Verlag GmbH & Co. KGaA, Weinheim 1433-7851/03/4203-0337 $ 20.00+.50/0

titration curves are in agreement with those reported for [Pt(en){d(GpG)-*N7(1),N7(2)*}]$^{2+}$ (**6**).[21,22] The lack of a high frequency shift in the pH range 3–4 indicates platinum binding at *N7* of G^1 and G^2. The only major species present after 1.8 h irradiation was [Pt^{II}(^{15}N-en){d(G^1pG^2)-$N7^1$,$N7^2$}]$^{2+}$ (**6**), which is indicative of a rapid stereospecific reaction.

The photoreaction pathway was elucidated by following the photoreaction of **4** alone in water (Figure 3 a/b). After 4 h irradiation (λ_{irr} = 457.9 nm, 20 mW), ^{1}H/^{15}N cross-peaks were present at δ(^{15}N) −6 (**G**), −16 (**H**), and −48 ppm (**J**). The δ(^{15}N) value for **G** is characteristic of {$Pt^{IV}NH_2$(en)} *trans* to N, that for **H** of {$Pt^{IV}NH_2$(en)} *trans* to O, and that for **J** of {$Pt^{II}NH_2$(en)} *trans* to O.[23] The cross-peaks of **G** and **H** can be assigned to stereoisomers of complex **4** on the basis of their chemical shifts and coupling constants (Table 1), and cross-peaks **J** must arise from {$Pt^{II}NH_2$(en)} *trans* to OH/OH_2 because of the absence of any other oxygen donors except OH_2/OH in solution. Pt^{II}–aqua complexes are known to be very reactive towards strong donor atoms such as 5′-GMP-*N7* or d(G^1pG^2)-$N7^1$,$N7^2$ which are the reactive sites toward cisplatin.[24] Under physiological conditions, this photoreaction therefore transforms a stable Pt^{IV} complex into a highly reactive Pt^{II} species which can bind to nucleotides and hence has the potential to kill cancer cells. The site of the drug release could be chosen using site-specific irradiation, and the rate of the drug release could be adjusted by varying the light power.

Red light (λ_{irr} = 647.1 nm, 75 mW), which penetrates better through tissue than blue light, and is preferred for use in photochemotherapy, was also employed for irradiation of **4**. Such low-energy light also induced d(G^1pG^2)-$N7^1$,$N7^2$ binding, which illustrates the potential of this type of Pt^{IV} complex as a photochemotherapeutic agent.[25]

Similar photoreactions were also carried out with the [Pt^{IV}(diammine)(diazide)] complex **2** in the presence of d(GpG). The nucleotide adduct *cis*-[Pt(NH_3)$_2${d(GpG)-$N7^1$,$N7^2$}]$^{2+}$ (**5**) was identified as a photoproduct by 1D ^{1}H and 2D [^{1}H,^{15}N] HSQC NMR, and the pH-dependence of the H8 chemical shifts confirmed *N7* platination (see Table 1 for δ(^{1}H,^{15}N) values of **5**; 1D/2D NMR spectra are shown in the Supporting Information). Hence, this photoactivation strategy should be generally applicable to Pt^{IV}–diazido complexes containing a variety of monodentate and chelated diamine ligands and may allow the site-specific delivery of a wide range of Pt^{II}–diamine drugs. This approach could therefore be used to target many commonly used Pt^{II}-containing anticancer drugs and has the potential to strongly reduce unwanted side-effects often associated with platinum chemotherapy.

Experimental Section

K_2[$PtCl_4$] was purchased from Alfa-Johnson Matthey plc., NaN_3 from BDH, $^{15}NH_4Cl$ and ^{15}N-potassium phthalimide from Aldrich, dibromoethane from Fisons, H_2O_2 (30 %) from Prolabo, GSH and 5′-GMP from Acros and 2′-deoxyguanylyl (3′→5′)-2′-deoxyguanosine sodium salt (d(GpG)) from Sigma. Human blood plasma (leucocyte depleted, blood group 0 Rh D positive) was provided by the Western General Hospital, Edinburgh.

1: KI (0.4 g, 24 mmol) was added to an aqueous solution (50 mL) of K_2[$PtCl_4$] (1 g, 2.41 mmol). After stirring for 30 min at ambient temperature, $^{15}NH_4Cl$ (0.26 g, 4.88 mmol) was added and the pH adjusted to 11 with 1M NaOH. The yellow precipitate (*cis*-[PtI_2($^{15}NH_3$)$_2$]) was filtered off, washed with water, ethanol, and diethyl ether, and dried under vacuum. $AgNO_3$ (2 mol equiv, 0.146 g, 0.86 mmol) was added to a suspension of *cis*-[PtI_2($^{15}NH_3$)$_2$] (0.2 g, 0.43 mmol) in water (20 mL) and then stirred in the dark for 24 h. The AgI precipitate was filtered off using an inorganic membrane filter (Whatman, Anotop 10, 0.02 μm). NaN_3 (20 mol equiv, 0.57 g, 8.77 mmol) was added and the solution stirred for 30 min in the dark at ambient temperature. The volume was reduced to 10 mL and the flask was stored at 277 K overnight. The yellow precipitate was washed with diethyl ether and dried in air. Yield: 97 mg (72 %). Crystals suitable for X-ray crystal-structure determination were obtained from an aqueous solution at 277 K.

2: H_2O_2 (40 mol equiv, 1.2 mL of 30 % H_2O_2, 11.75 mmol) was added to a suspension of *cis*-[Pt^{II}(N_3)$_2$(NH_3)$_2$] (0.086 g, 0.27 mmol) in water (10 mL) which was stirred in the dark at ambient temperature for 24 h. The volume of the solution was reduced, and on cooling to 277 K, complex **2** formed as a yellow precipitate which was filtered and washed with water and diethyl ether, yield: 32.8 mg (35 %). Crystals suitable for X-ray crystal-structure determination were grown from a water/ethanol (1/1 v/v) mixture at 277 K. Elemental analysis calcd for $H_8N_8O_2Pt$: H 2.30, N 32.28; found: H 2.64, N 31.85.

3: ^{15}N-labeled ethylenediamine was synthesized as previously described.[26] K_2[$PtCl_4$] (0.162 g, 0.39 mmol) was added to an aqueous solution of ^{15}N-en·2 HCl (0.052 g, 0.39 mmol, pH 8) and the solution stirred at ambient temperature. The yellow precipitate ([$Pt^{II}Cl_2$(^{15}N-en)]) was washed with water and diethyl ether and dried under vacuum. [$Pt^{II}Cl_2$(^{15}N-en)] (0.04 g, 0.12 mmol) and $AgNO_3$ (0.041 g, 0.24 mmol, 2 mol equiv) were stirred in water in the dark at room temperature for 24 h. The AgCl precipitate was filtered off and NaN_3 (25 mol equiv, 0.208 g, 3.2 mmol) was added to the solution. The volume was reduced and a yellow precipitate was obtained on cooling the solution to 277 K. This was washed with water and diethyl ether. Yield: 23.5 mg (57 %). Crystals suitable for X-ray crystal-structure determination were obtained from an aqueous solution at 277 K.

4: H_2O_2 (50 mol equiv, 0.3 mL of 30 % H_2O_2, 2.9 mmol) was added to a solution of [Pt(en)(N_3)$_2$] (0.021 g, 0.06 mmol) in water (5 mL). This was then stirred in the dark at ambient temperature for 24 h. The yellow precipitate was filtered off and washed with water and diethyl ether, yield 10 mg (40 %). Crystals suitable for X-ray crystal-structure determination were obtained from an aqueous solution at 277 K. Elemental analysis calcd for $C_2H_{10}N_8O_2Pt$: C 6.43, H 2.68, N 30.03; found: C 6.54, H 2.37, N 30.18.

Uv/Vis spectra of complexes **2** and **4** as well as the Raman spectra of complexes **1**–**4** are shown in the Supporting Information.

Irradiation was carried out using an argon-krypton ion laser (Coherent Innova 70C Spectrum) equipped with a fibre optic (FT-600-UMT, ∅ 600 μm; Elliot Scientific Ltd.) to deliver light (λ = 457.9 nm, 488 nm, 647.1 nm) directly into the sample within the magnet of the NMR spectrometer. The laser output, after the fiber, was in the range of 10 to 75 mW, as measured by a Coherent 210 power meter. 1D ^{1}H, 2D [^{1}H,^{15}N] HSQC and 2D [^{1}H,^{15}N] HSQC-TOCSY NMR spectra were recorded on a Bruker DMX 500 NMR spectrometer (^{1}H: 500.13 MHz, ^{15}N: 50.7 MHz) at pH 5 using sodium 3-(trimethylsilyl)-[2,2,3,3-D_4]-propionate (TSP, 0 ppm) as the internal δ(^{1}H) standard. All δ(^{15}N) values were referenced externally to $^{15}NH_4^+$ at δ = 0. pH values were measured with a pH meter (Orion 710A) equipped with a microcombination electrode (Aldrich) calibrated with Aldrich standard buffers (pH 4, 7, and 10) and were adjusted with dilute solutions of $HClO_4$ and NaOH. No correction was made for ^{2}H isotope effects on the glass electrode.

Received: July 30, 2002 [Z19849]

 © 2003 Wiley-VCH Verlag GmbH & Co. KGaA, Weinheim 1433-7851/03/4203-0338 $ 20.00+.50/0

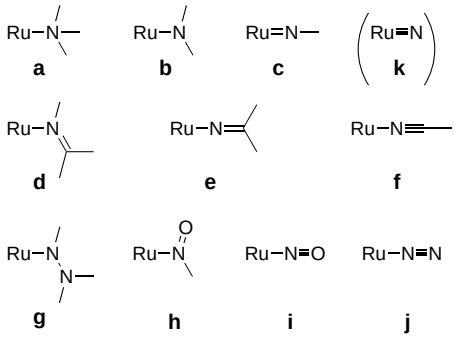
[1] L. Milgrom, S. MacRobert, *Chem. Br.* **1998**, *34*, 45.
[2] N. A. Kratochwil, J. A. Parkinson, P. J. Bednarski, P. J. Sadler, *Angew. Chem.* **1999**, *111*, 1566; *Angew. Chem. Int. Ed.* **1999**, *38*, 1460.
[3] N. A. Kratochwil, P. J. Bednarski, H. Mrozek, A. Vogler, J. K. Nagle, *Anti-Cancer Drug Des.* **1996**, *11*, 155.
[4] N. A. Kratochwil, M. Zabel, K.-J. Range, P. J. Bednarski, *J. Med. Chem.* **1996**, *39*, 2499.
[5] N. A. Kratochwil, Z. J. Guo, P. D. Murdoch, J. A. Parkinson, P. J. Bednarski, P. J. Sadler, *J. Am. Chem. Soc.* **1998**, *120*, 8253.
[6] A. Vogler, A. Kern, B. Fusseder, *Z. Naturforsch. B* **1978**, *33*, 1352.
[7] A. Vogler, J. Hlavatsch, *Angew. Chem.* **1983**, *95*, 153; *Angew. Chem. Int. Ed. Engl.* **1983**, *22*, 154.
[8] Diffraction data were collected with $Mo_{K\alpha}$ X-rays ($\lambda = 0.71073$ Å) on a Bruker Smart APEX diffractometer equipped with an Oxford Cryosystems low-temperature device operating at 150 K, with the exception of **2**, for which data were collected at 100 K. Absorption corrections were applied using the program SADABS; the structures were solved either using Patterson methods (DIRDIF)[9] or direct methods (Shelxtl)[10] and refined by full-matrix least-squares against F^2 (Shelxtl) using all unique data. H atoms were treated either as part of a rotating rigid group (NH_3 and OH ligands), or with a riding model. Other analyses were carried out using Platon.[11] Crystal data for **1** (H_6N_8Pt), $M_r = 313.22$, yellow rod, $0.13 \times 0.06 \times 0.03$ mm^3, monoclinic, space group $P2_1/n$, $a = 8.6327(10)$, $b = 7.1432(8)$, $c = 10.5689(12)$ Å, $\beta = 104.323(2)°$, $V = 631.47(12)$ Å^{-3}, $\rho_{calcd} = 3.295$ Mg m^{-3}, 3431 reflections measured, of which 1270 were independent, $\theta_{max} = 26.38°$, $R_{int} = 0.024$, $\mu = 22.145$ mm^{-1} (range of transmission = 0.161–0.556), 84 parameters, $R = 0.0229$ (based on F and 1219 data with $F > 4\sigma(F)$), $R_w = 0.0532$ (based on F^2 and all data), the final difference map extremes were +1.40 and −1.79 e Å^{-3}. Crystal data for **2** ($H_8N_8O_2Pt$), $M_r = 347.23$, colorless plate, $0.13 \times 0.07 \times 0.04$ mm^3, triclinic, space group $P\bar{1}$, $a = 6.3232(11)$, $b = 7.9816(14)$, $c = 8.1663(14)$ Å, $\alpha = 82.247(3)$, $\beta = 67.294(2)$, $\gamma = 68.885(2)°$, $V = 354.67(11)$ Å^{-3}, $\rho_{calcd} = 3.251$ Mg m^{-3}, 2624 reflections measured, of which 1251 were independent, $\theta_{max} = 24.99°$, $R_{int} = 0.036$, $\mu = 19.752$ mm^{-1} (range of transmission = 0.18–0.51), 105 parameters, $R = 0.0339$ (based on F and 1144 data with $F > 4\sigma(F)$), $R_w = 0.0786$ (based on F^2 and all data), the final difference map extremes were +2.69 and −2.32 e Å^{-3} (all intense peaks were in the region of the Pt atom). Crystal data for **3** ($C_2H_8N_8Pt$), $M_r = 339.25$, yellow needle, $0.12 \times 0.06 \times 0.02$ mm^3, monoclinic, space group $P2/n$, $a = 7.778(8)$, $b = 3.405(3)$, $c = 14.139(14)$ Å, $\beta = 100.848(15)°$, $V = 367.8(6)$ Å^{-3}, $\rho_{calcd} = 3.063$ Mg m^{-3}, 2377 reflections measured, of which 726 were independent, $\theta_{max} = 26.50°$, $R_{int} = 0.066$, $\mu = 19.025$ mm^{-1} (range of transmission = 0.22–1.00), 77 parameters, $R = 0.0426$ (based on F and 718 data with $F > 4\sigma(F)$), $R_w = 0.0982$ (based on F^2 and all data), the final difference map extremes were +3.57 and −2.42 e Å^{-3} (all intense peaks were in the region of the Pt atom). The molecule is disordered about a crystallographic twofold axis, with common positions for the ligating nitrogen atoms; there appeared to be no weak diffraction spots that might have indicated a larger unit cell. This determination can reasonably be said to determine connectivity, but it should not be used for detailed analysis. Crystal data for **4**, $C_2H_{10}N_8O_2Pt$, $M_r = 373.27$, pale yellow chip, $0.20 \times 0.09 \times 0.06$ mm^3, monoclinic, space group $P2_1/c$, $a = 15.8580(12)$, $b = 6.2374(5)$, $c = 17.5220(13)$ Å, $\beta = 102.0720(10)°$, $V = 1694.8(2)$ Å^{-3}, $\rho_{calc} = 2.926$ Mg m^{-3}, 10251 reflections measured, of which 4093 were independent, $\theta_{max} = 29.11°$, $R_{int} = 0.021$, $\mu = 16.545$ mm^{-1} (range of transmission = 0.454–1.00), 240 parameters, $R = 0.0263$ (based on F and 3881 data with $F > 4\sigma(F)$), $R_w = 0.0601$ (based on F^2 and all data), the final difference map extremes were +1.04 and −1.44 e Å^{-3}. Further details of the crystal-structure investigations may be obtained from the Fachinformationszentrum Karlsruhe, 76344 Eggenstein-Leopoldshafen, Germany (fax: (+49) 7247-808-666; e-mail: crysdata@fiz-karlsruhe.de), on quoting the depository numbers CSD-412675 (**1**) and CSD-412674 (**2**). CCDC-190266 (**3**) and CCDC-190265 (**4**) contain supplementary crystallographic data for this paper. These data can be obtained free of charge via www.ccdc.cam.ac.uk/conts/retrieving.html (or from the Cambridge Crystallographic Data Centre, 12 Union Road, Cambridge CB21EZ, UK; fax: (+44) 1223-336-033; or deposit@ccdc.cam.ac.uk).
[9] P. T. Beurskens, G. Beurskens, W. P. Bosman, R. de Gelder, S. Garcia-Granda, R. O. Gould, R. Israel, J. M. M. Smits, Crystallography Laboratory, University of Nijmegen, The Netherlands, **1996**.
[10] G. M. Sheldrick, SHELXTL, version 5, Bruker AXS, Madison WI, **1995**.
[11] A. L. Spek, *Acta Crystallogr. Sect. A* **1990**, *46*, C34. PLATON, A Multipurpose Crystallographic Tool, Utrecht University, Utrecht, The Netherlands. Incorporated into the WinGX suite: L. J. Farrugia, *J. Appl. Crystallogr.* **1999**, *32*, 837.
[12] A. F. Holleman, E. Wiberg, *Lehrbuch der anorganischen Chemie*, Walter de Gruyter, Berlin, **1985**.
[13] S. Schröder, W. Preetz, *Z. Anorg. Allg. Chem.* **2000**, *626*, 1757.
[14] S. Schröder, W. Preetz, *Z. Anorg. Allg. Chem.* **2000**, *626*, 1915.
[15] S. Schröder, W. Preetz, *Z. Anorg. Allg. Chem.* **2001**, *627*, 390.
[16] B. Neumueller, F. Schmock, S. Schlecht, K. Dehnicke, *Z. Anorg. Allg. Chem.* **2000**, *626*, 1792.
[17] S. J. Berners-Price, J. D. Ranford, P. J. Sadler, *Inorg. Chem.* **1994**, *33*, 5842.
[18] S. J. Berners-Price, U. Frey, J. D. Ranford, P. J. Sadler, *J. Am. Chem. Soc.* **1993**, *115*, 8649.
[19] H. Sigel, S. S. Massoud, N. A. Corfu, *J. Am. Chem. Soc.* **1994**, *116*, 2958.
[20] K. H. Scheller, V. Scheller-Krattiger, R. B. Martin, *J. Am. Chem. Soc.* **1981**, *103*, 6833.
[21] J.-P. Girault, G. Chottard, J.-Y. Lallemand, J.-C. Chottard, *Biochemistry* **1982**, *21*, 1352.
[22] E. L. M. Lempers, M. J. Bloemink, J. Reedijk, *Inorg. Chem.* **1991**, *30*, 201.
[23] S. J. Berners-Price, P. J. Sadler, *Coord. Chem. Rev.* **1996**, *151*, 1.
[24] J. Reedijk, *Chem. Commun.* **1996**, 801.
[25] A. M. Rouhi, *Chem. Eng. News* **1998**, *76*(31), 22.
[26] E. Zang, P. J. Sadler, *Synthesis* **1997**, 410.

Aminations with Ru Porphyrins

Nitrido Ruthenium Porphyrins: Synthesis, Characterization, and Amination Reactions with Hydrocarbon or Silyl Enol Ethers**

Sarana Ka-Yan Leung, Jie-Sheng Huang, Jiang-Lin Liang, Chi-Ming Che, and Zhong-Yuan Zhou*

Ruthenium porphyrins constitute an unmatched family of metalloporphyrin that exhibits extraordinary versatility in binding N-donating ligands at the axial sites.[1–5] A wide variety of ruthenium porphyrins featuring axial Ru–N bonds have been prepared, including those bearing amine,[1c,3a,3b] amido,[3b–d,g] imido,[3a,c–e,g,j] imine,[3h,4] methyleneamido,[3h] nitrile,[1a,2] hydrazido,[3f] nitrosoarene,[1b,3i] nitrosyl,[5] and dinitrogen[1d] axial ligands (Scheme 1, **a**–**j**). This makes the lack of



Scheme 1. Axial Ru–N bonds in ruthenium porphyrins.

isolable ruthenium porphyrins with terminal nitrido axial ligands (Scheme 1, **k**) especially conspicuous.[6,7]

Our interest in nitrido ruthenium porphyrins stems from the particular importance of nitrido–metal (M≡N) complexes in C–N bond-formation reactions.[8] In a pioneering work by Groves and Takahashi, a nitrido manganese porphyrin, upon activation with trifluoroacetic anhydride (TFAA) to form a trifluoroacetylimido manganese (Mn=NCOCF$_3$) species, underwent NCOCF$_3$ group transfer with *cis*-cyclooctene to give an aziridine product.[8a] Subsequent works by Carreira and co-workers demonstrate that several nitrido manganese Schiff base complexes can be activated with TFAA and undergo NCOCF$_3$ group transfer with silyl enol ethers, glycols, and styrene to afford amination or aminohydroxylation products.[8b–e] Recently, Komatsu and co-workers reported asymmetric aziridination of alkenes and asymmetric amination of silyl enol ether with chiral nitrido manganese Schiff base complexes upon (*p*-MeC$_6$H$_4$SO$_2$)$_2$O or TFAA activation.[8f]

Surprisingly, all the aziridination/amination reactions of nitrido metal complexes have to date been confined to nitrido complexes of manganese, although numerous nitrido complexes of other transition metals have been reported.[9] The amination by nitrido manganese Schiff base complexes only occurred for unsaturated C–H bonds. No nitrido metalloporphyrins have been found to undergo C-H insertion reactions to afford amination products.

Herein we report the syntheses and amination reactions of nitrido ruthenium(VI) porphyrins [Ru^{VI}(por)(N)(OH)] (**1a**: por = tmp, **1b**: por = 3,4,5-MeO-tpp; see Scheme 2).[10] These nitrido ruthenium complexes were prepared by employing an unprecedented synthetic strategy for nitrido metal complexes, that is, reaction of oxo–metal complexes with an imine compound. Upon activation with TFAA, both **1a** and **1b** can aminate silyl enol ethers to give *N*-trifluoroacetylated α-amino ketones. Especially interesting is that the "**1a**/**1b** + TFAA" system can undergo C–H insertion reaction with indan to form *N*-trifluoroacetyl indan-1-ylamine. This reaction, to our knowledge, is the first amination of saturated C–H bonds of a hydrocarbon with nitrido metal complexes.

Treatment of dioxoruthenium(VI) porphyrin [Ru^{VI}(por)(O)$_2$] (por = tmp[11a] or 3,4,5-MeO-tpp[3b]) generated in situ from [Ru^{II}(por)(CO)] and excess *m*-CPBA[10] (see Scheme 2, reaction (1)) with excess HN=C*t*Bu$_2$ in dichloromethane for ≈40 min afforded a green solution, workup of which gave **1a** or **1b** as a dark purple solid in ≈85% yield (reaction (2) in Scheme 2). Both **1a** and **1b** are stable to moist air for several months in the solid state and can exist for several hours in dichloromethane solutions exposed to the atmosphere.

We found that reaction (2) shows surprisingly strong dependence on the electronic properties of the porphyrin ligand.[12] Attempts to extend reaction (2) to less electron-rich porphyrins (such as tpp[10] and ttp[10]) and electron-deficient porphyrins (such as tpfpp[10]) did not lead to formation of nitrido ruthenium porphyrins; instead, μ-oxo and nitrosyl ruthenium porphyrins were obtained, respectively.

The reaction between [Ru^{VI}(3,4,5-MeO-tpp)(O)$_2$] and HN=C*t*Bu$_2$ to form **1b** contrasts sharply with that between the same dioxo complex and HN=CPh$_2$, the latter reaction has been reported to produce bis(methyleneamido) ruthenium(IV) porphyrin [Ru^{IV}(3,4,5-MeO-tpp)(N=CPh$_2$)$_2$] in ≈65% yield under similar conditions.[3h]

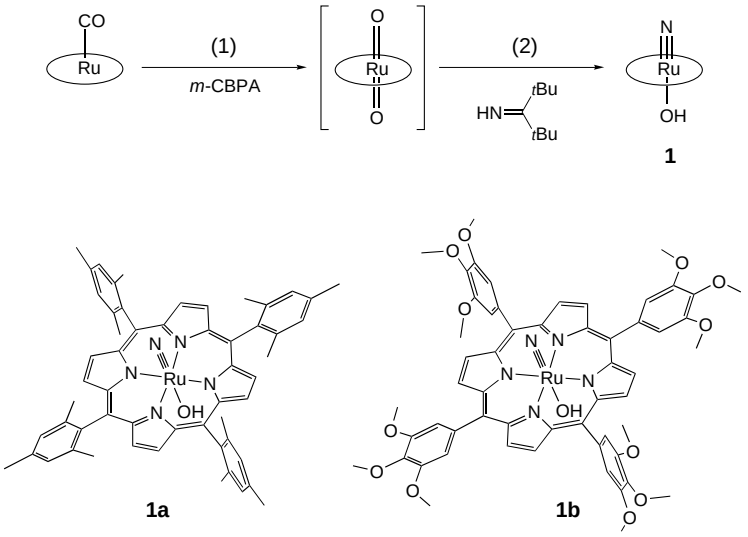
Efforts were once made to prepare **1a**/**1b** or their analogues by employing known synthetic strategies such as cleavage of the N–R bond in imido metal (M=NR) complexes and oxidation of coordinated ammines.[9b] However, these synthetic strategies did not lead to isolation of pure nitrido

[*] Prof. Dr. C.-M. Che, S. K.-Y. Leung, Dr. J.-S. Huang, J.-L. Liang
Department of Chemistry and Open Laboratory of Chemical Biology of the Institute of Molecular Technology for Drug Discovery and Synthesis
The University of Hong Kong, Pokfulam Road (Hong Kong)
Fax: (+852) 2857-1586
E-mail: cmche@hku.hk
Prof. Z.-Y. Zhou
Department of Applied Biology and Chemical Technology
The Hong Kong Polytechnic University, Hung Hom, Kowloon (Hong Kong)

[**] This work was supported by The University of Hong Kong, the Hong Kong University Foundation, the Hong Kong Research Grants Council, and the University Grants Committee of the Hong Kong SAR of China (Area of Excellence Scheme, AoE/P-10/01).

Supporting information for this article is available on the WWW under http://www.angewandte.org or from the author.

 © 2003 Wiley-VCH Verlag GmbH & Co. KGaA, Weinheim 1433-7851/03/4203-0340 $ 20.00+.50/0



Scheme 2. Synthesis of the nitrido ruthenium(VI) porphyrins **1**. *m*-CPBA = *meta*-chloroperoxybenzoic acid.

ruthenium porphyrins. For example, autodegradation of in situ formed bis(tosylimido) ruthenium(VI) porphyrin [Ru^{VI}(tmp)$(NTs)_2$][3d] in aerobic dichloromethane gave [Ru^{VI}(tmp)(N)(NHTs)] (**2**; reactions (3) and (4) in Scheme 3) contaminated with NH_2Ts; oxidation of the isolated bis(ammine) ruthenium(II) porphyrin [Ru^{II}(ttp)$(NH_3)_2$] (prepared from [Ru^{VI}(ttp)$(O)_2$][11b] and excess NH_3, reaction (5) in Scheme 3) with 4 equivalents of NBS[10] in dichloromethane under argon afforded [Ru^{VI}(ttp)(N)Br] (**3**; reaction (6)) contaminated by NBS.

The nitrido ruthenium(VI) porphyrins **1**–**3** are all diamagnetic and feature "oxidation-state marker" bands[3a,b] at $> 1015\ cm^{-1}$ in their IR spectra, like dioxo, oxo(imido) or bis(imido) ruthenium(VI) porphyrins.[3a,d] The following spectral features of **1**–**3** are distinctive. First, the signals of the pyrrole protons (H_β) in the ^1H NMR spectra are at $\delta = 9.00$ (**1a**), 9.09 (**2**), 9.33 (**1b**), and 9.36 ppm (**3**), which are all downfield from those of their dioxo,[3b,11] oxo(imido),[3a,g] or bis(imido)[3c,d] ruthenium(VI) counterparts. Second, the β bands in the UV/Vis spectra appear at 485–488 nm, which are substantially blue-shifted from those of other ruthenium porphyrins reported.[1–5]

In the electrospray mass spectra (ESI–MS) of **1**–**3**, intense cluster peaks corresponding to the fragments $[Ru(por)(N)]^+$ were located. The ESI–MS of **1a**, **1b**, and **3** also show prominent peaks ascribable to their parent ions. Complex **2** did not give parent-ion peaks in the ESI–MS; its axial NHTs ligand was identified on the basis of the ^1H NMR spectrum. In the IR spectra, conversion of [Ru^{II}(tmp)(CO)] into **1a** and **2** led to the appearance of a new band at $1038\ cm^{-1}$, which we tentatively assigned to the Ru≡N group.[13] Identification of the Ru≡N band for **1b** and **3** was hampered by either intense signals of the porphyrin ligand in the region of interest or impurities in the sample.

The structure of **1b** has been determined by X-ray crystallography (Figure 1),[14] and features a

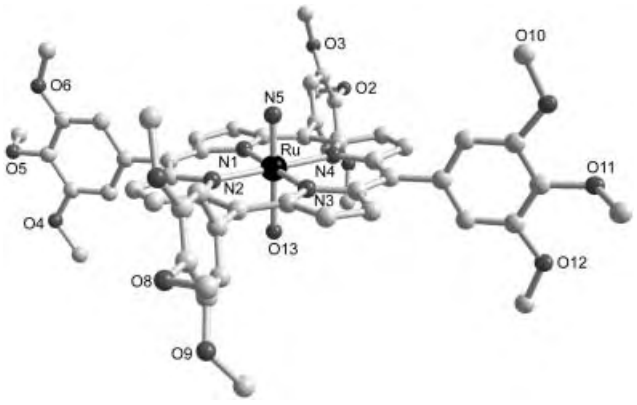
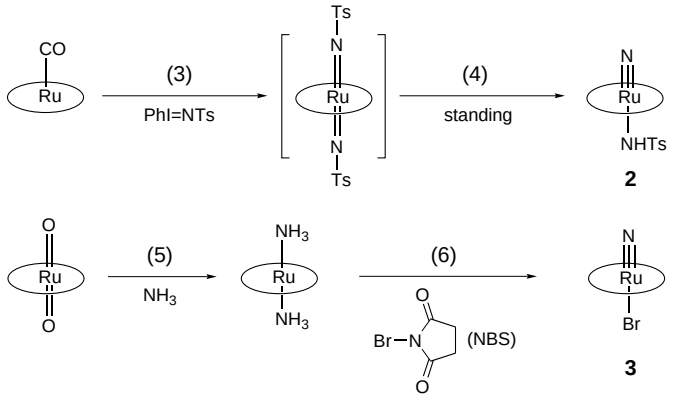


Figure 1. Molecular structure of **1b** determined by X-ray crystallography (hydrogen atoms are not shown). Selected bond lengths [Å] and bond angles [°]: Ru-N1 2.046(6), Ru-N2 2.086(6), Ru-N3 2.001(6), Ru-N4 2.026(7), Ru-N5 1.656(5), Ru-O13 2.086(7); N1-Ru-N2 92.7(2), N2-Ru-N3 88.5(2), N3-Ru-N4 88.5(3), N4-Ru-N1 90.3(3), N5-Ru-O13 177.8(3).



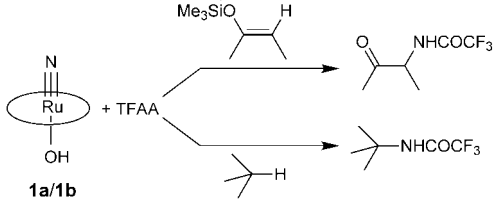
Scheme 3. Formation of the nitrido ruthenium(VI) porphyrins **2** and **3** from autodegradation of a bis(tosylimido)ruthenium(VI) porphyrin or from NBS oxidation of a bis(ammine)ruthenium(II) porphyrin.

planar porphyrin ring and a Ru–N(nitrido) distance of 1.656(5) Å, slightly longer than those of nitrido ruthenium complexes with tri- or tetradentate non-porphyrin ligands (1.594–1.615 Å).[15] The Ru–O(OH) distance of 2.086(7) Å in **1b** is longer than that in [Ru(ttp)(NO)(OH)] (1.943(5) Å).[5g]

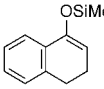
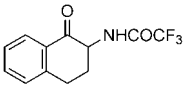
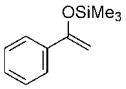
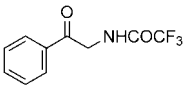
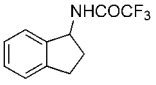
Note that the above nitrido ruthenium porphyrins can be readily converted into hexacoordinate {Ru(NO)} complexes. For example, reactions of **1b** with PhIO and MeOH in dichloromethane gave [Ru(3,4,5-MeO-tpp)(NO)(OH)] and [Ru(3,4,5-MeO-tpp)(NO)(OMe)], respectively. In an attempt to purify **3** by chromatography on an alumina column, the complex was converted into [Ru(ttp)(NO)Br] (see Supporting Information).

Interestingly, treatment of **1a** or **1b** with silyl enol ethers and TFAA in dichloromethane containing pyridine under argon for ≈5 h afforded respective *N*-trifluoroace-

Table 1: Amination reaction of **1a** or **1b** with silyl enol ethers and indan.



1a/1b

Entry	Substrate	Product	Yield [%]
1			68 (**1a**)
2			75 (**1b**)
3			70 (**1a**)
4			84 (**1b**)
5			52 (**1a**)
6			63 (**1b**)

tylated α-amino ketones in 68–84 % yields of isolated product (entries 1–4 in Table 1). By employing indan instead of silyl enol ethers, the same reactions gave *N*-trifluoroacetyl indan-1-ylamine in 52 (**1a**) or 63 % (**1b**) yield (determined by GC), as shown in entries 5 and 6 in Table 1. These reactions are very striking, because many non-porphyrin nitrido ruthenium complexes have been isolated, but none of these is reported to be reactive toward hydrocarbons or silyl enol ethers.[6,15,16]

The reaction of "**1a**/**1b** + TFAA" with indan to form *N*-trifluoroacetyl indan-1-ylamine is a unique approach to *N*-trifluoroacetyl amines from direct intermolecular amination of hydrocarbon saturated C–H bonds. Previous formation of *N*-substituted amines from metal-mediated stoichiometric or catalytic intermolecular amination of saturated C–H bonds of hydrocarbons was successful only for *N*-SO_2R or *N*-COPh amines.[17] We envision that the nitrido ruthenium(VI) porphyrin **1a** or **1b**, upon proper activation, might also be useful for the synthesis of other types of *N*-substituted amines by direct amination of saturated C–H bonds; such studies, together with the mechanisms of reaction (2) and the $NCOCF_3$ group-transfer reactions between "**1a**/**1b** + TFAA" and indan/silyl enol ethers, are under current investigation in our laboratory.

Received: September 10, 2002 [Z50138]

[1] a) N. Farrell, D. H. Dolphin, B. R. James, *J. Am. Chem. Soc.* **1978**, *100*, 324; b) C. Crotti, C. Sishta, A. Pacheco, B. R. James, *Inorg. Chim. Acta* **1988**, *141*, 13; c) A. J. Bailey, B. R. James, *Chem. Commun.* **1996**, 2343; d) M. J. Camenzind, B. R. James, D. Dolphin, J. W. Sparapany, J. A. Ibers, *Inorg. Chem.* **1998**, *37*, 3054.

[2] J.-T. Groves, K.-H. Ahn, R. Quinn, *J. Am. Chem. Soc.* **1988**, *110*, 4217.

[3] a) J.-S. Huang, C.-M. Che, C.-K. Poon, *J. Chem. Soc. Chem. Commun.* **1992**, 161; b) J.-S. Huang, C.-M. Che, Z.-Y. Li, C.-K. Poon, *Inorg. Chem.* **1992**, *31*, 1313; c) S.-M. Au, W.-H. Fung, M.-C. Cheng, C.-M. Che, S.-M. Peng, *Chem. Commun.* **1997**, 1655; d) S.-M. Au, J.-S. Huang, W.-Y. Yu, W.-H. Fung, C.-M. Che, *J. Am. Chem. Soc.* **1999**, *121*, 9120; e) X.-G. Zhou, X.-Q. Yu, J.-S. Huang, C.-M. Che, *Chem. Commun.* **1999**, 2377; f) X.-R. Sun, J.-S. Huang, K.-K. Cheung, C.-M. Che, *Inorg. Chem.* **2000**, *39*, 820; g) J.-S. Huang, X.-R. Sun, S. K.-Y. Leung, K.-K. Cheung, C.-M. Che, *Chem. Eur. J.* **2000**, *6*, 334; h) J.-S. Huang, S. K.-Y. Leung, K.-K. Cheung, C.-M. Che, *Chem. Eur. J.* **2000**, *6*, 2971; i) J.-L. Liang, J.-S. Huang, Z.-Y. Zhou, K.-K. Cheung, C.-M. Che, *Chem. Eur. J.* **2001**, *7*, 2306; j) J.-L. Liang, J.-S. Huang, X.-Q. Yu, N. Zhu, C.-M. Che, *Chem. Eur. J.* **2002**, *8*, 1563.

[4] a) C. Morice, P. Le Maux, G. Simonneaux, *Tetrahedron Lett.* **1996**, *37*, 6701; b) C. Morice, P. Le Maux, C. Moinet, G. Simonneaux, *Inorg. Chim. Acta* **1998**, *273*, 142.

[5] a) A. Antipas, J. W. Buchler, M. Gouterman, P. D. Smith, *J. Am. Chem. Soc.* **1978**, *100*, 3015; b) K. M. Kadish, V. A. Adamian, E. V. Caemelbecke, Z. Tan, P. Tagliatesta, P. Bianco, T. Boschi, G.-B. Yi, M. A. Khan, G. B. Richter-Addo, *Inorg. Chem.* **1996**, *35*, 1343; c) D. S. Bohle, P. A. Goodson, B. D. Smith, *Polyhedron* **1996**, *15*, 3147; d) S. J. Hodge, L.-S. Wang, M. A. Khan, V. G. Young, Jr., G. B. Richter-Addo, *Chem. Commun.* **1996**, 2283; e) K. M. Miranda, X. Bu, I. Lorkovic, P. C. Ford, *Inorg. Chem.* **1997**, *36*, 4838; f) G.-B. Yi, M. A. Khan, D. R. Powell, G. B. Richter-Addo, *Inorg. Chem.* **1998**, *37*, 208; g) D. S. Bohle, C.-H. Hung, B. D. Smith, *Inorg. Chem.* **1998**, *37*, 5798; h) I. M. Lorkovic, K. M. Miranda, B. Lee, S. Bernhard, J. R. Schoonover, P. C. Ford, *J. Am. Chem. Soc.* **1998**, *120*, 11674; i) J. Lee, G.-B. Yi, M. A. Khan, G. B. Richter-Addo, *Inorg. Chem.* **1999**, *38*, 4578; j) G. B. Richter-Addo, R. A. Wheeler, C. A. Hixson, L. Chen, M. A. Khan, M. K. Ellison, C. E. Schulz, W. R. Scheidt, *J. Am. Chem. Soc.* **2001**, *123*, 6314.

[6] L. Bonomo, E. Solari, R. Scopelliti, C. Floriani, *Angew. Chem.* **2001**, *113*, 2597; *Angew. Chem. Int. Ed.* **2001**, *40*, 2529.

[7] Ruthenium porphyrins bearing a bridging nitrido ligand have been isolated, see: W.-H. Leung, J. L. C. Chim, W. Lai, L. Lam, W.-T. Wong, W. H. Chan, C.-H. Yeung, *Inorg. Chim. Acta* **1999**, *290*, 28. We noticed that in a previous synthesis of a terminal nitrido complex of ruthenium(VI) porphyrin, [Ru^{VI}(4-Cl-tpp)(N)(OH)] (H_2(4-Cl-tpp) = *meso*-tetrakis(4-chlorophenyl)-porphyrin), from a biphasic (CH_2Cl_2/H_2O) reaction of in situ formed [Ru^{VI}(4-Cl-tpp)$(O)_2$] with $NH_3 \cdot H_2O$ (see: Z.-Y. Li, C.-M. Che, C.-K. Poon, *Wuhan Univ. J. Nat. Sci.* **1996**, *1*, 89), the "nitrido" species (which was not structurally characterized) should be reformulated as a hexacoordinate {Ru(NO)} complex, [Ru(4-Cl-tpp)(NO)(X)], according to its UV/Vis spectral data (Soret band: 412 nm, β band: 558 nm).

[8] Selected examples: a) J. T. Groves, T. Takahashi, *J. Am. Chem. Soc.* **1983**, *105*, 2073; b) J. Du Bois, J. Hong, E. M. Carreira, M. W. Day, *J. Am. Chem. Soc.* **1996**, *118*, 915; c) J. Du Bois, C. S. Tomooka, J. Hong, E. M. Carreira, *J. Am. Chem. Soc.* **1997**, *119*, 3179; d) J. Du Bois, C. S. Tomooka, J. Hong, E. M. Carreira, *Acc. Chem. Res.* **1997**, *30*, 364; e) J. Du Bois, C. S. Tomooka, J. Hong, E. M. Carreira, M. W. Day, *Angew. Chem.* **1997**, *109*, 1722; *Angew. Chem. Int. Ed. Engl.* **1997**, *36*, 1645; f) S. Minakata, T. Ando, M. Nishimura, I. Ryu, M. Komatsu, *Angew. Chem.* **1998**, *110*, 3596; *Angew. Chem. Int. Ed.* **1998**, *37*, 3392.

[9] a) W. A. Nugent, J. M. Mayer, *Metal-Ligand Multiple Bonds*, Wiley, New York, **1988**; b) K. Dehnicke, J. Strähle, *Angew. Chem.* **1992**, *104*, 978; *Angew. Chem. Int. Ed. Engl.* **1992**, *31*, 955.

 © 2003 Wiley-VCH Verlag GmbH & Co. KGaA, Weinheim 1433-7851/03/4203-0342 $ 20.00+.50/0

[10] Abbreviations: H_2tmp: *meso*-tetrakis(2,4,6-trimethylphenyl)-porphyrin, H_2(3,4,5-MeO-tpp): *meso*-tetrakis(3,4,5-trimethoxyphenyl)porphyrin, *m*-CPBA: *m*-chloroperoxybenzoic acid, H_2tpp: *meso*-tetraphenylporphyrin, H_2ttp: *meso*-tetrakis(*p*-tolyl)porphyrin, H_2tpfpp: *meso*-tetrakis(pentafluorophenyl)porphyrin, NBS: *N*-bromosuccinimide, Ts = *p*-toluenesulfonyl.
[11] a) J. T. Groves, R. Quinn, *J. Am. Chem. Soc.* **1985**, *107*, 5790; b) C. Ho, W.-H. Leung, C.-M. Che, *J. Chem. Soc. Dalton Trans.* **1991**, 2933.
[12] As tmp is a sterically encumbered porphyrin, whereas 3,4,5-MeO-tpp is basically a sterically unencumbered porphyrin ligand (the latter can not prevent formation of dinuclear μ-oxo ruthenium porphyrins), yet both of them gave nitrido ruthenium porphyrin **1** in similar yields, the steric properties of porphyrin ligands should have a minor effect on the Ru≡N formation from reaction (2).
[13] The frequency of this new band is comparable to the Ru≡N stretching frequency of 1023 cm^{-1} reported for the non-porphyrin nitrido ruthenium(VI) complex $[Ru^{VI}(N)Cl_3(AsPPh_3)_2]$ (a neutral, six-coordinate nitrido ruthenium(VI) species, like **1a** and **2**). See: D. Pawson, W. P. Griffith, *Inorg. Nucl. Chem. Lett.* **1974**, *10*, 253.
[14] CCDC-193042 (**1b**) contains the supplementary crystallographic data for this paper. These data can be obtained free of charge via www.ccdc.cam.ac.uk/conts/retrieving.html (or from the Cambridge Crystallographic Data Centre, 12 Union Road, Cambridge CB2 1EZ, UK; fax: (+44) 1223-336-033; or deposit @ccdc.cam.ac.uk).
[15] P. M. Chan, W.-Y. Yu, C.-M. Che, K.-K. Cheung, *J. Chem. Soc. Dalton Trans.* **1998**, 3183.
[16] We treated $[NnBu_4][Ru^{VI}(N)Cl_4]$ (prepared as described in W. P. Griffith, D. Pawson, *J. Chem. Soc. Dalton Trans.* **1973**, 1315) and $[Ru^{VI}(N)(L)Cl]$ (H_2L = 2,6-bis(2-hydroxy-2,2-diphenylethyl)-pyridine, prepared as described in ref. [15]) with TFAA and the silyl enol ethers shown in Table 1 under the conditions similar to those for **1a**/**1b** but obtained no amination products from the reaction mixtures.
[17] Selected examples: a) R. Breslow, S. H. Gellman, *J. Chem. Soc. Chem. Commun.* **1982**, 1400; b) J. P. Mahy, G. Bedi, P. Battioni, D. Mansuy, *Tetrahedron Lett.* **1988**, *29*, 1927; c) I. Nägeli, C. Baud, G. Bernardinelli, Y. Jacquier, M. Moran, P. Müller, *Helv. Chim. Acta* **1997**, *80*, 1087; d) S.-M. Au, J.-S. Huang, C.-M. Che, W.-Y. Yu, *J. Org. Chem.* **2000**, *65*, 7858, and references therein; e) Y. Kohmura, T. Katsuki, *Tetrahedron Lett.* **2001**, *42*, 3339.

Synthesis of a marine macrolide

Stereocontrolled Total Synthesis of (+)-Leucascandrolide A**

Ian Paterson and Matthew Tudge*

Leucascandrolide A (**1**, Scheme 1) was isolated in 1996 from the calcareous sponge *Leucascandra caveolata*, collected off the east coast of New Caledonia, by Pietra and co-workers.[1] This polyoxygenated 18-membered macrolide features two trisubstituted tetrahydropyran rings, one of which has an unusual oxazole-bearing unsaturated side chain. To date, the true biosynthetic origin of this unique polyketide is uncertain.[2] Subsequent reisolation attempts proved unsuccessful which indicates that leucasandrolide A may be produced by opportunistic microbial colonization of the sponge.[2] Preliminary biological studies revealed potent cytotoxic activity against a range of cancer cell lines (IC_{50} = 0.05 and 0.25 $\mu g\,mL^{-1}$ against KB oral epidermoid carcinoma and P388 leukemia cell lines, respectively), as well as pronounced antifungal activity. Since the natural supply of leucascandrolide A is unreliable, an efficient synthesis is paramount to enable further biological studies and, furthermore, to provide access to analogues. Consequently, leucascandrolide A has attracted considerable synthetic attention,[3–5] with the first total synthesis reported by Leighton and co-workers.[3] Herein, we report an expedient total synthesis of (+)-leucascandrolide A in which essentially complete control over all of the stereochemistry is achieved.

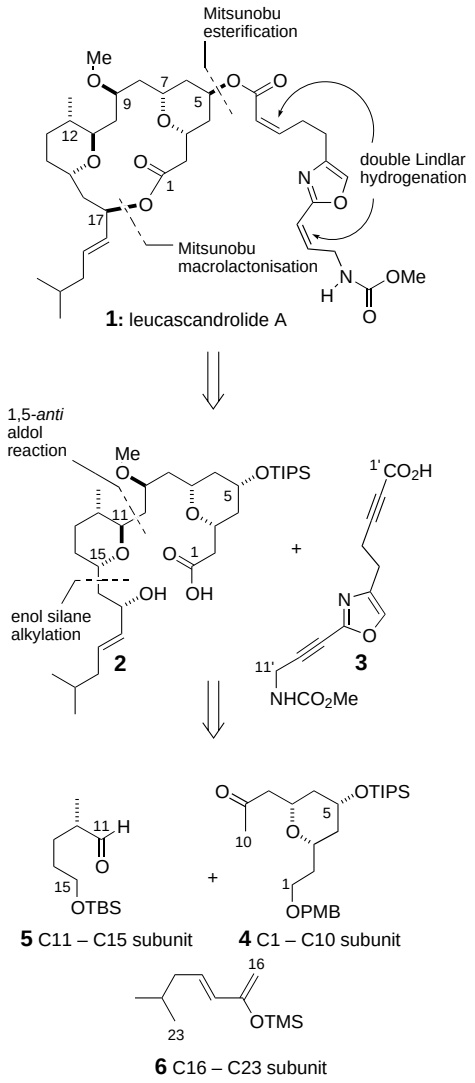
As outlined in Scheme 1, our approach relies on two Mitsunobu reactions—the first is employed to cyclize the *seco*-acid **2** and the second to append the heterocyclic side chain **3** at C5. A double Lindlar hydrogenation should then install the two *Z*-configured alkenes to provide leucascandrolide A directly. By exploiting the high degree of 1,3-dioxygenation embodied within the *seco*-acid **2**, we planned to introduce all the oxygenated stereocenters from tetrahydropyran **4** by using only substrate control. In light of the *anti* configurational relationship between C7 and C11, *seco*-acid **2** should be accessible from the β-oxygenated ketone **4** and aldehyde **5** by using our 1,5-*anti* aldol methodology.[5b,6,7] Furthermore, the resulting C11 stereocenter could then serve, in turn, to direct an alkylation with silyl enol ether **6** to install the full C15 side chain.

As shown in Scheme 2, the synthesis of the trisubstituted tetrahydropyran **4** began with a Jacobsen asymmetric hetero

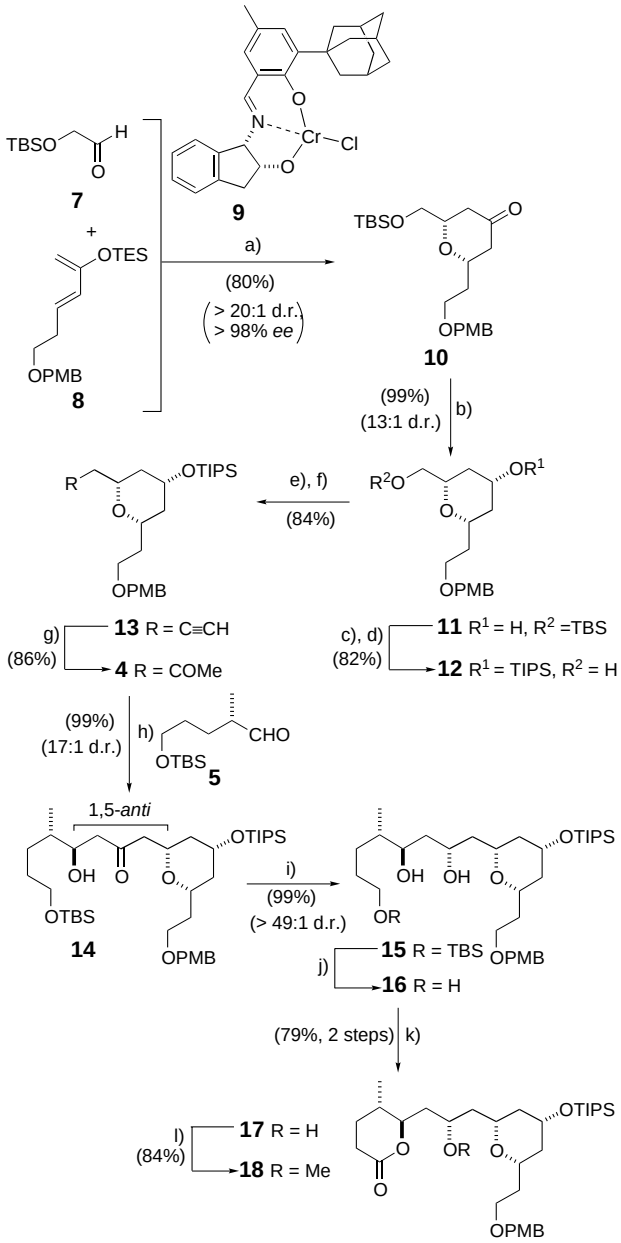
[*] Prof. I. Paterson, M. Tudge
University Chemical Laboratory
Lensfield Road, Cambridge, CB2 1EW (UK)
Fax: (+44) 1223-336-362
E-mail: ip100@cus.cam.ac.uk

[**] We thank the EPSRC (studentship to M.T. and GR/N08520), the EU (Network HPRN-CT-2000-00018), and Merck, Pfizer, and Novartis for support.

Supporting information for this article is available on the WWW under http://www.angewandte.org or from the author.



Scheme 1. Retrosynthesis of leucascandrolide A (**1**) leading to key building blocks **2**–**6**. TIPS = triisopropylsilyl; TBS = *tert*-butyldimethylsilyl; TMS = trimethylsilyl; PMB = *p*-methoxybenzyl.

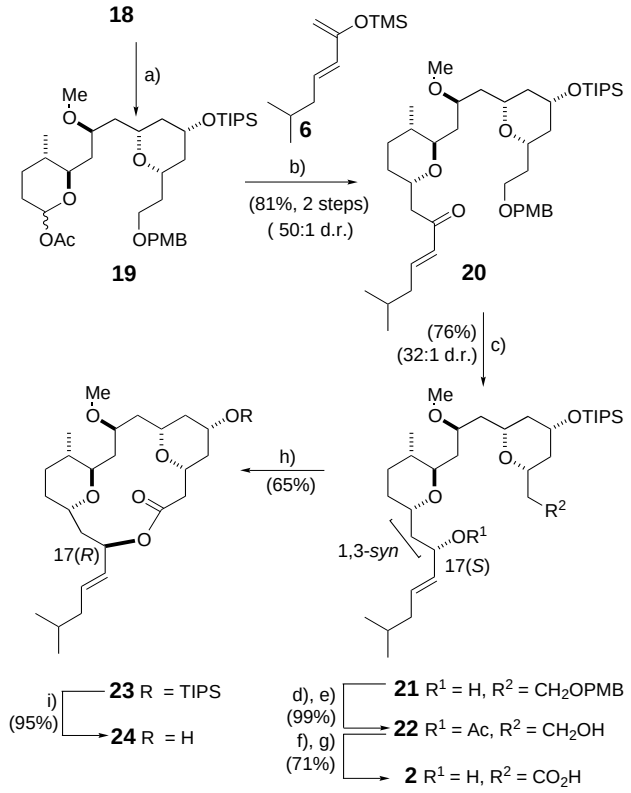


Scheme 2. Preparation of advanced intermediate **18**. a) **9** (10 mol%), 4 Å molecular sieves, 20°C, 20 h; acidified $CHCl_3$, 20°C, 4 h; b) $NaBH_4$, MeOH, 20°C, 2 h; c) TIPSOTf, lut, CH_2Cl_2, −78°C, 2 h; d) CSA, 2:1 MeOH/CH_2Cl_2, 20°C, 1 h; e) Tf_2O, pyr, CH_2Cl_2, −10°C, 1 h; f) LDA, TMSC≡CH, HMPA, −78→20°C, 1 h; K_2CO_3, MeOH, 20°C, 12 h; g) cat. $Hg(OAc)_2$, PPTS, wet THF, 40°C, 1 h; h) *c*Hex_2BCl, NEt_3, Et_2O, 0°C, 30 min; **5**, −78°C, 2 h; −78→−30°C, 24 h; i) $Me_4NBH(OAc)_3$, 3:1 MeCN/AcOH, −40→−20°C, 24 h; j) CSA, 2:1 MeOH/CH_2Cl_2, 25°C, 1 h; k) TEMPO, $PhI(OAc)_2$, CH_2Cl_2, 20°C, 12 h; l) Me_3OBF_4, proton sponge, CH_2Cl_2, 0→20°C, 1 h. OTf = trifluoromethane sulfonate; lut = 2,6-lutidine; Tf_2O = trifluoromethane sulfonic anhydride; pyr = pyridine; LDA = lithium diisopropylamide; HMPA = hexamethyl phosphoramide; PPTS = pyridinium *p*-tolunesulfonate; CSA = 10-camphorsulfonic acid; TEMPO = 2,2,6,6-tetramethyl-1-piperidinyloxyl.

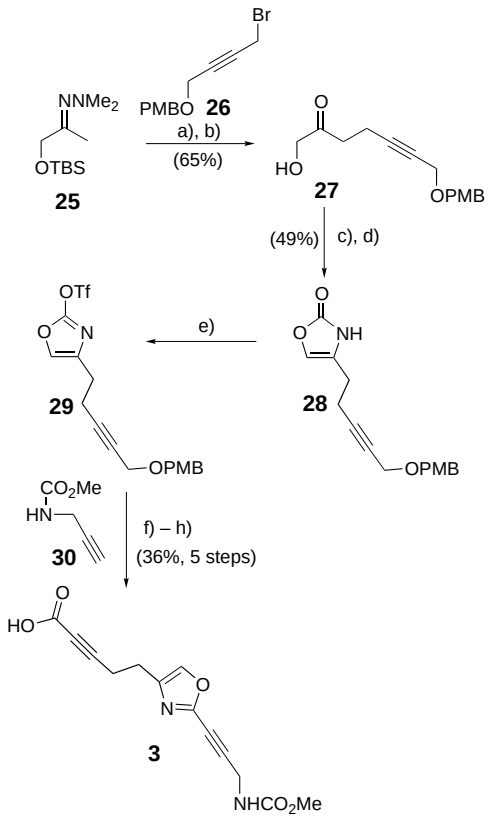
Diels–Alder reaction of aldehyde **7** and readily available 2-siloxydiene **8**,[8] promoted by the chromium tridentate catalyst **9**.[9a] This generated the corresponding [4+2] cycloadduct,[9b] which, upon workup with mild acid, led to isolation of 2,6-*cis*-pyranone **10** in 80% yield with >20:1 d.r. and >98% *ee*. Installation of the equatorial C5 hydroxy group was achieved by treatment with $NaBH_4$ in MeOH to give secondary alcohol **11** in 99% yield and 13:1 d.r. Following TIPS ether formation, selective acidic removal of the TBS group gave primary alcohol **12** (82%). Homologation[10] to the methyl ketone **4** involved activation of alcohol **12** as its triflate derivative, displacement with lithium trimethylsilyl acetylide and basic methanolysis to give alkyne **13** (84%). Subsequent Hg^{II}-mediated hydration gave the methyl ketone **4** cleanly (86%). This efficient reaction sequence was performed to produce multigram quantities of enantiopure **4**.

The key 1,5-*anti* aldol coupling reaction of β-alkoxy ketone **4** with aldehyde **5**[11] proceeded smoothly under our

 © 2003 Wiley-VCH Verlag GmbH & Co. KGaA, Weinheim 1433-7851/03/4203-0344 $ 20.00+.50/0



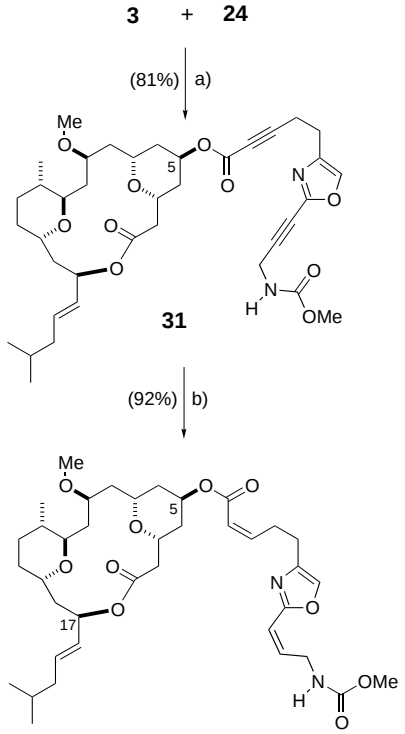
Scheme 3. Elaboration to the macrocyclic core **24**. a) DIBAL, CH_2Cl_2, then Ac_2O, pyr, DMAP, −78→−20°C, 15 h; b) $ZnBr_2$, CH_2Cl_2, 20°C, 4 h; c) $LiAlH(OtBu)_3$, CH_2Cl_2, −78→−10°C, 1.5 h; d) Ac_2O, pyr, DMAP, CH_2Cl_2, 0→20°C, 15 h; e) DDQ, 10:1 CH_2Cl_2/pH 7 buffer, 20°C, 1 h; f) TEMPO, $PhI(OAc)_2$, CH_2Cl_2, 20°C, 1 h; $NaClO_2$, $NaHPO_4$, methyl-2-butene, aq. *t*BuOH, 0→20°C, 1 h; g) K_2CO_3, MeOH, 20°C, 18 h; h) DEAD, PPh_3, PhH, 20°C, 5 min; i) HF·pyr, THF, 0→20°C, 5 h. DIBAL = diisobutylaluminum hydride; DMAP = 4-(dimethylamino)pyridine; DDQ = 2,3-dichloro-5,6-dicyano-1,4-benzoquinone; DEAD = diediethylazodicarboxylate.



Scheme 4. Preparation of the oxazole-bearing side chain **3**. a) LDA, HMPA, THF, −78→20°C, 2 h; b) TBAF, THF, 20°C, 1 h; c) $Cl_3CC(O)NCO$, CH_2Cl_2, 20°C, 1 h; K_2CO_3, MeOH, 20°C, 1 h; d) 4 Å molecular sieves, PhMe, 90°C, 2 h; e) Tf_2O, lut, CH_2Cl_2, −78→−10°C, 1 h; f) $[Pd(PPh_3)_4]$, **30**, lut, 1,4-dioxan, 20°C, 6 h; g) DDQ, 10:1 CH_2Cl_2/pH 7 buffer, 20°C, 1 h; h) TEMPO, $PhI(OAc)_2$, CH_2Cl_2, 20°C, 1 h; then $NaClO_2$, $NaHPO_4$, methyl-2-butene, aq. *t*BuOH, 0→20°C, 1 h. TBAF = tetrabutylammonium fluoride.

standard conditions.[5b,6] Thus, treatment of **4** with *c*Hex_2BCl and Et_3N in Et_2O generated the corresponding less substituted enolate, which on addition of aldehyde **5** provided, after oxidative workup, aldol adduct **14** in 99% yield and 17:1 d.r.[12] With the required 11*R* configuration installed, efforts were now focused towards constructing the second tetrahydropyran ring and installing the C9 stereocenter. To this end, 1,3-*anti* reduction of β-hydroxy ketone **14** with $Me_4NBH(OAc)_3$[13] provided diol **15** in 99% yield and ≥50:1 d.r. Next, acidic removal of the TBS group gave triol **16**, which was oxidized selectively at the primary hydroxy group by using catalytic TEMPO and iodobenzene diacetate[14] to give δ-lactone **17** (79%); by this procedure, the 1,5,7-triol was discriminated and the second pyran ring closed in a highly effective manner. This constitutes one of the first examples of a TEMPO-mediated procedure for achieving chemoselective lactone formation from open-chain polyols. Methylation of the isolated C9 hydroxy group with Me_3OBF_4 and proton sponge gave advanced intermediate **18** (84%).

Effective anomeric allylation procedures for the stepwise installation of the C15 side chain have been reported by both Leighton et al.[3] and Rychnovsky et al.[4] In both these cases, however, following ozonolysis of the terminal alkene, the addition of either an alkenyl[3] or an alkynyl[4] organozinc to the derived aldehyde resulted in modest control over the C17 hydroxy stereocenter, that is, typically 3–3.5:1 in favor of the 1,3-*anti* stereochemistry (followed by a Yamaguchi macrolactonization). In contrast, we set about installing the full C16–C23 side chain with concomitant generation of the C15 stereocenter. As shown in Scheme 3, suitable activation of the anomeric position was achieved by treating δ-lactone **18** with DIBAL followed by in situ acetylation[15] to afford acetate **19**. Treatment of **19** with an excess of silyl enol ether **6**[16] in the presence of catalytic $ZnBr_2$[17] afforded ketone **20** cleanly in 81% yield and ≥50:1 d.r. Next, a 1,3-*syn* reduction directed by the C15 pyran oxygen atom was envisioned to configure the C17 stereocenter ready for the planned Mitsunobu macrolactonization. Several reducing agents were screened in the presence of $ZnBr_2$ to induce metal chelation, but only $LiAlH(OtBu)_3$ provided a satisfactory selectivity (5:1 d.r.) in favor of the *syn* isomer. However, use of $LiAlH(OtBu)_3$ alone gave allylic alcohol **21** with much improved *syn* diastereose-



1: (+)-leucascandrolide A

Scheme 5. Completion of the total synthesis of leucascandrolide A. a) DEAD, PPh_3, 1.5:1 THF/PhMe, 0→20 °C, 18 h; b) H_2, 5% Pd/$CaCO_3$ poisoned with lead (Lindlar catalyst), quinoline, EtOAc, 20 °C, 2 h.

lectivity (76%, >32:1 d.r.) which indicates the operation of a nonchelation pathway possibly following the Evans polar model.[18] Acetylation of the resultant (17*S*)-hydroxy group followed by oxidative removal of the PMB group gave alcohol **22** in 99% yield. Oxidation to the corresponding acid and saponification afforded *seco*-acid **2** (71%) which set the stage for the Mitsunobu macrolactonization.[19] Pleasingly, treatment of **2** with DEAD and Ph_3P in degassed benzene for 5 min proceeded to give the desired macrocycle **23** in 65% yield with clean inversion of configuration. Cleavage of the equatorial C5 TIPS ether was achieved by HF·pyr in THF to furnish macrocycle **24** in 95% yield in readiness for the introduction of the axially oriented side chain at C5.

As shown in Scheme 4, preparation of the bis-alkyne side chain **3** relied on a Sonogashira coupling, in which the required oxazolyl triflate **29** was derived from alcohol **27**, the α-alkylation product of hydrazone **25**[20] and bromide **26**.[21] Treatment of **27** with trichloroacetyl isocyanate, followed by basic hydrolysis and heating the resulting intractable mixture to 90 °C, in the presence of 4 Å molecular sieves, produced the required oxazolone **28** (49%). Reaction with triflic anhydride provided oxazolyl triflate **29** which was treated with alkyne **30**[3] under Sonogashira coupling conditions, as developed by Panek and co-workers,[22] to provide the side-chain precursor. Removal of the PMB group, followed by oxidation of the resulting alcohol to the carboxylic acid, then gave the required oxazole-bearing side chain **3**.

With the two key fragments in hand, we were now poised to test the Mitsunobu coupling on the equatorial C5 hydroxy group. As detailed in Scheme 5, reaction of acid **3** and macrocycle **24** in the presence of DEAD and PPh_3 in 1.5:1 PhMe/THF resulted in the smooth formation of the axial ester **31** in 81% yield. Finally, Lindlar hydrogenation of the triple bonds enabled the stereospecific introduction of the two *Z*-alkenes to provide a 92% yield of (+)-leucascandrolide A (**1**). This had spectroscopic data[23] in full accord with those reported by Leighton[3] and Pietra.[1]

In summary, we have completed a highly stereocontrolled synthesis of the potent cytotoxic macrolide leucascandrolide A, proceeding in 23 steps from **8** (longest linear sequence) and 5.3% overall yield. Key features include a Jacobsen asymmetric hetero Diels-Alder reaction to configure the right-hand tetrahydropyran ring, a 1,5-*anti* aldol coupling, control over the C17 hydroxy center, and two sequential Mitsunobu reactions, to close the 18-membered macrolactone and append the oxazole-bearing side chain, respectively.

Received: September 12, 2002 [Z50143]

[1] M. D'Ambrosio, A. Guerriero, C. Debitus, F. Pietra, *Helv. Chim. Acta* **1996**, *79*, 51.

[2] M. D'Ambrosio, M. Tato, G. Pocsfalvi, C. Debitus, F. Pietra, *Helv. Chim. Acta* **1999**, *82*, 347.

[3] K. R. Hornberger, C. L. Hamblett, J. L. Leighton, *J. Am. Chem. Soc.* **2000**, *122*, 12894.

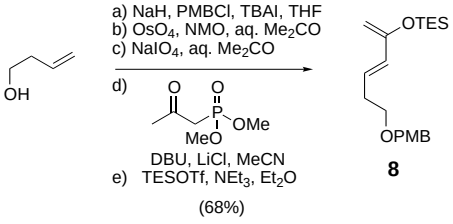
[4] For formal syntheses based on the endgame of Leighton, see: a) D. J. Kopecky, S. D. Rychnovsky, *J. Am. Chem. Soc.* **2001**, *123*, 8420; b) P. Wipf, J. T. Reeves, *Chem. Commun.* **2002**, 2066. c) After submission of this manuscript, we were informed by Professor Carreira of his completed synthesis of leucascandrolide A, see: A. Fettes, E. M. Carreira, *Angew. Chem.* **2002**, *114*, 4272; *Angew. Chem. Int. Ed.* **2002**, *41*, 4098.

[5] For the synthesis of fragments of leucascandrolide, see: a) M. T. Crimmins, C. A. Carroll, B. W. King, *Org. Lett.* **2000**, *2*, 597; b) S. A. Kozmin, *Org. Lett.* **2001**, *3*, 755; c) P. Wipf, T. H. Graham, *J. Org. Chem.* **2001**, *66*, 3242.

[6] I. Paterson, K. R. Gibson, R. M. Oballa, *Tetrahedron Lett.* **1996**, *37*, 8585.

[7] D. A. Evans, P. J. Coleman, B. Coté, *J. Org. Chem.* **1997**, *62*, 788.

[8] Diene **8** was prepared from 3-buten-1-ol [Eq. (1); DBU = 1,8-diazabicyclo[5.4.0]undec-7-ene, TES = triethylsilyl].



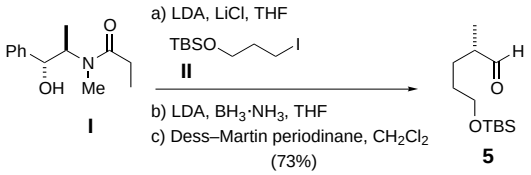
(1)

[9] a) A. G. Dossetter, T. F. Jamison, E. N. Jacobsen, *Angew. Chem.* **1999**, *111*, 2549; *Angew. Chem. Int. Ed.* **1999**, *38*, 2398. b) This reaction is believed to proceed through a highly ordered [4+2] cycloaddition in contrast to a Mukaiyama aldol/hetero-Michael pathway. For a review, see: K. A. Jorgensen, *Angew. Chem.* **2000**, *112*, 3702; *Angew. Chem. Int. Ed.* **2000**, *39*, 3559.

[10] This homologation sequence was adapted from Evans and coworkers: D. A. Evans, D. M. Fitch, T. E. Smith, V. J. Cee, *J. Am. Chem. Soc.* **2000**, *122*, 10033.

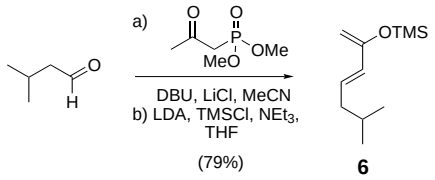
 © 2003 Wiley-VCH Verlag GmbH & Co. KGaA, Weinheim 1433-7851/03/4203-0346 $ 20.00+.50/0

[11] Aldehyde **5** was prepared by diastereoselective alkylation of the Myers chiral amide **I** with iodide **II** [Eq. (2)]. A. G. Myers, L. McKinstry, *J. Org. Chem.* **1996**, *61*, 2428.



(2)

[12] The corresponding aldol addition with achiral aldehydes led to comparably high levels of 1,5-*anti* stereoinduction which indicates that chiral aldehyde **5** contributed only negligibly to 1,2-induction.
[13] D. A. Evans, K. T. Chapman, E. M. Carreira, *J. Am. Chem. Soc.* **1988**, *110*, 3560.
[14] A. De Mico, R. Margarita, L. Parlanti, A. Vescovi, G. Piancatelli, *J. Org. Chem.* **1997**, *62*, 6974.
[15] V. H. Dahanukar, S. D. Rychnovsky, *J. Org. Chem.* **1996**, *61*, 8317.
[16] Enol silane **6** was prepared from isovaleraldehyde [Eq. (3)].



(3)

[17] I. Paterson, *Tetrahedron Lett.* **1979**, 1519.
[18] D. A. Evans, M. J. Dart, J. L. Duffy, M. G. Yang, *J. Am. Chem. Soc.* **1996**, *118*, 4322.
[19] O. Mitsunobu, *Synthesis* **1981**, 1. A Mitsunobu macrolactonization strategy was independently reported by Wipf et al.[4b] while this manuscript was in preparation.
[20] C. W. Jefford, J.-C. Rossier, J. Boukouvalas, P. Huang, *Helv. Chim. Acta* **1994**, *77*, 661.
[21] L. Banfi, G. Guanti, A. Basso, *Eur. J. Org. Chem.* **2000**, 939.
[22] N. F. Langille, L. A. Dakin, J. S. Panek, *Org. Lett.* **2002**, *4*, 2485.
[23] $[\alpha]_D^{20} = +40.0$ ($c = 0.29$, EtOH) [ref. [1], $[\alpha]_D^{20} = +41.0$ ($c = 0.29$, EtOH)]. For copies of ^1H and ^{13}C NMR spectra, see the Supporting Information.

Yttria-Zirconia Thin Films

Controlled Formation of Highly Ordered Cubic and Hexagonal Mesoporous Nanocrystalline Yttria–Zirconia and Ceria–Zirconia Thin Films Exhibiting High Thermal Stability**

*Eduardo L. Crepaldi, Galo J. de A. A. Soler-Illia, Anne Bouchara, David Grosso, Dominique Durand, and Clément Sanchez**

Zirconia-based mixed oxides are current targets of intensive research as a result of their applications in strategic technologies, such as yttria-stabilized zirconia (YSZ) in solid-oxide fuel cells (SOFCs),[1] and ceria–zirconia in the latest generation of automotive exhaust three-way catalysts,[2,3] the latter having the potential to be applied in the next generation of compact SOFCs.[3] In view of these applications, controlling the porosity of these systems is highly desirable. The "supramolecular template approach" offers precise control of the material porosity on the mesoscale (20–200 Å).[4] Ozin and co-workers[5] were the first to extend this method to the synthesis of YSZ by using cetyltrimethylammonium bromide (CTAB) templated glycolate-modified inorganic precursors. Gedanken and co-workers[6] reported the synthesis of mesoporous YSZ using metallic salts or oxides as inorganic sources and anionic surfactants as templates. All of these precipitation methods yield disordered wormlike mesoporous powders. However, to the best of our knowledge, periodically organized mesoporous ceria–zirconia and even yttria–zirconia materials are yet to be reported.

The present work reports the first examples of periodically organized mesoporous yttria–zirconia (YZ) and ceria–zirconia (CZ) ($R = M/(M+Z) = 0.05$–0.30, where Z is the amount of Zr and M is the amount of Y or Ce present in the material). Moreover, these materials are processed as thin films. The procedure is simple and reproducibly gives highly ordered mesoporous nonsilicate mixed oxides, which retain their structure (order and porosity) after crystallization of the inorganic walls and subsequent thermal treatment to temperatures as high as 700 °C. This advantageous one-step method can replace the usual precipitation of particles/deposition/

[*] Dr. C. Sanchez, Dr. E. L. Crepaldi, Dr. G. J. de A. A. Soler-Illia, A. Bouchara, Dr. D. Grosso
Laboratoire de Chimie de la Matière Condensée
UMR 7574, Université Pierre et Marie Curie (Paris VI)
4 place Jussieu, 75252 Paris CEDEX 05 (France)
Fax: (+33) 1-4427-4769
E-mail: clems@ccr.jussieu.fr
Dr. D. Durand
LURE Bât 209D, Centre Universitaire
B.P. 34, 91898 Orsay Cedex (France)

[**] This work was financially supported by the French Ministry of Research, CNRS, CNPq (Brazil, grant no. 200636/00-0), CONICET, and Fundación Antorchas (Argentina). Rhodia is greatly acknowledged for financial support of A.B.

Supporting information for this article is available on the WWW under http://www.angewandte.org or from the author.

sintering process that is applied to construct zirconia-based mixed-oxide porous coatings. The mesostructured hybrids (precursors to the mesoporous solids) were templated by poly(ethylene oxide) (EO) based amphiphilic block copolymers (ABCs), and were produced by an evaporation-induced self-assembly (EISA) derived method,[7] which uses anhydrous metal chlorides in ethanol/water solutions (see Experimental Section).

Figure 1 shows a schematic view of the film processing technique. Time-resolved small-angle X-ray scattering (SAXS) and interferometry analysis (SAXS beamline of Elettra, Trieste, Italy; details elsewhere[8]) showed that organization starts just after the drying line. A diffraction ring, characteristic of polyoriented domains, is initially observed. For SiO_2[9] and TiO_2-based[10] ABC-templated systems, the organization occurs through a "disorder-to-order" transition, which for the ZrO_2-based systems does not run to completion as a result of the formation of extended metal–oxo polymers, which "freeze" the intermediate worm-like mesophase. The quenched system has poor optical quality (see Figure 1a) after the first drying process (FD) at low relative humidity (RH). These freshly formed olated metal–oxo polymers (olation is kinetically favored[11]) can be "rearranged" by a short (10–20 s) water-vapor treatment (WVT), which promotes the diffusion of water within the coating to allow the reorganization of the organic species into a highly ordered mesophase. The second drying process (SD) then takes place homogeneously, which results in smooth crack-free coatings (see Figure 1b). This formation path takes place for all zirconia-based systems, and was also observed for Brij 58-templated mesostructured ZrO_2 films.[12]

At this stage, the inorganic framework is far from being fully condensed (see Supporting Information). We observed that one can take advantage of structural "flexibility" to tailor the final mesophase at a fixed template/inorganic molar ratio. Figure 2 shows 2D synchrotron SAXS patterns (recorded at the D43 line of LURE, Orsay, France; transmission mode, incidence of 4° to the substrate) that correspond to two different mesostructures obtained for different RHs during SD and aging. For pure ZrO_2, a 2D hexagonal mesostructure is obtained under all conditions. The loading of less acidic trivalent metal cations ($R = 5$–$30\,\%$) induces a higher flexibility of the inorganic framework and allows for the formation of cubic mesophases. The low tendency of such cations to condense in acidic media is likely to reduce the condensation rate and the extension of the ZrO_2-based inorganic polymers (creation of "dead ends"). In addition, the different size and coordination of these cations (when compared to the Zr^{4+} ion) can alter the polyhedral linking. Each of these effects can contribute, either individually or in association, to give a better adjustment of the inorganic framework to the more curved organic–inorganic interface of the cubic mesophase.[8b]

For films with R greater than 5% that were dried and aged under "dry" conditions (RH = 10%), the SAXS patterns show six defined spots that can be indexed as the {10} reflections of a 2D hexagonal (*P6m* space group) mesostructure (Figure 2a) with the channels, and more precisely the (01) planes, preferentially aligned parallel to the substrate. The same orientation has already been observed for CTAB or F127-templated 2D hexagonal mesoporous silica films.[9,13] The unit-cell parameters are displayed in Table 1. Drying and aging under a humid atmosphere (RH = 50%) favors the formation of a cubic mesophase (Figure 2b). The resulting SAXS patterns show eight spots with angles in agreement

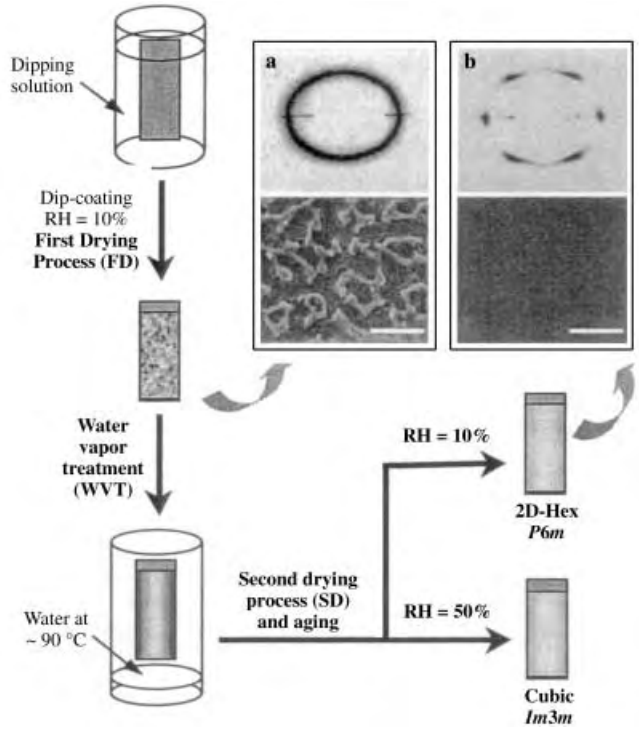


Figure 1. Schematic representation of film processing by dip-coating. Parts (a) and (b) are in situ SAXS patterns (top) and SEM images (bottom) acquired respectively before and after water vapor treatment. Scale bars are 10 μm.

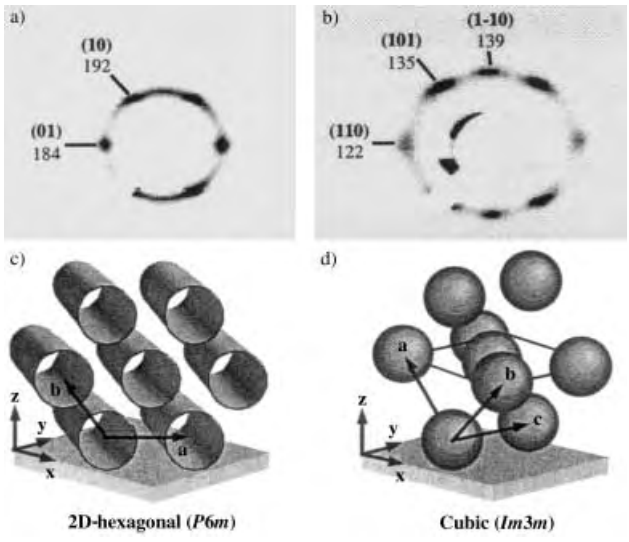


Figure 2. 2D SAXS patterns for F127-templated films: a) 2D hexagonal mesostructured CZ (drying and aging at RH = 10%); b) cubic mesostructured YZ (drying and aging at RH = 50%); c) and d) orientation scheme for the 2D hexagonal and cubic mesophases. Distances in parts (a) and (b) are given in Å.

 © 2003 Wiley-VCH Verlag GmbH & Co. KGaA, Weinheim 1433-7851/03/4203-0348 $ 20.00+.50/0

Table 1: Aging conditions and structural characteristics of Pluronic F127-templated films.

Inorganic framework	M/(M+Z)	RH [%]	Structure	*a* [Å]
ZrO_2	–	10	2D hexagonal	211
ZrO_2	–	50	2D hexagonal	218
ZrO_2–Y_2O_3	0.20	10	2D hexagonal	222
ZrO_2–Y_2O_3	0.20	50	cubic	197
ZrO_2–ceria	0.20	10	2D hexagonal	231
ZrO_2–ceria	0.20	50	cubic	213

with those between the {110} planes of a body-centered cubic mesophase (*Im*3*m* space group) with the (110) planes parallel to the substrate (see Figure 2c). A complete indexation for such a phase in the same orientation can be found elsewhere for F127-templated silica films.[14] This orientation seems to be the same as that reported for the Pluronic P123 (EO_{20}-$PO_{70}EO_{20}$, PO = propylene oxide) templated *Im*3*m* mesoporous silica and titania films.[15] Another orientation for this same structure, with the (100) planes parallel to the substrate, was also reported for F127-templated silica films.[16] For both 2D-hexagonal and cubic mesophases, SAXS patterns taken at incidence normal to the substrate displayed diffraction rings that show that the *c* vector (for both structures) does not have preferential orientation with respect to the deposition direction (*xy* plane, as represented in Figure 2c).

Transmission electron microscopy (TEM) images of calcined cubic and hexagonal films are presented in Figure 3.

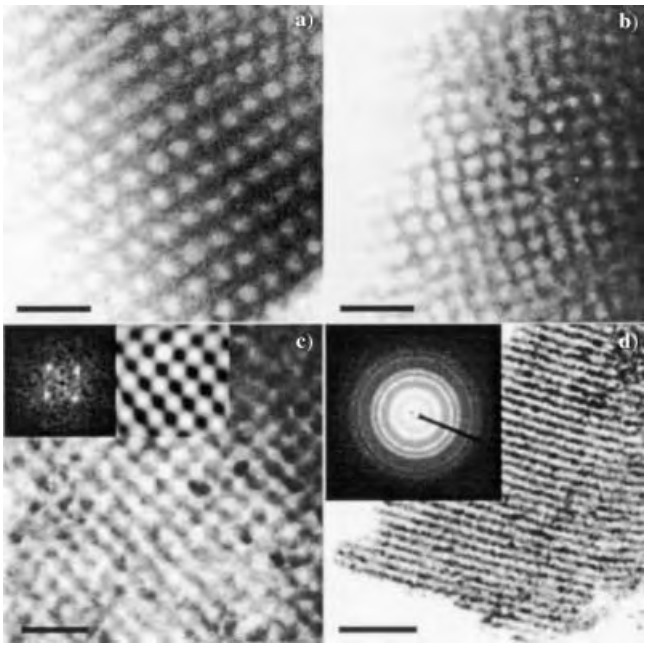


Figure 3. TEM images for F127-templated films: a) 2D hexagonal ZrO_2 treated at 300 °C; b) cubic CZ treated at 300 °C; c) and d) cubic YZ treated at 700 °C. The images are projections parallel to the following directions; [001] (a), [100] (b) and (c), and [211] (d). The insets in part (c) show the modulus of a Fourier-transform of the full image, and a reconstructed image of a selected region. The inset in part (d) is an electron diffraction pattern showing that the inorganic framework is composed of crystalline cubic YZ. Scale bars are: a) 25 nm, b) and c) 50 nm, and d) 100 nm.

Periodic distances are in agreement (within 10%) with those found by 2D SAXS (because of tilting or sample shrinking under calcination, see below). For cubic YZ and CZ, *a* values of 183 and 195 Å are found, respectively. In the case of hexagonal phases, an a_{TEM} value of around 200 Å was found for all compositions, which is in good agreement with the SAXS values, when considering the contraction upon thermal treatment.

The results described above show that for zirconia-based mixed-oxide systems, the final mesophase can be tailored by aging the film at controlled humidity. At high humidity, water is encouraged to remain inside the coating and is located within the inorganic network (through hydrogen bonding with OH groups and/or coordination to the metal cations), between the ABC hydrophilic chains, and at the organic–inorganic interface. These factors contribute to increase: 1) the inorganic/template volume ratio, 2) the curvature of the ABC micelles, and 3) the amount of interface.[14] During aging, further condensation progressively takes place (oxolation is thermodynamically favored),[11] which stabilizes the mesophase with varying quantities of water within the hybrid framework, to give three-dimensional (cubic, "humid" conditions) or two-dimensional (hexagonal, "dry" conditions) mesostructures. The results reported for silica–CTAB[17] and silica–F127 mesostructured films[14] are in agreement with the results reported here. It is recognized that the choice of the template[16] and the inorganic/template volume ratio are both important factors that determine the final mesostructure.[15] However, the results shown here and elsewhere[14,17] demonstrate clearly that the water content in the system is a crucial variable, and working without taking this parameter into account could lead to irreproducible results.

Films aged for 24 h are stable enough to be calcined without mesostructural transition. Heating induces further condensation, which stabilizes the coating and causes structural contraction. As a result of the adhesion of the film to the substrate, all the contraction should occur in the direction perpendicular to the substrate (*z* axis, as represented in Figure 2c). Such preferential (often uniaxial) contraction is well documented for mesostructured films exhibiting 2D hexagonal mesostructure (*P*6*m*),[13,18] but it has never been displayed for a cubic *Im*3*m* mesophase. The *P*6*m* distorted hexagonal structure can be described as a 2D-centered rectangular mesophase (*C*2*m*). The uniaxial contraction of the cubic *Im*3*m* mesostructure (Figure 1c) results in a considerable loss of symmetry. Formally, a triclinic unit cell can be found inside the distorted body-centered cubic mesostructure (see Supporting Information). For simplicity, the parameters of the cubic lattice (even after distortion), instead of those of the triclinic lattice, will be used here for the description of the structural changes.

SAXS data showed that the YZ and CZ cubic (or triclinic after contraction) mesostructures (Figure 4) are stable at temperatures as high as 700 °C. The (110) spots (the in-plane spots) become weak at 500 °C and above, which can be

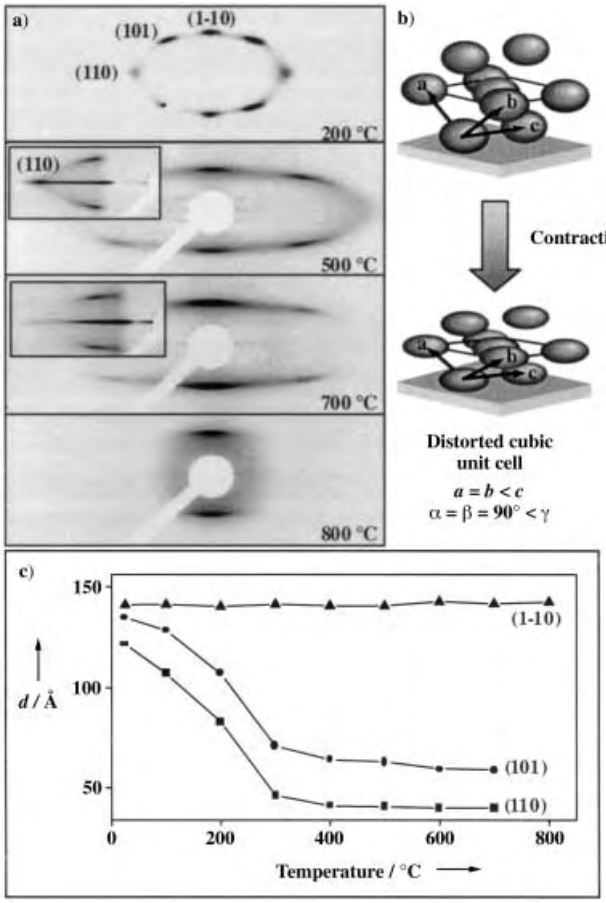


Figure 4. Typical results obtained during the calcination of films exhibiting a cubic mesostructure; the example here is a F127-templated YZ film. a) 2D SAXS patterns (4° incidence angle) of the film treated at different temperatures. The insets are patterns taken at a grazing incidence; b) schematic representation of the distorted cubic structure observed after the anisotropic contraction (the *c* parameter is constant); c) variation of *d* spacing as a function of temperature, which clearly displays the uniaxial contraction.

partially explained by the exponential decay of the reflection intensity on increasing Bragg angle for these large diffraction domains, and also by a reduction in structural order along the direction parallel to the substrate (remembering that such planes are subject to higher degrees of contraction). SAXS patterns collected in grazing incidence (see insets in Figure 4a) showed that the (110) spots are still present at 700 °C, although they are very weak. TEM images of films treated at 700 °C (Figure 3c and d) showed that the cubic (or triclinic) mesostructure is fully preserved. The inorganic framework remains continuous, and the cage-like pores (approximately 80 Å in diameter) can be observed throughout the sample (see Figure 3a). These values are close to those reported for SBA-16 (cavities of 95 Å),[19] and to those reported for F127-templated cubic (*Im*3*m*) silica films (85 Å).[16] In fact, after contraction the cage-like pores present themselves as ellipsoids of about 80 × 40 Å (parallel and perpendicular to the substrate, respectively). Such a high thermal stability for periodically organized transition-metal-oxide mesoporous materials has never been reported. Only disordered wormlike mesoporous metal oxides, such as YSZ,[5] Nb_2O_5,[20] and tungsten oxide–zirconia[21] are known to be stable after heating to temperatures in excess of 500 °C. Examples of nonsilicate periodically organized mesostructures stable up to 600 °C are only found for zirconium oxophosphates.[4,22] By 800 °C, only the (1–10) spots are still present in the SAXS patterns, which indicates that the initial order was retained only in the direction normal to the substrate. This loss of order can be seen by TEM (see Supporting Information), which shows a wormlike disordered structure, but with a constant correlation distance in one direction. Even though most of the order was lost, the porosity is still present at 800 °C.

2D hexagonal mesophases display lower thermal stability. At 400 °C a diffraction ellipse, together with the spots, can be observed in the SAXS patterns, independent of the inorganic composition, which indicates the presence of mixed organized and disorganized domains. The mesostructure degrades with increasing temperature, and completely polyoriented domains (only a diffraction ellipse is observed) are obtained after treatment at 700 °C for both YZ and CZ. For these 2D hexagonal mesophases, TEM investigations of films heated to 700 °C showed that the structure is really composed of disordered domains, and that the films are still porous.

For all inorganic compositions, electron diffraction (see inset in Figure 3d) and wide-angle X-ray diffraction (XRD) showed that crystallization commences at 300 °C. Very small crystallites (smaller than 2 Å) are initially detected (see Supporting Information). At 400 °C the inorganic walls are composed of cubic YZ (JCPDS 82–1245) or tetragonal CZ[23] crystallites with dimensions of 7–9 nm. These nanocrystallites do not significantly grow at temperatures up to 700 °C; the growth is likely to be hindered by the wall–pore boundaries. Heating to 800 °C causes the crystallites to grow to approximately 11 nm. The cubic or tetragonal zirconia-based mixed-oxide crystalline phase (respectively for YZ or CZ) is stable at temperatures above 1000 °C, and no phase segregation is observed. Stabilization of the cubic or tetragonal crystalline structure indicates that Y or Ce cations are well-dispersed inside the zirconia matrix.

A key to the high stability of the cubic mesophase seems to be the presence of large inorganic domains (which can be seen in the center of each four-pore square in Figure 3b and c). These domains, with dimensions of approximately 100–120 Å, can accommodate the large crystallites formed in the 400–700 °C temperature range.

For the 2D hexagonal mesophase, the lower thermal stability (of the structural order) can be attributed to the presence of inorganic walls with a thickness of around 80 Å. Notably, the main degradation of such a mesostructure occurs together with the crystallite growth (400–500 °C, where polyoriented domains begin to appear). Therefore, the mesostructural degradation can be directly related to the formation of crystallites that exceed the size of the inorganic framework domains.

Thermogravimetric and differential scanning calorimetry analysis (TGA–DSC) showed that in air, most of the template is lost from 200 to 400 °C for all inorganic compositions. FT-IR investigations confirmed that films treated at 400 °C are free of organic compounds (see Supporting Information). The

 © 2003 Wiley-VCH Verlag GmbH & Co. KGaA, Weinheim 1433-7851/03/4203-0350 $ 20.00+.50/0

thickness of these films was estimated by SEM and TEM to be around 300 nm (for a withdrawal rate of 1.5 mm s^{-1}). Successive coatings can be applied (four coatings have been achieved) after stabilization at 130–150 °C, which gives rise to crack-free films that exhibit good optical quality. Preliminary results showed that other templates, such as Brij 56 or 58 surfactants (C_nEO_m), are suitable for the preparation of mesoporous YZ and CZ thin films, which allow the formation of smaller pores (20–40 Å) than those obtained with F127.

In summary, the formation of highly organized mesoporous yttria–zirconia and ceria–zirconia thin films is demonstrated for the first time. The mesostructure can be controlled by the conditions applied in the post-processing of the film; cubic or 2D hexagonal mesophases are formed by varying the quantity of water inside the coating during aging. 2D hexagonal mesostructures are stable to 400–500 °C. In addition to the loss of periodicity, the porosity is conserved up to at least 800 °C (the highest temperature investigated) for both mesophases. The cubic mesostructures are stable to 700 °C, which represents the highest thermal stability reported so far for periodically organized mesoporous transition-metal-oxide materials. The resulting porous inorganic framework is highly crystalline, and is composed of cubic YZ or tetragonal CZ. These robust, 3D-interconnected porous coatings, which are prepared by a very convenient one-pot sol-gel method, are very promising. Moreover, the chemical concepts developed in this work can be easily extended to the preparation of YZ and CZ mesoporous particles at the micron or submicron scale[24] as we have demonstrated that the methods developed to prepare mesoporous transition-metal-oxide thin films could feasibly be employed for the formation of spherical particles using aerosol techniques.[25] Therefore, this study presents new opportunities for designing shape-tailored mesoporous materials for applications such as heavy-duty conductive membranes, catalysis, sensors, and electrode materials.

Experimental Section

The dipping solutions were prepared by reacting a mixture of metal chlorides (MCl_3 + $ZrCl_4$, M = Y or Ce; 0.01 mol) with an ABC solution (Pluronic F127 ($EO_{106}PO_{70}EO_{106}$), 0.005 mol) in EtOH (0.4 mol). Water was added to this mixture (20:1 H_2O/metal molar ratio), which resulted in very acidic (less than pH 0) solutions that prevented precipitation. Films were prepared by dip-coating glass or silicon substrates at a constant withdrawal rate (1–5 mm s^{-1}) under controlled relative humidity (RH = 10 %) and temperature (20–23 °C). Immediately after the first drying process (see Figure 1), films were submitted to a water-vapor treatment for 10–20 s. Subsequently, the second drying process took place inside the chamber of the dip-coater under controlled RH (either 10 or 50 %) in flowing air for 1 h. Thereafter, films were transferred to an RH-controlled (using saturated solutions of different salts) closed chamber and aged for between 12 h and 2 weeks. SD and aging were carried out at a controlled temperature (20–22 °C). After aging, films were calcined in static air at temperatures in the 100–800 °C range (ramping rate of 1 °C min^{-1}) for 4 h.

Received: September 12, 2002 [Z50147]

[1] T. Takahashi, N. Q. Minh, *Science and Technology of Ceramic Fuel Cells*, Elsevier, New York, **1995**.

[2] M. Daturi, C. Binet, J.-C. Lavalley, A. Galtayries, R. Sporken, *Phys. Chem. Chem. Phys.* **1999**, *1*, 5717, and references therein.

[3] B. C. H. Steele, *Nature* **1999**, *400*, 619.

[4] a) C. T. Kresge, M. E. Leonowicz, W. J. Roth, J. C. Vartuli, J. S. Beck, *Nature* **1992**, *359*, 710; b) C. G. Göltner, M. Antonietti, *Adv. Mater.* **1997**, *9*, 431; c) J. Y. Ying, C. P. Mehnert, M. S. Wong, *Angew. Chem.* **1999**, *111*, 58; *Angew. Chem. Int. Ed.* **1999**, *38*, 56; d) F. Schüth, *Chem. Mater.* **2001**, *13*, 3184; e) G. J. de A. A. Soler-Illia, C. Sanchez, B. Lebeau, J. Patarin, *Chem. Rev.* **2002**, in press.

[5] a) M. Mamak, N. Coombs, G. Ozin, *Adv. Mater.* **2000**, *12*, 198; b) M. Mamak, N. Coombs, G. Ozin, *J. Am. Chem. Soc.* **2000**, *122*, 8932.

[6] a) Y. Wang, L. Yin, O. Palchik, Y. Rosenfeld Hacohen, Y. Koltypin, A. Gedanken, *Chem. Mater.* **2001**, *13*, 1248; b) Y. Q. Wang, L. X. Yin, O. Palchik, Y. Rosenfeld Hacohen, Y. Koltypin, A. Gedanken, *Langmuir* **2001**, *17*, 4130.

[7] a) C. J. Brinker, Y. Lu, A. Sellinger, H. Fan, *Adv. Mater.* **1999**, *11*, 579; b) P. Yang, D. Zhao, D. I. Margolese, B. F. Chmelka, G. D. Stucky, *Nature* **1998**, *395*, 583; c) G. J. de A. A. Soler-Illia, A. Louis, C. Sanchez, *Chem. Mater.* **2002**, *14*, 750.

[8] a) D. Grosso, F. Babonneau, P.-A. Albouy, H. Amenitsch, A. R. Balkenende, A. Brunet-Bruneau, J. Rivory, *Chem. Mater.* **2002**, *14*, 931; b) E. L. Crepaldi, D. Grosso, G. J. de A. A. Soler-Illia, P.-A. Albouy, H. Amenitsch, C. Sanchez, *Chem. Mater.* **2002**, *14*, 3316.

[9] D. Grosso, A. R. Balkenende, P.-A. Albouy, A. Ayral, H. Amenitsch, F. Babonneau, *Chem. Mater.* **2001**, *13*, 1848.

[10] E. L. Crepaldi, G. J. de A. A. Soler-Illia, D. Grosso, P.-A. Albouy, H. Amenitsch, C. Sanchez, *Stud. Surf. Sci. Catal.* **2002**, *141*, 235.

[11] E. M. Larsen, in *Advances in Inorganic Chemistry and Radiochemistry, Vol. 13* (Eds.: H. J. Emeléus, A. G. Sharpe), Academic Press, New York, **1970**, p. 1.

[12] E. L. Crepaldi, G. J. de A. A. Soler-Illia, D. Grosso, P.-A. Albouy, C. Sanchez, *Chem. Commun.* **2001**, 1582.

[13] M. Klotz, P.-A. Albouy, A. Ayral, C. Ménager, D. Grosso, A. Van der Lee, V. Cabuil, F. Babonneau, C. Guizard, *Chem. Mater.* **2000**, *12*, 1721.

[14] G. J. de A. A. Soler-Illia, E. L. Crepaldi, D. Grosso, D. Durand, C. Sanchez, *Chem. Commun.* **2002**, 2298.

[15] P. C. A. Alberius, K. L. Frindell, R. C. Hayward, E. J. Kramer, G. D. Stucky, B. F. Chmelka, *Chem. Mater.* **2002**, *14*, 3284.

[16] D. Zhao, P. Yang, N. Melosh, J. Feng, B. F. Chmelka, G. D. Stucky, *Adv. Mater.* **1998**, *10*, 1380.

[17] F. Cagnol, D. Grosso, G. J. de A. A. Soler-Illia, E. L. Crepaldi, C. Sanchez, *J. Mater. Chem.*, **2003**, in press.

[18] D. Grosso, G. J. de A. A. Soler-Illia, F. Babonneau, C. Sanchez, P.-A. Albouy, A. Brunet-Bruneau, A. R. Balkenende, *Adv. Mater.* **2001**, *13*, 1085.

[19] Y. Sakamoto, M. Kaneda, O. Terasaki, D. Y. Zhao, J. M. Kim, G. Stucky, H. J. Chin, E. Ryoo, *Nature* **2000**, *408*, 449.

[20] B. Lee, T. Yamashita, D. Lu, J. N. Kondo, K. Domen, *Chem. Mater.* **2002**, *14*, 867.

[21] M. S. Wong, E. S. Jeng, J. Y. Ying, *Nano Lett.* **2001**, *1*, 637.

[22] U. Ciesla, M. Fröba, G. Stucky, F. Schüth, *Chem. Mater.* **1999**, *11*, 227.

[23] S. Rossignol, Y. Madier, D. Duprez, *Catal. Today* **1999**, *50*, 261.

[24] Preliminary results showed that by using the same conditions that were applied to prepare mesoporous thin films, mesoporous CZ submicronic particles can be obtained by aerosol processing (see Supporting Information).

[25] D. Grosso, G. J. de A. A. Soler-Illia, E. L. Crepaldi, C. Sanchez, *Adv. Funct. Mater.* **2003**, in press.

 © 2003 Wiley-VCH Verlag GmbH & Co. KGaA, Weinheim 1433-7851/03/4203-0351 $ 20.00+.50/0

Glycobiology

Thioglycoligases: Mutant Glycosidases for Thioglycoside Synthesis**

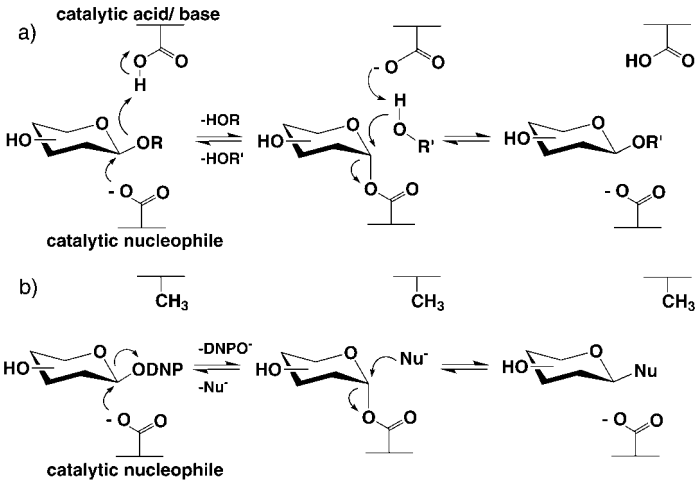
*Michael Jahn, Jennifer Marles, R. Antony J. Warren, and Stephen G. Withers**

Carbohydrate mimetics that are resistant towards enzymatic hydrolysis have proven to be useful as competitive glycosidase inhibitors and therefore have potential as therapeutics. Thioglycosides, in which the glycosidic oxygen atom has been replaced by a sulfur atom, have been especially valuable as stable glycoside analogues in a range of studies of glycosidases, both as competitive inhibitors, for example, for α-L-fucosidases,[1] pancreatic α-amylase,[2] or for cellulases,[3] and recently in the formation of stable complexes for X-ray crystallographic analysis, for example, with endoglucanase Cel7B from *Fusarium oxysporum*,[4] maize β-glucosidase ZMGlu1,[5] barley β-D-glucan glucohydrolase,[6] endoglucanase Cel5A,[7] or *E. coli* maltodextrin phosphorylase (MalP),[8] and they are gaining increasing interest as targets for the pharmaceutical industry.[9]

Thioglycosides have been synthesized by glycosylation of thioacceptors with activated glycosyl donors,[10–12] by the S_N2 reaction of 1-thio sugars with activated acceptors,[13] and by Michael-like addition of 1-thiosugars to α,β-unsaturated systems;[14] all routes involve numerous protection and deprotection steps and require good control of anomeric stereochemistry.

The few naturally occurring thioglycosides belong to the family of glucosinolates and are found in cruciferous plants.[15] The enzymes that catalyze the formation of the thioglycosidic linkages, *S*-glucosyltransferases, have been purified from plant extracts,[16] as well as cloned into and expressed from *E. coli*.[17] There are a few examples of transfer to simple thiols.[18–20] However, no useful enzymatic syntheses of thioglycosidic linkages in oligosaccharides in vitro have been reported—such approaches would be valuable.

The action of retaining glycosidases on glycosides is in most instances mediated by two key active site amino acid residues, the catalytic nucleophile and the catalytic acid/base. We have previously reported on the efficient synthesis of *O*-glycosidic linkages in oligosaccharides by the use of retaining glycosidases that lack the catalytic nucleophile, glycosynthases, in conjunction with activated donors of the opposite anomeric configuration to that of the natural substrate.[21–23] Herein we present a novel strategy for the synthesis of *S*-glycosidic linkages in oligosaccharides by the use of retaining glycosidases that lack the catalytic acid/base amino acid residue. The choice of appropriate donors and acceptors to be used in such an approach becomes apparent by considering the double displacement mechanism of retaining glycosidases



Scheme 1. Mechanism of a retaining glycosidase: Glycosylation and deglycosylation with wild-type (a) and acid/base mutant (b). DNP = dinitrophenyl, Nu = nucleophile.

first proposed by Koshland (Scheme 1).[24] In the glycosylation step the concerted action of the catalytic acid/base (protonated, acting as an acid) and the catalytic nucleophile (deprotonated) leads to the departure of the aglycon group and to the formation of the covalent glycosyl–enzyme intermediate (a). Use of a mutant glycosidase in which the catalytic acid/base residue has been replaced by a noncatalytically active residue necessitates glycosyl donors with good leaving groups that do not need acid catalysis, for example, dinitrophenyl groups, to allow formation of the glycosyl–enzyme intermediate (b). However, turnover of that intermediate via transglycosylation to an oxygen acceptor is impractically slow, since general base catalysis is required to speed this step (a). The acid/base mutant therefore requires strong nucleophiles as acceptors that do not need general base catalysis (b).

Earlier experiments revealed that small anionic molecules, such as N_3^-, AcO^-, HCO_2^-,[25] and F^-,[26] rescue the reaction by enhancing the rate of the deglycosylation step. In the present study we exploit this concept to allow the synthesis of thiooligosaccharides by use of deoxythio sugars as nucleophilic acceptors that do not need base catalysis in the deglycosylation step. In summary, our approach requires activated donor glycosides, such as dinitrophenyl glycosides, and chemically synthesized deoxythio sugars as acceptors in conjunction with mutant glycosidases modified at the acid/base position.

[*] Prof. Dr. S. G. Withers, Dr. M. Jahn
Department of Chemistry
University of British Columbia
2036 Main Mall, Vancouver, B.C. V6T 1Z1 (Canada)
Fax: (+1) 604-822-2847
E-mail: withers@chem.ubc.ca
J. Marles, Prof. Dr. R. A. J. Warren
Department of Microbiology
University of British Columbia (Canada)

[**] M. J. was financed by a DFG fellowship.

Supporting information for this article is available on the WWW under http://www.angewandte.org or from the author.

 © 2003 Wiley-VCH Verlag GmbH & Co. KGaA, Weinheim 1433-7851/03/4203-0352 $ 20.00+.50/0

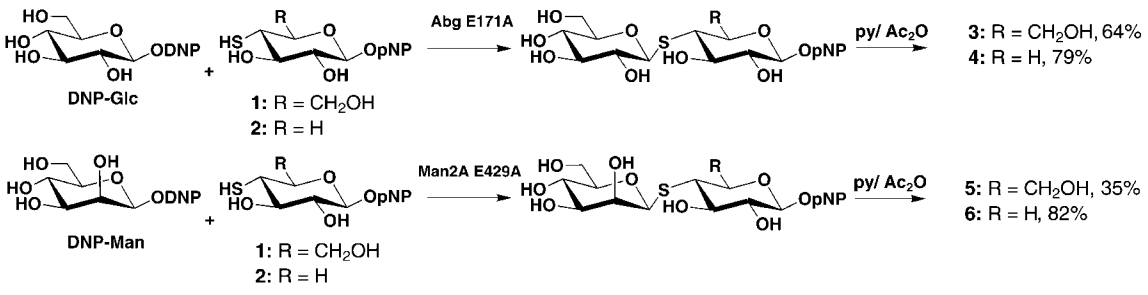
We have probed our strategy using the alanine acid/base mutants of two retaining β-glycosidases, the β-glucosidase from *Agrobacterium sp.* Abg E171A and the β-mannosidase from *Cellulomonas fimi* Man2A E429A. The mutant Abg E171A was generated by site-directed mutagenesis by a "megaprimer" PCR method by using three oligonucleotide primers, one containing the mutation, as described for the Abg E358S mutant.[22] The purified product of the first PCR reaction served as a megaprimer in the second PCR reaction. The purified gene was subcloned into an expression vector, and after expression the protein was purified in a single step by Ni^{2+}-chelation chromatography. The mutant Man2A E429A was the same protein sample described by Zechel et al.[26]

As donors we chose the readily available dinitrophenyl glycosides: 2,4-dinitrophenyl β-D-glucopyranoside (DNP-Glc) for studies with the mutant glucosidase and 2,5-dinitrophenyl β-D-mannopyranoside (DNP-Man) for experiments involving the mutant mannosidase.[26] The low pK_a values of 3.96 for 2,4-dinitrophenol and 5.15 for 2,5-dinitrophenol render acid catalysis for the glycosylation step unnecessary.[27] As an acceptor we initially chose *para*-nitrophenyl 4-deoxy-4-thio-β-D-glucopyranoside (**1**) since the parent sugar *para*-nitrophenyl β-D-glucopyranoside (pNP-Glc) acts as an excellent acceptor for both wild type and nucleophile mutant forms of Abg[21] and Man2A[23] undergoing transfer preferentially to the 4-hydroxy group. The deoxythio sugar **1** was readily synthesized by regioselective protection of the *galacto* sugar, activation of the unprotected axial alcohol by formation of the triflate, nucleophilic substitution with thioacetate with inversion of configuration, and finally Zemplen deprotection under exclusion of oxygen (in the presence of DTT). Anaerobic conditions, even during the enzymatic reactions, are compulsory to prevent oxidation of the thiols to the corresponding disulfides.

Upon incubation of **1** (20 mM) with the appropriate donor (45 mM) and mutant enzyme (~1 mg mL^{-1}) in phosphate buffered solutions at pH 6.8 TLC analysis revealed that a new product with the expected mobility of a disaccharide was formed quite rapidly in each case. These products were stable towards hydrolysis by both the wild-type and mutant enzymes. By contrast, incubation of the wild-type enzymes with the appropriate DNP sugar donors and thiosugar acceptor **1** resulted in no detectable formation of disaccharide. It was therefore suspected that a novel enzymatic coupling reaction was occurring involving specific thiolinkage formation. This was confirmed by isolation of the products of the enzymatic reactions by silica gel chromatography after acetylation. Analysis of the products by ^{1}H and ^{13}C NMR spectroscopy and mass spectrometry revealed that they were indeed sulfur-linked disaccharides (Scheme 2).

These extremely encouraging results led us to question whether the regiochemical outcome of the transglycosylation reaction could be controlled by virtue of the location of the thiol group within the acceptor sugar. We therefore synthesized and tested *para*-nitrophenyl 4-deoxy-4-thio-β-D-xylopyranoside (**2**) as an acceptor for the two enzymes. Previous studies with both the wild-type Abg and its nucleophile mutant had revealed that *para*-nitrophenyl β-D-xylopyranoside (pNP-Xyl) is an excellent acceptor substrate, but that transfer, surprisingly, occurred exclusively to the 3-position.[21] Use of **2** as an acceptor would reveal whether the greater nucleophilicity of the thiol group controls the reaction outcome. Indeed, incubation of **2** with Abg E171A and DNP-Glc resulted in an excellent yield (79%) of the sulfur-linked disaccharide, as revealed by ^{1}H and ^{13}C NMR spectroscopy and ESI-MS. Similarly, incubation of **2** with Man2A E429A and DNP-Man produced, in 82% yield, the β(1–4)-linked thiodisaccharide product (Scheme 2).

Interestingly, control reactions, in which the parent sugars *para*-nitrophenyl β-D-xylopyranoside (pNP-Xyl) and *para*-nitrophenyl β-D-glucopyranoside (pNP-Glc) were used as acceptors for Man2A E429A in the presence of DNP-Man, showed the formation of disaccharide products, but only very slowly. This is in contrast to Abg E171A where no formation of disaccharides was observed when using pNP-Glc or pNP-Xyl in the presence of DNP-Glc as donor. To assess the relative rates of transfer to the oxygen and sulfur nucleophiles in the case of Man 2A E429A we established a competition reaction in which equimolar amounts of pNP-Xyl and its 4-thio analogue **2** were incubated together with DNP-Man as donor and Man2A E429A (Figure 1). When the concentration of donor was limiting (one third of the concentration of acceptors) we saw exclusive formation of the S-linked disaccharide **6** (a). However, upon addition of further donor to a final concentration twice that of the acceptors the O-linked disaccharides (indicated by arrows) were formed (b). Isolation and characterization after acetylation showed that the β(1→3)- and β(1→4)-linked disaccharides were formed.[28] Integration of HPLC peaks indicates that transfer



Scheme 2. Enzymatic synthesis of thioglycosides **3**–**6**. Experimental details and spectroscopic data are provided in the Supporting Information. DNP = dinitrophenyl, pNP = *para*-nitrophenyl.

 © 2003 Wiley-VCH Verlag GmbH & Co. KGaA, Weinheim 1433-7851/03/4203-0353 $ 20.00+.50/0

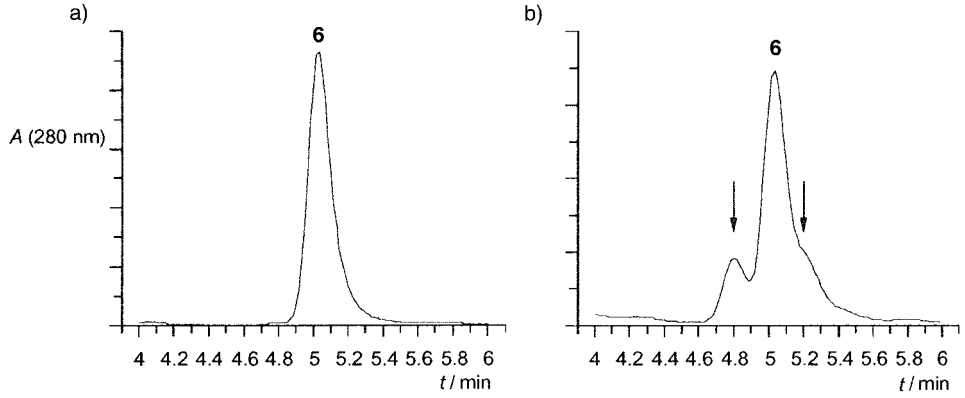


Figure 1. HPLC traces of the Man2A E429A-catalyzed reaction of the two competing acceptors pNP-Xyl (5.5 mM) and its thio analogue **2** (5.5 mM) with varying concentrations of DNP-Man: a) 3.75 mM, b) 22 mM. Arrows indicate the elution of the β(1→3)- and β(1→4)-O-linked disaccharides, **6** is the S-linked disaccharide. Experimental details are provided in the Supporting Information.

to the thiosugar acceptor is at least 100-fold faster than transfer to its oxygen analogue. These results were confirmed by ESI-MS analysis.

The glycosynthases have proven to be powerful tools for the synthesis of O-linked oligosaccharides. Herein we have shown again that the concept of engineering glycosidases on mechanistic grounds in conjunction with use of appropriately modified substrates can lead to novel synthetic methodologies. We anticipate that the outlined approach is general, as demonstrated with two different enzymes from two separate glycosidase families, and will prove to be of considerable value in the specific assembly of thiooligosaccharides for mechanistic and possibly therapeutic use.

Received: September 13, 2002 [Z50153]

[1] Z. J. Witczak, D. Boryczewski, *Bioorg. Med. Chem. Lett.* **1998**, *8*, 3265–3268.
[2] M. Blanc-Meusser, L. Vigne, H. Driguez, J. Lehmann, J. Steck, K. Urbahns, *Carbohydr. Res.* **1992**, *224*, 59–71.
[3] C. Schou, G. Rasmussen, M. Schuelein, B. Henrissat, H. Driguez, *J. Carbohydr. Chem.* **1993**, *12*, 743–752.
[4] G. Sulzenbacher, H. Driguez, B. Henrissat, M. Schuelein, G. J. Davies, *Biochemistry* **1996**, *35*, 15280–15287.
[5] M. Czjzek, M. Cicek, V. Zamboni, W. P. Burmeister, D. R. Bevan, B. Henrissat, A. Esen, *Biochem. J.* **2001**, *354*, 37–46.
[6] M. Hrmova, J. N. Varghese, R. De Gori, B. J. Smith, H. Driguez, G. B. Fincher, *Structure* **2001**, *9*, 1005–1016.
[7] A. Varrot, M. Schulein, S. Fruchard, H. Driguez, G. J. Davies, *Acta Crystallogr. Sect. D* **2001**, *57*, 1739–1742.
[8] K. A. Watson, C. McCleverty, S. Geremia, S. Cottaz, H. Driguez, L. N. Johnson, *EMBO J.* **1999**, *18*, 4619–4632.
[9] Z. J. Witczak, *Curr. Med. Chem.* **1999**, *6*, 165–178.
[10] J. S. Andrews, B. M. Pinto, *Carbohydr. Res.* **1995**, *270*, 51–62.
[11] L. X. Wang, N. Sakairi, H. Kuzuhara, *J. Chem. Soc. Perkin Trans. 1* **1990**, 1677–1682.
[12] M. Blanc-Muesser, J. Defaye, H. Driguez, *Carbohydr. Res.* **1978**, *67*, 305–328.
[13] S. Fort, A. Varrot, M. Schulein, S. Cottaz, H. Driguez, G. J. Davies, *ChemBioChem* **2001**, *2*, 319–325.
[14] Z. J. Witczak, J. M. Sun, R. Mielguj, *Bioorg. Med. Chem. Lett.* **1995**, *5*, 2169–2174.
[15] J. W. Fahey, A. T. Zalcmann, P. Talalay, *Phytochemistry* **2001**, *56*, 5–51.
[16] J. W. D. GrootWassink, D. W. Reed, A. D. Kolenovsky, *Plant Physiol.* **1994**, *105*, 425–433.
[17] E. F. Marillia, J. M. MacPherson, E. W. T. Tsang, K. Van Audenhove, W. A. Keller, J. W. D. GrootWassink, *Physiol. Plant.* **2001**, *113*, 176–184.
[18] T. Dintinger, D. Dutheil-Bouedec, M. Bouchonneau, C. Tellier, *Biotechnol. Lett.* **1994**, *16*, 689–692.
[19] G. Vic, D. H. G. Crout, *Tetrahedron: Asymmetry* **1994**, *5*, 2513–2516.
[20] J. B. Kempton, S. G. Withers, *Biochemistry* **1992**, *31*, 9961–9969.
[21] L. F. Mackenzie, Q. P. Wang, R. A. J. Warren, S. G. Withers, *J. Am. Chem. Soc.* **1998**, *120*, 5583–5584.
[22] C. Mayer, D. L. Zechel, S. P. Reid, R. A. J. Warren, S. G. Withers, *FEBS Lett.* **2000**, *466*, 40–44.
[23] O. Nashiru, D. L. Zechel, D. Stoll, T. Mohammadzadeh, R. A. J. Warren, S. G. Withers, *Angew. Chem.* **2001**, *113*, 431–434; *Angew. Chem. Int. Ed.* **2001**, *40*, 417–420.
[24] D. E. Koshland, *Biol. Rev.* **1953**, *28*, 416–436.
[25] Q. Wang, D. Trimbur, R. Graham, R. A. J. Warren, S. G. Withers, *Biochemistry* **1995**, *34*, 14554–14562.
[26] D. L. Zechel, S. P. Reid, O. Nashiru, C. Mayer, D. Stoll, D. L. Jakeman, R. A. J. Warren, S. G. Withers, *J. Am. Chem. Soc.* **2001**, *123*, 4350–4351.
[27] We used 2,5-dinitrophenyl β-D-mannopyranoside instead of 2,4-dinitrophenyl β-D-mannopyranoside as the latter is impractically unstable due to aryl migration. We also tested the appropriate pNP-glycosides as donors, but prolonged reaction times make those less attractive.
[28] The physical data of the compounds were identical to those described by Nashiru et al.[23]

 © 2003 Wiley-VCH Verlag GmbH & Co. KGaA, Weinheim 1433-7851/03/4203-0354 $ 20.00+.50/0

A Cytotoxic Proteasome Inhibitor

Salinosporamide A: A Highly Cytotoxic Proteasome Inhibitor from a Novel Microbial Source, a Marine Bacterium of the New Genus *Salinospora***

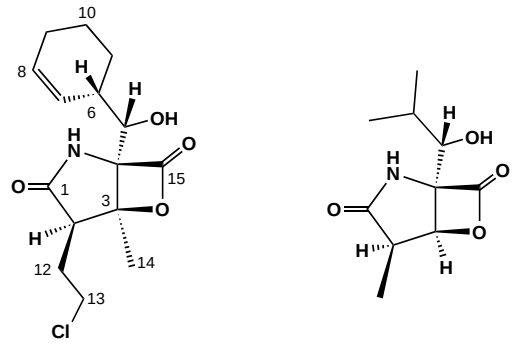
*Robert H. Feling, Greg O. Buchanan, Tracy J. Mincer, Christopher A. Kauffman, Paul R. Jensen, and William Fenical**

In memory of D. John Faulkner

We recently reported the cultivation and phylogenetic characterization of a new group of obligate marine actinomycete bacteria that is widely distributed in ocean sediments.[1] Analogous soil-derived actinomycetes have been the single most significant source of naturally occurring microbial antibiotics,[2] thus the discovery of a major new group of these bacteria in marine sediments suggests that the ocean represents an overlooked habitat from which to isolate these important microorganisms. Given that the rate of discovery of new biologically active compounds from common soil actinomycetes has been falling,[3] obligate marine actinomycetes represent a new resource for structurally diverse secondary metabolites.

To date, we have isolated in excess of 2500 strains belonging to this new taxon for which we have proposed the genus name "*Salinospora*" (a formal taxonomic description is in progress). "*Salinospora*" strains, with previously undescribed 16S rRNA gene sequences, have been recovered from five distinct tropical/subtropical ocean systems[1] and from depths as great as −1100 m, which indicates that they represent a widely distributed and taxonomically diverse group of sediment bacteria. All isolates display an obligate requirement of ionic sodium for growth, thus indicating a high level of marine adaptation.

In preliminary screening, a high percentage of the organic extracts of cultured "*Salinospora*" strains possessed antibiotic and anticancer activities, which suggests that these bacteria are an excellent resource for drug discovery. Herein we report the results of our first chemical investigation of a member of the "*Salinospora*" group and show that strain CNB-392 produces the chemically unique and highly bioactive metabolite salinosporamide A (**1**, Scheme 1). Salinosporamide A exhibits potent cancer cell cytotoxicity and appears to exert its cytotoxic effects through inhibition of the 20S proteasome.



1 **2**

Scheme 1. Structures of salinosporamide A (**1**) and *clasto*-lactacystin-β-lactone (omuralide, **2**).

"Salinospora" strain CNB-392 was isolated from a heat-treated marine sediment sample that was plated on a seawater-based agar nutrient medium. Liquid shake flask cultivation of this strain, followed by solid-phase extraction with Amberlite resin (XAD-16) and elution with acetone, resulted in a crude extract that was highly cytotoxic in vitro toward HCT-116 human colon carcinoma (IC_{50} ca. 80 ng mL^{-1}). Cytotoxicity-guided fractionation of the crude extract led to the isolation of salinosporamide A (**1**) as a colorless crystalline solid (yield: 7 mg L^{-1}). The complete structural assignment of **1** was accomplished by spectral analysis and by a single-crystal X-ray diffraction study.

Analysis of the low-resolution mass spectrum of salinosporamide A showed a characteristic $[M+2]^+$ peak indicative of the presence of a chlorine atom. High-resolution mass-spectral analysis provided the molecular formula $C_{15}H_{21}{}^{35}ClNO_4$ (calcd for $[M+H]^+$: m/z 314.1160, obsd: m/z 314.1144) for salinosporamide A. The infrared spectrum of **1** showed bands characteristic of amide and β-lactone carbonyl groups ($\tilde{\nu}$ = 1702 and 1819 cm^{-1}). Analysis of the ^{1}H NMR spectrum of **1** showed the presence of two protons on a *cis*-double bond (δ = 6.42 ppm, d and δ = 5.88 ppm, m, ^3J = 9.6 Hz), an amide proton (δ = 10.60 ppm), and one hydroxy proton (δ = 4.99 ppm, br s). Also evident was a single oxygen atom bearing a methine proton (δ = 4.24 ppm, t), an isolated methyl group (δ = 2.07 ppm, s), and a chloroethyl substituent.

Comprehensive analysis of 2D NMR data, including the results of COSY, HMQC, and HMBC experiments, enabled the complete planar structure of salinosporamide A to be assigned, as in **1**, to a 2-aza-6-oxabicyclo[3.2.0]heptane-3,7-dione skeleton substituted with cyclohexenylcarbinol and chloroethyl side chains.

Portions of the relative stereochemistry of salinosporamide A were readily assigned by NOE NMR spectral methods. However, several attempts to solve the absolute configuration by derivatization of the secondary hydroxy group with Mosher's reagent and esterification with *p*-bromobenzoic acid for CD analysis were unsuccessful, presumably because of steric hindrance at the C-5 hydroxy

[*] Prof. W. Fenical, Dr. R. H. Feling, Dr. G. O. Buchanan, T. J. Mincer, C. A. Kauffman, P. R. Jensen
Center for Marine Biotechnology and Biomedicine
Scripps Institution of Oceanography
University of California, San Diego
La Jolla, CA 92093-0204 (USA)
Fax: (+1) 858-558-3702
E-mail: wfenical@ucsd.edu

[**] Financial support was provided by the National Cancer Institute, US National Institutes of Health (under grant CA44848). We thank Dr. Peter Gantzel, University of California, San Diego, for assistance with X-ray diffraction experiments.

 © 2003 Wiley-VCH Verlag GmbH & Co. KGaA, Weinheim 1433-7851/03/4203-0355 $ 20.00+.50/0

group. Subsequently, the absolute stereochemistry of **1**, and confirmation of the overall structure of salinosporamide A, was achieved by single-crystal X-ray diffraction analysis.

Crystallization of **1** from ethyl acetate/*iso*-octane resulted in single, cubic crystals, which diffracted as a monoclinic system P2(1). The unusual high unit-cell volume of 3009 Å[4] hosted four independent molecules in which different conformational positions were observed for the flexible chloroethyl substituent. The assignment of the absolute structure from the diffraction anisotropy of the chlorine substituent resolved the absolute stereochemistry of Salinosporamide A (**1**) as 2*R*,3*S*,4*R*,5*S*,6*S* (Figure 1) with a Flack parameter of 0.01 and an esd of 0.03.

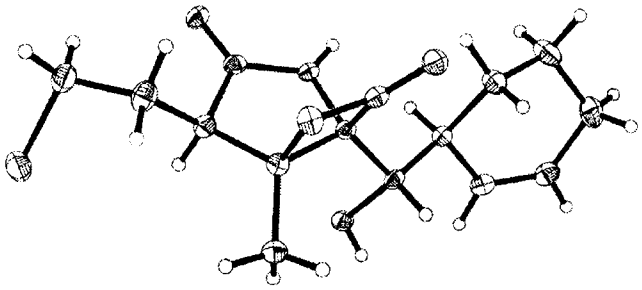


Figure 1. ORTEP plot of the final X-ray structure of salinosporamide A (**1**) depicting the absolute stereochemistry.

Salinosporamide A shares its fused γ-lactam-β-lactone bicyclic ring structure with *clasto*-lactacystin-β-lactone (**2**), a transformation product of the microbial metabolite lactacystin[5] originally isolated by Ōmura and co-workers from cultures of a terrestrial *Streptomyces* sp.[6a,b] *Clasto*-lactacystin-β-lactone, also called omuralide,[7] is remarkable since it was the first molecule discovered to be a truly specific inhibitor of the proteasome, a multicatalytic proteinase complex responsible for most nonlysosomal protein degradation in the cell. Omuralide is unique in that it specifically inhibits the proteolytic activity of the 20S subunit of the proteasome without inhibiting any other protease activities of the cell.[8] For this reason **2** has proven to be a valuable tool in the elucidation of the role of the proteasome in the degradation of regulatory proteins that control fundamental cellular processes, and selective proteasome inhibition has become an important target for drug discovery.

Although salinosporamide A (**1**) shares an identical bicyclic ring structure with omuralide (**2**, Scheme 1), it is uniquely functionalized. More specifically, **1** is methylated at the C-3 ring juncture, possesses a chloroethyl group instead of a methyl group at C-2, and, significantly, is functionalized with a cyclohexene instead of an isopropyl group at the C-5 position. The structural features of omuralide that are responsible for its activity have been studied in detail by Corey and co-workers who demonstrated that the C-5 isopropyl group (see Scheme 1) is required for activity and that substitution with a phenyl ring at this position completely abolished activity.[9] The fact that salinosporamide A (**1**) incorporates a cyclohexene substituent at this position, yet retains activity, suggests that it may interact with the proteasome in a manner that is different from omuralide. Future studies on the structure–activity relationships of salinosporamide A derivatives, or co-crystallization of **1** with purified 20S proteasome, may help elucidate these differences.

Salinosporamide A seems to be a direct product of the fermentation rather than a subsequent transformation product of a precursor similar in structure to that of lactacystin. Further, while some ring opening does occur in methanol during chromatography on silica gel, the β-lactone functionality seems to be somewhat stabilized in this molecule.

Salinosporamide A (**1**) displayed potent in vitro cytotoxicity against HCT-116 human colon carcinoma with an IC_{50} value of 11 ng mL^{-1}. This compound also displayed potent and highly selective activity in the NCI's 60-cell-line panel with a mean GI_{50} value (the concentration required to achieve 50% growth inhibition) of less than 10 nM and a greater than 4 log LC_{50} differential between resistant and susceptible cell lines. The greatest potency was observed against NCI-H226 non-small cell lung cancer, SF-539 CNS cancer, SK-MEL-28 melanoma, and MDA-MB-435 breast cancer (all with LC_{50} values less than 10 nM). Salinosporamide A was tested for its effects on proteasome function because of its structural relationship to omuralide (**2**). When tested against purified 20S proteasome (Calbiochem, cat. no. 539158), salinosporamide A inhibited proteasomal chymotrypsin-like proteolytic activity with an IC_{50} value of 1.3 nM.[10] This compound is approximately 35 times more potent than omuralide (IC_{50} = 49 nM in our assay) which was tested as a positive control in the same assay. Thus, the unique functionalization of the core bicyclic ring structure of salinosporamide A appears to have resulted in a molecule that is a significantly more potent proteasome inhibitor than omuralide.

Experimental Section

Cultivation of strain CNB-392: Strain CNB-392 was isolated from a sediment sample collected at a depth of about 1 m in June 1989 from a mangrove environment in Chub Cay, Bahamas. The strain was cultured in 2.8-L Fernbach flasks (20 × 1 L) in a seawater-based medium (0.2% chitosan, 0.2% kelp powder, 0.2% menhaden meal, 0.2% fish solubles, 0.5% starch) and shaken at 230 rpm at 27 °C). After nine days of cultivation, sterilized Amberlite XAD-16 resin (20 g L^{-1}) was added and the resin was collected 24 h later by filtration, washed with deionized water, and eluted with acetone to afford 5 g of a cytotoxic, crude organic extract after removal of solvent under reduced pressure.

1: The crude extract was partitioned between ethyl acetate and water, and the organic fraction was purified by flash column chromatography on silica gel, using increasing concentrations of acetone in CH_2Cl_2, to yield 250 mg of a fraction enriched in salinosporamide A (**1**). Recrystallization of the semi-purified fraction from ethyl acetate/*iso*-octane (3/1) provided 150 mg of **1** as colorless needles: m.p. 169–171 °C. $[\alpha]_D^{25} = -72.9°$ (c = 0.55, MeOH); NMR data ([D$_5$]pyridine): see Table 1; IR (NaCl): $\tilde{\nu}$ = 2920, 1819 m, 1702 s, 1255 m, 1085 s, 1020 s, 797 s cm^{-1}; UV (MeOH): λ_{max} nm (logε) = 225 (3.3), 205 (4.03); LC/(+)ESI-MS (70 eV, 3500 eV): R_t = 10.1 min (acetonitrile/water, 15 min gradient): m/z 314.1 $[M+H]^+$, 336 $[M+Na]^+$; HR-MALDI: m/z 314.1144 $[M+H]^+$, calcd for $C_{15}H_{21}{}^{35}ClNO_4$, m/z 314.1159.

Received: October 4, 2002 [Z50299]

 © 2003 Wiley-VCH Verlag GmbH & Co. KGaA, Weinheim 1433-7851/03/4203-0356 $ 20.00+.50/0

Table 1: NMR spectral data for salinosporamide A (**1**).

C no.	δ_C	δ_H, mult., int., J [Hz]	COSY correlations	HMBC correlations
1	176.4 C			
2	46.2 CH	3.17, t, 1H, 7.0	H-12	C-1, 3, 12, 13, 14
3	86.1 C			
4	80.2 C			
5	70.9 CH	4.24, d, 1H, 9.0	H-6	C-3, 6, 7
6	39.2 CH	2.85, m, 1H	H-5, H-11a/b	
7	128.4 CH	6.42, d, 1H, 9.6	H-6, 8, 9	C-9
8	128.8 CH	5.88, m, 1H	H-7, 9	
9	25.3 CH_2	1.91, m, 2H	H-8, 10b	C-11
10	21.7 CH_2	a 1.66, m, 1H	H-9, 10b	C-6, 8, 9
		b 1.38, m, 1H	H-9, 10a	
11	26.5 CH_2	a 2.37, m, 1H	H-6, 11b	C-6, 7, 9, 10
		b 1.66, m, 1H	H-6, 10b	C-5, 6
12	29.0 CH_2	a 2.48, m, 1H	H-2, 12b, 13	C-1, 2, 3, 13
		b 2.32, m, 1H	H-2, 12a, 13	C-1, 2, 3, 13, 14
13	43.2 CH_2	a 4.14, m, 1H	H-12a/b, 13b	C-2, 12
		b 4.01, m, 1H	H-12a/b, 13a	C-2, 12
14	20.0 CH_3	2.07, s, 3H		C-2, 3, 4, 15
15	169.0 C			
NH		10.60, brs		C-2, 3, 4
OH		4.99, brs		

[1] T. J. Mincer, P. R. Jensen, C. A. Kauffman, W. Fenical, *Appl. Environ. Microbiol.* **2002**, *68*(10), 5005–5011.

[2] Y. Okami, K. Hotta in *Actinomycetes in Biotechnology*, (Eds.: M. Goodfellow, S. T. Williams, M. Mordarski), Academic Press, New York, **1988**, pp. 33–67.

[3] A. T. Bull, A. C. Ward, M. Goodfellow, *Microbiol. Mol. Biol. Rev.* **2000**, *64*, 573–604.

[4] Crystal Data for **1**: $C_{15}H_{21}ClNO_4$, $M_r = 313.11$, monoclinic space group, $P21$, $a = 10.4805(6)$, $b = 24.2085(13)$, $c = 12.5163(7)$ Å, $\beta = 108.603(10)°$, $V = 3009.7(3)$ Å^3, $Z = 8$, $\rho_{calcd} = 1.385$ g cm^{-3}; $Mo_{K\alpha}$ radiation, $\lambda = 0.71073$ Å, $\mu = 0.269$ mm^{-1}, $T = -100$ K. 25627 data (13056 unique, $R_{int} = 0.0146$, $\theta < 27.52°$) were collected on a Bruker SMART APEX CCD X-ray diffractometer. The structure was solved by direct methods and refined by full-matrix least-squares on F^2 values of all data (G. M. Sheldrick, SHELXTL Manual) to give $wR2 = 0.0824$, conventional $R = 0.0313$ for F values of 12747 reflections, $S = 1.037$ and 773 parameters. Residual electron density max/min 0.448/ -0.232 e Å^{-3}. CCDC-183413 (**1**) contains the supplementary crystallographic data for this paper. These data can be obtained free of charge via www.ccdc.cam.ac.uk/conts/retrieving.html (or from the Cambridge Crystallographic Data Centre, 12 Union Road, Cambridge CB21EZ, UK; fax: (+44) 1223-336-033; or deposit@ccdc.cam.ac.uk).

[5] L. R. Dick, A. A. Cruikshank, L. Grenier, F. D. Melandri, S. L. Nunes, R. L. Stein, *J. Biol. Chem.* **1996**, *271*, 7273–7276.

[6] a) S. Ōmura, T. Fujimoto, K. Otoguro, K. Matsuzaki, R. Moriguchi, H. Tanaka, Y. Sasaki, *J. Antibiot.* **1991**, *44*, 113–116; b) S. Ōmura, T. Fujimoto, K. Otoguro, K. Matsuzaki, R. Moriguchi, H. Tanaka, Y. Sasaki, *J. Antibiot.* **1991**, *44*, 117–118.

[7] E. J. Corey, W.-D. Z. Li, *Chem. Pharm. Bull.* **1999**, *47*, 1–10.

[8] a) G. Fenteany, S. L. Schreiber, *J. Biol. Chem.* **1998**, *273*, 8545–8548; b) H. Tomoda, S. Ōmura, *Yakugaku Zasshi* **2000**, *120*, 935–949.

[9] E. J. Corey, W.-D. Z. Li, T. Nagamitsu, G. Fenteany, *Tetrahedron* **1999**, *55*, 3305–3316.

[10] We gratefully acknowledge K. Lloyd, S. Glaser, B. Miller, Nereus Pharmaceuticals Inc., for providing proteasome inhibition data.



Molybdenum–Silicon Multiple Bonds

Multiple Bonding Between Silicon and Molybdenum: A Transition-Metal Complex with Considerable Silylyne Character**

*Benjamin V. Mork and T. Don Tilley**

The 2p elements carbon, nitrogen, and oxygen readily form multiple bonds to many other elements, and such bonds contribute strongly to the chemical behavior of organic compounds. In contrast, the heavier main-group elements (with principal quantum numbers of three or greater) reluctantly participate in multiple bonding,[1] and this aspect of main-group chemistry has been the focus of considerable fundamental research. A number of stable compounds with

[*] Prof. T. D. Tilley, B. V. Mork
Department of Chemistry
University of California, Berkeley
Berkeley, CA 94720-1460 (USA)
Fax: (+1) 510-642-8940
E-mail: tdtilley@socrates.berkeley.edu

[**] Acknowledgment is made to the National Science Foundation for their generous support of this work.

Supporting information for this article is available on the WWW under http://www.angewandte.org or from the author.

double bonds to p-block elements have been isolated,[2] but examples of the corresponding triply bonded compounds are quite rare. The first compounds containing triple bonds to a Group 14 element (germanium) were the transition-metal complexes $[Cp(CO)_2M{\equiv}Ge(C_6H_3\text{-}2,6\text{-}Ar_2)]$ ($Cp = \eta^5$-cyclopentadienyl; M = Cr, Mo, W; Ar = Mes, Trip; Mes = 2,4,6-trimethylphenyl; Trip = 2,4,6-triisopropylphenyl), reported by Power and co-workers.[3] Recently, Filippou et al. described another class of complexes featuring triple-bonding to germanium, $[X(dppe)_2M{\equiv}Ge(\eta^1\text{-}Cp^*)]$ (X = Cl, Br, I; M = Mo, W; Cp* = pentamethylcyclopentadienyl; dppe = 1,2-bis(diphenylphosphanyl)ethane).[4] In addition, Power has recently reported the heavy Group 14-element analogues of alkynes, $[(2,6\text{-}Ar_2H_3C_6)EE(C_6H_3\text{-}2,6\text{-}Ar_2)]$ (E = Ge, Sn, Pb; Ar = Trip, Dipp; Dipp = 2,6-diisopropylphenyl).[5] The lead dimer is described as having primarily metal–metal single-bond character with lone pairs of electrons localized at each lead center; the germanium and tin species are postulated to have electronic structures intermediate between the singly- and triply-bonded extremes.

Efforts to prepare stable triple bonds to silicon have not yet been successful, although results from the work of Wiberg suggest that the disilyne $[t\text{Bu}_3\text{SiSi}{\equiv}\text{SiSi}t\text{Bu}_3]$ may be an unobserved intermediate in a reaction which forms its dimer, the tetrasilatetrahedrane $[(t\text{Bu}_3\text{SiSi})_4]$.[6] West's research group has also proposed the intermediacy of the disilyne species $[(2,6\text{-}Mes_2H_3C_6)Si{\equiv}Si(C_6H_3\text{-}2,6\text{-}Mes_2)]$, which decomposes through the cleavage of two C–C bonds in the terphenyl groups.[7] Thus, the synthesis of the first stable compound with a formal triple bond to silicon remains a key synthetic challenge. Here we report the isolation and characterization of $[\{Cp^*(dmpe)(H)MoSiMes\}\{B(C_6F_5)_4\}]$ (dmpe = 1,2-bis(dimethylphosphanyl)ethane), a complex that possesses considerable silylyne character.

Routes that have been developed to prepare silylene complexes include the abstraction of a group bound to silicon,[8] [Eq. (1)] and the activation of two Si–H bonds of a

$$L_nM\text{—}SiR_2X \xrightarrow{-X^-} L_nM{=}SiR_2^{+} \qquad (1)$$

hydrosilane by oxidative addition and subsequent α-hydrogen elimination (silylene extrusion; [Eq. (2)]).[9] The availability of these different methods for the generation of metal–silicon multiple bonds suggested the possibility of combining them in

$$L_nM\text{—}R + H_2SiR_2 \xrightarrow{-RH} \left[\begin{array}{c} L_nM\text{—}SiR_2 \\ \quad\quad | \\ \quad\quad H \end{array}\right] \longrightarrow \begin{array}{c} L_nM{=}SiR_2 \\ \quad\quad | \\ \quad\quad H \end{array} \qquad (2)$$

the synthesis of a silylyne complex. This approach involves silylene extrusion to produce a silylene complex with a potential leaving group, followed by abstraction of the leaving group from silicon. Ideally, the silylene-extrusion step in this scheme would produce a neutral silylene complex, since the subsequent abstraction necessarily produces a cation.

A suitable system for the application of this strategy was discovered in studies of the interactions of silanes with $[Cp^*(dmpe)Mo(\eta^3\text{-}CH_2Ph)]$ (**2**), prepared by the reaction of $[Cp^*(dmpe)(PMe_3)MoCl]$ (**1**)[10] with one equivalent of $PhCH_2MgCl$ in benzene. Complex **2**, which appears to be in equilibrium with its more reactive $[Cp^*(dmpe)Mo(\eta^1\text{-}benzyl)]$ form, reacts with chloromesitylsilane to produce the neutral silylene complex $[Cp^*(dmpe)(H)Mo{=}Si(Cl)Mes]$ (**3**). This reaction proceeds with the elimination of toluene, and presumably an α-hydrogen migration in the putative 16-electron intermediate $[Cp^*(dmpe)MoSi(H)(Cl)Mes]$. Benzyl complex **2** reacts with a variety of hydrosilanes to eliminate toluene, and these reactions are currently being investigated.

Silylene complex **3** was isolated as dark-red crystals in 88% yield. ^{1}H NMR spectroscopy shows that the complex has mirror symmetry, with a hydride resonance at $\delta = -12.50$ ppm ($J_{H\text{-}P} = 19$ Hz, $J_{H\text{-}Si} = 38$ Hz). The $^{31}P\{^1H\}$ NMR spectrum of **3** exhibits a single resonance at $\delta = 64.9$ ppm, and the silylene silicon center resonates at $\delta = 182$ ppm in the $^{29}Si\{^1H\}$ NMR spectrum. The molecular structure of **3**, as determined by X-ray crystallography (Figure 1),[11] features a very short Mo–Si separation of 2.288(2) Å, and the sum of the angles about the silicon center is 359.8(3)°. These values are consistent with what is expected for base-free silylene complexes and sp^2 hybridization at silicon centers. The Mo–Si separation may be reduced somewhat by the presence of the chloride substituent, as has been observed in chloro-substituted silyl complexes.[12] The location of the hydride ligand was not determined, however, the spectroscopic data is consistent with a position *trans* to the centroid of the Cp* ring.

The conversion of **3** to a cationic silylyne–hydride complex required exchange of the chloride ion for an inert, noncoordinating anion, such as $[B(C_6F_5)_4]^-$. The reaction of **3** with $[Li(OEt_2)_3B(C_6F_5)_4]$ occurred immediately upon mixing the reagents in fluorobenzene, and the reaction solution changed from dark red to dark green/amber. The ^{1}H NMR spectrum of the resultant mixture in fluorobenzene/$[D_6]$benzene (10:1) revealed the quantitative conversion of **3** to a new product that has a hydride resonance at $\delta = -9.78$ ppm ($J_{H\text{-}P} = 20$ Hz). The new complex also exhibits a downfield-shifted resonance in the $^{29}Si\{^1H\}$ NMR spectrum at $\delta = 289$ ppm. The downfield-shifted ^{29}Si resonance, coupled with the very low $J_{Si\text{-}H}$ value of 15 Hz suggested the formulation of the new product as the silylyne complex, $[\{Cp^*(dmpe)(H)MoSiMes\}\{B(C_6F_5)_4\}]$ (**4**, [Eq. (3)]). The extent to which the

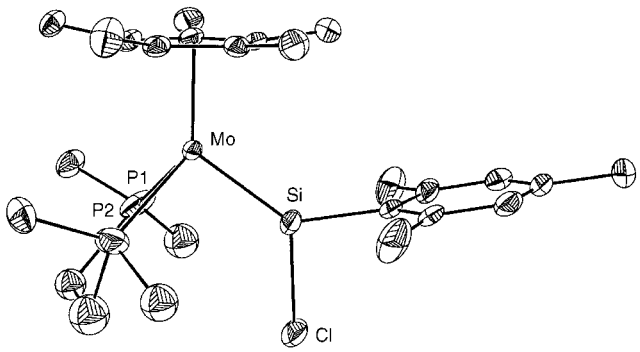


Figure 1. ORTEP diagram of the chloromesityl silylene complex **3**.

 © 2003 Wiley-VCH Verlag GmbH & Co. KGaA, Weinheim 1433-7851/03/4203-0358 $ 20.00+.50/0

$$[Cp^*(dmpe)(H)Mo{=}Si(Cl)Mes] \xrightarrow[\substack{PhF\\-LiCl}]{LiB(C_6F_5)_4} [\{Cp^*(dmpe)(H)MoSiMes\}\{B(C_6F_5)_4\}] \quad (3)$$

hydride ligand interacts with the silicon center in this complex is difficult to determine, although the low $J_{Si\text{-}H}$ value suggests that the interaction is minimal.[12]

Amber crystals of **4**, suitable for X-ray crystallography, were grown by layering a solution of the compound in fluorobenzene with pentane in a glass tube stored under nitrogen. The structure of the complex, determined by X-ray diffraction techniques, was found to exhibit an Mo–Si bond, which at 2.219(2) Å is the shortest bond of this type reported to date. An ORTEP diagram of the cation in **4** is shown in Figure 2. The Mo-Si-C angle of 170.9(2)° is approximately linear and in the range of M-C-C bond angles observed in carbyne complexes.[13] Additional geometric parameters of interest are the P-Mo-Si angles (99.66(6) and 87.14(6)°) for P1 and P2, respectively. The significantly wider P1-Mo-Si angle suggests that the hydride ligand adopts a position as the fourth leg of the "piano stool"-type structure (**A**, Scheme 1). This limiting case, suggested by the relatively low $J_{Si\text{-}H}$ coupling constant, bears no Si–H interaction. However, a peak in the Fourier-difference electron-density map could be refined as a hydride ligand in a bridging position between the molybdenum and silicon atoms. The H–Mo and H–Si bond lengths of 1.85(5) and 1.39(5) Å, respectively, represent reasonable separations for bonds of these types. Although X-ray diffraction is not a reliable method for determining hydride positions in the vicinity of a heavy metal, the refined position for the hydride ligand of **4** suggests that in the solid state an H···Si interaction may be present (**B**, Scheme 1). A third possible structure bears a hydride ligand that caps the P-Si-P face below the piano stool (**C**, Scheme 1). This structure is in agreement with the mirror symmetry observed for **4** by NMR spectroscopy.

In principle, it should be possible to differentiate between the mirror-symmetric structure **C** and structures **A** and **B** by NMR spectroscopy. Although the solid-state structure of **4** does not possess mirror symmetry, in solution at room temperature the cation of **4** exhibits C_s symmetry on the NMR timescale. However, an asymmetric structure is observed at −30 °C (in fluorobenzene) by NMR spectroscopy. For example, **4** exhibits a single resonance at $\delta = 47.9$ ppm in its $^{31}P\{^1H\}$ NMR spectrum at room temperature, while at low temperature, two doublets at $\delta = 49.5$ and 46.3 ppm are observed ($J_{P\text{-}P'} = 20$ Hz). Additionally, the ^1H NMR spectrum of **4** at −30 °C exhibits four peaks for the inequivalent dmpe methyl groups at $\delta = 1.48$, 1.31, 1.05, and 0.87 ppm. The resonance for the hydride ligand at $\delta = -10.03$ ppm is a multiplet resulting from coupling to inequivalent phosphorous nuclei. Thus, it appears that **4** adopts structure **A** or **B** and undergoes a rapid dynamic process that exchanges the phosphorous atoms of the dmpe ligand. This process could involve migration of the hydride ligand to the silicon center, followed by rotation about the Mo–Si bond, or a pseudorotation (for **A**).

Preliminary computational studies on the cation of **4** using DFT methods (at the B3LYP/LACVP** level of theory) resulted in an energy-minimized structure that closely resembles the crystallographically determined one. Most importantly, the calculated structure features the hydride ligand in a bridging position across the Mo–Si bond. This is further evidence that the complex bears a nonclassical Si–H interaction, as in structure-type **B** (Scheme 1). Studies are in progress to locate energy minima which correspond to structure-type **A.** If such a minimum is found, a comparison of the energies of these two structures will be informative.

Initial reactivity studies of complex **4** show that its silicon center is electrophilic. Reaction of the complex with $Me_3Si\text{-}CH_2Li$ in fluorobenzene resulted in an immediate color change of the solution to purple/red. A new product formed

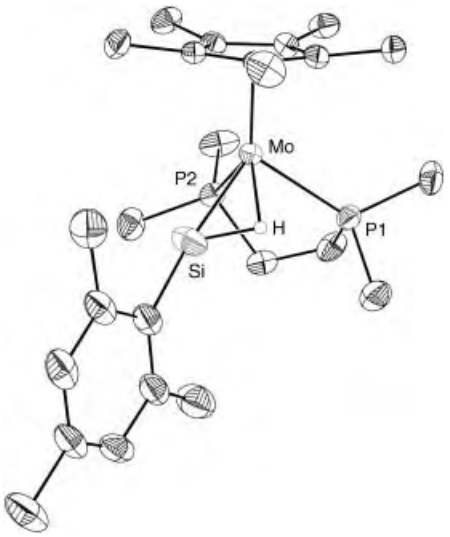
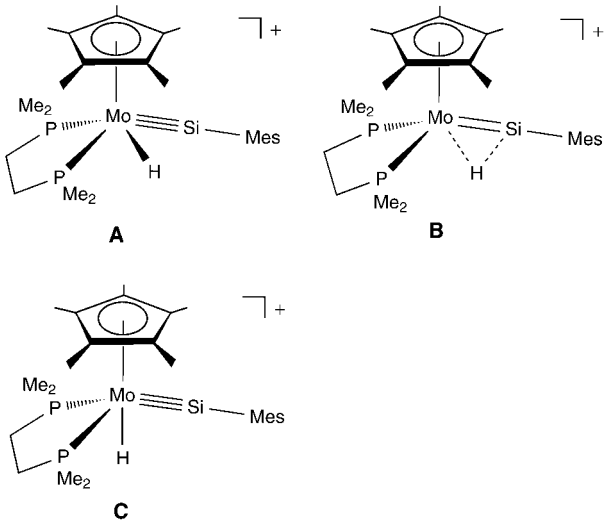


Figure 2. ORTEP diagram of the cation in **4**.



Scheme 1. Structural models discussed for the cation in **4**.

 © 2003 Wiley-VCH Verlag GmbH & Co. KGaA, Weinheim 1433-7851/03/4203-0359 $ 20.00+.50/0

cleanly (as given by ^{1}H, $^{31}P\{^{1}H\}$, and $^{29}Si\{^{1}H\}$ NMR spectroscopy), and was identified as the neutral silylene complex [Cp*(dmpe)(H)Mo=Si(CH_2SiMe_3)Mes] (**5**). The silylene and trimethylsilyl silicon centers resonate at $\delta = 243$ and -2 ppm in the $^{29}Si\{^{1}H\}$ NMR spectrum, respectively. Preliminary experiments have shown that weaker nucleophiles such as pyridine and bipyridine will also coordinate to the silicon center of **4** (as shown by ^{1}H NMR spectroscopy). The electrophilicity observed for the silylyne center is consistent with what has been observed for silylene complexes of transition metals.[8,9]

Complex **4** is the first example of an isolable compound that has silylyne (M≡Si) character.[14] The electrophilic silicon center in this complex may be stabilized by an interaction with the molybdenum hydride, although this interaction is likely to be weak considering the very low $J_{H\text{-}Si}$ coupling constant, and the exact location of the hydride ligand has not been firmly established. The metal–silicon bond order in this complex is difficult to ascertain, and the models used to describe bonding in second-row-element species often break down in heavy-element systems. However, it is interesting to make comparisons with [{Cp($P(OMe)_3$)$_2$(H)Mo≡C-CH_2CMe_3}{BF_4}], prepared by Green and co-workers,[15] which was reported to have strictly carbyne hydride character. Future efforts are planned to probe the bonding in **4** and in related compounds.

Received: October 10, 2002 [Z50334]

[1] a) A. G. Massey, *Main Group Chemistry*, 2nd ed., Wiley, Chichester, **2000**; b) P. P. Power, *Chem. Rev.* **1999**, *99*, 3463.

[2] a) R. West, M. J. Fink, J. Michl, *Science* **1981**, *214*, 1343; b) A. G. Brook, S. C. Nyburg, F. Abdesaken, B. Gutekunst, G. Gutekunst, R. K. M. R. Kallury, Y. C. Poon, Y.-M. Chang, W. Wong-Ng, *J. Am. Chem. Soc.* **1982**, *104*, 5667; c) M. Weidenbruch, *J. Organomet. Chem.* **2002**, *646*, 39; d) B. Twamley, C. D. Sofield, M . M. Olmstead, P. P. Power, *J. Am. Chem. Soc.* **1999**, *121*, 3357; e) B. Twamley, P. P. Power, *Chem. Commun.* **1998**, *1998*, 1979; f) T. Sasamori, N. Takeda, N. Tokitoh, *Chem. Commun.* **2000**, *2000*, 1353; g) T. Sasamori, N. Takeda, M. Fujio, M. Kimura, S. Nagase, N. Tokitoh, *Angew. Chem.* **2002**, *114*, 147; *Angew. Chem. Int. Ed.* **2002**, *41*, 139.

[3] a) R. S. Simons, P. P. Power, *J. Am. Chem. Soc.* **1996**, *118*, 11966; b) L. H. Pu, B. Twamley, S. T. Haubrich, M. M. Olmstead, B. V. Mork, R. S. Simons, P. P. Power, *J. Am. Chem. Soc.* **2000**, *122*, 650.

[4] a) A. C. Filippou, A. I. Philippopoulos, P. Portius, D. U. Neumann, *Angew. Chem.* **2000**, *112*, 2881; *Angew. Chem. Int. Ed.* **2000**, *39*, 2778; b) A. C. Filippou, P. Portius, A. I. Philippopoulos, *Organometallics* **2002**, *21*, 653.

[5] a) L. H. Pu, B. Twamley, P. P. Power, *J. Am. Chem. Soc.* **2000**, *122*, 3524; b) A. D. Phillips, R. J. Wright, M. M. Olmstead, P. P. Power, *J. Am. Chem. Soc.* **2002**, *124*, 5930; c) M. Stender, A. D. Phillips, R. J. Wright, P. P. Power, *Angew. Chem.* **2002**, *114*, 1863; *Angew. Chem. Int. Ed.* **2002**, *41*, 1785.

[6] N. Wiberg, C. M. M. Finger, K. Polborn, *Angew. Chem.* **1993**, *105*, 1140; *Angew. Chem. Int. Ed. Engl.* **1993**, *32*, 1054.

[7] R. Pietschnig, R. West, D. R. Powell, *Organometallics* **2000**, *19*, 2724.

[8] a) T. D. Tilley in *The Silicon–Heteroatom Bond*, (Eds.: S. Patai, Z. Rappoport), Wiley, New York, **1991**, chap. 9; b) S. K. Grumbine, G. P. Mitchell, D. A. Straus, T. D. Tilley, A. L. Rheingold, *Organometallics* **1998**, *17*, 5607; c) P. W. Wanandi, P. B. Glaser, T. D. Tilley, *J. Am. Chem. Soc.* **2000**, *122*, 972.

[9] a) J. C. Peters, J. D. Feldman, T. D. Tilley, *J. Am. Chem. Soc.* **1999**, *121*, 9871; b) S. R. Klei, T. D. Tilley, R. G. Bergman, *J. Am. Chem. Soc.* **2000**, *122*, 1816; c) J. D. Feldman, G. P. Mitchell, J. O. Nolte, T. D. Tilley, *J. Am. Chem. Soc.* **1998**, *120*, 11184; d) G. P. Mitchell, T. D. Tilley, *Angew. Chem.* **1998**, *110*, 2602; *Angew. Chem. Int. Ed.* **1998**, *37*, 2524; e) B. V. Mork, T. D. Tilley, *J. Am. Chem. Soc.* **2001**, *123*, 9702; f) K. Ueno, S. Asami, N. Watanabe, H. Ogino, *Organometallics* **2002**, *21*, 1326.

[10] The preparative procedures and data for compounds **1**–**5** are explained in detail in the Supporting Information.

[11] CCDC-194946 (**3**) and -194947 (**4**) contains the supplementary crystallographic data for this paper. These data can be obtained free of charge via www.ccdc.cam.ac.uk/conts/retrieving.html (or from the Cambridge Crystallographic Data Centre, 12 Union Road, Cambridge CB21EZ, UK; fax: (+44)1223-336-033; or deposit@ccdc.cam.ac.uk).

[12] J. Y. Corey, J. Braddock-Wilking, *Chem. Rev.* **1999**, *99*, 175.

[13] H. P. Kim, R. J. Angelici, *Adv. Organomet. Chem.* **1987**, *27*, 51.

[14] We previously reported a base-stabilized silylyne complex of ruthenium, [Cp*(Me_3P)$_2$Ru{Si(2,2′-bipyridyl)(S-Tol)}]$^{2+}$, which is likely to have metal–silicon single-bond character: S. D. Grumbine, R. K. Chadha, T. D. Tilley, *J. Am. Chem. Soc.* **1992**, *114*, 1518.

[15] a) M. Bottrill, M. Green, *J. Am. Chem. Soc.* **1977**, *99*, 5795; b) M. Bottrill, M. Green, A. G. Orpen, D. R. Saunders, I. D. Williams, *J. Chem. Soc. Dalton Trans.* **1989**, 511.

 © 2003 Wiley-VCH Verlag GmbH & Co. KGaA, Weinheim 1433-7851/03/4203-0360 $ 20.00+.50/0

Cover Picture



Ryo Kitaura, Kenji Seki, George Akiyama, and Susumu Kitagawa*

Flexible and dynamic channels created by an interdigitated framework of microporous coordination polymers are shown on the cover picture. The compound undergoes reversible crystal-to-crystal transformation from a nonporous (closed-form) to a microporous (open-form) structure, which is triggered by adsorption of supercritical gases. A hysteretic isotherm, shown bottom left, displays abrupt adsorption at a gate-opening pressure and equally sharp desorption at a gate-closing pressure. More about this coordination polymer is reported in the Communication by S. Kitagawa et al. on page 428 ff.

Contents

News

Leibniz Award 2003 to Ferdi Schüth ____ 378

Jay Siegel and Kim Baldridge move to the University of Zurich ____ 378

Strasbourg: New Building for Supramolecular Chemistry ____ 378

Meeting Reviews

The 50th Birthday of the Organocuprates ____ 379 – 380 | International Symposium on Modern Organocopper Chemistry | *N. Krause*

Books

Essentials of Computational Chemistry ____ 381 | Christopher J. Cramer | *F. M. Bickelhaupt*

Biomineralization ____ 381 – 382 | Stephen Mann | *M. Epple*

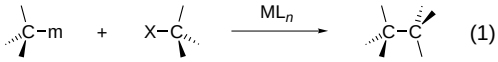
Highlights

Cross-Coupling Developments

D. J. Cárdenas* ____ 384 – 387

Advances in Functional-Group-Tolerant Metal-Catalyzed Alkyl–Alkyl Cross-Coupling Reactions

Keywords:
alkanes · boranes · cross-coupling · nickel · palladium



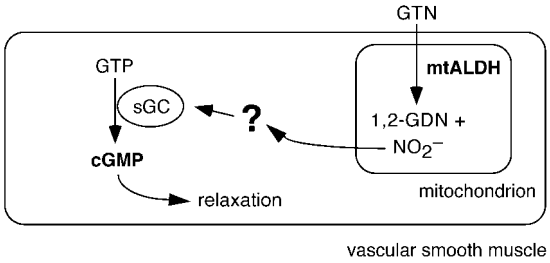
Methods for the general formation of C(sp^3)–C(sp^3) bonds by cross-coupling reactions in the presence of functional groups (see Equation (1)) are important but uncommon synthetic organometallic tools. Recent developments in the metal-catalyzed reactions of mild alkyl nucleophiles and alkyl electrophiles have yielded new methodologies for the formation of this type of C–C bond. M = Ni, Pd. m = Li, Mg, Zn, Al, Sn, B, Si.

Nitroglycerin Bioactivation

B. Mayer* ____ 388 – 391

Bioactivation of Nitroglycerin—A New Piece in the Puzzle

Keywords:
aldehyde dehydrogenase · nitrate metabolism · nitric oxide · vasodilation



Even after more than a century it is not completely understood how nitroglycerin (GTN) functions in the treatment of ischemic heart disease (angina pectoris). Recent work by Jonathan Stamler and co-workers (Duke University) now suggests that bioactivation of nitroglycerin, which is essential to the vascular action of the drug, is catalyzed by mitochondrial aldehyde dehydrogenase (mtALDH; see scheme). These important findings are discussed with special emphasis given to their pharmacological and clinical implications.

© 2003 Wiley-VCH Verlag GmbH & Co. KGaA, Weinheim

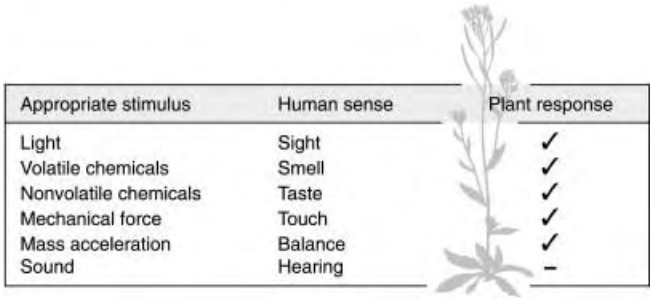
1433-7851/03/4204-0370 $ 20.00+.50/0

Reviews

Plant Biochemistry

E. W. Weiler* ——— 392 – 411

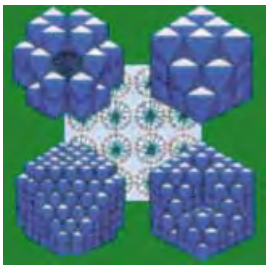
Sensory Principles of Higher Plants



Plants constantly monitor their environment and the situation of their interior by using a stunning array of highly specific and sensitive sensoric systems that can respond to the same stimuli, with the exception of sound, as animals and man (see picture). Plant sensoric systems, however, are very different from those of animals and man.

Keywords:
genetic engineering · hormones · membrane proteins · receptors · signal transduction

Communications



Crystals as building blocks: Self-assembled crystals are obtained through hierarchical and self-similar growth. Using microscopic, polyhedral, self-assembled crystals as building blocks, large crystals and open mesophase structures which preserve the shape and orientation of the basic structural units are spontaneously formed. A wide range of morphologies can be derived by different stacking, or by truncating the crystals on different surfaces (see picture).

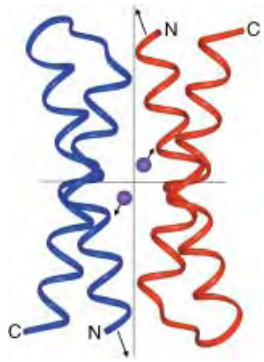
Self-Assembly with Crystals

Z. R. Tian, J. Liu,* J. A. Voigt, B. Mckenzie, H. Xu ——— 414 – 417

Hierarchical and Self-Similar Growth of Self-Assembled Crystals

Keywords:
crystal growth · inorganic–organic hybrid materials · mesoporous materials · self-assembly · silicon

An artificial four-helix-bundle metalloprotein was shown to have two different dimanganese coordination environments with bridging or terminal solvent molecules. A sliding-helix mechanism, by which metalloproteins can accommodate changes in their coordination environment, is demonstrated (see picture).



Metalloprotein Conformation

W. F. DeGrado, L. Di Costanzo, S. Geremia,* A. Lombardi, V. Pavone, L. Randaccio ——— 417 – 420

Sliding Helix and Change of Coordination Geometry in a Model Di-Mn^{II} Protein

Keywords:
bioinorganic chemistry · conformation analysis · metalloproteins · protein design · structure elucidation

For the USA and Canada:
ANGEWANDTE CHEMIE International Edition (ISSN 1433-7851) is published weekly by Wiley-VCH PO Box 191161, D 69451 Weinheim, Germany. Air freight and mailing in the USA by Publications Expediting Inc. 200 Meacham Ave., Elmont, NY 11003. Periodicals postage paid at Jamaica NY 11431. US POSTMASTER: send address changes to *Angewandte Chemie*, Wiley-VCH, 605 Third Ave, New York, NY 10158-0012. Annual institutional subscription price for institutions: Europe € 2998.00/3148.00. Outside Europe US$ 3718.00/3904.00 (valid for print or electronic/print and electronic delivery); for individuals who are personal members of a national chemical society, or whose institution already subscribes, or who are retired or self-employed consultants, print only (including postage and handling charges): Europe € 248.00/Outside Europe US$ 348.00.

 © 2003 Wiley-VCH Verlag GmbH & Co. KGaA, Weinheim 1433-7851/03/4204-0371 $ 20.00+.50/0

Contents

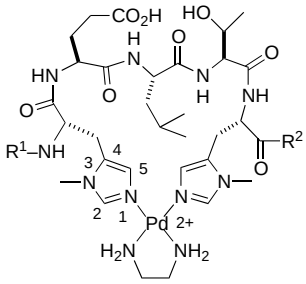
Helix-Folding Templates

M. J. Kelso, H. N. Hoang, W. Oliver, N. Sokolenko, D. R. March, T. G. Appleton, D. P. Fairlie* ——— 421 – 424

A Cyclic Metallopeptide Induces α Helicity in Short Peptide Fragments of Thermolysin

Keywords:
helical structures · NMR spectroscopy · palladium · peptides · peptidomimetics

Coordination of $[Pd(en)]^{2+}$ to histidine residues in 5-, 10-, and 15-residue peptides results in α-helical structures that mimic the Zn^{2+}-binding domain of thermolysin. The novel 22-membered metallacycle **1** (e.g. $R^1 = Ac$, $R^2 = NH_2$) is an α-helix-inducing template.



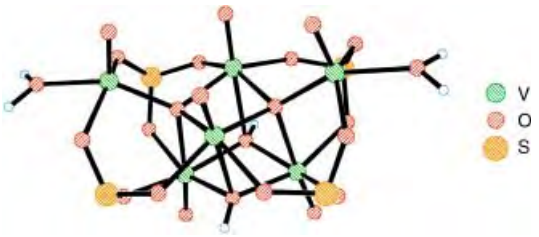
1

Vanadium–Sulfite Polyoxometalates

M. J. Manos, H. N. Miras, V. Tangoulis, J. D. Woollins, A. M. Z. Slawin,* T. A. Kabanos* ——— 425 – 427

Polyoxovanadium(IV) Sulfite Compounds: Synthesis, Structural, and Physical Studies

Keywords:
bridging ligands · cluster compounds · polyoxometalates · sulfite ions · vanadium



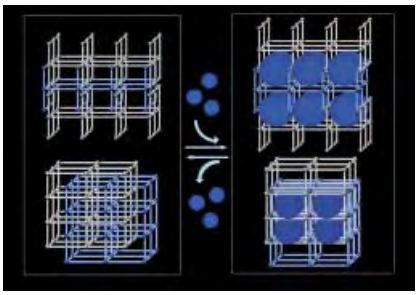
An unexplored family of polyoxometalates has evolved through the synthesis and structural characterization of vanadium(IV) sulfite heteropolyanions. The hexanuclear vanadium(IV) compound, which is ferromagnetic down to 2 K, exhibits a unique structural motif for such metal species, with a central cubic $\{M_4O_2(OH)_2\}$ fragment and metal centers at two of the corners of the cluster (see figure).

Flexible Coordination Polymers

R. Kitaura, K. Seki, G. Akiyama, S. Kitagawa* ——— 428 – 431

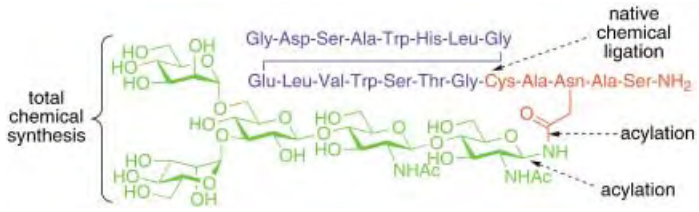
Porous Coordination-Polymer Crystals with Gated Channels Specific for Supercritical Gases

Keywords:
copper · crystal engineering · microporous materials · phase transitions · supercritical fluids



Flexible and dynamic coordination polymers based on interpenetration and interdigitation have been synthesized and characterized. Reversible crystal-to-crystal transformation from a nonporous structure (24 $m^2 g^{-1}$) to a microporous structure (at least 320 $m^2 g^{-1}$) is triggered by adsorption of various supercritical gases (see picture).

© 2003 Wiley-VCH Verlag GmbH & Co. KGaA, Weinheim
1433-7851/03/4204-0372 $ 20.00+.50/0



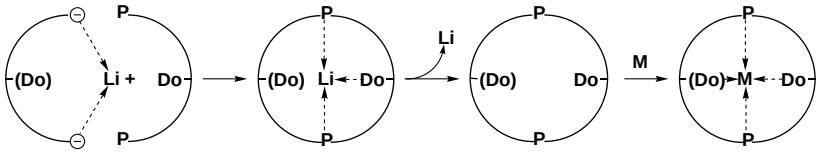
Substantial quantities of fully synthetic, homogeneous, *N*-linked glycopeptides may be accessed by a highly convergent and flexible protocol. Only four transformations are required to generate naturally linked glycopeptides in high yield. Amination of a free glycan is followed by acylation with an asparagine residue of a peptide and Fmoc deprotection; native chemical ligation completes the puzzle to afford *N*-linked glycopeptides (see scheme). Fmoc = 9-fluorenylmethoxycarbonyl.

Glycopeptide Synthesis

J. S. Miller, V. Y. Dudkin, G. J. Lyon, T. W. Muir, S. J. Danishefsky* ——— **431 – 434**

Toward Fully Synthetic *N*-Linked Glycoproteins

Keywords: carbohydrates · glycopeptides · glycosylation · peptides · synthetic methods



The shape of rings to come! The novel synthetic strategy for macrocycles containing differently functionalized ligands is based on a coupling reaction between two alkali-metal-fixed carbanionic centers **I** and two specifically connected, electrophilic phosphorus centers **II** (see scheme, Do = donor atom). Twofold P–C-bond formation first results in a metallamacrocycle **III**, which is subsequently converted by protonation into the neutral ring system **IV**. The formation of unprecedented coordination geometries of Cu^{I} and Ni^{0} centers is shown by the X-ray crystal structures of the complexes **V**.

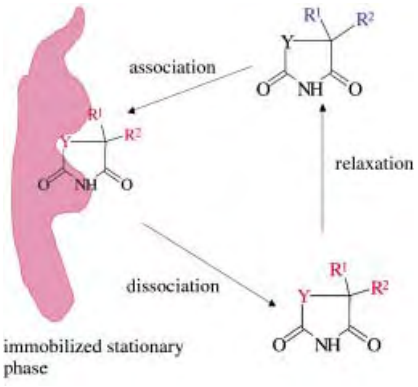
Complexes of P,N Macrocycles

S. Ekici, M. Nieger, R. Glaum, E. Niecke* ——— **435 – 438**

A Strategy for the Synthesis of Phosphorus-Containing Macrocycles—Ligands for Exceptional Coordination Geometries

Keywords: copper · macrocyclic ligands · N ligands · nickel · P ligands

Towards an understanding of chromatographic separation processes: The effect of the solvent composition on the strength of interaction between a chromatographic support and different organic substrates can be monitored by the relative intensity of the intramolecular negative transferred NOE effect (trNOE). The strength of interaction of different synthetic stationary phases with model substrates could be evaluated as changes in the observed trNOE (see picture Y = CH_2 or NH, R^1 = CH_3, R^2 = phenyl).



HRMAS NMR Spectroscopy

H. Händel, E. Gesele, K. Gottschall, K. Albert* ——— **438 – 442**

Application of HRMAS ^{1}H NMR Spectroscopy To Investigate Interactions between Ligands and Synthetic Receptors

Keywords: analytical methods · liquid chromatography · molecular recognition · NMR spectroscopy

 © 2003 Wiley-VCH Verlag GmbH & Co. KGaA, Weinheim 1433-7851/03/4204-0373 $ 20.00+.50/0

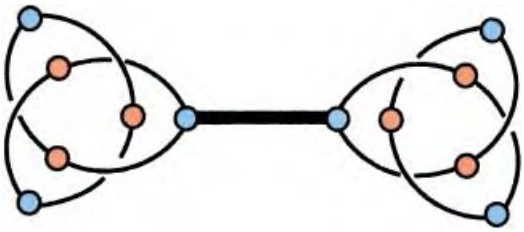
Contents

Molecular Knots

O. Lukin, J. Recker, A. Böhmer, W. M. Müller, T. Kubota, Y. Okamoto, M. Nieger, R. Fröhlich, F. Vögtle* ——— **442 – 445**

A Topologically Chiral Molecular Dumbbell

Keywords:
knots · macrocycles · molecular devices · topological chirality



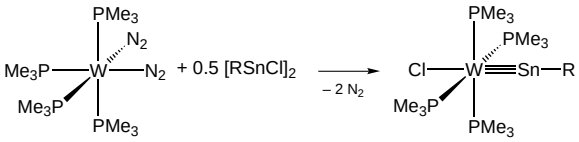
"Knotanes", that is knots that have been selectively monosubstituted and linked by a spacer unit to form the first topologically chiral dumbbell (see picture). The three isomers formed, a *meso* form and a DL enantiomeric pair, were separated completely by using covalently linked chiral chromatographical material. The chirality of the pure enantiomers of the dumbbell was proved from their circular dichroism spectra.

Triple Bond to Tin

A. C. Filippou,* P. Portius, A. I. Philippopoulos, H. Rohde ——— **445 – 447**

Triple Bonding to Tin: Synthesis and Characterization of the Stannylyne Complex *trans*-[Cl(PMe$_3$)$_4$W≡Sn–C$_6$H$_3$-2,6-Mes$_2$]

Keywords:
dinitrogen complexes · multiple bonds · stannylyne ligands · tin



1 **2** **3**

Straightening out tin: The reaction of the dinitrogen complex **1** with the aryl tin(II) chloride **2** affords selectively the stannylyne complex **3**. The molecular structure of **3** shows a very short W–Sn bond of 2.4902(8) Å and a linear coordinated tin atom (W-Sn-C = 178.2(1)°). R = C$_6$H$_3$-2,6-Mes$_2$, Mes = C$_6$H$_2$-2,4,6-Me$_3$.

Aggregating Gold Nanoparticles

W. Cheng, S. Dong,* E. Wang* ——— **449 – 452**

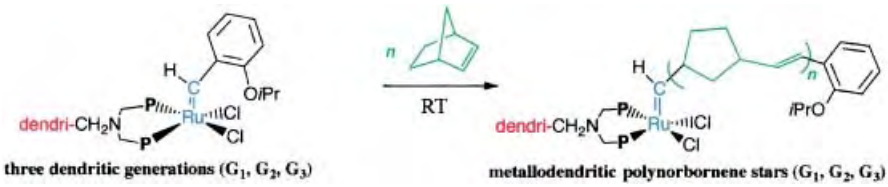
Iodine-Induced Gold-Nanoparticle Fusion/Fragmentation/Aggregation and Iodine-Linked Nanostructured Assemblies on a Glass Substrate

Keywords:
aggregation · chemisorption · gold · iodine · nanostructures



Iodine glue! Spontaneous iodine chemisorption on gold nanoparticles is demonstrated. The concomitant electron injection into gold nanoparticles results in particle fusion, fragmentation, and aggregation, excess KI addition leads to the formation of nanocrystals (see scheme). Surprisingly, iodine-"glued" surface-bound nanostructured assemblies of gold nanoparticles can be constructed on an amino-functionalized solid support by stepwise derivatization with colloidal Au and KI solution.

© 2003 Wiley-VCH Verlag GmbH & Co. KGaA, Weinheim
1433-7851/03/4204-0374 $ 20.00+.50/0



A star in the making: A new ruthenium–carbene complex has been synthesized by using a diphosphane ligand that models the dendritic branch of poly(diphosphane) dendrimers. First, second, and third generation metallodendrimers derived from diaminobutane polyamines, with 4, 8, and 16 ruthenium-containing branches, respectively, have been synthesized and shown to initiate the ring-opening-metathesis polymerization (ROMP) of norbornene at room temperature to form metallodendritic polymer stars (see scheme; **P** = PCy_2).

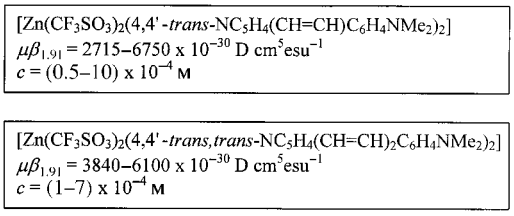
Ruthenium Metallodendrimers

S. Gatard, S. Nlate, E. Cloutet, G. Bravic, J.-C. Blais, D. Astruc* ——— **452 – 456**

Dendritic Stars by Ring-Opening-Metathesis Polymerization from Ruthenium–Carbene Initiators

Keywords:
carbenes · dendrimers · metathesis · polymerization · ruthenium

---



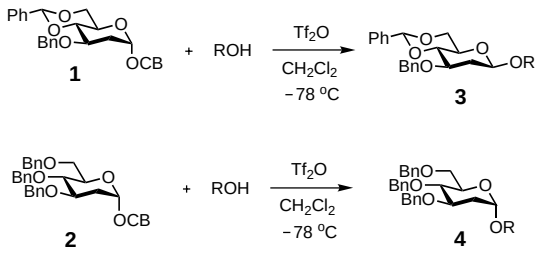
An unexpected dependence on concentration was found for the quadratic hyperpolarizability β of Zn complexes with stilbazole and $CF_3SO_3^-$ ligands (see values given), which reaches very large values on dilution. This is surprising, because the concentration used for determining β is traditionally not given in the literature, probably because it is a molecular property that should not vary with concentration. The origin of this effect is also reported.

Concentration Affects NLO Behavior

F. Tessore, D. Roberto,* R. Ugo, P. Mussini, S. Quici, I. Ledoux-Rak, J. Zyss ——— **456 – 459**

Large, Concentration-Dependent Enhancement of the Quadratic Hyperpolarizability of $[Zn(CH_3CO_2)_2(L)_2]$ in $CHCl_3$ on Substitution of Acetate by Triflate

Keywords:
N ligands · nonlinear optics · solvolysis · zinc



Different protecting groups on the glycosyl donor changes the stereoselectivity of the new glycosylation reaction shown in the scheme. Glycosylation of CB 4,6-*O*-benzylidene-2-deoxyglycoside **1** with secondary alcohol acceptors gave predominantly β-disaccharides **3**, whereas the same reaction with CB tri-*O*-benzyl-2-deoxyglycoside **2** afforded α-disaccharides **4**. CB = (2′-carboxy)benzyl.

Stereoselective Glycosylations

K. S. Kim,* J. Park, Y. J. Lee, Y. S. Seo ——— **459 – 462**

Dual Stereoselectivity of 1-(2′-Carboxy)-benzyl 2-Deoxyglycosides as Glycosyl Donors in the Direct Construction of 2-Deoxyglycosyl Linkages

Keywords:
carbohydrates · glycosides · glycosylation · protecting groups

 © 2003 Wiley-VCH Verlag GmbH & Co. KGaA, Weinheim 1433-7851/03/4204-0375 $ 20.00+.50/0

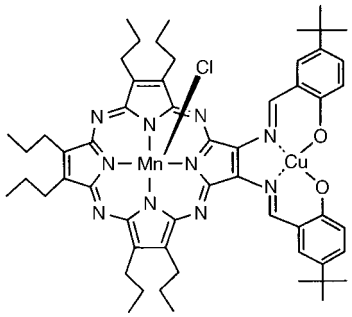
Contents

Spin Coupling between Metal Ions

M. Zhao, C. Stern, A. G. M. Barrett,* B. M. Hoffman* ——— **462 – 465**

Porphyrazines as Molecular Scaffolds: Periphery–Core Spin Coupling between Metal Ions of a Schiff Base Porphyrazine

Keywords:
copper · EPR spectroscopy · macrocyclic ligands · manganese · Schiff bases



1

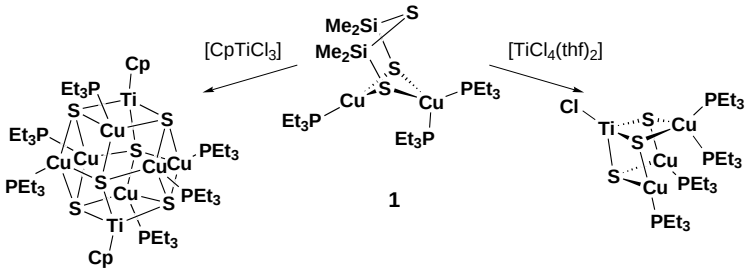
Strong Heisenberg exchange between the core Mn^{III} ion ($S=2$) and peripheral Cu^{II} ion ($S=^1/_2$) creates $S=^3/_2$ and $^5/_2$ total-spin manifolds in a $ClMn^{III}$-complexed porphyrazine (tetraazaporphyrin) to which a Cu^{II}-complexed Schiff base is rigidly linked through nitrogen atoms attached to the macrocycle periphery (**1**). EPR spectroscopy and magnetic susceptibility measurements have been used to characterize these spin manifolds and to determine the exchange-splitting ($\Delta/k_B=23$ K) between them.

Cu and Ag Silanethiolato Complexes

T. Komuro, T. Matsuo, H. Kawaguchi,* K. Tatsumi ——— **465 – 468**

Copper and Silver Complexes Containing the $S(SiMe_2S)_2^{2-}$ Ligand: Efficient Entries into Heterometallic Sulfido Clusters

Keywords:
cluster compounds · copper · S ligands · Si ligands · titanium



1

Thermally stable silanethiolato complexes of copper (**1**) and silver can be prepared readily by using cyclotrisilathiane. Complex **1a** reacts with titanium–chloride complexes under mild conditions to produce copper–titanium sulfido clusters.

Communications labeled with this symbol have been judged by two referees as being "very important papers".

The publication of Communications labeled with this symbol has been accelerated because of their topical or highly competitive nature.

Supporting information for articles labeled with this symbol can be found at www.angewandte.org or www.interscience.wiley.com.



News in *Angewandte Chemie*?

The aim of this section is to bring the scientific community closer together. The focus will be on international and interdisciplinary events, moves and awards. News items will include references to current articles in our family of journals.

Service

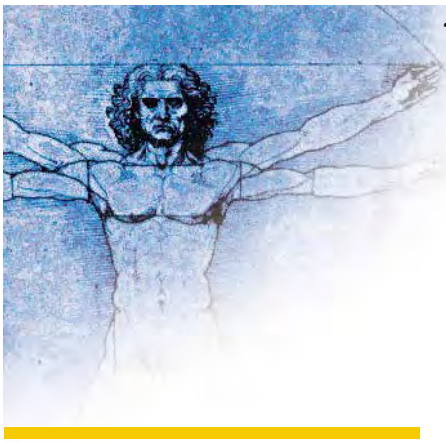
Classified ——— *377*

Keywords ——— *470*

Authors ——— *471*

Preview ——— *473*

© 2003 Wiley-VCH Verlag GmbH & Co. KGaA, Weinheim
1433-7851/03/4204-0376 $ 20.00+.50/0



Leibniz Award 2003 to Ferdi Schüth

To be among the winners of the Gottfried Wilhelm Leibniz Program of the German Research Foundation (DFG) is an honor and a privilege for any researcher, last but not least because it allows one to spend those extra 1.55 M€ over five years. This year, Ferdi Schüth (Max Planck Institute for Coal Research, Mülheim, Germany) is among the ten honorees.

His research is mainly devoted to the synthesis of solids with tailor-made properties and functions, especially for catalysis. Mesoporous solids and crystal growth from solution are of central importance to his work.

Schüth received his PhD in 1988 from the University of Münster under the guidance of Wicke and spent his post-doc time in 1989 with L. D. Schmidt in Minneapolis, MN. The same year, he graduated from law school. In 1993, he was a Visiting Assistant Professor in the group of Stucky (Santa Barbara, CA). He earned his Habilitation in Mainz (Germany) to become a professor in Frankfurt am Main in 1995 and a Director at the Max Planck Institute in Mülheim an der Ruhr (Germany) in 1998.

His most recent Communication in *Angewandte Chemie* deals with "Taking Nanocasting One Step Further: Replicating CMK-3 as a Silica Material".[1] Schüth is a co-editor of the "Handbook of Porous Solids".

Jay Siegel and Kim Baldridge to Move from California to Switzerland

This spring, Jay Siegel and Kim Baldridge (University of California, San Diego) will assume professorships for Organic Chemistry and Computational Chemistry, respectively, at the University of Zurich.

Siegel received his PhD from Princeton University in 1985 (supervisor: Kurt Mislow). After postdoctoral studies with Jean-Marie Lehn, he started his academic career in San Diego in 1986. His research is focused on the stereochemistry of organic and organometallic compounds and reactions as well as chemical synthesis directed toward the elucidation of molecular topologies and physical properties.[2] Among other commitments, Siegel is a member of the Editorial Board of the *European Journal of Organic Chemistry*.

Baldridge received her PhD from North Dakota State University. She joined the San Diego Supercomputer Center in 1988 and became adjunct professor of chemistry in 1997. She is currently director of the "Integrative Computational Sciences" at the San Diego Supercomputer Center. With her group, she develops theoretical methods for the description of the electronic structure of molecules, such as the GAMESS package, and specializes in problems of solvation, following reaction pathways and predictions of physical properties.

New Building for Supramolecular Chemistry in Strasbourg

The Institut des Sciences et d'Ingénierie Supramoléculaires (ISIS) in Strasbourg, France, has a new building (see picture). It was inaugurated on December 9 with a scientific symposium with prominent speakers, including two Nobel Prize winners: Pierre-Gilles de Gennes (ESPCI Paris), François Diederich (ETH Zurich), and Hartmut Michel (MPI Biophysics, Frankfurt). The formal inauguration ceremony was held in the afternoon in the presence of representatives of the Université Louis Pasteur, the city of Strasbourg, the region Alsace, and the French government.



The new ISIS building in Strasbourg by Claude Vasconi. Photo: Florence Schaeffer.

The new building was conceived by Nobel Prize winner Jean-Marie Lehn to be an excellent place for high-level international researchers to work and communicate on the interface of physics and chemistry. It will accommodate the research groups of Jean-Marie Lehn, Thomas Ebbesen, Nicolas Winssinger, and Michel Granet with a total of 150 people. Work on the building started in November 2000 and cost a total of 15 M€ plus 2 M€ for equipment.

Jean-Marie Lehn is the founding Chairman of the Editorial Boards of *Chemistry—A European Journal* and, together with Alan Fersht, of *ChemBioChem*.

[1] A.-H. Lu, W. Schmidt, A. Taguchi, B. Spliethoff, B. Tesche, F. Schüth, *Angew. Chem.* **2002**, *114*, 18, 3639, *Angew. Chem. Int. Ed.* **2002**, *41*, 3489.

[2] J. C. Loren, J. S. Siegel, *Angew. Chem.* **2001**, *113*, 776; *Angew. Chem. Int. Ed.* **2001**, *40*, 754.

 © 2003 Wiley-VCH Verlag GmbH & Co. KGaA, Weinheim 1433-7851/03/4204-0378 $ 20.00+.50/0

The 50th Birthday of the Organocuprates**

Norbert Krause*

In 1952, Henry Gilman described the first preparation of an organocuprate, namely lithium dimethylcuprate (Me_2CuLi).[1] Gilman was not only the founder of organometallic chemistry in the United States, but also one of the most eminent organometallic chemists of the 20th century, and many of his discoveries are now fundamental to this important branch of chemistry. It is interesting to note that the high preparative potential of these cuprates (which are nowadays known as Gilman cuprates) was not recognized initially, but only much later in the groundbreaking work of Corey, House, and others. This triggered the rapid development of new preparative procedures and their application toward the synthesis of natural and non-natural target molecules, as well as investigations dedicated to acquiring a better understanding of the structures and mechanisms of copper-promoted transformations.[2] The current protagonists in the field (as well as many young researchers) met at the University of Dortmund on October 9–11, 2002, to coincide with the 50th anniversary of Gilman's discovery, for the "International Symposium on Modern Organocopper Chemistry", which was organized by N. Krause and supported by the Volkswagen Foundation and other industrial sponsors.

What is hot in organocopper chemistry?

What is hot in organocopper chemistry? The symposium made it clear that substantial progress can be expected in the implementation of new environmentally friendly catalytic procedures (in particular in stereoselective synthesis), in the understanding of reaction mechanisms and the role of copper in biological systems (mostly metalloproteins), and in the development of new materials with the aid of organocopper compounds. A highlight regarding the use of copper in stereoselective synthesis is the enantioselective 1,4-addition of organozinc reagents to enones and other Michael acceptors. The lectures held by A. Alexakis (Geneva), B. L. Feringa (Groningen), and K. Tomioka (Kyoto) demonstrated the high standard now reached with the aid of chiral phosphorus ligands and new experimental conditions, allowing routine applications of the reaction in natural-product synthesis. In spite of this tremendous success, the use of stoichiometric amounts of chiral auxiliaries may still be advantageous, as shown by B. Breit (Freiburg) in copper-catalyzed Michael addition and S_N2' substitution reactions with the aid of the *o*-diphenylphosphanylbenzoyl group. Further new and seminal preparative methods were presented by (among others) R. K. Dieter (Clemson; aminoalkyl cuprates) and B. H. Lipshutz (Santa Barbara; catalysis with copper hydride).

The fundamental role of copper in metalloproteins was described in an impressive lecture by P. M. H. Kroneck (Konstanz). Copper proteins play a fundamental role in many biological processes, in particular in photosynthesis and the reduction of dioxygen.[3] In this case, the redox properties of copper are of utmost importance since it exists not only in oxidation states I and II, but also as a binuclear Cu(1.5) complex. Still, nature can provide surprises, as demonstrated by the unexpected discovery of copper in carbon monoxide dehydrogenase/acetyl-CoA made recently by Drennan and coworkers:[4] Copper was found in an unprecedented complex together with a nickel and a Fe_4S_4 cluster, which may suggest a new role of copper in biology.[5]

Another highlight of the symposium was the lecture by E. Nakamura (Tokyo) on the "Organocopper Way to Material Science". By taking advantage of a regioselective, fivefold addition of organocopper compounds to C_{60}, several functionalized fullerenes were prepared which could be transformed into metal complexes with fullerene cyclopentadienide units. In water, certain "buckyferrocenes" form spheric, bilayered vesicles with diameters in the nanometer range, whereas fullerenes with five long-chained "feathers" can be aggregated like shuttlecocks.[6] These fascinating complexes form liquid crystalline phases that depend not only on the temperature but also on the concentration. It is expected that these new materials will exhibit intriguing optical and electronic properties.

The fourth important subject area of the symposium was dedicated to the structures of organocopper reagents and the mechanisms of their reactions. J.-E. Bäckvall (Stockholm) presented experimental evidence for the existence of (hitherto putative) copper(III) intermediates, which was obtained by mathematical analysis of the mixtures of homo- and heterocoupling products formed by S_N2' substitution reactions of allylcuprates with allylic electrophiles. Just as fascinating was the lecture by G. Boche (Munich) about the life and scientific work of Henry Gilman and subsequent investigations into the structure of organocuprates in the solid state as well as in solution. Thus, the latent controversy about "higher-order cyanocuprates" was resolved with the aid of X-ray crystallography,[7] and it could be shown that Michael additions of organocuprates proceed via solvent-separated ion pairs. Very recent NMR spectroscopic investigations presented by R. M. Gschwind (Bonn) document an even more complicated behavior of cuprates in solution: Besides monomers and dimers, much larger aggregates were

Thus, the latent controversy about "higher-order cyanocuprates" was resolved with the aid of X-ray crystallography, and it could be shown that Michael additions of organocuprates proceed via solvent-separated ion pairs.

[*] Prof. Dr. Norbert Krause
Organische Chemie II, Universität Dortmund, 44221 Dortmund (Germany)

[**] International Symposium on Modern Organocopper Chemistry, Dortmund University (Germany), October 9–11, 2002.

 © 2003 Wiley-VCH Verlag GmbH & Co. KGaA, Weinheim 1433-7851/03/4204-0379 $ 20.00+.50/0

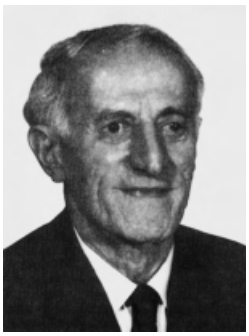


Photo of Henry Gilman. Reprinted with permission from Biographical Memoirs, Vol. 36. Copyright 1990 National Academy of Sciences.

detected, and the reactivity may strongly depend on equilibria between these species.

[1] H. Gilman, R. G. Jones, L. A. Woods, *J. Org. Chem.* **1952**, *17*, 1630 – 1634.

[2] N. Krause (Ed.), *Modern Organocopper Chemistry*, Wiley-VCH, Weinheim, **2002**.

[3] P. M. H. Kroneck, Binuclear Copper A, in: *Handbook of Metalloproteins* (Eds.: K. Wieghardt, R. Huber, T. Poulos, A. Messerschmidt), Wiley, Chichester **2001**, p. 1333 – 1341.

[4] T. I. Doukov, T. M. Iverson, J. Seravalli, S. W. Ragsdale, C. L. Drennan, *Science* **2002**, *298*, 567 – 572.

[5] E. I. Solomon, P. Chen, M. Metz, S.-K. Lee, A. E. Palmer, *Angew. Chem.* **2001**, *113*, 4702 – 4724; *Angew. Chem. Int. Ed.* **2001**, *40*, 4570 – 4590.

[6] M. Sawamura, K. Kawai, Y. Matsuo, K. Kanie, T. Kato, E. Nakamura, *Nature* **2002**, *419*, 702 – 705.

[7] N. Krause, *Angew. Chem.* **1999**, *111*, 83 – 85; *Angew. Chem. Int. Ed.* **1999**, *38*, 79 – 81.

 © 2003 Wiley-VCH Verlag GmbH & Co. KGaA, Weinheim 1433-7851/03/4204-0380 $ 20.00+.50/0

Cross-Coupling Developments

Advances in Functional-Group-Tolerant Metal-Catalyzed Alkyl–Alkyl Cross-Coupling Reactions**

*Diego J. Cárdenas**

Keywords:
alkanes · boranes · cross-coupling · nickel · palladium

The efficient formation of C(sp^3)–C(sp^3) bonds from organic electrophiles and mild nucleophiles, compatible with a wide variety of functional groups, represents one of the subjects remaining to be solved in transition-metal-catalyzed synthetic organometallic chemistry. The development of methods directed to achieve this goal (Scheme 1) may virtually complete the scope of metal-catalyzed cross-coupling reactions.[1,2]

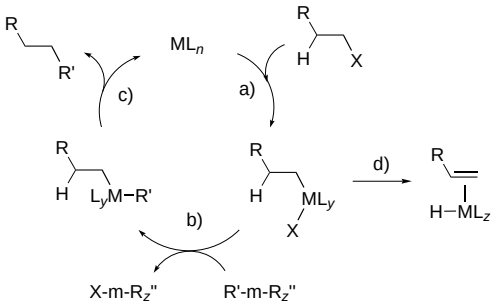
Whereas main group organometallic derivatives with nucleophilic C(sp^3), C(sp^2), and C(sp) atoms can be used in this type of reaction, alkyl halides or sulfonates have been rarely used. The general catalytic cycle for metal-catalyzed cross-coupling reactions (Scheme 2) involves an oxidative addition of the organic electrophile to a coordinatively unsaturated metal complex, followed by transmetalation from the nucleophile to the intermediate



Scheme 1. A general metal-catalyzed alkyl–alkyl cross-coupling reaction. M = Ni, Pd, etc.; m = Li, Mg, Zn, Al, Sn, B, Si, etc.; X = halide, sulfonate.

[*] Dr. D. J. Cárdenas
Departamento de Química Orgánica
Facultad de Ciencias
Universidad Autónoma de Madrid
Cantoblanco, 28049 Madrid (Spain)
Fax: (+34) 91-397-3966
E-mail: diego.cardenas@uam.es

[**] dba = (*E*,*E*)-dibenzylideneacetone, Cy = cyclohexyl, 9-BBN = 9-borabicyclo[3.3.1]nonane, cod = (*Z*,*Z*)-1,5-cyclooctadiene, acac = acetylacetonate. Prof. Antonio M. Echavarren is gratefully acknowledged.



Scheme 2. General mechanism for transition-metal-catalyzed cross-coupling reactions between alkyl electrophiles and organometallic nucleophiles. Catalytic cycle steps: a) oxidative addition, b) transmetalation, and c) reductive elimination. β-Hydride elimination (d) prevents the coupling process.

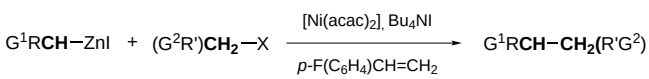
species formed in the first step, to give a diorganometal derivative. A fast C–C reductive elimination yields the coupled product and usually regenerates the active catalyst.

In the case of alkyl halides or sulfonates, the first step is relatively slow and, in contrast, gives rise to an alkyl metal complex that may suffer a fast β-hydride elimination that prevents the coupling process (Scheme 2). For these reasons the coupling between sp^3-carbon atoms has not been developed as well as other C–C bond-forming reactions.[3]

Some years ago, the first efficient coupling between alkyl carbons in the presence of a variety of functional groups was published,[4,5] and the importance of such an achievement was highlighted.[6] Diorganozinc derivatives were coupled with alkyl halides in a Ni- catalyzed reaction taking advantage of a rapid reductive elimination induced by the coordination of suitable π-acceptor ligands to the intermediate diorganonickel complex. During the last year, several relevant works on alkyl–alkyl cross-coupling have been reported with both Pd and Ni complexes used as catalysts. Knochel et al. have extended the above mentioned method to the less reactive and more functional-group-tolerant alkylzinc iodides.[7] Another Ni-catalyzed process, the coupling of alkyl Grignard reagents with alkyl electrophiles, has been reported by Kambe et al.[8] Using an alternative strategy, Fu et al. have succeeded in coupling alkyl halides and tosylates by utilizing alkyl boranes with Pd catalysts, [9–11] thus extending the highly versatile Suzuki reaction.

The new Ni-catalyzed coupling of iodoalkylzinc reagents[12] and alkyl halides is summarized in Scheme 3. Ethers, ketones, nitriles, and tertiary amides are compatible with the nucleophilic reagents, in a process that takes place at low temperature (−5 °C).

In addition to 4-fluorostyrene, which accelerates the reductive elimination, Bu_4NI has to be added to promote the reaction of these derivatives, although

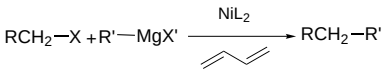


Scheme 3. Ni-catalyzed cross-coupling of haloalkanes and alkylzinc iodides. X = Br, I; G^1 = alkyl, ester; G^2 = ketone, ester, amide.

 © 2003 Wiley-VCH Verlag GmbH & Co. KGaA, Weinheim 1433-7851/03/4204-0384 $ 20.00+.50/0

its role is not clear.[13] The reaction has been extended to alkyl bromides and to secondary diorganozinc derivatives, which widens the scope of this process.

In the other recently reported Ni-catalyzed process, alkyl chlorides, bromides, and tosylates are coupled with alkyl or aryl Grignard reagents.[8] Besides the precatalyst ($NiCl_2$, $[Ni(acac)_2]$, or $[Ni(cod)_2]$), the presence of 1,3-butadiene or isoprene is necessary for the coupling to take place (Scheme 4).

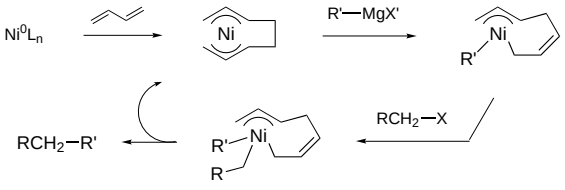


Scheme 4. Ni-catalyzed reaction between Grignard reagents and alkyl electrophiles. R′ = alkyl, aryl; X = Cl, Br, TsO; X′ = Cl, Br; L = Cl, acac, cod.

In the absence of a diene, both reduction of the organic electrophile to the alkane or elimination to the alkene are observed. Although the scope of this reaction is severely limited by the high reactivity of the nucleophiles (Table 1), it has interesting mechanistic implications. Probably, the actual catalysts are diallyl–Ni^{II} complexes.[14] These derivatives are proposed to first transmetalate with the alkylmagnesium halide to give a more nucleophilic species, which then undergoes an oxidative addition of the alkyl halide to give a formal Ni^{IV} intermediate. Reductive elimination from this complex yields the coupled product and regenerates the active Ni^{II} catalyst (see Scheme 5).

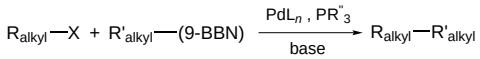
This procedure contrasts with the Ni-catalyzed cross-couplings between Grignard reagents and aryl or vinyl halides, which are thought to proceed through a catalytic cycle involving Ni^0 and Ni^{II} intermediates, and with the homocoupling of haloarenes, which has been demonstrated to take place through Ni^I and Ni^{III} radical species.[15] Related Pd^{II}–Pd^{IV} catalytic cycles probably operate in some reported alkylations of arenes.[16] This work suggests that new mechanisms are still to be discovered in the field of cross-coupling reactions.

An important contribution from the organosynthetic point of view has been made by Fu et al. They have succeeded in coupling primary bromides,[9] chlorides,[10] and tosylates[11] with organoboranes in a Suzuki- type reaction.[17] The catalytic species are generated from $Pd(OAc)_2$ or $[Pd_2(dba)_3]$ (for the coupling of bromo- or chloroalkanes, respectively), and PCy_3 (Scheme 6). In the case of alkyl tosylates, $Pd(OAc)_2$ and $PtBu_2Me$ gives the best results. The reactions of alkyl bromides and tosylates take place even at room temperature.



Scheme 5. Possible reaction mechanism for the Ni-catalyzed cross-coupling of alkylmagnesium halides and alkyl electrophiles.

This process takes advantage of the high tolerance of boron derivatives with most functional groups (Table 1), which makes this reaction a powerful synthetic tool. In addition, the alkyl boranes can be prepared by hydroboration of alkenes, thus avoiding the use of highly reactive organolithium and organomagnesium reagents in the preparation of the nucleophilic partners used in the coupling reactions.



Scheme 6. Pd-catalyzed cross-coupling of alkyl electrophiles and alkylboranes. $PdL_n = Pd(OAc)_2$, $PR''_3 = PCy_3$, and base = $K_3PO_4 \cdot H_2O$ for X = Br; $PdL_n = [Pd_2(dba)_3]$, $PR''_3 = PCy_3$, and base = $CsOH \cdot H_2O$ for X = Cl; $PdL_n = Pd(OAc)_2$, $PR''_3 = PtBu_2Me$, and base = NaOH for X = OTs.

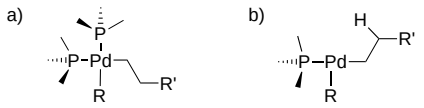
A strict choice of the Pd source, the phosphane, and even the base is necessary for the reactions to give the desired products. PCy_3 affords the best yields and minimizes the extent of β-hydride elimination in the case of bromides and chlorides. For the latter, P(cyclopentyl)$_3$ and P(*i*Pr)$_3$ are less effective but still give the coupled products. P(*t*Bu)$_3$ and dcpe (1,2-bis(dicyclohexylphosphanyl)-ethane)[18] favor the β-elimination process, whereas triarylphosphanes, phosphites, and arsanes are not effective. These results indicate that the ligands must have a high electron-donating ability,[19] which in the case of phosphanes, depends on the nature of the substituents and on the Tolman angle. Additionally, the cone angle is related to the steric hindrance imposed by the ligand. The experimentation suggests that a delicate balance of steric and electronic features has to be attained for the ligand to be adequate in this case.[11] Thus, for the coupling of alkyl tosylates, PCy_3 is less effective than $PtBu_2Me$. If a good donor ligand is too large (for example, P(*t*Bu)$_3$), the key dialkyl–Pd^{II} precursor of the reductive elimination may only coordinate to a single phosphane group,[20] and the resulting coordinatively unsaturated Pd^{II} complex[21] would be

Table 1: Comparison of the reported $C(sp^3)$–$C(sp^3)$ cross-coupling reactions.

Nucleophile	Nucleophile type	Alkyl electrophile	Catalyst	Compatible with
R—MgX	primary, secondary	primary	Ni^{II}/Ni^{IV}	ether, acetal[a]
R_2Zn, RZnX	primary, secondary	primary	Ni^0/Ni^{II}	ether, acetal,[a] ketone, ester, tertiary amide, nitrile, thioether,[b] thioacetal, carbamate[c]
$R—BR'_2$	primary	primary	Pd^0/Pd^{II}	alkyne, ether, acetal, silyl, tertiary amine, ketone,[a] ester, amide,[a] nitrile, thioether,[a] thioacetal,[a] sulfone,[a] carboxylic acid,[a] tertiary alcohols,[d] and aqueous solvents

[a] Functional groups usually compatible with the reactions but not included in the mentioned articles. [b] In the reactions with R_2Zn. [c] The presence of an NH bond requires an excess of the organozinc reagent. [d] In the case of alkyl tosylates.

 © 2003 Wiley-VCH Verlag GmbH & Co. KGaA, Weinheim 1433-7851/03/4204-0385 $ 20.00+.50/0



Scheme 7. Possible diorganopalladium precursors of the reductive elimination. a) Square planar 16-electron species; b) coordinatively unsaturated metal complexes that may afford β-elimination products.

more likely to undergo β-elimination[22,23] (Scheme 7).

Suzuki cross-coupling reactions usually require the addition of base to increase the nucleophilicity of the borane species and to promote the transmetalation step. The choice of these reagents is also critical, since it may affect the functional group compatibility. Alkyl bromides react in the presence of $K_3PO_4 \cdot H_2O$, but not if the anhydrous salt is employed. In the case of alkyl chlorides and tosylates, $CsOH \cdot H_2O$ and NaOH are, respectively, more convenient. KOH is suitable for both types of halides and minimizes the extent of hydrolysis when esters are present among the reagents. Regarding the Pd precatalyst, $Pd(OAc)_2$ is effective for the coupling of bromides and tosylates. For the reaction of chlorides, which takes place at 90 °C, $[Pd_2(dba)_3]$ gives better results. In spite of the higher strength of the C–Cl bond (compared with C–Br and C–I bonds),[10] the extension of the reaction to choloroalkanes was probably expected not to be difficult to achieve considering the usual S_N2-type mechanism of the oxidative addition for alkyl substrates. In fact, a wide array of ligands and conditions for the coupling of the less reactive chloroarenes in a variety of reactions has been reported.[24] The subsequent mechanistic study on the stereochemistry of the oxidative addition of alkyl tosylates to Pd^0 complexes demonstrated that this step and the overall coupling process take place with inversion of the carbon configuration in the electrophile, which supports this mechanism.[11] In summary, the fine tuning of the reaction catalysts and additives has allowed the development of an extremely important Pd-catalyzed reaction. The avoidance of the β-elimination process by a careful choice of the conditions widens the scope of the Suzuki reaction and opens up the possibility of utilizing alkyl halides in other reactions that are catalyzed by this metal.

A common limitation of the above-mentioned methods is that they are restricted to primary alkyl electrophiles. New processes have to be developed to extend the scope of the reaction to secondary and tertiary substrates. This will probably imply the participation of complexes of other transition metals and the utilization of new mechanisms. The development of methods based on mild nucleophiles (boranes and boronates, stannanes, silanes, etc.) is of particular interest because of their functional-group tolerance. Future advances on this kind of $C(sp^3)$–$C(sp^3)$ bond formation will provide useful synthetic tools, and will make it possible to design new routes for the synthesis of highly functionalized organic molecules.

[1] *Metal-catalyzed Cross-coupling Reactions* (Eds.: F. Diederich, P. J. Stang), Wiley-VCH, Weinheim, **1998**.

[2] *Transition Metals for Organic Synthesis, Vol. 1* (Eds.: M. Beller, C. Bolm), Wiley-VCH, Weinheim, **1998**, chap. 2.10, pp. 128–183.

[3] This does not include the formation of allyl–allyl bonds, which are much easier to make because of both a more facile oxidative addition and the occurrence of a different reductive elimination mechanism: M. Méndez, J. M. Cuerva, E. Gómez-Bengoa, D. J. Cárdenas, A. M. Echavarren, *Chem. Eur. J.* **2002**, *8*, 3620–3628.

[4] R. Giovannini, T. Stüdemann, G. Dussin, P. Knochel, *Angew. Chem.* **1998**, *110*, 2512–2515; *Angew. Chem. Int. Ed.* **1998**, *37*, 2387–2392.

[5] R. Giovannini, T. Stüdemann, A. Devasagayaraj, G. Dussin, P. Knochel, *J. Org. Chem.* **1999**, *64*, 3544–3553.

[6] D. J. Cárdenas, *Angew. Chem.* **1999**, *111*, 3201–3203; *Angew. Chem. Int. Ed.* **1999**, *38*, 3018–3020.

[7] A. E. Jensen, P. Knochel, *J. Org. Chem.* **2002**, *67*, 79–85.

[8] J. Terao, H. Watanabe, A. Ikumi, H. Kuniyashu, N. Kambe, *J. Am. Chem. Soc.* **2002**, *124*, 4222–4223.

[9] M. R. Netherton, C. Dai, K. Neuschütz, G. C. Fu, *J. Am. Chem. Soc.* **2001**, *123*, 10099–10100.

[10] J. H. Kirchhoff, C. Dai, G. C. Fu, *Angew. Chem.* **2002**, *114*, 2025–2027; *Angew. Chem. Int. Ed.* **2002**, *41*, 1945–1947.

[11] M. R. Netherton, G. C. Fu, *Angew. Chem.* **2002**, *114*, 4066-4068; *Angew. Chem. Int. Ed.* **2002**, *41*, 3910–3912.

[12] Pd-catalyzed homocoupling of alkylboranes and alkylzinc iodides: A. Lei, X. Zhang, *Org. Lett.* **2002**, *4*, 2285–2288.

[13] It may coordinate the alkylzinc iodide to give a more nucleophilic anionic species or may just change the medium ionic strength.

[14] These are formed by reaction of the dienes with either the Ni^0 complexes directly used as precatalysts, or the Ni^0 species generated from the Ni^{II} precursors by reduction with the Grignard reagents.

[15] J. P. Collman, L. S. Hegedus, J. R. Norton, R. G. Finke, *Principles and Applications of Organotransition Metal Chemistry*, University Science Books, Mill Valley, CA, **1987**, pp. 310–314 and 710–712.

[16] a) M. Catellani, F. Frignani, A. Rangoni, *Angew. Chem.* **1997**, *109*, 142–145; *Angew. Chem. Int. Ed. Engl.* **1997**, *36*, 119–122; b) M. Lautens, S. Piguel, *Angew. Chem.* **2000**, *112*, 1087–1088; *Angew. Chem. Int. Ed.* **2000**, *39*, 1045–1046; c) M. Lautens, J.-F. Paquin, S. Piguel, *J. Org. Chem.* **2002**, *67*, 3972–3974.

[17] Alkyl boron derivatives in cross-coupling reactions: S. R. Chemler, D. Trauner, S. J. Danishefsky, *Angew. Chem.* **2001**, *113*, 4676–4701; *Angew. Chem. Int. Ed.* **2001**, *40*, 4544–4568.

[18] Ligand dcpe is mentioned in ref. [9] to be a bicyclic analogue of PCy_3. Donor properties may be affected through changes in the cone angle (see examples in ref. [19]).

[19] The donor character of these ligands has been estimated from the CO stretching frequency in several phosphane carbonyl metal complexes: D. Woska, A. Prock, W. P. Giering, *Organometallics* **2000**, *19*, 4629–4638.

[20] Semiempirical calculations at the PM3 level show that in the model complex $[cis\text{-}Pd(Et)_2\{P(t\text{Bu})_3\}_2]$ the square planar geometry is strongly distorted (P-Pd-P angle = 129.6°), which may destabilize the complex and make one of the ligands easy to dissociate, thus favoring the competing β-elimination. The comparable value for the $P(i\text{Pr})_3$ analogue (101.5°) is much closer to a right angle (D. J. Cárdenas, unpublished results).

[21] A complex with a single hindered monodentate phosphane may not necessarily be coordinatively unsaturated. An agostic interaction has been recently observed in an aryl–Pd^{II} complex containing $P(t\text{Bu})_3$: J. P. Stambuli, M. Bühl, J. F. Hartwig, *J. Am. Chem. Soc.* **2002**, *124*, 9346–9347.

[22] Tricoordinate 14-electron complexes of d^8 metals have also been proposed as precursors of certain reductive eliminations: J. P. Collman, L. S. Hegedus, J. R.

Norton, R. G. Finke, *Principles and Applications of Organotransition Metal Chemistry*, University Science Books, Mill Valley, CA, **1987**, p. 322 – 333.
[23] Coordinatively unsaturated Pd^{II} complexes may be formed in the transmetalation step of the Stille reaction: a) A. L. Casado, P. Espinet, A. M. Gallego, *J. Am. Chem. Soc.* **2000**, *122*, 11771 – 11782; b) A. L. Casado, P. Espinet, *J. Am. Chem. Soc.* **1998**, *120*, 8978 – 8985.
[24] The oxidative addition mechanism involved in this case is different. Some leading references on aryl chlorides functionalization: a) J. P. Wolfe, R. A. Singer, B. H. Yang, S. L. Buchwald, *J. Am. Chem. Soc.* **1999**, *121*, 9550 – 9561; b) A. F. Littke, L. Schwarz, G. C. Fu, *J. Am. Chem. Soc.* **2002**, *124*, 6343 – 6348; c) A. F. Littke, G. C. Fu, *J. Am. Chem. Soc.* **2001**, *123*, 6989 – 7000; d) A. Furstner, A. Leitner, *Synlett* **2001**, 290 – 292.

Nitroglycerin Bioactivation

Bioactivation of Nitroglycerin—A New Piece in the Puzzle

*Bernd Mayer**

Keywords:
aldehyde dehydrogenase · nitrate metabolism · nitric oxide · vasodilation

Introduction

Nitroglycerin (glyceryl trinitrate, GTN), an explosive constituent of Alfred Nobel's dynamite, has been used since the second half of the 19th century for the treatment of angina pectoris, the primary symptom of ischemic heart disease, which is caused by an insufficient supply of oxygen to the myocardium (for a short history of GTN see reference [1]). Besides an apparent genetic predisposition, high blood pressure, diabetes mellitus, hyperlipidemia, lack of exercise, and smoking are major risk factors for the development of coronary atherosclerosis, a predominant cause of ischemic heart disease. GTN dilates most types of blood vessels including arterioles and veins. At low doses, venodilation, which causes a reduction of cardiac preload and oxygen consumption, prevails over arterial dilation. At higher doses arterial resistance and cardiac output are decreased as well, resulting in a drop of diastolic and systolic blood pressure, respectively.

The molecular basis of the cardiovascular effects of GTN and other organic nitrates (e.g. isosorbide mono- and dinitrates) has remained a mystery for a long period of time. In the mid 1970s Ferid Murad and co-workers discovered that vasodilation by organic nitrates requires enzymatic release of nitric oxide (NO), a free radical that triggers increased synthesis of the cellular messenger molecule cyclic GMP (cGMP) by the enzyme soluble guanylate cyclase (sGC) in vascular smooth muscle.[2] Then believed to be a pathway of vasodilation unique to the so-called nitrovasodilators (GTN and other NO-releasing drugs), activation of sGC by NO has later been recognized as an important endogenous signaling mechanism in a number of mammalian tissues, including blood vessels, platelets, and brain (for review see reference [3]). The discovery of "NO as a signaling molecule in the cardiovascular system" was awarded with the Nobel Prize for Physiology or Medicine in 1998.[4] The major pathways of NO/cGMP-mediated vascular relaxation are illustrated in Figure 1.

GTN Metabolism Catalyzed by Mitochondrial Aldehyde Dehydrogenase

The biological action of GTN requires enzymatic bioactivation of the nitrate in vascular smooth muscle, which presumably explains both the therapeutically desired venoselectivity of GTN as well as the unwanted loss of vasodilation upon long-term administration of the drug ("nitrate tolerance"). Despite this clinical relevance, the mechanism by which GTN becomes activated to stimulate sGC in vascular smooth muscle has remained elusive. In a recent study Chen et al.[5] report on the con-

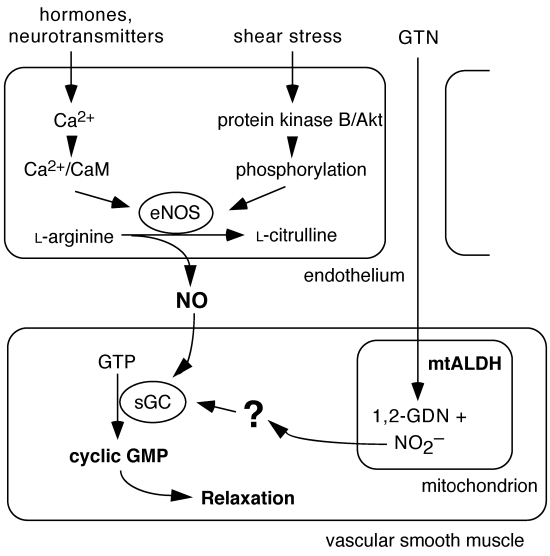


Figure 1. Schematic illustration of the major pathways involved in vascular relaxation by endothelium-derived NO and GTN. Circulating hormones and transmitters released from neurons that innervate blood vessels induce Ca^{2+}/calmodulin(CaM)-dependent activation of endothelial NO synthase (eNOS), an enzyme that converts the amino acid L-arginine to L-citrulline and NO. Fluid shear stress of the circulation activates the protein kinase B/Akt pathway, resulting in Ca^{2+}-independent stimulation of eNOS through serine phosphorylation. The latter pathway appears to modulate the basal NO release in the vasculature that is required to keep the organism in a state of continuous active vasodilation. Binding of endothelium-derived NO to the regulatory heme group of sGC in the adjacent smooth muscle layer leads to accumulation of cGMP, an intracellular messenger molecule that triggers vascular relaxation by decreasing the intracellular concentration of free Ca^{2+}. GTN provokes accumulation of cGMP in the vascular smooth muscle in an endothelium-independent manner. The study by Chen et al.[5] suggests metabolism to 1,2-GDN and nitrite by mtALDH as a crucial step of GTN bioactivation. The link between enzymatic nitrite formation and sGC activation is elusive yet but may involve conversion of nitrite to NO or another reactive intermediate.

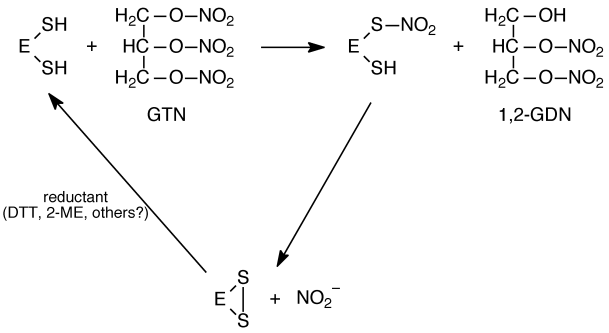
[*] Prof. Dr. B. Mayer
Institut für Pharmakologie und Toxikologie
Universitätsplatz 2, 8010 Graz (Austria)
Fax: (+43) 316-380-9890
E-mail: mayer@kfunigraz.ac.at

 © 2003 Wiley-VCH Verlag GmbH & Co. KGaA, Weinheim 1433-7851/03/4204-0388 $ 20.00+.50/0

version of GTN to 1,2-glyceryl dinitrate (1,2-GDN) and stoichiometric amounts of nitrite by mitochondrial aldehyde dehydrogenase (mtALDH), an enzyme which may be involved in detoxification of acetaldehyde leaking from acetyl-CoA synthesis by the nonoxidative activity of pyruvate dehydrogenase.

Following their observation that the murine macrophage RAW 264.7 cell line resembles vascular smooth muscle cells with respect to GTN metabolism, Chen et al. used an enormously large number of the macrophages (ca. 10^{10} cells corresponding to a wet weight of 50 g) as starting material for purification of the GTN-metabolizing enzyme and obtained 3.6 mg of a 53 kDa protein identified as mtALDH. The enzyme produced 1,2-GDN and nitrite with a specific activity of 30 nmol h^{-1} mg^{-1}. Similar results were obtained with mtALDH purified from bovine liver, indicating that GTN metabolism by mtALDH is not a function of tissue type or species. The bovine liver enzyme exhibited a specific activity of 3 nmol min^{-1} mg^{-1}, which was increased 10-fold by addition of NAD^+; the reaction followed classical Michaelis–Menten kinetics with a K_m of 12 μM and was inhibited by the natural mtALDH substrate acetaldehyde as well as the classical mtALDH inhibitor chloral hydrate with IC_{50} values of about 0.1 and 0.8 mM, respectively.

A number of early studies suggested that cellular thiols are essentially involved in GTN bioactivation, but the precise role of this thiol dependence has never been settled.[6] The study by Chen et al. may provide an explanation for those earlier observations, as it shows that GTN metabolism by mtALDH is dependent on the availability of a reductant. (The authors used the nonphysiological thiols dithiothreitol (DTT) and sulfanylethanol (2-ME), leaving the identity of the natural reductive cofactor unrevealed). Based on these results, Chen et al. proposed a model according to which mtALDH functions as GTN reductase in the presence of reductants. As illustrated in Scheme 1 (adapted from Scheme 1 in reference [5]), GTN reacts with one of two cysteine residues located in proximity to the active site of mtALDH to form a thionitrated intermediate (E–S–NO_2) and 1,2-GDN, followed by disulfide formation and release of nitrite. The oxidized enzyme is then reduced back to the native dithiol form by exogenous thiols or other reductants. This model predicts that the reaction of mtALDH with GTN would result in enzyme inactivation in the absence of the final reductive step. Intriguingly, such a mechanism-based inactivation of mtALDH has been reported previously for the interaction of the enzyme with classical inhibitors and NO-donor compounds (see citations in reference [5]).



Scheme 1. Metabolism of GTN by mtALDH according to Chen et al.[5] For details see text. The nonphysiological thiols DTT and 2-ME are suitable as reductant; however, reduction of the enzyme was not observed with the physiologically most abundant thiol GSH, suggesting that an as yet unknown reductant is required to support the GTN reductase activity of mtALDH in vivo.

Involvement of mtALDH in GTN-Induced Vascular Relaxation and Hypotension

Chen et al. used rings of isolated rabbit aorta to investigate the involvement of mtALDH in GTN-induced vascular relaxation and cyclic GMP accumulation. Having confirmed that the mtALDH inhibitors chloral hydrate, cyanamide, and acetaldehyde attenuated 1,2-GDN formation in blood vessels, the authors performed perfused organ bath experiments to test the effects of these agents on vascular relaxation induced by increasing concentrations of GTN. All three inhibitors led to the rightward shift of GTN concentration–response curves, suggesting that mtALDH contributes to GTN bioactivation in vascular smooth muscle. However, other mechanisms appear also relevant, because inhibitor-treated blood vessels showed complete relaxation at higher concentrations of GTN. To further test the physiological role of mtALDH in GTN bioactivation, Chen et al. assessed the effects of cyanamide and chloral hydrate in anesthetized rabbits. Infusions of increasing concentrations of GTN led to a progressive drop in mean arterial blood pressure, and this hypotensive effect of GTN was significantly diminished, albeit not abolished, when the animals were infused with the mtALDH inhibitors 20 min before application of GTN. In control experiments, Chen et al. showed that cyanamide had no effect on hypotension caused by sodium nitroprusside which stimulates vascular sGC directly, that is, without requirement for enzymatic activation. Similar results were obtained in rats, suggesting that mtALDH-catalyzed bioactivation resulting in vascular relaxation is a general mechanism of mammalian GTN metabolism. As illustrated in Figure 1, this pathway may lead to formation of an endogenous activator of sGC (presumably NO or a related species) mediating the beneficial cardiovascular effects of GTN.

Does GTN Bioactivation by mtALDH Explain GTN Tolerance?

The essential role of a thiol or another reductant to prevent inactivation of mtALDH by GTN may provide an interesting explanation for nitrate tolerance, that is, the loss of vasodilation that occurs upon long-term administration of GTN or other organic nitrates. The results of Chen et al. demonstrate that 30 min exposure of blood vessels to a relatively high GTN concentration of 0.3 mM resulted in impaired vascular relaxation (evident as rightward shift of the GTN concentration–response curve), abolished GTN-induced cGMP accumulation, and decreased formation of 1,2-GDN. (The observation of vascular relaxation in the absence of a detect-

 © 2003 Wiley-VCH Verlag GmbH & Co. KGaA, Weinheim 1433-7851/03/4204-0389 $ 20.00+.50/0

able increase in cGMP accumulation confirms previous data on a cGMP-independent component of GTN action[7]). Based on these results, the authors propose that GTN inhibits its own bioactivation by depleting the reductant that is essential for reactivation of mtALDH. This model revives early suggestions invoking GTN-triggered depletion of cellular thiols[6] and/or impaired bioactivation[8] to explain nitrate tolerance.

Thiol depletion of vascular smooth muscle cells as a possible cause of nitrate tolerance is still controversial.[9] The study by Chen et al. may resolve this controversy, as it invokes the essential role of an unknown reductant different from GSH or cysteine, whereas previous studies have focused on these most abundant physiological thiols. However, the widely held view of impaired bioactivation of GTN as a primary cause of nitrate tolerance has also been challenged.[10] The apparent conflict between the clinically important phenomenon of nitrate tolerance in patients and the impaired response to GTN of isolated blood vessels exposed to relatively high, presumably unphysiological concentrations of GTN has led to the suggestion that counter-regulatory forces, for example, elevated plasma catecholamines or increased activity of the renin system, become activated in GTN-treated patients.[11] Reflectory activation of the renin system (in response to decreased mean arterial blood pressure and cardiac output) results in increased plasma levels of angiotensin-II, which may activate vascular NADPH oxidase and thereby trigger the generation of superoxide radicals that efficiently scavenge free NO to yield the potent cytotoxin peroxynitrite ($ONOO^-$). Notably, in animal experiments nitrate tolerance was reported to be largely prevented by administration of selective angiotensin-II receptor antagonists or the antioxidant vitamin C (for review see reference [12]). However, activation of the renin system is a general response of the organism to vasodilation, suggesting that this process may not fully account for the unique characteristics of GTN tolerance.

Long-term treatment with GTN appears to be associated with endothelial dysfunction, apparent as increased superoxide generation, decreased NO bioavailability, and reduced response of blood vessels to endothelium-dependent vasodilators.[13–16] Superoxide production by uncoupled endothelial NO synthase was suggested as a potential cause of this phenomenon.[14] The findings of Chen et al.[5] do not explain how GTN could affect endothelial NO biosynthesis. However, if NO is indeed released from GTN in mitochondria, sustained nitrate metabolism could lead to NO-mediated inhibition of cytochrome c oxidase and increased superoxide production through uncoupling of the respiratory chain in vascular smooth muscle.[17] At present, it appears likely that in vivo tolerance to GTN is caused by multiple factors; a definitive judgment on the potential contribution of mtALDH awaits further insights into the mechanism of GTN-induced inactivation of mtALDH and the development of new strategies to interfere with this process in vivo.

Perspectives

The study by Chen et al. provides important new insights into the mechanism of GTN bioactivation but also raises a number of interesting questions for future research. The most puzzling issue is the link between GTN metabolism and sGC activation. Inhibition of cyclic GMP accumulation by three different inhibitors suggests that mtALDH is essential to activation of sGC in smooth muscle. According to the model of Chen et al (Scheme 1), nitrite is the initial product of mtALDH-catalyzed GTN metabolism, but at the expected low concentrations nitrite doesn't cause significant cGMP accumulation. In search of a process linking nitrite formation to sGC activation, the authors propose that nitrite may be converted to NO either enzymatically by components of the respiratory chain or nonenzymatically by low pH in the mitochondrial intermembrane space. However, the experimental evidence supporting these possibilities is weak. To address this issue, it appears essential to show release of NO from GTN by isolated mitochondria. Alternatively, an NO-independent mechanism of sGC activation could be involved. Intriguingly, sGC contains an NO-independent regulatory site,[18] which might be involved in the (presumably artificial) activation of sGC exposed to high concentrations of GTN in the presence of cysteine.[19]

As mentioned in the Introduction, GTN preferentially dilates veins as compared to arterial resistance vessels. This therapeutically desired venoselectivity could be reconciled with the essential role of mtALDH in GTN metabolism if this protein were enriched in veins. Alternatively, the venoselectivity of GTN could be a consequence of differences in the rates of endogenous NO formation in arteries and veins. Since NO inhibits vascular GTN bioactivation and veins produce significantly less NO than arteries, Kojda et al.[20] suggested that GTN bioactivation is inhibited in arteries but not in veins. The study by Chen et al. would be in line with this model if endogenous NO production led to inactivation of mtALDH, as reported for NO donors (see citations in reference [5]).

Further studies are required to settle the role of mtALDH in GTN bioactivation and tolerance in vivo. Hitherto, pharmacologists have not paid much attention to mtALDH, but the report by Chen et al. is expected to provoke the development of novel tools needed to further explore the biological and clinical relevance of this pathway. A large piece has been added to the puzzle of GTN bioactivation, raising hope that it won't take another 130 years to complete it.

[1] N. Marsh, A. Marsh, *Clin. Exp. Pharmacol. Physiol.* **2000**, *27*, 313–319.

[2] S. Katsuki, W. P. Arnold, C. K. Mittal, F. Murad, *J. Cyclic Nucleotide Res.* **1977**, *3*, 23–35.

[3] B. Mayer, B. Hemmens, *Trends Biochem. Sci.* **1997**, *22*, 477–481.

[4] W. W. Gibbs, S. Nemecek, G. Stix, *Sci. Am.* **1999**, *280*(1), 16–19; see also the Nobel Lectures from F. Murad, R. F. Furchgott, and L. J. Ignarro: *Angew. Chem.* **1999**, *111*, 1976–2013; *Angew. Chem. Int. Ed.* **1999**, *38*, 1856–1892.

[5] Z. Q. Chen, J. Zhang, J. S. Stamler, *Proc. Natl. Acad. Sci. USA* **2002**, *99*, 8306–8311.

[6] P. Needleman, *Annu. Rev. Pharmacol. Toxicol.* **1976**, *16*, 81 – 93.
[7] F. Brunner, K. Schmidt, E. B. Nielsen, B. Mayer, *J. Pharmacol. Exp. Ther.* **1996**, 277, 48 – 53.
[8] S. Forster, I. Woditsch, H. Schröder, K. Schrör, *J. Cardiovasc. Pharmacol.* **1991**, *17*, 867 – 872.
[9] S. Boesgaard, J. Aldershvile, H. E. Poulsen, S. Loft, M. E. Anderson, A. Meister, *Circ. Res.* **1994**, *74*, 115 – 120.
[10] J. B. Laursen, A. Mülsch, S. Boesgaard, P. Mordvintcev, S. Trautner, N. Gruhn, J. E. Nielsen-Kudsk, R. Busse, J. Aldershvile, *Circulation* **1996**, *94*, 2241 – 2247.
[11] J. O. Parker, J. D. Parker, *Am. J. Cardiol.* **1992**, *70*, 93B – 97B.
[12] T. Münzel, S. Kurz, T. Heitzer, D. G. Harrison, *Am. J. Cardiol.* **1996**, *77*, 24C – 30C.
[13] P. R. Caramori, A. G. Adelman, E. R. Azevedo, G. E. Newton, A. B. Parker, J. D. Parker, *J. Am. Coll. Cardiol.* **1998**, *32*, 1969 – 1974.
[14] T. Münzel, H. Li, H. Mollnau, U. Hink, E. Matheis, M. Hartmann, M. Oelze, M. Skatchkov, A. Warnholtz, L. Duncker, T. Meinertz, U. Förstermann, *Circ. Res.* **2000**, *86*, E7-E12.
[15] T. Gori, J. M. Burstein, S. Ahmed, S. E. S. Miner, A. AlHesayen, S. Kelly, J. D. Parker, *Circulation* **2001**, *104*, 1119 – 1123.
[16] T. Gori, S. S. Mak, S. Kelly, J. D. Parker, *J. Am. Coll. Cardiol.* **2001**, *38*, 1096 – 1101.
[17] G. C. Brown, *Biochim. Biophys. Acta* **2001**, *1504*, 46 – 57.
[18] J. P. Stasch, E. M. Becker, C. Alonso-Alija, H. Apeler, K. Dembowsky, A. Feurer, R. Gerzer, T. Minuth, E. Perzborn, U. Pleiß, H. Schröder, W. Schroeder, E. Stahl, W. Steinke, A. Straub, M. Schramm, *Nature* **2001**, *410*, 212 – 215.
[19] J. D. Artz, V. Toader, S. I. Zavorin, B. M. Bennett, G. R. J. Thatcher, *Biochemistry* **2001**, *40*, 9256 – 9264.
[20] G. Kojda, M. Patzner, A. Hacker, E. Noack, *Mol. Pharmacol.* **1998**, *53*, 547 – 554.

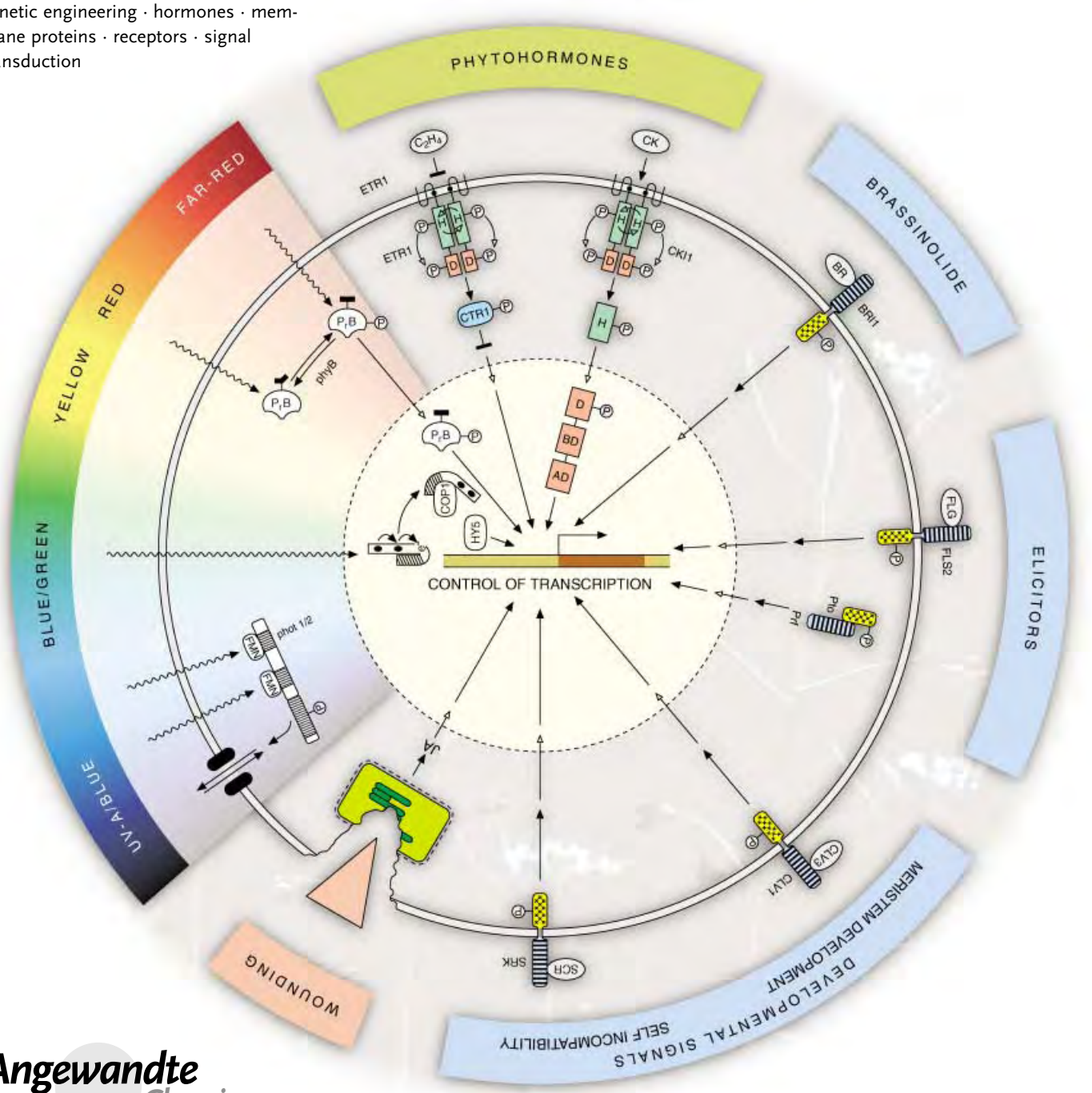
Plant Biochemistry

Sensory Principles of Higher Plants

*Elmar W. Weiler**

Dedicated to Professor Meinhart H. Zenk on the occasion of his 70th birthday

Keywords:
genetic engineering · hormones · membrane proteins · receptors · signal transduction



© 2003 Wiley-VCH Verlag GmbH & Co. KGaA, Weinheim
1433-7851/03/4204-0392 $ 20.00+.50/0

Plants respond to a broad variety of stimuli from the interior of their body and from the outside environment. A revolution in our knowledge of the sensory capabilities of plants took place during the last decade, thanks to the consequent application of the tools of molecular genetics and the focusing of most work, in a worldwide effort, on a single, representative, higher plant: Arabidopsis thaliana. This review concentrates on the complete sensory periphery of higher plants, with focus placed on the principles rather than the details, and such systems that have been functionally identified unambiguously. Higher plants are no less fascinating, no less complex, and no less sensitive than animals, even man, with respect to their sensory capabilities. Plants constantly monitor their environment and their interior situation by using a stunning array of sensory systems, that are mostly different from those of animals or man.

From the Contents

1. Introduction 393

2. Sensing and Processing Endogenous Signals 394

3. Sensing the Abiotic Environment 398

4. LRR Receptor Kinases in Pathogen Defense and Development 405

5. Cyclo-Oxylipins: Signaling Molecules from Plant Membranes 406

6. Modulating the Sensory Mechanisms of Higher Plants: Prospects for Improving Crops and Crop Protection 409

1. Introduction

The evolution of multicellular organisms from simple, unicellular ancestors has led to the perfection of two remarkably different types of body plans: on one side, to the motile animals (and to man), and on the other side, to the sessile plants. In order to master its life, a higher animal such as a vertebrate, is equipped with a variety of sensory organs, geared to pick up information from the body interior or—even more so—from its environment, and a brain of stunning complexity, designed to integrate all these incoming signals and to construct from them a representation of the outside world and a picture of the individual in it, thus allowing for its orientation and appropriate behavior.

However, plants are rooted in the soil and, to us, appear passive: aren't they simply chemical factories designed to convert CO_2 and some further inorganic compounds with the energy of light into carbohydrates and other organic molecules, the foodstuff needed by the animals?

Yet, no notion could be more misleading! Just because plants are sessile, they are exposed to much more variation in environmental conditions—including often extreme situations—compared to an animal: plants simply cannot move out of harsh or perilous situations and seek more favorable ones. In order to thrive or even survive, a plant probably has to acquire as much information from its environment as does an animal. Indeed, with the exception of sound, plants are able to perceive any other environmental signal a human being can (Figure 1). The sensory periphery by which a plant does so, the molecular structures involved, and the reactions triggered, however, have long remained unknown, and many still are. But the last couple of years have seen a dramatic gain in knowledge about molecular features of many sensory processes in higher plants. The picture which emerges reveals two things: the sensory processes of plants are highly distinct from those of animals, and the sensory periphery of a plant is no less complex, versatile, and sensitive than that of an animal. It allows the plant to adjust its growth and differentiation patterns and to orient its organs relative to subtle endogenous or environmental changes; it enables the plant to recognize and then to fight a huge number of potential pathogens and herbivores. In a rudimentary way, plants may even exchange signals between one another, and they certainly communicate—through chemical interactions—with other organisms during the establishment of associative or symbiotic relationships, just as they will send chemical alarm when attacked.

It is the purpose of this article to introduce the world of sensory processes in higher plants, with focus placed more on the principles than on the details. Understanding how plants sense (and react to) internal and external factors, both abiotic as well as biotic stimuli, will undoubtedly have profound consequences for all those dealing with plants from an applied perspective: the plant breeder, the farmer, and also the plant protection chemist.

Appropriate stimulus	Human sense	Plant response
light	sight	✓
volatile chemicals	smell	✓
nonvolatile chemicals	taste	✓
mechanical force	touch	✓
mass acceleration	balance	✓
sound	hearing	–

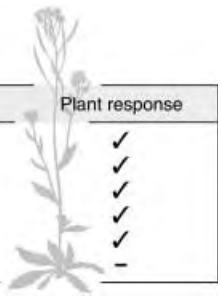


Figure 1. Comparison of human senses and their appropriate stimuli with the sensory abilities of a higher plant.

[*] Prof. Dr. E. W. Weiler
Lehrstuhl für Pflanzenphysiologie
Fakultät für Biologie
Ruhr-Universität
44780 Bochum (Germany)
Fax: (+ 49) 234-322-4291
E-mail: elmar.weiler@ruhr-uni-bochum.de

 © 2003 Wiley-VCH Verlag GmbH & Co. KGaA, Weinheim 1433-7851/03/4204-0393 $ 20.00+.50/0

2. Sensing and Processing Endogenous Signals

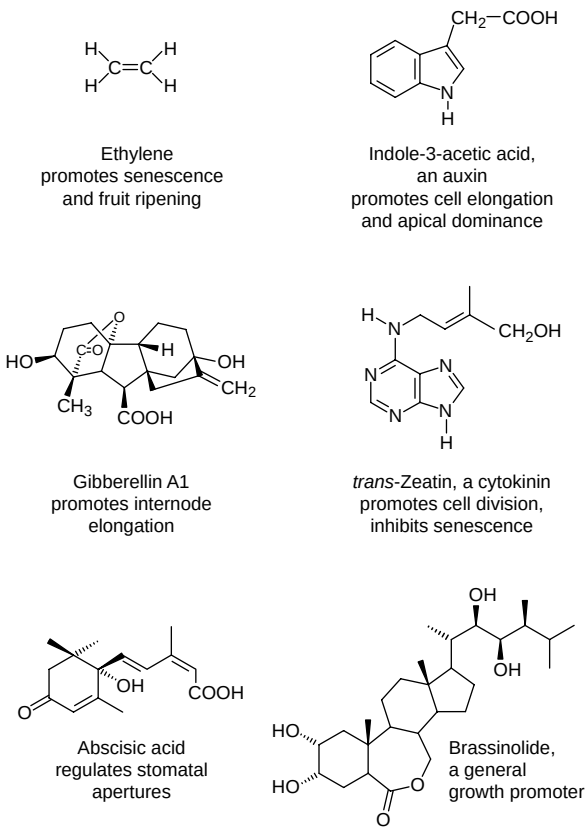
Intraorganismic communication in higher plants is largely—and in many cases exclusively—chemical, and serves to coordinate not only development, but also the orientation of organs, the mass flows of water, nutrients, and assimilates within the organism, as well as metabolism and molecular exchange at the plant surface.

Some of the signaling molecules involved are shown in Scheme 1; they belong to the group of endogenous plant growth regulators also termed phytohormones. These, like the auxins, may act over distances of only a few cells, for example, in meristems or developing embryos, but some may be translocated with the xylem or phloem flow and travel over long distances throughout a plant to correlate organ functions. For example, abscisic acid (ABA) is produced in a root system under conditions of water stress and translocated with the transpiration stream to the leaves where it reaches the epidermal guard cells and causes their osmotic potential (and, as a consequence, their cell volume) to decrease, which leads to closure of the stomatal pores and a sharp reduction in transpiration. The latter is an example of a phytohormone acting like a hormonal messenger in an animal; others also exist. However, more typically, phytohormones control growth and differentiation, that is, the process of development itself, rather than regulating metabolic functions of a developed organism—as typical animal hormones would. This observation suggests that we might envisage clear distinctions between the modes and mechanisms of action of phytohormones and animal hormones, a fact already indicated by the lack of structural similarity between animal and plant hormones.

Breakthroughs in the elucidation of how phytohormones act have only been obtained in recent years, largely because of the use of mutants and the progress in genome analysis of the master model of plant developmental biology, *Arabidopsis thaliana* (L.) Heynh. (Thal's Cress, a member of the family Brassicaceae, Figure 2). Its three genomes (the nucleome, plastome, and chondrome) have been sequenced completely,[1] and the nucleotide sequences of its approximately 25500 assigned genes are publicly accessible, as are large collections of mutants, genes, cDNAs, ESTs (expressed sequence tags), and other tools (TAIR, The Arabidopsis Information Resource: http://www.arabidopsis.org/).



Elmar W. Weiler was born in 1949. He studied Biology and Chemistry, and received his doctoral degree with Professor M. H. Zenk in 1977 from the Ruhr-University, Bochum, and habilitated in Botany in 1982. Since 1985 he has been head of the institute of Plant Physiology at the University Osnabrück, and since 1988 head of the institute of Plant Physiology at the Ruhr-University. He received the Gottfried-Wilhelm-Leibniz Award of the Deutsche Forschungsgemeinschaft in 1995. After several years of work in the field of natural plant products and immunological analysis of plant metabolites, his current research interests focus on plant developmental biology, membrane functions, and phytohormone biosynthesis.



Scheme 1. Typical examples of phytohormones of higher plants and of physiological processes controlled by these compounds. The list of physiological roles of phytohormones as given is by no means complete.

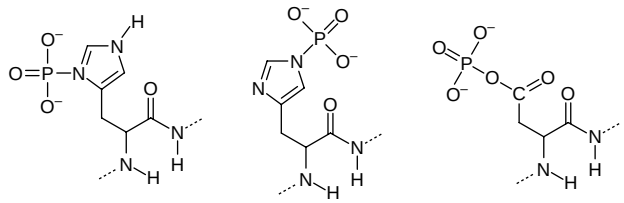
From the above, it follows that many, and perhaps most, of the actions of phytohormones involve controlling the activities of particular sets of hormone-responsive genes, and it is in this area that most of the progress has been made, thus opening the door for rational approaches to plant-growth control.

2.1. Phosphorelay Regulators in Phytohormone Perception and Signal Processing

The primary molecular targets of phytohormone action have resisted their identification by classical biochemical procedures. The way to their unveiling was paved when hormone-insensitive mutants, mainly of *Arabidopsis thaliana,* became available,[2] and techniques of positional cloning were sufficiently developed to allow the mutated gene(s) to be actually isolated. Still, unambiguous identification of the receptors as well as further components of the signaling pathway has been achieved for only two of the hormone classes to date—ethylene, the senescence promoter, and cytokinins, which are cell-cycle activators and senescence retarders.

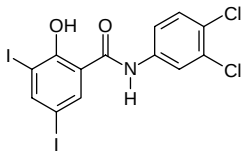


Figure 2. Habitus of eight-weeks-old flowering *Arabidopsis thaliana* (Thal's Cress), the only higher plant whose genome has been sequenced completely and made available publicly. The nuclear genome comprises 125 Mbp of DNA distributed over five chromosomes (1 n) and contains approximately 25 500 genes, only 10% of which have an unambiguously assigned function, while another 50% can be categorized according to known genes from other organisms. For the remaining 40% of all genes, the nucleotide sequences do not give any clues to potential functions of the encoded gene products.

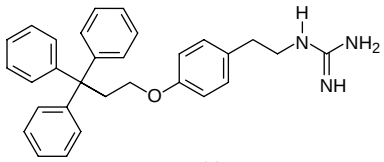


1-Phosphohistidine 3-Phosphohistidine Phosphoaspartate

Scheme 2. Phosphoamino acids involved in phosphorelay signal transduction pathways. Only segments of polypeptide chains are shown for clarity. In most cases, it is not known which phosphohistidine isomer is produced in a particular histidine kinase reaction.



Dichlorodiiodsalicylanilide



RWJ-49815

Scheme 3. Examples of histidine kinase inhibitors (reviewed in [3a]).

The results were surprising, as they revealed that the two sets of receptors for ethylene and cytokinins were homologous to bacterial histidine kinase phosphorelay systems, also known as two-component regulators, because the simplest ("classical") type comprises only two proteins, a sensor protein with histidine kinase activity (the receptor, typically a dimeric, transmembrane protein, although there are exceptions, see Section 3.1.1) and a response regulator to which the phosphate group is transferred from the phosphohistidine of the sensor protein.[3] The response regulator becomes phosphorylated at a specific aspartyl moiety and typically, in its phosphorylated form, is an active transcription regulator which directly interacts with DNA-promoter elements to alter the transcriptional activity of the respective genes. In most cases it is unknown which of the two isomeric histidine phosphates, 1-phosphohistidine or 3-phosphohistidine, is formed by the histidine kinase activity of the sensor protein. In the case of the histidine kinase CheA involved in bacterial chemotaxis, the thermodynamically more stable 3-phosphohistidine is formed (Scheme 2), as shown by ^{31}P NMR spectroscopic measurements.[4] Only a few inhibitors of histidine kinases have been described.[3a] These belong to two classes: salicylanilides, such as dichlorodiiodosalicylanilide, and hydrophobic tyramines, such as RWJ-49815. These inhibitors show IC_{50} values in the low micromolar range (Scheme 3).[3a]

Phosphorelay regulators are modular in their architecture and are now known to be widespread in prokaryotes (*Escherichia coli* possesses 30 sensor histidine kinase genes and 32 genes encoding response regulators of which 25 are transcription factors[3a,d]), fungi, and plants,[3g] but they have not been found in the completely sequenced genomes of *Drosophila melanogaster, Caenorhabditis elegans,* and man, and thus they appear to be absent in animals.[3d]

Several types of phosphorelay systems can be discriminated (Figure 3), which differ from the "classical" two-component regulators either by the involvement of hybrid-type sensor histidine kinases containing a response regulator domain (and sometimes a second phosphohistidine domain) or by the involvement of additional, intermediate phosphorelay proteins between the sensor kinase and the response regulator. It is evident that phosphorelay systems involving more modules allow for a much finer tuning of regulatory inputs, for more different inputs, and thus for a better integration into other regulatory pathways in the cell.

With two exceptions (the ethylene receptors ERS1 and ERS2), the eukaryotic phosphorelay systems so far known (Figure 4) comprise hybrid sensor kinases with a fused

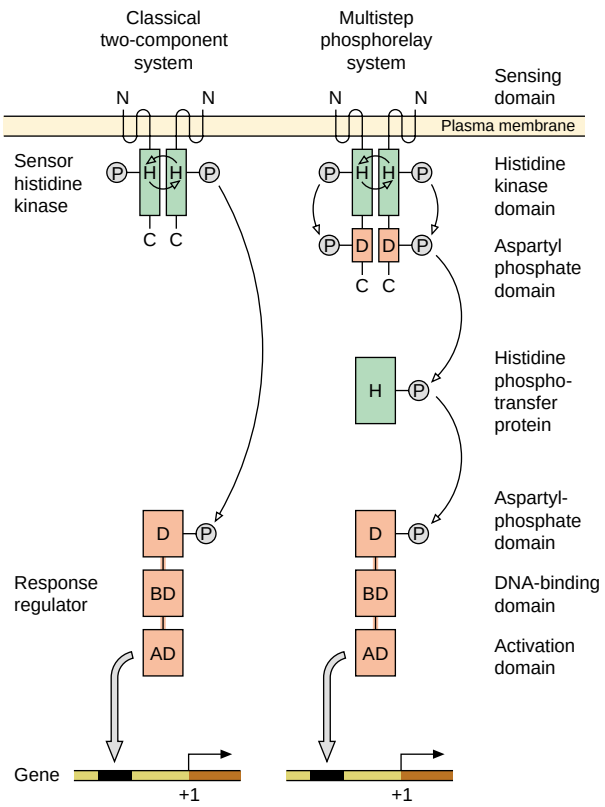


Figure 3. Types of two-component regulators. "Classical" two-component systems consist of a sensor histidine kinase (most often membrane-bound with two or more transmembrane segments) and a cytoplasmatic response regulator which receives its phosphate group from the phosphohistidine of the sensor histidine kinase at a conserved aspartyl moiety. Most—but not all—of the response regulators are transcription factors. Multistep phosphorelay systems typically consist of a hybrid histidine kinase with a fused response regulator domain and an intermittant histidine phosphotransfer protein acting between the sensor kinase and the final response regulator. Curved open arrows indicate phosphotransfer. The sensor kinases are homodimers which autophosphorylate the histidine of the respective opposite monomer using ATP. The multistep systems allow for more flexible regulation and networking. For example, several sensor kinases might act on the same phosphotransfer protein, or one phosphotransfer protein may act on more than one response regulator. An example of a "classical" two-component system is the EnvZ→OmpR system of *E. coli* involved in osmoregulation. Abbreviations: H: histidine, D: aspartate, P: phosphate, BD: DNA-binding domain, AD: activation domain, + 1: nucleotide one marking the start of transcription of a gene.

response regulator domain, which is rare in prokaryotes. Phylogenetic analysis reveals all of these hybrid sensor kinases to be most related to a single, clustered group of bacterial hybrid sensor kinases represented by ArcB, BarA, and ResC.[3f] Thus, it seems that all eukaryotic sensor histidine kinases evolved from a single prokaryotic ancestor, perhaps from the cyanobacterial endosymbiont that gave rise to the plastid organelles. Also, the presence of structurally similar phosphorelay systems in the sensory periphery of both fungi and plants and their complete absence in animals suggests that they had evolved before the separation of the fungal and the plant branch on the tree of life.[3b]

Three examples of eukaryotic phosphorelay signaling are shown in Figure 4, the two phytohormone signal pathways so far known and the yeast osmoregulatory signal pathway are aligned to make clear the similarities and differences in these pathways. All sensor histidine kinases in these pathways are membrane bound with either two or three N-terminal transmembrane domains. In all three cases the receptors are present as dimers in the membrane, a situation common to membrane-bound sensor kinases of phosphorelay systems. In the case of both cytokinins and ethylene, a family of receptors picks up the input signal.

Five ethylene receptors have been identified in *Arabidopsis thaliana* (the hybrid sensor kinases ETR1, ETR2, and EIN4, as well as ERS1 and ERS2, with the latter two lacking a fused response regulator domain).[5] Ethylene binds in the region of the transmembrane domain.[6] Cu^+ ions coordinated by histidine and cysteine ligands participate in ethylene binding (one per monomer),[7] but the precise nature of the interaction of the olefin with the metal is still a matter of speculation.[3a] The ethylene receptors interact with the CTR1 kinase, which is a negative regulator of the downstream signal pathway, as evident from the fact that mutations leading to a loss of CTR1 function show a constitutive ethylene response in the absence of ethylene. Most evidence favors a hypothesis in which, in the absence of ethylene, the ethylene receptors interact with the CTR1 kinase, thus keeping it active and repressing the downstream steps. According to this model,[8] binding of ethylene would disrupt the receptor–CTR1 interaction and derepress the pathway downstream of CTR1.

CTR1 is a Raf-kinase homologue, and is thus a member of the MAP kinase cascade equivalent to MAPKKK. This feature resembles the part of the yeast osmoregulatory pathway downstream of the response regulator SSK1 in which all members have been identified and form a typical MAP-kinase cascade (SSK2/22→PBS2→HOG1).[3b] However, no further members of such a cascade other than CTR1 have been detected so far in the ethylene response pathway.

Ethylene-dependent derepression of the downstream signaling pathway requires the activity of the transmembrane EIN2 protein. The precise function of the EIN2 is unknown, but its N-terminal domain shares homology with fungal and animal divalent cation transporters of the Nramp family, while the C-terminal domain is unique to EIN2. The protein could be a metal sensor. How it acts after being released from repression by CTR1 is unclear. Its activity, however, causes activation of a group of nuclear, dimeric transcription factors, such as EIN3, EIL1, and EIL2. These activate the transcription of the gene encoding the ethylene response factor ERF1, as well as other genes encoding transcriptional regulators. These, in turn, bind to their target sequences (ethylene-response elements) in a varity of ethylene-responsive promoters, which activates the transcription of an array of indirectly ethylene-regulated target genes.

Phosphorelay signaling of cytokinin receptors[9] is even more reminiscent of bacterial phosphorelay pathways than the ethylene signaling pathway, in which, as in the yeast osmoregulatory pathway, novel elements have been recruited during evolution and placed between the response regulator and the promoters of the regulated genes (Figure 4). Cyto-

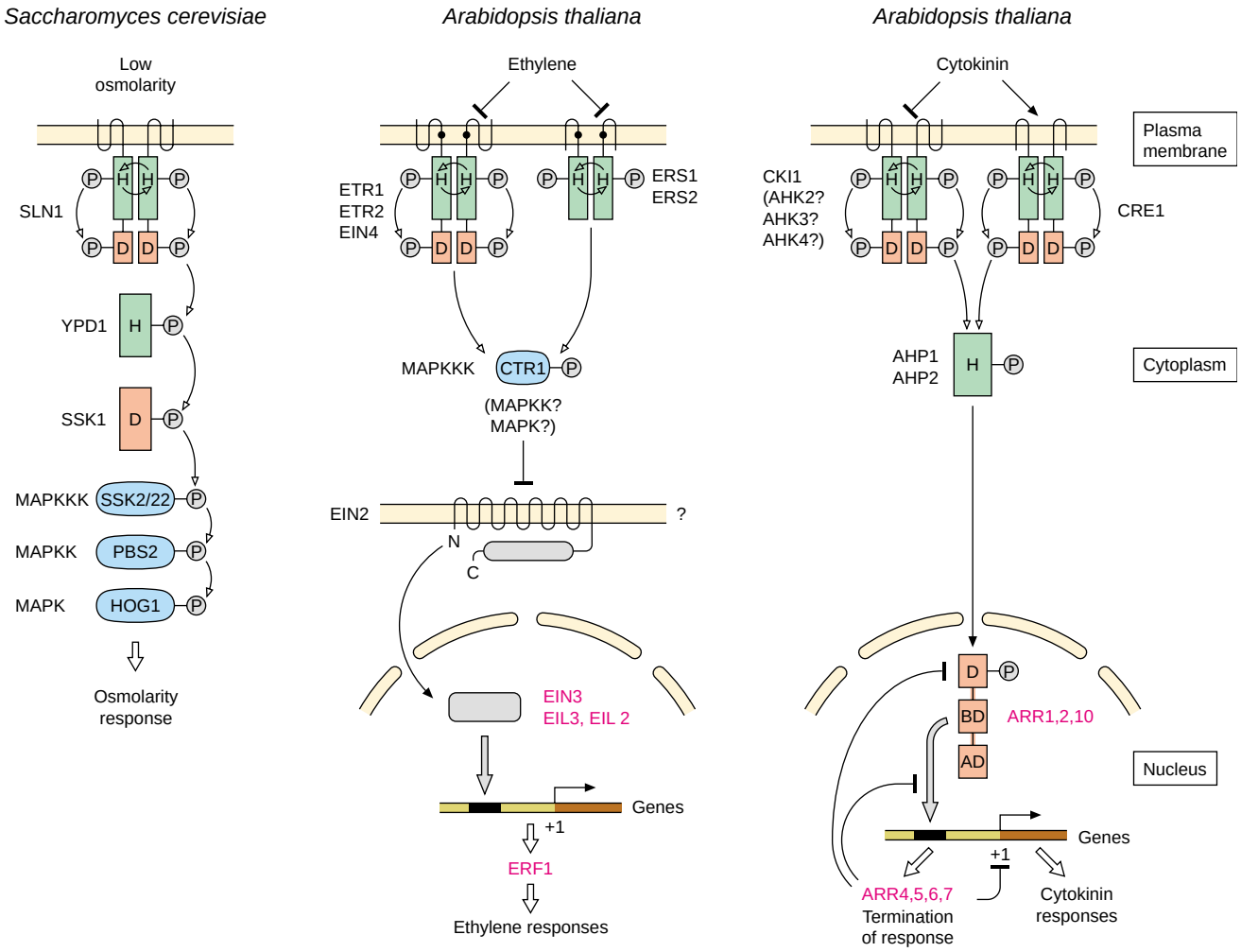


Figure 4. Comparison of the ethylene and cytokinin signaling pathways with the yeast osmoregulatory pathway.[3b,c,7,8] Phosphorelays are shown in red and green, components of MAP kinase pathways in blue. The acronyms of transcription factors are written in magenta. Curved arrows with open arrowheads denote phosphotransfers, gray arrows denote DNA binding, T arrows (⊥) symbolize inhibition or repression. MAPK: mitogen-activated protein kinase, MAPKK: MAPK kinase, MAPKKK: MAPKK kinase, H: histidine, D: aspartate, P: phosphate. AHP: *Arabidopsis* histidine phosphotransfer protein, ARR: *Arabidopsis* response regulator, ETR: ethylene resistant, EIN: ethylene insensitive, ERF: ethylene response factor, CKI: cytokinin insensitive, CRE: cytokinin resistant; other acronyms are explained in the cited literature. The black dots in the ethylene receptors represent Cu^{+} ions.

kinin signaling involves at least two transmembrane hybrid sensor histidine kinases (CKI1[10] and CRE1,[11] with further candidates being AHK2, AHK3, and AHK4[12]). CKI1 is probably active in the absence of cytokinin and inactivated by cytokinin while CRE1 appears to be activated upon cytokinin binding. The signal is transferred, through the histidine kinase domains, to the fused response regulator domains where the characteristic aspartyl phosphate is formed. From here, the phosphate group is transferred to the histidine–phosphorelay proteins AHP1 and AHP2. These, when phosphorylated, migrate into the nucleus and interact with several constitutively present response regulators (ARR1, ARR10, and particularly ARR2). Interaction of AHP with ARR causes the ARR proteins to become active, presumably by removal of a repressor protein whose identity is not yet known. Active (phosphorylated) ARR proteins bind to target sequences in multiple cytokinin-responsive genes involved in the control of transcription, the cell cycle, shoot formation, and the delay of senescence. Phosphorylated ARR proteins additionally activate a second cascade of genes encoding further response regulators (ARR4, 5, 6, 7). This latter group of transcriptional regulators acts to terminate the cytokinin response at multiple regulatory sites. Thus, as in the prokaryotic systems, the cytokinin signaling pathway contains only a short regulatory circuit composed entirely of phosphorelay components homologous to bacterial counterparts.

Next to nothing is known on how the other plant hormones, for example, auxins, gibberellins, abscisic acid, or the jasmonates, are perceived. The fact that the genome of *Arabidopsis thaliana* has revealed over 40 genes encoding sensor histidine kinases, phosphorelay proteins, and response regulators,[1,3g] leaves much room for further discoveries. Yet, in addition to phosphorelays, a second large family of chemosensors of completely different structure and function was discovered in plants a few years ago, and these are currently being analyzed intensively for their multiple roles in

pathogen recognition, brassinosteroid action, and other developmental processes. These receptor-like kinases with leucine-rich repeat domains will be discussed in Section 4.

3. Sensing the Abiotic Environment

The physical and chemical factors in a plant's environment may fluctuate rapidly and unpredictably, and adjustment to them may require immediate action. Examples for such processes are shading by the canopy, mechanical stresses caused by wind forces, or growth reactions in response to dislocation of the growth axis from its normal position. Additionally, seasonal fluctuations of climatic conditions occur in most regions of the world in a more systematic way, and unfavorable phases, such as periods of drought or cold winters, require an adjustment of the developmental program, such as the timing of flowering or fruit set, leaf abscission, or the filling of vegetative storage tissues with assimilate reserves. The physicochemical signals eliciting plant adaptations include light, temperature, humidity, even nutrient supply, as well as mechanical forces and mass acceleration in the earth's gravitational field. In many cases, the sensory mechanisms are not well understood at present, the notable exception being light-sensing. Work in this field has revealed an extraordinary complexity, and it is now clear that a higher plant operates a greater number of photoreceptors than man.

3.1. Plant Photoreceptors and Their Evolution

Three classes of photoreceptors, the phytochromes, the cryptochromes, and the phototropins, have been identified in higher plants by physiological, biochemical, photochemical as well as genetical means. The typical retinylidene photoreceptors[13] of animals and man (for example, rhodopsin) do not occur in plants, except for some lower flagellate algae, where sensorrhodopsins function as phototaxis receptors.[13,14] The evolutionary origin of this latter class of photoreceptors lies in the ancestors of the archaea, and members comprise the light-driven ion pumps bacteriorhodopsin and halorhodopsin as well as the phototaxis receptors sensorrhodopsin and phoborhodopsin of the extant archaeal halobacteria.[13,15] Since *Arabidopsis thaliana* is the best-studied species, the following discussion of molecular properties of higher plant photoreceptors and the photoreceptor classification will be based on this species. It should, however, be noted that the physiology of light-perception has a long tradition in the plant sciences and many different plants have been studied by physiologists in great detail.

Phytochromes are red-light-absorbing, cryptochromes are blue-light- and UV-A-absorbing chromoproteins, and phototropins are blue-light-absorbing chromoproteins. They act either alone or in cooperation to induce a large number of physiological processes (Table 1). Five phytochromes (phyA, B, C, D, E), two cryptochromes (cry1, 2), and two phototropins (phot 1, 2) have been identified in *A. thaliana*. Within each class, the chromophores are identical, while the apoproteins are somewhat different, though clearly homologous. Although the number of photoreceptor isoforms within each class may differ somewhat between species, current knowledge suggests the situation found in *A. thaliana* to be typical for angiosperms. Although much functional redundancy has been found among the photoreceptor isoforms within each group, it has nevertheless become evident that each of the photoreceptors also plays some particular role in triggering specific plant responses after being activated by the absorption of light energy. A further characteristic of plant photosensors is the considerable degree of cooperation among different classes of photoreceptors (Table 1).

Table 1: General and physiological characteristics of light-dependent processes in higher plants and of the photoreceptors involved. The terminology of individual photoreceptors is that for *Arabidopsis thaliana*. The list is by no means complete and, for clarity, the complex interactions between different photoreceptors are listed in a simplified manner. Dominant interaction partners are italicized.

Photoreceptor(s)	Chromophore(s)	Examples of physiological response(s) triggered	Cooperation with
phytochromes:			
class I (phyA)	phytochromobilin	● photomorphogenesis of the etiolated seedling	*cry1*, cry2
		● circadian clock control in low light	cry1
class II (*phyB*,C,D,E)	phytochromobilin	● photomorphogenic processes in the light	
		● light-induction of seed germination	
		● photoperiodic processes (e.g., induction of flowering)	*cry2*, cry1
		● shade-avoidance response and neighbor sensing	
		● photomodulations (e.g., leaf movements)	
cryptochromes:			
cry1 (high-light-intensity receptor)	pterin, FAD	● circadian clock control	phyA (in low light)
		● photomorphogenesis of the etiolated seedling	*phyA*, cry2
cry2 (low-light-intensity receptor)	pterin, FAD	● photoperiodic processes	*phyB*, cry1
phototropins:			
phot 1 (low-light-intensity receptor)	FMN	● phototropism in low light	
		● chloroplast movement in low light	
		● blue-light-dependent stomatal opening	
phot 2 (high-light-intensity receptor)	FMN	● as phot 1, but mediates high-light-intensity responses	

3.1.1. Phytochromes

Phytochromes were originally thought to occur only in plants, but are now known to occur in all photoautotrophic eukaryotes and prokaryotes as well as in several nonphototrophic bacteria, such as *Deinococcus radiourans* and *Pseudomonas aeruginosa*.[16] Phytochromes are relatively large proteins of over 1000 amino acids with a bipartite structure: an N-terminal photoperception domain and a C-terminal output domain (Figure 5),[16,17] and all phytochromes carry a covalently bound linear tetrapyrrole synthesized from heme as the chromophore and as such classify as biliproteins. Attachment of the chromophore occurs autocatalytically through the bilin–lyase activity of the N-terminal domains of the phytochrome apoproteins. In the case of plants, phytochromobilin (PϕB) serves as the chromophore; cyanobacterial phytochromes contain phycocyanobilin (PCB), and the bacteriophytochromes of nonphototrophic bacteria were recently shown to utilize biliverdin as the chromophoric group (Scheme 4).[18] The 3*E* isomers of PϕB and PCB react with the thiol group of a conserved cysteine in plants and cyanobacteria, respectively, while the bacteriophytochromes lack this acceptor cysteine. It has been shown that the biliverdin chromophore binds (likely through a Schiff's base type reaction) to a histidine residue located directly to the C-terminal side of the position occupied by the cysteine of the plant and cyanobacterial phytochromes to which the chromophore is attached (Figure 6).[18] Sequence comparisons have yielded clues for the occurrence of bacteriophytochrome-like polypeptides in many other species of nonphototropic bacteria, as well as cyanobacteria and even fungi (Figure 6).[18] Their physiological functions remain to be elucidated.

Phytochromes and bacteriophytochromes act as red-light-operated, reversible switches (Scheme 5). The phytochromes, when synthesized in the dark, attach their chomophore so as to form the 15*Z* isomer. This isomer absorbs red light (absorption maxima of the chromoproteins are in the range from 660 to 667 nm) and, in doing so, switches to the 15*E* conformation. This latter conformation can, in turn, be converted into the 15*Z* isomer with far-red light (absorption maxima of (15*Z*)-phytochromes are in the region of 730 nm).

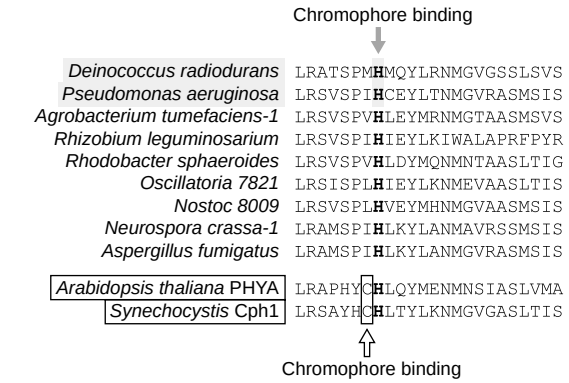


Figure 6. Comparison of amino acid sequences around the chromophore attachment sites (arrows), which are cysteine (C) moieties in the case of phytochromes and histidine (H) moieties in the case of bacteriophytochromes. Sequence analysis has identified polypeptides showing sequence similarity to bacteriophytochromes in many other nonphototrophic organisms, including fungi, and also in cyanobacteria.[18]

In most (but not in all) cases, the (15*Z*)-phytochromes (also termed P_{fr} because of their absorption maxima in the far-red region) are the active photoreceptors and the 15*E* isomers (P_r forms) are inactive. Photoreversibility is a characteristic feature of all phytochromes. The considerable overlap of the absorption spectra of P_r and P_{fr} results in a photoequilibrium always being established between the two forms. This photoequilibrium is dependent on the spectral quality of the light impinging on the plant and has several physiological implications: 1) Some processes (for example, the seed germination of some species) require only a very small amount of active P_{fr}, and thus are triggered even when far-red light is used (giving approximately 2.5 % of P_{fr} at photoequilibrium). These processes cannot be suppressed by treatment with far-red light after a pulse of red light. 2) Changes in the red:far-red light ratio have drastic consequences for the activation state of phytochrome. Such changes occur in the natural environment of a plant: during dusk and dawn (the ratio decreases, that is, there is more far-red light relative to full sunlight), in the shade of a canopy (the ratio drastically decreases because of the large overlap of the absorption of

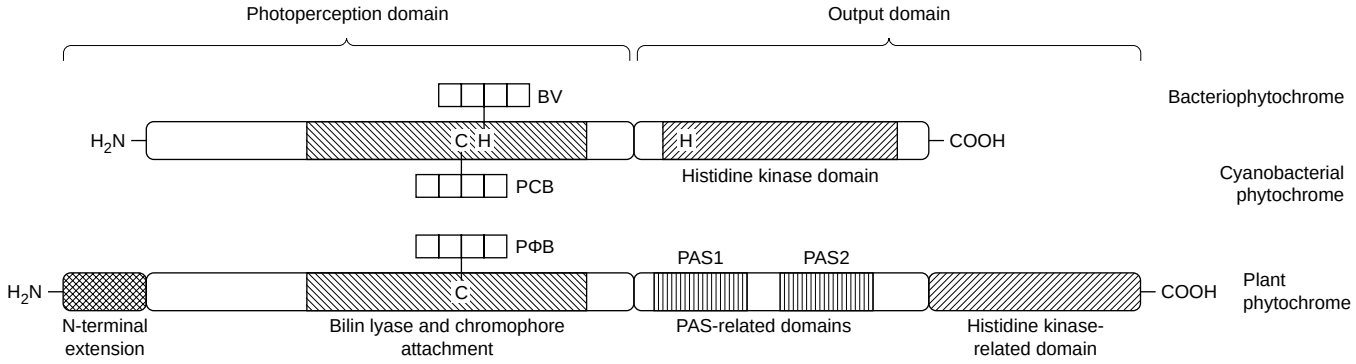
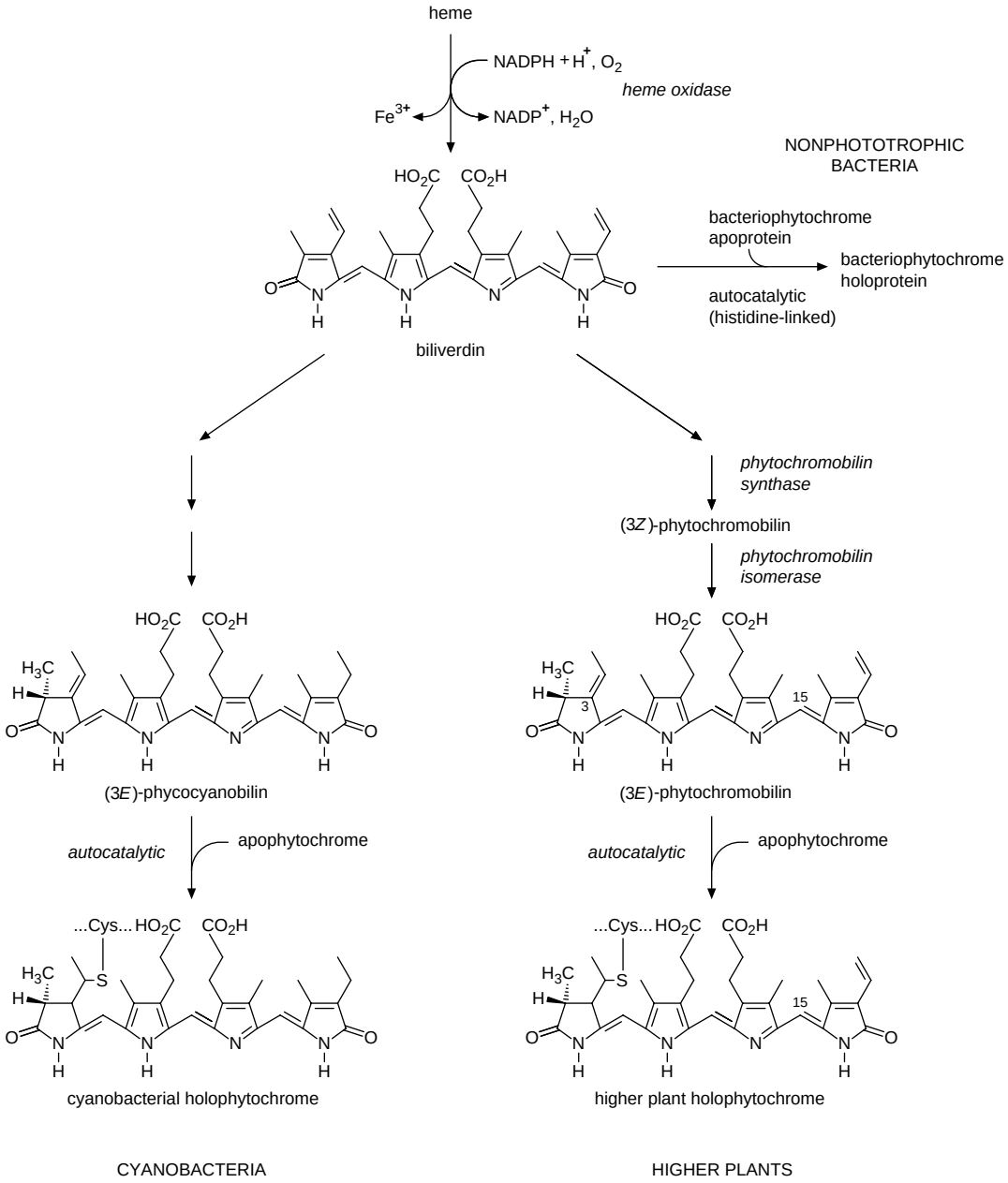


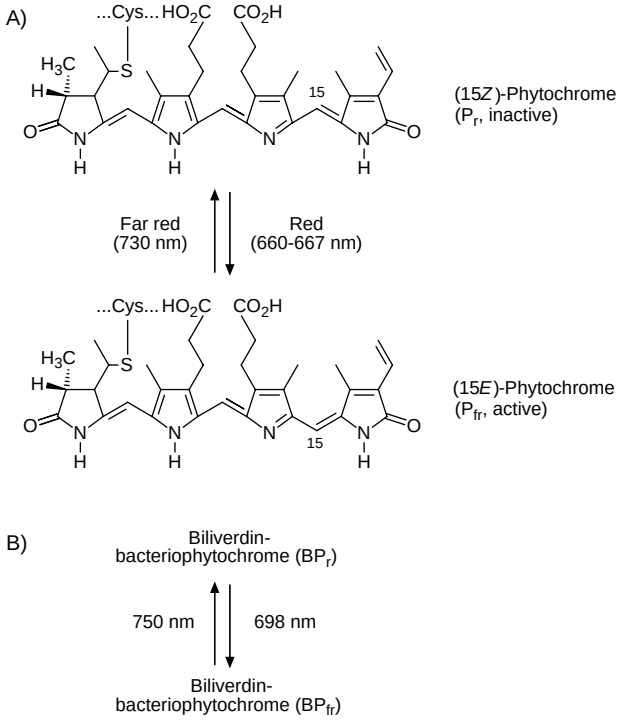
Figure 5. Comparison of the modular composition of bacteriophytochrome and the phytochromes of cyanobacteria and plants. BV: biliverdin, PCB: phycocyanobilin, PϕB: phytochromobilin, C: cysteine, H: histidine.



Scheme 4. Structures and attachment of chromophores to the bacteriophytochrome or phytochrome apoproteins.

phytochromes and the chlorophylls), and—for the same reason—in the light reflected from a nearby green plant. Thus, phytochrome is an ideal photoreceptor to determine day length, green-shade, and plant neighbors, and—in combination with the endogenous circadian clock—even the seasons (through changes in the length of the photoperiod).

Also the bacteriophytochromes are red/far-red reversible switches, but their absorption spectra are strongly red-shifted relative to the phytochromes of the photoautotrophs (Scheme 5). They would not work properly in the environmental situations outlined in the last paragraph. This may be the reason for the evolution of the blue-shifted phytochromes in the photoautotrophic organisms which have spectra overlapping those of chlorophylls. Originally, phytochromes may have evolved to help photoautotrophic organisms to find optimum conditions for photosynthesis (as chemotaxis receptors and/or, in excess light, to trigger protective reactions such as the synthesis of shade pigments).[19] Later (during the evolution of the land plants), the phytochromes then acquired many other functions. The most recent expansion of phytochrome functions occurred during the evolution of the angiosperms. This group, in contrast to all other photoautotrophs, possesses class I phytochrome as well as class II phytochromes (the latter found in all photoautotrophs).[17] Class I phytochrome (represented by a single isoform, phyA, in *A. thaliana*), in contrast to the light-stable class II photoreceptors, is very light-sensitive and rapidly degraded by the ubiquitin–proteasome system in the light. In addition, the *PHYA* gene is transcriptionally downregulated in the light (by phyA itself and by phyB, a class II phytochrome).



Scheme 5. Photoreversible isomerization of phytochromobilin (A) and bacteriophytochrome (B) containing biliverdin as the chromophore.[18]

The evolution of class I phytochrome in the angiosperms occured in conjunction with the evolution of skotomorphogenesis, a unique developmental program repressing normal development of seedlings in the absence of light. Dark-grown angiosperm seedlings look very different from light-grown ones (think of potato sprouts grown in the dark versus those grown in daylight): they lack chlorophyll, leaf expansion, and normal gravitropic behavior and show greatly enhanced elongation growth—all processes which help the seedling, when germinating and growing in the soil in the absence of light, to reach the sunlight as rapidly and effectively as possible, before its storage reserves are depleted. Light, via phyA (which acts together with the blue-light receptor cry1 in this high-light-intensity response, Table 1) induces removal of the repressor complex and thus allows for the transcription of the derepressed genes to start photomorphogenesis (for example, the differentiation of chloroplasts to initiate photosynthesis). In the light, phyA is degraded and the transcription of its gene downregulated so that the level of phyA falls to 10% or less of its dark level. Class II phytochromes now take over to regulate most phytochrome-dependent processes in the plant growing in the light. However, phyA is still active in the light, for example, to transmit a low-intensity red light signal, in cooperation with the blue-light receptor cry1, to the circadian clock. In this function, it complements phyB, which, together with cry2, regulates circadian clock functions under higher light intensities.

The modular representation of the phytochrome and the bacteriophytochrome apoproteins (Figure 5) shows that the output domain (and thus probably the transduction pathway) has also undergone significant changes during evolution of this class of photoreceptors. The cyanobacterial phytochromes and the bacteriophytochromes are typical, but cytoplasmatic, soluble components of two-component phosphorelay regulators (Figure 3), and their output domain contains the histidine kinase function (Figure 5). In some cases, the response regulators of these directly light-regulated sensor histidine kinases have been identified (for example, Rcp in the case of the cyanobacterial phytochrome Cph1).[20] Plant phytochromes contain a bipartite output domain consisting of a C-terminal domain with weak sequence similarity to a histidine kinase domain but with no detectable histidine kinase activity and a second domain which bears two PAS-related motifs. PAS-domains can have diverse functions, for example, in protein–protein interactions, and may be involved in phytochrome dimerization. The name PAS is an acronym derived from the names of three proteins bearing such domains: The *Drosophila* circadian clock protein PERIOD (PER), the vertebrate aryl hydrocarbon receptor nuclear translocator (ARNT, **a**ryl hydrocarbon **r**eceptor **n**uclear **t**ranslocator), and the *Drosophila* SINGLE-MINDED protein SIM. Rather than being histidine kinases, plant phytochromes are Ser/Thr kinases and they do not transmit their output signal through a phosphorelay mechanism. Rather, they appear to be directly involved in controlling transcription, as has recently been shown for phyB of *A. thaliana* (Figure 7).[21] The P_r form of phyB is localized in the cytoplasm, whereas the P_{fr} form is rapidly translocated into the nucleus where it interacts with the G-box-binding protein PIF3 (**p**hytochrome-**i**nteracting **f**actor 3), and results in transcriptional activation of the corresponding genes. There is evidence that also phyA, upon illumination, is translocated to the nucleus where it may act either alone or by interacting with the nuclear-localized cryptochromes. By extending this hypothesis, the basis for the interaction of

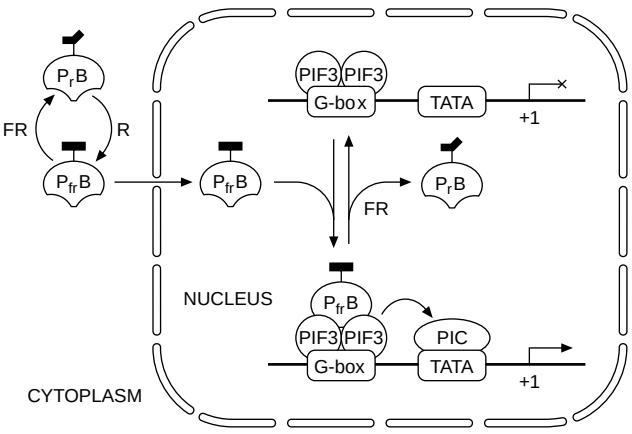


Figure 7. Model of the control of gene activity by phyB. $P_{fr}B$: far-red(FR)-absorbing, active form of phyB, P_rB: red(R)-absorbing, inactive form of phyB, PIF3: phytochrome-interacting factor 3, a G-box binding protein interacting with $P_{fr}B$. This interaction results in activation of the genes controlled by the respective promoters. PIC: transcriptional preinitiation complex, TATA, TATA-box: nucleotide sequence where the pre-initiation complex is being assembled, + 1: nucleotide where transcription starts.

phyB with cryptochromes (for example, in the control of circadian processes, Table 1) may involve the physical interaction of both photoreceptors to control gene regulation.[17] There is evidence that cryptochromes are substrates of the Ser-/Thr kinase activity of phytochrome in vitro. It is thus conceivable that the phytochrome–cryptochrome interaction involves phosphorylation of cryptochrome by light-activated phytochrome. Phytochromes (and cryptochromes) can thus be categorized as directly light-switchable transcriptional regulators, and provide a very straightforward transduction of a light signal into the nucleus to alter the activity of light-regulated genes.

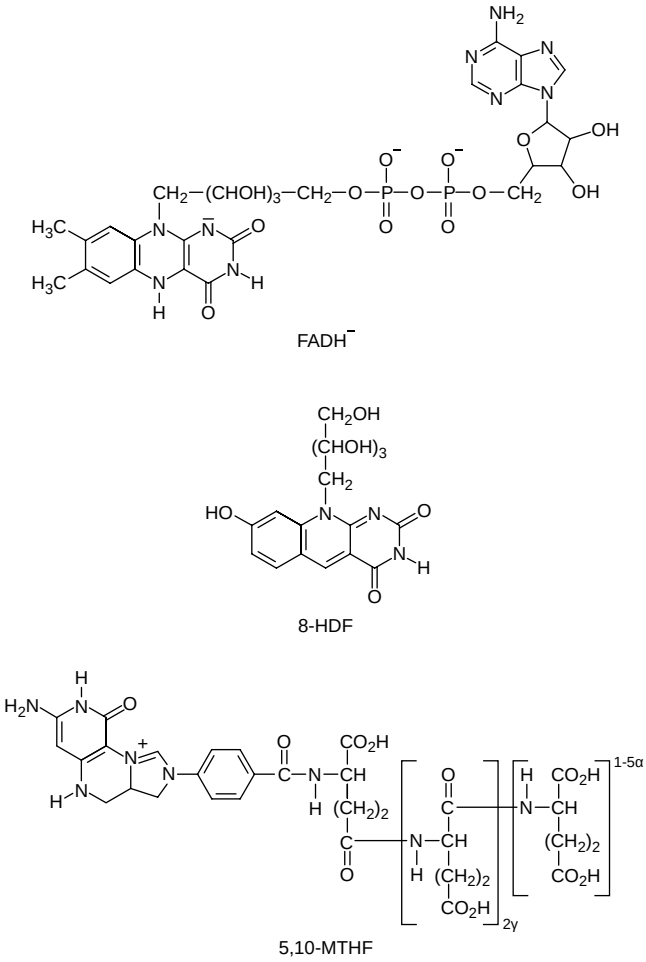
However, not all phytochrome-dependent responses may involve gene regulation. Photomodulated processes which are fully reversible, such as phytochrome-dependent alterations of leaf position (day and night positioning) or chloroplast movements in some lower plants (weak-light versus high-light positioning of some algal chloroplasts, for example, in the genus *Mougeotia*) occur within minutes and may reflect further, as yet unknown, modes of action of phytochrome.

3.1.2. Cryptochromes

The evolution of the cryptochrome photoreceptors can be traced back to ancestors of the prokaryotic DNA-repair enzymes, the photolyases (deoxyribocyclobutadipyrimidine pyrimidine lyase, EC 4.1.99.3), which are found in archaea, bacteria, and eukaryotes. Photolyases catalyze the blue-light- and UV-A-dependent repair of UV-B-damaged DNA. The class I and class II photolyases repair cyclobutane pyrimidine dimers whereas the (6-4)-photolyases catalyze the repair of pyrimidine-(6-4)-pyrimidone adducts.[22] Light energy is absorbed by either a 5,10-methenyltetrahydrofolate (MTHF) poly($n = 3$-8)glutamate or a 8-hydroxy-7,8-didemethyl-5-deazariboflavin, which compound is utilized is dependent on the particular enzyme (Scheme 6). These cofactors are tightly, but noncovalently bound to their respective apoproteins. The absorbed light energy (in the blue/UV-A region) is transferred to a second cofactor, a semireduced flavinadeninedinucleotide ($FADH^-$) which is noncovalently, but very tightly ($K_D < 10^{-11}$ M) bound to the apoprotein. Excited $FADH^-$ ($^*FADH^-$) then transfers one electron to the pyrimidine dimer (pyr-pyr), which results in splitting of the 5–5 and 6–6 bonds of the cyclobutane ring of the dimer to produce pyr + $pyr^{-\bullet}$. The latter donates one electron back to the flavin to regenerate the $FADH^-$ in the ground state, and the enzyme dissociates from the DNA (Scheme 7).[22]

Cryptochromes[23,24] have now been found in all groups of green plants, from algae to angiosperms. They were later shown to occur also in animals and man. The apoproteins of the animal/man cryptochromes resemble more the (6-4)-photolyases, while the plant cryptochromes are more similar to the class I photolyases. Thus, cryptochromes have evolved separately from different photolyases in the animal and plant kingdoms.

All the plant and animal cryptochromes so far analyzed are devoid of photolyase activity and have acquired an additional, C-terminal domain necessary for eliciting their physiological responses (Figure 8). Their N-terminal, photo-



Scheme 6. Structures of photolyase cofactors.[22] All photolyases contain $FADH^-$ as the electron donor and either 8-hydroxy-7,8-didemethyl-5-deazariboflavin (8-HDF) or 5,10-methenyltetrahydrofolatepolyglutamate (5,10-MTHF) as the light-absorbing chromophore.

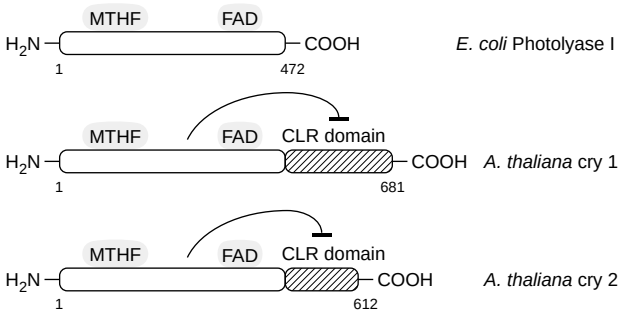
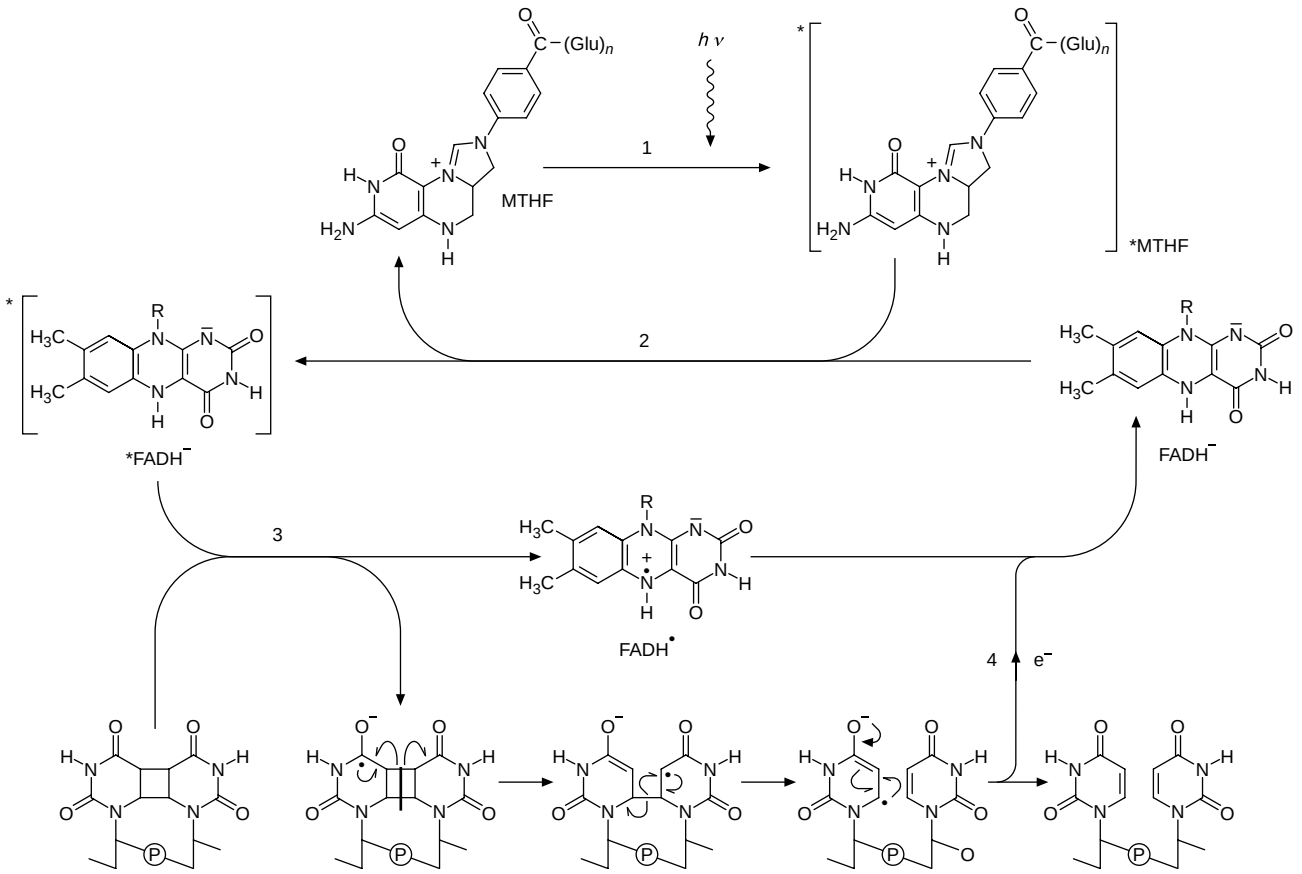


Figure 8. Comparison of the domain structure of cryptochromes of *Arabidopsis thaliana* with photolyase I of *E. coli*. Open bar: light-absorbing domain indicating the position of the two noncovalently bound cofactors, MTHF and FAD (for abbreviations, see Scheme 6). The CLR domain alone is able to confer a constitutive light response. In the dark, the light-absorbing domain represses the activity of the CLR domain (⊥).[22,26] The numbers indicate the number of amino acids.



Scheme 7. Reaction mechanism of photolyase.[22] 1) Absorption of a photon by the chromophore, in this case MTHF; 2) transfer of energy from excited MTHF (*MTHF) to the $FADH^-$ electron donor; 3) excited $FADH^-$ (*$FADH^-$) donates one electron to the pyrimidine dimer and catalyzes the cycloreversion; 4) regeneration of $FADH^-$ by electron back transfer from $pyr^{-\bullet}$.

lyase-related domains bind, as do the photolyases, two chromophores in vitro: MTHF and $FADH^-$. Although most experiments were conducted with recombinant apoproteins expressed in *Escherichia coli*, action spectra of cryptochrome-dependent physiological responses suggest this cofactor complement also to be characteristic for the in vivo situation.

Arabidopsis thaliana has two cryptochromes, cry1 and cry2, which overlap considerably in their physiological roles, but also have some unique functions in the plant (Table 1). Although the N-terminal, photolyase-like, chromophore-binding domains of cry1 and cry2 are clearly homologous, their C-terminal effector domains (CLR domains, Figure 8) are very different. However, the CLR domains of cry1 and cry2 are functionally equivalent (hence the overlapping spectrum of physiological responses) and interchangeable. Both CLR domains mediate a **c**onstitutive **l**ight **r**esponse when expressed in the absence of the photolyase-like domain.[25] Thus, in darkness, the photolyase-like domain appears to block the action of the CLR domain of cryptochrome. The absorption of a photon—presumably through an intramolecular redox reaction involving the $FADH^-$ cofactor—is believed to result in a conformational change of the apoprotein, thus relieving the CLR domain from the intramolecular repression.[25,26] The C-terminal extensions of animal cryptochromes, when expressed in the plant, give no physiological response, which suggests that they have an unrelated mode of action. Nevertheless, it is intriguing that—although evolved separately—the animal cryptochromes mediate light input to the circadian clock,[27] as does plant cry1 (Table 1).

The molecular basis of the functional redundancy of the two cryptochromes in the cryptochrome-mediated blue-light regulation of seedling photomorphogenetic development has recently been elucidated (Figure 9).[26] As in the case of the phytochromes, it turned out that cryptochromes are light-controlled switches that affect transcription in a very direct way, though rather differently from the phytochromes (compare with Figure 7). Both cryptochromes affect the structure and/or activity of a central regulator of photomorphogenesis, the E3-ubiquitin ligase COP1, by binding to COP1 after absorbing a photon. Binding results in inactivation of COP1, which allows the transcriptional regulator HY5 to bind to target promoter sequences of a range of light-regulated genes and activate their transcription and thus initiate photomorphogenesis. COP1 is a repressor of photomorphogenesis in that it prevents the transcription factor HY5 to accumulate in the nucleus by targeting HY5 for ubiquitination and degradation by the 26S-proteasome (Figure 9). Mutations in *COP*1 leading to a loss of function of COP1 show a **co**nstitutive **p**hotomorphogenesis, hence the particular name of this E3-ubiquitin ligase, which plays a central role in the control of angiosperm photomorphogenesis.[26]

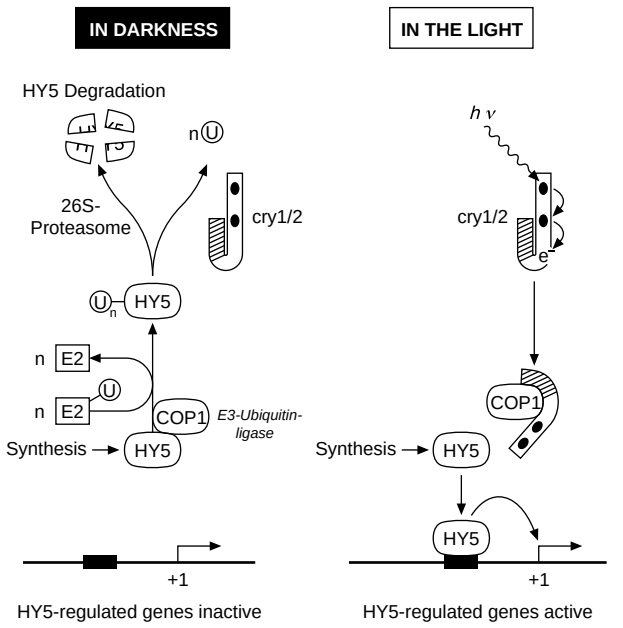


Figure 9. Model of the regulation of photomorphogenesis by the cryptochromes.[26] The bZIP-type transcription factor HY5 was originally isolated by positional cloning from a mutant of *Arabidopsis thaliana* showing long hypocotyls when irradiated with blue light. Wild-type etiolated seedlings show blue-light-dependent inhibition of hypocotyl elongation, a typical photomorphogenic response of angiosperm seedlings to blue light. U: ubiquitin, E2: ubiquitinating enzyme, E3: ubiquitin protein ligase.

Both cry1 and cry2 are localized in the cell nucleus.[24,28] However, while cry2 is found predominantly in the nucleus, only a fraction of cry1 is nuclear localized: the majority of this photoreceptor occurs in the cytoplasm, a fact probably related to those parts of cryptochrome action that are different among the two photoreceptors. Intriguingly, circadian clock models involve transcriptional regulators that move in and out of the nucleus periodically.[29] The function of cry1, which regulates the plant circadian clock,[30] may be related to such processes. In the simplest (hypothetical) model, cry1 by itself would slowly translocate between the nucleus and the cytoplasm in a light-dependent fashion.

3.1.3. ***Phototropins***

During work on the cryptochrome mutant *cry*1 (formerly designated *hy*4),[31] it became apparent that, while lacking the blue-light-dependent hypocotyl growth-inhibition response characteristic of the wild type, the mutant still showed a normal phototropic behavior (bending toward a unilateral source of blue light).[24,31] In contrast, the mutant *nph*1 lacked this phototropic behavior (nph, ***n****on****p****hototropic*** ***h****ypocotyl*), but showed the normal photomorphogenic blue-light-induced inhibition of hypocotyl elongation.[32] This genetic evidence gave the first clear-cut proof for the existence of a second blue-light photoreceptor in higher plants distinct from cryptochrome.

Cloning of the *nph*1 locus allowed the identification of *NPH*1 in the genome of *A. thaliana*,[33] and a second NPH1-like gene (NPL1) was soon also identified.[34] The two genes (now renamed *PHOT*1 and *PHOT*2) indeed encode a different class of photoreceptors, the phototropins, which are light-regulated Ser-/Thr protein kinases structurally and functionally unrelated to the cryptochromes.[24,33,34]

The most prominent characteristic features evident from the amino acid sequences of the two homologous phototropins, phot1 and phot2, are the presence of a C-terminal 11-amino acid motif characteristic of Ser/Thr protein kinases and of two LOV domains, LOV1 and LOV2, each spanning approximately 110 amino acids, in either of the two proteins (Figure 10). LOV domains constitute a subset of PAS domains (Section 3.1.1) characteristic of eukaryotic and prokaryotic sensor proteins responsive to **l**ight, **o**xygen, or **v**oltage.[33] In the phototropins each LOV domain binds one molecule of FMN noncovalently.[35] Recombinant, isolated LOV domains bind the FMN chromophore and undergo a characteristic photocycle. Spectroscopic examination of such isolated, reconstituted domains has provided evidence of a reversible, covalent photoadduct between C(4a) of the flavin and a cysteinyl residue of the polypeptide chain.[35,36] This result has been corroborated by the crystal structure of an isolated LOV domain[36a] and furthermore, by NMR spectroscopic analysis of the recombinant *Avena sativa* phototropin 1 LOV2 domain reconstituted with various $^{13}C/^{15}N$-labeled isotopomers of the cofactor FMN (Scheme 8).[37] Irradiation with blue light induces the formation of the FMN-C(4a)–cysteinyl adduct which spontaneously, but slowly, reverts in the dark. Adduct formation results in conformational modification of the LOV domain. It is hypothesized that LOV domains are optomechanical transducers that mediate structural changes in the phototropin apoprotein, thereby activating its autokatalytic kinase and initiating phosphotransfer to (as yet unidentified) target proteins.[24,37] Since irradiation with blue light results in an increase in the cytosolic Ca^{2+} level of guard cells, and this increase is lacking in the *nph*1 mutant, Ca^{2+}-influx channels could be targets of regulation by the phototropin kinase in the process of blue-light-induced stomatal opening.[24] Indeed, phototropins are membrane-associated, though not transmembrane, proteins.[32]

Since the isolated LOV domains LOV1 and LOV2 differ considerably in light sensitivity, and phot1 and phot2 differ again in their light sensitivity (phot1 being activated by much lower light intensities than phot2) the cooperation of the two photoreceptors helps the plant to cope with a broad range of different light intensities. A unifying theme of both phototropins is their involvement in several responses that permit the plant to position itself in such a way as to allow for optimum photosynthesis to occur: 1) phototropism, which orients the shoot towards the sun, 2) chloroplast movements,

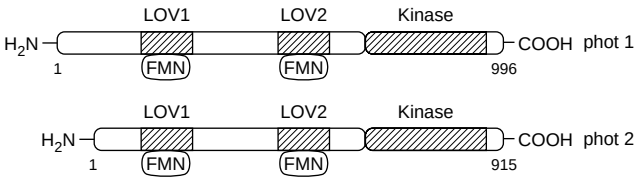
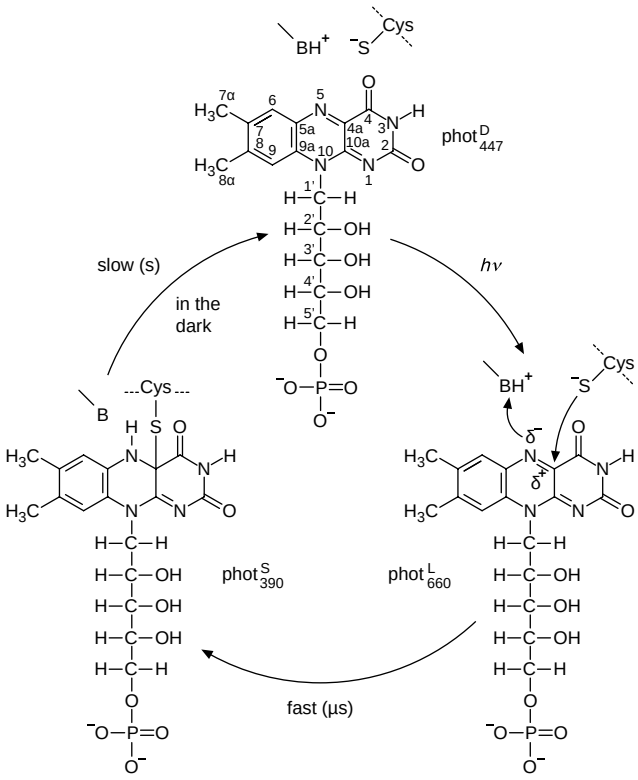


Figure 10. Domain structure of phototropins of *A. thaliana*.[24] LOV: **l**ight, **o**xygen, **v**oltage domain; the numbers indicate the number of amino acids.



Scheme 8. The phototropin photocycle. The indices give the absorption maxima of the intermediates; phot: phototropin, D: dark form, L: light-activated form, S: signaling form of phototropin. Experiments were carried out with recombinant, isolated LOV2 domains of *Avena sativa* reconstituted with FMN.[36b]

which orient the chloroplasts in the cell relative to the intensity of light, and 3) stomatal opening movements which regulate the passage of CO_2 into the leaf in the light.[24,38] As yet, no prokaryotic relatives of the phototropins have been reported, but it is only a matter of time.

4. LRR Receptor Kinases in Pathogen Defense and Development

The availability of a vast amount of nucleotide data from various organisms now permits insights into the evolution of many sensor mechanisms. One of the emerging themes is to understand the evolution and functional diversification of the very large superfamily of the eukaryotic receptor kinases, which encompasses thousands of members; to date 610 genes have been found in *Arabidopsis thaliana* alone.[39]

The relay of a signaling event into the cell through changes in the phosphorylation status of receptors as well as of further signal transducers acting downstream of the receptors has proven so versatile that, during evolution, a large number of signaling pathways involving protein phosphorylation has developed, some examples of which have already been mentioned (Figures 3 and 4). These, like the ethylene and cytokinin receptors, have arisen from prokaryotic phosphorelay regulators that are not found in animals.

A family of receptors typical for animals and man (not found in plants) are the receptor tyrosine kinases (RTKs) which are localized in the cell membrane to monitor the presence or absence of many different signals, such as nerve growth factor, platelet-derived growth factor, fibroblast and epidermal growth factors, and insulin. These receptors consist of two large domains, an extracellular sensor domain and a cytoplasmic tyrosine kinase domain, linked by a single transmembrane domain. The same basic structure (extracellular sensor domain, kinase domain, and a single transmembrane domain) characterizes a large group of plant kinases, the LRR receptor kinases (LRR, leucine-rich repeat), represented by 216 genes in the genome of *Arabidopsis thaliana*.[39] This group is characterized by the occurrence of leucine-rich amino acid motifs which are repeated several times and thought to mediate protein–protein interactions. Only for a few of these LRR receptor kinases (LRR-RKs) have the functions and/or ligands been found recently. These functionally characterized LRR receptor kinases include the receptor for the steroid growth factor brassinolide (Figure 1), BRI1,[40] the receptor for the CLAVATA3 peptide CLAVATA1 (CLV1) involved in regulating shoot meristem development,[41] and the receptors for bacterial elicitor peptides Xa21[42] and FLS2[43] that mediate pathogen defense responses (Figure 11).[44] Most recently, it has been shown that the receptor for the tomato octadecapeptide systemin (SR160)

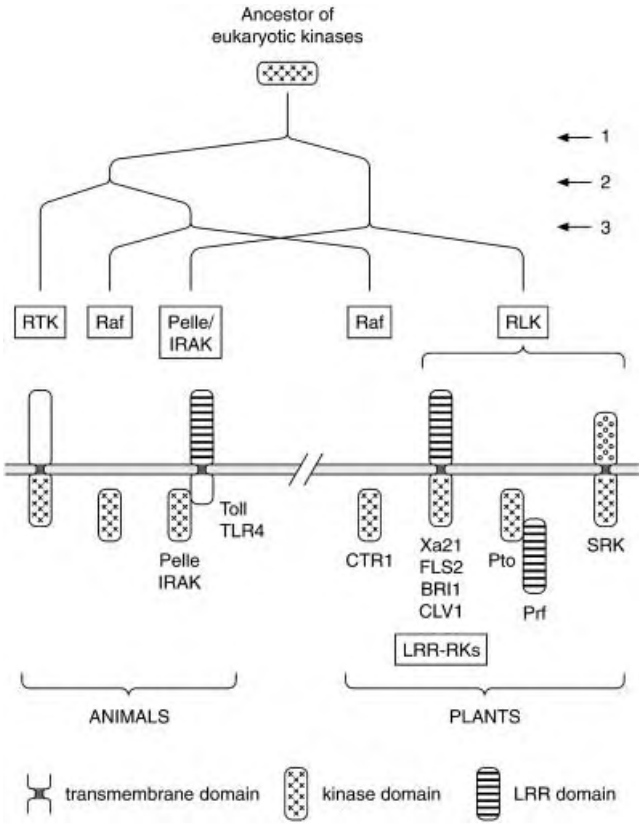


Figure 11. Module composition and evolutionary relationships[39b] of animal and plant receptor kinases. 1, 2) gene duplication events in common ancestors of the plants and animals leading to the divergence of the RLK + Pelle/IRAK from the RTK + Raf groups of kinases (1) and the RTK kinases from the Raf kinases (2). 3) Divergence of the animal and plant kinases separating ancestral sequences that further evolved into the extant kinase families.

involved in the elicitation of herbivore defense reactions[45a] and the receptor for the *Rhizobium* Nod factors (NORK),[45b] as well as the receptor SYMRK which is involved in the establishment of both bacterial and fungal symbioses with the higher plant *Lotus*[45c] also belong to the LRR receptor kinase family.

These two classes, the animal RTKs and the plant LRR-RKs, cluster within the superfamily of eukaryotic receptor kinases as a monophyletic group together with a class of soluble kinases, the Raf kinases—of which members have been found in animals and plants (CTR1 belongs to this group, see Section 2.1, Figure 4) and with a second class of soluble kinases represented by the *Drosophila* kinase Pelle, the mammalian interleukin-1-receptor-associated kinase (IRAK), and the tomato kinase Pto, all of which are involved in triggering pathogen defense reactions.[39,44b]

It is now possible to trace the coarse evolutionary history of the receptor kinase families from an ancestral, soluble kinase which gave rise, by an ancient gene duplication event, to the RTK/Raf branch and the branch leading to both the plant receptor-like kinases and the Pelle/IRAK group. Since Raf kinases are also found in plants (for example, CTR1), the divergence of the RTK group from the Raf group must have taken place before the separation of the animals and the plants. At the animal/plant junction, the evolutionary separation of the two groups of Raf kinases on one side and the divergence of the Pelle/IRAK-type kinases on the other side from the plant receptor-like kinases took place, this latter group then evolved—concurrent with considerable expansion of gene numbers—into the individual RLK families (see Figure 11).

Repeated gene fusion events during the course of evolution have resulted in the recruitment of different extracellular sensor domains, and have led to the LRR receptor kinase family, the self-incompatibility receptor kinase SRK,[46] and, in the animal line, to the RTK family. Other receptor kinases have retained a—presumably evolutionary more ancient—separation from the sensor component, as is the case for Pelle (interacting with the transmembrane peptide receptor Toll) and IRAK (interacting with TLR4; Figure 11). A similar situation exists in the plant LRK family for the receptor kinase Pto which interacts noncovalently with the cytoplasmatic LRR protein Prf to mediate the cellular response against the *Pseudomonas syringae* pv. tomato AvrPto elicitor protein.[44b,47] Both Toll and TLR4 also belong to the group of LRR proteins, which proves that the interaction of Pelle/IRAK/Pto-type kinases with LRR domain proteins is evolutionary ancient and dates back in time before the animal/plant divide. The gene fusion events leading to the LRR-RKs in plants apparently occurred at a later stage during evolution.[39]

The regulatory complexity suggested by the presence of 610 genes in *Arabidopsis thaliana* that encode receptor-like kinases, of which 216 are LRR receptor kinases by structure, is still unimaginable. The few receptors which have been functionally characterized at least in some detail reveal that their ligands are steroidal growth factors (BRI1: brassinolide[40]), lipochitooligosaccharides (NORK: Nod factors[45b]), regulatory peptides (phytosulfokines;[54d] CLV1: CLAVATA3-peptide,[48] SR160: systemin[45a]), peptide elicitors from bacterial cells (FLS2: a short, 22-amino acid fragment of bacterial flagellin[43]), or small proteins (Pto: AvrPto;[44b] SRK: pollen-borne, cysteine-rich S-locus proteins (SCRs)[49]). The biggest surprise perhaps is not so much the fact that there can be considerable similarity between animal and plant pathways triggering defenses against pathogens,[44b,50] but rather the importance of peptide regulators in higher plants. It has long been assumed that peptides would be ineffective regulators for plants, partly because of diffusion constraints imposed by the walls of plant cells. However, a number of regulatory peptides has been identified in addition to those already mentioned (Table 2), and this list will undoubtedly expand further.[51]

The signaling pathway initiated by the mammalian, IRAK-dependent, TLR4 receptor and that initiated by the *Drosophila*, Pelle-dependent, Toll-receptor—both of the LRR receptor type—involves MAP kinase cascades which regulate the activity of transcription factors (Jun/Fos and NF-κB in the case of the IRAK-dependent pathways). It was recently found that a typical MAP kinase cascade also mediates between the plant LRR receptor kinase FLS2 and the transcription factors WRKY22 and WRKY29.[52a] Thus, there exists an intriguing conservation of LRR-receptor-dependent signaling pathways which trigger pathogen defense responses in animals, *Drosophila*, and higher plants. A MAP kinase has also been found in the signaling pathway of the brassinolide receptor BRI1,[52b] which suggests there is a common mode of action of LRR receptor kinases.

5. Cyclo-Oxylipins: Signaling Molecules from Plant Membranes

The destruction of cellular integrity accompanies many adverse situations a plant may encounter. Damage may be

Table 2: Regulatory peptides from higher plants.

Peptide	Size	Receptor	Function	Species	Ref.
Systemins	18 aa[a]	SR160[45a][e]	systemic wound response	*Lycopersicon, Solanum, Capsicum, Nicotiana*[b]	[45a, 53a–53c]
RALF[c]	49 aa	unknown	root growth and developmental arrest	*Nicotiana*, other species	[53d]
CLAVATA 3	96 aa	CLV1[e]	shoot meristem organization	*Arabidopsis*	[48]
Phytosulfokines	4, 5 aa[d]	PSK-RK[54d][e]	cell-cycle regulation	*Arabidopsis, Asparagus, Oryza*	[54]
S-locus, cystein-rich proteins (SCRs)	$<$8 kDa	SRK[e]	self-incompatibility	*Brassicaceae*	[49]
ENOD 40	13, 27 aa	unknown	root nodulation	legumes, *Oryza*	[55]

[a] aa, amino acids. [b] *Nicotiana* systemins are glycosylated. [c] **R**apid **al**kalinization **f**actor. [d] With sulphotyrosine. [e] Members of the LRR receptor kinase family.

caused by mechanical stresses, such as by herbivore feeding, or by an invading parasite or pathogen. In both cases, it is essential for a plant to mount appropriate defenses, local as well as systemic ones. Cellular decompartmentation leads to disintegration of cellular membranes and mixing of components separated from one another in the intact cell. It has become evident during recent years that local, as well as systemic, signaling is initiated at a wound site, which leads to drastic and complex defense reactions of the plant. Pioneering work has been carried out on tomato plants,[56] but the signaling system detected in this species has relevance for all higher plants—with variations.

In the tomato plant, wounding (either mechanical or as a consequence of insect feeding) leads to the production and accumulation of several proteinase inhibitors which are highly toxic to insects when ingested.[56,57] Initiation of the synthesis of the proteinase inhibitor is effected locally through oligogalacturonides, which are breakdown products of plant cell walls, and systemically through the phloem-mobile octadecapeptide systemin which is proteolytically cleaved off a precursor protein, prosystemin (Figure 12).[58] Both oligogalacturonides and systemin induce the accumulation of proteinase inhibitors via the lipid-derived signaling compound jasmonic acid (JA, Scheme 9). Even before the biosynthesis of JA is induced by these elicitors, decompartmentation of membranes produces free fatty acids (including α-linolenic acid), from which JA is produced within minutes by the pathway's enzymes which are constitutively present at low levels in the cell. The function of JA is evident because mutant tomato plants unable to accumulate JA, no longer produce

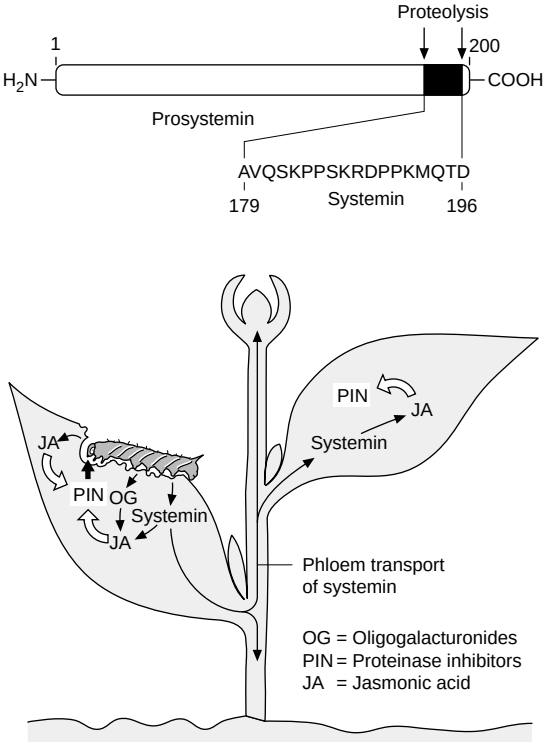
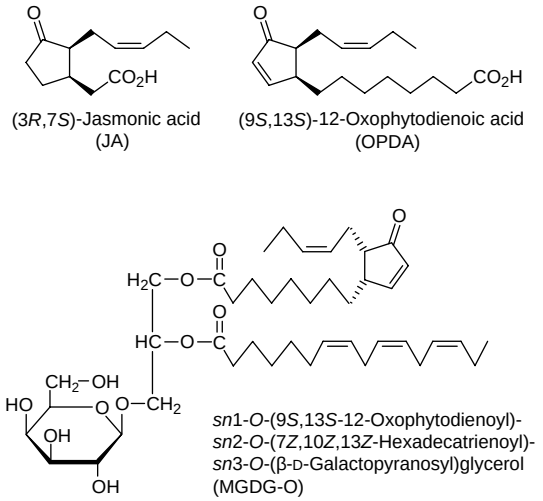


Figure 12. Local and systemic induction of proteinase inhibitor formation in tomato. Systemin is released by proteolytic processing of prosystemin, as shown in the upper panel.[58b]



Scheme 9. Structures of cyclic oxylipins from higher plants.

proteinase inhibitors when wounded and are defenseless—hence the mutant's designation *def*1.[59] Earlier it had been shown in a pioneering paper that airbone methyl jasmonate would induce the accumulation of proteinase inhibitors in an unwounded plant.[60] Wounding leads to drastic increases in the level of JA in wounded tissue.[61] Likewise, plants with mutations in the jasmonate biosynthetic pathway, or jasmonate-insensitive mutants, are hypersusceptible to insect attack, but also less resistant against pathogen attack.[62] Jasmonic acid is, thus, an important inducer of plant defenses.

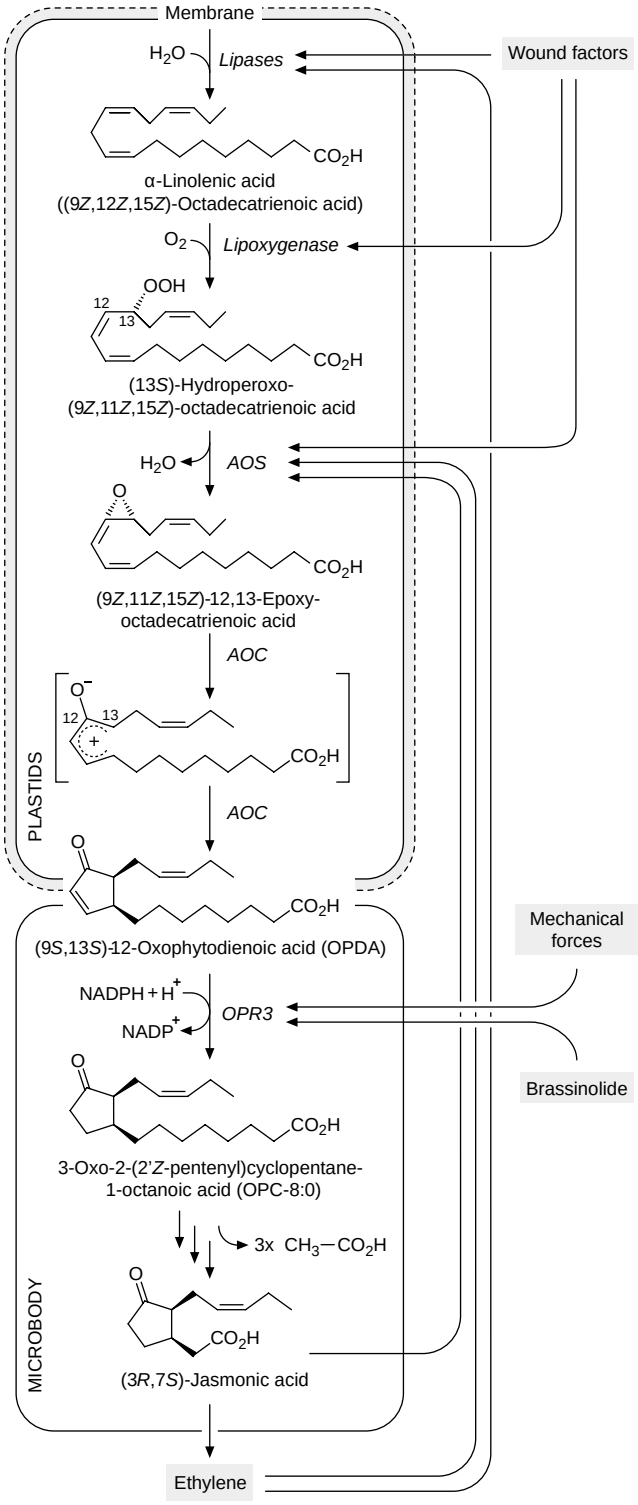
The biosynthesis of JA was worked out in the early 1980s,[63] and the pathway's enzymes have been cloned with the exception of the terminal step, which is believed to be carried out by the plant's system for β-oxidizing fatty acids.[64] It is now evident that JA is not a highly mobile molecule, in fact, it seems to act locally at the site of production or application, and can thus be regarded as a second messenger of defense reactions. For example, when JA is applied locally from the outside, the induced gene transcription is confined to the site of application.[65] JA is required for pollen maturation and dehiscence of the flower organs in *Arabidopsis thaliana*, and these processes coincide with a highly local accumulation of JA biosynthetic enzymes in pollen or abscission zones.[65,66]

In the intact cell, JA biosynthesis is presumably limited by substrate availability, but decompartmentation liberates α-linolenic acid from membrane lipids through the action of lipases or esterases, and initiates an early first peak of JA accumulation. In addition, key enzymes of JA biosynthesis, mainly allene oxide synthase (AOS) and 12-oxophytodienoate reductase 3 (OPR3), are subject to transcriptional control by a number of regulatory processes. Most of these processes serve to increase the biosynthetic capacity of the pathway provided enough substrate is available. Substrate is probably produced by lipases which are also upregulated in cells under conditions inducing the pathway's enzymes (Scheme 10).

Two recent findings add to the complexity of the jasmonate signaling system, but may help to ultimately understand how this system could work in regulating such a variety of physiological responses as diverse as, for example,

mechanotransduction, pollen maturation, pathogen, or herbivore defenses.[67]

1. JA is not the only active compound in this group. In fact, there is now compelling evidence that 12-oxophytodienoic acid (OPDA) is an active signaling molecule in its own right. OPDA, rather than JA, is involved in mechanotransduction, as has been shown by detailed structure–response analyses of JA and OPDA analogues.[68] Mutant *Arabidopsis thaliana* plants defective in OPR3, and thus unable to produce JA, have been used to demonstrate that applied JA or OPDA induce sets of genes which are overlapping, but not identical.[69] Although the mutant has even higher than normal levels of OPDA, it is male sterile;[62] thus, JA, but not OPDA, is required for male fertility. However, the mutant doesn't show reduced herbivore defences, which suggests that OPDA can substitute for many JA responses in this physiological context.
2. A major twist in understanding what jasmonates do in a cell may come from the recent identification of a novel plastid membrane lipid, MGDG-O, in which the *sn*1 fatty acid is replaced by (9*S*,13*S*)-OPDA and for which the presence of a 16:3-fatty acid in the *sn*2 position suggests a plastidic biosynthesis.[70] The discovery of this metabolite, which is of widespread occurrence in plants (M. Dettenberg and E. W. Weiler, unpublished results), necessitates a re-evaluation of how OPDA is actually produced in vivo. There are several options (Figure 13), with the most likely being that MGDG-O is actually synthesized from monogalactosyldiglyceride (MGDG), a dominant plastid lipid, by conversion of α-linolenic acid at the *sn*1 position of MGDG into OPDA in situ. This sequence would explain why allene oxide synthase (AOS) occurs membrane-bound in the plastid.[71] If that is so, then there may be a very short way to initiate defense signaling—via OPDA released from the membrane directly. It is interesting that the lipases which most effectively mobilize OPDA from the lipid precursor, are those from the phytopathogenic fungi *Mucor javanicus* and *Rhizopus arrhizus*.[70] Thus, the release of an OPDA signal (or JA precursor) may be an immediate plant response at sites of fungal attack. Clearly, we have not yet penetrated to the depths of understanding many facets of oxylipin signaling in plants, and the molecular mechanisms that initiate and regulate the synthesis of these potent regulators as well as the mechanisms by which they act to regulate transcription, are almost completely obscure.



Scheme 10. Pathway, compartmentation, and regulation of jasmonic acid biosynthesis from free α-linolenic acid. AOC: allene oxide cyclase, AOS allene oxide synthase, OPR3 isoform 3 of oxophytodienoate reductase.

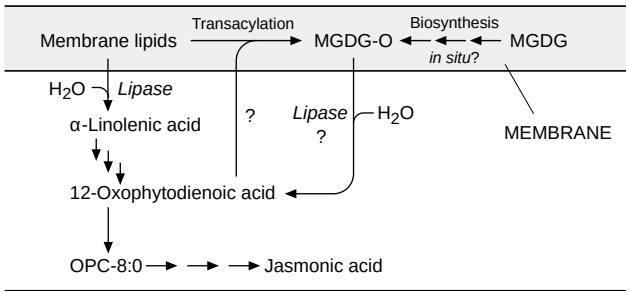


Figure 13. Possible relationships between free and lipid-bound 12-oxophytodienoic acid in chloroplasts. MGDG: monogalactosyl diglyceride, O: 12-oxophytodienoyl-moiety, OPC-8:0: 3-oxo-2-(2′Z-pentenyl)-cyclopentane-1-octanoic acid.

One facet of oxylipin signaling which cannot be discussed here in detail is the herbivore-induced production of plant volatiles,[72a] many of which can also be induced by treating plants with JA.[72b] These volatiles attract carnivorous animals to their herbivorous prey and this represents a unique form of plant–carnivore mutualism in a tritrophic interaction,[73] which may be more widespread in nature than currently anticipated. Herbivory-induced plant volatiles have been shown, for example, in lima beans, to elicit genes for plant defense,[74] and at least some of these compounds act on the plant itself. Consequently, there must be a mechanism by which such volatiles can be perceived in the plant. Whether herbivore-induced volatiles act as "phytopheromones" and thus serve as a signal to a plant community that some of its members are under attack by herbivores, is an open question.[75] The control of plant defense gene activity by external chemical signals derived from naturally occurring lead compounds is a promising strategy in plant protection.

6. Modulating the Sensory Mechanisms of Higher Plants: Prospects for Improving Crops and Crop Protection

The sensory capabilities of a higher plant are stunning and of an unexpected complexity. Yet, we know about only a few processes in some detail. The bewildering number of receptor-like kinases without known functions, the large number of phosphorelay components encoded in the genome—only a few of which have an assigned function—the emergence of peptide signals—undoubtedly only the tip of an iceberg—together with indications of a large family of genes encoding peptide–transporter-like proteins[1,76] are only a few indications of the uniqueness of higher plants. Further examples encompass the transcriptional regulators: Of the known 26 families of transcriptional regulators, 19 are unique to plants.[1] In addition, there is an indication that many more genes encode cell-cycle-related proteins in *Arabidopsis thaliana* than even in man.[77] Another area of plant expertise is in target-protein-specific proteolysis, as evident by the large number of E3-type ubiquitin protein ligases in the *Arabidopsis* genome. Such mechanisms appear to be intimately involved in the control of transcription in higher plants mediating both light responses and hormonal responses.[77]

On the other hand, many important signaling devices of animals and man are absent, or nearly absent in the plant: there are no receptor tyrosine kinases, only very few—highly divergent—7-transmembrane-receptor-like proteins and G-protein-subunit-like proteins encoded in the *Arabidopsis thaliana* genome, and there are no retinylidene photoreceptors in higher plants, to name but a few examples.[1]

The earlier notion that understanding the biology of animals and yeast cells will suffice to understand that of plants, can no longer be upheld. The physiological uniqueness of higher plants has now become clear, even in such basic mechanisms as the regulation of the cell cycle or transcriptional control.[39a] This is even more true with respect to the plant's sensory mechanisms, which are almost completely different from those of animals and mostly different from those of fungi. Besides justifying intensive research in the physiology of the plant cell and the multicellular plant organism at all levels, the molecular uniqueness of plants provides many chances of modulating plant processes either chemically and/or genetically in a plant-selective manner.

It is easy to foresee that future plant breeding will target plant sensory mechanisms to improve growth, productivity, and health; in addition, plant protection may benefit from the knowledge of such processes.

As an early example, the constitutive expression of phyA in tobacco has been used to generate shorter plants.[78] In contrast to phyB, which, when activated, increases internode length (shade avoidance response, Table 1), phyA induces the reverse effect (photomorphogenic reduction of stem growth in the light). Tobacco plants constitutively expressing a higher than normal level of *phyA* against the normal background of *phyB* indeed show a reduction in growth rate in the light caused by a physiological dominance of phyA over phyB.[78] In an interesting experiment, again using tobacco, Gan and Amasino[79] transformed plants with the *Agrobacterium ipt* gene controlled by the senescence-activated promoter of the SAG12 gene (pSAG12). The onset of senescence activates the transcription of the *ipt* gene whose gene product, isopentenyl transferase, catalyzes the initial step of cytokinin biosynthesis (the prenyl transfer from isopentenyl pyrophosphate to 5′-AMP) to give isopentenyladenosine-5′-monophosphate. Cytokinins (Scheme 2) are phytohormones that retard senescence. The accumulation of cytokinins as a result of *ipt* activity terminates the senescence process and this down-regulates the transcription of pSAG12-controlled *ipt*. Plants expressing this self-attenuating control circuit designed to counteract senescence, indeed, show a dramatically retarded leaf senescence concurrent with much longer productive photosynthetic CO_2 fixation, but they flower and fruit normally.[79] With the phytohormones so deeply involved in regulating plant development, the modulation of hormone homeostasis in a time- and tissue-controlled manner holds great promise for the breeding of improved agricultural varieties such as shorter cereals which are less prone to topping down.

Working out the individual functions of the hundreds of LRR receptor kinases of a higher plant will undoubtedly allow genetic approaches to be greatly focussed on altering plant development and pathogen resistance, the latter by establishing combinations of resistance genes with particularly broad effectivity. A new area of chemical pest control may even lie ahead of us which is targeted more towards activating plant resistance rather than to eradicating the pest. Such strategies will perhaps combine a higher degree of selectivity for plants with less side effects on other organisms, including man, and might be a powerful complement to today's tools of plant protection.

The jasmonate signaling system is a potential target for the deliberate control of inducible plant resistance. Jasmonate itself or its methyl ester are not suitable as such, because of their volatility and adverse side effects (reduction of transpiration, growth inhibition, promotion of senescence). It was thus of importance to see if chemical design of the jasmonate lead structure would allow adverse side effects to be reduced

while retaining the desired biological activity. Using the elicitation of antimicrobial benzophenanthridine alkaloids in an *Eschscholzia californica* tissue culture system, Blechert and colleagues have indeed provided clear evidence for this notion. They have designed synthetic jasmonates with strong elicitation capacity, which, however, show considerably reduced senescence promotive properties, do not affect stomatal function (transpiration), and have almost no inhibitory side effects on growth.[68]

In conclusion, higher plants are nothing less than simply light-driven chemical factories, slowly growing and passively dwelling in their habitat. Moreover, they permanently monitor their environment using a stunningly complex array of unique, specific, and highly sensitive sensors perfectly adapted to their needs. Thus, they are as highly evolved as animals and man, no less complex, no less fascinating, no less important. The (simple) ability of an animal or of man to move around has often been perceived as an (intuitive) indicator of evolutionary achievement in contrast to the immobile plant, but we are now well advised to abandon this notion.

This work was funded by the Deutsche Forschungsgemeinschaft and Fonds der Chemischen Industrie. The author wishes to express his apologies to all those whose work could not be cited or discussed, because of space constraints and the task of providing a broad overview over the highly diversified field of plant sensorics with a very substantial body of original publications within the last couple of years alone. For these reasons, recent reviews have been cited wherever possible.

Received: March 12, 2002 [A525]

[1] The Arabidopsis Genome Initiative, *Nature* **2000**, *408*, 796 – 815.
[2] K. A. Feldmann, R. L. Malenberg, C. Dean in *Arabidopsis* (Eds.: E. M. Meyerowitz, C. R. Somerville), Cold Spring Harbor Laboratory Press, Cold Spring Harbor, **1994**, pp. 137 – 172.
[3] a) M. C. Pirrung, *Chem. Biol.* **1999**, *6*, R167-R175; b) P. Thomason, R. Kay, *J. Cell Sci.* **2000**, *113*, 3141 – 3150; c) G. E. Schaller, *Adv. Bot. Res.* **2000**, *32*, 109 – 148; d) A. M. Stock, V. L. Robinson, P. N. Goudreau, *Annu. Rev. Biochem.* **2000**, *69*, 183 – 215; e) T. Urao, K. Yamaguchi-Shinozaki, K. Shinozaki, *Trends Plant Sci.* **2000**, *5*, 67 – 74; f) G. M. Pao, M. H. Saier, Jr., *J. Mol. Evol.* **1997**, *44*, 605 – 613; g) I. Hwang, H.-C. Chen, J. Sheen, *Plant Physiol.* **2002**, *129*, 500 – 515.
[4] M. G. Surette, M. Levit, Y. Liu, G. Lukat, E. G. Ninfa, A. Ninfa, J. B. Stock, *J. Biol. Chem.* **1996**, *271*, 939 – 945.
[5] a) C. Chang, S. F. Kwok, A. B. Bleecker, E. M. Meyerowitz, *Science* **1993**, *262*, 539 – 544; b) J. Hua, C. Chang, Q. Sun, E. M. Meyerowitz, *Science* **1995**, *269*, 1712 – 1714; c) J. Hua, H. Sakai, S. Nourizadeh, Q. G. Chen, A. B. Bleecker, J. R. Ecker, E. M. Meyerowitz, *Plant Cell* **1998**, *10*, 1321 – 1332; d) H. Sakai, J. Hua, Q. G. Chen, C. Chang, L. J. Medrano, A. B. Bleecker, E. M. Meyerowitz, *Proc. Natl. Acad. Sci. USA* **1998**, *95*, 5812 – 5817.
[6] G. E. Schaller, A. B. Bleecker, *Science* **1995**, *270*, 1809 – 1811.
[7] a) T. Hirayama, J. M. Alonso, *Plant Cell Physiol.* **2000**, *41*, 548 – 555; b) F. I. Rodriguez, J. J. Esch, A. E. Hall, B. M. Binder, G. E. Schaller, A. B. Bleecker, *Science* **1999**, *283*, 996 – 998.
[8] C. Chang, J. A. Shockey, *Curr. Opin. Plant Biol.* **1999**, *2*, 352 – 358.
[9] a) J. Hwang, J. Sheen, *Nature* **2001**, *413*, 383 – 389; b) C. Fankhauser, *Trends Plant Sci.* **2002**, *7*, 143 – 145.
[10] T. Kakimoto, *Science* **1996**, *274*, 982 – 985.
[11] T. Inoue, M. Higuchi, Y. Hashimoto, M. Seki, M. Kobayashi, T. Kato, S. Tabata, K. Shinozaki, T. Kakimoto, *Nature* **2001**, *409*, 1060 – 1063.
[12] C. Ueguchi, S. Sato, T. Kato, S. Tabata, *Plant Cell Physiol.* **2001**, *42*, 751 – 755.
[13] a) J. L. Spudich, C.-S. Yang, K.-H. Jung, E. N. Spudich, *Annu. Rev. Cell Dev. Biol.* **2000**, *16*, 365 – 392; b) O. A. Sineshchekov, K.-H. Jung, J. L. Spudich, *Proc. Natl. Acad. Sci. USA* **2002**, *99*, 8689 – 869.
[14] a) P. Hegemann, W. Gartner, R. Uhl, *Biophys. J.* **1991**, *60*, 1477 – 1489; b) P. Hegemann, *Planta* **1997**, *203*, 265 – 274; c) G. Nagel, D. Ollig, M. Fuhrmann, S. Kateriya, A. M. Musti, E. Bamberg, P. Hegemann, *Science* **2002**, *296*, 2395 – 2398.
[15] H. Kandori, K. Shimono, Y. Sudo, M. Iwamoto, Y. Shichida, N. Kamo, *Biochemistry* **2001**, *40*, 9238 – 9246, and references therein.
[16] a) C. Fankhauser, J. Chory, *Annu. Rev. Cell Dev. Biol.* **1997**, *13*, 203 – 229; b) S. J. Davies, A. V. Vener, R. D. Vierstra, *Science* **1999**, *286*, 2517 – 2520.
[17] a) C. Fankhauser, *J. Biol. Chem.* **2001**, *276*, 11453 – 11456; b) P. Más, P. F. Devlin, S. Panda, S. A. Kay, *Nature* **2000**, *408*, 207 – 211.
[18] S.-H. Bhoo, S. J. Davies, J. Walker, B. Karniol, R. D. Vierstra, *Nature* **2001**, *414*, 776 – 779.
[19] C. W. Mullineaux, *Mol. Microbiol.* **2001**, *41*, 965 – 971.
[20] K. C. Yeh, S. H. Wu, J. T. Murphy, J. C. Lagarias, *Science* **1997**, *277*, 1505 – 1508.
[21] J. F. Martinez-Garcia, E. Huq, P. H. Quail, *Science* **2000**, *288*, 859 – 863.
[22] A. Sancar, *Biochemistry* **1994**, *33*, 2 – 9.
[23] a) W. R. Briggs, E. Huala, *Annu. Rev. Cell Dev. Biol.* **1999**, *15*, 33 – 62; b) C. Lin, *Trends Plant Sci.* **2000**, *8*, 337 – 342; M. Ahmad, *Curr. Opin. Plant Biol.* **1999**, *2*, 230 – 235; W. Marwan, *BIOspektrum* **1999**, *5*, 443 – 448.
[24] a) J. M. Christie, W. R. Briggs, *J. Biol. Chem.* **2001**, *276*, 11457 – 11460; W. R. Briggs, J. M. Christie, *Trends Plant Sci.* **2002** *7*, 204 – 210.
[25] H.-Q. Yang, Y.-J. Wu, R.-H. Tang, D. Liu, Y. Liu, A. R. Cashmore, *Cell* **2000**, *103*, 815 – 827.
[26] H. Wang, L.-G. Ma, J.-M. Li, H.-Y. Zhao, X. W. Deng, *Science* **2001**, *294*, 154 – 158.
[27] G. T. J. van der Horst, M. Muijtjens, K. Kobayashi, R. Takano, S.-I. Kanno, M. Takao, J. de Wit, A. Verkerk, A. P. M. Eker, D. van Leenen, R. Buijs, D. Bootsma, J. H. J. Hoeijmakers, A. Yasui, *Nature* **1999**, *398*, 627 – 630.
[28] a) O. Kleiner, S. Kircher, K. Harter, A. Batschauer, *Plant J.* **1999**, *19*, 289 – 296; b) H. Go, H. Duong, N. Ma, C. Lin, *Plant J.* **1999**, *19*, 279 – 287.
[29] T. Kondo, M. Ishiura, *Trends Plant Sci.* **1999**, *4*, 171 – 176.
[30] D. E. Somers, P. F. Devlin, S. A. Kay, *Science* **1998**, *282*, 1488 – 1490.
[31] M. Ahmad, A. R. Cashmore, *Nature* **1993**, *366*, 162 – 166.
[32] E. Liscum, W. R. Briggs, *Plant Cell* **1995**, *7*, 473 – 485.
[33] E. Huala, P. W. Oeller, E. Liscum, I.-S. Han, E. Larsen, W. R. Briggs, *Science* **1997**, *278*, 2120 – 2130.
[34] J. A. Jarillo, M. Ahmad, A. R. Cashmore, *Plant Physiol.* **1998**, *117*, 719.
[35] M. Salomon, J. M. Christie, E. Knieb, U. Lempert, W. R. Briggs, *Biochemistry* **2000**, *39*, 9401 – 9410.
[36] a) S. Crosson, K. Moffat, *Proc. Natl. Acad. Sci. USA* **2001**, *98*, 2995 – 3000; b) T. E. Swartz, S. B. Corchnoy, J. M. Christie, J. W. Lewis, J. Szundi, W. R. Briggs, R. A. Bogomolni, *J. Biol. Chem.* **2001**, *276*, 36493 – 36500.
[37] M. Salomon, W. Eisenreich, H. Dürr, E. Schleicher, E. Knieb, V. Massey, W. Rüdiger, F. Müller, A. Bacher, G. Richter, *Proc. Natl. Acad. Sci. USA* **2001**, *98*, 12357 – 12361.

[38] a) J. A. Jarillo, H. Gabrys, J. Capel, J. M. Alonso, J. R. Ecker, A. R. Cashmore, *Nature* **2001**, *410*, 952 – 954; b) T. Kagawa, T. Sakai, N. Suetsugu, K. Oikawa, S. Ishiguro, T. Kato, S. Tabata, K. Okada, M. Wada, *Science* **2001**, *291*, 2138 – 2141; c) T. Sakai, T. Kagawa, M. Kasakava, T. E. Swartz, J. M. Christie, W. R. Briggs, M. Wada, K. Okada, *Proc. Natl. Acad. Sci. USA* **2001**, *98*, 6969 – 6974; d) T. Kinoshita, M. Doi, N. Suetsugu, T. Kayawa, M. Wada, K.-J. Shimazaki, *Nature* **2001**, *414*, 656 – 660.

[39] a) E. Meyerowitz, *Science* **2002**, *294*, 1482 – 1485; b) S.-H. Shiu, A. B. Bleecker, *Proc. Natl. Acad. Sci. USA* **2001**, *98*, 10763 – 10768.

[40] a) K. Schumacher, J. Chory, *Curr. Opin. Plant Biol.* **2000**, *3*, 79 – 84; b) J. Li, J. Chory, *Cell* **1997**, *90*, 929 – 938; c) Z.-Y. Wang, H. Seto, S. Fujioka, S. Yoshida, J. Chory, *Nature* **2001**, *410*, 380 – 383.

[41] S. E. Clark, R. W. Williams, E. M. Meyerowitz, *Cell* **1997**, *89*, 575 – 585.

[42] W.-Y. Song, G.-L. Wang, L.-L. Chen, H.-S. Kim, T. Holsten, J. Gardner, B. Wang, W.-X. Zhai, L.-H. Zhu, *Science* **1995**, *270*, 1804 – 1806.

[43] L. Gomez-Gomez, T. Boller, *Mol. Cell* **2000**, *5*, 1003 – 1011.

[44] a) K. U. Torii, *Curr. Opin. Plant Biol.* **2000**, *3*, 361 – 367; b) T. Nürnberger, D. Scheel, *Trends Plant Sci.* **2001**, *6*, 372 – 379.

[45] a) J. M. Scheer, C. A. Ryan, Jr., *Proc. Natl. Acad. Sci. USA* **2002**, *99*, 9585 – 9590; b) G. Ender, A. Kereszt, Z. Kevei, S. Mihacea, P. Kalo, G. B. Kiss, *Nature* **2002**, *417*, 962 – 966; c) S. Stracke, C. Kistner, S. Yoshida, L. Mulder, S. Sato, T. Kaneko, S. Tabata, N. Sandal, J. Stougaard, K. Szczyglowski, M. Parniska, *Nature* **2002**, *417*, 959 – 962..

[46] J. Nasrallah, M. Nasrallah, *Plant Cell* **1993**, *5*, 1325 – 1335.

[47] T. Romeis, *Curr. Opin. Plant Biol.* **2001**, *4*, 407 – 414.

[48] a) J. C. Fletcher, U. Brand, M. P. Running, R. Simon, E. M. Meyerowitz, *Science* **1999**, *283*, 1911 – 1914; b) A. E. Trotochaud, T. Hao, G. Wu, Z. Yang, S. E. Clark, *Plant Cell* **1999**, *11*, 393 – 405.

[49] a) C. Schopfer, M. Nasrallah, J. Nasrallah, *Science* **1999**, *286*, 1697 – 1700; b) S. Takayama, H. Shiba, M. Iwano, H. Shimosato, F.-S. Che, N. Kai, M. Watanabe, G. Suzuki, K. Hinata, A. Isogai, *Proc. Natl. Acad. Sci. USA* **2000**, *97*, 1920 – 1925.

[50] M. Zasloff, *Nature* **2002**, *415*, 389 – 395.

[51] a) K. Lindsey, S. Casson, P. Chilley, *Trends Plant Sci.* **2002**, *7*, 78 – 83; b) C. A. Ryan, G. Pearce, *Plant Physiol.* **2001**, *125*, 65 – 68; b) J. M. Cock, S. McCormick, *Plant Physiol.* **2001**, *126*, 939 – 942.

[52] a) T. Asai, G. Tena, J. Plotnikova, M. R. Willmann, W.-L. Chiu, L. Gomez-Gomez, T. Boller, F. M. Ausubel, J. Sheen, *Nature* **2002**, *415*, 977 – 983; b) A. Sharma, M. Matsuoka, H. Tanaka, S. Komatsu, *FEBS Lett.* **2001**, *507*, 346 – 350.

[53] a) G. Pearce, D. Strydom, S. Johnson, C. A. Ryan, *Science* **1991**, *253*, 895 – 897; b) C. P. Constabel, L. Yip, C. A. Ryan, *Plant Mol. Biol.* **1998**, *26*, 55 – 62; c) G. Pearce, D. S. Moura, J. Stratmann, C. A. Ryan, *Nature* **2001**, *411*, 817 – 820; d) G. Pearce, D. S. Moura, J. Stratmann, C. A. Ryan, *Proc. Natl. Acad. Sci. USA* **2001**, *98*, 12843 – 12847.

[54] a) Y. Matsubayashi, Y. Sakagami, *Proc. Natl. Acad. Sci. USA* **1996**, *93*, 7623 – 7627; b) Y. Matsubayashi, A. Morita, E. Matsunaga, A. Furuya, N. Hanai, Y. Sakagami, *Planta* **1999**, *207*, 559 – 565; c) T. Kobayashi, C. H. Eun, H. Hanai, Y. Matsubayashi, Y. Sakagami, H. Kamada, *J. Exp. Bot.* **1999**, *50*, 1123 – 1128; d) Y. Matsubayashi, M. Ogawa, A. Morita, Y. Sakagami, *Science* **2002**, *296*, 1470 – 1472.

[55] H. Röhrig, J. Schmidt, E. Miklashevichs, J. Schell, M. John, *Proc. Natl. Acad. Sci. USA* **2002**, *99*, 1915 – 1920.

[56] C. A. Ryan, *Plant Mol. Biol.* **1992**, *19*, 123 – 133.

[57] C. A. Ryan, *Annu. Rev. Plant Physiol.* **1973**, *24*, 173 – 196.

[58] a) C. A. Ryan, G. Pearce, *Annu. Rev. Cell Dev. Biol.* **1998**, *14*, 1 – 17; b) A. Schaller, C. A. Ryan, *BioEssays* **1995**, *18*, 27 – 33.

[59] G. A. Howe, J. Lightner, J. Browse, C. A. Ryan, *Plant Cell* **1996**, *8*, 2067 – 2077.

[60] E. E. Farmer, C. A. Ryan, *Proc. Natl. Acad. Sci. USA* **1990**, *87*, 7713 – 7716.

[61] T. Albrecht, A. Kehlen, K. Stahl, H.-D. Knöfel, G. Sembdner, E. W. Weiler, *Planta* **1993**, *191*, 86 – 94.

[62] a) P. M. Sanders, P. Y. Lee, C. Biesgen, J. D. Boone, T. P. Beals, E. W. Weiler, R. B. Goldberg, *Plant Cell* **2000**, *12*, 1041 – 1061; b) A. Stintzi, J. Browse, *Proc. Natl. Acad. Sci. USA* **2000**, *97*, 10625 – 10630.

[63] B. A. Vick, D. C. Zimmermann, *Plant Physiol.* **1984**, *75*, 458 – 461.

[64] F. Schaller, *J. Exp. Bot.* **2001**, *52*, 11 – 23.

[65] I. Kubigsteltig, D. Laudert, E. W. Weiler, *Planta* **1999**, *208*, 463 – 471.

[66] S. Ishiguro, K.-O. Akido, J. Ueda, I. Nishida, K. Okada, *Plant Cell* **2001**, *13*, 2191 – 2209.

[67] a) E. W. Weiler, *Naturwissenschaften* **1997**, *84*, 340 – 349; b) E. W. Weiler, D. Laudert, B. A. Stelmach, P. Hennig, C. Biesgen, I. Kubigsteltig in *Insect-plant interactions and induced plant defence* (Ed.: J. A. Pickett), Wiley, Chichester, **1999**, pp. 191 – 204.

[68] a) S. Blechert, O. Brümmer, M. Füsslein, S. Hölder, C. Bockelmann, T. Kutchan, E. W. Weiler, M. H. Zenk, *J. Chem. Soc. Perkin 1* **1997**, 3549 – 3559; b) S. Blechert, C. Bockelmann, M. Füsslein, T. von Schrader, B. A. Stelmach, U. Niesel, E. W. Weiler, *Planta* **1999**, *207*, 470 – 479.

[69] A. Stintzi, H. Weber, P. Reymond, J. Browse, E. E. Farmer, *Proc. Natl. Acad. Sci. USA* **2001**, *98*, 12837 – 12842.

[70] B. A. Stelmach, A. Müller, P. Hennig, S. Gebhardt, M. Schubert-Zsilavecz, E. W. Weiler, *J. Biol. Chem.* **2001**, *276*, 12832 – 12838.

[71] W. Song, C. D. Funk, A. R. Brash, *Proc. Natl. Acad. Sci. USA* **1993**, *90*, 8519 – 8523.

[72] a) E. E. Farmer, *Nature* **2001**, *411*, 854 – 856; b) W. Boland, J. Hopke, J. Donath, J. Nüske, F. Bublitz, *Angew. Chem.* **1995**, *107*, 1715 – 1717; *Angew. Chem. Int. Ed. Engl.* **1995**, *34*, 1600 – 1602.

[73] J. Takabayashi, M. Dicke, *Trends Plant Sci.* **1996**, *1*, 109 – 113.

[74] G. Arimura, R. Ozawa, T. Shimoda, T. Nishioka, W. Boland, J. Takabayashi, *Nature* **2000**, *406*, 512 – 515.

[75] J. A. Pickett, G. M. Poppy, *Trends Plant Sci.* **2001**, *6*, 137 – 139.

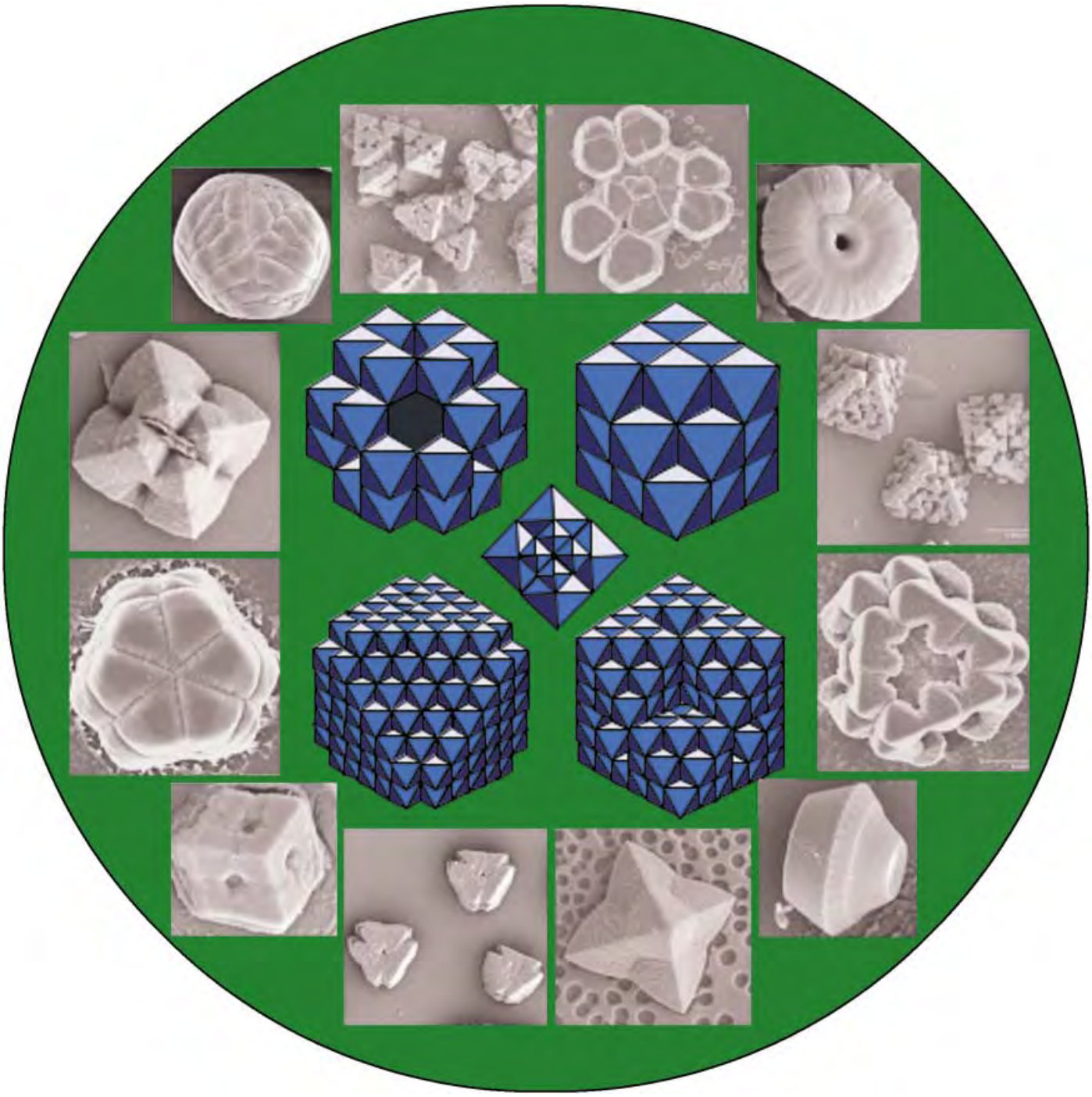
[76] a) F. F. Assaad, *Curr. Opin. Plant Biol.* **2001**, *4*, 478 – 487; b) H. Schoof, H. W. Mewes, *BioSpektrum* **2001**, *7*, 234 – 238; c) G. Stacey, S. Koh, C. Granger, J. M. Becker, *Trends Plant Sci.* **2002**, *7*, 257 – 263.

[77] a) A. Bachmair, M. Novatchkova, T. Potuschak, F. Eisenhaber, *Trends Plant Sci.* **2001**, *6*, 463 – 470; b) A. Ciechanover, A. Orian, A. L. Schwartz, *BioEssays* **2000**, *22*, 442 – 451; c) O. Leyser, *Curr. Opin. Plant Biol.* **2001**, *4*, 382 – 386; d) J. C. del Pozo, M. Estelle, *Trends Plant Sci.* **1999**, *4*, 107 – 112; e) C. Schwechheimer, G. Serino, J. Callis, W. L. Crosby, S. Lyapina, R. J. Deshaies, W. M. Gray, M. Estelle, X.-W. Deng, *Science* **2001**, *292*, 1379 – 1382; f) C. Schwechheimer, X.-W. Deng, *Trends Cell Biol.* **2001**, *11*, 420 – 426.

[78] P. R. H. Robson, A. C. MacCormac, A. S. Irvine, H. Smith, *BioTechnology* **1996**, *14*, 995 – 998.

[79] S. Gan, R. M. Amasino, *Science* **1995**, *270*, 1986 – 1988.

Communications



Using microscopic, polyhedral, self-assembled crystals as building blocks, large crystals and open mesophase structures that preserve the shape and orientation of the basic structural units are spontaneously formed. These structures are found to correlate well with those of simple geometrical models. For further information see the article by Liu and co-workers on the following pages.

 © 2003 Wiley-VCH Verlag GmbH & Co. KGaA, Weinheim 1433-7851/03/4204-0413 $ 20.00+.50/0

Self-Assembly with Crystals

Hierarchical and Self-Similar Growth of Self-Assembled Crystals**

Zhengrong R. Tian, Jun Liu, James A. Voigt, Bonnie Mckenzie, and Huifang Xu*

Biomaterials, such as seashells[1,2] and diatoms[3] display rich morphologies and multiple-scale ordering. Recently remarkable biomaterial-like morphologies were reported in synthetic, self-assembled mesophase silicates.[4–8] The formation of these unusual shapes is related to curvature effects and is independent of the basic structural units.[4,5] Hierarchical mesoporous oxides and patterned films were prepared by combining micropatterning with surfactant self-assembly.[9–13] In addition, ordered patterns and open structures were assembled from millimeter-sized objects.[14–16] Synthetic materials containing biological patterns were also prepared using pre-existing templates.[17–19] Furthermore, fractal growth has been investigated in some simple crystalline systems.[20–22] Herein, we report a novel hierarchical and self-similar crystal-growth process leading to the spontaneous formation of large objects with controlled morphology and ordering from nano- to macro-scale. To our knowledge this is the first report of true hierarchical and self-similar crystal growth for self-assembled materials based on the assembly of microscopic polyhedral single crystals.

Self-assembled periodic silicates were first reported in 1992 from silicic acid and quaternary ammonium surfactants.[23,24] Since then hybrid silanes and bridged organic silsesquioxanes have been used to prepare mesoporous powders[25–28] and films.[29,30] Recently Inagaki and co-workers prepared well-defined hybrid mesoporous crystals using 1,2-bis(trimethoxysilyl)ethane (BTME) as a silica source and hexadecyltrimethylammonium chloride (CTAC) as a surfactant.[31] Herein, we use the hybrid organic silane BTME along with CTAC to create a new class of supported hierarchical mesophase crystals (that is, large mesophase structures formed from crystalline building blocks) through heterogeneous nucleation and growth.[32] BTME and CTAC were mixed in basic aqueous solutions and heated in a Teflon container. A microscope glass slide was placed vertically in the container to allow the crystals to nucleate and grow on the surface.

Well-defined and oriented mesophase crystals were formed on the glass surface within 30 minutes. Figure 1a shows a typical scanning electron microscopy (SEM) image of large arrays of the mesophase crystals. These crystals are rather uniform in shape and size (12 μm wide). Low-angle X-ray diffraction (XRD) and transmission electron microscopy (TEM) indicate that these mesophase crystals have a cubic structure (*Pm3n*, $a_o = 98$ Å) as reported in the literature.[31] Figure 1b shows a TEM image of the $<001>$ zone axis square lattice of the cubic structure. As will be discussed later, the crystals in Figure 1a are secondary octahedral structures formed from primary octahedral crystals, and are oriented with one of the {111} planes parallel to the substrate. We further demonstrated that these mesocrystals can be patterned on preformed polystyrene lines on glass substrates (Figure 1c). The formation of oriented mesophase crystals is significant for practical applications, but to date there have been few reports on how to prepare uniform and oriented self-assembled crystals. In contrast, the particles that precipitated from the solutions under similar conditions have a wide range of morphologies and have poorly defined shapes (Figure 1d).

Hierarchically ordered large crystals and open structures can be constructed through multiple and self-similar growth. Figure 2 and Figure 3 show some examples of the high-order structures and schematic representations of how they are formed. Figure 2a and 3a are the primary 5 μm octahedral crystals formed by the {111} planes of the cubic phase. Figure 2b shows a commonly observed rosette-like structure viewed from different angles, and indicate that these crystals

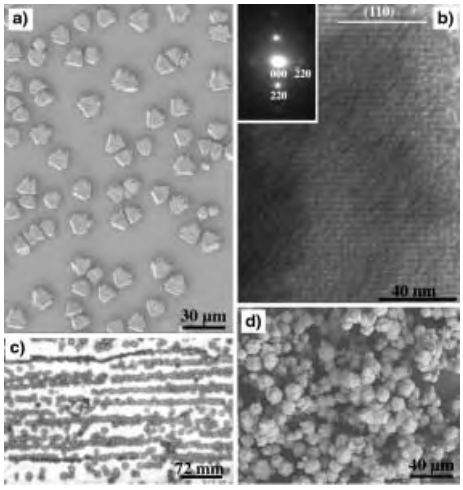


Figure 1. Oriented mesophase crystals on a glass substrate: a) large arrays of oriented mesophase crystals. One of the {111} planes of the mesocrystals is parallel to the glass surface, b) TEM image of the square lattice in the $<001>$ orientation, c) aligned mesophase crystals on patterned glass surface, d) heterogeneous particles precipitated from the solution.

[*] Dr. J. Liu, Dr. Z. R. Tian, Dr. J. A. Voigt, B. Mckenzie
Biomolecular Materials and Interfaces Department
Sandia National Laboratories
Albuquerque, NM 87185 (USA)
Fax: (+1) 505-844-5470
E-mail: jliu@sandia.gov
Dr. H. Xu
Department of Earth and Planetary Sciences
The University of New Mexico, Albuquerque, NM 87131 (USA)

[**] This work is supported by the Sandia National Laboratories Laboratory-Directed Research and Development Program (LDRD), and by the Materials Sciences and Engineering Division of the Basic Energy Science Office of the US Department of Energy. Sandia is a multiprogram national laboratory operated by Sandia Corporation, a Lockheed Martin Company, for the United States Department of Energy under contract DE-AC04-94AL85000. H.X. thanks NSF for supporting the TEM and XRD work. We would like to thank Dr. C. J. Brinker from Sandia National Laboratories for valuable discussions on the preparation of this manuscript.

 © 2003 Wiley-VCH Verlag GmbH & Co. KGaA, Weinheim 1433-7851/03/4204-0414 $ 20.00+.50/0

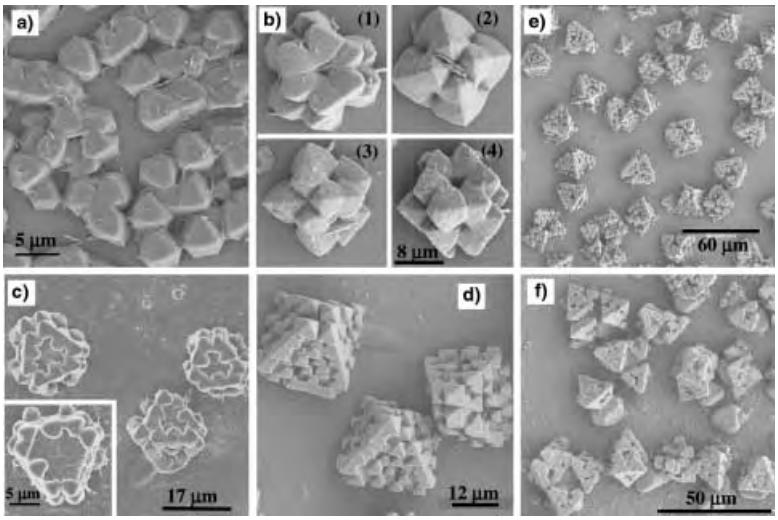


Figure 2. Hierarchically ordered octahedral open crystal structures: a) primary octahedral crystals, b) secondary octahedral crystals: 1) face-on, 2) top view from one corner, 3) edge-on, 4) tilted edge-on, c) tertiary octahedral crystals. The insert shows small octahedral units nucleated on a secondary rosette crystal, d) large open octahedral objects containing five primary octahedral units on each side, e) large area view of high-order open structures, f) large open structures assembled from tertiary units.

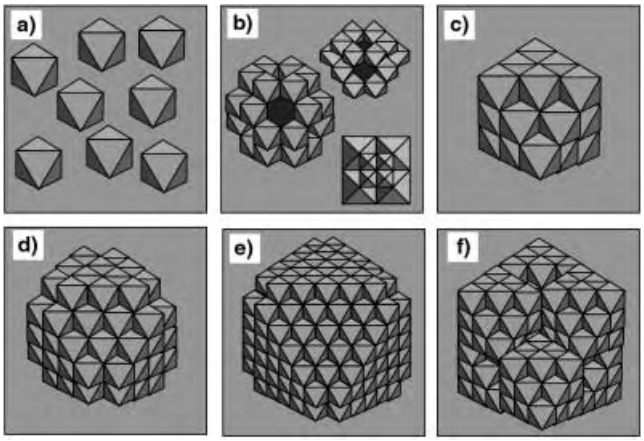


Figure 3. Schematic illustrations of edge-sharing stacking: a) primary octahedral units, face-on configurations, b) quartet-octahedron model for the secondary structure, c) tertiary structure with filled corners, d) tertiary structure with unfilled corners, e) a high-order structure from primary octahedra, f) a high-order structure from tertiary units.

are secondary structures made of primary octahedral subunits shown in Figure 2a. The secondary structure is about 11 μm in width, two times the size of the primary structure, and is based on a quartet-octahedron model with 24 edge-sharing octahedral primary subunits (Figure 3b). The model contains four surfaces made of six subunits and six corners made of four subunits. This model differs from the real crystal slightly in that the real crystal appears denser (no large voids at the center) than the model, which is not surprising because the open structure would have a tendency to grow to a higher density. The mesophase crystals can also become truncated by the substrate on certain orientations. For example, the face-on rosette (Figure 2b(1)) can be reproduced by truncating the quartet-octahedron model in the middle plane and by allowing the octahedral units to deform to permit denser packing. Similarly, the end-on (top) configuration (Figure 2b(2)) can be derived if only one third of the quartet-octahedron structure (8 units) is allowed to grow and the quartet on the bottom is allowed to grow to a larger size.

On a large length scale, high-order structures can be derived by edge-sharing growth. These large mesophase crystals are remarkable in several ways. First, these structures are not close-packed and contain large empty spaces (cages), but they still have almost perfect octahedral shapes. Second, the octahedral subunits in the large structure are all about 5 μm in size and are fairly uniform. These subunits are also well aligned throughout the crystal by edge sharing. Finally, the high-order octahedral mesophase crystals are also rather uniform in size. Figure 2c and Figure 3d show the tertiary octahedral structures containing three subunits on each side. The width of the tertiary structure is 16 μm, roughly three times the size of the primary crystal. Figure 2d (high magnification), 2e, and Figure 3e illustrate even higher order structures about 25 μm in width, which contain five units on each side. Furthermore, large open octahedral structures are not only formed from primary octahedral units, but can be also derived from secondary and tertiary structures. Figure 2f and Figure 3f show a high-order structure consisting of filled tertiary octahedral units (Figure 3c) that still preserve the overall octahedral shape.

Currently the detailed growth mechanism is still under investigation, but there is strong evidence that the large structures are formed through step-wise nucleation from the edges of previous crystals. The insert in Figure 2c is an incomplete tertiary structure, clearly showing new octahedral crystals formed on the edge of secondary crystals. Here, one side of the secondary structure is yet not covered with new crystals.

By systematically varying the experimental conditions, such as the temperature, surfactant concentration, and reaction time, a wide range of morphologies were observed based on polyhedral crystal stacking. Among these crystals (Figure 4) are triangular rosettes, round rosettes, flowerlike patterns, stars, cubelike cages, large rhombic dodecahedral structures.[33] Although the morphologies shown in Figure 4 appear to be complex, they are based on similar cubic crystal stacking and can be controlled. For example, a higher temperature and a higher surfactant concentration favor the formation of better defined, and more facetted crystals. Figures 4a and 4b are high magnification images of Figure 1a. These secondary crystals were formed after 3 h as compare to 30 minutes for the rosette crystals in Figure 2b. The crystals are almost octahedral in shape, but the individual octahedral units are no longer obvious. However, the tips of the individual octahedral units can still be observed when the crystals are tilted and it is possible to envision how these

 © 2003 Wiley-VCH Verlag GmbH & Co. KGaA, Weinheim 1433-7851/03/4204-0415 $ 20.00+.50/0

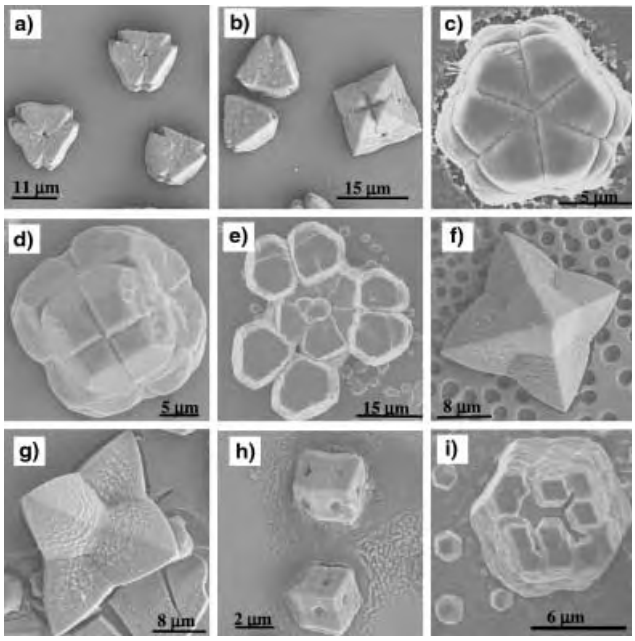


Figure 4. Various morphologies of mesophase crystals formed on glass surfaces through polyhedral stacking: a) triangular rosettes, b) tilted triangular rosettes, c) rounded rosettes, d) tilted rounded rosettes, e) flowerlike patterns, f) stars, g) tilted stars, h) cubelike cages by face-sharing growth, i) large rhombic dodecahedra by face-sharing growth.

crystals can be derived from the quartet-octahedron. Similarly, the morphologies in Figure 4c and Figure 4d share the same origin as the quartet model, except here some surfaces of the octahedral subunits are truncated. The flowerlike pattern in Figure 4e is formed by growing truncated octahedral crystals on the tips of the octahedral subunits in the rosette.

We have also shown that different mesophase crystals can be formed through different stacking patterns, and grown with different orientations. For example, the starlike particles shown in Figure 4f and 4g are derived from six edge-sharing octahedral units with some deformation of the primary crystals. The cubelike cages and the large rhombic dodecahedron in Figure 4h and Figure 4i are formed through face-on stacking of different kinds of subunits. The formation of different crystal shapes with different orientations will be the subject of future publications.

In conclusion, we have demonstrated true multiscale hierarchical structures through self-similar assembly of polyhedral mesophase crystals. This work shows that complex structures and morphologies can be derived from the fundamental microscopic building units, and the final morphologies are correlated with the structure and shape of the basic crystal. Octahedral edge-sharing stacking is commonly observed in true atomic crystals,[34] but extensive and continuous 3D open structures through edge sharing as reported herein are rare. The unusual hierarchical structures and the complex morphologies may shed new light on self-assembly and crystal growth. These results also point to how one can start with basic structural units to design and build large hierarchical structures with controlled size, orientation, and morphology. This approach can be adapted for large-scale preparation on patterned substrates. In nature, hierarchical ordering is critical for the functional needs of biomaterials. Synthetic materials containing biomimetic patterns mostly involve using a pre-existing patterns and template.[14–19] Some of the morphologies observed show similarities with those from diatoms, and therefore may lead to new thinking on how these biominerals are formed. The ability to spontaneously form such ordered hierarchical structures could lead to novel applications of self-assembled materials.

Experimental Section

A typical molar ratio for BTME:CTAC:NaOH:H_2O is 1:*x*:2.36:353, where *x* (the concentration of the surfactant) was varied from 0.45 to 1.70. After BTME, CTAC , NaOH, and H_2O were mixed together, the resulting solutions were stirred and aged overnight. Only solutions that became clear after aging were used for our experiments. The aged solution was transferred to a Teflon container. A microscope glass slide (or tin oxide coated glass slide) was placed vertically in the Teflon container. The reaction temperature ranged from room temperature to 115°C. High-order crystals, such as shown in Figures 2c to 2f were formed by repeated growth under the same conditions.

The XRD results were obtained on a Scintag PADV diffractometer at the University of New Mexico, with six peaks at 69, 48, 45, 40, 31, and 25 Å assigned to the 110, 200, 210, 211, 310, and 400 reflections of the *Pm3n* structure ($a_o = 98$ Å). The TEM image was obtained on a JEOL 2010 high-resolution microscope at 200 keV.

Received: August 16, 2002 [Z19982]

[1] A. P. Kackson, J. F. V. Vincent, R. M. Turner, *Proc. R. Soc. London Ser. B* **1998**, *234*, 415.
[2] A. M. Belcher, X. H. Wu, R. J. Christensen, P. K. Hansma, G. D. Stucky, D. E. Morse, *Nature* **1996**, *381*, 56.
[3] M. Sumper, *Science* **2002**, *295*, 2430.
[4] H. Yang, N. Coombs, G. A. Ozin, *Nature* **1997**, *386*, 692.
[5] G. A. Ozin, *Can. J. Chem.* **1999**, *77*, 2001.
[6] D. Zhao, J. Sun, Q. Li, G. D. Stucky, *Chem. Mater.* **2000**, *12*, 275.
[7] C. H. Lee, S. S. Park, S. J. Choe, D. H. Park, *Microporous Mesoporous Mater.* **2001**, *46*, 257.
[8] A. Sayari, S. Hamoudi, Y. Yang, I. L. Moudrakovski, J. R. Ripmeester, *Chem. Mater.* **2000**, *12*, 3857.
[9] H. Yang, M. Coombs, G. A. Ozin, *Adv. Mater.* **1997**, *9*, 811.
[10] M. Trau, N. Yao, E. Kim, Y. Xia, G. M. Whitesides, I. A. Aksay, *Nature* **1997**, *390*, 674.
[11] P. Yang, T. Deng, D. Zhao, P. Feng, D. Pine, B. F. Chmelka, G. M. Whitesides, G. D. Stucky, *Science* **1998**, *282*, 2244.
[12] P. Yang, G. Wirnsberger, H. C. Huang, S. R. Cordero, M. D. McGehee, B. Scott, T. Deng, G. M. Whitesides, B. F. Chmelka, S. K. Buratto, G. D. Stucky, *Science* **2000**, *287*, 465.
[13] D. A. Doshi, N. K. Heusing, M. Lu, H. Fan, Y. Lu, K. Simmons-Potter, B. G. Potter, Jr., A. J. Hurd, C. J. Brinker, *Science* **2000**, *290*, 107.
[14] N. Bowden, A. Terfort, J. Carbeck, G. M. Whitesides, *Science* **1997**, *276*, 233.
[15] T. L. Breen, J. Tien, S. J. Oliver, T. Hadzic, G. M. Whitesides, *Science* **1999**, *284*, 948.
[16] D. H. Gracias, J. Tien, T. L. Breen, C. Hsu, G. M. Whitesides, *Science* **2000**, *289*, 1170.
[17] S. Mann, D. D. Archibald, J. M. Didymus, T. Douglas, B. R. Heywood, F. , C. Meldrum, N. J. Reeves, *Science* **1993**, *261*, 1286.

 © 2003 Wiley-VCH Verlag GmbH & Co. KGaA, Weinheim 1433-7851/03/4204-0416 $ 20.00+.50/0

[18] S. S. Kim, W. Zhang, T. J. Pinnavaia, *Science* **1998**, *282*, 1302.
[19] Y. Shin, J. Liu, J. H. Chang, Z. Nie, G. J. Exarhos, *Adv. Mater.* **2001**, *13*, 728.
[20] M. Wu, X.-Y. Liu, C. S. Strom, P. Bennema, W. van Enckevort, N.-B. Ming, *Phys. Rev. Lett.* **1998**, *80*, 3089.
[21] S. Busch, H. Dolhaine, A. DuChesne, S. Heinz, O. Hochrein, F. Laeri, O. Podebrad, U. Vietze, T. Weiland, R. Kniep, *Eur. J. Inorg. Chem.* **1999**, 1643.
[22] C. S. Strom, P. F. P. Grimbergen, P. Bennema, H. Meekes, M. A. Verheijen, L. J. P. Vogels, M. Wang in *Molecular Modeling Applications in Crystallization* (Ed.: A. S. Myerson), Cambridge University Press, Cambridge, **1999**, pp. 228–312.
[23] C. T. Kresge, M. E. Leonowicz, W. J. Roth, J. C. Vartuli, J. S. Beck, *Nature* **1992**, *359*, 710.
[24] J. S. Beck, J. C. Vartuli, W. J. Roth, M. E. Leonowicz, C. T. Kresge, K. D. Schmitt, C. T.-W. Chu, D. H. Olson, E. W. Sheppard, S. B. McCullen, J. B. Higgins, J. L. Schlenker, *J. Am. Chem. Soc.* **1992**, *114*, 10834.
[25] S. Inagaki, S. Guan, Y. Fukushima, T. Ohsuna, O. Terasaki, *J. Am. Chem. Soc.* **1999**, *121*, 9611.
[26] M. H. Lim, A. Stein, *Chem. Mater.* **1999**, *11*, 3285.
[27] T. Asefa, M. J. MacLachlan, N. Coombs, G. A. Ozin, *Nature* **1999**, *402*, 867.
[28] Many papers have been published in this area by many groups, which include those of Professors Ozin, Stein, Sayari, Inagaki. A complete list of publications is beyond the purpose of this paper, but Professor Stein published a good review article: A. Stein, B. J. Melde, R. C. Schroden, *Adv. Mater.* **2000**, *12*, 1403.
[29] O. Dag, C. Yoshina-Ishii, T. Asefa, M. J. MacLachlan, H. Grondey, N. Coombs, G. A. Ozin, *Adv. Funct. Mater.* **2001**, *11*, 213.
[30] H. Y. Fan, S. Reed, T. Baer, R. Schunk, G. P. Lopez, C. J. Brinker, *Microporous Mesoporous Mater.* **2001**, *44*, 625.
[31] S. Guan, S. Inagaki, T. Ohsuna, O. Terasaki, *J. Am. Chem. Soc.* **2000**, *122*, 5660.
[32] B. C. Bunker, P. C. Rieke, B. J. Tarasevich, A. A. Campbell, G. E. Fryxell, G. L. Graff, S. Song, J. Liu, J. W. Virden, *Science* **1994**, *264*, 48.
[33] Other curved morphologies such as discoids, doughnuts, and cupcakes were also observed at a lower surfactant concentration. The curved geometry is consistent with the curved shapes reported in hexagonal mesophase materials and will not be discussed here.
[34] A. F. Wells, *Structural Inorganic Chemistry Clarendon Press*, 5th ed., Oxford University Press, Oxford, **1984**.

Metalloprotein Conformation

Sliding Helix and Change of Coordination Geometry in a Model Di-Mn^{II} Protein**

William F. DeGrado, Luigi Di Costanzo, Silvano Geremia, Angela Lombardi, Vincenzo Pavone, and Lucio Randaccio*

In metalloenzymes, the protein matrix tunes the dynamic and structural properties of their metal ion cofactors to catalyze a wide range of reactions with remarkable catalytic efficiencies.[1] As the reaction proceeds, the metal ions must cycle between different ligation and sometimes also oxidation states;[2] the protein plays an active role in stabilizing and catalyzing the interconversion of these intermediates.[3–5] Shifts of key carboxylate side chains and other localized motions are often observed in response to changes in oxidation state and the binding of exogenous ligands.[6–8] The de novo design of novel artificial proteins that have predictable structures and functions is the most challenging goal in protein design and mimicry. Creating functional artificial metalloproteins requires a detailed understanding of the protein-folding mechanism as well as of the coordination chemistry of the metal centers. Herein we demonstrate a sliding-helix mechanism for stabilizing a change in the ligand environment of DF1, a model di-Mn^{II} protein.

Recently, we designed DF1 as a highly simplified model for diiron/dimanganese proteins.[9] This class of protein includes a number of functionally diverse structures including diiron proteins such as the radical-forming R2 subunit of ribonucleotide reductase[10] and methane monooxygenase,[11] as well as dimanganese proteins[12] such as catalase[13] and arginase.[14] DF1 is a dimer of helix-loop-helix motifs with a dimetal site near the center of the four-helix-bundle structure. As in natural diiron proteins, two Glu side chains bridge both metal ions, while the other two carboxylates interact with a

[*] Prof. S. Geremia, Dr. L. Di Costanzo, Prof. L. Randaccio
Center of Excellence in Biocrystallography
Department of Chemical Sciences, University of Trieste
Via L. Giorgieri 1, 34127 Trieste (Italy)
Fax: (+39) 040-558-3903
E-mail: geremia@univ.trieste.it
Prof. W. F. DeGrado
Department of Biochemistry and Biophysics
School of Medicine, University of Pennsylvania
Philadelphia, PA 19104-6059A (USA)
Prof. A. Lombardi, Prof. V. Pavone
Department of Chemistry, University of Naples "Federico II"
Complesso Universitario Monte S'Angelo
Via Cynthia 45, 80126 Naples (Italy)

[**] This work was supported by the MIUR (PRIN MM03185591), NIH grant GM54616, and by the MRSEC program of the NSF (award DMR0079909. We thank Ben North for many helpful discussions and preliminary calculations.

Supporting information for this article is available on the WWW under http://www.angewandte.org or from the author.

single metal ion in a bidentate, chelating interaction. Two His residues form additional monodentate ligands. The minimalist design of DF1 renders it an excellent candidate for determining how the tertiary and quaternary structures respond to changes in the ligation of dimetal centers. Direct access to the dimetal site of DF1 is controlled by the nature of the side chain at positions 13 and 13′ of equivalent monomers; with Leu at these positions, the protein binds two Co^{II}, Zn^{II}, or Mn^{II} ions without exogenous ligands.[9] Reducing the bulk of residue 13 and 13′ to Ala allows access of small molecules to the active site, and the X-ray structure of the di-Mn^{II} revealed a bridging DMSO group, whose sulfoxide oxygen atom is in direct contact with both manganous ions.[15] Herein we report the crystal structure of DF1–L13G–DF1, in which the active-site cavity has been expanded by further reducing the bulk of residue 13 to Gly.

The structure of di-Mn^{II}–L13G–DF1 displays four crystallographically independent dimers in the asymmetric unit. The individual dimers are closely related to the structure of di-Mn^{II}–L13A–DF1, with the exception that the water-filled access channel has been expanded in the expected manner. The most striking feature found in di-Mn^{II}–L13G–DF1 is the presence of two different dimanganese coordination environments. In three of the four dimers (AB, CD, and EF) a solvent molecule bridges the two metal ions (Figure 1 a), while in the fourth dimer (GH) two terminal solvent molecules are coordinated to the two manganese ions *trans* to the histidine ligands (Figure 1 b). The electron density of the four dimetal centers is well-defined, and there is no evidence for a mixture of binding modes within a given active site. Dimanganous derivatives of analogues of DF1 are very resistant to air oxidation in solution (unpublished data), and the observed coordination geometries observed in the crystal structure are consistent with the Mn^{II} oxidation state.

The bridging solvent molecules in AB, CD, and EF have been tentatively assigned as water molecules, based on the Mn–Mn and Mn–O distances, and in view of the pH value at which the crystals were grown.[16] The solvent-bridged centers show an intermetal distance of 3.59 Å (mean value), which is close to the value of 3.61 Å observed in small-molecule complexes for water-bridged di-Mn^{II} centers that are also bridged by two 1,3-carboxylate groups.[17] A significantly shorter distance would be expected for higher oxidation states of Mn ions in the presence of bridging exogenous anions.[13] In di-Mn^{II}–L13G–DF1 the Mn–O distances of the bridging solvent ligand range from 2.3 to 2.5 Å, which is somewhat larger than the 2.2-Å distance generally observed in analogous small-molecule H_2O–Mn^{II}_2 complexes.[17–19] In the GH dimer with two terminal solvent molecules, the intermetal distance increases to 4.20 Å. The two axial Mn–solvent

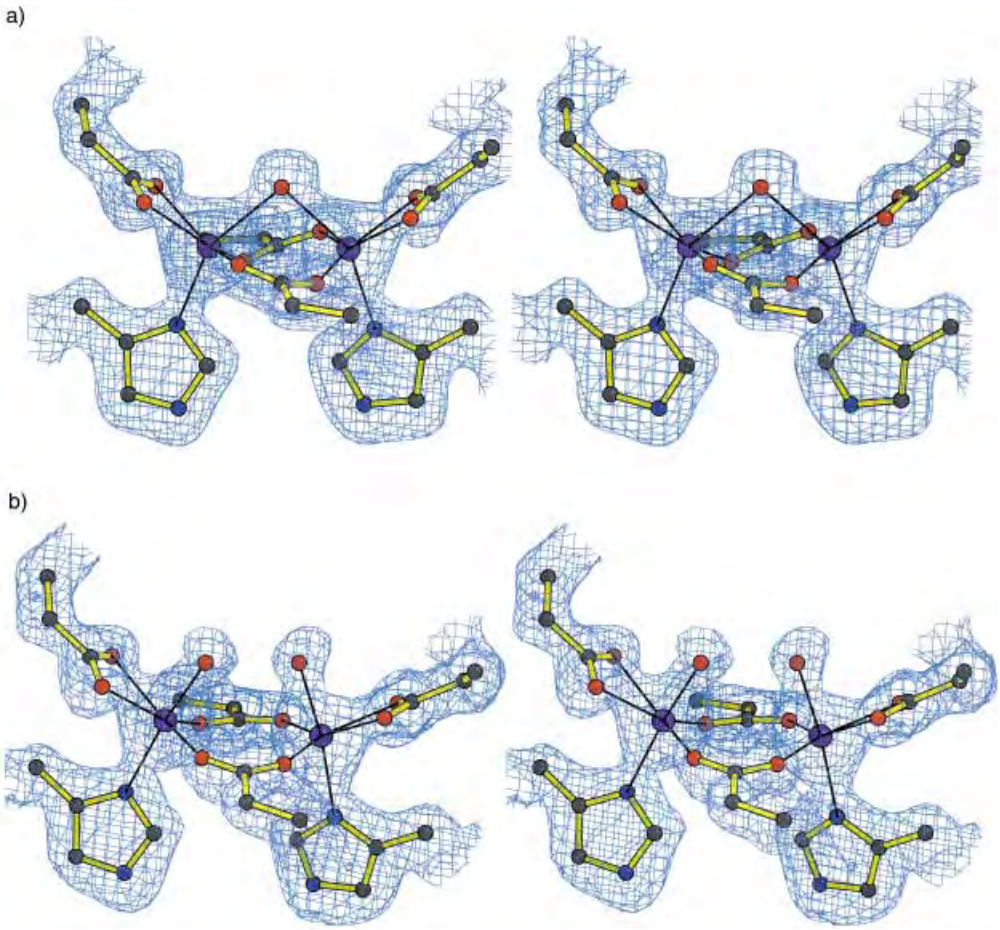


Figure 1. Stereoview of 2*Fo-Fc* electron-density maps (contour levels are 1.5σ) of the dinuclear metal-binding site of di-Mn–L13G–DF1 in the AB dimer (a) and in the GH dimer (b). These figures were generated with Bobscript.[29]

 © 2003 Wiley-VCH Verlag GmbH & Co. KGaA, Weinheim 1433-7851/03/4204-0418 $ 20.00+.50/0

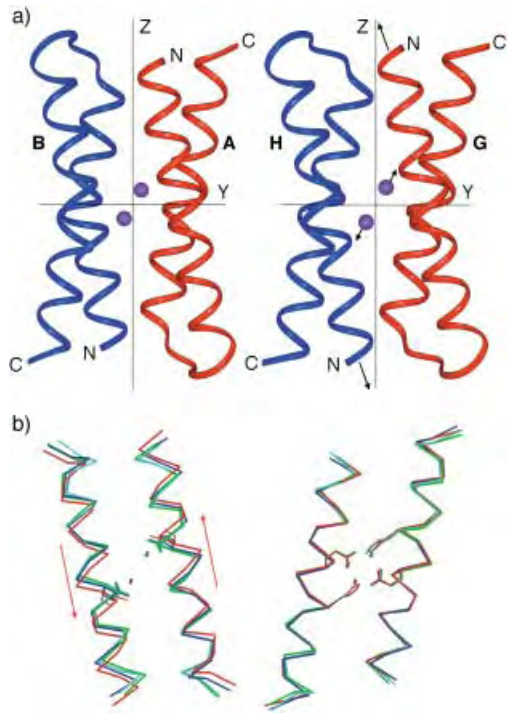


Figure 2. a) Crystallographically independent dimers of di-Mn–L13G–DF1, AB (left) and GH (right), viewed along the x axis of a common orthogonal reference system. The arrows in the GH dimer indicate the shifts of N-terminal helices and metal ions with respect to the other dimers. This figure was generated with InsightII (BIOSYM, San Diego, CA). b) Superimposition of helices 1 and 1′ (left) and helices 2 and 2′ (right) of the four crystallographically independent dimers of di-Mn^{II}–L13G–DF1. Note the movement of helices 1 and 1′ of the GH pair (red) relative to the remaining helices (AB blue; CD green; EF cyan). The Figure was generated with Rasmol.[30]

distances are 2.0 and 2.1 Å, which are significantly shorter than the corresponding distances found in simpler dinuclear manganese aqua complexes (ca. 2.3 Å).[20,21] We also observe a close approach of the two terminal solvent molecules (2.7 Å), which suggests that the pair of solvent molecules might actually be a more tightly chelated $H_3O_2^-$.[6]

To investigate the structural consequences of the different modes of binding, we analyzed crystal packing, local shifts in side-chain conformations, as well as global shifts in tertiary structure. The analysis of the differences in crystal-lattice packing among the four-helix bundles (see Supporting Information) revealed no significant relationship between the packing environment and the different structural behavior of these molecules. In GH, the carboxylate planes are rotated with respect to each other by an angle of 20°; in the other dimers small changes in the Glu side-chain torsions result in more acute carboxylate plane angles ranging from 32 to 40°. A more deep-seated change in quaternary structure was discovered when the bundles were examined in a common Cartesian coordinate system in which the central axis of the bundle is aligned along the z axis and the approximate C_2 axis of symmetry of the metal-binding site is aligned along the x axis (Figure 2). The C-terminal helices (2 and 2′), which contain the His-Xxx-Xxx-Glu liganding site, are virtually invariant among the structures (Table 1 and Figure 2). In contrast, the N-terminal helices (1 and 1′), each of which contains only a single liganding Glu side chain, occupy different positions in the GH dimer relative to the other structures. In GH the two copies of helix 1 undergo a shift in opposite directions (approximately 0.7 Å) along the Z axis, away from the metal-binding site (Table 1 and Figure 2). Indeed, this shift accompanies the lengthening of the metal–metal distance observed in the GH dimer.

In summary, this analysis has revealed a novel, sliding-helix mechanism by which metalloproteins can accommodate changes in their coordination environment. Although similar mechanisms have been shown to be important for signal transduction,[22,23] such motions have not been observed in the dimetal class of metalloenzymes. Instead, previous studies of catalytically active metalloproteins have focused on more localized carboxylate shifts and changes to isolated regions of the backbone.[6] Indeed, the idealized structure of DF1 has facilitated this analysis, which might have been more difficult to observe in a complex, large protein. Our data show that more collective motions provide an attractive mechanism for dynamic conformational tuning in designed metalloproteins. It will be interesting to determine whether this mechanism contributes to the catalytic activities of natural metalloproteins as well.

Table 1: Angles formed by each axis of helices for the four dimers of Mn^{II}–L13G–DF1 with the axes of the reference system, together with the coordinates of the center of mass of the individual helices. The only significant deviation between the equivalent helices of GH relative to the other dimers lies within helix 1 of G and H (bold values).

Helix	Angles			Centre of mass		
	x [°]	*y* [°]	*z* [°]	*x* [Å]	*y*[Å]	*z*[Å]
HEL 1-A	−97	−78	−166	4.52	5.41	0.13
HEL 1-C	−102	−78	−163	4.52	5.07	−0.13
HEL 1-E	−102	−78	−163	4.59	5.14	−0.07
HEL 1-G	−97	−77	−165	4.62	5.32	**0.68**
HEL 1′-B	99	102	15	4.53	−5.38	−0.03
HEL 1′-D	101	104	18	4.33	−5.16	0.17
HEL 1′-F	99	101	14	4.35	−5.16	0.15
HEL 1′-H	97	103	14	4.56	−5.40	**−0.78**
HEL 2-A	82	78	−15	−4.55	5.85	2.08
HEL 2-C	76	76	−20	−4.40	5.95	1.93
HEL 2-E	77	78	−18	−4.47	5.89	2.06
HEL 2-G	81	77	−16	−4.51	6.00	2.12
HEL 2′-B	−80	−102	164	−4.45	−5.91	−2.18
HEL 2′-D	−79	−102	163	−4.48	−5.81	−1.91
HEL 2′-F	−80	−101	165	−4.65	−5.85	−2.10
HEL 2′-H	−82	−103	164	−4.59	−5.93	−2.03

 © 2003 Wiley-VCH Verlag GmbH & Co. KGaA, Weinheim 1433-7851/03/4204-0419 $ 20.00+.50/0

Experimental Section

Crystallization and data collection: Single crystals of the complex di-Mn^{II}–L13G–DF1 were grown at 277 K using the hanging-drop vapor-diffusion method. The protein was solubilized as described previously,[15] and drops were prepared by adding 2 μL of protein (10 mg mL^{-1}) to 2 μL of reservoir solution containing PEG 400 (34%), $Mn(CH_3COO)_2$ (0.03 M), Tris–HCl (0.1 M of pH 7.5). Diamond-shaped crystals of di-Mn^{II}–L13G–DF1 ($0.3 \times 0.3 \times 0.2$ mm^3) grew within 10 days at 277 K. X-ray diffraction data were collected at the Elettra Synchrotron (Trieste, Italy) using a monochromatic radiation ($\lambda =$ 1.200 Å) and a MAR Research 345-mm imaging plate as detector. The crystal used in the collection data was harvested into mother liquor with a small loop of fine rayon fiber and flash-frozen in a stream of N_2 at 100 K. The data were collected at a resolution of 1.91 Å, fixing the crystal–detector distance at 180 cm. The crystal belongs to the space group $P2_12_12_1$ with unit-cell parameters of $a =$ 38.22, $b = 89.27$, $c = 146.29$ Å. The determination of unit-cell parameters, integration of reflection intensities, and data scaling were performed using MOSFLM and SCALA from the CCP4 program suite.[24] The data set consists of 94932 measured reflections and provides a unique data set of 38634 reflections with an $R_{merge} = 0.125$ and an overall completeness to 1.91 Å of 0.966. R_{merge} in the 2.01–1.91 resolution shell is 0.463.

Structure determination: the V_M values suggested the presence of 32 or 40 monomer chains in the unit cell and 8 or 10 monomers in the asymmetric unit. The structure of the complex di-Mn–L13G–DF1 was solved by molecular replacement with the program AMORE[25] using the coordinates of one dimer of the crystal structure of di-Mn^{II}–L13A–DF1[15] as the starting model. Four rotation/translation solutions were found for the independent dimers, compatible with the complete crystal packing. The first rigid body refinement of the four dimers gave an R factor of 0.420. The structure was refined with the REFMAC program[26] using 36674 unique reflections following a process of manual model building by using the program O[27] (5% of the data set was selected for the calculation of the R_{free}). The final R factor was 0.201 and $R_{free} = 0.244$.

Structure analysis: each four-helix bundle was positioned in a common orthogonal coordinate system using the following algorithm: 1) The regression line passing through the midpoints of pseudoequivalent C_α pairs of the N-terminal helices (residues 1–22) and of C-terminal helices (residues 27–48) defines the direction of the x axis, which coincides with the approximate, noncrystallographic twofold axis of the dimer. 2) The regression line passing through the midpoints of pseudoequivalent C_α pairs of diagonally opposing helices (the N-terminal helix of one monomer with the C-terminal helix of the other monomer) projected on the plane orthogonal to the x direction defines the z axis, which coincides with the super-helix axis. 3) The equation of the best line passing through the point of origin[28] of one helix in this reference system describes the position of the single helices (Table 1). Crystallographic data have been deposited in the Protein Data Bank, access number 1 LT1.

Received: May 29, 2002
Revised: October 11, 2002 [Z19403]

[1] L. Que, Jr., *Nat. Struct. Biol.* **2000**, *7*, 182.
[2] E. I. Solomon, T. C. Brunold, M. I. Davis, J. N. Kemsley, S. K. Lee, N. Lehnert, F. Neese, A. J. Skulan, Y. S. Yang, J. Zhou, *Chem. Rev.* **2000**, *100*, 235.
[3] S. J. Lippard, *Nature* **2002**, *416*, 587.
[4] R. H. Holm, P. Kennepohl, E. I. Solomon, *Chem. Rev.* **1996**, *96*, 2239.
[5] D. E. Wilcox, *Chem. Rev.* **1996**, *96*, 2435.
[6] D. A. Whittington, S. J. Lippard, *J. Am. Chem. Soc.* **2001**, *123*, 827.
[7] M. I. Davis, A. M. Orville, F. Neese, J. M. Zaleski, J. D. Lipscomb, E. I. Solomon, *J. Am. Chem. Soc.* **2002**, *124*, 602.
[8] R. L. Rardin, W. B. Tolman, S. J. Lippard, *New J. Chem.* **1991**, *15*, 417.
[9] A. Lombardi, C. M. Summa, S. Geremia, L. Randaccio, V. Pavone, W. F. DeGrado, *Proc. Natl. Acad. Sci. USA* **2000**, *97*, 6298.
[10] M. Hogbom, Y. Huque, B. M. Sjoberg, P. Nordlund, *Biochemistry* **2002**, *41*, 1381.
[11] M. Merkx, D. A. Kopp, M. H. Sazinsky, J. L. Blazyk, J. Muller, S. J. Lippard, *Angew. Chem.* **2001**, *113*, 2860; *Angew. Chem. Int. Ed.* **2001**, *40*, 2782.
[12] C. F. Yocum, V. L. Pecoraro, *Curr. Opin. Chem. Biol.* **1999**, *3*, 182.
[13] V. V. Barynin, M. M. Whittaker, S. V. Antonyuk, V. S. Lamzin, P. M. Harrison, P. J. Artymiuk, J. W. Whittaker, *Structure* **2001**, *9*, 725.
[14] D. E. Ash, J. D. Cox, D. W. Christianson, *Met. Ions Biol. Syst.* **2000**, *37*, 407.
[15] L. Di Costanzo, H. Wade, S. Geremia, L. Randaccio, V. Pavone, W. F. DeGrado, A. Lombardi, *J. Am. Chem. Soc.* **2001**, *123*, 12749.
[16] M. C. Wilce, C. S. Bond, N. E. Dixon, H. C. Freeman, J. M. Guss, P. E. Lilley, J. A. Wilce, *Proc. Natl. Acad. Sci. USA* **1998**, *95*, 3472.
[17] S.-B. Yu, S. J. Lippard, I. Shweky, A. Bino, *Inorg. Chem.* **1992**, *31*, 3502.
[18] In small-molecule complexes, typical bridging bond distances are 2.18–2.25 Å in μ-H_2O–Mn^{II}_2, 2.05–2.09 Å in μ-OH–Mn^{II}_2, and 1.78–1.81 Å in μ-O–Mn^{III}_2.
[19] B. Ye, T. Mak, I. D. Williams, X. Li, *Chem. Commun.* **1997**, 1813.
[20] K. Wieghardt, *Angew. Chem.* **1989**, *101*, 1179; *Angew. Chem. Int. Ed. Engl.* **1989**, *28*, 1153.
[21] Z. Shirin, V. G. Young, Jr., A. S. Borovik, *Chem. Commun.* **1997**, 1967.
[22] J. J. Falke, G. L. Hazelbauer, *Trends Biochem. Sci.* **2001**, *26*, 257.
[23] J. J. Chou, S. Li, C. B. Klee, A. Bax, *Nat. Struct. Biol.* **2001**, *8*, 990.
[24] COLLABORATIVE COMPUTATIONAL PROJECT, NUMBER 4, *Acta Crystallogr. D* **1994**, *50*, 760.
[25] J. Navaza, *Acta Crystallogr. A* **1994**, *50*, 157.
[26] G. N. Murshudov, A. A. Vagin, E. J. Dodson, *Acta Crystallogr. D* **1997**, *53*, 240.
[27] T. A. Jones, J. Y. Zou, S. W. Cowan, M. Kjeldgaard, *Acta Crystallogr. A* **1991**, *47*, 110 *(Pt2)*.
[28] H. Sugeta, T. Miyazawa, *Biopolymers* **1967**, *5*, 673.
[29] R. M. Esnouf, *Acta Crystallogr. D* **1999**, *55*, 938 *(Pt4)*.
[30] R. A. Sayle, E. J. Milner-White, *Trends Biochem. Sci.* **1995**, *20*, 374.

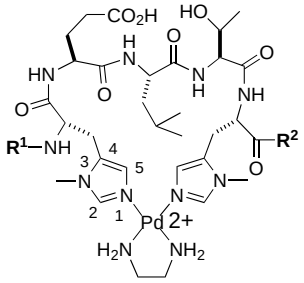
 © 2003 Wiley-VCH Verlag GmbH & Co. KGaA, Weinheim 1433-7851/03/4204-0420 $ 20.00+.50/0

Helix-Folding Templates

A Cyclic Metallopeptide Induces α Helicity in Short Peptide Fragments of Thermolysin**

*Michael J. Kelso, Huy N. Hoang, Warren Oliver, Nikolai Sokolenko, Darren R. March, Trevor G. Appleton, and David P. Fairlie**

About 30% of all amino acids in proteins are found in α helices.[1] When buried in the hydrophobic interiors of proteins, helices are important in stabilizing tertiary structures, promoting protein folding, and molding active sites of enzymes. However, short peptides (< 15 amino acids) corresponding to such helices are usually unstructured outside of their hydrophobic protein environments.[2] Attempts to produce short, stable α helices by using noncovalent side chain constraints (e.g., salt bridges, hydrophobic interactions),[3a,b] covalent side chain linkers (e.g., disulfide,[3c] hydrazone,[3d] aliphatic,[3e] lactam[3f] bridges) have met with some success. However, little is known about the capacity of metal ions to stabilize α helicity in short peptides,[4] even though metals are often bound to the helical regions of metalloproteins.[5] Here we report that at 300 K $[Pd(en)]^{2+}$ induces helicity in 5-, 10-, and 15-residue nonhelical peptides corresponding to the Zn^{2+}-binding α helix of the active site of thermolysin (Figure 1). Formation of an unusual 22-membered macrocycle in the metallopentapeptides **1**–**3**, by metal



1 (**R**^{1} = Ac, **R**^{2} = NH_2)
2 (**R**^{1} = Ac, **R**^{2} = AVTDY-NH_2)
3 (**R**^{1} = Ac-IDVVA, **R**^{2} = AVTDY-NH_2)

[*] Prof. D. P. Fairlie, M. J. Kelso, W. Oliver, N. Sokolenko, Dr. D. R. March
Centre for Drug Design and Development
Institute for Molecular Bioscience
University of Queensland
Brisbane, Qld 4072 (Australia)
Fax: (+61) 73365-1990
E-mail: d.fairlie@imb.uq.edu.au
H. N. Hoang, Prof. T. G. Appleton
Department of Chemistry
University of Queensland
Brisbane, Qld 4072 (Australia)

[**] We thank the Australian Research Council for financial support.
Supporting information for this article is available on the WWW under http://www.angewandte.org or from the author.



Figure 1. Crystal structure[6] of the metalloprotease thermolysin highlighting the α helix of the active site (yellow) containing two, $i,i+4$-spaced histidines (green/blue) bound through their N1 nitrogen atoms to tetrahedral Zn^{2+} (white).

coordination to two histidine residues spaced three residues apart (i.e. $i,i+4$), results in helical structures in solution that are analogous to those in the thermolysin crystal structure.[6]

Reaction of $[Pd(^{15}NH_2CH_2CH_2{}^{15}NH_2)(ONO_2)_2]$ with one equivalent of each of the following thermolysin fragments[7] Ac-H*ELTH*-NH_2 (**4**), Ac-H*ELTH*-AVTDY-NH_2 (**5**) and Ac-IDVVA-H*ELTH*-AVTDY-NH_2 (**6**) (Ac = acetyl) in DMF (or water) exclusively led to the respective metallopeptide products **1**–**3**, which were unambiguously characterized by multinuclear (^{1}H, ^{15}N, ^{13}C) and 2D NMR spectroscopy (see Supporting Information). Formation of a $[Pd(en)(peptide)]^{2+}$ product **1**, with 1:1 en:peptide stoichiometry, from **4** was supported by an unambiguously assigned single set of peptide ^{1}H NMR resonances (Figure 2a). The resonances of the imidazole protons H2 and H5 of both histidine residues (H*1H2, H*5H2, H*1H5, H*5H5) are shifted significantly after palladium addition. The ^{15}N NMR spectrum of **1** exhibited just two resonances (Figure 2b), both upfield of the resonance of $[Pd(^{15}NH_2CH_2CH_2{}^{15}NH_2)(solvent)_2]$ (~ −26 ppm; $\delta(NH_4^+) = 0.0$ ppm) and both with chemical shifts characteristic of inequivalent ethylenediamine nitrogen atoms *trans* to nitrogen donors.[8] The only other possible N donors (amide nitrogen atoms) were not coordinated to Pd since all amide-NH protons were accounted for in the one set of ^{1}H NMR resonances observed (Figure 2a).

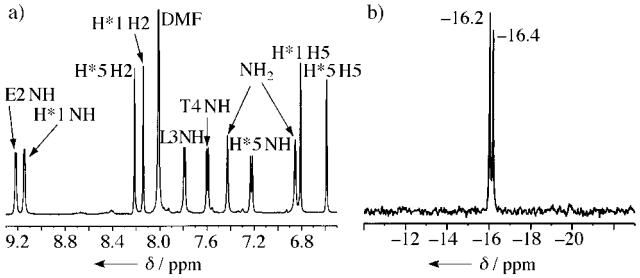


Figure 2. a) 500 MHz ^{1}H NMR spectrum (amide region) of reaction product **1** (obtained from ~3 μmol $[Pd(^{15}NH_2CH_2CH_2{}^{15}NH_2)(ONO_2)_2]$ and ~3 μmol **4** in 0.5 mL $[D_7]$DMF). b) 40.5 MHz ^{15}N NMR spectrum of the same mixture corroborating formation of **1**.

 © 2003 Wiley-VCH Verlag GmbH & Co. KGaA, Weinheim 1433-7851/03/4204-0421 $ 20.00+.50/0

Alternative Pd coordination to the oxygen atoms of amide units or of Asp/Thr/Tyr side chains would instead be characterized by ^{15}N NMR chemical shifts of −24 to −26 ppm for the *trans*-en ligand.[8] ^{13}C NMR chemical shifts also indicated imidazole coordination to palladium, a large increase in δ_{C5} of each imidazole ring in **1** relative to **4** being diagnostic of N1 bound to Pd^{II}.[9] Finally, ROESY spectra and the structures calculated from the NMR data further confirmed the chemical identity of **1**.

Free peptide **4** was unstructured in solution as evidenced by 2D ROESY spectra which showed only intra-residue and sequential cross peaks (see Supporting Information). In contrast, metallopeptide **1** showed ^{1}H NMR parameters characteristic of defined structure, specifically of helicity (see Supporting Information). Helicity in **1** was supported by a) characteristic upfield shifts of the CHα signals[10] relative to free peptide **4**, b) multiple $^3J_{NHCH\alpha}$ coupling constants of ≤ 6 Hz,[11] c) amide-NH chemical shifts with low temperature dependence ($\Delta\delta/T \leq 4$ ppb K^{-1}), consistent with the presence of hydrogen bonds,[12] and d) characteristic[13] nonsequential cross peaks in the ROESY spectra ($d_{\alpha N(i,i+3)}$, $d_{\alpha N(i,i+4)}$, $d_{\alpha\beta(i,i+3)}$, Figure 3a,b). Variable temperature NMR data suggest the presence of three hydrogen-bonded amide protons (His5, Thr4, and Leu3), supportive of a 3_{10} helix, whereas only two hydrogen bonds (His5-NH···OC-His1, Thr4-NH···OC-Ac) would be expected for an α helix. On the other hand, the presence of $d_{\alpha N(i,i+4)}$ ROEs supports α rather than 3_{10} helicity for **1**.[13] Most likely there is rapid interconversion between the two helical forms,[14] but the metallacycle is certainly α-helical within longer peptides (see below).

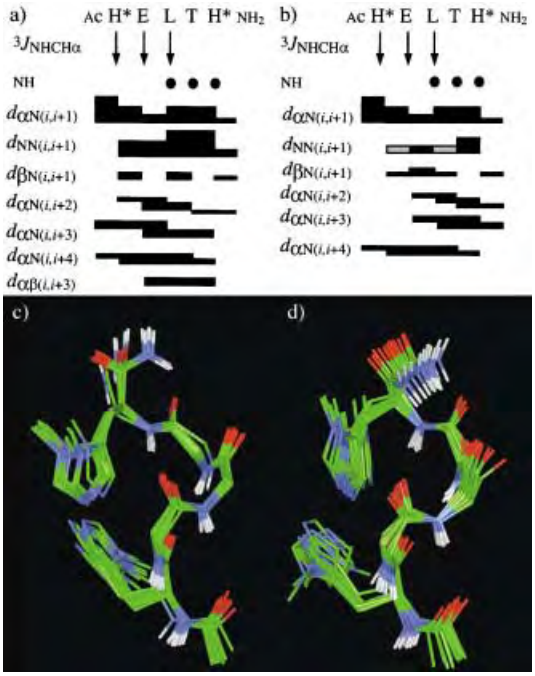


Figure 3. Top: Summary of sequential and medium-range ROE data for **1** in a) [D$_7$]DMF, b) H$_2$0/D$_2$O (9/1). Residues with $^3J_{NHCH\alpha} \leq 6$ Hz marked by ↓, amide protons with temperature coefficients $\Delta\delta/T = 4$ ppb K^{-1} by ●. The ROE intensities are symbolized by different bar thicknesses, which correspond to distances ≤2.7, ≤3.5, ≤5.0, and ≤6.0 Å. Shaded bars represent ROEs obscured by spectral overlap. Bottom: Backbone superimposition of the 14 lowest-energy refined structures calculated for **1** in c) [D$_7$]DMF and d) H$_2$0/D$_2$O (9/1). (average backbone pairwise rmsd 0.21 Å and 0.33 Å, respectively). Side chains of His* residues only are shown for clarity.

Structures were initially calculated for **1** in [D$_7$]DMF (74 ROE distance restraints: 35 intra-residue, 22 sequential, 17 medium-range; 3 backbone ϕ angles from $^3J_{NHCH\alpha}$ values) and H$_2$O/D$_2$O (9/1) (48 ROEs: 24 intra-residue, 15 sequential, 9 medium-range; 3 backbone ϕ angles) using a dynamic simulated-annealing and energy-minimization protocol in X-PLOR (3.851)[15] without explicit hydrogen bond or [Pd(en)$^{2+}$] restraints to prevent structure biasing. Since the N1 atoms of the two His* residues were correctly oriented and spaced to coordinate Pd in the initial calculations, they were constrained in the final calculations to within 2.7 Å of each other, this being the known separation between nitrogen atoms of N-Pd-N units (Pd-N 1.90 Å).[16] The resulting structures (Figure 3c,d) were helical and similar in the two solvents, although the structures were less ordered in water as indicated by the higher backbone root mean square deviation (rmsd). Their stability is attributed to His5-N1···Pd···N1-His1 bonds and intramolecular constraints imposed by hydrogen bonds.

Can the helical metallopentapeptide **1** propagate helicity when incorporated in longer peptides corresponding to the α helix in the active site of thermolysin? All of the NMR data for **1** suggest less helicity in water than in DMF. For this reason, and also because the corresponding thermolysin sequence is buried within the hydrophobic interior of the protein, we chose to examine helix induction by [Pd(en)]$^{2+}$ for the longer thermolysin fragments **5** and **6** in the aprotic solvent DMF, rather than in water.[17] We report that [Pd(en)]$^{2+}$ selectively coordinates N1 of the two $(i,i+4)$ histidine residues in **5** and **6** to exclusively form metallopeptides **2** and **3**, respectively, despite **5** and **6** being functionalized with many potential metal-binding sites. The chemical identities of metallopeptides **2** and **3** were confirmed using multinuclear and 2D NMR spectroscopy as described above for **1** (see Supporting Information).

2D ROESY spectra revealed that the free peptides **5** and **6** were unstructured in solution (see Supporting Information), whereas the metallopeptides **2** and **3** showed characteristic parameters for α-helical conformations. Both **2** and **3** exhibited many features that are consistent with helicity: upfield shifts of the CHα signals relative to the free peptides, low temperature dependence of the amide proton signals, low $^3J_{NHCH\alpha}$ coupling constants (≤6.0 Hz), medium-range NOEs (Figure 4a,b), and the calculated solution structures (Figure 4c–f). Multiple $d_{\alpha N(i,i+4)}$ NOEs, both within the metallacyclic components and throughout **2** and **3**, strongly favor α rather than 3_{10} helicity in these longer peptides.

The three-dimensional solution structures (in [D$_7$]DMF) for **2** (derived from 133 NOE distance restraints: 61 intra-residue, 46 sequential, 26 medium-range, and 5 torsion angle restraints: for $^3J_{NHCH\alpha} \leq 6$ Hz, $\phi = -60$ to $-25°$) and **3** (derived from 234 NOE distance restraints: 95 intra-residue, 65 sequential, 74 medium-range and 10 ϕ angle restraints) were calculated as for **1** using X-PLOR.[15] The backbone superimposition of the final 14 lowest-energy structures for **2**

 © 2003 Wiley-VCH Verlag GmbH & Co. KGaA, Weinheim 1433-7851/03/4204-0422 $ 20.00+.50/0

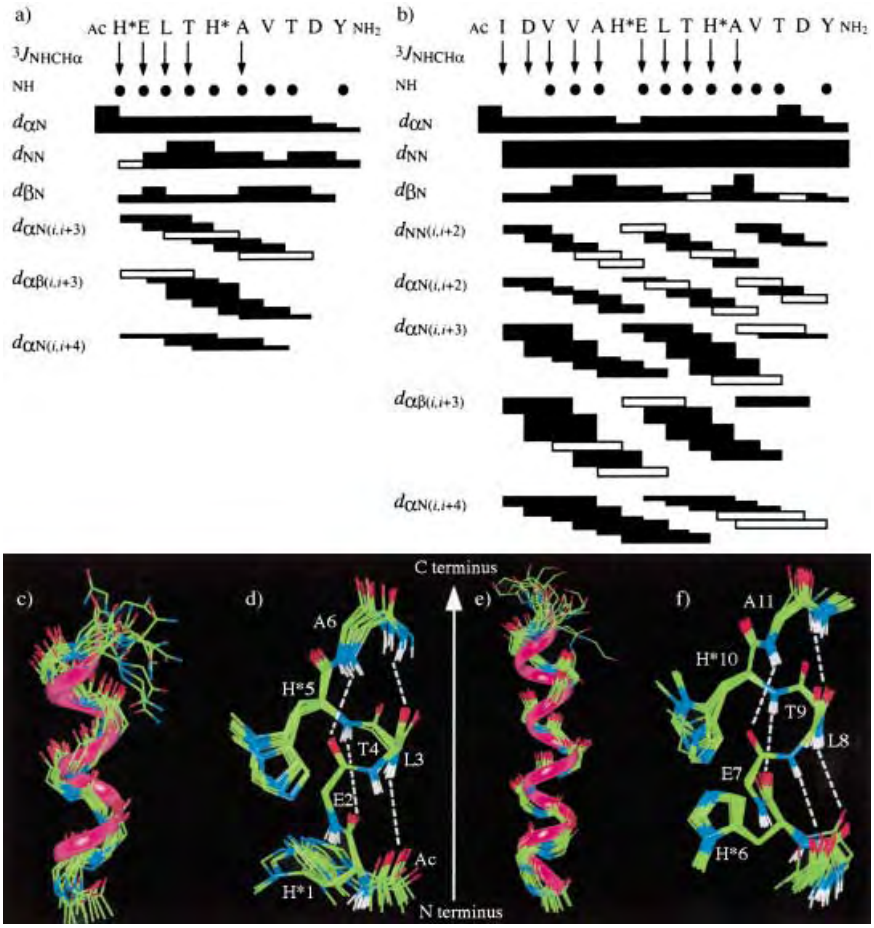


Figure 4. Top: Summary of sequential and medium-range NOE data for a) **2** and b) **3** in [D_7]DMF. (cf. Figure 3). Bottom: Backbone superimposition of c) the 14 lowest-energy refined structures of **2** (green; average backbone pairwise rmsd 1.37 Å; side chains omitted for clarity), d) residues H1* to A6 showing the helical metallacycle, four intrahelical hydrogen bonds, and imidazole locations, e) the 20 lowest-energy refined structures of **3** (green; average backbone pairwise rmsd 0.81 Å), f) residues H1* to A11 showing the helical metallacycle, five intrahelical hydrogen bonds, and imidazole locations. The purple ribbon in (c) and (e) is the superimposed backbone of the analogous α helix of thermolysin.[6]

(Figure 4c,d) indicates the formation of an α helix that closely mimics the α-helical counterpart in thermolysin, except for some fraying at the exposed C terminus. Its cyclic metallopeptide component forms a well defined α-helical turn featuring the hydrogen bonds Ac-CO···HN-Thr4, His1-CO···HN-His5, Glu2-CO···HN-Ala6, Leu3-CO···HN-Val7, and Thr4-CO···HN-Thr8, the first four being shown in Figure 4d.

The backbone superimposition of the final 20 lowest-energy structures representing **3** (Figure 4e,f) also indicates a regular α helix which closely mimics its 15-residue α-helical counterpart in thermolysin, except for some fraying at the C terminus. Some of the hydrogen bonds in the metallacycle are marked in Figure 4f. The metallacycle is the most highly structured α-helical region of **3** and does propagate α helicity in both directions towards the N and C termini. In contrast to the disorder at the C terminus, there was ordered α-helical structure extending to the N terminus of **3**. This difference may be the result of better C-terminal α helix nucleation by the metallacycle, or alternatively the N-terminal sequence may simply have a lower helical propensity.

It has been demonstrated here that Pd^{2+} preferentially binds imidazole N1 atoms over alternative peptide components including carboxylate, alcohol, amide, and phenol units. The resulting 22-membered metallacycle, while uncommon for inorganic complexes in which metals (even Pd^{2+}) normally favour 5- or 6-membered rings,[18] is not an uncommon chelate ring size in metalloproteins.[19] Although structure calculations on small cyclic peptides can be notoriously misleading, because they assume the presence of a single conformation when many rapidly interconverting structures are more likely in solution, we have clearly identified helicity for **1** in both DMF and water. While the distinction between α and 3_{10} helicity was not unequivocal for **1**, the fact that we do observe α-helix induction in the longer peptides **2** and **3** (incorporating **1**) supports α helicity in **1** as well.

Helicity in the $[Pd(en)(HxxxH)]^{2+}$ metallacycle enables it to act as a template, propagating α helicity through at least one additional helical turn (3.6 residues) at either side of the metallacycle. Disorder at the C terminus of peptides **2** and **3** may have obscured the true extent of this helix induction, which might be transmitted even further in longer peptides. No compound has been reported to nucleate an α helix from the C terminus of a short peptide, and only a few N-terminal nucleators have been described,[20] those being organic scaffolds that are difficult to synthesize and require covalent linking to peptides thereby limiting their applications. Metallacycles like $[Pd(en)(HxxxH)]^{2+}$ may find wider applications due to their ease of formation and successful helix propagation in both N- and C-terminal directions. It remains to be seen whether moieties such as $[Pd(en)]^{2+}$ can be used as metal clips to reversibly fold peptide and protein domains. Although we have not observed hydrolysis of these histidine-containing peptides in solution, this side reaction has been reported in other systems[21] and could potentially affect the utility of these metal clips.

HxxxH is a common signature in proteins and raises the possibility that metal ions may play important roles as helix-folding templates. This could be true not only in metalloproteins, but also in other proteins to which first-row transition metals may only be transiently coordinated. The use of the diamagnetic $[Pd(en)]^{2+}$ moiety has enabled us to detect thermodynamically stable structures in solution by

NMR spectroscopy. More labile metal complexes only form transient metallopeptides that are kinetically labile and more difficult to study. For example, adding Zn^{2+} to solutions of these peptides results only in broad NMR signals, and CD spectra showed negligible structure. Less labile metal complexes may alternatively capture donor atoms other than N1 of a His imidazole ring, forming kinetically inert nonhelical metallopeptides. This work demonstrates that small metallopeptides may have potential for seeding α helicity in peptides and proteins, for studying α-helical turns outside proteins, and for producing artificial models of the active sites of metalloproteins.

Received: July 31, 2002 [Z19863]

[1] D. J. Barlow, J. M. Thornton, *J. Mol. Biol.* **1988**, *201*, 601.

[2] a) B. Zimm, J. Bragg, *J. Chem. Phys.* **1959**, *31*, 526; b) A. Scholtz, R. L. Baldwin, *Annu. Rev. Biophys. Biomol. Struct.* **1992**, *21*, 95.

[3] a) L. Mayne, S. W. Englander, R. Qiu, J. Yang, Y. Gong, E. J. Spek, N. R. Kallenbach, *J. Am. Chem. Soc.* **1998**, *120*, 10643; b) J. S. Albert, A. Hamilton, *Biochemistry* **1995**, *34*, 984; c) D. Y. Jackson, D. S. King, J. Chmielewski, S. Singh, P. G. Schultz, *J. Am. Chem. Soc.* **1991**, *113*, 9391; d) E. Cabezas, A. C. Satterthwait, *J. Am. Chem. Soc.* **1999**, *121*, 3862; e) H. E. Blackwell, J. D. Sadowsky, R. J. Howard, J. N. Sampson, J. A. Chao, W. E. Steinmetz, D. J. O'Leary, R. H. Grubbs, *J. Org. Chem.* **2001**, *66*, 5291; f) C. Bracken, J. Gulyas, J. W. Taylor, J. Baum, *J. Am. Chem. Soc.* **1994**, *116*, 6431.

[4] a) M. R. Ghadiri, H. Fernholz, *J. Am. Chem. Soc.* **1990**, *112*, 9633; b) M. R. Ghadiri, C. Choi, *J. Am. Chem. Soc.* **1990**, *112*, 1630; c) F. Ruan, Y. Chen, P. B. Hopkins, *J. Am. Chem. Soc.* **1990**, *112*, 9403; d) W. D. Kohn, C. M. Kay, B. D. Sykes, R. S. Hodges, *J. Am. Chem. Soc.* **1998**, *120*, 1124; e) M. Kohtani, B. S. Kinnear, M. F. Jarrold, *J. Am. Chem. Soc.* **2000**, *122*, 12377; f) M. J. Kelso, H. N. Hoang, T. G. Appleton, D. P. Fairlie, *J. Am. Chem. Soc.* **2000**, *122*, 10488.

[5] *Metalloproteins in Bioactive Molecules, Vol. 8* (Eds. S. Otsuka, T. Yamanaka), Elsevier, Tokyo, **1988**.

[6] D. R. Holland, A. C. Hausrath, D. Juers, B. W. Matthews, *Protein Sci.* **1995**, *4*, 1955.

[7] Each His (H) residue was substituted by a His-containing N3-methylated imidazole (H*) to block formation of linkage isomers of $[Pd(en)(peptide)]^{2+}$ with different coordinating atoms (N1 or N3 imidazole nitrogen atoms) of the two histidine residues.

[8] T. G. Appleton, A. J. Bailey, D. R. Bedgood Jr., J. R. Hall, *Inorg. Chem.* **1994**, *33*, 217.

[9] a) T. G. Appleton, F. J. Pesch, M. Wienken, S. Menzer, B. Lippert, *Inorg. Chem.* **1992**, *31*, 4410; b) T. N. Parac, N. M. Kostić, *Inorg. Chem.* **1998**, *37*, 2141; c) T. N. Parac, G. M. Ullman, N. M. Kostić, *J. Am. Chem. Soc.* **1999**, *121*, 3127.

[10] D. S. Wishart, B. Sykes, F. Richards, *Biochemistry* **1992**, *31*, 1647.

[11] H. J. Dyson, P. E. Wright, *Annu. Rev. Biophys. Biophys. Chem.* **1991**, *20*, 519.

[12] H. Kessler, *Angew. Chem.* **1982**, *94*, 509; *Angew. Chem. Int. Ed. Engl.* **1982**, *21*, 512.

[13] a) K. Wüthrich, *NMR of Proteins and Nucleic Acids*, Wiley, New York, **1986**; b) K. Wüthrich, M. Billeter, W. Braun, *J. Mol. Biol.* **1984**, *180*, 715; c) A. Pardi, M. Billeter, K. Wüthrich, *J. Mol. Biol.* **1984**, *180*, 741.

[14] A. Dehner, E. Planker, G. Gemmecker, Q. B. Broxterman, W. Bisson, F. Formaggio, M. Crisma, C. Toniolo, H. Kessler, *J. Am. Chem. Soc.* **2001**, *123*, 6678.

[15] a) A. T. Brünger, X-PLOR Manual Version 3.1, **1992**, Yale University, New Haven, CT; b) M. Nilges, A. M. Gronenborn, A. T. Brünger, G. M. Clore, *Protein Eng.* **1988**, *2*, 27; c) B. R. Brooks, R. E. Bruccoleri, B. D. Olafson, D. J. States, S. Swaminathan, M. Karplus, *J. Comput. Chem.* **1983**, *4*, 187.

[16] M. Wienken, E. Zangrando. L. Randaccio, S. Menzer, B. Lippert, *J. Chem. Soc. Dalton Trans.* **1993**, 3349.

[17] At μM concentrations helicity is also observed in water by CD spectroscopy (see Figure S16 in the Supporting Information), although this is considered to be less relevant to the hydrophobic active site of the metalloprotein thermolysin.

[18] a) M. Hahn, D. Wolters, W. S. Sheldrick, F. B. Hulsbergen, J. Reedijk, *J. Biol. Inorg. Chem.* **1999**, *4*, 412; b) P. Tsiveriotis, N. Hadjiliadis, G. Savropoulos, *Inorg. Chim. Acta* **1997**, *261*, 83; c) S. U. Milinkovic, T. N. Parac, M. I. Djuran, N. M. Kostic, *J. Chem. Soc. Dalton Trans.* **1997**, 2771; d) I. Sovago in *Biocoordination Chemistry, Coordination Equilibria in Biologically Active Systems*, Ellis Horwood, London, **1990**; e) P. Tsiveriotis, N. Hadjiliadis, *J. Chem. Soc. Dalton Trans.* **1999**, 459; f) C. E. Livera, L. D. Pettit, M. Battaaille, B. Perly, H. Kozlowski, B. Radomska, *J. Chem. Soc. Dalton Trans.* **1987**, 661; g) R. P. Agarwal, D. D. Perrin, *J. Chem. Soc. Dalton Trans.* **1976**, 89; h) J. Ueda, N. Ikota, A. Hanaki, K. Koga, *Inorg. Chim. Acta* **1987**, *135*, 43; i) H. Kozlowski, W. Bal, M. Dyba, T. Kowalik-Jankowska, *Coord. Chem. Rev.* **1999**, *184*, 319.

[19] For example: a) E. Morgunova, A. Tuuttila, U. Bergmann, M. Isupov, Y. Lindqvist, G. Schneider, K. Tryggvason, *Science* **1999**, *284*, 1667; b) M. Elrod-Erickson, M. A. Rould, L. Nekludova, C. O. Pabo, *Structure* **1996**, *4*, 1171; c) K. A. Magnus, B. Hazes, H. Ton-That, C. Bonaventura, J. Bonaventura, W. G. Hol, *Proteins* **1994**, *19*, 302.

[20] Reviews: a) D. Fairlie, M. West, A. Wong, *Curr. Med. Chem.* **1998**, *5*, 29; b) M. J. L. Andrews, A. B. Tabor, *Tetrahedron* **1999**, *55*, 11711; articles: c) D. Kemp, T. Curran, J. Boyd, T. Allen, *J. Org. Chem.* **1991**, *56*, 6683; d) K. Müller, D. Obrecht, A. Knierzinger, C. Stankovic, C. Spiegler, W. Bannwarth, A. Trzeciak, G. Englert, A. M. Labhardt, P. Schoenholzer, *Perspect. Med. Chem.* **1993**, 513; e) R. Austin, R. A. Maplestone, A. M. Sefler, K. Liu, W. N. Hruzewicz, C. Liu, H. S. Cho, D. Wemmer, P. Bartlett, *J. Am. Chem. Soc.* **1997**, *119*, 6461; f) E. Cabezas, A. Satterthwait, *J. Am. Chem. Soc.* **1999**, *121*, 3862.

[21] N. M. Milovic, N. M. Kostic, *J. Am. Chem. Soc.* **2002**, *124*, 4759.

 © 2003 Wiley-VCH Verlag GmbH & Co. KGaA, Weinheim 1433-7851/03/4204-0424 $ 20.00+.50/0

Vanadium–Sulfite Polyoxometalates

Polyoxovanadium(IV) Sulfite Compounds: Synthesis, Structural, and Physical Studies**

Manolis J. Manos, Haralampos N. Miras, Vassilis Tangoulis, J. Derek Woollins, Alexandra M. Z. Slawin, and Themistoklis A. Kabanos**

Dedicated to Professor Dieter Rehder on the occasion of his 60th birthday

The current interest in polyoxometalate chemistry is representative of the diverse nature of this family of inorganic clusters, which exhibit a wide variety of compositions and have considerable structural versatility,[1] as well as important magnetic,[2] optical,[1] and catalytic properties.[1] Much attention has been paid to heteropolyanions that contain tetrahedral phosphate groups.[3] While a number of research groups have focussed on polyoxomolybdenum and vanadium phosphates, fewer studies have been carried out on polyoxoanions that incorporate the pyramidal sulfite anion.[4,5] The sulfite anion has C_{3v} symmetry and contains a nonbonding, but stereochemically active pair of electrons, and their metal complexes may potentially display nonlinear optical (NLO) properties,[6] which are observed in the metal-selenites[7] and metal-iodates.[8] Herein, we report the isolation, X-ray crystal structures, and some properties of the first vanadium–sulfite species $(n\mathrm{Bu_4N})_2[(\mathrm{V^{IV}O})_6(\mu_4\text{-}\mathrm{O})_2(\mu_3\text{-}\mathrm{OH})_2(\mu_3\text{-}\mathrm{SO_3})_4(\mathrm{H_2O})_2]$ (**1**), $(\mathrm{NH_4})_2[(\mathrm{V^{IV}O})_6(\mu_4\text{-}\mathrm{O})_2(\mu_3\text{-}\mathrm{OH})_2(\mu_3\text{-}\mathrm{SO_3})_4(\mathrm{H_2O})_2]$ (**2**), and $(\mathrm{NH_4})[\mathrm{V^{IV}O(SO_3)_{1.5}(H_2O)}]\cdot 2.5\,\mathrm{H_2O}$ (**3**). Compounds **1** and **2** are polyoxovanadium(IV)–sulfite heteropolyanions that exhibit a unique structural motif with a central cubic $\{\mathrm{V_4^{IV}O_2(OH)_2}\}$ fragment and two vanadium(IV) ions located at two of the corners of the cluster. Compound **3** exhibits an open-framework structure. Open-framework materials have recently received great interest because of their applications in shape-selective catalysis, separation science, and ion-exchange.[9]

The reaction of $[\mathrm{V^{IV}OCl_2(thf)_2}]$ in an HCl solution (37% HCl in water, 1:3 v/v, approximately pH 1) with an aqueous solution (approximately pH 9) containing $\mathrm{Na_2SO_3}$ and $\mathrm{Bu_4NBr}$ (final pH value of the solution was approximately 2.5) resulted in the formation of compound **1** [Eq. (1)].

$$6\,[\mathrm{V^{IV}OCl_2(thf)_2}] + 4\,\mathrm{NaSO_3} + 2\,\mathrm{Bu_4NBr} + 6\,\mathrm{H_2O} \rightarrow (\mathrm{Bu_4N})_2[(\mathrm{V^{IV}O})_6\mathrm{O_2(OH)_2(SO_3)_4(H_2O)_2}] + 8\,\mathrm{NaCl} + 4\,\mathrm{HCl} + 2\,\mathrm{HBr} + 12\,\mathrm{THF} \quad (1)$$

Compound **2** was isolated by replacing sodium sulfite and tetra-*n*-butylammonium bromide in the above synthetic procedure with ammonium sulfite. The synthesis of compound **3** was achieved by treating $\mathrm{NH_4V^VO_3}$, in an HCl solution (37% HCl in water, 1:4 v/v, approximately pH 1), with $(\mathrm{NH_4})_2\mathrm{SO_3}$ in the presence of magnesium oxide (final pH value was approximately 3) [Eq. (2)].

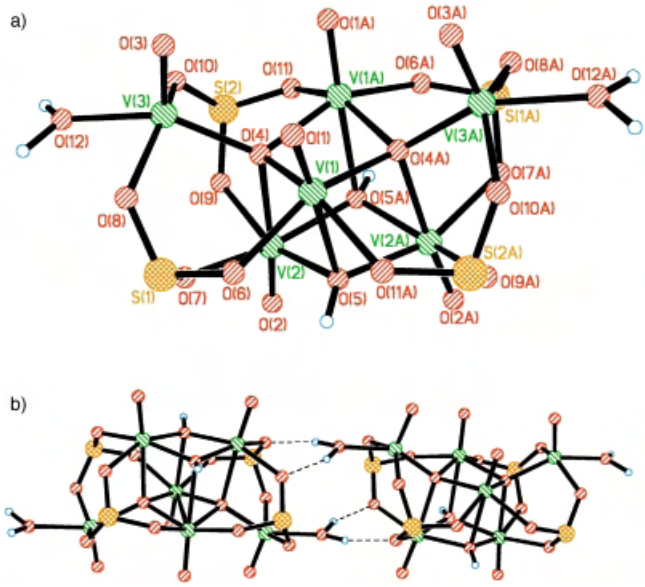


Figure 1. a) Ball-and-stick representation of **1a**. Average bond lengths (Å): V=O 1.577(6), V-O (μ_3-OH^-) 2.202(3), V-O (μ_4-O^{2-}) 2.073(4), V-O (μ_3-SO_3^{2-}) 2.024(3), V-O(H_2O) 2.052(2), S-O (μ_3-SO_3^{2-}) 1.532(8), V(1)···V(1A) 2.933(1), V(2)···V(2A) 3.185(2); b) Ball-and-stick representation of the hydrogen-bonded dimer formed between two adjacent **1a** anions.

$$2\,\mathrm{NH_4V^VO_3} + 4\,(\mathrm{NH_4})_2\mathrm{SO_3} + 4\,\mathrm{H_2O} \xrightarrow{\mathrm{MgO}} 2\,\mathrm{NH_4}[(\mathrm{V^{IV}O})(\mathrm{SO_3})_{1.5}(\mathrm{H_2O})]\cdot 2.5\,\mathrm{H_2O}\ \mathbf{3} + (\mathrm{NH_4})_2\mathrm{SO_4} + 6\,\mathrm{NH_3} \quad (2)$$

In the latter reaction, absence of MgO results in the isolation of **2**. The role of MgO in the formation of **3** remains as yet unknown. Our reason for adding MgO to the reaction was to attempt to replace the V(3) and V(3A) atoms in **2** (see Figure 1) with $\mathrm{Mg^{II}}$ ions, to modify the complicated magnetic properties of compound **2**.

X-ray structural analysis of **1**[10] revealed the presence of the $[(\mathrm{V^{IV}O})_6(\mu_4\text{-}\mathrm{O})_2(\mu_3\text{-}\mathrm{OH})_2(\mu_3\text{-}\mathrm{SO_3})_4(\mathrm{H_2O})_2]^{2-}$ anion (**1a**; Figure 1a) as well as two $\mathrm{Bu_4N^+}$ counterions. The core of the hexanuclear anion **1a** consists of a distorted cubane unit, $\{\mathrm{V_4^{IV}O_2(OH)_2}\}$, which is comprised of four, triply edge-sharing

[*] Dr. T. A. Kabanos, M. J. Manos, H. N. Miras
Department of Chemistry
Section of Inorganic and Analytical Chemistry
University of Ioannina, 45110 Ioannina (Greece)
Fax: (+30) 651-0-98795
E-mail: tkampano@cc.uoi.gr
Dr. A. M. Z. Slawin, Prof. J. D. Woollins
Department of Chemistry, University of St.Andrews
St. Andrews, Fife KY16 9ST (UK)
Fax: (+44) 1334-463384
E-mail: jdw3@st-andrews.ac.uk
Dr. V. Tangoulis
Department of Science of Materials, University of Patra, 26504 Patra (Greece)

[**] We thank the central laser facility of the University of Ioannina for the NLO measurements.

 © 2003 Wiley-VCH Verlag GmbH & Co. KGaA, Weinheim 1433-7851/03/4204-0425 $ 20.00+.50/0

$V^{IV}O_6$ octahedra, each having an oxo group (V=O 1.58 Å) in a position *trans* to a long V–O bond (2.36 Å); the four equatorial V–O bonds are similar in length, at approximately 2.02 Å. The two square-pyramidal O_5–V^{IV} units are coordinated to the vanadium ions of the core through one μ_4-O^{2-} and two μ_3-SO_3^{2-} bridges. The two μ_4-oxygen atoms O(4) and O(4A) connect the network of six vanadium(IV) ions and possess almost a trigonal pyramidal geometry. There are moderate-to-strong hydrogen bonds between the two hydrogen atoms of O(12)[11a] and the sulfite oxygen atoms O(7′) and O(9′), along with the symmetry-related interactions between the hydrogen atoms of O(12′) and the sulfite oxygen atoms O(7) and O(9) (Table 1). These combine to form a hydrogen-bonded dimer of two adjacent anions about a center of symmetry (Figure 1b). There is further bonding between the hydrogen atoms of O(12A) and O(7″)/O(9″) and, by symmetry, the hydrogen atoms of O(12′A) with O(7‴)/O(9‴), etc., which links the dimeric units in 1D chains along the *a* axis. In addition, the hydroxylic hydrogen atoms H(O(5)) and H(O(5A)) form weak hydrogen bonds with the sulfite oxygen atoms O(6) and O(6A), respectively (Table 1). Although the $\{M_4(\mu_4\text{-}O)_2(\mu_3\text{-}OH)_2\}$ cubane core has been reported in the literature,[12] the connection of the $\{V_4^{IV}(\mu_4\text{-}O)_2(\mu_3\text{-}OH)_2\}$ unit with two other metals through the oxygen atoms of the core represents a novel motif, not only for vanadium species, but for any metal. In addition, there are no known examples where the $\{M_4O_4\}$ cubane core is connected to two other metals.

The structure of **2**[10] is similar to that of **1**. However, **2** crystallizes in the noncentrosymmetric space group $P2_1$, while **1** crystallizes in the centrosymmetric *I*2/*a* space group. This demonstrates the crucial role of the counterion concerning the formation of noncentrosymmetric structures.[8a] The NLO properties of compound **2** were studied in aqueous solution using 1 cm- and 1 mm-thick glass cells. Under laser irradiation at 590 nm, with a 5 ns pulse duration, the NLO properties of **2** were found to be limited; experiments using lasers in the picosecond time domain are underway. Compound **3** crystallizes in the orthorhombic space group *Pbcm*[10] and exhibits a two-dimensional open-framework structure. The crystallographically unique vanadium ion of **3** resides in a distorted octahedron comprised of four equatorial sulfite oxygen atoms, as well as an oxygen atom from a water molecule and an oxo group, which occupy the axial positions (Figure 2). The 2D structure of **3** can be described as a layered net of isolated VO_6 octahedra, each sharing four corners with four adjacent SO_3 trigonal pyramids. The connectivity between the VO_6 octahedra and the SO_3 pyramids creates eight- and four-ring "windows". Each eight-ring results from four VO_6 octahedra linked by four SO_3^{2-} pyramids. In contrast, the four-rings are formed from two VO_6 octahedra that are connected through two SO_3 pyramidal units. To the best of our knowledge, the preparation of **3** represents the first example of the isolation of an open-framework compound under mild conditions.

Table 1: Hydrogen bonds for **1**.

D–H···A	*d*(D–H)	*d*(H···A)	*d*(D···A)	∢ (DHA)
O12–H(12D)···O7′	0.976(5)	1.794(15)	2.702(3)	153(3)
O12–H(12E)···O9′	0.976(5)	1.916(16)	2.825(3)	154(3)
O5–H···O6	0.976(5)	2.33(4)	2.675(2)	100(2)

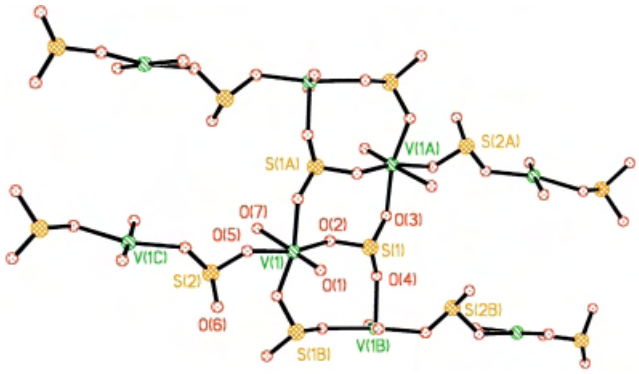


Figure 2. Structural building unit of **3** and the atomic numbering scheme. Selected interatomic distances (Å): V(1)-O(1) 1.580(7), V(1)-O(5) 1.984(6), V(1)-O(4A) 2.024(5), V(1)-O(2) 2.029(6), V(1)-O(3A) 2.057(5), V(1)-O(7) 2.280(7), S(1)-O(4) 1.548(6), S(1)-O(3) 1.548(6), S(1)-O(2) 1.551(7), S(2)-O(6) 1.506(11), S(2)-O(5) 1.549(6).

The temperature dependence of the susceptibility data for compound **1** is shown in Figure 3 in the form of χT versus T, where an overall ferromagnetic behavior is revealed. The χT value of 2.24 $cm^3 mol^{-1}$ K at room temperature is higher than the value expected for six uncorrelated $S = 1/2$ spins, and increases with decreasing temperature to a maximum value of 3.1 $cm^3 mol^{-1}$ K at 2 K.

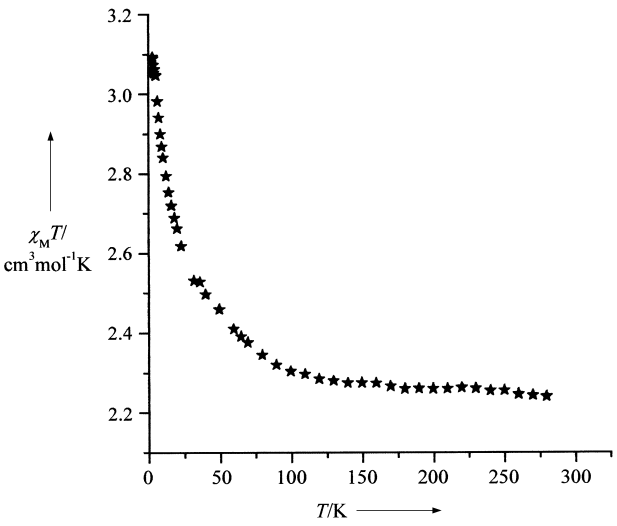


Figure 3. Temperature dependence of magnetic susceptibility given by measurements of $\chi_M T$ at 0.1 T over a temperature range of 2–300 K

Experimental Section

1: An aqueous solution (approximately 10 mL, pH 9) containing Na_2SO_3 (1.5 g, 12.0 mmol) and Bu_4NBr (7.5 g, 24.0 mmol) was added in one portion to a stirred solution of $[V^{IV}OCl_2(thf)_2]$[12] (1.5 g, 5.5 mmol) in an HCl solution (37% HCl in water, 1:4 v/v, 15 ml, pH ~ 1). Upon addition of Na_2SO_3 and Bu_4NBr the light-blue color of the solution immediately changed to dark blue and the pH value of the solution changed to approximately 2.5. Blue-green orthogonal

 © 2003 Wiley-VCH Verlag GmbH & Co. KGaA, Weinheim 1433-7851/03/4204-0426 $ 20.00+.50/0

crystals of **1** were isolated from the resulting solution after one day. Yield: 0.48 g (40% based on V). IR: $\tilde{\nu}$ = 2964 [ν(C_{But}–H)], 1000, 1021, 987, 953 [ν(V=O)], 823, 636, 508 cm^{-1} [ν(SO_3^{2-})]; UV/Vis (H_2O): λ/nm (ε/$dm^3 mol^{-1} cm^{-1}$) = 238(sh, 14258) 862 (547); TGA: percentage weight loss (temperature (°C)) = 6.8 (187, assigned to H_2O), 36.5 (208, assigned to C_xH_y and NH_3), 3.6 (306, assigned to SO_x); elemental analysis calcd (%) for $C_{32}H_{78}N_2O_{24}S_4V_6$ (1308.83): C 29.37, H 6.00, N 2.14, S 9.80, V 23.35; found: C 29.68, H 6.04, N 2.17, S 9.63, V 23.50.

2: Compound **2** was prepared in 60% yield in a similar fashion to **1**, except that $(NH_4)_2SO_3$ was used instead of Na_2SO_3 and Bu_4NBr. IR: $\tilde{\nu}$ = 3239 [ν(N-H)], 1019, 989, 953 [ν(V=O)], 895, 644, 492 cm^{-1} [ν(SO_3^{2-})]; UV/Vis (H_2O): λ/nm (ε/$dm^3 mol^{-1} cm^{-1}$) = 380 (1757), 266 (9034), 889 (580); TGA: percentage weight loss (temperature (°C)): 6.2 (170, assigned to H_2O), 3.9 (352, assigned to NH_3), 24.1 (501, assigned to SO_x); elemental analysis calcd (%) for $H_{14}N_2O_{24}S_4V_6$ (860.01): H 1.64, N 3.26, S 14.92, V 35.54; found: H 1.75, N 3.10, S 15.10, V 35.85.

3: Solid MgO (7.0 g, 174 mmol) was added in one portion to a stirred solution of NH_4VO_3 (1.5 g, 12.8 mmol) in diluted HCl (37% HCl in water, 1:4 v/v, 20 mL, pH ~ 1.5). Upon addition of MgO, the yellow color of the solution did not change. Solid $(NH_4)_2SO_3$ (1.5 g, 15.3 mmol) was then added to the solution, the color of which immediately turned blue, and the pH value changed to approximately 3.0. Blue hexagonal crystals of **3** were precipitated from the solution after 2 days. Yield: 2.06 g (60% based on V). IR: $\tilde{\nu}$ = 3262 [ν(NH_4^+)], 1019, 987, 953 [ν(V=O)], 904 cm^{-1} [ν(SO_3^{2-})]; UV/Vis (H_2O): λ/nm (ε/$dm^3 mol^{-1} cm^{-1}$) = 896 (2230), 235(sh, 6750); TGA: percentage weight loss (temperature (°C)): 26.8 (270, assigned to H_2O), 6.3 (361, assigned to NH_3) 35.8 (519.9, assigned to SO_2); elemental analysis calcd (%) for $H_{11}NO_9S_{1.5}V$ (268.13): H 4.13, N 5.22, S 17.94, V 19.00; found: H 4.20, N 5.10, S 18.05, V 18.80.

Received: August 19, 2002
Revised: October 29, 2002 [Z50002]

[1] a) M. T. Pope, *Heteropoly and Isopoly Oxometalates*, Springer, New York, **1983**; b) M. T. Pope, A. Müller, *Angew. Chem.* **1991**, *103*, 56; *Angew. Chem. Int. Ed. Engl.* **1991**, *30*, 34; c) *Polyoxometalates: From Platonic Solids to Anti-Retroviral Activity* (Eds.: M. T. Pope, A. Müller), Kluwer Academic, Dordrecht, **1994**; d) guest editor: C. L. Hill, *Chem. Rev.* **1998**, *98*, 8; e) M. Farahbakhsh, H. Schmidt, D. Rehder, *Chem. Ber.* **1997**, *130*, 1123; f) M. Farahbakhsh, P. Kagerler, H. Schmidt, D. Rehder, *Inorg. Chem. Commun.* **1998**, *1*, 111.

[2] J. M. Clemente-Juan, E. Coronado, *Coord. Chem. Rev.* **1999**, *193–195*, 361, and references therein.

[3] a) A. K. Cheetham, G. Férey, T. Loiseau, *Angew. Chem.* **1999**, *111*, 3466; *Angew. Chem. Int. Ed.* **1999**, *38*, 3268, and references therein; b) R. C. Haushalter, L. A. Mundi, *Chem. Mater.* **1992**, *4*, 31; c) C. du Peloux, A. Dolbecq, P. Mialane, J. Marrot, E. Riviere, F. Secheresse, *Angew. Chem.* **2001**, *113*, 2521; *Angew. Chem. Int. Ed.* **2001**, *40*, 2455.

[4] K. Y. Matsumoto, M. Kato, Y. Sasaki, *Bull. Chem. Soc. Jpn.* **1976**, *49*, 106.

[5] M. J. Manos, J. D. Woollins, A. M. Z. Slawin, T. A. Kabanos, *Angew. Chem.* **2002**, *114*, 2925; *Angew. Chem. Int. Ed.* **2002**, *41*, 2801.

[6] a) *Materials for Non-Linear Optics: Chemical Perspectives* (Eds.: G. D. Stucky, S. R. Marder, J. E. Sohn), American Chemical Society, Washington, DC, **1991**; b) *Novel Optical Materials and Applications* (Eds.: I.-C. Khoo, F. Simoni, C. Umeton), Wiley, New York, **1997**.

[7] a) W. T. A. Harrison, M. L. F. Phillips, J. Stanchfield, T. M. Nenoff, *Angew. Chem.* **2000**, *112*, 3966; *Angew. Chem. Int. Ed.* **2000**, *39*, 3808; b) M. G. Johnston, W. T. A. Harrison, *Inorg. Chem.* **2001**, *40*, 6518; c) W. T. A. Harrison, *Acta Crystallogr. Sect. C* **1999**, *55*, 1980; d) P. S. Halasyamani, D. O'Hare, *Chem. Mater.* **1998**, *10*, 646, and references therein; e) W. T. A. Harrison, L. L. Dussack, A. J. Jacobson, *J. Solid State Chem.* **1996**, *125*, 234.

[8] a) R. E. Sykora, K. M. Ok, P. S. Halasyamani, T. E. Albrecht-Schmitt, *J. Am. Chem. Soc.* **2002**, *124*, 1951; b) A. C. Bean, S. M. Pepper, T. E. Albrecht-Schmitt, *Chem. Mater.* **2001**, *13*, 1266; c) A. C. Bean, C. F. Campana, O. Kwon, T. E. Albrecht-Schmitt, *J. Am. Chem. Soc.* **2001**, *123*, 8806; d) R. E. Sykora, D. M. Wells, T. E. Albrecht-Schmitt, *Inorg. Chem.* **2002**, *41*, 2697.

[9] A. K. Cheetham, G. Férey, T. Loiseau, *Angew. Chem.* **1999**, *111*, 3466, *Angew. Chem. Int. Ed.* **1999**, *38*, 3268, and references therein.

[10] Crystal data for **1**: $C_{32}H_{78}N_2O_{24}S_4V_6$, M_w = 1308.83, monoclinic, space group *I*2/*a*, *a* = 20.48910(10), *b* = 16.6679(4), *c* = 18.0218(3) Å, β = 111.3460(10)°, *V* = 5732.42(17) Å^3, *Z* = 4, ρ_{calc} = 1.517 $Mg m^{-3}$, *T* = 293(2) K; *R*1(final) = 0.0274, *wR*2 = 0.0693. Crystal data for **2**: $H_{14}N_2O_{24}S_4V_6$, M_W = 860.01, monoclinic, space group $P2_1$, *a* = 7.596(3), *b* = 20.033(9), *c* = 7.624(3) Å, β = 91.157(8)°, *V* = 1159.9(9) Å^3, *Z* = 2, ρ_{calc} = 2.463 $Mg m^{-3}$, *T* = 293(2) K; *R*1(final) = 0.1226, *wR2* = 0.3021. The structure of **2** was determined using different crystals under a variety of conditions (including two determinations at 125 K); the reported data are the best that were obtained. Crystal data for **3**: $H_{11}NO_9S_{1.5}V$, *M* = 268.13, orthorhombic, space group *Pbcm*, *a* = 7.0680(17), *b* = 12.536(3), *c* = 19.968(5), *V* = 1769.2(7) Å^3, *Z* = 8, ρ_{calc} = 2.013 $Mg m^{-3}$, *T* = 293(2) K. *R*1(final) = 0.0586, *wR2* = 0.1140. CCDC-179446 (**1**) contains the supplementary crystallographic data for this paper. These data can be obtained free of charge via www.ccdc.cam.ac.uk/conts/retrieving.html (or from the Cambridge Crystallographic Data Centre, 12, Union Road, Cambridge CB21EZ, UK; fax: (+44) 1223-336-033; or deposit@ccdc.cam.ac.uk). Further details on the crystal structure investigations for **2** and **3** may be obtained from the Fachinformationszentrum Karlsruhe, 76344 Eggenstein-Leopoldshafen, Germany (fax: (+49) 7247-808-666; e-mail: crysdata@fiz-karlsruhe.de), on quoting the depository numbers CSD-412712 and -412713.

[11] a) Bond valence sum (BVS) calculations for compound **1**: BVS calculations for O(5) and O(12) gave values of 1.24 and 0.47, respectively, while calculations for the crystallographically independent vanadium and sulfur ions gave values very close to 4. b) BVS calculations for compound **3**: BVS calculations for O(7) and O(1) gave values of 0.23 and 1.2, respectively, while calculations for the crystallographically independent vanadium and sulfur ions gave values very close to 4 [I. D. Brown in *Structure and Bonding in Crystals, Vol. II* (Ed.: M. O'Keefe, A. Navrotdsky), Academic Press, New York, **1981**, p. 1–30].

[12] a) K. Dimitrou, K. Folting, W. E. Streib, G. Christou, *J. Chem. Soc. Chem. Commun.* **1994**, 1385; b) K. Dimitrou, A. D. Brown, K. Folting, W. E. Streib, G. Christou, *Inorg. Chem.* **1999**, *38*, 1834.

[13] R. J. Kern, *J. Inorg. Nucl. Chem.* **1962**, *24*, 1105.

 © 2003 Wiley-VCH Verlag GmbH & Co. KGaA, Weinheim 1433-7851/03/4204-0427 $ 20.00+.50/0

Flexible Coordination Polymers

Porous Coordination-Polymer Crystals with Gated Channels Specific for Supercritical Gases**

*Ryo Kitaura, Kenji Seki, George Akiyama, and Susumu Kitagawa**

Considerable effort has been devoted to the synthesis and characterization of new crystalline nanosized porous materials, such as coordination polymers and inorganic zeolites, because of their versatile applicability to gas storage, molecular sieves, size- or shape-selective catalysis, and ion exchange.[1–7] For successful performance of these functions, robustness and stability of the porous frameworks are essential. In contrast, flexible host frameworks that respond to guest molecules, for example, induced-fit recognition between a protein and its substrate, have high selectivity for guest inclusion. Coordination polymers, in spite of their crystalline form, are suitable for creating flexible and dynamic porous frameworks, so-called third-generation compounds,[8] because the wide variety of architectures and topologies are based not only on coordinative bonds, but also on hydrogen bonds and/or π–π stacking, which are weaker than the Si–O and Al–O bonds in zeolites.[9–13] Hence, we focused on the preparation of two new types of flexible and dynamic nanoporous frameworks created by coordination polymers with interdigitation and interpenetration, and examined the gas-adsorption properties (CO_2, CH_4, O_2, and N_2) at high pressure and ambient temperature.

Our strategy for functional coordination polymers that respond to guest molecules is to assemble rigid motifs with a degree of freedom in displacement to provide two types of integrated frameworks (Figure 1): framework A with mutually interdigitated two-dimensional (2D) motifs, and framework B with mutually interpenetrated three-dimensional (3D) motifs. Both the rigidity of a structural motif and a degree of freedom in displacement could give rise to flexibility of the whole framework and thus improve porous properties. A coordination polymer of type A, namely, $[Cu(dhbc)_2(4,4'\text{-bpy})]\cdot H_2O$ (**1a**), was prepared from Cu^{II} nitrate, 2,5-dihydroxybenzoic acid (Hdhbc), and 4,4′-bipyridine (4,4′-bpy). The copper ions are connected by 4,4′-bpy to produce straight chains, and linked by dhbc to give a 2D sheet motif (Figure 2a and b, respectively). The motif has interlocking ridges and hollows constructed by the dhbc benzene planes in an upright fashion. The distance of 3.443 Å between the planes of the nearest-neighbor dhbc ligands indicates the presence of π–π stacking interactions, and the motifs are mutually interdigitated to create 1D channels along the *a* axis with a cross section of 3.6 × 4.2 Å (Figure 2c), in which one water molecule is included per copper ion. The type B coordination polymer **2** was obtained by using Cu^{II}, benzene-1,4-dicarboxylate (bdc), and 4,4′-bpy. Two-dimensional grid-type sheets composed of Cu^{II} and bdc are linked by 4,4′-bpy to produce a 3D jungle-gym-like framework, similar to the structure of Prussian Blue. Two independent 3D structures interpenetrate each other to form a 3D framework with cylindrical channels with approximate dimensions of 3.4 × 3.4 Å along the *c* axis (Figure 3).[14]

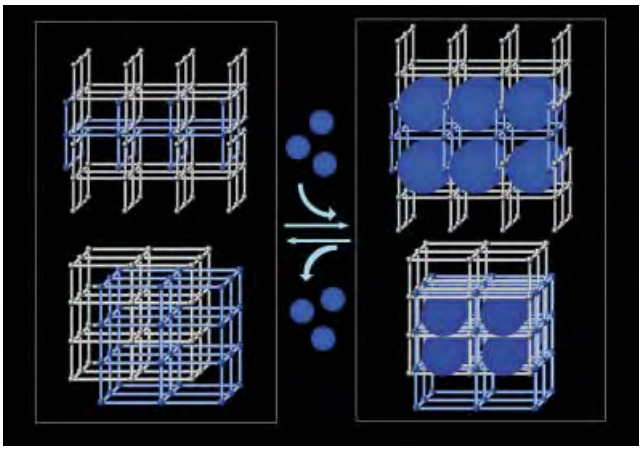


Figure 1. Schematic representation of dynamic frameworks. Above: Interdigitated framework of layers whose gap depends on the guest molecules. Below: Interpenetrated framework whose interunit space depends on the guest molecules.

Thermogravimetric analysis of **1a** shows the release of water molecules of crystallization with increasing temperature up to 120 °C to give guest-free anhydrous **1b**. No further weight loss was observed between 120 °C and 170 °C, that is, the guest-free phase is stable. Since the X-ray powder diffraction (XRPD) pattern of **1b** (Figure 4) shows sharp diffraction peaks similar to those of **1a**, the porous framework is largely maintained, even without water molecules. Detailed comparison of the two XRPD patterns reveals that only small shifts were observed for the peaks (010) and (100), which are attributed to the *ac* and *bc* planes, respectively. Therefore, the 2D layer motif is retained during dehydration. On the other hand, peaks corresponding to the relative position of the layer motifs show an apparent shift to the higher angle region between 15 and 20°. This result clearly indicates shrinking of the layer gap along the *c* axis, which is attributable to a gliding motion of the two π-stacked rings, which decreases the channel cross section.

[*] Prof. Dr. S. Kitagawa, R. Kitaura, G. Akiyama
Department of Synthetic Chemistry and Biological Chemistry
Graduate School of Engineering
Kyoto University
Yoshida, Sakyo-ku, Kyoto 606-8501 (Japan)
Fax: (+81) 75-753-4979
E-mail: kitagawa@sbchem.kyoto-u.ac.jp
K. Seki
Energy Conversion and Storage Technology
Applied Research Centre
Research and Development Department
Osaka Gas Co., Ltd.
6-19-9, Torishima, Konohana-ku, Osaka 554-0051 (Japan)

[**] This work was supported by Grant-in-Aid for Creative Scientific Research (No. 13GS0024), Ministry of Education, Culture, Sports, Science, and Technology, Japan.

Supporting information for this article is available on the WWW under http://www.angewandte.org or from the author.

 © 2003 Wiley-VCH Verlag GmbH & Co. KGaA, Weinheim 1433-7851/03/4204-0428 $ 20.00+.50/0

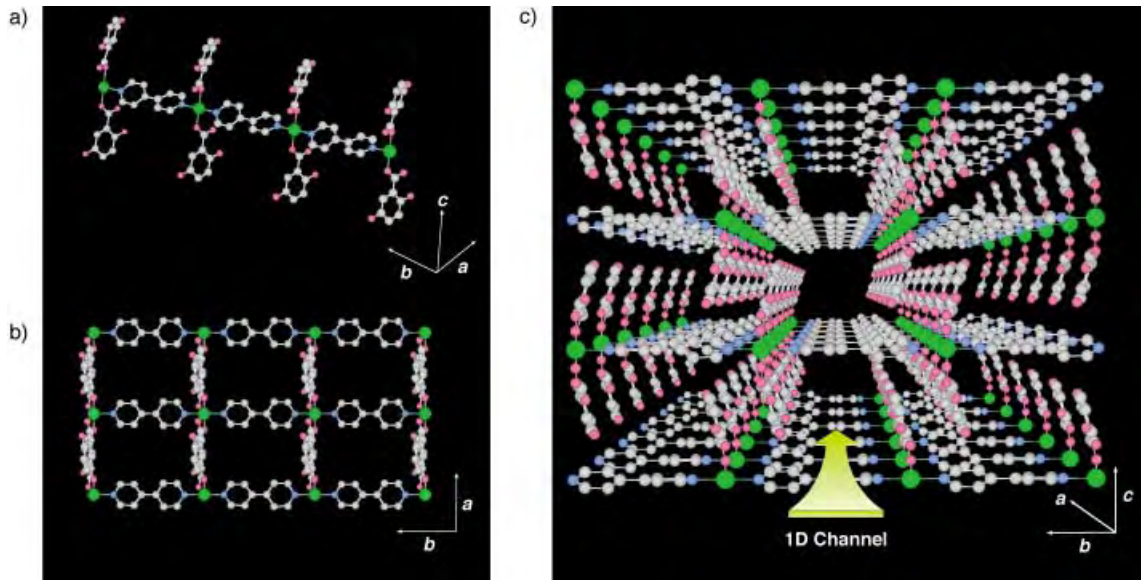


Figure 2. Crystal structure of **1a**. a) 1D chain structure constructed by Cu^{II}, 4,4′-bpy, and dhbc along the *b* axis (Cu, green; O, red; C, gray; N, blue). b) 2D layer structure along the *ab* plane. c) 3D π-stacked pillared layer structure of **1a**. Hydrogen atoms and water molecules are omitted for clarity.

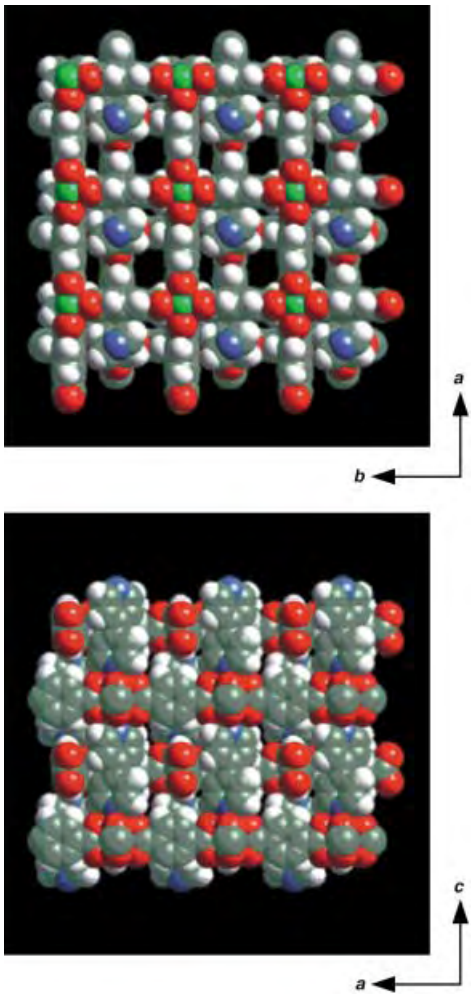


Figure 3. Space-filling model of the crystal structure of **2**. The structure model was optimized by molecular mechanics (MM) with the program package Cerius2.

Compound **1b** shows a type II nitrogen adsorption isotherm at 77 K, and the calculated BET specific surface area is 24 $m^2 g^{-1}$ (see Supporting Information). This low specific surface area leads to the conclusion that nitrogen molecules (molecular size 3.3 Å) could not diffuse into the micropores at all. If the original cross section of **1a** were retained, the nitrogen molecules would readily diffuse into the channels. This also indicates pore contraction on dehydration, as was demonstrated by XRPD. Figure 5a shows the N_2 adsorption isotherm of **1b** in the pressure range between 1 and 120 atm at 298 K. Unlike the adsorption profile at 77 K, the isotherm shows a profile unlike the usual adsorption patterns—a flat curve indicative of no adsorption in the lower pressure region, with an abrupt increase at a pressure of 50 atm (point a), as if channels large enough for the molecule already existed. Langmuir plots are almost linear in the higher pressure region and give a specific surface area of 320 $m^2 g^{-1}$. This high specific surface area clearly shows that nonporous phase **1b** was transformed into microporous phase **1a**. This onset pressure at which the channels of **1b** change into open gates is referred to as the gate-opening pressure.[15] Interestingly, the desorption isotherm shows an abrupt decrease at 30 atm (gate-closing pressure, point b), indicative of hysteresis in the adsorption and desorption isotherms. This hysteretic profile could be repeated many times. This hysteretic sorption behavior is well reproduced by the sum of the isotherms for nonporous phase **1b** and porous phase **1a**. Red and blue dashed lines in Figure 5a represent the estimated adsorption isotherms for nonporous phase and microporous phase, respectively. Below the gate-opening pressure, the adsorption isotherm coincides with the red line for the nonporous phase. Above the gate-opening pressure, the adsorption isotherm starts to approach the blue line (porous phase), and they coincide above 100 atm. At the gate-opening pressure, nitrogen molecules result in transformation

 © 2003 Wiley-VCH Verlag GmbH & Co. KGaA, Weinheim 1433-7851/03/4204-0429 $ 20.00+.50/0

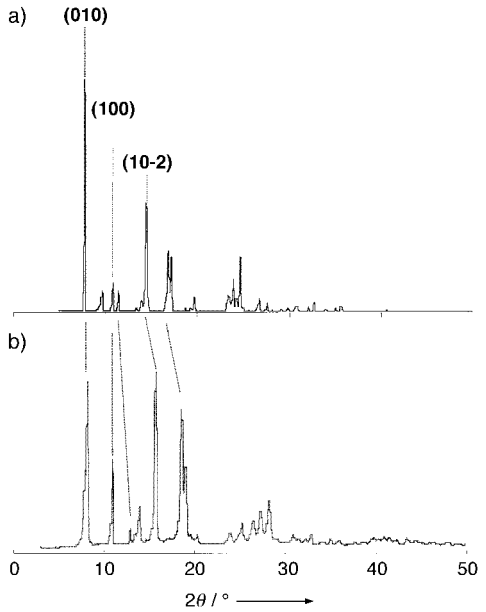


Figure 4. a) Observed XRPD pattern for the as-synthesized sample of **1a**. b) XRPD pattern for the anhydrous sample **1b** (dried at 110 °C under reduced pressure for 5 h). Estimated channel size based on the peak shift of (10−2) is 3.0×3.6 Å.

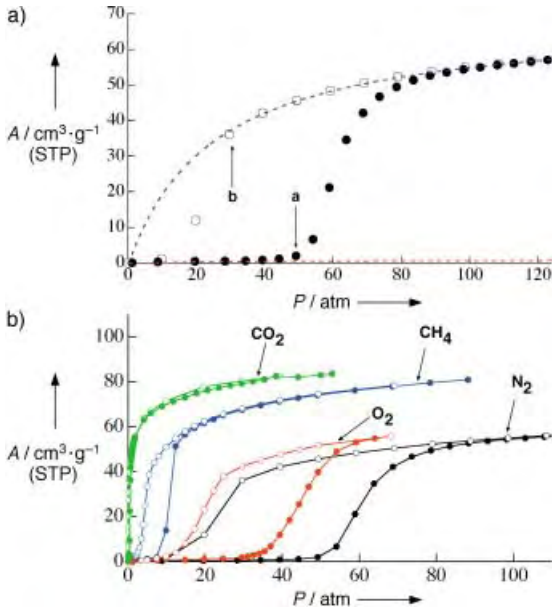


Figure 5. a) Nitrogen adsorption (filled circles) and desorption isotherms (open circles) for **1b** at 298 K. Blue and red dashed lines were determined by fitting the linear parts of the Langmuir plots in the higher (from 83 to 122 atm) and lower (from 8 to 34 atm) pressure ranges, respectively. b) Adsorption (filled circles) and desorption (open circles) isotherms of N_2, CH_4, CO_2 and O_2 at 298 K.

of crystalline "closed" form **1b** into crystalline "open" form **1a**.[15,16] Once nitrogen gas is adsorbed into the micropores of **1a**, nitrogen molecules stabilize the porous phase. Therefore, in the desorption isotherm, the porous phase was maintained until the pressure reached 30 atm (gate-closing pressure). This crystal structure transformation triggered by guest molecules was confirmed by an XRPD measurement on **1b** containing adsorbed methanol (molecular size 4.2 Å; see Supporting Information). To the best of our knowledge, this is the first example of hysteretic sorption behavior of supercritical nitrogen gas at ambient temperature under high pressure. Structural transformation triggered by a supercritical gas, which only exhibits weak dispersive interactions in this system, is facilitated by the unusual framework flexibility provided by displacement of π–π stacked moieties. Figure 5b shows the adsorption isotherms for various gases on **1b** in the pressure range between 1 and 100 atm at 298 K. All of the isotherm profiles are essentially similar to that for N_2 at 298 K, but a clear difference is observed for the gate-opening and gate-closing pressures. The gate-opening pressures for nitrogen, oxygen, and carbon dioxide are 50, 35, and 0.4 atm, and the gate-closing pressures 30, 25, and 0.2 atm, respectively. This difference should be attributable to differences in the intermolecular interaction force of the guest molecules. Similar adsorption behavior was observed for **2** (see Supporting Information).

Many coordination polymers have been synthesized with the aim of achieving stable microporous structures like those of zeolites; however, the goal here is not to mimic zeolites but to create new properties characteristic of coordination polymers. A coordination polymer is the best candidate for realizing of the unique nanostructure reported here. Guests are permitted to pass the gate at a specific gate-opening pressure that depends on the strength of the intermolecular interaction. We expect that such coordination polymers will find applications in gas separation, sensors, switches, and actuators. This flexible and dynamic coordination network opens up a new field in porous coordination materials.

Experimental Section

Synthesis of **1a**: A diethyl ether solution (20 mL) containing a mixture of 4,4′-bpy (0.13 g, 0.8 mmol) and Hdhbc (0.50 g 3.2 mmol) was carefully layered on the top of an aqueous solution (20 mL) of $Cu(NO_3)_2{\cdot}3H_2O$. Platelike green crystals began to form over a few days. One of these crystals was used for X-ray crystallography. The green crystals were collected by filtration, washed with ethanol, and dried under reduced pressure for 2 h. Yield: 0.18 g (0.32 mmol, 41 %). Elemental analysis (%) calcd for $C_{24}H_{14}N_2O_{10}Cu$: C 54.81, H 3.45, N 5.33; found: C 54.64, H 4.04, N 5.12. IR (KBr pellet): $\tilde{\nu}$ = 2810m, 1613s, 1492s, 1383w, 1279w, 1241m, 1131w, 1073w, 820s, 785s, 688m, 648w 554w and 493m cm^{-1}.

Single-crystal X-ray structure determination on **1a**: intensities were measured at 298 K with a graphite-monochromatized $Mo_{K\alpha}$ radiation source (λ = 0.71069 Å). 2198 independent reflections (8955 total measured) were analyzed by a direct method using the SIR92 program and expanded by Fourier techniques. Hydrogen atoms of hydroxy groups were located in the Fourier difference map. Hydrogen atoms except for those of hydroxy groups were placed in idealized positions, and their parameters were not refined. Crystal data: $C_{24}H_{22}CuN_2O_{10}$, M_r = 561.99, monoclinic, space group $P2/c$ (No. 13), a = 8.167(4), b = 11.094(8), c = 15.863(2) Å, β = 99.703(4)°, V = 1416(1) Å^3, Z = 2, R = 0.068, wR = 0.088. CCDC-191853 contains the supplementary crystallographic data for this paper. These data can be obtained free of charge via www.ccdc.cam.ac.uk/conts/retrieving.html (or from the Cambridge Crystallographic Data Centre, 12, Union Road, Cambridge CB21EZ, UK; fax: (+44) 1223-336-033; or deposit@ccdc.cam.ac.uk).

 © 2003 Wiley-VCH Verlag GmbH & Co. KGaA, Weinheim 1433-7851/03/4204-0430 $ 20.00+.50/0

Coordination polymer **2** was synthesized according to a published procedure. Elemental analysis (%) calcd for $C_{13}H_8NO_4Cu$: C 51.06, H 2.62, N 4.58; found C 50.62, H 2.45, N 4.60.

Gas adsorption measurements: Sorption isotherms were measured at 298 K on an FMS-BG (BEL inc.) automatic gravimetric adsorption measurement system with Rubotherm magnet coupling balance incorporated in a SUS steel pressure chamber. A known weight (200–300 mg) of the as-synthesized sample was placed in the aluminum sample cell in the chamber, and the sample was dried under high vacuum at 373 K for 5 h to remove the host water molecules. The adsorbate was dosed into the chamber, and the change in weight was monitored. After correction for buoyancy, the absorbed amount was determined.

Received: August 27, 2002 [Z50052]

[1] G. A. Ozin, A. Kuperman, A. Stein, *Angew. Chem.* **1989**, *101*, 373–390; *Angew. Chem. Int. Ed. Engl.* **1989**, *28*, 359–376.
[2] A. Corma, *Chem. Rev.* **1997**, *97*, 2373–2419.
[3] M. Eddaoudi, D. B. Moler, H. Li, B. Chen, T. M. Reineke, M. O'Keeffe, O. M. Yaghi, *Acc. Chem. Res.* **2001**, *34*, 319–330.
[4] M. Eddaoudi, J. Kim, N. Rosi, D. Vodak, J. Wachter, M. O'Keeffe, O. M. Yaghi, *Science* **2002**, *295*, 469–472.
[5] B. Moulton, M. J. Zaworotko, *Chem. Rev.* **2001**, *101*, 1629–1658.
[6] J. S. Seo, D. Whang, H. Lee, S. I. Jun, J. Oh, Y. J. Jeon, K. Kim, *Nature* **2000**, *404*, 982.
[7] S. Noro, S. Kitagawa, M. Kondo, K. Seki, *Angew. Chem.* **2000**, *112*, 2162–2164; *Angew. Chem. Int. Ed.* **2000**, *39*, 2082–2084.
[8] S. Kitagawa, M. Kondo, *Bull. Chem. Soc. Jpn.* **1998**, *71*, 1739–1753.
[9] R. Robson, *J. Chem. Soc. Dalton Trans.* **2000**, *21*, 3735–3744.
[10] A. J. Fletcher, E. J. Cussen, T. J. Prior, M. J. Rosseinsky, C. J. Kepert, K. M. Thomas, *J. Am. Chem. Soc.* **2001**, *123*, 10001–10011.
[11] D. V. Soldatov, J. A. Ripmeester, S. I. Shergina, I. E. Sokolov, A. S. Zanina, S. A. Gromilov, Y. A. Dyadin, *J. Am. Chem. Soc.* **1999**, *121*, 4179–4188.
[12] L. C. Tabares, J. A. R. Navarro, J. M. Salas, *J. Am. Chem. Soc.* **2001**, *123*, 383–387.
[13] M. Albrecht, M. Lutz, A. L. Spek, G. van Koten, *Nature* **2000**, *406*, 970–974.
[14] K. Seki, *Phys. Chem. Chem. Phys.* **2002**, *4*, 1968–1972.
[15] D. Li, K. Kaneko, *Chem. Phys. Lett.* **2001**, *335*, 50–56.
[16] R. Kitaura, K. Fujimoto, S. Noro, M. Kondo, S. Kitagawa, *Angew. Chem.* **2002**, *114*, 141–143; *Angew. Chem. Int. Ed.* **2002**, *41*, 133–135.

Glycopeptide Synthesis

Toward Fully Synthetic *N*-Linked Glycoproteins**

*Justin S. Miller, Vadim Y. Dudkin, Gholson J. Lyon, Tom W. Muir, and Samuel J. Danishefsky**

The structural and biological consequences of cellular protein modification through posttranslational glycosylation are central issues in the rapidly growing field of glycobiology.[1] The availability of homogeneous glycopeptides, both *O*-linked (serine, threonine, or tyrosine α-glycosides) and *N*-linked (asparagine β-glycosides), could greatly enhance insight into glycobiology.[2] It became our view that the prospect of total synthesis of homogeneous glycoproteins provides the best chance for gaining such access.

Numerous methods exist for glycopeptide synthesis: glycans have been introduced into peptides by means of amino acid "cassettes" with pendant protected saccharides,[3] through enzymatic manipulations of glycopeptides,[4] or by conjugation of fully elaborated, complex saccharides to short synthetic peptides.[5] Larger *O*-linked glycopeptides have been synthesized by using ligation techniques[6] such as expressed protein ligation.[7] Bertozzi and co-workers extended the scope of the "cassette" approach by applying native chemical ligation to the synthesis of a biologically active glycoprotein with two single-residue *O*-linked glycans.[8] Tolbert and Wong described the ligation of a 392-residue intein-generated peptide thioester and a dipeptide functionalized with a single *N*-acetylglucosamine residue.[7c] Using a different fragment condensation protocol, Hojo et al. reported the synthesis of a glycopeptide domain of Emmprin that contains an *N*-linked chitobiose unit, but the saccharide was not entirely stable to the conditions required for resin cleavage in their solid-phase synthesis.[9]

[*] Prof. S. J. Danishefsky, Dr. J. S. Miller, Dr. V. Y. Dudkin
Laboratory for Bioorganic Chemistry
Sloan-Kettering Institute for Cancer Research
1275 York Avenue, New York, NY 10021 (USA)
Fax: (+1) 212-772-8691
E-mail: s-danishefsky@ski.mskcc.org
Prof. S. J. Danishefsky
Department of Chemistry, Columbia University
Havemeyer Hall, New York, NY 10027 (USA)
G. J. Lyon, Prof. T. W. Muir
Laboratory of Synthetic Protein Chemistry
The Rockefeller University
1230 York Avenue, New York, NY 10021 (USA)

[**] This work was supported by the NIH (AI16943). The receipt of a Pfizer Award to S.J.D. for Creative Work in Organic Synthesis is gratefully acknowledged. We thank Drs. Andrzej Zatorski and Ulrich Iserloh for the preparation of starting materials and for helpful discussions, and Dr. George Sukenick and Ms. Sylvi Rusli (NMR Core Facility, CA-02848) for mass spectral analyses.

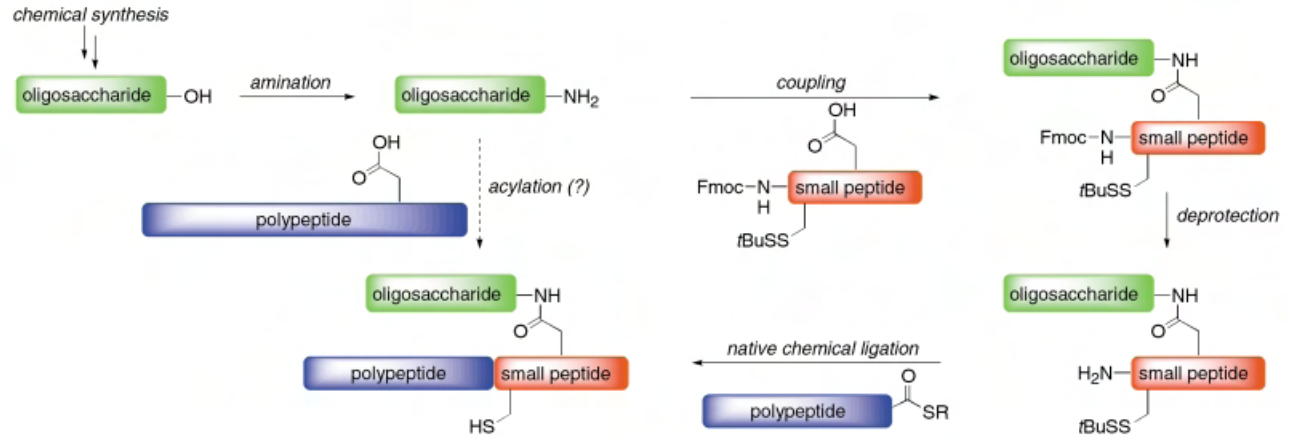
Supporting information for this article is available on the WWW under http://www.angewandte.org or from the author. Experimental details include the preparation of and mass spectral characteristics for **2**–**6, 8**, and **10**–**12**; and NMR spectra for **5, 6, 8**, and **10**.

Our goal was to set the stage for fully synthetic routes to complex glycoproteins. It would thus be necessary to harmonize *all* of the components of the undertaking. This includes building a complex glycodomain and incorporating it into a polypeptide setting. Herein we show how the pieces of the puzzle can be interfaced. In launching our program we took particular note of the work of Kochetkov and co-workers,[10] applied by Lansbury and co-workers,[5b] involving direct anomeric β-amination of unprotected saccharides followed by acylation with a peptide carboxylic acid.

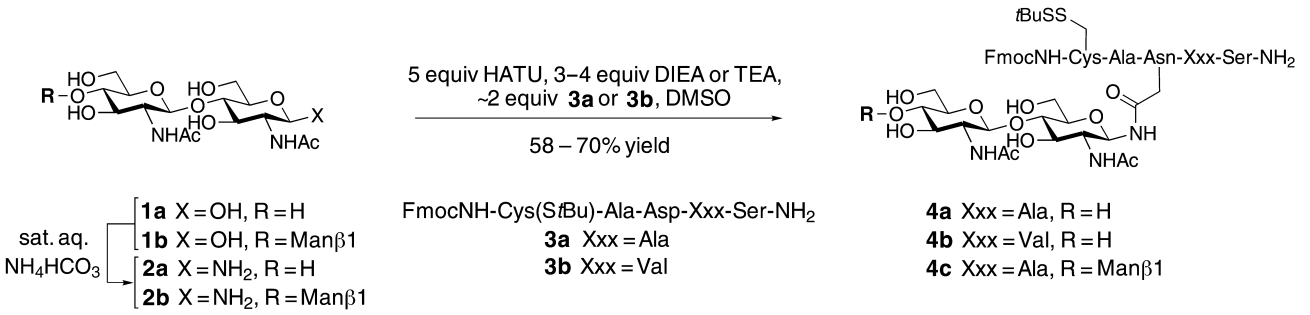
Our program focuses on natural *O*- and *N*-linkages as opposed to non-natural arrangements. Furthermore, as our oligosaccharides are assembled by total chemical synthesis,[11] there is, in principle, no limit to the structural complexity of the carbohydrate sectors of our glycopeptide targets, even as homogeneity is maintained.

The scenario for an ultimately convergent protocol involves merging fully mature oligosaccharide and polypeptide domains in one grand acylation event (dashed arrow, Scheme 1). For the moment, we favored the slightly less convergent, but in the end more practical and certainly more flexible, route shown in Scheme 1. In this case, the anomeric amine function of an oligosaccharide domain is acylated with a more manageable small peptide; native chemical ligation is then used to anneal this construct to a larger polypeptide segment. Critical for our long-term goals was the requirement that the precious, fully synthetic glycan be the limiting reagent in the chemical mergers. As shown in Scheme 1, this boundary condition has been attained.

We began our investigation as shown in Scheme 2. Treatment of known[12] unprotected saccharides **1a–b** (generated by total synthesis) with saturated aqueous ammonium hydrogen carbonate followed by lyophilization to a constant mass afforded glycosylamines **2a–b**. As a consequence of the known instability of anomeric glycosylamines and our desire to maximize yields, the resulting white powders were used without further purification or analysis, aside from mass spectrometry. The results of Kochetkov amination are well-documented,[13] and could in any case be confirmed by ^{1}H NMR coupling constants after peptide conjugation. Using optimized conditions developed for this purpose, glycosylamines **2a–b** were acylated with pentapeptides **3a** or **3b** by adding to the glycosylamine a twofold excess of peptide preactivated with HATU (5 equiv) and a tertiary amine (3–4 equiv) in DMSO. Upon completion of the reactions after only 2–4 h as monitored by analytical HPLC or LCMS, the reaction mixtures were purified by semipreparative HPLC. Two major side products were observed, showing molecular ions of 1 Da and 18 Da less than the starting aspartate-containing peptides. These are consistent with conversion of Asp into Asn through acylation of spurious ammonia and aspartimide formation as shown in Scheme 3,[14] which several other authors also note and seek to avoid by various methods. Though these processes are competitive with glycopeptide formation in terms of rate, their products are solely peptide-derived. Thus an excess of peptide starting material avoids most losses caused by these processes, even with an Ala residue immediately towards the C-terminus of the activated

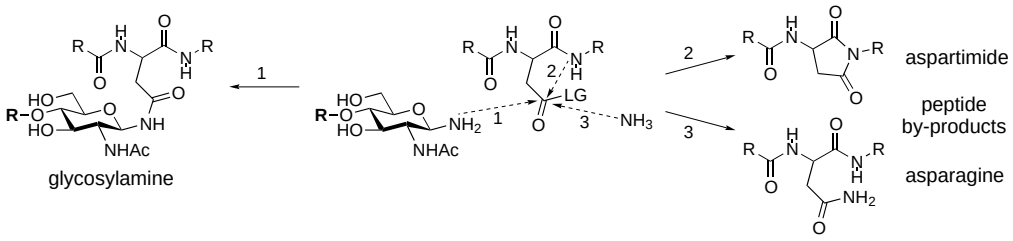


Scheme 1. Convergent approach to *N*-linked glycopeptides. Fmoc = 9-fluorenylmethoxycarbonyl.



Scheme 2. Glycan preparation and peptide conjugation. HATU = *N*-[(dimethylamino)-1*H*-1,2,3-triazole[4,5-*b*]-pyridin-1-ylmethylene]-*N*-methylmethanaminium hexafluorophosphate, DIEA = diisopropylethylamine, TEA = triethylamine, DMSO = dimethyl sulfoxide.

 © 2003 Wiley-VCH Verlag GmbH & Co. KGaA, Weinheim 1433-7851/03/4204-0432 $ 20.00+.50/0



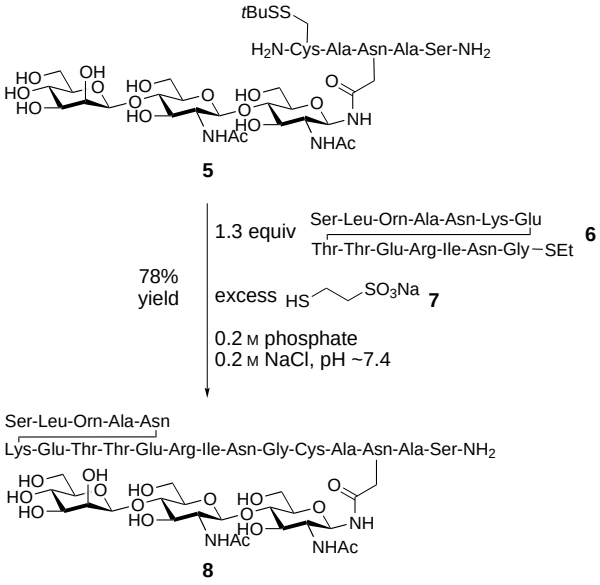
Scheme 3. Peptide byproducts of aspartate acylation.

Asp.[15] The yields of the combined amination and acylation products **4a–c** upon isolation were in the range of 58 to 70% based on starting glycan,[16] representing a significant improvement over the best yields previously reported.

Deprotection of Fmoc-glycopeptide **4c** with 20% piperidine in DMF followed by purification by HPLC afforded free glycopeptide **5** as a cysteine thiol *tert*-butyl disulfide in 68% yield. Additional products were observed with molecular ions identical to that of the desired material, perhaps as a result of epimerization of cysteine or the anomeric amide. The purified, isolated material at this stage was characterized by ^{1}H NMR spectroscopy, electrospray ionization (ES) MS, and liquid chromatography (LC) MS as a single isomer with an anomeric ^{1}H NMR shift ($\delta = 5.04$) and coupling constant ($J =$ 9.6 Hz) indicating the presence of a β-linked anomeric glycosylamide, thus validating the results of the Kochetkov–Lansbury amination.

We next extended glycopeptide **5** through native chemical ligation on a sizable (~15 mg) scale as shown in Scheme 4. As an independent test of the methodology, we synthesized tetradecapeptide thioester **6** employing the Fmoc/*t*Bu solid-phase peptide synthesis method recently reported by Hilvert and co-workers.[17] After automated peptide synthesis on a PEG-type Wang resin,[18] cleavage with trimethylaluminum and ethanethiol in dichloromethane afforded the desired thioester along with several (presumably Glu side chain) thioester derivatives. We noted a significant improvement in the purity of our peptide when the cleavage was quenched by filtration of the cleavage mixture (to remove resin) into a stirred mixture of trifluoroacetic acid, water, and phenol over an ice bath rather than pouring the entire cleavage reaction mixture into the TFA mixture at room temperature; in fact, we observed no side chain thioesters at all when the cleavage was quenched as described.

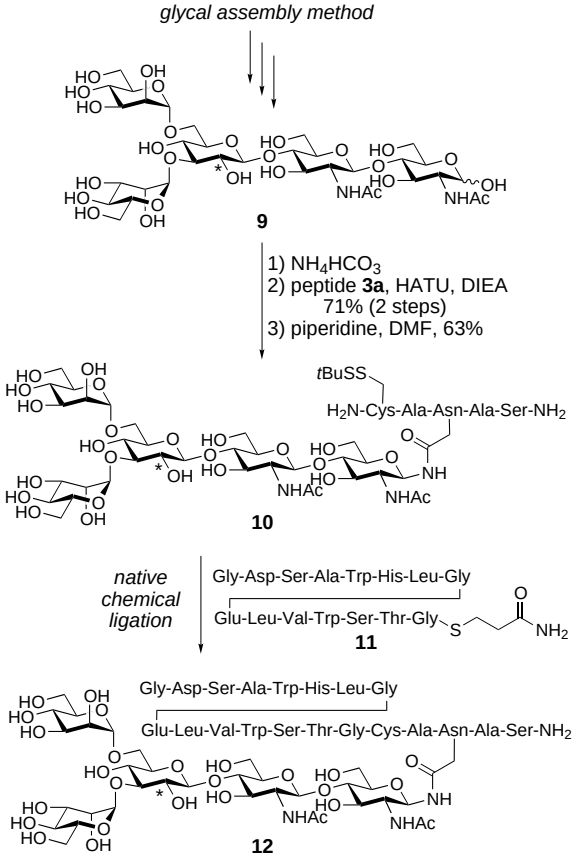
Ligation of **5** and **6** was carried out in aqueous PBS, 0.2 M in both saline and phosphate, pH ~7.4, in the presence of excess sulfanylethane-2-sulfonate (**7**) as illustrated in Scheme 4. Global disulfide reduction with the water-soluble phosphane TCEP[19] followed by semipreparative HPLC afforded the desired, fully unprotected glycopeptide **8** in 78% yield based on starting glycopeptide. Characterization of glycopeptide **8** by ESMS, LCMS, and ^{1}H and ^{13}C NMR spectroscopy in D_2O (Supporting Information) was consistent with a single compound containing a β-linked glycosylamide.



Scheme 4. High-yielding ligation of an *N*-linked glycopeptide.

As an example of the power of this method for complex glycopeptide synthesis, we employed pentasaccharide **9** (Scheme 5), prepared by chemical synthesis.[11] The compound differs from a characteristic high mannose pentasaccharide at one of its 25 stereogenic centers (asterisk, Scheme 5).[20] Amination followed by our peptide acylation conditions with pentapeptide **3a** and Fmoc removal yielded pentasaccharide glycopeptide **10** as a single, β-linked isomer, confirmed by HPLC and ^{1}H NMR spectroscopy ($\delta =$ 5.01 ppm, $J = 9.6$ Hz). Native chemical ligation with **10** and excess pentadecapeptide thioester **11** synthesized by Boc chemistry[21] afforded glycopeptide **12** as evidenced by HPLC and ESMS, again demonstrating proof of principle.

In summary, we have presented a highly convergent route for the production of substantial quantities of homogeneous glycopolypeptides. In this effort we retain the full flexibility accruing from total chemical synthesis of the oligosaccharide (see compound **9**). Of course, the same flexibility is also retained in the polypeptide.[22] Although unexpected difficulties will no doubt be encountered, we presently see no insuperable boundary to progression towards fully synthetic,



Scheme 5. Native chemical ligation of a pentasaccharide glycopeptide and a pentadecapeptide. DMF = *N*,*N*-dimethylformamide.

homogeneous, complex glycoproteins. Applications of the advances recorded above to critical biological goal systems are well underway, and will be described in due course.

Received: September 23, 2002
Revised: November 11, 2002 [Z50217]

[1] a) B. Imperiali, S. E. O'Connor, *Curr. Opin. Chem. Biol.* **1999**, *3*, 643 – 649; b) B. Imperiali, S. E. O'Connor, T. Hendrickson, C. Kellenberger, *Pure Appl. Chem.* **1999**, *71*, 777 – 787; c) P. M. Rudd, T. Elliott, P. Cresswell, I. A. Wilson, R. A. Dwek, *Science* **2001**, *291*, 2370 – 2376; d) J. W. Dennis, M. Granovsky, C. E. Warren, *Biochim. Biophys. Acta* **1999**, *1473*, 21 – 34; e) J. R. Allen, C. R. Harris, S. J. Danishefsky, *J. Am. Chem. Soc.* **2001**, *123*, 1890 – 1897.

[2] C. R. Bertozzi, L. L. Kiessling, *Science* **2001**, *291*, 2357 – 2364.

[3] a) X. T. Chen, D. Sames, S. J. Danishefsky, *J. Am. Chem. Soc.* **1998**, *120*, 7760 – 7769; b) N. Bezay, G. Dudziak, A. Liese, H. Kunz, *Angew. Chem.* **2001**, *113*, 2350 – 2353; *Angew. Chem. Int. Ed.* **2001**, *40*, 2292 – 2295; c) N. Bezay, G. Dudziak, A. Liese, H. Kunz, *Angew. Chem.* **2001**, *113*, 2350 – 2353; d) J. van Ameijde, H. B. Albada, R. M. J. Liskamp, *J. Chem. Soc. Perkin Trans. 1* **2002**, 1042 – 1049; e) M. Ciommer, H. Kunz, *Synlett* **1991**, 593 – 595; f) M. V. Chiesa, R. R. Schmidt, *Eur. J. Org. Chem.* **2000**, 3541 – 3554; g) E. Meinjohanns, M. Meldal, K. Bock, *Tetrahedron Lett.* **1995**, *36*, 9205 – 9208.

[4] a) C. Unverzagt, *Tetrahedron Lett.* **1997**, *38*, 5627 – 5630; b) K. Witte, P. Sears, R. Martin, C. H. Wong, *J. Am. Chem. Soc.* **1997**, *119*, 2114 – 2118; c) L. X. Wang, M. Tang, T. Suzuki, K. Kitajima, Y. Inoue, S. Inoue, J. Q. Fan, Y. C. Lee, *J. Am. Chem. Soc.* **1997**, *119*, 11137 – 11146; d) G. Arsequell, G. Valencia, *Tetrahedron: Asymmetry* **1999**, *10*, 3045 – 3094; e) M. Mizuno, K. Haneda, R. Iguchi, I. Muramoto, T. Kawakami, S. Aimoto, K. Yamamoto, T. Inazu, *J. Am. Chem. Soc.* **1999**, *121*, 284 – 290; f) K. M. Koeller, M. E. B. Smith, R. F. Huang, C. H. Wong, *J. Am. Chem. Soc.* **2000**, *122*, 4241 – 4242; g) O. Blixt, K. Allin, L. Pereira, A. Datta, J. C. Paulson, *J. Am. Chem. Soc.* **2002**, *124*, 5739 – 5746.

[5] a) S. T. Anisfeld, P. T. Lansbury, *J. Org. Chem.* **1990**, *55*, 5560 – 5562; b) S. T. Cohen-Anisfeld, P. T. Lansbury, *J. Am. Chem. Soc.* **1993**, *115*, 10531 – 10537; c) E. Meinjohanns, M. Meldal, H. Paulsen, R. A. Dwek, K. Bock, *J. Chem. Soc. Perkin Trans. 1* **1998**, 549 – 560.

[6] a) T. Wieland, *Chimia* **1974**, *28*, 496 – 499; b) P. E. Dawson, T. W. Muir, I. Clark-Lewis, S. B. H. Kent, *Science* **1994**, *266*, 776 – 779; c) C. F. Liu, J. P. Tam, *Proc. Natl. Acad. Sci. USA* **1994**, *91*, 6584 – 6588.

[7] a) T. W. Muir, D. Sondhi, P. A. Cole, *Proc. Natl. Acad. Sci. USA* **1998**, *95*, 6705 – 6710; b) D. Macmillan, C. R. Bertozzi, *Tetrahedron* **2000**, *56*, 9515 – 9525; c) T. J. Tolbert, C. H. Wong, *J. Am. Chem. Soc.* **2000**, *122*, 5421 – 5428.

[8] Y. Shin, K. A. Winans, B. J. Backes, S. B. H. Kent, J. A. Ellman, C. R. Bertozzi, *J. Am. Chem. Soc.* **1999**, *121*, 11684 – 11689.

[9] H. Hojo, J. Watabe, Y. Nakahara, Y. Ito, K. Nabeshima, B. P. Toole, *Tetrahedron Lett.* **2001**, *42*, 3001 – 3004.

[10] L. M. Likhosherstov, O. S. Novikova, V. A. Derevitskaja, N. K. Kochetkov, *Carbohydr. Res.* **1986**, *146*, C1 – C5.

[11] S. J. Danishefsky, S. Hu, P. F. Cirillo, M. Eckhardt, P. H. Seeberger, *Chem. Eur. J.* **1997**, *3*, 1617 – 1628.

[12] a) T. Usui, M. Suzuki, T. Sato, H. Kawagishi, K. Adachi, H. Sano, *Glycoconjugate J.* **1994**, *11*, 105 – 110; b) G. M. Watt, L. Revers, M. C. Webberley, I. B. H. Wilson, S. L. Flitsch, *Angew. Chem.* **1997**, *109*, 2445 – 2447; *Angew. Chem. Int. Ed. Engl.* **1997**, *36*, 2354 – 2356.

[13] D. Vetter, M. A. Gallop, *Bioconjugate Chem.* **1995**, *6*, 316 – 318.

[14] M. Bodanszky, S. Natarajan, *J. Org. Chem.* **1975**, *40*, 2495 – 2499.

[15] See Supporting Information for details.

[16] Though aspartimides are prone to open at either imide carbonyl center, it is extremely unlikely that such a side reaction could account for β-peptide product corresponding to more than half of the starting glycosylamine. That the isolated yield here reflects a majority of the starting glycosylamine countermands the possibility that the product derives from nucleophilic (glycosylamine) aspartimide opening.

[17] a) D. Swinnen, D. Hilvert, *Org. Lett.* **2000**, *2*, 2439 – 2442; b) A. Sewing, D. Hilvert, *Angew. Chem.* **2001**, *113*, 3503 – 3505; *Angew. Chem. Int. Ed.* **2001**, *40*, 3395 – 3396.

[18] Solid-phase synthesis of this peptide met with difficulties that were overcome by using a pseudoproline dipeptide monomer; see Supporting Information for details.

[19] J. A. Burns, J. C. Butler, J. Moran, G. M. Whitesides, *J. Org. Chem.* **1991**, *56*, 2648 – 2650.

[20] Chemical synthesis of glycopeptides offers the ability to introduce structural modifications for the purpose of understanding the role of stereochemistry in glycoconjugate recognition. Evaluation of such stereochemical issues will be reported in due course. The implications of such a point mutation on binding to high mannose lectins is but one example of a fascinating question that can now be answered.

[21] See Supporting Information.

[22] a) B. L. Nilsson, L. L. Kiessling, R. T. Raines, *Org. Lett.* **2000**, *2*, 1939 – 1941; b) E. Saxon, J. I. Armstrong, C. R. Bertozzi, *Org. Lett.* **2000**, *2*, 2141 – 2143; c) J. P. Tam, J. X. Xu, K. D. Eom, *Biopolymers* **2001**, *60*, 194 – 205.

 © 2003 Wiley-VCH Verlag GmbH & Co. KGaA, Weinheim 1433-7851/03/4204-0434 $ 20.00+.50/0

Complexes of P,N Macrocycles

A Strategy for the Synthesis of Phosphorus-Containing Macrocycles—Ligands for Exceptional Coordination Geometries**

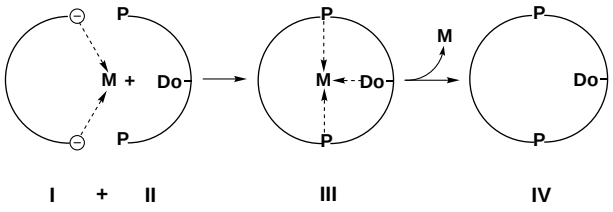
*Sahir Ekici, Martin Nieger, Robert Glaum, and Edgar Niecke**

In memory of Othmar Stelzer

On the basis of its simple implementation and high efficiency template-directed synthesis is of central importance for the assembly of macrocyclic structures.[1] Milestones of this discipline, which is situated on the interface between organic and supramolecular chemistry, include the syntheses of crown ethers, cryptands, and polyazamacrocycles which have potential applications in catalysis and electron transfer.[2] The macrocyclization is realized by a condensation or oxidative coupling reaction, where in particular the ions of alkali metals and late transition metals, respectively, proved their general usability.[1]

Template-directed syntheses of phosphamacrocycles normally proceed by 1,2-addition of primary or secondary phosphanes to vinylic or allylic double bonds, respectively.[3] However, examples of ring-closure reactions by alkylation of *cis* oriented PH units bound to a transition metal[4] or by reactions of bipodal, aliphatic, secondary phosphanes with β-carbonyl compounds are also present in the literature.[5] Unfortunately the access to such compounds is severely restricted by the limited availability of PH functionalized phosphanes.[6] Macrocycles containing additional donor atoms (N, O, S) besides the phosphorus fragment were obtained only in particular cases using high-dilution conditions or condensation reactions; template-directed ring closure is the exception.[7]

In the context of the synthesis of tridental hybrid ligands containing a PC_2EC_2P (E = N, O, S)[8,9] backbone with low-coordinated phosphorus centers we succeeded in developing a novel synthetic approach to macrocyclic structures. The strategy is based on a coupling reaction between two alkali-metal-fixed, carbanionic centers **I** (template) and two specifically connected, electrophilic phosphorus centers **II** (substrate). Twofold P–C bond formation first results in a metallamacrocycle **III** (in the form of a phosphamethanide complex), that is subsequently converted by protonation into the neutral ring system **IV** (Scheme 1). The reaction sequence



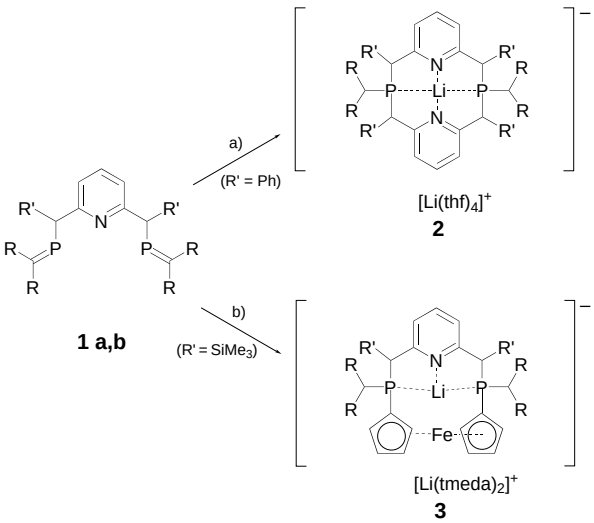
Scheme 1. Concept for the synthesis of macrocycles with phosphorus donor centers.

I + II→III→IV is supported by two examples: the synthesis of a) a 2,11-diphospha[3.3]-2,6-pyridinophane and b) a 1,10-diphospha(2)-2,6-pyridino(2)-1,1′-ferrocenophane incorporating a redox active metal center (Fe^{II}/Fe^{III}) in the framework.

The equimolar reaction of the bis(methylene)phosphane compounds **1a**[10] (R = $SiMe_3$, R′ = Ph) or **1b**[9](R = R′ = $SiMe_3$) with the lithium salts obtained from the deprotonation of 2,6-dibenzylpyridine and ferrocene, respectively,[11] yielded the respective ate complexes that were isolated in the form of their respective lithium salts **2** and **3** as red crystals (Scheme 2). Protonation (Et_3NHCl/THF) transforms the ate-complexes **2** and **3** to the respective neutral macrocycles **4** and **5**, that were also isolated as crystalline solids (Scheme 3).[12] The diazapyridinophane analogues of **4** and **5** are well documented in the literature.[13]

Starting from **4** a mononuclear, cationic complex can be obtained by reaction with $(Cu^{I}OTf)_2 \cdot C_6H_6$ (OTf = $CF_3SO_3^-$), which could be isolated as the yellow, crystalline salt **6**-OTf. Compound **5** reacts with tetracarbonyl nickel under displacement of three molecules of CO to yield the complex **7** as a red, crystalline solid (Scheme 3).

Figure 1 depicts the molecular structure of the anion **3**.[14,15] The macrocycle adopts a *syn*-conformation with a boat/

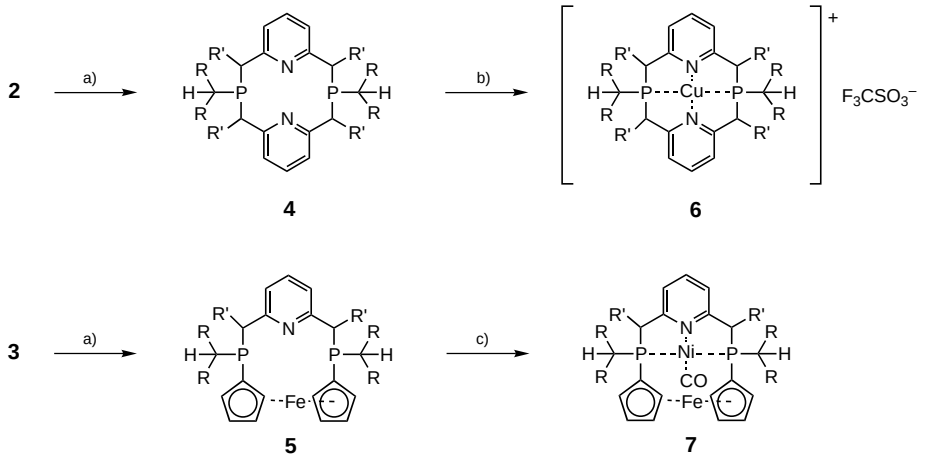


Scheme 2. Synthesis of **2** (**1a, 2**: R = $SiMe_3$, R′ = Ph) and **3** (**1b, 3**: R′ = R = $SiMe_3$); a) 2,6-di(lithiumbenzyl)pyridine, THF −78 °C; b) 1,1′-dilithiumferrocene, Et_2O/tmeda, −78 °C. tmeda = *N,N,N′*,N′-tetramethyl-1,2-ethanediamine.

[*] Prof. Dr. E. Niecke, Dipl.-Chem. S. Ekici, Dr. M. Nieger, Prof. Dr. R. Glaum
Anorganisch Chemisches Institut
Universität Bonn
Gerhard-Domagk-Strasse 1, 53121 Bonn (Germany)
Fax: (+49) 228-73-5792
E-mail: e.niecke@uni-bonn.de

[**] This work was supported by the Deutsche Forschungsgemeinschaft (SFB 624) and the Fonds der Chemischen Industrie. M.N. thanks the DAAD for financial support. We thank the group of Professor J. Beck, Bonn, for recording the fluorescence spectrum.

 © 2003 Wiley-VCH Verlag GmbH & Co. KGaA, Weinheim 1433-7851/03/4204-0435 $ 20.00+.50/0



Scheme 3. Syntheses and reactions starting from **4** (**2, 4, 6**: R = $SiMe_3$, R′ = Ph) and **5** (**3, 5, 7**: R,R′ = $SiMe_3$); reagents: a) Et_3NHCl (2 equiv), THF, 0 °C; b) $(CuOTf)_2C_6H_6$ (0.5 equiv), toluene, RT; c) $[Ni(CO)_4]$, Et_2O, −30 °C.

boat-arrangement of the phosphorus atoms. The lithium atom is coordinated in a trigonal-pyramidal geometry by the three donor atoms. The P–C bond lengths of the phosphanylmethanide fragment **3** (P–C 174 pm) correspond to those in analogously substituted compounds.[16] This is also the case for the Li–P and Li–N bonds,[17] that do not show any unusual features. As expected, the macrocyclic ring of the Cu^I complex **6**-OTf derived from **4** features the same conformation as **3** (Figure 2). The copper ion, however, forms a "seesaw" arrangement with the two phosphorus and nitrogen atoms. Such a coordination geometry with a quasilinear P-Cu-P (169°) and right-angle N-Cu-N alignment is without precedent in the chemistry of the copper(I) ion[18,19] and possibly explains the observed fluorescence of the complex ($\lambda_{ex} = 400$ nm, $\lambda = 515$ nm). Absorption bands in the region $\lambda = 400$ nm, combined with a shoulder at $\lambda = 455$ nm, are also observed in polarized UV/Vis single-crystal absorption spectra (polarization parallel to the crystalographic *a* axis).[20] On polarizing the incident light perpendicularly to the crystallographic *a* axis the intensity of the absorption band at $\lambda =$ 400 nm distinctly diminishes and the shoulder at $\lambda = 455$ nm almost entirely disappears, which indicates the pronounced anisotropy of the metal-to-ligand charge transfer (MLCT) transitions. UV/Vis absorption spectra of single crystals of the free ligand **4** do not feature any absorption bands in the range 800–350 nm and only at $\lambda \leq 350$ nm display a rise of the absorption curve that could, however, not be resolved in more detail (Figure 3).

Also without precedent is the virtually trigonal-monopyramidal coordination geometry of the nickel center in the complex **7**, where the two phosphorus centers and the CO ligand occupy the equatorial positions (P-Ni-CO 121°, 121°, P-Ni-P 116°; Figure 2). The short P–Ni and the long C–O bonds (172 vs. 117 pm) conform with an effective Ni→CO interaction that is also reflected by the redshift of the CO vibration ($\tilde{\nu} = 1867$ cm^{-1}).[21]

The $\{^1H\}^{31}P$ and $\{^1H\}^7Li$ NMR spectra (25 °C) confirm the coordination of the lithium center to two phosphorus atoms (**2**: $\delta^{31}P = 41.7$ ppm, q; $\delta^7Li = 4.2$ ppm, t, $^1J(P,Li) = 90$ Hz; **3**: $\delta^{31}P = 11.8$ ppm, q; $\delta^7Li = 3.1$ ppm, t, $^1J(P,Li) = 107$ Hz) and consequently the preservation of the ate-complex structure in solution. Intermolecular Li-exchange reactions which would lead to a loss of the ^{31}P–^7Li interaction are not observed between 25 and 60 °C.

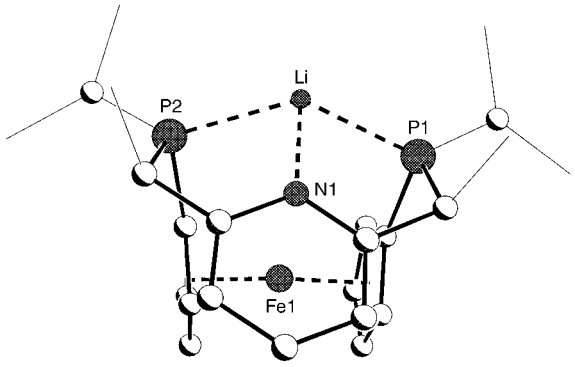


Figure 1. Molecular structure of **3** in the solid state (without H-atoms and peripheral groups). Selected bond lengths [pm] and angles [°]: Li1-N1 203.9(4), Li1-P1 236.5(4), Li1-P2 237.8(4), Li1···Fe1 397.4(4); P1-Li1-P2 128.9(2), N1-Li1-P1 84.7(2), N1-Li1-P2 83.8(2).

Experimental Section

Syntheses of **2, 3**: A suspension of 2,6-di(lithiumbenzyl)pyridine (0.80 g, 1.6 mmol) in THF (20 mL) or 1,1′-dilithioferrocene (0.50 g, 1.6 mmol) in Et_2O/tmeda (10/1; 20 mL) was added dropwise to a solution of bismethylenephosphane **1a** or **1b** (1.0 g 1.6 mmol) in diethyl ether (20 mL) at −78 °C and the mixture stirred for 2 h at this temperature. Upon storage at −30 °C for 2 days the products form as crystalline solids. Yield **2**: 1.72 g (85 %) **3**: 1.26 g (65 %); **3** features a reversible electron transfer: $E^P = 338$ mV (233 K).[22]

4, 5: At 0 °C a solution of **2** (1.0 g, 0.8 mmol) or **3** (1.0 g, 0.9 mmol) in THF (20 mL) was added dropwise to a suspension of triethylamine hydrochloride (0.10 g, 1.8 mmol) in CH_2Cl_2 (30 mL) at 0 °C. Under stirring the reaction solution was allowed to warm to room temperature and then stirred for 2 h. The solvent was removed under reduced pressure and the residue dissolved in diethyl ether (30 mL) to precipitate the lithium chloride which was removed by filtration. The filtrate was concentrated and upon storage at 0 °C for 2–3 days the products crystallize in the form of **4**: colorless **5**: orange crystals. Yield **4**: 0.66 g (92 %) **5**: 0.52 g (71 %); $\{^1H\}^{31}P$ NMR (THF, 25 °C) $\delta =$ 37.7(**4**), $\delta = -15.6$ ppm (**5**); MS (16 eV): m/z (%) = 894 (9.4) $[M]^+$, 636 (100) [M^+–2,6-dibenzylpyridine] (**4**); 813 (53) $[M]^+$, 654 (100) $[M-CH(SiMe_3)_2]^+$ (**5**); **5** features a reversible electron transfer: $E^P =$ 393 mV (298 K).[22]

6-OTf: A solution of **4** (0.30 g, 0.34 mmol) in toluene (15 mL) was added to a suspension of $(CuOTf)_2{\cdot}C_6H_6$ (0.08 g, 0.17 mmol) in toluene (20 mL) at room temperature under stirring. The solution was stirred for 2 h whereupon the product precipitates. After recrystallization from acetonitrile **6** was obtained as yellow to green crystals. Yield: 0.32 g (85 %); $\{^1H\}^{31}P$ NMR (THF, 25 °C): $\delta = 20.7$ ppm; **6** features a reversible electron transfer: $E^P = 970$ mV (298 K).[22]

 © 2003 Wiley-VCH Verlag GmbH & Co. KGaA, Weinheim 1433-7851/03/4204-0436 $ 20.00+.50/0

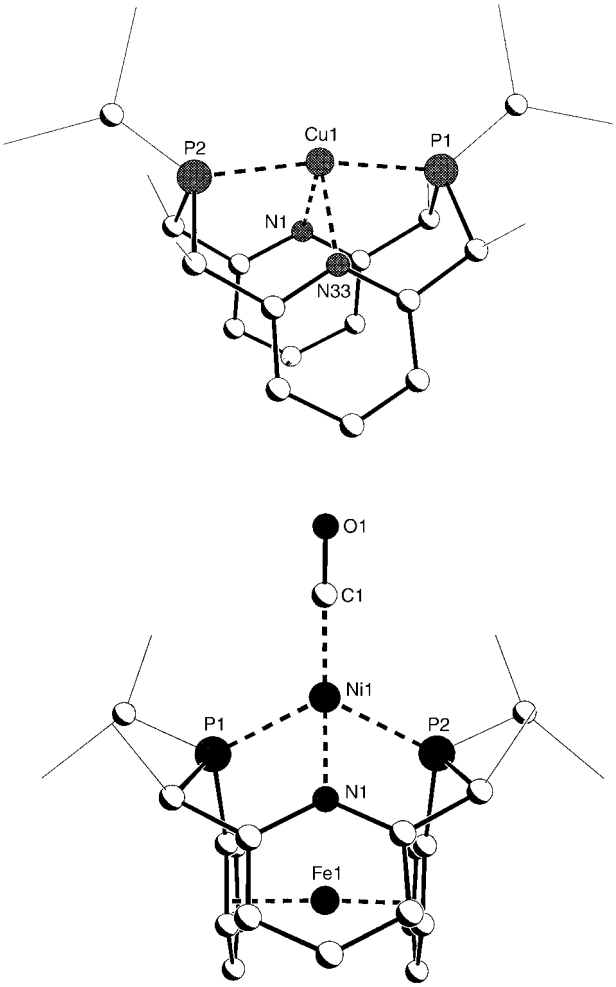


Figure 2. Top: molecular structure of **6** (H atoms and peripheral groups omitted for clarity). Selected bond lengths [pm] and angles [°]: Cu1-N1 214.6(6), Cu1-N33 212.5(6), Cu1-P1 223.8(2), Cu1-P2 223.6(3); N1-Cu1-N33 85.92, N1-Cu1-P1 85.6(2), N1-Cu1-P2 85.9(2), N33-Cu1-P1 85.8(2), N33-Cu1-P2 86.4(2), P1-Cu1-P2 168.9(1), bottom: molecular structure of one independent molecule of **7** in the solid state (H atoms and peripheral groups are omitted for clarity). Selected bond lengths [pm] and angles [°]: Ni1-P1 220.6(1) [220.2(1)], Ni1-P2 221.7(1) [221.1(1)], Ni1-N1 203.1(2) [204.1(2)], Ni1-C1 172.2(3) [172.6(3)], C1-O1 116.6(4) [116.6(4)], Ni1···Fe1 418.9(1) [416.5(1)]; N1-Ni1-P1 81.7(1) [82.3(1)], N1-Ni1-P2 81.6(1) [80.9(1)], N1-Ni1-C1 120.7(1) [121.6(1)], C1-Ni1-P1 121.1(1) [116.0(1)], C1-Ni1-P2 120.8(1) [124.8(1)], P1-Ni1-P2 115.7(1) [116.7(1)].

7: At −30 °C [Ni(CO)$_4$] (0.20 g, 1.17 mmol) was added dropwise to a solution of **5** (0.50 g, 0.61 mmol) in diethyl ether (30 mL) and the solution was stirred for 12 h at room temperature. The excess of [Ni(CO)$_4$] and the solvent were removed under reduced pressure and the residue dissolved in a small amount of diethyl ether. At 0 °C **7** crystallizes within two days in the form of red crystals. Yield: 0.45 g (83 %). MS (16 eV): *m*/*z* (%) 872 (10) [*M*−CO]$^+$, 73 (100) [SiMe$_3$]; {^{1}H}^{31}P NMR (Et$_2$O, 25 °C) $\delta = 32.4$ ppm; $\tilde{\nu} = \nu(\mathrm{CO}) = 1878.6\ \mathrm{cm}^{-1}$; **7** features two reversible electron transfers: $E^{P} = -556$ and 192 mV (298 K).[22]

Received: March 7, 2002
Revised: November 11, 2002 [Z18847]

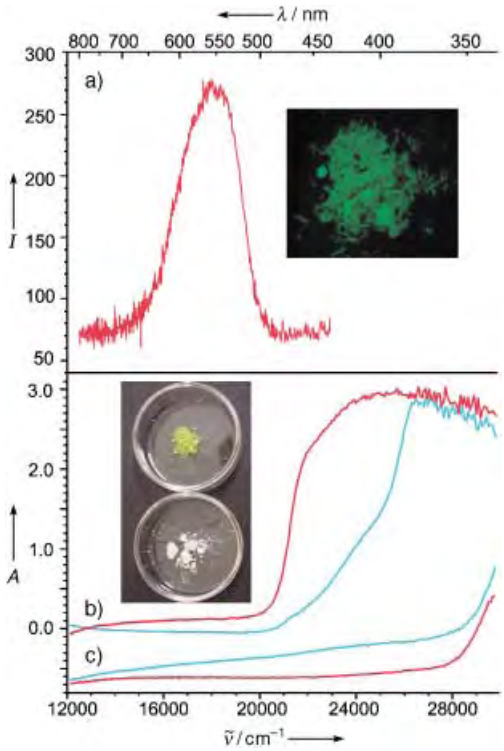


Figure 3. a) Fluorescence spectra of **6**-OTf and photographs of the fluorescing compounds, b) polarized single-crystal UV/Vis spectra of **6** (yellow crystal) and, c) the free ligand **4** (white crystal) on polarization parallel (red spectrum) and perpendicular (blue spectrum) to the *a* axis.

[1] a) N. V. Gerbeleu, V. B. Arion, J. Burgess, *Template Synthesis of Macrocyclic Compounds*, Wiley-VCH, Weinheim, **1999**; b) F. Diederich, P. J. Stang, *Templated Organic Synthesis*, Wiley-VCH, Weinhiem, **2000**.
[2] J.-M. Lehn, *Supramolekularer Chemistry, Concepts and Perspectives*, VCH, Weinheim, **1995**.
[3] a) B. N. Diel, P. F. Brandt, R. C. Haltiwanger, A. D. Norman, *J. Am. Chem. Soc.* **1982**, *104*, 4700–4701; b) P. G. Edwards, P. D. Neuman, D. E. Hibs, *Angew. Chem.* **2000**, *112*, 2834–2836, 3044; *Angew. Chem. Int. Ed.* **2000**, *39*, 2722; P. G. Edwards, P. D. Newman, K. M. A. Malik, *Angew. Chem.* **2000**, *112*, 3044–3046; *Angew. Chem. Int. Ed.* **2000**, *39*, 2922–2924.
[4] T. A. DelDonno, W. Rosen, *J. Am. Chem. Soc.* **1977**, *99*, 8051–8052.
[5] R. Bartsch, S. Hietkamp, S. Morton, O. Stelzer, *Angew. Chem.* **1982**, *94*, 367–368; *Angew. Chem. Int. Ed. Engl.* **1982**, *21*, 375.
[6] A template-free synthesis of macrocycles with planar coordinated phosphorus centers has been realized starting from 1,3,2-diazaphosphinines by a sequence of [4+2] cycloadditions/cycloreversions: N. Avarvari, N. Mezailles, L. Ricard, P. Le Floch, F. Mathey, *Science* **1998**, *280*, 1587–1589.
[7] "Metal Template Synthesis" in *Phosphorus-Carbon Heterocyclic Chemistry: The Rise of a New Domain* (Ed.: F. Mathey), Pergamon, Oxford, **2001**, pp. 652–655.
[8] S. Ekici, M. Bozkurt, M. Nieger, E. Niecke, unpublished results.
[9] S. Ekici, D. Gudat, M. Nieger, L. Nyulaszi, E. Niecke, *Angew. Chem.* **2002**, *114*, 3515–3519; *Angew. Chem. Int. Ed.* **2002**, *41*, 3367–3371.
[10] Synthesis of **1a**: At −78 °C a 1.6 M solution of *n*BuLi in *n*-hexane (4.8 mL, 7.7 mmol) was added to a solution of 2,6-dibenzylpyridine (1.0 g, 3.86 mmol) in THF (30 mL) and tmeda (1.2 mL,

 © 2003 Wiley-VCH Verlag GmbH & Co. KGaA, Weinheim 1433-7851/03/4204-0437 $ 20.00+.50/0

7.7 mmol). The solution was stirred 0.5 h at −78 °C and then another 5 h at RT. The resulting solution was added dropwise at −78 °C to a solution of ClP=C(SiMe$_3$)$_2$ (1.74 g 7.7 mmol) in diethyl ether (30 mL). After stirring for 1 h at low temperature the solvent was removed under reduced pressure. The residue dissolved in *n*-hexane and then filtrated. After concentration of the filtrate solution **1a** precipitates in crystalline form as isomeric mixture *rac*/*meso*-**1a** = 4:1. MS (16 eV): *m*/*z* (%) = 636 (8) $[M]^+$, 562 (66) $[M-SiMe_3]^+$, 73 (100) $[SiMe_3]^+$; ^{31}P NMR(CH_2Cl_2, 25 °C): δ = 386.2, 388.1 ppm (*rac*/*meso*-**1a**).

[11] a) D. Jerchel, S. Noetzel, K. Thomas, *Chem. Ber.* **1960**, *93*, 2966 – 2970; b) M. D. Rausch, D. J. Ciapenelli, *J. Organomet. Chem.* **1967**, *10*, 127 – 136.

[12] The free L-$N_2P_2[CH(SiMe_3)_2]_2$ ligand **4** prefers a *syn*-chair-chair conformation in the solid state.[8] The ligand **5** retains the conformation of the ate-complex **3**. S. Ekici, M. Nieger, E. Niecke, unpublished results.

[13] H. J. Krüger, *Chem. Ber.* **1995**, *128*, 531 – 539.

[14] Selected bond lengths [pm] and angles [°] of **2**. Li1-N1 209.7(8), Li1-N33 211.8(7), Li1-P1 244.5(7), Li1-P2 250.1(7); N1-Li1-N33 86.9(3), N1-Li1-P1 87.3(3), N1-Li1-P2 86.9(3), N33-Li1-P1 86.2(3), N33-Li1-P2 87.4(2), P1-Li1-P2 171.6(3). The analogous phosphamethanide-complex bearing four $SiMe_3$ groups instead of the four phenyl groups in **2** has a similar structure.[9]

[15] Crystal data: **3**: $C_{55}H_{115}ClFeLi_3N_7P_2Si_6$, M_r = 1217.14, triclinic, space group $P\bar{1}$ (no. 2), a = 13.6549(1), b = 14.6901(2), c = 19.2675(2) Å, α = 102.043(1), β = 92.848(1), γ = 103.988(1)°, V = 3647.28(7) Å^3, Z = 2, $\mu(Mo_{K\alpha})$ = 0.422 mm^{-1}, $F(000)$ = 1320, 43 173 reflections ($2\theta_{max}$ = 50°), thereof 12 849 unique, $wR2(F^2)$ = 0.1142, $R(F)$ = 0.0406, 670 parameters, 309 restraints. **2**: $C_{72}H_{106}Li_2N_2O_5Si_4$, M_r = 1267.77; orthorhombic, space group $P2_12_12_1$ (no. 19), a = 16.8587(2), b = 20.3906(3), c = 21.2944(3) Å, V = 7320.1(2) Å^3, Z = 4, $\mu(Mo_{K\alpha})$ = 0.173 mm^{-1}, $F(000)$ = 2736, 70 978 reflections ($2\theta_{max.}$ = 50°), thereof 12 972 unique, $wR2(F^2)$ = 0.2342, $R(F)$ = 0.0766, 759 parameters, 505 restraints. The absolute configuration could not be determined reliably (x = 0.40(14)). **6**: $C_{52}H_{68}CuN_2P_2Si_4^+$ $CF_3SO_3^-$, M_r = 1107.99, triclinic, space group $P\bar{1}$ (no. 2), a = 11.2089(5), b = 15.2256(7), c = 18.0123(10) Å, α = 99.324(2), β = 91.194(2), γ = 111.352(2)°, V = 2814.5(2) Å^3, Z = 2, $\mu(Mo_{K\alpha})$ = 0.619 mm^{-1}, $F(000)$ = 1164, 13085 reflections ($2\theta_{max.}$ = 50°), thereof 9316 unique, $wR2(F^2)$ = 0.2148, $R(F)$ = 0.0802, 606 parameters, 581 restraints (disordered $CHTms_2$ groups). **7**: $C_{38}H_{69}NOP_2Si_6FeNi{\cdot}Et_2O$, M_r = 975.10, triclinic, space group $P\bar{1}$ (no. 2), a = 15.0304(1), b = 18.0995(2), c = 20.0055(2) Å, α = 85.709(1), β = 88.418(1), γ = 69.915(1)°, V = 5097.0(1) Å^3, Z = 4, $\mu(Mo_{K\alpha})$ = 0.891 mm^{-1}, $F(000)$ = 2088, 65 240 reflections ($2\theta_{max}$ = 50°), thereof 17 943 unique, $wR2(F^2)$ = 0.1170, $R(F)$ = 0.0424, 986 parameters, 92 restraints (disordered solvent Et_2O). All structure data were collected on a Nonius KappaCCD diffractometer using $Mo_{K\alpha}$-radiation. The structures were solved by direct methods (SHELXS-97) and refined anistropically on F^2, the H-atoms were refined using a riding model (SHELXL-97). CCDC-181615 (**2**), CCDC-181616 (**3**), CCDC-190910 (**6**), and CCDC-190911 (**7**) contains the supplementary crystallographic data for this paper. These data can be obtained free of charge via www.ccdc.cam.ac.uk/conts/retrieving.html (or from the Cambridge Crystallographic Data Centre, 12 Union Road, Cambridge CB2 1EZ, UK; fax: (+44) 1223-336-033; or deposit @ccdc.cam.ac.uk). SHELXS-97: G. M. Sheldrick, *Acta Crystallogr. Sect. A* **1990**, *46*, 467 – 473 SHELXL-97: G. M. Sheldrick, Universität Göttingen, **1997**.

[16] a) H. H. Karsch, G. Müller, *J. Chem. Soc. Chem. Commun.* **1984**, 569 – 570; b) W. Clegg, S. Doherty, K. Izod, P. O'Shaughnessy, *Chem. Commun.* **1998**, 1129 – 1130, and references therein.

[17] "Structures of Lithium Salts of Heteroatom Compounds": F. Pauer, P. P. Power in *Lithium Chemistry* (Eds.: A.-M. Saspe, P. von Ragué Schleyer), Wiley-Interscience, New York, **1995**, p. 295.

[18] M. Melnik, L. Macaskova, C. E. Holloway, *Coord. Chem. Rev.* **1993**, *126*, 71 – 92.

[19] Cu^I-complexes of diazapyridinophanes do not display geometries that are comparable to **6**; H. J. Krüger, personal communication.

[20] The polarized UV/Vis absorption spectra were recorded using a particular micro single-crystal UV/Vis spectrometer. Details about this instrument are prevalent in the literature: E. Krausz, *Aust. J. Chem.* **1993**, *46*, 1041 – 1054. The investigated crystal of compound **6** had a cross-section of 0.20 × 0.08 mm^2, (thickness 0.05 mm), the crystal of compound **4** was notably smaller with a cross-section of 0.10 × 0.05 mm^2 (thickness = 0.05 mm).

[21] J. Grobe, N. Krummen, R. Wehmschulte, B. Krebs, M. Läge, *Z. Anorg. Allg. Chem.* **1994**, *620*, 1645 – 1658.

[22] CV: ν = 200 mV s^{-1}; CH_2Cl_2/$n$$Bu_4NBF_4$ 0.1 M; calomel/GCE/Pt (GCE = glassy carbon electrode). MeCN/$n$$Bu_4NPF_6$; reference electrode: calomel E = 0.24 V; IR-compensation (kΩ) **3**: 2.5; **5, 6**: 0.2; **7**: 4.5.

HRMAS NMR Spectroscopy

Application of HRMAS ^{1}H NMR Spectroscopy To Investigate Interactions between Ligands and Synthetic Receptors**

*Heidi Händel, Elke Gesele, Klaus Gottschall, and Klaus Albert**

Dedicated to Professor Günther Jung on the occasion of his 65th birthday

Molecular recognition processes are predicted to become the basis of all advanced separation techniques. The investigation of intermolecular interactions in the interphase between a chromatographic support and a substrate dissolved in a mobile phase is the crucial condition for understanding chromatographic separation mechanisms and for the design of tailored stationary phases. In solution and also in suspension ligand–receptor interactions can be studied using methods of high-resolution (HR) NMR spectroscopy, for example by employing the nuclear Overhauser enhancement (NOE)

[*] Prof. Dr. K. Albert, Dr. H. Händel, Dr. E. Gesele
Institut für Organische Chemie
Universität Tübingen
Auf der Morgenstelle 18, 72076 Tübingen (Germany)
Fax: (+49) 7071-295-875
E-mail: klaus.albert@uni-tuebingen.de
Dr. K. Gottschall
Dr. Gottschall INSTRUCTION
Gesellschaft für Technische Chromatographie mbH
Donnersbergweg 1, 67059 Ludwigshafen (Germany)

[**] This work was funded by Dr. Gottschall INSTRUCTION mbH, Ludwigshafen. HRMAS = high-resolution magic-angle spinning.

 © 2003 Wiley-VCH Verlag GmbH & Co. KGaA, Weinheim 1433-7851/03/4204-0438 $ 20.00+.50/0

or 2D NOESY technique.[1] The NOE can provide information on the distance between protons in close spatial proximity[1] within a given molecule and can also be used to detect ligand–receptor interactions in complex mixtures (bioaffinity NMR spectroscopy)[2] and in solutions of chiral selectors and optical isomers.[3] Specific interactions between macromolecules and low-molecular-weight compounds (ligands or substrates) with equilibrium constants K in the mM to μM range, the so-called fast-exchange regime, are revealed by the transferred NOE (trNOE) effects.

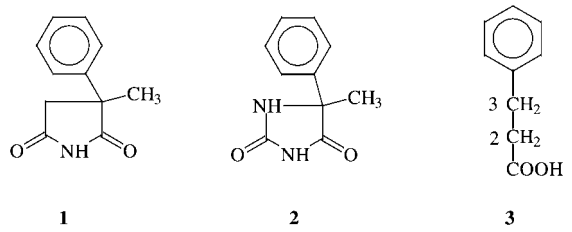
High-molecular-weight compounds, such as proteins or polymers, exhibit a strong negative NOE effect with a fast build-up rate. If a low-molecular-weight compound binds to a macromolecule, it acquires the motional correlation time τ_C of the macromolecule thus developing a negative NOE in the bound state. This negative NOE will be transferred to the NOE cross-peaks associated with the free ligand (in fast exchange within the NMR time scale) to an extent which depends on the lifetimes in the free and bound states and the spin-lattice relaxation times in the free state.

If there is a binding equilibrium between a small-molecule ligand and a polymeric support, the intramolecular NOEs normally observed for free ligands alone (typically weak positive NOEs) will exhibit increased negative amplitudes because of the trNOE effect. The trNOE effect, however, vanishes for weak affinities as well for high affinities. A particular advantage of the trNOE is that it can be detected even in the presence of a large free-ligand excess. Furthermore, since the trNOE derives from the bound state, it strongly depends on the interproton distance providing information upon the geometry of the ligand in the bound state.[1] Thus, a weaker trNOE could be the result of a slightly increased interproton distance or of a weaker binding affinity between the ligand the polymeric support.

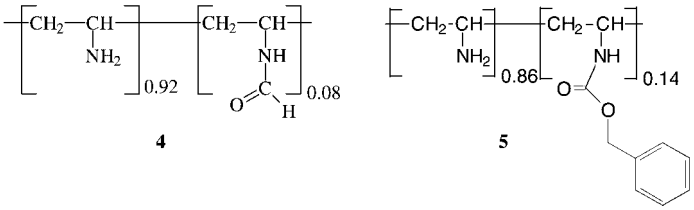
trNOE measurements are performed for the detection of interactions between biologically active compounds (e.g. saccharides and their derivatives) and proteins and for the fast screening of substance libraries for new active compounds.[4–7]

In the field of separation science NMR spectroscopic investigations have been performed mainly for the characterization of stationary phases. Here, the application of solid-state NMR spectroscopy resulted in a deeper understanding of the structure and dynamics of stationary phases.[8–14] The investigation of interactions between analytes and chromatographic supports in the presence of a mobile phase is feasible with the help of HR magic-angle spinning (HRMAS) NMR spectroscopy. This technique allows the application of HR NMR spectroscopy to suspended solid- or gel-like samples. Under MAS conditions spectral resolution can approach the typical values obtainable in the liquid state. Thus, an insoluble sample swollen in an appropriate solvent can be rapidly characterized by HRMAS ^{1}H NMR spectroscopy.[15–20]

We have utilized 2D NOESY techniques together with HRMAS ^{1}H NMR spectroscopy to characterize the interactions between new chromatographic supports and the following low-molecular-weight compounds containing secondary amine, carbonyl, and carboxy groups: methylphenylsuccinimide (**1**), methylphenylhydantoin (**2**), and phenylpropionic acid (**3**). The current investigations are focussed at obtaining a qualitative insight into the role of hydrogen-bonding, ionic, and hydrophobic interactions. Two new coated silica-gel chromatographic supports have been investigated: **4** with a polyvinylamine coat containing 8% formamide groups and **5** with a polyvinylamine coat containing 14% benzylcarbamate groups.[21]



1 **2** **3**



4 **5**

Figure 1 shows the HRMAS 2D NOESY spectrum in D_2O for a suspension of **1** and silica gel coated with **4**. The ligand in solution (fast exchange between free and bound forms) shows well-resolved narrow signals while the polymer gel gives broad signals for CH and CH_2 protons. The strongest cross-peak is that between the unresolved phenyl-group signal ($\delta =$ 7.3 ppm) and the singlet of the methyl group ($\delta = 1.65$ ppm) of the ligand, and is negative because of the trNOE effect and the binding equilibrium. If the ring CH_2 group in **1** is replaced by an NH group as in **2**, the interaction between ligand and polymer is increased, as reflected in a twofold increase in the negative amplitude for the phenyl—CH_3 cross-peak observed for ligand **2** versus ligand **1**.

Hydrophobic interactions between receptor and ligand are expected to dominate with water as a solvent. Therefore, the binding energy observed for **1** should exceed that of **2** because **1** is less polar, less soluble in water, and has a larger hydrophobic contact area. Despite the aqueous environment, hydrogen bonds seem to be responsible for the observed binding energies of the investigated ligands: the hydantoin can engage in more hydrogen bonds simultaneously than the succinimide.

The interaction of **2** with the silica-gel coating **5** is also sensitive to changes in the solvent composition of the mobile phase. Various D_2O/[D_3]acetonitrile mixtures (100/0, 90/10, 10/90, and 0/100) were investigated, and the phenyl–CH_3 cross-peak integrals for ligand **2** were evaluated (Figure 2). The negative cross-peak integral is three-times larger in 100% D_2O than in 100% [D_3]acetonitrile, which indicates that water increases the equilibrium constant for binding in **2**. However, the minimum NOE amplitude was obtained in D_2O/[D_3]acetonitrile 10/90 The same solvent effect is also reflected in the chromatographic retention data for **2**, for

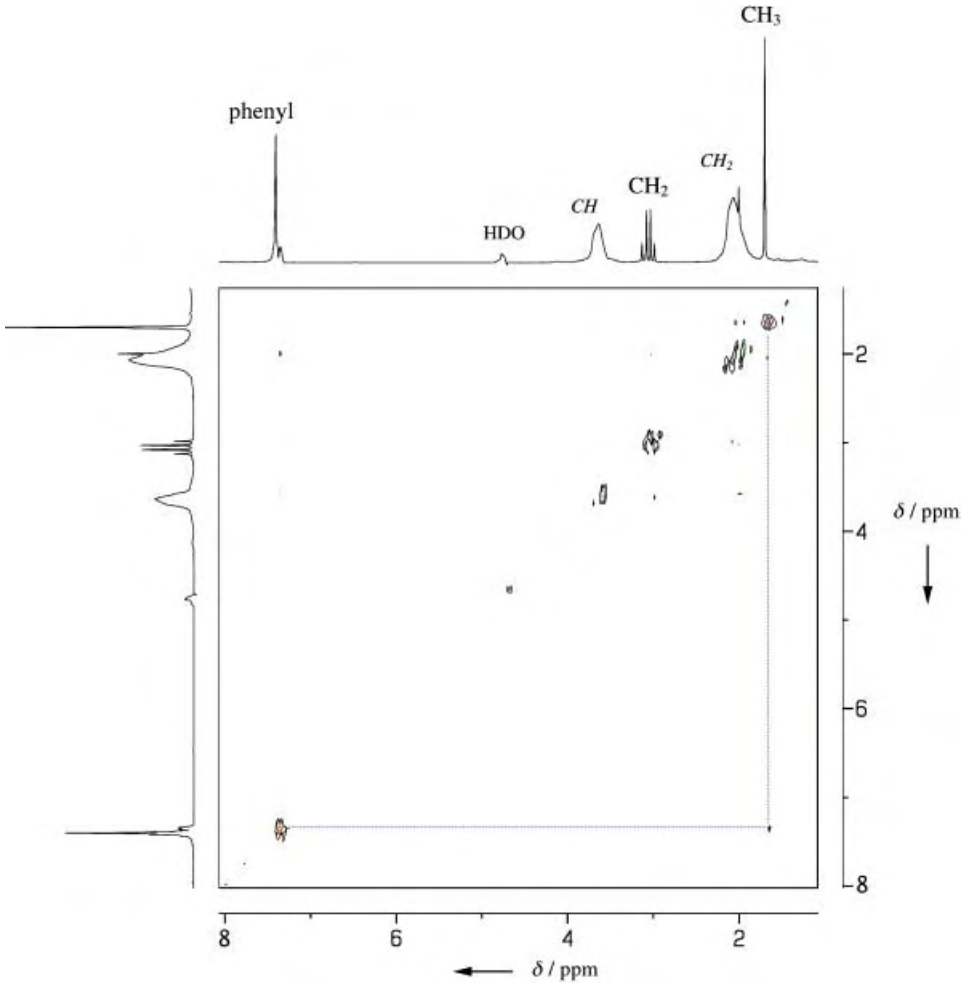


Figure 1. HRMAS 2D NOESY spectrum (400 MHz) of a suspension containing **1** and silica gel coated with the **4** in D_2O (300 K, mixing time 100 ms). The 1D HRMAS ^1H NMR spectrum of **1** together with the stationary phase **4** is depicted in the F_2 and the F_1 directions. The narrow signals of the substrate are labeled in the 1D trace with roman letters; the broad signals of the coating **4** of the swollen polymeric phase are labeled with italic letters. Only a negative intramolecular phenyl–CH_3 cross-peak (trNOE) was observed (correlation depicted in blue).

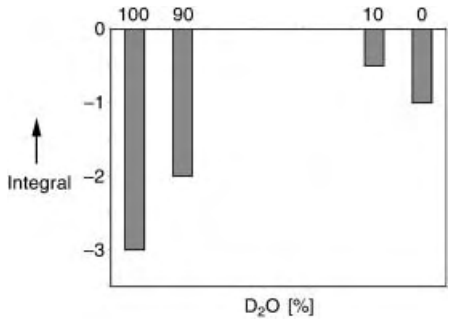


Figure 2. Relative integrals for the negative intramolecular NOE cross-peak between the phenyl and methyl groups of **2** in a suspension of **2** and silica gel coated with the **5** in D_2O/[D_3]acetonitrile solvent mixtures.

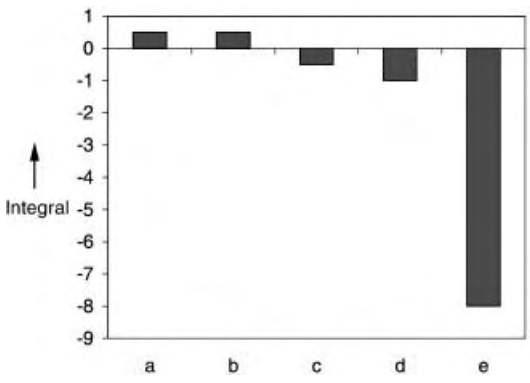


Figure 3. Relative integrals for the intramolecular phenyl–CH_2 NOE cross-peak recorded in D_2O for **3** alone (a) and in suspensions containing: silica gel (b), aminopropyl silica gel (c), polyvinylamine **5** (M_r = 10000–20000 Dalton) (d), silica gel coated with **5** (e).

which a maximum retention occurs at 100% water.[21] To discriminate between polar and nonpolar binding contributions as a function of the solvent composition is a major objective of ongoing investigations.

NOE measurements can also be used to investigate the efficiency of various stationary phases for binding **3**. Dissolved in D_2O compound **3** exhibits a weak positive NOE between the aromatic *ortho* protons of the phenyl rings and the neighboring methylene protons at C-3 (Figure 3a). This

 © 2003 Wiley-VCH Verlag GmbH & Co. KGaA, Weinheim 1433-7851/03/4204-0440 $ 20.00+.50/0

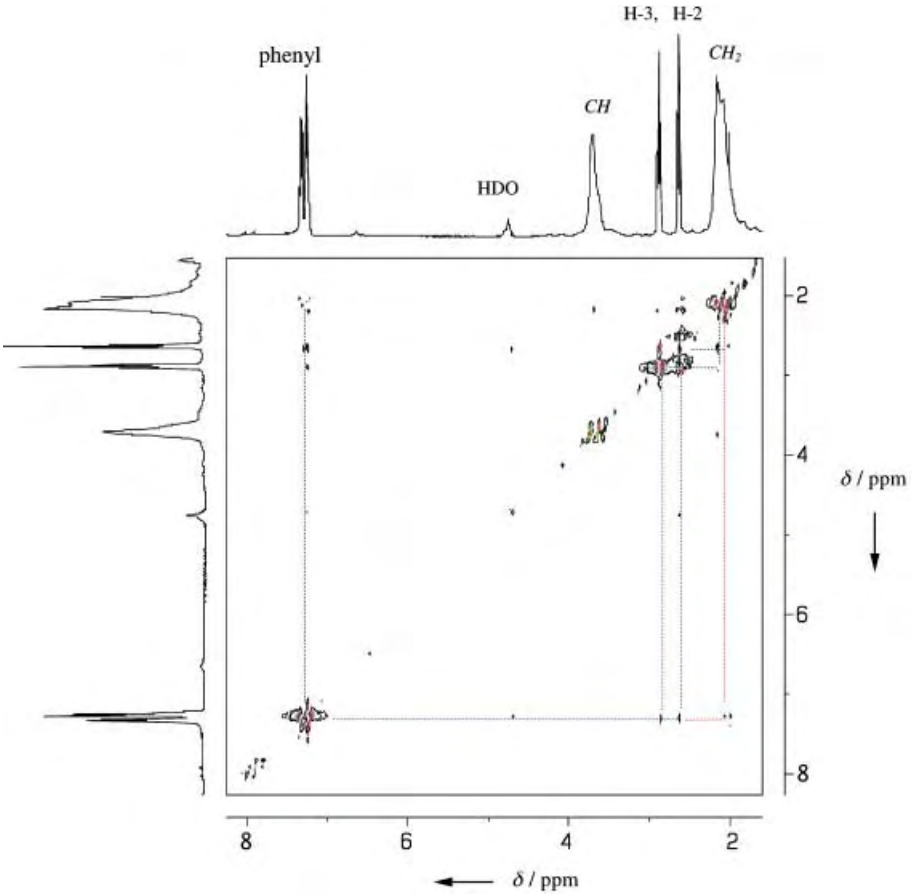


Figure 4. HRMAS 2D NOESY spectrum (400 MHz) of a suspension containing dissolved **3** and silica gel coated with **4** in D_2O (300 K, mixing time 100 ms). Substrate and are labeled with roman letters and polymer signals with italic letters. Only negative intramolecular (correlation depicted in blue) and intermolecular (correlation depicted in red) trNOE cross-peaks are observed.

NOE did not change when underivatized silica gel was added (Figure 3b), which indicates very weak or even no binding of ligand **3**. With aminopropyl silica gel coated in **4** as the stationary phase a weak negative NOE is observed (Figure 3c), corresponding to a trNOE effect as a result of a moderate ligand–polymer interaction. A slightly larger negative NOE is observed in the presence of the pure derivatized **5** which had not been immobilized to silica gel (Figure 3d). Finally, when polymer **5** was immobilized on silica gel, the negative phenyl–CH_2 cross-peak intensity increased eightfold (Figure 3e). This phenomenon may be explained by the increase in the effective correlation time τ_C for the polymer when bound to the silica gel together with an significant increase of the equilibrium constant K for the ligand–receptor complex.

The interaction between **3** and silica gel coated with the **4** was illustrated in more detail by the HRMAS 2D NOESY experiment shown in Figure 4. Negative intramolecular NOEs were observed for the phenyl protons to methylene protons on C-2 and C-3 of the ligand. In addition, a negative intermolecular cross-peak was observed arising from the phenyl protons (also from the protons on C-2 and C-3) of the ligand to CH_2 groups of the polymer backbone of the stationary phase.

Isooctane was used as a reference ligand which did not interact with the investigated stationary phases and exhibited no trNOEs for any of the systems studied. This result indicates that a hydrophilic interaction may be prerequisite for additional hydrophobic effects.

The model ligands employed here and the 2D NOESY data obtained in the presence of several stationary phases illustrate how the trNOE can be used to evaluate ligand binding affinities of novel synthetic receptors developed for separation or binding purposes. We could show that HRMAS ^{1}H NMR spectroscopy and 2D NOESY experiments can be efficiently used to observe interactions between the analyte and the stationary phase as well as the influence of chemical modifications of the stationary phase and the contribution of solvent effects. Thus, the trNOE effect can provide valuable information for the design and implementation of novel, task-specific or tailored stationary phases. In addition, HRMAS 2D NOESY NMR may become a potent method for visualizing the binding epitopes in molecular recognition processes.

Experimental Section

All NMR spectroscopic studies were conducted at 400 MHz with a Bruker ARX-400 NMR spectrometer equipped with an HRMAS accessory. HRMAS ^{1}H NMR spectra were recorded with 4 mm ZrO_2 rotors (detection volume 60 μL) at a rotation rate of 4500 Hz at 300 K. Ligand concentrations in stock solutions were 0.1 mol L^{-1} (the concentration of ligand **3** was lower for solubility reasons). Suspensions were prepared by adding the stationary phase (3.5 mg) to the stock solution (60 μL). According to the total number of monomer units in the polymer the receptor concentration was approximately 145 mM, the amount of strong binding sites was estimated to 1–3%.

The standard phase-sensitive 2D NOESY pulse sequence was modified to include solvent suppression, either by presaturation for a single solvent peak (D_2O) or using frequency-selective 90° pulses (Gaussian) for multicomponent solvents. 2D NOESY spectra of ligands alone were recorded with a mixing time of 900 ms; for ligand–polymer mixtures a mixing time of 100 ms was used. A total of 512 increments with 128 transients and 1 K data points with a spectral width (SW) of 8 kHz were acquired in both dimensions for the 2D NOESY spectra. A zero filling up to 1 K data points in the F_1 dimension and multiplication with a shifted sine bell function (factor 2) in both dimensions were performed. Phase correction was performed to give negative absorption lineshapes for diagonal peaks in both dimensions. Positive and negative NOEs then result in positive and negative cross-peaks, respectively.

Received: August 5, 2002 [Z19893]

 © 2003 Wiley-VCH Verlag GmbH & Co. KGaA, Weinheim 1433-7851/03/4204-0441 $ 20.00+.50/0

[1] D. Neuhaus, M. P. Williamson, *The Nuclear Overhauser Effect in Structural and Conformational Analysis*, Wiley-VCH, Weinheim, **2000**.
[2] W. Jahnke, H. C. Kolb, M. J. J. Blommers, J. L. Magnani, B. Ernst, *Angew. Chem.* **1997**, *109*, 2715 – 2719; *Angew. Chem. Int. Ed. Engl.* **1997**, *36*, 2603 – 2607.
[3] N. M. Maier, S. Schefzick, G. M. Lombardo, M. Feliz, K. Rissanen, W. Lindner, K. B. Lipkowitz, *J. Am. Chem. Soc.* **2002**, *124*, 8611 – 8629.
[4] a) B. Meyer, T. Weimar, T. Peters, *Eur. J. Biochem.* **1997**, *246*, 705 – 709; b) T. Peters, B. Meyer, DE-B 19649359 **1996**; [*Chem. Abs.* **1998**, *128*, 177880z].
[5] D. Henrichson, B. Ernst, J. L. Magnani, W.-T. Wang, B. Meyer, T. Peters, *Angew. Chem.* **1999**, *111*, 106 – 110; *Angew. Chem. Int. Ed.* **1999**, *38*, 98 – 102.
[6] H. Maaheimo, P. Kosma, L. Brade, H. Brade, T. Peters, *Biochemistry* **2000**, *39*, 12778 – 12788.
[7] F. Casset, T. Peters, M. Etzler, E. Korchagina, N. Nifant'ev, S. Pérez, A. Imberty, *Eur. J. Biochem.* **1996**, *239*, 710 – 719.
[8] H. O. Fatunmbi, M. D. Bruch, M. J. Wirth, *Anal. Chem.* **1993**, *65*, 2048 – 2054.
[9] A. B. Scholten, J. W. de Haan, H. A. Claessens, L. J. van de Ven, C. A. Cramers, *Langmuir* **1996**, *12*, 4741 – 4757.
[10] K. Albert, T. Lacker, M. Raitza, M. Pursch, H.-J. Egelhaaf, D. Oelkrug, *Angew. Chem.* **1998**, *110*, 809 – 812; *Angew. Chem. Int. Ed.* **1998**, *37*, 777 – 780.
[11] K. Albert, *TrAC Trends Anal. Chem.* **1998**, *17*, 648 – 658.
[12] M. Pursch, L. C. Sander, K. Albert, *Anal. Chem.* **1999**, *71*, 733A-741A.
[13] M. Raitza, J. Wegmann, S. Bachmann, K. Albert, *Angew. Chem.* **2000**, *112*, 3629 – 3632; *Angew. Chem. Int. Ed.* **2000**, *39*, 3486 – 3489.
[14] S. Bachmann, C. Hellriegel, J. Wegmann, H. Händel, K. Albert, *Solid State Nucl. Magn. Reson.* **2000**, *17*, 39 – 51.
[15] P. C. Anderson, M. A. Jarema, M. J. Shapiro, J. P. Stokes, M. Ziliox, *J. Org. Chem.* **1995**, *60*, 2650 – 2651.
[16] P. A. Keifer, L. Baltusis, D. M. Rice, A. A. Tymiak, J. N. Shoolery, *J. Magn. Reson. Ser. A* **1996**, *119*, 65 – 75.
[17] P. A. Keifer, *J. Org. Chem.* **1996**, *61*, 1558 – 1559.
[18] M. Pursch, G. Schlotterbeck, L.-H. Tseng, K. Albert, W. Rapp, *Angew. Chem.* **1996**, *108*, 3034 – 3036; *Angew. Chem. Int. Ed. Engl.* **1996**, *35*, 2867 – 2869.
[19] L.-H. Tseng, D. Emeis, M. Raitza, H. Händel, K. Albert, *Z. Naturforsch. B* **2000**, *55*, 651 – 656.
[20] J. Klein, R. Meinecke, M. Mayer, B. Meyer, *J. Am. Chem. Soc.* **1999**, *121*, 5336 – 5337.
[21] Dr. Gottschall Instruction, DE-19855173 **2000**, PCT/EP99/09200 (WO 0032649), **2000**, PCT/EP/09199 (WO 0032648), **2000**, [*Chem. Abs.* **2000**, *133*, 18027p], [*Chem. Abs.* **2000**, *133*, 31037m].
[22] G. Gottschall, unpublished results.

Molecular Knots

A Topologically Chiral Molecular Dumbbell**

*Oleg Lukin, Janosch Recker, Athanasia Böhmer, Walter M. Müller, Takateru Kubota, Yoshio Okamoto, Martin Nieger, Roland Fröhlich, and Fritz Vögtle**

"Knotaxanes",[1] as we call the hitherto unknown rotaxanes bearing knots as stoppers, are an as yet unrealised dream in topological chemistry.[2] A prerequisite for these systems is a "dumbbell"[3] in which at least one molecular knot forms the topologically chiral stoppers. To connect two molecular knots in such a way necessitates the availability of a monosubstituted knot. Our recent efforts involved removal of one to three benzyl groups from the periphery of tris(benzyloxy)knotane to yield an inseparable mixture of hydroxyknotanes.[4] We have now extended the idea of protecting-group chemistry in the knotane architecture to synthesize the tris(allyloxy)knotane **1** in 5% yield by utilizing our already well-developed one-pot procedures for the preparation of amide-based knots.[5,6]

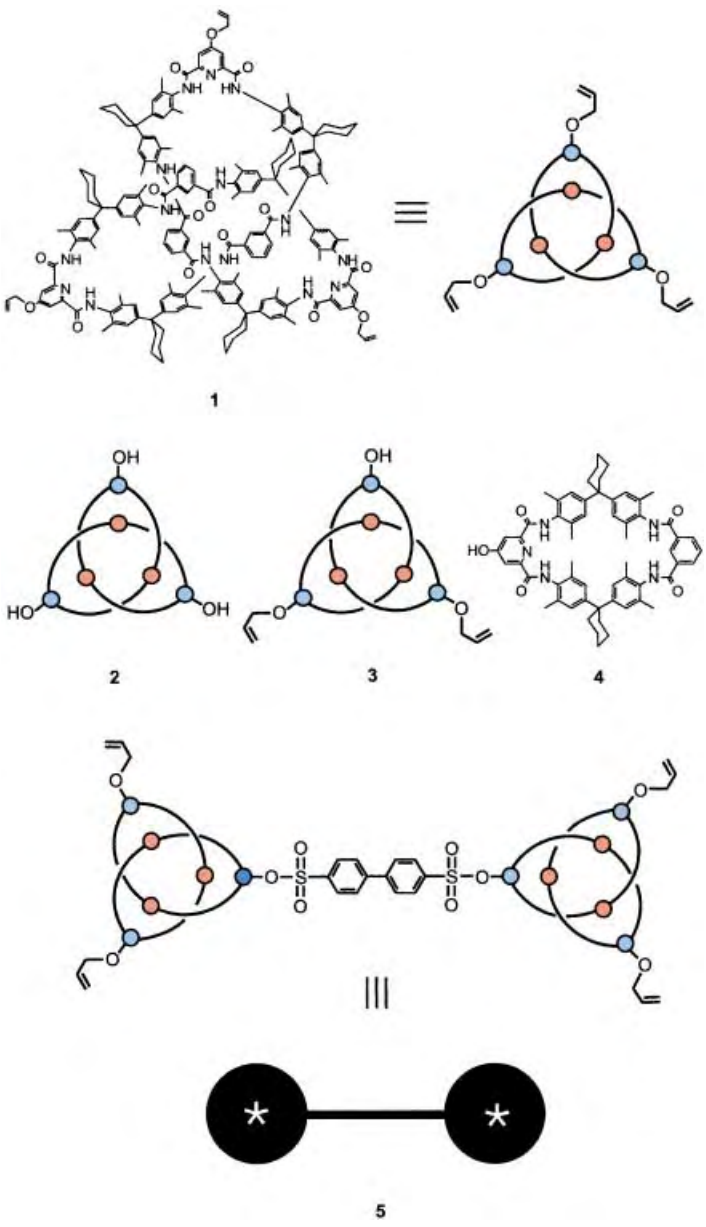
Twelve of the reaction batches were collected and purified by column chromatography and resulted in 1 g of the knotane **1**, which gave diffraction-quality crystals upon recrystallization from $CHCl_3/CH_3OH$. Single-crystal X-ray analysis[7] revealed (Figure 1) that molecule **1** is indeed a chiral knotted structure and adopts a conformation which is very similar to that of the unsubstituted knot:[5] all the 2,6-pyridindicarbamide moieties form outer edges of the three loops of the

[*] Prof. Dr. F. Vögtle, Dr. O. Lukin, Dr. J. Recker, Dipl.-Chem. A. Böhmer, W. M. Müller
Kekulé-Institut für Organische Chemie und Biochemie
Rheinische Friedrich-Wilhelms-Universität Bonn
Gerhard-Domagk-Strasse 1, 53121 Bonn (Germany)
Fax: (+49) 228-73-5662
E-mail: voegtle@uni-bonn.de
Dr. T. Kubota, Prof. Dr. Y. Okamoto
Department of Applied Chemistry
Graduate School of Engineering, Nagoya University
Chikusa-ku, Nagoya, 464-8603 (Japan)
Dr. M. Nieger
Institut für Anorganische Chemie
Rheinische Friedrich-Wilhelms-Universität Bonn
Gerhard-Domagk-Strasse 1, 53121 Bonn (Germany)
Dr. R. Fröhlich
Organisch-chemisches Institut
Universität Münster
Corrensstrasse 40, 48149 Münster (Germany)

[**] A part of this work was presented on September 9, 2002 at the "14th International Symposium on Chirality" in Hamburg. Financial assistance by the Deutsche Forschungsgemeinschaft is gratefully acknowledged (Sonderforschungsbereich 624). O.L. thanks the Alexander von Humboldt Foundation for a fellowship. We would also like to express our thanks to Mr. S. Bitter and Mr. S. Buschbeck for recording MALDI-TOF mass spectra and Dr. C. A. Schalley for helpful discussions.

Supporting information for this article is available on the WWW under http://www.angewandte.org or from the author.

 © 2003 Wiley-VCH Verlag GmbH & Co. KGaA, Weinheim 1433-7851/03/4204-0442 $ 20.00+.50/0



knot while the isophthaloyl diamide fragments are "hidden" inside the knot. A transoid orientation of the carbonyl groups at one isophthaloyl diamide unit (I2; cisoid in the unsubstituted knot) and one additional methanol molecule located at the pyridinedicarbamide loop (P3) constitute the only noticeable differences between these two solid-state structures.

Regulating the amount of the reducing agent (Bu_3SnH in the presence of 1% $[PdCl_2(PPh_3)_2]$, see Experimental Section) allows for the complete and partial removal of the allyl groups of **1** and enables formation of the first pure trihydroxy- and monohydroxyknotanes **2** and **3,** respectively. These mono- and trifunctionalized knotanes have been isolated as pure substances in high yields.

The coupling of two units of the monohydroxy derivative **3** with 1,10-diiododecane was then attempted to obtain the dumbbell structure. The reaction was carried out in DMF with Cs_2CO_3 as a base (30% yield), analogously to that reported for the coupling of monohydroxycryptophanols.[8] However, the reaction proved unsuccessful in our case and neither traces of the desired product nor starting monohydroxyknotane **3** were detected in the MALDI-TOF spectra. This failure was surprising as the analogous reaction involving macromonocyclic **4**—which lacks allyl groups—proceeds smoothly to give the expected axle with two macrocyclic stoppers ($[M^+] = 1980.9$). This observation suggests that the allyl groups are intolerant to the basic conditions and can be cleaved off.[9]

Finally we decided to investigate acylation, since it requires milder conditions than alkylation. Indeed, the reaction of monohydroxyknotane **3** with biphenyl-4,4′-disulfonyl chloride in the presence of Et_3N in acetonitrile yields the desired molecular dumbbell **5** as a white powder in 75% yield (after column chromatography).

The new knotanes **1**–**3** and the dumbbell **5** were all fully characterized (MALDI-TOF-MS, FABMS, ^{1}H NMR). ^{1}H NMR spectroscopy was especially useful both for determining the purity and for interpreting the substitution patterns in the knotanes. The twelve sharp amide proton signals in the spectra of knotanes **1** and **2** were assigned by deuterium exchange experiments in $[D_6]$DMSO/CD_3OD (85:15) solutions; this assignment shows that the rigid unsymmetrical conformation found in the solid state also remains in DMSO solution. The amide protons located on the 2,6-pyridindicarbamide units are most sensitive to the substituent on the phenolic pyridine-O atom: upfield shifts are evident upon transformation of the allyl substituent on **1** into a hydroxy group in **2** or **3** and downfield shifts are observed upon sulfonylation of the hydroxypyridine fragment to give **5**. The splittings observed in the amide area of the proton spectra of monohydroxyknotane **3** and the dumbbell **5** are brought about by the presence of equal amounts of three different knotane conformers in solution.

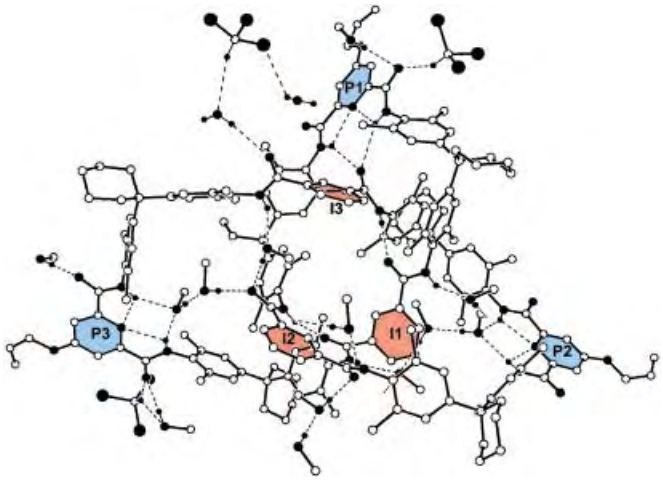


Figure 1. Single-crystal X-ray structure of allyloxyknotane **1**. The isophthaloyl rings are marked orange and the 2,6-pyridinedicarbamide units blue.

 © 2003 Wiley-VCH Verlag GmbH & Co. KGaA, Weinheim 1433-7851/03/4204-0443 $ 20.00+.50/0

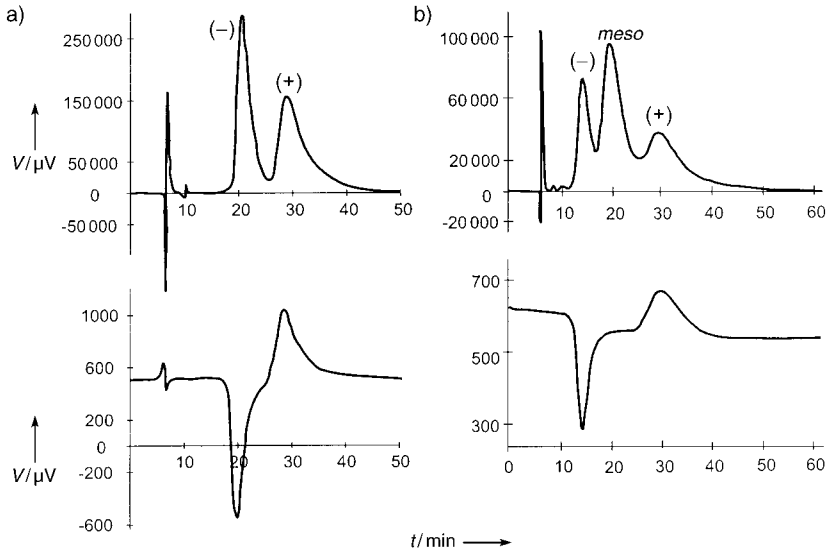


Figure 2. a) Separation of the enantiomers of **1** (top: UV detection, bottom: CD detection; column: Chiralpak AD, eluent: hexane/chloroform/isopropanol = 60:40:1, CD detection at 254 nm); b) separation of the enantiomers and the *meso* form of **5** (top: UV detection, bottom: CD detection; column: Chiralpak AD, eluent: hexane/chloroform = 45:55, CD detection at 254 nm).

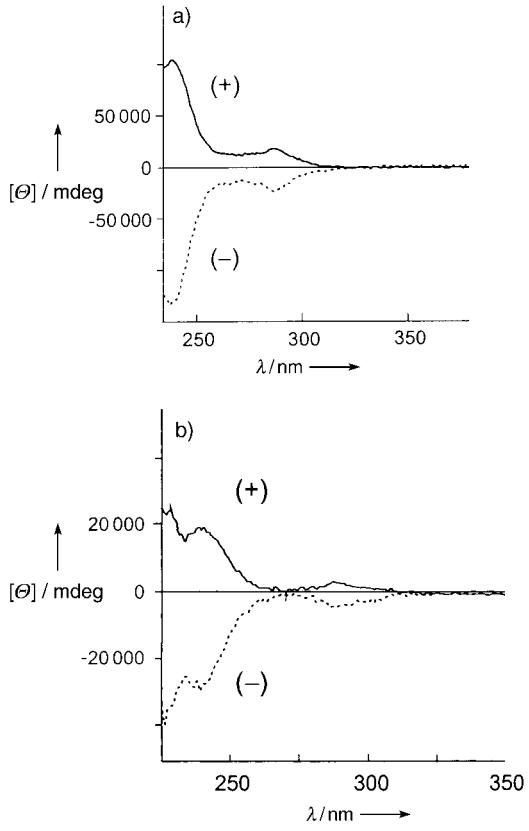


Figure 3. Circular dichroism spectra obtained in chloroform of a) allyloxyknotane **1** ((+) enantiomer $c = 1.1 \times 10^{-3}$ M, (−) enantiomer $c = 7.4 \times 10^{-4}$ M); b) dumbbell **5** ((+) enantiomer $c = 2.6 \times 10^{-4}$ M, (−) enantiomer $c = 1.4 \times 10^{-4}$ M); $[\Theta]$ = molar ellipticity.

Although our early attempts to separate the expected *meso* form and the DL pair of dumbbell **5**—as well as the racemate of the tris(allyloxy)knotane **1**—on noncovalent commercial material failed,[10] they could be completely separated on noncommercial Chiralpak AD column material[11] containing tris(3,5-dimethylphenylcarbamate)amylose covalently linked to the silica gel support.

Figure 2 shows the successful complete separation of **1** and **5**. Interestingly, the *meso* form of **5** appears between its D and L isomers. The circular dichroism (CD) spectra were recorded after the preparative separation of the enantiomers. Figure 3 shows the CD spectra of the enantiomers of **1** and **5**. The mirror-symmetrical circular dichroisms found for the enantiomers confirm the purity of the compounds and of the enantiomers.

Dumbbells of this kind seem to be the key axles for future rotaxanes in which the molecular knot stoppers render them topologically chiral. The topological chirality of the stoppers combined with their large size (ca. 3 nm) is expected to force the unidirectional rotational movement[12] of the rotaxane constituent parts that is important for molecular machines[13] and to prevent virtually any molecular ring from de-slipping. It should also be interesting to study how the chirotopic properties of such dumbbells can be affected by modifying the length and flexibility of the spacer in between.

Our preliminary efforts to prepare such a rotaxane from monohydroxyknotane **3** by the "phenolate-trapping method"[14] proved unsuccessful because of the above-mentioned instability of the allyloxy groups in the basic solution. Currently we are exploring other templation procedures which could possibly lead to the knotaxane.

Experimental Section

The preparation of knotanes **1**–**3** can be found in the Supporting Information.

Synthesis of **5:** Triethylamine (20 mg, 0.2 mmol) and dry dichloromethane (2 mL) were added to a stirred suspension of **3** (50 mg, 0.018 mmol) in dry acetonitrile (8 mL). A solution of biphenyl-4,4′-disulfonyl chloride (3 mg, 0.009 mmol) dissolved in dry acetonitrile (0.5 mL) was added after the suspension had become a homogenous solution. The reaction mixture was allowed to stir for 30 min at reflux and then at room temperature overnight. The solvent was removed under reduced pressure and the crude product was purified by column chromatography on silica gel with dichloromethane/ethyl acetate (3:1) as the eluent to give a colorless solid ($R_f = 0.80$). Yield: 40 mg (75%); m.p. > 300 °C. ^{1}H NMR (400 MHz, [D$_6$]DMSO): δ = [0.05, 0.86, 0.95] (ArCH$_3$), 1.24, 1.36, 1.48, 1.56, 1.82, 1.99, 2.14, 2.19, 2.24, 2.28, 2.32, 4.88 (m, 8H, OCH$_2$), 4.99 (m, 2H, ArH), 5.31–5.46 (m, 8H, C*H*$_2$=CH), 6.07 (m, 4H, C*H*=CH$_2$), [6.42, 6.50, 6.63, 6.79, 6.89, 6.95, 6.98, 7.16, 7.34, 7.50, 7.52, 7.56, 7.77, 7.80, 7.82, 7.87, 7.90, 7.92, 7.98, 8.02, 8.05, 8.09, 8.11, 8.20] (ArH), [8.27, 8.58, 9.06, 9.13, 9.31, 9.35, 9.47, 9.57, 9.78, 9.79, 10.21, 10.48, 10.52, 10.57, 10.99, 11.00, 11.04, 11.06 ppm] (NH); MALDI-TOF-MS: *m/z* 5972.1 [M^+], 5995.7 [M+Na$^+$]; calcd for $C_{378}H_{400}N_{30}O_{34}S_2$: *m/z* 5971.5 [$M^+$].

Received: October 7, 2002 [Z50315]

 © 2003 Wiley-VCH Verlag GmbH & Co. KGaA, Weinheim 1433-7851/03/4204-0444 $ 20.00+.50/0

[1] Knotaxane is used here for the first time; it is comprised from the words "knot" and "rotaxane". For known rotaxane stoppers possessing central chirality, see a) A. Archut, W. M. Müller, S. Baumann, M. Habel, F. Vögtle, *Liebigs Ann.* **1997**, 495 – 499; b) T. Schmidt, R. Schmieder, W. M. Müller, B. Kiupel, F. Vögtle, *Eur. J. Org. Chem.* **1998**, 2003 – 2007; c) P. R. Ashton, J. A. Bravo, F. M. Raymo, J. F. Stoddart, A. J. P. White, D. J. Williams, *Eur. J. Org. Chem.* **1999**, 899 – 908.

[2] J.-P. Sauvage, C. Dietrich-Buchecker, *Molecular Catenanes, Rotaxanes and Knots, A Journey Through the World of Molecular Topology*, Wiley-VCH, Weinheim, **1999**.

[3] For an explanation of molecular dumbbells, see M. Belohradsky, F. M. Raymo, J. F. Stoddart, *Collect. Czech. Chem. Commun.* **1996**, *61*, 1 – 43.

[4] J. Recker, W. M. Müller, U. Müller, T. Kubota, Y. Okamoto, M. Nieger, F. Vögtle, *Chem. Eur. J.* **2002**, *8*, 4434 – 4442.

[5] O. Safarowsky, M. Nieger, R. Fröhlich, F. Vögtle, *Angew. Chem.* **2000**, *112,* 1699 – 1701; *Angew. Chem. Int. Ed.* **2000**, *39,* 1616 – 1618.

[6] F. Vögtle, A. Hünten, E. Vogel, S. Buschbeck, O. Safarowsky, J. Recker, A. Parham, M. Knott, W. M. Müller, U. Müller, Y. Okamoto, T. Kubota, W. Lindner, E. Francotte, S. Grimme, *Angew. Chem.* **2001**, *113*, 2534 – 2537; *Angew. Chem. Int. Ed.* **2001**, *40*, 2468 – 2471.

[7] Crystal data for **1**: $C_{186}H_{201}N_{15}O_{15}\cdot 3\,CHCl_3\cdot 13\,MeOH\cdot 2\,H_2O$, colorless crystals, crystal dimensions $0.50\times 0.30\times 0.10$ mm; $M_r = 3697.28$ (2886.70 + 810.58 (solvent)); monoclinic, space group $P2_1/n$ (No. 14), $a = 20.2432(1)$, $b = 39.5892(3)$, $c = 25.2668(2)$ Å, $\beta = 91.830(1)°$, $V = 20238.8(2)$ Å^3, $Z = 4$, $\mu(Mo_{K\alpha}) = 0.195$ mm^{-1}, $T = 198(2)$ K, $F(000) = 7872$. Nonius Kappa CCD, 62070 reflections collected ($2\theta = 50°$), of which 35289 were unique; $wR2(F^2) = 0408$ (all data), $R_1 = 0.131$ ($I > 2\sigma(I)$), 2247 parameters, 2282 restraints. CCDC-193813 contains the supplementary crystallographic data for this paper. These data can be obtained free of charge via www.ccdc.cam.ac.uk/conts/retrieving.html (or from the Cambridge Crystallographic Data Centre, 12 Union Road, Cambridge CB21EZ, UK; fax: (+44) 1223-336-033; or deposit@ccdc.cam.ac.uk).

[8] M. Darzac, T. Brotin, D. Bouchu, J.-P. Dutasta, *Chem. Commun.* **2002**, 48 – 49.

[9] A. Arduini, G. Giorgi, A. Pochini, A. Secchi, F. Ugozzoli, *J. Org. Chem.* **2001**, *66*, 8302 – 8308.

[10] a) Y. Okamoto, M. Kawashima, K. Hatada, *J. Am. Chem. Soc.* **1984**, *106*, 5357 – 5359; b) Y. Okamoto, M. Kawashima, K. Hatada, *J. Chromatogr.* **1986**, *363*, 173 – 186.

[11] N. Enomoto, S. Furukawa, Y. Ogasawara, H. Akano, Y. Kawamura, E. Yashima, Y. Okamoto, *Anal. Chem.* **1996**, *68*, 2798 – 2804.

[12] a) N. Koumura, R. W. J. Zijlstra, R. A. van Delden, N. Harada, B. L. Feringa, *Nature* **1999**, *401*, 152 – 155; b) N. Koumura, E. M. Geertsema, A. Meetsma, B. L. Feringa, *J. Am. Chem. Soc.* **2000**, *122*, 12005 – 12006; c) N. Koumura, E. M. Geertsema, A. Meetsma, M. B. van Gelder, B. L. Feringa, *J. Am. Chem. Soc.* **2002**, *124*, 5037 – 5051; d) C. A. Stanier, S. J. Alderman, T. D. W. Claridge, H. L. Anderson, *Angew. Chem.* **2002**, *114*, 1847 – 1850; *Angew. Chem. Int. Ed.* **2002**, *41*, 1769 – 1772; e) J.-P. Sauvage, lecture at the *EuroConference on Supramolecular Chemistry: Molecular Rods, Wires and Switches* (San Feliú de - Guixols, Spanien), **2002**.

[13] a) A. R. Pease, J. Jeppesen, J. F. Stoddart, Y. Luo, C. P. Collier, J. R. Heath, *Acc. Chem. Res.* **2001**, *34*, 433 – 444; b) R. Ballardini, V. Balzani, A. Credi, M. Gandolfi, M. Venturi, *Acc. Chem. Res.* **2001**, *34*, 445 – 455; c) A. Harada, *Acc. Chem. Res.* **2001**, *34*, 456 – 464; d) C. A. Schalley, K. Beizai, F. Vögtle, *Acc. Chem. Res.* **2001**, *34*, 465 – 476; e) J.-P. Collin, C. Dietrich-Buchecker, P. Gavina, M. C. Jiménez-Molero, J.-P. Sauvage, *Acc. Chem. Res.* **2001**, *34*, 477 – 487; f) V. Amendola, L. Fabbrizzi, C. Mangano, P. Pallavicini, *Acc. Chem. Res.* **2001**, *34*, 488 – 493.

[14] a) G. M. Hübner, J. Gläser, C. Seel, F. Vögtle, *Angew. Chem.* **1999**, *111*, 395 – 398; *Angew. Chem. Int. Ed.* **1999**, *38*, 383 – 386; b) C. Seel, F. Vögtle, *Chem. Eur. J.* **2000**, *6*, 21 – 24.

Triple Bond to Tin

Triple Bonding to Tin: Synthesis and Characterization of the Stannylyne Complex *trans*-[Cl(PMe$_3$)$_4$W≡Sn–C$_6$H$_3$-2,6-Mes$_2$]**

Alexander C. Filippou, Peter Portius, Athanassios I. Philippopoulos, and Holger Rohde*

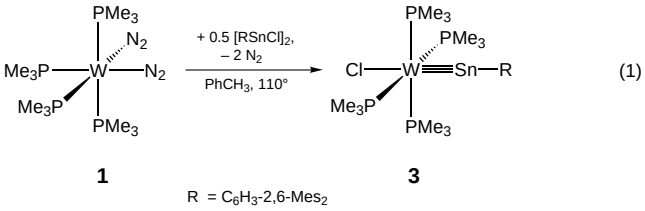
Dedicated to Professor Dieter Fenske on the occasion of his 60th birthday

The discovery of transition-metal carbyne complexes was a landmark in organometallic chemistry.[1] Numerous stoichiometric and catalytic transformations were accomplished with these compounds.[2] In comparison, studies on the heavier Group-14-element analogues of carbyne complexes [L$_n$M≡E–R] (L = ligand, M = transition metal, E = Si, Ge, Sn, Pb, R = organic group) are very rare. In fact, silylyne,[3] stannylyne, and plumbylyne complexes are currently unknown and for germanium only the germylyne complexes [(η^5-C$_5$H$_5$)(CO)$_2$M≡Ge–R] (M = Cr, Mo, W, R = C$_6$H$_3$-2,6-Mes$_2$, C$_6$H$_3$-2,6-Trip$_2$ where Mes = C$_6$H$_2$-2,4,6-Me$_3$ and Trip = C$_6$H$_2$-2,4,6-*i*Pr$_3$)[4] and *trans*-[X(L$_2$)$_2$M≡Ge(η^1-C$_5$Me$_5$)] (X = Cl, Br, I; L$_2$ = R$_2$PCH$_2$CH$_2$PR$_2$ (R = Et (depe), R = Ph (dppe)) or 2 PMe$_3$, M = Mo, W)[5] could be isolated to date. This situation is not surprising given the reluctance of the heavier Group 14 elements to form triple bonds, which makes this one of the most challenging areas in main-group chemistry.[6] In a continuation of our work in this field, we describe herein the synthesis and structure of the first stannylyne complex *trans*-[Cl(PMe$_3$)$_4$W≡Sn–C$_6$H$_3$-2, 6-Mes$_2$] (**3**).

[*] Prof. Dr. A. C. Filippou, Dr. A. I. Philippopoulos, Dipl.-Chem. H. Rohde
Institut für Chemie
Humboldt-Universität zu Berlin
Brook-Taylor Strasse 2, 12489 Berlin (Germany)
Fax: (+49) 30-2093-6939
E-mail: filippou@chemie.hu-berlin.de
Dr. P. Portius
University of Nottingham, University Park
Nottingham, NG7 2RD (United Kingdom)

[**] This work was supported by the Deutsche Forschungsgemeinschaft and the Humboldt Universität zu Berlin. We thank Dr. B. Ziemer and P. Neubauer for the X-ray crystallography and W.-D. Bloedorn, all of the Humboldt Universität zu Berlin, for recording the ^{119}Sn NMR spectrum of **3**. Mes = C$_6$H$_2$-2,4,6-Me$_3$.

Treatment of *cis*-$[W(N_2)_2(PMe_3)_4]$ (**1**)[7] with the *meta*-terphenyl tin(II) chloride $[\{Sn(Cl)(C_6H_3\text{-}2,6\text{-}Mes_2)\}_2]$ (**2**)[8] in refluxing toluene is accompanied by a rapid color change to dark red-brown to afford the stannylyne complex **3** [Eq. (1)]. No intermediates could be detected by IR spectroscopy during the fast reaction, which is completed within a few minutes. In addition, the ^1H and $^{31}P\{^1H\}$ NMR spectra of the crude product, which was obtained after evaporation of toluene, revealed the selective formation of **3**.[9] The stannylyne complex was isolated after workup and crystallization from pentane as a red-brown, microcrystalline, very air-sensitive solid in 47% yield. Upon exposure to air the dark red pentane solutions of **3** immediately turn yellow and a white solid precipitates. Complex **3** shows a remarkable thermal stability and decomposes only above 165°C turning gradually to a black-brown mass.



1 **3**

R = C_6H_3-2,6-Mes_2 (1)

The solid-state structure of **3** was determined by single-crystal X-ray diffraction.[10] Two independent molecules with marginally different bonding parameters were found in the unit cell.[11] The structure of one molecule is depicted in the Figure 1 and the mean values of the two molecules are used in the following discussion. The molecular structure reveals a distorted octahedral coordination environment around the tungsten atom and a *trans* arrangement of the chloro and the stannylyne ligand (Cl-W-Sn 179.3°). Two *trans* PMe_3 ligands (P2 and P4 in Figure 1) are inclined by 11.2° to the chloro ligand, whereas the other two PMe_3 ligands (P1 and P3) are bent by 1.7° towards the stannylyne ligand. Notably, the same geometric distortion of the $M(PMe_3)_4$ moiety from square-planar to flat tetrahedral is observed in the carbyne complexes *trans*-$[Cl(PMe_3)_4W{\equiv}C{-}R]$ (R = H, Me)[12] and the germylyne complex *trans*-$[Cl(PMe_3)_4Mo{\equiv}Ge{-}(\eta^1\text{-}C_5Me_5)]$.[5c] The W–Sn bond of **3** (2.4902(8) Å) is 0.2–0.3 Å shorter than W–Sn single or double bonds (2.71–2.81 Å).[13] The 0.188 Å difference in the W–E triple bond lengths of the stannylyne complex **3** and the germylyne complex *trans*-$[Cl(dppe)_2W{\equiv}Ge{-}(\eta^1\text{-}C_5Me_5)]$[5a] compares well with the difference of the element radii (0.19 Å) calculated from the E–E separation in the alkyne homologues REER (E = Ge, Sn, R = C_6H_3-2,6-$Dipp_2$, Dipp = C_6H_3-2,6-*i*Pr_2)[6e,f] or the difference of the single-bond covalent radii (0.20 Å) of tin and germanium.[14] Another striking structural feature of **3** is the linear coordination of the tin atom (W-Sn-C_{aryl} 178.2(1)°). Thus, complex **3** differs from the "distannyne" RSnSnR (R = C_6H_3-2,6-$Dipp_2$), which has a *trans*-bent structure with a Sn-Sn-C_{aryl} angle of 125.24(7)°.[6e]

The solution ^1H, $^{13}C\{^1H\}$, $^{31}P\{^1H\}$, and $^{119}Sn\{^1H\}$ NMR spectra of **3** are consistent with the structure determined by X-ray crystallography (see Experimental Section). Thus, the $^{31}P\{^1H\}$ NMR spectrum of **3** displays one singlet at $\delta = -27.7$ ppm for the chemically equivalent PMe_3 ligands, which is accompanied by two pairs of satellites arising from coupling with the ^{183}W ($^1J(W,P) = 256.7$ Hz) and $^{117}Sn/^{119}Sn$ nuclei ($^2J(Sn,P) = 129.6$ Hz). In addition, the $^{119}Sn\{^1H\}$ NMR spectrum of **3** shows a quintet $\delta = 340.1$ ppm ($^2J(^{119}Sn,^{31}P) = 133.8$ Hz) at higher field than the corresponding resonance signal of **2** ($\delta = 562$ ppm)[8] or of other stannylenes.[15]

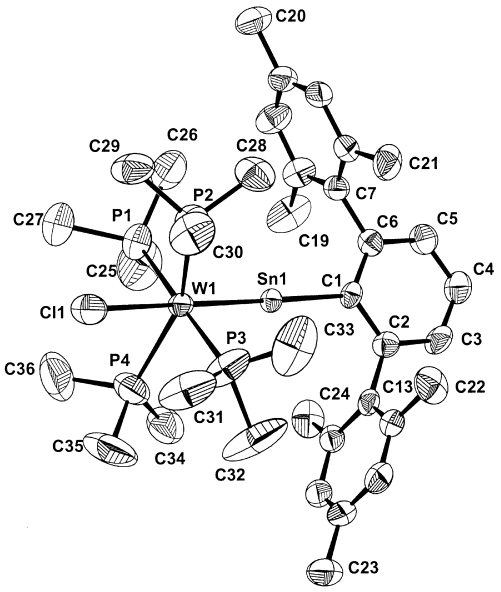


Figure 1. DIAMOND plot of the structure of one of the two independent molecules of **3** in the crystal lattice. The thermal ellipsoids are set at 50% probability. The hydrogen atoms are omitted for clarity. Selected bond lengths [Å] and angles [°]: W1-Sn1 2.4901(7), W1-Cl1 2.507(2), W1-P1 2.470(2), W1-P2 2.454(2), W1-P3 2.425(2), W1-P4 2.500(2), Sn1-C1 2.179(5), W1-Sn1-C1 178.2(1), Sn1-W1-Cl1 179.52(7), Sn1-W1-P1 87.23(5), Sn1-W1-P2 101.42(5), Sn1-W1-P3 90.02(6), Sn1-W1-P4 100.25(5), Cl1-W1-P1 93.20(8), Cl1-W1-P2 78.39(7), Cl1-W1-P3 89.55(9), Cl1-W1-P4 79.96(7), Sn1-C1-C2 119.9(4), Sn1-C1-C6 121.3(4).

The synthesis of the first complex featuring a triple bond to a linear-coordinated tin atom[16] corroborates the efficiency of the dinitrogen elimination method in the formation of triple bonds to heavier homologues of carbon. Furthermore, ongoing studies confirm the broad scope of this method with the syntheses of the related molybdenum–stannylyne complexes *trans*-$[Cl(L_2)_2Mo{\equiv}Sn{-}C_6H_3\text{-}2,6\text{-}Mes_2]$ (L_2 = dppe, 2 PMe_3) and the tungsten compounds *trans*-$[Cl(dppe)_n(PMe_3)_mW{\equiv}Sn{-}C_6H_3\text{-}2,6\text{-}Mes_2]$ ($n = 1$, $m = 2$; $n = 2$, $m = 0$).[16] The usefulness of the stannylyne complexes as SnR-transfer reagents is currently being investigated.

Experimental Section

For experimental conditions and analytical methods see ref. [5b] All NMR spectra were recorded in $[D_8]$THF at 25°C (Bruker AM-300 spectrometer); the ^1H and ^{13}C NMR signals of the *meta*-terphenyl substituent in **3** were assigned by H,H-COSY, H,C-COSY, and HMBC experiments. The $^{119}Sn\{^1H\}$ NMR spectrum of **3** was calibrated against an external solution of $SnMe_4$ in $[D_8]$THF.

3: Toluene (ca. 20 mL) was added by trap-to-trap condensation to a stoichiometric mixture of orange **1** (0.217 g, 0.399 mmol) and of yellow **2** (0.187 g, 0.200 mmol). The resulting dark red solution was stirred in the glove box at ambient temperature. An IR spectrum of

 © 2003 Wiley-VCH Verlag GmbH & Co. KGaA, Weinheim 1433-7851/03/4204-0446 $ 20.00+.50/0

the solution, recorded after several hours, showed only a slight decrease in intensity of the $\tilde{\nu}(N_2)$ absorption bands at 1984 and 1923 cm^{-1} of **1**, which indicated the slow progress of the reaction. The reaction mixture was then immersed in a preheated oil bath (150 °C) and heated under reflux. The solution rapidly turned dark red-brown. Completion of the reaction within 4 min was confirmed by IR spectroscopy. In the dark the solvent was evaporated to give a red-brown oil, which crystallized to a red-brown block of matted thin needles upon storage overnight in a freezer at −30 °C. The crystalline block was dried at 45 °C in vacuo for 0.5 h, and pentane (ca. 30 mL) was added by trap-to-trap condensation. The cloudy dark red solution was separated from a tiny amount of an insoluble khaki material by filtration, this khaki material fumed upon exposure to air. The filtrate was concentrated under vacuum until crystallization began and stored at −30 °C in a freezer and then on dry ice. The mother liquor was removed at low temperature and the crystals allowed to warm to ambient temperature under vacuum and dried for 1 h. Yield 178 mg (47 % based on **1**) as red-brown microcrystalline solid, m.p. 165 °C (decomp). Elemental analysis calcd (%) for $C_{36}H_{61}ClP_4SnW$ (955.78): C 45.24, H 6.43, Cl 3.71, N 0.00; found: C 44.84, H 6.03, Cl 3.92, N 0.00; ^{1}H NMR: $\delta = 1.39$ (m, 36 H, $4 \times P(CH_3)_3$), 2.06 (s, 12 H, $4 \times o$-CH_3, Mes), 2.31 (s, 6 H, $2 \times p$-CH_3, Mes), 6.87 (d, $^3J(H,H) = 7.5$ Hz, 2 H, *m*-H, C_6H_3), 6.87 (s, 4 H, *m*-H, Mes), 7.29 ppm (t, $^3J(H,H) = 7.5$ Hz, 1 H, *p*-H, C_6H_3); ^{13}C{^{1}H} NMR: $\delta = 21.3$ (s, $2 \times p$-CH_3, Mes), 21.8 (s, $4 \times o$-CH_3, Mes), 30.2 (m, $4 \times P(CH_3)_3$), 128.1 (s, *p*-C, C_6H_3), 129.9 (s, $4 \times m$-C, Mes), 130.6 (s, $2 \times m$-C, C_6H_3), 136.7 (s, $4 \times o$-C, Mes), 137.4 (s, $2 \times p$-C, Mes), 142.4 (s, $2 \times ipso$-C, Mes), 146.2 (quint, $^4J(P,C) = 1.4$ Hz, $2 \times o$-C, C_6H_3), 191.8 ppm (quint, $^3J(P,C) = 0.8$ Hz, $1 \times ipso$-C, C_6H_3); ^{31}P{^{1}H} NMR: $\delta = -27.7$ ppm {s, $^1J(^{183}W,^{31}P) = 256.7$ Hz, $^2J(^{117}Sn/^{119}Sn,^{31}P) = 129.6$ Hz (coupling to the ^{119}Sn and ^{117}Sn nuclei could not be resolved because of the broadness of the tin satellite signals)}; ^{119}Sn{^{1}H} NMR: 340.1 ppm (quint, $^2J(^{119}Sn,^{31}P) = 133.8$ Hz).

Received: August 26, 2002 [Z50045]

[1] E. O. Fischer, G. Kreis, C. G. Kreiter, J. Müller, G. Huttner, H. Lorenz, *Angew. Chem.* **1973**, *85*, 618 – 620; *Angew. Chem. Int. Ed. Engl.* **1973**, *12*, 564 – 565.

[2] Selected review articles on carbyne complexes: a) H. Fischer, P. Hofmann, F. R. Kreißl, R. R. Schrock, U. Schubert, K. Weiss, *Carbyne Complexes*, VCH, Weinheim, **1988**; b) A. Mayr, H. Hoffmeister, *Adv. Organomet. Chem.* **1991**, *32*, 227 – 324; c) R. R. Schrock, *Chem. Rev.* **2002**, *102*, 145 – 179.

[3] A donor-stabilized silylyne complex containing a four-coordinate silicon atom, $[Cp^*(PMe_3)_2RuSi\{(2,2'\text{-bpy})(SC_6H_4\text{–}4\text{-Me})\}](OTf)_2$ ($Cp^* = C_5Me_5$, bpy = bipyridyl) has been reported: S. D. Grumbine, R. K. Chadha, T. D. Tilley, *J. Am. Chem. Soc.* **1992**, *114*, 1518 – 1520.

[4] a) R. S. Simons, P. P. Power, *J. Am. Chem. Soc.* **1996**, *118*, 11966 – 11967; b) L. Pu, B. Twamley, S. T. Haubrich, M. M. Olmstead, B. V. Mork, R. S. Simons, P. P. Power, *J. Am. Chem. Soc.* **2000**, *122*, 650 – 656.

[5] a) A. C. Filippou, A. I. Philippopoulos, P. Portius, D. U. Neumann, *Angew. Chem.* **2000**, *112*, 2881 – 2884; *Angew. Chem. Int. Ed.* **2000**, *39*, 2778 – 2781; b) A. C. Filippou, P. Portius, A. I. Philippopoulos, *Organometallics* **2002**, *21*, 653 – 661; c) A. C. Filippou, A. I. Philippopoulos, P. Portius, D. U. Neumann, XXXVth International Conference on Coordination Chemistry (ICCC35), Heidelberg, Germany, **2002**, Book of Abstracts, p. 129.

[6] Recent experimental work on heavier Group-14-element analogues of alkynes: a) L. Pu, B. Twamley, P. P. Power, *J. Am. Chem. Soc.* **2000**, *122*, 3524 – 3525; b) R. Pietschnig, R. West, D. R. Powell, *Organometallics* **2000**, *19*, 2724 – 2729; c) C. Bibal, S. Mazieres, H. Gornitzka, C. Couret, *Angew. Chem.* **2001**, *113*, 978 – 980; *Angew. Chem. Int. Ed.* **2001**, *40*, 952 – 954; d) N. Wiberg, W. Niedermayer, H. Nöth, M. Warchhold, *Z. Anorg. Allg. Chem.* **2001**, *627*, 1717 – 1722; e) A. D. Phillips, R. J. Wright, M. M. Olmstead, P. P. Power, *J. Am. Chem. Soc.* **2002**, *124*, 5930 – 5931; f) M. Stender, A. D. Phillips, R. J. Wright, P. P. Power, *Angew. Chem.* **2002**, *114*, 1863 – 1865; *Angew. Chem. Int. Ed.* **2002**, *41*, 1785 – 1787.

[7] E. Carmona, A. Galindo, M. L. Poveda, R. D. Rogers, *Inorg. Chem.* **1985**, *24*, 4033 – 4039.

[8] R. S. Simons, L. Pu, M. M. Olmstead, P. P. Power, *Organometallics* **1997**, *16*, 1920 – 1925.

[9] According to NMR spectroscopy small amounts of PMe_3 and C_6H_4-2,6-Mes_2 were also liberated.

[10] Crystal-structure determination of **3**: $C_{36}H_{61}ClP_4SnW$, $M_r = 955.72$; dark red single crystals from a concentrated pentane solution by slow evaporation and cooling from 20 → −23 °C, monoclinic, space group $P2_1/a$, $a = 24.926(5)$, $b = 27.909(5)$, $c = 12.290(5)$ Å, $\alpha = \gamma = 90$, $\beta = 93.98(3)°$, $V = 8529(3)$ Å^3, $Z = 8$, $\rho_{calcd} = 1.489$ g cm^{-1}, $2\theta_{max} = 50.00°$, STOE-IPDS diffractometer with area detector, $T = 180(2)$ K, $\lambda(Mo_{K\alpha}) = 0.71073$ Å, $\mu = 3.515$ mm^{-1}, $F(000) = 3824$, 54394 reflections, 14246 unique reflections, 812 parameters, GOF = 1.025, $R_1 = 0.0383$ [$I > 2\sigma(I)$], $wR_2 = 0.1022$ (all data), largest differential peak and hole 1.473/−1.742 e Å^{-1}. CCDC-192090 (**3**) contains the supplementary crystallographic data for this paper. These data can be obtained free of charge via www.ccdc.cam.ac.uk/conts/retrieving.html (or from the Cambridge Crystallographic Data Centre, 12 Union Road, Cambridge CB2 1EZ, UK; fax: (+44) 1223-336-033; or deposit@ccdc.cam.ac.uk).

[11] The two molecules differ in the orientation of the *meta*-terphenyl substituent relative to the $WCl(PMe_3)_4$ fragment. In one molecule (Figure 1) the terphenyl substituent adopts an almost staggered conformation as shown by the interplane angle of 49.2° between the central aryl ring and the least-square plane defined by the atoms Cl1, W1, P2, and P4, whereas in the second molecule the corresponding interplane angle is 12.9°.

[12] a) M. R. Churchill, A. L. Rheingold, H. J. Wasserman, *Inorg. Chem.* **1981**, *20*, 3392 – 3399; b) L. M. Atagi, J. M. Mayer, *Polyhedron* **1995**, *14*, 113 – 125.

[13] Selected references for complexes with W–Sn single and double bonds: a) W. Petz, *Chem. Rev.* **1986**, *86*, 1019 – 1047; b) M. S. Holt, W. L. Wilson, J. H. Nelson, *Chem. Rev.* **1989**, *89*, 11 – 49; c) O. Kircher, G. Huttner, B. Schiemenz, K. Heinze, L. Zsolnai, O. Walter, A. Jakobi, A. Driess, *Chem. Ber.* **1997**, *130*, 687 – 699; d) T. Szymanska-Buzar, T. Glowiak, *Polyhedron* **1998**, *17*, 3419 – 3426; e) H. Nakazawa, M. Kishishita, T. Ishiyama, T. Mizuta, K. Miyoshi, *J. Organomet. Chem.* **2001**, *617–618*, 453 – 463.

[14] R. Blom, A. Haaland, *J. Mol. Struct.* **1985**, *128*, 21 – 27.

[15] a) B. Wrackmeyer, *Annu. Rep. NMR Spectrosc.* **1999**, *38*, 203 – 264; b) B. E. Eichler, B. L. Phillips, P. P. Power, M. P. Augustine, *Inorg. Chem.* **2000**, *39*, 5450 – 5453.

[16] Quantum-chemical calculations of the model complexes *trans*-$[Cl(PR_3)_4W{\equiv}SnR']$ (R = H, Me, R′ = Me, Ph) at different levels of theory (RI-MP2/TZVP, B3LVP/TZVP, RI-BP86/TZVP, HF/TZVP) reveal a good agreement of the calculated and experimental bonding parameters. Furthermore, charge decomposition (CDA) and natural bond orbital (NBO) analyses show that the W≡Sn bonds are composed of one σ and two degenerate, polar π bonds. The stannylyne complexes *trans*-$[Cl(L_2)_2Mo{\equiv}Sn\text{–}C_6H_3\text{-}2,6\text{-}Mes_2]$ (L_2 = dppe, $2PMe_3$) and *trans*-$[Cl(dppe)_n(PMe_3)_mW{\equiv}Sn\text{–}C_6H_3\text{-}2,6\text{-}Mes_2]$ ($n = 1$, $m = 2$; $n = 2$, $m = 0$) have been characterized by X-ray crystallography and display the same structural features as **3**: A. C. Filippou, G. Schnakenburg, A. I. Philippopoulos, H. Rohde, P. Portius, unpublished results.

Aggregating Gold Nanoparticles

Iodine-Induced Gold-Nanoparticle Fusion/Fragmentation/Aggregation and Iodine-Linked Nanostructured Assemblies on a Glass Substrate**

Wenlong Cheng, Shaojun Dong, and Erkang Wang**

Recently, molecularly bridged nanoparticle aggregates[1] have been attracting growing interest as a result of their collective electronic, optical, and magnetic properties being distinctly different from a corresponding collection of individual nanoparticles (NPs) or the extended solid. The 2D/3D control over the spatial arrangement of NPs is primarily based on the thiol-amphilic nature[1b,e] of metal NPs, hydrogen-bonding interactions,[1a] the highly specific recognition interaction of antigens/antibodies, and specific base-pairing interactions[1f] between DNA and its complementary strand.[1c,d] In addition, by careful linker-molecule design, spatially and symmetrically well-defined NP aggregates have been reported.[2] Such aggregated nanostructures can also be constructed on a solid support.[3] A remaining question is whether atoms can also "glue" NPs together?

A monolayer of iodine atoms has been known to form spontaneously on immersing a bulk-gold surface in dilute iodide solution.[4] Herein, we demonstrate that such chemisorption also takes place on tiny citrate-stabilized gold NPs. As a result of electron donation, these gold NPs undergo fusion and fragmentation in solution. Also, iodine adsorption on NPs displaces citrate ions from the surface of the NPs and lowers the surface potential, as a result, increasing van der Waals attractive forces between these I-coated gold NPs drive the formation of aggregates in a controlled manner both in solution and on solid support.

The idea that iodide spontaneously chemisorbed on gold NPs was supported by electrochemistry and optical spectra. Using the strategy of Natan and co-workers,[5] we can prepare highly reproducible NPs submonolayers on 3-aminopropyltrimethoxysilane (APTMS) modified ITO (indium–tin oxide) substrate. The gold NPs submonolayers are rather robust, resistant of electrochemical scanning in the potential range 0–1.5 V (Figure 1a, curve 1). Interestingly, after the NPs submonolayers are immersed into aqueous 1 mM KI solution for several minutes, the submonolayers exhibited characteristic voltammetry of desorption and oxidation of iodine to iodate (a five-electron process; Figure 1a, curve 2), which is extremely similar to the results obtained with bulk gold.[4] Thus, it is thought that these APTMS-tethered gold NPs behave in the same way as bulk gold, and a similar chemisorptive process of iodide should take place. The coulometric analysis indicated that a monolayer of adsorbed iodine formed on the exposed surface of the immobilized gold NPs, which is again consistent with the case for bulk gold. This result is also supported by spectral studies. Immersion of gold NP submonolayers in dilute KI leads to gold-surface plasmon-band damping and a red-shift of the peak position (Figure 1b: curve 1)[6] relative to the original gold plasmon band (Figure 1b: dotted line), which indicates iodine adsorbsion on these immobilized NPs (see below). Similar spectral responses were also observed for interactions between iodide and free solution-state gold NPs (Figure 1c), which is indicative of similar iodine chemisorptive events on these not-immobilized gold NPs. For confirmation of this result, a control experiment for KCl addition to colloidal Au was performed (Figure 1d); it is clear that no second absorbance band appearance even after 100 μL of 0.2 M KCl was added. Previous studies[7] have shown that the interaction of chloride with gold nanoparticles is the result of salt effects. The distinctly different optical responses for KI addition show that iodine interaction must follow a different mechanism. The only reasonable explanation is that a chemisorptive process takes place.

It is expected that the adsorbed iodine on the gold NPs would displace the stabilizing citrate ions, neutralize surface charge, lower "ζ potential", thus, paving way for gold-NP aggregation and fusion. This speculation was supported by the optical spectra and transmission electron microscopy (TEM). When controlled amounts of 0.2 M KI were added to ruby-colored colloidal-Au suspension[8] at room temperature, color changes were observed within several minutes.[9] The spectral changes are shown in Figure 1c. It is clearly seen that the absorbance is highly dependent on the quantity of KI added. The native-surface plasmon band at 520 nm weakens and an absorption band in the red/infrared region (λ_{max} ca. 760 nm) appears and becomes more intense with increasing addition of KI solution. The weakening of the plasmon band is attributed to damping effects,[6] whereas the new band indicates aggregation[10a] and/or changes in the shape[10b] of gold NPs.

TEM[11] results correlate with the KI addition-dependent spectroscopic observations as shown in Figure 2. The native gold NPs are monodispersed, nearly spherical in shape, with an average diameter of 12 nm, and well separated (see Supporting Information). When a small amount of KI was added, the TEM image shows the presence of NP aggregates, each consisting of hundreds of individual NPs that are in close contact (Figure 2a–c). These individual NPs of aggregates are predominantly spherical with a diameter of 20–30 nm. However, in some domains we found some gold NPs smaller than the original spherical gold NPs (Figure 2c). We attribute these changes in the dimensions of the gold NPs to energetic injection, and the energy source is electron injection by the reductive chemisorption of iodide ions[3] ($I^- - e^- \rightarrow I_{(adsorbed)} + e^-$). Similar energetic-injection-induced fusion,[12] fragmentation,[13] and dissolution[14] of NPs has been described. Upon

[*] Prof. S. Dong, Prof. E. Wang, W. Cheng
State Key Laboratory of Electroanalytical Chemistry Changchun Institute of Applied Chemistry
Chinese Academy of Sciences, Changchun, Jilin 130022 (P.R. China)
Fax: (+86) 431-5689711
E-mail: dongsj@ciac.jl.cn
ekwang@ns.ciac.jl.cn

[**] This work was supported by the National Natural Science Foundation of China. (No. 29835120, No. 29975028).

Supporting information for this article is available on the WWW under http://www.angewandte.org or from the author.

 © 2003 Wiley-VCH Verlag GmbH & Co. KGaA, Weinheim 1433-7851/03/4204-0449 $ 20.00+.50/0

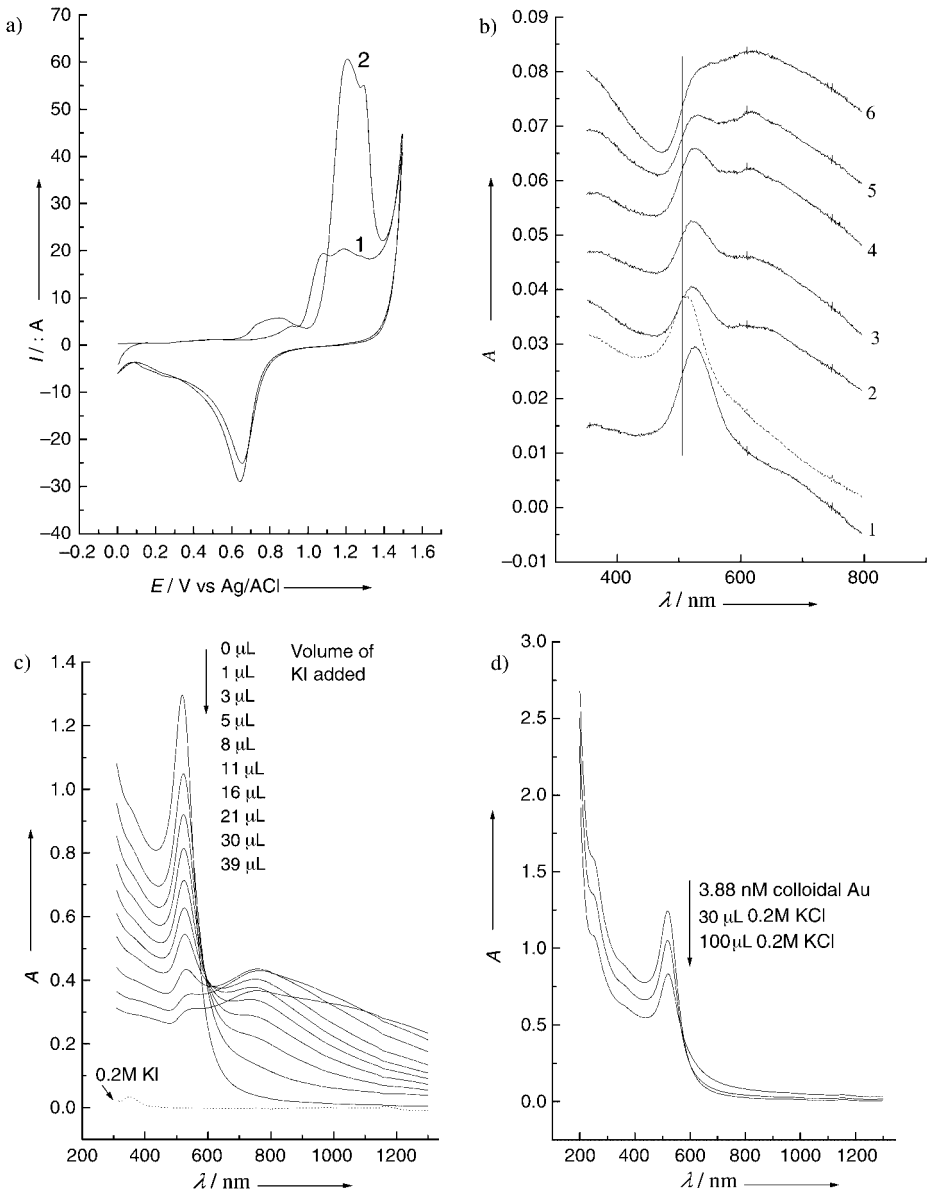


Figure 1. a) Cyclic voltammograms in 0.5 M H_2SO_4 of NP submonolayers on APTMS-modified ITO before (1) and after (2) iodine adsorption. Scan rate is 50 mVs^{-1}. b) Absorbance spectra monitoring of the construction of iodine-bound ITO-surface-bound-NP nanostructured assemblies. The stepwise derivatizing cycles with Au colloid and 1 mM KI are labeled beside curves. The doted line shows the absorbance of NP submonolayers on APTMS-modified ITO. c) UV/Vis absorption changes of colloidal Au (1 mL, 3.88 nM) upon addition of different amounts of aqueous 0.2 M KI solutions. d) UV/Vis absorption changes of colloidal Au (1 mL, 3.88 nM) upon addition of different amounts of aqueous 0.2 M KCl solutions.

increasing the KI addition, the aggregation becomes more extensive (Figure 2 d, e). Excess KI addition ($\geq$ 50 μL) leads to a decrease of both absorption bands, and the whole broad absorption band is extended into infrared region.[15] Under these conditions, many nanocrystals with various geometries could be seen in the TEM (Figure 2 f). Comparison of the optical response with the corresponding TEM morphology reveals that the appearance of the broad absorbance band is actually mirrored by the appearance of the anisometric nanocrystals.[10b] Previous studies indicate that collective optical, electronic properties[1–3] are dictated by aggregate size,[10a] particle shape,[10b] interparticle distance,[10a,16] and damping effects.[6] Here, optical spectra and TEM, support the idea that coupling aggregation and damping effects dictate optical responses in low KI concentration and anisometric nanocrystal shape determines the optical responses in high KI concentration.

It is clearly noted from TEM that iodine-induced gold-NP aggregation is different from that described in reference [1]. It resembles photoinduced conversion[17] of silver nanospheres into nanoprisms, where an energetic injection process was also involved. In our system, the energy source is the electron injection which results from iodide reduction. Such electron-transfer processes are not unusual, and it has been indicated in C_{60}-mediated aggregation.[18] Based on these experimental results and the previous studies,[17,18] an iodine chemisorption-induced aggregating/fusing mechanism is given in Figure 3. The chemisorbed iodine atoms on NPs would neutralize NP surface charge, and as a result, increase the van der Waals attractive forces among these iodine-coated NPs which would lead to aggregate generation. The iodine atoms might be still associated with these NP aggregates to keep structural stability. The fusion/fragmentation is at the expense of the original gold NPs, this situation is supported by the presence of an isosbestic point in Figure 1 c. Excess KI addition results in nearly complete fusion of the gold NPs. The fusing process is similar to Ostwald ripening (i.e. particle growth through the exchange of "monomer" between particles), and KI addition enhances the rate of the Ostwald ripening process. Thus, small amounts of a water-soluble gold-iodide/iodine might exist.

Strong interaction of iodides and gold NPs is reminiscent of the strategy of Willner and co-workers [3a,10a] for the fabrication of surface-bound nanostructured assemblies on solid supports. Interestingly, repeated treatment of APTMS-modified ITO with citrate-stabilized colloidal Au and 1 mM KI results in similar nanostructure generation, which is shown by spectral observations (Figure 1 b). The above discussion demonstrates that the immersion of primary gold NPs

 © 2003 Wiley-VCH Verlag GmbH & Co. KGaA, Weinheim 1433-7851/03/4204-0450 $ 20.00+.50/0

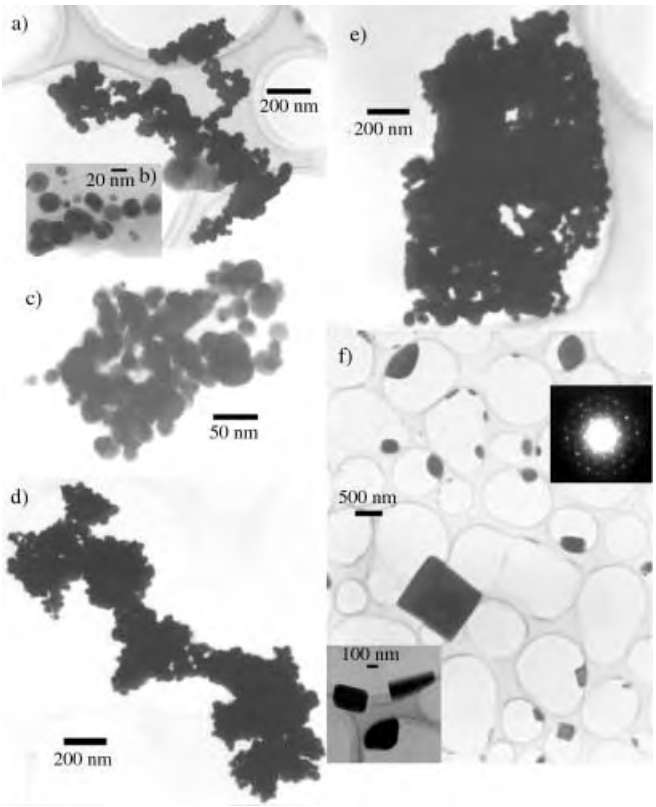


Figure 2. Representative morphological changes of TEM micrographs for colloid Au (1 mL, 3.88 nM) upon addition of different amounts of 0.2 M KI solutions: 6 μL (a–c), 18 μL (d–e), 60 μL (f). Inset of (f) top: electron diffraction pattern analysis. The spot array, diagnostic of a hexagonal structure, is from the [111] orientation of the largest cubic platelet lying flat on the substrate with the top facet perpendicular to the electron beam, bottom: enlargement.

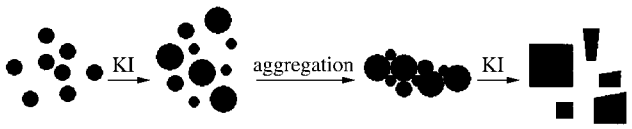


Figure 3. Schematic aggregating/fusing mechanism of gold NPs upon KI addition.

submonolayers into dilute KI leads to iodine-atom-monolayer formation on these immobilized NPs (Figure 1b, curve 1). This adsorbed iodine lowers the surface charge of the immobilized NPs significantly, as a result, additional gold NPs can be "glued" together upon immersing them in Au colloid. Formation of a second NP layer is demonstrated by the decrease of the plasmon absorbance and the appearance of second coupled plasmon absorbance band arising from the close contact of NPs (curve 2).[3,10a] As the treating times are increased, the coupled-band strengthens (curves 3–6), which indicates that the coupling interactions become longer-range.[3,10a] Previously, fabrication of surface-bound nanostructures was based on electrostatic or covalent interactions, whereas van der Waals attractive forces could be the driving forces for the surface-bound nanostructure formation in this study.

In conclusion, this study demonstrates for the first time that iodine chemisorption takes place on gold NPs. Compared with previous aggregating studies,[1,2] both aggregation and fusion/fragmentation of NPs were observed by TEM upon KI addition. We propose that the physical origin of the fusion/fragmentation of gold NPs is energetic injection, which fits with these previous studies.[12–14,17] The driving force of aggregation should be van der Waals attractive force. It is found that I-linked surface-bound-NP nanostructure can be fabricated by a layer-by-layer deposition techniques. This observation shows that crosslinkers are not confined to oligocations.[3,10a] It is expected that this study might be instructive for testing the relationship between collective optical responses of metal NPs[1–3] and individual NPs, and could find application in nanoscale electronics and photonics.

Experimental Section

Reagents: analytical grade $[HAuCl_4]\cdot 3H_2O$, trisodium citrate, KI, and KCl were all purchased from commercial vendors (Aldrich) and used as received. Solutions were prepared from ultrapure water purified with Milli-Q plus system (Millipore Co.), its resistivity was over 18 MΩcm.

Instrumentation: all electrochemical experiments were carried out on Autolab PGSTAT30 potentiostat (Utrecht, Netherlands) in a conventional one-compartment cell. The cell was housed in a homemade Faraday cage to reduce stray electrical noise. The electrochemical measurements were performed using standard three-electrode systems. A Ag/AgCl electrode was used as the reference electrode, a Pt foil as the counter electrode, and the O-rings with 6 mm inner diameter were used to seal the ITO slides for all electrochemical experiments (geometry area is ca. 0.283 cm^2). Optical spectra were acquired using Cary 500 UV-visible NTR spectrometer (Varian, USA). TEM samples were examined by using JEOL 2010 transmission electron microscopy operated at 200 kV.

Synthesis of 3.88 nM colloidal Au: Typically, aqueous solutions of $[HAuCl_4]$ (≈0.5 mL 1%) were diluted (to 70 mL), then the mixed solutions were heated to nearly boiling. Afterwards, aqueous trisodium citrate solutions (≈1.3 mL) were injected into the stirring system. The color changes were noted within several minutes, and a ruby-colored solution was obtained finally. The concentration of gold NPs was calculated to be ≈3.88 nM by assuming an average 12 nm diameter for all NPs.

Received: May 17, 2002
Revised: August 23, 2002 [Z19327]

[1] a) A. K. Boal, F. Ilhan, J. E. DeRouchey, T. Thurn-Albrecht, T. P. Russell, V. M. Rotello, *Nature* **2000**, *404*, 746–748; b) R. P. Andres, J. D. Bielefeld, J. I. Henderson, D. B. Janes, V. R. Kolagunta, C. R. Kubiak, W. J. Mahoney, R. G. Osifchin, *Science* **1996**, *273*, 1690–1693; c) C. A. Mirkin, R. L. Letsinger, R. C. Mucic, J. J. Storhoff, *Nature* **1996**, *382*, 607–609; d) A. P. Alivisatos, K. P. Johnsson, X. G. Peng, T. E. Wilson, C. J. Loweth, Jr., M. P. Bruchez, P. G. Schultz, *Nature* **1996**, *382*, 609–611; e) M. Brust, D. Bethell, D. J. Schiffrin, C. J. Kiely, *Adv. Mater.* **1995**, *7*, 795–797; f) S. Mann, W. Shenton, M. Li, S. Connolly, D. Fitzmaurice, *Adv. Mater.* **2000**, *12*, 147–150; g) Y. Jin, S. Dong, *Angew. Chem.* **2002**, *114*, 1082–1086; *Angew. Chem. Int. Ed.* **2002**, *41*, 1040–1044.
[2] J. P. Novak, D. L. Feldheim, *J. Am. Chem. Soc.* **2000**, *122*, 3979–3980.

 © 2003 Wiley-VCH Verlag GmbH & Co. KGaA, Weinheim 1433-7851/03/4204-0451 $ 20.00+.50/0

[3] a) A. N. Shipway, E. Katz, I. Willner, *ChemPhysChem* **2000**, *1*, 18 – 52; b) W. Cheng, J. Jiang, S. Dong, E. Wang, *Chem. Commun.* **2002**, *16*, 1706.
[4] H. O. Finklea in *Electroanalytical Chemistry, Vol. 19* (Eds.: A. J. Bard), Marcel Dekker, New York, **1996**, pp. 185 – 187.
[5] R. G. Freeman, K. C. Grabar, K. J. Allison, R. M. Bright, J. A. Davis, A. P. Guthrie, M. B. Hommer, M. A. Jackson, P. C. Smith, D. G. Walter, M. J. Natan, *Science* **1995**, *267*, 1629 – 1632.
[6] P. Mulvaney, *Langmuir* **1996**, *12*, 788 – 800.
[7] a) S. I. Cumberland, G. F. Strouse, *Langmuir* **2002**, *18*, 269 – 276; b) F. W. Vance, B. I. Lemon, J. T. Hupp, *J. Phys. Chem. B* **1998**, *102*, 10091 – 10093.
[8] Gold colloids were prepared by the conventional citrate reduction of $[HAuCl_4]$ in water at near-boiling temperature. See G. Frens, *Nature* **1973**, *241*, 20.
[9] The colloid became light-blue upon addition of a small amount of KI and light-gray upon addition of excess KI.
[10] a) A. N. Shipway, M. Lahav, R. Gabai, I. Willner, *Langmuir* **2000**, *16*, 8789 – 8795; b) J. Wiesner, A. Wokaun, *Chem. Phys. Lett.* **1989**, *157*, 569 – 575.
[11] TEM examination was conducted by applying a drop of the samples to carbon-coated copper grids in contact with filter paper. The solvent was quickly wicked away by the filter paper, preventing particle agglomeration.
[12] Y. Takeuchi, T. Ida, K. Kimura, *J. Phys. Chem. B* **1997**, *101*, 1322 – 1327.
[13] a) H. Kurita, A. Takami, S. Koda, *Appl. Phys. Lett.* **1998**, *72*, 789; b) A. Takami, H. Yamada, K. Nakano, S. Koda, *Jpn. J. Appl. Phys.* **1996**, *35*, L781.
[14] Y. Nakao, *J. Chem. Soc. Chem. Commun.* **1994**, 2067.
[15] Precipitation is not found, even after several days later.
[16] a) B. Kim, S. L. Tripp, A. Wei, *J. Am. Chem. Soc.* **2001**, *123*, 7955 – 7956; b) J. J. Storhoff, A. A. Lazarides, R. C. Mucic, C. A. Mirkin, R. L. Letsinger, G. C. Schatz, *J. Am. Chem. Soc.* **2000**, *122*, 4640 – 4650.
[17] R. C. Jin, Y. W. Cao, C. A. Mirkin, K. L. Kelly, G. C. Schatz, J. G. Zheng, *Science* **2001**, *294*, 1901 – 1903.
[18] M. Brust, C. J. Kiely, D. Bethell, D. J. Schiffrin, *J. Am. Chem. Soc.* **1998**, *120*, 12367 – 12368.

Ruthenium Metallodendrimers

Dendritic Stars by Ring-Opening-Metathesis Polymerization from Ruthenium–Carbene Initiators

*Sylvain Gatard, Sylvain Nlate, Eric Cloutet, Georges Bravic, Jean-Claude Blais, and Didier Astruc**

Dendrimers are a rich and appealing field of polymer chemistry.[1] Organic polymerization from dendritic initiators also offers a route to highly branched polymers, and indeed these have been obtained, amongst other methods, by atom transfer radical polymerization (ATRP), anionic polymerization at a focal point of dendrons,[2] and cationic polymerization of styrene using star-shaped initiators.[3] Our goal was to synthesize dendritic stars by polymerization at the branch termini of a core. Therefore, we investigated the synthesis of new stable ruthenium–carbene[4–8] dendrimers[9,10] that would be able to catalyze subsequently the ring-opening-metathesis polymerization (ROMP) of norbornene.[11] Only a few metal–carbene dendrimers are known: these are tetrabranched ruthenium catalysts recently reported by the groups of Hoveyda,[4] van Koten,[5] and Verdonck.[6]

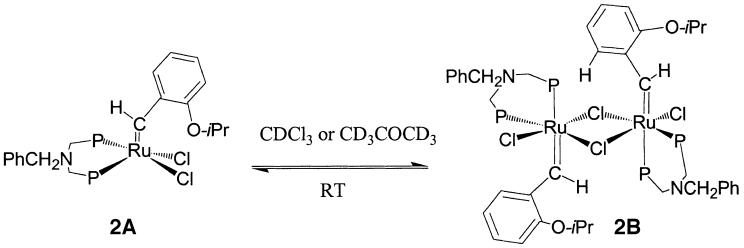
Herein, we report: a) the synthesis of new ruthenium–carbene complexes containing a chelating diphosphane, b) by modeling a dendritic branch, the reversible dimerization of these complexes in concentrated solutions, c) the extension of this synthetic route to three generations of dendritic ruthenium–carbene complexes, d) the ROMP reactions of the latter with norbornene to form metallodendritic stars, and e) the remarkable dendritic effects on the dimerization and polymerization reactions.

We designed a system that should be stable enough to support the dendritic structure and yet be reactive enough for ROMP. Therefore, we selected a chelating diphosphane-ruthenium-carbene framework. The strategy is based on recent breakthroughs. Hoveyda[4] modified the Grubbs catalyst $[RuCl_2(PCy_3)_2](CHPh)]$[7,10] (Cy = cyclohexyl) by introducing an isopropoxy substituent at the *ortho* position of the benzylidene ligand such that the hemilabile chelating ether ligand replaces one phosphane. We chose the PPh_3 version of this system as the PPh_3 group can be substituted by a chelating diphosphane unit containing a dendritic branch. Hofmann

[*] Prof. Dr. D. Astruc, Dr. S. Gatard, Dr. S. Nlate
LCOO, UMR CNRS 5802
Université Bordeaux I
33405 Talence Cedex (France)
Fax: (+33) 5-5684-6646
E-mail: d.astruc@lcoo.u-bordeaux.fr
Dr. E. Cloutet
LCPO, ENSCPB
Université Bordeaux I, 33607 Pessac Cedex (France)
Dr. G. Bravic
ICMCB, 33608 Pessac Cedex (France)
Dr. J.-C. Blais
LCSOB, UMR CNRS 7613
Université Paris VI, 75252 Paris (France)

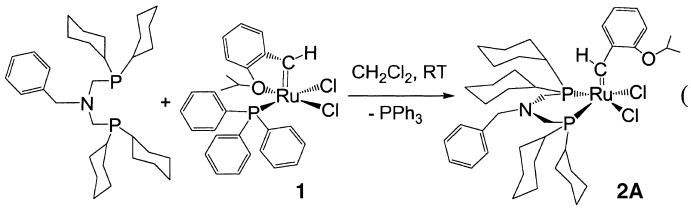
 © 2003 Wiley-VCH Verlag GmbH & Co. KGaA, Weinheim 1433-7851/03/4204-0452 $ 20.00+.50/0

and co-workers showed that the chelating diphosphanes $t\mathrm{Bu_2P(CH_2)}_n\mathrm{P}t\mathrm{Bu_2}$ ($n=1$ or 2) could form ruthenium metathesis catalysts for ring-closing metathesis (RCM) and ROMP after activation with a Lewis acid,[12] and the groups of Fog[13] and Leitner[14] demonstrated that some neutral *cis*-bisphosphane–ruthenium complexes could also be active ROMP catalysts without the addition of a Lewis acid. The dendritic diphosphanes of Reetz et al. have already been used in catalysis[15] and for the attachment of triruthenium carbonyl clusters at the periphery.[16]



(3)

Starting from benzyl amine, we synthesized the new diphosphane model $\mathrm{PhCH_2N(CH_2PCy_2)_2}$, **1**, and the corresponding air-stable green monoruthenium-carbene complex **2** [Eq. (1)], as well as the three first generations of dendritic deep-green alkylidene complexes: **3** (G_1, Ru_4P_8), **4** (G_2, Ru_8P_{16}), and **5** (G_3, $Ru_{16}P_{32}$) in which the Ph group of **1** is replaced by the dendritic branch [Eq. (2)]. The X-ray crystal structure of **2A**[17] (Figure 1; there is a second isomer **2B**, see below) shows the geometry about the Ru center is a distorted tetragonal pyramid. It also shows that the ether group of the hemilabile ligand is not coordinated, unlike in Hoveyda's complex,[4] and confirms the chelation of the diphosphane ligand. The angle of the carbenic carbon atom with the Ru center and the aryl carbon atom is slightly larger (127°) than the classic 120° angle expected for an sp^2-hybridized carbon center. The ^{1}H NMR spectrum of **2A** in dilute $CDCl_3$ shows a triplet ($^3J_{H,P}=15.7$ Hz) at $\delta=15.66$ ppm arising from the carbene hydrogen atom. The spectrum of a concentrated $CDCl_3$ solution of **2A** indicates the presence of an additional carbene hydrogen atom ($\delta=16.96$ ppm; $^3J_{H,P}=13.3$ Hz). Likewise, the ^{31}P NMR spectrum of this concentrated solution contains, in addition to the major singlet, a doublet of doublets suggesting the presence of another ruthenium carbene complex **2B** in which the two phosphorus groups are not equivalent. The equilibrium found between these two carbene complexes **2A** and **2B** in a concentrated solution is independent of the nature of the solvent (CD_3COCD_3, $CDCl_3$) and on the addition of $n\mathrm{Bu_4NCl}$. The equilibrium constant (being the same at different concentrations) fits that of a monomer–dimer equilibrium [Eq. (3), $K=5.5\pm0.5$ mol^{-1}L at 25 °C] and is strongly temperature dependent. This equilibrium is displaced, as expected for entropic reasons, towards the dimer at −40 °C ($K=117\pm10$ mol^{-1}L). The downfield shift of the resonance



(1)

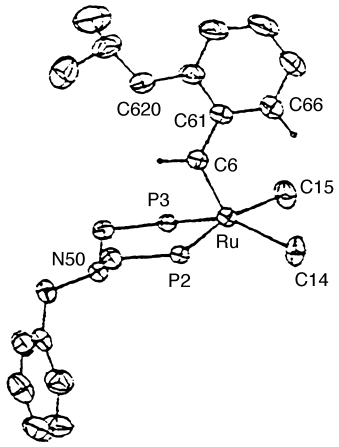
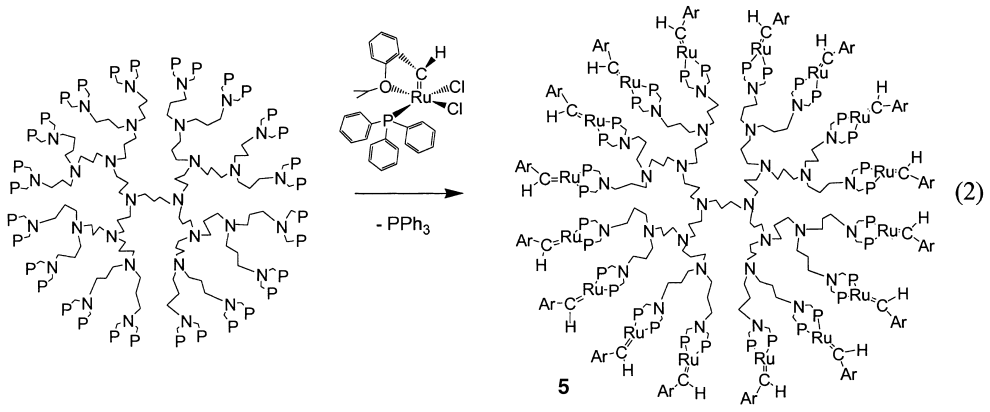


Figure 1. ORTEP diagram of the solid-state structure of **2A** (thermal ellipsoids set at 50% probability). Selected interatomic distances [Å] and angles [°]: Ru···O620, 4.565(2), Ru-P2 2.3211(6), Ru-P3 2.2798(6), Ru-Cl4 2.3889(8), Ru-Cl5 2.3975(8), C6-C61 1.464(4), Ru-C6 1.860(3); Ru-C6-C61 127. The Cy groups are omitted for clarity.



(2)

 © 2003 Wiley-VCH Verlag GmbH & Co. KGaA, Weinheim 1433-7851/03/4204-0453 $ 20.00+.50/0

Table 1: ^{1}H NMR chemical shift and relative intensities for the carbene proton of the monomeric and dimeric forms of **2** and dendritic ruthenium complexes **3**–**5**. The relative intensities are given at two concentrations to show the dilution effect.

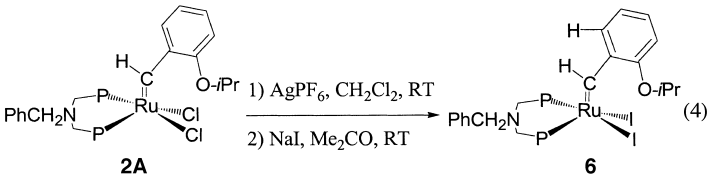
Ru complex	Monomeric form δ[a]	Rel. int.[%][b]	Rel. int.[%][c]	Dimeric form δ[a]	Rel. int.[%][b]	Rel. int.[%][c]
2	15.66	70	56	16.96	30	44
3	15.63	58	87	16.87	42	13
4	15.63	55	81	16.90	45	19
5	15.63	48	77	16.95	52	23

[a] chemical shift δ [ppm] vs $SiMe_4$ in $CDCl_3$ of the carbenic proton. [b] Diluted solution (13 mg Ru complex **2** or 5 mg dendrimer **3**–**5** in 0.3 mL $CDCl_3$). [c] Concentrated solution (34 mg Ru complex **2** or 20 mg dendrimer **3**–**5** in 0.3 mL $CDCl_3$).

signal of the phenyl hydrogen atoms of the carbene ligand found in the ^{1}H NMR spectra of the Grubbs-type complexes[8,11] is not observed in the ^{1}H NMR spectrum of Hoveyda's complex,[4] that is, when the oxygen atom of the aryl ether is coordinated to the Ru atom. This shift is observed for both species of the equilibrium of **2A** and **2B**, which discards the possibility of oxygen coordination. Evidence of similar dimeric Ru–carbene species is also found in the ^{1}H NMR spectrum of **3**, **4**, and **5** ($\delta \approx 16.9$ ppm; Table 1) as a minor signal in addition to the major signal from the monomeric Ru–carbene species ($\delta =$ 15.63 ppm). Remarkably, the intensity of the signal arising from the dimer in the ^{1}H NMR spectrum of the metallodendrimers **3**, **4**, and **5** increases with dilution contrary to that observed for **2** (**2A** + **2B** Table 1). The difference in behavior between the model complex and the dendridrimers implies the two following phenomena: 1) intradendritic dimerization between two branches is dominant over intermolecular dendritic dimerization (which is reasonable for entropic reasons), 2) the conformation of the dendritic branches depends on the concentration so that the branches expand more easily, and so have more freedom to dimerize in dilute solutions than in concentrated solutions.

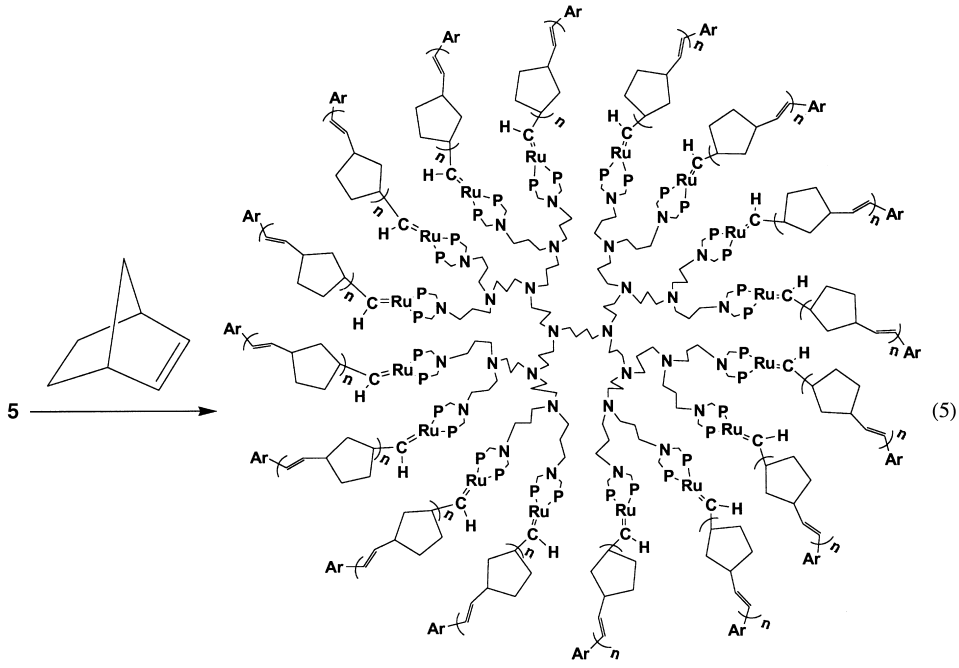
At low temperature (−40 °C), the monomer–dimer equilibrium is not changed, which is not surprising since the entropic factor present for the model is not applicable in the intradendrimer dimerization.

Addition of two equivalents of $AgPF_6$ to a solution of **2** in CH_2Cl_2 at room temperature followed by the addition of NaI in acetone gives the diiodo analogue **6** [Eq. (4)]. Dimerization in concentrated solution also occurs for **6**, and is even more marked (dimerization constant: $K = 20 \pm 2$ mol^{-1} L at 25 °C) than for the dichloro complex **2**. Thus, a new family of ruthenium carbene complexes is accessible using this sequence.



2A 6 (4)

ROMP of norbornene was found to proceed with **2** and the dendritic Ru–carbene complexes **3**–**5** at room temperature [Eq. (5); concentration 1.9×10^{-4} mol L^{-1}], although no coordination site next to the benzylidene ligand is available to generate the active metallacyclobutane intermediate in the ground state of these complexes.[18] Complex **6** is much less reactive than **2** and, for instance, no ROMP activity is observed for **6** at room temperature. These results support the



(5)

 © 2003 Wiley-VCH Verlag GmbH & Co. KGaA, Weinheim 1433-7851/03/4204-0454 $ 20.00+.50/0

idea that the primary coordination of an olefin is disfavored by the increased *trans* effect of iodo substituent (compared to chloro substituent) as shown by Grubbs for his catalyst.[11,18] Remarkably, ROMP proceeds more rapidly with the metallodendritic Ru–carbene complexes than for the monomeric model **2**. For instance, after 3.5 h at 25 °C in $CDCl_3$, the conversions are: **3** (G_1):94 %, >**4** (G_2):65 %, >**5** (G_3):59 %, >**2** (model):traces. A reason for the dramatically increased rate of polymerization with the dendrimers compared to **2** is that the metal–ligand bonds are more labile in the dendrimers because of interbranch collisions of the metal groups. For instance, phosphane dissociation plays an important role in the Grubbs catalyst.[18] More mechanistic and theoretical studies are needed to get a better insight into this phenomenon. Among the dendrimers, it is also interesting that the rate decreases when the generation number is increased. We believe that this negative dendritic effect arises from the increased bulk around the ruthenium centers when the generation number increases, a classic phenomenon in metallodendrimers. Indeed, the solubility of the metallodendritic carbene complex of this series drops at the fourth generation, which is also a sign of steric congestion. On the other hand, the variation of the monomer:dimer ratio upon dendritic generation increase from G_1 to G_3 is very weak and largely insufficient to explain the decrease in polymerization activity.

Gratifyingly, the molar masses of each branch could be determined after cleavage of the metallodendritic cores (Table 2). From this, we checked the number of "arms" in all cases. The fact that the observed number-average molecular weight ($\bar{M}_{n(obs)}$) are similar to the theoretical values is an excellent indication that all the Ru–carbene species of the dendrimers are efficient initiators, that is, they are converted into propagating species yielding metallodendritic stars.

In conclusion, we have synthesized new ruthenium–carbene complexes that have a chelating diphosphane ligand and characterized them thoroughly including by X-ray crystalographic studies, and we have shown that these complexes reversibly dimerize in concentrated solution. Metallodendritic analogues were synthesized for three generations, and the influence of the concentration on their dimerization was shown to be the opposite of that observed for the (nondendritic) complex **2**. This observation is consistent with an essentially intradendritic dimerization that is favored by expansion of the wedges allowed by dilution. ROMP of norbornene is much faster with the metallodendrimers than with the model, probably because interbranch collisions make the metal–ligand bonds more labile, but the polymerization rates decrease as the generation number increases as a result of the inhibiting steric effects. These dendritic effects are of interest, because they play a key role in understanding the chemistry, the catalytic properties, and the physico-chemistry of branched macromolecules.

Table 2: SEC data for the norbornene polymers obtained by cleavage of the metallodendritic stars using ethyl vinyl ether after polymerization with various norbornene (nb):Ru ratios.

Complex	nb:Ru	$\bar{M}_n$ obs[a]	$\bar{M}_w/\bar{M}_n$	$\overline{DP}_n$[a]	conv.[b]	*trans*[c]
2	100:1	5300	2.7	53.2	63	82
3	400:1	8000	3.4	85.1	100	77
4	800:1	9500	3.2	101.1	98	86
5	1600:1	9541	2.2	101.5	98	80

SEC = size exclusion chromatography, [a] Polymerization in $CDCl_3$ (4 mL); $\bar{M}_{n(obs)}$: observed number-averaged molecular weight; $\bar{M}_n$: weight-average molecular weight. $\overline{DP}_n$: average number of norbornene units in the polymer in THF based on polystyrene standard (detector: refraction indice). [b] Conversion [%] determined by ^{1}H NMR spectroscopy. [c] *trans*/*cis* Proportions: *trans* [%] determined by ^{1}H NMR spectroscopy.

Experimental Section

General procedure for the synthesis of the metal–carbene complexes: the mixture of di or dendritic phosphane DAB-dendrimer-$(N(CH_2PCy_2)_2)_{16}$ (DAB = diaminobutane) and $[RuCl_2(=CH\text{-}o\text{-}O\text{-}iPrC_6H_4)PPh_3]$ was stirred at room temperature under nitrogen for 72 h (24 h for the diphosphane). The reaction mixture was concentrated under reduced pressure to about 2 mL, and pentane (20 mL) was added. A green powder precipitated, and was then dried under high vacuum.

2: Yield: 86 %. ^{1}H NMR ($CDCl_3$, 400 MHz): δ = 0.91–2.60 (m, Cy), 1.32 (d, J = 6.5 Hz; $OCH(CH_3)_2$), 2.94 (m; NCH_2P), 3.69 (s; NCH_2Ph), 4.79 (m; $OCH(CH_3)_2$), 6.70–7.63 (m; H arom), 9.33 (d, $^1J_{H,H}$ = 7.2 Hz, 1H; H arom), 9.55 (d, $^1J_{H,H}$ = 7.2 Hz, 2H; H arom.), 15.66 (t, $^3J_{H,P}$ = 15.7 Hz; Ru=CH), 16.96 ppm (t, $^3J_{H,P}$ = 13.3 Hz; Ru=C*H* **2B**). ^{13}C NMR ($CDCl_3$,100 MHz): δ = 22.8 (s; $OCH(CH_3)_2$), 26.3–30.2 (m; Cy), 34.6 (d, $^2J_{C,P}$ = 23.2 Hz; Cy,), 35.4 (t, $^3J_{C,P}$ = 11.6 Hz; NCH_2Ph), 36.6 (d, $^2J_{C,P}$ = 23.2 Hz, Cy), 37.7 (t, $^3J_{C,P}$ = 11.6 Hz; NCH_2Ph), 38.9 (dd, $^1J_{C,P}$ = 52.6 Hz, $^3J_{C,P}$ = 23.2 Hz; Cy), 41.6 (dd, $^1J_{C,P}$ = 154.8 Hz, $^3J_{C,P}$ = 38.7 Hz; Cy), 45.5 (NCH_2P), 69.3 (NCH_2P), 70.0 (s; $OCH(CH_3)_2$), 70.5 (s, $OCH(CH_3)_2$), 112.0, 112.7, 120.7, 122.1, 128.6, 130.5, 131.1, 132.4, 134.0, 134.2, 135.0, 135.4, 135.7, 136.9, 137.2, 140.5, 143.7, 148.1, 150.4 (C arom), 291.5 (t, $^2J_{C,P}$ = 80.1 Hz; Ru=*C*H), 308.8 ppm (t, $^2J_{C,P}$ = 80.1 Hz, Ru=*C*H); ^{31}P{^{1}H,^{13}C} NMR ($CDCl_3$, 81.03 MHz): δ = 40.9 (s; CH_2PCy_2), 36.8, 412 ppm (dd, $^2J_{P,P}$ = 375 Hz, $^4J_{P,P}$ = 45.9 Hz; CH_2PCy_2); concentration of NMR sample: 0.62 mol L^{-1}; mass (*m*/*z*) calcd for $C_{43}H_{67}P_2OCl_2RuN$: 847.92; found: 812.45 (M^+−Cl), elemental analysis calcd (%) for $C_{43}H_{67}P_2OCl_2RuN$: C 60.91, H 7.96; found: C 60.42, H 7.91.

G_1 Ru_4P_8, **3**: Yield: 65 %; ^{1}H NMR ($CDCl_3$, 200 MHz): δ = 0.52–4.14 (m; $OCH(CH_3)_2$, Cy, $NCH_2CH_2CH_2N$, $NCH_2CH_2CH_2CH_2CH_2N$, NCH_2–P), 4.70 (m; $OCH(CH_3)_2$), 6.45–7.88 (m; H arom), 9.40 (d, $^1J_{H,H}$ = 9,1 Hz, 4H, H arom), 9.67 (m; H arom), 15.63 (t, $^3J_{H,P}$ = 15,6 Hz, 4H; Ru=CH monomer), 16.87 (m; Ru=CH dimer). ^{31}P{^{1}H,^{13}C} NMR ($CDCl_3$, 81.03 MHz): δ = 40.9 (s, CH_2PCy_2), 38.6–42,1 (m, not well resolved, CH_2PCy_2);concentration of NMR sample: 2×10^{-2} mol L^{-1}; elemental analysis calcd (%) for $C_{160}H_{272}Cl_8N_6O_4P_8Ru_4$: C 58.59, H 8.36; found: C 57.64, H 8.35.

G_2 Ru_8P_{16}, **4**: Yield: 63 %. ^{1}H NMR ($CDCl_3$, 200 MHz): δ = 0.52–4.15 (m; $OCH(CH_3)_2$, Cy, $NCH_2CH_2CH_2N$, $NCH_2CH_2CH_2CH_2CH_2N$, NCH_2-P), 4.71 (m; $OCH(CH_3)_2$), 6.45–8.07 (m; H arom), 9.40 (d, 8H; H arom), 9.63 (m, 16H; H arom), 15.63 (br., 8H, Ru=CH monomer), 16.90 ppm (br.; Ru=CH dimer). ^{31}P{^{1}H,^{13}C} NMR ($CDCl_3$, 81.03 MHz): δ = 40.89 (s; CH_2PCy_2), 38.6–42,1 (m, not well resolved; CH_2PCy_2);concentration of NMR sample: 1.23×10^{-2} mol L^{-1}; elemental analysis calcd (%) for $C_{328}H_{560}Cl_{16}Ru_8O_8P_{16}N_{14}$: C 58.80, H 8.42; found: C 58.64, H 8.25.

G_3 $Ru_{16}P_{32}$, **5**: Yield: 60 %. ^{1}H NMR ($CDCl_3$, 200 MHz): δ = 0.24–4.25 (m; $OCH(CH_3)_2$, Cy, $NCH_2CH_2CH_2N$, $NCH_2CH_2CH_2CH_2CH_2N$, NCH_2-P), 4.71 (m; $OCH(CH_3)_2$), 6.45–8.07 (m; H arom.), 9.40 (m, 16H; H arom.), 9.63 (m, 32H; H arom.), 15.63 (br., 16H; Ru=CH monomer), 16.95 ppm (br.; Ru=CH dimer). ^{31}P{^{1}H,^{13}C} NMR ($CDCl_3$, 81.0 MHz): δ = 40.9 (s; CH_2PCy_2), 38.6–42,1 (m, not well resolved; CH_2PCy_2); concentration of NMR sample: 5.0×10^{-3} mol L^{-1}; ele-

mental analysis calcd (%) for $C_{664}H_{1136}Cl_{32}Ru_{16}O_{16}P_{32}N_{30}$: C 58.90, H 8.46; found: C 58.73, H 8.61.

Received: July 9, 2002
Revised: September 30, 2002 [Z19698]

[1] G. R. Newkome, C. N. Moorefield, F. Vögtle, *Dendrimers and Dendrons, Concepts, Synthesis and Applications*, VCH-Wiley, Weinheim, **2001**.
[2] a) M. R. Leduc, C. J. Hawker, J. Dao, J. M. J. Fréchet, *J. Am. Chem. Soc.* **1996**, *118*, 11111; b) I. Gitsov, P. T. Ivanova, J. M. J. Fréchet, *Macromol. Rapid Commun.* **1994**, *15*, 387.
[3] E. Cloutet, J.-L. Fillaut, Y. Gnanou, D. Astruc, *J. Chem. Soc. Chem. Commun.* **1994**, 2433.
[4] S. B. Garber, J. S. Kingsbury, B. L. Gray, A. H. Hoveyda, *J. Am. Chem. Soc.* **2000**, *122*, 8168.
[5] P. Wijkens, J. T. B. H. Jastrzebski, P. A. van der Schaaf, R. Kolly, A. Hafner, G. van Koten, *Org. Letters* **2000**, *2*, 1621.
[6] a) H. Beerens, F. Verpoort, L. Verdonck *J. Mol. Catal.* **2000**, *151*, 279; b) H. Beerens, F. Verpoort, L. Verdonck *J. Mol. Catal.* **2000**, *159*, 197.
[7] Metal–carbene complexes in catalysis: a) K. H. Doetz, *Transition Metal Carbene Complexes*, Verlag Chemie, Weinheim, **1983**; b) M. Brookhart, W. B. Studabaker, *Chem. Rev.* **1987**, *87*, 411; c) K. J. Ivin, J. C. Mol, *Olefin Metathesis and Metathesis Polymerization*, Academic Press, San Diego, **1997**; d) R. R. Schrock, J. S. Murdzek, G. C. Bazan, J. Robbins, M. DiMare, M. O'Regan, *J. Am. Chem. Soc.* **1990**, *112*, 8378; e) J. P. A. Harrity, M. S. Visser, J. D. Gleason, A. H. Hoveyda, *J. Am. Chem. Soc.* **1997**, *119*, 1488; f) R. H. Grubbs, S. Chang, *Tetrahedron* **1998**, *54*, 4413; g) *Alkene Metathesis in Organic Synthesis*, (Ed.: A. Fürstner), Springer, Berlin, **1998**; h) J. Kingsbury, J. P. A. Harrity, P. J. Bonitatebus, A. H. Hoveyda, *J. Am. Chem. Soc.* **1999**, *121*, 791; i) A. Fürstner, *Angew. Chem.* **2000**, *112*, 3140; *Angew. Chem. Int. Ed.* **2000**, *39*, 3012.
[8] Grubbs ruthenium–carbene catalysts of olefin-metathesis including ROMP and RCM: a) S. T. Nguyen, R. H. Grubbs, J. W. Ziller, *J. Am. Chem. Soc.* **1993**, *115*, 9858; b) P. Schwab, R. H. Grubbs, J. W. Ziller, *J. Am. Chem. Soc.* **1996**, *118*, 100; c) T. M. Trnka, R. H. Grubbs, *Acc. Chem. Res.* **2001**, *34*, 18.
[9] Reviews on dendritic catalysts: a) G. E. Oosterom, J. N. H. Reek, P. C. J. Kamer, P. W. N. M. van Leeuwen, *Angew. Chem.* **2001**, *113*, 1878; *Angew. Chem. Int. Ed.* **2001**, *40*, 1828; b) R. Kreiter, A. W. Kleij, R. J. M. Klein Gebbink, G. van Koten, *Top. Curr. Chem.*, **2001**, *217*, 163; c) D. Astruc, F. Chardac, *Chem. Rev.* **2001**, *101*, 2991.
[10] Comprehensive reviews on metallodendrimers: a) G. R. Newkome, E. He, C. N. Moorefield, *Chem. Rev.* **1999**, *99*, 1689; b) H. M. Janssen, E. W. Meijer, *Chem. Rev.* **1999**, *99*, 1665; c) I. Cuadrado, M. Morán, C. M. Casado, B. Alonso, J. Losada, *Coord. Chem. Rev.* **1999**, *189*, 123; d) M. A. Hearshaw, J. R. Moss, *Chem. Commun.* **1999**, 1. See also reference [9].
[11] P. Schwab, M. B. France, J. W. Ziller, R. H. Grubbs, *Angew. Chem.* **1995**, *107*, 2179; *Angew. Chem. Int. Ed. Engl.* **1995**, *34*, 2039.
[12] S. M. Hansen, M. A. O. Volland, F. Rominger, F. Eisenträger, P. Hofmann, *Angew. Chem.* **1999**, *111*, 1360; *Angew. Chem. Int. Ed.* **1999**, *38*, 1273; S. Hansen, F. Rominger, M. Metz, P. Hofmann, *Chem. Eur. J.* **1999**, *5*, 557; C. Adlhart, M. A. O. Volland, P. Hofmann, P. Chen, *Helv. Chim. Acta* **2000**, *83*, 3306.
[13] D. Amoroso, D. E. Fogg, *Macromolecules* **2000**, *33*, 2815.
[14] C. Six, K. Beck, A. Wegner, W. Leitner, *Organometallics* **2000**, *19*, 4639.
[15] M. T. Reetz, G. Lohmer, R. Schwickardi, *Angew. Chem.* **1997**, *109*, 1529; *Angew. Chem. Int. Ed. Engl.* **1997**, *36*, 1526.
[16] E. Alonso, D. Astruc, *J. Am. Chem. Soc.* **2000**, *122*, 3222.
[17] Single crystals of **2A** from CH_2Cl_2/pentane at 4 °C; monoclinic; space group $P2_1/c$; $a = 25.0209(4)$, $b = 9.3092(1)$, $c = 18.5033(2)$ Å; $\beta = 93.8485(5)°$; $V = 4300.2(2)$ Å^3, $\rho_{calcd} = 1.304$ mg m^{-3} for $Z = 4$; $R_1 = 0.034$; $wR_2 = 0.105$; $R_{int} = 0.0235$. CCDC-194781 (**2A**) contains the supplementary crystallographic data for this paper. These data can be obtained free of charge via www.ccdc.cam.ac.uk/conts/retrieving.html (or from the Cambridge Crystallographic Data Centre, 12 Union Road, Cambridge CB21EZ, UK; fax: (+44) 1223-336-033; or deposit @ccdc.cam.ac.uk).
[18] M. S. Sanford, M. Ulman, R. H. Grubbs, *J. Am. Chem. Soc.* **2001**, *123*, 749.

Concentration Affects NLO Behavior

Large, Concentration-Dependent Enhancement of the Quadratic Hyperpolarizability of $[Zn(CH_3CO_2)_2(L)_2]$ in $CHCl_3$ on Substitution of Acetate by Triflate**

Francesca Tessore, Dominique Roberto, Renato Ugo, Patrizia Mussini, Silvio Quici, Isabelle Ledoux-Rak, and Joseph Zyss*

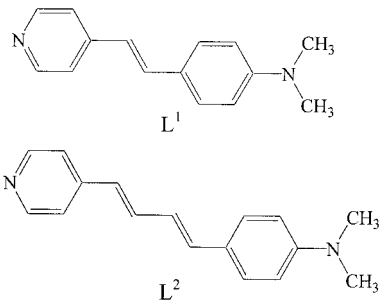
Organometallic and coordination compounds can offer a great diversity of tunable electronic properties that act on their second-order nonlinear optical (NLO) response.[1] The quadratic hyperpolarizability, measured by the electric field

[*] Prof. D. Roberto, Dr. F. Tessore, Prof. R. Ugo
Dipartimento di Chimica Inorganica Metallorganica e Analitica dell'Università di Milano
INSTM UdR di Milano and
Istituto di Scienze e Tecnologie Molecolari del CNR (ISTM)
Via G. Venezian, 21, 20133 Milano (Italy)
Fax: (+39) 02-5031-4405
E-mail: dominique.roberto@unimi.it
Prof. P. Mussini
Dipartimento di Chimica Fisica ed Elettrochimica dell'Università di Milano
Via G. Venezian, 21, 20133 Milano (Italy)
Dr. S. Quici
Istituto di Scienze e Tecnologie Molecolari del CNR (ISTM)
Via C. Golgi 19, 20133 Milano (Italy)
Prof. I. Ledoux-Rak, Prof. J. Zyss
LPQM, Ecole Normale Supérieure de Cachan
61 avenue du Président Wilson, 94230 Cachan (France)

[**] L = 4,4′-*trans*-$NC_5H_4(CH{=}CH)C_6H_4NMe_2$ or *trans*,*trans*-$NC_5H_4(CH{=}CH)_2C_6H_4NMe_2$. This work was supported by the MIUR and by the CNR (Progetto Finalizzato Materiali Speciali per Tecnologie Avanzate II, year 2000, Research Title: *Sintesi e sviluppo di composti molecolari organometallici e di coordinazione con proprietà di ottica non lineare (NLO) e con proprietà elettriche anisotropiche e isotropiche*).

 © 2003 Wiley-VCH Verlag GmbH & Co. KGaA, Weinheim 1433-7851/03/4204-0456 $ 20.00+.50/0

induced second harmonic (EFISH) generation technique,[2] of push–pull stilbazole ligands such as 4,4′-*trans* or *trans*,*trans*-$NC_5H_4(CH{=}CH)_nC_6H_4NMe_2$ ($n = 1$ and 2 for $L = L^1$ and L^2, respectively) usually increases on coordination to various acceptor centers.[3] According to both theoretical[3b] and



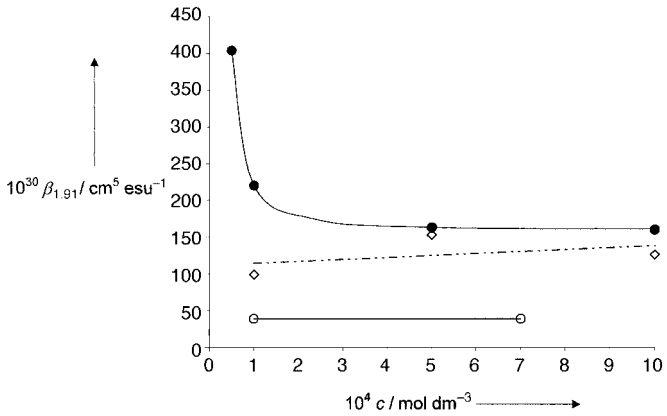


Figure 1. Dependence of $\beta_{1.91}$ on concentration for $[Zn(CH_3COO)_2L_2^1]$ (○), $[Zn(CF_3SO_3)_2L_2^1]$ (●), and NPP (reference; ◇) in anhydrous $CHCl_3$.

solvatochromic[3e] investigations, this enhancement mainly originates from the red shift of the intraligand charge transfer (ILCT) n→π* transition, which is often controlled by the increased Lewis acceptor properties of the metal atom[3d] and therefore by the ancillary ligands that tune these properties.[3e] However, up to now the effect of a very strong electron-withdrawing ancillary ligand such as the triflate anion has not been investigated.

A large enhancement of the dipole moment μ of $[ZnX_2L_2]$ complexes ($X = CH_3CO_2$, CF_3CO_2, CF_3SO_3) in anhydrous $CHCl_3$[4] occurs on coordination of the triflate ligand, together with a red shift of the ILCT transition of the stilbazoles L^1 or L^2 that is much larger ($\Delta\lambda_{max} = 116$–$123$ nm) than usually occurs on coordination to "$Zn(CH_3CO_2)_2$" or "$ZnCl_2$" ($\Delta\lambda_{max} = 2$–36 nm, Table 1)[3e] or, despite the well-known positive effect of chelation,[3e] on coordination to the Zn^{II} complexes of electronically related chelating ligands such as 4-dialkylaminostyryl-2,2′-bipyridine (59–72 nm)[5a,b] or 4,4′-bis(dialkylaminophenylazo)-2,2′-bipyridine and 4,4′-bis(dialkylaminophenylimino)-2,2′-bipyridine ($\Delta\lambda_{max} = 45$–58 nm).[5c] Consistent with such a large red shift, the quadratic hyperpolarizability $\beta_{1.91}$, measured in anhydrous $CHCl_3$ at an incident wavelength of 1.907 μm by the EFISH technique,[2] of $[Zn(CF_3SO_3)_2L_2]$ ($L = L^1$, L^2) complexes is much higher than that of related Zn^{II} complexes with Cl, CH_3CO_2, and CF_3CO_2 ancillary ligands (Table 1).[3e] This increase in the second-order NLO response is far higher than those reported up to now for the coordination of these push–pull stilbazoles to various metal centers or even to the very strong Lewis acid BF_3.[3a–e]

Surprisingly, the $\beta_{1.91}$ value of these triflate complexes is dependent on concentration (Table 1). At concentrations below about 10^{-4} M, it increases abruptly with decreasing concentration, and reaches very large values (Figure 1), an effect that is not observed for the acetate or trifluoroacetate complexes (Table 1). This large increase does not result from inappropriate EFISH measurements owing to high dilution, since $\beta_{1.91}$ of *N*-(4-nitrophenyl)-L-prolinol (NPP), taken as reference and measured under the same conditions by the EFISH technique,[2] remains unchanged even at a concentration of 10^{-4} M (Figure 1).

Given the weak nucleophilicity of the triflate anion, these results could be explained by some solvolysis of strong ion pairs, as suggested by the fact that it was not possible to carry out EFISH[2] or capacitance measurements[4] when $CHCl_3$ was not completely anhydrous, because traces of water lead to dissociation of strong ion pairs into ionic species which hinder EFISH and capacitance measurements. Careful investigations of the electrical conductivity of anhydrous $CHCl_3$ solutions (Figure 2) of $[ZnX_2L_2]$ complexes ($X = CH_3CO_2$, CF_3CO_2, CF_3SO_3) are in agreement with this proposal. According to Figure 2, both $[Zn(CH_3CO_2)_2L_2^1]$ and $[Zn(CH_3CO_2)_2L_2^2]$ are practically undissociated in the concentration range 10^{-3}–10^{-4} M, while the complexes with the triflate ligand show a slightly higher conductivity, but much lower than that of reference ionic species such as tetrabutylammonium triflate and acetate. The conductivities of these two salts are comparable, so that we can safely assume that in anhydrous $CHCl_3$ both triflate and acetate anions have comparable ionic mobilities.

Table 1: Electronic spectra, dipole moments, and $\beta_{1.91}$ values of various $[ZnX_2L_2^1]$ and $[ZnX_2L_2^2]$ complexes ($X = CH_3CO_2$, CF_3CO_2, CF_3SO_3).

Complex	$10^4 c$ [M]	λ_{max} [nm][a]	μ [D][a]	$10^{30}\mu\beta_{1.91}$ [D cm^5 esu^{-1}][a]	$10^{30}\beta_{1.91}$ [cm^5 esu^{-1}][a]	EF[b]
$[Zn(CH_3CO_2)_2L_2^1]$	1–7	376[3e]	8.0[3e]	316	39	–
$[Zn(CF_3CO_2)_2L_2^1]$	1–7	420[3e]	10.5[3e]	512	49	1.3
$[Zn(CF_3SO_3)_2L_2^1]$	10	490	16.7	2715	163	4.2
	5			2720	163	4.2
	1			3670	220	5.6
	0.5			6750	404	10.4
$[Zn(CH_3CO_2)_2L_2^2]$	1–7	406	6.7	680	101	–
$[Zn(CF_3SO_3)_2L_2^2]$	7	519	14.7	3840	261	2.6
	1			6100	415	4.1

[a] In anhydrous chloroform. [b] EF is $\beta_{1.91}$ enhancement factor with respect to the related $[Zn(CH_3CO_2)_2L_2]$ complex, that is, $\beta_{1.91}([ZnX_2L_2])/\beta_{1.91}([Zn(CH_3CO_2)_2L_2])$.

 © 2003 Wiley-VCH Verlag GmbH & Co. KGaA, Weinheim 1433-7851/03/4204-0457 $ 20.00+.50/0

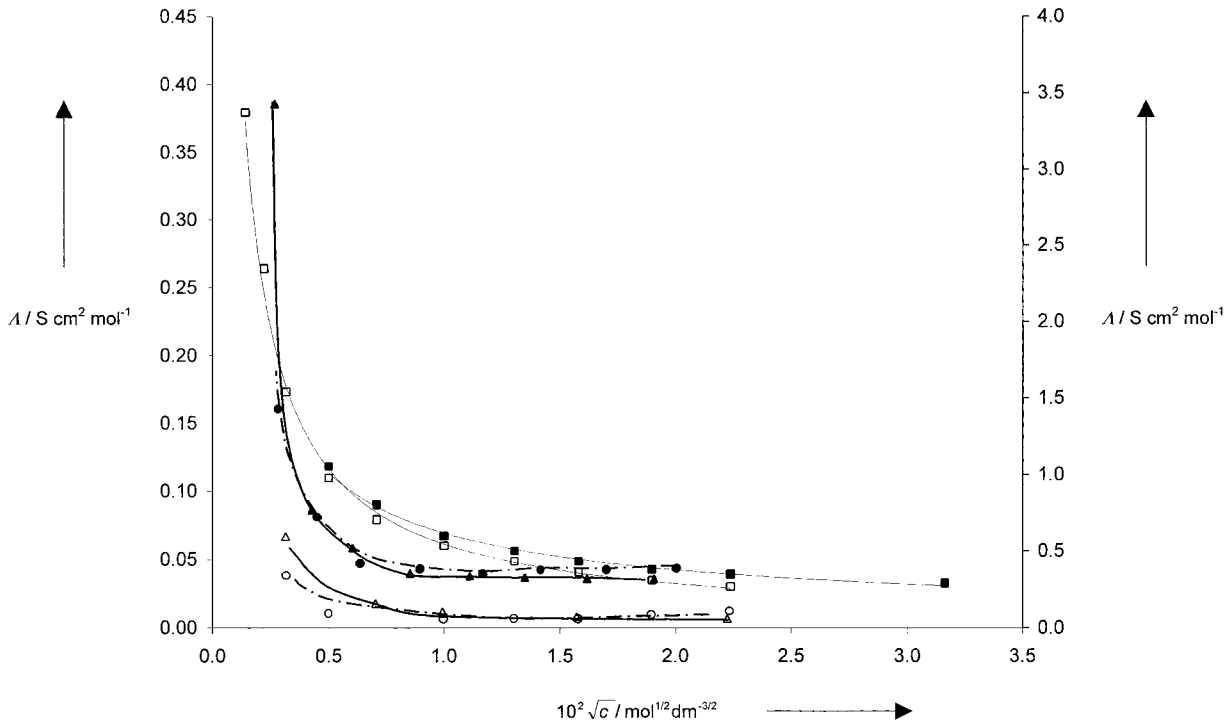


Figure 2. Dependence of molar conductances Λ of zinc acetate and triflate complexes of ligands L^1 and L^2 (left y axis) and of tetrabutylammonium acetate and triflate salts (right y axis) on the square root of the concentration c in anhydrous $CHCl_3$ at 298 K. ○ = $[Zn(CH_3COO)_2L^1_2]$, △ = $[Zn(CH_3COO)_2L^2_2]$, ● = $[Zn(CF_3SO_3)_2L^1_2]$, ▲ = $[Zn(CF_3SO_3)_2L^2_2]$; □ = $[Bu_4N]CH_3COO$, ■ = $[Bu_4N]CF_3SO_3$.

Therefore, the slight but significant conductivity enhancement observed on passing from acetate to triflate ancillary ligands (Figure 2) confirms the hypothesis of some solvolysis of the triflate anion with concomitant strong ion pairing. Strong ion pairing in anhydrous $CHCl_3$ was already proposed to explain the significant second-order NLO response, measured by the EFISH technique,[2] for the iodide salt of the alkylated cation of 4,4′-*trans*-$NC_5H_4CH{=}CHC_6H_4NBu_2$.[6] Accordingly, the sharp conductivity increase towards limiting values for triflate complexes at concentrations below 10^{-4} M indicates a sharp increase in the degree of ionization, as expected for increased dissociation of ion pairs with increasing dilution. It is noteworthy that the molar conductivity versus concentration trend (Figure 2) is similar to that of $\beta_{1.91}$ versus concentration (Figure 1). Therefore, the large increase in $\beta_{1.91}$ at very low concentrations must be attributed to increased dissociation of strong ion pairs owing to solvolysis of the triflate ligand.

Nevertheless, the $\beta_{1.91}$ values of $[Zn(CF_3SO_3)_2L_2]$ complexes at concentrations above 10^{-4} M are already three to six times higher than those of the related acetate or trifluoroacetate complexes (Table 1). This unusual result supports a mechanism for increasing the positive charge on the stilbazole system, such as ion pairing, which should favor the unusually high red shift of their ILCT transitions. In fact this increase cannot be explained solely by the stronger inductive electron-withdrawing effect of triflate relative to trifluoroacetate. Consequently, an increased concentration (albeit still very low, because the EFISH measurement is possible) of the free cation $[Zn(CF_3SO_3)L_2]^+$, which, as expected for a localized positive charge, must have a very high $\beta_{1.91}$ value, is the origin of the large $\beta_{1.91}$ value at high dilution.

A possible general role of the triflate ligand in increasing the quadratic hyperpolarizability, measured in anhydrous $CHCl_3$ solution, of complexes of ligands L^1 or L^2 with other metals or of Zn^{II} complexes with chelating nitrogen-donor π-delocalized ligands[3e,5] is under investigation, as is the effect on the second-order NLO response of Zn^{II} complexes of ligands L^1 or L^2 and less strongly electron withdrawing sulfonated ancillary ligands, to determine whether the strong increase in the quadratic hyperpolarizability results only from the sulfonate nature of the ligand, or whether it also requires a strongly electron-withdrawing CF_3 group. Although the concentration used for the experimental determination of the quadratic hyperpolarizability is traditionally not reported, probably because it is a molecular property which should not vary with concentration, here we have provided clear evidence that quadratic hyperpolarizabilities can be strongly concentration dependent.

Experimental Section

Complexes $[ZnX_2L_2]$ ($X = CH_3CO_2$, CF_3CO_2, CF_3SO_3; $L = L^1$ or L^2) were prepared[3e] by allowing a stoichiometric mixture of $ZnX_2{\cdot}x\,H_2O$ (kept under vacuum at 100 °C for 3 h) and L in CH_2Cl_2 to stir at room temperature in the dark for 3 h. Removal of the solvent under vacuum and recrystallization from dichloromethane/pentane afforded the complexes, which were stored under N_2 in the dark and characterized by elemental analysis, ^{1}H NMR spectroscopy, and mass spectrometry (FAB +). EFISH measurements[3d,e] were carried out in anhydrous $CHCl_3$ (purchased from Fluka and used without further

 © 2003 Wiley-VCH Verlag GmbH & Co. KGaA, Weinheim 1433-7851/03/4204-0458 $ 20.00+.50/0

treatment) at an incident wavelength of 1.907 μm. Dipole moments μ were determined in anhydrous $CHCl_3$ by the Guggenheim method.[4] All solutions for EFISH, conductivity, and capacitance measurements were used immediately after preparation.

Received: August 2, 2002 [Z19874]

[1] a) N. J. Long, *Angew. Chem.* **1995**, *107*, 37 – 55; *Angew. Chem. Int. Ed. Engl.* **1995**, *34*, 21 – 38; b) *Optoelectronic Properties of Inorganic Compounds* (Eds.: D. M. Roundhill, J. P. Fackler, Jr.), Plenum, New York, **1999**; c) J. Heck, S. Dabek, T. Meyer-Friedrichsen, H. Wong, *Coord. Chem. Rev.* **1999**, *190–192*, 1217 – 1254; d) H. Le Bozec, T. Renouard, *Eur. J. Inorg. Chem.* **2000**, 229 – 239; e) P. G. Lacroix, *Eur. J. Inorg. Chem.* **2001**, 339 – 348; f) S. Di Bella, *Chem. Soc. Rev.* **2001**, *30*, 355 – 366.

[2] a) B. F. Levine, C. G. Bethea, *Appl. Phys. Lett.* **1974**, *24*, 445 – 447; b) J. L. Oudar, *J. Chem. Phys.* **1977**, *67*, 446 – 457; c) K. D. Singer, A. F. Garito, *J. Chem. Phys.* **1981**, *75*, 3572 – 3580; d) I. Ledoux, J. Zyss, *Chem. Phys.* **1982**, *73*, 203 – 213.

[3] a) D. W. Bruce, A. Thornton, *Mol. Cryst. Liq. Cryst.* **1993**, *231*, 253 – 256; b) D. R. Kanis, P. G. Lacroix, M. A. Ratner, T. J. Marks, *J. Am. Chem. Soc.* **1994**, *116*, 10089 – 10102; c) M. J. G. Lesley, A. Woodward, N. J. Taylor, T. B. Marder, I. Cazenobe, I. Ledoux, J. Zyss, A. Thornton, D. W. Bruce, A. K. Kakkar, *Chem. Mater.* **1998**, *10*, 1355 – 1365; d) D. Roberto, R. Ugo, S. Bruni, E. Cariati, F. Cariati, P. C. Fantucci, I. Invernizzi, S. Quici, I. Ledoux, J. Zyss, *Organometallics* **2000**, *19*, 1775 – 1788; e) D. Roberto, R. Ugo, F. Tessore, E. Lucenti, S. Quici, S. Vezza, P. C. Fantucci, I. Invernizzi, S. Bruni, I. Ledoux-Rak, J. Zyss, *Organometallics* **2002**, *21*, 161 – 170.

[4] a) E. A. Guggenheim, *Trans. Faraday Soc.* **1949**, *45*, 714 – 720; b) H. B. Thompson, *J. Chem. Educ.* **1966**, *43*, 66 – 73.

[5] a) M. Bourgault, C. Mountassir, H. Le Bozec, I. Ledoux, G. Pucetti, J. Zyss, *J. Chem. Soc. Chem. Commun.* **1993**, 1623 – 1624; b) M. Bourgault, K. Baum, H. Le Bozec, G. Pucetti, I. Ledoux, J. Zyss, *New J. Chem.* **1998**, 517 – 522; c) A. Hilton, T. Renouard, O. Maury, H. Le Bozec, I. Ledoux, J. Zyss, *Chem. Commun.* **1999**, 2521 – 2522.

[6] V. Alain, M. Blanchard-Desce, I. Ledoux-Rak, J. Zyss, *Chem. Commun.* **2000**, 353 – 354.

Stereoselective Glycosylations

Dual Stereoselectivity of 1-(2′-Carboxy)benzyl 2-Deoxyglycosides as Glycosyl Donors in the Direct Construction of 2-Deoxyglycosyl Linkages**

Kwan Soo Kim, Jin Park, Yong Joo Lee, and Yong Sung Seo*

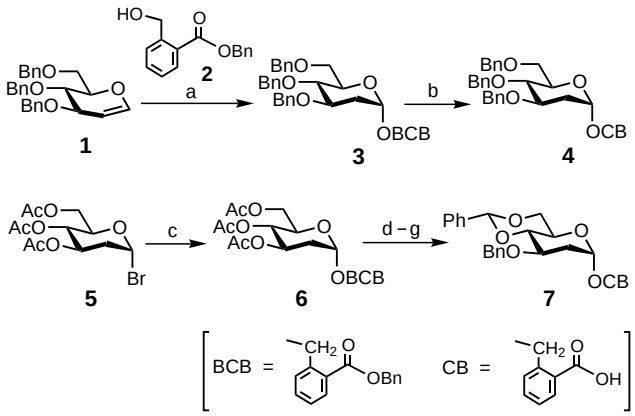
2-Deoxyglycosides are found as the integral part of many important natural products.[1] The stereocontrolled construction of 2-deoxyglycosyl linkages is more challenging than that of usual glycosyl linkages as the 2-deoxyglycosyl donors lack the stereodirecting substituent at C2 and the resulting glycosides are more acid-labile. Although the synthesis of 2-deoxy-α-glycopyranosides is relatively easier, the construction of 2-deoxy-β-glycopyranosyl linkages is a far more challenging problem[2] as the axial addition of a glycosyl acceptor to the oxocarbenium ion intermediate is a favorable process owing to the anomeric effect.[3] Therefore, the frequently used method for the synthesis of 2-deoxy-β-glycopyranosides employs the glycosyl donors with equatorial heteroatom substituents at C2 that can participate during glycosylation to direct the incoming acceptor to the β-face and are removed at a later stage.[4] Nevertheless, a direct and efficient method for the construction of the 2-deoxy-β-glycopyranosyl linkage by using a 2-deoxyglycopyranosyl donor would be more efficient and practical than the indirect methods. Although a few methods (e.g. glycosylation mediated by silver silicate[5] or silver zeolite,[6] the 2-deoxyglycosyl phosphite/TMSOTf (TMSOTf = trimethylsilyl trifluoromethanesulfonate) method,[7] and the glycosylation of 2-deoxyglycosyl fluoride with TiF_4[8] or $SnCl_2$,[9]) have been devised, the direct synthesis of 2-deoxy-β-glycopyranosides from 2-deoxyglycosyl donors still remains a difficult task. We have previously introduced (2′-carboxy)benzyl (CB) glycosides as glycosyl donors for the efficient β-mannopyranosylation.[10] We applied this CB glycoside methodology to the direct synthesis of 2-deoxyglycopyranosides and herein report the preparation of CB 2-deoxyglycosides from glycals and their α- or β-stereoselectivity (dual stereoselectivity) as glycosyl donors in the glycosylation reaction, depending on their protecting groups.

CB 2-deoxyglucoside **4** was readily obtained from the tribenzylglucal **1** as shown in Scheme 1. CB 4,6-*O*-benzylidene-2-deoxyglucoside **7**, on the other hand, was prepared from a 3,4,6-tri-*O*-acetyl-D-glucal via 2-deoxyglycosyl bromide **5**.[13] Glycosylations of the CB 2-deoxyglycosyl donors **4** and **7** were performed with primary alcohol acceptors **8**–**12** and with secondary alcohol acceptors **13**–**17**. Glycosylation of the benzyl-protected donor **4** with primary alcohol acceptors

[*] Prof. Dr. K. S. Kim, J. Park, Y. J. Lee, Y. S. Seo
Department of Chemistry, Yonsei University
Seoul 120-749 (Korea)
Fax: (+82) 2-364-7050
E-mail: kwan@yonsei.ac.kr

[**] This work was supported by a grant from KOSEF-CMDS (Center for Molecular Design and Synthesis).

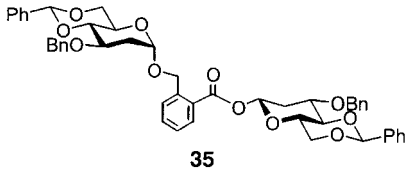
 © 2003 Wiley-VCH Verlag GmbH & Co. KGaA, Weinheim 1433-7851/03/4204-0459 $ 20.00+.50/0



Scheme 1. Synthesis of CB 2-deoxyglycosides **4** and **7**: a) **2** (2.5 equiv), $Ph_3P{\cdot}HBr$[11] (0.05 equiv), 0→40 °C, 1 h, 89%; b) H_2, Pd/C (10%), NH_4OAc[12] (3.5 equiv), MeOH, 1 h, 90%; c) **2** (1.2 equiv), $Hg(CN)_2$, $HgBr_2$, CH_3CN, molecular sieves (4 Å), 0 °C, 20 min, 90%; d) NaOMe, MeOH, 20 min; e) $PhCH(OMe)_2$, CSA, DMF, 50 °C, 1 h, 90% over two steps; f) BnBr, NaH, DMF, 1 h, 84%; g) same as b), 92%. CSA = (±)-camphorsulfonic acid, DMF = *N*,*N*-dimethylformamide, Bn = benzyl.

8–**12** exhibited no significant stereoselectivity (Table 1, entries 1–5). For example, the dropwise addition of Tf_2O (1.2 equiv) to a stirred solution of **4** (1.0 equiv), the acceptor **8** (1.5 equiv), and 2,6-di-*tert*-butyl-4-methylpyridine (DTBMP, 2.4 equiv) in CH_2Cl_2 at −78 °C for 1 h led to the isolation of equal amounts of α- and β-disaccharides **18** in 98% yield (Table 1, entry 1). Some β-selectivity was observed when primary alcohols **10** (α/β 1:1.2), **11** (α/β 1:1.5), and **12** (α/β 1:1.7) were employed as the glycosyl acceptors (Table 1, entries 3–5). On the other hand, glycosylation of **4** with secondary alcohol donors **13**–**15** afforded the α-disaccharides exclusively (Table 1, entries 6–8) and with the secondary alcohol **16** afforded predominantly the α-disaccharide **26** (α/β 9.4:1; Table 1, entry 9).

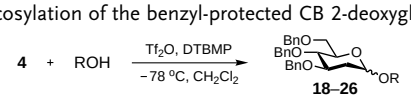
Under the same reaction conditions, glycosylation of the benzylidene-protected donor **7** with primary alcohol acceptors **8** and **9** provided a mixture of almost equal amounts of α- and β-anomers of disaccharides **27** (α/β 1:1) and **28** (α/β 1:1.2), respectively, together with a minor amount of the self-condensed ester **35**, which must be derived from two



35

molecules of the glycosyl donor **7** (Table 2, entries 1 and 2). When primary alcohols **11** and **12** were used as glycosyl acceptors, the ratio of the resulting disaccharides increased substantially in favor of the β-anomer; α/β 1:2 for **29** and 1:5.1 for **30** (Table 2, entries 3 and 4). The highly β-selective glycosylation of **7** could be carried out with secondary alcohol acceptors. Thus, the β/α ratio in the reactions of **7** with acceptors **13** and **15** was 10:1 and that with **17** was 8:1

Table 1: Glycosylation of the benzyl-protected CB 2-deoxyglycoside **4**.



18–**26**

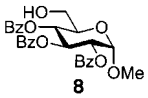
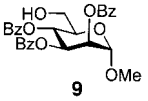
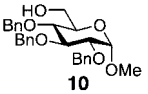
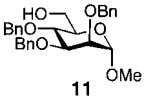
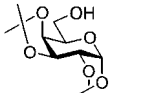
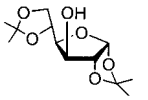
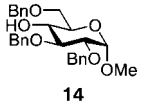
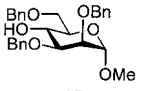
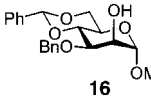
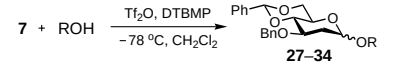
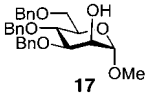
Entry	ROH	Product	Yield [%]	Ratio [α/β]
1	 **8**	**18**	98	1:1
2	 **9**	**19**	93	1:1
3	 **10**	**20**	94	1:1.2
4	 **11**	**21**	78	1:1.5
5	 **12**	**22**	93	1:1.7
6	 **13**	**23**	91	α only
7	 **14**	**24**	91	α only
8	 **15**	**25**	88	α only
9	 **16**	**26**	94	9.4:1

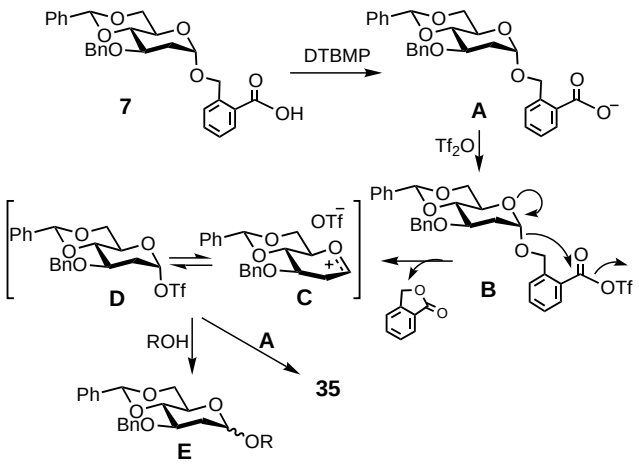
Table 2: Glycosylation of the benzylidene-protected CB 2-deoxyglycoside **7**.



27–**34**

Entry	ROH	Product	Yield [%]	Ratio [α/β]	Ester **35** [%]
1	**8**	**27**	92	1:1	8
2	**9**	**28**	80	1:1.2	16
3	**11**	**29**	83	1:2	14
4	**12**	**30**	85	1:5.1	12
5	**13**	**31**	76	1:10	14
6	**14**	**32**	72	β only	16
7	**15**	**33**	78	1:10	16
8	 **17**	**34**	71	1:8	17

 © 2003 Wiley-VCH Verlag GmbH & Co. KGaA, Weinheim 1433-7851/03/4204-0460 $ 20.00+.50/0



Scheme 2. Plausible mechanism for the formation of disaccharides and the self-condensed ester **35**.

(Table 2, entries 5, 7, and 8). Glycosylation of **7** with **14**, on the other hand, afforded the β-anomer of disaccharide **32** exclusively (Table 2, entry 6) in 72% yield along with the self-condensed ester **35** in 16% yield.

Formation of the self-condensed ester **35** probably resulted from the coupling between the carboxylate anion **A**, which was generated by deprotonation of **7** by DTBMP, and the oxocarbenium ion **C** or the C-1 triflate intermediate **D** as shown in Scheme 2. Generation of a substantial amount of ester **35** led us to postulate that the conversion of the carboxylate **A** into the triflate **B** was slower than the formation of **C** or **D** by the lactonization of the mixed anhydride **B**. We envisaged that if the conversion rate of **A** into **B** was enhanced or the concentration of **A** was kept at a minimum during the glycosylation, the formation of the ester **35** would be suppressed. We therefore ran several glycosylation reactions under modified conditions. Other bases such as triethylamine, pyridine, and 4-dimethylaminopyridine were rather detrimental to the glycosylation reaction, whereas a three- to fivefold excess of the glycosyl acceptor did not decrease the amount of the ester **35**. On the other hand, slow addition of either the glycosyl donor **7** or DTBMP to the mixture of all other reactants greatly affected the course of the reaction to give only the disaccharide without the formation of the ester **35**, although the α/β selectivity was lost. For example, slow addition of the donor **7** to a solution of the acceptor **13**, DTBMP, and Tf_2O in CH_2Cl_2 at −78 °C afforded only the disaccharide **31** (α/β 1:1.5) in 92% yield, whereas slow addition of DTBMP to a solution of **7**, **13**, and Tf_2O in CH_2Cl_2 at −78 °C gave exclusively **31** (α/β 1:1) in 90% yield.

Complete reversal of the stereoselectivity from α to β simply by changing the protecting group of the 2-deoxyglycosyl donor from a benzyl to a benzylidene in the present glycosylation reaction is unprecedented. The precise mechanistic details underlying this reversal of selectivity and the lack of selectivity with primary alcohol acceptors are not yet clear. Nevertheless, it is quite reasonable to assume that in the glycosylation of the benzylidene-protected CB 2-deoxyglycoside **7** with secondary alcohols, the β-disaccharides were formed by S_N2-like displacement of the α-triflate **D** (or a tight ion pair) by the acceptor alcohol ROH (Scheme 2). In this case, the equilibrium might highly favor the α-triflate **D** over the oxocarbenium ion **E** owing to the 4,6-*O*-benzylidene protective group. Previously, highly β-selective mannopyranosylations with 4,6-*O*-benzylidene-protected mannosyl donors have been reported[10,14] and the S_N2-like displacement of the α-triflate by the acceptor has been suggested for the β-selectivity by Crich and Sun.[15] No or poor β-selectivity in the reaction of **7** with primary alcohols might be interpreted by assuming that more reactive primary alcohols reacted with both the α-triflate **D** and the oxocarbenium ion **C** (Scheme 2) before the equilibrium was established. In this respect, it is also noteworthy that the more hindered primary alcohol donor **13** showed a substantial β-selectivity (α/β 1:5.1). The α-selectivity in the glycosylation of the benzyl-protected CB 2-deoxyglycoside **4** with secondary alcohols might be explained if the β-triflate exists in equilibrium. It has been suggested that the α-glucoside was formed by the S_N2-like displacement of the β-halide[16] found in equilibrium and was less stable but more reactive than the corresponding α-anomer.

In conclusion, we have developed a highly α- and β-stereoselective (dual stereoselective) method for the synthesis of 2-deoxyglycosides by employing CB 2-deoxyglycosides as glycosyl donors. Glycosylation of the 4,6-*O*-benzylidene-protected glycosyl donor **7** with secondary alcohols afforded predominantly β-glycosides whereas glycosylation of the benzyl-protected glycosyl donor **4** with secondary alcohols afforded α-glycosides.

Experimental Section

Typical procedure (**34**): A mixture of **7** (40 mg, 0.084 mmol, 1 equiv), **17** (59 mg, 0.127 mmol, 1.5 equiv), DTBMP (41 mg, 0.202 mmol, 2.4 equiv), and activated molecular sieves (4 Å) in dichloromethane (8 mL) was stirred at room temperature for 30 min. Tf_2O (17.0 μL, 0.101 mmol, 1.2 equiv) was added to this mixture at −78 °C. The resulting mixture was stirred at −78 °C for 1 h before the addition of saturated aqueous $NaHCO_3$ (10 mL). The reaction mixture was filtered and the organic layer was separated, washed with saturated aqueous sodium chloride solution (10 mL), dried, filtered, and concentrated. The residue was purified by means of silica-gel flash-column chromatography to afford the separable disaccharides β-**34** (42 mg, 63%), α-**34** (5 mg, 8%), and the self-condensed ester **35** (6 mg, 17%). β-**34**: $R_f = 0.70$ (hexane/ethyl acetate 2:1); $[\alpha]_D = +0.74$ ($c = 0.20$ in $CHCl_3$); ^{1}H NMR (250 MHz, $CDCl_3$): $\delta = 1.68$–1.81 (m, 1H), 2.25 (ddd, $J = 2.1$, 4.5, 13.6 Hz, 1H), 3.24–3.33 (m, 1H), 3.30 (s, 3H), 3.58–3.90 (m, 8H), 4.12 (d, $J = 9.8$ Hz, 1H), 4.29 (dd, $J = 4.9$, 10.4 Hz, 1H), 4.66 (dd, $J = 2.0$, 9.8 Hz, 1H), 4.56 and 4.81 (q, $J = 12.1$ Hz, 2H), 4.59 (s, 2H), 4.69 and 4.93 (q, $J = 11.3$ Hz, 2H), 4.71 (s, 2H), 4.74 (d, $J = 1.6$ Hz, 1H), 5.58 (s, 1H), 7.21–7.57 ppm (m, 25H); ^{13}C NMR (63 MHz, $CDCl_3$): $\delta = 37.7$, 54.8, 66.7, 68.9, 69.1, 71.5, 72.2, 72.6, 72.7, 74,6, 75.1, 77.4, 80.4, 83.2, 99.0, 101.0, 101.4, 126.2, 127.8, 128.0, 128.4, 128.5, 129.0, 137.7, 138.4, 138.6, 138.7 ppm; elemental analysis (%): calcd for $C_{48}H_{52}O_{10}$ (788.9): C 73.08, H 6.64; found: C 73.10, H 6.70. α-**34**: $R_f = 0.60$ (hexane/ethyl acetate 2:1); $[\alpha]_D = +0.94$ ($c = 0.20$ in $CHCl_3$); ^{1}H NMR (250 MHz, $CDCl_3$): $\delta = 1.76$ (ddd, $J = 3.6$, 11.3, 13.2 Hz, 1H), 2.33 (dd, $J = 5.1$, 13.2 Hz, 1H), 3.27 (s, 3H), 3.64–3.93 (m, 10H), 4.21 (dd, $J = 4.5$, 9.8 Hz, 1H), 4.57 (d, $J = 10.9$ Hz, 1H), 4.62 (s, 2H), 4.63 (d, $J = 11.6$ Hz, 1H), 4.67 and 4.77 (q, $J = 11.9$ Hz, 2H), 4.72–4.76 (m, 2H), 4.94 (d, $J = 11.0$ Hz, 1H), 5.06 (d, $J =$

3.0 Hz, 1H), 5.61 (s, 1H), 7.21–7.51 ppm (m, 25H); ^{13}C NMR (63 MHz, $CDCl_3$): $\delta = 36.5$, 54.8, 63.2, 69.3, 71.5, 72.2, 72.8, 74.8, 74.9, 75.2, 77.2, 80.4, 84.1, 98.2, 98.9, 101.5, 124.3, 126.3, 127.6, 127.7, 127.8, 127.9, 128.0, 128.3, 128.4, 128.5, 129.0, 138.4, 138.6, 138.8 ppm; elemental analysis (%): calcd for $C_{48}H_{52}O_{10}$ (788.9): C 73.08, H 6.64; found: C 73.06, H 6.69. **35**: $R_f = 0.55$ (hexane/ethyl acetate 2:1); $[\alpha]_D = +0.15$ ($c = 0.20$ in $CHCl_3$); ^{1}H NMR (250 MHz, $CDCl_3$): $\delta =$ 1.86 (ddd, $J = 3.8$, 11.3, 13.2 Hz, 1H), 1.99 (m, 1H), 2.36 (dd, $J = 5.3$, 13.2 Hz, 1H), 2.45 (ddd, $J = 2.4$, 4.8, 13.2 Hz, 1H), 3.50–3.60 (m, 1H), 3.69–3.94 (m, 6H), 4.04–4.16 (m, 1H), 4.25 (dd, $J = 4.2$, 9.5 Hz, 1H), 4.37 (dd, $J = 4.8$, 9.8 Hz, 1H), 4.70 and 4.87 (q, $J = 11.8$ Hz, 2H), 4.72 and 4.85 (q, $J = 12.1$ Hz, 2H), 4.91 and 5.03 (q, $J = 14.5$ Hz, 2H), 5.05 (d, $J = 2.7$ Hz, 1H), 5.61 (s, 1H), 5.63 (s, 1H), 6.00 (dd, $J = 2.2$, 9.9 Hz, 1H), 7.24–7.64 (m, 23H), 8.03 ppm (d, $J = 7.8$ Hz, 1H); ^{13}C NMR (63 MHz, $CDCl_3$): $\delta = 36.4$, 36.7, 63.5, 67.3, 67.5, 68.8, 69.3, 72.9, 73.2(2), 74.3, 82.8, 84.1, 92.6, 98.0, 101.5, 101.6, 126.2, 127.1, 127.5, 127.7, 127.8, 127.9, 128.0, 128.4(2), 128.5, 128.6, 129.0, 129.1, 131.2, 133,3, 137.5, 137.7, 138.3, 138.9, 140.8, 164.8 ppm; calcd for $C_{48}H_{48}O_{11}$ (800.9): C 71.98, H 6.04; found: C 71.78, H 6.10.

Received: August 30, 2002 [Z50069]

[1] D. A. Johnson, H.-W. Liu, *Comprehensive Natural Products Chemistry, Vol. 3* (Eds.: D. Barton, K. Nakanishi, O. Meth-Cohn), Elsevier, Oxford, **1999**, chap. 12.

[2] For reviews, see: a) C. H. Marzabadi, R. W. Franck, *Tetrahedron* **2000**, *56*, 8385–8417; b) A. Veyrieres, *Carbohydrates in Chemistry and Biology, Vol. 1* (Eds.: B. Ernst, G. W. Hart, P. Sinay), Wiley-VCH, Weinheim, **2000**, chap. 15; c) J. Thiem, W. Klaffke, *Top. Curr. Chem.* **1990**, *154*, 285–333.

[3] a) P. Deslongchamps, *Stereoelectronic Effects in Organic Chemistry*, Pergamon, Oxford, **1983**; b) E. Juaristi, G. Cuevas, *The Anomeric Effect*, CRC, Boca Raton, **1995**.

[4] For selected references, see: a) K. C. Nicolaou, T. Ladduwahetty, J. L. Randall, A. Chucholowski, *J. Am. Chem. Soc.* **1986**, *108*, 2466–2467; b) J. Thiem, B. Schottmer, *Angew. Chem.* **1987**, *99*, 591; *Angew. Chem. Int. Ed. Engl.* **1987**, *26*, 555–557; c) M. Perez, J.-M. Beau, *Tetrahedron Lett.* **1989**, *30*, 75–78; d) M. Trumtel, P. Taveccchia, A. Veyrieres, P. Sinay, *Carbohydr. Res.* **1989**, *191*, 29; e) W. R. Roush, B. W. Gung, C. E. Bennett, *Org. Lett.* **1999**, *1*, 891–893; f) W. R. Roush, C. E. Bennett, *J. Am. Chem. Soc.* **1999**, *121*, 3541–3542.

[5] a) R. W. Binkley, *J. Carbohydr. Chem.* **1990**, *9*, 507–511; b) R. W. Binkley, M. R. Sivik, *J. Carbohydr. Chem.* **1991**, *10*, 399–416; c) R. W. Binkley, D. J. Koholic, *J. Org. Chem.* **1989**, *54*, 3577–3581; d) Z. Zhang, G. Magnusson, *J. Org. Chem.* **1996**, *61*, 2383–2393.

[6] P. J. Garegg, S. Kopper, P. Ossowski, J. Thiem, *J. Carbohydr. Chem.* **1986**, *5*, 59–65.

[7] S. Hashimoto, A. Sano, H. Sakamoto, M. Nakajima, Y. Yanagiya, S. Ikegami, *Synlett* **1995**, 1271–1273.

[8] J. Junnemann, I. Lundt, J. Thiem, *Liebigs Ann. Chem.* **1991**, 759–764.

[9] K. Toshima, M. Misawa, K. Ohta, K. Tatsuta, M. Kinoshita, *Tetrahedron Lett.* **1989**, *30*, 6417–6420.

[10] K. S. Kim, J. H. Kim, Y. J. Lee, J. Park, *J. Am. Chem. Soc.* **2001**, *123*, 8477–8481.

[11] V. Bolitt, C. Mioskowski, *J. Org. Chem.* **1990**, *55*, 5812–5813.

[12] H. Sajiki, *Tetrahedron Lett.* **1995**, *36*, 3465–3468.

[13] M. Michalska, J. Borowiecka, P. Lipka, T. Rotkita-Trygubowicz, *J. Chem. Soc. Perkin Trans. 1* **1989**, 1619–1622.

[14] a) D. Crich, S. Sun, *J. Org. Chem.* **1997**, *62*, 1198–1199; b) D. Crich, S. Sun, *J. Am. Chem. Soc.* **1998**, *120*, 435–436.

[15] D. Crich, S. Sun, *J. Am. Chem. Soc.* **1997**, *119*, 11217–11223.

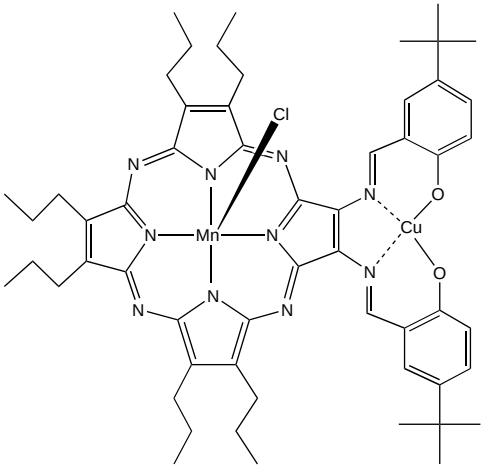
[16] R. U. Lemieux, K. B. Hendriks, R. V. Stick, K. James, *J. Am. Chem. Soc.* **1975**, *97*, 4056–4062.

Spin Coupling between Metal Ions

Porphyrazines as Molecular Scaffolds: Periphery–Core Spin Coupling between Metal Ions of a Schiff Base Porphyrazine**

Min Zhao, Charlotte Stern, Anthony G. M. Barrett, and Brian M. Hoffman**

The periphery of a metalloporphyrazine (pz) can be readily functionalized with heteroatoms that coordinate additional metal ions, and this opens the way to high-spin molecules and molecular arrays based on exchange coupling between the metal ions.[1] We previously reported evidence for core–periphery spin coupling when a metal ion is bound to a peripheral dithiolene.[1–3] We show here that the pz molecule can be used as a scaffold on which to build complex peripheral chelating ligands, and that the resulting dimetallic complex shows some remarkable core–periphery spin coupling. We have synthesized the Schiff base appended porphyrazine (**1**) where the core metal ion is Mn^{III} with spin $S = 2$, and the peripheral ion is Cu^{II} with $S = 1/2$; have obtained its crystal structure, and characterized the $S = 3/2$ and 5/2 total-spin manifolds created by strong core–periphery M_1–M_2 spin coupling; and have

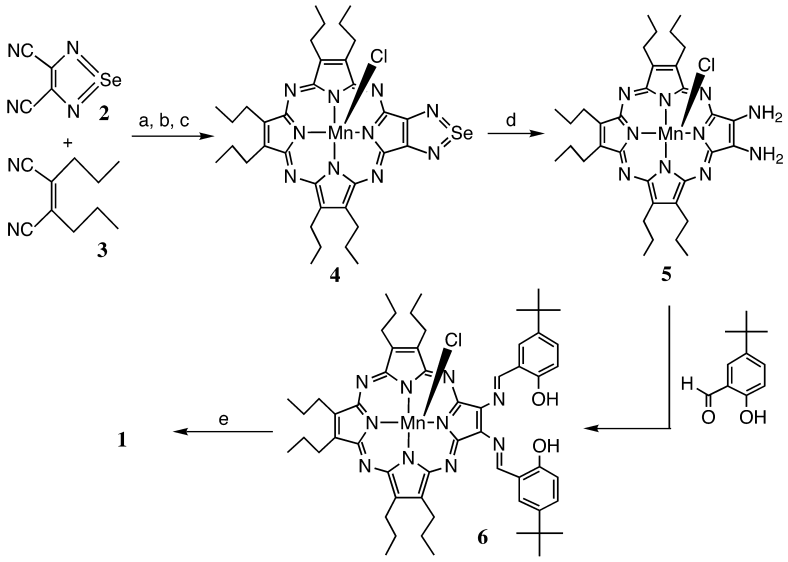


1

[*] Prof. A. G. M. Barrett
Department of Chemistry
Imperial College of Science, Technology, and Medicine
London SW7 2AY (UK)
Fax: (+44) 207-594-5805
E-mail: agmb@ic.ac.uk
Prof. B. M. Hoffman, M. Zhao, Dr. C. Stern
Department of Chemistry
Northwestern University
2145 Sheridan Road
Evanston, IL 60208 (USA)
Fax: (+1) 847-491-7713
E-mail: bmh@northwestern.edu

[**] This work was supported by the National Science Foundation (CHE-0091364, B.M.H.), the EPSRC (A.G.M.B.), and through the NU Materials Research Center (DMR-0076097).

 © 2003 Wiley-VCH Verlag GmbH & Co. KGaA, Weinheim 1433-7851/03/4204-0462 $ 20.00+.50/0



Scheme 1. a) $Mg(OBu)_2$/BuOH, reflux; b) trifluoroacetic acid; c) $MnCl_2$, chlorobenzene/*N*,*N*-dimethylformamide, 100 °C; d) H_2S/pyridine; e) $CuCl_2$, $MeOH/CHCl_3$.

determined the exchange-splitting between them through the use of EPR spectroscopy and magnetic susceptibility measurements.

The synthesis of **1** follows the procedures shown in Scheme 1. It involves the reaction of the [ClMn(pzdiamine)] (**5**) with two equivalents of 5-*tert*-butyl-2-hydroxybenzaldehyde to give **6**, followed by metalation of the Schiff base. Attempts to prepare **5** by a route that involves cocyclization of diaminomaleonitrile (DAMN) with dipropyl maleonitrile (**3**) were unsatisfactory, so we utilized the procedure devised by Baum et al.[4] in which DAMN is protected as 3,4-dicyano-1,2,5-selenodiazole (**2**) by oxidation with SeO_2 following the approach of Ercolani and co-workers.[5] This was cocyclized then with **3** by reaction with $Mg(OBu)_2$ in BuOH, demetalated in TFA to give the free-base form, which was metalated with $MnCl_2$ and air-oxidized to form **4**.[6] Deprotection with H_2S/pyridine generated **5**, which was treated in situ with 5-*tert*-butyl-2-hydroxybenzaldehyde to give the desired ligand **6**; the MnCu complex **1** was formed by stirring **6** with $CuCl_2$ in methanol/chloroform overnight.[7] Complex **1** was crystallized from dichloromethane/toluene/acetonitrile, and X-ray diffraction analysis[8] confirmed the structure (Figure 1).

Compound **1** crystallizes in the space group $P\bar{1}$, along with a molecule of CH_3CN and CH_2Cl_2 solvent. The pz core is planar to within 0.002 Å. As with other $ClMn^{III}$-complexed porphyrazines,[9] the manganese ion has a distorted square-pyramidal geometry, with the Mn center raised out of the N_4 coordination plane toward the apical chloride ion by 0.31 Å. The coordination environment of the copper ion of the Schiff base is planar to within 0.06 Å; the bonds to the O atoms are nearly equal in length, with an average value of 1.910 Å, which is slightly shorter than those to the N atoms, whose average value is 1.972 Å.

Figure 2 displays an X-band EPR spectrum of **1** taken at 77 K. It shows two overlapping "perpendicular" features at $g_\perp = 6$ and $g_\perp = 4$, each of which displays a sextet splitting from interaction with the ^{55}Mn ion ($I = 5/2$); the spectrum further shows unresolved intensity from the associated $g_\parallel$ features around $g = 2$. The hyperfine splittings show that these signals are associated with the Mn^{III} ion. However, an "isolated" Mn^{III} ion incorporated in a [$ClMn^{III}$pz] has a high-spin ($S = 2$), d^4 configuration and at X-band is EPR silent; high-field EPR spectra show that an axial zero-field splitting (zfs) interaction resolves the four $S = 2$ spin sublevels into $\pm 1/2$ and $\pm 3/2$ doublets that are separated in zero field by $2D^{Mn} = -4.6\ cm^{-1}$, which is far greater than the X-band microwave quantum.[10] The d^9 Cu^{II} ion in an isolated Schiff base complex has $S^{Cu} = 1/2$; its frozen-solution EPR spectrum shows a quartet of $^{63/65}Cu$ ($I = 1/2$) hyperfine lines centered at $g_\parallel = 2.2$, and a broad, but unsplit, "perpendicular" feature at $g_\perp \approx 2.05$.[11] Thus, the spectrum shown in Figure 2 cannot be associated with

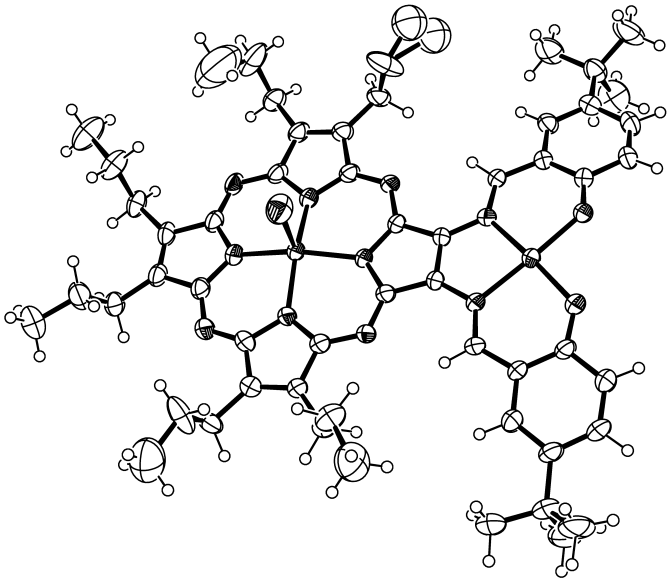


Figure 1. Crystal structure of **1**.

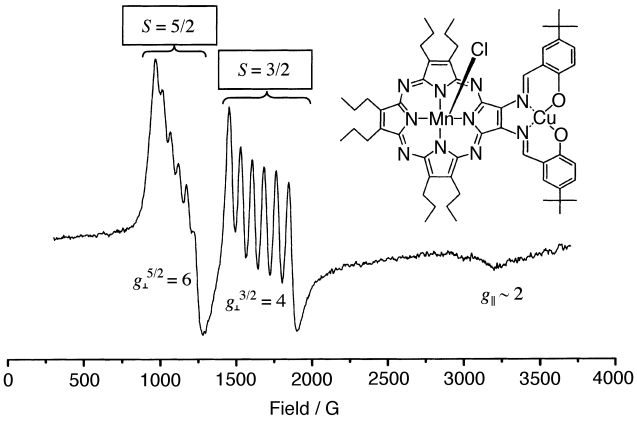


Figure 2. Frozen-solution X-band EPR spectrum of **1** dissolved in toluene/pyridine (1/1) (77 K).

 © 2003 Wiley-VCH Verlag GmbH & Co. KGaA, Weinheim 1433-7851/03/4204-0463 $ 20.00+.50/0

either uncoupled spin center and must reflect interactions between them.

Heisenberg exchange coupling between the $S=2$ and $S=1/2$ individual spins ($\hat{H}_{ex}=JS^{Mn}S^{Cu}$) would produce two total-spin manifolds with $S=3/2$ and 5/2 which are separated by $\Delta=5J$. Each of these manifolds exhibits an axial zfs interaction whose principal value (D^S) is determined by that of the uncoupled Mn^{III} ion: $D^{3/2}=(3/5)D^{Mn}$, $D^{5/2}=(7/5)D^{Mn}$. As these zfs parameters are much larger than the X-band microwave quantum one expects the X-band spectra to display only transitions within the $m_s=\pm 1/2$ doublet for each total-spin manifold. These would be characterized by g tensors with $g_{\perp}^{3/2}=4$, $g_{\perp}^{5/2}=6$, and $g_{\parallel}^{3/2}=g_{\parallel}^{5/2}=2$. The spectrum shown in Figure 2 is clearly a superposition of the spectra expected for the $S=3/2$ and $S=5/2$ total-spin manifolds, and the observation of such a superposition at 77 K establishes the existence of a strong Heisenberg coupling between the partner spins, while implying there is thermal population of both manifolds at this temperature.

This interpretation is confirmed by the observed ^{55}Mn hyperfine splittings. It is straightforward to show that the exchange-coupled system should exhibit splittings of $A_{Mn}^{3/2}=(6/5)A_{Mn}$ and $A_{MMn}^{5/2}=(4/5)A_{Mn}$, where A_{Mn} is the coupling for the isolated Mn^{III} ion. The resulting prediction that $A_{Mn}^{3/2}/A_{Mn}^{5/2}=3/2$, clearly matches the ratio of the observed couplings $A_{Mn}^{3/2}/A_{Mn}^{5/2}=80\ G/53\ G=1.51$; the resulting hyperfine interaction for the uncoupled Mn^{III} ion ($A_{Mn}=66$ G) is typical for such ions.[12] Despite the assignment of these signals to an exchange-coupled MnCu center, they surprisingly show no hyperfine splittings by the $^{63/65}Cu$ ion. This too, however, is explained by the exchange model: The resolved features are "perpendicular", and $A_{\perp}^{Cu}$ value for a $^{63/65}Cu$ ion ($I=3/2$) of a Schiff base is normally small ($A_{\perp}^{Cu}=$ ca. 30 G).[11] A coupling of this magnitude would still give substantial hyperfine broadening and indeed would preclude resolution of the ^{55}Mn couplings, especially for the $S=5/2$ state of **1**. However, spin-coupling calculations further show that the hyperfine coupling of the copper ion is sharply reduced in the total-spin manifolds generated by the spin exchange: $A_{\perp}(Cu)^{3/2}=A_{\perp}(Cu)^{5/2}=\pm(1/5)A_z(Cu)$. These considerations explain why the ^{55}Mn splittings are well resolved in the EPR spectra associated with the $S=3/2$, 5/2 spin manifold, and why no evidence of $^{63/65}Cu$ splittings is detectable.

The detailed analysis of the spectrum in Figure 2 shows definitively that **1** exhibits strong Heisenberg spin exchange between the partner metal-ion spins, but cannot yield a value of the exchange parameter Δ that splits the $S=3/2$ and $S=5/2$ manifolds. The magnetic susceptibility of **1** was measured between temperatures of 2 and 300 K using a SQUID magnetometer to determine the value of Δ (Figure 3). The high-temperature limiting value is $\chi T\approx 3.5\ cm^3 mol^{-1} K$, which is consistent with the presence of partners with $S=2$ and $S=1/2$ spins, each having intrinsic g values of roughly 2. The fall-off with decreasing temperature is indicative of antiferromagnetic coupling ($J>0$ for the $\hat{H}_{ex}$ condition defined above), which places the $S=3/2$ manifold lower in energy than the $S=5/2$ one. The measured $\chi(T)$ value was fit to the theoretical expression for such a spin-coupled center, [Eq. (1)].[13]

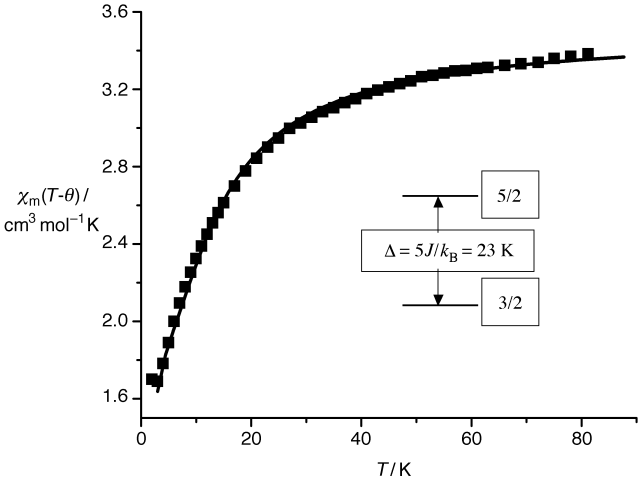


Figure 3. Plot of the molar magnetic susceptibility of a powdered sample of **1** plotted as (χT), which corresponds to the effective moment squared. The solid line is a fit to the data by Eq. (1), with $\theta=-8$ K, $g=2.05$, $D^{3/2}=(3/5)D^{Mn}=-1.38\ cm^{-1}$, and $\Delta/k_B=23$ K.

$$\chi=\chi^{3/2}\frac{2}{2+3e^{-\Delta/k_B T}}+(C/4)\frac{35e^{-\Delta/k_B T}}{2+3e^{-\Delta/k_B T}} \quad (1)$$

$C=N\mu_B^2 g^2/k_B(T-\theta)$ and the symbols have their usual meanings; the function $\chi^{3/2}$ is associated with the $S=3/2$ manifold and incorporates the effects of the zero-field splitting, where $D^{3/2}$ is fixed as described above [Eq. (2)].

$$\chi^{3/2}=C\left[\frac{1}{3}\frac{1+9e^{-2D^{3/2}/k_B T}}{4(1+e^{-2D^{3/2}/k_B T})}+\frac{2}{3}\frac{4+\frac{3k_B T}{D^{3/2}}(1-e^{-2D^{3/2}/k_B T})}{4(1+e^{-2D^{3/2}/k_B T})}\right] \quad (2)$$

The fits give $\Delta/k_B=23$ K and the Curie–Weiss constant $\theta=-8$ K.

The present results show that the pz macrocycle can be used as a scaffold on which to build a peripheral chelate, and that exchange coupling between core and peripheral metal ions with different intrinsic spin values yields a spin-coupled "ferrimagnetic" system with high residual spin. Other combinations of metal ions are being examined so as to define the systematics of spin coupling within this system, and we further anticipate that systems being prepared with more than one peripheral chelate will show exciting new features.

Received: August 30, 2002 [Z50078]

[1] S. L. J. Michel, B. M. Hoffman, S. Baum, A. G. M. Barrett, *Prog. Inorg. Chem.* **2001**, *50*, 473–590.
[2] S. L. J. Michel, D. P. Goldberg, C. Stern, A. G. M. Barrett, B. M. Hoffman, *J. Am. Chem. Soc.* **2001**, *123*, 4741–4748.
[3] D. P. Goldberg, S. L. J. Michel, A. J. P. White, D. J. Williams, A. G. M. Barrett, B. M. Hoffman, *Inorg. Chem.* **1998**, *37*, 2100–2101.
[4] S. M. Baum, A. A. Trabanco, A. G. Montalban, A. S. Micallef, A. J. P. White, D. J. Williams, A. G. M. Barrett, B. M. Hoffman, *J. Org. Chem.* submitted .
[5] E. M. Bauer, C. Ercolani, P. Galli, I. A. Popkova, P. A. Stuzhin, *J. Porphyrins Phthalocyanines* **1999**, *3*, 371–379.

 © 2003 Wiley-VCH Verlag GmbH & Co. KGaA, Weinheim 1433-7851/03/4204-0464 $ 20.00+.50/0

[6] Yield: 59%. UV/Vis (CH_2Cl_2) $\lambda_{max} = 361, 618, 679$ nm; FAB MS: m/z 725.5 $[M-Cl]^+$, calcd for $C_{34}H_{42}N_{10}SeMn$: m/z 725.2.
[7] Yield: 41%. UV/Vis (CH_2Cl_2) $\lambda_{max} = 344$, 381, 656, 694 nm; atmospheric pressure CI-MS: m/z 1066.5 $[M+H]^+$, 1030.5 $[M-Cl]^+$; calcd $C_{56}H_{69}N_{10}O_2MnCuCl$: m/z 1066.4, calcd $C_{56}H_{68}N_{10}O_2MnCu$: m/z 1030.4; elemental analysis calcd for $C_{56}H_{71}N_{10}O_3MnCuCl$ (**1**+H_2O): C 61.98, H 6.50, N 12.91; found: C 62.01, H 6.27, N 13.12.
[8] Crystal data for **1**, $C_{59}H_{73}Cl_3CuMnN_{11}O_2$: triclinic, space group $P\bar{1}$, $a = 13.009(3)$, $b = 14.273(4)$, $c = 17.856(6)$ Å, $\alpha = 104.66(2)$, $\beta = 104.964(16)$, $\gamma = 104.781(14)°$, $V = 2910.9(14)$ Å^3, $Z = 2$, $\rho_{calcd} = 1.358$ Mg m^{-3}, final $R1$ value of 0.0581 and wR_2 value of 0.1363 were based on 13690 independent reflections ($I > 2\sigma(I)$) out of 27297 reflections collected and 678 variable parameters. The data collection were performed at 153 K on a Bruker SMART-1000 CCD area detector, by using graphite monochromated Mo_K radiation ($\lambda = 0.71073$ Å), by the ϕ and ω-scan mode, within the limits $1.57 < \theta < 28.84°$. The linear absorption coefficient μ is 0.770 mm^{-1}. An integration absorption correction was applied. Minimum and maximum transmission factors were 0.8337 and 0.9801, respectively. The data were corrected for Lorentz and polarization effects. The structure was solved by direct methods (SHELXS-97), expanded by using Fourier techniques (SHELXS-97), and refined by full-matrix least-squares on F^2. The non-hydrogen atoms were refined anisotropically except those on the disordered C33 methyl group. Hydrogen atoms were included in idealized positions, except those on the disorder carbon atoms, but not refined. The program Squeeze (A. L. Spek, *Acta Crystallogr. Sect. A* **1990**, *46*, C-34) was used to take out 84 electrons which correspond to the dichloromethane molecule. This solvent was refined as a diffuse contribution without specific atom positions, but the density and absorption coefficient reflect the full formula. All calculations were performed using the Bruker SHELXTL crystallographic software package. CCDC-190473 contains the supplementary crystallographic data for this paper. These data can be obtained free of charge via www.ccdc.cam.ac.uk/conts/retrieving.html (or from the Cambridge Crystallographic Data Centre, 12 Union Road, Cambridge CB21EZ, UK; fax: (+44) 1223-336-033; or deposit@ccdc.cam.ac.uk).
[9] a) D. P. Goldberg, A. G. Montalban, A. J. P. White, D. J. Williams, A. G. M. Barrett, B. M. Hoffman, *Inorg. Chem.* **1998**, *37*, 2873–2879; b) G. Ricciardi, A. Bavoso, A. Bencini, A. Rosa, F. Lelj, F. Bonosi, *J. Chem. Soc. Dalton Trans.* **1996**, *13*, 2799–2807.
[10] J. Krzystek, J. Telser, L. A. Pardi, D. P. Goldberg, B. M. Hoffman, L.-C. Brunel, *Inorg. Chem.* **1999**, *38*, 6121–6129.
[11] C. E. Tauber, H. C. Allen, Jr., *J. Phys. Chem.* **1979**, *83*, 1391–1393.
[12] J. M. Peloquin, K. A. Campbell, D. W. Randall, M. A. Evanchik, V. L. Pecoraro, W. H. Armstrong, R. D. Britt, *J. Am. Chem. Soc.* **2000**, *122*, 10926–10942.
[13] C. J. O'Connor, *Prog. Inorg. Chem.* **1982**, *29*, 203–283.

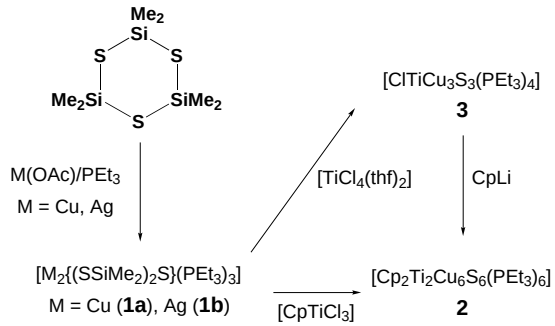
Cu and Ag Silanethiolato Complexes

Copper and Silver Complexes Containing the $S(SiMe_2S)_2^{2-}$ Ligand: Efficient Entries into Heterometallic Sulfido Clusters

Takashi Komuro, Tsukasa Matsuo, Hiroyuki Kawaguchi, and Kazuyuki Tatsumi*

The development of synthetic routes to mixed-metal sulfido clusters is a critical prerequisite to study these important materials.[1] It is well known that $(Me_3Si)_2S$ is a good sulfur-transfer reagent, and can replace a halide, alkoxide, acetate, or oxide with a sulfido ligand through the formation of energetically favorable Si–Cl or Si–O bonds.[2] Therefore, the corresponding M–$SSiMe_3$ species have the potential to be synthetic precursors of sulfido clusters.[3,4] However, because of the high lability of Si–S bond, there is a tendency to restrict the use of silanethiolato complexes. Thus, the stabilization of these complexes is required if they are to be used in the development of cluster syntheses. Cyclotrisilathiane has received less attention than $(Me_3Si)_2S$ for use in preparations of sulfido clusters.[5] In exploring of the utility of this reagent, we discovered the formation of thermally stable copper and silver complexes containing the intriguing $S(SiMe_2S)_2^{2-}$ ligand. Herein we report the synthesis of these complexes, and their reactions with titanium–chloride complexes.

Treatment of Cu(OAc) with cyclotrisilathiane in the presence of PEt_3 at room temperature generated $[Cu_2\{(SiMe_2)_2S\}(PEt_3)_3]$ (**1a**) as colorless crystals in 74% yield (Scheme 1). The silver congener **1b** was obtained as colorless



Scheme 1. Synthesis of **1** and reactions with titanium chloride complexes to give **2** and **3**.

[*] Prof. Dr. H. Kawaguchi, Dr. T. Matsuo
Coordination Chemistry Laboratories
Institute for Molecular Science
Myodaiji, Okazaki, 444-8585 (Japan)
Fax: (+81) 564-55-5245
E-mail: hkawa@ims.ac.jp
T. Komuro, Prof. Dr. K. Tatsumi
Research Center for Materials Science and
Department of Chemistry
Graduate School of Science
Nagoya University
Furo-cho, Chikusa-ku, Nagoya 464-8602 (Japan)

 © 2003 Wiley-VCH Verlag GmbH & Co. KGaA, Weinheim 1433-7851/03/4204-0465 $ 20.00+.50/0

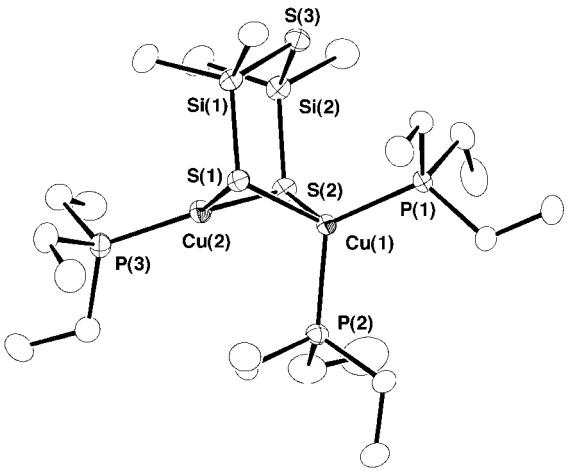


Figure 1. Molecular structure of **1a**. Selected interatomic distances [Å] and angles [°]: Cu(1)-Cu(2) 2.715(1), Cu(1)-S(1) 2.440(1), Cu(1)-S(2) 2.480(1), Cu(2)-S(1) 2.339(1), Cu(2)-S(2) 2.305(1), Cu(1)-P(1) 2.258(1), Cu(1)-P(2) 2.266(1), Cu(2)-P(3) 2.209(1), S(1)-Si(1) 2.099(1), S(2)-Si(2) 2.102(1), S(3)-Si(1) 2.161(1), S(3)-Si(2) 2.163(1); S(1)-Cu(1)-S(2) 97.45(4), S(1)-Cu(2)-S(2) 105.56(3), Cu(1)-S(1)-Cu(2) 69.21(3), Cu(1)-S(2)-Cu(2) 69.05(2), P(1)-Cu(1)-P(2) 118.46(3).

crystals in 75% yield from the analogous reaction. The X-ray study revealed that **1a** is a bicyclic structure (Figure 1).[6] The silanedithiolato ligand bridges two Cu atoms, one of which is three-coordinate and the other four-coordinate. Because of these different coordination geometries, the average Cu(1)–S bond length (2.460 Å) is elongated relative to the average Cu(2)–S bond length (2.322 Å). The S(3) atom is oriented toward the tetrahedral Cu(1) center to avoid steric crowding. The Cu_2S_2 quadrilateral is folded, the dihedral angle between the two CuS_2 planes is 127.4°, and the two Cu atoms are separated by 2.715(1) Å. The thioether-like S(3)–Si(1) and S(3)–Si(2) bonds are about 0.06 Å longer than the thiolato S(1)–Si(1) and S(2)–Si(2) bonds, which may be attributed to the hyperconjugative interaction between the occupied p orbital of the $S_{thiolato}$ atom and the vacant antibonding σ* ($Si–S_{thioether\text{-}like}$) orbital. Although the solid-state molecular structure of **1a** is unsymmetrical, the resonance signal from the methyl protons of the silanedithiolato ligand appears as a sharp singlet in the ^1H NMR spectrum at room temperature, which indicates that the structure is fluxional in solution by means of dynamic processes involving a rapid ring inversion of the $Cu_2(SSiMe_2)_2S$ core and a fast exchange of the PEt_3 ligands between two Cu centers. In the $^{29}Si\{^1H\}$ NMR spectrum, the resonance signal arising from the $S(SiMe_2S)_2^{2-}$ ligand shifts upfield considerably, relative to the starting silyl sulfide ($\delta = 21.4$ ppm).

The stability of **1a** deserves comment. The related complex $[Cu(SSiMe_3)(PEt_3)_3]$ is unstable in solution above 0°C resulting in formation of sulfidocopper clusters.[3a] In contrast, **1a** did not show any signs of decomposition in C_6D_6 at room temperature over two days when monitored by ^1H NMR spectroscopy. However, **1a** reacts with metal halides under mild conditions to afford mixed-metal clusters in high yields. For example, the addition of 0.5 equivalents of $[CpTiCl_3]$ to **1a** in toluene at −50°C gave a dark red solution, from which we isolated $[Cp_2Ti_2Cu_6S_6(PEt_3)_6]$ (**2**) as dark red crystals after suitable workup (Scheme 1). Analogously, the reaction of **1a** with 0.5 equivalents of $[TiCl_4(thf)_2]$ afforded $[ClTiCu_3S_3(PEt_3)_4]$ (**3**) as yellow crystals. Both compounds are diamagnetic, and the elemental analyses were in agreement with the structures elucidated by X-ray crystallography.

In the molecular structure of **2**, the centrosymmetric octanuclear core is a distorted Ti_2Cu_6 cube with a μ_4-S^{2-} ligand occupying the position above the center of each of the six faces (Figure 2).[6] Two Cp and six PEt_3 ligands also coordinate to the titanium and the copper sites, respectively. All Cu atoms assume a tetrahedral geometry. Alternatively, the core structure can be viewed as a $[Cu_6S_6(PEt_3)_6]^{6-}$ prismane, which is capped at each of the two Cu_3S_3 hexagonal chairs by $[CpTi^{3+}]$ units. The cluster core of **2** is structurally analogous to the dodecahedral skeletons found in $[Co_8S_6(SPh)_8]^{4-}$,[7] $[Fe_8S_6I_8]^{3-}$,[8] and $[Fe_6S_6X_6\{M(CO)_3\}_2]^{n-}$ (X = Cl, Br, I; M = Mo, W; $n = 3$, 4).[9] The Cu–S bond lengths and the Cu–Cu distances fall within the ranges that are typical for sulfido-bridged copper(I) clusters.[10] The average Cu–Ti distance of 2.869 Å suggests the existence of a dative bond between the d^{10} Cu atom and the d^0 Ti atom.[11]

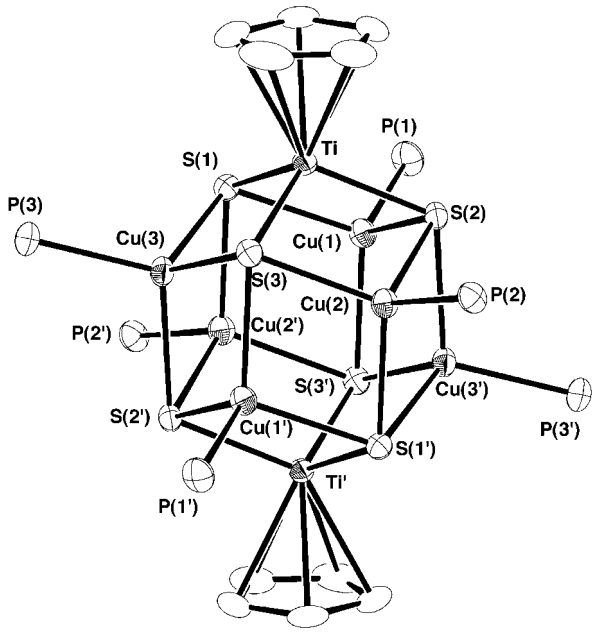


Figure 2. Molecular structure of **2**; ethyl groups of phosphane ligands have been omitted for clarity. Selected interatomic distances [Å] and angles [°]: Cu-Cu 2.743(1)–2.769(1), Cu-Ti 2.865(1)–2.876(2), Cu-S 2.328(1)–2.442(2), Ti-S 2.310(2)–2.314(2), Cu-P 2.253(2)–2.260(2); S-Ti-S 104.74(5)–105.06(5), S-Cu-S 102.49(7)–110.13(5).

The molecular structure of **3** (Figure 3) consists of a tetranuclear $TiCu_3S_3$ core analogous to half of the octanuclear core found in **2**, and a crystallographic mirror plane passes through the molecule.[6] One Cl atom bound to a Ti center remains after completion of the cluster forming reaction. There are two different copper coordination environments in **3**. As expected, the Cu–Ti distances, and the Cu–S, and Cu–P bond lengths of the Cu(1) and Cu(1′) atoms in the trigonal-

 © 2003 Wiley-VCH Verlag GmbH & Co. KGaA, Weinheim 1433-7851/03/4204-0466 $ 20.00+.50/0

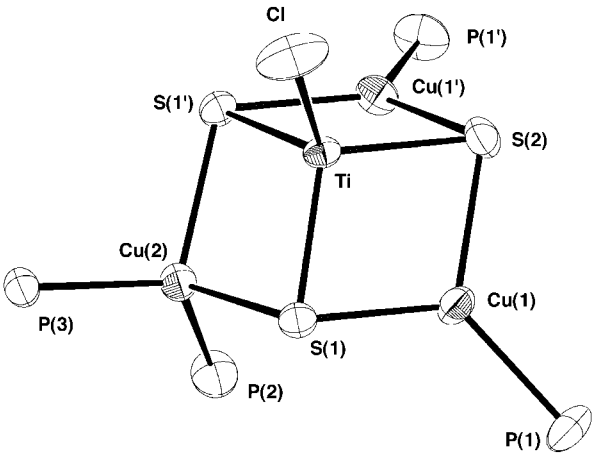


Figure 3. Molecular structure of **3**; ethyl groups of phosphane ligands have been omitted for clarity. Selected interatomic distances [Å] and angles [°]: Cu(1)-Ti 2.702(1), Cu(2)-Ti 2.863(2), Cu(1)-S(1) 2.243(1), Cu(1)-S(2) 2.256(1), Cu(2)-S(1) 2.360(1), Ti-S(1) 2.252(1), Ti-S(2) 2.263(2), Cu(1)-P(1) 2.202(1), Cu(2)-P(2) 2.248(2), Cu(2)-P(3) 2.266(2), Ti-Cl 2.288(2); S(1)-Cu(1)-S(2) 106.59(6), S(1)-Cu(2)-S(1′) 99.83(6), S(1)-Ti-S(2) 106.05(5), S(1)-Ti-S(1′) 106.64(7), P(1)-Cu(1)-S(1) 126.65(5), P(1)-Cu(1)-S(2) 126.51(6), P(2)-Cu(2)-P(3) 121.11(7).

planar coordination environments are shorter than the corresponding distances of the tetrahedrally coordinated Cu(2) atom. Although **3** is stable in solution, addition of one equivalent of CpLi to solution of **3** in THF resulted in the formation of **2** concomitant with a small amount of unidentified copper compounds. This result implies that the steric and electronic properties of the ligand bound to the Ti atom are related to the observed cluster sizes and shapes.

In conclusion, we have described new dimetallic silanedithiolato complexes of copper and silver that are stable in solution at room temperature and react readily with titanium–chloride complexes under mild conditions to afford mixed-metal sulfido clusters. We are extending our work to prepare other silanethiolato complexes by using cyclotrisilathiane, and to study their potential utility in the synthesis of ternary clusters .

Experimental Section

All manipulations were carried out under an argon atmosphere using standard Schlenk techniques, all solvents were dried, and deoxygenated before use.

1a: A solution of $(Me_2SiS)_3$ (0.92 g, 3.4 mmol) in hexane (2.3 mL) was added to a solution of Cu(OAc) (0.69 g, 5.6 mmol) and PEt_3 (7.8 mL, 11 mmol: 1.41M toluene solution) in Et_2O (20 mL), which gave a yellow solution. After the mixture had been stirred for 3 h at room temperature, the solvent was removed in vacuo. Recrystallization from hexane afforded **1a** as colorless crystals (1.44 g, 74%). ^{1}H NMR (500 MHz, C_6D_6): $\delta = 1.36$ (dq, 18H; PCH_2CH_3), 1.03 (dt, 27H; PCH_2CH_3), 0.96 ppm (s, 12H; $SiMe_2$); ^{31}P{^{1}H} NMR (202.35 MHz, C_6D_6): $\delta = -14.6$ ppm (br, $\Delta\nu_{1/2} = 48$ Hz); ^{29}Si{^{1}H} NMR (99.25 MHz, C_6D_6): $\delta = 16.0$ ppm (s); elemental analysis calcd (%) for $C_{22}H_{57}Cu_2P_3S_3Si_2$: C 38.07, H 8.28, S 13.86; found: C 37.69, H 8.42, S 13.15. **1b**: ^{1}H NMR (C_6D_6): $\delta = 1.21$ (dq, 18H; PCH_2CH_3), 1.06 (s, 12H; $SiMe_2$), 0.97 ppm (dt, 27H; PCH_2CH_3); ^{31}P{^{1}H} NMR (C_6D_6): $\delta = -5.2$ ppm (br, $\Delta\nu_{1/2} = 110$ Hz); elemental analysis calcd (%) for $C_{22}H_{57}Ag_2P_3S_3Si_2$: C 33.76, H 7.34, S 12.29; found: C 33.28, H 7.42, S 12.07.

2: A solution of $[CpTiCl_3]$ (0.10 g, 0.46 mmol) in toluene (10 mL) was added to a solution of **1a** (0.64 g, 0.92 mmol) in toluene (10 mL) at −50°C. The resulting dark red mixture was stirred overnight at room temperature. This solution was concentrated to a small volume, then hexane was added. Cooling the solution to −30°C gave a brown polycrystalline solid of **2** (0.29 g, 84% based on Ti). ^{1}H NMR ($CDCl_3$): $\delta = 5.96$ (s, 10H; C_5H_5), 1.54 (dq, 36H; PCH_2CH_3), 1.08 ppm (dt, 54H; PCH_2CH_3); ^{31}P{^{1}H} NMR ($CDCl_3$): $\delta = 2.7$ ppm (br, $\Delta\nu_{1/2} = 94$ Hz); elemental analysis calcd (%) for $C_{46}H_{100}Cu_6P_6S_6Ti_2$: C 36.62, H 6.68, S 12.75; found: C 36.56, H 6.72, S, 12.81.

3: A solution of **1a** (0.42 g, 0.60 mmol) in toluene (4.5 mL) was added to a solution of $[TiCl_4(thf)_2]$ (0.10 g, 0.30 mmol) in toluene (15 mL) at −50°C. Workup similar to that used for **2** yielded **3** as a yellow powder (0.21 g, 83% based on Ti). ^{1}H NMR ($CDCl_3$): $\delta = 1.56$ (m, 24H; PCH_2CH_3), 1.09 ppm (dt, 36H; PCH_2CH_3); ^{31}P{^{1}H} NMR ($CDCl_3$): $\delta = -3.1$ ppm (br, $\Delta\nu_{1/2} = 1100$ Hz); elemental analysis calcd (%) for $C_{24}H_{60}ClCu_3P_4S_3Ti$: C 34.20, H 7.18, S 11.41; found: C 34.10, H 7.17, S 10.95.

Received: October 10, 2002 [Z50336]

[1] a) D. Coucouvanis, *Acc. Chem. Res.* **1991**, *24*, 1–8; b) H. Weller, *Angew. Chem.* **1993**, *105*, 43–55; *Angew. Chem. Int. Ed. Engl.* **1993**, *32*, 41–53; c) M. Hidai, S. Kuwata, Y. Mizobe, *Acc. Chem. Res.* **2000**, *33*, 46–52; d) M. A. Casado, M. A. Ciriano, A. J. Edwards, F. J. Lahoz, J. J. Pérez-Torrente, L. A. Oro, *Organometallics* **1998**, *17*, 3414–3416; e) U. Riaz, O. Curnow, M. D. Curtis, *J. Am. Chem. Soc.* **1991**, *113*, 1416–1417.

[2] a) S. Dehnen, A. Eichhöfer, D. Fenske, *Eur. J. Inorg. Chem.* **2002**, 279–317; b) D. Fenske, J. Ohmer, J. Hachgenei, K. Merzweiller, *Angew. Chem.* **1988**, *100*, 1300–1321; *Angew. Chem. Int. Ed. Engl.* **1988**, *27*, 1277–1296; c) E. Nordlander, S. C. Lee, W. Cen, Z. Y. Wu, C. R. Natoli, A. Di Cicco, A. Filipponi, B. Hedman, K. O. Hodgson, R. H. Holm, *J. Am. Chem. Soc.* **1993**, *115*, 5549–5558; d) J.-F. You, B. S. Snyder, G. C. Papaefthymiou, R. H. Holm, *J. Am. Chem. Soc.* **1990**, *112*, 1067–1076.

[3] a) D. T. T. Tran, J. F. Corrigan, *Organometallics* **2000**, *19*, 5202–5208; b) P. A. Shapley, H.-C. Liang, N. C. Dopke, *Organometallics* **2001**, *20*, 4700–4704; c) H.-C. Liang, P. A. Shapley, *Organometallics* **1996**, *15*, 1331–1333.

[4] D. T. T. Tran, N. J. Taylor, J. F. Corrigan, *Angew. Chem.* **2000**, *112*, 965–967; *Angew. Chem. Int. Ed.* **2000**, *39*, 935–937.

[5] a) T. Komuro, T. Matsuo, H. Kawaguchi, K. Tatsumi, *Chem. Commun.* **2002**, 988–989; b) D. M. Giolando, T. B. Rauchfuss, G. M. Clark, *Inorg. Chem.* **1987**, *26*, 3080–3082.

[6] Crystal data for **1a**: $C_{22}H_{57}S_3P_3Si_2Cu_2$ ($M_r = 694.06$); $P2_1/c$ (no. 14), $a = 15.985(5)$, $b = 11.309(3)$, $c = 19.712(5)$ Å, $\beta = 96.792(4)°$, $V = 3538.5(17)$ Å^3, $\rho_{calcd} = 1.303$ g cm^{-3}, $Z = 4$, $\mu = 15.93$ cm^{-1}, 27340 measured, 7840 unique, 346 variables, GOF = 1.05, $R1 = 0.035$ ($I > 2\sigma(I)$), $wR_2 = 0.088$ (all unique reflections). For **2**: $C_{46}H_{100}S_6P_6Ti_2Cu_6 \cdot C_6H_{14}$ ($M_r = 1594.75$); $P2_1/n$ (no. 14), $a = 12.450(7)$, $b = 14.061(8)$, $c = 20.683(12)$ Å, $\beta = 92.557(7)°$, $V = 3617.1(35)$ Å^3, $\rho_{calcd} = 1.464$ g cm^{-3}, $Z = 2$, $\mu = 22.74$ cm^{-1}, 28735 measured, 8211 unique, 327 variables, GOF = 1.00, $R1 = 0.047$, $wR_2 = 0.120$. For **3**: $C_{24}H_{60}S_3P_4ClTiCu_3$ ($M_r = 842.80$); *Pnma* (no. 62), $a = 20.772(8)$, $b = 16.653(6)$, $c = 11.356(4)$ Å, $V = 3928.1(25)$ Å^3, $d_{calc} = 1.425$ g cm^{-3}, $Z = 4$, $\mu = 22.02$ cm^{-1}, 31867 measured, 4651 unique, 199 variables, GOF = 1.03, $R1 = 0.043$, $wR_2 = 0.122$. Diffraction data of **1a, 2**, and **3** were collected at −100°C on a Rigaku Mercury CCD diffractometer ($Mo_{K\alpha}$ radiation). The structures were solved by direct methods and refined by full-matrix least-squares on F^2 by using the CrystalStructure software package. All non-hydrogen atoms

were refined anisotropically, and hydrogen atoms were located at calculated positions. Ethyl groups of the phosphane ligands in **2** and **3** were partly disordered, and their carbon atoms were refined isotropically. CCDC-194040 (**1a**), CCDC-194041 (**2**) and CCDC-194042 (**3**) contains the supplementary crystallographic data for this paper. These data can be obtained free of charge via www.ccdc.cam.ac.uk/conts/retrieving.html (or from the Cambridge Crystallographic Data Centre, 12 Union Road, Cambridge CB21EZ, UK; fax: (+44) 1223-336-033; or deposit @ccdc.cam.ac.uk).

[7] G. Christou, K. S. Hagen, J. K. Bashkin, R. H. Holm, *Inorg. Chem.* **1985**, *24*, 1010 – 1018.

[8] S. Pohl, W. Saak, *Angew. Chem.* **1984**, *96*, 886 – 887; *Angew. Chem. Int. Ed. Engl.* **1984**, *23*, 907 – 908.

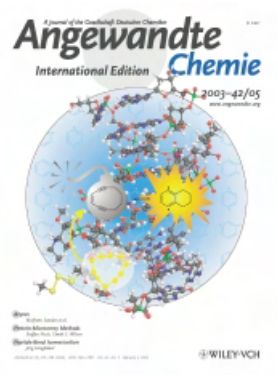
[9] D. Coucouvanis, A. Salifoglou, M. G. Kanatzidis, W. R. Dunham, A. Simopoulos, A. Kostikas, *Inorg. Chem.* **1988**, *27*, 4066 – 4077.

[10] a) S. Dehnen, A. Schäfer, D. Fenske, R. Ahlrichs, *Angew. Chem.* **1994**, *106*, 786 – 790; *Angew. Chem. Int. Ed. Engl.* **1994**, *33*, 764 – 768; b) S. Dehnen, D. Fenske, *Chem. Eur. J.* **1996**, *2*, 1407 – 1416; c) P. Betz, B. Krebs, G. Henkel, *Angew. Chem.* **1984**, *96*, 293 – 294; *Angew. Chem. Int. Ed. Engl.* **1984**, *23*, 311 – 312.

[11] a) T. Amemiya, S. Kuwata, M. Hidai, *Chem. Commun.* **1999**, 711 – 712; b) Y. Huang, R. J. Drake, D. W. Stephan, *Inorg. Chem.* **1993**, *32*, 3022 – 3028.

 © 2003 Wiley-VCH Verlag GmbH & Co. KGaA, Weinheim 1433-7851/03/4204-0468 $ 20.00+.50/0

Cover Picture



Hans Henning Wenk, Michael Winkler, and Wolfram Sander*

A century of aryne chemistry has not dampened the interest in this class of reactive intermediates. The cover picture shows the structure of a calicheamicin–DNA complex, the "warhead" of which is a cyclic enediyne unit (highlighted). The biological activity of the enediyne cytostatics is based on the depicted Bergman cyclization of the enediyne to a didehydrobenzene biradical. More about these short-lived species is given by Sander et al. on pp. 502 ff.

Contents

Web Sites

http://www.dnaftb.org/dnaftb/ —— 487 From Mendel to the Postgenomic Era *A. Marx*

Books

Organometallics in Synthesis —— 488 Manfred Schlosser *N. Krause*

Global Environmental Change —— 489 Ronald E. Hester, Roy M. Harrison *J. Hahn*

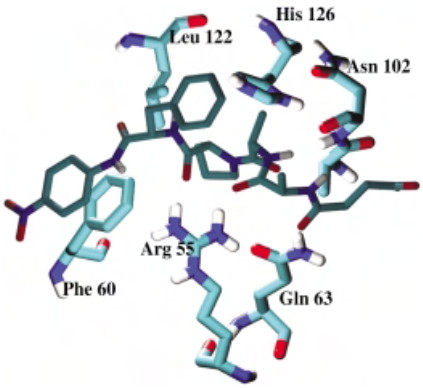
Highlights

Peptide Bond Isomerization

J. Fanghänel* —— 490 – 492

Enzymatic Catalysis of the Peptidyl–Prolyl Bond Rotation: Are Transition State Formation and Enzyme Dynamics Directly Linked?

Keywords:
cyclophilin · enzyme catalysis · molecular dynamics · PPIase · proteins



The search for the answer to the question posed in the title has been helped by results by Eisenmesser et al. on the cyclophilin 18-catalyzed peptidyl–prolyl *cis*/*trans* isomerization. Here their results are discussed in connection with previously published data about the catalytic mechanism of this enzyme class. For several of the amino acid side chains (see picture) present in the active center of the enzyme it could be shown that they are involved in substrate binding or in formation of the transition state.

Minireviews

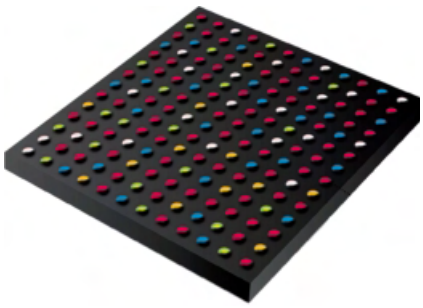
Protein Microarray Methods

D. S. Wilson, S. Nock* —— 494 – 500

Recent Developments in Protein Microarray Technology

Keywords:
drug development · immunoassays · multiplexed analysis · proteomics · proteins

Small and fast: The miniaturization and parallelization of protein microarrays has made it possible to measure simultaneously the interactions between proteins and numerous analytes in a small biological sample. These microarrays consist of numerous, about 50–200 μm, spots with surface-bound proteins (see picture). This will enable the throughput of proteomic analysis to be increased dramatically.



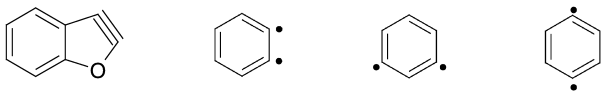
Reviews

100 Years of Arynes

H. H. Wenk, M. Winkler, W. Sander* —— 502 – 527

One Century of Aryne Chemistry

Keywords:
arynes · cyclization · enediynes · matrix isolation · quantum chemistry



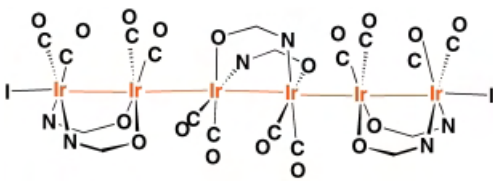
1 **2** **3** **4**

One century the after postulation of the first aryne (didehydrobenzofuran **1**) as a reactive intermediate, research activities in this area are more prevalent than ever before. The discovery of the endiyne cytostatics in particular has promoted a renaissance of aryne chemistry. Despite considerable progress during the last few years many questions still remain unanswered and, therefore, interest in aryne chemistry—parent systems **2**–**4**—is expected to continue far into the future.

© 2003 Wiley-VCH Verlag GmbH & Co. KGaA, Weinheim

1433-7851/03/4205-0478 $ 20.00+.50/0

Communications



Electrons in chains: A novel metallic chain made up of six iridium atoms (see picture) with an average oxidation state of +1.33 has been found in the complex HH,HT,HH-$[Ir_6(\mu\text{-}OPy)_6(I)_2(CO)_{12}]$ (Opy = 2-pyridonate, H = head, T = tail). This complex provides a new link in the electronic sequence connecting dinuclear Ir^{I} and Ir^{II} complexes.

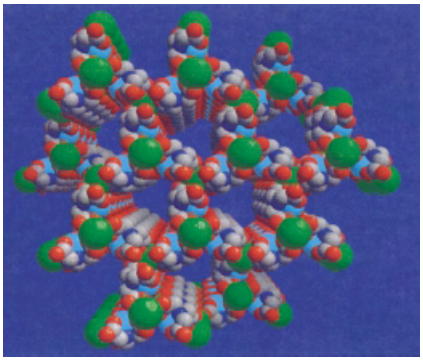
Chains of Metal Atoms

C. Tejel, M. A. Ciriano,* B. E. Villarroya, J. A. López, F. J. Lahoz, L. A. Oro* ——— **529 – 532**

A Hexanuclear Iridium Chain

Keywords:
chain structures · electronic structure · iridium · metal–metal interactions · N,O ligands

Water shortage: The structures of the three-dimensional coordination polymers $[\{M_2(Cu_3(iminodiacetate)_6)\}\cdot 8\,H_2O]_n$ (M = La (**1**), Nd (**2**), and Eu (**3**)) contain water molecules that are located within channels throughout the lattice structure (see picture). Investigation of their thermal stability shows that the frameworks remained intact when the guest water molecules were removed. Rehydration of the La and Eu species leads to polymers with only five lattice water molecules per polymer unit, which corresponds to a change in the bonding characteristics of the water molecules.

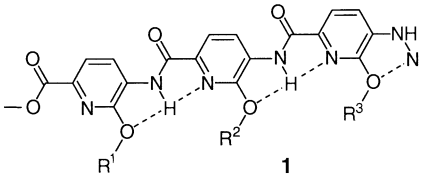


Nanoporous Coordination Polymers

Y.-P. Ren, L.-S. Long,* B.-W. Mao, Y.-Z. Yuan, R.-B. Huang, L.-S. Zheng ——— **532 – 535**

Nanoporous Lanthanide–Copper(II) Coordination Polymers: Syntheses and Crystal Structures of $[\{M_2(Cu_3(iminodiacetate)_6)\}\cdot 8\,H_2O]_n$ (M = La, Nd, Eu)

Keywords:
copper · lanthanides · nanostructures · polymers · structure elucidation



1

The prevention of cell death by the anti-apoptotic protein Bcl-xL has been linked to a number of cancers. Bcl-xl binds to the BH3 domain of the proapoptotic protein Bak, thus preventing programmed cell death. A competitive assay and docking studies have shown that the polyamide scaffold **1**, which was synthesized based on a rational structure-based design, interferes with the Bak BH3/Bcl-xl complexation.

Protein-Protein Interactions

J. T. Ernst, J. Becerril, H. S. Park, H. Yin, A. D. Hamilton* ——— **535 – 539**

Design and Application of an α-Helix-Mimetic Scaffold Based on an Oligoamide-Foldamer Strategy: Antagonism of the Bak BH3/Bcl-xL Complex

Keywords:
amides · helical structures · peptidomimetics · protein models · proteins

For the USA and Canada:
ANGEWANDTE CHEMIE International Edition (ISSN 1433-7851) is published weekly by Wiley-VCH PO Box 191161, D 69451 Weinheim, Germany. Air freight and mailing in the USA by Publications Expediting Inc. 200 Meacham Ave., Elmont, NY 11003. Periodicals postage paid at Jamaica NY 11431. US POSTMASTER: send address changes to *Angewandte Chemie*, Wiley-VCH, 111 River Street, Hoboken, NJ 07030. Annual institutional subscription price for institutions: Europe € 2998.00/3148.00. Outside Europe US$ 3718.00/3904.00 (valid for print or electronic/print and electronic delivery); for individuals who are personal members of a national chemical society, or whose institution already subscribes, or who are retired or self-employed consultants, print only (including postage and handling charges): Europe € 248.00/Outside Europe US$ 348.00.

 © 2003 Wiley-VCH Verlag GmbH & Co. KGaA, Weinheim 1433-7851/03/4205-0479 $ 20.00+.50/0

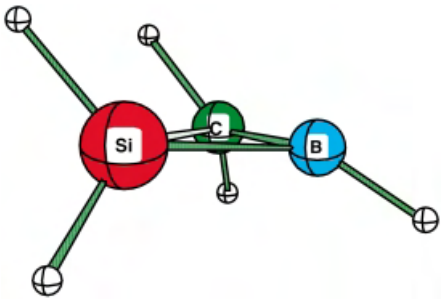
Contents

Theory of Pyramidal Boron

K. T. Giju, A. K. Phukan, E. D. Jemmis* ——— 539 – 542

Stabilization of Tricoordinate Pyramidal Boron: Theoretical Studies on $CBSiH_5$, BSi_2H_5, $CBGeH_5$, and $CBSnH_5$

Keywords: boron · computer chemistry · density functional calculations · small ring systems



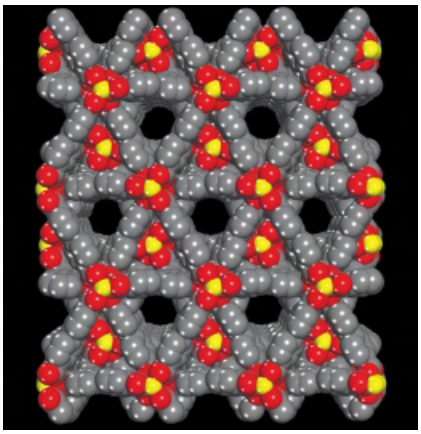
Discovery of new pyramids: Theoretical studies have characterized $CBSiH_5$, BSi_2H_5, $CBGeH_5$, and $CBSnH_5$, all of which have a tricoordinate pyramidal boron atom as minima on their respective potential energy surfaces (see picture). The extent of pyramidalization, as well as the energy for inversion through the planar structure, is dependent on the substituents of the boron atom.

Ship-in-Bottle Photochemistry

L. Pan, H. Liu, X. Lei, X. Huang, D. H. Olson, N. J. Turro, J. Li* ——— 542 – 546

IRPM-1: A Recyclable Nanoporous Material Suitable for Ship-In-Bottle Synthesis and Large Hydrocarbon Sorption

Keywords: cobalt · coordination polymers · host-guest systems · photochemistry · zeolite analogues



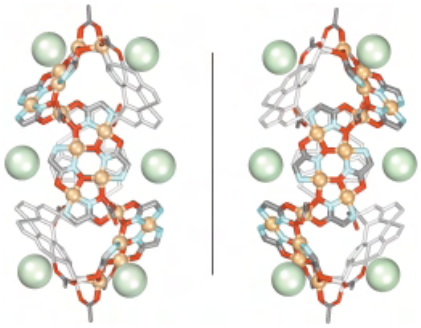
Narrow windows and large supercavities comprise the novel nanoporous coordination organometallic structure IRPM-1, which has a two-fold interpenetrating 3D network containing unique open channels (see picture). IRPM-1 exhibits a high sorption capacity for large hydrocarbons and superior size/shape selectivity for the photolysis of *ortho*-methyl dibenzyl ketone (*o*-MeDBK; 100% cage effect). A completely reversible structural transformation takes place between IRPM-1 and a nonporous 1D compound, which allows a full recovery of the *o*-MeDBK derived products (100% mass balance).

Chiral Metallahelicates

J. A. Johnson, J. W. Kampf, V. L. Pecoraro* ——— 546 – 549

The Preparation of a Double Metallahelicate Containing 28 Copper Atoms

Keywords: copper · helical structures · macrocycles · self-assembly · supramolecular chemistry



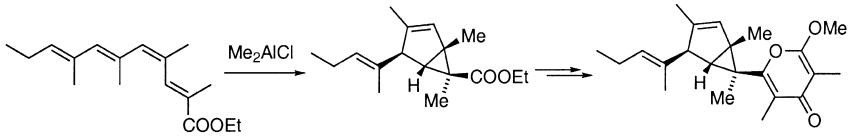
Both L- or D-norvaline hydroxamic acids undergo one-step reactions with acetate, chloride, and Cu^{II} ions to form self-assembled metallahelicates that contain 20 chiral carbon and four chiral metal centers. Enantiopure complexes of over three nanometers in length, and composed of either *P*- or *M*-type double-stranded helical oligomers (see scheme), have been isolated.

Lewis Acids in Total Synthesis

A. K. Miller, D. Trauner* ——— 549 – 552

Total Synthesis of (±)-Photodeoxytridachione through a Lewis Acid Catalyzed Cyclization

Keywords: cyclization · cycloaddition · homogeneous catalysis · Lewis acids · total synthesis

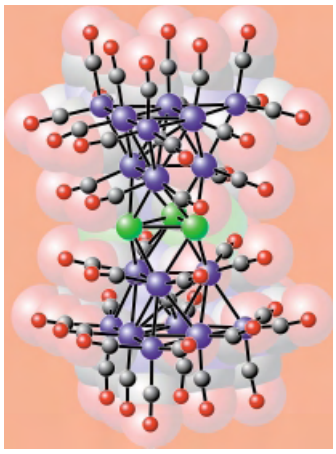


1 **2** **3**

Concerted or stepwise: The concise total synthesis of the molluscan polypropionate photodeoxytridachione (**3**) features a Lewis acid catalyzed cyclization of tetraenoic ester **1** to form bicylo[3.1.0]hexene **2** as a key step. The stereochemistry of the cyclization can be rationalized in terms of a stepwise or a concerted mechanism.

© 2003 Wiley-VCH Verlag GmbH & Co. KGaA, Weinheim
1433-7851/03/4205-0480 $ 20.00+.50/0

Palladium-filled sandwiches: The reaction between the $[Os_{10}(\mu_6\text{-}C)(CO)_{24}]^{2-}$ ion and $[Pd(NCMe)_4](BF_4)_2$ yields the osmium–palladium mixed-metal cluster, $[\{N(PPh_3)_2\}_2\{Os_{18}Pd_3(\mu_6\text{-}C)_2(CO)_{42}\}]$, which has the highest nuclearity known for such clusters, and has been shown by single-crystal X-ray analysis to be a "metal sandwich" with two Os_9 units connected by a triangular Pd_3 subcluster (see picture); five reversible cathodic waves have been observed through cyclic voltammetry.

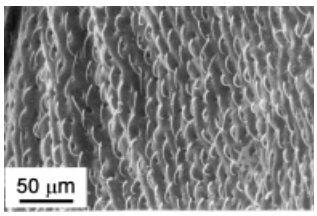


Osmium–Palladium Clusters

K.-F. Yung, W.-T. Wong* —— **553 – 555**

$[\{N(PPh_3)_2\}_2\{Os_{18}Pd_3(\mu_6\text{-}C)_2(CO)_{42}\}]$: An Osmium–Palladium Mixed-Metal High-Nuclearity Carbonyl Cluster

Keywords:
cluster compounds · electrochemistry · osmium · palladium · redox chemistry



Silica coats for butterfly wings: The oxidation of silane with hydrogen peroxide is conducted on the surface of delicately structured biological specimens (templates), to produce a thin silica coating that leaves the underlying structure unharmed. Removal of the template by calcination leaves a precise replica of the original specimen (see SEM image of a silica replica obtained from a fly wing). The method is also proposed as a novel means of conservation for sensitive archaeological specimens.

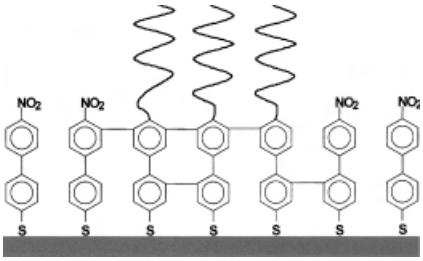
Biomimetic Structures Through CVD

G. Cook, P. L. Timms, C. Göltner-Spickermann* —— **557 – 559**

Exact Replication of Biological Structures by Chemical Vapor Deposition of Silica

Keywords:
biomimetics · coating · CVD · replication · silicates

Patterned polymer brushes can be produced on the micrometer and nanometer scale by a combination of self-assembly and lithography. Self-assembled monolayers of biphenyl thiols were structured by chemical lithography. The patterns were amplified by surface-initiated polymerization.



Patterned Polymer Brushes

U. Schmelmer, R. Jordan,* W. Geyer, W. Eck, A. Gölzhäuser,* M. Grunze, A. Ulman —— **559 – 563**

Surface-Initiated Polymerization on Self-Assembled Monolayers: Amplification of Patterns on the Micrometer and Nanometer Scale

Keywords:
azo compounds · lithography · polymerization · polymers · self-assembly

 © 2003 Wiley-VCH Verlag GmbH & Co. KGaA, Weinheim 1433-7851/03/4205-0481 $ 20.00+.50/0

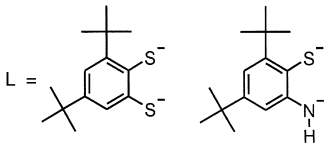
Contents

Radical Anion Complexes

P. Ghosh, A. Begum, D. Herebian, E. Bothe, K. Hildenbrand, T. Weyhermüller, K. Wieghardt* ——— **563 – 567**

Coordinated *o*-Dithio- and *o*-Iminothiobenzosemiquinonate(1−) π Radicals in $[M^{II}(bpy)(L^{\bullet})](PF_6)$ Complexes

Keywords:
electronic structure · palladium · platinum · radical ligands · S ligands



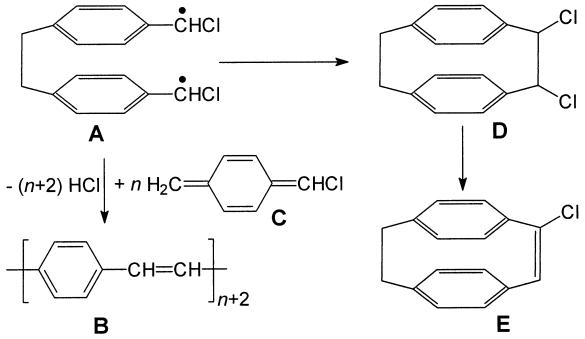
Reversible ligand-centered one-electron oxidation of square-planar neutral complexes of palladium(II) and platinum(II) [M(bpy)(L)] (bpy = bipyridine, L: see picture) leads to the paramagnetic complexes $[M(bpy)(L^{\bullet})]^+$. Thus, the existence of S,S-coordinated *o*-dithiobenzosemiquinonate(1−) π radical ions has been proven unequivocally.

Polymerization Mechanism Determined

J. Wiesecke, M. Rehahn* ——— **567 – 570**

[2.2]Paracyclophanes with Defined Substitution Pattern—Key Compounds for the Mechanistic Understanding of the Gilch Reaction to Poly(*p*-phenylene vinylene)s

Keywords:
cyclophanes · Gilch reaction · radical reactions · reaction mechanisms



Radical reassessment: [2.2]Paracyclophanes **D** and **E** have been identified as the main side-products of the Gilch reaction leading to poly(*p*-phenylene vinylene)s (PPV **B**). The constitution of the cyclic dimers allows the conclusion to be drawn that the PPV formation occurs by free-radical polymerization of **C**, initiated by diradicals **A**. Anionic chain growth, often discussed as an alternative to the radical process, can be excluded.

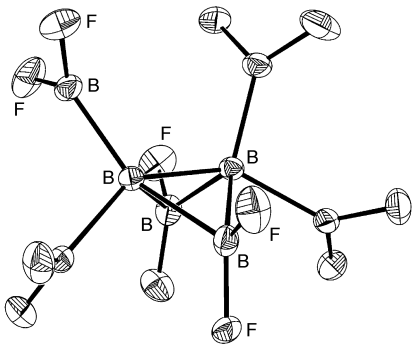
Structures of Polyboron Fluorides

J. A. J. Pardoe, N. C. Norman, P. L. Timms,* S. Parsons,* I. Mackie, C. R. Pulham, D. W. H. Rankin ——— **571 – 573**

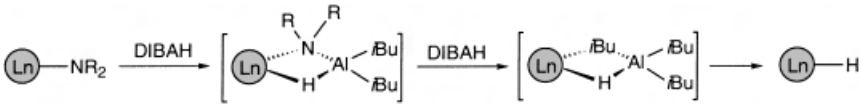
The Surprising Structures of B_8F_{12} and $B_{10}F_{12}$

Keywords:
boron · bridging ligands · cluster compounds · fluorides · X-ray diffraction

Unstable, reactive, and yellow: Compound B_8F_{12}, assumed for 30 years to have a diborane-like structure $B_2(BF_2)_6$, has now been shown also to contain a short, central B—B bond. Across the B—B bond are two bridging BF_2 groups, which are bent out of the plane by long-range, intramolecular F···B interactions. The B-(μ-BF_2) bonds are long and, surprisingly, asymmetric, but calculations confirm that this structure is intrinsic to the molecule.



© 2003 Wiley-VCH Verlag GmbH & Co. KGaA, Weinheim
1433-7851/03/4205-0482 $ 20.00+.50/0



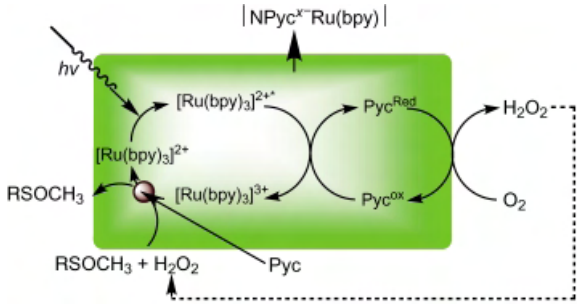
Unsolvated hydride derivatives [Me_2Si-(2-Me-C_9H_5)$_2$LnH] (Ln = Y, Ho) are available from *ansa*-lanthanidocene complexes *rac*-[{Me_2Si(2-Me-C_9H_5)$_2$}Ln{N($SiHMe_2$)$_2$}] by utilizing a novel [N($SiHMe_2$)$_2$]/[H] transformation inititated by diisobutylaluminumhydride (DIBAH; see scheme; R = $SiHMe_2$). The molecular structure of the THF adduct reveals a "flyover" dimer of composition [{Y(thf)}$_2${μ_2-[(η^5-2-Me-C_9H_5)$SiMe_2$(η^5-2-Me-C_9H_5)]}$_2$(μ_2-H)$_2$].

Amide/Hydride Transformation

M. G. Klimpel, P. Sirsch, W. Scherer, R. Anwander* ——— 574 – 577

DIBAH-Mediated Amide/Hydride Transformation in *ansa*-Lanthanidocene(III) Complexes

Keywords:
BIBAH · holmium · hydrides · metallocenes · silylamide · yttrium



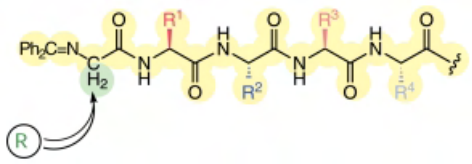
A heterogenous nafion membrane containing lead ruthenate pyrochlore (Pyc) and $[Ru(bpy)_3]^{2+}$ (designated as |NPyc^{x-}Ru(bpy)|) photochemically catalyzes the selective oxidation of organic sulfide to sulfoxide in the presence of O_2 through formation of H_2O_2 as an intermediate (see scheme, R = Ph, $PhCOCH_3$, $PhOCH_3$).

Photocatalytic Oxidation

J.-M. Zen,* S.-L. Liou, A. S. Kumar, M.-S. Hsia ——— 577 – 579

An Efficient and Selective Photocatalytic System for the Oxidation of Sulfides to Sulfoxides

Keywords:
heterogeneous catalysis · membranes · photochemistry · ruthenium · sulfoxidation



Virtually complete chirality transfer has been realized in the N-terminal alkylation of small, Schiff-base activated peptides under mild phase-transfer conditions, in which finely tuned chiral quaternary ammonium salts are used as catalysts. Repeated extension and alkylation of the N-terminal position can lead selectively to nonnatural oligopeptides (see picture).

Stereoselective Alkylation

T. Ooi, E. Tayama, K. Maruoka* ——— 579 – 582

Highly Stereoselective N-Terminal Functionalization of Small Peptides by Chiral Phase-Transfer Catalysis

Keywords:
alkylation · asymmetric catalysis · peptides · phase-transfer catalysis · synthetic methods

VIP Communications labeled with this symbol have been judged by two referees as being "very important papers".

The publication of Communications labeled with this symbol has been accelerated because of their topical or highly competitive nature.

Supporting information for articles labeled with this symbol can be found at www.angewandte.org or www.interscience.wiley.com.

 © 2003 Wiley-VCH Verlag GmbH & Co. KGaA, Weinheim 1433-7851/03/4205-0483 $ 20.00+.50/0

Sources

Product and Company Directory

You can start the entry for your company in "Sources" in any issue of *Angewandte Chemie*.

If you would like more information, please do not hesitate to contact us.

Wiley-VCH Verlag – Advertising Department
Tel.: 0 62 01 - 60 65 65
Fax: 0 62 01 - 60 65 50
E-Mail: MSchulz@wiley-vch.de

Service

Keywords ____ *584*

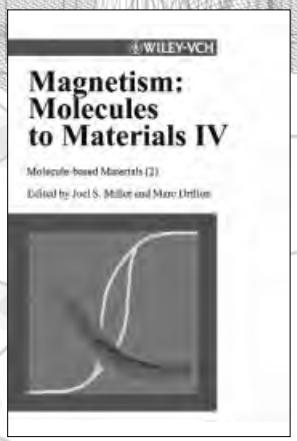
Authors ____ *585*

Angewandte's Sister Journals ____ *586*

Sources ____ *A7 – A8*

Preview ____ *587*

Magnetism: Molecules to Materials



J.S. MILLER, University of Utah, Salt Lake City, USA; **M. DRILLON**, Inst. de Physique et Chimie des Materiaux de Strasbourg, France (Eds)

John Wiley & Sons, Ltd.
Baffins Lane Chichester, West Sussex, PO 19 1UD, UK
Fax: +44 (0)1243-775878

WILEY

As a depository of contemporary knowledge on key topics related to magnetism, this open series of volumes provides a much-needed comprehensive overview of this growing interdisciplinary field. In topical reviews written by foremost scientists trends and recent advances focusing on the correlations between electronic structure and magnetic properties are explained in a clear and detailed way. The balance between theory and experiment within this series will guide advanced students and specialists alike to this research area. It will help evaluate own experimental observations and serve as a base for the design of new magnetic materials. A unique reference work, indispensable for everyone concerned with the phenomena of magnetism!

Reviews for Volume II:
"... presents a good ... current overview of an active and diverse research area."
Journal of the American Chemical Society

NEW: Magnetism: Molecules to Materials IV
Molecule-based Materials (2)
2002. XI, 492 pp. 300 fig. HC
€ 159.-/£ 95.-/US$ 125.-
3-527-30429-0

Magnetism: Molecules to Materials III
Nanosized Magnetic Materials
2001. XV, 388 pp. 209 fig. 14 tab. HC
€ 139.-/£ 80.-/US$ 125.-
3-527-30302-2

Magnetism: Molecules to Materials II
Molecule-Based Materials
2001. XIV, 489 pp. 323 fig. 43 tab. HC
€ 159.-/£ 95.-/US$ 125.-
3-527-30301-4

Magnetism: Molecules to Materials I
Models and Experiments
2001. XVI, 437 pp. 270 fig. 33 tab. HC
€ 139.-/£ 80.-/US$ 125.-
3-527-29772-3

WILEY-VCH · P.O. Box 10 11 61 · 69451 Weinheim, Germany · Fax: +49 (0) 62 01-60 61 84 · e-mail: service@wiley-vch.de · http://www.wiley-vch.de

WILEY-VCH

 © 2003 Wiley-VCH Verlag GmbH & Co. KGaA, Weinheim 1433-7851/03/4205-0484 $ 20.00+.50/0

Peptide Bond Isomerization

Enzymatic Catalysis of the Peptidyl–Prolyl Bond Rotation: Are Transition State Formation and Enzyme Dynamics Directly Linked?**

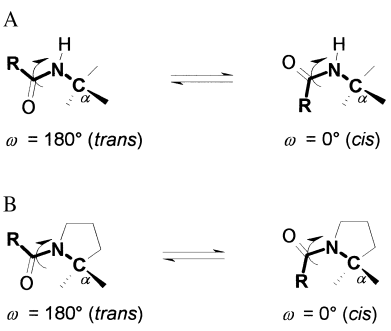
*Jörg Fanghänel**

Keywords:
cyclophilin · enzyme catalysis · molecular dynamics · PPIase · proteins

How do enzymes achieve the extraordinary decrease in activation energy for the conversion of substrates to their products? This question has been discussed extensively since the beginning of enzymological research. Five catalytic mechanisms have been determined to be particularly important:[1]

1) catalysis by preorientation and proximity of reactants
2) covalent catalysis
3) general acid-base catalysis
4) catalysis through complementarity of the active site with the transition state
5) catalysis through conformational distortion of the reactants.

It has been speculated for 25 years that the internal motion of the protein backbone and of amino acid side chains could contribute not only to the the formation of the enzyme–substrate complex, but also to the substrate conversion and therefore to all five of the mentioned catalytic mechanisms.[2] Based on Kramers' theory, the viscosity dependence of the acceleration of the reaction catalyzed by carboxypeptidase A was demonstrated and explained through the reduced protein flexibility in highly viscous solutions.[2] NMR spectroscopic methods for measuring nuclear relaxation rates have been employed to gain further insight into protein dynamics and have changed our view of enzymes from that of a rigid polymer to a dynamic macromolecule.[3,4] Eisenmesser et al. have recently published the first direct evidence showing that the dynamics of certain amino acid residues are linked to the formation of the enzyme-bound transition state. Using the cyclophilin 18 (Cyp18)-catalyzed reaction as a model, the authors showed that the dynamics of an amino acid residue in the active site of the enzyme changes with the catalytic cycle.[5] The investigated protein is a member of the enzyme class of peptidyl–prolyl *cis*/*trans* isomerases (PPIases, EC 5.2.1.8), which were first described in 1984.[6] Owing to its partial double-bond character, the peptide bond is planar and the two thermodynamically most stable conformers with torsion angles of $\omega = 0°$ (*cis*) and $\omega = 180°$ (*trans*) (Scheme 1, A) are separated by an activation barrier of 75–100 kJ mol^{-1}. PPIases can lower this activation barrier for peptidyl–prolyl bonds and thus catalyze the conversion of *cis* and *trans* conformers in oligopeptides and proteins.[7] They accelerate the refolding of proteins, which contain a *cis*-peptidyl–prolyl bond in the folded state, as well as the isomerization of this bond in the native state of proteins.[7–9]



Scheme 1. The *cis* and *trans* conformations of a secondary amide peptide bond (A) and of a peptidyl–prolyl bond (B).

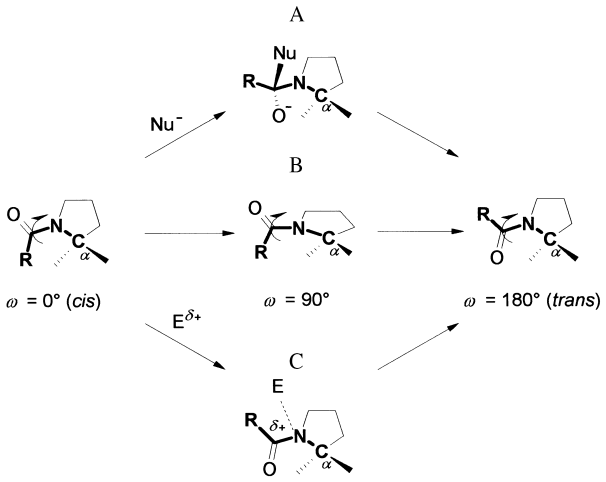
Investigations of oligo- and dipeptides as well as of *N*-methylacetamide showed that the *trans* conformer of a secondary amide peptide bond is about 10–16 kJ mol^{-1} more stable than the *cis* conformer. For the imidic peptidyl–prolyl bond the stabilization of the *trans* conformer is only about 2–6 kJ mol^{-1}, which leads to an increased concentration of the *cis* conformer of between 5 and 30% (Scheme 1, B).[10,11] Because the *cis*/*trans* isomerization is one of the simplest chemical reactions, PPIases are particularly suitable for basic enzymological research. Scheme 2 summarizes the three main catalytic mechanisms of PPIases described in the literature.

Fischer et al. observed that Cyp18 is inactivated by thiol-modifying reagents and concluded that during catalysis a thiol group attacks the carbonyl carbon atom of the peptidyl–prolyl bond in a nucleophilic manner to form a tetrahedral intermediate which leads to a reduction of the partial double-bond character of the peptide bond (Scheme 2, A).[6] Enzyme kinetic and crystallographic data for Pin1, another PPIase, led to the conclusion that such a tetrahedral intermediate is likely.[12] In contrast, based on secondary kinetic deuterium isotope effects, Harrison and Stein, concluded that the transition state of Cyp18 catalysis cannot be tetrahedral,[13] and proposed a new model:

[*] Dipl. Biochem. J. Fanghänel
Max-Planck-Forschungsstelle für Enzymologie der Proteinfaltung
Weinbergweg 22, 06120 Halle/Saale (Germany)
Fax: (+49) 345-551-1972
E-mail: fanghaenel@enzyme-halle.mpg.de

[**] I thank Prof. Dr. Gunter Fischer, Halle, for helpful discussions during the preparation of the manuscript.

 © 2003 Wiley-VCH Verlag GmbH & Co. KGaA, Weinheim, 1433-7851/03/4205-0490 $ 20.00+.50/0



Scheme 2. Overview of the three most important mechanisms of catalysis for PPIase-catalyzed peptidyl–prolyl *cis*/*trans* isomerization as discussed in the literature. A: Nucleophilic attack (Nu^-) of the carbonyl carbon atom; B: formation and stabilization of a transition state in which the carbonyl oxygen atom is perpendicular to the plane of the proline ring; C: destabilization of the partial double-bond character by interaction of the imide nitrogen atom with an electrophile (E). (Scheme adapted from G. Fischer).[19]

polar resonance structures are destabilized through hydrophobic interactions of the peptidyl–prolyl bond within the active site, thus decreasing the double-bond character. It is then forced from its planar structure into a transition state in which the carbonyl oxygen atom is perpendicular to the prolyl ring ($\omega = 90°$, Scheme 2, B). However, studies with inhibitors mimicking this transition state as well as NMR spectroscopic measurements with an enzyme-bound oligopeptide did not support this mechanism.[14,15]

The determination of the crystal structure of a Cyp18–substrate complex by Y. Zhao and H. Ke confirmed a third catalytic mechanism, first proposed by Kofron et al. The latter observed a close proximity of the guanidine group of Arg 55 to the imide-nitrogen atom of the substrate proline and concluded that a hydrogen bond could be formed in the enzyme-bound transition state.[16,17] This would decrease the rotational barrier for the *cis*/*trans* isomerization (Scheme 2, C). Figure 1 shows the active site of Cyp18 as derived from the crystal structures. In accordance with the mechanism proposed by Kofron et al., the Arg-55-Ala variant of Cyp18 retains only 0.1% of the activity of the wild-type enzyme.

On the other hand, these crystal structures represent only the thermodynamically most stable ground state of the enzyme–substrate complex under the given crystallization conditions and provide little information about the transition state during catalysis. This ground state might be far off the reaction coordinate and constitute a dead-end complex. As another disadvantage, crystal structures generally do not offer much insight into enzyme dynamic processes. NMR spectroscopy provides us with tools that allow these limitations to be overcome. The Cyp18-catalyzed reaction suits these experiments for the following reasons:

1) The reaction is completely reversible and proceeds without side products.
2) The equilibrium concentrations of substrates and products are similar.
3) The parameters of the catalysis are on the same time scale as that for NMR spectroscopic methods to analyze the protein dynamics.
4) The structure of the enzyme in solution has already been determined by NMR spectroscopy.
5) The enzyme has been well characterized by a broad range of methods.

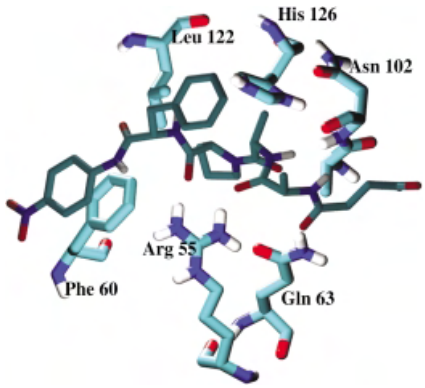


Figure 1. Active site of Cyp18 derived from the crystal structure.[17] The amino acid residues in the vicinity of the substrate peptidyl–prolyl bond are highlighted. The C-terminus of the bound substrate peptide (Suc-Ala-Ala-Pro-Phe-NH-Np) is on the left-hand side. The following protein variants are described in the literature: Arg-55-Ala (0.1% residual activity), Phen-60-Ala (0.32%), His-126-Glu (0.5%).

NMR spectroscopic line shape analysis of oligopeptide signals during catalysis showed that both the *cis* and *trans* conformer bind to the active site of Cyp18 with similar affinity.[18] The same experiments indicated that the isomerization proceeds by rotation of the C-terminal part of the peptide, while the N-terminus remains bound to Cyp18. Eisenmesser et al. estimated the change in protein backbone dynamics by measuring the longitudinal and transversal autocorrelation parameters $R1$ and $R2$, respectively, as a function of the substrate concentration.[5] Protein-dynamic processes such as substrate binding and turnover occurring in a micro- and millisecond time frame, affect the autocorrelation parameter $R2$, while $R1$ depends on structural fluctuations in the picosecond range. For ten backbone nitrogen atoms of Cyp18 (Arg 55, Thr 68, Gly 72, Lys 82, Leu 98, Ser 99, Ala 101, Asp 102, Ala 103, and Gly 109), a change of $R2$ but not $R1$ is observed upon addition of substrate. All identified backbone nitrogen atoms are in close proximity to the substrate molecule, even though only some of the corresponding amino acid side chains are known to be in direct contact with the substrate in its *cis* conformation (Arg 55, Asp 102, and Ala 103).

Both substrate binding and catalysis can have an influence on the environment of the observed ^{15}NH–H bond of the protein backbone and thus affect $R2$. To separate both effects, $R2$ was measured as a function of substrate concentration. Enzyme amino acid residues that are exclusively involved in substrate binding would show the greatest change in $R2$ when equal amounts of free and bound enzyme molecules are present in the solution. The substrate dependence of $R2$ for nine out of the ten amino acid residues mentioned above can be described by a model that takes only binding of the substrate with Cyp18, but not catalysis, into consideration. For the peptide nitrogen atom of Arg 55 on the other hand, the biggest change in $R2$ occurs under saturated conditions. The authors argued that this type of behavior

 © 2003 Wiley-VCH Verlag GmbH & Co. KGaA, Weinheim, 1433-7851/03/4205-0491 $ 20.00+.50/0

cannot be explained by binding processes alone. They conclude that catalysis of the *cis*/*trans* isomerization of the bound substrate molecule by the enzyme must be the reason for this peculiar change in dynamics of Arg 55. Additional evidence for this assumption comes from the fact that the dynamics of Arg 55 changes with the same rate as the substrate conversion. In another publication Bosco et al.[9] demonstrated the crucial role of Arg 55 in the Cyp18-catalyzed *cis*/*trans* isomerization of proline-containing oligopeptides, and extended these findings to a native protein substrate of cyclophilin: They showed that the *cis*/*trans* conversion of the glycyl-89–prolyl bond in the folded HIV-1 coat protein is accelerated by catalytic amounts of Cyp18, and that the Arg 55-Ala mutant of Cyp18 no longer displays PPIase activity against this substrate.

The experiments performed by Eisenmesser et al. provide the first direct evidence that the change of the dynamics of a peptide nitrogen atom is coupled with the formation of the enzyme-bound transition state. Furthermore, they confirm the participation of Arg 55 in Cyp18 in the catalysis of the *cis*/*trans* isomerization of peptidyl–prolyl bonds both in oligopeptides as well as in native proteins. However, these measurements do not permit insight into the molecular details of all amino acids involved in catalysis. Extending the investigations from backbone to side chain dynamics could now substantially improve our understanding of Cyp18 action. Despite the new insights into protein dynamics, it remains to be shown to what extent active site residues and some tightly bound water molecules visible in the crystal structure are involved in transition state formation. It is important to note that the available crystal structures of Cyp18–substrate complexes do not represent the transition state and are therefore of limited use for identifying all amino acid residues for catalysis. The ten residues identified by Eisenmesser et al. provide valuable clues in this respect.

[1] R. A. Copeland, *Enzymes*, Wiley-VCH, New York, **2000**.
[2] B. Gavish, M. M. Werber, *Biochemistry* **1979**, *18*, 1269.
[3] L. E. Kay, *Biochem. Cell. Biol.* **1998**, *76*, 145.
[4] A. J. Wand, *Nat. Struct. Biol.* **2001**, *8*, 926.
[5] E. Z. Eisenmesser, D. A. Bosco, M. Akke, D. Kern, *Science* **2002**, *295*, 1520.
[6] G. Fischer, H. Bang, C. Mech, *Biomed. Biochim. Acta.* **1984**, *43*, 1101.
[7] S. F. Gothel, M. A. Marahiel, *Cell. Mol. Life. Sci.* **1999**, *55*, 423.
[8] K. N. Brazin, R. J. Mallis, D. B. Fulton, A. H. Andreotti, *Proc. Nat. Acad. Sci. USA* **2002**, *99*, 1899.
[9] D. A. Bosco, E. Z. Eisenmesser, S. Pochapsky, W. I. Sundquist, D. Kern, *Proc. Natl. Acad. Sci. USA* **2002**, *99*, 5247.
[10] A. Jabs, M. S. Weiss, R. Hilgenfeld, *J. Mol. Biol.* **1999**, *286*, 291.
[11] M. S. Weiss, A. Jabs, R. Hilgenfeld, *Nat. Struct. Biol.* **1998**, *5*, 676.
[12] R. Ranganathan, K. P. Lu, T. Hunter, J. P. Noel, *Cell* **1997**, *89*, 875.
[13] R. K. Harrison, R. L. Stein, *J. Am. Chem. Soc.* **1992**, *114*, 3464.
[14] H. C. Wang, K. Kim, R. Bakhtiar, J. P. Germanas, *J. Med. Chem.* **2001**, *44*, 2593.
[15] L. T. Kakalis, I. M. Armitage, *Biochemistry* **1994**, *33*, 1495.
[16] J. L. Kofron, P. Kuzmic, V. Kishore, E. Colon-Bonilla, D. H. Rich, *Biochemistry* **1991**, *30*, 6127.
[17] Y. Zhao, H. Ke, *Biochemistry* **1996**, *35*, 7356.
[18] D. Kern, G. Kern, G. Scherer, G. Fischer, T. Drakenberg, *Biochemistry* **1995**, *34*, 13594.
[19] G. Fischer, *Chem. Soc. Rev.* **2000**, *29*, 119.

Protein Microarray Methods

Recent Developments in Protein Microarray Technology

*David S. Wilson and Steffen Nock**

Keywords:
drug development · immunoassays · multiplexed analysis · proteomics · proteins

The sequencing of the human genome and the advent of DNA chips and sophisticated bioinformatics platforms have enabled molecular biologists to take a more global view of biological systems and to analyze naturally occurring genetic variation. Microarrays of antibodies can measure the concentrations of many proteins quickly and simultaneously. Microarrays of genomically encoded proteins allow scientists to screen entire genomes for proteins that interact with particular factors, catalyze particular reactions, or act as substrates for protein-modifying enzymes or as targets of autoimmune responses. The new protein microarray platforms will prove invaluable to basic biological research, and will dramatically accelerate the pace of discovery of drug targets and diagnostic biomarkers.

Introduction

During the last two decades, protein biochemists have envied molecular biologists working with nucleic acids for their rapid and tangible scientific progress, the most notable example being the sequencing of the human genome. The latest triumph of nucleic acid biotechnology has been the invention of DNA microarrays, which allow for the simultaneous monitoring of the expression, at the mRNA level, of thousands to tens of thousands of genes in a single experiment. These accomplishments have been enabled by significant improvements in the core technologies of nucleic acid biochemistry—oligonucleotide synthesis, DNA sequencing, and hybridization-based detection of DNA and RNA—as well as in bioinformatics. In particular, the ability to miniaturize, multiplex, and automate these basic operations has radically increased the rate of data generation.

Despite the clear technical advantages of analyzing nucleic acids over proteins, the latter are the functional products of most genes and the targets of pharmaceutical intervention, so there is a clear need for protein analysis tools to "catch up" with those for examining nucleic acids. One avenue in this direction has been the development of protein microarrays, which have been reviewed in depth.[1–5] As in the case of nucleic acid microarrays, both multiplexation and miniaturization are achieved relative to traditional methods, thus dramatically increasing the amount of data that can be obtained per volume of biological sample. For example, when 100 μL of sample is applied to a flat surface with 10000 spatially and biochemically distinct features (for example, each one being derivatized with a different antibody—see Figure 1), then it would be possible to obtain up to 10000 data points in one experiment. By comparison, a conventional 96-well ELISA type assay would only produce a single data point from the same amount of sample.

Identification of Molecular Patterns

This ability of protein microarrays to increase the quantity of data points per amount of biological sample is critical for protein expression profiling since the protein samples are often very limited in supply and (unlike nucleic acids) cannot be amplified. If the goal of expression profiling is to identify molecular markers for pathological conditions, protein microarrays will allow for more potential markers to be screened than would be possible using conventional, serial biochemical analysis. This not only offers a higher likelihood of finding a suitable marker, but also opens up the possibility of finding diagnostic patterns ("biosignatures") of protein levels that would be missed if one were taking a more traditional, reductionist approach of attempting to correlate individual protein levels with disease states. The possibility that pathological states can be correlated to patterns of gene expression, as opposed to correlation to single markers, has been clearly demonstrated for various types of cancer at the mRNA level.[6–12] These reports also demonstrated that gene expres-

[*] S. Nock, D. S. Wilson
Department of Biochemistry
Zyomyx, Inc.
26101 Research Road, Hayward, CA 94545 (USA)
Fax: (+1) 510-784-2569
E-mail: snock@zyomyx.com

 © 2003 Wiley-VCH Verlag GmbH & Co. KGaA, Weinheim 1433-7851/03/4205-0494 $ 20.00+.50/0

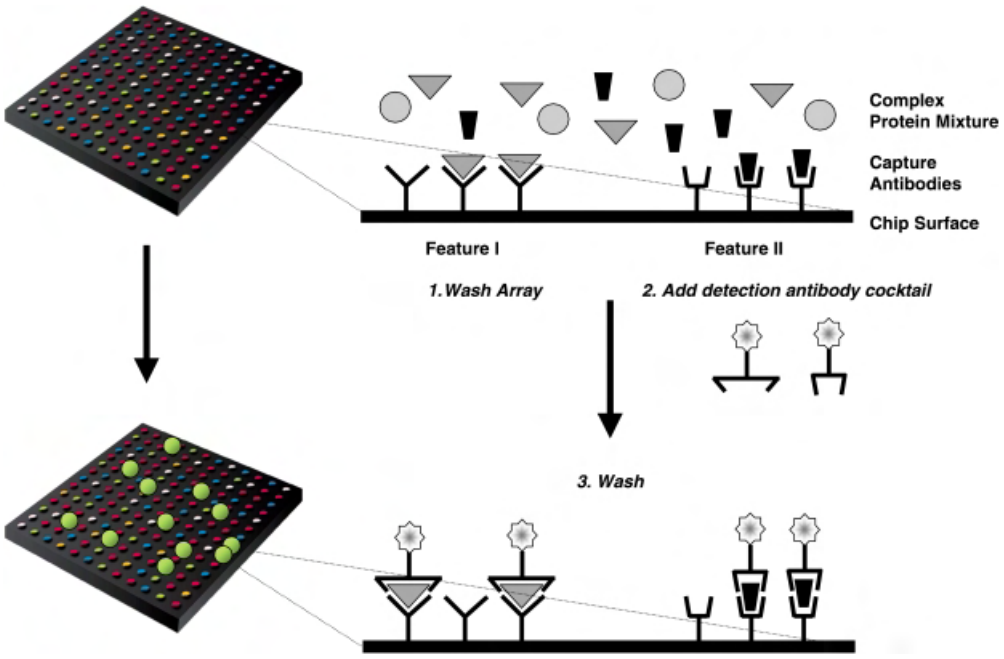


Figure 1. The use of protein microarrays in protein expression profiling. A schematic representation of a 12×14 antibody array is shown top left. Each feature is derivatized by a distinct antibody specifically (top right), making it possible to measure the concentrations of up to 168 proteins simultaneously. First, a complex protein mixture (biological sample) is brought into contact with the antibody array. Each feature on the array captures a single protein species from the complex mixture. After equilibration, the array is washed to remove unbound proteins. At this point, the bound proteins on the array can be directly measured in cases where the analyte proteins have been labeled by fluorescent compounds, for example (this is not explicitly shown). Alternatively, a cocktail of labeled detection antibodies can be added to the array, thus forming sandwich complexes on the features that have captured analyte protein (bottom right). After washing, the signal on the array can be quantified.

sion patterns could taxonomically stratify histologically indistinguishable tumor types, and that these molecular distinctions could correlate to disease prognosis and therapeutic responsiveness.

Patterns of protein levels have also been proven to correlate with pathological states. Petricoin et al.[13] performed surface-enhanced laser desorption and ionization (SELDI) mass spectrometry on hydrophobically enriched serum proteins and peptides from patients with ovarian cancer, and compared the patterns of mass/charge (m/z) signals to those from healthy individuals. The data were analyzed by a novel pattern–recognition method that combines elements from genetic algorithms and cluster analysis to correlate patterns of peak intensities to the pathological condition. The algorithm uncovered a pattern of intensities at five different m/z ratios that was capable of diagnosing malignant ovarian cancer in all diseased patients tested, and had a false positive rate of 5%. This method led to a much higher positive predictive value (94%) than diagnosis based on the most widely used serum biomarker for ovarian cancer, cancer antigen 125 (CA125), which has a positive predictive value of only 10%.

This study demonstrates the benefits of being able to measure concentration differences for numerous proteins in parallel. Mass spectrometry offers one method for making such a comparison, and retains the advantage that patterns



Steffen Nock, born in 1967, studied Biochemistry at the University of Bayreuth (Germany). In 1993 he started his PhD work on guanine nucleotide binding proteins in prokaryotes under the supervision of Prof. M. Sprinzl (Bayreuth), in collaboration with Prof. Roger Goody at the Max-Planck Institut für Molekulare Physiologie in Dortmund. After completion of his doctorate in 1996, he was awarded a fellowship from the Deutsche Forschungsgemeinschaft to carry out research in the Department of Biochemistry at Stanford University. In 1998 he co-founded Zyomyx, Inc., a biotechnology company that develops protein microarrays.



David S. Wilson was born in 1965 in New York, and earned his B.S. in Biochemistry from the University of California, Berkeley. He received his Ph.D. from the Rockefeller University in Biochemistry and Biophysics under the supervision of Claude Desplan and John Kuriyan. In 1996, he received a post-doctoral fellowship from the Cancer Research Foundation of the Damon Runyon-Walter Winchell Foundation in the laboratory of Jack W. Szostak at the Massachusetts General Hospital/Harvard Medical School. He moved to Zyomyx, Inc., in 2000, and is currently the Manager of Protein Engineering.

 © 2003 Wiley-VCH Verlag GmbH & Co. KGaA, Weinheim 1433-7851/03/4205-0495 $ 20.00+.50/0

can be obtained without knowledge of the proteins that correspond to the *m*/*z* signals. Disadvantages of this method include low throughput relative to immunoassays, and difficulty in molecular identification of the markers. When markers can be identified, however, antibodies could be developed and incorporated into multiplexed immunoassays, which are compatible with much higher throughput and offer greater sensitivity and accurate quantification. A powerful synergy therefore exists between discovery technologies such as mass spectrometry and high-throughput, quantitative immunoassays for testing thousands of samples from different patient populations.

Miniturized Immunoassays

The ability to miniaturize and multiplex immunoassays for measuring protein abundance has been the subject of numerous studies and reviews.[3–5] Recently, Schweitzer et al.[14] demonstrated a microarray system with antibodies that can be used for the simultaneous measurement of 75 cytokines (soluble signaling proteins involved in immune response). Antibodies of known specificities were arrayed onto a glass slide, which was subsequently incubated with biological samples, washed, and then exposed to a cocktail of detection antibodies (Figure 1). The detection antibodies were also of known specificity, and could bind to different regions (epitopes) of the cytokines than those bound by the surface-immobilized antibodies. Therefore, cytokines in the biological sample could be "sandwiched" between the surface-attached and detection antibodies, thus causing retention of the detection antibodies after washing. Detection antibodies are typically labeled with fluorescent dyes, which allows for measurement by confocal fluorescent scanners designed for reading DNA microarrays. The sensitivity of this method, unfortunately, may be insufficient in some cases to measure proteins present at very low concentrations such as cytokines.

To address this limitation, a powerful signal-enhancement method called rolling circles amplification (RCA) was used. The mechanism of this clever method is beyond the scope of this review, but consists of using a sandwich immunoassay in which the detection antibodies are conjugated to DNA sequences. Once the detection antibodies are localized to the antigens on the protein array features, their DNA sequences are extended by a DNA polymerase in situ, thus forming long DNA polymers of defined sequence that are tethered to the detection antibody and therefore to the appropriate feature of the microarray. After this polymerization step, the extended DNA sequence is allowed to hybridize to fluorescently labeled DNA oligonucleotides of complementary sequence. Since the extended DNA polymers are very long, multiple oligonucleotides, and therefore fluorophores, are attached to each detection antibody.

By using this RCA–sandwich approach, Schweitzer et al.[14] were able to detect cytokine concentrations in the pico- and subpicomolar ranges, which should be sufficient to measure biological levels of these proteins. This technology was used to monitor the expression levels of 51 cytokines in cultured dendritic cells in response to stimulation by either lipopolysaccharide or tumor necrosis factor α. Cytokine concentrations were measured on only a few microliters of cell culture supernatant at multiple time points, a project that would have required thousands of times more sample using standard ELISA methods. The authors observed the upregulation of several cytokines, and validated the data by comparison to standard ELISA methods, which showed comparable sensitivity.

As an alternative to using methods based on nucleic acid amplification to obtain sufficient assay sensitivity to measure biologically relevant analyte concentrations, we have obtained comparable sensitivity by using an extremely bright fluorescent label (phycoerythrin) for the detection of antibodies and by optimizing the surface chemistry and antibody engineering (Figure 2). In this way, it is possible to create a protein-resistant surface with a densely packed monolayer of oriented antibody fragments that are nearly 100% active.[15]

Commercial antibody arrays with hundreds of distinct antibodies are now available from BD Biosciences Clontech (Palo Alto, CA) and Hypromatrix (Millbury, MA). To use these products, one must label the proteins in the biological sample (with a fluorophore, for example), expose them to the array, wash, and then detect the labeled proteins that bind to the corresponding antibody features. Alternatively, one can compare two different samples (such as normal versus pathological) by labeling the proteins from each sample with a different fluorophore, mixing the samples, and then applying them to the arrays[16] (Figure 3). In this case, one compares the relative fluorescence intensity at each antibody feature so as to identify differences in protein levels between the two samples. Two drawbacks of this type of approach are that sensitivity is generally not very high, which makes it difficult to detect proteins present at low concentration, and sample-labeling efficiency is often variable.[16]

Antibody–antigen interactions can also be used to study immune responses by applying patient serum to microarrays of immobilized antigens (Figure 4), thus providing information on the patient's exposure to pathogens, allergic reactions, or the presence of autoimmune disorders. Robinson et al.[17] created a microarray of 196 known autoantigens and tested serum from patients with 6 different autoimmune disorders, and found a pattern of reactivity that could differentiate the syndromes from each other and from normal individuals. Furthermore, the results matched those obtained by conventional ELISA methods. The isotype subclass of the autoantibodies could also be determined by developing the arrays by using different subclass-specific antibodies with distinct fluorophores. For most of the autoantigens it was possible to detect physiological concentrations of autoantibodies, with lower limits of detection than could be obtained by conventional ELISA methods. Some of the antigens were unrecognizable, however, presumably because of denaturation resulting from the immobilization method. The authors suggest that this problem could be overcome by replacing the surface (polylysine-coated glass, which binds proteins nonspecifically) with one that is more biocompatible. Nitrocellulose-coated glass slides have been successfully used to array carbohydrate-based antigens and monitor human

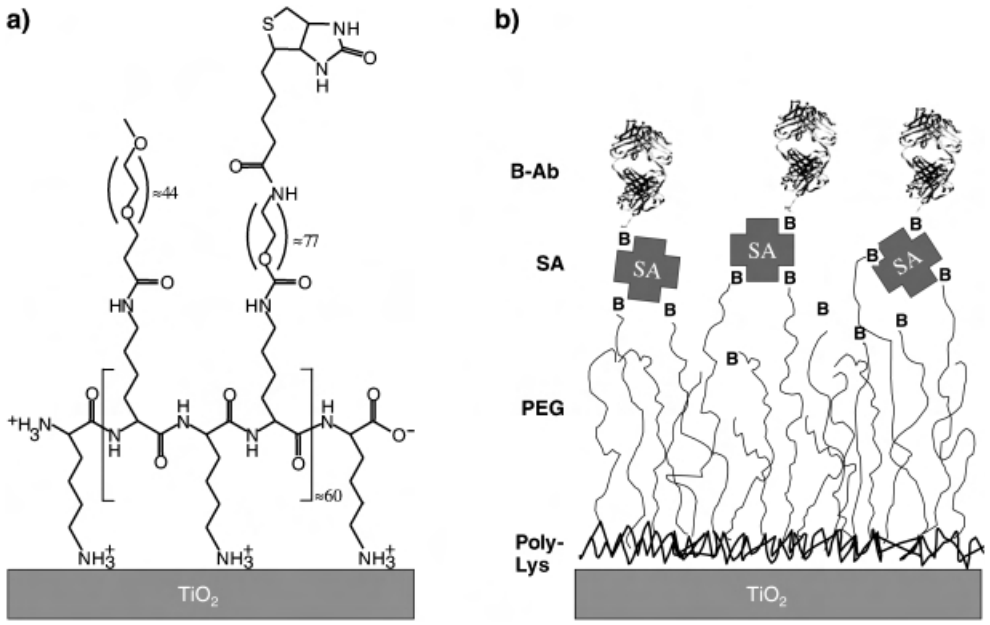


Figure 2. A surface chemistry that is highly resistant to nonspecific protein binding, but allows for derivitization with antibodies. a) Structure of a poly(L-lysine-PEG-biotin) copolymer adsorbed onto a negatively charged surface such as TiO_2. The methoxy-PEG and biotin-PEG chains are grafted onto about 20 and 9% of the lysine side chains, respectively. b) Schematic representation of this surface after derivitization with streptavidin (SA). Since SA is tetravalent, biotinylated antibodies (B-Ab) or Fab fragments (as shown) can be attached through the free biotin-binding sites of SA.

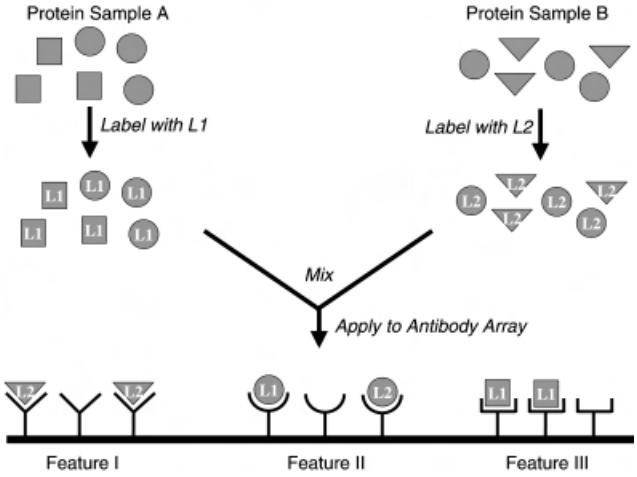


Figure 3. Differential protein expression profiling. Two different protein samples (normal and pathological) are labeled with two different fluorescent dyes, L1 and L2. The two samples are then mixed and applied to an antibody array, which allows the labeled proteins from each sample to be captured by antibodies. Feature I will display a high signal for L2 but not L1, which indicates that protein sample B has a higher concentration of the corresponding protein than does sample A. The opposite is true for Feature III. Feature II shows equal activity of L1 and L2, which indicates there are equal concentrations of the corresponding proteins in the samples.

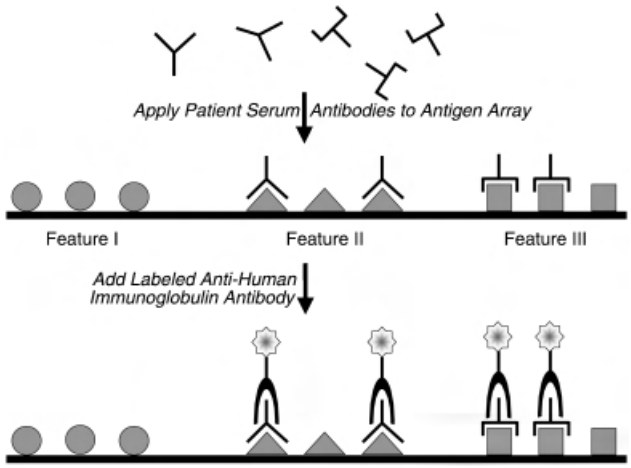


Figure 4. Probing immune responses with antigen arrays. These arrays are inverted with respect to those shown in the previous figures. Patient serum, which contains immunoglobulins (antibodies), is exposed to an antigen array so that antibodies specific for the different antigens are captured at specific locations on the array. After washing away unbound immunoglobulins, a labeled anti-human immunoglobulin antibody is added, and binds to the human antibodies on the array, thus indirectly revealing the antibody response to the various antigens in the patient serum.

immune responses.[18] This result is important since polysaccharides frequently constitute the most immunogenic components of infectious agents.

Other possible applications of antigen arrays could include discovery of cancer-specific autoantigens, which could lead to novel diagnostic methods and to drug target candidates. Antigen arrays could also enable a more systematic approach to vaccine development.

New Microarray Formats

In addition to measuring the abundance of proteins and antibodies, arrays can also be used to study protein activity. Zhu et al.[19] created expression constructs for virtually all of the 5800 genes in yeast, and then expressed and purified small quantities of them in parallel, and finally arrayed them onto glass slides. These "proteome chips" were subsequently

incubated with labeled molecules to identify yeast proteins with which they interact. As a result, they identified several proteins that bind to the protein calmodulin and to certain lipids.

Enzymatic activity can also be studied in microarray format. Arrays of peptide substrates and kinases were used to characterize the specificity of virtually all of the known yeast protein kinases, for example.[20] Recently, Houseman et al.[21] described a system for studying enzyme–substrate interactions on a type of surface that provides the chemical characteristics consistent with quantitative assays: it is protein-repellent and has a defined density and homogeneous presentation of covalently immobilized substrates. This was achieved by self-assembly of organic thin films composed of alkanethiols with polyethyleneglycol (PEG) groups, which are known to be resistant to nonspecific protein binding, onto gold surfaces. A fraction of the PEG groups on this surface contain an ω-benzoquinone functionality that can form a covalent bond with cyclopentadiene-conjugated peptides. The peptide substrates are thereby immobilized on a well-characterized and homogeneous surface, thus minimizing the influence of the surface on the enzyme–substrate interactions. The authors showed that the peptides could be enzymatically phosphorylated by a protein kinase, thus providing information about substrate specificity and phosphorylation kinetics. Phosphorylation was measured either directly, by incubating the immobilized peptides with the kinase and radiolabeled [γ-^{32}P]ATP (ATP = adenosine 5′-triphosphate), or indirectly, by using a fluorescently labeled antibody against phosphotyrosine. This system was also used to quantify inhibitory constants of different kinase inhibitors.

One of the greatest challenges in the protein microarray field will be the incorporation of membrane proteins, which collectively represent about half of the current drug targets.[22] A method for immobilizing membrane proteins onto microarrays has recently been described. Fang et al.[22] showed that aminopropylsilane-derivatized glass slides could be used to immobilize lipid bilayers in such a way that they were stable against washing in aqueous buffers and against dehydration, but retained the capacity to support long-range lateral fluidity. The authors demonstrated that G-protein-coupled receptors, which constitute one of the most important classes of drug targets, could be immobilized on the glass slides and retain their ligand-binding affinity and specificity.

Ion channels are one of the most important classes of membrane proteins, and microarray formats for measuring current through such channels are being developed. The membranes must be immobilized in such a way as to maintain their insulation properties so that conductance of ions is largely the result of the embedded channel proteins rather than of defects in the bilayer structure.[23] Arrays of different channel proteins embedded in such supported membranes, in which each feature could be independently monitored by a microelectrode, would enable the screening of compounds for their ability to modulate the conductive properties of numerous channel proteins in parallel.

Another new concept in the protein microarray field is referred to as "affinity contact printing."[24] The basis for this technology is to use a three-dimensional chip in which raised, flat structures (mesas) protrude from the base of the chip (Figure 5). Different proteins can then be covalently attached to the different raised features. The chip is then brought into contact with a complex protein solution so that the covalently attached proteins on the tops of the mesas can capture proteins from the complex mixture. The chip thereby acts as a purifying and concentrating device. Next, the mesa chip is removed from the protein solution, washed, and then used as a stamp: it is brought into contact with a surface that has a high, nonspecific affinity for proteins. The specifically bound proteins are thereby transferred to the new surface (the "printed surface"), while the covalently attached proteins are left on the stamp. The printed surface can then be analyzed by mass spectrometry or other methods. Some of the printed proteins retain their biological activity.

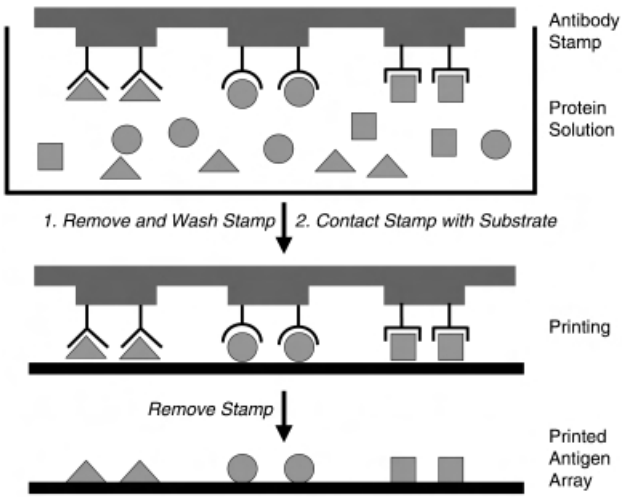


Figure 5. Affinity contact printing. A stamp is prepared whereby antibodies (or other affinity agents) are covalently attached to protruding structures. This stamp is then "inked" by being brought into contact with a protein solution. After washing, the inked stamp is brought into contact with a substrate that binds to proteins with a higher affinity than that of antibody–antigen interactions, which results in the printing of specific proteins in defined patterns onto a substrate.

Use of Protein Microarrays in Drug Development

The advanced target discovery technologies of genomics and proteomics have led to a vast amount of potential drug targets. Nearly all of these molecules are proteins. This situation has created an immediate need for tools that help to validate and prioritize these potential targets. New tools also need to address other bottlenecks in drug development—the preclinical and clinical stages, which have to be streamlined and made more efficient.

Protein microarrays hold great promise for accelerating the development of both therapeutic and diagnostic biomarkers. Figure 6 outlines the different stages of these processes and highlights the areas where protein biochips could be most relevant.

Protein microarrays currently have minor impact on the initial phase of target discovery, since there are a limited

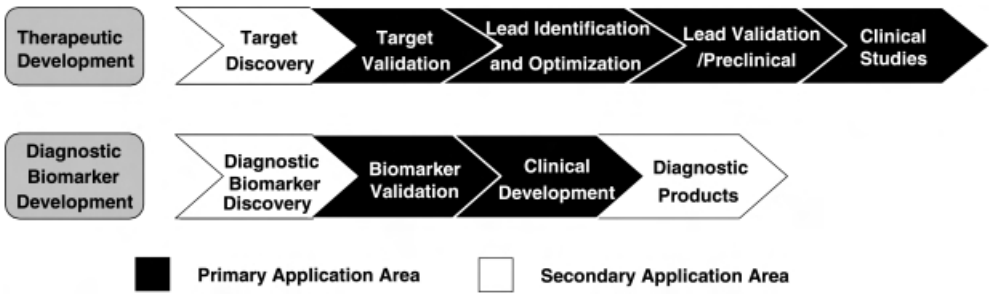


Figure 6. The use of protein microarrays for the development of drug and diagnostic biomarkers.

number of antibodies available to profile potential targets. Rather, genomics and proteomics technologies, such as DNA arrays for mRNA expression profiling, and two-dimensional gel electrophoresis in combination with mass spectrometry, are uncovering numerous drug target candidates. Once these targets have been defined, they must be placed into a biological context, for example, into certain pathways. A combination of mass spectrometry and protein chips with immobilized targets that can act as bait proteins to capture protein complexes will help to streamline and multiplex the placement of these proteins into pathways, and will also further define pathways and cross-talk between them. Once the biological context of a target has been defined, a statistical validation across different tissues of many patients has to be performed. This is an area where protein expression profiling chips based on simple, quantitative readout (such as fluorescence) could take over from the lower throughput, less quantitative techniques based on two-dimensional gels and mass spectrometry.

Protein microarrays will also help to speed up lead identification as well as downstream processes such as lead optimization and validation. The inhibitory properties of lead compounds on enzymatic drug targets, and also on related nontarget enzymes, can be analyzed in chip-based systems.[21,25,26] Substantial savings could be made both in terms of time and precious reagents by multiplexing and miniaturizing these assays. Generic chips to assess toxic side effects of drug candidates early on in the development process will potentially help to prevent failures during the ever more costly later stage clinical studies.

Biomarker discovery, which is tightly linked to the drug development process, constitutes a second area where protein arrays could dramatically accelerate the pace of research. Biomarkers can support preclinical and clinical development, help identify focused subgroups in the clinical patient population with predispositions relating to efficacy or toxicity, and be used to monitor efficacy and toxicity of drug compounds. Examples of the utility of protein chips as tools to discover biomarkers in autoimmunity[17] and cancer[13] were discussed above. We and other research groups are developing antibody arrays to measure cytokines and other mediators of the immune response with the hope of finding patterns that will aid in the diagnosis and treatment of inflammatory diseases.

In conclusion, protein microarrays have the potential to revolutionize many stages of drug and biomarker development. This will lead to significant savings in cost, time, and reagents. Furthermore the use of protein biochips will enable pharmaceutical companies to personalize therapeutic regimens to the appropriate patient groups.

Summary and Outlook

Protein microarrays have gained popularity over the last two to three years, with dozens of reports in the literature of their use (reviewed in references [1–5]). Several basic platforms have been established, especially for expression profiling applications. The most significant challenge for the future will be to obtain the biological content with which to load the chips.[2,27] Expression profiling requires at least one specific antibody for each protein that is to be monitored. Polyclonal antibodies may not be specific enough for use in multiplexed immunoassays, but the development of monoclonal antibodies requires a great deal of time (usually about six months) and labor. One attractive alternative is to use phage display of recombinant antibody fragments, an artificial in vitro selection process by which high affinity binding agents can be obtained from large, naïve libraries.[28–31] The time required to perform binding selections is much shorter than that to generate a robust immune response in an animal, and there is no problem with toxic or self proteins.

Other artificial selection methods include microbial display[32] and ribosome display[33] of antibody fragments, mRNA display of artificial protein libraries,[34] the two-hybrid systems,[35] and systematic evolution of ligands by exponential enrichment (SELEX) of nucleic acid libraries.[36,37] These are all relatively new systems with the potential to be automated.

Before one can generate a binding agent by any of these methods, the target protein must be synthesized and purified. Most mammalian proteins can be expressed at high levels in *E. coli*, or in vitro using *E. coli* extracts, but they usually precipitate as insoluble, misfolded proteins. For most human proteins, it will therefore be necessary to access alternative expression systems or identify robust, high-throughput protein-refolding protocols for bacterially expressed proteins.

An easier route to antigen generation would be to use short synthetic peptides, but antibodies for short peptides are generally lower in affinity than are those that are raised against folded proteins. The development of detection methods applicable to protein arrays with large numbers (hundreds to thousands) of different antibody specificities is

another area in need of innovation. One can chemically label the complex mixtures to be analyzed with fluorescent compounds, but this may provide insufficient sensitivity for proteins present at low concentrations because of a poor signal-to-noise ratio. Many important signaling molecules (such as cytokines) can be present in human serum at about a billionfold lower concentrations than other proteins in the same mixture, and so even high-quality immobilized antibodies will generally not be capable of distinguishing the specific signal from the general noise arising from nonspecific protein binding. The signal-to-noise ratio can be dramatically improved by utilizing a sandwich assay, but this requires the development of two binding reagents per target protein.

The last few years have witnessed intense innovation in the field of protein microarrays, but substantially more development will be required before this technology reaches its zenith in contributing to both basic biological research and drug development.

Received: July 16, 2002 [M1587]

[1] R. E. Jenkins, S. R. Pennington, *Electrophoresis* **2001**, *1*, 13 – 29.
[2] T. Kodadek, *Chem. Biol.* **2001**, *8*, 105 – 115.
[3] D. J. Cahill, *J. Immunol. Methods* **2001**, *250*, 81 – 91.
[4] D. S. Wilson, S. Nock, *Curr. Opin. Chem. Biol.* **2001**, *6*, 81 – 85.
[5] D. Stoll, M. F. Templin, M. Schrenk, P. C. Traub, C. F. Vohringer, T. O. Joos, *Front. Biosci.* **2002**, *7*, c13-c32.
[6] T. R. Golub, D. K. Slonim, P. Tamayo, C. Huard, M. Gaasenbeek, J. P. Mesirov, H. Coller, M. L. Loh, J. R. Downing, M. A. Caligiuri, C. D. Bloomfield, E. S. Lander, *Science* **1999**, *286*, 531 – 537.
[7] A. A. Alizadeh, M. B. Eisen, R. E. Davis, C. Ma, I. S. Lossos, A. Rosenwald, J. C. Boldrick, H. Sabet, T. Tran, X. Yu, J. I. Powell, L. Yang, G. E. Marti, T. Moore, J. Hudson, Jr., L. Lu, D. B. Lewis, R. Tibshirani, G. Sherlock, W. C. Chan, T. C. Greiner, D. D. Weisenburger, J. O. Armitage, R. Warnke, L. M. Staudt, *Nature* **2000**, *403*, 503 – 511.
[8] C. M. Perou, T. Sorlie, M. B. Eisen, M. van de Rijn, S. S. Jeffrey, C. A. Rees, J. R. Pollack, D. T. Ross, H. Johnsen, L. A. Akslen, O. Fluge, A. Pergamenschikov, C. Williams, S. X. Zhu, P. E. Lonning, A. L. Borresen-Dale, P. O. Brown, D. Botstein, *Nature* **2000**, *406*, 747 – 752.
[9] T. Sorlie, C. M. Perou, R. Tibshirani, T. Aas, S. Geisler, H. Johnsen, T. Hastie, M. B. Eisen, M. van de Rijn, S. S. Jeffrey, T. Thorsen, H. Quist, J. C. Matese, P. O. Brown, D. Botstein, L. P. Eystein, A. L. Borresen-Dale, *Proc. Natl. Acad. Sci. USA* **2001**, *98*, 10869 – 10874.
[10] S. M. Dhanasekaran, T. R. Barrette, D. Ghosh, R. Shah, S. Varambally, K. Kurachi, K. J. Pienta, M. A. Rubin, A. M. Chinnaiyan, *Nature* **2001**, *412*, 822 – 826.
[11] T. O. Nielsen, R. B. West, S. C. Linn, O. Alter, M. A. Knowling, J. X. O'Connell, S. Zhu, M. Fero, G. Sherlock, J. R. Pollack, P. O. Brown, D. Botstein, M. van de Rijn, *Lancet* **2002**, *359*, 1301 – 1307.
[12] S. L. Pomeroy, P. Tamayo, M. Gaasenbeek, L. M. Sturla, M. Angelo, M. E. McLaughlin, J. Y. Kim, L. C. Goumnerova, P. M. Black, C. Lau, J. C. Allen, D. Zagzag, J. M. Olson, T. Curran, C. Wetmore, J. A. Biegel, T. Poggio, S. Mukherjee, R. Rifkin, A. Califano, G. Stolovitzky, D. N. Louis, J. P. Mesirov, E. S. Lander, T. R. Golub, *Nature* **2002**, *415*, 436 – 442.
[13] E. F. Petricoin, A. M. Ardekani, B. A. Hitt, P. J. Levine, V. A. Fusaro, S. M. Steinberg, G. B. Mills, C. Simone, D. A. Fishman, E. C. Kohn, L. A. Liotta, *Lancet* **2002**, *359*, 572 – 577.
[14] B. Schweitzer, S. Roberts, B. Grimwade, W. Shao, M. Wang, Q. Fu, Q. Shu, I. Laroche, Z. Zhou, V. T. Tchernev, J. Christiansen, M. Velleca, S. F. Kingsmore, *Nat. Biotechnol.* **2002**, *20*, 359 – 365.
[15] a) L. A. Ruiz-Taylor, T. L. Martin, F. G. Zaugg, K. Witte, P. Indermuhle, S. Nock, P. Wagner, *Proc. Natl. Acad. Sci. USA* **2001**, *98*, 852 – 857; b) P. Peluso, D. S. Wilson, D. Do, H. Tran, M. Venkatasubbaiah, D. Quincy, B. Heidecker, K. Poindexter, N. Tolani, M. Phelan, K. Witte, P. Wagner, S. Nock, *Anal. Biochem.* **2003**, *312*, 113 – 124
[16] B. B. Haab, M. J. Dunham, P. O. Brown, *Genome Biol.* **2001**, *2*, research 0004.1 – 0004.13.
[17] W. H. Robinson, C. DiGennaro, W. Hueber, B. B. Haab, M. Kamachi, E. J. Dean, S. Fournel, D. Fong, M. C. Genovese, H. E. de Vegvar, K. Skriner, D. L. Hirschberg, R. I. Morris, S. Muller, G. J. Pruijn, W. J. van Venrooij, J. S. Smolen, P. O. Brown, L. Steinman, P. J. Utz, *Nat. Med.* **2002**, *8*, 295 – 301.
[18] D. Wang, S. Liu, B. J. Trummer, C. Deng, A. Wang, *Nat. Biotechnol.* **2002**, *20*, 275 – 281.
[19] H. Zhu, M. Bilgin, R. Bangham, D. Hall, A. Casamayor, P. Bertone, N. Lan, R. Jansen, S. Bidlingmaier, T. Houfek, T. Mitchell, P. Miller, R. A. Dean, M. Gerstein, M. Snyder, *Science* **2001**, *293*, 2101 – 2105.
[20] H. Zhu, J. F. Klemic, S. Chang, P. Bertone, A. Casamayor, K. G. Klemic, D. Smith, M. Gerstein, M. A. Reed, M. Snyder, *Nat. Genet.* **2000**, *26*, 283 – 289.
[21] B. T. Houseman, J. H. Huh, S. J. Kron, M. Mrksich, *Nat. Biotechnol.* **2002**, *20*, 270 – 274.
[22] Y. Fang, A. G. Frutos, J. Lahiri, *J. Am. Chem. Soc.* **2002**, *124*, 2394 – 2395.
[23] G. Wiegand, N. Arribas-Layton, H. Hillebrandt, E. Sackmann, P. Wagner, *J. Phys. Chem. B* **2002**, *106*, 4245 – 4254.
[24] A. Bernard, D. Fitzli, P. Sonderegger, E. Delamarche, B. Michel, H. R. Bosshard, H. Biebuyck, *Nat. Biotechnol.* **2001**, *19*, 866 – 869.
[25] C. B. Cohen, E. Chin-Dixon, S. Jeong, T. T. Nikiforov, *Anal. Biochem.* **1999**, *273*, 89 – 97.
[26] P. Arenkov, A. Kukhtin, A. Gemmell, S. Voloshchuk, V. Chupeeva, A. Mirzabekov, *Anal. Biochem.* **2000**, *278*, 123 – 131.
[27] A. Abbott, *Nature* **2002**, *415*, 112 – 114.
[28] T. J. Vaughan, A. J. Williams, K. Pritchard, J. K. Osbourn, A. R. Pope, J. C. Earnshaw, J. McCafferty, R. A. Hodits, J. Wilton, K. S. Johnson, *Nat. Biotechnol.* **1996**, *14*, 309 – 314.
[29] M. D. Sheets, P. Amersdorfer, R. Finnern, P. Sargent, E. Lindquist, R. Schier, G. Hemingsen, C. Wong, J. C. Gerhart, J. D. Marks, E. Lindqvist, *Proc. Natl. Acad. Sci. USA* **1998**, *95*, 6157 – 6162.
[30] H. J. de Haard, N. van Neer, A. Reurs, S. E. Hufton, R. C. Roovers, P. Henderikx, A. P. de Bruïne, J. W. Arends, H. R. Hoogenboom, *J. Biol. Chem.* **1999**, *274*, 18218 – 18230.
[31] A. Knappik, L. Ge, A. Honegger, P. Pack, M. Fischer, G. Wellnhofer, A. Hoess, J. Wolle, A. Plückthun, B. Virnekäs, *J. Mol. Biol.* **2000**, *296*, 57 – 86.
[32] K. D. Wittrup, *Curr. Opin. Biotechnol.* **2001**, *12*, 395 – 399.
[33] J. Hanes, C. Schaffitzel, A. Knappik, A. Plückthun, *Nat. Biotechnol.* **2000**, *18*, 1287 – 1292.
[34] D. S. Wilson, A. D. Keefe, J. W. Szostak, *Proc. Natl. Acad. Sci. USA* **2001**, *98*, 3750 – 3755.
[35] P. Colas, B. Cohen, T. Jessen, I. Grishina, J. McCoy, R. Brent, *Nature* **1996**, *380*, 548 – 550.
[36] E. N. Brody, L. Gold, *J. Biotechnol.* **2000**, *74*, 5 – 13.
[37] M. P. Robertson, A. D. Ellington, *Nat. Biotechnol.* **2001**, *19*, 650 – 655.

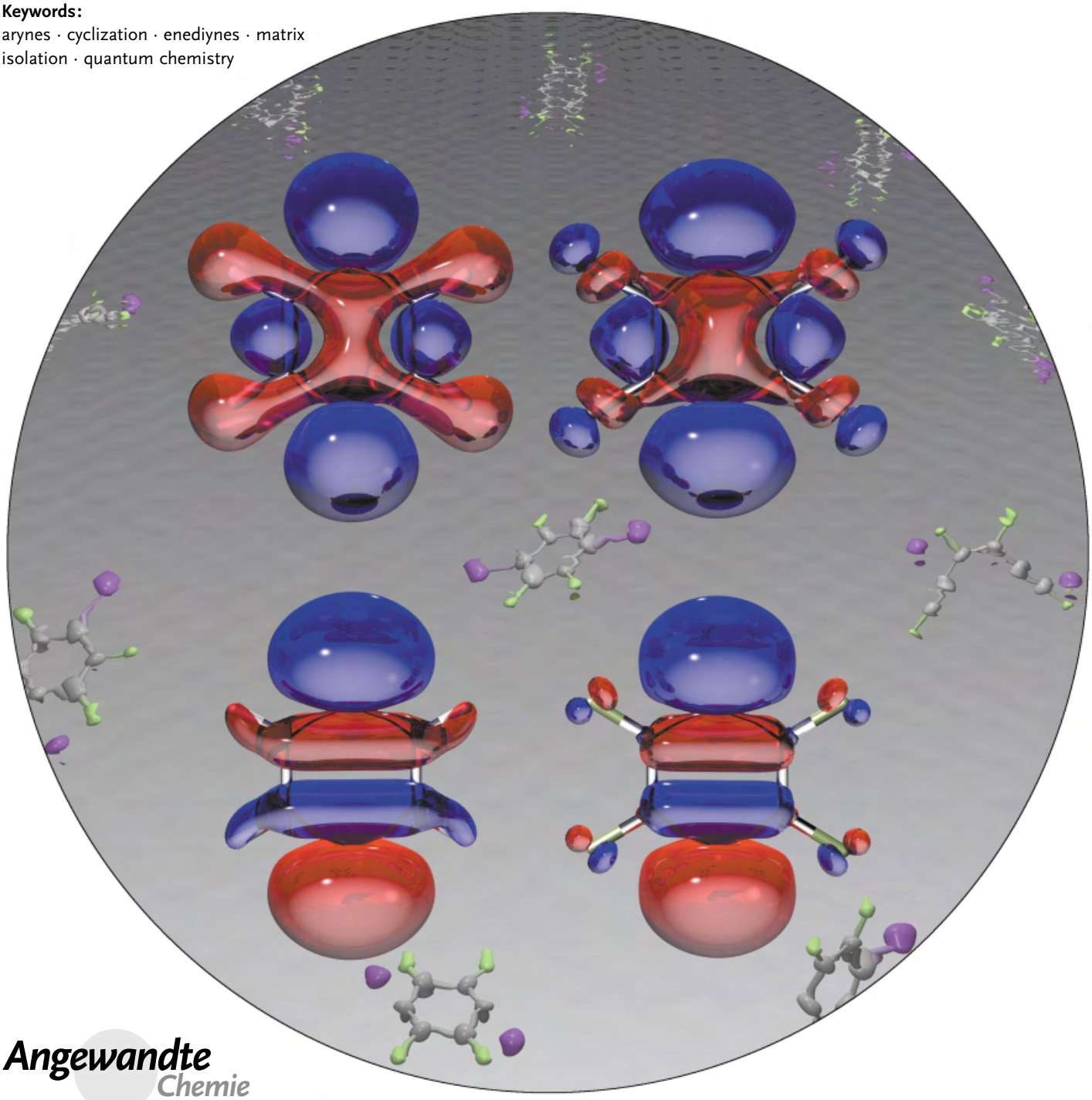
100 Years of Arynes

One Century of Aryne Chemistry

*Hans Henning Wenk, Michael Winkler, and Wolfram Sander**

Dedicated to Professor Günther Maier on the occasion of his 70th birthday

Keywords:
arynes · cyclization · enediynes · matrix isolation · quantum chemistry



 © 2003 Wiley-VCH Verlag GmbH & Co. KGaA, Weinheim 1433-7851/03/4205-0502 $ 20.00+.50/0

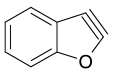
Arynes, which are formally derived from aromatic rings by abstraction of two hydrogen atoms, have been a focus of organic chemistry for 100 years. In contrast to ortho-benzyne, which is mentioned in almost every introductory textbook on organic reaction mechanisms as a reactive intermediate of nucleophilic aromatic substitution, the meta and para isomers were regarded as rather exotic until recently. This situation has changed dramatically with the discovery of the enediyne antibiotics, a promising new class of antitumor drugs, and has aroused the interest of research groups from all branches of chemistry. Nowadays, arynes and related compounds are among the most intensively studied systems in chemistry. However, many aspects of the chemistry of these reactive intermediates are not well understood yet. In this review we outline the historical developement with an emphasis on recent progress in this challenging field of research.

From the Contents

1. Introduction	503
2. ortho-Arynes	503
3. meta-Arynes	507
4. para-Arynes and the Bergman Cyclization	511
5. Other Dehydroarenes	521
6. Perspective	522

1. Introduction

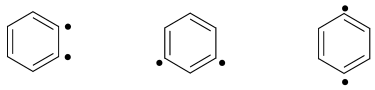
First evidence for the existence of an aryne was reported 100 years ago from the Chemical Institute of the University of Rostock: Stoermer and Kahlert observed the formation of 2-ethoxybenzofuran on treatment of 3-bromobenzofuran with bases in ethanol and postulated the formation of *ortho*-didehydrobenzofuran (2,3-didehydrobenzofuran, **1**) as a reactive intermediate (Figure 1).[1]



1

Despite occasional speculation about arynes in the following years,[2] it took several decades until Roberts,[3] Huisgen,[4] and Wittig[5] could obtain definitive evidence for the existence of these reactive intermediates. Numerous reviews have been published since,[6–11] and it is impossible to cover the entire spectrum of aryne chemistry within a single article.

This review is therefore not intended to give a complete survey of the topic, but to emphasize general trends and recent developments with a focus on the parent systems **2**–**4**.



2 **3** **4**

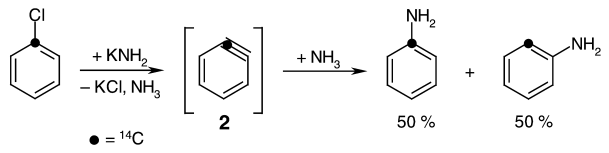
In line with the research interests of our laboratory we concentrate on direct (spectroscopic and theoretical) investigations, whereas indirect evidence, as, for example, from trapping reactions, is only dealt with occasionally.

2. ortho-Arynes

2.1. ortho-Benzyne

ortho-Benzyne (**2**) was first suggested as a reactive intermediate in 1927,[12] and Wittig corroborated the existence of this species in the following years.[5] In a classical investigation in 1953 Roberts et al. found compelling evidence for the intermediate formation of **2** in the reaction of ^{14}C-labeled chlorobenzene with sodium amide (Scheme 1).[3]

In 1963 Fisher and Lossing investigated the pyrolysis of the three isomeric diiodobenzenes using mass spectrometry and identified **2** on the basis of the measured ionization potential.[13] At approximately the same time Berry et al. studied the photoinitiated decomposition of benzenediazonium carboxylates in the gas phase and characterized **2** by its UV and mass spectra.[14]

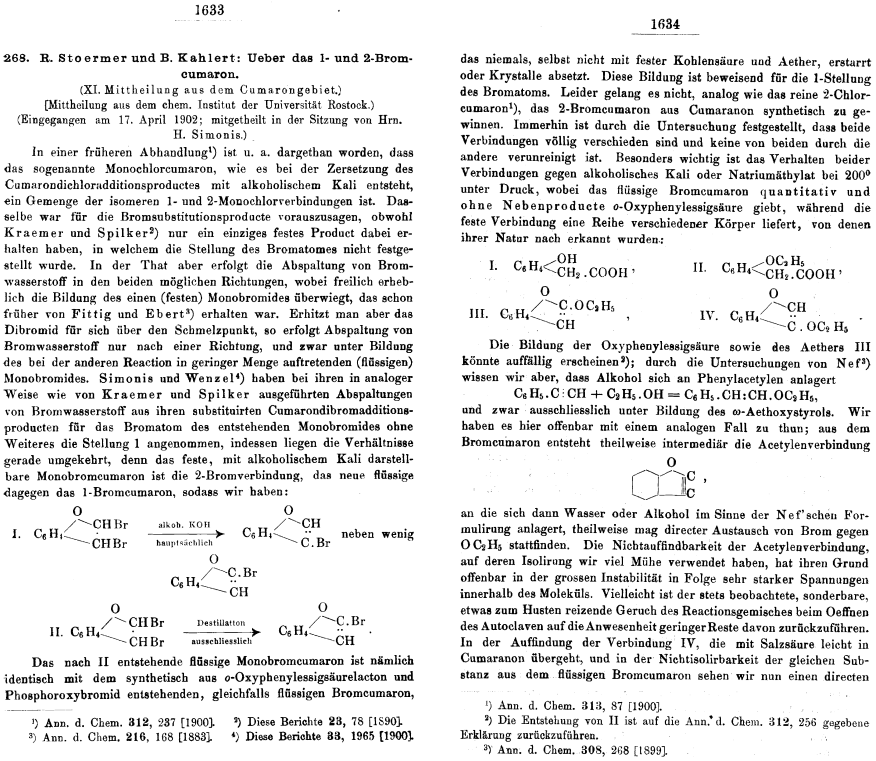


Scheme 1. In a classical isotopic labeling experiment Roberts et al. demonstrated the involvement of **2** in nucleophilic aromatic substitution. The product distribution can only be understood by assumption of a symmetrical intermediate.[3]

The first direct IR spectroscopic detection of *ortho*-benzyne was accomplished by Chapman et al., using matrix isolation spectroscopy at very low temperatures to generate **2** starting from phthaloyl peroxide (**5**) and benzocyclobutenedione (**6**; Scheme 2).[15] High yields of **2** were also obtained by using phthalic anhydride (**7**) as a precursor. The comparatively complex reactions of the molecules involved in this photochemistry led to some controversy concerning the frequency of the C≡C stretching vibration.[16] This was settled in 1992 by Radziszewski et al., who finally was able to assign this vibration to an absorption at 1846 cm^{-1} by thorough analysis of the spectra of **2** obtained from different isotopomers of phthalic anhydride.[16h] As expected, the formal C–C

[*] Prof. Dr. W. Sander, Dr. H. H. Wenk, Dipl.-Chem. M. Winkler
Lehrstuhl für Organische Chemie II der Ruhr-Universität Bochum
Universitätsstrasse 150, 44780 Bochum (Germany)
Fax: (+49) 234-32-14353
E-mail: Wolfram.Sander@ruhr-uni-bochum.de

 © 2003 Wiley-VCH Verlag GmbH & Co. KGaA, Weinheim 1433-7851/03/4205-0503 $ 20.00+.50/0



1633

268. R. Stoermer und B. Kahlert: Ueber das 1- und 2-Bromcumaron.

(XI. Mittheilung aus dem Cumarongebiet.)

[Mittheilung aus dem chem. Institut der Universität Rostock.)

(Eingegangen am 17. April 1902; mitgetheilt in der Sitzung von Hrn. H. Simonis.)

In einer früheren Abhandlung[1]) ist u. a. dargethan worden, dass das sogenannte Monochlorcumaron, wie es bei der Zersetzung des Cumarondichloradditionsproductes mit alkoholischem Kali entsteht, ein Gemenge der isomeren 1- und 2-Monochlorverbindungen ist. Dasselbe war für die Bromsubstitutionsproducte vorauszusagen, obwohl Kraemer und Spilker[2]) nur ein einziges festes Product dabei erhalten haben, in welchem die Stellung des Bromatomes nicht festgestellt wurde. In der That aber erfolgt die Abspaltung von Bromwasserstoff in den beiden möglichen Richtungen, wobei freilich erheblich die Bildung des einen (festen) Monobromides überwiegt, das schon früher von Fittig und Ebert[3]) erhalten war. Erhitzt man aber das Dibromid für sich über den Schmelzpunkt, so erfolgt Abspaltung von Bromwasserstoff nur nach einer Richtung, und zwar unter Bildung des bei der anderen Reaction in geringer Menge auftretenden (flüssigen) Monobromides. Simonis und Wenzel[4]) haben bei ihren in analoger Weise wie von Kraemer und Spilker ausgeführten Abspaltungen von Bromwasserstoff aus ihren substituirten Cumarondibromadditionsproducten für das Bromatom des entstehenden Monobromides ohne Weiteres die Stellung 1 angenommen, indessen liegen die Verhältnisse gerade umgekehrt, denn das feste, mit alkoholischem Kali darstellbare Monobromcumaron ist die 2-Bromverbindung, das neue flüssige dagegen das 1-Bromcumaron, sodass wir haben:

I. C_6H_4(O, CHBr, CHBr) —alkoh. KOH, hauptsächlich→ C_6H_4(O, CH, C.Br) neben wenig C_6H_4(O, C.Br, CH)

II. C_6H_4(O, CHBr, CHBr) —Destillation, ausschliesslich→ C_6H_4(O, C.Br, CH)

Das nach II entstehende flüssige Monobromcumaron ist nämlich identisch mit dem synthetisch aus *o*-Oxyphenylessigsäurelacton und Phosphoroxybromid entstehenden, gleichfalls flüssigen Bromcumaron,

[1]) Ann. d. Chem. **312**, 237 [1900]. [2]) Diese Berichte **23**, 78 [1890].
[3]) Ann. d. Chem. **216**, 168 [1883]. [4]) Diese Berichte **33**, 1965 [1900].

1634

das niemals, selbst nicht mit fester Kohlensäure und Aether, erstarrt oder Krystalle absetzt. Diese Bildung ist beweisend für die 1-Stellung des Bromatoms. Leider gelang es nicht, analog wie das reine 2-Chlorcumaron[1]), das 2-Bromcumaron aus Cumaranon synthetisch zu gewinnen. Immerhin ist durch die Untersuchung festgestellt, dass beide Verbindungen völlig verschieden sind und keine von beiden durch die andere verunreinigt ist. Besonders wichtig ist das Verhalten beider Verbindungen gegen alkoholisches Kali oder Natriumäthylat bei 200° unter Druck, wobei das flüssige Bromcumaron quantitativ und ohne Nebenproducte *o*-Oxyphenylessigsäure giebt, während die feste Verbindung eine Reihe verschiedener Körper liefert, von denen ihrer Natur nach erkannt wurden:

I. C_6H_4(OH, CH_2.COOH), II. C_6H_4(OC_2H_5, CH_2.COOH),

III. C_6H_4(O, C.OC_2H_5, CH), IV. C_6H_4(O, CH, C.OC_2H_5).

Die Bildung der Oxyphenylessigsäure sowie des Aethers III könnte auffällig erscheinen[2]); durch die Untersuchungen von Nef[3]) wissen wir aber, dass Alkohol sich an Phenylacetylen anlagert

$C_6H_5.C{:}CH + C_2H_5.OH = C_6H_5.CH{:}CH.OC_2H_5$,

und zwar ausschliesslich unter Bildung des ω-Aethoxystyrols. Wir haben es hier offenbar mit einem analogen Fall zu thun; aus dem Bromcumaron entsteht theilweise intermediär die Acetylenverbindung

an die sich dann Wasser oder Alkohol im Sinne der Nef'schen Formulirung anlagert, theilweise mag directer Austausch von Brom gegen OC_2H_5 stattfinden. Die Nichtauffindbarkeit der Acetylenverbindung, auf deren Isolirung wir viel Mühe verwendet haben, hat ihren Grund offenbar in der grossen Instabilität in Folge sehr starker Spannungen innerhalb des Moleküls. Vielleicht ist der stets beobachtete, sonderbare, etwas zum Husten reizende Geruch des Reactionsgemisches beim Oeffnen des Autoclaven auf die Anwesenheit geringer Reste davon zurückzuführen. In der Auffindung der Verbindung IV, die mit Salzsäure leicht in Cumaranon übergeht, und in der Nichtisolirbarkeit der gleichen Substanz aus dem flüssigen Bromcumaron sehen wir nun einen directen

[1]) Ann. d. Chem. **313**, 87 [1900].
[2]) Die Entstehung von II ist auf die Ann. d. Chem. **312**, 256 gegebene Erklärung zurückzuführen.
[3]) Ann. d. Chem. **308**, 268 [1899].

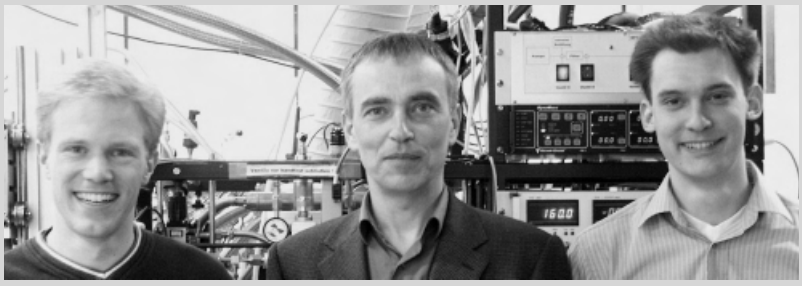
Figure 1. First evidence for the existence of an *ortho*-aryne was presented in this paper by Stoermer and Kahlert in 1902.[1]

triple bond in **2** is significantly weaker than in unstrained alkynes, whose C≡C stretching vibrations usually occur in the range about 2150 cm^{-1}. Nevertheless, *ortho*-benzyne is better described as a strained alkyne than as a biradical, which is evident from both the large singlet–triplet splitting of (37.5 ± 0.3) kcal mol^{-1}[16e,17] and the alkyne-like reactivity (e.g. Diels–Alder reactions). The enthalpy of formation of **2** was determined to be (106.6 ± 3.0) kcal mol^{-1} by Squires and Wenthold.[18] For the C≡C bond length in **2** a value of (124 ± 2) pm was found experimentally,[19] which comes closer to a typical C–C triple bond (120.3 pm in acetylene) than to a C–C double bond (133.9 pm in ethylene).

In a remarkable piece of work Warmuth et al. were able to isolate *ortho*-benzyne in a hemicarcerand as a "molecular container" and to measure its NMR spectrum in solution.[20,21] Whereas previous theoretical work[22,16f] concerning the structure of **2** had to rely solely on IR spectra, there were now additional experimental data available to judge the quality of the theoretical predictions. The experimental ^1H and ^{13}C chemical shifts were most accurately reproduced by using the B3LYP/6-311G** structure (d(C1–C2) = 124.5 pm), while calculations on the basis of CASSCF(8,8)/DZP or CCSD(T)/6-31G** geometries led to poorer agreement with experiment.[23,16i] Furthermore, it was concluded that **2** more closely resembles a cyclic alkyne rather than a cumulene.[23]

2.2. Substituted ortho-Benzynes

Numerous nucleophilic aromatic substitution reactions take place by an elimination–addition mechanism via intermediate formation of arynes.[24] To understand the regiose-

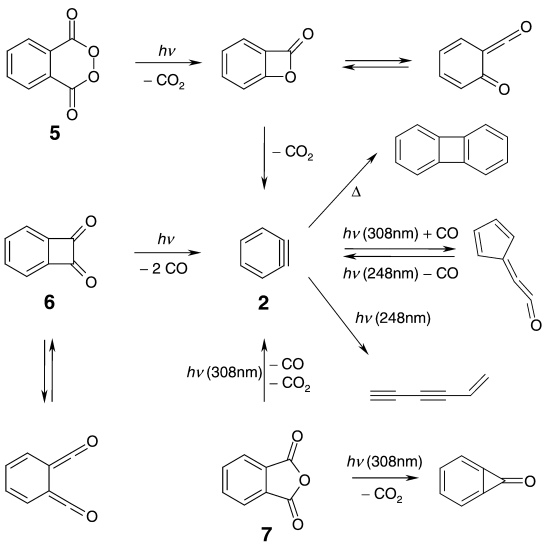


From left to right: H. H. Wenk, W. Sander, M. Winkler

Hans Henning Wenk was born in 1973 in Munich, Germany. During his diploma thesis at the Ruhr-Universität Bochum he worked on the synthesis and characterization of arynes. He is currently continuing his studies in the research group of Prof. Wolfram Sander, where he recently finished his Ph.D. work. For his thesis on the matrix isolation of fluorinated benzynes and biradicals he received the book award of the Faculty of Chemistry of the Ruhr-Universität Bochum. His research interests are the photochemical generation and spectroscopy of reactive intermediates, especially arynes, in low-temperature matrices.

Michael Winkler, born 1974 in Gelsenkirchen, Germany, finished his diploma thesis in 1999 in the research group of Prof. Wolfram Sander at the Ruhr-Universität Bochum. Currently he is preparing his Ph.D. thesis in the same group. His research interests focus on the theoretical and experimental characterization of reactive intermediates and unusual molecules. For his research activities he was awarded stipends of the Fonds der Chemischen Industrie and the Ruth und Gert Massenberg-Stiftung, and in 2000 he received the "Preis an Studierende" of the Ruhr-Universität Bochum.

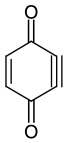
Wolfram Sander was born in Heidelberg, Germany, in 1954. He received his doctoral degree from the University of Heidelberg in 1982 under the guidance of Prof. R. Gleiter and completed his Habilitation in 1989. He was introduced to the matrix isolation technique as a postdoc with Prof. O. L. Chapman at the University of California in Los Angeles (1982–1984). His research interests in the field of physical organic chemistry focus on the characterization of reactive intermediates using matrix isolation spectroscopy and time-resolved techniques. In 1990 he joined the Institute of Organic Chemistry at the University of Braunschweig as Associate Professor, and since 1993 he has been Full Professor of Chemistry at the Ruhr-Universität Bochum. In 1988 he was awarded the Karl-Freudenberg-Preis of the Heidelberger Akademie der Wissenschaften, and in 1990 he received a Heisenberg-Stipendium and a Winnacker-Stipendium.



Scheme 2. Photochemistry of **2** and the corresponding precursor.

lectivity of these reactions it is essential to take substituent effects into account.[25] Several substituted didehydrobenzenes have been investigated theoretically.[26,22v] A systematization of substituent effects with respect to structure and reactivity of **2** is all but trivial, since the substituents act on the σ as well as the π system of *ortho*-benzyne, resulting in a complex interplay of inductive and resonance effects.[26] However, substituent effects can often be discussed approximately in terms of an increase or decrease of the contribution of zwitterionic structures to the resonance hybrid.[26,22v] Generally, substituent effects are significantly more pronounced in 2,3-arynes (polarization of the triple bond) than in the 3,4-didehydro isomers.[26] The interpretation of experimental reactivity data is often complicated by the fact that the attack of approaching nucleophiles is not solely charge controlled.[22v] It appears that more systematic studies on a reliable level of theory are necessary for an extensive understanding of substituent effects on **2.** Experimental data (such as C≡C stretching vibrational frequencies or gas-phase structures) to compare the theoretical results with are rare.

The perfluorinated *ortho*-benzyne could be isolated in cryogenic matrices by photolysis of the corresponding phthalic anhydride.[27] According to CASSCF calculations the singlet–triplet gap of tetrafluoro-*ortho*-benzyne is larger than in **2** by several kcal mol^{-1}. The fluorine substituents only have a minor influence on the length of the C≡C bond.[27] Interestingly, a nonplanar C_2-symmetrical structure is found with DFT methods (BLYP, B3LYP) for the triplet state, whereas CASSCF predicts a planar C_{2v}-symmetrical geometry.[27]



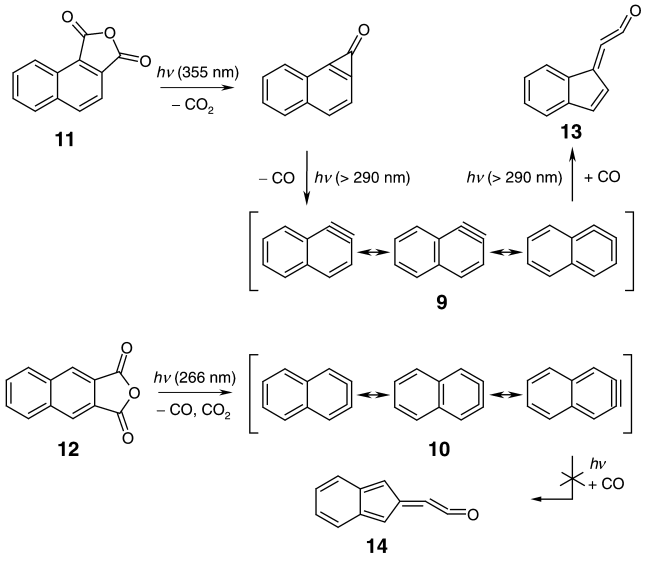
8

Another interesting compound related to **2** is 2,3-didehydro-1,4-benzoquinone (**8**), a quinoid didehydrobenzene analogue, which has been investigated theoretically by Cramer et al.,[28] and experimentally by negative-ion photoelectron spectroscopy (NIPES) by Davico et al.[29]

2.3. Annelated ortho-Benzynes

Didehydronaphthalenes (naphthynes) were studied theoretically by Squires and Cramer.[30] The bond length alternation observed for naphthalene is retained in the *ortho*-naphthynes. The 1,2-bond in naphthalene is well known to be shorter than the 2,3-bond.[31] The preference for the singlet state in the 1,2-naphthyne (**9**) is higher than in **2** by about 2 kcal mol^{-1}, while it is lower in the 2,3-isomer **10** by approximately the same amount (CASPT2/cc-pVDZ). This was interpreted in terms of the lower energy necessary for the distortion towards the formal triple bond in **9** than in **10** (for relative stabilities of the naphthynes, see Table 3, Section 4.5).[30]

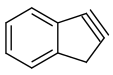
Several naphthynes were already synthesized in the early 1970s. Grützmacher et al. generated some derivatives by pyrolysis of different precursors and measured the ionization potentials of the pyrolysis products.[32] At about the same time Lohmann investigated the photochemistry of the isomeric naphthalenedicarboxylic anhydrides **11** and **12** using laser flash photolysis (LFP) and found that dimerization of 2,3-didehydronaphthalene (**10**) is significantly faster than that of **2**, whereas the 1,2-isomer **9** hardly dimerizes at all.[33] Matrix isolation of **10** was described for the first time by Weltner et al.[34] and has been the subject of a recent investigation by Sato et al.[35,36] Compounds **9** and **10** are accessible photolytically from the anhydrides **11** and **12** when the photolysis conditions are selected carefully.[36] Noteworthy is again the difference of both isomers compared with **2**: Whereas—in analogy to the parent system (see Scheme 2)—**9** is photochemically carbonylated to cyclopentadienylideneketene **13** (albeit irreversibly, in contrast to **2**), photocarbonylation of **10** to **14** is not observed at all (Scheme 3).[36] This finding was



Scheme 3. Photochemical generation of **9** and **10** from anhydrides **11** and **12**. The mesomeric structures imply a short, acetylene-like C–C bond for **9**, while a longer, cumulenic C–C bond is expected in the case of **10**. Compound **9** is photocarbonylated to cyclopentadienylideneketene **13**, the analogous reaction of **10** to ketene **14** was not observed.[35,36]

attributed to the different stability of the ketenes. A similar alternance is observed for the calculated frequencies of the C≡C stretching vibration (**2**: 1953; **9**: 1994; **10**: 1922 cm^{-1}; B3LYP/6-31G**), which could not be detected experimentally due to their low intensity, as well as for the calculated C≡C bond lengths (**2**: 125.1; **9**: 124.1; **10**: 126.0 pm; B3LYP/6-31G**).[36] These differences can be rationalized qualitatively by the mesomeric structures for **9** and **10** (Scheme 3).[36]

Didehydroindenes were also the subject of theoretical investigations.[37] The three isomers bearing the formal C≡C bond within the six-membered ring hardly differ in their stability and singlet–triplet gaps. This is in accordance with the fact that indene (in contrast to naphthalene) displays essentially no bond length alternation within the six-membered ring.[37] The enthalpy of formation of the highly strained 5,6-didehydroindene (**15**) is approximately 17 kcal mol^{-1} higher.[37]



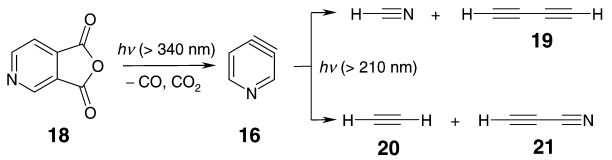
15

2.4. Heterocyclic ortho-Arynes

Although the history of hetarynes is older than that of the benzynes (see **1**), physical data on these compounds are scarce. Numerous trapping experiments furnished evidence for the formation of biradicaloid intermediates in the field of five-membered heterocycles (didehydrofurans, -thiophenes, and -pyrroles).[10] Direct spectroscopic data of these species, however, are not available, which is attributable to the increased ring strain in the five-membered *ortho*-arynes, associated with a strong tendency to undergo ring-opening reactions.

Investigations of six-membered heteroarynes have concentrated on didehydropyridines, which will be dealt with exclusively in this section. The influence of the nitrogen lone pair on the structural and electronic properties of the didehydropyridines was investigated by Cramer and Debbert.[38,39] In agreement with earlier calculations[40] at low levels of theory it could be shown, that 3,4-pyridyne (**16**) is significantly more stable than the 2,3-isomer **17**.[38] The formal C–C triple bond length is similar in **2** and **16**, while it is markedly lengthened in **17** (**2**: 124.1; **16**: 124.8; **17**: 126.7 pm; B3LYP/cc-pVTZ).[41] In addition, the singlet–triplet gap of **2** and **16** is comparable, whereas it is reduced by several kcal mol^{-1} in **17**.[38,39] This difference is caused by a cumulative effect of both, destabilization of the singlet ground state, and stabilization of the triplet state of **17**, as is evident from the biradical stabilization energies (BSE), derived from isodesmic equations.[38,39] The triplet state gains stability from the efficient delocalization to the third center (the calculated ^{14}N hyperfine coupling constant of 37 G in **17** is significantly larger than in the 2,4- and 2,5-isomers with 32 and 31 G, respectively). On the other hand, the singlet state of **17** is destabilized by an unfavorable three-center, four-electron interaction, which makes the major contribution to the difference in ΔE_{ST} between **16** and **17** (a comparable interaction destabilizes the 2,6- and 3,5-isomers, see Section 3.4.; additionally, an anomeric effect of the nitrogen lone pair on the vicinal C–C bonds is likely to be operative in **17**, see Figure 11).[38,39] The effect of protonation of the nitrogen atom in the pyridynes was also investigated.[39] Replacement of CH by N in benzynes has a large impact on the singlet states (rather than on the triplets), which is attenuated by protonation.[39]

In 1972 Berry et al. detected 3,4-pyridyne (**16**) by mass spectrometry.[42] Trapping experiments also provided evidence for the existence of this intermediate, although the chemistry of **16** differs considerably from that of *ortho*-benzyne.[10] Thus, neither anthracene[10a] nor dimethylfulvene[43] form Diels–Alder adducts with **16**. Nam and Leroi were able to generate **16** in nitrogen matrices at 13 K and characterize it by IR spectroscopy.[44] Irradiation of 3,4-pyridinedicarboxylic anhydride (**18**) ($\lambda > 340$ nm) results in formation of **16**, which upon photolysis with light of short wavelength ($\lambda > 210$ nm) fragments to give buta-1,3-diyne (**19**) and HCN, and acetylene (**20**) and cyanoacetylene (**21**; Scheme 4). The assignment of an intense absorption at



18 **16** **19** **20** **21**

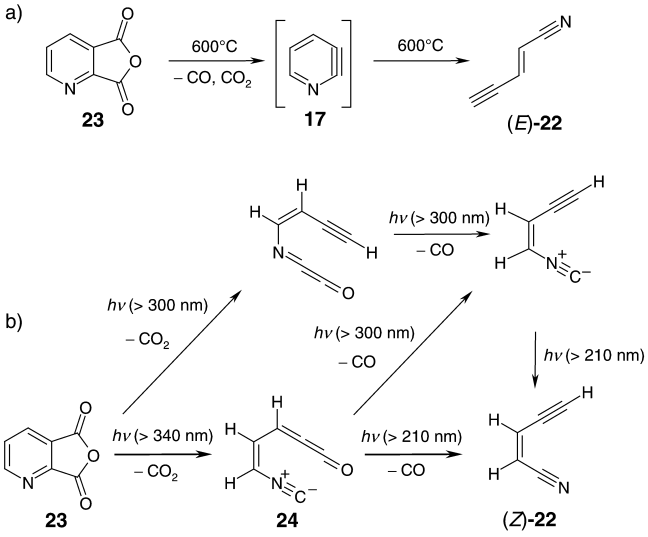
Scheme 4. Generation and photofragmentation of **16** in a nitrogen matrix at 13 K.[44]

2085 cm^{-1} to the C≡C stretching mode in **16**[44] might have to be revised in view of the reinterpretation of the *ortho*-benzyne spectrum by Radziszewski et al.; ketene structures are apparently formed in this case as well.[16]

2,3-Didehydropyridine (**17**) is less well investigated, and the existence of this intermediate is not yet established definitively. Compound **17** has been postulated as an intermediate of the gas-phase pyrolysis of 2,3-pyridinedicarboxylic anhydride (**23**) at 600 °C, which finally yields β-ethynylacrylonitrile (**22**).[45] Indirect evidence stems from trapping experiments with benzene and thiophene.[10g] Photolysis of matrix-isolated **23**, however, does not produce **17** (Scheme 5 a).[46] Nam and Leroi suggested that loss of CO_2 leads initially to the 3-acyl-2-pyridyl biradical, which undergoes ring opening to **24** significantly faster than the second radical center at the aromatic ring is formed by CO release (Scheme 5 b).[46]

2.5. Concluding Remarks on ortho-Arynes

Except for the parent *ortho*-benzyne (**2**), direct spectroscopic data on *ortho*-arynes are scarce. Theoretical results are often subject to differences related to method and basis set, which make it difficult to separate physical effects from artefacts. Despite enduring efforts, much remains to be done to gain a fundamental understanding of the effect of substitution, annelation, and heteroatoms on the structure and reactivity of **2**. Even more difficult is the situation for



Scheme 5. a) 2,3-Pyridyne was postulated as an intermediate in the gas-phase pyrolysis of **23** that finally leads to **22**.[45] Direct proof for the existence of this species could not be achieved yet. b) The reaction scheme of the photolysis of **23** in a nitrogen matrix at 13 K suggested by Nam and Leroi.[46]

meta-arynes, which have been focused upon only recently and which will be described in more detail in the following chapter.

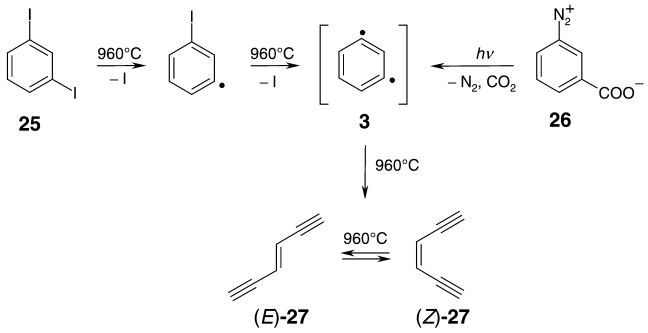
3. meta-Arynes

3.1. meta-Benzyne

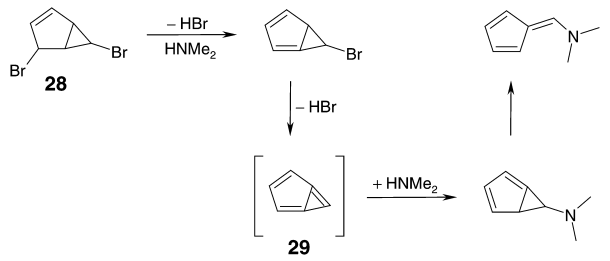
Early attempts to generate and characterize *meta*-benzyne (**3**) described in literature comprise pyrolysis of 1,3-diiodobenzene (**25**)[13] and flash photolysis of benzenediazonium 3-carboxylate (**26**).[47] While in the former case only enediynes (*E*)- and (*Z*)-**27** were in accordance with the ionization potentials determined (pyrolysis temperature: 960 °C), the results of the latter work remain unclear. A transient with *m*/*z* 76 and a lifetime of 400 μs was observed, however, it was not possible to unambiguously assign this species to **3** due to the complexity of the product spectrum (Scheme 6). Indirect evidence for the existence of **3** stems from trapping experiments.[48–50]

In 1975 Washburn et al. investigated the dehydrohalogenation of 2,6-dibromobicyclo[3.1.0]hex-3-ene (**28**) with bases and postulated the intermediate formation of bicyclo[3.1.0]-hexatriene (**29**; Scheme 7).[51]

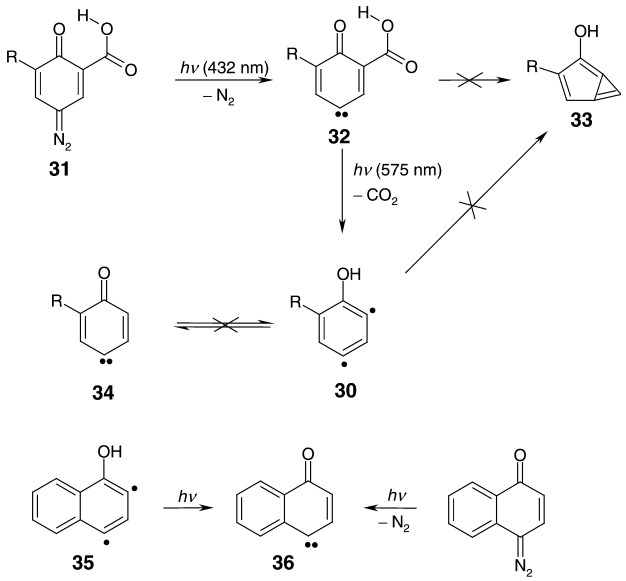
The first spectroscopic evidence for a derivative of **3** was presented by Bucher and Sander in 1992, who were able to isolate 2,4-didehydrophenol **30** in cryogenic matrices (Scheme 8).[52] Irradiation of matrix-isolated quinone diazide **31** with monochromatic light ($\lambda = (432 \pm 10)$ nm) yields carbene **32**, which is photochemically converted to didehydrophenol **30** by long wavelength irradiation ($\lambda = (575 \pm 10)$ nm). The existence of an OH group in **30** was confirmed by isotopic labeling using $[D]_1$-**31**.[52] Evidence for a bicyclic



Scheme 6. Early attempts to generate *meta*-benzyne did not yield conclusive evidence for existence and structure of **3**.

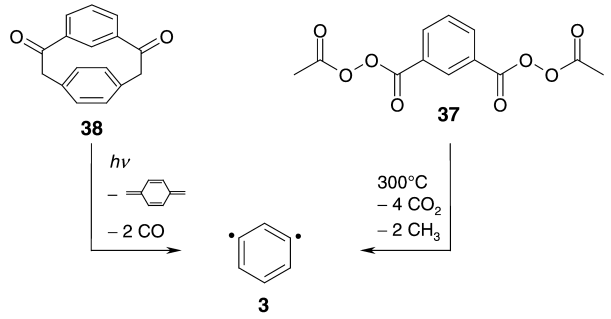


Scheme 7. Dehydrohalogenation of **28** with the postulated bicyclic intermediate **29** instead of a *meta*-benzyne **3**.[51] The question whether **29** exists has been the subject of some controversy until recently.



Scheme 8. Didehydrophenol **30** was the first derivative of **3** that could be isolated in an argon matrix at 8 K. Comparison of measured and calculated spectra supports the assignment to a monocyclic structure **30**. Evidence for bicyclic isomer **33** was not found.[52–54] Similarly, a tautomerization to **34** was not observed. In contrast to **30**, derivative **35** can be converted photochemically to carbene **36**.[54]

isomer **33** was not found.[52,53,54] Benzannelated didehydrophenol **35** tautomerizes photochemically to carbene **36**, in contrast to didehydrophenol **30**, which yields ring-opened products of unknown constitution upon irradiation.



Scheme 9. The first IR spectroscopic characterization of **3** was achieved in 1996 by FVP of **37** with subsequent trapping of the products in argon at 10 K, and, alternatively, by irradiation of **38** in an argon matrix.[55]

The isolation of the parent *meta*-benzyne (**3**) in a cryogenic matrix was finally achieved in 1996 starting from diacetyl peroxide **37** as a thermal, and *meta-para*-cyclophane-9,10-dione (**38**) as a photochemical precursor (Scheme 9).[55]

In a recent work the IR measurements on **3** were extended to the FIR region ($>200\,cm^{-1}$) and additional precursors were employed.[56] In particular, it was shown that pyrolysis of 1,3-diiodobenzene at 600 °C gives good yields of *meta*-benzyne, together with (*Z*)- and (*E*)-hex-3-ene-1,5-diyne (**27**), the latter being formed exclusively at temperatures above 650 °C, in accordance with the results obtained earlier by Fisher and Lossing.[13] Flash vacuum pyrolysis (FVP) of 1,3-dinitrobenzene also yields small amounts of **3**.[56] By using these four different routes to *meta*-benzyne all of the more intense IR absorptions of **3** were unambiguously identified. The IR spectrum of the perdeuterated isotopomer $[D]_4$-**3** was also obtained.[56]

The vibrational spectrum of **3** is nicely reproduced by quantum-chemical calculations at the CCSD(T) level of theory,[56,57] whereas DFT shows a variable performance depending on the functional employed.[57,58] This holds especially for the distance between the radical centers and the question of whether the matrix-isolated species can be assigned to the bicyclic structure **29**.[59] In more recent theoretical and experimental investigations it was shown that **3** has a monocyclic structure with a distance of (205 ± 5) pm between the radical centers (Table 1).[56–58] Nevertheless, the potential energy suface along the 'cyclization coordinate' is rather flat.[57,58] Despite the significant distance of the radical centers the biradical character of **3** is low (19–32 %, depending on the definition of this quantity).[22q,53,57,58] The electronic structure of **3** is most appropriately described as a σ-allylic system (Figure 2), in which primarily the C–H-σ* orbital, located between the dehydrocarbons, participates in the interaction of the radical lobes.[60]

NIPES experiments also support a monocyclic structure of *meta*-benzyne, although the spectra of **3** are considerably more complex than in the case of *ortho*- and *para*-benzyne.[17]

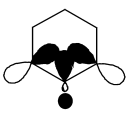


Figure 2. The electronic structure of **3**.

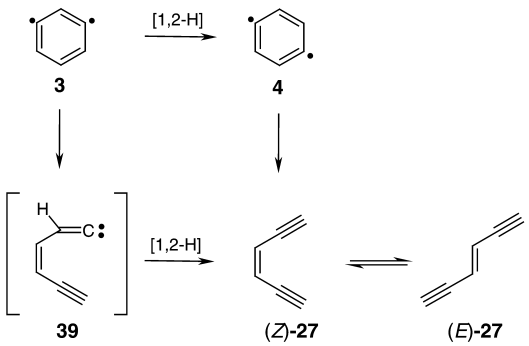
Table 1: Calculated equilibrium distances *d*(C1–C3) of the radical centers in *meta*-benzyne.[a]

Method	Basis set		
	cc-pVDZ	cc-pVTZ	cc-pVQZ
SPW91	155.0	154.0	154.0
MPW1PW91	155.9	154.9	154.9
B3PW91	157.3	156.2	156.2
B3P86	157.4	156.3	156.2
SVWN	158.1	156.9	157.0
SLYP	158.0	157.0	157.1
SVWN5	158.6	157.5	157.6
MPW1LYP	160.1	159.0	159.1
B3LYP	161.5	160.3	160.4
BPW91	187.8	184.3	182.2
BP86	193.3	190.4	189.9
BLYP	202.1	199.7	199.5
BVWN	203.4	200.7	200.4
BVWN5	204.1	201.4	201.2
BCCD(T)[b]	211 ± 1	204 ± 1	203 ± 1
RCCSD(T)[b]	211 ± 1	205 ± 1	203 ± 1
CAS(8,8)-RS3[b]	211 ± 1	205 ± 1	203 ± 1
CAS(8,8)-CISD + Q[b]	213 ± 1	207 ± 1	
CAS(8,8)-CISD[b]	215 ± 1	210 ± 1	
CAS(8,8)-RS2[b]	215 ± 1	210 ± 1	209 ± 1

[a] Ref. [41] and [58]. Distances *d*(C1–C3) in pm. [b] Lowest-energy structure determined for (U)B3LYP/cc-pVTZ-optimized geometries with constrained distances *d*(C1–C3).

The singlet–triplet energy gap was determined to be (21.0 ± 0.3) kcal mol^{-1}, confirming the low biradical character of **3**.[17]

The mechanism of the rearrangement of *meta*-benzyne **3** to (*Z*)-hex-3-ene-1,5-diyne ((*Z*)-**27**) has been elucidated recently. Possible isomerization pathways include ring-opening to a vinylidene **39** with subsequent hydrogen shift or rearrangement to the *para* isomer **4** followed by retro-Bergman reaction (Scheme 10, and Section 4.3).[56,61] Experimental data obtained by Zewail et al. using femtosecond time-resolved spectroscopy with mass spectrometric detection on the photolysis of 1,2-, 1,3-, and 1,4-dibromobenzene were interpreted by the authors in terms of a rapid equilibrium between *ortho-*, *meta-*, and *para*-benzyne via quantum-mechanical tunneling of H atoms, from which the *para* isomer reacts to the entropically favored enediyne **27**.[62] Investigations by Sander and Cremer, however, favor an



Scheme 10. Possible pathways for the rearrangement **3**→**27**.

alternative mechanism of direct ring opening of **3**. According to DFT calculations the vinylidene **39** does not occupy a stationary point on the potential energy surface, and ring opening and hydrogen migration proceed in one step. Additional support for this mechanism is provided by the fact no *ortho*-benzyne is formed in pyrolysis of 1,3-diiodobenzene. The rearrangment **3**→**27** could also be induced photochemically.[56]

A new method for the investigation of reactions of *meta*-benzyne derivatives in the gas phase using FT ion cyclotron resonance mass spectrometry has recently been described by Kenttämaa et al.[63] It could be shown that the reactivity of *meta*-benzyne is reduced compared to that of the phenyl radical due to strong coupling of the radical centers. It was also noted that **3** possesses electrophilic properties.[63]

3.2. Substituted meta-Benzynes

Photolysis of cyclophanediones was applied for the generation of several derivatives of **3**. Thus, 5-fluoro- and 5-methyl-1,3-didehydrobenzene were isolated in argon matrices and characterized by their IR spectra.[64] The synthesis of 2-substituted derivatives of **3** is not feasible with this method, since the corresponding cyclophanediones could not be synthesized. The perfluorinated *meta*-didehydrobenzene **40** was generated by photolysis of 1,3-diiodotetrafluorobenzene (**41**) in solid neon (but not in argon) at very low temperature, whereas the pyrolysis of **41** results in complete fragmentation of the ring system.[27,65]

One important parameter for understanding substituent effects on structure and reactivity of **3** is the distance between the radical centers. Despite the flat potential between **3** and **29**, the effect of substitution on the structure of *meta*-benzyne seems to be limited.[26] The data obtained with theoretical methods could again be interpreted in terms of varying weights of mesomeric structures (Scheme 11).[66]

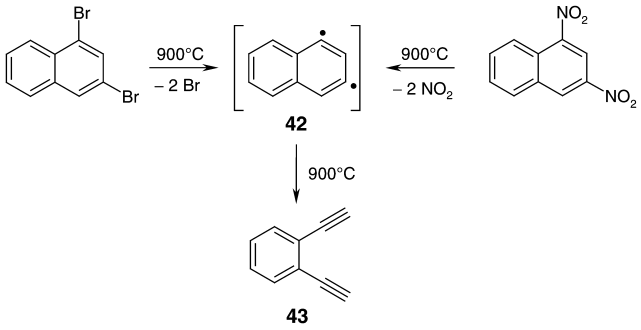
For the bicyclic structure **29** two resonance structures may be drawn; apart from the anti-Bredt form **29A** a charge-separated structure **29B** contributes to the resonance hybrid.[26] Substituents, which stabilize the cyclopropenyl cation or allyl anion unit, are expected to favor the bicyclic structure and to decrease the distance between the radical centers.[26] Accordingly, calculations show that donor substituents (NH_2, SiH_3) decrease, acceptor substituents (CN, NH_3^+) increase the C2–C6 distance in 2,6-didehydro isomers.[26] In 2,4-isomers the substituents interact with a negative partial charge, and therefore donor substituents result in increased, acceptor substituents in decreased distances. For 3,5-isomers the shortest C3–C5 distances are predicted for σ-acceptor–π-donor substituents, since the central carbon atom (C1) of the allyl anion unit is positively polarized (significant negative charge density at the termini of the allyl anion).[26] The influence of substituents on biradical stabilization energies in singlet *meta*-benzynes is small, and slight variations have been rationalized on the basis of electrostatic arguments.[26] The triplet states are even less affected by substitution.[26] It remains to be noted that the high structural flexibility is obviously characteristic for all *meta*-benzynes.[17,22q,u,26,30,37–39,53,57,58] It can therefore not be taken for granted that calculated tendencies (and in particular those obtained with DFT methods) represent actual physical trends instead of just reflecting deficiencies of the respective level of theory.



Scheme 11. Mesomeric forms of **29**; the transition to **3** is characterized by a flat potential.

3.3. Annelated meta-Arynes

In contrast to the situation with the *ortho* derivatives, Grützmacher et al. identified on the basis of the high ionization potential ((8.96 ± 0.02) eV) diethynylbenzene (**43**) instead of 1,3-didehydronaphthalene (**42**) as the pyrolysis product of 1,3-dinitro- and 1,3-dibromonaphthalene.[32b] Evidently, a rearrangement analogous to the ring opening of *meta*-benzyne takes place for the annelated derivative as well (Scheme 10 and 12).

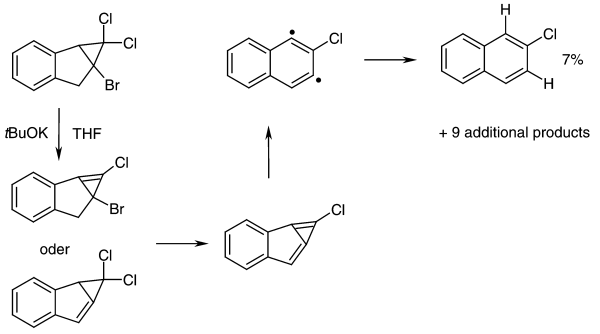


Scheme 12. Pyrolysis with mass spectrometric detection of 1,3-dibromo- and 1,3-dinitronaphthalene indicates that **42** is thermally not stable at 900 °C. The measured ionization potential suggests that the ring-opened product **43** is formed under these conditions (see also Scheme 10).[32b]

A derivative of 1,3-naphthyne was postulated by Billups et al. as an intermediate of the dehydrohalogenation of the dichlorocarbene adduct of 2-bromoindene with potassium *tert*-butoxide, however, the complex product mixture did not allow to conclusively elucidate the reaction mechanism (Scheme 13).[67]

In a broader sense, 1,8-naphthyne (**44**) may also be regarded as a derivative of *meta*-benzyne, since the radical centers are separated by the same number of bonds as in **42**. However, whereas 1,3-naphthyne (**42**) displays a strong

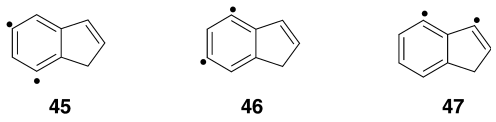




Scheme 13. 2-Chloro-1,3-didehydronaphthalene was postulated as an intermediate of a complex dehydrohalogenation reaction by Billups et al.[67]

preference for the singlet state (17.3 kcal mol^{-1}, comparable to that of *meta*-benzyne; Table 3, Section 4.5), singlet and triplet states are almost degenerate in the 1,8-isomer (ΔE_{ST} = 0.9 kcal mol^{-1}).[30] The ionization potential (IP) of **44** (7.92 eV) is lower than that of naphthalene (8.26 eV), while the IPs of most other naphthynes are higher.[32] Attempts to generate **44** by irradiation of 1,8-naphthalenedicarboxylic anhydride in an argon matrix were unsuccessful.[68]

A similar situation is observed for the didehydroindenes. The singlet–triplet gaps of **45** and **46** (ca. (15 ± 2) kcal mol^{-1}) are closer to that of **3**, while the separation in **47** is

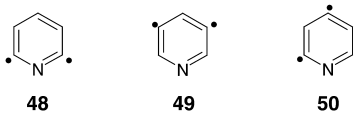


significantly lower (1–2 kcal mol^{-1}).[37] The strong dependence of the calculated structures on the level of theory employed was also pointed out for all of the annelated *meta*-benzynes.[30,37]

3.4. meta-Pyridynes

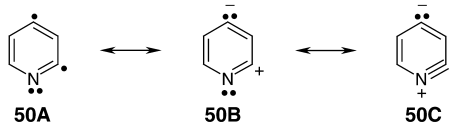
So far the three isomeric *meta*-pyridynes eluded experimental observation,[41] although the properties of **48**–**50** are of some interest from a theoretical point of view.[38,39]

Compound **48** is the least stable of all six pyridynes and its lowest singlet and triplet states are essentially degenerate. It is less stable than the singlet ground state of *ortho* isomer **16** by approximately 20 kcal mol^{-1}.[38] The structural flexibility of **48** is even more pronounced than in the case of the other *meta*-arynes (see Sections 3.1–3.3). In addition to mono- and bicyclic structures analogous to **3** and **29** an allylic structure

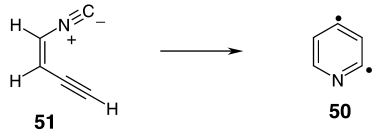


with a widened C2-N-C6 angle is found depending on the level of theory applied.[38,39,40d,41] The 3,5-isomer **49**, which lies energetically above **16** by 15–18 kcal mol^{-1}, is the second least stable pyridyne. The singlet–triplet gap of **49** is about 18 kcal mol^{-1}, still below that of *meta*-benzyne **3**.[38,39] The unprecedented properties of the *meta*-pyridynes, and in particular of **48**, result from a strong σ-allylic interaction, as schematically depicted in Figure 3.[38]

2,4-Pyridyne (**50**) is the most stable of the three isomers, and, in contrast to **48** and **49**, has a higher preference for the singlet ground state than **3**. This suggests the participation of



nitrilium ion structure **50B** and possibly **50C** in the resonance hybrid, which is also evident from the shortening of the N–C2 bond compared to the N–C6 bond. On the other hand, the triplet state of **50** is less stable than that of **3**, which has been attributed to the ring contraction generally observed for heterocycles.[38,39] An interesting route to **50** was suggested by Cramer et al.:[39] Cyclization of isonitrile **51** could lead to **50** in a rearrangement analogous to the Bergman cyclization (see Section 4). The activation enthalpy for the only slightly



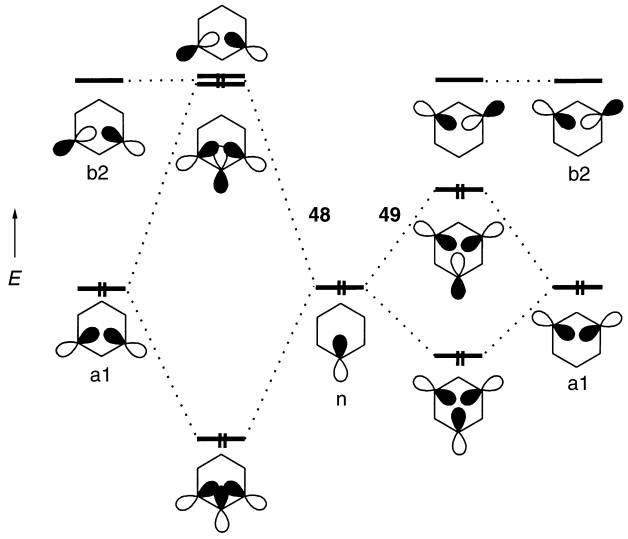
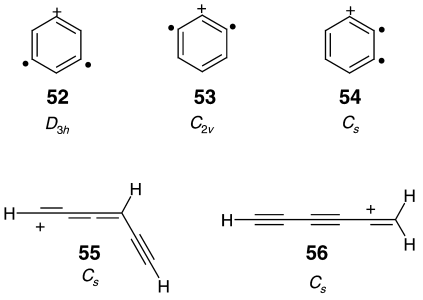


Figure 3. σ-Allylic interaction of the lone pair (n) at the nitrogen atom with the bonding (a1) and antibonding (b2) combination of the p orbitals in **48** and **49**. Owing to the stronger overlap the SOMOs (HOMO and LUMO) in **48** are essentially degenerate, which results in a very small singlet–triplet gap. In **49** ΔE_{ST} is only slightly decreased by about 3 kcal mol^{-1} compared to that in **3** (see also Section 3.5).[38,39]

exothermic reaction was estimated to 18 kcal mol^{-1},[39] however, this novel access to *meta*-arynes could not be realized experimentally so far.

3.5. Didehydroaryl Cations

A three-center interaction similar to that in *meta*-pyridynes **48** and **49** results in substantial stabilization in the two-electron case. 3,5-Didehydrophenyl cation (**52**), the classic example[69] for "in-plane aromaticity",[70] is the global minimum of the $C_6H_3^+$ hypersurface.[71] Remarkably, the 2,6-isomer **53** and 2,3-isomer **54** are less stable than **52** by 11.7 and 23.2 kcal mol^{-1}, respectively.[71] Evidently, for the two-electron case the 1,3,5-topology (comparable to that in the trishomocyclopropenium cation) is favored over the 1,2,3-topology, while for the four-electron, three-center systems the destabilization is most pronounced in the second case (see Figure 3). In addition to its remarkable stability **52** also fulfils magnetic aromaticity criteria.[70,71] At the same level of theory (MP4(SDTQ)/6-31G*//MP2/6-31G* + ZPE) open chain isomers **55** and **56** are less stable by 11.8 and 30.4 kcal mol^{-1}, respectively.[71] In contrast to the Jahn–Teller distorted, C_{2v}-symmetric 1,3,5-tridehydrobenzene (see Section 5.1), cation **52** has D_{3h} symmetry,[71] and the structure of the molecule clearly reflects the influence of the three-center interaction (Figure 4).



Although the experimental generation of **52** has been claimed several times, a definitive structural characterization of this interesting system has not been realized yet.[72] Another molecule for which a similar three-center interaction has been discussed is cyclo[6]carbon, which will be dealt with in more detail in Section 5.3.[71]

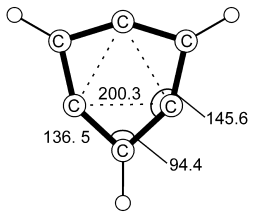


Figure 4. The structure of **52**, calculated at the BLYP/cc-pVTZ level of theory, reflects the in-plane interaction of the hydrogen-free carbon atoms.[41] Bond lengths are in pm, bond angles in degrees.

3.6. Concluding Remarks on meta-Arynes

A common feature of all *meta*-arynes is their pronounced structural flexibility, which complicates theoretical investigations of these systems. Within the last few years we have began to develop a basic understanding of the structure and reactivity of this class of compounds. The discussion concerning the structure of the parent *meta*-benzyne (**3**) emphasizes the importance of verifying theoretical results by comparison with experimental data. Interesting molecules like **52**, which seemed out of reach until recently, have now become attractive synthetic targets. Investigations of the exceptional properties and bonding within these systems will undoubtly help to further improve our understanding of structure and reactivity in general.

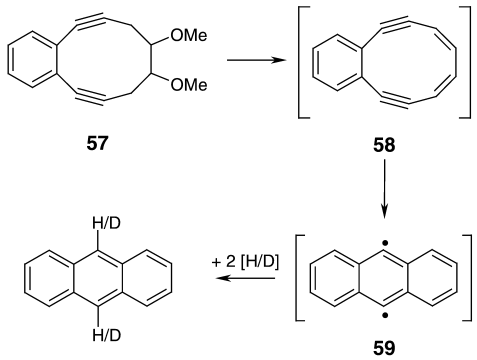
4. para-Arynes and the Bergman Cyclization

4.1. Historical Survey

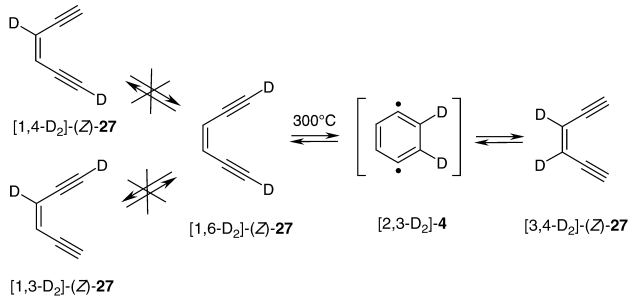
Experimental access to *para*-benzyne (**4**) turned out to be even more difficult than to *meta*–benzyne (**3**). Pyrolysis of 1,4-diiodobenzene results in exclusive formation of hex-3-ene-1,5-diyne (**27**).[13] Attempts by Berry et al. to generate **4** by photoinitiated decomposition of benzenediazonium 4-carboxylate in the gas phase gave dubious results.[47] The authors postulated the formation of **4**, however, a lifetime of more than two minutes was measured for the product observed, which is incompatible with a reactive biradical, in particular since the lifetime of *ortho* and *meta* isomers **2** and **3** are reported to be in the order of milliseconds and microseconds, respectively.[47]

The first example of a cycloaromatization analogous to the **27**→**4** reaction (Bergman cyclization) was reported by Masamune et al. Attempts under various experimental conditions to generate didehydro[10]annulene **58** yielded anthracene instead.[73] In deuterated solvents 9,10-dideuteroanthracene was isolated, indicating the intermediate formation of 9,10-didehydroanthracene (**59**) (Scheme 14).[73]

However, it was not before the classic experiments of Jones and Bergman in 1972 that *para*-benzyne (**4**) came into the focus of mechanistic organic chemistry.[74] The authors



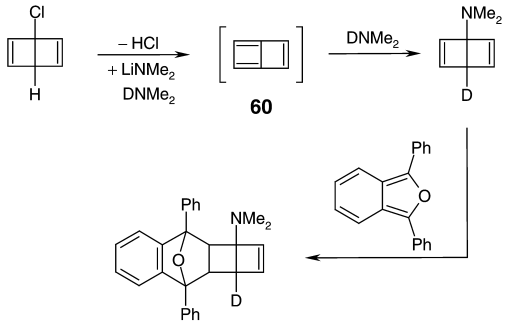
Scheme 14. First experimental evidence for the existence of a *para*-aryne was obtained by Masamune et al. in 1971.[73]



Scheme 15. At 300 °C [1,6-D_2]-**27** equilibrates with [3,4-D_2]-**27**, but not with the 1,4- or 1,3-deuterated isotopomers. The simultaneous migration of the deuterium atoms from acetylenic to vinylic positions can only be explained by supposition of a cyclic, symmetric intermediate [2,3-D_2]-**4**.[74]

observed that [1,6-D_2]-(*Z*)-hex-3-ene-1,5-diyne ([1,6-D_2]-**27**) rapidly reacts to a mixture of [3,4-D_2]- and [1,6-D_2]-**27** at 300 °C. The fact that no [1,3-D_2]- or [1,4-D_2]-**27** is formed can only be explained by presumption of a cyclic, symmetrical intermediate (Scheme 15).[74] Numerous trapping experiments supported the hypothesis of the thermal formation of *para*-benzyne from (*Z*)-**27**. In CCl_4, for example, thermolysis of the enediyne yields 1,4-dichlorobenzene.[74,75]

While the majority of trapping experiments favors a biradicaloid structure, evidence for a bicyclic intermediate (butalene (**60**)) was also found.[76] Breslow et al. reported the formation of **60** (the possible existence of which had been



Scheme 16. Breslow et al. postulated the formation of a butalene intermediate **60** in 1975.[76]

pointed out by Dewar before[77]) upon dehydrohalogenation of 3-chloro[2.2.0]bicyclohexadiene (Scheme 16).[77d] The bicyclic nature of the intermediate was inferred from the observed Diels–Alder type reactivity with activated dienes.[76]

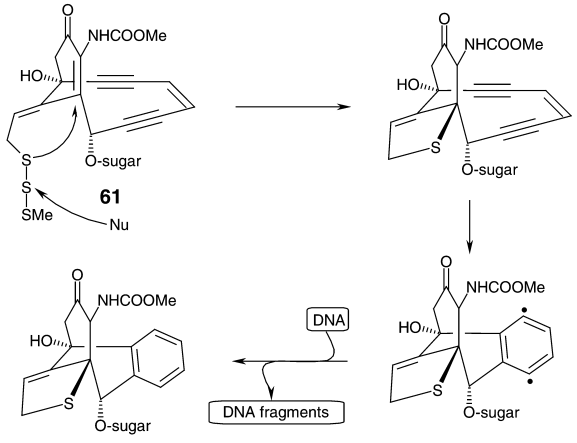
The energy profile of the reaction **4**⇌**60** and the question of whether butalene exists at all have been a matter of controversy until recently.[77] According to DFT calculations the biradical structure **4** is more stable by 37 kcal mol^{-1} than the highly strained butalene.[77a] The barrier for ring opening of butalene **60** is 3–6 kcal mol^{-1}, which could be sufficient to allow its isolation in cryogenic matrices.[77a]

4.2. Enediyne Cytostatics

One of the most important motivations for the investigation of *para*-benzyne and the Bergman reaction was the discovery of the enediyne cytostatics, namely calicheamicins, esperamicins, and dynemicins, which are able to cleave the DNA double-strand sequence specifically in vivo.[78] These substances have in common a (*Z*)-hex-3-ene-1,5-diyne moiety, usually embedded in a complex cyclic system, which, upon activation, cyclizes to form an aromatic biradical. In the case of calicheamicin (**61**) a *para*-benzyne derivative is formed, while similar compounds yield didehydroindene or α,3-didehydrotoluene derivatives (see Section 4.5).[78]

The sophisticated mechanism of the biological activity of these substances has been elucidated in detail (Scheme 17). The sugar moiety of **61** coordinates to the minor groove of the DNA double helix (the binding energy has been estimated to be ca. 10 kcal mol^{-1}), pyrimidine-rich sequences (e.g. TCCT or CTCT) being preferred.[78] Nucleophilic attack at the S–S bond of the trisulfide group and subsequent intramolecular addidtion to the α,β-unsaturated ketone embedded in the adjacent six-membered ring initiates a reaction cascade: Rehybridization ($sp^2 \rightarrow sp^3$) of the attacked carbon atom results in a decreased distance between the terminal acetylenic carbon atoms in the enediyne moiety, triggering the Bergman cyclization already at room temperature.[78] The newly formed biradical attacks the DNA strand by abstracting a hydrogen atom from the sugar. The phenyl radical generated thereby is significantly more reactive than *para*-didehydrobenzene and rapidly abstracts another hydrogen atom from the neighboring DNA strand.[80] Reaction with oxygen and reduction of the hydroperoxide formed results in cleavage of both DNA chains.[78]

Since the naturally occurring enediyne cytostatics turned out to be highly toxic in animal experiments, much effort was spent on the design of more selective derivatives to achieve high biological activity towards tumor cells in combination with a minimum toxicity towards normal cells.[78–81] One approach to increase the selectivity is to decrease the reactivity of the biradical intermediate in hydrogen-abstraction reactions.[80,81] In this regard Chen et al. have established

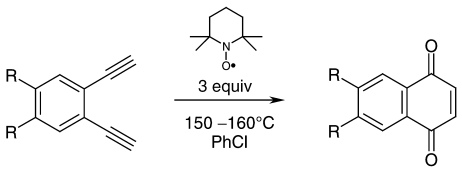


Scheme 17. Mechanism of the DNA cleavage by calicheamicin γ_1^I.[78]

a simple model which correlates the reactivity of singlet biradicals with their singlet–triplet gap ΔE_{ST}.[80] This model is based on the assumption that the reactivity of the triplet biradical is comparable to that of the monoradical, while effects stabilizing the singlet state have to be overcome in the transition state of the hydrogen abstraction. Accordingly, an increased singlet triplet gap is expected to raise the barrier for hydrogen abstraction and (possibly) the selectivity of the reaction.[80] An interesting method to estimate ΔE_{ST} based on the isotropic hyperfine coupling constant of the radical center in the respective monoradical with the proton at the second center has been developed by Cramer and Squires.[82] Since this approach provides reliable results already with DFT methods it can be applied to larger systems such as potential antitumor drugs.

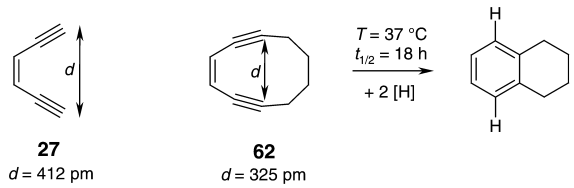
In this context it is noteworthy that the pH value of tumor cells (6.2 to 6.6) is lower than that of normal cells (7.5),[78,83] which could be used to control the Bergman cyclization of substituted and/or heterocyclic derivatives of **4** by protonation/deprotonation or to control the hydrogen abstraction depending on the pH value. In an exhaustive theoretical study Cremer and Kraka investigated a large number of substituted and hetetrocyclic enediynes and the corresponding benzynes and proposed potential candidates for future anticancer drugs.[81] Aza-Bergman reactions, which were initially discussed in this context by Chen et al.[80] and later by Cramer[84] as well as Kraka and Cremer,[81] will be referred to in Section 4.3.

Recently, the suggestion that a quinone (formed by oxygen trapping of the biradical) rather than the biradical itself could act as the "warhead" of the enediyne cytostatics attracted much attention among chemists.[85] While the formation of quinoid systems from *para*-benzynes has already been established (Scheme 18),[86] Lerner, Janda, and co-



Scheme 18. The formation of quinoid systems by oxygen transfer to *para*-arynes was established in 1995.[86]

workers demonstrated that trapping by oxygen can occur even in the presence of suitable hydrogen donors, and that the resulting quinone is even more toxic toward tumor cells than the enediyne.[85a] This reaction is intriguing, not only because the quinone is formed at all, but in particular because the rate of quinone formation depends on the oxygen concentration. The mechanism by which oxygen is involved in the rate-determining step of the reaction is still unclear, since calculations by Jones and Warner found neither a significant activation barrier for the reaction of the biradical with O_2, nor a feasible reaction path for direct reaction of the enediyne with oxygen.[85b] Thus, it is to be awaited, whether this mechanistic view is going to be widely accepted.



27
d = 412 pm

62
d = 325 pm

Scheme 19. The transition from the acyclic enediyne **27** to the cyclic enediyne **62** leads to a drastic reduction of the barrier for cycloaromatization.[78h,87] However, the distance *d* between the acetylenic carbon atoms seems to be only one of the factors governing the activation enthalpy of the Bergman cyclization.[88]

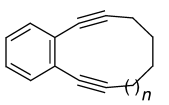
4.3. The Bergman Cyclization

4.3.1. The Thermal Bergman Cyclization

Since the enediyne moiety of most naturally occurring enediynes is embedded in a larger (nine- or ten-membered) ring system, much attention has been paid to the influence of the distance *d* between the terminal acetylenic carbon atoms on the cyclization temperature in different cyclic enediynes: While parent enediyne (*Z*)-**27** cyclizes only at about 200 °C ($t_{1/2} = 30$ s), cyclization in 3-cyclodecen-1,5-diyne (**62**) already starts at 37 °C ($t_{1/2} = 18$ h, Scheme 19).[78h,87]

This interatomic distance dependence has also been the subject of theoretical investigations.[88] It was suggested that Nicolaou's "critical distance",[78h,87] at which cyclization occurs at room temperature, should be extended from 320–331 pm to 290–340 pm; apart from this *no* direct correlation between *d* and the activation enthalpy of the cyclization was found in that work.[88] Instead, the difference in ring strain between ground and transition state apparently is an important factor influencing the energetics of the cycloaromatization of monocyclic enediynes, which was also proposed by Magnus et al.[89] and Snyder et al.[90] Nevertheless, no enediynes with $d < 310$ ppm that are stable at room temperature have been synthesized so far, and, on the other hand, systems with $d > 370$ ppm do not cyclize spontaneously.[91] Therefore, the distance of the alkyne carbon atoms seems to be at least one important factor determining the kinetic stability of the enediynes.[91] Experiments carried out by Semmelhack et al. also indicate that *d* influences the cylization temperature.[92] While **63** cyclizes at 84 °C with a half life of 24 h, the 11-membered ring system **64** fails to undergo a thermal Bergman reaction.[92]

In this context, the gas-phase structure of acyclic enediyne (*Z*)-**27** is noteworthy (Figure 5), which was determined by analyzing the microwave spectra of seven isotopomers.[93] Interestingly, the C–C≡CH units are not linear, but are tilted outwards by 1.2°, which possibly accounts for a part of the activation barrier for cyclization and can be overcome by integration into a cyclic system.



63: *n* = 1
64: *n* = 2

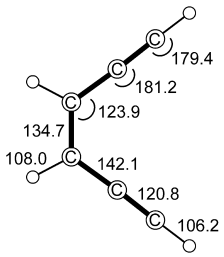
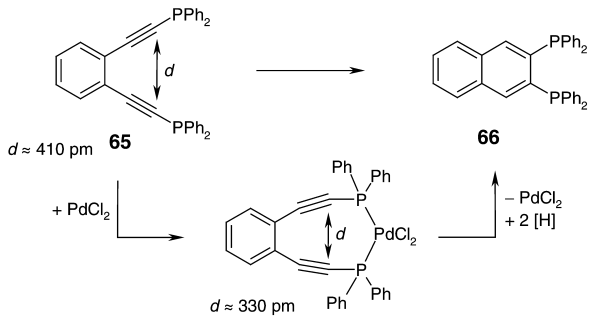


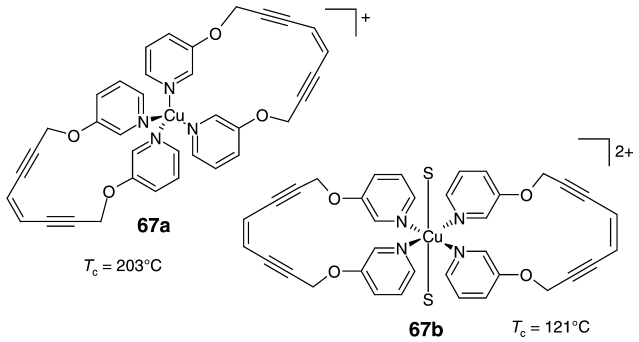
Figure 5. Gas-phase structure of enediyne (*Z*)-**27**.[93] Bond lengths in pm, bond angles in degree.

An elegant method to raise the ground-state energy of an enediyne by shortening the distance between the acetylenic carbon atoms and thereby lowering the barrier for cyclization (the term "new base camp" strategy has been established for this method)[94,95] is complexation by transition metals. In 1995 Buchwald et al. were able to demonstrate that the cyclization of diphosphanylenediyne **65** to **66** is accelerated by a factor of more than 30000 by chelatization with $PdCl_2$, corresponding to a decrease in activation energy of at least 6 kcal mol^{-1} (Scheme 20).[96] By using different metal ions, this method allows one to control the distance of the alkyne termini by means of the ionic radii.[96,97]

Major improvements in this direction for practical applications were achieved by Zaleski et al.[91,98] For copper complex **67** (Scheme 21) the cyclization temperature can be controlled by changing the oxidation state of the Cu ion and thereby the coordination geometry (square-planar or octahedral for Cu^{II}, tetrahedral for Cu^{I}).[91,98] In a more recent work,



Scheme 20. The cyclization temperature of **65** is drastically reduced by metal complexation.[95]



Scheme 21. Bergman cyclization of the flexible enediyne ligands depicted is not accelerated by metals that prefer a tetrahedral ligand field (Cu^{I}, Pd^{0}, Hg^{II}), while planar metallocycles (Cu^{II}, Pd^{II}) exhibit significantly lowered cyclization barriers.[91,97,98] This change is of interest for the potential redox control, as, for example, in Cu^{I}/Cu^{II} complexes of the type **67**.[91,97,98] Cyclization temperatures were measured in the solid state by differential scanning calorimetry (DSC), and analogous reactivity trends were observed in solution.[91,97,98]

enediyne ligands could also be activated by using non-hazardous Mg^{2+} salts.[99] Without donor substitution the activation of enediynes could only be achieved by π complexation using transition metals,[100] however, inhibition of the cyclization by complexation of the alkyne moiety has also been reported.[101] The emerging field of metalloenediynes is developing rapidly, and thus a more detailed overview is beyond the scope of this article.[102]

In addition to metal complexation electronic effects on the energetics of the Bergman cyclization were investigated in detail.[95] However, the interpretation of experimental results is often nontrivial. Benzannelation of the enediyne unit, for example, results in acceleration of the cyclization for some systems, while in other cases inhibition is observed. Additionally, factors like concentration of hydrogen donors can affect the measured rates and often have to be taken into account.[95]

Detailed thermochemical data for the Bergman rearrangement were determined by Roth et al. from gas-phase NO-trapping experiments.[103] The activation barrier for ring opening of **4** to enediyne (*Z*)-**27** was reported as 19.8 kcal mol^{-1}, and the enthalpy of formation of (*Z*)-**27** ($\Delta H^0_{f,298} = 129.5$ kcal mol^{-1}) is lower than that of *para*-benzyne ($\Delta H^0_{f,298} = (138 \pm 1)$ kcal mol^{-1}) by 8.5 kcal mol^{-1} (Figure 6). The too low value for the enthalpy of formation of **4** determined in an earlier work by Squires et al. using collision-induced dissociation (CID) measurements[18a] was corrected to (137.8 ± 2.9) kcal mol^{-1} in a recent reinvestigation, now in perfect agreement with Roth's data.[17] The thermal cyclization of 1,2-diethynylbenzene (**43**) to 1,4-didehydronaphthalene (**68**) was also investigated by Roth et al.[104] The influence of benzannelation on the potential energy surface of the Bergman reaction is depicted in Figure 6. The barrier of 25 kcal mol^{-1} for the cyclization of **43** is lower than for (*Z*)-**27**. This value is in excellent agreement with the activation parameters determined by Grissom et al. for the reaction **43**→**69** (E_a = 25.1 kcal mol^{-1}).[105] The reaction enthalpy for cyclization of the benzannelated system is higher, that is, the reaction is more endothermic, which has been rationalized by the smaller amount of resonance energy released by formation of the second six-membered ring in naphthalene compared to benzene.[104] Accordingly, the barrier for the reverse (ring-

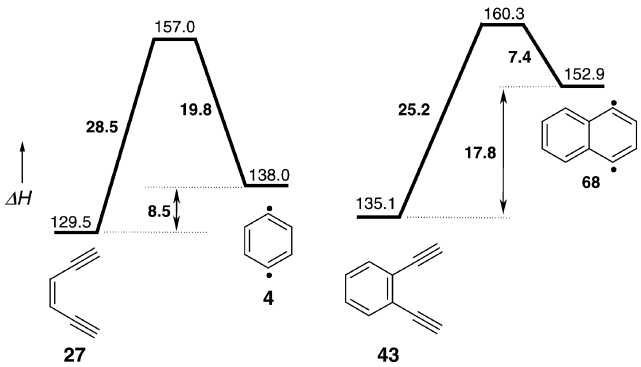
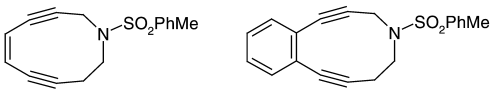


Figure 6. The energy profiles of the Bergman reaction of **27** and **43** as measured by Roth et al.[103,104] ΔH in kcal mol^{-1}.

opening) reaction **68**→**43** is lower than for *para*-benzyne (**4**; 19.8 kcal mol^{-1}).[104]

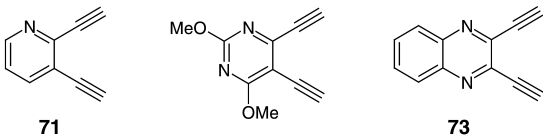
A different situation is encountered when comparing the cyclic enediynes **62** and **63**. In this case benzannelation apparently decelerates the Bergman reaction.[87e,92] A similar effect was reported for aza-enediynes **69** ($t_{1/2}$ = 72 h, T = 23 °C) and **70** ($t_{1/2}$ = 52 h, T = 65 °C).[106]



69 **70**

A thorough investigation of the effect of benzannelation by Hirama et al. demonstrated that kinetic measurements are not solely determined by the rate of the Bergman reaction, but the rates of the retro-Bergman reaction and hydrogen abstraction have to be considered as well.[107] Thus for the systems **62**/**63** a change of the rate-determining step (cyclization for **62**, hydrogen abstraction for **63**) was observed, which (confirmed by MCSCF calculations) was explained by a significantly *lowered* cyclization barrier for **63**. If hydrogen abstraction is rate-determining, the observed reaction rate depends on the concentration of hydrogen donor (which usually varies from one study to another).[107] In recent investigations a large excess of reactive hydrogen donors (such as cyclohexadiene) is therefore generally applied.

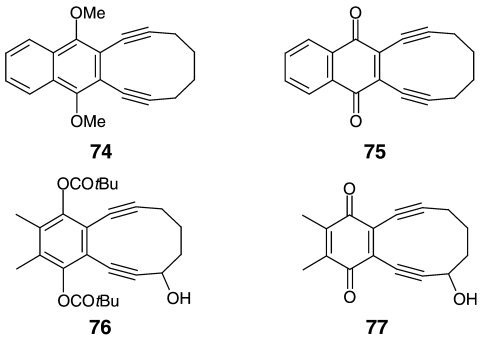
Difficult to interpret are results concerning the effect of annelation with heteroarenes by Kim and Russell.[108] While pyridine derivative **71** and pyrimidine **72** cyclize faster than **43**, quinoxaline **73** is less reactive.[108]



71 **72** **73**

E_a = 21.5 kcal mol^{-1} E_a = 16.1 kcal mol^{-1} E_a = 33.6 kcal mol^{-1}

Remarkably large differences in reaction rates were also observed for **74** and **75**, which was attributed to the different double-bond character of the ene moiety.[92] Semmelhack et al. suggested a possible redox-triggering mechanism to initiate the Bergman reaction under physiological conditions (see also Scheme 21).[92] However, the reactivity of the related systems **76** and **77** has been found to be almost identical.[109]



74 **75**

76 **77**

Solvent effects on the rate of the Bergman cyclization have been less well investigated. While early studies of substituted enediynes by Nicolaou et al. did not reveal a substantial influence of the medium (comparable rates were measured in benzene and THF),[87b] recent experiments with benzannelated systems by Russell et al. indicate, that the solvent can significantly affect their reactivity. Depending on the solvent, half-lives ranging from 16 (THF) to 361 min (acetonitrile) were measured for **73**.[110]

Substituent effects on the energetics of the cycloaromatization were also investigated theoretically[81,95,111a] as well as experimentally.[112] Substitution in the acetylenic positions generally seems to affect the energetics of the Bergman cyclization more than in the vinylic positions.[95] The effect of substitution of the acetylenic hydrogen was rationalized on the basis of a simple MO analysis:[111] Depending on the substituent the HOMO of the transition state of the cyclization can be of the σ- or of the π-type (Figure 7). π-Donating substituents decrease the cyclization barrier by increasing the occupation of the bonding orbital; σ acceptors facilitate the Bergman reaction by decreasing the occupation of the antibonding σ orbital.[111] Fluorine substitution is particularly effective in activating the enediyne.[113] When both acetylenic positions bear substituents, steric effects in the transition state (repulsion of the substituents en route to the 2,3-disubstituted 1,4-benzyne) must also be taken into account.[111]

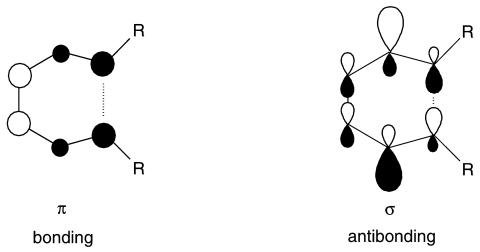
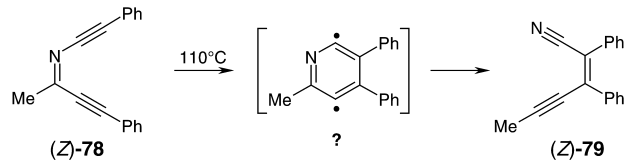


Figure 7. Schematic representation of HOMO and HOMO-1 for the transition state of the Bergman reaction of substituted enediynes.[111] The occupation of both orbitals plays an important role in determining the activation barrier of the reaction.[111]

Substitution in the vinyl position is comparably uneffective in changing the energetics of the Bergman cyclization.[95] Substituents that lower the electron density generally seem to increase the cyclization barrier, while σ donors result in a slightly decreased activation energy. π-Conjugative interaction has hardly any effect in the vinyl position.[95] These (primarily theoretical) results were also supported by experimental evidence.[112]

The aza-Bergman rearrangement of *C,N*-dialkynylimines to β-alkynylacrylonitriles has also been studied intensively. In 1997 David and Kerwin investigated the thermochemistry of (*Z*)-**78** in solution and observed rearrangement to (*Z*)-**79** (Scheme 22).[114] However, a 2,5-didehydropyridine inter-



Scheme 22. Rearrangement of *C,N*-dialkynylimine **78** to β-alkynylacrylonitrile **79**.[114]

mediate could not be detected or trapped, which was attributed to the low barrier for ring opening of this species (a mechanism involving an aza-butalene structure was also not excluded).[114]

One year later Hoffner et al. reported trapping experiments of protonated 2,5-pyridyne.[80d] Detectable hydrogen abstraction rates were only observed under pH conditions, which suggest the existence of a protonated 2,5-pyridyne derivative.[80d] Theoretical investigations by Cramer et al.[38,39,84] show that—in contrast to *para*-benzyne (**4**) and enediyne (*Z*)-**27** (Figure 6)—2,5-didehydropyridine **81** is stabilized relative to imine **80** (Figure 8); the relative stability of the nitrile (*Z*)-**22** is also increased significantly.[84] However, the barrier for ring opening of 2,5-pyridyne (**81**) to (*Z*)-**22** was determined to be only 0.9 kcal mol^{-1} (see reference [84] for numerical details). The singlet–triplet separation was calculated to be 11.6 kcal mol^{-1}, which, in addition to the short lifetime, accounts for the poor hydrogen abstraction ability of **81**.[80d,84] Protonation does not only decrease the singlet–triplet gap significantly (to a value comparable to that of **4**), but also increases the barrier for the retro-Bergman reaction of **81-H**$^+$ to (*Z*)-**22-H**$^+$ to more than 10 kcal mol^{-1}.[39,81,84] Thus, protonation partially cancels the perturbation introduced by the heteroatom, as has been described in Section 2.4. While replacing CH in **27** by N allows pH-dependent control of the Bergman cyclization (see Section 4.2.), calculations by Kraka and Cremer indicate that the proton affinity of **81** is not sufficient to achieve efficient protonation under physiological conditions (see reference [81] for details).

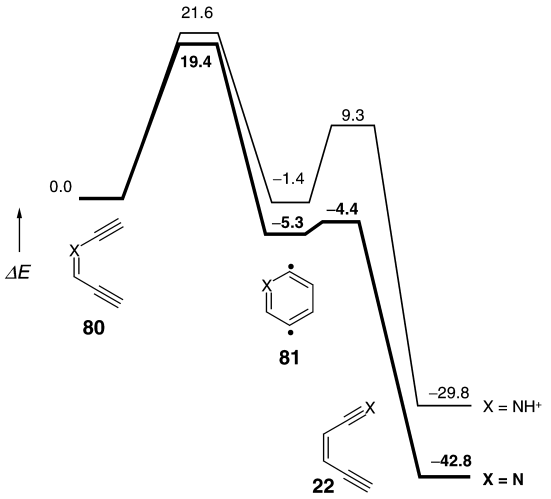
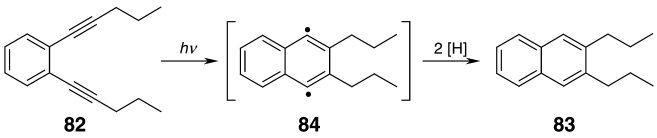


Figure 8. Calculated energy profile of the Bergman cyclization of imine **80** and its protonated form **80-H**$^+$ and of the subsequent retro-Bergman cyclization to nitrile **22** (**22-H**$^+$). ΔH in kcal mol^{-1}.[84]

4.3.2. The Photochemical Bergman Reaction

The photochemical Bergman reaction is one of the less well understood aspects of the chemistry of didehydrobenzenes, despite the fact that this reaction has been known since 1968 (and thus longer than its thermal counterpart).[115] The photochemical enediyne cyclization has attracted some attention since the observation that in the presence of suitable sensitizers acyclic enediynes do not only undergo *cis–trans* isomerization, but also display DNA-cleaving activity.[116] While photocyclization of the unsubstituted enediyne (*Z*)-**27** has not been observed yet,[74] several examples of this type of reaction have been reported since 1994. Turro et al. found that 1,2-dipropylnaphthalene (**83**) is formed upon irradiation of 1,2-di(pent-1-ynyl)benzene (**82**) in hexane in the presence of a photosensitizer, which suggests the intermediate formation of the 1,4-didehydronaphthalene derivative **84** (Scheme 23).[117a]

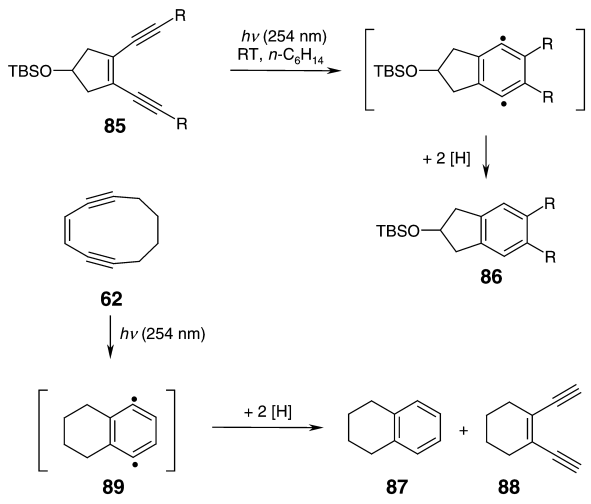


Scheme 23. Photochemical Bergman cyclization of **82**.[117]

In 1996 Funk et al. reported the photochemical cycloaromatization of several *ortho*-dialkynylarenes (pyrenes, phenanthrenes, etc.) and investigated their DNA-cleaving properties.[118] Proteins were also envisaged as potential targets of photochemically activated enediynes. In one case cleavage of the protein was observed, in others dimerization occurred. For this study enediynes were synthesized the enediyne unit of which was embedded in rings of different size. The influence of ring size on the yield of cyclization products was also determined.[119]

The first example of a photo-Bergman reaction of a nonbenzannelated enediyne was described by Hirama et al. in 1999 (Scheme 24).[120] On irradiation with 254 nm light enediyne **85** (R = Me) is converted to the indane derivative **86** in 71% yield. Irradiation with light of longer wavelengths does not result in cyclization, even in the presence of a triplet sensitizer. Derivatives of **85** (R = H, Ph, TMS) yielded only 0–3% of cyclized product upon irradiation at 254 nm.[120] Irradiation of cyclic enediyne **62** in various solvents yields tetrahydronaphthalene (**87**) and diethynylcyclohexene **88** in different ratios depending on the solvent.[120] The formation of **88**, which is also photolabile under the experimental conditions, supports the postulated formation of the biradical intermediate **89**. Photochemical reaction of **62** to **88** could also be observed in an argon matrix, however, the biradical **89** was not observed under any photolysis conditions.[68] Meanwhile, several examples of photo-Bergman reactions have been reported in the literature.[121]

Recently, the electronic details of the photochemical enediyne cycloaromatization were investigated with theoretical methods.[117b,122] The low-lying excited states of enediyne **27** can be described as a linear combination of the config-



Scheme 24. Various photochemical Bergman reactions reported by Hirama et al.[120]

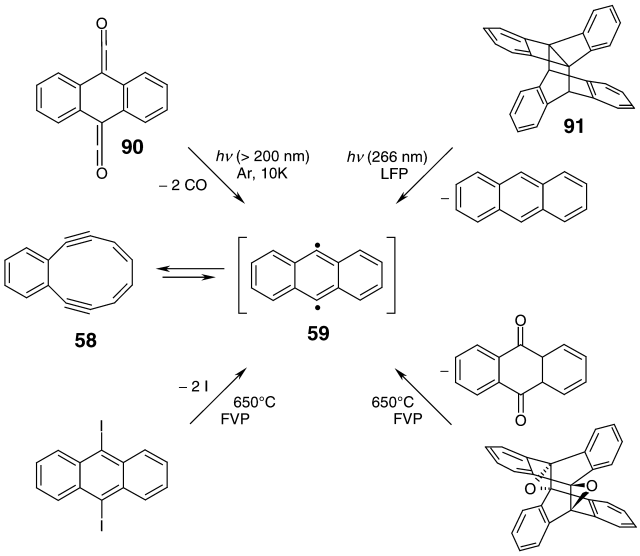
urations of weakly interacting ethylene and acetylene units. According to this model, excitation of the ethylene fragment induces *cis–trans* isomerizations and hydrogen-abstractions in addition to Bergman cyclization, and the photochemical cycloaromatization is most likely initiated by excitation of the acetylene unit.[117b,122] Moreover, the cyclization is more likely to occur on the 2^1A potential energy surface than in the 1^3B state. Although the reaction is more exothermic in the latter case ($-42\ kcal\,mol^{-1}$ compared to $-18\ kcal\,mol^{-1}$ at the CASMP2 level), the probability of *cis–trans* isomerization and hydrogen abstraction is increased concurrently.[122] Consistently, Hopf et al. observed photochemical *cis–trans* isomerization of **27** in the presence of a triplet sensitizer (Michler's ketone).[123]

In conclusion, it is noted that a systematic understanding of the factors (substituents or sensitizers) that facilitate the photochemical ring closure or inhibit competing reaction pathways is hardly recognizable so far, although this reaction is of potential interest for tumor therapy (see Section 4.2).

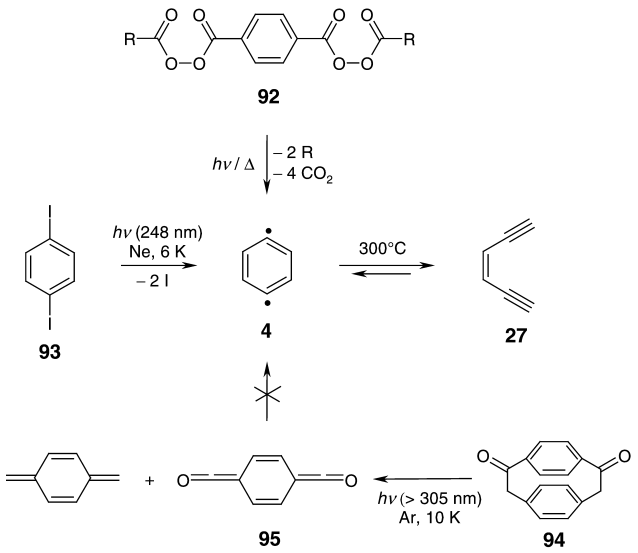
4.4. *para*-Arynes

The first direct observation of a derivative of *para*-benzyne was reported by Chapman et al. in 1976.[124] Irradiation of anthraquinone bisketene **90** in organic glasses at 77 K produced a new species with UV absorptions in the range from 256 to 449 nm. After subsequent warming to room temperature, anthracene was isolated from the solution. An analogous experiment in the presence of 5% CCl_4 yielded 9,10-dichloroanthracene. In an argon matrix at 10 K two IR absorptions at 710 and 760 cm^{-1} were observed for the new species. Based on the trapping reactions and the absence of an ESR signal, the photolysis product was identified as 9,10-didehydroanthracene ($^1A_1$-**59**; Scheme 25).[124] In 1996 Chen et al. investigated the photochemistry of dehydrodianthracene (**91**) using laser flash photolysis (LFP) and were able to identify two transients: a short-lived species with a lifetime of 2.1 μs and an absorption maximum at 295 nm, and a long-lived species (500 μs) with an absorption at 335 nm.[80a,b] The short-lived transient was assigned to 9,10-didehydroanthracene (**59**), the long-lived photolysis product was identified as 3,4-benzocyclododeca-3,7,9-triene-1,5-diyne (**58**).[80a] Since the UV spectroscopic data of **91** from the LFP study were in disaccord with the earlier study by Chapman et al., Sander et al. reinvestigated the photochemistry of bisketene **90** in argon matrices. By using alternative precursors and by (meanwhile possible) comparison with DFT-calculated IR spectra it could be demonstrated that 9,10-didehydroanthracene (**59**) is labile even under matrix isolation conditions, and that the IR absorptions observed by Chapman et al. are due to cyclic diyne **58**.[125] Pyrolysis of various precursors also gave only **58** (Scheme 25).[125,126] According to the DFT calculations and LFP measurements, the barrier for ring opening of **59** was estimated to be 10–12 $kcal\,mol^{-1}$, diyne **59** is approximately 6–8 $kcal\,mol^{-1}$ more stable than didehydroanthracene **59**.[125,126]

The comparatively low barrier for the retro-Bergman cyclization of **4** accounts for the numerous unsuccessful attempts to directly detect *para*-benzyne (see Section 4.1). Still, the barrier is significantly higher than in the case of didehydroanthracene **59**. Photochemical cyclization of **27** could not be achieved in solution or under matrix isolation conditions. The breakthrough came in 1998 with experiments by Sander, Radziszewski, and co-workers.[11,127] Photolysis of diacetylterephthaloyldiperoxide **92** in argon matrices at 10 K yields (in addition to large amounts of CO_2) alkyl radicals and various further compounds (Scheme 26). Characteristic IR absorptions were observed at 724.8 and 980.0 cm^{-1}, which (as well as the bands of the monoradicals) disappeared upon annealing of the matrix at 40 K. Apart from these absorptions the IR spectrum of **4**, calculated at the UB3LYP level of theory, predicted only two other bands of comparable intensity: An absorption at 427 cm^{-1}, which could not be identified due to the low signal-to-noise ratio in this spectral region, and a band at 886 cm^{-1}, which was obscured by other



Scheme 25. Generation of 9,10-Didehydroanthracene (**59**) from various precursors; **59** rapidly rearranges to cyclic diyne **58**.

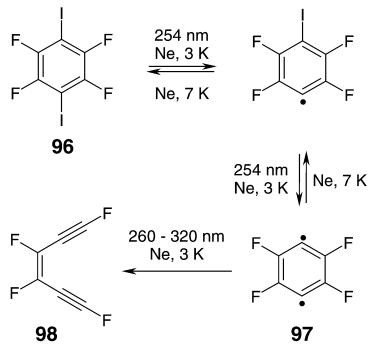


Scheme 26. Matrix isolation of *para*-benzyne (**4**).[127]

intense bands.[127] The identification of **4** was confirmed by photolysis of partially deuterated derivatives of **92**. Independently, Radziszewski et al. observed the same IR bands after photolysis of 1,4-diiodobenzene (**93**) at 248 nm in solid neon at 6 K.[127] Despite the low overall intensity they were able to assign all IR active absorptions of **4** up to 2000 cm^{-1}. The experimental vibrational spectrum was further completed by NIPES measurements by Wenthold, Squires, and Lineberger, which allowed the identification of the frequencies of two totally symmetric (and therefore IR-inactive) modes at about 600 and 1000 cm^{-1}, again in good agreement with the DFT-calculated spectrum.[17]

Recently, the assignment of the band at 980 cm^{-1} to **4** has been doubted based on new calculations (this band is shifted by 4 cm^{-1} to 976 cm^{-1} if **4** is generated from 1,4-diiodobenzene (**93**), which, however, is not unusual due to the presence of iodine atoms and to the change of the matrix host from argon to neon[65]).[127,128] However, the ab initio calculation of the IR spectrum is complicated by the existence of orbital instabilities, the effect of which may often be negligible for first-order properties (such as geometry and energy), but can result in severe deviations for second-order properties (vibrational frequencies, IR intensities).[128] In further matrix isolation studies cyclophanedione **94** was envisaged as a precursor, which upon long wavelength irradiation fragments quantitatively to *para*-xylylene and bisketene **95** (Scheme 26).[129] In contrast to the benzannelated derivative **90**, however, the latter turned out to be photochemically stable under matrix isolation conditions.[129]

The method developed by Radziszewski and co-workers to generate aromatic biradicals by photolysis of the corresponding diiodoarenes in neon matrices turned out to be suitable for the synthesis of substituted derivatives of **4** as well, although the reason for the different photochemistry in neon and argon matrices could not be concludingly elucidated yet.[65] Thus, irradiation of 1,4-diiodotetrafluorobenzene (**96**) in solid neon at 3 K generates tetrafluoro-*para*-didehydrobenzene (**97**) in good yield (Scheme 27).[130] According to



Scheme 27. Photochemistry of **96** in a neon matrix at 3 K.[130]

calculations, this derivative still has a singlet ground state. However, the lowest triplet state is only 0.5 kcal mol^{-1} higher in energy (CASPT2/cc-pVDZ). Definitive experimental evidence for the ground state of **97** is not available yet, since the calculated IR spectra of the singlet and triplet states are essentially identical, and an ESR spectrum of the photolysis products in solid neon could not be measured so far.[130] Interestingly, longer wavelength irradiation (260–320 nm) converts **97** to the ring-opened 1,3,4,6-tetrafluorohex-3-ene-1,5-diyne(**98;** Scheme 27). This observation is particularly remarkable, since the high electronegativity of the fluorine substituents destabilizes the enediyne relative to the biradical (see Section 4.3.1), so that the ring opening of **97** is endothermic by 8 kcal mol^{-1} (UB3LYP/6-311 + + G(d,p)), and the barrier for retro-Bergman cyclization is significantly increased (37.5 kcal mol^{-1}) relative to that of **4**.[113,130]

In 1968 Hoffmann, Imamura, and Hehre systematized the properties of the benzynes by formally separating the interaction of the radical centers into through-space and through-bond contributions.[60] Specifically, this concept predicts that in *para*-benzyne the antisymmetric combination (b_{1u}) of the p orbitals at C1 and C4 is lowered beyond the symmetric combination (a_g), which has been confirmed by high-level calculations (Figure 9).[60,128,131] The partial occupation of the antibonding C2–C3- and C4—C5-σ* orbitals results in lengthening of these bonds, while the other C–C bonds are shortened (Figure 10).[60,131] The coupling of the electrons in *para*-benzyne described above stabilizes the singlet state relative to the triplet state. Experimentally a

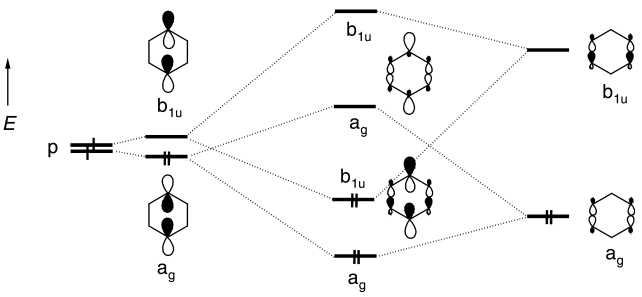


Figure 9. Schematic MO representation of through-bond coupling in *para*-benzyne.[60,128,131]

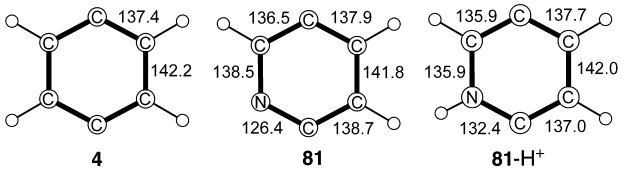


Figure 10. The structures of *para*-benzyne (**4**), 2,5-pyridyne (**81**), and **81**-H$^+$, calculated at the UB3LYP/6-31G(d,p) level of theory.[81c] Bond lengths in pm.

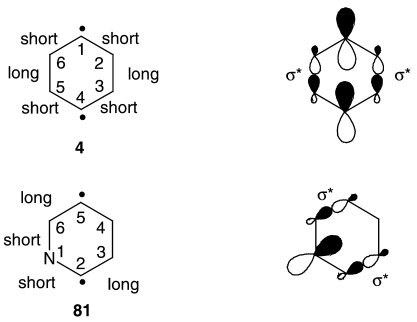


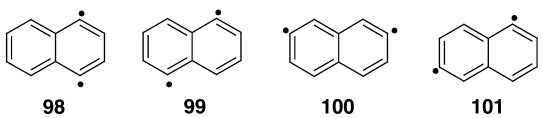
Figure 11. In **81** the shortened C2–N bond (anomeric delocalization of the lone pair) and energy lowering of the σ*(C6–N) orbital (compared with σ*(C–C) orbitals) results in increased through-bond coupling in **4**. This effect is attenuated by protonation of the nitrogen atom.[81c]

singlet ground state with a singlet–triplet splitting of (3.8 ± 0.5) kcal mol^{-1} was determined by using NIPES.[17]

Substituent effects on geometry and singlet–triplet splitting in *para*-didehydroaromatic compounds were investigated in several theoretical studies and can often be rationalized in terms of amplification or attenuation of through-bond coupling. In **97**, for example, the fluorine substituents stabilize the a_g-symmetric orbital relative to the b_{1u}-symmetric combination.[130]

In didehydronaphthalene **99** the separation of A- and S-orbitals is larger than in **98**, since in the former there is no *t*hrough-space interaction counteracting the through-bond coupling.[30] A more complex situation is encountered in **100** and **101**. For the "W-shaped" configuration **100** the splitting of the orbital energies is comparably large (large "zigzag coupling" is well known in NMR[132] and ESR spectroscopy[133]);[30] the preference for the singlet state amounts to approximately 3 kcal mol^{-1} in **100**, while both states are essentially degenerate in **101**.[30] However, it should be noted that state energies do not necessarily correlate with orbital energy differences, since the former are not one-electron properties. Thus, in 1,8-didehydronaphthalene (**44**; Section 3.3) a comparatively large HOMO–LUMO energy difference is found, while on the other hand the singlet and triplet states are almost degenerate (Table 3, Section 4.5).[30]

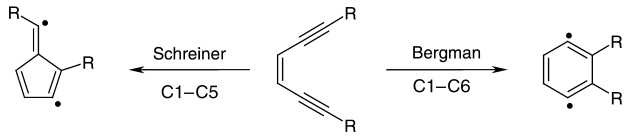
Another point of interest is the comparison of **4** with 2,5-didehydropyridine (**81**) and its protonated form **81**-H$^+$.[38,39,80d,81c,84] In these compounds the singlet–triplet gaps are calculated to be 2.5, 8.2, and 2.8 kcal mol^{-1}, respectively (UB3LYP/6-31G(d,p), different methods predict at least similar trends[38,39,80d,84]).[81c] A detailed interpretation of these energy differences has been given by Kraka and Cremer.[81c] Anomeric delocalization of the lone pair at the nitrogen atom into the vicinal C–C bonds results in shortening of the N–C2 and N–C6 bonds (Figure 11); the shortened C2–N bond enhances through-bond coupling by increasing the overlap of the interacting orbitals. Additionally, the σ*(C6–N) orbital is lower in energy than the σ*(C–C) orbital (due to the higher electronegativity of nitrogen compared to carbon), which also increases the through-bond interaction.[81c] Thus, the efficient coupling of the electrons in **81** takes place primarily through the C6–N bond.[81c] In **81**-H$^+$ the anomeric effect is switched off, which is also reflected in the calculated geometries (Figure 10).[81c]



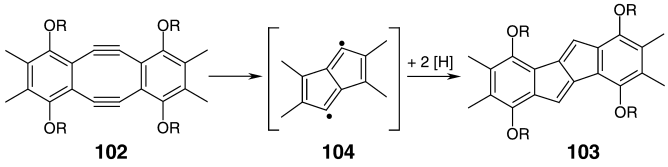
4.5. Cycloaromatizations analogous to the Bergman Reaction

Apart from the well known Bergman cyclization some closely related cycloaromatization reactions were described more recently, which will be dealt with briefly here for the sake of completeness. The possibility of an alternative C1–C5 cyclization of enediynes yielding fulvenediyls was recently proposed by Schreiner et al. (Scheme 28).[134] However, the reaction is endothermic with approximately 40 kcal mol^{-1} (R = H), and the cyclization barrier amounts to about 42 kcal mol^{-1}.[134] Still, an experimental realization of this cyclization might be facilitated by introducing sterically demanding substituents R into the terminal positions.[134] Experimentally accomplished was the closely related rearrangement of dibenzocyclin **102** to indeno[2.1-a]indene **103**, which possibly proceeds via a biradical intermediate **104** (Scheme 29).[135]

As already noted in Section 4.2., there exists a group of biologically active molecules, which are closely related to the enediyne cytostatics, namely the neocarcinostatins,[136] in

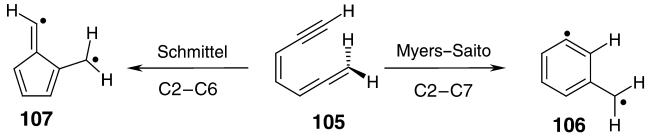


Scheme 28. A C1—C5 cyclization of enediynes as proposed by



Scheme 29. The rearrangement of **102** to **103**[135] possibly proceeds in a manner similar to the C1–C5 cyclization suggested by Schreiner et al.[134]

Schreiner et al. could not be realized experimentally yet.[134]



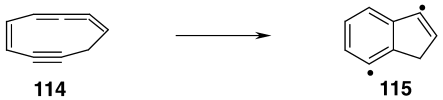
Scheme 30. Myers–Saito and Schmittel cyclizations.

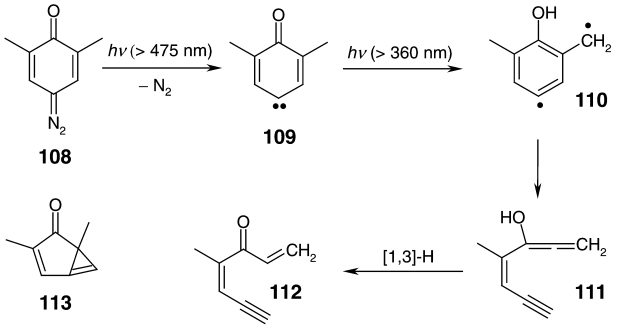
which a similar cycloaromatization (Myers–Saito cyclization)[137] results in formation of didehydroarenes (α,3-didehydrotoluenes or 1,5-didehydroindenes). Prototype of the Myers—Saito reaction is the rearrangement of the eneyne–allene (*Z*)-hepta-1,2,4-triene-6-yne (**105**) to α,3-didehydrotoluene (**106**). This C2–C7 cyclization yields a benzylic π-conjugated σ,π-diradical and is therefore exothermic by (15 ± 3) kcal mol^{-1} (Scheme 30).[137] The reaction barrier was determined to be approximately 22 kcal mol^{-1}.[137a,b] Also known in the literature is the alternative C2–C6 cyclization (Schmittel cyclization), which generates the less stable fulvenediyl **107**.[138] According to calculations, the Schmittel cyclization is endothermic by about 10 kcal mol^{-1} with an activation barrier of about 35 kcal mol^{-1}.[139] Replacing the acetylenic hydrogen atoms by sterically demanding substituents (*t*Bu, TMS), however, favors the C2–C6 over C2–C7 cyclization.[138e,f] Phenyl groups also reverse the energetics by benzylic stabilization in the transition state of the Schmittel cyclization.[138a,b] Substituted aryl groups in the acetylenic positions seem to have no systematic effect on the barrier of the Schmittel reaction (which remains favored over C2–C7 cyclization).[140]

The interesting α,3-didehydrotoluene diradical (**106**) has not yet been matrix-isolated and structurally characterized. Experimentally, it could be shown by CID measurements in the gas phase that **106** (in contrast to α,2- and α,4-didehydrotoluene) possesses a singlet ground state.[141] According to these experiments the lowest triplet state is approximately 3 kcal mol^{-1} higher in energy,[141] in reasonable agreement with photoelectron spectroscopic data by Chen et al. (5 kcal mol^{-1})[142] and quantum-chemical calculations.[143]

The first isolation of a derivative of **106** was reported by Sander et al. in 1998.[144] Irradiation of quinone diazide **108** with light of wavelength $\lambda > 475$ nm in an argon matrix at 10 K quantitatively yields 2,6-dimethylcyclohexa-2,5-diene-1-one-4-ylidene (**109**). Short wavelength irradiation ($\lambda > 360$ nm) converts **109** to the substituted α,3-didehydrotoluene derivative **110** (Scheme 31). Upon prolonged irradiation **111** and (presumably) **112** are formed by Myers cycloreversion. No evidence was found for the formation of bicyclic **113**.[144]

The chromophore of the naturally occurring neocarcinostatins is the cyclic system **114**. The activation enthalpy for cyclization to 1,5-didehydroindene (**115**) was calculated to be approximately 18 kcal mol^{-1}, the reaction is slightly exothermic with about 1 kcal mol^{-1} (in contrast to acyclic system **106, 105** does not profit from benzylic stabilization).[145] The



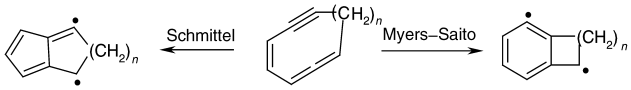


Scheme 31. Matrix isolation of the first (and so far only) α,3-didehydrotoluene derivative **110** and its photochemical rearrangement to **111**.[144]

singlet–triplet separation of about 6 kcal mol^{-1} in **115** is somewhat larger than in **4**.[145] Myers et al. were able to demonstrate that synthetic eneyne–allenes (combining an acyclic (*Z*)-eneyne–allene with a unit, that selectively binds to the minor groove of DNA) can cause sequence-specific DNA cleavage as well.[146]

Systematic investigations by Schreiner and Prall concerning the influence of ring size on the barrier ot the Myers–Saito and the Schmittel cyclization of cyclic eneyne–allenes are summarized in Scheme 32 and Table 2.[139b] All cyclic systems possess lower cyclization barriers than the open-chain system **105**, since the reactants are highly strained.[139b] For the seven-membered ring ($n = 0$) Myers–Saito cyclization is not expected to occur, since the reverse reaction proceeds without any activation barrier; for $n = 1$ the energy profiles of both reactions are similar. Larger rings apparently favor the Myers–Saito cyclization.[139b]

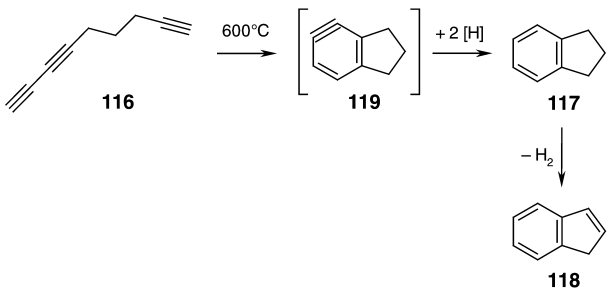
Apart from the reactions mentioned above, several processes generating didehydroarenes starting from unsaturated systems have been reported. Thus, FVP of nona-1,3,8-triyne (**116**) yields indane (**117**) and indene (**118**; which is formed from **117** by loss of H_2).[147] Results from isotopic labeling suggest an unusual (1,3-diyne + alkyne)-[2+4] cycloaromatization resembling a Diels–Alder reaction, forming 1,2-didehydroindane (**119**; Scheme 33).[147]



Scheme 32. Myers–Saito and Schmittel cyclizations in cyclic eneyne–allenes.[139b]

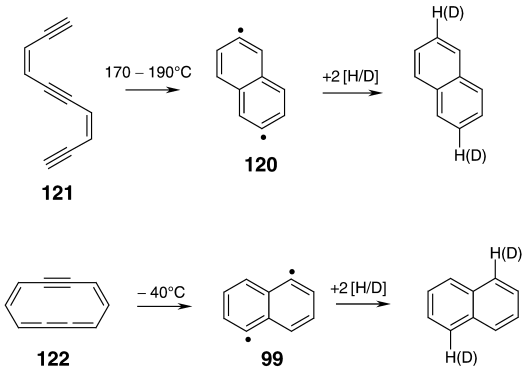
Table 2: Free activation ($\Delta G^{\ddagger}_{298}$) and reaction enthalpies (ΔG_{298}) for Myers–Saito and Schmittel cyclizations of cyclic eneyne–allenes (Scheme 32). Energies (BLYP/6-31G(d)) in kcal mol^{-1} relative to the eneyne–allenes.[139b]

n	Schmittel		Myers–Saito	
	$\Delta G^{\ddagger}_{298}$	ΔG_{298}	$\Delta G^{\ddagger}_{298}$	ΔG_{298}
0	24.0	14.0	9.0	9.0
1	15.2	2.6	17.8	3.8
2	12.3	4.2	14.2	−11.8



Scheme 33. Thermolysis of **116** results in formation of indane **117**, presumably via intermediate formation of didehydroindane **119**.

The trapping chemistry of 2,6-naphthyne **120**, generated by a cyclization cascade from (*Z*,*Z*)-deca-3,7-diene-1,5,9-triene (**121**), was investigated by Bergman and co-workers, who thereby turned towards the cycloaromatization reactions again after a longer period of time.[148] In a similar fashion, Myers et al. were able to trap 1,5-naphthyne (**99**) in solution, which is formed from 1,2,6,7-tetradehydro[10]annulene (**122**) already at −40 °C.[149] In both cases the intermediate formation of the naphthynes was confirmed by formation of 2,6- and 1,5-dideuterated derivatives in deuterated solvents (Scheme 34). Relative energies of the lowest singlet and triplet states of all naphthynes are summarized in Table 3.



Scheme 34. Formation of naphthynes **99** and **120** by cycloaromatization of **122** and **121**.[148,149]

Table 3: Calculated energies of the naphthynes relative to the singlet ground state of 1,2-naphthyne (**9**) (CASPT2(12,12)/cc-pVDZ + ZPE(BPW91/cc-pVDZ)).[30] All values in kcal mol^{-1}.

Isomer	Compound	*E*(singlet)	*E*(triplet)	ΔE_{ST}
1,2	**9**	0.0	32.2	32.2
1,3	**42**	10.8	28.1	17.3
1,4	**98**	21.5	27.1	5.6
1,5	**99**	19.4	27.3	7.9
1,6	**101**	24.8	25.6	0.8
1,7	**139**	24.4	26.0	1.6
1,8	**44**	25.5	26.4	0.9
2,3	**10**	2.1	30.5	28.4
2,6	**120**	24.0	25.8	1.8
2,7	**100**	23.0	25.9	2.9

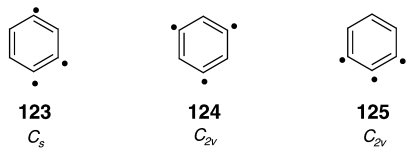
4.6. Concluding Remarks on para-Arynes

The chemistry of *para*-arynes is developing rapidly at the moment, and many aspects could not be discussed in detail here. This field is characterized by a close interplay of experiment and theory. The problems encountered with an exact quantum-chemical treatment of biradicals (and in particular their reactions) requiring a balanced treatment of dynamic and nondynamic (near-degeneracy) contributions to the correlation energy on one hand, and the availability of precise experimental data on the other made *para*-benzyne and the Bergman cyclization a benchmark test for ab initio and (in recent years) DFT methods.[150] It can be expected that scrutiny of these systems will continue to inspire not only physical-organic chemistry, but also quantum and synthetic chemistry.

5. Other Dehydroarenes

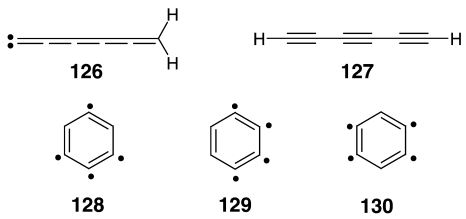
5.1. Tridehydrobenzenes

In contrast to benzynes and benzdiynes (see Section 5.2) knowledge about tridehydrobenzene derivatives is scarce. According to calculations by Bettinger et al. 1,2,4-tridehydrobenzene (**123**) and 1,3,5-tridehydrobenzene (**124**) are less stable than the 1,2,3-isomer **125** by 4.0 and 11.8 kcal mol^{-1}, respectively.[16i] In contrast to the didehydrophenyl cation **52** (see Section 3.5), **124** possesses C_{2v} symmetry; the calculated C1–C3 and C1–C5 distances are different (194 and 230 pm, respectively at the CCSD/DZP level of theory).[16i] For the 1,2,3-isomer **125** a significantly shorter C1–C3 distance (ca. 170 pm) is predicted by various methods.



5.2. Benzdiynes

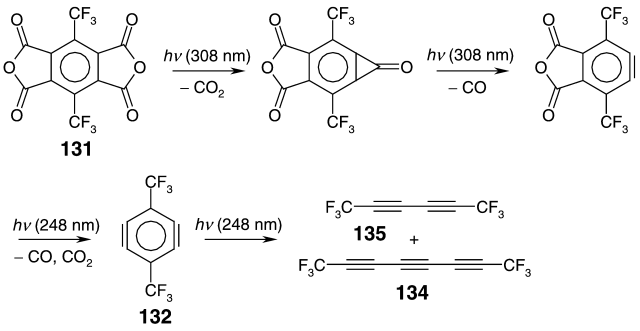
Polar carbon-rich species such as hexapentaeneylidene (**126**)[151] have been identified in interstellar clouds,[152] which has attracted some attention and raised interest in C_6H_2 compounds.[16i,153,154] The existence of **126** in interstellar space is remarkable, since this structure is 50 kcal mol^{-1} (CCSD(T)/cc-pVTZ) less stable than hexatriyne (**127**),[153] which, how-



ever, is nonpolar and, therefore, difficult to observe radioastronomically. At the same level of theory the three isomeric benzdiynes **128**–**130** are higher in energy than **127** by 39.4, 46.3, and 56.2 kcal mol^{-1}, respectively.[153]

The C1–C3 distance of 176 pm in **128**[16i,153,154] is rather low, which has been attributed to a strong σ-allylic interaction as in the case of *meta*-benzyne (**3;** see Section 3.1).[16i] Like *ortho*-benzyne (**2**), **129** and **130** possess C–C bonds with triple-bond character. Due to the increased ring strain the singlet–triplet gaps in **129** and **130** are lower than in **2** by 9.5 and 17.5 kcal mol^{-1}, respectively.[16i] In contrast, the difference of both states is increased by 2 kcal mol^{-1} in **128** compared to the value for *ortho*-benzyne. The LUMO (which is singly occupied in the triplet state) has not only a bonding interaction with C1 and C3, but also a strong antibonding interaction with C5, resulting in a large HOMO–LUMO gap and destabilization of the triplet state ($BSE = -7$ kcal mol^{-1}, ref. [16i]).

Despite early mention of benzdiynes as reactive intermediates,[155] the first direct evidence for the existence of a substituted derivative of **130** was not achieved before 1997.[156] Upon irradiation in an argon matrix 1,4-bis(trifluoromethyl)-2,3,5,6-benzenetetracarboxylic dianhydride (**131**) loses CO_2 and CO in a stepwise manner. A photoproduct with IR absorptions at 1466, 1183, 1127, and 798 cm^{-1} was assigned the structure of 1,4-bis(trifluoromethyl)-2,3,5,6-benzdiyne (**132**) on the basis of its chemistry and comparison with the calculated spectrum (Scheme 35).[156] The difluoro derivative **133** could be generated in a similar fashion.[156b] Prolonged irradiation converts **132** to bis(trifluorormethyl)hexatriyne (**134**) and -butadiyne (**135**).[156] An analogous fragmentation pathway is found for **133**.[156b]

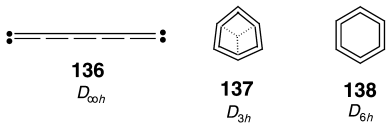


Scheme 35. First synthesis and chemistry of a benzdiyne derivative (**132**) by Yabe et al.[156]

The parent systems **129** and **130** are not accessible by this route. Photolysis of 1,2,3,4- and 1,2,4,5-benzenetetracarboxylic dianhydride with light of different wavelengths invariably results in formation of hexatriyne (**127**) and butadiyne as final products.[156,157] The preparation of 1,2,5,6- and 2,3,6,7-tetradehydronaphthalene by photolysis of the corresponding tetracarboxylic dianhydrides failed as well, and only acetylenic products could be detected.[158] These careful investigations show that tetradehydroaromatic systems are highly photolabile, but can be stabilized by fluorine or CF_3 substitution.[156–158]

5.3. Cyclo[6]-carbon

Aside from fullerene research, carbon clusters have always attracted much interest among scientists.[159] Linear cumulene-like C_6 ($D_{\infty h}$) **136** is well known theoretically as well as experimentally.[160] Cyclic C_6, which will be considered as the extreme case of a dehydrobenzene here, has a long and varied history.[161] In particular, two cyclic isomers possessing D_{3h} and D_{6h} symmetry (**137** and **138**) have been discussed.[161] According to the most recent calculations **137** ($^1A_1'$) is lowest in energy; **138** ($^1A_{1g}$) and **136** ($^3\Sigma_g^-$) are less stable by approximately 8 and 10 kcal mol^{-1}, respectively.[161e]



The IR spectrum of **137** was obtained by laser vaporization of graphite and subsequent trapping of the reaction products in solid argon at 10 K. Only the most intense vibrational mode at 1695 cm^{-1} could be detected.[162] The antisymmetric stretching vibration of the linear isomer **136** is observed at 1952 cm^{-1}.[160b,e] The assignment could be corroborated by measuring the spectra of isotopically labeled compounds. In a more recent theoretical work the UV spectra of **137** and **138** were calculated;[163] experimental data are lacking so far.

6. Perspective

The interest in arynes has changed the status of these molecules from laboratory curiosities to well established reactive intermediates. Yet our knowledge of this class of compounds is still incomplete and many aspects of their chemistry remain to be investigated. This pertains in particular to the photo-Bergman cylization, ring-opening and ring-closing mechanisms as well as a systematic account for substituent and heteroatom effects.

The last point leads over to a more abstract systematization of the interplay of different perturbations in aromatic systems in terms of *n*-electron, *m*-center interactions for different topologies, to scrutinize isoelectronic analogies but also differences. Figure 12 shows potential structural motifs for the $m = 3$ case. Although the synthesis of some of these molecules may never be realized, they represent attractive targets for future research projects.

Whether investigation of dehydroarenes is going to facilitate the developement of novel antitumor drugs is not foreseeable at the moment, and undue optimism is certainly not justified. Nevertheless, the concerted efforts of many research groups have contributed to the refinement of the experimental and theoretical tools of physical-organic chemistry, and it is no exaggeration to state that the arynes are prototypical examples for the interplay of experiment and theory in modern chemistry.

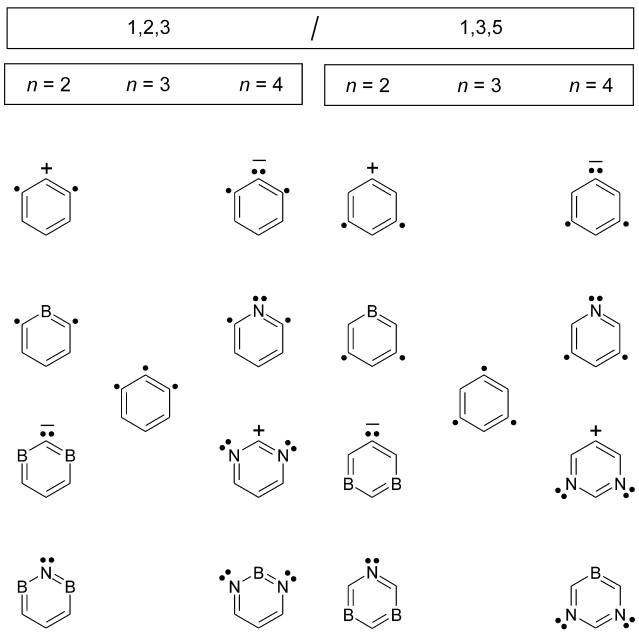


Figure 12. *n*-Electron, three-center interaction for 1,2,3- and 1,3,5-topology in various isoelectronic structures.

Addendum

After submission of the manuscript several studies of relevance to the field appeared in print and the most important ones will be briefly discussed here:

In the realm of *ortho*-benzyne derivatives a high-resolution IR-spectroscopic investigation of 3-flouro- and tetrafluoro-*ortho*-benzyne by Radzsizewski et al. deserves special mention.[164] The observed frequency shifts of the C≡C stretching vibration upon substitution are not reproduced by DFT calculations (B3LYP, BLYP), however, which casts additional doubt on the reliability of these methods for studies on biradicaloids and strained systems.

A rather new but promising area is the coordination of *ortho*-benzynes to transition-metal surfaces. An ordered layer of *ortho*-benzyne on Ir{100} has recently been prepared by thermal decomposition of adsorbed benzene, and characterized by low-energy electron diffraction (LEED).[165] It has been demonstrated that the benzyne is di-σ-bonded to the surface with its ring plane at 47.2° to the surface normal. In a theoretical study it has been shown that this tilt arises from a backbonding interaction of the aromatic π system with the surface d orbitals.[166]

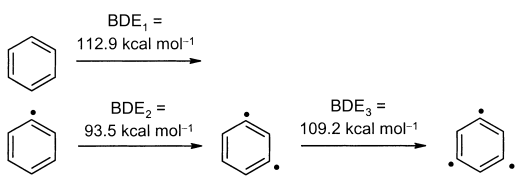
A number of perfluorinated *meta*-benzyne derivatives bearing different substituents in the 5-position has been prepared by photolysis of the corresponding diiodo compounds in neon matrices at 3 K.[167] The effect of substitution on the structural and spectroscopic properties turned out to be rather small. The 5-chloro-*meta*-benzyne heat of formation has been determined by Wenthold et al. to be (116.2 ± 3.7) kcal mol^{-1} and is thus approximately 6 kcal mol^{-1} lower than that of unsubstituted *meta*-benzyne, indicating that substitution at the 5-position has little effect on the stability of the *meta*-benzynes.[168] In the same work the heat of formation of the 1,3,5-tridehydrobenzene is given as (179 ± 4.6) kcal mol^{-1}, which results in the bond dissociation energies (*BDE*) given in Scheme 36 for successive hydrogen removal from benzene.

These data (in conjunction with stabilization energies derived from isodesmic equations) show that the triradical is most appropriately described as a *meta*-benzyne moiety interacting only weakly with the third radical center.[168] The electronic structure of the triradical is thus very different from that of the 3,5-didehydro phenyl cation, which has also been the subject of a recent investigation.[169] By carefully analyzing the ion–molecule reactivity in a FT-ICR mass spectrometer the molecular structure of this fundamental system could be established for the first time.[169] New intermolecular reactions of charged benzyne derivatives have also been investigated by mass spectrometry.[170] These reactivity data show that *para*-benzyne derivatives are weaker electrophiles than the corresponding *meta* isomers.[170]

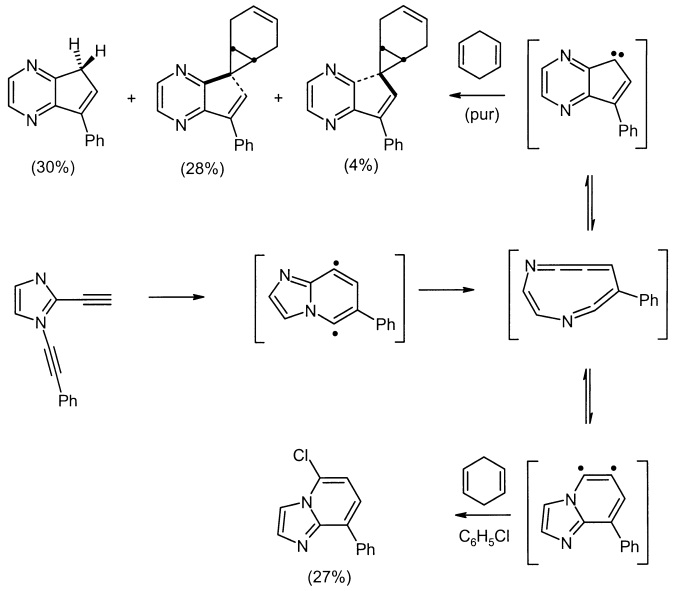
A number of recent studies apply arguments based on magnetic or energetic aromaticity criteria to cycloaromatization reactions to rationalize the calculated or observed course of these reactions.[171] Whereas the Bergman and the Myers–Saito reaction seem to profit from a cyclic electron delocalization, this is not the case for the alternative formation of five-membered biradicals.[171] In earlier investigations it was proposed that interactions of in-plane orbitals occur early along the reaction path and thus determine the barrier of the Bergman cyclization.[172] In contrast, dissected NICS values suggest that cyclic electron delocalization in the transition state occurs predominantly in the out-of-plane system.[171] In a careful study of the Bergman cyclization Alabugin et al. concluded that four-electron repulsion of filled in-plane orbitals is the main factor governing the barrier height and suggested that this might efficiently be reduced by introduction of electron acceptors in proximity to the acetylenic units; out-of-plane interactions occur at a later reaction stage.[173] Relative aromaticities of the parent benzynes have been compared as well and seem to increase in the order *ortho*- < *meta*- < *para*-benzyne.[174] In related work it has been proposed that butalene is less antiaromatic than cyclobutadiene.[175]

An interesting variant of the aza-Bergman cyclization has been described by Kerwin et al. (Scheme 37).[176] The product distribution points at a highly complex reaction mechanism that involves a ring-opening/ring-closure step of a 2,5-pyridyne intermediate to form a 2,3-pyridyne derivative (in chlorobenzene) or a carbene (in neat cyclohexadiene). Trapping products, indicative of the primary 2,5-pyridyne intermediate could not be isolated.[176]

A new cycloaromatization, reminiscent of the Bergman reaction, has been proposed by Kawatkar and Schreiner



Scheme 36.



Scheme 37.



Scheme 38.

(Scheme 38).[177] For X=OH$^+$ the reaction has a barrier of approximately 35 kcal mol^{-1} (BLYP) and is slightly exothermic. Therefore, an experimental realization might be achieved (e.g. by activation of 3-oxo-penta-1,4-diyne with suitable Lewis acids at higher temperatures).[177]

We thank the Deutsche Forschungsgemeinschaft and the Fonds der Chemischen Industrie for financial support.

Received: February 5, 2002 [A515]

[1] R. Stoermer, B. Kahlert, *Ber. Dtsch. Chem. Ges.* **1902**, *35*, 1633.
[2] A. Lüttringhaus, G. Saaf, *Justus Liebigs Ann. Chem.* **1930**, *592*, 250.
[3] a) J. D. Roberts, H. E. Simmons, L. A. Carlsmith, C. W. Vaughan, *J. Am. Chem. Soc.* **1953**, *75*, 3290; b) J. D. Roberts, D. A. Semenow, H. E. Simmons, L. A. Carlsmith, *J. Am. Chem. Soc.* **1956**, *78*, 601, 611; c) M. Panar, J. D. Roberts, *J. Am. Chem. Soc.* **1960**, *82*, 3629.
[4] a) R. Huisgen, H. Rist, *Naturwissenschaften* **1954**, *41*, 358; b) R. Huisgen, H. Rist, *Ann. Chem.* **1955**, *594*, 137; c) R. Huisgen, R. Knorr, *Tetrahedron Lett.* **1963**, 1017.
[5] a) G. Wittig, *Naturwissenschaften* **1942**, *30*, 696; b) G. Wittig, G. Harborth, *Ber. Dtsch. Chem. Ges.* **1944**, *77*, 306, 316; c) G. Wittig, L. Pohmer, *Chem. Ber.* **1956**, *89*, 1334.
[6] For early reviews (before 1970) on aryne chemistry, see, for example: a) G. Wittig, *Angew. Chem.* **1957**, *69*, 245; b) J. F. Bunnett, *J. Chem. Educ.* **1961**, *38*, 278; c) H. Heany, *Chem. Rev.* **1962**, *62*, 81; d) G. Wittig, *Angew. Chem.* **1965**, *77*, 752; *Angew. Chem. Int. Ed. Engl.* **1965**, *4*, 731; e) R. W. Hoffmann: *Dehydrobenzene and Cycloalkynes*, Academic Press, New York, **1967**; f) E. K. Fields, S. Meyerson, *Adv. Phys. Org. Chem.* **1969**, *6*, 1; g) H. Heany, *Fortschr. Chem. Forsch.* **1970**, *16*, 35.
[7] "Arene und Arine": C. Grundmann, *Methoden der Organischen Chemie (Houben-Weyl), 4th ed 1952–, Vol. 5*, **1981**.
[8] J. A. Zoltewicz, *International Review of Science, Org. Chem.*, *Ser. 2, Vol. 3* (Ed.: H. Zollinger), Butherworth, London, **1976**, Chapter 3.
[9] S. V. Kessar, *Acc. Chem. Res.* **1978**, *11*, 283.
[10] Special reviews on heteroarynes: a) T. Kauffmann, *Angew. Chem.* **1965**, *77*, 557; *Angew. Chem. Int. Ed. Engl.* **1965**, *4*, 543; b) H. J. den Hertog, H. C. van der Plas, *Adv. Heterocycl. Chem.* **1965**, *4*, 121; c) H. J. den Hertog, H. C. van der Plas, *Chemistry of Acetylenes* (Ed.: H. G. Viehe), Marcel Dekker, New York, **1969**, Chapter 17; d) T. Kaufmann, R. Wirthwein, *Angew. Chem.* **1971**, *83*, 21; *Angew. Chem. Int. Ed. Engl.* **1971**, *10*, 20; e) M. G. Reinecke, *Reactive Intermediates, Vol. 2* (Ed.: R. A. Abramovitch), Plenum, New York, **1982**, Chapter 5; f) H. C. van der Plas, *The Chemistry of Triple Bonded Groups*, Supplement C of *The Chemistry of Functional Groups* (Eds.: S. Patai, Z. Rappoport), Wiley-Interscience, New York, **1982**; g) M. G. Reinecke, *Tetrahedron* **1982**, *38*, 427.
[11] W. Sander, *Acc. Chem. Res.* **1999**, *32*, 669.
[12] W. E. Bachman, H. T. Clarke, *J. Am. Chem. Soc.* **1927**, *49*, 2089.
[13] I. P. Fisher, F. P. Lossing, *J. Am. Chem. Soc.* **1963**, *85*, 1018.
[14] a) R. S. Berry, J. Clardy, M. E. Schafer, *J. Am. Chem. Soc.* **1964**, *86*, 2738; b) R. S. Berry, G. N. Spokes, M. Stiles, *J. Am. Chem. Soc.* **1962**, *84*, 3570.
[15] a) O. L. Chapman, K. Mattes, C. L. McIntosh, J. Pacansky, G. V. Calder, G. Orr, *J. Am. Chem. Soc.* **1973**, *95*, 6134; b) O. L. Chapman, C. C. Chang, J. Kolc, N. R. Rosenquist, H. Tomioka, *J. Am. Chem. Soc.* **1975**, *97*, 6586.
[16] Chapman and co-workers assigned a band at 2085 cm^{-1} to the C≡C stretching vibration and this assignment was confirmed afterwards, see, for example: a) I. R. Dunkin, J. G. MacDonald, *J. Chem. Soc. Chem. Commun.* **1979**, 772. Wentrup et al. identified the band at 2080 cm^{-1} in a phthalic anhydride matrix at 77 K. On annealing of the matrix a second overlapping absorption at the same position was observed, which was assigned to cyclopentadienylideneketene: b) C. Wentrup, R. Blanch, H. Briehl, G. Gross, *J. Am. Chem. Soc.* **1988**, *110*, 1874. The assignment to the C≡C stretching vibration in **2** was supported theoretically as well: c) J. W. Laing, R. S. Berry, *J. Am. Chem. Soc.* **1976**, *98*, 660; d) N.-H. Nam, G. E. Leroi, *Spectrochim. Acta A* **1985**, *41*, 67. Doubts arose, when Leopold, Miller, and Lineberger identified the position of this vibration at 1860 cm^{-1} from the gas-phase photoelectron spectrum: e) D. G. Leopold, A. E. Stevens-Miller, W. C. Lineberger, *J. Am. Chem. Soc.* **1986**, *108*, 1379. To clarify this discrepancy Schaefer et al. calculated the IR spectrum of **2** and proposed that the absorption should be found in the range from 1965 to 2010 cm^{-1}: f) A. C. Scheiner, H. F. Schaefer III, B. Liu, *J. Am. Chem. Soc.* **1989**, *111*, 3118. In 1990 Schweig et al. were able to demonstrate that an absorption at 2087 cm^{-1} should be assigned to cyclopentadienylideneketene rather than **2**: g) J. G. G. Simon, N. Muenzel, A. Schweig, *Chem. Phys. Lett.* **1990**, *170*, 187. Finally, Radziszewski et al. proved in an exhaustive investigation that the C≡C stretching vibration is observed at 1846 cm^{-1}: h) J. G. Radziszewski, B. A. J. Hess, R. Zahradnik, *J. Am. Chem. Soc.* **1992**, *114*, 52. Quantum-chemical calculations of the frequency of this vibration display a pronounced dependence on the level of theory and the basis set employed, see for exapmle: i) H. F. Bettinger, P. von R. Schleyer, H. F. Schaefer III, *J. Am. Chem. Soc.* **1999**, *121*, 2829, and ref. [22].
[17] P. G. Wenthold, R. R. Squires, W. C. Lineberger, *J. Am. Chem. Soc.* **1998**, *120*, 5279.
[18] a) P. G. Wenthold, R. R. Squires, *J. Am. Chem. Soc.* **1994**, *116*, 6401. For earlier work concerning the enthalpy of formation of

2, see: b) P. G. Wenthold, J. A. Paulino, R. R. Squires, *J. Am. Chem. Soc.* **1991**, *113*, 7414: $\Delta H^0_{f,298} = (106 \pm 3)$ kcal mol^{-1}; c) J. M. Riveros, S. Ingemann, N. M. M. Nibbering, *J. Am. Chem. Soc.* **1991**, *113*, 1053: $\Delta H^0_{f,298} = (105 \pm 3)$ kcal mol^{-1}; d) Y. Guo, J. J. Grabowski, *J. Am. Chem. Soc.* **1991**, *113*, 5923: $\Delta H^0_{f,298} = (105 \pm 5)$ kcal mol^{-1}.

[19] A. M. Orendt, J. C. Facelli, J. G. Radziszewski, W. J. Horton, D. M. Grant, J. Michl, *J. Am. Chem. Soc.* **1996**, *118*, 846.

[20] R. Warmuth, *Angew. Chem.* **1997**, *109*, 1406; *Angew. Chem. Int. Ed. Engl.* **1997**, *36*, 1347.

[21] a) R. Warmuth, *Eur. J. Org. Chem.* **2001**, 423; b) R. Warmuth, J. Yoon, *Acc. Chem. Res.* **2001**, *34*, 95.

[22] From the numerous studies until 1998 the following are mentioned here exemplarily: a) E. Haselbach, *Helv. Chim. Acta* **1971**, *54*, 1981; b) M. J. S. Dewar, W.-K. Li, *J. Am. Chem. Soc.* **1974**, *96*, 5569; c) W. Thiel, *J. Am. Chem. Soc.* **1981**, *103*, 1420; d) M. J. S. Dewar, G. P. Ford, C. H. Reynolds, *J. Am. Chem. Soc.* **1983**, *105*, 3162; e) C. W. Bock, P. George, M. Trachtman, *J. Phys. Chem.* **1984**, *88*, 1467; f) M. J. S. Dewar, T.-P. Tien, *J. Chem. Soc. Chem. Commun.* **1985**, 1243; g) L. Radom, R. H. Nobes, D. J. Underwood, L. Wai-Kee, *Pure Appl. Chem.* **1986**, *58*, 75; h) K. Rigby, I. H. Hillier, M. A. Vincent, *J. Chem. Soc. Perkin Trans. 2* **1987**, 117; i) I. H. Hillier, M. A. Vincent, M. F. Guest, W. von Niessen, *Chem. Phys. Lett.* **1987**, *134*, 403; j) A. C. Scheiner, H. F. Schaefer III, *Chem. Phys. Lett.* **1991**, *177*, 471; k) R. Liu, Z. Xuenfeng, P. Pulay, *J. Phys. Chem.* **1992**, *96*, 259; l) H. U. Sutter, T.-K. Ha, *Chem. Phys. Lett.* **1992**, *198*, 259; m) A. Nicolaides, W. T. Borden, *J. Am. Chem. Soc.* **1993**, *115*, 11951; n) S. G. Wierschke, J. J. Nash, R. R. Squires, *J. Am. Chem. Soc.* **1993**, *115*, 11958; o) P. B. Karadahov, J. Gerrat, G. Raos, D. L. Cooper, M. Raimondi, *Isr. J. Chem.* **1993**, *33*, 253; p) E. Kraka, D. Cremer, *Chem. Phys. Lett.* **1993**, *216*, 333; q) E. Kraka, D. Cremer, *J. Am. Chem. Soc.* **1994**, *116*, 4929; r) R. Lindh, B. J. Persson, *J. Am. Chem. Soc.* **1994**, *116*, 4963; s) R. Lindh, T. J. Lee, A. Bernhardsson, B. J. Persson, G. Karlström, *J. Am. Chem. Soc.* **1995**, *117*, 7186; t) J. J. Nash, R. R. Squires, *J. Am. Chem. Soc.* **1996**, *118*, 11872; u) C. J. Cramer, J. J. Nash, R. R. Squires, *Chem. Phys. Lett.* **1997**, *277*, 311; v) W. Langenaeker, F. De Proft, P. Geerlings, *J. Phys. Chem. A* **1998**, *102*, 5944.

[23] Additional spectroscopic data are available, which have, however, less frequently been used for comparison with theoretical calculations. These comprise the UV spectrum (ref. [16g]) and in particular the microwave spectrum of **2**: a) R. D. Brown, P. D. Godfrey, M. J. Rodler, *J. Am. Chem. Soc.* **1986**, *108*, 1296. The dipolar ^{13}C NMR spectrum of [1,2-$^{13}C_2$]-**2** in an argon matrix was measured and analyzed to determine the C≡C distance., see ref. [19]. A detailed comparison of measured and calculated chemical shifts is found in: b) H. Jiao, P. von R. Schleyer, B. R. Beno, K. N. Houk, R. Warmuth, *Angew. Chem.* **1997**, *109*, 2929; *Angew. Chem. Int. Ed. Engl.* **1997**, *36*, 2761.

[24] For example: a) F. A. Carey, R. J. Sundberg, *Advanced Organic Chemistry*, 4th ed. part A, Plenum, New York, **2000**, S. 593; b) J. March, *Advanced Organic Chemistry*, 4th ed., Wiley, New York **1992**, S. 646; b) "Aromatic Nucleophilic Substitution": J. Miller in *Reaction Mechanisms in Organic Chemistry* (Eds: C. Eaborn, N. B. Chapman), Elsevier, Amsterdam, **1968**.

[25] For investigations of the regioselectivity of the addition to unsymmetrical arynes, see, for example: a) E. R. Biehl, E. Nieh, K. C. Hsu, *J. Org. Chem.* **1969**, *34*, 3595; b) M. Tielemans, V. Areschka, J. Colomer, R. Promel, W. Langenaeker, P. Geerlings, *Tetrahedron* **1992**, *48*, 10575 as well as ref. [6e], [22v], and references therein.

[26] a) W. T. G. Johnson, C. J. Cramer, *J. Phys. Org. Chem.* **2001**, *14*, 597; b) W. T. G. Johnson, C. J. Cramer, *J. Am. Chem. Soc.* **2001**, *123*, 923.

[27] H. H. Wenk, W. Sander, *Chem. Eur. J.* **2001**, *7*, 1837.

[28] C. J. Cramer, *J. Chem. Soc. Perkin. Trans. 2* **1999**, 2273.

[29] G. E. Davico, R. L. Schwartz, T. M. Ramond, W. C. Lineberger, *J. Am. Chem. Soc.* **1999**, *121*, 6047.

[30] R. R. Squires, C. J. Cramer, *J. Phys. Chem. A* **1998**, *102*, 9072.

[31] G. P. Ford, E. R. Biel, *Tetrahedron Lett.* **1995**, *36*, 3663.

[32] a) H.-F. Grützmacher, J. Lohmann, *Liebigs Ann. Chem.* **1970**, *733*, 88; b) H.-F. Grützmacher, J. Lohmann, *Liebigs Ann. Chem.* **1975**, 2023.

[33] J. Lohmann, *J. Chem. Soc. Perkin Trans. 1* **1972**, *68*, 814.

[34] H. A. Weimer, B. J. McFarland, S. Li, W. Weltner, Jr., *J. Phys. Chem.* **1995**, *99*, 1824.

[35] T. Sato, M. Moriyama, H. Niino, A. Yabe, *Chem. Commun.* **1999**, 1089.

[36] T. Sato, H. Niino, A. Yabe, *J. Phys. Chem. A* **2001**, *105*, 7790.

[37] C. J. Cramer, J. Thompson, *J. Phys. Chem. A* **2001**, *105*, 2091.

[38] C. J. Cramer, S. Debbert, *Chem. Phys. Lett.* **1998**, *287*, 320.

[39] S. L. Debbert, C. J. Cramer, *Int. J. Mass Spectrom.* **2000**, *201*, 1.

[40] a) T. Yonezawa, H. Konishi, H. Kato, *Bull. Chem. Soc. Jpn.* **1969**, *42*, 933; b) W. Adam, A. Grimison, R. Hoffmann, *J. Am. Chem. Soc.* **1969**, *91*, 2590; c) M. J. S. Dewar, G. P. Ford, *J. Chem. Soc. Chem. Commun.* **1977**, 539; d) H. H. Nam, G. E. Leroi, J. F. Harrison, *J. Phys. Chem.* **1991**, *95*, 6514; e) R. Liu, D. R. Tate, J. A. Clark, P. R. Moody, A. S. Van Buren, J. A. Krauser, *J. Phys. Chem.* **1996**, *100*, 3430.

[41] M. Winkler, W. Sander, unpublished results.

[42] J. Kramer, R. S. Berry, *J. Am. Chem. Soc.* **1972**, *94*, 8336.

[43] T. Sasaki, K. Kanematsu, M. Uchide, *Bull. Chem. Soc. Jpn.* **1971**, *44*, 858.

[44] H.-H. Nam, G. E. Leroi, *J. Am. Chem. Soc.* **1988**, *110*, 4096.

[45] a) M. P. Cava, M. J. Mitchell, D. C. DeJongh, R. Y. van Fossen, *Tetrahedron Lett.* **1966**, 2947. Compare: b) I. R. Dunkin, J. G. MacDonald, *Tetrahedron Lett.* **1982**, *23*, 4839.

[46] H. H. Nam, G. E. Leroi, *Tetrahedron Lett.* **1990**, *31*, 4837.

[47] a) R. S. Berry, J. Clardy, M. E. Schafer, *Tetrahedron Lett.* **1965**, *415*, 1011; b) R. S. Berry, J. Clardy, M. E. Schafer, *Tetrahedron Lett.* **1965**, *415*, 1003.

[48] H. E. Bertorello, R. A. Rossi, R. Hoyos de Rossi, *J. Org. Chem.* **1970**, *35*, 3332.

[49] W. E. Billups, J. D. Buynak, D. Butler, *J. Org. Chem.* **1979**, *44*, 4218.

[50] S. V. Luis, F. Gavina, V. S. Safont, M. C. Torres, M. I. Burguete, *Tetrahedron* **1989**, *45*, 6281.

[51] a) W. N. Washburn, *J. Am. Chem. Soc.* **1975**, *97*, 1615; b) W. N. Washburn, R. Zahler, *J. Am. Chem. Soc.* **1976**, *98*, 7827, 7828.

[52] G. Bucher, W. Sander, E. Kraka, D. Cremer, *Angew. Chem.* **1992**, *104*, 1225; *Angew. Chem. Int. Ed. Engl.* **1992**, *31*, 1230.

[53] E. Kraka, D. Cremer, G. Bucher, H. Wandel, W. Sander, *Chem. Phys. Lett.* **1997**, *268*, 313.

[54] W. Sander, G. Bucher, H. Wandel, E. Kraka, D. Cremer, W. S. Sheldrick, *J. Am. Chem. Soc.* **1997**, *119*, 10660.

[55] R. Marquardt, W. Sander, E. Kraka, *Angew. Chem.* **1996**, *108*, 825; *Angew. Chem. Int. Ed. Engl.* **1996**, *35*, 746.

[56] W. Sander, M. Exner, M. Winkler, A. Balster, A. Hjerpe, E. Kraka, D. Cremer, *J. Am. Chem. Soc.* **2002**, *124*, 1307.

[57] E. Kraka, J. Anglada, A. Hjerpe, M. Filatov, D. Cremer, *Chem. Phys. Lett.* **2001**, *348*, 115.

[58] M. Winkler, W. Sander, *J. Phys. Chem. A* **2001**, *105*, 10422.

[59] The IR spectrum of **3** has been interpreted in favor of a bicyclic structure **29** based on B3LYP calculations: a) B. A. Hess, Jr., *Eur. J. Org. Chem.* **2001**, 2185; b) B. A. Hess, Jr., *Chem. Phys. Lett.* **2002**, *352*, 75. Regarding this interpretation it should be mentioned that 1) the measured IR spectrum of **3**, ref. [55], is not reproduced correctly. Two additional bands were assigned to *meta*-benzyne, which are unequivocally due to other species (cf. refs. [56] and [57]). 2) As is evident from the data in Table 1, hybrid functionals fail to give even a qualitatively accurate

description of *meta*-benzyne. Only the BLYP-, BVWN, and BVWN5 functionals are in good agreement with high-level ab initio calculations. The IR spectra, calculated with these methods, excellently reproduce the experimental spectrum as well as that calculated at the CCSD(T) level of theory. Therefore, the equilibrium distance of the radical centers in **3** is expected to be around 205 pm (refs. [56–58]).

[60] This type of coupling has already been mentioned in early work by Hoffmann et al., see: R. Hoffmann, A. Imamura, W. J. Hehre, *J. Am. Chem. Soc.* **1968**, *90*, 1499. It was later applied by Cramer et al. to systematize the properties of several *meta*-arynes, (see refs. [30, 38]). For a detailed investigation of **3**, see reference [58].

[61] W. Sander, R. Marquardt, G. Bucher, H. Wandel, *Pure Appl. Chem.* **1996**, *68*, 353.

[62] E. W. G. Diau, J. Casanova, J. D. Roberts, A. H. Zewail, *Proc. Natl. Acad. Sci. USA* **2000**, *97*, 1376.

[63] a) K. K. Thoen, H. I. Kenttämaa, *J. Am. Chem. Soc.* **1997**, *119*, 3832; b) K. K. Thoen, H. I. Kenttämaa, *J. Am. Chem. Soc.* **1999**, *121*, 800; c) E. D. Nelson, A. Artau, J. M. Price, S. E. Tichy, L. Jing, H. I. Kenttämaa, *J. Phys. Chem. A* **2001**, *105,* 10155.

[64] W. Sander, M. Exner, *J. Chem. Soc. Perkin Trans. 2* **1999**, 2285.

[65] The reason for the different photochemistry of aromatic iodides and diiodides in neon and argon could not be elucidated concludingly so far. The lower viscosity of neon compared to argon cannot account for this difference alone, since aromatic diiodides do not undergo any photochemistry in argon matrices around 35 K, although the viscosity is similar to that of solid neon at 4 K. Whether the different atom radii are responsible for the different behavior cannot be determined due to the lack of suitable matrix host materials for comparison. Frequently, other physical effects are also important. Thus, in nitrogen matrices photolysis products are often isolated, which in argon matrices undergo further fragmentation. This is attributable to a more efficient coupling to the matrix, which improves the transfer of excess energy to the lattice (photolysis products are often generated in highly excited vibrational states). In contrast, the difference between photochemistry in xenon and argon is often caused by heavy atom effects. A systematic comparison of the photochemistry in neon and argon matrices is a subject of ongoing research in our laboratory.

[66] Reproduced from ref. [26] with minor changes. In the authors' opinion a resonance arrow between **3** and **29** is not appropriate, since the position of atoms is altered in this representation. Also, the authors wish to avoid the term "bond stretch isomers", ref. [57], in this context.

[67] W. E. Billups, J. D. Buynak, D. Butler, *J. Org. Chem.* **1979**, *44*, 4218.

[68] H. H. Wenk, W. Sander, unpublished results.

[69] J. Chandrasekhar, E. D. Jemmis, P. von R. Schleyer, *Tetrahedron Lett.* **1979**, 3707.

[70] Concerning this special form of aromaticity, see: a) M. N. Glukhovtsev, V. I. Minkin, B. Y. Simkin, *Russ. Chem. Rev.* **1985**, *54*, 86; b) M. Feyereisen, M. Gutowski, J. Simons, *J. Chem. Phys.* **1992**, *96*, 2926. For a more general discussion of the concept of aromaticity, see: c) V. I. Minkin, M. N. Glukhovtsev, B. Y. Simkin: *Aromaticity and Antiaromaticity*, Wiley, New York, **1994**, especially chapter 8; d) P. von R. Schleyer, *Chem. Rev.* **2001**, *101*, 1115 (Special Issue: *Aromaticity*).

[71] P. von R. Schleyer, H. Jiao, M. N. Glukhovtsev, J. Chandrasekhar, E. Kraka, *J. Am. Chem. Soc.* **1994**, *116*, 10129.

[72] a) Y. V. Gal'perin, G. M. Bogolyubov, N. N. Grishin, A. A. Petrov, *Russ. J. Gen. Chem.* **1969**, *39*, 1567; b) J. Momigny, A. M. Wirtz-Cordier, *Ann. Soc. Sci. Bruxelles* **1962**, *76*, 164. The results of these studies are not conclusive, particularly with regard to the structures of the species detected.

[73] a) N. Darby, C. U. Kim, J. A. Salaün, K. W. Shelton, S. Takada, S. Masamune, *J. Chem. Soc. Chem. Commun.* **1971**, 1516; b) S. Masamune, N. Darby, *Acc. Chem. Res.* **1972**, *5*, 272.

[74] a) R. R. Jones, R. G. Bergman, *J. Am. Chem. Soc.* **1972**, *94*, 660; b) R. G. Bergman, *Acc. Chem. Res.* **1973**, *6*, 25.

[75] T. P. Lockhart, P. B. Comita, R. G. Bergman, *J. Am. Chem. Soc.* **1981**, *103*, 4082; T. P. Lockhart, P. B. Comita, R. G. Bergman, *J. Am. Chem. Soc.* **1981**, *103*, 4091.

[76] a) R. Breslow, J. Napierski, T. C. Clarke, *J. Am. Chem. Soc.* **1975**, *97*, 6275. Compare also: b) R. Breslow, P. L. Khanna, *Tetrahedron Lett.* **1977**, 3429.

[77] For quantum-chemical studies on butalene, see: a) P. M. Warner, G. B. Jones, *J. Am. Chem. Soc.* **2001**, *123*, 10322; b) K. Ohta, T. Shima, *Chem. Phys. Lett.* **1994**, *217*, 7; c) M. J. S. Dewar, G. P. Ford, C. H. Reynolds, *J. Am. Chem. Soc.* **1983**, *105*, 3162; d) M. J. S. Dewar, W.-K. Li, *J. Am. Chem. Soc.* **1974**, *96*, 5569. See also ref. [22m].

[78] For reviews on this topic, see: a) Z. Xi, I. H. Goldberg in *Comprehensive Natural Products Chemistry, Vol. 7* (Eds.: D. H. R. Barton, K. Nakanishi), Pergamon, Oxford, **1999**, S. 553; b) M. E. Maier, F. Boße, A. J. Niestroj, *Eur. J. Org. Chem.* **1999**, 1; c) A. G. Fallis, *Can. J. Chem.* **1999**, *77*, 159; d) W. K. Pogozelski, T. D. Tullius, *Chem. Rev.* **1998**, *98*, 1089; e) S. J. Danishefski, M. D. Shair, *J. Org. Chem.* **1996**, *61*, 16; f) *Endiyne Antibiotics as Antitumor Agents* (Eds.: D. B. Borders, T. W. Doyle), Marcel Dekker, New York, **1995**; g) K. C. Nicolaou, A. L. Smith, *Acc. Chem. Res.* **1992**, *25*, 497; h) K. C. Nicolaou, W.-M. Dai, *Angew. Chem.* **1991**, *103*, 1453; *Angew. Chem. Int. Ed. Engl.* **1991**, *30*, 1387.

[79] A. L. Smith, K. C. Nicolaou, *J. Med. Chem.* **1996**, *39*, 2103.

[80] a) M. J. Schottelius, P. Chen, *J. Am. Chem. Soc.* **1996**, *118*, 4896; b) C. F. Logan, P. Chen, *J. Am. Chem. Soc.* **1996**, *118*, 2113; c) P. Chen, *Angew. Chem.* **1996**, *108*, 1584; *Angew. Chem. Int. Ed. Engl.* **1996**, *35*, 1478; d) J. H. Hoffner, M. J. Schottelius, D. Feichtinger, P. Chen, *J. Am. Chem. Soc.* **1998**, *120*, 376. For a more recent discussion of the Chen model and detailed investigations of hydrogen abstractions by benzynes, see: e) A. E. Clark, E. R. Davidson, *J. Am. Chem. Soc.* **2001**, *123*, 10691.

[81] a) E. Kraka, D. Cremer, *J. Am. Chem. Soc.* **2000**, *122*, 8245; b) E. Kraka, D. Cremer, *J. Mol. Struct. (Theochem)* **2000**, *506*, 191; c) E. Kraka, D. Cremer, *J. Comput. Chem.* **2001**, *22*, 216.

[82] C. J. Cramer, R. R. Squires, *J. Phys. Chem. A* **1997**, *101*, 9191. This correlation has been successfully applied to various didehydroarenes, see, for example, refs. [30, 37–39].

[83] a) M. von Ardenne, *Adv. Pharmacol. Chemot. (San Diego)* **1972**, *10*, 339; b) I. F. Tannock, D. Rotin, *Cancer Res.* **1989**, *49*, 4373; c) E. M. Sevick, R. K. Jain, *Cancer Res.* **1988**, *48*, 1201; see also ref. [80d], and references therein.

[84] C. J. Cramer, *J. Am. Chem. Soc.* **1998**, *120*, 6261.

[85] a) L. H. Jones, C. W. Harwig, P. Wentworth Jr. , A. Simeonov, A. D. Wentworth, S. Py, J. A. Ashley, R. A. Lerner, K. D. Janda, *J. Am. Chem. Soc.* **2001**, *123*, 3607; b) G. B. Jones, P. M. Warner, *J. Org. Chem.* **2001**, *66*, 8669.

[86] J. W. Grissom, G. U. Gunawardena, *Tetrahedron Lett.* **1995**, *36*, 4951.

[87] a) K. C. Nicolaou, G. Zuccarello, Y. Ogawa, E. J. Schweiger, T. Kumazawa, *J. Am. Chem. Soc.* **1988**, *110*, 4866; b) K. C. Nicolaou, Y. Ogawa, G. Zuccarello, H. Kataoka, *J. Am. Chem. Soc.* **1988**, *110*, 7247; c) K. C. Nicolaou, G. Zuccarello, C. Riemer, V. A. Estevez, W.-M. Dai, *J. Am. Chem. Soc.* **1992**, 114, 7360; d) K. C. Nicolaou, A. L. Smith, E. E. Yue, *Proc. Natl. Acad. Sci. USA* **1993**, *90*, 5881; e) K. C. Nicolaou, W.-D. Dai, Y. P. Hong, S.-C. Tsay, K. K. Baldrige, J. S. Siegel, *J. Am. Chem. Soc.* **1993**, *115*, 7944.

[88] a) P. R. Schreiner, *Chem. Commun.* **1998**, 483; b) P. R. Schreiner, *J. Am. Chem. Soc.* **1998**, *120*, 4184.

[89] a) P. Magnus, R. T. Kewis, J. C. Huffman, *J. Am. Chem. Soc.* **1988**, *110*, 1626; b) P. A. Carter, P. Magnus, *J. Am. Chem. Soc.* **1988**, *110*, 6921; c) P. Magnus, S. Fortt, T. Pitterna, J. P. Snyder, *J. Am. Chem. Soc.* **1990**, *112*, 4986.

[90] a) J. P. Snyder, *J. Am. Chem. Soc.* **1989**, *111*, 7630; b) J. P. Snyder, *J. Am. Chem. Soc.* **1990**, *112*, 5367.

[91] P. J. Benites, D. S. Rawat, J. M. Zaleski, *J. Am. Chem. Soc.* **2000**, *122*, 7208.

[92] a) M. F. Semmelhack, T. Neu, F. Foubelo, *Tetrahedron Lett.* **1992**, *33*, 3277; b) M. F. Semmelhack, T. Neu, F. Foubelo, *J. Org. Chem.* **1994**, *59*, 5038.

[93] a) R. J. McMahon, R. J. Halter, R. L. Fimmen, R. J. Wilson, S. A. Peebles, R. L. Kuczkowski, J. F. Stanton, *J. Am. Chem. Soc.* **2000**, *122*, 939. The gas-phase structure of (*Z*)-**22** has recently been determined with the same method: b) R. J. Halter, R. L. Fimmen, R. J. McMahon, S. A. Peebles, R. L. Kuczkowski, J. F. Stanton, *J. Am. Chem. Soc.* **2001**, *123*, 12353.

[94] T. R. Kelly, R. A. Silva, H. De Silva, S. Jasmin, Y. Zhao, *J. Am. Chem. Soc.* **2000**, *122*, 6935.

[95] G. B. Jones, P. M. Warner, *J. Am. Chem. Soc.* **2001**, *123*, 2134, and references therein.

[96] B. P. Warner, S. P. Millar, R. D. Broene, S. L. Buchwald, *Science* **1995**, *269*, 814.

[97] a) B. König, W. Pitsch, I. Thondorf, *J. Org. Chem.* **1996**, *61*, 5258; b) A. Basak, J. C. Shain, *Tetrahedron Lett.* **1998**, *39*, 3029; c) E. W. Schmitt, J. C. Huffman, J. M. Zaleski, *Chem. Commun.* **2001**, 167.

[98] D. S. Rawat, P. J. Benites, C. D. Incarvito, A. L. Rheingold, J. M. Zaleski, *Inorg. Chem.* **2001**, *40*, 1846, and references therein.

[99] D. S. Rawat, J. M. Zaleski, *J. Am. Chem. Soc.* **2001**, *123*, 9675.

[100] J. M. O'Connor, L. I. Lee, P. Gantzel, *J. Am. Chem. Soc.* **2000**, *122*, 12057.

[101] P. Magnus, *Tetrahedron*, **1994**, *50*, 1397.

[102] B. König, *Eur. J. Org. Chem.* **2000**, 381; see also ref. [91, 96–100].

[103] W. R. Roth, H. Hopf, C. Horn, *Chem. Ber.* **1994**, *127*, 1765.

[104] W. R. Roth, H. Hopf, T. Wasser, H. Zimmermann, C. Werner, *Liebigs Ann.* **1996**, 1691.

[105] J. W. Grissom, T. L. Calking, H. A. McMillen, Y. Jiang, *J. Org. Chem.* **1994**, *59*, 5833.

[106] A. Basak, J. C. Shain, U. K. Khamrai, K. R. Rudra, A. Basak, *J. Chem. Soc. Perkin Trans. 1* **2000**, 1955.

[107] a) T. Kaneko, M. Takahashi, M. Hirama, *Tetrahedron Lett.* **1999**, *40*, 2015; b) S. Koseki, Y. Fujimura, M. Hirama, *J. Phys. Chem. A* **1999**, *103*, 7672.

[108] C.-S. Kim, K. C. Russell, *J. Org. Chem.* **1998**, *63*, 8229. According to one of the referees the results for **72** are questionable.

[109] D. L. Boger, J. Zhou, *J. Org. Chem.* **1993**, *58*, 3018.

[110] C.-S. Kim, K. C. Russell, *Tetrahedron Lett.* **1999**, *40*, 3835.

[111] a) M. Prall, A. Wittkopp, A. F. Fokin, P. R. Schreiner, *J. Comput. Chem.* **2001**, *22*, 1605. For an investigation of the transition state of the Bergman cyclization, see: b) J. M. Galbraith, P. R. Schreiner, N. Harris, W. Wei, A. Wittkopp, S. Shaik, *Chem. Eur. J.* **2000**, *6*, 1446.

[112] From the large number of experimental data only a few can be mentioned here: Vinylic chlorine substituents decelerate the Bergman reaction in a number of cyclic enediynes: a) G. B. Jones, G. W. Plourde II, *Org. Lett.* **2000**, *2*, 1757. However, donors in the vinylic position may result in a slower cycloaromatizaion as well, for example: b) M. E. Maier, B. Greiner, *Liebigs Ann. Chem.* **1992**, 855. Hydroxy and carbonyl groups in the vicinity of the acetylenic carbon atoms seem to accelerate the Bergman cyclization: c) N. Choy, B. Blanko, J. Wen, A. Krishan, K. C. Russell, *Org. Lett.* **2000**, *2*, 3761; d) B. König, W. Pitsch, M. Klein, R. Vasold, M. Prall, P. R. Schreiner, *J. Org. Chem.* **2001**, *66*, 1742; e) M. F. Semmelhack, J. Gallagher, *Tetrahedron Lett.* **1993**, *34*, 4121. *para*-acceptor-substituted phenyl substituents at the alkyne termini also increase the cyclization rate: f) M. Schmittel, S. Kiau, *Chem. Lett.* **1995**, 953.

[113] Fluorine generally avoids acetylenic positions. Thus, in addition to stabilization of the transition state, destabilization of the enediyne has to be taken into account as well. See also ref. [130]. This strategy has been applied successfully to the synthesis of difluorovinylidene from difluoroacetylene: J. Breidung, H. Bürger, C. Kötting, R. Kopitzky, W. Sander, M. Senzlober, W. Thiel, H. Willner, *Angew. Chem.* **1997**, *109*, 2072; *Angew. Chem. Int. Ed. Engl.* **1997**, *36*, 1986. The direct photochemical rearrangement of acetylene to vinylidene, in contrast, has never been reported.

[114] W. M. David, S. M. Kerwin, *J. Am. Chem. Soc.* **1997**, *119*, 1464.

[115] I. D. Campbell, G. Eglington, *J. Chem. Soc. C* **1968**, 2120.

[116] J. Kagen, X. Wang, X. Chen, K. Y. Lau, I. V. Batac, R. W. Tuveson, J. B. Hudson, *J. Photochem. Photobiol. B* **1993**, *21*, 135.

[117] a) N. J. Turro, A. Evenzahav, K. C. Nicolaou, *Tetrahedron Lett.* **1994**, *35*, 8089; b) A. Evenzahav, N. J. Turro, *J. Am. Chem. Soc.* **1998**, *120*, 1835.

[118] R. L. Funk, E. R. R. Young, R. M. Williams, M. F. Flanagan, T. L. Cecil, *J. Am. Chem. Soc.* **1996**, *118*, 3291.

[119] G. B. Jones, J. M. Wright, G. Plourde II, A. D. Purohit, J. K. Wyatt, G. Hynd, F. Fouad, *J. Am. Chem. Soc.* **2000**, *122*, 9872.

[120] T. Kaneko, M. Takahashi, M. Hirama, *Angew. Chem.* **1999**, *111*, 1347; *Angew. Chem. Int. Ed.* **1999**, *38*, 1267.

[121] D. Ramkumar, M. Kalpana, B. Varghese, S. Sankararaman, M. N. Jagadeesh, J. Chandrasekhar, *J. Org. Chem.* **1996**, *61*, 2247; see also ref. [112c].

[122] A. E. Clark, E. R. Davidson, J. M. Zaleski, *J. Am. Chem. Soc.* **2001**, *123*, 2650.

[123] L. Eisenhuth, H. Siegel, H. Hopf, *Chem. Ber.* **1981**, *114*, 3772.

[124] O. L. Chapman, C. C. Chang, J. Kolc, *J. Am. Chem. Soc.* **1976**, *98*, 5703.

[125] H. H. Wenk, W. Sander, *Eur. J. Org. Chem.* **1999**, 57.

[126] C. Koetting, W. Sander, S. Kammermeier, R. Herges, *Eur. J. Org. Chem.* **1998**, 799.

[127] R. Marquardt, A. Balster, W. Sander, E. Kraka, D. Cremer, J. G. Radziszewski, *Angew. Chem.* **1998**, *110*, 1001; *Angew. Chem. Int. Ed.* **1998**, *37*, 955.

[128] a) T. D. Crawford, E. Kraka, J. F. Stanton, D, Cremer, *J. Chem. Phys.* **2001**, *114*, 10638. For a general treatment of orbital instabilities, see: b) T. D. Crawford, J. F. Stanton, W. D. Allen, H. F. Schaefer III, *J. Chem. Phys.* **1997**, *107*, 10626.

[129] R. Marquardt, W. Sander, T. Laue, H. Hopf, *Liebigs Ann.* **1995**, 1643.

[130] H. H. Wenk, A. Balster, W. Sander, D. A. Hrovat, W. T. Borden, *Angew. Chem.* **2001**, *113,* 2356; *Angew. Chem. Int. Ed.* **2001**, *40*, 2295.

[131] For a general treatment of through-bond interactions, see: a) R. Hoffmann, *Acc. Chem. Res.* **1971**, *4*, 1; b) R. Gleiter, *Angew. Chem.* **1974**, *86*, 770; *Angew. Chem. Int. Ed. Engl.* **1974**, *13*, 696; c) M. N. Paddon-Row, *Acc. Chem. Res.* **1982**, *15*, 245; d) H.-D. Martin, B. Mayer, *Angew. Chem.* **1983**, *95*, 281; *Angew. Chem. Int. Ed. Engl.* **1983**, *22*, 283. A detailed treatment of through-bond interactions in **4** is found in ref. [128a].

[132] S. Sternhell, *Q. Rev. Chem. Soc.* **1969**, *23*, 236.

[133] F. W. King, *Chem. Rev.* **1976**, *76*, 157.

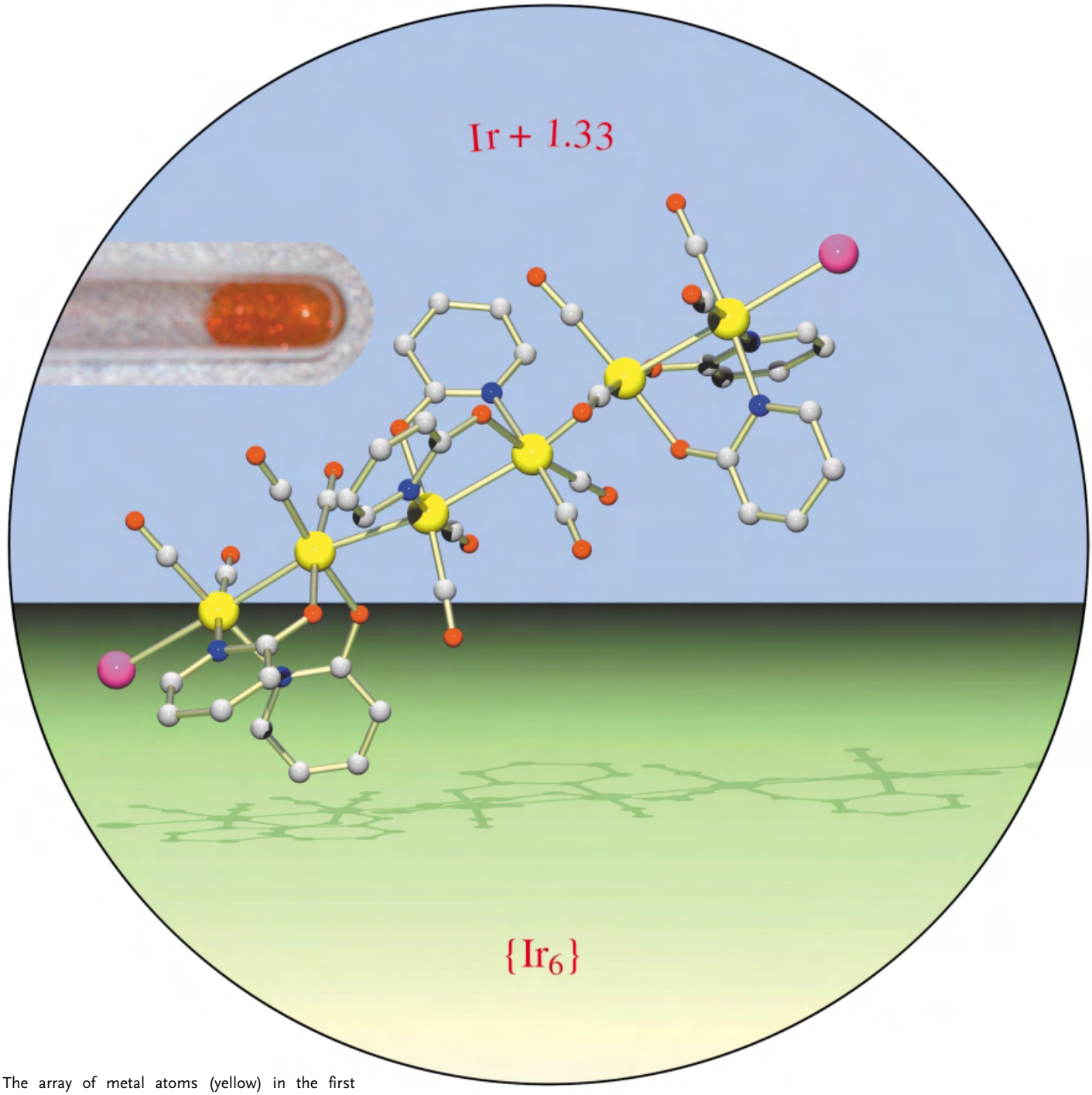
[134] M. Prall, A. Wittkopp, P. R. Schreiner, *J. Phys. Chem. A* **2001**, *105*, 9265.

[135] M. Chakraborty, C. A. Tessier, W. J. Youngs, *J. Org. Chem.* **1999**, *64*, 2947.

[136] For reviews on neocarcinostatin cytostatics, see for example: K. Edo, Y. Koide in *Neocarzinostatin: The Past, the Present and Future of an Anticancer Drug* (Eds.: H. Maeda, K. Edo, N.

Ishida), Springer, Tokyo, **1997**, pp. 23–45. See also refs. [78,146].
[137] a) A. G. Myers, E. Y. Kuo, N. S. Finney, *J. Am. Chem. Soc.* **1989**, *111*, 8057, 9130; b) A. G. Myers, P. S. Dragovich, E. Y. Kuo, *J. Am. Chem. Soc.* **1992**, *114*, 9369; c) R. Nagata, H. Yamanaka, E. Okazaki, I. Saito, *Tetrahedron Lett.* **1989**, *30*, 4995; d) R. Nagata, Y. Hidenori, E. Murahashi, I. Saito, *Tetrahedron Lett.* **1990**, *31*, 2907.
[138] a) M. Schmittel, M. Strittmatter, S. Kiau, *Tetrahedron Lett.* **1995**, *36*, 4975; b) M. Schmittel, S. Kiau, T. Siebert, M. Strittmatter, *Tetrahedron Lett.* **1996**, *37*, 999, 7691; c) M. Schmittel, M. Strittmatter, S. Kiau, *Angew. Chem.* **1996**, *108*, 1952; *Angew. Chem. Int. Ed. Engl.* **1996**, *35*, 1843; d) M. Schmittel, M. Keller, S. Kiau, M. Strittmatter, *Chem. Eur. J.* **1997**, *3*, 807; e) T. Gillmann, T. Hülsen, W. Massa, S. Wocadlo, *Synlett* **1995**, 1257; f) J. G. Garcia, B. Ramos, L. M. Pratt, A. Rodriguez, *Tetrahedron Lett.* **1995**, *36*, 7391.
[139] a) B. Engels, M. Hanrath, *J. Am. Chem. Soc.* **1998**, *120*, 6356; b) P. R. Schreiner, M. Prall, *J. Am. Chem. Soc.* **1999**, *121*, 8615; c) C. J. Cramer, B. L. Kormos, M. Seierstad, E. C. Sherer, P. Winget, *Org. Lett.* **2001**, *3*, 1881; d) S. P. de Visser, M. Filatov, S. Shaik, *Phys. Chem. Chem. Phys.* **2001**, *3*, 1242.
[140] M. Schmittel, M. Maywald, *Chem. Commun.* **2001**, 155.
[141] a) P. G. Wenthold, S. G. Wierschke, J. J. Nash, R. R. Squires, *J. Am. Chem. Soc.* **1993**, *115*, 12611; b) P. G. Wenthold, S. G. Wierschke, J. J. Nash, R. R. Squires, *J. Am. Chem. Soc.* **1994**, *116*, 7378.
[142] C. F. Logan, J. C. Ma, P. Chen, *J. Am. Chem. Soc.* **1994**, *116*, 2137.
[143] For quantum-chemical studies on **106** and related open-shell singlet biradicals, see: a) J. Gräfenstein, D. Cremer, *Phys. Chem. Chem. Phys.* **2000**, *2*, 2091; b) J. Cabrero, N. Ben-Amor, R. Caballol, *J. Phys. Chem. A* **1999**, *103*, 6220; see also ref. [139].
[144] W. Sander, H. Wandel, G. Bucher, J. Gräfenstein, E. Kraka, D. Cremer, *J. Am. Chem. Soc.* **1998**, *120*, 8480.
[145] a) C. J. Cramer, R. R. Squires, *Org. Lett.* **1999**, *1*, 215; see also: b) P. W. Musch, B. Engels, *Angew. Chem.* **2001**, *113*, 3951; *Angew. Chem. Int. Ed.* **2001**, *40*, 3833.
[146] A. G. Myers, C. A. Parrish, *Bioconjugate Chem.* **1996**, *7*, 322.
[147] A. Z. Bradley, R. P. Johnson, *J. Am. Chem. Soc.* **1997**, *119*, 9917.
[148] K. N. Bharucha, R. M. Marsh, R. E. Minto, R. G. Bergman, *J. Am. Chem. Soc.* **1992**, *114*, 3120.
[149] a) A. G. Myers, N. S. Finney, *J. Am. Chem. Soc.* **1992**, *114*, 10986; b) A. G. Myers, P. S. Dragovich, *J. Am. Chem. Soc.* **1993**, *115*, 7021.
[150] See, for example, refs. [22,81,84,88,95,111,134] as well as: a) R. Lindh, A. Bernhardsson, M. Schütz, *J. Phys. Chem. A* **1999**, *103*, 9913; b) J. Gräfenstein, A. Hjerpe, E. Kraka, D. Cremer, *J. Phys. Chem. A* **2000**, *104*, 1748, and references therein.
[151] W. D. Langer, T. Velusamy, T. B. H. Kuiper, R. Peng, M. C. McCarthy, M. J. Travers, A. Kovacs, C. A. Gottlieb, P. Thaddeus, *Astrophys. J.* **1997**, *480*, L63.
[152] An up-to-date list of the molecules detected in the interstellar medium is found on the homepage of the Thaddeus group: http://cfa-www.harvard.edu/cfa/mmw/mmwlab/ismmolecules_-carbon.html.
[153] K. W. Sattelmeyer, J. F. Stanton, *J. Am. Chem. Soc.* **2000**, *122*, 8220.
[154] S. Arulmozhiraja, T. Sato, A. Yabe, *J. Comput. Chem.* **2001**, *22*, 923.
[155] E. K. Fields, S. Meyerson, *J. Org. Chem.* **1966**, *31*, 3307.
[156] a) M. Moriyama, T. Ohana, A. Yabe, *J. Am. Chem. Soc.* **1997**, *119*, 10229; b) T. Sato, S. Arulmozhiraja, H. Niino, S. Sasaki, T. Mutsuura, A. Yabe, *J. Am. Chem. Soc.* **2002**, *124*, 4512.
[157] a) M. Moriyama, T. Ohana, A. Yabe, *Chem. Lett.* **1995**, 557; b) M. Moriyama, A. Yabe, *Chem. Lett.* **1998**, 337; see also: c) M. Moriyama, T. Sato, T. Uchimaru, A. Yabe, *Phys. Chem. Chem. Phys.* **1999**, *1*, 2267.
[158] T. Sato, H. Niino, A. Yabe, *J. Photochem. Photobiol. A* **2001**, *145*, 3.
[159] a) W. Weltner, Jr., R. J. van Zee, *Chem. Rev.* **1989**, *89*, 1713; b) J. M. L. Martin, J. P. Franccois, R. J. Gijbels, *Mol. Struct.* **1993**, *294*, 21.
[160] a) K. R. Thompson, R. L. DeKock, W. Weltner, Jr., *J. Am. Chem. Soc.* **1971**, 93, 4688; b) M. Vala, T. M. Chandrasekhar, J. Szcepanski, R. Pellow, *High Temp. Sci.* **1990**, *27*, 19; c) D. W. Arnold, S. E. Bradforth, T. N. Kitsopoulos, D. N. Neumark, *J. Chem. Phys.* **1991**, *95*, 8753; d) C. C. Arnold, Y. Zhao, T. N. Kitsopoulos, D. N. Neumark, *J. Chem. Phys.* **1992**, *97*, 6121; e) R. H. Kranze, W. R. M. Graham, *J. Chem. Phys.* **1993**, *98*, 71; f) H. J. Hwang, A. van Orden, K. Tanaka, E. W. Kuo, J. R. Heath, R. J. Saykally, *Mol. Phys.* **1993**, *79*, 769.
[161] Relative stabilities of **136, 137**, and **138** have been calculated at different levels of theory: a) K. Raghavachari, R. A. Whiteside, J. A. Pople, *J. Chem. Phys.* **1986**, *85*, 6623; b) K. Raghavachari, J. S. Binkley, *J. Chem. Phys.* **1987**, *87*, 2191; c) J. Hutter, H. P. Lüthi, *J. Chem. Phys.* **1994**, *101*, 2213; d) J. Hutter, H. P. Lüthi, F. Diederich, *J. Am. Chem. Soc.* **1994**, *116,* 750. The historical developement of calculations on C_6 is outlined in: e) J. M. L. Martin, P. R. Taylor, *J. Phys. Chem.* **1996**, *100*, 6047. Concerning the aromaticity of **137** and **138**, see ref. [71].
[162] S. L. Wang, C. M. L. Rittby, W. R. M. Graham, *J. Chem. Phys.* **1997**, *107*, 6032.
[163] F. Grein, J. Franz, M. Hanrath, S. D. Peyerimhoff, *Chem. Phys.* **2001**, *263*, 55.
[164] J. G. Radziszewski, J. Waluk, P. Kaszynski, J. Spanget-Larsen, *J. Phys. Chem. A* **2002**, *106*, 6730.
[165] K. Johnson, B. Sauerhammer, S. Titmuss, D. A. King, *J. Chem. Phys.* **2001**, *114*, 9539.
[166] S. Yamagishi, S. J. Jenkins, D. A. King, *J. Chem. Phys.* **2002**, *117*, 819.
[167] H. H. Wenk, W. Sander, *Eur. J. Org. Chem.* **2002**, 3927.
[168] H. A. Lardin, J. J. Nash, P. G. Wenthold, *J. Am. Chem. Soc.* **2002**, *124*, 12612.
[169] E. D. Nelson, H. I. Kenttämaa, *J. Am. Soc. Mass Spectrom.* **2001**, *12*, 258.
[170] F. S. Amegayibor, J. J. Nash, A. S. Lee, J. Thoen, C. J. Petzold, H. I. Kenttämaa, *J. Am. Chem. Soc.* **2002**, *124*, 12066.
[171] F. Stahl, D. Moran, P. von R. Schleyer, M. Prall, P. R. Schreiner, *J. Org. Chem.* **2002**, *67*, 1453.
[172] Compare Ref. [111b] in the main text and, for example: G. Haberhauer, R. Gleiter, *J. Am. Chem. Soc.* **1999**, *121*, 4664.
[173] a) I. V. Alabugin, M. Manoharan, *J. Phys. Chem. A*, in press; b) I. V. Alabugin, M. Manoharan, S. V. Kovalenko, *Org. Lett.* **2002**, *4*, 1119.
[174] F. De Proft, P. von R. Schleyer, J. H. van Lenthe, F. Stahl, P. Geerlings, *Chem. Eur. J.* **2002**, *8*, 3402.
[175] B. A. Hess, Jr., L. J. Schaad, *Org. Lett.* **2002**, *4*, 735.
[176] A. K. Nadipuram, W. M. David, D. Kumar, S. M. Kerwin, *Org. Lett.* **2002**, *4*, 4543.
[177] S. P. Kawatkar, P. R. Schreiner, *Org. Lett.* **2002**, *4*, 3643.

Communications



The array of metal atoms (yellow) in the first hexanuclear Ir-chain compound is almost linear. This 1D oligomer is a molecular piece of a "metal wire" related to the infinite mixed-valence metal chains, such as the Krogmann salts. Crystalline samples of the Ir complex have a copper-like appearance. For more information see the Communication by Oro, Ciriano, and co-workers on the following pages....

 © 2003 Wiley-VCH Verlag GmbH & Co. KGaA, Weinheim 1433-7851/03/4205-0529 $ 20.00+.50/0

Chains of Metal Atoms

A Hexanuclear Iridium Chain**

Cristina Tejel, Miguel A. Ciriano, B. Eva Villarroya, José A. López, Fernando J. Lahoz, and Luis A. Oro**

Compounds containing discrete chains of metal-bonded atoms are interesting not only from a theoretical point of view but also because of their potential applications, particularly as nanoscale electronic devices. Reproducible and well-defined syntheses for these compounds include ligand-assisted reactions with conjugated polyenes[1] and polydentate ligands, such as oligo-α-pyridylamino ligands.[2] In these cases, the number of available coordination sites of the ligand determines the length of the metallic chain. Another interesting approach involves the formation of metallic chains by oxidation of dinuclear complexes containing d^8 square-planar metal centers or by reduction of d^7 metal compounds. With this methodology there are, in principle, no limitations to the chain length other than the thermodynamic stability of the compound, provided that the steric encumbrance between the links is kept at minimum. To date, this method has allowed the isolation of only two rare 1D rhodium-chain compounds[3] and the platinum,[4] rhodium,[5] and iridium[6] blues, which typically consist of tetrametallic chains.[7] Between both situations only a remarkable octanuclear platinum chain, reported by Matsumoto and co-workers, is known.[8] Moreover, while several fractional oxidation states of the metal centers have been found for the platinum blues, only the averaged oxidation state of +1.5 has been reported for the tetranuclear rhodium and iridium blues. Herein we describe the novel iridium compound HH,HT,HH-$[Ir_6(\mu\text{-}OPy)_6(I)_2(CO)_{12}]$ containing an unprecedented linear metal chain made up of six iridium atoms in a formal oxidation state of +1.33.

Oxidation of a toluene solution of the dinuclear complex $[Ir_2(\mu\text{-}OPy)_2(CO)_4]$[6a] (**1**; Opy = 2-pyridonate) with diiodine (in a 3:1 molar ratio) at 0 °C immediately gave an EPR-silent, dark-blue solution from which a crystalline solid having a copper-like aspect (**2**) was isolated in good yield (75%) on addition of hexanes.[9] The crystal structure of **2**[10] (Figure 1), revealed the hexametallic chain formed by an almost linear array in which two HH-$[Ir_2(\mu\text{-}OPy)_2(I)(CO)_4]$ units sandwich an HT-$[Ir_2(\mu\text{-}OPy)_2(CO)_4]$ complex. The six iridium atoms are linked by metal–metal bonds, two of which are unsupported by bridging ligands. The bonds of the latter (range 2.7757(14)–2.7929(14) Å) are longer than the ligand-bridged metal–metal bonds (range 2.6849(14)–2.7096(14) Å) in the two independent molecules. The relative conformation of the dinuclear complexes around the unsupported metal–metal bonds is staggered and almost *transoid* with mean torsion angles around these bonds in the range 142.2(10)–147.7(12)°. These structural features are similar to those found in the tetranuclear complex HT,HH-$[Ir_4(\mu\text{-}OPy)_4(I)_2(CO)_8]$.[6a]

Remarkably, the hexanuclear chain which was found to be stable in the solid state, remained intact in solution under 0 °C. Moreover, the observation of resonance signals corresponding to three inequivalent α-pyridonate bridging ligands in the ^{1}H NMR spectrum indicates a C_2 symmetry of the species in solution, this symmetry is accessible by a slight rotation of the three dinuclear moieties around the unsupported iridium–iridium bonds.

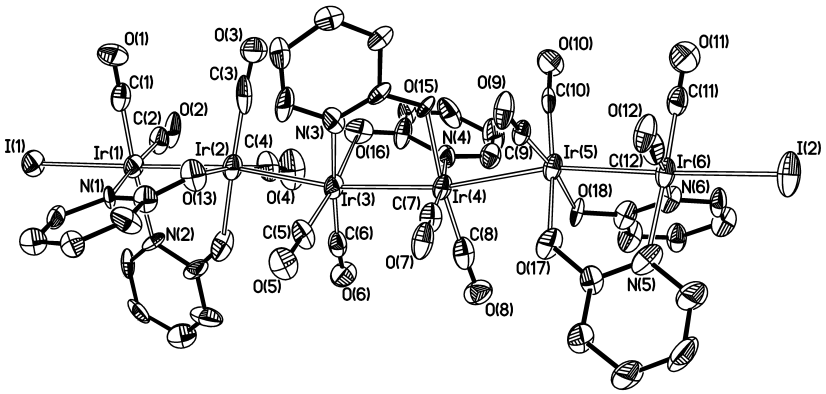


Figure 1. Molecular representation of one of the two independent molecules of the hexanuclear complex **2**. Selected bond lengths [Å] and angles [°] for both molecules: Ir(1)-Ir(2) 2.6971(15), 2.6849(14), Ir(2)-Ir(3) 2.7929(14), 2.7757(14), Ir(3)-Ir(4) 2.7031(14), 2.6899(14), Ir(4)-Ir(5) 2.7927(14), 2.7887(15), Ir(5)-Ir(6) 2.7096(14), 2.7088(15), Ir(1)-I(1) 2.860(2), 2.846(2), Ir(6)-I(2) 2.857(2), 2.850(2), Ir-O range 1.994(17)–2.084(15), Ir-N range 2.08(2)–2.13(2), Ir-C(O) range 1.73(3)–1.93(3); I(1)-Ir(1)-Ir(2) 178.53(6), 176.76(6), Ir(1)-Ir(2)-Ir(3) 169.75(5), 165.00(5), Ir(2)-Ir(3)-Ir(4) 166.02(5), 168.51(5), Ir(3)-Ir(4)-Ir(5) 167.33(5), 168.78(5), Ir(4)-Ir(5)-Ir(6) 167.26(5), 166.70(5), Ir(5)-Ir(6)-I(2) 177.53(7), 175.65(7).

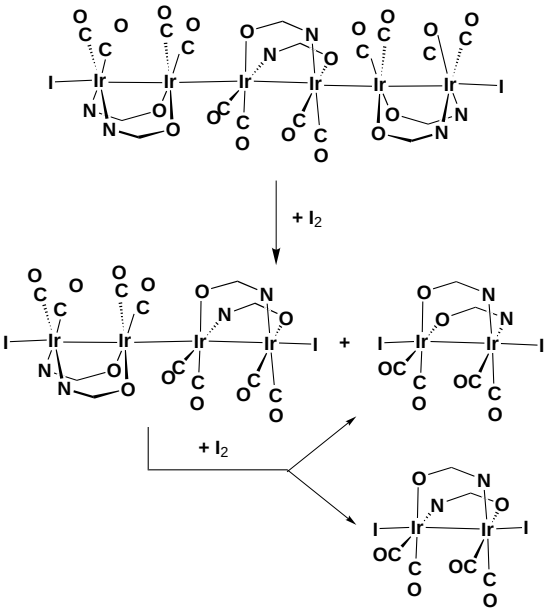
Also remarkable was the selectivity in the assembly of the dinuclear links in the correct configuration to form the hexametallic chain found in **2** (HH,HT,HH). Indeed, since the starting material **1** was found to be in equilibrium between the **1**-HH and **1**-HT isomers in solution, six different hexametallic isomers could be formed. Therefore, the location of the HT configuration as the central link indicates a specific pathway for the growth of the metal chain or a predetermined reaction mechanism. For example, a possible reaction mechanism is the oxidation of the **1**-HH to the paramagnetic species HH-$[Ir_2(\mu\text{-}OPy)_2I(CO)_4]$, these molecules then sandwich a molecule of unreacted **1**-HT, although alternative mechanisms are also plausible.

[*] Dr. M. A. Ciriano, Prof. L. A. Oro, Dr. C. Tejel, Dr. B. E. Villarroya, Dr. J. A. López, Dr. F. J. Lahoz
Departamento de Química Inorgánica
Instituto de Ciencia de Materiales de Aragón
Universidad de Zaragoza-C.S.I.C., 50009-Zaragoza (Spain)
Fax: (+34) 976761143
E-mail: mciriano@posta.unizar.es
oro@posta.unizar.es

[**] Financial support from DGES (Project PB98-641) is gratefully acknowledged.

 © 2003 Wiley-VCH Verlag GmbH & Co. KGaA, Weinheim 1433-7851/03/4205-0530 $ 20.00+.50/0

Moreover, the hexametallic chain in complex **2** was broken up, step by step, while maintaining the configuration of the individual links (Scheme 1). Thus, the addition of diiodine to **2** produced HT,HH-$[Ir_4(\mu\text{-}OPy)_4(I)_2(CO)_8]$ along with the diiridium(II) complex HH-$[Ir_2(\mu\text{-}OPy)_2(I)_2(CO)_4]$ (**3**-HH). A further reaction of HT,HH-$[Ir_4(\mu\text{-}OPy)_4(I)_2(CO)_8]$ with diiodine gave an equimolar mixture of **3**-HH and its configurational isomer **3**-HT. The HH and HT configurations were established from the single-crystal X-ray structure determination of **3**-HH[11] (Figure 2) and the ^{1}H NMR spectrum of this mixture.



Scheme 1. Sequential cleavage of diiridium units from **2**.

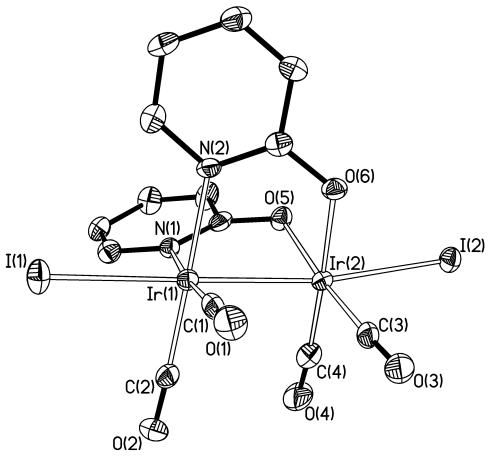


Figure 2. Molecular representation of one of the two independent molecules of the dinuclear complex **3**-HH. Selected bond lengths [Å] and angles [°] for both molecules: Ir(1)-Ir(2) 2.6426(4), 2.6353(4), Ir(1)-I(1) 2.7831(5), 2.7852(5), Ir(2)-I(2) 2.7379(5), 2.7424(5), Ir-O range 2.042(4)–2.060(4), Ir-N range 2.098(5)–2.112(5), Ir-C(O) range 1.856(7)–1.903(6); I(1)-Ir(1)-Ir(2) 177.721(14), 179.400(14), Ir(1)-Ir(2)-I(2) 170.808(13), 170.342(13).

As a result of the single iridium–iridium bonds, the Ir–Ir separations (2.6426(4) and 2.6353(4) Å) in **3**-HH are shorter than those in **2**. However, the stability of the hexanuclear complex **2** which has a six-center two-electron bond is remarkable. Noteworthy is also the oxidation state +1.33 for the iridium atoms in **2**, which provides a new link in the electronic sequence shown in Scheme 2. Another remarkable

$$\{Ir(+1)\}_2 \longrightarrow \{Ir(+1.33)\}_6 \longrightarrow \{Ir(+1.5)\}_4 \longrightarrow \{Ir(+2)\}_2$$

Scheme 2. Oxidation states and compositions of compounds containing iridium–iridium bonds.

feature is that the HT-pyridonate complex is the linker between two HH-$[Ir_2(\mu\text{-}OPy)_2(I)(CO)_4]$ units when the HT configurations had been declared inappropriate to engage in the tetrametallic chains of the platinum blues.[4d,12]

In conclusion, the HT-pyridonate dinuclear complexes are found to be a key building block for the construction of hexa- and tetranuclear chains containing metal centers with different fractional oxidation states.

Received: August 8, 2002 [Z19927]

[1] a) T. Murahashi, T. Nagai, Y. Mino, E. Mochizuki, Y. Kai, H. Kurosawa, *J. Am. Chem. Soc.* **2001**, *123*, 6927; b) T. Murahashi, T. Nagai, T. Okuno, T. Matsutani, H. Kurosawa, *Chem. Commun.* **2000**, 1689.

[2] Selected references: a) R. Clérac, F. A. Cotton, K. R. Dunbar, T. B. Lu, C. A. Murillo, X. P. Wang, *J. Am. Chem. Soc.* **2000**, *122*, 2272; b) Y. H. Chen, C. C. Lee, C. C. Wang, G. H. Lee, S. Y. Lai, F. Y. Li, C. Y. Mou, S. M. Peng, *Chem. Commun.* **1999**, 1667; c) S. Y. Lai, T. W. Lin, Y. H. Chen, C. C. Wang, G. H. Lee, M. H. Yang, M. K. Leung, S. M. Peng, *J. Am. Chem. Soc.* **1999**, *121*, 250; d) F. A. Cotton, D. M. Daniels, T. B. Lu, C. A. Murillo, X. P. Wang, *J. Chem. Soc. Dalton Trans.* **1999**, 517.

[3] a) F. P. Pruchnik, P. Jakimowicz, Z. Ciunik, K. Stanislawek, L. A. Oro, C. Tejel, M. A. Ciriano, *Inorg. Chem. Commun.* **2001**, *4*, 19; b) F. P. Pruchnik, P. Jakimowicz, Z. Ciunik, *Inorg. Chem. Commun.* **2001**, *4*, 726; c) M. E. Prater, L. E. Pence, R. Clérac, G. M. Finnis, C. Campana, P. Auban-Senzier, D. Jerome, E. Canadell, K. R. Dunbar, *J. Am. Chem. Soc.* **1999**, *121*, 8005.

[4] a) K. Matsumoto, K. Sakai, *Adv. Inorg. Chem.* **2000**, *49*, 375; b) B. Lippert, *Cisplatin: Chemistry and Biochemistry of a Leading Anticancer Drug* (Ed.: B. Lippert), VHCA and Wiley-VCH, Zürich and Weinheim, **1999**, pp. 379–403; c) K. Sakai, M. Takeshita, Y. Tanaka, T. Ue, M. Yanagisawa, M. Kosaba, T. Tsubomura, M. Ato, T. Nakano, *J. Am. Chem. Soc.* **1998**, *120*, 11353; d) K. Sakai, Y. Tanaka, Y. Tsuchiya, K. Hirata, T. Tsubomura, S. Iijima, A. Bhattacharjee, *J. Am. Chem. Soc.* **1998**, *120*, 8366; e) A. P. Ginsberg, T. V. O'Halloran, P. E. Fanwick, L. S. Hollis, S. J. Lippard, *J. Am. Chem. Soc.* **1984**, *106*, 5430.

[5] a) C. Tejel, M. A. Ciriano, J. A. López, F. J. Lahoz, L. A. Oro, *Angew. Chem.* **1998**, *110*, 1647; *Angew. Chem. Int. Ed.* **1998**, *37*, 1542; b) K. R. Mann, M. J. DiPierro, T. P. Gill, *J. Am. Chem. Soc.* **1980**, *102*, 3965.

[6] a) C. Tejel, M. A. Ciriano, B. E. Villarroya, R. Gelpi, J. A. López, F. J. Lahoz, L. A. Oro, *Angew. Chem.* **2001**, *113*, 4208; *Angew. Chem. Int. Ed.* **2001**, *40*, 4084; b) M. A. Ciriano, S. Sebastián, L. A. Oro, A. Tiripicchio, M. Tiripicchio-Camellini, *Angew. Chem.* **1988**, *100*, 406; *Angew. Chem. Int. Ed. Engl.* **1988**, *27*, 402.

[7] C. Tejel, M. A. Ciriano, L. A. Oro, *Chem. Eur. J.* **1999**, *5*, 1131.
[8] a) K. Matsumoto, K. Sakai, K. Nishio, Y. Tokisue, R. Ito, T. Nishide, Y. Schichi, *J. Am. Chem. Soc.* **1992**, *114*, 8110; b) K. Sakai, K. Matsumoto, *J. Am. Chem. Soc.* **1989**, *111*, 3074.
[9] Selected analytical and spectroscopic data for the new complexes: Complex **2**, elemental analysis (%) calcd for $C_{42}H_{24}N_6O_{18}I_2Ir_6{\cdot}0.5(C_6H_{14})$: C 22.99, H 1.33, N 3.57; found: C 23.12, H 1.39, N 3.49; IR (Nujol): $\tilde{\nu}=2101$ (sh), 2079 (s), 2061 (sh), 2042 (s), 2023 (sh), 2007 cm^{-1} (sh) (CO); ^1H NMR ([D$_8$]toluene, −50 °C): $\delta=9.74$ (dd, $J=6.3$, 1.8 Hz, 2H), 9.68 (d, $J=6.3$ Hz, 2H), 9.56 (dd, $J=6.3$, 1.8 Hz, 2H), 6.58 (td, $J=8.4$, 2.1 Hz, 2H), 6.49 (m, 4H), 6.35 (td, $J=7.2$, 1.5 Hz, 2H), 6.17 (d, $J=8.4$ Hz, 2H), 6.10 (d, $J=8.1$ Hz, 2H), 5.98 (td, $J=7.2$, 1.3 Hz, 2H), 5.69 ppm (m, 4H). Complex **3**-HH; elemental analysis (%) calcd for $C_{14}H_8N_2O_6I_2Ir_2$: C 17.92, H 0.86, N 2.98; found: C 18.17, H 1.03, N 2.89; IR (toluene): $\tilde{\nu}=2123$ (s), 2095 (m), 2071 (s), 2050 cm^{-1} (w) (CO); ^1H NMR (C_6D_6, 23 °C): $\delta=8.90$ (ddd, $J=6.6$, 1.8, 0.6 Hz, 2H), 6.34 (ddd, $J=8.7$, 6.6, 1.8 Hz, 2H), 6.22 (ddd, $J=8.7$, 1.2, 0.6 Hz, 2H), 5.61 ppm (td, $J=6.6$, 1.2, 0.6 Hz, 2H). Complex **3**-HT; elemental analysis (%) calcd for $C_{14}H_8N_2O_6I_2Ir_2$: C 17.92, H 0.86, N 2.98; found: C 18.07, H 0.96, N 2.91; IR (toluene): $\tilde{\nu}=2123$ (s), 2096 (m), 2070 cm^{-1} (s) (CO); ^1H NMR (C_6D_6, 23 °C): $\delta=9.30$ (dd, $J=6.6$, 1.8 Hz, 2H), 6.35 (ddd, $J=8.7$, 6.6, 1.8 Hz, 2H), 6.19 (dd, $J=8.7$, 1.5 Hz, 2H), 5.67 ppm (td, $J=6.6$, 1.5 Hz, 2H).
[10] a) Crystal data for **2**·0.5(C_6H_{14}): $C_{42}H_{24}I_2Ir_6N_6O_{18}{\cdot}0.5(C_6H_{14})$, $M_r=2350.76$, laminar crystal ($0.09\times0.035\times0.008$ mm), triclinic, space group $P\bar{1}$, $a=14.2642(18)$, $b=20.927(3)$, $c=21.153(3)$ Å, $\alpha=68.369(2)$, $\beta=81.169(2)$, $\gamma=82.126(2)$°, $V=5777.8(14)$ Å^{-3}, $Z=4$, $\rho_{calcd}=2.702$ g cm^{-3}, $F(000)=4220$, $T=100(2)$ K, $Mo_{K\alpha}$ radiation ($\lambda=0.71073$ Å, $\mu=14.905$ mm^{-1}). Data collected with a Bruker SMART APEX CCD diffractometer. Of 49364 measured reflections (2θ: 5–50°, ω scans 0.3°), 20135 were unique ($R_{int}=0.0892$); a multi-scan absorption correction was applied (SADABS program) with min./max. transmission factors of 0.455/0.825. Structure solved by Patterson and difference-Fourier maps; refined using SHELXTL. Two independent complex molecules and disordered hexane solvent were found in the asymmetric unit. Final agreement factors were $R1=0.0660$ (10409 observed reflections, $F^2>4\sigma(F^2)$) and $wR2=0.1912$; data/restrains/parameters 20135/309/1381; GOF = 0.970. Largest peak and hole in the final difference map 2.912 and −2.980 e Å^{-3}. The limited quality of the structural data (also the merging and agreement factors) should be necessarily associated to the very small dimensions of the crystal, and to the associated diffracting weakness. b) CCDC-191178 (**2**) and CCDC-191179 (**3**-HH) contains the supplementary crystallographic data for this paper. These data can be obtained free of charge via www.ccdc.cam.ac.uk/conts/retrieving.html (or from the Cambridge Crystallographic Data Centre, 12 Union Road, Cambridge CB2 1EZ, UK; fax: (+44) 1223-336-033; or deposit @ccdc.cam.ac.uk).
[11] Crystal data for **3**-HH·0.25(C_7H_8)·0.25(C_6H_{14}): $C_{14}H_8I_2Ir_2N_2O_6{\cdot}0.25(C_7H_8){\cdot}0.25(C_6H_{14})$, $M_r=983.00$, triclinic, space group $P\bar{1}$, $a=11.9579(12)$, $b=12.6320(13)$, $c=16.2249(16)$ Å, $\alpha=104.439(2)$, $\beta=99.257(2)$, $\gamma=93.659(2)$°, $V=2328.6(4)$ Å^{-3}, $Z=4$, $\rho_{calcd}=2.804$ g cm^{-3}, $F(000)=1756$, $T=100(2)$ K, $Mo_{K\alpha}$ radiation ($\lambda=0.71073$ Å, $\mu=14.103$ mm^{-1}). Data collected as described for **2** with a prismatic block ($0.27\times0.25\times0.09$ mm). Of 27550 measured reflections (2θ: 5–54°, ω scans 0.3°), 10076 were unique ($R_{int}=0.0360$); a multi-scan absorption correction was performed (SADABS program) with min./max. transmission factors of 0.092/0.244. Structure solution and refinement as described for **2**. Two independent complex molecules and disordered toluene and hexane solvents were found in the asymmetric unit. Final agreement factors were $R1=0.0279$ (9002 observed reflections) and $wR2=0.0638$. Data/restrains/parameters 10076/37/518; GOF = 1.051. Largest peak and hole in the final difference map 1.652 and −1.107 e Å^{-3}.[10b]
[12] a) T. V. O'Halloran, P. K. Mascharak, I. D. Williams, M. Roberts, S. J. Lippard, *Inorg. Chem.* **1987**, *26*, 1261; b) T. Wienkötter, M. Sabat, G. Fusch, B. Lippert, *Inorg. Chem.* **1995**, *34*, 1022.

Nanoporous Coordination Polymers

Nanoporous Lanthanide–Copper(II) Coordination Polymers: Syntheses and Crystal Structures of $[\{M_2(Cu_3(iminodiacetate)_6)\}{\cdot}8H_2O]_n$ (M = La, Nd, Eu)**

Yan-Ping Ren, La-Sheng Long, Bing-Wei Mao, You-Zhu Yuan, Rong-Bin Huang, and Lan-Sun Zheng*

Designing and constructing three-dimensional (3D) coordination polymers with well-defined pores is of current interest for the creation of new zeolite-type materials with potential applications in catalysis, gas storage, chemical separation, and ion exchange.[1–3] Up to now, a great many porous three-dimensional coordination polymers have been synthesized and characterized.[4–6] However, the synthetic focus in this rapidly expanding area of research has been centered on monometallic porous coordination polymers,[1–6] while the chemistry, as well as the synthetic strategy toward porous heterometallic coordination polymers has received much less attention.[7–9]

It is well known that heterometallic coordination polymers have potentially interesting physical properties, such as conductivity or magnetic ordering, that result from interactions between two distinct metal centers connected by a suitable linker.[10,11] Moreover, the structural preference of different metal centers in a mixed-metal system often leads to a broader palette of polymer structural motifs than can be achieved with monometallic systems, and thus makes the obtained structures more diverse.[7a] In particular, the incorporation of different metals may enhance the catalytic properties of the coordination polymers. By using this approach, we now report the syntheses and crystal structures of three 3D lanthanide–transition metal coordination polymers of the form $[\{M_2(Cu_3(iminodiacetate)_6)\}{\cdot}8H_2O]_n$, where M = La (**1**),Nd (**2**), and Eu (**3**). Investigation of the thermal

[*] Dr. L.-S. Long, Y.-P. Ren, B.-W. Mao, Y.-Z. Yuan, R.-B. Huang, Prof. Dr. L.-S. Zheng
State Key Laboratory for Physical Chemistry of Solid Surface and Department of Chemistry, Xiamen University
Xiamen 361005 (P.R. China)
Fax: (+86) 592-218-3047
E-mail: lslong@jingxian.xmu.edu.cn.

[**] This work was supported by the NNSF of China (Nos. 20271044, 20273052, 20021002, and 20023001) and NSF of Fujian Province, P.R. China (E0110001).

 © 2003 Wiley-VCH Verlag GmbH & Co. KGaA, Weinheim 1433-7851/03/4205-0532 $ 20.00+.50/0

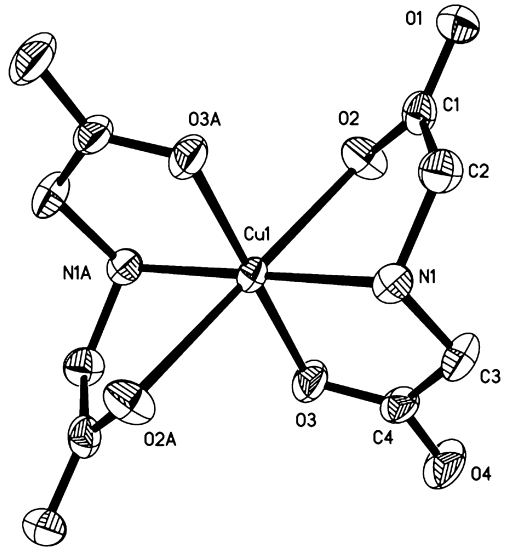


Figure 1. ORTEP diagram of the metalloligand.

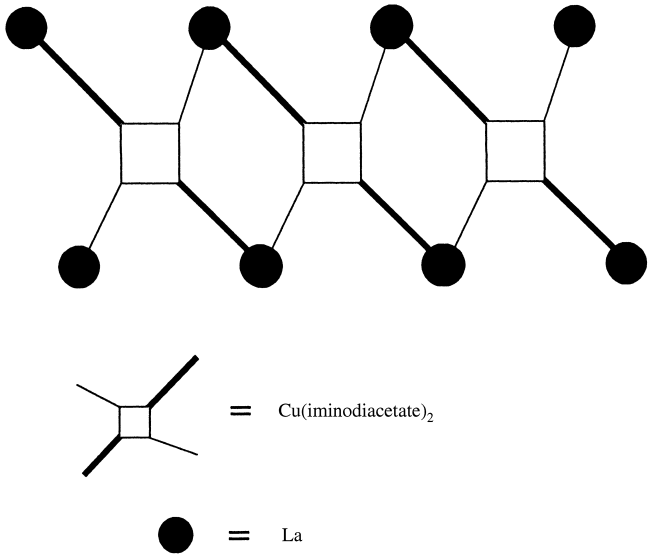


Figure 2. A schematic of the infinite band-like structure, with Cu(iminodiacetate)$_2$ anions connected to La^{III} ions. The bold lines represent carboxylate groups of iminodiactate units that bind to a La^{III} ion in a bidentate fashion, while the narrow lines represent carboxylate groups that exhibit a monodentate binding mode.

stability of the coordination polymers shows that their frameworks retained their stability when the guest molecules were removed.

The synthetic strategy of this study is to use a metalloligand to construct the coordination polymers.[7a,12] As shown in Figure 1, the iminodiacetate anions form complexes with copper(II) centers, in which four noncoordinated oxygen atoms can act as potential donors for other metal ions. If these donors do coordinate with another metal ion, an assembly process will occur, which leads to the formation of a heterometallic coordination polymer.

Compounds **1**, **2**, and **3** were obtained by the reaction of $LaCl_3 \cdot 9H_2O$, $NdCl_3 \cdot 9H_2O$, or $EuCl_3 \cdot 9H_2O$, respectively, with a mixture of iminodiacetic acid and $Cu(NO_3)_2 \cdot 3H_2O$ in a 2:6:3 molar ratio in aqueous solution, at a pH value of 5–6. X-ray diffraction analysis[13] reveals that the three compounds are isomorphous. In **1**, the copper(II) ion is chelated by two iminoacetate ligands to form the metalloligand (Figure 1), which acts as a tetradentate ligand, with each of the uncoordinated oxygen atoms coordinating to one La(III) ion, which leads to the formation of an infinite band-like structure, as illustrated in Figure 2. Connection of the bands in C_3 symmetry through sharing La^{III} ions gives rise to an edge-shared 3D structure with a chair-shaped hexagonal channel along the crystallographic *c* axis, as shown in Figure 3. Each channel in **1** is formed by six CuO_4N_2 polyhedra and six LaO_9 polyhedra. The diameter of the hexagonal channels is 16.8 Å, with lattice water molecules located within the channels. To the best of our knowledge, the pores in **1** are the largest among heterometallic coordination polymers reported to date.

Each copper(II) ion in **1** is six-coordinated in a distorted octahedral geometry by four oxygen atoms and two nitrogen atoms from iminoacetate ligands, while each La^{III} ion is nine-coordinated through interactions with carboxylate groups from six metalloligands; three ligands exhibit bidentate chelation, while the remaining three chelate in a monodentate

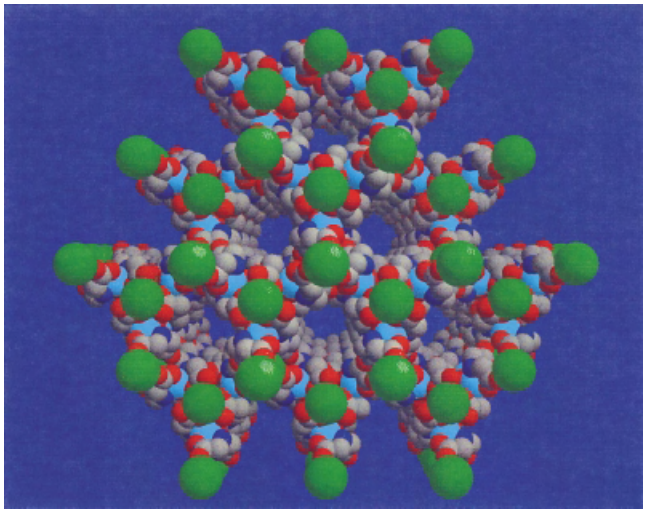


Figure 3. Space-filling representation of the 3D structure of **1**, viewed along the crystallographic *c* axis. La: green, Cu: cyan, O: red, N: deep blue and C: grey.

fashion. The bond lengths of Cu–N, Cu–O, and La–O are 2.022(3), 1.960(3)–2.373(3), and 2.449(3)–2.775(3) Å, respectively, which is comparable to those bonds found in the lanthanide–copper(II)–iminoacetate complex previously reported.[14] The shortest Cu···Cu, Cu···La, and La···La separations in **1** are 6.370, 4.640, and 7.461 Å, respectively.

The crystal structures of **2** and **3** are very similar to that of **1**. In **2**, the Cu–N bond length is 2.009(3) Å, while the length of the Cu–O bonds range from 1.950(3) to 2.378(2) Å, and the Nd–O bond lengths are between 2.397(2) and 2.741(3) Å. The shortest Cu···Cu, Cu···Nd, and Nd···Nd distances are 6.071, 4.594, and 7.335 Å, respectively, slightly shorter than those of

 © 2003 Wiley-VCH Verlag GmbH & Co. KGaA, Weinheim 1433-7851/03/4205-0533 $ 20.00+.50/0

1. In **3**, the Cu–N bond length is 2.019(3) Å, while the Cu–O bond lengths range from 1.952(2) to 2.401(3) Å, and the Eu–O bond lengths of between 2.339(3)–2.721(3) Å. The shortest Cu···Cu, Cu···Eu, and Eu···Eu distances are 6.064, 4.552, and 7.264 Å, respectively, slightly shorter than those of **2**.

Owing to the similarity of the structures for **1**, **2,** and **3**, compound **1** was selected for thermogravimetric analysis (TGA) to examine the thermal stability of the complexes. The TGA curve for **1** (Figure 4) displays an initial weight loss of 11.16% between 50 and 141.6 °C, which corresponds to the loss of lattice water molecules. Between 141.6 and 300 °C, **1** shows no weight loss, which is an indication of its stability up to 300 °C, comparable to that of $[Zn_4O(O_2C{-}C_6H_4{-}CO_2)]_n$ (300 °C),[1e] and significantly higher than for $[Cu_3(TMA)_2(H_2O)_3]_n$ (240 °C, TMA = benzene-1,3,5-tricarboxylate)[2a], and $[Cu_3(BTB)_2(H_2O)_2]_n$ (250 °C, BTB = 4,4′,4″-benzene-1,3,5-triyl-tribenzocarboxylate).[3a] The higher thermal stability of **1** is mainly attributed to the coordination of cooper(II) ions, which solidifies the flexible organic ligand.

In light of the results of the TGA study of **1**, we decided to investigate the crystal structures of samples that had been heated to 200 °C overnight under reduced pressure. Although TGA proved such samples to be anhydrous, they were extremely hygroscopic and, thus, the structure of an anhydrous sample of **1** could not be obtained. However, we were able to collect and fully analyze data from structures of **1** that were reloaded with water (hereafter named **1a**) and **3** (hereafter named **3a**). Structural characterization[13] reveals that the frameworks of **1a** and **3a** are very similar to that of **1** and **3**, respectively, but the number of water molecules in **1a** and **3a** is significantly less than that in **1** and **3**; both structures now only containing five lattice water molecules per polymer unit.

Interestingly, the TGA of **1a** (Figure 4) shows that the dehydration temperature for the reloaded water molecules in **1a** (approximately 100 °C) is much lower than that in **1** (approximately 150 °C). Crystal structure analysis reveals that the significant difference in dehydration temperature between the two samples can be attributed to different arrangements of the water molecules in **1** and **1a**. The O2W and O3W

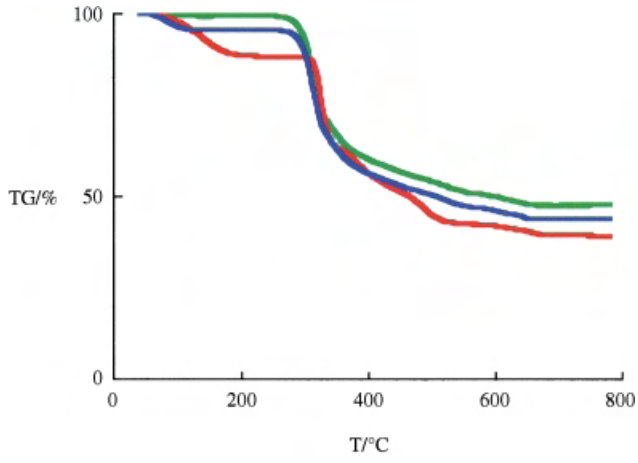


Figure 4. TGA curves for **1** (red), guest-free **1** (green), and **1a** (blue).

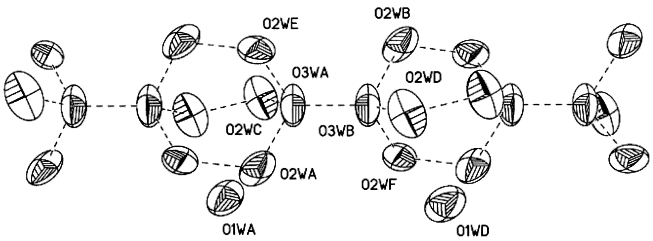


Figure 5. An ORTEP plot showing the Chinese-lanternlike water cluster in **1**.

lattice water molecules in **1** form a Chinese-lanternlike water cluster through water–water hydrogen bonds (Figure 5), with the O1W water molecules forming weak hydrogen bonds with the oxygen atoms of carboxylate groups. In contrast, the lattice water molecules in **1a** are hydrogen-bonded only to oxygen atoms of carboxylate groups; there are no water–water hydrogen bonds observed, as a consequence of the O2W water molecules being absent in the structure of **1a**.

In conclusion, we have reported the crystal structures and thermal properties of three nanoporous 3D lanthanide–copper(II) coordination polymers. Since the coordination polymers possess high thermal and structural stability, they may be promising materials for applications in catalysis, separation, gas storage, and molecular recognition. Investigations of molecular recognition, as well as potential catalytic properties of the materials are underway.

Experimental Section

1: An aqueous solution of $Cu(NO_3)_2{\cdot}3H_2O$ (0.36 g, 1.5 mmol) was added to an aqueous solution of iminodiacetic acid (0.40 g, 3.0 mmol). After the pH value of the mixture had been adjusted to approximately 6, an aqueous solution of $LaCl_3$ (1.0 mmol) was added. The resulting mixture was allowed to stand in air at room temperature for one week. Blue hexagonal column-shaped crystals of **1** suitable for X-ray crystallography were obtained in 83% yield. Compounds **2** and **3** were prepared in a similar way to **1**, except that $NdCl_3$ and $EuCl_3$ were used instead of $LaCl_3$.

Received: February 4, 2002
Revised: November 8, 2002 [Z18635]

[1] a) L.-S. Long, X.-M. Chen, M.-L. Tong, Z.-G. Sun, Y.-P. Ren, R.-B. Huang, L.-S. Zheng, *J. Chem. Soc. Dalton Trans.* **2001**, 2888; S.-Y. Yang, L.-S. Long, R.-B. Huang, L.-S. Zheng, *Chem. Commun.* **2002**, 472; S.-Y. Yang, L.-S. Long, Y.-B. Jiang, R.-B. Huang, L.-S. Zheng, *Chem. Mater.* **2002**, *14*, 3229; M. J. Zaworotko, *Nature* **1997**, *386*, 220; b) T. E. Mallouk, *Nature* **1997**, *387*, 350; c) G. B. Gardner, D. Venkataraman, J. S. Moore, S. Lee, *Nature* **1995**, *374*, 729; d) O. M. Yaghi, G. Li, H. Li, *Nature* **1995**, *378*, 703; e) H. Li, M. Eddaoudi, M. O'Keeffe, O. M. Yaghi, *Nature* **1999**, *402*, 276; f) J. S. Seo, D. G. Wheng, S. I. Jun, J. H. Oh, Y. J. Jeon, K. K. Kim, *Nature* **2000**, *404*, 982.
[2] a) S. S.-Y. Chui, S. M.-F. Lo, J. P. H. Charmant, A. G. Orpen, I. D. Williams, *Science* **1999**, *283*, 1148; b) C. R. Kagan, D. B. Mitzi, C. D. Dimitrakopoulos, *Science* **1999**, *286*, 954.
[3] a) B. L. Chen, M. Eddaoudi, S. T. Hyde, M. O'Keeffe, O. M. Yaghi, *Science* **2001**, *291*, 1021; b) M. Eddaoudi, J. Kim, N. Rosi,

 © 2003 Wiley-VCH Verlag GmbH & Co. KGaA, Weinheim 1433-7851/03/4205-0534 $ 20.00+.50/0

D. Vodak, J. Wachter, M. O'Keeffe, O. M. Yaghi, *Science* **2002**, *295*, 469.

[4] P. S. Halasyamani, M. J. Drewitt, D. O'Hare, *Chem. Commun.* **1997**, 867; P. J. Hagraman, J. Zubieta, *Angew. Chem.* **1999**, *111*, 2798; *Angew. Chem. Int. Ed.* **1999**, *38*, 2634; S. A. Bourne, J. J. Lu, A. Mondal, B. Moulton, M. J. Zaworotko, *Angew. Chem.* **2001**, *113*, 2171; *Angew. Chem. Int. Ed.* **2001**, *40*, 2111; J. J. Lu, A. Mondal, B. Moulton, M. J. Zaworotko, *Angew. Chem.* **2001**, *113*, 2174; *Angew. Chem. Int. Ed.* **2001**, *40*, 2113.

[5] J. Kim, B. L. Chen, T. M. Reineke, H. L. Li, M. Eddaoudi, D. B. Moler, M. O'Keeffe, O. M. Yaghi, *J. Am. Chem. Soc.* **2001**, *123*, 8239; M. Eddaoudi, D. B. Moler, H. L. Li, B. L. Chen, T. M. Reineke, M. O'Keeffe, O. M. Yaghi, *Acc. Chem. Res.* **2001**, *34*, 133.

[6] R. Kitaura, K. Fujimoto, S.-I. Noro, M. Kondo, S. Kitagawa, *Angew. Chem.* **2002**, *114*, 141; *Angew. Chem. Int. Ed.* **2002**, *41*, 113; A. Escuer, R. Vicente, F. A. Mautner, M. A. S. Goher, M. A. M. Abu-Youssef, *Chem. Commun.* **2002**, 64; D. T. Vodak, M. E. Braun, J. Kim, M. Eddaoudi, O. M. Yaghi, *Chem. Commun.* **2001**, 2534.

[7] a) Y.-B. Dong, M. D. Smith, H.-C. zur Loye, *Angew. Chem.* **2000**, *112*, 4438; *Angew. Chem. Int. Ed.* **2000**, *39*, 4271; b) R. J. Doedens, E. Yohannes, M. I. Khan, *Chem. Commun.* **2002**, 62; c) D. M. Ciurtin, M. D. Smith, H.-C. zur Loye, *Chem. Commun.* **2002**, 74.

[8] Z. Shi, S.-H. Feng, S. Gao, L, -R. Zhang, G. Y. Yang, J. Hua, *Angew. Chem.* **2000**, *112*, 2415; *Angew. Chem. Int. Ed.* **2000**, *39*, 2325.

[9] Y.-C. Liang, R. Cao, W.-P. Su, M.-C. Hong, W.-J. Zhang, *Angew. Chem.* **2000**, *112*, 3442; *Angew. Chem. Int. Ed.* **2000**, *39*, 3304; Y.-C. Liang, M.-C. Hong, W.-P. Su, R. -Cao, W.-J. Zhang, *Inorg. Chem.* **2001**, *40*, 4574.

[10] D. M. J. Doble, C. H. Benison, A. J. Blake, D. Fenske, M. S. Jackson, R. D. Kay, W.-S. Li, M. Schröder, *Angew. Chem.* **1999**, *111*, 2042; *Angew. Chem. Int. Ed.* **1999**, *38*, 1915; Y. Pei, P. Bergerat, O. Kahn, *J. Am. Chem. Soc.* **1994**, *116*, 3866; E. Coronado, J.-R. Galán-Mascarós, C.-J. Gómez-García, J. Ensling, P. Gütlich, *Chem. Eur. J.* **2000**, *6*, 552; E. Coronada, C.-J. Gómez-García, *Chem. Rev.* **1998**, *98*, 273; R. Sieber, S. Decurtins, H. Stoeckli-Evans, C. Wilson, D. Yufit, J. A. K. Howard, S. C. Capelli, A. Hauser, *Chem. Eur. J.* **2000**, *6*, 361; G. Ballester, E. Coronado, C. Giménez-Saiz, F. Romero, *Angew. Chem.* **2001**, *113*, 814; *Angew. Chem. Int. Ed.* **2001**, *40*, 792; E. Coronado, J. R. Galăn-Mascarós, C. J. Gómez-García, J. M. Martínez-Agudo, *Inorg. Chem.* **2001**, *40*, 113; F. Bellourard, M. Clemente-León, E. Coronado, J. R. Galăn-Mascarós, C. J. Gómez-García, F. Romero, K. R. Dunbar, *Eur. J. Inorg. Chem.* **2002**, 1603.

[11] B.-Q. Ma, S. Gao, G. Su, G.-X. Xu, *Angew. Chem.* **2001**, *113*, 448; *Angew. Chem. Int. Ed.* **2001**, *40*, 434.

[12] J. M. Dominguez, F. Camara, J. M. Moreno, E. Colacio, H. Sroeckli, *Inorg. Chem.* **1998**, *37*, 3046.

[13] X-ray crystal structure analysis: The data were collected at 293(2) K on a CAD4 diffractometer ($Mo_{K\alpha}$ radiation; $\lambda = 0.71073$ Å). The structure was solved by direct methods (SHELXTL Version 5.10) and refined by full-matrix least-squares on F^2. All non-hydrogen atoms were refined anisotropically. Crystal data for $[C_{24}H_{46}Cu_3La_2N_6O_{32}]_n$ (**1**): $0.50 \times 0.40 \times 0.40$ mm, trigonal, space group $P\bar{3}c1$ (no. 165), $a = 13.4713(19)$, $c = 14.922(3)$ Å, $\gamma = 120°$, $V = 2345.3(7)$ Å^3, $Z = 2$, $\rho_{calcd} = 1.958$ g cm^{-3}, $\mu(Mo_{K\alpha}) = 3.223$ mm^{-1}, $M_W = 1398.98$. Of the 2615 reflections measured ($2 < 2\theta < 56$), 1708 symmetry-independent reflections were used to solve the structure. Based on these data and 108 refined parameters, $R_1 = 0.0410$ (all data), $wR_2 = 0.0757$, GOF (F^2) = 1.111. Crystal data for $[C_{24}H_{46}Cu_3Nd_2N_6O_{32}]_n$ (**2**): $0.52 \times 0.40 \times 0.40$ mm, trigonal, space group $P\bar{3}c1$ (no. 165), $a = 13.4027(19)$, $c = 14.669(3)$ Å, $\gamma = 120°$, $V = 2282.0(6)$ Å^3, $Z = 2$, $\rho_{calcd} = 2.019$ g cm^{-3}, $\mu(Mo_{K\alpha}) = 3.699$ mm^{-1}, $M_W = 1409.64$. Of the 1854 reflections measured ($2 < 2\theta < 56$), 1189 symmetry-independent reflections were used to solve the structure. Based on these data and 114 refined parameters, $R_1 = 0.0642$ (all data), $wR_2 = 0.0870$, and GOF (F^2) = 1.011. Crystal data for $[C_{24}H_{46}Cu_3Eu_2N_6O_{32}]_n$ (**3**): $0.33 \times 0.18 \times 0.17$ mm, trigonal, space group $P\bar{3}c1$ (no. 165), $a = 13.306(5)$, $c = 14.528(5)$ Å, $\gamma = 120°$, $V = 2227.6(14)$ Å^3, $Z = 2$, $\rho_{calcd} = 2.101$ g cm^{-3}, $\mu(Mo_{K\alpha}) = 4.291$ mm^{-1}, $M_W = 1425.08$. Of the 1533 reflections measured ($2 < 2\theta < 56$), 1468 symmetry-independent reflections were used to solve the structure. Based on these data and 107 refined parameters, $R_1 = 0.0497$ (all data), $wR_2 = 0.1143$, GOF (F^2) = 1.127. Crystal data for $[C_{24}H_{38}Cu_3La_2N_6O_{29}]_n$ (**1a**): $0.32 \times 0.24 \times 0.22$ mm, trigonal, space group $P\bar{3}c1$ (no. 165), $a = 13.5588(3)$, $c = 14.9986(6)$ Å, $\gamma = 120°$, $V = 2387.94(12)$ Å^3, $Z = 2$, $\rho_{calcd} = 1.857$ g cm^{-3}, $\mu(Mo_{K\alpha}) = 3.157$ mm^{-1}, $M_W = 1344.98$. Of the 9010 reflections measured ($2 < 2\theta < 56$), 1721 symmetry-independent reflections were used to solve the structure. Based on these data and 100 refined parameters, $R_1 = 0.1017$ (all data), $wR_2 = 0.2352$, GOF (F^2) = 1.155. Crystal data for $[C_{24}H_{38}Cu_3Eu_2N_6O_{29}]_n$ (**3a**): $0.30 \times 0.22 \times 0.20$ mm, trigonal, space group $P\bar{3}c1$ (no. 165), $a = 13.3031(2)$, $c = 14.5660(3)$ Å, $\gamma = 120°$, $V = 2232.42(7)$ Å^3, $Z = 2$, $\rho_{calcd} = 2.025$ g cm^{-3}, $\mu(Mo_{K\alpha}) = 4.273$ mm^{-1}, $M_W = 1369.08$. Of the 9618 reflections measured ($2 < 2\theta < 48$), 1170 symmetry-independent reflections were used to solve the structure. Based on these data and 107 refined parameters, $R_1 = 0.0359$ (all data), $wR_2 = 0.0881$, GOF (F^2) = 1.091. CCDC-193487–193491 contains the supplementary crystallographic data for this paper. These data can be obtained free of charge via www.ccdc.cam.ac.uk/conts/retrieving.html (or from the Cambridge Crystallographic Data Centre, 12, Union Road, Cambridge CB2 1EZ, UK; fax: (+44) 1223-336-033; or deposit @ccdc.cam.ac.uk).

[14] Q.-D. Liu, S. Gao, J.-R. Li, Q.-Z. Zhou, K.-B. Yu, B.-Q. Ma, S.-W. Zhang, X.-X. Zhang, T.-Z. Jin, *Inorg. Chem.* **2000**, *39*, 2488.

Protein-Protein Interactions

Design and Application of an α-Helix-Mimetic Scaffold Based on an Oligoamide-Foldamer Strategy: Antagonism of the Bak BH3/Bcl-xL Complex**

*Justin T. Ernst, Jorge Becerril, Hyung Soon Park, Hang Yin, and Andrew D. Hamilton**

The design of low-molecular-weight ligands (< 750 Da) that recognize protein surfaces and subsequently disrupt protein–protein interactions is an area of intense research.[1] Current strategies for identifying small-molecule protein-surface antagonists primarily involve the use of combinatorial methods.

[*] Prof. A. D. Hamilton, J. T. Ernst, J. Becerril, Dr. H. S. Park, H. Yin
Department of Chemistry, Yale University
P.O. Box 208107, New Haven, CT 06520-8107 (USA)
Fax: (+1) 203-432-6144
E-mail: andrew.hamilton@yale.edu

[**] We thank the National Institutes of Health for support of this work.

However, more recently, rational structure-based-design approaches have been presented.[1] Given the ubiquitous role of α helices in mediating protein–protein interactions, we sought to explore the de novo design of scaffolds that present side-chain functionality with similar distance and angular constraints to that found along one face of an α-helical secondary structure.[2] Herein we report a new class of proteomimetics based on a novel oligoamide foldamer; these structures serve as surface mimetics of the Bak BH3 domain. Analogues were identified by means of a fluorescence polarization assay and shown to bind Bcl-xL protein with low micromolar affinity and disrupt the Bak BH3/Bcl-xL complex.

The critical interactions for α-helix recognition often involve the side chains of the *i*, $i+3$ and/or $i+4$, and $i+7$ positions, which constitute one face of the helix. The goal of a designed helix mimetic is to provide a rigid preorganized framework from which functional groups are projected in such a way to resemble these key residues closely. Other criteria for mimetic design include a modular synthesis and moderate aqueous solubility.

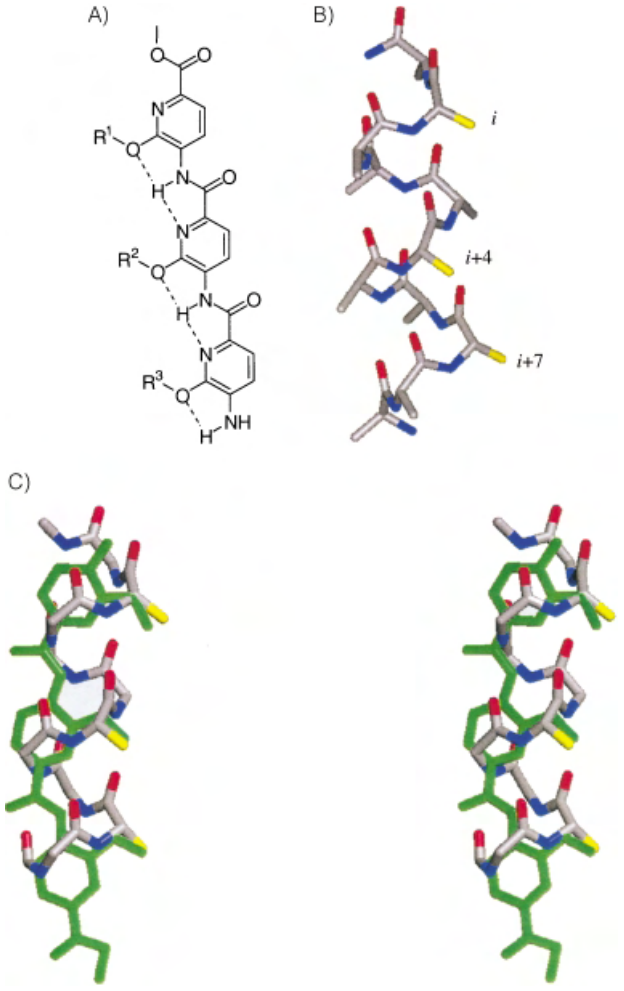


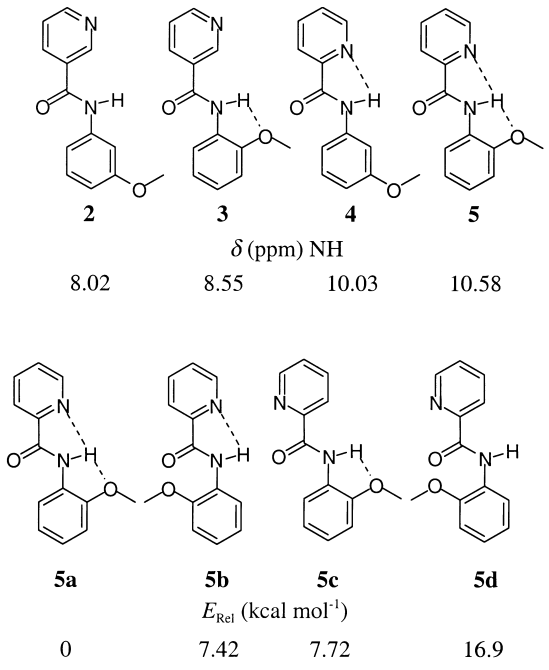
Figure 1. A) Structure of **1**. B) Polyalanine α-helix (the *i*, $i+4$, and $i+7$ side chains are shown in yellow). C) Stereoview of the rms difference overlay of a polyalanine α-helix (*i*, $i+4$, and $i+7$ positions) and **1a** (green).

A trispyridylamide scaffold **1** was designed as an α-helix mimetic. The structure assumes a preferred conformation in which all three functional groups are projected on the same face of the molecule. This preorganization is accomplished through a stabilizing bifurcated hydrogen-bonding network as well as through the minimization of destabilizing alternative conformations (Figure 1 A).

To probe this unique arrangement of noncovalent bonding, model systems **2**–**5** were synthesized and studied by means of ^{1}H NMR spectroscopy (1 mM in $CDCl_3$). The resonance for the amide hydrogen of **5** is concentration-independent and also shifted downfield relative to the corresponding NH signals of **3** and **4** ($\delta = 8.55$ and 10.03 ppm, respectively), each containing one potential hydrogen bond, and **2** ($\delta = 8.02$ ppm), which lacks hydrogen-bonding potential altogether (Scheme 1). Molecular-mechanics calculations (MM2) gave relative energies for the different planar conformations of **5** and these confirmed that **5a** is substantially preferred over **5b**–**5d**, which have unfavorable electrostatic interactions in addition to decreased hydrogen bonding.

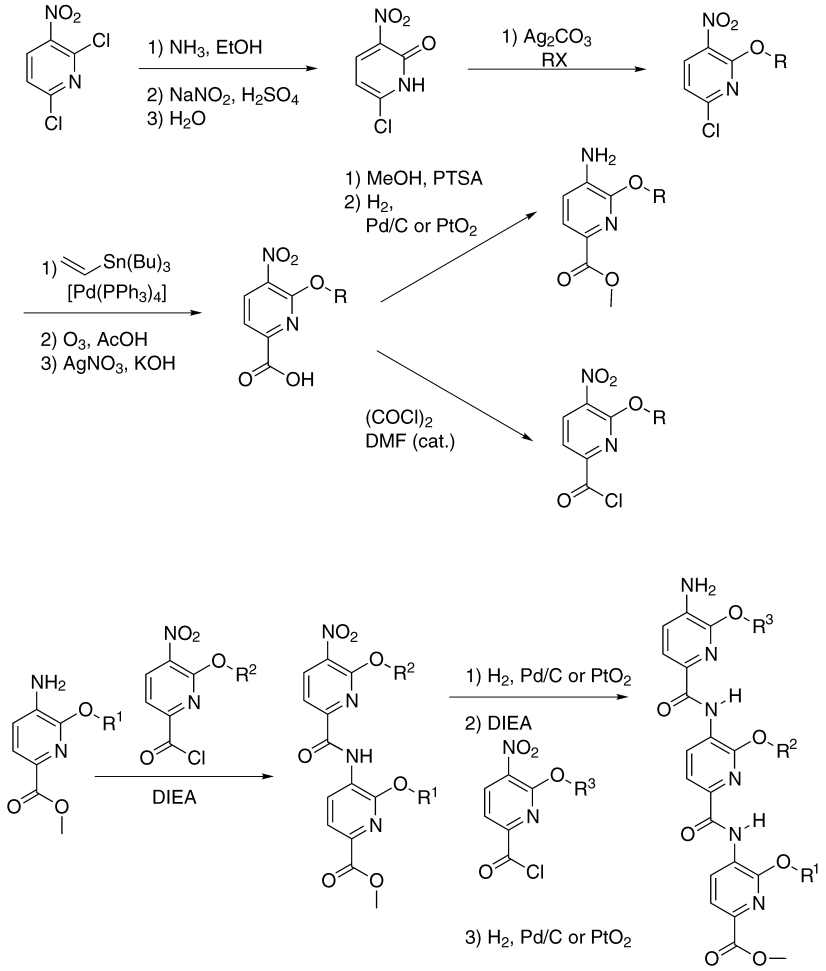
MM2 energy minimization of **1a** (R_1, R_2, R_3 = Me) showed the polyamide backbone to be quite planar. The alkoxy side chains, however, are rotated approximately 45° out of the plane of the carboxamide backbone, presumably to optimize the position of the lone pairs of electrons on the oxygen atom of the ether functionalities for hydrogen bonding. Overlaying the α and β positions of the *i*, $i+4$, and $i+7$ alanine methyl groups of an α helix (Figure 1 B) with the corresponding side-chain atoms of a low-energy conformation of **1a** shows close correspondence of the two structures (Figure 1 C, root-mean-square deviation = 0.94 Å).

The modular synthesis of derivatives of **1** (**1a**–**1e**) is shown in Scheme 2. The different monomers can be easily



Scheme 1. Analogues of **1** used in model studies.

 © 2003 Wiley-VCH Verlag GmbH & Co. KGaA, Weinheim 1433-7851/03/4205-0536 $ 20.00+.50/0



1a: R^1, R^2, R^3 = Me
1b: R^1, R^2, R^3 = *i*Pr
1c: R^1, R^2, R^3 = Bn
1d: R^1, R^3 = *i*Pr; R^2 = Bn
1e: R^1, R^2 = Bn; R^3 = *i*Pr

Scheme 2. Synthesis of derivatives of **1**. DIEA = diisopropylethylamine.

prepared through *O*-alkylation of 6-chloro-3-nitro-2(1*H*)-pyridone with the desired electrophile.[3] Assembly of the pyridyl trimers is accomplished through iterative amide bond formation between the aryl amines and aryl acid chlorides by using standard coupling conditions.

An X-ray crystal structure of nitro derivative **6** shows that the polyamide backbone is indeed planar and that the molecule adopts the expected conformation in which all the isopropoxy side chains are projected from one side of the molecule (Figure 2). The distances between the amide hydrogen atoms and the pyridine nitrogen atoms (2.1 Å) and the oxygen atoms of the side chains (2.2 Å) are consistent with the formation of four five-membered hydrogen-bonding rings within the structure. The torsional angles of the alkoxy side chains in the solid state are 4°, 0°, and 15° out of the plane of the aromatic backbone. Although these angles are less than that predicted by computational analysis, it is assumed that the side chains will be more flexible in solution.

NOESY ^{1}H NMR spectroscopy experiments (20 mM in $CDCl_3$) were conducted to probe the conformation of **6** in solution. Cross peaks were observed between the amide protons and the methine and methyl protons of the isopropoxy side chains. However, no cross peaks were observed between the amide protons and the pyridine 4-protons. Furthermore, variable-temperature ^{1}H NMR spectroscopy experiments from 20 to 125 °C using **1b** (1 mM in CD_2Cl_2) revealed only a 0.12 ppm upfield shift for the signal from the amide protons. Repeating the experiment in [D_6]DMSO also resulted in only a slight upfield shift ($\Delta\delta = -0.95$ ppm). These results suggest that the backbone conformation in which all the alkoxy groups project from the same face of the molecule is adopted, even in a polar solvent. The presence of NOE cross peaks between the side-chain methyl groups and the backbone amide hydrogen atoms suggests that the side chains have some flexibility, enabling the structure to adopt the desired conformations for α-helix mimicry (Figure 1).

To test the trispyridylamides as proteomimetic scaffolds, we studied the complex formed between the BH3 domain of the proapoptotic protein Bak and the antiapoptotic protein Bcl-xL.[4] Bak and Bcl-xL belong to the Bcl-2 family of proteins, which regulates cell death through an intricate balance of homodimer and heterodimer complexes formed within this class of proteins.[5] Overexpression of antiapoptotic proteins such as Bcl-xL and Bcl-2 prevent cells from triggering programmed death pathways and has been linked to a variety of cancers.[5c] A current strategy for developing new anticancer agents is to identify

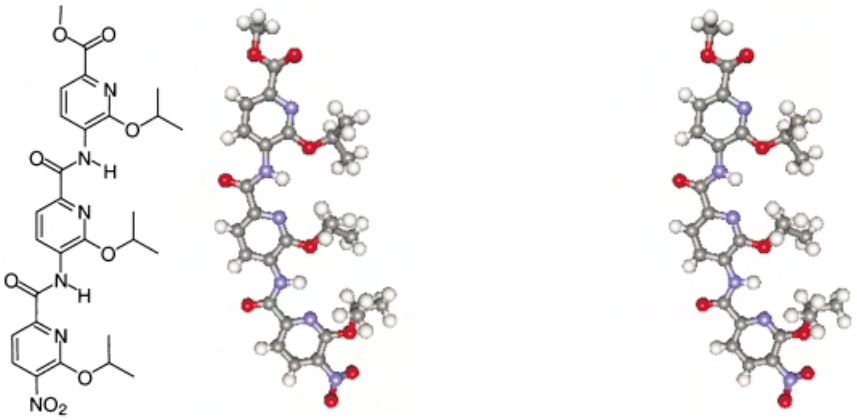


Figure 2. Crystal structure of **6**.

 © 2003 Wiley-VCH Verlag GmbH & Co. KGaA, Weinheim 1433-7851/03/4205-0537 $ 20.00+.50/0

molecules that bind to the Bak-recognition site on Bcl-xL, disrupting the complexation of the two proteins and therefore antagonizing Bcl-xL function.[2a] To date, there have been several reports of small molecules, identified from screening large libraries, that disrupt the Bak BH3/Bcl-xL complex, with the best inhibitors having K_i values in the low micromolar range.[6]

The structure determined by NMR spectroscopy[4] shows the 16 residue BH3 domain peptide from Bak (aa 72 to 87, $K_d \approx 300$ nM) bound in a helical conformation to a hydrophobic cleft on the surface of Bcl-xL, formed by the BH1, BH2, and BH3 domains of the protein. The crucial residues for binding were shown by alanine scanning to be V74, L78, I81, and I85,[4] which project in an i, $i+4$, $i+7$, $i+11$ arrangement from one face of the α-helix. The Bak peptide is a random coil in solution but adopts an α-helical conformation when complexed to Bcl-xL. Studies utilizing stabilized helices of the Bak BH3 domain have shown the importance of this conformation for tight binding.[7]

Molecule **1b** represented our initial design for a Bcl-xL antagonist in which the isopropoxy side chains serve to mimic the key hydrophobic residues of the Bak BH3 domain. Analogues **1a**, and **1c**–**1e** were also prepared to probe the degree of hydrophobicity of the scaffold side chains (Scheme 2). The BH3 domain of another proapoptotic Bcl-2 family member (Bad) has larger hydrophobic groups at these positions (Tyr, Phe) and binds with a higher affinity than Bak to Bcl-xL.[8]

To study the ability of **1a**–**1e** to bind Bcl-xL and disrupt the Bak BH3/Bcl-xL complex, we employed a previously reported fluorescence polarization assay.[8d] Displacement of a fluorescein-labeled Bak BH3 peptide from the Bcl-xL complex by competitive binding of a small molecule will lead to a reduction in polarization. Taking into account the known binding affinity of the Bak peptide, the change in polarization can be used to calculate the binding affinity of the inhibitor. Using this assay, compounds **1b, 1d**, and **1e** (Scheme 2) were found to inhibit the Bak BH3/Bcl-xL complex successfully, binding to Bcl-xL with low micromolar affinity (K_i values of 2.3, 9.8, and 1.6 μM, respectively).[9] Molecule **1c** (Scheme 2), which contains three benzyloxy side chains, showed reduced affinity ($K_i > 20$ μM) for the hydrophobic pocket of Bcl-xL. Finally, the trismethoxy derivative **1a** as well as the isopropoxy dimer **7** (Scheme 3) showed no observed binding below a concentration of 25 μM.

To probe the mode of binding of **1b**, molecular-docking studies were completed using the structure of Bcl-xL present in the Bak BH3/Bcl-xL complex. The conformational flexibility of the side chains in **1b** was taken into account and the different binding modes were ranked using an energy-scoring function. The results of this study suggest that molecule **1b** binds into the same hydrophobic cavity as Bak (Figure 3).

The initial success of trimer **1b** suggested that extending the design to include four isopropoxy subunits would improve binding, since the tetramer **8** (Scheme 3) would have the potential to mimic all the key hydrophobic residues of Bak used for binding (V74, L78, I81, I85). Computational docking studies suggested that the preferred mode of binding of **8** is in the hydrophobic pocket with the isopropoxy side chains

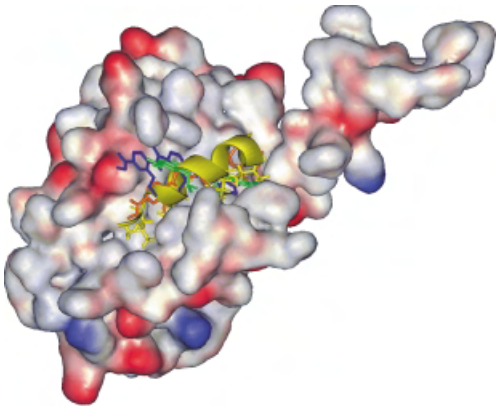
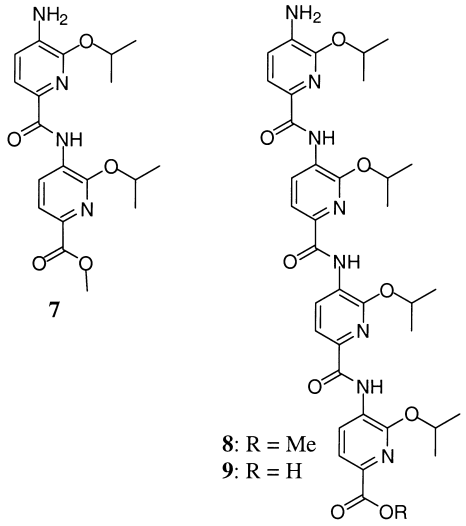


Figure 3. Results of the molecular-docking studies of **1b** and Bcl-xL. The three highest-ranked binding modes are shown: green (rank 1), orange (rank 2), and blue (rank 3). The Bak BH3 peptide (yellow) is overlayed with the docked structures. The key hydrophobic side chains of Bak are shown as stick representations (V74, L78, I81, I85).



Scheme 3. Dimeric (**7**) and tetrameric (**8, 9**) analogues of **1.**

having an analogous spatial arrangement to the four key alkyl side chains of Bak. Unfortunately, **8** proved to be insoluble under the experimental conditions of the fluorescence polarization assay. To improve the aqueous solubility of this system, the methyl ester was hydrolyzed to yield the free acid derivative **9**. Although compound **9** mimics all four key hydrophobic side chains of Bak, it shows a slightly lower affinity ($K_i = 4.17$ μM) for Bcl-xL than does trimer **1b**.

In summary, a new scaffold for mimicking the surface functionality of an α helix was designed using a novel polyamide foldamer. The mimetic strategy was applied to the synthesis of antagonists of the Bak BH3/Bcl-xL complex. Results from fluorescence polarization experiments suggest that three trimer analogues (**1b, 1d**, and **1e**) have a low micromolar affinity for Bcl-xL and inhibit its interaction with Bak. Extension of the design to include four pyridyl subunits (i.e. **9**) failed to improve the binding affinity of the mimetic

 © 2003 Wiley-VCH Verlag GmbH & Co. KGaA, Weinheim 1433-7851/03/4205-0538 $ 20.00+.50/0

system. Molecular-docking studies suggest that the inhibitors bind into the Bak-recognition site on the surface of Bcl-xL.

Received: May 21, 2002
Revised: October 22, 2002 [Z19346]

[1] a) P. L. Toogood, *J. Med. Chem.* **2002**, *45*, 1–16; b) A. G. Cochran, *Curr. Opin. Chem. Biol.* **2001**, *5*, 654–659.
[2] For examples of α-helix mimetics, see: a) O. Kutzki, H. S. Park, J. T. Ernst, B. P. Orner, H. Yin, A. D. Hamilton, *J. Am. Chem. Soc.* **2002**, *124*, 11832–11839; b) J. T. Ernst, O. Kutzki, A. K. Debnath, S. Jiang, H. Lu, A. D. Hamilton, *Angew. Chem.* **2002**, *114*, 288–291; *Angew. Chem. Int. Ed.* **2002**, *41*, 278–281; c) B. P. Orner, J. T. Ernst, A. D. Hamilton, *J. Am. Chem. Soc.* **2001**, *123*, 5382–5383; d) H. Xuereb, M. Maletic, J. Gildersleeve, I. Pelczer, D. Kahne, *J. Am. Chem. Soc.* **2000**, *122*, 1883–1890; e) W. P. Nolan, G. S. Ratcliffe, D. C. Rees, *Tetrahedron Lett.* **1992**, *33*, 6879–6882.
[3] G. C. Hopkins, J. P. Jonak, H. J. Minnemeyer, H. Tieckelmann, *J. Org. Chem.* **1967**, *32*, 4040–4044.
[4] M. Sattler, H. Liang, D. Nettesheim, R. P. Meadows, J. E. Harlin, M. Eberstadt, H. S. Yoon, S. B. Shuker, B. S. Chang, A. J. Minn, C. B. Thompson, S. W. Fesik, *Science* **1997**, *275*, 983–986.
[5] a) M. C. Raff, *Science* **1994**, *264*, 668–669; b) D. T. Chao, S. J. Korsmeyer, *Annu. Rev. Immunol.* **1998**, *16*, 395–419; c) C. B. Thompson, *Science* **1995**, *267*, 1456–1462; d) L. L. Rubin, K. L. Philpott, S. F. Brooks, *Curr. Biol.* **1993**, *3*, 391–394.
[6] a) I. J. Enyedy, Y. Ling, K. Nacro, Y. Tomita, X. Wu, Y. Cao, R. Guo, B. Li, X. Zhu, Y. Huang, Y.-Q. Long, P. P. Roller, D. Yang, S. Wang, *J. Med. Chem.* **2001**, *44*, 4313–4324; b) A. Degterev, A. Lugovskoy, M. Cardone, B. Mulley, G. Wagner, T. Mitchison, J. Yuan, *Nat. Cell Biol.* **2001**, *3*, 173–182; c) S.-P. Tzung, K. M. Kim, G. Basanez, C. D. Giedt, J. Simon, J. Zimmerberg, K. Y. J. Zhang, D. M. Hockenbery, *Nat. Cell Biol.* **2001**, *3*, 183–191; d) J.-L. Wang, D. Liu, Z.-J. Zhang, S. Shan, X. Han, S. M. Srinivasula, C. M. Croce, E. S. Alnemri, Z. Huang, *Proc. Natl. Acad. Sci. USA* **2000**, *97*, 7124–7129.
[7] J. W. Chin, A. Schepartz, *Angew. Chem.* **2001**, *113*, 3922–3925; *Angew. Chem. Int. Ed.* **2001**, *40*, 3806–3809.
[8] A. M. Petros, D. G. Nettesheim, Y. Wang, E. T. Olejniczak, R. P. Meadows, J. Mack, K. Swift, E. D. Matayoshi, H. Zhang, C. B. Thompson, S. W. Fesik, *Protein Sci.* **2000**, *9*, 2528–2534;b) A. Kelekar, B. S. Chang, J. E. Harlan, S. W. Fesik, C. B. Thompson, *Mol. Cell. Biol.* **1997**, *17*, 7040–7046.
[9] The protein-binding experiments were carried out by diluting a solution of the helix mimetic in DMSO into an aqueous buffer solution (25°, 10 mM PBS, pH 7.4) of Bcl-xL and the fluorescently labeled Bak peptide.

Theory of Pyramidal Boron

Stabilization of Tricoordinate Pyramidal Boron: Theoretical Studies on $CBSiH_5$, BSi_2H_5, $CBGeH_5$, and $CBSnH_5$**

*Kalathingal T. Giju, Ashwini Kumar Phukan, and Eluvathingal D. Jemmis**

The dramatic computational discoveries[1] and experimental realizations[2] of planar tetracoordinate carbon and planar tetracoordinate boron[3] species have set the stage for other rule-breaking structures. Preference for the trigonal planar arrangement in carbenium ions and tricoordinate boron species is one of the tenets of main-group chemistry that remains unchallenged. An unconstrained pyramidal carbenium ion or its boron equivalent has, so far, remained elusive. We report here, for the first time, the computational[4] discovery of a neutral-ground-state molecule, silaborirane **1**, which contains a tricoordinate pyramidal boron center. The conventional planar geometry **2** is a transition state with the imaginary frequency corresponding to pyramidalization around the boron atom. Similar results are obtained when the Si atom in **1** is replaced by Ge and Sn.

Structure **1** is derived from the C_{2v} cyclopropyl cation **3**, which is calculated to be a transition state.[5a,b] Replacement of $\{CH\}^+$ by $\{BH\}$ leads to borirane **4**, which is a minimum with a trigonal planar boron center.[5c] Replacement of one CH_2 group by an SiH_2 group yields a three-membered ring comprised of three different atoms. Its conventional structure (**2**), with a planar tricoordinate boron atom, is calculated to be a transition state with an imaginary frequency (331.4 cm^{-1} at B3LYP/6-311 + G**);[6] this leads to the minimum-energy structure **1** with a pyramidal arrangement at the boron center, which is lower in energy by 2.4 kcal mol^{-1}. This energy difference increases to 4.1 kcal mol^{-1} at the CCSD(T)/6-311 + G**level of theory.[7–9]

Pyramidalization at the boron center causes substantial changes in the structure (Figure 1). In order to understand these changes, the structures **1** and **2** are visualized from different perspectives. While there is very little change in the H-Si-H and H-C-H angles of **1** and **2**, the H-Si-C and H-C-Si angles change on the transition from **2** to **1**, which is indicative of an unusual twisting of the CH_2 and SiH_2 groups with respect to each other (Table 1).

By symmetry, the pairs of angles H-Si-C (116.8°), H-C-Si (119.7°), and H-Si-B (122.2°) are the same in **2**. However in **1**,

[*] Prof. Dr. E. D. Jemmis, Dr. K. T. Giju, A. K. Phukan
School of Chemistry
University of Hyderabad
Hyderabad – 500 046 (India)
Fax: (+91) 40-301-2460
E-mail: jemmis@uohyd.ernet.in

[**] This work was supported by the Board of Research in Nuclear Sciences, Mumbai, Department of Science and Technology, and the University with Potential for Excellence Program of the University Grants Commission, New Delhi, India. A.K.P. thanks CSIR for a Senior Research Fellowship.

Table 1: Geometric parameters of [Cy(CH_2)(SiH_2)(B–H)] calculated at the CCSD(T)/6-311+G** level of theory. Bond lengths are in Å and angles are in degrees. The numbers in italics indicate the Wiberg Bond Index (WBI).

Molecule	B–C	B–Si	C–Si	H-Si-H	H-C-H	H1-Si-C	H2-Si-C	H3-C-Si	H4-C-Si
$CBSiH_5$ (**1**, C_1)	1.498	1.912	2.107	110.2	111.8	99.5	125.2	86.7	137.9
	1.303	*1.115*	*0.601*						
$CBSiH_5$ (**2**, C_s)	1.573	1.971	1.903	113.5	110.4	116.8		119.7	
	0.946	*0.986*	*0.828*						

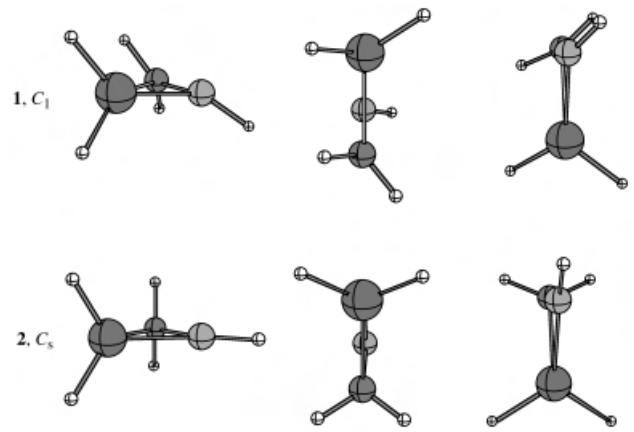


Figure 1. Structures of **1** and **2** viewed from different angles. The top row represents structure **1** with a pyramidal boron atom. The corresponding view of **2** with a trigonal planar boron atom is given below for comparison.

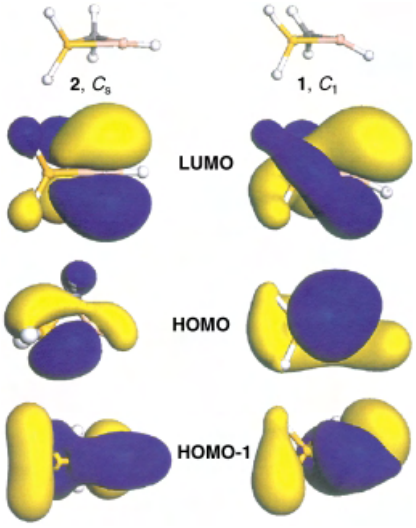


Figure 2. Frontier MOs corresponding to the planar (**2**) and pyramidal (**1**) structure: B (pink); Si (yellow); C (gray); H (white).

one of the H atoms attached to the silicon center moves closer to the CH_2 group and the other H atom moves away from it (H1-Si-C = 99.5°; H2-Si-C = 125.2°). A similar change is noticed at the CH_2 moiety. In addition, the SiH_2 group rotates by a few degrees around a hypothetical axis perpendicular to the SiH_2 plane and passing through the Si atom, so that the two H-Si-B angles are 125.9 and 123.2°. In this process the nature of the C–Si bonding changes considerably. What was nearly an sp^3–sp^3 bond in $CSiBH_5$ now becomes an almost pure p–p bond (Table 2), which leads to an elongation of the C–Si bond to 2.109 Å. Correspondingly there is an increase in the s character of the C–B and Si–B bonds, which corresponds to a reduction in their bond lengths.

A bonding description of structures **1** and **2** can be obtained in terms of Walsh orbitals.[10] The planar C_s structure **2** has two Walsh orbitals along the periphery of the ring (HOMO and HOMO-1, Figure 2). The LUMO is a p orbital on the boron center, which is perpendicular to the C-Si-B plane. There is a hyperconjuagative stabilization of the π-type CH_2 and SiH_2 orbitals by the boron p orbital (not indicated in the Figure). One of the Walsh orbitals of structure **1** is stabilized by bringing the vacant boron p orbital (the LUMO of **2**) into a bonding form. This is achieved by reorienting the SiH_2 group as a whole, so that the sp hybrid on SiH_2 can interact with the new sp hybrid on the boron atom, which is pyramidalized (HOMO of **1**, Figure 2). Pyramidalization, therefore, is an attempt to involve the vacant p orbital on the boron atom in bonding to the Si atom. This behavior leads to the structural reorganizations that are shown in Figure 1. Such a process is not attractive in borirane (C_2BH_5) as the strong C–C bond determines the structure. An equivalent description of the bonding in **1** can be constructed by dividing **1** into SiH_2 and $H_2C{=}BH$ fragments (Scheme 1a) and b)). The empty p_π orbital on SiH_2 receives electrons from the π MO of $H_2C{=}BH$, which are concentrated on the carbon atom (Scheme 1c). The second interaction involves the donation of

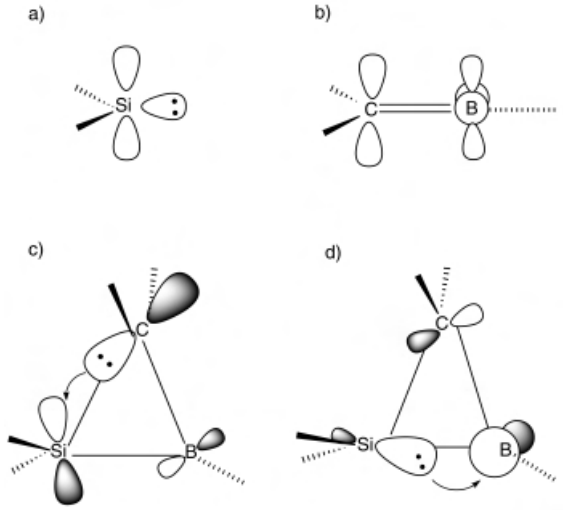
Table 2: Hybridization of the B–C, B–Si, and C–Si bonds in **1** and **2** at the B3LYP/6–311+G** level of theory using the NBO method.[11]

Molecule	Bond X–Y	Occupancy	%X	%s (X)	%p (X)	%Y	%s (Y)	%p (Y)
$CBSiH_5$ (**1**, C_1)	B–C	1.98	33.2	31.7	67.9	66.8	39.2	60.6
	B–Si	1.96	48.5	27.6	71.9	51.5	34.2	65.3
	C–Si	1.68	70.8	8.6	91.1	29.2	8.6	90.0
$CBSiH_5$ (**2**, C_s)	B–C	1.98	32.2	28.5	71.2	67.8	28.7	71.1
	B–Si	1.97	51.6	28.6	71.1	48.4	24.4	75.0
	C–Si	1.97	70.1	21.3	78.5	29.9	17.9	81.0

 © 2003 Wiley-VCH Verlag GmbH & Co. KGaA, Weinheim 1433-7851/03/4205-0540 $ 20.00+.50/0

Table 3: Total energies (including zero-point vibrational energy (ZPVE) correction) of the planar (**2**), allyl (**5**), and pyramidal (**1**) isomers of [Cy(CH_2)(SiH_2)(B–H)] calculated at various level of theory. Values in parentheses indicate the number of imaginary frequencies. E_{rel} (kcal mol^{-1}) is the energy difference between the planar and pyramidal isomers. θ is the pyramidalization angle at boron, given in degrees.

	Planar (**2**)	Allyl (**5**)	Pyramidal (**1**)	E_{rel}	θ
HF/6-31G*	−354.23407 (1)	−354.21118 (1)	−354.23387 (0)	−0.1	0.5
HF/6-311+G**	−354.27551 (1)	−354.25660 (1)	−354.27518 (0)	−0.2	1.5
MP2/6-31G*	−354.51730 (1)	−354.50932 (1)	−354.52106 (0)	2.4	19.0
B3LYP/6-31G*	−355.32435 (1)	−355.31846 (1)	−355.32781 (0)	2.2	17.3
B3LYP/6-311+G**	−355.37132 (1)	−355.36744 (1)	−355.37513 (0)	2.4	16.5
B3LYP/LANL2DZ	−69.69861 (1)	−69.69574 (1)	−69.69843 (0)	−0.1	14.1
CCSD(T)/6-311+G**	−354.71997(1)	−354.71749 (1)	−354.72653 (0)	4.1	18.2



Scheme 1.

the lone pair on SiH_2 to the vacant hybridized orbital on the boron atom (Scheme 1d).

In view of the novelty of these results, we have carried out the optimization of **1** and **2** at the following levels of theory: HF/6-31G*, HF/6-311+G**, MP2/6-31G*,[5b] B3LYP/6-31G*, B3LYP/6-311+G**, B3LYP/LANL2DZ,[6] and CCSD(T)/6-311+G**.[7–9] At all of these levels the C_1 structure with a pyramidal geometry is found to be a minimum (Table 3). At the HF/6-31G* and HF/6-311+G** levels, the pyramidalization angle θ (calculated as 360° minus the sum of the three angles around boron) is 0.5 and 1.5°, respectively, which makes the energy difference between **1** and **2** negligible. An allyl-type structure **5** is also calculated because the allyl cation **6** is more stable than the cyclopropyl cation **3**. At all levels, **5** is calculated to be higher in energy than either **1** or **2**.

If the incentive for pyramidalization at the boron center is to involve the p orbital of B into Si–B bonding, substituents on boron, that donate electrons to the vacant p orbital, and thus make it less available for bonding, must reduce pyramidalization. We have calculated (B3LYP/6-311+G**)[6] the geometries of the derivatives of **1** and **2** where the hydrogen atom attached to boron is replaced by SiH_3, CH_3, and F (Table 4). The pyramidalization angle at the boron center decreases in going from H to F (H (16.5°) > SiH_3 (14.7°) > CH_3 (11.1°) > F (8.8°)). Thus, electron donation through π or pseudo-π orbitals decreases the tendency to pyramidalize.

Table 4: Geometric parameters and relative energies (including ZPVE correction) of [Cy(CH_2)(SiH_2)-(B-R)] (R = H, SiH_3, CH_3, and F) calculated at the B3LYP/6-311+G** level of theory. Bond lengths are in Å and angles are in degrees; WBI values are in parentheses.

Bond		R = H	SiH_3	CH_3	F
B–C	C_1	1.481 (1.331)	1.482 (1.369)	1.502 (1.20)	1.515 (1.082)
	C_s	1.551 (1.000)	1.557 (0.985)	1.553 (0.976)	1.539 (0.988)
B–Si	C_1	1.911 (1.117)	1.916 (1.114)	1.943 (1.043)	1.947 (1.000)
	C_s	1.966 (0.980)	1.982 (0.959)	1.977 (0.964)	1.955 (0.983)
C–Si	C_1	2.109 (0.617)	2.103 (0.573)	2.023 (0.680)	1.988 (0.749)
	C_s	1.904 (0.856)	1.894 (0.848)	1.912 (0.837)	1.943 (0.816)
θ	C_1	16.5	14.7	11.1	8.8
	C_s	0.0	0.0	0.0	0.0
E_{rel}	C_1	0.0	0.0	0.0	0.0
	C_s	2.4	2.2	0.5	−0.1

Table 5: Total energies (including ZPVE correction) of [Cy(SiH_2)(SiH_2)(B–H)] isomers calculated at various levels of theory. Values in the parentheses indicate the number of imaginary frequencies. E_{rel} (kcal mol^{-1}) is the energy difference between the planar and pyramidal isomers. θ is the pyramidalization angle at boron, given in degrees.

	Planar	Allyl	Pyramidal	E_{rel}	θ
HF/6-31G*	−605.27179 (0)	−605.27199 (1)	−605.27310 (0)	0.8	22.8
HF/6-311+G**	−605.32475 (0)	−605.32671 (1)	−605.32765 (0)	1.8	21.4
MP2/6-31G*	−605.50241 (1)	−605.52265 (1)	−605.52333 (0)	13.1	17.0
B3LYP/6-31G*	−606.70217 (2)	−606.71952 (1)	−606.71932 (0)	10.8	8.1
B3LYP/6-311+G**	−606.76040 (1)	−606.77952 (0)	–	[a]	
B3LYP/LANL2DZ	−35.46612 (1)	−35.48618 (0)	–	[a]	
CCSD(T)/6-311+G**	−605.71564	−605.73714	−605.73842	14.3	14.4

[a] Leads to the allyl structure.

 © 2003 Wiley-VCH Verlag GmbH & Co. KGaA, Weinheim 1433-7851/03/4205-0541 $ 20.00+.50/0

Table 6: Relative energies (in kcal mol^{-1}) of [Cy(CH_2)(B-H)(YH_2)] (Y = Si, Ge, Sn) with pyramidal (C_1) and planar (C_s) boron atoms, calculated at the B3LYP/LANL2DZ level of theory. θ is the pyramidalization angle at boron, given in degrees.

		Si	Ge	Sn
E_{rel} + ZPVE	C_1	0	0.0	0.0
	C_s	−0.1	6.5	11.2
θ	C_1	14.1	7.7	6.5

If one Si atom causes pyramidalization, two of them should enhance the effect. We have calculated the Si_2BH_5 structure at various levels and found it to have a C_s structure (**7**) with a pyramidal boron atom. The corresponding C_{2v} structure (**8**) with a planar boron center is found to be higher in energy. The calculated value of θ is larger than that of **1**. The energy differences are also found to be considerably higher (Table 5).

The heavier group 14 elements, Ge and Sn, must also influence the pyramidalization of boron. Calculations at the B3LYP/LANL2DZ level show that θ decreases as Si (14.1°) is replaced by Ge (7.7°) or Sn (6.5°; Table 6). However, the inversion barrier increases in going from Si (0.7) to Ge (7.5) to Sn (12.7 kcal mol^{-1}). The unexpected nonplanar arrangement of the tricoordinate boron center in **1** provides another demonstration of the many novel structural patterns that the heavier elements of the main group can contribute to the first-row elements, and invites experimental verification.

Received: July 4, 2002
Revised: October 22, 2002 [Z19666]

[1] a) R. Hoffmann, R. W. Alder, C. F. Wilcox, Jr., *J. Am. Chem. Soc.* **1970**, *92*, 4992; b) J. B. Collins, J. D. Dill, E. D. Jemmis, Y. Apeloig, P. v. R. Schleyer, R. Seeger, J. A. Pople, *J. Am. Chem. Soc.* **1976**, *98*, 5419; c) D. R. Rasmussen, L. Radom, *Angew. Chem.* **1999**, *111*, 3051; *Angew. Chem. Int. Ed.* **1999**, *38*, 2875; d) Z.-X. Wang, P. von R. Schleyer, *J. Am. Chem. Soc.* **2001**, *123*, 994.

[2] a) D. Röttger, G. Erker, *Angew. Chem.* **1997**, *109*, 840; *Angew. Chem. Int. Ed. Engl.* **1997**, *36*, 812; b) W. Siebert, A. Gunale, *Chem. Soc. Rev.* **1999**, *28*, 367; c) X. Li, L. S. Wang, A. I. Boldyrev, J. Simons, *J. Am. Chem. Soc.* **1999**, *121*, 6033; d) L. S. Wang, A. I. Boldyrev, X. Li, J. Simons, *J. Am. Chem. Soc.* **2000**, *122*, 7681; e) *Chem. Eng. News* **2000**, *78* (34), 8.

[3] a) C. Präsang, A. Mlodzianowska, Y. Sahin, M. Hofmann, G. Geiseler, W. Massa, A. Berndt, *Angew. Chem.* **2002**, *114*, 3529; *Angew. Chem. Int. Ed.* **2002**, *41*, 3380; b) C. Präsang, M. Hofmann, G. Geiseler, W. Massa, A. Berndt, *Angew. Chem.* **2002**, *114*, 1597; *Angew. Chem. Int. Ed.* **2002**, *41*, 1526; c) A. Maier, M. Hofmann, H. Pritzkow, W. Siebert, *Angew. Chem.* **2002**, *114*, 1600; *Angew. Chem. Int. Ed.* **2002**, *41*, 1529.

[4] Gaussian 94, M. J. Frisch, G. W. Trucks, H. B. Schlegel, P. M. W. Gill, B. G. Johnson, M. A. Robb, J. R. Cheeseman, T. Keith, G. A. Petersson, J. A. Montgomery, K. Raghavachari, M. A. Al-Laham, V. G. Zakrzewski, J. V. Ortiz, J. B. Foresman, J. Cioslowski, B. B. Stefanov, A. Nanayakkara, M. Challacombe, C. Y. Peng, P. Y. Ayala, W. Chen, M. W. Wong, J. L. Andres, E. S. Replogle, R. Gomperts, R. L. Martin, D. J. Fox, J. S. Binkley, D. J. Defrees, J. Baker, J. P. Stewart, M. Head-Gordon, C. Gonzalez, J. A. Pople, Gaussian Inc., Pittsburgh, PA, **1995**.

[5] a) L. Radom, P. C. Hariharan, J. A. Pople, P. v. R. Schleyer, *J. Am. Chem. Soc.* **1973**, *95*, 6531; b) W. A. Hehre, L. Radom, P. v. R. Schleyer, J. A. Pople, *Ab Initio Molecular Orbital Theory*, Wiley, New York, **1986**; c) M. Bühl, P. von R. Schleyer, M. A. Ibrahim, T. Clark, *J. Am. Chem. Soc.* **1991**, *113*, 2466.

[6] a) A. D. Becke, *J. Chem. Phys.* **1993**, *98*, 5648; b) A. D. Becke, *Phys. Rev. A* **1988**, *38*, 3098; c) C. Lee, W. Yang, R. G. Parr, *Phys. Rev. B* **1988**, *37*, 785; d) P. J. Hay. W. R. Wadt, *J. Chem. Phys.* **1985**, *82*, 299.

[7] G. D. Purvis, R. J. Bartlett, *J. Chem. Phys.* **1982**, *76*, 1910.

[8] K. Raghavachari, G. W. Trucks, J. A. Pople, M. Head-Gordon, *Chem. Phys. Lett.* **1989**, *157*, 479.

[9] R. J. Bartlett, J. D. Watts, S. A. Kucharski, J. Noga, *Chem. Phys. Lett.* **1990**, *165*, 513.

[10] a) A. D. Walsh, *Nature* **1947**, *159*, 712; b) A. D. Walsh, *Trans. Faraday Soc.* **1949**, *45*, 179.

[11] a) A. E. Reed, R. B. Weinstock, F. Weinhold, *J. Chem. Phys.* **1985**, *83*, 735; b) A. E. Reed, F. Weinhold, *J. Chem. Phys.* **1983**, *83*, 1736; c) A. E. Reed, F. Weinhold, L. A. Curtiss, *Chem. Rev.* **1988**, *88*, 899.

Ship-in-Bottle Photochemistry

ℝPM-1: A Recyclable Nanoporous Material Suitable for Ship-In-Bottle Synthesis and Large Hydrocarbon Sorption**

*Long Pan, Haiming Liu, Xuegong Lei, Xiaoying Huang, David H. Olson, Nicholas J. Turro, and Jing Li**

Zeolites and related molecular sieves, which contain rigid frameworks and accessible internal channels and/or cages, have been dominating the porous material world for a long time, because of their widespread applications in catalytic and separation science.[1,2] Although there is an increasing demand for materials with tunable structures, the structural design of zeolites is limited by their requirement for

[*] Prof. J. Li, Dr. L. Pan, X. Huang
Department of Chemistry and Chemical Biology
Rutgers University
Piscataway, NJ 08854 (USA)
Fax: (+1) 732-445-5312
E-mail: jingli@rutchem.rutgers.edu
Dr. H. Liu, Prof. D. H. Olson
Department of Chemical Engineering
University of Pennsylvania
Philadelphia, PA 19104 (USA)
Dr. X. Lei, Prof. N. J. Turro
Department of Chemistry
Columbia University
New York, NY 10027 (USA)

[**] The Rutgers University team is grateful to the National Science Foundation for its generous support (MDR-0094732). This work was supported in part by the MRSEC Program of the National Science Foundation under Award Number DMR-9809687, and by the National Science Foundation and the Department of Energy under Grant No. NSF CHE9810367 to the Environmental Molecular Sciences Institute at Columbia University.

 © 2003 Wiley-VCH Verlag GmbH & Co. KGaA, Weinheim 1433-7851/03/4205-0542 $ 20.00+.50/0

tetrahedral oxide skeletons. Another impediment in the applications of zeolites is the difficulty in framework dissolution or removal, which is required for ship-in-bottle synthesis.[3] In such a reaction, synthesis is conducted within the internal framework of the zeolite to produce a product (ship) that is difficult to remove from the pores of the zeolite internal surface (bottle) for some technical reason. In most of these cases, concentrated acids or bases must be used to "break the bottle", that is, to remove or dissolve the host framework. Such a harsh processes may not only rupture the framework but also cause severe damage to the products.[4,5]

Recently, organometallic materials have demonstrated great potential as zeolite mimics, with some properties of the mimic being superior to those of zeolites. For example, highly porous organometallic structures can be rationally synthesized and tuned by a suitable choice of organic ligands and metal ions to control their framework architecture and functionality.[6,7] However, it remains a challenge to synthesize reversibly recyclable systems in which the frameworks can be effectively removed and rebuilt. We have met this challenge through the synthesis of a thermally stable, 3D nanoporous organometallic material, IRPM-1 (Rutgers Recyclable Porous Materials) via a nonporous 1D precursor. This compound has demonstrated a strong capability in sorption of large hydrocarbons and outstanding shape selectivity in the photolysis of *ortho*-methyldibenzylketone (*o*-MeDBK), to give a cage effect of 100% of the α-cleavage products, and a high yield of the cyclization product. By breaking the framework of IRPM-1, a mass balance of 100% is achieved. Thus, not only does IRPM-1 demonstrate a similar (or better) performance in sorption and catalysis than some of the most commonly used zeolites (ZSM-5, X, and Y), but it is also the first recyclable organometallic nanoporous compound whose framework (the bottle) can be completely broken down under mild conditions to allow a full recovery of photochemical products (the ship; see Figure 1).

The targeted 3D network was prepared from a previously reported 1D structure, $[Co(bpdc)(H_2O)_2]\cdot H_2O$ (bpdc = biphenyldicarboxylate).[8] A key earlier observation was that all materials, 1D or 2D, which belong to a Co–bpdc–py (py = pyridine) family readily convert to this 1D compound when immersed in water, regardless of their initial dimensionality.[8] This remarkable feature is highly desirable for designing a recyclable process in which 1) an open 3D framework is made from the nonporous 1D $[Co(bpdc)(H_2O)_2]\cdot H_2O$ phase (hereafter referred to as the precursor) by substitution of an ancillary water molecule in the precursor with a bpy ligand (bpy = 4,4′-bipyridine) and 2) the open 3D framework is readily broken down and converted back into the precursor when immersed in water.

$[Co_3(bpdc)_3(bpy)]\cdot 4DMF\cdot H_2O$ (hereafter referred to as IRPM-1) was synthesized by a solvothermal reaction. The product, IRPM-1, remained stable in common organic solvents. When immersed in water, IRPM-1 quickly and quantitatively converted into the precursor. Upon heating the precursor in DMF and bpy, IRPM-1 was recovered in high yield [Eq. (1)].

$$\underset{\text{(precursor)}}{[Co(bpdc)(H_2O)_2]\cdot H_2O + bpy} \underset{H_2O,\ RT}{\overset{DMF,\ 150^\circ C}{\rightleftharpoons}} \underset{\text{(RPM-1)}}{[Co_3(bpdc)_3bpy]\cdot 4DMF\cdot H_2O} \quad (1)$$

An X-ray structural analysis performed on a single crystal of IRPM-1 revealed a structure possessing a two-fold interpenetrating 3D network constructed with a unique building block, $[Co_3(bpdc)_6]$, as shown in Figure 2.[9] The structure

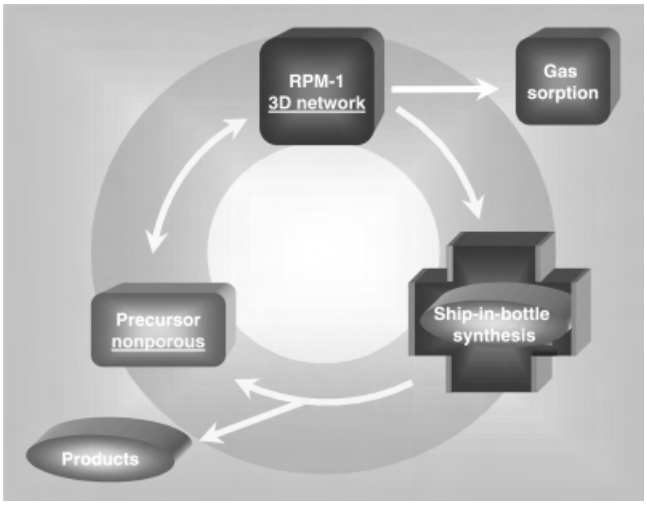


Figure 1. Schematic representation of the recycling process involving IRPM-1.

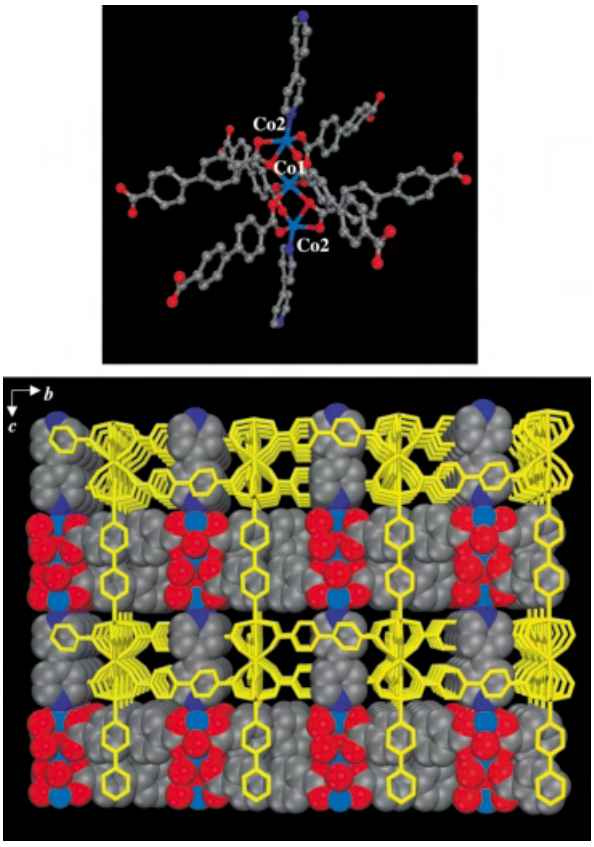


Figure 2. Single crystal structure of IRPM-1. Top: the $[Co_3(bpdc)_6(bpy)_2]$ building unit. Bottom: View down the *a* axis showing two interpenetrating 3D networks. Co (light blue), O (red), N (blue), C (gray).

 © 2003 Wiley-VCH Verlag GmbH & Co. KGaA, Weinheim 1433-7851/03/4205-0543 $ 20.00+.50/0

contains two crystallographically independent cobalt centers. The octahedrally coordinated Co1 is located on the two-fold rotation axis and is connected to two adjacent Co2 centers with distorted trigonal bipyramidal geometry, through six bpdc ligands (Figure 2, top). Each of the two Co1···Co2 pairs is connected through three carboxylate groups by two μ_2 and one μ_3 bonding modes. The Co_3 unit, which acts as a node, is connected to six adjacent nodes through six bpdc ligands to form a 2D layer parallel to the *ab* (*xy*) plane. The remaining coordination sites of the two Co2 centers in each building block are occupied by nitrogen atoms of bpy ligands that act as pillars, and which bind the adjacent 2D layers to generate a pillared 3D framework. Such a pillared 3D structure composed of "double" metal–carboxylate layers (Figure 2, bottom) is rare. Two of these pillared 3D motifs, identical in structure, interpenetrate to yield a new type of catenated network consisting of large, open, 1D channels (Figure 3). All aromatic rings self-assemble to line up approximately with their planes parallel to the *z* axis, and act as sidewalls of the channels. The free space accommodates four DMF molecules and one H_2O molecule per formula unit. As illustrated in Figure 3a, these channels contain large diameter supercages (approximately $11 \times 11 \times 5$ Å, based on the van der Waals radius of carbon atoms) and smaller windows (triangular, with an effective maximum dimension of about 8 Å), and thus are shaped dramatically differently from most other organometallic open frameworks, which usually have straight channels.[10]

IRPM-1 has demonstrated an unusually high thermal stability with respect to organometallic materials.[6] Thermogravimetric (TG) analyses were performed both in air and nitrogen atmosphere. A weight loss of $\approx$22.7% was observed at around 180°C in both cases, which corresponds to the weight of all guest solvents (calcd 22.7%). Upon further heating in air, the desolvated samples showed no signs of decomposition up to 400°C (see Supporting Information). The crystal structure of the evacuated sample of IRPM-1 was determined from a single crystal after the removal of all the guest molecules at 300°C. The structure remained essentially unchanged.[9]

The adsorption and catalytic properties of IRPM-1 were examined under experimental conditions that are identical or similar to those employed with conventional zeolites. IRPM-1 displays a high sorption capacity for hydrocarbons, in accordance with the large channels observed. A pore volume of 0.25 $cm^3 g^{-1}$ is estimated for IRPM-1, based on the *n*-hexane ($p = 90$ Torr, $p/p_o = 0.48$) sorption capacity (17 wt%) at 30°C. This volume is between those for the large-pore zeolite H-Y (0.32 $cm^3 g^{-1}$)[11a] and medium-pore zeolite H-ZSM-5 (0.19 $cm^3 g^{-1}$).[11b] At 80°C, the sorption capacity for cyclohexane ($p = 55$ Torr, $p/p_o = 0.074$) of IRPM-1 is 19 wt% (corresponding to 2.4 molecules per cage, see Supporting Information), which exceeds that of H-Y (17 wt%), one of the most widely used large-pore zeolites; this demonstrates the high porosity of this material. The higher uptake of cyclohexane in IRPM-1, despite its lower pore volume, may be caused by more efficient packing of the molecules and/or their stronger interaction with the walls than in the case of H-Y. IRPM-1 is capable of adsorbing even larger hydrocarbon molecules: The sorption capacities at 80°C for mesitylene (7 Å, $p = 1.4$ Torr, $p/p_o = 0.27$) and triisopropylbenzene (8.5 Å) are 17 and 12 wt%, respectively. From these pore-gauging data, a pore window with a maximum dimension of $\approx$8 Å is deduced. A series of sorption isotherms for *n*-hexane at various temperatures are shown in Figure 4a. IRPM-1 demonstrates remarkable stability on repetitive gas sorption and desorption trials, even at high temperatures up to at least 250°C. To our knowledge, this study represents the first

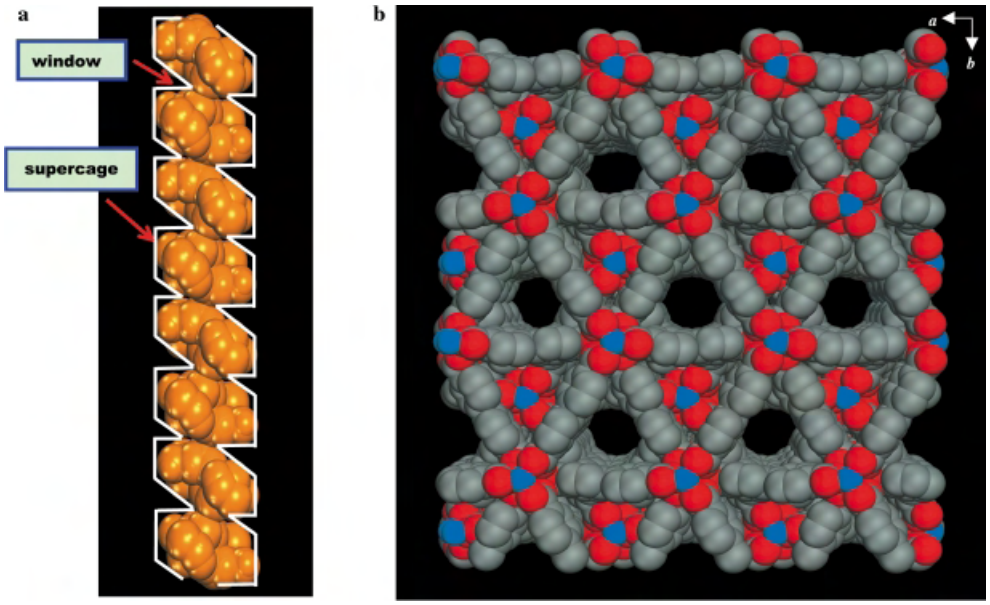


Figure 3. a) Side view (100) of one-dimensional channel in IRPM-1 with solvent molecules (gold). The narrower window has an effective maximum dimension of about 8 Å (calculated based on the van der Waals radius of carbon atoms), and the size of the supercage is $11 \times 11 \times 5$ Å; b) top view (001) of the channels showing the window openings. The same labeling scheme as in Figure 2 is used here.

 © 2003 Wiley-VCH Verlag GmbH & Co. KGaA, Weinheim 1433-7851/03/4205-0544 $ 20.00+.50/0

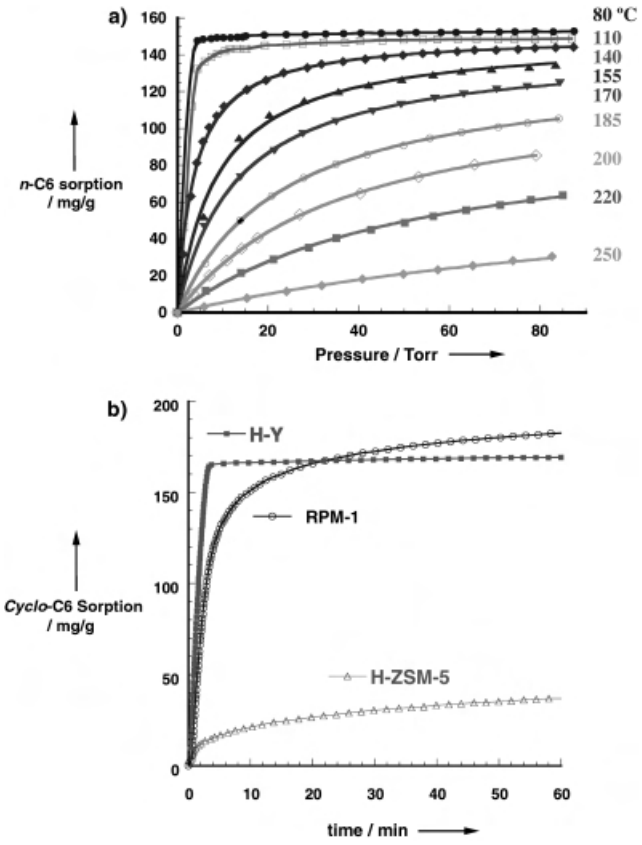
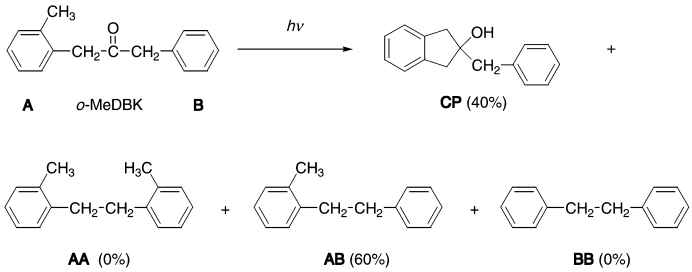


Figure 4. a) The *n*-hexane sorption isotherms of IRPM-1 measured at various temperatures; b) the cyclohexane uptake on H-Y, IRPM-1, and H-ZSM-5 as a function of sorption time, measured at 80 °C

investigation of zeolite-like sorption properties of a organometallic compound at temperatures above 100 °C. The heat of *n*-hexane sorption on IRPM-1 (66 kJ mol^{-1}) is considerably larger than that of H-Y (45.5 kJ mol^{-1}), and is close to that of H-ZSM-5 (68.8 kJ mol^{-1}).[12] The high isosteric heat, unexpected for the large pore size of IRPM-1, suggests the strong sorption of these hydrocarbons in the channels. Comparison of Henry constants[13] of *n*-hexane sorption isotherms measured at 250 °C: 0.0070, 0.0060, and 0.0038 Torr^{-1} for H-ZSM-5, IRPM-1, and H-Y, respectively, confirms the strong hydrocarbon molecule–pore-wall interaction in IRPM-1. The sorption rate can be used to estimate the size of the effective pore windows in porous materials.[2] As clearly seen in Figure 4b, the sorption rate of cyclohexane in IRPM-1 is slower than that in H-Y, which contains 12-membered ring windows with openings of 7.4 × 7.4 Å, and faster than that in H-ZSM-5, which has 10-membered ring windows with apertures of 5.3 × 5.6 Å. The retardation in rate for IRPM-1 for the nearly spherical cyclohexane molecule (kinetic diameter 6.0 Å) suggests a minimum window dimension of $\leq$6 Å. Another interesting feature of IRPM-1 is that it is hydrophobic (1 wt% water sorption at 15 Torr at 30 °C). We attribute this hydrophobicity to the hydrophobic surface of the pores in IRPM-1, which are composed mainly of aromatic carbon and hydrogen atoms. It is also worth noting that IRPM-1 retains its porous framework against water vapor (15 Torr) in the temperature range of 30 to 80 °C.

IRPM-1 was examined for its ability to serve as a host for photochemical reactions.[14] The photochemistry of dibenzylketone (DBK) and its derivatives adsorbed on classical FAU and MFI zeolites has been thoroughly investigated.[3] *o*-MeDBK was selected as a test substrate in consideration of the specific shape of the 1D channels of IRPM-1. This molecule, when adsorbed on FAU or MFI zeolites, undergoes two photoreactions as shown in Scheme 1: 1) α cleavage,



Scheme 1. The ship-in-bottle photochemical reaction.

followed by loss of carbon monoxide to form a geminate pair of hydrocarbon radicals, which undergo geminate (product AB) or random combination (products **AA**, **AB**, and **BB**), and 2) an intramolecular hydrogen abstraction followed by cyclization to form a cyclopentanol, **CP**. Photolysis of *o*-MeDBK@IRPM-1 produced only **AB** with 60% yield in reaction 1, which corresponds to a "cage effect" of 100% (compared to a cage effect of 70% for photolysis of *o*-MeDBK in NaX). The yield of **CP** is 40% in reaction 2. This yield of **CP** is much higher than the values found in other zeolites (e.g. NaX) where the maximum yield is approximately 10%. More significantly, only ≈50% of the overall products could be extracted before breaking the IRPM-1 framework.[14] The remaining 50% of the products were recovered only after IRPM-1 was immersed in water and completely converted into a nonporous 1D precursor, to give a 100% mass balance (compared to ca. 60–70% mass balance of NaX). The results from the photolysis demonstrate the unique potential of IRPM-1 to serve as "smart" porous host for "ship-in-bottle" photochemistry and other reactions.[14]

In conclusion, IRPM-1 is a thermally stable, nanoporous, organometallic structure containing unique open channels formed by narrower windows and larger supercavities. It exhibits a high sorption capacity for large hydrocarbons over a wide temperature range. IRPM-1 also possesses superior size/shape selectivity for the in situ photolysis of *o*-MeDBK. Most notably, the 3D framework of IRPM-1 can be readily broken down into a nonporous structure under mild conditions. This would allow a full recovery of product molecules in a ship-in-bottle synthesis application. Such a structural conversion is completely reversible. The structural reversibility of IRPM-1 may provide significant economic and technical advantages for recyclable use of this material.

 © 2003 Wiley-VCH Verlag GmbH & Co. KGaA, Weinheim 1433-7851/03/4205-0545 $ 20.00+.50/0

Experimental Section

Synthesis of IRPM-1: In a typical synthesis, $[Co(bpdc)(H_2O)_2]\cdot H_2O$ (0.3 mmol, white-gray), prepared as previously reported[8], and bpy (0.1 mmol) were stirred in DMF (10 mL) and well mixed. The solution was then transferred into an acid digestion bomb, which was closed and heated at 150 °C for 3 days, giving rise to deep-purple columnar crystals of IRPM-1 in high yield (129.1 mg, ≈94.5 %). IRPM-1 can also be synthesized solvothermally by direct reaction of $Co(NO_3)_2\cdot 6H_2O$ with bpy and bpdc in a DMF solution at 150 °C for three days. A 13.5 mg of the ground product was immersed in distilled water for 30 min, yielding $[Co(bpdc)(H_2O)_2]\cdot H_2O$ in quantitative yield (10.4 mg, calcd 10.5 mg). Powder X-ray diffraction (PXRD) analysis of the product was in excellent agreement with the calculated PXRD pattern produced by single crystal data.

Sorption Experiments: The sorption studies were conducted on a computer-controlled DuPont Model 990 TGA. The hydrocarbon partial pressure was varied by changing the blending ratios of hydrocarbon-saturated nitrogen and pure nitrogen gas streams. The zeolite and IRPM-1 samples were initially activated at 500 and 200 °C in nitrogen, respectively. At 80 °C, the measured sorption capacities for propylene ($p = 600$ Torr, $p/p_o = 0.023$), *n*-hexane ($p = 90$ Torr, $p/p_o = 0.084$), and cyclohexane $p = 55$ Torr, $p/p_o = 0.074$) of IRPM-1 are 12, 15, and 19 wt %, respectively, where p is the sorption pressure of the sorbate and p_o is the calculated vapor pressure at the sorption temperature. Measurements of cyclohexane sorption rate on IRPM-1, H-Y, and H-ZSM-5 samples were performed at 80 °C.

Photolysis of *o*-MeDBK: IRPM-1 (about 50 mg) was prepared as a slurry in pentane, and transferred to a branched quartz cell. Argon was used to evaporate the solvent, and the sample was then heated to 150 °C for an hour at 1 Torr. A sample of *o*-MeDBK (2 mg) in pentane/ether (0.3 mL; 1:1) was added to IRPM-1 at room temperature under Ar. The mixture was allowed to soak for 2 h, then flushed with Ar, and pumped to 2×10^{-5} Torr and left overnight. It was then irradiated with a 500 W medium-pressure mercury lamp for one hour. Procedure 1: The irradiated sample was then extracted with ether. Procedure 2: After procedure 1 sample was soaked in water until the color turned to white–gray and then extracted with an excess amount of ether. Procedures 1 and 2 gave ≈30 % and ≈30 % **AB**, respectively, and >40 % of the alcohol (**CP**).

Received: August 5, 2002 [Z19888]

[1] D. W. Breck, *Zeolite Molecular Sieves: Structure, Chemistry and Use*, Wiley, New York, **1974**.

[2] R. M. Barrer, *Zeolites and Clay Minerals as Sorbents and Molecular Sieves*, Academic Press, London, **1978**.

[3] a) N. Turro, *Acc. Chem. Res.* **2000**, *33*, 637; b) V. Ramamurthy, M. Garcia-Garibay, Zeolites as Supramolecular Hosts for Photochemical Transformations in *Comprehensive Supramolecular Chemistry, Vol. 7* (Ed.: T. Bein) Pergamon, Oxford, UK, **1996**.

[4] A. Corma, V. Fornés, H. García, M. A. Miranda, M. J. Sabater, *J. Am. Chem. Soc.* **1994**, *116*, 9767.

[5] W. DeWilde, G. Peeters, J. H. Lunsford, *J. Phys. Chem.* **1980**, *84*, 2306.

[6] M. Eddaoudi, J. Kim, N. Rosi, D. Vodak, J. Wachter, M. O'Keeffe, O. M. Yaghi, *Science* **2002**, *295*, 469.

[7] J. S. Seo, D. Whang, H. Lee, S. I. Jun, J. Oh, Y. J. Jeon, K. Kim, *Nature* **2000**, *404*, 982.

[8] L. Pan, N. Ching, X.-Y. Huang, J. Li, *Inorg. Chem.* **2000**, *39*, 5333.

[9] $[Co_3(bpdc)_3(bpy)]\cdot 4DMF\cdot H_2O$ (IRPM-1) crystallizes in the orthorhombic crystal system, space group *Pbcn*, with $a = 14.195(3)$, $b = 25.645(5)$, $c = 18.210(4)$ Å, $V = 6629(2)$ Å^3, $Z = 4$, and $d_{calc} = 1.367\ g\,cm^{-3}$. Analysis was done at wavelength λ ($Mo_{K\alpha}$) = 0.71073 Å. The structure was solved by direct methods and successive Fourier difference syntheses. The refinement by full-matrix least squares gave a final value $R = 0.056$ from 3662 reflections with intensity $I \geq 2\sigma(I)$ for 384 variables. The analytical data for IRPM-1 are as follows: calcd C 57.11, H 4.53, N 6.02 %; found C 56.4, H 4.58, N 6.16 %. The evacuated IRPM-1, $[Co_3(bpdc)_3(bpy)]$, crystallizes in the orthorhombic crystal system, space group *Pbcn*, with $a = 13.950(3)$, $b = 25.999(5)$, $c = 18.089(4)$ Å, $V = 6561(2)$ Å^3, $Z = 4$ and $d_{calc} = 1.067\ g\,cm^{-3}$. The analytical data for $[Co_3(bpdc)_3(bpy)]$ are as follows: calcd C 59.3, H 3.06, N 2.66 %; found C 59.24, H 3.27, N 2.75 %. CCDC-188406 (IRPM-1) contains the supplementary crystallographic data for this paper. These data can be obtained free of charge via www.ccdc.cam.ac.uk/conts/retrieving.html (or from the Cambridge Crystallographic Data Centre, 12 Union Road, Cambridge CB2 1EZ, UK; fax: (+44) 1223-336-033; or deposit@ccdc.cam.ac.uk).

[10] The pore sizes reported here are approximate because of the complicated linkage and orientation of the aromatic rings that form the surface of the pore structure, which results in a highly irregular pore shape.

[11] a) E. L. Wu, G. R. Landolt, A. W. Chester in *Proc. 7th Inter. Zeolite Conf.* (Eds.: Y. Murakami, A. Iijima, J. W. Ward), Elsevier, Kodanska, **1986**, p. 547; b) D. H. Olson, G. T. Kokotailo, S. L. Lawton, W. M. Meier, *J. Phys. Chem.* **1981**, *85*, 2238.

[12] J. F. , Denayer, W. Souverijns, P. A. Jacobs, J. A. Martens, G. V. Varon, *J. Phys. Chem. B* **1998**, *102*, 4588.

[13] Henrys constants, K_h, were calculated from the linear regions of the adsorption isotherms and are expressed as $Q/Q^\circ = K_hP$, where Q is the amount adsorbed and Q° is the equilibrium sorption capacity.

[14] X. Lei, Jr., C. E. Doubleday, M. B. Zimmt, N. J. Turro, *J. Am. Chem. Soc.* **1986**, *l08*, 2444.

Chiral Metallahelicates

The Preparation of a Double Metallahelicate Containing 28 Copper Atoms

*James A. Johnson, Jeff W. Kampf, and Vincent L. Pecoraro**

Molecules of great complexity that are prepared by the self-organization of simple components have garnered considerable recent attention. Among these compounds are metallamacrocycles such as the helicates,[1a–d] molecular squares,[2a,b] and the metallacrowns.[3a–e] The latter molecular class is reminiscent of organic crown ethers; however, the $\{O\text{-}C\text{-}C\}_n$ repeat unit is substituted by heteroatoms, such as $\{O\text{-}M\text{-}N\}_n$. Metallacrowns have been prepared with ring sizes ranging from 9-metallacrown-3 (9-MC-3) to 30-MC-10.[4a–c] The 15-

[*] Prof. V. L. Pecoraro, J. A. Johnson, Dr. J. W. Kampf
Department of Chemistry
Willard H. Dow Laboratories
The University of Michigan
Ann Arbor, MI 48109-1055 (USA)
Fax: (+1) 734-936-7628
E-mail: vlpec@umich.edu.

 © 2003 Wiley-VCH Verlag GmbH & Co. KGaA, Weinheim 1433-7851/03/4205-0546 $ 20.00+.50/0

MC-5 complexes, in particular, have been of interest as these can be prepared using α-amino acid-derived ligands. As such they are inherently chiral and can form cavities capable of selective anion recognition[5a] or resolved, fourfold symmetric, amphiphilic metallahelices.[5b] Herein, we demonstrate that a new class of self-assembled complex, a metallahelicate, can also be isolated by our synthetic strategy.

The standard preparation of a 15-MC-5 complex entails the addition of a stoichiometric ratio (5:5:2) of copper acetate, an α-aminohydroxamic acid, and ammonium chloride, respectively, followed by the addition of one equivalent of a lanthanide(III) salt. Before the addition of the lanthanide, a slightly soluble green material can be observed in the aqueous solvent. Recent work by Dallavalle and Tegoni,[6] in which L-phenylalanine hydroxamic acid (L-H_2pheha) was employed, proposed a 12-MC-4 model for this green material. Such a structure, however, should be relatively unstable, as the ring of a 12-MC-4 complex is highly strained when composed of ligands with fused 5,5-membered chelate rings.

In an attempt to improve our understanding of the nature of this green intermediate, we adjusted the copper/L-norvaline hydroxamic acid (L-H_2norvalha)/chloride ratios to 5:4:2, and changed our solvent system to pure methanol. Crystalline material was observed after three weeks of slow methanol evaporation.

The compound ion $[\mathbf{1}]^{2+}$[7,8] ($M_W = 5328.7$) contains copper atoms in seven different donor environments (Figure 1), with an overall stoichiometry of $[Cu_{28}L_{20}(OAc)_{10}Cl_4(MeOH)_5(H_2O)_3]$. Additional unbound solvent molecules and anions ($2\,Cl^-$) are present in the crystal structure, to give an overall molecular weight of 5952.1. This remarkable molecule is over three nanometers long and is constructed from two $\{Cu_{14}L_{10}(OAc)_4\}$ strands that are related by a noncrystallographic twofold symmetry axis. Each strand contains three structural domains; a central "body" (composed of four Cu^{II} atoms and four [L-norvalha]$^{2-}$ ligands), two sets of "wings" (each composed of four Cu^{II} atoms and three [L-norvalha]$^{2-}$ ligands) and two $[Cu(OAc)]^+$ bridges that link together the body and wing domains. The relationship between the body, the "hinge" copper atom, and the wing is illustrated in Figure 2. The coordination of the copper ions is, with the exception of the hinges, essentially square planar with a weaker interaction perpendicular to the plane. The body of the metallahelicate contains two collapsed 12-MC-4 units[9] oriented cofacially, with *n*-propyl groups pointing away from the central plane of the body, thus forming two pockets (one on each side) that each surround a chloride counterion (Figure 3). The wings that form the upper and lower domains of the structure are capped by dicopper sites, which display simultaneous μ-alkoxy (using the oxygen atom of the carbonyl hydroxamate) and μ-acetato bridged copper centers

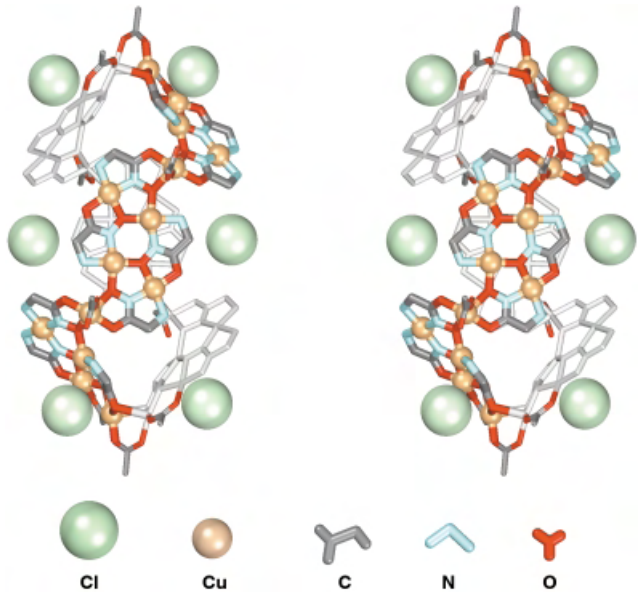


Figure 1. A stereoview of **1**·2Cl with lattice solvent, coordination solvent, and alkyl groups removed for clarity.

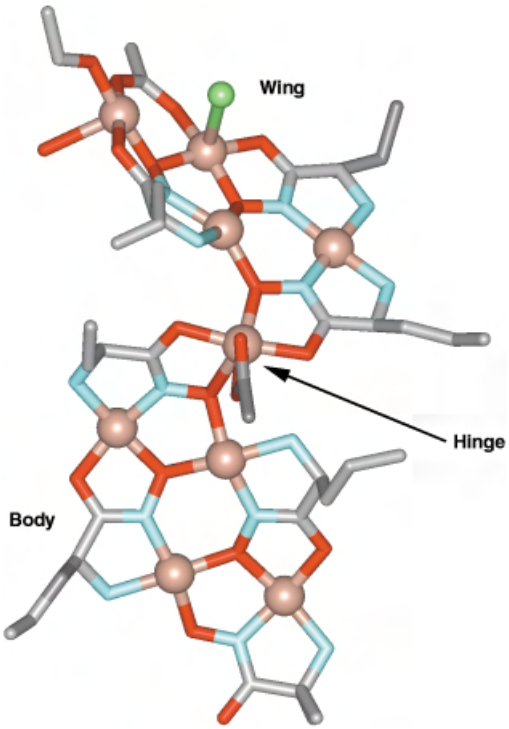


Figure 2. A side view of the collapsed metallacrown core of the "body" portion of **1**·2Cl.

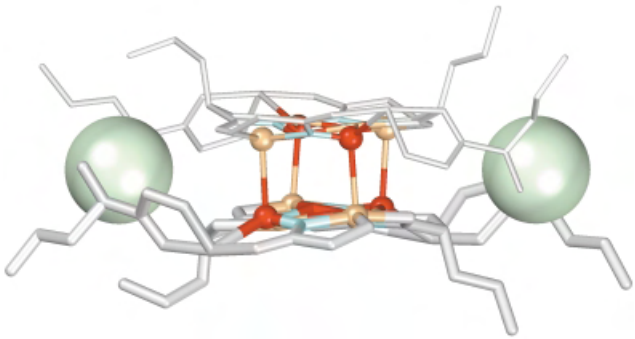


Figure 3. A minimal representation of the connectivity in the metallahelicate showing one body unit, one wing unit, and one hinge Cu^{II} center of the complex.

 © 2003 Wiley-VCH Verlag GmbH & Co. KGaA, Weinheim 1433-7851/03/4205-0547 $ 20.00+.50/0

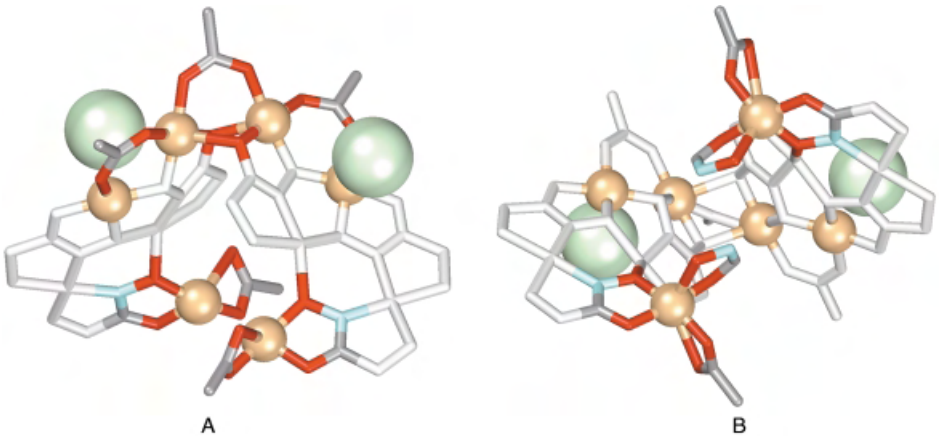


Figure 4. A) A side view of the top "wing" of the $[\mathbf{1}]^{2+}$ unit displaying the binuclear copper centers with bridging acetate groups and coordinated chloride ions; B) a view along the pseudo-twofold axis of the $[\mathbf{1}]^{2+}$ unit showing two of the unique "hinge" copper atoms and their pseudo-Δ propeller geometry.

(Figure 4 A). There is a nearly planar tetranuclear fragment on either side of the wing, related by a twofold axis, with each wing containing one of these binuclear copper atoms. To satisfy the coordination geometry about the capping copper dimer, the planes of the two tetranuclear fragments must twist with respect to one another. One of the three remaining Cu^{II} ions has a coordinated chloride ion. The conformational complexity of the $[\mathbf{1}]^{2+}$ ion is further defined by the absolute stereochemical configurations of the four chiral copper atoms (hinge atoms) that form the links between the body and wings of the structure. In the $[\mathbf{1}]^{2+}$ unit, all four Cu^{II} ions have a Δ configuration (Figure 4 B) while in the $[\mathbf{2}]^{2+}$ ion, prepared from D-H_2norvalha,[10] they have a Λ configuration.

Finally, upon combining all structural domains and stereochemical restrictions, a metallahelicate topology is generated if one begins at one of the top binuclear copper atoms and traces the connectivity of adjacent copper atoms throughout the molecule. This suggests that helicate-like molecules should be accessible using a binuclear cap with an appropriate helix-inducing organic ligand.

This new supermolecule[11] offers a unique set of potential attachment points for a variety of ligand sets, as well as providing a potential synthon for metallacrown formation. Currently, we are exploring the incorporation of mesogenic groups onto the periphery of these noncentrosymmetric metal clusters to observe possible nonlinear optical phenomena that may be apparent as a result of liquid-crystalline ordering.[12a–c]

Experimental Section

The syntheses of L-H_2norvalha and D-H_2norvalha were accomplished by a literature method.[13] m.p. = 168–171 °C (L-H_2norvalha); m.p. = 163–168 °C (D-H_2norvalha).

Compound **1**·2 Cl was synthesized by the addition of L-norvalha (0.67 mmol) to a stirred slurry of $Cu^{II}(OAc)_2 \cdot H_2O$ (0.93 mmol) in predried methanol (10 mL). After stirring the capped reaction solution for 30 min, NH_4Cl (0.20 mmol) was added. The mixture was then stirred for 2 h to give a dark-green solution, which was subsequently filtered by gravity into a vial (27 × 165 mm) and allowed to stand uncapped for 48–72 h. Suitable green blocks were obtained for X-ray diffraction study. Yield 28.6 %; m.p. = 198–200 °C (decomp); elemental analysis (%) calcd for $C_{131}H_{320}Cl_6Cu_{28}N_{40}O_{94}$: C 26.43, H 5.42, N 9.41; found: C 26.62, H 4.94, N 9.66.

Compound **2**·2 Cl was prepared in the same manner as **1**·2 Cl, but with D-H_2norvalha as the ligand. Yield 8.1 %; m.p. = 196–199 °C (decomp); elemental analysis (%) calcd for $C_{135}H_{330}Cl_6Cu_{28}N_{40}O_{95}$: C 26.91, H 5.52, N 9.30; found: C 25.05, H 4.71, N 9.37.

Received: September 16, 2002 [Z50160]

[1] a) M. Albrecht, *Chem. Rev.* **2001**, *101*, 3457; b) C. Piguet, G. Bernardelli, G. Hopfgartner, *Chem. Rev.* **1997**, *97*, 2005; c) J.-M. Lehn, *Supramolecular Chemistry*, VCH, Weinheim, **1995**; d) A. V. Davis, R. M. Yeh, K. N. Raymond, *Proc. Natl. Acad. Sci. USA* **2002**, *99*, 4793.

[2] a) M. Fujita in *Comprehensive Supramolecular Chemistry, Vol. 9* (Ed.: J.-M. Lehn), Elsevier Science, New York, **1996**, pp. 253–282; b) P. J. Stang, B. Olenyuk, *Acc. Chem. Res.* **1997**, *30*, 502.

[3] a) M. S. Lah, V. L. Pecoraro, *J. Am. Chem. Soc.* **1989**, *111*, 7258; b) V. L. Pecoraro, A. J. Stemmler, B. R. Gibney, J. J. Bodwin, H. Wang, J. W. Kampf, A. Barwinski, *Prog. Inorg. Chem.* **1997**, *45*, 83–177; c) R. W. Saalfrank, N. Löw, F. Hampel, H.-D. Stachel, *Angew. Chem.* **1996**, *108*, 2353; *Angew. Chem. Int. Ed. Engl.* **1996**, *35*, 2209; d) A. J. Stemmler, A. Barwinski, M. J. Baldwin, V. Young, V. L. Pecoraro, *J. Am. Chem. Soc.* **1996**, *118*, 11962; e) A. D. Cutland, R. G. Malkani, J. W. Kampf, V. L. Pecoraro, *Angew. Chem.* **2000**, *112*, 2801; *Angew. Chem. Int. Ed.* **2000**, *39*, 2689.

[4] a) B. R. Gibney, A. J. Stemmler, S. Pilotek, J. W. Kampf, V. L. Pecoraro, *Inorg. Chem.* **1993**, *32*, 6008; b) D. Gaynor, Z. A. Starikova, W. Haase, K. B. Nolan, *J. Chem. Soc. Dalton Trans.* **2001**, 1578; c) S.-X. Liu, S. Lin, B.-Z. Lin, C.-C. Lin, J.-Q. Huang, *Angew. Chem.* **2001**, *113*, 1118; *Angew. Chem. Int. Ed.* **2001**, *40*, 1084.

[5] a) A. D. Cutland, J. A. Halfen, J. W. Kampf, V. L. Pecoraro, *J. Am. Chem. Soc.* **2001**, *123*, 6211; b) A. D. Cutland-Van Noord, J. W. Kampf, V. L. Pecoraro, *Angew. Chem.* **2002**, *114*, 4861; *Angew. Chem. Int. Ed.* **2002**, *41*, 4667.

[6] F. Dallavalle, M. Tegoni, *Polyhedron* **2000**, *20*, 2697.

[7] CCDC-193213 and -193214 (**1**·2 Cl and **2**·2 Cl) contains the supplementary crystallographic data for this paper. These data can be obtained free of charge via www.ccdc.cam.ac.uk/conts/retrieving.html (or from the Cambridge Crystallographic Data Centre, 12, Union Road, Cambridge CB2 1EZ, UK; fax: (+44) 1223-336-033; or deposit@ccdc.cam.ac.uk).

 © 2003 Wiley-VCH Verlag GmbH & Co. KGaA, Weinheim 1433-7851/03/4205-0548 $ 20.00+.50/0

[8] Crystal data for **1**·2Cl ($[Cu_{28}L_{20}(OAc)_{10}Cl_6(MeOH)_{11}(H_2O)_{23}]$): $M_W = 5952.09$, monoclinic, space group $P2_1$, $a = 14.2512$, $b = 26.9615(19)$, $c = 34.476(3)$ Å, $\alpha = 90.00$, $\beta = 90.049(2)$, $\gamma = 90.00°$, $V = 13246.8(16)$ Å^3, $Z = 2$; $\rho_{calcd} = 1.492$ g cm^{-3}; $2.73 < \theta < 28.34°$; crystal dimensions $0.24 \times 0.38 \times 0.42$ mm^3; $\mu = 23.35$ cm^{-1}; $T = 123(2)$ K; 172045 reflections collected; 63307 unique reflections and 2727 parameters were used for the full-matrix least-squares refinement on F^2; $R1 = 0.0394$, $wR2 = 0.1012$.

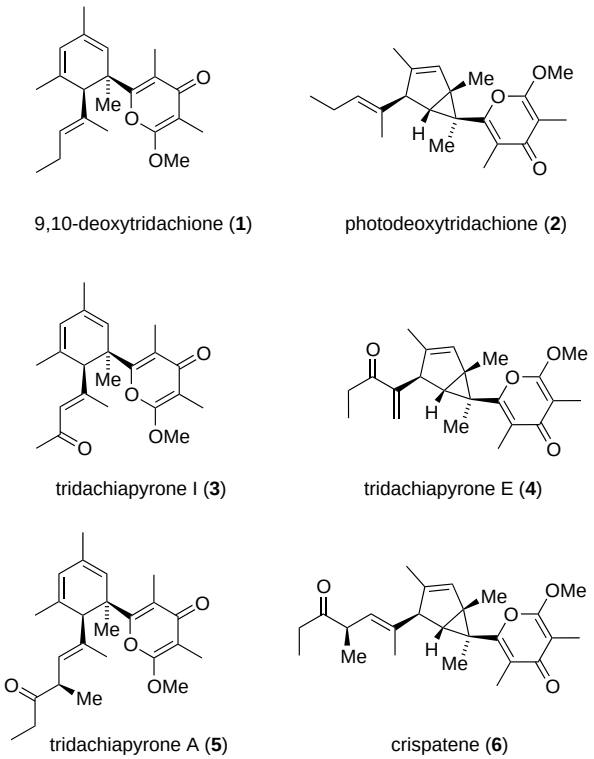
[9] G. Psomas, A. J. Stemmler, C. Dendrinou-Samara, J. J. Bodwin, M. Schneider, M. Alexiou, J. W. Kampf, D. P. Kessissoglou, V. L. Pecoraro, *Inorg. Chem.* **2001**, *40*, 1562.

[10] Crystal data for **2**·2Cl ($[Cu_{28}L_{20}(OAc)_{10}Cl_6(MeOH)_{15}(H_2O)_{20}]$): $M_W = 6026.21$, monoclinic, space group $P2_1$, $a = 14.1740(12)$, $b = 26.753(2)$, $c = 34.535(3)$ Å, $\alpha = 90.00$, $\beta = 90.314(3)$, $\gamma = 90.00°$, $V = 13095.7(19)$ Å^3, $Z = 2$; $\rho_{calcd} = 1.528$ g cm^{-3}; $2.70 < \theta < 22.78°$; crystal dimensions $0.10 \times 0.14 \times 0.22$ mm^3; $\mu = 23.63$ cm^{-1}; $T = 150(2)$ K; 84037 reflections collected; 34295 unique reflections and 2767 parameters were used for the full-matrix least-squares refinement on F^2; $R1 = 0.0651$, $wR2 = 0.1270$. Note that **2**·2Cl differs from **1**·2Cl in that the bound solvent composition is 6 MeOH and 2 H_2O for the former and 5 MeOH and 3 H_2O for the latter.

[11] Here we define a "supermolecule" (see ref. [1c]) as composed of receptors (that is, α-aminohydroxamic anions and acetates) and substrates (copper and chloride ions) held together weakly by intermolecular forces, thus giving a larger discreet superstructure.

[12] a) A.-M. Giroud-Godquin, *Coord. Chem. Rev.* **1998**, *178*, 1485; b) *Metallomesogens: Synthesis, Properties, and Applications* (Ed.: J. L. Serrano), VCH, Weinheim, **1996**; c) A.-M. Giroud-Godquin, P. M. Maitlis, *Angew. Chem.* **1991**, *103*, 370; *Angew. Chem. Int. Ed. Engl.* **1991**, *30*, 375.

[13] A. H. Blatt, *Organic Syntheses Collection, Vol. 2*, Wiley, New York, **1943**, pp. 67–68.



Scheme 1. Molluscan polypropionates. The absolute stereochemistry shown is arbitrary.

Lewis Acids in Total Synthesis

Total Synthesis of (±)-Photodeoxytridachione through a Lewis Acid Catalyzed Cyclization**

*Aubry K. Miller and Dirk Trauner**

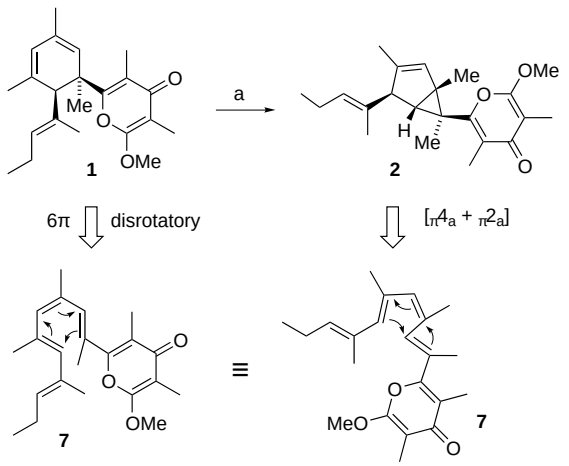
Certain sacoglossan molluscs sequester active chloroplasts from algae and use these organelles to carry out photosynthesis in their own tissues.[1] These fascinating animals lack a protective shell and thus rely on chemical defense against predators. Not surprisingly, they have yielded a range of interesting biologically active natural products.[2] Many of these are highly unsaturated polypropionates that feature an α-methoxy-γ-pyrone moiety (Scheme 1).

Architecturally, these natural products, which have been largely ignored by the synthetic community,[3] fall into two categories. Whereas 9,10-deoxytridachione (**1**), tridachiapyrone I (**3**), and tridachiapyrone A (**5**) are cyclohexadiene derivatives, photodeoxytridachione (**2**), tridachiapyrone E (**4**), and crispatene (**6**) feature a bicyclo[3.1.0]hexene core. The isomeric nature of these ring systems raises questions about their mutual biogenetic relationship.[4] In 1979, Ireland and Scheuer demonstrated that 9,10-deoxytridachione (**1**) can be photochemically converted in vivo and in vitro into photodeoxytridachione (**2**).[1] This transformation could proceed through conrotatory photochemical retro-electrocyclization followed by a "photochemical Diels–Alder reaction"—that is a $[_\pi 4_a +_\pi 2_s]$ cycloaddition.[5] However, since no racemization occurs, the reaction was proposed to proceed as a photochemical $[_o 2_a +_\pi 2_a]$ rearrangement.[4]

Although these results suggest that **2** is biosynthesized via **1**, it is also, at least in principle, conceivable that both compounds are *directly* derived from a common acyclic precursor **7** (Scheme 2). The cyclohexadiene **1** may originate from this hypothetical intermediate through thermal disrotatory 6π electrocyclization. In contrast, the bicyclo[3.1.0]hexene **2** could arise in one step from a thermal $[_\pi 4_a +_\pi 2_a]$ cycloaddition of the same precursor. Provided that such a reaction could be realized in the laboratory, a unified synthetic approach toward both classes would be possible, since 6π electrocyclizations of hexatrienes are well-prece-

[*] Prof. D. Trauner, A. K. Miller
Center for New Directions in Organic Synthesis
Department of Chemistry, University of California, Berkeley
Berkeley, CA 94720-1460 (USA)
Fax: (+1) 510-643-9480
E-mail: trauner@cchem.berkeley.edu

[**] The Center for New Directions in Organic Synthesis is supported by Bristol-Myers Squibb as a sponsoring member and Novartis as a supporting member.



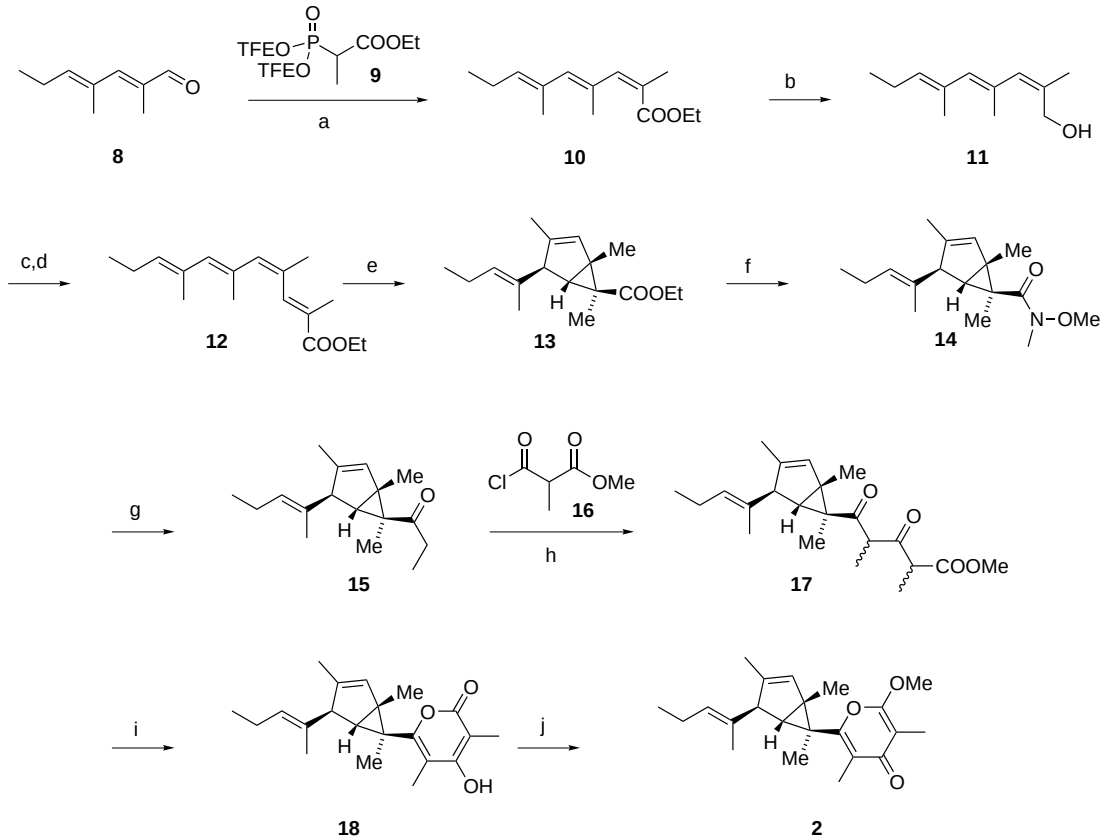
Scheme 2. Biosynthetic relationship and retrosynthetic analysis of **1** and **2**. a) hν.[4]

dented. We present herein the development of a Lewis acid catalyzed cyclization of hexatrienes to bicyclo[3.1.0]hexenes and the application of this novel reaction toward the total synthesis of **2**.

Our synthesis started with the known unsaturated aldehyde **8** (Scheme 3).[6] Still–Gennari condensation with trifluoroethyl phosphonate **9** yielded intermediate (*E,E,Z*)-**10** with excellent diastereoselectivity (≈20:1 in favor of the diastereomer shown).[7] Reduction with DIBAH then afforded alcohol **11**. A subsequent oxidation with TPAP/NMO followed by Horner–Wadsworth–Emmons condensation under Masamune–Roush conditions yielded the tetraenoic ester **12** (see Table 1 for selected data) and set the stage for the key step of the synthesis.[8]

After extensive experimentation (see below) it was found that treatment of **12** with catalytic amounts of dimethylaluminum chloride afforded bicylo[3.1.0]hexene **13** as the only isolated diastereomer in good yield (73%, Table 1). Thus, the bicyclo[3.1.0]hexene core of the natural product with its two adjacent quaternary stereocenters was formed from an acyclic precursor in a single step.[9]

The installment of the α-methoxy-γ-pyrone moiety proved to be more difficult than anticipated, presumably as a result of steric hindrance of the neopentylic ester function. Despite many attempts, **13** could not directly be converted into the desired tricarbonyl compound **17** by cross-Claisen condensation with a corresponding dianion.[10] To circumvent this obstacle, **13** was transformed into the Weinreb amide **14** and then exposed to ethyl magnesium bromide to afford ethyl ketone **15**. Deprotonation with excess base and addition of malonyl chloride **16** gave **17** in good yield (95% based on



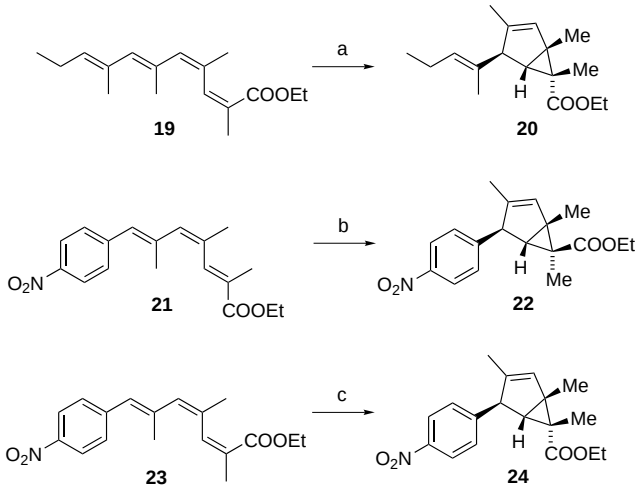
Scheme 3. Total synthesis of **2**. Reagents and conditions: a) **9**, KHMDS, 18[crown]-6, THF, −78°C, 79%; b) DIBAH, CH_2Cl_2, 0°C, 93%; c) TPAP, NMO, CH_2Cl_2; d) $(EtO)_2P(O)CH(Me)COOEt$, LiCl, DBU, MeCN, 43% from **11**; e) Me_2AlCl (0.2 equiv), CH_2Cl_2, 73%; f) MeHNOMe·HCl, *i*PrMgCl, THF, 0°C, 63%; g) EtMgBr, THF, 87%; h) LiHMDS (3 equiv), **16**, THF, hexanes, −78°C, 59% (95% based on recovered starting material); i) DBU, benzene, reflux, 78%; j) FSO_2OMe, CH_2Cl_2, 77%. HMDS = hexamethyldisilazide, DIBAH = diisobutylaluminum hydride, TPAP = tetra *n*-propylammonium perruthenate, NMO = *N*-methylmorpholine-*N*-oxide, DBU = 1,8-diazabicyclo[5.4.0]undec-7-ene, TFE = trifluoroethyl.

 © 2003 Wiley-VCH Verlag GmbH & Co. KGaA, Weinheim 1433-7851/03/4205-0550 $ 20.00+.50/0

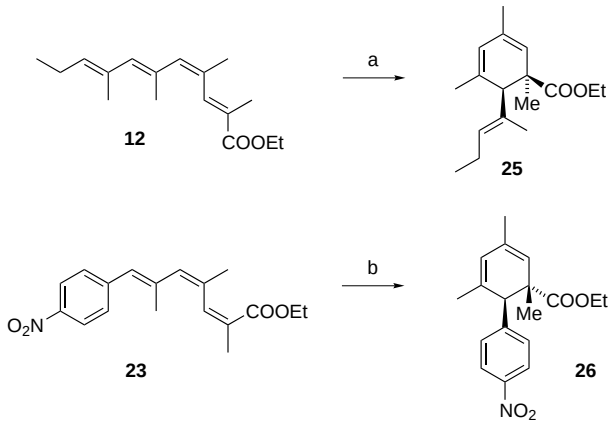
recovered starting material).[11] Cyclization of **17** under basic conditions resulted in the formation of the pyrone **18**.[10] Finally, regioselective methylation of this ambident nucleophile under the conditions of Beak et al. afforded **2**.[12] The NMR spectra of our synthetic material corresponded in all respects to the published data,[2f] and the high-resolution mass spectrum confirmed the molecular formula (Table 1).

To explore the scope and limitations of the key cyclization and to gain more insight into its mechanism, we studied the reactions of several compounds related to **12** in the presence of various Lewis acids. In addition to Me_2AlCl, other catalysts such as $Sc(OTf)_3$, $BF_3{\cdot}OEt_2$, and $TiCl_4$ were found to effect the isomerization, albeit in lower yields. Importantly, all reactions were found to proceed stereospecifically (Scheme 4). For instance, tetraenoic ester **19**, a diastereomer of **12**, gave bicyclo[3.1.0]hexene **20**, which is an epimer of **14** (Table 1).[13] Similarly, **21** cyclized to **22**, whereas its isomer **23** afforded **24**.[14]

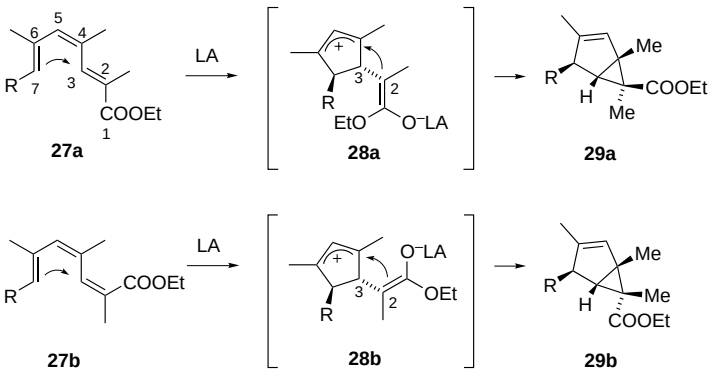
Notably, in the absence of a Lewis acid these substrates underwent regular disrotatory 6π electrocyclization to afford cyclohexadienes (Scheme 5).[14] Compound **25** may serve as an intermediate in the total synthesis of **1** and its congeners.



Scheme 4. Stereospecific formation of bicyclo[3.1.0]hexenes. Reagents and conditions: Me_2AlCl (0.2 equiv), CH_2Cl_2; a) 61%; b) 84%; c) 68%.



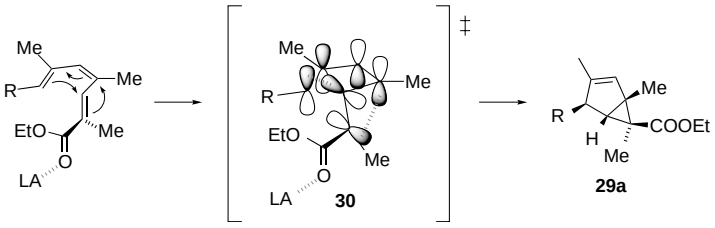
Scheme 5. Stereospecific formation of cyclohexadienes. Conditions: a) benzene, 80°C, 95%; b) toluene, 60°C, 98%.



Scheme 6. Proposed stepwise mechanism.

Mechanistically, the Lewis acid catalyzed cyclization could either proceed in a stepwise fashion or as a concerted cycloaddition. In the stepwise mechanism, coordination of the Lewis acid (LA) to the carbonyl group of trienoic ester **27a** or its isomer **27b** triggers a stereoselective ring formation, placing the two substituents *anti* with respect to each other (Scheme 6). The resulting zwitterionic intermediates **28a**/**28b** stabilize themselves by C–C-bond formation to yield bicyclo[3.1.0]hexenes **29a** or **29b**. Provided that this last step is considerably faster than rotation around the C2–C3 bond, the reactions could proceed stereospecifically.

Alternatively, a concerted cycloaddition mechanism that involves only one transition state **30** could be formulated (Scheme 7). The severe $A^{1,3}$ strain between the methyl groups



Scheme 7. Proposed concerted mechanism.

at C2 and C4 forces the triene to adopt a conformation in which it is effectively dissected into a diene and a dienophile moiety. Assisted by the C6 methyl group, the diene can assume an s-*cis* conformation, which allows for an intramolecular $[_{\pi}4_a+_{\pi}2_a]$ cycloaddition.[5a,15] The highest occupied molecular orbital (HOMO) of the diene and the lowest unoccupied molecular orbital (LUMO) of the dienophile are oriented more or less perpendicular to each other and overlap in such a way that bond formation occurs in an antarafacial sense with respect to both components. Coordination of a Lewis acid to the carbonyl group decreases the energy level of the LUMO, enabling this reaction to compete effectively with a 6π electrocyclization. The stereospecificity of the reaction is nicely explained by this concerted mechanism. Nevertheless, based on the currently available experimental data, no firm conclusion can be drawn as to the actual mechanism of the reaction.

 © 2003 Wiley-VCH Verlag GmbH & Co. KGaA, Weinheim 1433-7851/03/4205-0551 $ 20.00+.50/0

Table 1: Selected physical properties of **12, 13, 20**, and **2**.

12: $R_f = 0.45$ (silica, 5% Et_2O in hexanes); IR (thin film): $\tilde{\nu} = 2954, 2932, 2873, 1709\ cm^{-1}$; ^1H NMR (400 MHz, $CDCl_3$, 25 °C): $\delta = 7.45$ (s, 1H), 6.01 (s, 1H), 5.78 (s, 1H), 5.34 (t, $J = 7.2$ Hz, 1H), 4.20 (q, $J = 7.2$ Hz, 2H), 2.10 (quint, $J = 7.2$ Hz, 2H), 1.95 (s, 3H), 1.89 (d, $J = 1.2$ Hz, 3H), 1.83 (s, 3H), 1.73 (s, 3H), 1.29 (t, $J = 7.2$ Hz, 3H), 0.98 ppm (t, $J = 7.2$ Hz, 3H); ^{13}C NMR (100 MHz, $CDCl_3$, 25 °C): $\delta = 168.9, 140.6, 137.5, 136.4, 133.4, 132.3, 132.1, 131.1, 127.2, 60.7, 31.8, 24.2, 21.8, 18.4, 17.0, 14.4, 14.2$ ppm; HRMS (EI): calcd for $C_{17}H_{26}O_2$ [M^+]: 262.1933, found: 262.1931

13: $R_f = 0.34$ (silica, 5% Et_2O in hexanes); IR (thin film): $\tilde{\nu} = 2961, 2930, 2872, 1717\ cm^{-1}$; ^1H NMR (400 MHz, $CDCl_3$, 25 °C): $\delta = 5.25$ (m, 2H), 4.13 (q, $J = 7.2$ Hz, 2H), 2.60 (s, 1H), 2.02 (quint, $J = 7.6$ Hz, 2H), 1.92 (s, 1H), 1.53 (s, 3H), 1.47 (s, 3H), 1.30 (s, 3H), 1.26 (t, $J = 7.2$ Hz, 3H), 1.05 (s, 3H), 0.96 ppm (t, $J = 7.6$ Hz, 3H); ^{13}C NMR (100 MHz, $CDCl_3$, 25 °C): $\delta = 174.2, 144.1, 134.1, 129.3, 128.9, 60.5, 59.1, 43.1, 37.9, 33.6, 21.4, 14.6, 14.5, 14.5, 13.8, 12.5, 10.1$ ppm; HRMS (EI): calcd for $C_{17}H_{26}O_2$ [M^+]: 262.1933, found: 262.1937; elemental analysis: calcd for $C_{17}H_{26}O_2$: C 77.82, H 9.99; found: C 78.16, H 10.20

20: $R_f = 0.34$ (silica, 5% Et_2O in hexanes); IR (thin film): $\tilde{\nu} = 2961, 2928, 2872, 1729\ cm^{-1}$; ^1H NMR (400 MHz, $CDCl_3$, 25 °C): $\delta = 5.30$ (t, $J = 7.2$ Hz, 1H), 5.28 (s, 1H), 4.08 (dq, $J = 10.8, 7.2$ Hz, 1H), 3.99 (dq, $J = 10.8, 7.2$ Hz, 1H), 3.24 (s, 1H), 2.01 (dq, $J = 7.6, 7.2$ Hz, 2H), 1.43 (s, 6H), 1.30 (s, 3H), 1.28 (s, 3H), 1.18 (t, $J = 7.2$ Hz, 3H), 0.97 (s, 1H), 0.95 ppm (t, $J = 7.6$ Hz, 3H); ^{13}C NMR (100 MHz, $CDCl_3$, 25 °C): $\delta = 173.0, 140.5, 134.9, 131.2, 128.7, 60.1, 59.3, 39.4, 39.1, 36.1, 29.9, 21.4, 18.2, 14.6, 14.0, 13.9, 12.2$ ppm; HRMS (EI): calcd for $C_{17}H_{26}O_2$ [M^+]: 262.1933, found: 262.1928

2: $R_f = 0.50$ (silica, 5% MeOH in CH_2Cl_2); IR (thin film): $\tilde{\nu} = 1661\ cm^{-1}$; ^1H NMR (400 MHz, $CDCl_3$, 25 °C): $\delta = 5.33$ (s, 1H), 5.30 (t, $J = 7.2$ Hz, 1H), 3.96 (s, 3H), 2.73 (s, 1H), 2.04 (dq, $J = 7.6, 7.2$ Hz, 2H), 1.97 (s, 3H), 1.84 (s, 3H), 1.57 (s, 3H), 1.48 (s, 3H), 1.42 (s, 1H), 1.19 (s, 3H), 1.10 (s, 3H), 0.97 ppm (t, $J = 7.6$ Hz, 3H); ^{13}C NMR (100 MHz, $CDCl_3$, 25 °C): $\delta = 181.8, 162.5, 160.7, 144.2, 134.2, 129.0, 128.8, 120.6, 99.7, 58.6, 55.5, 40.9, 37.0, 32.0, 21.4, 17.3, 14.5, 13.9, 12.9, 11.0, 7.1$ ppm; HRMS (EI): calcd for $C_{21}H_{30}O_3$ [M^+]: 343.2229, found: 343.2248

In summary, a new Lewis acid catalyzed cyclization has been developed and applied to a concise total synthesis of photodeoxytridachione (ten steps from the known aldehyde **8**). Future work will focus on the scope and limitations of the reaction and the development of a catalytic asymmetric version using a chiral Lewis acid. Concurrently, the detailed mechanism of the reaction will be further investigated experimentally and computationally. Total syntheses of other molluscan polypropionates are well underway in our laboratories and will be reported in due course.

Received: September 18, 2002
Revised: October 15, 2002 [Z50192]

[1] C. Ireland, P. J. Scheuer, *Science* **1979**, *205*, 922.
[2] a) M. T. Davies-Colman, M. J. Garson, *Nat. Prod. Rep.* **1998**, *15*, 477, and references therein; b) C. Ireland, D. J. Faulkner, B. A. Solheim, J. Clardy, *J. Am. Chem. Soc.* **1978**, *100*, 1002; c) M. B. Ksebati, F. J. Schmitz, *J. Org. Chem.* **1985**, *50*, 5637; d) X. Fu, E. P. Hong, F. J. Schmitz, *Tetrahedron* **2000**, *56*, 8989; e) R. D. Gawe, J. L. C. Wright, *Tetrahedron Lett.* **1986**, *27*, 2559; f) M. Gavagnin, A. Spinella, F. Castelluccio, G. Cimino, A. Marin, *J. Nat. Prod.* **1994**, *57*, 298.
[3] For synthetic studies directed toward molluscan polypropionates, see: R. P. Alexander, C. Morley, G. R. Stephenson, *J. Chem. Soc. Perkin Trans. 1* **1988**, 2069.
[4] C. Ireland, J. Faulkner, *Tetrahedron* **1981**, *37*, 233 (Supplement 1).
[5] a) R. B. Woodward, R. W. Hoffmann, *The Conservation of Orbital Symmetry*, VCH, Weinheim, **1970**; b) W. G. Dauben, M. S. Kellogg, J. I. Seemann, N. D. Vietmeyer, P. H. Wendschuk, *Pure Appl. Chem.* **1973**, *33*, 197; c) D. H. R. Barton, A. S. Kende, *J. Chem. Soc.* **1958**, 688.
[6] G. Dahmann, R. W. Hoffmann, *Liebigs Ann. Chem.* **1994**, 837.
[7] W. C. Still, C. Gennari, *Tetrahedron Lett.* **1983**, *24*, 4405.
[8] M. A. Blanchette, W. Choy, J. T. Davis, A. P. Essenfeld, S. Masamune, W. R. Roush, T. Sakai, *Tetrahedron Lett.* **1984**, *25*, 2183.
[9] **13**: A solution of dimethylaluminum chloride in hexanes (1.0 M; 0.35 mL, 0.35 mmol) was added dropwise to a solution of **12** (425 mg, 1.62 mmol) in CH_2Cl_2 (16 mL) at 0 °C. The reaction mixture was allowed to warm to room temperature and quenched after 8 h with H_2O (15 mL). The two layers were separated, the aqueous layer was extracted with CH_2Cl_2 (2 × 15 mL), and the combined organic layers were dried ($MgSO_4$), filtered, and concentrated in vacuo. The product was purified by column chromatography (silica gel, 5% Et_2O in hexanes) to afford **13** (312 mg, 73.4%) as a clear, colorless oil.
[10] a) W. Oppolzer, R. Moretti, G. Bernardinelli, *Tetrahedron Lett.* **1986**, *27*, 4713; b) A. A. Birkbeck, D. Enders, *Tetrahedron Lett.* **1998**, *39*, 7823.
[11] This reaction presumably proceeds via an acyl ketene intermediate: D. Garey, M. L. Ramirez, S. Gonzales, A. Wertsching, S. Tith, K. Keefe, M. R. Pena, *J. Org. Chem.* **1996**, *61*, 4853.
[12] P. Beak, J. K. Lee, B. G. McKinnie, *J. Org. Chem.* **1978**, *43*, 1367.
[13] The relative stereochemistry of bicyclo[3.1.0]hexenes **13** and **20**, as well as of **23** and **24** was elucidated by reduction to the corresponding primary alcohols and extensive NOE measurements.
[14] Compounds **21, 23**, and **26** were available from our program directed at the immunosuppressants SNF4435 C and D: C. M. Beaudry, D. Trauner, *Org. Lett.* **2002**, *4*, 2221.
[15] M. V. George, A. Mitra, K. B. Sukumaran, *Angew. Chem.* **1980**, *92*, 1005.

 © 2003 Wiley-VCH Verlag GmbH & Co. KGaA, Weinheim 1433-7851/03/4205-0552 $ 20.00+.50/0

Osmium–Palladium Clusters

$[\{N(PPh_3)_2\}_2\{Os_{18}Pd_3(\mu_6\text{-}C)_2(CO)_{42}\}]$: An Osmium–Palladium Mixed-Metal High-Nuclearity Carbonyl Cluster**

*Ka-Fu Yung and Wing-Tak Wong**

Dedicated to Professor The Lord Lewis on the occasion of his 75th birthday

High-nuclearity mixed-metal clusters have aroused considerable attention because of their ability to act as an "electron reservoir", the potential to precisely control the ratio and geometry of the two metals involved,[1] and their potential application in catalysis.[2] Reactions of cluster anions with palladium–halide complexes were found to be effective in producing high-nuclearity mixed-metal clusters, for example, $[Fe_6Pd_6(CO)_{24}H]^{3-}$,[3] $[Ru_{10}Pd_8C_2(CO)_{27}(C_3H_5)_4]$,[4] and $[Ni_9Pd_{33}(PPh_3)_6(CO)_{41}]^-$.[5] However, high-nuclearity osmium–palladium mixed-metal clusters prepared by a similar approach are rare.[6] We recently established a reliable route to preparing such species in moderate yield using a decaosmium cluster anion and a palladium cation as the starting materials. Herein, we report the synthesis and structural characterization of the novel high-nuclearity sandwich osmium–palladium mixed-metal cluster $[\{N(PPh_3)_2\}_2\{Os_{18}Pd_3(\mu_6\text{-}C)_2(CO)_{42}\}]$ (**1**).

An excess of $[Pd(NCMe)_4](BF_4)_2$[7] was treated with $[\{N(PPh_3)_2\}_2\{Os_{10}(\mu_6\text{-}C)(CO)_{24}\}]$[8] in CH_2Cl_2 at room temperature to yield the novel osmium–palladium cluster anion $[Os_{18}Pd_3(\mu_6\text{-}C)_2(CO)_{42}]^{2-}$, which was isolated as its $[N(PPh_3)_2]^+$ salt (**1**) in 37% yield. An insoluble black solid was also obtained from the reaction mixture; IR spectroscopy indicated that the solid material may consist of high-nuclearity carbonyl–metal clusters.

Single crystals of **1** suitable for X-ray analysis were obtained as dark-green blocks by slow evaporation of the CH_2Cl_2/MeOH solution mixture at 0°C. The molecular structure, together with some important bond parameters, is depicted in Figure 1. The structure of **1** can be described as a giant dumbbell-shaped bimetallic nanocluster. The cluster core-geometry can be divided into three metallic domains. A triangular Pd_3 metal unit is sandwiched between two tricapped octahedral $\{Os_9(\mu_6\text{-}C)(CO)_{21}\}$ subclusters, which combine to give an overall D_{3h} symmetry. The five ABABA close-packed layers of metal ions (6:3:3:3:6) that are shown in Figure 2 are unprecedented in existing Os–Pd mixed-metal clusters. The central $\{Os_3Pd_3Os_3\}$ unit, which consists of the Os7, Os8, Os9, Pd1, Pd2, Pd3, Os10, Os11, and Os12 metal ions, forms a face-sharing bioctahedron that is reminiscent of the Rh_9 geometry observed in the $[Rh_9(CO)_{19}]^{3-}$ ion.[9] The palladium ions, which form the edge-sharing face of the bioctahedron only possess metal–metal bonding character; there are no bonds to carbonyl ligands, which is very unusual. This naked metal triangle is relatively exposed, which may facilitate the coordination of nucleophiles. For the two osmium domains, two Os_9 units are in an eclipsed conformation, which is contrary to the closely related osmium–mercury mixed-metal cluster, $[\{N(PPh_3)_2\}_2\{Os_{18}Hg_3(\mu_6\text{-}C)_2(CO)_{42}\}]$.[10]

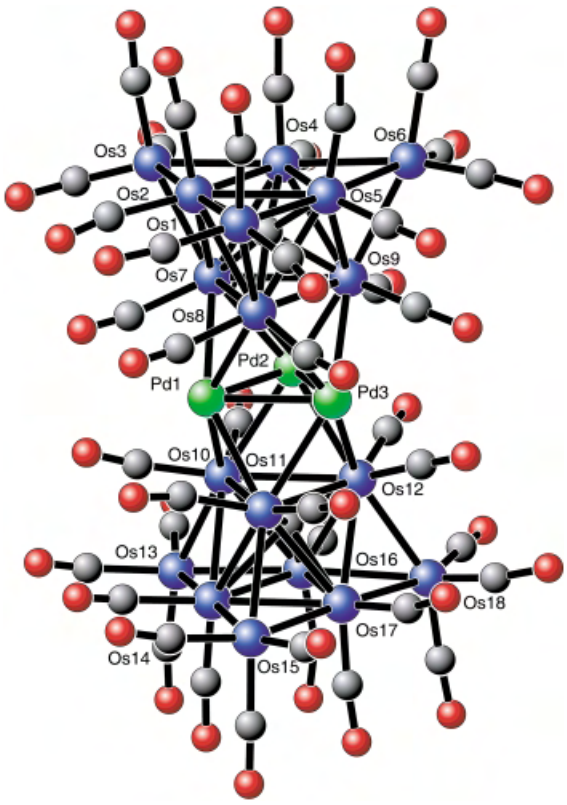


Figure 1. Molecular structure of cluster anion **1** showing the atomic numbering scheme (with osmium in blue and palladium in green). Selected Os–Os bond lengths (Å): Os1-Os2 2.772(3), Os1-Os4 2.785(3), Os1-Os7 2.778(2), Os2-Os3 2.780(3), Os2-Os4 2.852(3), Os2-Os5 2.840(3), Os2-Os7 2.875(3), Os2-Os8 2.843(3), Os3-Os5 2.772(3), Os3-Os8 2.803(4), Os4-Os5 2.870(3), Os4-Os6 2.774(3), Os4-Os7 2.838(3), Os4-Os9 2.859(3), Os5-Os6 2.772(3), Os5-Os8 2.864(3), Os5-Os9 2.850(3), Os6-Os9 2.814(3), Os7-Os8 2.953(3), Os7-Os9 2.956(3), Os8-Os9 2.951(2), Os10-Os11 2.964(3), Os10-Os12 2.951(3), Os10-Os13 2.811(3), Os10-Os14 2.858(3), Os10-Os16 2.853(3), Os11-Os12 2.969(2), Os11-Os14 2.852(3), Os11-Os15 2.817(3), Os11-Os17 2.831(3), Os12-Os16 2.855(3), Os12-Os17 2.860(3), Os12-Os18 2.822(3), Os13-Os14 2.764(3), Os13-Os16 2.774(3), Os14-Os15 2.773(3), Os14-Os16 2.858(3), Os14-Os17 2.846(3), Os15-Os17 2.785(3), Os16-Os17 2.874(3), Os16-Os18 2.792(3), Os17-Os18 2.779(3); Pd–Pd bonds: Pd1-Pd2 2.733(5), Pd1-Pd3 2.728(5), Pd2-Pd3 2.717(5); Os–Pd bonds: Os7-Pd1 2.751(4), Os7-Pd3 2.770(4), Os8-Pd1 2.773(5), Os8-Pd2 2.744(4), Os9-Pd2 2.774(4), Os9-Pd3 2.764(5), Os10-Pd1 2.777(5), Os10-Pd3 2.766(4), Os11-Pd1 2.732(4), Os11-Pd2 2.766(4), Os12-Pd2 2.768(5), Os12-Pd3 2.777(4).

[*] Prof. W.-T. Wong, K.-F. Yung
Department of Chemistry
The University of Hong Kong
Pokfulam Road, Hong Kong (P.R. China)
Fax: (+852) 2547-2933
E-mail: wtwong@hku.hk

[**] We gratefully acknowledge financial support from the Hong Kong Research Grants Council and the University of Hong Kong. K.-F.Y. acknowledges the receipt of a postgraduate studentship and a Swire Scholarship (2000–2001), administrated by the University of Hong Kong.

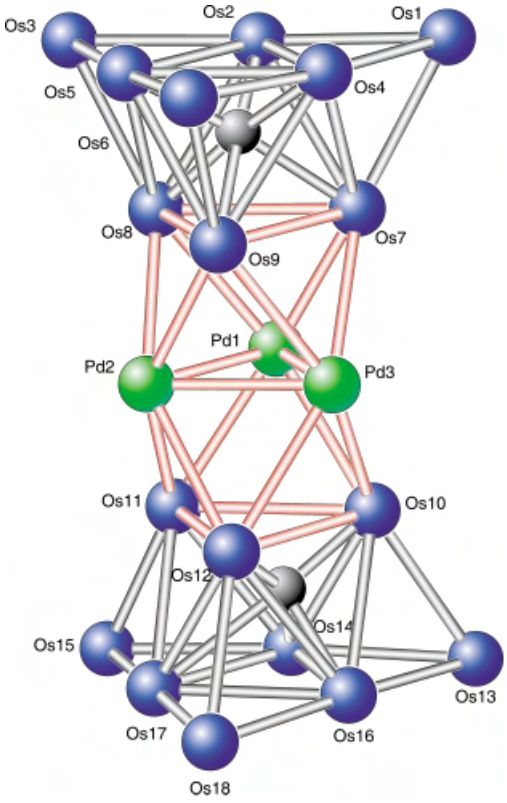


Figure 2. The metal core-geometry of cluster **1** illustrating the position of the carbide ions, which are located above and below the central bimetallic face.

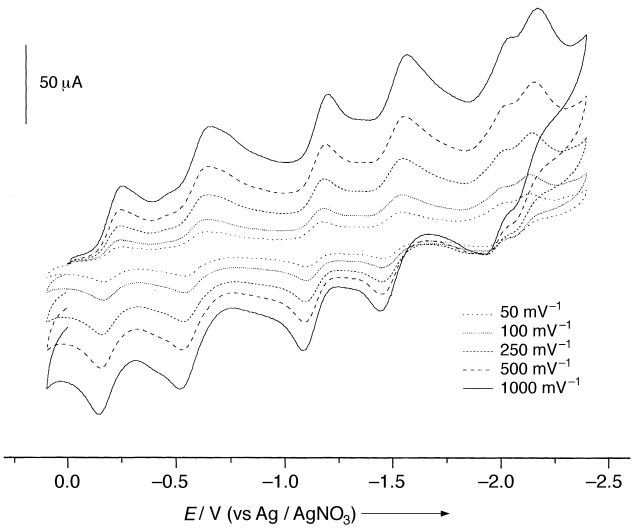


Figure 3. Cyclic voltammogram of $[\{N(PPh_3)_2\}_2\{Os_{18}Pd_3(\mu_6\text{-}C)_2(CO)_{42}\}]$ in acetone containing 0.1 M tBu$_4$NPF$_6$; glassy carbon working electrode, platinum auxiliary electrode, and Ag/AgNO$_3$ reference electrode; the scan rate was varied from 50 to 1000 mV s^{-1}.

The average Os–Pd bond length is 2.764(5) Å, which falls well within the normal range for Os–Pd bonds (2.6–2.9 Å).[6] The Os–Os bonds in the two layers either side of Pd_3 subcluster are elongated (2.958(3) Å) when compared to the remaining Os–Os bonds (av. 2.806(5) Å). This phenomenon is also observed in the $[Os_{18}Hg_3(\mu_6\text{-}C)_2(CO)_{42}]^{2-}$ [11] and $[Ru_{18}Hg_3(\mu_6\text{-}C)_2(CO)_{42}]^{2-}$ ions.[12] All carbonyl groups are terminally bound to the cluster, as suggested by solution IR spectroscopy. In addition, ^{1}H NMR spectroscopy confirms that there are no associated hydride species, since there are no signals detected between −40 and 10 ppm; such species are common in high-nuclearity clusters. The UV/Vis spectrum of **1** shows an absorption peak at 664 nm, which is believed to be a charge-transfer band, and is commensurate with its dark-green color. The negative FAB mass spectrum of **1** shows a signal for the parent monoanion centered at m/z 4944 (calcd 4944) and another at m/z 2472 (calcd 2472) for the dianionic species. Cluster **1** contains 57 metal–metal bonds and 268 cluster valence electrons (CVE). However, this structure cannot be rationalized by common electron-counting rules.[13] This is not entirely unexpected, as many Os–Pd or Os–Pt mixed-metal clusters do not obey such as alternative stable 16-electron configurations of Pd and Pt can exist. Nevertheless, this bimetallic system can be viewed as having two $[Os_9(\mu_6\text{-}C)(CO)_{21}]^{2-}$ ions sandwiching the central $\{Pd_3^{2+}\}$ unit.

To investigate the redox properties of this new mixed-metal cluster anion, the electrochemistry of **1** at room temperature was examined (Figure 3); the electrochemical data are summarized in Table 1. Cluster **1** exhibits five reversible cathodic waves at $E_{pc} = -0.14$, -0.52, -1.08, -1.51, and -2.02 V versus a Ag/AgNO$_3$ electrode in acetone. The cathodic wave at $E_{pc} = -1.94$ V results from the presence of the $[N(PPh_3)_2]^+$ ion, which is the counterion of the cluster, and cannot be removed. Analysis of the cyclic voltammetric responses relating to these five peaks, with the scan rate varying from 50 to 1000 mV s^{-1}, indicates that the peak current ratio i_{pa}/i_{pc} remains close to unity. The current function is essentially constant and the peak-to-peak separation lies between 50–80 mV, which is comparable with that of ferrocene under the same experimental conditions. The increase in anionic charge on the cluster does not prevent the cluster from accepting electrons, as the gaps between the cathodic waves do not increase significantly. The trend of these reversible cathodic waves shows that this mixed-metal nanocluster can act as an electron reservoir, with the ability to gain or lose electrons without significant decomposition. The observed electrochemical behavior is significantly different to that of the analogous mercury cluster. Upon receiving electrons, a Hg ion is eliminated to form a more stable

Table 1: Electrochemical data[a] for cluster **1**.

Reduction potential [V][b]		Oxidation potential [V][b]	
E_{pa1}	(−0.14)[c]	E_{pc2}	0.48
E_{pa2}	(−0.52)	E_{pc1}	0.29
E_{pa3}	(−1.08)		
E_{pa4}	(−1.51)		
E_{pa5}	(−2.02)		

[a] Approximately 10^{-3} M of **1** in acetone containing 0.1 M tBu$_4$NPF$_6$ at 298 K; the working electrode was a glassy carbon electrode, the auxiliary electrode was platinum, and the reference electrode was Ag/AgNO$_3$ (0 V, calibrated with ferrocene); the scan rate was 100 mV s^{-1}. [b] E_{pa} and E_{pc} are the anodic and cathodic potentials, respectively. [c] The values in parentheses are half-wave potential ($E_{1/2}$) values.

 © 2003 Wiley-VCH Verlag GmbH & Co. KGaA, Weinheim 1433-7851/03/4205-0554 $ 20.00+.50/0

cluster, $[\{N(PPh_3)_2\}_2\{Os_{18}Hg_2(\mu_6\text{-}C)_2(CO)_{42}\}]$.[14] The average separation between the cathodic waves is 0.47 V, which is consistent with the trend observed for the average separation of the electrode potentials of consecutive redox couples, with respect to cluster nuclearity.[15] With regard to oxidation, cluster **1** exhibits two irreversible anodic waves at $E_{pa} = +0.29$ and $+0.48$ V versus the $Ag/AgNO_3$ electrode in acetone. Thus, the oxidation process leads to a breakdown of the cluster.

The coordination of further ligands to cluster **1** is possible as a result of its ability to exhibit various reversible electronic states, in addition to possessing an exposed naked palladium site for the coordination of targeted substrate molecules. Further study on the reactivity of this cluster is in progress.

Experimental Section

All experiments were carried out under a nitrogen atmosphere with dry deoxygenated solvents. $[\{N(PPh_3)_2\}_2\{Os_{10}(\mu_6\text{-}C)(CO)_{24}\}]$ was stirred with an excess of $[Pd(NCMe)_4](BF_4)_2$ in CH_2Cl_2 at room temperature for one hour. The $[Os_{18}Pd_3(\mu_6\text{-}C)_2(CO)_{42}]^{2-}$ ion, which was isolated as the $[\{N(PPh_3)_2\}]^+$ salt, is obtained in 37% yield. Cluster **1** was fully characterized by spectroscopic techniques (IR, FAB MS, ^{1}H NMR) and X-ray crystallography.

1: IR (CH_2Cl_2): $\tilde{\nu} = \nu(CO) = 2060$ (s), 2008 cm^{-1} (s); ^{1}H NMR (300 MHz, CD_2Cl_2): no hydride signal detected; negative FAB mass spectrum: $m/z = 4944$ (monoanion; calcd 4944), 2472 (dianion; calcd 2472); UV/Vis (CH_2Cl_2): $\lambda_{max} = 664$ nm $\varepsilon = 40100$ mol dm^{-3} cm^{-1}; elemental analysis (%) calcd for $C_{116}H_{60}N_2O_{42}P_4Pd_3Os_{18}$: C 23.139, H 1.004, N 0.465, P 2.057; found: C 23.151, H 1.023, N 0.472, P 2.086.

Crystal data of **1**: $C_{116}H_{60}N_2O_{42}P_4Os_{18}Pd_3$, $M_W = 6020.43$, triclinic, space group $P\bar{1}$ (no. 2), $a = 15.607(1)$, $b = 18.357(1)$, $c = 25.350(2)$ Å, $\alpha = 85.14(1)$, $\beta = 83.08(1)$, $\gamma = 76.95(1)°$, $V = 7011.2(9)$ Å^3, $Z = 2$, $\rho_{calcd} = 2.852$ g cm^{-3}, $F_{(000)} = 5344$, $\mu(Mo_{K\alpha}) = 167.15$ cm^{-1}, dimensions $0.12 \times 0.13 \times 0.15$ mm. 40769 reflections were collected with 29169 unique reflections and merged to give 13454 ($R_{int} = 0.119$) observed data [$I > 1.50\sigma(I)$]. The data were collected on a Bruker SMART 1K CCD diffractometer. Structures were solved by direct methods (SHELXS86) and Fourier-difference techniques, refined by full-matrix least-squares analysis to give $R = 0.098$ and $R_w = 0.094$. CCDC-194450 contains the supplementary crystallographic data for this paper. These data can be obtained free of charge via www.ccdc.cam.ac.uk/conts/retrieving.html (or from the Cambridge Crystallographic Data Centre, 12, Union Road, Cambridge CB2 1EZ, UK; fax: (+44) 1223-336-033; or deposit@ccdc.cam.ac.uk).

Received: October 4, 2002 [Z50295]

[1] *Clusters and Colloids From Theory to Applications*, (Ed.: G. Schmid), VCH, New York, **1994**; *Physics and Chemistry of Metal Cluster Compounds* (Ed.: L. J. de Jongh), Kluwer, Dordrecht, **1994**.

[2] B. C. Gates, *Chem. Rev.* **1995**, *95*, 511 – 522; *Catalysis by Di- and Polynuclear Metal Cluster Complexes*, (Eds.: R. D. Adams, F. A. Cotton), Wiley-VCH, New York, **1998**; N. Toshima, T. Yonezawa, *New J. Chem.* **1998**, *22*, 1179 – 1201; *Metal Clusters in Chemistry* (Eds.: P. Braunstein, L. A. Oro, P. R. Raithby), Wiley-VCH, New York, **1999**; *Handbook of Heterogeneous Catalysis* (Eds.: G. Ertl, H. Knözinger, J. Weitkamp), Wiley-VCH, New York, **1994**; *Applied Homogeneous Catalysis with Organometallic Compounds, Vol. 1 (Applications), Vol. 2 (Developments)* (Eds.: B. Cornils, W. A. Herrmann), VCH, New York, **1996**.

[3] G. Longoni, M. Manassero, M. Sansoni, *J. Am. Chem. Soc.* **1980**, *102*, 3242 – 3244.

[4] T. Nakajima, A. Ishiguro, Y. Wakatsuki, *Angew. Chem.* **2000**, *112*, 1175 – 1177; *Angew. Chem. Int. Ed.* **2000**, *39*, 1131 – 1134.

[5] M. Kawano, J. W. Bacon, C. F. Campana, B. E. Winger, J. D. Dudek, S. A. Sirchio, S. L. Scruggs, U. Geiser, L. F. Dahl, *Inorg. Chem.* **2001**, *40*, 2554 – 2569.

[6] J. W.-S. Hui, W.-T. Wong, *J. Cluster Sci.* **1999**, *10*, 91 – 108; S.-M. Lee, W.-T. Wong, *J. Cluster Sci.* **1998**, *9*, 417 – 444; J. W.-S. Hui, W.-T. Wong, *J. Chem. Soc. Dalton Trans.* **1998**, *12*, 2065 – 2070; J. W.-S. Hui, W.-T. Wong, *Chem. Commun.* **1997**, *20*, 2009 – 2010; J. W.-S. Hui, W.-T. Wong, *J. Chem. Soc. Dalton Trans.* **1997**, 2445 – 2450; J. W.-S. Hui, W.-T. Wong, *J. Chem. Soc. Dalton Trans.* **1997**, 1515 – 1520; J. W.-S. Hui, W.-T. Wong, *J. Chem. Soc. Dalton Trans.* **1996**, 2887 – 2888; S. Chan, S.-M. Lee, Z. Lin, W.-T. Wong, *J. Organomet. Chem.* **1996**, *510*, 219 – 231; S. Chan, W.-T. Wong, *J. Chem. Soc. Dalton Trans.* **1995**, 3987 – 3994; S. Chan, W.-T. Wong, *J. Organomet. Chem.* **1995**, *489*, C78-C80; S. Chan, W.-T. Wong, *J. Chem. Soc. Dalton Trans.* **1994**, 1605 – 1606.

[7] R. F. Schramm, B. B. Wayland, *J. Chem. Soc. Chem. Commun.* **1968**, 898 – 899.

[8] P. F. Jackson, B. F. G. Johnson, J. Lewis, M. McPart, *Chem. Commun.* **1980**, 224 – 226.

[9] S. Martinengo, A. Fumagalli, R. Bonfichi, G. Ciani, A. Sironi, *J. Chem. Soc. Chem. Commun.* **1982**, 825 – 826.

[10] L. H. Gade, B. F. G. Johnson, J. Lewis, M. McPartlin, H. R. Powell, *J. Chem. Soc. Chem. Commun.* **1990**, 110 – 113.

[11] L. H. Gade, B. F. G. Johnson, J. Lewis, M. McPartlin, T. Kotch, A. J. Lees, *J. Am. Chem. Soc.* **1991**, *113*, 8698 – 8708.

[12] P. J. Bailey, B. F. G. Johnson, J. Lewis, M. McPartlin, H. R. Powell, *J. Chem. Soc. Chem. Commun.* **1989**, 1513 – 1515.

[13] D. M. P. Mingos, *Acc. Chem. Res.* **1984**, *17*, 311 – 319; D. M. P. Mingos, *J. Chem. Soc. Chem. Commun.* **1983**, 706 – 708.

[14] L. H. Gade, B. F. G. Johnson, J. Lewis, G. Conole, M. McPartlin, *J. Chem. Soc. Dalton Trans.* **1992**, 3249 – 3254.

[15] F. F. de Biani, C. Femoni, M. C. Iapalucci, G. Longoni, P. Zanello, A. Ceriotti, *Inorg. Chem.* **1999**, *38*, 3721 – 3724.

Biomimetic Structures Through CVD

Exact Replication of Biological Structures by Chemical Vapor Deposition of Silica**

*Gary Cook, Peter L. Timms, and Christine Göltner-Spickermann**

Biological species produce a rich variety of structures or forms that serve their needs of adaptation and survival. The success of these forms often depends on the underlying organization of their structure from the nanometer scale upwards.[1,2] The superb performance of biologically derived inorganic materials is usually not reproduced in synthetic analogues, which is why the biomimetic or bio-inspired approach towards new functional materials is currently a topic of research interest.[3,4] The mechanisms of formation of most biological structures are often extremely complex, therefore the exact imitation of biological form in a chemistry laboratory is difficult. However, the synthetic replication of evidently useful biological structures by a simple casting process is expected to introduce some of the superb properties of biological structures into man-made materials. Wet-chemistry techniques, as applied to polymer gels[5] or microfibers,[6] can cause considerable damage to a delicate biological specimen, but chemical vapor deposition (CVD) has greater potential. Herein we demonstrate that the controlled vapor-phase oxidation of silanes on the surface of biological structures produces an exact, inorganic oxide replica of the natural form.

At room temperature and under pressures in the range between 1 and 5 hPa, silane reacts with an excess of vaporized hydrogen peroxide to deposit silica on almost any material by a surface-phase process.[7–9] This reaction was initially developed for depositing a smooth dielectric layer of silica on silicon wafers, but is now shown to be an outstandingly effective way of coating delicate biological specimens. Conventional CVD processes create a stream of oxide particles in gas-phase reactions, which cannot uniformly coat a three-dimensional object because of shadowing. Other techniques employ surface reactions, but at elevated temperatures detrimental to delicate (biological) specimens. The apparatus for the reaction of hydrogen peroxide and silane is shown in Figure 1. The CVD of silica is known to produce silica primary clusters. These clusters have extraordinary flow properties and are capable of "creeping" into smallest gaps within the substrate,[9] which makes the method promising for the replication of intricately structured objects. The biological specimens used in this study were chosen for their structure-related function, for example, optical properties, mechanical stability, or surface energy.

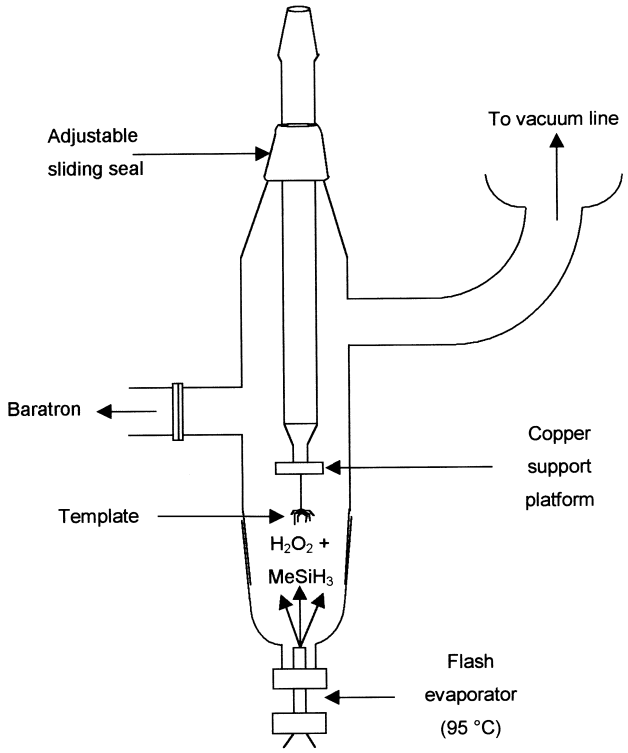


Figure 1. Experimental apparatus for the chemical vapor deposition of silica.

In all cases the relatively soft templates are substantially harder after the deposition of silica and brittle after removal of the biological structure through calcination (combustion of the organic material at 500 °C in air). However, the coated materials as well as the calcined, all-inorganic products can be handled easily with tweezers. Depending on the thickness of the silica layer, the film is either invisible, translucent, or white. The true character of the replication process is revealed by scanning electron microscopy (SEM). The beautifully iridescent 2D-photonic bandgap material[10] of a butterfly wing (Figure 2a), designed by nature for aerodynamics, light weight, protection, and finding a suitable mate (color!), can be replicated by CVD of silica. Figure 2b shows the hollow silica replica obtained from a Peacock butterfly. The overall dimension of the wing is reduced by 25% due to shrinkage during calcination, which also causes slight creasing, but the structural features of the 100–150 nm thick replica are clearly visible (Figure 2b, inset). In contrast, if the same type of butterfly wing is subjected to dip-coating with a sol–gel precursor solution, there is a very evident lack of compatibility (dewetting) between the wing and the inorganic coating, and catastrophic cracking of the coating occurs because of shrinkage (not shown here).

More interestingly, this process can be applied to replicate hierarchical structure, such as the hairy, protective surface of a

[*] C. Göltner-Spickermann, G. Cook, P. L. Timms
School of Chemistry
University of Bristol
Bristol BS8 1TS (UK)
Fax: +44 1179251295
E-mail: goltner@supanet.com

[**] The authors would like to thank Stratford Butterfly Farm and Alan Stealey from Bristol Gardens for the generous supply of naturally deceased butterflies and live plants, respectively. Prof. Fritz Vollrath is gratefully acknowledged for supplying the spider silk. G.C. gratefully acknowledges the Engineering and Physical Sciences Research Council (EPSRC) for a studentship.

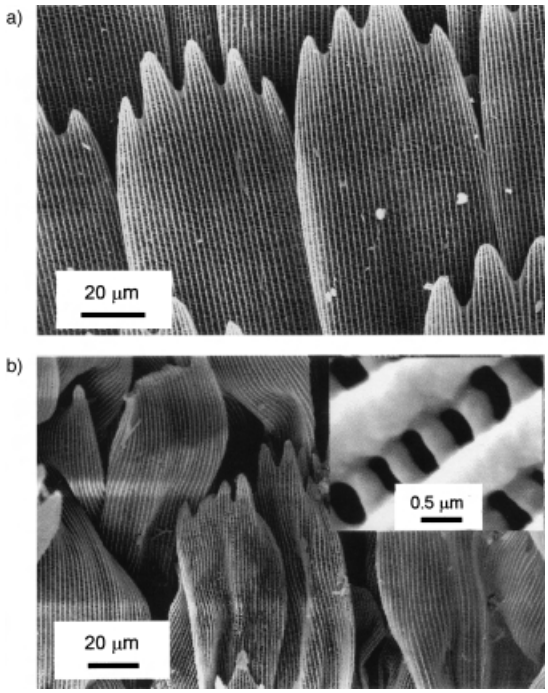


Figure 2. a) Details of a peacock butterfly wing revealed by SEM. b) Calcined silica replica showing a slight degree of creasing as a consequence of heat treatment. Insert: high-magnification image.

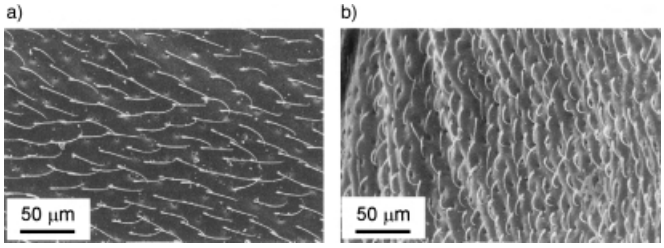


Figure 3. The hairy wing of a housefly can be replicated precisely by CVD of silica. a) Original specimen, b) The hollow silica replica not only maintains structural identity, but is also macroscopically iridescent.

housefly wing, a structure designed by nature to be self cleaning in that dust particles are repelled from the wing. The specimen (see Figure 3a) consists of a smooth surface with periodic indentations 2 μm wide and almost 2-μm-thick hairs protruding from it, which are periodically spaced, approximately 20 μm apart. This structure is precisely replicated (Figure 3b) in a hollow silica cast, again allowing for a slight degree of shrinkage as a result of heat treatment (calcination). It can be imagined that the function of such surfaces (optical properties, repellency) could be preserved in the inorganic replica, which in turn would introduce specific properties, such as a particular refractive index or sorption behavior. Indeed, the all-inorganic replica of the house-fly wing shows the same iridescence as the biological specimen.

The replication of ultrahydrophobic, self-cleaning plant leaves (*colocasia esculenta*, see Figure 4a, and common pond weed, Figure 4b) is equally successful and produces an exact cast of the leaf structure.[11] The comparison of contact angles

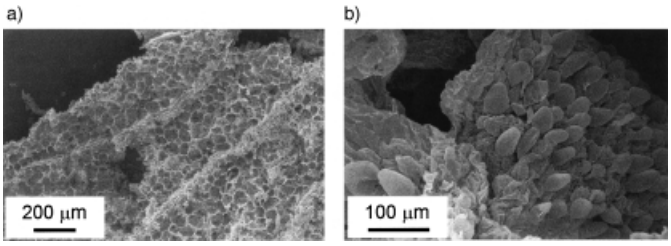


Figure 4. a) Figure 4a: SEM image of a silica cast obtained from the leaf surface of *colocasia esculenta*, a self-cleaning plant. b) SEM image of the silica replica obtained from a common pond-weed leaf, likewise an ultrahydrophobic surface.

of water on a silica layer structured like this with those of water on a smooth blank is expected to provide information on the extent of structural contribution to the ultrarepellency of rough surfaces (lotus effect). Regardless of surface polarity, the CVD of silica from silane provides a means of faithfully replicating the most intricately structured biological specimens without the occurrence of artifacts. This universal behavior can be explained in two ways, partly by the reaction conditions, as the vacuum in the reaction chamber would remove nanoscopic air bubbles, which are held responsible for the ultrahydrophobic character of many surfaces[12] and partly by the variety of ways hydrogen peroxide can bind to surfaces, creating sites at which the oxidation of silane can occur.

Using this technique organic fibers of many types can be successfully coated with silica and then calcined to leave silica tube replicas of 200 nm thick nylon, spider silk of 2 μm diameter, sucrose-based "candyfloss" fibers of 5–10 μm diameter (not shown here). Even more complex, three-dimensional structures, such as the chitin skeleton of cuttlefish bone[13] can also be replicated precisely.

The thickness of the ceramic layer is controlled by the amount of silane added to the deposition chamber and the reaction time. Typical thicknesses are between 100 nm and 2 μm. Depending on the size of the object and the thickness of the layer the degree of shrinkage observed as a consequence of calcination lies between 5 and 40%, which is little compared with materials of similar dimensions derived by sol–gel processing. In addition, removal of the underlying template by heat treatment in air does not cause cracking of the inorganic coating, which is a common problem in sol–gel derived ceramic coatings.

The method presented here is chemically flexible, as mixing the silane with varying amounts of diborane, phosphane, or germane produces borosilicate, phosphosilicate, or germanosilicate coatings with maximum Si:B, Si:P, or Si:Ge ratios of about 3:1, 3:4 or 1:4, respectively.

We also propose this CVD technique as a novel tool for the generation of intricate and hierarchical structures on several length scales. As specimens do not appear to change shape, we propose the coating of biological structures with an invisibly thin film of silica as a possible means of conservation of delicate biological specimens (fixing). Nature provides an abundance of shapes which can be synthetically modified and preserved by this facile and inexpensive process.

 © 2003 Wiley-VCH Verlag GmbH & Co. KGaA, Weinheim 1433-7851/03/4205-0558 $ 20.00+.50/0

Experimental Section

Liquid 60% hydrogen peroxide (3 mmol $H_2O_2\,min^{-1}$) was sucked through fine teflon tubing into a flash evaporator at 90 °C. The peroxide vapor mixed with gaseous silane (0.1–03 $mmol\,min^{-1}$) a few centimeters below where the template (substrate) was suspended in a pyrex glass reaction chamber. The sample and all internal surfaces of the reaction chamber became coated with silica at a rate of 50–200 $nm\,min^{-1}$. The layer thickness was adjusted through the amount of silane precursor and the reaction time. Subsequent pumping on the reaction chamber at 0.01 hPa assisted in removing side products as well as giving a highly condensed silica network. The organic template was removed by calcination at 500 °C in air. As known from earlier studies of the deposition on silicon wafers, silane can be replaced by the less pyrophoric methylsilane to give silica containing only a very small amount of organic groups.[6]

Received: April 26, 2002
Revised: September 23, 2002 [Z19180]

[1] *Biomineralization: Chemical and Biochemical Perspectives* (Eds.: S. Mann, J. Webb, R. J. P. Williams), VCH Weinheim, **1989**.
[2] S. Mann, *Biomineralization, Principles and Concepts in Bioinorganic Materials Chemistry*, Oxford University Press, **2001**.
[3] S. Mann, *Angew. Chem.* **2000**, *112*, 3532; *Angew. Chem. Int. Ed.* **2000**, *39*, 3392.
[4] *Biomimetic Materials Chemistry* (Ed.: S. Mann), VCH, Weinheim, **1996**.
[5] R. A. Caruso, J. H. Schattka, A. Greiner, *Adv. Mater.* **2001**, *13*, 1577.
[6] R. A. Caruso, M. Antonietti, *Chem. Mater.* **2001**, *13*, 3272.
[7] M. P. Taylor, P. L. Timms, G. C. Allen, S. R. Church, *J. Mater. Chem.* **1998**, *8*, 1769.
[8] D. L. Moore, P. L. Timms, G. C. Allen, S. R. Church, *J. Chem. Soc. Dalton Trans.* **2000**, *16*, 2673.
[9] M. P. Taylor, P. L. Timms, *J. Chem. Soc. Dalton Trans.* **1997**, *6*, 1049.
[10] H. Tada, S. E. Mann, I. N. Miaoulis, P. Y. Wong, *Opt. Express* **1999**, *5*, 87.
[11] W. Barthlott, C. Neinhuis, *Planta* **1997**, *202*, 1.
[12] P. Attard, J. W. G. Tyrell, *Phys. Rev. Lett.* **2001**, *87*, 176104.
[13] W. Ogasawara, W. Shenton, S. A. Davis, S. Mann, *Chem. Mater.* **2000**, *12*, 2835.

Patterned Polymer Brushes

Surface-Initiated Polymerization on Self-Assembled Monolayers: Amplification of Patterns on the Micrometer and Nanometer Scale**

Ursula Schmelmer, Rainer Jordan, Wolfgang Geyer, Wolfgang Eck, Armin Gölzhäuser,* Michael Grunze, and Abraham Ulman*

The application of highly ordered self-assembled monolayers (SAMs) as initiator systems for surface-initiated polymerization (SIP) allows the preparation of uniform and densely grafted polymer brushes. This so-called "grafting from" technique was demonstrated for nearly all types of polymerization,[1] including living anionic[2] and cationic SIP.[3] One important aspect offered by the use of SAM systems as two-dimensional initiator systems is the possibility to control the locus of the initiator sites within a SAM, for example, to finetune the grafting density of the resulting polymer brush by using mixed SAMs,[4] to prepare two-component gradients,[5] or to fabricate complex spatial structures at various length scales. The latter can be formed by various techniques, in particular by microcontact printing (μCP) for structures ranging from 0.1 to several hundred micrometers.[6,7] For patterning on the nanometer scale, SPM-based techniques for the manipulation of SAMs such as "dip-pen nanolithography",[8] "nanografting", or "nanoshaving"[9] were recently developed.

A combination of directed deposition of functionalized areas of SAMs and consecutive SIP allows a superior control of pattern formation and amplification of the patterns by creating polymer-brush layers at predefined sites. Surface defects, present in all SAM systems, as well as topological features of the substrate are covered by a significantly thicker layer of a flexible polymer brush. The resulting structures display a better contrast between the functionalized and

[*] Dr. R. Jordan, U. Schmelmer
Lehrstuhl für Makromolekulare Stoffe
Technische Universität München
Lichtenbergstr. 4, 85747 Garching (Germany)
Fax: (+49) 89-289-13562
E-mail: rainer.jordan@ch.tum.de
Dr. A. Gölzhäuser, Dr. W. Geyer, Dr. W. Eck, Prof. Dr. M. Grunze
Angewandte Physikalische Chemie, Universität Heidelberg
Im Neuenheimer Feld 253, 69120 Heidelberg (Germany)
Fax: (+49) 6221-546-199
E-mail: goelzhaeuser@uni-hd.de
Dr. R. Jordan, Prof. Dr. A. Ulman
Department of Chemistry, Chemical Engineering, and Materials Science, Polytechnic University
Six Metrotech Center, Brooklyn, NY 11201 (USA)

[**] We thank K. Edinger (University of Maryland) for the production of the high-resolution stencil mask. Financial support from the Deutsche Forschungsgemeinschaft and the Fonds der Chemischen Industrie is gratefully acknowledged. R.J. is thankful for financial support by the Dr. Hermann-Schnell-Stiftung.

unfunctionalized areas in terms of their chemical and physical properties (e.g. interfacial roughness, wetting behavior, thermal stability, etch resistance, etc.). The wide variety of recently developed combined SAM/SIP systems allows the production of tailor-made surfaces for a given technological application.

This approach was first demonstrated by using contact-printed SAMs of ω-functionalized alkane thiols, passivation of the uncovered areas by inert *n*-alkyl thiols, and subsequent SIP of *N*-carboxy anhydrides,[10] ε-caprolactone,[11] or norbornene derivatives.[12] The created polymer-brush layers amplified the originally printed SAM structures. The lateral resolution of features obtained with this technique ranged from 2–50 μm. With the same technique, spatially resolved free[13] and controlled[14] radical SIP as well as step polymerization for the preparation of hyperbranched polymers[15] was carried out on printed SAMs. The advantages of SAM structure amplification by SIP was demonstrated by an improved etch resistance as a function of the brush-layer thickness and by the selective adsorption of cells.

In another approach, surface patterns can be created by selective UV irradiation of homogeneous SAMs of photoinitiators through a mask or processed photo resists.[16] Although the lateral resolution is limited, this approach allows a repetitive SIP on the same substrate, resulting in chemically heterogeneous polymer-brush surfaces.[17] Both techniques, however, are intrinsically limited by means of the obtainable structure size and the stability of the original SAM system.

Recently, some of us developed chemical lithography, a technique that utilizes specific reactions between the SAMs and electron beams for nanopatterning.[18,19] The name was chosen, since electron irradiation of SAMs of, for example, 4′-nitro-1,1′-biphenyl-4-thiol (NBT) results in selective and quantitative reduction of the nitro functionalities to amino groups,[20] while the aromatic biphenyl layer is dehydrogenated and cross-linked.[21] Hence, the local irradiation of SAMs can be used for the chemically selective binding of functional entities by using the terminal amino group.

In contrast to the above-mentioned techniques based on scanning probe microscopy and microcontact printing, chemical lithography is not restricted to any length scale since the use of electron-flood guns in combination with adequate stencil masks allows an efficient patterning of large areas. For high-resolution patterning, electron beams can be focused to nanometer-sized spots, and the resolution is only limited by secondary electrons that are generated during irradiation. The smallest SAM structures that have been generated with electron beams are about 5 nm in size;[22] thus far, the smallest chemical nanostructures obtained by chemical lithography had lateral dimensions of ~20 nm.[18,19]

The selectivity, flexibility, high throughput, and superior resolution of chemical lithography make it an ideal technological platform for the preparation of structured, functionalized SAM patterns that can be amplified by SIP. Herein we present a facile method for the conversion of patterns created by irradiation of NBT SAMs through a mask into patterned polymer-brush systems.

The preparation of initiator sites and a consecutive polymerization was first carried out without structuring: A SAM of NBT on Au(111) was converted into cross-linked 4′-amino-1,1′-biphenyl-4-thiol (cABT) SAM by irradiation with electron beams, as previously reported (50 eV with an electron dose of 20000 μC cm^{-2} or 300 eV with 40000 μC cm^{-2}).[20] The terminal amino groups were then diazotized and treated with methylmalonodinitrile to give a surface-bound monolayer of the 4′-azomethylmalonodinitrile-1,1′biphenyl-4-thiol (cAMBT) (Figure 1). Phenyldiazenylalkylmalonodinitriles and their derivatives are suitable second-generation initiators for the radical polymerization of a broad variety of vinyl compounds to prepare graft copolymers in solution,[23] as well as for SIP.[17,24] In contrast to commonly used symmetric azo initiators, thermal or photoinitiated decomposition yields a highly reactive, bound (in our case) phenyl radical and a free, stable malonodinitrile radical, which is not capable of initiating radical polymerization owing to its resonance stabilization. In other words, by the decomposition of the surface-bound, asymmetric phenylazoalkyl initiator, the polymerization is only initiated at the surface and not by a cleaved free radical in solution, as is the case with dialkylazo initiators.[25] Furthermore, previous results indicate that the radical polymerization initiated by phenylazomethylmalonodinitrile follows a controlled polymerization mechanism: in "grafting from" reactions the degree of polymerization of the side chains can be varied with the reaction time and the typical polydispersity index is significantly lower ($M_w/M_n \sim 1.4$) than in free-radical polymerization.[26]

The monolayer of cAMBT was then exposed to a solution of styrene in toluene and heated to 80 °C, and the polymerization was thus started by thermal decomposition of the SAM initiator system. After a reaction time of 6 hours, unbound polystyrene was removed from the substrate surface by Soxhlet extraction. Inspection of the substrate surface with FTIR spectroscopy, scanning probe microscopy (SPM), and ellipsometry revealed that the surfaces were homogeneously covered by a polystyrene brush layer of 6.3 nm.[27,28] The surface modification proved to be surprisingly stable at elevated temperatures and resistant to solvent extraction (Soxhlet) as a result of the cross-linked SAM support and the known stabilization effect of the polymer brush itself.[2,3a] The SPM scans of the polymer brush, contrary to those of the native polycrystalline gold substrate, showed the rendering of the single gold crystals, with a decrease in the step height of individual crystals from ~2.5 nm to approximately 1 nm and a small decrease in the root-mean-square roughness value to 0.7 nm (from 0.9 nm for the original surface roughness of the gold substrate).

The structured polystyrene brushes were prepared by following the same procedures (Figure 1 a–d), but the irradiation was performed through a stencil mask with circular openings of 800-nm radii[29] which was placed on the NBT-covered substrate. Figure 2 a shows an scanning electron micrograph recorded at an electron energy of 3 keV using the "in-lens" detector, which is particularly sensitive to secondary electrons emitted from the sample surface. The contrast results from the differences in the secondary electron yield from the original SAM/gold substrate and the thin polystyrene film. The dark dots represent areas where NBT was

 © 2003 Wiley-VCH Verlag GmbH & Co. KGaA, Weinheim 1433-7851/03/4205-0560 $ 20.00+.50/0

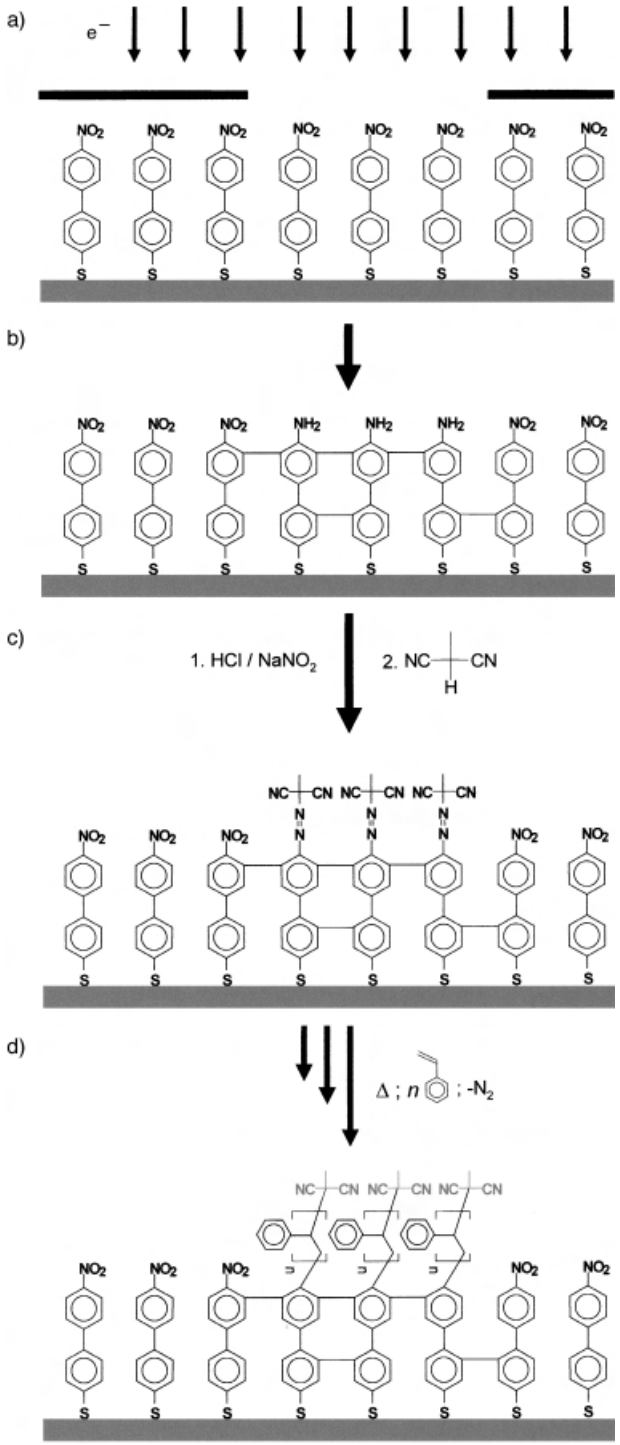


Figure 1. Reaction scheme starting from SAMs of NBT on Au(111). a) Exposure of the monolayer to electron beams. b) This irradiation results in intralayer cross-linking and conversion of the terminal nitro groups into amino groups, thus forming cABT. c) Diazotization and coupling with malonodinitrile gives a SAM that bears an asymmetric azo initiator (cAMBT). d) Finally, by exposure to a vinyl monomer (styrene) and heating at 80 °C, the radical polymerization results in a polymer brush layer at the irradiated areas.

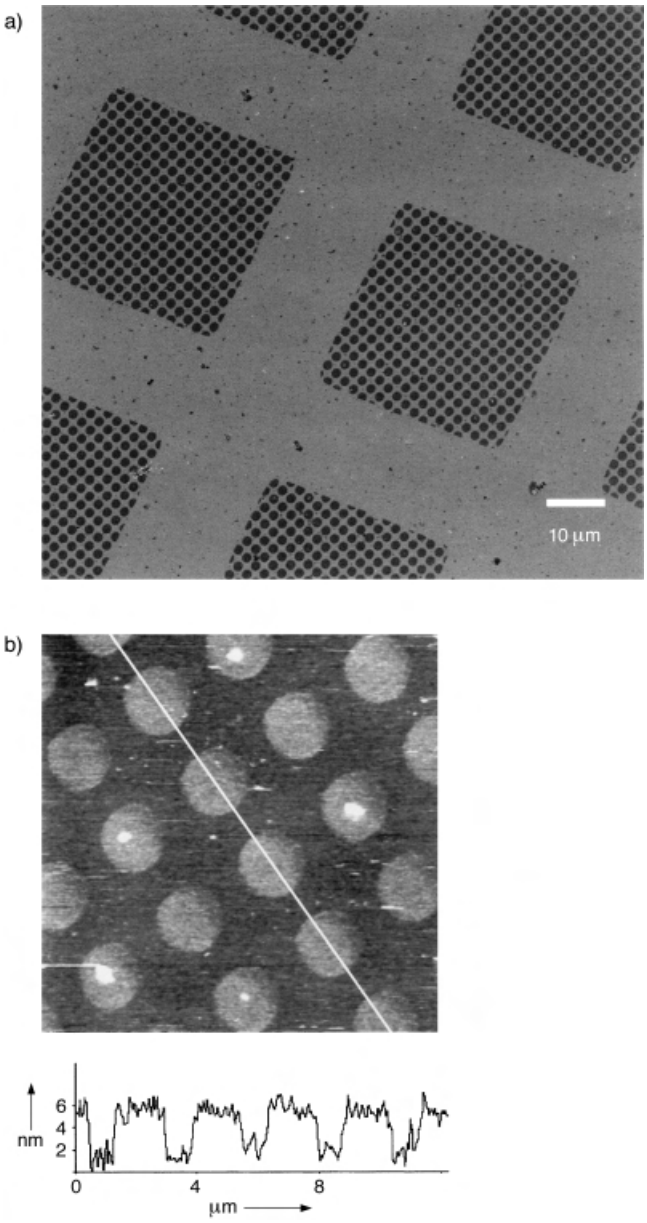


Figure 2. a) Scanning electron micrograph of polystyrene brushes generated by SIP on a substrate that was irradiated through a stencil mask with a coarse grid with a 60-µm periodicity. Each square contains an array of circular holes (1.6-µm diameter, 2.5-µm periodicity). b) SPM image of a small area of the same substrate, together with a height profile along the indicated line.

converted into cABT by irradiation, which reacted further to form cAMBT, and where SIP of styrene took place. The selectivity and uniformity of the process on this large scale is significant. We further investigated the surface topography by SPM (Figure 2b), which revealed typical heights of the polystyrene spots of 6 nm, a diameter of 1.6 µm; the spots were spaced with a periodicity of 2.5 µm. This pattern reflects a one-to-one translation of the original mask at the surface. Investigation of different areas by SPM showed nearly no variation of the structures.

As a test of the potential of our approach, a stencil mask made by focused ion-beam milling[21] with slits between 50 and 300 nm wide, was also used for the selective irradiation and amplification by SIP. The SPM micrographs of the

 © 2003 Wiley-VCH Verlag GmbH & Co. KGaA, Weinheim 1433-7851/03/4205-0561 $ 20.00+.50/0

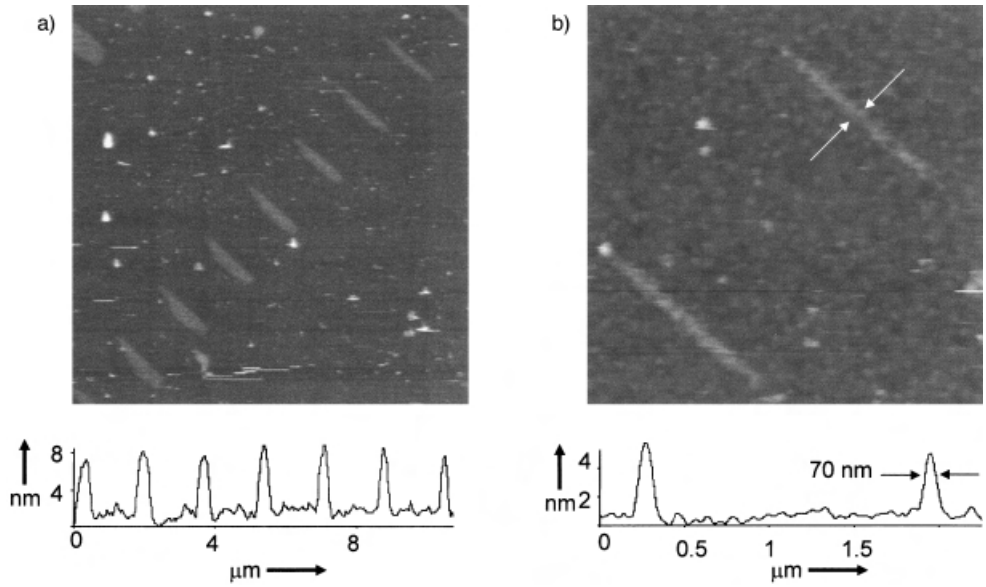


Figure 3. AFM micrographs of polystyrene brushes, which were generated by irradiation of an NBT SAM with a stencil mask with a slit pattern and subsequent SIP. The height profiles show an average profile with lines of width ~200 nm (a) and ~70 nm (b).

resulting polystyrene brush-line structures together with averaged height profiles are depicted in Figure 3. Again, SIP was limited to the NBT SAM originally exposed to radiation, resulting in a one-to-one translation of the mask pattern in the nanometer range.

These structures created by the combination of chemical lithography and SIP are significantly smaller than features produced by using previously known techniques.[10–15] This approach allows the choice of surface structures that can be created and the material contrast that can be realized by the combination of chemical lithography and amplification with SIP. Furthermore, micrometer- as well as nanometer-sized features can be generated in a single step.

Experimental Section

The polycrystalline gold films on silicon were obtained from Albert Coatings.[30] The preparation of the SAMs as well as the irradiation by low-energy electrons was performed as previously reported.[18,20,21] FTIR spectra were recorded on a Bruker IFS55 spectrometer equipped with an FT-80 external reflection setup from SpectraTech. AFM images were obtained in the tapping mode with a Nanoscope IIIa scanning probe microscope from Digital Instruments or with an Autoprobe CP scanning probe microscope from Park Scientific. Scanning electron micrographs were obtained with a LEO 1530 electron microscope with a primary electron energy of 3 kV and an in-lens detector for secondary-electron detection.

Preparation of the cAMBT/Au initiator system: The irradiated substrates bearing SAMs of cross-linked cABT were diazotized at 4 °C by treatment with an aqueous solution of HCl (0.5 mL $HCl_{conc.}$ in 2 mL water) and subsequent treatment with sodium nitrite (1 mmol) in water (2 mL). Finally, the azo initiator was prepared by the reaction of the substrate with methylmalonodinitrile[31] and sodium acetate (1 g) in water/ethanol (2.5 mL:1.5 mL) for at least 15 min.

Polymerization: A freshly prepared functionalized substrate was added to an oxygen-free solution of toluene (2 mL) and styrene (1 mL) and heated at 80 °C (for polymerization times, see text). After the reaction, all substrates were cleaned by Soxhlet extraction with toluene for at least 12 h.

Received: June 19, 2002
Revised: September 3, 2002 [Z19565]

[1] a) B. Zhao, W. J. Brittain, *Prog. Polym. Sci.* **2000**, *25*, 677, and references therein; b) R. Jordan in *Polymeric Materials in Organic Chemistry and Catalysis* (Ed.: M. Buchmeiser), Wiley-VCH, Weinheim, in print.
[2] R. Jordan, A. Ulman, J. F. Kang, M. Rafailovich, J. Sokolov, *J. Am. Chem. Soc.* **1999**, *121*, 1016.
[3] a) R. Jordan, A. Ulman, *J. Am. Chem. Soc.* **1998**, *120*, 243; b) R. Jordan, N. West, A. Ulman, Y.-M. Chou, O. Nuyken, *Macromolecules* **2001**, *34*, 1606.
[4] S. Yamamoto, M. Ejaz, Y. Tsujii, T. Fukuda, *Macromolecules* **2000**, *33*, 5608.
[5] B. Liedberg, P. Tengvall, *Langmuir* **1995**, *11*, 3821.
[6] H. Schmid, B. Michel, *Macromolecules* **2000**, *33*, 3042.
[7] Y. Xia, G. Whitesides, *Angew. Chem.* **1998**, *110*, 568; *Angew. Chem. Int. Ed.* **1998**, *37*, 550.
[8] R. D. Piner, J. Zhu, F. Xu, S. Hong, C. A. Mirkin, *Science* **1999**, *283*, 661.
[9] G. Y. Liu, S. Xu, Y. Qian, *Acc. Chem. Res.* **2000**, *33*, 457.
[10] T. Kratzmüller, D. Appelhans, H.-G. Braun, *Adv. Mater.* **1999**, *11*, 555.
[11] M. Husemann, D. Merreceyes, C. J. Hawker, J. L. Hedrick, R. Shah, N. L. Abbot, *Angew. Chem.* **1999**, *111*, 685; *Angew. Chem. Int. Ed.* **1999**, *38*, 647.
[12] N. L. Jeon, I. S. Choi, G. M. Whitesides, N. Y. Kim, P. Laibinis, Y. Harada, K. R. Finnie, G. S. Girolami, R. G. Nuzzo, *Appl. Phys. Lett.* **1999**, *75*, 4201.
[13] J. Hyun, A. Chilkoti, *Macromolecules* **2001**, *34*, 5644.
[14] R. R. Shah, D. Merreceyes, M. Husemann, I. Rees, N. L. Abbot, C. J. Hawker, J. L. Hedrick, *Macromolecules* **2000**, *33*, 597.
[15] a) W. M. Lackowski, P. Ghosh, R. M. Crooks, *J. Am. Chem. Soc.* **1999**, *121*, 1419; b) R. M. Crooks, *ChemPhysChem* **2001**, *2*, 644, and references therein.
[16] a) O. Prucker, M. Schimmel, G. Torvar, W. Knoll, J. Rühe, *Adv. Mater.* **1998**, *10*, 1073; b) H. J. Lee, Y. Nakayama, T. Matsuda,

 © 2003 Wiley-VCH Verlag GmbH & Co. KGaA, Weinheim 1433-7851/03/4205-0562 $ 20.00+.50/0

Macromolecules **1999**, *32*, 6989; c) R. Schmidt, T. Zhao, J.-B. Green, D. J. Dyer, *Langmuir* **2002**, *18*, 1281.
[17] O. Prucker, J. Habicht, I.-J. Park, J. Rühe, *Mater. Sci. Eng. C* **1999**, *8–9*, 291.
[18] A. Gölzhäuser, W. Eck, W. Geyer, V. Stadler, Th. Weimann, P. Hinze, M. Grunze, *Adv. Mater.* **2001**, *13*, 806.
[19] W. Geyer, V. Stadler, W. Eck, A. Gölzhäuser, M. Grunze, M. Sauer, T. Weimann, P. Hinze, *J. Vac. Sci. Technol. B* **2001**, *19*, 2732.
[20] W. Eck, V. Stadler, W. Geyer, M. Zharnikov, A. Gölzhäuser, M. Grunze, *Adv. Mater.* **2000**, *12*, 805.
[21] A. Gölzhäuser, W. Geyer, V. Stadler, W. Eck, M. Grunze, K. Edinger, T. Weimann, P. Hinze, *J. Vac. Sci. Technol. B* **2000**, *18*, 3414.
[22] M. J. Lercel, H. G. Craighead, A. N. Parikh, K. Seshadri, D. L. Allara, *Appl. Phys. Lett.* **1996**, *68*, 1504.
[23] O. Nuyken, R. Weidner, *Adv. Polym. Sci.* **1986**, *73–74*, 147, and references therein.
[24] N. Fery, R. Hoene, K. Hamann, *Angew. Chem.* **1972**, *84*, 359; *Angew. Chem. Int. Ed.* **1972**, *11*, 337.
[25] Another strategy to obtain this is to immobilize both termini of the azo compound: a) G. Boven, M. L. C. M. Oosterling, G. Challa, A. J. Schouten, *Polymer* **1990**, *31*, 2377; b) E. Carlier, A. Guyot, A. Revillon, M.-F. Llauro-Darricades, R. Petiaud, *React. Polym.* **1991**, *16*, 41.
[26] It is suspected that the resonance-stabilized methylmalonodinitrile radical acts as a reversible termination agent in the polymerization (P. C. Wieland, O. Nuyken, M. Schmidt, K. Fischer, *Macromol. Rapid Commun.* **2001**, *22*, 1255). Related studies are currently underway in our laboratories.
[27] The external reflection FTIR spectra of the purified surfaces (Soxhlet extraction, toluene, 12 h) confirmed that in all cases a layer of covalently attached polystyrene was formed (typical absorption bands: ($\tilde{\nu}$ in cm^{-1}): CH aromatic stretching: 3102, 3018, 3060, 3026, 2999; CH aliphatic stretching: 2922, 2848; overtones of CH out-of-plane fundamentals for monosubstituted aromatic rings: 1945, 1867, 1795; ring breathing: 1602, 1493, 1452, CH deformation modes (out-of-plane): 758, 698.
[28] Quantitative analysis of the film thickness as a function of the polymerization time and irradiation conditions are currently underway. However, the film thickness steadily increases with the time of polymerization, although not as rapidly as reported in reference [17] for the photoinitiated polymerization in the presence of a similar initiator.
[29] The stencil mask was obtained from Quantifoil Micro Tools, Jena, Germany.
[30] Georg Albert PVD-Coatings, Heidelberg, Germany (GeorgAlbert@web.de).
[31] Methylmalonodinitrile was obtained by ammonolysis (R. Meyer, P. Bock, *Justus Liebigs Ann. Chem.* **1906**, *347*, 98) and subsequent dehydration (S. Starck, *Ber. Dtsch. Chem. Ges. A* **1934**, *67*, 42) of methylmalonic acid diethyl ester.

Radical Anion Complexes

Coordinated *o*-Dithio- and *o*-Iminothiobenzosemiquinonate(1−) π Radicals in $[M^{II}(bpy)(L^{\bullet})](PF_6)$ Complexes**

*Prasanta Ghosh, Ameerunisha Begum, Diran Herebian, Eberhard Bothe, Knut Hildenbrand, Thomas Weyhermüller, and Karl Wieghardt**

Dedicated to Professor Gottfried Huttner on the occasion of his 65th birthday

o-Benzosemiquinonate(1−) π-radical anions are archetypical open-shell, bidentate ligands in the coordination chemistry of transition-metal ions[1] but for their *o*-dithio derivatives the situation is not clear. The existence of S,S-coordinated *o*-dithiobenzosemiquinonate(1−) radical anions (rather than their closed-shell, aromatic *o*-dithiolate dianions) has occasionally been suggested[2] to occur in some complexes but—at times—has also been explicitly denied.[3] Clear experimental evidence is lacking to date. Similarly, recently it has been shown indirectly that *o*-iminobenzosemiquinonate(1−) π radical ions[4] and their sulfur analogues[5] as well as *o*-diiminobenzosemiquinonate(1−)[6] π radical anions (Scheme 1) are coordinated in diamagnetic, square-planar complexes $[Ni^{II}(X^{\bullet})_2]$. Density functional theoretical (DFT) calculations have shown that the electronic structure of these species is in accord with the description as singlet diradicals.[7]

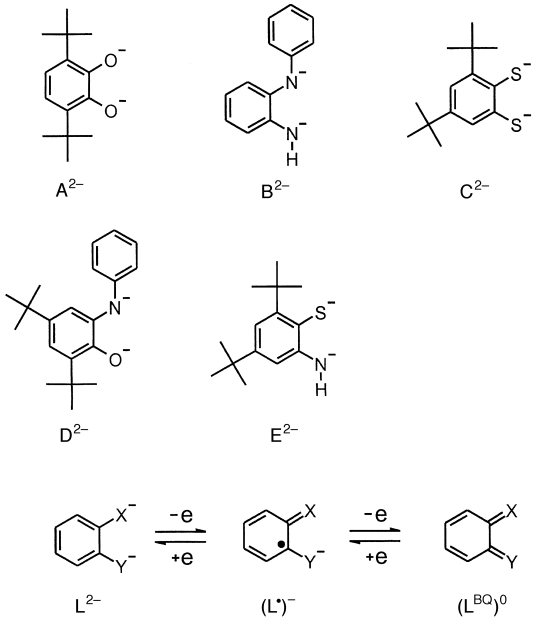
Here we report the synthesis and characterization of diamagnetic square-planar neutral complexes of Pd^{II} and Pt^{II} containing a *single* aromatic $(L)^{2-}$ ligand and a 2,2′-bipyridine ligand (Scheme 1): $[M^{II}(bpy)(X)]^0$ (**1**–**5**). We show that complexes **1**–**5** undergo a reversible, ligand-centered one-electron oxidation yielding paramagnetic complexes $[M^{II}(bpy)(X^{\bullet})](PF_6)$ (**1a**–**5a**) with a $S = {}^1/_2$ ground state and a coordinated π radical anionic ligand $(L^{\bullet})^-$.

The following complexes have been isolated as solid materials: $[Pd^{II}(bpy)(A)]$ (**1**), $[Pd^{II}(bpy)(A^{\bullet})](PF_6)$ (**1a**), $[Pd^{II}bpy)(B^{\bullet})](PF_6)$ (**2a**), [Pd(bpy)(C)] (**3**), $[Pd^{II}(bpy)(D)]$ (**4**), $[Pd^{II}(bpy)(D^{\bullet})](PF_6)$ (**4a**), $[Pt^{II}(bpy)(E)]$ (**5**), and $[Pt^{II}(bpy)(E^{\bullet})](PF_6)$ (**5a**).

The reaction of $[M(bpy)Cl_2]$ (M = Pd, Pt) and the respective ligand $H_2[A]$, …$H_2[E]$ (1:1) in CH_3CN or THF in the presence of two equivalents of a base ($NaOCH_3$, BH_4^-, or NEt_3) under argon led to the formation of the neutral species **1, 3**, and **5**, which were isolated as dark blue needles (**1**) or dark green crystals (**3** and **5**). The oxidized species **1a** (dark

[*] Prof. Dr. K. Wieghardt, Dr. P. Ghosh, Dr. A. Begum, Dr. D. Herebian, Dr. E. Bothe, Dr. K. Hildenbrand, Dr. T. Weyhermüller
Max-Planck-Institut für Strahlenchemie
Stiftstrasse 34-36, 45470 Mülheim an der Ruhr (Germany)
Fax: (+49) 208-306-3952
E-mail: wieghardt@mpi-muelheim.mpg.de

[**] This work was supported by the Fonds der Chemischen Industrie. P. Ghosh thanks the Alexander von Humboldt Foundation for a stipend. M^{II} = Pd, Pt; bpy = 2,2′-bipyridine.



Scheme 1. Structures and redox scheme of the ligands L^{2-} employed.

green) and **5a** (orange) were prepared by oxidation of the neutral complexes **1** and **5** in CH_2Cl_2 with one equivalent of ferrocenium hexafluorophosphate; **2a** was obtained by oxidation with air of the reaction mixture of **2** (after addition of $[N(n\mathrm{Bu})_4](PF_6)$). Complexes **4** and **4a** were described previously.[8] Owing to its extreme O_2-sensitivity it was not possible to prepare a pure sample of **2; 3a** was generated electrochemically at 20 °C in CH_2Cl_2 solution and frozen immediately with liquid nitrogen.

The crystal structures of **1, 5** (Figure 1), and **2a** (Figure 2) were determined by X-ray structure analysis; those of **4, 4a**,[8] and $[Pd^{II}(bpy)(C_6H_4S_2)]$[9] as an analogue of **3** are known. Table 1 summarizes the bond lengths in the coordinated dianions L^{2-} and in their oxidized π-radical anions$(L^{\bullet})^{-}$. It is clearly established, that the same geometric changes occur upon oxidation of L^{2-} to $(L^{\bullet})^{-}$: 1) In the dianions L^{2-} the six C–C bonds of the ring are equidistant within 3σ but in the corresponding radicals these rings adopt a quinoid-type structure with two alternating short C–C distances (ca. 1.37 Å) and four longer C–C distances (ca. 1.41 Å). This is also true for the *o*-aminothiophenolates $(E^{\bullet})^{-}$ and, as shown here for the first time, for the *o*-dithiobenzosemiquinonates $(C^{\bullet})^{-}$. 2) The C–X and C–Y bonds are always ~0.04 Å longer in X,Y-coordinated dianions (single bonds) than in the radical anions (double-bond character).

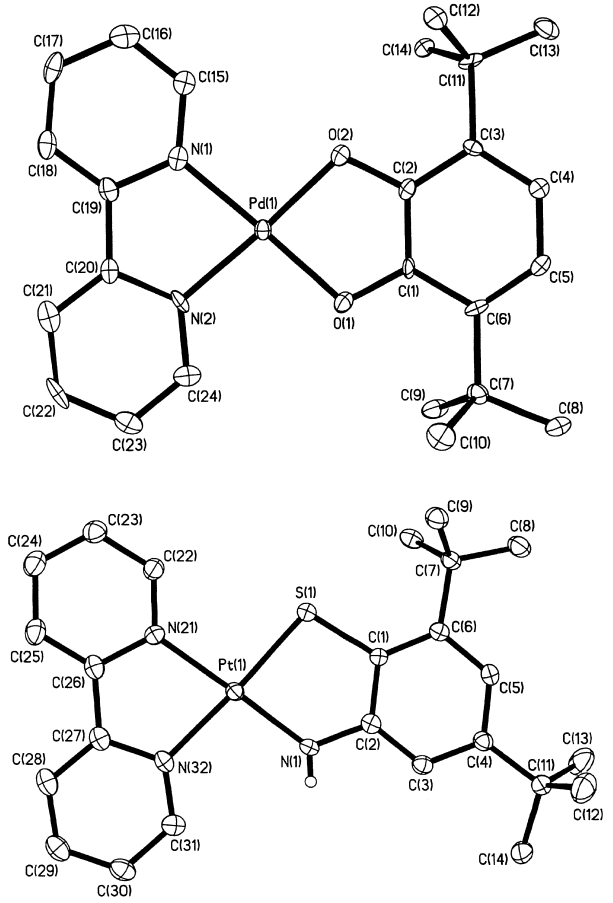
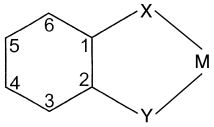


Figure 1. Structures of the neutral molecules in crystals of **1**·CH_3CN (top) and **5** (bottom). Selected bond lengths [Å] in **1**: Pd-O(1) 1.973(4), Pd-O(2) 1.959(4), Pd-N(1) 2.001(5), Pd-N(2) 1.999(5) and in **5**: Pt-N(1) 1.950(3), Pt-N(21) 2.013(3), Pt-N(32) 2.048(3), Pt-S(1) 2.2566(8).

Table 1: Bond lengths [Å] of X,Y-coordinated dianions L^{2-} and of their radical anions $(L^{\bullet})^{-}$.



Complex	C–X	C–Y	C(1)–C(2)	C(2)–C(3)	C(3)–C(4)	C(4)–C(5)	C(5)–C(6)	C(1)–C(6)
1·CH_3CN	1.351(6)	1.371(6)	1.423(7)	1.404(7)	1.392(7)	1.403(7)	1.390(7)	1.411(7)
$[Pd(A^{\bullet})_2]$ [16]	1.307(4)	1.302(5)	1.435(5)	1.420(5)	1.368(5)	1.436(5)	1.366(5)	1.407(5)
$[W(CO)_3(HNC_6H_4NH)]^{2-}$ [17]	1.372(6)	1.418(6)	1.420(7)	1.432(7)	1.396(8)	1.382(8)	1.390(8)	1.390(8)
2a	1.326(2)	1.348(2)	1.453(2)	1.422(2)	1.374(2)	1.423(2)	1.373(2)	1.420(2)
$[Pd(bpy)(C_6H_4S_2)]$[9]	1.756(2)	1.759(2)	1,396(5)	1.399(5)	1.378(5)	1.394(5)	1.375(5)	1.399(5)
$[Ni(C^{\bullet})_2]$[3b]	1.723(2)	1.731(2)	1.419(3)	1.409(3)	1.373(3)	1.422(3)	1.375(3)	1.429(3)
4[8]	1.348(2)	1.387(2)	1.421(3)	1.406(2)	1.405(3)	1.398(3)	1.402(2)	1.395(2)
4a[8]	1.309(2)	1.346(2)	1.450(2)	1,428(3)	1.382(3)	1.437(2)	1.366(3)	1.420(3)
5	1.379(4)	1.772(4)	1.418(4)	1.406(5)	1.386(5)	1.408(5)	1.396(5)	1.419(5)
$[Ni(E^{\bullet})_2]$[5]	1.348(4)	1.724(3)	1.418(4)	1.411(4)	1.364(4)	1.424(4)	1.384(4)	1.431(4)

 © 2003 Wiley-VCH Verlag GmbH & Co. KGaA, Weinheim 1433-7851/03/4205-0564 $ 20.00+.50/0

The structure of **2a** is interesting because two ion pairs of $[Pd(bpy)(B^{\bullet})]PF_6$ form a "dimer" through π-stacking of two $(B^{\bullet})^-$ radical anions (Figure 2). The centroid of the six-membered ring of one $(B^{\bullet})^-$ ligand is only 2.923 Å above the carbon atom C(1) of the second ring. This accounts for the observed diamagnetism of **2a** in the solid state.[10] In contrast, in CH_2Cl_2 solution **2a** is paramagnetic (see below).

Figure 3 displays the cyclic voltammograms of **1, 2a, 3**, and **5** in CH_2Cl_2 (0.1 M $[(n\text{Bu})_4\text{N}](PF_6)$); that of **4** was reported previously.[8] Table 2 gives the redox potentials versus the ferrocenium/ferrocene couple (Fc^+/Fc). All complexes exhibit at least two, ligand-centered reversible one-electron transfer waves, $E^1_{1/2}$ and $E^2_{1/2}$, and a similar third wave, $E^3_{1/2}$, which is irreversible for **1** and **3**. These waves are assigned to processes shown in Scheme 2, in which $(bpy^{\bullet})^-$ is the radical anion of 2,2′-bipyridine (bpy) and $(L^{BQ})^0$ is the neutral benzoquinone form of the ligand L^{2-}.

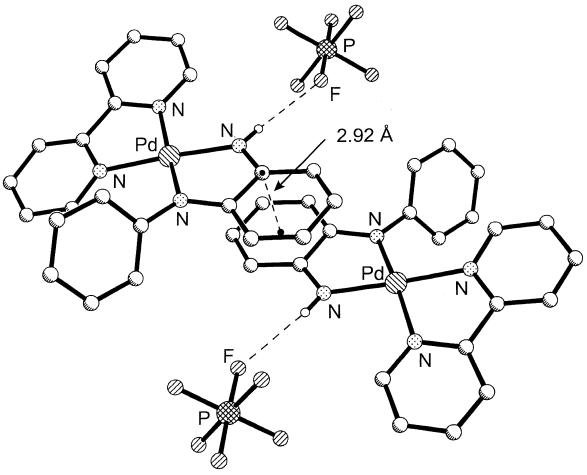


Figure 2. Structure of **2a** in the crystal showing an ion pair dimer $\{[Pd(bpy)(B^{\bullet})]^+(PF_6^-)\}_2$. Selected bond lengths [Å]: Pd-N_{bpy} 2.054(1), 2.025(1), Pd-$N_{B^{\bullet}}$ 1.976(1), 2.012(1). The dotted line represents the shortest distance between the atom C(1) of the first $(B^{\bullet})^-$ ligand and the centroid of the six-membered ring of the second $(B^{\bullet})^-$ ligand.

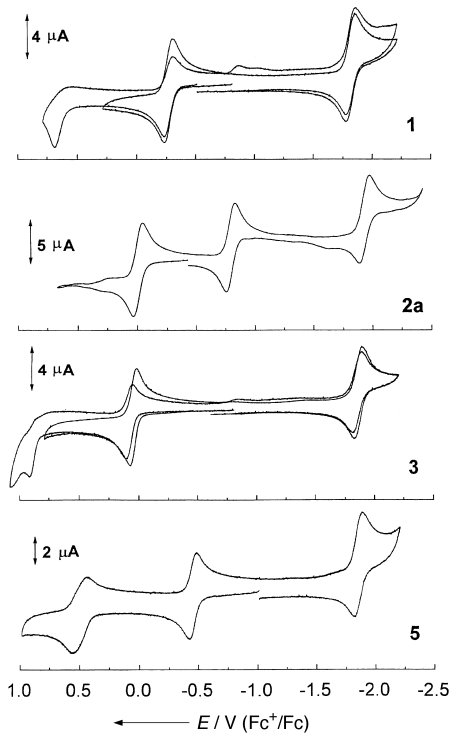


Figure 3. Cyclic voltammograms of **1, 2a, 3**, and **5** in CH_2Cl_2 (0.10 M $[(n\text{Bu})_4\text{N}](PF_6)$) at a glassy carbon working electrode at a scan rate of 200 mV s^{-1}.

Table 2: Redox potentials of complexes **1, 2a, 3–5**, and $[Pt^{II}(bpy)Cl_2]$.[a]

Complex	$E^1_{1/2}$ [V]	$E^{21}_{1/2}$ [V]	$E^3_{1/2}$ [V]
1	−1.80 (r)	−0.18 (r)	+0.70 (irr)
2a	−1.91 (r)	−0.79 (r)	−0.01 (r)
3	−1.87 (r)	0.04 (r)	+0.90 (irr)
4[8]	−1.90 (r)	−0.58 (r)	+0.42 (r)
5	−1.86 (r)	−0.46 (r)	+0.49 (r)
$[Pt^{II}(bpy)Cl_2]$[11]	−1.61 (in DMF)		

[a] Measured in CH_2Cl_2 (0.1 M $[(n\text{Bu})_4\text{N}](PF_6)$) versus Fc^+/Fc at 20 °C and and a scan rate of 200 mV s^{-1}. r = reversible, irr = irreversible.

$$[M(bpy^{\bullet})(L)]^- \underset{-e}{\overset{+e}{\rightleftharpoons}} [M(bpy)(L)] \underset{-e}{\overset{+e}{\rightleftharpoons}} [M(bpy)(L^{\bullet})]^+ \underset{-e}{\overset{+e}{\rightleftharpoons}} [M(bpy)(L^{BQ})]^{2+}$$

$$E^1_{1/2} \qquad E^2_{1/2} \qquad E^3_{1/2}$$

Scheme 2. Electron transfer processes of the complexes investigated by cyclic voltammetry.

Interestingly, $E^1_{1/2}$ is nearly constant throughout the series at ~ −1.87 V which is also observed for the reduction of $[Pt^{II}(bpy)Cl_2]$ to EPR-active $[Pt^{II}(bpy^{\bullet})Cl_2]^-$.[11] $E^2_{1/2}$ and $E^3_{1/2}$ involve the successive oxidations of the aromatic dianions L^{2-} (Scheme 1) to the semiquinonate radical anions $(L^{\bullet})^-$, and further to the quinones $(L^{BQ})^0$. Interestingly, the *o*-dithiolate species **3** is the most difficult neutral species to oxidize,[12] followed by the catecholate complex **1**, whereas the *o*-diimino species **2** is the easiest to oxidize.

The electronic spectra of the neutral complexes **1–5** (Figure 4) are dominated by a charge-transfer band in the visible which was assigned to a "mixed metal–ligand (M(L)) to ligand (bpy)" transition,[13] LLCT. Accordingly, the HOMO involves contributions from the metal ion and the $C_6H_4XY^{2-}$ system, while the LUMO is localized on the bpy ligand (π* orbital). Therefore, the energy of the LUMO should be approximately constant throughout the series. If this is the case, the redox potential $E^2_{1/2}$ for the couple [neutral complex]/[monocation]$^+$ should correlate with the energy of this LLCT transition as shown in Figure 5.

Temperature-dependent (3–298 K) magnetic susceptibility measurements (SQUID magnetometer, 1 T) established that solid samples of **1a, 4a**,[8] and **5a** are paramagnetic with an effective magnetic moment (μ_{eff}) of 1.6–1.8 μ_B at 298 K corresponding to one unpaired electron per formula unit. In contrast, solid **2a** is diamagnetic ($\mu_{eff} = 0.2\,\mu_B$ (10 K) and 0.8 μ_B per Pd center at 298 K corresponding to temperature-independent paramagnetism, χ_{TIP}) because the N,N-coordinated ligands $(B^{\bullet})^-$ form dimers through π-stacking in the solid state.

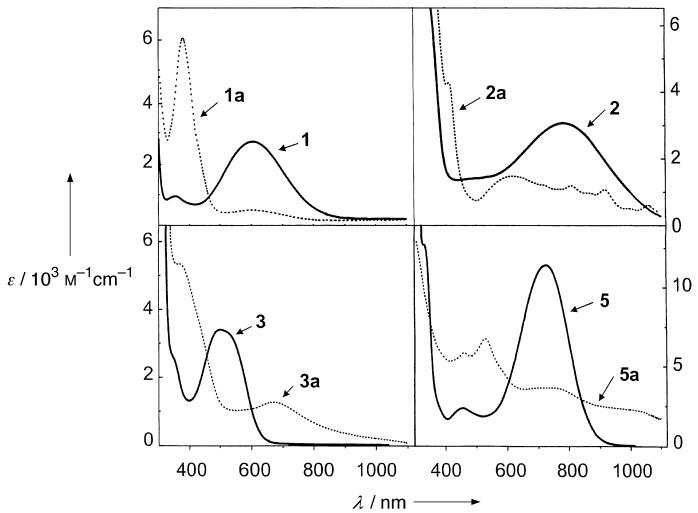


Figure 4. Electronic spectra of the neutral species **1, 2, 3**, and **5** and their electrochemically generated one-electron oxidized forms **1a, 2a, 3a**, and **5a** (0.10 M [(*n*Bu)$_4$N](PF$_6$)).

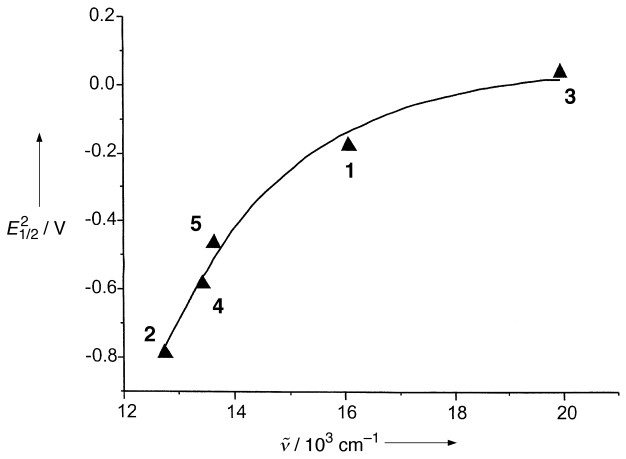


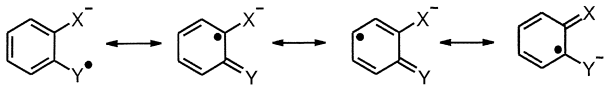
Figure 5. Correlation between the redox potential $E^2_{1/2}$ for the couple [neutral complex]/[monocation]$^+$ and the energy of the LLCT transitions of the neutral complexes.

CH_2Cl_2 solutions of **1a, 2a, 4a**, and **5a** as well as an electrochemically generated solution of **3a** display typical π-radical signals at $g \sim 2.0$ in the X-band EPR spectra. The observed g values and hyperfine coupling constants are summarized in Table 3. The spectrum of **3a** could only be recorded in frozen solution below 60 K;[14] a rhombic signal with very small g anisotropy and without detectable hyperfine splitting is observed. This π-radical anion is predominantly S-centered,[15] whereas in $(A^{\bullet})^-$, $(B^{\bullet})^-$, $(D^{\bullet})^-$, and $(E^{\bullet})^-$ the unpaired electron is delocalized over the six-membered ring (Scheme 3).

Table 3: X-band EPR spectra of [M(bpy)(X$^{\bullet}$)]$^+$ complexes in CH_2Cl_2 solution at 298 K.

Complex	g_{iso}	Hyperfine coupling constant [G]
1a	2.002	$a_H = 3.5$ (2H); $a_{^{105}Pd} = 2.4$
2a	1.999	$a_N = 6.2$, 5.8, $a_H = 5.1$, 3.2
3a	2.0057[a]	n.o.[b]
4a[8]	2.002	$a_N = 7.7$; $a_H = 4.6$; $a_{^{105}Pd} = 3.56$
5a	1.99	$a_{^{195}Pt} = 50$

[a] Measured in frozen solution (CH_2Cl_2, 0.10 M [(*n*Bu)$_4$N](PF$_6$)) at 60 K; rhombic signal $g_1 = 2.018$, $g_2 = 2.006$, $g_3 = 1.993$. [b] n.o. no hyperfine coupling observed.



Scheme 3. Resonance structures of the π-radical ligands $(A^{\bullet})^-$, $(B^{\bullet})^-$, $(C^{\bullet})^-$, $(D^{\bullet})^-$, and $(E^{\bullet})^-$.

In summary, we have presented spectroscopic evidence for the existence of the S,S- and N,S-coordinated π-radicals *o*-dithiobenzosemiquinonates(1−) and *o*-iminothiobenzosemiquinonates(1−), respectively, in [M(bpy)(L$^{\bullet}$)]$^+$ complexes. These results necessitate a reformulation of oxidation states and ligand oxidation levels of a number of *o*-dithiolato transition-metal ion complexes.

Experimental Section

Detailed procedures for the synthesis of complexes and their characterizations using mass spectrometry and ^{1}H NMR spectroscopy will be reported later in a full paper. All new compounds **1, 1a, 2a, 3, 5**, and **5a** gave satisfactory elemental analyses (C, H, N, S).

Crystal structure analysis data for **1**: $C_{24}H_{28}N_2O_2Pd \cdot CH_3CN$, $M_r = 523.94$, monoclinic, $P2_1/c$, $a = 6.7891(6)$, $b = 14.053(1)$, $c = 25.259(3)$ Å, $\beta = 91.57(1)°$, $V = 2409.0(4)$ Å^3, $Z = 4$, $\rho_{calcd} = 1.445$ Mg m^{-3}, $\mu(Mo_{K\alpha}) = 0.797$ mm^{-1}, $F(000) = 1080$, 12870 reflections collected at 100(2) K, 4212 independent reflections, 290 parameters, GOF = 1.028, $R_1 = 0.066$, $wR_2 = 0.1074$. Crystal structure analysis data for **2a**: $C_{22}H_{18}F_6N_4PPd$, $M_r = 589.77$, triclinic, $P\bar{1}$, $a = 8.9146(3)$, $b = 10.8276(4)$, $c = 12.2280(4)$ Å, $\alpha = 76.34(1)$, $\beta = 83.24(1)$, $\gamma = 66.57(1)°$, $V = 1051.97(6)$ Å^3, $Z = 2$, $\rho_{calcd} = 1.862$ Mg m^{-3}, $\mu(Mo_{K\alpha}) = 1.031$ mm^{-1}, $F(000) = 586$, 39386 reflections collected, 8052 independent reflections, 310 parameters, GOF = 1.032, $R_1 = 0.030$, $wR_2 = 0.0606$. Crystal structure analysis data of **5**: $C_{24}H_{29}N_3SPt$, $M_r = 586.65$, monoclinic, $P2_1/c$, $a = 10.4225(6)$, $b = 12.6824(9)$, $c = 16.4985(9)$ Å, $\beta = 91.00(1)°$, $V = 2180.5(2)$ Å^3, $Z = 4$, $\rho_{calcd} = 1.787$ Mg m^{-3}, $\mu(Mo_{K\alpha}) = 6.546$ mm^{-1}, $F(000) = 1152$, 24351 reflections collected, 8271 independent reflections, 271 parameters, GOF = 1.033, $R_1 = 0.036$, $wR_2 = 0.079$. CCDC-187891 (**1**), CCDC-187892 (**2a**), and CCDC-187893 (**5**) contain the supplementary crystallographic data for this paper. These data can be obtained free of charge via www.ccdc.cam.ac.uk/conts/retrieving.html (or from the Cambridge Crystallographic Data Centre, 12, Union Road, Cambridge CB21EZ, UK; fax: (+44) 1223-336-033; or deposit@ccdc.cam.ac.uk).

Received: June 21, 2002
Revised: October 10, 2002 [Z19586]

[1] C. G. Pierpont, C. W. Lange, *Prog. Inorg. Chem.* **1994**, *41*, 331.
[2] D. T. Sawyer, G. S. Srivatsa, M. E. Bodini, W. P. Schaefer, R. M. Wing, *J. Am. Chem. Soc.* **1986**, *108*, 936.
[3] a) D. Sellmann, M. Geck, F. Knoch, G. Ritter, J. Dengler, *J. Am. Chem. Soc.* **1991**, *113*, 3819; b) D. Sellmann, H. Binder, D. Häussinger, F. W. Heinemann, J. Sutter, *Inorg. Chim. Acta* **2000**, *300–302*, 829.

 © 2003 Wiley-VCH Verlag GmbH & Co. KGaA, Weinheim 1433-7851/03/4205-0566 $ 20.00+.50/0

[4] P. Chaudhuri, C. N. Verani, E. Bill, E. Bothe, T. Weyhermüller, K. Wieghardt, *J. Am. Chem. Soc.* **2001**, *123*, 2213.
[5] D. Herebian, E. Bothe, E. Bill, T. Weyhermüller, K. Wieghardt, *J. Am. Chem. Soc.* **2001**, *123*, 10012.
[6] H.-Y. Cheng, C.-C. Lin, B.-C. Tzeng, S.-M. Peng, *J. Chin. Chem. Soc.* **1994**, *41*, 775.
[7] V. Bachler, G. Olbrich, F. Neese, K. Wieghardt, *Inorg. Chem.* **2002**, *41*, 4179.
[8] X. Sun, H. Chun, K. Hildenbrand, E. Bothe, T. Weyhermüller, F. Neese, K. Wieghardt, *Inorg. Chem.* **2002**, *41*, 4295.
[9] T. M. Cocker, R. E. Bachman, *Inorg. Chem.* **2001**, *40*, 1550.
[10] For a similar π-stacking of a metalloporphyrin π-radical cation $[Zn(tpp^{\bullet})(OClO_3)]_2$ see: H. Song, N. P. Rath, C. A. Reed, W. R. Scheidt, *Inorg. Chem.* **1989**, *28*, 1839.
[11] E. J. L. McInnes, R. D. Farley, S. A. Macgregor, K. J. Taylor, L. J. Yellowlees, C. C. Rowlands, *J. Chem. Soc. Faraday Trans.* **1998**, *94*, 2985.
[12] In line with this observation it was recently reported that a (thiophenolato)cobalt(III) and its (phenolato)cobalt(III) analogue are oxidized at 0.55 and 0.36 V versus Fc^+/Fc, respectively to generate the coordinated thinyl and phenoxy radicals. S. Kimura, E. Bill, E. Bothe, T. Weyhermüller, K. Wieghardt, *J. Am. Chem. Soc.* **2001**, *123*, 6025.
[13] a) J. A. Zuleta, J. M. Bevilacqua, D. M. Proserpio, P. D. Harvey, R. Eisenberg, *Inorg. Chem.* **1992**, *31*, 2396; b) A. Vogler, H. Kunkely, J. Hlavatsch, *Inorg. Chem.* **1984**, *23*, 506; c) A. Vogler, H. Kunkely, *J. Am. Chem. Soc.* **1981**, *103*, 1559; d) T. R. Miller, G. Dance, *J. Am. Chem. Soc.* **1973**, *95*, 6970.
[14] We rationalize this behavior by a fast dimerization at ambient temperature of the radical **3a** with S–S bond formation; however, **3a** is stable in frozen solution at < 77 K.
[15] The EPR spectrum of the 2,4,6-tris(*tert*-butyl)phenylthiyl radical is similar; it also lacks observable hyperfine splitting. Z. B. Alfassi in *S-Centered Radicals*, Wiley, New York, **1999**, p. 7.
[16] G. A. Fox, C. G. Pierpont, *Inorg. Chem.* **1992**, *31*, 3718.
[17] D. Darensbourg, K. K. Klausmeyer, J. H. Reibenspiess, *Inorg. Chem.* **1996**, *35*, 1535.

Polymerization Mechanism Determined

[2.2]Paracyclophanes with Defined Substitution Pattern—Key Compounds for the Mechanistic Understanding of the Gilch Reaction to Poly-(*p*-phenylene vinylene)s**

*Jens Wiesecke and Matthias Rehahn**

Since the discovery of (semi)conductivity in organic polymers in 1976,[1,2] and electroluminescence in semiconducting polymers in the early 1990s,[3] much effort has been made to determine the structure–property relationships in conjugated macromolecular systems. The knowledge of these correlations is essential for further systematic development for application in light-emitting diodes (LEDs),[4] photovoltaic cells,[5] and field-effect transistors (FETs).[6] Poly(*p*-phenylene vinylene) (PPV) **1** is one of the most promising polymers for LED applications. Furthermore, it can be prepared by many synthetic methods in good to excellent yields.[7] The Gilch route[8] has a few advantages compared to other routes such as the Heck,[9] Wessling,[10] and Knoevenagel reactions.[11] These advantages include easily accessible starting materials, mild reaction conditions, and formation of film-forming products. To be suitable for LED applications, the PPVs must be free of structural defects.[12] Unfortunately, it is well-known that the Gilch process generates a variety of characteristic defects within the polymer chains, such as saturated ethylene bridges, rodlike ethynylene subunits, and halogenated chain ends.[13] Lowering the occurrence of such defects to a minimum level is therefore of crucial importance and requires a profound understanding of the Gilch reaction's mechanism. If one ignores some rather speculative ideas about mechanisms occurring via carbene intermediates,[14] just one general reaction scheme remains (Scheme 1): using KO*t*Bu as the base, the starting material **2** eliminates one HCl molecule. The resulting "real" monomer **3** polymerizes, leading to the nonconjugated but chlorinated poly(*p*-xylylene) (PPX; **4**). It is particularly the mechanism of this chain growth process which is presently under controversial discussion, although the mechanisms of chain initiation, chain termination, and cross-linking in this reaction are also unclear. For the final step, there is agreement that **4** converts into PPV **1** by elimination of a second equivalent of HCl.

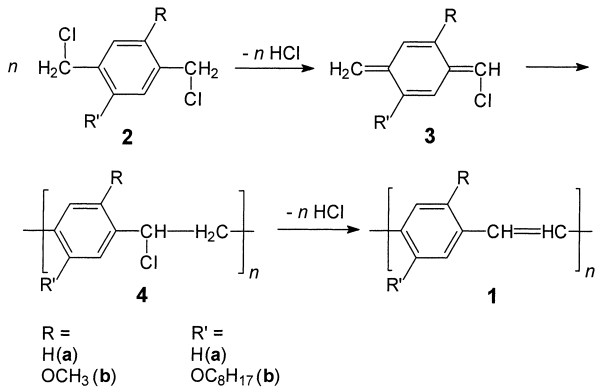
For the polymerization reaction anionic,[15] radical,[16] and simultaneous anionic and radical chain-growth processes

[*] Prof. Dr. M. Rehahn, Dipl.-Chem. J. Wiesecke
Technische Universität Darmstadt
Institut für Makromolekulare Chemie
Petersenstrasse 22, 64287 Darmstadt (Germany)
Fax: (+49) 6151-16-4670
E-mail: mrehahn@dki.tu-darmstadt.de

[**] We thank the Fonds der Chemischen Industrie e.V. (FCI) and the Vereinigung der Freunde der TU Darmstadt e.V. for financial support.

Supporting Information (experimental and analytical details) for this article available on the WWW under http://www.angewandte.org or from the author.

 © 2003 Wiley-VCH Verlag GmbH & Co. KGaA, Weinheim 1433-7851/03/4205-0567 $ 20.00+.50/0



Scheme 1. General representation of the Gilch process leading to PPV.

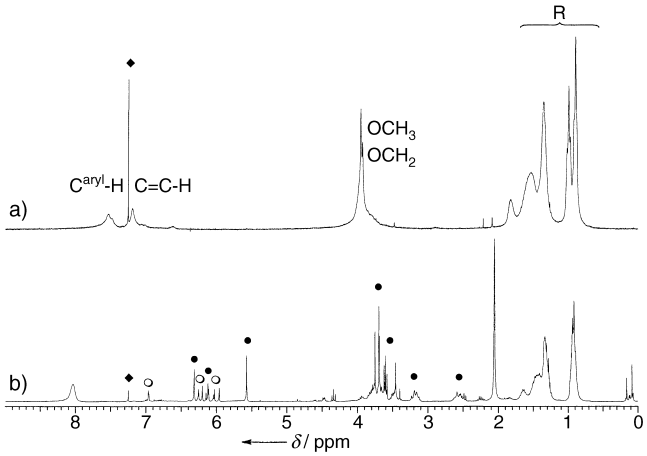


Figure 1. ^{1}H NMR spectrum of a) MEH-PPV (**1b**) and b) the methanol-soluble product fraction; recorded in $CDCl_3$ (◆) at room temperature.

have been proposed.[14,17] For each of these positions, there is some experimental evidence, but to the best of our knowledge, no final proof.

Whereas most conclusions have been drawn mainly on the basis of a comprehensive polymer analysis, we focus our attention on the low-molecular-weight side products formed during the Gilch reaction. Herein, we report first results that allow clear statements concerning 1) the reactive monomer, 2) the chain-initiating process, and 3) whether an anionic or a radical chain growth is dominant under the tested conditions. Poly[2-methoxy-5-(β-ethylhexoxy)phenylene vinylene] (MEH-PPV; **1b**) was selected as the readily soluble target polymer, KO*t*Bu was selected as the base and THF as the solvent. All polymerization reactions were carried out at room temperature. *tert*-Butyl alcohol is formed during the polymerization process as a product of HCl elimination. Its quantity increases during the conversion from zero to 2 mole per mole **2b**. This could cause a change in the reaction mechanism from anionic at the start to radical at later stages. Thus *tert*-butyl alcohol (2 mole per mole **2b**) was added to most of the reaction mixtures to avoid such a change in mechanism. No further compounds, such as chain-transfer or chain-initiating agents, were added to the reaction mixtures.

When the conversions were complete, the mixtures were acidified with acetic acid, and poured into methanol to precipitate the formed polymer. The soluble part of the precipitated polymer was subsequently analyzed using NMR spectroscopy (see Figure 1a for a typical ^{1}H NMR spectrum). All NMR spectra were found to be identical to those described for MEH-PPV (**1b**) in the literature.[14] In full agreement with the literature, the yields of polymer **1b** were of the order 60–75 %.[16]

The ^{1}H NMR spectrum of the methanol-soluble and thus presumably low-molecular-weight part of the product mixture (Figure 1b) showed no evidence of remaining starting material **2b**. This is clear from the lack of a singlet at $\delta = 3.90$ ppm corresponding to the benzylic CH_2Cl protons of **2b**. Furthermore, there is no evidence of significant ether formation by nucleophilic substitution: the CH_2OtBu protons should give rise to a singlet at $\delta \approx 4.50$ ppm. On the other hand, there are some characteristic new signals in the range of $\delta = 2.5$–3.5 ppm and $\delta = 5.5$–6.5 ppm (Figure 1b; indicated by ○ and ●) which do not correspond to PPX substructures **4b** nor to oligomeric species **1b**. Because of the complexity of the patterns, it was impossible to assign them to specific molecules at this stage. By column chromatography it was finally possible to obtain some pure product fractions (silica gel as the stationary phase and toluene/hexane as the eluent). As the first fraction, a colorless oil was isolated and then analyzed by mass spectrometry which gave a value of m/z 592.30. This is exactly twice the molar mass of the singly dehydrohalogenated starting material **2b**. Moreover, this first fraction has a characteristic ^{1}H NMR spectrum, that coincides with the signals marked with ● in Figure 1b. Comparison with literature NMR data supported the intuitive first interpretation that a [2.2]paracyclophane was obtained.[18] The ^{1}H and ^{13}C NMR spectra of most of the later chromatographic fractions pointed towards these also being cyclodimerized products. These results suggest that dimerization is the second most important reaction occurring during the Gilch process—a conclusion with potentially far-reaching consequences for the polymerization process.

For more detailed analysis 2D NMR techniques were applied, such as ^{1}H-^{1}H (gs-COSYDF) and ^{1}H-^{13}C correlations (gs-HSQC, gs-HMBC). From the spectra obtained it was conclusion that 1,2-dichloro-[2.2]paracyclophane (**5a**) is the material that elutes first from the column (Figure 2). Analysis of the gs-HMBC spectrum (Figure 3 shows the relevant

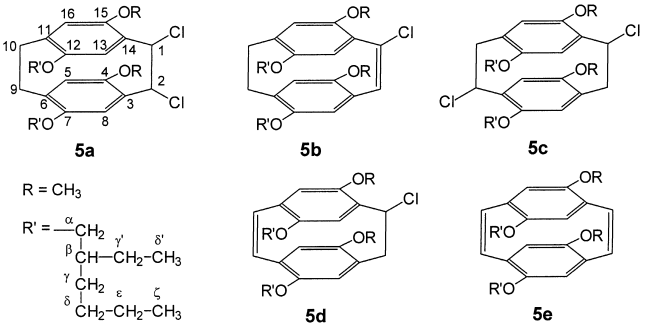


Figure 2. [2.2]Paracyclophanes potentially formed during the Gilch reaction.

 © 2003 Wiley-VCH Verlag GmbH & Co. KGaA, Weinheim 1433-7851/03/4205-0568 $ 20.00+.50/0

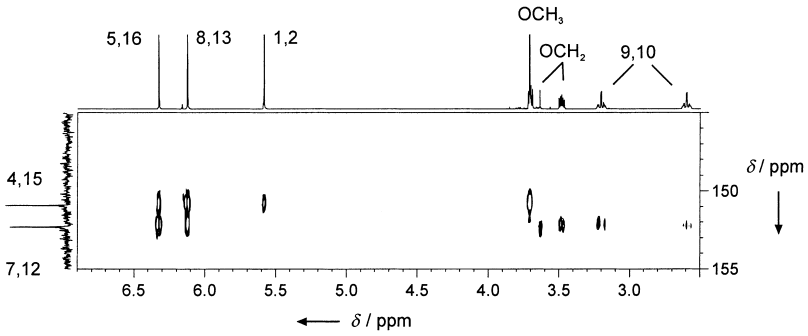


Figure 3. Relevant region of the gs-HMBC spectrum of **5a** (^{1}H-^{13}C long-range coupling), recorded in $CDCl_3$ at room temperature; the signal assignment is made according to the numbering given in Figure 2.

region) even allows conclusions concerning the neighborhood of the OCH_3 and OC_8H_{17} groups to be drawn: the ^{13}C NMR spectrum shows two base-line separated absorptions for the C^{ar}-OC_xH_y carbons at $\delta = 153.3$ and 151.9 ppm. By means of the ^{13}C NMR spectra of monomer **2b** and related compounds it can be shown that this difference in chemical shifts is not caused by the directly attached side chains OR and OR′ but by differences in the substituents attached to the aromatic carbon atoms *ortho* to the C^{ar}-$OR^{(\prime)}$ carbon atoms. In this specific case, the splitting of the signals arising from the C^{ar}-OC_xH_y carbon atoms must be caused by the two different bridges, that is, CH_2-CH_2 and CHCl-CHCl. This situation allows to use—in pairs—specific $^3J_{H,C}$ long-range couplings to determine the precise positions of the respective alkoxy groups within **5a**.

Let us consider the H_3C-O-C^{ar}-C^{ar}-CHCl coupling in combination with the H_3C-O-C^{ar}-C^{ar}-CHCl coupling, and the corresponding coupling between the CH_2-CH_2 bridges and the branched side chain OCH_2-C_7H_{15} as the cross-check. Careful analysis of Figure 3 leads to the conclusion that the H_3C-O-C^{ar} carbon atom *only* couples with the protons of the CHCl-CHCl bridges but does not couple with those of the CH_2-CH_2 bridges. Similarly, the C^{ar}-O-CH_2-C_7H_{15} carbon atom couples exclusively with the CH_2-CH_2-bridge protons and the C^{ar}-O-CH_2-C_7H_{15} protons in **5a**. From this analysis it can be concluded that all the OCH_3 groups are *ortho* to the CHCl-CHCl bridges, whereas the more bulky β-ethylhexoxy groups are *ortho* to the CH_2-CH_2 bridges. Hence the activation of **2b** occurs by HCl elimination, and this step clearly starts with deprotonation of the CH_2Cl group which is *ortho* to the sterically less-demanding OCH_3 substituent.

In the subsequent fractions it was possible to identify 1-chloro[2.2]paracyclophan-1-ene (**5b**) as a further cyclic side product. Its ^{1}H NMR resonance signals are those marked by ○ in Figure 1b, and Figure 4 shows the ^{1}H NMR spectrum of the compound **5b** together with the signal assignments. It is reasonable to assume that **5b** is formed from **5a** by dehydrohalogenation. Altogether, **5a** and **5b** represent approximately 95% of the methanol-soluble material. The remaining 5% of methanol-soluble material might be larger rings or short linear oligomers, but we can exclude any trace of 1,9-dichloro-[2.2]paracyclophanes, such as **5c** and its elimination products such as **5d** or **5e**.

Identical results were obtained when no *tert*-butyl alcohol was added at the beginning of the experiment, which allows a change of reaction mechanism to be ruled out. Thus, a more detailed mechanistic picture of the Gilch reaction can be proposed (Scheme 2): in the first step, starting material **2** is dehydrohalogenated, giving **3** as the "real monomer". The CHCl group *ortho* to the sterically less demanding side group OR is deprotonated. The subsequent cyclodimerization leads *only* to **5a**, and *does not* give **5c** or its deviatives. From this result it can be concluded that no anionic species are involved in the chain initiation and growth processes—or at best only to a very small extent. If **5a** were to be formed via an anionic intermediate, this is only possible via route A (Scheme 2) which leads to the formation of the dimeric anionic intermediate **6**. But the anionic "chain end" in intermediate **6** is less stabilized than that in **7**. So route B should be favored instead of route A, but this would lead to **5c** and not to **5a** as observed.

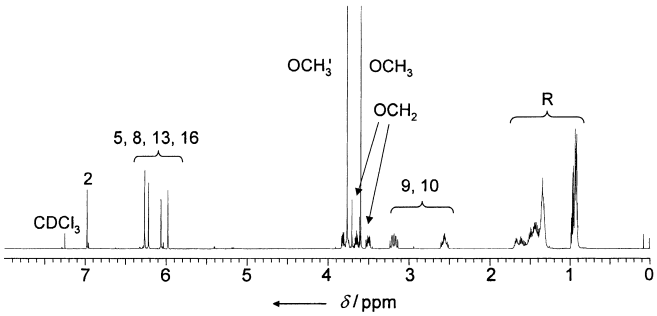
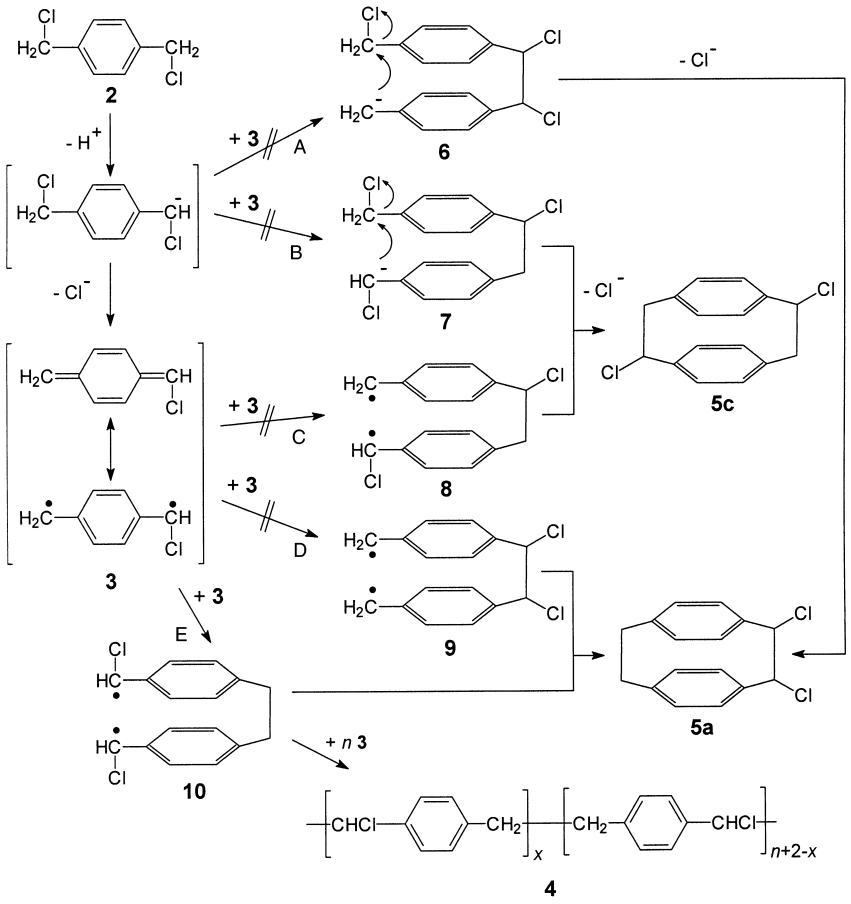


Figure 4. ^{1}H NMR spectrum of **5b;** the numbering scheme is given in Figure 2.

On the other hand, if one assumes a radical mechanism, intermediate **8** (formed by route C in Scheme 2) can be excluded because **8** would also lead to the formation of paracyclophane **5c**. The remaining two routes D and E would both lead to **5a**. But the formation of **9** is also highly improbable because—as in conventional free-radical polymerizations—the radical is (nearly) always at the carbon center which allows its most efficient stabilization, and the radical center on the Cl-substituted carbon atom in **10** would be more effectively stabilized. In contrast to **3** for which the diradical picture is given just to represent the mesomerism, dimer **10** is a real diradical which is able to initiate the chain growth leading to PPV as well as the observed cyclodimerization leading to **5a**. Larger cyclic oligomers are seldom because, as the chain length increases, ring-closure becomes more and more improbable. The fact that exclusively 1,2-dichloro-[2.2]paracyclophane **5a** and its following products are found as cyclooligomers under the applied conditions also allows exclusion of polyrecombination of **10**: if such a mechanism were involved, alternating copolymers

 © 2003 Wiley-VCH Verlag GmbH & Co. KGaA, Weinheim 1433-7851/03/4205-0569 $ 20.00+.50/0



Scheme 2. Proposed reaction mechanism leading to **5a, 5b**, and PPV **1** (route E) and reactions that clearly do not occur during the Gilch polymerization (routes A to D); side chains -OR and -OR′ are omitted for clarity.

$[\text{-Ar-CH}_2\text{-CH}_2\text{-Ar-C}\equiv\text{C-}]_n$ would be obtained in the limiting case, or at least highly "disordered" polymers, but not PPV **1**.

In conclusion, the Gilch reaction is a (nearly) exclusive radical chain growth reaction under the applied conditions. Species **3** is the reactive monomer, diradical **10** is the initiator, and each PPV macromolecule contains at least one saturated ethylene bridging unit and presumably two chloromethylene end groups. Last but not least, the Gilch process is clearly a convenient and very efficient source of [2.2]paracyclophanes.

Received: August 1, 2002 [Z19868]

[1] a) H. Shirakawa, *Angew. Chem.* **2001**, *113*, 2642 – 2648; *Angew. Chem. Int. Ed.* **2001**, *40*, 2574; b) A. G. MacDiarmid, *Angew. Chem.* **2001**, *113*, 2649 – 2659; *Angew. Chem. Int. Ed.* **2001**, *40*, 2581; c) A. J. Heeger, *Angew. Chem.* **2001**, *113*, 2660 – 2682; *Angew. Chem. Int. Ed.* **2001**, *40*, 2591.

[2] a) H. Shirakawa, E. J. Louis, A. G. MacDiarmid, C. K. Chiang, A. J. Heeger, *J. Chem. Soc. Chem. Commun.* **1977**, 578; b) C. K. Chiang, C. R. Fincher, Jr., Y. W. Park, A. J. Heeger, H. Shirakawa, E. J. Louis, *Phys. Rev. Lett.* **1977**, *39*, 1098.

[3] J. H. Burroughes, D. D. C. Bradley, A. R. Brown, R. N. Marks, K. Mackay, R. H. Friend, L. Burns, A. B. Holmes, *Nature* **1990**, *347*, 539.

[4] J. C. Scott, G. G. Malliaras in *Semiconducting Polymers* (Eds.: G. Haziioannou, P. F. van Hutten), Wiley-VCH, Weinheim, **2000**, pp. 411 – 461.

[5] C. J. Brabec, N. Serdar Sariciftci in *Semiconducting Polymers* (Eds.: G. Haziioannou, P. F. van Hutten), Wiley-VCH, Weinheim, **2000**, pp. 515 – 560.

[6] G. Horowitz in *Semiconducting Polymers* (Eds.: G. Haziioannou, P. F. van Hutten), Wiley-VCH, Weinheim, **2000**, pp. 499 – 514.

[7] A. Kraft, A. C. Grimsdale, A. B. Holmes, *Angew. Chem.* **1998**, *110*, 416 – 443; *Angew. Chem. Int. Ed.* **1998**, *37*, 402 – 428.

[8] H. G. Gilch, W. L. Wheelwright, *J. Polym. Sci. Part A* **1966**, *4*, 1337.

[9] Z. Bao, Y. Chen, R. Chai, L. Yu, *Macromolecules* **1993**, *26*, 5281 – 5286.

[10] R. A. Wessling, *J. Polym. Sci. Polym. Symp.* **1985**, *72*, 55 – 66.

[11] N. C. Greenham, S. C. Moratti, D. D. C. Bradley, R. H. Friend, A. B. Holmes, *Nature* **1993**, *365*, 628 – 630.

[12] H. Becker, H. Spreitzer, W. Kreuder, E. Kluge, H. Vestweber, H. Schenk, K. Treacher, *Synth. Met.* **2001**, *122*, 105.

[13] H. Becker, H. Spreitzer, K. Ibrom, W. Kreuder, *Macromolecules* **1999**, *32*, 4925.

[14] J.-Q. Pan, Z.-K. Chen, Y. Xiao, W. Huang, *Chin. J. Polym. Sci.* **2000**, *18*, 541 – 549.

[15] a) B. R. Hsieh, Y. Yu, A. C. VanLaeken, H. Lee, *Macromolecules* **1997**, *30*, 8094; b) C. J. Neef, J. P. Ferraris, *Macromolecules* **2000**, *33*, 2311 – 2314; c) C. Yin, C.-Z. Yang, *J. Appl. Polym. Sci.* **2001**, *82*, 263 – 268.

[16] L. Hontis, V. Vrindts, L. Lutsen, D. Vanderzande, J. Gelan, *Polymer* **2001**, *42*, 5793 – 5796.

[17] Z.-K. Chen, J.-Q. Pan, Y. Xiao, N. H. S. Lee, S.-J. Chua, W. Huang, *Thin Solid Films* **2000**, *363*, 98 – 101.

[18] H. Hopf, M. Psiorz, *Chem. Ber.* **1986**, *119*, 1836 – 1844.

 © 2003 Wiley-VCH Verlag GmbH & Co. KGaA, Weinheim 1433-7851/03/4205-0570 $ 20.00+.50/0

Structures of Polyboron Fluorides

The Surprising Structures of B_8F_{12} and $B_{10}F_{12}$**

Jennifer A. J. Pardoe, Nicholas C. Norman, Peter L. Timms, Simon Parsons,* Iain Mackie, Colin R. Pulham, and David W. H. Rankin*

Much is known about the structure of polyboron chlorides, bromides, and iodides[1,2] and of cluster compounds of other Group 13 elements derived from their monohalides.[3–5]

However, with the exception of B_2F_4,[6] experimental structures of the polyboron fluorides are unknown. It is notable that no report of a theoretically predicted structure of B_8F_{12} has appeared since the molecule was first postulated to adopt a borane-like structure, $B_2(BF_2)_6$, in 1972.[7] Herein we describe the experimentally determined structures of B_8F_{12} and of a completely new boron subhalide $B_{10}F_{12}$, both obtained by means of X-ray crystallography at low temperatures.

The yellow liquid B_8F_{12} was prepared, as earlier reported, by low-temperature decomposition of $(BF_2)_2BF$, which had been made by condensing gaseous BF with the vapor of B_2F_4 at 77 K.[8] The colorless compound $B_{10}F_{12}$ was discovered by X-ray crystallography as a component of the mixture of the less volatile boron fluorides formed by the condensation of BF. The thermal stability of $B_{10}F_{12}$ seems comparable to or higher than that of B_8F_{12}, but both compounds decompose quite rapidly at 273 K. Samples of B_8F_{12}, and the fraction containing $B_{10}F_{12}$ were sealed in glass capillaries and crystals were grown at low temperatures on a diffractometer by using the laser technique employed by Boese and Nussbaumer.[9] Structures were determined by X-ray crystallography for pure B_8F_{12},[10] $B_8F_{12}{\cdot}0.5\,BF_3$, and $B_{10}F_{12}$[11] Molecular structures of B_8F_{12} and of B10F12 are shown in Figure 1 and Figure 2, respectively.

There are two crystallographically independent molecules of B_8F_{12} in the structure of $B_8F_{12}{\cdot}0.5\,BF_3$, and four in that of pure B_8F_{12}. However, the structures of all six of these molecules are essentially the same. It is interesting to view the structure of B_8F_{12} in relation to earlier attempts to understand the structure of diborane.[12] It has both bridge bonds and a short central B–B bond, that is, it combines all the structural elements once considered diborane. Unlike the equivalent $B(\mu\text{-}H)_2B$ unit of diborane, however, the core $B(\mu\text{-}BF_2)_2B$ unit of B_8F_{12} is both nonplanar, with average angles between the B1-B2-B4 and B2-B3-B4 planes of 123.1° (range 121.6–125.7°), and markedly asymmetric, with the four B–B bridge bonds varying in length in all the six crystallographically independent molecules in the range of 1.79(2) to 2.11(4) Å in the sequence B2–B3 < B2–B1 < B3–B4 ≪ B1–B4. Overall, these bond lengths are consistent with there being less electron density available for bridge bonding than in the classic three-center, two-electron bridge bonds of diborane, and with substantial electron density associated with the short, central B2–B4 bond (av 1.667(6) Å). The bond lengths and fold angles within the core B_4 unit might be expected to be easily deformed within a crystal, but all six independent molecules have very similar structures. The results of molecular orbital calculations at the MP2/6-31G* level[13–15] show that this distorted and folded structure does indeed lie in an energy minimum in the gas phase. The optimized C_{2v} (*mm*2) structure with a nonplanar B_4 unit, in which the core B–B bond lengths are constrained to be equal, is not a potential energy minimum and is 8.77 kJ mol^{-1} higher in energy than the distorted structure.

More detailed and extensive calculations (which will be the subject of a subsequent full paper) are needed to fully understand the origin of the observed unsymmetrical structure, but preliminary results indicate that intramolecular F···B interactions play a critical role. For example, for the

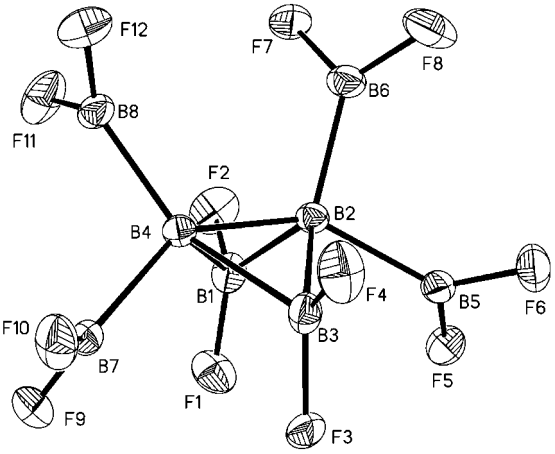


Figure 1. Structure of B_8F_{12} in the crystal. The numbering scheme shown was used for all molecules of B_8F_{12} observed in this study. In the supplemental data,[10b] atoms in molecule 1 are labeled B11, B21 etc. Molecules 1–4 occur in B_8F_{12}, 5–6 in $B_8F_{12}{\cdot}0.5\,BF_3$. Average distances [in Å]: B1-F1 1.303(3), B1-F2 1.301(5), B3-F3 1.335(4), B3-F4 1.316(4), B5-F5 1.311(5), B5-F6 1.313(10), B6-B7 1.328(6), B6-F8 1.315(6), B7-F9 1.309(7), B7-F10 1.312(9), B8-F11 1.316(7), B8-F12 1.311(9), B1-B4 2.11(4), B1-B2 1.86(2), B2-B3 1.792(18), B3-B4 1.92(4), B2-B5 1.745(6), B2-B6 1.714(6), B4-B7 1.736(5), B4-B8 1.717(8), B2-B4 1.667(6). The errors quoted are unweighted sample standard deviations based on the dimensions of the six independent molecules observed crystallographically in B_8F_{12} and $B_8F_{12}{\cdot}0.5\,BF_3$; individual B–B and B–F distances in these structures had standard uncertainties of around 0.002 Å and 0.003 Å, respectively. Thermal ellipsoids are drawn at the 30% probability level.

[*] Dr. P. L. Timms, J. A. J. Pardoe, Dr. N. C. Norman
School of Chemistry
University of Bristol
Bristol, BS8 1TS (UK)
Fax: (+44) 117-925-1295
E-mail: peter.timms@bris.ac.uk
Dr. S. Parsons, I. Mackie, Dr. C. R. Pulham, Prof. Dr. D. W. H. Rankin
Department of Chemistry
University of Edinburgh
King's Building
West Main Road, Edinburgh EH9 3JJ (UK)
Fax: (+44) 131-650-4743
E-mail: s.parsons@ed.ac.uk

[**] This research was supported by the Engineering and Physical Sciences Research Council, and help from the UK Computational Facility is gratefully acknowledged.

compound B_8F_{12} a long bifurcated interaction between F3 and the boron atoms B5 and B7 in two of the terminal BF_2 groups pulls the B3 atom out of the plane of B1, B2, and B4 (Figure 1; observed experimental ranges 2.603(2)–2.675(2) Å for F3···B5 and 2.620(2)–2.693(2) Å for F3···B7; calculated ab initio values 2.572 and 2.587 Å, respectively). These interactions also affect the B3–F3 bond which, at an average of 1.335(4) Å (calcd 1.361 Å), is longer than other such bonds in the molecule. Furthermore, the atoms B2, B4, B5, B7, and B8 are coplanar, but B6 is displaced from this plane by an average of 0.43(7) Å to accommodate an interaction between F7 and B8. The longest B···F interaction (obs. 2.733(2)–2.942(2) Å; calcd 2.855 Å) is formed between F5 and B1. This contact may be responsible for the lengthening of the B1–B4 bridge bond. While the results of calculations at the MP2/6-31G* level point to some polarity in the B2–B4 bond (Mulliken charges; B2 −0.95, B4 −0.41), the very high volatility of B_8F_{12} indicates a compound with negligible intermolecular dipole–dipole interactions.

Calculations[13–15] on the model compound $B_8H_4F_8$, in which the bridging BF_2 groups are replaced by bridging BH_2 groups, reveal a symmetrically bridged structure with a planar central B_4 unit and overall D_2 (222) symmetry. The calculations also indicate a twisting of the planes of the BH_2 groups with respect to the central B_4 unit, which can be attributed to intramolecular interactions between the highly electron-deficient bridging boron atoms and the fluorine atoms of terminal BF_2 groups. The π-donating ability of fluorine atoms means that BF_2 is less electron deficient than BH_2. However, in B_8F_{12} the fluorine atoms of both the bridging and terminal BF_2 groups seem to be involved in long-range interactions with the boron atoms of other BF_2 groups. Clearly both the observed intramolecular interactions and the inherent electronic properties are critical in determining the precise structures adopted.

As pointed out by a referee, unsymmetrical bridging is well-known in carbocation chemistry, where there is a continuum of hyperconjugation, asymmetric bridging, and symmetric bridging, depending on the strength of interaction between a σ donor and a center of electron deficiency. To quote the referee, "B_8F_{12} would seem to belong to the world between pure classical and pure nonclassical structures". The detailed calculations referred to above should shed light on these structural issues (as well as the reasons for the intense yellow color of the compound) and we are currently trying to refine gas-phase electron-diffraction data for the molecule.

The structure of $B_{10}F_{12}$ (Figure 2) has crystallographic S_4 symmetry and is based on a central distorted tetrahedron of boron atoms (B1 and its symmetry equivalents B1A, B1B, and B1C) each with a terminal BF_2 substituent, similar to the known B_4X_4 tetrahedra,[1] but with BF_2 bridges across the B1–B1B and B1A–B1C edges. If each BF_2 group is replaced by an H atom, this structure equates to $B_4H_4(\mu\text{-}H)_2$. Organic derivatives of $B_4H_4(\mu\text{-}H)_2$ of type $B_4R_4(\mu\text{-}H)_2$ have been reported[16,17] and while the structures were not established by X-ray crystallography, there seems little doubt that they have a similar B_4 core to $B_{10}F_{12}$ but with bridging H atoms across opposite edges of the tetrahedron. Nevertheless, such organoboron compounds and related derivatives of tetraborane (6)[18,19] are much more electron rich and thus more stable than $B_{10}F_{12}$, which depends on relatively weak F–B π-bonding to compensate for its electron deficiency.

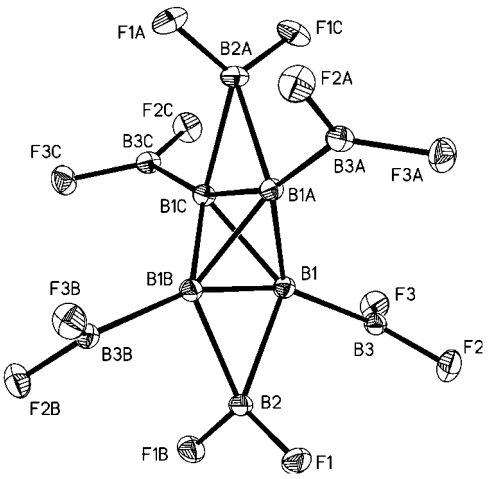


Figure 2. Structure of $B_{10}F_{12}$ in the crystal. Bond lengths [Å]: B1-B1A 1.7583(14), B1-B1B 1.6053(18), B1-B2 1.8070(15), B1-B3 1.7037(13), B2-F1 1.3266(9), B3-F2 1.3052(11), B3-F3 1.3191(11). Thermal ellipsoids are drawn at the 30% probability level.

Exchange reactions of BCl_3 with B_8F_{12} and $B_{10}F_{12}$ were studied, and are a route to the formation of new polyboron chlorides.[20] Polyboron fluorides less volatile than $B_{10}F_{12}$ are also formed by the condensation of BF, and efforts are being made to determine their molecular structures by X-ray crystallography.

Experimental Section

The volatile products, obtained from the condensation of gaseous BF (1.5 g, 50 mmol) with excess gaseous B_2F_4 at 77 K, were fractionated on a low-temperature distillation column[21] to yield $(F_2B)_2BF$ (ca. 0.35 g, 2.7 mmol), which came off the column at about 200 K, and a fraction (ca. 0.2 g) that was partly liquid, partly crystalline on the column, which came off slowly at about 235 K. The $(F_2B)_2BF$ was held at 250 K to allow it to disproportionate to B_8F_{12} (ca. 0.17 g, 0.54 mmol) and B_2F_4, which were easily separated. Both B_8F_{12} and the 235 K fraction were sealed in Pyrex capillaries (ca. 0.3 mm bore) on a vacuum line. Crystals of the compounds were grown in these capillaries, which were mounted on a Bruker AXS Smart Apex diffractometer equipped with an Oxford Cryosystems Cryostream and an OHCD IR laser-assisted crystallization device. Crystal growth of B_8F_{12} was hampered by glass formation, but crystals were grown from a sample that had been annealed into a polycrystalline powder at 160 K, by moving the point of focus along the capillary over a period of 13 h, then ramping down the laser power from 1.9 W to zero over 1 h. Prior to this study, crystallization of B_8F_{12} had never been observed to occur; when it was handled at low temperature on a vacuum line, it always formed a glassy solid.

A crystal of $B_{10}F_{12}$ was grown without difficulty by establishing a stable solid–liquid equilibrium at 200 K with a laser power of 2.5 W at one end of the sample. The position of the phase boundary was moved along the length of the sample over the course of 5 min, then the laser power was ramped down to zero over another 5 min.

Received: July 16, 2002
Revised: November 5, 2002 [Z19745]

 © 2003 Wiley-VCH Verlag GmbH & Co. KGaA, Weinheim 1433-7851/03/4205-0572 $ 20.00+.50/0

[1] J. A. Morrison, *Chem. Rev.* **1991**, *91*, 35.
[2] W. Hönle, Y. Grin, A. Burkhardt, U. Wedig, M. Schultheiss, H. G. von Schnering, *J. Solid State Chem.* **1997**, *133*, 59.
[3] C. Dohmeier, D. Loos, H. Schnöckel, *Angew. Chem.* **1996**, *108*, 141; *Angew. Chem. Int. Ed. Engl.* **1996**, *35*, 129.
[4] A. Rodig, G. Linti, *Angew. Chem.* **2000**, *112*, 3076; *Angew. Chem. Int. Ed.* **2000**, *39*, 2952.
[5] A. Schnepf, H. Schnöckel, *Angew. Chem.* **2001**, *113*, 734; *Angew. Chem. Int. Ed.* **2001**, *40*, 712.
[6] L. Trefonas, W. N. Lipsomb, *J. Chem. Phys.* **1958**, *28*, 54.
[7] R. W. Kirk, D. L. Smith, W. Airey, P. L. Timms, *J. Chem. Soc. Dalton Trans.* **1972**, 1392.
[8] P. L. Timms, *J. Am. Chem. Soc.* **1967**, *89*, 1629.
[9] R. Boese, M. Nussbaumer in *Correlations, Transformations and Interactions in Organic Crystal Chemistry,* IUCr Crystallographic Symposia, *Vol. 7* (Eds.: D. W. Jones, A. Katrusiak), Oxford University Press, Oxford, UK, **1994**, pp. 20–37.
[10] a) Crystal structure analysis of B_8F_{12}: $M_r = 1257.86$, monoclinic $P2/c$, $a = 24.577(3)$, $b = 7.3341(8)$, $c = 24.493(3)$ Å, $\beta = 106.708(2)°$, $V = 4401.1(9)$ Å^3, $T = 120$ K, $\rho_{cald} = 1.898$ g cm^{-3}, $\lambda = 0.71073$ Å. Yellow cylinder, $0.30 \times 0.30 \times 1.0$ mm, $\mu(Mo_{K\alpha}) = 0.244$ mm^{-1}. An absorption correction was performed by the multiscan method using the program SADABS ($0.76 < T < 0.93$). Data were collected to $2\theta_{max} = 57.6°$ comprising 39515 measured and 10721 unique data, of which 7462 with $F > 4\sigma(F)$ were used for refinement. The structure was solved by direct methods using SHELXTL[22] and refined by full-matrix least-squares against F, with anisotropic displacement parameters on all atoms and a Chebychev three-term polynomial weighting scheme (CRYSTALS).[23] The final R factor was 0.0298, $R_w = 0.0334$, for 721 parameters. The final difference map max. and min were $+0.36$ and -0.19 e Å^{-3}, respectively. Further analyses were performed with PLATON.[24] b) Further details on the crystal structure investigations may be obtained from the Fachinformationszentrum Karlsruhe, 76344 Eggenstein-Leopoldshafen, Germany (fax: (+49) 7247-808-666; email: crysdata@fiz-karlsruhe.de), on quoting the depository numbers CSD-412616 (B_8F_{12}), CSD-412617 ($B_{17}F_{27}$), and CSD-412618 ($B_{10}F_{12}$).
[11] Crystal structure analysis of $B_{10}F_{12}$: $M = 336.08$, tetragonal $I4_1/a$, $a = 6.4118(8)$, $c = 25.551(5)$ Å, $V = 1132.6(3)$ Å^3, $T = 150$ K, $\rho_{cald} = 1.971$ g cm^{-3}, $\lambda = 0.71073$ Å. Colorless cylinder, o. d. 0.36 mm, $\mu(Mo_{K\alpha}) = 0.242$ mm^{-1}. An absorption correction was performed by the multiscan method using the program SADABS ($0.762 < T < 1$). Data were collected to $2\theta_{max} = 58°$ comprising 3613 measured and 728 unique data, of which 685 with $F > 4\sigma(F)$ were used for refinement. The structure was solved by direct methods and refined as a merohedral twin using a twofold axis about [110] as the twin law by full-matrix least-squares against F, with anisotropic displacement parameters on all atoms and a Chebychev three-term polynomial weighting scheme. The final R factor was 0.0219, $R_w = 0.0252$, for 52 parameters. The final difference map max. and min. were $+0.22$ and -0.15 e Å^{-3}, respectively, and the twin-component scale factors were 0.5841 and 0.4186(16).[10b] The programs used were the same as those in reference [10a].
[12] P. Laszlo, *Angew. Chem.* **2000**, *112*, 2151; *Angew. Chem. Int. Ed.* **2000**, *39*, 2071.
[13] All calculations were performed by using the GAUSSIAN 98 computer program[14] using resources of the UK Computational Chemistry Facility, on a DEC 8400 superscalar cluster equipped with 10 fast processors, 6 GB of memory, and 150 GB disc. Calculations were performed at the MP2/6-31G* level of theory.[14] Calculations were carried out starting with the crystal coordinates of B_8F_{12}, and a similar structure, whereby the central four B–B distances were constrained to be equal. Calculations were also carried out on the structure of $(F_2B)_2B(\mu\text{-}BH_2)_2(BF_2)_2$ to determine how removing fluorine atoms from the bridging groups affects the structural symmetry in B_8F_{12}. Frequency calculations allowed the nature of any stationary points to be determined, which confirms the structures as either local minima, transition states, or saddle points on the potential energy surfaces.
[14] GAUSSIAN 98 (Revision A.7), M. J. Frisch, G. W. Trucks, H. B. Schlegel, G. E. Scuseria, M. A. Robb, J. R. Cheeseman, V. G. Zakrzewski, J. A. Montgomery, R. E. Stratmann, J. C. Burant, S. Dapprich, J. M. Millam, A. D. Daniels, K. N. Kudin, M. C. Strain, O. Farkas, J. Tomasi, V. Barone, M. Cossi, R. Cammi, B. Mennucci, C. Pomelli, C. Adamo, S. Clifford, J. Ochterski, G. A. Petersson, P. Y. Ayala, Q. Cui, K. Morokuma, D. K. Malick, A. D. Rabuck, K. Raghavachari, J. B. Foresman, J. Cioslowski, J. V. Ortiz, B. B. Stefanov, G. Liu, A. Liashenko, P. Piskorz, I. Komaromi, R. Gomperts, R. L. Martin, D. J. Fox, T. Keith, M. A. Al-Laham, C. Y. Peng, A. Nanayakkara, C. Gonzalez, M. Challacombe, P. M. W. Gill, B. G. Johnson, W. Chen, M. W. Wong, J. L. Andres, M. Head-Gordon, E. S. Replogle, J. A. Pople, Gaussian, Inc., Pittsburgh, PA, **1998**.
[15] C. Møller, M. S. Plesset, *Phys. Rev.* **1934**, *46*, 618; P. Hohenburg, W. Kohn, *Phys. Rev. B* **1964**, *136*, 864.
[16] A. Neu, T. Mannekes, U. Englert, P. Paetzold, M. Hoffman, P. von Schleyer, *Angew. Chem.* **1997**, *109*, 2211; *Angew. Chem. Int. Ed. Engl.* **1997**, *36*, 2117.
[17] A. Neu, T. Mannekes, U. Englert, P. Paetzold, M. Hoffman, P. von Schleyer, *Inorg. Chim. Acta* **1999**, *289*, 58.
[18] C. Präsang, M. Hofmann, G. Geiseler, W. Massa, A. Berndt, *Angew. Chem.* **2002**, *114*, 1597; *Angew. Chem. Int. Ed.* **2002**, *41*, 1526.
[19] A. Maier, M. Hofmann, H. Pritzkow, W. Siebert, *Angew. Chem.* **2002**, *114*, 1600; *Angew. Chem. Int. Ed.* **2002**, *41*, 1529.
[20] J. A. J. Pardoe, N. C. Norman, P. L. Timms, *Polyhedron* **2002**, *21*, 543.
[21] See: D. F. Shriver, *Manipulation of Air Sensitive Compounds*, McGraw-Hill, New York, **1969**, p. 91.
[22] G. M. Sheldrick, SHELXTL version 5, Bruker-AXS, Madison, Wisconsin, **1995**.
[23] D. J. Watkin, C. K. Prout, J. R. Carruthers, P. W. Betteridge, R. I. Cooper, CRYSTALS Issue 11. Chemical Crystallography Laboratory, Oxford, UK, **2001**.
[24] A. L. Spek, PLATON, a Multipurpose Crystallographic Tool, Utrecht University, Utrecht, The Netherlands, **2002**. PC version part of the WINGX suite: L. J. Farrugia, *J. Appl. Crystallogr.* **1999**, *32*, 837.

Amide/Hydride Transformation

DIBAH-Mediated Amide/Hydride Transformation in *ansa*-Lanthanidocene(III) Complexes**

*Michael G. Klimpel, Peter Sirsch, Wolfgang Scherer, and Reiner Anwander**

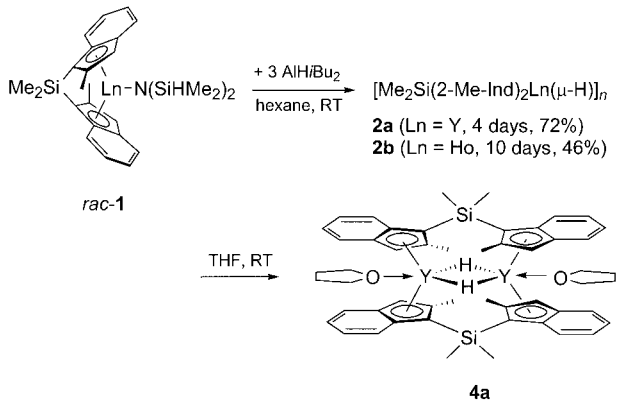
Lanthanidocene(III) hydride derivatives are classified as highly efficient precatalysts for a variety of olefinic transformations,[1] such as the polymerization of ethylene[2] and methylmethacrylate[3] as well as hydrogenation[4] and hydrosilylation reactions.[5] Such highly reactive discrete molecular hydride complexes are commonly synthesized, both on a preparative scale or in situ, by hydrogenolysis of lanthanidocene alkyl complexes.[6] Less cumbersome synthetic routes comprise: a) thermal decomposition[7] or silanolysis of alkyl derivatives,[8] b) salt metathesis of lanthanidocene(III) chloride complexes with NaH or $LiAlH_4$,[9,10] and c) oxidation of samarocene(II) complexes with $AlH_3(NEt_3)$.[11] Recently, we applied an "extended silylamide route"[12] to generate heteroleptic lanthanidocene(III) bis(dimethylsilyl)amide complexes, including the first Brintzinger-type, indenyl-derived *ansa*-lanthanidocene derivatives.[13] Here we report that the silylamide moiety in *rac*-[{Me_2Si(2-Me-$C_9H_5)_2$}Ln{$N(SiHMe_2)_2$}] (Ln = Y, Ho) can be easily hydrogenated with diisobutylaluminumhydride (DIBAH). Although the hydrogenating power of DIBAH is well-established in organic synthesis,[14] it has been scarcely used as a hydrogenating reagent in organometallic chemistry.[15]

Inspired by the ease of the $[N(SiHMe_2)_2]\rightarrow[AlR_4]$ transformation which occurs in the reaction of rare earth metal silylamide complexes with an excess of trialkylaluminum reagents,[16] we were intrigued by the feasibility of other $[N(SiHMe_2)_2]\rightarrow[X]$ transformations by exploiting the formation of a thermodynamically very stable Al–N bond. Accordingly, a suspension of *rac*-[{Me_2Si(2-Me-$C_9H_5)_2$}Y{$N(SiHMe_2)_2$}] (*rac*-**1a**) in *n*-hexane was treated with an excess (3 equiv) of a commercially available sample of DIBAH (Scheme 1). The initially formed clear solution gradually produced a pale yellow precipitate. After four days, the yield of the hydrogenated species **2a** was 72%.

[*] Dr. R. Anwander, Dr. M. G. Klimpel
Anorganisch-chemisches Institut
Technische Universität München
Lichtenbergstrasse 4, 85747 Garching (Germany)
Fax: (+49) 89-289-13473
E-mail: reiner.anwander@ch.tum.de
P. Sirsch, Prof. W. Scherer
Institut für Physik
Universität Augsburg
Universitätsstrasse 1, 86159 Augsburg (Germany)

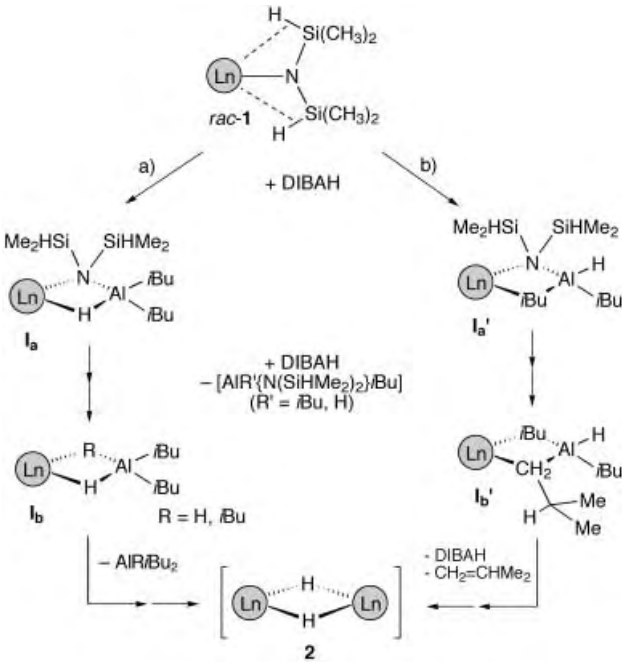
[**] Financial support from BAYER AG, the Deutsche Forschungsgemeinschaft, the Fonds der Chemischen Industrie, and Prof. W. A. Herrmann is gratefully acknowledged.

Supporting information for this article is available on the WWW under http://www.angewandte.org or from the author.



Scheme 1. Synthesis of **2** and **4a**. Only one enantiomer of *rac*-**1a** is depicted.

Both microanalytical (no nitrogen detected) and IR spectroscopic data (disappearance of the characteristic silylamide vibration $\tilde{\nu}$(SiH) at 1804 cm^{-1}) were indicative of the formation of a hydrogenated product. The recording of NMR spectra of yttrium complex **2a** was hampered by its low solubility in aliphatic and aromatic hydrocarbons. However, additional preparative investigations provided important details of the mechanism of the $[N(SiHMe_2)_2]\rightarrow[H]$ transformation. The proposed reaction sequence is shown in Scheme 2a. Initial formation of heterobimetallic complex *rac*-[{Me_2Si(2-Me-$C_9H_5)_2$}Y{μ-N$(SiHMe_2)_2$}(μ-H)Al*i*Bu_2] as reaction intermediate $\mathbf{I}_a$ is plausible since similar Lewis acid/base adducts have been isolated in the form of homoleptic complexes such as $[Yb\{N(SiMe_3)_2\}_2(AlMe_3)_2]$.[17] Additionally, a bridging mode of the small hydride ligand should be favored compared with a bridging isobutyl group (as in $\mathbf{I}_a'$) for



Scheme 2. Proposed reaction pathways for the formation of hydride dimer **2**.

 © 2003 Wiley-VCH Verlag GmbH & Co. KGaA, Weinheim 1433-7851/03/4205-0574 $ 20.00+.50/0

steric and thermodynamic reasons (Scheme 2b).[18,19] Steric considerations also suggest that the formation of intermediate $\mathbf{I}_a$ is the rate-determining step. In the present system, intermediate $\mathbf{I}_a$ could not be isolated, and was most likely converted via intermediate $\mathbf{I}_b$ into the kinetically favored hydride complex **2**. The second intermediate $\mathbf{I}_b$ is formed upon interaction of $\mathbf{I}_a$ with additional DIBAH. In accordance with this scenario is the exclusive formation of **2** along with recovered *rac*-**1a** from an equimolar reaction of *rac*-**1a** with DIBAH, as shown in Scheme 1. Moreover, intermediate $\mathbf{I}_b$ with R = *i*Bu could be isolated as the only stable reaction product ([$(Ph_4C_5H)_2$La(μ-H)(μ-*i*Bu)Al*i*Bu_2] (**3**)) from the reaction of sterically highly encumbered [$(Ph_4C_5H)_2$La{N$(SiHMe_2)_2$}][20] with two equivalents of DIBAH. The presence of a bridging hydride ligand in complex **3** is clearly visible in the ^{1}H NMR spectrum at $\delta = 5.19$ ppm ($\delta(H_{DIBAH}) = 3.05$ ppm). Finally, rapid conversion of intermediate $\mathbf{I}_b$ into the bridged hydride complex **2** most likely proceeds by dissociation of weakly coordinated Al$RiBu_2$ (R = H, *i*Bu) and irreversible dimerization of mononuclear metallocene hydride units (which precipitate from hexane and toluene); intermediate $\mathbf{I}_b$ is not formed, however, in the presence of a large excess of Al*i*Bu_3. Formation of lanthanide hydride complex **2** by β-H-elimination of a doubly *i*Bu-bridged intermediate $\mathbf{I}_b'$ would be an optional reaction pathway.[7] The availability of two μ-*i*Bu groups in lanthanidocene complexes was recently evidenced for [Cp_2^*Sm(μ-*i*Bu)$_2$Al*i*-Bu_2] and *rac*-[{Me_2Si(2-Me-$C_9H_5)_2$}Y(μ-*i*Bu)$_2$Al*i*Bu_2].[21,22] The involvement of *ansa*-ligand rearrangement (see below) might further complicate such a DIBAH-mediated [N$(SiHMe_2)_2$]→[H] transformation.[23,24] The strong dependency of the reaction on stereoelectronic factors could be further demonstrated by the isolation of **2b** containing the similarly sized holmium center, while the corresponding lutetium derivative did not form under these conditions.

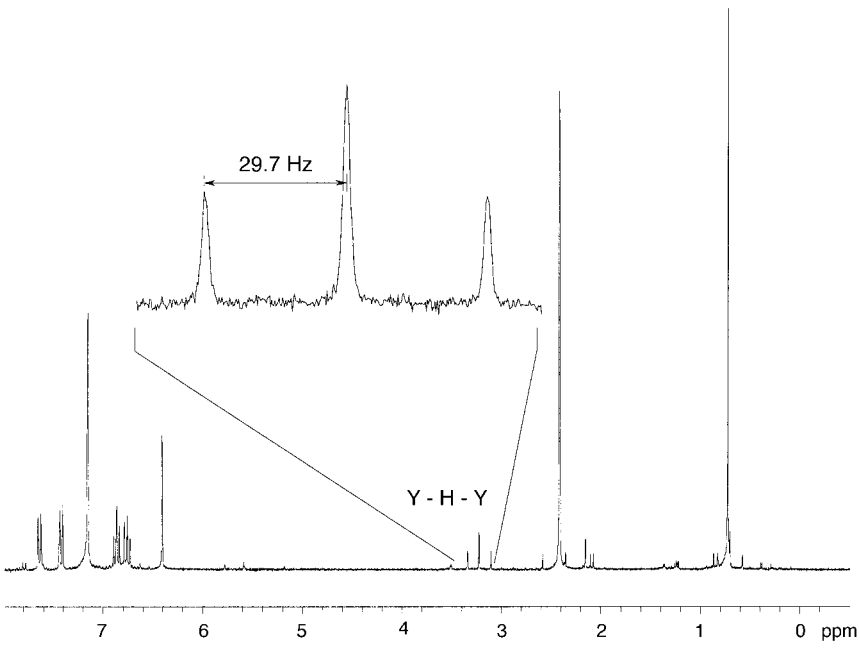


Figure 1. ^{1}H NMR spectrum of **4a** recorded in C_6D_6 at 25 °C.

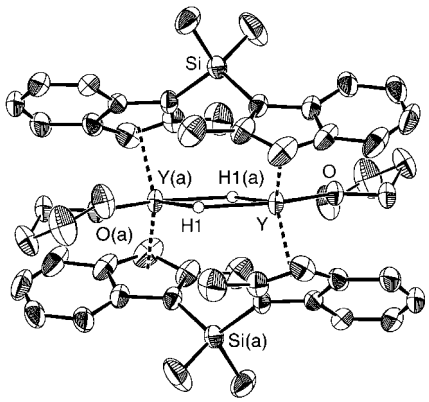


Figure 2. PLATON drawing of complex **4a**. Atoms are represented by atomic displacement ellipsoids at the 50% level. Except for the bridging H and H(a) atoms, all hydrogen atoms are omitted for clarity. For selected bond lengths and angles see Table 1.

Complex **2a** readily dissolves in benzene on addition of a small amount of a donor solvent such as tetrahydrofuran and yields complex **4a** (Scheme 1). The formulation of **4a** as a symmetrically bridged hydride dimer is based on the 1:2:1 triplet structure of the bridging hydride ligands at $\delta =$ 3.22 ppm in the ^{1}H NMR spectrum (Figure 1; two equivalent ^{89}Y nuclei, $^1J_{YH} = 29.7$ Hz).[25]

An X-ray structure analysis of complex **4a**[26] revealed the presence of a "flyover dimer"[23] of composition [{Y(thf)}$_2${μ$_2$-[(η^5-2-Me-C_9H_5)SiMe_2(η^5-2-Me-C_9H_5)]}$_2$(μ$_2$-H)$_2$] as the predominant structural motif (Scheme 1, Figure 2). It is known that single-atom-linked *ansa*-lanthanidocene complexes tend to abandon the chelating "wedge-type" binding mode (as shown for *rac*-**1** in Scheme 1) in favor of this "spanning" coordination mode. Structurally characterized examples featuring this binding mode comprise [{Me_2Si$(C_5H_4)_2$Yb-(μ-Cl)}$_2$],[27a] [{Me_2Si$(C_5H_4)_2$Yb}$_2$(μ-H)(μ-Cl)],[27b] [{Et_2-Si(C_5H_4)(3,4-Me_2-C_5H_2)Lu(μ-H)}$_2$] (**5**),[24] [{Et_2Si(C_5H_4)(3,4-Me_2-C_5H_2)Lu}$_2$(μ-H)(μ-Et)],[24] and [{Me_2Si(3-SiMe$_3$-$C_5H_3)_2$Sm(thf)(μ-H)}$_2$] (**6**).[3a] The spanning mode is particularly favored in the presence of small ligands such as H or Cl and sterically demanding linked cyclopentadienyl ligands.

Table 1 summarizes selected bond lengths and angles by comparing those of complex **4a** with the relevant "flyover" dimers **5** and **6**. The bonding parameters of the {Ln(μ-H)$_2$Ln} core respond extremely sensitively to repulsive metal···metal interactions, that is, they are sensitive to the metal size. The Y···Y distances and Y–H bond lengths of **4a** fall in the range of those observed in other dimeric hydrido complexes,[6,28–33] for example, [{(Me-$C_5H_4)_2$Y(thf)(μ-H)}$_2$] (3.66(1); 2.17(8), 2.19(8) Å),[6] [{(1,3-Me_2-$C_5H_3)_2$Y(thf)(μ-H)}$_2$] (3.68(1); 2.03(7), 2.27(6) Å),[28] [{(2,4,7-$Me_3C_9H_4)_2$Y(μ-H)}$_2$] (2.09(4)–2.14(7) Å),[29] [{$SiMe_2$(C_5Me_4)(NCMe_3)Y(thf)(μ-H)}$_2$] (3.672(1); 1.98(6)–2.48(4) Å),[30] [{[PhC(N$SiMe_3$)$_2$]$_2$Y(μ-H)}$_2$]

Table 1: Selected structural parameters in "flyover" lanthanidocene hydride complexes [{$Me_2Si(2\text{-}Me\text{-}C_9H_5)_2Y(thf)(\mu\text{-}H)\}_2$] (**4a**), [{$Et_2Si(C_5H_4)(3,4\text{-}Me_2\text{-}C_5H_2)Lu(\mu\text{-}H)\}_2$] (**5**), and [{$Me_2Si(3\text{-}SiMe_3\text{-}C_5H_3)_2Sm(thf)(\mu\text{-}H)\}_2$] (**6**).

Feature[a]	**4a** (Ln = Y)	**5** (Ln = Lu)[24]	**6** (Ln = Sm)[3a]
	Bond lengths [Å]		
Ln(1)···Ln(1a)	3.6524(3)	3.390(1)	3.762(1)
Ln–C_g(1)	2.480(1)	2.27	2.46
Ln–C_g(2)	2.447(2)	2.29	2.48
Ln–C(range)	2.656(3)–2.844(3)	2.551(4)–2.608(4)	2.706(7)–2.813(7)
Ln–H(1)	2.09(3)	2.15(4)	1.91
Ln–H(1a)	2.13(3)	2.12(4)	2.15
	Bond angles [°]		
C_g(1)-Ln-C_g(2)	127.51(5)	130.2	132.4
H(1)-Ln-H(1a)	60(1)	75.2	39
Ln(1)-H(1)-Ln(1a)	120(1)	104.8	141

[a] C_g(1) and C_g(2) = ring centroid. Ln–H bond lengths have to be discussed carefully because of the location of the hydrogen atoms close to two heavy atoms.

(2.11(3)–2.19(3) Å),[31] and [{(dadmb)Y(thf)(μ-H)}$_2$] (3.6652(8); 2.22(4), 2.27(4) Å (dadmb = 2,2′-bis-((*tert*-butyldimethylsilyl)amido)-6,6′-dimethylbiphenyl)).[32] The spanning geometry of the μ-[$Me_2Si(2\text{-}Me\text{-}C_9H_5)_2$] ligand results in the C-Si-C angle of 115.3(1)° in **4a** being markedly widened relative to that of synthetic precursor *rac*-**1a** (100.9(1)°).

These preliminary results show that *ansa*-lanthanidocene hydride derivatives can be synthesized by treatment of the silylamide precursor with DIBAH at ambient temperature. We are currently examining the scope of DIBAH-mediated amide/hydride transformation reactions in organolanthanide and early transition metal chemistry.

Experimental Section

Representative syntheses of **2a** and **4a**: A 1M solution of diisobutylaluminumhydride (3 equiv) in *n*-hexane was added to a suspension of *rac*-**1a** (535 mg, 1.00 mmol) in *n*-hexane (10 mL) at ambient temperature in an argon-filled glovebox. The lemon yellow suspension immediately became a pale yellow solution and after about 5 min a pale yellow precipitate formed. The reaction mixture was then stirred for 4 days at ambient temperature. The suspension was then centrifuged and the residue washed twice with *n*-hexane (5 mL) and dried in high vacuum to leave **2a** as a pale yellow powder (292 mg, 72%). Complex **4a** was obtained upon addition of a small amount of THF to a suspension of **2a** in benzene. Colorless prisms of **4a** suitable for X-ray analysis were obtained from a saturated benzene solution at ambient temperature. IR (nujol) of **2a**: $\tilde{\nu}$ = 1351 s, 1276 s, 1201 s, 1036 m, 874 m, 834 m, 806 m, 773 m, 737 s, 641 w, 461 w, 427 m cm^{-1}. ^{1}H NMR (400 MHz, C_6D_6, 25 °C) of **4a**: δ = 7.66 (d, $^3J_{H,H}$ = 8.4 Hz, 2H, indenyl), 7.54 (d, $^3J_{H,H}$ = 8.0 Hz, 2H, indenyl), 6.81 (dd, 2 × $^3J_{H,H}$ = 7.3 Hz, 2H, indenyl), 6.72 (dd, 2 × $^3J_{H,H}$ = 8.4 Hz, 2H, indenyl), 6.52 (s, 2H, indenyl), 3.22 (t, $^1J_{Y,H}$ = 29.7 Hz, 1H, Y-H-Y), 2.45 (s, 6H, indenyl-CH_3), 0.71 ppm (s, 6H, Si(CH_3)$_2$). ^{13}C{^{1}H} NMR (100 MHz, C_6D_6, 25 °C) of **4a**: δ = 140.3, 124.0, 123.6, 122.8, 121.4, 120.9, 120.1, 106.6, 105.4 (s, indenyl-C), 19.2 (s, indenyl-CH_3), 4.2 ppm (s, Si(CH_3)$_2$). Elemental analysis calcd for $C_{22}H_{23}SiY$ (**2a**): C 65.34, H 5.73; found: C 64.50, H 6.20. Full experimental and spectroscopic details for complexes **2b** and **3** are available in the Supporting Information.

Received: July 16, 2002 [Z19748]

[1] For recent reviews, see a) F. T. Edelmann, *Top. Curr. Chem.* **1996**, *179*, 247; b) R. Anwander in *Applied Homogeneous Catalysis with Organometallic Compounds* (Eds.: B. Cornils, W. A. Herrmann), Wiley-VCH, Weinheim, **2002**, pp. 974; c) H. Yasuda, *Top. Organomet. Chem.* **1999**, *2*, 255.

[2] a) G. Jeske, H. Lauke, H. Mauermann, P. N. Swepston, H. Schumann, T. J. Marks, *J. Am. Chem. Soc.* **1985**, *107*, 8091; b) G. Jeske, L. E. Schock, P. N. Swepston, H. Schumann, T. J. Marks, *J. Am. Chem. Soc.* **1985**, *107*, 8103.

[3] a) G. Desurmont, Y. Li, H. Yasuda, T. Maruo, N. Kanehisa, Y. Kai, *Organometallics* **2000**, *19*, 1811; b) G. Desurmont, T. Tokimitsu, H. Yasuda, *Macromolecules* **2000**, *33*, 7679.

[4] M. A. Giardello, V. P. Conticello, L. Brard, M. R. Gagne, T. J. Marks, *J. Am. Chem. Soc.* **1994**, *116*, 10241.

[5] P.-F. Fu, L. Brard, Y. Li, T. J. Marks, *J. Am. Chem. Soc.* **1995**, *117*, 7157.

[6] W. J. Evans, J. H. Meadows, A. L. Wayda, W. E. Hunter, J. L. Atwood, *J. Am. Chem. Soc.* **1982**, *104*, 2008.

[7] W. J. Evans, J. H. Meadows, A. L. Wayda, W. E. Hunter, J. L. Atwood, *J. Am. Chem. Soc.* **1982**, *104*, 2015.

[8] A. Z. Voskoboynikov, I. N. Parshina, A. K. Shestakova, K. P. Butin, I. P. Beletskaya, L. G. Kuz'mina, J. A. K. Howard, *Organometallics* **1997**, *16*, 4041.

[9] H. Schumann, W. Genthe, *J. Organomet. Chem.* **1981**, *213*, C7.

[10] G. L. Soloveichik, S. Y. Knyazhanskii, B. M. Bulychev, V. K. Bel'skii, *Organomet. Chem. USSR* **1992**, *5*, 73, and references therein.

[11] G. L. Soloveichik, *New J. Chem.* **1995**, *19*, 597, and references therein.

[12] R. Anwander, *Top. Organomet. Chem.* **1999**, *2*, 1.

[13] J. Eppinger, M. Spiegler, W. Hieringer, W. A. Herrmann, R. Anwander, *J. Am. Chem. Soc.* **2000**, *122*, 3080.

[14] J. J. Eisch in *Comprehensive Organometallic Chemistry II, Vol. 11* (Eds.: G. Wilkinson, F. G. A. Stone, E. W. Abel), Pergamon, Oxford, **1995**, chap. 6.

[15] W. P. Neumann, H. Niermann, *Justus Liebigs Ann. Chem.* **1962**, *653*, 164.

[16] a) R. Anwander, O. Runte, J. Eppinger, G. Gerstberger, M. Spiegler, E. Herdtweck, *J. Chem. Soc. Dalton Trans.* **1998**, 847; b) M. G. Klimpel, R. Anwander, M. Tafipolsky, W. Scherer, *Organometallics* **2001**, *20*, 3983.

[17] J. M. Boncella, R. A. Andersen, *Organometallics* **1985**, *4*, 205.

[18] For examples, see a) L. J. Guggenberger, F. N. Tebbe, *J. Am. Chem. Soc.* **1973**, *95*, 7870; b) R. B. Waymouth, B. D. Santarsiero, R. J. Coots, M. J. Bronikowski, M. J. Grubbs, *J. Am. Chem. Soc.* **1996**, *118*, 1427; c) R. H. Siedle, R. A. Newmark, J. N. Schroepfer, P. A. Lyon, *Organometallics* **1991**, *10*, 400.

[19] S. P. Nolan, D. Stern, T. J. Marks, *J. Am. Chem. Soc.* **1989**, *111*, 7844.

[20] M. G. Klimpel, H. W. Görlitzer, M. Tafipolsky, W. Scherer, M. Spiegler, R. Anwander, *J. Organomet. Chem.* **2002**, *647*, 236.

[21] W. J. Evans, J. T. Leman, R. D. Clark, J. W. Ziller, *Main Group Chem.* **2000**, *23*, 163.

[22] Reaction of complex *rac*-**1a** with an excess of Al*i*Bu$_3$ also produced the Lewis acid base adduct *rac*-[{$Me_2Si(2\text{-}Me\text{-}C_9H_5)_2$}Y(μ-*i*Bu)$_2$Al*i*Bu$_2$] as the final product. Under these conditions, Al*i*Bu$_3$, which is often employed as a latent hydride

 © 2003 Wiley-VCH Verlag GmbH & Co. KGaA, Weinheim 1433-7851/03/4205-0576 $ 20.00+.50/0

source, does not form a lanthanide-bonded hydride ligand and isobutene by β-H-elimination: M. G. Klimpel, J. Eppinger, P. Sirsch, W. Scherer, R. Anwander, *Organometallics* **2002**, *21*, 4021.

[23] E. B. Coughlin, L. M. Henling, J. E. Bercaw, *Inorg. Chim. Acta* **1996**, *242*, 205.

[24] D. Stern, M. Sabat, T. J. Marks, *J. Am. Chem. Soc.* **1990**, *112*, 9558. *Ansa*-ligand rearrrangement and formation of hydride-bridged "flyover"dimers seems to have drastic consequences on the catalytic activity in olefin polymerization. For example, the reaction of $[\{Et_2Si(C_5H_4)(3,4\text{-}Me_2\text{-}C_5H_2)Lu(\mu\text{-}H)\}_2]$ (**5**) with ethylene, propylene, and 1-hexene gave quantitatively μ-hydride/μ-alkyl mono-insertion products at ambient temperature. However, similar complexes such as **6** were also shown to be highly efficient in the block copolymerization of ethylene and polar monomers.[3]

[25] A comprehensive survey of the ^{1}H NMR chemical shifts (δ = 1.85–8.31 ppm) and ^{89}Y-^{1}H coupling constants (23.8–35.3 Hz) of dimeric yttrium hydrido complexes is presented in: K. C. Hultzsch, P. Voth, K. Beckerle, T. P. Spaniol, J. Okuda, *Organometallics* **2000**, *19*, 228.

[26] Compound **4a** ($C_{52}H_{62}O_2Si_2Y_2{\cdot}2\,C_6D_6$) crystallizes from benzene in the monoclinic space group $P2_1/c$ with a = 11.7875(2), b = 14.0396(3), c = 16.8378(4) Å, β = 104.2053(12)°, V = 2701.31(10) Å^3, and ρ_{calcd} = 1.364 g cm^{-3} for Z = 2. Data were collected at 193 K on a Nonius Kappa-CCD system. The structure was solved by Patterson methods, and least-square refinement of the model based on 3682 reflections ($I > 2.0\sigma(I)$) converged to a final $R1$ = 4.0 % ($wR2$ = 8.1 %). Except H(1), all hydrogen atoms were placed in calculated positions. H(1) was located in difference Fourier maps and refined with isotropic thermal parameters. CCDC-188842 (**4a**) contains the supplementary crystallographic data for this paper. These data can be obtained free of charge via www.ccdc.cam.ac.uk/conts/retrieving.html (or from the Cambridge Crystallographic Data Centre, 12 Union Road, Cambridge CB2 1EZ, UK; fax: (+44) 1223-336-033; or deposit@ccdc.cam.ac.uk).

[27] a) N. Höck, W. Oroschin, G. Paolucci, R. D. Fischer, *Angew. Chem.* **1986**, *98*, 748; *Angew. Chem. Int. Ed. Engl.* **1986**, *25*, 738; b) K. Qiao, R. D. Fischer, G. Paolucci, *J. Organomet. Chem.* **1993**, *456*, 185.

[28] W. J. Evans, D. K. Drummond, T. P. Hanusa, R. J. Doedens, *Organometallics* **1987**, *6*, 2279.

[29] W. P. Kretschmer, S. I. Troyanov, A. Meetsma, B. Hessen, J. H. Teuben, *Organometallics* **1998**, *17*, 284.

[30] a) K. C. Hultzsch, T. P. Spaniol, J. Okuda, *Angew. Chem.* **1999**, *111*, 163; *Angew. Chem. Int. Ed.* **1999**, *38*, 227; b) S. Arndt, P. Voth, T. P. Spaniol, J. Okuda, *Organometallics* **2000**, *19*, 4690.

[31] R. Duchateau, C. T. van Wee, A. Meetsma, P. T. van Duijnen, J. H. Teuben, *Organometallics* **1996**, *15*, 2279.

[32] T. I. Gountchev, T. D. Tilley, *Organometallics* **1999**, *18*, 2896.

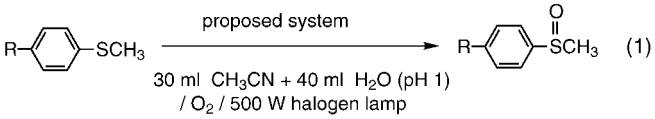
[33] J. P. Mitchell, S. Hajela, S. K. Brookhart, K. I. Hardcastle, L. M. Henling, J. E. Bercaw, *J. Am. Chem. Soc.* **1996**, *118*, 1045.

Photocatalytic Oxidation

An Efficient and Selective Photocatalytic System for the Oxidation of Sulfides to Sulfoxides**

Jyh-Myng Zen, Shiou-Ling Liou, Annamalai Senthil Kumar, and Mung-Seng Hsia*

The selective oxidation of organic sulfides to sulfoxides without any overoxidation to sulfones is a challenging research interest in synthetic organic chemistry, partly because of the importance of sulfoxides as intermediates in biologically active compounds.[1] Of the many classical oxidants, H_2O_2-based systems are considered to be relatively clean and free of pollution.[2] Nevertheless, under catalytic conditions, the choice of H_2O_2 conditions and the stoichiometry with respect to the catalyst are critical to the selectivity of the reaction. Herein, we report a novel heterogeneous photochemical system for the selective transformation of organic sulfides to sulfoxides in the presence of oxygen using a nafion membrane doped with a lead ruthenate pyrochlore (Pyc) catalyst and a $[Ru(bpy)_3]^{2+}$ photosensitizer (designated as $|NPyc^{x-}Ru(bpy)|$). Figure 1a illustrates the typical procedure for the incorporation of Pyc into a nafion membrane.[3] The membrane (5 × 5 cm) was first soaked with a mixture of Pb^{2+} and Ru^{3+} ions (1.5:1), which led to electrostatic exchange of ions into the hydrophilic sites of nafion. The precipitation of Pyc (designated as $|NPyc^{x-}|$) was done by treating the ion-exchanged membrane in 1.1 M KOH at 53 °C for 24 h with continuous purging of O_2.[3a] The formation of Pyc was confirmed by X-ray diffraction analysis.[3a] The $|NPyc^{x-}|$ membrane was found to be highly stable in organic media.[4] Finally, a suitable amount of $[Ru(bpy)_3]^{2+}$ was doped into the $|NPyc^{x-}|$ membrane simply by an ion-exchange process from a solution containing 1 mM $[Ru(bpy)_3]^{2+}$. This membrane (designated as $|NPyc^{x-}Ru(bpy)|$) was then used in organic syntheses. Very few photochemical reactions have so far been reported for the sulfide oxidation reaction (SOR), and all the cases resulted in a mixture of products from C–S bond breakage and overoxidation through radical combination reactions.[5] In the present study a clean reaction [Eq. (1)] occurs, and the controlled catalytic oxygen reduction reaction (ORR) to H_2O_2 at the Pyc active sites is essential to the SOR (see below).



(1)

[*] Prof. Dr. J.-M. Zen, S.-L. Liou, Dr. A. S. Kumar, M.-S. Hsia
Department of Chemistry
National Chung Hsing University
Taichung 402 (Taiwan)
Fax: (+886) 4-2286-2547
E-mail: jmzen@dragon.nchu.edu.tw

[**] The National Science Council of the Republic of China is gratefully acknowledged for financial support of this work.

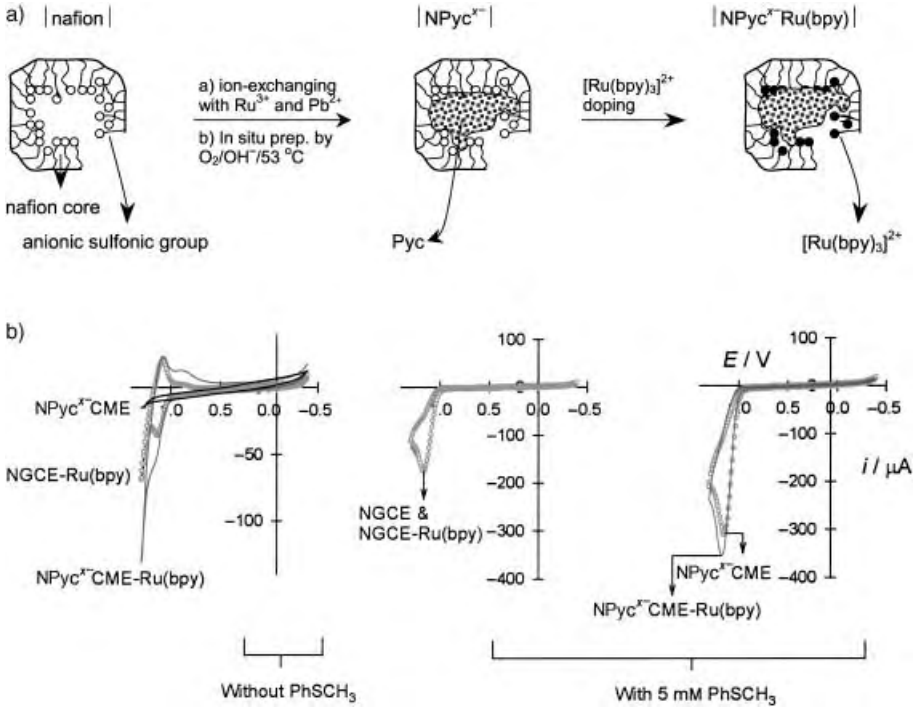


Figure 1. a) Conceptional representation for the preparation of $|NPyc^{x-}Ru(bpy)|$. b) Cyclic voltammetric response of various chemically modified electrodes at pH 1 in a supporting electrolyte consisting of a mixture of CH_3CN and H_2O (3:4) without and with 5 mM $PhSCH_3$ at $\upsilon = 50\ mV s^{-1}$.

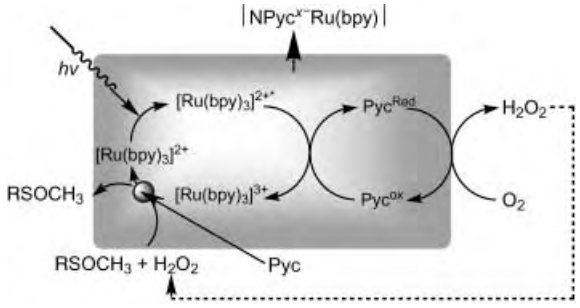
To electrochemically characterize the multicomposite $|NPyc^{x-}Ru(bpy)|$ membrane and to study the photoconversion of $[Ru(bpy)_3]^{2+} \rightarrow [Ru(bpy)_3]^{3+}$ (via $[Ru(bpy)_3]^{2+*}$) in the presence of Pyc, a simulated chemically modified electrode (designated as $NPyc^{x-}$CME-Ru(bpy)) was prepared. The only difference in preparing the $NPyc^{x-}$CME was that a nafion-coated glassy carbon electrode (NGCE) was first prepared by dip coating with 5 μL of a 5 wt% solution of nafion. As shown in Figure 1b, a well-defined redox peak at approximately 1.1 V versus Ag/AgCl corresponding to the $[Ru(bpy)_3]^{3+}/[Ru(bpy)_3]^{2+}$ couple was observed at the $NPyc^{x-}$CME.[6] The anodic peak current (i_{pa}) was much higher than that observed at the $[Ru(bpy)_3]^{2+}$-doped NGCE (NGCE-Ru(bpy)). The increase in the current response clearly has something to do with the existence of active Pyc catalyst inside nafion. The catalyst can somehow assist the reaction of $[Ru(bpy)_3]^{2+} \rightarrow [Ru(bpy)_3]^{3+}$ via $[Ru(bpy)_3]^{2+*}$. The importance of the active Pyc site in nafion was further demonstrated by the following two experiments. First, an irreversible oxidation peak at the redox potential of the $[Ru(bpy)_3]^{3+}/[Ru(bpy)_3]^{2+}$ couple with a much higher i_{pa} value with $NPyc^{x-}$CME than with NGCE was observed on addition of 5 mM $PhSCH_3$. Secondly, virtually no change in the i_{pa} value was observed on using NGCE and NGCE-Ru(bpy); while a net increase of approximately 60 μA in the i_{pa} value was observed at the $NPyc^{x-}$CME-Ru(bpy) than that at the $NPyc^{x-}$CME. In other words, there is no intrinsic effect on the SOR by using $[Ru(bpy)_3]^{2+}$ without the assistance of the active Pyc site in nafion. These preliminary electrochemical results can indeed help to explain the reaction mechanism of the photochemical oxidation of $RSCH_3$ (R = Ph, $PhCOCH_3$, and $PhOCH_3$) at the $|NPyc^{x-}Ru(bpy)|$ membrane (see below).

Controlled experiments were carried out under various experimental conditions (Table 1) to rationalize the reaction mechanism. It is clear that the success of the system lies in the proper combination of catalyst, photosensitizer, solvent composition, pH value, O_2, and light illumination. A possible reaction mechanism based on these results is shown in Scheme 1, where Pyc plays a dual catalytic role both in the ORR (dark reaction) and the SOR (light reaction). It is noteworthy that, since the Pyc is opaque, only $[Ru(bpy)_3]^{2+}$ can be involved in light

Table 1: The influence of the reaction conditions on the selective photochemical oxidation of $RPhSCH_3$ to $RPhSOCH_3$.[a]

Entry	Membrane catalyst		Solution					
	Pyc	$[Ru(bpy)_3]^{2+}$	$CH_3CN:H_2O$	pH[b]	O_2	$h\nu$[c]	t [h]	yield [%]
1	+	–	3:4	1	+	+	8	–
2	–	+	3:4	1	+	+	8	–
3	+	+	3:4	1	+	–	8	–
4	+	+	1:4	ca. 7	+	+	8	–
5	+	+	3:4	1	–	+	8	23
6	+	+	14:1	1	+	+	8	37
7	–	–	3:4	1	1 mL of 30% H_2O_2 added	–	3	47
8	+	+	3:4	ca. 7	+	+	8	49
9	+	+	3:4	1	+	+	3	>97

[a] +: presence, –: absence, [$RPhSCH_3$: R = H, $COCH_3$, OCH_3] = 17 mM, Entries 1–8 tested with $PhSCH_3$. [b] Adjusted with dilute HCl. [c] A 500-W halogen lamp was used as the light source. As for entry 9, the yields for the substituted organic sulfides are: $R = COCH_3$: 96% and $R = OCH_3$: 90%.



Scheme 1. Reaction mechanism for the photochemical sulfide oxidation reaction.

 © 2003 Wiley-VCH Verlag GmbH & Co. KGaA, Weinheim 1433-7851/03/4205-0578 $ 20.00+.50/0

absorption in the membrane. The active Pyc site was reported to be an efficient catalyst for the ORR,[3b,7] and hence, the purging O_2 is essential for the formation of H_2O_2 during the reaction. The control experiment in pure H_2O_2 gave only about 47% conversion with poor selectivity (Table 1). However, the assistance of Pyc and $[Ru(bpy)_3]^{2+}$ in the SOR was supported by the indirect electrochemical studies mentioned earlier. The efficiency of the SOR was then evaluated by putting a 4.5×2 cm $|NPyc^{x-}Ru(bpy)|$ in a mixture of CH_3CN (30 mL), H_2O (40 mL), and 17 mM $RSCH_3$ (R = Ph, $PhCOCH_3$, and $PhOCH_3$) at pH 1, with constant purging of O_2 under illumination (500 W halogen lamp) for 3 h. The products were analyzed simply by evaporation of the solution of the separated reaction product in $CHCl_3$ with a rotary-vacuum system. All reactions gave a single product of sulfoxide (that is, no sulfone was observed on the TLC plate and was further confirmed by NMR and mass spectroscopic studies) in >90% yield. The high selectivity of the current approach was clearly demonstrated. Finally, three repeated experiments were performed with $PhSCH_3$ to test the recyclability of the $|NPyc^{x-}Ru(bpy)|$ system, and almost the same yield was observed.

In conclusion, we have demonstrated a clean and highly selective photochemical oxidation of sulfide to sulfoxide on a novel heterogeonous multicomponent nafion membrane containing a Pyc catalyst and a $[Ru(bpy)_3]^{2+}$ photosensitizer. The high sulfoxide selectivity, lack of pollution, ease of product separation, and recyclable nature of the muticomponent membrane has a clear advantage over classical approaches. Further investigations are currently underway to expand the scope of this reaction to sulfide compounds containing more complicated organic structures and to a macroscale synthesis.

Experimental Section

Photochemical experiments were carried out at pH 1 (adjusted with HCl) in a mixture of CH_3CN and H_2O (3:4, ca. 70 mL) in a closed round-bottomed flask sealed with a gasket-septum under constant purging of O_2 gas. Cyclic voltammetric (CV) experiments were performed using a CHI workstation with a three-electrode system of working (0.071 cm^2), reference (Ag/AgCl), and counter (Pt disc, 0.071 cm^2) electrodes between −0.4 to 1.4 V. A negative current in the cyclovoltammograms denotes an anodic response, while a positive current denotes a cathodic current. The oxidized product was separated into $CHCl_3$ and then analyzed by NMR spectroscopic (in $CDCl_3$) and mass spectrometric techniques after rotary-vacuum evaporation. The yield of the products was determined on the basis of the ratio between the molar weight of the reactant and the product.

Received: July 17, 2002
Revised: August 27, 2002 [Z19755]

[1] a) M. C. Carreño, *Chem. Rev.* **1995**, *95*, 1717; b) *Sulfur Centered Reactive Intermediates in Chemistry and Biology*, (Eds.: C. Chatgilialoglu, K. D. Asmus), Nato ASI series, Plenum, New York, **1990**; c) M. Hudlický, *Oxidations in Organic Chemistry, ACS Monograph 186*, American Chemical Society, Washington, DC, **1980**.

[2] a) H. S. Schultz, H. B. Freyermuth, S. R. Bu, *J. Org. Chem.* **1963**, *28*, 1140; b) T. Indrasena, R. S. Varma, *Chem. Commun.* **1997**, 471; c) J. M. Fraile, J. I. García, B. Lázaro, J. A. Mayoral, *Chem. Commun.* **1998**, 1807; d) R. S. Varma, K. P. Naicker, *Org. Lett.* **1999**, *1*, 189; e) J. Brinksma, R. L. Crois, B. L. Feringa, M. I. Donnoli, C. Rosini, *Tetrahedron Lett.* **2001**, *42*, 4049; f) K. Sato, M. Hyodo, M. Aoki, X.-Q. Zheng, R. Noyori, *Tetrahedron* **2001**, *57*, 2469; g) S. Choi, J.-D. Yang, M. Ji, H. Choi, M. Kee, K.-H. Ahn, S.-H. Byeon, W. Baik, S. Koo, *J. Org. Chem.* **2001**, *66*, 8192.

[3] a) J.-M. Zen, A. S. Kumar, *Acc. Chem. Res.* **2001**, *34*, 772; b) J.-M. Zen, A. S. Kumar, C.-C. Chen, *J. Mol. Cat. A* **2001**, *165*, 177; c) J.-M. Zen, C.-B. Wang, *J. Electrochem. Soc.* **1994**, *141*. L51; d) J.-M. Zen, C.-B. Wang, *J. Electroanal. Chem.* **1994**, *368*, 251–256; e) J.-M. Zen, A. S. Kumar, C.-C. Chen, *Anal. Chem.* **2001**, *73*, 1169, and references therein.

[4] The stability experiment was checked by continuously stirring the $|NPyc^{x-}|$ membrane (ca. 0.1 cm^2) in a solution of about 99% ethanol for 90 days. The membrane did not show any change in weight, which illustrates the Pyc-modified nafion membrane has a relatively rigid structure.

[5] a) W. Adam, J. E. Argüello, A. B. Peñéñory, *J. Org. Chem.* **1998**, *63*, 3905; b) N. Somasundaram, C. Srinivasan, *J. Photochem. Photobiol.* **1998**, *115*, 169; c) K. Chiba, Y. Yamaguchi, M. Tada, *Tetrahedron Lett.* **1998**, *39*, 9035; d) E. L. Clennan, A. Aebisher, *J. Org. Chem.* **2002**, *67*, 1036.

[6] K. C. Pillai, A. S. Kumar, J.-M. Zen, *J. Mol. Catal. A* **2000**, *160*, 277.

[7] a) J. B. Goodenough, R. Manoharan, M. Parandhaman, *J. Am. Chem. Soc.* **1990**, *112*, 2076; b) J.-M. Zen, R. Manoharan, J. B. Goodenough, *J. Appl. Electrochem.* **1992**, *22*, 140.

Stereoselective Alkylation

Highly Stereoselective N-Terminal Functionalization of Small Peptides by Chiral Phase-Transfer Catalysis**

*Takashi Ooi, Eiji Tayama, and Keiji Maruoka**

Peptide modification is an essential yet flexible synthetic concept for screening targets efficiently and optimizing lead structures in the application of naturally occurring peptides as pharmaceuticals.[1,2] The introduction of side chains directly to a peptide backbone is a powerful method for preparing nonnatural peptides. The achiral glycine subunit has generally been used for this purpose[3] and glycine enolates,[4–8] radicals,[9–11] and glycine cation equivalents[12,13] have been ex-

[*] Prof. K. Maruoka, Dr. T. Ooi, E. Tayama
Department of Chemistry, Graduate School of Science
Kyoto University, Sakyo, Kyoto, 606-8502 (Japan)
Fax: (+81) 75-753-4041
E-mail: maruoka@kuchem.kyoto-u.ac.jp

[**] This work was supported in part by a Grant-in-Aid for Scientific Research from the Ministry of Education, Culture, Sports, Science and Technology, Japan.

Supporting information for this article is available on the WWW under http://www.angewandte.org or from the author.

ploited as reactive intermediates. However, controlling the stereochemical outcome of these processes in an absolute sense is difficult, especially in the modification of linear peptides, and hence the development of an efficient, practical, and general approach to establish sufficient stereoselectivity has been eagerly awaited.[7d,14] Although the stereoselective phase-transfer alkylation of Schiff-base-activated small peptides **2**, which involves chirality transfer between two adjoining amino acid residues, appears to be an attractive method,[6] it has never been developed to a useful level due to the lack of well-designed chiral catalysts.[15,16] Here we present the first solution to this problem, in which the optically pure, C_2-symmetric quaternary ammonium salt **1** is used as the catalyst (Scheme 1).[17] By fine-tuning the catalyst structure, a variety of new side chains can be attached to the growing peptide N terminus with remarkable stereoselectivity. This newly created chirality can be transferred efficiently to an adjacent amino acid residue, allowing the asymmetric construction of nonnatural oligopeptides.

We initially examined the alkylation of the dipeptide Gly-L-Phe derivative **2a** as a representative system and evaluated the critical importance of the chiral phase-transfer catalyst in obtaining high stereoselectivity (Table 1). When a mixture of **2a** and tetrabutylammonium bromide (2 mol%) as a typical achiral ammonium salt in toluene was treated with 50% KOH aqueous solution and benzyl bromide (1.1 equiv) at 0°C for 4 h, the corresponding benzylation product **3a** was obtained in 85% yield. The diastereomer ratio (D,L-**3a**:L,L-**3a**) was determined to be 54:46 (8% diastereomeric excess (*de*)) by chiral HPLC analysis (entry 1 in Table 1). In contrast, the reaction with the chiral quaternary ammonium bromide (*S*,*S*)-**1a** as the catalyst under similar conditions gave rise to **3a** with a D,L:L,L ratio of 77.5:22.5 (55% *de*, 88% yield, entry 2). Here, use of enantiomeric (*R*,*R*)-**1a** led to the preferential formation of L,L-**3a** in 20% *de* (entry 3), indicating that (*R*,*R*)-**1a** is a mismatched catalyst for this diastereofacial differentiation of **2a**. Significantly, the stereoselectivity was increased dramatically when the aryl substituent (Ar) on the 3- and 3′-positions of the catalyst was changed. Almost complete diastereocontrol was achieved with the catalyst (*S*,*S*)-**1d**, which has 3,5-bis(3,5-di-*tert*-butylphenyl)phenyl groups (97% *de*, entries 4–6).[18] It is worthy of comment that neither racemization of the preexisting chiral center nor N-alkylation was observed under the present biphasic conditions.

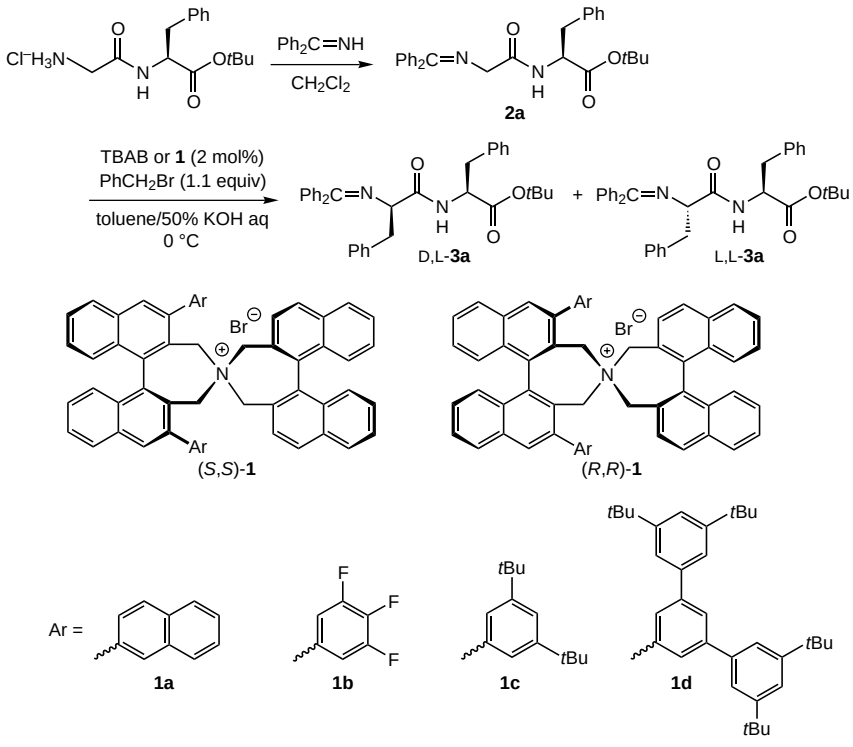
Table 1: Effect of the chiral C_2-symmetric quaternary ammonium salts on the diastereoselectivity of the phase-transfer benzylation of **2a**.[a]

Entry	Catalyst	Reaction time [h]	Yield [%][b]	*de* [%][c]
1	TBAB	4	85	8
2	(*S*,*S*)-**1a**	4	88	55
3	(*R*,*R*)-**1a**	6	83	20
4	(*S*,*S*)-**1b**	8	43	81
5	(*S*,*S*)-**1c**	4	98	86
6	(*S*,*S*)-**1d**	6	97	97

[a] The reactions were carried out with 1.1 equivalents $PhCH_2Br$ in the presence of 2 mol% TBAB or **1** in 50% aqueous KOH/toluene (volume ratio = 1:3) at 0°C under argon. [b] Yield of isolated product. [c] The diastereomeric excess of **3a** (R = CH_2Ph) was determined by ^1H NMR spectroscopy and by HPLC analysis with a chiral column (Daicel Chiralcel OD) and hexane/2-propanol as solvent. The absolute configuration of **3a** was determined by comparison of the ^1H NMR spectrum and the HPLC retention time with those of the independently synthesized authentic sample.

In a similar manner a variety of alkyl halides can be employed as the electrophile in this alkylation (Table 2, entries 1–5), where excellent stereoselectivities were uniformly observed. The efficiency of the transmission of stereochemical information was not affected by the side-chain structure of the preexisting amino acid residues, as clearly demonstrated in the phase-transfer benzylation of various dipeptides derived from natural α-amino acids (Table 2, entries 6–9). Interestingly, sterically less demanding (*S*,*S*)-**1c** was found to be a suitable catalyst for the substrate with the L-proline *tert*-butyl ester moiety (entry 10).

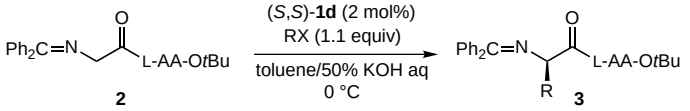
We further examined the stereoselective alkylation of the dipeptide L-Ala-L-Phe derivative **4**, which would enable the asymmetric construction of noncoded α,α-dialkyl-α-amino acid residues at the peptide terminal (Scheme 2).[19] Thus, reaction of a mixture of **4**, benzyl bromide (1.1 equiv), and the catalyst (*S*,*S*)-**1d** (2 mol%) in toluene with $CsOH\cdot H_2O$ (5 equiv) as a solid base at 0°C for 1 h

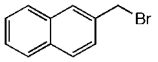
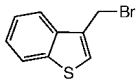


Scheme 1. Catalytic asymmetric alkylation of Schiff-base-activated dipeptide **2a** under phase-transfer conditions. TBAB = tetrabutylammonium bromide.

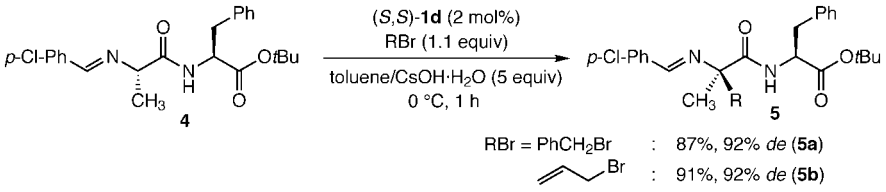
 © 2003 Wiley-VCH Verlag GmbH & Co. KGaA, Weinheim 1433-7851/03/4205-0580 $ 20.00+.50/0

Table 2: Stereoselective N-terminal alkylation of dipeptides by chiral phase-transfer catalysis.[a]

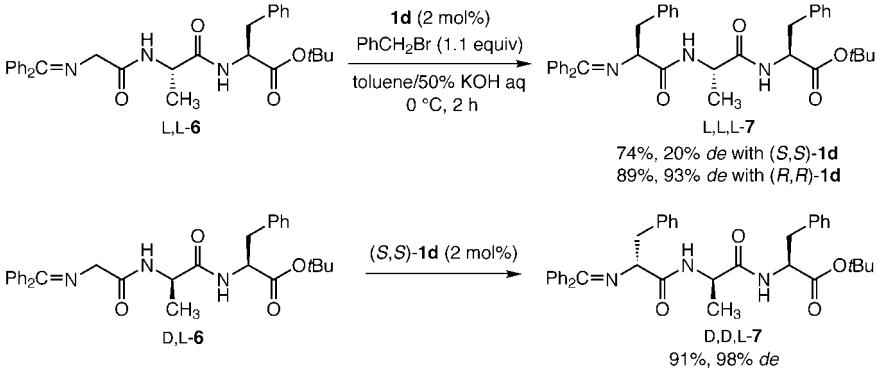


Entry	AA	RX	Reaction time [h]	Yield [%][b]	*de* [%][c]
1	Phe (**2a**)		6	89	98
2			6	80	96
3[d]		CH_3CH_2I	12	90	98
4			8	92	96
5[d]			6	95	91
6	Leu	$PhCH_2Br$	6	91	96
7	Val		12	85	93
8	Tyr(Bn)		8	90	98
9	Ala		6	92	93
10	Pro		8	80	90[e]

[a] Unless otherwise specified, the reactions were carried out with 1.1 equivalents RX in the presence of 2 mol% (*S*,*S*)-**1d** in 50% aqueous KOH/toluene (volume ratio = 1:3) under the given reaction conditions. [b] Yield of isolated product. [c] Diastereomeric excess of **3** was determined by ^{1}H NMR spectroscopy and HPLC analysis of the alkylated peptide with a chiral column (Daicel Chiralpak AD (entries 1, 3, and 8–10) and Chiralcel OD (entries 2, 4, and 5–7)) and hexane/2-propanol or hexane/ethanol as solvent. [d] A saturated solution of CsOH was used as the aqueous base. [e] With (*S*,*S*)-**1c** as catalyst.



Scheme 2. Asymmetric construction of terminal α,α-dialkyl-α-amino acid residues.



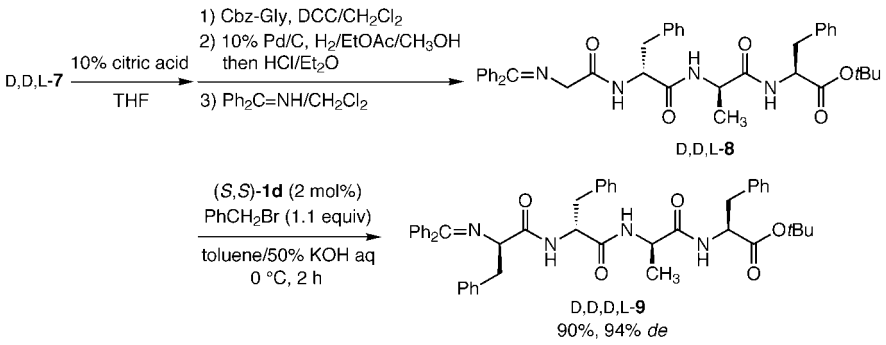
Scheme 3. Reversal of stereochemical preference in the asymmetric phase-transfer catalytic alkylation of tripeptide derivative **6**.

afforded **5a** in 87% yield and 92% *de*. The reaction with allyl bromide under similar conditions also proceeded smoothly with high diastereoselectivity (**5b**; 91% yield, 92% *de*).

Encouraged by the results, we extended the chiral phase-transfer catalysis with (*S*,*S*)-**1d** to the stereoselective N-terminal alkylation of Gly-Ala-Phe derivative **6**, that is, asymmetric synthesis of tripeptides (Scheme 3). To our surprise, the benzylation of L,L-**6** with (*S*,*S*)-**1d** under the optimized biphasic conditions resulted in poor diastereoselectivity (20% *de*) with L,L,L-**7** as the major product; however, the selectivity was enhanced to 93% *de* (89% yield) by the use of (*R*,*R*)-**1d** as a catalyst. The observed stereochemical relationship was totally opposite to that in the reactions of dipeptides. This interesting fact was further supported by the benzylation of D,L-**6**, where (*S*,*S*)-**1d** turned out to be a matched catalyst leading to almost exclusive formation of D,D,L-**7** under similar conditions (Scheme 3).

Furthermore, we found that this tendency for stereochemical communication was consistent in the phase-transfer alkylation of D,D,L-**8**, which can be readily prepared from D,D,L-**7** by means of hydrolysis and successive introduction of a new glycine subunit by well-established methods. The corresponding protected tetrapeptide D,D,D,L-**9** was obtained in 90% yield with excellent stereochemical control (94% *de*) as illustrated in Scheme 4. We also confirmed that similar alkylation of L,L,L-**8** with (*R*,*R*)-**1d** as the catalyst furnished L,L,L,L-**9** in 87% yield and 92% *de*, suggesting that (*R*,*R*)-**1d** is suitable for the stereoselective N-terminal alkylation of naturally occurring polypeptides.

Our approach based on the use of chiral quaternary ammonium salts enables the asymmetric phase-transfer catalytic alkylation of peptides. This provides a general procedure not only for the highly stereoselective N-terminal functionalization of peptides but also



Scheme 4. Asymmetric synthesis of tetrapeptides by chiral phase-transfer catalysis of (*S*,*S*)-**1d**. Cbz = benzyloxycarbonyl, DCC = 1,3-dicyclohexylcarbodiimide.

for the sequential asymmetric construction of nonnatural oligopeptides, which play a vital role in the development of peptide-based drugs.

Received: September 2, 2002 [Z50088]

[1] A. N. Eberle, *Chimia* **1991**, *45*, 145.

[2] V. De Filippis, D. Quarzago, A. Vindigni, E. Di Cera, A. Fontana, *Biochemistry* **1998**, *37*, 13507.

[3] R. M. Williams in *Synthesis of Optically Active α-Amino Acids, Vol. 7* (Eds.: J. E. Baldwin, P. D. Magnus), Pergamon, Oxford, **1989**.

[4] For a comprehensive review, see: a) D. Seebach, A. K. Beck, A. Studer in *Modern Synthetic Methods, Vol. 7* (Eds.: B. Ernst, C. Leumann), VCH, Weinheim, **1995**, p. 1. See also b) D. Seebach, A. K. Beck, H. G. Bossler, C. Gerber, S. Y. Ko, C. W. Murtiashaw, R. Naef, S. Shoda, A. Thaler, M. Krieger, R. Wenger, *Helv. Chim. Acta* **1993**, *76*, 1564; c) T. Matt, D. Seebach, *Helv. Chim. Acta* **1998**, *81*, 1845, and references therein.

[5] D. J. Ager, D. E. Froen, R. C. Klix, B. Zhi, J. M. McIntosh, R. Thangarasa, *Tetrahedron* **1994**, *50*, 1975.

[6] a) M. J. O'Donnell, T. P. Burkholder, V. V. Khau, R. W. Roeske, Z. Tian, *Pol. J. Chem.* **1994**, *68*, 2477; b) M. J. O'Donnell, C. Zhou, W. L. Scott, *J. Am. Chem. Soc.* **1996**, *118*, 6070; c) M. J. O'Donnell, M. D. Drew, R. S. Pottorf, W. L. Scott, *J. Comb. Chem.* **2000**, *2*, 172.

[7] a) U. Kazmaier, *Angew. Chem.* **1994**, *106*, 1096; *Angew. Chem. Int. Ed. Engl.* **1994**, *33*, 998; b) U. Kazmaier, *J. Org. Chem.* **1994**, *59*, 6667; c) U. Kazmaier, S. Maier, *Chem. Commun.* **1998**, 2535; d) U. Kazmaier, S. Maier, *J. Org. Chem.* **1999**, *64*, 4574.

[8] a) M. Ricci, L. Madariaga, T. Skrydstrup, *Angew. Chem.* **2000**, *112*, 248; *Angew. Chem. Int. Ed.* **2000**, *39*, 242; b) M. Ricci, P. Blakskjær, T. Skrydstrup, *J. Am. Chem. Soc.* **2000**, *122*, 12413.

[9] For a recent review, see: a) C. J. Easton, *Chem. Rev.* **1997**, *97*, 53. See also b) C. J. Easton, I. M. Scharfbillig, E. W. Tan, *Tetrahedron Lett.* **1988**, *29*, 1565; c) C. J. Easton, E. W. Tan, M. P. Hay, *J. Chem. Soc. Chem. Commun.* **1989**, 385; d) V. A. Burgess, C. J. Easton, M. P. Hay, *J. Am. Chem. Soc.* **1989**, *111*, 1047.

[10] a) D. Elad, J. Sperling, *J. Chem. Soc. Chem. Commun.* **1969**, 1579; b) D. Elad, J. Sperling, *J. Chem. Soc. Chem. Commun.* **1969**, 234; c) J. Sperling, D. Elad, *J. Am. Chem. Soc.* **1971**, *93*, 967; d) J. Sperling, D. Elad, *J. Am. Chem. Soc.* **1971**, *93*, 3839.

[11] A. Papadopoulos, B. Lewall, E. Steckhan, K.-D. Ginzel, F. Knoch, M. Nieger, *Tetrahedron* **1991**, *47*, 563.

[12] a) G. Apitz, W. Steglich, *Tetrahedron Lett.* **1991**, *32*, 3163; b) W. Steglich, M. Jager, S. Jaroch, P. Zistler, *Pure Appl. Chem.* **1994**, *66*, 2167.

[13] a) P. Renaud, D. Seebach, *Angew. Chem.* **1986**, *98*, 836; *Angew. Chem. Int. Ed. Engl.* **1986**, *25*, 843; b) P. Renaud, D. Seebach, *Helv. Chim. Acta* **1986**, *69*, 1704; c) D. Seebach, R. Charczuk, C. Gerber, P. Renaud, H. Berner, H. Schneider, *Helv. Chim. Acta* **1989**, *72*, 401.

[14] For reviews on selective alkylation of peptides, see: a) D. Seebach, *Angew. Chem.* **1988**, *100*, 1685; *Angew. Chem. Int. Ed. Engl.* **1988**, *27*, 1624; b) D. Seebach, *Aldrichimica Acta* **1992**, *25*, 59. See also refs. [3–13].

[15] For recent reviews on asymmetric phase-transfer catalysis, see: a) T. Shioiri, S. Arai in *Stimulating Concepts in Chemistry* (Eds.: F. Vögtle, J. F. Stoddart, M. Shibasaki), Wiley-VCH, Weinheim, **2000**, p. 123; b) M. J. O'Donnell in *Catalytic Asymmetric Synthesis*, (Ed.: I. Ojima), Wiley, New York, **2000**, chap. 10.

[16] For recent reports on the development of new chiral catalysts, see for example: a) T. Kita, A. Georgieva, Y. Hashimoto, T. Nakata, K. Nagasawa, *Angew. Chem.* **2002**, *114*, 2956; *Angew. Chem. Int. Ed.* **2002**, *41*, 2832; b) H.-g. Park, B.-S. Jeong, M.-S. Yoo, J.-H. Lee, M.-k. Park, Y.-J. Lee, M.-J. Kim, S.-s. Jew, *Angew. Chem.* **2002**, *114*, 3162; *Angew. Chem. Int. Ed.* **2002**, *41*, 3036.

[17] a) T. Ooi, M. Kameda, K. Maruoka, *J. Am. Chem. Soc.* **1999**, *121*, 6519; b) T. Ooi, M. Takeuchi, M. Kameda, K. Maruoka, *J. Am. Chem. Soc.* **2000**, *122*, 5228; c) T. Ooi, M. Kameda, H. Tannai, K. Maruoka, *Tetrahedron Lett.* **2000**, *41*, 8339; d) T. Ooi, M. Takeuchi, K. Maruoka, *Synthesis* **2001**, 1716; e) T. Ooi, Y. Uematsu, M. Kameda, K. Maruoka, *Angew. Chem.* **2002**, *114*, 1621; *Angew. Chem. Int. Ed.* **2002**, *41*, 1551; f) T. Ooi, M. Takahashi, K. Doda, K. Maruoka, *J. Am. Chem. Soc.* **2002**, *124*, 7640.

[18] Attempted benzylations of **2a** with *O*-allyl-*N*-(9-anthracenylmethyl)cinchonidinium bromide and *O*-allyl-*N*-(9-anthracenylmethyl)cinchonium bromide (E. J. Corey, F. Xu, M. C. Noe, *J. Am. Chem. Soc.* **1997**, *119*, 12414) as catalyst were sluggish under similar phase-transfer conditions and produced **3a** in 12% yield with 43% *de* (L,L major product) and 22% yield with 59% *de* (D,L major product), respectively.

[19] K. Miyashita, H. Iwaki, K. Tai, H. Murafuji, N. Sasaki, T. Imanishi, *Tetrahedron* **2001**, *57*, 5773.

 © 2003 Wiley-VCH Verlag GmbH & Co. KGaA, Weinheim 1433-7851/03/4205-0582 $ 20.00+.50/0

Cover Picture



Hong Meng, Dmitrii F. Perepichka, and Fred Wudl*

The solid-state synthesis of a conducting polymer was achieved by gentle heating of 2,5-dibromo-3,4-ethylenedioxythiophene, the colorless crystals of which are characterized by intermolecular Br–Br contacts of just 3.45 Å. The bromine-doped black poly(3,4-ethylenedioxythiophene) crystals show a high conductivity of 80 $S\,cm^{-1}$. Thin films of the conducting polymer can also be easily fabricated. For more information see the communication by Wudl et al. on page 658 ff.

Contents

News

Simulations: Max Planck Award to van Gunsteren ——— 600

Asymmetric Synthesis: Kagan Receives Noyori Prize ——— 600

Chemistry in Europe: Bäckvall Leads the Way ——— 600

Books

Handbook of Green Chemistry and Technology ——— 601 – 602

James Clark and Duncan Macquarrie

Reviewed by: *Jürgen O. Metzger*

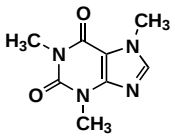
Highlights

Caffeine

S. R. Waldvogel* ——— 604 – 605

Caffeine—A Drug with a Surprise

Keywords:
alkaloids · heterocycles · natural products · reaction mechanisms



1

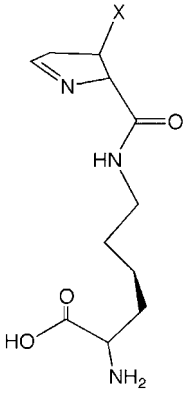
Over 180 years after its isolation caffeine (**1**) still has some surprises in store: As a repellent for snails and slugs, as a stimulating agent with a molecular mode of action, for enhancing performance, its habituation, and as an artificial receptor.

Coded Amino Acid No. 22

C. Fenske, G. J. Palm, W. Hinrichs* ——— 606 – 610

How Unique Is the Genetic Code?

Keywords:
amino acids · enzymes · genetic code · pyrrolysine · RNA



Sometimes, less is more. The genetic code seems to be reduced and was probably optimized during evolution. This idea is supported by the newly discovered amino acid pyrrolysine (see scheme, X = Me, NH_2, OH) as an essential side chain in the active site of a methyl transferase in Archaea. The chemical and structural properties of pyrrolysine, which is directly encoded by redefining a stop codon, are discussed with regard to the "universality" of the genetic code.

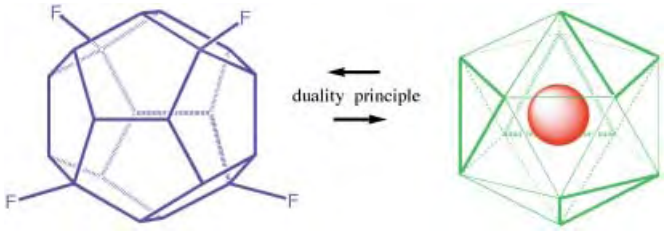
Correspondence

Duality Principle and Chirality

A. Rassat* ——— 611 – 613

Application of the Duality Principle to Chiral Icosahedral Metal Complexes

Keywords:
cage compounds · chirality · duality · symmetry

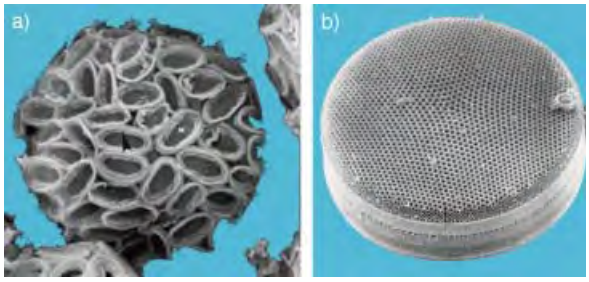


By application of the duality principle, the type of chirality recently reported in icosahedral barium, strontium, or lanthanum complexes can be found in a tetrafluorododecahedrane of the same *T* symmetry (see scheme).

© 2003 Wiley-VCH Verlag GmbH & Co. KGaA, Weinheim

1433-7851/03/4206-0592 $ 20.00+.50/0

Reviews



Long seen as difficult to determine, the mechanisms of the biomineralization of species-specific nanostructures of magnetic bacteria, calcareous algae (a), and diatoms (b) are now within reach. Modern methods in molecular biology have in the last few years provided much insight into these biomineralization processes.

Biomineralization

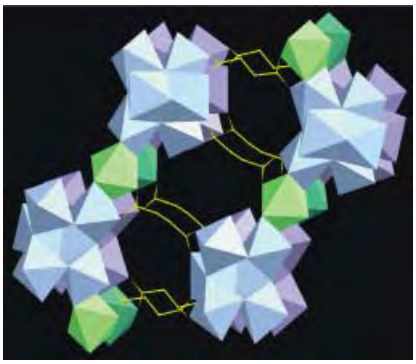
E. Bäuerlein* ——— **614 – 641**

Biomineralization of Unicellular Organisms: An Unusual Membrane Biochemistry for the Production of Inorganic Nano- and Microstructures

Keywords:
biomineralization · magnetosomes · unicellular organisms · vesicles

Communications

Despite the presence of 55 nonequivalent atoms the structure of the layered nickel succinate $[Ni_7(C_4H_4O_4)_4(OH)_6(H_2O)_3]\cdot 7H_2O$ was solved by ab initio methods from powder-diffraction data. The structure contains unprecedented Ni_6 units (blue in the picture) linked by further Ni-centered octahedra (green) and succinate ions (yellow).



Microporous Nickel Succinate

N. Guillou,* C. Livage, W. van Beek, M. Noguès, G. Férey ——— **644 – 647**

A Layered Nickel Succinate with Unprecedented Hexanickel Units: Structure Elucidation from Powder-Diffraction Data, and Magnetic and Sorption Properties

Keywords:
carboxylate ligands · hydrothermal synthesis · magnetic properties · microporous materials · nickel · X-ray powder diffraction



Discrimination of isomeric anions: The selective, shape-controlled colorimetric sensing of dicarboxylate ions has been achieved and represents a development in the "naked-eye" detection of certain organic isomers. The photograph shows the diverse colors of solutions of a 1,3,5-triarylpent-2-en-1,5-dione in dioxane/water solution (70:30 v/v) at approximately pH 6, in the presence of either maleate (*cis* isomer, magenta) or fumarate (*trans* isomer, yellow) ions.

Colorimetric Isomer Probes

F. Sancenón, R. Martínez-Máñez,* M. A. Miranda, M.-J. Seguí, J. Soto ——— **647 – 650**

Towards the Development of Colorimetric Probes to Discriminate between Isomeric Dicarboxylates

Keywords:
carboxylate ligands · hydrogen bonding · ion–molecule reactions · receptors · sensors

For the USA and Canada:
ANGEWANDTE CHEMIE International Edition (ISSN 1433-7851) is published weekly by Wiley-VCH PO Box 191161, D 69451 Weinheim, Germany. Air freight and mailing in the USA by Publications Expediting Inc. 200 Meacham Ave., Elmont, NY 11003. Periodicals postage paid at Jamaica NY 11431. US POSTMASTER: send address changes to *Angewandte Chemie*, Wiley-VCH, 111 River Street, Hoboken, NJ 07030. Annual institutional subscription price for institutions: Europe € 2998.00/3148.00. Outside Europe US$ 3718.00/3904.00 (valid for print or electronic/print and electronic delivery); for individuals who are personal members of a national chemical society, or whose institution already subscribes, or who are retired or self-employed consultants, print only (including postage and handling charges): Europe € 248.00/Outside Europe US$ 348.00.

 © 2003 Wiley-VCH Verlag GmbH & Co. KGaA, Weinheim 1433-7851/03/4206-0593 $ 20.00+.50/0

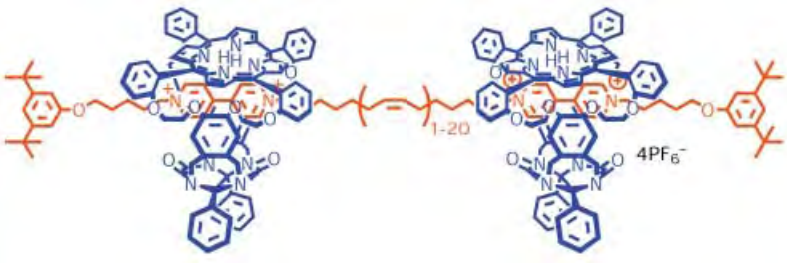
Contents

Porphyrin-Containing [3]Rotaxanes

R. G. E. Coumans, J. A. A. W. Elemans, P. Thordarson, R. J. M. Nolte, A. E. Rowan* ——— **650 – 654**

Synthesis of Porphyrin-Containing [3]Rotaxanes by Olefin Metathesis

Keywords:
host–guest systems · metathesis · porphyrinoids · ring-opening polymerization · rotaxanes



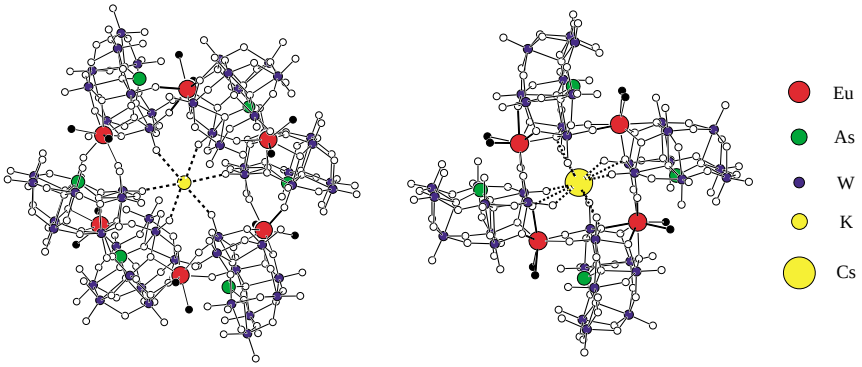
A ruthenium-carbene-stoppered [2]rotaxane acts an intermediate in the synthesis of porphyrin-containing [3]rotaxanes by an olefin-metathesis protocol. The thread of these [3]rotaxanes can be extended to a polybutadiene strand by using them as chain-transfer agents in the ring-opening-metathesis polymerization of cyclooctadiene to give macromolecular porphyrin rotaxanes (see picture).

Crown-Shaped Ln Polyoxometalates

K. Fukaya, T. Yamase* ——— **654 – 658**

Alkali-Metal-Controlled Self-Assembly of Crown-Shaped Ring Complexes of Lanthanide/$[\alpha\text{-AsW}_9O_{33}]^{9-}$: $[K\subset\{Eu(H_2O)_2(\alpha\text{-AsW}_9O_{33})\}_6]^{35-}$ and $[Cs\subset\{Eu(H_2O)_2(\alpha\text{-AsW}_9O_{33})\}_4]^{23-}$

Keywords:
host–guest systems · lanthanides · polyoxometalates · self-assembly · tungsten



Crowning glory: The L-shaped $[Ln(H_2O)_2(\alpha\text{-AsW}_9O_{33})]^{6-}$ (Ln = lanthanide) building unit provides an elegant approach to develop crown-shaped structures of $[\{Ln(H_2O)_2(\alpha\text{-AsW}_9O_{33})\}_n]^{6n-}$ (n = even number of ≥ 4) which can encapsulate a cation. The watermill-propeller structure, left, is a K^+ ion encapsulated by six $[\alpha\text{-AsW}_9O_{33}]^{9-}$ ligands, whereas the windmill structure, right, is a Cs^+ ion encapsulated by four $[\alpha\text{-AsW}_9O_{33}]^{9-}$ ligands.

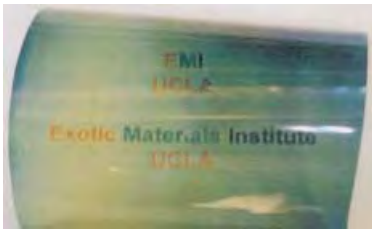
Conducting Polymers

H. Meng, D. F. Perepichka, F. Wudl* ——— **658 – 661**

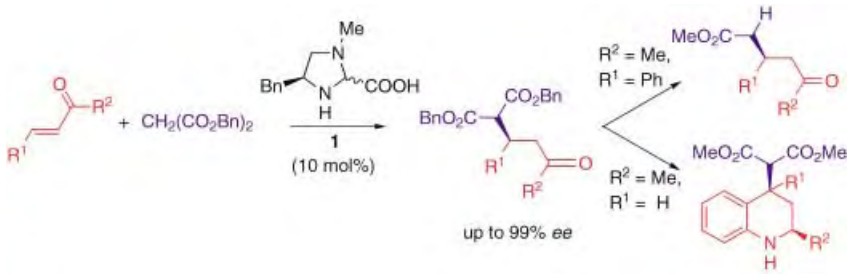
Facile Solid-State Synthesis of Highly Conducting Poly(ethylenedioxythiophene)

Keywords:
C–C coupling · conducting materials · polymerization · polythiophenes · solid-state reactions

Gentle heating of crystalline 2,5-dibromo-3,4-ethylenedioxythiophene affords a highly conducting, bromine-doped poly(3,4-ethylenedioxythiophene) (PEDOT). The conductivity of the polymer can be further increased by doping with iodine. By using this approach, thin films of PEDOT with a conductivity as high as 20 $S\,cm^{-1}$ can be easily fabricated on insulating plastic surfaces (see picture).



© 2003 Wiley-VCH Verlag GmbH & Co. KGaA, Weinheim
1433-7851/03/4206-0594 $ 20.00+.50/0



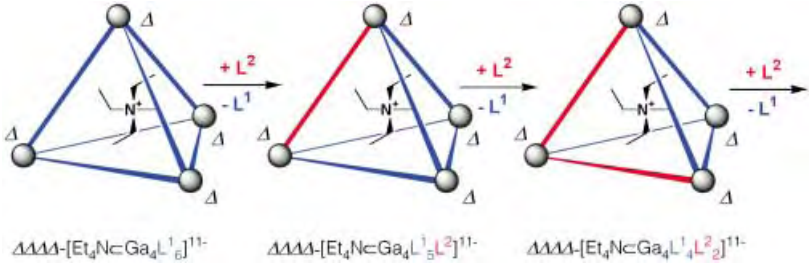
Asymmetric Michael Addition

N. Halland, P. S. Aburel, K. A. Jørgensen* ——— 661 – 665

Highly Enantioselective Organocatalytic Conjugate Addition of Malonates to Acyclic α,β-Unsaturated Enones

An imidazolidine easily prepared from phenylalanine is the catalyst for the highly enantioselective Michael addition shown. A great diversity of α,β-unsaturated enones was transformed with excellent enantioselectivities. The scope of the reaction is further demonstrated by the synthesis of two optically active compounds, a δ-ketoester and a tetrahydroquinoline (see scheme).

Keywords:
asymmetric catalysis · enones · ketoesters · malonates · tetrahydroquinolines



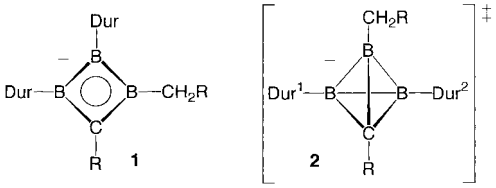
Structural Memory Reporters

M. Ziegler, A. V. Davis, D. W. Johnson, K. N. Raymond* ——— 665 – 668

Supramolecular Chirality: A Reporter of Structural Memory

Non-tetrahedron-forming L^2 ligands insert into a resolved $\Delta\Delta\Delta\Delta$-$[Ga_4L^1_6]^{12-}$ tetrahedral assembly of labile metal and ligand components without compromising its supramolecular structure (see scheme). Preservation of the chirality of the initial architecture verifies its structural memory.

Keywords:
chiral memory · circular dichroism · self-assembly · structural memory · supramolecular chemistry



Fluctuating Skeletal Bonds

Y. Sahin, C. Präsang, P. Amseis, M. Hofmann, G. Geiseler, W. Massa, A. Berndt* ——— 669 – 671

Triboracyclobutanides: Four-Membered Two-Electron Aromatic Compounds with Fluctuating Skeletal Bonds

A distorted triboratetrahedrane anion, 2, is proposed as the transition state of the fluctuation of the skeletal bonds of triboracyclobutanide **1**, a two-electron aromatic compound, B3LYP/6-31G* computations support this suggestion (R = $SiMe_3$, Dur = 2,3,5,6-tetramethylphenyl).

Keywords:
boron · density functional calculations · enantiomerization · ring inversion · small ring systems

 © 2003 Wiley-VCH Verlag GmbH & Co. KGaA, Weinheim 1433-7851/03/4206-0595 $ 20.00+.50/0

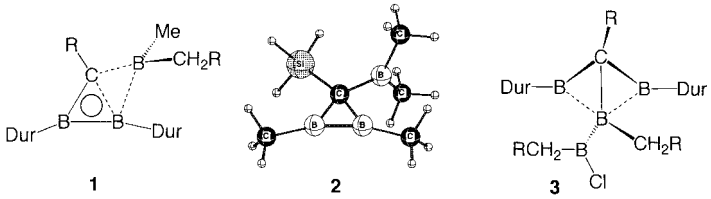
Contents

Boron-Containing Rings

Y. Sahin, C. Präsang, M. Hofmann, G. Subramanian, G. Geiseler, W. Massa, A. Berndt* _____ **671 – 674**

A Diboracyclopropane with a Planar-Tetracoordinate Carbon Atom and a Triborabicyclobutane

Keywords:
anti-van't-Hoff/Le Bel compounds · boron · density functional calculations · multicenter bonds · small ring systems



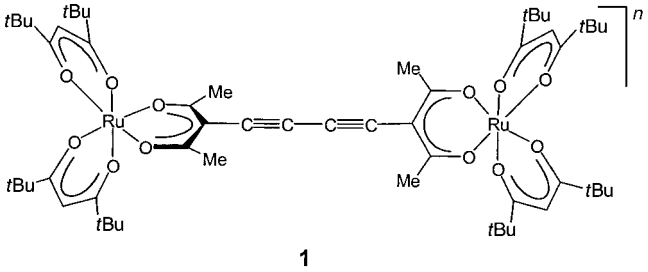
Four-coordinate in a three-membered ring and thereby planar: The chemical shift of the skeletal carbon atom of **1**, which was generated and spectroscopically characterized at −90 °C, agrees very well with that computed for the model **2**, but differs by 70 ppm from that of the similarly substituted, but distorted-tetrahedral carbon atom in **3**. R = $SiMe_3$, Dur = 2,3,5,6-tetramethylphenyl.

Long-Range Electronic Coupling

Y. Hoshino,* S. Higuchi, J. Fiedler, C.-Y. Su, A. Knödler, B. Schwederski, B. Sarkar, H. Hartmann, W. Kaim* _____ **674 – 677**

Long-Range Electronic Coupling in Various Oxidation States of a C_4-Linked Tris(β-diketonato)ruthenium Dimer

Keywords:
alkynyl ligands · mixed-valent compounds · ruthenium · spectroelectrochemistry



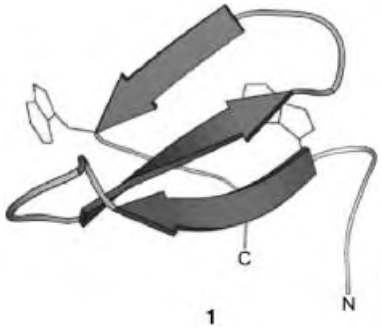
Getting the message across: Strong electronic coupling over a distance of 1.3 nm is observed for the $Ru_2^{IV,III}$ state of the complex $\mathbf{1}^n$ ($n = +$). The fully delocalized system $\mathbf{1}^+$ is distinguished by an extremely intense intervalence charge-transfer (IVCT) band and a single intense vibrational band.

Peptides Composed of D-Amino Acids

N. Wehofsky, S. Thust, J. Burmeister, S. Klussmann, F. Bordusa* ___ **677 – 679**

all-D-Polypeptides: Novel Targets for Semisynthesis

Keywords:
clostripain · peptides · proteases · semisynthesis · substrate mimetics



The chemoenzymatic synthesis of all-D-polypeptides such as the all-D version of the WW domain of hPin1 (**1**) was achieved by applying the substrate mimetics strategy and clostripain as the biocatalyst. Ironically all-D-peptides are better synthesis targets for proteases than their all-L analogues, although nature designed these enzymes for the cleavage of all-L-peptides.

© 2003 Wiley-VCH Verlag GmbH & Co. KGaA, Weinheim
1433-7851/03/4206-0596 $ 20.00+.50/0



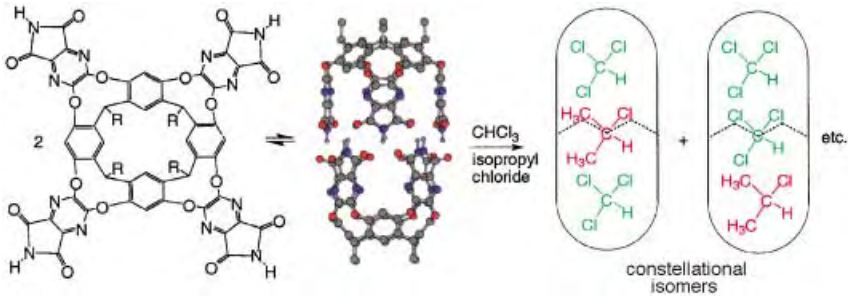
Electron Transfer in Rotaxanes

N. Watanabe, N. Kihara, Y. Furusho, T. Takata,* Y. Araki, O. Ito* ___ **681 – 683**

Photoinduced Intrarotaxane Electron Transfer between Zinc Porphyrin and [60]Fullerene in Benzonitrile

A through-space superexchange mechanism appears to be responsible for charge recombination (CR) following photoexcitation and charge separation (CS) in rotaxanes containing zinc porphyrin and C_{60} moieties (see picture), as suggested by the low activation energy of this process. Furthermore, the charge-separated state is relatively long-lived.

Keywords:
charge transfer · fluorescence · fullerenes · porphyrinoids · rotaxanes



New Form of Isomerism

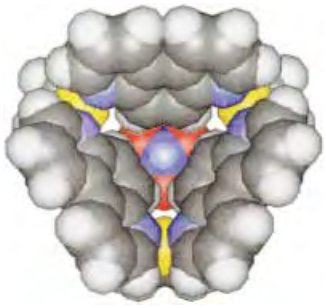
A. Shivanyuk, J. Rebek, Jr.* ___ **684 – 686**

Isomeric Constellations of Encapsulation Complexes Store Information on the Nanometer Scale

The limited mobilities of two different guests present during the self-assembly of a cylindrical capsule give rise to a new form of isomerism (see scheme).

Keywords:
data storage · encapsulation · isomerism · nanostructures · self-assembly

A [3+3] modular self-assembly gives rise to the formation of a molecular bowl or crown with *syn,syn,syn* conformation (see picture). These structures are analogues of calix[3]arenes and can function as anion receptors. Interestingly, an NO_3^- ion is found to distort from a trigonal plane into a trigonal pyramid when binding to the bottom of the molecular bowl.



Modular-Assembled Bowls and Crowns

S.-Y. Yu,* H. Huang, H.-B. Liu, Z.-N. Chen, R. Zhang, M. Fujita _____ **686 – 690**

Modular Cavity-Tunable Self-Assembly of Molecular Bowls and Crowns as Structural Analogues of Calix[3]arenes

Keywords:
metallacycles · palladium · platinum · self-assembly · supramolecular chemistry

 © 2003 Wiley-VCH Verlag GmbH & Co. KGaA, Weinheim 1433-7851/03/4206-0597 $ 20.00+.50/0

Contents

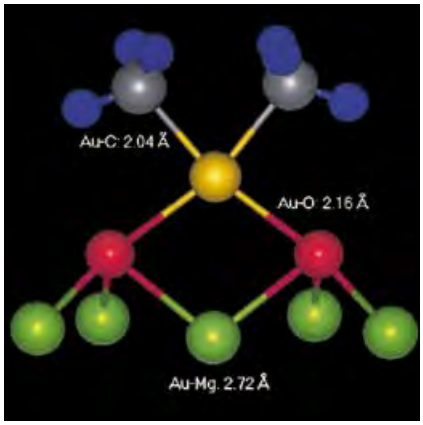
Supported Gold Catalysts

J. Guzman, B. C. Gates* ——— **690 – 693**

Structure and Reactivity of a Mononuclear Gold-Complex Catalyst Supported on Magnesium Oxide

Keywords:
cluster compounds · EXAFS spectroscopy · gold · hydrogenation · supported catalysts

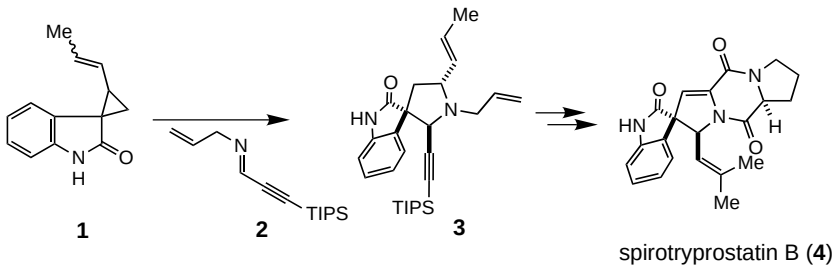
A golden age of catalysis? A structural model of a MgO-supported complex $[Au^{III}(CH_3)_2\{OMg\}_2]$ (where the MgO ligands are part of the MgO support) has been established based on distances and coordination numbers determined by EXAFS spectroscopy (see picture). This compound is the precursor of a mononuclear gold complex that catalyzes ethene hydrogenation. For comparison, a family of supported gold clusters was also prepared.



Spiro Alkaloids

C. Meyers, E. M. Carreira* ——— **694 – 696**

Total Synthesis of (−)-Spirotryprostatin B



Keywords:
alkaloids · Julia–Kociensky reaction · ring expansion · spiro compounds · total synthesis

Rapid assembly of the backbone of spirotryprostatin B (**4**) was achieved by employing a MgI_2-catalyzed ring-expansion reaction of spiro[cyclopropane-1,3′-oxindole] **1** and alkynyl imine **2** to yield advanced intermediate **3**. Introduction of the prenyl side chain was accomplished by aldehyde olefination through a Julia–Kociensky reaction, a transformation that greatly facilitates late-stage derivatization for biological studies. TIPS = triisopropylsilyl.

VIP Communications labeled with this symbol have been judged by two referees as being "very important papers".

The publication of Communications labeled with this symbol has been accelerated because of their topical or highly competitive nature.

Supporting information for articles labeled with this symbol can be found at www.angewandte.org or www.interscience.wiley.com.

The issues for January 2003 appeared online on the following dates:
Issue 1: January 14. · Issue 2: January 16. · Issue 3: January 20. · Issue 4: January 28

Sources

Product and Company Directory

You can start the entry for your company in "Sources" in any issue of *Angewandte Chemie*.

If you would like more information, please do not hesitate to contact us.

Wiley-VCH Verlag – Advertising Department
Tel.: 0 62 01 - 60 65 65
Fax: 0 62 01 - 60 65 50
E-Mail: MSchulz@wiley-vch.de

Service

Keywords ——— *698*

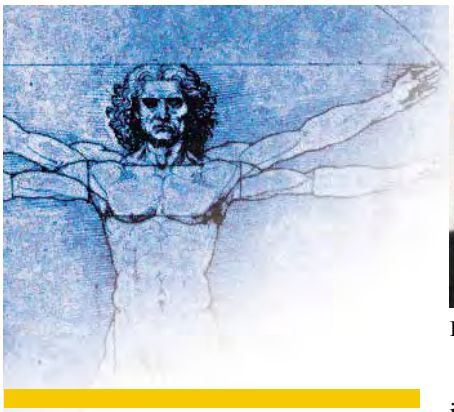
Authors ——— *699*

Preview ——— *701*

Events ——— *702*

© 2003 Wiley-VCH Verlag GmbH & Co. KGaA, Weinheim

1433-7851/03/4206-0598 $ 20.00+.50/0



Max Planck Research Award to van Gunsteren



W. van Gunsteren

The Max Planck Society and the Alexander von Humboldt Foundation annually award the Max Planck Research Award donated by the German Research Ministry. It is worth € 125 000. This year, the award for chemistry and pharmacy was given jointly to Wilfried van Gunsteren (ETH Zurich) and Franz Hofmann (TU Munich).

Van Gunsteren was recognized for the development of new computer dynamics simulation methods in the field of biomolecular systems. He thus contributed to the understanding of the relationship between structure, dynamics, and function of molecular processes in terms of interactions on an atomic level. He received his doctorate in 1977 from the Free University Amsterdam (The Netherlands) and spent postdoc time in Groningen, Harvard, and Amsterdam. Since 1990, he has held the chair for computer-aided chemistry at the ETH Zurich. The software company Biomos he founded distributes the biomolecular simulation program GROMOS.

His most recent Communication "The Key to Solving the Protein-Folding Problem Lies in an Accurate Description of the Denatured State" led to the publication of a Correspondence and a Reply.[1]



H. Kagan

Henri Kagan Wins Noyori Prize 2002, Call for Nominations 2003

The Ryoji Noyori Prize is given to scientists in recognition and as an encouragement for outstanding contributions to research in asymmetric synthetic chemistry in its broadest sense. Each year, the International Prize Committee selects a winner to receive the US$ 10 000 prize money sponsored by Takasago International Corporation.

In 2002, the committee has selected Henri B. Kagan (Institut de Chimie Moléculaire, Paris, France) for his leadership in the field, for example the first asymmetric synthesis by means of circularly polarized light, a chiral bidentate diphosphane ligand (DIOP), and a chiral "homogeneous" supported catalyst. He graduated from the Sorbonne and ENS Chimie in Paris in 1954 and received his doctorate for work on modified steroids under the guidance of J. Jacques. He became a full professor in Orsay near Paris in 1973 and was elected a member of the French academy of sciences in 1991. In 1998, he reviewed "Nonlinear Effects in Asymmetric Synthesis and Stereoselective Reactions: Ten Years of Investigation".[2] His most recent communication in Angewandte Chemie describes a "Highly Efficient Catalytic Synthesis of α-Amino Acids under Phase-Transfer Conditions with a Novel Catalyst/Substrate Pair".[3] Kagan is a member of the Academic Advisory Board of Advanced Synthesis & Catalysis.

At the same time, the committee asks for nominations for the year 2003 until May 1, 2003. The nomination form may be downloaded from the website of the Society of Synthetic Organic Chemistry, Japan.[4]

J.-E. Bäckvall for President



J.-E. Bäckvall

The year 2003 will be full of new commitments for Jan-Erling Bäckvall. The professor of Organic Chemistry at the University of Stockholm (Sweden) just took over chairmanship of the editorial board of *Chemistry—A European Journal* from founding chairman Jean-Marie Lehn, and he will be the president of this year's Bürgenstock Conference on Stereochemistry (April 27 to May 2) near Luzern (Switzerland).

The research of Bäckvall's group is focused on enantioselective transition-metal and enzyme catalysis, in particular oxidations with environmentally friendly reagents such as O_2 and H_2O_2 and Pd catalysis, as well as the chemistry of sulfonyldienes. See for example his recent Full Paper "Ruthenium-Catalyzed Transfer Hydrogenation of Imines by Propan-2-ol in Benzene".[5] Bäckvall received his doctorate from the Swedish Royal Institute of Technology in 1975 and spent his postdoc time with Barry Sharpless at the MIT. He has held the Chair of Organic Chemistry in Stockholm since 1997.

[1] a) W. F. van Gunsteren, R. Bürgi, C. Peter, X. Daura, *Angew. Chem.* **2001**, *113*, 363; *Angew. Chem. Int. Ed.* **2001**, *40*, 351; b) A. R. Dinner, M. Karplus, *Angew. Chem.* **2001**, *113*, 4751; *Angew. Chem. Int. Ed.* **2001**, *40*, 4615; c) W. F. van Gunsteren, R. Bürgi, C. Peter, X. Daura, *Angew. Chem.* **2001**, *113*, 4753; *Angew. Chem. Int. Ed.* **2001**, *40*, 4616.

[2] C. Girard, H. B. Kagan, *Angew. Chem.* **1998**, *110*, 3088; *Angew. Chem. Int. Ed.* **1998**, *37*, 2922.

[3] Y. N. Belokon, K. A. Kochetkov, T. D. Churkina, N. S. Ikonnikov, O. V. Larionov, S. R. Harutyunyan, Š. Vyskočil, M. North, H. B. Kagan, *Angew. Chem.* **2001**, *113*, 2002; *Angew. Chem. Int. Ed.* **2001**, *40*, 1948.

[4] http://wwwsoc.nii.ac.jp/ssocj/

[5] J. S. M. Samec, J.-E. Bäckvall, *Chem. Eur. J.* **2002**, *8*, 2955.

 © 2003 Wiley-VCH Verlag GmbH & Co. KGaA, Weinheim 1433-7851/03/4206-0600 $ 20.00+.50/0

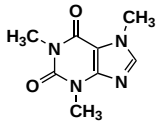
Caffeine

Caffeine—A Drug with a Surprise

*Siegfried R. Waldvogel**

Keywords:
alkaloids · heterocycles · natural products · reaction mechanisms

The first reported caffeine consumers in history were the members of the Galla tribe in Ethiopia, who were enjoying coffee 1000 years ago. In 1819 Friedlieb Ferdinand Runge isolated caffeine for the first time as a pure compound from coffee beans. The first total synthesis of caffeine was accomplished by Emil Fischer in 1895. Despite the extensive consumption of caffeinated nutrients in our daily lives over the last 1000 years, caffeine received only scant attention by scientists. Large portions of the textbook knowledge were based on common experiences with that particular drug. The speculative nature of these half-truths about caffeine were recently corrected by different sources.[1] Caffeine (**1**) is one of the most frequently consumed alkaloidal compounds and is omnipresent in many plants. The traditional significant sources of caffeine in our daily lives are coffee, black tea, and cocoa. The alkaloid is also an ingredient of cola beverages and energy drinks.[2] Many analgesics sold over the counter contain caffeine.[3] Caffeine is currently gathering increasing attention because of its wide range of applications and the potential of new analytical tools.



1

The extensive consumption of caffeinated beverages can be attributed to their stimulating effects. After a long time of speculation concerning the low concentrations of caffeine on the mechanism of action, a Swedish–American research group was able to prove why caffeine gives, despite its low affinity to the receptors, a good buzz. The efficacy of action is caused by a feedback loop in the nerve cells. As already known from previous investigations in mice, caffeine binds and inhibits the adenonsine A_{2A} receptor, which is important for voluntary movements. Inhibition causes a preferential phosphorylation of a particular threonine residue of a protein (DARPP-32). A key player in the signaling cascade is protein kinase A; when the adenosine A_{2A} receptor is blocked the activity of the kinase A to dephosphorylate DARPP-32 is drastically reduced, which leads to an increased DARPP-32 level, thereby amplifying the initial effect of caffeine. Mice that lack DARPP-32 were only slightly affected by caffeine.[4]

A caffeine-containing diet is a widespread practice for many endurance athletes. How caffeine intake causes a substantial improvement of endurance performance was not scientifically clear. However, two recent studies have shed light on this particular area. In conjunction with a carbohydrate-rich diet, an intake of caffeine leads to a clear improvement of endurance performance (riding a cycle ergometer). The Australian study reports an increase in performance of around 3% by a single dose of caffeine as well as by multiple smaller intakes. The researchers have also taken a look at cola beverages, which are held in high esteem by many athletes. A remarkable effect was obtained after increasing the concentration to fourfold that of commercial products. A caffeine intake of 6 mg kg^{-1} for the tested individuals led to good results.[5]



An American research group investigated in this context the use of caffeine and habituation to it. An increased performance was found in all of the 21 persons involved. Regular users of caffeine experienced a less stimulating effect and the time to exhaustion was much shorter than for individuals who were considered as non-users. Caffeine produced a significant rise in oxygen consumption after 15 minutes of exercise in all cases.[6]

Since caffeine is not appropriate for a permanent increase in performance, nonregular users will find the best energetic boost or kick in a cup of coffee or black tea. For the frequent consumers of coffee, who scarcely experiences the stimulating effect of coffee, it might be of some consolation that caffeine in coffee probably substantially lowers the risk of clinical type 2 diabetes. A study of 17000 Dutch people indicated there was a significant decrease in the risk of diabetes when more than seven cups coffee were consumed per day.[7] It is important to mention the irritants in coffee, such as the chlorogenic acids, which cause adverse affects on the state of health.

Caffeine even offers some unexpected perspectives for amateur gardeners. The drug can be used as an efficient repellent for slugs and snails. Researchers from Hawaii accidentally found that

[*] Dr. S. R. Waldvogel
Organisch-Chemisches Institut
Westfälische Wilhelms-Universität Münster
Corrensstrasse 40
48149 Münster (Germany)
Fax: (+49) 251-83-39772
E-mail: waldvog@uni-muenster.de

 © 2003 Wiley-VCH Verlag GmbH & Co. KGaA, Weinheim 1433-7851/03/4206-0604 $ 20.00+.50/0

surfaces of cabbage leaves heavily disturb the appetite of these gluttonous molluscs. Higher concentrations of caffeine led to uncoordinated writhing, while further increased levels of caffeine killed the critters. The up-take of the alkaloidal compound by the mucous layer of the slug probably happens very fast and initiates a couple of physiological responses. However, the good solubility of caffeine in water means that an application for deterring slugs and snails in an outdoor trial will be challenging, but represents a remarkable alternative to the commercially used metaldehyde treatments. Amelioration by mixing with an appropriate agricultural polymer, which could increase the water resistance of the applied drug, offers the prospect of controlled release.[8]

The extensive and diverse consumption of caffeine requires further analytical tools to be developed for enhanced product safety. Many naturally occurring materials, especially those containing electron-rich aromatic moieties, have a certain affinity to caffeine. The polyphenolic ingredients of black tea are typical representatives which mask the caffeine and considerably obstruct the analysis. Therefore, several concepts for the selective recognition of this particular drug were developed. Artificial receptors and adaptamers often prefer the demethylated derivatives of caffeine.[9] Only a few systems are actually known which recognize and bind caffeine with high affinity and selectivity. The methyl groups at the hypoxanthin structure often prevent the formation of a successful hydrogen-bonding pattern. Molecular imprinting of polymers offers new possibilities.[10] A combination of adsorption on silanes and a quartz microbalance was used for the detection of caffeine in aqueous media, but yielded results which are still not satisfactory for an analytical application.[11]

Recently, several research groups accomplished the synthesis of artificial caffeine receptors.[12] All the systems described, however, were only investigated in organic solvents; a significant selectivity and high affinity for the target molecule in aqueous media will be of particular interest for a promising application in caffeine detection. Important scientific progress is expected in the near future in this field. Although caffeine was isolated from coffee beans for the first time 183 years ago by Runge, it still has some surprises in store.

[1] http://www.cosic.org/caffeine/index.html, **2002**.

[2] Caffeinated Beverages: T. H. Parliment, C. T. Ho, P. Schieberle, *ACS Symp. Ser.* **2000**, *754*.

[3] G. A. Spiller, *Caffeine*, CRC, Boca Raton, **1998**.

[4] M. Lindskog, P. Svenningsson, L. Pozzi, Y. Kim, A. A. Flenberg, J. A. Bibb, B. B. Fredholm, A. C. Nairn, P. Greengard, G. Fisone, *Nature* **2002**, *418*, 774–778.

[5] G. R. Cox, B. Desbrow, P. G. Montgomery, M. E. Anderson, C. R. Bruce, T. A. Macrides, D. T. Martin, A. Moquin, A. Roberts, J. A. Hawley, L. M. Burke, *J. Appl. Physiol.* **2002**, *93*, 990–999.

[6] D. G. Bell, T. M. McLellan, *J. Appl. Physiol.* **2002**, *93*, 1227–1234.

[7] R. M. van Dam, E. J. M. Feskens, *Lancet* **2002**, *360*, 1477–1478.

[8] R. G. Hollingsworth, J. W. Armstrong, E. Campbell, *Nature* **2002**, *417*, 915–916.

[9] C. Frauendorf, A. Jäschke, *Bioorg. Med. Chem.* **2001**, *9*, 2521–2524.

[10] F. A. Villamena, A. A. De La Cruz, *J. Appl. Polym. Sci.* **2001**, *82*, 195–205; S. R. Carter, S. Rimmer, *Adv. Mater.* **2002**, *14*, 667–670.

[11] T. Kobayashi, Y. Murawaki, P. S. Reddy, M. Abbe, N. Fujii, *Anal. Chim. Acta* **2001**, *435*, 141–149.

[12] S. R. Waldvogel, C. A. Schalley, R. Fröhlich, *Angew. Chem.* **2000**, *112*, 2580–2583; *Angew. Chem. Int. Ed.* **2000**, *39*, 2472–2475; P. Ballester, M. A. Barcelo, A. Costa, P. M. Deya, J. Morey, M. Orell, C. A. Hunter, *Tetrahedron Lett.* **2000**, *41*, 3849–3853; S. Goswami, A. K. Mahapatra, R. Mukherjee, *J. Chem. Soc. Perkin Trans. 1* **2001**, 2717–2726.

 © 2003 Wiley-VCH Verlag GmbH & Co. KGaA, Weinheim 1433-7851/03/4206-0605 $ 20.00+.50/0

Coded Amino Acid No. 22

How Unique Is the Genetic Code?**

*Christiane Fenske, Gottfried J. Palm, and Winfried Hinrichs**

Keywords:
amino acids · enzymes · genetic code · pyrrolysine · RNA

In memory of Max Perutz

Introduction

In two recent publications in *Science*, a new type of gene-encoded amino acid has been described by the groups of Krzycki and Chan, extending the genetic code to 22 amino acids. This modified lysine side chain was identified by genetic[1] and crystallographic[2] investigations and is clearly the active site in enzymes that play an essential role in catabolizing methylamines in methanogenic Archaea. Carbon assimilation and methanogenesis in *Methanosarcina* species rely on specific methyl transferases, which use mono-, di-, or trimethylamines as substrates.

In the first paper it is shown that this new amino acid is added to the growing polypeptide chain on the ribosome at the position of an UAG stop codon, which usually interrupts translation during protein synthesis. A specific tRNA is used which is charged by its own tRNA synthetase. The second paper describes the characterization of the monomethylamine methyl transferase (458 amino acid residues) from *Methanosarcina barkeri* by X-ray crystallography and identifies residue 201 as a 4-methyl-pyrroline-5-carboxylate-modified lysine called pyrrolysine.

The discovery that a stop codon does not always mean "stop", but may encode a nonstandard amino acid in some organisms urged us to reconsider the universality of the genetic code. Could it be that in former times every codon defined a different amino acid and after millions of years of evolution some rare amino acids were replaced by common ones that now have up to six different codons? If this holds true, it could be compared with the loss of languages in the world: Chinese, English, and Arabic are spoken by more and more people, whereas each year many languages become extinct because indigenous people are no longer able to uphold their traditions.

Structure and Chemistry of Pyrrolysine

X-ray crystallography reveals the three-dimensional folding pattern of biological macromolecules (polypeptides, polynucleotides, etc.) and the interaction of these macromolecules with other biologically relevant molecules. This method opens the door to understanding of the chemistry of biological processes at the atomic level, for example, regulation mechanisms, chemical reactions, or transport phenomena. The chemical composition of the crystallized compounds is usually known, but not the conformation of the building blocks and the specific type of interactions within the protein or polynucleotide and their recognition of ligands. This information can still not be predicted very well from the sequence by ab initio methods, and thus high-resolution structures are only provided by crystallography or NMR spectroscopy.

Monomethylamine methyl transferase (MtmB) transfers the methyl group of monomethylamine to the corrinoid cofactor of another associated methyl transferase, MtmC. The crystal-structure analysis of MtmB from the archaea *Methanosarcina barkeri* at 1.55 Å resolution revealed the chemical structure of a previously unknown amino acid residue in the polypeptide.[2] The electron density observed for the new residue was interpreted as a lysine side chain connected to 4-methyl-pyrroline-5-carboxylate through an amide linkage (Figure 1). Therefore the authors suggested the name L-pyrrolysine for this novel amino acid (three-letter code: Pyl; our suggested one-letter code: O). The direct precursor of L-proline, the Δ^1-pyrroline-5-carboxylate, does not fit to the diffraction data because of the D chirality and the substituent at C4.

Electrospray mass spectrometry of the MtmB/MtmC complex supports the assignment as pyrroline-5-carboxylate with an additional methyl substituent at C4, and excludes the alternative interpretation of the corresponding electron density as an amino or hydroxy substituent. The enzyme adopts an α/β TIM barrel fold.[3,4] Although there is no significant sequence identity of MtmB to other corrinoid-cofactor-associated enzymes, the authors point out that the topology is reminiscent of tetrahydrofolate:corrinoid/iron–sulfur methyl transferases, diol hydratase, and racemases/mutases.[5–8]

As in the case of other methyl transferases, the barrel of MtmB features a deep, negatively charged cavity, which is clearly required to bind the methylammonium cation substrate. The position of the newly identified residue at the bottom of this typical cavity suggests its function in the catalytic mechanism. Pyrrolysine positions and displays the methyl group of the substrate for attack by the corrinoid cofac-

[*] Prof. Dr. W. Hinrichs, Dipl.-Biol. C. Fenske, Dr. G. J. Palm
Institut für Chemie und Biochemie
Ernst-Moritz-Arndt-Universität Greifswald
Soldmannstraße 16
17489 Greifswald (Germany)
Fax: (+49) 3834-86-4373
E-mail: hinrichs@uni-greifswald.de

[**] Financial support to W.H. by Fonds der Chemischen Industrie is gratefully acknowledged.

 © 2003 Wiley-VCH Verlag GmbH & Co. KGaA, Weinheim 1433-7851/03/4206-0606 $ 20.00+.50/0

tor. The proposed methylamine-activation mechanism is based on the two different conformations of the active site seen in the crystal forms obtained with NaCl and $(NH_4)_2SO_4$ as precipitating agents, diffracting to 1.55 Å and 1.70 Å, respectively. As a reaction intermediate an amine substituent at C2 of the pyrroline ring was found in the crystal obtained by precipitation with $(NH_4)_2SO_4$, but not in the other crystal structure. This substituent undergoes hydrogen bonding to Glu and Gln side chains and most probably represents the ammonium group, which is the product after methyl transfer from methylamine to the corresponding corrinoid protein, MtmC.

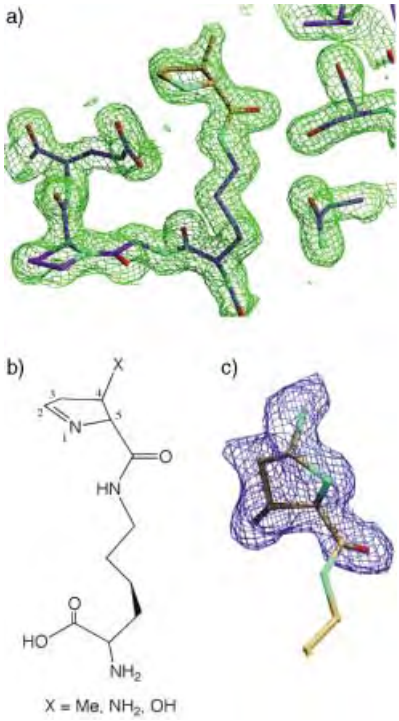


Figure 1. a) Modeling of (4*R*,5*R*)-4-substituted-pyrroline-5-carboxylate to the $2F_O-F_C$ electron density (3σ) of the NaCl crystal form (orientation 1). The substituent at C4 is shown as a methyl, but it could also be an ammonium or an hydroxy group. b) Structure of the proposed L-pyrrolysine amino acid. c) Residual F_O-F_C electron-density-difference map of the $(NH_4)_2SO_4$ crystal form after incorporation of a 40%-occupancy model consisting of L-pyrrolysine in orientation 1 and an exogenous ammonium ion. This remaining difference density suggests that L-pyrrolysine adopts a different orientation (orientation 2) at 60% occupancy in $(NH_4)_2SO_4$ with an amine at C2 of the pyrroline ring. Reprinted with permission from reference [2]. Copyright 2002 American Association for the Advancement of Science.

The challenge in the interpretation of electron-density maps at the borderline of atomic resolution is the disorder of the pyrroline moiety in both structures. The pyrroline head group is found in two orientations rotated approximately 90° relative to each other. The relative occupancies of the alternate orientations differ in the two crystal forms, because different sets of hydrogen-bonding interactions with the protein determine the dominant conformation of the pyrrolysine side chain. However, the observed disorder in the two structures also provides additional information on possible active-site conformations, which hints at the catalytic mechanism shown in Scheme 1 and supports the assigned imine double bond (N1=C2).

Genetic Background for Pyrrolysine Coding

All known organisms synthesize the polypeptide chains of their proteins out of a subset of 20 different L-amino acids. The sequence of each protein is stored in the DNA sequences and is copied to mRNA (transcription) for polypeptide syntheses, which determines the sequence-specific peptide bond formation in the ribosomal machinery (translation). The fundamental textbook coding system is based on 20 proteinogenic amino acids, which are determined by the variation of four different RNA nucleotides. For almost 50 years it has been known that each amino acid residue is encoded by a triplet of nucleotides in the polynucleotide chain of the DNA and RNA molecules.

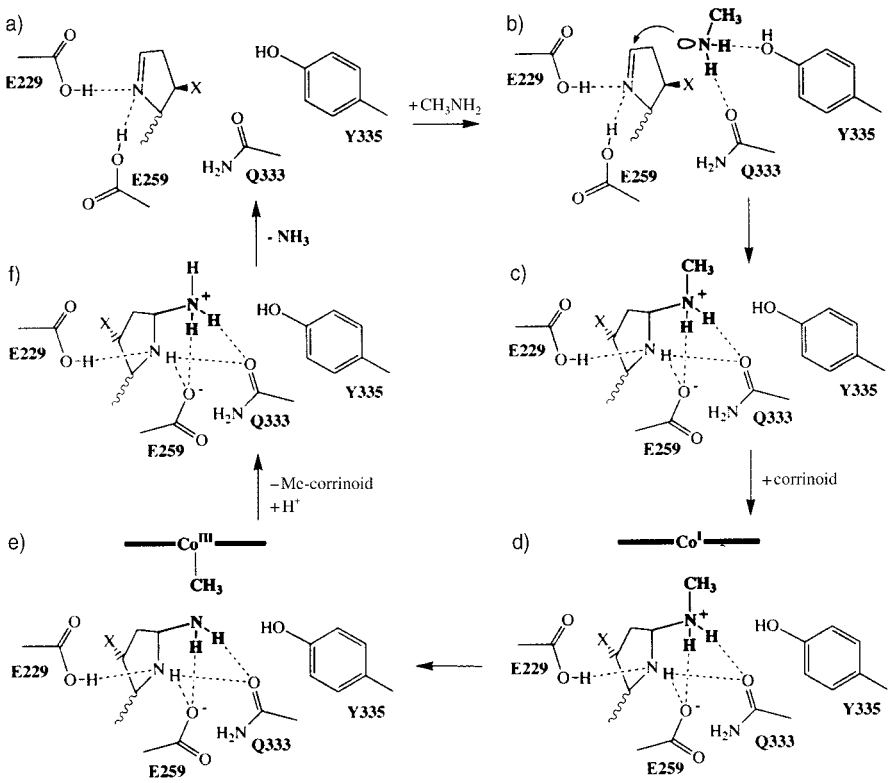
Hundreds of nonstandard amino acids in proteins are known,[9] but these are all formed by chemical modification after ribosomal polypeptide syntheses or in nonribosomal processes. The first observed exception was selenocysteine, which is found in proteins of various organisms, from Archaea to mammals.[10–13] Selenocysteine is not formed by posttranslational modification as is the case for all nonstandard amino acids, but is encoded by UGA, the so-called opal stop codon.[14,15] Now, more than one decade later, pyrrolysine has been found as another example.[1,2] Krzycki and co-workers identified an uncommon $tRNA^{Pyl}$ and a corresponding lysyl-$tRNA^{Pyl}$ synthetase (PylS), which enable the translation of the stop codon as pyrrolysine in various methane-producing Archaea. The genes that encode these methyl transferases have an in-frame stop codon (UAG, so-called amber stop codon), which does *not* stop ribosomal polypeptide elongation. Dimethyl and monomethyl methyl transferases have very similar genes in the same genome, and the read-through is very efficient, unlike other stop-codon overrunning events.[16] The function of UAG as a sense codon for this specific type of protein was unknown in archaeal genes. The translation of the stop codon as pyrrolysine is made possible by a specific $tRNA^{Pyl}$ that can be charged with lysine by a corresponding lysyl-tRNA synthetase (LysRS).

The 20 standard aminoacyl synthetases can be divided into two structurally conserved classes. Interestingly, LysRS enzymes are the only examples that feature nonhomologous members in both class I and class II.[17,18] In *M. barkeri*, two other LysRS enzymes were identified: one belongs to class I and the other to class II. Sequence alignment of the newly identified synthetase suggests that PylS represents a third type of LysRS that probably belongs to a new subclass of class II. There is no evidence for modification of the mRNA (transcript editing) prior to translation.

Based on all the genetic and biochemical results, Krzycki and co-workers concluded that pyrrolysine is inserted into the polypeptide chain of MtmB during translation. Unfortunately, pyrrolysine itself has not yet been synthesized chemically and could not be tested as a substrate for PylS, which shows a high affinity but a low reaction rate for lysine. Pyrrolysyl-$tRNA^{Pyl}$ is probably synthesized by enzymatic condensation of pyrroline-5-carboxylate to the amino group of the lysine side chain of the charged $tRNA^{Pyl}$.

Alternatively, $tRNA^{Pyl}$ might be charged with preformed pyrrolysine. Both routes would allow direct translation of the UAG codon as pyrrolysine in ribosomal polypeptide elongation. However, an enzyme for either pathway

 © 2003 Wiley-VCH Verlag GmbH & Co. KGaA, Weinheim 1433-7851/03/4206-0607 $ 20.00+.50/0



Scheme 1. Hypothetical model for the role of the amber-encoded residue in the catalytic cycle. The proposed intermediates for a), b), c), and f) are based on the structures of L-pyrrolysine (X = CH_3, NH_2, or OH) in orientation 1 (85% occupancy) in the NaCl crystal form and on both orientations of L-pyrrolysine in the $(NH_4)_2SO_4$ crystal form. Intermediates d) and e) are based on a preliminary docking model of MtmB with the corresponding corrinoid protein, MtmC. (Reprinted with permission from reference [2]. Copyright 2002 American Association for the Advancement of Science.

remains to be identified. Since sustaining both pathways would require two enzymes and pyrrolysine would compete with lysine as substrate for PylS, Krzycki et al. favor the route in which Pyl synthesis occurs on the tRNA molecule.

A strong analogy between pyrrolysine and selenocysteine is observed because both are identified at positions encoded by canonical stop codons. Moreover, for both selenocysteine and pyrrolysine, an uncommon tRNA (which deviates structurally from the predicted secondary structure) is involved.[19]

It has been noted that the readthrough of the selenocysteine "stop" codon is only possible with the special sequence and the structural organization of the corresponding mRNA, which permits continuous decoding of two separated open reading frames and, of course, only this very subset of stop codons will not terminate polypeptide elongation.[20] The same mechanism can be expected for pyrrolysine.

Deviation from the "Universal" Code

Variations in the reading of the genetic code (as a result of a redefinition of codons) can lead to the formation of different products. This is possible by the interaction of a specific tRNA with the corresponding aminoacyl-tRNA synthetase supported by specific features of the mRNA. There are two possibilities to introduce amino acid modifications prior to translation:

1. Instead of aminoacylating a tRNA directly with a new amino acid, a standard amino acid is attached to a specific tRNA and modified enzymatically. This procedure is described for selenocysteinyl-tRNA, which is loaded with serine and enzymatically converted into selenocysteine.[21]By the criteria discussed for Sec and Pyl we have at least 23 encoded amino acids, because the long known formylmethionine (fMet) in bacteria can also be considered as an encoded amino acid: its AUG codon is recognized as a special codon with help of the preceding Shine–Dalgarno sequence; $tRNA^{fMet}$ is exclusively used for the start codon, charged with methionine and enzymatically formylated to fMet-$tRNA^{fMet}$ prior to translation. For methionines in other than start positions a different tRNA (Met-$tRNA^{Met}$) is used, which cannot be formylated. Modifications of standard amino acids attached to specific tRNAs are known from various examples. The use of tRNA in the synthesis of amino acids is not restricted to Sec, Pyl, and fMet. In some instances, the amide side chains of Asn and Gln are formed only after their corresponding acids (Asp, Glu) have been loaded onto their tRNAs.[21]
2. In certain organisms or organelles, the meaning of a subset of codons is reassigned—that is, it differs from the "universal" code—and holds for all mRNAs in which these codons occur. It is well-known that the

mitochondrial and nuclear reading of mRNA is different. For example, in humans and other mammals, UGA is a stop codon in nuclear mRNA, but encodes Trp in mitochondrial mRNA. Other examples and differences within various species are reported[22] and can be found in databases.[23]

RNA and Convergent Evolution

The involvement of RNA not only in translation but also in amino acid synthesis might be a relict of an RNA world. The distribution of Sec in all kingdoms and of fMet in bacteria points to an ancient origin. It is likely that the substrate of the methylamine methyl transferases was already available in the primordial soup. The corrinoid methyl acceptor has also been hypothesized to be accessible for prebiotic chemical reactions.[24]

Most of the 20 standard amino acids have degenerated codons. For example, the four triplets for alanine could be the simplified pool of several different aliphatic amino acids that behave similarly. Of the small, aliphatic L-amino acids (up to C_5), only the linear 2-aminobutanoic and -pentanoic acids are missing today; they may have been replaced by alanine, which shows similar helix-forming propensity.

The reason to keep an amino acid during evolution should be either structural or functional, and indeed Sec and Pyl are catalytic residues. Apparently, organisms with a reduced set of coded amino acids were able to survive evolution because of more efficient metabolic pathways. Based on these statements, the approximately 20 amino acids today seem to be a reduced set rather than an expanded one; as genome sequencing and proteome analysis progresses further, more relicts may be found.

Entry to an Expanded Set of Encoded Amino Acids

Special tRNA and aminoacyl-tRNA synthetases are the key to modify the transcription signal. This might be a general approach to design proteins for biotechnological applications by increasing the actual genetic repertoire with a variety of amino acids with novel physical, structural, and chemical properties, which are not found in the standard set of 20–23 amino acids.

Novel amino acids have been introduced into proteins by using the biosynthetic machinery of the *Escherichia coli* ribosome. In *E. coli* mutants that charge $tRNA^{Val}$ incorrectly with cysteine, 20% of the valine in the cellular protein could be replaced by the noncanonical aminobutyrate, sterically similar to cysteine.[25] Modified pairs of tRNA/aminoacyl-tRNA synthetases were used to incorporate in vivo synthetic *O*-methyl- or *O*-allyl-L-tyrosine into enzymes in response to an amber stop codon.[26]

Moreover, it happens that a gene that is transferred into another organism is not read with the expected efficiency by the new host, because a certain codon for an amino acid is not as well-recognized. These codons, which are not used often, support the hypothesis that in former times more than 23 amino acids were encoded by distinct base triplets.

Genetic Variability on All Levels

Whereas in humans the combination of XY or XX defines male or female, respectively, in some bugs (Insecta: Heteroptera) only the X chromosome is required: the females have two (XX) and the males only one (X0). In butterflies, some fish, amphibians, reptiles, and birds, the females are heterogametic (WZ) and the males homogametic (ZZ).[27]

Thus, not only words (codons) of the genetic code can be read with different meanings. Even whole books (chromosomes) of the library (genome) can be interpreted with surprising variations. It is not only the written genetic information (DNA sequence), but also the biochemistry of the reading system (mRNA, tRNA, synthetases, ribosomes), that determines the sequence and the biological function of the gene products.

[1] G. Srinivasan, C. M. James, J. A. Krzycki, *Science* **2002**, *296*, 1459–1462.
[2] B. Hao, W. Gong, T. K. Ferguson, C. M. James, J. A. Krzycki, M. K. Chan, *Science* **2002**, *296*, 1462–1466.
[3] D. W. Banner, A. C. Bloomer, G. A. Petsko, D. C. Phillips, C. I. Pogson, I. A. Wilson, P. H. Corran, A. J. Furth, J. D. Milman, R. E. Offord, J. D. Priddle, S. G. Waley, *Nature* **1975**, *255*, 609–614.
[4] C. A. Orengo, A. D. Michie, S. Jones, D. T. Jones, M. B. Swindells, J. M. Thornton, *Structure* **1997**, *5*, 1093–1108.
[5] T. Doukov, J. Seravalli, J. J. Stezowski, S. W. Ragsdale, *Structure* **2000**, *8*, 817–830.
[6] J. Masuda, N. Shibata, Y. Morimoto, T. Toraya, N. Yasuoka, *Structure* **2000**, *8*, 775–788.
[7] F. Mancia, N. H. Keep, A. Nakagawa, P. F. Leadlay, S. McSweeney, B. Rasmussen, P. Bosecke, O. Diat, P. R. Evans, *Structure* **1996**, *4*, 339–350.
[8] R. Reitzer, K. Gruber, G. Jogl, U. G. Wagner, H. Bothe, W. Buckel, C. Kratky, *Structure* **1999**, *7*, 891–902.
[9] G. C. Barrett in *Amino acid derivatives: a practical approach* (Ed.: G. C. Barrett), Oxford University Press, New York, NY, **1999**, pp. 15–30.
[10] J. F. Atkins, A. Böck, S. Matsufuji, R. F. Gesteland in *The RNA World* (Eds.: R. F. Gesteland, T. R. Cech, J. F. Atkins), Cold Spring Harbor Laboratory Press, Cold Spring Harbor, NY, **1999**, pp. 637–673.
[11] A. Böck, K. Forchhammer, J. Heider, W. Leinfelder, G. Sawers, B. Veprek, F. Zinoni, *Mol. Microbiol.* **1991**, 5, 515–520.
[12] M. Rother, R. Wilting, S. Commans, A. Böck, *J. Mol. Biol.* **2000**, *299*, 351–358.
[13] M. J. Berry, R. M. Tujebajeva, P. R. Copeland, X. M. Xu, B. A. Carlson, G. W. Martin 3rd, S. C. Low, J. B. Mansell, E. Grundner-Culemann, J. W. Harney, D. M. Driscoll, D. L. Hatfield, *Biofactors* **2001**, 14, 17–24.
[14] I. Chambers, J. Frampton, P. Goldfarb, N. Affara, W. McBain, P. R. Harrison, *EMBO J.* **1986**, *5*, 1221–1227.
[15] F. Zinoni, J. Heider, A Böck, *Proc. Natl. Acad. Sci. USA* **1990**, *87*, 4660–4664.
[16] L. Paul, D. J. Ferguson, J. A. Krzycki, *J. Bacteriol.* **2000**, *182*, 2520–2529.
[17] D. Moras, *Trends Biochem. Sci.* **1992**, *17*, 159–164.
[18] M. Ibba, S. Morgan, A. W. Curnow, D. R. Pridmore, U. C. Vothknecht, W. Gardner, W. Lin, C. R. Woese, D. Söll, *Science* **1997**, *278*, 1119–1122.
[19] S. Commans, A. Böck, *FEMS Microbiol. Rev.* **1999**, 23, 335–351.
[20] R. F. Gesteland, J. F. Atkins, *Annu. Rev. Biochem.* **1996**, *65*, 741–768.

[21] M. Ibba, D. Söll, *EMBO Rep.* **2001**, *2*, 382 – 387.
[22] S. Osawa in *Evolution of the Genetic Code*, Oxford University Press, Oxford, UK, **1995**.
[23] http://www.ncbi.nlm.nih.gov/Taxonomy/Utils/wprintgc.cgi?mode = c.
[24] G. Ksander, G. Bold, R. Lattmann, C. Lehmann, T. Früh, Y.-B. Xiang, K. Inomata, H.-P. Buser, J. Schreiber, E. Zass, A. Eschenmoser, *Helv. Chim. Acta* **1987**, *70*, 1115 – 1172.
[25] V. Döring, H. D. Mootz, L. A. Nangle, T. L. Hendrickson, V. de Crécy-Lagard, P. Schimmel, P. Marlière, *Science* **2001**, *292*, 501 – 504.
[26] a) L. Wang, A. Brock, B. Herberich, P. G. Schultz, *Science* **2001**, *292*, 498 – 500; b) Z. Zhang, L. Wang, A. Brock, P. G. Schultz, *Angew. Chem.* **2002**, *114*, 2964 – 2966; *Angew. Chem. Int. Ed.* **2002**, *41*, 2840 – 2842.
[27] Rolf Siewing, *Lehrbuch der Zoologie, Vol. 1, Allgemeine Zoologie*, Gustav Fischer, Stuttgart, **1980**, p. 297.

Duality Principle and Chirality

Application of the Duality Principle to Chiral Icosahedral Metal Complexes

*André Rassat**

Keywords:
cage compounds · chirality · duality · symmetry

Symmetry lowering from I_h to T symmetry in mononuclear complexes was the subject of a recent communication by Hegetschweiler and co-workers[1] and of a corrigendum[2] quoting two other complexes of this type previously obtained by Prinzbach and co-workers.[3] These complexes are made up of a central ion surrounded by twelve atoms in an idealized icosahedral I_h symmetry. Because of the presence of four tripodal ligands in a tetrahedral arrangement, the (idealized) symmetry group of the complex is lowered to T.

I would like to draw attention to the occurrence of the same symmetry lowering in a dodecahedrane derivative $C_{20}H_{16}F_4$ reported by Schulman and Disch,[4] and to the fact that their example is exactly related to the more recent cases by application of the "duality principle" to the ligands of these polyhedral molecules. In three dimensions, the duality principle[5] expresses the fact that, with appropriate changes, similar properties are obtained upon interchanging points and planes. In the case of polyhedra, this corresponds to an exchange of vertices and faces. The dual or reciprocal of a polyhedron[5d,6] is thus the new polyhedron obtained by connecting the centers of the adjacent faces of the first one: the numbers of faces and of vertices are interchanged, and the number of edges remains the same. The permutation representation of the vertices of one member of the pair is identical with that of the faces of the other and the permutation representation of the edges is the same for both members. For instance, as is well known for the platonic solids,[5d,6] the cube and the dodecahedron are duals of the octahedron and the icosahedron, respectively, and the tetrahedron is its own dual. Table 1 presents the relationships between the vertices, edges, and faces of these solids, and Figure 1 shows how a regular octahedron is obtained by connecting the centers of the faces of a cube.

Theoretical consequences of the relationships between dual polyhedra have been explored in the theoretical chemistry of fullerenes,[7] boron hydrides,[8] and transition-metal–silicon clusters.[9] Experimentally, dual polyhedral backbones of molecular assemblies have been found in intermetallic crystals,[10] and dual infinite networks have also been reported.[11]

Apparently, the duality principle has not been extended to ligands. A monovalent substituent on a polyhedral molecule can be considered as a label attached to a vertex, producing a labeled face in the dual. It thus seems legitimate to consider that the dual of a monovalent substituent on a trivalent vertex of a polyhedral molecule is a tridentate ligand connected to the atoms of a triangular face of the dual, the symmetry of the labeled dual being maintained when the tridentate ligand is C_3-symmetric. Precisely this situation exists in the molecules described in references [1,3], in which tripodal ligands are connected to triangular faces of the

Table 1: Relationship between the numbers v of n-coordinated vertices, f of m-sided faces and e of edges in the platonic polyhedra. These numbers obey Euler's formula $v-e+f=2$

Polyhedron	Symmetry group	v	n	f	m	e
Tetrahedron	T_d	4	3	4	3	6
Octahedron	O_h	6	4	8	3	12
Cube	O_h	8	3	6	4	12
Icosahedron	I_h	12	5	20	3	30
Dodecahedron	I_h	20	3	12	5	30

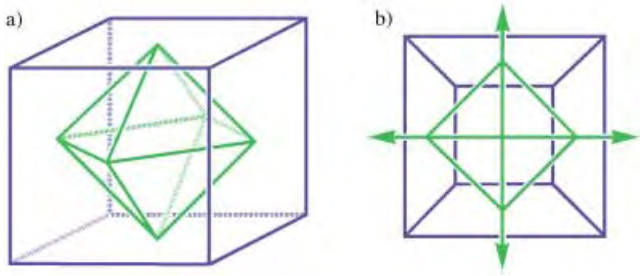


Figure 1. By connecting the centers of the faces of a cube, the dual octahedron is obtained; the dual of a three-coordinated vertex is a triangular face and the dual of a square face is a four-coordinated vertex. a) Perspective view. b) Corresponding Schlegel diagram; the four arrows represent a single vertex at infinity.

[*] Prof. Dr. A. Rassat
UMR CNRS 8640, Département de Chimie
École Normale Supérieure, 24 rue Lhomond
F75231 Paris CEDEX 05 (France)
Fax: (+33) 1-44-32-33-25
E-mail: andre.rassat@ens.fr

 © 2003 Wiley-VCH Verlag GmbH & Co. KGaA, Weinheim 1433-7851/03/4206-0611 $ 20.00+.50/0

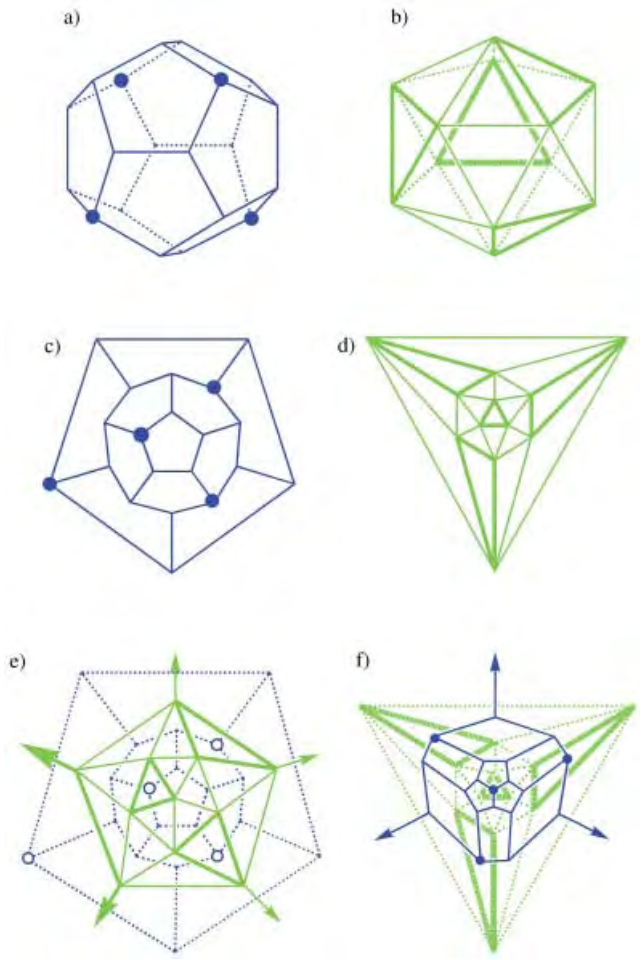


Figure 2. a) Perspective view of a labeled dodecahedron: symmetry is lowered from I_h to T by labeling four vertices (dots) in a regular tetrahedral arrangement. When dots and unlabeled vertices are taken as CF and CH respectively, the figure represents $C_{20}H_{16}F_4$. b) Schlegel diagram corresponding to a). c) Schlegel diagram of the dual icosahedron (in green) superimposed on b): the dual is obtained from b) by connecting the centers of the adjacent faces and labeling the faces corresponding to the four labeled vertices with thick lines. The five arrows represent a single pentavalent vertex at infinity. d) Perspective view of a labeled icosahedron: symmetry is lowered from I_h to T by labeling four faces (thick lines) in a regular tetrahedral arrangement, as in Figure 1b of reference [1]. e) Schlegel diagram corresponding to d). f) Schlegel diagram of the dual dodecahedron (in blue) superimposed on e): the dual is obtained from e) by connecting the centers of the adjacent faces and labeling the vertices corresponding to the four labeled faces with dots. The three arrows represent a single trivalent vertex at infinity.

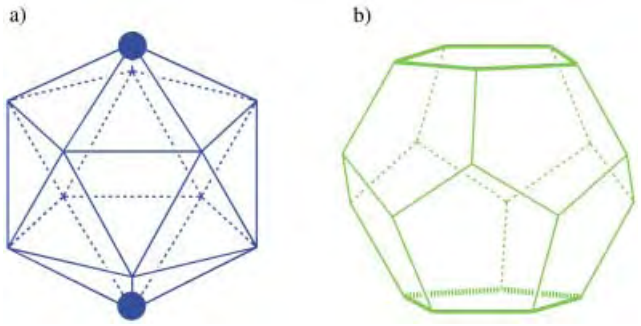


Figure 3. Symmetry lowering from I_h to D_{5d} by labeling a) two vertices (dots) in an icosahedron, and b) the dual faces (thick lines) in a dodecahedron. In a), when labeled and unlabeled vertices represent CH and BH, respectively, the figure represents *p*-$B_{10}C_2H_{12}$. In b), when vertices on the labeled faces are taken as CH, and the unlabeled faces as C, the figure represents the aromatic $C_{20}H_{10}$ of reference [13].

coordination polyhedron. The symmetry characteristics of these molecules may be represented by a regular icosahedron with faces labeled in such a way that the total object has T symmetry (Figure 2d). The dual of this schematic figure is a dodecahedron with labeled vertices at the symmetrical tetrahedral positions (Figure 2a).[12]

As mentioned above, a molecule of this type, $C_{20}H_{16}F_4$ (Figure 2), was studied more than twenty years ago,[4] so that the experimental examples of references [1, 3] are dual transpositions of this symmetry lowering from I_h to T.

A transposed version of this vertex/face duality exists (Figure 3): in *para*-dicarbaclosododecaborane (Figure 3a), the I_h symmetry of $(B_{12}H_{12})^{2-}$ is lowered to D_{5d} by vertex labeling, whereas the dodecahedrapentaene of Schleyer and co-workers[13] (Figure 3b) represents a dual molecule in which the symmetry of the smallest fullerene has been lowered by labeling the upper and lower faces with ten hydrogen atoms. Other D_{5d} dodecahedral molecules such as (the unknown) $C_{20}H_{10}F_{10}$, with its ten fluorine substituents either on the upper and lower rings or on the "equatorial" ring, are similarly related to *para*-dicarbaclosododecaborane.

Application of the duality principle is not restricted to labeled vertices and faces of dual polyhedra: examples of symmetry lowering by labeling corresponding edges in a pair of dual polyhedra can also be envisaged. I would like to suggest that this principle, a useful heuristic tool in geometry,[5] could play a similar role in structural chemistry.

[1] J. Sander, K. Hegetschweiler, B. Morgenstern, A. Keller, W. Amrein, T. Weyhermuller, I. Muller, *Angew. Chem.* **2001**, *113*, 4307–4310; *Angew. Chem. Int. Ed.* **2001**, *40*, 4180–4182.

[2] J. Sander, K. Hegetschweiler, B. Morgenstern, A. Keller, W. Amrein, T. Weyhermuller, I. Muller, *Angew. Chem.* **2002**, *114*, 16–16; *Angew. Chem. Int. Ed.* **2002**, *41*, 16–16.

[3] a) R. Schwesinger, K. Piontek, W. Littke, O. Schweikert, H. Prinzbach, C. Kruger, Y. H. Tsay, *Tetrahedron Lett.* **1982**, *23*, 2427–2430; b) R. Schwesinger, K. Piontek, W. Littke, H. Prinzbach, *Angew. Chem.* **1985**, *97*, 344–345; *An-*

 © 2003 Wiley-VCH Verlag GmbH & Co. KGaA, Weinheim 1433-7851/03/4206-0612 $ 20.00+.50/0

gew. Chem. Int. Ed. Engl. **1985**, *24*, 318 – 319.

[4] J. M. Schulman, R. L. Disch, *J. Am. Chem. Soc.* **1978**, *100*, 5677 – 5681.

[5] For the duality principle in space, see: a) D. Hilbert, S. Cohn-Vossen, *Geometry and the Imagination* (Transl.: P. Nemenyi), Chelsea Publishing Company, New York, **1952**, p. 92 and b) D. Hilbert, S. Cohn-Vossen, *Geometry and the Imagination* (Transl.: P. Nemenyi), Chelsea Publishing Company, New York, **1952**, pp. 119 – 121; c) H. S. M. Coxeter, *Introduction to Geometry*, Wiley, New York, **1961**, p. 256 and d) H. S. M. Coxeter, *Introduction to Geometry*, Wiley, New York, **1961**, pp. 157 – 159.

[6] For example, see: A. Holden, *Shapes, Space and Symmetry*, Columbia University Press, New York, **1971**, p. 4.

[7] a) P. W. Fowler, J. I. Steer, *J. Chem. Soc. Chem. Commun.* **1987**, 1403 – 1405; b) D. L. D. Caspar, *Philos. Trans. R. Soc. London Ser. A* **1993**, *343*, 133 – 144; c) P. W. Fowler, D. E. Manolopoulos, *An Atlas of Fullerenes*, Oxford University Press, Oxford, **1995**, p. 17.

[8] a) A. Burkhardt, U. Wedig, H. G. von Schnering, A. Savin, *Z. Anorg. Allg. Chem.* **1993**, *619*, 437 – 441; b) A. A. Quong, M. R. Pederson, J. Q. Broughton, *Phys. Rev. B* **1994**, *50*, 4787 – 4794; c) A. Gindulyte, N. Krishnamachari, W. N. Lipscomb, L. Massa, *Inorg. Chem.* **1998**, *37*, 6546 – 6548, and references therein; d) R. B. King, *J. Math. Chem.* **1998**, *23*, 197 – 227; e) R. B. King, *Chem. Phys. Lett.* **2001**, *338*, 237 – 240.

[9] R. B. King, *Z. Phys. D* **1991**, *18*, 189 – 191.

[10] R. Nesper, *Angew. Chem.* **1991**, *103*, 805 – 834; *Angew. Chem. Int. Ed. Engl.* **1991**, *30*, 789 – 817 (see Figure 9a therein).

[11] M. Eddaoudi, J. Kim, M. O'Keeffe, O. M. Yaghi, *J. Am. Chem. Soc.* **2002**, *124*, 376 – 377.

[12] For a description of these symmetrical "tetrahedral positions", see: A. Rassat, *Chirality* **2001**, *13*, 395 – 402.

[13] a) A. B. MacEwen, P. von R. Schleyer, *J. Org. Chem.* **1986**, *51*, 4357 – 4368; b) A. A. Fokin, H. Jiao, P. von R. Schleyer, *J. Am. Chem. Soc.* **1998**, *120*, 9364 – 9365; c) R. W. A. Havenith, A. Rassat, P. W. Fowler, *J. Chem. Soc. Perkin Trans. 2* **2002**, 723 – 727.

 © 2003 Wiley-VCH Verlag GmbH & Co. KGaA, Weinheim 1433-7851/03/4206-0613 $ 20.00+.50/0

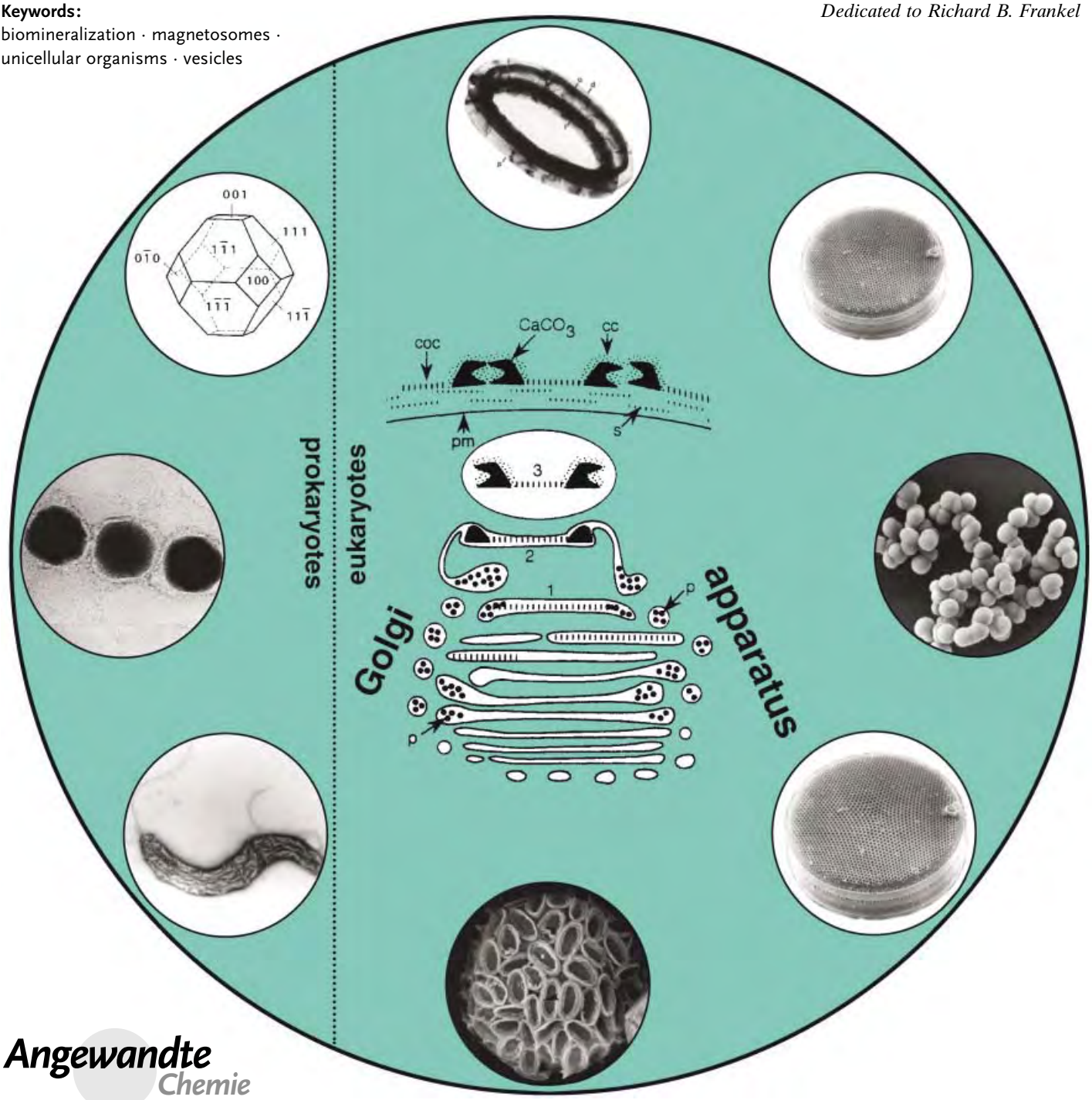
Biomineralization

Biomineralization of Unicellular Organisms: An Unusual Membrane Biochemistry for the Production of Inorganic Nano- and Microstructures

*Edmund Bäuerlein**

Keywords:
biomineralization · magnetosomes · unicellular organisms · vesicles

Dedicated to Richard B. Frankel



© 2003 Wiley-VCH Verlag GmbH & Co. KGaA, Weinheim
1433-7851/03/4206-0614 $ 20.00+.50/0

With evolution, Nature has ingeniously succeeded in giving rise to an impressive variety of inorganic structures. Every organism that synthesizes biogenic minerals does so in a form that is unique to that species. This biomineralization is apparently biologically controlled. It is thus expected that both the synthesis and the form of every specific biogenic mineral is genetically determined and controlled. An investigation of the mechanism of biomineralization has only become possible with the development of modern methods in molecular biology. Unicellular organisms such as magnetic bacteria, calcareous algae, and diatoms, all of which are amongst the simplest forms of life, are particularly suited to be investigated by these methods. Crystals and composites of proteins and amorphous inorganic polymers are formed as complex structures within these organisms; these structures are not known in conventional inorganic chemistry.

From the Contents

1. Introduction 615
2. Biomineralization on Bacterial Surfaces 616
3. Formation of Nanocrystal Forms from Fe_3O_4 in Magnetic Bacteria 618
4. The Formation of Complex Crystal Morphologies of $CaCO_3$ in Unicellular Algae 624
5. The Formation of Nanostructured Cell Walls of Amorphous Polysilicic Acid in Diatoms 629
6. Summary and Outlook 636

1. Introduction

There is much to indicate that bacteria or archaea (formerly called archaebacteria), which can be assigned to the prokaryotes, appeared in the late Archean and Proterozoic eons as the first life forms on Earth.[1] Microfossils[2] suggest that they existed prior to about 3.6 Ga (Ga = giga years, 10^9 years). Even today both can survive or live under such extreme conditions that rarely occur in the inhabited world. Such extremophiles[3] thrive very well at high or low temperatures (thermo- or psychrophiles), under highly acidic or alkaline conditions (acido- or alkalophiles), high salt concentrations (halophiles), and high levels of γ radiation (radiation-resistant microorganisms).

Even though fossils of microbial life forms of carbon-like material exist, the oldest fossils are found in petrified forms and correspond to the morphologies of bacteria, magnetite crystals can be regarded as the most reliable direct evidence of early life (Figure 1A). This applies only if they display the five most important characteristics of biologically controlled magnetite,[4] as found in today's magnetic bacteria.[5] These properties are:

1) crystal dimensions of a single magnetic domain and restricted anisotropic width/length ratios
2) chemical purity
3) crystallographic perfection
4) unusual crystal morphologies
5) crystallographic direction of extension of magnetic crystals (described in detail in reference [4b,c]).

The ability to form linear chains is an important additional property of biogenic magnetite crystals, which in living magnetobacteria are surrounded by a special phospholipid membrane and are thus called magnetosomes.[6] Biogenic magnetite crystals were also found in "magnetofossils" in terrestrial sediments up to two billion years old[7a–c] and possibly in meteorites from Mars (Figure 1B).[7d] After their isolation from a culture of *Magnetospirillum gryphiswaldense*, magnetosomes were arranged in parallel for the electron microscope with a bar magnet to obtain information on their purity and magnetosomal membrane.[7ef] As long chains were found in the presence of the bar magnet instead of the original short chains (Figure 1C), this experiment could be a model for the formation of magnetite crystal chains on Mars, provided short chains were released after the death of the bacterial cells.

During the period between two billion years ago to the Precambrian Era about 550 million years ago, the terrestrial "magnetofossils" were the only witnesses to biomineralization, until evidence was found at the end of this eon for a "matrix-mediated" formation of a calcium mineral by an invertebrate, *Cloudina*.[8] Several hundred million years previously the main animal phyla appear to have already divided.[9,10] In the early Cambrian Period (525–510 million years ago) a tremendous increase in biomineralization occurred, called the Cambrian Explosion. In the first 10 million years, a plethora of biomineralizing animal species was formed almost exponentially.[4a 11–13] Most of the more important skeletal materials were then produced. Thereafter only corals, a few algae, and the vertebrates in marine habitats formed new skeletons.[13]

This knowledge prompted Kirschvink and Hagedorn to formulate a bold and comprehensive hypothesis:[14] The complex mineral structures of animals and plants as they occur today could have evolved from an already existing, simpler system. Thus gene patterns that developed for a special function would have been changed through gene duplication, mutation, and adaptation in another biological system for a new role, a new mineral structure.[15] The palaeontological findings suggested that the formation of

[*] Prof. em. Dr. E. Bäuerlein
Abteilung Membranbiochemie, Max-Planck-Institut für Biochemie
Am Klopferspitz 18 A, 82152 Martinsried (Germany)
Fax: (+49) 89-8578-3777
E-mail: e_baeuerlein@yahoo.de

 © 2003 Wiley-VCH Verlag GmbH & Co. KGaA, Weinheim 1433-7851/03/4206-0615 $ 20.00+.50/0

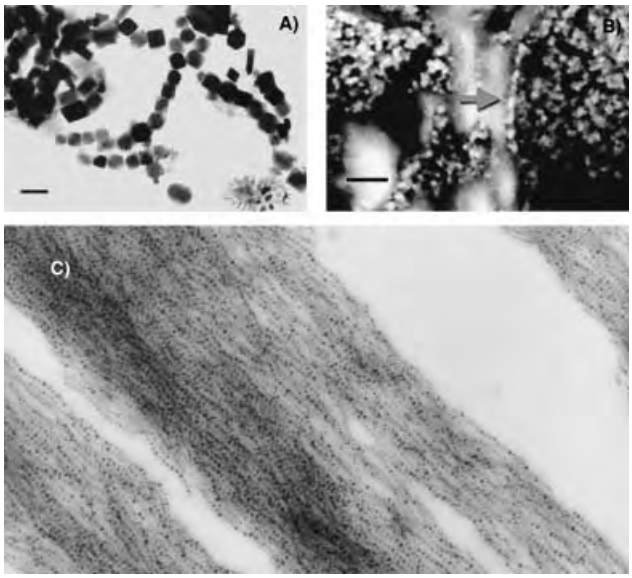


Figure 1. Fossil chains of magnetite crystals of magnetotactic bacteria (magnetofossils): A) terrestrial magnetofossils from marine sediments. They originate from cores from the South Atlantic (*Deep Sea Drilling Project* (Leg 73), Angola Basin); their age is about 50 million years, length of the bar represents 100 nm. (Unpublished electron microscope image (TEM), with kind permission of N. Petersen and M. Hanzlik, LMU Munich). B) Magnetofossils in the Mars meteorite ALH 84001. Electron microscope image (SEM-BSE) of a long chain of magnetite crystals (arrow) which were taken through the intact surface of a freshly fractured specimen. The magnetite crystals are located on the rim of carbonate globules in ALH 84001. The length of the bar represents 200 nm. (Section from Figure 4A of reference [7d] with kind permission of I. Friedman and the National Academy of Science, USA). c) Long magnetosome chains. Electron microscope image of isolated magnetosomes from *Magnetospirillum gryphiswaldense* which during arrangement for electron microscopy had formed long chains in the weak magnetic field. (From reference [7d] with kind permission of D. Schüler.) SEM = scanning electron microscopy, BSE = back-scattered electron mode.

magnetite crystals of magnetic bacteria could be the preliminary stage of biogenic mineral formation in eukaryotes. This assumption finds support in that magnetite crystals have also been found in unicellular eukaryotic organisms such as Euglena algae (*Euglenophyta*)[16] and dinoflagellates[4b] as well as in higher species such as salmon,[17] trout,[18] carrier pidgeons,[19] army ants,[19] and also in the human brain.[20] But not only the ability to form magnetite crystals is clearly present in many higher organisms. The system based on intracytoplasmic vesicles through which biominerals are formed could also have been transferred from the magnetotactic bacteria to the unicellular eukaryotic organisms. If this hypothesis were to be verified, the explanation of the mechanisms that lead to the formation of complex structures, including bones and teeth, would be simpler.



Edmund Bäuerlein was born in 1932 in Höchst (Germany). He studied chemistry in Saarbrücken, Munich, and Frankfurt (Germany) and he completed his PhD with Prof. Th. Wieland on biologically relevant hydroquinones. He then moved to the Max-Planck-Institut für medizinische Forschung, Heidelberg (Germany), as a research group leader. He completed his Habilitation at the Fakultät für Chemie, Universität Heidelberg in 1974, where he was appointed Professor in 1980. In 1984 he moved to the Max-Planck-Institut für Biochemie in Munich, Abteilung Membranbiochemie, where he was research group leader until the end of his active service in 1997.

2. Biomineralization on Bacterial Surfaces

2.1. Immobilization of Ions

Bacterial cells have a volume of 1.5–2.5 μm^3,[21] and consequently a high surface/volume ratio. To give an idea of what this means, a cube with an edge of 1 cm can be divided into 10^{12} cubes with an edge of 1 μm. Thus the whole surface of these 10^{12} small cubes is 10000 times larger than that of the large cube.[22] The large surface area of a bacterial cell is suitable primarily for the uptake of nutrients and the elimination of waste materials, as both processes are totally dependent on the diffusion gradients of the respective substances.

Moreover, the different structures of the cell walls of the two groups of bacteria, which were originally named Gram positive or Gram-negative depending on their color behavior with Gram coloration, provide a large number of possibilities to bind cations and also anions. Thus the cell wall of Gram-positive bacteria is made up of a highly crosslinked polymer, a 25-nm-thick peptidoglycan layer, also known as murein sacculus, which is rich in carboxylate groups. Secondary polymers, such as teichoic acid, chains of 8–50 glycerol or ribitol molecules that are esterified with each other through phosphate bridges, or teichuronic acid, which is essentially based on uronic acid, extend the arsenal of negatively charged compounds (phosphate and further carboxylate groups). In contrast, the cell wall of Gram-negative bacteria are made up of a thin peptidoglycan layer of 4 nm which is protected from the environment by the lipid/protein bilayer of its outer membrane. Therefore the externally extending lipopolysaccharides (LPS), which are anchored to the outer membrane with the lipophilic ends, are probably the preferred centers of cation binding as a result of their many phosphate and frequently also carboxylate groups.

Additional layers of the outer surface of both the Gram-positive and the Gram-negative bacteria are formed from acid mucopolysaccharides: as capsules if they are bound to the cell walls,[23] or as a slime if they can move freely between the bacteria.[23] Sheaths (hollow cylinders of filament-forming bacteria) are made up of a heteropolysaccharide. This heteropolysaccharide contains gluconic acid cations through which the sheaths bind. Such an immobilization can also occur actively through enzymes that are located in the sheaths: for example, they oxidize Mn^{II} to Mn^{IV}, which precipitates as MnO_2.[23]

Many bacteria and archaea form paracrystalline surface layers with a two-dimensional protein arrangement, the S layer (surface layer).[24] The polar amino acid functions

appear to be buried mainly within the S-layer proteins. However, such functions in the channels that penetrate through the S-layer network can explain the observed biomineralization.[23] Remarkably, the S-layer proteins are the first glycoproteins to be found in prokaryotes, initially in the archaeon *Halobacterium salinariun* (previously *H. halobium*).[25]

From this overview of all important bacterial surfaces, a negative surface charge ensues from the COOH and PO(OH) groups at the neutral pH of the environment. Thus in the simplest case the positively charged metal ions are bound by electrostatic interactions. However, because of the complex structure of the surfaces there is little concrete evidence of actual metal complexes. A three-pK model for the cell walls of bacilli obtained from acid–base titration suggests not only the participation of carboxy and phosphoryl groups, but that participation of hydroxy groups may be involved in complex formation.[23,26] Stability constants of the metal carboxylates have been determined for Cd^{II}, Cu^{II}, Pb^{II}, and Al^{III}.[26]

Although the surfaces of many bacteria are negatively charged, anions such as carbonate and silicate can be bound at neutral to acidic pH values. Diaminopimelic acid, which is present in the peptidoglycan of Gram-positive bacteria such as *Bacillus subtilis*, and *N*-acetylfucosamine, which is present in the lipopolysaccharide (LPS) of Gram-negative bacteria such as *Pseudomonas aeroginosa*, provide a limited number of positively charged functional groups after protonation.

Since the binding of silicate is high relative to the number of positive groups, it is assumed that multivalent metal ions such as Fe^{III} exercise a bridging function in which they first bind to negatively charge sites and then immobilize the silicate ion. If no multivalent metal ions are present in solution it is highly probable that the positive groups bind the silicate ions.[27]

2.2. Nucleation and Crystal Growth of Biominerals

Living bacteria that are partially or totally covered in minerals are found in many, principally aqueous, environments. Microfossils[2] consist mainly of a special mineral layer around a volume that resembles that of bacteria. Extensive investigations into their formation on living bacteria have been carried out to corroborate the biogenic origin of these fossils.[2] Bacteria are able not only to bind ions, but are also able to produce minerals on their highly reactive surface. To produce the necessary local supersaturation, they can decrease the amount of free energy required for precipitation. This is possible when they change the pH value or redox potential on their surface by means of their metabolism. The ion-binding sites are assumed to be the centers of this growth.[28] In this case, poorly ordered to crystalline phases of iron or manganese oxides can be precipitated several orders of magnitude more rapidly by enzymatic redox reactions than by chemical redox reactions from a solution without bacteria.[23] Metal ions such as Fe^{III}, alone or together with Al^{III}, form not only bridges between the silicates and carboxy or phosphate groups of the surface, but are also critical for the formation of amorphous to poorly ordered, fine-grained polysilicates.[23,27] An unusual example of nucleation and crystal growth, in this case of carbonate minerals, has been found on the S layer of photosynthetic bacteria.[29] In this case, the S layer consists of copies of a 104-kDa protein in an hexagonal configuration. S layers are to date the best-known organic matrices, although not in but on the surface of an organism. In weak light, gypsum ($CaSO_4$) is formed on these layers; however, during photosynthesis, calcite ($CaCO_3$) is formed through an increase in the pH value in the immediate neighborhood.

2.3. Biomolecules as Matrices

The stability of the extended two-dimensional lattice of S layers allows the isolation and use of these biomolecules as matrices for the preparation of molecular-templated nanostructures.[24e,30,31] Thus metallic platinum could be deposited on an isolated S layer by reduction of K_2PtCl_4 in such a way that it forms highly ordered and periodically arranged metal clusters. Well-separated and almost spherical particles (dark) are arranged along the crystalline protein matrix, and the tetragonal structure of the S layer is reproduced (Figure 2).[31a]

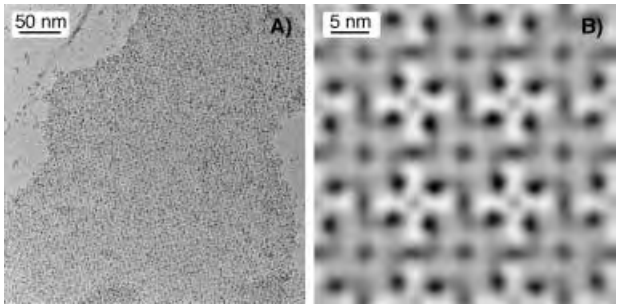


Figure 2. Platinum nanocluster, highly ordered on a crystalline bacterial S layer (surface layer). A) TEM image of platinum clusters produced on isolated S layers of *Sporosarcina urea* by reduction of a platinum salt. B) Distribution of platinum clusters (black) with an average diameter of 1.9 ± 0.6 nm on the two-dimensional protein matrix, visualized by image processing. The unit cell of the cluster lattice has a size of 13.2×13.2 nm^2. (From reference [31a] with kind permission of W. Pompe and H. Engelhardt, and Springer Verlag, Heidelberg.)

2.4. Metal or Mineral Formations inside Bacteria—A Transition from the Outside to the Inside?

All previously described minerals are formed on the surface of bacteria (Section 2.1).[2a] In the following section, the biomineralization of magnetite (Fe_3O_4) crystals in special phospholipid vesicles of the cell interior (cytoplasm) is discussed. The question arises as to whether on a pathway from the exterior to the interior, a primitive stage of biomineralization occurs in the cytoplasm, that is, without a membrane. Indeed, gold ions in the form of Au^{III} or $AuCl_4^-$ can actually penetrate into the cytoplasm of endospores, that is, metabolically resting bacteria, and form numerous metallic gold nanoparticles with a diameter of 5–20 nm diameter in a redox reaction (Figure 3).[2a] Although Au^{III} ions are strong

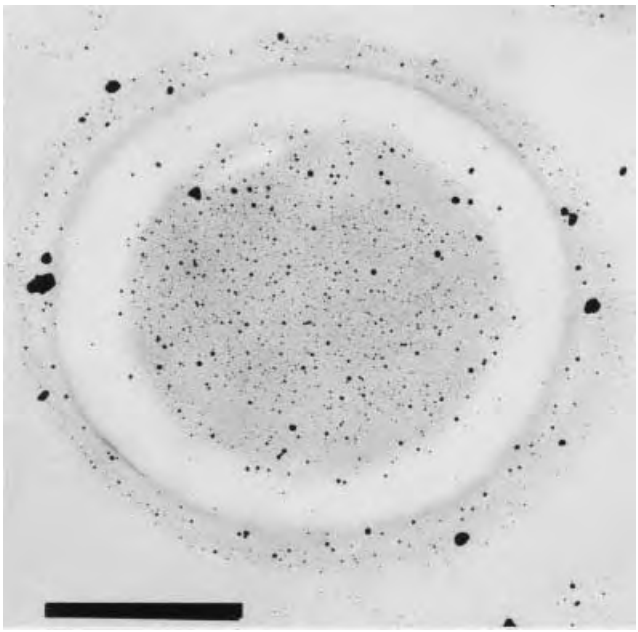


Figure 3. Formation of gold nanoparticles in the cytoplasm of the endospores of *Clostridium botulinum*. If these endospores are suspended in a solution of $AuCl_3$ for 10 min at room temperature gold particles with a diameter of 5–20 nm are formed. In a thin section without negative contrasting the gold particles are found by electron microscopy almost exclusively in the cytoplasm. The length of the bar represents 500 nm. (From reference [2a] with kind permission of T. J. Beveridge.)

oxidizing agents, in contrast to Hg^{II} ions, their conversion into metal in the cytoplasm[32] resembles the detoxification and resistance behavior of bacteria towards Hg^{II} ions. However, metallic gold is deposited, whereas elemental mercury, which in this case actually first arises through the action of *cytosolic* mercury reductase, diffuses out of the bacteria as vapor.[33]

Intracellular particlelike iron sulfide deposits, which were irregularly distributed and consist of amorphous material, have been found in a few sulfate-reducing bacteria. They are probably not surrounded by a membrane since after lysis of the cells they could not be isolated by density-gradient centrifugation.[34] Moreover, spherical particles have been found in a few purple bacteria in which anaerobic photosynthesis occurs—that is, they originate from the earliest stages of photosynthesis development—when cultured in media with relatively high concentrations of iron. These particles, which were surrounded by a kind of membrane and formed a chain within the cell, were probably responsible for the magnetic reaction of the bacteria. Such purple bacteria could thus be an earlier stage of biomineralization in vesicles.[34]

A bacterium has recently been described as a "missing link" between bacterial biomineralization on the surface on the one hand and in the cytoplasm or intracytoplasmic vesicles on the other, as it probably allows both at the same time.[35a] This bacterium, *Shewanella putrifaciens CN 32*, a Gram-negative and facultatively anaerobic bacterium that can reduce Fe^{III} as electron acceptor to Fe^{II} in its anaerobic energy generation (dissimilatory iron reduction, see also Section 3.4). Under the strict anaerobic conditions of an H_2/Ar atmosphere and only in the presence of the Fe^{III} oxide ferrihydrite (2-line ferrihydrite[35]) these bacteria not only produce magnetite (Fe_3O_4) outside the bacteria. When after a short time Fe^{II} is detectable in the reaction mixture, they form about 60 iron oxide particles of 30–50-nm diameter in their cytoplasm. These are very probably surrounded by a lipid bilayer membrane and give rise to reflections in selected-area electron-diffraction (SAED) experiments, which may be attributed to magnetite or maghaemotite.[35] In contrast to the previously described experiment,[34] these minerals were formed at iron concentrations similar to those found in soils and sediments.[35a]

3. Formation of Nanocrystal Forms from Fe_3O_4 in Magnetic Bacteria

3.1. Occurrence of Magnetic Bacteria

Magnetic bacteria, also known as magnetotactic bacteria, are widespread in aqueous habitats and prefer microaerophilic regions (oxic-anoxic transition zone, OATZ).[36,37] Such characteristic habitats exist mainly at the water–sediment interface of fresh-water pools, lakes, and rivers, where most magnetic bacteria have also been found. The Chiemsee (Bavaria) is an excellent example.[7f] Numerous magnetotactic bacteria have also been found in the OATZ in transitions from brackish water to sea water, which are characterized by special layers (for example, vertically arranged chemical layers that exhibit oxidizing conditions above, but have a reducing environment below).[38] Although unusual, these magnetotactic bacteria are found a few meters deep in a water column, which depending on the season, moves in a vertical direction. Even in the salt water of the South Atlantic, magnetotactic bacteria have been discovered in surface sediments up to a depth of 3000 m at the continental edges of both the eastern part (Angola) and the western part (Brazil).[39]

The magnetotactic bacteria are found in all significant morphotypes, as cocci, spirilli, vibrios, rod bacteria, and also as multicellular bacteria[40] in the different habitats. As is the case with many other sediment bacteria, they are usually difficult to culture. For this reason, since the isolation of the first magnetotactic bacteria in 1979, today called *Magnetospirillum magnetotacticum* MS-1[41] (previously *Aquaspirillum magnetotacticum*[42]) only ten pure cultures have been described.[7f,43] It was, however, still possible to describe an ecology and an initial phylogenetic pedigree of the magnetotactic bacteria, thanks to an elegant method that combines the comparative sequence analysis of ribosomal ribonucleic acid (rRNA)[44] with in situ hybridization of fluorescent oligonucleotide probes (FISH) for bacteria that could previously not be cultured (Figure 4).[45]

3.2. Species-Specific Magnetite Crystals

Electron microscopic studies have shown that magnetite crystals with specific sizes and morphologies are found in the numerous forms of bacteria (morphotypes); both size and

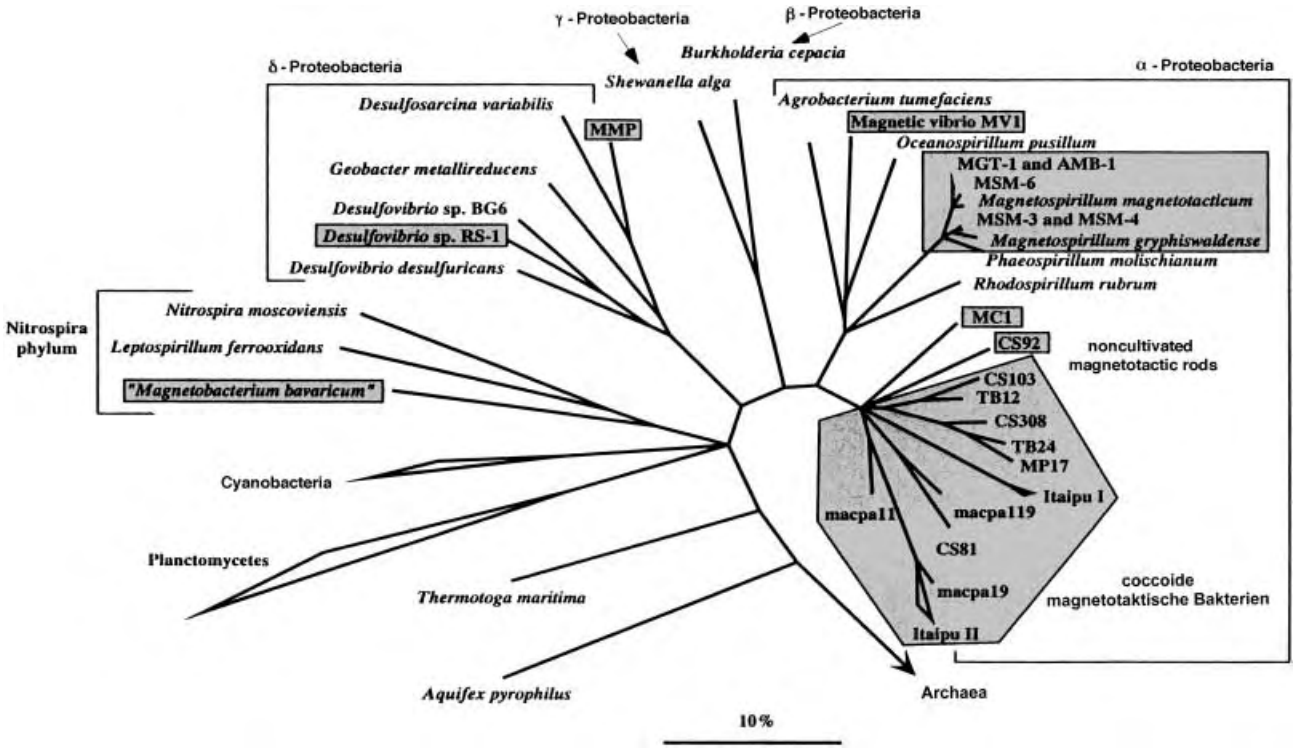


Figure 4. 16S rRNA-based tree reconstruction showing the phylogeny of magnetotactic bacteria (shadowed region). The tree was prepared with the ARB software package and is based on a "parsimony" analysis. It was corrected in accordance with the results of "maximum likelihood"—and "neighbor joining" analysis, when unstable branches were indicated by multifurcations. The tree topology is based on almost full-length 16S rRNA sequences. The partial sequences of the strains CS103, MC-1, MV-1, MMP, and RS-1 have been added with the parsimony algorithm without allowing changes to the overall tree topology. (From reference [45] with kind permission of R. Amann.)

morphology seem to be specific to the respective species of bacteria. This assumption was confirmed by the isolation and culturing of pure specimens: their "mature" crystals correspond in size (maximum dimension) and morphology.[5b] In contrast to the above essentially undistorted "mature" crystals, a number of deviations were conspicuous when the isolates were obtained from natural habitats;[46] these deviations are probably brought about by changes in the bacterial environment, for example changes in iron concentration, oxygen content, and temperature. As a simplification, the crystal morphologies found in magnetotactic bacteria can be classified into: 1) cubooctahedral, 2) pseudohexagonal, and 3) bullet-shaped (Figure 5). It should be emphasized here that all the magnetite crystals found have the cubic face-centered crystal lattice of magnetite, but species-specific crystal morphologies.[4b,c] Idealized crystal morphologies of these biogenic crystals are shown in Figure 6. In addition, the morphologies found for greigite (Fe_3S_4), the magnetic sulfur analogue of magnetite, is also shown.[4b,c]

The unexpected and unusual features of these biogenic magnetite crystals is not only a narrow size distribution, but above all, a diameter range of 40–120 nm, which thus allocates them the highest magnetic moment. This diameter range corresponds to magnetite crystals with a single magnetic domain.[47] Since magnetite crystals from inorganic synthesis offer neither a similarly narrow size distribution (and thus also no such uniform magnetic properties) nor such a variety of crystal morphologies, the formation of these biogenic magnetite and greigite crystals is probably under strict biological control. Research into this control has not yet been reported.

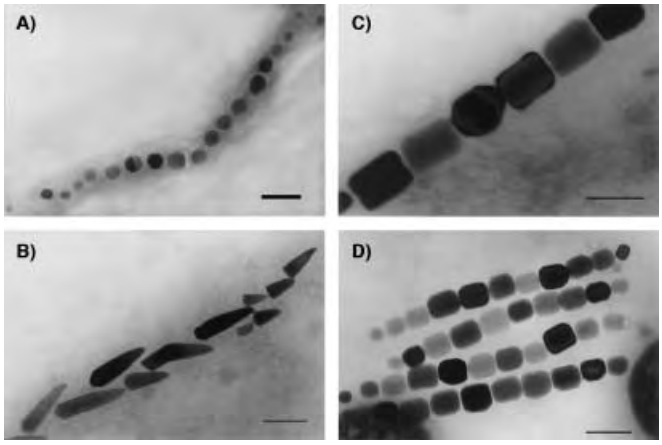


Figure 5. Crystal morphologies and intracellular organization of magnetosomes from magnetotactic bacteria: A) cubooctahedral; b) bullet-shaped; c–d) pseudohexagonal. The magnetosomes are arranged in one (C) or more (D) chains. The lengths of the bars represents 100 nm.

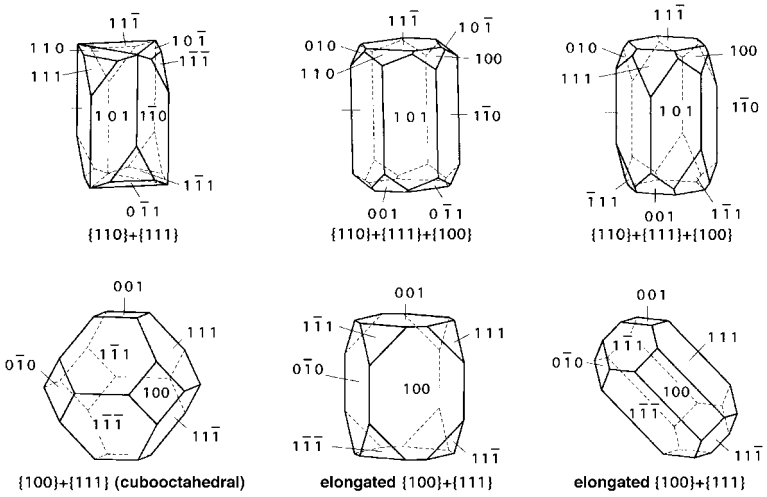


Figure 6. Idealized crystal morphologies of magnetite (Fe_3O_4) and greigite (Fe_3S_4) derived from high-resolution TEM investigations on magnetosomes from magnetotactic bacteria. Top row: variations of pseudohexagonal prisms; bottom row (from left to right): cubooctahedra, which occurs with magnetite and greigite in magnetosomes; elongated cube with angular truncated corners, which was found only in magnetosomes with greigite; elongated cubooctahedra present in a few magnetosomes with magnetite. (Modified from Devouard et al.[4c] with kind permission of R. B. Frankel).

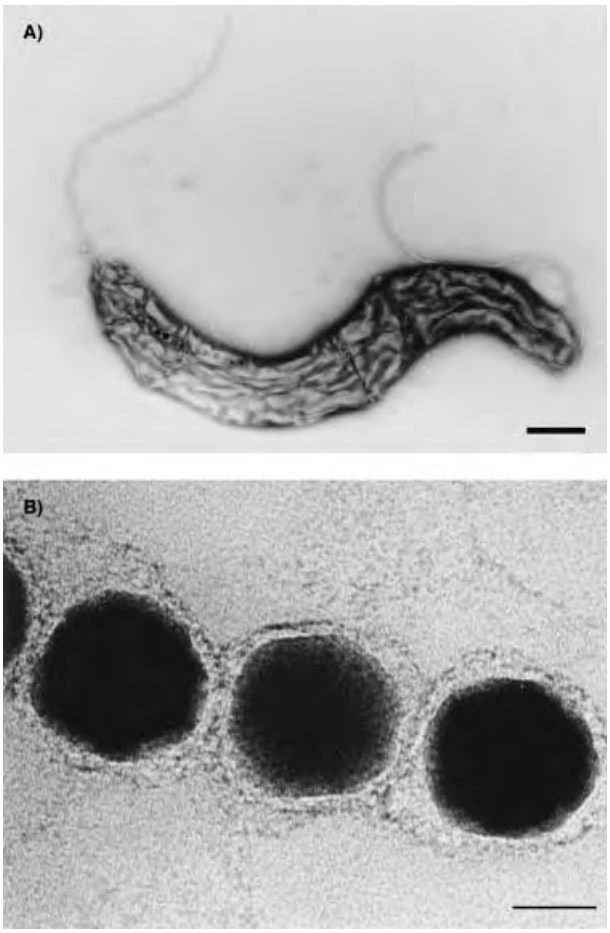


Figure 7. TEM image of A) *Magnetospirillum gryphiswaldense* with a chain of cubooctahedral magnetite crystals and one flagellum at each pole (the length of the bar represents 500 nm) and b) its isolated and purified magnetosomes enveloped by a membrane (the length of the bar represents 20 nm).

3.3. The Magnetosome: a Phospolipid Vesicle for the Production of Species-Specific Magnetite Crystals.

3.3.1. The Magnetosome Membrane

In their pioneering work, Blakemore, Frankel, and coworkers were not only successful in the isolation[36a] and cultivation[42] of *Magnetospirillum magnetotacticum*, but also in the identification of the magnetite crystals.[5b] With the assistance of transmission electron microscopy (TEM) they were also able to show that almost all these crystals are surrounded by an electron-dense layer, probably a lipid bilayer. The term magnetosome was therefore introduced for such enveloped, magnetic, inorganic crystals.[6] An initial analysis of the lipids of small quantities of isolated magnetosomes revealed the presence of neutral lipids, free fatty acids, glycolipids, sulfolipids, and phospholipids.[48] A pure culture was obtained with the phylogentically related *Magnetospirillum gryphiswaldense* (Figure 7 A, B) which, unlike the highly oxygen-sensitive *M. magnetotacticum*, was essentially oxygen tolerant.[41,49] A magnetotactic bacterium that provided the highest yields of highly purified magnetosomes could be developed. A new technique in which magnetic columns are used allowed the isolation of the magnetosomes in a highly pure form.[50] As a result, the lipid composition of the magnetosome membrane, as well as that of the outer and cytoplasmic membrane, was determined quantitatively (Table 1).[7f,51] Contrary to what was previously thought,[48] the lipid profile of the magnetosome membrane differed from that of the other two membranes. The amount of phosphatidylglycerol was about three times larger than in the external and cytoplasmic membrane, whereas the amount of phosphatidylcholine was eight times larger. In contrast, ornithinamide lipid and another, previously unknown lipid ($X\text{-}NH_2$), which also contained no phosphate group, could only be found in the outer and cytoplasmic membranes, but not in the magnetosome membrane. Both lipids were valuable markers in the separation of the membranes. These results suggest at least that the magnetosome membrane follows its own synthesis pathway, and could also be responsible for the maximum size of the crystals as a deformation of the phospholipid vesicle by crystals that were too large has not been previously observed.

Table 1: Lipid composition of the membranes of *M. gryphiswaldense*

Lipid	Outer membrane [mol%]	Cytoplasmic membrane [mol%]	Magnetosome membrane [mol%]
Phosphatidyl ethanolamine	59.9 ± 5.1	70.7 ± 0.5	52.8 ± 5.5
Phosphatidyl glycerol	13.9 ± 0.9	12.6 ± 1.9	38.3 ± 5.7
Ornithineamide lipid	18.6 ± 5.8	4.7 ± 0.4	–
Phosphatidyl choline	–	1.1	8.9 ± 0.5
XNH_2	7.6 ± 0.7	7.2 ± 1.9	–

Also, varying the compositions of the phospholipids of the membrane and thus its surface could also play a role in the respective crystal morphology of magnetite crystals.

Functionally even more important than phospholipids are the proteins of the magnetosome membrane; it is presumed that the latter are involved in the mechanism of magnetite crystal formation. They should be associated in a biologically controlled biomineralization,[4a,52] whose first principle is the intracellular spatial compartmentalization with the lipid bilayer of the magnetosome. Iron transport proteins that produce local saturation in the magnetosomes, proteins that catalyze crystal nucleation, and redox proteins that produce a Fe^{III}/Fe^{II} stoichiometry of 2:1 for magnetite (Fe_3O_4) are expected to control this mechanism.

Consequently, interest in the chemistry of proteins and in molecular biology has been directed at the proteins of the magnetosome membrane;[48,53] these proteins are probably of pivotal importance for the simplest mechanism of a controlled biomineralization. Because of the electrostatic properties of their membrane, isolated magnetosomes form stable suspensions. Detergents are able to dissolve the magnetosome membrane, upon which the magnetite crystals immediately agglomerated.[7f] By means of sodium dodecyl sulfate polyacrylamide gel electrophoresis (SDS-PAGE), nine specific protein bands were initially found in these extracts from the magnetosomes of *M. gryphiswaldense*,[54] whereas in those of *M. magnetotacticum* either two[48] or three[53a] protein bands were found for the respective magnetosome membrane. In the most recent investigations on *M. gryphiswaldense*, the number of specific bands has risen to thirteen.[55]

3.3.2. Cloning and Sequence Analysis of the Genes of Magnetosome Membrane Proteins

The first step in the molecular biology of magnetosome membranes, carried out by Y. Fukumori and co-workers seven years ago with SDS-polyacrylamide gel on the N-terminal amino acid sequence of a 22-kDa protein (MAM22) from *M. magnetotacticum,* led to the cloning and sequence analysis of the corresponding gene.[53a] Likewise, the amino acid sequence of a 24-kDa protein (MamA) from *M. gryphiswaldense* was determined, and was found to have a 91% similarity to the protein from *M. magnetotacticum*.[54] Although very different protein compositions were found in the magnetosome membranes of a number of *Magnetospirillum* strains by SDS-PAGE, Western blots (identification of the protein by a specific antibody) showed that this 24-kDa protein occurred in all membranes.[53b] It showed significant homology with the tetratricopeptide repeat (TPR) family of thus far at least 25 proteins.[56] The primary structure of the TPR motif is a degenerate tetratrico (34) amino acid repeat that is arranged mostly in tandems of up to nine single motifs. This motif appears in many organisms, from bacteria to humans. TPR proteins can exercise numerous biological functions, which range from transcription control to protein folding, and include protein transport and cell division. The tetratricopeptide motif is repeated up to six times and appears to play an important role in protein–protein interactions. Unlike typical membrane proteins, MamA does not contain a hydrophobic membrane-spanning segment, and it can thus be assumed that it is bound electrostatically to the magnetosome membrane.[54] The homologous MAM22 protein has been suggested to act as a receptor as well as playing a role in the interaction with the cytoplasmic proteins.[57]

The recent investigations on *M. gryphiswaldense*[55] mentioned in Section 3.3.1 have led to the cloning and sequencing of four further genes of important proteins of the magnetosome membrane. These genes (*mamB, mamC, mamD, mamE*) and their derived proteins have thus far not been associated with the formation of magnetite crystals in any other magnetic bacterium. The *mamB* gene codes for a protein whose band in SDS-PAGE corresponds to a molecular mass of 33.3 kDa.[55] The significant sequence homology with proteins of the ubiquitous cation-diffusion facilitation (CDF) family[58] makes MamB a candidate for iron transport, as this protein family is not only responsible for the transport of heavy metals, but also for resistance to certain heavy metals. Such a resistance can lead to their export (for example, the evaporation of mercury whose ions are initially converted into elemental mercury by a mercury reductase in the bacterial cytoplasm[33]) or equally to deposition of heavy metals in the vesicles.[59] The *mamC* gene encodes a 15.5-kDa protein, the main protein in the magnetosome membrane. The *mamD* gene encodes a protein that corresponds to a protein of 21.9 kDa.[55] No information on proteins homologous to MamC and MamD has been found in data banks.

During this work the genome of the two magnetic bacteria *Magnetospirillum magnetotacticum* and *Magnetococcus MC-1* (together with those of 13 nonmagnetic bacteria) were published almost fully sequenced (that is, more than 95%) within four weeks by the Joint Genome Institute (JGI) of the U.S. Department of Energy and immediately made accessible in the public domain.[60] Thus, the homologous genes with significant similarity to *mamA* and *mamB* from *M. gryphiswaldense* could be identified in the genome sequences of the two magnetic bacteria.[55] The Mam proteins from *M. gryphiswaldense* and *M. magnetotacticum* have almost identical sequences (91–97% similarity), whereas the similarity between the amino acid sequences of Magnetospirillum species and Magnetococci-MC1 lies at 46–67%. By means of a further comparative analysis it was possible to assign the fourth new gene, mamE, to the N-terminal sequence of the 36.3-kDa protein from *M. gryphiswaldense*.[55]

3.3.3. The mamAB Gene Cluster in M. Gryphiswaldense, M. Magnetotacticum, and Magnetococcus MC-1

Not only are genes homologous to *mamA* and *mamB* from *M. gryphiswaldense* found in the two genomes of *M. magnetotacticum* and *Magnetococcus MC-1*, but additionally the neighboring genes, open reader frames (ORFs), are also arranged collinearly in all three bacterial strains (Figure 8). Furthermore, the corresponding ORFs belong predominantly to the same known protein families, or have nothing in common with known proteins.[55] Clearly, the

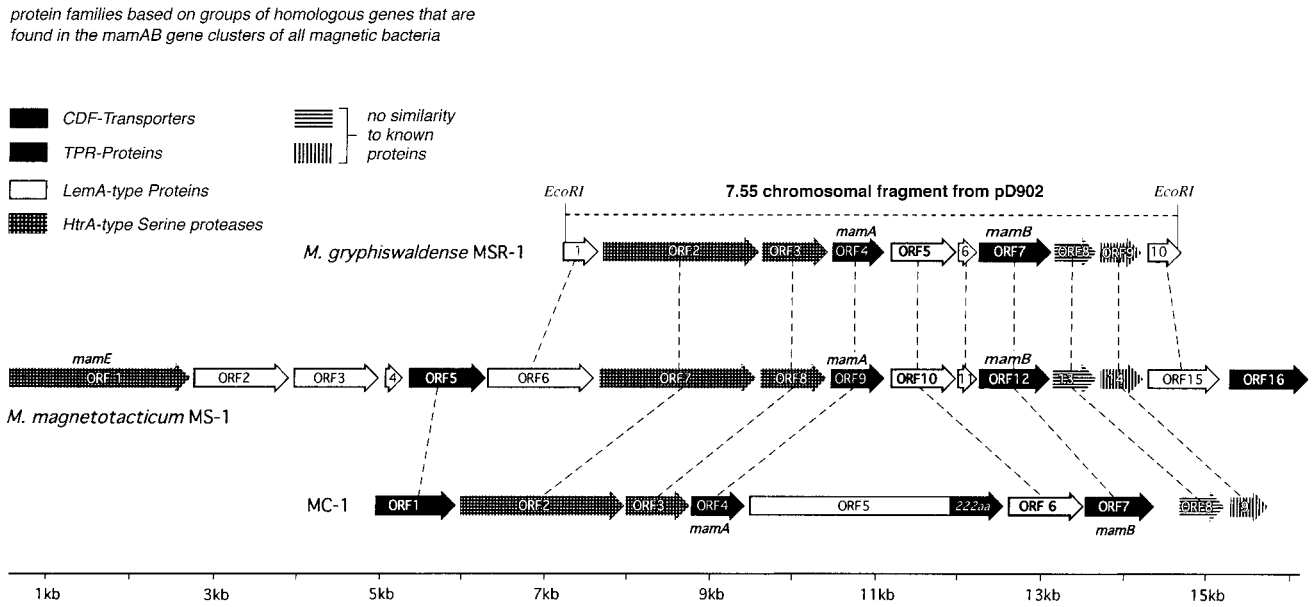


Figure 8. Molecular organization of the *mamAB* gene cluster in *M. gryphiswaldense, M. magnetotacticum*, and *Magnetococcus* MC-1. The arrows indicate the direction of gene transcription. The different marking of the graphically depicted arrows ORFs (open reader frames), which belong to the respective homologous families of genes. These families occur in every *mamAB* cluster of the three magnetotactic bacteria investigated. The dashed lines connect equivalent genes, that is, the most similar homologues. (From reference[55a] with kind permission of D. Schüler and the American Society of Microbiology.)

following protein families in the *mamAB* cluster may be assigned to these three, possibly also to all known, magnetic bacterial strains (Figure 8):

1) TPR ProteinsThe *mamA* genes in all three strains show similarities to the genes of the TPR proteins (Section 3.3.2).
2) CDF ProteinsNot only are the proteins of the mamB genes in all three strains (Section 3.3.2) homologous to the CDF proteins, but additional CDF homologues have also been found in the *mamAB* clusters of *M. magnetotacticum* and *Magnetococcus MC-1* (Figure 8)
3) HtrA-like Serine ProteasesIn addition to the *mamE* gene of *M. magnetotacticum*, additional genes whose proteins are similar to these serine proteases[61] have been found in the *mamAB* clusters of all three strains: ORF2 in *M. gryphiswaldense*, ORF7 in *M. magnetotacticum*, and ORF2 in *Magnetococcus MC-1* (Figure 8).
4) LemA-like ProteinsIn each of the three bacterial strains, an ORF has been found, with a similar sequence to that of the *lemA*-like genes, between the *mamA* and *mamB* genes. The functions of this protein family[62] are currently unknown.

In parallel, two further classes of genes occur in the *mamAB* clusters of all three magnetic bacteria: the ORFs 8 and 9 in *M. gryphiswaldense*, the ORFs 13 and 14 in *M. magnetotacticum*, and the ORFs 8 and 9 in *Magnetococcus MC-1* (Figure 8).[55] As no significant sequence similarities have been found for the derived proteins of prokaryotes or eukaryotes, they could represent important functions of magnetite biomineralization. In addition to these details, it can be concluded from a glance at Figure 8 that the current genes probably have an operon-like organization and are connected functionally with each other. Thus they could play a specific role in magnetite biomineralization.

As is now known (D. Schüler, personal communication) the genes *mamC*[55] and *mamD*[55] are found in a second gene cluster.

3.4. The Mechanism of Magnetite Crystal Formation in Magnetosomes

Before the detailed mechanism of magnetite crystal formation is uncovered by switching off of individual genes (knock-out method) the results of classical microbiology on magnetite biomineralization will be addressed once more at this point.

The unusually high iron uptake of the magnetotactic bacteria under microaerobic conditions and 10–20 μM $FeSO_4$ leads to a maximum in both magnetism and cell growth. The iron content ranges from about 3% in most bacteria to 10% of dry weight in *Magnetobacterium bavaricum*.[37,45a] Iron ions are not taken up as Fe^{II} but as Fe^{III}, which is formed from Fe^{II} by rapid oxidation in the medium, although the maximum solubility of Fe^{III} in water at biological pH is only about 10^{-18} M. This is possible without precipitation because this enormous Fe^{III} uptake take place in a medium in which a stationary culture of *M. gryphiswaldense* was previously cultured under moderate iron deficiency and which greatly stimulates Fe^{III} uptake.[63] However, there is no indication that the complexing agent is one of the known siderophores[64] (Fe^{III}-specific complexing agent, MW. ca. 1000 Da, stability

constant $K_f = 10^{30}$–10^{50}) as synthesized by many, primarily aerobic, nonmagnetic bacteria under the stress of low iron concentrations. This was also observed with the equally air-tolerant *Magnetospirilium sp.* AMB-1.[65] The Fe^{III} uptake of *M. gryphiswaldense* follows Michaelis–Menton kinetics, with the constants $K_M = 3\ \mu M$ Fe^{III} and $V_{max.} = 0.86$ nmol $Fe^{III} min^{-1} mg^{-1}$ (dry weight). These data correspond to a transport system of low affinity and high rate.[66]

Also of considerable importance for the mechanism is whether and when Fe^{III} is reduced to Fe^{II} during transport across the three membranes (outer, cytoplasmic, and magnetosome membranes), that is, whether in the final instance Fe^{III} or Fe^{II} ions arrive at the "empty" magnetosome vesicles (here, empty means without magnetite). A ferrireductase such as that isolated from the *external membrane* of a dissimilatory iron-reducing bacterium[67a,b] and identified in *Candida albicans*[67c] has hitherto not been found in magnetotactic cells. However, a *soluble* and *cytoplasmic* ferrireductase, which is bound loosely to the cytoplasmic membrane and is inhibited by Zn^{II} ions, has been isolated from *M. magnetotacticum*. In that way the average magnetosome count falls and the number of nonmagnetic cells increase.[57,68] If Fe^{II} ions were transported into the empty magnetosome vesicles, two protons would be formed by the oxidation of two Fe^{II} ions to give two Fe^{III} ions [Eq. (1)], since Fe_3O_4 contains stoichiometrically two Fe^{III} and one Fe^{II}.

$$2\,Fe^{2+} + 2\,H_2O \rightarrow 2\,[Fe(OH)]^{2+} + 2\,H^+ + 2\,e^- \qquad (1)$$

Formally this would be associated with an acidification of the intravesicular medium. In analogy to the coccolith vesicles of coccolithophores, in which calcification (calcite formation) also leads to the formation of protons (Section 4.4.2), here too the protons would have to be transported from the magnetosomes to produce a defined, alkaline microenvironment for magnetite crystal formation.

Y. Fukumori and co-workers were the first to discover Fe^{II} oxidation activity in a culture of *M. magnetotacticum*, which uses nitrate as electron acceptor. They were able to attribute the high Fe^{II} nitrite oxidoreductase activity to a nitrite reductase, a cytochrome cd_1, in the periplasma.[57,68] As Fe^{III} is clearly taken up by bacteria (Section 5.4) it could be reduced to Fe^{II} by this enzyme and transported into the empty vesicle. However, if this enzyme oxidizes Fe^{II} to Fe^{III} the divalent ions would have to be (re)transported into the periplasma.

The formation of magnetite crystals and thus magnetism has provided the unique opportunity to develop a simple spectroscopic method by which to measure the time-resolved formation of a mineral, magnetite, in living magnetic bacteria.[69] In a differential light scattering induced by magnetism, a light beam is passed through a suspension of cells of *M. gryphiswaldense* subjected to a strong homogeneous magnetic field both parallel (E_{max}) and vertical to (E_{min}) to the light beam. The ratio of the two scattering intensities ($C_{mag} = E_{max}/E_{min}$) correlates well with the average number of magnetic particles of different cell populations.[69] This sensitive and rapid method makes it possible to investigate the magnetism in parallel with the iron uptake as well as with bacterial cell growth and the oxygen concentration in the medium.

When radioactive $^{55}FeCl_3$ is added to a culture of nonmagnetic *M. gryphiswaldense* when the oxygen concentration for magnetite biomineralization is reached,[50] the extensive iron uptake, clearly closely coupled with the parallel increase in magnetism, begins immediately (Figure 9A). As a concentration of 1 μM iron in the medium is sufficient for cell growth, this result supports the assumption that most of the added iron (final concentration 30 μM) is transported into the vesicles, the empty magnetosomes (Figure 9B). No clusters of stored iron are found in the cytoplasm.

With magnetically induced light scattering, magnetism is detected just 5–10 min after the addition of iron. If after a total of 30 min cells are removed and killed, particles are

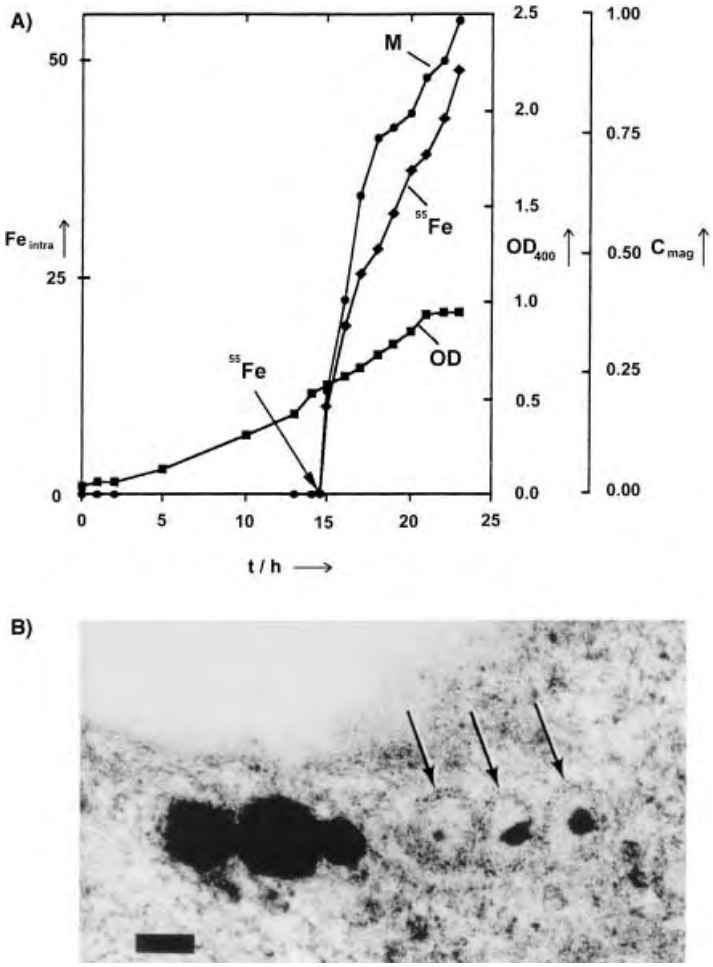


Figure 9. Close coupling of increased iron transport and magnetism during the growth of *M. gryphiswaldense*: A) iron was added as $^{55}FeCl_3$ after 14.5 h (arrow) and adjusted to an initial concentration of 30 μM. Under microaerobic conditions, iron uptake (Fe_{intra}) takes place almost parallel to the formation of magnetism (M): ■ cell density (OD), ● cellular magnetism (M), and ◆ intracellular iron content (Fe_{intra} corresponds to nmol Fe per mg dry weight). (Modified from reference [50]). B) Representation of empty vesicles. Thin section of *M. magnetotacticum* after iron deficiency over several generations. Three almost magnetite-free magnetosomes (empty vesicles) clearly show a bilayer membrane (arrow). The length of the bar represents 20 nm. (From reference [2a] with kind permission of T. J. Beveridge.)

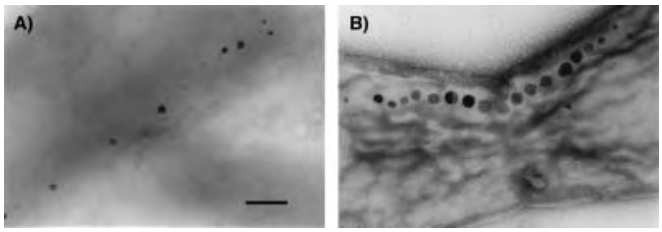


Figure 10. TEM images of the formation of magnetite crystals in *M. gryphiswaldense*: A) Magnetite particles 30 min after induction of Fe_3O_4 biomineralization by the addition of 30 μM $FeCl_3$ (see Figure 9A. These early particles, which already have a chainlike alignment, have a diameter of 5–20 nm and correspond mostly to the order of magnitude of superparamagnetic crystals.[47] B) Chain of magnetosomes of a cell that has grown for several hours in the presence of 30 μM $FeCl_3$. The "mature" crystals, which are mostly situated in the middle of the chain, are cubooctahedral and have a maximum diameter of 42–45 nm.

found in the transmission electron microscope image which, even though spatially separated, begin to indicate a chain (Figure 10A).[50] The initial particles are 5–20 nm in size and consequently exhibit superparamagnetism,[47] that is, they do not have a permanent magnetic dipole moment. This rapid, local supersaturation and crystal formation presumes the existence of empty vesicles. The chain of essentially "mature" crystals, which in comparison to inorganic magnetite are of surprising regularity and have a diameter of 42–45 nm (Figure 10B), is the result of this biomineralization. The elemental assignment of iron and oxygen was carried out by electron microscopy, which operates under low-dose conditions and uses the automatic three-window method of energy spectroscopy imaging (ESI).[69b,70]

3.5. Magnetotaxis

Magnetotactic bacteria are so named because they typically align themselves 80–90% like a magnetic needle in the Earth's magnetic field of 50 μT (Tesla).[71] This alignment is possible because they have a permanent magnetic dipole, which is large enough within the Earth's magnetic field to overcome the thermal forces that would otherwise produce a statistical disorder. Such a dipole is made up of the above-mentioned magnetosomes, intracellular phospholipid vesicles in which single-magnetic-domain magnetite crystals organize themselves along a chain through magnetic interactions. This chain is probably bound to the inside of the cytoplasmic membrane with the help of each individual magnetosome and a protein of the TPR family[55] (Section 3.3.2). In this way the bacterial cell as a whole acquires a magnetic dipole moment, which corresponds approximately to the sum of the individual magnetic moments of the magnetosomes[72] and is orientated parallel to their axis of rotation. Aligned passively in the Earth's magnetic field, the bacterial cells then swim along the magnetic field lines. They are driven by their flagella motors and steered by an aerotaxis, that is, by a movement that follows an oxygen concentration gradient, possibly to more favorable microaerobic habitats. Discussion can therefore only be of a magnetically supported aerotaxis,[73] not of magnetotaxis.

However, because magnetic bacteria already require microaerobic conditions to synthesis their magnetite crystals, as was demonstrated experimentally with *M. gryphiswaldense* (Figure 9A), the above-mentioned aim of a magnetically supported aerotaxis also appears questionable.

However, one new development should be mentioned briefly here. There are at least two theories to describe the mechanism of a biological compass in animals: a) the magnetic–mechanical interaction of the Earth's magnetic field with minute magnetic crystals (< 100 nm) in tissues,[74] and b) the effect of changes in magnetic fields on biochemical reactions.[75] Although both theories are similarly well-corroborated, the former theory is currently preferred because it has been possible to identify magnetite in the tissues of different animals. For example, superparamagnetic magnetite particles (grain size < 20 nm) have been found in carrier pigeons and soldier ants,[19] and with grain sizes that are typical of magnetic bacteria (30–120 nm) in, for example, salmon[17] and trout[18] (Section 1). For the latter, a mechanism with a certain analogy to the formation of the magnetosome chain has been proposed, that is, an orientation of the chain in the magnetic field. The following theory has been developed for the accumulation of superparamagnetic magnetite particles: In an external magnetic field, a membrane vesicle of a few μm diameter which contains a number of superparamagnetic particles is extended in parallel to the magnetic field axis and contracted across it. As this effect can be reinforced by a change in osmotic pressure, these membrane vesicles, also known as *ferrovesicles*, have been called magnetic osmometers.[76] There are probably at least two types of magnetoreception in animals. It would be of interest to know whether vesicle-dependent magnetoreception is the older of the two, and whether it developed from the magnetosomes of magnetic bacteria.

4. The Formation of Complex Crystal Morphologies of $CaCO_3$ in Unicellular Algae

4.1. The Occurrence of Coccolithophores (Calcareous Algae)

The best-known species of marine algae, mainly unicellular, which form a large part of the phylum Haptophyta (Prymnesiophyta)[77] are the coccolithophores (also called coccolithophorides). They are covered by a shield, the coccolithosphere, a frequently spherically-shaped aggregation of shells, platelets, or rods which are called coccoliths and are made of unusual calcite crystals. Together with the foraminifera, which do not contain any chlorophyll, the calcareous algae form a main part of marine plankton and are the most important carbonate source for the deep-sea sediments of the oceans.

Fossil coccolithophores from the late Triassic Period and the Palaeozoic Era are thus far known in only a few examples and in a small number of species.[78] However, they are found abundantly in a larger variety of species in the widespread deposits of light calcareous rocks of the early Jurassic Period (190–170 million years ago) and above all in the earlier

Cretaceous Period (95–63 million years ago). The end of the Cretaceous Period and the transition to the Tertiary Period was characterized by the extinction of about two thirds of the 50 genera of the coccolithophores of that time. New species developed during the Tertiary Period to reach a new high-point during the Eocene Epoch (50 million years ago).[78,79] On the basis of coccolith ultrastructure, attempts have been made to draft a type of phylogeny for the coccolithophores.[79c]

4.2. Holo- and Heterococcoliths

A differentiation is made between holo- and heterococcoliths with respect to their calcite crystal morphology. Holococcoliths are composed merely of simple calcite elements of rhombohedral or prismatic crystal forms. They are generally formed as extracellular structures.[80]

In analogy to the magnetite crystals in the magnetosomes, the calcite crystals of the heterococcoliths are likewise species-specific, and their complicated and complex morphologies are not found in inorganic chemistry.[81] Moreover, the property of the *heterococcoliths*, rare for eukaryotes, to also form their calcite structure intracellularly and in membrane vesicles suggests an evolutionary relationship to bacterial biomineralization.

Although the two unicellular algae *Emiliana huxleyi* and *Pleurochrysis carterae* have been intensively investigated to a similar extent, only the latter is described here, as *coccolith* vesicles have hitherto only been isolated from *Pleurochrysis* carterae (Figure 11).[82] Moreover, it has been possible to find or produce mutants of this calcareous alga with which the respective function of (now) three acid polysaccharides in the formation of the complex crystal morphologies have been explained (see also Section 4.5.1).[83]

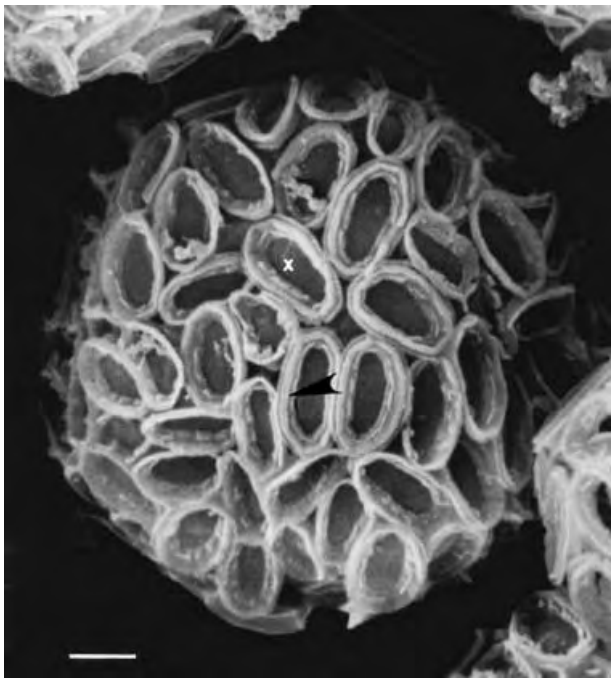


Figure 11. SEM image of a *Pleurochrysis* cell showing the mineralized scales of the coccosphere (the calcareous shield). These scales, called coccoliths, consist of an oval, organic base plate (x) and two discs of $CaCO_3$ crystals on their rim (arrow points). The length of the bar represents 1.0 μm. (From reference [89] with kind permission of M. E. Marsh and Springer Verlag, Vienna).

4.3. Heterococcolith Structures of the Unicellular Alga, *Pluerochrysis carterae*

On the surface of *Pleurochrysis*, the heterococcoliths consist of an oval organic base plate and, attached to it at the rim, a ring of calcite crystals. These crystals form two parallel discs, which extend radially from the rim of the coccolith (Figure 12A,B).[81] The ring itself is formed by the interlocking of individual crystals with alternate radial (R) or vertical (V) alignment (Figure 13). This R and V orientation corresponds to the alignment of the crystallographic c axis of the crystals to the plane of the coccolith. With the exception of the distal shield element, the disc element that is more distant from the base plate and unusually appears as a rather curved crystal surface (Figure 12B), all other surfaces are sheetlike elements (Figure 13).[81]

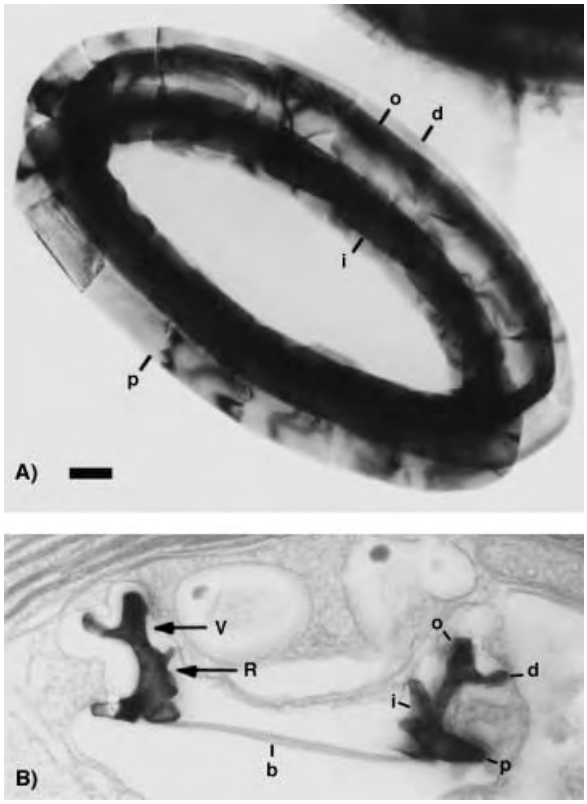


Figure 12. A) TEM images of an isolated, mature coccolith from *Pleurochrysis* whose plane is tilted about 30°; B) thin section which shows a cross-sectional view of a mature coccolith of *Pleurochrysis* in its vesicle prior to secretion into the coccosphere. The V and R crystal units are located on the rim of the base plate (b). The distal shield (d), the proximal shield (p), the inner tube (i), and the outer tube (o) as elements of the mineral ring are indicated. The length of the bar represents 100 nm. (From reference [81b] with kind permission of M. E. Marsh and Springer Verlag, Vienna)

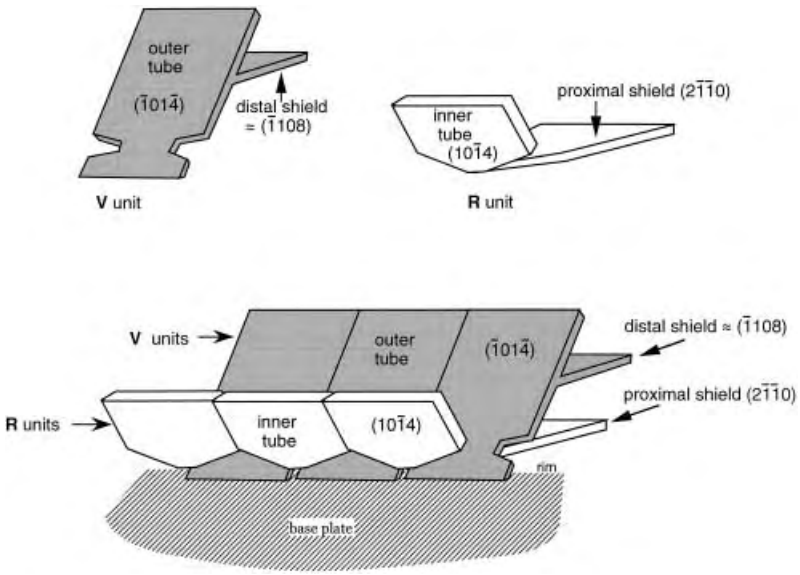


Figure 13. Schematic representation of the V and R crystal units and their precisely fitted and mutually interlocking structure on the rim of the coccolith of *Pleurochrysis* viewed from the interior of the coccolith. For simplicity the crystal elements are represented as if they consist of thin plates. The crystal surfaces, which correspond to the distal and proximal shield, and the outer and inner tubes are identified. (From reference [81b] with kind permission of M. E. Marsh and Springer Verlag, Vienna.)

4.4. Biomineralization in Coccolith Vesicles of Pleurochrysis Carterae

4.4.1. Membrane Proteins of the Coccolith Vesicles

The exceptional difficulties in isolating coccolith vesicles have hitherto been overcome only with *Pleurochrysis carterae*.[82] A successful combination of a) dissolution of the cytoskeleton, which connects the organelles of the coccolithophores, with b) an elaborate sucrose gradient centrifugation, which is possible thanks to the somewhat higher density of the coccolith vesicles, c) the possible differentiation of the coccolith vesicles from the outer coccoliths, and d) the selective dissolution of these free, outer coccoliths has led to the first isolation of purified coccolith vesicles (Figure 14 A, B).

Similar to the magnetosome membrane from the magnetic bacterium *M. gryphiswaldense,*[55] a whole range of polypeptides (in this case as many as 20) have been found by SDS-PAGE during the analysis of the purified coccolith vesicles. This large number is explained primarily by the now confirmed presence of a V(vacuole)-ATPase, whose total complex in many species contains between 12 and 13 subunits.[84]

Of the polypeptides, whose apparent molecular weights lie close to the most important subunits of the V_1(A–E) and V_0(a,c) part, two have been identified: 1) The subunit B, which reacted specifically with the 2E7-monoclonal antibody raised against the corresponding subunit B from oats.[85] The isolated and purified vesicles were made visible on the basis of the same antibody (Figure 14 A).[82] 2) The "16-kDa subunit", which in well-founded analogy to the c subunit of the ATP synthase was named "proteolipid".[84b] It was established by cloning and sequencing that its ORF has a derived molecular weight of 16.2 kDa. Its apparent molecular weight was, however, 24 kDa. Immunoblotting and immunofluorescence microscopy confirmed that this 24-kDa protein corresponds to the 16.2 kDa protein and was apparently modified post-translationally.[86]

4.4.2. Proton, Hydrogen Carbonate, and Calcium Transport in the Coccolith Vesicles

The formation of calcium carbonate leads to the release of many protons in the coccolith vesicles. Depending upon whether hydrogen carbonate [Eq. (2)] or carbon dioxide [Eq. 3] is transported into the vesicle, this amounts to one or two protons per molecule. Both the coccolithophore cell and the magnetic bacterial cell must produce a precise pH within a defined microenvironment of their vesicles which leads to crystal nucleation, crystal growth, and the mature end product, of which the crystal morphology and size are specific to the coccolith and magnetite crystal, respectively (Section 3.4).

$$HCO_3^- + Ca^{2+} \rightarrow CaCO_3 + H^+ \quad (2)$$

$$CO_2 + H_2O + Ca^{2+} \rightarrow CaCO_3 + 2\,H^+ \quad (3)$$

Extensive ATPase activities have been found in the coccolithophore cell,[87], for example, a Ca^{II}-dependent ATPase of the P type on the plasma membrane and a V-ATPase in the coccolith vesicles. As the coccolith vesicles stem from the trans-Golgi network, (Figure 15) V-ATPases are also found in the latter.[84b] An ATP-dependent proton transport that is inhibited by nitrate has been found in purified isolated

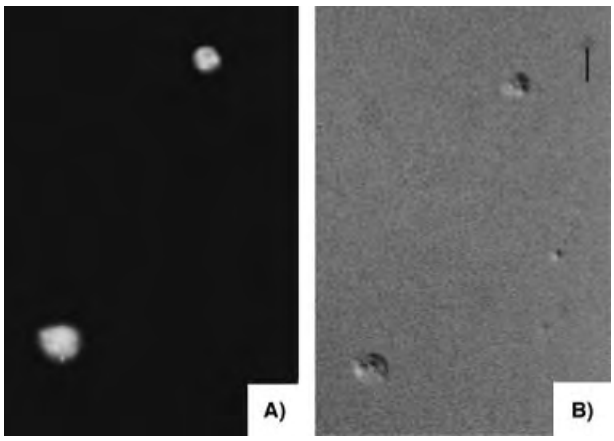


Figure 14. Immunofluorescence microscopy of coccolith vesicles. Isolated and aldehyde-fixed vesicles were exposed to 2E7 monoclonal and secondary antibodies, which had been labeled with FITC fluorochromium. Vesicles visualized by epifluorescence (A) and by Normaski optics (B). The length of the bar represents 1 μm. (From reference [82a] with kind permission of E. L. Gonzalez.)

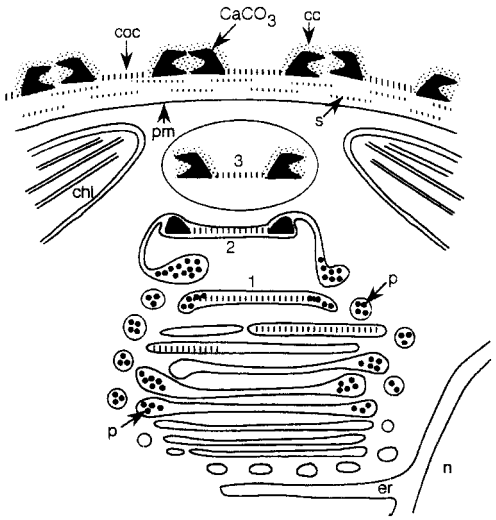


Figure 15. Schematic representation of coccolith formation in the Golgi apparatus of *Pleurochrysis*. A coccolith vesicle is shown before (1), during (2), and after (3) mineral deposition. Ca–PS1/PS2 complexes are formed in medial Golgi cisternae. These complexes are present as single 20-nm particles (p) before and during mineralization (1 and 2). After the mineralization ceases (3 and coccosphere) the crystal surfaces are surrounded by an amorphous polyanion coat (cc). (The coccolith base plate (hatched marks), coccoliths (coc), unmineralized scales (s), chloroplasts (chl), endoplasmic reticulum (er), nucleus (n), plasma membrane (pm).) (From reference [97] with kind permission of M. E. Marsh and Springer Verlag, Vienna.)

coccolith vesicles. In this way the function of the previously identified V-ATPases could also be established.[86] Furthermore, with an antibody against its subunit c of the V_0 part the V-ATPase could be localized on the coccolith vesicles. However, against expectation, the protons were pumped into and not out of the vesicles. This orientation of the V-ATPase corresponds to that found in secretory vesicles in all eukaryote cells, which likewise arise out of the trans-Golgi network.[84b] It is thus still an open question as to how the protons are transported out of the vesicles. An antiporter, which for example transports two protons out and one calcium ion in, has so far not been found.

Little is known about the molecular mechanism of the transport of HCO_3^- or CO_2, generally known as dissolved inorganic carbon (DIC). However, the release of protons during calcite formation appears to be an important requirement the for the carbon-concentrating mechanism (CCM) in chloroplasts, which in spite of the low concentration of dissolved DIC in the ocean allows a higher photosynthesis rate than would be expected at this lower DIC concentration.[88]

Even today the mechanism of Ca^{II} transport into the coccolith vesicles is also essentially unknown. The hope that one of the two Ca^{II}-dependent ATPases—the P-type or V-type, which represents the widespread ATPase activity in *Pleurochrysis*—could be connected with Ca^{II} transport is still unfulfilled, both for the plasma membrane and the coccolith vesicles.[82] However, the assumption that in place of diffusion by the cytosol, calcium ions are also transported, immobilized in vesicles, into the coccolith vesicles is becoming more firmly established: in *Pleurochrysis*, calcium ions form 25-nm particles in which the ions complex with the polysaccharides PS1 and PS2.[89] A large number of these particles, the coccolithosomes,[89] are formed in the middle Golgi cisterns and are probably infiltrated to and into the outermost trans-Golgi cisterns in small vesicles of Golgi membranes. They are present in these coccolith vesicles both during calcite nucleation and during the whole crystal growth (Figure 15).[81]

4.4.3. ***Formation of a Heterococcolith in a Coccolith Vesicle***

Before crystal formation begins, many coccolithosome-containing vesicles attach themselves to the outer rim of the basal plate (Figure 16A). This rim is covered by a small ring of a special organic material called the coccolith ribbon. The first crystallites form in accumulations of coccolithosomes (Figure 16B); in each case, a crystallite corner is in contact with the coccolith ribbon (Figure 16C) and each developing crystal is firmly attached. A ring of 24 small crystals of parallelepipeds, which exhibit alternating radial (R) or vertical (V) orientation relative to their crystallographic c axis, is formed from the crystallites (Figure 17A). A single fold of the coccolith ring that would run parallel to the rim of the basal plate can explain why crystals of similar structure form on both sides of the fold with different orientation.[81b] The maturing of crystals to their complex structures begins at the V unit (Figure 17B) with the extension of a $(10\bar{1}4)$ surface, which forms the platelike surface of the outer tube elements (Figure 17C), and ends with the structure of parallel double discs, which is characteristic of mature coccoliths. The detailed crystallographic analysis[81b] is not discussed here.

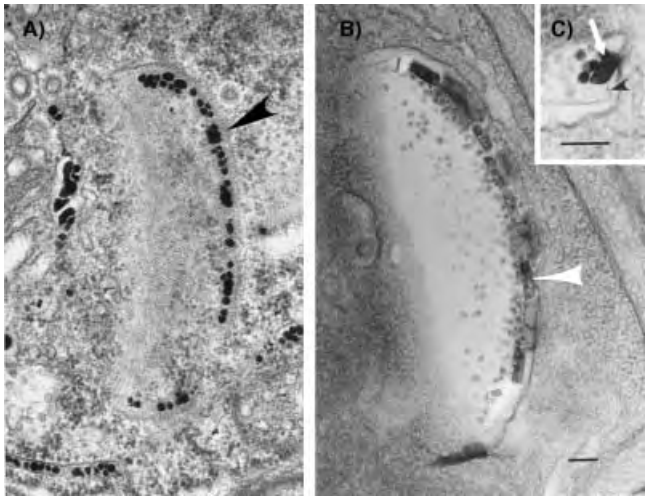


Figure 16. Thin sections showing successive early stages of mineralization in *Pleurochrysis* with a grazing view of the coccolith rim: A) Base plate with dense, polyanion-rich particles (coccolithosomes) associated with their rim (arrow head). B) Base plate with a ring of small, rectangular crystals between the polyanion-rich particles (arrow point). Sections without negative contrasting. C) Cross-section showing a small crystal (arrow) above the base plate. It is clearly attached to a small band of organic material, the coccolith ribbon, which is located on the distal rim of the base plate. The lengths of both bars represent 100 nm. (From reference [81a, b] with kind permission of M. E. Marsh and Springer Verlag, Vienna.)

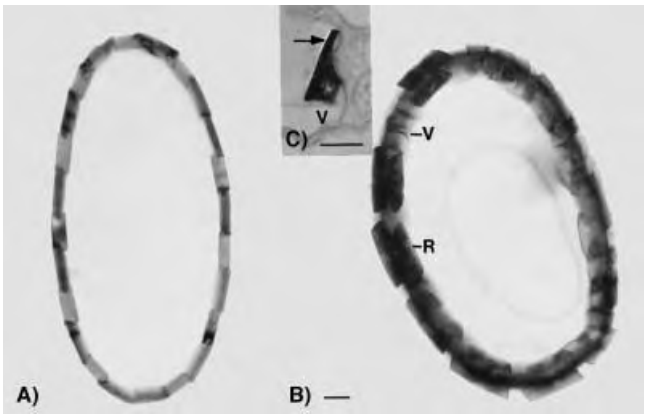


Figure 17. a) Electron microscope image of an isolated protococcolith from *Pleurochrysis*. It consists of a ring of 24 small crystals in the shape of rectangular parallelepipeds. The crystals have alternating V and R unit orientation. B) An isolated, still immature coccolith at a later development stage. As observed in projection, the R elements have the structure of double parallelograms, which will develop into the inner tube and proximal shield elements. C) Cross-section of a coccolith at a similar stage showing an immature V element on the rim of the coccolith base plate. The lengths of all bars represent 100 nm. (From reference [81a, b] with kind permission of M. E. Marsh and Springer Verlag, Vienna.)

The process of mineralization is apparently stopped by the pronounced swelling[89] of the coccolith vesicle (Figure 15), probably when the amount of ion product of the calcium carbonate is so greatly decreased by the huge influx of fluid that no further precipitation is possible. *Pleurochrysis* crystal growth also ends with dissociation of the polyanion-rich particles, the coccolithosomes. In addition, the residual calcium ions and numerous polyanions are released; the latter then form a protective layer on the crystal surface.[90] Subsequently the "mature" coccolith is transported to the upper surface of the algae, the coccolithosphere, by exocytosis.

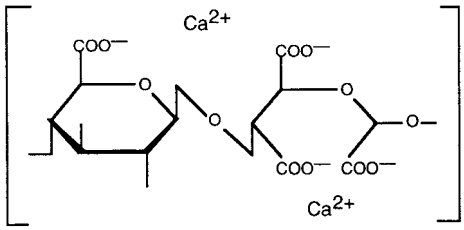
4.5. Mechanism of Formation of Complex Crystals in the Coccolith Vesicles of Pleurochrysis carterae

For some time it has been assumed that highly acidic macromolecules play an important role in the biomineralization of eukaryotes. Of these, those that can bind a large number of calcium ions and occur in high concentrations at the centers of mineralization of a number of tissues have aroused special interest.[91,92] For example, the phosphophoryn proteins, which are associated with the dentin of vertebrates, are rich in aspartic acid and phosphoserine.[93] In the presence of calcium ions, they form 25-nm particles, as does one of the acidic polysaccharides.[94] The considerable difficulties associated with the elucidation of the biomineralization of multicellular organisms because of the growing number of sequenced proteins and because of their different possible activities[95] can be judged from the mother-of-pearl of crustacean shell, which has been extensively investigated because of its hardness and fracture resistance. Therefore work on unicellular eukaryotic organisms has gained in importance. In particular, the pioneering investigations of Marsh et al. on *Pleurochrysis carterae*[81a,96] have for the first time allowed the localization of crystal nucleation in a unicellular organism, in this case calcite, and an unusual crystal growth. The isolation of acidic polysaccharides,[90a] the production of associated antibodies,[89,96] and a mutant analysis[83,96] of these polysaccharides, together with morphological studies, have also contributed.

4.5.1. The Acidic Polysaccharides PS1, PS2, and PS3

The three acidic polysaccharides PS1, PS2, and PS3, have been isolated from the coccoliths of *Pleurochrysis* and purified.[90a] In polyacrylamide gel without SDS, PS1 and PS3 migrate as relatively narrow bands that appear to represent a narrow molecular weight range. The fact that, in contrast, PS2 forms a ladder of many discrete bands over the whole gel suggests a broad variation in the degree of polymerization. PS2 is the most abundant coccolith polyanion in *Pleurochrysis*. The mass ratio of PS2/PS1 is 77:22. The smaller but very important fraction[96] of PS3 lies close to 2%.

PS2 is made up essentially of the repeating motif [→4)D-glucuronate(β1→2)*meso*-tartrate(3→1)glyoxylate(1-]$_n$ (formula of the calcium salt of PS2 reproduced from references [89, 90a] with kind permission of M. E. Marsh), a motif



that has not previously been found in any other polysaccharides. With its four carboxylate groups or four negative charges per motif, PS2 is the most acidic polyanion that has thus far been described for mineral storage.[90,97] The primary structures of PS1 and PS3 are still unknown. PS1 is a polyuronide that consists essentially of glucuronic acid and galacturonic acid (1:3 ratio).[90] PS3 is a galacturonomannan with a significant number of sulfate ester groups.[81a]

The fate of PS1 and PS2 was followed during the whole mineralization process by TEM with well-characterized antibodies and immunogold labeling of thin sections; the analysis began with crystal nucleation and continued to the end of crystal growth.[89] The many detailed electron microscope images cannot be shown here for reasons of space. Their results, which are also discussed together with the following mutation experiments, will be summarized briefly here (see Figure 15 for a schematic representation).

The polysaccharides PS1 and PS2 are synthesized in the central cisterns of the Golgi apparatus. There, together with calcium ions, they form numerous individual 25-nm particles called coccolithosomes. Vesicles that contain a series of these particles are derived from the edges of the central cisterns. These PS1/PS2–Ca particles are then transported in these

small vesicles to the coccolith vesicles, with which they fuse[81a] The coccolith vesicles contain an oval basal plate on the rim of which the PS1/PS2–Ca particles now attach themselves. The mineralization process then begins there during which these particles and thus also the polyanions PS1 and PS2 are present, from crystal nucleation to shortly before the end of crystal growth. In the end phase of coccolith maturing, the crystal receive a polysaccharide coating of PS1 and PS2, which is not detectable on them during the growth phase.

Until recently no well-characterized antibodies for the localization of PS3 by immunogold labeling could be produced. However, it was possible to show by pulse-chase experiments with radioactive carbonate, sulfate, and calcium in kinetic experiments[97] that the cellular half-life of PS3 is more than three times that of PS1 and PS2. It is concluded from this that PS3 is synthesized and secreted in a different way to that of PS1 and PS2.[81a,97]

4.5.2. Mutants from Pleurochrysis that do Not Synthesize These Acidic Polysaccharides

More than 100 spontaneous and chemically induced mutants have been isolated from *Pleurochrysis*. The respective polysaccharides were isolated from the cells after pulse labeling with ^{14}C carbonate and ^{35}S sulfate and characterized by gel autoradiography.

The coccoliths of a *ps1* mutant, which had been induced chemically with *N*-methyl-*N'*-nitro-*N*-nitrosoguanidine (MNNG) and no longer expresses PS1, are clearly similar in every respect to the wildtype coccoliths.[81] That means that PS1 probably does not play a role in the formation of these coccoliths, which possess the morphology of the wildtype.

The hypothesis that PS2 is a functional intermediate of calcite biomineralization in *Pleurochrysis* was supported by three independent mutants.[83] Two of these *ps2* mutants formed spontaneously, a third was induced chemically with MNNG. All three are phenotypically identical and do not express PS2. The mineral content of each of these mutants is less than 5% of the content of the wildtype, which also means that most of their coccoliths are not mineralized. It is extremely important for the functional analysis of the *ps2* mutants, however, that they deposit the small amount calcium carbonate not only on the rim of the basal plate as calcite, like the wildtype, but also that they form the V and R structures of the wildtype crystal with the more mature crystals. Thus PS2 has no influence on the crystal morphologies of this specific crystal form. Moreover, the merely reduced calcite mineralization on the coccolith rim in the absence of PS2 indicates that PS2 is not absolutely necessary for crystal nucleation, and that the PS1/PS2–Ca particles are clearly not the only source of calcium for coccolith formation.

How does PS2 contribute to the formation of unusual, anvillike calcite crystal? On a small ribbon of organic material (Figure 16C) a large number of PS1/PS2–Ca particles are bound to the outer rim of the basal plate in the wildtype (Figure 16A). The result is a local concentration of 6 M polyanion-bound calcium ions[90b] before crystal formation begins.[89] In contrast to the *ps2* mutants, the PS1/PS2–Ca particles in the wildtype clearly accelerate the rate of calcite crystal nucleation. It is still not known whether the PS1/PS2–Ca complex exercises its action through its structure, that is, as part of a postulated crystal nucleation complex, or through its capacity as a buffer for calcium ions.

Mutant analysis, the ideal pathway for an understanding of the mechanisms of complex biological systems, has, as previously described, come close to an explanation of crystal nucleation. The particular potential of this method was plain to see in the first described *ps3* mutants,[81a] which were induced by MNNG and were now termed $ps3^{-1}$:[96] when PS3 was no longer expressed, the complex anvillike calcite crystals were also not formed; instead, only simply orientated crystals that resemble the rectangular parallelepipeds of the protococcoliths of the wildtype were found (Figure 17A). Amongst 500 new mutants of Pleurochrysis, a second mutant (named $ps3^{-2}$) has been recently found that also exhibits the protococcolith phenotype and does not express PS3. In addition, it was also now possible to produce monospecific anti-PS3 antibodies. In this way it was possible to demonstrate that PS3, unlike PS1 and PS2, is localized between the membrane of the coccolith vesicle and the crystal surface and is directly associated with the growth and the shaping of the calcite crystals to their complex anvillike morphologies (M. Marsh, personal communication).[96]

5. The Formation of Nanostructured Cell Walls of Amorphous Polysilicic Acid in Diatoms

5.1. Occurrence of Diatoms

Diatoms are unicellular eukaryotic organisms, algae of the class Bacillariophyceae. The number of living species known today is about 100000.[98] They are found in sea water, brackish water, and in fresh water. These diatoms make up the dominant part of phytoplankton, which together with other marine organisms such as silicoflagellates, radiolaria, and sponges, converts annually the exceptional amount of 6.7 gigatons (giga $= 10^9$) of silicon biogenically during the formation of their silica skeletons.[99]

According to recent age estimates, the oldest fossil diatoms could not have existed earlier than 266–238 Ma (million years) ago.[100] Based on the discovery of the hitherto earliest fossil diatoms (dated to the early Jurassic Period, 185 Ma ago),[101] the rRNA clock developed for this purpose shows that the diatoms must have originated between 266–238 Ma and 185 Ma ago. In spite of this, it is still an open question whether or not these unicellular diatoms could have originated during the Cambrian Explosion of biomineralization[4a,11,12,14] (Section 1) between about 525–510 Ma ago, that is, much earlier than the Permo-Triassic boundary of around 250 Ma ago. According to this timescale, about 96% of all marine species, 70% of all terrestrial vertebrates, and many main groups of terrestrial plants were, amongst other factors, destroyed by the most violent period of continental volcanic activity in the Earth's history.[100,102] Thus, unlike the coccolithophores,[78] no fossil diatoms have yet been found which survived the Permian–Triassic Periods mass extinction to allow a new age estimation (Section 4.1).

5.2. The Structure of Diatoms

Diatoms can be readily recognized by their characteristic ornamented cell walls, which are made of amorphous polysilicic acid, opal. Such a silica cell is also known as the frustule. Since the morphologies are species specific, a genetic control of this biogenic structure formation is very likely.

The architecture of the diatoms (class Bacillariophyceae) allows this class of algae to be subdivided into two orders.[98] Thus the silica shells of *Pennales* are extended and bilaterally symmetrical (lancet-shaped or elliptical). *Cylindrotheca fusiformis* is shown here as an example which for about the last ten years has become established as a model organism for molecular biological investigations of biomineralization processes (Figure 18A).[103,104] The silica shells of *Centrales* on the other hand are often radially symmetrical, but with many deviations. An almost perfect example of central diatoms is *Cosconodiscus granii* (Figure 18B).

Common to all diatom cell walls (frustule) is that they consist of the hypotheca, the box, and the epitheca, the lid (Figure 19). The epitheca for its part consists of two parts, the flat upper part, called the epivalve, the upper box and a ring-shaped side wall, which consists one or more girdle bands. This bipartition applies also to the hypotheca, in this case the hypovalve and the lower girdle bands with the difference that the girdle bands of the lid overlap those of the box.[98] In this way the protoplast is completely enclosed and protected. This concept is strengthened in that organic layers probably join the silica shells (valves) and the girdle bands exactly. In addition, all silicified components are protected by a casing of organic material, probably for protection against desilification.[105]

As was recently shown by atomic force microscopy (AFM) on living, hydrated *Pinnularia viridis* (Nitzsch),[106] their cell walls (frustules) are coated with a thick mucilaginous material that is only interrupted in the vicinity of the raphe fissure (Figure 20A).[107] (The raphes are probably responsible for the rapid, gliding motion of diatoms; maximum of about 20 $\mu m\,s^{-1}$).[108]

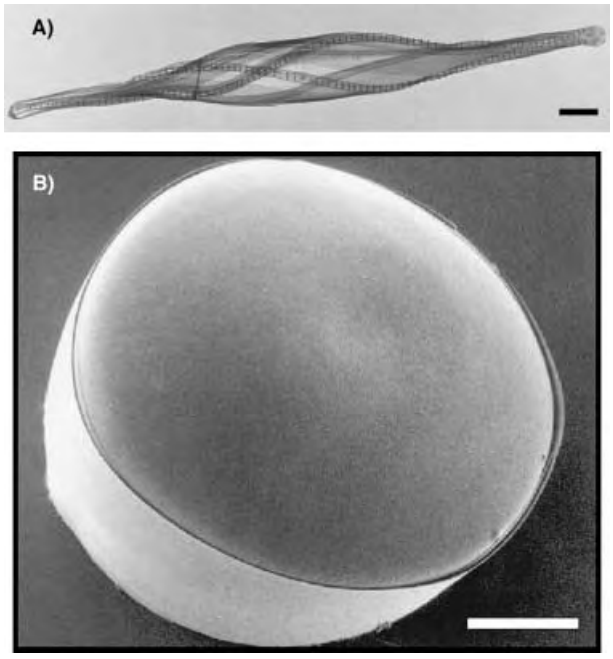


Figure 18. Morphologies of diatom cell walls: a) TEM image of *Cylindrotheca fusiformis*. The length of the bar represents 2.5 μm. b) SEM image of *Coscinodiscus granii*. The length of the bar represents 50 μm. (From reference [109] with kind permission of M. Sumper.)

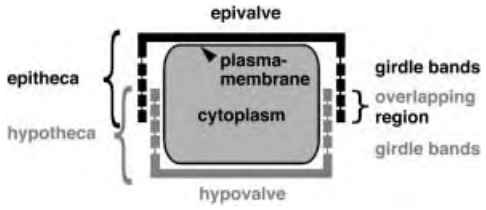


Figure 19. Structure of the diatom cell wall (from reference [109] with kind permission of M. Sumper.)

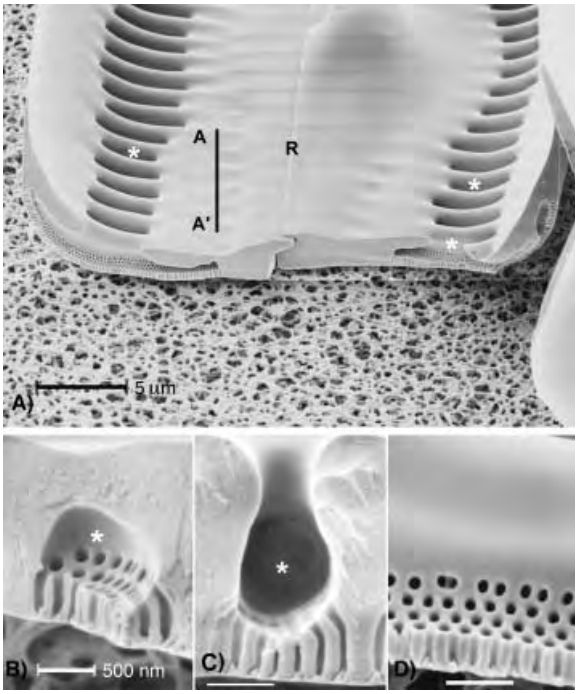


Figure 20. Images of *Pinnularia sp.* obtained by field emission scanning electron microscopy (FESEM): A) Cross-section of fractured valve with a view of the surface that faces the concealed cytoplasm. B, C) The enclosed chambers (stars) result from a cleavage along the AA′ axis, which is labeled in (A). D) High enlargement of the region framed in (A) shows tiny pores organized in precise arrays. The lengths of the bars represent: A) 5 μm, B–D) 500 nm. (From reference [105c] with kind permission of R. Wetherbee)

Since the cells are constantly in contact with their environment, the shells (valves) and to a lesser extent the girdle bands are equipped with numerous holes such as pores, slits, etc. which allow the necessary exchange reactions. At the same time these holes form the fascinating ornamentation of the diatoms (Figure 20B–D).

5.3. Biomineralization of the Cell Wall in Silica Deposition Vesicles (SDV)

Extensive electron microscope studies on a variety of different diatoms of both orders, the *Pennales* and the *Centrales*, have established the different morphological stages of the biomineralization process,[105a] which is summarized schematically (Figure 21).[109] Similar to the coccolithophores (calcareous algae), whose biomineralization takes place in specialized vesicles, the coccolith vesicles (Figure 15); special vesicles, called silica deposition vesicles (SDV), were also found in diatoms.[105] It has been concluded from investigations on other unicellular eukaryotic organisms (protists) that the SDV is the common organelle for their silica ($SiO_2 \cdot n\,H_2O$) biomineralization process.[110] The ornamented silica shell (frustule) is formed in the SDV, whose membrane, called the silicalemma, consists of a typical lipid bilayer. The origins for the species-specific ornamentation of the silica shells is thus sought in the SDV, their components, and their structure.

5.3.1. Silicic Acid Transport and Cell Wall Synthesis

Transport proteins of the cytoplasmic membrane for the formation of the silica walls in diatoms, its silicic acid transporters (SITs), have already been characterized and sequenced.[103,111,112] Thus the first proteins that specifically bind silicon, whose predominant form in sea water is as undissociated orthosilicic acid $[Si(OH)]_4$, and transport it into the cells have been described. This transport is coupled with and controlled by the incorporation of orthosilicic acid into the cell wall,[112] the frustule, a relationship also found between the transport of Fe^{III} ions and the formation of magnetite crystals in magnetic bacteria (Figure 9A, B).

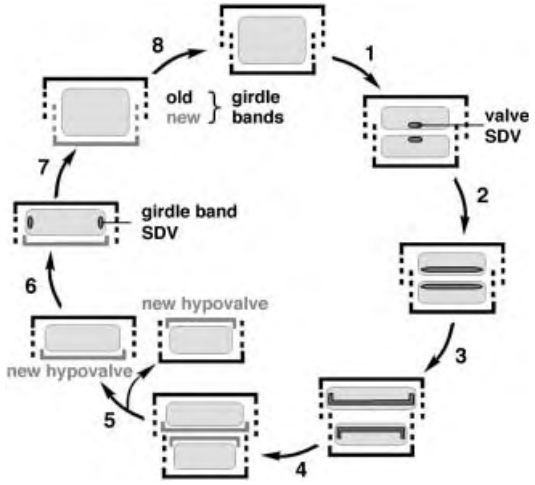


Figure 21. Diatom cell cycle: 1) cytokinesis (division of the cytoplasm) and formation of an SDV for a valve (silica shell) in each daughter protoplast; 2) and 3) expansion of the SDV and formation of a new hypovalve within each SDV; 4) exocytosis of the contents (hypovalves of each SDV); 5) separation of daughter cells; 6) formation of the first girdle band SDV; 7) consecutive formation and secretion of girdle bands; 8) DNA replication. (From reference [109] with kind permission of M. Sumper.)

In the cytoplasm the orthosilicic acid must find the path to its deposition for the construction of the hypotheca in the SDV under clearly stringent structural conditions. These conditions differ from those in magnetic bacteria and coccolithophores as the new silica wall is first formed after cytokinesis (division of the cytoplasm) and before cell division (Figure 21). The daughter cells thus remain in close proximity in the region in which the two silica deposition vesicles (SDVs) form the new hypovalves (Figure 22), a region that is thus shielded from the extracellular space. For that reason the orthosilicic acid can only be transported through the cytoplasmic membrane when the latter is still connected with the surroundings. Since many diatoms form their silica walls within one to two hours,[113] large amounts of orthosilicic acid must be transported through the cytoplasm without being polymerized.

The orthosilicic acid uptake of the diatom cells follows Michaelis–Menten kinetics with the kinetic parameters $K_M = 0.2\text{–}7.7\ \mu M$ and $V_{max} = 1.2\text{–}950\ fmol\,Si\,cell^{-1}\,h^{-1}$.[114] The transport of $Si(OH)_4$ in marine diatoms is coupled with sodium ions in the form of a sodium/orthosilicic acid symporter.[103,111]

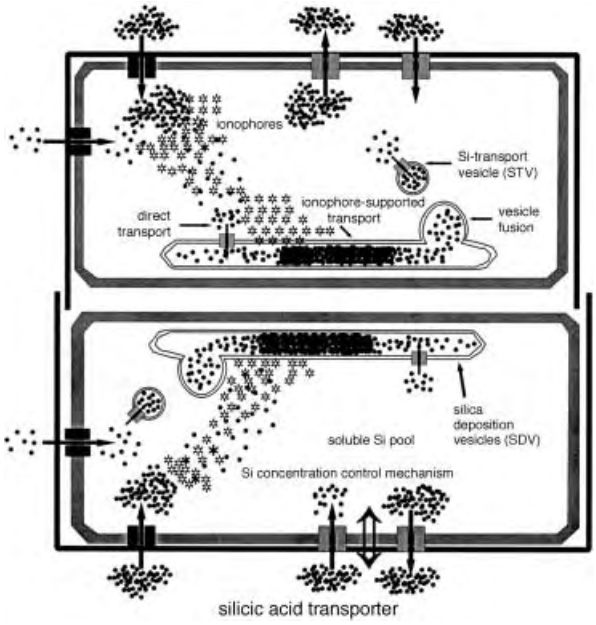


Figure 22. Features of silicic acid uptake, its intracellular transport, and its deposition in a dividing cell. The scheme shows these three activities after separation of the cytoplasm (cytokinesis) into two daughter cells, which are still located in the silica shell, the epi- and hypotheka, of the mother cell during the synthesis of their silicic acid walls. The outer black lines represent the silica wall of the mother cell. The plasma membrane of each of the two daughter cells forms the respective large rectangle with shaded borders. Other components are labeled. Black dots represent silicic acid. The lower daughter cell illustrates three main components of transport into the cell and polysilicic acid formation: the silicic acid transporter, the soluble silicon pool, and SDVs. The upper daughter cell illustrates three possible means of *intracellular* transport into the SDVs: direct transport by intracellularly localized silicic acid transporting proteins, ionophore-mediated transport by silicate ionophoretic activities, and transport by silicon transport vesicles (STVs). (From reference [112a] with kind permission of M. Hildebrand.)

If the orthosilicic uptake is investigated in diatom cells that have been cultured for an extended period under substrate deficiency and their intracellular stores have then been essentially emptied, after addition to the medium $Si(OH)_4$ is taken up at maximum rate with replenishment of the stores. This massive increase in orthosilicic acid transport occurs in a manner similar to that when DNA synthesis starts.[115] On this basis cDNA libraries were set up from *C. fusiformis*, and five cDNAs with identical common sequences were identified and sequenced (SIT 1–5).[112] As no significant homologies for the derived proteins were found in either prokaryotes or eukaryotes, SIT 1–5 represent a new class of transporters,[112a] although they have a signature sequence (AX_3LX_3GR) for sodium symporters at amino acids 216–225 (Figure 23).[116] The transmembrane domain is highly conserved with 87–99% amino acid identity, as is seen from a comparison of the five SITs,[112a] and is probably the region in which the undissociated orthosilicic acid is transported through the membrane.

As the C-terminal domains in other transporters probably control their activity,[117] it is assumed that the five SITs display respectively different activities in different regions of the cytoplasmic membrane (Figure 23.[111b] In the intracellular stores, which depending on the conditions are filled by these orthosilicic acid transporters, up to 50% of the total silicon is present as soluble orthosilicic acid.[118] Not only do the concentrations vary from 19–340 mM soluble orthosilicic acid,[112] but they are maintained far above the saturation limit of the respective solubility for orthosilicic acid.[119]

Two mechanisms have been proposed for this observation:First, on the basis of investigations in which it was possible to precipitate 80% of the soluble orthosilicic acid with trichloroacetic acid, it was suggested that organic orthosilicic acid binding components inhibited its polymerization.[120] The capacity of these components can also determine the extent of the silicic acid stores. It was possible to extract the silicic acid ionophores form *Nitzschia alba* with organic solvents, but they could not be characterized. These ionophore activities were induced sixfold in cells that had been cultivated under orthosilicic acid deficiency. This indication of their direct relationship with orthosilicic acid metabolism has led to the prediction that they serve to maintain high intracellular concentrations of unpolymerized orthosilicic acid.[121] Thus catechol and its derivatives, for example, catecholamines such as epinephrine, bind and dissolve orthosilicic acid rapidly. This class of compounds is synthesized by bacteria in the form of the catechol siderophores; during iron deficiency, these compounds capture extracellular Fe^{III} under aerobic conditions or dissolve Fe^{III} from its oxides. In these catechol siderophores, 2,3-dihydroxybenzoic acid groups are bound to 1,4-diaminobutane (putrescine) or *N*-(3-aminopropyl)-1,4-diaminobutane (spermidine)—two amines that play an important role in silaffins, which were isolated from the cell walls of diatoms and will be described later (Section 5.3.3).[122] However, during the biomineralization of magnetite by magnetic bacteria an ionophore is secreted that holds the available Fe^{III} in solution, is not a siderophore, and stimulates iron uptake.[63,65] The chemical nature of this compound is also unknown (Section 3.4).

Second, as an alternative mechanism it has been suggested that intracellular transport of orthosilicic acid takes place through small vesicles in which it is stored, either solubilized or undissolved.[123–125] These vesicles have been named silicon transport vesicles (STVs) by Schmid and Schulz.[123] They were found during several electron microscope studies in the region of active silica deposition vesicles (SDVs).[123,125,126]

These STVs correspond to the highly characterized, small transport vesicles of coccolithophores (Section 4.5.1). The size of the STVs corresponds to that of the polysilicic acid particles, which attach themselves to the growing silica shells. This indicates that these particles are used as building blocks. Their size is probably determined by polyamine-modified polypeptides, called silaffins, or by their polyamines alone (Section 5.3.3). Such polysilicic acid particles were already found by AFM in *Pinnularia viridis* with remarkably low variation in their size: 44.8 ± 0.7 nm in the valves and 40.3 ± 0.8 nm in the girdle bands.[106] Whether orthosilicic acid is contained in STVs has not yet been investigated by X-ray microanalysis.[127]

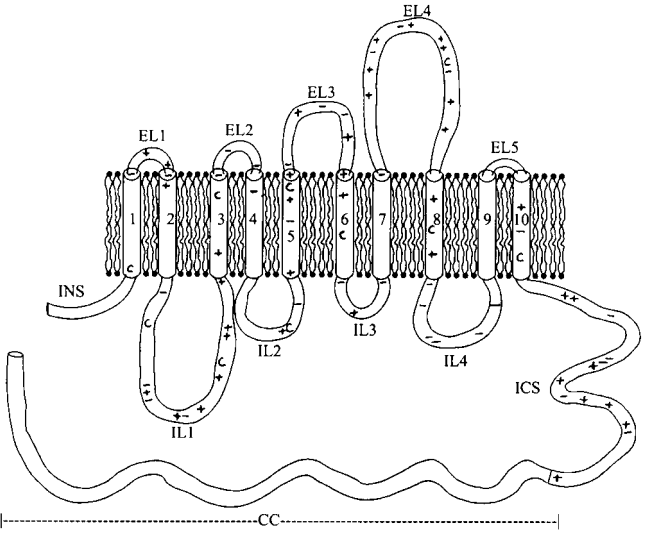


Figure 23. Topological model of the silicic acid transporters (SITs) from *C. fusiformis*, based on SIT4, in a lipid bilayer membrane. Bottom = intracellular. IL = intracellular loops, EL = extracellular loops, INS = intracellular amino segment, ICS = intracellular carboxy segment, CC = coiled coil, (+) and (−) orders the charged amino acids, C = cystein residue. (From reference [112a] with kind permission of M. Hildebrandt.)

5.3.2. *Silica Deposition Vesicles*

It was recognized quite early that morphogenesis of structures containing silicic acid takes place in silica deposition vesicles not only in diatoms but also in other unicellular eukaryotic organisms.[105a,110,128] In spite of this their formation in diatoms is still a matter of debate, mainly because of the plethora of different vesicles. However, there are numerous indications that the SDVs originate in the Golgi apparatus, both in the central diatoms[123,126,129] and in the pennate diatoms.[130] The analogy to the coccolith vesicles (Section 4) supports these findings (Figure 15).

A methodologically important step was made with the introduction of the cationic, lipophilic fluorescent dye rhodamin 123 (R123), which depending on the electrochemical potential accumulates in the SDVs and there indicates an acidic pH value.[131] R123 is also incorporated into actively polymerizing polysilicic acid and this process can be monitored quantitatively.[105c,112a,131]

The extraordinarily extensive and until now mainly morphological studies by electron microscopy suggest that orthosilicic acid is directed to the site of morphogenesis, the SDVs, either by ionophore supported diffusion[121] (Figure 22) or by transport vesicles (STVs)[123,126] as particles of a certain size (Section 5.2.2). However, it has thus far not been possible to isolate the SDVs to investigate orthosilicic acid transport through their membranes, the silicalemma, because of the difficulty in removing the silica shell.

5.3.3. *Proteins of the Diatom Cell Wall: Frustulins, Pleuralins, Silaffins*

If the cell walls of the diatoms are compared with those of the coccolithphores, whose complex structures are made up of either amorphous silica (opal) or crystalline calcium carbonate, it is immediately clear when searching for analogies that many more organic components are found during work-up of the diatom cell walls. This difference is attributed to the fact that unlike the coccoliths, diatom cell walls possess pores and slits from an ornamentation process, also called micromorphogenesis.[105c,121] Whereas the three polysaccharides PS1, PS2, and PS3 of the coccolithophore cells can be isolated most simply by treatment with trichloroacetic acid, or even with EDTA,[90a] the diatom cell wall must be treated with anhydrous hydrogen fluoride (HF) to release the very firmly bound and incorporated components.[104,105b,132,133] Three groups of proteins has been isolated from the cell wall of *C. fusiformis* and characterized: frustulins,[104,105b,132] pleuralins,[133] and silaffins.[134]

Frustulins are found everywhere on the cell wall and clearly form a protective protein coating deep into the internal space (Section 5.3.1; see also reference [106]). The protein coating can be completely destroyed with EDTA, a complexing agent for calcium ions.[104,105b,132] The frustulins resemble the polysaccharides PS1 and PS2 in both properties; the latter also cover the calcite crystals of the coccoliths as a protective coat and can be released with EDTA (Section 4.5.1). Furthermore, the frustulins in *C. fusiformis* are a family of four, essentially glycosylated proteins, which are found together with apparent molecular weights of 75–200 kDa.[104,105b,132] The frustulins are conspicuous for, amongst other properties, five to six repeated domains that are rich in acids and cystein.

Pleuralins, the second family of proteins of diatom cell walls from *C. fusiformis*, could only be obtained by dissolving the silica cell wall with hydrogen fluoride, which is why they were originally called HEPs (HF-extractable proteins).[133] Three pleuralins, called pleuralin 1 (200 kDA), pleuralin 2 (180 kDa), and pleuralin 3 (150 kDa), have been isolated and sequenced (Figure 24 A). Like the frustulins, these proteins

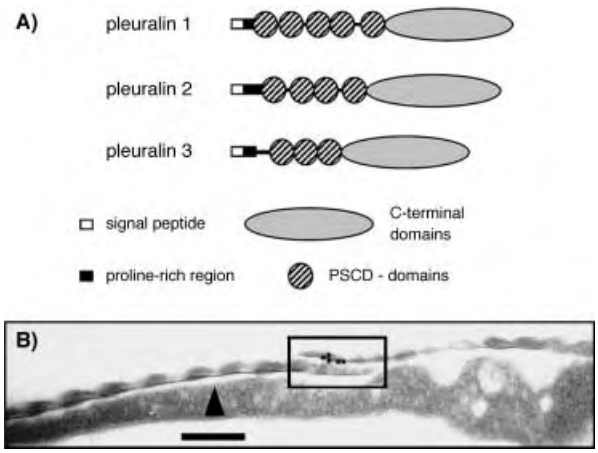


Figure 24. A) Schematic primary structures of the three pleuralins. b) Immunogold labeling of a thin section of *C. fusiformis*. The TEM image shows the overlapping region of the girdle bands (framed). The black arrow indicates the plasma membrane and points towards the extracellular space. The rows of oval structural elements outside the protoplasts represent the girdle bands, from the left of the hypotheka and from the right of the epitheka. An anti-pleuralin 1 antibody was used for indirect immunogold labeling. The length of the bar represents 200 nm. (Adapted from reference [109, 133b] with kind permission of M. Sumper and N. Kröger.)

contain repeated special domains, in this case the PSC domains (proline-serine-cystein domains).

The important discovery of the (hitherto) only signal sequence of proteins of biomineralization (the pleuralins), which is important for an entry into the endoplasmic reticulum, points to a relationship or analogy between biomineralization in eukaryotes and the secretory transport pathways of proteins, exocytosis. This analogy is extensively supported by the biomineralization of the coccoliths of *Pleurochrysis carterae*, in which almost all processes previously described take place in the Golgi system (Figure 15). However, no proteins were detected; without exception, acid polysaccharides have hitherto been found.

With immunogold labeling, all pleuralins have been identified at a specific site of the diatom cell wall that corresponds to their cell-cycle-dependent development. With this method it was first found that the protein composition of the two theka, the epitheka and the hypotheka, are clearly different. During cell division the pleuralins bind to the newly formed girdles of the hypotheka, whereas previously they were still found on those of the epitheka (Figure 24 B). This process runs parallel to the simultaneous conversion of the former hypotheka into the epitheka of the daughter cell[133] (Figure 21). Clearly, this development-controlled cooperation of the pleuralins with the diatom cell wall is involved in the hypotheka–epitheka differentiation.

The silaffins make up the third family of proteins of the diatom cell wall in *C. fusiformis*. Like the pleuralins, they could also only be found after dissolution with anhydrous hydrogen fluoride. They are three polypeptides of low molecular weight: silaffin 1A (4 kDA), silaffin 1B (8 kDa), and silaffin 2 (17 kDa). With the help of the *N*-terminal amino acid sequence of silaffine 1B the corresponding *sil1* gene was

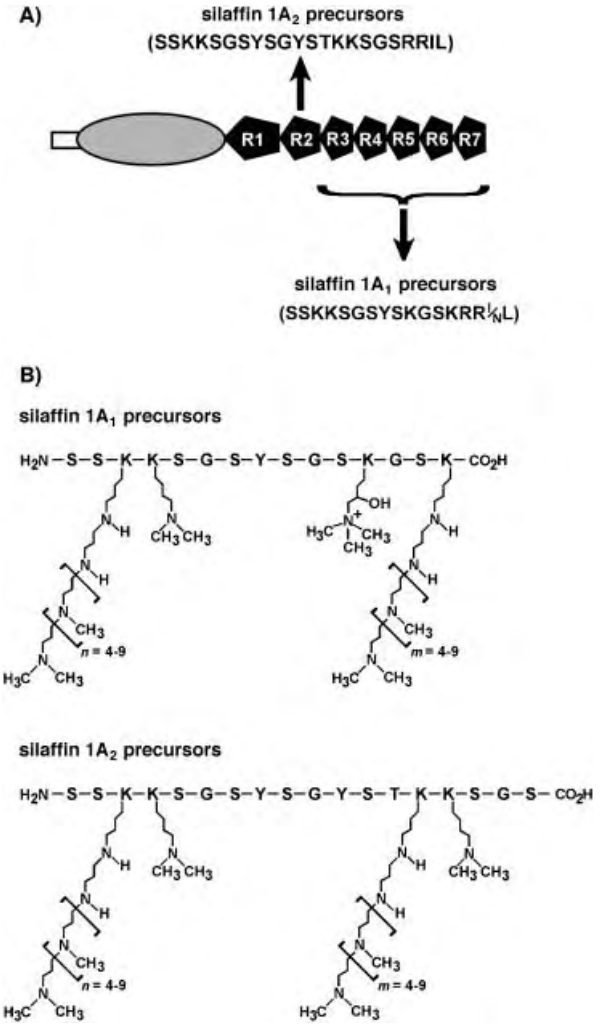


Figure 25. Formation of the silaffin 1A isoforms: A) Schematic structure of the precursor of all silaffins, the polypeptide sil1p. The black pentagons show the repeating R1–R7 elements from which all silaffins are formed. The amino acid sequences of the elements R2 and R3–R7 are shown in parenthesis. Silaffin B is formed from element R1. The white bar represents the signal sequence, the gray ellipse the highly acidic prosequence.[134b] B) Chemical structure of silaffin $1A_1$ and silaffin $1A_2$. The chemical structures of the side chains are only illustrated for the modified lysine residues. (From reference [134b] with kind permission of M. Sumper and N. Kröger and the American Society for Biochemistry and Molecular Biology.)

cloned. As is the case with the frustulins[104,105b,132] and the pleuralins (Figure 24 A), the protein sil1p coded there shows a series of repeating sequences (Figure 25 A), which are termed R1–R7. Unlike the frustulins and the pleuralins, sil1p is not used in the cell in this repetitive structure, but is cleave proteolytically. The R1–R7 units are released as single peptides, R1 corresponds to the precursor of sillafin 1B whereas R2–R7 correspond to the precursors of the isoforms of silaffin 1A (Figure 25 A).[134]

The active peptides, the silaffins, are formed in the cell by a unique posttranslational modification of four lysine residues of their precursors, which are present as two pairs or as one pair and two individual residues (Figure 25 A). This modification is an alkylation of each of two lysine units by linear polyamines, which consist of 5–10 methylated propylamine groups, and by *ε-N,N*-dimethylation of the other two lysine residues. In the silaffin $1A_1$ isoform, one of these dimethyllysines is replaced by a *δ*-hydroxy-*ε-N,N,N*-trimethyllysine (Figure 25 B).[134,136]

The unique property of the silaffins to form polysilicic acid in vitro suggests that they probably play a pivotal role in the construction of the silica cell wall. Whereas in the absence of silaffins a solution of orthosilicic acid at an end concentration of 1 M (freshly prepared from tetramethyl orthosilicate in 1 mM hydrochloric acid) is stable for at least a few hours, each silaffin as well as the mixture of silaffins can precipitate polysilicic acid from this orthosilicic acid solution within seconds. Although the amount of polysilicic acid is essentially proportional to the amount of individual silaffins or their mixture (Figure 26 A), spherical particles of very different diameters are formed. Thus silaffin 1A induces the formation of particles with diameters of 500–700 nm (Figure 26 B), whereas the natural mixture of silaffin 1A, silaffin B, and silaffin 2 produces much smaller particles (diameter < 50 nm). This relationship between different silaffins and particle size, which can also be of considerable interest to materials science, has led to even more detailed investigations. Recently, the complete chemical structures of silaffin $1A_1$ and silaffin $1A_2$ were elucidated: they are made up of 15 and 18 amino acid residues, respectively (Figure 25 B).[134] In the modifications of their respective four lysine units, they differ only in the *δ*-hydroxy-*ε-N,N,N*-trimethyl residue; the quaternary ammonium ion has hitherto been found only in silaffin $1A_1$.[134,136] However, this difference has practically

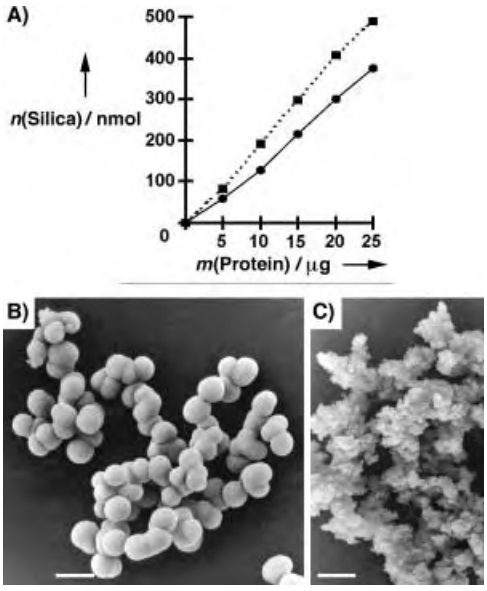


Figure 26. Silaffin-induced silica precipitation: A) Correlation between the silaffin concentrations (µg protein in 0.1 M silica solution) and the amount of polysilicic acid (nmol) that is precipitated from the silicic acid solution. Dotted line: silaffin mixture. Solid line: pure silaffin 1A. B, C) SEM image of silica precipitated (B) by silaffin 1A and (C) by the natural silaffin mixture. The diameter of the particles is 500–700 nm (B) and < 50 nm (C). The length of the bar represents 1 µm. Modified from reference [109] with kind permission of M. Sumper and N. Kröger.)

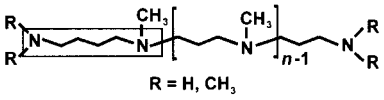
no influence on the amount of polysilicic acid precipitated over the pH range of 5–8, nor on the diameter of the spherical particles produced.[134]

Moreover, since the unmodified peptide pR5 cannot induce polysilicic acid precipitation in an acid solution with a pH value lower than 6,[134] but polysilicic acid deposition in vitro takes place in the acid plasma of the SDVs, the polyamine side chains clearly play a crucial role in the biological system.

5.3.4. *Species-Specific Polyamines, Structure, and In Vitro Production of Polysilicic Acid Nanoparticles*

Until now, almost all investigations have been carried out on *C. fusformis*, the model organism for diatom research. Since the formation of valves with their pores, slits, and other openings in the SDVs (Figures 19, 20 A–C) leads to species-specific structures, it is probable that each species has different silaffins or silaffin-like molecules.

To test this hypothesis, organic cell-wall components of six different diatoms from a broad range of species were isolated.[135a] In a special SDS-PAGE, which also has the ability to separate compounds of low molecular weight,[137] the assumption has already been confirmed that, in comparison to *C. fusiformis*, each of the five other species has a respectively specific silaffin composition.[135a] In addition, compounds were also discovered whose molecular weights are smaller than 3.5 kDA and, with the exception of *C. fusiformis*, appear to be either one of or the main components of all other diatoms. After purification and mass spectrometric analysis, a different number of polyamines were found for each type, in each case with different molecular weights. All compounds are linear polyamines composed of *N*-methylaminopropyl or aminopropyl units, that is, they exhibit a different degree of methylation. As in the polyamine synthesis of bacteria and eukaryotes,[135b] ornithine (2,5-diaminopentanoic acid) and its decarboxylation product putrescine (1,4-diaminobutane) form the basis of the alkylation with aminopropyl residues. These two residues as well as the amino groups of the terminal aminopropyl residue can be methylated differently. A simplified polyamine structure is shown schematically. The aminopropyl groups and



ornithine are not added here, and putescine is shown within a frame. (Reproduced with kind permission of M. Sumper and N. Kröger.)

The assumption that in addition to the silaffins these polyamines are also major components of biological polysilicic acid formation can be also confirmed by in vitro experiments. The largest number of polyamines has been isolated from *Nitzschia angularis*.[135a] Their molecular weights vary between 600–1250 Da. They were investigated with respect to both the molecular weight and to their ability to precipitate polysilicic acid at different pH values. Thus spherical polysilicic acid particles of mainly 0.8–1 μm were produced with polyamines of 1000–1250 Da at pH 5 (Figure 27 A). With polyamines of 600-700 Da, spherical polysilicic acid particles of only 100–200 nm were found (Figure 27 B). A close relationship between the morphology of polysilicic acid particles and pH emerges when the pH value of the orthosilicic acid is increased in the presence of the natural polyamine mixture from *N. angularis*. The diameter falls from 700 nm to 50 nm with increasing pH value (Figure 27 C–F). An additional potential for structure formation is presented by three silaffins from *N. angularis*, as can be deduced from the formation of blocklike structures In vitro,[135] which have also been found in vivo as areolae (honeycomb) walls.[138] When the silaffins are combined with the polyamines from *N. angularis*, these blocklike structures vary in that a flat side with oblate polysilicic acid particles is formed.[135]

Recently it was possible to isolate a SP41 protein (SP41 = scale protein 41 kDa) from the silica-containing platelets and spines of *Mallomonas slendens*, a photosynthetic Chrysophycee (gold–brown alga), which is closely related to the diatoms. With the help of polyclonal anti-SP41 antibodies it was possible to show for the first time that during the biogenesis of platelets and spines SP41 is deposited together with polysilicic acid in special SDVs.[139] Thus a whole arsenal of compounds is available to investigate the relationship between polysilicic acid polymerization, particle size, and structure formation, and ornamentation.

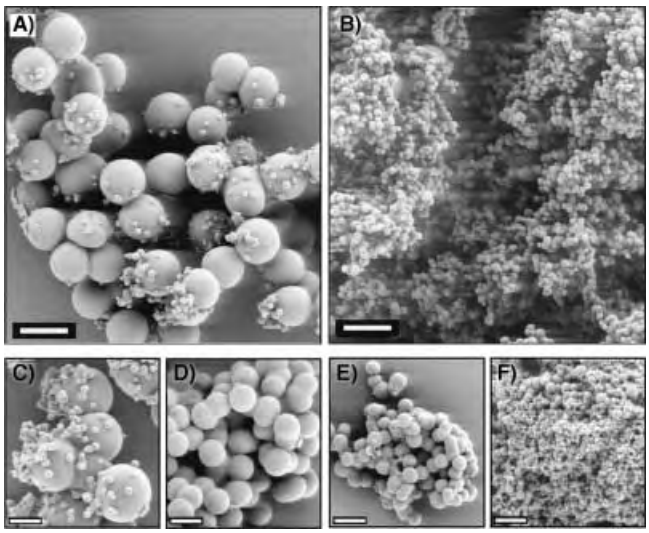


Figure 27. Silica precipitates induced with polyamines from *Nitzschia angularis*. Polyamines of molecular weight M_W 1000–1250 Da (A) and 600–750 Da (B) were used. The natural mixture of polyamines (M_W = 600–1250 Da) was used to investigate the pH dependence of the polyamine-induced silica precipitation: (C) pH 5.4, (D) pH 6.3, (E) pH 7.2, (F) pH 8.3. The polyamine concentration in each solution was 0.85 mg ml^{-1}. The length of the bars represents 1 μm in (A) and (B), 500 nm in (C), (D), (E), and (F). (From reference [135a] with kind permission of M. Sumper and N. Kröger and the National Academy of Science USA.)

Based on the structural investigations,[105a,138] the isolation of organic compounds from the silica cell walls,[109,135,139] and the chemical syntheses for the preparation of inorganic materials from polysilicic acid with defined porosity—with the use of organic substrates with defined shape[140–144c]—a series of model concepts were proposed.[105a,145] These revolve around either preformed structures of the mould-prepattern hypothesis[145e,f] or the phenomena of phase separation.[146] Recently Sumper[146a] outlined a simple phase-separation model for the formation of honeycomblike structures (areolae) frequently found in diatoms and also formed by chemical synthesis.[144b,c] His model describes repeated phase separation in the SDVs through which emulsions of micro- and subsequently nanodroplets or micelles are produced as centers of polysilicic acid deposition. Volkmer et al. used an in situ video microscope to monitor time-resolved phase separation during the formation of radial silica shells. [146b] Lipophilic, detergent-stabilized drops with limited amounts of a mixed titanium silicon oxide developed the ability to form and shape an inorganic matrix in a dynamic dissipation process, that is, in a spontaneous formation of increasingly smaller drops. However, thus far only spinelike shapes have been found (honeycomb shapes were not observed). The choice of mixture of anionic and cationic surfactants is critical for the success of such investigations. Moreover, van Blaaderen et al were able to show that colloidal crystals, three-dimensional periodic structures from small, suspended colloidal particles, can also develop into particles whose sizes are dependent on the periodic distance of the hollow sections in a polymer layer.[147a] This process was named colloidal epitaxis.[147b]

The importance and utility of silicate compounds in biological systems has been discussed for quite some time.[148a] The question has been raised as to whether the biomineralization of silicic acid offers any ecological advantages. Several proposals have been put forward about the function of the silicic acid cell wall of the diatoms, for example, as a UV filter or as a form of protection against zooplankton (eukaryotic unicellular organisms that do not contain chlorophyll). However, none of these hypotheses have been verified experimentally. On the contrary, Milligan and Morel have shown that the polysilicic acid plays an active role as a pH buffer in the cell walls of diatoms.[148b] Diatoms have extracellular carboanhydrase on their surfaces that catalyzes the reaction between HCO_3^- and CO_2. The high catalytic rate of this enzyme allows it to act as a pH buffer by either providing or rapidly binding protons. The buffer action of polysilicic acid could be verified in studies on cells of *Thalassiosira weissflogii* or in the presence of isolated polysilicic cell walls with isolated soluble carboanhydrase (bovine): the polysilicic acid accelerates the reaction of the enzyme. It has been postulated that the increased release of CO_2 by the extracellular carboanhydrase is part of the carbon-concentrating (CCM). This results in the increase of the concentration of CO_2 in the vicinity of the most important carboxylase, the ribulose-1,5-diphosphate carboxylase oxygenase (RubisCO), and thus in an increase in the rate of photosynthesis, even though the concentration of CO_2 in sea water is only 1/100 that required for the full activity of the enzyme. In this way, the global cycle of silica (essentially the biomineralization of polysilicic acid) can be coupled to that of carbon (that is, photosynthesis) in diatoms. This could be proven directly in the diatomaceous *Phaeodactylum tricornutum*, which can be isolated as both silicified and nonsilicified morphotypes. The silicified morphotype preferentially fixes carbon.

6. Summary and Outlook

A great deal of new information on biomineralization is currently being obtained rapidly by the methods of molecular biology. What for a long time appeared to be extremely difficult to achieve (an understanding of the mechanism of biomineralization at least in stages) has already been achieved by Marsh et al. with the unicellular coccolithophores (calcareous algae). A type of multicomponent complex was revealed in which the fixation of a first crystallite edge is associated with an accumulation of 25-nm-large PS1/PS2–Ca particles which release the polyanion-bound calcium ions in high concentrations. Here the first crystals are produced as small rectangles. The acid polysaccharide PS3, which is associated both with the coccolith vesicle membrane and with the above crystals, then induces the growth of the respective protocrystal to the unusual anvil-shaped crystals of *Pleurochrysis* (Figure 12).[96]

Unfortunately as yet no coccolithophore genome has been sequenced. In contrast, two genome sequences have been known for the magnetic bacteria since April 2001. This has contributed to the observation that according to the extensive work of Schüler and co-workers on proteins of the magnetosome membrane, not only are these proteins found in two gene clusters, but in addition a series of protein families has now been found there in a similar arrangement. (Figure 8). Thus, it is now possible to investigate the mechanism of magnetite crystal formation in the magnetosome vesicles by switching off individual genes. Furthermore, the accompanying empty vesicles could now be isolated and investigated.

The magnetosome vesicles have also led to a comprehensive and discussion-stimulating hypothesis of biomineralization by Kirschvink and co-workers in which they propose evolution of the genes of bacterial magnetite biomineralization through doubling, mutation, adaptation, and variation up to bone formation.[14] However, the work of Schüler has demonstrated that until now all genes of proteins from the magnetosome membrane occur solely in magnetic bacteria. Moreover, no homologues has been found in other organisms.[55]

The analogy of coccolith formation to the transport of proteins through the endoplasmic reticulum (ER) and Golgi apparatus to exocytosis has in this article led to the working hypothesis that the magnetosome vesicles, as perhaps the first intracytoplasmic vesicles in bacteria, could be the prokaryotic precursors of the endomembrane system of the ER and the Golgi apparatus. The formation of the magnetosome membrane is unknown, endocytosis stands against de novo synthesis. The absence of the endomembranes in early eukaryotes, the diplomonads, is conspicuous.[149] Endosymbiotic

events of such early protists with a magnetic bacterium could have led to the formation of the endomembranes.

The previously described parts of biomineralization machineries are clearly too complicated when isolated in full to be used in vitro for production. As already shown by polyamines and silaffins (Section 5), the use of parts is of considerable interest for the chemist, but only methodological simplification and variation of these compounds can open up new areas. Probably the first example was shown by Stone and co-workers[150] who used the unmodified polycationic precursor peptide pR5 of silaffin $1A_1$ that does not precipitate polysilicic acid at physiological acidic pH, but does so at neutral pH. This peptide was incorporated in a mixture of a hydrophilic and a lipophilic acrylate by photopolymerization: a hologram with a periodicity of 1.33 μ was imprinted into the polymer by means of a holographic process (Figure 28 A, C). The peptide is clearly fixed in the H_2O-enriched depression as by slow addition of ≈ 0.1 M $[Si(OH)_4]$ a two-dimensional arrangement of polysilicic acid particles with a mean diameter of 452 nm (± 81 nm) formed in the periodicity of the hologram (Figure 28 B, D).

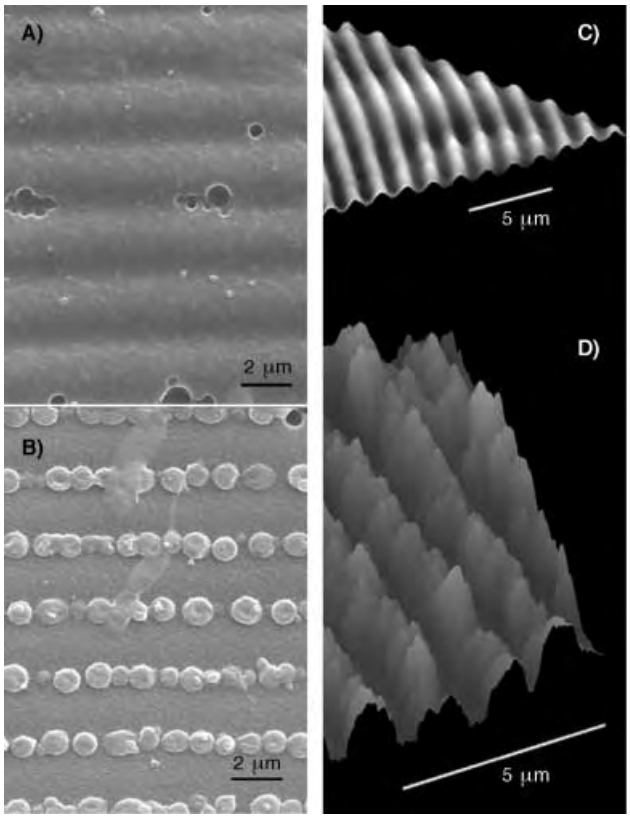


Figure 28. Two-dimensional array of ordered silica nanospheres formed within a hologram (lattice) that had previously been produced by a holographic process in an exceptionally clear and colorless polymer: A) SEM images of the control hologram after being treated with dissolved silicic acid; B) the polysilicic acid nanostructure formed by reaction of polysilicic acid with the peptide-modified hologram; C) AFM images of the control polymer *before* and d) the hybrid structure *after* treatment with silicic acid. (Modified from reference [150] with kind permission of M. O. Stone and Nature.)

In a fascinating analogy to studies on the surfaces of semiconductors and metals[151] Stone and co-workers[152] introduced a "combinatorial phage display library" to biomimetic material science in order to discover peptides that precipitate polysilicic acid. Thus a very large number of peptides were expressed from twelve amino acids as fusion proteins with a phage coat protein. The peptide with the highest yield of spherical particles contains a serine residue and five histidine units. As with the silaffins, the amount of silicic acid was proportional to the amount of peptide phage particles (Figure 25),[152] so that such polysilicic acid particles are a mixture of organic and inorganic compounds.

A different and novel method to produce spherical polysilicic acids particles is the previously described experiment of Stone and co-workers.[150] Only parts of the pR5 peptide, which probably catalyze the precipitation of the polysilicic acid, extend out of the hydrophilic part of the polymer. The resulting particles contain only small amounts of organic substances and are not a composite. The comparison of both methods may contribute to a clarification of the question of what determines the diameter of the particles and how a preparation of more narrow diameter variations may be obtained.

Addendum

Important progress in biosilica morphogenesis was published recently by Sumper and co-workers.[146c] Ammonium fluoride was used instead of anhydrous hydrogen fluoride to extract silaffins (Section 5.3.3.) by dissolving diatom biosilica under mild conditions. The apparently native silaffins were obtained, all of whose serine residues were found to be phosphorylated. In silaffin molecules, therefore, not only are many positive charges accumulated by the modification with polyamines, but also many negative charges by the above-mentioned phosphoryl groups. These zwitterionic molecules are able to self-assemble, probably forming a template that promotes silica precipitation in large units.

I thank Dr. Dirk Schüler (Bremen, Germany), Professor Mary E. Marsh (Houston, TX), as well as Dr. Susan Glasauer and Professor T. J. Beveridge (Guelph, Canada) who shortly before the conclusion of this article provided me with preprints of their highly relevant publications. I have received critical help from my colleagues Professor Lars-Oliver Essen (Marburg, Germany), Professor Nicolai Petersen (Munich, Germany), Dr. Dirk Schüler (Bremen, Germany), and Dr. Michael Winkelhofer (Southampton, UK), who kindly reviewed the manuscript. I thank wholeheartedly Professor Dieter Oesterhelt, who in my active retirement gave me the opportunity as a guest in his department to be able to dedicate myself to this article and more. This article would not have been completed without the inestimable support of my wife Cornelia and my son Felix, who as computer specialists made almost everything possible, including the presentation of the many figures.

Received: February 18, 2002 [A519]

[1] M. R. Walter in *Earths Earliest Biosphere: Its Origin and Evolution* (Ed.: J. W. Schopf), Princeton University Press, Princeton **1983**, pp. 187 – 213.
[2] a) T. J. Beveridge, in *Metal Ions and Bacteria* (Eds.: T. J. Beveridge, R. J. Doyle), Wiley, New York **1989**, p. 1 – 29; b) F. G. Ferris, W. Shotyk, W. S. Fyfe in *Metal Ions and Bacteria* (Eds.: T. J. Beveridge, R. J. Doyle), Wiley, New York **1989**, p. 415 – 442.
[3] a) K. Hausmann, B. P. Kremer, *Extremophile, Mikroorganismen in ausgefallenen Lebensräumen,* VCH, Weinheim, **1995**; b) K. O. Stetter, *FEMS Microbiol. Rev.* **1990**, *75*, 117 – 124.
[4] a) H. A. Lowenstam, *Science* **1981**, *211*, 1126 – 1131; b) D. A. Bazylinski, R. B. Frankel in *Biomineralization* (Ed.: E. Baeuerlein), Wiley-VCH, Weinheim **2000**, p. 41 – 43; c) B. Devouard, M. Pósfai, X. Hua, D. A. Bazylinski, R. B. Frankel, P. R. Busek, *Am. Mineral.* **1998**, *83*, 1387 – 1398; d) K. L. Thomas-Kerpta, D. A. Bazylinski, J. L. Kirschvink, S. J. Clemett, D. S. McKay, S. J. Wentworth, H. Vali, E. K. Gibson, Jr., C. S. Romanek, *Geochim. Cosmochim. Acta* **2000**, *64*, 4049 – 4081.
[5] a) R. P. Blakemore, *Science* **1975**, *190*, 377 – 379; b) R. B. Frankel, R. P. Blakemore, R. S. Wolfe, *Science* **1979**, *203*, 1355 – 1356.
[6] D. Balkwill, D. Marata, R. P. Blakemore, *J. Bacteriol.* **1980**, *141*, 1399 – 1408.
[7] a) N. Petersen, T. von Dobeneck, H. Vali, *Nature* **1986**, *320*, 611 – 615; b) J. F. Stolz, S.-B. R. Chang, J. L. Kirschvink, *Nature* **1986**, *321*, 849 – 850; c) S.-B. R. Chang, J. L. Kirschvink, *Annu. Rev. Earth Planet Sci.* **1989**, *17*, 169 – 195;d) E. I. Friedmann, J. Wierzchos, C. Ascaso, M. Winklhofer, *Proc. Natl. Acad. Sci. USA* **2001**, *98*, 2176 – 2181; e) D. Schüler, Dissertation, Technische Universität München, **1994**; f) D. Schüler, E. Baeuerlein in *Transitions Metals in Microbial Metabolism* (Eds.: G. Winkelmann, C. J. Carrano), Harwood Academic Press, Amsterdam, **1997**, pp. 159 – 185.
[8] S. W. F. Grant, *Am. J. Sci.* **1990**, *290A*, 261.
[9] A. H. Knoll, S. B. Caroll, *Science* **1999**, *284*, 2129.
[10] F. J. Ayala, A. Rzhetsky, *Proc. Natl. Acad. Sci. USA* **1998**, *95*, 606.
[11] H. A. Lowenstam, L. Margulis, *Biosystems* **1980**, *12*, 27.
[12] S. Bengtson, Y. Zhao, *Science* **1992**, *257*, 367.
[13] K. Simkiss, K. M. Wilbur, *Biomineralization*, Academic Press, San Diego, **1989**.
[14] J. L. Kirschvink, J. W. Hagedorn in *Biomineralization* (Ed.: E. Baeuerlein), Wiley-VCH, Weinheim, **2000**, p. 139 – 149.
[15] S. J. Gould, E. S. Vrba, *Paleobiology* **1982**, *8*, 4.
[16] F. F. Torres de Araujo, M. A. Pires, R. B. Frankel, C. E. M. Bicudo, *Biophys. J.* **1986**, *50*, 375 – 378.
[17] S. Mann, N. H. C. Sparks, M. M. Walker, J. L. Kirschvink, *J. Exp. Biol.* **1988**, *140*, 35 – 49.
[18] a) M. M. Walker, C. E. Diebel, C. V. Haugh, P. M. Pankhurst, J. C Montgomery, C. R. Green, *Nature* **1997**, *390*, 371 – 376; b) C. E. Diebel, R. Proksch, C. R. Green, P. Neilson, M. M. Walker, *Nature* **2000**, *406,* 299 – 302.
[19] a) E. Holtkamp-Rötzler, G. Fleissner, M. Hanzlik, N. Petersen, *Ann. Geophys.* **1997**, *15 (Suppl. IC),* 117; b) M. Hanzlik, Ch. Heunemann, E. Holtkamp-Rötzler, M. Winklhofer, N. Petersen, G. Fleissner, *BioMetals* **2000**, *13*, 325 – 331; c) D. Acosta-Avalos, E. Wajnberg, P. S. Oliveira, I. Leal, M. Farina, D. S. Esquivel, *J. Exp. Biol.* **1999**, *202*, 2687 – 2692.
[20] a) J. L. Kirschvink, A. Kobayashi-Kirschvink, B. J. Woodford, *Proc. Natl. Acad. Sci USA* **1992**, *89*, 7683; b) J. Dobson, P. P. Grassi, *Brain Res. Bull.* **1996**, *39*, 255 – 259; c) P. P. Schultheiss-Grassi, R. Wessiken, J. Dobson, *Biochem. Biophys. Acta* **1999**, *1426*, 212 – 216; d) P. P. Schultheiss-Grassi, J. Dobson, *BioMetals* **1999**, *12*, 67 – 72.
[21] T. J. Beveridge, in *Bacteria in Nature* (Eds: J. S. Pointdexter, E. R. Leadbetter), Plenum Press, New York, **1989**, pp. 1 – 65.
[22] *Allgemeine Mikrobiologie*, (Ed.: H. G. Schlegel) *7th ed.*, Thieme, Stuttgart **1992**, p. 14.
[23] a) F. G. Ferris in *Metal Ions and Bacteria* (Eds.: T. J. Beveridge, R. J. Doyle), Wiley, New York, **1989**, p. 295 – 323; b) D. Fortin, T. J. Beveridge in *Biomineralization* (Ed.: E. Baeuerlein), Wiley-VCH, Weinheim **2000**, p. 7 – 22.
[24] a) T. J. Beveridge, *Int. Rev. Cytol.* **1981**, *72*, p. 229 – 317; b) W. Baumeister, G. Lembcke, G. Dürr, B. Phipps in *Electron Crystallography of Organic Molecules* (Eds.: J. R. Freyer, D. L. Dorset), Kluwer Academic, Dordrecht, **1990**, p. 283 – 296; c) M. Engelhardt, J. Petres, *J. Struct. Biol.* **1998**, *125,* 276 – 302; d) T. J. Beveridge, P. H. Pouwels, M. Sara, A. Kotiranta, K. Lonnatmaa, K. Kari, E. Kerosuo, M. Haapasalo, E. M. Egelseer, I. Schocher, U. B. Sleytr, *FEMS Microbiol. Rev.* **1997**, *20*, 99 – 149; e) U. B. Sleytr, P. Messner, D. Plum, M. Sara, *Angew. Chem.* **1999**, *111*, 1099 – 1120; *Angew. Chem. Int. Ed.* **1999**, *38,* 1035 – 1054.
[25] M. Sumper, *Biochim. Biophys. Acta* **1987**, *906*, 69 – 79.
[26] C. J. Daughney, J. B. Fein, N. Yee, *Chem. Geol.* **1998**, *144*, 161 – 176.
[27] M. M. Urrutia, T. J. Beveridge, *Chem. Geol.* **1994**, *116*, 261 – 280.
[28] D. Fortin, T. J. Beveridge, *Geomicrobiol. J.* **1997**, *14*, 1 – 21.
[29] S. Schultze-Lam, G. Harauz, T. J. Beveridge, *J. Bacteriol.* **1992**, *174*, 7971 – 7981.
[30] S. Mann in *Biomimetic Materials Chemistry*, VCH, New York **1996**, p. 1 – 40.
[31] a) M. Mertig, R. Kirsch, W. Pompe, H. Engelhardt, *Eur. Phys. J. D* **1999**, *9*, 45 – 48; b) S. R. Hall, W. Shenton, H. Engelhardt, S. Mann, *ChemPhysChem.* **2001**, *3,* 184 – 186.
[32] G. Southam, T. J. Beveridge, *Geochim. Cosmochim. Acta* **1994**, *58*, 4527 – 4530.
[33] a) D. H. Nies, *Appl. Microbiol. Biotechnol.* **1999**, *51, 730–750*; b) S. Silver, *Ann. Rev. Microbiol.* **1996**, *50*, 753 – 789.
[34] a) H. E. Jones, P. A. Trudinger, L. A. Chambers, N. A. Pyliotis, *Z. Allg. Microbiol.* **1976**, *16*, 425 – 435; b) M. Vainshtein, N. Suzina, V. Sorokin, *Syst. Appl. Microbiol.* **1997**, *20*, 182 – 186.
[35] a) S. Glasauer, S. Langley, T. J. Beveridge, *Science,* **2001**, *295*, 117 – 119; b) U. Schwertmann, R. M. Cornell, *Iron Oxides in the Laboratory*, VCH, Weinheim, **1991**.
[36] a) R. B. Frankel, R. B. Blakemore, *Iron Biominerals*, Plenum Press, New York, **1991**; b) S. Mann, R. B. Frankel in *Biomineralization, Chemical and Biochemical Perspectives* (Eds.: S. Mann, J. Webb, R. J. P. Williams), VCH, Weinheim **1989**, pp. 389 – 426.
[37] S. Spring, R. Amann, W. Ludwig, K.-H. Schleifer, H. van Gemerden, N. Petersen, *Appl. Environ. Microbiol.* **1993**, *59*, 2397 – 2403.
[38] D. A. Bazylinski, R. B. Frankel, B. R. Heywood, S. Mann, J. W. King, P. L. Donaghay, A. K. Hanson, *Appl. Environ. Microbiol.* **1995**, *61*, 3232 – 3239.
[39] H. Petermann, Berichte Fachbereich Geowissenschaften Univ. Bremen, Nr. 56, Bremen, **1994**; Fahrten M16/2, M20/2, M23/1, M23/2 des Forschungsschiffes Meteor.
[40] a) M. Farina, H. Lins des Barros, D. M. S. Esquival, J. Danon, *Biol. Cell.* **1983**, *48*, 85 – 88; b) E. F. De Long, R. B. Frankel, D. A. Bazylinski, *Science* **1993**, *259,* 803 – 806.
[41] K. H. Schleifer, D. Schüler, S. Spring, M. Weizenegger, R. Amann, W. Ludwig, M. Köhler, *Syst. Appl. Microbiol.* **1991**, *14,* 379 – 385.
[42] R. P. Blakemore, D. Maratea, R. Wolfe, *J. Bacteriol.* **1979**, *140*, 720 – 729.
[43] D. Schüler, S. Spring, D. A. Bazylinski, *Syst. Appl. Microbiol.* **1999**, *22*, 466 – 471.
[44] C. R. Woese, *Microbiol. Rev.* **1987**, *51*, 221 – 271.

[45] a) R. Amann, R. Rosello-Mora, D. Schüler in *Biomineralization* (Ed.: E. Baeuerlein), Wiley-VCH, Weinheim **2000**, p. 47–59; b) O. Strunk, O. Gross, B. Reichel, M. May, S. Hermann, N. Stuckmann, B. Nonhoff, M. Lenke, A. Ginhart, A. Vilbig, T. Ludwig, A. Bode, K. H. Schleifer, W. Ludwig, http://www.mikro.biologie.tu-muenchen.de/pub/ARB, Department of Microbiology, Technische Universität München, Germany, **1999**; c) W. Ludwig, O. Strunk, S. Klugbauer, N. Klugbauer, M. Weizenegger, J. Neumaier, M. Bachleitner, K. H. Schleifer, *Electrophoresis* **1998**, *19*, 554–568; d) R. Amann, W. Ludwig, K. H. Schleifer, *Microbiol. Rev.* **1995**, *59*, 143–169.

[46] D. A. Bazylinski, A. J. Garrett-Reed, R. B. Frankel, *Microsc. Res. Tech.* **1994**, *27*, 389–401.

[47] R. F. Butler, S. K. Banerjee, *J. Geophys. Res.* **1975**, *80*, 4049–4058.

[48] Y. A. Gorby, T. J. Beveridge, R. P. Blakemore, *J. Bacteriol.* **1988**, *170*, 834–841.

[49] D. Schüler, M. Köhler, *Zentralbl. Mikrobiol.* **1992**, *147,* 150–151.

[50] D. Schüler, E. Baeuerlein, *J. Bacteriol.* **1998**, *180*, 156–162.

[51] a) M. Gassmann, Diplomarbeit, Universität Tübingen (Germany), **1996**; b) E. Baeuerlein, D. Schüler, R. Reszka, S. Päuser, DE 197 16 732 **1997**; E. Baeuerlein, D. Schüler, R. Reszka, S. Päuser, PCT/DE 98/00668 **1998**; E. Baeuerlein, D. Schüler, R. Reszka, S. Päuser, US 6251365 **2001**.

[52] H. A. Lowenstam, S. Weiner, *On Biomineralization*, Oxford University Press, Oxford, **1989**.

[53] a) Y. Okuda, K. Denda, Y. Fukumori, *Gene* **1996**, *171*, 99–102; b) D. Schüler, E. Baeuerlein, D. A. Bazylinski, *Abstracts of the General Meeting of the ASM,* Miami, USA, **1997**, p. 332.

[54] D. Schüler, in *Biomineralization* (Ed.: E. Baeuerlein), Wiley-VCH, Weinheim, **2000**, p. 109–118.

[55] a) K. Grünberg, C. Waver, B. M. Tebo, D. Schüler, *Appl. Environ. Microbiol.* **2001**, *67*, 4573–4582; b) D. Schüler, C. Waver, K. Grünberg, *Jahrestagung der VAAM*, **2001,** Oldenburg, Abstract KSB 11.

[56] G. L. Blatch, M. Lassle, *Bioassays* **1999**, *21,* 932–934.

[57] Y. Fukumori in *Biomineralization* (Ed.: E. Baeuerlein), Wiley-VCH, Weinheim, **2000**, p. 93–107.

[58] I. T. Paulsen, M. H. Saier, *J. Membr. Biol.* **1997**, *156*, 99–103.

[59] O. H. Nies, S. Silver, *J. Ind. Microbiol.* **1995**, *14*, 186–199.

[60] http://www.jgi.doe.gov/temweb/JGI microbial/html/index.html.

[61] M. J. Pallen, B. W. Wren, *Mol. Microbiol.* **1997**, *26*, 209–221.

[62] L. Lenz, B. Dere, M. Bevan, *Immunology* **1996**, *5*, 63–72.

[63] D. Schüler, E. Baeuerlein, *Arch. Microbiol.* **1996**, *166*, 301–307.

[64] a) J. B. Neilands, *J. Biol. Chem.* **1995**, *270*, 26723–26726; b) G. Winkelmann in *CRC Handbook of Microbial Iron Chelates* (Ed.:G. Winkelmann), CRC Press, Boca Raton, **1991**, pp. 65–106.

[65] C. Nakamura, T. Sakaguchi, S. Kudo, I. G. Burgess, K. Sude, T. Matsunaga, *Appl. Biochem Biotechnol.* **1993**, *39*/40, 169–171.

[66] A. Hartmann, V. Braun, *Arch. Microbiol.* **1981**, *130*, 353–356.

[67] a) T. S. Magnuson, A. L. Hodges-Myerson, D. R. Lovely, *FEMS Microbiol. Lett.* **2000**, *185*, 205–211; b) D. R. Lovely, J. D. Coates, D. A. Saffarini, D. J. Lonergan in *Transition Metals in Microbial Metabolism* (Eds.: G. Winkelmann, C. J. Carrano), Harwood Academic Press, Amsterdam, **1997**, pp. 187–215; c) S. A. B. Knight, E. Lesuisse, R. Stearman, R. D. Klausner, A. Dencis, *Microbiology* **2000**, *148,* 29–40; d) M. Fontecave, J. Covès, J. L. Pierre, *BioMetals* **1994**, *7*, 3–8; e) L. C. Paoletti, R. P. Blakemore, *Curr. Microbiol.* **1998**, *17,* 339–342.

[68] a) Y. Noguchi, T. Fujiwara, K. Yoshimatsu, Y. Fukumori, *J. Bacteriol.* **1999**, *181*, 2142–2147; b) M. Abe, Y. Tamaura, *Jpn. J. Appl. Phys.* **1983**, *22*, L511; c) T. Yamazaki, H. Oyanagi, T. Fujiwara, Y. Fukumori, *Eur. J. Biochem.* **1995**, *233*, 665–671.

[69] a) D. Schüler, R. Uhl, E. Baeuerlein, *FEMS Microbiol. Lett.* **1995**, *132*, 139–145; b) E. Baeuerlein in *Biomineralization* (Ed.: E. Baeuerlein), Wiley-VCH, Weinheim, **2000**, pp. 61–79.

[70] D. Grimm, A. J. Koster, U. Ziese, D. Typke, W. Baumeister, *J. Microsc.* **1996**, *183*, 60–68.

[71] R. P. Blakemore, N. A. Blakemore in *Iron Biominerals* (Eds.: R. Frankel, R. P. Blakemore), Plenum Press, New York **1991**, pp. 51–67.

[72] R. E. Dunin-Borkowski, M. R. Mc Cartney, R. B. Frankel, D. A. Bazylinski, M. Pósfai, P. R. Busek, *Science* **1998**, *282*, 1868–1870.

[73] a) D. A. Bazylinski, R. B. Frankel in *Biomineralization* (Ed.: Baeuerlein), Wiley-VCH, Weinheim **2000**, p. 36–37; b) R. B. Frankel, D. Bazylinski, M. S. Johnson, B. L. Taylor, *Biophys. J.* **1997**, *73*, 994–1000.

[74] R. Wiltschko, W. Wiltschko, *Magnetic orientation in animals, Zoophysiology, Vol. 33*, Springer, Berlin, **1995**.

[75] J. C. Weaver, T. E. Vaughan, D. Astumian, *Nature* **2000**, *405*, 707–709.

[76] a) V. P. Shcherbakov, M. Winklhofer, *Eur. Biophys. J.* **1999**, *28*, 380–392; b) M. Winklhofer, *Modelle hypothetischer Magnetfeldrezeptoren auf der Grundlage biogenen Magnetits*, M. Leidorf GmbH, Rahden, **1999**; c) M. Winklhofer, E. Holtkamp-Rötzler, M. Hanslik, G. Fleissner, N. Petersen, *Eur. J. Mineral.* **2001**, *13*, 659–669.

[77] a) J. C. Green, K. Perch-Nielsen, P. Westbroek in *Handbook of Protoctista* (Eds.: L. Margulis, J. O. Corliss, M. Melkonian, D. J. Chapman), Jones & Bartlett, Boston, **1990**, pp. 293–317; b) C. van den Hoek, H. M. Jahns, D. G. Mann, *Algen, 3rd ed.*, Thieme, Stuttgart, **1993**, pp. 167–179.

[78] a) H. Trappan, *Paleobiology in Plant Protists,* W. H. Freeman and Co., San Francisco, **1980**; b) A. S. Jafar, *Neues Jahrb. Geol. Palaeontol., Abh.*, **1983**, *166*, 218–258.

[79] a) P. R. Brown, *Calcareous Nanofossils Biostratigraphy*, British Micropaleontology Society Series, Chapman & Hall, London, **1998**; b) L. Cros, A. Kleijne, A. Zeltner, C. Billiard, J. R. Young, *Mar. Micropaleontol.* **2000**, *39*, 1–34; c) J. R. Young, S. A. Davis, P. R. Brown, S. Mann, *J. Struct. Biol.* **1999**, *126*, 195–215.

[80] J. D. Rowson, B. S. C. Leadbeater, J. C. Green, *Br. Phycol. J.* **1986**, *21*, 359–370.

[81] a) M. E. Marsh in *Biomineralization* (Ed.: E. Baeuerlein), Wiley-VCH, Weinheim, **2000**, pp. 251–268; b) M. E. Marsh, *Protoplasma* **1999**, *207*, 54–66; c) I. R. Young, I. M. Didymus, P. R. Brown, N. Prins, S. Mann, *Nature* **1992**, *356*, 516–518; d) P. van der Wal, E. W. de Jong, P. Westbrock, W. C. de Bruijn, A. A. Hulder-Stapel, *J. Ultrastruct. Res.* **1983**, *85*, 139–158.

[82] a) E. L. Gonzalez, in *Biomineralization* (Ed.: E. Baeuerlein), Wiley-VCH, Weinheim, **2000**, pp. 269–282; b) Y. Araki, PhD thesis, University of California, Los Angeles, **1997**.

[83] M. E. Marsh, D. P. Dickinson, *Protoplasma* **1997**, *199*, 9–17.

[84] a) M. E. Finbow, M. A. Harrison, *Biochem. J.* **1997**, *324*, 697–712; b) N. Nelson, *Organellar Proton-ATPases,* Springer, Heidelberg, **1995**.

[85] J. M. Ward, A. Reinders, H.-T. Hsu, H. Sze, *Plant Physiol.* **1992**, *99*, 161–169.

[86] P. L. A. M. Corstjens, Y. Araki, E. L. Gonzales, *J. Phycol.* **2001**, *37*, 71–78.

[87] a) Y. Araki, E. L. Gonzalez, *J. Phycol.* **1998**,*34*, 79–88; b) D.-K. Kwon, E. L. Gonzalez, *J. Phycol.* **1994**, *30,* 689–695.

[88] A. A. Israel, E. L. Gonzalez, *Mar. Ecol. Prog. Ser.* **1996**, *137*, 243–250.

[89] M. E. Marsh, *Protoplasma* **1994**, *177*, 108–122.

[90] a) M. E. Marsh, D. K. Chang, G. C. King, *J. Biol. Chem.* **1992**, *267*, 20507–20512; b) P. van der Wal, E. W. de Jong, P. Westbrock, W. C. de Bruiyn, in *Environmental Biogeochemistry,*

Vol. 35 (Ed.: R. Hallberg), Swedish Research Council, Stockholm, **1983**, pp. 251 – 258.
[91] a) S. L. Lee, A. Veis, T. Gloneck, *Biochemistry* **1977**, *16*, 2971 – 2979; b) W. G. Stetler-Stevenson, A. Veis, *Calcif. Tissue Int.* **1987**, *40*, 97 – 102.
[92] M. E. Marsh, R. L. Sass, *J. Exp. Zool.* **1983**, *226*, 193 – 203.
[93] M. T. Dimuzo, A. A. Veis, *Calcif. Tissue Res.* **1978**, *25*, 169 – 178.
[94] M. E. Marsh, *Biochemistry* **1989**, *28*, 339 – 345.
[95] a) H. Miyamoto, T. Miayashita, M. Okushima, S. Nakano, T. Morita, A. Matsushiro, *Proc. Natl. Acad. Sci. USA* **1996**, *93*, 9657 – 9660; b) B. L. Smith, T. Schäffer, M. Viani, J. B. Thompson, N. A. Frederick, J. Kindt, A. M. Belcher, G. D. Stucky, D. E. Morse, P. K. Hansma, *Nature* **1999**, *399*, 761 – 763; c) M. Kono, N. Hayashi, T. Samata, *Biochem. Biophys. Res. Commun.* **2000**, *269*, 213 – 218; d) A. M. Belcher, E. E. Gooch in *Biomineralization* (Ed.: E. Baeuerlein), Wiley-VCH, Weinheim, **2000**, pp. 221 – 249; e) K. Mann, I. M. Weiss, S. André, H.-J. Gabius, M. Fritz, *Eur. J. Biochem.* **2000**, *267*, 5257 – 5264; f) I. M. Weiss, W. Göring, M. Fritz, K. Mann, *Biochem. Biophys. Res. Commun.* **2000**, *285*, 244 – 249.
[96] M. E. Marsh, A. L. Ridall, P. Azadi, P. J. Duke, *J. Struct. Biol.* **2003**, *139*, 39 – 45.
[97] M. E. Marsh, *Protoplasma* **1996**, *190*, 181 – 188.
[98] a) C. van den Hoek, D. G. Mann, H. M. Jahns, *Algae*, Cambridge University Press, Cambridge, **1998**; b) F. E. Round, R. M. Crawford in *Handbook of Protoctista* (Eds.: L. Margulis, J. O. Corliss, M. Melkonian, D. J. Chapman), Jones & Bartlett, Boston, **1990**, pp. 574 – 596.
[99] a) R. Tacke, *Angew. Chem.* **1999**, *111*, 3197 – 3200; *Angew. Chem. Int. Ed.* **1999**, *38*, 3015 – 3018; b) P. Tréguer, D. M. Nelson, A. J. van Bennekom, D. J. DeMaster, A. Leynaert, B. Quéguiner, *Science* **1995**, *268*, 375 – 379.
[100] a) L. K. Medlin, W. H. C. F Kooistra, R. Gersonde, P. A. Sims, U. Welbrock, *Nova Hedwigia* **1997**, *65*, 1 – 11; b) W. H. C. F. Kooistra, L. K. Medlin, *Mol. Phylogenet. Evol.* **1996**, *6*, 391 – 407.
[101] A. Rothpletz, *Z. Dtsch. Geol. Ges.* **1986**, *48*, 854 – 914.
[102] a) D. H. Erwin, *Rev. Ecol. Syst.* **1990**, *21*, 69 – 91; b) D. H. Erwin, *Nature* **1994**, *367*, 231 – 236; c) P. R. Renne, Z. Zichao, M. A. Richards, M. T. Black, A. R. Basu, *Science* **1995**, *269*, 1413 – 1416; d) G. J. Retallack, *Science* **1995**, *267*, 77 – 80.
[103] M. Hildebrand, D. R. Higgins, K. Busser, B. E. Volcani, *Gene* **1993**, *132*, 213 – 218.
[104] N. Kröger, C. Bergsdorf, M. Sumper, *EMBO J.* **1994**, *13*, 4676 – 4683.
[105] a) J. D. Pickett-Heaps, A.-M. M. Schmid, L. A. Edgar in *Progress in Phycological Research, Vol. 7* (Eds.: F. E. Round, D. J. Chapman), Biopress, Bristol, **1990**, p. 2 – 168; b) N. Kröger, M. Sumper, *Protist* **1998**, *149*, 213 – 219; c) R. Wetherbee, S. Crawford, P. Mulvaney in *Biomineralization* (Ed.: E. Baeuerlein), Wiley-VCH, Weinheim, **2000**, p. 189 – 206.
[106] A. S. Crawford, J. M. Higgins, P. Mulvaney, R. Wetherbee, *J. Phycol.* **2001**, *37,* 543 – 554.
[107] C. van den Hoek, D. G. Mann, H. M. Jahns, *Algen, 3rd ed.* Thieme, Stuttgart, **1993**, p. 115.
[108] L. A. Edgar, J. D. Pickett-Heaps in *Progress in Phycological Research, Vol. 3*, Biopress, Bristol, **1984**, pp. 47 – 88.
[109] N. Kröger, M. Sumper in *Biomineralization* (Ed.: E. Baeuerlein), Wiley-VCH, Weinheim, **2000**, p. 151 – 170.
[110] R. W. Drum, H. S. Pankratz, *J. Ultrastruct. Res.* **1964**, *10*, 217 – 223.
[111] a) M. Hildebrand, B. E. Volcani, W. Gassmann, J. I. Schröder, *Nature* **1997**, *385,* 688 – 689; b) M. Hildebrand, K. Dahlin, B. E. Volcani, *Mol. Gen. Genet.* **1998**, *260,* 480 – 486.
[112] a) M. Hildebrand in *Biomineralization* (Ed.: E. Baeuerlein), Wiley-VCH, Weinheim, **2000**, pp. 171 – 188; b) H. L. Conway, P. J. Harrison, C. O. Davies, *Mar. Biol.* **1976**, *35*, 187 – 199; c) H. L. Conway, P. J. Harrison, *Mar. Biol.* **1977**, *43*, 33 – 43.
[113] M. A. Brzezinski, R. J. Olson, S. W. Chisholm, *Mar. Ecol. Prog. Ser.* **1990**, *67*, 83 – 96.
[114] V. Martin-Jezequel, M. Hildebrand, M. A. Brzezinski, *J. Phycol.* **2000**, *36*, 821 – 840.
[115] C. W. Sullivan, *J. Phycol.* **1977**, *13*, 86 – 91.
[116] a) J. Reizer, A. Reizer, M. J. Saier, Jr., *Biochim. Biophys. Acta* **1994**, *1197*, 133 – 166; b) Y. Deguchi, I. Yamoto, Y. Anraku, *J. Biol.Chem.* **1990**, *265*, 21 704 – 21 708.
[117] a) T. Caspari, R. Stadler, N. Sauer, W. Tanner, *J. Biol.Chem.* **1994**, *269*, 3498 – 3502; b) A. D. Due, Q. Zhinchao, J. M. Thomas, A. Buchs, A. C. Powers, J. M. May, *Biochemistry* **1995**, *34*, 5462 – 5471; c) H. Katagiri, T. Asano, H. Ishihara, K. Tsukuda, J.-L. Lin, K. Inukai, M. Kikuchi, Y. Yazaki, Y. Oka, *J. Biol. Chem.* **1992**, *267*, 22 550 – 22 555.
[118] C. W. Sullivan, *J. Phycol.* **1979**, *15*, 210 – 216.
[119] R. K. Iler, *The Chemistry of Silica: Solubility, Polymerization, Colloid and Surface Properties, and Biochemistry*, Wiley, New York, **1979**.
[120] a) D. Werner, *Arch. Microbiol.* **1966**, *55*, 278 – 308; b) F. Azam, B. B. Hemmingsen, B. E. Volcani, *Arch. Microbiol.* **1974**, *97*, 103 – 114.
[121] P. Bhattacharyya, B. E. Volcani, *Biochem. Biophys. Res. Commun.* **1983**, *114*, 365 – 372.
[122] H. Drechsel, G. Winkelmann in *Transition Metals in Microbial Metabolism* (Eds.: G. Winkelmann, C. J. Carrano), Harwood Academic Press, Amsterdam, **1997**, pp. 1 – 51.
[123] A.-M. Schmid, D. Schulz, *Protoplasma* **1979**, *100*, 267 – 288.
[124] M. Lee, C.-W. Li, *Bot. Bull. Acad. Sin.* **1992**, *33*, 317 – 325.
[125] J. D. Pickett-Heaps, A. M. Schmid, L. A. Edgar, in *Progress in Phycological Research, Vol. 7*, Biopress, Bristol, **1990**, p. 127 – 133.
[126] a) C.-W. Li, B. E. Volcani, *Philos. Trans. R. Soc. London, Ser. B* **1984**, *304*, 519 – 528; b) C.-W. Li, B. E. Volcani, *Protoplasma* **1985**, *124*, 10 – 29; c) D. Schulz, G. Drebes, H. Lehmann, R. Jank-Ladwig, *Eur. J. Cell. Biol.* **1984**, *33*, 43 – 51.
[127] C. W. Mehard, B. E. Volcani, *Cell Tissue Res.* **1976**, *166*, 255 – 263.
[128] a) B. E. F. Reimann, J. C. Lewin, B. E. Volcani, *J. Phycol.* **1966**,*2*, 74 – 84; b) A. M. Schmid, M. A. Borowitzka, B. E. Volcani in *Cytomorphogenesis in Plants* (Ed.: O. Kiermayer), *Cell. Biol. Mon.* **1981,** *8*, 63 – 97; c) R. M. Crawford, A. M. Schmid in *Biomineralization in Lower Plants and Animals* (Eds.: B. S. C. Leadbeater, R. Riding), The Systematics Association special volume **1986,** *30*, 291 – 314.
[129] E. Schnepf, G. Deichgräber, G. Drebes, *Plant Syst. Evol.* **1980**, *135*, 265 – 277.
[130] a) B. E. F. Reimann, *Exp. Cell Res.* **1964**, *34*, 605 – 608; b) E. F. Stoermer, H. S. Pankratz, C. C. Bowen, *Am. J. Bot.* **1965**, *52*, 1067 – 1078; c) J. Coombs, I. A. Lauritis, W. M. Darly, B. E. Volcani, *Z. Pflanzenphysiol.* **1968**, *59*, 124 – 152; d) P. A. Dawson, *J. Phycol.* **1973**, *9*, 353 – 365.
[131] a) C. W. Li, S. Chu, M. Lee, *Protoplasma* **1989**, *151*, 158 – 163; b) M. A. Brzezinski, D. J. Conley, *J. Phycol.***1994**, *30*, 45 – 55; c) E. G. Vrieling, W. W. C. Gieskes, T. P. M. Beelen, *J. Phycol.* **1999**, *35*, 548 – 559.
[132] N. Kröger, C. Bergsdorf, M. Sumper, *Eur. J. Biochem.* **1996**, *239*, 259 – 264.
[133] a) N. Kröger, G. Lehmann, R. Rachel, M. Sumper, *Eur. J. Biochem.* **1997**, *250*, 99 – 105; b) N. Kröger, R. Wetherbee, *Protist* **2000**, *151*, 263 – 273.
[134] a) N. Kröger, R. Deutzmann, M. Sumper, *Science* **1999**, *286*, 1129 – 1132; b) N. Kröger, R. Deutzmann, M. Sumper, *J. Biol. Chem.* **2001**, *276*, 26 066 – 26 070.
[135] a) N. Kröger, R. Deutzmann, C. Bergsdorf, M. Sumper, *Proc. Natl. Acad. Sci. USA* **2000**, *97*, 14 133 – 14 138; b) D. R. Morris,

L. J. Marton, *Polyamines in Biology and Medicine*, Dekker, New York, **1981**.

[136] T. Nakajima, B. E. Volcani, *Biochem. Biophys. Commun.* **1970**, *39*, 28 – 33.

[137] H. Schägger, G. von Jagow, *Anal. Biochem.* **1987**, *166*, 368 – 379.

[138] A. M. M. Schmid, B. E. Volcani, *J. Phycol.* **1983**, *19*, 387 – 402.

[139] T. F. Schultz, L. Egerton-Warburton, S. Crawford, R. Wetherbee, *Protist* **2001**, *152*, 315 – 327.

[140] a) C. T. Kresge, M. E. Leonowicz, W. J. Roth, J. C. Vartuli, J. S. Beck, *Nature* **1992**, *359*, 710 – 712; b) S. Mann, G. A. Ozin, *Nature* **1996**, *382*, 313 – 318; c) H. P. Lin, C. H. Mou, *Science* **1996**, *273*, 765 – 767; d) H. Yang, N. Coombs, G. A. Ozin, *Nature* **1997**, *386*, 692 – 695.

[141] a) S. S. Kim, W. Z. Zhang, T. J. Pinnavia, *Science* **1998**, *282*, 1302 – 1305; b) P. T. Tauer, T. J. Pinnavia, *Science* **1996**, *271*, 1267 – 1269.

[142] a) F. Caruso, R. A. Caruso, H. Möhwald, *Science* **1998**, *282*, 1111 – 1114; b) B. T. Holland, C. F. Blanford, T. Do, A. Stein, *Chem. Mater.* **1999**, *11*, 795 – 805.

[143] a) J. N. Cha, G. D. Stucky, D. E. Morse, T. J. Demning, *Nature* **2000**, *403*, 289 – 292; b) C. Göltner, S. Henke, M. C. Weißenberger, M. Antonietti, *Angew. Chem.* **1998**, *110*, 633 – 636; *Angew. Chem. Int. Ed.* **1998**, *37,* 613 – 616; c) D. Y. Zhao, J. J. Feng, Q. S. Huo, N. Melosh, G. H. Frederickson, B. F. Chmelka, G. D. Stucky, *Science* **1998**, *279,* 548 – 552; d) M. Templin, A. Frank, A. DuChesne, H. Leist, Y. M. Zhang, R. Ulrich, V. Schadler, U. Wiesner, *Science* **1997**, *278*, 1795 – 1798.

[144] a) P. Schmidt-Winkel, W. W. Lukens, Jr., P. Yang, D. I. Margolese, I. S. Lettow, J. Y. Ying, G. D. Stucky, *Chem. Mater.* **2000**, *12*, 686 – 696; b) S. Schacht, Q. Huo, I. G. Voigt-Martin, G. D. Stucky, F. Schüth, *Science* **1996**, *273*, 768 – 771; c) A. Imhof, D. J. Pine, *Nature* **1997**, *389*, 948 – 951.

[145] a) E. G. Vrieling, T. P. M. Beelen, R. A. van Santen, W. W. C. Gieskes, *Angew. Chem.* **2002**, *114*, 1613 – 1616; *Angew. Chem. Int. Ed.* **2002**, *41*, 1543 – 1546; b) A. R. Hemsley, P. C. Griffith, *Philos. Trans. R. Soc. London, Ser. A* **2000**, *358*, 547 – 564; c) R. Gordon, R. W. Drum, *Int. Rev. Cytol.* **1994**, *150*, 243 – 372; d) J. Parkinson, Y. Brechet, R. Gordon, *Biochim. Biophys. Acta* **1999**, *1452,* 89 – 102; e) A. M. M. Schmid, *Protoplasma* **1994**, *181,* 43 – 60; f) A. M. M. Schmid, R. K. Eberwein, M. Hesse, *Protoplasma* **1996**, *193*, 144 – 173.

[146] a) M. Sumper, *Science* **2002**, *295*, 2430 – 2433; b) D. Volkmer, S. Tugulu, M. Fricke, T. Nielsen, *Angew. Chem.* **2003**, *115*, 60 – 64; *Angew. Chem. Int. Ed.* **2003**, *42*, 38 – 61; c) N. Kröger, S. Lorenz, E. Brunner, M. Sumper, *Science* **2002**, *298*, 584 – 586.

[147] a) A. van Blaaderen, R. Ruel, P. Wiltzins, *Nature* **1997**, *385*, 321 – 324; b) A. McPherson, *Crystallization of Biological Macromolecules*, Cold Spring Harbor Laboratory Press, Cold Spring Harbor, New York **1999**.

[148] a) E. Epstein, *Annu. Rev. Plant Physiol. Plant Mol. Biol.* **1999**, *50*, 641 – 644; b) A. J. Milligan, F. M. M. Morel, *Science* **2002**, *297*, 1848 – 1850.

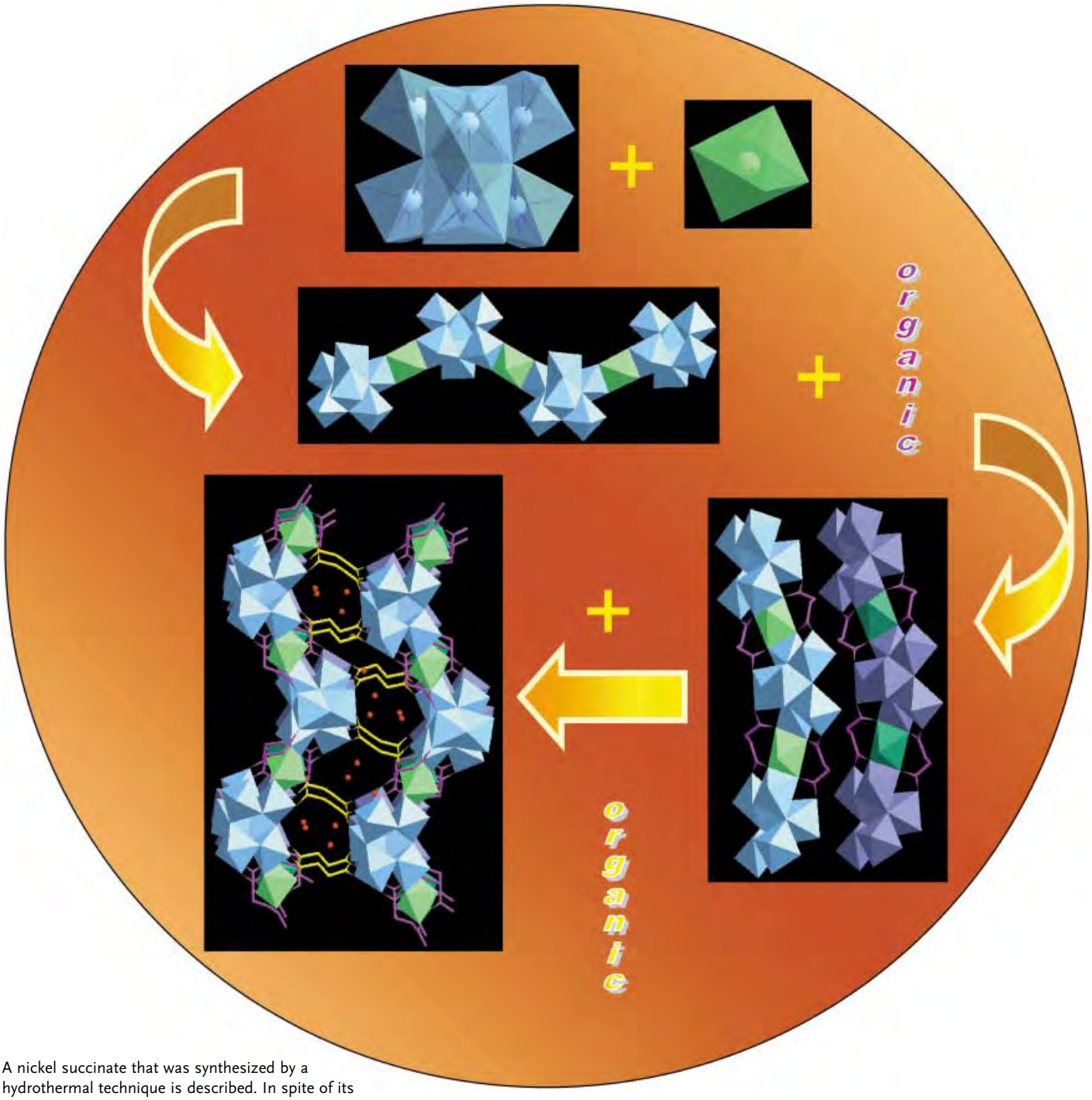
[149] R. D. Adam, *Clin. Microbiol. Rev.* **2001**, *14*, 447 – 475.

[150] L. L. Brott, R. R. Naik, D. J. Pikas, S. M. Kirkpatrik, D. W. Tomlin, P. W. Whitlock, S. J. Clarson, M. O. Stone, *Nature* **2001**, *413*, 291 – 293.

[151] a) S. Brown, *Nat. Biotechnol.***1997**, *15*, 269 – 274; b) S. R. Whaley, D. S. English, E. L. Hu, P. F. Barbara, A. M. Belcher, *Nature* **2000**, *405*, 665 – 668.

[152] R. R. Naik, L. L. Brott, S. J. Clarson, M. O. Stone, *J. Nanosci. Nanotechnol.* **2002**, *2*, 95 – 100.

Communications



A nickel succinate that was synthesized by a hydrothermal technique is described. In spite of its complexity and the presence of 55 nonequivalent atoms, the structure was completely solved ab initio from synchrotron powder-diffraction data. The structure was found to contain a unique hexanickel unit with interesting magnetic interactions; the compound is ferrimagnetic below 20 K. For more information see the article by Guillou et al. on the following pages.

 © 2003 Wiley-VCH Verlag GmbH & Co. KGaA, Weinheim 1433-7851/03/4206-0643 $ 20.00+.50/0

Microporous Nickel Succinate

A Layered Nickel Succinate with Unprecedented Hexanickel Units: Structure Elucidation from Powder-Diffraction Data, and Magnetic and Sorption Properties**

Nathalie Guillou, Carine Livage, Wouter van Beek, Marc Noguès, and Gérard Férey*

During the last decade, synthesis of hybrid organic–inorganic compounds based on transition metals has been actively investigated. It allows the wide-ranging functionality of transition metals (e.g., magnetic and optical properties, electrical conductivity, and ferroelectricity) to be associated with the ability of the organic moiety to modulate structural arrangements.[1] Moreover, the use of hydrothermal conditions can considerably enlarge the range of possible architectures that may arise from a metal and an organic molecule. It is even more efficient when the organic molecule is flexible, for example, the linear dicarboxylic acid succinic acid.[2] In general terms, coordination polymers obtained with divalent metal ions such as Mn^{II}, Fe^{II}, Co^{II}, Cu^{II}, and Zn^{II} often exhibit interesting architectures, but metal/oxide condensation is essentially "classical", with edge- and sometimes corner-sharing octahedra.[3] By contrast, with nickel, inorganic condensation is more diverse: Our first investigations on nickel phosphates showed that Ni could generate microporous materials with novel M–O–M connectivities in which polyhedra can share faces, edges, and/or corners.[4] This was followed by the first hydrothermally synthesized nickel succinate,[5] which forms a remarkable honeycomb nickel oxide network, and by two new nickel carboxylates with rigid linkers.[6] Here we describe the second nickel succinate, the structure of which, in spite of its complexity and the presence of 55 nonequivalent atoms, was completely solved ab initio from synchrotron powder-diffraction data. It forms a novel network with an unusual hexanuclear building block that confers peculiar ferrimagnetic properties on the material. To our knowledge this unit has never been observed, neither in solid-state chemistry nor in the rich domain of polyoxometalates.[7]

The nickel succinate was synthesized by classical hydrothermal reaction.[8] Synchrotron powder data were collected on the Swiss-Norwegian beamline at the ESRF.[9] A monoclinic solution ($a = 7.8597(1)$, $b = 18.8154(3)$, $c = 23.4377(4)$ Å, $\beta = 92.0288(9)°$, $V = 3463.9(4)$ Å^3) was consistent with the $P2_1/c$ space group. In the angular range $2\theta = 1$–$44°$, 2921 integrated intensities were extracted for direct-methods calculations, and 252 phases were observed for $|E|$ values greater than 1.2 and refined by using 4213 unique triplets. By increasing the number of direct-methods attempts to 256, the most probable E map revealed all nickel atoms, most of the surrounding oxygen atoms and a few carbon atoms. Subsequent Rietveld refinement converged approximately to $R_B = 0.30$ and $R_F = 0.20$. Successive difference Fourier maps alternated with profile refinements then completed the inorganic framework. The use of soft distance and angular constraints gradually differentiated electron-density maps and allowed the location of the organic moieties and the free water molecules. At the final stage, the structural model contained 55 non-hydrogen atoms, and soft constraints were maintained for the organic molecules. The final Rietveld refinement ($2\theta = 2.5$–$40°$, 2266 reflections, 170 structural parameters; Figure 1) corresponds to satisfactory model indicators ($R_B = 0.063$ and $R_F = 0.066$) and profile factors ($R_P = 0.049$ and $R_{WP} = 0.062$).

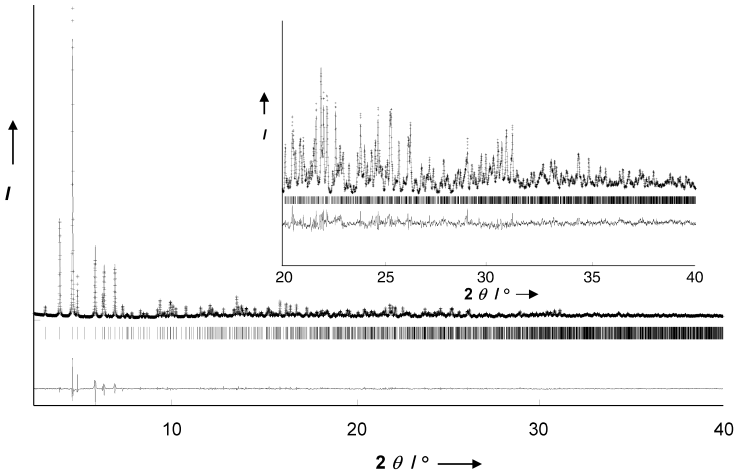


Figure 1. Final Rietveld plot of MIL-73. A zoom at high angles is shown as inset.

This new nickel succinate, denoted MIL-73, is built up from organic–inorganic (100) layers. Nickel oxide corrugated chains running along the b axis are connected by succinate ions along the c axis (Figure 2a). All carboxy groups of the four independent succinate anions are deprotonated. Half of the organic molecules decorate the chains, and the other half covalently connect them. Nickel atoms occupy seven independent crystallographic sites with octahedral geometry. The Ni atoms are cooordinated by two μ_4-, two μ_3-, and three μ_2-O atoms; two terminal water molecules; and O atoms of four succinate ions. Bond valence calculations give values very close to 1 for the two μ_4-O atoms, and values in the range 0.77(5)–0.61(3) for the three μ_2-O atoms.[10] This leads to assignment of the μ_4-O atoms to hydroxo groups, as were already observed in nickel(II) complexes,[11] and to the

[*] Dr. N. Guillou, Dr. C. Livage, Dr. M. Noguès, Prof. G. Férey
Institut Lavoisier-Franklin, FR 2483
Université de Versailles Saint-Quentin-en-Yvelines
45 avenue des Etats-Unis, 78035 Versailles Cedex (France)
Fax: (+33) 1-3925-4358
E-mail: guillou@chimie.uvsq.fr
Dr. W. van Beek
SNBL at ESRF
6 Rue Jules Horowitz, 38043 Grenoble (France)

[**] We thank the ESRF for allowing us access to their synchrotron facilities.

Supporting information for this article is available on the WWW under http://www.angewandte.org or from the author.

 © 2003 Wiley-VCH Verlag GmbH & Co. KGaA, Weinheim 1433-7851/03/4206-0644 $ 20.00+.50/0

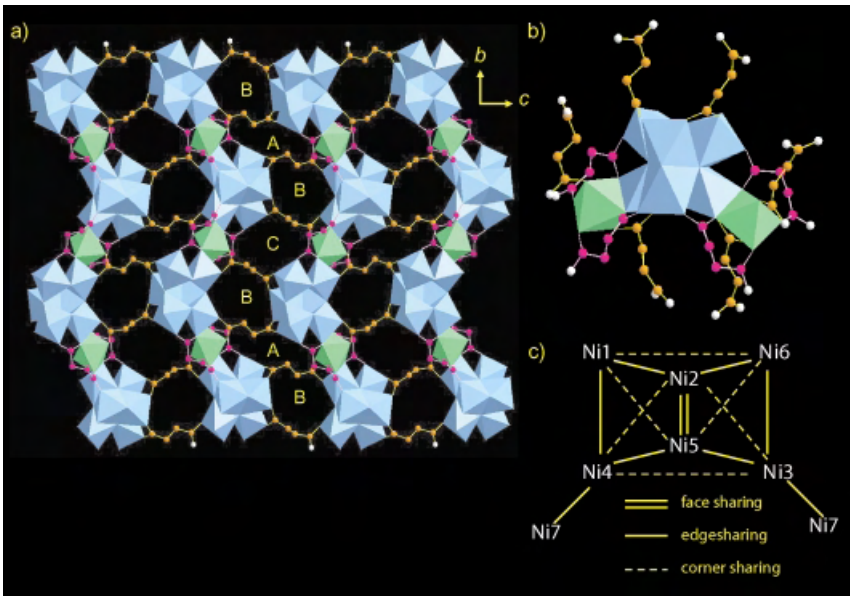


Figure 2. a) Projection of the structure along the *a* axis showing the three types of channels A–C. b) Polyhedral view of the hexanickel unit (blue) connected to two bridging Ni7 octahedra (green). Decorating succinate ions are represented in purple and bridging ones in orange. c) Schematic view of the connectivity of the Ni-centered octahedra.

assumption that the three μ_2 sites are statistically occupied by two hydroxo ligands and one water molecule. This corresponds to the chemical formula $[Ni_7(C_4H_4O_4)_4(OH)_6(H_2O)_3]\cdot 7H_2O$. Inorganic chains are built up from unusual hexanickel units connected by a seventh octahedron (Ni7, green in Figure 2). This polyhedron shares two *trans* edges with two neighboring Ni_6 units. In the Ni_6 unit a dimer of face-sharing octahedra is grafted onto a tetramer formed by two dimers of edge-sharing octahedra (Ni1, Ni4 and Ni6, Ni3) whose corners are connected via hydroxide ions. The face-sharing Ni atoms are connected to the tetramer by sharing edges with the two adjacent nickel octahedra, and corners with the opposite ones (Figure 2c). The cohesion of successive layers is ensured by strong hydrogen bonds involving one of the three μ_2-"hydroxo/water" and the two terminal water molecules (d (O···O) = 2.73(4), 2.88(4) Å). A pseudo-three-dimensional hybrid framework is thus formed in which three types of channels (A–C in Figure 2a) contain seven water molecules, connected to the framework by hydrogen bonds.

The thermal behavior of $[Ni_7(C_4H_4O_4)_4(OH)_6(H_2O)_3]\cdot 7H_2O$ was investigated by X-ray thermodiffraction (in air) and gravimetric analysis (under flowing nitrogen).[12] A gradual weight loss of 3.4% up to 45 °C corresponds to the loss of 2.4 adsorbed water molecules without any structural change. Then, the loss of the seven occluded water molecules (found: 9.9 wt%, calcd: 10.5 wt%) occurs with three successive crystallographic changes at 60, 110, and 180 °C (Figure 3). This dehydration is reversible, but rehydra-

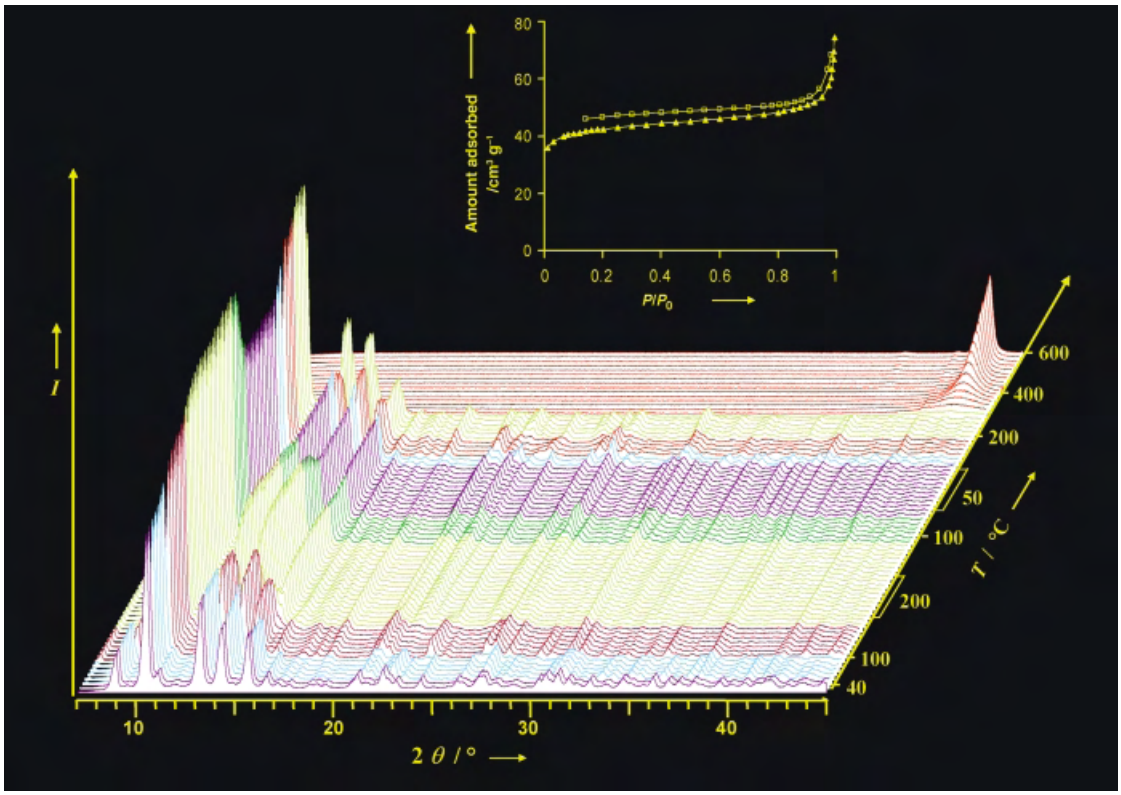


Figure 3. Thermal evolution of diffractograms during dehydration–rehydration (40–200–50 °C) and decomposition (up to 600 °C) of MIL-73. Adsorption (lower curve) and desorption (upper curve) isotherms for nitrogen at 77 K are shown in the inset. A = amount adsorbed.

 © 2003 Wiley-VCH Verlag GmbH & Co. KGaA, Weinheim 1433-7851/03/4206-0645 $ 20.00+.50/0

tion is characterized by progressive changes in the diffractogram between 120 and 60 °C, instead of successive steps. This behavior may indicate sorption properties. The weight loss between 225 and 300 °C was attributed to the three coordinated water molecules (found: 4.3 wt %, calcd: 4.5 wt %). The structure collapses at 280 °C in air with the loss of the hydroxo groups and combustion of the organic moieties. A sample activated at 170 °C under vacuum gave a typical type-1 N_2 adsoption isotherm (Figure 3, inset) and a surface area of 135(4) $m^2 g^{-1}$, which clearly indicates considerable porosity for this compound.[13]

$[Ni_7(C_4H_4O_4)_4(OH)_6(H_2O)_3]\cdot 7H_2O$ is ferrimagnetic below 20 K. The paramagnetic part of the $1/\chi(T)$ curve follows a Curie–Weiss law (150–300 K) with $C = 9.65$ K emu mol^{-1}, $\theta_p = -101$ K, and $\mu_{eff} = 3.3\ \mu_B$ per atom. The difference between zero-field and field-cooled (100 G) curves provides a good estimation of the magnetic ordering temperature of 20 K.[14] Magnetization data versus applied field H below T_N confirm this assessment and the extrapolated saturation magnetization was estimated to be 4.7 μ_B per formula unit. The high θ_p value relative to those currently obtained for Ni compounds indicates very strong antiferromagnetic interactions.[4–6] The complexity of the Ni-O-Ni connectivity, in which polyhedra can be linked by faces, edges, and corners, means that the compound is magnetically frustrated. Indeed, if only vertex connections with large angles, which favor antiferromagnetic superexchange, are taken into account, antiferomagnetic interactions are expected in the Ni1-Ni5-Ni6 and Ni4-Ni2-Ni3 triangles (Figure 2c), and hence spin frustration is inevitable. A saturation magnetization of 4.7 μ_B suggests the coexistence of two magnetic networks with five spin-up and two spin-down centers. This experimental value is, of course, lower than that calculated for cooperative ferrimagnetism ($M_s = 6\ \mu_B$ assuming $g = 2$) resulting from the strong spin frustration, which often decreases magnetic moments.[15]

In summary, a nickel succinate was synthesized by a hydrothermal technique. Its structure contains a unique hexanickel unit with interesting magnetic interactions: The compound is ferrimagnetic below 20 K. The novelty of the structure illustrates the flexibility of nickel oxide networks and confirms the versatility of nickel inorganic condensation under hydrothermal conditions.[5,6] Moreover, after removing the water of hydration, it also becomes porous (135(4) $m^2 g^{-1}$) and can reversibly reabsorb water molecules. Finally, the structure determination (55 atoms and 165 atomic coordinates) from synchrotron-powder diffraction data reaches the limits of "traditional" ab initio methods.[16] Above this limit and for larger cells, a new way of collecting data[17] or "direct-space" strategies in the case of organic materials,[18] must be used, as was shown recently.

Received: September 26, 2002 [Z50247]

[1] a) G. Férey, *Chem. Mater.* **2001**, *13*, 3084–3098; b) S. Feng, R. Xu, *Acc. Chem. Res.* **2001**, *34*, 239–247; c) M. Eddaoudi, H. Li, O. M. Yaghi, *J. Am. Chem. Soc.* **2000**, *122*, 1391–1397.

[2] a) C. Livage, C. Egger, G. Férey, *Chem. Mater.* **2001**, *13*, 410–414; b) L.-S. Long, X.-M. Chen, M.-L. Tong, Z.-G. Sun, Y.-P. Ren, R.-B. Huang, L.-S. Zheng, *J. Chem. Soc. Dalton Trans.* **2001**, *19*, 2888–2890; c) F. Serpaggi, G. Férey, *J. Mater. Chem.* **1998**, *8*, 2737–2741.

[3] a) Y. Kim, E. Lee, D.-Y Jung, *Chem. Mater.* **2001**, *13*, 2684–2690; b) M. Riou-Cavellec, C. Albinet, J.-M. Grenèche, G. Férey, *J. Mater. Chem.* **2001**, *11*, 3166–3171; c) C. Livage, N. Guillou, J. Marrot, G. Férey, *Chem. Mater.* **2001**, *13*, 4387–4392; d) E. Lee, Y. Kim, D.-Y. Jung, *Inorg. Chem.* **2002**, *41*, 501–506; e) M. Kurmoo, H. Kumagai, M. A. Green, B. W. Lovett, S. J. Blundell, A. Ardavan, J. Singleton, *J. Solid State Chem.* **2001**, *159*, 343–351; f) S. S.-Y. Chui, S. M.-F. Los, J. P. H. Charmant, A. G. Orpen, I. D. Williams, *Science* **1999**, *283*, 1148–1150; g) H. Li, M. Eddaoudi, M. O'Keeffe, O. M. Yaghi, *Nature* **1999**, *402*, 276–279.

[4] a) N. Guillou, Q. Gao, M. Noguès, R. E. Morris, M. Hervieu, G. Férey, A. K. Cheetham, *C. R. Acad. Sci. Ser. IIc* **1999**, *2*, 387–392; b) N. Guillou, Q. Gao, P. M. Forster, J.-S Chang, M. Noguès, S.-E. Park, G. Férey, A. K. Cheetham, *Angew. Chem.* **2001**, *113*, 2913–2916; *Angew. Chem. Int. Ed.* **2001**, *40*, 2831–2834.

[5] P. M. Forster, A. K. Cheetham, *Angew. Chem.* **2002**, *114*, 475–477; *Angew. Chem. Int. Ed.* **2002**, *41*, 457–459.

[6] a) H. Kumagai, Y. Oka, M. M. Akita-Tanaka, K Inoue, *Inorg. Chim. Acta* **2002**, *332*, 176–180; b) S. Konar P. S. Mukherjee, E. Zangrando, F. Lloret, N. R. Chaudhuri, *Angew. Chem.* **2002**, *114*, 1631–1633; *Angew. Chem. Int. Ed.* **2002**, *41*, 1561–1563; c) N. Guillou, S. Pastre, C. Livage, G. Férey, *Chem. Commun.* **2002**, 2358–2359.

[7] J.-P. Jolivet, *Metal Oxide Chemistry and Synthesis*, J. Wiley, New York, **2000**.

[8] Reactions were carried out in a Teflon container (23 mL) at 180 °C for 2 d under autogenous pressure. The reaction mixture contained $NiCl_2\cdot 6H_2O$ (0.550 g), succinic acid (0.411 g), KOH (0.534 g), and H_2O (5 mL) in the molar ratio 1:1.5:4.1:120. After cooling (pH 6), the pale green powder was washed with distilled water. Elemental analysis (%): calcd: C 16.60, H 3.66, Ni 35.49; found: C 16.65, H 3.66, Ni 33.80.

[9] High-resolution synchrotron data were measured with a Debye–Scherrer diffractometer geometry and a Si(111) analyzer crystal ($\lambda = 0.7999$ Å). The powder was introduced in a 1.5 mm capillary and the pattern was scanned in the range $2\theta = 1$–60° with a step length of $2\theta = 0.0035°$ and a counting time of 1 s per step. To improve the counting statistics at high angles, the pattern was then divided in two 2θ regions (1–15 and 15–45°), with times per step of 1 and 3 s, respectively. Pattern indexing was carried out with DICVOL91 (A. Boultif, D. Louër, *J. Appl. Crystallogr.* **1991**, *24*, 987–993). Direct methods and Fourier difference calculations were performed with SHELXTL (G. M. Sheldrick, **1997**). Pattern matching and Rietveld refinements were performed by using FullProf (J. Rodriguez-Carvajal in *Collected Abstract of Powder Diffraction Meeting* (Toulouse), **1990**, p. 127) and integrated in WinPlotr (T. Roisnel, J. Rodriguez-Carvajal, *Mater. Sci. Forum* **2001**, *378–381*, 118–123). CCDC-194049 contains the supplementary crystallographic data for this paper. These data can be obtained free of charge via www.ccdc.cam.ac.uk/conts/retrieving.html (or from the Cambridge Crystallographic Data Center, 12, Union Road, Cambridge CB21EZ, UK; fax: (+44) 1223-336-033; or deposit@ccdc.cam.ac.uk).

[10] N. Brese, M. O'Keeffe, *Acta Crystallogr. Sect. B* **1991**, *47*, 192–196.

[11] A. J. Edwards, B. F. Hoskins, E. H. Kachab, A. Markiewicz, K. S. Murray, R. Robson, *Inorg. Chem.* **1992**, *31*, 3585–3591.

[12] X-ray thermodiffractometry was performed under static air in an Anton Parr HTK16 high-temperature device of a Siemens D-5000 diffractometer (θ/θ mode, $Co_{K\alpha}$ radiation) equipped with an M Braun linear position-sensitive detector (PSD). The dehydration–rehydration process was studied at 10 °C intervals (40–200–50 °C), and decomposition at 20 °C intervals up to 600 °C; temperature ramp of 0.1 °C s^{-1}; several hours at 200 and 50 °C. Thermogravimetric analysis was performed using a TA

 © 2003 Wiley-VCH Verlag GmbH & Co. KGaA, Weinheim 1433-7851/03/4206-0646 $ 20.00+.50/0

Instruments TGA-2050 apparatus (nitrogen flow 60 ml min^{-1}, 2 °C min^{-1}).
[13] The BET surface area of the sample activated at 170 °C under vacuum for 64 h was studied on a Micromeritics ASP200 porosimeter.
[14] Magnetization measurements were performed on a Quantum Design Squid magnetometer (MPMS-5).
[15] G. Férey, R. de Pape, M. Leblanc, J. Pannetier, *Rev. Chim. Miner.* **1986**, *23*, 474 – 484.
[16] a) R. E. Morris, J. J. Owen, J. K. Stalick, A. K. Cheetham, *J. Solid State Chem.* **1994**, *111*, 52 – 57; b) L. B. McCusker, R. W. Grosse-Kunstleve, C. Bearlocher, M. Yoshikawa, M. E. Davis, *Microporous Mater.* **1996**, *6*, 295 – 309; c) D. M. Poojary, A. Cabeza, M. A. G. Aranda, S. Bruque, A. Clearfield, *Inorg. Chem.* **1996**, *35*, 1468 – 1473; d) M. Louër, C. Le Roux, J. Dubac, *Chem. Mater.* **1997**, *9*, 3012 – 3016.
[17] T. Wessels, C. Baerlocher, L. B. McCusker, E. J. Creyghton, *J. Am. Chem. Soc.* **1999**, *121*, 6242 – 6247.
[18] a) K. D. M. Harris, M. Tremayne, B. M. Kariuki, *Angew. Chem.* **2001**, *113*, 1674 – 1700; *Angew. Chem. Int. Ed.* **2001**, *40*, 1626 – 1651; b) E. Tedesco, G. W. Turner, K. D. M. Harris, R. L. Johnston, B. M. Kariuki, *Angew. Chem.* **2000**, *112*, 4662 – 4665; *Angew. Chem. Int. Ed.* **2000**, *39*, 4488 – 4491; c) E. Y. Cheung, E. E. McCabe, K. D. M. Harris, R. L. Johnston, E. Tedesco, K. M. P. Raja, P. Balaram, *Angew. Chem.* **2002**, *114*, 512 – 514; *Angew. Chem. Int. Ed.* **2002**, *41*, 494 – 496; d) R. B. Von Dreele, P. W. Stephens, G. D. Smith, R. H. Blessing, *Acta Crystallogr. Sect. D* **2000**, *56*, 1549 – 1553.

Colorimetric Isomer Probes

Towards the Development of Colorimetric Probes to Discriminate between Isomeric Dicarboxylates**

Felix Sancenón, Ramón Martínez-Máñez, Miguel Angel Miranda, Maria-Jesus Seguí, and Juán Soto*

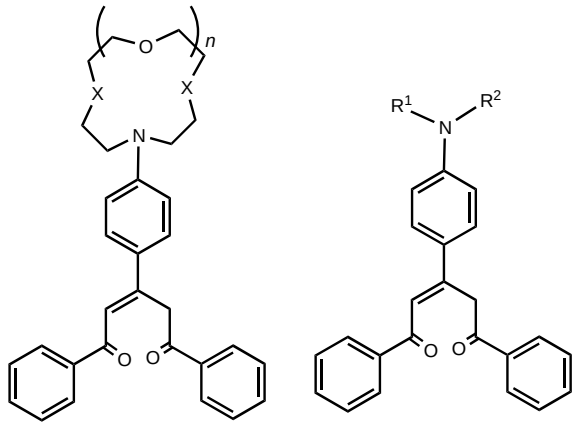
The development of new chemosensors based on supramolecular concepts is a field of current interest.[1] A significant amount of work has been devoted to obtain specific chemosensors that are able to change, upon complexation with the target guests, one or several macroscopic properties in response to the molecular coordination event. Changes in fluorescence[2] and in absorbance[3] are the output signals used in the development of optical chemosensors. Although a number of chromogenic receptors for the sensing of metal ions have been developed,[4] very few chromogenic receptors for anions have been described in the literature that are based on recognition approaches.[5] Most of the receptors have been developed for the colorimetric sensing of inorganic anions,[6] whereas very few have been designed for recognition of organic anions,[7] particularly in aqueous environments. Thus, the development of chromogenic reagents for such species remains a challenge. In this context, and as an advancement of this field, we wish now to report a chromogenic system for the colorimetric discrimination between certain organic isomers (*cis*/*trans* and *ortho*/*meta*/*para* dicarboxylates). Differentiation of isomers is, in general, a difficult task because of their rather similar chemical and physical properties. To the best of our knowledge, the examples we show here are the first supramolecular-based colorimetric probes for the detection of isomeric anions.

Most of the known colorimetric anion chemosensors are based on host molecules containing anion coordination sites coupled to chromogenic signaling units. In those receptors, coordination of the anion usually modifies the charge-transfer band of the chromogenic group resulting in "naked-eye" anion detection. A different approach involves the use of anion-induced reactions that can be either reversible or irreversible.[8] We have recently reported the use of one such anion-induced reversible reaction for the selective detection of ATP in water/organic solvent mixtures.[9] The system was based on the cyclization of yellow 1,3,5-triarylpent-2-en-1,5-diones to the magenta pyrylium cation. A family of 1,3,5-triarylpent-2-en-1,5-diones were synthesized by electrophilic aromatic substitution of the corresponding aniline derivative with 2,6-diphenylpyrylium perchlorate in DMF at 150 °C. Subsequent column chromatography on aluminum oxide afforded the receptors L^1–L^8 in approximately 35 % yield. The UV/Vis spectra of L^1–L^8 are very similar, with a band centered at around 370–380 nm, which is indicative of their brightly yellow color. The structures of the compounds L^1–L^8 are shown in Scheme 1.

Figure 1 shows a photograph of buffered dioxane/water (70:30 v/v) solutions of L^8 at approximately pH 6 (0.01 M HEPES buffer, HEPES = 4-(2-hydroxyethyl)-1-piperazineethanesulfonic acid) containing an equimolar amount of certain carboxylate (acetate, benzoate) and dicarboxylate anions (terephthalate, $^-OOC–(CH_2)_n–COO^-$, $n = 0$ to 7, oxalate, malonate, succinate, glutarate, adipate, pimelate, suberate). The solution remains yellow upon addition of all the above mentioned species, except for the oxalate and malonate ions, whereby the solutions turn red-magenta. This remarkable color change is, as stated above, a result of the anion-induced selective cyclization of L^8 to give the colored 2,4,6-triphenylpyrylium cation (absorption maximum at approximately 550 nm). Figure 1 also shows the color variation observed upon addition of maleate or fumarate dicarboxylate ions to buffered solutions of L^5 (0.01 M HEPES buffer, approximately pH 6). The solution is yellow in the presence

[*] Prof. R. Martínez-Máñez, F. Sancenón, Prof. M. A. Miranda, M.-J. Seguí, Dr. J. Soto
Departamento de Química
Universidad Politécnica de Valencia
Camino de Vera s/n, 46071 Valencia (Spain)
Fax: (+34) 96-387-9349
E-mail: rmaez@qim.upv.es

[**] This research was supported by the Ministerio de Ciencia y Tecnología (proyecto PB98-1430-C02-02, and AMB99-0504-C02-01). F.S. thanks the Ministerio de Ciencia y Tecnología for a Doctoral Fellowship. M.-J.S. thanks the Universidad Politécnica de Valencia for a Doctoral Fellowship.



L^1, X = O, n = 1
L^2, X = O, n = 2
L^3, X = O, n = 3
L^4, X = S, n = 2

L^5, $R^1 = R^2 = CH_3$
L^6, $R^1 = CH_2CH_2OH$, $R^2 = (CH_2CH_2O)_2CH_2CH_2OH$
L^7, $R^1 = CH_2CH_2OH$, $R^2 = (CH_2CH_2O)_3CH_2CH_2OH$
L^8, $R^1 = CH_2CH_2OH$, $R^2 = (CH_2CH_2O)_4CH_2CH_2OH$

Scheme 1. Schematic representation of L^1–L^8.

of the *trans* isomer, but changes color to magenta in the presence of the *cis* isomer. As far as we know, this is the first reported example of *cis*/*trans* discrimination using colorimetric reagents. In fact, there are very few reports in the literature dealing with the use of synthetically constructed receptors for the colorimetric sensing of carboxylic acids. One such study, by Hamilton and co-workers, was carried out in dichloromethane[10] and, more recently, two reports by Anslyn and coworkers have described chromogenic competition assays for the colorimetric determination of citrate and tartrate species in aqueous organic solvents.[11]

In addition to the use of L^8 and L^5 as receptors (Figure 1), similar results are obtained when using the remaining compounds outlined in Scheme 1, which strongly suggests that the interaction of the anions with the receptors involves a fragment that is common to all of them. This points to the pent-2-en-1,5-dione group, rather than the aza-oxa- or aza-thia-oxa-polyazaalkane fragments, acting as the anion binding site. Thus, although diones can not bind to carboxylates, the corresponding enol tautomers can form hydrogen bonds with the anions (see the upper part of Scheme 2). From all the dicarboxylates studied, only oxalate, malonate, and maleate ions gave color variation. The special feature that these three anions have in common is the presence of carboxylate groups in close proximity. In this context, the potential ability of these guests to bind the hydroxyl group of the receptor by using both carboxylate groups would result in the formation of stronger hydrogen bonds and, therefore, in an enhancement of the nucleophilic character of the hydroxylic oxygen atom. One might refer to this action as "tweezers-like" behavior, in the sense that only diacids shaped like "tweezers" are able to act as chelating ligands towards the OH group, whereas other diacids or monoacids do not. Hence, the recognition process conforms to the supramolecular concept that guests (in our case anions) do not only have charge or size, but also a certain shape (in this case, proximity between carboxylate groups).[12] Scheme 2 describes the steps in the shape-induced recognition process; the tweezers-like carboxylate groups serve to disrupt the hydrogen atom from the hydroxy oxygen atom, which induces nucleophilic attack at the C1 carbon, with subsequent cyclization occuring to give the magenta pyrylium cation.

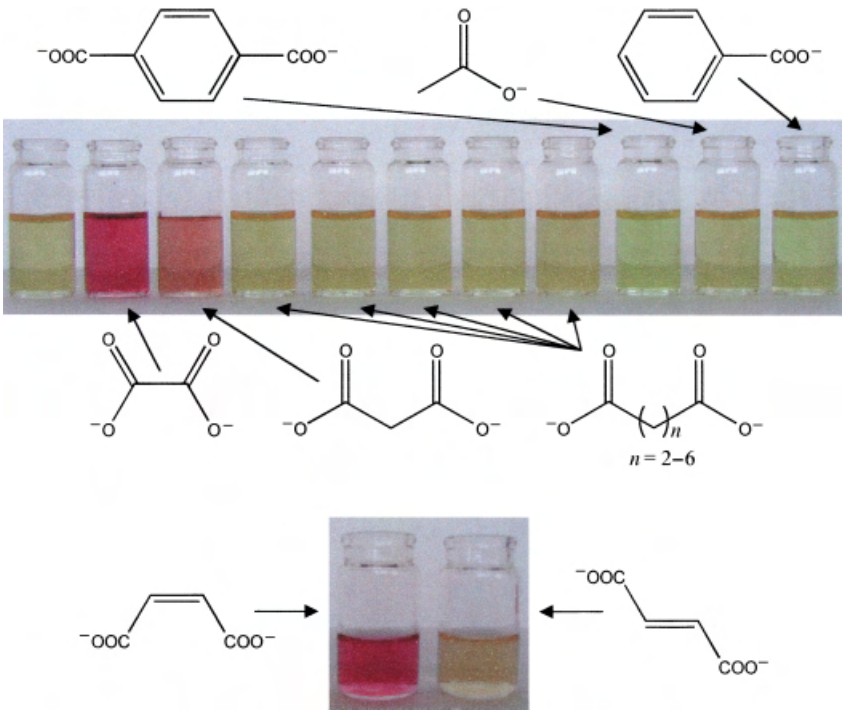
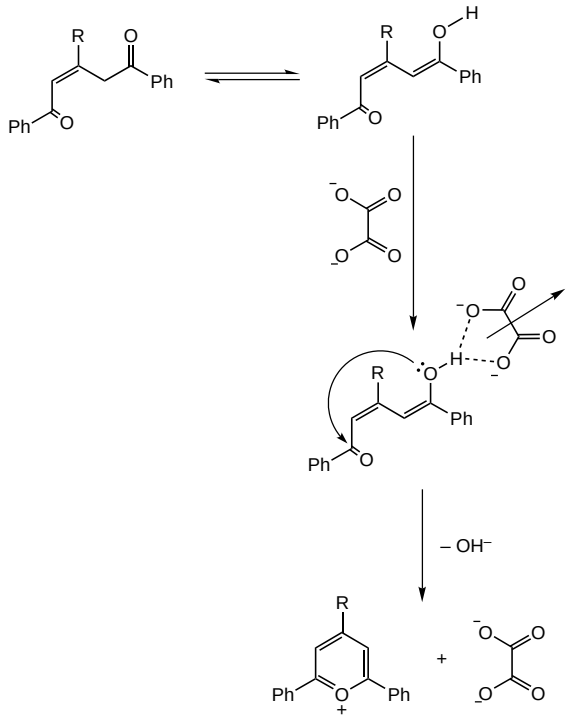


Figure 1. a) Color changes induced on L^8 (5×10^{-5} mol dm^{-3}) at pH 6 (buffered with 0.01 M HEPES) in dioxane/water (70:30 v/v) in the presence of (from left to right): no anion, oxalate, malonate, succinate, glutarate, adipate, pimelate, suberate, terephthalate, acetate, and benzoate anions. b) Color changes induced on L^5 under the same conditions, in the presence of (from left to right) maleate and fumarate anions.

Further studies also appear to support the mechanism outlined in Scheme 2. Thus, if that mechanism is correct, then the anions should be acting as catalysts for the cyclization. This has been confirmed, and we have found rate constants for the process anion + $L^5 \rightarrow L^5$(cy) + anion of 149.3, 62.6, and 148.7 M^{-1} s^{-1} for oxalate, malonate, and maleate ions, respectively. Furthermore, when kinetic studies were carried out in D_2O/dioxane mixtures, the rate constants were found to be 3–4 times smaller than when water/dioxane was used as solvent. Such an isotope effect suggests that the rate-determining step of the cyclization reaction involves cleavage of the O–H (O–D) bond.

Additionally, molecular modeling calculations to study the interaction of the enol tautomer of L^5 with different anions[13] have shown that when a carboxylate is placed near the hydroxyl group of the enol tautomer, a hydrogen bond is formed. However, the strength of the hydrogen bond depends on the nature of the anions. The calculations show that the oxalate, malonate, and maleate anions tend to

 © 2003 Wiley-VCH Verlag GmbH & Co. KGaA, Weinheim 1433-7851/03/4206-0648 $ 20.00+.50/0



Scheme 2. Proposed mechanism of cyclization by nucleophilic attack of the oxygen atom to the C1 carbon. The Scheme also shows the proposed formation of hydrogen bonds between the dianion and the hydroxy group.

form strong hydrogen bonds, significantly enhancing the electron density of the oxygen atom of the hydroxyl group. This is shown in Figure 2, where the charge on the enolic oxygen atom (from PM3 calculations) of the L^5 receptor bound to the corresponding anion is plotted against the

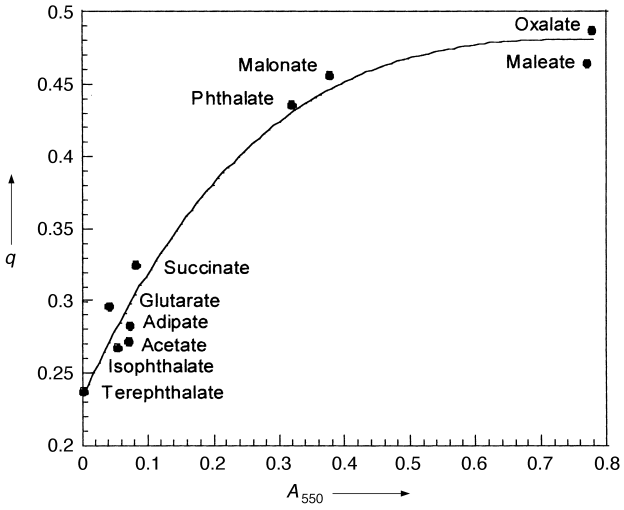


Figure 2. Plot of the charge (q) on the oxygen atom of the hydroxyl group in the enol tautomer of L^5 after forming hydrogen bonds with certain anions, as a function of the absorbance of the 550 nm band. The charge q is calculated from PM3 calculations of the interaction of L^5 and the corresponding anion. All the anions studied form hydrogen bonds with the hydroxyl group.

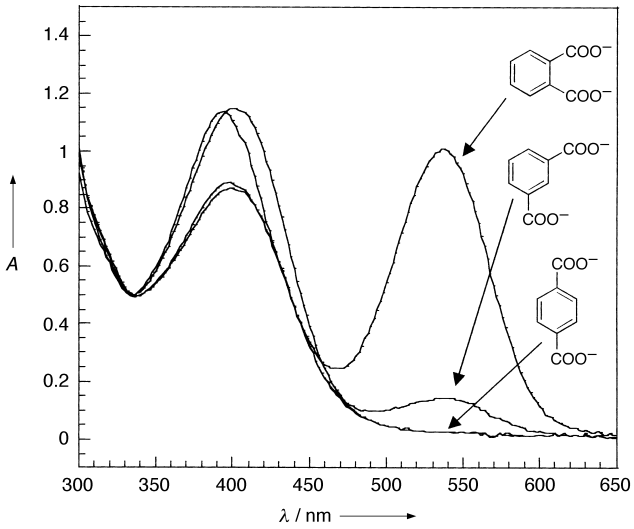


Figure 3. Visible spectra of L^5 (5×10^{-5} mol dm^{-3}) at pH 6 (buffered with 0.01 M HEPES) in dioxane/water (70:30 v/v) in the presence of phthalate, isophthalate, and terephthalate anions.

experimental absorbance of the band at 550 nm after a reaction time of 30 min (this absorbance indicates the extent to which the magenta pyrylium cation is obtained). In fact, a very good correlation is found. It is interesting that carboxylates showing the above-described tweezers-like shape tend to induce a significant increase in negative-charge density at the oxygen atom of the hydroxyl group.

Colorimetric recognition of the tweezers-like dicarboxylates appears to be of general application (Figure 3), as the yellow L^1–L^8 receptors also change color to magenta in the presence of phthalate anions, whereas they remain yellow in the presence of isophthalate or terephthalate anions (dioxane/water (70:30 v/v) solutions, 0.01M HEPES buffer, approximately pH 6).

In summary, the use of relatively simple receptors combined with a specific anion shape allows remarkable colorimetric recognition of certain organic guests in water/dioxane mixtures. The recognition process, which is based on the cyclization of 1,3,5-triarylpent-2-en-1,5-diones, has proved to be very sensitive to the presence of tweezers-like carboxylates. Thus, for the first time, shape-induced cyclization allows for the design of probes for the selective colorimetric recognition of certain organic isomers. For instance, receptors L^1–L^8 are suitable chromogenic reagents for selective discrimination between *cis*/*trans* dicarboxylates and *ortho*/*meta*/*para* dicarboxylates in water/organic solvent mixtures at nearly neutral pH values. We believe that the interaction of target molecules with suitable chemical reactions, associated with a color change, can play a significant role in the development of a new generation of colorimetric sensors or reagents for the detection of target organic guests.

Received: September 3, 2002
Revised: November 7, 2002 [Z50095]

 © 2003 Wiley-VCH Verlag GmbH & Co. KGaA, Weinheim 1433-7851/03/4206-0649 $ 20.00+.50/0

[1] a) "Chemosensors for Ion and Molecular Recognition": J. P. Desvergne, A. W. Czarnik, *NATO ASI Ser. Ser. C* **1997**, *492*; b) A. Bianchi, K. Bowman-James, E. García-España, *Supramolecular Chemistry of Anions*, Wiley-VCH, New-York, **1997**.
[2] See for example: a) A. P. de Silva, H. Q. N. Gunaratne, T. Gunnlaugsson, A. J. M. Huxley, C. P. McCoy, J. T. Rademacher, T. E. Rice, *Chem. Rev.* **1997**, *97*, 1515–1566; b) C. Bargossi, M. C. Fiorini, M. Montalti, L. Prodi, N. Zaccheroni, *Coord. Chem. Rev.* **2000**, *208*, 17–32; c) A. B. Descalzo, D. Jimenez, M. D. Marcos, R. Martínez-Máñez, J. Soto, J. El Haskouri, C. Guillem, D. Beltrán, P. Amorós, M. V. Borrachero, *Adv. Mater.* **2002**, *14*, 966–969.
[3] a) H. G. Löhr, F. Vögtle, *Acc. Chem. Res.* **1985**, *18*, 65–72; b) M. Inouye, *Color. Non-Text. Appl.* **2000**, 238–274; c) S. L. Wiskur, H. Aït-Haddou, J. J. Lavigne, E. V. Anslyn, *Acc. Chem. Res.* **2001**, *34*, 963–972.
[4] a) O. Brümmer, J. J. La Clair, K. D. Janda, *Bioorg. Med. Chem.* **2001**, *9*, 1067–1071; b) B. Valeur, I. Leray, *Coord. Chem. Rev.* **2000**, *205*, 3–40; c) K. Fuji, K. Tsubaki, K. Tanaka, N. Hayashi, T. Otsubo, T. Kinoshita, *J. Am. Chem. Soc.* **1999**, *121*, 3807–3808.
[5] V. Amendola, L. Fabbrizzi, C. Mangano, P. Pallavicini, A. Poggi, A. Taglietti, *Coord. Chem. Rev.* **2001**, *219–*221, 821–837;b) P. D. Beer, P. A. Gale, *Angew. Chem.* **2001**, *113*, 502–532; *Angew. Chem. Int. Ed.* **2001**, *40*, 486–516; c) H. Miyaji, J. L. Sessler, *Angew. Chem.* **2001**, *113*, 158–161; *Angew. Chem. Int. Ed.* **2001**, *40*, 154–157.
[6] a) D. H. Lee, H. Y. Lee, K. H. Lee, J. I. Hong, *Chem. Commun.* **2001**, 1188–1189; b) P. Anzenbacher, Jr., A. C. Try, H. Miyaji, K. Jursíková, V. M. Lynch, M. Marquez, J. L. Sessler, *J. Am. Chem. Soc.* **2000**, *122*, 10268–10272; c) H. Miyaji, W. Sato, J. L. Sessler, *Angew. Chem.* **2000**, *112*, 1847–1850; *Angew. Chem. Int. Ed.* **2000**, *39*, 1777–1780; d) F. Sancenón, R. Martínez-Máñez, J. Soto, *Angew. Chem.* **2002**, *114*, 1474–1477; *Angew. Chem. Int. Ed.* **2002**, *41*, 1416–1419; e) D. Jiménez, R. Martínez-Máñez, F. Sancenón, J. Soto, *Tetrahedron Lett.* **2002**, *43*, 2823–2825.
[7] a) K. Niikura, A. Metzger, E. V. Anslyn, *J. Am. Chem. Soc.* **1998**, *120*, 8533–8534; b) L. A. Cabell, M. K. Monahan, E. V. Anslyn, *Tetrahedron Lett.* **1999**, *40*, 7753–7756; c) H. Aït-Haddou, S. L. Wiskur, V. M. Lynch, E. V. Anslyn, *J. Am. Chem. Soc.* **2001**, *123*, 11296–11297; d) R. Kato, S. Nishizawa, T. Hayashita, N. Teramae, *Tetrahedron Lett.* **2001**, *42*, 5053–5056.
[8] When the color change is coupled to an irreversible chemical reaction the term "sensor" should not be applied, and should instead be replaced by terms such as "chromogenic reagent" or "chromogenic dosimeter" (or "chemodosimeter").
[9] F. Sancenón, A. B. Descalzo, R. Martínez-Máñez, M. A. Miranda, J. Soto, *Angew. Chem.* **2001**, *113*, 2710–2713; *Angew. Chem. Int. Ed.* **2001**, *40*, 2640–2643.
[10] M. S. Goodman, A. D. Hamilton, J. Weiss, *J. Am. Chem. Soc.* **1995**, *117*, 8447–8455.
[11] a) A. Metzger, E. V. Anslyn, *Angew. Chem.* **1998**, *110*, 862–865; *Angew. Chem. Int. Ed.* **1998**, *37*, 649–652; b) J. J. Lavigne, E. V. Anslyn, *Angew. Chem.* **1999**, *111*, 3903–3906; *Angew. Chem. Int. Ed.* **1999**, *38*, 3666–3669.
[12] a) C. Seel, A. Galan, J. De Mendoza, *Top. Curr. Chem.* **1995**, *175*, 102–132; b) R. Fitzmaurice, G. M. Kyne, D. Douheret, J. D. Kilburn, *J. Chem. Soc. Perkin Trans. 1* **2002**, 841–864.
[13] Hyperchem 6.0. Molecular Modeling System, Hypercube, Inc.

Porphyrin-Containing [3]Rotaxanes

Synthesis of Porphyrin-Containing [3]Rotaxanes by Olefin Metathesis**

*Ruud G. E. Coumans, Johannes A. A. W. Elemans, Pall Thordarson, Roeland J. M. Nolte, and Alan E. Rowan**

Rotaxanes are fascinating examples of interlocked molecules. Their synthesis is now well-established, and a large variety of interesting rotaxane-based architectures have been reported.[1,2] Our interest in rotaxanes partly arises from the reports by others on the synthesis of these molecules and their application in molecular devices, but predominantly by the impressive way nature makes use of catalytically efficient (pseudo)rotaxane structures in processes such as DNA replication and degradation.[3] In these structures the enzyme (for example, DNA polymerase III)[3] completely encircles the DNA strand and performs numerous rounds of catalysis (for example, template polymerization or hydrolysis) on the macromolecular substrate before dissociating from it. These so-called processive enzymes are therefore very efficient. Inspired by this concept, we have initiated a research project to construct synthetic analogues of these processive enzymes. For this purpose we have designed porphyrin host **1** (see Scheme 1), which can form very stable 1:1 host–guest complexes with viologen derivatives ($K_{ass} > 10^6\,M^{-1}$),[4] and have synthesized simple porphyrin-containing [2]rotaxanes.[5] It was also shown that the manganese derivative of **1** is a very active epoxidation catalyst.[6] A polymeric rotaxane with double bonds in the polymeric thread and host **1** as the circular component is needed to be able to construct a processive mimic. The latter molecule can then slide over the thread and epoxidize the double bonds (Figure 1). Herein we report the synthesis of such a rotaxane molecule by using olefin metathesis protocols.

Grubbs and co-workers have developed an elegant and efficient route to synthesize end-functionalized polybutadienes. They showed that an acyclic olefin can act as a chain transfer agent (CTA) in the ring opening metathesis polymerization (ROMP) of 1,5-cyclooctadiene (COD), using ruthenium carbenes **2** and **3** (Scheme 1) as initiators.[7] The CTA is incorporated at both ends of the polymer, with the average number of end groups per polymer chain (F_n) being close to 2. We decided to apply this protocol to synthesize the desired

[*] Dr. A. E. Rowan, R. G. E. Coumans, Dr. J. A. A. W. Elemans, Dr. P. Thordarson, Prof. R. J. M. Nolte
Department of Organic Chemistry, NSRIM
University of Nijmegen
Toernooiveld, 6525 ED Nijmegen (The Netherlands)
Fax: (+31) 24-3652929
E-mail: rowan@sci.kun.nl

[**] National Research School Combination Catalysis (NRSCC) is acknowledged for financial support.

Supporting information for this article is available on the WWW under http://www.angewandte.org or from the author.

 © 2003 Wiley-VCH Verlag GmbH & Co. KGaA, Weinheim 1433-7851/03/4206-0650 $ 20.00+.50/0

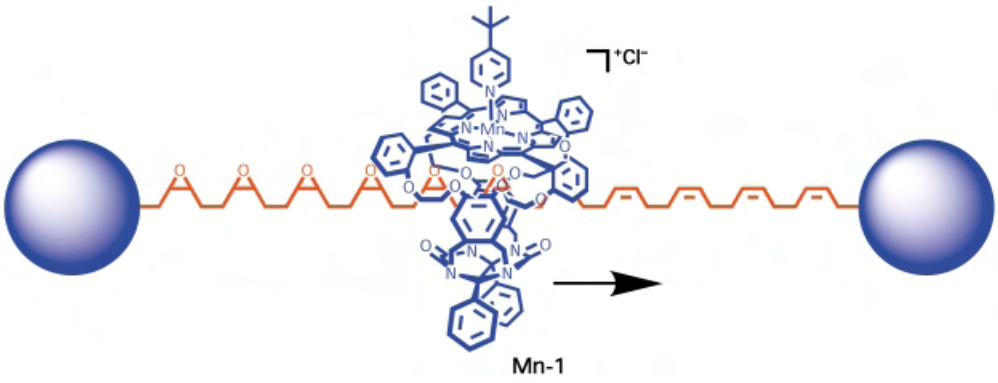
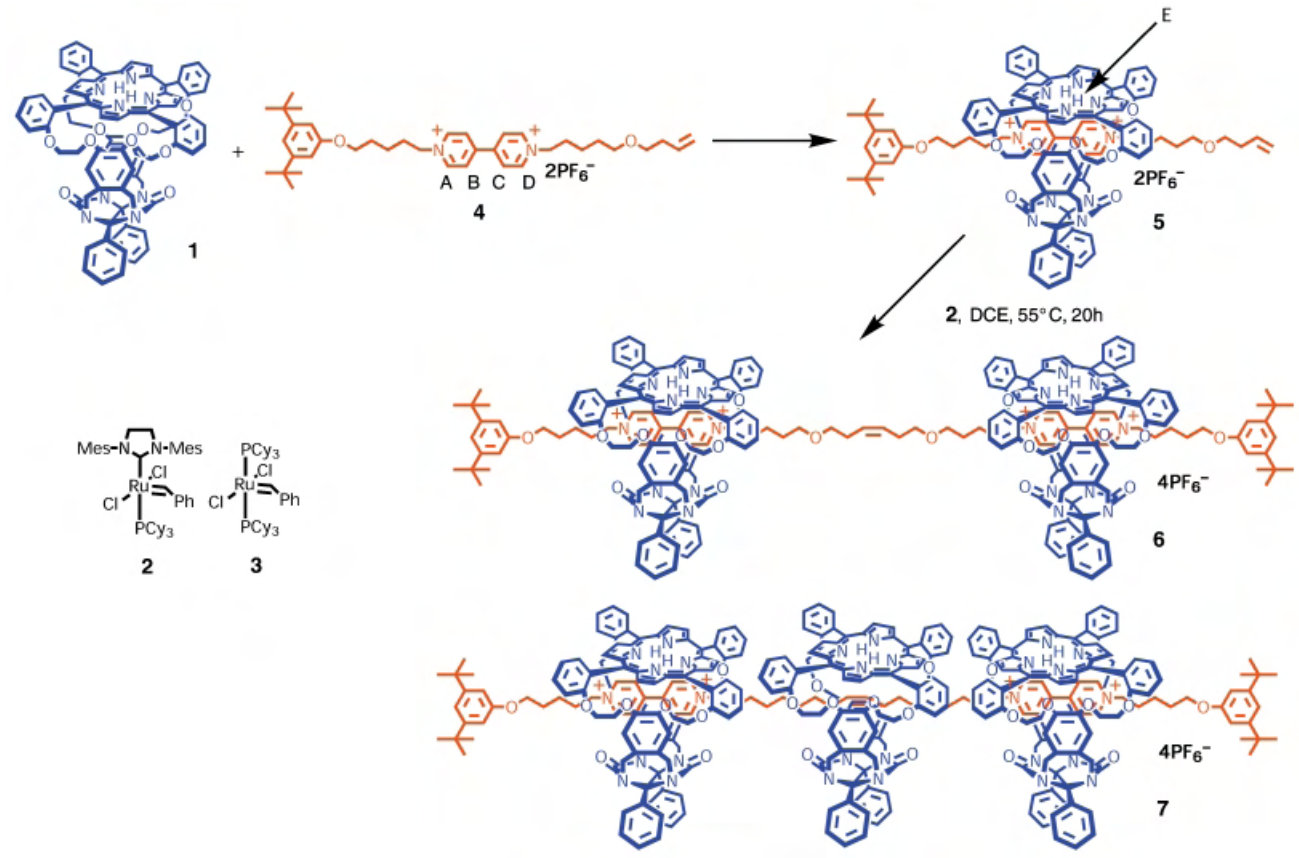


Figure 1. Schematic representation of an oxidative processive enzyme mimic, which involves a synthetic porphyrin threaded on a polymeric chain containing double bonds. The manganese porphyrin catalyst is shielded on the outside by a bulky 4-(*tert*-butyl)pyridine group and converts the double bonds into epoxides on the inside.



Scheme 1. Synthesis of [3]rotaxane **6** and [4]rotaxane **7**.

rotaxane by using a [3]rotaxane which contains a double bond as the CTA. The latter compound is synthesized by olefin self-metathesis. To the best of our knowledge there is only one example in the literature where olefin metathesis has been used to synthesize [2]rotaxanes, one in which the double bond is in the macrocyclic part.[8,9]

As a first step in the synthesis, viologen derivative **4** was synthesized which contains a blocking group on one end and a terminal alkene on the other end (Scheme 1). As expected, complexation of this guest molecule with host **1** afforded [2]pseudorotaxane **5**, which was soluble in solvents such as dichloromethane and 1,2-dichloroethane (DCE). The formation of **5** was evidenced by the large upfield complexation-induced shifts (CIS) of the bipyridinium protons A–D in the ^{1}H NMR spectra (Table 1) and by the presence of NOE contacts between these protons and the pyrrole NH protons E of the porphyrin.

It was envisioned that the addition of the second generation Grubbs' catalyst **2** (20 mol%) to a solution of **5** in DCE at 55°C would give rise to a homodimerization

 © 2003 Wiley-VCH Verlag GmbH & Co. KGaA, Weinheim 1433-7851/03/4206-0651 $ 20.00+.50/0

Table 1: Complexation-induced shifts for viologen protons A–D of [2]pseudorotaxane **5**.[a]

Proton	**4** (δ [ppm])	**5** ($\Delta\delta$ [ppm])
A	8.97	−2.48
B	8.44	−4.04
C	8.44	−4.30
D	8.94	−2.81

[a] 500 MHz, 298 K, $CDCl_3$/MeCN (1/1, v/v), 4×10^{-3} M.

reaction and yield [3]rotaxane **6** (Scheme 1). MALDI-TOF analysis of the reaction mixture after 20 h indeed showed peaks at *m/z* 4243.6, 4097.1, 3952.4, and 3807.2, which correspond to $[M^+-n\,PF_6]$ ($n=1,2,3,4$; Figure 2a). However, only a 25% conversion to **6** was observed (as judged by ^{1}H NMR spectroscopy). Therefore, an excess (five equivalents) of host **1** was used to drive the equilibrium more to the direction of **6** to improve the conversion of the reaction. Disappointingly, the conversion did not increase, but to our surprise MALDI-TOF analysis now clearly showed the presence of [4]rotaxane **7** ($[M^+-n\,PF_6]$ ($n=1,2,3,4$) at *m/z* 5588.1, 5443.2, 5298.2, and 5153.2) in addition to the [3]rotaxane (Scheme 1), which were inseparable (Figure 2a). This result suggests that viologen **4** is capable of forming a 2:1 host–guest complex with **1**.[10]

Interestingly, MALDI-TOF analysis showed, in addition to the expected masses for the rotaxanes **6** and **7**, peaks with values *m/z* 14 lower than the expected masses (Figure 2a). We believe that these peaks arise from a product that is formed from an initial isomerization reaction of a terminal alkene to an internal alkene, which can react with a second terminal olefin (with liberation of propene) to yield a [3]rotaxane with one methylene group less than in the expected product. Previous reports have demonstrated that catalyst **2** indeed is active in isomerization reactions of terminal alkenes to internal alkenes and leads to similar results.[11] Moreover, the isomerization of homoallyl ethers by **2** to yield vinyl ether species has been described in a recent report.[12] This observation can explain the rather low yield in the rotaxane synthesis, since the generated vinyl ether species can react with the metathesis catalyst to yield a Fisher carbene, which has already been shown to be inactive in cross-metathesis.[13] A signal at $\delta=13.74$ ppm arising from Ru=CHOR was observed in the ^{1}H NMR spectrum, which definitively supports the presence of this Fisher-carbene species.[13]

It was decided to use catalyst **3** instead of **2** to induce a metathesis reaction between the [2]pseudorotaxanes because of this interfering isomerization side-reaction. However, in a recent report by Grubbs and co-workers on cross-metathesis

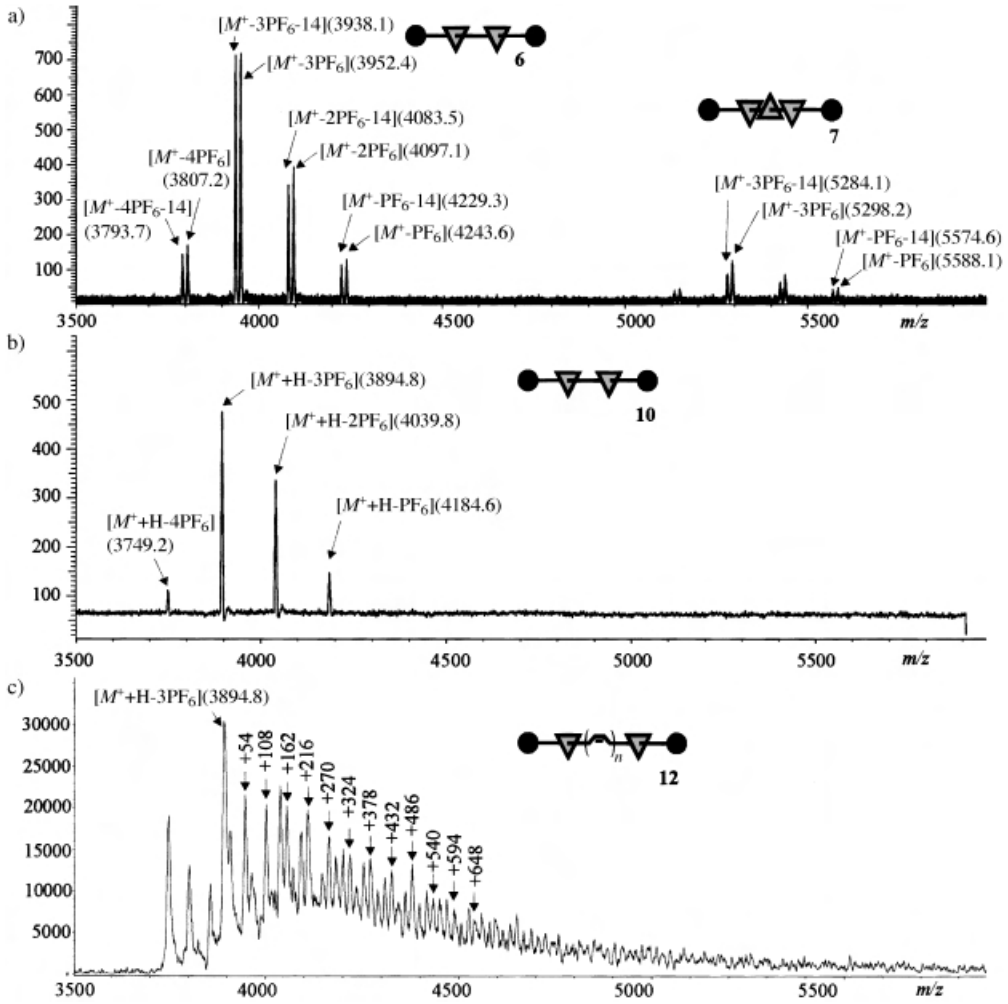
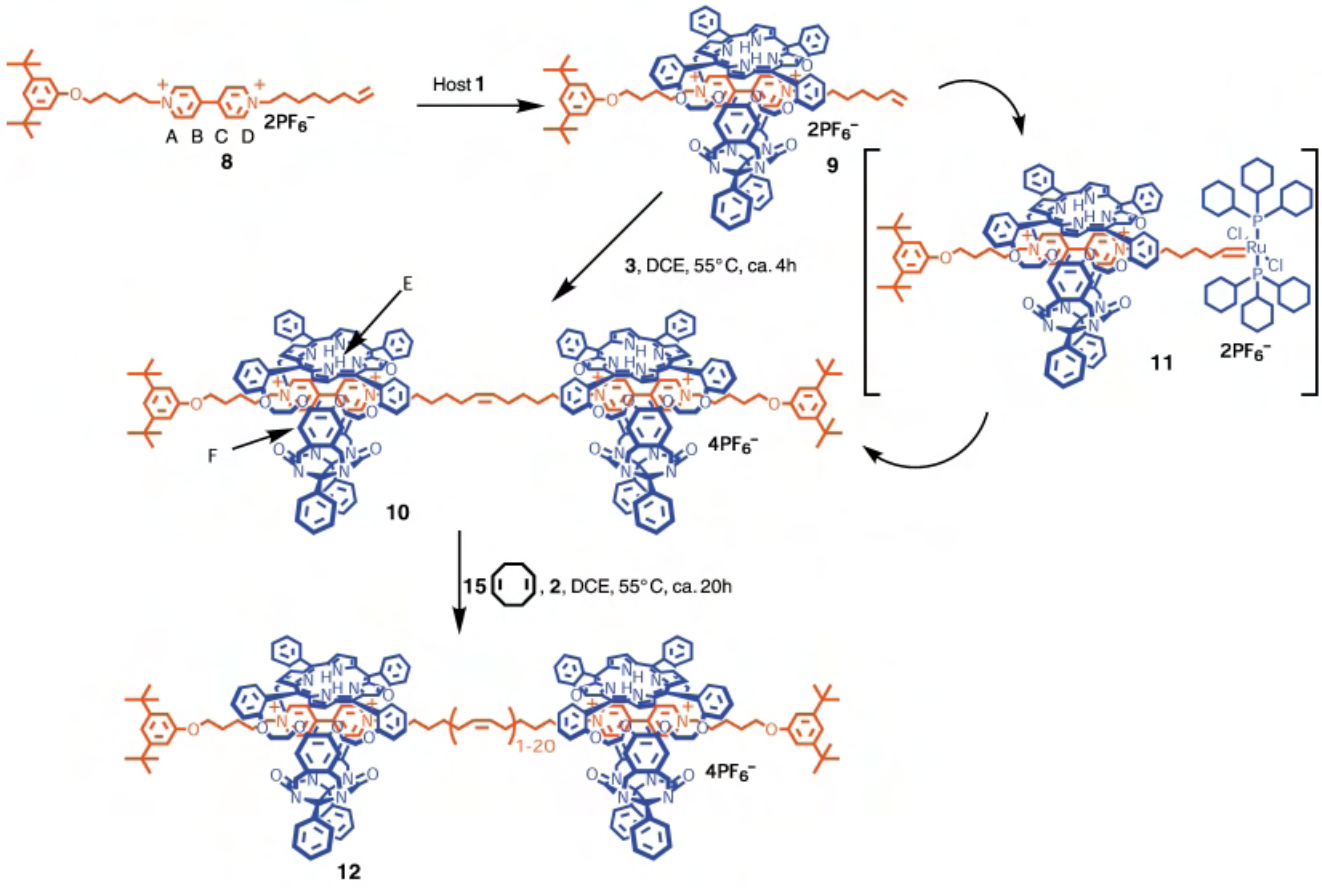


Figure 2. MALDI-TOF spectra of: a) [3]rotaxane **6** and [4]rotaxane **7**, b) [3]rotaxane **10**, and c) polymeric [3]rotaxane **12**.

 © 2003 Wiley-VCH Verlag GmbH & Co. KGaA, Weinheim 1433-7851/03/4206-0652 $ 20.00+.50/0



Scheme 2. Synthesis of [3]rotaxanes **10** and **12**.

using catalyst **3**, it was demonstrated that 4,4-diethoxy-1-butene is not very active in self-metathesis.[14] We, therefore, switched to using viologen **8**, in which the oxygen atom is omitted from the alkene part of the molecule (Scheme 2).

A solution of [2]pseudorotaxane **9** was treated with 16 mol% of **3** in DCE at 55°C for approximately 4 h to reach a conversion of approximately 60% into [3]rotaxane **10** (as judged by ^{1}H NMR spectroscopy; Scheme 2). Small amounts of [2]rotaxane, styrene-cross coupled [2]pseudorotaxane, and **9** were observed as side-products. MALDI-TOF analysis revealed peaks at *m*/*z* 4184.6, 4039.8, 3894.8, and 3749.2, which correspond to $[M^+ + H - n\,PF_6]$ ($n = 1, 2, 3, 4$; Figure 2b). No peaks for any isomerized product were visible, which probably accounts for the increase in the conversion relative to that in the previous reaction using **2**. Purification of the product was possible by chromatography: firstly on silica gel and and then on a size-exclusion column, and afforded [3]rotaxane **10** in 40% yield as a mixture of *cis* and *trans* isomers in a 2:3 ratio. The accepted mechanism for olefin self-metathesis is that catalyst **3** reacts with a terminal alkene to give an intermediate alkylidene complex.[15] This complex further reacts with another terminal alkene to give the homodimer and a propagating methylidene complex. In our case, the intermediate alkylidene complex is **11**, which is already a [2]rotaxane since the bulky PCy_3 groups bound to the ruthenium center prevent porphyrin host **1** from sliding off the thread. This intermediate could be oberved by ^{1}H NMR spectroscopy, namely, by the presence of a characteristic triplet at 19.26 ppm (Ru=CHR).

^{1}H NMR spectroscopic analysis showed that the resonances of protons A–D in **10** were dramatically shifted relative to those in [2]pseudorotaxane **9** (Table 2). The data suggest that the porphyrin beads in [3]rotaxane **10** are pulled towards each other, which results in downfield shifts for resonances A and B and upfield shifts for resonances C and D relative to those in the spectrum of the [2]pseudorotaxane **9**. Furthermore, NOE contacts of viologen protons A–D with porphyrin protons E and side-wall protons F are indicative of a rotaxane geometry.[5] The *cis* or *trans* geometry at the double bond is

Table 2: Comparison of chemical shifts of viologen protons A–D in [2]pseudorotaxane **9** and [3]rotaxane **10**.[a]

Proton	**9** (δ [ppm])	*cis*-**10** ($\Delta\delta$ [ppm])	*trans*-**10** ($\Delta\delta$ [ppm])	Δ(*cis* − *trans*) [ppm]
A	6.46	+0.90	+0.71	+0.19
B	5.08	+0.44	+0.35	+0.09
C	4.73	−0.76	−0.68	−0.08
D	5.91	−0.98	−0.79	−0.19

[a] 500 MHz, 298 K, $CDCl_3$, 4×10^{-3} M.

 © 2003 Wiley-VCH Verlag GmbH & Co. KGaA, Weinheim 1433-7851/03/4206-0653 $ 20.00+.50/0

reflected in the differences in the chemical shift of the resonances arising from the viologen protons A–D in the ^{1}H NMR spectrum of **10** (Table 2). These differences can be explained from the fact that the porphyrin beads are slightly more shifted towards the central double bond in the *cis* isomer than in the *trans* isomer, which results in downfield shifts for resonances A and B, and upfield shifts for resonances C and D.

Compound **10** was used as a chain transfer agent in the polymerization of cyclooctadiene catalyzed by **2** to synthesize a [3]rotaxane containing a polymeric thread (Scheme 2). Initial studies using 15 equivalents of COD showed that up to 10 units of COD are inserted (Figure 2c). This observation means that [3]rotaxane **10** can successfully be extended to [3]rotaxane **12**. Since **2** is a very active catalyst, chain transfer results in a stepwise increase in mass of *m*/*z* 54 (Figure 2c).

In conclusion, we have presented a novel procedure to synthesize porphyrin-containing [3]rotaxanes starting from [2]pseudorotaxanes through a self-metathesis reaction using Grubbs' catalyst **3**. These [3]rotaxanes can be extended to [3]rotaxanes containing a polymeric thread by using them as a CTA in the polymerization of COD by **2**. Further studies will be focused on the catalytic epoxidation of the double bonds in the manganese porphyrin derivative of [3]rotaxane **12**, with the intention of mimicking a natural processive enzyme.

Received: September 10, 2002 [Z50137]

[1] D. B. Amabilino, J. F. Stoddart, *Chem. Rev.* **1995**, *95*, 2725–2828.
[2] A. R. Pease, J. O. Jeppesen, J. F. Stoddart, Y. Luo, C. P. Collier, J. R. Heath, *Acc. Chem. Res.* **2001**, *34*, 433–444.
[3] a) W. A. Breyer, B. W. Matthews, *Protein Sci.* **2001**, *10*, 1699–1711; b) S. J. Benkovic, A. M. Valentine, F. Salinas, *Annu. Rev. Biochem.* **2001**, *70*, 181–208; c) E. T. Kool, J. C. Morales, K. M. Guckian, *Angew. Chem.* **2000**, *112*, 1026–1044; *Angew. Chem. Int. Ed.* **2000**, *39*, 990–1009.
[4] J. A. A. W. Elemans, M. B. Claase, P. P. M. Aarts, A. E. Rowan, A. P. H. J. Schenning, R. J. M. Nolte, *J. Org. Chem.* **1999**, *64*, 7009–7016.
[5] A. E. Rowan, P. P. M. Aarts, K. W. M. Koutstaal, *Chem. Commun.* **1998**, 611–612.
[6] J. A. A. W. Elemans, E. J. A. Bijsterveld, A. E. Rowan, R. J. M. Nolte, *Chem. Commun.* **2000**, 2443–2444.
[7] a) M. A. Hillmyer, S. T. Nguyen, R. H. Grubbs, *Macromolecules* **1997**, *30*, 718–721; b) C. W. Bielwaski, O. A. Sherman, R. H. Grubbs, *Polymer* **2001**, *42*, 4939–4945.
[8] D. A. Leigh, A. J. Wilson, T. J. Kidd in *Abstracts (Part 2) of the 218th American Chemical Society National Meeting* (New Orleans), **1999**, ORGN 0243.
[9] Olefin metathesis has been used in the synthesis of [2]catenanes and knots; see a) B. Mohr, M. Weck, J.-P. Sauvage, R. H. Grubbs, *Angew. Chem.* **1997**, *109*, 1365–1367; *Angew. Chem. Int. Ed. Engl.* **1997**, *36*, 1308–1310; b) T. J. Kidd, D. A. Leigh, A. J. Wilson, *J. Am. Chem. Soc.* **1999**, *121*, 1599–1600; c) D. G. Hamilton, N. Feeder, S. J. Teat, J. K. M. Sanders, *New J. Chem.* **1998**, *22*, 1019–1021; d) D. A. Leigh, P. J. Lusby, S. J. Teat, A. J. Wilson, J. K. Y. Wong, *Angew. Chem.* **2001**, *113*, 1586–1591; *Angew. Chem. Int. Ed.* **2001**, *40*, 1538–1543; e) C. O. Dietrich-Buchecker, G. Rapenne, J.-P. Sauvage, *Chem. Commun.* **1997**, 2053–2054.
[10] Detailed investigations concerning this novel binding mode are under investigation and will be reported elsewhere.
[11] a) A. Furstner, O. R. Thiel, L. Ackermann, H. J. Schanz, S. P. Nolan, *J. Org. Chem.* **2000**, *65*, 2204–2207; b) D. Bourgeois, A. Pancrazi, S. P. Nolan, J. Prunet, *J. Organomet. Chem.* **2002**, *643–644*, 247–252; c) S. S. Kinderman, J. H. van Maarseveen, H. E. Schoemaker, H. Hiemstra, F. P. J. T. Rutjes, *Org. Lett.* **2001**, *3*, 2045–2048.
[12] C. Cadet, P. I. Dalko, J. Cossy, *Tetrahedron Lett.* **2002**, *43*, 1839–1841.
[13] A. K. Chatterjee, J. P. Morgan, M. Scholl, R. H. Grubbs, *J. Am. Chem. Soc.* **2000**, *122*, 3783–3784.
[14] H. E. Blackwell, D. J. O'Leary, A. K. Chatterjee, R. A. Washenfelder, D. A. Bussmann, R. H. Grubbs, *J. Am. Chem. Soc.* **2000**, *122*, 58–71.
[15] M. S. Sanford, J. F. Love, R. H. Grubbs, *J. Am. Chem. Soc.* **2001**, *123*, 6543–6554.

Crown-Shaped Ln Polyoxometalates

Alkali-Metal-Controlled Self-Assembly of Crown-Shaped Ring Complexes of Lanthanide/$[\alpha\text{-}AsW_9O_{33}]^{9-}$: $[K\subset\{Eu(H_2O)_2(\alpha\text{-}AsW_9O_{33})\}_6]^{35-}$ and $[Cs\subset\{Eu(H_2O)_2(\alpha\text{-}AsW_9O_{33})\}_4]^{23-}$**

*Keisuke Fukaya and Toshihiro Yamase**

Polyoxometalates that are formed by self-assembly combine their nanoscopic size with the electronic, magnetic, or optical properties of the metal atoms, which should lead to interesting new materials.[1] The incorporation of the lanthanide ions Ln^{3+} in such polyoxometalates is of interest in supramolecular chemistry because of their luminescent and magnetic properties.[1c,2] With the aim of producing large clusters, much attention has focused on developing Ln^{3+}-incorporated polyoxometalates (polyoxometallolanthanoates), in which the Ln^{3+} ions are used as linkers in the self-assembled structure. Recently it was demonstrated that nano-sized polyoxometallolanthanoates, such as $\{Pr_6Mo_{120}\}$,[3] $\{Eu_4Mo_{128}\}$,[4] and

[*] Prof. Dr. T. Yamase, K. Fukaya
Chemical Resources Laboratory
Tokyo Institute of Technology
4259 Nagatsuta, Midori-ku, Yokohama 226-8503 (Japan)
Fax: (+81) 45-924-5260
E-mail: tyamase@res.titech.ac.jp

[**] This work was supported by Grants-in-Aid for Scientific Research, No. 10304055 and 14204067 from the Ministry of Education, Science, Sports, and Culture and No. 99P01201 from RFTF/JSPS, and by Core Research for Evolutional Science and Technology (CREST) of the Japan Science and Technology Corporation. Approximately 50% of this work was presented at the Conference of "Metal-assembled Complexes, Grant-in-Aid for Scientific Research on Priority Area" in Sendai, on December 11–13, 2001 and written up in the proceedings (P117) of that meeting.

Supporting information for this article is available on the WWW under http://www.angewandte.org or from the author.

 © 2003 Wiley-VCH Verlag GmbH & Co. KGaA, Weinheim 1433-7851/03/4206-0654 $ 20.00+.50/0

$\{Ce_{16}W_{148}\}$ [5] can be constructed through the coordination of Ln^{3+} ions by the outer oxygen atoms of polyoxometalate ligands. The modular construction of these analogues allows a flexible and rational design, as the architecture and chemical functionality of the polyoxometallolanthanoates can be, in principle, precisely controlled.[6,7] In a continuing project on the development of chelating agents for the Ln^{3+} ions, we have investigated the intramolecular energy transfer between the polyoxometalate ligands and the Ln^{3+} ions.[1c,8] Herein we report how use of the simple ligand, $[\alpha\text{-}AsW_9O_{33}]^{9-}$, leads to a unique supramolecular crown-shaped ring architecture containing Eu^{3+} ions, which is controlled by the alkali-metal ions. These are the first examples of polyoxometallolanthanoates with a crown-shaped ring structure that encapsulates a single alkali-metal cation in the center. Compound **1a** was isolated as the mixed Cs^+/K^+ salt **1** and **2a** as the mixed Cs^+/Na^+ salt **2**.

$[K \subset \{Eu(H_2O)_2(\alpha\text{-}AsW_9O_{33})\}_6]^{35-}$ **1a**

$Cs_{22}K_{13}[K \subset \{Eu(H_2O)_2(\alpha\text{-}AsW_9O_{33})\}_6] \cdot 44\,H_2O$ **1**

$[Cs \subset \{Eu(H_2O)_2(\alpha\text{-}AsW_9O_{33})\}_4]^{23-}$ **2a**

$Cs_{16.75}Na_{6.25}[Cs \subset \{Eu(H_2O)_2(\alpha\text{-}AsW_9O_{33})\}_4] \cdot 24.5\,H_2O$ **2**

Compound **1a** is a cyclic, K^+-ion-encapsulated hexamer of $[Eu(H_2O)_2(\alpha\text{-}AsW_9O_{33})]^{6-}$ ions, with idealized S_6 symmetry and a diameter of about 2.6 nm (Figure 1a), and **2a** is Cs^+-ion-encapsulated tetramer of $[Eu(H_2O)_2(\alpha\text{-}AsW_9O_{33})]^{6-}$ ions, with idealized C_{4h} symmetry and a diameter of about 2.2 nm (Figure 1b). The arrangement of the six $[\alpha\text{-}AsW_9O_{33}]^{9-}$ ligands in **1a** gives a hexagonal-chair conformation which resembles a watermill propeller, whereas **2a** resembles the vanes of a windmill. The distances between each Eu^{3+} ion of **1a** and **2a** range from 6.5 to 6.6 Å and the ions are located approximately on the As···As axis between $[\alpha\text{-}AsW_9O_{33}]^{9-}$ ligands (9.1 Å between neighboring As atoms; $\sphericalangle$ As···As···As $\approx 90°$). Each $[\alpha\text{-}AsW_9O_{33}]^{9-}$ ion is a hexadentate ligand and coordinates to two Eu^{3+} ions through four three-coordinate and two two-coordinate oxygen atoms. The residual coordination sites of the eight-coordinate Eu^{3+} ions are occupied by the oxygen atoms of two water molecules, which together with two two-coordinate oxygen atoms form the least-squares plane of the square-antiprismatic coordination environment (mean distance between neighboring oxygen atoms 2.9 Å); the $W\text{–}O_{\text{two-coordinate}}$ bond lengths range from 1.74 to 1.82 Å. The angle between the plane (plane 1) described by the four tungsten atoms of the W_4O_4 cavity that coordinates an Eu^{3+} ion, and the plane that is formed by six tungsten atoms that enclose an arsenic center (plane 2) is about 56°(see Figure 2). The mean distance between neighboring oxygen atoms of the W_4O_4 cavity is 2.6 Å. The coordination of each $[\alpha\text{-}AsW_9O_{33}]^{9-}$ ligand to two Eu^{3+} ions is asymmetric and nonequivalent, and results in Eu···As···Eu angles of approximately 90° and asymmetric distances of 5.1 and 4.0–4.1 Å between neighboring Eu and As atoms (for the coordination through the three-coordinate and two-coordinate oxygen atoms, respectively). These factors are instrumental in the construction of the crown-shaped ring. The approximate Eu···Eu···Eu angles among neighboring Eu^{3+} ions in **1a** and **2a** were 120° and 90°, respectively. In **1a** the diameter of the pseudohexagon, that is, the distance between two opposing Eu^{3+} ions, is 13.0 Å, and the central K^+ ion is eight coordinate, being bound by a two-coordinate oxygen atom from each of the six $[\alpha\text{-}AsW_9O_{33}]^{9-}$ ions (K–O 2.9 Å) and two disordered oxygen atoms from apical water molecules (K–O 2.7 Å). As a result, the $[K(H_2O)_2]^+$ ion is bonded to six $[Eu(H_2O)_2(\alpha\text{-}AsW_9O_{33})]^{6-}$ units to give an overall hexagonal-bipyramidal geometry (Figure 3a). In **2a** the central Cs^+ ion is 12 coordinate, being bound by two two-coordinate oxygen atoms (mean Cs–O 3.3 Å) and one three-coordinate oxygen atom (mean Cs–O 3.4 Å) from each of the four $[\alpha\text{-}AsW_9O_{33}]^{9-}$ ligands, with no coordinated water molecules. The Cs^+ ion enclosed in the molecular cavity of $[\{Eu(H_2O)_2(\alpha\text{-}AsW_9O_{33})\}_4]^{24-}$ is shown in Figure 3b. Interestingly, the molecular cavity of the $[\{Eu(H_2O)_2(\alpha\text{-}AsW_9O_{33})\}_4]^{24-}$ ring is too large to accommodate a single K^+ ion. The exchange of one type of Ln^{3+} ion for another demonstrates that the same crown architecture, with almost the same crystal-lattice parameters, could be obtained for other smaller lanthanide ions (across the periodic table until Yb^{3+}). Unfavorable coordination of the four three-coordinate oxygen atoms of the W_4O_4 cavity to large lanthanide ions implies that the high charge density of the Ln^{3+} ion affects the electrostatic interaction of the three-coordinate oxygen atoms in the formation of the crown. It has been established that two

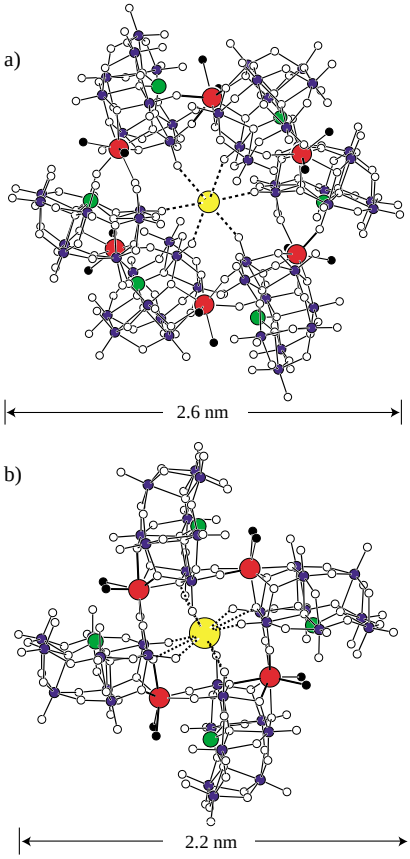


Figure 1. Molecular structures of a) **1a** and b) **2a**: green = As, red = Eu, yellow = K or Cs, blue = W, black = water O, and ○ = O.

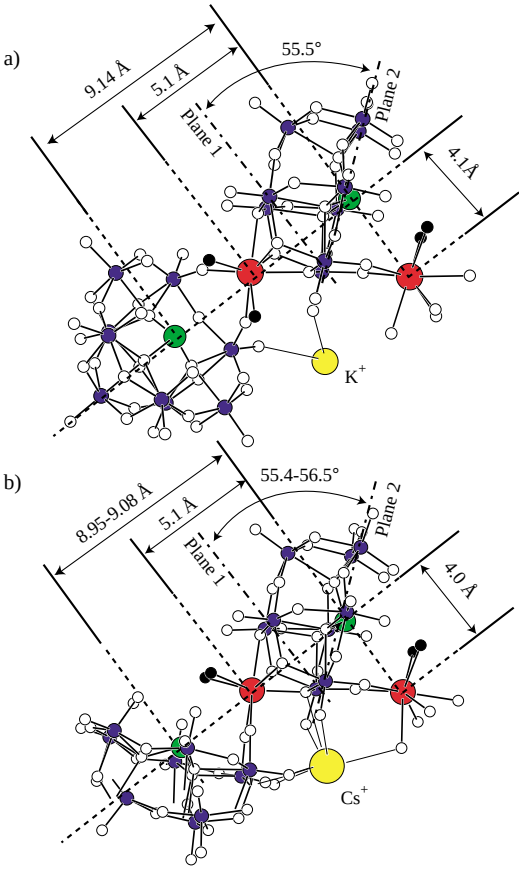


Figure 2. $[Eu(H_2O)_2]^{3+}$ ion coordinated by two hexadentate $[\alpha\text{-}AsW_9O_{33}]^{9-}$ ligands for a) **1a** and b) **2a**: Color code as in Figure 1. Ranges of the bond lengths [Å] and mean values in parentheses for **1a** and **2a**: Eu—$O_{three\text{-}coordinate}$ 2.31–2.52 (2.45 for **1a** and 2.43 for **2a**), Eu—$O_{two\text{-}coordinate}$ 2.30–2.39 (2.34 for **1a** and 2.36 for **2a**), Eu—O_{water} 2.36–2.55 (2.42 for **1a** and 2.45 for **2a**).

threefold symmetric $[\alpha\text{-}AsW_9O_{33}]^{9-}$ ligands can sandwich three transition-metal (TM) ions with TM···TM distances of 4.7–5.5 Å.[9] In these complexes the TM ions are coordinated through two two-coordinate oxygen atoms bonded to two of the six equatorial W atoms of the $[\alpha\text{-}XW_9O_{33}]^{9-}$ ligand (X = As, Sb, Bi) which results in an approximate D_{3h} symmetry. The coordination of the $[\alpha\text{-}AsW_9O_{33}]^{9-}$ ligands to metal ions through two two-coordinate oxygen atoms was also observed for Ln^{3+}-ion complexes, such as $\{Ce_{16}W_{148}\}$,[5] **3**,[7a] **4**,[10a] and **5**.[10b] The coordination of the $[\alpha\text{-}XW_9O_{33}]^{9-}$ ligand to the Ln^{3+} ion through the four three-coordinate oxygen atoms of the W_4O_4 cavity has been recently shown for **6** [6] where one of two square-antiprismatic LnO_8 coordination sites consists of four three-coordinate oxygen atoms of the $[\alpha\text{-}SbW_9O_{33}]^{9-}$ ligand and four two-coordinate oxygen atoms from $[W_5O_{18}]^{6-}$ (and the other site consists of six two-coordinate oxygen atoms from the $[W_5O_{18}]^{6-}$, and $[\alpha\text{-}SbW_9O_{33}]^{9-}$ ligands, and two water molecules). Interestingly, the coordination of three three-coordinate oxygen atoms to an Ln^{3+} ion has been shown for the highly negative charged $[Nb_6O_{19}]^{8-}$ ligand in **7**, where each Ln^{3+} ion has an approximately bicapped-trigonal-prismatical coordination environment, and is coordinated by three three-coordinate O atoms (mean O···O 2.7 Å) of the

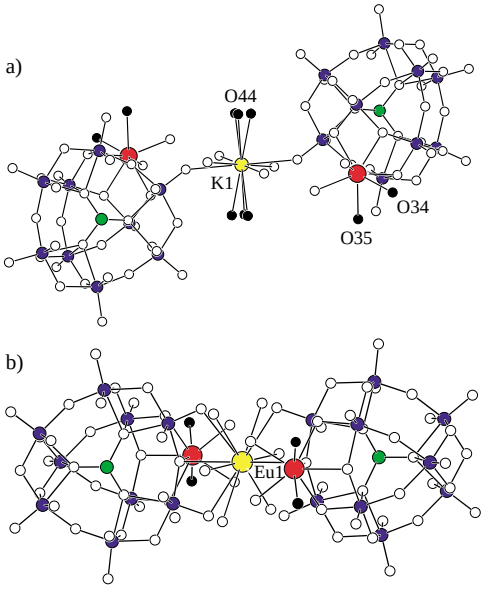


Figure 3. The coordination environment of a central alkali-metal a) **1a** b) **1b**: Color codes as in Figure 1. Apical O44 atoms in **1a** are related by C_3 symmetry in the interatomic O···O distances of 0.87(8) Å fixed at 1/3 occupancy . K—$O_{hexagonal}$; 2.92 Å, K—O_{apical}; 2.68 Å. Cs—$O_{three\text{-}coordinate}$; 3.31–3.45 Å (mean, 3.40 Å), Cs—$O_{two\text{-}coordinate}$; 3.11–3.44 Å (mean, 3.26 Å).

Nb_3O_3 cavity for the equatorially positioned $[Nb_6O_{19}]^{8-}$ ligand, one two-coordinate oxygen atom from an adjacent equatorially positioned Nb_6O_{19} ligand, an oxygen atom from a water molecule, two oxygen atoms shared by two Eu and Al atoms, and one oxygen atom shared by three Eu atoms in the central $\{Ln_3O(OH)_3(H_2O)_3\}_2$ core.[11]

$[Ce(Ce_2OH)(H_2O)_{10}(WO_2)_4(\alpha\text{-}AsW_9O_{33})_4]^{20-}$ **3**

$[\{Eu(H_2O)\}_3(\alpha\text{-}SbW_9O_{33})(W_5O_{18})_3]^{18-}$ **4**

$[Ce_3(CO_3)(\alpha\text{-}SbW_9O_{33})(W_5O_{18})_3]^{20-}$ **5**

$[(W_5O_{18})Ln(\alpha\text{-}SbW_9O_{33})Ln(H_2O)_2(W_5O_{18})]^{12-}$
(Ln = Eu, Dy, Er) **6**

$[\{Ln_3O(OH)_3(H_2O)_3\}_2Al_2(Nb_6O_{19})_5]^{26-}$ (Ln = Eu, Er, Lu) **7**

The fact that **1** and **2** were also obtained by mixing solutions containing $[\alpha\text{-}AsW_9O_{33}]^{9-}$ and Eu^{3+} ions with an aqueous solution containing alkali-metal ions at approximately 80 °C reveals that the $[Eu(H_2O)_2(\alpha\text{-}AsW_9O_{33})]^{6-}$ ion is the simple building unit for the crown-shaped ring structure. In the absence of any alkali-metal cations other than Na^+, no crown-shaped ring structure was formed, which suggests that the structure is stabilized by Cs^+ ions,[12] since the crystallization of **1a** was possible by treatment of a solution containing ligand, KCl, and Ln^{3+} with an aqueous solution containing Cs^+ ions. The structures of **1a** and **2a** originate from the approximately 90° Eu···As···Eu angle of the hexadentate $[\alpha\text{-}AsW_9O_{33}]^{9-}$ ligands coordinated to the $[Eu(H_2O)_2]^{3+}$ ions through the four three-coordinate and the

 © 2003 Wiley-VCH Verlag GmbH & Co. KGaA, Weinheim 1433-7851/03/4206-0656 $ 20.00+.50/0

two two-coordinate oxygen atoms which leads to the asymmetric position of the Eu^{3+} ion (Eu···As separations of 5.1 and 4.0–4.1 Å) on the almost linear As···Eu···As axis of the crown-shaped ring. The formation of the crown-shaped ring results from the cyclic polymerization of the $[Eu(H_2O)_2(\alpha\text{-}AsW_9O_{33})]^{6-}$ units which is governed by the radius of the encapsulated alkali-metal cation. Such an L-shaped $[Ln(H_2O)_2(\alpha\text{-}AsW_9O_{33})]^{6-}$ building unit provides an elegant approach to allow the development of the crown-shaped ring $[\{Ln(H_2O)_2(\alpha\text{-}AsW_9O_{33})\}_n]^{6n-}$ (n is an even number ≥ 8), which could encapsulate a large cation (such as C_{60}^+ or C_{70}^+ ion with the radius larger than Cs^+) which may form extended structures.

Experimental Section

1: A solution of $Na_2WO_4 \cdot 2H_2O$ (19.8 g, 60 mmol) and $NaAsO_2$ (0.87 g, 6.7 mmol) in water (60 mL) was heated at approximately 80 °C, thereafter acidified with 6 M HCl (20 mL, 120 mmol), and a solution of $Eu(NO_3)_3 \cdot 4H_2O$ (2.23 g, 5.0 mmol) in water (10 mL) was added. The solution pH was adjusted to 7–8 by the addition of KOH (8.0 g) in water (40 mL). The resulting cloudy solution was warmed again to approximately 80 °C and stirred for 30 min, then solid KCl (10 g) was added to precipitate the white product (21.8g), which was isolated by filtration. Recrystallization of the crude product (1.0 g) from a solution of CsCl (0.2 g) in water (40 mL) gave colorless hexagonal columnar crystals of **1**, which were isolated after the solution was left to stand at room temperature overnight. Yield: 0.18 g (18 % based on W). Elemental analysis (%) calcd: Cs 15.44, K 2.89, Eu 4.81, W 52.43, As 2.37; found: Cs 15.42, K 2.97, Eu 4.68, W 50.17, As 2.37. IR (KBr disk) metal–oxygen stretches at $\tilde{\nu} = 939$ (m), 883 (s), 795 (s), 715 cm^{-1} (s). For details of the synthesis of **2**, see Supporting Information.

Compounds **1** and **2** were also obtained by the reaction between the $[\alpha\text{-}AsW_9O_{33}]^{9-}$ ligand and the Ln^{3+} ion in an aqueous solution containing alkali-metal cations: For **1**, solid KCl (1.0 g, 13.4 mmol) was added to a solution of $Na_9(\alpha\text{-}AsW_9O_{33}) \cdot 19.5H_2O$ (1.4 g, 0.50 mmol)[13] and $Eu(NO_3)_3 \cdot 6H_2O$ (0.22 g, 0.50 mmol) in water (55 mL) at pH 6.2. The solution was warmed to approximately 80 °C for 30 min then cooled to room temperature to yield a white precipitate. After isolation of the crude product by filtration (1.5 g), a portion (1.0 g) was recrystallized from a solution of CsCl (0.2 g, 1.2 mmol) in water (30 mL) with a yield of 0.46 g.

Data for the single crystal X-ray studies of **1** and **2** were collected on a Rigaku RAXIS-RAPID imaging plate diffractometer with a graphite monochromatized $Mo_{K\alpha}$ radiation ($\lambda = 0.71069$ Å) at −130° and −100 °C, respectively. Lorentz polarization effects and numerical absorption corrections (by using the program Numabs and Shape, T. Higashi, *Program for Absorption Correction*, Rigaku Corporation, Tokyo, **1999**) were applied to the intensity data, and H atoms were not indicated in the calculation. Na, K, and Cs atoms (except for disordered atoms) and As, Eu, and W atoms were refined anisotropically, and all the O atoms and the disordered atoms were refined isotropically.

For **1** a total of 53693 reflections (ω scan and $2\theta_{max} = 54.9°$) was collected of which 11261 unique reflections ($R_{int} = 0.11$) were used. Crystal data: $M_r = 19045.31$, Space group $P\bar{3}$ (No. 147), $a = 23.560(1)$, $c = 15.370(1)$ Å, $Z = 1$, $V = 7388.6(6)$ $Å^3$, $\rho = 4.26$ g cm^{-3}, $\mu = 258.3$ cm^{-1}, $F(000) = 8192$. Crystal size = 0.20 × 0.15 × 0.15 mm. Transmission factors of 0.03–0.40. The structure was solved by a direct method (SIR92) and refined based on 5521 observed reflections with $I > 3\sigma(I)$ and 330 parameters to $R_1 = 0.066$ (refined against $|F|$) and $R_w = 0.170$ (refined against $|F^2|$). The highest residual electron density was 6.0 e $Å^{-3}$. All calculations were performed using the teXsan software package (teXsan: Crystal Structure Analysis Package, Molecular Structure Corporation **1998**–**1999**). The site occupancies of two Cs atoms (Cs4 and Cs5) and one K (K3) were fixed at 1/3, since distances between these atoms related by the C_3 symmetry are very short (< 3.0 and < 2.8 Å for Cs^+ and K^+, respectively), which may be brought about the disorder of these atoms. Similarly, the occupancy of O44 (apical coordination to K1) was also fixed at 1/3 because of the short distance (0.87(8) Å) between C_3-symmetric atoms. Furthermore, two water O atoms O42 and O43 were fixed at an occupancy of 1/2 because of their large thermal displacement parameters and short interatomic distance (2.4(1) Å), and the site occupancy of K4 was fixed at 5/6 to balance the charge of the molecule, which suggests the formula of **1** given.[14] A total of 22 Cs^+ (Cs1–Cs5) and 13 K^+ (K2–K4) counter cations are in the lattice coordinated by 5–14 oxygen atoms belonging to anion and lattice water molecules with Cs–O and K–O bond lengths of < 3.7 and < 3.2 Å, respectively. For details of **2**, see Supporting Information

Received: September 13, 2002 [Z50158]

[1] a) A. Müller, F. Peter, M. T. Pope, D. Gatteshi, *Chem. Rev.* **1998**, *98*, 239; b) E. Coronado, C. J. Gómez-Garcia, *Chem. Rev.* **1998**, *98*, 273; c) T. Yamase, *Chem. Rev.* **1998**, *98*, 307.

[2] R. C. Howell, F. G. Perez, S. Jain, W. D. Horrocks, Jr., A. L. Rheingold, L. C. Francesconi, *Angew. Chem.* **2001**, *113*, 41558; *Angew. Chem. Int. Ed.* **2001**, *40*, 4031.

[3] $\{Pr_6Mo_{120}\} = [\{Pr(H_2O)_5\}_6Mo_{120}O_{366}H_{12}(H_2O)_{48}]^{6-}$ A. Müller, C. Beugholt, H. Bögge, M. Schmidtmann, *Inorg. Chem.* **2000**, *39*, 3112.

[4] $\{Eu_4Mo_{128}\} = [\{Eu_4Mo_{128}O_{388}H_{10}(H_2O)_{81}\}_2]^{20-}$, L. Cronin, C. Beugholt, E. Krickemeyer, M. Schmidtmann, H. Bögge, P. Kögerler, T. Kim, K. Luong, A. Müller, *Angew. Chem.* **2002**, *114*, 2929; *Angew. Chem. Int. Ed.* **2002**, *41*, 2805.

[5] $\{Ce_{16}W_{148}\} = [Ce_{16}(H_2O)_{36}(WO_2)_4(W_2O_6)_8(W_5O_{18})_4(\alpha\text{-}AsW_9O_{33})_{12}]^{76-}$, K. Wassermann, M. H. Dickman, M. T. Pope, *Angew. Chem.* **1997**, *109*, 1513; *Angew. Chem. Int. Ed. Engl.* **1997**, *36*, 1445.

[6] a) H. Naruke, T. Yamase, *Bull. Chem. Soc. Jpn.* **2001**, *74*, 1289; b) H. Naruke, T. Yamase, *Bull. Chem. Soc. Jpn.* **2002**, *75*, 1275.

[7] a) K. Wassermann, M. T. Pope, *Inorg. Chem.* **2001**, *40*, 2763; b) M. Sadakane, M. H. Dickman, M. T. Pope, *Inorg. Chem.* **2001**, *40*, 2715; c) M. Sadakane, M. H. Dickman, M. T. Pope, *Angew. Chem.* **2000**, *112*, 3036; *Angew. Chem. Int. Ed.* **2000**, *39*, 2914.

[8] T. Yamase, H. Naruke, *J. Phys. Chem. B* **1999**, *103*, 8850.

[9] a) For $[Cu_3(H_2O)_2(\alpha\text{-}AsW_9O_{33}$ or $\alpha\text{-}SbW_9O_{33})_2]^{12-}$, F. Robert, M. Leyrie, G. Hervé, *Acta Crystallogr. Sect. B* **1982**, *38*, 358; b) For $[(VO)_3(\alpha\text{-}AsW_9O_{33})_2]^{11-}$, P. Mialane, J. Marrot, E. Rivière, J. Nebout, G. Hervé, *Inorg. Chem.* **2001**, *40*, 44; c) For $[\{Cu(H_2O)\}_3(\alpha\text{-}AsW_9O_{33}$ or $\alpha\text{-}SbW_9O_{33})_2]^{12-}$ and $[\{Mn(H_2O)\}_3(\alpha\text{-}AsW_9O_{33})_2]^{12-}$, U. Kortz, N. K. Al-Kassem, M. G. Savelieff, N. A. Al Kadi, M. Sadakane, *Inorg. Chem.* **2001**, *40*, 4742; d) For $[\{Mn(H_2O)\}_3(\alpha\text{-}SbW_9O_{33})_2]^{12-}$, M. Bösing, A. Nöh, I. Koose, B. Krebs, *J. Am. Chem. Soc.* **1998**, *120*, 7252; e) For $[(VO)_3(\alpha\text{-}SbW_9O_{33})_2]^{12-}$, T. Yamase, B. Botar, E. Ishikawa, K. Fukaya, *Chem. Lett.* **2001**, 56; f) For $[(VO)_3(BiW_9O_{33})_2]^{12-}$, B. Botar, T. Yamase, E. Ishikawa, *Inorg. Chem. Commun.* **2000**, *4*, 551; g) For $[\{PhSn\}_3(\alpha\text{-}SbW_9O_{33})_2]^{9-}$, G. Sazani, M. H. Dickman, M. T. Pope, *Inorg. Chem.* **2000**, *39*, 939.

[10] a) T. Yamase, H. Naruke, Y. Sasaki, *J. Chem. Soc. Dalton Trans.* **1990**, 1687; b) H. Naruke, T. Yamase, *J. Alloys Compd.* **1998**, *268*, 100.

[11] a) T. Ozeki, T. Yamase, H. Naruke, Y. Sasaki, *Inorg. Chem.* **1994**, *33*, 409; b) H. Naruke, T. Yamase, *Acta Crystallogr. Sect. C* **1996**, *52*, 2655; c) H. Naruke, T. Yamase, *J. Alloys Compd.* **1997**, *255*, 183.

[12] Preliminary results showed that Na^+ ions in the absence of other alkali-metal cations formed the hamburger-type sandwiched

$[Yb_2(H_2O)_5(\alpha\text{-}AsW_9O_{33})_2]^{12-}$ ion, where the Yb^{3+} ion is seven-coordinate, being bound by two two-coordinate O atoms from each $[\alpha\text{-}AsW_9O_{33}]^{9-}$ ligand and five (including one Yb–O–Yb bridging) water molecules. Single-crystal X-ray analysis is in progress. For $Na_{12}[Yb_2(H_2O)_6(\alpha\text{-}AsW_9O_{33})_2]\cdot m H_2O$ IR (KBr disk): $\tilde{\nu}$ = 938 (m), 887 (s), 788 (m), 724 cm^{-1} (s).

[13] C. Tourné, A. Revel, G. Tourné, M. Vendrell, *C. R. Seances Acad. Sci. Ser. C* **1973**, *277*, 643. IR (KBr disk): $\tilde{\nu}$ = 931 (m), 903 (s), 781 (s), 725 cm^{-1} (s).

[14] The existence of a broad asymmetric peak (at 579.4 and 580.3 nm with approximately 1:4 intensity ratio) for the $^5D_0 \rightarrow {}^7F_0$ transition in the 77 K photoluminescence spectrum (under the exposure to the 396 nm light corresponding to the $^7F_0 \rightarrow {}^5L_6$ transition) of solid **1** indicated the existence of at least two different sites (with approximate occupancy ratio of 1:4) for the Eu^{3+} luminescence. This supports the disorder (with 5/6 occupancy) for the K4 atom which is coordinated by water O atoms (O34 and O35) for $[Eu(H_2O)_2]^{3+}$, since the $^5D_0 \rightarrow {}^7F_0$ transition at about 580 nm cannot be split by any crystal field, see Supporting Information.

[15] Further details on the crystal structure investigations may be obtained from the Fachinformationszentrum Karlsruhe, 76344 Eggenstein-Leopoldshafen, Germany (fax: (+49) 7247-808-666; e-mail: crysdata@fiz-karlsruhe.de), on quoting the depository numbers CSD-391197 **1** and CSD-391198 **2**.

Conducting Polymers

Facile Solid-State Synthesis of Highly Conducting Poly(ethylenedioxythiophene)**

*Hong Meng, Dmitrii F. Perepichka, and Fred Wudl**

Conducting polymers continue to be a rapidly expanding, significant research area, attracting scientists from different disciplines.[1–3] Though synthesis has had a major role, a large effort has been focused on materials processing in organic electronics. Thin-film organic electronic devices such as light-emitting diodes, field effect transistors, solar cells, high-storage capacitors, and various other types of semiconductor devices have been widely investigated.[4–6] Efforts have also been directed toward developing new processing techniques and exploring new materials with a higher degree of molecular order.[2,7] However, the existence of very few single-crystalline polymers and the defects associated with the usual synthetic methods constitute a serious problem for the in-depth investigation of molecular order in conducting polymers.[8]

In general, it is not possible to obtain well-defined polymer structures unless the conducting polymers can be synthesized by endogenous polymerization routes, that is, without addition of initiators or catalysts. A possible solution for this problem lies in the solid-state polymerization of a structurally pre-organized crystalline monomer. The idea of solid-state polymerization of a suitable monomer in a well-ordered crystalline state was already realized in the 1960s and 1970s with polydiacetylenes and $(SN)_x$.[9–11] However, there were no reports on the solid-state synthesis of the most widely investigated conducting polymers—the polythiophenes. The importance of this goal is emphasized by the high potential of polythiophenes for industrial applications, as compared to other conducting polymers.[12] For example, the synthesis of poly(3,4-ethylenedioxythiophene), one of the most successful conducting polymers used in industry, is still confined to chemical or electrochemical oxidation of monomer solutions.[13] As a consequence, defect sites and a relatively low degree of intermolecular order limit the number of possible applications.

On the other hand, solid-state polymerization could give rise to a nearly defect-free, highly ordered or even "single-crystalline" conjugated polymer. With this in mind, while our discovery fall short of the mark regarding high degree of order, we report the first solid-state synthesis of conducting PEDOT by facile polymerization of 2,5-dibromo-3,4-ethylenedioxythiophene (DBEDOT) in the solid state.

The monomer DBEDOT[14] is a white, crystalline solid, melting at 96 °C and very soluble in all common organic solvents. Its solutions in solvents such as tetrahydrofuran, hexane, xylene, chloroform, ethanol, acetone, dimethylformamide, 1,4-dioxane, and 1,2-dichlorobenzene are very stable, even on heating to reflux. However, prolonged storage of DBEDOT in the solid state at room temperature results in transformation of the sample to blue-black "crystals" or "fibers" with metallic luster, while retaining the morphology of the starting material (Figure 1). To our surprise, the blue-

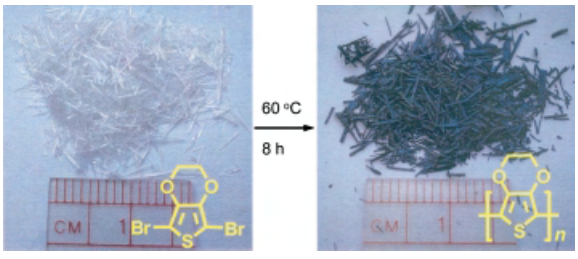


Figure 1. Photographs of crystals of DBEDOT (left) and PEDOT (right), formed on heating the crystals of the monomer at 60 °C for 8 h.

[*] Prof. F. Wudl, H. Meng, Dr. D. F. Perepichka
Department of Chemistry and Biochemistry
and
Exotic Materials Institute
University of California, Los Angeles, CA 90095-1569 (USA)
Fax: (+1) 310-825-0767
E-mail: wudl@chem.ucla.edu

[**] We thank the United States Air Force Office of Scientific Research for support through F49620-00-1-0103 and the Army Research Office for support of a MURI through DAAD19-99-1-0316. The authors thank Dr. M. Bendikov, Dr. R. Helgeson at EMI, UCLA, and Dr. Z. Bao, Lucent Technologies, for many valuable discussions. We are grateful to Mr. J. Huang for TEM measurements, Dr. S. I. Khan for the X-ray crystallographic analysis, Dr. R. E. Taylor for help with solid-state ^{13}C NMR and ESR measurements (Department of Chemistry and Biochemistry, UCLA), Dr. G. Z. Pan, of the Microfabrication Lab (UCLA), Mr. W. Yu, Mr. W. Dong, and Prof. S. Brown of the Department of Physics (UCLA) for help with conductivity measurements.

 © 2003 Wiley-VCH Verlag GmbH & Co. KGaA, Weinheim 1433-7851/03/4206-0658 $ 20.00+.50/0

black solid showed high conductivity, and its elemental analysis revealed that a clean polymerization reaction affording PEDOT took place (see below).

The reaction is dramatically accelerated on heating (Table 1) and is not affected by air, vacuum, or light; it can even be performed in hot water, and occurs only in the solid

Table 1: Conductivity σ_{rt} [$S\,cm^{-1}$] of PEDOT samples measured at room temperature.

	SSP PEDOT				$FeCl_3$-PEDOT
Temperature [°C]	ca. 20	60	80	120	0–5
Reaction time	2 years[a]	24 h	4 h	24 h	24 h
"crystals"/"fibers"	80	33	20	–	–
pellets as synthesized	30	18	16	0.1	–
pellets after I_2-doping	53	30	27	5.8	7.6
thin films	–	23	–	–	–
thin films after I_2-doping	–	48	–	–	–

[a] The monomer was stored in a closed jar for 2 years at room temperature (~20°C).

state. The resulting bromine-doped polymer[15] is infusible and insoluble in organic solvents and exhibits conductivity in the range of 20–80 $S\,cm^{-1}$ ("crystals") and 16–30 $S\,cm^{-1}$ (compressed pellets, as determined by the four-probe method), higher than that of conventional, commercial material (e.g., $FeCl_3$-synthesized PEDOT, Table 1). The conductivity showed a slight temperature dependence, with no semiconductor–metal transition down to 20 K.[16] The "as-formed" doped polymer was dried in vacuum (0.1 Torr) at 150°C and treated with 50% hydrazine monohydrate in acetonitrile to afford a brown, dedoped polymer (which is also insoluble in organic solvents) possessing a much lower conductivity ($< 10^{-4}\,S\,cm^{-1}$). Re-doping with iodine vapor restored the conductivity to essentially the original level (~20 $S\,cm^{-1}$).

The composition of the blue-black solid was determined by elemental analysis after vacuum drying at ambient temperature. The analysis corresponds to an empirical formula of $C_6H_4Br_{1.2}O_2S$, which suggests two Br_3^- anions and, therefore, a bipolaron per every five thiophene units.[17] Hydrazine treatment (as above) results in the almost complete removal of bromine (0.4% Br by elemental analysis).

A powdered, dedoped sample of polymerized DBEDOT was characterized by solid-state ^{13}C NMR and FT-IR spectroscopies. The comparison of the spectra of solid-state polymerized (SSP) material with a PEDOT sample prepared by traditional $FeCl_3$ oxidation of EDOT,[13] clearly demonstrates an essentially identical structure for both materials (Figure 2). The absence of a signal at $\delta = 84.6$ ppm, characteristic for CBr (as observed for DBEDOT), and the presence of a resonance at $\delta = 108.8$ ppm, typical of C–C bonds formed at the C-2 atoms of the thiophene rings, confirm the structure.

The conductivity of polymers prepared at different temperatures is listed in Table 1. The polymers synthesized at lower temperatures show a higher conductivity, which may reflect a higher degree of order in the polymerization for these conditions. Indeed, the highest conductivity was found for the SSP sample polymerized at room temperature; however, a very long reaction time from months to about 2 years was required. On the other hand, heating above the

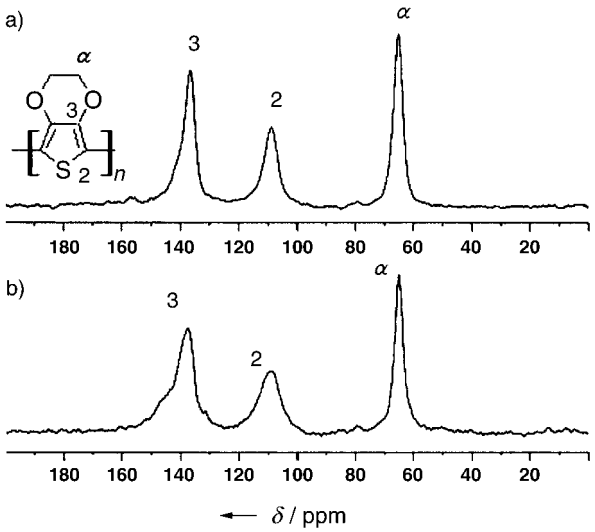


Figure 2. Solid-state ^{13}C NMR CP-MAS spectra of PEDOT prepared by a) solid-state polymerization of DBEDOT at 60°C and b) oxidative polymerization of EDOT in solution with $FeCl_3$, after dedoping with hydrazine monohydrate in acetonitrile solution (50%).

melting point of the monomer significantly inhibits the reaction and results in dramatically reduced conductivities (0.1 $S\,cm^{-1}$).

This observation implies that some aspects of the crystal structure may be responsible for the polymerization.[10] Figure 3 shows a crystal packing diagram of DBEDOT. Though the reaction cannot be topotactic since bromine is liberated, it does take advantage of the solid-state packing. Particularly, a short intermolecular Br–Br distance of 3.45 Å [vs the sum of van der Waals (vdW) radii of 3.9 Å] favors solid-state polymerization through the expulsion of molecular bromine and concomitant C–C bond formation at the 2- and 5-positions of the thiophene rings.[18] The molecular bromine, being a strong oxidant, dopes the formed polythiophene, providing a driving force for this unusual coupling reaction. Although the exact mechanism of the polymerization is not clear, there is a growth and decay of a free-radical species as a function of time, determined by ESR spectroscopy.[15,16] However, there is also an induction period which is ESR silent, leading us to believe that the ESR signal may not be associated with the polymerization but due to the formation of polarons in the polymer.

The approach described here offers a unique opportunity for the preparation of highly conductive, relatively well-ordered polymer films on an insulating support, which, in principle, can be utilized in the fabrication of all-organic LEDs.[5] High-vacuum (~10^{-4}–10^{-5} mbar) sublimation of DBEDOT with gentle heating of the substrate results in in-situ deposition of transparent, dark green to blue, uniform PEDOT films onto glass slides or a poly(ethyleneterephthalate) substrate (Figure 4). The average surface resistance of the films on a glass slide (average film thickness 2700 Å) is $2.1 \times 10^3\,\Omega_\square^{-1}$ ($\square = 1\,cm^2$) and on a plastic substrate (average film thickness 1300 Å) $3.6 \times 10^3\,\Omega_\square^{-1}$. The conductivity reaches 20 $S\,cm^{-1}$ and can be increased by almost a factor of 2 on further doping with iodine vapor. The very low value of

 © 2003 Wiley-VCH Verlag GmbH & Co. KGaA, Weinheim 1433-7851/03/4206-0659 $ 20.00+.50/0

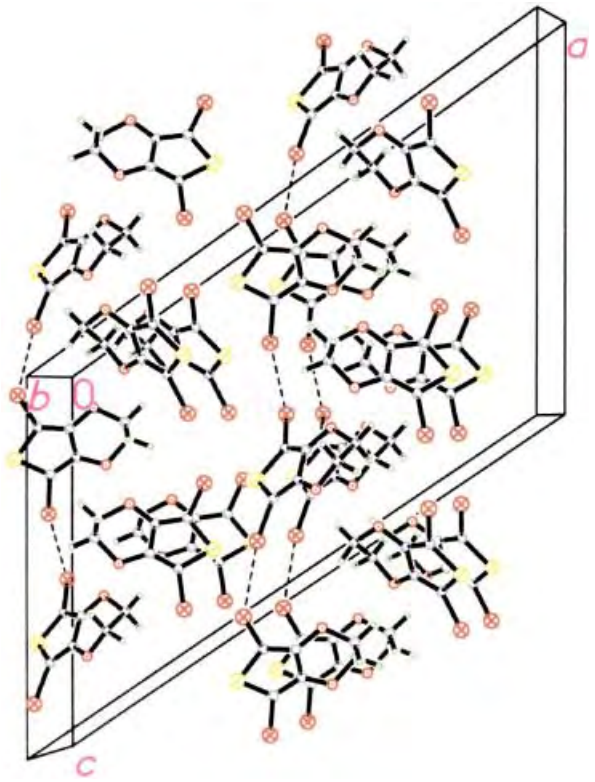


Figure 3. View of the X-ray crystallographically determined (monoclinic) structure of monomer DBEDOT: (⊗) bromine, (○) carbon, (○) hydrogen, (○) sulfur, (-----) short contacts between neighboring bromine atoms. The unit cell parameters are: $a = 25.27$, $b = 5.01$, $c = 15.67$ Å, $\alpha = 90$, $\beta = 123.96$, $\gamma = 90°$.

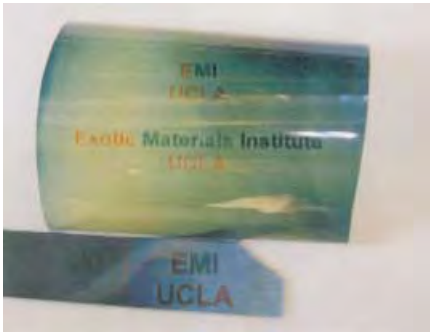


Figure 4. Photographs of transparent conducting films made by in-situ sublimation solid-state polymerization onto a plastic substrate (top) and a glass slide (bottom).

the surface resistance of the present thin films is comparable with that of recently reported films of PEDOT processed with glycerol or sorbitol (surface resistance: $\sim 10^3\ \Omega_{\square}^{-1}$, conductivity: $\sim 10\ \mathrm{S\,cm^{-1}}$).[19]

Figure 5 shows the UV-Vis spectra of the PEDOT films "as formed" and after "dedoping" (incomplete, note broad band at 1800 nm). The onset absorption at ca. 750 nm corresponds to an optical bandgap of 1.65 eV. This value is in the range of values reported for PEDOT samples synthesized by other methods (1.6–1.7 eV).[13]

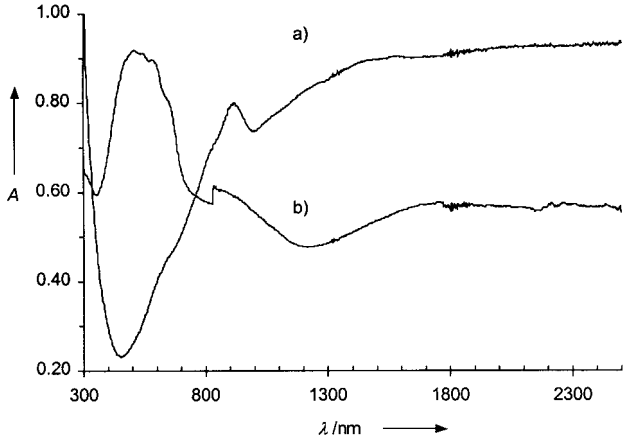


Figure 5. UV-Vis-NIR spectra of polymer films on glass slide substrates: a) "as-formed" on sublimation, b) after dedoping with hydrazine monohydrate in acetonitrile (50%).

The cyclic voltammogram (CV) of the as-prepared film on a platinum plate (Figure 6) shows an oxidation peak (*p* doping) at +0.07 V vs Ag/Ag^+, and the corresponding dedoping peak at −0.62 V. The film is very stable to repeated scanning from −1.0 to +0.2 V (less than 1% drop in current on 50 scans, without special precautions such as inert atmosphere). The bandgap determined from the onset of E^{pa} and E^{pc} potentials is 1.65 eV, in full agreement with the optical bandgap value.

In conclusion, we described an unprecedented catalyst-free coupling reaction of heteroaromatic halides, which provides a facile synthesis of highly conducting poly(ethylenedioxythiophene)s through solid-state polymerization of a substituted dibromothiophene derivative. This method allows fabrication of conducting films, which may be utilized in a variety of electronic devices. Although there are many challenges ahead, the present example of solid-state polymerization can be regarded as an important step towards the synthesis of a higher quality, solid-state polymerized conducting polythiophene derivative. Research directed to achieve a higher degree of order in the condensed state of conducting polymers using this strategy is in progress in our group.

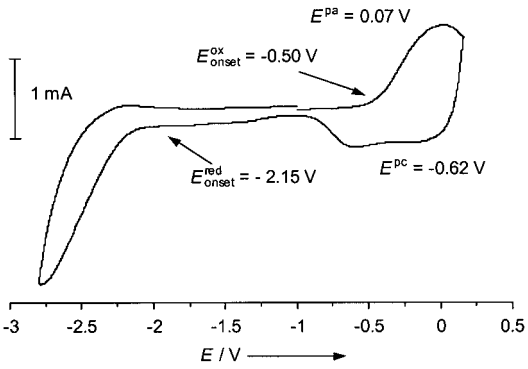


Figure 6. CV of a solid-state polymerized thin film deposited on a platinum plate. 0.1 M Bu_4NPF_6 in MeCN; scan rate 50 $mV\,s^{-1}$. Fc/Fc^+ shows + 0.14 V under these conditions.

 © 2003 Wiley-VCH Verlag GmbH & Co. KGaA, Weinheim 1433-7851/03/4206-0660 $ 20.00+.50/0

Experimental Section

DBEDOT was obtained according to ref. [14] with 76% yield: m.p. 96°C; ^{1}H NMR (500 MHz, $CDCl_3$, 25°C, TMS): $\delta = 4.27$ ppm (s, 4H); ^{13}C NMR (125 MHz, $CDCl_3$, 25°C, TMS): $\delta = 139.6$, 85.4, 64.9 ppm; CP-MAS ^{13}C NMR (75 MHz, solid state, 25°C, TMS): $\delta = 140.3$, 84.6, 65.1 ppm; MS (70 eV): m/z (%): 302 (55) [M^+], 300 (100), 298 (55); elemental analysis: found: C 23.79, H 1.28, Br 53.00, S 10.86; calcd for $C_6H_4Br_2O_2S$: C 24.02, H 1.34, Br 53.27, S 10.69.

PEDOT: In a typical experiment, DBEDOT (0.01–2 g) was incubated at 60°C for 24 h and dried in vacuum (0.1 mbar) at room temperature to give black crystals of bromine-doped PEDOT; elemental analysis: found: C 28.87, H 1.65, Br 38.42, S 12.90; calcd for $C_6H_4Br_{1.2}O_2S(H_2O)_{0.6}$: C 28.01, H 3.50, Br 38.73, S 12.45.

The well-ground material was additionally dried in vacuum (0.1 mbar) at 150°C overnight, then stirred with hydrazine hydrate (50% aqueous solution, in MeCN) overnight, filtered, and washed with neat MeCN. Vacuum drying afforded a nearly fully dedoped PEDOT; elemental analysis: found: C 46.84, H 2.42, N ~2, Br 0.42, S 19.04; calcd for $C_6H_4O_2Br_{0.01}S(NH_2NH_2{\cdot}3H_2O)_{0.12}$: C 47.63, H 3.44, N 2.22, Br 0.53, S 21.19. CP-MAS ^{13}C NMR (75 MHz, solid state, 25°C, TMS): $\delta_c = 136.5$, 108.7, 64.9 ppm; IR (KBr): $\tilde{\nu} = 1650$, 1431, 1358, 1203, 1066, 984, 918, 832, 690 cm^{-1}.

Received: September 24, 2002 [Z50225]

[1] a) C. K. Chiang, C. R. Fincher, Jr., Y. W. Park, A. J. Heeger, H. Shirakawa, E. J. Louis, S. C. Gau, A. G. MacDiarmid, *Phys. Rev. Lett.* **1977**, *39*, 1098; b) A. J. Heeger, *Angew. Chem.* **2001**, *113*, 2660; *Angew. Chem. Int. Ed.* **2001**, *40*, 2591.

[2] *Handbook of Conducting Polymers*, 2nd ed. (Eds.: T. A. Skotheim, R. L. Elsenbaumer, J. R. Reynolds), Marcel Dekker, New York, **1998**.

[3] G. Yu, J. Gao, J. C. Hummelen, F. Wudl, A. J. Heeger, *Science* **1995**, *270*, 1789.

[4] a) Q. Pei, G. Yu, C. Zhang, Y. Yang, A. J. Heeger, *Science* **1995**, *269*, 1086; b) J. H. Burroughes, D. D. C. Bradley, A. R. Brown, R. N. Marks, K. Mackay, R. H. Friend, P. L. Burns, A. B. Holmes, *Nature* **1990**, *347*, 539.

[5] a) J. A. Rogers, Z. Bao, K. Baldwin, A. Dodabalapur, B. Crone, V. R. Raju, V. Kuck, H. Katz, K. Amundson, J. Ewing, P. Drzaic, *Proc. Natl. Acad. Sci. USA* **2001**, *98*, 4817; b) H. Sirringhaus, T. Kawase, R. H. Friend, T. Shimoda, M. Inbasekaran, W. Wu, E. P. Woo, *Science* **2000**, *290*, 2123.

[6] a) S. Ghosh, O. Inganäs, *Adv. Mater.* **1999**, *11*, 1214; b) C. J. Brabec, N. S. Sariciftci, J. C. Hummelen, *Adv. Funct. Mater.* **2001**, *11*, 15; c) W. H. Kim, A. J. Mäkinen, N. Nikolov, R. Shashidhar, H. Kim, Z. H. Kafafi, *Appl. Phys. Lett.* **2002**, *80*, 3844.

[7] a) B. W. Maynor, S. F. Filocamo, M. W. Grinstaff, J. Liu, *J. Am. Chem. Soc.* **2002**, *124*, 522; b) R. P. Kingsborough, T. M. Swager, *J. Am. Chem. Soc.* **1999**, *121*, 8825.

[8] *Handbook of Organic Conductive Molecules and Polymers, Vol. 3* (Ed.: H. S. Nalwa), Wiley, New York, **1997**.

[9] a) M. Magat, *Polymer* **1962**, *3*, 449; b) R. H. Baughman, *J. Polym. Sci. Polym. Phys. Ed.* **1974**, *12*, 1511.

[10] a) G. Wegner, *Z. Naturforsch. B* **1969**, *24*, 824; b) G. Wegner, *Makromol. Chem.* **1971**, *145*, 85; c) V. Enkelmann, G. Schleier, G. Wegner, *Chem. Phys. Lett.* **1977**, *52*, 314; d) K. C. Yee, R. R. Chance, *J. Poly. Sci. Poly. Phys. Ed.* **1978**, *16*, 431.

[11] a) V. V. Walatka, Jr., M. M. Labes, J. H. Perlstein, *Phys. Rev. Lett.* **1973**, *31*, 1139; b) M. J. Cohen, A. F. Garito, A. J. Heeger, A. G. MacDiarmid, C. M. Mikulski, M. S. Saran, J. Kleppinger, *J. Am. Chem. Soc.* **1976**, *98*, 3844.

[12] *Handbook of Organic Conductive Molecules and Polymers, Vol. 2* (Ed.: H. S. Nalwa), Wiley, New York, **1997**.

[13] a) L. B. Groenendaal, F. Jonas, D. Freitag, H. Pielartzik, J. R. Reynolds, *Adv. Mater.* **2000**, *12*, 481; b) F. Jonas, L. Schrader, *Synth. Met.* **1991**, *41–43*, 831.

[14] DBEDOT was first reported by Reynolds et al.: G. A. Sotzing, J. R. Reynolds, P. J. Steel, *Chem. Mater.* **1996**, *8*, 882. It was used for a Ni^0-mediated coupling in solution to give oligo-EDOT: F. Tran-Van, S. Garreau, G. Louarn, G. Froyer, C. Chevrot, *J. Mater. Chem.* **2001**, *11*, 1378.

[15] In-situ ESR monitoring of the polymerization at 65°C showed the development of a symmetric ESR signal ($g = 2.006$), which reached a maximum after 4 h (corresponding to the formation of a polaron) and then gradually decreased to 65% of the maximum intensity (and changed shape, as a result of bipolaron formation).[16,17]

[16] H. Meng, F. Wudl, G. Z. Pan, W. Yu, W. Dong, S. Brown, unpublished results.

[17] A. O. Patil, A. J. Heeger, F. Wudl, *Chem. Rev.* **1988**, *88*, 183.

[18] 2,5-Dichoro-3,4-ethylenedioxythiophene, the intermolecular Cl–Cl distance of which (3.58 Å) is larger than the double vdW radius of chlorine (3.4 Å), does not polymerize under these conditions.

[19] F. Zhang, M. Johansson, M. R. Andersson, J. C. Hummelen, O. Inganäs, *Adv. Mater.* **2002**, *14*, 662.

Asymmetric Michael Addition

Highly Enantioselective Organocatalytic Conjugate Addition of Malonates to Acyclic α,β-Unsaturated Enones**

*Nis Halland, Pompiliu S. Aburel, and Karl Anker Jørgensen**

Even though the first reports of enantioselective organocatalysis by Wiechert et al. and Hajos and Parrish appeared almost three decades ago,[1] the field of asymmetric catalysis has been dominated by metal catalysis. It is only recently that asymmetric organocatalysis has received renewed attention and become the focus of intense research efforts.[2] This is primarily due to the operational simplicity, the cheap catalysts, and the obvious industrial applications.

Recently, a number of reports on organocatalytic transformations has appeared covering a wide range of reactions including Diels–Alder reactions,[3] aldol reactions,[4] Mannich

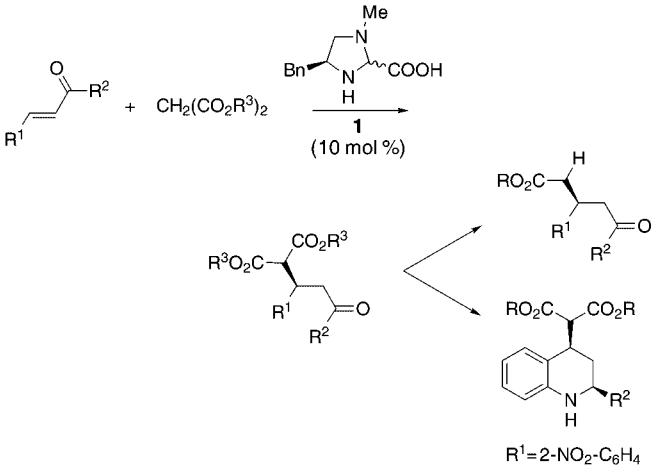
[*] K. A. Jørgensen, N. Halland, P. S. Aburel
Danish National Research Foundation: Center for Catalysis
Department of Chemistry
Aarhus University
8000 Aarhus C (Denmark)
Fax: (+45) 86196199
E-mail: kaj@chem.au.dk

[**] This work was supported by a grant from The Danish National Research Foundation. We are grateful to Dr. R. G. Hazell for X-ray crystallographic analysis.

Supporting information for this article is available on the WWW under http://www.angewandte.org or from the author.

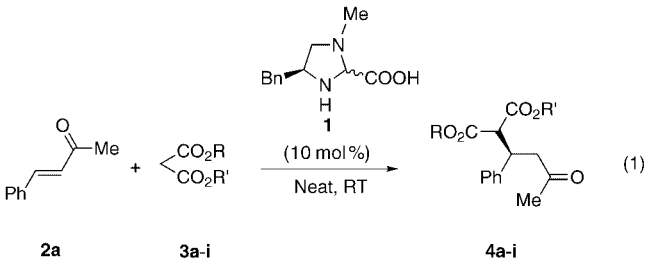
reactions,[5] 1,3-dipolar cycloadditions,[6] α amination,[7] synthesis of electron-rich benzene systems,[8] Robinson annulation,[9] Michael reaction,[10] Strecker reaction,[11] and others.[12] Although impressive results have been achieved in many organocatalytic asymmetric reactions, reports on enantioselective Michael addition reactions with excellent enantioselectivities (>90% *ee*) have until recently[10l] been limited to cyclic substrates[10e] or reactions with very low yields.[10f]

Herein we report the first enantioselective Michael addition of malonates to acyclic enones in excellent yields and enantioselectivities using an imidazolidine catalyst easily prepared from phenylalanine.[13] The potential of this new catalytic enantioselective C–C bond-forming reaction is demonstrated by an easy synthetic route to optically active δ ketoesters after a simple decarboxylation procedure and the formation of optically active tetrahydroquinolines (Scheme 1). This organocatalytic approach compares favorably to Lewis acid catalyzed[14] and indirect Lewis acid catalyzed[15] Michael additions to acyclic substrates in terms of ease of handling, yields, and enantioselectivities.



Scheme 1. Enantioselective Michael addition of malonates to acyclic enones.

The imidazolidine catalyst **1** is an efficient catalyst for the Michael addition of malonate nucleophiles to α,β-unsaturated enones [Eq. (1)], and a test reaction of benzylideneacetone (**2a**) with diethyl malonate (**3b**) and 10 mol% of catalyst **1** yielded the Michael adduct **4b** in high yield and 91% *ee* (Table 1, entry 2). A series of malonates were tested as it is known that the ester group has a large effect on the asymmetric induction of the reaction.[10a] The results of the screening of malonates **3a–i** in the reaction with **2a** in the presence of 10 mol% of **1** are presented in Table 1.



It turned out that the ester functionality has a large influence on the yield and enantioselective induction. The use of dimethyl malonate (**3a**) afforded only 73% *ee* (Table 1, entry 1), which is substantially lower than the 91% *ee* obtained in the initial test reaction with **3b** (Table 1, entry 2). For the sterically more hindered malonates **3c, 3d**, and **3i**, the reaction rate was decreased considerably and only low yields were obtained (Table 1, entries 3, 4, 9). The reactions of the medium-sized malonates **3e–h** all proceeded with excellent yields and enantioselectivities. For example, dibenzyl malonate (**3f**) afforded the Michael adduct in 93% yield and higher than 99% *ee* (Table 1, entry 6). Unfortunately the diastereoselectivities with the nonsymmetrical malonates **3g,h** were rather low (Table 1, entries 7, 8) as almost equal amounts of the isomers at the α-carbon atom were formed. This has been observed previously in amine-catalyzed Michael additions of nitroalkanes to enones.[10b,13]

To further explore the scope of the reaction, a series of α,β-unsaturated enones **2a–o** were reacted with dibenzyl malonate (**3f**) in the presence of 10 mol% of catalyst **1** [Eq. (2)]. The results are presented in Table 2. The aromatic

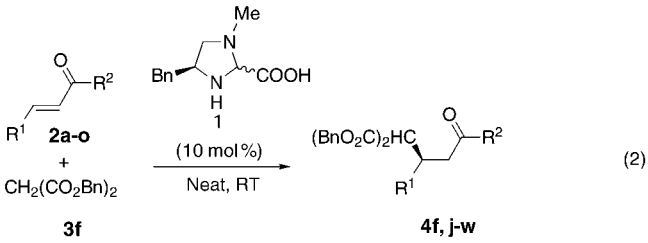


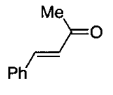
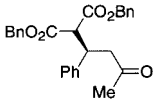
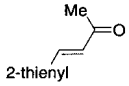
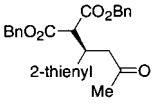
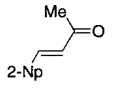
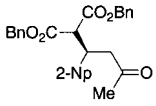
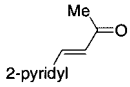
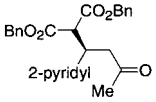
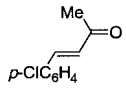
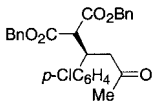
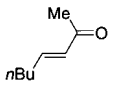
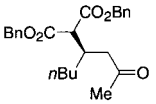
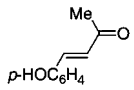
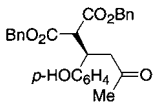
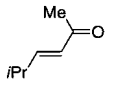
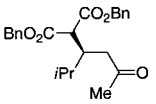
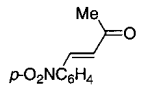
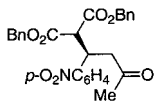
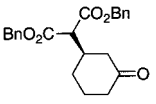
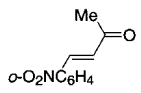
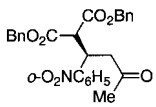
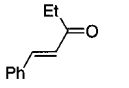
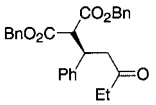
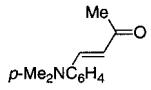
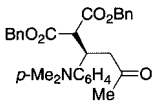
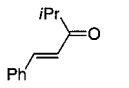
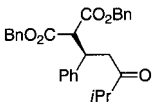
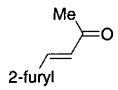
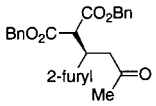
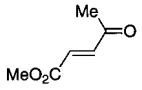
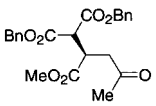
Table 1: Enantioselective Michael addition of malonates **3a-i** to benzylideneacetone (**2a**) catalyzed by **1** [Eq. (1)].[a]

Entry	Malonate	R	R′	*t* [h]	d.r.	Yield of **4** [%][b]	*ee* [%][c]
1	**3a**	Me	Me	120	–	66	73
2	**3b**	Et	Et	120	–	73	91
3	**3c**	*i*Pr	*i*Pr	210	–	26	71
4	**3d**	*t*Bu	*t*Bu	210	–	<5	nd
5	**3e**	allyl	allyl	150	–	92	89
6	**3f**	Bn	Bn	150	–	93	>99
7	**3g**	Bn	Me	150	1:1.5	92	98/97
8	**3h**	Bn	Et	150	1:1	90	90[d]
9	**3i**	Et	*t*Bu	150	1:1.3	<10	nd

[a] Experimental conditions: **2a** (0.5 mmol) and **1** (0.05 mmol) were added to **3** (1.0 mL) and the reaction mixture was stirred at ambient temperature for the time indicated in the table. [b] Unoptimized yields determined by GC. [c] Determined by chiral stationary-phase HPLC, see Supporting Information; nd: not determined. [d] Determined by chiral stationary-phase HPLC after decarboxylation, see Supporting Information.

 © 2003 Wiley-VCH Verlag GmbH & Co. KGaA, Weinheim 1433-7851/03/4206-0662 $ 20.00+.50/0

Table 2: Enantioselective Michael addition of dibenzyl malonate (**3f**) to **2a–o** catalyzed by **1** [Eq. (2)].[a]

Entry	Enone	Product	*t* [h]	Yield [%][b]	*ee* [%][c]	Entry	Enone	Product	*t* [h]	Yield [%][b]	*ee* [%][c]
1	 **2a**	 **4f**	165	86	99	9	 **2i**	 **4q**	165	75	92
2	 **2b**	 **4j**	165 165	99 74	90 93[d]	10	 **2j**	 **4r**	165	95	88
3	 **2c**	 **4k**	165	75	98	11	 **2k**	 **4s**	250	61	91[f]
4	 **2d**	 **4l**	165	75	93	12	 **2l**	 **4t**	170	33	84
5	 **2e**	 **4m**	165	84	89[e]	13	 **2m**	 **4u**	150	78	83
6	 **2f**	 **4n**	150	87	86	14	 **2n**	 **4v**	250	66	95[f]
7	 **2g**	 **4o**	170	58	77	15	 **2o**	 **4w**	170	2	94
8	 **2h**	 **4p**	150	75	92	16	 **2p**	 **4x**	288	59	59[e]

[a] Experimental conditions: Enone **2** (0.5 mmol) and **1** (0.05 mmol) were added to **3f** (1.0 mL) and the reaction mixture was stirred at ambient temperature for the time indicated in the table. [b] Yields after flash chromatography. [c] Determined by chiral stationary-phase HPLC, see Supporting Information. [d] Performed at 10 °C. [e] Performed at 0 °C. [f] Performed by using 20 mol% of catalyst.

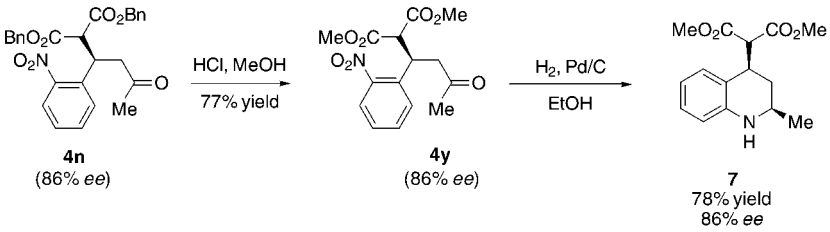
enones **2a–f** reacted very well with **3f** and the Michael adducts **4f,j–n** were all formed in high yields and enantioselectivities (Table 2, entries 1–6). Both electron-withdrawing (NO_2, Cl) and -donating substituents (OH) can be introduced on the aromatic ring without compromising the yield or enantioselectivity of the reaction (Table 2, entries 3–6). The only exception to the generally high yields and enantioselectivities with aromatic enones was the *N,N*-dimethylaniline derivative **2g** (58% **4o** with 77% *ee*, Table 2, entry 7). The heteroaromatic enones **2h–j** were also successfully used in this Michael reaction (Table 2, entries 8–10). The alkyl-substituted enones **2k,l** were found to react quite slowly and with lower yields even when longer reaction times and higher catalyst loadings were employed (Table 2, entry 11), however high enantioselectivities were still obtained (Table 2, entries 11, 12).

It should be noted that no by-products were observed in any of the reactions, that the yields for the slowly reacting substrates **2k,l,n,o** are a consequence of the reaction time, and that higher yields could be obtained at longer reaction times. Higher yields[16] could also be achieved at elevated reaction temperatures, but generally accompanied by slightly decreased enantioselectivies: for instance, compound **4v** was formed in 82% yield and 87% *ee* at 60 °C (10 mol% of **1** and shorter reaction time). For the sterically more hindered enones **2n,o**, the reaction rate was decreased and lower yields resulted. This seems to be an effect of the added steric bulk on the ketone, hindering the catalyst approach, and thus slowing

 © 2003 Wiley-VCH Verlag GmbH & Co. KGaA, Weinheim 1433-7851/03/4206-0663 $ 20.00+.50/0

down the reaction rate. The reduced reaction rate did not affect the asymmetric induction (Table 2, entries 14, 15). An ester-substituted enone, **2p**, was also tested; the Michael adduct **4x** was formed, although in moderate yield and enantioselectivity (Table 2, entry 16).

The absolute configuration of the Michael adduct **4k** was determined to be *R*.[17] This is in complete agreement with an iminium ion intermediate **5** (Figure 1),[18] obtained from activation of enone **2a** by the chiral catalyst. The *Re* face of the enone in this intermediate is shielded by the benzyl group of the chiral catalyst allowing the malonate to approach the open *Si* face of the enone as outlined in Figure 1.



Scheme 2. Synthesis of an optically active tetrahydroquinoline from **4n**.

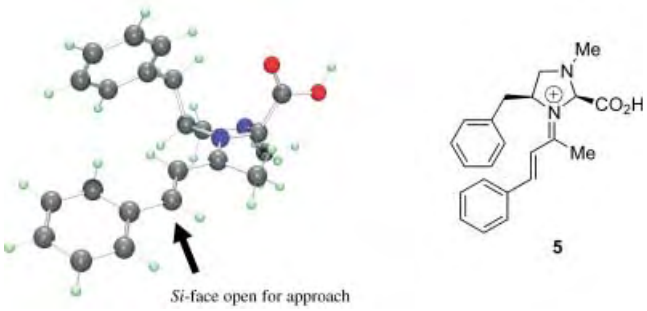
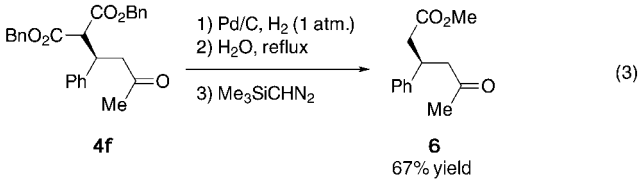


Figure 1. PM3-minimized structure and formula of the proposed iminium ion intermediate **5**.

The Michael adducts **4** could easily undergo a simple one-pot decarboxylation–transesterification procedure to give the corresponding optically active δ ketoesters **6** as shown in Equation (3) for Michael adduct **4f** which is decarboxylated in 67% yield (unoptimized) and without detectable loss of optical activity.



(3)

Michael adduct **4n** could be used for a facile synthesis of the biologically interesting optically active tetrahydroquinoline **7** (Scheme 2).[19] The transformation of dibenzyl ester **4n** into the corresponding dimethyl ester **4y** was followed by reductive amination giving tetrahydroquinoline **7** as a single diastereomer in 78% yield and without loss of otical purity.

In summary, we have developed the first highly enantioselective organocatalytic Michael addition of malonates to α,β-unsaturated enones using an imidazolidine catalyst easily prepared from phenylalanine. The reaction proceeds for a great diversity of α,β-unsaturated enones with excellent enantioselectivities. The scope of the reaction is demonstrated by the synthesis of optically active δ ketoesters and tetrahydroquinolines.

Received: October 10, 2002 [Z50341]

[1] a) U. Eder, G. Sauer, R. Wiechert, *Angew. Chem.* **1971**, *83*, 492; *Angew. Chem. Int. Ed. Engl.* **1971**, *10,* 496; b) Z. G. Hajos, D. R. Parrish, *J. Org. Chem.* **1974**, *39*, 1615.

[2] For recent reviews on asymmetric organocatalysis, see: a) B. List, *Tetrahedron* **2002**, *58*, 5573; b) H. Gröger, J. Wilken, *Angew. Chem.* **2001**, *113*, 545; *Angew. Chem. Int. Ed.* **2001**, *40,* 529; c) P. I. Dalko, L. Moisan, *Angew. Chem.* **2001**, *113*, 3840; *Angew. Chem. Int. Ed.* **2001**, *40,* 3726; d) E. R. Jarvo, S. J. Miller, *Tetrahedron* **2002**, *58*, 2481.

[3] a) A. B. Northrup, D. W. C. MacMillan, *J. Am. Chem. Soc.* **2002**, *124*, 2458; b) K. A. Ahrendt, C. J. Borths, D. W. C. MacMillan, *J. Am. Chem. Soc.* **2000**, *122*, 4243.

[4] a) A. Córdova, W. Notz, C. F. Barbas III, *J. Org. Chem.* **2002**, *67*, 301; b) K. Sakthivel, W. Notz, T. Bui, C. F. Barbas III, *J. Am. Chem. Soc.* **2001**, *123*, 5260; c) B. List, R. A. Lerner, C. F. Barbas III, *J. Am. Chem. Soc.* **2000**, *122*, 2395; d) A. Bøgevig, N. Kumaragurubaran, K. A. Jørgensen, *Chem. Commun.* **2002**, 620; e) A. B. Northrup, D. W. C. MacMillan, *J. Am. Chem. Soc.* **2002**, *124*, 6798.

[5] a) A. Córdova, S. Watanabe, F. Tanaka, W. Notz, C. F. Barbas III, *J. Am. Chem. Soc.* **2002**, *124*, 1842; b) A. Córdova, W. Notz, G. Zhong, J. M. Betancort, C. F. Barbas III, *J. Am. Chem. Soc.* **2002**, *124*, 1866; c) B. List, *Synlett* **2001**, 1687; d) B. List, P. Pojarliev, W. T. Biller, H. J. Martin, *J. Am. Chem. Soc.* **2002**, *124*, 827.

[6] a) W. S. Jen, J. J. M. Wiener, D. W. C. MacMillan, *J. Am. Chem. Soc.* **2000**, *122*, 9874; b) S. Karlsson, H. Högberg, *Tetrahedron: Asymmetry* **2002**, *13*, 923.

[7] a) B. List, *J. Am. Chem. Soc.* **2002**, *124*, 5656; b) A. Bøgevig, K. Juhl, N. Kumaragurubaran, W. Zhuang, K. A. Jørgensen, *Angew. Chem.* **2002**, *114*, 1868; *Angew. Chem. Int. Ed.* **2002**, *41*, 1790; c) N. Kumaragurubaran, K. Juhl, W. Zhuang, A. Bøgevig, K. A. Jørgensen, *J. Am. Chem. Soc.* **2002**, *124*, 6254.

[8] a) N. A. Paras, D. W. C. MacMillan, *J. Am. Chem. Soc.* **2001**, *123*, 4370; b) J. F. Austin, D. W. C. MacMillan, *J. Am. Chem. Soc.* **2002**, *124*, 1172; c) N. A. Paras, D. W. C. MacMillan, *J. Am. Chem. Soc.* **2002**, *124*, 7894.

[9] T. Bui, C. F. Barbas III, *Tetrahedron Lett.* **2000**, *41*, 6951.

[10] a) M. Yamaguchi, T. Shiraishi, M. Hirama, *J. Org. Chem.* **1996**, *61*, 3520; b) M. Yamaguchi, Y. Igarashi, R. S. Reddy, T. Shiraishi, M. Hirama, *Tetrahedron* **1997**, *53*, 11223; c) M. Yamaguchi, T. Shiraishi, Y. Igarashi, M. Hirama, *Tetrahedron Lett.* **1994**, *35*, 8233; d) T. E. Horstmann, D. J. Guerin, S. J. Miller, *Angew. Chem.* **2000**, *112*, 3781; *Angew. Chem. Int. Ed.* **2000**, *39*, 3635; e) S. Hanessian, V. Pham, *Org. Lett.* **2000**, *2*, 2975; f) J. M. Betancort, K. Sakthivel, R. Thayumanavan, C. F. Barbas III, *Tetrahedron Lett.* **2001**, *42*, 4441; g) J. M. Betancort, C. F. Barbas III, *Org. Lett.* **2001**, *3*, 3737; h) B. List, P. Pojarliev, H. J.

 © 2003 Wiley-VCH Verlag GmbH & Co. KGaA, Weinheim 1433-7851/03/4206-0664 $ 20.00+.50/0

Martin, *Org. Lett.* **2001**, *3*, 2423; i) D. Enders, A. Seki, *Synlett* **2002**, 26; j) A. Alexakis, O. Andrey, *Org. Lett.* **2002**, *4*, 3611; k) H. Brunner, C. Krumey, *J. Mol. Catal. A* **1999**, *142*, 7; l) D. J. Guerin, S. J. Miller, *J. Am. Chem. Soc.* **2002**, *124*, 2134.

[11] P. Vachal, E. N. Jacobsen, *J. Am. Chem. Soc.* **2002**, *124*, 10012.

[12] a) A. E. Taggi, A. M. Hafez, H. Wack, B. Young, W. J. Drury III, T. Lectka, *J. Am. Chem. Soc.* **2000**, *122*, 7831; b) B. R. Sculimbrene, A. J. Morgan, S. J. Miller, *J. Am. Chem. Soc.* **2002**, *124*, 11653.

[13] N. Halland, R. G. Hazell, K. A. Jørgensen, *J. Org. Chem.* **2002**, *67*, 8331.

[14] For reviews of enantioselective conjugate addition reactions, see: a) *Comprehensive Asymmetric Catalysis* (Eds.: E. N. Jacobsen, A. Pfaltz, H. Yamamoto), Springer, Berlin, **1999**; b) M. P. Sibi, S. Manyem, *Tetrahedron* **2000**, *56*, 8033; for examples of Lewis acid catalyzed enantioselective Michael additions of 1,3-dicarbonyl compounds to acyclic substrates, see: c) Y. Hamashima, D. Hotta, M. Sodeoka, *J. Am. Chem. Soc.* **2002**, *124*, 11240; d) N. End, L. Macko, M. Zehnder, A. Pfaltz, *Chem. Eur. J.* **1998**, *4*, 818; e) J. Ji, D. M. Barnes, J. Zhang, S. A. King, S. J. Wittenberger, H. E. Morton, *J. Am. Chem. Soc.* **1999**, *121*, 10215; f) J. Christoffers, U. Rößler, T. Werner, *Eur. J. Org. Chem.* **2000**, 701.

[15] For examples of Lewis acid catalyzed enantioselective Mukaiyama–Michael additions, see: a) D. A. Evans, T. Rovis, M. Kozlowski, C. W. Downey, J. S. Tedrow, *J. Am. Chem. Soc.* **2000**, *122*, 9134; b) D. A. Evans, K. A. Scheidt, J. N. Johnston, M. C. Willis, *J. Am. Chem. Soc.* **2001**, *123*, 4480.

[16] H_2O was also tried as an additive in the reactions to affect turnover, but it was found that the addition of 5 or 10 equiv of H_2O to the reaction mixture did not affect yield or enantioselectivity.

[17] CCDC-194337 contains the supplementary crystallographic data for this paper. These data can be obtained free of charge via www.ccdc.cam.ac.uk/conts/retrieving.html (or from the Cambridge Crystallographic Data Centre, 12, Union Road, Cambridge CB21EZ, UK; fax: (+44) 1223-336-033; or deposit@ccdc.cam.ac.uk).

[18] The calculations have been performed for the protonated carboxylic acid form of **5**.

[19] For a recent racemic synthesis of tetrahydroquinolines and their biological activity, see R. A. Bruce, D. M. Herron, L. B. Johnson, S. V. Kotturi, *J. Org. Chem.* **2001**, *66*, 2822, and references therein.

Structural Memory Reporters

Supramolecular Chirality: A Reporter of Structural Memory**

*Marco Ziegler, Anna V. Davis, Darren W. Johnson, and Kenneth N. Raymond**

Dedicated to Dr. Jide Xu
on the occasion of his 60th birthday

Herein we describe a molecular structure, formed from labile components, that exhibits structural memory. The macroscopic model in Figure 1 demonstrates this principle. The wooden icosohedral puzzle retains its structure (without any glue) despite dissociation of several pieces. These labile pieces can be removed and replaced without disassembly of the original structure. The structure itself is retained, or remembered, throughout the process of component substitution. In short, structural memory describes the substitution process itself and not merely the starting and ending states of the system.



Figure 1. A 3D puzzle made of labile wooden components retains its structure despite dissociation of several pieces.

Like the wooden puzzle, discrete supramolecular assemblies exhibit well-defined topologies, specified by the arrangement and connectivity of the constituent molecular components. If these molecular components can be substituted in a stepwise fashion and the supramolecular structure still persists, then there is structural memory. We describe such structural memory—as reported by retention of chirality—in

[*] Prof. K. N. Raymond, M. Ziegler, A. V. Davis, D. W. Johnson
Department of Chemistry
University of California
Berkeley, CA 94720-1460 (USA)
Fax: (+1) 510-486-5283
E-mail: raymond@socrates.berkeley.edu

[**] Coordination Number Incommensurate Cluster Formation, Part 23. Financial support for this work was provided by NSF CHE-9709621. We thank the Miller Foundation for a fellowship to M.Z. Part 22: D. W. Johnson, K. N. Raymond, *Inorg. Chem.* **2001**, *40*, 5157–5161.

 © 2003 Wiley-VCH Verlag GmbH & Co. KGaA, Weinheim 1433-7851/03/4206-0665 $ 20.00+.50/0

a chiral metallo-supramolecular assembly composed exclusively of labile *achiral* components. Although the molecular composition of the assembly is altered, chirality of the original assembly serves as a structural reporter, confirming that the original structure is preserved.

Chiral memory of self-assembled structures has been described previously.[2] In each of those examples, *chiral* molecular components induce supramolecular chirality in the original structure. Replacement of the chiral components by achiral analogues then creates a resolved structure, which is stable from days to years at room temperature. Importantly, without the initial chirally templated structure, the achiral components would assemble racemic, structural analogues. In contrast, we began with a resolved chiral assembly of achiral components in which chirality exists only at the supramolecular level. Stepwise replacement of the achiral components results in preservation of the original supramolecular chirality.

We have described the $[Ga_4L^1_6]^{12-}$ tetrahedron as the product of a rational design strategy; its labile metal and ligand components are programmed to form one predetermined structure.[3,4] The C_3 symmetry of trisbidentate chelation at the four octahedral metal centers and the C_2 symmetry of the six naphthyl-biscatecholamide L^1 ligands drive formation of an $M_4L^1_6$ tetrahedral cluster (Figure 2).[1] An isolated cavity exists within the structure, and it encapsulates guest molecules such as tetraethylammonium. The assembly is truly supramolecular: the lability of the Ga^{III}–catecholate interactions insures that self-assembly of the discrete structure is under thermodynamic control.

The chirality of the $[Ga_4L^1_6]^{12-}$ tetrahedron results from trisbidentate coordination of the metal ion. A simple $[GaL_3]^{3-}$ catecholate complex exists in solution as two rapidly interconverting enantiomers (Λ and Δ).[5] Mechanical coupling of two such metal centers in a $[Ga_2L_3]^{6-}$ helicate complex slows the isomerization rate by a factor of 100 (Figure 3).[6]

Assembly of the $[Ga_4L^1_6]^{12-}$ tetrahedron produces a racemic mixture of homochiral ($\Lambda\Lambda\Lambda\Lambda$ and $\Delta\Delta\Delta\Delta$) structures. We have shown that these assemblies can be resolved by using chiral countercations.[7] Most remarkably, after exchange of the resolving agent for achiral countercations, an aqueous solution of the $\Delta\Delta\Delta\Delta$-$[(Et_4N)\subset Ga_4L^1_6]^{11-}$ cluster retains its enantiopurity for at least eight months, even after extended boiling of the solution. The chirality of this structure, as measured from the circular dichroism spectra, persists even though there is evidence that partial dissociation of the complex occurs on the time scale of seconds.

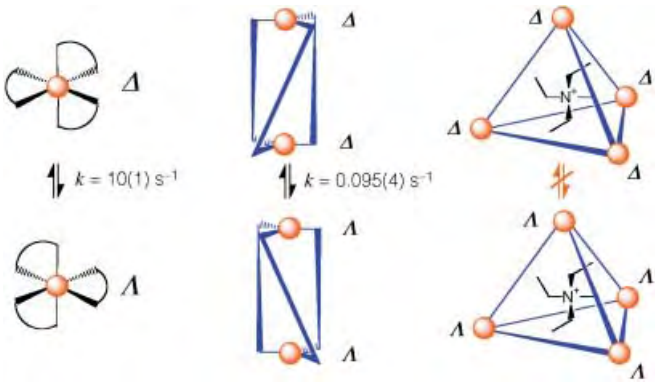


Figure 3. Racemization of a mononuclear $[GaL_3]^{3-}$ catecholate complex occurs 100 times faster than for $[Ga_2L_3]^{6-}$, while mechanical coupling of vertices in $[Ga_4L^1_6]^{12-}$ completely inhibits racemization.

The phenyl biscatecholamide L^2 ligand does not form a tetrahedral structure itself but rather only forms an M_2L_3 helicate when combined with octahedral metal ions (Figure 4).[8] However, ligands L^1 and L^2 share very similar coordination chemistries, as both are biscatecholates. That such supramolecular components are programmed with the information specific to the formation of one self-assembled structure is a central tenet of supramolecular chemistry. In violation of this principle, the robustness of the $[Ga_4L^1_6]^{12-}$ tetrahedral framework is subjected to a radical test. Its ligands are replaced with the nontetrahedral L^2 components in a stepwise fashion. Consequently, the formation of a series of $[Ga_4L^1_nL^2_{6-n}]^{12-}$ mixed-ligand tetrahedra from the homoleptic $[Ga_4L^1_6]^{12-}$ is followed in aqueous solution over time.

The L^1 tetrahedral cluster was prepared and isolated as the $\Delta\Delta\Delta\Delta$-$(Et_4N)_{11}[(Et_4N)\subset Ga_4L^1_6]$ salt, and the ligand L^2 was introduced as the helicate complex $K_6[Ga_2L^2_3]$ (Figure 4).

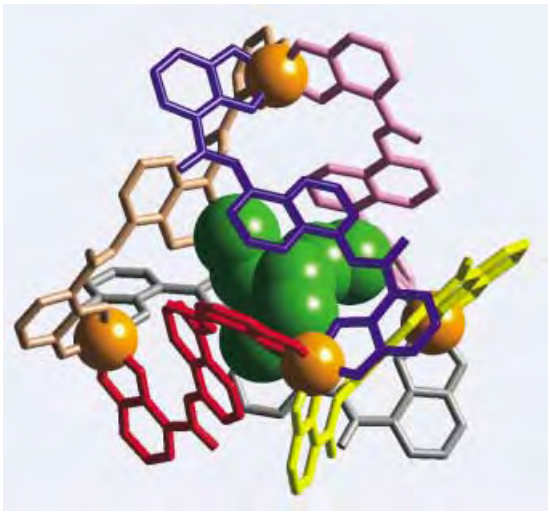


Figure 2. $M_4L^1_6$ tetrahedral assembly composed of biscatecholamide ligands and octahedrally coordinated metal ions.[1] The structure encapsulates guests such as Et_4N^+ ions.

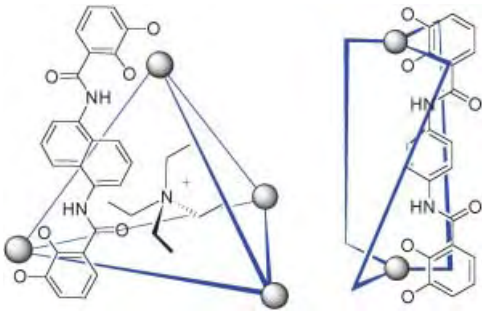


Figure 4. $\Delta\Delta\Delta\Delta$-$[(Et_4N^+)\subset Ga_4L^1_6]^{11-}$ and $[Ga_2L^2_3]^{6-}$ complexes used in the ligand-substitution experiment. Gray spheres represent Ga^{III} ions, while the blue lines represent the ligands of each structure.

 © 2003 Wiley-VCH Verlag GmbH & Co. KGaA, Weinheim 1433-7851/03/4206-0666 $ 20.00+.50/0

A D_2O solution of an equimolar ratio of the two complex (5.5 mM each) was prepared and buffered at pD 7.8. (The $K_6[Ga_2L^2_3]$ helicate provides a soluble source of L^2.)[9] This solution was heated to 75 °C, and the ligand-exchange reaction was monitored over 24 h by ^{1}H NMR and CD spectroscopies (Figure 5 and Figure 6, respectively).

The encapsulated Et_4N^+ ion acts as a structural probe in these experiments—it is only encapsulated in the M_4L_6 tetrahedra, as demonstrated by a large, characteristic upfield shift of its ^{1}H NMR resonance signals. The initial ^{1}H NMR spectrum of this reaction solution shows only one type of encapsulated Et_4N^+ ion, corresponding to the *ΔΔΔΔ*-$[(Et_4N)\subset Ga_4L^1_6]^{11-}$ starting material. The ^{1}H NMR data reveal formation of *ΔΔΔΔ*-$[(Et_4N)\subset Ga_4L^1_nL^2_{6-n}]^{11-}$ species over time, as new resonance signals for the encapsulated Et_4N^+ ion grow into the ^{1}H NMR spectra. (Identification of these species is corroborated by MS data.[10]) These mixed-ligand structures are the result of stepwise ligand replacement of L^1 by L^2 in the initial *ΔΔΔΔ*-$[(Et_4N)\subset Ga_4L^1_6]^{11-}$ tetrahedron. The CD spectra recorded at each time point show that the L^2-substituted *ΔΔΔΔ*-$[(Et_4N)\subset Ga_4L^1_nL^2_{6-n}]^{11-}$ tetrahedra maintain their full chirality throughout the substitution reaction. Stepwise ligand replacements do not compromise the structural or chiral memory of the initial tetrahedron! In fact at 24 h, little of the initial $[(Et_4N)\subset Ga_4L^1_6]^{11-}$ remains, while the initial tetrahedral structure and *ΔΔΔΔ* configuration are fully preserved in the L^2-substituted products.[11]

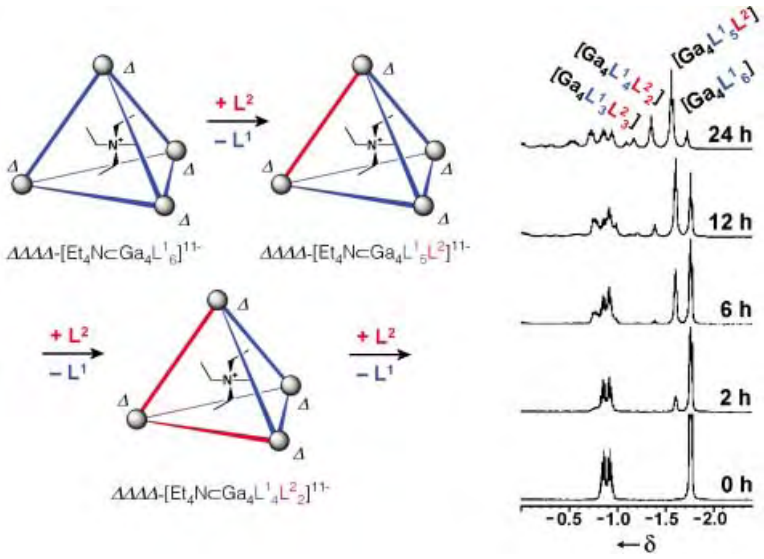


Figure 5. Left: schematic representation of L^2 ligand substitution into *ΔΔΔΔ*-$[(Et_4N)\subset Ga_4L^1_6]^{11-}$. Right: ^{1}H NMR spectral region showing signals of the Et_4N^+ guest. New guest signals appear as tetrahedra with different ligand combinations are formed. The methyl resonance signals of these guest species are labeled with the composition of the host tetrahedron.

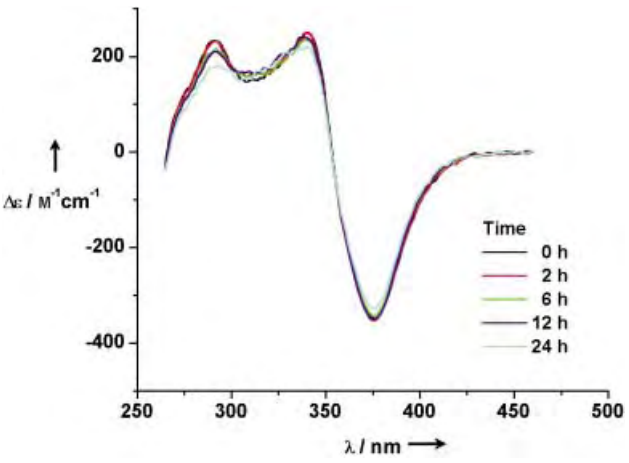


Figure 6. The chirality of the $[(Et_4N)\subset Ga_4L^1_nL^2_{6-n}]^{11-}$ tetrahedra is monitored by CD over time. Some change in the CD spectra is seen in the ligand-based absorptions due to the difference in chromophoric groups of the L^1 and L^2 ligands. However, these spectra show very little change in CD activity, demonstrating retention of chirality and thus structural memory of the tetrahedral system.

We have previously described the formation of libraries of mixed-ligand M_4L_6 tetrahedra, created from combinations of ligands, some of which form homoleptic tetrahedra and some of which do not; the formation of mixed-ligand supramolecular assemblies is not itself unprecedented.[10] However, we present here a different phenomenon: a tetrahedral assembly undergoes ligand substitution to generate a mixture of hybrid assemblies that retain the originally imprinted *chiral* tetrahedral structure. The chirality of the original structure—a property of the structure itself and not of its constituent components—acts as a structural reporter; retention of chirality throughout the substitution reaction distinguishes substitution into the original structure from disassembly of the original structure and *de novo* assembly of the new mixed species. This result is a consequence of the inertness of the resolved homochiral structure to racemization. Just as resolved *ΔΔΔΔ*-$[(Et_4N)\subset Ga_4L^1_6]^{11-}$ is not the thermodynamic product of the self-assembly of L^1 and Ga^{III}, resolved *ΔΔΔΔ*-$[(Et_4N)\subset Ga_4L^1_nL^2_{6-n}]^{11-}$ cannot be simply the thermodynamic product of the current substitution reaction. Therefore, we assert that the *ΔΔΔΔ*-$[(Et_4N)\subset Ga_4L^1_nL^2_{6-n}]^{11-}$ tetrahedra retain the structure, and consequently the chirality, of their *ΔΔΔΔ*-$[(Et_4N)\subset Ga_4L^1_6]^{11-}$ progenitors. This is a remarkable demonstration of structural and chiral memory in a single molecular species.

Experimental Section

General: ^{1}H NMR spectra were recorded on a Bruker DRX 500 MHz spectrometer. Circular dichroism spectra were measured with a Jasco J-500C spectropolarimeter, equipped with an IF-500 II A/D converter, and a Varian Cary 300 spectrophotometer was used to collect UV/Vis spectra. *ΔΔΔΔ*-$(Et_4N)_{11}[(Et_4N)\subset Ga_4L^1_6]$ and $K_6[Ga_2L^2_3]$ were synthesized as previously reported.[1,7,8]

Ligand substitution: A solution of $K_6[Ga_2L^2_3]$ (5.5 mM) and *ΔΔΔΔ*-$(Et_4N)_{11}[(Et_4N)\subset Ga_4L^1_6]$ (5.5 mM) was prepared in a KD_2PO_4/D_2O buffer adjusted to pD 7.8 with NaOD. The solution was heated in an NMR tube at 75 °C. At each time point the tube was cooled to room temperature, and an NMR spectrum was recorded.

 © 2003 Wiley-VCH Verlag GmbH & Co. KGaA, Weinheim 1433-7851/03/4206-0667 $ 20.00+.50/0

For CD spectral measurements, aliquots of the reaction solution were removed at each time point and diluted to 0.52 mM with 2 mM KOH(aq). CD samples were measured in a 0.1 mm quartz cell. The absorption spectrum of each diluted aliquot was measured to verify aliquot concentration. Some material precipitated from the D_2O solution over the course of the reaction. This material was redissolved and was found to contain the same mixture of species as the reaction solution (as evidenced by ^1H NMR spectroscopy) and the same CD spectrum.

Received: October 15, 2002 [Z50366]

[1] a) D. L. Caulder, R. E. Powers, T. N. Parac, K. N. Raymond, *Angew. Chem.* **1998**, *110*, 1940; *Angew. Chem. Int. Ed.* **1998**, *37*, 1840; b) D. L. Caulder, C. Brückner, R. E. Powers, S. König, T. N. Parac, J. A. Leary, K. N. Raymond, *J. Am. Chem. Soc.* **2001**, *123*, 8923.

[2] a) Y. Furusho, T. Kimura, Y. Mizuno, T. Aida, *J. Am. Chem. Soc.* **1997**, *119*, 5267; b) Y. Mizuno, T. Aida, K. Yamaguchi, *J. Am. Chem. Soc.* **2000**, *122*, 5278; c) E. Bellacchio, R. Lauceri, S. Gurrieri, L. Monsù Scolaro, A. Romeo, R. Purrello, *J. Am. Chem. Soc.* **1998**, *120*, 12353; d) R. Purrello, A. Raudino, L. Monsù Scolaro, A. Loisi, E. Bellacchio, R. Lauceri, *J. Phys. Chem. B* **2000**, *104*, 10900; e) E. Yashima, K. Maeda, Y. Okamoto, *Nature* **1999**, *399*, 449; f) L. J. Prins, F. De Jong, P. Timmerman, D. N. Reinhoudt, *Nature* **2000**, *408*, 181.

[3] D. L. Caulder, K. N. Raymond, *Acc. Chem. Res.* **1999**, *32*, 975.

[4] a) J.-M. Lehn, *Supramolecular Chemistry: Concepts and Perspectives*, VCH, Weinheim, **1995**; b) M. Fujita, *Chem. Soc. Rev.* **1998**, *27*, 417; c) S. R. Seidel, P. J. Stang, *Acc. Chem. Res.* **2002**, *35*, 972; d) G. F. Swiegers, T. J. Malefetse, *Chem. Rev.* **2000**, *100*, 3483.

[5] B. Kersting, J. R. Telford, M. Meyer, K. N. Raymond, *J. Am. Chem. Soc.* **1996**, *118*, 5712.

[6] M. Meyer, B. Kersting, R. E. Powers, K. N. Raymond, *Inorg. Chem.* **1997**, *36*, 5179.

[7] A. J. Terpin, M. Ziegler, D. W. Johnson, K. N. Raymond, *Angew. Chem.* **2001**, *113*, 161; *Angew. Chem. Int. Ed.* **2001**, *40*, 157.

[8] D. L. Caulder, K. N. Raymond, *Angew. Chem.* **1997**, *109*, 1508; *Angew. Chem. Int. Ed. Engl.* **1997**, *36*, 1440.

[9] $[Ga_2L^2_3]^{6-}$ was used as the L^2 source because of the poor D_2O solubility of H_4L^2 itself. The excess Ga^{III} introduced as a result presumably forms oligomeric products with the exchanged L^1 ligand and excess L^2. Regardless of the composition of these side products, they produce no CD signal since racemic $[Ga_2L^2_3]^{6-}$ helicate was used. Hence there is no change in CD activity.

[10] M. Ziegler, J. Miranda, U. N. Andersen, D. W. Johnson, J. A. Leary, K. N. Raymond, *Angew. Chem.* **2001**, *113*, 755; *Angew. Chem. Int. Ed.* **2001**, *40*, 733.

[11] The CD spectra are cut off at 260 nm, because the bands at higher energies result from ligand π–π^* transitions that are highly sensitive to the nature of the ligand present (L^1 versus L^2) rather than the configuration (Λ or Δ) of the metal centers.

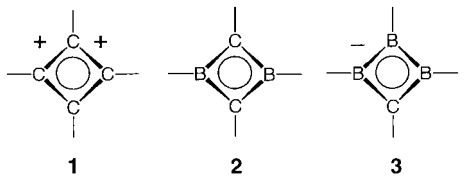
 © 2003 Wiley-VCH Verlag GmbH & Co. KGaA, Weinheim 1433-7851/03/4206-0668 $ 20.00+.50/0

Fluctuating Skeletal Bonds

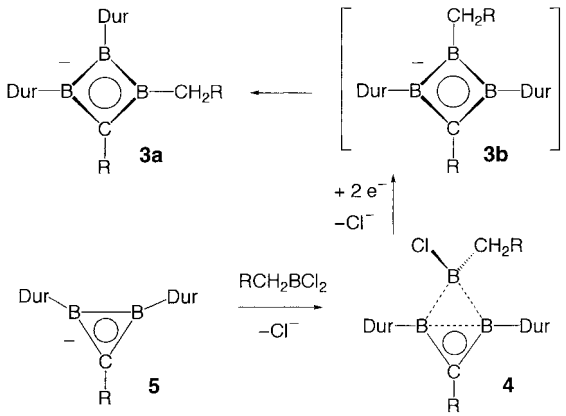
Triboracyclobutanides: Four-Membered Two-Electron Aromatic Compounds with Fluctuating Skeletal Bonds**

*Yüksel Sahin, Carsten Präsang, Peter Amseis, Matthias Hofmann, Gertraud Geiseler, Werner Massa, and Armin Berndt**

Among the series of isoelectronic four-membered, two-electron aromatic compounds **1**–**3** (Scheme 1), to date derivatives of the dicationic and uncharged skeletons **1**[1] and **2**,[2–4] respectively, have been realized experimentally. The barriers of their ring inversions, which are a measure of the stabilization of the folded over the planar rings, have not been determined experimentally for any example. We report herein the synthesis, crystal structure, and the ring inversion barrier of the anion **3a** (Scheme 2), and show, based on line shape analyses of its temperature-dependent NMR spectra, that its skeletal bonds fluctuate via a distorted triboratetrahedrane anion **6a** (see Scheme 3) as transition state. B3LYP computations[5] on model molecules support this proposal.



Scheme 1. Frameworks of isoelectronic four-membered two-electron aromatic compounds **1**–**3**. Circles denote two cyclic delocalized electrons.



Scheme 2. Synthesis of the triboracyclobutanide **3a** by ring expansion of the diboracyclopropanide **5** via **4**. The compound **3b**, expected as the primary product of the reaction of **4** with lithium, was not detected. (R = $SiMe_3$, Dur = 2,3,5,6-tetramethylphenyl).

The unsymmetrically substituted triboracyclobutanide **3a** is obtained by reaction of lithium in diethyl ether with the symmetrically substituted derivative **4**, which is accessible from **5**[6] and dichloro(trimethylsilylmethyl)borane (Scheme 2). Attempts to detect the symmetrically substituted compound **3b** by NMR spectroscopic monitoring of the reaction of **4** with lithium naphthalenide in [D_8]THF at −80 °C proved unsuccessful. The constitutions of **3a** and **4** are in accord with their NMR data (Table 1) and are confirmed unambiguously by their crystal structure determinations[7] (Figure 1).

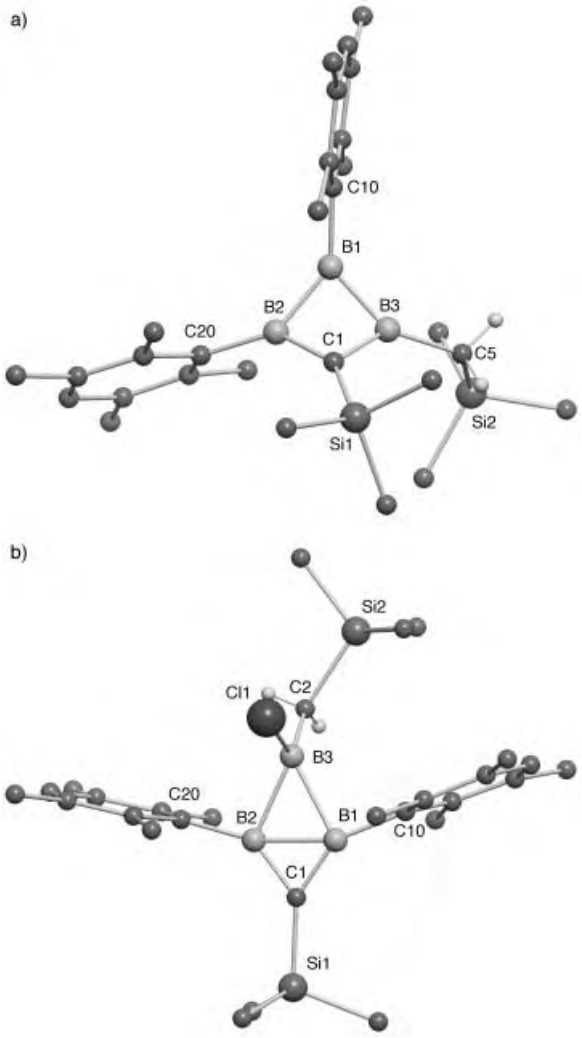


Figure 1. Structures of the anion **3a** (a) and of **4** (b) in the crystal. Hydrogen atoms were omitted for clarity, except those of the methylene groups. Selected bond lengths [pm] and angles [°]. **3a**: C1-B2 150.6(5), B2-B1 162.7(5), B1-B3 162.8(5), B3-C1 152.2(5), C1-B1 199.8(4), B2-B3 214.0(5), C1-Si1 182.7(3); C1,B2,B3/B3,B2,B1 59.3(3)°. **4**: C1-B1 142.8(8), C1-B2 145.4(7), B2-B1 169.5(9), B1-B3 192.6(8), B2-B3 189.0(9), C1-Si1 183.7(5), B1-C10 156.9(8), B2-C20 156.8(8), B3-C2 153.9(8), B3-Cl1 179.0(6); C1,B1,B2/B3,B2,B1 0.8(6)°.

[*] Prof. Dr. A. Berndt, Dr. Y. Sahin, Dr. C. Präsang, Dr. P. Amseis, G. Geiseler, Prof. Dr. W. Massa
Fachbereich Chemie
Universität Marburg
35032 Marburg (Germany)
Fax: (+49) 6421-282-8917
E-mail: berndt@chemie.uni-marburg.de
Dr. M. Hofmann
Anorganisch-Chemisches Institut
Universität Heidelberg
Im Neuenheimer Feld 270, 69120 Heidelberg (Germany)

[**] This work was supported by the Deutsche Forschungsgemeinschaft and the Fonds der Chemischen Industrie.

 © 2003 Wiley-VCH Verlag GmbH & Co. KGaA, Weinheim 1433-7851/03/4206-0669 $ 20.00+.50/0

The anion **3a** forms a solvent-separated ion pair with a lithium ion, which is coordinated by three molecules of diethyl ether. The four-membered ring of the triboracyclobutanide **3a** is strongly (by 59°) folded, as expected for an isoster of the 1,3-dihydro-1,3-diborete[2–4] **2** and the cyclobutadienyl dication[1] **1**. The substitution pattern of the boron atoms of **3a** does not correspond to the symmetric substitution pattern of its precursor **4**. Evidently, the initially formed, symmetrically substituted triboracyclobutanide **3b** rapidly isomerizes to **3a**. Line width phenomena in the NMR spectra of **3a** provide a hint for the mechanism of this isomerization. At low temperature there are ^{1}H and ^{13}C NMR signals for two different Duryl substituents, at higher temperatures their broadenings and coalescences are observed. The ^{11}B NMR spectrum of **3a** in [D$_8$]THF at 27 °C shows three signals at $\delta =$ 16, 38, and 42 ppm, of which that at $\delta = 42$ ppm remains unchanged at higher temperatures, whereas the other two signals broaden. This shows that not only the Duryl substituents but also the boron atoms to which they are attached participate in the exchange. The barrier for the exchange of the environments of the Duryl substituents, that is the topomerization in **3a**, was determined to be 19.9 kcal mol^{-1} based on the line shape analysis of the signals of the *o*-Me, *m*-Me, and *p*-H atoms.[8] For the diastereotopic methylene protons of the Me_3SiCH_2 substituents, which reveal the planar chirality of **3a**, a more rapid exchange than for the Duryl substituents is determined from the line shape analysis of their signals. This is plausible, if one considers, that two pathways are available for the enantiomerization of **3a**: one by ring inversion via the planar transition state **7a** (Scheme 3b) and a second by rearrangement of the framework via a distorted triboratetrahedrane anion **6a**,[9,10] which *also* leads to an enantiomerization, however, without ring inversion (see Scheme 3a). The barrier of the enantiomerization by ring inversion is calculated to be 13.2 kcal mol^{-1}.[8]

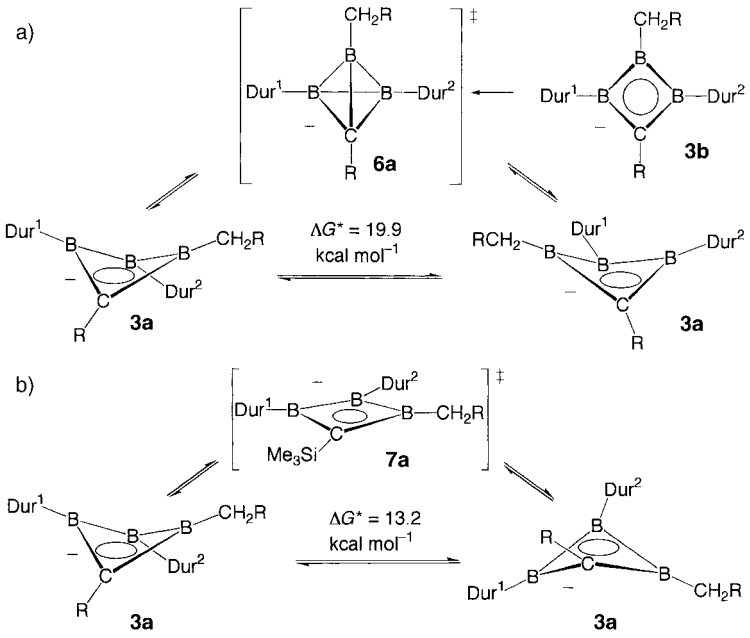
B3LYP/6-311+G** computations[5] reveal that the transition state **6c** (Scheme 4) lies 17.2 kcal mol^{-1} above **3c**, and planar **7c** is 9.6 kcal mol^{-1} higher in energy than **3c**. The distorted tetrahedral transition state of the isomerization of the 1,2-dihydro-1,2-diborete to the unsubstituted 1,3-dihydro-1,3-diborete **2u**, which is isoelectronic to the framework of **6**, lies 22.9 kcal mol^{-1} above **2u** according to computations by McKee; planarization of **2u** requires only

Table 1: Selected physical and spectroscopic properties of **3a**·Li(DME)$_2$ and **4**.[a]

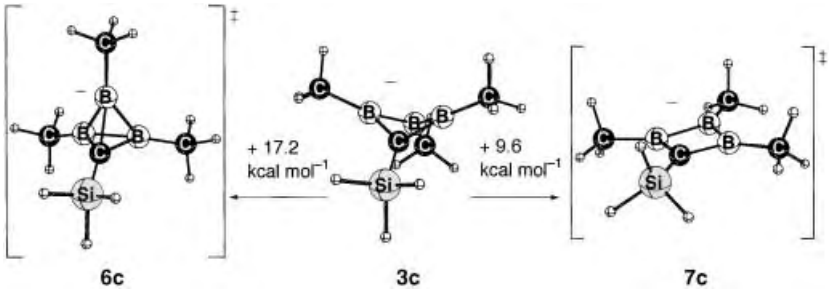
3a·Li(DME)$_2$: pale yellow solid, m.p. 73–75 °C (without decomp), yield 90%. ^{1}H NMR (500 MHz, [D$_8$]THF, −23 °C): $\delta = 6.36$, 6.20 (each s, each 1H, *p*-H, $T_{coal} = 40$ °C); 3.41, 3.26 (each DME); 2.04, 2.02 (each s, each 6H, *o*- or *m*-CH$_3$, $T_{coal} = 17$ °C); 1.98, 1.94 (each s, each 6H, *o*- or *m*-CH$_3$, $T_{coal} = 27$ °C); 0.92, 0.43 (each d, each 1H, BCH$_2$, $T_{coal} = 37$ °C); −0.05, −0.08 ppm (each s, each 9H, Me$_3$Si); ^{13}C NMR (75 MHz, [D$_8$]THF, 27 °C): $\delta = 156.4$, 155.6 (each br. s, each 1C, *i*-C); 133.4, 131.9, 130.4, 130.0 (each s, each 2C, *o*- and *m*-C); 129.0 (br. s, 1C, CB$_2$); 126.6, 124.5 (each d, each 1C, *p*-C); 20.7, 20.0 (each q, each 4C, *o*- and *m*-CH$_3$); 9.7 (br. t, 1C, BCH$_2$), 2.4, 1.8 ppm (each q, each 3C, Me$_3$Si); ^{11}B NMR (160 MHz, [D$_8$]THF, 27 °C): $\delta = 42$, 38, 16 ppm

4: colorless solid, m.p. 133–134 °C (decomp), yield 55%. ^{1}H NMR (500 MHz, C$_6$D$_6$, 27 °C): $\delta = 7.04$ (s, 2H, *p*-H); 2.54, 2.19 (each s, each 12H, *o*- and *m*-CH$_3$); 1.49 (s, 2H, BCH$_2$); 0.32, −0.21 ppm (each s, 9H, Me$_3$Si); ^{13}C NMR (125 MHz, C$_6$D$_6$, 27 °C): $\delta = 137.2$, 134.6 (each s, each 4C, *o*- and *m*-C); 134.0 (br. s, 2C, *i*-C); 132.9 (d, 2C, *p*-C); 22.0 (br. t, 1C, BCH$_2$); 22.2, 19.7 (each q, each 4C, *o*- and *m*-CH$_3$); 0.6, 0.3 ppm (each q, each 3C, Me$_3$Si); ^{11}B NMR (160 MHz, C$_6$D$_6$, 27 °C): $\delta = 71$ (1B), 38 ppm (2B)

[a] DME = 1,2-dimethoxyethane.



Scheme 3. a) Distorted triboratetrahedrane anions of the type **6a**[9] as transition states of the isomerization **3b**→**3a** and of the enantiomerization of **3a** without ring inversion but with topomerization, that is exchange of the boron atoms with the Duryl substituents. There are only ten electrons available for the six skeletal bonds of the tetrahedron. b) Enantiomerization of **3a** with ring inversion the planar transition state **7a**.



Scheme 4. Computed[5] energy differences between **3c** and distorted tetrahedral **6c** and planar **7c**, respectively.

 © 2003 Wiley-VCH Verlag GmbH & Co. KGaA, Weinheim 1433-7851/03/4206-0670 $ 20.00+.50/0

16.9 kcal mol^{-1}.[4] For the dianion of B_4Me_4[10] the distorted tetrahedral form according to our computations lies only 4.9 kcal mol^{-1} above the folded two-electron aromtic compound; its planarization requires 7.3 kcal mol^{-1}. Thus, an increasing number of boron atoms in four-membered two-electron aromatic compounds facilitates the planarization as well as the fluctuation of the skeletal bonds.

Received: August 6, 2002 [Z19899]

[1] M. Bremer, P. von R. Schleyer, U. Fleischer, *J. Am. Chem. Soc.* **1989**, *111*, 1147, and references therein.

[2] M. Hildenbrand, H. Pritzkow, W. Siebert, *Angew. Chem.* **1985**, *97*, 769; *Angew. Chem. Int. Ed. Engl.* **1985**, *24*, 759, and references therein.

[3] P. H. M. Budzelaar, K. Krogh-Jespersen, T. Clark, P. von R. Schleyer, *J. Am. Chem. Soc.* **1985**, *107*, 2723.

[4] M. McKee, *Inorg. Chem.* **2000**, *39,* 4206, and references therein.

[5] All geometries were optimized by employing the B3LYP hybrid functional together with the 6-31G(d) basis set, and the nature of the stationary points was characterized by analytical frequency calculations. Relative energies are based on energy calculations with 6-311+G(d,p) and are corrected for zero-point energies. a) Gaussian 98, Revision A.7, M. J. Frisch, G. W. Trucks, H. B. Schlegel, G. E. Scuseria, M. A. Robb, J. R. Cheeseman, V. G. Zakrzewski, J. A. Montgomery, Jr., R. E. Stratmann, J. C. Burant, S. Dapprich, J. M. Millam, A. D. Daniels, K. N. Kudin, M. C. Strain, O. Farkas, J. Tomasi, V. Barone, M. Cossi, R. Cammi, B. Mennucci, C. Pomelli, C. Adamo, S. Clifford, J. Ochterski, G. A. Petersson, P. Y. Ayala, Q. Cui, K. Morokuma, D. K. Malick, A. D. Rabuck, K. Raghavachari, J. B. Foresman, J. Cioslowski, J. V. Ortiz, A. G. Baboul, B. B. Stefanov, G. Liu, A. Liashenko, P. Piskorz, I. Komaromi, R. Gomperts, R. L. Martin, D. J. Fox, T. Keith, M. A. Al-Laham, C. Y. Peng, A. Nanayakkara, C. Gonzalez, M. Challacombe, P. M. W. Gill, B. Johnson, W. Chen, M. W. Wong, J. L. Andres, C. Gonzalez, M. Head-Gordon, E. S. Replogle, und J. A. Pople, Gaussian, Inc., Pittsburgh PA, **1998**; b) A. D. Becke, *J. Chem. Phys.* **1993**, *98*, 1372; A. D. Becke, *J. Chem. Phys.* **1993**, *98*, 5648; c) C. Lee, W. Yang, R. G. Parr, *Phys. Rev. B* **1988**, *37*, 785.

[6] The synthesis of **5** will be described elsewhere.

[7] Crystal structure analyses: **3a**·Li(Et$_2$O)$_3$: A colorless crystal ($0.45\times0.35\times0.25$ mm^3) was measured at 193 K on an IPDS area detector system (Stoe) with $Mo_{K\alpha}$ radiation. $C_{40}H_{76}B_3LiO_3Si_2$, monoclinic, space group $P2_1/c$, $Z=4$, $a=1183.4(1)$, $b=2277.6(2)$, $c=1756.7(1)$ pm, $\beta=98.32(1)°$, $V=4685.0(6)\times10^{-30}$ m^3, $\rho_{calcd}=0.993$ Mg m^{-3}, 50384 reflections up to $\theta=25.84°$, 8557 independent ($R_{int}=0.1160$), 3910 with $I>2\sigma(I)$. The structure was solved with direct methods and refined against F^2 with full matrix. Hydrogen atoms were considered as riding at calculated positions, $wR_2=0.1527$ for all reflections, $R=0.0691$ for observed reflections. Limited accuracy due to the disorder of the diethyl ether in the Li(Et$_2$O)$_3$ cation. **4**: Pale yellow crystal ($0.30\times0.15\times0.05$ mm^3) $C_{28}H_{46}B_3ClSi_2$, monoclinic, space group $C2/c$, $Z=8$, $a=3031.1(2)$, $b=988.1(1)$, $c=2217.6(1)$ pm, $\beta=111.06(1)°$, $V=6198.1(8)\times10^{-30}$ m^3, $\rho_{ber}=1.086$ Mg m^{-3}, measurement as for **3a**·Li(Et$_2$O)$_3$, 12475 reflections up to $\theta=24.0°$, 4627 independent ($R_{int}=0.1414$), 1857 with $I>2\sigma(I)$ (only very thin platelets available). The structure was solved analogously to that of **3a**, resulting in $wR_2=0.1144$ for all reflections, and $R=0.0539$ for the observed reflections. CCDC-187178 (**3a**·Li(Et$_2$O)$_3$) and CCDC-187179 (**4**) contain the supplementary crystallographic data for this paper. These data can be obtained free of charge via www.ccdc.can.ac.uk/conts/retrieving.html (or from the Cambridge Crystallographic Centre, 12 Union Road, Cambridge CB21EZ, UK; Fax: (+44) 1223-336033; or deposit @ccdc.cam.ac.uk).

[8] The line shape analysis was carried out with WIN-DYNA 32, Bruker Analytik GmbH, Version 1.01; the changes in the chemical shifts in the investigated temperature interval were considered to be linear and the line widths of the trimethylsilyl groups were used as the reference line widths. The rate constants of the ring inversion k_{RInv} were computed from the difference in rate constants of the enantiomerization without ring inversion k_{tet} (coalescence of the methyl groups and protons at the aromatic group) and the enantiomerization with ring inversion k_{total} (coalescence of the methylene protons) according to $k_{RInv}=k_{total}-k_{tet}$.

[9] Tetrahedra of CB_3 anions are, like those of the isoelectronic B_4 dianions, distorted.[10] There are three forms for distorted tetrahedra of the type **6a**: two enantiomers with short C–BDur edges (the transition state between **3b** and **3a**), and one with a short C–BCH$_2$R edge (the transition state of the degenerate rearrangement of **3a**).

[10] A. Neu, T. Mennekes, U. Englert, P. Paetzold, M. Hofmann, P. von R. Schleyer, Angew. Chem. **1997**, *109*, 2211; *Angew. Chem. Int. Ed. Engl.* **1997**, *36*, 2117.

Boron-Containing Rings

A Diboracyclopropane with a Planar-Tetracoordinate Carbon Atom and a Triborabicyclobutane**

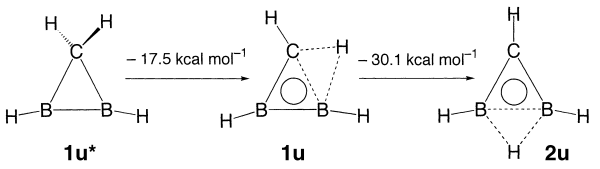
*Yüksel Sahin, Carsten Präsang, Matthias Hofmann, Govindan Subramanian, Gertraud Geiseler, Werner Massa, and Armin Berndt**

Dedicated to Professor Paul von Ragué Schleyer

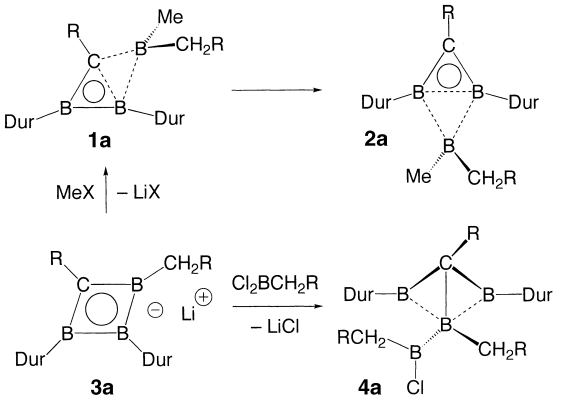
Known molecules with a planar-tetracoordinate carbon atom[1] contain metal centers.[2] According to computations[3] the prototype of such molecules *without* metal centers is the diboracyclopropane **1u** (Scheme 1). Derivatives of the lower energy isomer **2u** with planar-tetracoordinate *boron* atoms[4]

[*] Prof. Dr. A. Berndt, Dr. Y. Sahin, Dr. C. Präsang, Dr. G. Subramanian, G. Geiseler, Prof. Dr. W. Massa
Fachbereich Chemie
Universität Marburg
35032 Marburg (Germany)
Fax: (+49) 6421-282-8917
E-mail: berndt@chemie.uni-marburg.de
Dr. M. Hofmann
Anorganisch-Chemisches Institut
Universität Heidelberg
Im Neuenheimer Feld 270, 69120 Heidelberg (Germany)

[**] This work was supported by the Deutsche Forschungsgemeinschaft and the Fonds der Chemischen Industrie.



Scheme 1. Structures and energy differences computed at the B3LYP/6-31G* level for classical diboracyclopropane **1u*,** its lower energy form with a planar-tetracoordinate carbon atom **1u**, and for **2u** with two planar-tetracoordinate boron atoms.[3b,c] A solid line denotes a 2c2e bond, a dashed triangle a 3c2e σ bond, a circle a 3c2e π bond: **1u** and **2u** are two-electron aromatic compounds.

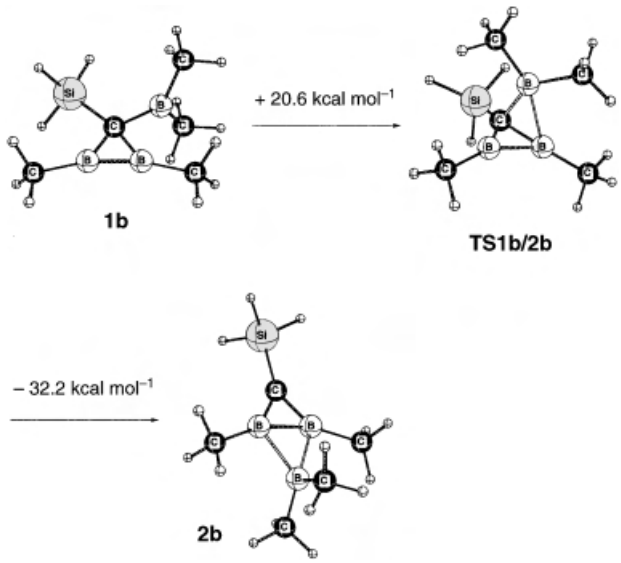


Scheme 2. Synthesis of the *C*-boryldiboracyclopropane **1a** by methylation of **3a**, its isomerization to **2a,** and the synthesis of **4a**. R = $SiMe_3$, Dur = 2,3,5,6-tetramethylphenyl, MeX = $MeOSO_2CF_3$.

are known experimentally, the classical form **1u*** with a tetrahedral carbon atom does not represent an energy minimum. We report herein on the synthesis, NMR spectroscopic characterization, and facile isomerization of the derivative **1a** to **2a** at low temperature (Scheme 2). To compare the chemical shift of the planar-tetracoordinate carbon atom of **1a** with that of a similarly substituted carbon atom without a planar environment, we describe in addition **4a,** the first derivative of triborabicyclobutane. Density functional computations[5] for the models **1b** and **2b** (Scheme 3) as well as for the transition state **TS1b/2b** of the isomerization **1b**→**2b** support our argumentation.

The reaction of the triboracyclobutanide **3a**[6] in [D_8]THF with methyl trifluoromethanesulfonate in an NMR tube at −90 °C affords a mixture of the *C*-boryldiboracyclopropane **1a** and of **2a** (ca. 3:1).[7] At this temperature **1a** does not rearrange appreciably into **2a**. In contrast, at −70 or −65 °C this isomerization occurs with half lives of 61 and 7 min, respectively. Compound **3a** reacts with dichloro(trimethylsilylmethyl)borane to give a product mixture, from which **4a** can be separated by crystallization (Scheme 2). Its constitution and that of **2a**[8] are confirmed by X-ray structure analyses[9] (Figure 1). Compound **4a** contains a folded CB_3 four-membered ring with relatively short C–B distances and a short C–B diagonal to the pentacoordinate boron atom bearing the trimethylsilylmethyl and the chloroboryl groups.

The constitution of **1a** is derived from its NMR-spectroscopic data (Table 1), in particular from the comparison of the chemical shift of its skeletal carbon atom with that computed for **1b** (Scheme 3). Figure 2 shows the relevant section of the ^{13}C NMR spectrum of the above-mentioned mixture. Ten sharp signals are observed (eight singlets and two doublets) in the region between $\delta = 140$ and 132 ppm, which show that the Duryl groups are not equivalent and are bound to a ring with different sides. Three additional, broad singlets at $\delta = 143.7$, 133.2, and 126.4 ppm need to be assigned to boron-bound carbon atoms, one of which is the skeletal carbon atom of the diboracyclopropane ring, the other two the *ipso*-carbon atoms of the Duryl groups.[10] Independent of the assignment of these signals, the skeletal carbon atom of **1a** is deshielded by at least 53 ppm as compared to the quite similarly substituted, distorted-tetrahedral carbon atom in **4a** ($\delta(^{13}C) = 73.3$ ppm). GIAO-NMR computations gave a chemical shift of $\delta =$ 143.6 ppm for the exactly planar-tetracoordinate carbon atom of the model molecule **1b**. This agrees very well with the experimental value of $\delta = 143.7$ ppm for **1a**, which shows that the skeletal carbon atom of the diboracyclopropane ring of **1a**



Scheme 3. Computed[5] energy diferences between **1b, 2b**, and the transition state **TS1b/2b**.

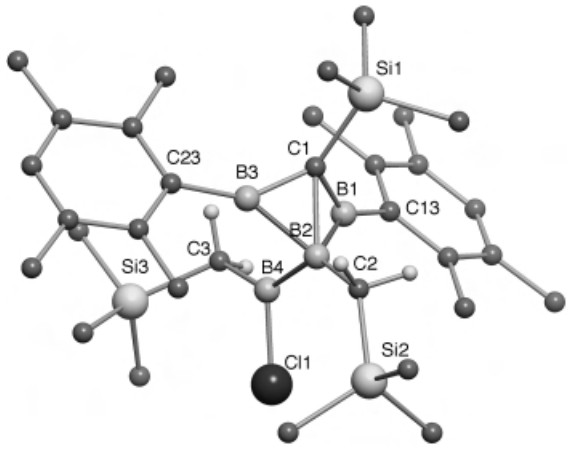


Figure 1. Structure of **4a** in the crystal. Selected bond lengths [pm] and angles [°]: C1-B1 150.2(3), B1-B2 173.9(3), B2-B3 173.3(3), B3-C1 149.4(3), C1-B2 174.5(3), B2-B4 169.4(3); B1-C1-B3 105.7(2), C1-B1-B2 64.7(1), C1-B3-B2 65.0(1), B1-B2-B3 87.0(1), C2-B2-B4 134.2(2), C1-B2-B4 102.2(1), B1-C1-B2-B3 −124.7(2).

 © 2003 Wiley-VCH Verlag GmbH & Co. KGaA, Weinheim 1433-7851/03/4206-0672 $ 20.00+.50/0

Table 1: Selected physical and spectroscopic properties of **1a, 2a**, and **4a**.

1a: yield estimated by NMR spectroscopy 75%; ^{1}H NMR (500 MHz, [D$_8$]THF, −90°C): δ = 6.88, 6.87 (each s, each 1H, *p*-H), 3.40 (s, 4H, DME), 3.24 (s, 6H, DME), 2.28, 2.18, 2.15, 2.12, 1.97, 1.84, 1.24, 1.00 (each s, each 3H, *o*- and *m*-Me), 1.21, 0.73 (each d, each 1H, B-CH$_2$Si), 1.10 (s, 3H, B-Me), 0.23, 0.03 ppm (each s, each 9H, SiMe$_3$); ^{13}C NMR (125 MHz, [D$_8$]THF, −90°C): δ = 143.7 (br. s, 1C, CB$_3$), 139.7, 139.6, 138.2, 137.6, 134.5, 134.4, 134.2, 134.0, 133.3, 132.5 (each s, each 1C, *o*- and *m*-C), 133.4, 132.5 (each d, each 1C, *p*-C), 133.2, 126.4 (each br. s, each 1C, *i*-C), 72.4, 58.8 (each 2C, DME), 22.0, 21.8, 21.3, 12.1, 20.9, 20.1, 19.6, 19.4 (each q, each 1C, *o*- and *m*-Me), 16.6 (br. q, 1C, MeB), 9.1 (br. t, 1C, BCH$_2$Si), 1.1, 1.0 ppm (each q, each 3C, SiMe$_3$)

2a: colorless crystals; m.p. 109°C (decomp); yield 78%; ^{1}H NMR (500 MHz, [D$_8$]THF, −90°C): δ = 6.90 (s, 2H, *p*-H), 2.24, 2.23, 2.16 (each s, in total 24H, *o*- and *m*-CH$_3$), 0.88 (br. s, 2H, BCH$_2$), 0.76 (br. s, 3H, BCH$_3$), −0.04, −0.5 ppm (each s, each 9H, Me$_3$Si); ^{13}C NMR (125 MHz, [D$_8$]THF, −90°C): δ = 137.2, 137.1, 134.8, 134.7 (each s, each 2C, *o*- and *m*-C), 134.2 (br. s, 2C, *i*-C), 133.0 (br. s, 1C, CB$_2$), 132.3 (d, 2C, *p*-C), 22.6, 20.1, 20.0 (in total 8C, *o*- and *m*-CH$_3$), 19.8 (br. t, 1C, BCH$_2$), 13.4 (br. q, 1C, BCH$_3$), 0.9, 0.4 ppm (each q, each 3C, Me$_3$Si); ^{11}B NMR (96 MHz, [D$_{10}$]Et$_2$O, 27°C): δ = 80 (1B), 40 ppm (2B)

4a: colorless crystals; m.p. 118°C; yield ca. 50%; ^{1}H NMR (500 MHz, CD$_2$Cl$_2$, −40°C): δ = 7.10 (s, 2H, *p*-H), 2.52, 2.46, 2.20(each s, in total 24H, *o*- and *m*-Me), 0.23, 0.03, (each s, each 2H, H$_2$CSi, localized by C/H correlation), 0.08, −0.04, −0.57 ppm (each s, each 9H, Me$_3$Si); ^{13}C NMR (125 MHz, CD$_2$Cl$_2$, −40°C): δ = 142.2, 140.5, 133.7, 133.6 (each s, each 2C, *o*- and *m*-C), 135.0 (d, 2C, *p*-C), 132.1 (br. s, 2C, *i*-C), 73.3 (br. s, 1C, CB$_3$), 21.4, 21.1, 20.3, 20.2 (each q, in total 8C, *o*- and *m*-Me), 18.1, 12.8 (each br. t, each 1C, CH$_2$Si), 2.1, 1.1, 0.2 ppm (each q, each 3C, Me$_3$Si); ^{11}B NMR (96 MHz, CDCl$_3$, −20°C): δ = 58 (br. s, 3B), 5.8 ppm (1B). Above −20°C **4a** is converted partly to an isomer with δ(^{11}B) = −1.0 ppm, crystallization of the mixture leads to the re-formation of **4a**

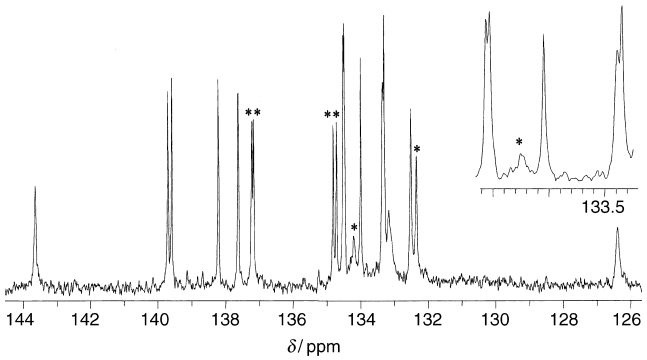


Figure 2. Section (145 to 125.5 ppm) of the ^{13}C NMR spectrum of a 3:1 mixture of **1a** and **2a**. The insert shows an expansion of the region between δ = 133.2 and 136.6 ppm. The signals of **2a** are marked by an asterisk (*); their intensities increase as the temperature is raised, those of the other signals decrease: after 30 min at −65°C only the signals of **2a** are observed.

is planar-tetracoordinate. DFT computations[5] for the models **1b, 2b**, and the transition state **TS1b/2b** of the isomerization **1b**→**2b** reveal that **2b** is 11.6 kcal mol^{-1} lower in energy than **1b**[11] and that the barrier of the isomerization (20.6 kcal mol^{-1}) is low.[12] The facile isomerization to **2a** thus provides additional support for the structure of **1a**.

Received: August 6, 2002 [Z19909]

[1] R. Hoffmann, R. G. Alder, C. F. Wilcox, *J. Am. Chem. Soc.* **1970**, *92*, 4992; J. B. Collins, J. D. Dill, E. D. Jemmis, Y. Apeloig, P. von R. Schleyer, R. Seeger, J. A. Pople, *J. Am. Chem. Soc.* **1976**, *98*, 5419.

[2] D. Röttger, G. Erker, *Angew. Chem.* **1997**, *109*, 841; *Angew. Chem. Int. Ed. Engl.* **1997**, *36*, 812, and references therein; W. Siebert, A. Gunale, *Chem. Soc. Rev.* **1999**, *28*, 367; M. Driess, J. Aust, K. Merz, C. van Wüllen, *Angew. Chem.* **1999**, *111*, 3967; *Angew. Chem. Int. Ed.* **1999**, *38*, 3677; Y. Sahin, M. Hartmann, G. Geiseler, D. Schweikart, C. Balzereit, G. Frenking, W. Massa, A. Berndt, *Angew. Chem.* **2001**, *113*, 2725; *Angew. Chem. Int. Ed.* **2001**, *40*, 2662, and references therein.

[3] a) K. Krogh-Jespersen, D. Cremer, D. Poppinger, J. A. Pople, P. von R. Schleyer, J. Chandrasekhar, *J. Am. Chem. Soc.* **1979**, *101*, 4843; b) K. Sorger, P. von R. Schleyer, *THEOCHEM* **1995**, *338*, 317, and references therein; Z.-X. Wang, P. von R. Schleyer, *J. Am. Chem. Soc.* **2001**, *123*, 994, and references therein; c) S. Fau, G. Frenking, *THEOCHEM* **1995**, *338*, 117.

[4] M. Menzel, D. Steiner, H.-J. Winkler, D. Schweikart, S. Mehle, S. Fau, G. Frenking, W. Massa, A. Berndt, *Angew. Chem.* **1995**, *107*, 368; *Angew. Chem. Int. Ed. Engl.* **1995**, *34*, 327.

[5] All geometries were optimized by employing the B3LYP hybrid functional together with the 6-31G(d) basis set. The transition state **TS1b/2b** was characterized by its intrinsic reaction coordinate. Relative energies are corrected for zero-point energies and are based on energy computations with 6-311+G(d,p), likewise the computed chemical shifts (GIAO-NMR). a) Gaussian 98 (Revision A.7), M. J. Frisch, G. W. Trucks, H. B. Schlegel, G. E. Scuseria, M. A. Robb, J. R. Cheeseman, V. G. Zakrzewski, J. A. Montgomery, R. E. Stratmann, J. C. Burant, S. Dapprich, J. M. Millam, A. D. Daniels, K. N. Kudin, M. C. Strain, O. Farkas, J. Tomasi, V. Barone, M. Cossi, R. Cammi, B. Mennucci, C. Pomelli, C. Adamo, S. Clifford, J. Ochterski, G. A. Petersson, P. Y. Ayala, Q. Cui, K. Morokuma, D. K. Malick, A. D. Rabuck, K. Raghavachari, J. B. Foresman, J. Cioslowski, J. V. Ortiz, B. B. Stefanov, G. Liu, A. Liashenko, P. Piskorz, I. Komaromi, R. Gomperts, R. L. Martin, D. J. Fox, T. Keith, M. A. Al-Laham, C. Y. Peng, A. Nanayakkara, C. Gonzalez, M. Challacombe, P. M. W. Gill, B. G. Johnson, W. Chen, M. W. Wong, J. L. Andres, M. Head-Gordon, E. S. Replogle, J. A. Pople, Gaussian, Inc., Pittsburgh, PA, **1998**; b) A. D. Becke, *J. Chem. Phys.* **1993**, *98*, 1372; A. D. Becke, *J. Chem. Phys.* **1993**, *98*, 5648; c) C. Lee, W. Yang, R. G. Parr, *Phys. Rev. B* **1988**, *37*, 785.

[6] Y. Sahin, C. Präsang, P. Amseis, M. Hofmann, G. Geiseler, W. Massa, A. Berndt, *Angew. Chem.* **2003**, 115, 693; *Angew. Chem. Int. Ed.* **2003**, *42*, 669.

[7] The methylating reagent was added to a solution of **3a** in [D$_8$]THF at −120°C, which had been frozen in an NMR tube with the aid of liquid nitrogen. Thereafter the components were warmed to −90°C in the NMR spectrometer.

[8] The structure of **2a** in the crystal resembles that of the starting material of **3a**,[6] which bears a chlorine atom instead of the methyl group at the boron atom of the boryl bridge of **2a**. Selected distances in **2a** [pm]: C1−B1 145.5(7), C1−B2 143.9(8), B1−B2 167.7 (10), B1−B3 192.4(9), B2−B3 192.8(8).

[9] Crystal structure analysis of **4a**: A colorless crystal (0.60 × 0.30 × 0.05 mm^3) was measured on at 193 K on an IPDS area detector system (Stoe) with Mo$_{K\alpha}$ radiation. $C_{32}H_{57}B_4ClSi_3$, monoclinic, space group *P2/c*, Z = 4, a = 1186.3(1), b = 1185.9(1), c = 2697.2(1) pm, β = 91.55(1)°, V = 3793.1(5) × 10^{-30} m^3, ρ_{calcd} = 1.059 Mg m^{-3}, 29451 reflections up to θ = 25.94°, 6979 independent (R_{int} = 0.0584), 4901 with $I > 2\sigma(I)$. The structure was solved with direct methods and refined against all F^2 data with full matrix, wR_2 = 0.0997 for all reflections, R = 0.0391 for the observed reflections. CCDC-185030 (**4a**) contains the supplementary crystallographic data for this paper. These data can be

obtained free of charge via www.ccdc.cam.ac.uk/conts/retrieving.html (or from the Cambridge Crystallographic Data Centre, 12, Union Road, Cambridge CB21EZ, UK; fax: (+44) 1223-336-033; or deposit@ccdc.cam.ac.uk).

[10] The other broad signals of the boron-bound carbon atoms at $\delta =$ 16.6 and 9.1 ppm are not singlets, and thus clearly not assignable to the skeletal carbon atom.

[11] For the classical **1b*** with a distorted tetrahedral coordinate ring carbon atom computations at this level give two imaginary frequencies and an energy 8.9 kcal mol^{-1} higher than for **1b**. The chemical shift of the ring carbon atom computed at the level used for **1b** was $\delta = 103.6$ ppm.

[12] The barrier of the isomerization of **1u** to **2u** was computed to be 22.0 kcal mol^{-1}.[3c]

Long-Range Electronic Coupling

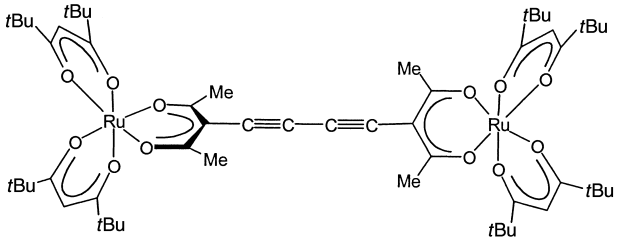
Long-Range Electronic Coupling in Various Oxidation States of a C_4-Linked Tris(β-diketonato)ruthenium Dimer**

Yoshimasa Hoshino, Seiichiro Higuchi, Jan Fiedler, Cheng-Yong Su, Axel Knödler, Brigitte Schwederski, Biprajit Sarkar, Heiko Hartmann, and Wolfgang Kaim**

Despite an increasingly varied experimental data basis[1] and sophisticated theoretical approaches[2] there is still only a rudimentary understanding of which factors govern the extent of interaction between metal centers in formally symmetrical mixed-valent compounds. Such compounds can be considered as intermediates in "degenerate" inner-sphere metal-to-metal electron transfer. The interplay between metal configurations, the metal–ligand interface, and the properties of the ligand bridge has to be considered. Although the mere metal–metal distance has often been used as a guideline[3] in the absence of other, less accessible parameters, it is clear from several experiments[1] that the electronic properties of the ligands mediating the metal–metal interaction may be more relevant than the metal–metal separation. However, the correlation between metal configurations and the bridge type also requires consideration, especially when using alternatives to the often studied d^5/d^6 combination,[1,3] familiar from prototypes, such as the Creutz–Taube ion[3a] $[(H_3N)_5Ru(\mu\text{-pz})Ru(NH_3)_5]^{5+}$ (pz = pyrazine) or partially oxidized biferrocenyl species.[4]

Herein we describe the extraordinarily varied results for two different mixed-valent configurations that are accessible by single-electron transfer from the structurally characterized diruthenium(III) complex **1**.[5] The distinguishing feature of the ligand bridge is an unsaturated, cumulene-like, C_4 spacer which, in contrast to other C_4-bridged dinuclear systems,[6] interacts with the metals through conventional Werner-type coordination, namely through β-diketonato chelate ligation.[5]

The complex **1** could be characterized crystallographically,[7] it has an almost linear C_4 chain with localized single-bond/triple-bond alternation (Figure 1). At 13.1359(6) Å the metal–metal separation is much longer than in directly C_4-connected diruthenium complexes (ca. 8.0 Å),[6] and the chelate rings are virtually perpendicular (90.9°).



1

The crystallographically determined orthogonality agrees with the EPR spectroscopic observation at 4 K of a half-field signal at $g = 4.83$ in addition to the main broad resonance at about 2.00, which indicate a triplet state. Stepwise one-electron reduction of the metal centers in **1** occurs at closely spaced potentials,[5] yielding a relatively[1,3] small value of the comproportionation constant $K_c = 10^{1.9}$ [5] of the $Ru_2^{III,II}$ intermediate $\mathbf{1}^-$. No intervalence charge-transfer (IVCT) transition could be observed in the visible and near-infrared regions ($\varepsilon < 100\ M^{-1}cm^{-1}$), and the IR vibrational spectroelectrochemical study at −40 °C[8] clearly revealed the reversible emergence of distinctly split alkyne stretching bands (Figure 2a and b). The latter indicates dissymmetry and thus *localized valences* on the vibrational time scale of about 10^{-12} s, that is, Class II behavior according to the Robin and Day classification.[9] The EPR spectra taken at 4 K in CH_2Cl_2

[*] Prof. Dr. Y. Hoshino, Prof. Dr. S. Higuchi
Department of Chemistry
Faculty of Education
Nagasaki University
1-14 Bunkyo-machi, Nagasaki 852-8521 (Japan)
Fax: (+81) 95-840-0537
E-mail: hoshino@net.nagasaki-u.ac.jp
Prof. Dr. W. Kaim, Dr. A. Knödler, Dr. B. Schwederski, B. Sarkar, Dipl.-Chem. H. Hartmann
Institut für Anorganische Chemie
Universität Stuttgart
Pfaffenwaldring 55, 70550 Stuttgart (Germany)
Fax: (+49) 711-685-4165
E-mail: kaim@iac.uni-stuttgart.de
Dr. J. Fiedler
J. Heyrovsky Institute of Physical Chemistry
Academy of Sciences of the Czech Republic
Dolejškova 3, 18223 Prague (Czech Republic)
Prof. Dr. C.-Y. Su
School of Chemistry and Chemical Engineering
Zhongshan University
Guangzhou, 510275 (China)

[**] This work was supported by a Gastdozentenstipendium of Land Baden-Württemberg (Y.H.), by a Grant-in-Aid for Scientific Research (No. 13640562) from the Japan Society for the Promotion of Science, by an Alexander von Humboldt Research Fellowship (C.-Y.S.), by the Deutsche Forschungsgemeinschaft, and by the Fonds der Chemischen Industrie. We also thank Dr. Falk Lissner for X-ray crystallographic data collection.

 © 2003 Wiley-VCH Verlag GmbH & Co. KGaA, Weinheim 1433-7851/03/4206-0674 $ 20.00+.50/0

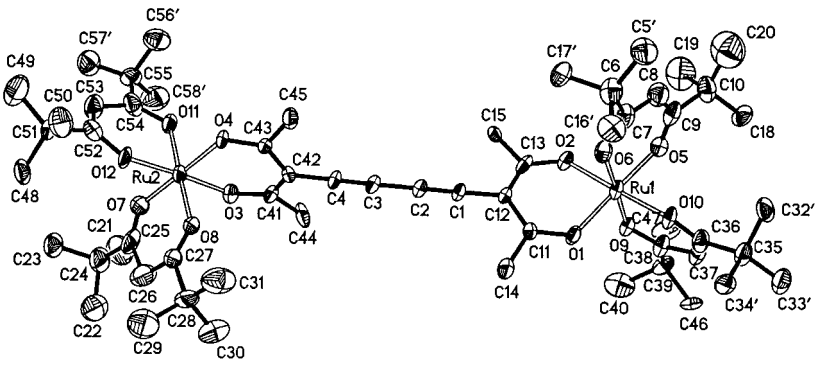


Figure 1. Molecular structure of **1**. Bond lengths [Å] and angles [°]: C42-C4 1.406(6), C4-C3 1.173(6), C3-C2 1.430(6), C2-C1 1.180(6), C1-C12 1.404(6); C42-C4-C3 178.0(5), C4-C3-C2 175.3(5), C3-C2-C1 178.5(6), C2-C1-C12 178.3(6).

confirm this interpretation, the g components at 2.35, 2.24, and 1.64 are very similar to those of mononuclear $[Ru^{III}(dpm)_3]$, dpm = dipivaloylmethanate (2,2,6,6-tetramethylheptan-3,5-dionate),[10] under the same conditions: $g_{1,2} = 2.27$, $g_3 = 1.69$.

A very different result is obtained on stepwise one-electron oxidation of the metal centers: At $10^{3.8}$ the K_c value of the $Ru_2^{IV,III}$ intermediate $\mathbf{1}^+$ is larger than for $\mathbf{1}^-$ but still far from the typical K_c value of about 10^6 for the Creutz–Taube ion[3a] and 1,4-dicyanamidobenzene-bridged species,[11] the K_c value of approximately 10^{10} for directly C_4-bridged compounds,[6] or even the $K_c > 10^{13}$ for tetrazine-bridged systems.[1,12] However, results from IR- and UV/Vis-NIR spectroelectrochemistry (Figures 2 and 3) clearly indicate strong electronic coupling across a distance of 1.3 nm.

An extremely intense, broad IVCT band is centered about 1730 nm ($\varepsilon = 25000\,M^{-1}cm^{-1}$, $\Delta\tilde{\nu}_{1/2} = 3400\,cm^{-1}$) for the formally d^4/d^5 mixed-valent intermediate (Figure 3a). Further oxidation to homovalent $\mathbf{1}^{2+}$ also produces a long-wavelength band at 1346 nm (Figure 3b) which we assign to an LMCT/MLCT mixed transition for the resonance alternatives $[Ru^{IV}(L^{2-})Ru^{IV}]^{2+} \leftrightarrow [Ru^{III}(L)Ru^{III}]^{2+}$ of $\mathbf{1}^{2+}$ (Scheme 1).[13]

The IR vibrational spectra are most revealing and show a single C_4 stretching band, of greatly enhanced intensity, at lower wavenumbers (Figure 2c). This result indicates valence delocalization (Class III behavior[9]), in agreement with the unusually strong IVCT transition. The enormous intensity increase points to considerable contributions from cumulene-type resonance structures as suggested by the (localized)

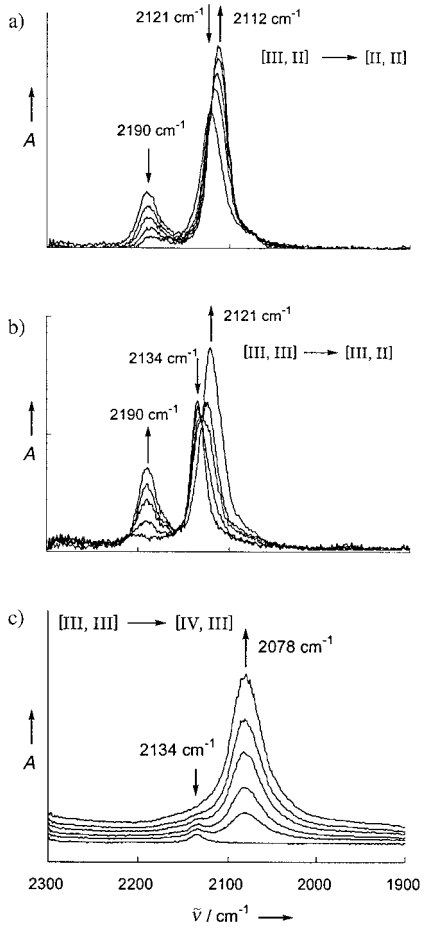


Figure 2. IR spectroscopic changes in the alkyne and cumulene stretching region from low-temperature spectroelectrochemistry measurements (−40 °C) of $\mathbf{1}^n$ in CH_2Cl_2/0.1 M Bu_4NPF_6. a) $(n=1-)\rightarrow(n=2-)$, b) $(n=0)\rightarrow(n=1-)$, c) $(n=0)\rightarrow(n=1+)$.

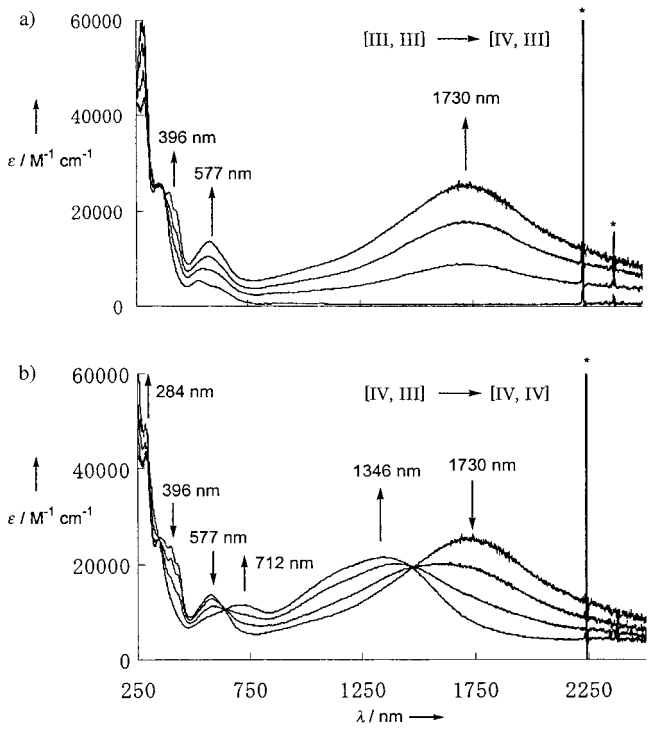
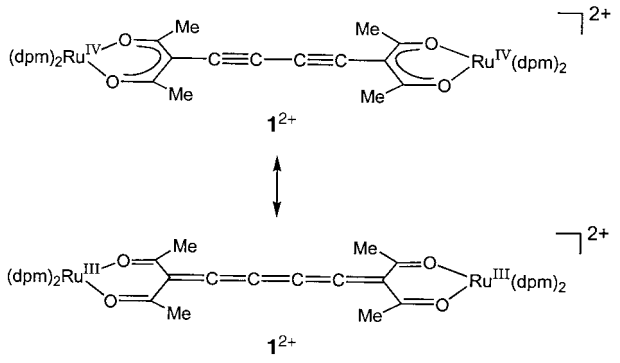


Figure 3. UV/Vis-NIR spectroscopic changes from low-temperature spectroelectrochemistry measurements (−40 °C) of $\mathbf{1}^n$ in CH_2Cl_2/0.1 M Bu_4NPF_6. a) $(n=0)\rightarrow(n=1+)$, b) $(n=1+)\rightarrow(n=2+)$ (*: artifact peaks).

 © 2003 Wiley-VCH Verlag GmbH & Co. KGaA, Weinheim 1433-7851/03/4206-0675 $ 20.00+.50/0

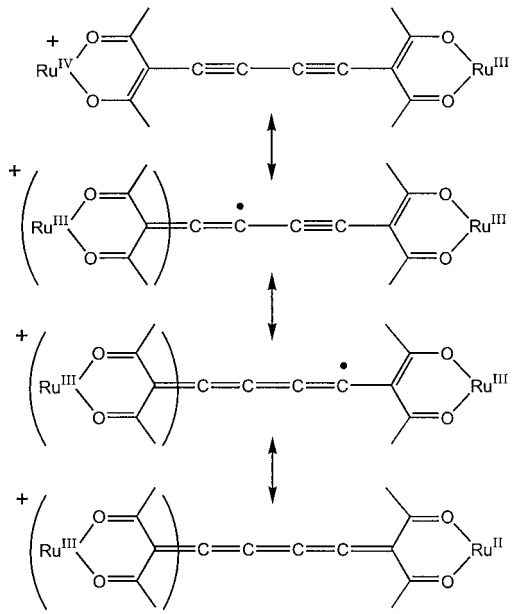


Scheme 1. Resonance alternatives of $\mathbf{1}^{2+}$.

formulations in Scheme 2, cumulenes exhibit much more intense stretching bands in the 2000 cm^{-1} region than alkynes.[14]

EPR spectroscopy at 4 K in CH_2Cl_2 confirms the Class III assignment for $\mathbf{1}^+$. With resonance signals at 2.34, 2.20, and 1.91 the *g* anisotropy is distinctly smaller than for $\mathbf{1}^-$ which would be expected for diminished metal and enhanced ligand participation at the singly occupied MO in $\mathbf{1}^+$ in accord with the two intermediate resonance formulations in Scheme 1.[13] In agreement with established concepts[1,11,13] this result points to a hole-transfer mechanism for the electronic coupling as would be expected for a dianionic ligand[13] and oxidized metal centers. Alternatively, a combination of a neutral ligand with $Ru_2^{III,II}$ mixed-valent centers may be considered which would be expected to exhibit a similar *g* anisotropy.[15] For the reduced state $\mathbf{1}^-$ the interaction is too weak for delocalized valences or detectable IVCT features to occur, possibly a result of a different geometry (orthogonal vs coplanar conformation of the bridge).

Application of the Hush formalism[2a] with the approximation $\Delta\tilde{\nu}_{1/2} = (2310\ \nu_{max})^{1/2}$ for the IVCT band of $\mathbf{1}^+$ gives a slightly higher calculated $\Delta\tilde{\nu}_{1/2} = 3650\ cm^{-1}$ than the experimental value at 3400 cm^{-1}. It is possible, however, that several transitions lie within that broad band envelope. The electronic coupling parameter H_{AB} would be calculated from the Hush formula[2a] for Class II systems to be 1090 cm^{-1}; assuming a Class III situation based on the IR spectroscopic behavior this number is estimated[3a] to be 2890 cm^{-1}.



Scheme 2. Resonance forms of $\mathbf{1}^+$ (localized formula).

In summary, we have demonstrated for a familiar mixed-valence situation[1,3,6a] (π-ligand bridged diruthenium compounds) that the long metal–metal separation may affect the Coulomb-determined K_c value as derived from the difference in electrochemical potential whereas the electronic interaction is more influenced by the correlation between the configurations of the metal centers and the properties of the bridging ligand. While the excellent electronic-interaction-mediating capability of cumulene-like C_n bridges is well established,[6] it remains remarkable that a rather strong interaction is transmitted through the polar, less covalent Ru–O junctions involving the β-diketonato ligand systems in what appears to be a rare $Ru_2^{IV,III}$ (d^4/d^5) mixed-valent configuration.[16] Clearly, C_n spacers can be combined with robust Werner-type coordination complexes to achieve variable, potentially very strong electronic coupling across large distances.

Received: August 21, 2002
Revised: November 20, 2002 [Z50020]

[1] W. Kaim, A. Klein, M. Glöckle, *Acc. Chem. Res.* **2000**, *33*, 755.
[2] a) N. S. Hush, *Prog. Inorg. Chem.* **1967**, *8*, 391; b) N. Sutin, *Prog. Inorg. Chem.* **1983**, *30*, 441.
[3] a) C. Creutz, *Prog. Inorg. Chem.* **1983**, *30*, 1; b) A.-C. Ribou, J.-P. Launay, K. Takahashi, T. Nihira, S. Tarutani, C. W. Spangler, *Inorg. Chem.* **1994**, *33*, 1325; c) C. Patoux, J.-P. Launay, M. Beley, S. Chaodorowski-Kimmes, J.-P. Colin, J. Stuart, J.-P. Sauvage, *J. Am. Chem. Soc.* **1998**, *120*, 3117.
[4] D. O. Cowan, F. Kaufmann, *J. Am. Chem. Soc.* **1970**, *92*, 219.
[5] Y. Kasahara, Y. Hoshino, M. Kajitani, K. Shimizu, G. P. Satô, *Organometallics* **1992**, *11*, 1968.
[6] a) M. I. Bruce, P. J. Low, K. Costuas, J.-F. Halet, S. P. Best, G. A. Heath, *J. Am. Chem. Soc.* **2000**, *122*, 1949, and references therein; b) N. Le Narvor, L. Toupet, C. Lapinte, *J. Am. Chem. Soc.* **1995**, *117*, 7129; c) M. Brady, W. Weng, Y. Zhou, J. W. Seyler, A. J. Amoroso, A. M. Arif, M. Bohme, G. Frenking, J. A. Gladysz, *J. Am. Chem. Soc.* **1997**, *119*, 775.
[7] Crystallization from CH_2Cl_2/C_2H_5OH (10/1, v/v). Crystal data for **1**: $M_r = 1179.42$, monoclinic, space group $P2_1/n$, $a = 12.0875(3)$, $b = 29.0406(8)$, $c = 20.8946(7)$ Å, $\beta = 106.175(1)°$, $V = 7044.3(4)$ Å^3, $T = 293(2)$ K, $Z = 4$, 7313 independent reflections measured, final $R1 = 0.0884$ and $wR2 = 0.1864$ for 5144 observed [$I > 2\sigma(I)$] reflections. Most of the methyl groups are disorderd and were refined with fractional occupancy. CCDC-191410 contains the supplementary crystallographic data for this paper. These data can be obtained free of charge via www.ccdc.cam.ac.uk/conts/retrieving.html (or from the Cambridge Crystallographic Data Centre, 12 Union Road, Cambridge CB21EZ, UK; fax: (+44) 1223-336-033; or deposit @ccdc.cam.ac.uk).
[8] a) The spectroelectrochemical experiments at low temperatures were performed with an improved version of a previously described thin-layer optically transparent electrochemical (OTTLE) cell: F. Hartl, H. Luyten, H. A. Nieuwenhuis, G. C. Schoemaker, *Appl. Spectrosc.* **1994**, *48*, 1522; b) The measurements were performed in CH_2Cl_2/0.1 M Bu_4NPF_6 at −40 °C.

 © 2003 Wiley-VCH Verlag GmbH & Co. KGaA, Weinheim 1433-7851/03/4206-0676 $ 20.00+.50/0

Higher temperatures or the use of CH_3CN led to slow decomposition reactions of $\mathbf{1}^{2-}$ and $\mathbf{1}^{2+}$ on the time scale of the experiment (1–5 minutes).

[9] M. B. Robin, P. Day, *Adv. Inorg. Chem. Radiochem.* **1967**, *10*, 247.
[10] Y. Hoshino, B. Schwederski, B. Sarkar, W. Kaim, unpublished results.
[11] C. E. B. Evans, G. P. A. Yap, R. J. Crutchley, *Inorg. Chem.* **1998**, *37*, 6161.
[12] a) W. Kaim, *Coord. Chem. Rev.* **2002**, *230*, 127; b) S. Chellamma, M. Lieberman, *Inorg. Chem.* **2001**, *40*, 3177.
[13] For π-donor-bridged $Ru_2^{III,II}$ and $Ru_2^{III,III}$ systems see: a) V. Kasack, W. Kaim, H. Binder, J. Jordanov, E. Roth, *Inorg. Chem.* **1995**, *34*, 1924; b) A. Dei, D. Gatteschi, L. Pardi, *Inorg. Chem.* **1990**, *29*, 1442.
[14] D. Lin-Vien, N. B. Colthup, W. G. Fateley, J. G. Grasselli, *The Handbook of Infrared and Raman Characteristic Frequencies of Organic Molecules*, Academic Press, San Diego, **1991**, p. 95 and 213.
[15] J. Heck, G. Lange, M. Malessa, R. Boese, D. Bläser, *Chem. Eur. J.* **1999**, *5*, 659.
[16] For oxo-bridged $Ru_2^{IV,III}$ systems see: a) J. A. Baumann, T. J. Meyer, *Inorg. Chem.* **1980**, *19*, 345, and a 1,4-dicyanamidobenzene-bridged $Ru_2^{IV,III}$ system: b) M. L. Naklicki, C. A. White, V. V. Kondratiev, R. J. Crutchley, *Inorg. Chim. Acta* **1996**, *242*, 63.

Peptides Composed of D-Amino Acids

all-D-Polypeptides: Novel Targets for Semisynthesis**

*Nicole Wehofsky, Sven Thust, Jens Burmeister, Sven Klussmann, and Frank Bordusa**

Although D-amino acids are found only rarely in nature, they play a prominent role in the structure and biological activity of the polypeptides in which they appear. For example, D-amino acids act as key building blocks for the cell wall in bacteria and in antibiotics,[1] while in mammals they are essential for maintaining the activity of a number of hormones and neural transmitters.[2] Beside these natural functions, synthetic all-D-polypeptides have found a significant application as mirror-image proteins in the screening of libraries of nucleic acids or genetically encoded proteins for specific binding ligands.[3] This variety in function along with their resistance toward proteolytic degradation has made D-amino acid containing polypeptides important as long-acting therapeutic agents and as tools in drug discovery, and has spurred great interest in their synthesis.

Presently, only chemical methods provide access to both short- and long-chain D-amino acid containing peptides. In contrast, approaches based on gene technology and enzymatic ligation are limited to the preparation of all-L- and L,D-peptides, respectively.[4] Exceptions are reported only rarely and utilize D-amino acid specific peptidases, esterases, and aminoacyltransferases[5] or solvent-engineered[6] and chemically mutant enzymes.[7] Although these enzymes show altered stereospecificities, their applicaction is limited to the coupling of single D-amino acid residues; the ligation of peptide fragments is not possible.

We report here on the first biocatalytic approach to the synthesis of D-amino acid containing peptides by the ligation of all-D-peptide fragments. The synthetic method is not restricted to special sequences or chain lengths of either the acyl donor or the acyl acceptor fragment. Mild reaction conditions, ease of practicability, and the possibility of using reactants with unprotected side chains are further hallmarks of this approach which, in principle, does not require either organic solvents or artificial mutant enzymes. Instead, an ordinary peptidase, the cysteine protease clostripain is used, and water serves as the solvent, which guarantees high enzyme activity and stability during synthesis. The acceptance of all-D-peptide donors by the inherently highly L-Arg-specific enzyme is easily achieved by using the substrate mimetics strategy.[8] The combination of this approach with the use of clostripain, which has a relaxed stereospecificity towards the acyl acceptor, finally enables the synthesis of a wide variety of all-D-peptides, compounds for which the enzyme is originally completely nonspecific.

Initially, we investigated the general reactivity of clostripain with both D-amino acid derived acyl donors and acyl acceptors. For this purpose, model reactions were performed with simple D-amino acid 4-guanidinophenyl esters (OGp) as acyl donors and amino acid amides and peptides of D-configuration as acyl acceptors. The OGp moiety was selected because it is known to mediate the acceptance of nonspecific acyl moieties by clostripain.[9] In addition, an analogous glycine ester was used, which owing to achirality of glycine, can appear in both all-L- and all-D-peptides.

The enzymatic reactions were performed in buffered aqueous solution at a pH and temperature optimal for the enzyme.[10] The concentrations of acyl donor and acyl acceptor were 2 mM and 10 mM, respectively (see the Supporting Information). In some cases 2.5% DMF was added to the reaction mixture to completely solubilize the reactants. As a control, parallel reactions without the enzyme were performed. Analysis by HPLC indicated that incubation times of less than 60 min sufficed for complete consumption of the

[*] Dr. F. Bordusa, Dr. N. Wehofsky
Max Planck Research Unit "Enzymology of Protein Folding"
Weinbergweg 22, 06120 Halle (Germany)
Fax: (+49) 345-5511-972
E-mail: bordusa@enzyme-halle.mpg.de
Dr. J. Burmeister, Dr. S. Klussmann
NOXXON Pharma AG
Max-Dohrn-Strasse 8–10, 10589 Berlin (Germany)
Dr. S. Thust
Department of Organic Chemistry, University of Leipzig
Johannisallee 29, 04103 Leipzig (Germany)

[**] This work was supported by the Deutsche Forschungsgemeinschaft (SFB610 and BO1770/1-1) and the Fonds der Chemischen Industrie (Liebig scholarship to F.B.). The authors thank Dr. G. Jahreis for his help in peptide synthesis and Prof. G. Fischer for his continuing support.

Supporting information for this article is available on the WWW under http://www.angewandte.org or from the author.

 © 2003 Wiley-VCH Verlag GmbH & Co. KGaA, Weinheim 1433-7851/03/4206-0677 $ 20.00+.50/0

ester when enzyme concentrations of 5 μM (for Bz-Gly-OGp) and 20 μM (for D-amino acid esters) were employed. During this time, no nonenzymatic synthesis could be detected, and the extent of spontaneous ester hydrolysis was less than 5%. The results obtained (Table 1) document that clostripain catalyzes the coupling of not only the achiral Gly ester but also of analogous D-amino acid esters. Furthermore, we found that the enzyme can acylate D-amino acid amides, a finding from earlier studies with L-Arg esters as the acyl donor,[11] and even all-D-peptides. Remarkably, the enzyme accepted H-D-Pro-NH_2, which did not react in studies with L-Arg esters.[11] This surprising result indicates that substrate mimetics broaden the enzyme's specificity towards not only the carboxy but also the amino component—a finding that may be of general significance beyond the application of clostripain and D-amino acid reactants. As is evident in Table 1, the yield depends on the nature of the acyl donor and the acyl acceptor. In general, the reactions of the D-amino acid amides and the tripeptide H-(D-Ala)$_3$-OH gave higher yields than those of the dipeptides. The low yields achieved with the latter are attributed to the unfavorable effects of the negatively charged terminal carboxylate group and were also found for the respective all-L analogues.[12] The affect of the acyl donor on the yield can be correlated to the bulk of the amino acid side chain. Generally, the enzyme prefers esters either without or with small side chains, while reactions with the bulky esters Bz-D-Leu-OGp and Bz-D-Phe-OGp give reduced product yields. But even here the yields are only slightly lower than those found for reactions with specific L-Arg esters and H-D-Leu-NH_2 or H-D-Phe-NH_2.[11]

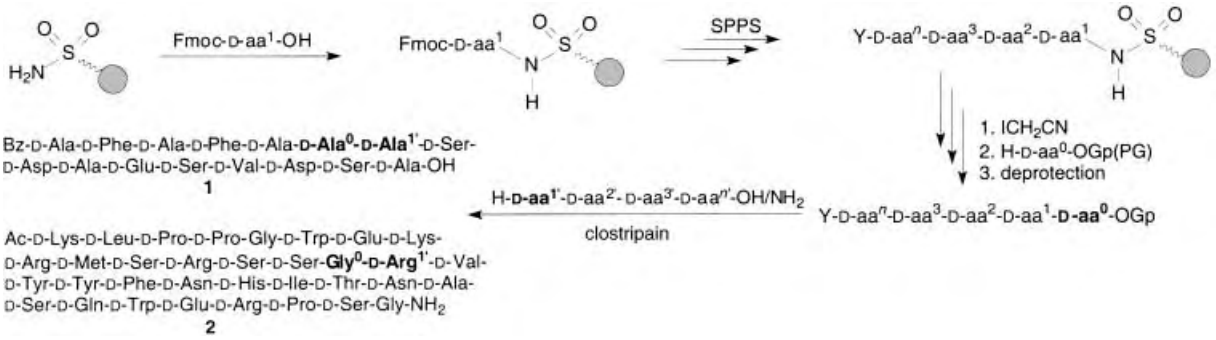
Table 1: Product yields for the clostripain-catalyzed synthesis of all-D-peptides.[a]

Acyl acceptor	Acyl donor			
	Bz-Gly-OGp	Bz-D-Ala-OGp	Bz-D-Leu-OGp[b]	Bz-D-Phe-OGp[b]
H-D-Pro-NH_2	72.6	60.7	46.2	44.0
H-D-Leu-NH_2	99.1	89.7	65.7	61.9
H-D-Phe-NH_2	98.4	90.5	66.3	67.4
H-(D-Met)$_2$-OH	43.6	43.1	37.3	38.1
H-(D-Leu)$_2$-OH	45.8	55.2	41.9	41.6
H-(D-Ala)$_3$-OH	62.4	64.8	45.8	46.6

[a] Synthesis conditions: 0.1 M HEPES buffer (4-(2-hydroxyethyl)piperazine-1-ethanesulfonic acid), 0.1 M NaCl, 0.01 M $CaCl_2$, pH 8.0, 25 °C. Concentrations: [donor] = 2 mM, [acceptor] = 10 mM, [clostripain] = 5 μM (Bz-Gly-OGp) or 20 μM (Bz-D-Xaa-OGp). [b] Reaction mixture contained 2.5% (v/v) DMF.

Finally, we tested this approach for the ligation of elongated all-D-peptide fragments. As targets we selected the model peptide **1** and the all-D version of the trifunctional 34-mer WW protein domain of the human peptidyl-prolyl-*cis*/*trans*-isomerase hPin1 (**2**, Scheme 1). Its biological relevance is based on the finding that proteins carrying WW domains play a role in numerous diseases such as Alzheimer disease, Huntington chorea, and Liddle syndrome.[13] Peptides **1** and **2** were synthesized by a single-step enzymatic coupling of appropriate N- and C-terminal fragments. The former were synthesized on 4-sulfamylbutyrylaminomethyl safety-catch resin while the latter were prepared by solid-phase peptide synthesis on Wang resin (cf. Scheme 1, for further details see the Supporting Information). After release, deprotection, and purification, the peptide fragments were used in the enzymatic ligations, which were performed under the same conditions and with the same concentrations as described above. For reasons of efficiency only in case of **2** was the ester concentration increased from 2 mM to 5 mM. To evaluate whether the approach also works with lower concentrations of reactants, we also synthesized **2** by using 2.5 mM acyl donor and 5 mM acyl acceptor. After 1 h and complete consumption of the ester, the reactions were terminated and analyzed by HPLC (Figure 1) and mass spectrometry. The yields were 58% (**1**) and ca. 50% (**2**), and the latter was independent of the reactant concentrations used. Importantly, besides hydrolyzed peptide esters, no further side products could be detected, which indicates that competitive peptide cleavages did not occur.

In summary, we have described a novel and promising method for the semisynthesis of D-amino acid containing peptides by the ligation of all-D-peptide fragments. The advantages of this approach are its broad tolerance towards the length and sequence of both the acyl donor and acceptor component, the mild reaction conditions, the avoidance of



Scheme 1. Synthesis of the all-D-hexadecapeptide **1** and the all-D version of the WW domain of hPin1 (**2**), which relies on substrate mimetics ligation and safety-catch solid-phase peptide synthesis (SPPS). Fmoc = 9-fluorenylmethyloxycarbonyl.

 © 2003 Wiley-VCH Verlag GmbH & Co. KGaA, Weinheim 1433-7851/03/4206-0678 $ 20.00+.50/0

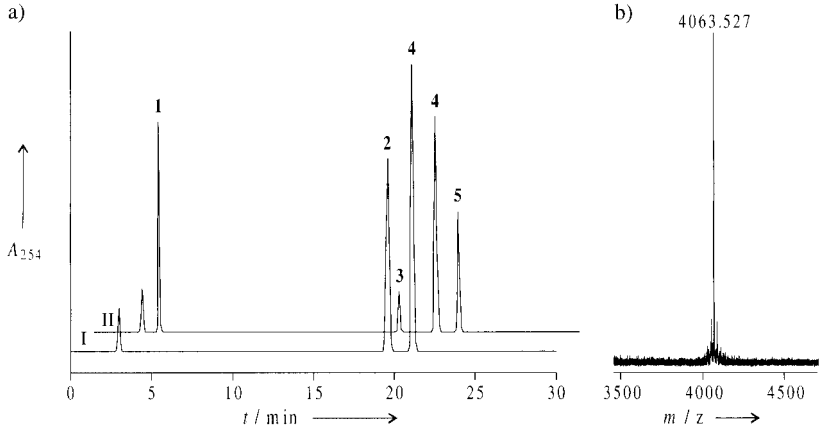


Figure 1. Analysis of the clostripain-catalyzed synthesis of the WW domain of hPin 1 by HPLC (a) and MALDI-TOF mass spectrometry (b). Synthesis conditions: 0.1 M HEPES buffer, 0.1 M NaCl, 0.01 M $CaCl_2$, pH 8.0, 2.5% (v/v) DMF, 25 °C, [donor] = 5 mM, [acceptor] = 10 mM, [clostripain] = 20 μM. aI) Before addition of enzyme; aII) after incubation for 60 min; 1: released OGp, 2: Ac-klppgwekrmsrssg-OGp, 3: Ac-klppgwekrmsrssg-OH, 4: H-rvyyfnhitnasqwerpsg-NH_2,5: Ac-klppgwekrmsrssgrvyyfnhitnasqwerpsg-NH_2. A_{254} = absorbance at 254 nm. b) calcd M_w = 4062.02.

organic solvents, and the possibility of using a highly active wild-type enzyme as the catalyst and unprotected peptides as the reactants. Proteolytic side reactions, which seriously limit the use of proteases for the conventional synthesis of all-L-peptides, are per se of no concern in the synthesis of all-D-peptides. The resulting irreversible course of synthesis ironically makes all-D-peptides even better synthesis targets for proteases than their all-L analogues, although nature designed these enzymes to be specific towards all-L-peptides. These hallmarks let one expect that this approach could gain significance for the production of even larger all-D-protein domains.

Received: August 30, 2002
Revised: November 14, 2002 [Z50072]

[1] G. Mignogna, M. Simmaco, D. Barra in *D-Amino Acids in Sequences of Secreted Peptides of Multicellular Organisms* (Ed.: P. Jolles), Birkhäuser, Basel, **1998**, pp. 29–36.
[2] a) E. C. Jimenez, B. M. Olivera, W. R. Gray, L. J. Cruz, *J. Biol. Chem.* **1996**, *271*, 28002–28005; b) G. Kreil, *Annu. Rev. Biochem.* **1997**, *66*, 337–345.
[3] a) T. N. M. Schumacher, L. M. Mayr, D. L. Minor, Jr., M. A. Milhollen, M. W. Burgess, P. S. Kim, *Science* **1996**, *271*, 1854–1857; b) D. M. Eckert, V. N. Malashkevich, L. H. Hong, P. A. Carr, P. S. Kim, *Cell* **1999**, *99*, 103–115; c) B. Wlotzka, S. Leva, B. Eschgfäller, J. Burmeister, F. Kleinjung, C. Kaduk, P. Muhn, H. Hess-Stumpp, S. Klussmann, *Proc. Natl. Acad. Sci. USA* **2002**, *99*, 8898–8902.
[4] a) C.-H. Wong, *Science* **1989**, *244*, 1145–1152; b) V. Schellenberger, H.-D. Jakubke, *Angew. Chem.* **1991**, *103*, 1440–1452; *Angew. Chem. Int. Ed. Engl.* **1991**, *30*, 1437–1449; c) F. Bordusa, *Chem. Rev.*, in press .
[5] a) A. Sugihara, Y. Shimada, S. Sugihara, T. Nagao, Y. Watanabe, Y. Tominaga, *J. Biochem.* **2001**, *130*, 119–126; b) A. Sugihara, Y. Shimada, S. Sugihara, T. Nakai, T. Kakuno, T. Nagao, Y. Watanabe, Y. Tominaga, *J. Biochem.* **2002**, *131*, 247–254, and references therein.
[6] a) J. B. West, C.-H. Wong, *J. Org. Chem.* **1986**, *51*, 2728–2735; b) A. L. Margolin, D.-F. Tai, A. M. Klibanov, *J. Am. Chem. Soc.* **1987**, *109*, 7885–7887; c) C. F. Barbas III, J. R. Matos, J. B. West, C.-H. Wong, *J. Am. Chem. Soc.* **1988**, *110*, 5162–5166.
[7] a) K. Matsumoto, B. G. Davis, J. B. Jones, *Chem. Commun.* **2001**, 903–904; b) K. Khumtaveeporn, A. Ullmann, K. Matsumoto, B. G. Davis, J. B. Jones, *Tetrahedron: Asymmetry* **2001**, *12*, 249–261.
[8] a) V. Schellenberger, H.-D. Jakubke, N. P. Zapevalova, Y. V. Mitin, *Biotechnol. Bioeng.* **1991**, *38*, 104–108; b) H. Sekizaki, K. Itoh, E. Toyota, K. Tanizawa, *Chem. Pharm. Bull.* **1996**, *44*, 1585–1587; c) F. Bordusa, D. Ullmann, C. Elsner, H.-D. Jakubke, *Angew. Chem.* **1997**, *109*, 2583–2585; *Angew. Chem. Int. Ed. Engl.* **1997**, *36*, 2473–2475; d) M. Thormann, S. Thust, H.-J. Hofmann, F. Bordusa, *Biochemistry* **1999**, *38*, 6056–6062.
[9] a) R. Günther, A. Stein, F. Bordusa, *J. Org. Chem.* **2000**, *65*, 1672–1679; b) R. Günther, F. Bordusa, *Chem. Eur. J.* **2000**, *6*, 463–467.
[10] D. Ullmann, F. Bordusa in *Handbook of Proteolytic Enzymes* (Eds.: A. J. Barrett, N. D. Rawlings, J. F. Woessner), Academic Press, London, **1998**, pp. 759–762.
[11] a) W. M. Mitchell, *Science* **1968**, *162*, 374–375; b) G. Fortier, S. L. MacKenzie, *Biotechnol. Lett.* **1986**, *12*, 873–876; c) D. Ullmann, H.-D. Jakubke, *Eur. J. Biochem.* **1994**, *223*, 865–872.
[12] V. Schellenberger, U. Schellenberger, Y. V. Mitin, H.-D. Jakubke, *Eur. J. Biochem.* **1990**, *187*, 163–167.
[13] a) P. W. Faber, G. T. Barnes, J. Srinidhi, J. Chen, J. F. Gusella, M. E. MacDonald, *Hum. Mol. Genet.* **1998**, *7*, 1463–1474; b) T. Russo, R. Faraonio, G. Minopoli, P. De Candia, S. De Renzis, N. Zambrano, *FEBS Lett.* **1998**, *434*, 1–7; c) S. Rentschler, H. Linn, K. Deininger, M. T. Bedford, X. Espanel, M. Sudol, *Biol. Chem.* **1999**, *380*, 431–442.

 © 2003 Wiley-VCH Verlag GmbH & Co. KGaA, Weinheim 1433-7851/03/4206-0679 $ 20.00+.50/0

Electron Transfer in Rotaxanes

Photoinduced Intrarotaxane Electron Transfer between Zinc Porphyrin and [60]Fullerene in Benzonitrile**

Nobuhiro Watanabe, Nobuhiro Kihara, Yoshio Furusho, Toshikazu Takata, Yasuyuki Araki, and Osamu Ito**

In the photosynthetic center of bacteria, charge separation proceeds by a series of electron-transfer steps between porphyrin(P)-like components and quinones that are spatially oriented in proteins. Numerous synthetic models for covalently connected donor–acceptor systems have been proposed,[1–4] based on coordinative bonds between donor and acceptor.[5] Recently, photoinduced electron transfer between donors and acceptors in rotaxanes was reported.[6,7] Rotaxanes containing ZnP (donor) and AuP (acceptor) show photoinduced superexchange forward electron transfer between noncovalently linked chromophores.[8] Imahori et al. reported that a ZnP–C_{60} linked dyad system shows a relatively long lifetime of the charge-separated state, in addition to high charge-separation efficiency.[3] We envisaged that the combination of a ZnP (donor), C_{60} (acceptor), and a rotaxane skeleton could mimic the photosynthesis reaction center. Herein we report on the ZnP/C_{60} rotaxane **7**, designed as shown in Scheme 1, in which through-space forward and backward electron transfer processes between the ZnP and C_{60} moieties and a relatively long charge-separation lifetime are expected.

Rotaxane **4** was synthesized by the hydrogen-bond-assisted method for *sec*-amide-based rotaxanes.[9,10] Thus, the condensation of isophthaloyl dichloride (**2**) and 5,10,15-tris(3,5-di-*tert*-butylphenyl)-20-(4-aminophenyl)porphyrin (**3**)[11] was carried out in chloroform in the presence of macrolactam **1**[9] at 0°C to afford **4** in 17% yield. The conversion of **4** into the corresponding zinc porphyrin rotaxane **5** was achieved by treatment with zinc acetate in refluxing chloroform. The Diels–Alder reaction of **4** and five equivalents of C_{60} was carried out in refluxing 1,2-dichlorobenzene to give rotaxane **6** in 69% yield. Finally, **6** was converted into zinc porphyrin rotaxane **7** in 82% yield by treatment with zinc acetate. The rotaxanes were characterized by satisfactory NMR and FAB-MS spectra corresponding to their structures. To our knowledge, these are the first rotaxane porphyrin–C_{60} conjugates, although such a pseudorotaxane has been reported.[12] On the other hand, some fullerene-containing catenanes have also been reported.[13]

The steady-state absorption spectrum of **7** is shown in Figure 1; the absorption bands at 420 and 500–600 nm are

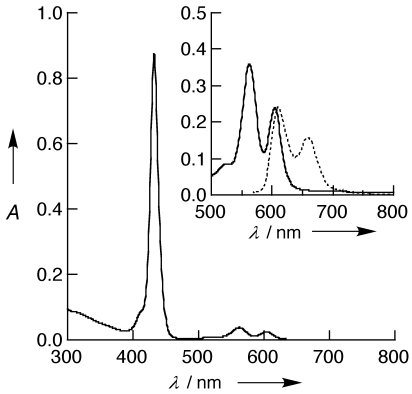


Figure 1. Steady-state absorption spectrum of **7** (1×10^{-6} M) in PhCN. Inset: steady-state absorption spectrum (solid line) and fluorescence spectrum (dashed line) of **7** (1×10^{-5} M).

mainly the Soret and Q bands, respectively, of ZnP moiety **5**. The absorption bands of the C_{60} moiety appear at 700 nm and below 350 nm. The absorption spectrum of **7** is almost a superimposition of those of **5** and C_{60}. Figure 1 also shows the fluorescence spectrum of **7** above 600 nm; the fluorescence peaks at 620 and 670 nm are attributed to the ZnP moiety **5**, while the fluorescence peak of C_{60}, which is expected to appear at 725 nm, may be hidden in the fluorescence bands of the ZnP moieties. The fluorescence intensity of **7** was quite weak compared to that of **5** in benzonitrile. Furthermore, an enhancement in the fluorescence of the C_{60} moiety at 725 nm was not observed, and this suggests that energy transfer from the excited singlet state of the ZnP moieties to the C_{60} moiety may not have taken place. These observations indicate that electron transfer predominantly takes place from the excited singlet state of the ZnP moieties to the C_{60} moiety.

The time profile of the fluorescence of rotaxane **7** shows biexponential decay in benzonitrile (Figure 2); the lifetimes of the ZnP moieties in **7** [$\tau_{f1}=93$ ps (80%) and $\tau_{f2}=1560$ ps (20%)] were evaluated by the curve-fitting method. The τ_{f1} value is small relative to that of **5** [$\tau_{fr}=1790$ ps (100%)], while the τ_{f2} value remained similar to that of τ_{fr}. From these lifetimes, the quantum yield Φ_{CS} and rate constant k_{CS} for charge separation were calculated to be 0.95 and 1.0×10^{10} s^{-1}, respectively, by using the ordinal equations [$\Phi_{CS}=1/\tau_{fr}/(1/\tau_{fr}-1/\tau_{f1})$ and $k_{CS}=(1/\tau_{fr}-1/\tau_{f1})$].[3]

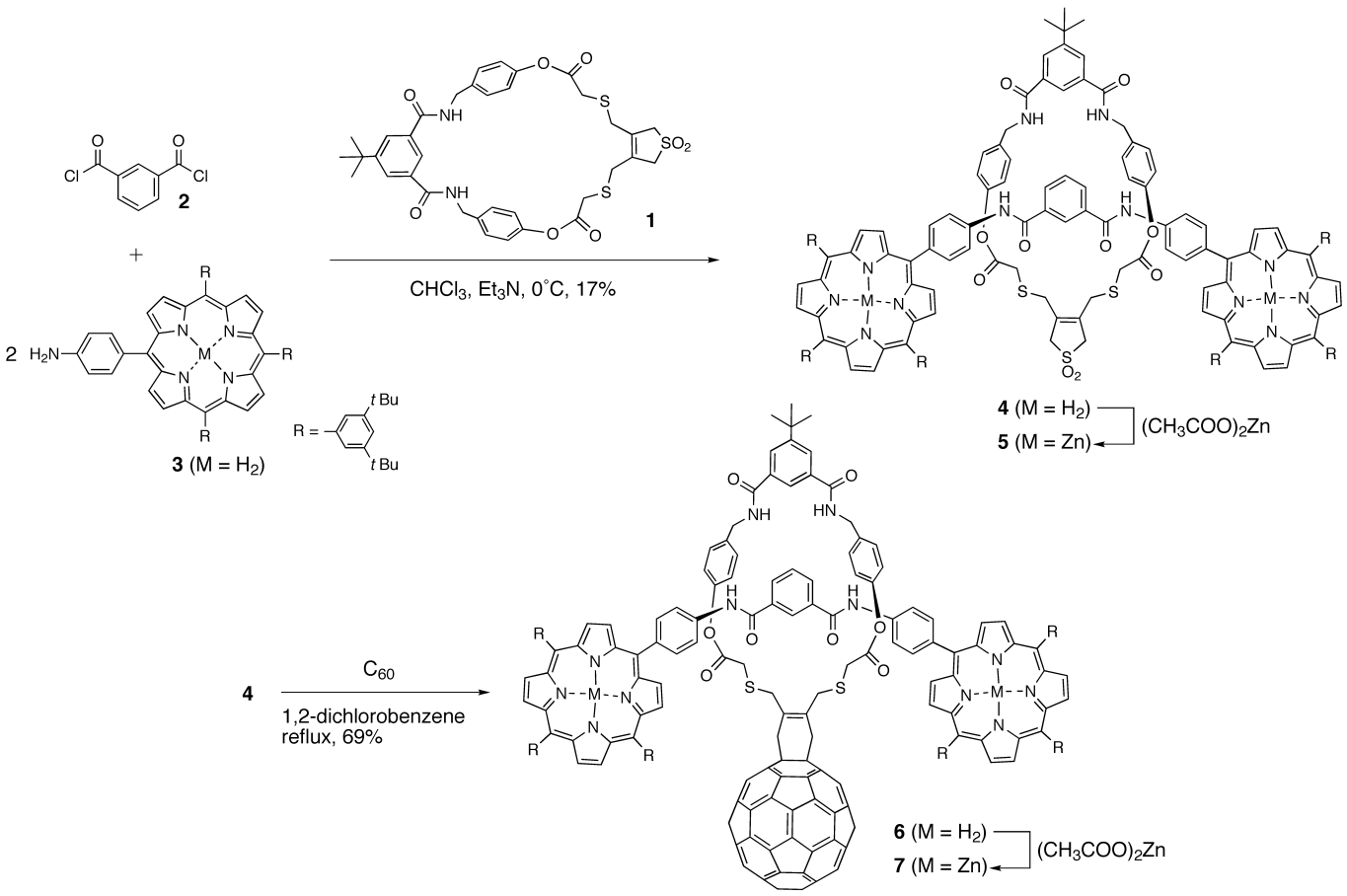
Figure 3 shows the nanosecond transient absorption spectra of rotaxane **7** in benzonitrile, observed by 532 nm laser excitation (6 ns laser pulse). The transient absorption band at 1000 nm observed immediately after laser pulse (6 ns)

[*] Prof. Dr. T. Takata, N. Watanabe, Dr. N. Kihara, Dr. Y. Furusho
Department of Applied Chemistry
Graduate School of Engineering
Osaka Prefecture University
1-1 Gakuen-cho, Sakai-shi, Osaka 599-8531 (Japan)
Fax: (+81) 72-254-9910
E-mail: takata@chem.osakafu-u.ac.jp
Prof. Dr. O. Ito, Dr. Y. Araki
Institute of Multidisciplinary Research for Advanced Materials
Tohoku University, CREST (JST)
Katahira, Aoba-ku, Sendai, Miyagi 980-8577 (Japan)
Fax: (+81) 22-217-5608
E-mail: ito@tagen.tohoku.ac.jp

[**] This work was partly supported by the Priority-Area-Research by the Ministry of Education, Science, Technology, Sports and Culture of Japan and by JSPS Research Fellowships for Young Scientists (N.W.) which is greatly acknowledged.

Supporting information for this article is available on the WWW under http://www.angewandte.org or from the author.

 © 2003 Wiley-VCH Verlag GmbH & Co. KGaA, Weinheim 1433-7851/03/4206-0681 $ 20.00+.50/0



Scheme 1. Synthesis of **4**–**7**.

was assigned to the anion radical of the C_{60} moiety; the absorption bands in the visible region, centered around 700 nm and 850 nm, were attributed to the triplet states of the C_{60} and ZnP moieties, respectively, with which the cation radical of the ZnP moieties may overlap.[3] These observations confirm that charge separation takes place immediately after laser exposure. The transient absorptions at 1000 ns were mostly attributed to the triplet states of C_{60} and ZnP in rotaxane **7**, which have longer lifetimes than the charge-separated state.

The inset time profile in Figure 3 shows the decay of the radical anion of C_{60} at 1000 nm. The decay obeys first-order kinetics with a rate constant of $5.5 \times 10^6\ s^{-1}$, which is the charge-recombination rate constant k_{CR}. This value corresponds to a lifetime τ_{RIP} of 180 ns for the charge-separated state (radical ion pair). This τ_{RIP} value is significantly larger

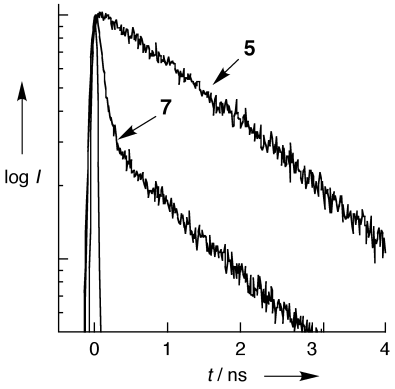


Figure 2. Time profiles of the fluorescence of rotaxane **7** (1×10^{-4} M) and ZnP moiety **5** (1×10^{-4} M) in PhCN. Excitation wavelength was 410 nm.

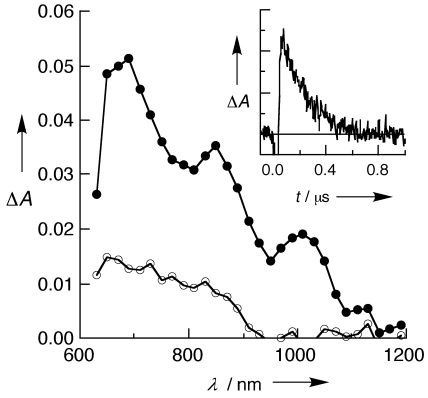


Figure 3. Nanosecond transient absorption spectra of **7** (1×10^{-4} M) observed by 532 nm laser excitation in PhCN after 100 (●) and 1000 ns (○). Inset: trace of the C_{60} radical anion at 1000 nm.

 © 2003 Wiley-VCH Verlag GmbH & Co. KGaA, Weinheim 1433-7851/03/4206-0682 $ 20.00+.50/0

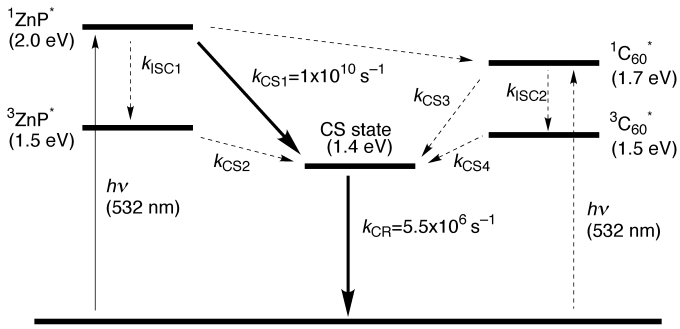


Figure 4. Energy diagram for charge separation (CS) and charge recombination (CR) of **7** after photoexcitation in PhCN. ISC = intersystem crossing.

than those reported for covalently connected dyad molecules; for example, C_{60}–dimethylaniline (< 1 ns),[14] C_{60}–β-carotene (< 1 ns),[15] and C_{60}-TTF (2 ns).[16] Rotaxane **7** has a τ_{RIP} value similar to that of covalently linked C_{60}–ZnP (770 ns).[3]

The energy diagram for the charge separation and recombination processes after photoexcitation is shown in Figure 4. The ion-pair state was evaluated from the first oxidation potential of the ZnP moiety (0.29 V vs ferrocene/ferrocene$^+$) and the first reduction potential of the C_{60} moiety (−1.1 V vs ferrocene/ferrocene$^+$) of rotaxane **7** in benzonitrile. The shortening of fluorescence lifetimes indicates that charge separation takes place mainly from the excited singlet state of the ZnP moiety to produce a radical ion pair. The rate of this charge-separation process was as high as 10^{10} s^{-1}. The slow recombination rate suggests that this process lies in an inverted region far more negative than the charge-separation process.

The charge-recombination rates k_{CR} showed slight temperature dependence; from the semiempirical Marcus equation,[3] the free-energy of activation $\Delta G^{\neq}_{CR}$ was evaluated to be 57 meV, which is somewhat smaller than for conventional dyad systems; for example, $\Delta G^{\neq}_{CR}$ of retinyl–C_{60} is 160 meV.[17] In general, a rather small $\Delta G^{\neq}_{CR}$ is expected for through-space electron transfer, while a considerably higher $\Delta G^{\neq}_{CR}$ is anticipated for through-bond electron transfer. Thus, the small $\Delta G^{\neq}_{CR}$ observed for rotaxane **7** suggests that charge recombination takes place by through-space electron transfer with a superexchange mechanism.[7] The $\Delta G^{\neq}_{CR}$ value of 57 meV for **7** is slightly larger than that expected for the complete through-space electron transfer system; hence, this slight increase in $\Delta G^{\neq}_{CR}$ of **7** can be attributed to the flexibility of the relative configuration of the ZnP and C_{60} moieties. The electronic coupling constant V, evaluated with the semiempirical Marcus equation, is 0.77 cm^{-1}, almost twice that of the retinyl–C_{60} dyad ($V = 0.34$ cm^{-1} in PhCN).[17] This difference in V value suggests that not only is the donor–acceptor distance smaller in **7** (center-to-center distance $r_{cc} \approx 10$ Å) than in retinyl–C_{60} dyad ($r_{cc} = 11.4$ Å), but also that **7** has a more suitable orientation for electron transfer. Further studies on electron transfer features are in progress.

Received: August 5, 2002 [Z19881]

[1] D. Gust, T. A. Moore, A. L. Moore, *Acc. Chem. Res.* **2001**, *34*, 40.

[2] S. Fukuzumi, D. M. Guldi in *Electron Transfer in Chemistry, Vol. 2* (Ed.: V. Balzani), Wiley-VCH, Weinheim, **2001**, pp. 270–337.

[3] H. Imahori, M. E. El-Khouly, M. Fujitsuka, O. Ito, Y. Sakata, S. Fukuzumi, *J. Phys. Chem. A* **2001**, *105*, 325.

[4] a) N. Armaroli, F. Diederich, C. O. Dietrich-Buchecker, L. Flamigni, G. Marconi, J.-F. Nierengarten, J.-P. Sauvage, *Chem. Eur. J.* **1988**, *4*, 406; b) N. Armaroli, G. Marconi, L. Echegoyen, J. P. Bourgeois, F. Diederich, *Chem. Eur. J.* **2000**, *6*, 1629; c) L. Flamigni, I. M. Dixon, J.-P. Collin, J.-P. Sauvage, *Chem. Commun*. **2000**, 2479.

[5] F. D'Souza, G. R. Deviprasad, M. E. El-Khouly, M. Fujitsuka, O. Ito, *J. Am. Chem. Soc.* **2001**, *123*, 5277.

[6] M.-J. Blanco, M. C. Jiménez, J.-C. Chambron, V. Heitz, M. Linke, J.-P. Sauvage, *Chem. Soc. Rev.* **1999**, *28*, 293.

[7] P. R. Ashton, R. Ballardini, V. Balzani, A. Credi, K. R. Dress, E. Ishow, C. J. Kleverlaan, O. Kocian, J. A. Preece, N. Spencer, J. F. Stoddart, M. Venturi, S. Wenger, *Chem. Eur. J.* **2000**, *6*, 3558.

[8] M. Andersson, M. Linke, J.-C. Chambron, J. Davidsson, V. Heitz, J.-P. Sauvage, L. Hammarström, *J. Am. Chem. Soc.* **2000**, *122*, 3526.

[9] N. Watanabe, N. Kihara, T. Takata, *Org. Lett.* **2001**, *3*, 3519.

[10] a) N. Kihara, T. Takata, *J. Synth. Org. Chem. Jpn.* **2001**, *59*, 206; b) Y. Furusho, J. Shoji, N. Watanabe, N. Kihara, T. Adachi, T. Takata, *Bull. Chem. Soc. Jpn.* **2001**, *74*, 139; c) N. Watanabe, Y. Furusho, N. Kihara, T. Takata, K. Kinbara, K. Saigo, *Chem. Lett.* **1999**, 915; d) R. Jäger, F. Vögtle, *Angew. Chem.* **1997**, *109*, 966; *Angew. Chem. Int. Ed. Engl.* **1997**, *36*, 930; e) F. Vögtle, T. Dünnwald, T. Schmidt, *Acc. Chem. Res.* **1996**, *29*, 451.

[11] H. Imahori, K. Hagiwara, M. Aoki, T. Akiyama, S. Taniguchi, T. Okada, M. Shirakawa, Y. Sakata, *J. Am. Chem. Soc.* **1996**, *118*, 11771.

[12] M. V. Martínez-Díaz, N. S. Fender, M. S. Rodríguez Morgade, M. Gómez-López, F. Diederich, L. Echegoyen, J. F. Stoddart, T. Torres, *J. Mater. Chem.* **2002**, *12*, 2095.

[13] P. R. Ashton, F. Diederich, M. Gómez-López, J.-F. Nierengarten, J. A. Preece, F. M. Raymo, J. F. Stoddart, *Angew. Chem.* **1997**, *109*, 1611; *Angew. Chem. Int. Ed. Engl.* **1997**, *36*, 1448.

[14] R. M. Williams, J. M. Zwier, J. W. Verhoeven, *J. Am. Chem. Soc.* **1995**, *117*, 4093.

[15] H. Imahori, S. Cardoso, D. Tatman, S. Lin, L. Noss, G. R. Seely, L. Sereno, C. Silber, T. A. Moore, A. L. Moore, D. Gust, *Photochem. Photobiol.* **1995**, *62*, 1009.

[16] N. Martín, L. Sánchez, M. A. Herranz, D. M. Guldi, *J. Phys. Chem. A* **2000**, *104*, 4648.

[17] M. Yamazaki, Y. Araki, M. Fujitsuka, O. Ito, *J. Phys. Chem. A* **2001**, *105*, 8615.

New Form of Isomerism

Isomeric Constellations of Encapsulation Complexes Store Information on the Nanometer Scale**

*Alexander Shivanyuk and Julius Rebek, Jr.**

Isomers in chemistry are defined through constitution. Further stereochemical relationships between two molecules can be assigned through configuration and conformation, but collections of molecules can also show isomerism through their arrangements in space. We report here a new form of isomerism resulting from the encapsulation of three small-molecule guests in a cylindrical, reversibly assembled host. The mobility of the guests within the host is limited: the guest molecules are held in different constellations within the confined space. The various combinations and isomeric constellations of capsules are nanoscale data storage devices.

Encapsulation complexes are reversibly formed assemblies in which small-molecule guests are surrounded by a multimolecular host. The systems are held together by weak intermolecular forces comprising metal–ligand interactions and hydrogen bonding. The assemblies are dynamic; they form and dissipate on time scales ranging from milliseconds to hours. The mechanical barriers that constrain the molecules within molecules offer new possibilities for isomerism, first observed in covalently bound carcerands.[1] In reversibly bound encapsulation complexes,[2] the lifetime of the array is determined by the mobility of the guests, either within the capsule or through exchange with molecules outside, in solution. We report here isomeric constellations—arrangements of several molecules in space—that emerge when two different guests, are encapsulated within a cylindrical host.[3] Specifically, all combinations of chloroform and isopropyl chloride in the encapsulation complexes (Figure 1) can be identified by NMR methods. The isomerism is an emergent property of the assembly, rather than that of individual molecules. The phenomenon hints at applications in mechanistic organic chemistry through the selective solvation of reactants[4] and information storage at the molecular level.

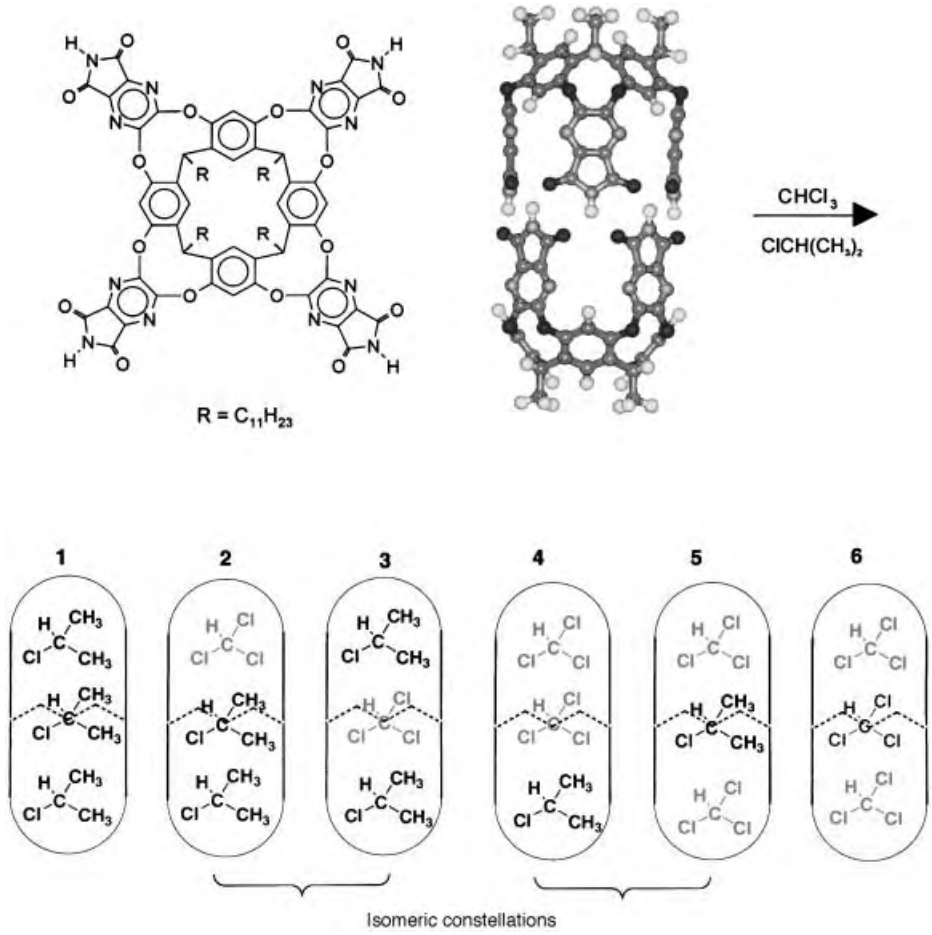


Figure 1. Top: Line drawing of the cavitand and a ball-and-stick representation of the self-assembled, cylindrical capsule. Bottom: the six different combinations of encapsulated $CHCl_3$ and $ClCH(CH_3)_2$.

The NMR spectrum of isopropyl chloride $ClCH(CH_3)_2$ in the capsule using deuterated mesitylene as the solvent is shown in Figure 2a. Mesitylene is too large to be encapsulated and cannot compete with appropriately sized guests present at lower concentrations. Accordingly, the spectrum represents array **1**. The sharp, widely separated signals for guests in the two locations reflect the sizable energetic barrier that prevents the guest molecules from exchanging positions: they are too large to slip past each other while within the capsule. The rate of the exchange process is slow on the NMR time scale. The assignments were confirmed by NOE experiments. Irradiation of the upfield doublet gave NOEs with the

[*] Prof. Dr. J. Rebek, Jr., Dr. A. Shivanyuk
The Skaggs Institute for Chemical Biology and
Department of Chemistry
The Scripps Research Institute, MB-26
10550 North Torrey Pines Road, La Jolla, CA 92037 (USA)
Fax: (+1) 858-784-2876
E-mail: jrebek@scripps.edu

[**] We are grateful to the Skaggs Institute of Research and the NIH (GM 50174) for support. A.S. is a Skaggs Postdoctoral Fellow. We are pleased to acknowledge illuminating discussions with Prof. A. Eschenmoser, Prof. P. Ballester, and Prof. J. Williamson. Technical help with NMR instrumentation was generously provided by Prof. M. Hennig.

 © 2003 Wiley-VCH Verlag GmbH & Co. KGaA, Weinheim 1433-7851/03/4206-0684 $ 20.00+.50/0

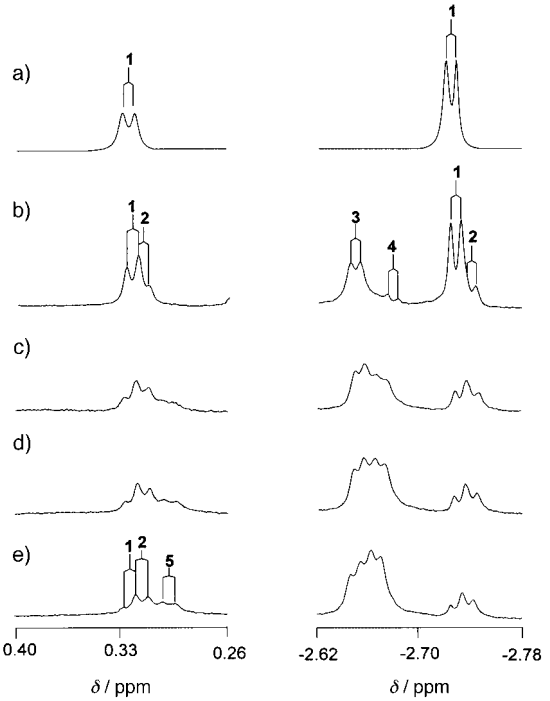


Figure 2. Upfield regions of the NMR spectra of the complexes (800 MHz; 298 K in $[D_{12}]$mesitylene (0.15 mL) and isopropyl chloride (0.3 mL)). The Initial concentration of the capsule is 2 mM. a) isopropyl chloride alone; array **1**. The furthest upfield doublet is assigned to the methyl groups of guests near the ends of the capsule, and the downfield doublet is assigned to methyl groups of the guest located near the middle. New arrays appear as the following volumes of $CDCl_3$ are added: b) addition of 0.05 mL $CDCl_3$. The isomeric constellations **2** and **3** arise as one guest is replaced and **4** appears as two guests are replaced from the $ClCH(CH_3)_2$-filled **1**; c) addition 0.15 mL $CDCl_3$. Array **4** increases at the expense of **1**, while the ratio **2**:**3** remains constant; d) addition of 0.3 mL $CDCl_3$; e) addition of 0.4 mL $CDCl_3$. Array **4** becomes the dominant $ClCH(CH_3)_2$-containing species, and its constellational isomer **5**, having a single $ClCH(CH_3)_2$ in the center of the capsule is identified.

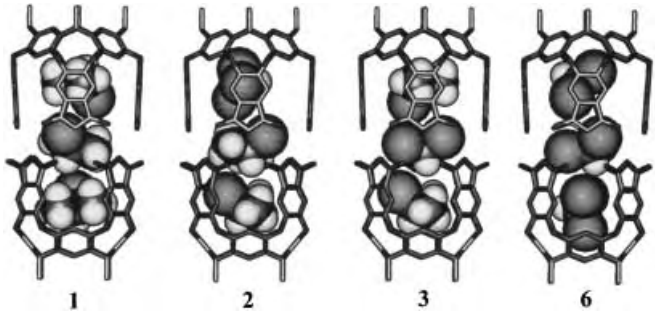


Figure 3. Energy-minimized structures of encapsulation complexes: **1**: $HCCl(CH_3)_2$ alone; **2** and **3**: constellational isomers of $CHCl_3 \cdot 2\,HCCl(CH_3)_2$; **6**: $CHCl_3$ alone. The van der Waals surfaces of the guests emphasize their inability to exchange places while within the capsule.

resorcinarene hydrogen atoms, while irradiation of the downfield doublet showed NOEs only with the imide N–H signals. An energy-minimized structure for array **1** is shown in Figure 3a, where the van der Waals surfaces featured on the guests emphasize the constraints on their mobility within the capsule.

Titration of $CDCl_3$ into the capsule filled with isopropyl chloride generated the 800 MHz spectra shown in Figure 2b–e. The identification of constellational isomers **2** and **3** was possible in the upfield regions of the spectra (the regions representing $ClCH(CH_3)_2$ guests at the ends and the middle of the capsule). The first to appear are those in which one $ClCH(CH_3)_2$ is replaced by $CDCl_3$ (arrays **2** and **3**). A key to the assignment of the signals lies in the identical stoichiometries of these constellational isomers: the relative amounts of **2** and **3** need not be equal, but their ratio remains constant throughout the titration. Integration of the signals shows this requirement is met by the assignments indicated, with **3**:**2** = 2.5:1. The next arrays that emerge during the titration are the isomers with one $ClCH(CH_3)_2$ and two $CDCl_3$ guests, (**4** and **5**) but only **4** appears in the furthest upfield region of the spectrum. Its constellational isomer **5** confines a single $ClCH(CH_3)_2$ guest to the middle of the capsule, and the appropriate region of the NMR spectrum is downfield (Figure 2c–e). Three arrays feature centrally located $ClCH(CH_3)_2$ guests: **1, 2**, and **5**. Identification of **5** follows from the known resonance signal for **1** and that deduced for **2**.

With $CHCl_3$ as the only guest (array **6**) under these conditions, the same exchange characteristics hold; a signal occurs at $\delta = 3.52$ ppm for $CHCl_3$ molecules at the ends of the capsule, and a signal occurs at $\delta = 6.46$ ppm for the $CHCl_3$ in the center. A reverse titration in which $ClCH(CH_3)_2$ was added to the $CHCl_3$-filled capsule showed the initial appearance of signals for **4** and **5** followed by those for **2** and **3** in the NMR spectra (data not shown).

In addition to all the upfield signals for capsules containing isopropyl groups (**1**–**5**) described above, an equimolar mixture of $CHCl_3$ and $ClCH(CH_3)_2$ showed the appropriate downfield signals for encapsulated $CHCl_3$. Even the $CHCl_3$-filled capsule **6** can be identified, that is, all six combinations coexist at comparable concentrations for this pair of guests. This may appear as an unlikely result because the six combinations are not expected to have equal free energies and appear at different concentrations. The attractive forces—van der Waals and dipole–dipole interactions—between the guests and the host, and between the guests themselves are different for each arrangement. If the energetic difference between the most favored and least favored combinations exceeds 3 kcal mol^{-1}, less than 1% of the least favored isomer will be present at equilibrium at ambient temperature; NMR methods would be hard-pressed to detect both combinations. Specifically, only five of the six combinations of $CHCl_3$ with $ClCH_2CH_2Cl$ in the capsule could be observed, and generally, other solvent pairs tested showed even fewer isomeric constellations coexist. Yet the energies for the $CHCl_3$/$ClCH(CH_3)_2$ combinations are, evidently, well within 1 kcal mol^{-1} and all appear simultaneously.

The explanation lies in the nearly identical properties of these two guests. Their shapes, dimensions, and volumes are practically superimposable. For example, the volume of $CHCl_3$ is 73 Å^3 and that of $ClCH(CH_3)_2$ is 74 Å^3; any combination of three guests occupies about 53% of the

 © 2003 Wiley-VCH Verlag GmbH & Co. KGaA, Weinheim 1433-7851/03/4206-0685 $ 20.00+.50/0

capsule's internal space of 420 Å^3. The proper filling of space is an essential determinant of reversible encapsulation: guests that fill slightly more than half of the available space lead to the most stable complexes.[5] Either guest can interact favorably with the polar seam of hydrogen bonds that hold the capsule together through their modest dipole moments (1.15 **D** for $CHCl_3$ and 2.1 **D** for $ClCH(CH_3)_2$).

The different combinations and isomeric constellations introduced here represent information, temporarily stored in the form of a binary code. The symmetry of the capsule reduces the capacity to six bits from the eight expected. Long-term storage of data on the nanometric scale may follow when their arrangements can be precisely controlled, maintained, and retrieved. In the meantime, reversible assembly provides access to capsules with volumes capable of surrounding numerous guests.[6,7] The well-defined sizes and shapes of the cavities impose limitations on the motions of the guests, both internal, such as ring inversion[8,9] or external, such as molecular translation and tumbling.[10–12] Guest–guest interactions[13] offer even more possibilities for information storage and we explore them in the sequel.

Received: August 5, 2002
Revised: October 29, 2002 [Z19884]

[1] P. Timmerman, W. Verboom, F. C. J. M. van Veggel, J. P. M. van Duynhoven, D. N. Reinhoudt, *Angew. Chem.* **1994**, *106,* 2437 – 2440; *Angew. Chem. Int. Ed. Engl.* **1994**, *33,* 2345 – 2347.
[2] F. C. Tucci, D. M. Rudkevich, J. Rebek, Jr., *J. Am. Chem. Soc.* **1999**, *121*, 4928 – 4929.
[3] T. Heinz, D. M. Rudkevich, J. Rebek, Jr., *Nature* **1998**, *394*, 764 – 766.
[4] C. K. Regan, S. L. Craig, J. I. Brauman, *Science* **2002**, *295*, 2245 – 2247.
[5] A. S. Mecozzi, J. Rebek, Jr., *Chem. Eur. J.* **1998**, *4*, 1016 – 1022.
[6] J. Chen, J. Rebek, Jr., *Org. Lett.* **2002**, *4*, 327 – 329.
[7] M. K. Ebbing, M.-J. Villa, J.-M. Malpuesta, P. Prados, J. de Mendoza, *Proc. Natl. Acad. Sci. USA* **2002**, *99*, 4962 – 4966.
[8] B. M. O'Leary, R. M. Grotzfeld, J. Rebek, Jr., *J. Am. Chem. Soc.* **1997**, *119*, 11701 – 11702.
[9] R. G. Chapman, J. C. Sherman, *J. Org. Chem.* **2000**, *65*, 513 – 516.
[10] D. J. Cram, J. M. Cram, J. M. *Container Molecules and Their Guests* (Ed.: F. Stoddart), The Royal Society of Chemistry, London, **1994**.
[11] A. Jasat, J. C. Sherman, *Chem. Rev.* **1999**, *99*, 931 – 968.
[12] M. M. Conn, J. Rebek, Jr., *Chem. Rev.* **1997**, *97*, 1647 – 1668.
[13] A. Shivanyuk, J. Rebek, Jr., *J. Am. Chem. Soc.* **2002**, *124*, 12074 – 12075.

Modular-Assembled Bowls and Crowns

Modular Cavity-Tunable Self-Assembly of Molecular Bowls and Crowns as Structural Analogues of Calix[3]arenes**

Shu-Yan Yu, Hui Huang, Hong-Bo Liu, Zhong-Ning Chen, Rongben Zhang, and Makoto Fujita*

The construction of container molecules is still an interesting topic in organic synthesis, particularly bowl-shaped molecules, such as calixarenes, because of their potential applications in a variety of areas of supramolecular chemistry.[1] In contrast to the inorganic approach, metal-directed self-assembly has been widely employed to construct well-defined metal–organic container molecules.[2] Metal-assembled bowl-shaped molecules that are structural analogues of calixarenes, such as metallacalix[3]arenes,[3] metallacalix[4]arenes,[4] and others[5,6] have attracted considerable attention. We obtained a metal–organic nanobowl by self-assembly,[7] which was found to assemble in aqueous media to form a dimeric capsule that contains a large hydrophobic pocket inside the framework.[8] This pocket served as a reaction container for a highly stereoselective [2+2] photodimerization of olefins.[9] These findings inspired us to develop structurally and functionally new container molecules with calixarene features to conform with certain molecular architectures, and various reactions. In addition, we noted that among the few inorganic analogues of calixarenes, conformational conversion usually occurred because of the flexibility of the ligand, and because of distortion of the coordination geometry, as found in some metallacalix[3]arenes (with partial cone conformer),[6] and metallacalix[4]arenes (with isomers).[4] Therefore, self-assembled metallacalixarenes with single rigid conformations (i.e., cone conformer, bowl form, and *all-syn* conformation) are

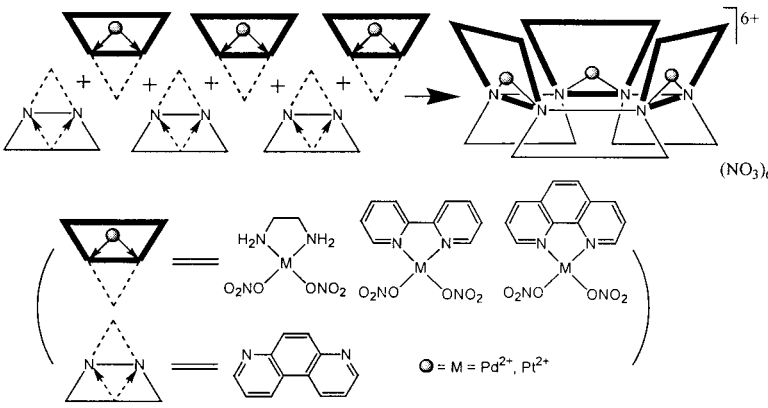
[*] Prof. Dr. S.-Y. Yu, H. Huang, Dr. H.-B. Liu, Prof. Dr. R. Zhang
State Key Laboratory of Polymer Physics and Chemistry
Center for Molecular Science
Institute of Chemistry
Chinese Academy of Sciences
Beijing 100080 (P.R. China)
Fax: (+86) 10-6255-9373
E-mail: syu@infoc3.icas.ac.cn
Prof. Dr. Z.-N. Chen[+]
State Key Laboratory of Structural Chemistry
Fujian Institute of Research on the Structure of Matter
Chinese Academy of Sciences
Fuzhou 350002 (P.R. China)
Prof. Dr. M. Fujita
Department of Applied Chemistry
Graduate School of Engineering
The University of Tokyo
bunkyo-ku, Tokyo 113-8656 (Japan)

[+] Crystal structure analysis.

[**] The project supported by National Natural Science Foundation of China No. 90206013.

Supporting information for this article is available on the WWW under http://www.angewandte.org or from the author.

 © 2003 Wiley-VCH Verlag GmbH & Co. KGaA, Weinheim 1433-7851/03/4206-0686 $ 20.00+.50/0



Scheme 1. Modular self-assembly of the crowns. See text for details.

rare.[3] To obtain the cone conformer, which is a structural analogue of calix[3]arenes, we prepared modular, cavity-tunable self-assembly molecular bowls and crowns with unique (*syn, syn, syn*) conformations, the basic principle of which is shown in Scheme 1.

These metallacalix[3]arenes are self-assembled from six planar modules, three metal-coordination-complex ions, and three rigid aromatic ligands (4,7-phenanthroline; L). The metal-coordination complexes are *cis*-protected metal centers that direct the coordination angle to 90°, such as $[Pd(NO_3)_2(en)]$, $[Pt(NO_3)_2(en)]$ (en = ethylenediamine), $[Pd(NO_3)_2(bpy)]$, $[Pt(NO_3)_2(bpy)]$ (bpy = 2,2′-bipyridine), $[Pd(NO_3)_2(phen)]$, and $[Pt(NO_3)_2(phen)]$ (phen = 1,10-phenanthroline). In the ideal case, the three L modules form rigid 60° corners, which favor coordination to three linear metal complexes to self-assemble into an equilateral triangle;[10] but in the examples reported herein, the three ligand modules form a cone to link the three metal-complex units, which results in the formation of a trimetal bowl or crown with a charge of 6+. The lower cavity (below the trimetal triangular plane) consists of the three modules of L; while the upper cavity (above the trimetal triangular plane) consists of the three modules of the square-planar-coordinated metal Pd or Pt. Both cavities exhibit *syn, syn, syn* orientation and cone conformation, confirmed by solution NMR spectroscopy and X-ray crystallographic studies.

The treatment of $[Pd(NO_3)_2(en)]$ with a solution containing one equivalent of L in D_2O at room temperature over several minutes leads to formation of $[\{Pd(en)\}_3L_3](NO_3)_6$ (**1**) in quantitative yield. The ^{1}H NMR spectra shown in Figure 1a are consistent with a highly symmetrical structure and are indicative of a single product in solution. The resonance signals labeled □ correspond to the ligand 4,7-phenanthroline. Surprisingly, the resonance signals at approximately $\delta =$ 3.0 ppm assigned to the CH_2 group of ethylenediamine are a pair of doublets, indicative of two different environments that cannot be averaged. This is characteristic of a cone conformer, as exemplified by *p-tert*-butylcalix[4]arene,[11] rather than metallacalix[4]arenes, where other isomers exist (1,3-alternate conformer, cone),[4] or metallacalix[3]arene (partial cone).[6] The Pt analogue, $[\{Pt(en)\}_3L_3](NO_3)_6$ (**1′**) was obtained at elevated temperature (100 °C, 24 h) by a similar route to that of **1**, and the resonance signals assigned to CH_2 of the ethylenediamine are similar to those of **1** (compare Figure 1a and Figure 1b). Therefore, **1′** has the same structure as **1**, that is, a trimetal-center molecular bowl with a charge of 6+. The self-assembly of **1′** is thermodynamically favored, since the slow transformation from the kinetic products into **1′** was observed at room temperature over 24 h (Figure 1c). NMR monitoring experiments showed that the addition of an excess quantity of a solution containing the nitrate anion to a solution of **1** or **1′** does not lead to any significant chemical shift, which indicates that the binding of the nitrate anion to the bowl reached saturation during the formation of the bowl. Furthermore, when the nitrate anion was replaced with the acetate anion as the leaving group in the starting material, again the bowl formed, which was confirmed by NMR spectroscopy. Three acetate anions were found to be encapsulated within the bowls resulting in a downfield shift of

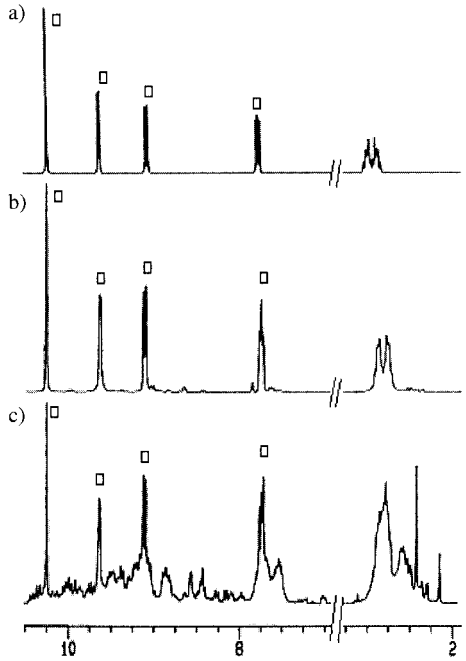


Figure 1. Self-assembly of **1** and **1′**. a) ^{1}H NMR spectrum of **1**, b) ^{1}H NMR spectrum of **1′**, c) ^{1}H NMR spectrum of a sample taken from the reaction of $[Pt(NO_3)_2(en)]$ with L in a 1:1 molar ratio at room temperature after 24 h.

1.0 ppm of the resonance signals associated with the acetate anion relative to those of the free acetate anion. It seems that the formation of the bowl is not affected by varying the counter anion.

The X-ray crystal structure analysis of **1**[12] shows that the solid-state structure is the same as that in solution. The structure of **1** (Figure 2) comprises a bowl with a binding nitrate anion, together with an empty bowl (omitted for clarity). The three rigid modules of L make up the bowl

 © 2003 Wiley-VCH Verlag GmbH & Co. KGaA, Weinheim 1433-7851/03/4206-0687 $ 20.00+.50/0

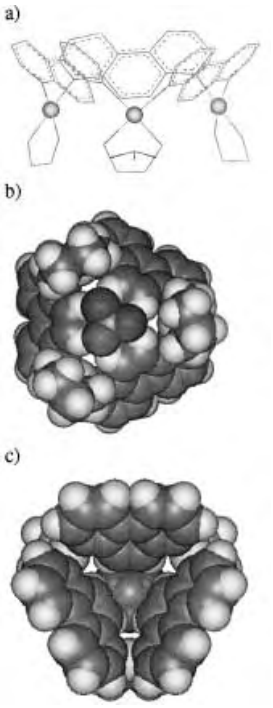


Figure 2. Crystal structure of **1** binding an NO_3^- ion (at the bottom; space-filling CPK presentation): a) side view, b) bottom view along the pseudo-C_3 axis, c) top view along the pseudo-C_3 axis.

framework; these L modules are bridged by three square-planar coordination modules [Pd(en)] in a *syn, syn, syn* orientation, thus the two methylene hydrogen atoms of each en group are in different environments. The bowl can be likened to a calix[3]arene with a cone conformation, in which each [Pd(en)] is related to a methylene group on the backbone of a calix[3]arene. In the metallacalix[3]arene **1**, the three Pd atoms build up an almost equilateral triangle with Pd···Pd distances of 7.64(1), 7.64(1), and 7.69(1) Å. The dimensions of the bowl are as follows: 8.63(1), 8.63(1), and 8.31(1) Å for the upper-rim lengths (i.e. the distances between the midpoints of the 1,10 position of L); 3.62(2) Å in depth; the dihedral angles between L and the tripalladium triangular plane are 52.0(2), 52.0(2), 45.9(1)°. The NO_3^- ion lies below the tripalladium triangular plane (at the bottom of the bowl) with Pd···O distances of 4.01(2), 4.01(2), and 3.78(1) Å, which are significantly longer than those reported by Lippert et al[3] for a complex in which the NO_3^- ion is situated at the center of a triplatinum plane (Pt···O 3.2(1)–3.5(1) Å). The strength of the binding between the NO_3^- ion and the Lewis acidic Pd atoms is limited because of the steric hindrance of the rigid L, since the (L)C···O(NO_3^-) distances of 3.31(2) Å are short (Figure 2b). The N atom of the NO_3^- ion is distorted by 0.337(4) Å out of the plane formed by the three O atoms towards the center of the tripalladium plane, to form a trigonal pyramid. Such a distortion arises from the equilibrium formed between the electrostatic interaction of the metal centers and the anion, and the steric hindrance. To our knowledge, similar examples have not been found in cationic receptors with soft, or symmetrical coordination environments.[13]

The anion binding for the SO_4^{2-} ion was investigated by NMR spectroscopic titration experiments. Increasing concentrations (0.5–2.5 equiv; 0.01–0.05 M) of an aqueous solution of Na_2SO_4, were added to an aqueous solution of the free bowl **1** (0.020 M). The results of NMR spectroscopy support the formation of a 1:1 host–guest complex in aqueous media. Downfield shifts for the signals associated with the 5-H and 6-H of 4,7-phenanthroline (Scheme 1) were observed with the addition of a solution of Na_2SO_4, indicating the substitution of the bound NO_3^- ion. The association constant (K_{ass})[14] for the 1:1 host–guest complex was estimated to be about 250, which is close to that previously reported.[3]

To enlarge the cavity size and to strengthen π-receptor function, aromatic ligands such as bpy and phen were coordinated *cis* to the Pd^{II} or Pt^{II} metal center. Unlike when [Pd(en)] or [Pt(en)] are employed as building blocks, the rigid aromatic-ligand metal complex can construct a second cavity by coupling with L, thus resulting in the formation of a molecular crown such as $[\{Pd(bpy)\}_3L_3(NO_3)_6$ (**2**), $\{[Pt(bpy)]_3L_3\}(NO_3)_6$ (**2′**), $\{[Pd(phen)]_3L_3\}(NO_3)_6$ (**3**), and $\{[Pt(phen)]_3L_3\}(NO_3)_6$ (**3′**).

Compound **2** or **3** readily self-assemble by the combination of $[Pd(NO_3)_2(bpy)]$ or $[Pd(NO_3)_2(phen)]$, respectively with L in a 1:1 molar ratio under mild conditions (40 °C, several minutes). However, the formation of the Pt analogues **2′** or **3′** require harsher conditions (100 °C, 24 h, excess $NaNO_3$). All reactions were monitored by NMR spectroscopy. The spectrum of **2** has highly symmetrical resonance signals, which indicate that the product is a unique tripalladium crown (Scheme 1). The self-assembly product formed under ambient conditions is kinetically favorable because of the labile Pd^{II}–N bonding. The NMR spectra indicate that the predominant species is the triplatinum crown **2′**, which occurs together with some oligomers. According to the concept of a molecular lock,[15] it is necessary to make the inert Pt^{II}–N bond labile if the Pt^{II} ion is to be involved in some self-assembly events. Under the harsher conditions used, the self-assembly gives the thermodynamically most favorable product **2′**, that is, the locked form (cycle closed) as the triplatinum crown. The completion of the self-assembly process is promoted not only by heating, but also by the interaction between NO_3^- ions and the Pt centers.

X-ray crystal structure analysis confirms the crown structure of **2** (Figure 3).[16] The three Pd atoms form an approximately equilateral triangle with Pd···Pd distances of 7.61(2), 7.62(1), and 7.71(3) Å. The lower cavity (below the tripalladium triangle consisting of the three modules of L) presents a bowl structure with a *syn, syn, syn* orientation and cavity size (7.99(1), 8.20(3), and 7.34(2) Å for the rim lengths; 3.6(2) Å in depth; dihedral angles between L and the tripalladium triangular plane are 62.7(2), 58.7(2), 47.4(2)°, slightly smaller than those of **1** because of the decreased flexibility within the metal-complex modules. The lower cavity (consisting of the three L modules) is quite stable, and therefore serves as a scaffold during the assembly process.

Significantly, the upper cavity (above the tripalladium triangle consisting of the three square-planar $(bpy)Pd^{2+}$ modules)has the following dimensions: 9.38(3), 9.34(2), and 10.16(4) Å for the rim lengths (i.e. the distances between two

 © 2003 Wiley-VCH Verlag GmbH & Co. KGaA, Weinheim 1433-7851/03/4206-0688 $ 20.00+.50/0

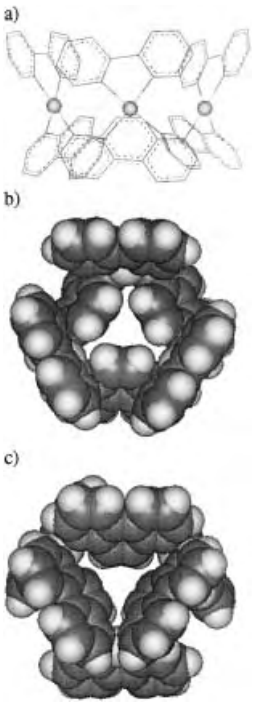


Figure 3. Crystal structure of **2** (space-filling CPK presentation): a) side view, b) bottom view along the pseudo-C_3 axis, c) top view along the pseudo-C_3 axis.

midpoints of the 6,6′ positions of bpy); 5.38(5) Å in depth; dihedral angles between the square planar (bpy)Pd^{2+} modules and the tripalladium triangular plane: 73.2(2), 72.7(2), and 74.7(2)°. The upper cavity, which contains the three Lewis acid centers, is larger than the lower cavity and is expected to exhibit more important receptor chemistry . Noteworthy, no NO_3^- ions are bound to any Pd atoms within the crown. As both the upper and the lower cavity are hydrophobic, the aqueous NO_3^- ions are unable to access the tripalladium Lewis acidic centers. This is in contrast to the situation in **1**, in which the [Pd(en)] modules are unable to form a hydrophobic cavity.

The modular self-assembly was successfully extended to the more rigid, planar, metal-complex modules [Pd(phen)] and [Pt(phen)]. Analysis by NMR spectroscopy confirms the formation of **3** under mild conditions. The resonance signals for **3** and **3′** are similar to those of **2** and **2′**, and again a crown structure is proposed as shown in Figure 4.

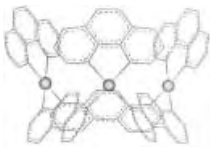


Figure 4. Side view of crown **3** or **3′**.

The dimensions of the upper cavity of the crowns **3** and **3′** are estimated to be about 1.1 nm for the rim lengths (i.e. the distances between the midpoints of the 5,6 positions of phen) and 0.65 nm for the cavity depth. The crowns **3** and **3′** behave as hosts to anions and neutral guests within the upper and lower cavities, which gives rise to strong host–guest interactions and color changes. Moreover, the crowns have strong aromatic receptor properties, and have potential for use as chemosensors for detecting mineral and biological anions. Further investigations will be extended to the self-assembly of calixarene-like metal-organic frameworks with deeper cavities by introducing square-planar coordinated metal complexes with luminescent ligands such as derivatives of 1,10-phenanthroline, as well as to the study of their luminescent responses to host–guest interactions.

Experimental Section

1–3: $[Pd(NO_3)_2(en)]$, $[Pd(NO_3)_2(bpy)]$, or $[Pd(NO_3)_2(phen)]$ (0.1 mmol) was added to an aqueous suspension of L (0.1 mmol, 2 mL), and the mixture was stirred for several minutes at room temperature. The resulting solution was allowed to stand at room temperature for several days during which crystals of the product were formed.

1′: $[PtCl_2(en)]$ (0.1 mmol) was added to an aqueous solution of $AgNO_3$ (0.1 mmol, 2 mL), and the mixture was stirred for 24 h at 80 °C. An aqueous suspension of L (0.1 mmol, 2 mL) was then added and the mixture was stirred for a further 24 h at 100 °C. The resulting clear solution was allowed to stand at room temperature for several days during which crystals of the product were formed.

2′ and **3′**: $[Pt(NO_3)_2(bpy)]$ or $[Pt(NO_3)_2(phen)]$ (0.1 mmol) was added to a suspended aqueous solution of L (0.1 mmol, 2 mL), and this mixture was stirred for 24 h at 100 °C. Excess $NaNO_3$ was added to the resulting clear solution, which was then stirred for a further 24 h at 100 °C. Excess KPF_6 was then added to the solution and the mixture was refluxed for a further 2 h. The hot solution was filtered and the collected solid was washed with several portions of water then dried in vacuo.

All ^{1}H NMR experiments were performed under the same conditions (300 MHz, D_2O, 25 °C, TMS).

1: Yield: 90 %. $\delta = 10.26$ (s, 6H), 9.66 (d, 6H, ^3J(H,H) = 5.3 Hz), 9.10 (d, 6H, ^3J(H,H) = 8.5 Hz), 7.83–7.78 (m, 6H), 3.04–2.89 ppm (m, 12H); **2**: Yield: 87 %. $\delta = 10.17$ (s, 6H), 9.92 (d, 6H, ^3J(H,H) = 5.4 Hz), 9.35 (d, 6H, ^3J(H,H) = 8.6 Hz), 8.27 (d, 6H, ^3J(H,H) = 8.1 Hz), 8.13–8.08 (m, 6H), 8.02–7.97 (m, 6H), 7.18–7.14 (m, 6H), 6.90 ppm (d, 6H, ^3J(H,H) = 2.8 Hz); **3**: Yield: 88 %. $\delta = 10.26$ (s, 6H), 10.02 (d, 6H, ^3J(H,H) = 5.4 Hz), 9.43 (d, 6H, ^3J(H,H) = 8.6 Hz), 8.63 (d, 6H, ^3J(H,H) = 8.3 Hz), 8.08–8.03 (m, 6H), 7.97 (s, 6H), 7.49–7.44(m, 6H), 7.28 ppm (d, 6H, ^3J (H,H) = 5.3 Hz). **1′**: Yield: 65 %. $\delta =$ 10.28 (s, 6H), 9.65 (d, 6H, ^3J(H,H) = 4.7 Hz), 9.14 (d, 6H, ^3J (H,H) = 8.6 Hz), 7.80–7.76 (m, 6H), 2.96–2.76 ppm (m, 12H). **2′**: Yield: 64 %. $\delta = 9.98$ (s, 6H), 9.80 (d, 6H, ^3J(H,H) = 5.4 Hz), 9.29 (d, 6H, ^3J(H,H) = 8.6 Hz), 8.16 (d, 6H, ^3J(H,H) = 8.2 Hz), 8.08–8.03 (m, 6H), 7.94–7.89 (m, 6H), 7.19–7.13 ppm (m, 12H); **3′**: Yield: 67 %. $\delta =$ 10.05 (s, 6H), 9.90 (d, 6H, ^3J(H,H) = 5.4 Hz), 9.39 (d, 6H, ^3J(H,H) = 8.4 Hz), 8.50 (d, 6H, ^3J(H,H) = 8.2 Hz), 8.01–7.97 (m, 6H), 7.76 (s, 6H), 7.51–7.42 ppm (m, 12H).

Received: August 16, 2002
Revised: October 15, 2002 [Z19979]

[1] Reviews on organic synthetic container molecules: a) D. J. Cram, J. M. Cram, *Container Molecules and Their Guests*, Royal Society of Chemistry, Cambridge, **1994**; b) D. Gutsche, *Calixarenes Revisited*, Royal Society of Chemistry, Cambridge, **1998**; c) *Calixarenes 2001*, (Eds.: Z. Asfari, V. Böhmer, J. Harrowfield, J. Vicens), Kluwer Academic Publishers, **2001**.

[2] For reviews on metal-directed self-assembled inorganic container molecules, see: a) J.-M. Lehn, *Supramolecular Chemistry, Concepts and Perspectives*, VCH, Weinheim, **1995**; b) C. J. Jones, *Chem. Soc. Rev.* **1998**, *27*, 289–299; c) M. Fujita, *Chem. Soc. Rev.* **1998**, *27*, 417–425; d) S. Leininger, B. Olenyuk, P. J. Stang, *Chem. Rev.* **2000**, *100*, 853–908; e) M. Fujita, K. Umemoto, M. Yoshizawa, N. Fujita, T. Kusukawa, K. Birada, *Chem. Commun.*

 © 2003 Wiley-VCH Verlag GmbH & Co. KGaA, Weinheim 1433-7851/03/4206-0689 $ 20.00+.50/0

2001, 509 – 518; f) F. A. Cotton, C. Lin, C. A. Murillo, *Acc. Chem. Res.* **2001**, *34*, 759 – 771.
[3] a) R.-D. Schnebeck, E. Freisinger, B. Lippert, *Angew. Chem.* **1999**, *111*, 235 – 238; *Angew. Chem. Int. Ed.* **1999**, *38*, 168 – 171; b) R.-D. Schnebeck, E. Freisinger, F. Glahe, B. Lippert, *J. Am. Chem. Soc.* **2000**, *122*, 1381 – 1390.
[4] a) H. Rauter, E. C. Hillgeris, B. Lippert, *J. Chem. Soc. Chem. Commun.* **1992**, 1385 – 1386; b) H. Rauter, E. C. Hillgeris, B. Lippert, *J. Am. Chem. Soc.* **1994**, *116*, 616 – 624; c) J. A. R. Navarro, M. B. L. Janik, E. Freisinger, B. Lippert, *Inorg. Chem.* **1999**, *38*, 426 – 432; d) J. A. R. Navarro, E. Freisinger, B. Lippert, *Inorg. Chem.* **2000**, *39*, 2301 – 2305.
[5] a) H. Chen, M. M. Olmstead, D. P. Smith, M. F. Maestre, R. H. Fish, *Angew. Chem.* **1995**, *107*, 1590 – 1593; *Angew. Chem. Int. Ed. Engl.* **1995**, *34*, 1514 – 1517; b) H. Piotrowski, G. Hilt, K. Severin, *J. Am. Chem. Soc.* **2001**, *123*, 2699 – 2700; M.-L. Lehaire, R. Scopelliti, H. Piotrowski, K. Severin, *Angew. Chem.* **2002**, *114*, 1477 – 1480; *Angew. Chem. Int. Ed.* **2002**, *41*, 1419 – 1422.
[6] a) S.-W. Lai, M. C.-W. Chan, S.-M. Peng, C.-M. Che, *Angew. Chem.* **1999**, *111*, 708 – 710; *Angew. Chem. Int. Ed.* **1999**, *38*, 669 – 671; b) P. Chaudhuri, I. Karpenstein, M. Winter, C. Butzlaff, E. Bill, A. X. Trautwein, U. Flörke, H.-J. Haupt, *J. Chem. Soc. Chem. Commun.* **1992**, 321 – 322.
[7] M. Fujita, S.-Y. Yu, T. Kusukawa, H. Funaki, K. Ogura, K. Yamaguchi, *Angew. Chem.* **1998**, *110*, 2192 – 2198; *Angew. Chem. Int. Ed.* **1998**, *37*, 2082 – 2085.
[8] S.-Y. Yu, T. Kusukawa, K. Biradha, M. Fujita, *J. Am. Chem. Soc.* **2000**, *122*, 2665 – 2666.
[9] M. Yoshizawa, Y. Takeyama, T. Kusukawa, M. Fujita, *Angew. Chem.* **2002**, *114*, 1403 – 1405; *Angew. Chem. Int. Ed.* **2002**, *41*, 1347 – 1349.
[10] 4,7-Phenanthroline is a simple and commercially available ligand that forms a rigid 60° corner, which was previously employed in the self-assembly of a molecular triangle with the linear bipalladium complexes (180° coordination angle), see: J. R. Hall, S. J. Loeb, G. K. H. Shimizu, G. P. A. Yap, *Angew. Chem.* **1998**, *110*, 130 – 133; *Angew. Chem. Int. Ed.* **1998**, *37*, 121 – 123.
[11] C. D. Gutsche in *Large Ring Molecules* (Ed.: J. A. Semlyen), Wiley, New York, **1996**, 309 – 343, and references therein.
[12] a) Crystal structure analysis of **1**. A single crystal with dimension of $0.25 \times 0.15 \times 0.05$ mm was coated with a sealing material and mounted on a glass fiber. All measurements were made on a Rigaku RAXIS Rapid IP detector equipped with a graphite monochromated $Mo_{K\alpha}$ radiation source. The data were collected at 293(2) K. The crystallographic molecule contains half a molecule of **1**. Crystal data: $C_{42}H_{48}N_{18}O_{18}Pd_3 \cdot 2H_2O$, $M_r = 1448.13$; orthorhombic, space group *Pmn*21, $a = 21.8807(4)$, $b = 14.7319(3)$, $c = 23.2315(2)$ Å, $V = 7488.5(2)$ Å^3, $\rho_{calcd} = 1182\ kg\,m^{-3}$. $Z = 8$, $F(000) = 2696$, $\mu(Mo_{K\alpha}) = 7.68\ mm^{-1}$, $\lambda = 0.71073$ Å. 19837 reflections measured, 7874 observed reflections ($I > 2\sigma(I)$); number of parameters 648; $R_1 = 0.1197$; $wR_2 = 0.3421$. Further refinement was unsuccessful because of the high degree of disorder of the counter anions and the water molecules. b) CCDC-191629 (**1**) and CCDC-191630 (**2**) contain the supplementary crystallographic data for this paper. These data can be obtained free of charge via www.ccdc.cam.ac.uk/conts/retrieving.html (or from the Cambridge Crystallographic Data Centre, 12 Union Road, Cambridge CB2 1EZ, UK; fax: (+44) 1223-336-033; or deposit@ccdc.cam.ac.uk).
[13] a) P. A. Gale, *Coord. Chem. Rev.* **2001**, *213*, 79 – 128; b) P. A. Gale, *Coord. Chem. Rev.* **2000**, *199*, 181 – 233; c) A. Bianchi, K. Bowman-James, E. García-España, *Supramolecular Chemistry of Anions*, Wiley-VCH, New York, **1997**.
[14] a) H. Sigel, K. H. Scheller, V. M. Rheinberger, B. E. Fischer, *J. Chem. Soc. Dalton Trans.* **1980**, 1022 – 1028; b) S. Shinkai, K. Araki, O. Manabe, *J. Am. Chem. Soc.* **1988**, *110*, 7214 – 7215.
[15] M. Fujita, F. Ibukuro, K. Yamaguchi, K. Ogura, *J. Am. Chem. Soc.* **1995**, *117*, 4175 – 4176.
[16] Crystal structure analysis of **2**. A single crystal with dimension of $0.25 \times 0.15 \times 0.05$ mm was coated with a sealing material and mounted on a glass fiber. All measurements were made on a Rigaku RAXIS Rapid IP detector equipped with a graphite monochromated $Mo_{K\alpha}$ radiation source. The data was collected at 293(2) K. The crystallographic molecule contains a molecule of **2**. Crystal data: $C_{66}H_{48}N_{18}O_{18}Pd_3 \cdot 2H_2O$, $M_r = 1736.40$, monoclinic, space group *C*2/*c*, $a = 39.366(8)$, $b = 24.887(5)$, $c = 18.217(4)$ Å, $\beta = 106.69(3)°$, $V = 17095(6)$ Å^3, $\rho_{calcd} = 1.544\ kg\,m^{-3}$, $Z = 32$, $F(000) = 8192$, $\mu(Mo_{K\alpha}) = 0.902\ cm^{-1}$, $\lambda = 0.71073$ Å; 19127 reflections measured, 7704 observed reflections ($I > 2\sigma(I)$); number of parameters 891; $R_1 = 0.0931$; $wR_2 = 0.2575$.[12b]

Supported Gold Catalysts

Structure and Reactivity of a Mononuclear Gold-Complex Catalyst Supported on Magnesium Oxide**

*Javier Guzman and Bruce C. Gates**

Oxide- and zeolite-supported mononuclear metal complexes are important industrial catalysts, for example, for alkene polymerization,[1] and some have properties not anticipated by known homogeneous catalysis.[2] Some supported transition-metal complexes are close analogues of molecular complexes, with the metal–support-oxygen bonds being as strong as metal–ligand bonds in common transition-metal complexes and strong enough to maintain anchoring during catalysis.[3]

Mononuclear gold complexes are used frequently in organometallic chemistry[4] and have been identified as catalysts for reactions including the addition of alcohols to alkynes,[5] asymmetric aldol reactions,[6] C–C bond formation,[7] oxidative carbonylation of amines,[8] and selective hydrosilylation of aldehydes.[9] Supported gold catalysts have recently been found to be surprisingly active and selective, for example, for CO oxidation and propene epoxidation.[10] Their unique properties have been variously attributed to the smallness of the gold clusters[10b] and to clusters adjacent to cationic gold species at the support surface.[11] Gold supported

[*] Prof. Dr. B. C. Gates, J. Guzman
University of California Davis
Department of Chemical Engineering and Materials Science
One Shields Ave., Davis, CA95616-5294 (USA)
Fax: (+1) 530-752-1031
E-mail: bcgates@ucdavis.edu

[**] This research was supported by DOE BES (FG02-87ER13790). We thank the Stanford Synchrotron Radiation Laboratory (Beamline 4-1), and the National Synchrotron Light Source (Beamline X-11A), both supported by DOE, for beam time.

 © 2003 Wiley-VCH Verlag GmbH & Co. KGaA, Weinheim 1433-7851/03/4206-0690 $ 20.00+.50/0

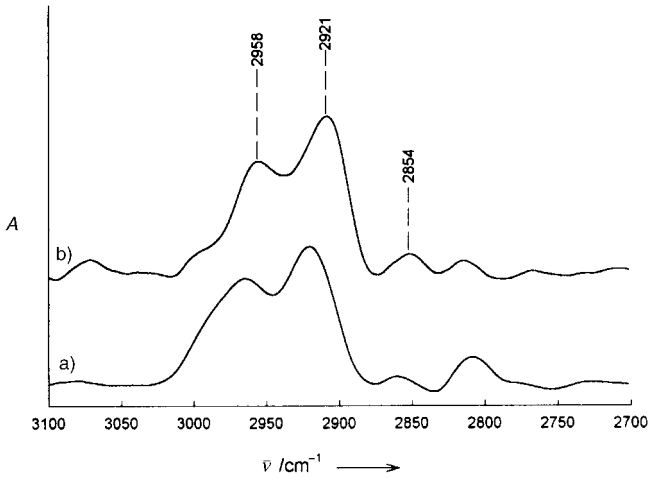


Figure 1. Infrared spectra in the ν_{CH} stretching region characterizing solid samples **2** (a) and **1** (b).

on SiO_2, Al_2O_3, or TiO_2 was observed to catalyze alkene hydrogenation,[12] and it was suggested that small gold clusters were the catalytically active species. However, the suggestion is unconfirmed, and, furthermore, there is a report[13] that the addition of gold to oxides makes the oxides even less active catalysts for ethene hydrogenation. The catalytic sites remain to be identified.

Herein we report the preparation and characterization of the first structurally simple supported gold complex, [Au-$(CH_3)_2${OMg}$_2$] (**1**) (where the braces denote ligands that are part of the MgO surface) and show that it is a precursor of a mononuclear gold complex that catalyzes ethene hydrogenation. To test the catalytic activity of supported gold in various forms, we also prepared a family of small gold clusters[14] on the MgO support.

Adsorption of [Au^{III}$(CH_3)_2$(acac)] (**2**; acac = acetylacetonate, $C_5H_7O_2$)[15] on MgO led to the formation of supported $Au(CH_3)_2$ species **1**, as shown by the IR bands (Figure 1) in the ν_{CH} region at 2958, 2854, and 1464 cm^{-1} (not shown), which nearly match those representing the CH_3 groups in solid **2**.[16] Furthermore, the changes in the ν_{OH} and ν_{COO} regions of the IR spectra characterizing **1** relative to those of bare MgO and of crystalline **2** indicate reaction of surface hydroxy groups of MgO and conversion of acac ligands, respectively, which results from the adsorption of **2**. The adsorption was confirmed by an increase in the intensity of the bands associated with hydrogen-bonded hydroxy groups (3689 and 3606 cm^{-1}) and a decrease in the intensity of bands associated with isolated hydroxy groups (3765 and 3749 cm^{-1}; Table 1).[17] The bands in the ν_{COO} region were shifted to higher frequencies and changed in intensity relative to those of solid **2**; moreover, new bands attributed to carbonaceous species, such as acetylacetone ($C_5H_8O_2$; 2921, 1708, and 1626 cm^{-1}), inferred to be formed during decomposition of **2**, were observed for **1** (Table 1). Thus, we infer release of the acac ligand from the gold center and its decomposition during adsorption of **2**.[18] The IR data suggest ligand exchange of the acac ligand with support oxygen atoms (basic surface sites, O^{2-} ions) and hydrogen-bonding of surface OH groups to the organic moiety, facilitating the formation of **1**.

Table 1: Infrared spectra representing samples **1** and **2**.

Sample	IR bands [cm^{-1}]
1	3765, 3749, 3689, 3606, 2958, 2854, 2921, 1708, 1626, 1517, 1464, 1420, 1285
2	2959, 2923, 2860, 1586, 1531, 1463, 1390, 1285

Other metal complexes containing nucleophilic ligands, such as acac, have also been shown to bond to metal-oxide surfaces by hydrogen bonding to hydroxy groups and by exchange of the ligands with support oxygen atoms.[3,19] The acid–base pair sites on a support surface may initiate an acid–base catalyzed decomposition of the complex as it comes in contact with the surface and releases the ligand to be replaced by a group from the surface, such as {OMg}$^{-1}$.[17,19] Ligand-exchange reactions of comparable metal complexes in solution (e.g., [Pt(acac)$_2$] and [Pd(acac)$_2$]) have also been reported.[20]

The X-ray absorption near-edge spectrum (XANES) characterizing **1** is virtually identical to that characterizing crystalline **2**. This comparison indicates that the gold retained its oxidation state of +III after the chemisorption of **2** (in which Au^{III} is bonded to $C_5H_7O_2$ through two oxygen atoms[21]).

Extended X-ray absorption fine structure (EXAFS) results characterizing **1** (measured at the Au L_{III} edge, 11919 eV, Table 2), show that in the surface complex the gold center was also bonded to two oxygen atoms. These are inferred to be part of the MgO surface (although the exact bonding sites are unknown), because the Au–O separation was found to be 2.16 Å (vs. 2.08 Å in **2**[21]), typical of M–O bonding distances in other zeolite- and oxide-supported mononuclear metal complexes (e.g., [Rh(CO)$_2${OAl}{OSi}] (supported on highly dealuminated zeolite Y), 2.15 Å;[3b] [Ru(CO)$_2${OAl}$_2$] (on γ-Al_2O_3), 2.17 Å;[22] and [Re(CO)$_3$-{OMg}{HOMg}$_2$] (on MgO), 2.13 Å[3a,23]). Another Au–O contribution in the EXAFS spectrum of **1** was found at a nonbonding distance of 2.85 Å (with a coordination number

Table 2: EXAFS parameters characterizing **1** and the species formed from it during ethene hydrogenation catalysis.[a]

Sample	Shell	N	R [Å]	$10^3 \times \Delta\sigma^2$ [Å^2]	ΔE_0 [eV]
1	Au-Au	–[b]	–	–	–
	Au-O$_s$	2.1	2.16	0.20	3.45
	Au-O$_l$	0.9	2.85	1.04	1.02
	Au-Mg	0.9	2.72	1.45	1.35
	Au-C	2.0	2.04	2.35	2.57
Working catalyst[c]	Au-Au	–[b]	–	–	–
	Au-O$_s$	2.0	2.18	2.14	2.34
	Au-O$_l$	0.9	2.87	3.13	4.62
	Au-Mg	0.9	2.73	2.46	3.17
	Au-C	–[b]	–	–	–

[a] Notation: N = coordination number; R = distance between absorber and backscatterer atoms; $\Delta\sigma^2$ = Debye–Waller factor; ΔE_0 = inner potential correction. The subscripts s = short and l = long. Typical errors are as follows: $N \pm 10\%$, $R \pm 0.02$ Å, $\Delta\sigma^2 \pm 20\%$, $\Delta E_0 \pm 20\%$. [b] Undetectable. [c] Catalytic reaction conditions stated in the Experimental Section.

 © 2003 Wiley-VCH Verlag GmbH & Co. KGaA, Weinheim 1433-7851/03/4206-0691 $ 20.00+.50/0

of 0.9), along with another (weak) contribution tentatively identified as Au–Mg ($N = 0.9$, 2.72 Å). The data also show a weak Au–C contribution ($N = 2.0$) at a distance of 2.04 Å (vs 2.05 Å in **2**[21]) that confirms the bonding of two carbon atoms to the gold center. The EXAFS data give no evidence of Au–Au contributions, consistent with the presence of site-isolated **1** on the MgO surface.

The catalytic activity[24] of the species formed from **1** and its stability in operation in a flow reactor were tested for hydrogenation of ethene. After a break-in period of about 30 min for attainment of steady state, the activity (measured at conversions less than 5%) was found to be unchanged during the measurements (12 h), corresponding to a reaction rate (determined from differential conversion data) of 2.9×10^{-3} molecules of ethene converted (Au atom)$^{-1}$ s^{-1}.

The reaction was also carried out under the same conditions when the reactor was an X-ray absorption cell[25] which allowed collection of spectra of the working catalyst. The spectra were unchanged during the period of steady-state operation, which confirmed the stability of the catalyst. The data (Table 2) identify mononuclear gold species, with no evidence of gold clusters (as shown by the absence of detectable Au–Au contributions). The oxidation state of the gold was found by XANES to be +III.[26] The EXAFS data show that the Au^{III} center was bonded to two oxygen atoms of the MgO unit with an Au–O bond of 2.18 Å. The data did not indicate any Au–C contribution, which demonstrates the removal of the CH_3 ligands before or during catalysis.[27]

IR data were collected during pretreatment of the catalyst in flowing ethene or H_2 and also during catalysis. After **1** had been treated in H_2 (at 1 bar and 300 K), the IR spectra did not show any evidence of CH_3 ligands bonded to the gold centers, consistent with the EXAFS results (data not shown). The IR spectra are not sensitive enough to determine whether gold hydride formed, and we do not rule out the possibility.[28] The IR spectra also show that ethene interacts with **1** (at 1 bar and 300 K) to form only physisorbed ethene. During steady-state ethene hydrogenation catalysis, supported mononuclear gold complexes were characterized by their IR bands (not observed with the catalyst in contact with H_2 or ethene alone) at 3085, 2961, 2920, and 2870 cm^{-1}, which suggest the formation of ethene-derived adsorbates (ligands) on the gold center. When H_2, ethene, or a catalytically reacting mixture of H_2, ethene, and He interacted with the MgO support without gold, no ethene-derived ligands were observed (the adsorption was negligible). Thus, the data are consistent with the inference that the mononuclear gold complexes are themselves the catalytically active species. Individual ligands on the gold centers observed by IR spectroscopy during steady-state ethene hydrogenation were characterized by varying the reaction conditions[26] and comparing against published spectra.[29] The 2961, 2920, and 2870 cm^{-1} bands suggest the formation of ethyl ligands on the gold, consistent with the IR bands characterizing ethyl on metal surfaces[29a,b,c] and with CH_3CH_2Cl.[29d] The 3085 cm^{-1} band is consistent with the formation of π-bonded ethene, as observed for Pt, Pd, Ir, and Rh complexes.[30]

The results point to supported mononuclear Au^{III} complexes as the catalytically active species for ethene hydrogenation. To test whether supported gold clusters might be catalysts for this reaction, catalysis experiments were also performed with a family of MgO-supported samples containing gold clusters of various sizes (made by adsorption of **2** on MgO, followed by treatment in flowing He at increasing temperatures).[14] The catalytic activity for ethene hydrogenation decreased as the Au–Au coordination number (thus, the average cluster size[31]) characterizing the gold clusters in the catalysts prior to use increased (Figure 2). The data imply that large gold particles are not catalysts for ethene hydrogenation, and the highest activity was observed for the sample containing only mononuclear gold complexes.

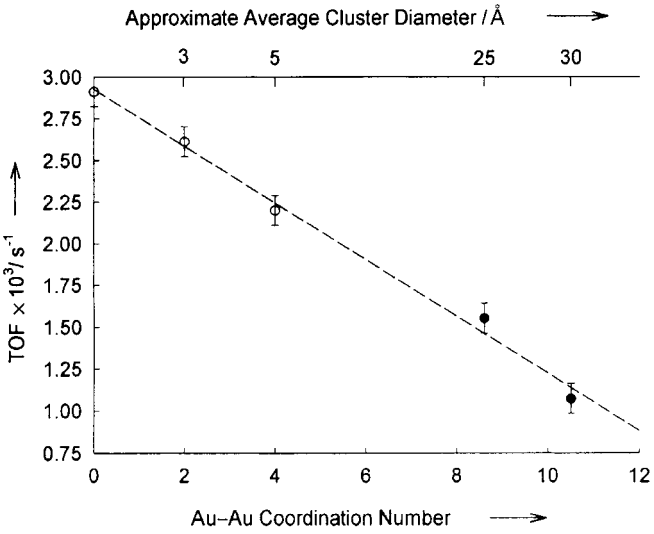


Figure 2. Activities of MgO-supported catalysts containing cationic gold and (except in the most active catalyst) gold clusters. Reaction conditions stated in Experimental Section. Note the nonlinearity of the scale at the top. XANES data were collected for the catalysts denoted by open symbols

XANES data indicate the presence of Au^{III} along with gold clusters in all the catalysts except the most active one, which contained Au^{III} complexes without detectable clusters. Thus, all the data are consistent with the inference that the catalytically active species in all the samples were mononuclear Au^{III} complexes; there is no evidence of the catalytic activity of gold clusters for ethene hydrogenation, consistent with the conventional wisdom about the lack of activity of samples containing zerovalent gold.[10b]

Experimental Section

The synthesis and sample handling were performed under anaerobic and anhydrous conditions. The MgO-supported gold complexes, containing 1 wt% Au, were prepared by slurrying **2** in dry and deoxygenated *n*-hexane with partially dehydroxylated MgO powder (pretreated at 673 K in vacuum; BET surface area 60 m^2 g^{-1}). The slurry was stirred for one day and the solvent removed by evacuation.

Transmission IR spectra of the solid samples were recorded with a Bruker IFS 66v spectrometer operated with a spectral resolution of 4 cm^{-1}. Samples were pressed into self-supporting wafers and loaded into a cell (In-situ Research Institute, Inc., South Bend, IN) in a drybox. The cell was connected to a vacuum/adsorption system with a base pressure of 1.334×10^{-7} bar, which allowed recording of spectra

 © 2003 Wiley-VCH Verlag GmbH & Co. KGaA, Weinheim 1433-7851/03/4206-0692 $ 20.00+.50/0

while the treatment gases flowed through and around the wafer at temperatures ranging from room temperature to 573 K.

The X-ray absorption experiments were performed on beamline 4-1 of the Stanford Synchrotron Radiation Laboratory (SSRL) at the Stanford Linear Accelerator Center, Stanford, CA, and on beamline X-11A of the National Synchrotron Light Source (NSLS) at Brookhaven National Laboratory, Upton, NY. The storage-ring electron energy was 3 GeV at SSRL and 2.5 GeV at NSLS; and the ring current varied within the range of 50–100 mA at SSRL and 140–240 mA at NSLS. The sample handling was as described elsewhere.[14] Data were recorded at the Au L_{III} edge (11 919 eV) during ethene-hydrogenation catalysis and also with the catalyst in flowing He, H_2, or C_2H_4 at atmospheric pressure and 353 K. Higher harmonics in the X-ray beam were minimized by detuning the Si(220) monochromator at SSRL or the Si(111) double-monochromator at NSLS by 20–25% at the Au L_{III} edge.

The catalytic activity[24] and stability of species formed from **1** were tested for the hydrogenation of ethene by contacting a mixture of He, ethene, and H_2 (ethene partial pressure, P_{ethene}, 0.0533 bar, $P_{hydrogen}$, 0.2134 bar, the balance He) with **1** in a flow reactor at 1.0135 bar, and 353 K.

Received: August 16, 2002 [Z19987]

[1] G. G. Hlatky, *Chem. Rev.* **2000**, *100*, 1347 – 1376.

[2] a) P. S. Kirlin, B. C. Gates, *Nature* **1987**, *325*, 38 – 40; b) V. Vidal, A. Théolier, J. Thivolle-Cazat, J.-M. Basset, *Science* **1997**, *276*, 99 – 102; c) B. J. O'Keefe, L. E. Breyfogle, M. A. Hillmyer, W. B. Tolman, *J. Am. Chem. Soc.* **2002**, *124*, 4384 – 4393.

[3] a) A. Hu, K. M. Neyman, M. Staufer, T. Belling, B. C. Gates, N. Rösch, *J. Am. Chem. Soc.* **1999**, *121*, 4522 – 4523; b) J. F. Goellner, B. C. Gates, G. N. Vayssilov, N. Rösch, *J. Am. Chem. Soc.* **2000**, *122*, 8056 – 8066.

[4] a) E. Cerrada, P. G. Jones, A. Laguna, M. Laguna, *Inorg. Chem.* **1996**, *35*, 2995 – 3000; b) K. Ortner, L. Hilditch, Y. Zheng, J. R. Dilworth, U. Abram, *Inorg. Chem.* **2000**, *39*, 2801 – 2806.

[5] J. H. Teles, S. Brode, M. Chabanas, *Angew. Chem.* **1998**, *110*, 1475 – 1478; *Angew. Chem. Int. Ed.* **1998**, *37*, 1415 – 1418.

[6] Y. Ito, M. Sawamura, T. Hayashi, *J. Am. Chem. Soc.* **1986**, *108*, 6405 – 6406.

[7] A. S. K. Hashmi, L. Schwarz, J.-H. Choi, T. M. Frost, *Angew. Chem. Int. Ed.* **2000**, *112*, 2382 – 2385; *Angew. Chem. Int. Ed.* **2000**, *39*, 2285 – 2288.

[8] F. Shi, Y. Deng, *Chem. Commun.* **2001**, *5*, 443 – 444.

[9] H. Ito, T. Yajima, J. Tateiwa, A. Hosomi, *Chem. Commun.* **2000**, *11*, 981 – 982.

[10] a) M. Haruta, S. Tsubota, T. Kobayashi, H. Kageyama, M. J. Genet, B. Delmon, *J. Catal.* **1993**, *144*, 175 – 192; b) M. Haruta, M. Daté, *Appl. Catal. A* **2001**, *222*, 427 – 437.

[11] a) H.-S. Oh, C. K. Costello, C. Cheung, H. H. Kung, M. C. Kung, *Stud. Surf. Sci. Catal.* **2001**, *139*, 375 – 381; b) J. Guzman, B. C. Gates, *J. Phys. Chem. B* **2002**, *106*, 7659 – 7665.

[12] P. A. Sermon, G. F. Bond, P. B. Wells, *J. Chem. Soc. Faraday Trans. 1* **1979**, *75*, 385 – 394.

[13] S. Lin, M. A. Vannice, *Catal. Lett.* **1991**, *10*, 47 – 62.

[14] J. Guzman, B. C. Gates, *Nano Lett.* **2001**, *1*, 689 – 692.

[15] Compound **2** was first used to prepare supported gold by M. Okumura, K. Tanaka, A. Ueda, M. Haruta, *Solid State Ionics* **1997**, *95*, 143 – 149. Pyrolysis of **2** was observed to occur, and the gold aggregated to form nanoparticles.

[16] The bands at 2958 and 2854 cm^{-1} are assigned to the asymmetric and symmetric CH_3 stretching vibrations, respectively, and that at 1464 cm^{-1} is attributed to the asymmetric bending vibrations of CH_3 groups.

[17] H. Knözinger, *NATO ASI Ser. Ser. C* **1988**, *231*, 35 – 46.

[18] We rule out the possibility that the acac ligand (or fragments, such as monoenols, formed from it) from the precursor compound was associated with the gold center, because the ν_{CH} region of our IR spectrum is virtually identical to that of similar samples made from salts that did not contain acac or related species. We conclude that the acac ligands were replaced by support oxygen ligands, and some acac ligands or fragments formed from them remained on the MgO surface.

[19] P. Van der Voort, M. B. Mitchell, E. F. Vansant, M. G. White, *Interface Sci.* **1997**, *5*, 169 – 197.

[20] a) R. G. Pearson, H. B. Gray, F. Basolo, *J. Am. Chem. Soc.* **1960**, *82*, 787 – 792; b) R. G. Pearson, D. A. Johnson, *J. Am. Chem. Soc.* **1964**, *86*, 3983 – 3989.

[21] S. Shibata, K. Iijima, T. H. Baum, *J. Chem. Soc. Dalton Trans.* **1990**, *4*, 1519 – 1520.

[22] K. Asakura, M. Yamada, Y. Iwasawa, H. Kuroda, *Chem. Lett.* **1985**, *4*, 511 – 514.

[23] J.-R. Chang, L. U. Gron, A. Honji, K. M. Sanchez, B. C. Gates, *J. Phys. Chem.* **1991**, *95*, 9944 – 9950.

[24] Reported as turnover frequency (TOF, rate of reaction per exposed gold atom), which for our catalysts is essentially the rate per total gold atom. There was no detectable catalytic activity in the absence of catalyst, and the MgO support alone was inactive.

[25] J. F. Odzak, A. M. Argo, F. S. Lai, B. C. Gates, K. Pandya, L. Feraria, *Rev. Sci. Instrum.* **2001**, *72*, 3943 – 3945.

[26] Reduction of Au^{III} to Au^0 was observed to occur only at a substantially higher temperature, 480 K, by XANES and temperature-programmed reduction in H_2 (J. Guzman, B. C. Gates, unpublished results).

[27] We do not rule out the possibility that ethene-derived adsorbates were formed on the gold center, but because of the noise in the signal it was not possible to isolate any such contribution in the EXAFS data.

[28] a) M.-J. Crawford, T. M. Klapötke, *Angew. Chem.* **2002**, *114*, 2373 – 2375; *Angew. Chem. Int. Ed.* **2002**, *41*, 2269 – 2271; b) X. Wang, L. Andrews, *J. Am. Chem. Soc.* **2001**, *123*, 12 899 – 12 900.

[29] a) H. E. Newell, M. R. S. McCoustra, M. A. Chesters, C. De La Cruz, *J. Chem. Soc. Faraday Trans.* **1998**, *94*, 3695 – 3698; b) P. S. Cremer, X. Su, Y. R. Shen, G. A. Somorjai, *J. Am. Chem. Soc.* **1996**, *118*, 2942 – 2949; c) B. E. Bent, C. M. Mate, C.-T. Kao, A. J. Slavin, G. A. Somorjai, *J. Phys. Chem.* **1988**, *92*, 4720 – 4726; d) T. Shimanouchi, *Tables of Molecular Vibrational Frequencies, Vol. 1*, Natl. Std. Ref. Data Ser., Natl. Bur. Std. (US) **1962**, p. 39; e) B. J. Bandy, M. A. Chesters, D. I. James, G. S. McDougall, M. E. Pemble, N, Sheppard, *Philos. Trans. R. Soc. London Ser. A* **1986**, *318*, 141 – 161.

[30] a) Y. Soma, *J. Chem. Soc. Chem. Commun.* **1976**, *24*, 1004 – 1005; b) W. Oberhauser, C. Bachmann, T. Stampfl, R. Haid, C. Langes, A. Rieder, P. Brüggeller, *Inorg. Chim. Acta* **1998**, *274*, 143 – 154.

[31] Calculated from Au–Au coordination numbers (first- and second-shell), geometrical shapes, and on the basis of a model proposed A. Jentys, *Phys. Chem. Chem. Phys.* **1999**, *1*, 4059 – 4063.

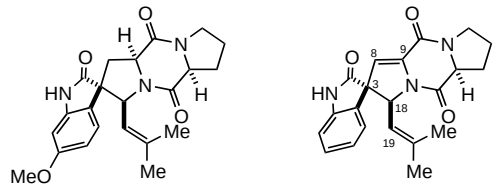
 © 2003 Wiley-VCH Verlag GmbH & Co. KGaA, Weinheim 1433-7851/03/4206-0693 $ 20.00+.50/0

Spiro Alkaloids

Total Synthesis of (−)-Spirotryprostatin B**

*Christiane Meyers and Erick M. Carreira**

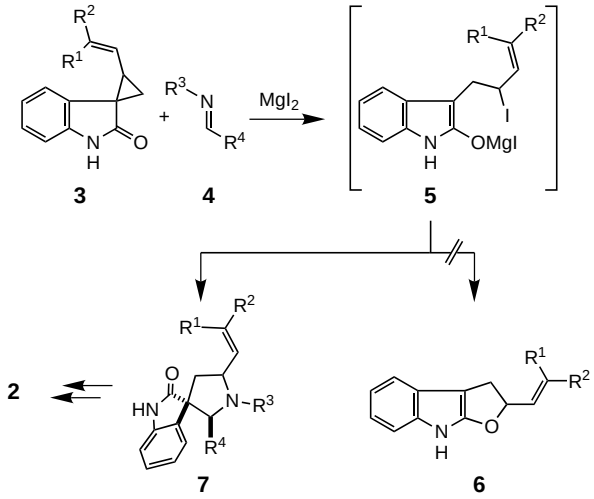
Spirotryprostatin A (**1**) and B (**2**), two powerfully bioactive indole alkaloids, were isolated in 1996 by Osada et al. from the fermentation broth of *Aspergillus fumigatus* BM939.[1] Only miniscule amounts of **1** and **2** (11 and 1 mg, respectively) were isolated from 400 L of fermentation medium. Both



1 spirotryprostatin A **2** spirotryprostatin B

compounds inhibit the cell cycle in the G2/M phase, and **2** shows cytotoxic activity on the growth of human leukemia cell lines. In this communication, we report a novel strategy towards the synthesis of spirotryprostatin B that is characterized by the MgI_2-catalyzed annulation reaction of a spiro[oxindole-3,1′-vinylcyclopropane] and an alkynyl imine. It is notable that in the context of our investigations we have developed the functionalization of an advanced aldehyde intermediate which enables the generation of biologically active congeners. The synthetic chemistry of the spirotryprostatins has recently been the subject of intense investigations by several groups. The various creative, distinct strategies have been devised to provide access to the spiro[oxindole-3,3′- pyrrolidine] core.[2–6]

We have recently developed a novel approach to spiro[oxindole-3,3′-pyrrolidines] by the MgI_2-catalyzed ring-expansion reaction of spiro[cyclopropane-1,3′-oxindoles] and aldimines.[7] The methodological studies we have carried out to date have left unaddressed a pertinent issue, which impacts the general applicability of the method to provide access to a wide range of related alkaloids. In particular, in none of the earlier studies had we or others examined the use of 1,2-disubstituted cyclopropanes, which would give access to 2,5-substituted pyrrolidines.[8] At the outset, there were two key questions we wished to address: the use of vinyl cyclopropane **3** in the ring-expansion reaction to yield **7** and the relative stereochemical outcome of the annulation. With respect to the former, it was not at all clear whether the intermediate allylic iodide/enolate **5** would be stable, as it could collapse by intramolecular cyclization to form a dihydrofuroindole **6** (Scheme 1).[9]

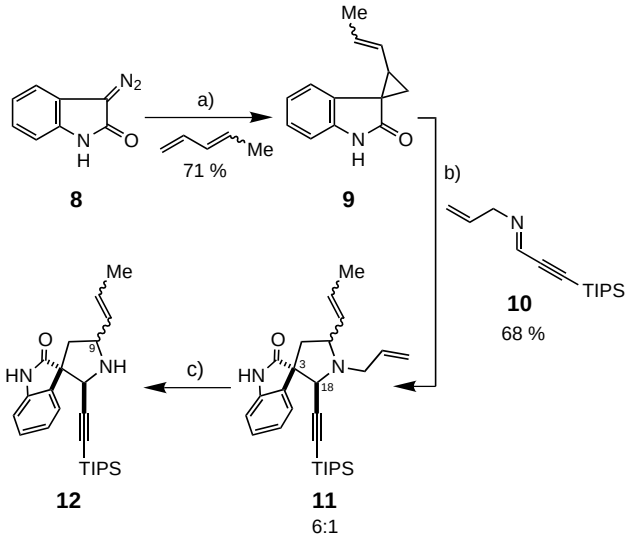


3 **4** **5** **7** **6**

Scheme 1. MgI_2-catalyzed ring-expansion reaction of spiro[cyclopropane-1,3′-oxindole], and a potential side reaction.

An additional problem we wished to explore was whether an aldehyde at C18 (spirotryprostatin B numbering) would serve as a useful precursor to the requisite prenyl side chain through an olefination reaction. Because earlier work in this area had concluded that olefination of a related aldehyde was unfeasible, revisting this strategic challenge was not without risk.

Our synthesis commenced with known diazoketone **8**, accessible in two steps and 79% yield from isatin (Scheme 2).[10] Rhodium-catalyzed cyclopropanation of



8 **9** **10** 68 % **12** **11** 6:1

Scheme 2. a) Piperylene, [{Rh(OAc)$_2$}$_2$] (1 mol%), benzene, reflux, slow addition of **8** in CH_2Cl_2; b) **10**, MgI_2 (1 equiv), THF, sealed tube, 75 °C; c) [Pd(PPh$_3$)$_4$] (6 mol%), NDMBA, CH_2Cl_2, 30 °C. TIPS = triisopropylsilyl, NDMBA = 1,3-dimethylbarbituric acid.

[*] Prof. Dr. E. M. Carreira, C. Meyers
Laboratorium für Organische Chemie
ETH Hönggerberg, HCI H335
8093 Zürich (Schweiz)
Fax: (+41) 1-632-1328
E-mail: carreira@org.chem.ethz.ch

[**] We thank the ETH, SNF, Eli Lilly, Merck, and F. Hoffmann-LaRoche for their generous support of our research program. We are grateful to Paul Seiler for the X-ray crystallographic analyses of compounds **14** and **21**.

Supporting information for this article is available on the WWW under http://www.angewandte.org or from the author.

 © 2003 Wiley-VCH Verlag GmbH & Co. KGaA, Weinheim 1433-7851/03/4206-0694 $ 20.00+.50/0

piperylene with diazoketone **8** afforded spiro[cyclopropane-1,3′-oxindole] **9** in 71 % yield as an inconsequential mixture of diastereomers.[11] The stage was set for investigation of the critical key step. When a solution of cyclopropane **9** and imine **10**[12] was heated in THF at 75 °C in a sealed tube in the presence of 1.0 equiv of MgI_2, **11** was isolated in combined 68 % yield, as a mixture of diastereomers favoring the desired relative stereochemistry at C3 and C18 found in the natural product in a ratio of 6:1. Deprotection of the secondary amine (cat. $[Pd(PPh_3)_4]$ and 1,3-dimethylbarbituric acid)[13] afforded **12**.[14]

Coupling of amine **13** with *N*-Boc-L-proline chloride[15] proceeded in 90 % yield and allowed the resolution of product **14** into two enantiomers which permitted its stereochemistry to be unambiguously determined by X-ray crystallographic analysis (Scheme 3; Figure 1). Oxidative cleavage of the olefin under standard conditions (see legend to Scheme 3) furnished aldehyde **15** (97 % yield over two steps),[16] which was oxidized to the corresponding acid by using the Lindgren protocol ($NaClO_2$, 2-methyl-2-butene, *t*BuOH, pH 3.6 buffer)[17] and converted to ester **16** (89 % yield over two steps).[18] Subsequent cleavage of the acetylenic C–Si bond was effected in 99 % yield to afford terminal alkyne **17**. The reaction sequence from **14** to **17** could be achieved with no significant decrease in the yield of **17** without purification of any intermediate (80 % overall yield over five steps). Semihydrogenation of alkyne **17** proceeded smoothly ($Pd/BaSO_4$, quinoline; 90 % yield)[19] to afford **18,** which in turn was oxidized to the corresponding aldehyde **19** in 77 % yield.

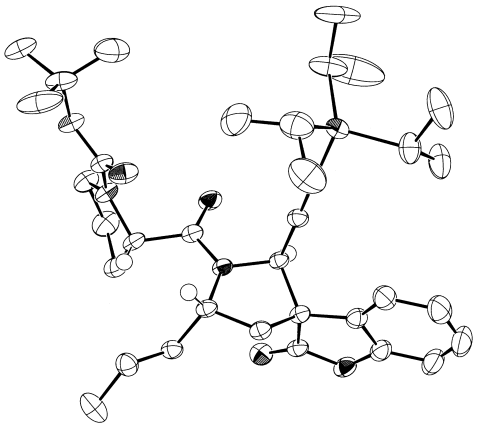
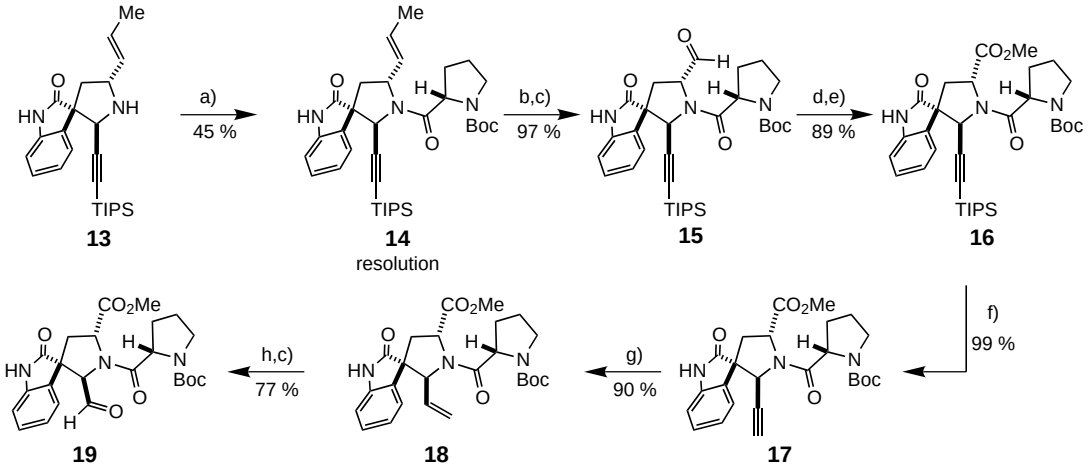


Figure 1. ORTEP drawing of **14**.[23]

In pioneering studies, Danishefsky et al. had noted the importance of intermediates bearing an aldehyde functionality at C18, as these would allow facile preparation of side chain analogues at a late stage in the synthesis of the spirotryprostatins. However, in an elegant study en route to spirotryprostatin A, a compound closely related to **19** was recalcitrant to a variety of olefination procedures.[20]

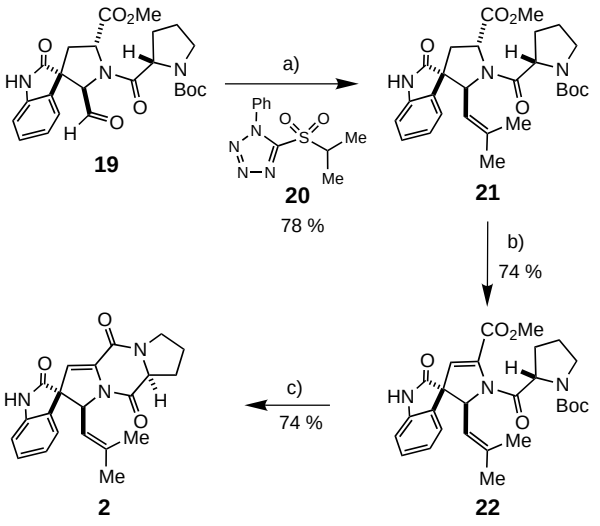
In a similar manner, severe difficulties were also encountered upon attempted olefination of **19**. However, a lead result was realized through the application of the Julia–Lythgoe olefination,[21] in which the desired trisubstituted olefin could be obtained, albeit in poor yield (11 % over three steps) and with extensive epimerization at C18. Further investigation revealed that the use of the Kociensky modification afforded the desired product **21** without scrambling at C18 in 78 % yield (Scheme 4).[22] The structure of compound **21** was confirmed by X-ray crystallographic analysis (Figure 2). From **21**, the synthesis of spirotryprostatin B was completed in four steps following the Danishefsky route. Thus, selenylation of **21** followed by elimination with DMDO afforded **22** (74 %) with introduction of the C8–C9 olefin. Deprotection of the proline and subsequent closure of the diketopiperazine ring led to spirotryprostatin B (**2**) in 74 % yield with analytical characteristics (^1H and ^{13}C NMR spectra, MS, IR, optical rotation) identical to those reported in the literature.[3]

In summary, we have described the total synthesis of spirotryprostatin B (16 steps from **8**). Our approach is highlighted by the rapid assembly of the spirotryprostatin core by employing the MgI_2-catalyzed ring-expansion reaction of



Scheme 3. a) NEt_3, Boc-L-ProCl, CH_2Cl_2, RT; b) $NMO{\cdot}H_2O$, OsO_4 (4 mol %), THF/*t*BuOH/H_2O 4:4:1, RT; c) $Pb(OAc)_4$, EtOAc, RT; d) $NaClO_2$, 2-methyl-2-butene, *t*BuOH, pH 3.6 buffer, RT; e) CH_2N_2, Et_2O, RT; f) TBAF, THF, RT; g) H_2, $Pd/BaSO_4$ (33 wt %), quinoline, EtOH, RT; h) $NMO{\cdot}H_2O$, OsO_4 (1 equiv), THF/*t*BuOH/H_2O 4:4:1, RT. Boc = *tert*-butoxycarbonyl, NMO = *N*-methylmorpholine-*N*-oxide, TBAF = tetrabutylammonium fluoride.

 © 2003 Wiley-VCH Verlag GmbH & Co. KGaA, Weinheim 1433-7851/03/4206-0695 $ 20.00+.50/0



Scheme 4. a) **20**, LHMDS, THF, −78 °C; b) 1. PhSeCl, LHMDS, THF, 0 °C; 2. DMDO, THF, 0 °C; c) 1. TFA, CH_2Cl_2, RT; 2. NEt_3, CH_2Cl_2, RT. LHMDS = lithium hexamethyldisilazide, DMDO = dimethyl dioxirane, TFA = trifluoroacetic acid.

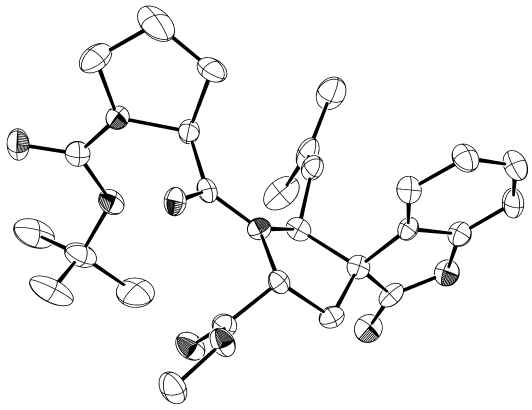


Figure 2. ORTEP drawing of **21**.[23]

spiro[oxindole-3,1′-vinylcyclopropane] **9** and an alkynyl imine **10** for the synthesis of substituted spiro[oxindole-3,3′- pyrrolidine] alkaloids. The study documents for the first time the use of substituted spiro[cyclopropane-1,3′-oxindoles] in the annulation reaction and thus considerably expands the scope of the method and its potential for additional applications in complex molecule synthesis. A key difficulty with the olefination of aldehyde **19** was overcome by using the Kociensky–Julia reaction. In principle, it is now possible to generate the related C18 aldehyde from the natural product which provides a handle for olefination. This opens up new avenues for the facile synthesis of analogues that should enable the elucidation of structure–activity relationships of this important class of natural products.

Received: November 11, 2002 [Z50515]

[1] a) C.-B. Cui, H. Kakeya, H. Osada, *J. Antibiot.* **1996**, *49*, 832–835; b) C.-B. Cui, H. Kakeya, H. Osada, *Tetrahedron* **1996**, *52*, 12651–12666.

[2] a) P. R. Shebahar, R. M. Williams, *J. Am. Chem. Soc.* **2000**, *122*, 5666–5667; b) P. R. Shebahar, H. Osada, T. Usui, R. M. Williams, *Tetrahedron* **2002**, *58*, 6311–6322.

[3] F. von Nussbaum, S. J. Danishefsky, *Angew. Chem.* **2000**, *112*, 2259–2262; *Angew. Chem. Int. Ed.* **2000**, *39*, 2175–2178.

[4] H. Wang, A. Ganesan, *J. Org. Chem.* **2000**, *65*, 4685–4693.

[5] L. E. Overman, M. D. Rosen, *Angew. Chem.* **2000**, *112*, 4768–4771; *Angew. Chem. Int. Ed.* **2000**, *39*, 4596–4599.

[6] T. D. Bagul, G. Lakshmaiah, T. Kawabata, K. Fuji, *Org. Lett.* **2002**, *4*, 249–251.

[7] a) P. B. Alper, C. Meyers, A. Lerchner, D. R. Siegel, E. M. Carreira, *Angew. Chem.* **1999**, *111*, 3379–3381; *Angew. Chem. Int. Ed.* **1999**, *38*, 3186–3189; for an application of this methodology, see: b) C. Fischer, C. Meyers, E. M. Carreira, *Helv. Chim. Acta* **2000**, *83*, 1175–1181; c) A. Lerchner, E. M. Carreira, *J. Am. Chem. Soc.* **2002**, *124*, 14826–14827.

[8] Several groups have employed this method to generate libraries of five- and six-membered heterocycles and substituted pyrrolidines from cyclopropyl ketones: a) M. Lautens, W. Han, *J. Am. Chem. Soc.* **2002**, *124*, 6312–6316; b) F. Bertozzi, M. Gustafsson, R. Olsson, *Org. Lett.* **2002**, *4*, 3147–3150.

[9] For a discussion of the mechanism of the MgI_2-catalyzed ring-expansion reaction, see ref. [7a].

[10] M. P. Cava, R. L. Litle, D. R. Napier, *J. Am. Chem. Soc.* **1958**, *80*, 2257–2263.

[11] T. Ye, M. A. McKervey, *Chem. Rev.* **1994**, *94*, 1091–1160, and references therein.

[12] Imine **10** was prepared from known triisopropylsilanyl propynal and allylamine. a) B. Alcaide, I. M. Rodríguez-Campos, J. Rodríguez-López, A. Rodríguez-Vicente, *J. Org. Chem.* **1999**, *64*, 5377–5387; b) M. Journet, D. Cai, L. M. DiMichele, R. D. Larsen, *Tetrahedron Lett.* **1998**, *39*, 6427–6428.

[13] F. Garro-Helion, A. Merzouk, F. Guibé, *J. Org. Chem.* **1993**, *58*, 6109–6113.

[14] At this stage, the various isomers of **12** can be separated by chromatography on silica gel. In parallel studies, we have converted the stereoisomers epimeric at C9 (*cis*/*trans* olefins) to spirotryprostatin B. For the purpose of clarity, in this communication we describe the synthesis from **13**.

[15] H. Buschmann, H.-D. Scharf, *Synthesis* **1988**, 827–830.

[16] a) V. VanRheenen, R. C. Kelly, D. Y. Cha, *Tetrahedron Lett.* **1976**, *17*, 1973–1976.

[17] B. O. Lindgren, T. Nilsson, *Acta Chem. Scand.* **1973**, *27*, 888–890.

[18] CH_2N_2 was prepared from *N*-methyl-*N*′-nitro-*N*-nitrosoguanidine as a Et_2O solution. H. M. Fales, T. M. Jaouni, J. F. Babashak, *Anal. Chem.* **1973**, *45*, 2302–2303.

[19] J. D. White, G. L. Bolton, A. P. Dantanarayana, C. M. J. Fox, R. N. Hiner, R. W. Jackson, K. Sakuma, U. S. Warrier, *J. Am. Chem. Soc.* **1995**, *117*, 1908–1939.

[20] S. Edmondson, S. J. Danishefsky, L. Sepp-Lorenzino, N. Rosen, *J. Am. Chem. Soc.* **1999**, *121*, 2147–2155.

[21] M. Julia, J.-M. Paris, *Tetrahedron Lett.* **1973**, *14*, 4833–4836.

[22] P. J. Kociensky, A. Bell, P. R. Blakemore, *Synlett* **2000**, 365–366.

[23] CCDC 196803 (**14**) and CCDC 196804 (**21**) contain the supplementary crystallographic data for this paper. These data can be obtained free of charge via www.ccdc.cam.ac.uk/conts/retrieving.html (or from the Cambridge Crystallographic Data Centre, 12, Union Road, Cambridge CB2 1EZ, UK; fax: (+44) 1223-336-033; or deposit@ccdc.cam.ac.uk).

 © 2003 Wiley-VCH Verlag GmbH & Co. KGaA, Weinheim 1433-7851/03/4206-0696 $ 20.00+.50/0